VOLUME 2: EXTENDED ABSTRACTS

12TH International Conference on Permafrost

PROCEEDINGS

EDITED BY RYLEY BEDDOE AND KUMARI KARUNARATNE

WHITEHORSE · YUKON · CANADA

16-20 June 2024

INTEGRATING PERSPECTIVES OF PERMAFROST THAW, CHANGE, AND ADAPTATION

Proceedings of the 12th International Conference on Permafrost
Whitehorse, Canada
16-20 June 2024

12th International Conference on Permafrost

Volume 2: Extended Abstracts

Edited by Ryley Beddoe and Kumari Karunaratne

Co-editors:

Karen MacFarlane, Sarah Gervais, Derek Cronmiller, Élise Devoie, Simon Dumais & Earl de Guzman

Recommended citation

Beddoe, R.A. and Karunaratne, K.C. (Eds.). 2024. 12th International Conference on Permafrost. 16-20 June 2024, Whitehorse, Canada: International Permafrost Association.

Cover Photo: Lake in ice-rich terrain in tundra uplands northwest of Inuvik, Northwest Territories. Ice wedge polygons are visible adjacent to the lake (Photo: Rachelle Landriau).

Cover Design: Inkit Communications Ltd.

12TH INTERNATIONAL CONFERENCE ON PERMAFROST
2024
XII
WHITEHORSE YUKON

INTEGRATING PERSPECTIVES OF PERMAFROST THAW, CHANGE, AND ADAPTATION

Preface

We are thrilled to share the contributions submitted for the 12th International Conference on Permafrost (ICOP2024) held 16-20 June 2024 in Whitehorse, Yukon, Canada. ICOP2024 is hosted by the Canadian Permafrost Association and is the first hybrid conference for the International Permafrost Association with live-streaming of oral presentations, a virtual poster hall, and facilitated online discussions. This innovative approach allows us to connect with participants from around the world, both in person and virtually, broadening the reach and impact of our collective knowledge.

The journey to ICOP2024 began with a call for solicited sessions 18 months before the conference. Session proposals required that the Session Chairs were from different countries and include an early career member. This community-driven approach encouraged international collaboration, mentoring, and the inclusion of both the classic permafrost topics as well as emerging issues in adjacent disciplines that are crucial to advancing permafrost science and engineering. We received a total of 50 session proposals. These submissions were evaluated by the International Scientific Committee and the Technical Program Committee and were organized into 13 distinct focus areas, which beautifully captured the ICOP2024 theme "Integrating Perspective of Permafrost Thaw, Change, and Adaptation".

We offered two conference submission options for ICOP2024: Full Papers (6-8 pages) and Extended Abstracts (2 pages). The response was impressive, receiving 72 Full Papers and over 450 Extended Abstracts. The session chairs were essential to the program development as they assigned two external reviewers to each paper, reviewed the extended abstracts, and made recommendations for presentation type. Following review of the submissions and confirmation of author registration, the ICOP2024 Conference Proceedings were compiled with Volume 1 comprising 64 Full Papers, and Volume 2 comprising 429 Extended Abstracts, organized according to the respective sessions. The ICOP2024 program included 227 oral presentations, 199 in-person posters, and 67 virtual posters. The keynote presentations and five concurrent sessions were live-streamed for virtual participants and recorded, allowing information to be shared for years to come.

We extend our heartfelt gratitude to everyone who contributed to the success of ICOP2024 program. Special thanks to Karen MacFarlane and Sarah Gervais, for their exceptional efforts in copyediting and formatting the proceedings, and the Technical Program Committee (Élise Devois, Derek Cronmiller, Simon Dumais, and EARL de Guzeman), whom we relied on to screen all submissions, complete reviews, draft instructions for authors and presenters, and advise on challenging decisions. And last, but not least, Lukas Arenson, our ICOP2024 Conference Chair. Lukas did a remarkable job convening an oversubscribed event in a small Northern city and we are extremely grateful for all his guidance, support, and camaraderie throughout this adventure.

Ryley Beddoe and Kumari Karunaratne

ICOP 2024 Organizing Committees

National Organizing Committee

Lukas Arenson, Chair, BGC Engineering

Ryley Beddoe, Technical Program Committee Chair, Royal Military College

Barb Fortin, Treasurer, Tetra Tech Canada Inc.,

Brian Horton, Local Organizing Committee Chair, Yukon University

Fabrice Calmels, Field Trips Committee Chair, Yukon University

Peter Morse, Secretary, Geological Survey of Canada

Nick Brown, Communications Committee Chair, Carleton University

Joseph Young, Early Career Representative, University of Alberta

Kumari Karunaratne, Publications Committee Chair, Northwest Territories Geological Survey

Technical Program Committee

Ryley Beddoe (Chair), Royal Military College
Élise Devoie, Queens University
Simon Dumais, Université Laval
Derek Cronmiller, Yukon Geological Survey
Earl de Guzman, Tetra Tech Canada Inc.
Kumari Karunaratne, NWT Geological Survey

Publication Committee

Kumari Karunaratne (Chair), NWT Geological Survey
Sarah Gervais, NWT Geological Survey
Karen MacFarlane, Yukon Geological Survey (retired)
Ryley Beddoe, Royal Military College

Local Organizing Committee

Brian Horton (Chair), Yukon University
Moya Painter, Yukon Geological Survey
Aaron Weber, BGC Engineering
Jay Dobson, Yukon University
Panya Lipovsky, Yukon Geological Survey
Muhammad Idrees, Yukon Government

Fieldtrip Committee

Fabrice Calmels (Chair), Yukon University
Louis-Philippe Roy, Yukon University
Duane Froese, University of Alberta
Steve Kokelj, NWT Geological Survey
Alice Wilson NWT Geological Survey
Jennifer Humphries, Aurora Research Institute

Communications Committee

Nick Brown (Chair), Carleton University
Astrid Schetselaar, Yukon Government

Sponsorship Committee

Robin McKillop, Palmer (SLR)
Emmanuel Herault, Université Laval
Lukas Arenson, BGC Engineering

International Advisory Committee

Antoni Lewkowicz (Chair), Canada
Anne Morgenstern, Germany
Karina Schollaen, Germany

ICOP 2024 Session Chairs

Lukas Arenson
Natalie Arpin
Michel Baraer
Prashant Baral
Helena Bergstedt
Frédéric Bouchard
Vincent Boulanger-Martel
Francesco Brardinoni
Sam Bratsman
Heather Brooks
Nick Brown
Fabrice Calmels
Bastien Charonnat
Lin Chen
Alexandre Chiasson
Derek Cronmiller
Julian Dann
Margaret Darrow
Earl de Guzman
Élise Devoie
Geoff Eichhorn
Saskia Eppinger
Jessica Ernakovich
Louise Farquharson
Daniel Fortier
Samuel Gagnon
Isabelle Gärtner-Roer
Sarah Gauthier
Raquel Granados Aguilar
Ed Grozic
Christopher Gruben
Stephan Gruber
Mauro Guglielmin
Charlotte Haugk
Liam Heffernan
Teddi Herring
Jennifer Humphries
Cornelia Inauen
Thomas Ingeman-Nielsen
Elchin Jafarov
Benjamin M. Jones
Andreas Kääb
Brandon Karchewski
Kaytan Kelkar
Anna Klene
Charles Klengenberg
Steve Kokelj
Michael Krautblatter
Julius Kunz
Emmanuel L'Hérault
Yuanming Lai
Mark Lara
Emma Lathrop
Mary-Cathrine Leewis
Susanne Liebner
Zhanju Lin
Rachel Mackelprang
Mahsa Malmir
Shawn Marshall
Jeffrey McKenzie
Robin McKillop
Burke Minsley
Lexi Mollica
Peter Morse
Marc Oliva
Laurent Orgogozo
Santosh Panda
Silvio Pastore
Anna Pekinasova
Cécile Pellet
Louis-Philippe Roy
Regina Plasken
Stefano Ponti
Youhua Ran
Mahya Roustaei
Line Rouyet
Pascale Roy-Léveillée
Wolfram Rühaak
Remya S.N.
Lutz Schirrmeister
Fabian Seemann
Antoine Séjourné
Ted Shuur
Ylva Sjöberg
Elliott Skierszkan
Sharon L. Smith
Andrea Soellinger
Emma Street
Tazio Strozzi
Matt C. Strzelecki
Dmitry A. Streletskiy
Zuzanna Swirad
Andy Take
Jing Tao
Carla Tapia Baldis
John Thornley
Claire Treat
Dario Trombotto Liaudat
Eole Valence
Aleksandra Veremeeva
Marja Vuorio
Anna Wagner
Ziyi Wang
Melissa Ward Jones
Niels Weiss
Juliane Wolter
Stephanie Wright
Mousong Wu
Ming Xiao
Brett Young
Joseph Young
Wenxin Zhang
Simon Zwieback

ICOP 2024 Sponsors, Partners, and Supporters

Arctic Foundations of Canada
Canadian National Committee for the IPA
NSERC PermafostNet
WSP
BGC Engineering Inc.
KGS Group
LogR Systems Inc.
Tetra Tech Inc.
TREK Geotechnical Inc.
Adaptive Baseline Geotechnical Ltd.
Arctic Gateway Group LP
Chance Oil and Gas Ltd.
Klondike Placer Miners' Association
Palmer Environmental Consulting Group
Permafrost Pathways
Hatch Ltd.
beadedstream Inc.
Center for Northern Studies
Mobile Augers and Research Ltd.
Quantum Machine Works Ltd.
Air North, Yukon's Airline
AM2 Geotechnical Inc.
Casino Mining Corporation
Core Geoscience Services Inc.
Winterlong Brewing Co.
Yukon Brewing
Yukon Government
Government of Northwest Territories
Transport Canada
Environment and Climate Change Canada
Natural Resources Canada
Canadian Geotechnical Society
Canadian Permafrost Association

International Scientific Committee

Andreas Kääb, Denmark
Andreas Kellerer-Pirklbauer, Austria
Anna Liljedahl, USA
Annett Bartsch, Germany
Antoine Sejourne, France
Arne Instanes, Norway
Britta Sannel, Sweden
Christian Hauck, Switzerland
Dario Trombotto Liaudat, Argentina
Ed Yarmak, USA
Francesca Casini, Italy
Frederick Nelson, USA
Gonçalo Vieira, Portugal
Guido Grosse, Germany
Hanne Christiansen, Norway
Hugues Lantuit, Germany
Isabelle Gärtner-Roer, Switzerland
Jambaljav Yamkhin, Mongolia
Jeanette Noetzli, Switzerland
John Zarling, USA
Lothar Schrott, Germany
Margaret Darrow, USA
Mauro Guglielmin, Italy
Megan Balks, New Zealand
Michael Krautblatter, Germany
Norikazu Matsuoka, Japan
Paul Overduin, Germany
Pavel Talalay, China
Phlippe Schöneich, France
Regula Frauenfelder, Norway
Thomas Douglas, USA
Thomas Ingeman-Nielsen, Denmark
Vladimir Romanovsky, USA
Ylva Sjöberg, Denmark

Summary of Contents

12TH INTERNATIONAL CONFERENCE ON PERMAFROST 2024 XII WHITEHORSE YUKON

INTEGRATING PERSPECTIVES OF PERMAFROST THAW, CHANGE, AND ADAPTATION

Table of Contents

1B — Permafrost Data Management and Climate Services

3: Permafrost Environments

3A — Extreme and Unique Environments: Antarctic and Beyond

3B — Characteristics of Permafrost in the Andes

3D — Joint session on Yedoma and Paleo Permafrost Records of Environmental Change

3F — Polar Coastlines in Transition: Arctic, Antarctic, Offshore and Shelf Perspectives

4B — Periglacial Geomorphology & Hazards

4E — Permafrost Mass-Wasting Processes and Slope Hazards

5: Permafrost Carbon Feedback

5A — Carbon Cycles in Cold Regions: Modelling and Observations

5B — Monitoring, Modelling, and Remote Sensing of the Permafrost Carbon Feedback

5C — Reducing Uncertainties for Permafrost Carbon Feedbacks

6: Permafrost Hydrology & Wetland Dynamics

6A — Implications of Thawing Permafrost on Water Resources in Cold Regions

6B — Drained Lake Basins in Lowland Permafrost Regions

6C — Arctic Wetlands in a Changing Climate

6D — The Hydrology of Mountain Permafrost

7: Permafrost Infrastructure

7A — Permafrost Railways

7B — Foundations and Infrastructure on Permafrost: Case Studies and Innovations

7C — Permafrost and Infrastructure Dynamics Along the Inuvik–Tuktoyaktuk Highway, NT

7D — Permafrost Engineering, Geomorphology, Hydrology for Northern Linear Infrastructure Resilience and Safety

8: Cold Region Engineering Modelling, Characterization, Observations & Testing

8A — Vulnerability of Cold-Region Infrastructure to Permafrost Degradation in a Changing Climate

8B — Advances in Numerical Modelling of Permafrost

8C — Geomechanics and Engineering Geophysics for Permafrost Characterization

8D — Investigating Permafrost Using Geophysical Techniques

8F — Laboratory Modelling and Testing of Permafrost Soils

9: Microbial Ecology in Permafrost

9A — Permafrost Microbiology: Combining -omics with Ecological Theory

9B — Microbial Pattern and Process in Permafrost Affected Ecosystems

10: Remote Sensing of Permafrost

10A — Remote Sensing of Permafrost Processes and Impacts on the Environment

10B — High Resolution Remote Sensing Applications in Permafrost Studies

11: Waste Containment in Permafrost

11A — Mining Geotechnics, Reclamation, Contaminant Behaviour and Nuclear Waste Safety in a Changing Climate

12: Monitoring Permafrost Conditions & Processes

12A — Monitoring Techniques and Feedback of Snow, Vegetation, and Permafrost

12B — Exploring the Roles of Ground Ice on Permafrost Dynamics

12D — Multiscale Observations of Permafrost Landscape Dynamics

13: Thaw, Change & Adaptation

13A — Permafrost Thaw, Change and Adaptation

1 Community

INTEGRATING PERSPECTIVES OF PERMAFROST THAW, CHANGE, AND ADAPTATION

1A — Communities, People, and Permafrost

Session Chairs: Alexandre Chiasson[1], Emma Street[2], Louis-Philippe Roy[3], Sarah Gauthier[4], Robin McKillop[5], Pascale Roy-Léveillée[4], Melissa Ward Jones[6] & Helena Bergstedt[7]

[1]*Department of Earth and Atmospheric Sciences, University of Alberta, Edmonton, Canada*
[2]*University of Victoria, Victoria, British Columbia, Canada*
[3]*Yukon University, Whitehorse, Yukon, Canada*
[4]*Université Laval, Québec City, Québec, Canada*
[5]*Palmer, Toronto, Ontario, Canada*
[6]*University of Alaska, Fairbanks, Alaska, United States*
[7]*b.geos, Vienna, Austria*

As climate change warms the Arctic four times faster than the rest of the planet, permafrost and the northern communities that rely upon it are facing times of immense transition. Permafrost thaw is rapidly changing landscape morphology, hydrological and biogeochemical regimes, and ecosystem services. These changes place existing infrastructure, including transportation and energy networks, at risk and threaten sociocultural well-being in northern communities. Understanding the complex nature of permafrost thaw and its consequences presents a major challenge requiring knowledge from multiple disciplines, sources, and traditions.

This session aims to address this collaboration by highlighting the importance of Indigenous community engagement in permafrost mapping, geohazard characterization, and land-use planning. We welcome contributions on community-based participatory methods, including participatory photography, ethnographic mapping, and interviews, and direct participation in research programs that provide opportunities for community members to share their perspectives and knowledge about their environment alongside Western scientific investigations.

Examples of collaborations include: the use of permafrost geomorphology for the identification, characterization, and communication of potential or ongoing permafrost-related threats to the safety and sustainability of northern communities, including their property, infrastructure, industries, traditional activities, and cultures; how changing permafrost conditions affect socioecological systems, communities, cultural practices, livelihoods, built environments and economic systems—including agriculture, and extractive industries. Interdisciplinary perspectives and research are needed to adequately study how human activities and built systems are impacted by changing permafrost conditions.

This session seeks to develop a comprehensive and nuanced understanding of the current state of permafrost at the community level. Community members, polar organizations, researchers, governments, and industry professionals are invited to share their experiences of permafrost change, and speak to knowledge sharing in permafrost research, community engagement, and permafrost and geohazard characterization in northern communities.

Modeled impacts of permafrost thaw and glacier melt on energy availability for fluvial fish across Alaska

Megan I. Behnke[1], J. Ryan Bellmore[2], Ryan Toohey[3], Jonathan O'Donnell[4], Joshua Koch[5], Michael Carey[5] & Jason B. Fellman[1]

[1]*Alaska Coastal Rainforest Center & Department of Natural Sciences, University of Alaska Southeast, Juneau, Alaska, United States*

[2]*Pacific Northwest Research Station, United States Forest Service, Juneau, Alaska, United States*

[3]*Alaska Climate Adaptation Science Center, United States Geological Survey, Anchorage, Alaska, United States*

[4]*Arctic Inventory and Monitoring Network, National Park Service, Anchorage, Alaska, United States*

[5]*Alaska Science Center, United States Geological Survey, Anchorage, Alaska, United States*

The Arctic is warming four times faster than the global average, transforming northern high-latitude ecosystems in unprecedented ways (Rantanen et al. 2022). Dramatic cryosphere changes like permafrost thaw and glacier melt are impacting ecological and human systems. One way that cryospheric change is manifesting in both systems is the myriad shifts in hydrology, chemistry, and ecosystem productivity that have the potential to modify energy flows to fluvial fish species of importance for human communities (e.g., Leppi et al. 2023).

The goal of this work is to use a food web model to explore how cryospheric change might alter the capacity of Alaska rivers to support fish. The model uses datasets of environmental parameters such as stream discharge, temperature, and nutrient regimes to explore drivers of periphyton, detritus, aquatic invertebrate, and fish growth, and how these patterns of productivity may change as the cryosphere thaws and environmental regimes shift.

To inform the modeling, we solicited input from local and regional experts, including river managers and researchers from tribal, state, and federal agencies that work in permafrost and glaciated ecosystems around Alaska. We sent out an open-ended questionnaire that gathered information on parameters they collected, use of parameters for management decisions or research applications, specific rivers of interest with their expected future drivers and changes, and expected use of modeling results. Participants identified the hydrologic, biological, chemical, and physical variables that are likely primary drivers of future capacity of riverine food webs to support fishes. After analyzing the responses, we held a virtual workshop with survey participants to further discuss the results within a group setting, to refine river selection and "future change" scenarios, and to identify additional data sets that could be used in model simulations. Several guiding ideas emerged involving which rivers were of greatest interest: 1) watersheds poised to transition between regimes (e.g., continuous to discontinuous permafrost, glacier to no glacier, etc.); 2) rivers with Chinook salmon (Oncorhynchus tshawytscha) runs which are experiencing temperature increases; and 3) rivers that would allow exploration of multiple possible future trajectories (e.g. catastrophic thaw slump v. gradual active layer deepening, wildfire). Further, hydrology and temperature were identified as the most studied variables that may control future shifts in energy flow and thus this study could add value by exploring the role of less frequently characterized parameters like nutrients, sediments, and riparian vegetation to food web capacity.

Based on participant input and dataset availability, we built models reflecting the current conditions of three watersheds from three cryospheric regimes experiencing great change: 1) a glacierized watershed (using data from 49% glacierized Herbert River in Southeast Alaska); 2) a watershed underlain by ice-rich discontinuous permafrost (using data from the C3 catchment in Caribou Poker Creek Watershed in interior Alaska); and 3) a watershed underlain by ice-poor continuous permafrost (using data from several small rivers within and surrounding the Noatak basin in Northwest Alaska). The following parameters were used to create our watershed models: discharge, water temperature, dissolved organic carbon (DOC) concentration, DOC percent bioavailability, total dissolved nitrogen (TDN), total dissolved phosphorus (TDP), turbidity, riparian vegetation cover and composition (i.e., deciduous versus coniferous), and stream shading. Where available, year-round datasets were used, while elsewhere, parameters were extrapolated based on existing data and expert knowledge of the watersheds. Data was sourced from published literature and data portals along with watershed observations and expert estimates.

We adapted the Aquatic Trophic Productivity (ATP) model to represent the physical and chemical characteristics of each river. The ATP model is a dynamic food web simulation model which explicitly links the bottom-up transfer of energy and nutrients

through a simplified river food web to the ability of the riverine ecosystem to support fish growth (Bellmore et al. 2017; Whitney et al. 2019). The model connects each food web attribute to the physical and hydraulic stream conditions and the vegetation structure and composition of the stream's riparian zone. The ATP model operates on the assumption that the general dynamics of a food web can be predicted if the environmental factors influencing that food web are understood (Bellmore et al. 2017). Thus, simulations can be used to explore how environmental changes due to climate change and cryospheric melt/thaw could impact food web dynamics and the energy available for fish growth.

Once we completed the present-day models representing current conditions, we simulated anticipated future scenarios for each river assuming continued warming and cryosphere loss. In the glacier watershed, we used published relationships between percent watershed glacierization and river chemistry to determine future trends in river chemistry with glacier melt (Hood and Berner 2009), and switched the riverine hydrograph from glacier-dominated to snowmelt-dominated. In the permafrost watersheds, the relationship between cryospheric change, hydrology, and chemistry is more complex due to different modes of thaw and subsequent impacts to groundwater flow and terrestrial-aquatic linkages. We use a combination of published data and recommendations from a working group of permafrost experts to envision future riverine scenarios. We convened this group virtually to discuss future trends and annual regimes in both the discontinuous and continuous watersheds and to assist us in parameterizing the future permafrost watershed models.

Each future model simulation begins with the equilibrated initial model and then runs for 100 years while experiencing continuing change in environmental input variables. Here we will assess the sensitivity of model output to each modified variable to better constrain controls on the future watershed trajectory and the capacity of each modeled river segment to support fish growth. For example, in this simulation (Figure 1), future changes to temperature and turbidity drove the greatest percent increase in fish biomass, while the largest percent decrease in fish biomass was attributed to declining phosphorus concentrations. We will present differences in how food webs respond to future changes in each cryospheric regime. We will also elucidate the variables predicted to be the most important to controlling future fish populations. By identifying important parameters and time scales of expected changes, these model findings can be used to develop monitoring recommendations for cryospheric rivers that support important fish species. Through our research, we will share with river managers and researchers which parameters may be most useful for monitoring and adapting to these changing conditions.

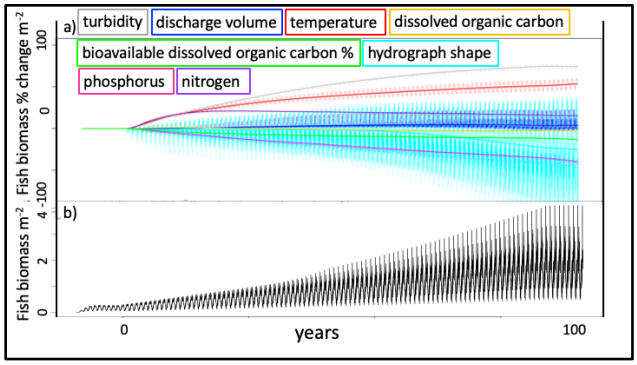

Figure 1. a) Initial results of the future glaciated model run demonstrating how the future changes in each specified variable influences the percent change in fish biomass per meter squared during the next 100 years. b) modeled fish biomass per meter squared during the next 100 years.

REFERENCES

Bellmore, J.R., Benjamin, J.R., Newsom, M., Bountry, J.A., and Dombroski, D. 2017. Incorporating food web dynamics into ecological restoration: a modeling approach for river ecosystems. Ecological Applications, 27(3), pp.814–832. https://doi.org/10.1002/eap.1486

Hood, E., and Berner, L. 2009. Effects of changing glacial coverage on the physical and biogeochemical properties of coastal streams in southeastern Alaska. Journal of Geophysical Research: Biogeosciences, 114(G3). https://doi.org/10.1029/2009JG000971

Leppi, J.C., Rinella, D.J., Wipfli, M.S., Liljedahl, A.K., Seitz, A.C., and Falke, J.A. 2023. Climate Change Risks to Freshwater Subsistence Fisheries in Arctic Alaska: Insights and Uncertainty from Broad Whitefish Coregonus nasus. Fisheries. https://doi.org/10.1002/fsh.10918

O'Donnell, J.A., Carey, M.P., Koch, J.C., Xu, X., Poulin, B.A., Walker, J., and Zimmerman, C.E. 2020. Permafrost hydrology drives the assimilation of old carbon by stream food webs in the Arctic. Ecosystems, 23, pp.435–453. https://doi.org/10.1007/s10021-019-00413-6

Rantanen, M., Karpechko, A.Y., Lipponen, A., Nordling, K., Hyvärinen, O., Ruosteenoja, K., Vihma, T., and Laaksonen, A. 2022. The Arctic has warmed nearly four times faster than the globe since 1979. Communications Earth & Environment, 3(1), p.168. https://doi.org/10.1038/s43247-022-00498-3

Whitney, E.J., Bellmore, J.R., and Benjamin, J.R. 2019. User manual for the aquatic trophic productivity model: a river food web simulation model for management and research. US Department of Agriculture, Pacific Northwest Research Station.

Slope stability monitoring in discontinuous permafrost

Blake Brodland[1] & A. James Morgan[2]
[1]*WSP Canada Inc., Calgary, Alberta, Canada*
[2]*WSP Canada Inc., Edmonton, Alberta, Canada*

The slopes above the Slave River, NT have a long history of instability posing a threat to some of the infrastructure in the Town of Fort Smith including the water intake pipeline, roads, walking trails, sewage lagoon and developed residential properties along the crest of the Slave River valley slope. The deadly landslide of 1968 spurred numerous geotechnical and geohazard studies. Previous geotechnical studies have identified possible causes of the previous slope instability as including the presence of weak clayey material at depth, shallow and deep aquifers, thawing icy permafrost, steep slope angles, and natural river erosion processes.

Recently, through Federal Government Grants, monitoring of this landslide complex has been brought closer to geotechnical standards using InSAR data, LiDAR data, RTK survey data, orthophotos, and visual slope inspections. Recent work has identified critical infrastructure and priority areas (e.g., culturally significant) to the Town of Fort Smith. The work has also focused on mapping areas that are actively moving and attempting to quantify slope movement. Future work proposes to add thermistors, piezometers and SAAs to provide near-real-time monitoring in key areas of the slope and to gain insight into how permafrost has degraded since the last borehole program on this slope in the 1980s.

The study site is located in the Town of Fort Smith (the Town), within the Northwest Territories, Canada. The Town is just across the northeast corner of the Alberta border. The Slave River flows northward on the limits of the Town of Fort Smith on the east and north.

The is a history of slope instability along the banks of the Slave River, documented as far back as 1937. In 1968, a significant movement of the slope took place which has been associated an earthquake. Several homes were destroyed as they moved down the slope and one person was died. A monument was erected near the slope to commemorate the damage to the Town and loss of life.

A number of studies have been undertaken by others between 1968 and 2012, some of which endeavoured to determine the driving factors leading to the ongoing slope instability. Some of the studies included the installation of instrumentation. Previous geotechnical studies have identified possible causes of the previous slope instability as including the presence of weak clayey material at depth, shallow and deep aquifers, thawing icy permafrost, steep slope angles, and natural river erosion processes.

Today the crest of the landslide complex impacting the Town is approximately 4.5 km long, with a crest to toe length ranging from 110 to 220 m. The overall landslide complex slope is approximately 40 to 50 m high and ranges from 8 to 18 degrees from horizontal. The slope instability continues to threaten the Town and its infrastructure including the water intake pipeline, roads, walking trails, sewage lagoon and developed residential properties along the crest of the Slave River valley slope.

PROPOSED REMEDIATION WORK AND INVESTIGATIONS BY OTHERS

Work by others between 1968 and 2012 has included drilling boreholes to determine stratigraphy, groundwater levels, presence of permafrost, installation of instrumentation, and site inspections. Some of the conceptual remediations previously proposed for this project include the following:

- Intercept water upland
- Intercept water on slope
- Riverbank erosion protection
- Safe Set back
- Pipe specific solutions
- Localized regrading
- Contingency planning

Approximately half of these proposed remediations that have been implemented to varied success. Difficulties impacting successful remediation of the site include a significant site area, challenging soil conditions, large length, tall slope, active erosion at the toe of the slope from the Slave River, environmental considerations, sporadic and melting permafrost, high ground water table, and existing infrastructure placements.

ONGOING WORK

Since the first studies of this site in 1968 the state of the art for permafrost and slope stability monitoring has improved, complemented by significant additions in available technology.

The work since 2019 has aimed to identify the most active areas of the landslide complex, to quantify moments, to identify key infrastructure in close proximity to the slope, and ultimately to focus monitoring on key areas to better understand the seasonality, triggers, rates and present ground conditions in these key areas.

Some of the technologies which have been commissioned for this site include InSAR, LiDAR, LiDAR change detection, orthophotos, RTK survey of installed pins, site walkthroughs with geolocated tracks/ photos/ observations.

For this site, InSAR data from 2017 through 2020, was provided free of charge from the Government of the Northwest Territories. The datasets included RADARSAT-2 and Sentinel-1 data, which showed limitations in penetrating certain areas of the site where vegetation was thick. On areas of the slope where vegetation had been cleared for existing infrastructure, the average higher movement rates were near 0.2 mm/day in the look direction.

The LiDAR for this site is shown in Figure 1, which provides an overview of the scale, magnitude and pervasiveness of the landslide complex adjacent to the Slave River.

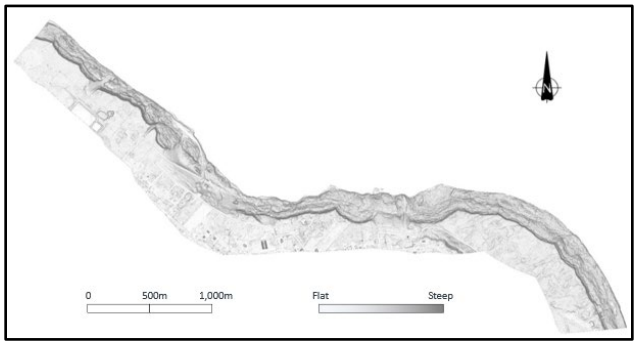

Figure 1. Overview of the Landslide Complex Adjacent to the Town of Fort Smith.

The LiDAR data highlighted the significant headscarp along the crest of the slope and allowed for the full extents of the heavily treed landslide complex to be realized. The LiDAR data also allowed for conceptual visualization of what localized regrading might look like.

Multiple years of LiDAR data have been acquired or commissioned for this landslide complex including 2009, 2021 and 2022. These data sets have been compared using LiDAR change detection and have identified locations of movement, particularly when compared to the oldest data set. These locations, as well as others were visited on the ground to document the conditions from year to year. Included in these areas is the location of the fatal 1968 landslide, which was locally regraded to establish stability and to provide a recreation area.

During one of the site visits previously installed geotechnical instrumentation locations were visited to determine if they were still existing, along with historical locations noted to have seepage.

A total of 37 steel monitoring pins were driven into the slope in three key locations to monitor the landslide complex adjacent to Town identified critical infrastructure. Each pin was approximately 1.5 m long and 127 mm in diameter. The pins were driven into the ground approximately flush to prevent tripping hazards and vandalism.

PATH FORWARD

With possible future influences to the site due to climate change, ongoing river erosion and other factors, this landslide complex remains at high priority for the Town.

The recommended path forward for this site is to continue on a regular basis monitoring through the use of LiDAR, site inspections and RTK survey of the installed pins. In parallel, additional funding is being sought to facilitate the installation of remotely monitored instrumentation in the key areas as identified by the Town. These new instruments, expected to consist of thermistors, piezometers and ShapeArrays will provide additional insight into the subsurface ground conditions, ground movement depths and rates. Of particular interest is how permafrost has changed at this site since the last borehole program in 1987, and the impacts that degrading or degraded permafrost will impact this slope going forward.

ACKNOWLEDGEMENTS

The authors would like to thank the following organizations: Town of Fort Smith, Government of Northwest Territories, and Climate Change Preparedness in the North Program. The authors would like to thank the following persons: Dr. Alexander Tchekhovski, En-Tzu (Peter) Hsieh, Curtis Treen, Ed McRoberts, Jim Hood, Cynthia White, Keith Morrison, Alex James, and Obrian Kydd.

Mapping of permafrost and ground hazards for community planning near Fort Good Hope Northwest Territories

Jeffrey Campbell[1,2], Alexandre Chiasson[1,2], Crystal Huscroft[3] & Duane Froese[1,2]

[1]*Department of Earth and Atmospheric Sciences, University of Alberta, Edmonton, Alberta, Canada*

[2]*Permafrost Archives Science Laboratory, Edmonton, Alberta, Canada*

[3]*Department of Environment, Culture and Society, Thompson Rivers University, Kamloops, British Columbia, Canada*

Permafrost, and associated ground ice distribution and abundance, is strongly dependent on near surface sediments and their properties. In order to understand the potential distribution of thaw sensitive terrain at local to regional scales, surficial geology mapping provides one of the most important tools available. This project focuses on mapping surficial geology, permafrost, and inferred ground ice conditions for the Fort Good Hope area in the Sahtu Region of the Northwest Territories. Initial mapping is at a scale of 1:50,000 and will inform a later, 1:10,000 scale map showing greater detail for the community.

Quaternary history

Understanding local Quaternary history is key to identifying the origin of surficial units as well as interpreting the presence and distribution of ground ice. Fort Good Hope has a complex Quaternary history as it is at the intersection between the two major drainage systems of the northwest edge of the retreating Laurentide Ice Sheet.

It is estimated that the Laurentide Ice Sheet boundary crosscut the map area at ~14 ka (Duk-Rodkin and Lemmen 2000; Stoker et al. 2022). As the ice retreated toward the south and east, glacial Lake Mackenzie, located to the southwest of the map area, began outflow via Dry Falls, in the western portion of the map area, approximately 12 ka (Smith 1992; Duk-Rodkin and Lemmen 2000).

Outflow from glacial Lake McConnell via the Hare Indian Channel, which encompasses the community site and is occupied by the modern day Rabbitskin (Hare Indian) River and Jackfish Creek, lasted from approximately 13 ka to 11.5 ka (Smith 1994). This likely commenced with a large, catastrophic outflow given the presence of boulder fields within the channel further to the east of the map area (Smith 1994).

It was initially unclear which units within the map area may be associated with this outflow until several exposures were found during ground truthing. North of the community, an exposure interpreted as slack water sediments was found against the north edge of the esker complex which runs east of the community. On the other side of the Hare Indian Channel, south of modern-day Jackfish Creek, reversely-graded sediments may reflect flood deposition. Both of these units are substantially higher than current high-water levels for any of the streams which intersect at Fort Good Hope

Surficial geology

A succession of landforms are recognized. Mega-scale glacial lineations, recording fast-flowing ice of the Bear Lake Ice Stream, from the ENE to WSW are present in uplands across the map extent. Proglacial and subglacial fluvial deposits are found largely east of the Mackenzie River, including a prominent esker complex that extends into the community. Significant portions of the glaciofluvial deposits are overlain by an eolian blanket which includes Late Pleistocene dunes, likely barchan forms, recording westerly winds. West of the Mackenzie River, fluvial deposits are present within former river channels incised into bedrock. Varying thicknesses of till and organics make up the remainder of the terrain immediately west of the Mackenzie River.

Interpretation of ground ice

The Fort Good Hope area is located at the southern boundary of the continuous permafrost zone, where significant ground ice is mostly found in organic terrain and glaciolacustrine units. In recent decades, permafrost disturbance in the form of thermokarst depressions suggest that ice-rich permafrost is widespread within the organic terrain that mantles upland till deposits across the region. Organic terrain shows evidence of recent thaw with prominent collapse bog scars and widening of fen channel networks.

Mackay and Mathews (1973) note that in the Fort Good Hope area, downstream of the Ramparts, ice wedges are present under stands of mature spruce but are absent in areas where cover is dominated by willows or other deciduous plants. While no ice wedges were observed during field work within finer grained units, there does appear to be a greater presence of ground ice in spruce dominated areas as opposed to willow, birch or tamarack dominated sites.

Field work also suggests major variation in active layer thickness, from approximately half a meter to several meters. This appears to be related to vegetation

density, plant community type and sediment type. Mature spruce forest sites with lichen dominated undergrowth and fine-grained soils tend to have the shallowest active layers and open, sandy sites show much deeper active layers.

COMMUNITY INVOLVEMENT AND PARTNERSHIPS

This project is conducted in partnership with the community of Fort Good Hope with significant involvement from the K'asho Got'ine Foundation Land Guardians. Our team conducted a permafrost science training course with the Guardians at one of their camps in the Ts'udé Niliné Tuyeta Protected Area. The training provided the guardians with an introduction to installing and maintaining permafrost monitoring infrastructure (ground temperature stations and active layer survey sites), and allowed our team to better understand areas of concern related to permafrost and recent environmental change with community members.

The Land Guardians were invaluable in facilitating outreach to the broader community. The guardians arranged for us to give two presentations to the high school students about permafrost while we were in the community conducting mapping. As well, the Guardians arranged a two-hour radio call in show. The radio show provided a platform to inform the community about our work and receive input from community members about places of interest or concern within the community.

CONTINUING WORK

Continuing work in Fort Good Hope focuses on further investigation of surficial units to confirm the characteristics of these deposits, in addition to continuing to gather input to develop data products that will be of maximum benefit to the community. As well, the work has allowed us to learn from the community as we develop further research questions for the area that will ultimately be transitioned to the Land Guardians monitoring network.

As part of the initial monitoring network, two sets of paired ground temperature stations have been established within Ts'udé Niliné Tuyeta. One set is comparing temperatures between cleared and uncleared ground at a K'asho Got'ine Foundation camp located within the lowland areas of the protected area. The other sites are monitoring ground temperatures between an historic burn and the adjacent unburned peat plateau in the northern reaches of the protected area.

Collectively, these data provide a strong foundation for community planning for Fort Good Hope, as well as for a broader, community-led permafrost monitoring program focused on areas of community concern.

REFERENCES

Duk-Rodkin, A., and Lemmen, D.S. 2000. Glacial history of the Mackenzie region; in The Physical Environment of the Mackenzie Valley, Northwest Territories: a Base Line for the Assessment of Environmental Climate Change. (ed.) L.D. Dyke & G.R. Brooks; Geological Survey of Canada, Bulletin 547, p. 11–20.

Mackay, J.R., and Mathews, W.H. 1973. Geomorphology and Quaternary History of the Mackenzie River Valley near Fort Good Hope, N.W.T., Canada. Can. J. Earth Sci., 10(26).

Smith, D.G. 1992. Glacial Lake Mackenzie, Mackenzie Valley, Northwest Territories, Canada. Can. J. Earth Sci., 29, 1756–1766.

Smith, D.G. 1994. Glacial Lake McConnell: Paleogeography, Age, Duration, and Associated River Deltas, Mackenzie River Basin, Western Canada. Quaternary Science Reviews, 13, 829–843.

Stoker, B.J., Margold, M., Gosse, J.C., Hidy, A.J., Monteath, A.J., Young, J.M., Gandy, N., Gregoire, L.J., Norris, S.L., and Froese, D. 2022. The collapse of the Cordilleran–Laurentide ice saddle and early opening of the Mackenzie Valley, Northwest Territories, Canada, constrained by 10Be exposure dating. The Cryosphere, 16, 4865–4886.

Transdisciplinary permafrost community-based research to handle permafrost thaw in Longyearbyen, Svalbard

Hanne H. Christiansen[1], Alexandra Meyer[2], Elisabeth Angell[3], Susanna Gartler[1], Thomas Ingeman-Nielsen[4], Leneisja Jungsberg[5], Heikki Lihavainen[6], Ilkka S.O. Matero[6], Olga Povoroznyuk[1], Arja Rautio[7], Aleksey Shestov[8], Anatoly O. Sinitsyn[9], Ulla Timlin[7] & Marjolaine Verret[10]

[1]*Department of Social and Cultural Anthropology, University of Vienna, Vienna, Austria*

[2]*Department of Arctic Geophysics, University Centre in Svalbard, Longyearbyen, Svalbard, Norway*

[3]*NORCE Norwegian Research Centre AS, Bergen, Norway*

[4]*Department of Environmental and Resource Engineering, Technical University of Denmark, Kgs. Lyngby, Denmark*

[5]*Nordregio, Stockholm, Sweden*

[6]*Svalbard Integrated Arctic Earth Observing System, Longyearbyen, Svalbard, Norway*

[7]*Arctic Health, Bioscience and Internal Medicine, University of Oulu, Finland*

[8]*Department of Arctic Technology, University Centre in Svalbard, Longyearbyen, Svalbard, Norway*

[9]*SINTEF AS, Trondheim, Norway*

[10]*Department of Arctic Geology, University Centre in Svalbard, Longyearbyen, Svalbard, Norway*

Two-thirds of all Arctic settlements are located on permafrost (Ramage 2019). There is an urgent need for knowledge about how changing permafrost conditions in the Arctic are affecting communities, and how these challenges can best be dealt with. We argue for a transdisciplinary approach to this problem. We use Longyearbyen (pop. 2500), Svalbard, to illustrate how permafrost thaw can be studied from a variety of disciplinary perspectives and in dialogue with the local community. Svalbard is considered a climate change hotspot as it has warmed around 4°C since meteorological recordings started 125 years ago (Nordli et al. 2020). Based on experiences from ongoing projects and discussions, we discuss locally identified challenges associated with permafrost thaw and outline recommendations for permafrost research and adaptation in Longyearbyen.

Permafrost thaw: Challenges and adaptation

Longyearbyen has some of the warmest permafrost this far north (Christiansen et al. 2021). Due to the town being confined in a narrow valley with steep mountain sides, permafrost thaw causes a high risk of rockfalls and landslides (active layer detachments and debris flows). The topography also represents a challenge for community infrastructure as there are only limited expansion possibilities, and the location along the coastline causes challenges related to coastal erosion. The town never had an indigenous population, and its economy is shifting from coal mining to tourism, academia and new business development, with corresponding social and demographic transformations. The population is highly international and experiences a frequent turnover. Most of the housing is owned and operated by two large Norwegian state companies.

Permafrost in Longyearbyen has been the subject of research for decades in natural and engineering sciences, and more recently in the health and social sciences. Lately, transdisciplinary, community-based projects have been developed, aiming to connect and foster dialogue with the local society. Based on these multiple research perspectives, we present a comprehensive picture of the various societal challenges related to permafrost thaw, and how these are perceived locally. These encompass impacts on the natural and built environment, including housing and infrastructure, cultural heritage, as well as other life domains such as health and well-being. Our results show that other issues, such as snow avalanches, are often overshadowing concerns about permafrost thaw, and that impacts may be indirect. Furthermore, it is difficult to distinguish between different possible causes of permafrost thaw impacts, especially related to infrastructure, such as climate change, improper maintenance, or poor engineering solutions. Therefore, more observations and infrastructure mapping are required to uncover the effects of a warming climate on the current infrastructures in Longyearbyen, specifically those with a lifespan exceeding the design period.

While Longyearbyen is well-adapted to permafrost thaw from an engineering perspective compared to many other Arctic communities, there are adaptation challenges related to the allocation of resources and prioritizations. Recently, there has been significant focus on enhancing avalanche protection in the area, following an incident in 2015 which claimed two lives and destroyed eleven homes. However, permafrost

thaw has garnered increased attention following two autumn rainstorms in 2016, which caused extensive active layer detachments sliding with associated debris flows, ultimately impacting the road infrastructure. Another challenge is the main water resource, which is confined by a road dam consisting of permafrost. The structural integrity of buildings is threatened by differential settlements. Adaptation measures include the reparation of foundations, with houses being put on the inbuilt frame and piles being replaced around the building. Road pavement surface is also subjected to uneven settlements affecting operational characteristic of the roads. Foundation designs of new infrastructure in town are increasingly chosen in favor of end bearing piles to the bedrock or artificial cooling plate foundations instead of traditional friction piles. Increased thaw will necessitate adapted foundations of new buildings and reparations of older buildings. Social challenges to adaptation relate to high staff and population turnover, limited space for urban development, and restricted local fate control and leeway for adaptation.

Regarding the management of permafrost-related challenges, there are close linkages between science and society in Longyearbyen, however, with room for improvement. Examples of successful collaborations include regular meetings between permafrost scientists and local authorities, co-produced collaborative projects, as well as elements of co-creation in community planning. Many of these collaborations depend on individuals, which presents a challenge in the context of high turnover. Another challenge is research and collaboration fatigue. Identified knowledge gaps include (1) knowledge about future climatic and environmental scenarios; (2) various types of mapping of existing infrastructure and their identified risks (deformation, settling, pollution, erosion) which can indicate where it is safe to build and not; (3) social variables (how is the society developing?); and (4) climate change and permafrost dynamics (what are the critical conditions to study seen from a local perspective).

IDENTIFIED SOLUTIONS, PRIORITIES AND WAYS FORWARD

There is presently a need locally for developing sensitive strategies for collaborations to meet the challenges related to permafrost thaw. Higher education has emerged as a crucial field. The next generation of scientists and professionals must be equipped with the necessary basic permafrost knowledge, and this challenge should be tackled in a pan-Arctic perspective. Relatedly, student internships with local communities, authorities and companies can be a mutually benefitting adaptive strategy. In the case of Longyearbyen, regular meetings between local permafrost scientists, the Community Council, the construction sector as well as state companies responsible for housing operations, should be systematically developed. Increased knowledge and awareness may support local residents in dealing with challenges. Engaging the community in a participatory manner is thus a logical progression. Adaptation efforts should be forward-looking and focus on innovation to develop construction practices better suited to Arctic environments. They shall further include the near real-time observation of landsliding and infrastructure, including a geotechnical slope modelling tool being built presently, using both local academic and commercial knowledge to innovate preparedness and develop resilience. Institutionalization and formalization of knowledge transfer might counteract the loss of knowledge due to turnover. This could include a best practice database where available permafrost meta data is gathered, possibly within the Svalbard Integrated Arctic Earth Observing System (SIOS) framework. This process has somewhat already started since permafrost has been identified as a thematic focus area to develop Shared Arctic Variables (SAV), following the Roadmap for Arctic Observing and Data system (ROADS) (Starkweather et al. 2021). To enhance the focus on and prioritization of permafrost challenges, permafrost-related concerns should be included into the local risk and vulnerability analysis. Risk maps could be complemented by mental maps developed by social scientists. Finally, outreach and dissemination towards local actors and media should be strengthened, to foster a more nuanced understanding of permafrost-related challenges within the broader society.

REFERENCES

Christiansen, H.H., et al. 2021. Ground ice content, drilling methods and equipment and permafrost dynamics in Svalbard 2016-2019 (PermaSval). In: Moreno-Ibáñez et al. (eds) SESS report 2020, Svalbard Integrated Arctic Earth Observing System, Longyearbyen, Norway, 259–275. https://doi.org/10.5281/zenodo.4294095

Nordli, Ø., et al. 2020 Revisiting the extended Svalbard Airport monthly temperature series, and the compiled corresponding daily series 1898-2018, Polar Research, 39 (3614). http://doi.org/10.33265/polar.v39.3614

Ramage, J. 2019. Settlements on permafrost in the Arctic, Nordregio. https://nordregio.org/maps/settlements-on-permafrost-in-the-arctic/

Starkweather, S., et al. 2021. Sustaining Arctic Observing Networks' (SAON) Roadmap for Arctic Observing and Data Systems (ROADS), Arctic, 74 (5). https://doi.org/10.14430/arctic74330

Key Risks from permafrost thaw – a comparative, trans- and interdisciplinary risk assessment

Susanna Gartler[1], Johanna Scheer[2] & Alexandra Meyer[1] with Nunataryuk Consortium Members

[1]*Department of Social and Cultural Anthropology, University of Vienna, Vienna, Austria*

[2]*Department of Environmental & Resource Engineering, Technical University of Denmark, Kongens Lyngby, Denmark*

Permafrost degradation has far-reaching consequences for the global climate and profound impacts on local and regional livelihoods (Doloisio and Vanderlinden 2020; Povoroznyuk and Schweitzer 2023; Ramage et al. 2022). We here present an inter- and transdisciplinary analysis of key risks associated with permafrost thaw across several sites along and near Arctic coasts. While the permafrost-climate feedback is well-documented (Schuur et al. 2015), the impacts on coupled socio-ecological systems of the permafrost region remain understudied. In addition to ongoing fast changes in the environment, the Arctic coastal region is characterised by strong geopolitical tensions and undergoes rapid societal transformations, making it essential to understand the implications of permafrost thaw on Arctic coastal communities. With this study, we aim to contribute to the growing body of research on climate-related hazard and risk assessments in the Arctic, as well as on vulnerability, resilience, and adaptation.

Methods and methodology

The "Nunataryuk" project, led by the Alfred Wegener Institute, has carried out a comprehensive six-year investigation into rapidly changing permafrost regions in the North. Between 2019 and 2023 Nunataryuk scientists in collaboration with local experts used a mixed-methods approach to collect extensive information on physical processes, uncertainties, and societal concerns in the following regions: Svalbard (Norway), the Avannaata Municipality (Greenland), the Beaufort Sea Region (Canada), and the Tiksi/Bykovskiy region (Russia). This pan-Arctic approach allowed us to include the perceptions of risk from diverse geo-political contexts and (Indigenous) populations (Ramage et al. 2022), who are confronted with distinct challenges due to varying physical properties of the prevailing permafrost soils (Irrgang et al. 2022). The qualitative data gathered during that period were firstly pooled through a series of workshops and discussions between the consortium members and local stakeholders. Secondly, we conducted a thematic (network) analysis to classify the data per component of risk, defined as key hazards, physical processes, societal consequences and adaptation practices. This laid the foundation for iteratively ranking the identified risks by engaging social, engineering, natural and health Nunataryuk scientists to scrutinize the results, derive and verify rankings. The results were then shared with Arctic communities in late 2022 and early 2023 through a series of workshops and interviews, who then further verified and/or modified the outcomes.

Aims and objectives

The novelty of our research is the comparative approach, spanning different environmental and societal contexts, as well as the multidisciplinary synthesis identifying risks across the case study areas. The primary objective of this study was to conduct an in-depth risk analysis of permafrost thaw, considering both physical processes and societal concerns. Harnessing an inter- and transdisciplinary approach, we drew understandings from diverse disciplines as well as from (Indigenous) land users, rights- and knowledge holders through multidirectional knowledge exchange processes. By synthesizing this information we contribute to a better understanding of the complex and interconnected risks across permafrost landscapes.

Definition of risk

We understand risk holistically, as a socio-natural phenomena defined by perceptions of multiple stakeholders (Larsen et al. 2021). Risks arise from the interaction between 1) physical processes, including anthropogenic global warming and pollution; 2) hazards which are set at the intersection of the natural and societal realms; and 3) socio-ecological consequences, corresponding to local perceptions of permafrost thaw impacts. Local perceptions vary significantly depending on socio-economic, political, environmental and other contexts. We define risks as dynamic and rooted in the interconnected relationship between humans and nature, encompassing various perspectives from stakeholders like scientists, regulators, and local landusers and residents (Larsen et al. 2021).

Results: Five key hazards

Through the comprehensive risk analysis, we identified five key hazards of permafrost thaw, namely:

1) infrastructure failure, 2) disruption of mobility and supply, 3) decreased water quality, 4) challenges for food security, and 5) increased risk of exposure to infectious diseases and contaminants. These key hazards have far-reaching impacts on ecosystems, socio-cultural dynamics, economies, governance and the health and wellbeing of Arctic communities. Their complex interconnectedness is highlighted in a composite overview (Figure 1).

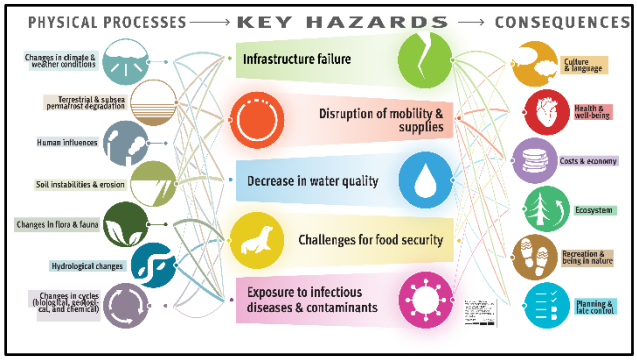

Figure 1. Key Hazards of Permafrost Thaw (adapted from Westerveld et al. 2023)

The risk assessment showed that infrastructure failure and disruption of mobility and supply chains have the largest impacts on costs and economy, and were generally perceived as having the highest societal impacts. Exposure to infectious diseases and contaminants was linked to the highest levels of perceived uncertainty. Challenges for food security, subsistence activities and decrease in water quality were perceived as central in the Beaufort Sea and in the Northeast Siberia regions, but not in Svalbard and Greenland. Hence, depending on factors such as livelihood strategies, socio-cultural and political context, structures of governance, available infrastructure and permafrost conditions, the perception of risks related to permafrost thaw entails significant place- and context-specific complexities, and exhibits substantial variation not only within individuals and communities, but also between regions.

Conclusion

The transdisciplinary risk analysis of permafrost thaw along and near Arctic coasts has revealed substantial impacts on the livelihoods of local communities. By synthesizing insights from various disciplines and involving stakeholders in multi-directional knowledge exchanges, our study enhances the understanding of the intricate factors driving risks in four focal areas. Our research provides pivotal insights into the key risks associated with permafrost thaw in Arctic coastal areas, a framework for future studies in this field, which are necessary to address uncertainties associated with permafrost thaw risks, and underscores the urgent need for proactive adaptive measures.

References

Doloisio, N., and Vanderlinden, J.P. 2020. The perception of permafrost thaw in the Sakha Republic (Russia): Narratives, culture and risk in the face of climate change, Polar Science, 26 (100589): 1–9. doi:10.1016/j.polar.2020.100589

Larsen, J.N., Schweitzer, P., Abass, K., Doloisio, N., Gartler, S., Ingeman-Nielsen, T., Ingimundarson, J.H., Jungsberg, L., Meyer, A., Rautio, A., Scheer, J., Timlin U., Vanderlinden, J.P., and Vullierme, M. 2021. Thawing Permafrost in Arctic Coastal Communities: A Framework for Studying Risks from Climate Change, Sustainability, 13 (2651): 1–17. doi:10.3390/su13052651

Povoroznyuk, O., and Schweitzer, P. 2023. Ignoring environmental change? On fishing quotas and collapsing coastlines in Bykovskiy, Northern Sakha (Yakutiya), Ambio, 52:1211–1220. doi:10.1007/s13280-023-01874-9

Ramage, J., Jungsberg, L., Meyer, A., and Gartler, S. 2022. 'No longer solid': perceived impacts of permafrost thaw in three Arctic communities, Polar Geography, 45(3): 226–239. doi:10.1080/1088937X.2022.2105973

Schuur, E.A., McGuire, A.D., Schädel, C., Grosse, G., Harden, J.W., Hayes, D.J., Hugelius, G., Koven, C.D., Kuhry, P., Lawrence, D.M., and Natali, S.M. 2015. Climate change and the permafrost carbon feedback, Nature, 520(7546): 171–179. doi:10.1038/nature14338

Irrgang, A.M., Bendixen, M., Farquharson, L.M., Baranskaya, A.V., Erikson, Li H., Gibbs, A.E., Ogorodov, S.A., Overduin, P.P., Lantuit, H., Grigoriev, M.N., and Jones, B.M. 2022. Drivers, dynamics and impacts of changing Arctic coasts, Nat Rev Earth Environ, 3: 39–54. doi:10.1038/s43017-021-00232-1

Westerveld, L., Kurvits, T., Schoolmeester, T., Mulelid, O.B., Eckhoff, T.S., Overduin, P.P., Fritz, M., Lantuit, H., Alfthan, B., Sinisalo, A., Miesner, F., Viitanen, L.-K., and the NUNATARYUK consortium 2023. Arctic Permafrost Atlas, GRID-Arendal, Arendal, Norway. https://url.grida.no/3S7Y762

Applied permafrost geomorphology in support of climate change adaptation at the municipal level

Sarah Gauthier[1,2], Michel Allard[1,2] & Pascale Roy-Léveillée[1,2]

[1]*CRYO-UL: Permafrost Research Laboratory, Université Laval, Québec City, Québec, Canada*

[2]*Centre d'études nordiques, Université Laval, Québec City, Québec, Canada*

There is a growing demand for research projects that address the concerns of northern communities regarding the impacts of permafrost thaw on infrastructure and related geohazards. Effective knowledge transmission and appropriation of research results by local and regional stakeholders is crucial for research results to become effective tools, and to be useful to northern communities in their efforts to mitigate and adapt to the effects of climatic warming and permafrost thaw. In the Inuit community of Salluit (Nunavik), extensive permafrost research has taken place over the last 30 years (Allard et al. 2023), yet the effective use of research results in support of landuse planning has been limited by data accessibility (Gauthier 2023).

Permafrost conditions within the municipal limits result in severe land use planning challenges that complicate community expansion, by imposing a lack of buildable space and forcing the community to expand farther from the coast. In partnership with local and regional stakeholders, this applied permafrost geomorphology project examined construction potential in an area of interest for community expansion, and used a multi-pronged knowledge transmission strategy to share decision-support tools to address existing and emerging needs for permafrost expertise in Salluit.

Methods

A key objective of this research was to respond to a request by the Kativik Regional Government (KRG) to carry a site-specific characterization in an area targeted for community development: ''Salluit-4''. This site was located at the southern fringe of the village, on a sloping plateau with a discontinuous cover of glacial till over bedrock, and for which very little information on subsurface conditions was available. This type of terrain is rarely selected for construction in Nunavik, as flat terrain is preferred, and current construction techniques are poorly suited to sloping terrain. GPR (Ground Penetrating Radar) surveys were used to map the thickness of frozen till over the bedrock and a monitoring station was installed to measure ground temperature through the till and up to the interface with bedrock, 3 m below the ground surface. A total of 8.5 km was surveyed following a tight grid pattern at the 100 Mhz frequency and two boreholes confirmed depth to bedrock. The signal penetration with the applied time-window setting was approximately 8 m. GPR results were interpolated to produce a map of till thickness on bedrock for the whole area, which yielded a mean error between measured and predicted values of 0.1 m.

Research results

The mapping of till thickness over bedrock and the ground thermal regime analysis were used to identify ice-rich areas to be avoided, areas with conditions potentially suitable for different types of foundations, and potentially problematic areas requiring careful geotechnical investigations.

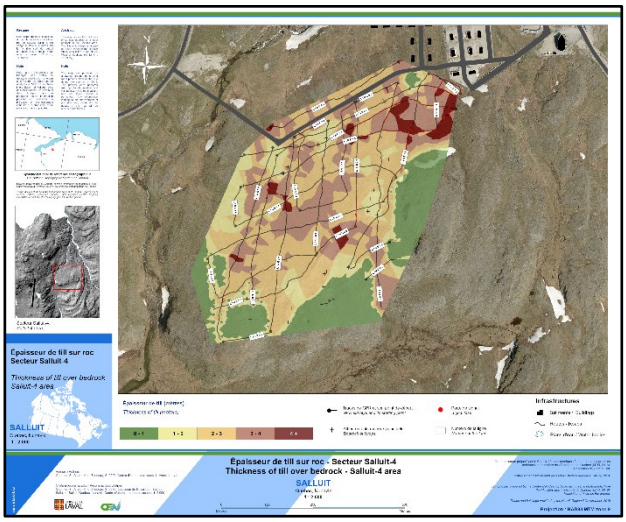

Figure 1. Map of the thickness of till over bedrock in Salluit-4 area with the GPR surveys grid (Gauthier 2020; Gauthier 2023).

Over large areas of the hillslope, the till cover was sparse and very thin, and the active layer was about 1.8 m, offering potentially suitable conditions for the use of piles. Upslope sections with heavily weathered bedrock outcrops offered good potential for cut-and-fill applications. Unsuitable zones showing signs of vulnerability to erosion, such as thermo-erosional gullying, were also identified as unsuitable.

Approach to knowledge transmission

The results obtained from the characterization of Salluit-4 were intended to support decision-making with regards to construction practices and foundation designs better suited to the geomorphological conditions of this area. But adapted communication strategies must be used to increase its potential use. As the technical nature of GPR data complicates the understanding of the results, maps enable the information to be visualized more effectively by the various stakeholders, as cartography is a powerful means of communicating geographical information. By mapping the thickness of till over bedrock, producing a summary map of field observations and general recommendations, and understanding the ground thermal regime in the till cover, we can determine essential geotechnical elements to highlight the various construction practices possible.

These results were made accessible to the community, the regional government, and other audience such as potential contractors using a multi-pronged knowledge transmission strategy. The map and GPR results where shared online on a bilingual (French and English) web platform made with ArcGIS Online (Gauthier 2020).

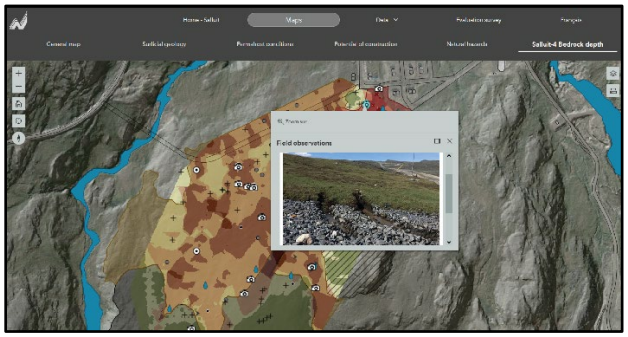

Figure 2. Screen capture of the maps available on the web platform, one of the methods used to share the results of the Salluit-4 terrain characterization (Gauthier 2020).

The translation of contents into Inuktitut is still in progress and the translated material is integrated as it becomes available. The maps and an information package were also shared directly with the KRG. This package is composed of maps in different formats, a map package with the produced shapefiles, GPR data (raw and interpreted), and ground temperature data.

The results were presented, shared and discussed with the Northern Village of Salluit municipal council and to the Qaqqalik Landholding Corporation (2019 and 2021). At the request of the regional partner (KRG, Renewable Resources, Environment, Lands and Parks Development), these results were then presented to the consulting firms hired to perform a prefeasibility study and preliminary plans for the new expansion zone Salluit-4 (2023). The KRG then mandated us to provide permafrost expertise and participate in the geotechnical investigations campaign that took place in Salluit-4 during October 2023.

Conclusion and outlooks

The objective of this project was to enhance the geomorphological knowledge on Salluit-4 in order to support the identification of practices better suited to the terrain. Despite the project's completion, communication efforts between researchers, regional governments, local communities, and other stakeholders are still needed to ensure that results are understood and well communicated and to promote the implementation of research projects. Ongoing communication also fosters collaborative relationships between researchers, professionals, and stakeholders involved in landuse planning. This may also facilitate continued scientific contributions in support of northern mitigation and adaptation to practical challenges related to permafrost.

References

Allard, M., L'Hérault, E., Aubé-Michaud, S., Carbonneau, A.-S., Mathon-Dufour, V., B.-St-Amour, A., and Gauthier, S. 2023. Facing the challenge of permafrost thaw in Nunavik communities: innovative integrated methodology, lessons learnt, and recommendations to stakeholders. Arctic Science. 9(3): 657–677. https://doi.org/10.1139/as-2022-0024

Gauthier, S. 2020 Permafrost Data Nunavik – Salluit: Data visualization on permafrost research in support of the land use planning of Salluit, Nunavik. [Online] Retrieved from https://bit.ly/Salluit-Permafrost-Data-English.

Gauthier, S. 2023. Géomorphologie appliquée du pergélisol et communication scientifique en appui à l'aménagement du territoire de Salluit, Nunavik (Doctoral dissertation, Université Laval, Québec, Canada). http://hdl.handle.net/20.500.11794/116084

Establishing a community-led permafrost monitoring program in the Ts'udé Niliné Tuyeta Indigenous and Territorial Protected Area, NWT

Buddy Gully[1,2], Twyla Edgi Masuzumi[1,2], John Tobac[1,2], Joseph Tobac[1,2], Danny Masuzumi[2], Alexa Scully[2], Jeffrey Campbell[3], Alexandre Chiasson[3], Michelle Landry[3], Ashley Rudy[4] & Duane Froese[3]

[1]*K'asho Got'ine Guardians, Fort Good Hope, Northwest Territories, Canada*

[2]*K'ahsho Got'ine Foundation, Fort Good Hope, Northwest Territories, Canada*

[3]*Department of Earth and Atmospheric Sciences, University of Alberta, Edmonton, Alberta, Canada*

[4]*Northwest Territories Geological Survey, Government of Northwest Territories, Yellowknife, Northwest Territories, Canada*

The vast wetlands of the Indigenous and Territorial Protected Area, Ts'udé Niljné Tuyeta, sits on the boundary between continuous and discontinuous permafrost, with peat bogs and fens, both major carbon sinks, and a landscape integral to the K'asho Got'ine (Hegginbottom et al. 1995; Aylsworth and Kettles 1999). We seek information to better understand recent changes and also the implications of these changes for the longterm stewardship of this land in the face of changing climate and fire regimes. Alongside Guardians, academic partners and community members, we will build research and monitoring capacity in Tuyeta to map permafrost and peatlands using remote sensing and drone-based approaches, and through drilling, to compare rate of permafrost accumulation (or loss) and quantify carbon storage across the diverse peatland landscape of Tuyeta. As well, we will monitor lakes and waters to assess the impacts of permafrost thaw on this landscape. Collectively, these data will drive our long-term vision of management of these natural resources and ecosystem services provided by these peatland landscapes.

In the first year, we were successful in training Guardians and hiring additional Guardians, in data gathering techniques, working closely with academic partners from the NWT Geological Survey and University of Alberta in permafrost research. We also made progress on developing our in-house database and research tools management, having connected with other Guardians programs doing similar work. A local research and data management protocol is near completion. The K'ahsho Got'ine Foundation is building the capacity needed to conduct research that is designed, analyzed, and shared by our community. We are working towards achieving sovereignty over research, monitoring, and data management in Tuyeta with direction from the Tuyeta Management Board.

Methods

In the first year, permafrost monitoring focused on skills development and an opportunity to discuss the types of questions that are of community concern with academic partners. From those discussions, we carried out a camp in late September 2023 at Turnitl'I Tue Lake (Figure 1). An area of the camp was cleared in 2019 of surface trees and shrubs to develop a helicopter landing site. Across this clearing, and into the undisturbed forest, active layer surveys were conducted with a goal of repeating these surveys in future years. Second, we established two ground temperature stations to 5 m depth, one in the clearing and one in the forested area adjacent to the camp. Third, we carried out Electrical Resistivity Tomography (ERT) surveys across the clearing and along the active layer survey line to assess permafrost thickness and continuity. A second site was investigated in the northern part of the Protected area (BL-01), looking at the changes between a caribou-lichen covered peat plateau, considered undisturbed, and an adjacent area that had burned in 1969.

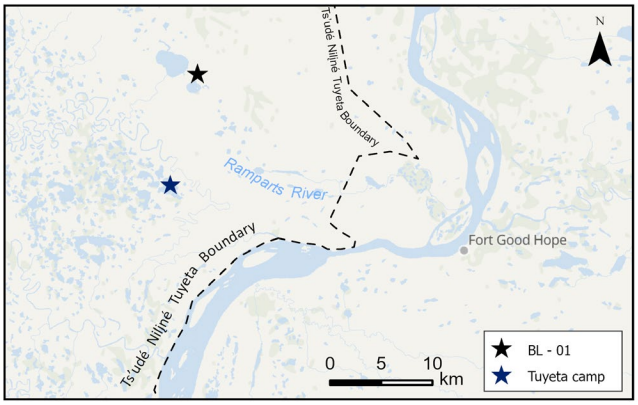

Figure 1. Location of the Ts'udé Niljné Tuyeta camp in the protected area.

Results

ERT surveys of 2-m and 4-m spacing were carried out at the protected area of Tuyeta, crossing an area cleared of vegetation and a forested boreal area. Frost probing set the average active layer depth at 63.9 ± 4.5 cm in the cleared area and 45.2 ± 14.0 cm

in the forested area. The ERT data from these profiles show low resistivity values (50-300 Ω.m) extending ~2 m in depth in the cleared area, while the forested area profile shows high resistivity values (1000-13000 Ω.m) which extends below the cleared area and estimate permafrost is at least 15 m thick at the site.

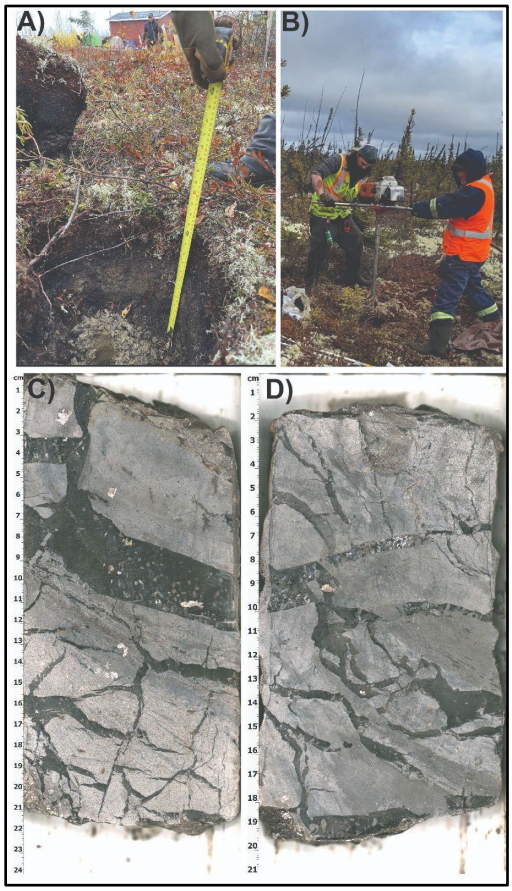

Figure 2. A) Measurement of the peat layer before drilling. B) K'ahsho Got'ine Guardian, Buddy Gully, and UofA permafrost researcher collecting permafrost cores. C-D) Ice-rich permafrost from glacial Lake Mackenzie characterizes much of the permafrost within Tuyeta.

Drilling near the camp showed that the Tuyeta area is underlain by ice-rich glaciolacustrine sediments (Figure 2). These sediments had ice contents that averaged near 50% with significant excess ice, and locally exceeded 70%. Peat thickness near the camp was relatively thin (~35-80 cm) above the lacustrine sediments. Peat thickness at the northern sites, however, was significantly thicker, at 400 cm in the undisturbed peat plateau and 150 cm in the area that was impacted by past fire. It is unclear whether this increased thickness of peat in the area recovering from past fires is a result of that disturbance and peatland recovery, or whether it is a local feature.

Figure 3. A) Guardians and UAlberta researchers drill into permafrost to establish a ground temperature monitoring station on 20/09/2023. B) Discussion about surficial geology and permafrost conditions in the vicinity of Fort Good Hope with the K'ahsho Got'ine Guardians.

Conclusions and Future Directions

The work in 2023 has shown that permafrost in the Tuyeta Protected Area is generally colder than in areas to the south within the Sahtu region. Peat thickness shows significant variations within the area but it is unclear why these thicknesses vary. Work in 2024 will target several different areas disturbed by fire to establish relations between peat thickness, ground temperatures and fire history, and continue to collect water samples to establish baseline data for Tuyeta. Developing a community-led permafrost monitoring program is a response to growing community concerns about changing permafrost conditions within the Protected Area and more broadly around the community of Fort Good Hope (Figure 3). The work we have begun is part of the longer-term work towards achieving sovereignty over research, monitoring, and data management in Tuyeta.

References

Aylsworth, J.M., and Kettles, I.M. 1999. Distribution of peatlands in the Mackenzie Valley, in The Physical Environment of the Mackenzie Valley: A Baseline Study for Environmental Change, edited by L.D. Dyke and G.R. Brooks, Bull. Geol. Surv. Can., 43–48.

Heginbottom, J.A., Dubreuil, M.A., and Harker, P.T. 1995. Permafrost Map of Canada. The National Atlas of Canada, 5th Edition,(1978-1995), published by Natural Resources Canada, sheet MCR, 4177(1), 7.

Permafrost research in the Arctic from a sociology of science perspective

Svenja Holste

Faculty of Sociology, Bielefeld University, Bielefeld, North Rhine-Westphalia, Germany

(Geo-)political worldviews of what the Arctic is or what it should be have shaped Arctic science since early times of polar explorations. By combining critical geopolitics and the sociology of science, this dissertation project studies how (western) knowledge is produced in the Arctic. It investigates two main research questions: What are the worldviews and role perceptions of permafrost researchers and glaciologists in the Arctic? How is indigenous knowledge perceived from a western scientists' perspective? Methodologically, a qualitative approach is applied, including literature analysis of Arctic strategies and research reports as well as semi-structured interviews. The focus lies on researchers at different career stages who work at Canadian, German and Norwegian institutions. This poster presents a preliminary analysis of permafrost research in the Arctic, discussing three key aspects: First, how (geo-)political worldviews are present in national scientific research agendas. Second, the perception of indigenous knowledge in western scientific research practices. Third, the notion of research on a vanishing object, by applying a framework of emotions.

Why permafrost research in the Arctic?

In critical geopolitics in the International Relations, traditional concepts of space are questioned. Space as such is regarded neither neutral nor objective, but socially constructed. While territoriality might be one important factor in constructing social and political space, it is not the only one (Albert et al. 2010, p. 552). Rather, identity, knowledge, indigeneity, and growing concerns about the environment and climate can be understood as geopolitical factors as well (Heininen 2019, p. 218). In other words, it is people's narratives, ideas, imaginations and perspectives that ascribe territorial realities a certain meaning. The increased (global) attention towards the Arctic, which is embedded in a context of increasing media coverage on Climate Change related issues, indicates a further consolidation of the image of the Arctic as a vulnerable region, including the making of a natural rather than a cultural region (Powell 2023). At national level, the researcher's perception of who should be doing science in the Arctic and why varies strongly. While the assumption can be made that science is neither neutral nor conducted in a vacuum, it lies at the heart of the sociology of science to unfold and deconstruct the process of doing science. Apart from funding, perceptions of the Arctic together with the researcher's individual motivation and background determine how research questions are shaped, whether they get addressed and if there are questions that never get asked. Studying the western Arctic scientific community, and individual scientists in particular, allows for valuable insights in the framing of permafrost as a research object and its implications for the regions. The poster presents the analysis of the 'doing of science' of a growing research community operating within the framework of (geo-)political conflicts, national Arctic strategies and funding priorities, institutional background and international scientific cooperation.

Perception of indigenous knowledge

Frozen ground, ice and snow are part of Arctic culture and so is the understanding of and encounters with frozen landscapes. Doing research in the Arctic and using data sets from ice cores or permafrost samples to understand large-scale global processes inevitable means to give ice a new role, to cultivate a 'New Arctic' – a region with "too little ice, too much glacial retreat, and insufficient frozen terrain" (Dodds and Smith 2022, p. 4). Thus, research on ice creates a narrative of a changing planet. Overall, it is argued that different ways of knowing construct an idea of the landscapes which can never claim to be exhaustive. Research interests and research questions are being constructed to serve different purposes. Different actors advocate for their Arctic, and their knowledge, to gain sovereignty about interpretation, and ultimately, political influence. Literature provides a richness of normative analysis why meaningful engagement and co-production of knowledge is important. A gap exists in the research practical analysis of how permafrost researchers feel they could learn from indigenous knowledge holders, and how their understanding of the Arctic could be enriched by applying other ways of knowing to their research. In this context, the question also arises as to where scientists perceive boundaries and how they argue in favour of these boundaries? The findings are scrutinised with regard to colonial legacies, logic and funding structures of the academic system, different research priorities, and degrees of interdisciplinarity.

RESEARCH ON A VANISHING OBJECT

Research on thawing permafrost could also be framed as research on a vanishing object. Acknowledging that Climate Change is one of several perceived challenges in the Arctic, its understanding, modelling, mitigation or adaptation is perceived as one main concern for the studied research field. A cross-cutting topic arises around the role of emotions. Therefore, it is important to observe how recent developments are changing the 'doing of science' as such. Living in an interglacial, we experience societal reception of ice in various forms (Knight 2019). Acknowledging the relationship between scientists and their research object provides insights into motivation, importance and challenges of fieldwork. On the one hand, the interviews depict an appreciation for the natural science behind the beauty of Arctic landscapes. On the other hand, scientists have to deal with negative emotions (feeling of loss, anger, disappointment, frustration, concern) in a rational context. A clear gap between scientific evidence and political action emerges, which leads to questioning the relationship between science, politics and society, and especially the role and responsibility of scientists. From the interviews, six – conscious or unconscious – coping mechanisms were noticeable, where scientists would stick to science, invest in public engagement, enhance training capabilities and invest in education, engage in sustainable/responsible science developments, turn to science activism or promote interdisciplinarity. Science communication is an important component of research projects, and especially in the case of cost- and logistics-intensive expeditions, a considerable amount of personnel and money is spent on communication and media coverage. Arguably, the Arctic is a thankful region for stories because it is easy to produce images that people like to look at. Art evokes emotion, and emotions speak to people and make them reflect and act. Thus, scientists are also using emotions to communicate their science to a broader public in an impactful way. This, however, comes with three main implications. First, creative approaches often succeed in providing more access to society. It can be questioned, however, in how far aesthetic approaches which are too artistic in a sense alienate the general public from arts and thus from science. Second, emotional science communication entails the danger of (re-)producing worldviews that are already old: a romanticised idea of the Arctic, that of an untouched region, waiting to be explored by a few adventurous and courageous scientists, maybe even reminding on early polar explorations. In fact, it opens a field of tension: What idea of the Arctic is to be disseminated? Has it changed? And what does the audience expect? Third, combining science, emotions and creative approaches sets the scene for interdisciplinary work which is much needed. For the relationship between science and politics it is important to acknowledge human's embeddedness in nature. Embracing the connection between humans and nature can open doors for an inter- and transdisciplinary understanding of permafrost research.

REFERENCES

Albert, M., Reuber, P., and Wolkersdorfer, G. 2010. Kritische Geopolitik. In Schieder, S. and Spindler, M. 2010. Theorien der Internationalen Beziehungen, 3rd ed., Barbara Budrich/UTB, Opladen, Germany, Farmington Hills, MI, USA: 551–578.

Dodds, K., and Smith, J.R. 2022. Against decline? The geographies and temporalities of the Arctic cryosphere, The Geographical Journal, 189(3): 388–397. doi:10.1111/geoj.12481

Heininen, L. 2019. Special Feature of Arctic Geopolitics – A Potential Asset for World Politics. In Finger, M. and Heininen, L. 2019. The GlobalArctic Handbook, 1st ed., Springer International Publishing AG, Cham, Switzerland: 215–234.

Knight, P. 2019. Glaciers. Nature and Culture, Reaktion Books, London, UK.

Powell, R.C. 2023. Geography, Anthropology, and Arctic Knowledge-Making. In Howkins, A. and Roberts, P. 2023. The Cambridge History of the Polar Regions, Cambridge University Press, Cambridge, UK: 279–301.

ILLUQ — Permafrost, pollution, health

Hugues Lantuit, Paul Overduin, Michael Fritz & Leena-Kaisa Viitanen
Alfred Wegener Institute Helmholtz Centre for Polar and Marine Research, Potsdam, Germany

Climate change is one of the most significant global challenges of our time, with far-reaching impacts on human and environmental health. Permafrost underlies 22% of the Northern Hemisphere's exposed land surface and is thawing at an alarming rate as a direct consequence of climate change. Permafrost thaw releases large quantities of organic matter and contaminants into the environment. In fact, permafrost soils store nearly twice as much mercury as all other soils, the ocean, and the atmosphere combined, and this mercury is vulnerable to release as permafrost thaws over the next century. Contaminants, including heavy metals, persistent organic pollutants and microbiological agents locked in permafrost, are a risk for both human and animal health. In addition, permafrost thaw dramatically impacts infrastructure in local communities with wide-ranging consequences for health, economy, and society. Yet the social, physical and health components of permafrost thaw have traditionally been studied in isolation, leading to inadequate policy options that ignore the holistic nature of the threat. For instance, contaminant release directly affects wildlife, which itself is harvested for food. Infrastructure failure directly threatens water and sanitation in communities, drastically impacting health and wellbeing. There is a need for an integrated and participatory approach to the complex issues at the overlap between climate change, permafrost thaw, infrastructure damage, contaminants, health and well-being and for solutions founded on the cultural, natural and social frameworks of local communities.

ILLUQ is an interdisciplinary project rooted in participatory research with local stake- and rightsholders. Its mission is to provide a holistic approach to permafrost thaw, pollution, One Health and well-being in the Arctic and delivering timely products on the threats from contaminant release, infrastructure failure and ecosystem changes to stakeholders. ILLUQ's endeavor is a direct answer to the pressing needs of communities located on permafrost. It targets the missing link between studies performed by scientists, engineers and consultants in local communities and solutions with local stake- and rightsholders focusing on the long-term implications of decision-making in the context of permafrost thaw, a time frame generally overlooked in existing governance frameworks. ILLUQ will focus on three main areas in the Arctic: Svalbard, West Greenland and the Mackenzie Delta area. In this presentation, we introduce the main activities of the project for years to come and show how it builds on the many outputs from the previous NUNATARYUK project conducted between 2017 and 2023.

Near real-time ground temperature monitoring networks using Low Power Wide Area Network (LoRaWAN): Challenges and opportunities in northern Québec and Yukon

Emmanuel L'Hérault[1,2,3,5], Mickael Lemay[1,5], Michel Allard[1,2], Fabrice Calmels[4] & Pascale Roy-Léveillée[1,2]

[1]*Centre d'études Nordiques, Université Laval, Québec City, Québec, Canada*

[2]*CRYO-UL: Permafrost Research Laboratory, Department of Geography, Université Laval, Québec City, Québec, Canada*

[3]*Department of Civil Engineering, Université Laval, Québec City, Québec, Canada*

[4]*Permafrost and Geoscience Research Chair, YukonU Research Centre, Yukon University, Whitehorse, Yukon, Canada*

[5]*LogR Systems Inc, Québec City, Québec, Canada*

The thaw of ice-rich permafrost is responsible for numerous transportation infrastructure failures in the North. In the most dramatic cases, thaw induced damage may render infrastructure unusable and, in the case of transportation infrastructure, completely disrupt on-site traffic (L'Hérault et al. 2012; Calmels et al. 2018; Hjort et al. 2022). Detection and monitoring systems can facilitate crucial, time-sensitive interventions to mitigate potential, incipient and evolving threats to infrastructure integrity. Latest technological advances can facilitate the effective detection and timely communication of potential and evolving hazards. The Centre d'études nordiques, Yukon University, the Québec Ministry of Transportation, Transport Canada and LogR Systems Inc. collaborated to develop and test near real-time geohazard surveillance systems based on star networks of sensors using the LoRa wireless transmission technology and the LoRaWAN communication protocol (Calmels et al. 2022). This work is part of larger initiatives aiming to provide stakeholders with real-time, pre-treated, meaningful data on infrastructure-permafrost interactions.

Methods

During summers 2021, four LoRaWAN networks of sensors were implemented in Nunavik (3) and in Yukon (1) at airports and road sites. In 2023, an additional two (2) LoRaWAN networks were implemented in Nunavik, bringing the total number to six fully operational networks (Figure 1).

LoRaWAN networks are composed of three primary components: data loggers equipped with LoRaWAN transmitters (end-nodes) (Figure 2), a gateway, and a network server. The network is based on a star topology where all end-nodes communicate directly to the gateway that manages and coordinates the communication with the network server. The overall architecture of the network server and client application has been structured using docker containers technology for easy packaging and transferability to the client server. Application Programming Interface (API) were developed to access and download data from the servers, enabling the execution of risk assessment algorithms and potential triggering of alarms.

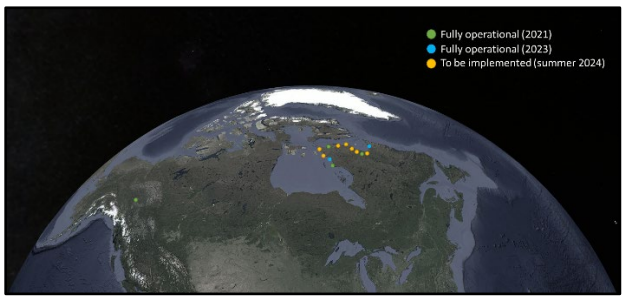

Figure 1. The six fully operational LoRaWAN networks implemented in northern Québec and Yukon, providing near-real time ground temperature along critical infrastructures.

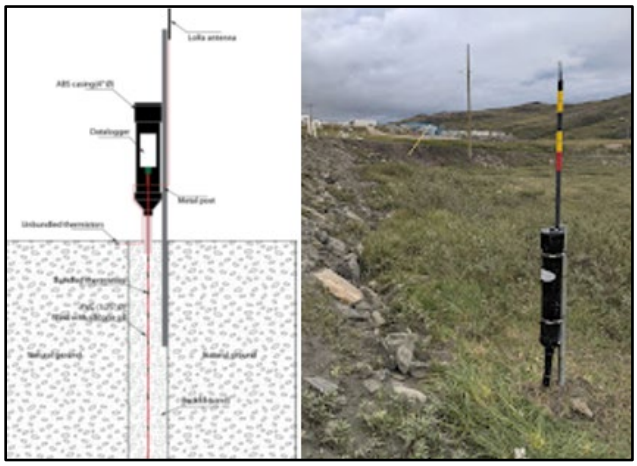

Figure 2. Ground temperature monitoring station equipped with LoRa datalogger that offers wireless data transmission capability.

Results and discussion

Performance assessments in the field demonstrated reliable wireless data transfer over a distance of up to 27 km, from the end node monitoring stations to the gateway. Using a single D-cell battery,

the power autonomy of the end-node monitoring station is estimated to 28 years with hourly data acquisition and transmission.

The organization of the data flow from the end nodes to the ultimate server were designed with safeguards to prevent data loss due to power outages and internet service interruptions (gateway) that may frequently occur in remote northern communities. For instance, during testing of the LoRaWAN network in Inukjuaq, Nunavik, an internet network failure occurred for approximately 120 hours. During that period, the end node monitoring stations were still transmitting data to the gateway, and data were temporarily saved in the gateway's internal memory. 6480 timesteps were saved, which correspond to over 300 days of hourly reading. When connection was reestablished between the gateway and the internet network, all data saved in the gateway were transmitted to the AWS server within 10 minutes.

Using the ground temperature data transmitted every hour, site-specific algorithms were developed to trigger alarms based on threshold values for warming or active layer depth increase (Figure 3).

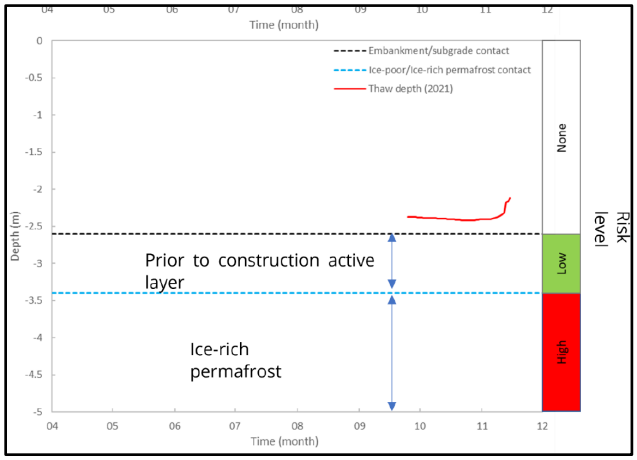

Figure 3. Thaw depth variations and the associated thaw settlement risk based on the site stratigraphy.

Moving forward, the system will benefit from technological upgrades and developments, including using different types of sensors, optimized data validation and cleansing algorithms, and customized user interfaces tailored to user preferences and needs.

Conclusions and Outlook

With near real-time acquisition, data validation and analyses can now be conducted periodically, and monitoring network component failures can now be remotely diagnosed leading to a "Know before you go" maintenance approach. With six fully functional LoRaWAN networks implemented to date and ground temperature data continuously being transmitted to the Centre d'études nordique's server at Université Laval, future work will focus on improving near real-time data processing and results visualization in order to build permafrost-related hazard warning systems to support fast decision-making processes, thus paving the way to a smarter northern infrastructure risk management.

Acknowledgements

Part of the funding for this project was provided by Transport Canada's Northern Transportation Adaptation Initiative (NTAI). Additional funding was provided by ArcticNet, as well as by Crown-Indigenous Relations and Northern Affairs Canada's (CIRNAC) Climate Change Preparedness in the North (CCPN) program, which was administered by the Government of Yukon's Department of Environment Climate Change Secretariat. In-kind contributions were also made by Yukon Geological Survey, Yukon University Research Centre, Centre d'Études Nordiques, Laval University, Yukon Government and MTQ partners listed above, and LogR Systems Inc.

References

Calmels, F., Roy, L.P., Grandmont, K., and Pugh, R. 2018. A Summary of Climate- and Geohazard-Related Vulnerabilities for the Dempster Highway Corridor. Yukon Research Centre, Yukon College, 200 p.

Calmels, F., Allard, M., Fortier, D., Amyot, F., L'Hérault, E., Sliger, M., Roy, L.-P., Laurent, C., and Gauthier, S. 2022. Design and implementation of early detection and warning systems for transportation infrastructure impacted by permafrost-related geohazards. Technical report, YukonU Research Centre, Yukon University, 203 p.

Hjort, J., Streletskiy, D., Doré, G., et al. 2022. Impacts of permafrost degradation on infrastructure. Nat Rev Earth Environ 3, 24–38. https://doi.org/10.1038/s43017-021-00247-8

L'Hérault, E., Allard, M., Barrette, C., Doré, G., and Sarrazin, D. 2012. Investigations géotechniques, caractérisation du pergélisol et stratégie d'adaptation dans un contexte de changements climatiques pour les aéroports d'Umiujaq, Inukjuak, Puvirnituq, Akulivik, Salluit, Quaqtaq, Kangirsuk et Tasiujaq, Nunavik. Technical report, Centre d'études nordiques, Université Laval, 224 p.

Mapping with the Land: Co-developing a Cumulative Impact Monitoring and Land Stewardship Framework with Sambaa K'é First Nation, Northwest Territories, Canada

Michael McPhee[1], Jessica Jumbo[3], Ruby Jumbo[2], Miguel Sioui[1] & William Quinton[1]

[1]*Department of Geography and Environmental Studies, Wilfrid Laurier University, Waterloo, Ontario, Canada*

[2]*Sambaa K'é First Nation, Senior Administrative Officer, Sambaa K' é, Dehcho, Northwest Territories, Canada*

[3]*Dehcho First Nations, Director of Lands and Resources, Łíídlı̨ Kúę́, Dehcho, Northwest Territories, Canada*

Across the Northwest Territories (NWT), Canada, Indigenous populations are striving to achieve effective environmental protection. Challenges arise when navigating complex methods, policies, and research relationships within co-management. Sambaa K'é First Nation (SKFN) is a member of the Dehcho First Nation (DFN) administrative government which unites 8 communities under traditional teachings of governance. SKFN utilizes a Two Walking as One (TWAO) ideology when managing land and people according to Dene Law. TWAO is a Dene ethos related to balancing two contrasting ways of living through a mixed approach which preserves the integrity of each and centers ideas of stewardship. Indigenous stewardship governance is the act of caring for the environment regardless of ownership according to Indigenous knowledge (IK) and ways of living utilizing one's local resources (Reed et al. 2020). This thesis addresses the question of how differing cultural systems, ecological change, and fractured multi jurisdictional partnerships may synergize into a cohesive land management strategy for the SKFN.

STUDY OBJECTIVE

Changes in SKFN's well-being and the mechanisms which cause, antagonize, or synergize these changes must be understood for effective Nation management and collaboration. Co-developed research questions with SKFN leadership yielded the following objectives: a) develop a new GIS-based method and logic model to manage, organize and mobilize environmental data; b) develop a new stewardship monitoring procedure so that users can apply the former while 'with the land" (WTL), and c) test the new methods developed in (a) and (b).

STUDY METHODOLOGY

This study embraced a mixture of methods to capture human and environmental dimensions of change while in SKFN from June 4th, 2022, to August 26th, 2022. Western scientific methods provided potential avenues of investigation equipped with tools and logic models to test hypotheses, analyze trends, and validate findings according to standardized knowledge. Indigenous methods provided actionable frameworks for cross-cultural collaboration based on perspectives of circular thinking, respect, and reciprocity. Scientific methods include employment of ArcMap Pro and Survey123 connect to develop a customized logic model. Local consultations, experiential learning, and academic literature informed theme creation. The logic model was then downloaded on mobile devices and populated with observations made while on excursions led by community members. Indigenous methods included co-development of research questions; situation of academic knowledge; learning the Dene Yahtie language; relationship building activities; and employment of protectionary protocols. This approach contextualized methods, databases, and solutions around SKFN's environment and culture increasing applicability and local engagement.

GIS MONITORING AND STEWARDSHIP DESIGN

Expanding on a mapping rubric, developed by Steve Kokeji et al. (2023) of the Thermokarst Collective (TKC) working group of the NWT Geologic Survey, this thesis created an Indigenous-led mapping framework to encourage youth-elder engagement with the land through monitoring cumulative environmental and cultural impacts. The original TKC template contained Mass Wasting, Hydrological, and Periglacial themes. New themes related to biological, cultural, and social change were added to increase engagement from audiences with diverse knowledge sets. This contributed to wider community goals. Mapping with the land along with youth-elder stewardship aim to facilitate community-driven data collection, analysis, and knowledge synthesis while providing pathways to cultural revitalization. A local database and community run monitoring framework improves interdisciplinarity between local, institutional, and government actors by bridging gaps in communication and research infrastructure.

MAPPING WITH THE LAND RESULTS

A total of 195 GPS-linked observations were recorded across 11 customized themes. Thematic distribution of observations can be seen in Table 1 and are filtered according to data collection method. These distributions reveal distinct differences in the themes collected when engaging directly with the land compared to removed aerial observations methods. Aerial methods favoured hydrological and periglacial features while ground based methods favoured a distribution centered around community-oriented variables in addition to environmental data.

Table 1. Thematic Distribution of Logic Model data collected in Sambaa K'é, NWT

Theme of Observation	Thematic Distribution (N=195)	Ground-Based Data (n=107)	Aerial Data (n=88)
Periglacial	32	2	30
Hydrological	37	4	33
Mass Wasting	11	9	2
Animal Data	23	17	6
Biological Process	11	6	5
Contamination & Waste	13	13	0
Cultural	27	25	2
Infrastructure & Community	14	12	2
Research	8	8	0
Vegetation Data	8	5	3

A LIVING RESEARCH FRAMEWORK

Through prioritizing Indigenous ways of living and being this thesis upheld central tenets of Dene Law and TWAO through a locally tailored framework which engages all ages and all voices through monitoring with the land. Sambaa K'é now has the capacity to consider multidimensional aspects of change affecting land use. Defined roles within the framework ensure the land and people are at the center, and not research agendas. This thesis project directly addressed gaps in holistic understandings of cumulative change while providing a user-friendly standard operating procedure and database for organizing grass roots action around Dene social frameworks. This situates land management around preserving traditional activities and intergenerational knowledge transfer systems.

LIMITATIONS AND NEXT STEPS

It is evident identities which characterize Sambaa K'é First Nation have undergone rapid and widespread change. Alterations to the land and people's relationship have manifested in the form of cumulative impacts which impede the foundations of Dene cultural praxis. This socio-political reality will be exacerbated by climate change indefinitely until SKFN is equipped with the proper tools and routes of expression. These includes ways to be understood, leaders, and innovators in cultural and environmental protection, revitalization, and mutualism. These gaps must be addressed through the utilization of Indigenous-led living research frameworks which ensure Indigenous ways of living are embodied when relating with the land. Dene law must be upheld through sacred protocols which sustain balanced relationships with the land and in management. This perspective illuminates how on the ground action, dispossession of autonomy, and diversity of cumulative impacts compound with disjunct research endeavours to undermine meaningful knowledge synthesis, contribution, and cohesive stewardship actualization in SKFN. Time is a major factor affecting limitations as the complexity and interdisciplinarity of the project requires many iterations to polish logic model design and reduce resistance to users. Thus, limitations primarily consist of receiving proper support in the socio-political actualization of this framework. Specifically, these include maintaining capacity given low local population, retaining funding needed to expand and integrate the project further, and access to scientific advisement on maintaining and improving the GIS logic model via quality assurance and control. More work is required to understand how local databases may be used to boost local capacity and interdisciplinarity between partnerships. Additional research is required to understand influences of mixed epistemological approaches may influence local land ethics through western techniques and data.

REFERENCES

Reed, G., Brunet, N.D., and Longboat, S. 2020. Indigenous Guardians as an emerging approach to indigenous environmental governance. In: Conservation Biology. 35 (1), S. 179–189. DOI:10.1111/cobi.13532.

Kokelj, S.V., Gingras-Hill, T., Daly, S., et al. 2023. The Northwest Territories Thermokarst Mapping collective: A northern-driven mapping collaborative toward understanding the effects of permafrost thaw. In: Arctic Science. DOI:10.1139/as-2023-0009

Application of a solution-orientated approach to support indigenous-led community-based monitoring

Louise Mercer[1], Deva-Lynn Pokiak[2], Dustin Whalen[3], Michael Lim[4] & Paul Mann[1]

[1]*Department of Geography and Environmental Sciences, Northumbria University, Newcastle-Upon-Tyne, Tyne and Wear, United Kingdom*

[2]*Hamlet of Tuktoyaktuk, Tuktoyaktuk, Northwest Territories, Canada*

[3]*Geological Survey of Canada Atlantic, Natural Resources Canada, Dartmouth, Nova Scotia, Canada*

[4]*Department of Mechanical and Structual Engineering, Northumbria University, Newcastle-Upon-Tyne, Tyne and Wear, United Kingdom*

Rapid Arctic warming (Rantanen et al. 2022) is causing multifaceted environmental and socio-ecological impacts to Indigenous and local communities over short and long-term timescales. Coastal landscape thaw and erosion, are of pressing concern across much of the Arctic including Inuit Nunangat (Inuit homeland in Canada). These dramatic changes to permafrost landscapes can increase the risk of mobilisation and toxic release of elements from contaminated sites through different means associated with permafrost thaw (Langer et al. 2023). There is a need for long-term measurements of contaminants across permafrost landscapes to track future risks and identify potential links between climate-driven environmental change and legacy infrastructure.

SOLUTION-ORIENTATED APPROACH

Community-based monitoring (CBM) is increasingly being seen as as a means of collecting valuable baseline environmental data that can contribute to our understanding of environmental change whilst supporting Indigenous governance and self-determination in research (Mercer et al. 2023a). However, there are specific limitations including funding constraints, organisational structures, and operational processes that impact program effectiveness and the progression of research stages beyond data collection. Exemplars from collaborative environmental research conducted in the acutely climate change impacted Hamlet of Tuktoyaktuk, Inuvialuit Settlement Region (ISR), Canada, fed into the co-development of a new solution-orientated model of environmental community-based research (CBR) (Figure 1) that works to ensure continuity between and community ownership in all research stages (Mercer et al. 2023b). Application of the model enables a more complete research workflow and greater equity in research outcomes. It is sufficiently general to be applied to different place-based and research contexts without losing specificity.

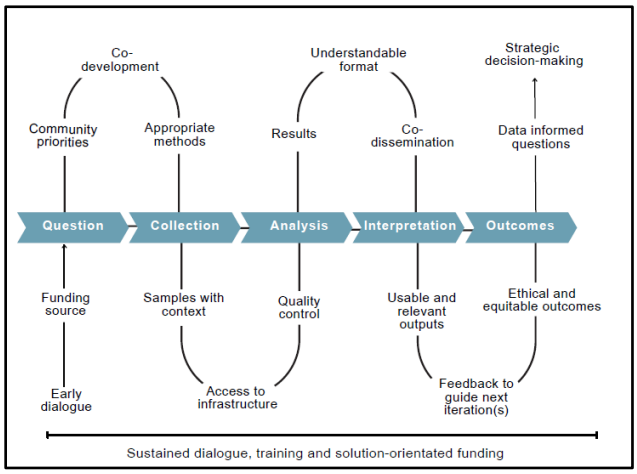

Figure 1. Solution-orientated research workflow (adapted from Mercer et al. 2023b).

CASE STUDY APPLICATION

We present a case study that applied a solution-orientated approach (Mercer et al. 2023b) to rapidly address key community concerns surrounding heavy metal release from different legacy source areas-industry, transport and waste- following a storm event in Tuktoyaktuk in 2022. We outline each stage of our research approach (question development, data collection, analysis, interpretation and outcomes). The approach taken monitored the short-range transport of contaminants and focused on appropriate data collection (i.e., accessible, and applicable sites), whilst proving feasible in terms of human, time and financial resources. To help guide future research collaborations we provide different perspectives from a cross-cultural collaborative partnership between an Indigenous and non-Indigenous ECR.

RESULTS

We highlight temporal trends in heavy metal release following a storm event in Tuktoyaktuk, August 2022. Responsive sampling captured a spike in zinc release from legacy industry source areas post storm event into

the marine environment that later returned to normal levels over the monitoring period. The initial outcomes from the pilot study fed into the proposal development of a larger community-based contaminant monitoring program that now supports a complete Indigenous-led research workflow from proposal development towards informing strategic-decision making.

Conclusion

Our results show that CBM can be used to capture temporal trends in contaminant release, contributing to a better understanding of the role of extreme weather events impact on contaminant release in the Arctic. The approach taken gives an example of the application of a solution-oriented research process that supported the development of an Indigenous-led research program. Collaboration between communities, researchers, funders and policy makers is important to ensure that CBM collected data is translated into decision-making processes. Equity in data collection requires a paralleled equity in capacity to complete later stages of research processes (collation, analysis etc.). Progress must be made to support later stages of research processes to facilitate longevity and continuity in CBM research. To do so requires flexibility, resources (time and financial) and focused training of both ECRs and Indigenous partners to support collaborative partnerships. Further support is required to drive Indigenous-led research from proposal development and aid the transition from externally driven approaches towards more collaborative and autonomous approaches. Doing so will require succession planning, partnership development and alignment of goals between communities, countries and funding agencies.

References

Langer, M., von Deimling, T.S., Westermann, S., Rolph, R., Rutte, R., Antonova, S., Rachold, V., Schultz, M., Oehme, A., and Grosse, G. 2023. Thawing permafrost poses environmental threat to thousands of sites with legacy industrial contamination. Nat Commun 14: 1721. doi:10.1038/s41467-023-37276-4

Mercer, L., Whalen, D., Lim, M., Cockney, K., Cormier, S., Irish, C., and Mann, P.J. 2023a. Towards more inclusive and solution orientated community-based environmental monitoring. Environ. Res. Lett. doi:10.1088/1748-9326/accfb0

Mercer, L., Whalen, D., Pokiak, D.-L., Lim, M., and Mann, P.J. 2023b. Ensuring continuity and impact in Arctic monitoring: a solution-orientated model for community-based environmental research. Environ. Res.: Ecology. doi:10.1088/2752-664X/ad0241

Rantanen, M., Karpechko, A.Y., Lipponen, A., Nordling, K., Hyvärinen, O., Ruosteenoja, K., Vihma, T., and Laaksonen, A. 2022. The Arctic has warmed nearly four times faster than the globe since 1979. Commun Earth Environ 3: 1–10. doi:10.1038/s43247-022-00498-3

Ground temperature and geotechnical data from ten new long-term ground temperature reference sites in five Yukon communities

Moya Painter, Derek Cronmiller & Panya Lipovsky
Yukon Geological Survey, Whitehorse, Yukon, Canada

During a drilling program conducted in the fall of 2023, ten new deep ground temperature monitoring stations were installed in Yukon communities at risk from permafrost thaw. These instrumented boreholes will serve as long-term reference sites in both undisturbed and developed locations within or adjacent to communities, and will fill key knowledge gaps including permafrost thickness and ground temperatures at the bottom of permafrost as well as depth of zero annual amplitude.

The approach for this project was modelled, where possible, on best practices for ground temperature monitoring as proposed by Noetzi et al. (2021), including recommendations for site selection, temperature sampling strategy and drilling procedures. Fifteen boreholes were drilled with a sonic drill in five different communities across the Yukon: Dawson, Ross River, Beaver Creek and Haines Junction. These communities were selected to provide extensive geographical distribution across the territory, while prioritizing the presence of thick permafrost. Within each community, sites were selected to be broadly representative of the permafrost conditions in the region and to provide local baseline data to inform future community and infrastructure development.

Prior to this program, only three of the 34 permafrost-monitoring boreholes managed by the Yukon Geological Survey (YGS) recorded temperatures through the bottom of permafrost, none of which are in the extensive discontinuous or continuous permafrost zones (Heginbottom et al. 1995). Additionally, only four of the preexisting sites were deeper than 10 m, and none surpassed 20 m (Figure 1).

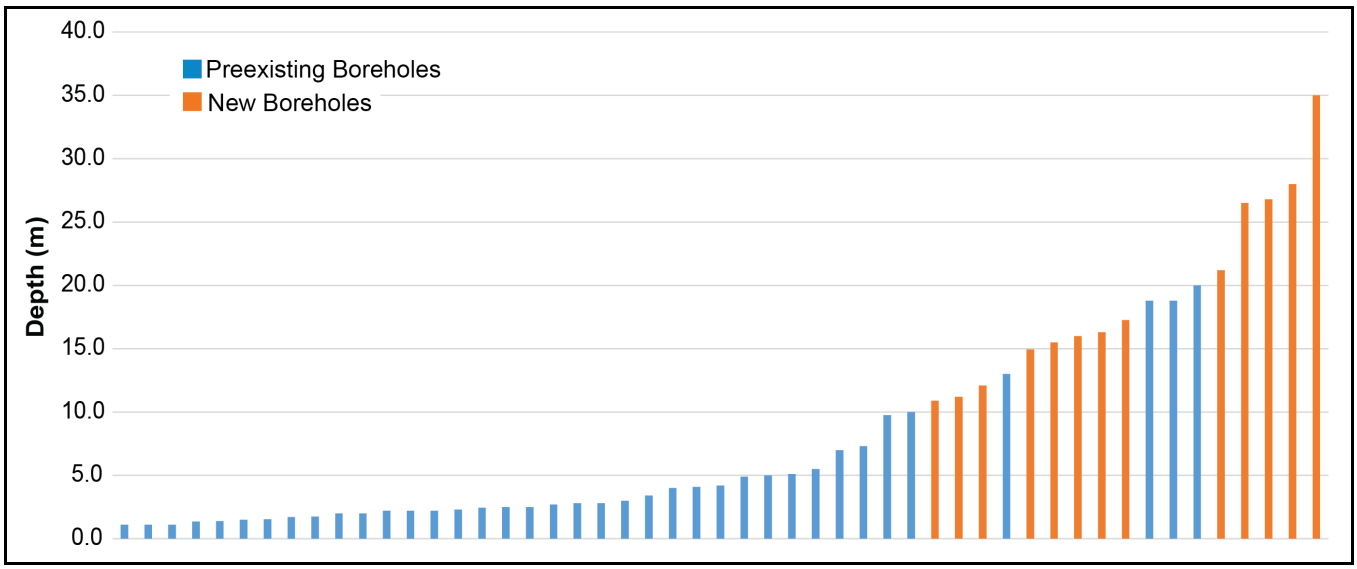

Figure 1. Depth of preexisting and new permafrost monitoring boreholes managed by YGS.

Permafrost was encountered in ten of the fifteen new boreholes, and five boreholes extended below the bottom of permafrost. Preliminary core logging was completed on site to document surficial material thickness, texture, colour, thermal state, ice-content, cryostructures and moisture. Samples were collected at selected representative intervals for laboratory analysis of ice content.

Figure 2A illustrates the stratigraphy from a borehole located in the community of Mayo. Extensive thermokarst ponds and tensions cracks from settlement show that widespread permafrost thaw is occurring in this area. The borehole is 15.5 m deep and materials at this site are primarily ice-rich glaciolacustrine silt and clay.

.

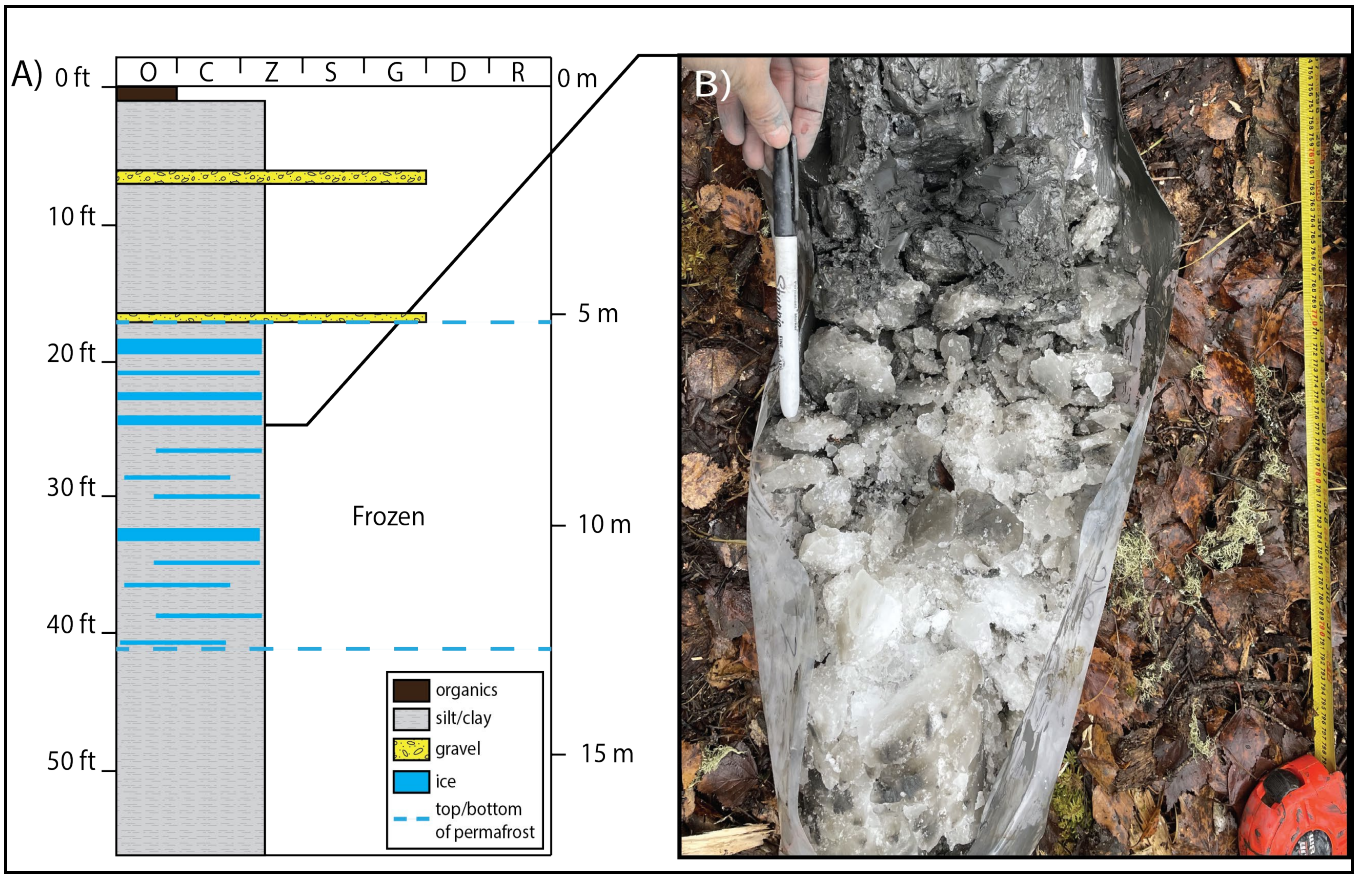

Figure 2. Mayo Group Home Road monitoring site: A) borehole log; and B) ice-rich core at 7.6 m depth.

Preliminary temperature data and drilling observations indicate permafrost begins at 5 m and extends to 12.5 m depth. Ice lenses up to 0.2 m thick were observed between 5 m and 12.5 m, and up to 80% ice was encountered from 5-8 m depth (Figure 2B). Samples taken at 5.2 m, 6.0 m and 6.7 m have excess ice volumes ranging from 51-60%

Customized thermistors strings will be installed to match thermistors with the depth of key permafrost horizons at each borehole. At this time, ground surface temperature loggers will be installed at sites adjacent to the borehole and an additional shallow borehole will be drilled at each site to determine the thermal impacts of site disturbance from drilling and borehole housing on near-surface ground temperatures.

Data and interpretations from each site will inform future development in the area and each site will serve as a reference of how ground temperatures respond to changes in air temperature and precipitation in different regions of the Yukon. Geotechnical data including ice-content measurements will provide more information on extent of ground subsidence expected as permafrost thaws and what the implications might be for existing and future development. Site information and monitoring data will be available on the Yukon Permafrost Database beginning in 2024, and will be updated on an annual basis.

https://service.yukon.ca/permafrost/

References

Heginbottom, J.A., Dubreuil, M.A., and Harker, P.A. 1995. Canada, Permafrost. National Atlas of Canada. Natural Resources Canada, 5th Edition, MCR, p. 4177. https://doi.org/10.4095/294672

Noetzli, J., Arenson, L.U., Bast, A., Beutel, J., Delaloye, R., Farinotti, D., Gruber, S., Gubler, H., Haeberli, W., Hasler, A., and Hauck, C. 2021. Best practice for measuring permafrost temperature in boreholes based on the experience in the Swiss Alps, Frontiers in Earth Science, vol. 9, p. 607875. https://doi.org/10.3389/feart.2021.607875

Electromagnetic signatures in glaciofluvial and glaciomarine deposits in permafrost, Nunavik.

Arianne B. St-Amour[1,2,3], Michel Allard[1,3] & Pascale Roy-Léveillée[1,2,3]

[1]*Center of Northern Studies, Québec City, Québec, Canada*

[2]*Department of Geography, Laval University, Québec City, Québec, Canada*

[3]*Cryo-UL lab, Québec City, Québec, Canada*

Ground penetrating radar (GPR) is often used in permafrost characterization studies. It takes advantage of dielectric contrasts, for instance between soil and rock or water and ice, to detect subsurface contacts such as the active layer/permafrost interface, ice-rich zones, depth to bedrock, stratigraphic contacts between layers of different permafrost properties, and geological structures. Conversely, the electromagnetic signal is attenuated in electrolytic media (e.g., water) which reduces visibility of soil patterns but allows to assess the presence of fine-grained sediments with a fraction of unfrozen water content (Allard et al. 2023; B. St-Amour 2021). GPR has been used extensively to map subsurface conditions in support of land use planning and permafrost conditions under roads and airport runways (Allard et al 2023). To facilitate interpretation, cryostructure and sedimentary structures found in permafrost soils need to be associated with specific electromagnetic signatures or image textures allowing their identification on GPR profiles. This presentation focuses on the interpretation of GPR profiles in glacio-marine sediments of Nunavik, with the support of boreholes and air photo interpretation, to identify structures common in these permafrost environments.

Study site

Inukjuak (Figure 1) is located on the eastern shore of the Hudson Bay and is in the continuous permafrost zone, with a mean annual air temperature of -5.6 °C. The main sedimentary unit in Inukjuak belongs to the Nastapoka drift belt complex, which is a series of submarine ice contact fans formed 8 ka ago during a standstill of the ice front of the Laurentide Ice Sheet near the Hudson Bay coast during deglaciation (Lajeunesse and Allard 2001). This sedimentary sequence is composed of fine sands alternating with clayey silt beds and can vary greatly depending on location, topography, and post-glacial geomorphological history. The general stratigraphy consists of deep-water fine-grained sediments overlain by thick sand and coarser deposits; however, layers of silt several meters thick are also interstratified in the top sandy formations. Important amounts of segregated ice are found in those silty and clayey facies, which are generally on the surface or at shallow depths forming thaw sensitive zones throughout the community.

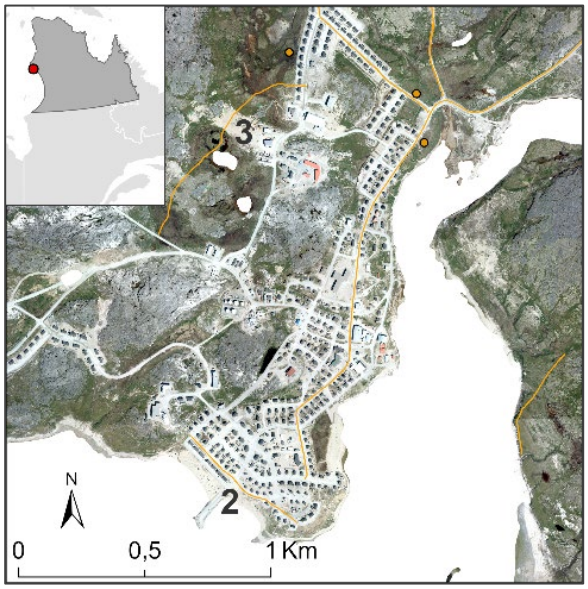

Figure 1. Community of Inukjuak, with GPR surveys collected in 2015 and 2017, shown in orange. The characters 2 and 3 on the map are the locations of excerpts in Figures 2 and 3.

Methodology

Locating both thaw stable and thaw sensitive areas was of primary importance for the purpose of supporting land-use planning. Estimating depth to bedrock was also useful to inform foundation design, particularly for setting piles. GPR profiles were collected in the summers of 2015 and using a Pulse Ekko from Sensors and Software Inc. fitted with antennas operating at the 50 and 100 MHz frequencies. The 100 MHz frequency was used in most of our surveys as it offers a good compromise between resolution of the active layer near the surface and provision of permafrost information to depths of several meters. Investigation depth varied from 3-4 m only, in clay soils, to more than 10 m, in sandy and gravelly deposits. The profiles were interpreted using surface deposit maps, aerial photographs, field observations,

boreholes, or natural stratigraphic sections along rivers as validation tools.

The various GPR patterns, or signatures, associated with different frozen sediments, were compiled to form a collection of signal types to be used as an interpretation key for GPR profiles interpretation in all the surveyed communities of Nunavik. Similarly, point reflectors created by discrete objects and generally producing hyperbolic reflectors, such as ice wedges, culverts, buried wires and boulders were also classified according to their specific signatures. Some stratified sediment types, for instances layered glacio-fluvial sand and gravel and layered raised marine sand in beaches could be identified by typical crossbedding or esker-like internal structures. A few electromagnetic signatures were identified along a GPR profile located near the top of a stratigraphic section along the Innuksuak river.

Results and Discussion

Many sedimentary structures in the sand and gravel layers of the Nastapoka drift complex have distinct electromagnetics signatures. For instance, figure 2 shows a characteristic scour and fill structure. Similar facies were identified in the literature in braided rivers (Ashworth et al. 2011)

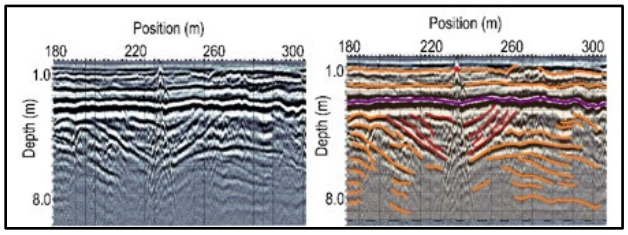

Figure 2. Scour and fill facies identified in red in fluvio-glacial deposits. Stratifications are identified in orange; top of permafrost is in purple. A metallic culvert making a hyperbolic reflector is shown with a red dot.

Glaciomarine deposits such as raised beaches and tombolos, deltaic deposits were also identified on GPR profiles (Figure 3).

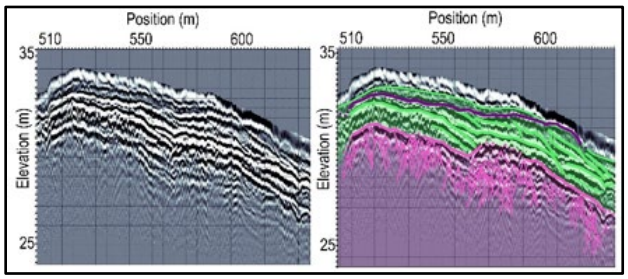

Figure 3. A tombolo in ancient littoral deposits identified in green. In this layered deposit structure, the top of permafrost is identified in purple. The bedrock is identified in pink with overlapping hyperbolic reflectors.

When it was within investigation depth, the underlying bedrock had a characteristic signature, consisting of a typical pattern of overlapping hyperbolic reflectors due to the abundant rock joints in granite-gneiss (Figure 3). This signature could easily be identified as many profiles were purposely run from bedrock outcrops to surrounding unconsolidated sediments.

Conclusion

GPR interpretation of thaw stable vs thaw sensitive permafrost soils was best achieved by delimiting the presence of sedimentary structures in coarse- grained glaciomarine formations favorable for electromagnetic signal travel. When they were near the surface, ice-rich thaw-sensitive fine-grained deposits limited signal penetration to just a few meters, but their spatial extent could nevertheless be determined along the profiles. When the bedrock surface was within reach of the equipment signal, i.e., down to 5-10 m, the characteristic signature of jointed rock allowed its identification, thus providing a critical information to consider construction on end-bearing piles.

References

Allard, M., L'Hérault, E., Aubé-Michaud, S., Carbonneau, A.-S., Mathon-Dufour, V., B. St-Amour, A., and Gauthier, S. 2023. Facing the challenge of permafrost thaw in Nunavik communities: innovative integrated methodology, lessons learnt, and recommendations to stakeholders, Arctic Science, 9, 657–677. doi:10.1139/as-2022-0024

Ashworth, P.J., Sambrook Smith, G.H., Best, J. L., Bridges, J.S., Lane, S.N., Lunt, I.A., Reesink, A.J.H., Simpson, C.J., and Thomas, R.E. 2011. Evolution and sedimentology of a channel fill in the sandy braided South Saskatchewan River and its comparison to the deposits of an adjacent compound bar, Sedimentology, 58, 1860–1883. doi:10.1111/j.1365-3091.2011.01242.x

B. St-Amour, A. 2021. Caractérisation du pergélisol à des fins d'aménagement à l'aide d'un géoradar, Inukjuak, Nunavik. Master's thesis, Laval University, Québec. http://hdl.handle.net/20.500.11794/71019

Lajeunesse, P., and Allard, M. 2002. Sedimentology of an ice-contact glaciomarine fan complex, Nastapoka Hills, eastern Hudson Bay, northern Québec, Sedimentary Geology, 152(3–4), 201–220. doi:10.1016/S0037-0738(02)00069-6

Exploring traditional knowledge of permafrost in the Gwich'in Settlement area and Inuvialuit Settlement Region

Emma Street & Trevor Lantz

School of Environmental Studies, University of Victoria, Victoria, British Columbia, Canada

Temperature increases four times faster than the global average are transforming Arctic landscapes at unprecedented rates (Ratanen et al. 2022). These changes drastically impact permafrost and cause concern for lake drainage, landslides, terrain subsidence, and peatland collapse; all of which have accelerated since the 1950s (Camill 2005; Jorgenson et al. 2010). Projections suggest a 70% reduction of near surface permafrost will occur by 2100 (IPCC 2018). Permafrost thaw will affect ecosystems, infrastructure, and socio-cultural wellbeing, as ground bearing capacity decreases, animal and vegetation patterns shift, and access to travel, hunting and fishing grounds are threatened. However, permafrost studies have historically focused on the ecological and geographic aspects of degradation and tell us little about impact at the community level.

This project seeks to address this research gap, which presents an opportunity to amplify the voices of land users. Indigenous Arctic communities have long been living on permafrost terrain and hold significant Traditional Knowledge and perspectives on frozen earth. This project looks to reshape contributions to permafrost knowledge by placing community experiences and needs at the forefront of conversation. Focusing within the Gwich'in Settlement Area and Inuvialuit Settlement Region in the western Canadian Arctic, this research places permafrost change in a longer-term context and studies the extent of thawing permafrost and its implications.

The goals of this project are to: (1) document Gwich'in and Inuvialuit Traditional Knowledge pertaining to permafrost, (2) map evidence of permafrost change in Gwich'in and Inuvialuit communities, and (3) work with Hunters and Trappers Committees and Renewable Resource Councils to co-develop projects that are responsive to local needs and will inform decision making.

METHODOLOGY

This project draws on 'Two-Eyed Seeing' as a guiding framework, seeing Indigenous knowledges and ways of knowing from one eye, seeing from Western knowledge with the other eye, and using both eyes together for a wholistic approach (Bartlett et al. 2012; Berkes 2012). Further, community based-participatory research drives this work, wherein community members are engaged in all phases of this research process and its outcomes as full and equal partners (Holkup et al. 2004).

As such, this project is in collaboration with local Hunters and Trappers Committees, Renewable Resource Councils, and members of each community. In the research design stage this collaboration involved co-developing research questions, interview procedures, and the research timeline. While conducting research, this collaboration involved hiring a local interview assistant, paying research participants for their time and expertise, and receiving feedback on research findings from each community. Further, all data will be shared and held by research partners, and the second stage of this research – co-developing community projects – will be led by interview outcomes and community interests.

METHODS

In pursuit of the first research goal – to document Gwich'in and Inuvialuit Traditional Knowledge pertaining to permafrost–110 semi-structured interviews have been conducted among the eight communities in the Gwich'in Settlement Area and Inuvialuit Settlement Region, including: Paulatuk, Sachs Harbour, Tuktoyaktuk, Ulukhaktok, Fort McPherson, Tsiigehtchic, Aklavik, and Inuvik. These interviews identified how permafrost knowledge is shared, how community interacts with permafrost, observed changes to permafrost terrain, and the effect of permafrost change.

To support the second research goal – to map evidence of permafrost change in Gwich'in and Inuvialuit communities - ethnographic mapping was incorporated into the semi-structured interviews to identify on maps: permafrost landscape features; land-use activities related to permafrost, including travel corridors, access to food sources, and community infrastructure; and anomalous permafrost conditions. Potential research participants were identified by local partners, through community board and social media postings, and through snowball recruiting techniques. Several participants were interviewed in each community for an approximate hour each.

Initial findings

Interview transcription and coding are currently underway to prepare data for analysis. Initial themes emerging from these interviews show that the effects of climate change are experienced in each community: summer is starting earlier, winter is starting later, storm and precipitation patterns are changing, and new plants and animals are making their way north. Community members were clear that these changes affect permafrost conditions and documented significant observations of permafrost change.

Emerging themes include concerns for the sustainability of infrastructure as houses and camps are requiring blocking and piling changes, more frequent changes, or relocation; cemeteries are challenged by thickening active layers, and water in and around graves, moving caskets and creating challenges for gravesites being dug; and concerns for roads both within and between communities that are developing dangerous hazards and requiring significant amounts of maintenance. Boating and traveling on the land were named as concerns as lakes drain; slump debris create sandbars and limit channel access; and hazards like thickening vegetation, erosion, and soft, uneven terrain threaten trails. Further, observations of changing access to traditional foods were shared, as warming waters render some fish meat too soft or mushy for cooking or drying; key fishing eddies or muskrat trapping spots are disappearing with slumping; and both animal and human travel routes are affected by changing ground. Traditional storage methods for this food have also been responding to permafrost degradation as many ice houses, community freezers, and fish pits have closed as they have started to fill with water and collapse.

Consultation is ongoing with community research partners to mobilize these initial themes into solutions-oriented permafrost projects. Some of this work may involve supporting observer-led monitoring programs, conducting a permafrost priorities and knowledge need assessment, or offering permafrost workshops and training programs. A full analysis of these data will be complete and ready to present at ICOP 2024, along with an initial implementation report of the community-directed permafrost projects.

As widespread permafrost thaw is projected to occur in the 21st century (IPCC 2018) such research and intervention are urgently needed now to protect permafrost environments and the communities that rely upon them.

References

Anisimov, O.A., and Reneva, S. 2006. Permafrost and Climate change: The Russian Perspective, Ambio Journal of the Human Environment, 35(4), 169–175. doi:10.1579/0044-7447(2006)35[169:pacctr]2.0.co;2

Bartlett, C., Murdena, M., and Marshall, A. 2012. Two-Eyed Seeing and other lessons learned within a co-learning journey of bringing together Indigenous and mainstream knowledges and ways of knowing, Journal of Environmental Studies and Sciences, 2, 331–340. doi: 10.1007/s13412-012-0086-8

Berkes, F. 2012. Sacred Ecology, Routledge, New York, New York, USA. Camill, P. 2005. Permafrost Thaw Accelerates in Boreal Peatlands During Late 20th Century Climate Warming, Climate Change, 68(1), 135–152. doi: 10.1007/s10584-005-4785y

Holkup, P.A., Tripp-Reimer, T., Salois, E.M., and Weinert, C. 2004. Community-based Participatory Research, Advancing in Nursing Science, 27(3), 162–175. doi:10.1097/00012272-200407000-00002

IPCC. 2018. Summary for Policymakers In Global Warming of 1.5°C. Cambridge University Press, Cambridge, UK and New York, NY, USA, 3–24.

Jorgenson, M.T., Romanovsky, V., Harden, J., Shur, Y., O'Donnell, J., Schuur, E.A.G., Kanevskiy, M., and Marchenko, S. 2010. Resilience and vulnerability of permafrost to climate change, Canadian Journal of Forest Research, 40(7), 1219–1236.

Ratanen, M., et al. 2022. The Arctic has warmed nearly four times faster than the globe since 1979, Communications Earth & Environment, 3(1), 1–10. doi:10.1038/s43247-022-00498-3

Permafrost thaw slump impacts on culturally and ecologically important fish habitat in the Peel River Watershed, Canada

Jackie Ziegler[1], Trevor Lantz[1], Mike Newton[1], Steven V. Kokelj[2], Sarah Lord[3,4] & Gwich'in Tribal Council Department of Culture and Heritage[5]

[1]*School of Environmental Studies, University of Victoria, Victoria, British Columbia, Canada*

[2]*Northwest Territories Geological Survey, Government of Northwest Territories, Yellowknife, Northwest Territories, Canada*

[3]*Gwich'in Renewable Resources Board, Inuvik, Northwest Territories, Canada*

[4]*Department of Fisheries and Oceans, Inuvik, Northwest Territories, Canada*

[5]*Gwich'in Tribal Council Department of Culture and Heritage, Fort McPherson, Northwest Territories, Canada*

In Northwestern Canada, increased temperatures and precipitation are intensifying forms of permafrost degradation like retrogressive thaw slumps (Segal et al. 2016). These disturbances can mobilize large quantities of sediment into adjacent rivers, creeks and lakes (Vonk et al. 2015). These thaw-driven landscape changes have the potential to impact fish spawning and migration areas, as well as Indigenous harvesting sites and travel routes critical to sustaining Indigenous cultures and access to traditional foods (Kokelj et al. 2013; Proverbs et al 2020b). However, very little information exists regarding the impacts of thaw slump expansion on culturally and ecologically important fish habitat in Canada's northern regions, including the Peel River Watershed. The objective of this study was to increase our understanding of thaw slump impacts on important food fish habitat in the portion of the Peel River Watershed within the Gwich'in Settlement Region using both Indigenous knowledge and western scientific knowledge.

Community Collaboration

This project is a collaboration among the University of Victoria, the Gwich'in Renewable Resources Board, the Gwich'in Tribal Council Department of Culture and Heritage, the Northwest Territories Geological Survey, and the Renewable Resource Councils of Aklavik, Inuvik, and Tetlit Zheh (Fort McPherson). This study was suggested as a next step during discussions of Proverbs et al.'s (2020a) study methods and results with Gwich'in partners in February 2018. Gwich'in fishers are concerned about the impact that high rates of permafrost slumping in the Peel River Watershed may have on culturally important fish habitat downstream and the Gwich'in Renewable Resources Board has identified this as a research priority.

Approach

We explored the potential to use GIS to assess the impacts of permafrost thaw on culturally and ecologically important fish habitat by undertaking a spatial overlay analysis using ArcGIS Pro 1.2 software (ESRI, USA). To complete this overlay analysis, we combined maps of: (1) the density and distribution of important fish habitat in the Peel River Watershed from interviews with Gwich'in knowledge holders, archived spatial data from the Gwich'in Tribal Council Department of Culture and Heritage, and a review of the scientific literature, and (2) the cumulative downstream impacts of thaw slumps in the area provided by the Northwest Territories Geological Survey (Kokelj et al. 2021) (Figure 1). By using both Indigenous and western scientific knowledge, we draw on multiple perspectives that provide a more complete understanding of these impacts.

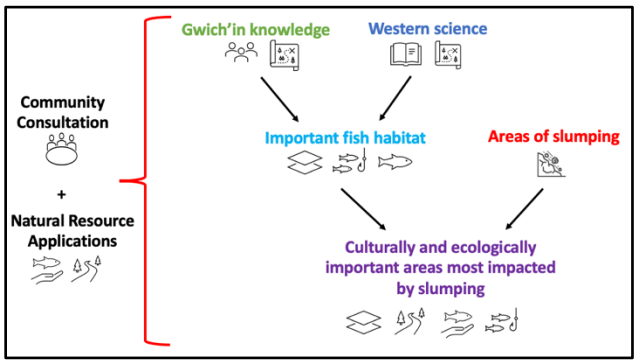

Figure 1. Overview of the methods used to assess the impacts of permafrost slumping on culturally and ecologically important fish habitat in the Peel River Watershed of the Gwich'in Settlement Region.

Results

We found that important fish habitat in the mainstem of the Peel River stretching from Tetlit Zheh (Fort McPherson) to the mouth of Tr'ineeditr'aii Njik (Wind River) is in the high and very high overlap category. This means that these areas are at high potential risk of experiencing the impact of sediment flow from the slumps upstream. Other areas of high

risk include large sections of the main tributaries including Gwatoh Taii Njik (Stony Creek), Vitreekwaa Viteetshìk (Vittrekwa River), Vihtł'òo Njik (Road River), Tr'atr'aataii Njik (Trail River), and Gyuu Dazhoo Njik (Snake River).

IMPORTANCE OF THIS RESEARCH

We hope that the findings of this project will inform regional decision-making and adaptation planning and help fill gaps in our knowledge of fish habitat and traditional use in the Peel River Watershed. To date, few cumulative environmental impact assessments adequately address impacts to cultural practices and livelihoods tied to impacted ecosystems (Adams et al. 2023). The methods developed in this project provide a model to include both Indigenous knowledge and scientific knowledge in cumulative impacts assessments. Our results highlight the importance of mixed methods to monitor ongoing landscape changes in areas that are inherently sensitive and culturally significant. The impacts of slumping across an entire watershed remain poorly understood and additional research is needed on a range of topics including fish health, water quality, and macroinvertebrate community structure.

REFERENCES

Adams, M.S., Tulloch V.J.D., Hemphill, J., Penn, B., Anderson, L.T., Davis, K., Avery-Gomm, S., Harris, A., and Martin, T.G. 2023. Inclusive approaches for cumulative effects assessments, People and Nature 5(2): 431–445. doi:10.1002/pan3.10447

Kokelj, S.V., Kokoszka, J., van der Sluijs, J., Rudy, A.C.A., Tunnicliffe, J., Shakil, S., Tank, S.E., and Zolkos, S. 2021. Thaw-driven mass wasting couples slopes with downstream systems, and effects propagate through Arctic drainage networks, The Cryosphere 15(7): 3059–3081. doi:10.5194/tc-15-3059-2021

Kokelj, S.V., Lacelle, D., Lantz, T.C., Tunnicliffe, J., Malone, L., Clark, I.D., and Chin, K.S. 2013. Thawing of massive ground ice in mega slumps drives increases in stream sediment and solute flux across a range of watershed scales, Journal of Geophysical Research: Earth Surface 118(2): 681–692. doi:10.1002/jgrf.20063

Proverbs, T.A., Lantz, T.C., and Gwich'in Tribal Council Department of Cultural Heritage. 2020a. Cumulative environmental impacts in the Gwich'in cultural landscape, Sustainability 12(11): 4667. doi:10.3390/su12114667

Proverbs, T.A., Lantz, T.C., Lord, S.I., Amos, A., Ban, N.C., and Gwich'in Tribal Council Department of Cultural Heritage. 2020b. Social-ecological determinants of access to fish and well-being in four Gwich'in communities in Canada's Northwest Territories, Human Ecology 48(2): 155–171. doi:10.1007/s10745-020-00131-x

Segal, R.A., Lantz, T.C., and Kokelj, S.V. 2016. Acceleration of thaw slump activity in glaciated landscapes of the western Canadian Arctic, Environmental Research Letters 11(3): 034025. doi:10.1088/1748-9326/11/3/034025

Vonk, J.E., Tank, S.E., Bowden, W.B., Laurion, I., Vincent, W.F., Alekseychik, P., Amyot, M., Billet, M.F., Canário, J., Cory, R.M., Deshpande, B.N., Helbig, M., Jammet, M., Karlsson, J., Larouche, J., MacMillan, G., Rautio, M., Walter Anthony, K.M., and Wickland, K.P. 2015. Reviews and syntheses: Effects of permafrost thaw on Arctic aquatic ecosystems, Biogeosciences 12(23): 7129–7167. doi:10.5194/bg-12-7129-2015

1B — Permafrost Data Management and Climate Services

Session Chairs: Cécile Pellet[1], Prashant Baral[2], Niels Weiss[3], Nick Brown[4], Shawn Marshall[5] & Stephan Gruber[4]

[1]*Department of Geosciences, University of Fribourg, Fribourg, Switzerland*
[2]*ICIMOD, Kathmandu, Nepal*
[3]*Northwest Territories Geological Survey, Government of Northwest Territories, Northwest Territories, Canada*
[4]*Carleton University, Ottawa, Ontario, Canada*
[5]*Environment and Climate Change Canada, Ottawa, Ontario, Canada*

Permafrost knowledge and data must be accessible and useable for people living on permafrost, planning adaptation, or conducting research. Yet few services concerning changing permafrost exist, and significant challenges and gaps remain in the management of permafrost data. In this session, we invite contributions that explore progress in the collection, management, and dissemination of permafrost data as well as envision and demonstrate permafrost climate services from diverse perspectives.

Permafrost data includes not only “traditional” permafrost observations such as ground temperature, active-layer thickness, and ground ice type or abundance, but also other types of permafrost data such as rock glacier velocity, traditional knowledge, landform inventories, or geophysical data. Corresponding contributions can describe (1) software or methods; (2) platforms and portals; (3) examples of applying the FAIR principles (findable, accessible, interoperable, reusable) to permafrost data; and (4) success stories in data sharing and collaborative workflows.

The concept of Permafrost Climate Services builds on the WMO Global Framework for Climate Services that emphasizes the importance of user needs and co-development. Climate services are understood as climate information prepared and delivered to meet user needs, and there is growing experience in delivering them. Permafrost Climate Services will have distinct attributes such as the combination of knowledge and data about the atmosphere, the land surface, and the subsurface.

Permafrost climate services for developing climate resilience guidelines for hydropower development in a Central Himalayan catchment

Prashant Baral & Miriam Jackson

International Centre for Integrated Mountain Development, Lalitpur, Bagmati Province, Nepal

Permafrost warming and thawing will lead to unstable mountain landscapes, changes in hydrologic processes and increases in river sediment in the high mountains of the Hindu Kush Himalaya (HKH) (Figure 1). However, information on permafrost extent is severely limited, as well as the status of the permafrost and projected changes in this region.

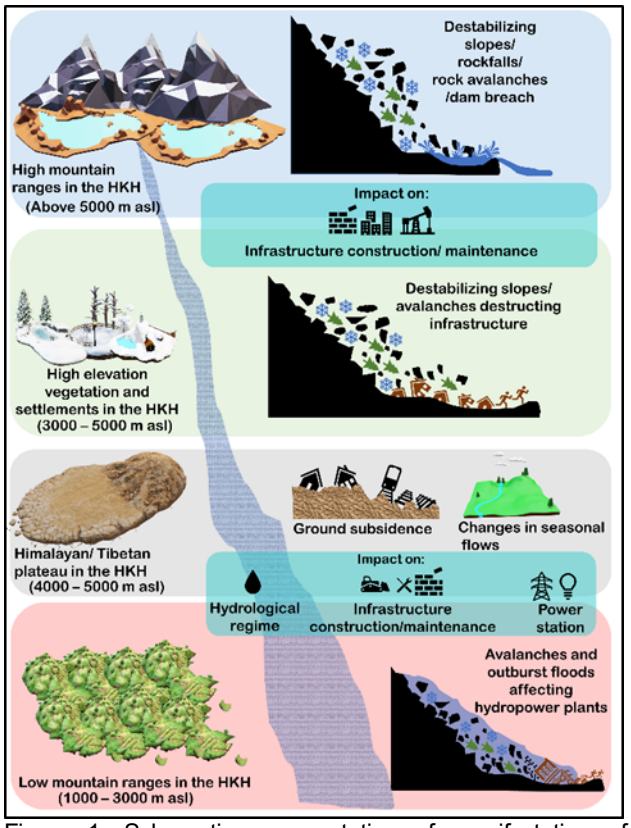

Figure 1. Schematic representation of manifestation of permafrost changes at different elevation ranges in the HKH and how it may affect the hydropower production.

Several large infrastructure projects, mainly hydropower plants, are being planned or constructed in close proximity to unstable mountain slopes without considering the implications of changing permafrost conditions and performing the necessary assessments. However, it is already well established that climate science knowledge should be incorporated into the planning, design, and operation of hydropower plants (Cherry et al. 2017; Li et al. 2021; Li et al. 2022).

Slope failure due to permafrost thaw can lead to cascading hazards, e.g. by triggering Glacial Lake Outburst Floods, further increasing the risk posed by thawing permafrost on the construction and maintenance of hydropower plants. Permafrost degradation is expected to influence the origin, magnitude, and distribution of cascading hazards, and could lead to substantial damage of hydropower development. To understand the consequences of changing permafrost requires comprehensive knowledge of permafrost extent, status, characteristics, and processes in the context of a changing climate

Permafrost climate services can provide readily accessible data on future permafrost conditions to assist in adaptation planning (Gruber et al. 2023). At present, permafrost information for the HKH is inadequate and limited to a few maps for permafrost probability in the Northern Hemisphere (e.g., Obu et al. 2019; Ran et al. 2022), a global permafrost zonation map (Gruber 2012) and limited sites with record of ground temperature (at shallow depths) and other geophysical measurements, although information on the neighbouring Qinghai-Tibet plateau is much more extensive.

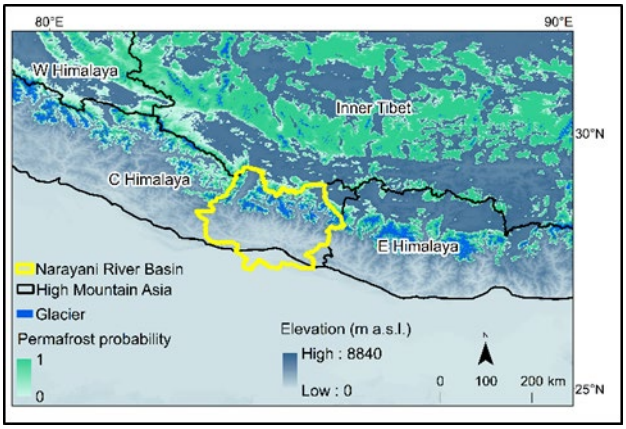

Figure 2. Narayani River Basin in the Central Himalayas. Spatial distribution of glaciers (from RGI Consortium. 2017) and permafrost probability (from Obu et al. 2019) shown in the background.

Some studies in the HKH have explored the application of global climate data, remote sensing data, local meteorological data, and computer models to estimate the geographic coverage of permafrost.

In the Narayani river basin in Central Himalaya, there is extensive hydropower development, with more under construction or in the planning stage (Figure 2). We have produced maps of modelled permafrost extent for this area using global climate data and a model of permafrost extent (Gruber 2012) (Figure 3). We have also developed permafrost probability maps using topoclimatic variables and machine learning techniques. These first-order estimates of permafrost extent are used to identify potential areas with possible marginal permafrost – areas that are vulnerable to small-scale increments of air temperature – in the basin.

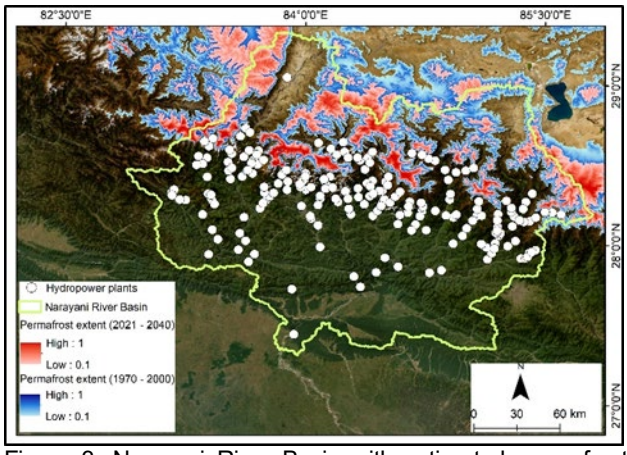

Figure 3. Narayani River Basin with estimated permafrost extent for 1970-2000 and 2021-2040, and locations for planned and operational hydropower plants in the catchment.

Note that the marginal permafrost areas are identified by subtracting model outputs from two equilibrium models, so uncertainties in data and estimates mean they may not be accurate, and results from marginal permafrost areas should be treated wth caution. However, in a region of limited data, the potential for a more robust analysis is limited. Furthermore, we note that the impact of permafrost thaw and resulting hazards often extend beyond identified marginal permafrost areas.

Our preliminary estimates of marginal permafrost areas are correlated with locations for planned and constructed hydropower plants, glacial lakes and potentially dangerous glacial lakes in the basin. As these estimates of permafrost extent are subject to significant uncertainties and there is a lack of field-based permafrost observations as well as quantitative estimates of hydrological response to changes in permafrost, the limited information available is used to develop qualitative recommendations for developing climate resilience guidelines for hydropower development in the catchment. These recommendations can serve as necessary preliminary climate resilient guidelines for hydropower development in the catchment and assist in selection of hydropower construction sites and preparedness for response to compound and cascading hazards, as well as suggest where further investigation of permafrost status should be explored.

References

Cherry, E.J., et al. 2017. Planning for climate change impacts on hydropower in the Far North, Hydrology and Earth System Sciences, 21(1): 133–151. doi:10.5194/hess-21-133-2017

Gruber, S. 2012. Derivation and analysis of a high-resolution estimate of global permafrost zonation, Cryosphere, 6(1): 221–233. doi:10.5194/tc-6-221-2012

Gruber, S., et al. 2023. 'Considerations toward a vision and strategy for permafrost knowledge in Canada, Arctic Science, 9(4): 4–8. doi:10.1139/as-2023-0016

Li, D., et al. 2021. 'Exceptional increases in fluvial sediment fluxes in a warmer and wetter High Mountain Asia, Science, 374(6567): 599–603. doi:10.1126/science.abi9649

Li, D., et al. 2022. High Mountain Asia hydropower systems threatened by climate-driven landscape instability, Nature Geoscience, 15(7), 520–530. doi:10.1038/s41561-022-00953-y

Obu, J., et al. 2019. Northern Hemisphere permafrost map based on TTOP modelling for 2000–2016 at 1 km^2 scale, Earth-Science Reviews, 193, 299–316. doi:10.1016/j.earscirev.2019.04.023

Ran, Y., et al. 2022. New high-resolution estimates of the permafrost thermal state and hydrothermal conditions over the Northern Hemisphere, Earth System Science Data, 14(2): 865–884. doi:10.5194/essd-14-865-2022

RGI Consortium. 2017. Randolph Glacier Inventory - A Dataset of Global Glacier Outlines, Version 6 [Data Set]. Boulder, Colorado USA. National Snow and Ice Data Center. https://doi.org/10.7265/4m1f-gd79. Date Accessed 12-07-2023.

Best-practices for permafrost data: Actionable recommendations for field scientists and database managers

Nicholas Brown[1,2], Stephan Gruber[2], Peter Pulsifer[2,3,4] & Amos Hayes[3,4]

[1]*NSERC PermafrostNet, Canada*

[2]*Department of Geography and Environmental Studies, Carleton University, Ottawa, Ontario, Canada*

[3]*Geomatics and Cartographic Research Centre, Carleton University, Ottawa, Ontario, Canada*

[4]*Canadian Consortium for Arctic Data Interoperability, Canada*

Permafrost data is hard to come by, despite its importance and the need for interoperable open data and modelling tools (Gruber et al. 2023). Permafrost databases increasingly provide access to large collections, but their holdings still only represent a fraction of what has been collected (Brown et al. 2020). Datasets in repositories or as part of journal publications are not standardized, reducing our ability to integrate data for broader-scale studies (Bavay 2020).

We attribute this, in part, to the set of challenges described below. To overcome these, we present a set of recommendations for streamlining permafrost data management from field collection to publication, leading to benefits for individuals collecting, distributing, and accessing permafrost data. We focus on field observations, particularly for monitoring ground temperature.

Challenges

Based on workshops in the permafrost community, and management of a large in-situ monitoring network (e.g., Gruber et al. 2018), we identify five challenges that limit the throughput of permafrost data from collection to publication, impacting both scientific research and other use of data for public good. (1) The varied nature of permafrost data means that they are often siloed, despite value in synergy. (2) Data management is difficult to scale up from site-level investigations. (3) There is a pervasive lack of resources for managing and distributing permafrost data. (4) Those interested in permafrost data have a diverse set of needs and wants. (5) Few ways exist to standardize or integrate datasets. The following sections outline recommendations to address these challenges.

Distinguish location and instrumentation

As monitoring networks grow larger and the number of individuals and instruments grow, rigorous sensor mapping—tracking sensor locations over time and attributing each data point to a location—can help ensure scientific quality and prevent misattribution.

Adopt and adapt existing standards

There are few dedicated standards for permafrost data. Instead, we recommend relying on existing broader standards, making modifications or contributions as necessary.

One such example are the Climate and Forecast (CF) Conventions, and the Attribute Convention for Data Discovery. Although these were originally designed for use with netCDF files and climatic data, there are many elements that are transferable to permafrost, including a rich metadata framework to recognize authorship and contributors to data, as well as a collection of standardized variable names which can be used to unambiguously identify what is contained within a dataset. Many permafrost-specific variables have recently been added to this list as part of *adapting* it for the permafrost community.

Existing permafrost databases and formats can also provide guidelines for data standardization. For those responsible for large permafrost data collections, consider that these can act as a model for others; we recommend *documenting* ad-hoc data formats and using versions when making changes over time.

Collaborate and build on shared tools

The adopt-and-adapt mentality is relevant beyond standardization. Effort is duplicated for many common tasks despite the lack of resources for data management and processing. This can be remedied through the collaborative development of tools.

As a demonstrator, we developed a python package titled tsp for working with ground temperature data. These data originate from a variety of sources and are highly heterogeneous, impeding the development of standardized workflows for quality control or publication. The tsp package reads ground temperature data from a variety of sensors and provide reusable functionality for the most common analysis and visualization tasks (Brown 2022). Contribution is encouraged to support additional data sources.

Consider multiple distribution pathways

To accommodate the different needs of the broader permafrost community, it is valuable to make data available in different ways, ranging from interactive graphs to GIS layers. However, it is unlikely that a single platform or organization will be able to accommodate all possible use cases. Instead, consider making data available through several different channels.

For example, make up-to-date data accessible in a way that provides value-added visualization or querying capabilities (such as through ERDDAP, which takes advantage of the existing standards discussed above), and periodically publish the entire collection as *snapshots* in a data repository with versioned DOIs (e.g., CPERS Collective 2023). Additional data access points can refer back to the latest publication to ensure appropriate attribution.

By providing access to data in a way that can be queried, it can be used by others to create services relevant to other stakeholders that you may not have considered. However, such a system is difficult to achieve with restrictive data licenses. For this reason, we recommend publishing data under permissive licenses requiring, at most, attribution of original authorship.

Balance technology and practice

Technological solutions are not a panacea, equally important is deciding on, documenting, and updating over time a strategy for data handling and ensuring this is part of the onboarding process for your team.

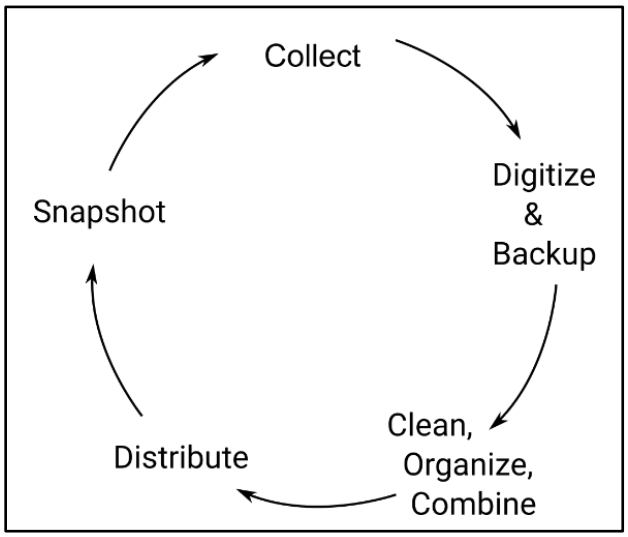

Figure 1. An example field-to-publication data process.

When considering long-term data collection campaigns, these recommendations can be summarized in Figure 1. Following data collection, relevant artefacts such as sensor output and digitized field notebooks should be backed up. Next, new data are integrated with existing data, creating a complete record at each site. This up-to-date dataset is made available using an interoperable endpoint. Optionally, a snapshot is published for long-term archival.

Summary and conclusion

No one database will solve our challenges with permafrost data. Instead, small and coordinated steps toward interoperability and shared tools will yield progress by meeting the short-term needs of those who generate data and advancing interoperable data and the incremental development of new products, services, and research benefiting from this data.

References

Bavay, M., Fiddes, J., and Godøy, Ø. 2020. Automatic Data Standardization for the Global Cryosphere Watch Data Portal, Data Science Journal 19(6). doi:10.5334/dsj-2020-006

Brown, N., Gruber, S., Pulsifer, P., and Stewart-Jones, E. 2020. Permafrost Data Workshop 2020: final report. Technical Report. Carleton University, Ottawa. doi:10.22215/pn/10120001

Brown, N. 2022. tsp ("Teaspoon"): A library for ground temperature data., Journal of Open Source Software, 7(77) :4704. doi:10.21105/joss.04704

CPERS Collective 2023. The Canadian Permafrost Electrical Resistivity Survey Database (CPERS). Nordicana D 121. doi:10.5885/45855XD-DC9883ABD609428B

Gruber, S., Brown, N., Stewart-Jones, E., Karunaratne, K., Riddick, J., Peart, C., Subedi, R., and Kokelj, S. 2018. Air and ground temperature, air humidity and site characterization data from the Canadian Shield tundra near Lac de Gras, Northwest Territories, Canada. Nordicana D, 39. doi:10.5885/45561XD-2C7AB3DCF3D24AD8.

Gruber, S., Hayley, J., Karunaratne, K., King, J., MacLean, T., Marshall, S., and Moore, D. 2023. Considerations toward a vision and strategy for permafrost knowledge in Canada. Arctic Science. doi:10.1139/as-2023-0016

Wilkinson, M., Dumontier, M., Aalbersberg, I., et al. 2016. The FAIR Guiding Principles for scientific data management and stewardship. Scientific Data, 3: 160018. doi:10.1038/sdata.2016.18

Permafrost legacy data: Making the most of a rich history of United States Geological Survey permafrost research

Alena Giesche, Eva Stephani & Elizabeth K. Drewes-Todd

Alaska Science Center, United States Geological Survey, Anchorage, Alaska, United States

Permafrost legacy data describe undigitized records, including hand or typewritten data log sheets, notes, and maps, that exist in various archives (Figure 1). Much of these data have never been released – perhaps only referenced in the text of a journal article, or partially appearing (often hand drawn) in a figure. Digital data releases became the standard practice for the United States Geological Survey (USGS) in 2018 (Order 3369), and this provides a mechanism for digitizing and releasing legacy datasets. For the community of permafrost researchers who work in a rapidly changing environment, legacy data are extremely valuable. For example, comparing modern conditions with an older baseline allows us to assess the degree of change, as well as the drivers and interactions behind this change. Legacy data such as daily borehole temperature logs over a period of months or years, sometimes paired with detailed daily descriptions of local climatological variables such as snow depth, wind, and ice thickness, can shed light on future permafrost thaw rates over various terrain types. The USGS Alaska Science Center is in the process of reviewing and digitizing legacy records for publication to help advance our understanding of permafrost, including data collected by the late USGS researcher Max Brewer while at the Naval Arctic Research Laboratory (NARL) in Utqiagvik (Barrow) Alaska in the 1950s and 1960s.

Max Brewer (1924-2012) was the longest serving director of the NARL from 1956-1971 after its establishment in 1947 (and closure in 1980). After serving in the US Army in World War II as a meteorologist, Brewer then studied to be a geological engineer at Washington University in St. Louis, MO, and joined a USGS project in 1948 to establish the technique of electrical resistivity to measure and map permafrost around Fairbanks, Alaska. Based on this experience, he was offered a posting in Utqiagvik (Barrow), which he accepted in September 1950 after finishing his University studies. As part of Brewer's work at the NARL, dozens of installations were set up in abandoned wells, with measurements (as deep as 30 m or more) taken on an approximately weekly basis for up to 12 years. In 1953, several installations were added in newly drilled boreholes with Navy support. Among other projects, Brewer oversaw the establishment of several research stations on ice floes in the Arctic Ocean in the late 1950s and 1960s in collaboration with the US Air Force and Navy, partly thanks to intensified research efforts spurred by the International Geophysical Year (1957-1958). After serving as the NARL director, Brewer became Alaska's first Commissioner of the Department of Environmental Conservation (1971-1974), authored the environmental impact statements for the National Petroleum Reserve in Alaska (NPRA) in 1975 and 1977, and then took on the role of Chief of Operations for the USGS in the NPRA in 1977. Brewer retired from the USGS in 1994.

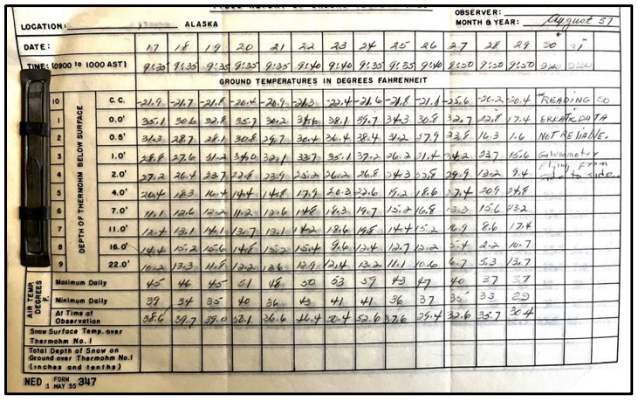

Figure 1. Example of handwritten daily ground and air temperature measurements from August 1957.

LEGACY DATA POTENTIAL

In a 2001 interview with the Byrd Polar Research Center, Brewer mentioned one of his regrets was not doing more writing. Indeed, given the massive volume of data collected under Brewer's leadership at the NARL, surprisingly few publications directly synthesize these data (e.g., Brewer et al. 1958a; Brewer et al. 1958b; Robinson and Brewer 1964). When initially collected, much of these data were mainly of interest to the military and engineering projects. Today, with permafrost thaw and climate change affecting Arctic communities, Brewer's legacy data have become even more valuable. The USGS archive holds more than 40 boxes of data, notes, and photos relating to this work. This includes weekly to monthly thermistor readings from "Camp Holes" #1-5 (1950-1951 and 1960), "Special Holes" #1-43 (covering date ranges between 1950 and 1961), and daily ground temperature measurements from the Barrow airport

weather station (1950-1957). Boreholes were in various terrain types, including by fresh or brackish lakes, wetlands, shore of the Arctic Ocean, the local airstrip, high centered polygons, and under various buildings. Many of these boreholes could be revisited, as was done 50 years later for one of these locations in the early 2000s (Romanovsky et al. 2002). We hope to undertake and facilitate studies to build upon this tremendous legacy data resource.

REFERENCES

Brewer, M.C. Interview by K.N. Brewster. 5 May 2001. Byrd Polar Research Center Archival Program. https://kb.osu.edu/items/f9304498-ae3c-551d-8b23-f65bf3ee181e. Accessed 5 December 2023.

Brewer, M.C. 1958a. Some results of geothermal investigations of permafrost in northern Alaska. Eos, Transactions American Geophysical Union, 39(1), 19–26. https://doi.org/10.1029/TR039i001p00019

Brewer, M.C. 1958b. The thermal regime of an Arctic lake. Eos, Transactions American Geophysical Union, 39(2), 278–284. https://doi.org/10.1029/TR039i002p00278

Robinson, F.M., and Brewer, M.C. 1964. Core tests, Simpson area, Alaska, with a section on temperature measurement studies. Geological Survey Professional Paper No. 305-L, 645–730. U.S. Geological Survey, Washington, DC, USA.

Romanovsky, V., Burgess, M., Smith, S., Yoshikawa, K., and Brown, J. 2002. Permafrost temperature records: Indicators of climate change. EOS, Transactions American Geophysical Union, 83(50), 589–594. https://doi.org/10.1029/2002EO000402

Permafrost climate services

Stephan Gruber

Department of Geography and Environmental Studies, Carleton University, Ottawa, Ontario, Canada

The IPCC Special Report on the Ocean and Cryosphere in a Changing Climate revealed the benefits of ambitious mitigation and effective adaptation for sustainable development and, conversely, the escalating costs and risks of delayed action (IPCC 2019). These costs and risks include those arising from permafrost thaw, projected, and already observed in polar and high-mountain regions. This contribution frames permafrost climate services as a key element of evidence-based support for decisions about adapting to permafrost thaw.

New knowledge and next practice are needed

There is a long history of living and working on and with permafrost. By contrast, permafrost thaw due to climate change is a new challenge for which we can only partially rely on past experience. A forward-looking next practice, extending best practice into anticipated future environments, is needed for living with and adapting to permafrost thaw (Figure 1).

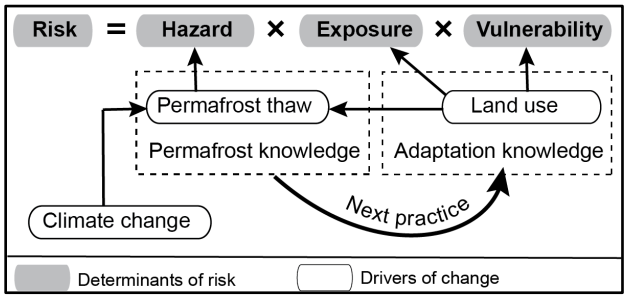

Figure 1. Permafrost thaw can increase risk via multiple and often cascading hazards. Adaptation of land use can reduce risk by lowering exposure and vulnerability and by reducing disturbance to permafrost. Climate change is an additional and persistent new driver.

The knowledge needed to support adaptation decisions differs between environments and types of land use. In some instances, common sense and past experience will suffice, and in others, geotechnical and geomorphological knowledge will help to stay clear of areas susceptible to thaw-related hazards. In other instances, quantitative information about the severity, timing, and location of permafrost thaw will be needed for informing the planning, design, and maintenance of structures. Some of this knowledge exists, some is emerging, and most of it needs to be better connected to support action (Gruber et al. 2023).

Services support decisions and research

To support decisions efficiently, knowledge needs to be available, suitable, and trustworthy. Weather prediction supports our everyday lives, from apps on smartphones to aviation forecasts supporting airlines and pilots. Climate services are now emerging to make information about future climate broadly available and to create a common basis that can be used in standards (e.g., BNQ 2023). Through these services, decades of research in atmospheric science and related fields are improving the lives of people. The capabilities created by operationalizing services have enabled new advances in research within and across disciplinary boundaries.

By comparison, few (if any) services exist for permafrost knowledge and for anticipating future permafrost changes. This is rooted in the remote and hidden nature of permafrost, as well as the importance of local site conditions, understanding which was often sufficient for the decisions to be made in the near-equilibrium climate of past decades. Today, quantifying the interaction of climate with site conditions requires new knowledge and capacity.

A gap exists between the need for forward-looking information and the ability to provide it. The relevant knowledge and methods are found across differing academic disciplines, locations, and sectors. Creating services will accelerate how permafrost knowledge can be connected and delivered for action.

Permfrost climate services

The Global Framework for Climate Services (WMO 2011) positions climate services as information and products that support individuals and organizations in forward-looking decision-making related to climate change and its consequences. Co-development (inclusive, collaborative, decisions driven, iterative) with the intended users has been shown to produce best results (Vincent et al. 2018).

In many jurisdictions around the world, research, operational capabilities, and institutions to generate and deliver climate services have emerged in the past decade. Information from climate models alone, however, cannot readily be interpreted to inform permafrost-related decision making.

Permafrost climate services will be distinct in three ways. (1) They will combine knowledge, data, and methods from the fields of geology, ecology, and

atmospheric science. (2) They will be built practically from scratch, as opposed to other climate services that grew from established institutions in numerical weather prediction and hydrology. (3) They may not be perceived as urgent or important as permafrost areas are sparsely populated and remote.

Permafrost climate services can be conceptualized inside the intersection of three domains (Figure 2). For each domain and their individual intersections, practices, services, and standards for risk reduction exist. For example, for determining snow loads or for hazard mapping. By contrast, the anticipation of future hazards controlled by permafrost thaw is novel. For example, how temporal change in mapped hazard zones can be derived in an evidence based and reproducible way.

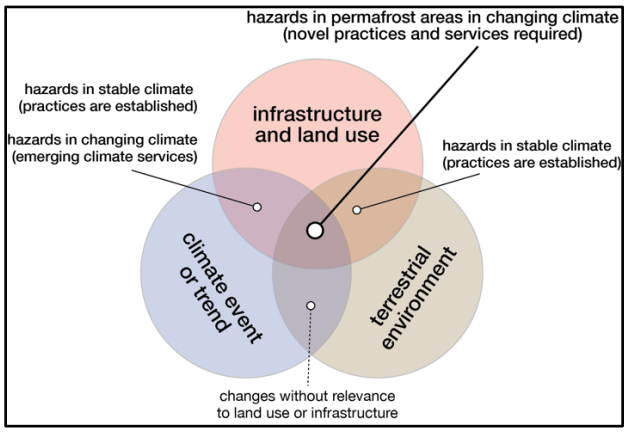

Figure 2. Permafrost climate services address challenges in a novel and expanding intersection of three domains. Permafrost affects most terrestrial systems in its environments. The reaction of permafrost to climate change often causes an unprecedented amplification of climate change into hazards.

The detailed requirements for permafrost climate services can only emerge and evolve from co-development with users. Nevertheless, some needs for information can be outlined: (A) Observed permafrost conditions and changes. This includes ground temperature and active-layer thickness but also ground-ice content and geomorphic change that is clearly related to ground-ice loss such as thermokarst (Kokelj et al. 2023). (B) Maps that can easily be related to local conditions (e.g., Allard et al. 2023; Boeckli et al. 2012). (C) Simulations of future permafrost conditions that can easily be related to local conditions. It will be important to balance information for the built (e.g., villages, roads, airports) and natural environment.

Conclusion

Establishing and co-developing permafrost climate services can advance and accelerate adaptation. They can provide an economy of scale where access to particular types of information is needed but few organizations have the capacity to deliver it. For example, for distributing monitoring data and for computer simulation products.

Services can help better connect distributed and networked capacity within a country and internationally. They are the missing link between permafrost reseach and the application of the knowledge generated.

Arctic nations like Canada have an opportunity to lead the way in building permafrost climate services, elevating permafrost research internationally and making it available for those who need it. Shared leadership, especially with Northerners and Indigenous peoples, will balance priorities toward local access to the best available climate data and services (Priority Area 1, in ITK 2019).

References

Allard, M., L'Hérault, E., et al. 2023. Facing the challenge of permafrost thaw in Nunavik communities: innovative integrated methodology, lessons learnt, and recommendations to stakeholders. Arctic Science, 9(3), 657–677.

Boeckli, L., Brenning, A., Gruber, S., and Noetzli, J. 2012. Permafrost distribution in the European Alps: calculation and evaluation of an index map and summary statistics. The Cryosphere, 6(4), 807–820.

Bureau de normalisation du Québec (BNQ) 2023. Canadian standard CAN/BNQ 9701-500 Risk-based approach for community planning in northern regions - requirements and guidance. Tech. rep.

Gruber, S., Hayley, J., Karunaratne, K., King, J., MacLean, T., Marshall, S., and Moore, D. 2023. Considerations toward a vision and strategy for permafrost knowledge in Canada. Arctic Science, 9(4), iv–viii.

IPCC 2019. Summary for Policymakers. In: IPCC Special Report on the Ocean and Cryosphere in a Changing Climate, Cambridge University Press, Cambridge, UK.

ITK. 2019. National Inuit Climate Change Strategy. Inuit Tapiriit Kanatami (ITK), Ottawa.

Kokelj, S. V., Gingras-Hill, T., et al. 2023. The Northwest Territories Thermokarst Mapping Collective: a northern-driven mapping collaborative toward understanding the effects of permafrost thaw. Arctic Science, 9(4), 886–918.

Vincent, K., Daly, M., Scannell, C., and Leathes, B. 2018. What can climate services learn from theory and practice of co-production? Climate Services, 12, 48–58.

World Meteorological Organization (WMO) 2011. Climate knowledge for climate action. Tech. rep.

Presenting land surface changes through the web-based Arctic Landscape EXplorer (ALEX) to permafrost communities – A permafrost service

Tillmann Lübker, Ingmar Nitze, Sebastian Laboor, Anna Irrgang, Hugues Lantuit & Guido Grosse
Alfred Wegener Institute, Helmholtz Centre for Polar and Marine Research, Potsdam, Germany

The EU-funded Arctic PASSION research project focuses on refining, improving and extending pan-Arctic scientific and community-based monitoring systems. The aim is to create a coherent and integrated Arctic observing system, tailored to the needs of the users or stakeholders. Within the project's Permafrost Service, we are developing a web-based portal, the 'Arctic Landscape EXplorer' (ALEX). In this online tool we present data on permafrost region land surface changes derived from remote sensing analysis. Using tailored visualizations and story maps as a means of more effectively communicating scientific observations of change, we specifically address non-scientific user communities, stakeholders, and rights holders in the Arctic.

Pan-Arctic land surface change data

Remote sensing analysis can be applied to detect and map permafrost disturbances at high spatial resolution over large regions to quantify landscape change, hydrological dynamics, and permafrost vulnerability. In the ERC PETA-CARB, ESA CCI Permafrost, and NSF Permafrost Discovery Gateway projects, a pan-Arctic time series of permafrost landscape change at 30m resolution and covering twenty years was produced using Landsat TM, ETM+, and OLI imagery (see Nitze and Grosse 2016).

To obtain robust trend parameters, the well-established Tasseled Cap transformation was applied to all cloud-free pixels in images with less than 80% cloud-cover for the months of July and August as part of the change analysis. Trends for each of the Tasseled Cap indices were calculated using a Theil-Sen regression (Sen 1968; Theil 1992), which considers the slope between each point in time and then calculates a median over the entire time period, which is defined as the master slope of the trend. The application of this approach is able to reliably detect and quantitatively assess key permafrost region disturbances such as lake drainage, coastal erosion, thermokarst lake expansion, retrogressive thaw slumps, fire scars, and infrastructure expansion, among many others, across continental-scale spatial domains (Nitze et al. 2018).

Within EU Arctic PASSION, the change algorithm and processing pipeline were further refined to provide even more robust results in areas where data sources are disrupted. The time series has also been updated to cover changes between 2003 and 2022.

The Arctic Landscape EXplorer (ALEX)

To make the scientific findings and the large remote sensing dataset more easily accessible, we have developed a tailored web-based portal, the Arctic Landscape EXplorer (ALEX, https://alex.awi.de, Figure 1). With the new portal, we provide interactive maps of recent information on land surface changes, hot spots of disturbance, and potential areas of active permafrost thaw and erosion.

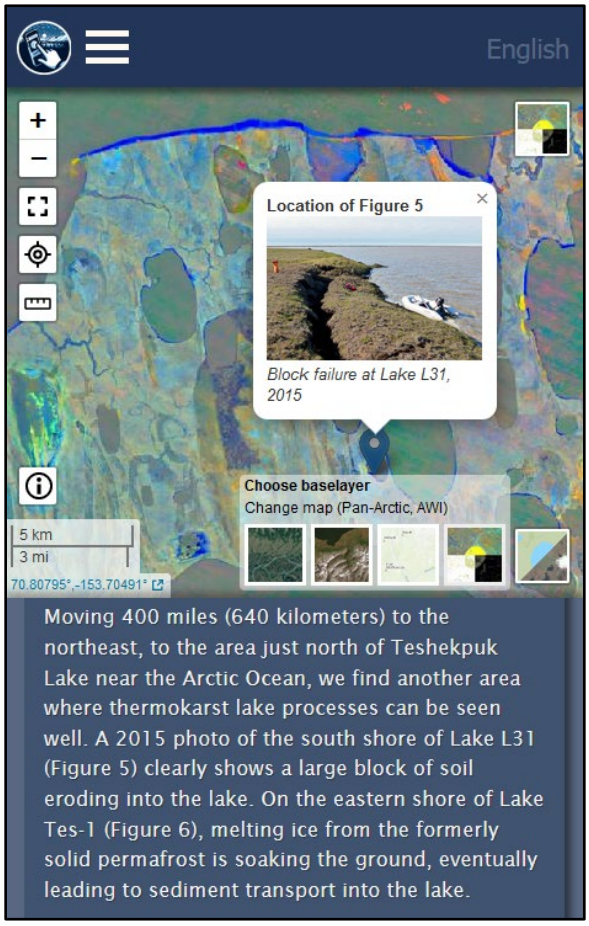

Figure 1. Screenshot of the Arctic Landscape EXplorer (ALEX) showing a story map in mobile device mode. In the change data (top), blue colors mark areas of lake expansion, coastal erosion, or flooding.

A series of short story maps are seamlessly integrated into the portal. This interactive approach combines map content with multimedia elements and narrative storytelling, encouraging users to engage more deeply with the map content. In a hands-on way, users are guided step-by-step to read and explore the map to gain a better understanding of the spatially explicit data. Tailored visualizations on topics such as coastal erosion, lake drainage, infrastructure expansion, and tundra fires are being implemented.

To ensure that user requirements are met, we build on mutually trusted collaboration with local permafrost communities. In recent consultations with local representatives and stakeholders from Alaska we received positive feedback and strong interest in the tool. The results of community evaluation and feedback are used to update the community-oriented maps.

Technical considerations and data dissemination

During the design and implementation of the tool, emphasis was placed on optimized page load times, the usability of the tool on mobile devices, and the ability to index the content. A set of simple to use controls helps the user to navigate to the current location and to compare different data sources. For the map component, we use the open source software library Leaflet, which is known to be one of the most popular open source JavaScript libraries for cartographic web applications (Edler & Vetter 2019). The library is very lightweight and offers an abundance of extensions that can be integrated to fulfill specific desired functionalities. For the layout, we use modern but well-established web standards such as the Cascading Style Sheets (CSS) Grid technology and Scalable Vector Graphics (SVG).

In addition to being visualized in the Arctic Landscape EXplorer, the surface change data can also be accessed via an OGC-compliant Web Map Service (WMS). Following the service-oriented architecture of a Spatial Data Infrastructure (SDI), publishing raster data via a WMS greatly facilitates data ruse. Using the appropriate service URL, a user can easily integrate the data into desktop geographic information systems (GIS; such as ArcMap or QGIS) as well as online map viewers based on standard map libraries (such as Leaflet or OpenLayers).

Conclusions

Publishing research data according to the FAIR data principles (Wilkinson et al. 2016) and by using open access information systems such as PANGAEA (Felden et al. 2023) can ensure that even large and complex scientific datasets are available in the long term and can be easily reused by the scientific community. However, these well-established information channels often do not reach local, regional, and state-level decision makers and community members living on permafrost.

With the ALEX tool, we strive to provide a permafrost landscape information tool that specifically addresses non-scientific audiences so that large and complex pan-Arctic permafrost change datasets become visible at the local and community level. The data presented through the tool can help to better understand the spatial explicitness of land surface changes and provide a valuable tool to support local decision making. Establishing a system to detect land surface changes caused by permafrost degradation is our contribution to a tailored, coherent, and integrated Arctic observing system.

References

Edler, D., and Vetter, M. 2019. The Simplicity of Modern Audiovisual Web Cartography: An Example with the Open-Source JavaScript Library leaflet.js, KN – Journal of Cartography and Geographic Information, 69: 51–62. doi:10.1007/s42489-019-00006-2

Felden, J., Möller, L., Schindler, U., Huber, R., Schumacher, S., Koppe, R., Diepenbroek, M., and Glöckner, F.O. 2023. PANGAEA — Data Publisher for Earth & Environmental Science, Scientific Data, 10(2023): 347. doi:10.1038/s41597-023-02269-x

Nitze, I., and Grosse, G. 2016. Detection of landscape dynamics in the Arctic Lena Delta with temporally dense Landsat time-series stacks, Remote Sensing of Environment, 181: 27–41. doi:10.1016/j.rse.2016.03.038

Nitze, I., Grosse, G., Jones, B.M., Romanovsky, V.E., and Boike, J. 2018. Remote sensing quantifies widespread abundance of permafrost region disturbances across the Arctic and Subarctic, Nature Communications, 9(1): 5423. doi:10.1038/s41467-018-07663-3

Sen, P.K. 1968. Estimates of the regression coefficient based on Kendall's tau. Journal of the American Statistical Association, 63(324): 1379–1389. doi:10.1080/01621459.1968.10480934

Theil, H. 1992. A rank-invariant method of linear and polynomial regression analysis. In Henri Theil's Contributions to Economics and Econometrics, 345–381. Springer, Netherlands.

Wilkinson, M., Dumontier, M., Aalbersberg, I., et al. 2016. The FAIR Guiding Principles for scientific data management and stewardship, Scientific Data, 3(2016): 160018. doi:10.1038/sdata.2016.18

Wildfires, permafrost thaw and permafrost carbon feedback – Exploring connections, interactions, research gaps and ways forward

Lina Madaj[1], Deniz Vural[2] & Scott Janzwood[3]

[1]*Department of Earth Sciences, Vrije Universiteit Amsterdam, Amsterdam, The Netherlands*

[2]*Alfred Wegener Institute for Polar and Marine Research, Potsdam, Germany*

[3]*Cascade Institute, Royal Roads University, Victoria, British Columbia, Canada*

Around 18 million km2 of the area in the northern high latitudes is characterised by permafrost (Turetsky et al. 2020). This permafrost stores as much as 1600 Pg of carbon, equal to twice the amount of carbon contained in the atmosphere and more than three times the carbon in all the forests on Earth (e.g., Hugelius et al. 2014). Rising atmospheric temperatures are causing these soils to thaw which is leaving the upper layers of soil to decompose and release greenhouse gasses (CO2 and CH4) into the atmosphere where it will further contribute to and accelerate atmospheric warming.

This positive feedback loop of enhanced greenhouse gas production through thawing permafrost and consequently exacerbating thaw is called the permafrost carbon feedback (PCF). The exact impacts of the PCF on the global climate are still deeply uncertain (Schuur et al. 2015).

One of the reasons for these uncertainties is the current challenge of including permafrost thaw and the PCF into earth system models. Those models that account for permafrost thaw focus primarily on gradual thaw (continuous thaw rates) (Walter Anthony et al. 2018). Abrupt thaw, however, is not yet covered within those predictions (Turetsky et al. 2020; Turetsky et al. 2019). Emissions from abrupt thaw could cause similar positive feedback on the same magnitude as expected from gradual thaw (Turetsky et al. 2020). One cause of abrupt thaw is wildfires. Not only do wildfires cause abrupt permafrost thaw but they also create more uncertainty about PCF.

The Permafrost Carbon Feedback Project

The Cascade Institute is a research institute based in Canada that investigates the causes of — and responses to — global systemic risks. The PCF project aims to shed light on PCF and to identify research gaps and goals. The project aims to deliver two stand-alone reports on the state of the art and future outlook of (1) the impacts of wildfire on permafrost thaw and (2) possible thaw mitigation strategies to preserve permafrost. Here, we will be focussing on the report identifying the impacts of wildfires on permafrost thaw.

The report will be put together through a combination of literature review and stakeholder interviews. These stakeholders include leading research teams in the field, policymakers, indigenous communities, and industry leaders. Through this approach, we will assess the state of the research, research gaps, and priorities for policy and action.

Wildfires and permafrost

An increasing number of wildfires in the Arctic and subarctic region have been reported in the past years. This growing number of wildfires can, like increased permafrost thaw, be attributed to rising global temperatures. Warmer temperatures in the atmosphere lead to a higher frequency of lightning, which in turn leads to a higher frequency in boreal forest and tundra fires in the higher latitudes (Chen et al. 2021; Veraverbeke et al. 2017).

In most publications permafrost and wildfires are separate topics, maybe mentioned alongside each other, but the focus is often on one of the topics or the other (Treharne et al. 2022). With this report, we will assess the literature on both topics, highlighting research that spans both issues (Figure 1).

What are the impacts of wildfires on permafrost thaw and are there any possible impacts of permafrost thaw on wildfires? How are both connected to the permafrost carbon feedback?

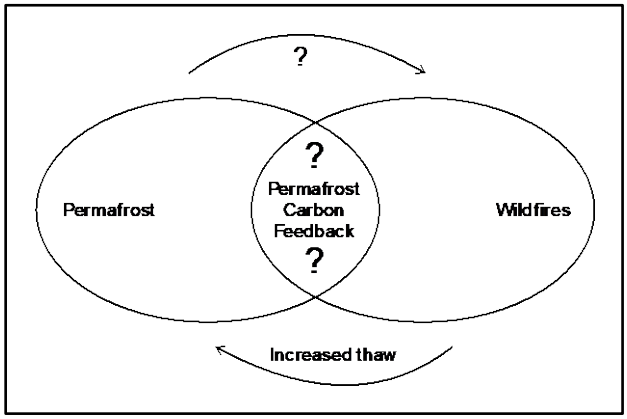

Figure 1. Schematic of report highlighting the impact of permafrost thaw and wildfires on each other, and the open question highlighted within the report.

The impacts of wildfires on permafrost can be direct and indirect; there is direct and abrupt thaw caused by the fire itself but there is also post-fire gradual thaw caused by the change in vegetation cover (Treharne et al. 2022). The main result of fire is a change in active layer thickness. Changes in vegetation cover that function as an insulating layer for the permafrost are far less easy to assess. Soil carbon that is locked away as long as the ground stays frozen can be mobilised through fires. Precisely how this process works is still an open question. Yet, we do not know the impact of wildfire on the permafrost active layer and the long-term carbon cycle.

The impact of wildfires on permafrost regarding the PCF is also strongly dependant on the specific area where the fire occurs – is the region characterised by discontinuous or continuous permafrost and what is the prevailing vegetation? Especially vulnerable areas, for example, are peatlands, which store vast amounts of carbon and nearly half of them are located above 60°N. Peatlands do not recover as quickly as boreal forest might, as carbon released from peatlands is lost to the atmosphere (Witze 2020).

Identifying the interplay of permafrost thaw and wildfires is crucial to quantify PCF, which in turn is an important parameter when estimating carbon emissions from these two sources – a pressing demand when addressing the global climate crisis (cf. Natali et al. 2021).

Preliminary findings

- There is an urgent need for collaboration between permafrost and fire researchers and policy makers.
- As with other fields of research, here especially about PCF impacts and future developments, there is a pressing need for more data and more observations on permafrost and wildfires.
- Abrupt permafrost thaw and combustion of soil organic matter need to be incorporated into (earth system) models.
- The full report on permafrost thaw and wildfire interactions is planned to be publicly available in summer 2024.

References

Chen, Y., Romps, D.M., Seeley, J.T., Veraverbeke, S., Riley, W.J., Mekonnen, Z.A., and Randerson, J.T. 2021. Future increases in Arctic lightning and fire risk for permafrost carbon, Nature Climate Change 11: 404–410. doi:10.1038/s41558-021-01011-y

Hugelius, G., Strauss, J., Zubrzycki, S., Harden, J.W., Schuur, E.A.G., Ping, C.-L., Schirrmeister, L., Grosse, G., Michaelson, G.J., Koven, C.D., O'Donnell, J.A., Elberling, B., Mishra, U., Camill, P., Yu, Z., Palmtag, J., and Kuhry, P. 2014. Estimated stocks of circumpolar permafrost carbon with quantified uncertainty ranges and identified data gaps, Biogeosciences 11: 6573–6593. doi:10.5194/bg-11-6573-2014

Natali, S.M., Holdren, J.P., Rogers, B.M., Treharne, R., Duffy, P.B., Pomerance, R., and MacDonald, E. 2021. Permafrost carbon feedbacks threaten global climate goals, Proceedings of the National Academy of Sciences 118(21): e2100163118. doi:10.1073/pnas.2100163118

Schuur, E.A.G., McGuire, A.D., Schädel, C., Grosse, G., Harden, J.W., Hayes, D.J., Hugelius, G., Koven, C.D., Kuhry, P., Lawrence, D.M., Natali, S.M., Olefeldt, D., Romanovsky, V.E., Schaefer, K., Turetsky, M.R., Treat, C.C., and Vonk, J.E. 2015. Climate change and the permafrost carbon feedback, Nature 520: 171–179. doi:10.1038/nature14338

Treharne, R., Rogers, B.M., Gasser, T., MacDonald, E., and Natali, S. 2022. Identifying Barriers to Estimating Carbon Release from Interacting Feedbacks in a Warming Arctic, Frontiers in Climate. 3: 716464. doi:10.3389/fclim.2021.716464

Turetsky, M.R., Abbott, B.W., Jones, M.C., Anthony, K.W., Olefeldt, D., Schuur, E.A.G., Grosse, G., Kuhry, P., Hugelius, G., Koven, C., Lawrence, D.M., Gibson, C., Sannel, A.B.K., and McGuire, A.D. 2020. Carbon release through abrupt permafrost thaw, Nature Geoscience 13: 138–143. doi:10.1038/s41561-019-0526-0

Turetsky, M.R., Abbott, B.W., Jones, M.C., Walter Anthony, K., Olefeldt, D., Schuur, E.A.G., Koven, C., McGuire, A.D., Grosse, G., Kuhry, P., Hugelius, G., Lawrence, D.M., Gibson, C., and Sannel, A.B.K. 2019. Permafrost collapse is accelerating carbon release, Nature 569: 32–34. doi:10.1038/d41586-019-01313-4

Veraverbeke, S., Rogers, B.M., Goulden, M.L., Jandt, R.R., Miller, C.E., Wiggins, E.B., and Randerson, J.T. 2017. Lightning as a major driver of recent large fire years in North American boreal forests, Natarue Climate Change 7: 529–534. https://doi.org/10.1038/nclimate3329

Walter Anthony, K., Schneider Von Deimling, T., Nitze, I., Frolking, S., Emond, A., Daanen, R., Anthony, P., Lindgren, P., Jones, B., and Grosse, G. 2018. 21st-century modeled permafrost carbon emissions accelerated by abrupt thaw beneath lakes, Nature Communications 9: 3262. doi:10.1038/s41467-018-05738-9

Witze, A. 2020. Why Arctic Fires are Bad News for Climate Change, Nature 585: 336–337. doi:10.1038/d41586-020-02568-y

Using k-means clustering to re-evaluate permafrost threats in Alaska

Santosh Muralidaran[1], Erin Trochim[2] & Nicole Jacobs[3]

[1]*Alaska Center for Energy and Power, University of Alaska Fairbanks, Fairbanks, Alaska, United States*

[2]*Institute of Northern Engineering, University of Alaska Fairbanks, Fairbanks, Alaska, United States*

[3]*Alaska Center for Energy and Power, University of Alaska Fairbanks, Fairbanks, Alaska, United States*

Data-driven approaches to evaluate risks to thawing permafrost for communities in the state of Alaska are a continually evolving process. One such study includes Kanevskiy et al. (2019) published five years ago by researchers at the University of Alaska Fairbanks (UAF) and the Cold Regions Research and Engineering Laboratory (CRREL). Kanevskiy et al. (2019) ranked 187 Alaskan communities based on five criteria (Table 1) as well as a "confidence" criteria which indicated the authors' confidence in the community-specific permafrost data.

Table 1. Kanevskiy et al. (2019) criteria and ranking meanings.

Criteria	Rank: 1	Rank: 2	Rank: 3
Permafrost Occurrence	Isolated	Discontin-uous	Continuous
Permafrost Temperature	Cold (MAGT* = < -5°C)	Cool (MAGT = -5 – -2°C)	Warm (MAGT = -2 – >0°C
Thaw Susceptibility	Low	Medium	High
Massive Ice Occurrence	Absent	Sparse	Abundant
Existing Infrastructure Problems	Minimal	Moderate	Severe

* MAGT = Mean Annual Ground Temperature

Kanevsky et al. (2019) then summed each of these individual ranks for all five categories to assign a rating score for each community. Using a theory-driven approach, the normalized scores of the communities were plotted against their respective percentiles on a cumulative distribution plot to categorize the communities into three risk categories: "High", "Medium", and "Low". The transitions between each ordinal group was discerned by visually identifying the gaps on the graph. The data from Kanevsky et al. (2019) greatly informed the Statewide Threat Assessment by the Denali Commission (2019) published several months later which used a similar three-point scale to assign risk indicators for permafrost, flooding, coastal erosion, as well as usteq, or "combined threat" of all conditions. For the permafrost rankings in Denali Commission (2019), the rankings from Kanevsky et al. (2019) were initially utilized as preliminary data. This data was later enriched with additional community-specific information (such as location, infrastructure distribution, etc.) to enhance risk assessment and refine the categorization of communities based on their vulnerability to the threat. The subsequent rankings produced by Denali Commission (2019) were also used in other studies to further develop permafrost-vulnerability indices (Alessa et al. 2023).

A common limitation in these studies is that while data visualization techniques used in the aforementioned reports can contribute to the reproducibility of data, machine learning techniques can enhance reproducibility by enabling the creation of predictive models or algorithms. For the categorization of communities in Alaska based on permafrost-related threats, data clustering algorithms can offer a more granular and accurate analysis of permafrost conditions by revealing relationships in the data that cannot be discerned otherwise. This paper uses a k-means clustering algorithm on the dataset in Kanevskiy et al. (2019) to assess a new method of separating the 187 Alaskan communities into risk categories based on existing data.

Methodology

Sixty communities had a ranking of "0" for each category in Table 1 because they are in regions with no permafrost (such as Southeast Alaska) and were eliminated from the dataset, resulting in 127 communities on or around permafrost. To preprocess the new dataset, all qualitative columns as well as the final risk scores and categories were temporarily removed from the data. The elbow method was then used to find an optimal number of clusters of three, leading to the development of a k-means model where k = 3. Each row was then assigned a cluster number of 1.0, 2.0, or 3.0 in a new "cluster" column and was joined with the original dataset of 127 communities to identify which communities belonged to each cluster.

Results and Analysis

The key difference between the clustered data and the original data in Kanevsky et al. (2019) lie in how the two grouped the communities with continuous permafrost differently. Both the "High" risk category in Kanvesky et al. (2019) and cluster 1.0 have a majority of high thaw susceptibility (82.35% and 77.78%,

respectively). In the "High" risk category of Kanvesky et al. (2019), there are 34 total communities and the majority have continuous permafrost (64.7%) and warm permafrost temperatures (76.47%). However, in cluster 1.0, there are only 9 communities in which all have continuous permafrost (100%) but the majority have cold permafrost temperatures (77.78%) while the remaining have cool permafrost temperatures (22.22%). Cluster 1.0 therefore further separated communities from the original "High" risk category that may not be expected to have high thaw susceptibility due to their cooler temperatures. A look into the distribution of massive ice occurrence between original risk levels and the new clusters offers further insights into this separation:

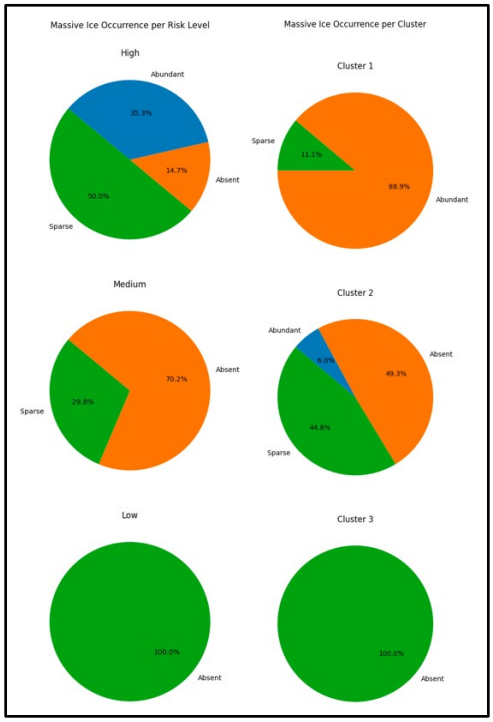

Figure 1. Comparison of massive ice per risk level versus massive ice per cluster in pie charts.

In Figure 1, it is seen that both the "Low" risk category and cluster 3.0 have no massive ice ("Absent"). It is also observed that the majority of cluster 1.0 has "Abundant" massive ice (88.9%, or 8 of the 9 communities) and only 1 has "Sparse" massive ice, while the "High" risk category of 34 communities is relatively distributed evenly with "Abundant" taking up only 35.3% and Sparse, 50.0% or half. With most of the "Sparse" massive ice communities gone from cluster 1.0, cluster 2.0 has approximately half "Sparse" massive ice communities. Many of those "Sparse" communities that were in the "High" risk category had warm permafrost, which contributed to the 76.47% of that category having warm permafrost; but without them, cluster 1.0 now highlights all continuous permafrost communities with cool or cold permafrost temperatures that still have a high susceptibility to permafrost thaw.

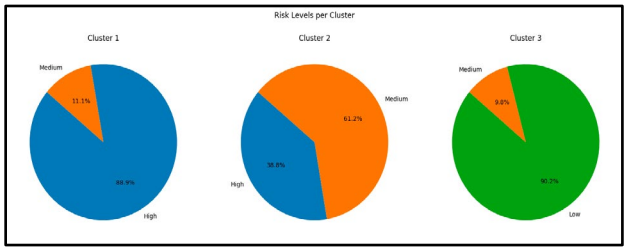

Figure 2. Risk levels per cluster in pie charts.

As seen in Figure 2, cluster 1.0 is overwhelmingly represented by the "High" risk when comparing the clustered data to original categories directly, highlighting that specific communities in the "High" category need to be individually grouped together. Figure 3 also shows the majority of cluster 1.0 (blue, left map) communities in the North Slope region while the "High" risk communities (blue, right map) also include communities in the southwest, indicating that the distinct separation of cluster 1.0 also exhibits a geographical rationale.

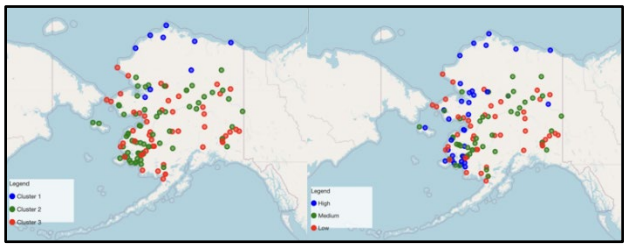

Figure 3. Alaska maps with clustered data (left) versus original risk levels (right).

This paper provides a case of how data-driven approaches with machine learning can be used to better assess degrees of permafrost risk between Alaskan communities compared to data visualization techniques.

References

Alessa, L., et al. 2023. Geographies, 2023, 3(3): 522–542. https://doi.org/10.3390/geographies3030027

Denali Commission. 2019. Statewide Threat Assessment: Identification of Threats from Erosion, Flooding, and Thawing Permafrost in Remote Alaska Communities (Report #INE 19.03).

Kanevskiy, M., et al. 2019. Risk Evaluation for Permafrost-Related Threats: Methods of Risk Estimation and Sources of Information (Report # INE 2019.10).

Delivering permafrost model data via flexible API infrastructure

Scott Rupp[1], Bruce Crevensten[1], Michael DeLue[1], Nancy Fresco[1], Sergey Marchenko[2] & SNAP tech team[1]

[1]*International Arctic Research Center, University of Alaska, Fairbanks, Alaska, United States*

[2]*Geophysical Institute, University of Alaska, Fairbanks, Alaska, United States*

Technical professionals, land managers, policy-makers, and local people in the North need up-to-date permafrost data that are relevant, trustworthy and easy to obtain. By building a flexible data infrastructure capable of handling diverse requests, an Application Program Interface (API) can be used as the foundation upon which permafrost data can be presented alongside other relevant variables for a variety of user audiences.

We will discuss the development of a geospatial data API and the web tools which have thus far been developed on that infrastructure, with a focus on two key examples: a tool designed for a general audience and land management professionals (Northern Climate Reports, or NCR), and a tool designed to deliver similar climate data formatted for engineering professionals (Arctic Environmental and Engineering Data and Design Support System, or Arctic-EDS).

Background

The Scenarios Network for Alaska and Arctic Planning (SNAP) is a research and development team at the International Arctic Research Center at the University of Alaska Fairbanks (UAF). Since 2007, SNAP has worked to make climate projections useful, readily available, and applicable for adaptation planning in the North.

SNAP datasets include dynamically downscaled and statistically downscaled climate projections as well as complex model outputs linking primary climate variables to projected changes in fire, vegetation, permafrost, and other variables. Our permafrost work has largely been in conjunction with colleagues at UAF's Geophysical Institute.

SNAP data and tools are used by diverse groups and individuals who are addressing different real-world issues. Different users need large datasets to be summarized, averaged, and presented across various spatial areas, timeframes, or climate scenarios. This has posed a technical challenge in terms of handling, sharing, and communicating about key aspects of the data.

Benefits of this approach

The development of an API to handle a variety of different data types and to expose them to public query has a number of advantages, from both data management and data access perspectives. This structure allows us to present diverse, gridded climate datasets in the contexts necessary for different audiences via relatively few queries. The API allows for the flexible integration of identical data into different web portals.

Currently, the API offers direct data access for technical users and provides the infrastructure for two different tools – described in more detail below – that utilize the API to return projected permafrost data. One tool, NCR, is targeted at general audiences seeking permafrost data for decision-making and planning. It presents returned results as mean annual ground temperature maps and a chart of active layer depth by multi-decade period. Another tool, Arctic-EDS, is designed for integration into Arctic engineering workflows. It returns identical results as tables of mean annual ground temperature at six depths alongside table summaries. Future tools may access the API to tailor permafrost data for other stakeholders such as agriculturalists.

While the API serves as the foundation of internally developed tools at SNAP, the public nature and documentation means that the underlying vector and raster data is available for query by anyone. Thorough documentation and open source code of all SNAP web applications distributed via Github allows the group to openly deliver complex data.

Underlying data infrastructure

Queries to the SNAP Geospatial Data API are checked against a cache of pre-populated point and area summaries (Figure 1). Vector data are stored in a database that allows values to be returned for named points or polygons. Examples of available area boundaries include First Nations traditional territories, areas managed by specific agencies such as the US or Canadian parks services, or game management units. This is done to speed up the delivery of commonly requested data endpoints across our suite of web tools.

Some pre-processing can be achieved for any given point by bounding the years requested, or requesting a summary of mean, min, and max values. A URL-based query of all datasets accessible via the API returns results in JSON format. Similar processes can be used on all data exposed through the API. Due to the size of the data available, SNAP makes use of a domain-independent array database management

system, rasdaman. for raster data management. Documentation is available within the API itself at earthmaps.io.

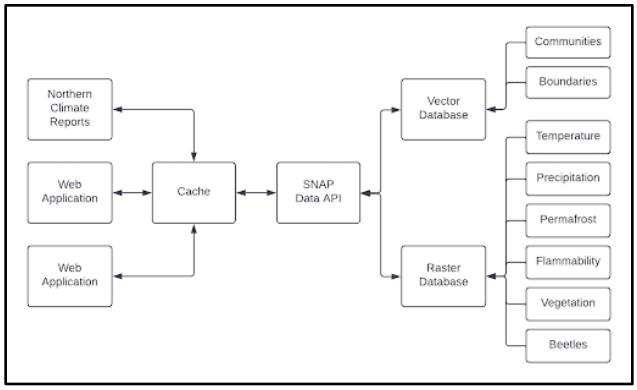

Figure 1. A rough abstraction of the structure of SNAP API and web tool interactions.

For permafrost, three datasets are available. Modeled data created in collaboration with the Geophysical Institute Permafrost Lab (Marchenko 2022) includes ten variables: mean annual ground temperature at the surface and at depths of 0.5, 1.0, 2.0, 3.0, 4.0, and 5.0 meters; plus, depths to the top and to the base of the permafrost layer, and talik thickness. Data from Jorgenson et al. (2008) includes permafrost extent and ground ice volume, and data from Obu et al. (2018) includes permafrost extent and mean annual ground temperature at the top of permafrost.

Example 1 - Arctic-EDS

One use case, and the use case for which the API was initially constructed, is the development of Arctic-EDS, a climate data tool built to better serve the needs of engineers building in the Arctic, particularly in Alaska.

The tool builds on past work performed by SNAP and partner researchers, and on the advisory expertise of participating engineers. Alongside permafrost-specific information are climate projections for temperature and precipitation, including hydrologic variables, freezing and thawing indices, heating degree days, and precipitation return interval modeling performed for the Alaska Department of Transportation and Public Facilities.

In this use case the focus of data delivery is on pixel-level data delivered in tabular form for export and integration into other engineering workflows. In some cases, interactive computational modules are available. The tool includes a direct link to the API; an interface searchable by community name or by point (lat/long); and selected statewide maps showcasing datasets suited to viewing in this format; this includes zoomable maps displaying permafrost extent, ground ice volume, and mean annual ground temperature at the top of the permafrost layer (Jorgenson 2008; Obu 2018).

Example 2 - Northern Climate Reports

A second example of successful development of a tool based on the API is the NCR web tool. Developed as the final product of a boundary-spanning long-term research project, the tool translates queries via the API to deliver a variety of climate model data, including projected changes in permafrost conditions and active layer thickness, in context for a more general audience. Other datasets available within this tool include temperature, precipitation, hydrology, wildfire and vegetation, and climate protection from bark beetles.

Here, the API stores both vector data (named point locations and “polygons of interest") and raster data (gridded climate model outputs). Permafrost projections, temperature projections, and other information can then be returned alongside accompanying interpretive text to assist in understanding or provide cautionary considerations.

This tool demonstrates how building flexible infrastructure via an API allows for reuse and repackaging of data for diverse users in order to meet current and future needs.

References

Jorgenson, M., Yoshikawa, K., Kanevskiy, M., Shur, Y., Romanovsky, V., Marchenko, S., and Jones, B. 2008. Permafrost Characteristics of Alaska + Map, In Ninth International Conference on Permafrost, Online Proceedings, 1: 121–122.

Marchenko, S., Romanovsky, V., and Tipenko, G. 2008. Numerical modeling of spatial permafrost dynamics in Alaska, In Ninth International Conference on Permafrost, Online Proceedings, 2: 1125–1130.

Marchenko, S. 2022. Arctic and Subarctic Engineering Design Tool: Technology Transfer UFC 3-130 (Year 1 Contract Report W913E5-21-C0010), Cold Regions Research & Engineering Laboratory, Hannover, NH, USA.

Obu, J., Westermann, S., Kääb, A., and Bartsch, A. 2018. Ground Temperature Map, 2000-2016, Northern Hemisphere Permafrost, Alfred Wegener Institute, Helmholtz Centre for Polar and Marine Research, Bremerhaven.

A monitoring network of ground surface temperature in the headwater area of the Yellow River

Raul-David Șerban[1,2], Huijun Jin[2,3], Mihaela Șerban[4], Ruixia He[2], Xiaoying Jin[3] & Jianjun Tang[3]

[1]*Faculty of Agricultural, Environmental and Food Sciences, Free University of Bozen-Bolzano, Bolzano, Italy*

[2]*National Key Laboratory of Cryosphere Science and Frozen Soils Engineering, Northwest Institute of Eco-Environment and Resources, Chinese Academy of Sciences, Lanzhou, China*

[3]*School of Civil Engineering and Transportation, Permafrost Institute, and China-Russia Joint Laboratory of Cold Regions Engineering and Environment, Northeast Forestry University, Harbin, China*

[4]*Applied Geomorphology and Interdisciplinary Research Centre, Department of Geography, West University of Timișoara, Timișoara, Romania*

Ground surface temperature (GST), measured at approximately 5 cm in depth, is an essential parameter that controls the subsurface biophysical processes at the land-atmosphere interaction. GST is important for better understanding the surface energy dynamics and flows, water cycles, ecohydrology, and climate change impacts in the Earth Critical Zone (Lin 2010). While the importance of GST in the cryosphere, ecosystem monitoring, and hazard mitigation has been emphasized (Hagedorn et al. 2019; Wani et al. 2020), GST is still scarcely monitored in alpine environments. In response to that, an observational network of GST was established across various spatial scales and under different land-cover types on the northeastern Qinghai-Tibet Plateau (QTP). The aim is to assess the spatial variability of GST under similar and different environmental conditions and its potential to detect the occurrence of permafrost.

Study area and monitoring design

The study area is located in the Headwater Area of the Yellow River (HAYR), one of the core water towers in China and a representative area of alpine discontinuous permafrost on northeastern QTP. The climate is cold and dry, with a mean annual air temperature below -4 °C, annual precipitation at 300–450 mm, and annual evaporation potential at 1000–1500 mm (Jin et al. 2009). The monitoring network covers spatial scales from fine (2 to 16 m) to local and landscape scales (2 and 50 km^2) and an 800-m elevational transect.

GST was recorded at 41 sites and 83 plots from 2019 to 2020 at three-hour intervals using the iButton temperature loggers DS1922L with an accuracy of ±0.5 ºC. The land-cover types are the alpine steppe, meadow, swamp meadow, and bare ground. GST is monitored mainly on flat terrains but also in disturbed grounds by highway construction, thermokarst depressions, or earth hummocks. Linear models and one-way analysis of variance were used to assess the relationship between GST and key variables (e.g., land-cover type, elevation).

Results and discussions

Mean annual GST (MAGST) was higher at sites in alpine meadows (-0.6 to 0.7 °C) than those in alpine swamp meadows (-1.4 to 0.7 °C) and bare grounds (-2.0 to -1.2 °C), (Șerban et al. 2023). This pattern was observed at both local and landscape scales but was not so clear along the elevational transect due to the influence of the highway. The intra-plot difference in MAGST was up to 0.5 °C for sites with similar land cover in both plots and up to 2 °C when vegetation was compared to the bare ground (Figure 1).

The decrease of MAGST with elevation was more obvious for the sites located in the bare ground (R^2 = 0.83, $p < 0.001$) than in meadow (R^2 = 0.64, $p < 0.003$) and swamp meadow (R^2 = 0.49, $p < 0.002$). These observations are supported by the statistical tests that reveal a significant positive correlation of MAGST with land cover (0.37, $p < 0.05$) and negative with elevation (-0.76, $p < 0.001$). These two predictors explain 70% of the MAGST variability (Șerban et al. 2023).

An elevational threshold was found at 4600–4700 m a.s.l., where MAGST turned from positive to negative. This corresponds well with the lower limit of continuous elevational permafrost (4660 m a.s.l.) validated by the borehole measurements (Luo et al. 2018). Sites with a MAGST < -1 °C corresponded with the stable permafrost, while sites with a MAGST > 1 °C matched the areas of seasonally frozen ground. The sites with a MAGST that ranged between -1 and 1 °C agreed with the lower elevation limits of discontinuous permafrost (Șerban et al. 2024).

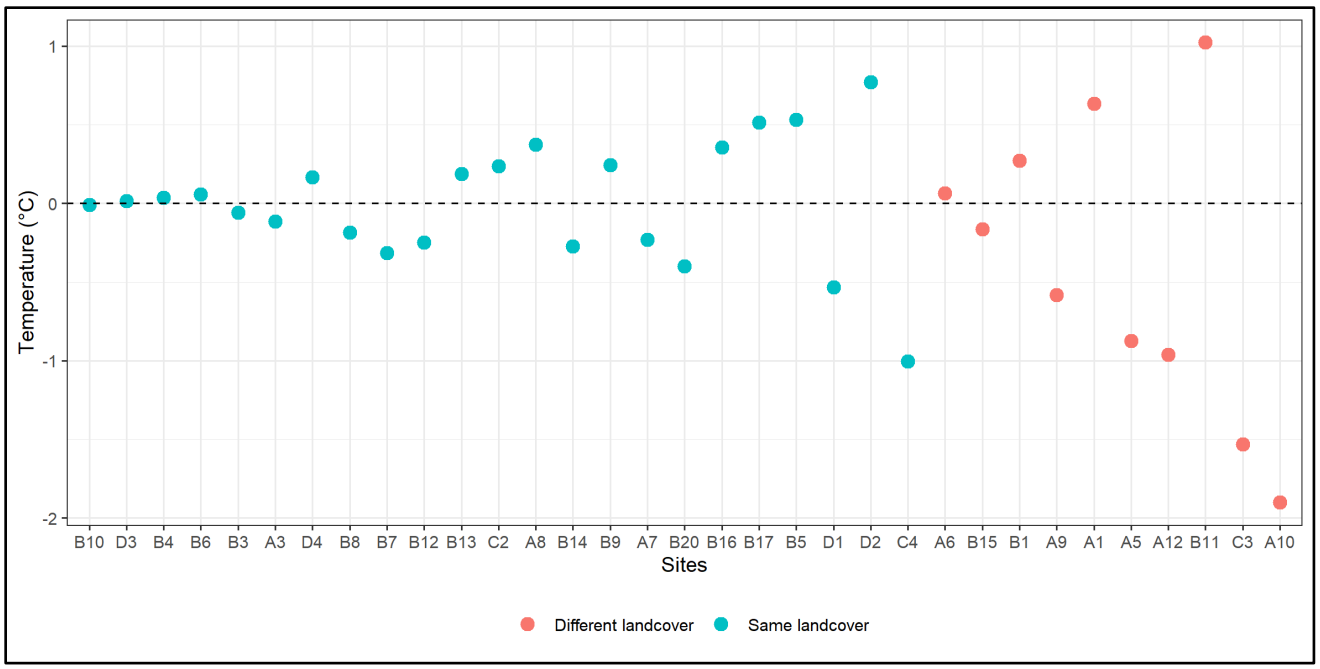

Figure 1. Intra-plot differences (fine scale) of mean annual ground surface temperature (MAGST) of all sites ordered according to similar and different landcover between plots.

Conclusions

Positive feedback of the vegetation on GST was observed in the HAYR with an obvious trend of higher MAGST at the vegetated sites than at those with bare ground. The GST showed the potential of detecting permafrost and permafrost thermal status at a high spatial resolution that cannot be detected through the sparse boreholes network or the coarse modelling approaches. This database is useful to validate the permafrost models, reanalysis and remote sensing products, and to improve the upper boundary conditions in physical models. This dataset is openly available in the Third Pole Environment Data Center (Șerban and Jin 2022).

Acknowledgements

This work was financially supported by the Autonomous Province of Bozen/Bolzano (Projects TEMPLINK and PERMAWAT, Grant Nos. D55F20002520003 and 13585/2023) and the Chinese Academy of Sciences (Grant Nos. XDA20100103 and 2018PE0007).

References

Hagedorn, F., Gavazov, K., and Alexander, J.M. 2019. Above- and belowground linkages shape responses of mountain vegetation to climate change. Science 365(6458), 1119–1123. doi:10.3929/ethz-b-000365795

Jin, H., He, R., Cheng, G., Wu, Q., Wang, S., Lü, L., et al. 2009. Changes in frozen ground in the Source Area of the Yellow River on the Qinghai–Tibet Plateau, China, and their eco-environmental impacts. Environmental Research Letters 4, 045206. doi:10.1088/1748-9326/4/4/045206

Lin, H. 2010. Earth's Critical Zone and hydropedology: Concepts, characteristics, and advances. Hydrology and Earth System Sciences 14(1), 25–45. doi:10.5194/hess-14-25-2010

Luo, D., Jin, H., Jin, X., He, R., Li, X, Muskett, R., et al. 2018. Elevation-dependent thermal regime and dynamics of frozen ground in the Bayan Har Mountains, northeastern Qinghai-Tibet Plateau, southwest China. Permafrost and Periglacial Processes 29(4), 257–270. doi:10.1002/ppp.1988

Șerban, R.D., Jin, H., Șerban, M., Bertoldi, G., Luo, D., Wang, Q., et al. 2024. An observational network of ground surface temperature under different land-cover types on northeastern Qinghai-Tibet Plateau. Earth System Science Data 16, 1425–1446. doi:10.5194/essd-16-1425-2024

Șerban, R.D., Bertoldi, G., Jin, H., Șerban, M., Luo, D. and Li, X. 2023. Spatial variations in ground surface temperature at various scales on the northeastern Qinghai-Tibet Plateau, China. Catena 222, 106811. doi:10.1016/j.catena.2022.106811

Șerban, R.D. and Jin, H. 2022. Multiscale observation of topsoil temperature below different landcover types on northeastern Qinghai-Tibet Plateau (2019-2020), National Tibetan Plateau/Third Pole Environment Data Center [data set]. doi:10.11888/Cryos.tpdc.272945

Wani, J.M., Thayyen, R.J., Gruber, S., Ojha, C.S.P. and Stumm, D. 2020. Single-year thermal regime and inferred permafrost occurrence in the upper Ganglass catchment of the cold-arid Himalaya, Ladakh, India. Science of the Total Environment 703, 134631. doi:10.1016/j.scitotenv.2019.134631

A framework for classifying permafrost terrain

Niek Speetjens[1], Stephan Gruber[2] & Trevor Lantz[1]

[1]*Department of Environmental Studies, University of Victoria, Victoria, British Columbia, Canada*

[2]*Department of Geography and Environmental Studies, Carleton University, Ottawa, Ontario, Canada*

Permafrost covers roughly 11% of the global land area and significantly influences hydrological processes, soil conditions, vegetation, and the global carbon budget. Rapid climate warming is triggering profound transformations in permafrost environments, impacting water resources, ecosystem services, infrastructure, and carbon and nutrient fluxes. Despite considerable advancements in permafrost science, the lack of a unified interdisciplinary framework hinders collaboration on pressing issues arising from changing permafrost environments.

Groups and individuals with an interest in permafrost have emphasized the importance of synthesizing multidisciplinary observations, creating data products characterizing permafrost change, establishing practices for data sharing, and setting up representative long-term monitoring (Laurie 2017). This is also reflected in elements of a vision forwarded for permafrost knowledge in Canada (Gruber et al. 2023). A foundational element in elevating permafrost science beyond individual sites and disciplines is a shared approach to identifying similar and dissimilar locations.

Permafrost knowledge spans multiple knowledge systems and an ever-increasing number of academic disciplines. This diversity of perspectives is a strength, but their integration is hampered by a range of approaches to classifying and describing permafrost environments. We aim to support incremental progress toward a more unified approach by proposing terminology and a classification framework specifically for permafrost terrain types.

The presence and dynamics of ground ice within permafrost terrain significantly influence its surface expressions and characteristics. Researchers commonly rely on surface features to guide their investigations and categorize, compare, and communicate their results. However, the importance of ground ice necessitates considerations that might not be reflected in terrain classification systems established in different contexts. While some consensus exists regarding pertinent terrain attributes and classes, substantial variations persist across different scales (e.g., The National Wetlands Working Group 1997; Grosse et al. 2006; Olefeldt et al. 2016; Kokelj et al. 2023). The absence of a standardized framework hinders synthesizing information across spatial scales and the comprehensive understanding of permafrost terrain dynamics.

We present a framework for classifying permafrost terrain. It consists of a nested hierarchy of classes for characterizing pattern and process across scales, from continental to local. We review existing classification methods from disciplines such as hydrology, ecology, geomorphology, glaciology, soil science and permafrost science. Based on this, we examine what classes are formed, which variables are used, and what application and purpose this serves. Subsequently we propose a framework that maximizes similarity and usage of existing approaches, employing an 'adopt and adapt' strategy.

The goal of this framework is to facilitate inventorying of permafrost-related stocks (e.g., carbon, nutrients, biodiversity), process domains (e.g., landforms), conditions (e.g., thermal state and ground-ice content), and projected change trajectories (e.g., various modes of permafrost degradation and their impacts). Successful implementation and adoption by permafrost stakeholders across scales will facilitate increased interoperability, enhanced data synthesis, and improved accessibility for modelers. Additionally, it will foster enriched communication with stakeholders outside academia, identifying urgent community, governmental, or industrial concerns and guiding scientific efforts accordingly.

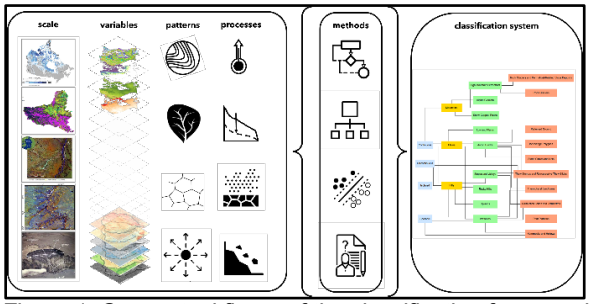

Figure 1. Conceptual figure of the classification framework.

References

Grosse, G., Schirrmeister, L., and Malthus, T.J. 2006. Application of Landsat-7 satellite data and a DEM for the quantification of thermokarst-affected terrain types in the periglacial Lena-Anabar coastal lowland. Polar Research, 25 (1). https://doi.org/10.1111/j.1751-8369.2006.tb00150.x.

Gruber, S., Hayley, J., Karunaratne, K., King, J., MacLean, T., Marshall, S., and Moore, D. 2023. Considerations toward a vision and strategy for permafrost knowledge in Canada. Arctic Science, 9 (4), 4–8. https://doi.org/10.1139/as-2023-0016

Kokelj, S.V, Gingras-Hill, T., Daly, S.V., Morse, P.D., Wolfe, S.A., Rudy, A.C.A., van der Sluijs, J., Weiss, N., Brendan O'neill, H., Baltzer, J.L., Lantz, T.C., Gibson, C., Cazon, D., Fraser, R.H., Froese, D.G., Giff, G., Klengenberg, C., Lamoureux, S.F., Quinton, W.L., et al. 2023. The Northwest Territories Thermokarst Mapping Collective: a northern-driven mapping collaborative toward understanding the effects of permafrost thaw. Arctic Science, 9 (4), 886–918. https://doi.org/10.1139/AS-2023-0009

Laurie, M. 2017. Workshop report: toward a Canadian Permafrost Network. Ottawa, Canada. doi:10.22215/pn/10117001

National Wetlands Working Group. 1997. The Canadian Wetland Classification System, 2nd Edition. Warner, B.G. and C.D.A. Rubec (eds.), Wetlands Research Centre, University of Waterloo, Waterloo, ON, Canada. 68 p.

Olefeldt, D., Goswami, S., Grosse, G., Hayes, D., Hugelius, G., Kuhry, P., Mcguire, A.D., Romanovsky, V.E., Sannel, A.B.K., Schuur, E.A.G., and Turetsky, M.R. 2016. Circumpolar distribution and carbon storage of thermokarst landscapes. Nature Communications, 7. https://doi.org/10.1038/ncomms13043

Mitigating permafrost thaw: Exploring strategies for sustainable solutions

Deniz Vural[1], Lina Madaj[2] & Scott Janzwood[3]

[1]*Alfred Wegener Institute, Helmholtz Centre for Polar and Marine Research, Potsdam, Germany*

[2]*Department of Earth Sciences, Vrije Universiteit Amsterdam, Amsterdam, The Netherlands*

[3]*Cascade Institute, Royal Roads University, Victoria, British Columbia, Canada*

The polar regions and the northern boreal zone play a vital role in the global climate system (IPCC 2019). Permafrost, characterized by perennially frozen ground, contains nearly twice the carbon present today in the entire Earth's atmosphere (Turetsky et al. 2020). Its susceptibility to environmental changes poses a significant threat to polar regions, a risk accentuated by the phenomenon of Arctic amplification, where warming occurs approximately three to four times faster in northern high latitudes (Serreze and Barry 2011). This phenomenon gives rise to the permafrost carbon feedback (PCF) cycle, wherein carbon emissions resulting from permafrost thaw contribute to further warming, thereby facilitating additional thawing (Schuur et al. 2015). PCF is a positive feedback loop that could, exacerbate the impact of climate change (Cox et al. 2000).

Recent regional climate changes in the Arctic and subarctic have had discernible impacts on both natural and human systems globally (IPCC 2021). Nevertheless, a definitive link between permafrost thaw and anthropogenic climate forcing, along with comprehensive solutions, is notably absent in current scientific discourse (Rosenzweig et al. 2018). Our study endeavors to address this gap by posing fundamental questions about permafrost thaw mitigation strategies, engaging with experts in the field, incorporating Indigenous perspectives, and conducting a systematic review and analysis of potential mitigation strategies. The assessment critically examines the feasibility and viability of these strategies, with a particular emphasis on tackling permafrost thaw and its associated consequences (Schuur et al. 2015), underscoring the urgent imperative to explore and implement effective solutions in response to this pressing environmental challenge.

Overview: Permafrost thaw and its implications for the climate crisis

This study is dedicated to creating an accessible report outlining novel strategies and policies for mitigation interventions. Additionally, it delves into the interconnectedness between permafrost thaw and boreal wildfire – another key outcome of the PCF Project, led by the Cascade Institute, a Canadian research centre addressing converging global crises.

The overarching goal of the PCF Project is to heighten awareness regarding the climate threat posed by the PCF. It aims to galvanize political will, clarify the investment and policy landscape for the development of technologies and strategies to decelerate permafrost thaw, and help bridge the communication gap between the scientific community and the public — all while elevating the unique perspectives and concerns of Indigenous and Northern communities.

Permafrost thaw mitigation strategies

While the IPCC process has been an outstanding model of science-policy collaboration and remains central to disseminating scientific knowledge to policy and other audiences, it is not ideal for disseminating highly relevant and rapidly updated knowledge (Natali et al. 2022), especially for the Arctic Indigenous peoples, whose livelihoods are detrimentally impacted by rapidly thawing permafrost, as well as reduced temporal and spatial extent and quality of sea ice (AMAP 2017b; Carson and Peterson 2016).

While various ideas for targeted geoengineering are emerging to preserve elements of the cryosphere, such as sea ice, permafrost, and ice sheets (Moore et al. 2021), the complexity of permafrost thaw requires concerted efforts in data gathering, policy change, and support for Arctic communities to mitigate permafrost thaw mitigation. This report will conduct a thorough and nuanced review of multiple identified mitigation strategies, employing diverse analysis and assessment approaches (Figure 1). The evaluation will encompass various perspectives, methodologies, and applications, ensuring a comprehensive analysis that will capture a wide spectrum of potential solutions for communities at different scales (e.g., local, regional, national, global).

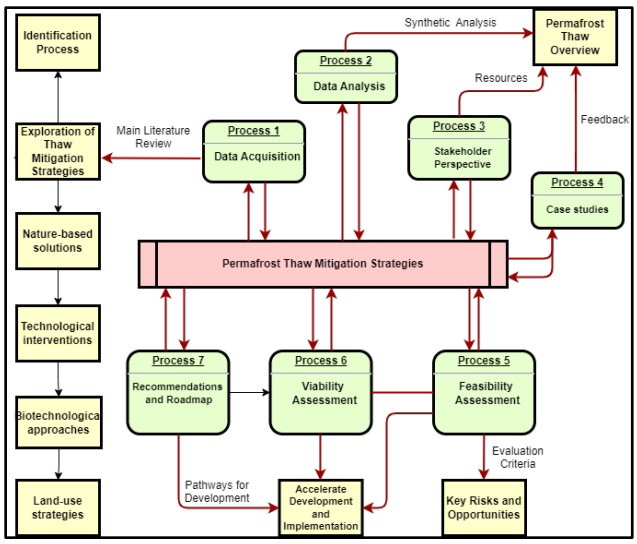

Figure 1. Workflow sequence based on literature review, engaging in discussions with scientists, and collecting insights from community experiences.

PRELIMINARY RESULTS

- This report will delve into the concept of an 'Arctic premium', emphasizing the vulnerability of the Arctic to warming, encompassing albedo and permafrost carbon feedbacks (Ted Parson): regionally or locally focused interventions may offer more cost-effective and immediately impactful results compared to global-scale efforts.
- This report will carefully address the topic of geoengineering, taking into account the associated "moral hazard". Insights from Moore et al. (2021), directly involved in geoengineering research, highlight a consensus on prioritizing conventional decarbonization efforts, including reducing fossil fuel consumption and addressing other climate drivers. Geoengineering, if considered, is seen as a supplementary or emergency measure, not a substitute for conventional decarbonization.
- There is an urgent need for research support and the development of human capacity in northern regions. This includes amplifying the voices of those already experiencing the impacts of climate change and permafrost loss.

REFERENCES

Alfthan, B., van Wijngaarden, A., Moore, J., Kullerud, L., Kurvits, T., Mulelid, O., and Husabø, E. 2023. Frozen Arctic: Horizon scan of interventions to slow down, halt, and reverse the effects of climate change in the Arctic and northern regions. A UArctic Rapid Response Assessment. UArctic, GRID-Arendal, and Arctic Centre/University of Lapland.

AMAP. 2017b. Adaptation Actions for a Changing Arctic: Perspectives from the Bering-Chukchi-Beaufort Region. Oslo: Arctic Monitoring and Assessment Programme (AMAP).

Carson, M., and Peterson, G. (eds.). 2016 Arctic Resilience Report. Stockholm: Arctic Council, Stockholm Environment Institute and Stockholm Resilience Centre.

Cox, P.M., et al. 2000. Acceleration of global warming due to carbon-cycle feedbacks in a coupled climate model. Nature, 408(6809), 184–187.

IPCC in Climate Change 2013: The Physical Science Basis. Contribution of Working Group I to the Fifth Assessment Report of the Intergovernmental Panel on Climate Change (eds. Stocker, T.F. et al.) 1535 (Cambridge Univ. Press, 2013).

IPCC Special Report on the Ocean and Cryosphere in a Changing Climate (2019).

IPCC. 2021. doi.org/10.1017/9781009157896.

Meinshausen, M., Lewis, J., McGlade, C., et al. 2022. Realization of Paris Agreement pledges may limit warming just below 2 C. Nature, 604(7905), 304–309.

Moore, J.C., Mettiäinen, I., Wolovick, M., Zhao, L., Gladstone, R., Chen, Y., Kirchner, S., and Koivurova, T. 2021. Targeted Geoengineering: Local Interventions with Global Implications. Glob Policy, 12: 108–118. https://doi.org/10.1111/1758-5899.12867

Natali, S.N., Bronen, R., Cochran, P., Holdren, J.P., Rogers, B.M., and Treharne, R. 2022. Incorporating permafrost into climate mitigation and adaptation policy. IOP Environ. Res. Lett., 17, 091001. https://doi.org/10.1088/1748-9326/ac8c5a

Serreze, M.C., and Barry, R.G. 2011. Processes and impacts of Arctic amplification: A research synthesis. Global and Planetary Change, 77(1-2), 85–96.

Schuur, E., McGuire, A., Schädel, C., et al. 2015. Climate change and the permafrost carbon feedback. Nature 520, 171–179.https://doi.org/10.1038/nature14338

Turetsky, M.R., et al. 2020. Permafrost collapse is accelerating carbon release. Nature, 569(7754), 32–34.

Designing a permafrost climate change response system in Longyearbyen, Svalbard, to equip Arctic societies with a management tool

Maaike F.M. Weerdesteijn, Hanne H. Christiansen & Marius O. Jonassen

Department of Geophysics, University Centre in Svalbard, Longyearbyen, Svalbard, Norway

The Arctic town of Longyearbyen on Svalbard is located at 79°N and is built on permafrost. Longyearbyen is situated in a narrow valley surrounded by steep mountain slopes. Longyearbyen is undergoing some of the strongest climatic warming recently. With rising air temperatures, the active layer thickness increases, and it stays unfrozen longer into the autumn. Thawing permafrost in Longyearbyen has two major consequences: (1) damage of the town's infrastructure and (2) an increase of landslide risk due to mountain slope instability.

Here, we give an example for each of the thawing permafrost consequences. (1) Lacking building foundation design has caused abrupt evacuation of buildings in recent years, thereby displacing people from their homes. There is minimal place for Longyearbyen to expand due to the limited unused and unprotected space between mountain slopes and the managed river flowing through the entire valley. Therefore, depreciated homes due to permafrost thaw cause a level of complexity on the already existing housing issue. (2) In October 2016, several landslides on the town's valley sides were triggered as the entire thawed active layer detached, due to a rainstorm with 20 mm of precipitation over 24 hours coming down with 2 mm/hour intensity. A 75 mm rainstorm in November the same year led to fewer and smaller landslides, because the active layer had started to freeze in November, and rainwater could not penetrate into the ground.

We focus on developing resilience in Arctic communities by providing a geoscientifically developed coupled permafrost climate change response system. This system will assist decision-making by providing real-time key geoscientific observations and access to short-term geotechnical slope modelling output. The aim is to achieve a better information basis for making decisions about infrastructure design and maintenance, and for use in preparedness situations in connection to potential landslides.

Data acquisition

Permafrost temperature and ground water content are measured by thermistor strings in boreholes and soil moisture sensors recording through the entire active layer in profiles on both sides of town near the boreholes. For the mountain slope stability modeling we require high resolution weather simulations that resolve the steep topography around Longyearbyen. These weather simulations are based on meteorological data from weather stations in and around town, of which some are co-located with the boreholes. Other inputs for the mountain slope stability modeling are a digital elevation model (DEM) and ground characteristics, such as ground ice content, thermal properties, and grain size of the sediment (see ICOP 2024 abstract by Knut I.L. Tveit). This information is obtained from borehole cores. The permafrost and meteorological data, and the weather simulation and mountain slope stability modeling output will all be fed into the response system.

The response system will also include static data, such as maps of ground ice content, sediment thickness, and landforms. Furthermore, deformation maps retrieved from interferometric synthetic aperture radar (InSAR) data processing over 2016–2022 will be available in the system to identify areas of concern.

Data flow and response system

The boreholes and co-located weather stations are equipped with a telemetric device (logging and sending data) that sends observations every 6 hours over 4G to a cloud storage by Amazon Web Services (AWS). This data is then fetched by the response system and visualized real-time. The response system is built in JavaScript and C# and utilizes a Python application programming interface (API), also to be hosted on AWS, to process data for visualization. The graphs are configurable depending on the type of data. We will also implement a dashboard with configurable widgets to make the system more user specific. Furthermore, more meteorological and borehole data that already exist in the Longyearbyen area run by other projects (e.g., SIOS, Svalbard Integrated Arctic Earth Observing System) or project partners (e.g., Longyearbyen local government) will be included, some of which are already providing data directly through the Norwegian Meteorological Institute. Other existing boreholes will need to be equipped with telemetric devices for the data to be available in our response system. Data will be available to download directly through the

response system or to fetch via the response system API.

The weather simulations and mountain slope stability modeling are work in progress and will be hosted on AWS, performing simulations at 6-hour intervals for 24 and 48 hours ahead. The landslide risk assessment will be based on flagging when certain parameters reach a threshold (e.g., 20 mm rain forecasted over the next 24 hours and ground temperatures down to 50 cm depth is above 0°C) and the output of the mountain slope stability modeling. This flagging system will aid the interpretation and thus increase the use of the data by the municipality and local authorities that do not have in-house permafrost and data handling expertise.

USERS

Through this response system we can:

1. Research and monitor permafrost and meteorological variables, both related to infrastructure and to geohazards such as landslides.
2. Educate the next generation of Arctic experts. Students are involved in the field component and the response system will enhance the amount of directly useful data and work experiences.
3. Inform the community on landslide risks in a changing climate for potential evacuation or roadblock measures and inform infrastructure companies and owners on the state of the permafrost for infrastructure building and maintenance (e.g., roads, housing, new infrastructure for renewable energy generation).

PERSPECTIVE

Whilst some of these features are implemented, the response system is under development and not yet operable. We develop the system in close collaboration with local partners that are future users, and we plan to host thematic workshops with users such that they can provide feedback throughout the development of the system, for a more user-friendly experience. This increases our cooperation locally and nationally with relevant partners and enables co-creation of resilience towards permafrost thaw. Finally, we have started to work on including participatory data into the response system by enabling data from private small weather stations to be sent into the system. This forms the first steps into adding a citizen science component into the response system. The ambition is to build the system to be translatable to other communities in Arctic regions built on permafrost.

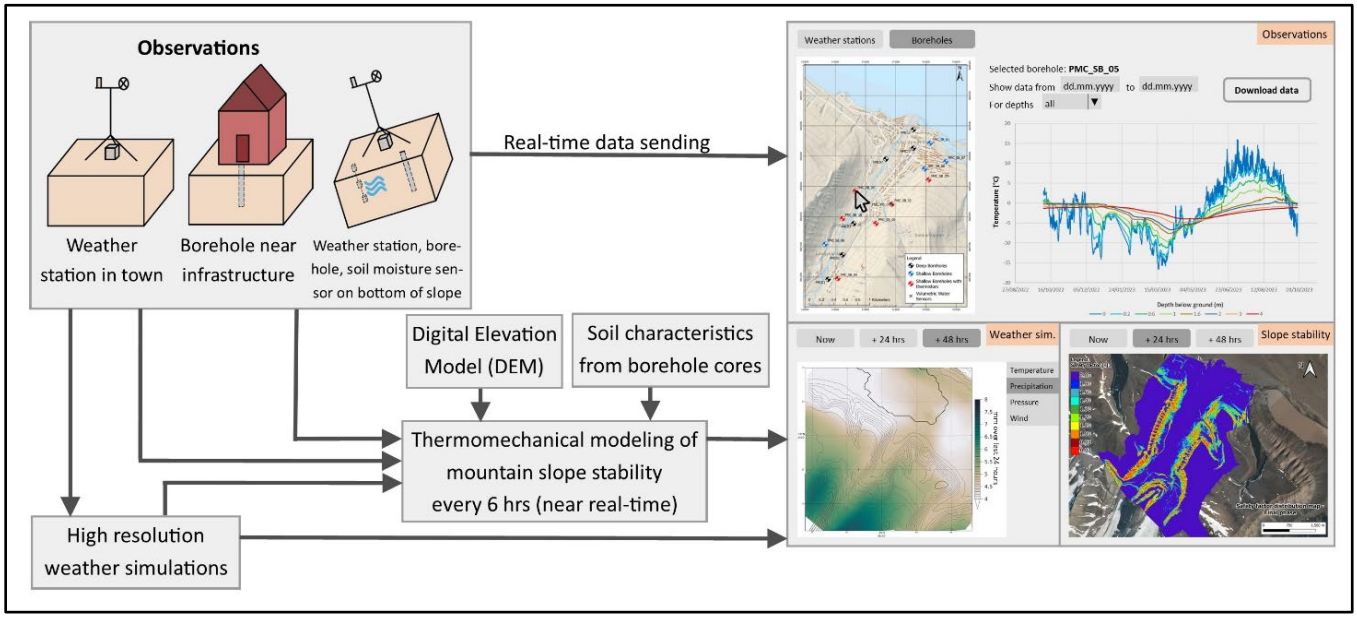

Figure 1. Schematic overview of the response system.

The Northwest Territories Permafrost Database

Niels Weiss[1], Steve Kokelj[1], Ashley Rudy[1], Kumari Karunaratne[1] & Jenny Tjhin[2]

[1]*Northwest Territories Geological Survey, Government of Northwest Territories, Yellowknife, Northwest Territories, Canada*

[2]*Northwest Territories Centre for Geomatics, Government of Northwest Territories, Yellowknife, Northwest Territories, Canada*

The stability of northern landscapes depends on permafrost conditions. Thermal and physical characterization is therefore crucial to understand and anticipate permafrost landscape change and its impacts on communities, infrastructure, and environment. Due to the overall extent and often challenging conditions, permafrost data collection requires a considerable physical and financial effort, and the amount of publicly available data remains relatively limited. The Northwest Territories Geological Survey (NTGS) aims to make data collected by the Government of Northwest Territories (GNWT) and through industry and academic partnerships available and discoverable. To facilitate data sharing and conservation, the NTGS developed the NWT Permafrost Database.

Data structure and templates

A collective comprising government, academic, and industry permafrost scientists and practitioners developed data and metadata templates for Ground temperature and Geotechnical information. Metadata tables contain project details (e.g., data ownership), site information (e.g., location, topographic position, general site description), details regarding the dataset (e.g., length of record, data completeness, thermistor depths), etc. The ground temperature data template comprises a single table for the ground temperature observations. The geotechnical data template includes tables for detailed geotechnical borehole records, such as sample record, soil description, and test results. Overall, the database comprises nearly 100 fields for ground temperature and 200 geotechnical fields.

Current datasets and contributions

The first datasets to be made available in the database were previously published as supplemental files with NTGS Open Reports. These reports include ground temperature and geotechnical data records related to the Inuvik to Tuktoyaktuk Highway and multiple collaborative research programs across the NWT. The NTGS is working on preparing hundreds of datasets derived from long-term monitoring sites and geotechnical investigations. Historic datasets will continue to be digitized, formatted, and made available in the database. Data from ongoing monitoring programs by the NTGS and partners will also be disseminated in the NWT Permafrost Database. Instructions on how to prepare ground temperature data are published as NTGS Open Reports (Northwest Territories Permafrost Database Technical Working Group 2019). A similar guide for geotechnical data preparation is being prepared.

Accessibility and interoperability

Data in the NWT Permafrost Database is accessible through a web interface developed with the GNWT Centre for Geomatics (NWTCG). The interface (dashboard) displays ground temperature and geotechnical borehole locations on a map and allows users to query or filter based on parameters such as project information, site conditions, and observation period. Data tables from selected sites can be exported in flat file format (.csv) or users can choose a Bulk download option to extract the entire dataset. In addition to filtering by expressions, sites can be selected in the map individually or using a polygon or custom extent. The dashboard allows users to display additional spatial data to the map, like point or polygon shapefiles, to help establish site selection. The dashboard supports base layers (topographic, satellite imagery, etc.) and thematic layers (e.g., permafrost zones or probability) and allows users to display custom web service layers. Data stored in NWT Permafrost database is accessible via ArcGIS map service REST API and WMS, hosted by the NWT Centre for Geomatics, for viewing in various GIS applications. This allows integration of NWT Permafrost Database site locations with metadata in synthesis products and other repositories while retaining the NWT Permafrost Database as the source.

References

Northwest Territories Permafrost Database Technical Working Group, 2019. Guide to Producing a Ground Temperature Report, Northwest Territories; Northwest Territories Geological Survey, NWT Open Report 2017-008. https://doi.org/10.46887/2017-008

2 Education


12TH INTERNATIONAL CONFERENCE ON PERMAFROST
2024
XII
WHITEHORSE YUKON

2A — Permafrost Education and Outreach for Everyone in a Warming World

Session Chairs: Ylva Sjöberg[1], Anna Klene[2] & Charlotte Haugk[3]

[1]Department of Geosciences and Natural Resource Management, University of Copenhagen, Copenhagen, Denmark
[2]Franke College of Forestry and Conservation, University of Montana, Missoula, Montana, United States
[3]Department of Environmental Science, Stockholm University, Stockholm, Sweden

Permafrost is not only a recognized topic of research in the context of continuing global warming and feedbacks but also has significant relevance for local societies and industry across the Arctic and in mountain permafrost areas. The teaching of permafrost to students in K-12 and higher education is of great importance for facing societal challenges locally and globally. As a topic, permafrost crosses disciplinary boundaries and may be integrated across educational programs in engineering, geosciences, and ecology. In this session, we will have a look at current education on permafrost from multidisciplinary perspectives and traditional knowledge. All educational levels, from elementary school to PhD level, are of interest.

Additionally, we welcome contributions focused on reaching audiences and communities outside the classroom. Projects advancing knowledge and understanding in communities on and far away from permafrost, those who live with its impacts on their lives, infrastructure, and agriculture, as well as those whose concerns are centred on the global climate system. New techniques and materials to reach small and large communities alike are welcome. Those targeting the general public, local stakeholders, policymakers, preschoolers, and elders are all welcome. We look forward to a dialogue and resource-sharing discussion among teaching and outreach enthusiasts, be they scientists, teachers, community members, or concerned citizens.

Permafrost education and outreach in Mongolia

Saruulzaya Adiya, Purevdulam Yondonrentsen, Undrakhbayar Enkhjargal, Maralmaa Ariunbold, Tsogt-Erdene Gansukh, Batzorig Batbold & Temuujin Khurelbaatar

Division of Permafrost Reseach, Institute of Geography and Geoecology, Mongolian Academy of Sciences, Ulaanbaatar, Mongolia

The Frozen Ground Cartoons project was initiated in 2015 by a core group stemming from the ECR collaboration (Fritz et al. 2015), and it aimed to develop a series of informative comics for students and teachers. The comics address important concepts about permafrost (e.g., distribution and dynamics of frozen ground, including human impacts, fieldwork activities) and were intended to be used for education and outreach of permafrost science worldwide, thus contributing to the recruitment of the next generation of permafrost scientists. Currently, the cartoons are translated into English, French, Swedish, German, Russian, Inuktitut, Luxembourgish, Danish, and Greenlandic. Then, in October of 2023, the Institute of Geography and Geoecology (IGG), Mongolian Academy of Sciences (MAS) and the IPA announced the release of Frozen Ground Cartoons in its 10th language: Mongolian.

Translation

The Division of Permafrost Research is implementing the project “Future projection of greenhouse gas emissions due to permafrost degradation using the model” at the IGG, MAS between 2022 and 2024. One of the main goals of the project is to disseminate knowledge sharing of permafrost by effectively engaging with students, schools, and educational communities. With this aim, the project combines traditional and innovative ways of communicating knowledge about permafrost. Under this project, A.Saruulzaya (Ph.D), head of Division of Permafrost Research in the IGG, contacted the Frozen Ground Cartoon Team and the IPA standing committee on Education and Outreach with a suggestion to translate the comic into Mongolian. Starting in 2023, she led translation work and the editing of the Mongolian version of the Frozen Ground Cartoons comic book. The translation process included several revisions to improve the comic as a tool for communications with a broad Mongolian audience. When translating this picture book, we paid special attention to the features of the Mongolian language in order to make it easy for children and young people to understand professional words.

Origination and publication

With the translation completed, the process of typesetting the original publication began. Graphic design of this work was carried out by researcher Purevdulam Yondontseren with Adobe Photoshop software. In October 2023, the electronic version of "Цэвдэг гэсэж байна!" comic book was finally ready. Thus, we uploaded the comic book in Mongolian version to official website of the frozengroundcartoon.com (Figure 1).

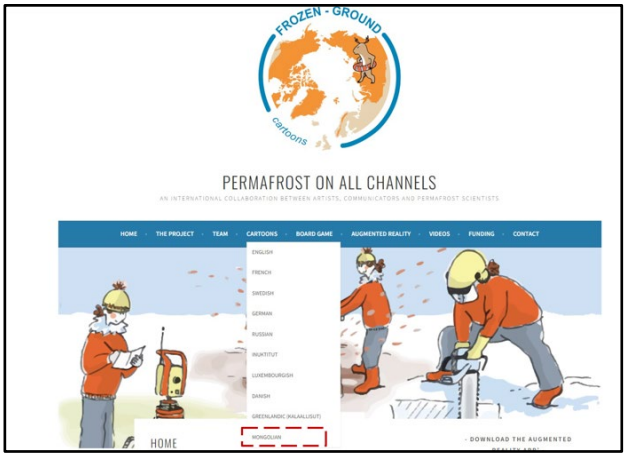

Figure 1. The electronic version of “Цэвдэг гэсэж байна!” comic book is updated on the official website of the Frozen Ground Cartoons.

The main goal of creating the Mongolian version of this comic book was to disseminate knowledge of permafrost/frozen ground to encourage dialogue between scientist and the general public, children and students. To effectively achieve this goal, we decided to expand the scope of our work. We introduced the comic book to experts of “The Nature Conservancy” in Mongolia, who decided to support our work by publishing the comic book in hard copy. In November 2023, “Цэвдэг гэсэж байна!” comic book was printed in hard copy with a total of 1000 copies (Figure 2), through the publishing company of Admon LLC. With the comic book carefully translated and printed, we were ready to present it to our audience.

Figure 2. A hardcopy of "Цэвдэг гэсэж байна!" comic book has been published in Mongolian version.

EDUCATION AND SCIENCE OUTREACH

During the translation process of "Цэвдэг гэсэж байна!" comic book, our outreach ambitions expanded. The researchers at the Division of Permafrost Research prepared a presentation of the "Цэвдэг гэсэж байна!" comic book (Figure 3) to disseminate and share the permafrost knowledge and education. After that, we presented it to approximately 500 children of Munkhkhairkhan's school in Khovd province, 24th school, 41st school, and Logarithm schools in Ulaanbaatar on 22-25 October and 24 November 2023 (Figures 4-6). In addition, we distributed "Цэвдэг гэсэж байна!" comic books for all childrens of these schools. Based on the comments received so far from scientists, teachers, and the general public, including children, the project seems to be moving in the right direction. Yet, there are still a lot of opportunities to extend this work and we provide future ideas and directions to bring our science to new audiences.

Figure 3. "Цэвдэг гэсэж байна!" presentation is upload in youtube.

Figure 4. The cartoons were presented in school of Logarithm in Ulaanbaatar on 22 November 2023.

Figure 5. The cartoons were presented in school of 41th in Ulaanbaatar on 23 November 2023.

Figure 6. The cartoons were presented in school of 24th in Ulaanbaatar on 24 November 2023.

AKNOWLEDGEMENT

We sincerely thank you to Dr. Ylva Sjöberg, Dr. Frédéric Bouchard, and Dr.Kenji Yoshikawa for helping and supports. Financial support was provided for material printing by the The Natural Conservancy (TNC) in Mongolia.

REFERENCES

Fritz, M., Deshpande, B.N., Bouchard, F., Högström, E., Malenfant-Lepage, J., Morgenstern, A., Nieuwendam, A., Oliva, M., Paquette, M., Rudy, A.C., et al. 2015. Brief Communication: Future avenues for permafrost science from the perspective of early career researchers. The Cryosphere 9, 1715–1720.

A collaboration to bring permafrost education into U.S. classrooms

Lauren Brase

American Geosciences Institute, Alexandria, Virginia, United States

In light of the fact that Earth's climate is warming, understanding permafrost is vitally important. Thawing permafrost presents immediate challenges for local communities residing atop soils containing permafrost, impacting infrastructure resilience. More broadly, it carries global implications because thawing permafrost releases greenhouse gases, exacerbating the positive feedback loop, thereby contributing to climate warming.

Communities built on top of or near permafrost areas are likely to be integrating permafrost into the curricula, since it impacts their population. But it is essential for all students to learn and understand permafrost to have a more comprehensive understanding of Earth's systems and the global implications of climate change, regardless of their geographic location. When permafrost-related educational activities are aligned with science education standards and are readily available, teachers can integrate permafrost into their existing classroom curricula.

The American Geosciences Institute (AGI) and the United States Department of Agriculture's Natural Resources Conservation Service (NRCS) are developing resources related to permafrost, and more broadly to many aspects of soil science.

Natural Resources Conservation Service

The NRCS is an agency that works to assist landowners with conservation practices. The primary goals of NRCS includes promoting sustainable land use, protecting natural resources, and addressing environmental concerns. As part of their work with soil conservation, the NRCS conducts soil surveys, assesses soil health, and operates Web Soil Survey.

Web Soil Survey is an invaluable online tool that provides comprehensive access to soil information across the United States. Offering a user-friendly interface, the Web Soil Survey enables landowners, farmers, policymakers, researchers, and the general public to explore detailed soil maps and access a wealth of soil-related data. Within Web Soil Survey, those interested in permafrost can analyze maps of the soil type in their area of interest. If the soil order Gelisols is present, such as in Figure 1, then permafrost is directly related to the community within the area of interest. (Gelisols are soils that contain permafrost within two meters of the surface.) Users can also explore Permafrost Sensitivity (Figure 2), which predicts the risk of permafrost thawing as a result of global climate change or removal of native vegetation by fire or human activities. Through these Web Soil Survey maps, important topics related to permafrost can be discussed and acted upon by educators, city planners, and others involved in land-use.

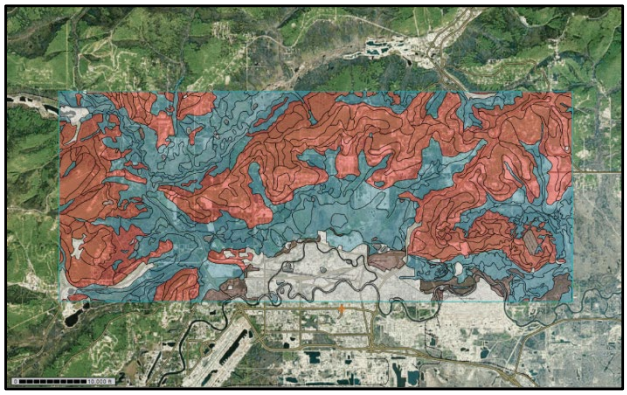

Figure 1. A map of soil orders near Fairbanks, AK. Blue areas identify where Gelisols are present and red areas identify Inceptisols. Created with Web Soil Survey.

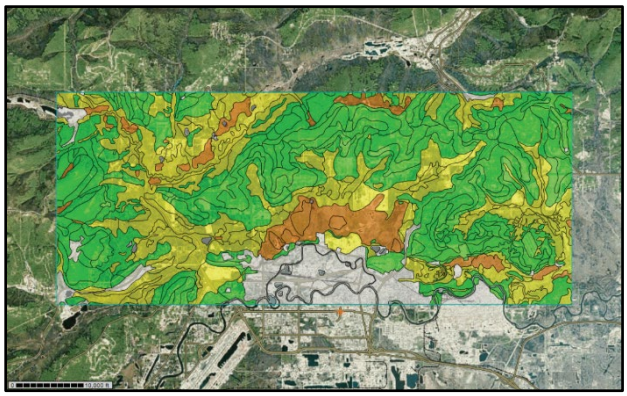

Figure 2. A map of permafrost sensitivity near Fairbanks, AK. Orange areas indicate high, yellow moderate, and green low or no sensitivity to thawing. Created with Web Soil Survey.

American Geosciences Institute

The American Geosciences Institute (AGI) is a nonprofit federation of geoscientific and professional associations that represents the interests of the geoscience community. AGI serves as a unifying force for the geosciences by fostering collaboration among its member societies and providing resources and

information to advance the understanding of Earth and its processes. The Education and Outreach Department of AGI supports initiatives to enhance Earth science education in pre-college schools and informal learning environments, such as museums and nature centers.

A large initiative of AGI is the annual Earth Science Week (ESW) celebration, during which a different theme is celebrated each year to promote awareness and understanding of the geosciences among students, educators, and the general public. The 2024 theme
for ESW is "Earth Science Everywhere." Educational materials related to permafrost will be included in this year's ESW toolkit, which as in past years will be distributed to 9,000 educators worldwide. AGI also plans to include a webinar speaker in the 2024 ESW webinar series to discuss permafrost and related topics. The webinar will be shared during ESW which takes place October 13-19, 2024.

PERMAFROST CLASSROOM MATERIALS

AGI and NRCS are partnering to create soil-related activities that are aligned with the Framework for K-12 Science Education (2011), which was developed by a group of lead states facilitated by the National Research Council (NRC) of the U.S. National Academy of Sciences, to raise awareness about the importance of soils and soil-related careers. (44/50 states in the U.S. have standards based on the Framework.) Aligning the permafrost lessons (and other soil-related activities) to the Framework is essential so that students everywhere learn about these important topics.

One activity recently developed for middle school students focuses on permafrost and its implications in a warming climate. Students begin by exploring how communities built on soil containing permafrost may be affected by atmospheric warming due to climate change with a hands-on model (Figure 3). Following the hands-on activity, students use soil maps created using Web Soil Survey (Figures 1 and 2) to analyze the extent of permafrost near Fairbanks, AK and consider its implications.

Soil-related lessons, including the permafrost activities, have been shared at science teaching conferences (National Science Teaching Association conference and Climate of HOPE conference) and at AGI/ExxonMobil's Teaching and Learning Academy for educators of children aged 5-14. The majority of educators who engaged in the conferences and academies primarily teach in regions absent of permafrost. They were enthusiastic to integrate permafrost and related activities into their instructional practices and recognized the benefits for all students regardless of geographic locations.

Figure 3. Setup of the hands-on activity in "Observing Impacts to Communities Built on Permafrost." Students pour hot water (simulating a warming climate) and observe changes to a model house sitting on ice and gravel (simulating soil containing permafrost).

In addition to soil-related lessons, AGI and NRCS are creating a teacher's guide to Web Soil Survey. Within the guide, there is a section about climate change and the Web Soil Survey interpretations that would be beneficial to examine with students, such as permafrost sensitivity. Teachers are guided on how to integrate soil data into their curriculum and on how to have authentic, specific conversations related to climate change, sustainable cities and communities, and infrastructure.

Complete lessons and guides can be found at www.americangeosciences.org/NRCS.

Additional permafrost-related activities are also in development and will be added to the website as they are released. Contact Lauren Brase, Education Specialist at AGI (lbrase@americangeosciences.org), for more information about the permafrost activities available from AGI and NRCS.

Exploration of changing high mountain areas in the central Andes within the framework of the PermaIntern internship with Chilean – Hungarian Cooperation

Viviána Jó[1,2], Sebastián Ruiz Pereira[2,3], László Mari[1,2] & Balázs Nagy[1,2]

[1]*Department of Physical Geography, Institute of Geography and Earth Sciences, ELTE Eötvös Loránd University, Budapest, Hungary*

[2]*PermaChile Network, Globe Foundation, Budapest, Hungary*

[3]*Pontificia Universidad Católica de Chile, Santiago, Chile*

A long-term Chilean-Hungarian cooperation (PermaChile Network, the research program of the Globe Foundation, Budapest, Hungary) was extended within the framework of the first international permafrost internship, which started this year. The current certified PermaIntern supervisor (second author, S. Ruiz Pereira) from the Pontificia Universidad Católica de Chile, in collaboration with the Eötvös Loránd University (Budapest, Hungary), started the internship in Santiago, Chile. The doctoral research of the first author focuses on changing high mountain environments, with a primary focus on changes in glacier movement. The internship has given her a good opportunity to broaden her research focus and deepen her understanding of permafrost, which change is also becoming more prominent today as glaciers retreat.

GOALS AND FIELDTRIPS

The fieldwork for the internship took place in October 2023 with the aim of understanding and studying the hydrological cycle of the Central Andes in the mountains, involving both glaciers and permafrost. In Chile, the Andes play a critical role in terms of available freshwater resources (Viviroli et al. 2007; Kinnard 2018). Two sites were visited where climate change-induced transformations are well observed, but the exact details (e.g., seasonal characteristics, long-term relationships) of the change is not yet fully known (Burger et al. 2019).

The Juncal Norte glacier and its surroundings (Figure 1) are very close to the Argentine border. The glaciers here, similar to other glaciers in the Central Andes, have decreased over the last decades (Ruiz Pereira et al. 2021). A large proglacial lake has been observed to form at the Juncal Norte front, making access to the glacier ice very difficult. The area before the front of the glacier is covered by buried ice to the east and west, covered by debris.

Figure 1. The Juncal Norte glacier. Proglacial lake from the meltwater and the Juncal River in the foreground, icefalls of the steep Juncal Norte glacier in the background. On the left you can see the buried ice.

The other fieldwork focused on the area around the Marmolejo, San José and Espíritu Santo volcanoes and the El Morado glacier (Figure 2), which are located in the Maipo River Basin. The glaciers in this area also show significant retreat and ice thinning (Farías-Barahona et al. 2020). The area is easily accessible. The Maipo River Basin supplies fresh water to Santiago and its surroundings, where 60% of the country's population lives (Jó et al. 2023). It is therefore important to understand as accurately as possible the hydrological cycle of the area, and to know and map all forms of ice present here.

Figure 2. From left to right: Marmolejo (in the back), Espíritu Santo and San José volcanoes covered with glaciers.

Benefits of the PermaIntern internship

The internship provided an opportunity for the first author to learn from an expert (S. Ruiz Pereira) of high mountain hydrological cycle also on the field. We believe that students do not have many opportunities for this kind of learning in a university setting. Fieldtrips and consultations help a lot in understanding these complex and extremely fragile processes.

Sponsors

The trip was supported by Erasmus+ scholarship and linked to the PermaChile Network (Globe Foundation).

References

Burger, F., Ayala, ´A., Farias, D., Shaw, T.E., MacDonell, S., Brock, B., McPhee, J., and Pellicciotti, F. 2019. Interannual variability in glacier contribution to runoff from a high-elevation Andean catchment: understanding the role of debris cover in glacier hydrology. Hydrol. Process. 33 (2), 214–229. https://doi.org/10.1002/hyp.13354

Farías-Barahona, D., Ayala, ´A., Bravo, C., Vivero, S., Seehaus, T., Vijay, S., Schaefer, M., Buglio, F., Casassa, G., and Braun, M.H. 2020. 60 years of glacier elevation and mass changes in the Maipo River Basin, Central Andes of Chile. Remote Sens. 12 (10), 1658. https://doi.org/10.3390/rs12101658

Jó, V., Van Wyk de Vries, M., Ignéczi, Á., Mari, L., and Nagy, B. 2023. Glacier slowdown and rapid ice loss in the Tinguiririca and Cachapoal Basin, Central Andes of Chile, Global and Planetary Change, 231(104287). https://doi.org/10.1016/j.gloplacha.2023.104287

Kinnard, C. 2018. Mass balance and meteorological conditions at Universidad Glacier, Central Chile. In: Rivera, D.A., Godoy-Faundez, A., and Lillo-Saavedra, M. (Eds.), Andean Hydrology. CRC Press Taylor & Francis Group, Boca Raton, USA, pp. 102–126.

Ruiz Pereira, S., Marquardt, C., Beriain, E., and Lambert, F. 2021. Permafrost evolution in a mountain catchment near Santiago de Chile, Journal of South American Earth Sciences, 109 (103293). https://doi.org/10.1016/j.jsames.2021.103293

Viviroli, D., Dürr, H.H., Messerli, B., Mexbeck, M., and Weingartner, R., 2007. Mountains of the world, water towers for humanity: Typology, mapping, and global significance. Water Resour. Res. 43 (7). https://doi.org/10.1029/2006WR005653

Fostering capacity sharing in permafrost research processes: Learnings from the APECS and Arctic PASSION's Sharing Circle

Fabian Seemann[1,2] & Louise Mercer[3]

[1]*Alfred Wegener Institute Helmholtz Centre for Polar and Marine Research, Permafrost Research Section, Potsdam, Germany*

[2]*Institute of Geosciences, University of Potsdam, Potsdam, Germany*

[3]*Department of Geography and Environmental Sciences, Northumbria University, Newcastle upon Tyne, United Kingdom*

Arctic research is moving towards being application-oriented to address the needs of those directly facing the impacts of accelerating change across permafrost landscapes. Capacity sharing is a two-way knowledge exchange process developed from a basis of reciprocity, communication and collaboration. Multi-directional knowledge exchange can exist in a variety of contexts including intercultural collaboration and the science-policy interface.

The Sharing Circle, a workshop organized by the Association of Polar Early Career Scientists (APECS) and the EU Horizon 2020 Arctic PASSION Project, took place in Sevettijärvi and Inari, Sápmi (northern Finland) in early October 2023. The event brought together Arctic youth and early career researchers (ECRs), with in total 18 participants. Hosted in the Skolt Sámi community, the event created a space that facilitated cross-cultural learning between each other and experienced collaborators (Indigenous and non-Indigenous) who have together co-created environmental monitoring and restoration projects.

The week was filled with a diverse range of activities including seminars circled around a wood fire and on the land learning activities. The program included both environmental and societal topics, contributing to the transdisciplinary nature of the event. Discussions and activities were centred around topics including: (1) a holistic understanding of the socio-ecological impacts of permafrost thaw (2) challenges and opportunities associated with fostering intercultural collaboration and (3) translating science into policy change.

Permafrost warming, a pressing challenge across the circumpolar Arctic (Biskaborn et al. 2019), and its associated impacts on environment and society was discussed heavily. This topic was introduced on an outdoor excursion to a palsa mire in Neiden, northern Norway. Participant-led presentations discussed the potential for co-created community-based monitoring approaches and challenges associated through the presentation of case studies from Tuktoyaktuk, Inuvialuit Settlement Region, Canada (Mercer et al. 2023a; Mercer et al. 2023b).

The concept of co-management was presented by the Snowchange Cooperative (See http://www.snowchange.org/). Due to high land-use pressure and climate change impacts, environmental degradation is evident in Sápmi. Long-term cross-cultural collaboration that addresses local priorities has led to successful management and restoration practices at regional scales. Learnings from Snowchange highlighted the need to weave together diverse knowledge systems to better preserve and restore biodiversity (Mustonen 2021; Ogar et al. 2020).

As permafrost scientists, we carry a responsibility to acknowledge the land and empower Indigenous-led research. Doing so can produce greater equity in research outcomes and contribute to a better understanding of the multifaceted impacts of rapid change across permafrost landscapes. Capacity sharing processes help to build long-term and co-created research projects. Therefore, providing opportunities for ECRs to attend events like the Sharing Circle are crucial to creating a step-change in the way research is conducted in the Arctic.

Figure 1. Participants of the Sharing Circle. Photo: Olivia Rempel/GRID-Arendal.

References

Biskaborn, B.K., Smith, S.L., Noetzli, J., Matthes, H., Vieira, G., Streletskiy, D.A., Schoeneich, P., Romanovsky, V.E., Lewkowicz, A.G., Abramov, A., Allard, M., Boike, J., Cable, W.L., Christiansen, H.H., Delaloye, R., Diekmann, B., Drozdov, D., Etzelmüller, B., Grosse, G., Guglielmin, M., Ingeman-Nielsen, T., Isaksen, K., Ishikawa, M., Johansson, M., Johannsson, H., Joo, A., Kaverin, D., Kholodov, A., Konstantinov, P., Kröger, T., Lambiel, C., Lanckman, J.-P., Luo, D., Malkova, G., Meiklejohn, I., Moskalenko, N., Oliva, M., Phillips, M., Ramos, M.,

Sannel, A.B.K., Sergeev, D., Seybold, C., Skryabin, P., Vasiliev, A., Wu, Q., Yoshikawa, K., Zheleznyak, M., and Lantuit, H. 2019. Permafrost is warming at a global scale. Nat Commun 10, 264. https://doi.org/10.1038/s41467-018-08240-4

Mercer, L., Whalen, D., Lim, M., Cockney, K., Cormier, S., Irish, C., and Mann, P.J. 2023a. Towards more inclusive and solution orientated community-based environmental monitoring. Environ. Res. Lett. 18, 064003. https://doi.org/10.1088/1748-9326/accfb0

Mercer, L., Whalen, D., Pokiak, D.-L., Lim, M., and Mann, P.J. 2023b. Ensuring continuity and impact in Arctic monitoring: a solution-orientated model for community-based environmental research. Environ. Res.: Ecology 2, 045001. https://doi.org/10.1088/2752-664X/ad0241

Mustonen, T. 2021. Indigenous Ecological Reconstruction After Industrial Ruin in Two Iconic Sámi Catchments: Ethics of Comanagement? American Journal of Evaluation 42, 254–275. https://doi.org/10.1177/1098214021997569

Ogar, E., Pecl, G., and Mustonen, T. 2020. Science Must Embrace Traditional and Indigenous Knowledge to Solve Our Biodiversity Crisis. One Earth 3, 162–165. https://doi.org/10.1016/j.oneear.2020.07.006

An international platform for internships focusing on permafrost — PermaIntern

Ylva Sjöberg[1,2], Iver Martens[3], Hanne H. Christiansen[4], Robin B. Zweigel[5,6], Julie Malenfant-Lepage[7], Thomas Ingeman-Nielsen[8], Wesley R. Farnsworth[9], A. Britta K. Sannel[10] & Mikkel Toft Hornum[1,11]

[1]*Department of Geoscience and Natural Resource Management, University of Copenhagen, Copenhagen, Denmark*
[2]*Department of Ecology and Environmental Science, Umeå University, Umeå, Sweden*
[3]*Department of Geoscience, UiT The Arctic University of Norway, Tromsø, Norway*
[4]*Arctic Geophysics Department, The University Centre in Svalbard, UNIS, Norway*
[5]*Department of Geosciences, University of Oslo, Norway*
[6]*Centre for Biogeochemistry of the Anthropocene, University of Oslo, Norway*
[7]*Department of Civil and Environmental Engineering, Norwegian University of Science and Technology, Trondheim, Norway*
[8]*Department of Environmental and Resource Engineering, Technical University of Denmark, Denmark*
[9]*Institute of Earth Sciences, University of Iceland, Reykjavík, Iceland*
[10]*Department of Physical Geography, Stockholm University, Stockholm, Sweden*
[11]*Arctic Geology Department, The University Centre in Svalbard, UNIS, Norway*

The Arctic is a complex region undergoing uniquely rapid changes in both nature and societies. These developments create new needs for professional competence to meet challenges related to thawing permafrost and changes in natural resource accessibility, as well as industrial and community development. We strongly believe that Arctic-specific professional competence needs to be built and maintained in the Arctic. Internships are learning forms that can help students realize knowledge as competence in a professional setting, and at the same time provide platforms connecting students, academics, and professionals with competence needed in the Arctic.

Aims

We are developing an international service for facilitating internships with a permafrost specific focus for all higher educational levels. Our aim is to provide a structure and system that are flexible enough to accommodate students in a wide range of educational programs and can support high-quality learning about permafrost from an internship experience. We hope to create an online platform which facilitates connections between internship hosts, supervisors, and students. This will provide a venue where hosts can post information about internship opportunities, where students are invited to share their internship experiences, and where supervisors with the necessary expertise are presented.

The project so far

The project is carried out by the UArctic Thematic Network on Permafrost and funded by UArctic for the period 2022 to 2024. The Nordic region is the pilot area for the internship service, and the project partners come from ten universities in the Nordic countries and from the Permafrost Young Researchers Network (PYRN). During fall 2022 and spring 2023, the partners developed the structure of the service through discussions and inventories of internship opportunities and needs at their respective universities (Figure 1.). The proposed service was presented and discussed at a workshop during EUCOP in June 2023, with international colleagues.

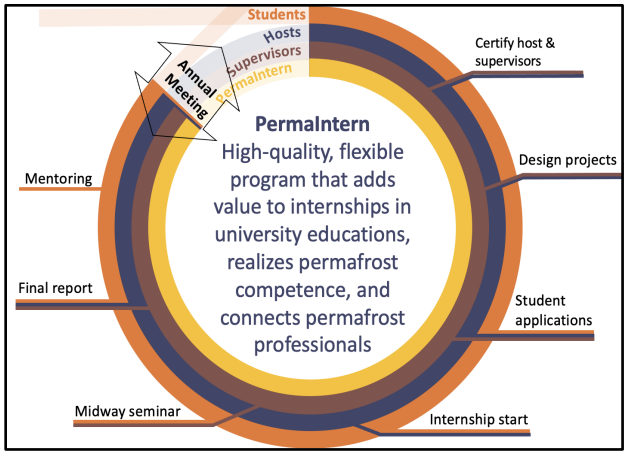

Figure 1. The basic structure of the PermaIntern program, including actors and mandatory elements.

The PermaIntern program

The service is called PermaIntern, short for permafrost internship. It includes certification of both internship hosts and supervisors (typically located at the student's home university or abroad if there is no

permafrost expertise that has been developed at the home university). The first supervisors and hosts were certified during the fall of 2023. The certification process includes information about the program and expectations on supervisors, hosts, and students in the program. Supervisors and hosts must also fill out forms with basic information needed to successfully take part in the program, and thereafter have a meeting (online) with a PermaIntern representative. The program includes certain mandatory elements for students (e.g., a project report and mid-term seminar), which are designed to overlap with the most common elements required from internship projects at the PermaIntern partners' educational programmes. Thereby, we strive to not create unnecessary extra work for students and supervisors, but instead provide guidance for high quality in existing educational elements.

Ongoing activities

During the fall of 2023 and spring 2024, we will continue the development of our online platform (www.permaintern.org). The platform will be used to connect hosts and students for pilot internships during the spring of 2024. And we aim to finish development to allow for the formal launch during ICOP in June 2024.

Launching PermaIntern

For our launch and presentation at ICOP2024, we will introduce the final online platform and present the experiences learned from the pilot internships in spring 2024. We will also provide future outlooks for PermaIntern as a resource for the international permafrost community.

Arctic Board Game: Tool for education, outreach, and discussion

Tetsuo Sueyoshi[1], Hajime Kimura[1], Eiji Watanabe[1], Jonaotaro Onodera[1], Makoto Sampei[2], Minoru Kitamura[1], Minori Takahashi[3], Satoshi Kimura[1] & Yuka Oishi[4]

[1]*Japan Agency for Marine-Earth Science and Technology (JAMSTEC), Yokosuka, Kanagawa, Japan*
[2]*Faculty of Fisheries Sciences, Hokkaido University, Hakodate, Hokkaido, Japan*
[3]*Department of Political Science, Hokkai Gakuen University, Sapporo, Hokkaido, Japan*
[4]*Department of Cultural-Interaction, Kobe University, Kobe, Hyogo, Japan*

The Arctic Board Game was developed as part of Japan's national Arctic research project, Arctic Challenge for Sustainability (ArCS, 2015-2020), in collaboration with the National Museum for Emerging Science and Innovation (Miraikan) in Japan. As an interdisciplinary research project, there was a need for a new outreach tool or method to illustrate the connection between research and society, as well as the interactions between research topics. A board game was chosen as the medium and was intended to be a learning/educational tool for the originally targeted high school students. It was also intended to be used for outreach purposes at public events. The game focused on the decline of Arctic sea ice and its far-reaching and complex impacts and consequences. Here, we present the concept and applications of our board game and suggest the permafrost community to contribute to/produce such game designs.

Background and Purpose

The Arctic Board Game was produced as a part of Japan's national Arctic research project, Arctic Challenge for Sustainability (ArCS, 2015-2020), in collaboration with the National Museum for Emerging Science and Innovation (Miraikan) in Japan. As an interdisciplinary research project, there was a need for a new tool or method of outreach to illustrate the connection between the research and society, as well as the interactions between the research topics. A board game was chosen as a medium and was aimed to be a learning/educational tool for the students originally targeted high school. It was also expected to be used for outreach purposes at public events.

The Game Design

The game is a tabletop role-playing game played by 4-6 people. In this game, there are three parameters or "Arctic Scores" of Environment, Culture, and Economy, ranging from 1 to 10. The aim of the game is to keep these scores as high as possible, with different goals (i.e., values of the three scores) for different players depending on their "role". There are six roles: Oceanographer, Cultural Anthropologist, Indigenous Worker, Industrial Worker, Fishery Worker, and Diplomat. For example, the Cultural Anthropologist must have Culture >6 and Environment >2, while the Industry Worker must have Economy >6 and Culture >2.

The game board consists of a main board and a side board. The main board shows the Arctic map for the sea ice tiles and the Arctic Score and Budget tracks. The budget is for all players. It represents the world's resources for Research/Policy in the game. The side board shows the Research/Policy panels and the phase track.

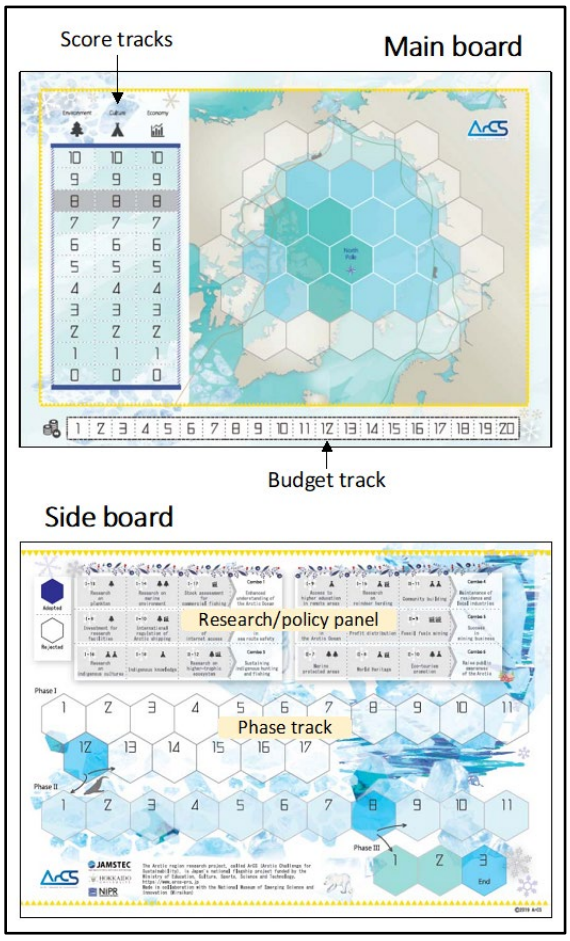

Figure 1. Main and Side Boards

The game progresses by the player flipping over the sea ice tiles one by one, which represents both the progression of time in the game and the decrease of sea ice due to the amplified climate warming. Players then follow the instructions on the back of the ice tile, which are explained in detail in the Event Book. Instructions are of three types: Events, Votes, and Decisions. Events are environmental or societal events that affect the Arctic Score. Votes and Decisions are opportunities for players to make some research or policy actions using the budget, which corresponds to actions or investments in the real world.

Sea ice tiles have three thicknesses: thin first-year ice on the outer side, thicker multiyear ice on the inner side, and thickest old ice in the central part, of the Arctic Ocean. The game ends when the three thickest ice tiles are flipped over. Many of the events written on these thick ice tiles are catastrophic and will severely damage the Arctic score, so it is required that players make an effort to 'prepare' by this stage to beat the game.

USING THE BOARD GAME IN CLASSROOM AND EVENTS

We have used the board game in several occasions, including 4 University lectures and 2 high school classes, one in private-tutoring school, as well as the public events in the science museum for students, including elementary school students. We have also made an English translation and used it in workshops and events for younger scientists at the international Arctic conferences. In all cases, the results were positive in general, being able to involve participants in the post-game discussion on the ongoing changes and challenges in the Arctic.

Figure 2. Using the Board Game in an outreach event.

DISCUSSIONS: ADVANTAGE OF THE "SERIOUS GAME" IN OUTREACH

This type of game is also called a "serious game" and its advantage as a learning tool is widely recognized in recent studies. We found that our board game can function as an effective learning aid in three ways. First, the game format promotes communication among players and thus deepens their understanding and broadens their thought processes as they share their knowledge, interests, opinions, and what they have learned. Second, the game helped players better grasp the complexity of the Arctic and the results of the ArCS research project and engage with these issues (as we can see from their feedback). Third, the game format allows workshop facilitators to respond to a variety of learning objectives by devising pre- and post-learning activities.

We strongly recommend the utilization of the gaming method as a learning tool, especially for younger generation and the indigenous communities. It can effectively lower the hurdles for seemingly boring scientific topics.

NEXT STEPS

We are also planning to update the game to reflect the latest situations of Arctic issues, including more terrestrial elements such as permafrost changes, landslides, and wildfires. Inputs/suggestions from the permafrost community in the development of the game are very welcome.

COMMERCIALISM

We don't sell this board game and therefore no commercialism is involved.

ACKNOWLEDGEMENT

The development of the board game "The Arctic" and related practices are supported by Japan's National Arctic research projects, the Arctic Challenge for Sustainability (ArCS), Program Grant Number JPMXD1300000000, and the Arctic Challenge for Sustainability II (ArCS II), Program Grant Number JPMXD142031886.

REFERENCES

Kimura, H., and Oishi, Y. 2022. Gaming for Arctic Sustainability, chapter 9 in Simulation and Gaming for Social Design, Kaneda, T., Hamada, R., and Kumazawa, T., Springer, Singapore.

Stanitsas, M., Kirytopoulos, K., and Vareilles, E. 2019. Facilitating sustainability transition through serious games: a systematic literature review. Journal of Cleaner Production 208: 924–936. doi:10.1016/j.jclepro.2018.10.157.hal-01918890

Arctic Permafrost Atlas

Levi Westerveld[1], Tina Schoolmeester[1], Oda Mulelid[1], Torjus Eckhoff[1], Paul Overduin[2], Michael Fritz[2], Hugues Lantuit[2], Björn Alfthan[1], Anna Sinisalo[1], Frederieke Miesner[2], Leena-Kaisa Viitanen[2] & Nunataryuk Consrotium[3]

[1]*Grid Arendal, Arendal, Norway*
[2]*Alfred Wegener Institute, Helmholtz Centre for Polar and Marine Research, Potsdam, Germany*
[3]*EU H2020 funded Nunataryuk research project Consortium*

The latest assessment report of the Intergovernmental Panel on Climate Change (IPCC) emphasizes the importance of permafrost for the Earth's climate. As permafrost thaws as a consequence of global warming, both its area and volume continue to decrease. Arctic ecosystems are changing irreversibly in ways that threaten not only flora and fauna but also the lives, livelihoods, and cultural identities of Arctic peoples.

As more attention is directed towards understanding the role of permafrost in the climate system and the various aspects of loss and damage associated with permafrost thaw, an ever-growing body of literature has emerged from both the natural and social sciences.

The primary goal of the Arctic Permafrost Atlas is to consolidate these findings and offer insights into the diverse aspects and impacts of permafrost and permafrost thaw. In doing so, it aims to provide deeper understanding of permafrost thaw, share knowledge to help mitigate uncertainties, and facilitate adaptation to changing conditions, especially with respect to infrastructure, food security, and mobility. It endeavours to be both informative and motivating while disseminating knowledge of this largely invisible yet vitally important component of the Earth's ecosystem. The Arctic Permafrost Atlas also strives to assess the effects of permafrost change on the Indigenous Peoples of the Arctic. While society throughout the Arctic is highly diverse, Indigenous Peoples continue to maintain close ties to the land as a means of preserving their culture, knowledge, and traditional food supply. However, the dramatic impacts of permafrost thaw on Arctic ecosystems now place thousands of years of cultural tradition and climate adaptation at risk.

The Arctic Permafrost Atlas was created within the European Union Horizon 2020 funded Nunataryuk project (2017–2023). Well over one hundred individuals, scientists, cartographers, science writers and people from the Arctic contributed to the making of the publication. It does a great job of describing permafrost with maps, prose, art, and personal stories. Far from being an academic product in the traditional sense, it gathers knowledge from the diverse voices of scientists, Indigenous Peoples, northern residents, and local practitioners to provide a holistic and inclusive view of today's challenges in the "country of permafrost".

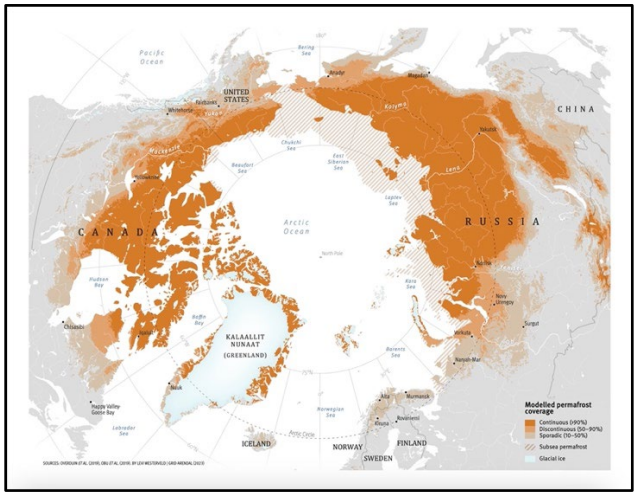

Figure 1. Modelled permafrost coverage. (from the Arctic Permafrost Atlas.) By Levi Westerveld / Grid Arendal (2023).

The Arctic Permafrost Atlas is freely available online at https://nunataryuk.org/news/atlas. A limited press run of hardcover editions will be available.

References

Westerveld, L., Kurvits, T., Schoolmeester, T., Mulelid, O. B., Eckhoff, T.S., Overduin, P.P., Fritz, M., Lantuit, H., Alfthan, B., Sinisalo, A., Miesner, F., Viitanen, L.-K., and the NUNATARYUK consortium. 2023. Arctic Permafrost Atlas. GRID-Arendal, Arendal, Norway.

3 Permafrost Environments

INTEGRATING PERSPECTIVES OF PERMAFROST THAW, CHANGE, AND ADAPTATION

3A — Extreme and Unique Environments: Antarctic and Beyond

Session Chairs: Mauro Guglielmin[1], Marc Oliva[2] & Stefano Ponti[1]

[1]*Insubria University, Varese, Italy*
[2]*Universidad de Barcelona, Barcelona, Catalonia, Spain*

The session is proposed within the SCAR Expert Group ANTPAS and it is focused on the climate change effects on geomorphologic and biologic processes of the periglacial and cryotic environment of the ice-free areas of Antarctica and SubAntarctic Islands. As highlighted by several recent studies, the recent climate change, as well as the significant climate change of the past, induce important and sometimes sudden changes in landform evolution, soil formation and vegetation development. The monitoring of the abiotic and biotic changes and the understanding of their mutual relationships and the relations with climate change and their feedbacks are the main issue to address in this session. All types of techniques to achieve these are welcome (geophysical investigations, thermal monitoring, vegetation and soil monitoring as well as remote sensing to monitor surface changes). Weathering changes on rock substrates and coastal evolution are also welcome.

Soil organic matter in soils of east Antarctica: insights from ^{13}C-NMR spectroscopy

Ivan Alekseev[1], Elena N. Grek[2,1] & Antonina Chetverova[1]

[1]*Arctic and Antarctic Research Institute, Saint Petersburg, Russia*
[2]*State Hydrological Institute, Saint Petersburg, Russia*

Recent studies indicated a significant variability in soil forming conditions and processes across the terrestrial ecosystems of Antarctica as well as considerable diversity of soil types. Our study provides a comprehensive investigation of soil organoprofiles in Antarctic terrestrial ecosystems and give informative insights into molecular composition of organic matter in soil and soil-like bodies of remote areas of East Antarctica - Larsemann Hills and Bunger Hills characterized by harsh environmental conditions. These soils showed predominantly coarse structure and low organic carbon content, which is connected with harsh climatic conditions and absence of vascular plants.

Soil pH in Bunger Hills varies from slightly acidic and acidic in the horizons under moss cushions in wind shelters to alkaline in places of active salt accumulation. Salt accumulation has a major environmental control on geomorphology, sediment geochemistry and biogeography of Bunger Hills. The major salts are halite (NaCl) and thenardite (Na_2SO_4), both of which are derived from seawater and marine salt spray (Gore and Leishman, 2020). It also occurs due to the active weathering of massive crystalline and friable rocks. It was found that the oasis seems to be divided by the "salt line" into two parts, affecting the intensity of rock weathering, as well as the spread and growth of salt-sensitive plants, such as mosses and lichens (Gore and Leishman 2020). Soil pH in soils of Larsemann Hills varies from slightly acidic to close to neutral. At the same time, both surface and subsurface horizons differed in the content of carbon (TC) and nitrogen (N). Thus, TC values varied in a wide range from 0.54% to 6.35%. Soils of wet valleys and wind shelters with developed moss cushions showed a higher carbon content compared to high dry valley slopes. In addition, high levels of organic matter accumulation and soil respiration are observed in localities influenced by the ornithogenic factor (nesting sites of small groups of penguins and their resting places). The bulk density of soils increases from topsoil horizons (the minimum is typical for peat horizons) to the sub-surface ones, which is associated with a varying content of fine-earth material and its weathering degree.

^{13}C-NMR spectra of humic acids investigated in typical soils from East Antarctica differ significantly from those from Maritime Antarctica (King George island). Differences in elemental composition and atomic ratios of O/C, H/C, and C/N as well as the dominance of the peripheral part over aromatic fragments in HAs of studied soils are reported. The C/N ratio in humic acids of soil from Bunger Hills is quite low, which is due to the low carbon content in the molecules of peripheral compounds with a significant proportion of nitrogen. This generally indicates a low degree of humification of organic matter. We also noticed very weak aromatic part in HA in studied Antarctic soils. This is due to the extremely low content of phenylpropane structural fragments caused by the dominance of organic residues of lower plants – mosses and lichens, consistent with previously published data (Beyer et al. 1997). There is also an increased content of aliphatic fragments, which also brings them closer to fulvic acids. Thus, the soils of Larsemann Hills are characterized by a reduced content of aromatic fragments compared to the soils of Fildes Peninsula (Figure 1). This is due to the different duration of the period of biological activity in these regions (20-30 days in case of Larsemann Hills, and more than 100 days in case of Fildes Peninsula and Ardley Island). The amount of liquid precipitation is also dramatically different, about 700 mm in liquid equivalent in Maritime Antarctica and only 100-200 mm in oases of Eastern Antarctica. These differences are related to the composition of humification precursor substances - in case of Antarctica, due to the absence of higher plants and weak development of plant communities in some landscapes, humic acids contain very few phenylpropane fragments at all.

In general, it is worth noting that these data indicate (at molecular level) the fundamental possibility of humification processes in soils of Antarctica. This confirms the fact that biogenic-abiogenic interactions occurring in the harsh conditions of the sixth continent still leads to the formation of soils.

All studied soil groups in Eastern Antarctica are characterized by the predominance of aliphatic structures. In addition, HAs contains significant amounts of carbohydrates, polysaccharides, esters and amino acids (Figure 1). At the same time, hydrophilic fragments predominate in HAs of soils.

It was shown that humification process occurs in soils and soil-like bodies of Eastern Antarctica and this process proceeds even in the case of almost complete absence of aromatic phenylpropane precursors. It was also shown that in harsh climatic conditions of Antarctica the formation of humic acids with a pronounced aromatic and peripheral part is possible.

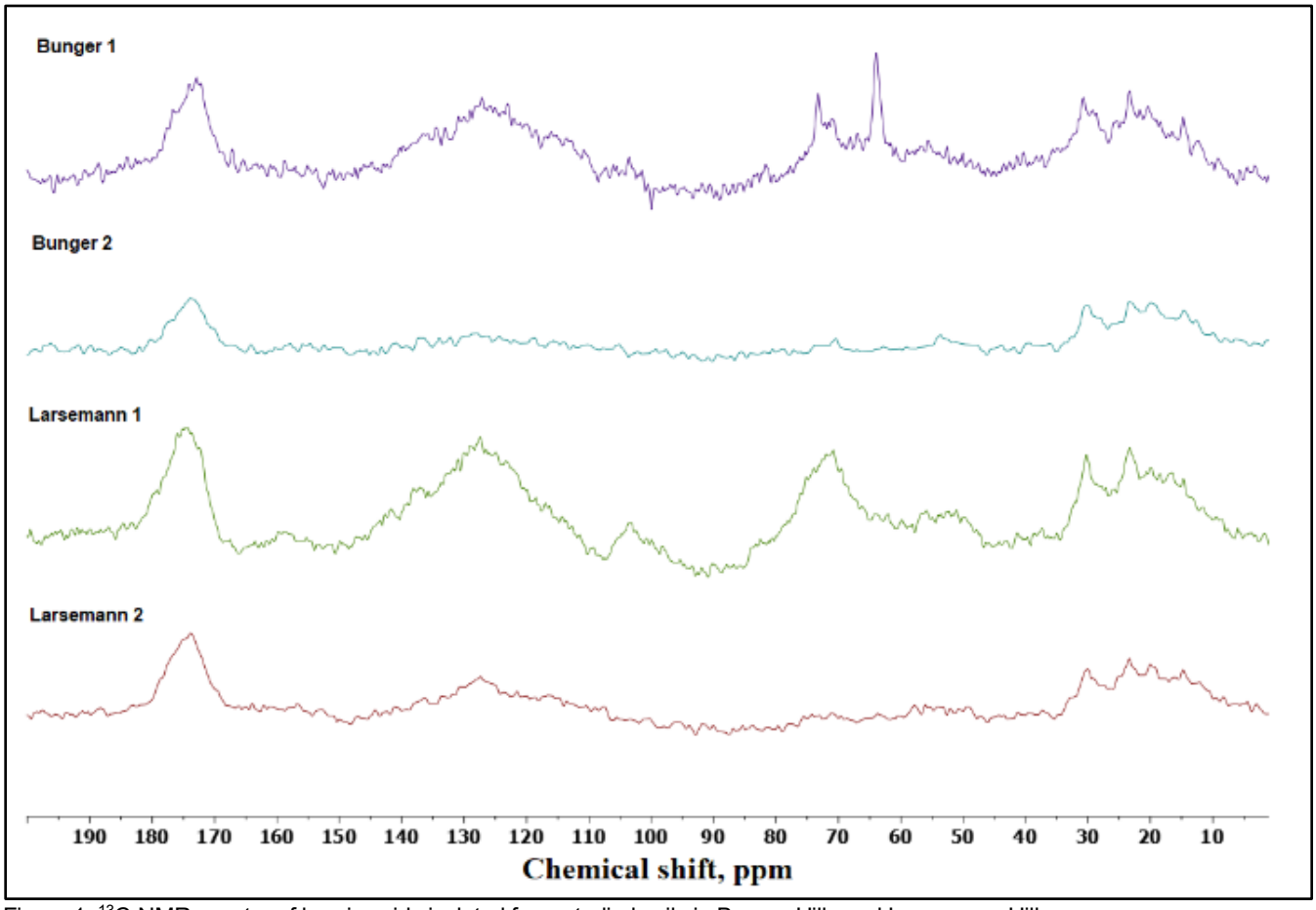

Figure 1. ^{13}C-NMR spectra of humic acids isolated from studied soils in Bunger Hills and Larsemann Hills.

Acknowledgement

This study has been supported by the grant of the Russian Scientific Foundation (project № 24-27-00361 «Soils in Eastern Antarctica oases: biogeochemistry, stability of organic matter and environmental risks»).

References

Beyer, L., Knicker, H., Blume, H.-P., Bölter, M., Vogt, B., and Schneider, D. 1997. Soil organic matter of suggested spodic horiozns in relic ornitogenic soils of coastal Continental Antarctica (Casey Station, Wilkes Land) in comparison with that of spodic soil horizons in Germany, Soil Sci. 7: 518–527.

Gore, D., and Leishman, M. 2020. Salt, sediments and weathering environments in Bunger Hills. Antarctic Science. 32(2),138–152. doi:10.1017/S0954102020000073

Geoelectric study in the area surrounding the Peruvian Antarctica Station of Machu Picchu, Maritime Antarctica

Cinthya Bello Chirinos[1], Wai Long Ng-Cutipa[2] & Antonio Correia[3]

[1]*Carrera de Biologia Marina, Universidad Científica del Sur, Lima, Peru*

[2]*Geological and Mining Institute of Spain, IGME-CSIC, Madrid, Spain*

[3]*Institute of Earth Sciences, University of Evora, Evora, Portugal*

In January 2018 a geoelectrical study was started in the Peruvian Antarctic Station of Machu Picchu to try to delineate the geoelectrical structure of the aquifer that provides water for domestic uses to the station. Machu Picchu station (62°05'49''S latitude and 58°28'23"W longitude) is located in Crepin Point, King George Island (South Shetland Islands, Antarctica) off the coast of Admiralty Bay. It is a summer station which was built in 1989. The study area is about 400 per 150 m above Quaternary deposits (Figure 1). The Machu Picchu Station area is limited to the south by lateral moraine and to the west by the Machu Picchu peak; beyond is Znosko Glacier. To the north and east is McKellar inlet.

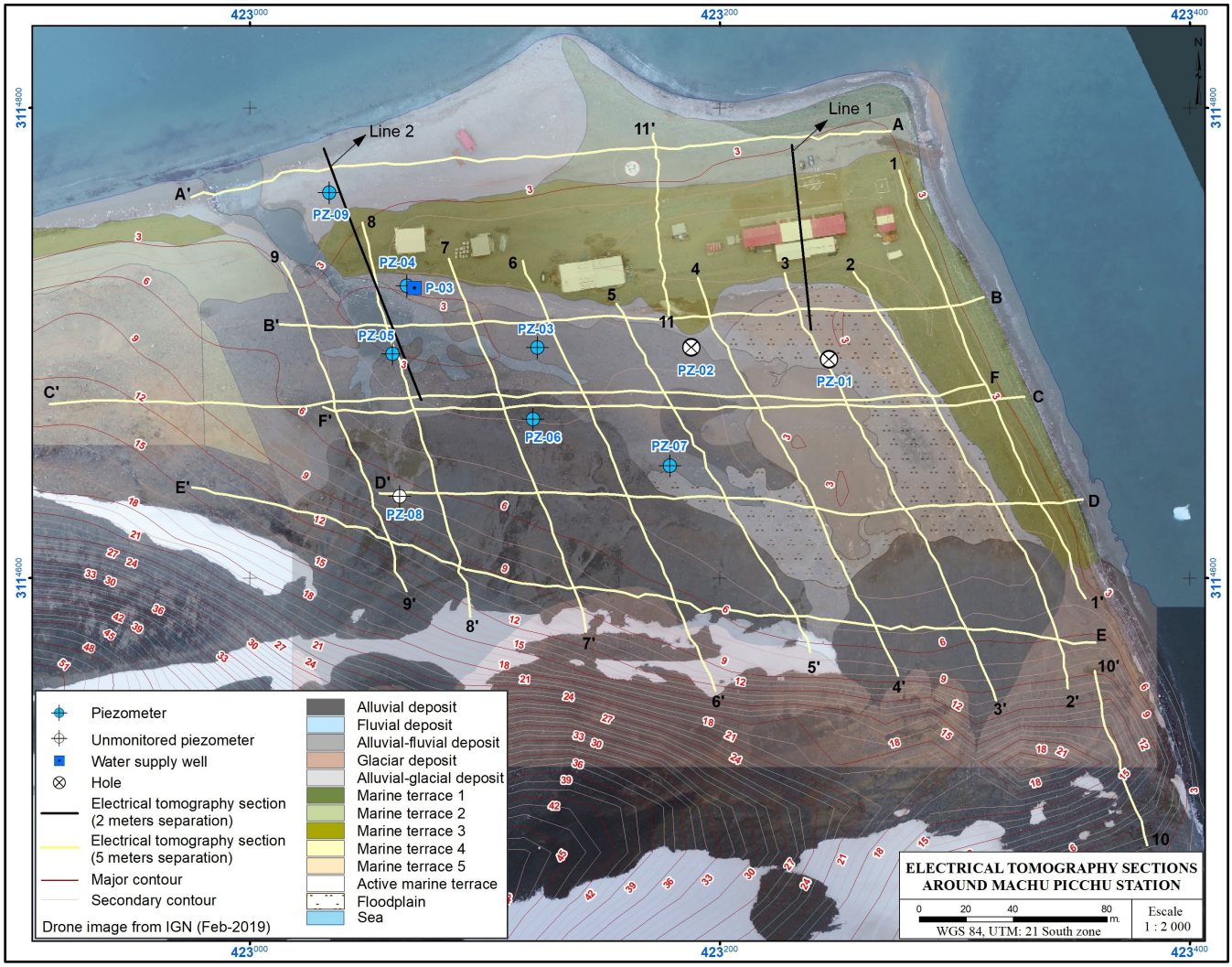

Figure 1. Crepin Point study area. Lines from 1-1' to 11-11' and A-A' to F-F' correspond to ERT profiles carried out in a first phase of the geoelectrical survey whereas Lines 1 and 2 correspond to ERT profiles carried out in a second phase.

The study aimed to try to delineate the aquifer's lateral and depth extensions so that a better water exploitation could be devised. Furthermore, the work also aimed at identifying areas of possible saline intrusion. As a matter of fact, Machu Picchu Station is planning to transform it into a permanent station which implies a more rigorous aquifer management. The study area (about 90,000 m^2) presents glacial, alluvial-glacial, alluvial, alluvial-fluvial, and marine sediments (mostly sandy and silty gravel layers); in the area where the aquifer is believed to exist several electric resistivity tomographies with lengths varying between 100 to 300 m long were carried out. Hydrogeological data was obtained from piezometers located within the area where electrical resistivity tomographies (ERTs) were done.

Geology and Geomorphology

The study area is on Barton horst oriented SW-NE with volcanic and volcanogenic rocks which are cut by dykes and intruded by calco-alkaline plutons. Around Machu Picchu station, the area is represented by Cardozo Cove Group, Wegger Peak Group and Quaternary deposits. Near to Crepin Point, Cardozo Cove Group consists of volcanic and volcanogenic successions (dacitic-andesitic) differentiated in three sub-units with ages from the Upper Cretaceous to the Paleocene. Wegger Peak Group consists of quarz-monzodiorites to grano-diorites dated 49.1 ± 0.4 Ma in diorite and quartz diorite rocks. Cerpa (2015) made a detailed description of Quaternary deposits in Crepin Point, recognizing glacial deposits, fluvial-alluvial system and six marine terraces (Figure 1). Geomorphology wise the zone has marine action geoforms (marine terraces, beach), modeled glaciar geoforms (glacial, morraines, erosioned/transported glacial-fluvial, gelifraction detritus) and mountain and denudational colin geoforms.

Materials and Methods

In a first phase, for each electrical resistivity tomography, with a Wenner-type configuration, 80 electrodes were used with a distance between consecutive electrodes of 5 m. To measure the apparent electrical resistivity, an ABEM Terrameter LS resistivity meter was used. The apparent electrical resistivity values were converted into two-dimensional electrical resistivity models (geoelectric sections) of the soil by mathematical inversion, using the RES2DINV software. The models obtained by inversion represent geoelectric sections with lengths between 100 and 400 m and depths between 13 and 29 m, approximately (example in Figure 2). In a second phase each ERT profile was done using 40 stainless electrodes spaced by 2 m. A LGM Resistivity Meter was used to control the measuring process and record the field data which were downloaded latter for processing. During the acquisition stage a few problems related with high electrical contact resistances between the ground and the stainless electrodes had to be solved. By eye inspection those problems were the result of frozen ground or dried moss roots. Those problems were solved watering with sea water the zone of the electrodes affected by high electrical contact resistance.

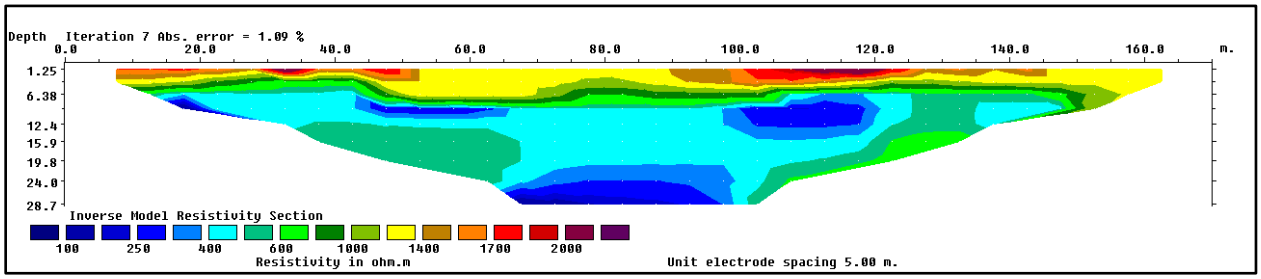

Figure 2. Geoelectrical model corresponding to ERT profil 5-5' of Figure 1. Bluish areas correspond to aquifer formations.

Conclusions

Processing and interpretation of the geoelectric data indicate that several tomographic profiles crossed the aquifer which appears to be several tens of meters deep; the bedrock appears to be deeper than 60 m according to seismic refraction studies carried out by Pari and Zavala (2000). The aquifer formation presents electrical resistivity values that range from about 100 to 400 Ω.m. Water samples from the piezometers present electrical resistivity values ranging from 25 to 50 Ω.m. At this stage two and three dimensional geoelectrical models are being constructed to try to have an idea of the aquifer's geometry.

References

Cerpa, L. 2015. Estratigrafía de Punta Crepín, isla Rey Jorge, islas South Shetland, Antártida, Boletín de la Sociedad Geológica del Perú, 110: 59–62.

Pari, W., and Zavala, B.L. 2000. Estudio geofísico de los suelos en Punta Crepin-Estación Científica Peruana Macchu Picchu (Isla Rey Jorge-Antártida). Comisión Nacional de Asuntos Antárticos. Consejo Nacional de Ciencia y Tecnología, p. 353–385.

Biogenic-abiogenic interactions in Cryosols of east Antarctica

Elena N. Grek[2,1] & Ivan Alekseev[1]

[1]*Arctic and Antarctic Research Institute, Saint Petersburg, Russia*
[2]*State Hydrological Institute, Saint Petersburg, Russia*

Levels of biogenic-abiogenic interactions and micromorphological features of Antarctic soils is poorly investigated. On the other hand, these information is highly crucialnot only for soil diagnostics and classification themselves, but also for identification of such important parameters as degree of biogenic transformation, decomposition of organic matter, formation of clay minerals and the accumulation of soluble salts etc.

Our research contributes with the results on investigation of initial soil-forming processes under harsh environmental conditions of Eastern Antarctic oases. This work is aimed at the investigation of levels of biogenic-abiogenic interactions in soil and soil-like bodies of Larsemann Hills and Bunger Hills by analyzing thin sections from soil micromonoliths to assess the intensity and trends of the pedogenic processes in selected soils.

Thin sections were investigated with use of polarization microscope Leica DM 750 p in plain and polarized light. Samples were air dried and then saturated with epoxy resin. The terminology used in this paper is published by Stoops (2003), Gagarina (2004) and Gerasimova et al. (2011), where micro-morphological organization of soils were described and classified in details (Stoops and Eswaran 1986; Stoops 2003, 2009). The following soil micromorphological indices have been investigated: soil microfabric, spatial arrangements of fabric units, soil particles distribution, elements of microstructure and character of organic matter.

Thin sections from soils in different locations of Larsemann Hills and Bunger Hills studied showed some differences in the microstructure, the distribution of the plasma and the amount and type of porosity. Microphotographs of sampled soils are summarized in Figure 1. It is usually seen that the grains of quartz, feldspars, and other primary minerals are characterized by angular shapes indicating to the relatively weak degree of their alteration. Soils from studied oases are highly influenced by cryogenic processes, which explains the presence of cracks and vertical orientation of minerals in the soil fabric. Thin sections of all the samples studied is composed of mineral and organic particles with abundant packing voids. Most of the quartz grains showed angular outline and sharp edges. Also, the features of the calcium carbonates neogenesis and redistribution could be seen as well as the microcrystallic calcareous aggregation and cementation of the skeletal particles (Figure 1).

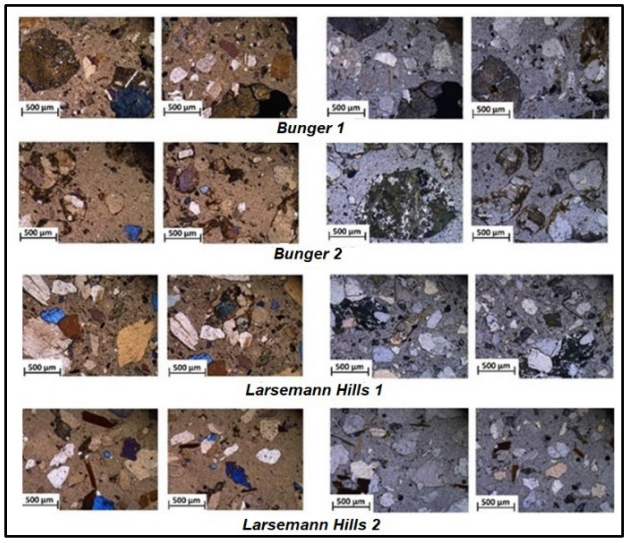

Figure 1. Microfabrics of investigated topsoils from Bunger Hills and Larsemann Hills: left–nicols X, polarized light; right–nicols II, plain light.

Studied soils generally have a sandy-skeletal textural class and feature strong oxidation of Fe-bearing minerals and some clay mineral alteration. Generally, small to medium-sized granular structure with ovoidal, subrounded forms is observed. Microfabrics of the topsoil horizons (Bunger 2, Larsemann 2) with the maximal biological activity show visible biofilms covering the most of the grains of quartz, feldspar, which are the dominant minerals. The presence of these microstructures (biofilms) on the surface of minerals creates a specific geochemical environment which may stimulate or slow down the weathering processes. Both studied oases– Larsemann Hills amd Bunger Hills– are characterized by harsh environmental conditions (strong winds, lack of moisture, ultraviolet radiation, sharp temperature changes), which determines the presence of more or less favourable environmental conditions in sporadic zones.

In such conditions the intense translocation of organic detritus take place, so organo-accumulative processes often are manifested as lichens residues (less often–moss) accumulation in rock cavities.

The micromorphological patterns of the studied thin sections also provide evidence on the activity of cryogenic weathering with the comminution of rock fragments.

This study has been supported by the grant of the Russian Scientific Foundation (project № 24-27-00361 «Soils in Eastern Antarctica oases: biogeochemistry, stability of organic matter and environmental risks»).

References

Gagarina, E.I. 2004. Micromorphological method of soil investigation. St. Petersburg Univ. Publ., Saint Petersburg, Russia (in Russian).

Stoops, G., and Eswaran, H. 1986. Soil micromorphology. Van Nostrands Reinhold Company, New York, USA.

Stoops, G. 2003. Guidelines for analysis and description of soil and regolith thin section. Soil Science Society of America Inc. Madison, Wisconsin, USA.

Stoops, G. 2009. Evaluation of Kubiena's contribution to micropedology. At the Occasion of the Seventieth Anniversary of His book "Micropedology", Eurasian Soil Science, 42(6): 693–698. doi:10.1134/S1064229309060155

A decade (2013-2022) of permafrost and active layer thickness monitoring in Antarctic Peninsula Area

Francesco Grifoni[1,2], Nicoletta Cannone[1,2], Peter Convey[3] & Mauro Guglielmin[1,2]

[1]*Insubria University, Department of Theoretical and Applied Science, Via Dunant, 3, 21100 Varese, Italy*

[2]*Climate Change Research Center, Insubria University,Via Dunant 3, 21100, Varese, Italy*

[3]*British Antarctic Survey, High Cross, Madingley Road, Cambridge CB3 0ET, United Kingdom*

Climate change had a detrimental effect on permafrost representing about 17% of the Earth's exposed land surface. This is due to rising air temperatures and changing snow regimes, which has been more rapid in polar and high elevation regions in recent decades. Even if global air temperatures rise no more than 2°C by 2100, there is still expected to be a significant area of permafrost degradation. Ecosystems, hydrological systems, and the integrity of infrastructure would all suffer greatly from such a shift (Biskaborn et al. 2019). The strong air temperature warming between the 1950s and 2016 in the Antarctic Peninsula region exceeded the global average warming with evident impacts on terrestrial ecosystems. After that,a short but intense cooling occurred from the Antarctic Peninsula to the South Orkney Islands (1999–2016) (Cannone et al. 2022).

STUDY AREA AND METHODS

Since 2013 the thermal profile of two intermediate deep boreholes (≥ 30 m) located approximately at the same elevation (ca. 30 m a.s.l.) and same distance from the coast respectively at Signy Island (60°43'S) (Figure 1) and Rothera (67°57'S) were monitored continuously (Figure 2).

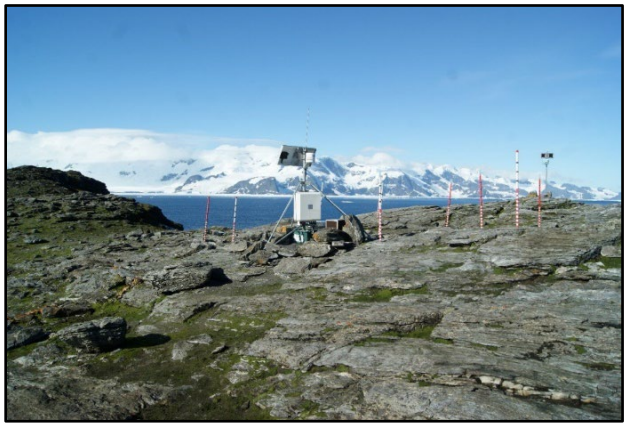

Figure 1. Photo of the Berntsen site on Signy Island, Antarctic Peninsula. (Photo from project 2013/C1.01).

Figure 2. Photo of the Rothera site on the Antarctic Peninsula. (Photo from project 2004/5.3).

Climatic and permafrost data were collected from micro-stations at the two sites, where air, ground surface and permafrost temperatures and snow cover data were recorded. The continuous snow field data was available only for Rothera obtained from a manual monitoring. The annual (Figure 3), seasons, and daily mean air and ground surface temperatures, and the climate TDD and FDD indices, were calculated through statistical analysis of the micro-stations climate data.

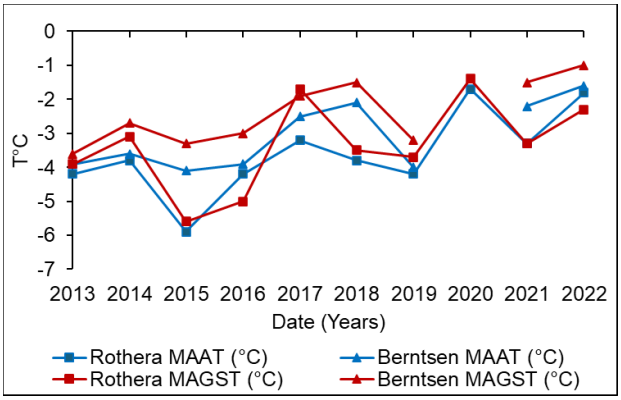

Figure 3. Mean annual air temperature (MAAT) mean annual ground surface temperature (MAGST) measured since 2013 at Rothera and Berntsen.

Active-layer thickness (ALT) defined as the maximum depth of the 0°C isotherm for each year was calculated from the interpolation of linear regression of the maximum temperature recorded at the borehole between the two depths in which the maximum daily temperature was closest to 0°C take both positive and negative temperature values (Adlam et al. 2010; Guglielmin et al. 2012). The mean annual temperature of permafrost's table was calculated from the active layer thickness data for each year, the average of the daily temperature values associated with the measured of the ALT was calculated (Muller 1947). Zero annual amplitude (ZAA) was the depth where the difference between the minimum and maximum temperature is smaller than 0.1 °C (instrument's accuracy) for all days of the year. The temperature of the ZAA was calculated from the depth and temperature values close to the ZAA by interpolating the linear regression obtained (Carlsaw and Jaeger 1959).

Results and discussion

Here we will present the main results of the trend of the ground surface temperature, the permafrost temperature at the zero annual amplitude (ZAA) depth and active layer thickness (ALT). Moreover, we analysed their relationships with the main climatic factors (air temperature, snow thickness) and finally with the latitude. The two sites both located in continuous permafrost areas showed different trends for the ALT with a substantial stability (β = 0.07; R^2 = 0.4) and a good correlation with summer air temperature (DJF) at Signy Island while a not statistically significant trend (β = 3.7; R^2 = 0.1) was recorded at Rothera. At the southern site ALT was very variable ranging between only 10 cm up to more than 130 cm while at the northern one between 270 cm and 360 cm. The temperature at ZAA at Rothera and Signy was substantially stable around the values of -3°C and -1.3°C respectively (Figure 4). The ALT variations were statistically correlated with the summer mean air temperature (R^2 = 0.7) at Signy Island and at Rothera where, in addition, a good regression has been found with thawing degree days index (R^2 > 0.5). The quite strong increase of the snow thickness (ca. 3 cm per year) at Rothera seems to not significantly affect the ALT. The significant stability of the two essential climate variables (ECV): ALT and temperature at ZAA in both sites may be related to the climate considered period, which includes both part of the cooling phase (1999-2016) and a portion of the following strong air warming. The interdecadal climatic changes impacts also on permafrost dynamics and require long term monitoring programs that are particularly rare in Antarctica, indeed only at Mario Zucchelli Station (74°S) started more than 25 years ago.

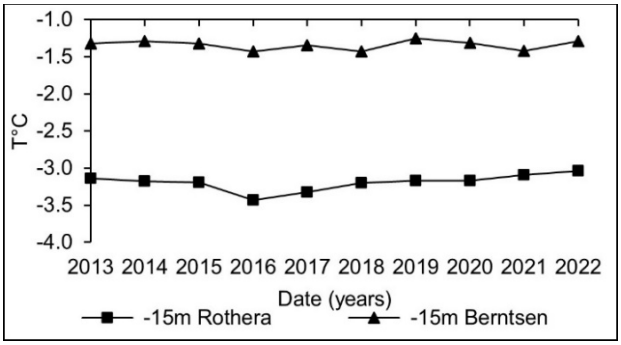

Figure 4. Mean annual permafrost temperature at 15 metres of depths close to the ZAA depth of the two boreholes measured since 2013 at Rothera and Berntsen.

References

Adlam, L.S., Balks, M.R., Seybold, C. A., and Campbell, D.I. 2009. Temporal and spatial variation in active layer depth in the McMurdo Sound Region, Antarctica. Antarctic Science, 22(01), 45. https://doi.org/10.1017/s0954102009990460

Biskaborn, B.K., Smith, S.L., Noetzli, J., Matthes, H., Vieira, G., Streletskiy, D.A., Schoeneich, P., Romanovsky, V.E., Lewkowicz, A.G., Abramov, A., Allard, M., Boike, J., Cable, W.L., Christiansen, H.H., Delaloye, R., Diekmann, B., Drozdov, D., Etzelmüller, B., Grosse, G., ... Lantuit, H. 2019. Permafrost is warming at a global scale. Nature Communications, 10(1). https://doi.org/10.1038/s41467-018-08240-4

Cannone, N., Malfasi, F., Favero-Longo, S.E., Convey, P., and Guglielmin, M. 2022. Acceleration of climate warming and plant dynamics in Antarctica. Current Biology, 32(7), 1599–1606.e2. https://doi.org/10.1016/j.cub.2022.01.074

Jaeger, J.C., and Carslaw, H.S. 1959. Conduction of Heat in Solids. Oxford University Press.

Guglielmin, M., Worland, M.R., and Cannone, N. 2012. Spatial and temporal variability of ground surface temperature and active layer thickness at the margin of maritime Antarctica, Signy Island. Geomorphology, 155-156, 20–33. https://doi.org/10.1016/j.geomorph.2011.12.016

Black, R.F., and Muller, S.W. 1948. Permafrost or Permanently Frozen Ground and Related Engineering Problems. Geographical Review, 38(4), 686. https://doi.org/10.2307/211462

Effect of surficial warming and drying on active layer thickness variability on CALM-S Berry Hill slopes, James Ross Island

Filip Hrbáček & Michaela Kňažková

Department of Geography, Faculty of Science, Masaryk university. Kotlářská 2, 611 37 Brno, Czech Republic

Soil moisture is one of the most important parameters affecting the dynamics of ice-free environments in Antarctica. The moisture content significantly affects soil thermal properties and heat flow, but also the abundance and health of the vegetation. The expected warming and thickening of the active layer can, therefore, cause drying of the surficial parts of the soil due to higher evaporation and water infiltration to the deeper parts of the soil (e.g., Andresen et al. 2020) and accelerate permafrost degradation. Notably, a sudden change in the hydric regime even in short-term period can rapidly worsen vegetation condition (Robinson et al. 2018). In this contribution we analyse the interactions between soil temperature, soil moisture and active layer thickness on a Circumpolar Active Layer Monitoring site (CALM-S) Berry Hill slopes in the period of 2011 to 2023 and discuss the possible implication on the overall environmental change of the area.

Study site and methods

Study area Berry Hill slope is located in the northern part of James Ross Island, Eastern Antarctic Peninsula. The site is elevated about 60 m a.s.l on a north-inclined slope shaped by patterned stripes and solifluction lobes. The site is equipped with an automatic weather station (AWS) with continuous monitoring of ground temperature down to 90 cm and air temperature since 2011. In this study, we used this data to determine the mean seasonal temperatures, thawing degree days and active layer thickness. In 2017, we established a CALM-S site with a size of 50 × 50 m. The active layer thaw depth on CALM-S is annually measured around 10th February using probing approach. Besides that, we measure surficial volumetric water content in the soil layer of ca. 0–15 cm.

Results

The mean annual air and ground temperature at the depth of 5 cm and active layer thickness exhibited an increasing tendency in the period 2011 to 2023.

Even though the warmest year (-3.7 °C) occured in 2016, we observed the maximum ALT of 98 cm in 2023 which was associated with the highest thawing degree days (533 °C/days). Mean thaw depth on CALM-S Berry Hill slope also increased from 83 cm in 2018 up to 98 cm in 2023. Unlike thaw depth, mean surficial soil moisture on CALM-S decreased from 36.1 % (2018) to 30.3 % (2023).

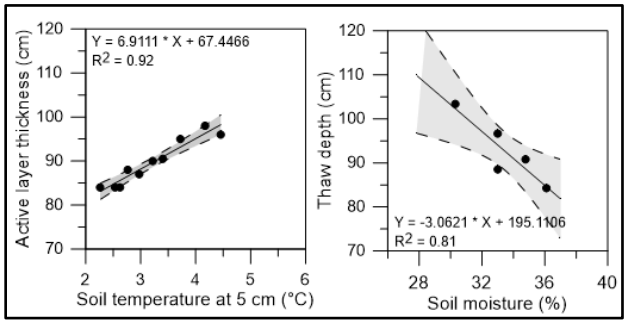

Figure 1. The relationship between summer ground temperature and active layer thickness (left) and mean surficial soil moisture and active layer thickness on CALM-S Berry Hill slope in the period 2011 to 2023. Grey color indicates the 95% confidence.

Interpretation and conclusion

The soil moisture threshold in the patches with vegetation was annually between ca. 37.5 and 40%. The bare ground surfaces exhibited moisture in the range from 25 to 35 %. The active layer thaw depth was annually about 15–25 cm thicker in the bare ground surfaces than vegetated ones. Observed strong negative correlation between soil moisture and active layer thaw depth (Figure 1) is in accordance with a recent analysis by Kňažková and Hrbáček (2024) from the Abernethy Flats site on James Ross Island. In the Berry Hill slope area, the effect of soil moisture is intensified by the presence of a basal form of vegetation, which is generally considered an effective insulator of heat transport to the ground.

We assume that the warming and drying climate scenario for the eastern AP can intensify the surficial drying. Such scenario will very likely lead to active layer deepening. Lack of surficial water can also have a huge impact on the worsening of health condition of the local vegetation which strongly depends on the amount of surficial water during the summer months.

References

Andresen, C.G., Lawrence, D.M., Wilson, C.J., McGuire, A.D., Koven, C., Schaefer, K., Jafarov, E., Peng, S., Chen, C., Gouttevin, I., Burke, E., Chadburn, S., Ji, D., Chen, G., Hayes, D., and Zhang, W. 2020. Soil moisture and hydrology projections of the permafrost region – a model intercomparison. The Cryosphere, 14, 445–459. doi.org/10.5194/tc-14-445-2020

Kňažková, M., and Hrbáček, F. 2024. Interannual variability of soil thermal conductivity and moisture on the Abernethy Flats (James Ross Island) during thawing seasons 2015–2023. Catena, 234, 107640. doi:10.1016/j.catena.2023.107640

Robinson, S.A., King, D.H., Bramley-Alves, J., Waterman, M.J., Ashcroft, M.B., Wasley, J., Turnbull, J.D., Miller, R.E., Ryan-Colton, E., Benny, T., Mullany, K., Clarke, L.J., Barry, L.A., and Hua, Q. 2018. Rapid change in East Antarctic terrestrial vegetation in response to regional drying. Nature Climate Change, 8(10), 879–884. doi:10.1038/s41558-018-0280-0

How geophysical observations of contrasting pingos in Alaska and the Canadian Arctic can inform the search for ground ice throughout the solar system

Kynan Hughson[1], Britney Schmidt[2], Matthew Siegfried[3], John Bradford[3], Alexia Kubas[2], Austin Routt[4], Venezia Follingstad[3], Roger Michaelides[5], Andrei Swidinski[6], Andrew Mullen[2], Enrica Quartini[2] & Hanna Sizemore[7]

[1]*University of New Brunswick, Fredericton, New Brunswick, Canada*

[2]*Cornell University, Ithaca, New York, United States*

[3]*Colorado School of Mines, Golden, Colorado, United States*

[4]*University of Alaska Fairbanks, Fairbanks, Alaska, United States*

[5]*Washington University in St. Louis, St. Louis, Missouri, United States*

[6]*University of Toronto, Toronto, Ontario, Canada*

[7]*Planetary Science Institute, Tucson, Arizona, United States*

The Earth's cryosphere is undergoing an unprecedented era of accelerated ground ice degradation, and pingos, ice-cored hills found in frozen environments, stand as crucial indicators of this transformation. The Pingo SubTerranean Aquifer Reconnaissance and Reconstruction (Pingo STARR) project employs a multi-physics-based survey approach to investigate the structure, composition, and evolution of large hydrostatic pingos across contrasting environments within Alaska's North Slope and the Tuktoyaktuk peninsula in Canada's western Arctic.

In addition to furthering our understanding of terrestrial pingos, this complementary survey approach also has potential applications in the exploration of planetary bodies such as Mars and Ceres, where pingo analogs have potentially been identified (e.g., Burr et al. 2008; Hughson et al. 2022; Soare et al. 2020). With increasing interest in the search for planetary ground ice, we turn to these geologically and geophysically distinct populations of pingos to help prepare us for the in situ geophysical investigation of periglacial terrains throught the solar system.

Field sites

The Pingo STARR project investigated four large hydrostatic pingos near the oil producing region of Prudhoe Bay, AK and nine within Pingo Canadian Landmark near the hamlet of Tuktoyaktuk, NT (Figure 1). These sites were selected due to a combination of their relative easy of access (as they are both situated near major aerodromes and road systems), their status as large easily identifiable landforms, and their contrasting hydrogeological settings. The pingos of Pingo Canadian Landmark exist either within or within a few hundred meters of the Arctic ocean, while our investigated pingos south of Prudhoe Bay are in excess of 50 km from the Arctic coast. The pingos of the Tuktoyaktuk peninsula as represent some of the most well observed examples of this landform on the planet (e.g., Mackay 1998).

Figure 1. Location of investigated pingos near Prudhoe Bay, AK (right image; spring 2021 field season) and within Pingo Canadian Landmark in Canada's Northwest Territories (left image; spring 2023 field season). Note the differences in proximity to the Arctic Ocean.

Methods

For all our investigated pingos in both Alaska and the Northwest Territories we deployed ground penetrating radar (GPR) and capacitively coupled resistivity (CCR) equipment to investigate surbsurface variations, both laterally and vertically, in electrical resistivity as well as cryostratigraphy (Figure 2). We used these observations to characterize subsurface pingo structure, delineate ice cores or core fragments from surrounding permafrost, and identify potential regions of groundwater activity.

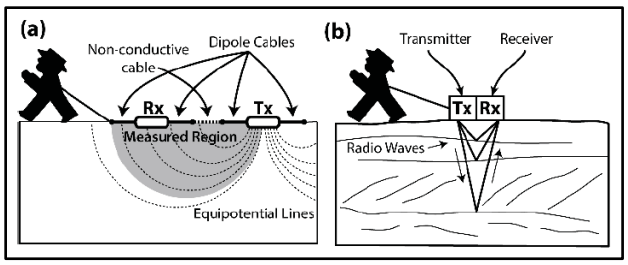

Figure 2. Schematic 55 depictions of our utilized geophysical techniques. (a) illustrates the electrical potential created by a CCR device, while (b) shows transmitted and reflected GPR waves.

Initial Results

The results of this geophysical investigation reveal significant differences in subsurface electrical resistivities between inland and coastal pingos, with coastal pingos exhibiting lower mean resistivities (Figure 3).

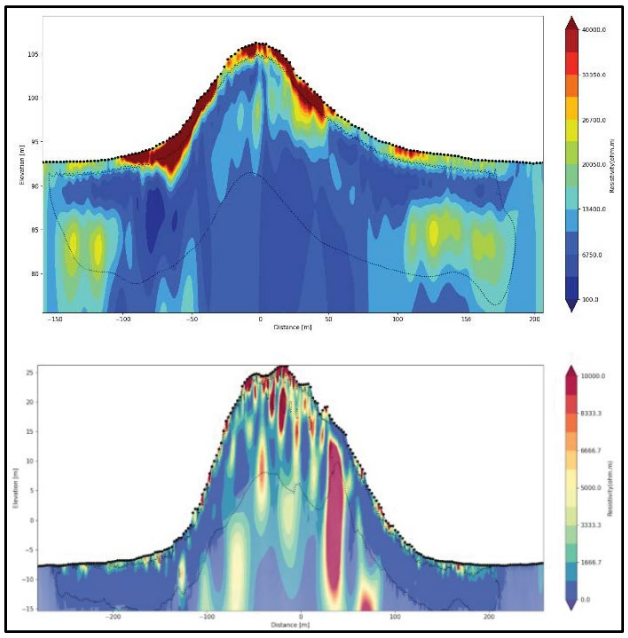
Figure 3. Resistivity inversion cross-sections for two pingos found south of Prudhoe Bay (top) and within Pingo Canadian Landmark (bottom). Note the high variability of resistivity within the bottom pingo.

Furthermore, we find that surface morphology is inconsistently linked to internal structure with some pingos displaying strong spatial correlations between elevated topography and massive ground ice while other similarly sized pingos appear relatively free of massive ice (Figure 4).

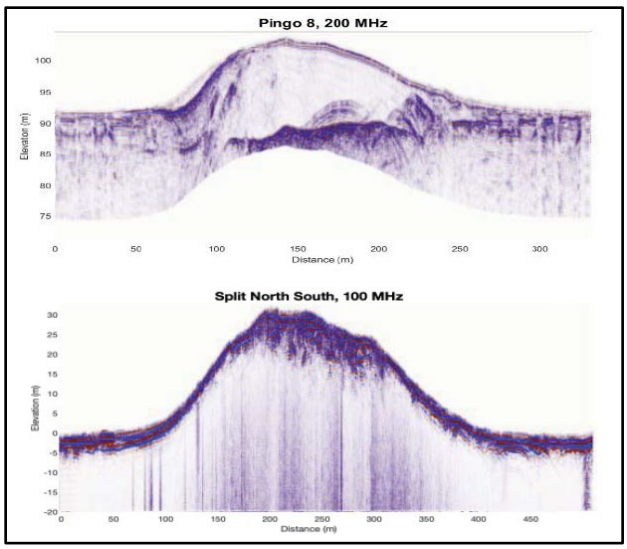

Figure 4. GPR cross-sections of the same pingos depicted in Figure 3. Note the strong basal reflector and clear transmission through the upper pingo from Alaska. This is highly suggestive of a massive ice core and is not seen in the lower pingo from ingo Canadian Landmark.

Discussion and Conclusions

Our observations demonstrate that a multi-physics approach to ground ice exploration can provide insights into the structure of periglacial features that significantly exceed those garnered from a single geophysical method. These observations also suggest that the processes responsible for pingo formation and evolution are likely more complex than what is commonly reported in the literature. This is particularly true of the role of marine influence on the development of massive ice structures within large hydrostatic pingos.

References

Burr, D.M., Tanaka, K.L., and Yoshikawa, K. 2008. Pingos on Earth and Mars. Planetary and Space Science, 57 (5-6): 541–555. https://doi.org/10.1016/j.pss.2008.11.003

Hughson, K.H.G., et al. 2022. Comparative morphometric analysis suggests ice-cored pingo shaped landforms on the dwarf planet Ceres. Geology, 50 (4): 522–527. https://doi.org/10.1130/G49321.1

Mackay, J.R. 1998. Pingo Growth and collapse, Tuktoyaktuk Peninsula Area, Western Arctic Coast, Canada: a long-term field study. Geogaphie physique et Quaternaire, 52 (3): 271–323. https.//doi.org/10.7202/004847ar

Soare, R.J., et al. 2020. Possible (closed system) pingo and ice-wedge/thermokarst complexes at the mid latitudes of Utopia Planitia, Mars. Icarus, v. 342, 113233. https://doi.org/10.1016/j.icarus.2019.03.010

Drilling into subglacial frozen bedrock in the north-western Elizabeth Land, east Antarctica

Pavel G. Talalay[1,2], Y. Sun[2], N. Zhang[1], G.L. Leitchenkov[3], X. Fan[1], I. Abdrahmanov[3], B. Li[2], D. Gong[1], Y. Yang[1], J. Hong[1], Y. Li[1], Y. Liu[1], Y. Sun[2] & Y. Chen[1]

[1]*Polar Research Center, Institute for Polar Science and Engineering, Jilin University, Changchun, China*

[2]*China University of Geosciences, Beijing, China*

[3]*All-Russian Scientific Research Institute for Geology and Mineral Resources of the World Ocean "Vniiokeangeologia", St-Petersburg, Russia*

Drilling to the bedrock of ice sheets and polar glaciers offers unique opportunities for examining processes acting at the bed (Talalay 2013). Samples of subglacial material contain important paleo-climatic and paleoenvironmental records, provide a unique habitat for life, and give significant information on subglacial geology and tectonics.

The base of Antarctic and Greenland ice sheets, polar ice caps and valley glaciers demonstrates alternating warm-based and cold-based areas. Drilling to subglacial aquatic environments requires environmental-friendly thermal drilling technologies (e.g., Priscu et al. 2021; Sun et al. 2023) while drilling to the frozen bedrock calls for mechanical drilling methods. Two types of mechanical drilling technologies are utilized: conventional pipe-string rotary drilling and electromechanical cable-suspended drilling.

The recent experience with subglacial conventional rotary drilling showed that drilling process was not routine and resulted in a large framework of problems associated with the removal of ice chips from the hole, separation of the chips from the drilling fluid at the surface, chip packing during wireline tool lowering and ice hydro-fracturing (Goodge et al. 2021; Kuhl et al. 2021).

The main feature of the electromechanical cable-suspended drills is that an armored cable with a winch is used instead of a pipe-string to provide power to the down-hole motor system and to retrieve the down-hole unit (Talalay 2022). The use of armored cable allows a significant reduction in power and material consumption, a decrease in the time of round-trip operations, and a simplification in the cleaning of the hole from the cuttings. Unlike conventional rotary drilling, where the fluid is normally pumped to the bottom of the hole from the surface, an electromechanical drill suspended on a cable uses a bottom circulation system with a downhole pump and chip chamber for filtering the fluid and collecting the cuttings. The chips are temporarily stored in a chamber within the drill, which is periodically withdrawn to the surface and emptied.

This report describes general concept of movable drilling rig with electromechanical cable-suspended drill, developed at Jilin University, China, results of experimental works, and future plans.

General concept of the drilling rig

The drilling facilities are divided into two groups: those associated with the movable drilling shelter and those associated with the movable workshop (Figure 1). Drilling shelter includes new, modified version of the cable-suspended Ice and Bedrock Electromechanical Drill (IBED), drilling winch with a cable, control desk, pipe handler with a fixed clamp, chip chamber vibrator, and centrifuge. Workshop includes two generators, logging winch with a cable, emergency devices, fitting and electrical tools.

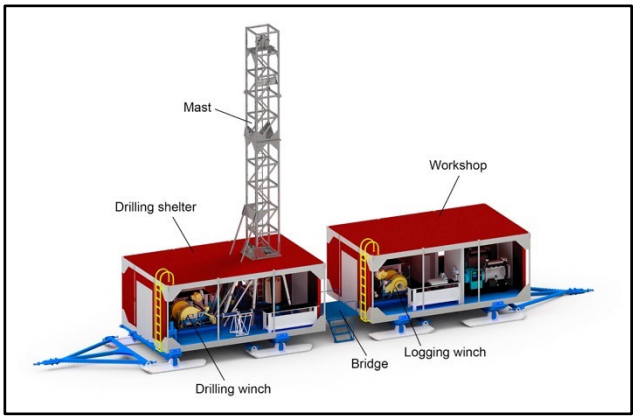

Figure 1. Schematic of the movable drilling shelter (from Talalay et al. 2021a).

The modules of the IBED can be changed for drilling in firn, ice, debris-containing ice and bedrock, which allows three different tasks to be accomplished: (1) auger drilling in the upper snow–firn layers with sequential reaming for casing installation; (2) coring in solid and debris-containing ice with near-bottom fluid circulation, and (3) bedrock-core drilling.

The different sections of the drill are easily replaced, as all of them have the same threaded joint

connections. The lower part of the bedrock variant is adapted for coring hard rocks using a toothed diamond bit and contains a 1 or 2 m-long conventional single-core or double-core barrel, a chip chamber for gravity separation of rock cuttings and adjustable deadweights (200 kg at maximum) to increase the load on the diamond drill bit. The ID/OD of the diamond bit is 41/60mm for the single-core barrel.

Field testing and targeted drilling

In December 2018–January 2019, drilling facilities were assembled and tested at the site ~12 km south of Zhongshan Station in the north-western Elizabeth Land, East Antarctica. The site was in an area where the subglacial topography is tracked to the highest point. The top of the subglacial hill was ~100 m a.s.l., ensuring dry, frozen-bed conditions for avoiding contamination of the subglacial hydrologic environment by drilling fluid.

Dry drilling using an IBED with an auger core barrel was performed to penetrate the permeable upper ice layers to a depth of 17.4 m. Then the hole was filled with drilling fluid (Jet A-1 fuel), and drilling was continued using the IBED with bottom reverse circulation. At a depth of 190.75 m, the first small black particles were found in the recovered ice core. At greater depths, the content of impurities (mainly silt, with some small rock fragments <8 mm in size) increased. Finally, from the depth of 198.11 m a 6 cm-long core of the true bedrock was recovered (Figure 2). The mineral material was brown-yellow metamorphosed gneiss. A total of 18 days was used to penetrate the ice sheet. The estimated temperature at the bottom was -4.5 °C (Talalay et al. 2023).

Figure 2. Recovered piece of the frozen subglacial bedrock core and impregnated diamond drill bit used for coring (from Talalay et al. 2021b).

In January-February 2024, drilling facilities were moved to the site 30 km from the cost in the central part of a high-amplitude (more than 800 nT), linear (E-W striking) magnetic anomaly crossing eastern and western flanks of the Lambert Rift Graben. The drill penetrated through 545 m thick ice and recovered 0.48 m of the frozen bedrock core sample. The basal ice was solidly frozen to the bedrock and measured temperature at the bottom of the borehole was -4.5 °C. The bedrock core is presented by metamorphosed mafic rocks (matagabbro) which may mark the suture zone formed during the amalgamation of the Rodinia Supercontinent in the early Neoproterozoic.

References

Goodge, J.W., Severinghaus, J.P., Johnson, J., et al. 2021. Deep ice drilling, bedrock coring and dust logging with the Rapid Access Ice Drill (RAID) at Minna Bluff, Antarctica. Annals of Glaciology, 62 (85–86): 324–339.

Kuhl, T., Gibson, C., Johnson, J., et al. 2021. Agile Sub-Ice Geological (ASIG) Drill development and Pirrit Hills field project. Annals of Glaciology, 62 (84): 53–66.

Priscu, J.C., Kalin, J., Winans, J., et al. 2021. Scientific access into Mercer Subglacial Lake: Scientific objectives, drilling operations and initial observations, Annals of Glaciology, 62 (84): 340–352.

Sun, Y., Li, B., Fan, X., et al. 2023. Brief communication: New sonde to unravel the mystery of polar subglacial lakes. The Cryosphere, 17: 1089–1095.

Talalay, P.G. 2013. Subglacial till and bedrock drilling. Cold Regions Science and Technology 86: 142–166.

Talalay, P.G. 2022. Geotechnical and exploration drilling in the polar regions. Springer Cham, Springer Nature, Switzerland.

Talalay, P., Sun, Y., Fan, X., et al. 2021a. Antarctic subglacial drilling rig: Part I. General concept and drilling shelter structure. Annals of Glaciology, 62 (84): 1–11.

Talalay, P., Li, X., Zhang, N., et al. 2021b. Antarctic subglacial drill rig. Part II: Ice and Bedrock Electromechanical Drill (IBED). Annals of Glaciology 62 (84–85): 12–22.

Talalay, P.G., Gong, D., Fan, X., et al. 2023. Geothermal heat flow from borehole measurements at the margin of Princess Elizabeth Land (East Antarctic Ice Sheet). Journal of Glaciology, 69 (277): 1524–1528.

3B — Characteristics of Permafrost in the Andes

Session Chairs: Dario Trombotto Liaudat[1], Silvio Pastore[2], Lukas Arenson[3] & Carla Tapia Baldis[1]

[1]*IANIGLA - CONICET, Mendoza, Argentina*
[2]*Universidad de San Juan, San Juan, Argentina*
[3]*BGC Engineering, Vancouver, British Columbia, Canada*

The Andes of South America are the longest continental mountain range in the world, with an average elevation of about 4,000 m. Due to this height, permafrost plays a crucial role in its morphology and local ecosystems. Similar to many cold regions around the world the Andes are currently facing unprecedented changes in climate conditions, which are leading to the degradation of permafrost and other related processes such as rock glaciers degradation, slope instabilities, and changes in local hydrology. However, today, our understanding of the spatial extent, thermal conditions and its characteristics, including ground ice content, and hydrological role, is still very limited, leading to large uncertainties when projecting future behaviour of permafrost conditions in the Andes.

This session will provide an opportunity for researchers and engineers from various disciplines to present their findings on the characteristics of permafrost in the Andes, specifically its spatial distribution, thickness, thermal state, presence of periglacial ice and paleopermafrost. Presenters will have the chance to share their knowledge, experiences, and ideas about the role of permafrost in this particular mountain ecosystems and how climate change impacts the current and future state of permafrost in the region.

The session accepts topics, such as permafrost mapping and modelling, ground temperature observations, use of remote sensing techniques, geomorphological and hydrological effects of permafrost degradation. It is expected that this session will contribute to the advancement of our understanding of permafrost in the Andes and provide opportunities for researchers from different disciplines and background to collaborate and exchange ideas.

Mountain permafrost in taluses and blockslopes in the Agua Negra Basin (Argentina) — towards a quantification using geophysics

Diana Agostina Ortiz[1], Manon Cramer[1],Tamara Koehler[1], Cristian D. Villarroel[2], Melanie A. Stammler[1], Lothar Schrott[1] & Dario Trombotto Liaudat[3]

[1]*Department of Geography, University of Bonn, Bonn, Germany*

[2]*Research Centre of the Geosphere and Biosphere (CIGEOBIO-CONICET), FCEN-UNCUYO, San Juan, Argentina*

[3]*Geocryology, IANIGLA, CCT CONICET Mendoza, Argentina*

Extensive areas in mountain regions are influenced by permafrost conditions (Caine 2010; Haeberli et al. 2010). In the Dry Andes of Argentina, permafrost bodies represent a solid-state water reserve, which holds special importance due to the strong dependence of Andean societies on meltwater. This work is motivated by the utmost significance of these water reserves as a source of water for irrigation, industry and domestic use in the area, which is enhanced by extreme droughts in the Andes that will have severe impacts on the availability of water in the lowlands.

The study area of the Agua Negra basin is located in the Western part of the San Juan Province, Argentina at ca. 30°S and 69°W. This area is part of the Cordillera Frontal and comprises areas of 57 km² (upper basin, see Figure 1) and approx. 1315 km² (entire Agua Negra basin). This basin belongs to a sector called Desert Andes (31°-17°30´S), which is characterized by extremely low mean annual precipitation (~ 250 mm) represented mainly by falls during winter months as snow or sleet above 4000 m a.s.l. (Minetti et al. 1986). Snow cover is comparatively thin and of short duration (~ 3 months) due to the effect of high incoming solar radiation throughout the year, controlling surface temperatures and upper ground thermal regimes (Schrott 1994; Lliboutry 1998).

Two field trips were carried out in austral summer 2022 and 2023 and there is one more planned for austral summer 2024. A combination of systematic two-dimensional measurements of Electrical Resistivity Tomography (ERT), Seismic Refraction Tomography (SRT) and Ground Penetrating Radar (GPR) were conducted in order to investigate the existence, distribution and internal structure of ground ice in taluses, block-slopes and protalus ramparts in the Upper Agua Negra Catchment. In total, more than 40 ERT, 20 SRT and 5 GRP profiles were measured along the entire upper catchment (and sourrandings), all distributed among the mentioned landforms (see Table 1).

Table 1. Summary of landforms and methodology applied.

Landform	Electrical Resistivity Tomography	Seismic Refraction Tomography	Ground Penetrating Radar
Talus Slope	12	8	2
Blockslope	20	5	2
Protalus Rampart	16	8	1

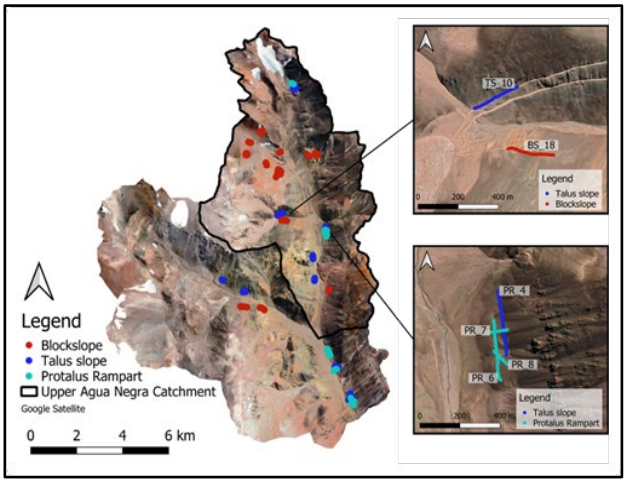

Figure 1. Spatial distribution of ERT, SRT and GPR measurements in the upper catchment and surroundings. The colors are indicating the three landforms: red for blockslopes, blue for talus slopes, and green for protalus ramparts. To the right a zoom to visualize some measurements of the mentioned landforms.

PRELIMINARY RESULTS

Results show a presence of permafrost within taluses and protalus ramparts, with differences in their distribution and ice- content. Talus slopes show resistivities up to 40kΩm and maximum seismic velocities of 3200 m/s, indicating a clear presence of ice-rich permafrost layers (See Figure 2). For most of the taluses analyzed, the presence of ground ice is indicated towards the lower and steepest part of the talus, as is also described by Lambiel and Pieracci (2008). For such landform, the boundary active layer-permafrost, is remarked by the threshold in resistivity

and seismic values, being the first one characterized by velocities up to 1700 m/s and resistivies< 8 kΩm.

Protalus ramparts show maximum resistivities of 12 kΩm and seismic velocities of around 2000 m/s. Those values may indicate the presence of a low-ice-content permafrost body.

On the other hand, maximum resistivities and velocities for block slopes are 1500 Ωm and 1600 m/s, respectively. ERT and SRT values remark absence of permafrost in this landform. Seimic velocities may indicate an internal structure of possibly weathered andesites and other volcanic rocks corresponding to the geological units of Choiyoi Group covering the area (Heredia et. al. 2002; Heo et. al. 2008; Maurer and Hauck 2007). GPR data results give detailed information on its internal stratigraphical structures, showing, in some cases, a discontinuous, irregular pattern of reflectors.

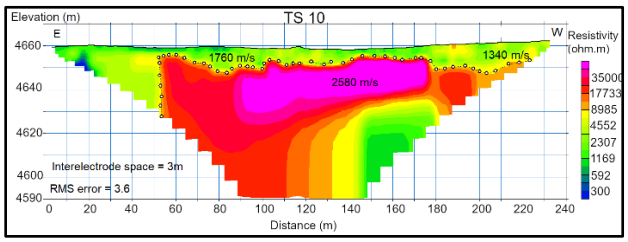

Figure 2. Example of talus profile (TS 10) measured at 4600 m a.s.l. The tomogram shows the ERT resistivities and the seismic velocities extracted from the SRT analysis. The dotted line indicates the boundary between the active layer and the permafrost body. For this profile, a Dipole-Dipole array and a spacing of 3 m was used.

The geophysical data is being used to estimate the volume of ice and water content using the Four Phase Modelling approach and its combination with hydrogeochemical measurements and remote sensing analyses(all together HyPerm Project*) aims to give an overview on the hydrological significance of taluses (including protalus ramparts) and blockslopes in the Agua Negra catchment.

* Spatial occurrence and Hydrological significance of Andean Permafrost (DFG funded project)

REFERENCES

Caine, N. 2010. Recent hydrologic change in a Colorado alpine basin: an indicator of permafrost thaw. Ann. Glaciol. 51 (56): 130–134. https://doi.org/10.3189/172756411795932074

Caminos, R. 1972. Upper paleozoic sedimentation and magmatism in the Cordillera frontal, Argentina. An. Acad. Bras. Ciencias S, 44: 77–86.

Gruber, S. 2012. Derivation and analysis of a high-resolution estimate of global permafrost zonation. The Cryosphere, 6(1): 221–233. https://doi.org/10.5194/tc-6-221-2012

Haeberli,W., Noetzli, J., Arenson, L., Delaloye, R., Gärtner-Roer, I., Gruber, S., and Isaksen, K. 2010. Mountain permafrost development and challenges of a young research field. Journal of Glaciology, 56 (200): 1043–1058. https://doi.org/10.3189/002214311796406121

Heredia, N., Fernández, L.R., Gallastegui, G., Busquets, P., and Colombo, F. 2002. Geological setting of the Argentine Frontal Cordillera in the flat slab segment 30 00 31 30 S latitude). Journal of South American Earth Sciences, 15(1): 79–99. https://doi.org/10.1016/S0895-9811(02)00007-X

Heo, S.K., HagSoo, C., YongKun, C., ManSup, C., and Kwan, Y. 2008. Case Study of Geotomography Survey of Civil Construction Field in Korea, 457(462). doi:10 3850 978 981 08 6396 8 _P 109

Lliboutry, L. 1998. Glaciers of Chile and Argentina. In: Williams, R.S., Ferrigno, J.G.(Eds.), Satellite Image Atlas of Glaciers of the World: South America. USGS Professional Paper 1386-I, Online version 1.02.

Lambiel, C., and Pieracci, K. 2008. Permafrost distribution in talus slopes located within the alpine periglacial belt, Swiss Alps. Permafrost and Periglacial Processes, 19(3): 293–304. https://doi.org/10.1002/ppp.624

Minetti, J.L., Barbieri, P.M., Carletto, M.C., Poblete, A.G., and Sierra, E.M. 1986. El régimen de precipitatiòn de la provincia de San Juan.–Informe técnico 8. CIRSAJ-CONICET, San Juan.

Maurer,H., and Hauck, C. 2007. Geophysical imaging of alpine rock glaciers.Journal of Glaciology, 53(180): 110–120.https://doi.org/10.3189/172756507781833893

Schrott, L. 1994. Die Solarstrahlung als steuernder Faktor im Geosystem der subtropischen semiariden Hochanden (Agua Negra, San Juan, Argentinien), Heidelberger Geographische Arbeiten, Heidelberg, Germany, 94: 199 S.

Study method of spatial distribution of non-soluble particles in permafrost ice

Lucía E. Arena[1,2] & Darío Trombotto Liaudat[3]

[1]*Faculty of Mathematics, Astronomy, Physics and Computing, National University of Córdoba, Córdoba, Argentina*

[2]*Hydro-Meteorological Observatory of Córdoba (OHMC), Córdoba, Argentina*

[3]*Instituto Argentino de Nivologia, Glaciologia y Ciencias Ambientales (IANIGLA) Mendoza, Argentina*

The crystallographic characterization of permafrost samples has implications of interest for paleoclimatic studies. Crystals, solid and gas inclusions, the chemical composition of the sample, tensions, among others, are studied. For example, the porosity as well as the size and orientation of the bubbles have a direct correlation with the age of the ice (Trombotto Liaudat et al. 2008). The same occurs with the crystal orientation and the size of the crystals: glacial or permafrost ice is generally older to the extent that the grains are smaller and textured, that is, the grains are oriented in a particular direction with respect to of the direction of forces acting on the sample (Arena et al. 2005). Also, it is important to determine the directions of the stresses to which the samples have been subjected (Gell 1978; Corte 1963). According to Trombotto Liaudat et al. (2008) and Arena et al. (2007), it is possible to determine a relationship between the pressures to which a glacial sample has been subjected and the density of crystallographic defects and dislocations. There are many techniques to study these parameters, in particular the combination of plastic replication of the sample surface and transmission microphotography of thin sections stands out (Arena and Nasello 1994; Carreras 1997; Arena et al. 2007; Trombotto Liaudat et al. 2008).

Finally we consider solid particles. The chemical composition and granulometry of the particles in the permafrost sample allow us to infer, depending on their size and other characteristics, glacial flow directions or interactions with the atmosphere such as ice condensation nuclei in the cloud (Barri et al. 2023). In general, the particles are isolated from the melting of permafrost ice and subsequent filtration. In this work, a simple methodology is presented that allows the separation of non-soluble particles from a permafrost sample using the adapted sublimation method (Arena 2023) to then determine the granulometry, the spatial distribution of particles in the sample and characterize the shape and elemental chemical composition of them.

METHODOLOGY

Ice sublimes easily at temperatures below and close to 0 °C. Therefore, non-soluble particles contained in an ice sample can be separated by sublimation. Simply prepare a thin sheet of the sample on a substrate (a glass) and wait for the ice to subside in a dry environment (for example a desiccator with silica gel), as illustrated in Figure 1. The particles are deposited in the substrate. This method of particle separation by sublimation was “adapted” to minimize sources of contamination during and after sublimation and to preserve the particles (Arena 2023). In this case, the sheet of ice is covered with a very thin layer of a porous plastic that, although it slows down the sublimation process, protects the trapped particles so that they are not dragged or contaminated while the sample is handled. This procedure is essential when a sample must be subjected to microscopy such as scanning electron microscopy, which requires the use of a vacuum both in the metallization stage and for the electron scanning itself. It has been proven that a plastic coating of polyvinyl formal dissolved in 1-2 dichloroethane (Formvar) in a low dilution (1-3%) is adequate (Arena 2023). In addition, for a 1mm thick sample, 2 days of exposure in a desiccator with siligcagel at -12 °C to complete the sublimation process and so that the particles are trapped between the glass and the formvar layer.

RESULTS AND DISCUSSION

Knowing the thickness of the thin sheet and its area, it is possible to determine the volume and establish:

- Number of particles per unit volume
- Surface spatial distribution of particles
- Granulometry: Particle size distribution
- Identification of shape, structure and elemental chemical composition (if electron and confocal microscopy are used, as an example)

This procedure has been used for samples of giant hailstones (5-12 cm in diameter), in the sub-zero laboratory of Atmospheric Physics Laura Levi, FAMAF-UNC , with very interesting results for the characterization of the particles that they capture. of the cloud during its growth (Bernal Ayala et al. 2023; Arena 2023).

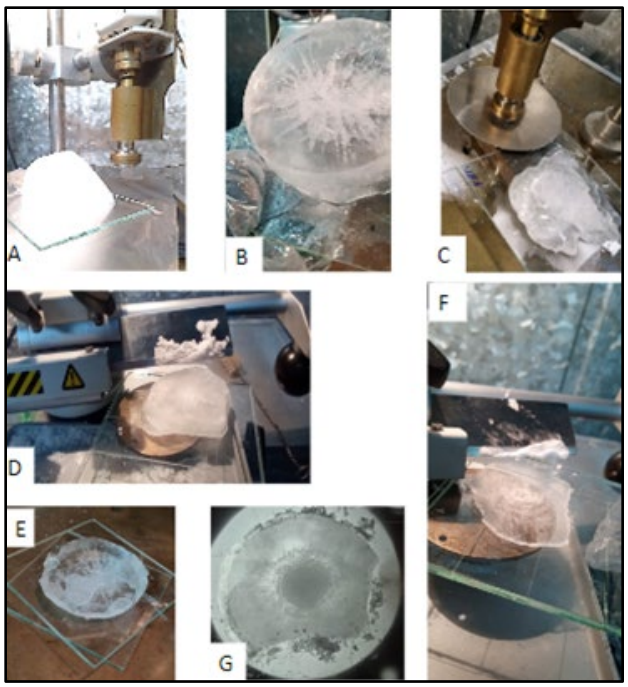

Figure 1. Procedure for sectioning the sample in an environment at -12 °C. A) to C) Sample glued by surface fusion and machined using a circular saw; D) Thick sheet whose surface is roughened to a mirror using a microtome; E) The thick sheet is glued to a slide, by fusion-solidification, of the surface; F) Roughing using a microtome to obtain the thin sheet to sublimate; and G) Sample with a maximum diameter of 9 cm.

The adapted sublimation particle separation method allows the identification of non-soluble particles from small volumes of permafrost samples while respecting the surface distribution of the particles. It also allows estimating the number of particles per unit volume. The limit of particle size is in the microscopic detection instruments, since it does not require the intervention of filters. Furthermore, by observing each isolated particle, its shape, structure and elemental chemical composition can be determined. Finally, the developed method is not very sensitive to sources of contamination from external agents since it always works in the solid phase of water.

The developed method is inexpensive and, with small considerations, can be used in the field and is easily transportable with minimal probability of contamination by external agents. Due to its sensitivity, precision and effectiveness, we consider it to be very interesting for the characterization of permafrost particulate matter. Furthermore, it can be implemented as a complement to plastic replication and thin film techniques to study the parameters of interest in permafrost samples such as texture, distribution and size of gas inclusions, and residual stresses.

References

Arena, L.E., and Nasello, O.B. 1994. Growth techniques for high-quality ice single crystals , ANALES AFA, 5(1).

Arena, L.E., Trombotto, D., and Caranti, G. 2005. Microcospical characterization of thermokarst ice from an area of Andean permafrost, Central Andes of Mendoza, Argentina" 2 nd European Conference on Permafrost. Terra Nostra Heft 2005/2: p. 55, Potsdam, Germany.

Arena, L.E., Caranti, G.M., Trombotto, D. 2007. Crystallographic study of thermocarst ice ,: ANALES AFA, 18(1).

Arena, L.E. 2023. Identification of particles included in natural ice (glaciers, permafrost, hail) by adapted sublimation. RDU -UNC, Argentina, 2023. https://rdu.unc.edu.ar/handle/11086/549250

Barry, K.R., Hill, T.C.J., Nieto-Caballero, M., Douglas, T.A., Kreidenweis, S.M., DeMott, P.J., and Creamean, J.M. 2023. Active thermokarst regions contain rich sources of ice-nucleating particles, Atmos. Chem. Phys., 23, 15783–15793. https://doi.org/10.5194/acp-23-15783-2023

Bernal Ayala A., Rowe, A.K., Arena, L.E., and Nachlas, W.O. 2023. What types of particles are trapped in hailstones from central Argentina? American Geophysics Union AGU 2023, San Francisco, USA.

Carreras, A.P., and Arena, L.E. 1997. Recrystallization in pure and doped ice. Anales de la AFA, 9,149–153.

Corte, A. 1963. Relationship between four ground patterns, structure of the active layer, and type and distribution of ice in the permafrost, Biuletyn peryglacjalny 12.

Gell, W. 1978. Fabrics of Icing-Mound and Pingo Ice in Permafrost. Journal of Glaciology, 20(84), 563–569. doi:10.3189 / S0022143000020967

Trombotto Liaudat, D., Arena, L.E., Caranti, G.M. 2008. Glacial Ice as Cryogenic Factor in the Periglaciation Zone of the Composed Rockglacier Brunettes Coloradas , Central Andes of Mendoza, Argentina Ninth International Conference on Permafrost Edited by D.L. Kane and K.M. Hinkel , Institute of Northern Engineering, University of Alaska. Fairbanks, Alaska, USA; p. 1781–1786.

A first approximation of water volume equivalent from rock glaciers in the Peruvian Andes

Edwin Badillo-Rivera[1], Katy Medina[2] & Edwin Loarte[2]

[1]*Centro de Investigación en Gestión del Riesgo de Desastre y Cambio Climático, National University of Callao, Bellavista-Callao, Peru*

[2]*Centro de Investigación Ambiental para el Desarrollo, National University Santiago Antunez de Mayolo, Huaraz, Ancash, Peru*

Rock glaciers (RG) are characteristic surface geoforms in the high mountain periglacial belt (Barsch 1996; Jones et al. 2018; Kofler et al. 2020; Lytkin 2020) and are considered to be climatically more resilient than glaciers because of the active layer that protects them (Jones et al. 2017), however, it is practically certain that the extent and volume of permafrost will decrease as climate temperature increases, which will generate changes in the extent, temperature and thickness of the active layer of rock glaciers (IPCC 2021). Therefore, it is necessary to have a clear understanding of their role as a component of the hydrological cycle of the high mountain cryosphere and the consequences of their projected degradation in a scenario of temperature increase, specifically in the Andes Mountains of the Tropical Andes, where in the last 60 years the temperature increased 0.17°/decade above 5000 m asl (Aguilar-Lome et al. 2019).

Regional rock glacier inventories have been constructed worldwide using geographic information technologies for various purposes, such as permafrost modeling, permafrost boundary inference, paleoclimatic studies, geohazard assessments, and estimation of hydrological significance (Angillieri 2017; Azocar 2013; Boccali et al. 2019; Brenning and Trombotto 2006; Kinworthy 2016; Marcer et al. 2017; Perucca and Esper Angillieri 2011; Seligman and Brown 2009; Wirz et al. 2016). The latter, for instance, aims to ascertain the water volume contained within them, as exemplified in the Peruvian, Bolivian, and Chilean Andes (Badillo-Rivera et al. 2021; Perucca and Esper Angillieri 2011; Rangecroft et al. 2015). In this study, we present a preliminary version of the water volume equivalent (WVE) of active, inactive, and intact RG within the scope of the Peruvian Andes using geographic information techniques.

Methodology

To estimate the ice content in RG (including protalus rampart), some variables that are not yet known will be assumed, based on active, inactive and intact RG, the paleo-WVE of relict RG is estimated, even though they no longer contain ice in their structure. The empirical formula proposed by Brenning (2005b) was used, which estimates the average thickness of RG according to Equation 1.

$$\text{Mean RG thickness } (h) = 50 \times (A[km^2])^{0.2} \quad [1]$$

Where A is the surface area of RG expressed in km^2, the value obtained is multiplied by the surface area of the glaciers (active, inactive and intact) and by the percentage of ice in the geoform. Several studies have estimated the volume of ice or equivalent volume of ice in RG assuming a percentage of ice present in the geoforms (Table 1), in this research a range of 10 - 30% as a maximum was used, this range is established according to the ranges assumed by different authors at the regional level. To convert to water equivalent, the final value is multiplied by the ice density 900 kg/m^3 (Rangecroft et al. 2015; Jones et al. 2018).

Table 1. Volume of ice content in rock glaciers.

% ice-content	Country	Method	Reference
Andes			
55.7	Chile	Geophysics	Croce y Milana (2002)
20.0 - 47.0	Chile	Geophysics	Milana y Guell (2008)
15 - 30	Chile	Geophysics, borehole	Monnier y Kinnard (2013)
40 - 60	Chile	Bibliography	Azocar (2013)
0.1 - 44.9	Chile	Bibliography	Janke et al. (2017)
50	Argentina	Borehole	Arenson et al. (2010)
50	Argentina	Bibliography	Perucca and Angillieri (2011)
40.0 - 60.0	Bolivia	Bibliography	Rangecroft et al. (2015)
Other regions			
40 - 60	Austria	Geophysics	Hausmann et al. (2007)
35- 40	Italia	Borehole	Krainer et al. (2015)
40 - 60	Nepal	Bibliography	Jones et al. (2018)
40 - 60	Italia/Slovenia	Bibliography	Boccali et al. (2019)

Results and discussion

The amount of ice volume in the RG of the Peruvian Andes was estimated based on empirical formulas relating ice thickness to surface area (10 to 30% ice content), the results show that the RGs have a thickness between 13.8 - 48.2 m, the amount of WVE in the GR was estimated in the range of 0.102 - 0.189 km^3 for active GR, and a range of 0.151 to 0.285 km^3 of WVE for inactive and intact GR in total, finally, the paleo-WVE content was estimated in the range of 0.044 to 0.083 km^3 for relict GR.

At the departmental level, it was estimated that 95% of the WVE of active, inactive and intact RG is found in the southern departments of Peru, specifically in Tacna, Puno, Moquegua and Arequipa, the latter accounting for 60% of the total WVE of active, inactive and intact RG in the Peruvian Andes. Finally, 84% of the total WVE of active, inactive and intact RG belong to the Pacific hydrographic region.

Tabla 2. WVE of peruvian GR.

Activity				
Department	Ice-content 10%		Ice-content 30%	
	Active	Inactive	Active	Inactive
Apurimac	0.000	0.001	0.001	0.002
Arequipa	0.061	0.077	0.184	0.231
Ayacucho	0.003	0.004	0.008	0.011
Cusco	0.001	0.006	0.003	0.019
Huancavelica	0.000	0.000	0.000	0.001
Huanuco	0.000	0.000	0.000	0.000
Junin	0.000	0.000	0.000	0.000
Lima	0.002	0.004	0.005	0.012
Moquegua	0.008	0.021	0.023	0.064
Puno	0.003	0.010	0.010	0.031
Tacna	0.024	0.028	0.073	0.083
Total	0.102	0.151	0.307	0.453
Region	Active	Inactive	Active	Inactive
Pacifico	0.088	0.125	0.265	0.376
Amazonas	0.003	0.009	0.009	0.026
Titicaca	0.011	0.017	0.033	0.050
Total	0.102	0.151	0.307	0.453

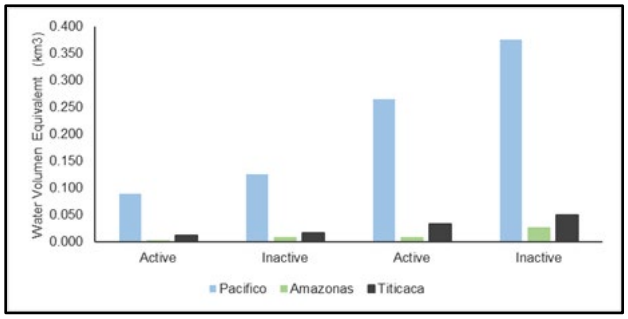

Figure 1. WVE of GR by hydrographic regions.

Of the 1785 RG identified in the Peruvian Andes of the active, inactive and intact type, it has been determined that approximately 98% of the total number of WVE are found in the mountain of southern Peru (Ampato, Apolobamba, Chila, Huanzo, La Raya, Urubamba, Vilcanota, Barroso and Volcanic), a region characterized by being the driest in Peru.

CONCLUSION

In this study, we present a first approximation of the WVE water content of the RG in the Peruvian Andes, reporting that there is a great potential for WVE in southern Peru, areas whose climatic characteristics are represented by low rainfall, therefore, the potential water reserve of the RG in these areas is positioned as a key element for water availability in a climate under the threat of climate change. It is worth noting that WVE values should not be considered as values to establish relationships between the hydrological contribution of RG in the study area; however, it is important to accompany these results with field studies to establish relationships of probable water contribution of RG in high mountain areas.

REFERENCES

Angillieri, M. 2017. Journal of South American Earth Sciences Permafrost distribution map of San Juan Dry Andes (Argentina) based on rock glacier sites. Journal of South American Earth Sciences, 73, 42–49. https://doi.org/10.1016/j.jsames.2016.12.002

Azocar, G. 2013. Modeling of Permafrost Distribution in the Semi-arid Chilean Andes.

Badillo-Rivera, E. 2022. Tecnologías de información geográfica para determinar la dinámica de los glaciares rocosos como formas de permafrost en los Andes Tropicales del Perú [Univerdidad Nacional del Callao]. In Univerdidad Nacional del Callao. http://repositorio.unac.edu.pe/handle/20.500.12952/6630

Badillo-Rivera, E., Medina, K., Loarte, E., Bodin, X., Azocar, G., and Cusicanqui, D. 2021. An estimation of past and present air temperature conditions, water equivalent, and surface velocity of rock glaciers in Cordillera Volcanica, Peru. Regional Conference Permafrost. https://doi.org/10.1061/9780784483589.01

Barsch, D. 1996. Rockglaciers: indicators for the present and former geoecology in high mountain environments. In Rockglaciers: indicators for the present and former geoecology in high mountain environments. https://doi.org/10.2307/3060377

Boccali, C., Žebre, M., and Colucci, R.R. 2019. Geometry and paleo-ice content of rock glaciers in the Southeastern alps (Ne Italy – NW Slovenia). Journal of Maps, 15(2), 346–355. https://doi.org/10.1080/17445647.2019.1595753

Brenning, A., and Trombotto, D. 2006. Logistic regression modeling of rock glacier and glacier distribution: Topographic and climatic controls in the semi-arid Andes. Geomorphology, 81(1–2), 141–154. https://doi.org/10.1016/j.geomorph.2006.04.003

IPCC. 2021. Ocean, Cryosphere and Sea Level Change. In: Climate Change 2021: The Physical Science Basis.

Jones, D.B., Anderson, K., Selley, H.L., Wood, J.L., and Betts, R.A. 2017. The distribution and hydrological significance of rock glaciers in the Nepalese Himalaya. Global and Planetary Change. https://doi.org/10.1016/j.gloplacha.2017.11.005

Jones, D.B., Harrison, S., Anderson, K., and Betts, R.A. 2018. Mountain rock glaciers contain globally significant water stores. Scientific Reports, 8(1), 1–10. https://doi.org/10.1038/s41598-018-21244-w

Kinworthy, B. 2016. New Mexico Rock Glacier Inventory : Analysis of Geomorphology and Paleogeography. University of New Mexico.

Kofler, C., Steger, S., Mair, V., Zebisch, M., Comiti, F., and Schneiderbauer, S. 2020. An inventory-driven rock glacier status model (intact vs. relict) for South Tyrol, Eastern Italian Alps. Geomorphology, 350, 106887. https://doi.org/10.1016/j.geomorph.2019.106887

Lytkin, V. 2020. Inventory and distribution of rock glaciers in northeastern yakutia. Land, 9(10), 1–18. https://doi.org/10.3390/land9100384

Marcer, M., Bodin, X., Brenning, A., and Schoeneich, P. 2017. Permafrost Favorability Index : Spatial Modeling in the French Alps Using a Rock Glacier Inventory. 5(December), 1–17. https://doi.org/10.3389/feart.2017.00105

Perucca, L., and Esper Angillieri, M.Y. 2011. Glaciers and rock glaciers ' distribution at 28°SL, Dry Andes of Argentina, and some considerations about their hydrological significance. https://doi.org/10.1007/s12665-011-1030-z

Rangecroft, S., Harrison, S., and Anderson, K. 2015. Rock glaciers as water stores in the Bolivian Andes : an assessment of their hydrological importance. 47(1), 89–98.

Wirz, V., Gruber, S., Purves, R.S., Beutel, J., Gärtner-Roer, I., Gubler, S., and Vieli, A. 2016. Short-term velocity variations at three rock glaciers and their relationship with meteorological conditions. Earth Surface Dynamics, 4(1), 103–123. https://doi.org/10.5194/esurf-4-103-2016

Crystalline misorientations in a permafrost sample

Carlos Leonardo Di Prinzio[1,2], Guillermo Aguirre Varela[1,2], Pastor Ignacio Achaval[1], Esteban Druetta[1] & Dario Trombotto Liaudat[3]

[1]*FAMAF (Facultad de Matemática, Astronomía, Física y Computación), Universidad Nacional de Córdoba, Medina Allende and Haya de la Torre, (5000) Ciudad Universitaria, Córdoba. Argentina*

[2]*IFEG-CONICET (Instituto de Física "Enrique Gaviola"), Universidad Nacional de Córdoba, Medina Allende and Haya de la Torre, (5000) Ciudad Universitaria, Córdoba. Argentina*

[3]*Geocryology, IANIGLA, CCT CONICET, Mendoza, Argentina*

Reference studies, environmental assessments and impact evaluations result from drillings conducted for the baseline study of different mining prospections located in the Andes, which provide samples of deep mountain permafrost rich in ice. Analyzing crystal orientation (CO) and crystal misorientation (CM) in the ice crystals of the sample will yield data on the changes and alterations experienced in their texture and crystallographic properties (Arena et al 2005; Corte 1962).

Sample preparation

In this work, a permafrost sample (PS) obtained from a drilling in an Andean rock glacier was studied (Trombotto Liaudat et al. 2024). The ice crystals in the sample have a hexagonal crystal structure characterized by three principal axes: a = $<11\bar{2}0>$, b = $<10\bar{1}0>$, and c = <0001>. As anticipated, the PS contains ice crystals with a significant presence of minerals, with volcanic glass and minerals derived from effusive igneous rocks being the most abundant. The PS was placed inside a refrigeration chamber at -20°C and polished using a LEITZ 1320 microtome. Polishing was performed on two planes perpendicular to the local vertical (Ve) of the PS extraction site (Pe) and on two planes perpendicular (Pa) to the former. A total of 43 ice grains were analyzed in the Pe samples and 33 grains in the Pa samples. The pairs of neighboring grains were 101 in the Pe samples and 119 in the Pa samples. Deflections φ, the angle between the principal axes a, b, and c with the normal to each polished surface, were determined. Plastic replicas were obtained from the polished surfaces following a methodology commonly implemented in ice studies (Matzuda et al. 1978; Di Prinzio et al. 2022). Figure 1 shows a region of a plastic replica of PS made in Pe. The ice grains are surrounded by minerals, exhibiting fairly regular shapes, and generally forming grain boundaries (GB). Figure 2 shows an enlarged area of Figure 1, where the chemical etching patterns are observed. These patterns are used to determine the CO and CM of the PS.

Experimental results

In Figure 3a and 3b, only the histograms of φ for the c-axes in the studied Pe and Pa samples, respectively, are presented. It can be clearly observed that the c-axis is parallel to the local vertical of the PS extraction, exhibiting a dynamic behavior very similar to that of samples extracted in polar ice (Di Prinzio et al. 2005).

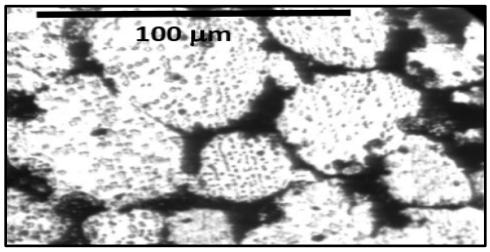

Figure 1. Plastic replica of the surface of the PS in the Pe plane. The white areas represent ice grains with chemical etching, while the black areas correspond to minerals.

In the Pa sample, the c-axis is preferentially perpendicular, correlating with the findings in Pe.

The φ angles were determined with a standard deviation of ±3°. The CMs are uniquely determined by a rotation axis <hklm> and a rotation angle θ, and they are defined as <hklm>/ θ.

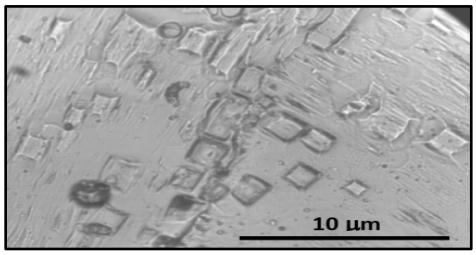

Figure 2. Plastic replica of the PS in a Pe plane. The nearly straight lines represent GB, the small circles denote bubbles, and the rectangular shapes depict chemical etching patterns.

In this study, CMs whose rotation axes were preferably a, b, and c are explored. Figure 4 presents histograms of θ for CMs around these preferential directions in the PS. In these histograms, the results of

CMs found for Pe and Pa were combined, as this property does not depend on Ve.

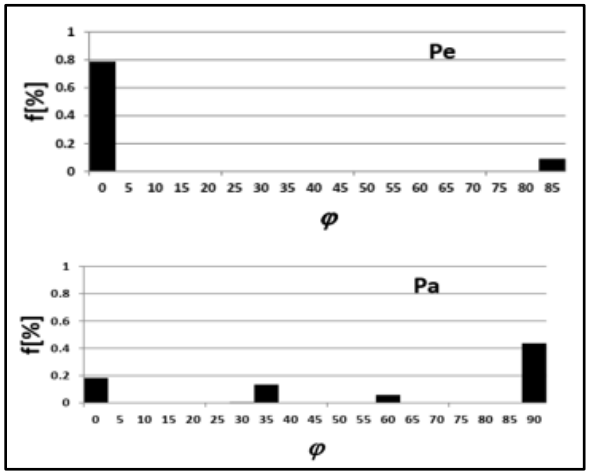

Figure 3. a) and b) Histograms of φ for the c-axes in the Pe and Pa samples, respectively.

Figure 4a displays the θ histogram for CMs around the a-axis. In general, many neighboring grains exhibit a CM <11$\bar{2}$0>/90°, as shown. Figure 4b presents the histogram of θ for CM around the b-axis.

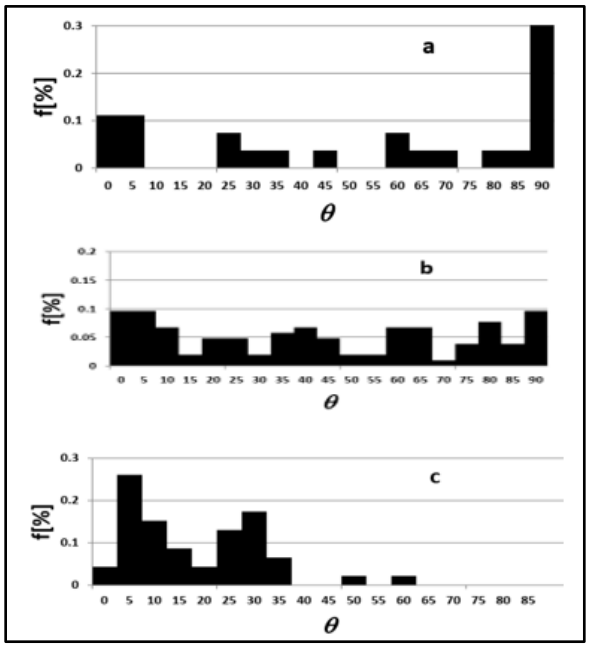

Figure 4. a) Histogram of θ for CM around the a-axis, b-axis and c-axis, respectively.

The CMs are more evenly distributed across the study interval. Consequently, the percentage of CMs for each angle is much lower than for the previous CM. However, this fact should not obscure the observation that groups of CMs can be seen around angles of <10$\bar{1}$0>/20°, <10$\bar{1}$0>/40°, <10$\bar{1}$0>/60°, and <10$\bar{1}$0>/80°. Figure 4c shows the histogram of θ for CM around the c-axis. Groups of CMs can be observed around angles of <10$\bar{1}$0>/5° and of <10$\bar{1}$0>/30°. The θ angles were determined with a standard deviation of ±3°. It is noteworthy that Di Prinzio et al. (2022) identified CMs with comparatively low relative energy. In the PS, the presence of CMs capable of forming GBs of very low-energy is observed. This presence could be linked to the gradual decrease in surface energy during the extensive thermal annealing of the PS.

Conclusion

It was observed that the grain basal plane is more frequently oriented perpendicular to the Ve. This observation may be related to the dynamics of permafrost rich in ice. Interestingly, the prismatic axes of the grains do not exhibit preferential inclinations. The presence of CMs capable of forming GBs with very low superficial energy was noted. This presence can be associated with the gradual decrease in surface energy that occurred over thousands of years in the creeping permafrost.

Future studies should compare these results with data obtained from simulations (Di Prinzio et al. 2023).

References

Arena, L.E., Trombotto Liaudat, D., and Caranti, G. 2005. Microcospical characterization of thermokarst ice from an area of Andean permafrost, Central Andes of Mendoza, Argentina. 2nd European Conference on Permafrost.Terra Nostra, 55.

Corte, A.E. 1962. Relationship Between Four Ground Patterns, Structure of the Active Layer and Type and Distribution of Ice in the Permafrost. U.S. Army. Cold Regions Research and Engineering Laboratory. Research Report 88. http://hdl.handle.net/11681/5867

Di Prinzio, C.L., Wilen, L.A., Alley, R.B., Fitzpatrick, J.J., Spencer, M.K., and Gow, A.J. 2005. Fabric and texture at siple dome, antarctica. Journal of Glaciology, 51(173), 281–290. doi:10.3189/172756505781829359

Di Prinzio, C.L., Stoler, D., Aguirre Varela, G., and Druetta, E. 2022. Tilt grain boundary energy in <0001>/φ bicrystals of pure ice. Canadian Journal of Physics, 100(9), 389–397. doi:10.1139/cjp-2021-0365

Di Prinzio, C.L., Achával, P.I., and Aguirre Varela, G. 2023. Evolution of Crystalline Misorientations in Polycrystalline Samples of Pure Ice. Chemical Physics, Manuscript accepted for publication.

Matsuda, M., and Wakahama, G. 1978. Crystallographic Structure of Polycrystalline Ice. Journal of Glaciology, 21(85), 607–620. doi:10.3189/S0022143000033724

Trombotto Liaudat, D., Arenson, L., Pecker Marcosig, I., Pastore, S., Wainstein, P., and Leach, M. 2024. Characteristics of Permafrost and Periglacial Environments in the Andes. ICOP 2024, Yukon, Canada.

First detailed case of study of a rock glacier in the Central Andes in Argentina

Silvio Pastore[1], Gabriela Álvarez Parma[1], Jorge Garcia[1], Santiago Graffigna[2], Sofia Cofone[1], Sol Trad[3] & Contanza Santori[2]

[1]*Department of Geology, Universidad Nacional de San Juan (UNSJ), Argentina*

[2]*Department of Geophysics, Universidad Nacional de San Juan (UNSJ), Argentina*

[3]*CONICET, Universidad Nacional de San Juan (UNSJ)*

This work constitutes the most detailed case study carried out for a rock glacier in Argentina to date, and one of the few cases worldwide that allow us to improve our understanding on the internal structure and behavior of a rock glacier. Additionally, this work intends to constitute an Andean reference case for physical parameters such as, electrical resistivities and seismic velocities (for geophysical investigations), ground temperatures at depth, volumetric ground ice contents, geotechnical and geothermal material properties. This will provide scientific evidence in support of resolving current precautionary and paralyzing environmental conflicts created by environmental legislation in Argentina. The work began in 2021 and to date the records continue.

The province of San Juan, Argentina has developed a local glacier inventory. As part of this inventorying work, detailed studies were completed on a rock glacier located at 31.7489°S/70.4278W 3.836 masl, in the San Juan River Basin. The objective of this detailed investigation is: i) to determine the physical parameters that control its geomorphological behavior; ii) estimate its volumetric ice content; iii) evaluate the contribution of permafrost degradation to surface runoff; and iv) project how the rock glacier responses to current and future weather conditions. For this, we completed multiple studies, including: a digital elevation model; geomorphological description; electrical resistivity tomography (ERT); seismic refraction tomography (SRT); geotechnical drilling (Sonic); ice content determination; lithological description; grain size distribution; ice dating; water quality analysis; and instrumentation of the borehole for ground temperature, deformation, and ground water level measurements.

These studies were carried out based on the agreement between the Government of the Province of San Juan and the UNSJ and are being continued with the Pites 37 project, also with the collaboration of the company Pachón S.A.

Results

According to its geomorphological features, the rock glacier was divided into three sectors that account for the complexity of its composition and ice content associated mainly with the contribution zones and the sub-base topography on which it lies (Figure 1). Five geophysical profiles were carried out combining the SRT and ERT methods in each of them and whose results for the drilling locations are shown in table 2.

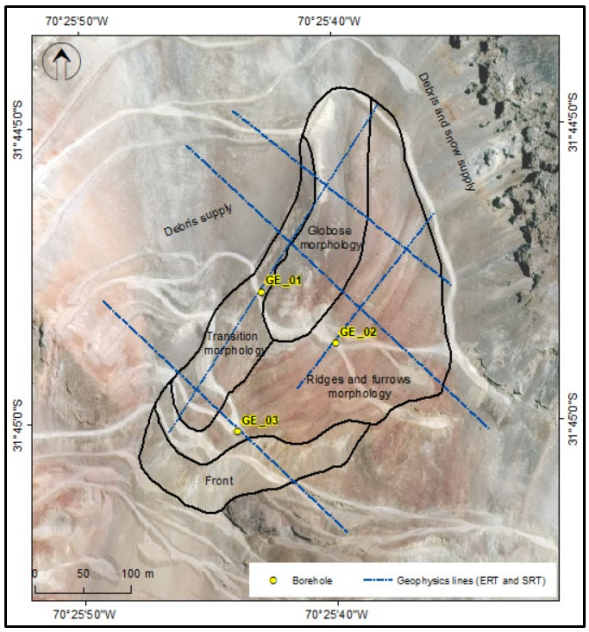

Figure 1. Rock glacier studied, morphologic description, location of geophysics lines (SRT-ERT), and boreholes.

Additionally, three sites were drilled to obtain samples for lithological description, calculation of ice content and granulometry (Table 1, Photography 1). These holes were instrumented with a thermistor, an inclinometer, and a vibrating wire piezometer. A sample of massive ice was obtained, which was prepared and sent to the laboratory for dating (Table 3) and water quality.

The equivalent water volume calculation was carried out, considering ground ice thicknesses from geophysics and ice volumes measured in the boreholes. Three possible combinations of thicknesses were used, and the maximum and minimum obtained were taken for these calculations, the results of which are shown in the table 4.

Table 1. Locations of borehole and main measured parameters.

Borehole	Height (masl)	Drilling length (m)	Permafrost table (m)	Permafrost base (m)	Ground ice thickness (m)	Average ice content (% Volumetric)
GE_01	3834	35	2	22,5	14.3	55
GE_02	3837	35	2	*	17.3	63
GE_03	3792	28	2	*	15.2	52

*Not data yet, activity in progress

Photography 1. GE_01 sonic drilling sample (ground ice).

Table 2. Vp and Resistivity values.

Borehole	SRT		ERT	
	Active layer (m/s)	Ground ice (m/s)	Active layer (kΩm)	Ground ice (kΩm)
GE_01	200-400	1600-3600		80-300
GE_02	200-800	1600-3800	5-25	100-300
GE_03	300-800	1700-4000		80-400

Table 3. Age ice sample.

Borehole	Ice sampling depth (m)		Mean age +-1σ (cal BP*)
	From	To	
GE_01	13.4	13.55	4080+-315

*BP refers to year before 1950

Table 4. Equivalent water volume calculation.

Maximum and minimum ice volume (hm^3)	Maximum and minimum equivalent water (hm^3)
0.26410729	0.23769656
0.32326913	0.29094221

CONCLUSIONS

From the drilling carried out and the combination of geophysical methods, it is concluded that the rock glacier is composed mainly of debris of angular rocks and gravel, with traces of sand and some fines, with interstitial ice, ice lenses and a cover, approximately two meters, of cobbles of that freezes seasonally (active layer). Its ice content varies between 52% and 63%, values like other rock glacier studied in the world.

The dating of an ice sample from rock glacier was carried out, resulting in an expected value that coincides with the distance from the debris and snow contribution area to the location of the drilling where the sample was obtained.

The age of 4080 ± 315 years of the ice sample from the rock glacier indicates that this mass of ground ice has not made any contribution to the historical water cycles of the basin at least in the last 3765 years.

The result of the water quality of the ice sample from the drilling indicates that it is not suitable for any type of consumption or use, due to its high values of metals and salts.

A representative understanding of the contribution to the water system was achieved, assuming the total melting of the contained ground ice by the year 2100 (conservative and unlikely case), considering 6 months per year of water contribution and without considering evaporation, between 0.19 l/s to 0.24 l/s.

REFERENCES

Jones, D.B., Harrison, S., Anderson, K., and Betts, R.A. 2021. Author Correction: Mountain rock glaciers contain globally significant water stores. Scientific reports, 11(1), 1–2.

Halla, C., Blöthe, J.H., Tapia Baldis, C., Trombotto Liaudat, D., Hilbich, C., Hauck, C., and Schrott, L. 2021. Ice content and interannual water storage changes of an active rock glacier in the dry Andes of Argentina. The Cryosphere, 15(2), 1187–1213.

Pastore, S., Álvarez Parma, G., and García, J. 2022. Cálculo del contenido de hielo y su contribución hídrica, en un glaciar de escombros en los Andes centrales de la República Argentina. In VII Congreso Argentino de Cuaternario y Geomorfología. San Juan. Acta Pag 42–43.

Evidence of rock-wall permafrost in the “Portillo Argentino” crossing (Dry-Central Andes of Argentina)

Carla Tapia Baldis[1], Ivanna Pecker[1], Mariano Castro[1], Noelia Sileo[2], Martín Mendoza[1] & Dario Trombotto Liaudat[1]

[1]*IANIGLA: Instituto Argentino de Nivología, Glaciología y Ciencias Ambientales, CCT Conicet, Mendoza, Argentina*

[2]*CNEA: Comisión Nacional de Energía Atómica PNGRR, Regional Cuyo, Mendoza, Argentina*

In high mountains, the air temperature and solar radiation control the likelihood of rock-wall permafrost occurrence. Due to the low ice content, which is primarily confined to discontinuities and joints within the rock massif, the thermal response to an external shift is usually quick. The permafrost degradation in rock-walls affects the geomechanical response of rock massifs, by reducing the resistance of the frozen rocks and joints once the 0 °C threshold is surpassed.

The "Portillo Argentino" is a narrow mountain pass, located above 4300 m asl between the Tunuyán and Tupungato valleys in Argentina (33°37’ S and 69°36’ W) (Figure 1). During the warm season it is used by riders and hikers, as it has historical, environmental, and esthetical significance.

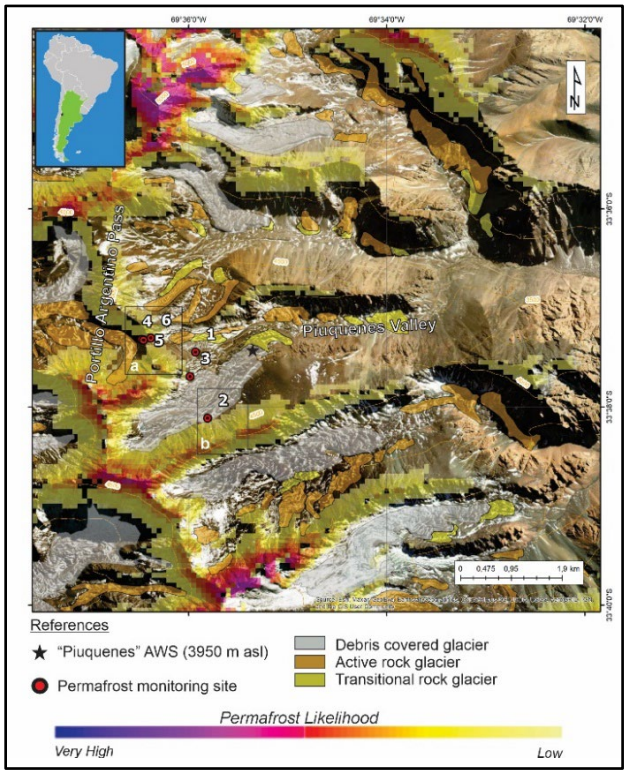

Figure 1. General overview of the “Portillo Argentino” pass. Permafrost in rock walls is expressed in terms of probability. Temperature data loggers are marked with red dots.

Annually, the thawing season with monthly mean air temperatures >0 °C extends from November to April, while the freezing season May to December. The precipitation patterns show a well-defined seasonal regime, with maximum precipitation during the cold season and scarce precipitation during the warm season. Precipitation falls as snow, with annual means ranging from 200 to 300 mm during the dry “La Niña” phases. The mean annual air temperature (MAAT) at approximately 3950 m asl (Piuquenes Automatic weather station – AWS – years 2019 to 2022) is -0.9 °C; during the thawing season MAAT ascends up to 9.1 °C, descending down to -16.9 °C during the cold season.

In the Piuquenes valley, the ice bodies are distributed altitudinally in a range that varies between 3200 and 5900 m asl, with an average height of 4500 m asl. According to the modeling provided by (Tapia-Baldis & Trombotto-Liaudat, 2020), there is a high probability of finding permafrost in the rock-wall outcrops above 4000 m asl (Figure 1). Nevertheless, this hyphotesis has never been tested before in the area.

Rock glaciers are located in the lowest altitude range up to approximately 5000 m asl, while glaciers and perennial snow patches are distributed from 3800 to 5900 m asl. Approximately 65% of the glaciers face south, southeast and east, coinciding with the coldest slope in the southern hemisphere and the main direction of runoff.

Since January 2022, eight temperature data loggers (iButtons ® DS1922L) were installed above 4100 m asl inside the rock outcrops, to verify the presence or absence of rock-wall permafrost (Figure 2). The temperature data in boreholes of 18 mm diameter, between 10-20 cm depth, are covering different topographic orientations (Figure 2c). Temperature measurements are recorded every 4 hours and were first retrieved in March 2023.

Figure 2. a) West-facing view from the Piuquenes Valley at the top of the "Portillo Argentino" pass. The rugged surface represents an active rock glacier landform. b) Near-vertical rock-wall outcrops above 4100 m asl. c) Drilling procedure using roto-percussion drilling.

Acording to the results from the first year of data collection (2022 to 2023), negative mean annual rock temperatures were obtained in P4, P5 and P6. These points are located at 4330 m asl, 4342 m asl and 4167 m asl, respectively (Table 1).

Despite having data only from one year, the results are promising for testing the presence of permafrost, which aligns with the expected permafrost likelihood model. Between 4100 and 4150 m asl, the mean rock temperature ranged from 3 to 7 °C, depending on the orientation of the rock walls. The results also indicate a strong coupling between the rock walls and air temperatures (in the absence of snow cover), with Pearson correlations ranging from 0.93 to 0.99 (Table 2 and Figure 3)

Table 1. Summary of rock-walls temperature data during 2022 and 2023, between 4100 and 4342 m asl.

Point	Aspect	Elevation (m asl)	Min T° (°C)	Max T° (°C)	Mean T° (°C)	Standard deviation
P1	NE	4100	-5.8	16.7	6.9	5.4
P2	S	4173	-8.4	14.4	2.9	5.6
P3	S	4145	-9.1	15.6	4.8	6.9
P4	W	4330	-17.7	7.8	-2.6	6.0
P5	Pass	4342	-16.3	6.2	-2.9	5.5
P6	S	4167	-8.9	8.2	-1.2	5.2
AIR T°	Valley	3950	-16.9	9.1	-0.9	5.6

Table 2. Pearson correlations between data points and air temperature. Bold numbers indicate higher correlations.

Variable	P1	P2	P3	P4	P5	P6	AIR T°
P1	**1.00**	**0.93**	0.92	0.91	0.91	0.79	0.88
P2	**0.93**	**1.00**	0.91	0.92	0.92	0.86	0.88
P3	0.92	0.91	**1.00**	**0.97**	**0.97**	**0.93**	0.90
P4	0.91	0.92	**0.97**	**1.00**	**0.99**	0.92	**0.95**
P5	0.91	0.92	**0.97**	**0.99**	**1.00**	**0.93**	**0.94**
P6	0.79	0.86	**0.93**	0.92	**0.93**	**1.00**	0.83
AIR T°	0.88	0.88	0.90	**0.95**	**0.94**	0.83	**1.00**

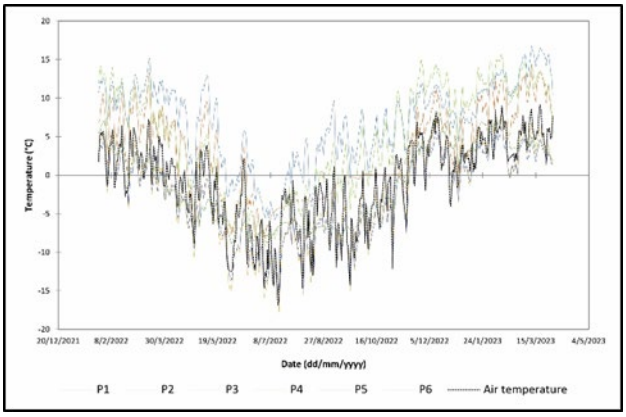

Figure 3. Temperature data correlation between rock-wall points.

REFERENCES

Tapia Baldis C, and Trombotto Liaudat D. 2020. Permafrost debris-model in Central Andes of Argentina (28°-33° S). Cuadernos de Investigación Geográfica 46. http://doi.org/10.18172/cig.3802

Characteristics of permafrost and periglacial environments in the Andes

Dario Trombotto Liaudat[1], Lukas U. Arenson[2], Ivanna Pecker Marcosig[1], Silvio Pastore[3], Pablo Wainstein[4] & Miguel Leach[5]

[1]*Geocryology, IANIGLA, CCT CONICET Mendoza, Argentina*

[2]*BGC Engineering Inc., Vancouver, British Columbia, Canada*

[3]*Universidad Nacional de San Juan, Argentina*

[4]*BGC Engineering Inc., Calgary, Alberta, Canada*

[5]*BGC Ingeniería Ltda., Mendoza, Argentina*

Periglacial environments in the Andes have been studied for decades, with much of the focus being on the presence of permafrost with pioneering works dating back nearly 100 years. However, later investigations shifted towards studying periglacial processes and mapping landforms, with limited deep ground temperature data that hindered an assessment of permafrost temperatures at depth throughout the Andes. Mining projects in the high Andes, through the regulatory requirement of developing environmental baseline studies and impact assessments, provide an opportunity to collect unique data on ground temperatures. Although such data have typically not yet been recorded for several years and some are not continuous, these data are believed to provide valuable information on the thermal state of the Dry Andes.

The Andean periglacial environment was studied long ago in the highest altitudes of Bolivia and southern Peru, in Chile, or in the northern hemispheric part of South America. The existence of permafrost was reported decades ago, from the pioneering works of Catalano (1926) and Corte in the 1970s (1976; 1978), and by Barsch's research in Argentina (Barsch 1983). However, in the matters of Andean cryospheric system and periglacial geomorphology efforts were still relatively small, having the main focus on rock glaciers. Cartography initiatives and the development of local rock glacier inventories in the Central Andes of Argentina were started and subsequently motivated regional inventories, followed by the development of a nationwide inventory. However, despite all the geomorphological initiatives, we found limited deep ground temperature data that hindered an assessment of permafrost temperatures at depth throughout the Andes. Mining projects in the high Andes, through the regulatory requirement of developing environmental baseline studies and impact assessments, provide an opportunity to collect unique data on ground temperatures, enabling researchers to assess permafrost conditions. Ground temperature data from four different mine sites and four non-mining sites with ice-rich permafrost are compared.

The selected sites are shown in Figure 1 according to their altitudes vs latitudes. It is remarkable that the permafrost lower limit descends with increasing aridity, as observed by Cheng Guodong (1983) for Tibet, as well as a shifting to lower latitudes in the Andes is observed. Aspect and local microclimatic conditions are additional important parameters for the existence of mountain permafrost. The lower elevation limit is not a single line but may vary by several hundred meters.

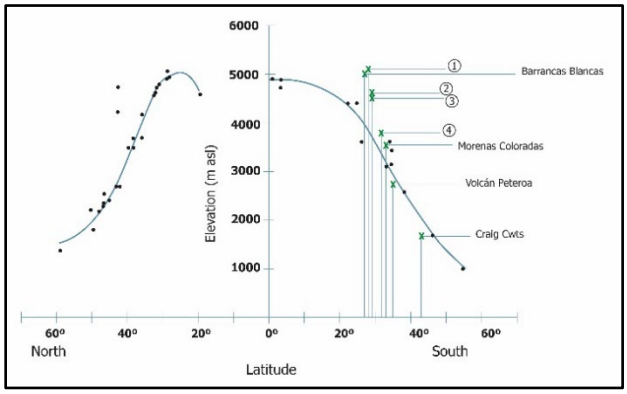

Figure 1. Locations of the sites presented, and permafrost lower limit compared to the average for the northern hemisphere (after Cheng Guodong 1983; Corte 1988).

Results

Figure 2 shows a series of trumpet curves derived from the ground temperature measured at the five sites. Depending on latitude and elevation, different temperatures are recorded. At nearly 5100 m, cold permafrost and a permafrost thickness of more than 200 m is recorded. At 5023 m but ~170 km to the north, temperatures are significantly warmer. The mean annual ground temperature at the first site is ~-6.1°C, but ~-2.5°C at the second.

Approximately 280 km to the south, the lower elevation boundary for permafrost is substantially lower, indicated by permafrost being measured at 3835 m (Figure 1). Recent shallow borehole temperature data indicate permafrost at that location to existence at elevations as low as 3600 m.

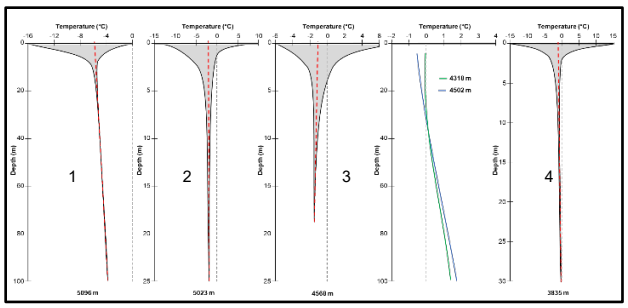

Figure 2. Trumpet curves based on the temperatures measured at the five sites.

In cases of non-mining sites it is worth noting that an important layer of ice-rich permafrost occurs in the Valley of Barrancas Blancas, Atacama, Chile. This area represents an extremely cold desert region with particular microclimatic characteristics on the bottom of the valley, which allow for an active layer of 30 to 45 cm at ~5000 m. Likewise, we do not know the permafrost thickness, but a rich periglacial geomorphology as Atacama pingos, permafrost dunes, rock glaciers or protalus, cryoplanation surfaces and gelifluction lobes among others can be identified (Trombotto Liaudat et al. 2023).

The Morenas Coloradas rock glacier is a well-known rock glacier in the Central Andes, with one of the oldest monitoring sites for active layers in South America. The ice-rich permafrost thickness showed thicknesses between 10 and 30 m (Halla et al. 2021). Permafrost on the slopes of the Peteroa volcano was identified through isolated ice bodies covered by volcanic sediments, active protalus lobes, and protalus ramparts, small rock glaciers, nivation hollows, gelifluction terraces, and cryogenic sedimentary slopes, identified starting at elevations of 2900 to 3000 m. In the Patagonian case of Craig Cŵts, permafrost is present at elevations below 1900 m due to special geomorphology conditions, narrow and shady valleys (Hughes and Trombotto Liaudat 2023).

Conclusions

Deep ground temperature measurements at various sites in the arid Andes confirm the local variability in ground thermal regimes (altitudinal zonation). The lower limit of permafrost decreases with increasing southern latitude. However, locally, the lower elevation limit can vary by several hundred meters. Deep boreholes at an elevation of nearly 5100 m record a permafrost thickness of more than 200 m.

Most temperature records indicate that there are no steady state conditions at depth, and that permafrost is slowly warming, i.e., adjusting to modern climate conditions. Ground temperatures at depths (e.g., >60 m) still represent colder conditions of past climates, whereas shallow ground temperatures (<20 m) have adjusted or, are currently adjusting to today's climate. By ignoring such transient thermal conditions, permafrost thicknesses are likely to be underestimated and the time needed for degradation wrongly projected.

An erroneous assessment of the permafrost conditions has impacts on environmental studies and engineering designs, which often result in additional costs. Because permafrost affects the time and spatial distribution of surface water runoff, and the temporary storage of water in the active layer during winter, a proper understanding of the heterogeneous distribution of permafrost helps in better appreciating regional ground water flows and assess potential impacts of a project. Further, a good understanding assists in avoiding problematic zones for infrastructure. It is therefore important to not only understand shallow ground temperatures at a few locations, but also the deep ground thermal regimes, including their topographic heterogeneity, of the mountainous arid or semiarid Andes.

References

Catalano, L. 1926. Contribución al conocimiento de los fenómenos geofísicos. Dirección General de Minas, Geología e Hidrología, Buenos Aires (24), 78 pp.

Corte, A. 1976. The hydrological significance of rock glaciers. Journal of Glaciology, 17: 157–158.

Corte, A. 1978. Rock glaciers as permafrost bodies with a debris cover as an active layer. A hydrological approach. Andes Mendoza, Argentine. In 3rd ICOP, 262–269.

Corte, A. 1988. Geocryology of the Central Andes and rock glaciers. In 5th ICOP, 718–723.

Cheng, G. 1983. Vertical and horizontal zonation of high altitude permafrost. In 4th ICOP, 136–141.

Halla, C., Blöthe, J.H., Tapia Baldis, C., Trombotto Liaudat, D., Hauck, C., and Schrott, L. 2021. Ice content and interannual water storage changes of an active rock glacier in the dry Andes of Argentina. The Cryosphere, 15: 1187–1213.

Hughes, E., and Trombotto Liaudat, D. 2023. Characteristics and geomorphological implications of the periglacial environment of Craig Cŵts, Patagonides, Chubut, Argentina. In 12th ICOP, Whitehorse. 2024.

Trombotto Liaudat, D., Buchroithmer, M., Mushkin, A., and Schröter, B. 2023. The Cold Desert of Atacama. Mapping Previously Unknown Cryophenomene in the Ojos del Salado Region. In 12th ICOP, Whitehorse. 2024.

3D — Joint session on Yedoma and Paleo Permafrost Records of Environmental Change

Session Chairs: Aleksandra Veremeeva, Fabian Seemann & Lutz Schirrmeister

Alfred Wegener Institute Helmholtz Centre for Polar and Marine Research, Potsdam, Germany

Permafrost and periglacial processes operate under cold-climate conditions, and in many regions of the world past climatic conditions were colder than at present. These include but are not limited to regions proximal and beyond the margins of the last glacial ice sheets. Relict permafrost and periglacial landforms provide indices for the extent of past cold-climate conditions, although the interpretation and significance of such features are commonly subject of debate. In addition, other forms of proxy data, including cryolithological parameters, flora and fauna fossil remains, DNA, microorganisms, as well as isotopic and chemical signatures in biological remains, ground ice and sedimentary deposits attest to past environmental conditions. Such geological and biological evidence provides insights into the extent of past climatic and environmental regimes, rates of change and provides context for impacts experienced under current climate change conditions.

One of the actively studied and discussed ancient permafrost deposits is the Yedoma Ice Complex (IC), a suite of ice-rich silty sandy sediments that accumulated in the Late Pleistocene. Formed in vast lowlands of Beringia, the Yedoma IC is widespread in Siberia, Alaska and northwestern Canada. The high ice content of Yedoma deposits, due to the presence of large ice wedges and excess ice, has led to large-scale development of thermokarst lakes and drained lake basins across Yedoma regions under climate warming conditions in the past and present times. Interest in Yedoma landscapes has been driven by: 1) the exceptional preservation of past environmental records, including the fossil remains of the mammoth steppe fauna and flora, biologically viable plants and microorganisms, cryostructures, stable water isotopes and biogeochemical characteristics; 2) the impact of thaw on these regions due to the Yedoma high ice content driving landscape changes; and 3) large amounts of buried freeze locked well-preserved organic matter in deposits which due to the permafrost thawing will be involved in modern biogeochemical processes and contribute to greenhouse gas formation. Significant questions remain about the origins and paleoenvironmental conditions of Yedoma formation, its microbiology, landscape changes and vulnerability to climate warming. Embracing the Yedoma and deep disturbance processes in models has been slow so far.

This joint session examines issues and evidence related to past permafrost and associated environmental conditions including paleoenvironmental records and microbiological studies of Yedoma, the current state and dynamics of landscapes formed by past and ancient permafrost, and the assessment of future landscape dynamics under different warming scenarios.

Geochemical characterization of massive tabular ground ice, ice wedges and thawed sediments of the Western Siberia Arctic lowlands

Nataliya Belova[1,2], Radik Makshaev[1], Lev Kuzyakin[1], Irina Streletskaya[1] & Gleb Oblogov[2]

[1]*Faculty of Geography, Lomonosov Moscow State University*

[2]*Earth's Cryosphere Institute, Tyumen Scientific Centre SB RAS*

Geochemical studies were carried out on 114 samples of massive tabular ground ice, ice wedges and thawed sediments from the Marre-Sale, Amderma and Vaskiny Dachi sections. In total, 88 ice samples with layers of silt-clay and sand were analyzed. All measurements of sediment and ice samples were carried out using an energy dispersive X-ray fluorescence analyzer (ED-XRF, Olympus Delta Pro). The following groups of elements were studied: Al, Si, P, S, Cl, Ca, Ti, Mn, Fe, Ni, Cu, Zn, Rb, Sr, Y, Zr, Nb, Mo, Pb, Th.

Measurements were carried out both for pure ice and for layers with the inclusion of silt-clay and impurities. To compare the geochemical composition of ice and inclusions in it, studies of sediments (26 samples) from the Marre-Sale section (alluvial-marine, lagoon-marine sediments) overlying and underlying massive ice layerswere carried out. Based on the results of studying samples with ice, two main groups of ground ice are distinguished based on the ratio of geochemical elements and dependent mineralogical inclusions in them. For the main part of ice samples, characteristic inclusions are the elements Si, Al, Fe, Ca, presented in small quantities (total content less than 0.7-0.9%) in ice without visible impurities. Silt-clay and sand layers in ice contains a larger amount of elements Si, Al, Ti, Fe, Ca, Cl, Sr, Th, Rb with a total content ranging from 2.7 to 8.4%. The elements Si, Al, Ca are predominate. Ice samples are characterized by an almost complete absence of the elements Ti, Cl, Rb, and Pb. In samples with inclusions, there is a noticeable increase in the concentration of Si, Al, Fe, Ca and the appearance of such elements as Sr, Mn, Th, Pb. The second group of ground ice is distinguished by the content of the elements Mo, Sr, Y, Nb and an increased amount of Si. The elemental composition of inclusions in ice samples from Marre-Sale, Amderma and Vaskiny Dachi has an almost identical composition. Samples from Amdrema are characterized by a lower content of silt-clay impurities and purer ice. These features suggest that the ices of Marre-Sale, Amderma and Vaskiny Dachi with a small amount of mineral inclusions without visible inclusions are presumably of identical origin, or that their origin can't be determined based just on the elemental composition of inclusions.

A comparison of the geochemical composition of ice and sediments demonstrates a clear differentiation in the composition of the studied samples. Sediments from the base of the Marre-Sale section are characterized by a predominance of the elements Si, Al, Ti, Fe, Ca, Mn, Ni, Cu, Sr, Zr, and Pb. The distribution of the elements Si, Al, Ti, Fe demonstrates a clear linear relationship and records the highest concentrations in samples from Marre-Sale sediments, and the minimum in ice without impurities. The suspended concentrations of elements (Si, Al, Ti, Fe, Mn) in sediments from the base of the Marre-Sale section suggest that these sediments accumulated in alluvial-marine, lagoonal conditions, with the periodic supply of more terrigenous components, which is also evidenced by the presence of a series sand layers (2-5 cm).

The study was supported by the Russian Science Foundation project No. 23-27-00218

Quartz grain micromorphology of relict sand wedge infillings from the Pannonian Basin, Central Europe

Beáta Farkas[1], Barbara Woronko[2], János Kovács[3] & Szabolcs Ákos Fábián[4]

[1]*Doctoral School of Earth Sciences, University of Pécs, Pécs, Hungary*

[2]*Department of Climate Geology, University of Warsaw, Warsaw, Poland*

[3]*Department of Geology and Meteorology, University of Pécs, Pécs, Hungary*

[4]*Department of Landscape and Environmental Geography, University of Pécs, Pécs, Hungary*

The Pannonian Basin was located ca. 600 km from the front of the Fennoscandian Ice Sheet during the Last Glacial Maximum, the latest cold period in the history of Earth. Due to the proximity of the ice sheet and the special basin-like environment, the Pannonian Basin is recognised as the southernmost limit of past permafrost. The cold-climate non-glacial environment resulted in sand-filled frost cracks throughout the northern part of the basin. These sand wedge polygons were detected earlier (Kovács et al. 2007; Fábián et al. 2014; Farkas et al. 2023), although their sedimentological properties were not studied in detail. To reconstruct periglacial conditions during the formation of sand-wedges, microtextures of sand-sized quartz grains were analyzed in a scanning electron microscope (SEM). This method has proven to be a useful tool for paleoenvironmental reconstructions. It gives us insight into the surface microtextures of grains and, therefore, information about transport and post-sedimentary processes.

Overall, 460 randomly selected quartz grains in the 250–500 µm size range were studied under a JEOL JSM IT500HR SEM. 15 samples were taken from the infilling of two relict sand wedges, while eight samples were collected from their host material, all of them from the Kemenshát area. 20 grains from each sample were analysed, as this amount is proven to be statistically representative of this grain size (Mahaney 2002). The type of grain edges (sharp/rounded), frequency of fractures (low/high), microrelief diversity (low/medium/high), and surface microtextures of the grains were analysed. Microtextures, described by Mahaney (2002), and extended by Goudie and Bull (1984), were categorised into six groups according to their frequency. Note that since SEM is a semi-quantitative method, only the presence or absence of the microtextures was described, not their quantity. Grains were classified into seven groups according to the last process detected on their surface (after Cailleux 1942; modified by Mycielska-Dowgiałło and Woronko 1998). For the infilling material, the degree of weathering and the frost action index were determined by counting all frost-induced, fresh microtextures (i.e., small [<10 µm] conchoidal fractures, big [>10 µm] conchoidal fractures, small [<10 µm] breakage blocks, big [>10 µm] breakage blocks).

After the SEM measurements, statistical analyses were applied in MATLAB environment. First, hierarchical cluster analysis was applied on the raw data to check if there are differences between the infilling and the host material. The average method and Euclidean distance were used. After data normalisation, principal component analysis was used to see what kind of microtextures (i.e., mechanical, chemical, polygenetic) were the most influential on the samples. 11 microtextures were selected as variables, while the 23 samples were the observations.

Scanning electron microscopy showed that most of the grains (42.50–58.33%) belong to the subangular roundness category, while subrounded being the second most frequent group (16.67–49.17%). The host samples are more angular, the biggest difference appears in the angular category (twice as many grains as from the infilling).

There is a huge difference in the grain types, as the host samples are mainly from fluvial environment (EM/EL), while the infilling is rather of eolian origin (EM/RM). Grains that were affected by intensive weathering (OTHER) appear in every sample in various amounts (8–22%). Cluster analysis reinforced this observation, as it sorted the samples into two categories (one exclusively with the host and one with all the infilling samples). PCA showed that chemical, mechanical and polygenetic microtextures influence the samples to a similar extent.

The quartz grain micromorphology helped us establish a transport history for the sediments. According to SEM, the grains probably are of Alpine origin. They were then transported in fluvial environment for a short period of time. Later, short yet intensive wind activity took place that deposited them into in-situ frost weathering conditions. Based on the frost action index, it is obvious that freeze-thaw cycles have affected the material after sedimentation. There is, however, no clear trend in the values along the vertical profiles. The most common frost-related microtexture is small conchoidal fracture, which points to an initial stage of frost weathering. It may suggest

that (1) periglacial conditions affected the studied area for a short time or (2) the studied deposits were within the permafrost and not in an active layer where the number of freeze-thaw cycles were low. Moreover, aeolian activity in the Pannonian Basin was short or weak during the formation and filling of the sand wedges, as it is marked only on the most concave parts of the grains.

Altogether, it can be concluded that quartz grain micromorphology can be used to detect and analyse periglacial sediments, however, there are limitations to its paleoenvironmental interpretations on its own.

Acknowledgements

Support of the National Research, Development and Innovation Office (Hungary) under contract ÚNKP-23-3 is gratefully acknowledged.

References

Cailleux, A. 1942. Les actions éoliennes périglaciaires en Europe. Mémoires de la Société Géologique de France 1–176.

Fábián, S.Á., Kovács, J., Varga, G., Sipos, G., Horváth, Z., Thamó-Bozsó, E., and Tóth, G. 2014. Distribution of relict permafrost features in the Pannonian Basin, Hungary. Boreas 43, 722–732. https://doi.org/10.1111/bor.12046

Farkas, B., Sipos, G., Bartyik, T., Józsa, E., Czigány, S., Balogh, R., Varga, G., Kovács, J., and Fábián, S.Á. 2023. Characterization and mapping of MIS-2 thermal contraction crack polygons in Western Transdanubia, Hungary. Permafrost & Periglacial 34, 11. https://doi.org/10.1002/ppp.2190

Goudie, A., and Bull, P.A. 1984. Slope process change and colluvium deposition in Swaziland: An SEM analysis. Earth Surf Processes Landf 9, 289–299. https://doi.org/10.1002/esp.3290090308

Kovács, J., Fábián, S.Á., Schweitzer, F., and Varga, G. 2007. A relict sand-wedge polygon site in north-central Hungary. Permafrost and Periglacial Processes 18, 379–384. https://doi.org/10.1002/ppp.600

Mahaney, W.C. 2002. Atlas of sand grain surface textures and applications. Oxford University Press, Oxford, England.

Mycielska-Dowgiałło, E., and Woronko, B. 1998. Analiza obtoczenia i zmatowienia powierzchni ziarn kwarcowych frakcji piaszczystej i jej wartosc interpretacyjna. Przeglad Geologiczny 46, 1275–1281.

Holocene ice wedges geochemistry: paleoenvironmental records from Central Yakutia

Nikolai Fedorov[1], Nayeon Ko[1], Jinho Ahn[1], Hyejung Jung[2], Yalalt Nyamgerel[2], Jeonghoon Lee[2], Moruot Skryabin[3] & Aleksander Fedorov[3]

[1]*Seoul National University, Seoul, South Korea*

[2]*Ewha Womans University, Seoul, South Korea*

[3]*Melnikov Permafrost Institute, Yakutsk, Russia*

Ice wedges are V-shaped bodies of ice formed by frost cracking of the sub-surface and infiltration by atmospheric precipitation, which subsequently freezes in the perennially frozen ground of the permafrost. Due to its specific way of accumulation and formation, they can preserve the records of the past environment and climate. For those reasons, we analyzed ice wedges from Central Yakutia for comprehensive geochemistry such as dissolved organic carbon (DOC) concentration, radiocarbon (^{14}C) age and stable carbon isotopes ($\delta^{13}C$) of DOC and plant remains, stable water isotopes ($\delta^{18}O$, δD, *d*-excess) of ground ice, greenhouse gases (GHGs) composition of the enclosed air bubbles (CO_2, CH_4, N_2O) and molar ratios of common gases (N_2, O_2, Ar) to obtain crucial information on the formation of the ground ice, ancient climate parameters, and biogeochemical conditions in the ground.

The DOC concentration was used to examine the abundance of organic matter in the ice, and we compared it with other reservoirs on Earth. The ^{14}C data were obtained to calculate the ages of ice wedge formation using two different proxies: entrapped plant remains tissue and DOC of ice, employing the accelerator mass spectrometry (AMS) technique. The $\delta^{13}C$ signature was applied to derive the origin of carbonic compounds inside the ice wedge, utilizing Isotope-ratio mass spectrometry (IRMS).

$\delta(N_2/Ar)$ and $\delta(O_2/Ar)$, are valuable tools for constraining the formation mechanisms of ground ice (St-Jean et al. 2011; Boereboom et al. 2013). Ice wedges formed by snow compaction or vapor sublimation should preserve occluded $\delta(N_2/Ar)$ and $\delta(O_2/Ar)$ values closer to atmospheric values. In contrast, the infiltration of meltwater is likely to affect these values, depending on the relative solubility of these gases in water. The analysis employs Gas Chromatography (GC) with a Thermal Conductivity Detector (TCD).

Stable O and H isotope ratios in water may provide information about temperature during winter and the source of atmospheric water vapor over climate history. The isotopic data was acquired using a Picarro L2140-i isotopic water analyzer via Wavelength-Scanned Cavity Ring-Down Spectroscopy.

GHGs mixing ratios can offer insight of microenvironmental conditions inside the ice wedges, which can be used to characterize in situ microbial production within the ice. Gas concentration data were derived using GC with a flame ionizing detector (FID) for CO_2 and CH_4 and an electron capture detector (ECD) for N_2O.

Using the multiproxy data, we conducted comprehensive investigations to understand the nature and genesis of ice wedges in Central Yakutia. Our goal is to address the following questions: (1) When were the ice wedges formed? (2) How were the ice wedges formed? (3) In what environmental conditions did they grow? (4) What internal processes controlled the composition of GHGs? Answers to these questions will offer fundamental insights into the microenvironment of ice wedges in Central Yakutia, contributing to precise paleoenvironmental interpretations for future studies involving ice wedges.

Ice wedge samples were collected from four study sites in Central Yakutia: Sylgacchi, Myndagai, Chabyda, and Kullaty (Figure 1). These study sites are relatively close to each other within the Lena-Amga rivers interfluve. Central Yakutia is renowned for its high abundance of Yedoma deposits. However, sampling focused on Holocene-aged sediments, primarily from the floodplains of contemporary water bodies, while Yedoma is defined by Late Pleistocene in age.

Samples were obtained from the underground environment by manually digging a vertical pit of 1.2–2.2 meters depth until reaching the cap of the permafrost layer. The frozen soil layer was then removed using a pickaxe, ultimately reaching the ice wedge cap. Blocks approximately 60 cm long, cut following the growth of the ice wedges, were obtained from each study site using a chainsaw. Additionally, adjacent ice was sampled separately for water stable isotopes analysis, and organic-rich soil material was collected for radiocarbon age determination. Fieldwork was conducted during the period of July to August 2022.

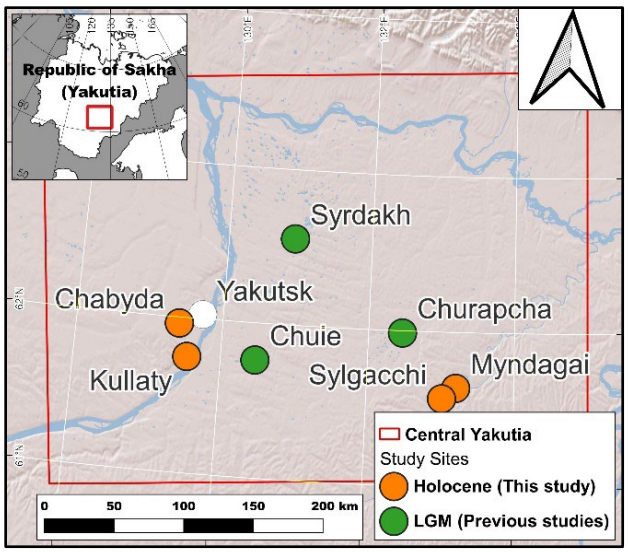

Figure 1. Location of the study sites. Orange circles represent the sites from this study and green circles – previous studies from Kim et al. (2018) and Yang et al. (2022).

We observed extremely high GHGs mixing ratios relative to atmospheric levels (Table 1): 4.83% to 14.04% for CO_2, 51.82 ppm to 16.82% for CH_4, and 163 ppb to 93.22 ppm for N_2O. The molar ratios of $\delta(O_2/Ar)$ varied between -98.26% to -40.92%, indicating an excess of oxygen depletion. The $\delta(N_2/Ar)$ ranged from -30.28% to 25.33%, suggesting that the ice wedges formed through both liquid water and snow compaction. Isotopic composition of O and H were -27.54‰ to -17.82‰ for $\delta^{18}O$, -214.93‰ to -138.16‰ for δD, and -0.35‰ to 9.50‰ for the *d*-excess, implying the changes in winter paleotemperatures ($\delta^{18}O$, δD) and/or changes in water vapor source (d-excess) during ice wedge formation.

Our results indicate that microbial production may have enriched the GHGs compositions. Further studies should include a comparison with ice wedges in the same region (Central Yakutia) but formed during the last glacial period (i.e., Yedoma ice wedges). This would contribute to a comprehensive understanding of the paleoenvironment during both glacial and interglacial periods.

Table 1. Geochemical properties of study sites (reported in mean ± 1σ, data count).

	Chabyda	Sylgacchi	Myndagai	Kullaty
DOC (mgC/L)	8.6, n=1	19.6, n=1	12.2, n=1	8.1, n=1
$\delta^{18}O$ (‰ vs VSMOW)	-18.93 ± 1.71, n=6	-26.40 ± 0.26, n=7	-27.17 ± 0.24, n=5	-26.37 ± 1.21, n=4
δD (‰ vs VSMOW)	-146.87 ± 13.41, n=6	-203.30 ± 1.60, n=7	-208.94 ± 1.90, n=5	-209.13 ± 9.37, n=4
d-excess (‰ vs VSMOW)	4.60 ± 0.33, n=6	7.93 ± 0.65, n=7	8.41 ± 0.63, n 5	1.83 ± 1.77, n=4
$\delta(N_2/Ar)$ (%)	-17.40 ± 12.16, n=5	-18.92 ± 4.56, n=7	-2.32 ± 2.45, n=6	6.76 ± 11.05, n=6
$\delta(O_2/Ar)$ (%)	-48.10 ± 9.51, n=5	-96.03 ± 2.86, n=7	-76.28 ± 10.81, n=6	-81.26 ± 14.26, n=6
CO_2 (%)	8.35 ± 1.37, n=5	12.12 ± 1.13, n=7	6.68 ± 1.20, n=6	9.40 ± 3.95, n=5
CH_4 (%)	5.31 ± 6.59, n=5	0.51 ± 0.41, n=7	0.05 ± 0.08, n=6	0.27 ± 0.29, n=6
N_2O (ppm)	37.20 ± 38.57, n=5	0.94 ± 0.12, n=7	30.31 ± 14.32, n=6	33.06 ± 43.46, n=6

REFERENCES

Boereboom, T., Samyn, D., Meyer, H., and Tison, J.-L. 2013. Stable isotope and gas properties of two climatically contrasting (Pleistocene and Holocene) ice wedges from Cape Mamontov Klyk, Laptev Sea, northern Siberia. The Cryosphere, 7(1), 31–46. https://doi.org/10.5194/tc-7-31-2013

Kim, K., Yang, J.W., Yoon, H., Byun, E., Fedorov, A., Ryu, Y., and Ahn, J. 2019. Greenhouse gas formation in ice wedges at Cyuie, central Yakutia. Permafrost and Periglacial Processes, 30(1): 48–57. https://doi.org/10.1002/ppp.1994

St-Jean, M., Lauriol, B., Clark, I.D., Lacelle, D., and Zdanowicz, C. 2011. Investigation of ice-wedge infilling processes using stable oxygen and hydrogen isotopes, crystallography and occluded gases (O_2, N_2, Ar). Permafrost and Periglacial Processes, 22(1), 49–64. https://doi.org/10.1002/ppp.680

Yang, J., Ahn, J., Iwahana, G., Ko, N., Kim, J., Kim, K., Fedorov, A., and Han, S. 2022. Origin of CO_2, CH_4, and N_2O trapped in ice wedges in central Yakutia and their relationship . Permafrost and Periglacial Processes, 34(1): 122–141. https://doi.org/10.1002/ppp.2176

Interpretation of radiocarbon ages and geochemistry in massive ground ice and underlying sediments of the Barrow Permafrost Tunnel, Alaska

Go Iwahana[1], Masao Uchida[2], Kazuho Horiuchi[3], Jody Deming[4], Hajo Eicken[1], Hiroshi Ohno[5], Kanako Mantoku[2], Toshiyuki Kobayashi[2] & Kazuyuki Saito[6]

[1]*International Arctic Research Center, University of Alaska Fairbanks, Fairbanks, Alaska, United States*

[2]*Earth system division, National Institute for Environmental Studies, Tsukuba, Ibaraki, Japan*

[3]*Graduate School of Science and Technology, Hirosaki University, Hirosaki, Aomori, Japan*

[4]*School of Oceanography, University of Washington, Seattle, Washington, United States*

[5]*Kitami Institute of Technology, Kitami, Hokkaido, Japan*

[6]*Japan Agency for Marine-Earth Science and Technology, Yokohama, Kanagawa, Japan*

Ground ice has been used to study past environmental and developmental history through its geochemistry, ground-ice structure (cryostructure), and relationship to the host deposits (Gilbert et al. 2016). Using ground ice as a paleoclimate proxy is especially important for studies in periglacial areas where paleo-records from ice cores, lake sediments, and tree rings are less available or absent in the vicinity.

The Barrow Permafrost Tunnel is located near the town of Utqiagvik and is a unique facility that provides access to massive ground ice distributed at depths of about 3 to 7 m and enables three-dimensional sampling of permafrost. The tunnel was created within the massive ground ice, with the dimension of the adit space being about 10 m long and 1.5 m wide (Figure 1). This permafrost research facility provides a unique opportunity to sample and observe massive ground ice and surrounding sediments three-dimensionally. Several studies were conducted using permafrost samples from this tunnel. Meyer et al. (2010a; 2010b) analyzed past environmental history using spatially sampled permafrost in the tunnel. Their research indicated that the massive ground ice in the tunnel developed as an ice wedge during the Late Glacial–Early Holocene (10–12 ka BP), recording winter climate information. Iizuka et al. (2019) conducted high-resolution sampling for ion concentration analysis in the ground ice along the Meyer et al. sampling transect. They found a high methanesulfonate ion concentration through the beginning of the Younger Dryas (YD) period, suggesting the existence of a nearby open sea surface during the coldest YD periods. A unique occurrence of cryopeg brines was found in this tunnel (Iwahana et al. 2021), and the microbiology of the brines was reported by Colangelo-Lillis et al. (2016), Cooper et al. (2019), etc.

To better constrain the age of permafrost development in the tunnel and to better interpret and understand the geochemistry information from the samples collected, we conducted additional radiocarbon dating for newly collected macro-plant remains obtained from the massive ground ice in the tunnel and underlying sediment layers. The objective of this study is to evaluate the origin and developmental history of the permafrost surrounding the Barrow Permafrost Tunnel with the new radiocarbon dating and geochemistry information together with previous microbiological and observational information.

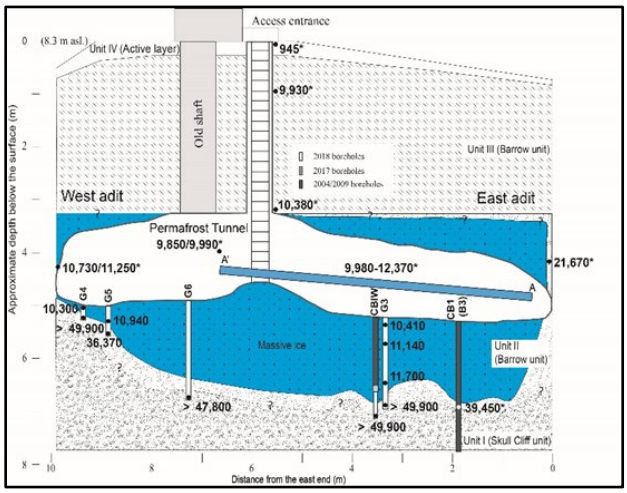

Figure 1. Cross section of the Barrow Permafrost Tunnel and sampling locations. Radiocarbon dates of the macro-plant remains sampled at the dot locations are displayed in uncalibrated BP. For transect A'-A, a range of the measured radiocarbon ages is displayed. Values with asterisks are from Meyer et al. (2010a).

MATERIALS AND METHODS

From 2016 to 2018, permafrost samples, including massive ground ice and frozen sediments, were collected at about 5 meters depth in the Barrow Permafrost Tunnel (71.294°N, 156.715°W). Fifteen block samples shaped like triangular prisms were cut along the A-A' transect, previously sampled by Meyer et al. (2010a). The sampling line was 6.2 meters long,

situated below the earlier sampling scars and above the tunnel floor. For sampling below the tunnel floor, a cordless drill with various corers, including a SIPRE corer, was used. To prevent cross-contamination, sampling tools were cleaned before each use. The methods and observations are detailed in Iwahana et al. (2021). The collected samples were labeled, packed, and kept frozen for further analysis at the University of Alaska Fairbanks.

Radiocarbon dating of macro-plant remains in the samples was conducted by Accelerator Mass Spectrometry at the University of Arizona and the National Institute for Environmental Studies, Japan. These remains were freeze-dried, washed, and analyzed using OxCal software and the IntCal20 atmospheric curve.

Result summary

Plant remains collected from the topmost sediment layer beneath the massive ground ice in the Barrow Permafrost Tunnel were dated as older than the radiocarbon dating limit. A significantly large radiocarbon age gap was found between plant remains in the massive ground ice (10–12 ka BP) and the topmost sediments (36 ka BP or older) of the underlying layer. Our confirmation of the age gaps (more than 24 ka) throughout at least a 7-m profile of the massive ground ice bottom could be attributed to the dislocation of the lower and older sediment layer due to upward thrusting at the boundary between ice and sediments while the growing ice wedge pushed the sediment sideways. Alternatively, the age gap indicates large-scale erosional events that removed the ground surface from the site before the development of Unit II with the massive ground ice at about 12–36 ka BP (14–41 cal ka BP).

Our dense sampling and radiocarbon dating of plant remains in the massive ground ice along the semi-horizontal profile in the tunnel showed several inversions and fluctuations up to about 1.5 ka within the profile. While the overall trend of the age change in the horizontal profile of the massive ice supported the ice-wedge hypothesis as the mechanism of the massive ice formation, the age resolution of the information that could be retrieved from the ice wedge might be coarser than that estimated from the previous studies considering the age inversions found in this study. Our dense radiocarbon dating of plant remains in the massive ground ice can also be interpreted as a step-wise change in the ages from one portion to another of the massive ground ice mass that coincides with a similar step-wise change in stable water isotopes. These newly interpreted distributions of the geochemistry and ages of plant remains in the massive ground ice can be explained by intermittent ice-wedge growth, a possible misalignment between sampling direction and the ice-wedge growth line, or else require the introduction of unknown processes of the ice mass development.

References

Colangelo-Lillis, J., et al. 2016. Evidence for marine origin and microbial-viral habitability of sub-zero hypersaline aqueous inclusions within permafrost near Barrow, Alaska, FEMS Microbiol Ecol, 92(5), p. fiw053. https://doi.org/10.1093/femsec/fiw053

Cooper, Z.S., et al. 2019. Distinctive microbial communities in subzero hypersaline brines from Arctic coastal sea ice and rarely sampled cryopegs, FEMS Microbiology Ecology, 95(fiz166). https://doi.org/10.1093/femsec/fiz166

Iizuka, Y., et al. 2019. Ion concentrations in ice wedges: An innovative approach to reconstruct past climate variability', Earth and Planetary Science Letters, 515, pp. 58–66. https://doi.org/10.1016/j.epsl.2019.03.013

Iwahana, G., et al. 2021. Intra-ice and intra-sediment cryopeg brine occurrence in permafrost near Utqiaġvik (Barrow), Permafrost and Periglacial Processes, 32(3), pp. 427–446. https://doi.org/10.1002/ppp.2101

Gilbert, G.L., Kanevskiy, M., and Murton, J.B. 2016. Recent advances (2008–2015) in the study of ground ice and cryostratigraphy, Permafrost and Periglacial Processes, 27(4), pp. 377–389. https://doi.org/10.1002/ppp.1912

Meyer, H., Schirrmeister, L., Andreev, A., et al. 2010a. Lateglacial and Holocene isotopic and environmental history of northern coastal Alaska - Results from a buried ice-wedge system at Barrow, Quaternary Science Reviews, 29(27–28), pp. 3720–3735. https://doi.org/10.1016/j.quascirev.2010.08.005

Meyer, H., Schirrmeister, L., Yoshikawa, K., et al. 2010b. Permafrost evidence for severe winter cooling during the Younger Dryas in northern Alaska, Geophysical Research Letters, 37, p. L03501. https://doi.org/10.1029/2009gl041013

Permafrost history in the sporadic zone as context for recent carbon loss using a cryostratigraphy, plant macrofossil, and stable isotope approach

Miriam C. Jones[1], Lesleigh Anderson[2], Eva Stephani[3] & Benjamin Jones[4]

[1]*U.S. Geological Survey Florence Bascom Science Center, Reston Virginia, United States*

[2]*U.S. Geological Survey Geoscience and Environmental Change Science Center, Denver Colorado, United States*

[3]*U.S. Geological Survey Alaska Science Center, Anchorage Alaska, United States*

[4]*University of Alaska Fairbanks, Fairbanks Alaska, United States*

Permafrost and landscape history, in addition to ground ice content, are increasingly identified as important components in predicting permafrost thaw trajectories. Together with cryostratigraphy, plant remains and stable isotopes can provide useful information about past permafrost aggradation and thaw. We applied these methods with radiocarbon dating on peat and permafrost cores in the sporadic zone on the Kenai Peninsula, Alaska, to provide a long-term framework for understanding recent thaw and implications for carbon loss.

Study Area

The Kenai Peninsula is in south-central Alaska (Figure 1). On the eastern side of the peninsula are the Kenai Mountains and the Harding icefield with glaciers terminating at or near sea-level. On the western side, in a leeward rain shadow, are lowlands characterized by a boreal forest mosaic of wetlands and kettle lakes where large glaciers coalesced. Regional mean annual temperatures exceed 0˚C and ecosystem-protected sporadic permafrost is only observed as isolated black spruce plateaus within carbon-rich peatlands, which developed following deglaciation in the late Pleistocene and early Holocene (Jones and Yu 2010). Jones et al. (2016) evaluated degrading permafrost plateaus in the Browns wetland complex from historic aerial imagery and found recent decreases in plateau extent of 60% primarily related to lateral thaw. A permafrost core was obtained from the center of a permafrost peat plateau and recently thawed collapse-scar bog for multi-proxy analyses.

Methods

The permafrost core collected from the Browns wetland complex in February 2015 with a 5-cm SIPRE core barrel was transported, stored, and sampled frozen. The permafrost core was cut into continuous 2-cm increments and analyzed for percent water by weight, percent organic matter by weight, and pore-water isotope ratios. Plant macrofossils were sampled every 10-cm for cellulose oxygen analyses. A peat core from a recently thawed area adjacent to the plateau where the 2015 permafrost core was taken was obtained in September 2019 with a Russian corer. The core was sampled continuously at 1-cm increments for organic matter content by weight and plant macrofossil analyses that were converted to organic carbon content based on a subset of CN analyses. A total of 13 radiocarbon ages were measured for select plant macrofossils for the permafrost core and 10 were measured for the collapse-scar bog core, and Bayesian methods were used to determined age-depth models for both cores.

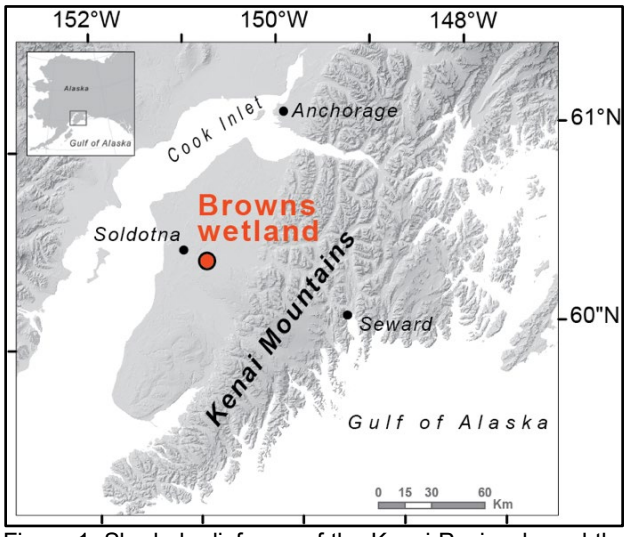

Figure 1. Shaded relief map of the Kenai Peninsula and the location of the Browns wetland complex in the western lowlands.

Results

The ~600-cm long active layer and permafrost core is primarily peat above and below a silt deposit between 290 and 390 cm depth. For the peat units, percent water and weight organic content is >95%. The silt has lower percent water (60 to 80%) and organic content (40%). The peat below the silt, which dates between 11,000 to 9500 calendar years before AD 1950 (cal yr BP) contains micro-lenticular to suspended cyrostructures and exceptionally well-preserved sphagnum and Tomenthypnum nitens moss dominates

the plant macrofossils assemblages. The permafrost peat above the silt, which spans 4500 cal yr BP to present, contains layered ice lenses and porphyritic structures and a macrofossil assemblage indicative of a rich fen peatland environment (e.g., Carex spp., Calliergon spp., Drepanocladus spp., Paludella squarrosa) that reflects early peatland succession. The plant macrofossil composition, lithostratigraphy, and age-depth model of the bog core is nearly identical to the permafrost core.

The liquid pore water isotope values are between -8 and -12 ‰VSMOW and deuterium excess (d-excess) values are between 0 and -20‰. The core values overlap the range of modern water values from the Browns wetland complex on a local evaporation line. Below the silt, $\delta^{18}O$ and $\delta^{2}H$ are relatively low (and d-excess is high) and gradually increase upcore. Immediately above the silt, $\delta^{18}O$ and $\delta^{2}H$ values are high before steady decline upcore to the base of the active layer at 50 cm depth. Values rise within the active layer to the core top. Water isotope values for each depth were used to calculate an epsilon factor derived by Lacelle et al. (2014) to trace thaw unconformities that were found to characterize the silt unit and depths above and below.

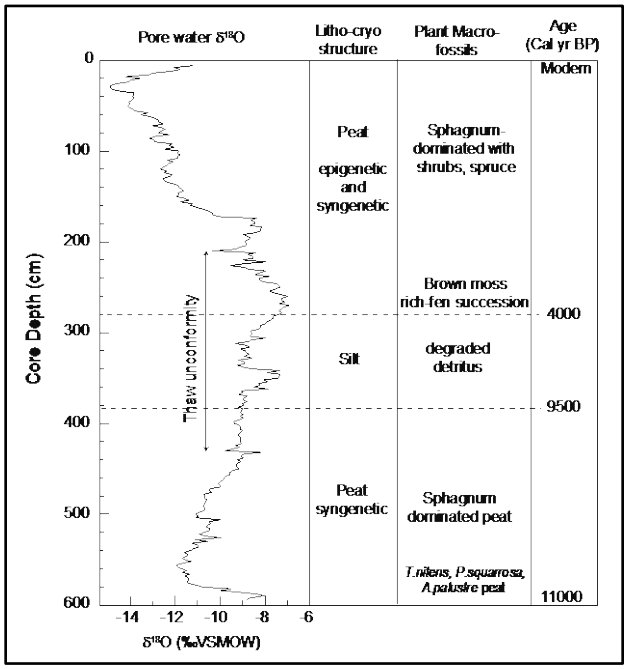

Figure 2. Summary interpretation diagram of the Browns permafrost and bog core data by depth and age range.

DISCUSSION

During the de-glacial and early Holocene, the Browns site underwent rapid peat accumulation, similar to regional patterns (Jones and Yu 2010) and syngenetic permafrost aggradation. This reflects the warming post-glacial climate with favorable growing seasons and annual average temperatures below freezing. The exceptional peat preservation and syngenetic cryostructures are supported by pore-ice oxygen and hydrogen isotope values indicative of equilibrium freezing conditions. The possibly unconformable silt unit, bracketed by peat dates of ~9500 and ~4000 cal yr BP reflects a thaw unconformity and annual temperatures above freezing. The subsequent late-Holocene peat accumulation reflects early successional, near-surface permafrost-free rich fen conditions until ~2000 cal yr BP. Epigenetic permafrost aggradation within the last ~1500 years are consistent with declines in mean annual air temperatures that reflect regional neoglacial cooling and amplification of North Pacific storm tracks and Aleutian Low strength and position.

The Holocene permafrost history of the Browns wetland complex indicates that past near-surface conditions have previously been permafrost free before permafrost re-aggraded. Similar macrofossil trends in the permafrost and thawed collapse-scar cores indicates negligible post-thaw decomposition. Thus, although the thawed portions of the permafrost plateau are currently losing surface peat (carbon) by oxidation, the Holocene permafrost history suggests that carbon loss is confined to the upper 1-2 m.

REFERENCES

Jones, M.C., and Yu, Z. 2010. Rapid deglacial and early Holocene expansion of peatlands in Alaska. Proceedings of the National Academy of Sciences, 107(16), 7347–7352.

Jones, B.M., Baughman, C.A., Romanovsky, V.E., Parsekian, A.D, Babcock, E.L., Stephani, E., Jones, M.C., Grosse, G., and Berg, E.E. 2016. Presence of rapidly degrading permafrost plateaus in south-central Alaska. The Cryosphere 10, 2673–2692.

Lacelle, D., Fontaine, M., Forest, A.P., and Kokelj, S. 2014. High-resolution stable water isotope tracers of thaw unconformities in permafrost: a case study from western Arctic Canada. Chemical Geology 368, 85–96.

Comparing gas geochemistry in the Holocene ice wedges between Zyryanka and Chokurdakh, Northeastern Siberia

Nayeon Ko[1], Hansu Park[1], Jeong-eun Kim[1], Nikolai Fedorov[1], Go Iwahana[2], Alexander Fedorov[3] & Jinho Ahn[1]

[1]*Seoul National University, Seoul, South Korea*

[2]*International Arctic Research Center (IARC), University of Alaska Fairbanks, United States*

[3]*Melnikov Permafrost Institute Siberian Branch RAS, Yakutsk, Russia*

Ice wedges are foliated ground-ice formed by repetitive infiltration of snow meltwater and/or hoarfrost into open thermal-contraction cracks. Greenhouse gases (GHGs) occluded in ice wedges recently draw attention because they may give us additional information on climate in the past and in-situ microbial metabolism within the ice wedges (Kim et al. 2019; Yang et al. 2022). Furthermore, mixing ratios of N_2/Ar and O_2/Ar of the occluded gas reflect the nature of infilling water phase and the effect of microbial respiration within ice-wedge ice, respectively.

In this study, analysis for multiple gas species was carried out to better understand the formation mechanism of the ice wedge and origin of greenhouse gas species. Compared to previous studies, this work takes an advantage of simultaneous analyses of three species of GHGs (CO_2, CH_4 and N_2O) and Ar-O_2-N_2 gas for the same single ice wedge subsamples. This procedure can help avoid bias from inhomogeneous distribution of chemicals and consequently better constrain the ice wedge formation process.

Geochemical study was conducted on ice wedge samples from Zyryanka and Chokurdakh, northeastern Siberia (Figure 1). Zyryanka is at 65°93′N, 150°89′E and located in the southern boreal region of the Kolyma River. Chokurdakh is located inland approximately 150 km from the Arctic sea coast, positioned at 70°56′N, 147°43′E, along the Indigirka River (Iwahana et al. 2014).

The primary difference between the two ice wedge samples lies in their geographical placement. The Zyryanka ice wedge is situated within a more inland region, whereas the Chokurdakh ice wedge is positioned closer to the sea coast. We have paid attention to understanding how these different conditions of formation might influence the physical and chemical composition of the ice wedge.

Assuming the atmospheric gas was equilibrated with liquid water at 0°C, δ(N_2/Ar) and δ(O_2/Ar) values in the occluded gas in ice wedges can be approximate -55.5% and -8.97%, respectively if the ratios did not change during freezing when the ice wedges formed. On the other hand, if ice wedge formed by either dry snow accretion or hoarfrost growing rather than meltwater freezing, both δ(N_2/Ar) and δ(O_2/Ar) should be close to the atmospheric value of 0 %.

δ(N_2/Ar) value of Zyryanka ice wedge ranges -17.5 ~ -3.5 %, which is less than zero in all samples (Figure 2). This results indicate that ice wedge was formed by mixing of liquid water and dry snow. δ(O_2/Ar) values exhibit a range from -72.8 to -37.6 %, implying that O_2 has partially been consumed within the ice. For the soils adjacent to ice wedge, δ(N_2/Ar) values range from -43.9 to -1.8 % and δ(O_2/Ar) shows a lower value range of -99.1 to -83.1 %.

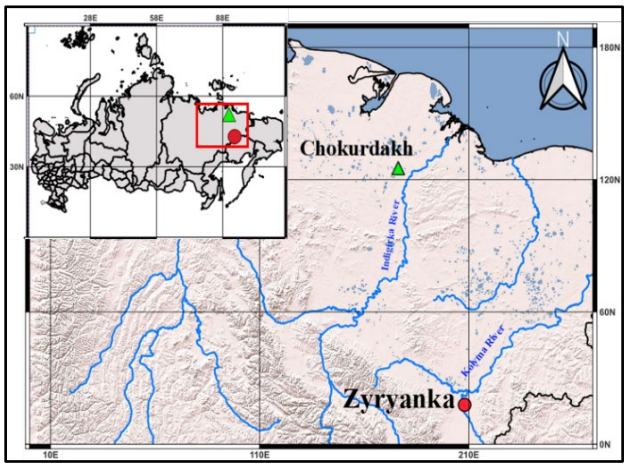

Figure 1. Map of the Zyryanka and Chokurdakh sampling site in Northeastern Siberia, Russia. The red box in the small insert map on the upper left shows the location of Zyryanka (red circle) and Chokurdakh (green triangle).

On the other hand, the Chokurdakh ice wedge shows that the δ(N2/Ar) value ranges from -3.5 ~ 2.4%, clearly surpassing the value of Zyryanka ice wedge and closer to atmospheric value of 0 %. This finding suggests that this ice wedge was dominantly formed by dry snow compaction. Additionally, δ(O2/Ar) ratios ranged from -97.8 ~ -79.2 % indicate near-complete consumption of oxygen within the ice wedge.

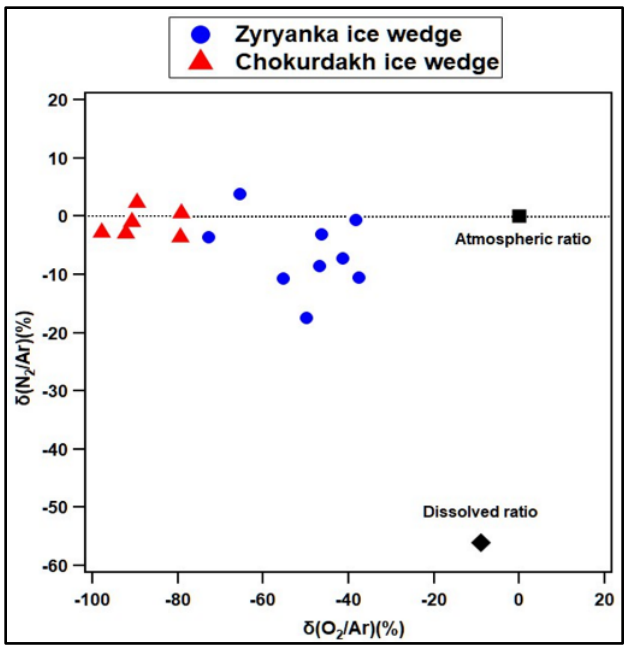

Figure 2. $\delta(N_2/Ar)$ and $\delta(O_2/Ar)$ mixing ratios of Zyryanka and Chokurdakh ice wedges. Blue circles and red triangles indicate Zyryanka and Chokurdakh ice wedges, respectively.

For the greenhouse gases(GHGs) composition (Figure 3), We observed that three GHG species (CO_2, CH_4, N_2O) of the trapped gas within both the Zyryanka and Chokurdakh ice wedges were significantly higher than those of the Holocene atmospheric level.

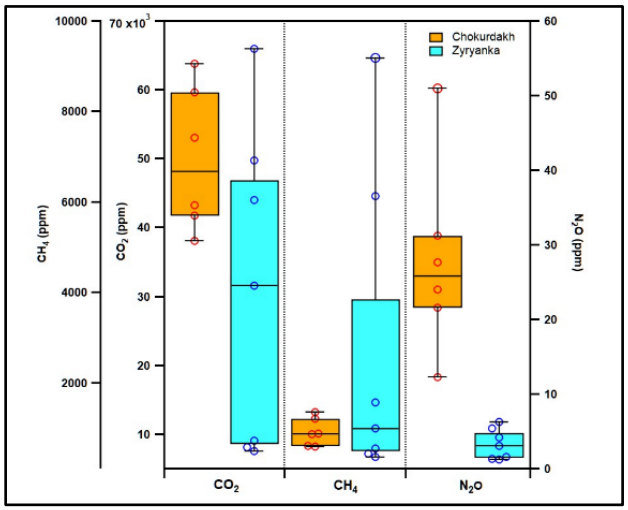

Figure 3. Boxplot of CO_2, CH_4 and N_2O mixing ratios of the Zyryanka and Chokurdakh ice wedges. Sky blue and orange colors are for Zyryanka and Chokurdakh ice wedges, respectively. The open circle symbol represents each measured data.

For the Zyryanka, the gas mixing ratios show a range of 0.76 to 6.60 % for CO_2, 356 to 9178 ppm for CH_4 and 1.25 to 6.26 ppm for N_2O, respectively. On the other hand, Chokurdakh exhibits ranges of 3.81 to 6.38 % for CO_2, 591.50 to 1355.20 ppm for CH_4 and 12.30 to 50.99 ppm for N_2O, respectively.

For the comparison between Zyryanka and Chokurdakh ice wedge, it is observed that slightly higher CO_2 compositions in Chokurdakh ice wedge. In addition to that, the Chokurdakh samples show a N_2O composition roughly one order of magnitude higher than that of Zyryanka samples. However, the Zyryanka ice wedge shows a CH_4 composition approximately twice that of the Chokurdakh sample.

In these results, it can be inferred that disparate regional environmental factors likely influenced the GHG compositions within the ice wedge, even if they were formed during the same geological period.

Future research may include the comparison of stable water isotope ratios within these two ice wedge samples, aiming to provide a more specific assessment and clarification regarding their origins.

References

Iwahana, G., Takano, S., Petrov, R.E., Tei, S., Shingubara, R., Maximov, T.C., Fedorov, A.N., Desyatkin, A.R., Nikolaev, A.N., Desyatkin, R.V., and Sugimoto, A. 2014. Geocryological characteristics of the upper permafrost in a tundra-forest transition of the Indigirka River Valley, Russia. Polar Science, 8(2), 96–113. https://doi.org/10.1016/j.polar.2014.01.005

Kim, K., Yang, J.W., Yoon, H., Byun, E., Fedorov, A., Ryu, Y., and Ahn, J. 2019. Greenhouse gas formation in ice wedges at Cyuie, central Yakutia. Permafrost and Periglacial Processes, 30(1): 48–57. https://doi.org/10.1002/ppp.1994

Yang, J., Ahn, J., Iwahana, G., Ko, N., Kim, J., Kim, K., Fedorov, A., and Han, S. 2022. Origin of CO_2, CH_4, and N_2O trapped in ice wedges in central Yakutia and their relationship. Permafrost and Periglacial Processes, 34(1): 122–141. https://doi.org/10.1002/ppp.2176

Permafrost aggradation and intra-permafrost processes in Svalbard using ground ice chemistry and radium isotopes

Dotan Rotem[1,2], Vladimir Lyakhovsky[3], Hanne Hvidtfeldt Christiansen[2], Yehudit Harlavan[3] & Yishai Weinstein[1]

[1]*Department of Environment, Planning and Sustainability, Bar-Ilan University, Ramat-Gan, 529002, Israel*

[2]*Arctic Geophysics Department, The University Centre in Svalbard, UNIS, N-9171 Longyearbyen, Norway*

[3]*Geological Survey of Israel, 32 Yesha'yahu Leibowitz, Jerusalem 9692100, Israel*

Svalbard is located in the continuous permafrost region (Obu et al. 2019). Deglaciation in Svalbard was followed in Early Holocene by seawater ingression and deposition of marine (deltaic) sediments in fjord valleys, while isostatic elastic rebound resulted in fast land uplift and the exposure of these sediment to the atmosphere (Forman et al. 2004). This was followed by epigenetic permafrost formation. Finally, alluvial and aeolian sediments were deposited during the Late Holocene, and they then underwent syngenetic permafrost aggradation (Gilbert et al. 2018).

We studied the chemistry and Ra isotopes in the ground ice of two permafrost cores, from the eastern end of the lower part of Adventdalen Valley, central Svalbard to get an insight into permafrost formation processes. The site is located 10 km from the local fjord, within the limits of post-deglaciation seawater ingression (Lønne and Nemec 2004). Chemistry analyses of the first core, retrieved in 2017 (ADE-17), showed that the ground ice in the syngenetic part of the profile is basically fresh. The epigenetic part demonstrates a frozen fresh-saline water interface (FSI), with chloride concentrations increasing from the top of the epigenetic part (at 5.5 m depth) to about 15% that of seawater at 11 m depth, and major elements ratios significantly different from that of seawater, indicating water-rock interaction.

We applied a one-dimensional freezing model to examine the rate of top-down permafrost formation, which could accommodate the observed saline ground ice at the top of the epigenetic section. The model examined permafrost development under different scenarios of mean average air temperature (MAAT), water-freezing temperature (WFT) and the degree of pore-water freezing. We found that even at relatively high air temperatures during Early to mid-Holocene of -4 °C (Park et al. 2019), permafrost could aggrade down to 20 to 37 m within 200 years (Figure 1a). This could prohibit flushing of the sub-surface freezing and the preservation of saline water despite the relatively fast rebound rate. Permafrost aggradation rate could even be enhanced if pore water freezing was not complete (Figure 1b), which is often observed in Adventdalen (Keating et al. 2018; Rotem et al. 2023). We conclude that freezing must have started immediately after the exposure of the marine sediment to atmospheric conditions, in the mid-Holocene.

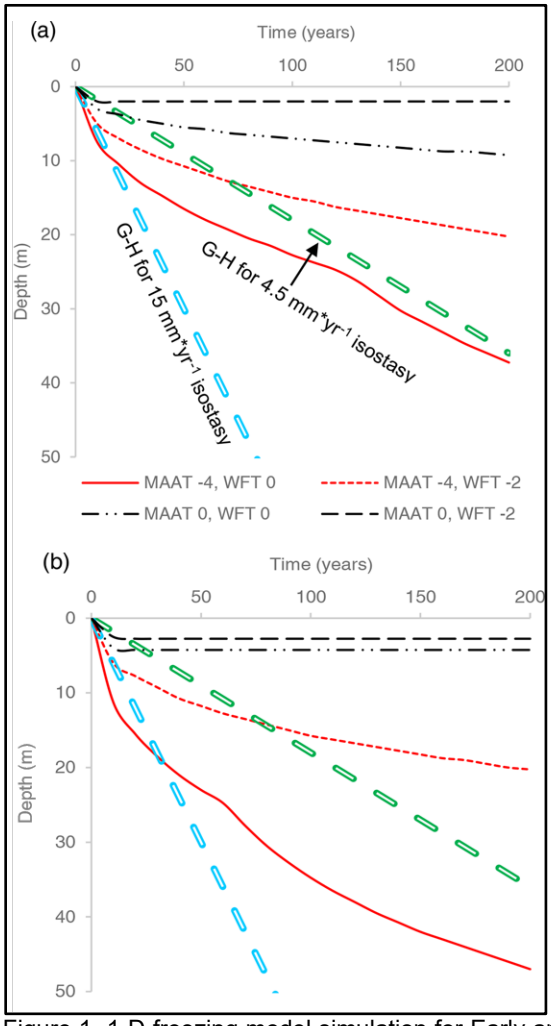

Figure 1. 1-D freezing model simulation for Early and mid-Holocene for the first 200 years with MAAT -4 °C and 0 °C; WFT of 0 and -2 °C. (a) 100% freezing, (b) 25% freezing. Also shown are curves of two scenarios of corresponding depths of the fresh-saline water interface, using a 1:40 Ghyben-Hertzberg (G-H) approximation for isostasy of 4.5 and 15 mm y^{-1}.

Another core (ADE-2) was retrieved in 2022, 30 m from ADE-17. In this case, the ground ice of the epigenetic section shows chloride concentrations up to 40% that of seawater, with no salinity gradient (FSI) and major elements ratios similar to seawater.

Long to short-lived Ra isotope ratios (e.g. $^{226}Ra/^{223}Ra$) in the ground ice of the two boreholes are also significantly different. While in ADE-17 ratios are similar to or exceeding the expected seqular equilibrium of 21.7 (the natural radioactive parents $^{238}U/^{235}U$ ratio), ratios at ADE-2 are <0.5 that of secular equilibrium (Figure 2). This indicates large local variability in the residence time of ground ice (i.e. the time since freezing) within tens of meter. While ground ice at ADE-17 could be several thousands of years old (considering the 1600 yr half-life of ^{226}Ra), the ground ice at ADE-2 could not be much older than 1,000 years. Together, the differences in chemistry and residence time suggest that the ADE site experienced a local saline water intrusion within the last ~1,000 years, which did not manage to react much with the sediment. The source of this water (seawater, deep old brines, other) should be further studied.

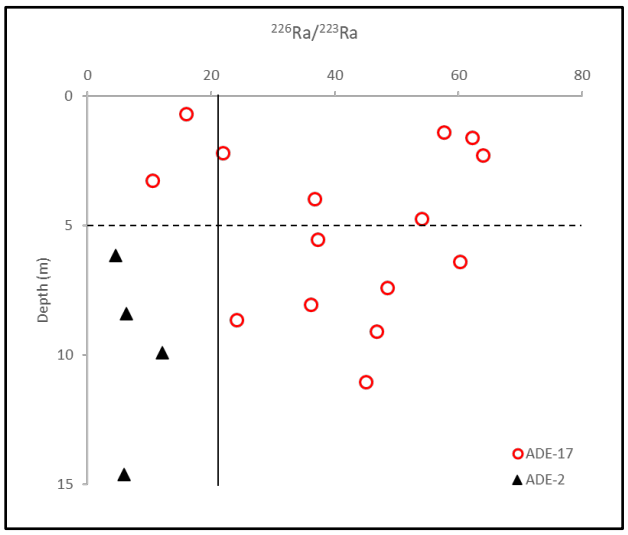

Figure 2. Ra isotopes ratios for two cores 30 m apart in Adventdalen. Dashed line indicate transition between syngenetic and epigenetic permafrost, following Gilbert et al. 2018. Vertical line indicates secular equilibrium of $^{235}U/^{238}U$ parents of $^{226}Ra/^{223}Ra$. Zero depth indicates permafrost table.

REFERENCES

Forman, S., Lubinski, D., Ingólfsson, Ó., Zeeberg, J., Snyder, J., Siegert, M., and Matishov, G. 2004. A review of postglacial emergence on Svalbard, Franz Josef Land and Novaya Zemlya, northern Eurasia, Quaternary Science Reviews, 23(11-13): 1391–1434. https://doi.org/10.1016/j.quascirev.2003.12.007

Gilbert, G.L., Nemec, W., Thiel, C., Christiansen, H.H., and Buylaert, P. 2018. Late Quaternary sedimentation and permafrost development in a Svalbard fjord-valley, Norwegian high Arctic, Sedimentology, 65(7): 2531–2558. https://doi.org/10.1111/sed.12476

Keating, K., Binley, A., Bense, V., Van Dam, R.L., and Christiansen, H.H. 2018. Combined Geophysical Measurements Provide Evidence for Unfrozen Water in Permafrost in the Adventdalen Valley in Svalbard, Geophysical Research Letters, 45(15): 7606–7614. https://doi.org/10.1029/2017GL076508

Lønne, I., & Nemec, W. 2004. High-arctic fan delta recording deglaciation and environment disequilibrium, Sedimentology, 51(3): 553–589. https://doi.org/10.1111/j.1365-3091.2004.00636.x

Obu, J., Westermann, S., Bartsch, A., Berdnikov, N., Christiansen, H.H., Dashtseren, A., Delaloye, R., Elberling, B., Etzelmüller, B., Kholodov, A., Khomutov, A., Kääb, A., Leibman, M.O., Lewkowicz, A.G., Panda, S.K., Romanovsky, V., Way, R.G., Westergaard-Nielsen, A., Wu, T., Yamkhin, J., and Zou, D. 2019. Northern Hemisphere permafrost map based on TTOP modelling for 2000–2016 at 1 km2 scale, Earth-Science Reviews, 193, 299–316. https://doi.org/10.1016/j.earscirev.2019.04.023

Park, S., Kim, J., Stewart, A.L., Son, W., and Seo, H. 2019. Mid-Holocene Northern Hemisphere warming driven by Arctic amplification, Science Advances. 5(12). https://doi.org/aax8203

Rotem, D., Lyakhovsky, V., Christiansen, H.H., Harlavan, Y., and Weinstein, Y. 2023. Permafrost saline water and Early to Mid-Holocene permafrost aggradation in Svalbard, The Cryosphere, 17(8): 3363–3381. https://doi.org/10.5194/tc-17-3363-2023

Yedoma and muck – New cryolithological studies of permafrost deposits in the Klondike Goldfields (Central Yukon, Canada)

Lutz Schirrmeister[1], Thomas Opel[2], Fabian Seeman[1], Trevor Porter[3], Jens Strauss[1], Hanno Meyer[2] & Duane Froese[4]

[1]*Permafrost Research Section, Alfred Wegener Institute for Polar and Marine Research, Bremerhaven, Germany*

[2]*Polar Terrestrial Environmental Systems, Alfred Wegener Institute for Polar and Marine Research, Bremerhaven, Germany*

[3]*Department of Geography, Geomatics and Environment, University of Toronto, Toronto, Ontario, Canada*

[4]*Department of Earth and Atmospheric Sciences, University of Alberta, Edmonton, Alberta, Canada*

Over the last 25 years, Canadian scientists have studied the permafrost environmental archives in the Klondike Goldfields south of Dawson City (e.g., Fraser and Burn 1997; Kotler and Burn 2010; Froese et al. 2009; Porter et al. 2016; Monteath et al. 2023). In 2023, a small Canadian-German team visited this area to sample mining exposures in the Klondike area (Figure 1). The goal was to conduct studies on ground ice (ice wedges and pore ice) and frozen sediments to reconstruct past landscape and climate conditions. Detailed profiles were sampled at three sites Little Blanche Creek, Whitman Gulch and Bear Creek (Figure 1).

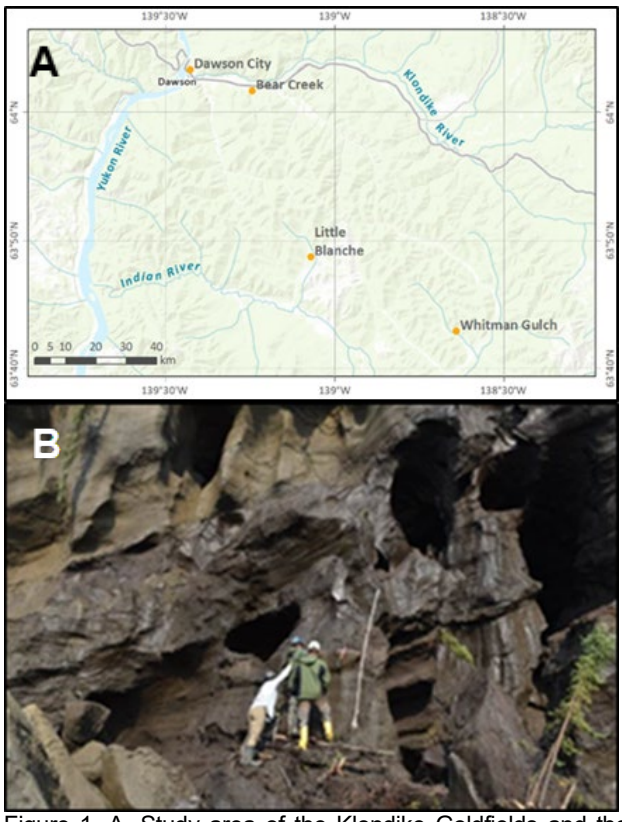

Figure 1. A. Study area of the Klondike Goldfields and the study sites. B. Study site at Whitman Gulch.

Ice wedges were described in terms of their size, the color of ice, internal structure, existence and form of gas bubbles and were sampled by chain saw as blocks. The frozen sediment was cleaned, and ice, sediment and cryostructures were described, followed by sediment sampling with an axe and hammer. Separately, sediment cores were collected with a battery driven drill for biomarker studies.

In our presentation, we present the first results of new field and laboratory studies. This concerns age determinations, sediment data, stable isotopes and hydrochemistry of the ground ice. The mean ice content measured was 38 ± 10 wt% (Figure 2).

We expect new knowledge regarding the reconstruction of Late Quaternary environment of Central Yukon.

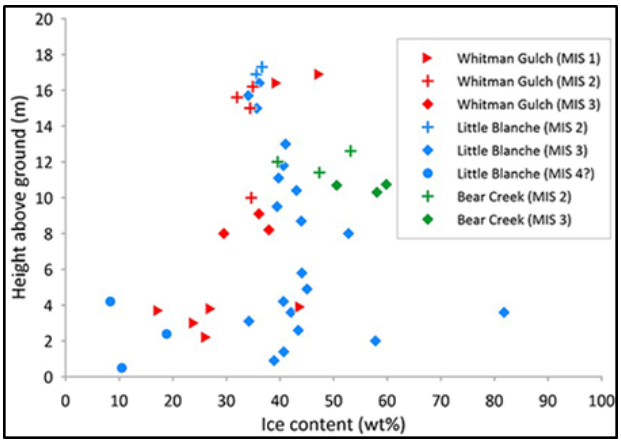

Figure 2. Gravimetric ice contents of permafrost samples with tentative age attribution from the three study sites measured in the field in 2023.

References

Fraser, T.A., and Burn, C.R. 1997. On the nature and origin of "muck" deposits in the Klondike area, Yukon Territory, Canadian Journal of Earth Sciences 34(10), 1333–1344. https://doi.org/10.1139/e17-106

Froese, D., Zazula, G., Westgate, J., Preece, S., Sanborn, P.A., Reyes, A., and Pearce, N. 2009. The Klondike goldfields and Pleistocene environments of Beringia, GSA Today, 19, 4–10. https://doi.org/10.1130/GSATG54A.1

Kotler, E., and Burn, C.R. 2000. Cryostratigraphy of the Klondike "muck" deposits, west-central Yukon Territory, Can. J. Earth Sci., 37, 849–861. https://doi.org/10.1139/e00-013

Monteath, A.J., Kuzmina, S., Mahony, M., Calmels, F., Porter, T., Mathewes, R., Sanborn, P., Zazula, G., Shapiro, B., Murchie, T.J., Poinar, H.N., Sadoway, T., Hall, E., Hewitson, S., and Froese, D. 2023. Relict permafrost preserves megafauna, insects, pollen, soils and pore-ice isotopes of the mammoth steppe and its collapse in central Yukon, Quaternary Science Reviews, 299, 107878. https://doi.org/10.1016/j.quascirev.2022.107878

Porter, T.J., Froese, D.G., Feakins, S.J., Bindeman, I.N., Mahony, M.E., Pautler, B.G., Reichart, G.J., Sanborn, P.T., Simpson, M.J., and Weijers, J.W.H. 2016. Multiple water isotope proxy reconstruction of extremely low last glacial temperatures in Eastern Beringia (Western Arctic), Quaternary Science Reviews, 137, 113–125. https://doi.org/10.1016/j.quascirev.2016.02.006

Role of retrogressive thaw slumps in release of sulfur into the environment and biosphere

Rhiannon E. Stevens[1], Simon H. Bottrell[2], Hazel Reade[1], Delphine Frémondeau[1] & Julian B. Murton[3]

[1]*UCL Institute of Archaeology, 31–34 Gordon Square, London, WC1H 0PY, United Kingdom*

[2]*School of Earth and Environment, University of Leeds, Leeds LS2 9JT, United Kingdom*

[3]*Permafrost Laboratory, Department of Geography, University of Sussex, Brighton BN1 9QJ, United Kingdom*

Recently, a high-magnitude Late Pleniglacial Sulfur Excursion (LPSE) has been reported in faunal δ34S values in Eurasia (Stevens et al. 2023). This LPSE is geographically widespread and is several orders of magnitude larger than could be caused by changing animal origins or diet, signalling that continental-scale environmental processes caused the LPSE. We argue that the LPSE is driven by a major change in the terrestrial sulfur cycle, which in this context relates to changing permafrost conditions. This high-magnitude excursion in faunal $\delta^{34}S$ values between approximately 30 and 15 kyr BP in some regions of Eurasia. This time period corresponds to the latter part of the last ice age and covers much of Marine Isotope Stage 2 (MIS 2, ~29–11.7 kyr BP), including the Last Glacial Maximum (LGM, ~26.5–19 kyr BP). The LPSE occurs in multiple species with differing dietary niches and mobility behaviours, suggesting that the signal is not driven by species-based differences. The magnitude of the LPSE is substantial (10 to 20 or more ‰), at least double that typically considered to indicate location-based differences. This suggests that underlying continental-scale environmental processes substantially impacted upon the terrestrial sulfur biogeochemical cycle during the Late Pleistocene.

Of four potential drivers of the LPSE, permafrost development and thaw are provisionally considered the most important. The LPSE is observed exclusively in regions where permafrost (or ice sheets / alpine glaciers) was present during the LGM but are now permafrost-free. Furthermore, the high-magnitude excursions appear to coincide with the suspected timing of regional permafrost development and thaw in NW and central Europe. Crucially, the LPSE is not observed in temporally comparable data from regions of Eurasia, where permafrost is present today and has persisted throughout the Late Pleistocene, nor in regions where permafrost was absent over the last 50 kyr. So far the LPSE is only observed in regions where permafrost developed and thawed during the last 50,000 years.

Several processes during permafrost growth and thaw have been shown to influence sulfur isotopes in alternative settings, but a key question remains as to the processes involved in the LPSE. Retrogressive thaw slumps are known to affect the hydrology and hydrochemistry of the catchments in which they occur (Kokelj et al. 2005; Tank et al. 2020) and can be associated with significant release of sulfate into the environment (Malone 2013; Kokelj et al. 2013). They thus represent an environment in which sulfur could be transferred from permafrost substrate to biosphere and thus a potential mechanism for (part of) the changes observed in the LPSE.

This Abstract discusses the results of sampling of thaw slump sites developed on different substrates. Sulfur concentration and isotopic data are compared between: sediment substrate, soil samples from slumped sites and soil samples at adjacent control sites. Where possible sulfate concentrations and sulfur isotopic compositions of drainage waters were also measured.

Samples were collected from retrogressive thaw slumps formed in different substrates on a N-S transect across Canadian permafrost from the Arctic Ocean coast near Tuktoyaktuk, NT, to southern Yukon and analyzed for content and sulfur isotopic composition of extractable sulfate and sulfide and concentration and sulfur isotopic composition of surface drainage where present. At Peninsula Point, on the coast, the superficial deposit is mapped as Toker Point Member till beneath rolling moraine (Rampton 1987). This till has isotopically light sulfide (0.05 to 1.83 mg/g, -7 to -25‰) with quite high concentrations of isotopically similar sulfate in the exposed section (presumably due to weathering of sulfide). At the control site mineral soils have sulfide 0.13 to 11.8 mg/g and light isotopes consistent with till substrate compositions and have very low sulfate (mean 0.007 mg/g, range 0 to 0.016). The soil organic fraction has 1.48 mg/g S and is heavier ($\delta^{34}S$ = -3.07‰) likely due to uptake of isotopically heavy sea-spray sulfur at this coastal site. Slumped till shows significantly elevated sulfate (320 mg/g) and waters draining slumps show elevated sulfate (1200 to 1300 mg/L); in both cases sulfur isotopes range from -20 to -34‰, consistent with the range in till substrate). A second slump on the Toker Point Member till, 4.5 km due west of Noell Lake, shows very similar characteristics with very low sulfate in mineral soil at

the control site, despite containing sulfide that has light sulfur isotopes (-11 to -14‰) consistent with the range of till substrate compositions here (-11 to -21‰), but this site is distant from the ocean and the soil organic fraction has 1.34 mg/g S and $\delta^{34}S$ = -12‰, consistent with derivation of S solely from the mineral soil below. Slumped till shows significantly elevated sulfate (1.0, 0.24 mg/g; -25 to -33‰) the very light isotopes, consistent with the sulfide in these soils. Waters draining slumps show elevated sulfate (1500 to 1900 mg/L) with very light sulfur isotopes (-27.4 to -28.8‰, consistent with the light end of the range in till substrate.

On the Peel Plateau the substrate is Late Wisconsin (MIS 2) till (Kokelj et al. 2017). Control site mineral soils both have sulfide 0.14 mg/g and light isotopes (-14, -17‰) and again have very low sulfate (0.002 and 0.009 mg/g). Soil organic fraction has 1.22 mg/g S and $\delta^{34}S$ = -10.5‰, consistent with derivation from sulfide in the mineral soil. Slumped till shows significantly elevated sulfate (0.25 mg/g) with very light isotopes (-26.9‰) and the water draining the slump shows elevated sulfate (820 mg/L) with very light sulfur isotopes (-23.5‰), consistent with oxidation of sulfide in the slumped soils ($\delta^{34}S$ = -32.6‰).

Two sites sampled in the Klondike are formed on a substrate of silt, silty fine sand, and sandy silt that tends to be rich in organic material, and collectively is termed 'muck'. Muck substrate contains sulfide and sulfate, both with S isotopic compositions close to 0‰. Control soils contain low concentrations of sulfate that generally reflect the isotopic composition of S in the substrate. Despite the presence of sulfide in the substrate there is little elevation of sulfate concentration in slumped soils or slump drainage. Potentially the presence of a high organic concentration in the muck substrate may inhibit oxidation of sulfide during slumping.

In the Takhini valley of southern Yukon the substrate comprises ice-rich glaciolacustrine silt and clay deposited in Glacial Lake Champagne during deglaciation ~10 – 9 ka (Calmels et al. 2021). The substrate here is low in sulfide compared to NWT till sites (max 0.053 mg/g, -11.6‰). Control soil has low sulfate and somewhat light isotopes – this sulfate and that in the substrate is consistent isotopically with oxidation of the small amount of sulfide in substrate. Slumps have low soil sulfate (and very low sulfide concentrations) and drainage has little elevation of sulfate concentration; in both cases sulfate isotopes are consistent with oxidation of the small amount of sulfide in the substrate.

Clearly substrate type exhibits a major control on the release of sulfur from substrate to environment during slumping. Formation of sulfate by sulfide oxidation is prevalent during slumping in sulfide-rich and organic-poor till materials but suppressed in the "muck" substrate of the Klondike slumps, likely because the high organic content maintains a more reducing environment. The Takhini valley substrate contains little sulfide (or sulfate) for release. Ongoing analyses will examine the relationships between the isotopic composition of the substrate and that of the main plant species growing in the slumps and available for herbivore grazing or browsing, and how these relationships may be modified by permafrost thaw relating to slumping.

REFERENCES

Calmels F., Roy, L.P., Laurent, C., Amyot, F., Cubley, J., and Lipovsky, P. 2021. Assessment and monitoring of a new retrogressive thaw slump at km 1456 of the Alaska Highway: a rare opportunity. YukonU Research Centre, Yukon University, 72 pp.

Kokelj, S.V., Jenkins, R.E., Milburn, D., Burn, C.R., and Snow, N. 2005. The influence of thermokarst disturbance on the water quality of small upland lakes, Mackenzie Delta Region, Northwest Territories, Canada. Permafrost and Periglacial Processes 16, 343–353.

Kokelj, S.V., Tunnicliffe, J.F., and Lacelle, D. 2017. The Peel Plateau of Northwestern Canada: an ice-rich hummocky moraine landscape in transition. In: O. Slaymaker (ed.), Landscapes and Landforms of Western Canada, World Geomorphological Landscapes. DOI:10.1007/978-3-319-44595-3_7

Malone, L. 2013. Impacts of retrogressive thaw slumps on the geochemistry of permafrost catchments, Stony Creek Watershed, NWT. MSc thesis, University of Ottawa.

Rampton, V.N. 1987. Surficial geology, Tuktoyaktuk Coastlands, Northwest Territories. Geological Survey of Canada, Map 1647A, scale 1:500 000.

Stevens, R.E., et al. 2023. Major excursions in sulfur isotopes linked to permafrost change in Eurasia during the last 50,000 years. Nature Geoscience preprint. https://doi.org/10.21203/rs.3.rs-2556240/v1

Tank, S.E., Vonk, J.E., Walvoord, M.A., McClelland, J.W., Laurion, I., and Abbott, B.W. 2020. Landscape matters: predicting the biogeochemical effects of permafrost thaw on aquatic networks with a state factor approach. Permafrost and Periglacial Processes 31(3), 358–370.

Major excursions in sulfur isotopes linked to permafrost changes in Eurasia during the last 50,000 years

Rhiannon E. Stevens[1], Hazel Reade[1], Julian B. Murton[2], Delphine Frémondeau[1] & Simon H. Bottrell[3]

[1]*UCL Institute of Archaeology, 31–34 Gordon Square, London, WC1H 0PY, United Kingdom*

[2]*Permafrost Laboratory, Department of Geography, University of Sussex, Brighton BN1 9QJ, United Kingdom*

[3]*School of Earth and Environment, University of Leeds, Leeds LS2 9JT, United Kingdom*

Sulfur isotope values ($\delta^{34}S$) of skeletal collagen are typically used as a tracer of animal living environment and diet. Studies use faunal $\delta^{34}S$ values either as a geolocator (because bioavailable sulfur varies spatially in relation to lithology and proximity to the ocean) or as a dietary indicator (because marine and terrestrial resources have relatively distinct $\delta^{34}S$ values). In both applications, animal and human $\delta^{34}S$ values are attributed to one or more sources, each with static sulfur isotope ratios. But this ignores potential temporal changes in biogeochemical sulfur cycling and associated fractionations.

Here we report a high-magnitude Late Pleniglacial Sulfur Excursion (LPSE) in faunal $\delta^{34}S$ values in Eurasia. We find that the LPSE is geographically widespread and is several orders of magnitude larger than could be caused by changing animal origins or diet, signalling that continental-scale environmental processes caused the LPSE. We argue that the LPSE is driven by a major change in the terrestrial sulfur cycle, which in this context relates to changing permafrost conditions. Our findings indicate animal $\delta^{34}S$ values may reflect local hydrological conditions, complicating the use of $\delta^{34}S$ values as a tool for food origin, animal migration, and archaeological palaeodiet and mobility research.

A total of 796 $\delta^{34}S$ isotope analyses was obtained from Late Pleistocene and Holocene fauna from Eurasia (Figure 1: 510 new and 286 collated from published literature). New accelerator mass spectrometry (AMS) radiocarbon determinations are reported for 25 samples, and 666 of the samples had previously been AMS dated.

Our results show a very high-magnitude excursion in faunal $\delta^{34}S$ isotope values between approximately 30 and 15 kyr BP in some regions of Eurasia (Figure 1). This time period corresponds to the latter part of the last ice age and covers much of marine isotope stage 2 (MIS 2, ~29–11.7 kyr BP), including the Last Glacial Maximum (LGM, ~26.5–19 kyr BP). The LPSE is particularly pronounced in regions where we have good temporal coverage within a discrete geographic area, such as in Britain and Belgium, and is also evident in other regions, such as central Europe north of the Alps. The LPSE occurs in multiple species with differing dietary niches and mobility behaviours, suggesting that the signal is not driven by species-based differences (Figure 1). The magnitude of the LPSE is substantial, at least double that typically considered to indicate location-based differences. This suggests underlying continental-scale environmental processes substantially impacted upon the terrestrial sulfur biogeochemical cycle during the Late Pleistocene.

Of several potential drivers of the LPSE, permafrost development and thaw are provisionally considered the most important. The LPSE is observed exclusively in regions where permafrost (or ice sheets / alpine glaciers) was present during the LGM but are now permafrost-free (Figure 1). Furthermore, the high-magnitude excursions appear to coincide with the suspected timing of regional permafrost development and thaw in NW and central Europe. Crucially, the LPSE is not observed in temporally comparable data from regions of Eurasia, where permafrost is present today and has persisted throughout the Late Pleistocene, nor in regions where permafrost was absent over the last 50 kyr (Figure 1). So far the LPSE is only observed in regions where permafrost developed and thawed during the last 50,000 years.

Several processes during permafrost growth and thaw have been shown to influence sulfur isotopes in alternative settings. Permafrost growth prevents or severely limits weathering of bedrock and sediments, limiting sulfide inputs until the active layer deepens sufficiently or until permafrost thaws. Alternative sources of sulfide are, however, likely to have become available due to permafrost growth. Permafrost exerts substantial control on hydrological processes across landscapes and impedes drainage. This can result in persistent or periodic waterlogged, anoxic soil conditions. Such conditions are known to alter soil redox status and result in the production and accumulation of sulfides as the end product of dissimilatory sulfate reduction (DSR) by bacteria and archaea which use sulfate as an electron recipient for redox reactions. This process can produce significant (–46 to –40‰) isotopic fractionation due to strong discrimination against ^{34}S. Some of these sulfides are re-oxidised to sulfate and can be taken up directly by plants. As minimal isotopic fractionation occurs with re-

oxidisation the sulfate produced is isotopically light, resulting in very low plant $\delta^{34}S$ values. In addition, the ^{34}S-depleted sulfides can be taken up directly by plants if they can tolerate sulfide toxicity or if they are able to re-oxidise the sulfides to SO_4^{2-} through transporting oxygen to their roots. Permafrost thaw and thermokarst activity also have a significant impact on hydrological processes across landscapes. Initially thermokarst can result in widespread soil waterlogging (anaerobic conditions) during thaw of fine-grained and poorly drained ice-rich soils, and then as the active layer deepens and permafrost disappears drainage improves resulting in a return to well-drained soils (aerobic conditions). Active-layer deepening can also introduce into newly thawed soils fresh sulfides from increased weathering of previously frozen sediments and bedrock.

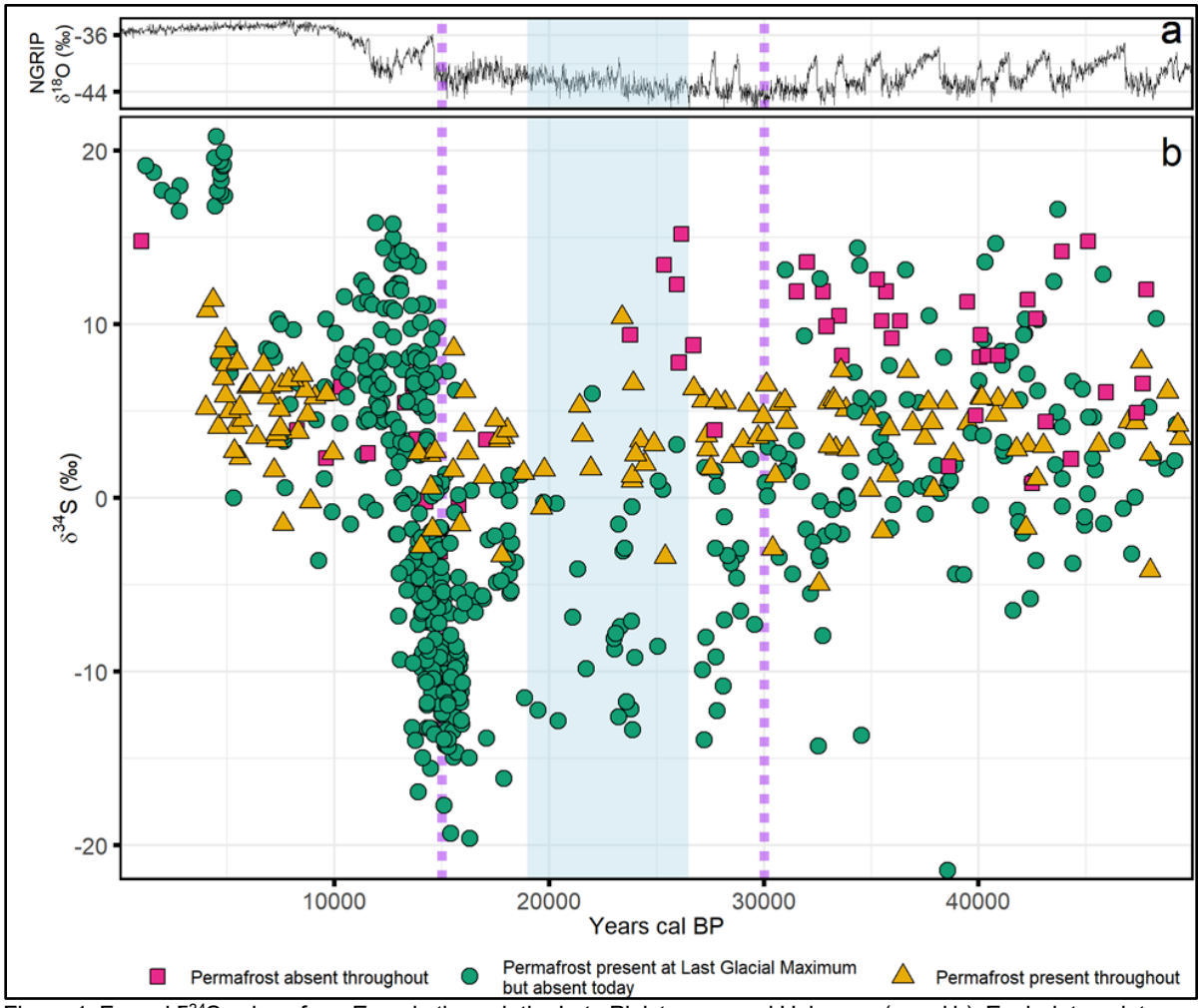

Figure 1. Faunal $\delta^{34}S$ values from Eurasia through the Late Pleistocene and Holocene (panel b). Each data point represents a single animal specimen that has been directly radiocarbon dated. Panel a shows the Greenland ice-core oxygen isotope record (NGRIP 2004), a proxy for global temperature. Shaded blue area indicates approximate duration of the Last Glacial Maximum. The dashed purple lines indicate the approximate timing of continuous permafrost development (~30 kyr BP) and thaw (~15 kyr BP) in western Eurasia. Pink squares = samples collected from regions where no permafrost was present during the last 50,000 years. Green circles = samples collected from areas that either had permafrost present at the LGM or were under ice sheets/glaciers at the LGM, but where permafrost/ice is absent today. Yellow triangles = samples collected from regions in which permafrost has been present throughout the past 50,000 years.

Reference

North Greenland Ice Core Project members. 2004. High-resolution record of Northern Hemisphere climate extending into the last interglacial period, Nature 431, 147–151. https://doi.org/10.1038/nature02805

Yedoma distribution in Arctic Alaska

Aleksandra Veremeeva[1], Benjamin Jones[2], Mikhail Kanevskiy[2], Yuri Shur[2] & Guido Grosse[1]

[1]*Alfred Wegener Institute Helmholtz Centre for Polar and Marine Research, Potsdam, Germany*

[2]*Institute of Northern Engineering, University of Alaska Fairbanks, Fairbanks, United States*

One of the most vulnerable permafrost regions under the global climate warming are unique landscapes formed by late Pleistocene ice-rich Yedoma Ice Complex which are widespread in unglaciated arctic lowlands of NE Eurasia, Alaska and NW Canada (Strauss et al. 2021). A specific characteristic of the Yedoma is the presence of large polygonal ice wedges, which may comprise up to 60-80% by volume of the entire deposit. This high ice content makes Yedoma highly vulnerable to thaw and subsequent relief changes, which is reflected in its drastically diminished areal extent since the end of the late Pleistocene - early Holocene warm period about 12,000 years ago (Kaplina 2009; Veremeeva and Glushkova 2016). In Yedoma regions, a typical yedoma-alas relief, characterized by yedoma uplands, thermokarst lakes, and drained thermokarst lake basins (alasses), formed as a result of partial thawing of Yedoma deposit. Recent climate warming, wildfires, and/or human activities have led to an intensification of Yedoma degradation processes resulting in surface subsidence, ice-wedge degradation, increase in thermokarst and thermal erosion intensity (Jones et al. 2011; Nitze et al. 2018; Veremeeva et al. 2021). The specific of Arctic Alaska in comparison with NE Siberia are natural fires that can occur much further north in the tundra (Miller et al. 2023) as well as the expansion of beavers to the north (Tape et al. 2022).

Yedoma deposits and their distribution are relatively well studied in NE Eurasia (e.g., Kaplina 1981; Sher et al. 1987; Schirrmeister et al. 2013; Grosse et al. 2013; Strauss et al. 2017; Strauss et al. 2021) but less studied in Alaska (Kanevskiy et al. 2011; Kanevskiy et al. 2016; Kanevskiy et al. 2022; Schirrmeister et al. 2016; Shur et al. 2004; Shur et al. 2021), where they also cover large areas (Jorgenson et al. 2008; Jorgenson et al. 2014) (Figure 1). Existing low-resolution maps (1:1,000,000) only show the possible Yedoma occurrence within the mapped area, but not the exact areas of Yedoma and alasses in Alaska. High-resolution map of Yedoma domain landscapes is the base for understanding the current distribution, patterns of Yedoma degradation in the past and present time, its impact for landscape habitat and characteristics as well as for a local land-use management. A high-resolution map of Yedoma distribution is necessary for the estimation of the organic matter content and prognosis of potential future the greenhouse gas emissions.

The aim of this study is to quantify the areas of Yedoma and alas deposits of Arctic Alaska based on high resolution remote sensing (RS) data.

The study region is Arctic Alaska including the North Slope of Alaska and the Seward Peninsula located within the tundra and continuous permafrost zones (Figure 1). The mapping of the yedoma-alas relief is based on the field data of the key sites located within various areas, including the Seward Peninsula, Teshekpuk Lake, Toolik field station, Anaktuvuk River Fire sites. The main approach for mapping is the manual digitization based on the analysis of high-resolution RS imagery (available e.g. in ArcGIS basemap layers) and digital elevation models (ArcticDEM). The approach was succesfully used in NE Siberia (Veremeeva and Glushkova 2016). Yedoma uplands are distinguishable from alasses and other terrain units by elevated position, specific baydzherakh relief formed on Yedoma upland slopes due to thawing of ice wedges, and more drained conditions detected by vegetation, which is reflected in spectral characteristics of optical satellite images.

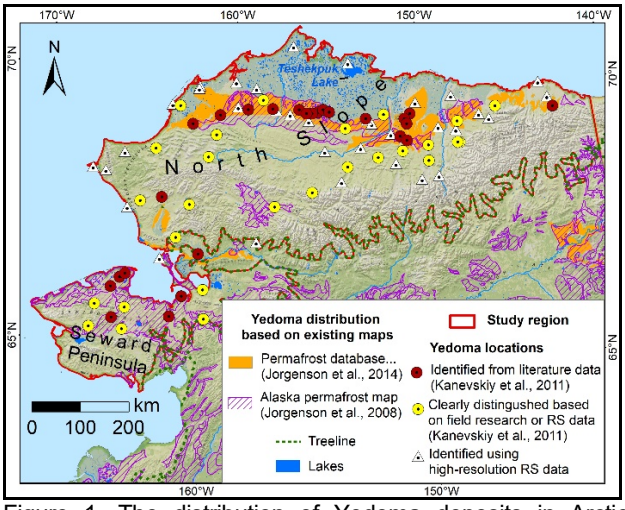

Figure 1. The distribution of Yedoma deposits in Arctic Alaska based on existing maps in comparison with high resolution remote sensing and fieldwork data.

Received map will be the base for testing the automated Yedoma uplands detection using the approach performed by Bergstedt et al. (2021) for the

drained lake basins detection in the North Slope Alaska region. Further geomorphological analysis will be performed in order to reveal spatial pattern of Yedoma degradation in the past and present time depending on geological, geomorphological, and climate conditions.

REFERENCES

Bergstedt, H., et al. 2021. Remote Sensing-Based Statistical Approach for Defining Drained Lake Basins in a Continuous Permafrost Region, North Slope of Alaska, Remote Sens., 13, 2539. doi.org/10.3390/rs13132539

Carter, L.D. 1988. Loess and deep thermokarst basins in Arctic Alaska, in Proceedings of the Fifth International Conference on Permafrost. Tapir Publishers, Trondheim, Norway: 706–711.

Jones, B.M., et al. 2011. Modern thermokarst lake dynamics in the continuous permafrost zone, northern Seward Peninsula, Alaska. J. Geophys. Res. Biogeosciences, 116. doi:10.1029/2011jg001666

Jorgenson, M.T., et al. 2008. Permafrost Characteristics of Alaska, in Proceedings of the 9th Intern. Conference on Permafrost, Fairbanks, Alaska: 121–122.

Jorgenson, M.T., et al. 2014. Permafrost Database Development, Characterization, and Mapping for Northern Alaska, Final Report Prepared for U.S. Fish and Wildlife Service, Anchorage, USA.

Kanevskiy, M., et al. 2011. Cryostratigraphy of late Pleistocene syngenetic permafrost (yedoma) in northern Alaska, Itkillik River exposure, Quat. Res. 75: 584–596. doi:10.1016/j.yqres.2010.12.003

Kanevskiy, M., et al. 2016. Patterns and rates of riverbank erosioninvolving ice-rich permafrost (yedoma) in northern Alaska, Geomorphology. doi.org/10.1016/j.geomorph.2015.10.023

Kanevskiy, M., et al. 2022. Yedoma Cryostratigraphy of Recently Excavated Sections of the CRREL Permafrost Tunnel Near Fairbanks, Alaska. Front. Earth Sci. 9:758800. doi:10.3389/feart.2021.758800

Kaplina, T.N. 1981. History of permafrost in Northern Yakutia during the late Cenozoic, in History of the Development of Perennial Frozen Deposits in Eurasia; Nauka: Moscow, Russia: 153–181 (in Russian).

Miller, E.A., et al. 2023. Unrecorded Tundra Fires of the Arctic Slope, Alaska USA, Fire, 6, 10. doi.org/10.3390/fire6030101

Nitze, I., et al. 2018. Remote sensing quantifies widespread abundance of permafrost region disturbances across the Arctic and Subarctic, Nat. Commun., 9, 5423. doi:10.1038/s41467-018-07663-3

Schirrmeister, L., et al. 2013. Permafrost and Periglacial Features | Yedoma: Late Pleistocene Ice-Rich Syngenetic Permafrost of Beringia, in The Encyclopedia of Quaternary Science. S.A. Elias (Ed) (Amsterdam: Elsevier): 542–552. doi:10.1016/ B978-0-444-53643-3.00106-0

Schirrmeister, L., et al. 2016. Late Quaternary paleoenvironmental records from the Chatanika River valley near Fairbanks (Alaska), Quatern. Sci. Rev. 5(147), 1. doi.org/10.1016/j.quascirev.2016.02.009

Sher, A.V., et al. 1987. Regional stratigraphic scheme of Quaternary deposits of the Yana-Kolyma Lowland and surrounding mountains, in Decisions of the Interdepartmental Stratigraphic Conf. for Quaternary System in the East of the USSR; N.A. Shilo (Ed) SVKNII DVO AN SSSR: Magadan, Russia: 29–69 (in Russian).

Shur, Y., et al. 2004. Syngenetic permafrost growth: cryostratigraphic observations from the CRREL tunnel near Fairbanks, Alaska, Permafr Periglac Proces. 4; 15 (4):339–347.

Shur, Y., et al. 2021. Fluvio-thermal Erosion and Thermal Denudation in the YedomaRegion of Northern Alaska: Revisiting the Itkillik River Exposure, Permafrost and Periglac Process 32: 277–298. doi:10.1002/ppp.2105

Strauss, J., et al. 2017. Deep Yedoma permafrost: A synthesis of depositional characteristics and carbon vulnerability, Earth-Science Reviews.,172: 75–86. doi:10.1016/j.earscirev.2017.07.007

Strauss, J., et al. 2021. Circum-Arctic Map of the Yedoma Permafrost Domain, Front. Earth Sci., 28. doi.org/10.389/feart.2021.758360

Tape, K.D., et al. 2022. Expanding beaver pond distribution in Arctic Alaska, 1949 to 2019, Sci Rep 12, 7123. doi.org/10.1038/s41598-022-09330-6

Veremeeva, A., and Glushkova N. 2016. Formation of relief in the regions of Ice Complex deposits distribution: remote sensing and GIS studies in the Kolyma Lowland tundra, Earth's Cryosphere, 20 (1):14–24.

Veremeeva, A., et al. 2021. Geomorphological and Climatic Drivers of Thermokarst Lake Area Increase Trend (1999–2018) in the Kolyma Lowland Yedoma Region, North-Eastern Siberia, Remote Sensing, 13, 178. doi.org/10.3390/rs13020178

3F — Polar Coastlines in Transition: Arctic, Antarctic, Offshore and Shelf Perspectives

Session Chairs: Matt C. Strzelecki[1], Louise Farquharson[2] & Zuzanna Swirad[3]

[1]*University of Wroclaw, Wrocław, Poland*
[2]*University of Alaska, Fairbanks, Alaska, United States*
[3]*Institute of Geophysics, Polish Academy of Sciences, Warsaw, Poland*

Polar coastlines make up over one-third of the global coastline total and are among the most dynamic in the world. Due to climate change polar coastlines are increasingly vulnerable to rapid change. Patterns of Arctic coastal change are mostly associated with decreased sea ice cover which is leaving coasts exposed to waves and storm action for longer each year. Additional influential factors include permafrost degradation, storm-surge flooding, and intensified sediment supply from glacierised catchments. These changes have wide-ranging impacts on circum-polar Arctic coastal communities through the destruction of culturally important sites and modern infrastructure.

In the Antarctic region accelerated deglaciation has led to the exposure of new coastlines where permafrost-related processes and fluxes of sediments from paraglacially transformed glacial landforms control coastal dynamics. In both regions, climate warming has triggered extreme processes including accelerated permafrost thermoerosion, destabilization of coastal slopes by periglacial processes or landslides leading to formation of tsunami waves that profoundly change the functioning of fragile polar coastal environments.

This session invites submissions that will improve our understanding of polar (Arctic and Antarctic) coastal dynamics on local and regional scales. We encourage submissions focusing on both sub-aerial and sub-aqueous processes driving changes to coastal morphology, and are also interested in submissions which discuss rates of change and socio-economic impacts. The objective of our session will be to raise interest in the topic and provide a platform for discussions on various aspects of coastal change and its impact on the resilience of polar environments and societies. We particularly encourage submission of contributions from members of ACD (Arctic Coastal Dynamics), CACOON (Circum-Arctic Coastal Communities KnOwledge Network), Permafrost Coastal Systems Network (Per-CS), Nunataryuk, and EO4PAC groups.

Multi-decadal shoreline evolution analysis of an unlithified permafrost coastline in the Coppermine River Delta, Nunavut

Samuel Binette[1], Richard Akana[2], Charles Jourdain-Bonneau[1], Émile Bujold[1], Béatrice Noël[1], Liam Mulgrew[2], Stéphanie Coulombe[3], Thomas Buffin-Bélanger[1] & David Didier[1]

[1]*Department of Biology, Chemistry and Geography, Université du Québec à Rimouski, Rimouski, Québec, Canada*

[2]*Kugluktuk Angoniatit Association, Hunters and Trappers Organization, Kugluktuk, Nunavut, Canada*

[3]*Polar Knowledge Canada, Cambridge Bay, Nunavut, Canada*

Very limited data is available regarding the state of the shoreline in western and central Nunavut, despite several coastal communities living in the area (Manson et al. 2005). Members of these communities witness their territories undergoing unprecedented changes due to the current climate trajectory (Ford et al. 2021).

In the Kitikmeot region, residents of Kugluktuk (67°49′36″N 115°05′36″W) report increased permafrost degradation affecting their cabins, significant beach erosion causing the disappearance of long-time off-road vehicle trails and abnormally low water levels in the river, making boat travel extremely challenging. Similar to other Arctic communities, beaches and rivers host important cultural heritage in Kugluktuk and are of paramount importance for the local culture. They are, however, highly threatened by erosion occurring at rates that are still unknown for this region (Smith 2014).

In the Coppermine River delta, an important cultural site for the Kugluktuk community sits on an island (Graveyard Island) characterized by bluffs of unlithified sediments, permafrost and well-developed ice-wedge polygon networks. In the estuary, locals have reported increasing erosion rates that are affecting the island where an old cemetery is located. This research presents a high-resolution analysis of Graveyard Island's shoreline changes and offers a contemporary understanding of the morphodynamic of this Arctic delta under a changing climate.

Between 2021 and 2023, in collaboration with community members and local HTO, a total of six field campaigns were conducted during the snow-free season (July to October) to assess coastal erosion and progradation, and to characterize the morphogenic processes at the river-coast interface. Several instruments were deployed on and around the island at study sites carefully selected with community members to monitor key controlling factors (permafrost monitoring, hydrodynamic and hydrological monitoring) and to document processes and morphological changes on the coast (drone mapping, time-lapse camera).

Historical aerial (Canadian National Air Photo Library) and satellite imagery (Quickbird, WorldView-1 and GeoEye), combined with very high resolution (VHR) Unmanned Aerial Vehicle surveys and Structure-from-Motion (UAV-SfM) processing allowed to conduct decadal analysis of planimetric changes (1952 to 2023), measured at 1-m intervals, and short-term (2021 to 2023) volumetric changes at 5-cm resolution, along a 1.4 km-long coastal segment of the island. Volumetric sediment gains and losses (m^3) were estimated through coastal elevation changes over time using digital elevation models (DEMs) produced at four dates between 2021 and 2023.

Analysis of shoreline movements (Figure 1), revealed a maximum shoreline retreat of 48.2 metres (Figure 1B), with average erosion rates of 0.22 m/yr over the decadal-scale period (Figure 1C). However, over the recent short-term period, high erosion rates are being measured with maximum of 3.14 m/yr and 2.04 m/yr for 2021-2022 and 2022-2023, respectively (Figure 1A). Volumetric analysis revealed a net loss of 814 m^3 between July 2021 and 2023, 75% of it occurring between July 2022 and July 2023 (614 m^3).

A thorough analysis of morphodynamics in the Coppermine estuary, based on time-lapse imagery, reveals the main erosional processes and patterns: (i) the increase of open-water period, followed by (ii) more frequent stormy events reaching the coast, combined with (iii) permafrost degradation, result in an increase in the impact of (iv) wave-induced basal erosion of the bluff.

These results show that unlithified permafrost coasts in western Nunavut are highly vulnerable to high rates of erosion, despite being in a fetch-limited and micro-tidal environment. This quantitative assessment of shoreline evolution is of crucial importance to the local community which can lead to coastal models of long-term shoreline evolution to better anticipate incremental and episodic impacts and plan adaptive strategies to adjust to future changes.

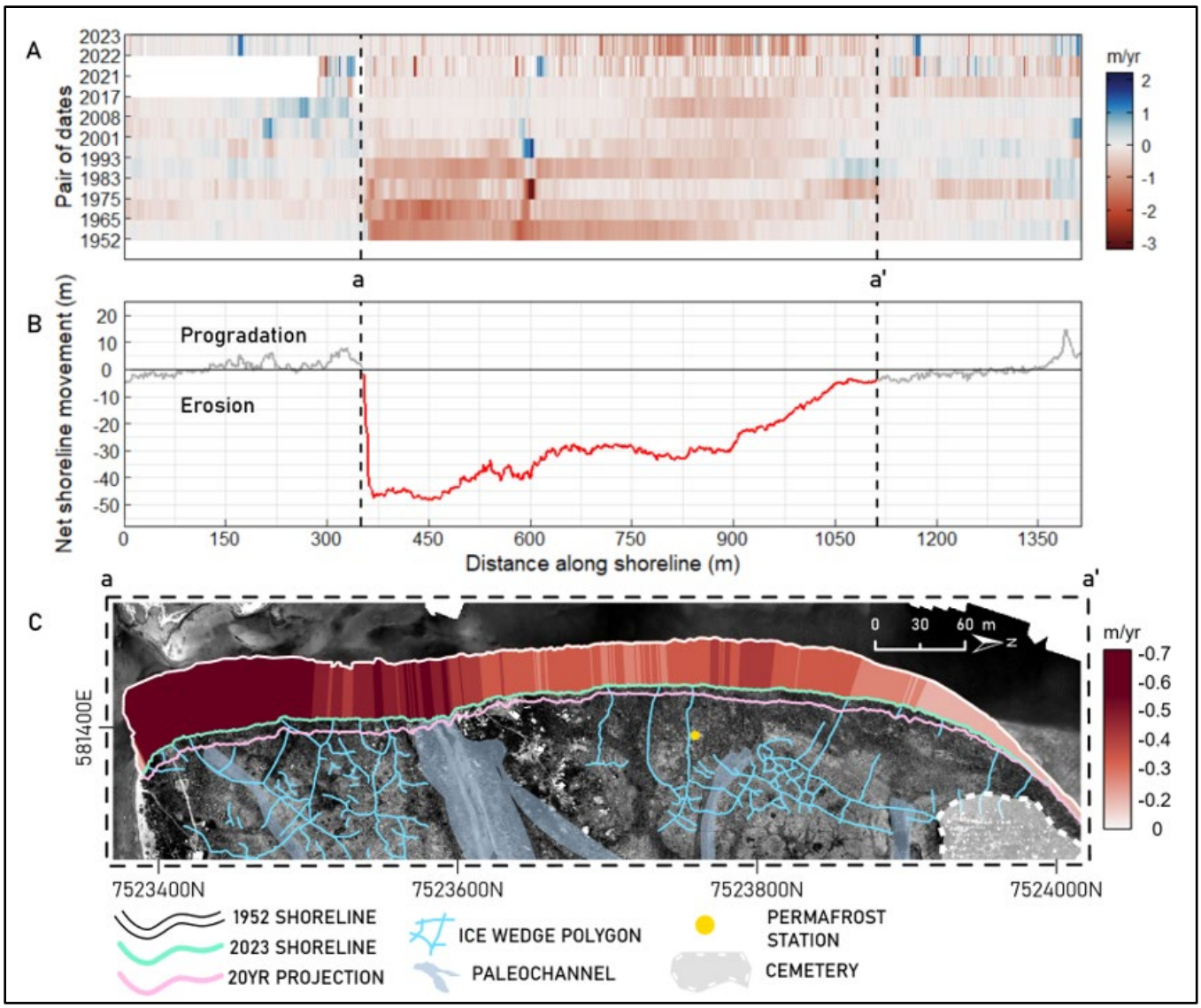

Figure 1. Shoreline evolution analysis of Graveyard Island's from shoreline position changes along analysed transects, digitized from acquired imagery over a period of 71 years (1952 to 2023). Panel A represent shoreline mobility rates over pairs of dates, in metre per year (m/yr), along linearized coastal segment (distance along the shoreline); B represents net shoreline movement (red line highlight a – a' data) for the decadal-scale period along linearized coastal segment; C shows actual spatial representation of shoreline changes over Graveyard Island's west coast (a – a') between 1952 (white line) and 2023 (green line) as well as rates (perpendicular transects with white to red colour gradient symbology), with the addition of the projected shoreline position in 20 years (pink line) using the averaged linear retreat rates of erosion per transect computed for the 70-year period. Additionally, panel C shows ice wedge polygon and inactive channels (paleochannels) position, as well as the cemetery and the position of the permafrost station. While panel A and B have the same scale in x (linearized shoreline distance), segments between dashed lines (a – a') highlight data over actual shoreline extent presented in panel C.

REFERENCE

Ford, J.D., Pearce, T., Canosa, I.V., and Harper, S. 2021. The rapidly changing Arctic and its societal implications. WIREs Climate Change. 12(6): e735. https://doi.org/10.1002/wcc.735

Manson, G.K., Solomon, S.M., Forbes, D.L., Atkinson, D.E., and Craymer, M.R. 2005. Spatial variability of factors influencing coastal change in the western Canadian Arctic. Geo-Marine Letters, 25(2-3), 138–145. https://doi.org/10.1007/s00367-004-0195-9

Smith, I.R. 2014. Reconnaissance assessment of landscape hazards and potential impacts of future climate change in Kugluktuk, western Nunavut. Canada-Nunavut Geoscience Office. http://cngo.ca/summary-of-activities/2013/

Nunavik's coastal permafrost environments: Synthesis and future research trajectories

Antoine Boisson, David Didier, Julie Major & Simon Bélanger
Université du Québec à Rimouski, Rimouski, Québec, Canada

Nunavik, the northernmost part of Québec containing a range of continuous to residual permafrost zones (Figure 1), is home to coastal Inuit communities who depend on their coastlines for traditional practices, food security, and transportation.

Arctic and subarctic coastlines of Nunavik are currently undergoing many climate-induced geomorphological changes across various spatial and temporal scales. These include changes in sea ice conditions, increased thermal and mechanical erosion, changing seasonality of open water periods, and increased exposure to swells and storm surges, all of which are often associated with permafrost thaw.

While coastal areas of Western Nunavik predominantly experienced progradation and permafrost aggradation due to glacio-isostatic uplift until the early 2010s, recent observations reveal contrasting trends with erosion rates of up to 1.5 meters per year in some regions. Natural variations, influenced by urbanization in coastal areas, introduce uncertainties regarding the trajectory of Nunavik's coastal systems amidst environmental changes.

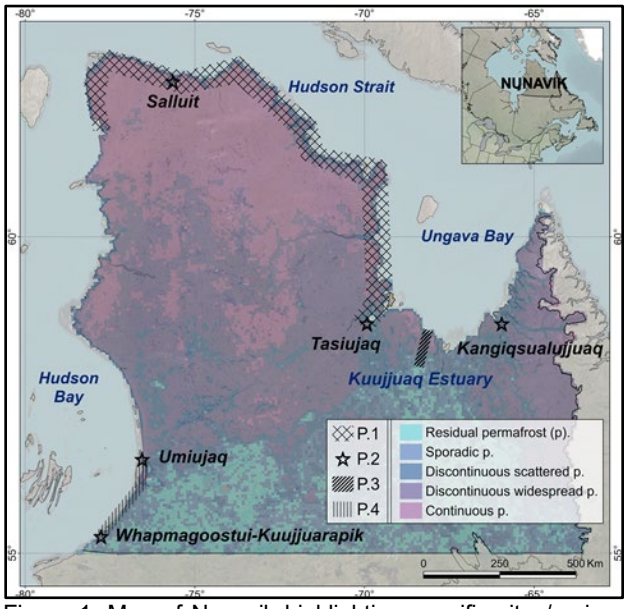

Figure 1. Map of Nunavik highlighting specific sites/regions chosen for coastal studies.

In light of the ever-growing necessity of developing mitigation and coastal adaptation strategies in Nunavik's permafrost zones, this paper seeks to synthesize findings from regional coastal projects conducted by the Northern and Arctic Coastal Research Lab (LNAR) since 2020, while outlining upcoming coastal research initiatives for Nunavik.

PAST PROJECTS (2020-2023)

Research in Nunavik's coastal permafrost environments has been mainly concentrated in the Whapmagoostui-Kuujjuarapik and Kangiqsualujjuaq regions, with a few studies conducted in other villages on the development of maritime infrastructures.

Assessment of Nunavik's coastal potential for deep-water port facilities: from Kovik Bay to Leaf Basin (P. 1; see figure 1)

The objective of this project was to identify suitable areas along the Nunavik coast for accommodating deep-water marine infrastructure. An atlas was developed to ensure ecosystem conservation, covering the northeast coast of Hudson Bay, the south coast of Hudson Strait, and the west coast of Ungava Bay.

Findings indicated that a substantial portion of the coastal zone lacks the necessary characteristics to support deep-water port facilities. Factors such as complex coastal processes, diverse and intricate landforms (e.g., fjords, tidal flats), as well as bathymetric, hydrodynamic, and permafrost conditions emerged as major limitations for such infrastructure.

Despite these limitations, this study provided valuable insights for future coastal development planning. By acknowledging these constraints and understanding the nuanced complexities of regional coastal dynamics, this assessment established a foundation for informed decision-making in the development of new parks and protected areas.

Towards a better understanding of coastal flooding in four Nunavik communities (Umiujaq, Salluit, Tasiujaq, and Kangiqsualujjuaq) (P. 2)

This project aimed to characterize coastal flooding hazards in four Nunavik communities. Different approaches were used, combining local Indigenous knowledge with scientific expertise to develop

mitigation strategies for anticipated coastal flood events.

Field surveys were conducted using cameras and drones, while meetings with community members allowed for the identification of local concerns about exposure and hazard levels.

Salluit is exposed to high coastal water levels, and a combination of adaptation strategies could be prioritized in the future to minimize risks to houses; the marine infrastructure and a road in Kangiqsualujjuaq are also affected, while Tasiujaq and Umiujaq have been experiencing episodic erosion events over the past decades.

Mapping the maritime vulnerability of the Kuujjuaq Estuary (P. 3)

To address the risks associated with potential oil spill incidents in response to increased marine shipping routes, a marine vulnerability map of the Kuujjuaq Estuary was developed using a methodology similar to the Environmental Sensitivity Index.

This focused study employed a participatory methodology that integrated local and indigenous knowledge to map the region's maritime vulnerability. This approach facilitated a comprehensive understanding of vulnerabilities and laid the foundation for effective risk mitigation strategies.

Diverse vulnerability indices, encompassing social, geomorphological, and biological dimensions, were established as part of this endeavor. Local and global vulnerabilities within the estuary were mapped and later validated on-site by community members.

Eco-geomorphological mapping and driving factors of the Whapmagoostui-Kuujjuarapik – Umiujaq region (P. 4)

An eco-geomorphological map was developed contributing to an increased understanding of these sensitive eco-geomorphological systems, while also facilitating the development of a Coastal Environmental Vulnerability Index (CVI).

This comprehensive study involved a detailed evaluation of shoreline evolution from 1954 to 2023. It precisely delineated coastal ecosystems by integrating various data sources, including historical aerial photographs, recent high-resolution satellite imagery, and drone-derived data.

The resulting high-resolution map shows geomorphological features along the coast and highlights hydro-sedimentary dynamics. Additionally, offshore wave climate data from the WAVEWATCH III model were used to analyze the spatial variability in offshore wave statistics and their influence on this subarctic coast.

UPCOMING PROJECTS (2024-2028)

Coastal dynamics in Nunavik

Coastal dynamics within Nunavik over time and their impacts on local communities will be analyzed in a newly started project at the regional scale. The approach involves empirical data collection, modeling, and collaborative analyses with Inuit. We will assess community vulnerability to coastal hazards, analyze morphological changes in the coastline, and establish a network of instruments to monitor environmental forcings. Additionally, annual changes in topo-bathymetry and hydrodynamics will be analyzed, and a framework will be developed for the assessment of potential impacts of extreme coastal events on Nunavik communities.

Coastal ecosystems atlas

An atlas detailing the coastal ecosystems in Nunavik is currently being developed. This atlas, primarily based on remote sensing analysis and field validations, aims to provide an encompassing overview of diverse ecosystems spanning from Ungava Bay to Hudson Bay and will contribute to informed conservation and management strategies.

CONCLUSION

The projects previously undertaken and those ongoing in Nunavik constitute a unified effort towards understanding, managing, and mitigating coastal risks and vulnerabilities comprehensively. By integrating scientific knowledge and local expertise, these initiatives play a significant role in developing sustainable coastal management strategies for the region.

ICESat-2 and satellite imagery highlight complex patterns of shoreline change on the Alaska Beaufort Sea Coast

Marnie Bryant[1], Adrian Borsa[1], Eric Anderson[2], Claire Masteller[3], Roger Michaelides[3], Matthew Siegfried[4] & Adam Young[1]

[1]*Scripps Institution of Oceanography, University of California San Diego, San Diego, California, United States*

[2]*Hydrologic Science and Engineering, Colorado School of Mines, Golden, Colorado, United States*

[3]*Department of Earth, Environmental and Planetary Sciences, Washington University in St. Louis, St. Louis, Missouri, United States*

[4]*Department of Geophysics, Colorado School of Mines, Golden, Colorado, United States*

Decreasing sea ice coverage, increasing air temperatures, and increasing storm intensity are driving rapid erosion rates along much of the Arctic coastline. This retreat threatens infrastructure, cultural sites, and economic development for coastal communities. Coastal erosion also results in the input of land-bound carbon into the ocean and atmosphere, with implications for ocean ecosystems and the global carbon budget (Irrgang et al. 2022). Accurately forecasting Arctic coastal erosion can be difficult since erosion rates are highly variable in both space and time and are not always well-correlated with environmental conditions (Jones et al. 2018). A better understanding of the shoreline properties and processes that modulate the coastal response to environmental forcings is needed to improve forecasts of future erosion rates.

Arctic coastlines are morphologically diverse, with different shore types dominated by different erosional and accretional processes. For example, steep, ice rich coastal bluffs are subject to thaw and erosion due to warm ocean and air temperatures, whereas gradually sloping beaches may erode or accrete depending on alongshore sediment transport patterns (Farquharson et al. 2018). Constraining the relationship between coastal morphology and retreat rates requires regular measurements of both the position and topography the shoreline. Satellite-based elevation measurements provide the opportunity to obtain annual to sub-annual repeat measurements of shoreline position and structure at a pan-Arctic scale.

With a 91-day revisit time, 13 m footprint, 0.7 m along-track sampling, vertical precision of 13 cm (Brunt et al. 2021), and single-photon counting technology (Neumann et al. 2019), ICESat-2 can provide high-resolution coastal elevation profiles on annual to sub-annual scales. This project aims to establish a framework for processing and interpreting cross-shore ICESat-2 elevation data and demonstrate how the derived elevation profiles can be leveraged with multispectral imagery and meteorological datasets to better understand the evolution of Arctic shorelines.

We focus on a case covering a ~7 km stretch of shoreline near Drew Point, Alaska, USA, where retreat rates have historically been high (up to ~-20 m/yr) and variable (Jones et al. 2018). We derived coastlines from the 2019-2021 open water seasons from 3 m four-band imagery from PlanetScope CubeSats using an automated classification approach, from which we estimate shoreline change at 10 m intervals along the coast. We discuss the spatiotemporal variability in the derived shoreline change and compare them with historical observations. We then considered repeat ICESat-2 measurements from 3 beams within this same time interval. We generated 2 m resolution elevation profiles using a customized version of the Land Ice Height Algorithm (Smith et al. 2019) for each track using the Sliderule Python client (Shean et al. 2023). From these elevation profiles, we identified the upper and lower boundaries of the backshore and estimated the annual change in position at both boundaries, backshore height, and backshore slope. We compared our ICESat-2- and Planet-derived shoreline positions and change rates to assess the consistency of shoreline estimates derived from these two datasets. We then considered the year-to-year evolution of our ICESat-2 elevation profiles and discuss specific processes that may be driving the observed change. We used available data on sea ice coverage, wave energy, and ocean and air temperatures to place our ICESat-2 and Planet observations in the context of time-varying environmental forcings.

Imagery-derived retreat rates show patterns of coastline change that are highly variable both in space and in time, with annual spatially-averaged shoreline change ranging from -11 m/yr to -29 m/yr, and local shoreline change as high as -78 m/yr occurring in 2019. While the year-to year variations in shoreline change are broadly consistent with year-to-year variations in open water days, wave energy, and

air and ocean temperature, the spatial response to these environmental forcings is not uniform. We observe the highest and most variable shoreline change rates in the headlands of our study region, and we observe the least shoreline change across the central portion of a large breached thermokarst lake.

We find that our Sliderule-derived ICESat-2 elevation profiles resolve the coastline with a high level of detail, with the ability to capture abrupt elevation changes over horizontal distances of 5 m or less. Inspection of the ATL03 photon data reveals process-sale features such as toppled blocks and small surface ponds. We estimate change rates from ICESat-2 (-7 to -60 m/y of retreat) that are consistent with those derived from imagery.

ICESat-2 profiles highlight a diversity in coastal morphology with each track revealing a different type of shoreline with different year-to-year retreat rates. Our first track consists of a steep coastal bluff that shows moderate year-to-year retreat (-7 to -22 m of shoreline change) without undergoing any major change in the shoreline shape. Our second ICESat-2 transect crosses a small drained lake basin that erodes and collapses over the course of three open water seasons, resulting in highly variable year-to-year change rates (-2 to -60 m/yr) and significant change in the shoreline structure. Our third ICESat-2 track consists of a ~1.5 m beach dune fronting crossing the stable portion of the large thermokarst lake identified from Planet imagery. At this location, we observe very little change in the shoreline position (< 10 m of retreat or advancement per year) and topography over our three-year study period. These ICESat-2 observations point to the role that localized erosion and accretion mechanisms that depend on the local topography may play in driving the spatiotemporal variability in shoreline observed with Planet.

In summary, ICESat-2 and multispectral imagery provide complimentary measurements of shoreline change. Multispectral imagery can provide regular scene-wide estimates of shoreline change that help place ICESat-2 observations in the context of the surrounding shoreline, while ICESat-2 provides more detailed information about the shoreline evolution than can be achieved with imagery alone. We discuss best practices and challenges when deriving coastal elevation profiles from ICESat-2 and consider strategies for extending this analysis to a regional scale and integrating additional elevation datasets.

REFERENCES

Brunt, K.M., Smith, B.E., Sutterley, T.C., Kurtz, N.T., and Neumann, T.A. 2021. Comparisons of Satellite and Airborne Altimetry With Ground-Based Data From the Interior of the Antarctic Ice Sheet. Geophys. Res. Lett. 48. https://doi.org/10.1029/2020GL090572

Farquharson, L.M., Mann, D.H., Swanson, D.K., Jones, B.M., Buzard, R.M., and Jordan, J.W. 2018. Temporal and spatial variability in coastline response to declining sea-ice in northwest Alaska. Mar. Geol. 404, 71–83. https://doi.org/10.1016/j.margeo.2018.07.007

Jones, B.M., Farquharson, L.M., Baughman, C.A., Buzard, R.M., Arp, C.D., Grosse, G., Bull, D.L., Günther, F., Nitze, I., Urban, F., Kasper, J.L., Frederick, J.M., Thomas, M., Jones, C., Mota, A., Dallimore, S., Tweedie, C., Maio, C., Mann, D.H., Richmond, B., Gibbs, A., Xiao, M., Sachs, T., Iwahana, G., Kanevskiy, M., and Romanovsky, V.E. 2018. A decade of remotely sensed observations highlight complex processes linked to coastal permafrost bluff erosion in the Arctic. Environ. Res. Lett. 13, 115001. https://doi.org/10.1088/1748-9326/aae471

Irrgang, A.M., Bendixen, M., Farquharson, L.M., Baranskaya, A.V., Erikson, L.H., Gibbs, A.E., Ogorodov, S.A., Overduin, P.P., Lantuit, H., Grigoriev, M.N., and Jones, B.M. 2022. Drivers, dynamics and impacts of changing Arctic coasts, Nature Reviews Earth & Environment, 3, 39–54. https://doi.org/10.1038/s43017-021-00232-1

Neumann, T.A., Martino, A.J., Markus, T., Bae, S., Bock, M.R., Brenner, A.C., Brunt, K.M., Cavanaugh, J., Fernandes, S.T., Hancock, D.W., Harbeck, K., Lee, J., Kurtz, N.T., Luers, P.J., Luthcke, S.B., Magruder, L., Pennington, T.A., Ramos-Izquierdo, L., Rebold, T., Skoog, J., and Thomas, T.C. 2019. The Ice, Cloud, and Land Elevation Satellite – 2 mission: A global geolocated photon product derived from the Advanced Topographic Laser Altimeter System. Remote Sens. Environ. 233, 111325. https://doi.org/10.1016/j.rse.2019.111325

Shean, D., Swinski, J.P., Smith, B., Sutterley, T., Henderson, S., Ugarte, C., Lidwa, E., and Neumann, T. 2023. SlideRule: Enabling rapid, scalable, open science forthe NASA ICESat-2 mission and beyond. J. Open Source Softw. 8, 4982. https://doi.org/10.21105/joss.04982

Smith, B., Fricker, H.A., Holschuh, N., Gardner, A.S., Adusumilli, S., Brunt, K.M., Csatho, B., Harbeck, K., Huth, A., Neumann, T., Nilsson, J., and Siegfried, M.R. 2019. Land ice height-retrieval algorithm for NASA's ICESat-2 photon-counting laser altimeter. Remote Sens. Environ. 233, 111352. https://doi.org/10.1016/j.rse.2019.111352

Short-term dynamics of a permafrost coastline on southern Victoria Island, Nunavut

Stephanie Coulombe[1], David Didier[2], Samuel Binette[2], Charles Jourdain-Bonneau[2], Jacob Stolle[3], Hatim Ben Said[3], Ivor Maksagak[4] & Joseph Evetalegak Jr.[4]

[1]*Polar Knowledge Canada, Cambridge Bay, Nunavut, Canada*

[2]*Department of biology, chemistry and geography – Université du Québec à Rimouski, Rimouski, Québec, Canada*

[3]*Eau-Terre-Environnement Research Centre – Institut national de la recherche scientifique, Québec City, Québec, Canada*

[4]*Ekaluktutiak Hunters and Trappers Organization, Cambridge Bay, Nunavut, Canada*

Permafrost coasts are highly diverse owing to spatial heterogeneity in environmental conditions. As such, they can be expected to show a broad range of responses to climate warming (Nitzbon et al. 2021). In western Nunavut, the intensity and trajectory of geomorphological changes in coastal environments remain poorly understood on a landscape scale because of the lack of historical baseline data in this region. In 2022, a research and monitoring project was launched in collaboration with the Ekaluktutiak Hunters and Trappers Organizations to investigate the permafrost conditions and short-term dynamics of an eroding permafrost coastline on southern Victoria Island. This study focuses on a 2 km long coastal stretch located at the foothills of an esker, to the east of Cambridge Bay (74°N, Nunavut, Canada). The area is widely used by community members to travel to their cabins and access traditional hunting and fishing grounds.

High-resolution satellite imagery was used together with repeated UAV surveys to document recent shoreline changes, surface disturbances and thermokarst processes along the coast between 2021 and 2023, thereby providing the first multiyear shoreline analysis (2021–2023) in this region. Permafrost exposures in coastal bluff were described and sampled vertically every 20 to 30 cm to investigate the sediment properties, ground-ice content, types and distribution of cryostructures, and presence of unconformities (French and Shur 2010). Ground temperature was measured using thermistor strings and a logging system.

In the studied area, permafrost is continuous and temperatures at 15 m depth typically have ranged between -9.9 and -8.6°C over the last four years. The bluffs range in height from ca. 1 m to more than 4 m high and modern thermo-erosional processes along the coastal bluff have exposed two cryostratigraphic units. Unit 1 consists of ice-rich marine silt and clay characterized by reticulate and ataxitic (suspended) cryostructures, covered by ice-poor sand and gravel (Unit 2) exhibiting a structureless cryostructure. Gravimetric moisture contents (GMC) in unit 1 are high, ranging between 30–195%, while GMC in unit 2 ranged between 27–28%.

Our results also showed that our study area is strongly impacted by thermo-erosional gullying and shoreline retreat. Between September 2021 and July 2023, the bluffs retreated an average of 5.1 ± 4.1 m, and a maximum of 17.7 m (Figure 1a). The average retreat rate for the whole 2 km long bluff was 2.6 ± 2.0 m y^{-1} and reached 8.9 m y^{-1} for the most actively eroded part of the bluff. This is higher than average rates observed in the western Canadian Arctic (Philipps et al. 2023). In addition to coastal erosion, permafrost degradation by thermal-erosion gullying is also altering the coastal landscape (Figure 1b). Of the seventeen gullies identified within a 200-m section, five were newly formed in 2023, and ten were actively eroding. The gully head sections have migrated upstream 0.6–30.5 m, with an average of 5.6 ± 7.0 m over 1 year. The overall eroded volume was estimated at 195 m^3 between 2022 and 2023.

This dynamic form of thermokarst can rapidly degrade ice-rich permafrost, induce surface subsidence and affect snow accumulation, ground temperature, local water flow and drainage while also mobilizing large amounts of sediment, organic matter, and nutrients from permafrost to the nearshore waters (Godin et al. 2014). Although temporal data are limited for now, this suggests that, combined with other meteorological and oceanographic drivers, thermo-erosion gullying may be an important factor controlling erosion patterns and sediment transport over time.

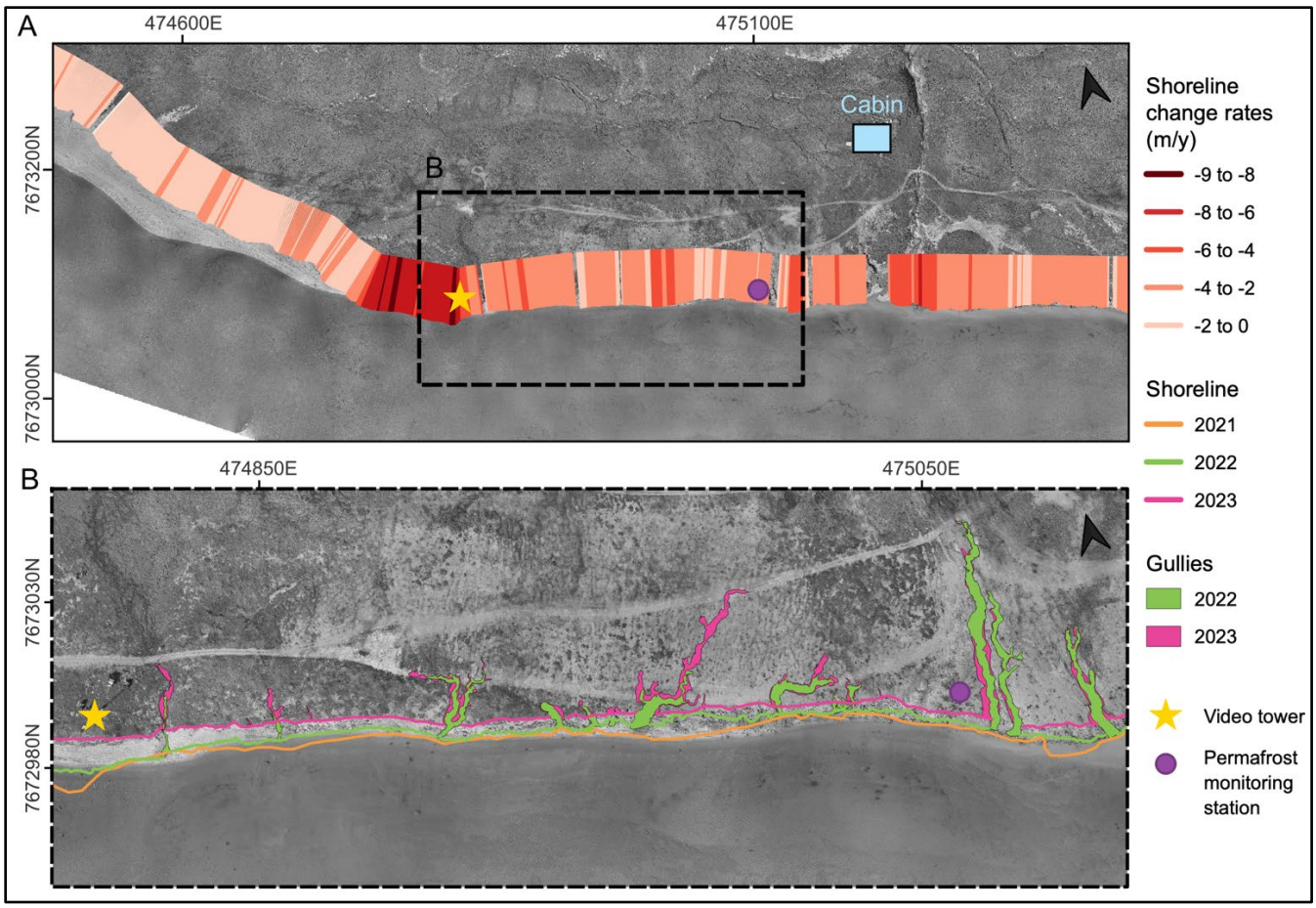

Figure 1. Shoreline evolution analysis (2021 to 2023) with the 2023 orthophotography shown as the basemap. A) Rates of shoreline changes along a 2-km long coastal section (Digital Shoreline Analysis System, v5.1, USGS 2021). B) Close up view of shoreline and gully positions for 2021, 2022 and 2023.

REFERENCE

Philipp, M., Dietz, A., Ullmann, T., and Kuenzer, C. 2023. A Circum-Arctic Monitoring Framework for Quantifying Annual Erosion Rates of Permafrost Coasts. Remote Sensing, 15(3): 818. doi:10.3390/rs15030818

Himmelstoss, E.A., Henderson, R.E., Kratzmann, M.G., and Farris, A.S. 2021. Digital Shoreline Analysis System (DSAS) version 5.1 user guide: U.S. Geological Survey Open-File Report 2021–1091, 104. doi:10.3133/ofr20211091.

Nitzbon, J., Langer, M., Martin, L.C.P., Westermann, S., Schneider von Deimling, T., and Boike, J. 2021. Effects of multi-scale heterogeneity on the simulated evolution of ice-rich permafrost lowlands under a warming climate. The Cryosphere, 15(3): 1399–1422. doi:10.5194/tc-15-1399-2021

Godin, E., Fortier, D., and Coulombe, S. 2014. Effects of thermo-erosion gullying on hydrologic flow networks, discharge and soil loss. Environmental Research Letters, 9(10): 105010. doi:10.1088/1748-9326/9/10/105010

Shur, Y., and French, H.M. 2010. The principles of cryostratigraphy, Earth-Science Reviews, 101(3-4): 190–206. doi:10.1016/j.earscirev.2010.04.002

Rising water, sinking land, slumping shores: permafrost thaw subsidence, sea-level rise, and coastal erosion are transforming the Alaska North Slope

Roger Creel[1], Julia Guimond[1], Benjamin Jones[2], David Nielsen[3], Paul Overduin[4], Tabatha Fuson[5], Craig Tweedie[5] & Emily Bristol[6]

[1]*Woods Hole Oceanographic Institution, Woods Hole, Massachusetts, United States*

[2]*Water and Environmental Research Center, University of Alaska Fairbanks, Fairbanks, Alaska, United States*

[3]*Max Planck Institut Für Meteorologie, Hamburg, Germany*

[4]*Alfred Wegener Institute, Potsdam, Germany*

[5]*University of Texas at El Paso, El Paso, Texas, United States*

[2]*University of Texas at Austin, Austin, Texas, United States*

Arctic coastal zones are increasingly threatened by climate change. Open water periods are extending. Sea ice extent is shrinking and multi-year ice is disappearing. Storms are becoming more frequent, more intense, and less predictable. Coastal ocean temperatures are increasing. Ocean acidification is making it harder for calcifying organisms to grow in Arctic waters. Wildfires are destabilizing tundra ecosystems. Shifting animal migration patterns are altering coastal landscapes. Wider precipitation extremes are influencing river flooding frequencies. Expanding oil and natural gas development are producing significant coastal zone noise pollution, adversely affecting marine mammals and the people who depend on them. River hydrographs are flattening. Permafrost is undergoing isotropic thaw subsidence in many regions across the Arctic; built infrastructure is in places exacerbating this thaw subsidence. Sea level rise is accelerating.

Half a century of satellite surveys of Arctic coastlines have demonstrated that coastal erosion is an acute hazard. However, other agents of coastal change, such as sea-level rise and land subsidence, are also at work, and these hazards have received substantially less study. For instance, scant attention has been paid to the additive effects that sea-level rise and isotropic permafrost thaw subsidence will have on Arctic coastlines over the 21st century, even as land subsidence along other parts of the world's coastlines receives significant recognition. This oversight has hindered comparisons of how impactful these processes may be relative to erosion. Northern Alaska's Arctic Coastal Plain (ACP) is an ideal region to perform such comparisons because of the relatively abundant remotely-sensed and in-situ observations of topography, rates of coastline retreat, permafrost characteristics, and records of past coastal features.

Here we present the first projections of 21st century shoreline position in the Arctic to include permafrost subsidence and relative sea-level rise in addition to shoreline erosion. Focusing on the ACP, we merge high-resolution (5 m) topography, satellite-derived maps of coastal lake depth, and empirical estimates of land subsidence due to isotropic permafrost thaw with projections of coastal erosion and sea-level rise for the range of emissions scenarios defined by the Intergovernmental Panel on Climate Change's Sixth Assessment Report (AR6). We find that by 2100, inundation due to thaw subsidence and sea level rise surpasses erosion to become the dominant agent of land loss even for low emissions scenarios. Our results underscore the additive hazards that compound climate change-related events pose to coastal communities and infrastructure, and highlight that communities within zones of 21st century land loss need support for adaptive planning.

Observing coastal change and permafrost dynamics in three Arctic communities

Louise Farquharson[1], Dmitry Nicolsky[2], Vladimir Romanovsky[1], Thomas Colby Wright[1] & Ming Xiao[2]
[1]*Geophysical Institute Permafrost Laboratory, University of Alaska Fairbanks, Alaska, United States*
[2]*Department of Civil and Environmental Engineering, Penn State, Pennsylvania, United States*

Permafrost thaw and coastal erosion are expected to cause widespread land loss (Nielsen et al. 2022), infrastructure damage (Hjort et al. 2018), the release of contaminants (Langer et al. 2023), lake drainage (Jones et al. 2020) and the destruction of important cultural sites across many Arctic coastal communities (Maslakov et al. 2020) within the next century. Permafrost degradation in ice-rich terrain results in ground subsidence and a decrease in soil sheer strength that can cause damage to building foundations (Liew et al. 2022). To date observations of permafrost degradation and coastal erosion in rural Alaskan communities has been limited. In order to create reliable projections of future change, baseline datasets of ground thermal dynamics and rates of coastline change are critical. Here we explore coastal change coupled with ground temperature measurements across three North Slope Borough coastal communities: Point Lay, Wainwright, and Utqiagvik. All three sites are underlain by continuous permafrost but are characterized by different coastal settings (e.g., barrier-island lagoon complex vs exposed, varying surficial geology types, and different coastal aspects).

MAPPING COASTAL CHANGE

We present a suite of observations including remote sensing derived rates of coastal change, coastal geomorphology maps, and in-situ ground temperature measurements across a wide range of conditions. Coastal geomorphology was mapped through field surveys, drone acquired orthoimages, and elevation from structure-from-motion based digital elevation models. We mapped coastal change between 1980 and 2022 using a combination of historic aerial photographs, satellite imagery and drone surveys. We compare rates of coastal erosion, and explore how coastal proximity, hydrological conditions and geomorphology influence the ground thermal regime. Rates of coastal erosion in Point Lay ranged from 0.1 to 1.1 m/yr and from 0.1- 1.34 in Wainwright (average based on 1950-2020, further analysis is needed to incorporate 2022 data) (Figures 1). In general rates of coastal erosion were faster in Wainwright, likely due to an absence of barrier island protection.

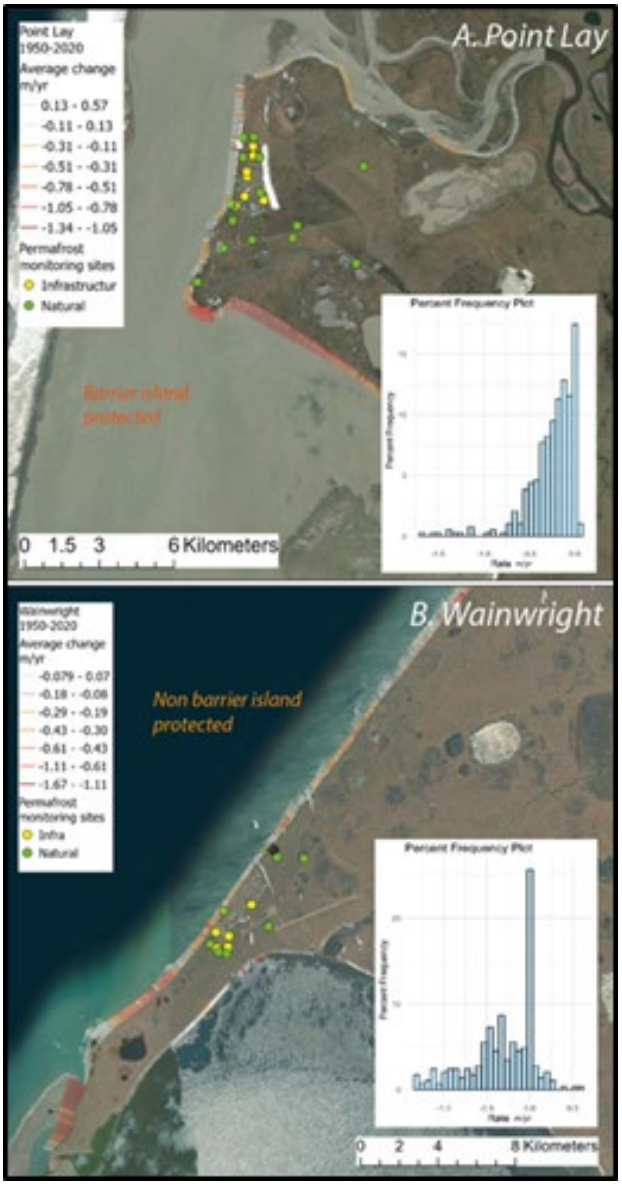

Figure 1. Shoreline change rates and associated frequency distribution plots for A. Point Lay and B. Wainwright in the North Slope Borough. Rates of change are based on changes in position of bluff edge. Green dots represent permafrost monitoring sites in natural conditions while yellow dots represent permafrost conditions in the build environment.

EXPLORING LOCAL VARIABILITY IN GROUND THERMAL REGIME

At seven coastal sites (four transects in the built environment and three in the natural environment), we installed a transect of two to four 1.5-meter-deep thermistors to monitor in-situ ground temperature within 1-100 meters of each coastal bluff (n=22 sites total) (for Wainwright and Point Lay sites see Figure 1). Transects were placed in a range of conditions including adjacent to homes, within thaw gullies, and on coastal bluffs (e.g., Figure 2, Utqiagvik Natural site 1). Coastal sites were accompanied by an additional 20 inland sites across a range of geomorphological and hydrological conditions. Mean annual ground temperature at 1.5 m depth in natural conditions range from -5 to -7°C in Point Lay,-5 to -7°C in Wainwright, and -3 to -7°C in Utqiagvik. Results from this study provide important baseline data for understanding the future evolution of Arctic landscapes and can improve our understanding of the interplay between coastal erosion, geomorphology, and permafrost thaw.

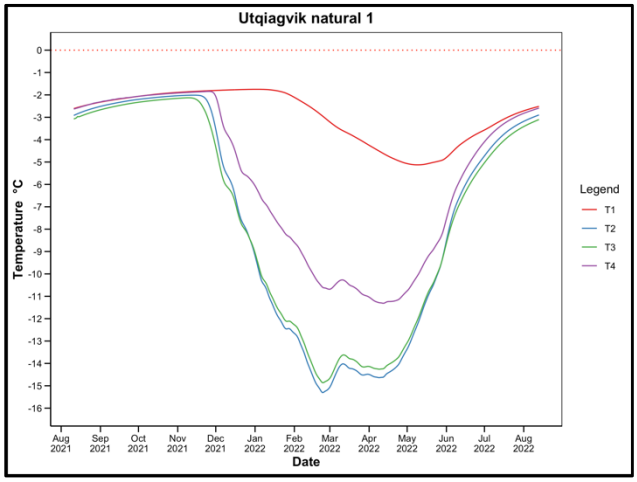

Figure 2. Ground temperature measurements for a coastal transect in natural conditions southwest of Utqiagvik for the August 2021 – August 2022. T1 is the bluff edge, T4 is a coastal thermoerosion gully and T2 and T3 are >50 m inland.

REFERENCES

Hjort, J., Karjalainen, O., Aalto, J., Westermann, S., Romanovsky, V.E., Nelson, F.E., Etzelmüller, B., and Luoto, M. 2018. Degrading permafrost puts Arctic infrastructure at risk by mid-century. Nature Communications, 9(1), 5147.

Jones, B.M., Arp, C.D., Grosse, G., Nitze, I., Lara, M.J., Whitman, M.S., Farquharson, L.M., Kanevskiy, M., Parsekian, A.D., Breen, A.L., and Ohara, N. 2020. Identifying historical and future potential lake drainage events on the western Arctic coastal plain of Alaska. Permafrost and Periglacial Processes, 31(1), 110–127.

Langer, M., von Deimling, T.S., Westermann, S., Rolph, R., Rutte, R., Antonova, S., Rachold, V., Schultz, M., Oehme, A., and Grosse, G. 2023. Thawing permafrost poses environmental threat to thousands of sites with legacy industrial contamination. Nature Communications, 14(1), 1721.

Liew, M., Ji, X., Xiao, M., Farquharson, L., Nicolsky, D., Romanovsky, V., Bray, M., Zhang, X., and McComb, C. 2022. Synthesis of physical processes of permafrost degradation and geophysical and geomechanical properties of permafrost. Cold Regions Science and Technology, 103522.

Maslakov, A.A., Nyland, K.E., Komova, N.N., Yurov, F.D., Yoshikawa, K., and Kraev, G.N. 2020. Community ice cellars in eastern chukotka: Climatic and anthropogenic influences on structural stability. Geography, Environment, Sustainability. https://doi.org/10.24057/2071-9388-2020-71

Nielsen, D.M., Pieper, P., Barkhordarian, A., Overduin, P., Ilyina, T., Brovkin, V., Baehr, J., and Dobrynin, M. 2022. Increase in Arctic coastal erosion and its sensitivity to warming in the twenty-first century. Nature Climate Change, 1–8.

The importance of the flocculation layer for permafrost degradation and cross-shelf transport

Lina Madaj[1], Kirsi Keskitalo[1,2], Örjan Gustafsson[3,4], Tommaso Tesi[5], Igor Semiletov[6,7,8], Oleg Dudarev[6,8], Jannik Martens[9], Lisa Bröder[10], Negar Haghipour[10,11] & Jorien Vonk[1]

[1]*Department of Earth Sciences, Vrije Universiteit Amsterdam, Amsterdam, The Netherlands*

[2]*Northumbria University, Newcastle, United Kingdom*

[3]*Stockholm University, Stockholm, Sweden*

[4]*Bolin Centre for Climate Research, Stockholm, Sweden*

[5]*National Research Council, Institute of Polar Sciences, Bologna, Italy*

[6]*Pacific Oceanological Institute, Russian Academy of Sciences, Vladivostok, Russia*

[7]*International Arctic Research Center, University of Alaska Fairbanks, Fairbanks, Alaska, United States*

[8]*National Research Polytechnic University, Tomsk, Russia*

[9]*Lamont-Doherty Earth Observatory, Columbia University, New York, New York, United States*

[10]*Geological Institute, Swiss Federal Institute of Technology (ETH), Zürich, Switzerland*

[11]*Laboratory of Ion Beam Physics, Swiss Federal Institute of Technology (ETH), Zürich, Switzerland*

The ongoing rise of atmospheric temperatures and sea level is exacerbating Arctic coastal permafrost thaw which leads to increased coastal erosion and input of organic carbon-rich permafrost soils into the Arctic Ocean. The East Siberian shelf is the world's largest shelf with ~600 km length and organic carbon (OC) transport across this shelf takes around 3600 years (Bröder et al. 2018). During lateral transport sediment-water interactions become crucial in the OC degradation process. These so-called flocculation layers (Figure 1) hold a high potential for sediment resuspension and therefore represent an environment favoring OC degradation thus preventing burial. The assumption of the continental shelf being a carbon sink has been challenged by studies assessing OC degradation impacted by e.g., CO_2 oversaturation within bottom waters (Semiletov et al. 2016).

With this study and the presented data, we want to gain new insights into how transport and degradation processes of terrestrial OC within the flocculation layer vary across the vast Siberian shelf.

Simulating the flocculation layer

To simulate flocculation at the sediment-water interface, surface sediment samples were collected with a multi-corer with overlying water preserved. The overlying water was stirred at a rotation speed of 130 rpm to mimic sediment resuspension. Following, the water was filtered through a 0.7 µm glass fiber filter and the captured suspended sediments were analyzed for OC properties. Measured parameters include total organic carbon (TOC), particulate organic carbon (POC), $\delta^{13}C$ and $\Delta^{14}C$ of the OC. Additionally, the two surface sediment layers underneath (0.0 to 0.5 cm and 0.5 to 1.0 cm) were analyzed for the same parameters along with sediment surface area to identify differences between flocculation and sediment layers. All samples were collected during ISSS-2020 expedition in late summer (September–October) of 2020 onboard R/V Akademik Msistlav Keldysh in the Laptev Sea (n=8), and the East Siberian Sea (n=4) along transects from the coast towards the shelf edge.

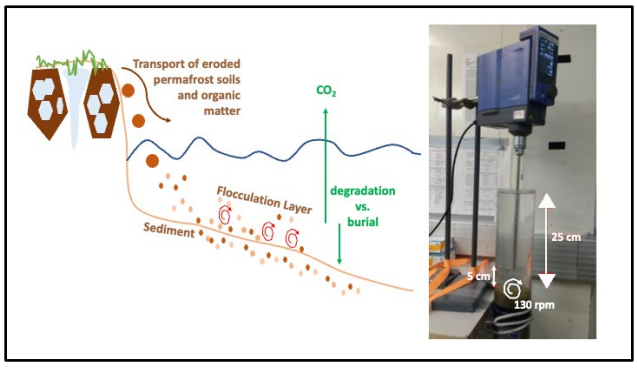

Figure 1. Schematic of sediment processes and sampling set up for simulating sediment entrainment at the sediment-water interface.

Differences in organic matter composition between flocculation and sediment layers

Results of this study show different trends with increasing distance from shore and increasing water depth within both, flocculation and sediment, layers. There is an overall decrease in OC when moving farther offshore. Based on the $\delta^{13}C$ and $\Delta^{14}C$ surface sediment data (Figure 2) the fraction of marine-

produced OC is increasing with distance from shore while the fraction of permafrost-derived OC is decreasing. This agrees with previous published data from the Laptev Sea (Figure 2; e.g., Bröder et al. 2016) and with the long transport time across the Siberian shelf fostering degradation, both lateral as well as vertical through the water column (Bröder et al. 2018).

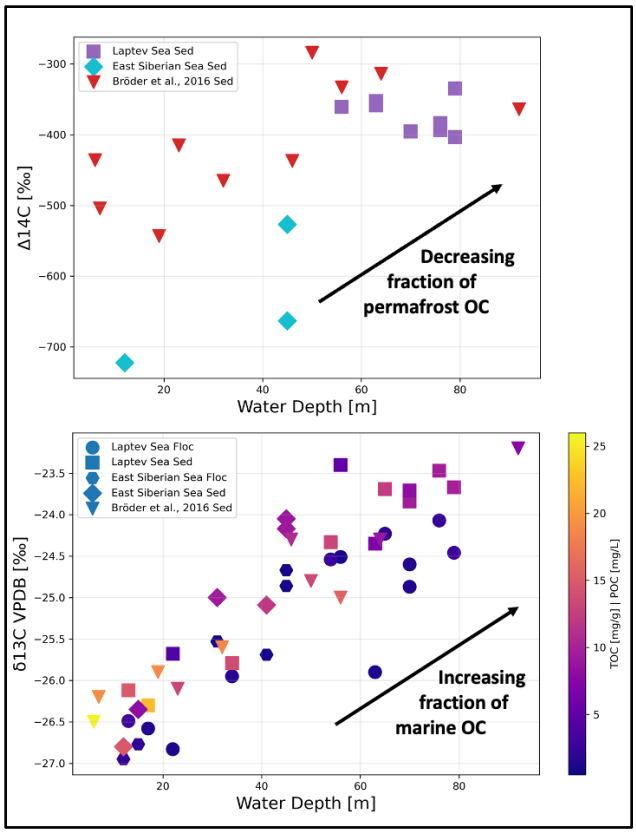

Figure 2. Organic carbon isotope data ($\Delta^{14}C$ and $\delta^{13}C$) and particulate organic carbon (POC) and total organic carbon (TOC) of flocculation (Floc) and surface sediment (Sed) samples, respectively, from the Laptev and East Siberian Sea. Samples from this study are plotted alongside sediment data from Bröder et al. 2016 from the Laptev Sea.

While the OC in the surface sediments in the East Siberian Sea appears older than in the Laptev Sea, the general trend of differences in OC composition between flocculation and surface sediment layers are similar. The fraction of permafrost derived OC is decreasing within both layers on the same scale. Overall lower OC content within the flocculation layer points towards faster degradation within this layer under resuspension and oxygen exposure. The data further emphasize the degradation potential of the flocculation layer, which may be particularly relevant on the vast Siberian shelf with its long sediment transport times.

Outlook

With increased OC input in the future caused by accelerated permafrost thaw and coastal erosion, across shelf transport patterns, including those at the sediment-water interface become more and more important, as they yield crucial information about sediment OC burial and degradation processes. Understanding these processes will improve estimations on fate of this OC upon entering the coastal waters.

References

Bröder, L., Tesi, T., Andersson, A., Semiletov, I., and Gustafsson, Ö. 2018. Bounding cross-shelf transport time and degradation in Siberian-Arctic land-ocean carbon transfer, Nature Communications, 9(806). doi:10.1038/s41467-018-03192-1

Bröder, L., Tesi, T., Salvadó, J.A., Semiletov, I.P., Dudarev, O.V., and Gustafsson, Ö. 2016. Fate of terrigenous organic matter across the Laptev Sea from the mouth of the Lena River to the deep sea of the Arctic interior, Biogeosciences, 13: 5003–5019. doi:10.5194/bg-13-5003-2016

Semiletov, I., Pipko, I., Gustafsson, Ö., Anderson, L.G., Sergienko, V., Pugach, S., Dudarev, O., Charkin, A., Gukov, A., Bröder, L., Andersson, A., Spivak, E., and Shakhova, N. 2016. Acidification of East Siberian Arctic Shelf waters through addition of freshwater and terrestrial carbon, Nature Geoscience 9: 361–365. doi:10.1038/ngeo2695

Morphological evolution of a young ice-marginal coastal system, Jakeman Glacier (Sirmialuk, ᓯᓚᐱᓗᒃ), Nunavut

Béatrice Noël[1], Samuel Binette[1], Charles Jourdain Bonneau[1], Terry Noah[2], Charlotte Stancu[1] & David Didier[1]

[1]*Department of Biology, Chemistery and Geography, Université du Québec à Rimouski, Rimouski, Québec, Canada*
[2]*Ausuittuq Adventure, Grise Fiord, Nunavut, Canada*

Arctic environments are particularly affected by climate change, causing rising air temperatures and the subsequent loss of ice masses (IPCC 2019). Rapid deglaciation in the Arctic is leading to the formation of new coastal landscapes by exposing glacial sediments that are reworked through various morphogenic processes (Strzelecki et al. 2020). The formation and transformation of these coasts in response to glacier retreat in the Canadian Arctic remains poorly studied. Unlike mid-latitude coasts, little is known about the possible impacts of climate change on high-latitude coastal systems (Overduin et al. 2014) and the understanding of the mechanisms governing their evolution remains limited (Lantuit et al. 2010). Moreover, the state of knowledge in polar coastal geomorphology focuses mainly on ice-rich permafrost coastlines and High Arctic research on coastal systems have mainly focused on Svalbard (Strzelecki et al. 2014; Strzelecki et al. 2017; Strzelecki et al. 2020).

Located in the Canadian Arctic Archipelago, south of Ellesmere Island and near Canada's northernmost community (Ausuittuq), Jakeman Glacier (76°27'40.03"N 80°52'14.49"W) is a pristine environment with a strong geomorphological response to changing climate and ocean forcing. From 1980 to 2020, an average retreat of 347 m was observed at the front margin of Jakeman Glacier, allowing the progradation of two ice-marginal coastal systems recently exposed to cryogenic and hydrodynamic processes. Southeast of the marine calving front, a moraine (Figure1A, circle #2), became detached from the glacier front between 2017–2018, and through morphodynamic processes, became a free spit formation (Moraine 2, M2). A 25-m eastward migration of the spit was observed between 2018 and 2022, with maximal movement rates of 35-m/yr occurring between 2019 and 2020 (da Silva et al. 2022). The west frontal deposits (Moraine 1, M1) (Figure 1A, circle #1), still attached to the glacier margin in 2023, is a 7-km long system with a maximal elevation reaching up to 33 m. A 400-m long supraglacial beach (Figure 1C) has developed on the southern end of the moraine system, adjacent to the glacier front. The aim of this project is to analyze the geomorphological changes at M1 between 2022–2023 and to provide new insights on the evolution of this peculiar system that contributes to sediment inputs in an Inuit hunting area.

Through community-led boat fieldwork, drone surveys were conducted in August 2022 and 2023. Digital elevation models (DEMs) were created using structure-from-motion photogrammetry. Interannual coastal elevation changes reveal more than 780-m^3 of sediment loss on the moraine seaward slope (Figure 1B), where the main retreat occurred along the bluff, suggesting a basal erosional niche followed by slope destabilization due to wave action at high tide and thickening of the active layer during warmer summer days. The analysis also reveals a reshaping of the beach profile (Figure 1C), where beachface erosion is balanced by backshore accretion behind the crest. Distinctive washover lobes indicate overwashing due to wave action and continuous overflow over the crest (Figure 1C). Migration of a drainage channel is also visible (Figure 1C).

To provide a better understanding of the processes controlling coastal evolution, moored pressure sensors were installed offshore of the glacier margin 10 m deep to measure waves and water levels. A LiDAR system has been deployed on the beach to quantify the wave regime and locate the maximal extend of wave runup. Better understanding of the hydrodynamic conditions leading to morphological changes within the site is particularly important considering the increase of the open-water period and frequency of storm-induced waves at the coast. Further campaigns will also include permafrost monitoring with thermal rods in order to assess the influence of thermal fluctuations on the morphological evolution and offshore sediment transport.

A deeper understanding of arctic coastal systems and their response to climate forcing is of prime importance in order to provide local communities with the information needed to adapt to climate changes. It also enables to highlight the impact of glacier retreat on sediment fate and biological productivity along marine-terminating glaciers, which are crucial areas for Inuit activities and subsistence hunting.

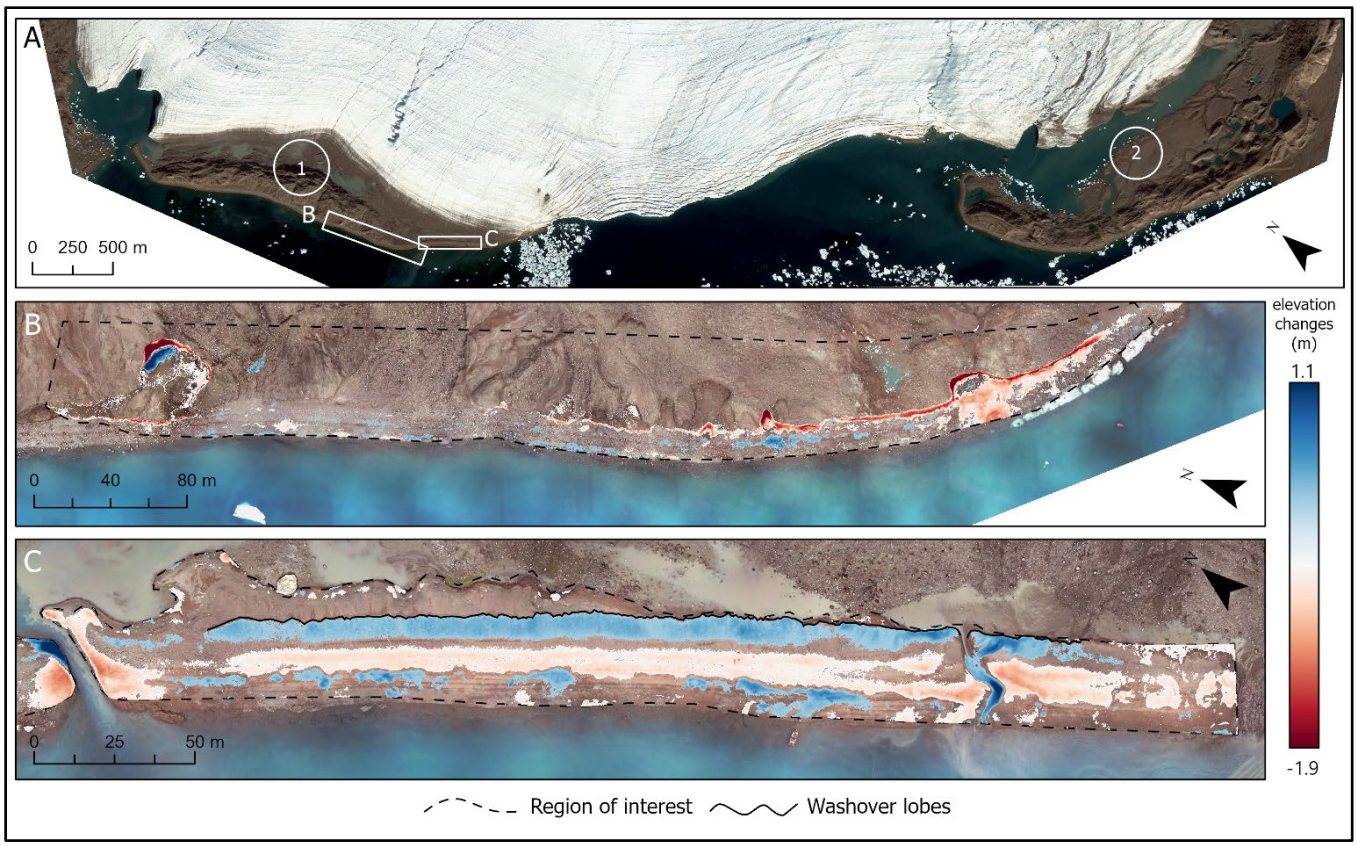

Figure 1. Jakeman Glacier ice-marginal coastal systems. Panel A locates two moraine systems (1, 2) on September 2022, as well as the two study sites (B, C) where topographic evolution analysis was conducted; Panels B and C represent elevation changes (m) on moraine 1 between 10/08/2022–08/08/2023. The regions of interest (ROI, dashed lines) corresponds to the spatial extension of analysed elevation changes. Washover lobes developed between 2022–2023 are delimited (plain line).

REFERENCES

IPCC. 2019. Summary for Policymakers. In: IPCC Special Report on the Ocean and Cryosphere in a Changing Climate [H.-O. Pörtner, D.C. Roberts, V. Masson-Delmotte, P. Zhai, M. Tignor, E. Poloczanska, K. Mintenbeck, A. Alegría, M. Nicolai, A. Okem, J. Petzold, B. Rama, N.M. Weyer (eds.)]. Cambridge University Press, Cambridge, UK and New York, NY, USA, pp. 3–35. https://doi.org/10.1017/9781009157964.001

Lantuit, H., Overduin, P., Solomon, S., and Mercier, D. 2010. Coastline dynamics in polar systems using remote sensing. In: Maanan M, Robin M (eds) Geomatic solutions for coastal environments. Nova Science Publishers, New York, 163–174 pp.

Overduin, P.P., Strzelecki, M.C., Grigoriev, M.N., Couture, N., Lantuit, H., St-Hilaire-Gravel, D., Günther, F., and Wetterich, S. 2014. Coastal changes in the Arctic. In: Martini IP, Wanless HR (eds) Sedimentary coastal zones from high to low latitudes: similarities and differences. Geological Society London Special Publications 388. http://dxdoi.org/101144/SP38813

Da Silva, A.O., et al. 2022. Glacier retreat leading to new coastal landforms in the Canadian high Arctic. [Poster]. In Arcticnet Annual Scientific Meeting 2022 Conference Book of Abstracts. https://doi.org/10.1139/as-2023-0007

Strzelecki, M.C., Long, A.J., and Lloyd, J.M. 2017. Post-Little Ice Age development of a High Arctic paraglacial beach complex. Permafrost and Periglacial Processes, 28(1), 4–17. https://doi.org/10.1002/ppp.1879

Strzelecki, M., Małecki, J., and Zagórski, P. 2014. The influence of recent deglaciation and associated sediment flux on the functioning of Polar Coastal Zone – Northern Petuniabukta, Svalbard. Coastal Research Library, Sediment Fluxes in Coastal Areas, 10, 23–45. https://doi.org/10.1007/978-94-017-9260-8_2

Strzelecki, M.C., Szczuciński, W., Dominiczak, A., Zagórski, P., Dudek, J., and Knight, J. 2020. New fjords, new coasts, new landscapes: The geomorphology of paraglacial coasts formed after recent glacier retreat in Brepollen (Hornsund, southern Svalbard). Earth Surface Processes and Landforms, 45(5), 1325–1334. https://doi.org/10.1002/esp.4819

Organic carbon composition and transport linked to wind forcing in the nearshore zone of Herschel Island, Qikiqtaruk (NW-Canada)

Pia Petzold[1,2], Hugues Lantuit[1,2] & Michael Fritz[1]

[1]*Section Permafrost at the Alfred-Wegener Institute Helmholtz Centre for Polar- and Marine Research, Potsdam, Germany*

[2]*Institute for Geosciences at the University of Potsdam, Potsdam, Germany*

Arctic coastal areas underlain by permafrost are significantly affected by the effects of global climate change. Rising permafrost temperatures, reduced sea ice cover and warmer seawater temperatures are all contributing to increased coastal erosion. This process releases carbon stored in permafrost into the adjacent coastal zone, where it is degraded, with the potential risk of releasing greenhouse gases (GHGs) into the atmosphere. However, the transport pathways and degradation processes of organic carbon (OC) in the nearshore zone are not well understood. To address this knowledge gap, we repeatedly sampled the nearshore zone of Herschel Island, Qikiqtaruk, Canada, for dissolved and particulate OC (DOC, POC) in order to capture the temporal intraseasonal variability of coastal biogeochemistry. The sampling was conducted along two transects in two consecutive weeks in July 2022. One transect was situated directly offshore of a retrogressive thaw slump, while the other was located in front of a permafrost cliff coast. Each transect comprised six sampling stations spanning from 10 to 1000 m offshore (Figure 1). Water temperature, water depth, electrical conductivity and salinity were determined using a CTD CastAway. For water depths less than 5 m, two water samples were collected at the surface and near the seafloor using a UWITEC water sampler. For depths exceeding 5 m, a third sample was obtained at the thermocline depth. Turbidity was recorded once per sample with a HACH 2100Q turbidity meter. Subsequently, the collected seawater was filtered through 0.7 µm GF/F filters. The filtrate was analyzed for DOC and total dissolved nitrogen (TDN) using a Shimadzu TOC-L with TNM-L module. Inorganic carbon was removed from the filter residues, which were then analyzed for POC and total particulate nitrogen (TPN) content, $\delta^{13}C$ and $\delta^{15}N$ using an elemental analyzer isotope mass spectrometer (EA-IRMS) at the University of California Stable Isotope Facility (Davis, USA). When feasible, the permafrost cliff transect was sampled for marine surface sediment. Those samples were analyzed for grain size, mercury, carbon and nitrogen content. The data shows a clear gradient in temperature, turbidity and organic carbon content (dissolved and particulate) in the water column, especially in the beginning of the sampling period. The influence of the Mackenzie River plume and the discharge from the slump is evident, with turbidity values between 3.8 and 205 FNU and salinities from 3.0 up to 31.9 PSU. Field parameters will be correlated with ERA5 wind data to indicate the variability in how geochemical properties are affected by wind direction and speed. Multivariate statistics will determine and quantify the relation between water/sediment properties and environmental forcing factors.

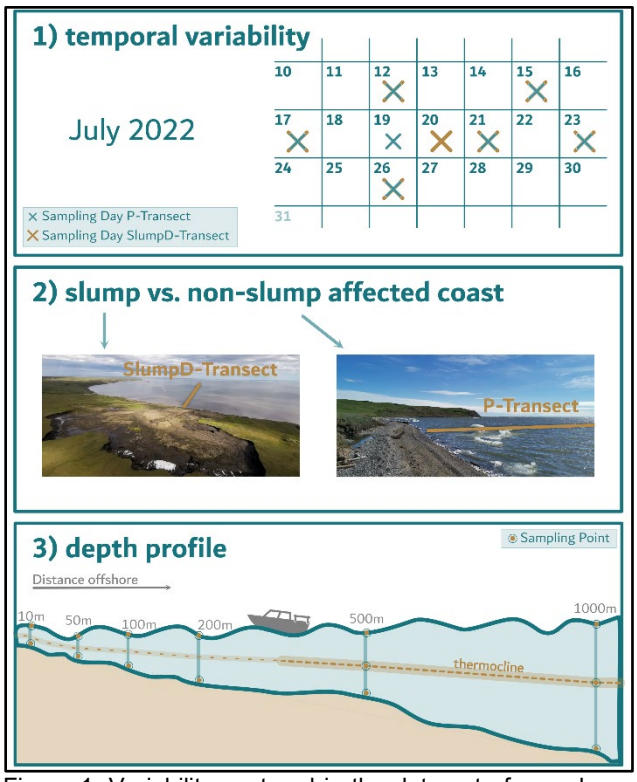

Figure 1. Variability captured in the data set of nearshore biogeochemical parameters.

Paraglacial coastal systems hit by big waves — Impacts, landforms, geohazard resilience

Mateusz C. Strzelecki[1], Malgorzata Szczypinska[1], Oskar Kostrzewa[1], Jan Kavan[2], Louise Farquharson[3], Mette Bendixen[4] & Alexandre Normandeau[5]

[1]*Alfred Jahn Cold Regions Research Centre, Institute of Geography and Regional Development, University of Wroclaw, Wroclaw, Poland*

[2]*Faculty of Science, University of South Bohemia, Ceske Budejovice, Czechia*

[3]*Permafrost Laboratory Geophysical Institute, University of Alaska, Fairbanks, Alaska, United States*

[4]*Department of Geography, McGill University, Montréal, Québec, Canada*

[5]*Geological Survey of Canada, Natural Resources Canada, Dartmouth, Canada*

Over the last century, rapid retreat of glaciers exposed vast areas of new land, particularly steep and unstable slopes along numerous Arctic and subarctic fjords and coasts (Kavan and Strzelecki 2023). Recent observations from Greenland and Alaska showed that landslides coming down those slopes may trigger massive tsunamis (Dahl-Jensen et al. 2004; Buchwal et al. 2015; Higman et al. 2018; Strzelecki and Jaskólski 2020; Svennevig et al. 2023). In contrast to tropical and mid-latitude tsunamis, the effects of cold region events remain on the landscape for long periods. Interestingly, there is no information on tsunami impact in regions deglaciated over the Holocene which experienced rapid paraglacial transformation destabilizing, not only terrestrial environments but also submarine landscapes of fjords.

At the same time, the coastal zones of rapidly deglaciating Arctic regions are influenced by other extreme processes. The calving of the glaciers often produce tsunami-like waves which pose a serious threat to coastal environments (e.g., Nielsen 1992; Lüthi and Vieli 2016). Those waves are able to move and redistribute icebergs, growlers or sea-ice across a fjord and flood and remodel local cliffs and beaches. In addition rolling of icebergs also may result in the formation of waves which in constraining topography of steep, bedrock shores may reach significant heights and pose environmental threat (Long et al. 2015).

Here we present the results of case studies carried out in western Greenland and concentred on the effects of two tsunamis that hit the coast of northern Disko Island (2000) and Karrat Fjord (2017). In both locations, tsunamis not only led to severe infrastructure damage but also destroyed tundra vegetation, eroded local beaches, and left on shore a diverse range of sediment accumulations.

In addition, we present the results of analyses of over 90 years of coastal zone changes (1929-2023) that occurred in front Equip Sermia, one of the best studied marine-terminating glaciers in Western Greenland. We show that calving-derived waves play a dominant role in the transformation of the lateral moraine and formation of the beach and spit system south of glacier front. Finally, we show examples of the role of iceberg roll waves in remodelling the relief of small pocket beaches scattered along the west coast of Greenland.

Importantly, in most of the studied coasts, human activity has concentrated and the current intensification of geohazards has a direct impact on the safety of the population and settlement infrastructure.

ACKNOWLEDGEMENTS

This study is the contribution to the National Science Centre project “GLAVE” (Award No. UMO-2020/38/E/ST10/00042) awarded to MCS. Andrzej and Halina Górajek are thanked for providing unique logistical service and a safe cruise to western Greenland on S/Y Ocean A.

REFERENCES

Buchwał, A.S., Szczuciński, W., Strzelecki, M.C., and Long, A.J., 2025. New insights into the 21 November 2000 tsunami in West Greenland from analyses of the tree-ring structure of Salix glauca, Polish Polar Research 36, 51–65. https://doi.org/10.1515/popore-2015-0005

Dahl-Jensen, T., Larsen, L.M., Pedersen, S.A.S., Pedersen, J., Jepsen, H.F., Pedersen, G., et al. 2004. Landslide and Tsunami 21 November 2000 in Paatuut, West Greenland, Nat. Hazards, 31, 277–287. https://doi.org/10.1023/b:Nhaz.0000020264.70048.95

Higman, B., Shugar, D.H., Stark, C.P., Ekstrom, G., Koppes, M.N., Lynett, P., et al. 2018. The 2015 landslide and tsunami in Taan Fiord, Alaska. Scientific Reports 8, 12993. https://doi.org/10.1038/s41598-018-30475-w

Kavan, J., and Strzelecki, M.C., 2023. Glacier decay boosts formation of new Arctic coastal environments – perspectives from Svalbard. Land Degradation & Development, 34 (12), 3467–3474. https://doi.org/10.1002/ldr.4695

Long, A.J., Szczuciński, W., and Lawrence, T. 2015. Sedimentary evidence for a mid-Holocene iceberg-generated tsunami in a coastal lake, west Greenland, Arktos, 1, 6. https://doi.org/10.1007/s41063-015-0007-7

Lüthi, M.P., and Vieli, A. 2016. Multi-method observation and analysis of a tsunami caused by glacier calving, The Cryosphere, 10, 995–1002. https://doi.org/10.5194/tc-10-995-2016

Nielsen, N. 1992. A boulder beach formed by waves from a calving glacier; Eqip Sermia, West Greenland. Boreas, 21, 159–168.

Strzelecki, M.C., and Jaskólski, M.W. 2020. Arctic tsunamis threaten coastal landscapes and communities -Survey of Karrat Isfjord 2017 tsunami effects in Nuugaatsiaq, western Greenland. Natural Hazards and Earth System Sciences, 20(9), 2521–2534. https://doi.org/10.5194/nhess-20-2521-2020

Svennevig, K., Keiding, M., Korsgaard, N.J., Lucas, A., Owen, M., Poulsen, M.D., et al. 2023. Uncovering a 70-year-old permafrost degradation induced disaster in the Arctic, the 1952 Niiortuut landslide-tsunami in central West Greenland. Science of the Total Environment, 859. https://doi.org/10.1016/j.scitotenv.2022.160110

Disentangling the fate of eroded carbon from permafrost coasts in the Canadian Beaufort Sea

Fleur van Crimpen[1], Lina Madaj[1], Joost van Genuchten[1], Deva-Lynn Pokiak[2], Dustin Whalen[3], Tommaso Tesi[4] & Jorien E. Vonk[1]

[1]*Department of Earth Sciences, Vrije Universiteit Amsterdam, Amsterdam, Noord-Holland, The Netherlands*
[2]*Hamlet of Tuktoyaktuk, Tuktoyaktuk, Northwest Territories, Canada*
[3]*Natural Resources Canada, Dartmouth, Nova Scotia, Canada*
[4]*National Research Council, Institute of Polar Sciences, Bologna, Emilia-Romagna, Italy.*

About one-third of the world's coastlines consist of Arctic permafrost (Lantuit et al. 2013). Due to amplified Arctic warming, coastal erosion has significantly intensified since the 2000s with as result thaw slumps and collapsing coasts (Jones et al. 2020). This process poses threats to Indigenous communities (Irrgang et al. 2018), due to subsidence and erosion. The erosion rate depends on factors such as cliff height, physical exposure, ground-ice content and, coastal morphology (Solomon 2005). External forces such as storms, sea-ice loss, and increased precipitation are becoming drivers of change. Additionally permafrost soils store vast amounts of organic carbon (OC) and the thawing and erosion of permafrost coasts release this carbon into the marine system (Figure 1; Hugelius et al. 2013; Jong et al. 2020).

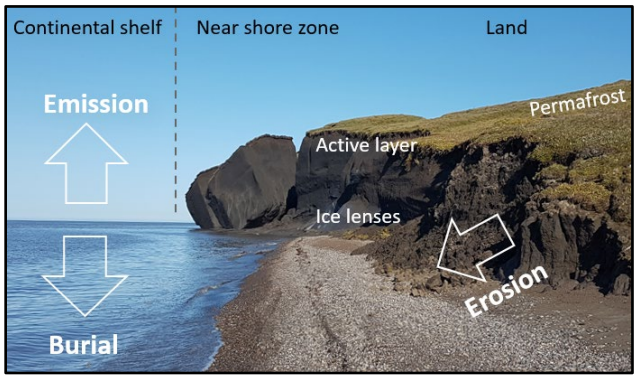

Figure 1. Schematic overview of thawing permafrost and its release into the marine system where it can be deposited on the sea floor or degraded into CO_2.

Studies estimated total OC released from eroding permafrost coasts by using bulk measurements (Irrgang et al. 2018; Lantuit et al. 2013). However, the behaviour and fate of thawed material upon release into the marine system, which depends on its hydrodynamic properties, remains poorly understood (Tesi et al. 2016a; Wakeham et al. 2009). In this study we sampled eroding permafrost coastal exposures at eight locations along the Canadian Beaufort Sea. We performed density and size-fractionation on all samples and subsequently analysed for geochemical properties to assess the characteristics and fate of the thaw-eroded material.

Study area and methods

The study area reaches from King Point in the west to McKinley Bay in the east and is located within the plume of the Mackenzie Delta. The eight sampling locations are representative for local variability in geomorphology, cliff height, ground ice content, and erosion rates. At each sampling location we collected parent material samples (actively eroding thaw slumps; n=5) and sediment and water samples (n=5 at each location). Water samples were collected in two parallel zones along the coast that we qualified as the resuspension zone (RZ) and the deposition zone (DZ) based on a combination of distance from shore, water depth, and turbidity. Both the sediment and parent material samples were fractionated based on density (cut-off 1.8 g/ml), enabling the separation of low-density (LD) and high-density (HD) fractions. The HD fraction was subsequently sieved over a >38µm, >63µm, and >200µm mesh. Each fraction was analysed for their OC, Total Nitrogen, $\delta^{13}C$ and $\Delta^{14}C$ content. This enables us to estimate the total coastal OC that enters the nearshore, and, based on the fractional partitioning of that OC, to identify the expected hydrodynamic pathways within the marine system. This provides novel insights into the transport and settling dynamics further offshore.

Preliminary results

Results reveal distinct weight and OC content partitioning between fractions. The HD<38µm fraction dominates by weight, yet the buoyant LD and HD<38µm together hold a substantial portion of OC content. With increasing grain size, we observe a decline in median OC-content. The LD fraction (median + IQR 29.1 ± 10.5 % OC) stands out but the sinking HD fractions, all significantly lower in OC% show a declining OC-content with increasing grain size

(0.96 OC ± 0.66% for HD<38µm to 0.23 ± 0.28% for HD>200µm) (Figure 2).

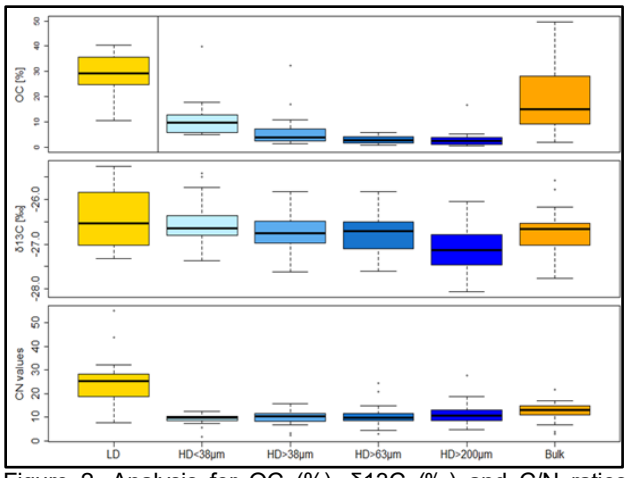

Figure 2. Analysis for OC (%), δ13C (‰) and C/N ratios shown for all analysed fractions (van Crimpen et al. in prep).

On average the LD and HD<38µm fractions, the fractions that remain mostly buoyant in the water column, together hold 77%-98% OC. The HD>38µm, HD>63µm and HD>200µm fractions hold 51% of the weight, yet only averaged per location between 1.5-23% of the total OC within the parent material.

The different fractions show varying stable carbon isotopic ratios ($\delta^{13}C$) and a range of radiocarbon isotopic ratios ($\Delta^{14}C$) which indicate a broad range of OC ages, emphasizing the heterogeneity of these permafrost sources (Figure 2). We observe that within one site, ages of different fractions are homogeneous, yet differences between different sites are significant

Discussion and conclusions

We found that the implication of fractional partitioning is of importance for marine degradation potential. Buoyant fractions, including LD and HD<38µm, constitute the majority of total OC and are more prone to degradation and CO_2 release. In contrast, sinking fractions (HD>38µm, >63µm, and >200µm) contribute less to the total OC and are expected to be buried in the nearshore zone, or transported offshore across the seabed.

Fractionation and geochemical analyses of the suspended matter and underlying sediments in the resuspension and deposition zone will allow for a comparison with hydrodynamic pathways based on hydrodynamic fractionation of the parent material samples. In conclusion, hydrodynamic fractionation provides a nuanced understanding of carbon release and expected pathways of coastal permafrost erosion. This study emphasises the importance of buoyant fractions in potential contribution to CO_2 evasion and allows for more accurate predictions of the fate and impact of eroding permafrost-derived carbon in the changing Arctic environment.

References

Hugelius, G., Tarnocai, C., Broll, G., Canadell, J.G., Kuhry, P., and Swanson, D.K. 2013. The northern circumpolar soil carbon database: Spatially distributed datasets of soil coverage and soil carbon storage in the northern permafrost regions. Earth System Science Data, 5(1), 3–13. https://doi.org/10.5194/essd-5-3-2013

Irrgang, A.M., Lantuit, H., Manson, G.K., Günther, F., Grosse, G., and Overduin, P.P. 2018. Variability in Rates of Coastal Change Along the Yukon Coast, 1951 to 2015. Journal of Geophysical Research: Earth Surface, 123(4), 779–800. https://doi.org/10.1002/2017JF004326

Jones, B.M., Irrgang, A.M., Farquharson, L.M., Lantuit, H., Whalen, D., Ogorodov, S., Grigoriev, M., Tweedie, C., Gibbs, A.E., Strzelecki, M.C., Baranskaya, A., Belova, N., Sinitsyn, A., Kroon, A., Maslakov, A., Vieira, G., Grosse, G., Overduin, P., Nitze, I., Romanovsky, V.E. (n.d.). NOAA Arctic Report Card 2020. https://doi.org/10.25923/e47w-dw52

Jong, D., Bröder, L., Tanski, G., Fritz, M., Lantuit, H., Tesi, T., Haghipour, N., Eglinton, T.I., and Vonk, J.E. 2020. Nearshore Zone Dynamics Determine Pathway of Organic Carbon from Eroding Permafrost Coasts. Geophysical Research Letters, 47(15). https://doi.org/10.1029/2020GL088561

Lantuit, H., Overduin, P.P., and Wetterich, S. 2013. Recent progress regarding permafrost coasts. Permafrost and Periglacial Processes, 24(2), 120–130. https://doi.org/10.1002/ppp.1777

Tesi, T., Semiletov, I., Dudarev, O., Andersson, A., and Gustafsson, Ö. 2016a. Matrix association effects on hydrodynamic sorting and degradation of terrestrial organic matter during cross-shelf transport in the Laptev and East Siberian shelf seas. Journal of Geophysical Research: Biogeosciences, 121(3), 731–752. https://doi.org/10.1002/2015JG003067

Solomon, S.M. 2005. Spatial and temporal variability of shoreline change in the Beaufort-Mackenzie region, northwest territories, Canada. Geo-Marine Letters, 25(2–3), 127–137. https://doi.org/10.1007/s00367-004-0194-x

Wakeham, S.G., Canuel, E.A., Lerberg, E.J., Mason, P., Sampere, T.P., and Bianchi, T.S. 2009. Partitioning of organic matter in continental margin sediments among density fractions. Marine Chemistry, 115(3–4), 211–225. https://doi.org/10.1016/j.marchem.2009.08.005

4 Permafrost Geomorphology & Hazards

INTEGRATING PERSPECTIVES OF PERMAFROST THAW, CHANGE, AND ADAPTATION

Permafrost Geomorphology & Hazards

4A — Rock Glaciers and Rock Slope Instability

Session Chairs: Kaytan Kelkar[1], Michael Krautblatter[2], Isabelle Gärtner-Roer[3], Francesco Brardinoni[4] & Regina Plasken[2]

[1]*Geophysical Institute Permafrost Laboratory, University of Alaska Fairbanks, Alaska, United States*
[2]*Technical University of Munich, Munich, Germany*
[3]*Glaciology and Geomorphodynamics Group, University of Zurich, Zurich, Switzerland*
[4]*Department of Biological, Geological and Environmental Sciences, University of Bologna, Bologna, Italy*

Mountain terrain is very sensitive to climate change. This is evident from observed shifts in mountain permafrost thermal regimes which is a precursor to trigger cascading geohazards from rock glacier destabilizations and rock slope failures. Rock glaciers are debris landforms generated by the former or current creep of frozen ground (permafrost), where creep refers to the variable combination of both internal deformation and shearing at depth. Their spatial distribution and dynamics are influenced by a combination of factors including topography, lithology, debris supply, internal structure as well as local-to-regional climatic conditions. In recent years, rock glaciers have received growing attention beyond permafrost investigation, involving disciplines such as geomorphology, hydrology, (paleo)climatology, ecology, and engineering. There is a growing need to better characterize unstable mountain permafrost slopes which is vital to ensure the safety of mountain communities and minimize damage to critical infrastructure in high-mountain areas.

Rock glacier velocity and changing active layer thickness impacting permafrost-affected rock slopes are listed as Essential Climate Variables (ECV) permafrost within the Global Climate Observing System (GCOS). Hence, reflecting both rock glaciers and rock slope instabilities as geomorphological indicators to indirectly track the evolution of mountain permafrost in a changing climate. Despite the growing number of studies highlighting the significance of rock glaciers and permafrost-affected rock slopes predisposed to cause cascading geohazards from destabilizations, or as key water stores in arid mountain environments, our understanding of the effects of climate-driven permafrost degradation on rock glacier state and evolution, and rock slope instability is limited.

This session aims to bring together experts from varied backgrounds to further advance our understanding of rock glaciers and rock slope instabilities in mountain permafrost environments. We welcome contributions addressing single rock glaciers, regional inventories, their kinematic or structural characterization and risk assessment, involving for example geophysical surveying, field observations, remote sensing or modelling approaches. The session accepts a wide range of topics, including rock mechanics, frozen soil engineering, hydrogeology, geothermal modelling, risk assessment, mitigation design, monitoring, climate change or the impact of human activities, with the objective of contributing to the advancement of our understanding of rock slope stability in mountain permafrost environments and reducing risk for vulnerable locations. Specifically, we are also encouraging the presentation of case studies.

We strive to promote discourse outlining novel techniques, monitoring, and multidisciplinary research between researchers, regional planners or public sector representatives, and partners to enhance our understanding of rock glacier evolution and rock slope instability in a warming climate.

Holocene cryo-geomorphological dynamics in the upper Río Limarí basin (30-31°S), Subtropical Andes of Chile: paleoclimatic implications for the origin of rock glaciers

Javiera Carraha[1,2], Juan-Luis García[1,2], Samuel U. Nussbaumer[3], Isabelle Gärtner-Roer[3] & Hans Fernández-Navarro[4]

[1]*Instituto de Geografía, Pontificia Universidad Católica de Chile, Santiago, Chile*

[2]*Centro UC Desierto de Atacama, Pontificia Universidad Católica de Chile, Santiago, Chile*

[3]*Department of Geography, University of Zurich, Zurich, Switzerland*

[4]*Instituto de Ciencias Agroalimentarias, Animales y Ambientales, Universidad de O´Higgins, San Fernando, Chile*

In the Subtropical Andes of Chile, the cryosphere is highly sensitive to climate changes (Bodin et al. 2010). This mountainous landscape, abundant in debris, showcases landforms resulting from the interplay between glacial and periglacial dynamics that have shaped the landscape from the Last Glacial Maximum (LGM) to the present. These well-preserved landforms present an excellent opportunity for better understanding the intricate atmosphere-cryosphere interactions concerning climate shifts (Fernández et al. 2023; García et al. 2014; Knight and Harrison 2014; Lira et al. 2022).

The headwaters of the Río Limarí basin (30-31°S; ~3000-5000 m a.s.l) are part of the semiarid Andes of Chile, which are still influenced by the mid-latitude westerly winds and intersect the Arid Diagonal in the south. Precipitation occurs mainly in winter associated with a weakened South Pacific Anticyclone, with its interannual variability influenced by the El Niño Southern Oscillation (ENSO) (Garreaud 2009). The dry and cold conditions lead to the ubiquitous presence of landforms associated with ice-rich permafrost, such as rock glaciers. In fact, rock glaciers in the Río Limarí basin cover an area of ~25.6 km^2 (DGA 2022). However, the origin and processes of rock glaciers as well as the evolution of the cryosphere since the last Glacial Termination (~18-11 ka; Denton et al. 2010) is an unresolved issue (Knight et al. 2019), and of increasing relevance due to the potential of rock glaciers as water reserves in these areas experiencing drought conditions (Azócar and Brenning 2010; Fernández and Ferrando 2018).

A mosaic of glacial, periglacial, and paraglacial landforms is identified in the Andean portion of the Río Limarí basin, accounting for the interaction and succession between glacial, paraglacial, and periglacial dynamics occurring since the Late Pleistocene to the present (Carraha et al. in press). The retreat of glaciers likely triggered periglacial dynamics in this Andean environment. In this context, our focus lies on interpreting the cryo-geomorphology and its climatic implications in the Río Limarí basin, specifically considering potential variations in glacial and periglacial domains throughout the Holocene. Our objective involves analyzing the origins of rock glaciers and the factors influencing their spatial distribution. This is acknowledging that the diversity, frequency, and distribution of rock glaciers serve as crucial indicators of regional cryosphere evolution dynamics (Frauenfelder and Kääb 2000). Additionally, we aim to assess the presence and distribution of permafrost in the valley while exploring the role of ENSO in influencing the glacial-periglacial domains controlling the landscape.

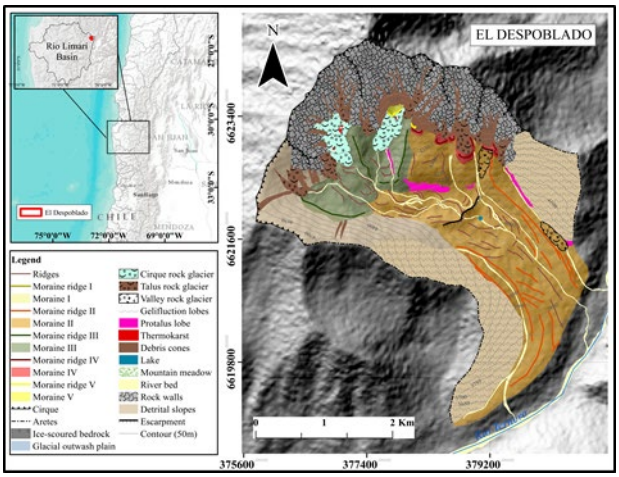

Figure 1. Geomorphological map of El Despoblado Valley.

Therefore, we present a detailed, field-based reconstruction of the geomorphology in the upper Río Limarí basin. Our methodology involves field work and remote sensing analysis to conduct detailed geomorphological mapping in El Despoblado valley (30°31'S; 3600-5400 m a.s.l) (Figure 1), a formerly glaciated valley situated in the head of the Río Limarí basin. Through the meticulous geomorphological mapping carried out in this valley, we have identified different types of rock glaciers, such as cirque, talus, and valley rock glaciers, as well as more complex

landforms including ‘debris rock glaciers’ (Barsch 1996) or moraine-derived rock glaciers (Lilleøren and Etzelmüller 2011), suggesting periglacial reworking of glacial deposits. We have also identified rock glaciers whose geomorphological features suggest different degrees of activity and which act as indicators for the occurrence of permafrost conditions in the valley (Barsch 1992; Buckel et al. 2021).

Our ongoing efforts aim to shed light on the causal relationship between glacial retreat and the formation of rock glaciers within this study area. Furthermore, surface exposure dating efforts have been made to establish temporal constraints for these geomorphic records. These findings from a barely explored region in the Andes, to be presented during the International Conference on Permafrost ICOP2024, provide valuable insights into understanding landscape transformations amidst regional climate changes and increasing aridity.

Acknowledgements

This work is supported by ANID Chile/ scholarship program/ Doctorado Nacional, and FONDECYT, Chile #1200935 awarded to J.-L.G. S.U.N and J.-L.G acknowledge support from the Swiss National Science Foundation (project IZSEZ0_215412).

References

Azócar, G.F, and Brenning, A. 2010. Hydrological and Geomorphological significance of rock glaciers in the Dry Andes, Chile (27–33°S), Permafrost and Periglacial Processes. 21, 42–53. https://doi.org/10.1002/ppp.669

Barsch, D. 1992. Permafrost creep and rockglaciers, Permafrost Periglacial Process, 3, 175–188. https://doi.org/10.1002/PPP.3430030303

Barsch, D. 1996. Rockglaciers: indicators for the present and former geoecology in high mountain environments, Springer, Berlin, Heidelberg.

Bodin, X., Rojas, F., and Brenning, A. 2010. Status and evolution of the cryosphere in the Andes of Santiago (Chile, 33.5°S.), Geomorphology, 118, 453–464. https://doi.org/10.1016/j.geomorph.2010.02.016

Buckel, J., Reinosch, E., Voigtländer, A., Dietze, M., Bücker, M., Krebs, N., Schroeckh, R., Mäusbacher, R., and Hördt, A. 2022. Rock glacier characteristics under semiarid climate conditions in the western Nyainqêntanglha range, Tibetan Plateau. Journal of Geophysical Research: Earth Surface,127. https://doi.org/10.1029/2021JF006256

Carraha, J., García, J.-L., Nussbaumer, S.U., Fernández-Navarro, H., and Gärtner-Roer, I. (In press). Late Pleistocene to Holocene glacial, periglacial and paraglacial geomorphology of the upper Río Limarí basin (30-31°S) in the Andes of central Chile, Journal of Maps. http://dx.doi.org/10.1080/17445647.2024.2329179

Denton, G.H., Anderson, R.F., Toggweiler, J.R., Edwards, R.L., Schaefer, J.M., and Putnam, A.E. 2010. The last glacial termination, Science, 328, 1652–1656. https://doi.org/10.1126/science.1184119

DGA. 2022. Inventario público de glaciares. Dirección General de Aguas, Santiago, Chile.

Fernández-Navarro, H., García, J.L., Nussbaumer, S.U., Tikhomirov, D., Pérez, F., Gärtner-Roer, I., Christl, M., and Egli, M. 2023. Fluctuations of the Universidad Glacier in the Andes of central Chile (34°S) during the latest Holocene derived from a 10Be moraine chronology, Quaternary Science Reviews, 300. https://doi.org/10.1016/j.quascirev.2022.107884

Fernández-Navarro, H.A., and Ferrando, F.J. 2018. Glaciares rocosos en la zona semiárida de Chile: relevancia de un recurso hídrico sin protección normativa, Cuadernos de Geografía: Revista Colombiana de Geografía, 27, 338–355. https://doi.org/10.15446/rcdg.v27n2.63370

Frauenfelder, R., and Kääb, A. 2000. Towards a palaeoclimatic model of rock-glacier formation in the Swiss Alps, Annals of Glaciology, 31, 281–286. https://doi.org/10.3189/172756400781820264

García, J.L., Pizarro, F., and Calcagni, V. 2014. Fluctuaciones glaciales holocénicas en el Cajón del Maipo, Andes Centrales de Chile: observaciones morfoestratigráficas de los glaciares Loma Larga y Nieves Negras in: Borsdorf, A., Sánchez, R., Hidalgo, R., and Zunino, H.M. (Eds.), Los riesgos traen oportunidades: Transformaciones globales en Los Andes sudamericanos. pp. 35–52.

Garreaud, R.D. 2009. The Andes climate and weather, Advances in Geosciences, 22, 3–11. https://doi.org/10.5194/adgeo-22-3-2009

Knight, J., and Harrison, S. 2014. Mountain glacial and paraglacial environments under global climate change: lessons from the past, future directions and policy implications, Geografiska Annaler: Series A, Physical Geography, 96, 246–264. https://doi.org/10.1111/geoa.12051

Lilleøren, K.S., and Etzelmüller, B. 2011. A regional inventory of rock glaciers and ice-cored moraines in Norway, Geografiska Annaler: Series A, Physical Geography, 93, 175–191. https://doi.org/10.1111/j.1468-0459.2011.00430.x

Lira, M.P., García, J.L., Bentley, M.J., Jamieson, S.S.R., Darvill, C.M., Hein, A.S., Fernández, H., Rodés, Á., Fabel, D., Smedley, R.K., and Binnie, S.A. 2022. The Last Glacial Maximum and deglacial history of the Seno Skyring Ice Lobe (52°S), Southern Patagonia, Frontiers in Earth Science (Lausanne), 10, 892316. https://doi.org/10.3389/feart.2022.892316

Deciphering the evolution of rockglacier Murtèl by a multi-methodological approach

Flurina Durisch[1], Isabelle Gärtner-Roer[1], Gwendolyn J.-M.C. Leysinger Vieli[1], Andreas Vieli[1], Alessandro Cicoira[1], Theo M. Jenk[2] & Margit Schwikowski[2]

[1]*Department of Geography, University of Zurich, Zurich, Canton of Zurich, Switzerland*
[2]*Paul Scherrer Institute, Villigen, Canton of Aargau, Switzerland*

Rockglaciers are distinct morphological indicators for the current and former occurrence of permafrost and act as important debris-transport systems in periglacial environments. For the enhanced use of these landforms as palaeoclimatic indicators, more insights are needed towards landform dynamics, genesis and evolution.

Rockglacier ages

In the European Alps, several attemps have been made in recent years to compile and reconstruct rockglacier ages; by description of flow-lines of horizontal surface velocities (Kääb et al. 1998), by surface-exposure dating (Haeberli et al. 2003, Amschwand et al. 2021), by ^{14}C dating of organic material from ice cores (Krainer et al. 2015), and modeling approaches (e.g. Müller et al. 2016).

Study site

Rockglacier Murtèl is located in Eastern Switzerland below the northern face of Piz Corvatsch (3300 m a.s.l.) and has a very long tradition in permafrost research as well as longterm monitoring (Gärtner-Roer and Hoelzle 2021, Hoelzle et al. 2002, PERMOS 2023). This ice-rich landform with distinct furrow-and-ridge topography has a length of 280 m and a mean slope of 12°. A new borehole was drilled in 2015 at about 160 m above the rockglacier front.

Methods

In a recent attempt, we follow a multi-method approach to decipher the evolution of rockglacier Murtèl in more detail (surface and depth). The corresponding data result from:

- Monitoring of subsurface deformation in a deep permafrost borehole (2015-2023).
- Geodetic surveys of selected boulders to quantify high-resolution annual horizontal velocities and vertical changes (2009-2023).
- Analysis of aerial images to compile multi-annual to decadal horizontal velocities and vertical changes (Fig. 1; Durisch 2023). The results build the basis for the streamline reconstruction (Fig. 2).
- 14C dating of water-insoluble organic carbon (14C-WIOC) by accelerator mass spectrometry from depths 11.4 m and 21.8 m in the rock glacier ice core taken in 2015 (Bella et al. 2020).
- Numerical age-layer modeling to analyse the age-depth profiles and thereby constrain the governing processes of flow and material accumulation patterns and rates.

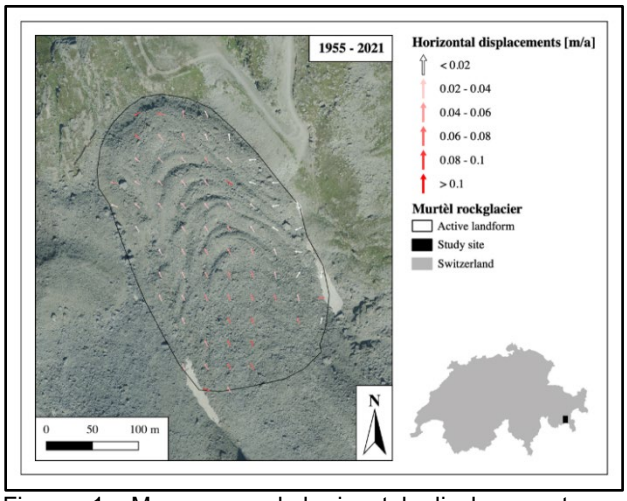

Figure 1. Mean annual horizontal displacements on rockglacier Murtèl of the period 1955 – 2021, compiled from digital photogrammetry. The location of the study site is indicated in the lower right.

Results

Borehole deformations show high rates at the shear horizon at 26 to 28 m depth and total displacement rates of 8-10 cm a^{-1} at the rockglacier surface. Repeated geodetic surveys between 2009 and 2023 indicate mean annual surface velocities between 7 and 15 cm ± 2 cm. Mean annual horizontal velocities derived from aerial images (1955-2021) are in the range of 2 to 10 cm. Kääb et al. (1998) provided first insight in the distribution of surface ages ranging from 6000 to 9000 years from flow trajectories derived from photogrammetry. Re-calculations of stream lines from recent in-situ and photogrammetric analyses (Durisch 2023) indicate ages of 5000 to 6000 years (Fig. 2). The two ^{14}C datings from different depths in

the rockglacier core yield ages of 2999 ± 646 cal yr BP (11.4 m) and 4736 ± 753 cal yr BP (21.8 m), which fit relatively well with findings from another Alpine rockglacier (Bella et al. 2020, Krainer et al. 2015). Constraining age-depth modelling with subsurface deformation, surface velocities and datings show that blockflow with a shear-horizon and a decreasing spatial pattern of material accumulation are the determining processes for the long-term evolution of Murtel rockglacier.

Discussion

Our multi-method approach provides insight into the recent dynamics as well as long-term evolution of rockglacier Murtèl. The combination of recent annual as well as decadal velocities indicates a possible range and temporal variability of creep rates over centuries and millennia. Nevertheless, distributed surface ages derived from surface velocities fit relatively well with the subsurface ages at a single location. Despite the fact that more datings are needed (and expected) from additional depths, the existing ages allow to determine the dominant processes for the genesis and long-term rockglacier evolution after deglaciation on this slope.

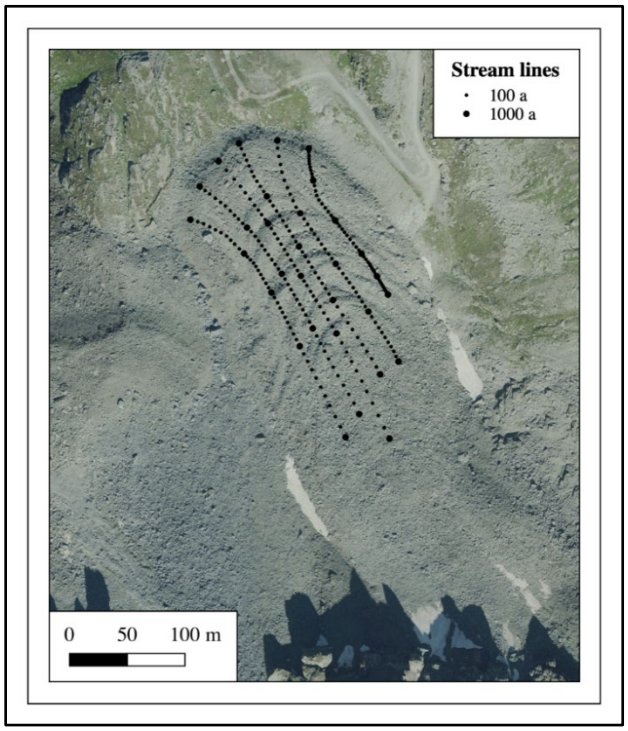

Figure 2. Streamlines reconstructed from mean annual horizontal displacements (1955-2021), indicating surfaces ages of 5-6 k years.

Acknowledgements

The aerial images were generously provided and processed (DEMs and orthophotos) by Swisstopo.

References

Amschwand, D., Ivy-Ochs, S., Frehner, M., Steinemann, O., Christl, M., and Vockenhuber, C. 2021. Deciphering the evolution of the Bleis Marscha rock glacier (Val d'Err, eastern Switzerland), The Cryosphere 15(4): 2057–2081.

Bella, V., Cicoira, A., Gärtner-Roer, I., Vieli, A., Jenk, T.M., and Schwikowski, M. 2020. Determining the age of the ice in the Murtèl rock glacier, Annual Report 2019, Laboratory of Environmental Chemistry, PSI: 32.

Durisch, F. 2023. Long-term evolution of different permafrost landforms on the northern slope of Piz Corvatsch, Engadin. Master's Thesis, Department of Geography, University of Zurich.

Gärtner-Roer, I., and Hoelzle, M. 2021. Rockglaciers of the Engadine. In: Reynard, E. Landscapes and landforms of Switzerland, Springer, Cham, Switzerland: 235–248.

Haeberli, W., Brandová, D., Burga, C., Egli, M., Frauenfelder, R., Kääb, A., Maisch, M. Mauz, B., and Dikau, R. 2003. Methods for absolute and relative age dating of rock-glacier surfaces in alpine permafrost. In: Phillips, Springman and Arenson. Permafrost: 343–348.

Hoelzle, M., Vonder Mühll, D., and Haeberli, W. 2002. Thirty years of permafrost research in the Corvatsch Furtschellas area, Eastern Swiss Alps: A review, Norsk Geografisk Tidsskrift 56: 137–145. doi:10.1080/ 002919502760056468

Kääb, A., Gudmundsson, G.H., and Hoelzle, M. 1998. Surface deformation of creeping mountain permafrost. Photogrammetric investigations on rock glacier Murtèl, Swiss Alps. Proceedings of the 7th International Conference on Permafrost, Yellowknife, Collection Nordicana 57:531–537.

Krainer, K, Bressan, D., Dietre, B., Haas, J.N., Hajdas, I., Lang, K., Mair, V., Nickus, U., Reidl, D., Thies, H., and Tonidandel, D. 2015. A 10,300-year-old permafrost core from the active rock glacier Lazaun, southern Ötztal Alps (South Tyrol, northern Italy), Quaternary Research 83(2): 324–335. doi:10.1016/j.yqres.2014.12.005

Müller, J., Vieli, A., and Gärtner-Roer, I. 2016. Rock glaciers on the run – understanding rock glacier landform evolution and recent changes from numerical flow modeling, The Cryosphere, 10(6): 2865–2886.

PERMOS 2023. Swiss Permafrost Bulletin 2022. Noetzli, J., and Pellet, C. (eds.). No. 4, 23 pp. doi:10.13093/permos-bull-23

Rockglacier dynamics on Disko Island, Western Greenland

Isabelle Gärtner-Roer[1], Andrea Kneib-Walter[1], Andreas Vieli[1], Alessandro Cicoira[1], Jan Beutel[2] & Tazio Strozzi[3]

[1]*Department of Geography, University of Zurich, Zurich, Switzerland*

[2]*Department of Computer Science, University of Innsbruck, Innsbruck, Austria*

[3]*GAMMA Remote Sensing, Gümligen, Switzerland*

Rockglaciers on Disko Island, Greenland

Different types of rock glaciers have been described for Disko Island: lobate, typically talus-derived and smaller landforms, as well as tongue-shaped landforms that reach greater lengths (up to several kilometers) and often indicate connections to present glaciers (Humlum 1982). By the analysis of InSAR data, 570 rock glaciers have been mapped on Disko Island, of which 68% are described as active, while 30% are in a transitional status (Bertone et al. 2022).

While many observations on rockglacier temperatures and kinematics, as well as related processes, are available from populated regions (e.g., the European Alps), Artic environments often lack these data due to remoteness and harsh conditions for instruments (and scientists).

Within the RockDynDisko (Rockglacier Dynamics on Disko Island) project, in-situ data on surface temperatures and displacements of rockglaciers are compiled for the first time on Disko Island, and probably also in Greenland. In combination with data from remote sensing, they allow for a thorough assessment of rockglacier dynamics and permafrost conditions under current and former climate conditions. The observations will be compared to landforms in other regions, in order to evaluate rockglacier dynamics on a global scale.

Study site

Within the project, we investigate three rockglaciers situated on the south coast of Disko Island, Central West Greenland, close to the village of Qequertarsuaq and in walking distance from the well-known Arctic Station (https://eu-interact.org/field-sites/arctic-station/). The geology of Disko Island is characterized by Precambrian gneisses and Tertiary basalts. The rockglacier material originates from the screeslopes below the basaltic cliffs. The area is influenced by a low arctic, coastal climate and lies in the transition zone between continuous and discontinuous permafrost. The rockglaciers show very different morphologies; Apostelfjeld rockglacier – for example - is about 1 km long and has two distinct tongues (Figure 1).

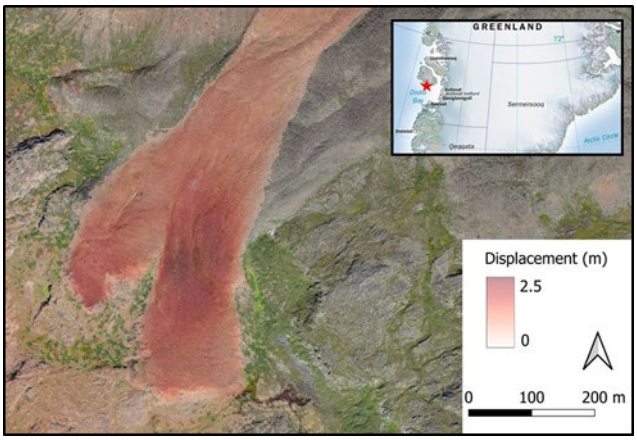

Figure 1. Total displacements (2019-2021) on Apostelfjeld rockglacier as derived from repeated UAV surveys. Study site location within Greenland (red star) is indicated in insert map (cut from SWmap.com).

Methods

The multi-method approach applied in this study is a proven combination of in-situ and remote-sensing techniques covering different spatio-temporal scales. The corresponding data result from:

- Assessment of rock glacier distribution and activity from InSAR (Spaceborne interferometric synthetic aperture radar) data from Sentinel-1 and ALOS-2 PALSAR-2 (2015-2019, Bertone et al. 2022).
- Analysis of repeated UAV (Unmanned Aerial Vehicle) surveys (2019, 2021, 2023) to compile distributed annual horizontal velocities and vertical changes for three landforms.
- Mapping of landforms and specific surface structures, such as active cracks indicating lateral shearing.
- Logging of GST (Ground Surface Temperature) on three different rockglaciers (2021-2023) with a resolution of < 0.1 °C and an accuracy of 0.1 °C at ± 20 °C (geotest.ch).
- Continuous GNSS (Global Navigation Satellite System) measurements (5 stations on 2 different rockglaciers (Figure 2); 2021-2023; Cicoira et al. 2022).

Figure 2. Surface of Apostelfjeld rockglacier with fixed GNSS station in the foreground.Results

The InSAR data did not only allow for the selection of the landforms to study in more detail, but provided basic information on kinematics. For the period 2015-2019, deformations of 0.1-0.3 m/yr are quantified for the upper part and 0.3-1 m/yr for the lower part of Apostelfjeld rockglacier (Bertone et al. 2022). These rates fit very well with the displacements derived from repeated UAV surveys in 2019 and 2021 (Figure 2). The UAV data additionally show the differences in displacement for the different lobes and zones of the rockglacier, which also explains the observed features of lateral shearing. The continuous GNSS stations were the first of its kind in Arctic environments (including e.g. the challenges related to the polar night) and proven to be feasible. The calculated rates for the selected positions also show good agreement with the data derived from remote sensing. In addition, they provide insight into seasonal patterns of horizontal displacements. The ground surface temperatures clearly indicate snow conditions and partly also reflect (rather discontinuous) permafrost conditions (when the snow cover was thick enough to decouple the ground from the atmosphere).

Discussion

Our study provides first in-situ data (temperatures and kinematics) for active rockglaciers in Greenland. The availability of this information allows for the validation of remote sensing data (e.g., InSAR data) and beyond that, provides insight into recent rockglacier dynamics. This insight builds the baseline for comparisons with other rockglaciers in the Arctic or in different environments as well as for the analysis of future changes in rockglacier dynamics.

Acknowledgements

The project RockDynDisko was kindly supported by the Swiss Polar Instiute (SPI) with an exploration grant (SPIEG-2019-003). We acknowledge the Arctic Station of University of Copenhagen for hosting us. The InSAR analysis was supported by the ESA Permafrost CCI project (grant number 4000123681/18/I-NB).

References

Bertone, A., Barboux, C., Bodin, X., Bolch, T., Brardinoni, F., Caduff, R., Christiansen, H.H., Darrow, M.M., Delaloye, R., Etzelmüller, B., Humlum, O., Lambiel, C., Lilleøren, K.S., Mair, V., Pellegrinon, G., Rouyet, L., Ruiz, L., and Strozzi, T. 2022. Incorporating InSAR kinematics into rock glacier inventories: insights from 11 regions worldwide. The Cryosphere 16: 2769–2792. https://doi.org/10.5194/tc-16-2769-2022

Cicoira, A., Weber, S., Biri, A., Buchli, B., Delaloye, R., Da Forno, R., Gärtner-Roer, I., Gruber, S., Gsell, T., Hasler, A., Lim, R., Limpach, P., Mayoraz, R., Meyer, M., Noetzli, J., Phillips, M., Pointner, E., Raetzo, H., Scapozza, C., Strozzi, T., Thiele, L., Vieli, A., Vonder Mühll, D., Wirz, V., and Beutel, J. 2022. In situ observations of the Swiss periglacial environment using GNSS instruments. Earth Syst. Sci. Data 14: 5061–5091. https://doi.org/10.5194/essd-14-5061-2022

Humlum, O. 1982. Rock glacier types on Disko, central West Greenland, Geogr. Tidsskr. J. Geogr. 82: 59–66.

A 75-year velocity time series of Cardinal Mountain rock glacier, Sierra Nevada, California

Andreas Kääb & Julie Røste
Department of Geosciences, University of Oslo, Norway

In this contribution we compile the, to our best knowledge, first multi-decadal time series of rock glacier speed in the United States, for one of the southern-most active rock glaciers on the continent. Our photogrammetric analysis for Cardinal Mountain rock glacier, Sierra Nevada, California, shows a significant increase in surface speeds between the periods 1947–1987 and 1987–2022. Analysing also airphotos from 2005 and 2016 we find no significant speed changes within the 1987–2022 period. Mean speeds increase from around 0.35 m/yr to around 1 m/yr, with local acceleration factors of up to 4, and maximum speeds of 2 m/yr. Our study demonstrates the feasibility of deriving long-term time series of rock glacier speed in the US based on USGS archive holdings of historic and modern airphotos.

Rock glacier velocity time series

Rock glacier velocity has recently become an associated product to the essential climate variable permafrost. Measured time series, in-situ observations, numerical models and theoretical considerations suggest that rock-glacier speed should be sensitive to a change in climatic boundary conditions, in particular air temperature and snow cover (Kääb et al. 2007; Pellet et al. 2023). There exist, however, only few long-term measurements of rock glacier speed globally, mostly in the European Alps, and only few elsewhere (Pellet et al. 2022). No such time series is available for North America despite the abundancy of rock glaciers across this continent.

Photogrammetric time series

Several methods exist today to build up time series of rock-glacier speed, such as ground-based surveys or GNSS, or satellite radar interferometry. None of the ground-based methods can be used, however, to reconstruct rock glacier speed time series, and archives of satellite radar images suitable for interferometric time series reach only one to two decades back in time. The only data source to reconstruct long-term time series of rock glacier speed consists in archives of photogrammetric-grade aerial photography (Kääb et al. 2021). Whereas difficult or expensive to access in many countries, such data are openly available in the US through the US Geological Survey (USGS). The purpose of this study is thus to explore the feasibility of USGS airphoto holdings to reconstruct the, to our best knowledge, first long-term time series of rock glacier speed in the contiguous US, and North America in general.

Our approach is based on standard automatic image matching between repeat orthoimages (Kääb and Vollmer 2000). We use pre-processed and already ortho-rectified airphotos for the years 1987, 2005, 2016, and 2022. The underlying original airphotos are not openly available and we thus have to rely on the given ortho-rectification quality. For the more recent image dates the data turn out to be of very good quality and well suited for our task. The older orthoimages are of reduced radiometric and geometric quality, which makes co-registration procedures necessary, reduces the number of surface features the displacement of which can be tracked, and increases the overall uncertainty of the displacement measurements.

For the year 1947 we use original scanned airphotos, obtained from USGS, reconstruct image orientation using ground-control points, and then ortho-rectify that data using the Copernicus global DEM as topographic reference.

Cardinal Mountain rock glacier

Cardinal Mountain rock glacier (lat 37.01°, lon -118.41°), Sierra Nevada, California, is one of the most southern active rock glaciers on the North-American continent (Johnson et al. 2021). Satellite interferometry based on ALOS PALSAR L-band radar images by Liu et al. (2013) and own interferometry based on recent Sentinel-1 C-band images confirm this rock glacier is highly active (0.6 m/yr estimated by Liu et al. 2013 for 2007). The rock glacier is approximately 1 km long and 150 m wide. Mean annual surface temperature is around 0.1 °C (Johnson et al. 2021). The global permafrost model by Obu et al. (2019) (which is, though, not particularly adjusted for mountain permafrost) indicates a mean annual ground temperature of 0 °C, and suggests the rock glacier is situated at the outer/lower boundary of the isolated permafrost zone.

VELOCITY FIELD AND TIME SERIES

Figure 1 shows the photogrammetric velocity field for the period 2016–2022 as derived from image matching between the 2016 and 2022 orthoimages. Maximum speeds are close to 2 m/yr.

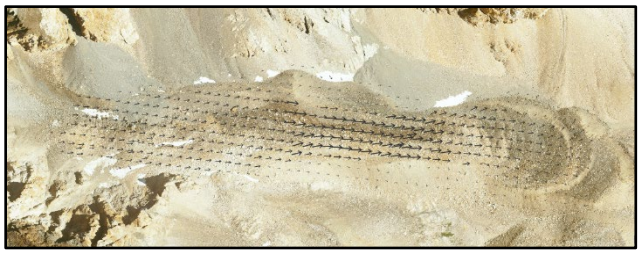

Figure 1. Photogrammetric velocity vectors 2016–2022 on Cardinal Mountain rock glacier, Sierra Nevada. Image width 1.3 km, grid distance between velocity vectors 20 m. Underlying airphoto of 2022, obtained from USGS. North to the top.

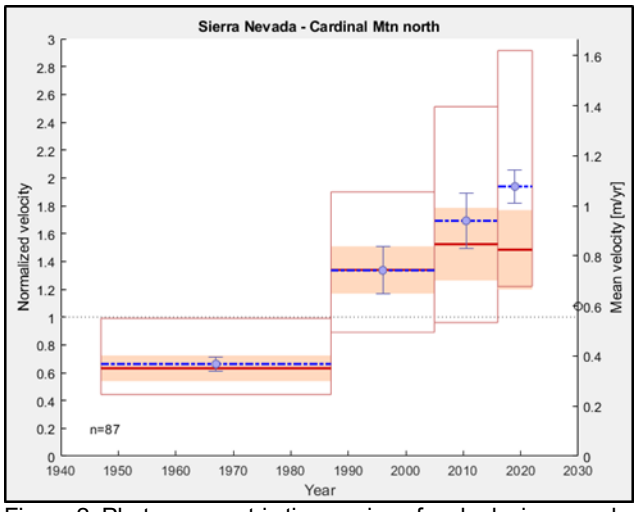

Figure 2. Photogrammetric time series of rock glacier speeds 1947–2022. Horizontal point-dashed blue bars for the individual periods are mean speeds, red bars are median speeds. Light red areas are the box-plot notches, red rectangles the interquartile range (25%–75%) of the individual measured speeds. Blue error bars are the mean stable ground offsets around the rock glacier. Left axis indicates normalized speeds relative to the mean speed over all periods, right axis the mean speed in m/yr. The y=1 dashed line refers to the median speed, the small circle on the right y-axis to the overall mean speed.

Figure 2 shows the results of our measured time series. Non-overlapping notches (light red areas) in the plot Figure 2 indicate that the individual period median speeds are significantly different at the >95% significance level. These notches and the non-overlapping errors bars (blue in Figure 2) from stable ground measurements indicate that the 1947–1987 speeds are significantly different from the 1987–2022 speeds. Within the latter period we observe no(medians) or only weakly significant (means) rock glacier acceleration. Figure 3 shows the ratios between 2016–2022 and 1947–1987 speeds, i.e. acceleration factors. We find acceleration all over the rock glacier, up to 4 times relative to the 1947–1987 speeds.

Figure 3. Acceleration factors between speeds 1947–1987 and 2015–2022. Maximum factors are 4, minimum ones around 1.7, meaning that at places with large blue circles speeds in the latter period are almost 4 times as high as in the first period. Underlying airphoto of 2022 from USGS.

REFERENCES

Johnson, G., Chang, H., and Fountain, A. 2021. Active rock glaciers of the contiguous United States: geographic information system inventory and spatial distribution patterns. Earth System Science Data. 13(8), 3979–3994.

Kääb, A., and Vollmer, M. 2000. Surface geometry, thickness changes and flow fields on creeping mountain permafrost: automatic extraction by digital image analysis. Permafrost and Periglacial Processes. 11(4), 315–326.

Kääb, A., Frauenfelder, R., and Roer, I. 2007. On the response of rockglacier creep to surface temperature increase. Global and Planetary Change. 56(1-2), 172–187.

Kääb, A., Strozzi, T., Bolch, T., Caduff, R., Trefall, H., Stoffel, M., and Kokarev, A. 2021. Inventory and changes of rock glacier creep speeds in Ile Alatau and Kungöy Ala-Too, northern Tien Shan, since the 1950s. The Cryosphere. 15(2), 927–949.

Liu, L., Millar, C.I., Westfall, R.D., and Zebker, H.A. 2013. Surface motion of active rock glaciers in the Sierra Nevada, California, USA: inventory and a case study using InSAR. Cryosphere. 7(4), 1109–1119.

Obu, J., Westermann, S., Bartsch, A., et al. 2019. Northern Hemisphere permafrost map based on TTOP modelling for 2000-2016 at 1 km^2 scale. Earth-Science Reviews. 193, 299–316.

Pellet C., Bodin, X., Cusicanqui, D., Delaloye, R., Kääb, A., Kaufmann, V., Noetzli, J., Thibert, E., Vivero, S., and Kellerer-Pirklbauer, A. 2023. Rock glacier velocity. In State of the Climate in 2022. Bull. Amer. Meteor. Soc., 104 (9), S41–S42. https://doi.org/10.1175/BAMS-D-23-0090.1

Alpine rock wall surface temperature in the southern British Columbia Coast Mountain

Lancelot Massé[1], Francis Gauthier[1,2], Jeff Crompton[2,3] & Stephan Gruber[2,4]

[1]*Departement of Biology, Chemistry and Geography, Université du Québec à Rimouski, Rimouski, Québec, Canada*

[2]*Centre d'étude nordique (CEN)*

[3]*Geological Survey of Canada, Vancouver, British Columbia, Canada*

[4]*Departement of Geography and Environmental Studies, Carleton University, Ottawa, Ontario, Canada*

On May 13 and 16, 2019, two rock avalanches totaling approximately 5 Mm^3 occurred on the north face of Joffre Peak in British Columbia (Friele et al. 2020). The magnitude of the events, the recreational and tourism use of the area, and their proximity to one of Canada's most popular hikes have raised questions and concerns about the risks associated with catastrophic mass movements. This event is part of a recent and well-publicized series of rock instabilities on the west coast of North America, with thawing permafrost cited as a likely cause (Friele et al. 2020; Geertsema et al. 2022).

The distribution of permafrost in the British Columbia Coast Mountains is poorly known. The only information available is derived from global (Gruber 2012) or preliminary (Hasler and Geertsema 2013) permafrost occurrence probability mapping, as well as a few observations reported by Mathews (1955). These products do not have the resolution required for local and event-based analysis. Permafrost in the southern British Columbia Coast Mountains is likely only present at high elevations where weather station data is sparse. This lack of quality weather data makes for a challenging estimate of alpine permafrost distribution and permafrost degradation.

OBJECTIVE

This project aims to characterize the thermal regime of alpine rock faces in the southern British Columbia Coast Mountains. The mean annual air temperature (MAAT), mean annual ground surface temperature (MAGST), and surface offset will be calculated. These results will be used to validate available permafrost occurrence probability maps (Hasler and Geertsema 2013) and improve knowledge of the distribution, state, and evolution of alpine rock wall permafrost.

STUDY SITES AND METHOD

Five sites distributed between latitudes 50°07'N – 52°21'N and elevations 1571 m – 2838 m have been selected through the southern British Columbia Coast Mountains (Figure 1A). The sites display contrasting climate patterns associated with differing levels of continentality.

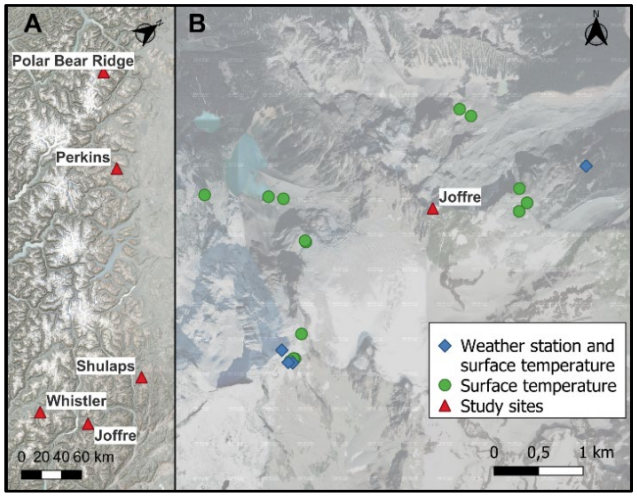

Figure 1. Study site location (A) and instruments position in the Joffre peak area (B).

The sites have been instrumented with thermistors, meteorological stations, and ground temperature probes. The site with the densest instrumentation is Joffre Lakes Provincial Park and Nlhàxten/Cerise Creek Conservancy (Figure 1B). A network of 15 surface temperatures with ground probes up to 45 cm, 2 weather stations, and 2 rock wall weather stations coupled with thermistor strings spaced at 30 cm to 1.5-m depth were deployed in the summer of 2021. The four sites outside of the Joffre area are equipped with air temperatures and a few rock wall surface temperatures at various orientations (roughly north and south exposure). Whistler was equipped in 2014, Joffre in 2021, and the remaining site in 2016.

Sites other than Joffre offer longer time series but multiple data gaps are present in the data due to sensor defects, empty batteries, and instrument damage. To allow the analysis of the inconsistent time series, data processing steps inspired by Hasler et al. (2015) will be taken. Statistics extracted from the running mean annual temperature will allow us to compute MAAT, MAGST, and surface offset as well as their incertitude

at all sites. Surface offset refers to the difference between MAAT and MAGST and allows us to describe the atmosphere/rock wall coupling. The extracted value will be analyzed against latitude, elevation, orientation, and slope angle to characterize the topoclimatic factor influence on the rock wall thermal regime. The result will then be compared with the available permafrost probability mapping product to validate the adequation between measurement and simulation.

PRELIMINARY RESULT AND PERSPECTIVE

The computation of the mean annual temperature for the 1.5-meter temperature probes at Slalok Peak shows that an important surface offset is present on the southeast face, making permafrost occurrence unlikely (Figure 2). On the northwest face, the small surface offset of 0.83 °C and the mean annual temperature of -0.85 °C at 1.5 m, suggest that permafrost is probable. These results are in line with the provisional permafrost map of British Columbia by Hasler and Geertsema (2013) as the south-east face is categorized as “no permafrost” and the north-west face is under “the only in very favourable condition” class. The results shown here account for only one year of data and must be analyzed with caution. Nevertheless, permafrost occurrence seems plausible and the investigation described further up will hopefully help clarify if and where permafrost is present.

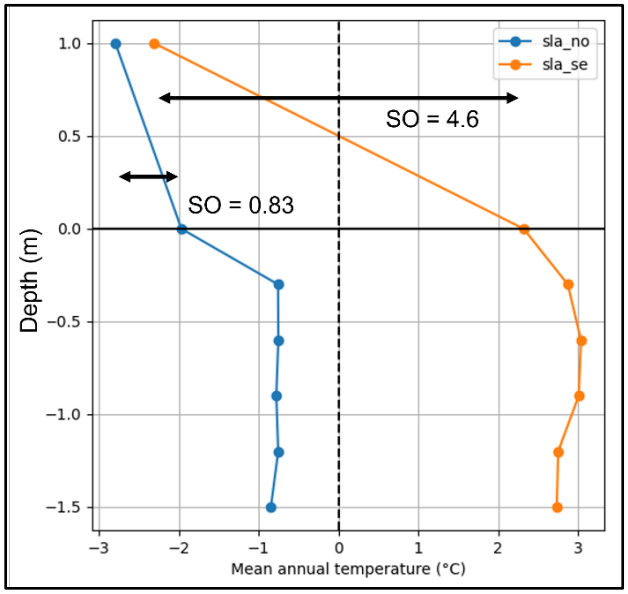

Figure 2. Mean annual air (1 m) and ground (0 to -1.5 m) temperature profile for northwest (no) and southeast (se) rock wall station on Slalok (Joffre Peak area).

REFERENCE

Friele, P., Millard, T.H., Mitchell, A., Allstadt, K.E., Menounos, B., Geertsema, M., and Clague, J.J. 2020. Observations on the May 2019 Joffre Peak landslides, British Columbia. Landslides 17, 913–930. https://doi.org/10.1007/s10346-019-01332-2

Geertsema, M., Menounos, B., Bullard, G., Carrivick, J.L., Clague, J.J., Dai, C., Donati, D., Ekstrom, G., Jackson, J.M., Lynett, P., Pichierri, M., Pon, A., Shugar, D.H., Stead, D., Del Bel Belluz, J., Friele, P., Giesbrecht, I., Heathfield, D., Millard, T., Nasonova, S., Schaeffer, A.J., Ward, B.C., Blaney, D., Blaney, E., Brillon, C., Bunn, C., Floyd, W., Higman, B., Hughes, K.E., McInnes, W., Mukherjee, K., and Sharp, M.A. 2022. The 28 November 2020 Landslide, Tsunami, and Outburst Flood – A Hazard Cascade Associated with Rapid Deglaciation at Elliot Creek, British Columbia, Canada. Geophysical Research Letters 49, e2021GL096716. https://doi.org/10.1029/2021GL096716

Gruber, S. 2012. Derivation and analysis of a high-resolution estimate of global permafrost zonation. The Cryosphere 6, 221–233. https://doi.org/10.5194/tc-6-221-2012

Hasler, A., and Geertsema, M. 2013. Provisional permafrost map of British Columbia.

Hasler, A., Geertsema, M., Foord, V., Gruber, S., and Noetzli, J. 2015. The influence of surface characteristics, topography and continentality on mountain permafrost in British Columbia. The Cryosphere 9, 1025–1038. https://doi.org/10.5194/tc-9-1025-2015

Mathews, W.H. 1955. Permafrost and its occurrence in the southern coast mountains of British Columbia. Canadian Alpine Journal 38.

Investigating potential earthquake-induced landslides in Kluane Lake area, southwest Yukon

Catalina Pino-Rivas, Sergio A. Sepúlveda & Brent C. Ward
Department of Earth Sciences, Simon Fraser University, Burnaby, British Columbia, Canada

The southwest Yukon presents a distinctive environment characterized by some of the highest rock uplift rates globally, along with extensive glaciation. These processes result in elevated erosion rates, active fault lines, and highly diverse microclimatic zones. Here, landslides are frequently triggered by several factors, including over-steepened slopes formed during glaciations, permafrost thaw, seismic activity, remobilization of slope materials, and loss of structural integrity on bedrock slopes.

Earthquake-induced landslides

Landslides triggered by earthquakes are common in regions with active tectonic activity, and they have global significance due to their destructive potential. The term "earthquake-induced landslide" is relatively recent. Keefer (1984) established a link between landslide initiation and earthquakes exceeding magnitude 4.0 for small slides and 6.0 for large slides and avalanches, with local geological conditions playing a crucial role. However, climate warming and permafrost degradation may reduce the minimum earthquake magnitude needed to trigger landslides, potentially expanding the affected area. This study in Southwestern Yukon aims to identify key landslide characteristics in various earthquake scenarios, considering local seismic factors like directivity and topographic amplification, and cryological factors, like deglaciation, permafrost distribution and the impact of climate change-induced thawing.

Study area

The study area in southwestern Yukon, part of the broader Kluane region, spans approximately 250 km from the White River to the Aishihik River and covers about 70 km from the southwestern tip of Kluane Lake to Gladstone Lakes in the north. It is intersected by the Alaska Highway Corridor which traverses northwest into Alaska. The area is characterized by granitic and metamorphic rocks in the mountain belt and volcanic rocks between the Denali and Duke River faults.

The area features glaciers in the mountain ranges, contributing to landscape shaping, and is underlain by over 80% permafrost (Bonnaventure et al. 2012). Prone to large-scale landslides, the region poses risks of harm, fatalities, and infrastructure damage. Given the significance of the Alaska Highway as a major corridor, there is a crucial need to deepen our understanding of landslides in this area.

The Southwest Yukon is recognized as one of Canada's most seismically active areas, experiencing regular earthquakes with magnitudes exceeding 6.0 Seismic activity is primarily concentrated along two zones: the Pacific-North American plate boundary and the Denali Fault System. Earthquakes along the plate boundary can reach up to magnitude 8.0, while segments of the Denali Fault System, including Dalton, Shakwak, and Duke River, have observed earthquakes up to magnitude 6.2.

The Denali fault system

The Denali Fault System, spanning over 2000 km from Alaska through Yukon to northwestern British Columbia, is an extensive intracontinental network of faults. This system involves strike-slip faulting and thrust portions, with varying intensity along segmented trunks. In Yukon, these trunks trend northwest-southeast, shifting to northeast-southwest as they extend into Alaska (Haeussler et al. 2017). The Duke River Fault section historically experiences a higher number of small to moderate earthquakes, particularly in the westward bend near the Duke River Depression to the Yukon-Alaska boundary. Despite the predominant right-lateral displacement on the Denali Fault System, the western part of the Duke River Fault is recognized as a transpressional bend, undergoing crustal shortening.

Discussion and concluding remarks

Although there are many observations of earthquakes and landslides in Southwest Yukon, fewer landslides have been successfully correlated with seismic events (e.g., Brideau et al. 2009; Whelan 2022).

In addition, climate change is driving a global phenomenon of glacial retreat and thinning, exposing unstable hillslopes. The reduction of glacial ice supporting steep terrain and the permafrost thawing in alpine regions increases the susceptibility to landslides.

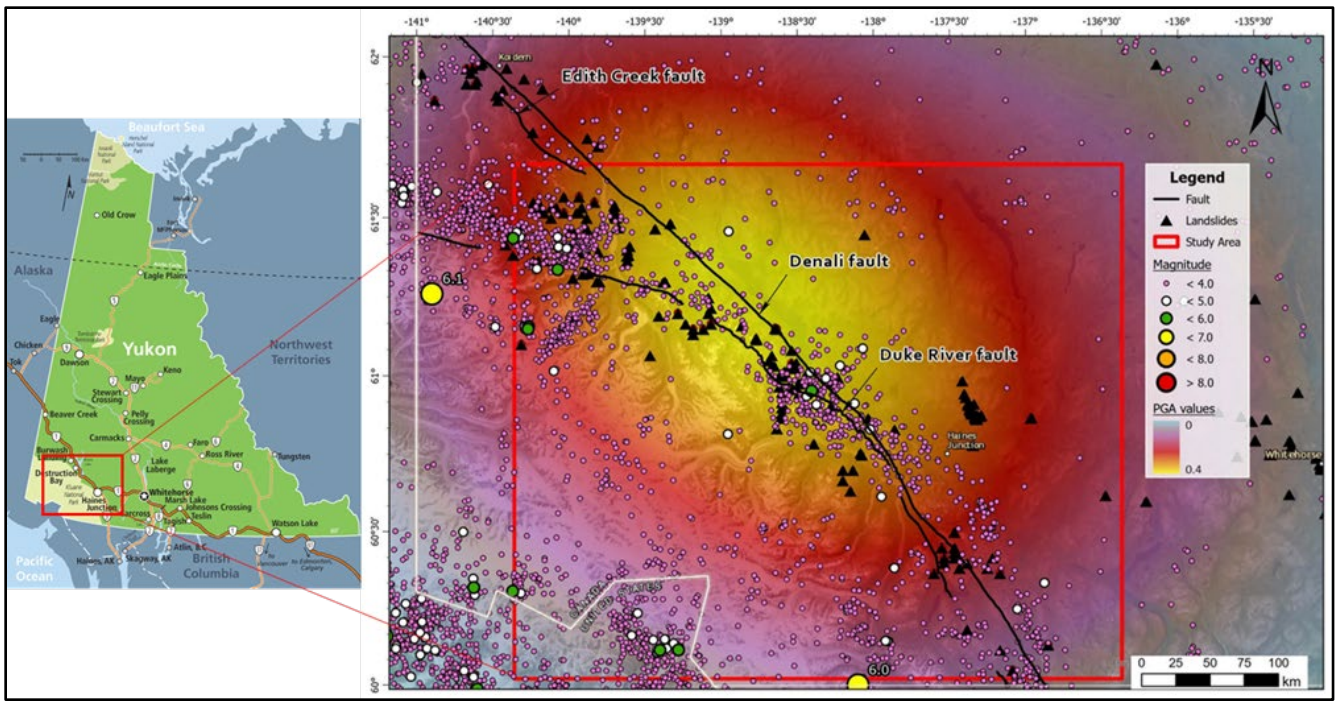

Figure 1. Study area, showing the seismicity between 1984-2019 (dots) and the hazard map (PGA values) modelled for an Mw 7.0 earthquake scenario. Preliminary landslide database (Brideau et al. 2023) and The Denali fault system is also shown.

In this regard, few studies have focused on how landslide hazards in existing permafrost areas might evolve with warmer climate conditions or the impact that different seismic scenarios could have on slope stability responses.

Therefore, this study proposes, firstly, an investigation into the landslides included within the current inventory for the region (Brideau et al. 2023) and their correlation with the Denali Fault System. This will allow the assessment of geomorphological features associated with the fault and the distance to it, as well as the evaluation of potential patterns linked to crustal seismicity, such as directivity effects in the nearby field and topographic amplification.

Secondly, an analysis will be conducted on selected landslides from Whelan (2022) to undertake a comprehensive geotechnical study and subsequent modeling. This aims to analyze earthquake-induced landslide susceptibility under the influence of deglaciation and permafrost over time, considering the climate change variable.

Hence, addressing these knowledge gaps holds significance for understanding landscape evolution and geohazard scenarios, as well as formulating appropriate development strategies in high-mountain settings and arctic and subarctic regions.

REFERENCES

Bonnaventure, P.P., Lewkowicz, A.G., Kremer, M., and Sawada, M.C. 2012. A permafrost probability model for the southern Yukon and northern British Columbia, Canada. Permafrost and Periglacial Processes, 23(1), 52–68.

Brideau, M.A., Stead, D., Lipovsky, P., Jaboyedoff, M., Hopkinson, C., Demuth, M., et al. 2009. Preliminary description and slope stability analyses of the 2008 Little Salmon Lake and 2007 Mt. Steele landslides, Yukon. Yukon exploration and geology, 110–133.

Brideau, M.-A., Lipovsky, P., and Brayshaw, D. 2023. Preliminary Canadian Landslide Database (6.0) [Data set]. Zenodo. https://doi.org/10.5281/zenodo.7962933

Haeussler, P.J., Matmon, A., Schwartz, D.P., and Seitz, G.G. 2017. Neotectonics of interior Alaska and the late Quaternary slip rate along the Denali fault system. Geosphere, 13(5), 1445–1463.

Keefer, D.K. 1984. Landslides caused by earthquakes. Geological Society of America Bulletin, 95(4), 406–421.

Whelan, N. 2022. Geochronology of landslides in the Kluane Lake Region, Southwest Yukon. M.Sc. thesis

Thermosyphons in Alpine environments – A feasibility study

Regina Pläsken[1], Khatereh Roghangar[2], Heather Brooks[3] & Lukas U. Arenson[4]

[1]*Chair of Landslide Research, Technische Universität München, Germany*

[2]*Schulich School of Engineering, Department of Civil Engineering, University of Calgary, Calgary, Alberta, Canada*

[3]*BGC Engineering Inc., Calgary, Alberta, Canada*

[4]*BGC Engineering Inc., Vancouver, British Columbia, Canada*

In the context of climate change, thermosyphons, widely used for stabilizing thermal conditions in lowland permafrost, can potentially find new applications in high mountain regions. As temperatures rise, infrastructure stability on permafrost rocks potentially reduces due to changing thermal dynamics and altered mechanical behaviour. We explore the practical use of thermosyphons in high alpine settings to stabilize thermal conditions in bedrock foundations and by that improving rock properties in naturally degrading permafrost rocks. The study aims to transfer approved solutions to new environments and promote sustainable infrastructure development in a changing climate.

Study site

Situated at an elevation of about 3050 meters in the mountains of Switzerland, our hypothetical study focuses on a generic building built on assumed gneissic bedrock foundation with typical rock properties. Emulating representative topographic conditions, we selected a simple peak-like geometry to capture the intricate shapes and their thermal implications typical of high alpine sites. The rock slope is assumed to be in warm, degrading permafrost conditions, as typical for such a location (e.g., Smith et al. 2022; PERMOS 2023). The building is chosen to be a simple, typical geometry and serves as a model for infrastructure in these environments, impacting the surrounding permafrost rock thermally as the bedrock would not be exposed to atmospheric conditions.

Thermosyphons

Thermosyphons are heat transfer devices that use the natural circulation of a working fluid to transfer heat from one location to another. They are frequently used in the Arctic to maintain permafrost conditions under buildings or road foundations. Passive thermosyphons rely on cold winter air temperature to initiate the natural convection of the fluid to circulate it for extracting heat, while active or hybrid thermosyphons use an active cooling mechanism so that the system also extracts heat when air temperatures are warmer than ground temperatures.

Data and methods

For this feasibility study, the commercially available thermal modelling software TEMP/W (Geostudio International, Seequent) is used to simulate thermal effects in a 2D cross-section. The model of the fictitious site incorporates representative input parameters derived from weather station data collected at two locations in the Swiss Alps: Lagrev (Lon 9.7331°, Lat 46.4489°, Ele. 3085 m) and Piz Bardella (Lon 9.7029°, Lat 46.4823°, Ele. 2838 m). Air temperature data is averaged and smoothed, using a sinusoidal fit, from 30-minute interval weather data as input data for the thermal modeling. The mean annual air temperature is -0.8 °C, the annual air freezing index is 1058 °C·days and the annual air thawing index is 764 °C·days. A constant windspeed of 10.8 km/h was chosen for this evaluation.

A rock temperature distribution, which is typical for such a high alpine location, is assumed as initial conditions in the model. Further, a uniform thermal conductivity of 2.03 W/(m·°C), frozen and unfrozen, and a low volumetric water content of 1% was chosen. We understand that in-situ conditions are more complex, but the assumptions selected provide a realistic baseline for evaluating thermal interactions and the feasibility of using thermosyphons.

Two passive thermosyphons are used to a depth of 10 m below the building that are 3 m apart (Figure 1). The thermosyphons were set to operate until a maximum temperature of -0.5 °C and with a constant thermal conductivity coefficient of 377 kJ/(d·m^2·°C). This simplified representation allows for the evaluation of the thermosyphon's effectiveness in maintaining thermal equilibrium below a heated building. Figure 1 further shows the extent of the constant temperature boundary condition (building) and the constant heat flux that was applied at the bottom boundary, representing a constant thermal gradient at depth. Ground surface temperatures were calculated using n-factors: 1.8 for thawing and 1.0 for freezing. This results in a mean annual ground surface temperature of +1.3 °C, conditions where permafrost would not be able to sustain.

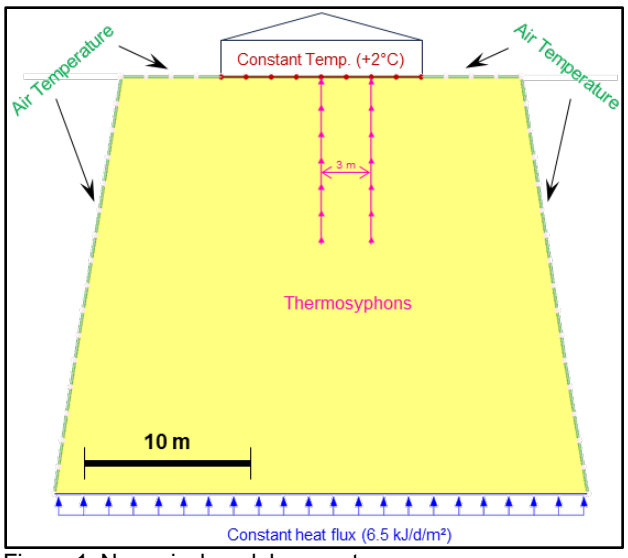

Figure 1. Numerical model geometry.

For the numerical analysis, a 5-year transient simulation is conducted following 20 years of model initiation with time steps of 4 hours. The finite element mesh consisted of about 2500 triangular elements.

Results and Discussion

Cooling of the bedrock below the building initiated immediately after the thermosyphons were activated. Figure 2 shows the difference in the ground thermal regime between a foundation with and without thermosyphons for the warmest and the coldest day of the year, five years into the simulation. The results demonstrate that the core remains frozen throughout the entire year, effectively maintaining permafrost conditions under a warm building foundation.

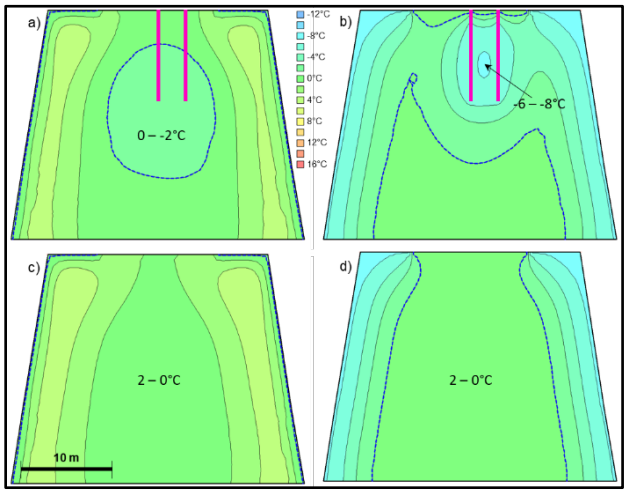

Figure 2. Ground temperatures for the warmest (a, c) and coldest (b, d) day during year 5 of modelling bedrock temperatures with (top) and without (bottom) thermosyphons.

The temperature trumpets (Figure 3) highlight the significant cooling that two passive thermosyphons generate in the bedrock under the building. While cooling continues past the modelled time, average temperatures at depths between 5 and 10 m cooled by more than 4 °C and remained frozen for the entire year, i.e., permafrost was generated.

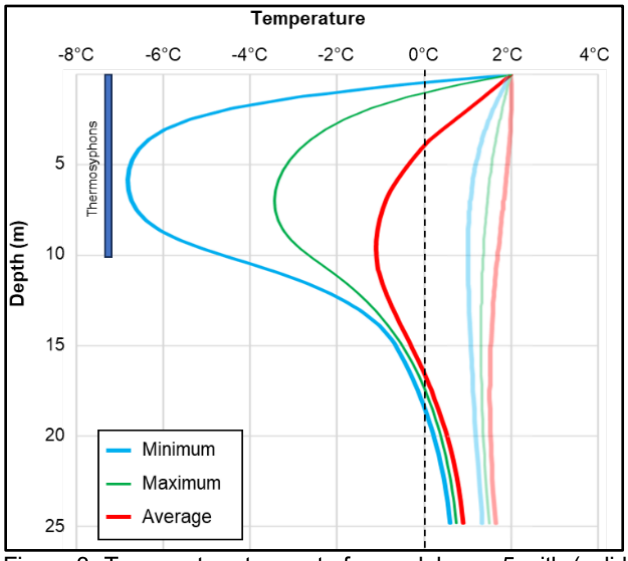

Figure 3. Temperature trumpets for model year 5 with (solid lines) and without (faded lines) thermosyphons.

Conclusion and Outlook

Temperatures in bedrock foundations in the Alps are increasing, potentially generating instable conditions for high mountain infrastructure. The use of passive thermosyphons, widely used in the Arctic, was evaluated through numerical modelling. The preliminary results demonstrated that permafrost can be maintained under climate conditions that are typical for the Alps. While project specific assessments and detailed geothermal modelling will be required for any detailed design, this initial evaluation has demonstrated that the use of passive thermosyphons in Alpine settings is a feasible mitigation measure against hazards from permafrost degradation in mountainous terrains.

References

Smith, S.L., O'Neill, H.B., Isaksen, K., Noetzli, J., and Romanovsky, V.E. 2022. The changing thermal state of permafrost. Nature Reviews Earth & Environment, 3(1), 10–23. doi:10.1038/s43017-021-00240-1

PERmafrost Monitoring Switzerland [PERMOS]. 2023. Swiss Permafrost Bulletin 2022. Noetzli, J., and Pellet, C. (eds.). No. 4, 23 pp. doi:10.13093/permos-bull-23

Multi-operator mapping exercise for consensus-based generation of rock glacier inventories (RoGI) in 12 areas worldwide

Line Rouyet[1,2], Reynald Delaloye[1], Tobias Bolch[3], Francesco Brardinoni[4], Rafael Caduff[5], Diego Cusicanqui[6,7], Margaret Darrow[8], Thomas Echelard[1], Christophe Lambiel[9], Lucas Ruiz[10], Flavius Sirbu[11] & Tazio Strozzi[5]

[1]*Department of Geosciences, University of Fribourg (UNIFR), Switzerland*
[2]*NORCE Norwegian Research Centre AS, Norway*
[3]*Institute of Geodesy, Graz University of Technology (TU Graz), Austria*
[4]*Department of Biological, Geological, and Environmental Sciences, University of Bologna (UniBo), Italy.*
[5]*GAMMA Remote Sensing AS, Switzerland*
[6]*Laboratoire EDYTEM, Université Savoie Mont-Blanc (USMB), France*
[7]*Institut des Sciences de la Terre (ISTerre), Université Grenoble Alpes (UGA), France*
[8]*Department of Civil, Geological, and Environmental Engineering, University of Alaska Fairbanks (UAF), United States*
[9]*Institute of Earth Surface Dynamics, University of Lausanne (UNIL), Switzerland*
[10]*Argentine Institute of Nivology, Glaciology and Environmental Sciences (IANIGLA), Argentina*
[11]*Department of Geography, West University of Timisoara (WUT), Romania*

The Rock Glacier Inventories and Kinematics community (RGIK) is defining standards for generating rock glacier inventories (RoGIs). We set up a multi-operator mapping exercise in 12 areas around the World. The operator teams performed similar steps individually and then discussed the results to provide consensus-based final products.

This unique cooperative initiative had three main objectives: 1) test common RoGI rules and identify discrepancies to refine the guidelines and procedure for generating consensus-based RoGIs, 2) develop standardized GIS tools for training the community to complete this work, and 3) encourage international exchanges from researchers and students with various backgrounds.

Here we present the multi-operator inventorying procedure, show examples of results and discuss the main findings of this unique international cooperation.

Background

Rock glaciers are characteristic landforms associated with mountain periglacial landscapes that attest the current or past presence of permafrost. Inventorying rock glaciers is relevant for many scientific fields (e.g., mapping current or paleo permafrost extent, understanding the mountain sediment cascade) and operational purposes (e.g., water storage or geohazard management). Rock glacier inventories (RoGIs) are not exhaustive worldwide, and existing RoGIs have been compiled with various methodologies. Consequently, merging and systematically comparing RoGIs is currently not possible. With the long-term objective of generating a homogenous open-access RoGI database, the IPA RGIK Action Group has developed standard guidelines to inventory rock glaciers (RGIK 2023a).

In a past study applying the guidelines at the regional scale (Bertone et al. 2022), we identified discrepancies that could not be systematically analysed due to the regional differences, the lack of interaction between the groups, and the subjectivity of a few involved persons in each region. As a follow-up, we designed a RoGI exercise with larger operator teams mixing institutions, countries and backgrounds.

Study areas and RoGI procedure

The exercise was performed in 12 areas selected in 10 countries and 5 continents (Table 1). A Principal Investigator (PI) was designated to coordinate the work in each area (Table 1). The inventory teams were composed of 5 to 10 operators (incl. the PI). The exercise involved 40 persons. The work was performed in similar QGIS projects, with common file structure, background data, and dialogue boxes for semi-automatic attribute filling.

The inventorying procedure follows up on prior work aiming to reduce discrepancies between different operators and produce homogenous consensus-based RoGIs (e.g., Brardinoni et al. 2019; Way et al. 2021). The work was performed in two steps between June and November 2023:

- Phase 1 (June-Sept. 2023): the operators individually identified rock glacier units (RGU) with primary markers (PM) and detected potential moving areas (MA) based on Synthetic Aperture Radar Interferometry (InSAR) data (RGIK 2023b). The PI compared the individual results and suggested a final solution. After discussion during an online meeting between operators, consensus-based PMs/MAs were adopted.
- Phase 2 (Sept-Nov. 2023): Based on the consensus-based results from Phase 1, the operators outlined and documented the morpho-kinematics characteristics of the RGUs. The PI compared the results and suggested

a final solution. After discussion during a second online meeting between operators, consensus-based PMs (incl. attributes) and outlines were adopted.

An example of multi-operator RoGI results from both phases is shown in Figure 1.

Table 1. Study areas of the multi-operator RoGI exercise (PI acronyms: see author list and affiliations).

RoGI area (approx. central lat/long location)	AOI km^2 *(# certain final RGU)*	PI (institution) *(# operators, incl. the PI)*
Western Alps (Switzerland) 46°11' N, 7°30' E	24 *(30)*	TE / UNIFR *(5 operators)*
Disko Island (Greenland) 69°51' N, 52°33' W	688 *(29)*	RC / GAMMA (6 operators)
Troms (Norway) 69°23' N, 20°26' E	377 *(15)*	LRo / NORCE (6 operators)
Finnmark (Norway) 70°45' N, 27°50' E	137 *(17)*	LRo / NORCE (7 operators)
Nordenskiöld Land (Norway) 77°53' N, 13°54' E	228 *(18)*	LRo / NORCE (6 operators)
Southern Venosta (Italy) 46°33' N, 10°36' E	39 *(40)*	FB / UniBo (10 operators)
Carpathians (Romania) 45°23' N, 22°53' E	36 *(18)*	FS / WUT (7 operators)
Vanois Massif (France) 45°19' N, 6°37' E	64 *(96)*	DC / USMB/UGA (6 operators)
Brooks Range (U.S.A.) 68°6' N, 149°58' W	149 *(14)*	MD / UAF (10 operators)
Central Andes (Argentina) 32°59' S, 69.34° W	78 *(71)*	LRu / IANIGLA (10 operators)
Tien Shan (Kazakhstan) 43°0' N, 77°1' W	110 *(16)*	TB / TU Graz (7 operators)
Southern Alps (New Zealand) 43°59' S, 170°3' E	13 *(24)*	CL / UNIL (7 operators)

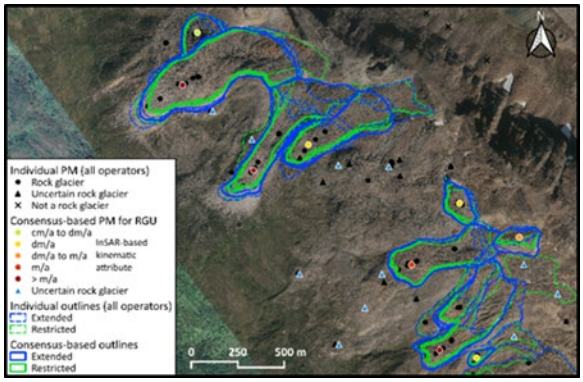

Figure 1. Examples of multi-operator RoGI results and final consensus-based results in Troms (Norway).

Examples of results

The results highlight the value of collaborative work, taking advantage of the strengths of several people with different backgrounds and perspectives to comprehensively map an area. The intitiative also showed the variety of cold mountain environments with a wide range of rock glacier types, highlighting different challenges to systematically apply common inventorying rules.

Various discrepancies were identified especially for complex cases, e.g., in case of continuum between different landforms (debris-covered glaciers, solifluction lobes or landslides), lack of clear limit between the talus slope and the rock glacier when outlining the landform, or unclear upslope connection. The contrasting data quality and variable use of the available data sources also explain differences between the operators and the regions.

Conclusion and prospects

This multi-operator mapping exercise is the first international initiative focusing on rock glacier inventories at such a scale. The involvement of 10 leading institutions and 40 people is a promising sign that the international rock glacier community is strengthening. In 2024, the differences between operators will be further analysed to identify the need for adjustments to the guidelines. The conclusions of the exercise will contribute to improve the initial regional RoGIs (Bertone et al. 2022). The dataset in all 12 areas will be openly disseminated. The GIS projects (incl. the suggested final results) will be released as training tools on the RGIK website.

Acknowledgements

We acknowledge the great effort of all operators of the RoGI exercise. The initative is funded by the European Space Agency Climate Change Initative on Permafrost (ESA CCI Permafrost). The Rock Glacier Inventories and Kinematics (RGIK) Action Group has been supported by the International Permafrost Association (IPA) and GCOS Switzerland.

References

Brardinoni, F., et al. 2019. Evaluating sources of uncertainty and variability in rock glacier inventories. Earth Surf. Processes and Landf., 44(12): 2450–2466. doi:10.1002/esp.4674

Bertone, A., et al. 2022. Incorporating InSAR kinematics into rock glacier inventories: insights from 11 regions worldwide. The Cryosphere, 16, 2769–2792. doi:10.5194/tc-16-2769-2022

RGIK 2023a. Guidelines for rock glacier inventories: baseline and practical concepts (version 1.0). IPA Action Group Rock Glacier Inventories and Kinematics, 25. doi:10.51363/unifr.srr.2023.002

RGIK 2023b. InSAR-based kinematic attribute in rock glacier inventories. Practical InSAR guidelines (v.4.0). IPA Action Group Rock glacier inventories and kinematics, 33.

Way, R.G., et al. 2021. Consensus-Based Rock Glacier Inventorying in the Torngat Mountains, Northern Labrador. RCOP 2021, Reston, VA, U.S.A., 130–141. doi:10.1061/9780784483589.012

Multi-annual Rock Glacier Velocity (RGV) products based on InSAR

Lea Schmid[1], Line Rouyet[1,2], Reynald Delaloye[1], Cécile Pellet[1], Nina Jones[3] & Tazio Strozzi[3]

[1]*Dept. of Geosciences, University of Fribourg (UNIFR), Fribourg, Switzerland*

[2]*NORCE Norwegian Research Centre Ås, Akershus county, Norway*

[3]*GAMMA Remote Sensing AG, Gümligen, Switzerland*

Rock glaciers are debris landforms resulting from the creep of mountain permafrost. Whereas motion rates are related to multiple structural, topographic and climatic factors, and range from a few cm/a to multiple m/a, their interannual variations are primarily linked to those of the thermal state of the permafrost. With the objective to provide novel climate change indicators tailored for mountain permafrost environments, the traditional parameters of the Essential Climate Variable (ECV) Permafrost have been complemented in 2022 by Rock Glacier Velocity (RGV) (WMO 2022). RGV is an annualized rock glacier velocity time series documenting the creep rate of mountain permafrost. RGV production on the basis of in-situ measurements is restricted to some specific sites. Data from multiple sites are needed to robustly relate the velocity trend to climate change.

Spaceborne Synthetic Aperture Radar Interferometry (InSAR) has proven to be well suited for measuring displacements in periglacial environments (Strozzi et al. 2020). With the launch of Sentinel-1, open access SAR data has become available every 12 days since 2015 worldwide, and every 6 days between 2017 and 2021 over Europe. Based on images acquired during the snow-free seasons, InSAR enables regular monitoring of rock glaciers moving between approx. 0.2 and 1.5 m/a. The European Space Agency (ESA) Climate Change Initiative (CCI) Permafrost project aims to develop a method to extract consistent RGV from spaceborne remote sensing. In parallel, the Rock Glacier Inventories and Kinematics Action Group (RGIK) has developed international recommendations to generate RGV products (RGIK 2023).

We apply these standards to develop an InSAR-based method to produce RGV. By averaging interferograms with short temporal baselines (stacking), extracting multiple spatially distributed velocity time series and identifying dominant trends through clustering, we produce InSAR-based RGV. To validate the results and assess the suitability of the approach, the time series are compared with in-situ GNSS-derived time series.

Data and methods

The pilot study has been conducted on four rock glaciers in the Swiss Alps: Becs-de-Bosson, Distelhorn, Steintälli and Bru. For the validation, depending on the sites, GNSS data from annual or bi-annual surveys and/or permanent GNSS is used.

Sentinel-1 SAR images (wavelength: approx. 5.55 cm) between 2015 and 2022 are used to produce RGV time series. First, the interferograms are computed and unwrapped using a minimum cost flow algorithm. In order to reduce the impact of atmospheric disturbances, removal of an atmospheric phase trend with respect to height and InSAR stacking are applied. Each stack consisting of images between July and October for every year and site is used to generate Line-Of-Sight (LOS) mean annual velocity maps. LOS velocities are then extracted for every pixel on the rock glacier, resulting in one value per year and pixel. Time series under the expected uncertainty limit (0.2 m/year) are filtered out. Based on the remaining dataset, the various trends are identified by clustering the relative velocity changes with a hierarchical clustering algorithm. Small clusters with trends deviating from the main one are discarded, allowing for the removal of outliers. The remaining velocity time series are averaged to extract the RGV. Validation of the InSAR-based RGV product is performed through the qualitative comparison of relative velocities with relative in-situ-based RGV.

Results

The four obtained InSAR-based RGV (relative velocity to the entire time series) are displayed in Figure 1. For three of the four sites, RGV is only calculated between 2017 and 2021 (6-day Sentinel-1 repeat), whereas for Bru, RGV was extracted between 2015 and 2022 (12-day Sentinel-1 repeat). All rock glaciers have a velocity peak in 2019-2020. Overall, three of the four rock glaciers have accelerated during the observation period, with maximum velocities observed in 2020 or 2021. Only Steintälli rock glacier has overall decelerated while also exhibiting a distinct velocity maximum in 2019. Figure 1 highlights that the acceleration occurring at Bru, the slow-moving site, is proportionally similar to the much faster moving rock

glaciers Distelhorn and Becs-de-Bosson. The average relative trend matches the trend observed on other rock glaciers surveyed by the University of Fribourg (dashed grey line in Figure 1), as well as in other studies, from 2017 to 2021.

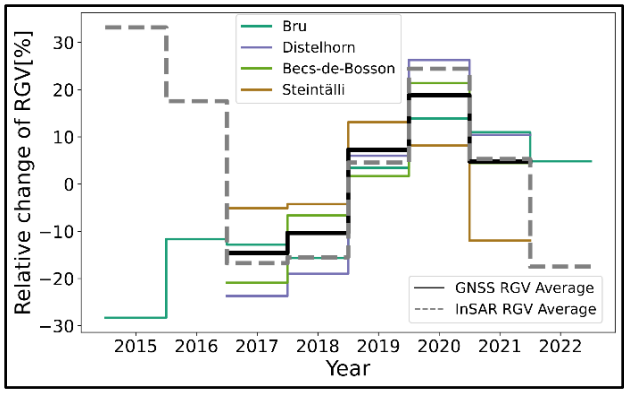

Figure 1. Relative change of RGV in %, relative to the period 2017-2021 (Mean annual velocities: Bru: 0.26 m/a; Distelhorn: 0.76 m/a; Becs-de-Bosson: 0.71 m/a; Steintälli 0.55 m/a). The GNSS average of the Western and Central Swiss Alps is marked by the dashed grey line and is based on 14 Sites.

Discussion

The presented InSAR-based method provides trends similar to the in-situ observations, showing an overall acceleration between 2018 and 2021 for rock glaciers in the European Alps. The additional years (2015, 2016 and 2022) for Bru rock glacier are not consistent with the observed interregional trend. The presented InSAR-based method is suited but subject to certain limitations. It can work well for rock glaciers moving between 0.2 and 1.5 m/year when the velocity field is relatively homogenous and with a good spatial continuity. Phase ambiguities can already occur at a quarter of the wavelength, which translates to a maximum detection capability of ca. 0.85 m/year for 6 days and 0.42 m/year for 12 days for Sentinel-1. Heterogeneous movement patterns can result in unwrapping errors, which affect the quality of the RGV products. Such unwrapping errors could not be resolved until now and are conditioning for instance the results in 2015 and 2016 for Bru. Therefore, not all rock glaciers are suited to be surveyed with InSAR. Rock glaciers moving faster than the upper detection limit require longer wavelength sensors. It is also important to note that the computed velocity is an extrapolated annual velocity based on summer images only (snow-free), which is only a fragment of the total movement. Velocities are faster during this period compared to the total annual velocity. When focusing on relative interannual changes, this should however have no significant major impact as the behavior is known as being repetitive over the years and if the observation time window (July-October) remains the same.

Conclusions and Perspectives

The presented method provides a way to extract RGV from InSAR data, which are comparable to RGV from in-situ measurements. Despite the existing limitations, the method makes it possible to systematically extract time series for a large amount of rock glaciers, thereby contributing to further use RGV as climate change indicator. Future research will first focus on testing the method on additional rock glaciers, with an emphasis on rock glaciers suitable for analysis with 12-day interferograms (current Sentinel-1 repeat-pass) and on solving unwrapping issues. We aim to produce time series in multiple mountain ranges worldwide, providing a comprehensive dataset of InSAR-RGV products for the characterization of various climate conditions.

Acknowledgements

This study is funded by the ESA CCI Permafrost project. The RGV guidelines have been developed by the RGIK, supported by the International Permafrost Association (IPA) and GCOS Switzerland. The annual and bi-annual GNSS data was provided by the University of Fribourg, partly supported by PERMOS. Permanent GNSS data was made available through Beutel et al. (2022)

References

Beutel, J., et al. 2022. Kinematic observations of the mountain cryosphere using in-situ GNSS instruments 2010-2021. PANGAEA. doi:10.1594/PANGAEA.948334

RGIK. 2023. Rock Glacier Velocity as associated product of ECV Permafrost: practical concepts (version 1.2). IPA Action Group Rock glacier inventories and kinematics. 17 pp.

Strozzi, T., et al. 2020. Monitoring Rock Glacier Kinematics with Satellite Synthetic Aperture Radar. Remote Sensing. 12 (3) 559 p. doi:10.3390/rs12030559.

WMO. 2022. The 2022 GCOS Implementation Plan. World Meteorological Organization. 98 pp.

Understanding the seasonal surface dynamics of a rock glacier through the assessment of ground ice content and origin

Julie Wee[1], Sebastián Vivero[1], Coline Mollaret[1], Christian Hauck[1], Christophe Lambiel[2] & Jan Beutel[3]

[1]*Department of Geosciences, University of Fribourg, Fribourg, Switzerland*

[2]*Institute of Earth Surface Dynamics, University of Lausanne, Lausanne, Switzerland*

[3]*Department of Computer Science, University of Innsbruck, Innsbruck, Austria*

The combination of geophysical data and geodetic measurements allowed to further the understanding of the spatial and temporal complexity of relations and interactions between glacial and periglacial processes through the assessment of ground ice properties and their influence on surface dynamics where glacier-permafrost interactions have occurred or still occur.

The high alpine environment is characterized by glacial and periglacial landforms, which express varying degrees of sensitivities to the current warming trend. The morphodynamical response of these landforms to this trend is not uniform in space nor in time as the occurrence of ice in high mountain environments can be found under a wide spectrum of possible origins, landform settings and assemblages.

In most contexts, there is a clear differentiation between debris-covered glacier and rock glaciers, as their morphologies and kinematic behaviour are distinctive (Haeberli et al. 2024). In environments where glacial and periglacial processes occurred or still occur simultaneously, the typology of the ice content and associated processes of the resulting landforms can be delicate to assess as they are the product of complex interconnected glacial and periglacial processes.

Study site

The Gruben site (46°10′22″N 7°58′09″E, Figure 1) is located in the Saas Valley in the southern Swiss Alps. It is characterized by the presence of the Gruben glacier forefield-connect rock glacier and the debris-covered cold tongue of the polythermal Gruben glacier, which were in interaction during the Little Ice Age (LIA) maximal extent of the latter (Gärtner-Roer et al. 2022). The morphological signature of this glacier-permafrost interaction is expressed in a complex contact zone by glaciotectonics and thermokarstic features, the latter inferring the presence of buried massive ground ice. Geometrical changes in this zone are expressed by lateral back-creeping and surface elevation changes mainly due to ice melt-induced subsidence.

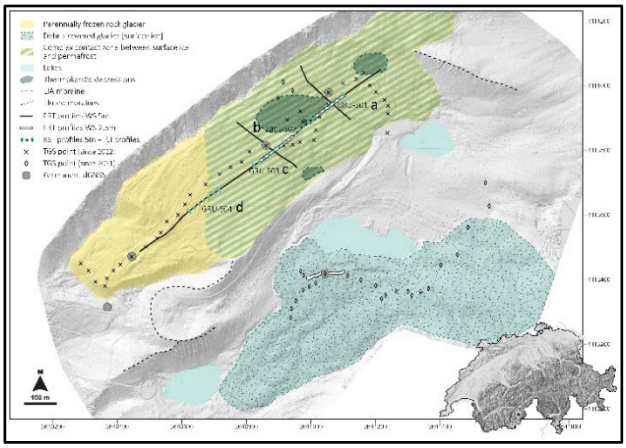

Figure 1. General geomorphological map of the Gruben site with an overview of the distribution of the geophysical and geodetic measurements. Background UAV-derived hillshade 06.10.2022.

Geophysical surveys and geodetic monitoring

In this study, the characterization of the subsurface is quantitively assessed using the petrophysical joint inversion (PJI) approach, based on electrical resistivity (ERT) and refraction seismic (RST) data. Surface dynamics are assessed through a geodetic approach, which relies on differential global navigation satellite system (dGNSS) observations for a high-temporal-resolution, and UAV-derived photogrammetry for a high-spatial-resolution.

Ground ice distribution and characterization

Geophysical data allowed to identify two zones of the rock glacier: the intact rock glacier zone (Figure 2d) and the complex contact zone (Figure 2a–c). In the complex contact zone, extremely high ice contents (up to 85%) are discernible. However, in the uppermost zone (Figure 2a), the liquid water-to-ice ratio is greater, which probably indicates an ongoing thermal degradation of the embedded surface ice.

In the intact permafrost zone of the Gruben rock glacier, the tomogram (Figure 2d) shows widespread supersaturated permafrost conditions below a 5 m thick active layer.

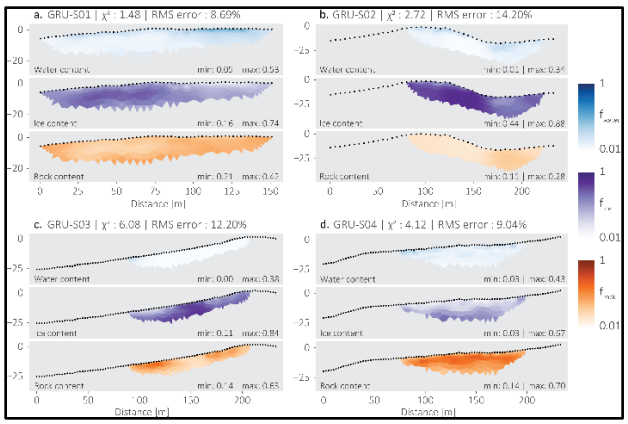

Figure 2. Ice, water and rock content estimated from the petrophysical joint inversion (PJI). The subpanels a–d correspond to the profiles shown in Figure 1.

SURFACE DISPLACEMENTS

A complex and heterogeneous kinematic pattern can be highlighted on the Gruben rock glacier, which reflects the distinction between the intact permafrost zone and the altered thermal regime, spatial distribution of ground ice and surface morphology of the complex contact zone (Figure 3).

Seasonal (summer) melt induces a subsidence which ranges between -0.5 m to -0.7 m. However, the melt directly stops once ground surface temperatures are below 0°C and starts again once the snow cover has melted. In contrast, surface displacements are rather constant through time in the intact rock glacier zone, where no abrupt changes in the kinematic behaviour are observed, aside from a gradual deceleration in winter.

PRELIMINARY CONCLUSIONS

Favouring a multi-method approach allowed a detailed representation of the spatial distribution of ground ice content and origin, which enabled to discriminate glacial from periglacial processes as their spatio-temporal patterns of surface change and geophysical signatures are (mostly) different.

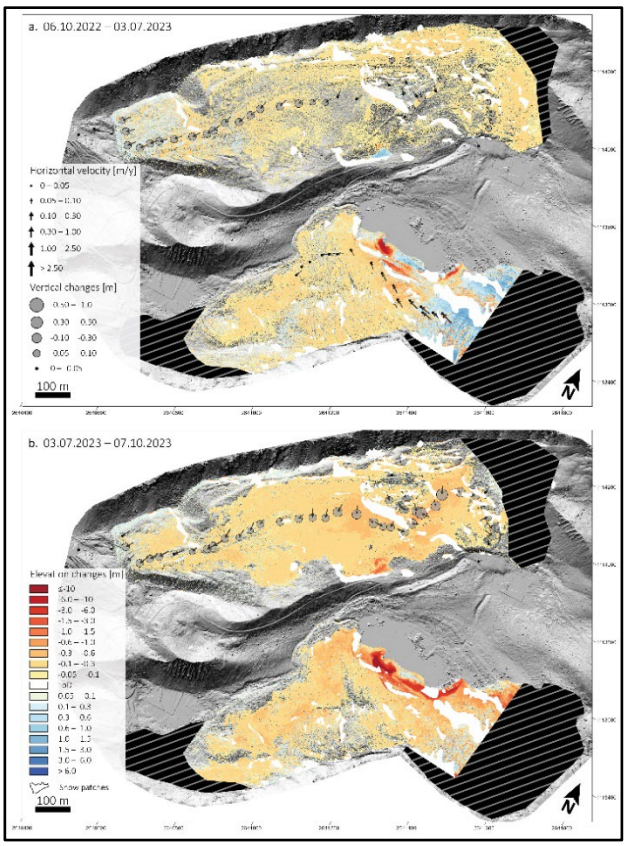

Figure 3. Horizontal surface and vertical changes (derived from dGNSS terrestrial ground surveys) and elevation changes (derived from UAV surveys) observed during the winter period (a) and summer period (b). Background UAV-derived hillshade 06.10.2022.

REFERENCES

Haeberli, W., Arenson, L.U., Wee, J., Hauck, C., and Mölg, N. 2023. Discriminating viscous creep features (rock glaciers) in mountain permafrost from debris-covered glaciers – a commented test at the Gruben and Yerba Loca sites, Swiss Alps and Chilean Andes, The Cryosphere [preprint]. https://doi.org/10.5194/egusphere-2023-1191

Gärtner-Roer, I., Brunner, N., Delaloye, R., Haeberli, W., Kääb, A., and Thee, P. 2022. Glacier–permafrost relations in a high-mountain environment: 5 decades of kinematic monitoring at the Gruben site, Swiss Alps, The Cryosphere, 16, 2083–2101. https://doi.org/10.5194/tc-16-2083-2022

4B — Periglacial Geomorphology

Session Chairs: Raquel Granados Aguilar[1], Marc Oliva[2] & Kaytan Kelkar[3]

[1]*Water Management & Hydrological Science, Texas A&M University, Texas, United States*
[2]*Antarctic, Arctic and Alpine Environments, University of Barcelona, Catalonia, Spain*
[3]*Geophysical Institute Permafrost Laboratory, University of Alaska, Fairbanks, Alaska, United States*

Periglacial landforms are observed in cold-climate environments, both at high latitudes and high elevations. Diverse processes such as physical and chemical weathering, mass-wasting, fluvial, aeolian, coastal, and paraglacial phenomena are common in such cold, non-glacial environments.

In periglacial regions, freeze-thaw cycles occur at varying times (i.e., diurnal, seasonal), and spatial scales (i.e., seasonal thawing of the active layer). Local factors including topography, snowfall, snow cover, aspect, and mean-annual ground and air temperatures, determine the presence and distribution of permafrost in periglacial areas. When permafrost is absent, frost-action processes dominate the periglacial environment.

Periglacial landforms can be highly susceptible to anthropogenic forcings and climate warming. Rising temperatures affect the thermal and geomorphological equilibrium of certain landforms. As a result, some areas are experiencing accelerated permafrost thaw and weathering, increased slope instability, thermokarst formation, and subsidence.

Periglacial geomorphology facilitates the integration of expertise from geomorphology, ecology, paleoclimatology, and engineering to address changing permafrost landscape dynamics. This session aims to foster discussions highlighting innovative approaches and multidisciplinary partnerships to improve our understanding of future permafrost thermal regimes within periglacial terrain. We welcome contributions outlining field observations, geophysical studies, laboratory testing, numerical modelling, and remote sensing techniques investigating the spatial and temporal evolution of periglacial landscapes.

Development of weathering rind in Midtre Lovénbreen foreland (Spitsbergen) – initial results

Ireneusz Badura & Maciej Dąbski

Faculty of Geography and Regional Studies, University of Warsaw, Warsaw, Poland

The aim of the study is to determine the rate of rock weathering in a proglacial glacial environment in front of a receding High Arctic glacier. The assumption underpinning this project is that freshly deglaciated rock surfaces at the glacier snout represent the onset stage of subaerial weathering. The increasing age of moraines allows us to register the subsequent development of weathering rinds. For the research, we selected rocks of the same petrography: fine-grained biotite gneiss.

The study was performed in NW Spitsbergen near Ny Ålesund, in the Midtre Lovénbreen foreland (Figure 1), developed 50-70 m asl in the zone of continuous permafrost (MAAT -8°C, MAP 400 mm).

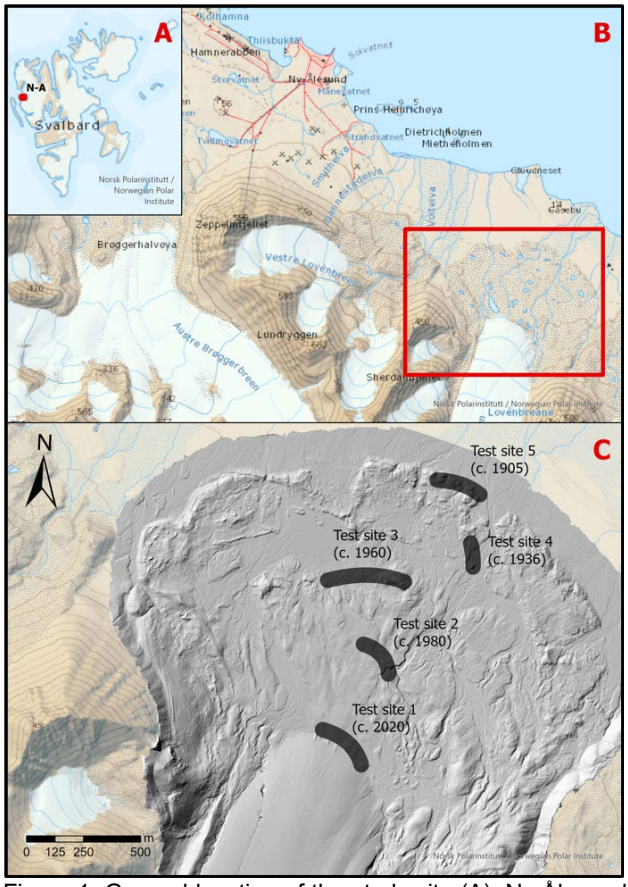

Figure 1. General location of the study site (A), Ny Ålesund area with marked Midtre Lovénbreen foreland (B), location of test sites with deglaciation ages (1-5) on the shaded relief DSM derived from UAV surveys (C).

Methods

We adopted a multidisciplinary approach and performed analyses of rock surface: i) micro-roughness, ii) hardness, iii) spectral reflectance, iv) petrographic and mineralogical characteristics (under optical microscopy, Scanning Electron Microscope – SEM, and X-ray Diffraction – XRD), vi) micro-biological content (SEM and isolation). Unmanned Aerial Vehicle (UAV) surveys allowed for precise documentation of the studied rock surfaces. Analyses i-iii were performed in situ in five test sites according to chronosequence: site 1 deglaciated c. 2020AD, site 2 – c. 1980AD, site 3 – c. 1960, site 4 – c. 1936AD and site 5 – c. 1905 (LIA – Little Ice Age glacial maximum), see Figure 1. Within each test site ten rock surfaces were selected for the measurements i-iii and the rest of the analyses were performed on rock samples under laboratory conditions. Rock surface micro-roughness was measured using a Handysurf+ profilometer, hardness using a Schmidt hammer N-type, and reflectivity using an ASD FieldSpec 4 (350-2500 nm).

Results

Rock surface micro-roughness increases from the glacier margin towards LIA moraines and this trend is accompanied by a delicate decrease in rock hardness. The differences and statistically significant, but the changes are not linear which is best visible by the leveling of micro-roughness on middle test sites and a slight elevation of rock hardness on the oldest moraine (Figure 2).

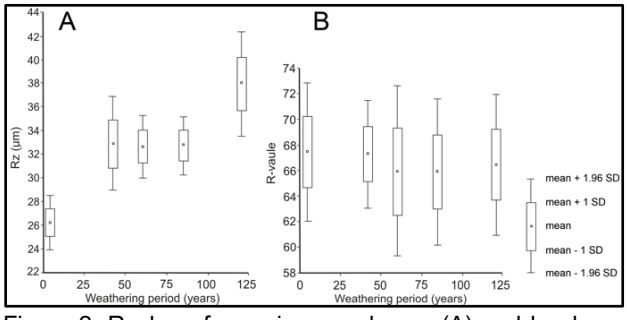

Figure 2. Rock surface micro-roughness (A) and hardness (Schmidt hammer tests) measurement values (B). Test sites sequence from left (site 1) to right (site 5).

The spectral reflectance curve obtained for test site 1 shows a significant elevation compared to the curves of the older sites. A general decrease in reflectance towards the older moraines is most apparent (and statistically significant) up to a wavelength of 1600 nm, and this trend is observable only when comparing sites 1 and 2 with the older moraines. The curves derived for sites 3-5 are very similar (Figure 3).

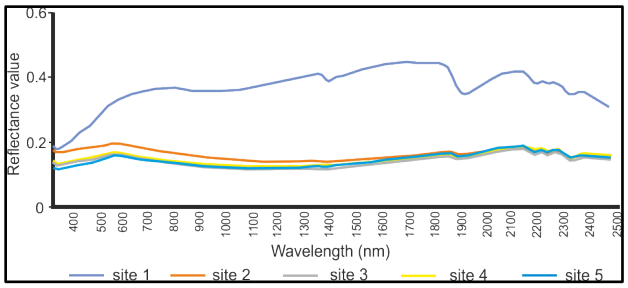

Figure 3. Reflectance values from test sites 1-5.

SEM images of the thin sections reveal the development of a weathering rind. The smooth textures, inherited from the glacier at test site 1 (Figure 4A), and much more porous textures, at test site 5 (Figure 4B).

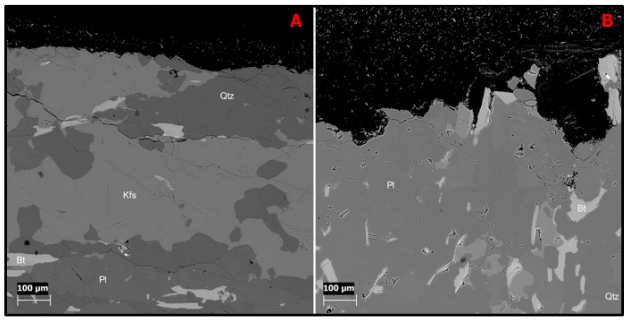

Figure 4. SEM images of the thin sections of the sample from test site 1 – c. 3 years of weathering (A), and test site 5 – c. 118 years of weathering (B).

We also performed SEM imaging of samples from the surfaces of the examined rocks, which revealed their colonization by lithobiontic microorganisms (Figure 5), known to potentially influence the weathering processes.

The rock samples were placed on various liquid and solid media for the isolation of bacteria and fungi. The cultures are currently being subjected to incubation and further passages.

For now, we have only obtained preliminary results from XRD analyses that are aimed at demonstrating changes in the mineral composition of the studied rock samples, both between the weathered rind and the parent rock, and across the different test sites. The results indicate quantitative changes in some minerals.

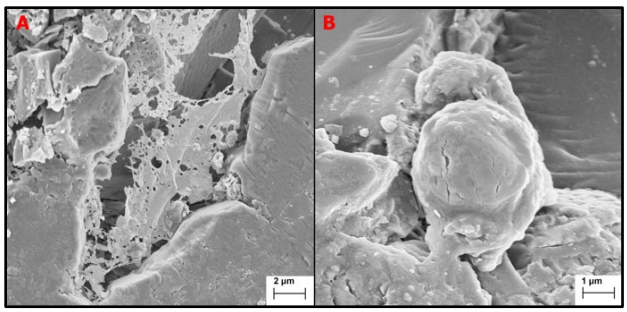

Figure 5. Examples of lithobiontic structures: a microbial biofilm on test site 2 (A) and cyanobacterial cells on test site 3 (B).

Discussion and conclusions

The research is a continuation of our previous study employing similar methods conducted in Hallstatter Glacier foreland (Alps) on limestone (Dąbski et al. 2022). On the foreland of the Midtre Lovénbreen, we focused on fine-grained biotite gneiss much harder than limestone. We are conducting investigations of weathering over a similar period, in different climates, and on various surfaces.

Results show a time-dependent increase in micro-roughness and strength, along with a decrease in spectral reflectivity. Rock structure varies with crystalline composition, and XRD analyses suggest the mineral weathering changes are mainly quantitative. Microorganisms were found at all test sites. Next, we aim to include DNA sequencing of environmental samples to further understand their role in micro-weathering processes.

Acknowledgements.

The authors express their gratitude to Marlena Kycko and Dominik Kopeć (MGGP Aero) for spectral reflectance measurements, Anna Grabarczyk (RM TERRA) for petrographic analysis, and Renata Matlakowska (Faculty of Biology, University of Warsaw) for microbiological analysis.

This research was authorized by the Governor of Svalbard (RiS ID: 12096) and funded by the National Science Centre, Poland [grant number 2020/39/O/ST10/01068].

References

Dąbski, M., Badura, I., Kycko, M., Grabarczyk, A., Matlakowska, R., and Otto, J.-C. 2023. The Development of Limestone Weathering Rind in a Proglacial Environment of the Hallstätter Glacier. Minerals 13(4) 530. doi:10.3390/min13040530

Permafrost degradation in dendritically-drained peat plateaus over the past 70 years in the central Mackenzie Valley, Northwest Territories

Alexandre Chiasson[1], Alejandro Alvarez[1], Jurjen van der Sluijs[2], Ashley C.A. Rudy[3], Steven V. Kokelj[3] & Duane G. Froese[1]

[1]*Department of Earth and Atmospheric Sciences, University of Alberta, Edmonton, Alberta, Canada*

[2]*NWT Centre for Geomatics, Government of Northwest Territories, Yellowknife, Northwest Territories, Canada*

[3]*Northwest Territories Geological Survey, Government of Northwest Territories, Yellowknife, Northwest Territories, Canada*

Permafrost thaw in ice-rich peatlands of subarctic regions usually transitions into wetland bog and fen complexes (Kokelj and Jorgenson 2013; Jones et al. 2016). This biophysical transition is associated with a myriad of significant impacts on vegetation, hydrology, aquatic ecosystems, and traditional lands (Kokelj et al. 2023). Despite extensive research on circumpolar peatlands, few studies have been carried out on the geomorphic dynamics and variability of permafrost peatlands in the central Mackenzie Valley of the Northwest Territories, where peatlands account for ~20% of the total peatland area in Canada (Tarnocai et al. 2000). In this study, we inventory the distribution of dendritic peat plateaus (DDPs) across the Mackenzie Valley and then, assess the rate of degradation using a combination of satellite data and field observations. The research aims to understand the spatial extent and controls on the distribution of dendritic peat plateau, their morphological characteristics, and change dynamics related to terrain, climate, permafrost thermal and ground conditions.

Methodology

A dendritic peat plateau is a type of peatland that exhibits a branching network of channelized fens which dissect the organic deposit and connect other similarly oriented channels, characterized by irregular branching tributaries. To assess the occurrence and spatial distribution of DPPs across the central Mackenzie Valley, we utilized a 7.5 x 7.5 km grid cell system in ArcGIS Pro 3.0 developed as part of the NWT Thermokarst Mapping Collective project (Kokelj et al. 2023). Elevations of the DPPs were retrieved using the ArcticDEM (Porter et al. 2018). To quantify changes in peat plateau extent and thermokarst expansion over the past ~70 years, aerial photographs from 1949 and 1970 were ordered at the National Air Photo Library (NAPL), and a 2008 black-and-white panchromatic QuickBird (0.52 m) was also acquired from Maxar Technologies (DigitalGlobe, Longmont, Colorado, United States). A high-resolution SPOT 6/7 (1.5 m) imagery from 2018 was used to map the most recent changes occurring within the peat plateau. Photographs were co-registered spatially using 50 tiepoints and the first-order polynomial transformation. Five classes of peatland features were manually digitized at a scale of 1:500 for four time points (ca. 1949, ca. 1970, ca. 2008, 2018): (1) waterbodies (ponds), (2) fens, (3) permafrost-free bogs, (4) forested peat plateaus (forest), and (5) peat plateaus. The annual average loss rate (AALR) was calculated using Olvmo et al. (2020) equation. Lateral and internal thaw were calculated using pixel-based comparison between raster (conversion of vector to raster).

Results

The total area covered by DPPs represented about 22,500 km^2. A total of 408 peatlands characterized by a dendritic drainage pattern have been identified throughout the valley. The majority of DPPs were located at relatively low elevations (μ = 276 m a.s.l., σ = 141, Median = 238 m a.s.l.) just above the boundary of the ancient glacial lakes Mackenzie and McConnell (Figure 1) (Smith 1994). A considerable number of dendritic peat plateaus were formed on gentle slopes with a gradient less than 0.25° (μ = 0.29°, σ = 0.37, Median = 0.17°).

Figure 2 illustrates the level of degradation measured as percentage of mapped surface areas occupied by waterbodies, fens, permafrost-free bogs, against the total area that also included forested peat plateaus and permafrost peat plateaus. The most notable changes occurred at the edges of the permafrost peat plateaus and the channel fens. The total peat plateau extent at the site was 2.1 km^2 in 1949 to 1.6 km^2 in 2018.

The decrease in peat plateau extent corresponds to a total permafrost loss of 26.2% during the last 69 years, and a 4.2% loss in the last 7 years (2011-2018). Since 1970, there has been a considerable increase in the annual average loss rate (AALR) with a rate of 0.48% a^{-1} from 1970 to 2011 and 0.55% a^{-1} from 2011 to 2018. The results show that lateral thaw is the dominant degradation process, from 91% of lateral loss in 1949 to 96% in 2018. Internal thaw

(bog expansion) is not prominent at this site despite relatively thin permafrost (5 m).

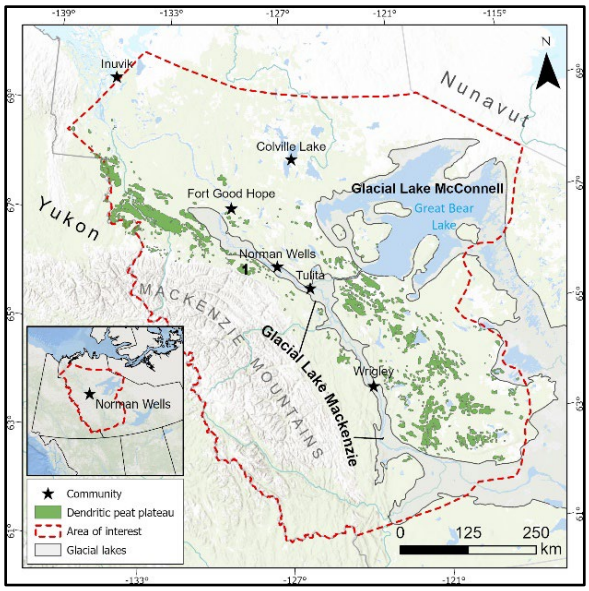

Figure 1. Distribution of dendritic peat plateaus in the central Mackenzie Valley. Number 1 shows the location of the studied DPP. Maximum extent of glacial Lakes Mackenzie and McConnell modified from Smith (1994).

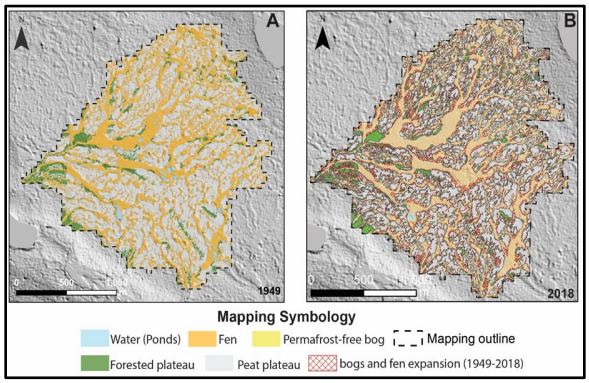

Figure 2. Dendritic peat plateau changes associated with permafrost degradation between 1949 (A) and 2018 (B). Waterbodies (blue), channel fens (orange), permafrost-free bogs (yellow), forested plateau (green) and permafrost peat plateau (grey) have been mapped for 1949 and 2018.

Discussion and Conclusion

The research provides the first detailed description of degrading dendritically-drained peat plateaus and degradation rates of the central Mackenzie Valley, Northwest Territories. The results show that the formation and intra-variability of DPPs are influenced by multiple factors and conditions.

Dendritic peat plateaus are mostly formed on gently sloping terrain (≤0.25°), which has contributed to the formation of the dendritic drainage system. These systems were relatively stable indicated by the undisturbed cover of reindeer lichens (moss) and in equilibrium with climate throughout most of the Holocene and started degrading after the 1970s following an increase in air temperature in the valley (Smith et al. 2010). Manual digitization of DPPs indicates that permafrost extent in these landforms has collectively decreased by ~25% over the last ~70 years, with lateral talik expansion being responsible for ~94% of the observed reduction in the areal extent of permafrost cover. However, the presence of channelized fens and permafrost-free bogs in aerial images from as early as 1949 indicates permafrost was probably always discontinuous within these important landscapes. Lateral expansion of fens and bog occurrences illustrates a long-term dynamic between unfrozen ground conditions (channel fens and bog) and permafrost peat plateaus. This suggests that the permafrost degradation has been ongoing for a longer period, prior to the 1940s.

References

Jones, B.M., Baughman, C.A., Romanovsky, V.E., Parsekian, A.D., Babcock, E.L., Stephani, E., et al. 2016. Presence of rapidly degrading permafrost plateaus in south-central Alaska. The Cryosphere, 10(6), 2673–2692. https://doi.org/10.5194/tc-10-2673-2016

Kokelj, S.V., Gingras-Hill, T., Daly, S.V., Morse, P., Wolfe, S., Rudy, A.C., et al. 2023. The Northwest Territories Thermokarst Mapping Collective: A northern-driven mapping collaborative toward understanding the effects of permafrost thaw. Arctic Science, 9(4): 886–918. https://doi.org/10.1139/as-2023-0009

Kokelj, S.V., and Jorgenson, M.T. 2013. Advances in thermokarst research. Permafrost and Periglacial Processes, 24(2), 108–119. https://doi.org/10.1002/ppp.1779

Olvmo, M., Holmer, B., Thorsson, S., Reese, H., and Lindberg, F. 2020. Sub-arctic palsa degradation and the role of climatic drivers in the largest coherent palsa mire complex in Sweden (Vissátvuopmi), 1955–2016. Scientific reports, 10(1), 8937. https://doi.org/10.1038/s41598-020-65719-1

Porter C, Morin P, Howat I, et al. 2018. ArcticDEM. Harvard Dataverse.

Smith, D.G. 1994. Glacial Lake McConnell: paleogeography, age, duration, and associated river deltas, Mackenzie River basin, western Canada. Quaternary Science Reviews, 13(9-10), 829–843. https://doi.org/10.1016/0277-3791(94)90004-3

Smith, S.L., Romanovsky, V.E., Lewkowicz, A.G., Burn, C.R., Allard, M., Clow, G.D., et al. 2010. Thermal state of permafrost in North America: a contribution to the international polar year. Permafrost and Periglacial Processes, 21(2), 117–135. https://doi.org/10.1002/ppp.690

Tarnocai, C., Kettles, I.M., and Lacelle, B. 2000. Peatlands of Canada: Geological Survey of Canada. Open File Report, 383.

The influence of rapidly changing permafrost conditions on geomorphological processes in the Nordic region

Bernd Etzelmüller[1], Justyna Czekirda[1], Ketil Isaksen[2], Karianne Lilleøren[1], Paula Snook[3] & Sebastian Westermann[1]

[1]*Department of Geosciences, University of Oslo, Oslo, Norway*

[2]*Meterological Institute of Norway, Oslo, Norway*

[3]*Department of Environmental Sciences, Western Norway University of Applied Sciences, Sogndal, Norway*

Mountain permafrost is widespread in the Nordic countries and on Svalbard. It is widely recognised that a change of the thermal state of permafrost is influencing geomorphological processes, and ultimately landscape development (Berthling og Etzelmuller 2011). A network of boreholes in Norway/Svalbard and Iceland witness about an accelerated warming during the last two decades, with the development of taliks documented both in Norway and Iceland (Etzelmüller et al. 2023). Global warming influences geomorphological processes in high mountains in the North. This presentation discusses examples from changes in relation to frost weathering, rock wall erosion, rock slope deformation rates and failure, and compare those with events dated to the Holocene Thermal Maximum (HTM). Finally, we discuss pathways of accelerated warming and its consequences on the mountainous environment.

Permafrost changes during the Holocene and present permafrost warming and degradation

Long-term modelling has revealed dramatic changes of permafrost distribution in mountainous terrain between deglaciation and the HTM, where probably most of the permafrost in Norway and Iceland was degraded (Etzelmüller et al. 2020; Lilleøren et al. 2012). After this period, during the neo-glaciation, permafrost aggraded and culminated during the Little Ice Age (LIA), after which we again see a degradation (Lilleøren et al. 2012). These changes influenced long-term geomorphological processes.

Systematic long-term monitoring of permafrost in northern Europe essentially began under the European Union-funded Permafrost and Climate in Europe (PACE) project (Harris et al. 2009) with ground temperature measuring instrumentation in deep boreholes in a transect from Sierra Nevada in Spain to Svalbard (Harris et al. 2009). Later, during other projects from 2004 and the International Polar Year (IPY) in 2007–2008, several boreholes were drilled in different sites in both Norway, Svalbard and Iceland, measuring temperatures along both altitudinal and latitudinal gradients (Christiansen et al. 2010, Etzelmuller et al. 2020; Isaksen et al. 2011). These data document that permafrost is warming at a high rate, including the development of taliks in both Norway and Iceland in response to climate change during the last 20 years (Etzelmüller et al. 2023). At most sites ground surface temperature (GST) is increasing stronger than surface air temperature (SAT). Changing snow conditions appear to be the most crucial factor for the higher GST rates (Etzelmuller et al. 2020; Etzelmüller et al. 2023).

Influence on frost weathering and rock slope erosion rates

Since 2012 we monitored rock wall temperatures at eight sites in Norway and generated a rock wall temperature map (Magnin et al. 2019). These data were used for the calibration of a 2D rock wall temperature modelling (Czekirda et al. 2022), providing unique insight into the permafrost distribution within mountains, and how the ground temperature react on climate forcing. With these temperature fields we forced Rempel's (Rempel et al. 2016) segregation ice weathering model to evaluate the potential of frost weathering in a changing climate, and identify sites of enhanced frost weathering, both in space (Iceland, Norway) and time (HTM, LIA). Furthermore, we estimate rock wall erosion based on differencing point clouds from terrestrial laser scanning and long-term erosion based on the quantification of sediment volumes in front of cirques (Czekirda 2023). The data indicate that short-term erosion rates during contemporary summers are considerably higher than average postglacial rates estimated for the Holocene (Figure 1).

Influence on rock slope movement and failure

We have done extensive research to decipher the influence of permafrost on sediment (Frauenfelder et al. 2018) and rock slope deformation and failure (Etzelmüller et al. 2022, Kristensen et al. 2021). We documented that rock slope failure activity peaked during certain periods associated to severe climate change in the Holocene (Hilger et al. 2021), including a geological crisis in western Norway (Hilger et al. 2018). Combining rock wall permafrost modelling with

present rock creep rates in Norway indicate that highest displacement rates are encountered at sites where permafrost is degrading since the LIA (Penna et al. 2023). The reconstruction of pre-historic displacement rates documents much higher displacement rates today than on average during the Holocene at many monitored sites in Norway (Hilger et al. 2021). All these observations indicate the strong influence of ground thermal regimes on these processes.

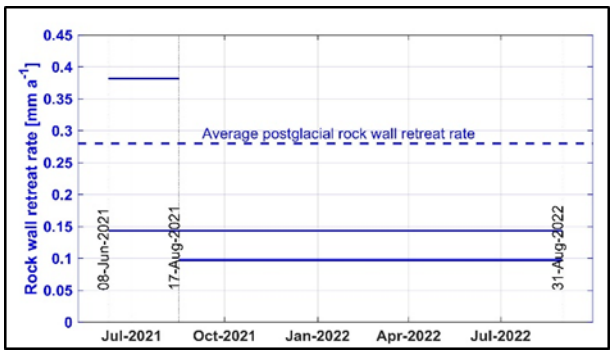

Figure 1. Rock wall retreat rate at Juvfonne (Kjelen), Jotunheimen, Norway. The average Holocene value is calculated by volume estimation from the ice-cored moraine. From Czekirda (2023).

SUMMARY

Ongoing global climate change influence the ground thermal regime in mountain environments. These changing conditions influence frost weathering, erosion rates, and unstable rock slopes. The conditions we encounter at present and will face during the near future are probably comparable with the HTM, where we documented widespread failure of steep slopes in Norwegian mountains.

REFERENCES

Berthling, I., and Etzelmuller, B. 2011. The concept of cryo-conditioning in landscape evolution. Quaternary Research, 75, 378–384.

Christiansen, H.H., Etzelmuller, et al. The Thermal State of Permafrost in Svalbard and Norway during IPY 2007-2009. PPP 21 (2), 156–181.

Czekirda, J. 2023. Ground thermal regime and periglacial slope processes in Norway and Iceland. PhD, Univeristy of Oslo.

Czekirda, J., Etzelmüller, B., Westermann, S., Isaksen, K., and Magnin, F. 2022. Post Little Ice Age rock wall permafrost evolution in Norway. The Cryosphere 17, 2022, 2725–2754.

Etzelmuller, B., et al. 2020. Twenty years of European mountain permafrost dynamics-the PACE legacy. Environmental Research Letters, 15.

Etzelmüller, B., Czekirda, J., et al. 2022. Permafrost in monitored unstable rock slopes in Norway – new insights from temperature and surface velocity measurements, geophysical surveying, and ground temperature modelling. Earth Surf. Dynam., 10, 97–129.

Etzelmüller, B., Isaksen, K., et al. 2023. Rapid warming and degradation of mountain permafrost in Norway and Iceland. The Cryosphere Discuss., 2023, 1–32.

Etzelmüller, B., Patton, H., et al. 2020. Icelandic permafrost dynamics since the Last Glacial Maximum–model results and geomorphological implications. Quaternary Science Reviews, 233, 106236.

Frauenfelder, R., Isaksen, K., et al. 2018. Ground thermal and geomechanical conditions in a permafrost-affected high-latitude rock avalanche site (Polvartinden, northern Norway). The Cryosphere, 12, 1531–1550.

Harris, C., et al., 2009. Permafrost and climate in Europe: Monitoring and modelling thermal, geomorphological and geotechnical responses. Earth-Science Reviews, 92, 117–171.

Hilger, P., et al.. 2021. Permafrost as a first order control on long-term rock-slope deformation in the (Sub-Arctic. Quaternary Science Reviews, 251, 106718.

Hilger, P., et al.. 2018. Multiple rock-slope failures from Mannen in Romsdal Valley, western Norway, revealed from Quaternary geological mapping and 10Be exposure dating. The Holocene, 28, 1841–1854.

Isaksen, K., et al. 2011. Degrading Mountain Permafrost in Southern Norway: Spatial and Temporal Variability of Mean Ground Temperatures, 1999-2009. Permafrost and Periglacial Processes, 22, 361–377.

Kristensen, L., Czekirda, J., et al.. 2021. Movements, failure and climatic control of the Veslemannen rockslide, Western Norway. Landslides. Journal of the International Consortium on Landslides, 18, 1963–1980.

Lilleøren, K.S., Etzelmuller, B., et al. 2012. The relative age of mountain permafrost - estimation of Holocene permafrost limits in Norway. Global and Planetary Change, 92–93, 209–223.

Magnin, F., Etzelmüller, B.,et al.. 2019. Permafrost distribution in steep rock slopes in Norway: measurements, statistical modelling and implications for geomorphological processes. Earth Surface Dynamics, 7, 1019–1040.

Penna, I.M., et al., 2023. Permafrost controls the displacement rates of large unstable rock-slopes in subarctic environments. Global and Planetary Change, 220, 104017.

Rempel, A.W., Marshall, J.A., and Roering, J.J. 2016. Modeling relative frost weathering rates at geomorphic scales. Earth and Planetary Science Letters, 453, 87–95.

Aufeis study of Ulaanbaatar city (A case study of Bumbat aufeis)

Ulambayar Ganbold[1,2], Dai Nakamura[1], Dashtseren Avirmed[2], Jambaljav Yamkhin[2] & Temuujin Khurelbaatar[2]

[1]*Graduate School of Engineering, Kitami Institute of Technology, Kitami, Hokkaido, Japan*

[2]*Institute of Geography and Geoecology, Mongolian Academy of Sciences, Ulaanbaatar, Mongolia*

Aufeis describes “a sheet-like mass of layered ice formed on the ground surface, or on river or lake ice, by freezing of successive flows of water that may seep from the ground, flow from a spring or emerge from below river ice through fractures” (Van Everdingen et al. 1998). Aufeis is a common phenomenon in Mongolia. Forming aufeis is essential for the water resources and regime of the environment. It positively affects the ecosystem by moistening the atmosphere and improving the environment and conditions for plant growth. This study examined the origin, spatial distribution, temperature regime, and characteristics of one aufeis in Ulaanbaatar. We conducted electrical resistivity tomography (ERT) measurements to determine the soil structure of the aufeis area. Some of the results are included in this extended abstract.

Study area

Mongolia is situated to the north of the Central Asian Plateau and placed on the southern boundary of the Northern Hemisphere's permafrost. The region experiences a continental climate with cold winters (a mean temperature of -21.3°C in January) and warm summers (with a mean temperature of 19.0°C in July). The average annual precipitation in the area is 273.2 mm.

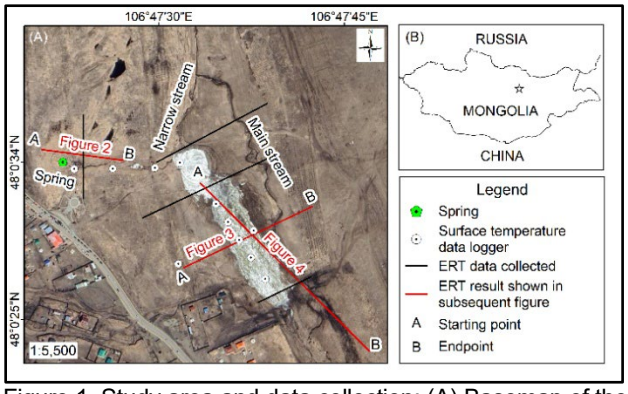

Figure 1. Study area and data collection; (A) Basemap of the Bumbat aufeis area showing ERT and surface temperature data collected in 2023; (B) Location of the study area within Mongolia.

The study area is located in Ulaanbaatar, the capital city of Mongolia (as shown in Figure 1B in the supporting information). This aufeis forms at the confluence of spring and river water and has a mixed origin. Its average area is 3.53 hectares, with a length of 485 meters and a width of 90 meters.

Methods

The geophysical electric resistivity tomography method determines the electrical resistivity properties of rocks beneath the surface and is a well-established method in near-surface characterization studies (Edwards 1977). The resistivity method is one of the oldest geophysical survey techniques. The aim of electrical resistivity measurement is to determine the subsurface resistivity distribution by measuring the ground surface. From these measurements, the true resistivity of the subsurface can be estimated. Ground resistivity is related to various parameters such as the mineral and moisture content, porosity, and water-saturation degree of the rock. Electrical resistivity surveys have been used for decades in hydrogeological, mining, geotechnical, environmental, and even hydrocarbon exploration (Loke 2015).

We used SYSCAL R1+ and SWITCH PRO tools from IRIS INSTRUMENTS company. Depending on the type and purpose of the study, the distance between the conductive stakes was adjusted to 3-5 meters. The acquired data were processed by Prosys-II software. Inversion analysis was conducted using RES2DINV software (Sasaki 1992; Barker 1992; Loke 2015). For the electrical resistivity method, we utilized the Wenner-Schlumberger array, which is particularly sensitive in detecting both horizontal and vertical soil structures.

Results

We conducted ERT measurements in October 2023 before aufeis formation. We took ERT profile-1 measurements behind the spring, which is the one source of aufeis. Profile-2 was measured along the cross-section of the aufeis area, while Profile-3 was measured along the longitudinal section.

In the ERT profile-1, two types of zones have been identified (Figure 2). The area on the left side of figure, which has a resistivity above 1000 ohm.m, is likely to be permafrost. On the other hand, the area on the right side, with a resistance of less than 80 ohm.m, is possibly a water-saturated zone. A geological fault has

been detected at the border of these two zones, and its location coincides with the source of the spring.

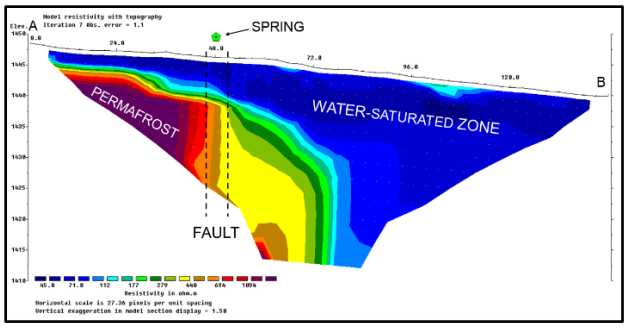

Figure 2. ERT profile-1.

According to the measurements of the ERT profile-2, we detected four different zones (Figure 3). As shown on the left and right sides of figure, the section with a resistivity less than 80 ohm.m is a water-saturated zones, while the sections between 112 ohm.m and 177 ohm.m in the centre of the figure may represent a moist zone. Zones with a resistivity between 177 ohm.m and 440 ohm.m may indicate a clay layer, while sections above 440 ohm.m can be permafrost.

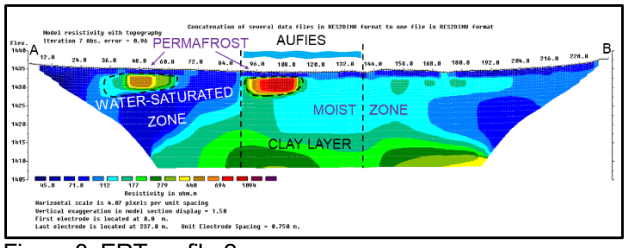

Figure 3. ERT profile-2.

ERT profile-3 measurements detected bedrock at a depth of about 22 meters below the surface, with a resistance value of higher than 1094 ohm.m (Figure 4).

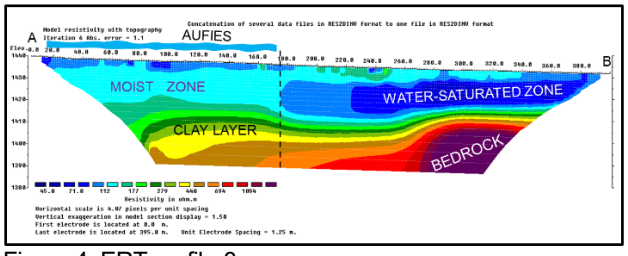

Figure 4. ERT profile-3.

Drone images of the surrounding area (Figure 5) taken by ERT Profile-2 show that the ground freezes, and the water-saturated zone beneath it is compressed and seeps to the surface.

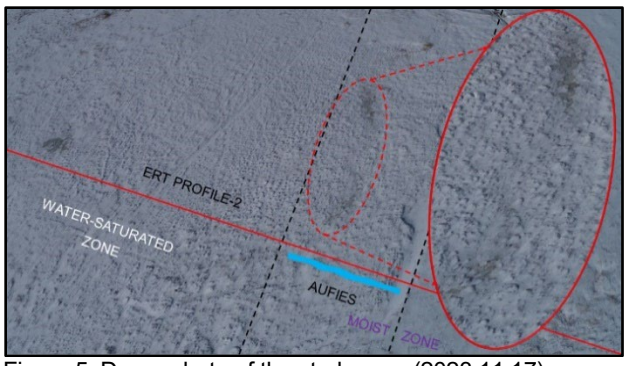

Figure 5. Drone photo of the study area (2023.11.17).

CONCLUSIONS

One source of the aufeis, the spring, is confirmed by our measured ERT profile-1 as a permanent flowing spring that comes to the surface through a geological fault. Generally, geological fault formation is the only groundwater source in hard rock terrain.

It appears that this aufeis is caused by spring and river water, but electrical resistivity tomography measurements and drone images show that soil water also contributes to its formation.

According to the results of the electrical resistivity tomography measurements, the resistance of the ground where the aufeis is formed is lower than that of the ground where the aufeis does not form, which is probably related to the aufeis formation.

REFERENCES

Barker, R.D. 1992. A simple algorithm for electrical imaging of the subsurface, First Break, 10(2). https://doi.org/10.3997/1365-2397.1992004

Edwards, L.S. 1977. A modified pseudosection for resistivity and ip, Geophysics, 42(5), pp. 1020–1036. https://doi.org/10.1190/1.1440762

Everdingen, V. 1998. Multi-language Glossary of Permafrost and Related Ground-ice Terms, National Snow and Ice Data Center, Boulder, CO, USA.

Loke, M.H. 2015. Tutorial: 2-D and 3-D electrical imaging surveys. www.geotomosoft.com

Sasaki, Y. 1992. Resolution of resistivity tomography inferred from numerical simulation1, Geophysical Prospecting, 40(4), pp. 453–463. https://doi.org/10.1111/j.1365-2478.1992.tb00536.x

Permafrost degradation and re-aggradation in the Beaver Creek Floodplain (Yukon Territory)

Emmanuèle Gautier[1], Daniel Fortier[2], Frédéric Gob[1], Marie Mousset[1], Thomas Dépret[1], Marc Pessel[3] & Rémi Lambert[3]

[1] *Department of Geography, University Paris 1 Panthéon-Sorbonne, CNRS, Laboratoire de Géographie Physique, Environnements Quaternaires et Actuels, 2 Rue Henri Dunant, F94320 Thiais, France*

[2]*Department of Geography, University of Montreal, Centre d'études Nordiques, Montréal, Québec, Canada*

[3]*Department of Earth Science, University Paris-Saclay, CNRS GEOPS, Rue du Belvédère, F91405 Orsay Cedex, France*

The Arctic amplification not only expresses a rise in air temperatures which is more than double the global average, but also greater precipitation and an increase in soil humidity. These changes have led to a cascade of reactions, the central element being permafrost degradation. While many publications have focussed on the hydrological and geomorphological consequences of permafrost degradation, it is only recently that attention has turned to the morphodynamic and sedimentary evolution of rivers draining permafrost regions (Tananaev and Lotsari 2022; Rowland et al. 2023). Thus, it is essential to determine to what extent permafrost degradation leads to changes in river morphodynamics. Conversely, the mechanical and thermal degradation of the permafrost by rivers has yet to be quantified. Furthermore it has been recently demonstrated that even in areas described as having a continuous permafrost cover, the presence of permafrost in alluvial plain may not be systematic (Gautier et al. 2021). If the absence of permafrost through alluvial plain is theoretically associated with recent deposits, it remains unclear how the spatial repartition of permafrost is controlled by fluvial dynamics as well as how long it takes for permafrost to re-aggrade in floodplains.

In this paper we will seek to gain a better understanding of the role of the river in the formation or degradation of permafrost. Through a case study of the middle Beaver Creek River (Yukon) we analyse the way fluvial dynamics control permafrost distribution at the alluvial plain scale and we try to determine the time needed for permafrost aggradation in undisturbed fluvial deposits.

STUDY AREA

The Beaver Creek River (Figure 1), a tributary of the White River, drains a 2308 km² basin (Yukon and Alaska) located in the north of the Kluane Range. The river flows east from a glacier and then north through the Wellesley basin where the study site is located. This middle part of the catchment remained unglaciated during the last glacial maximum. The area corresponds to the extensive discontinuous permafrost zone and the Pleistocene permafrost is ice-rich with networks of ice-wedges (Sliger et al. 2015).

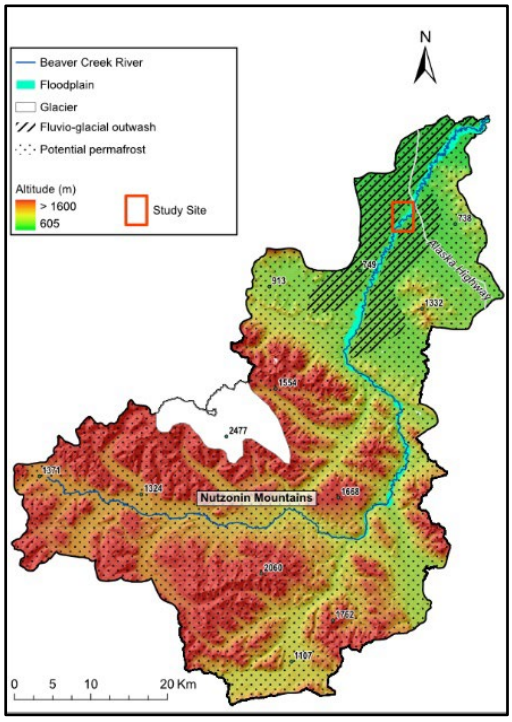

Figure 1. Beaver Creek River – Location map.

DATA AND METHODS

We combined different approaches at different spatial and temporal scales. First, we aim to determine the spatial distribution of the permafrost in different sites along the river. To do so, we associated, along two cross-sections perpendicular to the river, i) topographic surveys using a DGPS and ii) Electrical resistivity tomography (ERT) surveys together with iii) permafrost coring using a portable core-drill. The chronology of the various floodplain levels was obtained by radiocarbon dating and the presence of White River Ash in the soil (eruption in A.D. 803; Lerbekmo and Campbell 1969). Second, we

determined along a 18km-long reach of the river, the spatial distribution of the permafrost in the plain using the results obtained on the basis of i) the field surveys; ii) the reconstruction of the fluvial landform mobility since 1977 by remote sensing analysis and iii) the detrended Arctic DEM.

PERMAFROST SPATIAL DISTRIBUTION

The Beaver Creek is embedded in the eastern part of a glacio-fluvial outwash fan deposited during the Late Glacial Maximum in which permafrost is present. In the study area, no permafrost was observed under the river bed, as shown by the lowest value on the ERT cross-section of left riverside (Figure 2, U5). The recent proximal floodplain (U4), that has been stabilized and colonized by an alluvial vegetation since 1977-1986, has no permafrost either. In the active bed and in the proximal floodplain, the highest values (2000-5000 Ohm.m) measured on the ERT profile correspond to coarse fluvial deposits (sand, gravel and cobble). The large central unit (U3, undated), colonized by 12-15 m-high spruce trees is mostly permafrost free. Frozen ground in this unit was only observed at the contact with Unit 2, the highest (and probably the oldest) alluvial level. This unit 2 is entirely affected by permafrost as indicated by high resistivity values (> 5000 Ohm.m). Cores revealed a thaw depth of 30 – 45 cm deep at the beginning of September 2023.

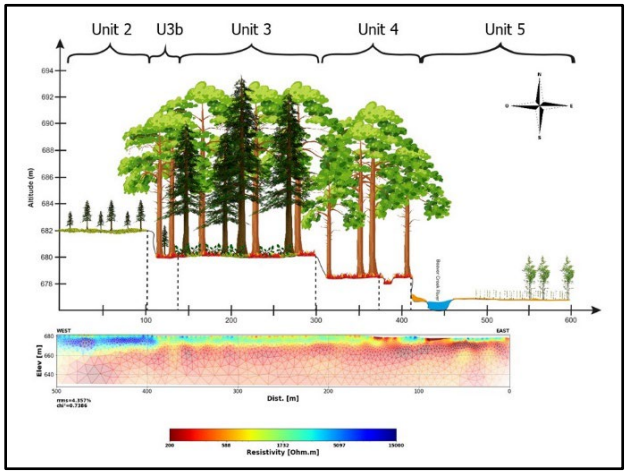

Figure 2. Cross-section of the left floodplain. Above: topographic units and below: ERT section. (Not the same vertical scale on both graphs).

U2 is present on both sides of the river. It can be relatively dated, as the White River Ash was preserved at a mean depth of 50 cm on the right side of the river under fine overbank deposits. Differently, on the left side, sand and gravel were found which let us suppose that this part of the plain corresponded to the active bed.

The diachronic study of the mobility of the fluvial forms since 1977 helps us to evaluate the impact of the river on permafrost erosion. For the last four-five decades, the Beaver Creek mainly eroded the unit 3, where no permafrost is present today. In 2023, erosion of the banks with permafrost represents less than 5% of the bank line.

CONCLUSION

This preliminar study highlights several points concerning interrelations between fluvial dynamics and permafrost. First, in the case of the Beaver Creek River, the aggradation of permafrost in abandoned fluvial sediments requires more than 40-50 years and likely a few centuries, as shown by the absence of permafrost within U4 stabilized since the late 1970's. The active lateral mobility of the river inhibits thus the formation of permafrost. Therefore the most part of the recent floodplain doesn't support permafrost. Second, U3 which is at least 100 years old according to the vegetation, contains isolated patches of permafrost. Finally, the oldest unit (U2) is entirely affected by permafrost, formed after the WRA deposits, *i.e.* younger than AD 800. These observations imply that the permafrost required more than one century to form. It differs from colder Arctic regions where the permafrost formation is faster (Gautier et al. 2021). These preliminary results need further investigations in order to better understand interactions between fluvial dynamics, permafrost and climate change.

REFERENCES

Gautier, E. et al. 2021. Fifty-year dynamics of the Lena River islands (Russia): Spatio-temporal pattern of large periglacial anabranching river and influence of climate change. Science of the Total Environment 783: 147020. https://doi.org/10.1016/j.scitotenv.2021.147020

Rowland, J.C. et al. 2023. Scale dependant influence of permafrost on riverbank erosion rate. JGR Earth Surface 28/7, e2023JF007101. https://doi.org/10.1029/2023JF007101

Tananaev, N., and Lotsari, E. 2022. Defrosting northern catchments: Fluvial effects of permafrost degradation. Earth Science Review, 228: 103096. https://doi.org/10.1016/j.earscirev.2022.103996

Sliger, M. et al. 2015. Incidence of Late Pleistocene-Holocene climate on the concurrent landscape and permafrost development of the Beaver Creek region. In Conference GeoQuebec 2015, Quebec, QC, Canada. https://doi.org/10.13140/RG.2.1.1008.1764

Lerbekmo, J.F., and Campbell, F.A. 1969. Distribution, composition and source of the White River Ash, Yukon Territory. Canadian Journal of Earth Sciences, 6: 109: 110–116. https://doi.org/10.1139/e69-011

COLDSPOTS: low temperatures of ground in the Central European Variscan Ranges (Sudetes, Bohemian Massif)

Marek Kasprzak

Faculty of Earth Sciences and Environmental Management, University of Wrocław, Wrocław, Poland

In Central Europe, evidence of modern permafrost in lower mountain ranges has yet to be confirmed. Nevertheless, negative temperatures of ground can persist all year round in specific conditions, mainly within coarse-grained sediments, rock crevices, and caves (e.g., Gude et al. 2003; Zacharda et al. 2007). I call such small-scale places of low ground temperature COLDSPOTS.

Knowledge about the ground thermic properties in seasonally frozen ground zones is limited (Kasprzak et al. 2022). Soil temperature measurements are carried out with WMO standards at meteorological stations, but their rare net does not reflect terrain diversity and topo- and microclimatic conditions.

This abstract provides project assumptions and preliminary research results on COLDSPOTS in the Sudetes, a medium–altitude range in Central Europe. The investigation should help determine or exclude the existence of mid-latitude permafrost and support ecological and geotechnical studies.

STUDY AREA

Sudetes, the northern part of a Bohemian Massif, is a mountainous area on the Polish-Czechian border (Figure 1). Its highest ranges rise above the tree line. Some of them, e.g., the Izera Mts, are characterised by an extremely harsh climate, enabling frosts to occur each month, and winter temperatures can drop below -37 °C. Also, year-round snow patches can survive here in rock clefts (Piekiełko cleft in the Stołowe Mts) and ice in the basaltic talus caves, such as the Naděje (641 m) and the no longer extant cave of Mt. Łysanka (444 m). Their altitude is 650–850 m lower than ice caves in the nearby Tatra Mts.

METHODS

Areas with specific microclimate (Figure 1, Table 1) are tested by thermistor strings (GEOprecison GmbH) embedded 1.5 m into the ground to measure ground temperature. Additional HOBO loggers, placed between the boulders, were also used to investigate the thermic properties of blockfields. As a background, ground–atmosphere heat flux conditions are monitored in a 15 m depth borehole. It was designed and drilled on Mt Szrenica (1,365 m) at the meteorological station operated by Karkonosze National Park. Thermistor strings were installed in the autumn of 2022. The Szrenica borehole ($OB_{Sz}1$) measurements began on June 22, 2023.

PRELIMINARY RESULTS

When submitting the abstract, a full-year data series had yet to be fully collected. However, a few conclusions can be drawn, which are unique due to the similar data deficit in the research area.

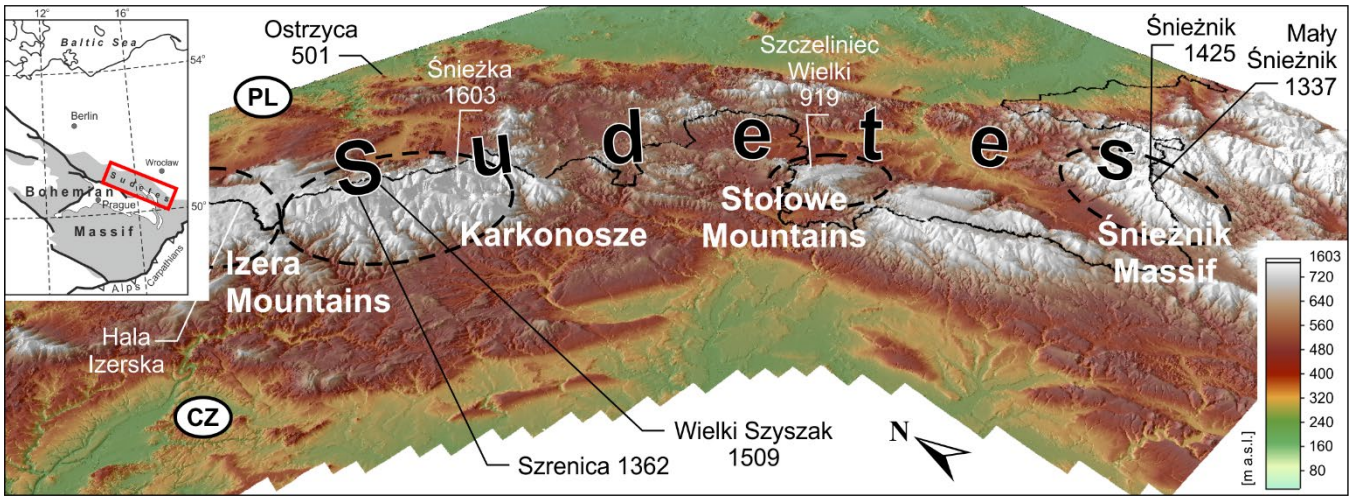

Figure 1. Mountain ranges under COLDSPOTS research in the Sudetes.

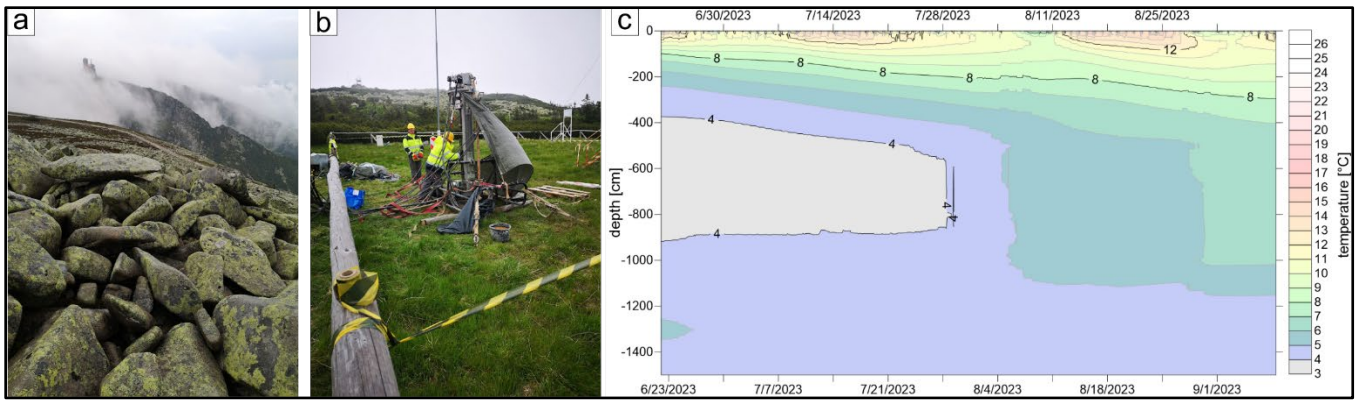

Figure 2. Investigation in the Karkonosze Mts: a – blockfields at altitudes 1200–1600 m a.s.l.; b – drilling of the 15 m depth borehole for thermistor string; c – temperature record from the borehole, preliminary results (June 22 – September 8, 2023).

Table 1. Sample results of ground temperature measurements on various surfaces.

Site	Range	Altitude	Characteristics	T min (0 cm)	T min (−50 cm)	T min (−100 cm)	T min (−150 cm)
Ostrzyca	Kaczawa Mts	470	scree slope	−2.28	0.05	1.76	3.71
Szczeliniec Wlk.	Stołowe Mts	880	soil in a rock cleft	−0.34	−0.03	0.08	0.28
Hala Izerska	Izera Mts	825	soil	−2.1	1.95	2.83	3.71
Mały Śnieżnik	Śnieżnik Massif	1320	soil (forested)	0.2 (no freezing)	1.11	malfunction	malfunction
Śnieżnik		1409	soil	−0.49	0.5	1.08	1.41
Szrenica	Karkonosze	1313	blockfield	−10.29	−10.95	−10.72	−9.81
Wielki Szyszak		1491	blockfield	−11.21	−12.29	−11.02	−10.13
Śnieżka		1550	blockfield	new installed	new installed	new installed	new installed

The measurements in the borehole concern the summer period (Figure 2). The lowest temperatures were 3–4 °C (min 3.3 °C on June 22) at depths of 4–9 m. Until September 8, an uninterrupted trend of heating the ground from the surface was noticed. The highest temperature of the grassed surface was 27.5 °C (Sept 15, 16:00).

Thermistors installed to a depth of 1.5 m (0, 5, 10, 20, 50, 100 and 150 cm) in test sites indicate significant temperature differences (Table 1).

Conclusions

The preliminary results show a variation in the thermal conditions of the ground determined by its structural features and water saturation, as well as a surface exposition on atmospheric factors, reduced by tree crowns, leaf litter and snow. The bedrock summer temperature, measured in the borehole in the highest parts of the Sudetes, was higher than 3 °C. The coldest part of the solid rock occurred at a depth of 4–9 m. At altitudes above 1000 m a.s.l., under tree crowns, it is possible that the ground, insulated with leaf litter and snow, can not freeze in winter. Within high-altitude blockfields, the air voids are characterised by low temperatures and large temperature amplitudes. After examining the annual values, whether the bedrock below blockfields is perennially frozen can be indicated.

Acknowledgements

The research was carried out with the financial support of the National Science Center (Poland) in the project "COLDSPOTS: low temperatures of ground in the Sudetes" (UMO-2021/43/B/ST10/00297).

References

Gude, M., Dietrich, S., Mäusbacher, R., et al. 2003. Probable occurrence of sporadic permafrost in non-alpine scree slopes in central Europe. *In* Phillips, Springman & Arenson (ed.) Permafrost. Swets & Zeitlinger, Lisse: 331–336.

Kasprzak, M., Traczyk, A., and Migała, K. 2022. Seasonally Frozen Ground. *In* Shroder, J.J.F. (ed.), Treatise on Geomorphology, vol. 4. Elsevier, Academic Press: 415–427. DOI:10.1016/B978-0-12-818234-5.00141-3

Zacharda, M., Gude, M., and Růžička, V. 2007, Thermal Regime of Three Low Elevation Scree Slopes in Central Europe, Permafrost and Periglacial Processes, 18: 301–308. DOI:10.1002/ppp.598

The 2023 Fluchthorn massive permafrost rock slope failure analysed

Michael Krautblatter[1], Samuel Weber[1,2], Michael Dietze[3,4], Markus Keuschnig[1,5], Georg Stockinger[1], Lisa Brückner[6], Jan Beutel[7], Thomas Figl[8], Claudia Trepmann[6], Robert Hofmann[9], Maximilian Rau[1], Felix Pfluger[1], Laura Barbosa Mejia[1,10] & Florian Siegert[10]

[1]*Chair of Landslide Research, Technical University of Munich, Munich, Germany*

[2]*WSL Institute for Snow and Avalanche Research SLF, Davos Dorf, Switzerland*

[3]*Institute of Geography, Georg-August University Göttingen, Göttingen, Germany*

[4]*German Research Center for Geosciences (GFZ), Potsdam, Germany*

[5]*GeoResearch Research Institute, Wals, Austria*

[6]*Professorship Geological Deformation and Transformation of Rocks, Ludwig-Maximilians-University Munich, Germany*

[7]*Department of Computer Science, University of Innsbruck, Innsbruck, Austria*

[8]*Geological Survey of Tirol, Innsbruck, Austria*

[9]*Geotechnical and Tunneling Engineering, University of Innsbruck, Innsbruck Austria*

[10]*3D RealityMaps, Munich, Germany*

Warming in the last two decades has caused massive rockfall activity with limited mobility in the range of 101-6 m³. However, only a few highly destructive and mobile rock avalanches above 1 Mio. m³ have been documented. Rock-ice mechanical models explaining high-magnitude rock slope failure in permafrost have been postulated but not validated on real failures.

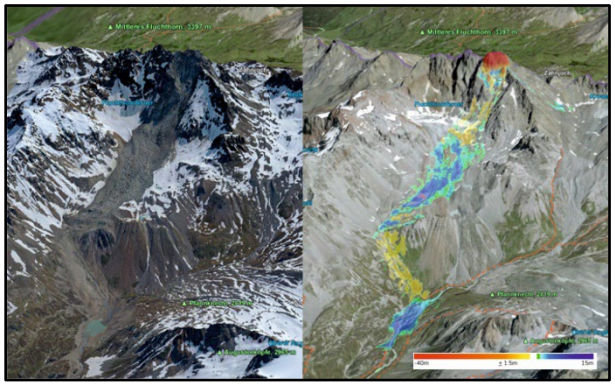

Figure 1. High-resolution Image of the Fluchthorn Massive Rock Slope (left) and altitudinal difference before and after the failure (right). With friendly permission from 3D reality solutions.

This manuscript combines complementary expert knowledge to decipher the 1 Mio. m³ Fluchthorn rock slope failure that detached on June 12, 2023, from the before 3399 m high summit causing a rock avalanche that additionally eroded ca. 120.000 m³ of ice. InSAR data shows deformation rates in the range 4.1 – 7.1 ± 0.13 cm/a from April 2021 to March 2023, but these are surprisingly linked to a westward deformation of the entire Silvretta nappe (in the range of 3 cm/a) over steepening the Fluchthorn. Mountain guides have observed singular failures before the event. IR drone flights immediately after the event indicate rock temperatures at the failure planes in the range of 0°C to -2°C and ice-filled fractures. Solid, scarcely fractured pseudotachilitic sequences in the summit regions may have contributed to the massive oversteepening of the Fluchthorn Westface without significant pre-failures. The grain size compositions shows massive material take up of fine grained material and fragmentation (Pudasaini and Krautblatter 2021).

In a seismic analysis we can exactly reconstruct the temporal and spatial trajectory, velocities and energy release during the 120-second rock avalanche propagation consistent with fragmentation and deposits. High-resolution photogrammetry highlights massive ice erosion and accumulation patterns during the rock avalanche propagation. In addition, we analyse all precursors in the last two years before the failure in detail (Leinauer et al. 2023): These include small prefailure volumes, seismic precursors, kinematic precursors, and kinematic precursors detected in UltraCam and LiDAR surveys.

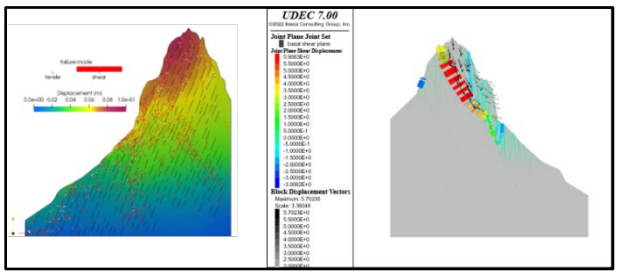

Figure 2. (i) Irazu and (ii) UDEC model of the Fluchthorn indicating (i) pre-failure preparation of a failure plane and (ii) permafrost influence on final failure plane with ice-filled fractures dependent on permafrost rock temperature.

In an IRAZU model, capable of nucleation and growth of fractures based on nonlinear fracture mechanics applied stresses act to produce a progressive fracturing path that closely resembles the real failure, and we can show the impact of the solid pseudotachilitic roof on the oversteepening. In a discontinuum model (UDEC) (Krautblatter et al. 2013; Draebing and Krautblatter 2019; Jia et al. 2017; Jia et al. 2019; Mamot et al. 2018; Mamot et al. 2020; Mamot et al. 2021), we can show the stabilizing effect of permafrost on developing fracturing patterns in a combined rock-ice mechanical approach.

In summary, we show a unique combination of datasets deciphering pre-failure tectonic and geological controls and forcing, syn-failure permafrost-related mechanics, and second-resolution data on rock avalanche evolution in a cryospheric terrain with massive ice uptake.

REFERENCES

Draebing, D., and Krautblatter, M. 2019. The Efficacy of Frost Weathering Processes in Alpine Rockwalls, Geophysical Research Letters, 46(12): 6516–6524. doi:10.1029/2019gl081981

Jia, H., Xiang, W., and Krautblatter, M. 2015. Quantifying rock fatigue and decreasing compressive and tensile strength after repeated freeze-thaw cycles, Permafrost and Periglacial Processes, 26(4): 368–377. doi:10.1002/ppp.1857

Jia, H., Leith, K., and Krautblatter, M. 2017. Path-Dependent Frost-Wedging Experiments in Fractured, Low-Permeability Granite, Permafrost and Periglacial Processes, 28(4): 698–709. doi: 10.1002/ppp.1950

Krautblatter, M., Funk, D., and Günzel, F.K. 2013. Why permafrost rocks become unstable: a rock-ice-mechanical model in time and space, Earth Surface Processes and Landforms, 38(8): 876–887. doi:10.1002/esp.3374

Krautblatter, M., and Leith, K. 2015. Glacier- and permafrost-related slope instabilities. Chapter 9 in Huggel, C., Carey, M., Clague, J., and Kääb, A., The High-Mountain Cryosphere, Cambridge University Press.

Leinauer, J., Weber, S., Cicoira, A., Beutel, J., and Krautblatter, M. 2023. An approach for prospective forecasting of rock slope failure time, Communications Earth and Environment, 4(1). doi:10.1038/s43247-023-00909-z

Mamot, P., Weber, S., Schröder, T., and Krautblatter, M. 2018. A temperature-and stress-controlled failure criterion for ice-filled permafrost rock joints, The Cryosphere, 12(10): 3333–3353. doi:10.5194/tc-12-3333-2018

Mamot, P., Weber, S., Lanz, M., and Krautblatter, M. 2020. Brief communication: The influence of mica-rich rocks on the shear strength of ice-filled discontinuities, The Cryosphere, 14(6): 1849–1855. doi:10.5194/tc-14-1849-2020

Mamot, P., Weber, S., Eppinger, S., and Krautblatter, M. 2021. A temperature-dependent mechanical model to assess the stability of degrading permafrost rock slopes, Earth Surface Dynamics, 9(5): 1125–1151. doi:10.5194/esurf-9-1125-2021

Pudasaini, S.P., and Krautblatter, M. 2021. The mechanics of landslide mobility with erosion, Nature Communications, 12(1). doi:10.1038/s41467-021-26959-5

Glacier-Permafrost Interactions and their influence on recent and sub-recent morphodynamics in alpine environments

Julius Kunz, Sebastian Buchelt, Tim Wiegand & Christof Kneisel
Institute of Geography and Geology, University of Wuerzburg, Germany

The presence of permafrost in glacier forefields during glacial advances can result in the formation of large thrust moraine complexes, also in high alpine environments (Haeberli 1979). However, in the European Alps, these oftentimes spectacular landforms are relatively rare due to the comparatively extensive glacial advances during the Little Ice Age (LIA), usually below the local lower permafrost boundary. Nevertheless, during the LIA, in some dry inner-alpine regions, glacier-permafrost interactions and the formation of comparatively large thrust moraine complexes occurred at some smaller cirque glaciers that did not advance beyond this local lower limit. Due to the complex formation, which may also be partly attributable to multiple glacial advances, permafrost-related ground ice, but also large amounts of sedimentary ice of glacial origin are often incorporated into these moraine complexes.

Especially the high amounts of ice within their internal structures make them very sensitive to external changes and particularly to climate warming. High ice contents also enable permafrost creep and internal deformation of the moraine complexes resulting in distinct morphodynamics. General spatial patterns of these and their temporal variations, but also their relationships to subsurface structures are key components to understand their origin and the future development of these landforms.

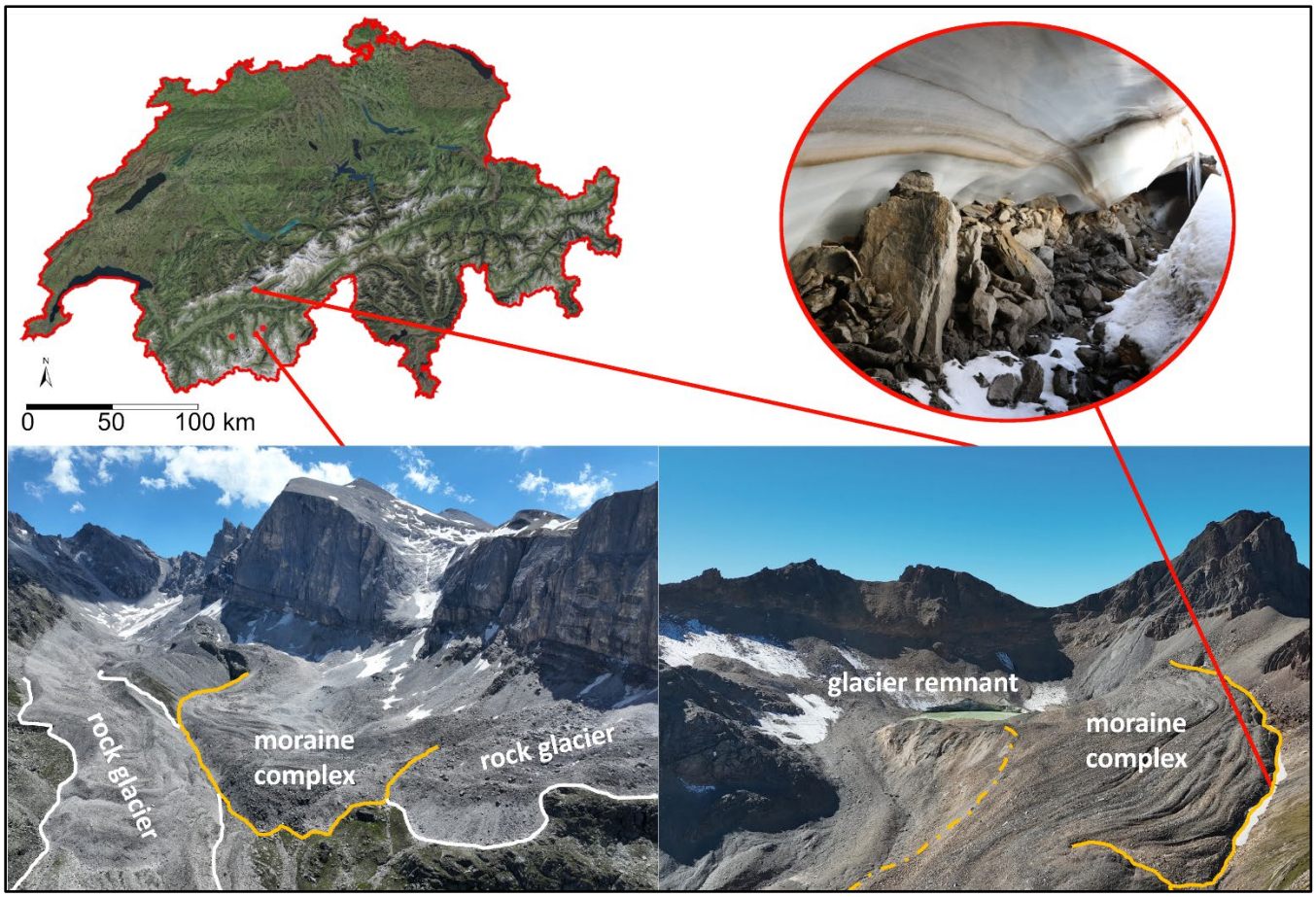

Figure 1. Thrust moraine complexes in the Piipjitelli (lower left) and Oberferden (lower right) glacier forefields in the Swiss Alps. In the upper right, a massive ice exposure in the distal flank of the Oberferden Moraine Complex is shown.

In the current research project, we investigate the internal structures of several thrust moraine complexes in the Swiss Alps (Figure 1) using geophysical methods to delineate zones with varying ice contents and different origin of ice types within the landforms. Especially the use of electrical resistivity tomography (ERT) and ground-penetrating radar (GPR) enables the detection of massive ice bodies and a differentiation between ice of glacial and periglacial origin (sedimentary and magmatic ice) in the subsurface of such landforms (e.g., Kunz et al. 2021). Additionally, Differential SAR Interferometry (DInSAR) based on Sentinel-1 data provides information about recent morphodynamics. Besides, the coexistence of thrust moraines and active rock glaciers at the study sites enables the comparison of morphodynamic similarities or differences between these landforms.

METHODS

To study the internal structure of the moraines, ERT and GPR were used. At the investigated sites, several 2D ERT surveys were measured using a Syscal Switch Pro (Iris Instruments) and 36 electrodes. At the Oberferden Moraine Complex (OMC), a quasi-three-dimensional approach was conducted measuring parallel profiles to invert them as a three-dimensional data set and to provide high spatial coverage within a sub-area of the moraine complex. Also, GPR measurements were conducted at OMC using a Sensors & Software Pulse Ekko Pro System and 50 MHz antennas. The recent morphodynamics were investigated using Sentinel-1 SAR data between 2017 and 2021 based on the approach developed by Buchelt et al. (2023). This approach enables the derivation of surface velocity on a 6-day interval as well as the investigation of movement seasonality.

PRELIMINARY RESULTS

The geophysical measurements revealed distinct heterogeneities within the moraine complexes and enabled a delineation of different structural zones. High electrical resistivities (> 1 MΩm) indicate the presence of massive ice of glacial origin within the moraine complexes. In other areas of the complexes, resistivity values of several kΩm but well below 1 MΩm also indicated the presence of permafrost with high amounts of ground ice, but probably not of glacial or sedimentary origin (cf. Haeberli and Vonder Mühll 1996). The general spatial distribution of resistivities also fits into the pattern of recent morphodynamics, which are concentrated to the areas where high electrical resistivities could be detected in the subsurface (e.g., Figure 2). In Piipjitelli, distinct differences between the internal structures of the Piipjitelli Moraine Complex (PMC) and the neighbouring rock glacier could be detected by geophysical surveying. The different internal structures also coincide with varying morphological dynamics of both features. While the PMC shows strong seasonality and large movements only in late summer, the surface displacement of the neighbouring rock glacier is more constant throughout the year.

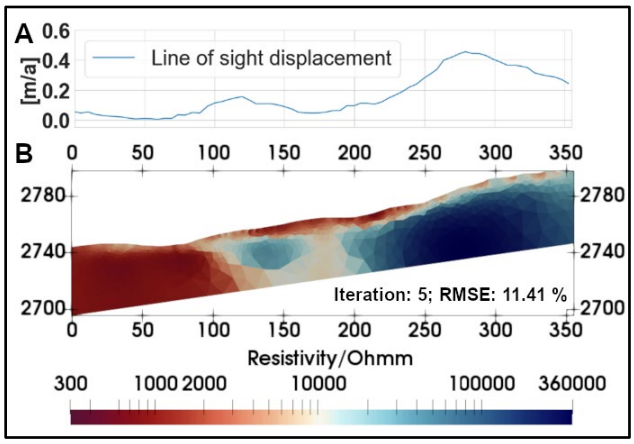

Figure 2. Line of sight displacement (A) along an ERT profile (B) in the proximal flank of OMC.

ACKNOWLEDGEMENTS

We gratefully thank Severin Scheib and Jannik Schönfeld for their assistance in the field. This study was funded by the German Research Foundation (DFG 506183115).

REFERENCES

Buchelt, S., Blöthe, J.H., Kuenzer, C., Schmitt, A., Ullmann, T., Philipp, M., and Kneisel, C. 2023. Deciphering Small-Scale Seasonal Surface Dynamics of Rock Glaciers in the Central European Alps Using DInSAR Time Series, Remote Sensing, 15(12): 2982. doi:10.3390/rs15122982

Haeberli, W. 1979. Holocene push-moraines in alpine permafrost, Geografiska Annaler: Series A, Physical Geography, 61(1-2): 43–48. doi:10.2307/520513

Haeberli, W., and Vonder Mühll, D. 1996. On the characteristics and possible origin of ice in rock glacier permafrost, Zeitschrift für Geomorphologie NF, Suppl.-Bd. 104: 43–57.

Kunz, J., Ullmann, T., and Kneisel, C. 2022. Internal structure and recent dynamics of a moraine complex in an alpine glacier forefield revealed by geophysical surveying and Sentinel-1 InSAR time series, Geomorphology, 398: 108052. doi:10.1016/j.geomorph.2021.108052

How do permafrost landforms in Svalbard respond to global warming?

Norikazu Matsuoka[1], Tatsuya Watanabe[2] & Hanne H. Christiansen[3]

[1]*College of Education, Ibaraki University, Mito, Japan*

[2]*Kitami Institute of Technology, Kitami, Japan*

[3]*Arctic Geophysics Department, The University Centre in Svalbard, Longyearbyen, Norway*

Having a variety of permafrost landforms within a small area that undergoes rapid warming, Svalbard offers excellent possibilities to study changing periglacial environments. Based on field observations during the last two decades in central Svalbard, we discuss contemporary dynamics and future changes of permafrost landforms, including ice-wedge polygons, mudboils, rock glaciers, and others. These landforms respond differently to continuous warming and resulting permafrost thawing.

Svalbard has undergone an extremely rapid ground warming at a rate of 0.1–0.2°C yr^{-1} and resulting thawing of the top of permafrost in sediments at a rate of about 1 cm yr^{-1} in the last few decades (Strand et al. 2021; Figure 1), which may rapidly change landforms and cause ground hazards.

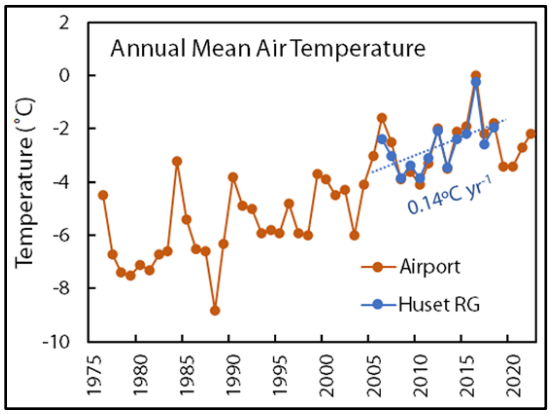

Figure 1. Warming trend in central Svalbard. Data from the meteorological station at Longyearbyen airport and from the Huset rock glacier in Longyearbyen valley.

We have conducted long-term monitoring of periglacial processes, including ice-wedge cracking, mudboil dynamics and rock glacier creep in Adventdalen, central Svalbard. Based on our observations and studies by other researchers, we summarize the present-day dynamics of permafrost landforms and prospect their near-future changes.

ICE-WEDGE POLYGONS

Ice-wedge polygons are abundant where winter snow cover is minimal, typically in sediment-filled valley bottoms. Fourteen years (2004-18) of monitoring of the dynamics of three polygon trough-ridge systems (opening-closing, heaving-settling, acceleration, cracking, air and ground temperature, and soil moisture) showed seasonal movements interlinked between troughs and ridges (Matsuoka et al. 2018). Rapid cooling in winter caused ground acceleration, opening (up to 1 cm) and cracking of the troughs. The opening was sometimes irreversible, which indicated the growth of ice wedge: e.g., 8 mm growth of ice wedge in the 2017/18 winter (Figure 2A).

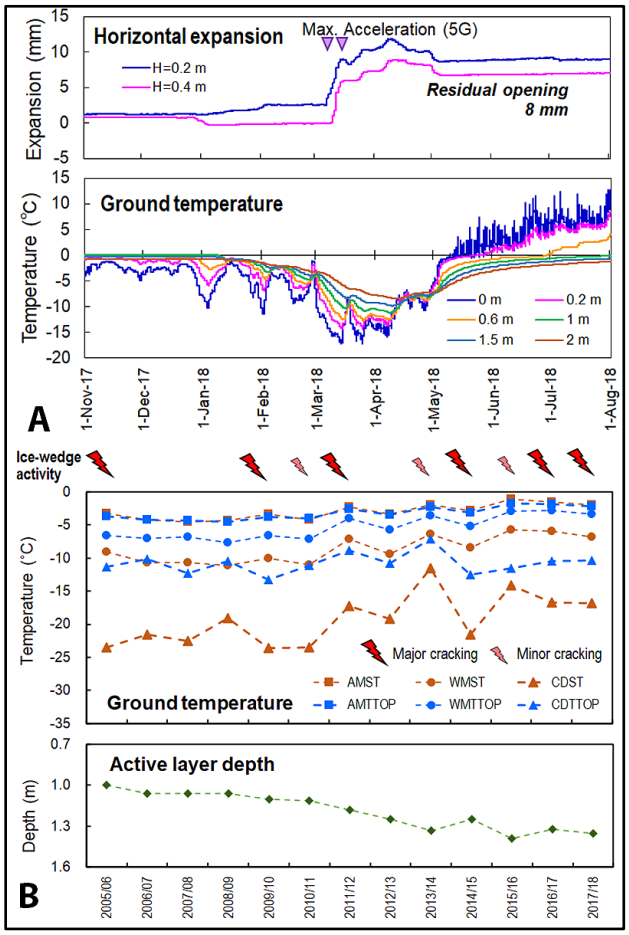

Figure 2. Ice-wedge dynamics in Adventdalen. (A) Rapid cooling in the 2017/18 winter led to trough expansion and ice wedge growth. (B) Summary of ground temperature and ice-wedge activity for 13 years. AM: annual mean. WM: winter mean. CD: coldest day. ST: surface temperature. TTOP: temperature at the top of permafrost.

Ice-wedge cracking showed interannual variability which did not correlate with annual mean or winter mean temperature. In fact, major cracking occurred in both cold (2005/06, 2009/10, 2014/15) and warm winters (2011/12, 2016/17, 2017/18), and despite the overall warming trend ice-wedge cracking did not decline (Figure 2B). This is because cracking is associated with intensive cold spells. If such periodical cold spells occur under further warming conditions, ice-wedge cracking may continue. However, a deepening active layer (AL) (Figure 2B) leads to thawing of the top of the ice wedge and may finally prevent cracking into the permafrost.

MUDBOILS

Four-years (2009–13) of monitoring of mudboil activity showed differential seasonal heave between the exposed centre (8–11 cm) and vegetated margin (2–4 cm), because of earlier freezing and moisture migration towards the centre. Drilling in winter revealed that segregated ice concentrated in the upper AL at the centre, suggesting that frost heave during downward freezing in early winter is most responsible for the mudboil formation (Watanabe et al. 2012). Continuous warming in the next decades can lead to progressive deepening of the AL and lowering of the water level. However, the activity of mudboils will continue if the AL is kept humid.

ROCK GLACIERS

Rock glaciers (RGs) in polar regions are relatively small and have only sporadically been monitored, although ongoing warming may activate permafrost creep and RGs. We observed surface displacements, internal deformation, and ground temperatures of a small talus-foot RG (called the Huset RG) in the Longyearbyen valley for 13 years (2006–19).

The permafrost temperature at the depths of 5–15 m fluctuated between −2.5°C and −4.5°C and showed overall warming at rates of 0.08–0.1°C yr^{-1} (Figure 3A). Surface markers moved downslope at velocities of 2.4–5.0 cm yr^{-1} with slight acceleration on average of 0.17 cm yr^{-1} in response to permafrost warming. Inclinometers at 5, 9 and 13 m depths in permafrost progressively tilted downslope (Figure 3B). Annual tilting amounts significantly correlated with annual mean ground temperatures at the same depths.

If permafrost warming continues at the same rate as in the last decade, the permafrost temperature at the Huset RG will reach −2.0°C to −2.5°C within the next decade, which is typical of active mid-latitude alpine RGs. Accordingly, RGs in Svalbard will gradually increase their velocities and might begin significant advance.

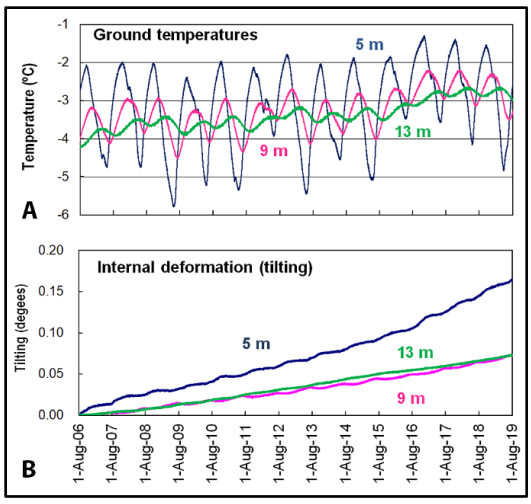

Figure 3. Thirteen years (2006-19) of permafrost temperature and deformation of the Huset rock glacier.

OTHER PERMAFROST AFFECTED LANDFORMS

Soil movement due to solifluction in Svalbard shows a significant interannual variation depending on the annual AL thickness, which affects whether an ice-rich layer produced by upward freezing from the permafrost table thaws or not (Harris et al. 2011). Long-term progressive warming may temporarily accelerate solifluction until the ice-rich layer completely thaws, but rising permafrost temperature would eventually disable upward freezing and confine the soil movement in the uppermost few decimeters.

Open system pingos may show a complex response to warming. Some pingos may subside by thawing of the uppermost part of their injection ice core, while subpermafrost hydraulics may support the growth of active pingos by adding new ice until the permafrost degrades.

REFERENCES

Harris, C., Kern-Luetschg M., Christiansen, H.H., and Smith, F. 2011. The Role of Interannual Climate Variability in Controlling Solifluction Processes, Endalen, Svalbard. Permafrost and Periglacial Processes, 22: 239–253.

Matsuoka, N., Christiansen, H.H., and Watanabe, T. 2018. Ice-Wedge Polygon Dynamics in Svalbard: Lessons from a Decade of Automated Multi-Sensor Monitoring. Permafrost and Periglacial Processes, 29: 210–227.

Strand, S.M., Christiansen, H.H., Johansson, M., Åkerman, J., and Humlum, O. 2021. Active Layer Thickening and Controls on Interannual Variability in the Nordic Arctic Compared to the Circum-Arctic. Permafrost and Periglacial Processes, 32: 47–58.

Watanabe, T., Matsuoka, N., and Christiansen, H.H. 2012. Mudboil and Ice-Wedge Dynamics Investigated by Electrical Resistivity Tomography, Ground Temperatures and Surface Movements in Svalbard. Geografiska Annaler, 94A: 445–457.

Periglacial processes and the formation of the Hickory Run Boulder Field, Carbon County Pennsylvania, U.S.A.

Raven Mitchell[1] & Frederick E. Nelson[1,2]

[1]*Department of Geography, Environment, and Spatial Sciences, Michigan State University, East Lansing, Michigan, United States*

[2]*Department of Earth, Environmental, and Geographical Sciences, Northern Michigan University, Marquette, Michigan, United States*

Boulder fields are open-work clast accumulations, often occupying low-angle surfaces. These features are nearly devoid of vegetation (except lichens and mosses) and have continuous spatial extents of several hundred to many thousands of square meters (Park Nelson et al. 2007). Boulder fields are among the best geomorphic expressions of long-term periglacial weathering (Ballantyne 2018) and are globally expressed in areas that escaped glaciation, including in Scandinavia, Scotland, Svalbard, Greenland, Arctic Canada, the United States, and Antarctica (Ballantyne 2018). Boulder fields occur in two forms: autochthonous (formed in situ) or allochthonous (formed by boulder emplacement) (Park Nelson et al. 2007).

Although the occurrence of boulder fields has been used to indicate paleoenvironments, there is contention surrounding the climates/processes responsible for their formation (Denn et al. 2018), a state of affairs that hinders the utility of boulder fields in paleoclimate reconstruction. One hypothesis states that boulder fields formed during the warmer, wetter conditions of the Neogene period and were only subtly modified by subsequent periglacial conditions (French and Millar 2014). An opposing hypothesis states that boulder fields are solely the result of periglacial processes operating throughout the Pleistocene (Ballantyne 2018).

Hundreds of boulder fields have been identified in the eastern United States but despite their prevalence in past and present periglacial regions, research on them has largely been the focus of descriptive analysis and has traditionally been situated in the larger context of periglacial climate/paleoclimate reconstruction studies. As such, processes leading to boulder field formation remain poorly understood (Denn et al. 2018).

Hickory Run Boulder Field

The Hickory Run Boulder Field (HRBF) (Figure 1) is located in the Pocono Plateau region, Carbon County, Pennsylvania (41°03’02”N, 75°38’44”W) approximately 1.5 km south of the Wisconsinan glacial border (Smith 1953). The HRBF is an exemplary relict boulder field and is the most impressive feature of its type in the eastern U.S. The boulder field is large, spanning over 500 meters in the long-axis dimension and is nearly devoid of vegetation. The outline of the boulder field is irregular and consists of a major unit and a minor limb. The 1°-degree slope of the boulder field accentuates its striking appearance.

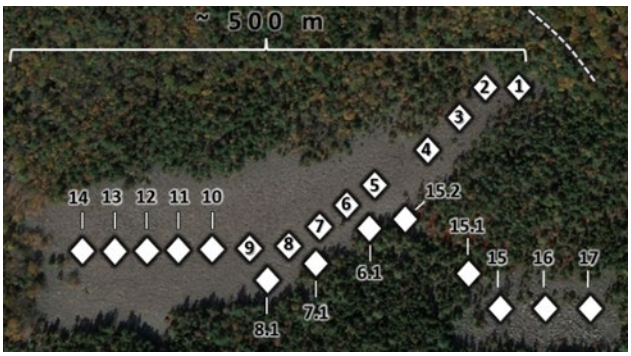

Figure 1. Aerial Imagery of the Hickory Run Boulder Field with sampling locations. Many of the boulders here are loosely packed and lack interstitial fine material.

A periglacial allochthonous interpretation has been advanced for HRBF’s formation (Smith 1953), emphasizing frost wedging on scarp-like bedrock source outcrops and slow movement of weathered material over an impermeable permafrost table during Pleistocene glacial advances. Under this interpretation, greater weathering of clasts furthest from the bedrock source area is expected due to longer exposure of the clasts to weathering processes (Smith 1953). Elaborations of this hypothesis attribute the formation of some boulder fields to periglacial mass movement in a fine-textured medium that was subsequently eluviated by wash (Ballantyne 2018, p. 191). This hypothesis remains a dominant explanation for the HRBF and is expressed through pamphlets and a sign placed by the Hickory Run State Park, although contention surrounding its formation exists (Denn et al. 2018).

Boulders within the field reach sizes of up to 6 meters and are primarily quarzitic sandstone and conglomerate that can be traced upslope as lithology trails from the boulder field to the bedrock source area. The boulder field is underlain by gently folded, resistant

Paleozoic sandstone and conglomerate (Denn et al. 2018). Vegetation in the form of forest is found only at the boulder field margins and a few “tree islands.

The abundance of clasts for sampling within the HRBF and the lack of consensus on its formation make the boulder field an opportune site for implementation and application of quantitative sedimentological analysis. The central concern is whether identifiable trends exist in clast weathering across HRBF and if any trends can be associated with periglacial conditions. Clast macrofabrics and relative weathering index data collected from HRBF were used to test the hypothesis that HRBF is allochthonous, and that clast weathering increases along the primary axis of the feature.

METHODS

Relative weathering indices (volume, shape parameters, and rebound) and clast macrofabric data were collected from 22 locations in the boulder field (Figure 1). Sampling sites were arranged to capture weathering trends along the primary axis of the main boulder field, in the adjoining area between the major and minor field, and primary axis of the smaller field. To minimize the impact of human interaction, twenty-five of the visibly largest clasts were measured from each sampling location, which are spaced 35 meters apart. Only sandstone conglomerate clasts (the dominant lithology in the boulder field) were sampled.

RESULTS

All the relative weathering indices show good agreement with one another and reveal dynamic trends in clast weathering with distance along the major axis of the boulder field (Figure 2). Anomalous values from samples in the intermediate portion of the field are in line with relative weathering values obtained from the minor boulder field. We interpret these trends as evidence for the contribution of clasts from the minor to the major field. The integration of clasts from the minor field appears to have been emplaced via “tributary” flow during the height of periglacial conditions in the Last Glacial Maximum. Macrofabric data reveal that clast orientation tends to align with the major axis of the field although statistically significant fabrics were found primarily in data obtained from the head and tail of the boulder field, with more chaotic patterns in the area where the two components of the field merge.

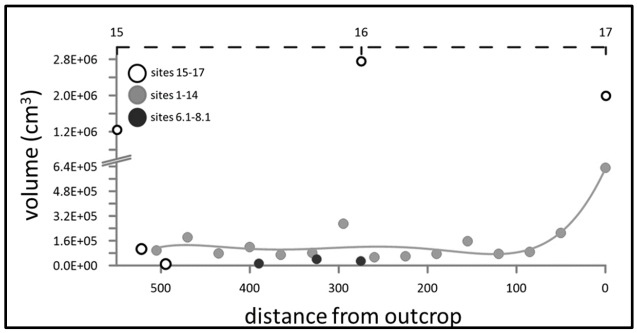

Figure 2. Volume data from the main and minor boulder fields, labelled.

SUMMARY AND CONCLUSION

The origin and evolution of the Hickory Run Boulder Field has remained contentious despite this feature being the subject of investigations for more than half a century (Smith 1953). Relative weathering indices reveal dynamic clast weathering and gradual increases in weathering with distance from local outcrops. Relative weathering indices indicate that the integration of clasts from the minor boulder field occurred, offering additional support for the interpretation of emplacement by mass movement. Macrofabrics show that clast orientation is in general agreement with the local slope and boulder field orientation. Overall, relative weathering and microfabric data lend support to the hypothesis that HRBF formed as an allocthonous feature. Future research will focus on obtaining additional samples from the boulder field to investigate clast dynamics along the intermediate axis of the boulder field.

REFERENCES

Ballantyne, C.K. 2018. Periglacial Geomorphology John Wiley & Sons.

Denn, A.R., Bierman, P.R., Zimmerman, S.R.H., Caffee, M.W., Corbett, L.B., and Kirby, E. 2018. Cosmogenic nuclides indicate that boulder fields are dynamic, ancient, multigenerational features. GSA Today, 4–10.

French, H.M., and Millar, S.W.S. 2014. Permafrost at the time of the Last Glacial Maximum (LGM) in North America. Boreas, 43(3), 667–677.

Park Nelson, K.J., Nelson, F.E., and Walegur, M.T. 2007. Periglacial Appalachia: Palaeoclimatic significance of blockfield elevation gradients, eastern USA. Permafrost and Periglacial Processes, 18(1), 61–73.

Smith, H.T.U. 1953. The Hickory Run boulder field, Carbon County, Pennsylvania. American Journal of Science, 251(9), 625–642.

Climate change, permafrost thaw, tipping points and landscape evolution

Brian J. Moorman

Department of Geography, University of Calgary, Calgary, Alberta, Canada

The Arctic is undergoing rapid climatic change, currently warming at four times that of the global average, and this is having a significant impact on the landscape. As increased amounts of energy are absorbed by the ground, permafrost warms and excess ice melts (Figure 1), the structural integrity of the surface can be lost (Figure 2) and long-term, irreversible consequences to the landscape may result. This is a dramatic tipping point in climate influenced landscape evolution.

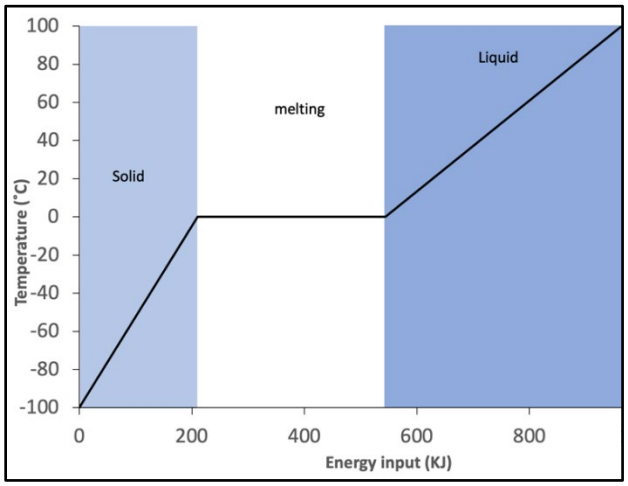

Figure 1. The large latent heat of fusion of water results in a large heat consumption to enable melting. However, this can also result in a tipping point in the physical properties of the ground if it is in the form of excess ground ice.

Figure 2. Example of the thawing of ice-rich permafrost core resulting in a muddy liquid.

The Earth's climate is warming - currently at a rate of 0.18-019 ˚C/decade (Rantanen et al. 2022), while arctic amplification is resulting in the northern regions warming at rates of 0.73 ˚C/decade (Biskaborn et al. 2019). And the ground is heating too. In the decade 2007-2016, circumpolar continuous permafrost was found to be warming at a rate of 0.39 ˚C/decade (Biskaborn et al. 2019) with cold permafrost (MAGT less than -2 ˚C) warming at rates up to 1 ˚C/decade (Smith et al. 2022). This is leading to thawing of the upper portion of the permafrost in many regions.

In areas of exposed bedrock or unsaturated sediment the increased heat added the ground has little impact. However, in areas where there is excess ice, whether it be segregated, buried, or wedge ice, this can lead to dramatic alterations to the landscape such as subsidence, active layer detachments or retrogressive thaw slumps (e.g., Figure 3 or Lewkowicz and Way 2019).

Figure 3. Dramatic landscape alteration created by a retrogressive thaw slump at Peninsula Point, NWT, Canada. For scale, the width slump is approximately 800 m long.

This research project involved quantifying the potential impact of warming on ice-rich permafrost and the resultant ramifications on permafrost landscapes with different ice content and of different ages.

The global average Earth Energy Imbalance is now estimated to be 1 W/m^2 (Figure 4). It is estimated that if all of this energy is propagated into the ground, it could lead to up to 9.4 cm of ground ice being melted per year. While this is a simplified estimation and there are many local and microclimatic factors that may affect it, it does indicate how significant the current climatic warming trends could be on the landscape.

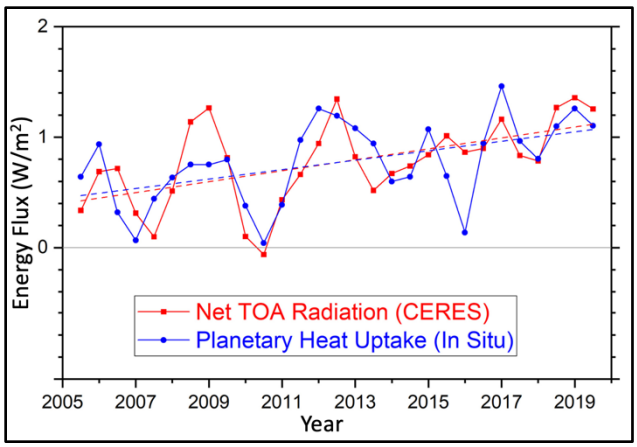

Figure 4. Earth's system energy balance trend over the last two decades including the Top of Atmosphere (TOA) net radiation and in situ observational estimate of uptake of energy by earth climate system (after Loeb et al. 2021).

Throughout the Holocene, northern landscapes have adjusted to changing climatic driving forces, with permafrost and ground ice replacing ice sheets and glaciers. During this time period, excess ground ice has accumulated in the top of permafrost in many regions. At colder, high latitudes where the active layer is thinner, this ice accumulation is found at shallower depths. The ice rich-layer just below the permafrost table is affected to a certain extent by interannual variability, however climatic stability has limited the depth of the short-term climate fluctuations.

Excess ground ice of different origins was mapped in several regions across the Canadian Arctic. This included massive ice bodies and ice-rich permafrost with ages ranging from less that 100 years old to greater than 50,000 years old. The one thing all these study sites had in common was that if the season energy flux was balanced and the depth of thaw stayed within the active layer, the ice below would stay frozen and the ground surface stable.

However, with atmospheric carbon dioxide concentrations now greater than any time in the last 300,000 years, the accelerated melt of recently formed and now older excess ground ice is currently underway. As the ground warms and the active layer thickens, excess ice in the top of permafrost is melting, leading to terrain instability at many sites. Estimates from glacierized regions in the eastern Canadian Arctic revealed up to 35% of the landscape could be subject terrain instability of some form, while in areas of the western Canadian Arctic, this number was much greater. The key being that the permafrost in much of the mid- to high-Arctic is now thawing for the first time in hundreds of thousands of years.

The result will be an order of magnitude increase in the rate of landscape evolution across much of the Arctic in the coming years. The average rate of landscape change in stable permafrost regions is in the order of millimeters to centimeters per year. Landscape change resulting from the melting of excess ice (or massive ice bodies) has been measured to be two orders of magnitude greater. This peak in geomorphic activity is estimated to occur for several hundred years, until a new steady(er) state non-permafrost environment is attained.

This increased geomorphic activity is dominated by increased terrain disturbance from mass movement, vegetation change, hydrological alteration, and increased fluvial erosion and transport.

As well as the rate of landscape evolution dramatically increasing, it is predicted to be of sufficient magnitude that it will represent a tipping point in the evolution of the landscape. Once the excess ice in the subsurface has melted, resulting in massive erosion and surface alteration, there will be no return to the arctic landscape that we have become accustom to since humans first started inhabiting the Arctic.

References

Biskaborn, B.K., et al. 2019. Permafrost is warming at a global scale. Nature Communications 10. doi.org/10.1038/s41467-018-08240-4

Lewkowicz, A.G., and Way, R.G. 2019. Extremes of summer climate trigger thousands of thermokarst landslides in a High Arctic environment. Nature Communications 10. doi.org/10.1038/s41467-019-09314-7

Loeb, N.G., et al. 2021. Satellite and ocean data reveal marked increase in Earth's heating rate. Geophysical Research Letters 48 (13). doi.org/10.1029/2021gl093047

Rantanen, M., et al. 2022. The Arctic has warmed nearly four times faster than the globe since 1979. Communications Earth & Environ 3 (168). doi.org/10.1038/s43247-022-00498-3

Smith, S.L., et al. 2022. The changing thermal state of permafrost. Nature Reviews Earth & Environment 3, 10–23. doi.org/10.1038/s43017-021-00240-1

Age of groundwater in Svalbard's pingos – Radium isotope insights

Dotan Rotem[1,2], Yishai Weinstein[1], Jurgen Sültenfuß[4], Hanne H. Christiansen[2] & Andrew Hodson[3]

[1]*Department of Environment, Planning and Sustainability - Bar-Ilan University, Ramat-Gan, Israel*

[2]*Arctic Geophysics Department, The University Centre in Svalbard, UNIS, N-9171 Longyearbyen, Norway.*

[3]*Arctic Geology Department, The University Centre in Svalbard, UNIS, N-9171 Longyearbyen, Norway.*

[4]*Institute of Environmental Physics, University of Bremen, Bremen, Germany*

Pingos are small hill landforms, up to several 10's meters high and up to hundred meter wide, which form due to the near-surface freezing of upwelling groundwater. There are open-system and closed-system pingos. The first are usually connected to the sub-permafrost groundwater system (Liestøl 1996), and are likely fed by meteoric water or glacial meltwater, while the latter are enclosed by permafrost, deriving their water from within-permafrost processes (i.e., thawing).

The pingos in Svalbard valleys (Figure 1) were traditionally considered as open-system style, owing to the scarcity of thermo-karst features and due to their location in valley bottoms surrounded by mountains, which could be the source for the sub-permafrost water. Hornum et al. (2020), suggested that the pingo-related groundwater discharge is due to the current downward aggradation of the permafrost. Hornum et al. (2021), argued that Svalbard pingos' groundwater does not solely arrive from the surrounding mountains, and that it is likely to include groundwater from a deeper fractured sandstone aquifer. Further, Hodson et al (2020) showed that the pingo springs represents a mixture of different groundwater types, including a more saline end member (relic of marine transgression or a regional brine, e.g., Demidov et al. 2021) and a freshwater endmember more akin to meteoric or glacial runoff. In spite of these insights, the travel history of this water remains obscure (e.g., Demidov et al. 2021).

Sediments have infilled central Svalbard's valleys during the Holocene after deglaciation. Freezing of most of the valley infill (marine sediments) occurred during 11-4 ka following isostatic rebound and exposure to the atmosphere, while the upper few meters (aeolian) froze syngenetically during 4-2 ka (Gilbert et al. 2018; Rotem et al. 2023). Water for pingo formation is assumed to arrive from sub-permafrost reservoirs (e.g., Hornum et al. 2020; Hornum et al. 2021; Demidov et al. 2022), although the possibility of intra-permafrost sources cannot be negated. Determining the residence time of this water in the sub-surface may provide insight into the open versus closed system pingo enigma.

We studied the activity (concentration) of radium isotopes (e.g., ^{226}Ra and ^{223}Ra) and ^{3}H in fresh to brackish groundwater discharging at eight pingos and nearby ice blisters in the central Svalbard valleys Adventdalen, Reindalen and Grøndalen (Figure 1). ^{3}H was relatively low, down to zero in two samples (Figure 2a), suggesting that most groundwater is older than 60 years, i.e. infiltrated into the sub-surface prior to the ^{3}H peak related to the nuclear bomb tests.

Figure 1. Location maps of study site at central Svalbard. Studied pingos are indicated as red dots. Bottom figure shows Innerhytta Pingo from the south.

Groundwater activities of radium isotopes, in particular long-lived to short-lived isotope ratios can be used to constrain water residence time in the aquifer (e.g., Kiro et al. 2015). At water-rock secular

equilibrium, activity ratio of $^{226}Ra/^{223}Ra$ in water should be 21.7, which is the natural activity ratio of these isotopes' radioactive parents $^{238}U/^{235}U$. Equilibrium time depends on (1) the half life of the long-lived isotope, ^{226}Ra (1600 years), (2) radium adsorption, which is high in fresh, oxygenated water. Assuming no adsorption, ratios would reach equilibrium ratios within 8-10 kyr. High adsorption may significantly shorten the equilibration time.

In most of the investigated water, $^{226}Ra/^{223}Ra$ was lower than 21.7 (Figure 2b), which suggests that the water did not arrive at equilibrium. Assuming no adsorption, residence times should be lower than 2000 years, while with adsorption >>0, times are reduced to hundreds of years, possibly lower. Equilibrium or higher than equilibrium ratios observed in some of the samples could be related to bedrock dissolution, as is evidenced by very high SO_4 concentrations in the water associated with one of the pingos.

The daughter to parent $^{224}Ra/^{228}Ra$ ratios (half-lives of 3.66 days and 5.75 years, respectively) are at steady state or lower (Figure 2c), which is common in water older than several decades.

Altogether, the above suggests that while most water is not modern, residence times are probably not older than hundreds years. This, in turn, is younger than permafrost formation (freezing) time in these valleys (>>2 ka), which suggests that despite of the continuous nature of Svalbard permafrost, the aquifer has been recharged post-permafrost formation. This could occur either from the base of glaciers or through faults in the mountains surrounding the studied valleys, which should be further studied.

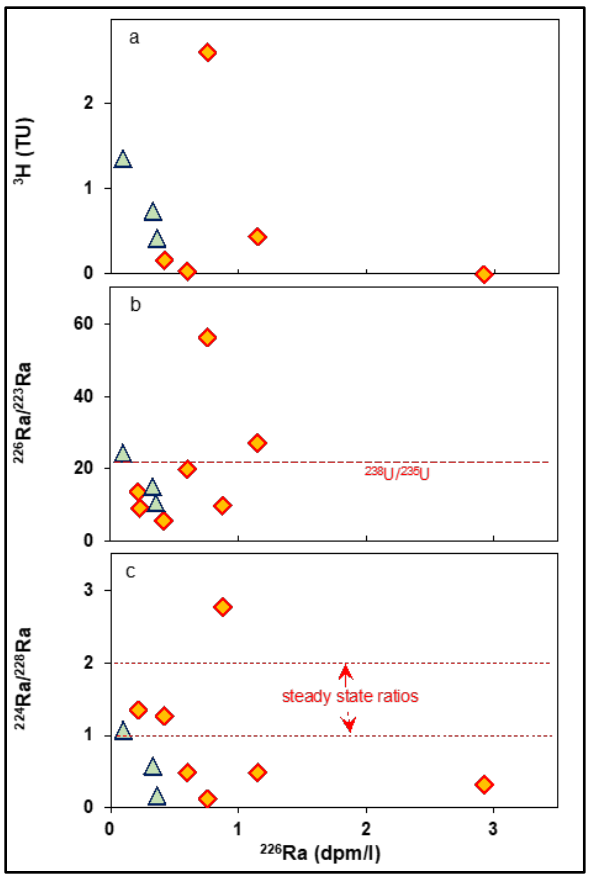

Figure 2. ^{3}H and Ra isotope ratios against the long-lived ^{226}Ra activities (dpm/l=disintegrations per minute per liter) in pingos' associated water. In (b), the natural activity ratios of $^{238}U/^{235}U$ (radioactive parents of ^{226}Ra and ^{223}Ra, respectively) is shown. In (c), common steady state daughter-parent ratios of $^{224}Ra/^{228}Ra$ (e.g., Kiro et al. 2015) are shown.

REFERENCES

Demidov, V., Demidov, N., Verkulich, S., and Wetterich, S. 2022. Distribution of pingos on Svalbard, Geomorphology, 412: 108326. doi.org/10.1016/j. geomorph.2022.108326

Gilbert, G.L., O'Neill, H.B., Nemec, W., Thiel, C., Christiansen, H.H., and Buylaert, J.P. 2018. Late Quaternary sedimentation and permafrost development in a Svalbard fjord-valley, Norwegian high Arctic, Sedimentology, 65(7): 2531–2558. doi.org/10.1111/sed.12476

Hodson, A.J., Nowak, A., Hornum, M.T., Senger, K., Redeker, K., Christiansen, H.H., et al. 2020. Sub-permafrost methane seepage from open-system pingos in Svalbard, The Cryosphere, 14(11): 3829–3842. doi.org/10.5194/tc-14-3829-2020

Hornum, M.T., Hodson, A.J., Jessen, S., Bense, V., and Senger, K. 2020. Numerical modelling of permafrost spring discharge and open-system pingo formation induced by basal permafrost aggradation, The Cryosphere, 14: 4627–4651. doi.org/10.5194/tc-14-4627-2020.

Hornum, M.T., Betlem, P., and Hodson, A. 2021. Groundwater flow through continuous permafrost along geological boundary revealed by electrical resistivity tomography. Geophysical Research Letters, 48: e2021GL092757. doi.org/10.1029/2021GL092757

Kiro, Y., Weinstein, Y., Starinsky, A., and Yechieli, Y. 2015. Application of radon and radium isotopes to groundwater flow dynamics: an example from the Dead Sea, Chemical Geology, 411: 155–171. doi.org/10.1016/j.chemgeo.2015.06.014

Liestøl, O. 1996. Open-system pingos in Spitsbergen, Norsk Geografisk Tidsskrift, 50: 81–84. doi.org/10.1080/00291959608552355

Rotem, D., Lyakhovsky, V., Christiansen, H.H., Harlavan, Y., and Weinstein, Y. 2023. Permafrost saline water and Early to Mid-Holocene permafrost aggradation in Svalbard. The Cryosphere, 17: 3363–3381. doi.org/10.5194/tc-17-3363-2023

Analysis of the internal structure of hydrostatic pingos in the Tuktoyaktuk Peninsula area with capacitively-coupled resistivity surveying

Austin Routt[1], Kynan Hughson[1], Alexia Kubas[2], Andrew Mullen[2], Enrica Quartini[2], Britney Schmidt[2], John Bradford[3], Venezia Follingstad[3], Matthew Siegfried[3], Roger Michaelides[4], Hanna Sizemore[5] & Andrei Swindinsky[6]

[1]*University of Alaska Anchorage, Anchorage, Alaska, United States*

[2]*Cornell University, Ithaca, New York, United States*

[3]*Colorado School of Mines, Golden, Colorado, United States*

[4]*Washington University in St. Louis, St. Louis, Missouri, United States*

[5]*Planetary Science Institute, Tuscon, Arizona, United States*

[6]*University of Toronto, Toronto, Ontario, Canada*

Pingos are ice-cored hills that form in permafrost as a result of freezing pressurized groundwater. The origin of water pressure defines whether a pingo is hydrostatic (confined groundwater following the drainage of surface water) or hydraulic (artesian pressure) (Mackay 1979). A dense concentration of hydrostatic pingos exists in the area of Tuktoyaktuk in the Northwest Territories, Canada. Despite nearly half a century of research, the internal structures of these pingos have been the subject of very few studies, and direct confirmation of the presumed formation mechanism and resulting ice cores has not been obtained.

METHODS

We surveyed nine pingos in Pingo Canadian Landmark with a variety of geophysical techniques including capacitively coupled resistivity (CCR), which emulates traditional DC resistivity surveying but without the need for galvanic contact of electrodes (Figure 1). We operated a Geometrics OhmMapper instrument in a dipole-dipole configuration using a sequence of increasing separation values to maximize depth of investigation.

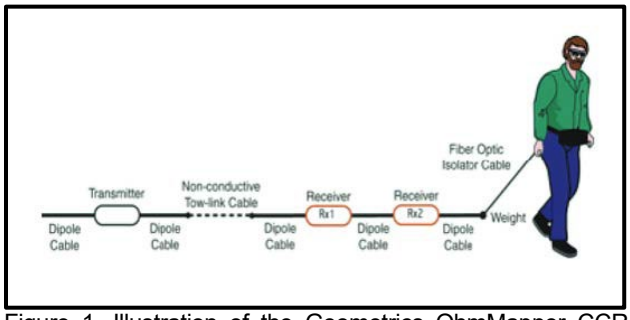

Figure 1. Illustration of the Geometrics OhmMapper CCR device with a dual-receiver dipole-dipole configuration. (schematic from Geometrics).

With a single receiver dipole and transmitter dipole, we hand-towed survey transects across each pingo of interest with the exception of the 49-meter tall Ibyuk Pingo, for which we could only complete a transect from the bottom to the summit on one side due to steepness.

RESULTS

Among the surveyed pingos, we found unexpected variability in resistivity structures. A small (~7 m), unnamed pingo in the landmark (dubbed “Mingo” by the team), for example, exhibits a highly resistive circular (r = ~2 m) core approximately 5 m below its apex, suggestive of a fresh ice core (Figure 2).

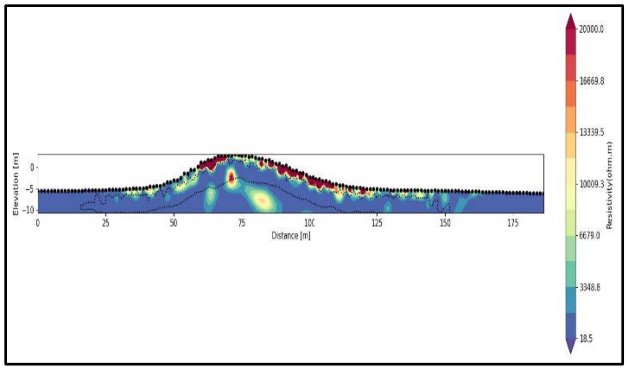

Figure 2. "Mingo" Pingo resistivity cross-section. Structure reveals areas of extremely high low resistivity (ρ = ~1Ωm) to a small, central, highly resistive core (ρ > 20,000Ωm)

In contrast, the well-known “Island” Pingo, which stands as an island in the Beaufort Sea just off the coast as per its namesake, has no such resistive core, but instead exhibits a fractured collection of resistive wedges and lenses (Figure 3).

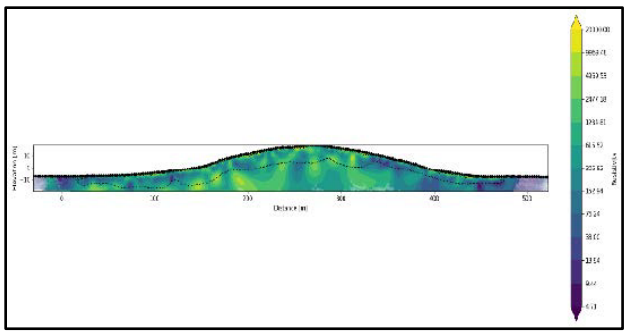

Figure 3: Resistivity cross-section of Island Pingo. Note the low resistivity values on both flanks over top of sea ice, and a mixtucture underneath its summit.

Conclusions

The resistive core found in “Mingo” pingo and others is supportive of the traditional model of pingo formation and structure as described by Mackay (1979) following lake drainage and the formation of an ice core. Many surveyed pingos, however, showed no such resistive core, and instead exhibited a complex admixture of highly resistive structures within strongly conductive coastal permafrost. We also find that average apparent resistivities for most pingos are very low (ρ = 980Ωm for one small pingo with fractured internal structure), which is inconsistent with massive freshwater ice, but consistent with a mixture of marine sediments and ice lenses, a finding in agreement with at least one study on hydraulic pingos in marine environments (Ross et al 2007).

We posit that the formation mechanism and internal structure of pingos in Pingo Canadian Landmark may not follow the traditional model, but instead rely on ice segregation in lenses and wedges, rather than the formation of massive ice cores. The role of segregated ice in other ground ice forms has been noted by Mackay (1972), and a pressure potential is key in both segregated ice and intrusive ice, such as pingo ice cores. This finding has implications for presumed ground ice quantities in regions with pingos and suggests further research will be required to understand pingo formation mechanisms and structures.

References

Mackay, J.R. 1972. The World of Underground Ice, Annals of the Association of American Geographers, 62 (1).

Mackay, J.R. 1979. Pingos of the Tuktoyaktuk Peninsula Area, Northwest Territories, Géographie physique et Quaternaire, 33 (1).

Ross, N., Brabham, P.J., Harris, C., and Christiansen, H.H. 2007. Internal Structure of Open System Pingos, Adventdalen, Svalbard: The Use of Resistivity Tomography to Assess Ground-Ice Conditions, Journal of Environmental and Engineering Geophysics 12: 113–126. https://doi.org/10.2113/JEEG12.1.113

Thermo erosional gully initiation near Tiksi settlement, Arctic Eastern Siberia

Anna Tarbeeva[1] & Yana Tikhonravova[2]

[1]*Lomonosov Moscow State University, Faculty of Geography, Moscow, Russia*

[2]*Melnikov Permafrost Institute of the Siberian Branch of the Russian Academy of Science, Yakutsk, Russia*

Thermo erosional gully (N 71.6319° E 128.8793°) was found in the lower part of the slope of Lyalkina Hill (206 m a.s.l.) in 2020. The upper part of Lyalkina Hill has a slope gradient up to 40 degrees and is composed of cobbles. The lower part of the slope at elevations of less than 40-50 m a.s.l. has gradients less than 10 degrees, is covered with a mantle of argillaceous deposits with ice wedges up to 4-5 m thick and has a pronounced polygonal relief. The head of the investigated gully is located at about 30 m a.s.l. and about 500 meters from the seashore. A few tens of meters above the gully at the base of the hill passes the winter road "Tiksi-Naiba". This road is indicated on the topographic maps of 1985, but local residents do not remember occurrences of any gullies before 2020. Observations on emergence and development of gully were conducted during 2020-2022.

The deposits exposed in gully's wall include ice wedges with young ice wedges. The roots of the ice wedges penetrate or abut on the weathered siltstones of the bottom. There are also remains of tunnel ice in the southern side of the gully's wall at about 1 m depth (top of the thermo-erosional tunnel). The tunnel ice was presumably formed by refreezing melt water in the underground tunnel (Fortier et al. 2008). There are thermo-erosional tunnels of 1-3 levels within the ice wedges (Figure 1).

Figure 1. Thermo-erosional tunnel within ice wedge.

During the first survey on August 15, 2020, the gully had steep sides and reached a maximum depth of 4.5 m with weathered bedrock exposed in the bottom, while the length and width of the gully were relatively small. A significant area of the gully sides exposed ice wedges, the uneven surface of which had traces of flowing water. Downstream the main gully, there was another erosional landform, with which the main gully was connected through a tunnel eroded in ice wedges (Figure 1).

Over the next 12 days, the gully doubled in length, merging with the neighboring erosional form due to the collapse of the roof of the connecting tunnel (Figure 2). At the head and the lower part of the gully, cavities and tunnels eroded in ice wedges were observed.

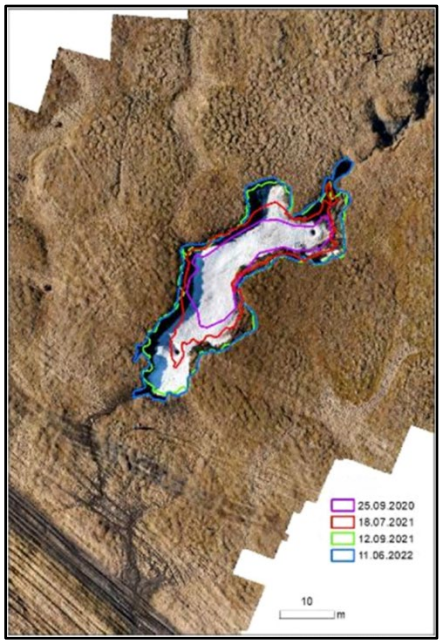

Figure 2. Spatial extent of the gully at different dates.

The head of the gully is confined to the water track and is a vertical scarp 3-4 m high, formed by the frontal part of ice wedge. The small branches of the gully are also confined to polygon throughs and had ice scarps at their heads. Since these polygon throughs were oriented across the slope, the waterflow through them was significantly less than through the water track at the head of the gully. The further growth of the

gully occurred mainly headward under the action of flowing water, to a lesser extent due to the retreat of scarps in the side branches. The growth of the side branches occurred only due to the subaerial melting of ice, and the collapsed material was not washed out beyond the base of the scarp. The depth of the gully was limited by the bedrock and did not exceed 4.5 m. The width of the gully changed insignificantly.

In 2022, despite the flood caused by heavy rainfall of 33 mm/day, the growth rate of the gully has significantly decreased. Melting of ice was observed in the tunnels below the gully, although the tunnels remained until the autumn of 2022.

The compared margins of the gully show that during snowmelt, when thaw depth is shallow, the runoff concentrate along the polygon troughs, and narrow incisions are formed at the head of the gully. In the end of the summer, the expansion of the gully due to slope sliding prevails.

Before the gully formation the surface flow on the slope passed through water tracks confined to polygonal troughs situated above partially melted wedge ice. At the site of the future gully, there was an elevated area, less prone to ice-wedge polygon degradation, where troughs were weakly expressed, and the reconstructed catchment area at the top of the ravine was minimal.

At least since 1985, there has been a winter road on the hillslope, the tracks of which intercept the flow from a significant part of the slope and divert it towards the Tiksi settlement. The winter road crosses several water tracks, and at some locations water overflows the winter road. Wedge ice under the road is not thick, since weathered bedrock is sometimes exposed in the road. The ratio of flow entering each water track and flow remaining in the road ruts varies depending on the water level, thawing depth and other reasons. One of the reasons is the deepening of the water tracks downslope the trail due to the melting of the tops of the ice wedges. The deepening of the troughs as a result of ice-wedge degradation contributes to an increase in water flow, which creates prerequisites for its further deepening and an increase in surface runoff along it. The redistribution of the runoff due to the uneven melting of ice-wedges is very characteristic of the tundra, where polygonal relief is widespread.

The formation of the gully was preceded by the formation of underground cavities: sinkholes and tunnels, which is confirmed by fragments of undestroyed tunnels downstream the gully, some of which survived at least until the autumn of 2022. The upper ones were formed at a depth of about 1 m from the surface, and then, when the flow cut in, they were displaced to lower levels until they reached the bedrock. The development of underground thermal erosion took place at least one year before the appearance of the open gully, as evidenced by the remains of tunnel ice in the gully sides. The existence of a tunnel for at least a year before the appearance of an erosion form on the surface was also described in Canada (Fortier et al. 2007).

The formation of underground cavities is facilitated by open frost cracks (Fortier et al. 2007). Probably, the gully in Tiksi also formed along a frost crack, since there were no signs of erosion on the surface before the appearance of the gully. We also did not observe surface erosion above the preserved tunnel downstream of the gully. In addition, frost cracks are namely formed along ice wedges (Romanovskiy 1977), which were mainly subjected to erosion at the initial stages of gully formation. However, for the development of a thermo-erosional sinkhole or tunnel along a crack, it is necessary to get a sufficient volume of water into it, which was provided by an increase in runoff through the deepened polygonal troughs.

The gully formed on one of the few sections of the slope where intact polygonal ice wedges were preserved, the volume of which was sufficient to form large tunnels. The gully appeared due to the collapse of the roof of the tunnel, which reached critical dimensions. During the first year after its appearance, the gully developed very quickly, and then its development gradually slowed down, which is also typical for other gullies (Fortier et al. 2007; Sidorchuk and Baranov 1999).

The depth of the gully is limited by underlying bedrock. Higher up the hillslope, the thickness of ice wedges decreases, because weathered mudstones are exposed in the road at a depth of 0.5 m below ground surface. In this regard, the headward grow of the gully will be limited to the nearest 20 meters. Neighboring watercourses are incised in the slope until bedrock, and the depth of their valleys does not exceed 1.5–2 m.

REFERENCES

Fortier, D., Allard, M., and Shur, Y. 2007. Observation of rapid drainage system development by thermal erosion of ice wedges on Bylot Island, Canadian Arctic Archipelago, Permafrost and Periglacial Processes, 18(3): 229–243. doi: https://doi.org/10.1002/ppp.595

Romanovskiy, N.N. 1977. Formation of Cryogenic Polygonal Structures, Nauka, Novosibirsk, Russia.

Sidorchuk, A.Y., Baranov, A.V. (Eds.) 1999. Erosion processes in the Central Yamal, RNII kul'turnogo i prirodnogo naslediya, St. Petersburg, Russia.

Short-term transformation of morphology of alluvial fans in periglacial (Svalbard) and non-periglacial (SE Iceland) settings quantified using UAV surveys

Aleksandra M. Tomczyk & Marek W. Ewertowski

Faculty of Geographical and Geological Sciences, Adam Mickiewicz University, Poznan, Poland

Alluvial fans are landforms which developed along mountain ranges in all climatic settings. Due to their location on the intersection between lithosphere, hydrosphere, and atmosphere, alluvial fans record long-term environmental changes. However, relatively little is known about their short-term dynamics and surface morphological changes in response to recent climate warming. This short-term dynamic is especially important from an anthropogenic standpoint because in many mountain areas fan-shaped landforms constitute land that is preferable for settlement and infrastructure development, while fan-related processes (like debris flows or avalanches) can threaten human life and infrastructure.

In this study, we have quantified annual (2015–2019) dynamics of debris-flow-dominated alluvial fans' surfaces located in periglacial (the central part of Spitsbergen, Svalbard) and non-periglacial (SE Iceland) settings. This Arctic location is especially important as it provides us with insights into the dynamics of fans located in the area where climate warming proceeds at one of the highest paces on Earth. Moreover, fans in the polar environment are exposed to many site-specific conditions related, among others, to the presence of permafrost and a relatively short period of annual geomorphic activity, which suggests that their dynamics might be different from fans located in warm and temperate settings (de Haas et al. 2015). The dynamics of Arctic fans is also important because (1) it can provide us with a model of how the fans will develop in other parts of the world; (2) fans in the polar environment are often used as analogues for extra-terrestrial landforms; (3) as the climate warms, the number of people living, working and visiting polar areas will increase, so we need to understand how the morphology of fans can change over a short period of time in the context of potential future human settlements and activities (Tomczyk 2021).

The main aims of this study were to: (1) quantify geomorphological changes that recently occurred on the fans' surfaces; and (2) analyse the spatial patterns of these geomorphological changes and suggest the key controls on them.

STUDY AREA

To quantify the short-term dynamics of alluvial fans in the Arctic environment, we selected four debris-flow-dominated fans in Central Svalbard, Svalbard Archipelago and three fans in the SE part of Iceland. In Svalbard, we studied four fans, which were located close to each other and subjected to the same regional climatic conditions. These fans were representative of different types of fan surfaces, varying from having a clear footprint of recent debris flows to demonstrating morphological footprints of mixed debris and fluvial flows. The melting season in Svalbard usually lasts for about three months, which restricts the time window for any potential geomorphological activity. Another limiting factor is the presence of continuous permafrost, which potentially limits the volume of sediments available for transport. For comparison, we studied three fans located in the SE part of Iceland, which is characterised by the absence of permafrost and much higher precipitation, reaching in the study area about 1,500 mm per year. Therefore, we presented these three cases as examples of sub-Arctic, non-permafrost settings.

METHODS

Our approach was based on a combination of analysis of unmanned aerial vehicle (UAV) surveys and geomorphological fieldwork. UAV-generated images were collected annually between 2015 and 2019 using small quadcopters. The external orientation of the models was established using a network of fixed ground control points (GCPs) surveyed with differential GNSS. UAV images were processed using a structure-from-motion approach following workflows used in previous studies (see Ewertowski et al. 2019 for details). The processing resulted in points of clouds with known 3D coordinates, which were then transformed into gridded DEMs with a cell size of 0.05 x 0.05 m. The digital elevation models of differences were produced by subtracting the DEMs from subsequent periods to detect surface changes. DEMs of Differences were used for the calculation of volumetric and planimetric changes.

RESULTS AND DISCUSSION

In general, large portions of studied fan surfaces were stable over the observation period; however, when the high-magnitude, low-frequency geomorphological processes occurred, the morphological changes were substantial. This response was very diversified over space (i.e., between fans as well as within single fans) and time (i.e., most of the changes occurred over one year, different for each fan, whereas the surface in the remaining years was stable). Based on five years of observations, we can distinguish four types of short-term surface transformations of alluvial fans:

- Scenario I – No significant changes (stable morphology). One of the studied fans did not change its surface over the studied period. There were some very minor transformations of surface morphology, but most parts were stable over the 2015–2019 period. Even some small clasts did not change their position and remained stable.
- Scenario II – Thermokarst modification of fan surface. Fan Bolterndalen-1 (Svalbard) exhibited rapid transformations related to the thermokarst modification of its surface. Over the first year, this transformation was relatively large and related mostly to the collapse of the small stream's permafrost banks. But then, over the next three years, only minor alterations were recorded.
- Scenario III – Reactivation of old debris flow channel. Fan Endalen-1 (Svalbard) and Breida-1 and 2 (Iceland) provided examples where an older, inactive debris flow channel was reactivated by a new debris flow, which led to a deepening of the channel and the development of new levees. Such a process was spatially restricted but clearly visible in both DEM (i.e., through elevation changes) and orthomosaics (through changes in texture).
- Scenario IV – Development of new debris flow channel. The fourth scenario includes the development of a new debris flow channel in the previously smooth (inactive) parts of the fans. This was also a single event, and after the construction of this new channel, the geomorphology in the remaining years was again stable.

Such variable geomorphological response resulted likely from a combination of factors, namely: (1) fan geometry; (2) composition of fan surface; (3) time of occurrence of specific events; (4) presence of permafrost; and (5) multitude and diversity of geomorphological processes. Our results indicate that the general response of slopes to global climate warming is strongly filtered by regional (such as the presence or lack of permafrost) and local (mainly topographic) factors. We speculate that the severity of the geomorphological impact relative to long-term low-magnitude processes could have been due to warming air temperatures that provided sediments from thawed permafrost and to an aggrading delta that raised the rivers' base levels and, in consequence, raised local erosional basis. Overall, we suggest that climate warming will not only make low-frequency, high-magnitude processes more likely in the Arctic but that those processes will achieve more geomorphological work with the mechanical erosion of permafrost (in the case of Svalbard). As mass-movement processes transforming fan surfaces will become more widespread and intense, it has clear implications for people settling in polar areas as well as tourism, transport and the mining industry, which might be more prone to negative impacts. Our finding also has implications for extra-terrestrial geomorphology, indicating that the surface morphology of fans can easily become variable even on annual temporal scales.

ACKNOWLEDGEMENTS

This research was funded by the National Science Centre, Poland, Grant Number 2016/21/B/ST10/01353.

REFERENCES

De Haas, T., Kleinhans, M.G., Carbonneau, P.E., Rubensdotter, L., and Hauber, E. 2015. Surface morphology of fans in the high-Arctic periglacial environment of Svalbard: Controls and processes, Earth-Science Reviews, 146: 163–182. doi:10.1016/j.earscirev.2015.04.004

Ewertowski, M.W., Tomczyk, A.M., Evans, D.J.A., Roberts, D.H., and Ewertowski, W. 2019. Operational Framework for Rapid, Very-high Resolution Mapping of Glacial Geomorphology Using Low-cost Unmanned Aerial Vehicles and Structure-from-Motion Approach, Remote Sensing, 11: 65. doi:10.3390/rs11010065

Tomczyk, A.M. 2021. Morphometry and morphology of fan-shaped landforms in the high-Arctic settings of central Spitsbergen, Svalbard, Geomorphology, 392: 107899. doi:10.1016/j.geomorph.2021.107899

Geoelectrical investigations of pingos and related permafrost mounds in the Tombstone Territorial Park, Yukon

Tim Wiegand, Julius Kunz & Christof Kneisel

[1]*Institute of Geography and Geology, University of Wuerzburg, Germany*

Pingos are the most prominent landforms in Arctic permafrost regions. They exist in a variety of shapes and sizes and are classified as either of hydraulic (open-system in terms of groundwater inflow) or hydrostatic (closed-system) origin. Along with a range of similar features such as palsas, lithalsas or frost blisters they are commonly subsumed as “permafrost mounds”. However, the differentiation often requires information about the internal structure and ground ice characteristics.

For those purposes, geophysical measurements have been proven successfully as they can provide multidimensional insights about frozen and unfrozen zones (Yoshikawa et al. 2006; Kunz and Kneisel 2021).

In northwestern Canada, apart from numerous closed-system pingos in the Inuvik-Tuktoyaktuk coastland area (Wolfe et al. 2023), several open-system pingos are described for the mountainous regions of Yukon (Hughes 1969).

The aim of this study is to investigate the interior and surrounding of different mounds containing permafrost in order to assess their origin and to discuss the findings with respect to the hydrological setting and the complex glaciation history of the Ogilvie Mountains.

Study sites

The Tombstone Territorial Park north-east of Dawson City, central Yukon, encompasses the two north-facing valleys of the East Blackstone River, along which the Dempster Highway crosses the park, and the Blackstone River (west fork).

Investigated landforms have diameters between 30 m and 280 m and heights between 4 m and 22 m (see Figure 1). The tallest mound, located about 5 km west of the river confluence near Chapman Lake, has remarkably steep slopes (>35°), a pronounced crack along the longitudinal axis and a crater-like depression at its top (see Figure 2). It has already been reported by Hughes (1969) and classified as one of the few closed-system pingos in the region.

However, this evaluation was mainly based on the topographic position. Considering geoelectrical in-situ measurements, there are indications for an open-system pingo on the opposite side of the valley (Kunz and Kneisel 2021).

A cluster of dome-shaped mounds of considerably smaller size is present in the valley bottom of the East Blackstone River close to Jaeger Lake. The surrounding area is part of a Pleistocene moraine complex.

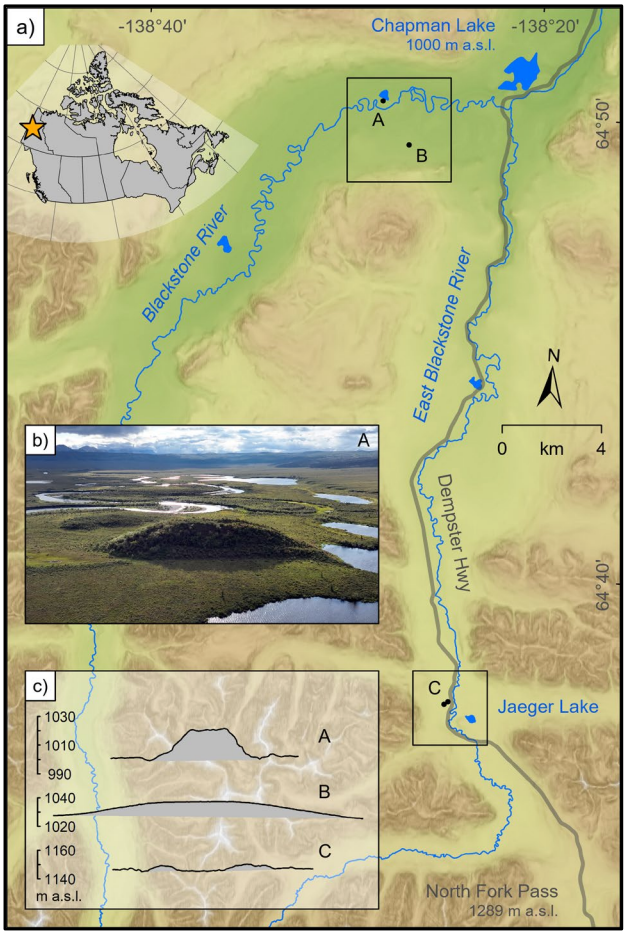

Figure 1. a) Study sites in the Tombstone Territorial Park. b) Blackstone riverside pingo. c) Shapes and sizes of investigated landforms (Vertical exaggeration: 1.5). Contains information licensed under the Open Government Licence – Canada.

Methods

2D and quasi-3D Electrical Resistivity Tomography (ERT) measurements were conducted at the mentioned sites using a Syscal Pro Switch device (IRIS Instruments) and up to 72 electrodes per line.

Several thousand recorded data points in both Wenner-Schlumberger and Dipole-Dipole array allow the generation of high-resolution 3D models. Additionally, active layer thicknesses were measured using a steel probe, whereas orthophotos and digital elevation models were generated by means of drone-based Structure-from-Motion. The surveys also address the surface and subsurface hydrological pattern in the catchments of the frost mounds.

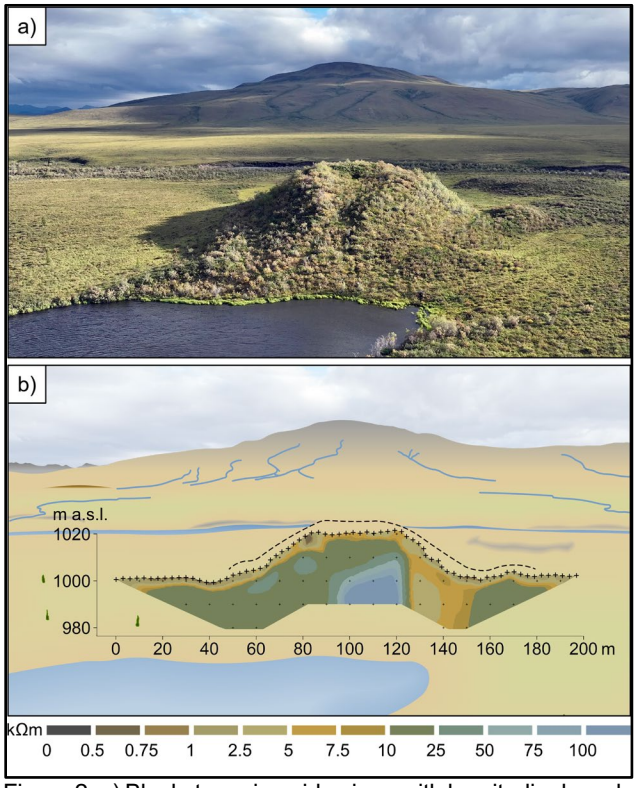

Figure 2. a) Blackstone riverside pingo with longitudinal crack and crater-like depression. b) Transversal 2D ERT profile (Measurement: Wenner-Schlumberger array; Inversion: Res2DInv, 5th Iteration, Abs. error: 4.0 %).

Results

Differences between the investigated landforms do not just exist in the outward appearance but also in the geophysical properties of the subsurface. For instance, the electrical resistivity values of the pingo at the west fork riverside significantly exceed those of the adjacent mound on the opposite side of the valley.

As shown for the Blackstone riverside pingo, geoelectrical measurements delineate the well conductive surface layer (active layer) from the high-resistive permafrost body beneath (see Figure 2). But even within the frozen part, resistivity values vary by up to an order of magnitude which likely reflects different ground ice characteristics. In the central core, values calculated by inversion reach those that have previously been interpreted as massive ice (e.g., Yoshikawa et al. 2006).

Low-resistivity zones that are presumably unfrozen were found in some of the mounds and also in the north-facing slope of the west fork valley. ERT soundings enable the detection of taliks that can serve as intra-permafrost water pathways. In the west fork the topographic and hydrological setting support the assumption that groundwater movement is connected to upwelling downslope enabling the formation of an open-system pingo (see Kunz and Kneisel 2021).

However, in the Tombstone Territorial Park, periglacial climate conditions, mountainous terrain, broad valley floors and the permanently changing channel pattern of the two main rivers leading to formation and drying of oxbow lakes, create environments that might have been suitable for both hydraulic and hydrostatic pingo formation.

For validation of the preliminary geophysical results borehole drillings and the monitoring of permafrost temperatures are intended.

Acknowledgements

We gratefully thank the Government of Yukon and the Tr'ondëk Hwëch'in Government for the issued research permits and Saskia Eppinger for the assistance in the field. This study was funded by the German Research Foundation (DFG 515411322).

References

Hughes, O.L. 1969. Distribution of open-system pingos in central Yukon Territory with respect to glacial limits, Geological Survey of Canada Paper, 69(34): 1-8.

Kunz, J., and Kneisel, C. 2021. Three-dimensional investigation of an open- and a closed-system Pingo in northwestern Canada, Permafrost and Periglacial Processes, 32(4): 541-557. doi:10.1002/ppp.2115

Wolfe, S.A., Morse, P.D., Parker, R., and Phillips, M.R. 2023. Distribution and morphometry of pingos, western Canadian Arctic, Northwest Territories, Canada, Geomorphology, 431: 108694. doi:10.1016/j.geomorph.2023.108694

Yoshikawa, K., Leuschen, C., Ikeda, A., Harada, K., Gogineni, P., Hoekstra, P., Hinzman, L., Sawada, Y., and Matsuoka, N. 2006. Comparison of geophysical investigations for detection of massive ground ice (pingo ice), Journal of Geophysical Research, 111(E6). doi:10.1029/2005je002573

Permafrost Geomorphology & Hazards

4D — Permafrost Temperature, Active Layer Thickness, and Rock Glacier Velocity

Session Chairs: Line Rouyet[1], Sharon L. Smith[2] & Dmitry A. Streletskiy[3]

[1]NORCE Norwegian Research Centre AS, Tromsø, Norway
[2]Geological Survey of Canada, Natural Resources Canada, Ottawa, Canada
[3]The George Washington University, Washington, D.C, United States

Permafrost temperature, active layer thickness, and rock glacier velocity (RGV) are key indicators of permafrost change as well as changes in the earth's climate system. Over the last three decades, the observational record of these key indicators has been extended in both length and extent. There have also been advances in our understanding of the permafrost-active layer system which has facilitated improved interpretation of trends and also led to improvements in measurement techniques and identification of new variables for monitoring.

10 m resolution circumpolar landcover as proxy for permafrost features

Annett Bartsch[1], Clemens von Baeckmann[1], Helena Bergstedt[1], Barbara Widhalm[1], Birgit Heim[2], Mareike Wieszorek[2] & Veronika Döpper[2]

[1]*b.geos, Korneuburg, Austria*

[2]*AWI, Potsdam, Germany*

A novel pan-arctic map of landcover at 10m nominal resolution has recently been released (Bartsch et al. 2023). The Circumpolar Landscape Units (CALU) dataset provides a comprehensive set of landcover units, including three wetland units and soil wetness specifications for various tundra units. While the map is static, the approach (fusion of Sentinel-1 and Sentinel-2 satellite data) can be applied annually in case of data availability. The CALU dataset is available for tundra regions underlain by permafrost and captures landscape heterogeneity associated with permafrost landscape features, including different stages of drained lake basin development (Figure 1).

The dataset has been developed to provide landscape heterogeneity measures and proxies for soil properties, specifically to aid parameterization of permafrost modelling. Documentation with in situ data of the units included volumetric water content, volumetric mineral content, soil organic carbon content etc. In a next step active layer thickness (ALT) properties in relation to the CALU dataset will be investigated.

Active layer thickness measurements

CALM ALT records were compiled and harmonized in the framework of the ESA Permafrost_cci project (Heim et al. 2021). In addition, thaw depth measurements were conducted during a field survey in July 2023 in the Inuvik region, NW Canada, during unusually dry conditions. Precise locations were determined using differential GPS measurements. Several complementary near surface moisture measurements were conducted and then averaged at each location.

Cross-comparison

Although the July 2023 thaw depth records only represent early season conditions and unusual dry surfaces, certain thaw depth ranges can be associated with different landscape units and reflect soil properties such as volumetric mineral soil content.

The comparison of CALU with CALM records is challenging due to geolocation issues in both the in situ records and satellite retrievals. The CALM grids represent transects or rectangular grids with measurements commonly at 10m distances. This matches the nominal resolution of CALU but shorter distances would be needed due to geolocation uncertainties.

The harmonized CALM ALT dataset and several examples which demonstrate the geolocation issues but also results of the cross-comparison will be presented.

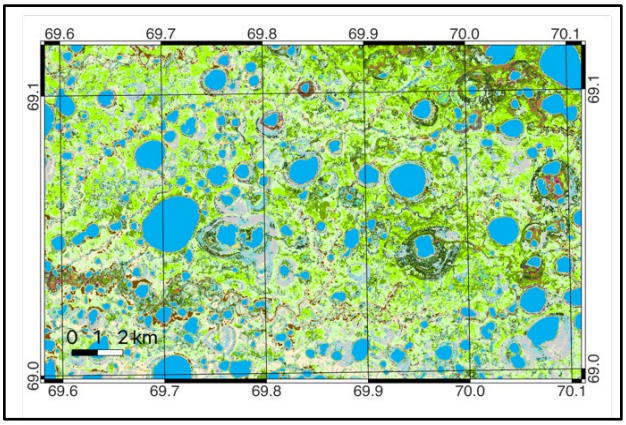

Figure 1. Example of the CALU dataset. Green shades represent different types of shrub tundra, growth form and moisture conditions (full legend details in Bartsch et al. 2023).

Acknowledgements

This work was supported by the European Space Agency CCI+ Permafrost and AMPAC-Net projects, the European Research Council project No. 951288 (Q-Arctic), and has received funding under the European Union's Horizon 2020 Research and Innovation Programme under Grant Agreement No. 869471 (CHARTER).

References

Bartsch, A., Efimova, A., Widhalm, B., Muri, X., von Baeckmann, C., Bergstedt, H., Ermokhina, K., Hugelius, G., Heim, B., and Leibmann, M. 2023. Circumarctic landcover diversity considering wetness gradients, EGUsphere [preprint]. https://doi.org/10.5194/egusphere-2023-2295

Bartsch, A., Efimova, A., Widhalm, B., Muri, X., von Baeckmann, C., Bergstedt, H., Ermokhina, K., Hugelius, G., Heim, B., and Leibmann, M. 2023. Circumpolar Landcover Units (1.0) [Data set]. Zenodo. https://doi.org/10.5281/zenodo.8399018

Heim, B., Lisovski, S., Wieczorek, M., Pellet, C., Delaloye, R., Bartsch, A., Jakober, D., Pointner, G., and Strozzi, T. 2021. ESA CCI+ Product Validation and Intercomparison Report, v3.0.

The impact of observation depth and depth of zero annual amplitude on the interpretation of permafrost warming

Nicholas Brown[1,2] & Stephan Gruber[1,2]

[1]*NSERC PermafrostNet, Canada*

[2]*Department of Geography and Environmental Studies, Carleton University, Ottawa, Ontario, Canada*

Warming rates in permafrost are strongly affected by the transfer of latent heat. In general, we observe reduced warming rates in warm permafrost (Biskaborn et al. 2019). This requires an additional and counter-intuitive interpretation step and further confounds the comparison of warming rates between locations.

Such comparisons usually calculate trends for boreholes grouped by temperature or by permafrost zone, but this ignores ground conditions. Within-group trends are affected by the spatial distribution of boreholes, which are not randomly sampled, and if a temperature criterion is used, individual sites may transition from cold to warm.

Permafrost thermal monitoring aims to track changes to mean annual ground temperature (MAGT) at the depth of zero annual amplitude (d_{za}). However, changes to climate or soil thermal properties mean the true d_{za} is a moving target. Increased latent heat release from melting ice can cause significant changes. Furthermore, monitoring depths depend on available sensor locations, meaning they are often not consistent between locations and may not coincide with d_{za}.

These challenges limit our ability to meaningfully interpret warming trends and should be expected to become more severe as permafrost warms. However, d_{za} trends and other temperature-derived metrics may allow us to create a more complete picture of permafrost thaw by providing additional information about changes to the ground thermal regime.

To this end, we address two questions: (1) How does monitoring depth affect observed warming rates? and (2) What additional insight can be obtained from other temperature-derived metrics, specifically estimated d_{za}?

Methods

We simulate 100 years of warming using a modified version of FreeThawXice1D (Tubini et al. 2021) which is capable of representing excess ice and subsequent surface lowering. We use GlobSim (Cao et al. 2019) to generate meteorological forcing data from the ERA5 reanalysis. Daily air temperature and precipitation were obtained for a site near Lac de Gras, Canada (64.7°N, 110.4°W). Latitudinal climatic variation is simulated by adding or subtracting a fixed offset to the temperature data. To simulate different ground conditions, we create distinct 40 m ground profiles. Two end-member simulations are presented here: the first corresponds to a thin till over bedrock, with an initial mean annual air temperature ($MAAT_0$) of -3 °C and ice-rich sediments with an excess ice ratio of 0.2 and $MAAT_0$ of -5 °C.

For model spin-up, we repeat the first year of input data. Future warming was simulated by repeating the last twelve years of input data and augmenting the values using climate projections from Climatedata.ca (Cannon 2015) assuming the SSP2-4.5 scenario.

For each year, annual amplitude was estimated as half the difference between the maximum and minimum daily averages. The d_{za} was calculated using the regression method described by Bonaventure et al. (2016) with a cutoff of 0.05 °C.

For each simulation, decadal warming rates are calculated on a 10-year rolling basis between 10 and 25 m. Variability is calculated as the range between the greatest and least warming rates for depths below d_{za}.

Results and Interpretation

In the ice rich soil profile, permafrost warming rates decline as the ground temperature approaches 0 °C (Figure 1). Estimates for d_{za} decline until 2040, then change relatively little until 2060, at which point, they increase again. We attribute the initial decline as corresponding to a decreasing apparent thermal diffusivity as more and more of the soil profile thaws and becomes isothermal. Once the d_{za} reaches its shallowest depth, the development and deepening of a suprapermafrost talik causes the reversal.

In profiles with no ice (Figure 2), warming rates do not decline as ground temperature approaches 0 °C and there is little trend in d_{za}.

Estimates for d_{za} exhibit significant interannual variability. Some of this can be attributed to inter-annual changes in surface temperature amplitude, but it may also be explained by warming rates at depth exceeding the 0.05°C threshold used to define d_{za}.

The difference in decadal warming rates between different observation depths varies from 0.01 °C dec^{-1} to 0.64 °C dec^{-1} (Figure 3). For the icy soil profile, this variability decreases as the profile approaches the melting point.

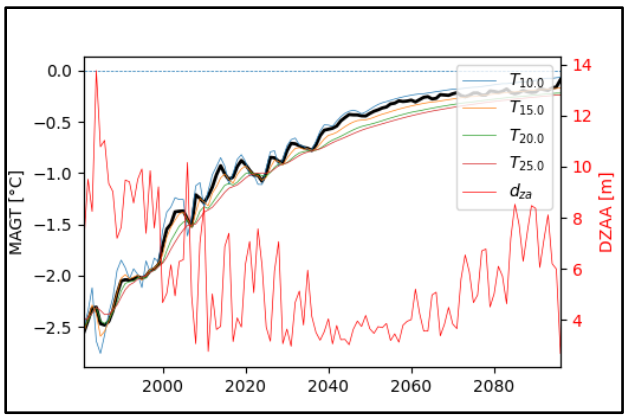

Figure 1. MAGT reported for multiple depths and d_{za} for 100 years of warming in an ice-rich soil. The black line represents the temperature at the estimated d_{za}.

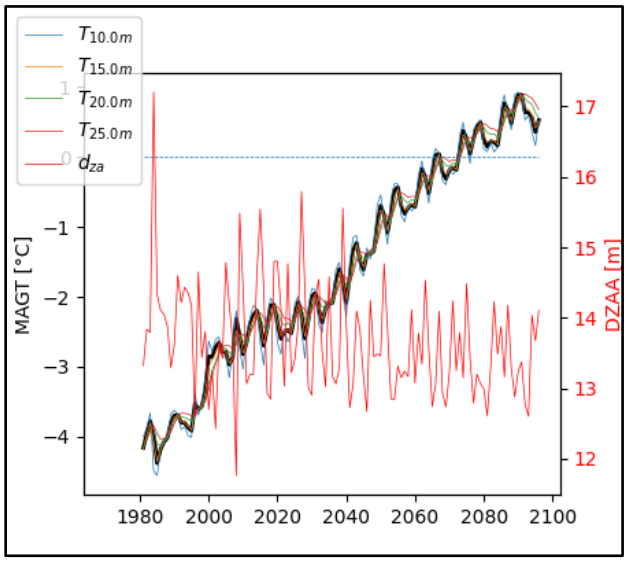

Figure 2. MAGT measured at multiple depths and d_{za} for 100 years of warming in bedrock. The black line represents the temperature at the estimated d_{za}.

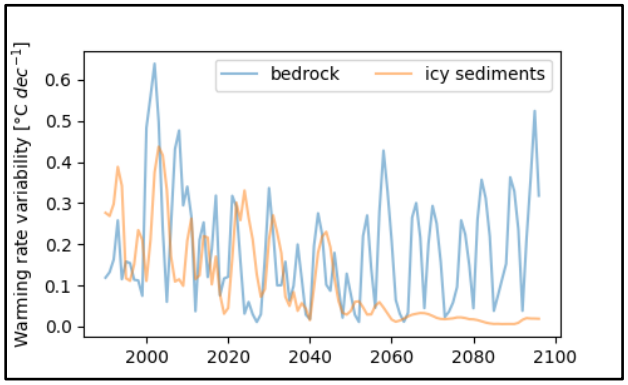

Figure 3. Variability in rolling 10-year warming trends for the two end-member simulations. Data are taken from observations between 10 and 25 m that are below the d_{za}.

Summary and Conclusions

Long-term trends in d_{za} are associated with ice loss in warm, ice-rich materials. Notably, the annual magnitude of d_{za} is less helpful because of deepening d_{za} during late-state permafrost thaw and talik development. Studies investigating permafrost warming rates should consider incorporating d_{za} trends in addition to the categorization of permafrost as warm and cold or continuous and discontinuous in order to distinguish reduced warming rates caused by latent heat transfer in warm permafrost. However, accurate estimation of d_{za} from yearly data is prone to high levels of uncertainty.

Observation depth has a notable effect on decadal warming rates, even when all depths are below d_{za}. This suggests there may be some benefit in multi-depth monitoring. Additional temperature-derived metrics may be able to further elucidate changes taking place in permafrost.

References

Cannon, A., Sobie, S., and Murdock, T. 2015. Bias correction of GCM precipitation by quantile mapping: How well do methods preserve changes in quantiles and extremes?, Journal of Climate, 28: 6938–6959. doi:10.1175/JCLI-D-14-2000754.1

Biskaborn, B., Smith, S., Noetzli, J. et al. 2019. Permafrost is warming at a global scale. Nature Communications 10(264). doi:10.1038/s41467-018-08240-4

Bonnaventure, P., Smith, S., Riseborough, D., Duchesne, C., and Ednie, M. 2015. The ground thermal regime across the Mackenzie Valley Corridor, Northwest Territories Canada. In GEOQuébec 2015 (68th Canadian Geotechnical Conference), Canadian Geotechnical Society, Québec, QC, Canada.

Cao, B., Quan, X., Brown, N., Stewart-Jones, E., and Gruber, S. 2019. GlobSim (v1.0): deriving meteorological time series for point locations from multiple global reanalyses, Geoscientific Model Development, 12: 4661–4679. doi:10.5194/gmd-12- 25

Tubini, N., Gruber, S., and Rigon, R. 2021. A method for solving heat transfer with phase change in ice or soil that allows for large time steps while guaranteeing energy conservation, The Cryosphere,15: 2541–2568. doi:10.5194/tc-15-2541-2021

Subsurface and meteorological measurements at seismic stations in Alaska

Joanne Heslop[1], Dmitry Nicolsky[2], Thomas Wright[2], Carolyn Parcheta[1], Michael West[1], Martin Stuefer[3] & The Alaska Earthquake Center[1]

[1]*The Alaska Earthquake Center, University of Alaska, Fairbanks, Alaska, United States*

[2]*Permafrost Laboratory, University of Alaska, Fairbanks, Alaska, United States*

[3]*The Alaska Climate Research Center, University of Alaska, Fairbanks, Alaska, United States*

Many change-based research questions require consistent and continuous long-term data that captures regional variability. Subsurface ground temperatures depend on many variables, including snow cover, vegetation, terrain, and soil properties. Recording temperatures across different ecotypes expands our understanding of subsurface thermal regimes under various ground conditions, in turn improving our characterization of changing permafrost regimes both in Alaska and across the Arctic. Since 2016, we have collected soil temperature data from 69 locations across Alaska (Figure 1). These stations complement existing ground temperature monitoring networks, allowing for better characterization of ground temperatures and permafrost conditions at remote locations across the state.

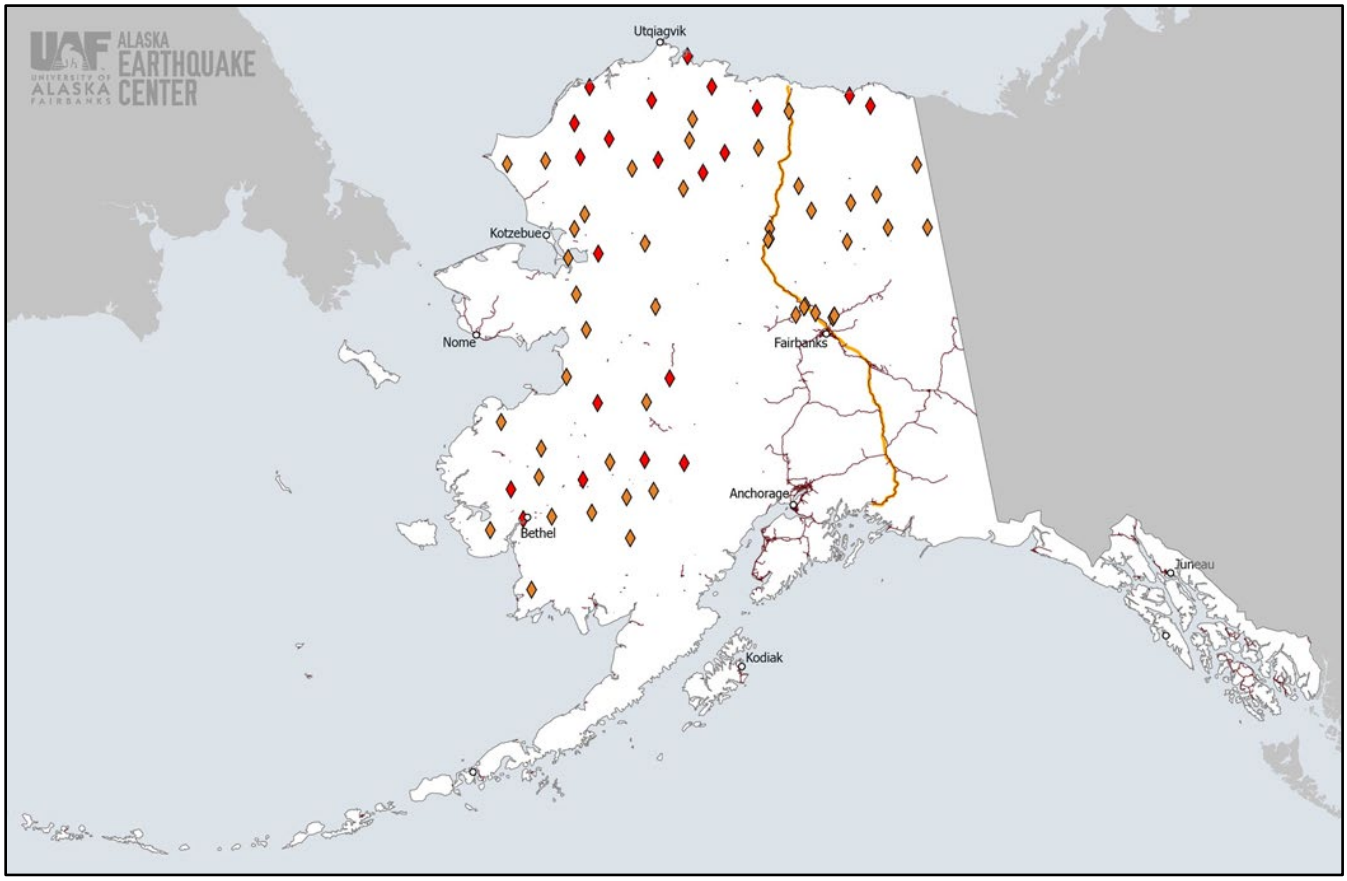

Figure 1. Locations of soil temperature profile data in Alaska collected as part of the USArray project (red) and currently deployed as part of the Alaska Geophysical Network (orange). Since 2016, we have collected soil temperature data from 69 locations across Alaska. Locations of the Trans-Alaska Pipeline (orange line) and major roadways (grey lines) are marked.

This network of soil temperature profiles was originally deployed in cooperation with the NASA Arctic-Boreal Vulnerability Experiment (ABoVE) (https://above.nasa.gov) and the USArray project (www.usarray.org). In Alaska, the USArray project, managed by the Incorporated Research Institutions for Seismology (IRIS) as part of the NSF EarthScope program, installed seismographs with co-located interdisciplinary instrumentation in a grid of 192 stations spaced 85 km apart between 2014 and 2017. Soil temperature profiles (< 1.5 m depth) were installed at 63 of these sites in northern and western Alaska during the 2016 and 2017 field seasons. Following the commencement of the USArray project, the Alaska Earthquake Center adopted 96 of the best-performing stations to become part of the Alaska Geophysical Network. We continue to collect soil temperature profiles and are actively expanding our spatial coverage to additional stations within our network.

Soil temperature data are collected using Onset TMCx-HD sensors attached to the HOBO (Onset UX120-006M) data logger. Following protocols developed within the scope of NASA ABoVE program, we use a slide hammer attached to a 1.5 m steel rod to make a ~1.6 cm diameter hole in the ground (www.youtube.com/watch?v=pQA7Mo70xCU). Calibrated temperature sensors are inserted into the hole, which is then filled and the cables and data logger were buried. A typical profile includes sensors at 0.01 m, 0.2 m, 1.0 m, and 1.5 m depths (depth uncertainty is ±0.025 m). Measurements vary in frequency from daily to every six hours. Metadata including site location, vegetation, slope, elevation, and soil type are recorded for each site.

As part of the Alaska Geophysical Network, all profiles are co-located with a 3-component broadband seismometer (Nanometrics T120PH or Kinemetrics STS-4B/5A) measuring ground movement; 32 of these profiles are co-located with weather instrumentation (Vaisala WXT520 or WXT536) that measure temperature, atmospheric pressure, relative humidity, wind speed and direction, and precipitation as part of the Alaska Mesonet. Concurrently collecting these different data types at the same locations allows for corresponding ground temperatures to air temperature and precipitation. Many of these sites are located at higher elevations (2 - 864 m above sea level), providing data which can be applied to slope stability studies.

We currently have 22 soil temperature probe profiles deployed across northern and western Alaska, with plans to expand deployments to additional stations during the 2024 field season. Soil temperature data collected through 2021 are publicly available through the Oak Ridge National Laboratory Distributed Active Archive Center (Nicolsky et al. 2022); weather data and soil temperature data collected on the Alaska Geophysical Network since 2022 are publicly available through the Arctic Data Center (West et al. 2023a; West et al. 2023b).

ACKNOWLEDGEMENTS

We acknowledge the Alaska Native nations upon whose land our study area resides and observe the stewardship of the traditional inhabitants of the region. All data collection was conducted in accordance with land permit and local government agreements. Funded by: The National Science Foundation as part of the EarthScope Transportable Array, and award number 2024208 as part of the Arctic Observing Network program; the National Oceanic and Atmospheric Administration as part of the National Mesonet Program; the NASA ABoVE program grant NNX16AH96G; and the State of Alaska.

REFERENCES

Nicolsky, D.J.,Romanovsky, V.E, Kholodov, A.L., Dolgikh, K., and Hasson, N. 2022. ABoVE: Soil Temperature Profiles, USArray Seismic Stations, 2016-2021. ORNL DAAC, Oak Ridge, Tennessee, USA. https://doi.org/10.3334/ORNLDAAC/1680

West, M., Ruppert, N., Nicolsky, D., Wright, T., Heslop, J., and Murphy, N. 2023a. Daily soil temperature profiles, the Alaska Geophysical Network, 2016-2022. Arctic Data Center. doi:10.18739/A2959C89K

West, M., Stuefer, M., Ruppert, N., Gardine, M., Holtkamp, S., Murphy, N., and Heslop, J. 2023b. Meteorological data around Alaska, provided by the Alaska Geophysical Network, 2020-Present. Arctic Data Center. doi:10.18739/A23N20G2N

Upgraded permafrost observations across periglacial landforms around Longyearbyen, Svalbard

Hanne H. Christiansen

Arctic Geophysics Department, The University Centre in Svalbard, UNIS, Norway

The IPY permafrost observation infrastructure in Svalbard has been upgraded through the Svalbard Integrated Earth Observing System (SIOS) infrastructure project SIOSInfraNOR. The upgrade includes permafrost drilling equipment, borehole depth and infrastructure, and dataflow and accessibility.

Since the establishment of the IPY Nordenskiöld Land Permafrost Observatory in 2008–2009 in central Svalbard (Christiansen et al. 2010), the SIOSInfraNOR project has allowed significant improvements to borehole drilling technology, observation technology, including data transmission capabilities. During the winters of 2019 and 2021 eight new boreholes were drilled down to 21 m and one to 101 m, using our UNIS based SIOS InfraNOR medium sized drill rig (Christiansen et al. 2021) (Figure 1). This was done as our existing IPY boreholes of 10 m depth, had shown that they did not reach the depth of zero annual amplitude (ZAA), and to upgrade the thermistor technology and to modernise the data recording and dataflow providing better and direct access to the data. The IPY boreholes were drilled using a commercial drill rig, unfortunately not able to collect cores, so we had no ground ice content information prior to the SIOS InfraNOR project from all our long-term permafrost thermal monitoring boreholes.

We have installed 20 m long thermistor strings with 25 sensors in all eight boreholes in the period from 2019 to 2021. In November 2021 a 100 m thermistor string was installed in the deepest borehole. Sensor spacing is highest in the top with 10 sensors down to 3 m, allowing for observing also the active layer thickness with good resolution. Due to the C-19 pandemic, the drilling operation was delayed by one year and subsequently the borehole instrumentation also suffered from delays in both production and transport following the pandemic.

RESULTS

We have drilled in total 218 m of borehole. Using the improved coring capacity of the UNIS medium-sized drill rig (Christiansen et al. 2021) the ambition for drilling was to obtain cores from all parts of the boreholes. The 100 m deep borehole was drilled mainly into sandstone bedrock using hammer drilling as there was not enough drilling time capacity to collect a full set of cores down to 100 m. Several of the other boreholes were drilled into diamict with large clast grain sizes, however, using a larger diameter core barrel, we were able to obtain some core samples even from blockfield sediments, but also from deeper located fine-grained marine sediments. In the fine-grained sedimentary infilled valley bottoms core recovering was close to 100%.

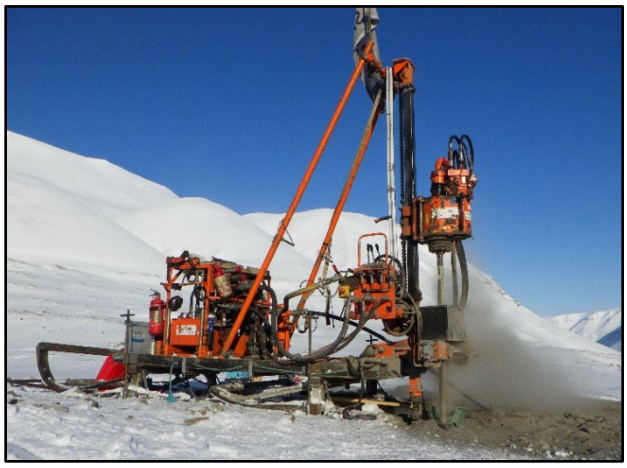

Figure 1. UNIS medium-sized 3m high permafrost drill rig (Photo Kolibri GeoServices, Ullrich Neumann).

With the extended boreholes the depth of zero annual amplitude (ZAA ≤°0.1C) have been reached in all borehole sites. The 20 m permafrost temperature recorded vary from -2.4°C to -5.8°C. Coldest are the highest located borehole drilled into a blockfield at 677 m asl. But also boreholes located in ice-wedges on a large alluvial fan and in a loess-covered fluvial terrace, both in the central part of the valley Adventdalen, have 20 m permafrost temperatures of -5.2°C and -5.8°C. However, the 20 m permafrost temperatures is only -2.6°C in a solifluction covered bedrock side in the sidevalley Endalen at 50 m asl., just 1500 m from the loess-covered fluvial terrace which is 3.1°C colder. Also the permafrost temperature in the fluvially infilled Longyeardalen valley bottom is around -2.6°C at 63 m asl. The warmest permafrost is found in the bottom of a mountain valley at 400 m asl. The geothermal gradient varies in the 100 m deep borehole in Endalen from 0°C/m from the depth of ZAA down to 50 m

depth (Figure 2), to a maximum of 0.037°C/m from 90 to 100m depth. The temperature profile clearly shows that warming has reached a depth of around 50 m at that site.

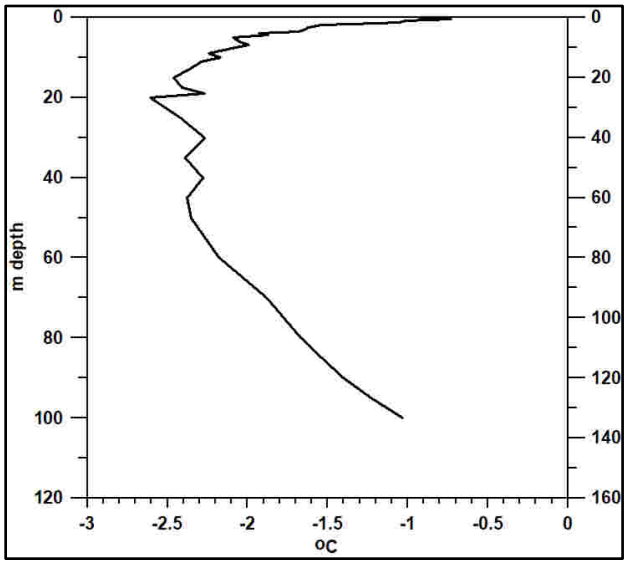

Figure 2. Average ground temperature showing the geothermal gradient down the 100 m deep borehole in Endalen. Data from the period November 2021 to November 2023.

The active layer thickness (ALT) can be interpolated based on the relatively dense spacing of thermistors in the top of the boreholes. ALT vary largely depending on landform and overall location. The thickest active layer is by far found in the Longyearbyen valley bottom of around 3 m. Whereas ALT is smallest with 80 cm in the blockfield borehole located highest at 677 m asl. All other sites have active layer thicknesses of between 100 to 160 cm. One borehole is located where there is also a CALM grid, and the borehole based ALT values of around 105 cm fits with the reported ALT for this period of time from the UNISCALM grid.

Data from all but one the SIOSInfraNOR boreholes are sent via the normal phone 5G network to the Norwegian Meteorological Institute's database in Oslo, and published in close to real time in the cryo web portal (https://cryo.met.no). Data is from there also included into the SIOS data management system, following the FAIR principles, as both permafrost temperature and ALT are SIOS core data.

Discussion

The 20 m permafrost temperature acquired from the eight new boreholes reflects the longer term climatic influence on the permafrost being well below the depth of ZAA in all the established boreholes. The large differences between the 20 m permafrost temperatures and ALT between the sites reflect both the influence of the landform and sediment type that the boreholes are drilled into, but it mainly reflect the influence of the local topography on the climatology of the periglacial landscape, including the influence of more or less snow cover.

The established permafrost drill rig is part of the SIOS infrastructure which can be rented for use, and it has already been used by both the local community in Longyearbyen, but also for other research and observation projects, such as e.g., establishing meteorological masts in remote parts of Svalbard for the Norwegian Meteorolical Institute.

Acknowledgements

The design of the UNIS based drill rig and its expansions, and the drilling of the new SIOS InfraNOR boreholes have been done in very close collaboration with Kolibri GeoServices operated by Ullrich Neumann. The collaboration agreement between the University Centre in Svalbard, UNIS and the Norwegian Meteorological Institute allows for ensuring the permafrost dataflow, and the collaboration with Ketil Isaksen from the Norwegian Meteorological Institute has been very important for this collaboration on permafrost data as part of the agreement.

References

Christiansen, H.H, Etzelmüller, B., Isaksen, K., Juliussen, H., Farbrot, H., Humlum, O., Johansson, M., Ingeman-Nielsen, T., Kristensen, L., Hjort, J, Holmlund, P., Sannel, A.B.K., Sigsgaard, C., Åkerman, H.J., Foged, N., Blikra, L.H., Pernosky, M.A., and Ødegård, R. 2010. The Thermal State of Permafrost in the Nordic area during the International Polar Year 2007-2009. Permafrost and Periglacial Processes, 21, 156–181.

Christiansen, H.H., Gilbert, G.L., Neumann, U., Demidov, N., Guglielmin, M., Isaksen, K., Osuch, M., and Boike, J. 2021. Ground ice content, drilling methods and equipment and permafrost dynamics in Svalbard 2016-2019 (PermaSval). In: Moreno-Ibáñez et al (eds) SESS report 2020, Svalbard Integrated Arctic Earth Observing System, Longyearbyen, pp 259–275. https://doi.org/10.5281/zenodo.4294095

How do thermal properties of a soil affect its response to climate change?

Michaela Kňažková & Filip Hrbáček

PolarGeoLab, Department of Geography, Masaryk University, Brno, Czech Republic

Soil thermal conductivity is a measure of heat transport capability of a soil. In permafrost-affected soils, the thickness of the active layer is largely dependent on how much heat can penetrate into the deeper layers of the soil and different types of soils therefore can either function in a way leading to acceleration or inhibition of the thawing propagation based on their thermal properties.

Thermal conductivity of a particular soil is determined by a variety of factors (Farouki 1981), some of which are inherent to the soil. However, thermal properties also vary in close connection with the natural variability of other parameters, of which the most prominent is the effect of soil moisture (Abu-Hamdeh and Reeder 2000).

The Antarctic Peninsula is currently one of the most rapidly warming parts of the Earth, where large areas of new ice-free terrain are predicted to emerge within the upcoming decades (Lee et al. 2017). While the ongoing climate change brings an increase in air temperature, it also affects precipitation rates or patterns and, subsequently, moisture conditions of soils.

In Antarctica, there is at present a significant gap in knowledge on the spatial and temporal variability of soil moisture and its connection to soil thermal properties. Better understanding of the current dynamics and the driving factors of change in these environments can help us gain an insight into how they will likely develop under different future scenarios.

Study site

The site for this study is situated on James Ross Island, off the north-eastern coast of the Antarctic Peninsula, in an area of flat terrain underlain by continuous permafrost with a semi-arid continental climate. This area, the Abernethy Flats, comprises of Cretaceous sandstones and siltstones and the soil texture is categorised as sandy clay loam. Over the years, instrumental measurements of air and ground temperature, soil heat flux and volumetric water content have been established on the site.

Methods

Data from the automatic weather station has been used in multiple studies, testing different approaches to active layer and soil thermal properties modelling (Hrbáček and Uxa 2020; Kňažková and Hrbáček 2024).

We collected soil samples from the site and subsequently measured their thermal conductivity in a laboratory experiment across the full range of water content from completely dry to fully saturated using a thermal properties analyser. In order to investigate how active layer thickness reacts to changes in temperature (represented by thawing degree days, or TDD) and the coupled effect of soil moisture and soil thermal conductivity, we employ the Stefan model (e.g., Hrbáček and Uxa 2020) to calculate active layer thickness for different soil moisture/conductivity scenarios in order to simulate possible future climate conditions.

Results

The laboratory experiment has shown that the soil thermal conductivity of our sample increases most rapidly within a relatively narrow window of soil moisture between 10 and 20 %. After this threshold, the further increase in thermal conductivity is slower (Figure 1).

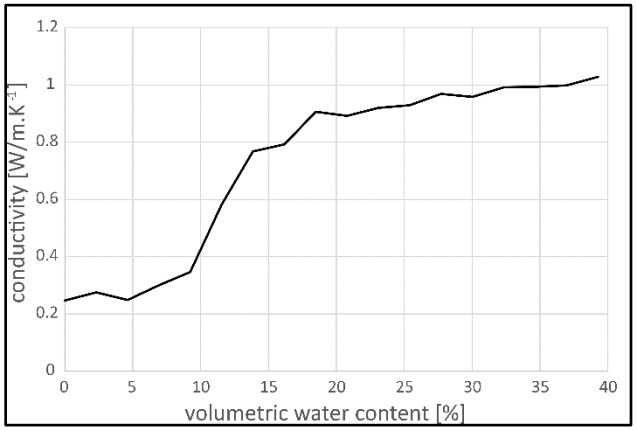

Figure 1. Variability of average soil thermal conductivity at different soil moisture based on laboratory experiment

The results of Stefan model for the different soil moisture/conductivity scenarios obtained from the laboratory experiment suggest that while atmospheric warming leads to thicker active layer in general, the increase is less pronounced for the wetter scenarios (Figure 2). To illustrate this, for TDD = 800 °C/days, the difference in soil moisture between 16 and 39 % translates into a difference in active layer thickness of over 30 cm.

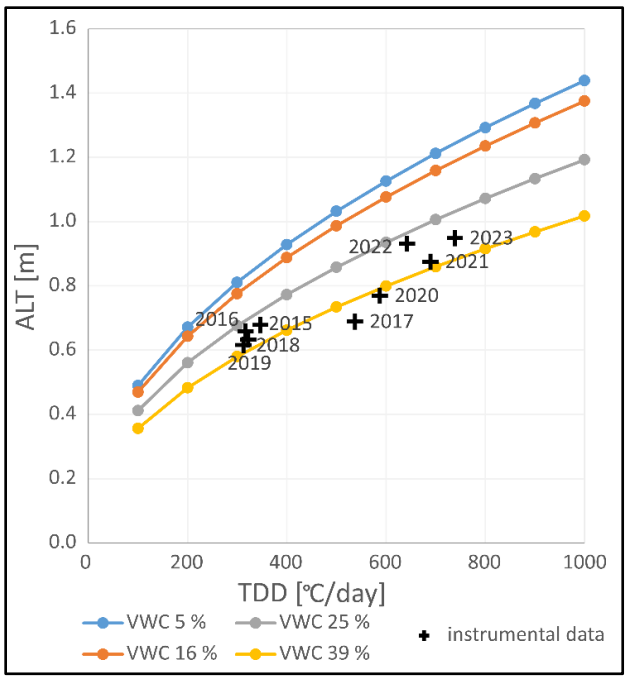

Figure 2. Modelled ALT thickness for different soil moisture/conductivity scenarios.

During the last several summer seasons since 2020 we have observed a rapid increase in active layer thickness on the Abernethy Flats based on instrumental data, while at the same time drying of the surficial part of the profile has been detected.

The loss of moisture might be attributed to atmospheric drying, as well as increased evaporation in the warmer climate or its migration downwards due to thicker active layer. In case of the drying propagating further down the profile, there is a potential for active layer thickness to increase at a much faster rate in the future.

Conclusions

This case study essentially underlines the role of soil moisture as a significant moderator of climate change effect on the active layer, due to the control that soil moisture exerts over soil thermal properties. The changing dynamics of soil moisture could have consequences such as permafrost degradation in areas experiencing the impacts of atmospheric drying. Additionally, the drying of the soil surface will very likely negatively influence the well-being of the sparse local biota, especially mosses.

References

Abu-Hamdeh, N.H., and Reeder, R.C. 2000. Soil Thermal Conductivity: Effects of Density, Moisture, Salt Concentration, and Organic Matter. Soil Science Society of America Journal, 64, 1285–1290. doi:10.2136/sssaj2000.6441285x

Farouki, O.T. 1981. Thermal Properties of Soil. U.S. Army Corps of Engineers, Cold Regions Research and Engineering Laboratory, Hanover, 136 pp.

Hrbáček, F., and Uxa, T. 2020. The evolution of a near-surface ground thermal regime and modeled active-layer thickness on James Ross Island, Eastern Antarctic Peninsula, in 2006–2016. Permafrost and Periglacial Processes, 31, 141–155. doi:10.1002/ppp.2018

Kňažková, M., and Hrbáček, F. 2024. Interannual variability of soil thermal conductivity and moisture on the Abernethy Flats (James Ross Island) during thawing seasons 2015–2023. Catena, 234, 107640. doi:10.1016/j.catena.2023.107640

Lee, J.R., Raymond, B., Bracegirdle, T.J., Chadès, I., Fuller, R.A., Shaw, J.D., and Terauds, A. 2017. Climate change drives expansion of Antarctic ice-free habitat. Nature, 547, 49–54. doi:10.1038/nature22996

Quantifying permafrost thaw in Canada using multiple metrics and temperature data from many boreholes

Olivia Meier-Legault[1], Stephan Gruber[1] & Nick Brown[1,2]

[1]*Department of Geography and Environmental Studies Carleton University, Ottawa, Ontario, Canada*

[2]*NSERC PermafrostNet, Ottawa, Ontario, Canada*

Permafrost underlies nearly half of Canada and is undergoing widespread thaw, primarily as a consequence of climate change. Locally, thaw can impact infrastructure, traditional ways of life and ecosystem health. Globally, the release of carbon from degrading permafrost further amplifies climate change. Monitoring permafrost change is important both for climate assessment and for developing permafrost climate services (Gruber et al. 2023).

Most studies and assessments of the permafrost thermal state in Canada use few boreholes and rely solely on temperatures measured at a single depth (e.g., Derksen et al. 2019). Changes measured by sensors at multiple depths are sometimes shown visually (e.g., Smith et al. 2022) but are not used quantitatively or in summary products. Monitoring mostly relies on two metrics: changes to the active layer thickness (ALT) and to the mean annual ground temperature (MAGT) near the depth of zero annual amplitude (DZA) (Smith et al. 2022; Romanovsky et al. 2019). While these metrics are important and established indicators, they reveal only some of the changes occurring in the soil column. For instance, ALT trends are confounded by subsidence (O'Neill et al. 2023) and do not necessarily reflect changes to the duration of thaw. Similarly, MAGT changes at the DZA in warm permafrost are subdued by latent-heat effects, requiring additional and counterintuitive interpretation.

Driven by the potential to complement these two metrics, and the low number of boreholes often reported on, this project aims to better quantify permafrost thaw and temperature change using multiple metrics and a larger set of borehole temperature data from across Canada.

This aim prompts two questions: (1) What new insight can additional metrics across multiple sensors in the boreholes offer? (2) What are the remaining obstacles for a semi-automated analysis of temperature data from numerous boreholes?

Data and Methods

We use openly available data from the Yukon Geological Survey, Northwest Territories Geological Survey, and in Nordicana D and are actively seeking additional collaborators and sources of data. To date, we have 69 boreholes with data spanning more than five years (Figure 1).

Using a semi-automated procedure and an interoperable framework for processing ground-temperature data (Brown 2022), we calculate an array of metrics for each borehole, including amplitude ratios, trends in the temperature-derived ALT, thaw depth duration ($\overline{D}$) (Harp et al. 2016), MAGT, mean monthly temperatures, duration of the zero curtain, date of maximum and minimum temperature, and DZA.

Trends and their significance are determined using two non-parametric methods: the Sen's slope estimate (Sen 1968) and the Mann-Kendall *p* value (Mann 1995; Kendall 1948). Procedures for temporally autocorrelated data are being established.

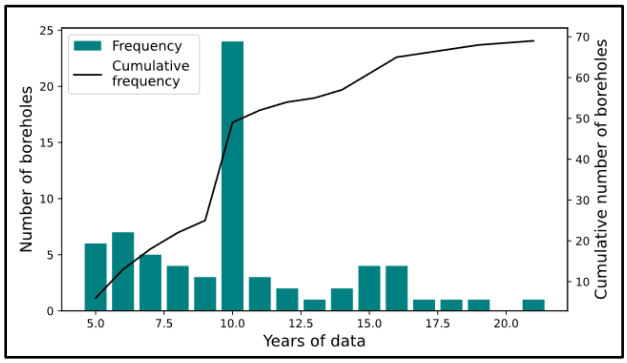

Figure 1. Number of boreholes with 5–20 years of usable data.

Results

Changing permafrost conditions at borehole CAS_DH1-23B in the Yukon depicted in Figure 2 is used as an example with data taken from Lipovsky et al. (2022). Table 1 shows that MAGT at 11.6 m, near the DZA, interpolated ALT, and $\overline{D}$ (i.e., the amount and duration of thawed soil in a given year) are all increasing (*p* value < 0.05). Both the annual minimum and maximum temperature trends at 2.6 m, the node directly beneath the active layer, are increasing (*p* value < 0.05), with the greater rise in minimum temperature providing an additional indication of thaw.

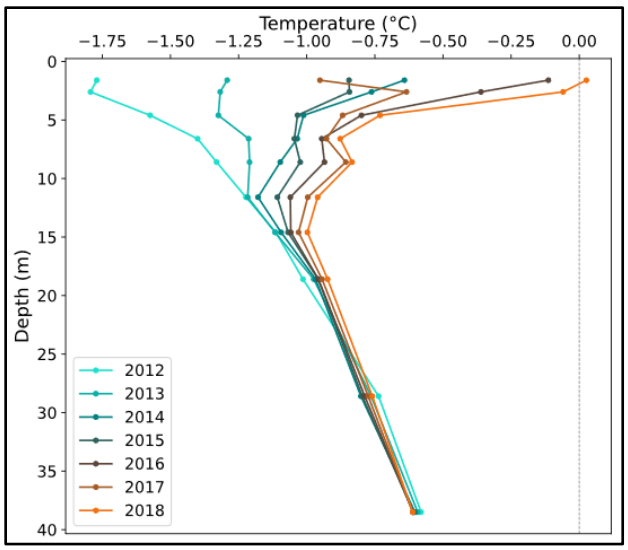

Figure 2. Change in the mean annual ground temperature between 2016 and 2018 at site CAS_DH1-23B. Data from Lipovsky et al. (2022).

Table 1. Trends in the MAGT at 11.6 m (°C), temperature-derived ALT (m), $\overline{\mathcal{D}}$ (m^3/m^2), annual minimum and maximum temperature at 2.6 m (°C) in borehole CAS_DH1-23B from 2012 until 2018. Data from Lipovsky et al. (2022).

	$MAGT_{11.6}$	ALT	$\overline{\mathcal{D}}$	$Min_{2.6}$	$Max_{2.6}$
Trend (unit/year)	0.050	0.38	0.23	0.54	0.13
p value	0.00267	0.00390	0.00981	0.0355	0.00267

These metrics are calculated for the entirety of the available data (Figure 1), allowing permafrost thaw and temperature change to be quantified at multiple depths and across many boreholes.

ACKNOWLEDGEMENTS

**NSERC PermafrostNet (NETGP 523228-18).

REFERENCES

Brown, N. 2022. tsp ("Teaspoon"): A Library for Ground Temperature. Journal of Open Source Software, 7(77). doi:10.21105/joss.04704

Derksen, C., Burgess, D., Duguay, C., Howell, S., Mudryk, L., Smith, S., Thackeray, C., and Kirchmeier-Young, M. 2019. Changes in Snow, Ice, and Permafrost across Canada. Canada's Changing Climate Report, 5: 194–260.

Gruber, S., Hayley, J., Karunaratne, K., King, J., MacLean, T., Marshall, S., and Moore, D. 2023. Considerations Toward a Vision and Strategy for Permafrost Knowledge in Canada. Arctic Science. doi:10.1139/as-2023-0016

Harp, D.R., Atchley, A.L., Painter, S.L., Coon, E.T., Wilson, C.J., Romanovsky, V.E., and Rowland, J.C. 2016. Effect of Soil Property Uncertainties on Permafrost Thaw Projections: A Calibration-Constrained Analysis, The Cryosphere, 10: 341–358. doi:10.5194/tc-10-341-2016

Kendall, M.G. 1948. Rank Correlation Methods. Griffin.

Lipovsky, P.S., Humphries, J.K., Stewart-Jones, E.T., and Cronmiller, D.C. 2022. Yukon Permafrost Database: A New Baseline Data Resource. Yukon Geological Survey.

Mann, H.B. 1945. Nonparametric Tests Against Trend. Econometrica, 13(3): 245–259. doi:10.2307/1907187

O'Neill, H.B., Smith, S.L., Burn, C.R., Duchesne, C., and Zhang, Y. 2023. Widespread Permafrost Degradation and Thaw Subsidence in Northwest Canada. Journal of Geophysical Research: Earth Surface, 128(8). doi:e2023JF007262.

Romanovsky, V.E., Smith, S.L, Isaksen, K., Shiklomanov, N.I., Streletskiy, D.A., Kholodov, A.L. Christiansen, H.H., Drozdov, D.S., Malkova, G.V., and Marchenko, S.S. 2017. Terrestrial Permafrost [in "State of the Climate in 2017"]. Bulletin of the American Meteorological Society, 100(9): S161–S165.

Sen, P.K. 1968. Estimates of the Regression Coefficient Based on Kendall's Tau. Journal of the American Statistical Association, 63(324): 1379–1389. doi:10.1080/01621459.1968.10480934

Smith, S.L., O'Neill, H.B., Isaksen, K., Noetzli, J., and Romanovsky, V.E. 2022. The Changing Thermal State of Permafrost. Nature Reviews Earth & Environment, 3(1): 10–23. doi:10.1038/s43017-021-00240-1

Strategic evaluation of the Swiss Permafrost Monitoring Network

Jeannette Noetzli[1], Cécile Pellet[2], Dominik Amschwand[2], Chloé Barboux[2], Jan Beutel[3], Reynald Delaloye[2], Daniel Farinotti[4,5], Isabelle Gärtner-Roer[6], Christian Hauck[2], Christin Hilbich[2], Martin Hoelzle[2], Christophe Lambiel[7], Coline Mollaret[2], Marcia Phillips[1], Cristian Scapozza[8], Andreas Vieli[6], Sebastián Vivero[2], Daniel Vonder Mühll[9], Samuel Weber[1], Julie Wee[2] & Jonas Wicky[2]

[1]*WSL Institute for Snow and Avalanche Research SLF, Davos, Switzerland*

[2]*Department of Geosciences, University of Fribourg, Fribourg, Switzerland*

[3]*Department of Computer Science, University of Innsbruck, Innsbruck, Austria*

[4]*Laboratory of Hydraulics, Hydrology and Glaciology (VAW), ETH Zurich, Zurich, Switzerland*

[5]*Swiss Federal Institute for Forest Snow and Landscape Research WSL, Birmensdorf, Switzerland*

[6]*Department of Geography, University of Zurich, Zurich, Switzerland*

[7]*Institute of Earth Surface Dynamics, University of Lausanne, Lausanne, Switzerland*

[8]*Institute of Earth Sciences, University of Applied Sciences and Arts of Southern Switzerland (SUPSI), Mendrisio, Switzerland*

[9]*Personalized Health and Related Technologies (PHRT), ETH Zurich, Zurich, Switzerland*

The Swiss Permafrost Monitoring Network PERMOS (www.permos.ch) was established in 2000 and has developed into an operational network documenting the state of permafrost in the Swiss Alps. The monitoring strategy, data management and network organisation have continuously been adapted to new results from research and technological progresses. A strategic evaluation of PERMOS was performed in 2021/2022 to (1) critically assess the strategy, structure, operation and cooperation of the network, (2) identify challenges and fields of action, and (3) decide on the support by the funding partners. Overall, the current monitoring strategy and organisation of PERMOS were evaluated as being successful. The key challenges identified are related to the continuation of existing measurements and the data curation, both crucial steps for the provision of coherent, robust, and comparable data over decades. The instruments maintenance in harsh environments, their timely renewal and continuous adaptation to technological progress are essential tasks for sustainable permafrost monitoring. Curation of the collected data, quality assessment (QA) and control (QC) as well as safe storage and open access are just as important.

The Swiss Permafrost Monitoring Network PERMOS started in the year 2000 and grew from an unconsolidated, science-driven collection of permafrost research sites into the operational network it is today. To systematically document state and changes of mountain permafrost in the Swiss Alps, PERMOS developed a comprehensive monitoring strategy over more than two decades of operation (see Table 1, PERMOS 2023).

Table 1. Methods applied within the PERMOS network.

Method (site nbr.)	Start/ End	Spat. Cover	Meas. Freq.	Derived information
Aerial photogra-mmetry	2000	Area	3–5 years	Rock glacier velocity, rock falls
Ground temperature in boreholes (26)	2000	Point *max. 100m depth*	1–24 hours	Permafrost temperature, active layer thickness, geothermal gradient, warming rates
Bottom temperature of the snow (BTS, disc.)	2000/ 2015	Multi-points	Annual	Permafrost occurrence and distribution
Ground surface temperature (GST, 230)	2000	Multi-points	1–3 hours	Ground surface temperature, ground freezing/thawing indices, snow cover duration
Electrical resistivity tomography (ERT, 5)	2006	Line *max. 40m depth*	Annual	Relative ground ice/water content and its changes, active layer thickness
Terrestrial geodetic survey (TGS,18)	2008	Multi-points	Annual	Permafrost creep velocity
Permanent GNSS (8)	2019	Point	1–24 hours	Permafrost creep velocity
Climate station (6)	2019	Point	10 minutes	Meteorological conditions, surface energy balance

The monitoring strategy focuses on three main observation elements (1) ground temperature near the surface (GST) and at depth (also used to derive Active Layer Thickness, ALT), (2) permafrost resistivity

as a proxy for changes in ground ice content, and (3) rock glacier velocities. They are complemented by recordings of meteorological conditions at key sites. The network includes 27 sites that are representative of the diversity of permafrost conditions in mountain regions in the Swiss Alps, with varying topography, snow regimes and (sub-)surface characteristics. These differences are considered more important for the evolution of permafrost at the scale of the country than those due to regional climate conditions.

Evaluation 2021/2022

The strategic priorities 2017–2026 of GCOS Switzerland state that Essential Climate Variables (ECV) and their associated monitoring networks must undergo regular evaluations. After smaller evaluations of particular parts of the network in 2007 and 2017, a comprehensive evaluation of the PERMOS network was performed in 2021/2022. The procedure included a self-assessment report and a review by three external international experts on behalf of the federal funding agencies. The external review was based on two workshops, where the network and its activities were presented and discussed to reach a common understanding with the external evaluators. The evaluation focused on the following fields of actions:

- Monitoring network (sites, variables, and methods)
- Conformity with GCOS objectives and requirements (data management)
- Data access
- (Inter)national exchange and cooperation
- User needs and benefits
- Public relations and communication
- Administration and finances

General assessment

The PERMOS set-up was considered to be successful and well adapted to achieve its goal and is in line with the GCOS objectives and requirements. PERMOS presently curates the largest and most comprehensive data set on mountain permafrost worldwide, with the longest time series covering 36 years. Over the past four-year period (2019–2022), the network continued to operationalize and standardize instrumentation and field work through systematic documentation and compilation of best practice guidelines for the measurements. Since 2020, a comprehensive overview of the PERMOS results is published annually online in the Swiss Permafrost Bulletin (e.g., PERMOS 2023). A quality-checked and updated data set is published each year.

Key challenges

The main goal of PERMOS is also its main challenge: obtaining permafrost data that are comparable and consistent over decades. Each year instruments deteriorate, field work conditions change and sometimes become hazardous, new technologies evolve, and data volume increases. Priorities of sites and tasks must be defined and site renovations proactively planned to optimise resource allocation.

The management, curation, and secure storage of a growing and diverse dataset is essential to ensure its quality and accessibility. The associated workload has increased significantly. To meet GCOS requirements and improve efficiency, standardization and automation of QA/QC procedures must be developed and implemented.

PERMOS benefits from substantial in-kind contributions (knowhow and time) from its academic partner institutions, which are not secured on a permanent basis. The training of young researchers and outreach should be further explored.

Finally, gaps in the monitoring network were identified, in particular the underrepresentation of cold high altitude bedrock sites (>3500 m asl).

Outlook and future activities

The continuation of PERMOS was defined based on the evaluation 2021/22 and a follow-up proposal for 2023–2026. Two key priorities will be addressed:

- Continuity of the network: sustained maintenance and data collection at the existing field sites to continue the long time series.
- Data management and quality: standardized processing and quality controls of the field data and their dissemination are essential to ensure their usability and quality.

PERMOS also aims to strengthen collaborations and increase synergies with stakeholders and other institutions involved in permafrost monitoring in Switzerland and internationally.

References

PERMOS. 2023. Swiss Permafrost Bulletin 2022. Noetzli, J., and Pellet, C. (eds.). No 4, 23 pp. doi:10.13093/permos-2023-01

On the influence of ground surface temperature on rock glacier velocity

Cécile Pellet[1], Reynald Delaloye[1], Isabelle Gärtner-Roer[2], Christophe Lambiel[3], Jeannette Noetzli[4], Marcia Phillips[4] & Cristian Scapozza[5]

[1]*Department of Geosciences, University of Fribourg, Fribourg, Switzerland*

[2]*Department of Geography, University of Zurich, Zurich, Switzerland*

[3]*Institute of Earth Surface Dynamics, University of Lausanne, Lausanne, Switzerland*

[4]*WSL Institute for Snow and Avalanche Research SLF, Davos*

[5]*Institute of Earth Sciences, University of Applied Sciences and Arts of Southern Switzerland (SUPSI), Mendrisio, Switzerland*

Rock glacier velocity (RGV) has been shown to react sensitively and synchronously to the evolution of ground temperatures. For this reason, it was adopted in 2021 as new associated product to the Essential Climate Variable (ECV) permafrost. Nevertheless, the physical processes governing RGV and the connection with external climate forcing remains incompletely understood. Using long-term observations from the Swiss Permafrost Monitoring Network, this study investigates the influence of Ground Surface Temperature (GST) on RGV across 13 sites in the Swiss Alps.

Introduction

Rock glaciers are debris landforms generated by the former or current creep of ice-rich permafrost which can be found in most mountain ranges worldwide. Since the early 2000s, an increasing number of studies investigated the kinematic behavior of rock glaciers and analysed the physical processes governing their evolution and response to climate change. Results show that regardless of size, morphology, velocity ranges, topographical and geological settings most of the rock glaciers within a specific region exhibit similar inter-annual and pluri-decadal kinematic behaviors, which mainly follows ground temperature changes and by extension climate change (e.g., PERMOS 2023). For this reason, Rock Glacier Velocity (RGV) was adopted in 2021 as new associated product to the Essential Climate Variable (ECV) Permafrost by the Global Climate Observing System (GCOS).

Although a connection between changes in RGV and ground temperature evolution has been observed, the physical processes controlling rock glacier dynamics as well as the interrelation with climate forcing remain incompletely understood. Studies show that the displacement at the surface of rock glaciers results from the internal deformation within the crystallin structure of the frozen ground (creep stricto sensu) combined with shearing in one or several discrete ground layers. The largest part of the deformation occurs within these shear horizons which are typically located at ~15-30 m depth. To appropriately use and interpret RGV as an ECV product, a better understanding of its connection with permafrost temperatures is required.

In this contribution we assess the influence of ground surface temperature (GST) as a proxy for permafrost temperature on RGV following the approach proposed by Staub et al. (2016) and expanding it to additional and longer time series.

Methods

Within the Swiss Permafrost monitoring Network (PERMOS), surface velocities are obtained by regularly measuring the position of 10–100 boulders on the rock glacier and the surrounding stable terrain using high precision differential GNSS or total stations. RGV is the annual site average of surface velocity (RGIK 2023) that is computed based on a subset of reference points selected for their spatial distribution (i.e., locations representative of permafrost creep) as well as data quality and completeness. For comparison with GST, we compute changes relative to the 2017–2021 reference period.

GSTs are recorded using spatially distributed temperature miniature data loggers (UTL-3) buried a few decimeters below the surface on and beside rock glaciers. Each site has 5–15 loggers measuring with a time resolution of 1–3 hours. GST time series are aggregated to daily mean values and gap filled. GSTs are used as proxy for deeper temperatures in this study since permafrost temperatures at greater depth are rarely available and challenging to obtain (e.g., due to shearing of boreholes). To account for the delay and filtering of the temperature signal with depth and to represent permafrost temperatures around the depth of the shear horizon, GSTs are averaged using a 2-year running window before computing the deviation to the 2017–2021 reference period. A site average of GST is computed based on time series selected for their location (i.e., underlain by permafrost conditions) as well as data quality and completeness.

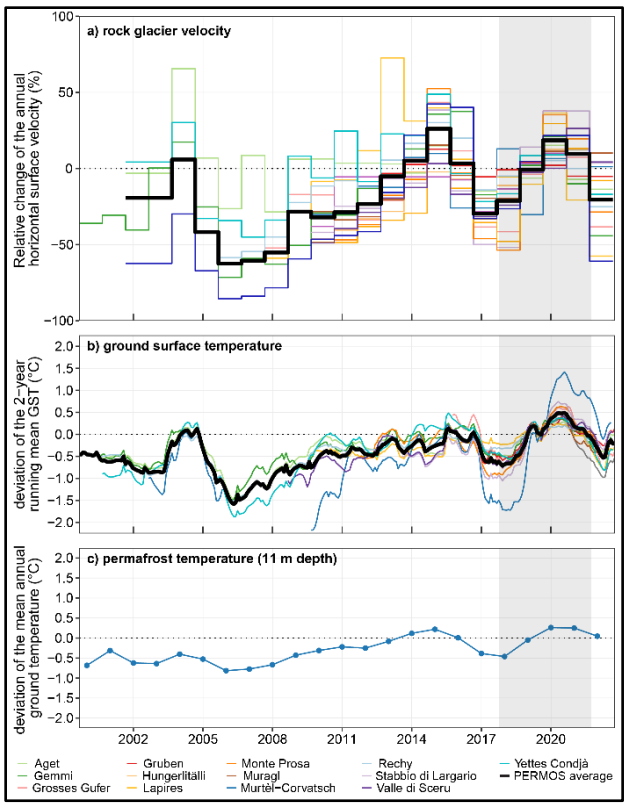

Figure 1. Relative changes of the mean annual horizontal surface velocity of 13 rock glaciers (a) compared to the deviation of the 2-year running mean ground surface temperature at the same sites (b) and the deviation of the hydrological mean annual permafrost temperature at 11 m depth at rock glacier Murtèl-Corvatsch (c). The used reference period (October 2017– September 2021) is indicated in grey, and the black line represents the average of all sites.

Results

Overall, a coherent signal of RGV evolution can be observed in the Swiss Alps (Figure 1a). It is characterized by marked inter-annual variability with RGV maxima reached in 2004, 2015 and 2020 as well as important velocity decrease in 2005–2006, 2016–2017 and 2021–2022. The RGV variations are synchronous with the changes of the 2-year running mean of GST (r2MGST, Figure 1b) and the mean annual ground temperature at 11 m depth measured at rock glacier Murtèl-Corvatsch (Figure 1c). RGV increase is typically observed during warming periods, and decreases are recorded during cooling periods, often because of snow-poor winters.

The systematic comparison of the relative RGV with the deviation of the r2MGST at the date of the velocity measurement shows a linear relation between the two variables (Figure 2). Considering the average of all sites, a statistically significant (>99%) relation is found, whereas for individual rock glaciers the significance levels range from <10% (Aget, Murtèl-Corvatsch, Gruben and Lapires) to >99% (Gemmi, Grosses Gufer, Rechy, Valle di Sceru and Yettes Condjà B and C).

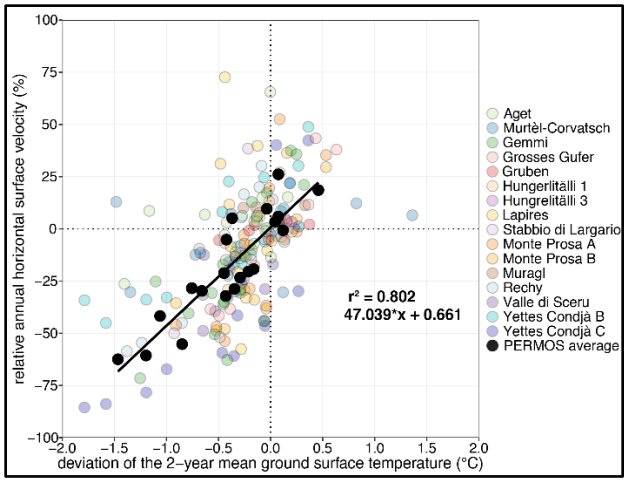

Figure 2. Relative annual horizontal surface velocity compared to the deviation of the 2-year running mean GST at the date of the velocity measurement for all rock glaciers. The linear relation based on PERMOS average data, related equation, and r-squared value are indicated.

Conclusion and Outlook

The changes in GST and ground temperature at ~15 m depth explain a large part of the inter-annual RGV variations. Based on the dataset presented, we aim to further develop and analyse the statistical temperature/RGV relation to better understand the interactions with climate forcing. Especially, the analysis of changes in RGV that are not explained by temperature variations could allow for identifying additional factors driving rock glacier velocity, such as water related processes, ice content, permafrost degradation or even rock glacier destabilization.

References

PERMOS. 2023. Swiss Permafrost Bulletin 2022. Noetzli, J. and Pellet, C. (eds.). No 4, 23 pp. doi:10.13093/permos-2023-01

RGIK. 2023. Rock Glacier Velocity as associated product of ECV Permafrost: practical concepts (version 1.2). IPA Action Group Rock glacier inventories and kinematics, 17 pp.

Staub, B., Lambiel, C., Delaloye, R., 2016. Rock glacier creep as a thermally-driven phenomenon: A decade of inter-annual observation from the Swiss Alps, In XI International Conference on Permafrost - Book of Abstracts, Bibliothek Wissenschaftspark Albert Einstein, Potsdam, Germany, 96–97.

Long-term landscape-specific responses of near-surface permafrost to climate change on the North Slope of Alaska

Nikolay I. Shiklomanov[1], Kelsey E. Nyland[1], Dmitry A. Streletskiy[1], Anna E. Klene[2] & Frederick E. Nelson[3,4]

[1]*Department of Geography, George Washinton University, Washington, District of Columbia, United States*

[2]*Franke College of Forestry & Conservation, University of Montana, Missoula, Montana, United States*

[3]*Department of Earth, Environmental, and Geographical Sciences, Northern Michigan University, Marquette, Michigan, United States*

[3]*Department of Geography, Environmental, and Spatial Sciences, Michigan State University, East Lansing, Michigan, United States*

Results of a 28-year (1995–2023) analysis for Active Layer Thickness (ALT) and air and soil-surface temperature observations are presented for a series of representative Circumpolar Active Layer Monitoring (CALM) sites on the North Slope of Alaska. All sites examined are within the continuous permafrost zone and distributed along the primary climatic gradient spanning the regional spectrum of vegetation and terrain conditions. Each site consists of a 1 ha plot representing homogeneous examples of the typical landscape categories within the Coastal Plain and Arctic Foothills physiographic provinces.

Methods

At each site, ALT was inferred from 71 thaw depth measurements conducted annually by mechanical probing at the end of the thawing season (end of August). For consistency, thaw depth measurements were made within the same calendar week of each year since 1995. Soil-surface temperatures under natural surface covers (e.g., vegetation, snow) were monitored continuously over the 1995–2023 period at nine locations representing different microtopographic landscape elements of each site. The air temperature was measured at standard meteorological height (~1.8 m) at each site. Periodic, spatially-oriented measurements of ground surface elevation were initiated in 2001 at three of these sites CALM sites using a Differential Global Position System (DGPS) and an explicitly spatial sampling scheme.

Results

Data show pronounced landscape-specific differences in long-term active-layer trends. Under similar climatic forcing observational sites dominated by shrubs demonstrate high rates of ALT increase while shrub-free tundra sites demonstrate relative long-term stability of the active layer. The stability of active-layer thickness can be partially explained by thaw settlement at the surface not accounted for in thaw depth measurements.

However, the analysis of long-term temperature measurements demonstrates divergent trends in air and ground-surface temperatures. These changes involve an overall increase in temperature differences between the air and soil surface. The multi-decadal increase in temperature offsets during summer months is observed at all sites suggesting an increase in the thermal insulating properties of vegetation attributable to long-term climate-induced biomass accumulation. Shrub-dominated landscapes also show a pronounced increase in air and soil surface temperature differences in winter however, not evident at shrub-free sites. This can be explained by enhanced snow retention due to increasing shrub height and density. This analysis indicates that in shrub-free tundra, vegetation change produces a negative feedback by increasing the summer temperature offset - partially explaining the relative stability of active-layer thicknesses here under a warming climate. Conversely, in shrublands, similar climatic forcing resulted in a positive (thickening) active-layer trend. Proliferating shrubs have contributed to the dominance of the positive winter feedback. Results suggest that the widely reported expansion of tundra shrubs can change from negative to positive vegetation-permafrost feedbacks.

Conclusions

Overall, long-term observations from the North Slope of Alaska demonstrate complex, non-linear responses of the active-layer/near-surface permafrost system to changes in climatic conditions. These data provide an empirical basis for the quantitative evaluation of complex interactions and feedback mechanisms between changing ecosystems and permafrost.CALM program data presented here are publicly available and offer a validation resource for modeled and remotely-sensed products.

The Verkhoyansk Range Permafrost Monitoring Network

Robert Sysolyatin, Sergei Serikov & Mikhail Zheleznyak
Melnikov Permafrost Institute, Yakutsk, Russia

Permafrost temperature regime in the East Siberian Mountain is less known overall than in other mountain permafrost areas, but it has crucial influence on hydrological, geomorphological, and biological processes. However, because of almost absence of the long-term permafrost temperature monitoring in this area, it is hard to correctly consider cryosphere response to climate warming. Since 2010 we have been running and expanding permafrost studies along the 63-64°N longitudinal transect that crossing the Verkhoyansk Range at elevation between 283 and 1821 m. Over study period, ground temperature at 1 m depth ranged between -1.1 to -10.1°C while maximum active layer thickness vary from 30 to 260 cm for different landscapes. Data have shown that mean soil temperatures and active layer thickness were generally stable during last decade. The 6.7m deep borehole was installed in August 2021 in floodplain terrace has showed first-time talik temperature regime for Verkhoyansk Range. It was revealed that sediments around large rivers under season freezing layer (~3 m) may warming to +6°C.

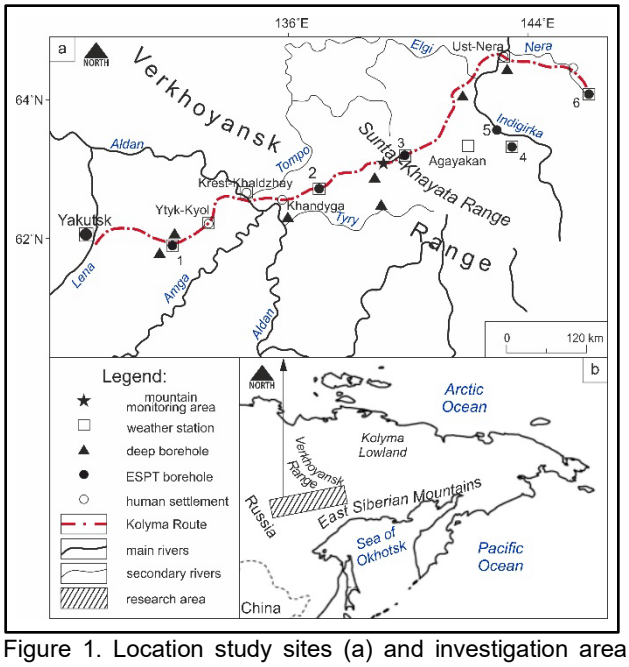

Figure 1. Location study sites (a) and investigation area (b) within Verkhoyansk Range and adjacent territory. ESPT boreholes: 1 – Churapcha; 2 – Tyoply Klyuch; 3 – Vostochnaya; 4 – Tomtor; 5 – Oymyakon; 6 – Delyankir.

Finally, five 30-m permafrost temperature-monitoring boreholes were established near weather stations in 2022 for designating depth of zero annual amplitude, ground structure, thermal properties, and ambient factors influencing on ground temperature regime. Additionally, permafrost thickness was 205 m and geothermal heat flux was about 0.052 Wm^{-2} that was determined by the deep borehole. Subsequently, it is anticipated that additional studies are expected to permafrost condition of the East Siberian Mountains.

This study focuses on the Verkhoyansk Range and adjacent territory, where the permafrost condition is still insufficiently studied (Figure 1). The mean air warming rate recorded by numerous weather stations shown rising around 0.3-0.4°C/10year, but the temperature regime of permafrost has remained unknown until recently.

Since the 1960s, the permafrost condition has been determining by deep boreholes. That investigation shows that permafrost is continuous with thickness from 100 to 600 m and D_{zaa} temperature ranging from -9 to -2°C.

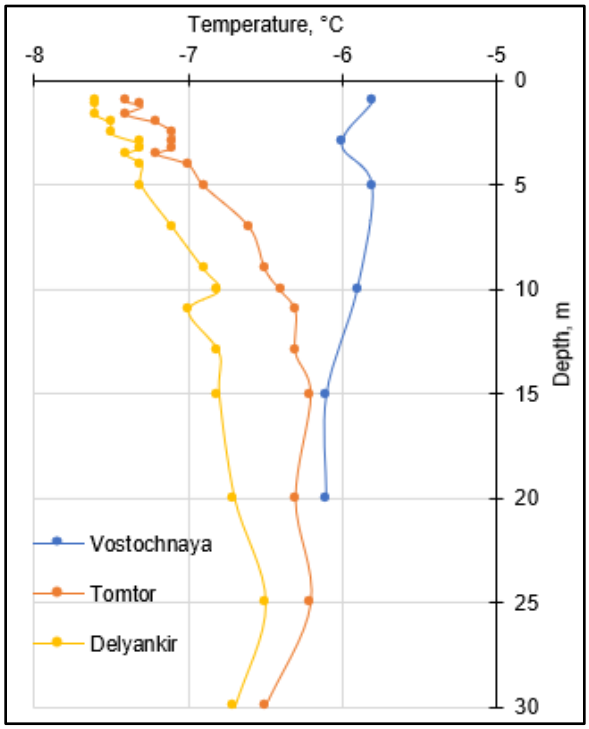

Figure 2. Vostochnaya, Tomtor and Delyankir mean temperature from period 15.09.2022 to 15.08.2023.

The key features of this region are extremely low air temperatures (down to -60°C), complex terrain and high geothermal heat flux (up to 100 Wm^{-2}).

The Verkhoyansk Range Network includes few permafrost onitoring sites - Vostochnaya, Tomtor, Oymyakon and Delyankir. Except Oymyakon site, these study sites are located nearby to the weather stations. The selected temperature profiles and main parameters from September, 2022 to August, 2023 are shown at the Figure 2 and the Table 1.

Vostochnaya site the highest located among others ones has more moderate air and permafrost temperature regime. Vegetation absence has lead to relatively thick active layer, although snow cover stays at this site the most part of year (7-8 months). From 5 m and downward to Dzaa temperature decrease to 6.0°C at 20 m depth.

Tomtor and Oymyakon study sites are located in the same condition within Oymyakon valley, but they relate to grass and forest vegetation types, respectively. This place characterized by extremely low air temperature and relatively thin snow cover. Open spaced Tomtor site has thinner active layer and colder permafrost temperature than Oymyakon site. At Tomtor site, downward to 11 m mean temperature rising, from 11 to 25 m permafrost temperature negligible oscillating and sharp decreasing to 0.3°C at 30 m.

Delyankir is coldest site among ESPT-project monitoring borehole at Verkhoyansk Range. The lowest air temperature, moss vegetation and short snow cover period lead to thin active layer (0.8 m) and to the coldest permafrost temperature at 1 m and Dzaa. Although Delyankir has the highest air temperature amplitude, the Dzaa at this site is the lowest.

Overall, type of temperature profile of D_{zaa} layer is similar for different environmental gradients at the end of thaw period (Figure 2). The mean permafrost table temperature ranges from -8 to -5°C, and D_{zaa} temperature veries around -6°C. The coldest temperature of air and permafrost for study period was measured at Delyankir site while the highest located Vostochnaya site refers to more moderate climate and permafrost condition.

The ground temperature at 1 m depth in particular sites can vary with an amplitude around 40°C. The average annual temperature ranges from -1.1°C to -10.6°C. The thickness of the active layer varies from 0.5-0.7 m to 1.8-2 m. The minimum values are characterized by wet areas with a moss cover. The thickness of the active layer within the moraine deposits varies within 1.5-1.7 m, whereas it does not exceed 1.2-1.4 m on the watersheds, due to the shortened period of action of positive temperatures.

Table 1. Main temperature parameter from 15.09.2022 to 15.08.2023.

Site	Altitude, m	Mean air temp., °C	Air temp. amplitude, °C	Max snow depth, cm	Days with snow cover	Active layer, m	D_{ZAA}, m	Mean surface temp. (0.2m), °C	Mean 1 m depth temp., °C	Temp., D_{ZAA}, °C
Tyoply Klyuch*	289	-12.2	89.9	82	215	7	13	-0.5	-1.1	-0.7
Vostochnaya	1288	-14.4	78	53	256	~ 2.4	>20	-5.4	-5.7	~6.0
Tomtor	740	-16.7	92.2	34	192	1.2	25	-6.5	-7.3	-6.1
Oymyakon**	682	~ -16.7	~ 92.2	~ 34	~ 192	~ 1.45	20	-	-	-5.3
Delyankir	801	-17.1	92.7	40	176	0.8	15	-7.0	-7.7	-6.7

*Tyoply Klyuch 1.6 sensor and downward failure 24.05.2023

**Oymyakon failure 06.06.2023

Active layer thickness database for the Lena Delta region (NE Siberia) and its analysis in relation with landscape parameters

Aleksandra Veremeeva[1], Anne Morgenstern[1], Evgeny Abakumov[2], Irina Adrian[3], Michael Angelopoulos[1], Sofia Antonova[1], Julia Boike[1], Niko Bornemann[1], Alexandra Cherepanova[4], Svetlana Evgrafova[5], Dmitry Fyedorov-Davydov[6], Matthias Fuchs[7], Mikhail Grigoriev[4], Frank Günther[8], Gustaf Hugelius[9], Alexander Kizyakov[10], Sebastian Laboor[1], Alexey Lupachev[6], Hanno Meyer[1], Frederieke Miesner[1], Jan Nitzbon[1], Pier Pau Overduin[1], Vyacheslav Polyakov[2], Elizaveta Rivkina[6], Alexandra Runge[11], Lutz Schirrmeister[1], Matthias Siewert[12], Georg Schwamborn[13], Anna Tarbeeva[10], Mathias Ulrich[14], Sebastian Wetterich[15], Sebastian Zubrzycki[16] & Guido Grosse[1]

[1]*Alfred Wegener Institute Helmholtz Centre for Polar and Marine Research, Potsdam, Germany*

[2]*Department of Applied Ecology, Faculty of Biology, St. Petersburg State University, St. Petersburg, Russia*

[3]*Ust-Lensky State Nature Reserve, Tiksi, Yakutia, Russia*

[4]*Melnikov Permafrost Institute, Siberian Branch, Russian Academy of Sciences, Yakutsk, Russia*

[5]*Sukachev Institute of Forest, Krasnoyarsk Science Centre, Siberian Branch, Russian Academy of Science, Krasnoyarsk, Russia*

[6]*Institute of Physicochemical and Biological Problems in Soil Science, Russian Academy of Sciences, Pushchino, Russia*

[7]*Renewable and Sustainable Energy Institute, University of Colorado Boulder, Boulder, United States*

[8]*Neubrandenburg University of Applied Sciences, Neubrandenburg, Germany*

[9]*Department of Physical Geography, Bolin Centre for Climate Research, Stockholm University, Stockholm, Sweden*

[10]*Faculty of Geography, Lomonosov Moscow State University, Moscow, Russia*

[11]*Arctic and Antarctic Research Institute, St. Petersburg, Russia*

[12]*Helmholtz Centre Potsdam GFZ German Research Centre for Geosciences, Potsdam, Germany*

[13]*Department of Ecology and Environmental Science, Umeå University, Sweden*

[14]*Eberswalde University for Sustainable Development, Faculty of Landscape Management and Nature Conservation, Eberswalde, Germany*

[15]*German Environment Agency, Dessau-Roßlau, Germany*

[16]*Technical University of Dresden, Institute of Geography, Dresden, Germany*

[17]*Center of Earth System Research and Sustainability (CEN), Universität Hamburg, Hamburg, Germany*

The active layer thickness (ALT) is one of currently two Essential Climate Variables (ECVs) related directly to permafrost regions as defined by the Global Climate Observing System at the World Meteorological Organization. Within the framework of the Circumpolar Active Layer Monitoring (CALM) program established in the 1990s, ALT is being monitored across the Arctic to better understand climate change impacts on landscape, permafrost, hydrology, vegetation, and soil biogeochemistry (Nelson et al. 2021). In addition to this standardized monitoring program at established sites, many ALT measurements are collected every year during other field work covering various research questions, field sites, and approaches. Usually, much of this ALT data remains unpublished. The Lena Delta region (NE Siberia) has been one of the Arctic focus regions of many Russian and international scientific teams for several decades. In a first step, we aimed to compile all available ALT measurements for the Lena Delta region, including both unpublished and published data collected during Russian and joint German-Russian expeditions since 1991, standardize them and make them accessible for further use. We adhere to the FAIR guiding principles for scientific data management and stewardship (Wilkinson et al. 2016) by publishing one comprehensive dataset in the PANGAEA Data Publisher for Earth & Environmental Science. In a second step, we will analyze this comprehensive dataset together with other data available for the region to reveal determining factors for spatial and temporal ALT variation.

Our Lena Delta ALT database contains ALT data collected by researchers during different tasks, such as sampling of exposures, drilling of boreholes, continuous measurements with soil temperature sensors and data loggers, soil and vegetation surveys, as well as for validation of remote sensing data. They include single measurements at individual locations as well as ALT transects across landforms and gridded measurements.

The ALT database contains about 6000 site measurements from different areas of the Lena Delta region with clustering in five research-intensive areas including Muostakh Island and Bykovsky Peninsula (Figure 1). 35 % of the ALT measurements were collected on Samoylov Island where the Samoylov Island Research Station has been operated since several decades (Hubberten et al. 2006), 22 % were measured on Kurungnakh Island, and 21 % on the Bykovsky Peninsula. Sobo-Sise Island and Muostakh Island represent 10 and 9 % of the number of ALT measurements, respectively. The remaining 3% were collected from other locations. ALT was measured mostly once per site, but some sites were measured 2-5 and more times in order to reveal microrelief and vegetation impact.

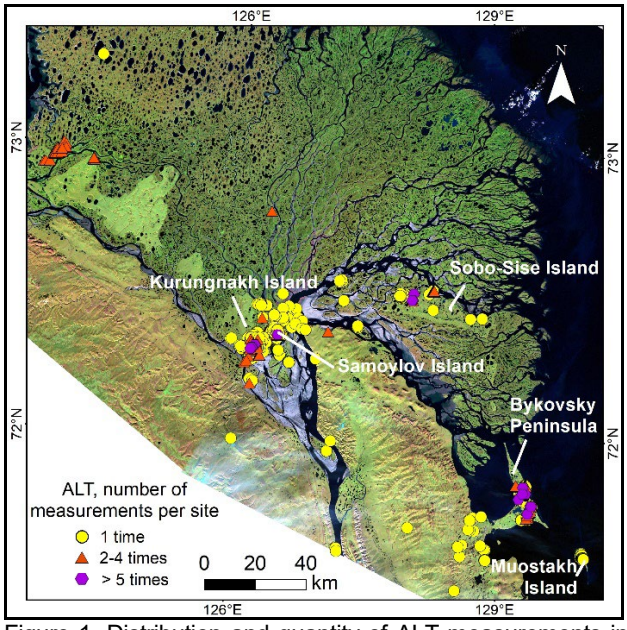

Figure 1. Distribution and quantity of ALT measurements in the Lena Delta region.

For several sites, repeated measurements of ALT profiles were conducted at the same locations in different years, e.g., on Samoylov Island from 2013 to 2022, on Sobo-Sise Island in 2015, 2016, and 2018, and on the Bykovsky Peninsula in 2015, 2016, and 2021. Repeated ALT measurements within one year were collected in 2010 and 2013 on Samoylov Island, in 2013 and 2014 on Kurungnakh Island and in 2017 on Bykovsky Peninsula.

The measurement sites represent various landscapes underlain by different types of deposits (Holocene Lena Delta terraces, remnants of Yedoma Ice Complex, slope deposits on the low-mountain relief, etc.), which are characterized by various relief positions, and different microtopography, soils, and vegetation cover.

Preliminary analyses indicate that the compiled ALT data show landscape unit-dependent variabilities, intraseasonal fluctuations, and long-term trends. Further in-depth spatial and temporal ALT analysis together with other existing datasets such as the ArcticDEM, a new habitat map for the Lena Delta (Lisovski et al. 2023), and climate parameters will be performed in order to reveal relationships with landscape characteristics and climate change.

Our new ALT database presents a valuable synthesis of permafrost and soil surface dynamics in the important Arctic region for the last decades in addition to established CALM sites and published literature data for other permafrost regions. The data may be useful for parametrization or validation of permafrost modeling results and remote sensing studies.

Acknowledgements

This study was supported by the Interact Virtual Access under EU-H2020 Grant Agreement No. 871120.

References

Hubberten, H.W., et al. 2006. The Russian-German Research Station Samoylov, Lena Delta - A Key Site for Polar Research in the Siberian Arctic, Polarforschung, Bremerhaven, 73 (2/3): 111-116.

Lisovski, S., et al. 2023. A new habitat map of the Lena Delta in Arctic Siberia based on field and remote sensing datasets, Earth Syst. Sci. Data Discuss. [preprint]. https://doi.org/10.5194/essd-2023-36 (in review)

Nelson, F.E., Shiklomanov, N.I., and Nyland, K.E. 2021. Cool, CALM, collected: the Circumpolar Active Layer Monitoring program and network, Polar Geography, 44:3, 155–166. doi: 10.1080/1088937X.2021.1988001

Wilkinson, M., et al. 2016. The FAIR Guiding Principles for scientific data management and stewardship, Sci Data 3, 160018. doi.org/10.1038/sdata.2016.18

Ground thermal regime and active layer depth at Irizar, a wind-exposed CALM site in Deception Island (Maritime Antarctica)

Gonçalo Vieira[1], Gabriel Goyanes[1], Joana Baptista[1], Miguel Angel de Pablo[2], Carla Mora[1], Mohammad Farzamian[1], Miguel Santos[1] & Miguel Ramos[3]

[1]*Centre of Geographical Studies and Associate Laboratory TERRA, Institute of Geography and Spatial Planning, University of Lisbon, Lisbon, Portugal*

[2]*Geology Unit, Faculty of Sciences, University of Alcalá, Alcalá de Henares, Spain*

[3]*Physics Unit, Faculty of Sciences, University of Alcalá, Alcalá de Henares, Spain*

The South Shetlands islands off-shore the northwest Antarctic Peninsula have been subject to numerous studies on permafrost and active layer, especially following the International Polar Year 2007–2008. The archipelago marks the northwestern boundary of continuous permafrost in the northwest Antarctic Peninsula, which depending on the geomorphological setting may be close to sea level (e.g., in Deception Island) or at up to about 150 m a.s.l. (e.g., in the rocky Livingston Island). Mean annual air temperatures in the islands are c. -2 ºC at sea level, which under a polar maritime climate result in mean permafrost table temperatures close to 0 ºC and of about -1.7 ºC at c. 275 m a.s.l. (e.g., Reina Sofia Peak). Several permafrost and active layer boreholes have been installed since 2000 from King George Island to the Palmer archipelago, integrating the PERMANTAR (Portugal) and PERMATHERMAL (Spain) networks. The rocky nature of the terrain in the islands limits the use of mechanic proving of the thaw depth and hence only 3 CALM observatories are operational within these networks: Limnopolar in Byers Peninsula (Livingston Island), Crater Lake and Irizar in Deception Island. Russia operates another CALM site in Fildes Peninsula, King George Island. In Deception Island, Crater Lake, is the reference CALM site with a longer time-series, an extensive set of instrumentation, and an easier access from the Spanish Station Gabriel de Castilla. In order to better understand the controls on the active layer characteristics in Deception Island, the Irizar CALM site was installed in 2009 in the vicinity of Collado Vapor, a wind-exposed col with the ground composed of a sandy-silty volcanic diamicton with numerous pebbles and boulders. A key difference to Crater Lake is the absence of a porous lappili pumice cover which results in different ground thermal properties.

In this study we present for the first an analysis of the active layer and permafrost thermal regimes and characteristics of the Irizar CALM site, framing it in interannual variability and the long-term climate trends.

STUDY AREA

Deception Island is an active stratovolcano with recent eruptions in 1956, 1967, 1967 and 1970, which covered wide areas of the island with thick pummice and ash deposits, generated new land areas and destroyed infrastructure. The island shows a crater rim with a horseshoe shape and has a diameter of about 15 km. The interior is a collapse caldera with up to 9 km in diameter open to the ocean in its southwest limit through a 500 m wide passage. The rim rise to 539 m in Mount Pond and shows an important glacier coverage. Due to the porosity and high insulating capacity of the volcanic soils, permafrost is widespread and continuous almost down to sea-level. However, boreholes and geophysical data show that the permafrost is only a few meters thick. The transient layer and permafrost table are ice-rich. The island shows several areas with geothermal anomalies, generally along fault lines and with temperatures reaching up to +90 ºC in some locations. However, the impacts of these anomalies on permafrost distribution are local, with permafrost being present a few hundred meters away from the anomalies (Goyanes et al. 2014).

The Irizar CALM site is located close to Collado Vapor at an elevation of c. 130 m and north of Irizar peak, which names the site. It is a wide col in the main crater rim, which bridges the ocean-side and the inner caldera slopes, making it very wind-exposed to the west. The slope is exposed to northwest promoting higher insolation.

METHODS AND TECHNIQUES

The CALM site was first installed in 2009 with the installation of a 100 x 100 m grid with nodes at 10 m intervals. Since then, the site is visited at least once every summer generally from the end of January to mid February, although in 2017 the visit was in early March. Thaw depth probing was conducted with a stainless steel rod. Unfortunately, the difficult access to the terrain limits selecting a later date in the summer for the measurements and it has also proven impossible to conduct the measurements at the same Julian day.

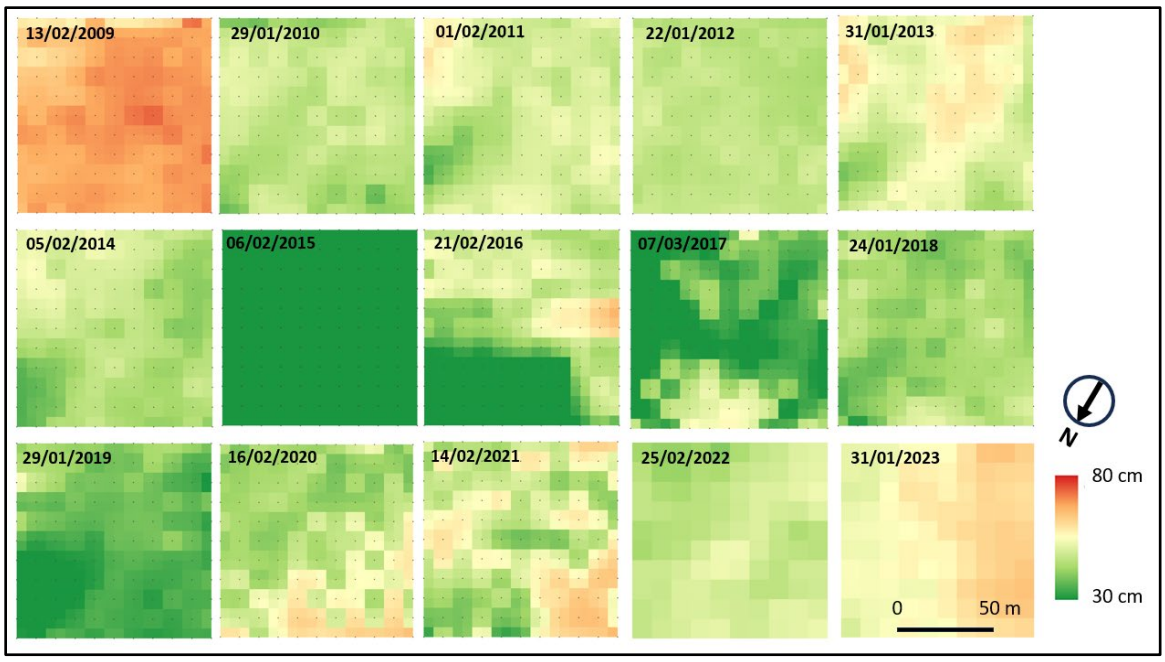

Figure 1. Thaw depth at the Irizar CALM site from 2009 to 2023.

In order to obtain a continuous dataseries, which also allows for framing the thaw probing, ground temperatures at 2, 5, 10, 15, 20, 40, 80 and 120 cm depths are measured at hour intervals in a borehole and complemented by air temperatures at a height of 150 cm. Currently, Geoprecision (Dallas) loggers calibrated at 0 ºC with an ice-water bath are used.

Here, we briefly present the results of the thaw depth variability, but at ICOP, we will perform an indepth analyses of several temperatures indexes, and compare with local and regional climate data.

Results

The average thaw depth varied between extremes of 67 cm in 2011 and 19 cm in 2015, with most years showing averages close to 50 cm. The interpolated thaw depth data for 2009–2023 (Figure 1) reveals that thaw depth varies significantly inside the grid, but that overall similar patterns are present between different years. From 2009 to 2015 thaw depth generaly decreased, while from then onwards, it tended to increase. The extreme shallow thaw depth in 2015 relates to the late lying snow cover in the summer. Actually, it has been shown for Crater Lake, as well as for other sites in the South Shetlands that the increase in the snow cover period until 2015 has been responsible for ground cooling and shallower thaw. Irizar shows a similar behaviour, but a higher interannual variability in thaw depth than Crater Lake, which relates to the lack of the insulating lappili layer.

Conclusions

The 14 year thaw depth data series from Irizar shows that the site represents the general regional variability recorded in Deception and Livingston islands, hence can be used as a regional value for the analysis of climate-permafrost interactions. It shows deeper annual thaw than Crater Lake due to the higher thermal diffusivity of the ground, and it also shows a higher interannual variability, which may indicate a higher sensitivity to changing conditions. This hypothesis still needs to be further investigated. The data also shows that despite the volcanic activity in the island, permafrost reacts clearly to climate forcing and has not been controlled by variations in geothermal fluxes.

Acknowledgements

This research was funded by PERMANTAR (PROPOLAR/FCT) and THAWIMPACT (FCT 2022.06628.PTDC). JB is funded by grant 2021.05119.BD. The Spanish Polar Committee, the Ejército de Tierra—Gabriel Castilla personnel, the Direccion Nacional del Antartico and Instituto Antartico Argentino, and the Base Decepción personnel are warmly thanked for the logistical support.

Reference

Goyanes, G. Vieira, G., Caselli, A., Cardoso, M., Marmy, A., Santos, F., Bernardo, I., and Hauck, C. 2014. Local influences of geothermal anomalies on permafrost distribution in an active volcanic island (Deception Island, Antarctica); Geomorphology, 225, pp. 57-68. https://doi.org/10.1016/j.geomorph.2014.04.010

Surface and thermal offsets in polar and mountain permafrost regions

Kenji Yoshikawa & Vladimir Romanovsky
University of Alaska Fairbanks, Fairbanks, Alaska, United States

Permafrost stability and its properties strongly depend on permafrost temperature. Mean annual temperature at the permafrost table directly relates to the mean annual air temperature through the so-called surface and thermal offsets. Surface offset is defined as the difference between mean annual ground surface and air temperatures. Thermal offset is defined as the difference between mean annual temperature at the bottom of the seasonally thawed/frozen layer and the mean annual ground surface temperature. Surface and thermal offsets were calculated from the permafrost and active layer temperature data collected at the selected 24 communities in Alaska (Figure 1) (out of over 400 monitored arctic and sub-arctic communities) and at currently established several tropical and arid mountain permafrost monitoring sites around the world.

METHODS

Active layer and permafrost temperature were measured with data loggers at various depths during the years 2005-2023. Typical permafrost monitoring boreholes were drilled to a depth of 3-6 m and temperature sensors were installed at 1 cm intervals in the active layer (typically upper 40 cm to 1 m depth, depending on the site). Deep permafrost temperatures were measured with thermistors and logged hourly, primarily with Onset dataloggers (UX-120) with thermistors (Sensor Scientific Inc. model-WM103Y). The accuracy of the temperature observations is approximately ±0.15°C after calibration. Active layer temperatures were measured using the DS18B20 digital thermometer (Dallas Semiconductor) and a central microprocessor programmable by Arduino. This study used a custom 40 cm to 1 m (1 cm interval of sensors at upper depth) probe with one microprocessor to control many sensors. The factory accuracy specification of the DS18B20 sensor is ±0.5°C (from -10°C to +85°C), however calibration has shown a higher stable accuracy of about ±0.12°C~0.18°C for most of the sensors.

RESULTS AND DISCUSSION

The thermal offset is generally caused by the difference in frozen/unfrozen thermal conductivities of the materials and depends on the thermal properties of the soil, the water content, and the ground surface temperature regime.

Southern most Alaskan community where permafrost temperature was measured is a village of Naknek located along the Bristol Bay, Southcentral Alaska, where the thermal offset was -2.4°C, active layer was slightly less than 1m (in 2009-14). Highest thermal offset of -2.8°C was measured in the village of Kaltag as well as at the Yoshikawa Reindeer Farm, interior Alaska.

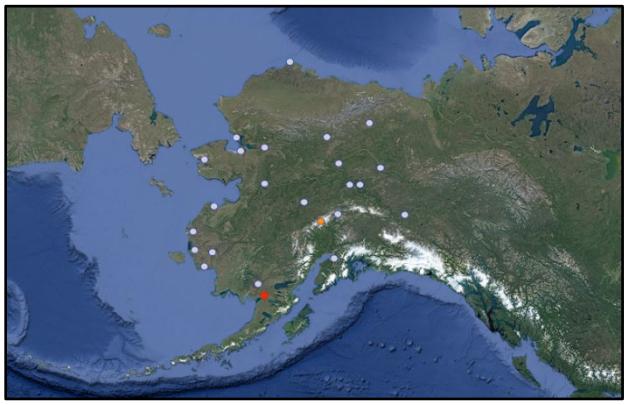

Figure 1. Random selection of Alaska ground temperature monitoring sites including the southernmost permafrost location at Naknek, Bristol Bay (red dot), and the summit of the Denali (orange dot).

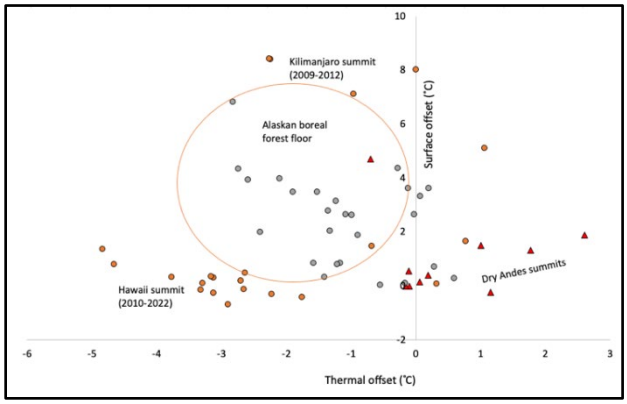

Figure 2. Thermal offset vs. surface offset of Alaskan boreal forest/ tundra communities (gray circles), tropical mountain permafrost (orange circles), and arid mountain permafrost (red triangles).

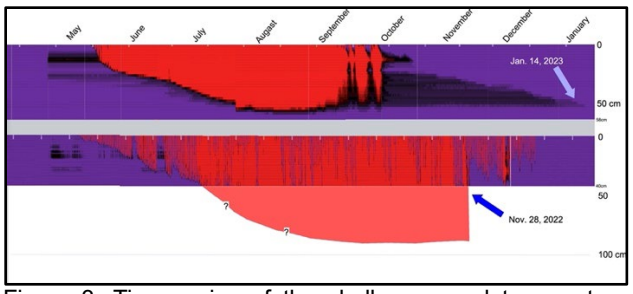

Figure 3. Time series of the shallow ground temperature distribution from spring 2022 to winter 2023 in interior Alaska (top) and Hawai'i (bottom). Red color indicates >0.2°C temperatures, purple <-0.2°C, and black color indicates near 0°C (<0.2°C, >-0.2°C) conditions, respectively. 50 and 100 cm thermistors in Hawai'i indicated that the maximum active layer thickness was about 80 cm.

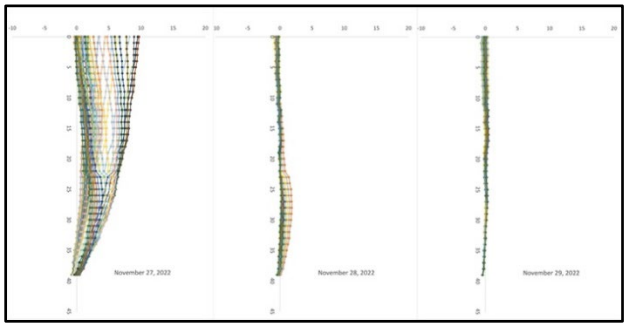
Figure 4. Three days (November 27-29, 2022) shallow (0-40 cm) ground temperature profiles at 30-minute time intervals show a sudden all-layer freeze up event on November 28, 2022 in Hawai'i.

The coldest permafrost was found near the summit of Denali in Alaska, -26°C (MAGT) and the thermal offset was almost zero at this site. Many interior Alaskan boreal forest sites typically have stronger thermal buffering and -1.5 to -2.8°C thermal offset (Figure 2). The summer ground surface temperature has a significant influence on the thermal offset in higher latitude regions, including these Alaskan communities. Where the active layer is deeper, the thermal offset is typically greater and the thawing index (or positive degree days) at the ground surface is also higher.

In high latitudes the surface offset mostly caused by the warming influence of the seasonal snow cover. However, in the high elevation regions the surface offset may also be governed by other physical processes. Thus, the largest positive surface offset (7.1-8.4°C) was found at the top of Mt. Kilimanjaro near the equator (3°S) (Figure 2), where a strong solar radiation produces a large difference between ground surface and air temperatures.

We examined detailed (1cm intervals temperature measurements) active layer temperature profiles over the last three years (2021-2023) at an Alaskan boreal forest site where the maximum active layer reached almost the same depth (52-54 cm) during the last 3 years and froze up in mid-January the following year (Figure 3 top). At the same time, we observed that a different type of thermal regime controls the thermal offset at tropical mountains such as Maunakea, Hawai'i (Figure 3 bottom). Tropical high elevation regions have greater diurnal than seasonal or interannual temperature variations. Here, the thawing index concept is not well suited and is rarely studied for active layer thermal properties. Our high-resolution temperature measurements reveal details of the freezing and thawing process of the tropical active layer and the thermal offset. When there is thawing period (e.g., spring to summer), ice-bonded layer slowly conducts heat and consumes latent heat similar like in the Arctic regions, but the early winter freezing is very sudden. Temperature of the entire active layer drops below 0°C in one day mostly by convective heat transfer (Figure 3 and 4), then, during the winter, water from partial snowmelt percolates to form ice bonded layers in frozen active layer. Figure 5 shows a summary of differences in the mechanism of thermal offset formation in arctic and tropical environments.

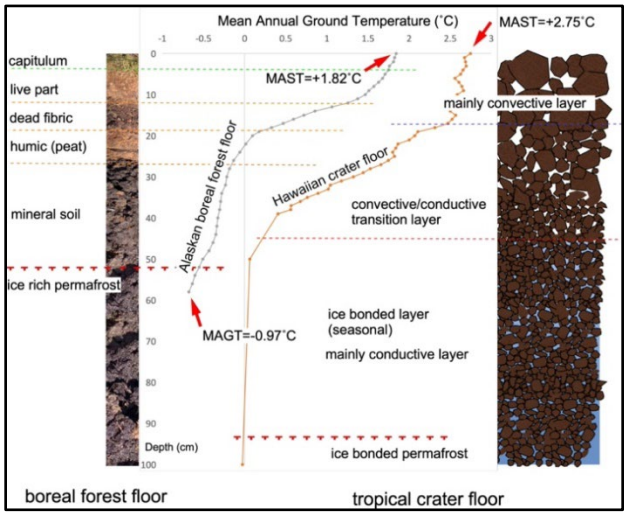

Figure 5. Two different types of thermal offset and ground profiles. Thermal offset is greater at the "dead fibric" layer in boreal forest profile in Alaska and just below the convective (large pore space) layer in Hawai'ian crater floor.

Permafrost Geomorphology & Hazards

4E — Permafrost Mass-Wasting Processes and Slope Hazards

Session Chairs: Steve Kokelj[1], Joseph Young[2] & Julius Kunz[3]

[1]Northwest Territories Geological Survey, Government of Northwest Territories, Yellowknife, Northwest Territories, Canada
[2]Department of Earth and Atmospheric Sciences, University of Alberta, Edmonton, Alberta, Canada
[3]Institute of Geography and Geology, University of Wuerzburg, Bavaria, Germany

Permafrost mass-wasting has increased in frequency and magnitude across permafrost slopes in the last two decades due to a changing climate. This recent acceleration of thaw-driven landscape change can rapidly alter hazards and risks to infrastructure and ecosystems. However, the diversity and variability of permafrost hillslopes make assessing the interactions between permafrost degradation, mass-wasting processes, and associated hazards a complex issue. Bridging these fundamental knowledge gaps remains essential in evaluating spatiotemporal thaw trajectories and the associated hazards of thawing permafrost slopes.

This session, therefore, aims to present developments in permafrost mass-wasting processes and their associated hazards. We welcome contributions from an array of scientific disciplines, timescales (past, current, future), and local- to circumpolar scales that assess permafrost mass-wasting processes and hazards from mountain and lowland settings. This includes studies on field and remote sensing observations, geomorphology, engineering geology, surface-subsurface hillslope interactions, big data processing, machine learning, mapping, and modelling, monitoring, and adaptation strategies.

Assessing hillslope reponses to permafrost thaw with InSAR-based mass movement inventories in two Alaska national parks

Kyra Bornong[1], Louise M. Farquharson[1], Daniel H. Mann[1] & Denny Capps[2]

[1]*University of Alaska Fairbanks, Fairbanks, Alaska, United States*

[2]*Geologic Resources Divison, U.S. National Park Service, Lakewood, Colorado, United States*

Warming climate is predicted to cause increased mass movement in permafrost areas (Huggel et al. 2012; Patton et al. 2019; Stoffel and Huggel 2012). However, the mechanisms driving hillslope failture and how they vary under different thermal and crolithoogical conditions, are not well understood. Investigating specific hillslope responses to warming permafrost will provide essential information on geologic hazards and on the processes that shape Alaska's mountainous landscapes.

This study focuses on mass movement inventories of Gates of the Arctic (GAAR) and Denali (DENA) National Parks. GAAR lies within Alaska's continuous permafrost zone, while Denali, further south, is located within the discontinuous permafrost zone (Jorgenson et al. 2008). Numerical modelling suggests that much of the permafrost in DENA is close to 0°C and that nearly all of it will thaw in the coming century (Panda et al. 2014).

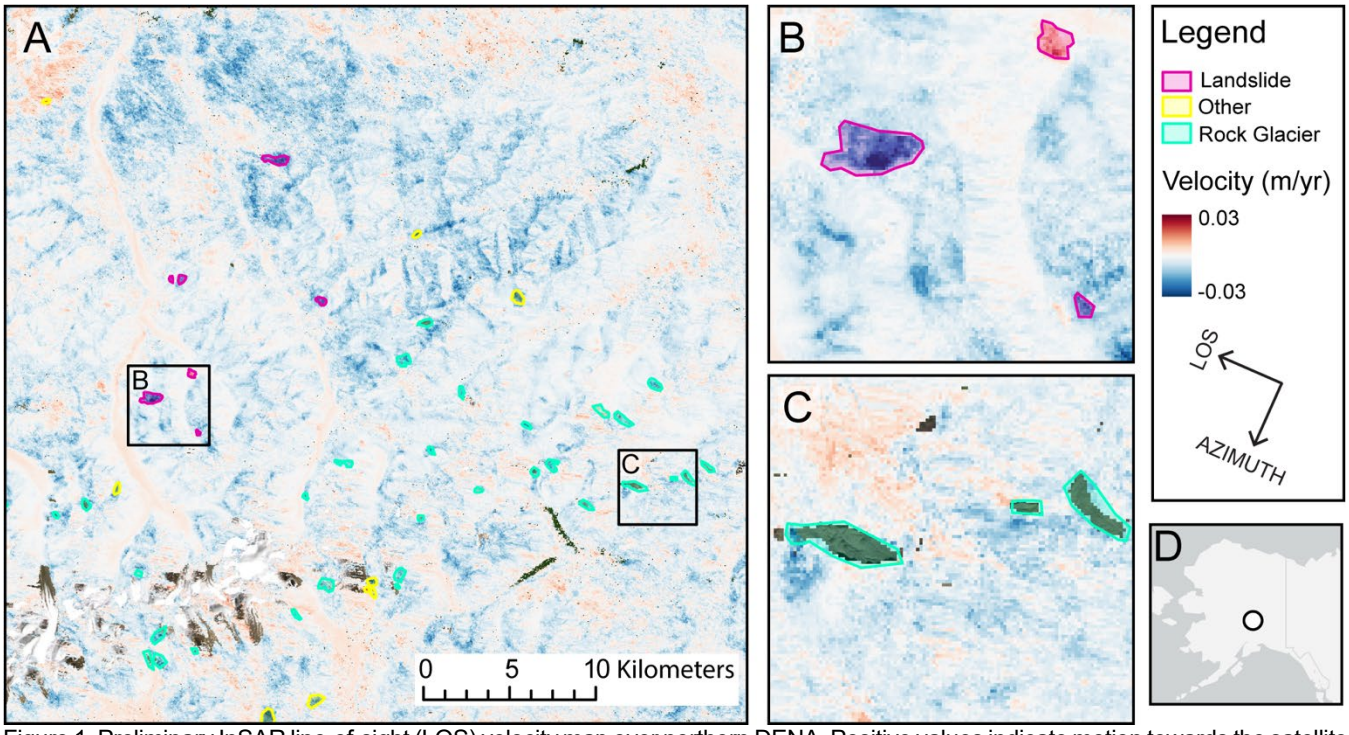

Figure 1. Preliminary InSAR line-of-sight (LOS) velocity map over northern DENA. Positive values indicate motion towards the satellite and negative values indicated motion away from the satellite. Pixels with a coherence of less than 0.3 are masked. A) shows broad overview with different features; B) shows clusters of high-velocity pixels that we have interpreted as actively creeping landslides with the aid of satellite imagery. In C) we interpret groups of low-coherence pixels that lie over rock glaciers that are visible in satellite imagery as moving too fast for accurate InSAR measurement. D) shows map location within Alaska.

Ground temperatures in GAAR are likely to remain below freezing, but warming is expected to drive active layer thickening and talik formation (Panda et al. 2016). Between 2014 and 2019, both DENA and GAAR experienced a nearly 2-degree increase in mean annual temperature relative to the preceding 30 years (Swanson et al. 2021).Here we describe mass movements in DENA and GAAR looking for differences that might indicate distinct responses related to differences in the nature of the underlying permafrost. We suspect that as continued warming brings DENA permafrost above freezing, larger and deeper mass

movements will occur in DENA, while mass movements in GAAR will continue to be shallower and of smaller size.

We use Sentinel-1 interferograms collected between 2017 and 2023 to create continuous time series measurements of hillslope deformation in DENA and GAAR. Using these deformation measurements together with inspection of optical imagery, we create a inventories of actively creeping hillslope features in both parks, including rock glaciers, landslides, and frozen debris lobes. The resolution of the InSAR data is such that the active features we can identify are relatively large (>10,000 m^2) and tend to be persistently unstable over the study period. In addition to classifying active features, the inventory contains topographic and geologic attributes for each features.

Through preliminary work in the northern half of DENA (Figure 1), we have identified 109 creeping hillslope features, while analysis of GAAR is in progress. Between 2017 and 2023, these mass movements had average annual velocities up to 2.8 cm/year. While underlying geology plays a significant role in the character and distribution of mass movements, (e.g., Patton et al. 2020), we suspect that this assessment of slope instability, in areas of permafrost, during a period of warming will provide some insight into the specific landscape changes in a warming climate.

REFERENCES

Huggel, C., Clague, J.J., and Korup, O. 2012. Is climate change responsible for changing landslide activity in high mountains? Earth Surf. Process. Landforms 37, 77–91. https://doi.org/10.1002/esp.2223

Jorgenson, T., Yoshikawa, K., Kanevskiy, M., Shur, Y., Romanovsky, V., Marchenko, S., Grosse, G., Brown, J., and Jones, B. 2008. Permafrost Characteristics of Alaska.

Panda, S., Romanovsky, V., and Marchenko, S. 2016. High-Resolution Permafrost Modeling in the Arctic Network National Parks, Preserves and Monuments (Natural Resource Report). https://doi.org/10.13140/RG.2.2.18127.89767

Panda, S.K., Marchenko, S.S., and Romanovsky, V.E. 2014. High-Resolution Permafrost Modeling in Denali National Park and Preserve (Natural Resource Technical Report). Geophysical Institute University of Alaska Fairbanks.

Patton, A.I., Rathburn, S.L., and Capps, D.M. 2019. Landslide response to climate change in permafrost regions. Geomorphology 340, 116–128. https://doi.org/10.1016/j.geomorph.2019.04.029

Patton, A.I., Rathburn, S.R., Capps, D., Brown, R.A., and Singleton, J.S. 2020. Lithologic, geomorphic, and permafrost controls on recent landsliding in the Alaska Range. Geosphere 16, 1479–1494. https://doi.org/10.1130/GES02256.1

Stoffel, M., and Huggel, C. 2012. Effects of climate change on mass movements in mountain environments. Progress in Physical Geography: Earth and Environment 36, 421–439. https://doi.org/10.1177/0309133312441010

Swanson, D.K., Sousanes, P.J., and Hill, K. 2021. Increased mean annual temperatures in 2014–2019 indicate permafrost thaw in Alaskan national parks. Arctic, Antarctic, and Alpine Research 53, 1–19. https://doi.org/10.1080/15230430.2020.1859435

Permafrost terrain disturbance mapping and susceptibility modeling in the Nacho Nyäk Tagé (Stewart River) watershed, Yukon

Frederic Brieger[1], Murray Richardson[1] & Shawn Kenny[2]

[1]*Department of Geography and Environmental Studies, Carleton University, Ottawa, Ontario, Canada*

[2]*Department of Civil and Environmental Engineering, Carleton University, Ottawa, Ontario, Canada*

The Nacho Nyäk Tagé (Stewart River) watershed is located in the traditional territory of the First Nation of Na-Cho Nyäk Dun within central Yukon. The region is characterized by variable topography, land cover, permafrost conditions, surficial geology, climatic history, and land use patterns. Consequently, the impact of wildfires, increasing air temperature, and changing precipitation patterns on the discontinuous permafrost landscape is spatially and temporally heterogenous.

Permafrost terrain disturbances (PTDs) including retrogressive thaw slumps (RTSs), thermoerosional gullies, and active layer detachments are common in the study area, but their spatial distribution, controlling factors, and temporal trends are poorly understood.

PTDs can impact terrestrial and aquatic habitats (Jin et al. 2021; Vonk et al. 2015), the ground thermal regime (Burn 2000), surface and sub-surface hydrology (Streletskiy et al. 2015), and lead to increased sediment and solute flux into rivers and lakes (Kokelj et al. 2013).

This study aims to map the current extent of regional permafrost landscape change and model terrain susceptibility to improve our understanding of predisposing factors using predictive modelling. The identification of areas that are particularly susceptible or resilient to climate change induced permafrost thaw can support evidence-based and community-driven regional land use planning that benefits traditional land use and the environment, while minimizing the impact on sensitive permafrost terrain from potential future development (e.g., public, mining, or energy infrastructure).

PTDs were manually identified in PlanetScope monthly cloud-free basemap satellite imagery (3 m resolution) from the summer of 2022 (76 RTSs and 262 other thermoerosion features). Shallow mass movements including active layer detachments and surficial debris flows (433 features) are abundant in recent wildfire scars but were excluded from the study because they cannot confidently be linked to permafrost disturbance and often revegetate within a few years without triggering further thermoerosion.

RTSs are indicators of ice-rich permafrost and have increased in frequency and activity across the watershed.

Random forest (RF) models were trained using the randomForest R-package (Liaw and Wiener 2002) to estimate PTD susceptibility towards thaw slumping and other mapped thermoerosion features.

Two presence data sampling strategies were compared. Area-based sampling considers all pixels in the digitized RTS scar zone for model training, therefore capturing all variability of known disturbed terrain. A second, point-based, method sampled 3 points per RTS-feature, giving RTSs of all sizes the same training weight. For each presence training point, one random disturbance-free point was generated within the study area.

Predictor variables were selected based on their potential to influence terrain response towards permafrost thermoerosion. The basis for all terrain variables is the FABDEM V1.2 (Neal et al. 2023) with a spatial resolution of ~22 m, which also dictated the resolution of the resulting susceptibility maps. From the DTM, slope angle, slope aspect, Topographic Wetness Index (TWI) (Sørensen et al. 2006), plan- and profile curvature, and Topographic Position Indices (TPI) at three scales (Weiss 2001) were extracted. Additionally, distance to water features (Geomatics Yukon 2019), Late Quaternary glacial limits (Duk-Rodkin 1999), and modelled permafrost probability (Bonnaventure et al. 2012) were used. Surficial geology is another important factor for the initiation of thaw slumps but not available for the entire study area.

The resulting susceptibility predictions were grouped into zones of very low (0-0.5), low (0.5-0.7), moderate (0.7-0.8), high (0.8-0.9), and very high (0.9-1) PTD susceptibility (Figure 1).

Model classification performance was assessed with 10-fold cross-validation (CV). For the area-based RF model, training observations belonging to the same RTS were kept together during data splitting to avoid bias stemming from large RTSs present in all CV splits. High average area under the receiver operating curve (AUROC) values (0.92 and 0.94 for area- and point-based models, respectively) indicate accurate classification of the validation data.

Predictor variable importance was assessed based on mean decrease in accuracy when permuting variables during bootstrapping. The most important predictors for both models are elevation, permafrost probability, glaciation history, distance to water, TPI (neighborhood radius = 3 km), and slope angle.

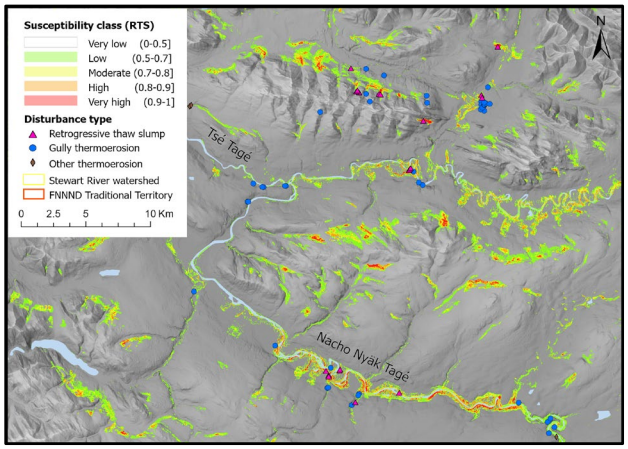

Figure 1. Permafrost terrain disturbances and RTS terrain susceptibility in the upper Nacho Nyäk Tagé (Stewart River) watershed.

Evaluating the results of both models revealed distinct spatial susceptibility patterns. RTSs are found almost exclusively within the limits of the McConnell glaciation (maximum extent ca. 18 ka), predominantly on gentle to moderate north-facing slopes and riverbanks in east-west oriented U-shaped valleys, as well as shaded, narrow, fluvially incised tributary valleys (Figure 1). Field visits along Nacho Nyak Tagé have confirmed that RTSs here are typically formed in glaciolacustrine sediments, glaciofluvial sediments, and sometimes till. This highlights the importance of closing gaps in regional surficial geology map coverage to further increase model accuracy.

Low susceptibility terrain typically encompasses wide, north-south oriented valleys, south-facing slopes, well-drained slopes, bedrock, and areas west of Mayo that weren't glaciated during the last regional glacial maximum.

Acknowledgement

This work would have not been possible without the support of FNNND Lands & Resources, field assistance by John Foster, and funding through the NSERC CREATE UTILI program.

References

Bonnaventure, P.P., Lewkowicz, A.G., Kremer, M., and Sawada, M.C. 2012. A Permafrost Probability Model for the Southern Yukon and Northern British Columbia, Canada. Permafrost and Periglacial Processes, 23(1), 52–68. doi:10.1002/ppp.1733

Burn, C.R. 2000. The thermal regime of a retrogressive thaw slump near Mayo, Yukon Territory. Canadian Journal of Earth Sciences, 37(7), 967–981. doi:10.1139/e00-017

Burn, C.R., and Friele, P.A. 1989. Geomorphology, Vegetation Succession, Soil Characteristics and Permafrost in Retrogressive Thaw Slumps near Mayo, Yukon Territory. Arctic, 42(1), 31–40.

Duk-Rodkin, A. 1999. Glacial Limits Map of Yukon Territory. Geological Survey of Yukon.

Geomatics Yukon. 2019. Yukon waterbody lines 250k.

Jin, X.Y., Jin, H.J., Iwahana, G., Marchenko, S.S., Luo, D.L., Li, X.Y., and Liang, S.H. 2021. Impacts of climate-induced permafrost degradation on vegetation: A review. Advances in Climate Change Research, 12(1), 29–47. doi:10.1016/j.accre.2020.07.002

Kokelj, S.V, Lacelle, D., Lantz, T.C., Tunnicliffe, J., Malone, L., Clark, I.D., and Chin, K.S. 2013. Thawing of massive ground ice in mega slumps drives increases in stream sediment and solute flux across a range of watershed scales. Journal of Geophysical Research, 118, 681–692. doi:10.1002/jgrf.20063

Liaw, A., and Wiener, M. 2002. Classification and Regression by randomForest. R News, 2(3), 18–22. cran.r-project.org/doc/Rnews/

Neal, J., Hawker, L., Uhe, P., Paulo, L., Sosa, J., Savage, J., and Sampson, C. 2023. FABDEM V1-2. University of Bristol. doi:10.5523/bris.s5hqmjcdj8yo2ibzi9b4ew3sn

Sørensen, R., Zinko, U., and Seibert, J. 2006. On the calculation of the topographic wetness index: Evaluation of different methods based on field observations. Hydrology and Earth System Sciences, 10(1), 101–112. doi:10.5194/hess-10-101-2006

Streletskiy, D.A., Tananaev, N.I., Opel, T., Shiklomanov, N.I., Nyland, K.E., Streletskaya, I.D., Tokarev, I., and Shiklomanov, A.I. 2015. Permafrost hydrology in changing climatic conditions: Seasonal variability of stable isotope composition in rivers in discontinuous permafrost. Environmental Research Letters, 10(9). doi:10.1088/1748-9326/10/9/095003

Vonk, J.E., Tank, S.E., Bowden, W.B., Laurion, I., Vincent, W.F., Alekseychik, P., Amyot, M., Billet, M.F., Canário, J., Cory, R.M., Deshpande, B.N., Helbig, M., Jammet, M., Karlsson, J., Larouche, J., Macmillan, G., Rautio, M., Walter Anthony, K.M., and Wickland, K.P. 2015. Reviews and syntheses: Effects of permafrost thaw on Arctic aquatic ecosystems. Biogeosciences, 12(23), 7129–7167. doi:10.5194/bg-12-7129-2015

Weiss, A. 2001. Topographic position and landforms analysis. Poster Presentation, ESRI User Conference, San Diego, CA, 64, 227–2.

Debris flows in permafrost areas of the Italian Alps in a context of climate change

Marta Chiarle[1], Marco Giardino[2], Laura Turconi[1] & Guido Nigrelli[1]

[1]*Research Institute for Geo-hydrological Protection, National Research Council of Italy, Torino, Italy*

[2]*Department of Earth Sciences, University of Torino, Italy*

Debris and mud flows (henceforth "debris flows") are extremely dangerous processes in Alpine valleys, where many settlements are located on the alluvial fans of small lateral catchments, also crossed by the main valley roads (Turconi et al. 2022). Furthermore, debris flow events occur especially in summer, when the tourist influx is maximum. Some major debris flows occurred in permafrost areas in the Italian Alps during summer 2023, threatening people and damaging buildings and infrastructure: for example, the 14 August debris flows in Bardonecchia (Susa Valley, Western Alps) and Valpelline (Aosta Valley, Western Alps), and on 27 August in Macugnaga (Valle Anzasca, Western Alps). This work aims to analyse, starting from case studies documented at high elevation in the Italian Alps, the current trends and possible impacts of ongoing permafrost degradation on debris flow occurrence.

Debris flow events in the Italian Alps

An inventory of mass movements that occurred at high altitudes (>1500 m a.s.l.) in the Italian Alps between 2000 and 2023 highlights how debris flows represent approximately 25% of the 826 documented events (Nigrelli et al. 2024). Debris flows occur primarily in July (39%), August (31%), and June (14%). The number of annual events is between 1 and 38 (2022), while the percentage of debris flows compared to other types of processes varies between 5% (2020) and 54% (2006 and 2022).

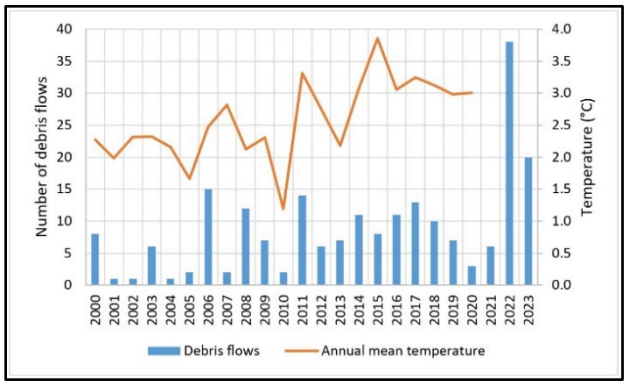

Figure 1. Number of debris flow events per year (blu bars) and annual mean temperature (orange line).

Both the number of events and the percentage of debris flows compared to other types of mass movements are highly variable from year to year. However, starting from 2011 there has been a change of pace, especially regarding the number of events per year which varies from an average of 5 in the period 2000-2010, to an average of 12 in the period 2011-2023 (Figure 1). This dichotomy is less evident when analyzing the percentage of debris flows compared to the totality of mass movements (Figure 2), which indicates that this increase applies to all types of mass movements at high elevation in the Italian Alps. However, the percentage of debris flows compared to the total events grows from 19% in the period 2000-2010 to 27% in the period 2011-2023. Finally, it is interesting to note that the percentage of events that occurred in August tripled in the period 2011-2023 (44%) compared to that in the period 2000-2010 (14%).

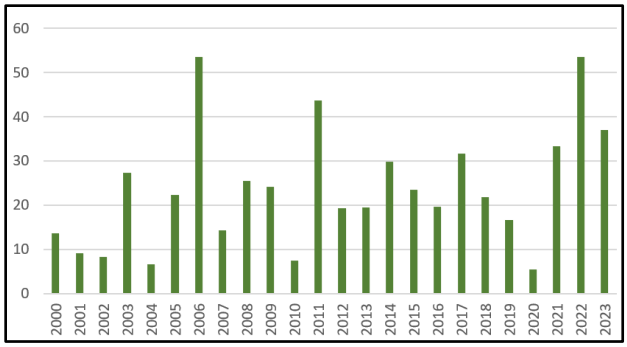

Figure 2. Percentage of debris flows compared to the totality of mass movements.

Discussion

The documentation of debris flow events is subject to a number of biases (e.g., debris flows are often reported only if they have caused some damage; if only the impact area was known, and it was below 1500 m a.s.l., the event was discarded), so the above-mentioned results must be considered with caution. However, the significant increase since 2011, compared to the previous decade, in the number of events, in the percentage of debris flows compared to the other types of mass movements, and the increasing number of cases occurred in August, are

all potential indicators of the impact of climate change on the frequency and timing of debris flows in high-elevation catchments, where permafrost degradation could play a key role. In fact, for the 2000-2020 time period, the annual mean temperature in the Italian Alps was 2.6 °C, with a warming trend of 0.6 °C/10 years (Nigrelli et al. 2023). However, for this time series, a detection test revealed a significant change point occurred in 2011 (Figure 1), also observed by the national and regional meteorological services and in many historical temperature time series. For supply-unlimited catchments, where debris flow triggering is controlled by rainfalls, the impact of climate change could be related primarily to the increase in frequency and intensity of extreme meteorological events; however, melt water resulting from permafrost degradation, and from cryosphere degradation in general, can increase the saturation degree of debris accumulations ready to be mobilized, thus reducing the amount of rain necessary to trigger debris flows. As regards supply-limited catchments, permafrost degradation may lead to an increase in the amount of debris available for transport. In fact, permafrost thawing, but also early thawing and late refreezing of permafrost active layer and its deepening can cause: 1) enhanced exposure of rock slopes to chemical/physical degradation processes linked to atmospheric agents and gravity (Viani et al. 2020; Hirschberg et al. 2021); 2) in debris accumulations, an increase in the volumes of debris that can be readily mobilized by precipitation.

Concluding remarks

Data collected in the Italian Alps show an increase in frequency and a change in seasonality of debris flows in high altitude catchments, which may partly depend on permafrost degradation due to climate change. However, compared to other mass movements, debris flow documentation, with the exception of some experimental basins that have been thoroughly studied and monitored, mainly focuses on flow characteristics and impacts, while source areas are often little investigated. This causes an information gap that needs to be filled to implement adequate management and mitigation measures for this type of risk in the context of ongoing and expected climate changes.

References

Hirschberg, J., Fatichi, S., Bennett, G.L., McArdell, B.W., Peleg, N., Lane, S.N., Schlunegger F., and Molnar, P. 2021. Climate change impacts on sediment yield and debris-flow activity in an alpine catchment, Journal of Geophysical Research: Earth Surface, 126(1): e2020JF005739. doi:10.1029/2020JF005739

Nigrelli, G., Luino, F., Turconi, L., Guerini, M., Paranunzio, R., Giardino, M., Mortara, G., and Chiarle, M. 2024. Catasto delle frane di alta quota nelle Alpi italiane. https://geoclimalp.irpi.cnr.it/catasto-frane-alpi/

Nigrelli, G., and Chiarle, M. 2023. 1991–2020 climate normal in the European Alps: focus on high-elevation environments, Journal of Mountain Science, 20(8): 2149–2163. doi:10.1007/s11629-023-7951-7

Turconi, L., Tropeano, D., Savio, G., Bono, B., De, S.K., Frasca, M., and Luino, F. 2022. Torrential hazard prevention in Alpine small basin through historical, empirical and geomorphological cross analysis in NW Italy, Land, 11(5): 699. doi:10.3390/land11050699

Viani, C., Chiarle, M., Paranunzio, R., Merlone, A., Musacchio, C., Coppa, G., and Nigrelli, G. 2020. An integrated approach to investigate climate-driven rockfall occurrence in high alpine slopes: the Bessanese glacial basin, Western Italian Alps, Journal of Mountain Science, 17: 2591–2610. doi:10.1007/s11629-020-6216-y

Properties of Tyrrell Sea glaciomarine silts and clays: State of knowledge and data gaps

Hemma Crisias[1,2] & Pascale Roy-Léveillée[1,2]

[1]*CRYO-UL: Permafrost Research Laboratory, Department of Geography, Université Laval, Québec City, Québec, Canada*

[2]*Centre d'études nordiques, Québec City, Québec, Canada*

In the last few years, flowslides and smaller mass movements have been observed in permafrost and non-permafrost areas of northern Quebec, Ontario, and Manitoba. As a result, the stability of glaciomarine deposits has become a concern for communities around the Hudson Bay. While the distribution and properties of fine glaciomarine deposits, in particular sensitive clays, have been extensively documented in temperate zones, glaciomarine silts and clays remain poorly studied in permafrost zones of central and eastern Canada. This research provides a regional overview and an analysis of the state of knowledge on Tyrrell Sea glaciomarine silts and clays to assess whether this region has the potential to develop sensitive clay behaviour and related slope instability hazards as permafrost warms and thaws.

Specifically, this project will: 1) critically review existing data on the marine transgression limit and the distribution of deep water deposits; 2) compare characteristics of fine glaciomarine Tyrrell Sea deposits with those of sensitive clays; 3) discuss frozen ground sustainability under current climatic conditions in fine grained Tyrrell Sea deposits.

Methods

This project involves a synthesis of existing data on the glaciomarine deposits of the area once submerged by the Tyrrell Sea, i.e., the coasts of Hudson Bay within the marine limits. This vast territory, covering several hundred thousand square kilometers, extends along the west coast of Québec, northern Ontario and Manitoba, and the southeastern coast of Nunavut (Figure 1). A map of the Tyrrell Sea marine limits was updated, incorporating data from recent geomorphological research concerned with west and east coasts of Hudson Bay (e.g., McMartin et al. 2022). Recent flowslides and flow-like mass-wasting events within the marine limits were inventoried. The region's major geomorphological zones are being identified and analyzed, with a more detailed investigation of the eastern coast. Boreholes from published reports and scientific papers that are within the marine limits were compiled in a database to facilitate the description and comparison of Tyrrell Sea fine grained deposit properties to known properties of sensitive clay deposits. Samples containing at least 20% clay (particles with a diameter of less than 2 µm) or presenting data on Atterberg limits were selected for further analysis on properties such as salinity, total fines and clay contents, as well as plastic and liquid limits. The database will be completed with data from recently acquired samples via on-going projects in Manitoba and Nunavik. Finally, existing data on temperature profiles, published in reports (e.g., Obu et al. 2019) and obtained directly from partners, will be compiled and compared to the expected distribution of sustainable permafrost in the region according to Ttop.

Preliminary results and conclusions

The database contains a synthesis of information for Kuujjuarapik (QC) and Moosonee (ON) sites, in addition to 274 samples, including 75 samples collected in 25 boreholes from 7 Nunavik communities, and 201 samples from 70 boreholes of the Polar Gas Pipeline project between Baker Lake (NU) and Fox Lake (MB) (Figure 1).

Of the 274 samples selected, 64 of the 95 with Atterberg limits data contain a liquidity index of at least 1.5, the minimum index that characterizes flowslides in eastern Canada (Demers 2014). 42 of the 44 PolarGas samples with grain size data contained at least 13% clay, the minimum amount of clay in flowslides surveyed in eastern Canada (Demers 2014). Clay contents up to 62% were reported. A majority of those are characterized as clay of low plasticity/lean clay (143), clayey silt (43) or silt (40), and some of them are also clayey or silty sands and contain between 23% and 57% sand.

Preliminary results suggest that recent flowslides and smaller mass-wasting events with flow components are concentrated near the southern limit of permafrost and in areas of continuous permafrost where conditions are expected to support only a sporadic distribution of permafrost. Isothermal temperature profiles are common in fine-grained sediment on the Nunavik and Ontario sides, indicating on-going thaw as heat exchanges at the surface are dominated by latent heat of fusion linked to increasing unfrozen water content in the sediment.

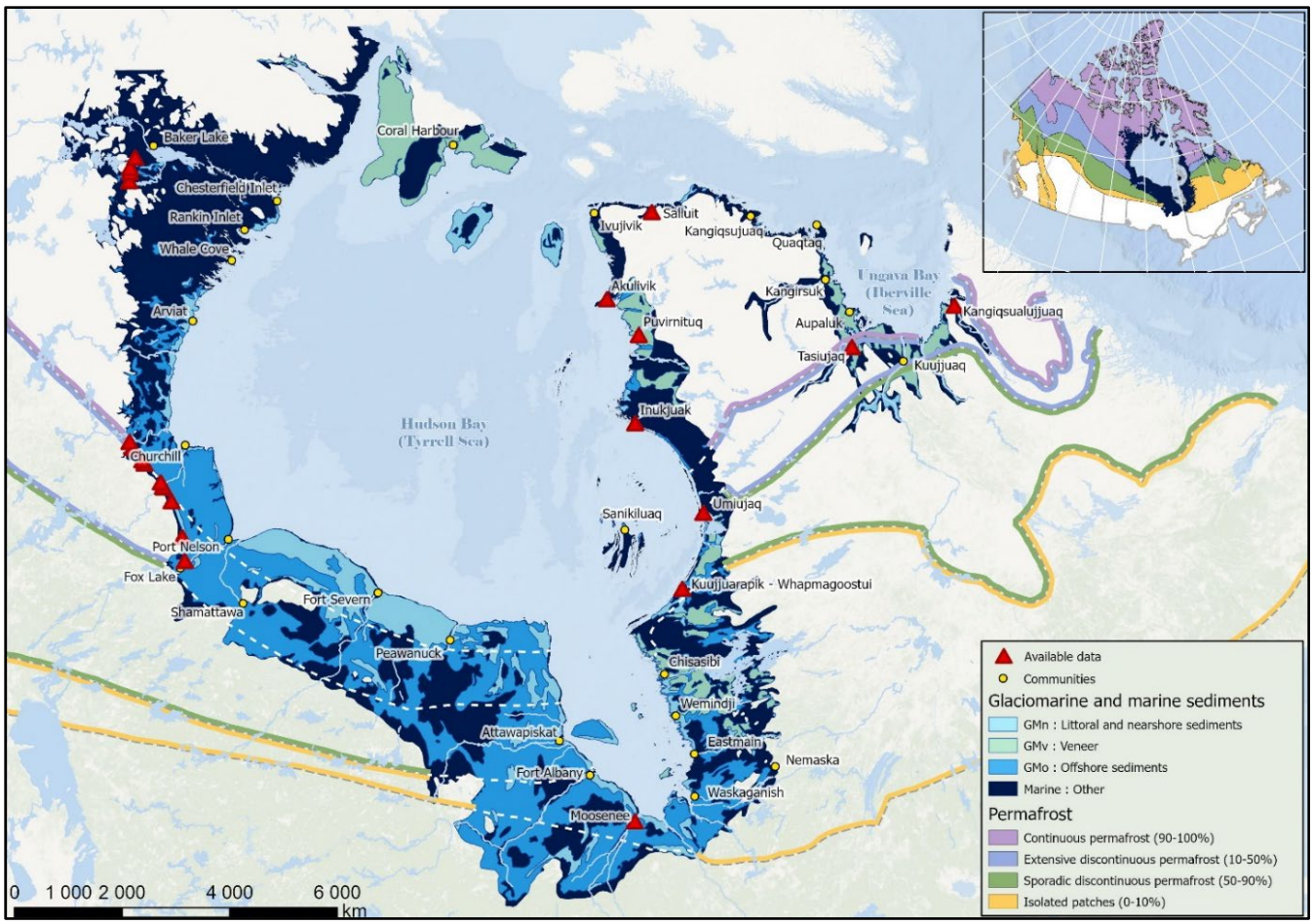

Figure 1. Glaciomarine and marine sediments of the Tyrrell Sea, modified from (Dredge and Cowan 1989; McMartin et al. 2022; Vincent 1989).

Preliminary results also highlight the need for inter-province collaboration in the mapping of surficial deposits to ensure compatibility of the data produced and to facilitate knowledge exchange. In the context of known imbalances in climate change preparedness between urban centres and remote areas, this work aims to facilitate remediation to the lack of geomorphological and geotechnical knowledge on fine grained glaciomarine deposits in permafrost regions by discussing whether some of these deposits could develop sensitive clay behaviour once thawed.

REFERENCES

Demers, D., Robitaille, D., Locat, P., and Potvin, J. 2014. Landslides in Sensitive Clays, in L'Heureux, J.-S., Locat, A., Leroueil, S., Demers, D. and Locat, J. (eds) Geosciences to Risk Management. Dordrecht: Springer Netherlands, 77–89.

Dredge, L.A., and Cowan, W.R. 1989. Le Quaternaire du sud-ouest du Bouclier canadien, in Fulton, R.J., Commission géologique du Canada and Geological Society of America (eds) Le Quaternaire du Canada et du Groenland. Ottawa: Commission géologique du Canada, 229–266.

McMartin, I., Gauthier, M., and Page, A. 2022. Updated postglacial marine limits along western Hudson Bay, central mainland Nunavut and northern Manitoba; GSC OF 8921: Natural Resources Canada.

Obu, J., Westermann, S., Bartsch, A., Berdnikov, N., Christiansen, H.H., Dashtseren, A., Delaloye, R., Elberling, B., Etzelmüller, B., Kholodov, A., Khomutov, A., Kääb, A., Leibman, M.O., Lewkowicz, A.G., Panda, S.K., Romanovsky, V., Way, R.G., Westergaard-Nielsen, A., Wu, T., Yamkhin, J., and Zou, D. 2019. Northern Hemisphere permafrost map based on TTOP modelling for 2000–2016 at 1 km^2 scale; Earth-Science Reviews, 193; 299–316.

Vincent, J.-S. 1989. Le Quaternaire du sud-est du Bouclier canadien, in Fulton, R.J., Commission géologique du Canada and Geological Society of America (eds) Le Quaternaire du Canada et du Groenland. Ottawa: Commission géologique du Canada, 266–295.

Widespread permafrost landslides caused by intense late-season rainfall in the Klondike, Yukon, a region at a climogeomorphic tipping point

Derek Cronmiller[1], Ghislain DeLaplante[2] & Peter Nagano[3]

[1]*Yukon Geological Survey, Whitehorse, Yukon, Canada*

[2]*Water Resources Branch, Department of Environment, Whitehorse, Yukon, Canada*

[3]*Transportation Maintenance Branch, Department of Highways and Public Works, Dawson City, Yukon, Canada*

The Klondike Valley, in west central Yukon, lies within the extensive discontinuous permafrost zone (Heginbottom et al. 1995; Figure 1). Deep, steep-sided valleys and strong surface-based inversions in this region cause permafrost distribution to be strongly controlled by slope aspect and topographic position, with north slopes and valley bottoms containing nearly continuous permafrost. Mean annual air temperature in Dawson City, the main population centre within the Klondike, has increased by approximately 3 °C since the 1970s. At the same time precipitation delivered as rainfall has also increased, in part due to an extended thaw season. Annual cumulative degree days of thaw, a metric thought to be correlated with active layer detachment (ALD) susceptibility (L'Hérault 2009), has exceeded the 75th-percentile every year since 2015, with 2017 being the warmest thaw season on record (Figure 2). Consistently higher than average snowfall over the last decade has compounded the effect on ground temperature increase.

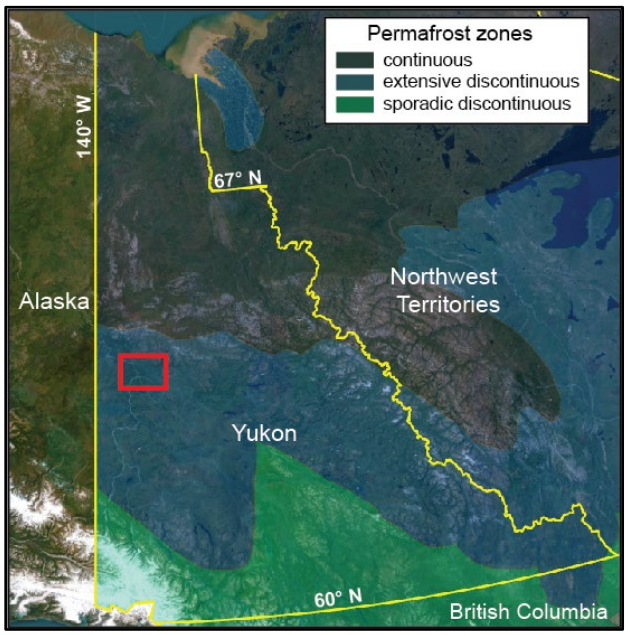

Figure 1. Location of Klondike Valley study area, permafrost zones by Higenbottom et al. (1995).

Regional destabilization

The rapid temperature increase in the region has likely raised temperatures beyond the previous Holocene Climate Optimum (Porter et al. 2019) and is causing correspondingly rapid warming and thawing of permafrost as observed in local ground temperature records (Figure 2) and in geomorphic manifestations including widespread thermal erosion and mass movements. At least nine prehistoric, relict, or very slow-moving landslides in permafrost terrain with volumes 10^5 – 10^7 m^3 show evidence of reactivation or acceleration in the last several decades (Figure 3), likely due to rapid warming and thawing of permafrost (cf. Hilger et al. 2021) caused by anthropogenic climate change.

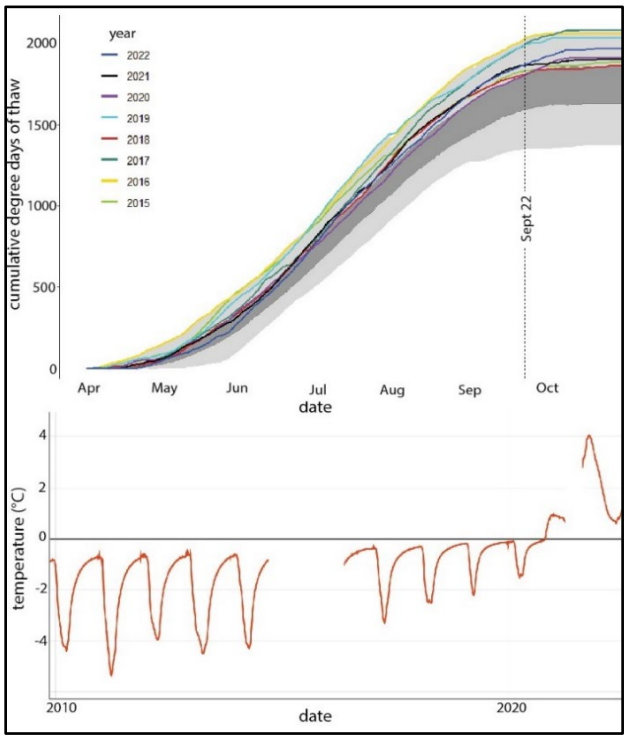

Figure 2. Upper – Cumulative degree days of thaw recorded near Dawson City, Yukon. Upper and lower quartiles are shown by light grey. Lower – Ground temperatures at 2 m recorded near Dawson City, indicating warming and thaw of permafrost.

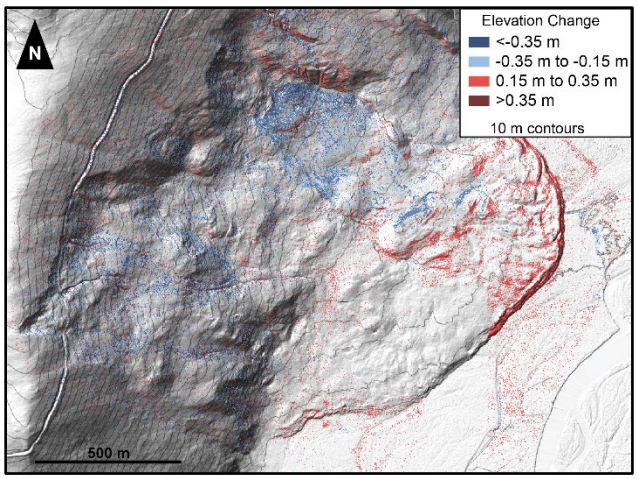

Figure 3. Partial reactivation of a large relict rockslide on NW slope of the Klondike River near Rock Creek shown through lidar change detection between 2014 and 2019.

EXTREME RAINFALL

On September 22nd, 2022, remnants of typhoon Merbok passed over central Yukon and produced extreme rainfall (over 35 mm in a 24/hr period) late in the thaw season in the Klondike Valley. This rainfall event has an ~15-year return interval when considering all rainfall events, but ranks as a 100-year return event if considering only the last two months of the thaw season. More than 260 ALD slides and flows occurred in the Klondike region during this rainfall with more than 60 occurring on the steep north-facing slopes immediately above the North Klondike Highway (Figure 4). Fourteen landslides impacted the road stranding 45 people between slide areas and requiring helicopter extraction. The North Klondike Highway was closed to the public for over 48 hours preventing the movement of people, fuel, and goods into the community.


Figure 4. Photograph of September 22, 2022 active layer detachment slides impacting km 694 of the North Klondike Highway.

POST-RAINFALL DECLINE IN ALD ACTIVITY

A novel dataset collected during repeat surveys of slide activity along the highway records a rapid decrease in ALD occurrence from approximately two ALDs per hour to zero by 48 hours after peak rainfall (Figure 5). This relationship between precipitation and frequency of landslide occurrence can inform highway operations emergency response efforts.

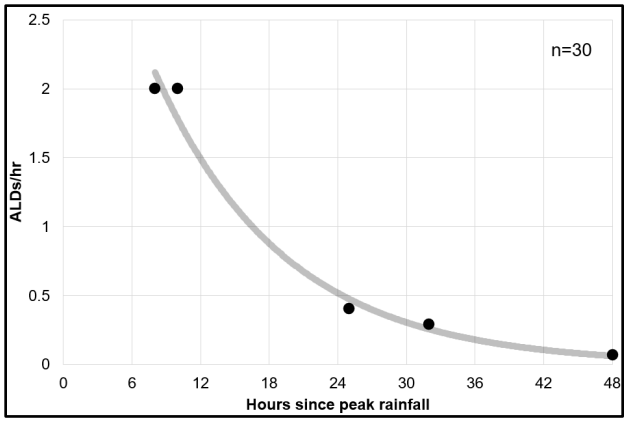

Figure 5. Decline in ALD occurrence after peak rainfall.

ONGOING RESEARCH

Efforts are underway to clarify the drivers of and acceleration trends in large landslides throughout the region. Several near real-time landslide monitoring networks have been established for both ALD-prone slopes and large slow-moving rockslides, with the intention of providing early-warning of landslides to decision-makers in the region once sufficient baseline data has been collected.

REFERENCES

Heginbottom, J.A., Dubreuil, M.A., and Harker, P.T. 1995. Canada, permafrost. The National Atlas of Canada, MCR Series no. 4177, 1 sheet. https://doi.org/10.4095/294672

Hilger, P., Hermann, R., Czekirda, J., Myhra, K., Gosse, J., and Etzelmüller, B. 2021. Permafrost as a first order control on long-term rock-slope deformation in (Sub-) Arctic Norway, Quaternary Sci. Rev., 251. https://doi.org/10.1016/j.quascirev.2020.106718

L'Hérault, E. 2009. Contexte climatique critique favorable au déclenchement de ruptures de mollisol dans la vallée de Salluit, Nunavik. MSc Thesis, Université Laval.

Porter, T.J., Schoenemann, S.W., Davies, L.J., et al. 2019. Recent summer warming in northwestern Canada exceeds the Holocene thermal maximum. Nat Commun 10, 1631. https://doi.org/10.1038/s41467-019-09622-y

Granular mechanics model of retrogressive thaw slumps

Cansu Culha[1], Alex Leonelli[2], Kathrin Maier[3], Philipp Bernhard[3], Mark Jellinek[1] & Eckart Meiburg[2]

[1]*Department of Earth, Ocean, Atmospheric Science, University of British Columbia, Vancouver, British Columbia, Canada*

[2]*Mechanical Engineering, University of California, Santa Barbara, Goleta, California, United States*

[3]*ETH Zürich, Zürich, Switzerland*

Retrogressive Thaw Slumps (RTSs) are an intermittent mass wasting process in permafrost environments that present acute risks to infrastructure and watersheds. They become active in the summer months when solar radiation can thaw the subsurface and they progressively expand both up and across topographic gradients. As climate change increases the intensity and longevity of high temperatures in the summer months, we beg the question: how will RTSs respond to these changes?

The extensive mapping efforts in Canada, Alaska, Siberia, and Tibetan Plateau reveal that the number of active RTSs is rising and their collective growth rates take on a bell curve distribution that can range from no growth to 10000 m^2/yr (Bernhard et al. 2022). However, the mechanical processes that set their growth rate and when they get activated is unclear. For example, large RTS-related scars, which have large surface area to erode, have yet to be shown to correlate with large growth rates, as some RTS initially grow fast then stabilize (Ward Jones et al. 2019). Furthermore, some permafrost landscapes like Axel Heiberg Island have a high density of RTS activity, whereas others like Devon Island do not, regardless of the fact that they are neighboring High Arctic Islands and subject to similar climate forcing.

These results suggest that the RTS failure characteristics hinge on a granular-scale comprehension of ice thawing, water drainage, and soil collapse processes along the headwalls. To this end, we employ the granular mechanics computational model, LIGGGHTS, to investigate ice thawing and soil collapse processes. We test the role of cohesion, segregated ice, headwall height, grain size, and water content on RTS erosion and growth rate. Our results show that while cohesion, heavily influenced by ice content and its phase state, can impede erosion, the increased potential energy due to headwall height can counteract the mitigating efforts by cohesion once triggered. A comparison of our computation results to the extensive site-specific observational data would suggest that cohesion could explain why there are fewer RTS features with slow growth rates; and limits around thaw depth, and thus headwall height, could explain why there are fewer RTS features with high growth rates (Bernhard et al. 2022). This introduces a sweet spot in RTS growth rates. We propose that the introduction of layers within the permafrost, be it through segregated ice, grain distribution, or water content variations, could amplify erosion and determine whether RTS accelerate or stabilize with thawing. This granular-scale modeling, exploring the mechanics behind RTS growth rates, enables us to better understand the mapping results put forth by the Permafrost Community.

REFERENCES

Bernhard, P., Zwieback, S., Bergner, N., and Hajnsek, I. 2022. Assessing volumetric change distributions and scaling relations of retrogressive thaw slumps across the Arctic. Cryosphere 16, 1–15.

Ward Jones, M.K., Pollard, W.H., and Jones, B.M. 2019. Rapid initialization of retrogressive thaw slumps in the Canadian high Arctic and their response to climate and terrain factors. Environ. Res. Lett. 14, 055006.

Solifluction processes in a warm permafrost Arctic landscape: Insights from a two-year monitoring period using a dense monitoring network

Sylvain Fiolleau, Sebastian Uhlemann, Ian Shirley, Chen Wang, Stijn Wielandt & Baptiste Dafflon
Lawrence Berkeley National Laboratory, Berkeley, California, United States

Solifluction processes inherent in Arctic environments introduce a layer of complexity when estimating both current and future soil carbon dynamics and fluxes. This intricacy extends to the assessment of hillslope stability and infrastructure resilience. Understanding the dynamic interplay of factors in the Arctic landscape requires a meticulous examination of triggers and drivers behind soil movement in hillslopes with discontinuous permafrost. In this study, we made use of a novel dense monitoring approach to obtain vertically resolved, continuous observations of soil movement and temperature at tens of locations across multiple adjacent hillslopes throughout two successive thawing seasons to better understand the mechanisms at play.

Study site

The study site is situated along the Nome-Teller highway, approximately 65 km northwest of Nome (Mile marker 47), on the western Seward Peninsula in Alaska (Figure 1). The study area includes south, south-east and east facing slopes over 1 km^2, separated by two main streams merging towards the bottom of the watershed (Fiolleau et al., submitted). The mean slope angle is 13°, ranging from 0 to 42°. The site is located in a region characterized by discontinuous permafrost and is predominantly covered by tussock tundra, dwarf shrubs and grasses with some patches of tall shrubs, especially near the streams (Uhlemann et al. 2023).

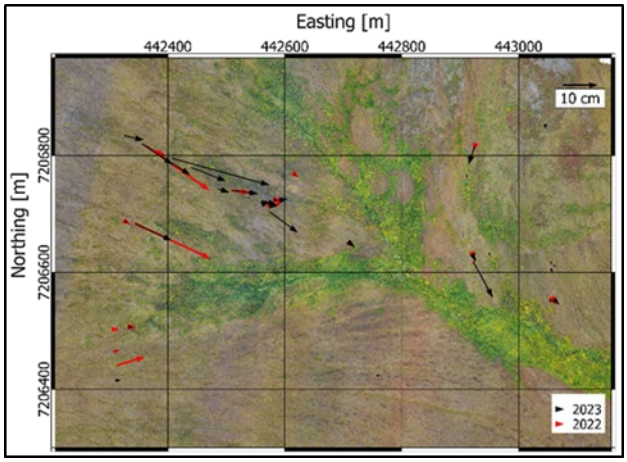

Figure 1. Study site map and fluxes for each probes location.

Methods

In this study, we conducted temperature (Dafflon et al. 2022) and movement monitoring using in-house sensor arrays and low-power consumption data loggers (Wielandt et al. 2022). 48 of these probes have been deployed across diverse hillslopes within a 1 km² watershed on the Seward Peninsula, AK. The data collection spanned over 2 years, from September 2021 to September 2023. The depth-resolved measurements, reaching down to 1.8 meters, provided insights into soil deformation processes during the two thawing seasons (May to September).

Results and discussion

Our monitoring strategy allowed us to quantify soil movements and understand the various factors influencing solifluction processes. The upper part of the watershed shows the largest movements (Figure 1). Over the two years of observation, we noted remarkably similar deformation patterns, with slight variations in thermal conditions, the second year being colder in winter and warmer in summer (Figure 2). We observed surface movements, reaching up to 334 mm in the first year and 344 mm in the second (Figure 1). All probes experiencing more than 10 cm of movements during a season show similar patterns, as shown by Figure 2. Deformation occurs once the thaw depth reaches around 50 cm, as indicated by the total angle gradient in Figure 2. Subsequently, the entire layer shifts cohesively along the deepening thawing front, as shown by the displacements (in green) in Figure 2.

A meticulous analysis of parameters identified three main factors guiding these soil movements: slope angle, soil thermal conditions, and thaw depth. The results highlight the central role of thaw depth, serving as both a trigger and driver of deformation by influencing the water column height and pressure at the thawing front. Soil temperature influences not only the thawing processes but also the freezing processes. It likely controls ice content, directly impacting fundamental soil properties such as cohesion and internal friction angle, which are essential for slope stability. The study also reveals the presence of a two-sided freeze process favoring plug-like flow solifluction.

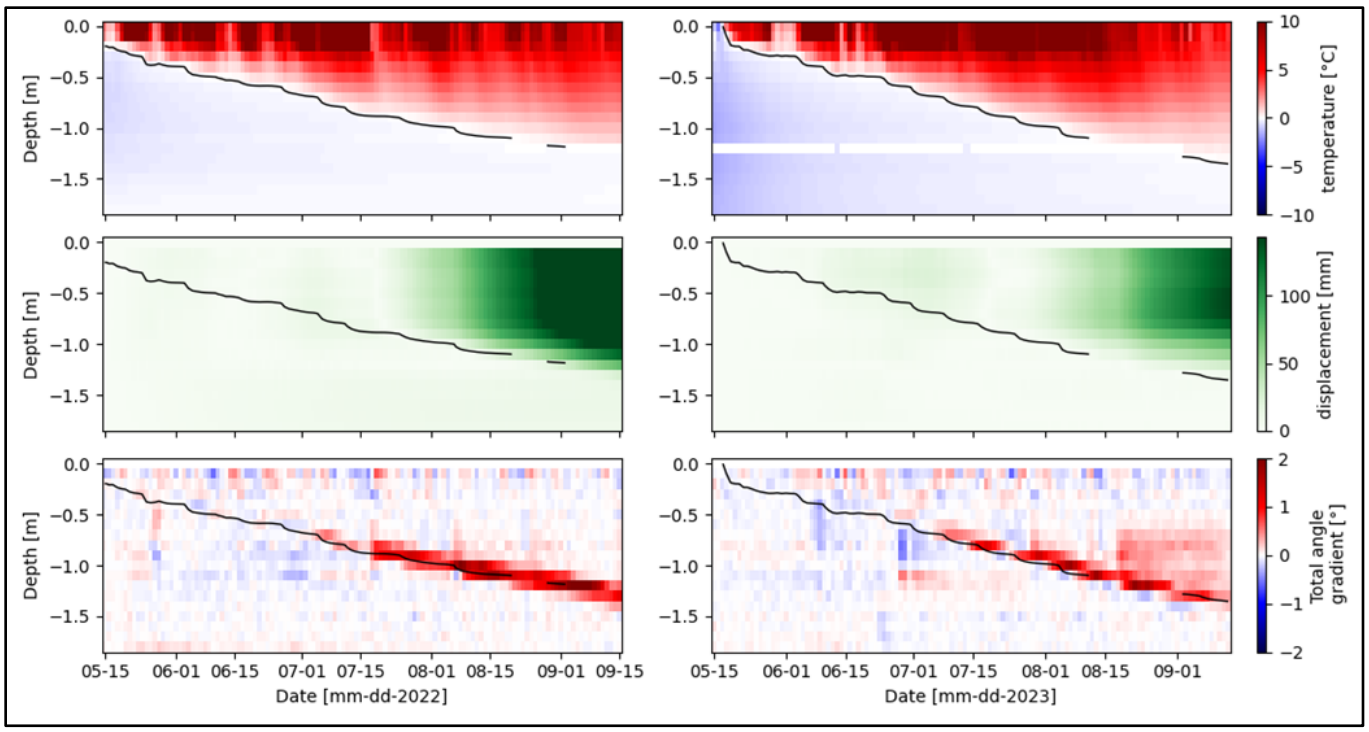

Figure 2. Monitoring data from May 15 to September 15, 2022 (left) and May 15 to September 15, 2023 at one location in East facing slope (Figure 1). From top to bottom: Temperature (°C), movement (mm), and the gradient of the total angle (°) for both period are plotted. Solid black lines show the thaw layer depth defined by the zero-degree isoline.

Building upon these insights, we developed a Factor of Safety proxy derived from our observations, consistently indicating levels below the triggering threshold for all probes experiencing displacements exceeding 50 mm. This innovative proxy serves as a practical tool for evaluating slope stability in the context of soil movements. Beyond its utility in assessing stability, this proxy allows us to improve our understanding of the impact of soil thermal conditions on slope deformation. This highlights the imperative of considering subsurface thermal states for precise assessments and predictions of slope instabilities.

By unraveling the intricate patterns and triggers of hillslope movements, our research provides a holistic perspective on the potential ramifications for soil redistribution in Arctic environments.

REFERENCES:

Fiolleau, S., Uhlemann, S., Wielandt, S., Shirley, I., Wang, C., Rowland, J., and Dafflon B. Insights on seasonal solifluction processes in warm permafrost Arctic landscape using a dense monitoring approach across adjacent hillslopes. ERL, submitted.

Dafflon, B., Wielandt, S., Lamb, J., McClure, P., Shirley, I., Uhlemann, S., Wang, C., Fiolleau, S., Brunetti, C., Akins, F.H., Fitzpatrick, J., Pullman, S., Busey, R., Ulrich, C., Peterson, J., and Hubbard, S.S. 2022. A distributed temperature profiling system for vertically and laterally dense acquisition of soil and snow temperature. The Cryosphere 16, 719–736. https://doi.org/10.5194/tc-16-719-2022

Uhlemann, S., Shirley, I., Wielandt, S., Ulrich, C., Wang, C., Fiolleau, S., Peterson, J., Lamb, J., Thaler, E., Rowland, J., Hubbard, S.S., and Dafflon, B., 2023. Estimating Permafrost Distribution Using Co-Located Temperature and Electrical Resistivity Measurements. Geophys. Res. Lett. 50. e2023GL103987. https://doi.org/10.1029/2023GL103987

Wielandt, S., Uhlemann, S., Fiolleau, S., and Dafflon, B. 2022. Low-Power, Flexible Sensor Arrays with Solderless Board-to-Board Connectors for Monitoring Soil Deformation and Temperature. Sensors 22, 2814. https://doi.org/10.3390/s22072814

Research on retrogressive thaw slumps: A synthesis of study regions and sites

Lingcao Huang[1], Nina Nesterova[2], Ilya Tarasevich[3,4,5], Brendan M. Rogers[6], Trevor C. Lantz[7], Alexander Kizyakov[3], Guido Grosse[2] & Alexandra Runge[8]

[1]*Institute of Space and Earth Information Science, The Chinese University of Hong Kong, Shatin, Hong Kong, China*

[2]*Alfred Wegener Institute, Helmholtz Centre for Polar and Marine Research, Potsdam, Germany*

[3]*Cryolithology and Glaciology Department, Faculty of Geography, Lomonosov Moscow State University, Moscow, Russia*

[4]*Earth Cryosphere Institute, Tyumen Scientific Centre Russian Academy of Sciences, Siberian Branch, Tyumen, Russia*

[5]*University of Tyumen, Laboratory of Polar and Subpolar geosystems, Tyumen, Russia*

[6]*Woodwell Climate Research Center, Falmouth, Massachusetts, United States*

[7]*School of Environmental Studies, University of Victoria, Victoria, British Columbia, Canada*

[8]*GFZ German Research Centre for Geosciences, Potsdam, Germany*

Increases in global air temperature and frequencies of extreme events have caused many changes in the Earth's system and environment, including accelerating permafrost thaw. Permafrost thaw can cause hydrologic and geomorphic changes that impact local communities and ecosystems and may release previously frozen carbon into the atmosphere, thereby further contributing to global warming. A retrogressive thaw slump (RTS) is a form of rapid mass wasting driven by permafrost thaw, that causes landscape transformation over timescales of a few days to years or decades. Intensifying RTS activities observed in local regions is concerning, but the RTS occurrences and affected areas in global permafrost regions are still poorly understood. To understand spatial gaps in monitoring RTS development and permafrost degradation, we compiled a map of study regions and research sites of all known RTS studies to date, highlighting hotspots of observations as well as data gaps.

METHODS

We exported records of publications that mentioned RTSs from the database of the Web of Science (WoS) on October 30, 2023, and manually added known reports/papers/data sets that were not in the WoS database. We used the keywords: permafrost and (thaw slump or landslide or (thermokarst & not lake & not pond)) and exported 1494 records from the WoS database. We further filtered the records by checking if “slump” or “landslide” were in their titles/keywords and manually added some. All records were uploaded to a shared spreadsheet in Google Drive, and a subset of members from the International Permafrost Association (IPA) RTSInTrain action group added latitudes and longitudes of research sites for each record. If the study area was very small (spanning a few kilometers), or the work only investigated one or a few RTSs close to each other, a point (latitude, longitude) was used to represent the research site. In the case of multiple points, we used semicolons (";") as delimiters to separate each point. If the paper showed the extent(s) of the study area, a bounding box (south to north, west to east) was used to represent the research site, and again, semicolons (";") were used to separate each extent if there were multiple. We downloaded and reviewed 153 records and used Python scripts to convert the latitudes and longitudes in the spreadsheet into either points or polygons and saved it to a vector file in the format of “ESRI Shapefile”.

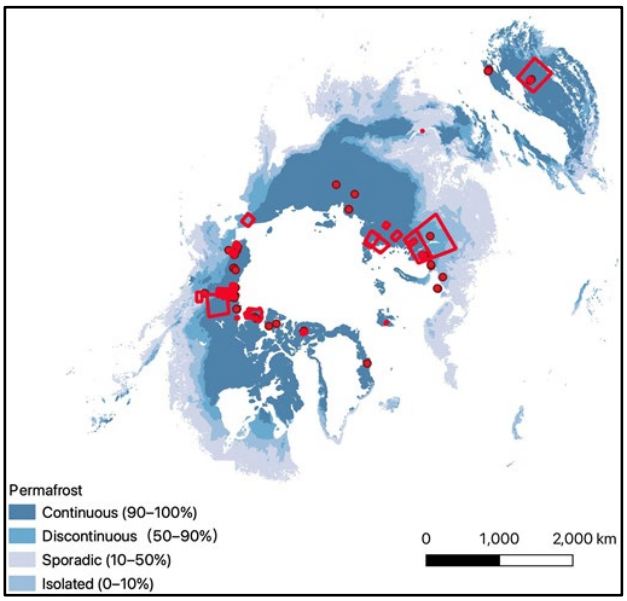

Figure 1. Research sites (points or polygons) where local studies mapped or investigated retrogressive thaw slumps in the northern hemisphere (N=218). The background is the permafrost distribution from Obu et al. (2019).

Results

Figure 1 shows a total of 168 points and 76 polygons representing research sites that have focussed on RTSs in permafrost regions. Local or regional studies only occupied a small portion of the entire permafrost region (Figure 1). A few regions including the western Canadian Arctic, West Siberia, and Beiluhe regions in Tibet contain many research sites. Studies in these regions directly mapped or investigated RTSs using remote sensing and/or fieldwork. Some of this research investigated vegetation, biochemistry, and sediment changes caused by the development of RTSs. To the best of our knowledge, we are not aware of any studies reporting RTSs in the southern hemisphere.

Recently, four continental-scale studies used very high-resolution imagery, time-series data of Landsat satellites, digital elevation models (i.e. ArcticDEM), and machine learning techniques to map RTSs (Figure 2). Luo et al. (2022) used Gaofen-1 and Gaofen-2 satellite images and manually identified 2669 RTSs in the Tibetan Plateau. Nitze et al. (2018) used time-series data of Landsat satellites and identified 465 RTSs in the four continental-scale transects. Runge et al. (2022) used time-series of Landsat images to identify 50895 RTSs and their annual thaw dynamics in North Siberia. Huang et al. (2023) used ArcticDEM to map RTSs at the pan-Arcitc scale and identified 2494 RTSs. The advance of machine learning techniques and availability of computing resources have facilitated the monitoring of RTSs at broad scales, but limitations among various steps in these methods and the dynamics and small size of RTSs have resulted in low overall mapping accuracy.

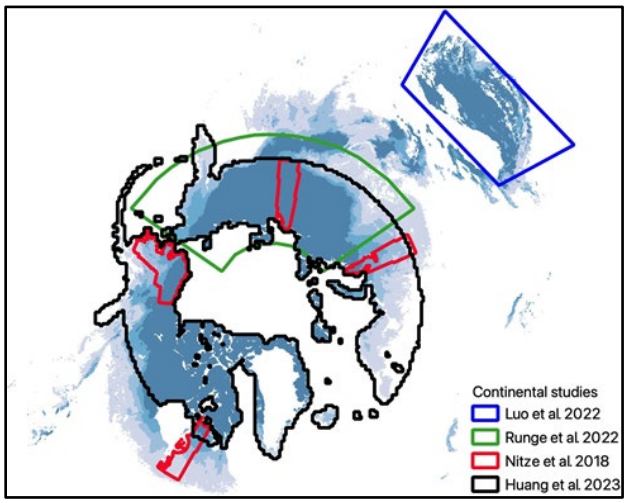

Figure 2. The extents of four studies focused on the mapping retrogressive thaw slumps at continental scales.

Discussion

As shown by our map, many unmapped regions need to be examined in more detail for RTS occurrences and development. Current local and regional studies only focused on a few regions. The four continental studies attempted to map RTSs at broad scales, but they still have not obtained a comprehensive map of RTSs. Our map serves as guidance for further research on monitoring of RTSs.

The RTS spatial occurrence is limited to permafrost areas with high-ice content and the presence of massive (tabular) ground ice or ice-wedges. This map of RTS distribution will also largely correspond to the Pleistocene permafrost history of these regions and can be used as one of the data sources for paleogeographic studies and reconstructions.

Our map only contains geographic extents or locations of research sites. More information such as the retreat rates and active periods of RTSs, ground ice content, vegetation, and soil type will be useful for the understanding of RTS development and permafrost degradation. We may miss some published RTS research and expect more results in the future. Therefore, the map will also be updated frequently (https://github.com/yghlc/rts-site-data-review).

References

Huang, L., Willis, M.J., Li, G., Lantz, T.C., Schaefer, K., Wig, E., Cao, G., Tiampo, K.F., 2023. Identifying active retrogressive thaw slumps from ArcticDEM. ISPRS J. Photogramm. Remote Sens. 205, 301–316. https://doi.org/10.1016/j.isprsjprs.2023.10.008

Luo, J., Niu, F., Lin, Z., Liu, M., Yin, G., Gao, Z., 2022. Inventory and Frequency of Retrogressive Thaw Slumps in Permafrost Region of the Qinghai–Tibet Plateau. Geophys Res Lett 49. https://doi.org/10.1029/2022gl099829

Nitze, I., Grosse, G., Jones, B.M., Romanovsky, V.E., Boike, J., 2018. Remote sensing quantifies widespread abundance of permafrost region disturbances across the Arctic and Subarctic. Nat Commun 9, 5423. https://doi.org/10.1038/s41467-018-07663-3

Obu, J., Westermann, S., Bartsch, A., Berdnikov, N., Christiansen, H.H., Dashtseren, A., Delaloye, R., Elberling, B., Etzelmüller, B., Kholodov, A., Khomutov, A., Kääb, A., Leibman, M.O., Lewkowicz, A.G., Panda, S.K., Romanovsky, V., Way, R.G., Westergaard-Nielsen, A., Wu, T., Yamkin, J., Zou, D., 2019. Northern Hemisphere permafrost map based on TTOP modelling for 2000–2016 at 1 km2 scale. Earth-sci Rev 193, 299–316. https://doi.org/10.1016/j.earscirev.2019.04.023

Runge, A., Nitze, I., Grosse, G., 2022. Remote sensing annual dynamics of rapid permafrost thaw disturbances with LandTrendr. Remote Sens Environ 268, 112752. https://doi.org/10.1016/j.rse.2021.112752

Are periglacial landslides in discontinuous permafrost more vulnerable to warming?

Kaytan Kelkar[1], Louise Farquharson[1], Margaret Darrow[2], Benjamin Gaglioti[3], Simon Zwieback[4], Dmitry Nicolsky[1] & Denny Capps[5]

[1]*Geophysical Institute Permafrost Laboratory, University of Alaska Fairbanks, Fairbanks, Alaska, United States*

[2]*Department of Civil, Geological, and Environmental Engineering, University of Alaska Fairbanks, Fairbanks, Alaska, United States*

[3]*Water and Environmental Research Center, University of Alaska Fairbanks, Fairbanks, Alaska, United States*

[4]*Geophysical Institute, University of Alaska Fairbanks, Fairbanks, Alaska, United States*

[5]*Denali National Park and Preserve, Denali Park, Alaska, United States*

Mass-movement in mountainous terrain poses a hazard to critical infrastructure and human activities. Rapid mountain permafrost degradation has further enhanced slope destabilizations of permafrost-affected slopes (Huggel et al. 2012). Large landslides in mountain regions of the cryosphere are increasing in frequency and magnitude as permafrost degradation becomes more acute in a warming climate (Coe et al. 2018). Such landslide activity is presently observed in high-latitude mountain ranges underlain by permafrost. The documented record of landslides in the Arctic is poor (Svennevig et al. 2022), which has presented a crucial knowledge gap in better understanding the mechanisms that cause these large landslides in the Arctic environment. Thus, interpretation of the mechanisms of permafrost-affected landslides requires identifying environmental conditions where mass-movements occur.

We examined three study sites in Alaska along a latitudinal transect for periglacial landslides: Wrangell Mountains, Alaska Range, and Brooks Range (Figure 1). The study of how landslide dynamics change over a North-South transect with varied permafrost conditions has received little attention (Smith et al. 2023). We hypothesize that landslides in discontinuous permafrost have a deeper depth to failure than landslides in continuous permafrost. (Figure 2).

We mapped landslide distribution at the selected study sites using high-resolution spectral satellite imagery in ArcGIS Pro. Each study site comprised of five landslides. For imagery with snow/cloud cover, 5-m resolution Planet Labs imagery was used. To quantify depth to failure and volume, we conducted Digital Elevation Model (DEM) subtraction pre and post slope failure of ArcticDEM datasets. Differencing of DEMs was conducted on failure scars for each landslide (Shugar et al. 2021). A time series of Planet Labs imagery and historical aerial photographs was constructed to constrain the timing of the date of landslide occurrence back to 1950. The role of continuous and discontinuous permafrost conditions derived from Obu (2021) in driving slope instability was identified by employing hindcast climate data (e.g., air temperature and snow depth from Scenarios Network for Alaska and Arctic Planning (SNAP) and the Geophysical Institute Permafrost Laboratory (GIPL) model. Due to poor constraints on snow depth and distribution, sensitivity tests were conducted with a range of snow depth and densities. As Alaska is seismically active, we determined if landslide movement was directly preceded by known earthquake events from the Alaska Earthquake Center (AEC) seismic stations within five days prior and after the date of landslide initiation.

Figure 1. A map of the landslide study sites on a north-south transect.

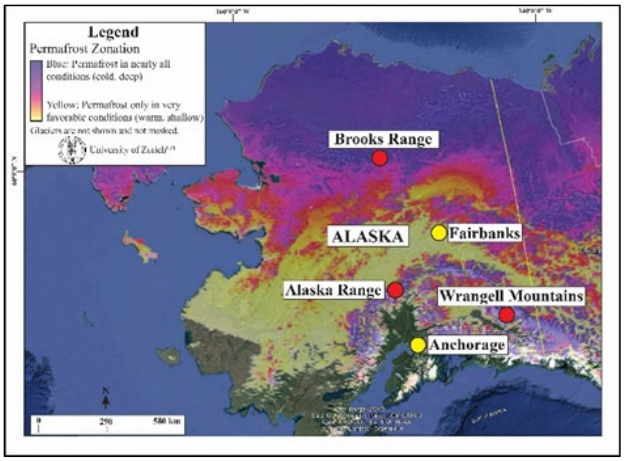

Figure 2. This map displays permafrost conditions underlying study site locations based on the Global Permafrost Zonation Index (GPZI) produced by Gruber (2012).

REFERENCES

Coe, J.A., Bessette-Kirton, E.K., and Geertsema, M. 2018. Increasing rock-avalanche size and mobility in Glacier Bay National Park and Preserve, Alaska detected from 1984 to 2016 Landsat imagery. Landslides, 15(3), pp.393–407. https://doi.org/10.1007/s10346-017-0879-7

Gruber, S. 2012. Derivation and analysis of a high-resolution estimate of global permafrost zonation. The Cryosphere, 6(1), pp.221–233. https://doi.org/10.5194/tc-6-221-2012

Huggel, C., Clague, J.J., and Korup, O. 2012. Is climate change responsible for changing landslide activity in high mountains? Earth Surface Processes and Landforms, 37(1), pp.77–91. https://doi.org/10.1002/esp.2223

Obu, J. 2021. How much of the earth's surface is underlain by permafrost? Journal of Geophysical Research: Earth Surface, 126(5), e2021JF006123. https://doi.org/10.1029/2021JF006123

Shugar, D.H., Jacquemart, M., Shean, D., Bhushan, S., Upadhyay, K., Sattar, A., Schwanghart, W., McBride, S., De Vries, M.V.W., Mergili, M., and Emmer, A. 2021. A massive rock and ice avalanche caused the 2021 disaster at Chamoli, Indian Himalaya. Science, 373(6552), pp.300–306. https://www.science.org/doi/10.1126/science.abh4455

Smith, W.D., Dunning, S.A., Ross, N., Telling, J., Jensen, E.K., Shugar, D.H., Coe, J.A., and Geertsema, M. 2023. Revising supraglacial rock avalanche magnitudes and frequencies in Glacier Bay National Park, Alaska. Geomorphology, 425, p.108591. https://doi.org/10.1016/j.geomorph.2023.108591

Svennevig, K., Hermanns, R.L., Keiding, M., Binder, D., Citterio, M., Dahl-Jensen, T., Mertl, S., Sørensen, E.V., and Voss, P.H. 2022. A large frozen debris avalanche entraining warming permafrost ground—the June 2021 Assapaat landslide, West Greenland. Landslides, 19(11), pp.2549–2567. https://doi.org/10.1007/s10346-022-01922-7

Mechanical modelling strategies for warming permafrost rock slopes

Michael Krautblatter[1], Georg Stockinger[1], Felix Pfluger[1], Philipp Mamot[1,2], Benjamin Jacobs[1] & Saskia Eppinger[1]
[1]*Chair of Landslide Research, Technical University of Munich, Munich, Germany*
[2]*Björnsen Beratende Ingenieure GmbH, Germany*

This paper discusses mechanical modelling strategies for instable permafrost bedrock. Modelling instable permafrost bedrock is a key requirement to anticipate magnitudes and frequency of rock slope failures in a changing climate but also to forecast the stability of high-alpine infrastructure throughout its lifetime.

High-alpine rock faces witness the past and present mechanical limit equilibrium. Rock segments where driving forces exceed resisting forces fall of the cliff often leaving a rock face behind which is just above the limit equilibrium. All significant changes in rock mechanical properties or significant changes in state of stress will evoke rock instability which often occurs with response times of years to 1000 years. Degrading permafrost will act to alter (i) rock mechanical properties such as compressive and tensile strength, fracture toughness and most likely rock friction, (ii) warming sub zero conditions will weaken ice and rock-ice interfaces and (iii) increased cryo- and (iv) hydrostatic pressures are expected. Laboratory experiments provide estimations of the serious impact of thawing and warming rock and ice-mechanical properties, which often lose 25-75% of their strength between -5°C and -0.5°C. Approaches to calculate cryostatic pressure (ad iii) have been published and are experimentally confirmed. However, the importance and dimension of extreme hydrostatic forces (ad iv) due to perched water above permafrost-affected rocks has been assumed but has not yet been quantitatively recorded.

This paper presents data and strategies how to obtain relevant (i) rock mechanical parameters (compressive and tensile strength and fracture toughness, lab) (Jia et al. 2015; Jia et al. 2017), (ii) ice- and rock-ice interface mechanical parameters (lab) (Mamot et al. 2018; Mamot et al. 2020), (iii) cryostatic forces in low-porosity alpine bedrock (lab and field) (Draebing and Krautblatter 2019) and (iv) hydrostatic forces in perched water-filled fractures above permafrost (field).

We demonstrate mechanical models that are based on the conceptual assumption of the rock ice mechanical (Krautblatter et al. 2013) and rely on frozen/unfrozen parameter testing in the lab and field. Continuum mechanical models (no discontinuities) can be used to demonstrate permafrost rock wall destabilization on a valley scale over longer time scales, as exemplified by progressive fjord rock slope failure in the Lateglacial and Holocene. Discontinuum mechanical models including rock fracture patterns can display rock instability induced by permafrost degradation on a singular slope scale, as exemplified for recent a recent ice-supported 10.000 m³ preparing rock at the Zugspitze (D) (Mamot et al. 2021). Discontinuum mechanical models also have capabilities to link permafrost slope stability to structural loading induced by high-alpine infrastructure such as cable cars and mountains huts, as exemplified for the Kitzsteinhorn Cable Car and its anchoring in permafrost rocks (A).

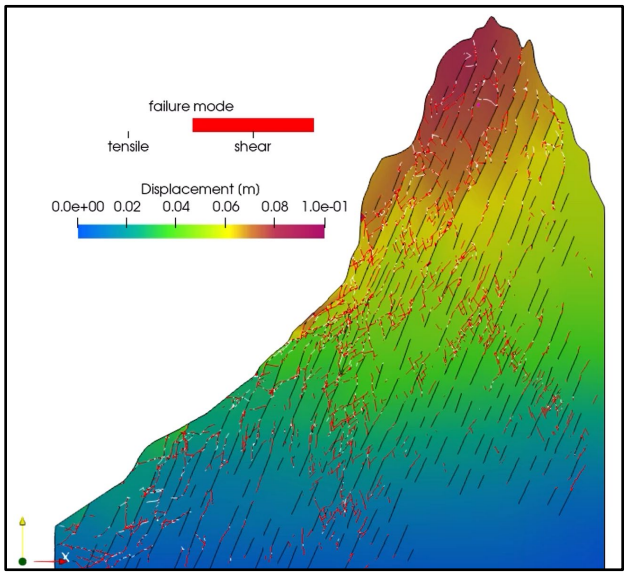

Figure 1: IRAZU model applied on the 1 Mio m³ Fluchthorn (Austria) permafrost Rock Slope Failure on June 12, 2023 capable of nucleation and growth of fractures based on nonlinear fracture mechanics applied stresses act to produce a progressive fracturing path that closely resembles the real failure

All these models have been recently combined to decipher the 1 Mio. m³ Fluchthorn rock slope failure that detached on June 12, 2023, from the before 3399 m high summit causing a rock avalanche that additionally eroded ca. 120.000 m³ of ice. In an IRAZU model, capable of nucleation and growth of fractures based on nonlinear fracture mechanics

applied stresses act to produce a progressive fracturing path that closely resembles the real failure, and we can show the impact of the solid pseudotachilitic roof on the oversteepening. In a discontinuum model (UDEC), we can show the stabilizing effect of permafrost on developing fracturing patterns in a combined rock-ice mechanical approach.

In this paper we discuss benchmark modelling approaches that try to implement laboratory-derived temperature-dependent weakening effects into real scale models and compare the explanatory power of different model approaches.

REFERENCES

Draebing, D., and Krautblatter, M. 2019. The Efficacy of Frost Weathering Processes in Alpine Rockwalls, Geophysical Research Letters, 46(12): 6516–6524. doi:10.1029/2019gl081981

Dwivedi, R.D., Soni, A.K., Goel, R.K., and Dube, A.K. 2000. Fracture toughness of rocks under sub-zero temperature conditions, International Journal of Rock Mechanics and Mining Sciences, 37(8): 1267–1275. doi:10.1016/S1365-1609(00)00051-4

Fischer, L., Kääb, A., Huggel, C., and Noetzli, J. 2006. Geology, glacier retreat and permafrost degradation as controlling factors of slope instability in a high-mountain rock wall: the Monte Rosa east face, Natural Hazards Earth System Sciences, 6(5): 761–772. doi:10.5194/nhess-6-761-2006

Jia, H., Xiang, W., and Krautblatter, M. 2015. Quantifying rock fatigue and decreasing compressive and tensile strength after repeated freeze-thaw cycles, Permafrost and Periglacial Processes, 26(4): 368–377. doi:10.1002/ppp.1857

Jia, H., Leith, K., and Krautblatter, M. 2017. Path-Dependent Frost-Wedging Experiments in Fractured, Low-Permeability Granite, Permafrost and Periglacial Processes, 28(4): 698–709. doi:10.1002/ppp.1950

Krautblatter, M., Funk, D., and Günzel, F.K. 2013. Why permafrost rocks become unstable: a rock-ice-mechanical model in time and space, Earth Surface Processes and Landforms, 38(8): 876–887. doi:10.1002/esp.3374

Krautblatter, M., and Leith, K. 2015. Glacier- and permafrost-related slope instabilities. Chapter 9 in Huggel C., Carey M., Clague J. and Kääb A., The High-Mountain Cryosphere, Cambridge University Press.

Leith, K., Moore, J.R., Amann, F., and Loew, S. 2014. In situ stress control on microcrack generation and macroscopic extensional fracture in exhuming bedrock, Journal of Geophysical Research: Solid Earth, 119 (1): 594–615. doi:10.1002/2012jb009801

Mamot, P., Weber, S., Schröder, T., and Krautblatter, M. 2018. A temperature-and stress-controlled failure criterion for ice-filled permafrost rock joints, The Cryosphere, 12(10): 3333–3353. doi:10.5194/tc-12-3333-2018

Mamot, P., Weber, S., Lanz, M., and Krautblatter, M. 2020. Brief communication: The influence of mica-rich rocks on the shear strength of ice-filled discontinuities, The Cryosphere, 14(6): 1849–1855. doi:10.5194/tc-14-1849-2020

Mamot, P., Weber, S., Eppinger, S., and Krautblatter, M. 2021. A temperature-dependent mechanical model to assess the stability of degrading permafrost rock slopes, Earth Surface Dynamics, 9(5): 1125–1151. doi:10.5194/esurf-9-1125-2021

Mellor, M. 1973. Mechanical Properties of Rocks at Low Temperatures, In Proceedings of the 2nd Int. Conference on Permafrost, Yakutsk, Russia, 334–344.

Murton, J., Kuras, O., Krautblatter, M., Cane, T., Tschofen, D., Uhlemann, S., Schober, S., and Watson, P. 2016. Monitoring rock freezing and thawing by novel geoelectrical and acoustic techniques, Journal of Geophysical Research: Earth Surface, 121(12): 2309–2332. doi: 10.1002/2016JF003948

Conceptual physical modeling of thaw slumps in a geotechnical centrifuge

Azin Mardani[1], Geoff N. Eichhorn[1], Ryley Beddoe[2] & Greg Siemens[2]

[1]*Department of Civil Engineering, Queen's University, Kingston, Ontario, Canada*

[2]*Department of Civil Engineering, Royal Military College of Canada, Kingston, Ontario, Canada*

Retrogressive thaw slumps are a well known arctic geohazard, which often occurs in ice-rich permafrost located near water bodies (Armstrong et al. 2018; Lacelle et al. 2015). Thaw slumps can be induced by climate warming and/or anthropogenic influences. Consequences of thaw slumps include changes to the landscape, impacts to infrastructure, sediment and solute loads to watersheds, and release of stored carbon, among other effects (Kokelj et al. 2017; Kokelj et al. 2021).

Most research studies on thaw slumps include external monitoring in the field through use of time-lapse photography, unmanned aerial vehicle (UAV), and lidar surveys. Digital recordings can then be processed to create Structure-from-Motion interpretations of ground movements with the aim to capture high temporal and spatial resolution data (Armstrong et al. 2018). While field studies using external monitoring equipment provide high quality information about the extent and consequence of thaw slumps, direct observations of thermal and mechanical mechanisms occurring behind the scarp normally remain hidden.

Recent advances at Royal Military College of Canada (RMC) have provided for physical modeling of cold regions phenomena using geotechnical centrifuge. Geotechnical centrifuges apply elevated gravity to small-scale models to create stress-equivalent environments. Clarkson et al. (2023) used this concept to test adfreeze piles in frozen ground and quantified pile capacity reduction with warming temperatures and increased thaw layer thickness.

Physical modeling of thaw slumps in a geotechnical centrifuge involves scaling a prototype (i.e., field case) to a reasonable model size, selecting the material to be tested, and then applying environmental warming conditions while at elevated gravity. A photo of the initially frozen block of soil is shown in Figure 1a. A typical 5.5-6 m tall thaw slump scarp was scaled down by a factor of 38 to fit in the RMC geotechnical centrifuge cradle. Field studies of thaw slumps that reported index properties showed that typical materials were classified as low plasticity clay. Thus, kaolin clay with approximately 38-40% moisture content was used as the initial state for thaw slump models. Blocks of kaolin are either compacted or consolidated to the required size, visual texture is added to the side of soil to allow for digital image correlation, and then the block is placed in the model cradle with insulation separating the soil from the aluminium base and sidewall.

Instrumentation for thaw slump models provide quantitative and qualitative information on the thermal and mechanical responses to warming. Digital cameras capture the changing side profile of the frozen block of soil as it thaws. A thermal camera is placed on the left side of the cradle (Figure 1a) to capture thermal maps of the block's front face. Thermal measurements are captured using a distributed fiber optic sensing method which provides sensing points every 2.6 mm (Litjens et al. 2024). Fiber optic cable is placed around and through the model to provide thermal measurements from within the frozen/thawing soil block, at the bottom and back boundaries, and in the air space.

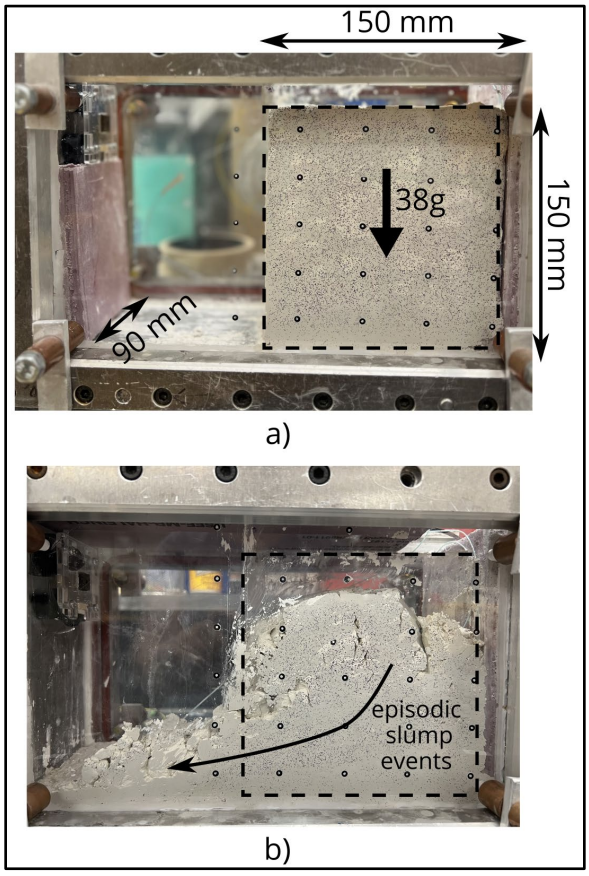

Figure 1. Photos from the thaw slump physical model showing: a) an initially frozen block with an exposed vertical face and b) post-model form after several episodic thaw slump events.

After physical model preparation and instrumentation installation, the model cradle is placed in a freezer set to -16°C for at least 24 hours to ensure thermal equilibrium. The model cradle is then removed and placed in the geotechnical centrifuge. The centrifuge is set to spin at 38*gravity to represent field stress conditions. Tests last 5-7 hours. Typically, warming driven thawing beginning at the face and surface leads to episodic thaw slump events. Failed material moves down and away from the face of the remaining frozen block. This repeats until the final slump occurs at the back face. A digital image following a thaw slump model is show in Figure 1b.

Preliminary observations indicate that the conceptual thaw slump physical models are capturing key behaviours observed from external field measurements. Future analysis will examine the internal and external thermal and mechanical response to warming.

REFERENCES

Armstrong, L., Lacelle, D., Fraser, R.H., Kokelj, S., and Knudby, A. 2018. Thaw slump activity measured using stationary cameras in time-lapse and Structure-from-Motion photogrammetry. Arctic Science, 4(4), 827–845.

Clarkson, C., Eichhorn, G.N., and Siemens, G. 2023. Centrifuge modelling of axially loaded steel piles in cold and warming permafrost. International Journal of Physical Modelling in Geotechnics, In press and available online: doi.org/10.1680/jphmg.22.00062.

Lacelle, D., Brooker, A., Fraser, R.H., and Kokelj, S.V. 2015. Distribution and growth of thaw slumps in the Richardson Mountains–Peel Plateau region, northwestern Canada. Geomorphology, 235, 40–51.

Litjens, C., Mardani, A., Eichhorn, G.N., Beddoe, R., and Siemens, G. 2024. Use of distributed fiber optic sensing for thermal mapping of laboratory permafrost samples. Extended abstract submitted to 12th International Conference on Permafrost. Whitehorse, YK.

Kokelj, S.V., Kokoszka, J., van der Sluijs, J., Rudy, A.C.A., Tunnicliffe, J., Shakil, S., et al. 2021. Thaw-driven mass wasting couples slopes with downstream systems, and effects propagate through Arctic drainage networks. The Cryosphere, 15(7), 3059–3081.

Kokelj, S.V., Lantz, T.C., Tunnicliffe, J., Segal, R., and Lacelle, D. 2017. Climate-driven thaw of permafrost preserved glacial landscapes, northwestern Canada. Geology, 45(4), 371–374.

Using deep learning to advance global monitoring of retrogressive thaw slumps at high spatio-temporal resolution

Ingmar Nitze[1], Konrad Heidler[2], Kathrin Maier[3], Sophia Barth[1,4], Anna Liljedahl[5] & Guido Grosse[1,4]

[1]*Permafrost Research, Alfred Wegener Institute Helmholtz Centre for Polar and Marine Research, Potsdam, Germany*

[2]*Data Science in Earth Observation, Technical University of Munich, Munich, Germany*

[3]*Institute of Environmental Engineering, ETH Zurich, Zurich, Switzerland*

[4]*Institute of Geosciences, University of Potsdam, Potsdam, Germany*

[5]*Woodwell Climate Research Center, Falmouth, Massachusetts, United States*

Retrogressive Thaw Slumps (RTS) are one of the most striking degradation landforms in permafrost regions. They are a geohazard on local to regional scales, are responsible for soil and carbon mobilization, and have a strong impact on local to regional hydrology. Over the past years they have been found to increase in abundance, area and eroded volume with an acceleration of dynamics exacerbated by further warming and wetting climate (Kokelj et al. 2015; Lewkowicz and Way 2019).

Their distribution is well known in several regions, e.g., the Peel Plateau in NW Canada (Kokelj et al. 2023; Kokelj et al. 2021). In the Eurasian Arctic and Subarctic there are datasets available (Runge et al. 2022), though in 30 m spatial resolution, which is coarse for RTS detections. This large knowledge gap leads to high uncertainties about their impact on the carbon cycle and other local- to regional-scale hazards related to permafrost thaw. Additionally, they are a good proxy for ground-ice distribution, which in turn is linked to permafrost vulnerability. Ground-ice distribution is one of the most important but poorly quantified permafrost properties.

Deep Learning (DL) has become an increasingly common method for the detection and segmentation of anthropogenic and natural objects in remote sensing imagery. Over the past years there have been significant advances in this field, with RTS mapping studies across several regions and scales with different methodologies and accuracies (Huang et al. 2021; Nitze et al. 2021; Witharana et al. 2022; Yang et al. 2023). In this study, we are expanding the work of Nitze et al. 2021 and aim to create a panarctic RTS monitoring system using high-resolution remote sensing and DL methodology.

Data and methods

We use an automated DL approach to identify and quantify individual RTS across the Arctic in high spatial resolution and annual to sub-annual temporal resolution using convolutional neural networks (UNet++).

We used multispectral PlanetScope data as base imagery in 3 m spatial resolution. Additionally, we used the ArcticDEM and derived data, such as slope or relative elevation as auxiliary data sources. We followed an iterative approach starting with a simple DL model, which we improved by adding new training labels and detailed evaluation of the output. Our training dataset currently contains more than 4500 mapped RTS footprints across different regions in the (Sub-) Arctic. This dataset is freely available and about to be included into a new meta-dataset of RTS ground-truth/labels (Yang et al. in prep).

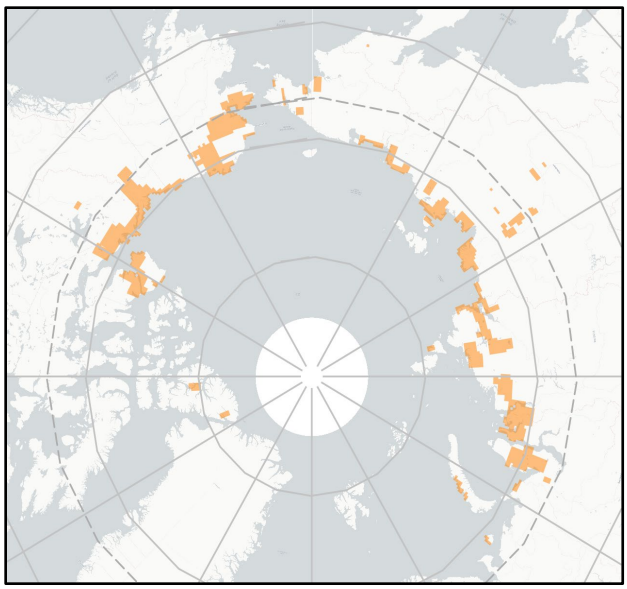

Figure 1. Current study areas with processed results.

To date, we applied our RTS detection model to an area of ~1 million km², for the years 2021 and 2022 (Figure 1). For several key sites (e.g., Peel Plateau, East Taymyr Peninsula, Banks Island) we processed a denser and longer time-series back to 2018 including multiple observations per year, which allows us to track the temporal dynamics with a high frequency (Figure 2). We analyze volumetric change information based on multitemporal DEMs generated from observations of the

TanDEM-X mission to better understand the highly relevant volumetric changes in addition to spatial dynamics to assess area to volume scaling.

For the DL model, we carried out exhaustive tuning, e.g., testing various model architectures, learning rate scheduling and further hyperparameter tests to improve the performance and ability to perform well in highly diverse environments.

Results

Generally, the DL based models exhibit a good performance (F1=0.80, IoU=0.66), particularly in areas with sufficient training data. In our current study area, we detected in total ~31,000 distinct RTS, many of them through multiple time steps.

On the individual object scale, they are well delineated along headwalls, where there is a clear boundary between RTS and surrounding terrain (Figure 2). In several key sites the output dataset has a great potential for the automatic retrieval of erosion rates in high temporal resolution. The lower boundary however can be fuzzy, leading to large variation in the affected area due to unclear distinction to the surrounding terrain. With the inclusion of the volumetric dimension in the next processing steps this effect will likely be reduced.

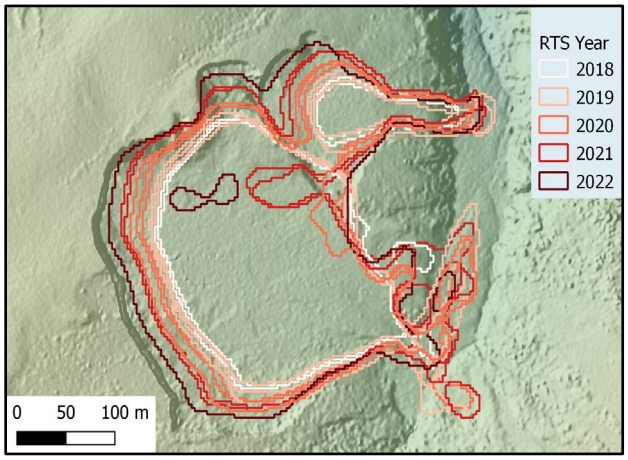

Figure 2. Automatically mapped RTS footprint of 11 individual observations from 2018 through 2022 on the Peel Plateau, NW Canada, overlaid on a high resolution DSM and Hillshade processed from aerial imagery, acquired in July 2023.

Outlook

Based on the current status and promising results of our processing, we aim to upscale this process to the entire Arctic region that is likely affected by hillslope thermokarst. As part of the new Permafrost AI project of the Google.org Impact Challenge, we aim to create a monitoring system for RTS to rapidly map and quantify their impact on permafrost landscapes and help to predict local to regional scale impacts in near real-time. We are working on an automated RTS monitoring model, which immediately detects RTS features once new datasets are available. This will provide the community with a much better understanding of the consequences of climate, ground ice distribution and predictions of future pathways of landscape dynamics.

References

Huang, L., Liu, L., Luo, J., Lin, Z., and Niu, F. 2021. Automatically quantifying evolution of retrogressive thaw slumps in Beiluhe (Tibetan Plateau) from multi-temporal CubeSat images. Int. J. Appl. Earth Obs. Geoinformation 102, 102399. https://doi.org/10.1016/j.jag.2021.102399

Kokelj, S.V., Gingras-Hill, T., Daly, S.V., Morse, P., Wolfe, S., Rudy, A.C.A., van der Sluijs, J., Weiss, N., O'Neill, B., Baltzer, J., Lantz, T.C., Gibson, C., Cazon, D., Fraser, R.H., Froese, D.G., Giff, G., Klengenberg, C., Lamoureux, S.F., Quinton, W., Turetsky, M.R., Chiasson, A., Ferguson, C., Newton, M., Pope, M., Paul, J.A., Wilson, A., and Young, J. 2023. The Northwest Territories Thermokarst Mapping Collective: A northern-driven mapping collaborative toward understanding the effects of permafrost thaw. Arct. Sci. AS-2023-0009. https://doi.org/10.1139/AS-2023-0009

Kokelj, S.V., Kokoszka, J., van der Sluijs, J., Rudy, A.C.A., Tunnicliffe, J., Shakil, S., Tank, S.E., and Zolkos, S., 2021. Thaw-driven mass wasting couples slopes with downstream systems, and effects propagate through Arctic drainage networks. The Cryosphere 15, 3059–3081. https://doi.org/10.5194/tc-15-3059-2021

Kokelj, S.V., Tunnicliffe, J., Lacelle, D., Lantz, T.C., Chin, K.S., and Fraser, R. 2015. Increased precipitation drives mega slump development and destabilization of ice-rich permafrost terrain, northwestern Canada. Glob. Planet. Change 129, 56–68. https://doi.org/10.1016/j.gloplacha.2015.02.008

Lewkowicz, A.G., and Way, R.G. 2019. Extremes of summer climate trigger thousands of thermokarst landslides in a High Arctic environment. Nat. Commun. 10, 1329. https://doi.org/10.1038/s41467-019-09314-7

Nitze, I., Heidler, K., Barth, S., and Grosse, G. 2021. Developing and Testing a Deep Learning Approach for Mapping Retrogressive Thaw Slumps. Remote Sens. 13. https://doi.org/10.3390/rs13214294

Runge, A., Nitze, I., and Grosse, G. 2022. Remote sensing annual dynamics of rapid permafrost thaw disturbances with LandTrendr. Remote Sensing of Environment 268, 112752. https://doi.org/10.1016/j.rse.2021.112752

Witharana, C., Udawalpola, M.R., Liljedahl, A.K., Jones, M.K.W., Jones, B.M., Hasan, A., Joshi, D., and Manos, E. 2022. Automated Detection of Retrogressive Thaw Slumps in the High Arctic Using High-Resolution Satellite Imagery. Remote Sens. 14, 4132. https://doi.org/10.3390/rs14174132

Yang, Y., Rogers, B.M., Fiske, G., Watts, J., Potter, S., Windholz, T., Mullen, A., Nitze, I., and Natali, S.M. 2023. Mapping retrogressive thaw slumps using deep neural networks. Remote Sens. Environ. 288, 113495. https://doi.org/10.1016/j.rse.2023.113495

Quantifying and characterising geomorphic signatures of active layer detachments in the Brooks Range, Alaska

Charlotte Pearson[1], Olly Bartlett[1], Alastair Curry[1], Phil Porter[1] & Ingmar Nitze[2]

[1]*Geography, Environment and Planning, School of Life and Medical Sciences, University of Hertfordshire, Hatfield, United Kingdom*

[2]*Alfred Wegener Institute, Helmholtz Centre for Polar and Marine Research, Potsdam, Germany*

Active-layer detachments (ALD) represent rapid mass-wasting phenomena triggered by the thawing of ice-rich sediments, leading to increased pore water pressure in shallow-angle hillslopes (Lewkowicz and Harris 2005a). These dynamic processes have significant implications for landscape evolution and stability, involving the mobilisation of organic carbon, redistribution of soils, and alterations in drainage patterns (Turetsky et al. 2020). Despite their importance, ALD are relatively understudied compared to other abrupt thaw features like retrogressive thaw slumps. This lack of attention is attributed to the complexity of their failure processes and the shorter, less dynamic disturbance periods, which hinder their long-term preservation (Harris and Lewkowicz 1993; Runge et al. 2022).

As Arctic temperatures and rainfall continue to rise, the frequency, extent, and magnitude of ALD are expected to increase (Lewkowicz and Harris 2005b). This is driven by the changing thermal properties of permafrost and heightened slope instability. Although individual ALD events may not result in substantial material displacement, their expansive spatial range contributes to widespread carbon release and thaw subsidence across High Arctic regions (Patton et al. 2021; Turetsky et al. 2020). However, these feedback mechanisms are inadequately represented in current climate models (Runge et al. 2022). Ongoing efforts are necessary to improve mechanistic understanding of ALD through remote sensing and automated processing across multiple platforms (Lissak et al. 2020).

Aims

This research focuses on quantifying and characterising the geomorphic signatures of ALD in the Brooks Range, Alaska. It employs a comprehensive approach, integrating remote sensing-derived datasets (ArcticDEM) and object-based random forest algorithms in the classification process in Google Earth Engine. This integration aims to enhance the mechanistic understanding of ALD and improve the identification of their widespread distribution and potential future impacts.

Methods

This methodology utilises high-resolution digital elevation data sourced from ArcticDEM within Google Earth Engine, alongside previously published auxiliary datasets (Figure 1). The attributes associated with known ALD locations, obtained from an existing dataset of over 2000 ALD polygons delineated by Swanson (2021), are extracted. Additionally, this process extends to randomly distributed points across the region, broadening the dataset used within the training and validation phases.

Random forest feature importances and SHAP values are calculated to identify distinct patterns and trends in each attribute. This approach facilitates the differentiation of ALD morphology from broader regional processes and establishes unique thresholds. These thresholds are crucial for training a classifier that can effectively detect ALD from the ArcticDEM.

Iterative development of a classification workflow aims to enhance and generate a process for extracting ALD locations and feature shapes from high-resolution (2 m) DEMs. Following the algorithm's development on Brooks Range data, its effectiveness will be validated by testing it in other Arctic regions where ALD exist.

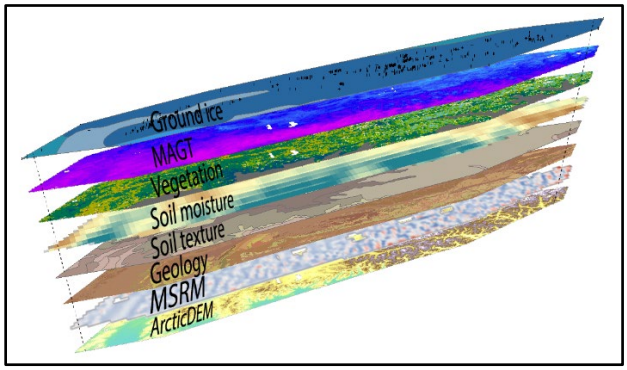

Figure 1. Datasets used to extract attributes to ALD and random point locations across the Brooks Range study region.

Results

A preliminary iteration of the algorithm, along with its associated results concerning model performance, will be presented. The classification is devised around

DEM terrain derivatives computed in Google Earth Engine which produce clear and discernible topographic signatures for ALD (Figure 2).

The geomorphic, lithologic and permafrost-condition-based signatures for ALD in the Brooks Range will be presented as a baseline for the development of classification algorithms and research into ALD in different Arctic locations.

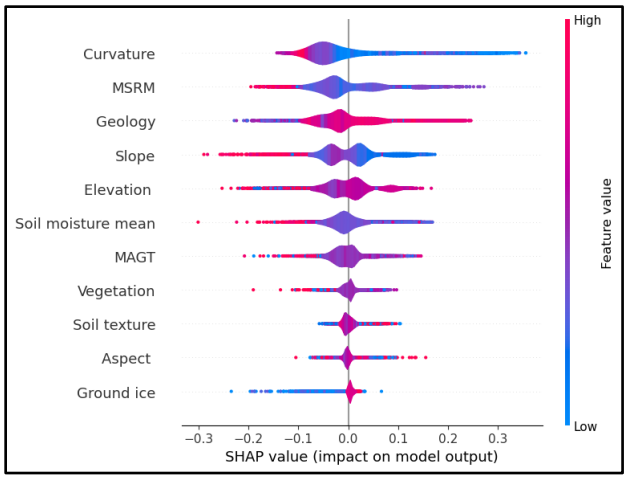

Figure 2. Distribution and density of SHAP values for each ALD, allowing for comparisons in attribute importance. Curvature is the most important variable, with negative values having greater importance for ALD formation.

SUMMARY

Ongoing efforts involve refining and optimising the algorithm through iterative processes. This involves not only fine-tuning the existing method but also integrating additional Arctic regions within the training dataset. The overarching goal is to improve the classifier's performance and enhance its transferability across diverse Arctic landscapes. Once fully developed, this automated mapping tool holds potential for widespread application across various Arctic regions. Its implementation could facilitate the pan-Arctic quantification of abrupt thaw through ALD, creating an invaluable inventory that forms the basis for developing susceptibility models.

REFERENCES

Harris, C., and Lewkowicz, A.G. 1993. Form and internal structure of active-layer detachment slides, Fosheim Peninsula, Ellesmere Island, Northwest Territories, Canada. Canadian Journal of Earth Sciences, 30(8), pp.1708–1714.

Lewkowicz, A.G., and Harris, C. 2005a. Morphology and geotechnique of active-layer detachment failures in discontinuous and continuous permafrost, northern Canada. Geomorphology, 69(1-4), pp.275–297.

Lewkowicz, A.G., and Harris, C. 2005b. Frequency and magnitude of active-layer detachment failures in discontinuous and continuous permafrost, northern Canada. Permafrost and Periglacial Processes, 16(1), pp.115–130.

Lissak, C., Bartsch, A., De Michele, M., Gomez, C., Maquaire, O., Raucoules, D., and Roulland, T. 2020. Remote sensing for assessing landslides and associated hazards. Surveys in Geophysics, 41: 1391–1435.

Patton, A.I., Rathburn, S.L., Capps, D.M., McGrath, D., and Brown, R.A. 2021. Ongoing landslide deformation in thawing permafrost. Geophysical research letters, 48(16), p.e2021GL092959.

Runge, A., Nitze, I., and Grosse, G. 2022. Remote sensing annual dynamics of rapid permafrost thaw disturbances with LandTrendr. Remote Sensing of Environment, 268, p.112752.

Swanson, D.K. 2021. Permafrost thaw-related slope failures in Alaska's Arctic National Parks, c. 1980–2019. Permafrost and periglacial processes, 32(3), pp.392–406.

Turetsky, M.R., Abbott, B.W., Jones, M.C., Anthony, K.W., Olefeldt, D., Schuur, E.A., Grosse, G., Kuhry, P., Hugelius, G., Koven, C., and Lawrence, D.M. 2020. Carbon release through abrupt permafrost thaw. Nature Geoscience, 13(2), pp.138–143.

Recent efforts in tracking permafrost-thaw driven landslides in the Northwest Territories via area-volume allometric scaling

Jurjen van der Sluijs[1], Steven V. Kokelj[2] & Jon F. Tunnicliffe[3]

[1]*Northwest Territories Centre for Geomatics, Government of Northwest Territories, Yellowknife, Northwest Territories, Canada*

[2]*Northwest Territories Geological Survey, Government of Northwest Territories, Yellowknife, Northwest Territories, Canada*

[3]*School of Environment, University of Auckland, Auckland, New Zealand*

Retrogressive thaw slumping (RTS) is the primary mass-wasting process modifying ice-rich glaciated terrain in the western Canadian Arctic. The climate-driven intensification of slump-related processes and feedbacks is increasing dynamics and diversity of landforms. This drives the need for better quantifying the evolution of RTS growth patterns across activity gradients and between regions. For example, the geomorphic consequences of RTS development requires that the volumetric displacement due to thaw-consolidation and sediment erosion can be estimated for regional- or catchment-scale RTS populations (Kokelj et al. 2021). The aim of this research is to explore the three-dimensional evolution of thaw-driven landslides. Here we overview recent methodological advances, evaluate regional relationships between area and volume, and examine the three-dimensional evolution of individual RTS through their activity lifecycle.

Methods

Determining RTS structural traits, such as volume, can be obtained for regional RTS populations through area-volume relationships, also known as allometric scaling (van der Sluijs et al. 2023). By leveraging high-resolution Digital Elevation Models (DEM) the expression of RTS diversity is no longer limited to two-dimensional morphometrics (e.g., length, area), but also more complex, time-integrated three-dimensional indicators such as allometric scaling coefficients.

To evaluate regional scaling relationships we integrated pre-disturbance topographies, slump digitisations, and DEMs to extract area and volume estimates of RTS along with activity ratings in the Mackenzie Delta region (northwestern Canada). Natural neighbour surface interpolation and undisturbed boundary elevations were used to reconstruct pre-disturbed slope topography from which volume estimates were derived through DEM differencing. A Multisource Slump Inventory (MSI) provided a temporally consistent geospatial database of RTS areas and associated attributes, capturing active RTS as well as more complex polycyclic or old/ancient RTS (n=1,415). To obtain scaling coefficients and examine the effect of activity or landscape position on these coefficients we established relationships using power-law models for RTS populations and subsets. Furthermore, to examine the effect of activity lifecycle on model scaling coefficients we established a dense temporal DEM time-series for a subset of RTS characterized by different activity levels and evolutionary stages.

Results

Results obtained through area-volume relationships indicate non-linearity in the geomorphic impacts of RTS intensification across scale. Regional analyses demonstrate increasing non-linear scaling coefficients with increases in slump activity. It implies climate-driven intensification of thaw slumping will cause disturbance concavities to increase in depth and volume at an increasingly greater rate than the enlargement of the disturbance area. Furthermore, model exponent variability among regions was related to differences in RTS landscape position and glacial legacies, whereby higher model exponents observed in fluvial environments indicated greater depth of material evacuation compared to lake-based RTS. For individual RTS we also observed that power-law exponents are positively correlated to increasing activity trends. The degree of vigorous incision into the landscape by individual RTS can now be quantified based on power-law coefficients and linked to slump processes and evolution stages.

Summary

Allometry is an important morphometric indicator to understand the impact of changing RTS dynamics on permafrost landscape evolution. Increasing rates of top-down thaw and terrain incision will intensify the observed and forecasted magnitude of RTS consequences to stream, lacustrine, deltaic, and coastal environments.

REFERENCES

Kokelj, S.V., Kokoszka, J., van der Sluijs, J., Rudy, A.C.A., Tunnicliffe, J., Shakil, S., Tank, S.E., and Zolkos, S. 2021. Thaw-driven mass wasting couples slopes with downstream systems, and effects propagate through Arctic drainage networks, The Cryosphere, 15: 3059–3081. doi:10.5194/tc-15-3059-2021

van der Sluijs, J., Kokelj, S.V., and Tunnicliffe, J.F. 2023. Allometric scaling of retrogressive thaw slumps, The Cryosphere, 17: 4511–4533. doi:10.5194/tc-17-4511-2023

Susceptibility mapping of active layer detachments using machine learning techniques

Jun Xiong[1], Derek Cronmiller[2], Tong Qiu[1] & Panya Lipovsky[2]

[1]*Department of Civil & Environmental Engineering, Pennsylvania State University, State College, Pennsylvania, United States*

[2]*Yukon Geological Survey, Whitehorse, Yukon, Canada*

Yukon Territory's Klondike region has seen an increasing frequency of active layer detachment (ALD) landslides as a result of wildfire disturbance and extreme precipitation superimposed on a long-term trend of warming climate and permafrost. ALDs in this region increasingly impact infrastructure, the environment, and the lives of Yukoners. As part of an effort to understand the risk these landslides pose and the controls on their distribution, we have developed a machine learning (ML) model of ALD susceptibility for the region.

LANDSLIDE INVENTORY

The database compiled for this study contains 438 manually-recorded ALDs in the Klondike region of Yukon, Canada. The spatial distribution of these ALDs is shown in Figure 1. ML requires both positive and negative labels for training algorithms to distinguish different classes; hence, the same number of non-ALDs are randomly sampled beyond a buffer zone of 1000 m from each ALD location. The buffer is used to avoid the possibility of coinciding with ALD locations in sampling.

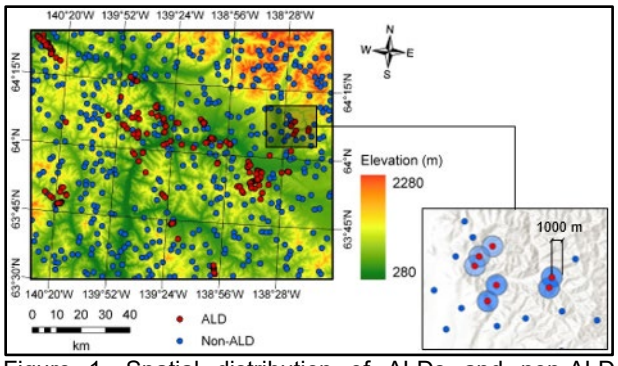

Figure 1. Spatial distribution of ALDs and non-ALDs sampled in the study area.

LANDSLIDE CAUSATIVE FACTORS

The selection of causative factors is a critical step in landslide susceptibility mapping (LSM) as the causative factors selected should be relevant to the geological conditions of the study area and have a high correlation with landslide occurrences (Kavzoglu et al. 2019). Based on the mechanisms of ALDs, sixteen landslide causative factors are selected in this study. They can be broadly categorized as follows:

- Topographic data: Elevation, slope, aspect, plan and profile curvature, topographic position index (TPI), topographic wetness index (TWI), and stream power index (SPI);
- Soil data: Soil texture, field capacity of soil, bulk density of soil, sand and clay contents;
- Land cover data: Normalized difference vegetation index (NDVI);
- Permafrost-related data: Wildfire, and annual potential incoming solar radiation (PISR).

The sources and spatial resolution of the aforementioned data are listed in Table 1.

Table 1. Causative factors of ALD.

Name	Sources	Spatial resolution
Topographic data	Canadian Digital Elevation Model (CDEM)	16-m
Soil data	OpenLandMap	250-m
Land cover data	NASA Landsat	30-m
Permafrost-related data	Yukon Geological Survey	16-m

ML ALGORITHMS AND EVALUATION METRICS

Four ML algorithms for classification problems are utilized in this study, including logistic regression (LR), support vector machine (SVM), random forest (RF), and gradient boosting machines (GBM). These models are popular for LSM applications and were chosen due to their applicability and reasonable results in previous studies (Merghadi et al. 2020).

Five common metrics are used for evaluating classification models, including Accuracy, Precision, Recall, F1 score, and AUC-ROC. These metrics help evaluate the model performance and can be used to improve the overall predictive power of ML models before these models are deployed on unseen data. To prevent overfitting and give better insight into how the models generalize to unknown datasets, five-fold cross-validation is used to evaluate and compare the model performance.

ML RESULTS AND LANDSLIDE SUSCEPTIBILITY MAP

Table 2 shows the model performance of four algorithms through five-fold cross-validation. It is found that RF yields the best performance with an AUC score of 0.96, which indicates a good performance in classifying ALDs and non-ALDs under different probability thresholds. A susceptibility map was constructed by applying the optimized RF model to the study area. As shown in Figure 2, the susceptibility zones of very low, low, moderate, high, and very high correspond to the landslide probability of 0-20%, 20-40%, 40-60%, 60-80%, and 80%-100%, respectively. The pattern of the susceptibility map indicates that there is a good performance in matching the modeled areas of high ALD susceptibility with the spatial distribution of actual ALD events.

Table 2. Model performance with five-fold cross-validation.

Model	Accuracy	Precision	Recall	F1 score	AUC score
LR	0.77	0.78	0.74	0.76	0.87
SVM	0.61	0.94	0.73	0.84	0.71
RF	0.90	0.89	0.90	0.90	0.96
GBM	0.89	0.88	0.90	0.89	0.95

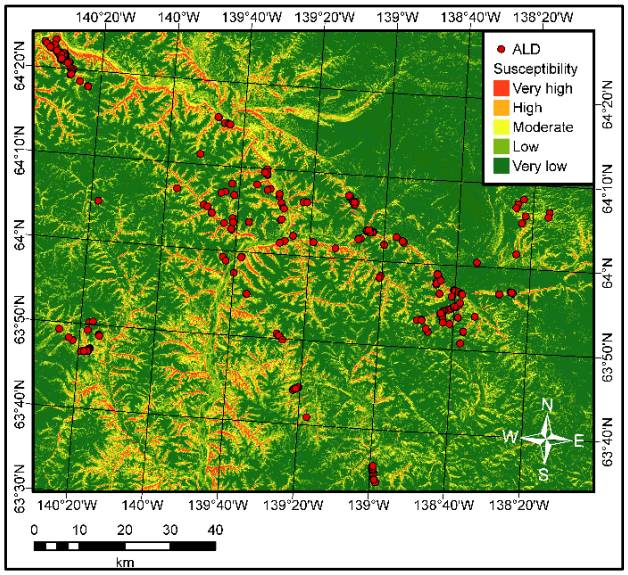

Figure 2. Landslide susceptibility map using RF model.

The SHapley Additive exPlanations (SHAP) method is used to interpret the ML results and explain the relationships between input factors and predicted outcomes (Figure 3). Elevation, PISR, and slope make the greatest contributions to the occurrence of ALDs. Specifically, the likelihood of ALDs increases with decreasing elevation, due to inverted surface lapse rates in the Klondike region (Bonnaventure et al. 2012). Lower elevation valley bottom positions have greater permafrost extent and thinner active layers which are more sensitive to destabilization from rapid warming, and precipitation. The same relationship between active layer thickness and sensitivity to disturbance likely explains the increased susceptibility to ALDs in areas with lower solar radiation. It also shows the steeper the slope, the greater the potential for ALDs. That is because increasing the slope angle decreases the factor of safety, which increases the likelihood of failure. Results in Figure 3 suggest that the ML model predictions are interpretable and consistent with relevant physical mechanisms of ALD.

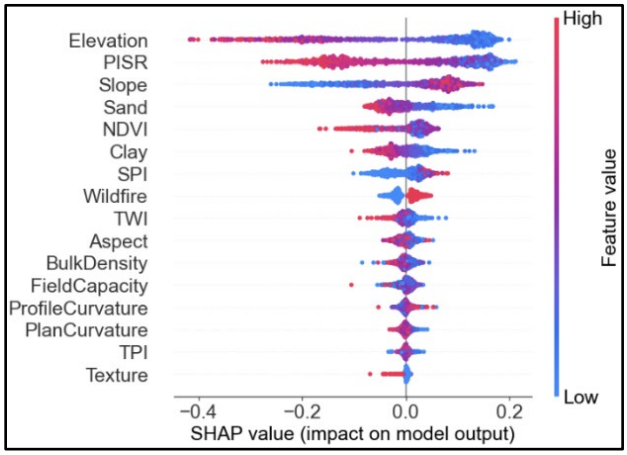

Figure 3. SHAP plot of RF model for LSM.

ACKNOWLEDGEMENTS

This research was supported by the U.S. National Science Foundation under Award No. ICER-2022444. This support is gratefully acknowledged.

REFERENCES

Bonnaventure, P.P., Lewkowicz, A.G., Kermer, M., and Sawada, M.C. 2012. A regional permafrost probability model for the southern Yukon and northern British Columbia, Canada. Permafrost and Periglacial Processes 23, 52–68.

Kavzoglu, T., Colkesen, I., and Sahin, E.K. 2019. Machine learning techniques in landslide susceptibility mapping: A survey and a case study. Landslides: Theory, Practice and Modelling. Advances in Natural and Technological Hazards Research, vol 50. Springer, Cham. https://doi.org/10.1007/978-3-319-77377-3_13

Merghadi, A., Yunus, A.P., Dou, J., Whiteley, J., ThaiPham, B., Bui, D.T., Avtar, R., and Abderrahmane, B. 2020. "Machine learning methods for landslide susceptibility studies: A comparative overview of algorithm performance." Earth-Science Reviews, 207: 103225. https://doi.org/10.1016/j.earscirev.2020.103225

Permafrost detachment slides: A novel high magnitude mass wasting process in warm discontinuous permafrost

Joseph M. Young[1], Jurjen van der Sluijs[2], Steven V. Kokelj[3], Stephan Gruber[4], Teddi Herring[5], Ashley C.A. Rudy[3] & Duane Froese[1]

[1]*University of Alberta, Edmonton, Alberta, Canada*

[2]*Northwest Territories Centre for Geomatics, Yellowknife, Northwest Territories, Canada*

[3]*Northwest Territories Geological Survey, Yellowknife, Northwest Territories, Canada*

[4]*Carleton University, Ottawa, Ontario, Canada*

[5]*University of Calgary, Alberta, Canada*

Warming permafrost in northern Canada is altering slope stability, resulting in abrupt geomorphic responses of permafrost landscapes. In particular, permafrost slope evolution through a cooling Holocene has increased the potential for thaw-driven transformation as recent warming alters the material properties of frozen slopes close to 0°C. These conditions can trigger failure, resulting in ice-rich permafrost landslides that involve processes and feedbacks operating at unexpected magnitudes. Our presentation focuses on large, deep-seated translational failures at the base of permafrost sediments that we term Permafrost Detachment Slides (PDS). These landslides are becoming more common throughout fluvially-incised glaciated terrain in the warm, thin permafrost of the central Mackenzie Valley, Northwest Territories. Understanding these evolving mechanisms of geomorphic change is important for better anticipating environmental and societal consequences of permafrost mass wasting and variation in associated hazards and risks.

Slope failures in ice-rich permafrost hillslopes have conventionally been classified as one of two prominent failure processes: thaw slumps involving ablation-dominated retrogression of an ice-rich headwall and downslope flow of thawed materials, or active layer detachment failures. Both styles of permafrost failure are the product of top-down permafrost thaw linked directly to increasing air temperature and precipitation driving disequilibrium slope failure (Kokelj and Jorgenson 2013). However, field and remote sensing inventories of permafrost landslides in warm discontinuous permafrost regions indicate the recent initiation (< 15 years) of large, deep-seated landslides in ice-rich sediments that do not conform to the existing framework of top-down, thaw-driven mass wasting (Young et al. 2022). To document geological controls, processes and feedbacks, and magnitudes of these emerging permafrost failures, we characterize in detail two recent PDS that occurred in the Johnson River (JR) (failure in August 2017; total landslide volume of ~25 x 10^6 m^3) and Redstone River (RR) (failure August 2018; total landslide volume of ~5.0 x 10^6 m^3) (Figure 1) valleys using litho- and cryostratigraphy, digital elevation models, thermal modeling, and electrical resistivity tomography (ERT) surveys and forward modeling.

Both landslides display similar failure patterns, morphological characteristics, and landscape preconditioning despite differences in ground ice and physiographic settings. The Johnson River PDS occurred in ice-rich glaciolacustrine sediments and the Redstone River PDS in clay-rich diamict. Satellite imagery indicates precursor slope thermokarst and tension crack formation at both sites in the toe and headscarp areas in the years before complete slope failure. Progressive enlargement of these features corresponded to increasing rates of pre-failure surface velocities throughout the landslide areas, up to 10s of meters per year. Failure at the JR and RR sites involved the planar translation of large, intact permafrost blocks (up to dozens of ha in size) into valley bottoms, depositing river-damming debris tongues 1.6 km (volume of 7.3 x 10^6 m^3) (Figure 2) and 1.2 km (volume 3.9 x 10^6 m^3) long, respectively, over a few days. A basal sliding surface at the RR slide was exposed in the upper portion of the scar zone at ~20 m depth. At the JR site, secondary thermokarst has covered the initial basal sliding surface, and we instead infer the surface from the presence of massive injection ice at the base of a lateral scarp at ~18 m depth. ERT surveys and geophysical forward modeling indicate permafrost thickness is consistent with the inferred depth of failure at both sites. In addition, thermal modeling from ground temperature data indicates a thermal response of climate disturbance at depth, with ice concentrations also diminishing near the base of warm permafrost (> -0.5°C), around 20 m from the surface.

Figure 1. Oblique view of the Redstone River PDS. The width of the scar zone is approximately 375 m.

Figure 2. Debris deposit of the Johnson River PDS. The width of the valley fill is approximately 500 m.

Our results indicate these landslides involved detachment of the entire permafrost body and we hypothesize the driver to be gradual thaw at the base of permafrost in response to climate-induced warming acting on burned terrain. The thermal response at depth may be accelerated by advective heat transfer as water moves through cracks. This may also alter thermal-mechanical properties of the permafrost body and increase pore water pressure at the base of permafrost.

The characterization of permafrost detachment slides highlights a geomorphic end-member of the thaw-driven mass-wasting continuum. We anticipate that the climate-driven destabilization of warm and thin ice-rich permafrost slopes will intensify the PDS slope failure regime, with the potential to rapidly modify Holocene slope morphologies of the central Mackenzie Valley, where PDS orders of magnitude larger and more rapid than retrogressive thaw slump counterparts have become a dominant style of permafrost failure.

REFERENCES

Kokelj, S.V., and Jorgenson, M.T. 2013. Advances in thermokarst research. Permafrost and Periglacial Processes, 24(2), pp.108–119.

Young, J.M., Alvarez, A., van der Sluijs, J., Kokelj, S.V., Rudy, A., McPhee, A., Stoker, B.J., Margold, M., and Froese, D. 2022. Recent Intensification (2004–2020) of Permafrost Mass-Wasting in the Central Mackenzie Valley Foothills Is a Legacy of Past Forest Fire Disturbances. Geophysical Research Letters, 49(24), p.e2022GL100559.

5 Permafrost Carbon Feedback

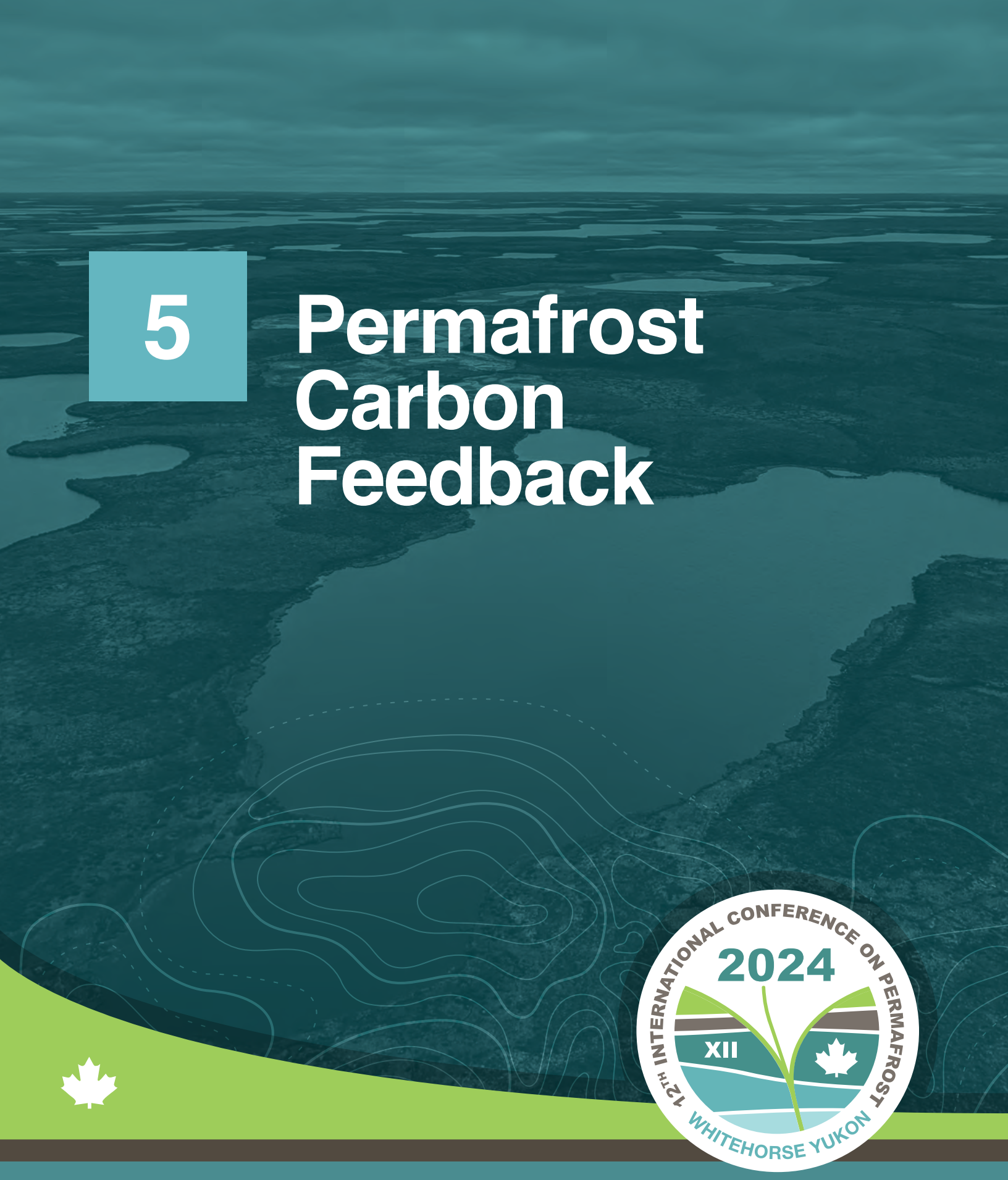

12TH INTERNATIONAL CONFERENCE ON PERMAFROST
2024
XII
WHITEHORSE YUKON

INTEGRATING PERSPECTIVES OF PERMAFROST THAW, CHANGE, AND ADAPTATION

5A — Carbon Cycles in Cold Regions: Modelling and Observations

Session Chairs: Mousong Wu[1], Wenxin Zhang[2] & Youhua Ran[3]

[1]*Nanjing University, Nanjing, Jiangsu, China*
[2]*Department of Physical Geography and Ecosystem Science, Lund University, Skåne, Sweden*
[3]*Chinese Academy of Sciences, Xicheng, Beijing, China*

This session focuses on understanding the response of carbon cycles to the rapid warming being experienced in cold regions of the world (the Arctic, Antarctic, Tibetan Plateau, and the alpines, etc.), where year-round or long-term measurements are often limited. We encourage presentations that share recent findings that improve our understanding of the mechanisms that drive the sensitivity of the carbon cycle, including modelling (both top-down and bottom-up approaches) and observations (both remote sensing and in-situ measurements).

This session aims to share current advances in respective research fields and to explore the possibilities of building tight collaborations on climate change and carbon cycle science in the world's climate-sensitive regions as an alliance. The topics of this session will include but are not limited to (1) Model development: improving or developing ecosystem models to improve our understanding of the ecosystem processes in the cold regions; (2) Remote sensing and in-situ observations: introducing new observations or datasets across different spatial and temporal scales, new techniques of measuring greenhouse gas and using remote sensing products that imply vegetation or land surface properties; and (3) Data assimilation methodologies and applications: the data assimilation methodologies used to combine model and observations to improve our understanding of ecosystem carbon cycles, as well as the applications of new observations to constrain ecosystem models.

Soil organic carbon stocks in permafrost zones of the Mongolian Plateau

Saruulzaya Adiya[1], Batzorig Batbold[1], Tonghua Wu[2], Xiaodong Wu[2], Tsogt-Erdene Gansukh[1], Ulambayar Ganbold[1], Purevdulam Yondontseren[1], Maralmaa Ariunbold[1]

[1]*Institute of Geography and Geoecology, Mongolian Academy of Sciences, Ulaanbaatar, Mongolia*

[2]*Cryosphere Research Station on the Qinghai-Tibet Plateau, State Key Laboratory of Cryospheric Science, Northwest Institute of Eco-Environment and Resources, Chinese Academy of Sciences, Lanzhou, Gansu 730000, China*

A huge amount of organic carbon is stored in the soil of the northern hemispheric permafrost regions. The soil organic carbon (SOC) stocks in the permafrost regions have been intensively studied in recent years (Hugelius et al. 2014). However, no reports of SOC stocks in the southern fringe of Siberian permafrost regions in the Mongolian Plateau are available. The total area of the country is approximately 156.6 × 106 km^2, with an average elevation of 1580 m above sea level. Mongolia has the largest environmental gradients from south to north. There are several mountain ranges, including Altai, Hangai, Hentii, and Huvsgul. This study presents the first detailed permafrost soil organic carbon (SOC) stocks in permafrost zones of the Mongolian Plateau. The area of the permafrost region is approximately 462,769.0 km^2 or approximately 29.3% of the Mongolian Plateau. Between 2020 and 2022, we estimated SOC content at 142 sites in permafrost zones of the Mongolian Plateau based on 1368 soil samples. We drilled five boreholes from the north to the southern part of Mongolia such as Arsai, Jaramtai, Chuluut, Galuut, and Erdene with depths up to 3 m, and collected samples. Furthermore, we used the method of Hugrlius et al. (2014) and the Northern Circumpolar Soil Carbon Database (NCSCD), a digital soil map database linked to extensive field-based SOC storage data in this study. As shown in the results, SOC stocks were estimated to be 7.89 Pg for the 0–100 cm depth, 2.38 Pg for the 100–200 cm depth, and 2.87 Pg for the 200–300 cm depth (Table 1). In total, permafrost zones of the Mongolian Plateau contain approximately ~13.14 Pg of SOC stocks. This 13.14 Pg of SOC stocks would account for approximately 1.01% of the estimated Northern hemispheric permafrost (Table 2).

Table 1. SOC stocks (Pg) in permafrost zones of the Mongolian Plateau.

Permafrost extent	Square (km^2)	0-30 cm	0-100 cm	100-200 cm	200-300 cm	0-300 cm
Continuous	118,306.0	0.80	1.70	0.97	0.97	3.64
Discontinuous	127,686.0	0.93	1.95	0.56	0.98	3.50
Sporadic	112,416.0	0.51	0.58	0.44	0.57	1.60
Isolated	104,362.0	0.47	0.94	0.41	0.34	1.69
Total	462,769.0	2.71	5.18	2.38	2.87	13.14

Table 2. SOC stocks (Pg) across Global and regional permafrost regions.

Region/Depth	0-30 cm	0-100 cm	100-200 cm	200-300 cm	0-300 cm	References
Northern hemisphere	191 Pg	495.8 Pg			1700 Pg	Tarnocai et al. 2009
Northern hemisphere	217 Pg	472 Pg	355 Pg	207 Pg	1300 Pg	Hugelius et al. 2014
Mongolia	6553.1 Mg	9937.3 Mg				Batkhishig et al. 2021
Mongolian permafrost region	2.7 Pg	5.2 Pg	2.9 Pg	2.4 Pg	13.14 Pg	Our study

REFERENCES

Hugelius, G., Strauss, J., Zubrzycki, S., Harden, J.W., Schuur, E.A.G., Ping, C.L., Schirrmeister, L., Grosse, G., et al. 2014. Estimated stocks of circumpolar permafrost carbon with quantified uncertainty ranges and identified data gaps, Biogeosciences, 11: 6573–6593. doi:10.5194/bg-11-6573-2014

Carbon dynamics in sub tropical eastern Himalayan permafrost region

Rahul Kumar Agrawal[1,2], Ranjan Kumar Mohanty[1], M.G. Yadava[1] & Amzad Hussain Laskar[1]

[1]*Physical Research Laboratory, Ahmedabad*

[2]*Indian Institute of Technology, Gandhinagar*

Soil organic carbon (SOC) stored in the permafrost region is a significant component of global carbon cycle. Approximately 33 % of the global soil carbon is stored in permafrost regions which is more than twice as that present in the atmosphere and is very sensitive to climate change (Hugelius et al. 2014). Permafrost is mainly present in the high latitude and high-altitude regions of world. As compared to arctic permafrost, data for understanding the carbon dynamics from mountain permafrost are scanty due to challenges associated with sampling. Various research work indicated the presence of permafrost in the Himalayan Mountain ranges (Gruber et al. 2017; Baral and Haq 2020), but those works were carried out using remote sensing and satellite data. The major objective of our present study is to understand carbon dynamics in Himalayan permafrost using radiocarbon dating of soil and soil CO_2.

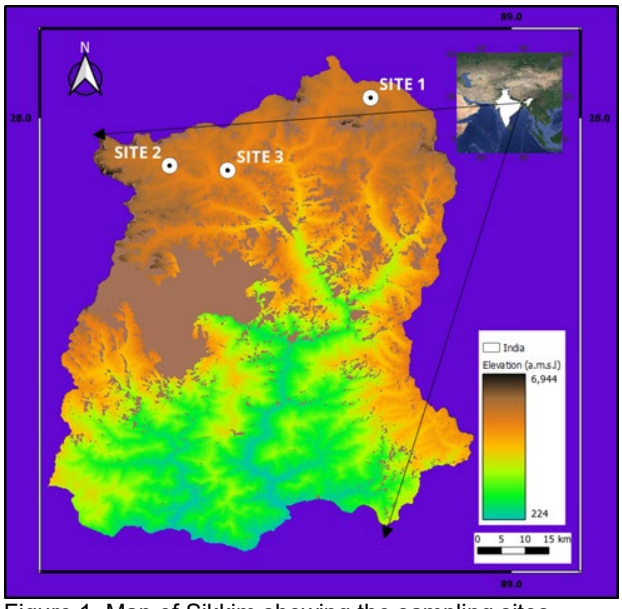

Figure 1. Map of Sikkim showing the sampling sites.

Study area and methodology

For this study we choose eastern Himalayan region (Sikkim, Figure 1). We collected soil and soil CO_2 samples from three locations in northern Sikkim (Figure 1) in September 2023. All the sites are located above 4000 m. At two locations (Site-1 and Site-3 in Figure 1) we found soil up to depth of more than 1.5 meter. We measured ^{14}C in bulk soil sample (peat) and soil CO_2 to estimate the soil organic residence time and the sources of the CO_2 in soils. The radiocarbon measurements were carried in Accelerator Mass Spectrometer (AMS) at Physical Research Laboratory, Ahmedabad. CO_2 was prepared from SOC by combustion and separated using cryogenic technique in vacuum system. CO_2 from soil air was also extracted using cryogenic technique. Pure CO_2 was reduced to graphite targets and the ^{14}C contents were measured in AMS.

Result and discussion

In all the locations, the temperature gradually decreased with increasing depth from the surface. However, within the soil zones, the summer temperature did not reach to zero indicating absence of permafrost up to the sampling depth. Baral and Haq (2020) reported presence of permafrost in this region by mapping the presence of rock glaciers using remote sensing data. Extrapolation of the temperature decrease with depth at site-2 and site-3 indicates that there can be permafrost in this region at depths of > 5 m below the surface (Figure 2). Probably it is not possible to get soils at such depths in this eastern Himalayan region. So, the permafrost in this region is basically rocky permafrost. The radiocarbon ages of SOC at site-3 are presented in Figure 3. Surface SOC are modern and deposited recently. Radiocarbon ages increases gradually reaching to a value of 10000 at a depth of 100 cm. The organic carbon strode in this high-altitude region is relatively old compared to the SOC in tropical and subtropical regions. We also measured the ^{14}C age of soil CO_2 at site-3 and got the age 780 cal BP near the surface (22 cm depth) and 2478 cal BP at a depth of ~80 cm. Unlike the most soil CO_2 profiles, here we observed older soil CO_2 even near the surface. This along with the ages of the SOC indicates that a large fraction of old SOC is decomposing to produce CO_2. Probably the recent increase in temperature due to climate change is destabilizing the old SOC in the region causing the decomposition of old SOC. With further increase in temperature, more CO_2 may get released causing positive feedback to climate change.

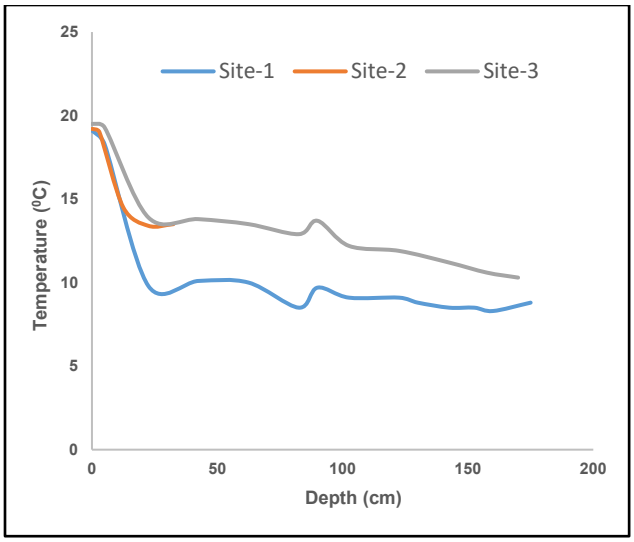

Figure 2. Variation of temperature with depth

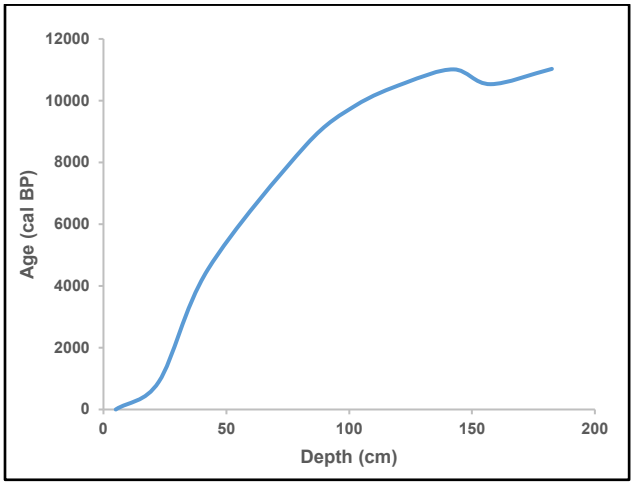

Figure 3. Variation of radiocarbon age with depth in Site-3

REFERENCES

Baral, P., and Haq, M.A. 2020. Spatial prediction of permafrost occurrence in Sikkim Himalayas using logistic regression, random forests, support vector machines and neural networks. Geomorphology, 371 (107331):1–21. https://doi.org/10.1016/j.geomorph.2020.107331

Gruber, S., Fleiner, R., Guegan, E., Panday, P., Schmid, M., Stumm, D., Wester, P., Zhang, Y., and Zhao, L. 2017. Review article: Inferring permafrost and permafrost thaw in the mountains of the Hindu Kush Himalaya region. The Cryosphere, 11:81–99. doi:10.5194/tc-11-81-2017

Hugelius G., Strauss, J., Zubrzycki, S., Harden, J.W., and Schuur, E.A.G. 2014. Estimated stocks of circumpolar permafrost carbon with quantified uncertainty ranges and identified data gaps. Biogeosciences, 11(23): 6573–6593.

Coupled modeling of subsurface processes to inform permafrost methane emissions predictions

Lisa Bigler, David Fukuyama, Rosie Leone & Jennifer Frederick
Sandia National Laboratories

We present the development of an ensemble modeling framework that drives coupled thermal-hydrologic-biogeochemical models to inform Arctic soil methane emission predictions. We demonstrate how the collaborative field, laboratory and modeling efforts informs the development of the software driving this workflow. We focus our discussion on the model development and framework, including model calibration and sensitivity studies aimed towards uncertainty quantification. We present work towards the project goal of modeling how environmental forcing changes would result in changes to the methane balance in terms of in situ methane production vs methane flux to the soil surface as a function of temperature, water content, and soil organic carbon content. This project is titled Coupled Hydro-thermo-biogeochemical modeling for Predicting Arctic Carbon Emissions (CH_4PACE) and is a collaboration between University of Alaska, Fairbanks (UAF), University of Texas, Austin (UT), and Sandia National Laboratories.

Modeling framework and software

Our modeling frameworks utilizes PFLOTRAN, a high performance, parallel, open-source code for subsurface processes. The governing equations are given by the conservation of mass and the conservation of energy with many supporting constitutive equations; details provided in Lichtner et al. (2020). The software is discretized using the finite volume in space and a fully implicit backward Euler approach in time and solved with a Newton-Rasphson solver.

The subsurface model requires soil properties such as porosity, thermal properties, saturation and permeability functions as well as initial and boundary conditions. We use an ecotype based approach where we assume soil properties and snow behaviors are constant for each ecotype. The ecotype classification used in our framework is that presented in Jorgenson et al. (2003) and Jorgenson et al. (2009).

Two additions to the subsurface model within the Arctic modeling framework are being developed. Both additions are ecotype based: one is a surface model and the other is a biogeochemistry model.

The surface model will take the inputs of ecotype, temperature and precipitation data. The ecotype will set snow accumulation and density properties which help determine the energy and mass flux at the boundary. The framework connects the surface model to the subsurface PFLOTRAN model.

A model for Arctic soil biogeochemistry process has been coupled to the reactive transport process model within PFLOTRAN using a Reaction Sandbox, see Hammond et al. (2022). The biogeochemistry model is based on with well known Monod equation. The development and full scope of the biogeochemistry model used within our frameworks will be discussed.

The ensemble for the framework is depicted in Figure 1. The framework entails preprocessing the data and formatting the simulation input, running the simulation, then postprocessing the output with the ultimate goal of upscaling the output or creating a surrogate based on the output to help inform earth system models. sensitivity analysis of the model are planned, which will help inform how we conduct uncertainty quantification.

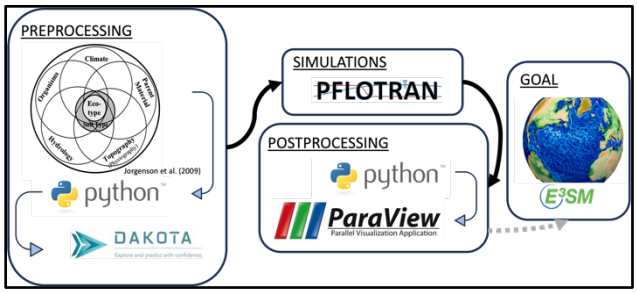

Figure 1. A depiction of the modeling framework for subsurface modeling in the Arctic, including software and data used for preprocessing, simulating, postprocessing and the ultimate goal of the project.

Model verification and validation

Initial model verification and validation have been conducted using data and benchmark problems.

For validations, an example at the Franklin Bluffs site was used. The soil properties found in Nicolsky et al. (2009) were used as well as data from Romanovsky (2016). The validation of the subsurface model was conducted using the air temperature as a surface boundary condition; the results showed the need to include a surface model to account for the insulating effect of the snow and other energy effecting processes. Developments toward the surface model are discussed.

For verification, we compare with a large benchmark case found in Grenier et al. (2018). This example is a two-dimension example of a square of ice encased in a rectangular domain of porous media. We see good qualitative agreement and results will be presented.

SUPPORTING FIELD AND LABORATORY RESEARCH

Core samples have been collected around the Fairbanks area. Two main sites are the focus of our studies: Smith Lake 1 warming permafrost, talik development mixed spruce, moss and Smith Lake 4, stable permafrost, black spruce tussocks. Figure 2. shows an overview of the Smith Lake sites and a map of Alaska with a reference point for Fairbanks. These Smith Lake sites were chosen due to their and difference in permafrost behavior, abundance of historical and current data, and their proximity to UAF for additional studies. Core samples taken at Smith Lake 1 and Smith Lake 4 were sent to UT, Austin and Sandia National Laboratories for soil and biogeochemistry analysis.

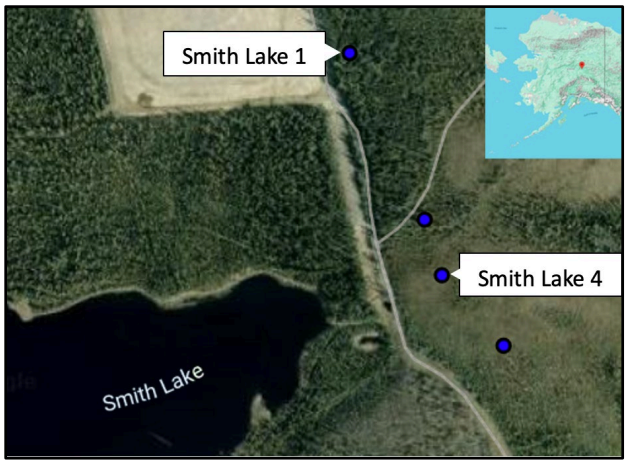

Figure 2. A picture of Smith Lake sites near UAF and a map of Alaska with a pin showing where Fairbanks is located. Both the image and map are from Google.

Subsurface models required a quality soil property data; UT has the means and expertise to conduct such research. Core samples sent to UT have been studied and grain size distributions for both Smith Lake 1 and Smith Lake 4 core samples have been conducted. Permeability experiments with synthetic sample of frozen soil have been conducted. Addition planned studies include characterization moisture and density, porosity, mineralogy, liquid limit and heat care samples from one end while performing CT scans and collection gas effluent for characterization.

For biogeochemical studies, samples were sent to Sandia National Laboratories. Scientists, experienced in Arctic soil biogeochemical studies, will incubate samples from Smith Lake 1 and Smith Lake 4 cores at different depths. The plan is to incubate duplicate samples near site temperatures in anoxic and oxic conditions and measure concentration of CH_4 and CO_2 produced and measure ^{12}C and ^{13}C of CH_4 and CO_2. Results will help calibrate and inform the biogeochemical model within the full subsurface model system.

CONCLUSION

We present efforts towards the CH_4PACE project goal of modeling how environmental forcing changes, including changes to temperature, water content, and soil organic carbon content, would result in changes of methane flux to the soil surface.

ACKNOWLEDGEMENT

SNL is managed and operated by NTESS under DOE NNSA contract DE-NA0003525. SAND2023-14434A

REFERENCES

Grenier, C., Anbergen, H., Bense, V., Chanzy, Q., Ethan, C., Collier, N., Costard, F., Ferry, A., Fredrick, J., Goncalves, J., Holmen, J., Jost, A., Kokh, S., et al. 2018. Groundwater flow and heat transport for systems undergoing freeze-thaw: Intercomparison of numerical simulators for 2D test cases. Advances in Water Resources, 114, 196–218.

Hammod, G. 2022. The PFLOTRAN Reaction Sandbox. Copernicus GmbH.

Jorgenson, M.T., Roth, J., Miller, F., Macander, M., Duffy, M., Wells, A., Frost, G., and Pullman, E. 2009. An Ecological Land Survey and Landcover Map of the Arctic Network. Natural Resource Technical Report NPS/ARCN/NRTR—2009/270.

Jorgenson, M.T., and Heiner, M. 2003. Ecosystems of Northern Alaska. 1:2.5 million-scale map produced by ABR, Inc., Fairbanks, AK and The Nature Conservancy, Anchorage, AK.

Lichtner, P., Hammond, G., Lu, C., Karra, S., Bisht, G., Andre, B., Mills, R., Kumar, J., and Frederick, J. 2020. PFLOTRAN Web page, http://www.pflotran.org.

Nicolsky, D., Romanovsky, V., and Tipenko, G. 2009. Estimation of soil thermal properties using in-situ temperature measurements in the active layer and permafrost. Cold Regions Science and Technology, 55.1, 120–129.

Nicolsky, D., Romanovsky, V., Wright, T., and Cable, W. 2022. Assessment of permafrost changes in the 21st century in the Alaskan Arctic and Brooks Range. In American Geophysical Union Fall Meeting.

Romanovsky, V. 2016. Updated North Slope air and ground temperatures, soil moisture (Excel). Arctic Data Center.

Measuring greenhouse gas emissions over discontinuous permafrost with UAV

Abdullah Bolek[1], Martin Heimann[1,2] & Mathias Goeckede[1]

[1]*Max Planck Institute for Biogeochemistry, Jena, Germany*

[2]*Institute for Atmospheric and Earth System Research, University of Helsinki, Helsinki, Finland*

The landscape heterogeneity in the Arctic permafrost region has broad scale separation ranges from less than a meter up to thousands of kilometers. This necessitates observations across different scales to comprehend the ecosystem processes and disturbances. The conventional ways of measuring greenhouse gas emissions over a region are accomplished either using flux chambers or eddy towers. However, flux chambers are not feasible for large scale measurements, while installing an eddy tower in such remote places requires a substantial amount of effort in logistics. In addition, due to the stationary installation the eddy towers only collect flux information from limited footprint areas, with sizes of several 100's to 1000's of m^2 depending on measurement height. Generally, these issues can be addressed by conducting aircraft based measurements. However, aircraft based measurements have high costs, have difficulties to fly near the sources at the ground and cannot be made regularly. Recently, unmanned aerial vehicles (UAVs) have developed into a promising approach for quantifying GHG emissions: UAVs are ubiquitous, convenient, and inexpensive compared to eddy towers and aircraft based measurements. Here, we present our recently developed UAV platform that carries two gas analyzers for CH_4 (Aeris Strato) and CO_2/H_2O (Licor Li-850) mixing ratio measurements on board as well as an ultrasonic anemometer (Trisonica Mini) that can measure 2-D wind speed, air temperature, pressure, and humidity (see Figure 1).

Our UAV platform is a hexacopter that can carry a payload of up to 7.5 kg. The flight time without payload is noted as 55 mins. It uses Cube Orange (Copter 4.2.2) as a flight controller and logs the flight data such as roll, pitch, yaw, and accelerations that can later be used to correct wind speed measurements. With our entire scientific payload weighing about 4.1 kg (the total take off mass is about 16.6 kg), the total flight time is about 20 mins per battery set. In addition, a custom-built data logger (Teensy 4.1) and a power distribution board are deployed to log the data from analyzers and anemometer, and power up the scientific payload, respectively. All data are synchronized and logged at 2 Hz.

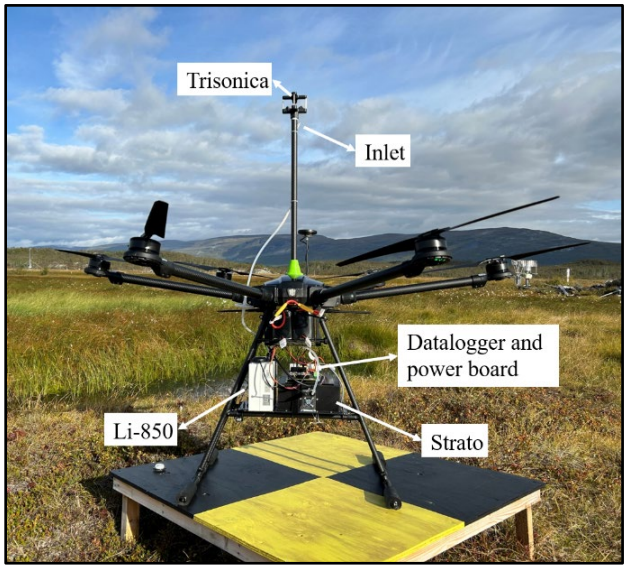

Figure 1. Instrumented UAV platform. Inlet of the gas analyzers and anemometer were placed about 65 cm over the rotor plane, and gas analyzers (Licor Li-850 for CO_2, and Aeris Strato for CH_4) were below the rotor plane.

After rigorous laboratory and field tests, the first field campaign was conducted over Stordalen Mire, Abisko, Sweden (68° 21' 20.574" N, 19° 2' 42.954"E) between 1 – 22 September 2023. The field site is within the sub-Arctic zone and with discontinuous permafrost (Sjögersten et al. 2023). During the field campaign, 33 independent flights (i.e., about 10 flight hrs) were conducted over different landscape features (dry and wet), altitudes, flight speeds, and flight modes.

Among different other flight modes, grid survey flights (flight tracks illustrated in Figure 2) were conducted on 11/09/2023. These flights were used to identify potential local GHG emission hot spots over the area of interest. The flight missions were planned using the landcover map of Varner et al. (2022). Three areas were defined, with two of them mostly wet (dominated by bog and fen) and one of them mostly dry (dominated by palsa). Area surveys (10 m AGL) started from the east-to-west direction first and continued from the north-to-south direction so that the same locations over the area were sampled twice at two different times. The flight tracks are shown as black solid circles in Figure 2, each of them representing a unique measurement point

separated by approximately 2 m based on the sampling frequency of 2 Hz, and the flight speed of 4 m s^{-1}.

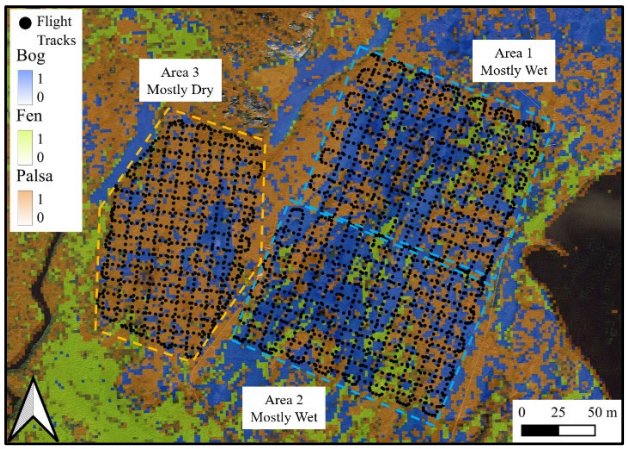

Figure 2. Flight tracks of grid surveys over three different areas. Here, the landcover map shows the vegetation distribution, and the border of areas were represented by dashed lines (blue for wet, orange for dry). Flight tracks are indicated with black solid circles.

Before and after each flight, two calibration gas tanks were sampled for about 5 mins to correct any offsets and drifts that might be present in the gas analyzers. After the correction procedure, the measured concentrations of CO_2 and CH_4 were first spatially averaged, subsequently concentration maps as presented in Figure 3 were created. This preliminary data analysis already reveals that the areas that are mostly wet (Areas 1 and 2) had higher atmospheric concentrations of CH_4 and CO_2 compared to the mostly dry area (Area 3).

In subsequent analyses, these concentration maps will later be combined with the measured wind speed, and a footprint analysis will be conducted to better identify the sources areas of local atmospheric hotspots. We will also present results based on additional flights in curtain and box flight modes over Stordalen Mire, which will be used to quantify the advection fluxes over the area of interest, and constrain net emissions within the target domains by employing a mass balance method. Taken together, the UAV experiments will allow us to evaluate the impact of the surface heterogeneity on regional carbon fluxes, and improve constraining net fluxes over structured Arctic wetland ecosystems.

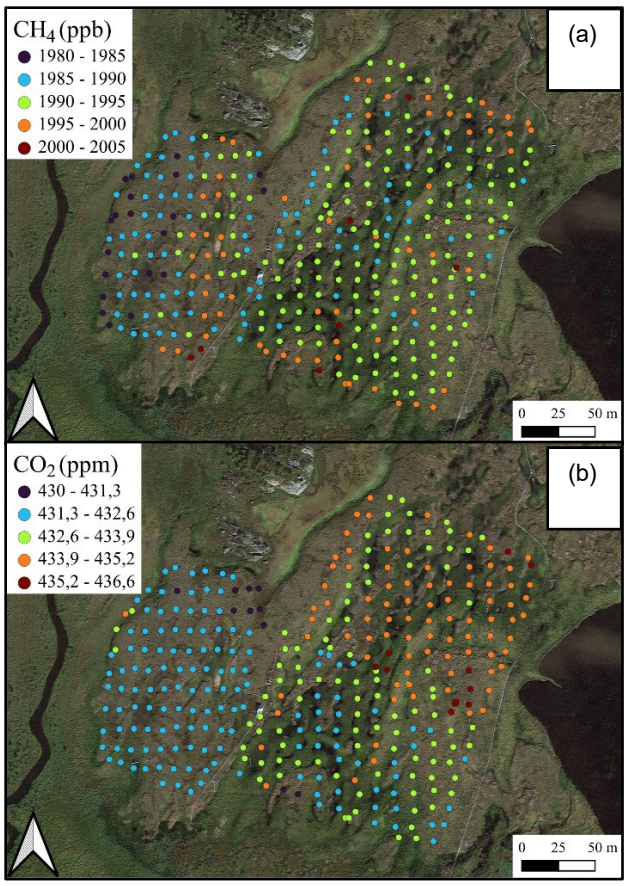

Figure 3. Spatially averaged CO_2 and CH_4 concentrations from grid surveys that were conducted on 11/09/2023.

References

Sjögersten, S., Ledger, M., Siewert, M., de la Barreda-Bautista, B., Sowter, A., Gee, D., Foody, G., and Boyd, D.S., 2023. Optical and radar Earth observation data for upscaling methane emissions linked to permafrost degradation in sub-Arctic peatlands in northern Sweden. Biogeosciences, 20(20): 4221–4239, https://doi.org/10.5194/bg-20-4221-2023

Varner, R.K., Crill, P.M., Frolking, S., McCalley, C.K., Burke, S.A., Chanton, J.P., Holmes, M.E., Isogenie Project Coordinators, Saleska, S., and Palace, M.W. 2022. Permafrost thaw driven changes in hydrology and vegetation cover increase trace gas emissions and climate forcing in Stordalen Mire from 1970 to 2014. Philosophical Transactions of the Royal Society A, 380(2215): p.20210022. https://doi.org/10.1098/rsta.2021.0022

Modelling the northern peatland methane fluxes with a process-based model

Wenzhuo Duan[1], Mousong Wu[2], Koffi D. Noumonvi[3], Joshua L. Ratcliffe[3], Mats.B. Nilsson[3], Matthias Peichl[3] & Per-Erik Jansson[4]

[1]*Nanjing University, Nanjing, Jiangsu, China*

[2]*International Institute for Earth System Science of Nanjing University, Nanjing, Jiangsu, China*

[3]*Department of Forest Ecology and Management, Swedish University of Agricultural Sciences, Umeå, Sweden*

[4]*KTH Royal Institute of Technology, Stockholm, Sweden*

Northern peatlands are significant in the global carbon cycle. Northern peatlands store a large amount of soil organic carbon (SOC) with a carbon stock of about 265-675 Pg, acting as a long-term atmospheric carbon dioxide sink and a source of methane and nitrogen dioxide. However, climate warming, peatland drainage, and agricultural conversion of peatlands could potentially disrupt this process and alter the cooling effect of peatlands on the climate (Frolking et al. 2011; Huang et al. 2021; Fewster et al. 2022; Helbig et al. 2022; Liu et al. 2022). Under drying and warming conditions, significant amounts of peat are more prone to decomposition. Currently, the carbon cycling process and the mechanism of its impact on Northern peatlands are not well understood. Therefore, optimal simulation and mechanistic analysis of key processes of carbon fluxes in peatlands are important for better predicting the climate effects of peatlands under future climate change scenarios. Our study is based on the CoupModel and almost 22 years of meteorological and flux data from the Degero site (SE-Deg), with the following objectives：

- To optimize simulation of surface CH4 emission fluxes, hydrothermal processes, and carbon fluxes at boreal minerotrophic mire.
- To explore groundwater table controls on methane flux emission.

METHODS

Degerö Stormyr (64.18°N, 19.56°E, 270m a.s.l) is a natural boreal nutrient-poor minerogenic mire, representing much of the mire areas in the boreal region, located in a highland in the county of Västerbotten, Sweden. The depth of the peat layer is generally 3-4m, reaching up to 8m. Vegetation around the study site area is dominated by mire lawn species with bog mosses dominating the bottom layer.

The model calibration is mainly divided into three steps: (1) a manual selection of parameters related to soil hydrothermal and plant growth processes and parameter sensitivity identification using the Morris method, machine learning, and Monte Carlo sampling; (2) optimized simulation and validation of model output variables, including soil temperature (TS), latent heat fluxes (LE), sensible heat fluxes (H), and net ecosystem carbon exchanges (NEE) were completed; (3) Screening and calibrating sensitive parameters related to methane fluxes (CH_4) and groundwater depth (WTD) with the same methodology as before.

PRELIMINARY RESULTS

312 out of 20000 groups of simulations were selected for demonstration using R^2 and RMSE as performance indicators. In the screening process, we found that, when the CH_4 simulation was constrained based on performance indexes, the WTD simulation was also constrained well. Therefore, the criteria on r^2 of CH_4 greater than 0.59 and RMSE of CH_4 less than 0.05 was chosen. Overall, the calibrated model captured the seasonal fluctuations of methane fluxes at the site well (CH_4, r^2_{mean} = 0.62), and the simulation accuracy for the groundwater table, although it needs to be improved, was also able to portray its overall changes (WTD, r^2_{mean} = 0.20), according to Figure 1. Among all the years, the simulated peak of methane fluxes in 2018 shows an overestimation relative to the observation, while at the same time, there is a certain deviation between the simulated and observed values of groundwater levels in this year compared to the other years. In addition, we note that the observed methane fluxes had a pulsed emission peak in the spring of each year, which may be due to surface snowmelt or thawing of the peat layer, but the model did not simulate this process well.

We take the average annual precipitation as the criterion, and years with more annual precipitation than average are considered wet years, and vice versa dry years. The fluxes of methane from production to emission in dry and wet years are demonstrated in Figure 2. Methane emissions as a proportion of total production do not differ significantly between dry and wet years. There are three pathways for the release of methane into the atmosphere: plant transport, surface emission, and ebullition. At this site, methane is emitted

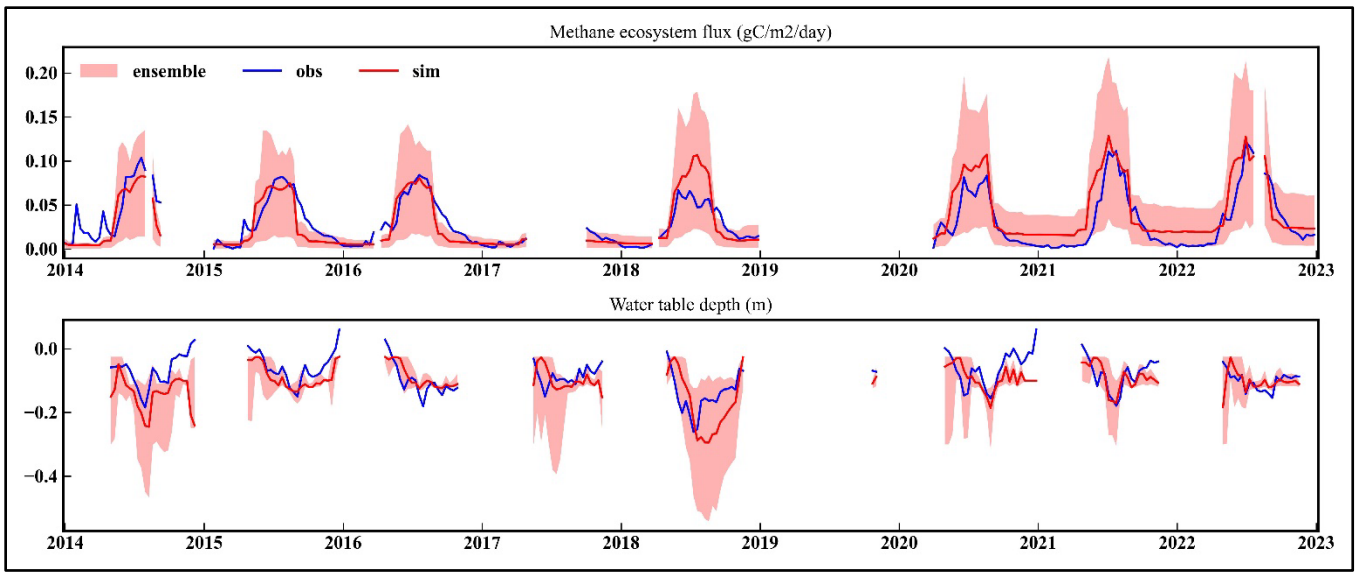

Figure 1. Simulation of the hourly methane ecosystem flux (CH_4) and water table depth (WTD) from 2014 to 2023. Red shading shows the upper and lower limits of the 314 groups of simulations. The time series in the figure are aggregated to a 10-day scale.

to the atmosphere mainly by convection and molecular diffusion through the soil pore space, and to a lesser extent as bubbles released at the water table, with a very small amount transported upwards from the soil in the root zone through plant rhizomes. In wet years, the proportion of methane emitted from the surface as a percentage of total emissions decreased slightly compared to dry years, while the proportion of bubbling release was nearly double that of dry years, and methane transported by vegetation was little changed.

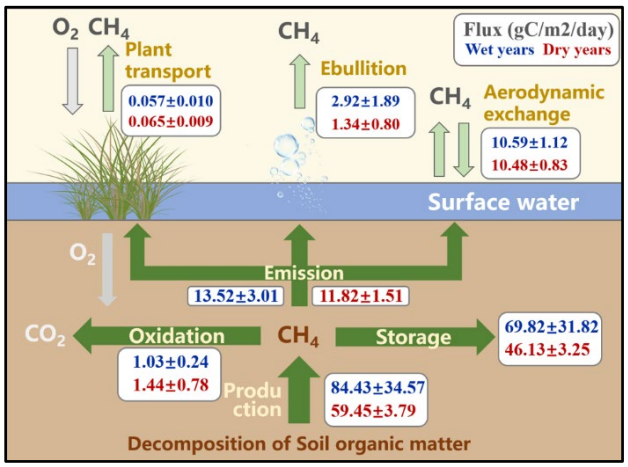

Figure 2. Schematic showing methane fluxes from production to emission under different water conditions.

References

Fewster, R.E., et al. 2022. Imminent loss of climate space for permafrost peatlands in Europe and Western Siberia, Nature Climate Change, 12(4): 373–379. doi:10.1038/s41558-022-01296-7

Frolking, S., et al. 2011. Peatlands in the Earth's 21st century climate system, Environmental Reviews, 19: 371–396. doi:10.1139/a11-014

Helbig, M., et al. 2011. Warming response of peatland CO2 sink is sensitive to seasonality in warming trends, Nature Climate Change, 12(8): 743–749. doi:10.1038/s41558-022-01428-z

Huang, Y., et al. 2021. Tradeoff of CO2 and CH4 emissions from global peatlands under water-table drawdown, Nature Climate Change, 11(7): 618–622. doi:10.1038/s41558-021-01059-w

Liu, L., et al. 2022. Carbon stock stability in drained peatland after simulated plant carbon addition: Strong dependence on deeper soil, Science of The Total Environment,848:157539. doi:10.1016/j.scitotenv.2022.157539

Beyond permafrost: The carbon cycle in the Arctic land-ocean continuum

Michael Fritz[1], Jorien Vonk[2], Marcel Babin[3], Annett Bartsch[4], Luana Basso[5], Lisa Bröder[6], Mathias Goeckede[5], Örjan Gustafsson[7], Gustaf Hugelius[7], Anna Irrgang[1], Bennet Juhls[1], Mckenzie Kuhn[8], Hugues Lantuit[1], Manfredi Manizza[9], Jannik Martens[10], Matt O'Regan[7], Niek Speetjens[11], Anya Suslova[12], Suzanne Tank[13], Jens Terhaar[14] & Scott Zolkos[12]

[1]*Alfred Wegener Institute Helmholtz Centre for Polar and Marine Research, Potsdam, Germany*

[2]*Vrije Universiteit Amsterdam, Amsterdam, The Netherlands*

[3]*Université Laval, Québec City, Québec, Canada*

[4]*b.geos, Korneuburg, Austria*

[5]*Max Planck Institute for Biogeochemistry, Hamburg, Germany*

[6]*ETHZ, Zurich, Switzerland*

[7]*Stockholm University, Stockholm, Sweden*

[8]*University of British Columbia, Vancouver, British Columbia, Canada*

[9]*University of California, San Diego, California, United States*

[10]*Columbia University, New York, New York, United States*

[11]*Department of Environmental Studies, University of Victoria, Victoria, British Columbia, Canada*

[12]*Woodwell Climate Research Center, Falmouth, Massachusetts, United States*

[13]*University of Alberta, Edmonton, Alberta, Canada*

[14]*University of Bern, Bern, Switzerland*

Northern high-latitude regions are experiencing climate warming at a rate of up to four times faster than the global average. Already in 2017, a report from the Arctic Council indicated a shift in the Arctic climate to a new state, marked by ongoing warming and an escalation in extreme events like heat waves and boreal fires. This trend is triggering a series of consequences affecting various components of the cryosphere and hydrosphere, including the melting of sea ice and ice sheets, increasing terrestrial discharge, thawing of frozen ground, and coastline collapse.

The Arctic is characterized by substantial continental land masses bordering the relatively small and shallow Arctic Ocean. Approximately 50% of the Arctic Ocean consists of shelf seas with a depth of less than 200 meters, comprising only 1% of the global ocean volume. Arctic fluvial systems contribute over 10% of global discharge to the Arctic Ocean, and the coast is subject to some of the highest erosion rates on earth. This underscores the profound connection between the Arctic Ocean and the terrestrial hinterland.

The terrestrial environment contributes large fluxes of organic matter to the Arctic Ocean. Arctic soils host significant belowground carbon pools, the majority being stored in permafrost. Warming in the Arctic leads to permafrost thaw, exposing large amounts of carbon to degradation into greenhouse gases and releasing other constituents into the environment. The increased input of organic carbon into the Arctic Ocean contributes to ocean acidification and serves as an additional food supply for heterotrophic organisms. In addition to emissions and biological uptake, long-term sequestration and natural carbon drawdown in marine sediments represent an important geological carbon sink.

This review focuses on the entire Arctic land-ocean continuum, spanning from continental headwaters to the seafloor sediments. In this entire region, rapid environmental changes are expected to strengthen the importance of the Arctic in global carbon cycling and climate feedbacks. However, the assessment of change becomes increasingly challenging in the absence of a clear baseline, and so it is crucial to provide a comprehensive overview of the current state.

This review presents a holistic yet detailed carbon budget for the Arctic land-ocean continuum, drawing mainly from recent or newly published data from international initiatives such as ARCADE, ArcticGro, CASCADE, GTN-P, NCSCD, and RECAPP2. The overview encompasses carbon stocks and fluxes in the pan-Arctic domain, including terrestrial and marine (sediment and water column) stocks, lateral fluxes from rivers and coastal erosion, as well as vertical fluxes on land (terrestrial and aquatic) and in the ocean (emission and accumulation). Additionally, the review identifies key knowledge gaps and outlines directions for future research priorities.

The eastern Siberian tundra, a highly variable and uncertain greenhouse gas source

Geert Hensgens[1], Luca B. Marchesini[2], Jorien E. Vonk[1], Josh F. Dean[3], Alex J.V. Buzacott[1], Roman Petrov[4], Sergei Karsanaev[4], Trofim V. Maximov[4] & Han J. Dolman[5]

[1]*Department of Earth and Climate, Vrije Universiteit Amsterdam, Amsterdam, the Netherlands*

[2]*Department of Sustainable Agro-Ecosystems and Bioresources, Edmund Mach foundation, San Michele all'Adige, Italy*

[3]*Department of Geographical Sciences, University of Bristol, Bristol, UK*

[4]*Inst. for Biological Problems of Cryolithozone, Siberian Division of Russian Academy of Science, Yakutsk, Russia*

[5]*Royal NIOZ, the Netherlands Institute for Sea Research, Den Burg, the Netherlands*

Following decades of warming at almost four times the average global rate (Rantanen et al. 2022), the Arctic is changing rapidly. The vast amounts of carbon stored in Arctic soils (Hugelius et al. 2014) present a potentially strong positive feedback loop. Siberia, home to a significant proportion of the global tundra, remains understudied and long-term greenhouse gas (GHG) monitoring using eddy covariance (EC) is scarce (Chu et al. 2017). With more than 15 years of data between 2003 and 2021, we present one of the longer EC monitoring series in eastern Siberia. We show that the eastern Siberian tundra is currently a highly variable and uncertain GHG source. Net CO_2 uptake in the growing season is offset by methane emissions, roughly half of which are emitted outside of the carbon uptake season. The cumulative CO_2 uptake has increased over the last decades. However, cumulative methane emissions are strongly coupled to carbon uptake, with roughly 1.97 g CO_{2eq}-C emitted as methane per 1 g CO_2-C taken up during the carbon uptake period. As a result, any future increase in tundra productivity is offset by enhanced methane release, strengthening the GHG source of the Siberian tundra.

Arctic tundra in a changing world

Current warming is changing the Arctic at an unprecedented rate, leading to 'greening' of the tundra and growing season lengthening (Piao et al. 2007). This affects primary production more than soil respiration (Forkel et al. 2016), increasing the carbon sink. However, not considered is the coupling with methane emissions, long-term measurements of which are rare, especially in Siberia. In this study we combine EC measurements with machine learning to analyse CO_2 and methane dynamics in an extremely remote site in northeastern Siberia.

Summer CO_2 uptake is offset by 'shoulder season' methane emissions

The average CO_2 uptake during the carbon uptake period was 120 ± 16 g·C·m^{-2}. Methane emissions were on average 104 ± 44 CO_{2eq} g·C·m^{-2}, rarely completely offsetting the CO_2 uptake, Figure 1. However, outside of the carbon uptake period both CO_2 and methane emissions were mostly positive. Previous research has established the importance of emissions within the so-called 'zero-curtain', the period in which soils remain unfrozen despite freezing surface temperatures, leading to emissions that offset the GHG balance (Oechel et al. 2014; Zona et al. 2016).

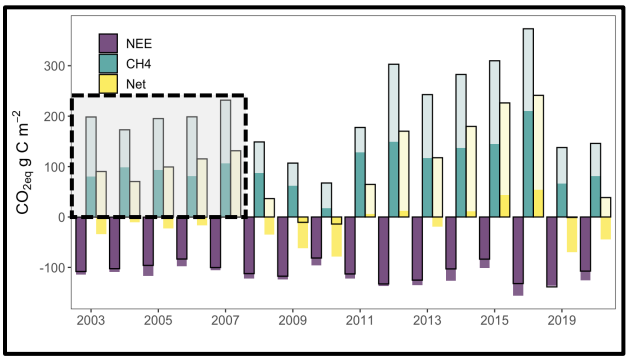

Figure 1. Cumulative greenhouse gas emissions of CO_2 (NEE, purple), CH_4 (green) and combined (Net, yellow) in CO_{2eq} g·C·m^{-2}. Methane and net fluxes in the grey box are modelled estimates. Dark shades show growing season and light tints 'shoulder season' cumulative fluxes.

However, keeping a constant power supply – a prerequisite to EC monitoring in winter – can be near impossible in remote areas with extreme winter conditions. This, together with other logistic considerations, led to the absence of winter flux measurements within this study. Instead, we have opted for careful and conservative estimation of 'shoulder season' fluxes, consisting of gap-filled or modelled data up to 45 days before snowmelt and 30 days after the first average sub-zero temperature day. These limits

avoid gap-filling outside of environments in which measurements are available, while providing estimates for years without 'shoulder season' data. Taking these fluxes and estimates into account show highly variable net GHG emissions of 97 ± 79 CO_{2eq} g·C·m^{-2} annually, reiterating the importance of non-growing season activity on annual fluxes (Zona et al. 2016), Figure 1.

The lack of winter measurements makes true annual GHG emissions uncertain, though likely to be higher. Years with data outside of the growing season (6 out of 11) unequivocally showed positive cumulative emission of methane. We found positive methane fluxes even outside of the 'zero curtain' and no indication of diminished strength with lower surface temperatures. Similarly, in Arctic tundra sites in Alaska methane is emitted year-round (Zona et al. 2016), and in other Russian Arctic tundra sites positive CO_2 measurements have been recorded throughout winter.

Trends GHG exchange

Since the 1990s, strong gradual surface temperature increases have advanced the start of the snow free period, resulting in an earlier onset of net carbon uptake, Figure 2A-B. Following an initial lag-phase of roughly 40 days after snowmelt, a strong positive trend can be seen in CO_2 uptake and incoming solar radiation (not shown). On average the start of the growing season occurs after the incoming solar radiation maximum, and thus an earlier carbon uptake period translates in a longer growing season. During the carbon uptake period CO_2 uptake is limited by sunlight and the end of the period coincides with diminishing sunlight, not temperature (not shown). As such, potential lengthening of positive temperatures at the end of the season will almost certainly not lead to increased annual CO_2 uptake.

Over the last decades a positive trend can be seen in the cumulative growing season carbon uptake, Figure 2C. However, cumulative growing season methane emissions are significantly related to cumulative growing season carbon uptake, Figure 2D. For every additional gram of carbon taken up as CO_2 during the carbon uptake period, almost 2 grams of CO_{2eq}-CH_4 is released. This strong coupling shows that greater carbon uptake in the growing season results in increased net GHG emissions.

Future Arctic tundra GHG exchange

Temperature increase is projected to continue, resulting in the earlier onset of snowmelt and a lengthening of the carbon uptake period. Our results show that while this lengthening of the growing season can lead to additional CO_2 uptake, the net GHG flux will increase through methane emission coupling. Local data shows that winter temperatures rise faster than annual averages (not shown), potentially creating favourable conditions for winter GHG release. Since no trend with temperature and 'shoulder season' emissions can be seen, it is not certain whether this will increase winter emissions. However, with minimum temperatures lower than -40 °C it does not seem unreasonable that emissions are indeed lower at these extreme conditions than what we measured in the 'shoulder season'. Other studies suggest that the lengthening of the 'zero-curtain' may increase emissions (Zona et al. 2016), a shortening of the 'extreme cold curtain' might do the same.

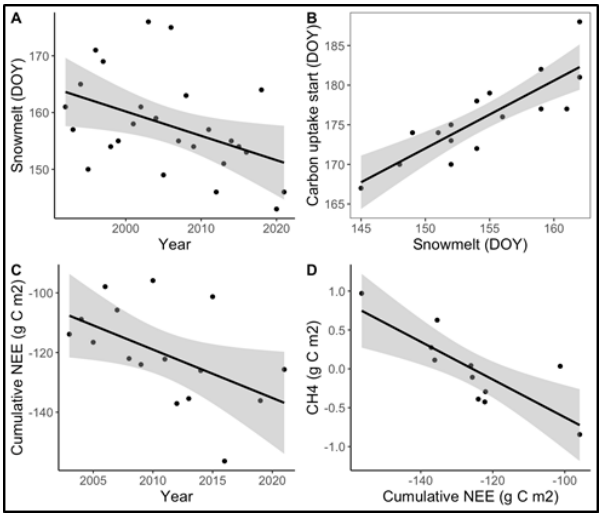

Figure 2. A) snowmelt (day of year), B) start of carbon uptake vs snowmelt (day of year), C) cumulative CO2 uptake (NEE) g·C·m^{-2}, D) methane emissions (g C-CO_{2eq} m^{-2}) vs CO_2 flux (NEE).

References

Chu, H., et al. 2017. Fluxes all of the time? A primer on the temporal representativeness of FLUXNET, Journal of Geophysical Research: Biogeosciences, 122(2): 289–307. doi:10.1002/2016JG003576

Forkel, M., et al. 2016. Enhanced seasonal CO_2 exchange caused by amplified plant productivity in northern ecosystems', Science, 351(6274): 696–699.

Hugelius, G., et al. 2014. Estimated stocks of circumpolar permafrost carbon with quantified uncertainty ranges and identified data gaps, Biogeosciences, 11(23): 6573–6593. doi:10.5194/bg-11-6573-2014

Oechel, W.C., et al. 2014. Annual patterns and budget of CO2 flux in an Arctic tussock tundra ecosystem, Journal of Geophysical Research-Biogeosciences, pp. 323–339.

Piao, S., et al. 2007. Growing season extension and its impact on terrestrial carbon cycle in the Northern Hemisphere over the past 2 decades, Global Biogeochemical Cycles, 21(3): 1–11.

Rantanen, M., et al. 2022. The Arctic has warmed nearly four times faster than the globe since 1979, Communications Earth and Environment, 3(1): 1–10.

Zona, D., et al. 2016. Cold season emissions dominate the Arctic tundra methane budget, Proceedings of the National Academy of Sciences of the United States of America, 113(1): 40–45.

Changing carbon fluxes in the Mackenzie Delta — southern Beaufort Sea river-sea system

Annabeth McCall[1], Lasse Sander[2], Vera Fofonova[3], Martin Hieronymi[4], Anne Morgenstern[1], Michael Fritz[1], Paul Overduin[1], Guido Grosse[1] & Bennet Juhls[1]

[1]*Alfred Wegener Institute Helmholtz Center for Polar and Marine Research, Potsdam, Germany*

[2]*Alfred Wegener Institute Helmholtz Center for Polar and Marine Research, Sylt, Germany*

[3]*Alfred Wegener Institute Helmholtz Center for Polar and Marine Research, Bremerhaven, Germany*

[4]*Institute of Carbon Cycles, Hemholtz-Zentrum Hereon, Geesthacht, Germany*

Intensification of climate change in the Arctic is shifting annual mass fluxes of rivers to coastal seas making them one of the most rapidly changing regions across the Arctic. Due to their inaccessibility, the flux and the fate of organic carbon (OC) and sediments in remote Arctic coastal waters is not well quantified and understood.

Along the Canadian Arctic coast, the Mackenzie River delivers the largest sedimentary load of all Arctic rivers to the Beaufort Sea via the Mackenzie Delta. Previous studies have found that freshwater discharge by the Mackenzie River has increased by ~25% since 2003, with a 39% increase in annual dissolved organic carbon (DOC) flux since the early 1970s (Tank et al. 2016) and an alarming 50% increase in the suspended load since 2009 (Doxaran et al. 2015). Recent findings from Matsuoka et al. (2022) show a decadal increase in late summer organic carbon in the Mackenzie Delta that can be related to a potential response to the current warming of permafrost within the watershed draining to the coastal waters. Such shifts in land-ocean fluxes have potentially crucial consequences for the biodiversity of, e.g., marine life in the coastal ecosystems on which local indigenous communities depend on.

The poor data coverage in these remote coastal regions presents a major knowledge gap to fill in order to achieve a true source-to-sink assessment of how land to sea fluxes of carbon and sediment are impacting coastal ecosystems and the greater pan-Arctic carbon budget. To fully assess seasonal variability of fluxes, hydrography, and fluvial-marine biogeochemistry in shallow Arctic coastal waters, high resolution satellite data along with in situ validation are needed to allow for broader remotely sensed monitoring.

To close the gap between terrestrial and marine observations, we started multiple projects and expeditions to the Mackenzie River - Beaufort Sea region. One of them - the “Fluxes from Land to Ocean: How Coastal Habitats in the Arctic Respond” (FLO CHAR) project - aims to provide valuable insights of changing Arctic land-ocean matter fluxes into the coastal waters and accumulation into sediments, permafrost thaw and associated impacts on the biodiversity in the Arctic coastal environment. In addition, a new high-frequency Mackenzie River sampling program (https://mackenzie-monitoring.awi.de/) will provide a full picture along the fresh to marine transition zone. Through these activities, we hope to resolve our understanding of the magnitude, variability, and impact of fluvial and coastal OC fluxes in river-sea systems utilizing advances in remote sensing that will ultimately allow for OC and sediment flux estimates independent of in situ observations.

This project employs an interdisciplinary approach that integrates field sampling, remote sensing, and modeling. Comprehensive water sampling, sediment coring, and other in situ measurements will be collected across the Mackenzie Delta and the southern Beaufort Sea. Applying new ocean color remote sensing (OCRS) techniques, Sentinel-3 OLCI and Sentinel-2 MSI optical remote sensing time series will be used to quantify DOC, particulate organic carbon (POC), and sediment concentrations throughout the study area. Additionally, NASAs surface water ocean topography (SWOT) will be the first satellite to provide high-resolution global surface water levels, yielding changes in freshwater budgets. Combining discharge observations with concentration retrievals of carbon and sediment will offer a new, unique, and globally available method to obtain land-ocean carbon fluxes (Figure 1). In addition to observational data, numerical simulations will be used to estimate carbon transport pathways, redistribution and deposition zones under different forcing scenarios using the FESOM-C model (Fofonova et al. 2021).

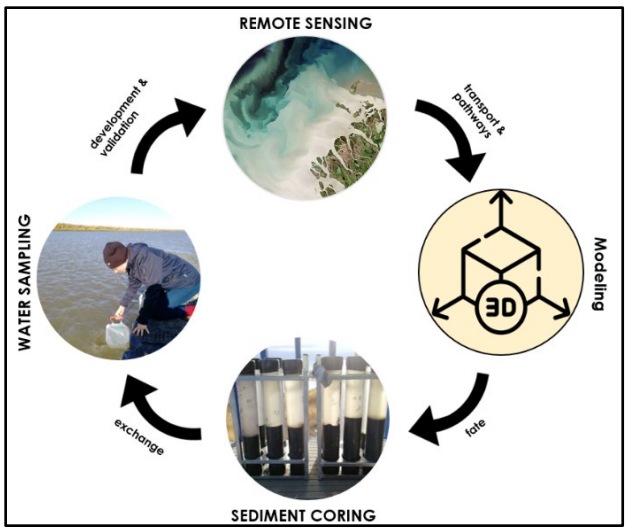

Figure 1. Scheme of how research addresses the interplay between coastal processes and marine ecosystems across the Arctic through novel remote sensing techniques, water sampling, sediment coring, and modeling across the river-sea system of the Mackenzie Delta.

This project will leverage existing observational datasets from AWI and Hereon field campaigns to the Mackenzie Delta and southern Beaufort Sea from 2019 (Lizotte et al. 2023) and 2021 (Bröder et al. 2022). FLO CHAR will conduct Arctic field campaigns to the near-shore and coastal waters of the Beaufort Sea beginning in April 2023 and last three years until April 2026.

Pioneering a new approach to monitor and estimate large river-sea system carbon fluxes, this study will employ combined remote sensing techniques, in situ observation, and modeling to better understand dynamics, pathways and fate of the organic carbon in the coastal Arctic waters.

REFERENCES

Bröder, L., O'Regan, M., Fritz, M., Juhls, B., Priest, T., Lattaud, J., Whalen, D., Matsuoka, A., Pellerin, A., Bossé-Demers, T., Rudbäck, D., Eulenburg, A., Carson, T., Rodriguez-Cuicas, M.E., Overduin, P., and Vonk, J.E. 2022. The Permafrost Carbon in the Beaufort Sea (PeCaBeau) Expedition of the Research Vessel CCGS AMUNDSEN (AMD2104) in 2021, Berichte zur Polar- und Meeresforschung = Reports on polar and marine research, Bremerhaven, Alfred Wegener Institute for Polar and Marine Research, 759, 120 p. doi:10.48433/BzPM_0759_2022

Doxaran, D., Devred, E., and Babin, M. 2015. A 50 % increase in the mass of terrestrial particles delivered by the Mackenzie River into the Beaufort Sea (Canadian Arctic Ocean) over the last 10 years, In Biogeosciences, 12, 3551–3565. https://doi.org/10.5194/bg-12-3551-2015.

Fofonova, V., Kärnä, T., Klingbeil, K., Androsov, A., Kuznetsov, I., Sidorenko, D., et al. 2021. Plume spreading test case for coastal ocean models, In Geoscientific Model Development, 14, 6945-6975. https://doi:10.5194/gmd-14-6945-2021

Lizotte, M., Juhls, B., Matsuoka, A., Massicotte, P., Mével, G., Anikina, D. O. J., Antonova, S., Bécu, G., Béguin, M., Bélanger, S., Bossé-Demers, T., Bröder, L., Bruyant, F., Chaillou, G., Comte, J., Couture, R.-M., Devred, E., Deslongchamps, G., Dezutter, T., Dillon, M., Doxaran, D., Flamand, A., Fell, F., Ferland, J., Forget, M.-H., Fritz, M., Gordon, T.J., Guilmette, C., Hilborn, A., Hussherr, R., Irish, C., Joux, F., Kipp, L., Laberge-Carignan, A., Lantuit, H., Leymarie, E., Mannino, A., Maury, J., Overduin, P., Oziel, L., Stedmon, C., Thomas, C., Tisserand, L., Tremblay, J.-É., Vonk, J., Whalen, D., and Babin, M. 2023. Nunataryuk field campaigns: understanding the origin and fate of terrestrial organic matter in the coastal waters of the Mackenzie Delta region, Earth Syst. Sci. Data, 15, 1617–1653. https://doi.org/10.5194/essd-15-1617-2023

Matsuoka, A., Babin, M., and Vonk, J.E. 2022. Decadal trends in the release of terrigenous organic carbon to the Mackenzie Delta (Canadian Arctic) using satellite ocean color data (1998–2019), In Remote Sensing of Environment, 283, 113322.

Tank, S.E., Striegl, R.G., McClelland, J.W., and Kokelj, S.V. 2016. Multi-decadal increases in dissolved organic carbon and alkalinity flux from the Mackenzie drainage basin to the Arctic Ocean, In Environmental Research Letters, 11 054015. https://doi.org/10.1088/1748-9326/11/5/054015

Soil development along soil hydrological gradients in a degrading permafrost landscape in Western Greenland

Tino Peplau[1], Patrick Liebmann[1], Amira Hildebrand[1], Timo Bastam[1], Niels Wobker[1], Claudia Bruhn[2], Susanne Liebner[2,3], Christian Knoblauch[4,5] & Georg Guggenberger[1]

[1]*Institute of Soil Science, Leibniz University of Hannover, Herrenhäuser Str. 2., 30419 Hannover, Germany*

[2]*GFZ German Research Centre for Geosciences, Geomicrobiology, Telegrafenberg, 14473 Potsdam, Germany*

[3]*Institute of Biochemistry and Biology, University of Potsdam, Karl-Liebknecht-Str. 24-25, 14476 Potsdam, Germany*

[4]*Institute of Soil Science, Universiät Hamburg, Hamburg, Germany*

[5]*Center for Earth System Research and Sustainability, Universität Hamburg, Hamburg, Germany*

Permafrost soils around the world are warming, exposing large amounts of soil organic matter (SOM) to decomposition and therefore releasing vast amounts of carbon (C) and nitrogen (N) as greenhouse gases. The positive feedback of such greenhouse gases is contributing to accelerated global climate change, but to date, there are big uncertainties concerning the amount and timing of greenhouse gas release from thawing permafrost. Despite intensive efforts in the quantification of SOM and its decomposition in arctic permafrost soils, it is still unclear to what extent methane (CH_4), carbon dioxide (CO_2) and other greenhouse gases are emitted upon permafrost thaw. Moreover, the interrelations between SOM and the mineral phase of permafrost soils and their relevance for the production of greenhouse gases are largely unknown. Soil development as well as environmental conditions in Arctic regions differ greatly from other biomes: Comparably low biological activity, enhanced physical weathering by freeze-thaw-cycles and a short time since the retreat of the glacial cover are characteristic for many Arctic ecosystems. To understand the processes that are relevant for carbon emissions from Arctic ecosystems, deeper knowledge of SOM stabilization, storage and mobilization in permafrost soils and of the kind and intensity of processes of soil development are required. Varying redox-regimes are of great importance for the formation of the different iron species, which in turn control the stabilization of SOM.

To answer the question, how the mineral phase contributes to the stabilization and mobilization of SOM in permafrost-affected tundra soils, we assessed the influence of the redox-regime on the formation of iron-(hydr)oxides and their interrelation with organic C under changing soil hydrological conditions.

Methodology

In our study, we examined soils on Disko Island, West Greenland, to study soil development and SOM storage under varying environmental conditions. The soils are Cryosols, originating from glacial till and basaltic rock with varying active layer depth between 30 and 60 centimeters. In total, seven sites along two transects were selected and three replicate soil profiles were sampled in September 2022. The two transects represent slope gradients with varying soil moisture (transect 1, three sites) and active layer thickness (transect 2, four sites). For a first characterization of the soils and soil forming processes in the research area, basic soil properties such as texture, C and N content, cation exchange capacity and pH have been measured. $\delta^{13}C$ and $\delta^{15}N$ have been determined to evaluate the degree of decomposition of SOM within the soil profile and along the transects. To unravel the relationship between SOM and soil mineralogy, we also conducted selective iron extractions using four extractants (water, sodium pyrophosphate, sodium dithionite, hydroxylamine) which were chosen to dissolve different iron phases (i.e., iron-organic complexes or iron minerals with varying crystallinity) in the soil. After each extraction, content of dissolved iron and carbon, which was previously associated with the respective iron minerals, were quantified. Furthermore, one transect has been equipped with soil monitoring stations, enabling continuous measurements of soil moisture, soil temperature and redox potential in both topsoil and subsoil. The year-round record of these parameters allows to directly observe spatial and temporal changes and patterns of the environmental conditions in the soils, which, in turn, are affecting decomposition of SOM and formation of Fe-organic associations.

Results and Discussion

First results show an increase in C stocks with increasing soil moisture, which is well in line with previous studies in the circumpolar permafrost region. Furthermore, we found a decline in C stocks with flattening active layer depth, which comes along with a decrease of the thickness of the organic layer and with a change in redox-conditions from oxic to anoxic. $\delta^{13}C$

and $\delta^{15}N$ increased with depth, but tend to decrease along the transects, showing that not only C stocks, but also patterns of SOM decomposition change with varying in-situ environmental conditions.

Records of the redox-regime in the soils revealed distinct spatial and temporal patterns between oxic (>700 mV Eh) and anoxic (~0 mV Eh) conditions within the soil, which can be related to alternating soil moisture. So far, records exist for a three months period but data logging continues and a long-term time-series is in progress.

The first promising results already show a distinct connection between SOM turnover and soil hydrological conditions. More data from selective iron and carbon extraction will be presented, as well as a detailed analysis of the first months of record from the soil monitoring stations. The assessment of the interplay between redox-regime and iron-(hydr)oxide formation in combination with SOM release and/or stabilization will provide new insights into the complex interactions in degrading permafrost soils.

FUNDING

This study is part of the 'MOMENT' project funded by the German Federal Ministry of Education and Research (BMBF), grant number 03F0931A.

Understanding the gas exchange mechanisms between permafrost soils and the atmosphere in Daring Lake (Canada): Implications to the climate change

Carlos Rufino Juarez-de-Leon[1], Guillaume Berthe[1], Philipp Schiffmann[1], Elyn Humprheys[2], David Sebag[1] & Maria-Fernanda Romero-Sarmiento[1]

[1]*IFP Energies Nouvelles (IFPEN), Rueil-Malmaison, Île-de-France, France*

[2]*Department of Geography and Environmental Studies, Carleton University, Ottawa, Ontario, Canada*

The carbon pool of arctic permafrost soils is estimated at about 1600 Gt, almost twice the concentration of carbon in the atmosphere (e.g., Miner et al. 2022). In these northern high latitudes, climate warming is responsible for several environmental changes leading to a potentially rapid decomposition of soil organic matter (SOM) and emissions of greenhouse gases (GHG) from the soil into the atmosphere (Schuur et al. 2015).

The principal aim of this study is to investigate the thermal properties of the SOM in permafrost-affected soils and evaluate the relationship between SOM stability and in-situ gas emissions.

For this study, two different ecosystem zones were defined near the Tundra Ecosystem Research Station (TERS) at Daring Lake (Canada) according to the predominate vegetation, soil moisture conditions, and relief (Humphreys and Lafleur 2011; Atlas of Canada) as shown in Figure 1: i) Mixed tundra (dwarf shrub/ sedge tundra) and ii) Wetlands. Mixed tundra soils are classified as turbic cryosols with some evidence of cryoturbation. They are characterized by non-calcareous coarse-textured mineral soils (sand to loamy sand) and good drainage. Wetlands are classified as organic cryosols, typically poor drainage soils showing a thick organic layer overlying silt loam sediment (Humphreys and Lafleur 2011).

An integrated analytical approach was tested here combining in-situ measurements as well as laboratory analysis. During the field campaign (August 2022), atmospheric concentrations of CO_2 and CH_4 and gaseous species associated with the GHG (H_2S, NO, NO_2, NH_3, SO_2) were continuously measured using both ABB® (infrared diode laser absorption spectroscopy) and Flair Box™ UV – DOAS (Ultraviolet –Differential Optical Absorption Spectroscopy) analyzers, respectively. The ABB® analyzer was coupled with an opaque flux chamber for measurements of GHG fluxes between the soil and the atmosphere (without any previous removal of ground cover vegetation). A total of 23 gas samples from the flux chamber were taken for a subsequent carbon isotopic analysis of the CH_4 using a Picarro® CRDS (Cavity Ring-Down Spectrometer) device. Soils were sampled at 23 point locations (15 and 8 locations for mixed tundra and wetlands, respectively). At each point, soil samples were taken every ~15 cm from the surface through the active layer until reaching the permafrost table. A total of 80 soil samples were described and provisionally assigned to a soil horizon. At the laboratory, soil samples were analyzed using the thermal Rock-Eval® method for SOM properties such as the thermolabile organic carbon, expressed in this case by the soil organic carbon (SOC in %wt), the Hydrogen index (HI in mg HC/gTOC), or the refractory index (R index) for the assessment of the quality and thermal stability of SOM.

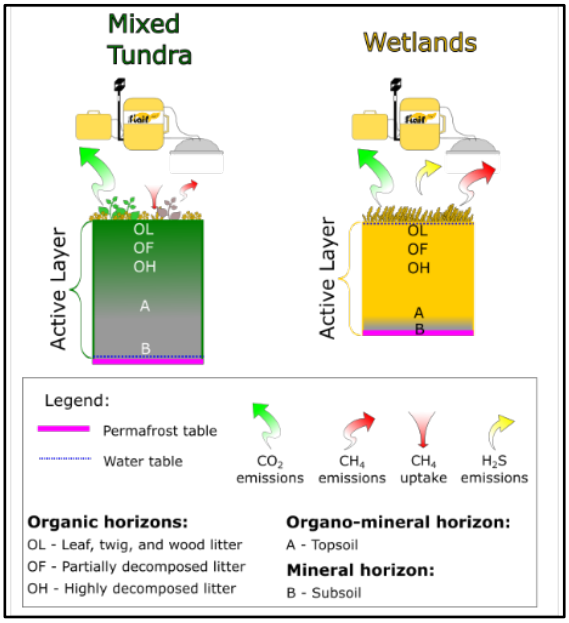

Figure 1. Diagram of the active layers of the two studied ecosystem zones at Daring Lake.

The mean atmospheric GHG concentration measured at Daring Lake was around 405 ppm and 2 ppm for CO_2 and CH_4, respectively, consistent with expected values for this latitude at this time of year (NOAA GHG data).

CO_2 emissions in the mixed tundra and wetlands were relatively similar (~1.3 µmol m^{-2} s^{-1}). Exchanges

of CH_4 are far more important. In the wetlands, anoxic conditions of flooded surfaces enhance emissions (~34 nmol m^{-2} s^{-1}). In the mixed tundra, uptakes dominate (~0.6 nmol m^{-2} s^{-1}) due to the oxic environment. These values are also consistent with reported fluxes in the literature at Daring Lake (Figure 2). This suggests that wetlands can be considered the main GHG source in the studied area, especially at the end of summer, during maximal soil thaw depth. However, heterogeneity in the region complicates the classification of emissions to specific oxic/anoxic conditions in each zone.

The stable carbon isotope analysis of $\delta^{13}CH_4$ revealed 3 different signatures: 1) The atmospheric isotope signature (~-47 ‰); 2) the anoxic conditions of acetoclastic methanogenesis (-50‰ to -60‰ for wetlands soil gas samples); 3) The shift from anoxic to oxic conditions of substrate (less than -40‰) (Whiticar et al. 1999). Due to an extreme dry summer period at Daring Lake, anoxic flooded areas were exposed to atmospheric conditions.

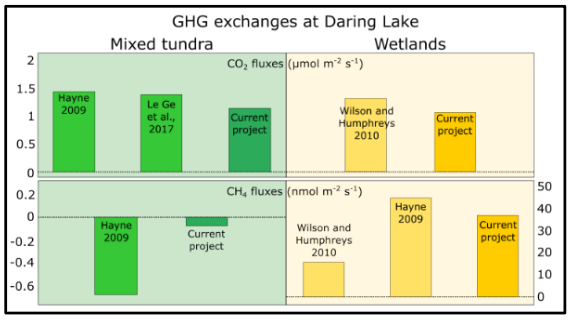

Figure 2. Overview of mean CO_2 and CH_4 fluxes reported in the literature for low-arctic ecosystems with dark flux chamber methodology in summer.

The rate of SOM degradation is mainly determined by SOM stability, quality, and quantity. Calculated Rock-Eval® parameters (Figure 3) indicate that topsoil horizons from the two zones are mainly dominated by thermolabile carbon forms. Obtained high HI values also suggests that the SOM from topsoils is mainly composed by rich-H molecules. Topsoil horizons from both zones are also characterized by high SOC and low R index, indicating that these intervals could be considered as the main potential source of GHG emissions.

In general, the stability of SOM increases as a function of the SOM accumulation and the geochemical interactions between organic and mineral horizons, depending on the anaerobic and aerobic conditions, respectively. Under oxic conditions, mixed tundra zones characterized by a good drainage, favors CO_2 emissions and CH_4 sinks. In contrast, wetlands zones show both higher CH_4 emissiosn with specific isotopic signatures and the presence of other associated gaseous molecules detected by Flai Box™ (H_2S), probably suggesting SOM decomposition under anaerobic conditions. In a warming climate scenario, constant fluctuations from anoxic to oxic conditions, SOM degradation can be followed by the integration between methane-isotopic signatures and the thermal stability of SOM, especially in a zone where spatial variation impacts on the GHG exchanges.

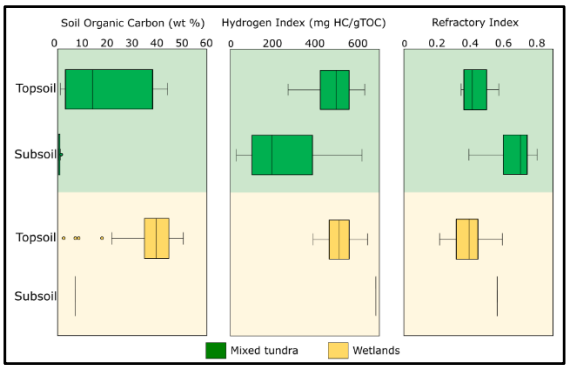

Figure 3. (From left to right) Soil Organic Carbon content, Hydrogen Index, and R index on topsoils (O and A horizons) and subsoils (B horizons) (see also Figure 1).

References

Ge, L., Lafleur, P.M., and Humphreys, E.R. 2017. Respiration from soil and ground cover vegetation under tundra shrubs, Arctic, Antarctic, and Alpine Research, 49 (4), 537–550.

Hayne, S.L. 2009. Controls on the atmospheric exchanges of carbon dioxide and methane for a variety of Arctic tundra types. Master of Science Dissertation, Carleton University.

Humphreys, E.R., and Lafleur, P.M. 2011. Does earlier snowmelt lead to greater CO_2 sequestration in two low Arctic tundra ecosystems?, Geophysical Research Letters, 38 (9), 1–5. doi:10.1029/2011GL047339

Miner, K.R., Turetsky, M.R., Malina,E., Bartsch,A., Tamminen, J., and McGuire, A.D. 2022. Permafrost carbon emissions in a changing Arctic, Nature Reviews Earth & Environment, 3 (1), 55–67. doi:10.1038/s43017-021-00230-3

Schuur E.A.G., McGuire, A.D., Schädel, C., Grosse, G., Harden, J.W., Hayes, D.J., Hugelius, G., Koven, C.D., Kuhry, P., Lawrence, D.M., Natali, S.M., Olefeldt, D., Romanovsky, V.E., Schaefer, K., Turetsky, M.R., Treat, C.C., and Vonk, J.E. 2015. Climate change and the permafrost carbon feedback, Nature, 520 (7546), 171–179. doi:10.1038/nature14338

Whiticar, M.J. 1999. Carbon and hydrogen isotope systematics of bacterial formation and oxidation of methane, Chemical Geology, 161 (1-3), 291–314. doi:10.1016/S0009-2541(99)00092-3

Wilson, K.S., and Humphreys, E.R. 2010. Carbon dioxide and methane fluxes from Arctic Mudboils, Canadian Journal of Soil Science, 90 (3), 441–449.

Enhancing E3SM Land Model (ELM) simulations of methane emissions at NGEE-Arctic sites

Jing Tao, William J. Riley, Qing Zhu, Baptiste Dafflon & Margaret S. Torn

Climate and Ecosystem Sciences Division, Lawrence Berkeley National Laboratory, Berkeley, California, United States

Permafrost thaw-induced hydrobiogeochemical dynamics play a crucial role in controlling the water-carbon-climate feedback across pan-Arctic landscapes. The intricate interplay between dynamic hydrological patterns (both vertical and horizontal) and biogeochemical pathways significantly influence the response of Arctic ecosystems and their feedbacks to climate change. However, current process-based global land models, including DOE's Energy Exascale Earth System Model (E3SM) land model (ELM), face challenges in accurately representing high-latitude hydrological dynamics, landscape inundation, ecosystem biogeochemistry, and permafrost carbon emissions.

Recent comprehensive field campaigns, e.g., the Next-Generation Ecosystem Experiments in the Arctic (NGEE Arctic), have generated many datasets relevant to the development and evaluation of permafrost modeling. However, the representation of fine-scale processes and interaction mechanisms of hydrological and biogeochemical cycling at regional to global scales remains challenging due to the unrepresented large sub-grid heterogeneity of plants, soil, topography, and drainage networks. Land models typically operate at resolutions larger than 0.5° x 0.5°, which limits the model's ability to capture these sub-grid heterogeneities. Consequently, the existing gaps between site-level understanding and large-scale modeling capabilities hinder model improvements across various spatial scales.

Method and Results

This work demonstrates an approach to bridge the gaps between fine-scale processes and coarse-scale modeling capabilities. Specifically, by leveraging the available NGEE-Arctic measurements from multiple representative sites that capture rapidly changing permafrost landscapes, we enhanced ELM's representation of permafrost wetland hydrobio-geochemistry to improve simulations of methane emissions at the site scale. Specifically, we enabled ELM's methane module to explicitly represent the wetland unit by distinguishing lowland geophysical processes (e.g., water, carbon, and energy fluxes and pools) from the upland unit. Then, we test the activated methane module at several NGEE-Arctic representative sites using a nested, hierarchical modeling strategy (Figure 1) to explore the best upscaling practice, and thus adequately represent critical processes across spatial resolutions. Our results highlight (1) the impact of aboveground snow-vegetation-hydrology interactions on belowground carbon and nutrient cycling and (2) how representing fine-scale wetland hydrogeochemical dynamics in coarse-resolution ELM simulations could improve methane emission estimates.

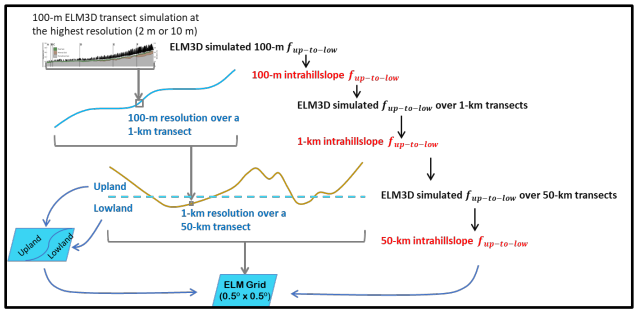

Figure 1. The upscaling process with the hierarchical nesting strategy. $f_{up\text{-}to\text{-}low}$ represents the upland-to-lowland transport flux relationship.

References

Riley, W.J., Subin, Z.M., Lawrence, D.M., Swenson, S.C., Torn, M.S., Meng, L., Mahowald, N.M., and Hess, P. 2011. Barriers to predicting changes in global terrestrial methane fluxes: analyses using CLM4Me, a methane biogeochemistry model integrated in CESM. Biogeosciences, 8(7), pp.1925–1953.

Tao, J., Zhu, Q., Riley, W.J., and Neumann, R.B. 2021. Improved ELMv1-ECA simulations of zero-curtain periods and cold-season CH_4 and CO_2 emissions at Alaskan Arctic tundra sites, The Cryosphere, 15, 5281–5307. https://doi.org/10.5194/tc-15-5281-2021

Stocks, origin, and future trajectories of hidden soil organic carbon in paleosols of blockfields in the high alpine permafrost region

Annegret Udke[1,2], Michele E. D`Amico[3], Michele Freppaz[4], Emanuele Pintaldi[4], Luisa Minich[1] & Frank Hagedorn[1]

[1]*Swiss Federal Institute for Forest, Snow and Avalance Research WSL, Birmensdorf, Zurich, Switzerland*

[2]*Department of Geography, University of Zurich, Zurich, Switzerland*

[3]*Department of Agricultural and Environmental Sciences, University of Milan, Milan, Italy*

[4]*Department of Agricultural, Forest and Food Sciences, University of Turin, Turin, Italy*

Permafrost is warming because of global temperature increase, which alters the carbon cycle in these environments. While research has primarily focused on arctic permafrost, we are lacking data on the timing and magnitude of potential C accumulation and release in the alpine permafrost zone. These environments contain blockfields on mountain tops (>2900 m) with and without patterned ground, which are mainly vegetation free and therefore thought to be free of soil organic carbon (SOC). Motivated by the fact that coarse and fine material separates with freezing and thawing, we aimed to test whether alpine blockfields without vegetation are indeed SOC-free or whether they contain hidden carbon which might represent a CO_2 source upon climatic warming. By sampling vegetated soils at the same or slightly lower elevation, we wanted to test how SOC stocks in blockfields will develop under climate warming in the near future.

On four mountain tops (2900 to 3200 m a.s.l.) in the periglacial zone of the Eastern Swiss and North-Western Italian Alps, we removed up to one-meter-deep thick stone layer and excavated eleven soil profiles. While one location was completely vegetation free, the three other locations were influenced by active patterned ground with non-vegetated and sparsely vegetated patches within the same blockfield.

At each site, we found dark and fine material beneath a stone cover of a few decimetres up to a meter. Preliminary results of the vegetation free location show a hidden SOC stock of 0.8 to 1.1 $kgC \cdot m^{-2}$ and narrow CN ratios of 9.0 to 10.1. Bulk soil ^{14}C dating revealed an age of 4,000 to 12,900 years right beneath the stone cover (0-20 cm) and at greater depth (>80 cm) respectively. In agreement with our finding, Pintaldi et al. (2021) observed “hidden” SOC stock beneath active patterned ground on a mountain top plateau in North-West Italy. There are two possible origins of the hidden carbon: 1) soot deposition by natural and anthropogenic processes throughout the Holocene and 2) carbon accumulation during warmer climatic conditions during the early to middle Holocene.

A first estimate of the soot deposition in high alpine environments indicates that soot input cannot explain the observed SOC stocks. OC concentrations from an ice core drilled at Fischerhorn glacier (Jenk et al. 2006) allows to calculate the input by soot deposition. Mean OC concentrations for the ice core were 33 $\mu gC \cdot kg^{-1}$ ice which would yield a soot deposition of about 70 $gC \cdot m^{-2}$ over 5000 years. Even when assuming the highest OC concentration of 80 $\mu gC \cdot kg^{-1}$ originating from wood combustion during mid-19th century, the soot input would range only around 165 $gC \cdot m^{-2}$ over 5000 years. Both estimates are far too little to explain the observed stocks of hidden SOC around 1 $kgC \cdot m^{-2}$.

We therefore presume that the hidden SOC primarily originates from SOC accumulation in a warmer climate during the early to middle Holocene. During the Holocene Thermal Maximum (5,000 to 11,000 years BP) temperatures were 0.5 to 3.1 °C higher compared to today’s conditions in the Alps (Badino et al. 2018; Heiri et al. 2003) which was associated with an upward shift of the treeline and a retreat of glaciers. Reconstructions of the treeline in the Western Italian (Badino et al. 2018), Central (Tinner and Theurillat 2003) and Central Eastern Alps (Nicolussi et al. 2005) show a 100 to 300 m higher tree line ecotone compared to the current situation. During this time, most high elevation peaks were also ice-free (Bohleber et al. 2020). Around 4,000 years, reconstructions indicate a drop in temperature by about 1.8 °C (Badino et al. 2018), a lowering of the treeline below present-day elevation (Badino et al. 2018; Nicolussi et al. 2005) and an elevation dependent development of the current neoglaciation (Bohleber et al. 2020). This strongly suggests that our sampled sites at 2900–3200 m a.s.l. carried a vegetation cover leading to soil development and carbon accumulation during the Holocene Thermal Maximum. Thereafter, soils became possibly covered by blocks due to reverse vertical sorting during the colder period from 4,000 years to present day. We will characterize the chemical composition of the hidden SOC to gain further insight into its origin.

To test the release of CO_2 from hidden paleosols, we measured CO_2 fluxes in the field using a CO_2

chamber installed onto the fine earth after stone removal. Results showed an average release rate of 2.6 ± 3.7 mg·CO_2-C·m^{-2}·h^{-1} from the four sites during the summer season. Rates were about a magnitude higher from the adjacent sparsely vegetated soils (27.7 ± 20.5 mg·CO_2-C·m^{-2}·h^{-1}). In conjunction with higher SOC stocks and younger ^{14}C ages (around 1,500 years) at slightly lower elevations measured at one of the sites, this indicates that upward plant migration has a strong impact on SOC cycling and leads (again) to carbon sequestration in the soil.

In summary, we show that high alpine blockfields in the permafrost region store a small amount of old carbon, which is now hidden below thick stone layers, and which most likely originates from past vegetation in these environments during warmer climates in the Holocene. In-situ soil CO_2 flux measurements give evidence that these paleosols are currently releasing small amounts of (possibly old) CO_2 to the atmosphere. Colonization with upward migrating plants will, however, lead to C sequestration in the soil. Further studies are needed to explore how widespread these paleosols are and to assess the magnitude of C losses and gains in high alpine terrain. The comparison of vegetated and non-vegetated plots presents the possibility of modelling the timing of carbon loss and uptake in these environments.

References

Badino, F., Ravazzi, C., Valle, F., Pini, R., Aceti, A., Brunetti, M., Champvillair, E., Maggi, V., Masero, F., Perego, R., and Orombelli, G. 2018. 8800 years of high-altitude vegetation and climate history at the Rutor Glacier forefield, Italian Alps. Evidence of middle Holocene timberlinerise and glacier contraction. Quaternary Science Reviews, 185: 41–68. doi.org/10.1016/j.quascirev.2018.01.022

Bohleber, P., Schwikowski, M., Stocker-Waldhuber, M., Fang, L., and Fischer, A. 2020. New glacier evidence for ice-free summits during the life of the Tyrolean Iceman. Nature Scientific Reports, 10: 20513. doi.org/10.1038/s41598-020-77518-9

Heiri, O., Lotter, A.F., Hausmann, S., and Kienast, F. 2003. A chironomid-based Holocene summer air temperature reconstruction from the Swiss Alps. Holocene, 13(4): 447–484. doi.org/10.1191/0959683603hl640ft

Jenk, T.M., Szidat, S., Schwikowski, M., Gäggeler, H.W., Brütsch, S., Brütsch, B., Wacker, L., Synal, H.-A., and Saurer, M. 2006. Radiocarbon analysis in an Alpine ice core: record of anthropogenicand biogenic contributions to carbonaceous aerosols in the past (1650–1940). Atmospheric Chemistry and Physics, 6: 5381–5390. doi.org/10.5194/acp-6-5381-2006

Nicolussi, K., Kaufmann, M., Patzelt, G., van der Plicht, J., and Thurner, A. 2005. Holocene tree-line veriability in the Kauner Valley, Central Eastern Alps, indicated by dendrochronological analysis of living trees and subfossil logs. Vegetation History and Archaeobotany, 14(3): 221–234. doi.org/10.1007/s00334-005-0013-y

Pintaldi, E., D`Amico, M., Colombo, N., Colombero, C., Sambuelli, L., De Regibus, C., Franco, D., Perotti, L., Paro, L., and Freppaz, M. 2021. Hidden soils and their carbon stocks at high-elevation in the European Alps (North-West Italy). Catena, 198: 105044. doi.org/10.1016/j.catena.2020.105044

Tinner, W., and Kaltenrieder, P. 2005. Rapid responses of high-mountain vegetation to early Holocene environmental changes in the Swiss Alps. Journal of Ecology, 93(5): 936–947. doi:10.1111/j.1365-2745.2005.01023.x

Carbon fluxes in Arctic and sub-Arctic freshwater ecosystems

Judith Vogt[1], Anna Virkkala[2], Isabel Wargowsky[2], McKenzie Kuhn[3] & Mathias Göckede[1]

[1]*Max Planck Institute for Biogeochemistry, Jena, Germany*

[2]*Woodwell Climate Research Center, Falmouth, Massachusetts, United States*

[3]*Department of Earth Sciences and Earth System Research Center, University of New Hampshire, Durham, New Hampshire, United States*

Arctic and sub-arctic regions experience severe impacts due to global warming. The most prominent example is permafrost thaw which leads to changes in landscape patterns and release of stored carbon to the atmosphere. These emissions create a positive feedback further amplifying global warming. Furthermore, the expected reduction in snow and ice cover will affect hydrology-driven carbon fluxes which can be substantial due to the large amount of freshwater ecosystems in these regions.

The greenhouse gases of interest concerning the carbon cycle are carbon dioxide (CO_2) and methane (CH_4). Estimates of global carbon budgets largely disregard emissions caused by permafrost thaw and budgets for freshwater ecosystems are highly uncertain to date. A general constraint in this field is data scarcity from remote northern regions. In addition, underlying processes specific to freshwater ecosystems remain poorly understood, especially given the landscape heterogeneity in high northern latitudes. To fill these gaps, we conduct new in-situ measurements of carbon fluxes in Arctic and sub-Arctic regions and synthesize newly gathered and existing carbon flux data accompanied by environmental parameters (temperature, pH, water depth, etc.) across the Arctic-boreal domain on a site-level and at monthly resolution.

The synthesis work is conceptually based on a range of previously published studies (Kuhn et al. 2021; Golub et al. 2023; Stanley et al. 2023) and will contribute to the Arctic-boreal carbon flux synthesis (ABCflux v2) that spans wetland and freshwater ecosystems. We work in close collaboration with scientists across the globe to collect requested data, extract data from the literature, and produce new datasets from recent field campaigns.

With the synthesized data, we aim to quantify the carbon budgets of freshwater ecosystems across the Arctic-boreal domain. The contribution of these ecosystems to the global carbon budget will be evaluated. Additionally, the impact of environmental controls including temperature, pH, and water depth on the carbon fluxes will be investigated.

Water bodies of interest comprise both lentic and lotic systems, including lakes, rivers, streams, reservoirs, ponds, and ditches. Methods used by the scientific community range widely from eddy covariance, manual and automated chamber measurements, and concentration-based techniques relying on the estimation of the gas transfer velocity. Figure 1 shows existing study sites across sub-Arctic and Arctic regions. Figure 2 provides the distribution of freshwater types studied across these sites.

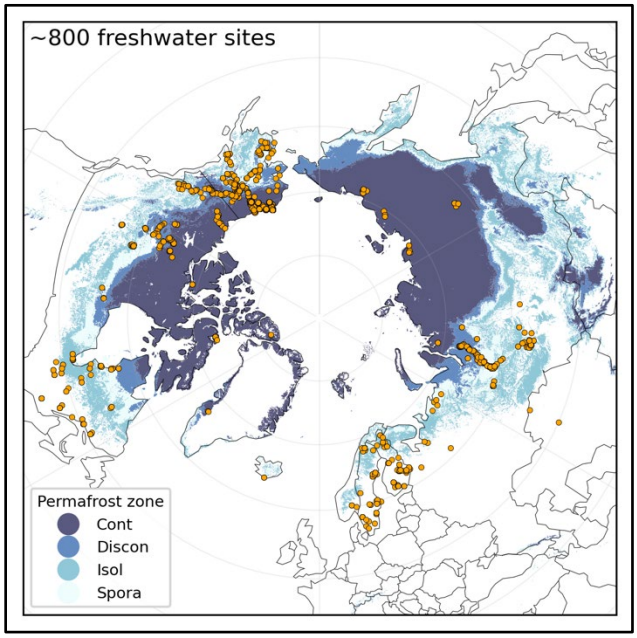

Figure 1. Map of known study sites (in orange) across the Arctic-boreal domain and different permafrost zones (continuous, discontinuous, isolated, sporadic).

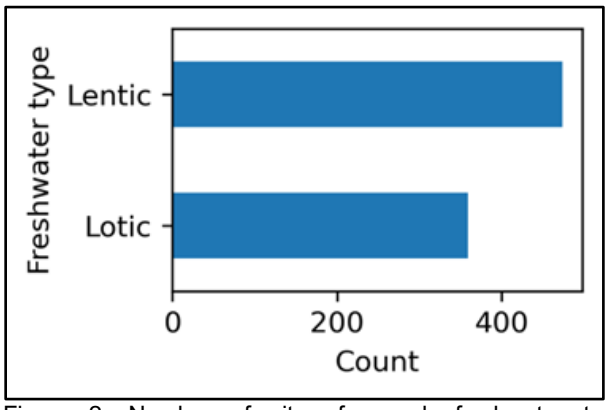

Figure 2. Number of sites for each freshwater type investigated.

With this synthesis, we will provide a public comprehensive dataset to the scientific community and foster collaboration within the network. In the future, upscaling studies will be conducted to reach set research aims. Furthermore, the dataset will provide a unique opportunity for benchmarking and verification of process-based models and remote sensing products.

ACKNOWLEDGEMENT

The presented research was supported by the European Climate, Infrastructure and Environment Executive Agency (CINEA) under the Horizon Europe Climate programme (grant agreement No 101056921, GreenFeedback), and by the European Research Council (ERC) under the European Union's Horizon 2020 research and innovation programme (grant agreement No 951288, Q-Arctic).

REFERENCES

Golub, M., et al. 2023. Diel, seasonal, and inter-annual variation in carbon dioxide effluxes from lakes and reservoirs, Environmental Research Letters, 18(3), 034046. doi:10.1088/1748-9326/acb834

Kuhn, M.A., et al. 2021. BAWLD-CH4: a comprehensive dataset of methane fluxes from boreal and arctic ecosystems, Earth System Science Data, 13(11), 5151–5189. doi:10.5194/essd-13-5151-2021

Stanley, E.H., et al. 2023. GRiMeDB: the Global River Methane Database of concentrations and fluxes, Earth System Science Data, 15(7), 2879–2926. doi:10.5194/essd-15-2879-2023

Climate warming benefits plant growth but net carbon uptake in Alaska tundra and needle leaf forest

Xiaodong Wu[1], Chuanhua Li[2] & Liangliang Li[1]

[1]*Cryosphere Research Station on the Qinghai-Tibet Plateau, State Key Laboratory of Cryospheric Science, Northwest Institute of Eco-Environment and Resources, Chinese Academy of Sciences, Lanzhou, China*

[2]*College of Geography and Environmental Science, Northwest Normal University, Lanzhou, China*

Climate warming has important effects on Arctic vegetation, but the roles of Arctic vegetation as a carbon sink or source in the future remain largely unknown. In this study, we selected the tundra and needle leaf forest areas in Alaska to examine the primary productivity of vegetation growth and carbon exchange using the LPJ-GUESS model.

We select two sites as representatives of the two land cover types in this area. One site is the tundra ecosystem, e.g., Atqasuk, with the site name US-ATQ (70.47°N, 157.41°W). The elevation is 15 meters above sea level. From 1989 to 2014 the average annual temperature is -9.7 °C, and the average annual precipitation is 93 mm. The vegetation communities at this site are dominated by sedges, grasses, mosses, and dwarf shrubs (<40 cm). The ATQ site belongs to the continuous permafrost region with high ground ice content. The other needle leaf forest site, e.g., the Poker Flat Research Range Black Spruce Forest, with the site name of US-PRR (65.12°N, 147.48°W). The elevation is 210 meters above the site level. At the US-PRR site, the average annual temperature is -2 °C, and the average annual precipitation is 275 mm. The land cover type belongs to the evergreen needleleaf (ENF), and this area is covered with extensive forest. The PRR site belongs to discontinuous permafrost regions with medium ground ice content.

The accuracy of the model is verified by linear regression of the measured data from 2004 to 2008, and the simulation results and ground-based observation data are correlated, with R^2 values of 0.51 and 0.46 for net ecosystem carbon exchange (NEE) at the tundra and needle leaf forest sites and Root Mean Square Error (RMSE) values of 22.85 and 23.40 gC/m^2/yr, respectively. For the gross primary production (GPP), the R^2 values were 0.66 and 0.85, and the RMSE values were 39.25 and 43.75 gC/m^2/yr at the tundra and needle leaf forest sites, respectively. The validation results suggested that the model is reliable.

There are clear seasonal changes in NEE and GPP. During December-March, vegetation was dormant, and the NEE values showed that the ecosystems in the tundra and needle-leaf forest sites were weak carbon sources. From May-August, the GPP at the tundra site was lower than that at the needle leaf forest site. The needle leaf forest was also a stronger carbon sink than the tundra.

We then simulated GPP and NEE using future climate scenarios of the CESM2, CESM2-WACCM, NorESM2-LM, NorESM2-MM and UKESM1-0-LL models, and calculated the mean values of the five models. Under future climate scenarios, both the GPP at the tundra and needle leaf forest sites showed increasing trends. The average GPP values from 1980 to 2100 at the tundra site under SSP1-2.6, SSP2-4.5 and SSP5-8.5 were 169.51, 342.88, and 387.11 gC/m^2/yr, respectively. The average GPP values from 1980 to 2100 at the needle leaf forest site under the three pathways were 1323.70, 1503.27 and 1923.15 gC/m^2/yr. For the NEE values, the tundra sites from 1980 to 2100 under SSP1-2.6, SSP2-4.5 and SSP5-8.5 were -102.68, -122.74 and -142.53 gC/m^2/yr, respectively. The average NEE values at the needle leaf forest site from 1980 to 2100 were -175.56, -193.60, and -266.44 gC/m^2/yr, respectively. The GPP increase rate at the PRR needle leaf forest site was the fastest under the SSP5-8.5 pathway. The NEE decrease rate at the ATQ tundra site was the fastest under the SSP5-8.5 pathway.

To explore the importance of climate variables on GPP and NEE, we re-drive the model based on the SSP1-2.6 scenario, changing the driving factor one by one, i.e., we changed air temperature, precipitation and solar radiation to the corresponding factors of SSP2-4.5 and SSP5-8.5 pathways, respectively. The results showed that the temperature has the greatest influence on GPP and NEE, under the SSP5-8.5 pathways. Increased temperatures had a positive effect on both GPP and NEE at the ATQ and PRR sites in Alaska.

Overall, our results showed that during the past decades, the GPP showed a faster increasing rate in the needle leaf forest site than in the tundra site, and the carbon uptake rates for the two areas fluctuated considerably, with nonsignificant increasing trends. Under the future emission pathways, the GPP values of the tundra and needle leaf forest were also higher,

while the carbon uptake showed no significant increasing trends in the future. Under the future emission pathways, the GPP of the high-emission SSP5-8.5 pathway increases faster and NEE decreases faster.

ACKNOWLEDGEMENTS

This work was supported by the National Natural Science Foundation of China (41941015, 32061143032), the State Key Laboratory of Cryospheric Science (SKLCS-ZZ-2023), and the West Light Foundation of the Chinese Academy of Sciences.

Modeling year-around CO_2 fluxes and winter subsurface CO_2 concentrations for an arctic heath ecosystem in West Greenland

Wenxin Zhang[1], Danielsen Birgitte Kortegaard[2] & Elberling Bo[2]

[1]*Departement of Physical Geography and Ecosystem Science, Lund University, Lund, Sweden*

[2]*Department of Geoscience and Nature Resource Management, University of Copenhagen, Copenhagne, Denmark*

The actual CO_2 production rates in nature may be very different and controlled by fluctuating temperatures and water contents. However, very few studies have discussed the influence of CO_2 or O_2 concentrations on the use of observed incubation results in modelling. In the permafrost regions, the active layer will thaw and potentially produce CO_2 by the end of the summer/autumn, but only until freezing of top layers and snow has effectively created a barrier for CO_2 release to the atmosphere. Based on the year-round Eddy Covariance (EC)-derived CO_2 fluxes, one-year chamber measurement of growing season CO_2 fluxes, and the winter-time subsurface CO_2 concentration, the process-oriented model (CoupModel) has been well constrained to simulate both winter-time sub-surface CO_2 concentration and year-round CO_2 fluxes. The model has accounted for abotic responses of soil CO_2 production, such as soil temperature, moisture and CO_2 concentration. Our model results indicate if the observed higher sub-surface CO_2 concentration in non-growing seasons than growing seasons is caused by the physical barriers of CO_2 diffusion in winter or higher CO_2 production due to relatively warmer winter. Model results regarding the effective diffusion of CO_2 in relation to fraction of air volume in frozen and unfrozen soil conditions will be demonstrated and evaluated using the lab experiments.

The CoupModel has been successfully calibrated to simulate Net Ecosystem Exchange (NEE), subsurface CO_2 concentrations, and other pertinent environmental variables. While higher CO_2 concentrations seem capable of reducing CO_2 production, their overall impact appears rather limited. During a year with an unusually deep snowpack, NGS CO_2 emissions showed a threefold increase compared to other years, resulting in a reduced CO_2 sink in the annual budget. Subsequently, the following growing season experienced warmer and wetter conditions, facilitating notably higher Gross Primary Production (GPP), Ecosystem Respiration (ER), and NEE.

According to the model, the current ecosystem acted as a sink for atmospheric CO_2. The model-data fusion approach presented here can fill data gaps in a manner that enables a more comprehensive understanding of annual CO_2 dynamics.

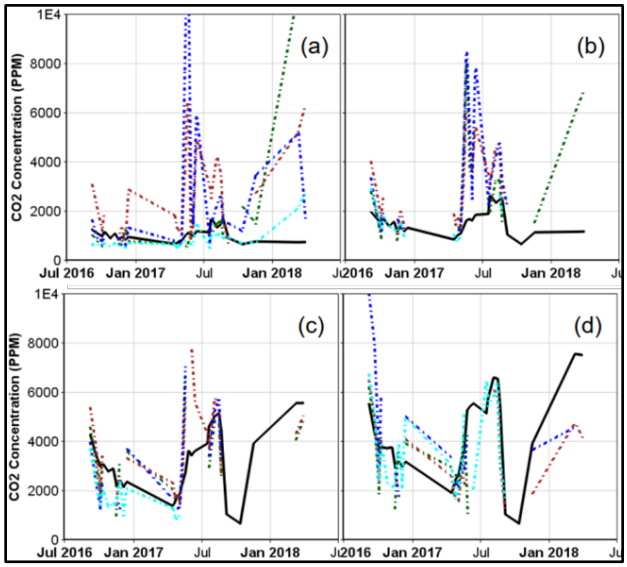

Figure 1. Soil CO_2 concentraiton simulated by CoupModel (Solid line, black) and measured at the field (dotted line, fourreplciates) for (a) 10 cm, (b) 20 cm, (c) 40 cm (d) 80 cm.

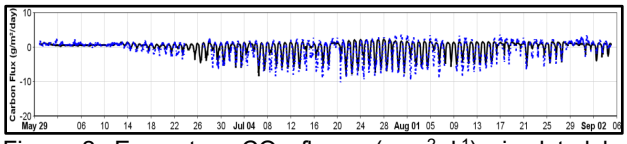

Figure 2. Ecosystem CO_2 fluxes ($g \cdot m^{-2} \cdot d^{-1}$) simulated by CoupModel (solid line, black) and measured by EC tower (dotted line, blue) at Østerlien, Disko Island, and West Greenland.

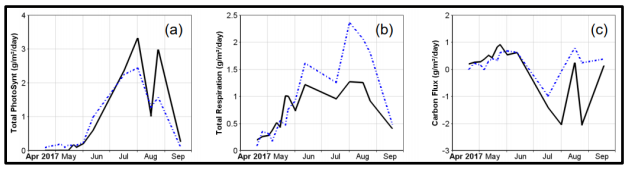

Figure 3. (a) Total photosynthesis ($g \cdot m^{-2} \cdot d^{-1}$), (b) total respiration ($g \cdot m^{-2} \cdot d^{-1}$) and (3) carbon fluxes ($g \cdot m^{-2} \cdot d^{-1}$) simulated by CoupModel (soilid line, black) and measured by the gas analyser.

5B — Monitoring, Modelling, and Remote Sensing of the Permafrost Carbon Feedback

Session Chairs: Elchin Jafarov[1], Ted Shuur[2] & Jing Tao[3]

[1]*Woodwell Climate Research Center, Falmouth, Massachusetts, United States*
[2]*Northern Arizona University, Flagstaff, Arizona, United States*
[3]*Lawrence Berkeley National Laboratory, Berkeley, California, United States*

The permafrost region stores 1440-1600 Pg organic carbon in soils, which represents nearly half of the world's soil organic carbon pool. Accelerated warming of the Arctic can impact the global climate system by thawing permafrost and exposing a substantial part of this carbon storage to decomposition and release as greenhouse gasses to the atmosphere. Our session is focused on advances in observations, modelling, and mapping techniques of the permafrost carbon feedback to climate change.

We invite modellers, observers, and remote sensing experts to share their research on permafrost carbon monitoring, modelling, and feedbacks in natural and urbanized settings. We solicit contributions related to in-situ, laboratory, model, and remote sensing observations to improve the understanding of uncertainties of the permafrost carbon feedback.

Carbon dioxide release from retrogressive thaw slumps in Siberia

Christian Beer[1,2], Alexandra Runge[3], Guido Grosse[4,5], Gustaf Hugelius[6,7] & Christian Knoblauch[1,2]

[1]*Department of Earth System Sciences, Institute of Soil Science, Universität Hamburg, Hamburg, Germany*

[2]*Center for Earth System Research and Sustainability, Universität Hamburg, Hamburg, Germany*

[3]*Helmholtz Centre Potsdam GFZ German Research Centre for Geosciences, Potsdam, Germany*

[4]*Permafrost Research Section, Alfred Wegener Institute Helmholtz Centre for Polar and Marine Research, Potsdam, Germany*

[5]*Institute of Geosciences, University of Potsdam, Potsdam, Germany*

[6]*Department of Physical Geography, Stockholm University, Sweden*

[7]*Bolin Centre for Climate Research, Stockholm University, Sweden*

Currently, only gradual permafrost thaw is accounted for in global climate models. However, rapid thawing of permafrost leading to features such as retrogressive thaw slumps (RTS) or thermokarst can lead to substantial additional permafrost organic carbon mobilization. To what extent this mobilization translates into greenhouse gas releases to the atmosphere today and in the future is unclear. The pan-Arctic area of such rapid ground failures and landscape changes due to permafrost thawing and the resulting alteration of the carbon cycle processes are still unclear. Combining broad-scale remote sensing approaches to determine landscape scale changes from permafrost thaw with modelling of carbon dynamics will help quantifying the impacts of abrupt thaw at continental scales.

RTS result from slope failure due to abrupt thawing of ice-rich permafrost. They mostly occur along shorelines of lakes, rivers, and coastlines, or along hillslopes with ice-rich permafrost. RTS are mass-wasting features, which after initial detachment failure and the exposure of ice-rich soils consist of a headwall, a muddy slump floor and often a drainage channel. The slope-failure processes associated with RTS formation and growth expose permafrost soil layers that have been frozen in the deep subsoil for hundreds or thousands of years. In RTS, these layers thaw and erode quickly due to the thermo-erosional processes driving RTS growth. Then, microbes will start to mineralize the organic matter that has been frozen for a long time and is exposed in RTS, releasing greenhouse gases such as carbon dioxide (CO_2) or methane. In this study, we focus on the CO_2 release from the RTS soils, i.e. material that has not been exported to aquatic systems.

At a continental to global scale, detailed estimates of CO_2 release from RTS based on combined field studies, remote sensing and models are lacking. In this study, we integrate a dynamic decomposition model with a recent remote sensing map and a soil carbon database to estimate recent carbon dioxide emissions from RTS in Northeast Siberia. The following research questions are addressed: 1) What is the amount of previously frozen soil organic matter available for mineralization due to recent retrogressive thaw slump development at the continental-scale in Siberia? 2) How much CO_2 has potentially been recently released from RTS to the atmosphere in Siberia in 1999-2020? 3) Has this estimated additional carbon release to the atmosphere any impact on the global carbon cycle?

Methods

We estimated the amount of annually mineralized organic matter which is released as CO_2 to the atmosphere using a dynamic 2-pool first-order decomposition model. To account for soil temperature seasonality and vertical distribution, we assumed the decomposition rate constant being temperature dependent following a Q10-model. We applied this dynamic model to all detected RTS across the entire study area in Siberia. The model required several variables as input (see sections below): location and area of the thaw slumps, mean soil temperature seasonality for topsoil and subsoil, and initial soil organic carbon stocks.

Active RTS were mapped across Northeast Siberia firstly to identify their distribution at continental scale, secondly to derive their annual thaw dynamics from 1999-2020, and thirdly to determine the terrestrial area currently impacted by rapid thaw from thaw slumps. To achieve this, we applied the Landsat-based detection of Trends in Disturbance and Recovery (LandTrendr) algorithm, which performs spectral-temporal segmentation from time series data to identify disturbance events and recovery periods from annual Landsat/Sentinel-2 mosaics.

The data on spatial distribution of soil organic carbon stocks is derived from the Northern Circumpolar Soil Carbon Database, version 2 (NCSCDv2). For the analyses in this study, data for 0-100 cm depth at a grid-cell resolution of 0.5 degrees was used. 30% and 70% of total 0-100 cm organic matter stocks were assigned to topsoil and subsoil stocks, respectively.

The time series of the temperature profile at 0.5 degree grid cells that show RTS during 1991-2010 has been estimated by a pan-Arctic simulation using the land surface model JSBACH. This model has recently been advanced by including cold regions processes. For this study, we run a model version that does not consider a layer of lichens and bryophytes because such layer is missing at the disturbed RTS sites. In total, five dynamic snow layers, and seven soil layers were used in an implicit numerical scheme to solve the heat conduction equation with phase change.

RESULTS AND DISCUSSION

When applying the dynamic decomposition model to the available soil organic matter with the specific topsoil and subsoil temperature, we estimate a mineralization of organic matter of 367 ± 213 gC $m^{-2}a^{-1}$ on average for all RTS (Figure 1). This corresponds to a total CO_2 release to the atmosphere of 0.42 ± 0.22 TgC a^{-1} from the area impacted by RTS in Siberia. Our results show that these RTS are a strong carbon source (local hotspot) to the atmosphere. The average emission of 367+/-204 gC $m^{-2}a^{-1}$ is in stark contrast to an otherwise small carbon sink of the tundra in this area. However, the recent RTS-affected area in Siberia of 868 km² is not large enough for emissions to be relevant for the global carbon cycle. The estimated carbon emission of 0.42 TgC a^{-1} from these Siberian thaw slumps is 4 orders of magnitude lower than the annual anthropogenic carbon emissions. Nevertheless, the large amount of CO_2 emitted from a relatively small, but rapidly increasing RTS area, is concerning for future scenarios should the currently observed RTS growing trend since 2016 continue.

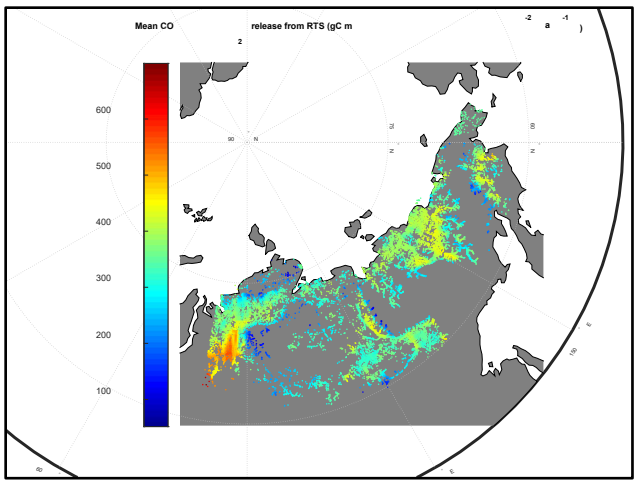

Figure 1. Estimated mean annual carbon dioxide release from RTS during the period 1991-2010.

FUNDING INFORMATION

CB acknowledges financial support by DFG-BE 6485/1-1 and DFG-BE 6485/4-1. CK was supported by the German Ministry of Education and Research (KOPF-Synthesis project 03F0834A) and the DFG excellence cluster CLICCS (EXC2037/1). We acknowledge the technical support by CEN-IT which is the central IT service provider of the Center for Earth System Research and Sustainability at Universität Hamburg. AR was supported by an ESA CCI Postdoctoral Fellowship. GG and AR acknowledge support by ESA CCI+ Permafrost, EU Horizon 2020 project Arctic Passion (grant no. 101003472), and the BMBF KoPf Synthesis project (03F0834B).

Impact of fire on future projections of permafrost degradation and carbon release

Eleanor J. Burke[1], Callum Christie[2], Noah D. Smith[2] & Norman Steniert[3]

[1]*Met Office, Exeter, United Kingdom*

[2]*Department of Mathematics, University of Exeter, Exeter, United Kingdom*

[3]*NORCE, Bergen, Norway*

Fires in the permafrost region will impact the underlying soil. They will burn the protective organic layer which leads to a reduced insulation of the soil. Consequently, this will degrade the permafrost further and increase the active layer thickness. This exposes more permafrost carbon to above zero temperatures and increased decomposition. Therefore, in the permafrost region, fire impacts the carbon cycle both directly via emissions from the burnt soil and vegetation and indirectly via increased permafrost degradation and permafrost carbon loss. Here we use the Joint UK Land Environment Simulator (JULES) to quantify these effects.

Model developments

This configuration of JULES utilises the Interactive Fire and Emission algorithm for Natural environments (INFERNO) fire model. INFERNO is a reduced complexity fire model which uses a combination of flammability and ignitions to quantify burnt area and carbon emissions from soil and vegetation (Mangeon et al. 2016; Burton et al. 2019). The soil organic carbon in this version of JULES is vertically resolved which enables the permafrost carbon to be defined separately to the soil carbon in the active layer (Burke et al. 2017). Furthermore, the inclusion of dynamic soil properties (Chadburn et al. 2020) means that any change in soil carbon will feed back onto the thermal and hydrological properties of the soil. The sub-surface component of INFERNO was modified to consider the vertically resolved soil carbon and dynamic properties. The burn depth was prescribed to 20 cm, so that any soil carbon above that depth was vulnerable to fire and any carbon below was not. In this initial study, the burn depth was just prescribed as a constant value, but later we will parameterise it as a function of soil moisture and temperature. A combustion factor was defined to represent incomplete combustion, initially set to 0.8. JULES has four soil carbon pools and the fire was assumed to burn equal proportions of carbon from each pool.

Modelling framework

Pan-arctic simulations of permafrost physics and the permafrost carbon cycle were carried out for the period from 1850 to 2100 using historical forcing and two Shared Socioeconomic Pathways, SSP1-26 (low greenhouse gas emissions) and SSP5-85 (very high greenhouse gas emissions). The model was initialised from a stable spun up state in 1850. Ignitions were prescribed using spatial distribution of cloud to ground lightning strikes and population. Both the climate and the ignitions followed the prescribed Shared Socioeconomic Pathways. We ran a set of factorial simulations (Table 1) to diagnose the direct and indirect impact of fire in the permafrost regions on the global carbon cycle. Two additional simulations were included to separate the impact of climate change and ignition change on the response of JULES-INFERNO.

Table 1. Factorial experiments.

Simulation	Description
FIRE_OFF	No fire
FIRE_1850IGN	Fire with 1850 ignitions
FIRE_DYN	Fire and dynamic soils
FIRE_DYN_1850CLIM	Fire with 1850 climate
FIRE_DYN_1850IGN	Fire with 1850 ignitions

Results

Figure 1 shows the simulated permafrost extent for FIRE_1850IGN. This shows a reduction of 14 million square km by 2100 for SSP5-85 and 7 million square km for SSP1-26. The simulated permafrost extent is similar for the FIRE_OFF runs, but FIRE_DYN is expected to show a greater loss of permafrost by 2100 alongside a further deepening of the active layer thickness.

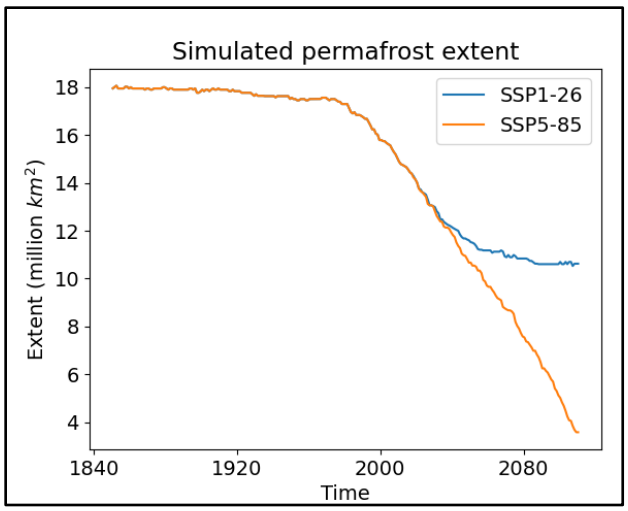

Figure 1. Time series of permafrost extent simulated by FIRE_1850IGN.

Figure 2 shows the vegetation carbon emissions simulated by FIRE_18750IGN. The 1850 emissions are 28 Tg C per year. This increases notably to 200 Tg C per year for SSP5-85 and approximately doubles to 56 Tg C per year for SSP1-26. There will be additional emissions from the soil carbon.

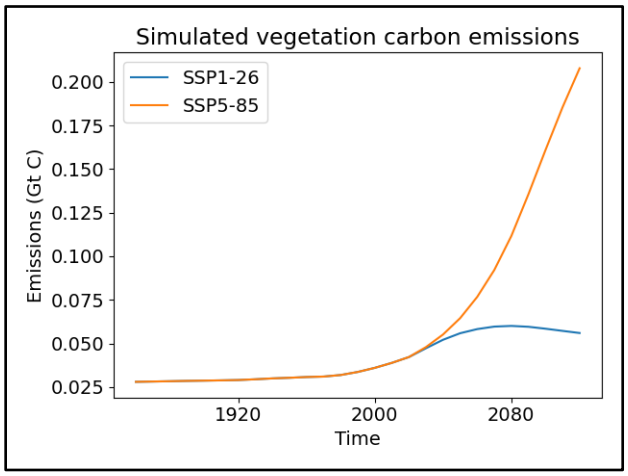

Figure 2. Time series of vegetation carbon fire emissions simulated by FIRE_1850IGN.

Conclusions

Here we present initial findings from JULES-INFERNO simulations. We aim to quantify both the direct effect of fire on carbon emissions from the permafrost region and the indirect effect caused by the loss of soil carbon insulation.

References

Burke, E.J., Chadburn, S.E., and Ekici, A. 2017. A vertical representation of soil carbon in the JULES land surface scheme (vn4. 3_permafrost) with a focus on permafrost regions. Geoscientific Model Development, 10(2), pp.959–975.

Burton, C., Betts, R., Cardoso, M., Feldpausch, T.R., Harper, A., Jones, C.D., Kelley, D.I., Robertson, E., and Wiltshire, A. 2019. Representation of fire, land-use change and vegetation dynamics in the Joint UK Land Environment Simulator vn4. 9 (JULES). Geoscientific Model Development, 12(1), pp.179–193.

Mangeon, S., Voulgarakis, A., Gilham, R., Harper, A., Sitch, S., and Folberth, G. 2016. INFERNO: A fire and emissions scheme for the UK Met Office's Unified Model. Geoscientific Model Development, 9(8), pp.2685–2700.

Chadburn, S.E., Burke, E.J., Gallego-Sala, A.V., Smith, N.D., Bret-Harte, M.S., Charman, D.J., Drewer, J., Edgar, C.W., Euskirchen, E.S., Fortuniak, K., and Gao, Y. 2022. A new approach to simulate peat accumulation, degradation and stability in a global land surface scheme (JULES vn5. 8_accumulate_soil) for northern and temperate peatlands. Geoscientific Model Development, 15(4), pp.1633–1657.

The impact of plant priming on C fluxes from permafrost soils after thaw: investigations of plant-microbe-mineral responses

Jessica Ernakovich[1,2,3], Sean Schaefer[1,2,3], Fernando Montaño-López[4], D.V. Bakke[1,3], Hannah Holland-Moritz[1,3], Nathan Alexander[1,3], Sarah Goldschmidt[4], Lukas Bernhardt[1,3], Else Schlerman[1,2,3], Elinor Cotter[3], Matthew Rozinski[3], Skylar Wilkins[4], William Wieder[5], A. Stuart Grandy[1,2,3] & Caitlin Hicks Pries[4]

[1]*Center for Soil Biogeochemistry and Microbial Ecology (SoilBioME), University of New Hampshire, Durham, New Hampshire, United States*

[2]*Natural Resources and Earth System Science Program, University of New Hampshire, Durham, New Hampshire, United States*

[3]*Department of Natural Resources and the Environment, University of New Hampshire, Durham, New Hampshire, United States*

[4]*Department of Biological Sciences, Dartmouth College, Hanover, New Hampshire, United States*

[5]*National Center for Atmospheric Research, Boulder, Colorado, United States*

Long-term projections of permafrost–climate feedbacks depend on recognizing complex biophysical and biogeochemical responses of terrestrial ecosystems to environmental change. Interactions among plant productivity, microbial communities, and soil minerals will determine the fate of the vast store of permafrost carbon (Hugelius et al. 2014), dictating whether carbon (C) is released to the atmosphere or stored below ground following permafrost thaw. Whether Arctic warming leads to a loss or gain in soils C depends on plant inputs and the interactions between plants, microbial activity, and mineral stabilization of organic matter.

Plants can be both sources of C accumulation and drive soil C decomposition. One key aspect of plant–microbe–mineral interactions is priming, a process where plants stimulate SOM decomposition—particularly from older, native SOM pools—via the addition of root exudates (Kuzyakov 2010). Despite observations that plant roots easily invade thawed permafrost (Blume-Werry et al. 2019), the drivers of priming by plants in arctic soils is an open question with global significance (Wild et al. 2014). Further, while it is known in temperate soils that elevated atmospheric CO_2 (eCO_2) increases root exudation (Kuzyakov et al. 2010) and therefore priming, the response of the arctic plant–soil system to eCO_2 has rarely been explored. Here we use a broader "systems view" to capture how the physico-chemical characteristics of newly exposed minerals and shifts in the microbial community composition and function tilt the balance of carbon accumulation and degradation following permafrost thaw.

We aim to address the question: How do feedbacks between plants, microbes, and minerals affect arctic soil carbon balance in response to global change (such as eCO_2 and a shift from sedge-dominated to shrub-dominated tundra)?

METHODS

In July/August 2021 and 2022, we sampled permafrost profiles (to ~85 cm, ~60 cm below the active layer-permafrost interface) using a Snow, Ice, and Permafrost Research Establishment (SIPRE) auger along a deglaciation gradient (Table 1) on the North Slope of Alaska. The soils are classified as turbels (cryoturbated mineral permafrost soils).

Table 1. Characteristics of soils along our deglaciation gradient, representative of landscape age. Fe_{ox}/Fe_{cd} is the ratio of oxalate and citrate diothionate extractable Fe, a proxy for the degree of weathering; lower values indicate more weathering. pH, %C, and Fe_{ox}/Fe_{cd} are averages along the soil profiles (0-85 cm).

Site/glacial drift	Deglaciation, years	pH	%C	Fe_{ox}/Fe_{cd}
Itkillik II	11.5-2.5K	5.1	12.5	1.03
Itkillik I	53-66K	4.6	4.6	0.99
Sagavanirktok Rvr	125-728K	4.3	8.2	0.92
Sagwon Hills/ unglaciated	4.5 million	5.4	6.7	1.08

We characterized the carbon (C) and nitrogen (N) content, pH, mineral characteristics, and microbial communities (identity and activity) in these soils. Mineral characteristics were assessed by measuring Fe and Al in crystalline, poorly-crystalline, and organically-complexed forms. Microbial communities were characterized with amplicon sequencing of bacteria and fungi, as well as by assessing the activity of three carbon degrading enzymes (cellobiohydrolase and β-xylosidase (hydrolytic) and phenol oxidase (oxidative)).

To assess the potential impact of mineralogy, vegetation type, and eCO_2 on the potential for plant inputs to prime microbial decomposition of permafrost organic matter, we grew Eriophorum angustifolium (sedge) and Betula nana (shrub) into a collar filled with 100 g permafrost soil from the end members along our deglaciation gradient (Itkillik II and Sagwon Hills). The

mesocosm experiment was conducted inside a climate-controlled continuous-labeling plant growth chamber for the length of one growing season (8 weeks) using ^{13}C-enriched CO_2 headspace (10 at %) under ambient (400 ppm) and elevated (700 ppm) atmospheric CO_2 concentrations. Respired CO_2 was captured in a collar and measured on a Picarro G220i. A mixing model was used to partition respiration into plant- and SOM-derived (eq 1 shows the derivation for SOM-derived respiration, Wild et al. 2014).

$$R_{SOM} = C_{Ttl} \times \frac{(at\%_{Ttl} - at\%_{roots})}{(at\%_{SOM} - at\%_{roots})} \quad [1]$$

C_{Ttl} is the concentration of headspace CO_2, and $at\%_{Ttl}$, $at\%_{roots}$, and $at\%_{SOM}$ are the enrichment of ^{13}C in the headspace, roots, and SOM, respecitively. Rhizodeposits have been tracked into various pools—including dissolved, particulate, mineral-associated, and microbial biomass—to be correlated with soil nutrients and microbial communities.

Results and Discussion

Along the 0-85 cm profile, soils from the most recent glacial retreat (Itkillik II) had the highest soil C (Table 1). As landscape age increased, pH and the Fe_{ox}/Fe_{cd} (iron activity) ratio decreased, which together are indicative of increased weathering. The oldest site (Sagwon Hills) was an exception to this trend, reflecting its geography. Microbial characterization (i.e., bacterial and archaeal composition and diversity, enzyme activities) have been performed at all sites, except for the oldest site. Bacterial diversity ranged from a Shannon Index (H) of 7.5 in the organic active layer to 2.6 in the deepest permafrost. Depth, but not glacial drift, played a role structuring the bacterial community ($p=0.001$) and diversity ($p<0.001$). Archaeal diversity (0.47 ± 0.50) wasn't affected by depth or glacial drift. Hydrolytic enzyme activities were variable with depth ($p<0.03$), and seemed responsive to soil C concentrations, whereas phenol oxidase activity was uniform through the soil profiles and across glacial drifts (meaning it was insensitive to carbon, mineral and ice content).

Soil mineralogy, plant type and eCO_2 all affected the magnitude and direction of the priming effect of permafrost organic matter (Figure 1). After seven weeks, the growth of B. nana into Sagwon Hills (oldest) permafrost resulted in more degradation of SOM-C to CO_2 when grown under ambient CO_2 conditions, but more utilization of plant-derived C under elevated CO_2 conditions. There was no effect of ambient versus elevated CO_2 on priming of SOM from our youngest site (Itkillik II) when grown with B. nana. However, when E. angustifolium grew into Itkillik II permafrost, eCO_2 resulted in more SOM-C degradation, and there was no effect of ambient versus eCO_2 at Sagwon Hills. Contribution of plants and SOM to respired CO_2 varied over the experiment, and at eight weeks many of the mesocosms were respiring more plant-derived C than SOM-C. However, the magnitude varied by location, indicating a context-dependency between minerals, carbon, and microbes that needs to be further explored.

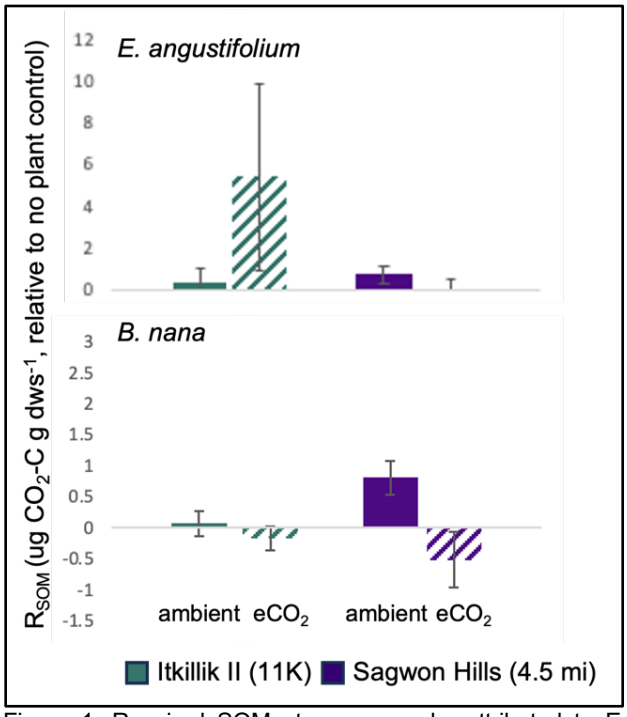

Figure 1. Respired SOM at seven weeks attributed to E. angustifolium (top) and B. nana (bottom). Data are represented as the difference between the plant treatment and the no plant control.

References

Blume-Werry, G., Milbau, A., Teuber, L.M., Johansson, M., and Dorrepaal, E. 2019. Dwelling in the deep – strongly increased root growth and rooting depth enhance plant interactions with thawing permafrost soil. New Phytologist, 223(3), 1328–1339. doi: 10.1111/nph.15903

Hugelius, G., Strauss, J., Zubrzycki, S., Harden, J.W., Schuur, E.A.G., et al. 2014. Estimated stocks of circumpolar permafrost carbon with quantified uncertainty ranges and identified data gaps. Biogeosciences, 11, 6573–6593. doi:10.5194/bg-11-6573-2014

Kuzyakov, Y. 2010. Priming effects: Interactions between living and dead organic matter. Soil Biology & Biochemistry, 42, 1363–1371. doi:10.1016/j.soilbio.2010.04.003

Wild, B., Schnecker, J., Alves, R., Barsukov, P., Barta, J., et al. 2014. Input of easily available organic C and N stimulates microbial decomposition of soil organic matter in arctic permafrost soil. Soil Biology & Biochemistry, 75, 143–151. doi:10.1016/j.soilbio.2014.04

Mineral-organic interactions may regulate dissolved organic matter bioavailability in the western Canadian Arctic

Gabrielle Hatten[1], Steven V. Kokelj[2], Duane G. Froese[3], Alejandro Alvarez[3], Joseph M. Young[3], Sophie Opfergelt[4] & Suzanne E. Tank[1]

[1]*Department of Biological Sciences, University of Alberta, Edmonton, Alberta, Canada*

[2]*Northwest Territories Geological Survey, Government of Northwest Territories, Yellowknife, Northwest Territories, Canada*

[3]*Department of Earth and Atmospheric Sciences, University of Alberta, Edmonton, Alberta, Canada*

[4]*Earth and Life Institute, Université catholique de Louvain, Louvain-la-Neuve, Belgium*

Increased land-water interactions, facilitated by permafrost thaw, are mobilizing terrestrial materials to aquatic networks and changing carbon and nutrient availability for microorganisms. A portion of this carbon is readily available for biological decomposition, resulting in carbon dioxide and methane emissions as by-products. However, other pathways for permafrost carbon have the potential to protect carbon from conversion into greenhouse gases. In non-permafrost soils, mineral-organic interactions are an established mechanism of sequestering carbon by reducing the bioavailability of organic matter via physico-chemical processes (McDowell and Wood 1984; Kaiser et al. 1996). In northern permafrost landscapes, where changing conditions are causing increases in that depth and thermokarst formation, interactions between organic-rich surface waters and newly exposed, mineral-rich sediment may facilitate similar effects.

Despite their potential to influence permafrost carbon pathways, few studies have directly evaluated mineral-organic interactions in northern systems; those studies are focused primarily on Eurasian permafrost (e.g., Gentsch et al. 2015). In the western Canadian Arctic, widespread mineral-rich soils (such as tills) and intensifying thaw-driven mass wasting (Kokelj et al. 2021) present substantial potential for mineral-organic interactions. Several regional studies have reported lower dissolved organic matter concentrations in lakes and rivers associated with increased permafrost disturbance (e.g., Kokelj et al. 2005; Shakil et al. 2022), suggesting mineral-organic interactions are likely impacting these aquatic systems. However, the potential for mineral-organic interactions and their variability across diverse permafrost landscapes affected by a wide range of thaw-driven processes are not well understood.

To examine the relationship between permafrost substrate properties and mineral sorption potential, we sampled sites across permafrost environments in northwestern Canada with contrasting geological legacy and climate history. Permafrost endmembers were targeted from three geographic regions in the western Canadian Arctic with a focus on areas of high thermokarst activity (Kokelj et al. 2021; Kokelj et al. 2023; Young et al. 2022). The Peel Plateau (Figure 1a; Gwich'in Settlement Area) is characterized by abundant mineral-rich tills in the continuous permafrost zone. An organic-rich paleo-active layer, reflective of early Holocene warming and subsequent cooling, lies immediately below the present-day active layer. Southeast of the Peel Plateau, the Sahtu Region (Figure 1b; Sahtú Dene and Métis Settlement Area) lies within the extensive discontinuous permafrost zone. With similar parent material to the Peel Plateau, the Sahtu region experienced more extensive warming in the early Holocene, leading to the loss of relict glacial ice and an accumulation of Holocene sedimentation. In the central Yukon, permafrost in the Klondike region (Figure 1c; Tr'ondëk Hwëch'in Traditional Territory) largely consists of loess and has remained unglaciated, providing a contrast to the permafrost landscapes found in the western Canadian Arctic.

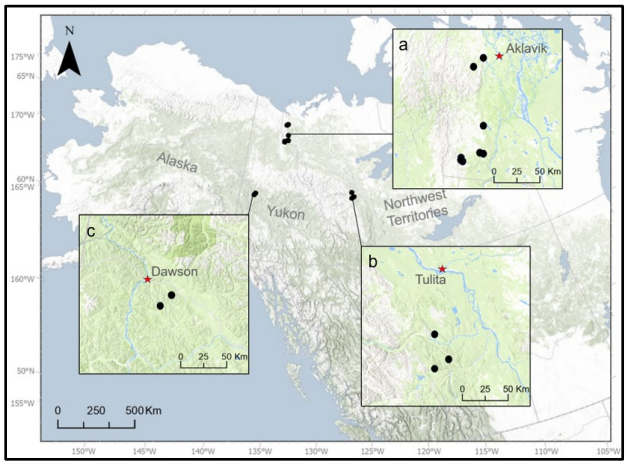

Figure 1. Study regions and sampling locations in the western Canadian Arctic: a – Peel Plateau; b – Sahtu Region; c – Klondike Region.

Sample collection was completed in the summer of 2023 to complement samples from past fieldwork available in the Permafrost Archives Laboratory at the University of Alberta. Permafrost endmembers

sampled included till, colluvium, and mineral-rich soils across stratigraphic boundaries, including paleo-active layer, relict talik, and contemporary active layer material.

Mineral sorption potential is being evaluated experimentally through batch sorption experiments. Organic-rich stock solutions, derived from active layer material, will be exposed to permafrost sediment for 48 hours; dissolved organic carbon concentration and organic matter composition of the stock solutions will be explored pre- and post-exposure to sediment. Sediment will then be characterized (e.g., pH, conductivity, grain size) based on soil metrics relevant to mineral sorption in non-permafrost soils to relate sediment properties to mineral sorption capacity.

Early results of batch sorption experiments show shifts in absorbance at 254 nm, a parameter closely tied to the aromatic content of dissolved organic matter (DOM). These results suggest that mineral-organic interactions influence the composition of the DOM pool and that the strength of these interactions varies between permafrost endmember types, likely reflecting differences in soil characteristics (Figure 2). Results of this study show the importance of considering mineral-organic interactions when predicting patterns in aquatic ecosystems and resulting CO_2 emissions in response to permafrost thaw.

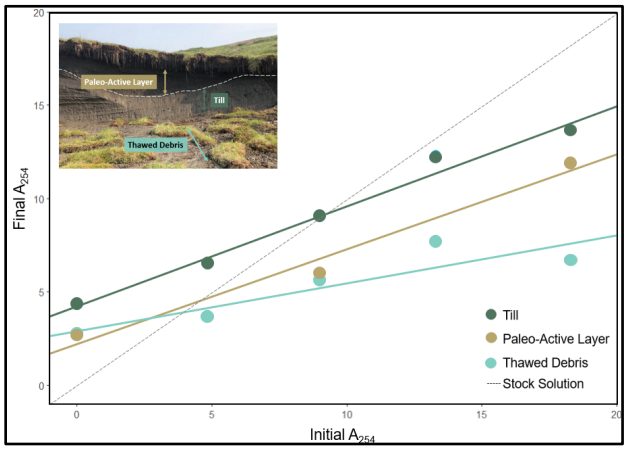

Figure 2. Relationship between the initial and final absorbance at 254 nm (A254), representing the aromaticity of dissolved organic matter of stock solutions following exposure to different permafrost endmembers in the Peel Plateau.

References

Gentsch, N., Mikutta, R., Shibistova, O., Wild, B., Schnecker, J., Richter, A., Urich, T., Gittel, A., Šantrůčková, H., Bárta, J., Lashchinskiy, N., Mueller, C.W., Fuß, R., and Guggenberger, G. 2015. Properties and bioavailability of particulate and mineral-associated organic matter in Arctic permafrost soils, Lower Kolyma Region, Russia: Organic matter stabilization in permafrost soils. European Journal of Soil Science, 66(4): 722–734. doi:10.1111/ejss.12269

Kaiser, K., Guggenberger, G., and Zech, W. 1996. Sorption of DOM and DOM fractions to forest soils. Geoderma, 74(3–4): 281–303. doi:10.1016/S0016-7061(96)00071-7

Kokelj, S.V., Gingras-Hill, T., Daly, S.V., Morse, P., Wolfe, S., Rudy, A.C.A., Van Der Sluijs, J., Weiss, N., O'Neill, B., Baltzer, J., Lantz, T.C., Gibson, C., Cazon, D., Fraser, R.H., Froese, D.G., Giff, G., Klengenberg, C., Lamoureux, S.F., Quinton, W., Turetsky, M.R., Chiasson, A., Ferguson, C., Newton, M., Pope, M., Paul, J.A., Wilson, A., and Young, J. 2023. The Northwest Territories Thermokarst Mapping Collective: A northern-driven mapping collaborative toward understanding the effects of permafrost thaw. Arctic Science, AS-2023-0009. doi:10.1139/AS-2023-0009

Kokelj, S.V., Jenkins, R.E., Milburn, D., Burn, C.R., and Snow, N. 2005. The influence of thermokarst disturbance on the water quality of small upland lakes, Mackenzie Delta region, Northwest Territories, Canada. Permafrost and Periglacial Processes, 16(4): 343–353. doi:10.1002/ppp.536

Kokelj, S.V., Kokoszka, J., van der Sluijs, J., Rudy, A.C.A., Tunnicliffe, J., Shakil, S., Tank, S.E., and Zolkos, S. 2021. Thaw-driven mass wasting couples slopes with downstream systems, and effects propagate through Arctic drainage networks. The Cryosphere, 15(7): 3059–3081. doi:10.5194/tc-15-3059-2021

Mcdowell, W.H., and Wood, T. 1984. Podzolization: Soil processes control dissolved organic carbon concentrations in stream water. Soil Science, 137(1): 23–32. doi:10.1097/00010694-198401000-00004

Shakil, S., Tank, S.E., Vonk, J.E., and Zolkos, S. 2022. Low biodegradability of particulate organic carbon mobilized from thaw slumps on the Peel Plateau, NT, and possible chemosynthesis and sorption effects. Biogeosciences, 19(7): 1871–1890. doi:10.5194/bg-19-1871-2022

Young, J.M., Alvarez, A., Van Der Sluijs, J., Kokelj, S.V., Rudy, A., McPhee, A., Stoker, B.J., Margold, M., and Froese, D. 2022. Recent intensification (2004–2020) of permafrost mass-wasting in the central Mackenzie Valley foothills is a legacy of past forest fire disturbances. Geophysical Research Letters, 49(24). doi:10.1029/2022GL100559

Recent advances in modeling permafrost dynamics and carbon cycling using terrestrial ecosystem model

Elchin Jafarov[1], Helene Genet[2], Valeria Briones[1], Benjamin Maglio[2], Joshua Randy[1], Andrew Mullen[1], Ruth Rutter[2], Tobey Carman[2], Joy Clien[2], Trevor Smith[1], Chu-Chun Chang[1], Brendan Rogers[1] & Susan Natali[1]

[1]*Woodwell Climate Research Center, Falmouth, Massachusetts, United States*

[2]*Institute of Arctic Biology, University of Alaska Fairbanks, Fairbanks, Alaska, United States*

Almost a quarter of the land in the Northern Hemisphere's vast expanse of land is covered by permafrost, which has been warming rapidly for the last 40 years. Integrating permafrost processes into Land System Models (LSMs) and Earth System Models (ESMs) is a complex and challenging task due to the intricate interplay between permafrost dynamics, hydrology, carbon cycling, and their impacts on climate. To tackle this complexity, our team is deploying an offline regional model to analyze permafrost carbon cycling and its future implications. To address disturbances that could lead to rapid permafrost thaw, our team is developing wildfire and thermokarst processes to include in the model. Leveraging data from the existing flux tower network in the Northern Hemisphere, we are enhancing model-data congruence. Our approach includes developing calibration and sensitivity analysis tools for automated parameter calibration using specific flux tower data. Additionally, we've created a tailored map of vegetation classes for more accurate spatial modeling and are developing a data assimilation tool aimed at reducing model biases. Here we highlight our recent advancements in modeling as part of the Permafrost Pathways project, which unites climate scientists, policymakers, and environmental justice advocates to devise strategies for adapting to and mitigating the impacts of permafrost thaw.

Parameter calibration

We utilized the MADS (Model Analysis and Decision Support) software for parameter calibration within the Terrestrial Ecosystem Model to reduce the gap between observed and modeled data at various sites (Vesselinov 2022). We use the Terrestrial Ecosystem Model with Dynamic Vegetation and Dynamic Organic Soil Layers (DVM-DOS-TEM), a process-based biosphere model designed to simulate biophysical and biogeochemical processes between the soil, vegetation, and atmosphere (Genet et al. 2018). MADS' user-friendly interface and robust optimization algorithms provided efficiency and flexibility, outperforming other tools like PEST and PECAN (Jafarov et al. 2020; Euskirchen et al. 2022). Additionally, a sensitivity analysis tool was developed to work in tandem with MADS, improving initial parameter estimates, constraining the parameter space, and aiding in understanding parameter interactions (Briones et al. in review). This semi-automated calibration approach streamlines the process, allowing for the handling of larger datasets and the use of parallel computing, thus enhancing efficiency. This method has been applied to five different sites, showcasing its effectiveness across diverse environmental conditions.

Thermokarst modeling

To address the cryohydrological impacts of thermokarst in the DVM-DOS-TEM, we analyzed changes at four sites in Alaska with varying drainage and permafrost conditions. The objective was to assess the model's accuracy in simulating carbon cycling and permafrost dynamics in ecosystems with varying moisture levels and permafrost continuity. The sites included a thermokarst bog and a black spruce permafrost plateau in boreal Alaska's discontinuous permafrost, as well as a wet sedge fen and moist tussock tundra in the continuous permafrost of the Alaskan Arctic. Comparisons of model outputs with field data showed that the model performed better in continuous permafrost areas, attributing to simpler thermal and hydrological dynamics during a shorter growing season. However, larger discrepancies were observed at the discontinuous permafrost and wetland sites, especially in carbon fluxes and active layer depth predictions. Attempts to correct hydrology in wetlands improved the active layer depth predictions but negatively affected carbon flux estimates, suggesting a need for better process representation. We found that soil moisture was consistently under-predicted, affecting respiration rates. Our findings highlight the need for improved hydrological and carbon cycling representations in models to more accurately simulate these complex and carbon-rich ecosystems (Maglio et al. 2024).

FIRE MODELING

We employed a DVM-DOS-TEM to study how black spruce and birch forests in Alaska respond to changes in fire frequency and how this impacts carbon cycling and permafrost interactions under shifting climate conditions. By simulating typical stands at Murphy Dome near Fairbanks and validating against field-measured carbon stocks, the study explored the effects of fire return intervals ranging from 50 to 250 years. The findings revealed that the model accurately reflects the distinct ecosystem dynamics of spruce and birch forests. More frequent fires were found to significantly decrease vegetation carbon, particularly in evergreen species, with soil organic carbon also severely impacted, and shorter intervals between fires hampering its recovery. Notably, soil carbon losses during moderate-severity fires were higher than those from vegetation. The study underscores the substantial role of fire in altering boreal forest composition and carbon reserves, which is critical for understanding landscape changes due to climate change. This work emphasizes the need to incorporate variations in fire frequency, moisture gradients, and changes in vegetation types into models to predict future carbon dynamics in boreal forests and calls for further investigation into the complex interplay between disturbance, succession, and carbon processes in this evolving ecosystem (Briones et al. 2024a).

SPATIAL MODELING

All existing model developments will be incorporated into spatial model simulations. Currently, our team is working on the development of the monthly input data at high spatial resolution. The input dataset will be used with a newly completed Pan-Arctic vegetation map customized for our model (Briones et al. 2024b). In parallel, we are working on spatial data assimilation that will be used to fine-tune model parameters and outputs using in-situ and remotely sensed data.

ACKNOWLEDGEMENTS

This study was made possible by funding catalyzed through the Audacious Project (Permafrost Pathways) and the Quadrature Climate Foundation (QCF Prime Grant Number 01-21-000094). We would also like to acknowledge great sources of data from the National Science Foundation (NSF) funded Bonanza Creek and Arctic members of the LTER Network, and the Circumpolar Active Layer Monitoring (CALM) Network. Additionally, we would like to thank the Department of Energy (DOE) Office of Biological and Environmental Research's (BER) AmeriFlux and its contributors, as well as the ABCFlux database available through the Oak Ridge National Laboratory (ORNL) Distributed Active Archive Center (DAAC).

REFERENCES

Briones, V., Jafarov, E., Genet, H., Rogers, B.M., Rutter, R., Carman, T.B., Clein, J., Euskirchen, E.S., Schuur, E.A.G., Watts, J.D., and Natali, S.M. in review. Modelling the linkage between soil thermal and hydrological regimes and its influence on ecosystem carbon dynamics in continuous and discontinuous permafrost, ERL.

Briones, V., Genet, H., Jafarov, E.E., Kabeer, A.K., Ritter, R., Carman, T., Rogers, B.M., and Natali, S.M. 2024a. Modeling the implications of post-fire alternative successional trajectory for boreal carbon and permafrost dynamics in Interior Alaska. 5B - Permafrost Carbon Feedback, International Conference on Permafrost.

Briones, V., Genet, H., Jafarov, E.E., Rogers, B.M., and Natali, S.M. 2024b. An integration approach to combine land cover products for improved ecosystem modeling across the pan-Arctic. 12D - Multiscale Observations of Permafrost Landscape Dynamics, International Conference on Permafrost.

Euskirchen, E.S., Serbin, S.P., Carman, T.B., Fraterrigo, J.M., Genet, H., Iversen, C.M., Salmon, V., and McGuire, A.D. 2022. Assessing dynamic vegetation model parameter uncertainty across Alaskan arctic tundra plant communities, Ecological Applications, 32. https://doi.org/10.1002/eap.2499.

Genet, H., He, Y., Lyu, Z., McGuire, A.D., Zhuang, Q., Clein, J., D'Amore, D., Bennett, A., Breen, A., Biles, F., Euskirchen, E.S., Johnson, K., Kurkowski, T., (Kushch) Schroder, S., Pastick, N., Rupp, T.S., Wylie, B., Zhang, Y., Zhou, X., and Zhu, Z. 2018. The role of driving factors in historical and projected carbon dynamics of upland ecosystems in Alaska. Ecol Appl, 28: 5–27. https://doi.org/10.1002/eap.1641

Jafarov, E.E., Harp, D.R., Coon, E.T., Dafflon, B., Tran, A.P., Atchley, A.L., Lin, Y., and Wilson, C.J. 2020. Estimation of subsurface porosities and thermal conductivities of polygonal tundra by coupled inversion of electrical resistivity, temperature, and moisture content data, The Cryosphere, 14, 77–91. https://doi.org/10.5194/tc-14-77-2020, 2020

Maglio, B.C., Rutter, R., Carman, T., Mullen, A., Briones, V., Edgar, C., Manies, K., Euskirchen, E.S., Jafarov, E.E., and Genet, H. 2024. Thermal and hydrological limitations on modeling carbon dynamics at wetland sites of discontinuous and continuous permafrost extent. 5A - Carbon cycles in the cold regions: modeling and observations, International Conference on Permafrost.

Vesselinov V.V. 2022. MADS: Model Analysis and Decision Support in Julia. https://github.com/madsjulia/Mads.jl

Changing sediment characteristics and greenhouse gas production within a thermokarst lagoon system, Reindeer Island, Mackenzie Delta, Canada

Maren Jenrich[1,2], Dustin Whalen[3], Susanne Liebner[4,5], Christian Knoblauch[6,7], Guido Grosse[1,2], Fiona Giebeler[2] & Jens Strauss[1]

[1]*Permafrost Research Section, Alfred Wegener Institute Helmholtz Center for Polar and Marine Research, Germany*

[2]*Institute of Geosciences, University of Potsdam, Potsdam, Germany*

[3]*Geological Survey of Canada Atlantic, Natural Resources Canada, Dartmouth, Nova Scotia, Canada*

[4]*GFZ German Research Center for Geosciences, Helmholtz Centre Potsdam, Section Geomicrobiology, Germany*

[5]*Institute of Biochemistry and Biology, University of Potsdam, Potsdam, Germany*

[6]*Institute of Soil Sciences, Faculty of Mathematics, Informatics and Natural Sciences, Universität Hamburg, Germany*

[7]*Center for Earth System Research and Sustainability, Universität Hamburg, Germany*

The permafrost carbon pool is an important storage of the terrestrial carbon cycle that is at risk as the Arctic rapidly warms. Accordingly, in 2019, the United Nations Environmental Program identified permafrost thaw as one of the top five emerging environmental issues of global concern (UNEP 2019).

In addition to increasing microbial decomposition of organic material and greenhouse gas release, permafrost thaw also leads to surface changes. Thermokarst lakes and basins are the result of the decrease in soil volume by melting ice in the subsurface. Rising sea levels and coastal erosion lead to the flooding of thermokarst lakes or drained lake basins along the ice-rich permafrost coasts of Siberia, Alaska and Canada, leading to the formation of thermokarst lagoons. These Arctic lagoons form a transition zone between the terrestrial and marine permafrost regime and represent an ideal research object for how permafrost carbon is affected by increasingly marine conditions. Due to current and future climate change in the Arctic, it is expected that the formation and development of thermokarst lagoons will accelerate (Jenrich et al. 2021). So far, thermokarst lagoons and their role in climate change have hardly been explored.

During one of the earliest studies on thermokarst lagoons Solomon et al. (2000) analyzed sediment cores taken in 1993 in a lagoon system at Reindeer Island at the North Head of the Mackenzie Delta, Canada (Figure 1). In 2021, we revisited this study area and took four sediment cores at the approximate same positions (3, 4, 5, 7) of this prior study and by comparing the same parameters (grain size, geochemistry, salinity, water and carbon content) we aim to investigate how sediment, carbon and porewater characteristics changed between 1993 to 2021. Further, we took additional sediment cores in the lagoon system (12-16).

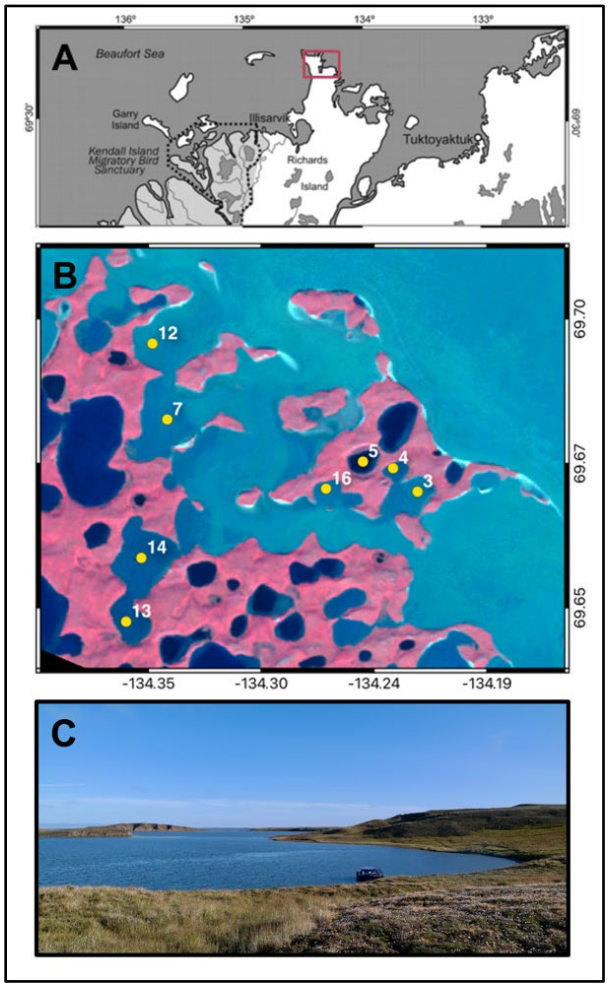

Figure 1. A: Location of the study site at the northern part of Richard Island, Mackenzie Delta, Canada. B: Coring locations (yellow dots) of this study. The locations 3, 4, 5 and 7 are comparable to the ones from Solomon et al. (2000). C: Photo taken from the western shore of Lagoon 4 overlooking lagoons 4 and 3. Source imagery: A: modified after Burn 2009, B: Sentinal 2 A false colour satellite image, aquired 2021-08-26, C: Photo by M. Jenrich 2021-08-21

To investigate the greenhouse gas production under varying degrees of seawater influence, and thus to assess whether the organic material in thermokarst lagoons is degraded on different temporal scales, we incubated the surface sediment below the lagoons with artificial sea water at two concentrations (brackish 13 g/L and marine 36 g/L) anaerobic at 4°C for 1 year. Here brackish conditions are considered as near natural conditions and represent the greenhouse gas production in the current state, while marine conditions represent the greenhouse gas production after the transition into a subsea state.

The investigation of sedimentological and biogeochemical changes between 1993 and 2021 has not yet been completed, but increased erosion of the permafrost coasts is expected to lead to increased sedimentation and carbon input at the sites.

First results of the incubation experiment show that the greenhouse gas production is depending more on the location, thus microbial community and/or carbon degradability, than the salinity treatment. Highest methane and carbon dioxide production was measured at location 13, which is the youngest lagoon, least connected to the sea.

In conclusion, we expect that coastal permafrost erosion is leading to higher sediment and organic carbon input and newly formed thermokarst lagoons produce more greenhouse gases than older, more connected lagoons.

REFERNECES

UNEP 2019. Frontiers 2018/19 Emerging Issues of Environmental Concern. United Nations Environment Programme, Nairobi.

Jenrich, M., Angelopoulos, M., Grosse, G., Overduin, P.P., Schirrmeister, L., Nitze, I., Biskaborn, B.K., Liebner, S., Grigoriev, M., Murray, A., Jongejans, L.L., and Strauss, J. 2021. Thermokarst Lagoons: A Core-Based Assessment of Depositional Characteristics and an Estimate of Carbon Pools on the Bykovsky Peninsula. Front. Earth Sci. 9, 637899. https://doi.org/10.3389/feart.2021.637899

Solomon, S., Mudie, P.J., Cranston, R., Hamilton, T., Thibaudeau, S.A., and Collins, E.S. 2000. Characterisation of marine and lacustrine sediments in a drowned thermokarst embayment, Richards Island, Beaufort Sea, Canada. International Journal of Earth Sciences 89, 503–521. https://doi.org/10.1007/s005310000126

Burn, C.R. 2009. The Mackenzie Delta: An Archetypal Permafrost Landscape. In: Migon, P. (eds) Geomorphological Landscapes of the World. Springer, Dordrecht. https://doi.org/10.1007/978-90-481-3055-9_1

Carbon-flux patterns in natural and disturbed ice-wedge-polygon tundra, Alaska

Anja Kade[1], Donald Walker[2], Martha Raynolds[2], Amy Breen[3] & Olivia Hobgood[2]

[1]*Biology and Wildlife Department, University of Alaska Fairbanks, United States*

[2]*Institute of Arctic Biology, University of Alaska Fairbanks, United States*

[3]*International Arctic Research Center, University of Alaska Fairbanks, United States*

Nearly half of the Arctic region is underlain by icerich permafrost, making it highly susceptible to changes in climate (Shur et al. 2012). Polygonal ice-wedge tundra, an indicator of ice-rich permafrost (Kanevskiy et al. 2017), is comprised of diverse microhabitats, including wet low-center polygons with elevated, drier rims and active ice-wedge troughs, as well as moist flat-center and dry high-center polygons lacking rims. The warming Arctic climate has resulted in the degradation of ice wedges and the deepening of troughs, leading to the redistribution and drainage of water, causing a shift from low-center to high-center polygons (Liljedahl et al. 2016; Jorgenson et al. 2015). In turn, soil conditions and vegetation in the various polygonal microhabitats are affected, impacting carbon-exchange dynamics (e.g., Lara et al. 2015; Wickland et al. 2020).

In addition to climate change, infrastructure development is causing significant degradation in ice-rich permafrost ecosystems. Activities associated with oilfield operations, such as the construction of gravel roads on thick pads, lead to dust deposition, change in vegetation composition, deep snow drifts and flooding caused by damming (Walker et al. 2022). The compounding effects of climate change and infrastructure development in the Arctic intensify changes in ice-rich polygonal tundra and need to be considered when predicting ecosystem changes in these susceptible landscapes.

Here, we studied the effects of (a) geologic landform and (b) infrastructure impacts caused by road dust and flooding on vegetation, soil and trace-gas fluxes in deteriorating polygonal ice-wedge tundra in arctic Alaska.

Methods

We measured plant species cover, soil properties of the upper mineral horizon and carbon fluxes at various microhabitats (i.e., polygon center, trough, rim) at a natural and a disturbed site within the Prudhoe Bay Oilfield, Alaska. At the natural site, we focused on different geologic landforms such as a residucal alluvial plain (RP), ice-rich drained thaw lake basin (ITB) and more recently drained, ice-poor thaw lake basin (PTB). At the disturbed site, which is underlain by the same residual alluvial plain deposits as the undisturbed RP plots, we investigated the effect road dust and increased flooding due to the damming effect of raised road infrastructure. We used chamber-based methods to measure ecosystem respiration (ER), the light response of net ecosystem exchange (NEE) and gross ecosystem productivity (GEP), and CH_4 flux at each study plot. Relationships among environmental parameters, plant species composition and trace-gas fluxes were evaluated using nonmetric multi-dimensional scaling. We used map extrapolations based on microhabitat and vegetation type to visually display the spatial variability of mid-summer ecosystem productivity and CH_4 efflux at the various geologic landforms.

Results

At the undisturbed study site, the different microhabitats on various landforms were correlated with environmental variables, plant functional types and carbon fluxes. The raised flat- and high-center polygons on the RP and elevated rims of the low-centered polygon tundra on the ITB supported moist nonacidic tundra dominated by sedges, evergreen and deciduous dward shrubs and mosses. In contrast, the low-centered polygon centers on the ITB and featureless plots on the PTB had wet sedge, moss tundra with deep organic layers. Average NEE was greater in polygon troughs than polygon centers on both the RP and ITB (Figure 1). NEE was highest in the aquatic polygon troughs on the ITB that were dominated by by *Carex aquatilis* and *Calliergon giganteum*. Interestingly, the wet featureless plots on the PTB showed net CO_2 emission at the peak of the growing season. Average CH_4 emissions were highest on the ITB.

At the disturbed site, the cumulative impacts of road dust and/or flooding had an effect of trace-gas fluxes. When compared to the polygon centers and troughs of the undisturbed RP, the road-affected plots had significantly lower ER but similar NEE. The deeply flooded polygon troughs along the road were characterized by aquatic sedge marsh and had significantly higher CH_4 than the other plots.

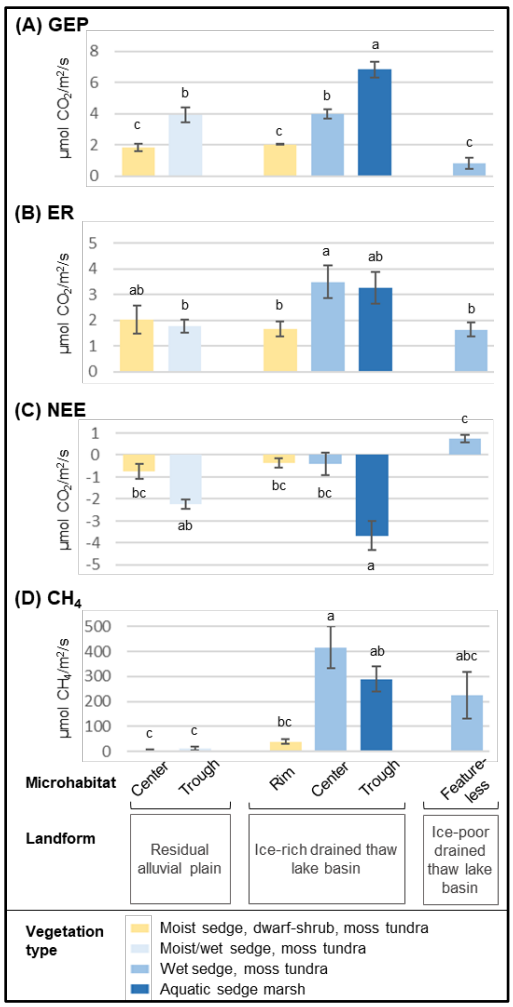

Figure 1. Means and standard errors for mid-summer (A) gross ecosystem productivity GEP, (B) ecosystem respiration ER, (C) net ecosystem exchange NEE and (D) methane CH_4 flux at the undisturbed study plots (n=3). Plots are arranged by landform and microhabitat, and different colors indicate vegetation types. Values for (A) and (C) are estimates at 600 µmol photons/m2/s. Negative NEE values indicate carbon uptake by the vegetation. Letters denote differences in fluxes among the microhabitats found on the various landforms as indicated by Tukey's HSD test at p=0.05.

Discussion

This study shows the importance of the intricate relationships among geologic landform, microhabitat, vegetation type and disturbance factors when assessing carbon-exchange dynamics in rapidly degrading, ice-rich permafrost environments. Aquatic, intermittently flooded polygon troughs with high sedge biomass had the greatest carbon-sequestration potential, while moist, shrubbier polygon centers exhibited intermediate productivity. The wetter site conditions due to road disturbance correlated with lower ER, which undermines the conventional understanding of disturbed areas acting as CO_2 sources. Also, the deeply flooded, minimally vegetated troughs close to the road were hot spots of CH_4 efflux, demonstrating the spatial variability in trace-gas fluxes due to the evolutionary stage of ice-wedge degradation.

References

Jorgenson, M.T., Kanevskiy, M., Shur, Y., Moskalenko, N., Brown, D.R.N., Wickland, K., Striegl, R., and Koch, J. 2015. Role of ground ice dynamics and ecological feedbacks in recent ice wedge degradation and stabilization, Journal of Geophysical Research Earth, 120: 2280–2297. https://doi.org/10.1002/2015JF003602

Kanevskiy, M., Shur, Y., Jorgenson, T., Brown, D.R.N., Moskalenko, N., Brown, J., Walker, D.A., Raynolds, M.K., and Buchhorn, M. 2017. Degradation and stabilization of ice wedges: Implications for assessing risk of thermokarst in northern Alaska, Geomorphology, 297: 20–42.

Lara, M.J., McGuire, A.D., Euskirchen, E.S., Tweedie, C.E., Hinkel, K.M., Skurikhin, A.N., Romansovsky, V.E., Grosse, G., Bolton, W.R., and Genet, H. 2015. Polygonal tundra geomorphological change in response to warming alters future CO2 and CH4 flux on the Barrow peninsula, Global Change Biology, 21: 1634–1651. https://doi.org/10.1111/gcb.12757

Liljedahl, A.K., Boike, J., Daanen, R.P., Fedorov, A.N., Frost, G.V., Grosse, G., Hinzman, L.D., Iijma, Y., Jorgenson, J.D., Matveyeva, N., Necsoiu, M., Raynolds, M.K., Romanovsky, V.E., Schulla, J., Tape, K.D., Walker, D.A., Wilson, C.J., Yabuki, H., and Zona, D. 2016. Pan-Arctic ice-wedge degradation in warming permafrost and its influence on tundra hydrology, Nature Geoscience, 9: 312–318.

Shur, Y., Kanevskiy, M., Jorgenson, T., Dillon, M., Stephani, E., Bray, M., and Fortier, D. 2012. Permafrost degradation and thaw settlement under lakes in yedoma environment, In Proceedings of the Tenth International Conference on Permafrost, Salekhard, Russia, 1: 383–388.

Walker, D.A., Raynolds, M.D., Kanevskiy, M.Z., Shur, Y.S., Romanovsky, V.E., Jones, B.M., Buchhorn, M., Jorgenson, M.T., Šibík, J., Breen, A.L., Kade, A., Watson-Cook, E., Matyshak, G., Bergstedt, H., Liljedahl, A.K., Daanen, R.P., Connor, B., Nicolsky, D., and Peirce, J.L. 2022. Cumulative impacts of a gravel road and climate change in an ice-wedge-polygon landscape, Prudhoe Bay, Alaska, Arctic Science, 8(4): 1040–1066. https://doi.org/10.1139/as-2021-0014

Wickland, K.P., Jorgenson, M.T., Koch, J.C., Kanevskiy, M., and Striegl, R.G. 2020. Carbon dioxide and methane flux in a dynamic Arctic tundra landscape: Decadal-scale impacts of ice degradation and stabilization, Geophysical Research Letters, 47: e2020GL089894. https://doi.org/10.1029/2020GL089

Taliks—an emerging source of old carbon export within a degrading permafrost watershed in interior Alaska

Allison K. Kelley, Zev Axler, Justin Ledman, Monica De La Torre, Christopher Ebert & Ted Schuur
Center for Ecosystem Science and Society, Northern Arizona University, Flagstaff, Arizona, United States

Warming and permafrost thaw in Arctic watersheds triggers previously-sequestered, old soil carbon release to both the atmosphere and streams. This study assesses the contribution that lateral pathways play in old carbon release by calculating the lateral carbon flux within a ~70 km^2 watershed, from soil pore waters to stream headwaters in interior Alaska. We use stream discharge and dissolved organic carbon (DOC) concentrations to calculate lateral DOC flux over time. These data are compared with known vertical fluxes and flux estimates (CO_2 and CH_4). Additionally, in order to assess increasing old, permafrost-derived carbon losses, we assess the radiocarbon signatures of each flux over time. In this process, we have also identified the radiocarbon signature of an evolving source of old carbon that may be exported from this watershed—taliks. Taliks are perennially unfrozen ground present overwinter between the seasonally-frozen active layer and the permafrost table which provide a new for prolonged old carbon release and export in a degrading permafrost system.

Results

To calculate stream discharge, we calculated a water budget for the watershed. Rainfall, measured using a HOBO weather station, averaged between 0.93 to 3.4 mm/day, with larger rain events of 20-30 mm/day during the growing season. Total rainfall (±SE) was between 141 ± 0.51 to 518 ± 0.97 mm between May and September (over a 7-year period). There was limited rainfall during the shoulders of the growing season (May and September) and rainfall peaked during the mid-late growing season (July and August).

Actual evapotranspiration (AET±SE), measured directly using an eddy flux tower, averaged 2 ± 0.01 mm/day and total average AET culminated in between 288 ± 1.8 to 430 ± 2.0 mm from May to September. Both precipitation and ET peaked in 2019.

Discharge at the second-order stream site was highest in May, due to snowmelt and in August, due to increased rainfall (Table 1). Concentrations of DOC within the second-order stream were also highest in May, during the high discharge period, leading May to have the greatest DOC export. Both DOC concentrations and discharge were lowest in July within the second-order stream.

Table 1. Average Monthly DOC Exports from the Second-Order Stream (2016-2023).

Month	Discharge (L H_2O / m^2)	DOC Concentration (g DOC/L)	DOC exported (g DOC / m^2)	Δ^{14}C-DOC (‰)
April	1	-	-	-316
May	35	0.015	0.51	14
June	17	0.014	0.25	-37
July	3	0.0073	0.02	-124
Aug	22	0.013	0.30	-57
Sept	2	-	-	-298

Note: Data analysis for April and September DOC concentrations is in process.

While the radiocarbon signature of May DOC was modern (more enriched), the radiocarbon signature of August DOC was more negative (older). Shoulder season DOC (April and September) was among the oldest of the DOC mixtures analyzed from the second-order stream location (Table 1). In combination with our lateral flux estimates, we hope to determine the magnitude of old carbon lost from this watershed across the season.

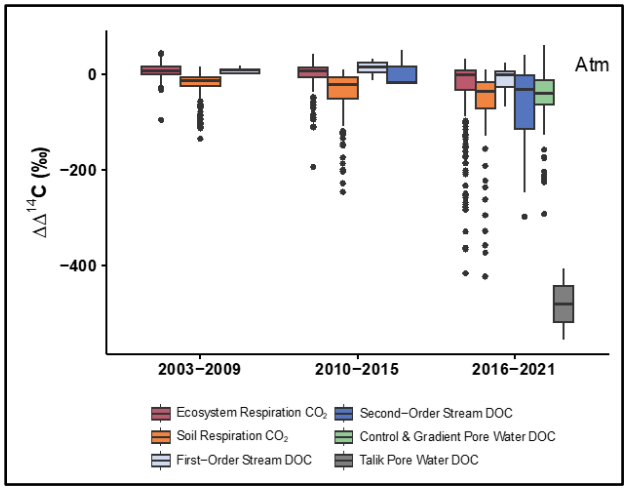

Figure 1. CO_2 and DOC radiocarbon signatures become increasingly negative over time, indicating more old carbon contributions (modified from Kelley et al. in prep; Schuur et al. 2023). Signatures are in comparison to the atmospheric radiocarbon signal over time.

Over time, the Δ^{14}C-DOC values of all carbon fluxes became more negative (Figure 1). This corresponds with increasing permafrost degradation across the same period and one new permafrost degradation feature present on the landscape are taliks. Taliks are one potential source of old carbon, driving the negative trend observed in each of the fluxes. The most negative DOC radiocarbon signatures measured (Δ^{14}C-DOC -180 to -573‰, mean: -365‰) were sourced from talik pore water (Figure 1). First detected in the ambient tundra in 2022, taliks are perennially unfrozen ground that may be sources of microbial respiration and DOC leaching overwinter (Figure 2).

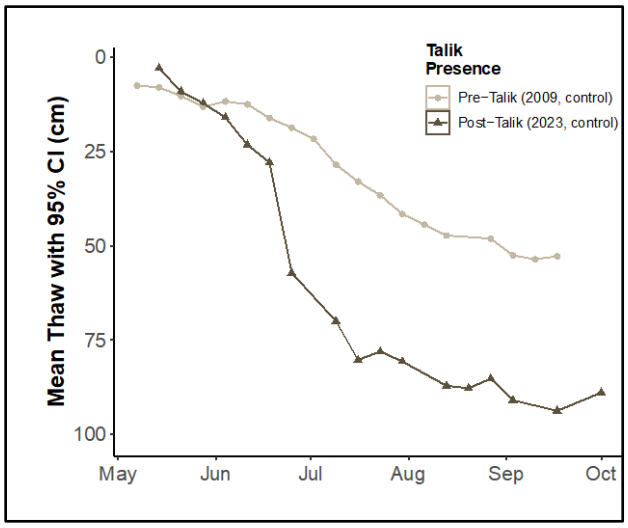

Figure 2. Talik conditions were documented within our watershed and pore water within this talik layer was analyzed for radiocarbon signature and DOC concentration.

Conclusions

Abrupt aging of DOC in large Arctic rivers was detected in 2018, and one potential cause of this abrupt aging was also attributed to taliks (Schwab et al. 2020), which were identified to be widespread the same year (Farquharson et al. 2022). We have identified taliks at our study site as well. In combination with our radiocarbon analyses and our lateral flux estimates, we hope to assess the contribution of talik pore water to old, lateral carbon losses.

To our knowledge, our study is the first to have dated the DOC present within taliks to provide direct evidence for the hypothesis that taliks contribute to old DOC losses. We combined these data with an overall lateral carbon flux from a second-order stream draining a landscape containing taliks. We hypothesize that the leaching of this exceptionally old DOC within talik features may explain a portion of the lower Δ^{14}C-DOC signal detected both in pore water and in surface waters over the course of our timeseries (Figure 1; Table 1).

The exceptionally old Δ^{14}C dissolved within talik pore spaces overwinter is also a likely contributor to the increasing proportion of permafrost-derived, terrestrial DOC that turned up within April second-order stream DOC, though further analysis is necessary (Table 1). April is a period where the seasonally frozen surface soil is still intact, but where taliks may create connected, subsurface pipes that allow for DOC export to second-order streams.

Farquharson et al. 2022, predicted that new taliks will form across 70% of this zone, regardless of snow conditions in the future. It is theorized that increasing talik formation will lead to a “slow leak” of old C in across the permafrost region in the future (Parazoo et al. 2018) and our data suggest that not only is this slow leak is possible, but that it could have large consequences for the whole ecosystem C balance if talik formation were to increase and shoulder season and overwinter DOC exports are not accounted for.

Equations

DOC Fluxes were calculated according to the following:

$$\text{Runoff}\left(\frac{\text{L } H_2O}{\text{m}^2\text{yr}}\right) \times \text{DOC Concentration}\left(\frac{\text{g DOC}}{\text{L } H_2O}\right) = \text{DOC Flux}\left(\frac{\text{g DOC}}{\text{m}^2\text{ yr}}\right) \quad [1]$$

$$\text{Total kg DOC exported yr}^{-1} = \text{DOC Flux}\left(\frac{\text{kg DOC}}{km^2\text{ yr}}\right) \times \text{Watershed Area } (km^2) \quad [2]$$

References

Farquharson, L. M., Romanovsky, V. E., Kholodov, A., and Nicolsky, D. 2022. Sub-aerial talik formation observed across the discontinuous permafrost zone of Alaska. Nature Geoscience, 1–7. https://doi.org/10.1038/s41561-022-00952-z

Parazoo, N.C., Koven, C.D., Lawrence, D.M., Romanovsky, V., and Miller, C.E. 2018. Detecting the permafrost carbon feedback: talik formation and increased cold-season respiration as precursors to sink-to-source transitions. The Cryosphere, 12(1), 123–144. https://doi.org/10.5194/tc-12-123-2018

Schuur, E.A.G., Hicks Pries, C., Mauritz, M., Pegoraro, E., Rodenhizer, H., See, C., and Ebert, C. 2023. Ecosystem and soil respiration radiocarbon detects old carbon release as a fingerprint of warming and permafrost destabilization with climate change. Philosophical Transactions of the Royal Society A: Mathematical, Physical and Engineering Sciences, 381(2261), 20220201. https://doi.org/10.1098/rsta.2022.0201

Schwab, M.S., Hilton, R.G., Raymond, P.A., Haghipour, N., Amos, E., Tank, S.E., et al. 2020. An Abrupt Aging of Dissolved Organic Carbon in Large Arctic Rivers. Geophysical Research Letters, 47(23), e2020GL088823. https://doi.org/10.1029/2020GL088823

Stabilization of plant derived organic matter in thawing permafrost of northern Siberia

Christian Knoblauch[1,2] & Christian Beer[1,2]

[1]*Institute of Soil Science, Universität Hamburg, Hamburg, Germany*

[2]*Center for Earth System Research and Sustainability, Universität Hamburg, Hamburg, Germany*

About 15 - 18% of the land area of the northern hemisphere is underlain by permafrost, which accumulated over millennia about 800 Pg of organic carbon. The strong warming of the Arctic causes permafrost thaw and the concomitant liberation of organic matter, which may be decomposed by microorganisms to carbon dioxide (CO_2) and methane (CH_4). However, warming of circumpolar landscapes and thawing of permafrost also cause increasing plant productivity and litter production that serve as source for the sequestration of soil organic carbon (SOC). Although an increasing number of studies have quantified the decomposition of permafrost organic matter the formation of SOC from fresh plant material in permafrost soils and the parameters determining its long-term stabilization are less well understood. To evaluate the decomposition and stabilization of fresh plant organic matter in thawing permafrost we conducted a 13 years incubation experiment with samples from Pleistocene and Holocene permafrost deposits of Siberia. After 4 years, we added to each of the incubations as much carbon as has been mineralised during the initial 4 incubation years in form of ^{13}C-labelled plant litter from Carex aquatilis (litter-C). During the following 9 years, we measured repeatedly CO_2 and CH_4 concentrations and their carbon stable isotope signatures to partition the gas production into its sources, i.e., SOC and litter-C. At the end of the incubations, we fractionated the organic carbon into the free particulate organic carbon (fPOC) and mineral associated organic carbon (MAOC) by density fractionation. These fractions were subsequently analysed for carbon content and carbon stable isotope signatures to quantify SOC and litter-C in these fractions separately. Finally, mean residence times (MRT) of labile and stabile carbon pools were calculated with a two pool carbon decomposition model that was calibrated with the long-term formation of CO_2 and CH_4 from SOC and litter-C.

The total release of CO_2 and CH_4 from SOC nine years after Liier addition was about 2.5 times higher than from litter-C, both under aerobic and anaerobic conditions. However, litter-C was still preferentially decomposed since the SOC pool was 26.7 ± 7.4 (mean ± SD) times higher than the litter-C pool in the aerobic incubations, while the anaerobic incubations contained even 85.2 ± 32.6 times more SOC than litter-C.

Although each of the incubations received as much litter-C as has been decomposed from SOC during the initial 4 years, a significantly lower fraction of added litter-C was decomposed under anaerobic conditions (mean 0.40 ± 0.12 SD) than under aerobic conditions (0.61 ± 0.21) (Figure 1), indicating a stronger stabilization of fresh plant litter under anaerobic conditions.

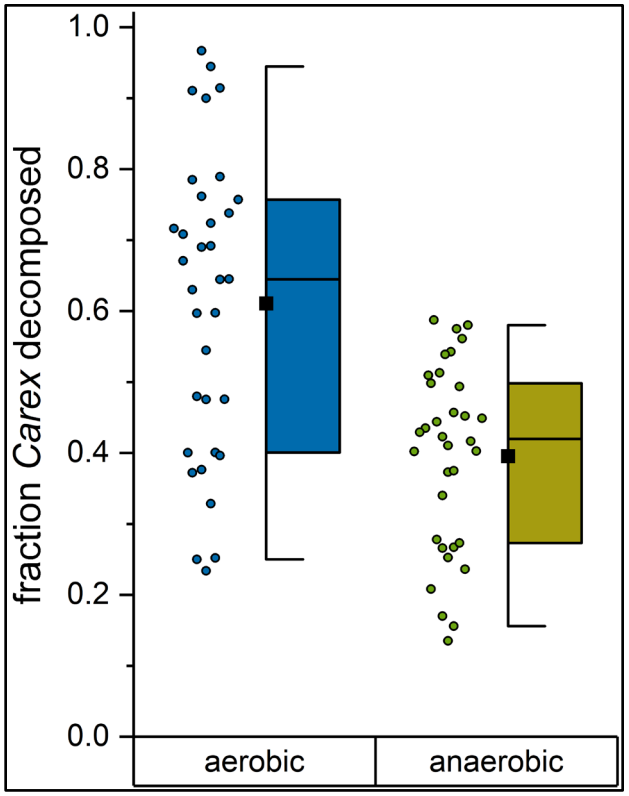

Figure 1. Fraction of organic carbon from added Carex decomposed during the incubations to CO_2 (aerobic) or CO_2 and CH_4 (anaerobic). The Box shows the 25/75 percentiles, the whiskers the 5/95 percentiles, the horizontal line the median and the square the mean. Single data points and the normal distribution are presented left of the boxplot.

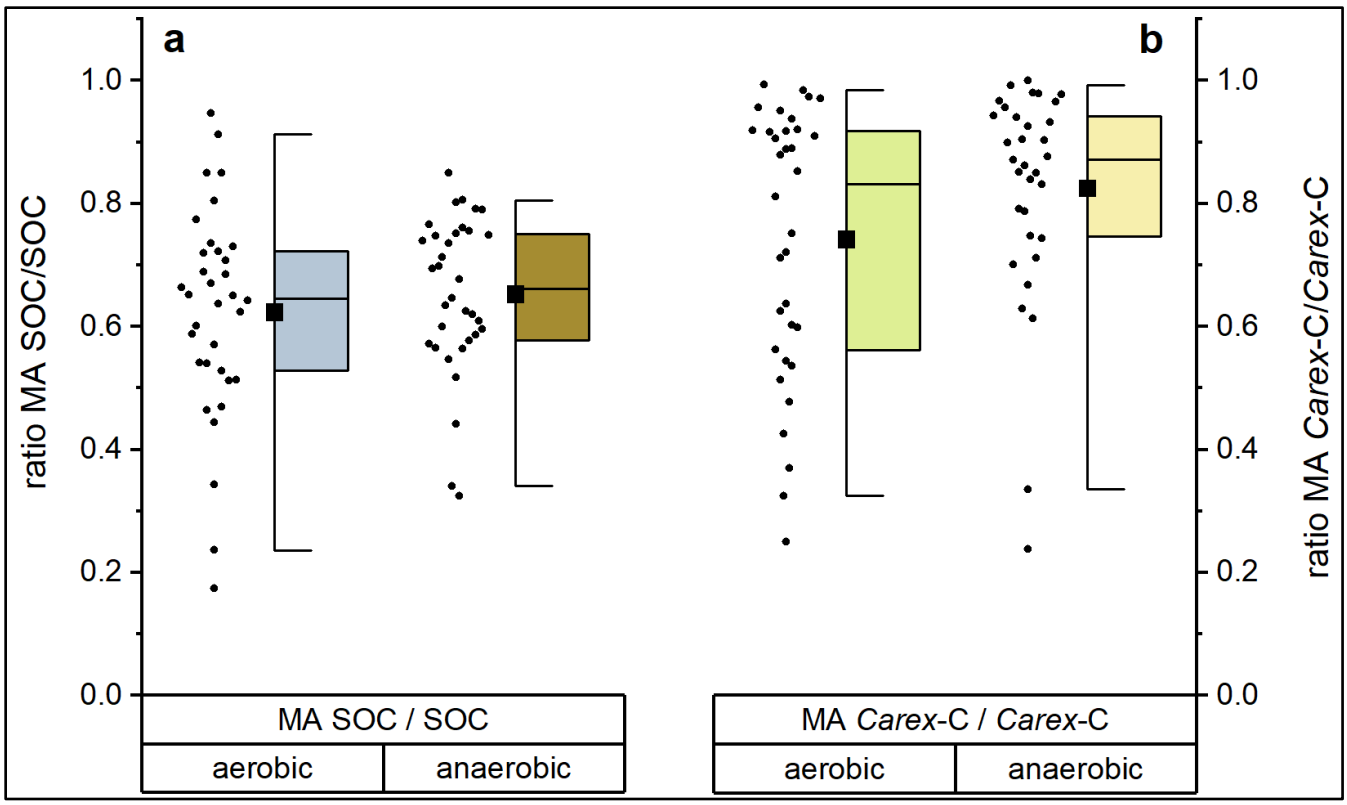

Figure 2. Ratio between mineral associated SOC (MA SOC) and total SOC (a) and between mineral associated Carex-C (MA Carex-C) and total Carex-C (b) at the end of a nine years incubation under aerobic and anaerobic conditions. The Box shows the 25/75 percentiles, the whiskers the 5/95 percentiles, the horizontal line the median and the open square the mean. Single data points are presented left of the boxplots.

Most of the organic carbon was associated with the mineral fraction (MAOC). However, we found a significantly higher fraction of mineral bound litter-C (average 0.74 ± 0.22 and 0.82 ± 0.18 aerobic and anaerobic incubations, respectively) than of SOC (average 0.62 ± 0.17 and 0.65 ± 0.13) (Figure 2), indicating a rapid stabilization of litter-C on mineral surfaces. The higher fraction of mineral associated litter-C under anaerobic conditions in comparison to aerobic conditions further supports a stronger stabilization of fresh plant litter in the absence of oxygen.

The fraction of litter-C decomposed to CO_2 under aerobic conditions showed a strong positive correlation with pH and with the fraction of mineral associated litter-C and a negative correlation with the MRT of the stable litter-C pool. Under anaerobic conditions texture was the strongest predictor for litter mineralisation with a positive correlation with the sand fraction and a negative correlation with the silt and clay fraction.

The MRT of the stable litter-C pools differed significantly from those of SOC with lowest values for the litter-C pool under aerobic conditions (median 17.6 yr) and highest values for the stable SOC pool under anaerobic conditions (median 905 yr). The MRT of the stable litter-C pool correlated negatively with the fraction of litter-C decomposed and the size of the sand fraction both under aerobic and anaerobic conditions.

The provided data indicate that the mineral fraction of thawing permafrost may stabilize a substantial fraction of fresh plant litter in the form of long-term stable mineral associations and my hence not only become a source of greenhouse gases by decomposing SOC but also a sink for carbon from fresh plant litter.

Improving temporal representation of Arctic-Boreal wetland carbon emissions through data flux synthesis efforts: ABCFlux V2 & BAWLD V2

McKenzie Kuhn[1,2,3], Anna M. Virkkala[3], Isabel Wargowsky[3], Judith Vogt[4], Tiffany Windholz[2], Mathias Göckede[4], David Olefeldt[5], Susan M. Natali[3] & Brendan M. Rogers[3]

[1]*University of British Columbia, Vancouver, British Columbia, Canada*

[2]*University of New Hampshire, Durham, New Hampshire, United States*

[3]*Woodwell Climate Research Center, Falmouth, Massachusetts, United States*

[4]*Max Planck Institute for Biogeochemistry, Jena, Germany*

[5]*University of Alberta, Edmonton, Alberta, Canada*

Methane (CH_4) emissions from Arctic-Boreal ecosystems make up a significant but uncertain portion of global wetland emissions (Saunois et al. 2020) and emissions are likely to increase due to warming and permafrost thaw. Ecosystem CH_4 fluxes have been measured from over 150 northern wetland sites starting back in the 1970s (Kuhn et al. 2021). Synthesis efforts have highlighted various widespread controls on wetland CH_4 fluxes including vegetation and microbial composition, hydrology, and soil types. However, thus far most CH_4 synthesis work has focused on average growing season fluxes, leaving out important temporal trends in fluxes that could help reduce uncertainties in regional emissions estimates. Further, CH_4 and carbon dioxide (CO_2) flux synthesis efforts for the region have long been done separate from one another, often using different land cover classifications, despite important ecological connections between the gases and a critical need for more uniform scaling approaches for the two greenhouse gases to better constrain Arctic-Boreal carbon emissions.

OBJECTIVE

Our goal is to collect and synthesize CH_4 and CO_2 fluxes (chamber, eddy covariance) and environmental parameters (e.g., air/soil temperatures, vegetation type, permafrost and disturbance conditions) from upland, wetland, and freshwater ecosystems across the Arctic-Boreal region. Our work builds off of previous synthesis efforts by Virkkala et al. (2019; ABCFlux V1- CO_2 fluxes) and Kuhn et al. (2021: BAWLD-CH_4). Our comprehensive approach includes chamber and eddy covariance CO_2 and CH_4 fluxes from terrestrial and freshwater ecosystems. We expand growing season flux data included in BAWLD-CH_4 to monthly time-steps. Using a uniform classification system, site-level ecosystems were defined based on their CH_4-emitting potentials. Terrestrial classifications include Upland Tundra, Boreal Forest, Fen, Bog, Marsh, Permafrost Bog, and Wet Tundra ecosystems (Kuhn et al. 2021). To compile flux data we reached out to >100 researchers and extracted data from available literature and databases. Ultimately, monthly carbon fluxes and associated environmental parameters will be openly available in one centralized database. Here we present preliminary CH_4 chamber flux results from wetland and upland ecosystems at a monthly resolution. As of November 2023, we have extracted or received contributer chamber flux data for 1400+ site-months and have added 25+ new sites not previously included in BAWLD-CH_4 (Figure 1).

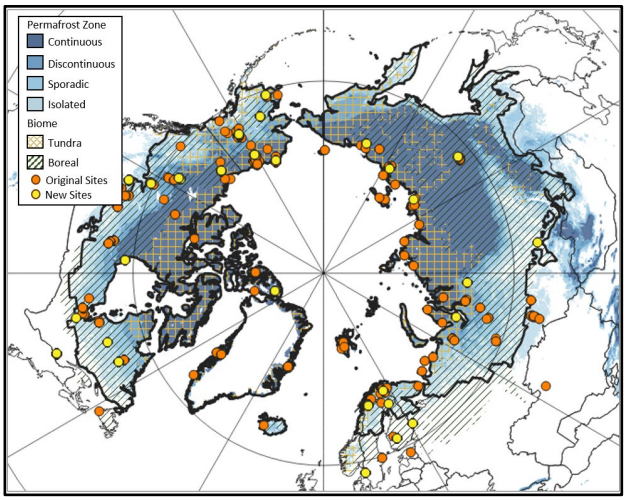

Figure 1. Map of original upland and wetland chamber CH_4 flux sampling locations in Kuhn et al. (2021; orange dots) and new sites included in this synthesis (yellow dots).

Ultimately, our aim with this highly collaborative synthesis effort is to improve our understanding of Arctic-Boreal carbon fluxes in order to better constrain ecosystem carbon budgets, including inprovements to non-growing season emissions estimates (Figure 2). Further this dataset can be used in model benchmarking and as a tool to inform future field research directions.

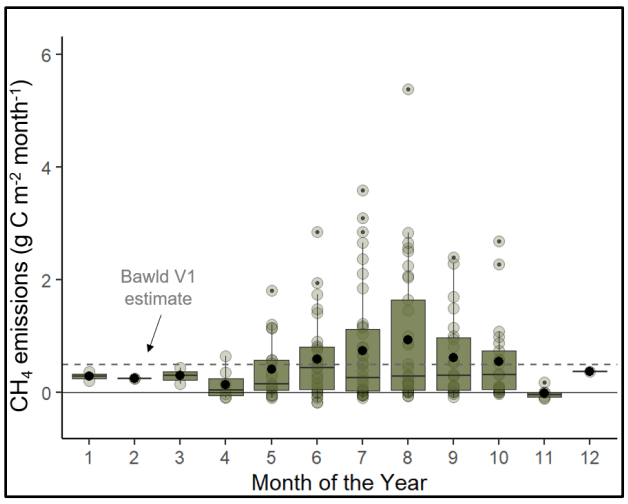

Figure 2. Preliminary synthesized fluxes from fen ecosystems, split into monthly timesteps. The dotted line represents the average monthly flux based on growing season data and a simplified non-growing season estimate using BAWLD-CH_4 v1.

REFERENCES

Kuhn, M.A., et al. 2021. BAWLD-CH_4: A Comprehensize Dataset of Methane Fluxes from Boreal and Arctic Ecosytems, Earth Systems Science Data, 13(11): 5151–5189. doi:10.5194/essd-13-5151-2021

Saunois, M., et al. 2020. The Global Methane Budget 2000-2017, Earth Systems Science Data, 12(3): 1561-1623. doi:10.18160/GCP-CH4-2019

Virkkala, A.M., et al. 2021, The ABCFlux database: Arctic-boreal CO_2 flux observations and ancillary information aggregated to monthly time steps across terrestrial ecosystems. Earth Systems Science Data, 14(1): 179–208. doi:10.5194/essd-14-179-2022

Change in soil carbon age and fractions during a permafrost warming experiment

Emma Lathrop, Christopher Ebert & Ted Schuur
Center for Ecosystem Science and Society, Northern Arizona University, Flagstaff, Arizona, United States

While they constitute only 15% of land area, permafrost soils contain approximately half of global soil organic carbon (SOC). Permafrost soils have the potential to release as much carbon as a developed country (Schuur et al. 2022) which could irreversibly alter the global carbon cycle by introducing old, previously sequestered carbon to the atmosphere. To understand the quantity of old carbon released as permafrost thaws, we measured the age of SOC pools from experimentally manipulated plots at the end of a 13-year permafrost warming experiment. Additionally, we examined SOC pools with a density fractionation to determine the proportions of SOC vulnerable to decomposition.

METHODS

Measurements were made at the Carbon in Permafrost Experimental Heating Research (CiPHER) plots housed at the ACCLIMATE site in Healy, Alaska, United States. Here, six snow fences insulate warming plots from low winter temperatures. Soil cores from 2009-2013 (n = 12 per year), 2017 (n = 24), and 2022 (n = 48) were collected using a SIPRE auger and split corer. Cores were split into 10 cm depth increments, dried, and ground to measure %C and %N on an elemental analyzer.

SOC pool change through time was calculated as a function of %C, bulk density, and mineral content of soil (mass remaining after burning at 550°C) content using the equivalent ash method (Plaza et al. 2019) to account for changes in depth related to ground surface subsidence during the warming experiment.

Radiocarbon (^{14}C) was measured on bulk SOC samples from 2022 cores to understand the proportion of old carbon released following permafrost thaw. Samples were graphitized and run on an accelerator mass spectrometer to determine the ^{14}C content.

Splitting bulk SOC into fractions gives insight into the vulnerability of permafrost carbon to decomposition. Light fraction carbon is relatively microbially available and has been found to have turnover times 1000 times shorter than heavy fraction carbon, making it more vulnerable to decomposition (Torn et al. 1997). SOC from a subset of 2022 soil cores (n = 21 cores) was fractionated into light and heavy fraction using a combination of density fractionation protocols from similar Arctic soils (Dutta et al. 2006; Gentsch et al. 2015). Here we define the light fraction as SOC that floats to the top of a dense (1.6 g/L) solution of sodium polytungstate following the breakup of occluded material with sonication, and the heavy fraction as any remaining SOC that sinks in the dense solution. Soils were fractionated and the %C from each fraction was measured on an elemental analyzer. Fraction stocks were calculated by multiplying the proportion of carbon in each fraction by the total carbon stock in each sample.

RESULTS

Preliminary results suggest a shift in the direction of the SOC pool change during the warming experiment at CiPEHR. From 2009-2013, pools declined 5% annually (Plaza et al. 2019). However, in 2017 and 2022, the pool size in control and warming plots increased and were 5-10 kg/m^2 greater than 2013.

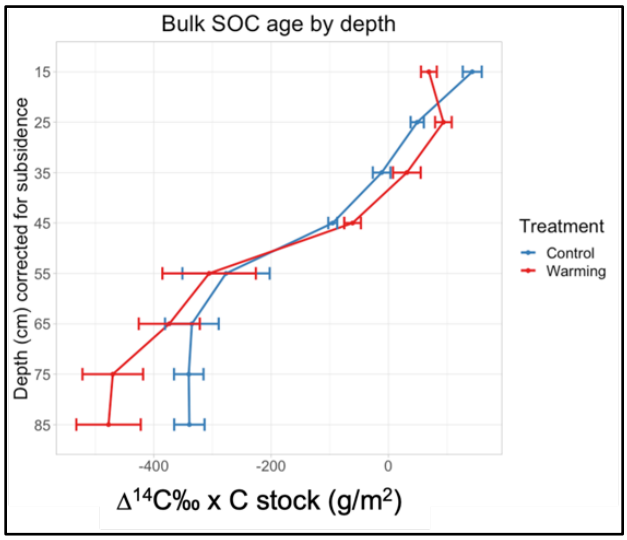

Figure 1. Age of carbon in bulk SOC samples from 2022 soil cores collected at CiPEHR in warming (red) and control (blue) plots. $\Delta^{14}C$ values greater than 0 represent modern carbon inputs, whereas smaller, negative $\Delta^{14}C$ values indicates older bulk SOC.

Bulk SOC age measurements from the end of the warming experiment (n = 5 per depth and treatment) indicate that in much of the shallow soil profile, warming plots have younger SOC than control plots following 13 years of warming (Figure 1).

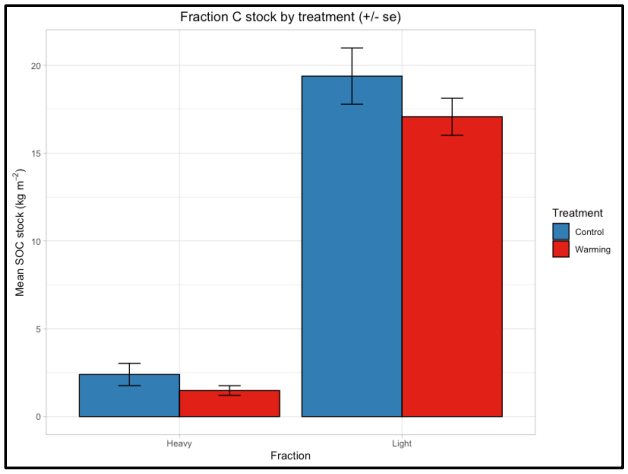

Figure 2. Stocks of light and heavy fraction carbon in control (blue) and warming (red) plots after 13 years of experimental warming at a permafrost.

SOC fractionation showed that in both control and warming plots, the light fraction dominated the SOC pools, even in deep soil (~35-55cm). Warmer plots had a smaller pool of both the light and heavy fraction, indicating the loss of both freely available light carbon, and mineral associated heavy carbon following permafrost thaw.

Discussion

Permafrost thaw altered bulk SOC, fractions and age in soils from the CiPEHR experimental warming site. Changes in plot CO_2 flux do not account for the increase in SOC pools observed in 2017 and 2022, indicating the importance of subsurface hydrologic and geochemical dynamics that control cycling of deep SOC. This unexpected pattern highlights the emergence of hydrologic and geochemical controls on SOC dynamics as the CiPHER site subsided and became saturated. Observed losses of old carbon following warming, particularly in the upper depths, highlight the potential for permafrost thaw to disrupt the global carbon cycle.

Results of the density fractionation suggest that stores of light fraction SOC in deep permafrost soils are larger than anticipated and particularly vulnerable to degradation following warming. These results are consistent with recent meta-analyses of cold-region density fractionation measurements (García-Palacios et al. 2024). Addtionally, the loss of heavy fraction carbon in warming plots means that carbon that is considered recalcitrant, or protected by mineral association is also vulnerable to loss in, likely as a function of redox changes in the soil environment (Opfergelt 2020).

Future work will include increasing the sample size of radiocarbon and SOC fractionation analyses and exploring environmental variables that drive changes in SOC dynamics.

References

Dutta, K., et al. 2006. Potential carbon release from permafrost soils of Northeastern Siberia, Global Change Biology, 12(12): 2336–2351. https://doi.org/10.1111/j.1365-2486.2006.01259.x

García-Palacios, P., et al. 2024. Dominance of particulate organic carbon in top mineral soils in cold regions, Nature Geoscience, pp. 1–6. https://doi.org/10.1038/s41561-023-01354-5

Gentsch, N., et al. 2015. Storage and transformation of organic matter fractions in cryoturbated permafrost soils across the Siberian Arctic, Biogeosciences, 12(14): 4525–4542. https://doi.org/10.5194/bg-12-4525-2015

Opfergelt, S. 2020. The next generation of climate model should account for the evolution of mineral-organic interactions with permafrost thaw, Environmental Research Letters, 15(9): 091003. https://doi.org/10.1088/1748-9326/ab9a6d

Plaza, C., et al. 2019. Direct observation of permafrost degradation and rapid soil carbon loss in tundra, Nature Geoscience, 12(8): 627–631. https://doi.org/10.1038/s41561-019-0387-6

Schuur, E.A.G., et al. 2022. Permafrost and Climate Change: Carbon Cycle Feedbacks From the Warming Arctic', Annual Review of Environment and Resources, 47(1): 343–371. https://doi.org/10.1146/annurev-environ-012220-011847

Torn, M.S., et al. 1997. Mineral control of soil organic carbon storage and turnover, Nature, 389(6647): 170–173. https://doi.org/10.1038/38260

Permafrost thaw effects on Arctic ecosystems: Insights from common substrate decomposition at ACCLIMATE in Healy, Alaska, USA

Megan McGroarty[1], Elaine Pegoraro[2] & Edward A.G. Schuur[1]

[1]*Center for Ecosystem Science and Society, Northern Arizona University, Flagstaff, Arizona, United States*

[2]*Lawrence Berkeley National Laboratory, Berkeley, California, United States*

The Arctic has warmed four times faster than the rest of the world over the past four decades (Rantanen et al. 2022). Permafrost, frozen soil, contains vast stores of organic carbon, and when thawed, this organic material microbially decomposes, emitting greenhouse gasses. Permafrost regions store 33% of the global soil carbon pool; however, this estimate does not account for carbon stored at depths below 3 meters, making it challenging to precisely calculate the extent of carbon release (Schuur et al. 2022). Decomposition of organic matter in thawing permafrost significantly influences soil nutrient availability, water balance, and plant growth, with cascading effects on the entire Arctic ecosystem. Understanding how permafrost thaw affects decomposition is essential for comprehending the impacts on soils and plants in this highly sensitive environment. We examined annual decomposition using a common substrate, cellulose paper, at both long-term sites Gradient and CiPEHR within the ACCLIMATE observatory.

Site Description

This study takes place at two sites within the Arctic Carbon and Climate (ACCLIMATE) observatory located in interior Alaska, which has two decades of observations of how northern landscapes are evolving with the changing climate. The first site, Gradient, comprises three varying sites of natural permafrost thaw established in 2004: minimal, moderate, and extensive. The second site, the Carbon in Permafrost Experimental Warming Project (CiPEHR), is a unique winter warming experiment that uses snow fences and snow drift to induce soil warming by creating an insulating blanket over the soil surface.

Methods

Mesh bags containing cellulose paper were annually incubated in situ at two depths, 0-10 and 10-20 cm. The bags were collected and replaced each fall at Gradient and CiPEHR. within two long-term monitoring sites from the beginning of their establishment (Gradient since 2004 and CiPEHR since 2008). Mass loss was determined by the difference in mass of the cellulose paper between the pre-incubation and post-incubation.

Results

Within Gradient, extensive thaw has experienced almost twice the mass loss compared to the moderate and minimal thaw sites (Figure 1). At CiPEHR, warming treatment impacts were observed through higher cellulose mass loss, though decomposition rates on average were 15-30% higher at shallower depths (Figure 2). At both sites, there were significant differences in percent averages of mass loss by year and depth ($p < 0.001$).

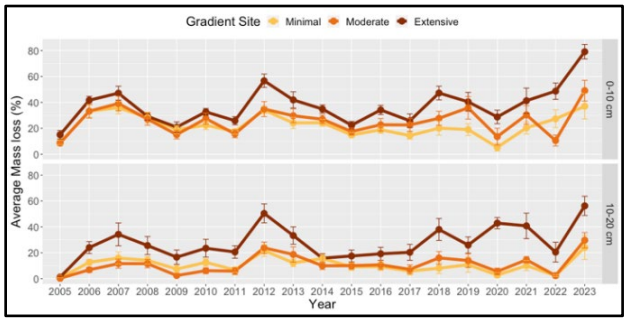

Figure 1. Gradient cellulose average mass loss time series data by year and depth.

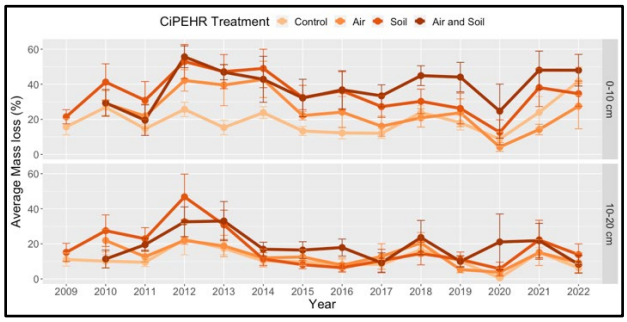

Figure 2. CiPEHR cellulose average mass loss time series data by year and depth.

Discussion

These preliminary results indicate that induced warming and extensive permafrost thaw lead to increased mass loss from decomposition in shallow soils, emphasizing the importance of investigating how thaw progression, hydrology, and vegetation

shifts control decomposition in the Arctic. These findings have critical implications on nutrient availability and the repercussions of ongoing warming to Arctic ecosystems.

Future work will include exploring environmental variables that could be driving these trends in decomposition.

REFERENCES

Rantanen, M., et al. 2022. The Arctic has warmed nearly four times faster than the globe since 1979, Communications Earth & Environment, 3, 168. https://doi.org/10.1038/s43247-022-00498-3

Schuur, E.A.G., et al. 2022. Permafrost and Climate Change: Carbon Cycle Feedbacks from the Warming Arctic, Annual Review of Environment and Resources, 47(1): 343–371. https://doi.org/10.1146/annurev-environ-012220-011847

Multi-objective soil organic carbon parameter optimization for more accurate quantification of the permafrost carbon feedback

Joe R. Melton[1], Charles B. Gauthier[2,3], Gesa Meyer[1] & Oliver Sonnentag[2]

[1]*Climate Research Division, Environment and Climate Change Canada, Victoria, British Columbia, Canada*

[2]*Département de Géographie, Université de Montréal, Montréal, Québec, Canada*

[3]*now at Ouranos Inc, Simulations et analyses climatiques, Montréal, Canada*

Process-based modelling of soil organic carbon (SOC) is a notoriously difficult problem. Models typically don't agree well with each other for both the present state of global SOC stocks and their future trajectory. Attempts to validate the models with observations are also challenging. Observations of SOC pools and respiratory fluxes are made at point-scales, adding ambiguity related to upscaling and sub-grid heterogeneity when comparing against gridded models. The uncertainty in modelled SOC presents a serious obstacle for attempts to quantify the permafrost carbon feedback under future climate change. Part of the difficulty stems from the highly parameterized nature of SOC modelling. Models typically have at least 10 to 30 parameters - just within their SOC schemes (Shi et al. 2018). These large numbers of parameters, along with equifinality, make it difficult to determine the correct values that will give the most accurate model response to changing environmental conditions.

Approach

To address these issues, we adopted a two-fold approach toward SOC scheme parameter optimization (Figure 1). First, we used sensitivity analysis to determine key parameters in the SOC parameterization of the Canadian Land Surface Scheme including Biogeochemical Cycles (CLASSIC; Melton et al. 2020). Then, using the most sensitive parameters, we conducted a Bayesian optimization where CLASSIC parameters were optimized against point-scale soil carbon measurements (World Soil Information Service; WoSIS, Batjes et al. 2020) and soil respiratory fluxes (Soil Respiration Database v. 5; SRDB, Jian et al. 2020). The optimization, conducted with a Tree of Parzen estimator, used two loss functions: "MO" focused on reproducing the observational mean and "EO", which prioritized being within a derived observational uncertainty range for each point. To manage computational cost, we used a stand-alone version of the soil C scheme run globally at T63 grid resolution. The optimized parameters were then used in full CLASSIC simulations over the historical period to compare to independent observation-based estimates and in future simulations to understand the impact upon model behaviour.

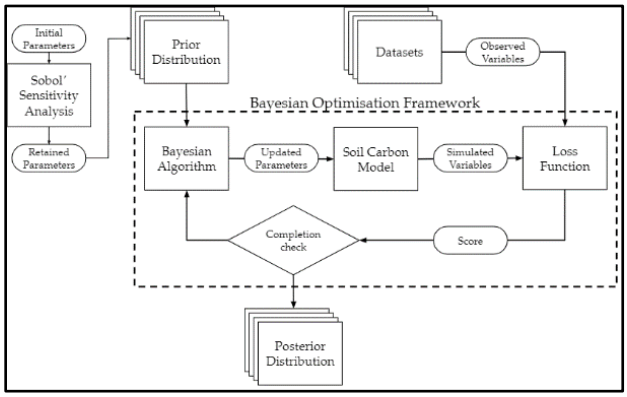

Figure 1. Study design.

Sensitivity analysis

Given the large number of parameters in a SOC scheme, it is advantageous to limit the optimization to only the parameters that most control the model response. To do this we performed a Sobol' global sensitivity analysis (Sobol` 2001) at three eddy covariance sites located in Finland (FI-Hyy), Canada (CA-TVC), and Ghana (GH-Ank) (Figure 2). From this we generated four parameter sets based on the first order sensitivity index across all sites and both heterotrophic respiration and SOC outputs.

Using radiocarbon to constrain turnover

To further constrain our optimization, we implemented a ^{14}C tracer into CLASSIC and used it to compare with measurements provided by the International Soil Radiocarbon Database (ISRaD; Lawrence et al. 2020). Radiocarbon measurements of SOC can be used to understand SOC turnover rates (e.g., He et al. 2016). Incorporation of ^{14}C into our framework gives a further constraint on a different aspect of the SOC system than provided by the WoSIS and SRDB data alone.

Bayesian parameter optimization

The optimization was performed on two loss functions and four different sets of parameters. Based upon the final loss scores and comparison with other observation-based datasets, a scenario with an

intermediate number of parameters optimized (5 general and 3 plant functional type (PFT) specific parameters) and the "EO" loss function was selected to give the largest improvement in model skill. Most parameter values were optimized well within the allowed range (±50% of original values) except one parameter particular to the needle-leaved deciduous tree PFT. Closer inspection revealed that CLASSIC litter inputs in eastern Russia were biased low, which the optimization scheme accommodated by greatly decreasing the base respiration rate of that region's dominant PFT and thus increasing the SOC stock closer to observations.

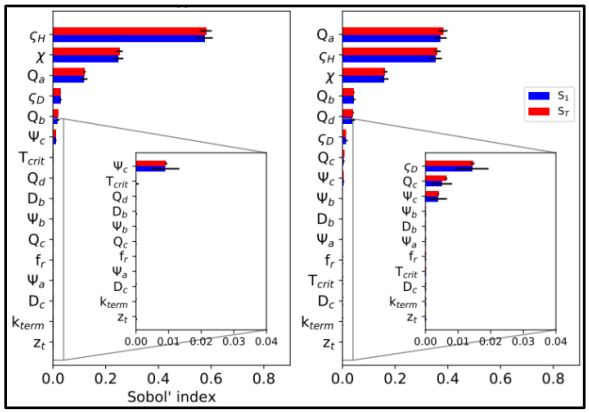

Figure 2. Parameter sensitivity depends on the conditions at the sites tested. When considering SOC, cold sites (e.g., FI-Hyy; left) are most sensitive to the base respiration of the humified pool (ς_H) and the humification transfer coefficient (χ) while at warm sites (e.g., GH-Ank; right) a coefficient of the Q_{10} function formulation (Q_a) becomes the most sensitive parameter.

Conclusions

Parameter optimization must be undertaken with great care. First, it is important to well understand the parameters used in the model to ensure the optimization is constrained and that the parameters with the greatest influence are optimized. Second, the loss function chosen can greatly influence the optimization. The formulation of the loss function should carefully consider the data used for evaluation and determine what aspect of the data is most important for the model to target. Third, any biases in the model inputs, to the soil C scheme or the model as a whole, should be addressed prior to optimization. As the optimization works to reduce biases in the outputs, the algorithm's search can lead to extreme parameter values that are unlikely to be reasonable when the bias is removed. Lastly, numerous aspects of the SOC system (e.g., SOC stocks, respiratory fluxes, ^{14}C-derived turnover) are needed to constrain SOC scheme parameter values most effectively. Once these prerequisites have been considered, Bayesian optimization approaches can be used effectively and lead to important changes in model behaviour. The optimization of CLASSIC led to a higher modern day SOC stock (top meter: 1328 Pg C) compared to the original parameterization (1203 Pg C). The new parameterization also changes the modelled carbon fluxes, e.g., if the optimized parameters are used in CLASSIC simulations with a bias-corrected Earth system model climate for Share Socioeconomic Pathway 370, CLASSIC simulates global soils giving off carbon across the 2015 – 2100 period, while the original parameter values simulated a small sink.

References

Batjes, N.H., Ribeiro, E., and van Oostrum, A. 2020. Standardised Soil Profile Data to Support Global Mapping and Modelling (WoSIS Snapshot 2019), Earth System Science Data, 12 (1): 299–320. doi:10.5194/essd-12-299-2020

He, Y., Trumbore, S.E., Torn, M.S., Harden, J.W., Vaughn, L.J.S., Allison, S.D., and Randerson. J.T. 2016. Radiocarbon Constraints Imply Reduced Carbon Uptake by Soils during the 21st Century. Science. 353 (6306): 1419–24. doi:10.1126/science.aad4273

Jian, J., Vargas, R., Anderson-Teixeira, K., Stell, E., Herrmann, V., Horn, M., Kholod, N., et al. 2021. A Restructured and Updated Global Soil Respiration Database (SRDB-V5), Earth System Science Data, 13 (2): 255–67. doi:10.5194/essd-13-255-2021

Lawrence, C.R., Beem-Miller, J., Hoyt, A.M, Monroe, G., Sierra, C.A, Stoner, S., Heckman, K., et al. 2020. An Open-Source Database for the Synthesis of Soil Radiocarbon Data: International Soil Radiocarbon Database (ISRaD) Version 1.0, Earth System Science, Data 12 (1): 61–76. doi:10.5194/essd-12-61-2020

Melton, J.R., Arora, V.K., Wisernig-Cojoc, E., Seiler, C., Fortier, M., Chan, E., and Teckentrup, L. 2020. CLASSIC v1.0: The Open-Source Community Successor to the Canadian Land Surface Scheme (CLASS) and the Canadian Terrestrial Ecosystem Model (CTEM) – Part 1: Model Framework and Site-Level Performance, Geoscientific Model Development, 13: 2825–50. doi:10.5194/gmd-13-2825-2020

Shi, Z., Crowell, S., Luo, Y., and Moore B. 2018. Model structures amplify uncertainty in predicted soil carbon responses to climate change, Nat. Commun., 9 (1): 2171–2176. doi:10.1038/s41467-018-04526-9

Sobol′, I.M. 2001. Global Sensitivity Indices for Nonlinear Mathematical Models and Their Monte Carlo Estimates. Mathematics and Computers in Simulation, 55 (1): 271–80. doi:10.1016/S0378-4754(00)00270-6

Implication of fire disturbance on soil carbon cycling and permafrost in black spruce forests of interior Alaska: A case study at Hess Creek

Christina Minions[1], Jennifer Watts[1], Claudia Czimczik[2], Shawn A. Pedron[2], Alexander Kholodov[3], Nicholas Hasson[3], Giselle Jimenez[2], Valeria Briones[1], Bradley Gay[4], Helene Genet[3], Andrew Mullen[1] & Susan Natali[1]

[1]*Woodwell Climate Research Center, Falmouth, Massachusetts, United States*

[2]*University of California Irvine, Irvine, California, United States*

[3]*University of Alaska Fairbanks, Fairbanks, Alaska, United States*

[4]*Biospheric Sciences Laboratory, NASA Goddard Space Flight Center, Greenbelt, Maryland, United States*

Arctic-boreal terrestrial ecosystems hold vast reservoirs of soil organic carbon (SOC) and are especially sensitive to climate warming. As air temperatures continue to rise across these regions, SOC within thawing permafrost soils becomes increasingly vulnerable to microbial communities and the subsequent transfer of carbon dioxide (CO_2) and methane (CH_4) to the atmosphere.

However, the impact of fire disturbance on the long-term trajectory of permafrost thaw and SOC is not well understood. Here we present a case study examining adjacent burned (2003) and mature black spruce (Picea mariana) dominated boreal forest stands within the Hess Creek River basin in interior Alaska (Figure 1).

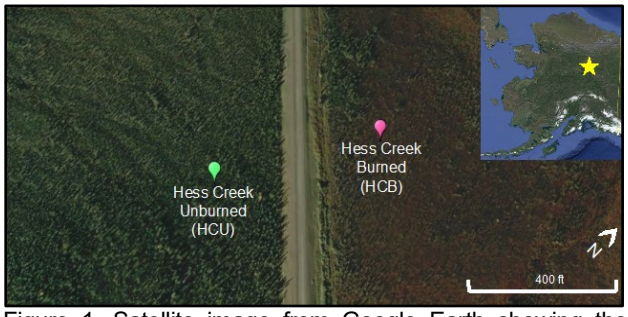

Figure 1. Satellite image from Google Earth showing the locations of the two study locations within the Hess Creek watershed in interior Alaska.

Long-term soil temperature and moisture

Soil temperature and soil moisture were continuously measured at a half-hour frequency from 2017 to 2021.vSoil temperatures at the burned site were significantly warmer throughout the winter months (November-April) compared to the unburned site, however throughout the growing season (May-September) the temperature difference between sites was variable (Figure 2A). Records of soil moisture were only available from April to November across all years. Soil moisture was significantly higher at the burned site across all months except for May (Figure 2B).

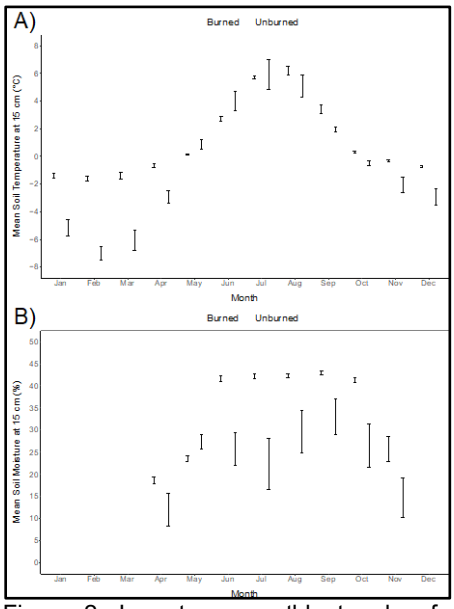

Figure 2. Long-term monthly trends of soil temperature (A) and soil moisture (B) at 15 cm depth within the unburned and burned black spruce stands from 2017 to 2021. Bars represent the monthly mean and error bars the standard error.

Soil CO_2 respiration

To monitor annual changes in soil respiration, and to better understand patterns of soil CO_2 respiration between undisturbed and fire-disturbed landscapes, automated Forced Diffusion (FD) surface chambers were used to track hourly changes in soil CO_2 flux (Watts et al. 2021).

Mean daily soil CO_2 flux rates at each site were compared for each month for years 2017 and 2018 (Figure 3). There were no significant differences in flux rates between sites expect for in November and December of 2017 where fluxes were significantly higher within the burned site compared to the unburned site. Fluxes were generally higher at the burned site during the shoulder seasons (Fall/Spring), whereas fluxes were generally higher at the unburned site during the summer months (June, July, August).

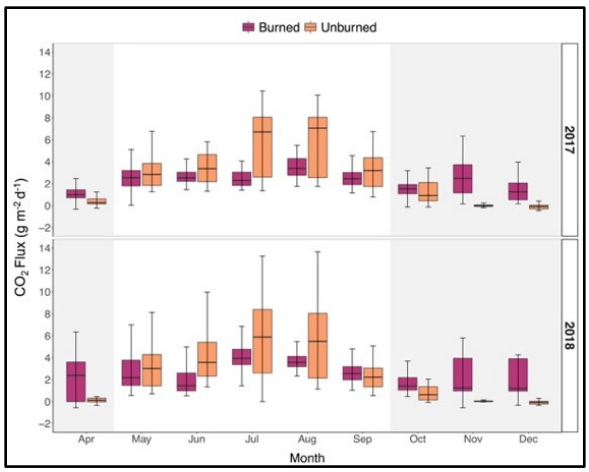

Figure 3. Box plots of daily mean CO_2 flux rates from FD chamber measurements for each month from the burned and unburned sites for years 2017 and 2018.

Soil Radiocarbon

Gas wells were installed at each site in 2021 to collect time-integrated samples of soil CO_2 for ^{14}C analysis to understand how the age of emitted CO_2 varies seasonally. Observations of radiocarbon were available at two depths within the soil profile: one within the organic layer (20 cm depth) and one within the mineral layer (50 cm depth) (Figure 4). The more negative values of delta ^{14}C indicate older sources of carbon. The decomposition and emission of much older carbon is occurring at the burned site compared to the unburned site.

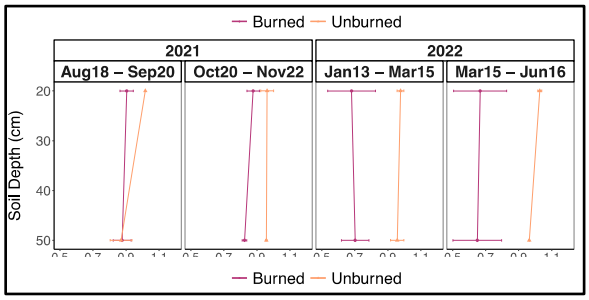

Figure 4. Radiocarbon observations from the unburned and burned sites for various sampling periods in 2021 and 2022. Points represent the mean and horizontal lines are the standard error.

Modeling Thaw Depth and Subsurface Mapping

Predictions of thaw depth were generated using the SIBBORK-TTE model (Figure 5). The model consistently simulated more abrupt thaw earlier in the growing season at the burned site, with current and future projections indicating a deepening of the active layer (Gay et al. 2022).

Very-low frequency electromagnetic (VLF-EM) subsurface mapping was conducted at the burned site (Figure 6). The scans show that sub-aerial taliks have formed within the severely burned areas of the 2003 burn. Sub-aerial taliks are a recent phenomenon, now widespread in Alaska, which can increase the hydrological conductivity throughout the subsurface, and impact CO_2 emissions (Farquharson et al. 2022).

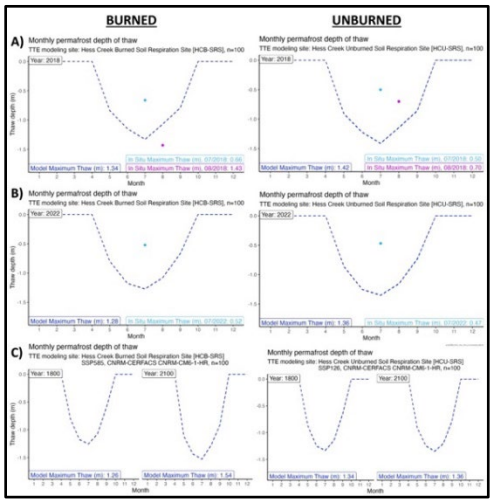

Figure 5. SIBBORK-TTE model predictions of thaw depth for years 2018 and 2022 at the burned and unburned sites (A and B), as well as long-term thaw depth predictions for the year 1800 and 2100 (C). Dashed lines show the predicted thaw depth throughout the year and points are in-situ measurements of thaw depth.

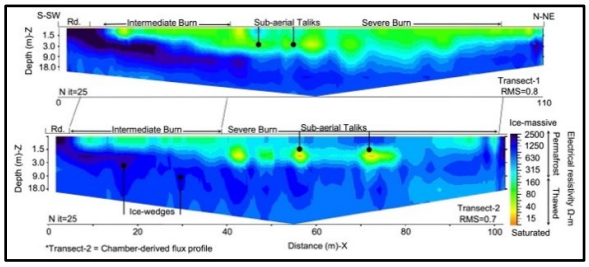

Figure 6. Two parallel geophysical transects of VLF-EM scans (scans are 20 meters apart). Lighter colours indicate thawed soils and areas of groundwater, whereas darker colours indicate ground ice and permafrost.

References

Gay, B.A. 2023. Investigating High-Latitude Permafrost Carbon Dynamics with Artificial Intelligence and Earth System Data Assimilation (Doctoral dissertation, George Mason University). doi:10.1061/(ASCE) 0733-9410(1983)109:7(883)

Farquharson, L.M., et al. 2022. Sub-aerial talik formation observed across the discontinuous permafrost zone of Alaska, Nat. Geosci, 15: 475–48. doi:10.1038/s41561-022-00952-z

Watts, J.D., et al. 2021. Soil Respiration Strongly Offsets Carbon Uptake in Alaska and Northwest Canada, Environ. Res. Letters, 16. doi:10.1088/1748-9326/ac1222

Simulating variably-saturated subsurface flow and reactive transport in thawing permafrost environments

Aaron A. Mohammed[1], Jeffrey M. McKenzie[2], Ruta Basijokaite[1] & Nathan L. Young[3]

[1]*Department of Earth and Environmental Sciences, Syracuse University, Syracuse, New York, United States*

[2]*Department of Earth and Planetary Sciences, McGill University, Montréal, Québec, Canada*

[3]*College of Environmental Science and Forestry, State University of New York, Syracuse, New York, United States*

Improved representations of subsurface water flow, energy transfer and solute transport processes in cold regions hydrogeological models are needed to constrain the response of arctic biogeochemical cycles to permafrost thaw and quantify terrestrial feedbacks to climate change (Vonk et al. 2015). Simulating the fate and transport of reactive chemical species such as carbon and nitrogen in permafrost-affected hydrogeologic systems is challenging however, due to multiple complex interactions and coupling between water, chemical, and energy transport processes (Mohammed et al. 2022). This work focuses on our efforts to develop SUTRA-solice, a new version of the SUTRA code (Voss and Provost 2002) that we have modified to include coupled variably-saturated porewater flow, advective-conductive heat transport with latent heat and freeze-thaw, and advective-dispersive reactive solute transport for multiple solute species. The new model integrates previous developments to the SUTRA code to simulate multiple transport species with SUTRA-MS (Hughs et al. 2006), and the inclusion of latent heat and freeze-thaw processes into the energy transport routine with SUTRA-ice (McKenzie et al. 2007), along with new couplings and constitutive relationships for both temperature and water-saturation dependent reaction rates. We adapt benchmark problems for groundwater and energy transport with freeze-thaw (Grenier et al. 2018) for the additional transport of conservative and reactive solutes and unsaturated conditions, and propose that these may be used by other researchers for future code comparison. We also present conceptual two-dimensional hillslope simulations investigating the fate and reactive transport of dissolved organic carbon mobilized by permafrost thaw. Simulating the effects of variable-saturation along arctic hillslopes is key to understanding the fate of permafrost carbon, as arctic soils contain ~1,700 Pg of organic carbon which is microbially-mineralized and vertically released as greenhouse gases more readily when active-layer and permafrost soils are warm and unsaturated (Schuur et al. 2015). Thus, the model developments presented here provide a physics-based framework for improved understanding and prediction of the fate of permafrost carbon, i.e., the vertical carbon release through mineralization reactions as a function of soil temperature and saturation, versus the lateral export as dissolved organic carbon with groundwater flow and discharge to surface waters in response to snowmelt and precipitation events. Continued model development and improvement, refining, and most critically, testing with field data at field sites in both continuous (Evans et al. 2020) and discontinuous (Koch et al. 2017) permafrost regions of Alaska are ongoing, and will be critical for further understanding coupled hydro-biogeochemical processes and their environmental impacts in warming permafrost landscapes.

References

Vonk, J.E., Tank, S.E., and Walvoord, M.A. 2019. Integrating hydrology and biogeochemistry across frozen landscapes. Nature Communications, 10(1).

Mohammed, A.A., Guimond, J.A., Bense, V.F., Jamieson, R.C., McKenzie, J.M., and Kurylyk, B.L. 2022. Mobilization of subsurface carbon pools driven by permafrost thaw and reactivation of groundwater flow: a virtual experiment. Environmental Research Letters, 17(12).

Grenier, C., Anbergen, H., Bense, V., Chanzy, Q., Coon, E., Collier, N., Costard, F., Ferry, M., Frampton, A., Frederick, J., and Gonçalvès, J. 2018. Groundwater flow and heat transport for systems undergoing freeze-thaw: Intercomparison of numerical simulators for 2D test cases. Advances in Water Resources, 114.

Voss, C.I., and Provost, A.M. 2002. SUTRA: A model for 2D or 3D saturated-unsaturated, variable-density ground-water flow with solute or energy transport. U.S. Geological Survey Open-File Report 2002-4231.

Hughes, J.D., and Sanford, W.E. 2005. SUTRA-MS a Version of SUTRA Modified to Simulate Heat and Multiple-Solute Transport: U.S. Geological Survey Open-File Report 2004-1207.

McKenzie, J.M., Voss, C.I., and Siegel, D.I. 2007. Groundwater flow with energy transport and water–ice phase change: numerical simulations, benchmarks, and application to freezing in peat bogs. Advances in Water Resources, 30(4).

Schuur, E.A., McGuire, A.D., Schädel, C., Grosse, G., Harden, J.W., Hayes, D.J., Hugelius, G., Koven, C.D., Kuhry, P., Lawrence, D.M., and Natali, S.M., 2015. Climate change and the permafrost carbon feedback. Nature, 520(7546).

Evans, S.G., Godsey, S.E., Rushlow, C.R., and Voss, C. 2020. Water tracks enhance water flow above permafrost in upland Arctic Alaska hillslopes. Journal of Geophysical Research: Earth Surface, 125(2), e2019JF005256.

Koch, J.C., Toohey, R.C., and Reeves, D.M. 2017. Tracer-based evidence of heterogeneity in subsurface flow and storage within a boreal hillslope. Hydrological Processes, 31(13).

Assessing the current and future carbon balance of the permafrost region through expanded measurements, data synthesis, and modeling

Susan M. Natali[1], Brendan Rogers[1], Anna-Maria Virkkala[1], Kyle Andreas Arndt[1], Jennifer Watts[1], Elchin Jafarov[1], Christina Schädel[1], Isabel Wargowsky[1], Mathias Goeckede[2], Torben R Christensen[3], Eugenie Susanne Euskirchen[4], Laure Gandois[5], Elyn Humphreys[6], Annalea Lohila[7], Trofim Maximov[8], Roman E. Petrov[8], Anatoly Stanislavovich Prokushkin[9], Alexandre Roy[10], Edward Schuur[11], Oliver Sonnentag[12], Margaret S. Torn[13], Andrej Varlagin[14], Donatella Zona[15], Martijn Pallandt[2], Greg Fiske[1], Marco Montemayor[1], Patrick Murphy[1] & Flux Synthesis Team

[1]*Woodwell Climate Research Center, Falmouth, Massachusetts, United States*
[2]*Max Planck Institute for Biogeochemistry, Jena, Germany*
[3]*Aarhus University, Department of Ecoscience, Arctic Research Centre, Roskilde, Denmark*
[4]*University of Alaska Fairbanks, Institute of Arctic Biology, Fairbanks, Alaska, United States*
[5]*Centre national de la recherche scientifique, Paris, France*
[6]*Carleton University, Ottawa, Ontario, Canada*
[7]*Finnish Meteorological Institute, Climate System Research, Helsinki, Finland*
[8]*Institute for Biological Problems of Cryolithozone, Yakutsk, Russia*
[9]*V.N. Sukachev Institute of Forest, Krasnoyarsk, Russia*
[10]*Université du Québec à Trois-Rivières, Trois-Rivières, Québec, Canada*
[11]*Northern Arizona University, Center for Ecosystem Science and Society, Flagstaff, Arizona, United States*
[12]*University of Montreal, Département de Géographie, Montréal, Québec, Canada*
[13]*Berkeley Lab/UC Berkeley, Berkeley, United States*
[14]*A.N. Severtsov Institute of Ecology and Evolution, Russian Academy of Sciences, Moscow, Russia,*
[15]*San Diego State University, San Diego, United States*

Rapid warming across the Arctic Boreal Zone is placing the large pool of soil and permafrost carbon at risk of being decomposed and released to the atmosphere in the form of carbon dioxide (CO_2) and methane (CH_4). At the same time, increased plant productivity—due to an extended growing season and nutrient fertilization following thaw—may offset these permafrost carbon emissions. While the Arctic Boreal Zone, much of which is underlain by permafrost, has been a carbon sink for tens of thousands of years, changes in carbon cycling associated with warmer temperatures, permafrost thaw, and hydrologic changes may alter the carbon balance of the region.

There are large uncertainties in assessing both current and future carbon fluxes from the Arctic Boreal Zone. This is in part due to rapidly changing environmental and ecological conditions, but also due to major gaps in carbon flux measurements and limited representation of permafrost processes into regional and global models. Despite increases in carbon cycling research across the permafrost region, outstanding data gaps persist and limit efforts to understand, upscale, and model carbon fluxes from the Arctic Boreal Zone. To address these gaps, we are strategically expanding carbon flux measurements across the permafrost region through the installation of new eddy covariance sites and support for expanded measurements at existing sites. We are also synthesizing and upscaling existing data to assess the current carbon balance of the Arctic Boreal Zone, and we will be integrating these data into a data model assimilation framework to reduce uncertainty in future carbon fluxes from the region. This large-scale effort is being undertaken through the Permafrost Pathways initiative, a collaborative effort to understand the local to global impacts of permafrost thaw and to integrate this knowledge into adaptation and climate mitigation policy

Approach

To assess the current carbon balance of the Arctic Boreal Zone, we are strategically expanding the existing network of eddy covariance sites, synthesizing new and existing carbon flux data, and using these data to upscale carbon fluxes across the region. During the next three years, the Permafrost Pathways initiative will support the installation of ten new eddy covariance towers and expanded measurements (during winter and for CH4) at existing towers to reduce uncertainty in the current carbon

balance of the region. To guide selection for new sites, we are using representativeness of the current tower network following the approach of Pallandt et al. (2022). New installations will fill critical data gaps areas that are underrepresented in terms of carbon flux measurements (e.g., Canadian High Arctic, Siberia, and Eastern Canada; Figure 1).

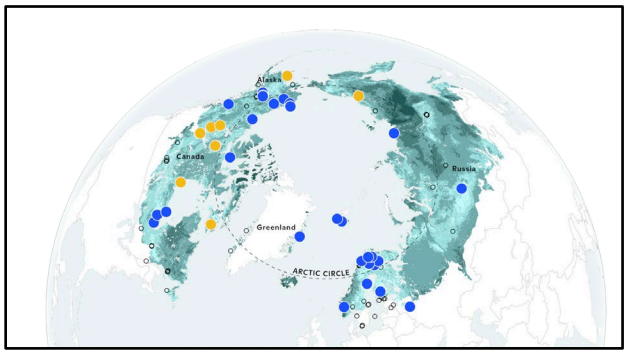

Figure 1. Locations of all eddy covariance towers in the Arctic Boreal Zone (open and closed symbols). Filled symbols show towers that measure both CO_2 and CH_4 and that run year round (Permafrost Pathways supported towers in yellow, all others in blue). The base layer (light to dark teal) shows the level of representativeness (good to poor) of the current tower network.

Here we will present an overview of the Permafrost Pathways project, an assessment of the representativeness of the current eddy covariance tower network, an overview of updates to the ABCFlux database (Virkkala et al. 2022), and estimates of current CO_2 flux budgets and trends based on upscaling of CO_2 exchange across the Arctic Boreal Zone. We will also discuss current needs and work toward integrating permafrost region carbon cycling data and permafrost processes into ecosystem and global climate models, and how we are using these data and models to inform climate policy.

REFERENCES

Virkkala, A.-M., Natali, S.M., Rogers, B.M., Watts, J.D., Savage, K., et al. 2022. The ABCflux database: Arctic–boreal CO2 flux observations and ancillary information aggregated to monthly time steps across terrestrial ecosystems, Earth Syst. Sci. Data, 14, 179–208. https://doi.org/10.5194/essd-14-179-2022

Pallandt, M.M.T.A., Kumar, J., Mauritz, M., Schuur, E.A.G., Virkkala, A.-M., Celis, G., Hoffman, F.M., and Göckede, M. 2022. Representativeness assessment of the pan-Arctic eddy covariance site network and optimized future enhancements, Biogeosciences, 19, 559–583. https://doi.org/10.5194/bg-19-559-2022

Permafrost degradation drives organic matter origin and composition in modern and Holocene thermokarst lakes in Central Yakutia, Eastern Siberia

Sarah Ollivier[1], Antoine Séjourné[1], Christine Hatté[2], Frédéric Bouchard[3], Aurélie Noret[1], François Costard[1] & Laure Gandois[4]

[1]*GEOPS, Université Paris-Saclay, Orsay, France*

[2]*LSCE, CEA-CNRS-UVSQ, Gif-sur-Yvette, France*

[3]*CARTEL, Université de Sherbrooke, Sherbrooke, Québec, Canada*

[4]*Laboratoire Ecologie Fonctionnelle et Environnement, CNRS, Université de Toulouse, Toulouse, France*

In Central Yakutia, Eastern Siberia, Russia, ice-rich continuous permafrost formed during the late Pleistocene is referred to as “Yedoma” (50 to 90% of ice in volume) (Strauss et al. 2021). In this region, air temperature is strongly increasing, where an augmentation of 3°C has been observed since the mid-1960s to 2010 (Skachkov 2010). It generates degradation of ice-rich permafrost leading to lakes inception by ground subsidence called thermokarst lakes (Soloviev 1973). Hydrology and geochemistry are also impacted with drainage modification and inputs of organic and inorganic elements previously stored in permafrost to aquatic ecosystems (Vonk et al. 2015). Ancient organic matter, yet not characterised, could be released, converted into greenhouse gases, and enhance the positive feedback on climate. This phenomenon is called the “permafrost carbon feedback” (Schuur et al. 2015). In this context, the PRISMARCTYC project aims at better understanding the impact of permafrost degradation on soils, surface and groundwater fluxes, carbon cycle in small understudied inland watersheds. Here, this study specifically focuses on organic matter origin and composition in modern and early Holocene thermokarst lakes in Central Yakutia, where strong spatial and seasonal patterns in greenhouse gases emissions have already been reported (Hughes-Allen et al. 2021).

Study site

Our study site is the watershed of the Syrdakh River, in Central Yakutia, a tributary of the Lena River. The river flows over Yedoma ice-rich permafrost syngenetically formed between 14 and 22 ka. Four lake types can be found in this area, partially retaking the classification of Hughes-Allen et al (2021): recent lakes, formed by thermokarst since the 50s by recent permafrost thaw, and residual lakes in large thermokarst basins, called alases, formed by thermokarst at early Holocene. Another type comprises alases connected with Syrdakh River. A 4th type corresponds to alases that have retrogressive thaw slumps forming along their banks (Séjourné et al. 2015).

Methods

From 4 to 15 lakes of each category have been studied in August 2019. Moreover, meltwater from a recently formed retrogressive thaw slump was sampled to characterize permafrost meltwater signature. Concentrations, $\delta^{13}C$ and ^{14}C carbon isotopic composition of dissolved (DOC) and particulate (POC) organic carbon have been analyzed. C/N ratio and specific ultraviolet absorbance (SUVA) provide information about the composition and dynamics of organic matter (OM) in aquatic systems.

Results and discussion

In all lake types, POC concentrations are low, ranging between 0.5 and 16 $mg \cdot L^{-1}$, and reaching 14 $mg \cdot L^{-1}$ for permafrost meltwater (Figure 1). DOC concentrations are very widespread, between 35 and 485 $mg \cdot L^{-1}$. The highest values are measured for permafrost meltwater and recent lakes, averaging about 350 $mg \cdot L^{-1}$ and 250 $mg \cdot L^{-1}$ respectively. Alases with retrogressive thaw slumps have intermediate DOC concentrations between those of recent lakes and alases. Connected alases show the lowest DOC concentrations (Figure 1).

The C/N and $\delta^{13}C$ signatures of DOC and POC reveal distinct OM compositions and origins. POC presents a C/N ratio between 4 and 8, and a large range of $\delta^{13}C$ values, between -35 and -19‰, suggesting autochthonous production by microorganisms or algae in lakes. The $\delta^{13}C$ of DOC, ranging from -24 and -28‰, and its C/N ratio between 27 and 37, are consistent with terrestrial photosynthesis, indicating OM inputs from soil banks. For alases, C/N values of DOC between 15 and 20 may correspond to more DOC production by algae in lakes.

The ^{14}C values of DOC and POC of permafrost meltwater show old ages (Figure 1), around 13 ka, consistent with the Yedoma age formation. Recent lakes and alases with retrogressive thaw slumps have old ages for both POC and DOC, while alases and connected alases show modern ^{14}C values (Figure 1).

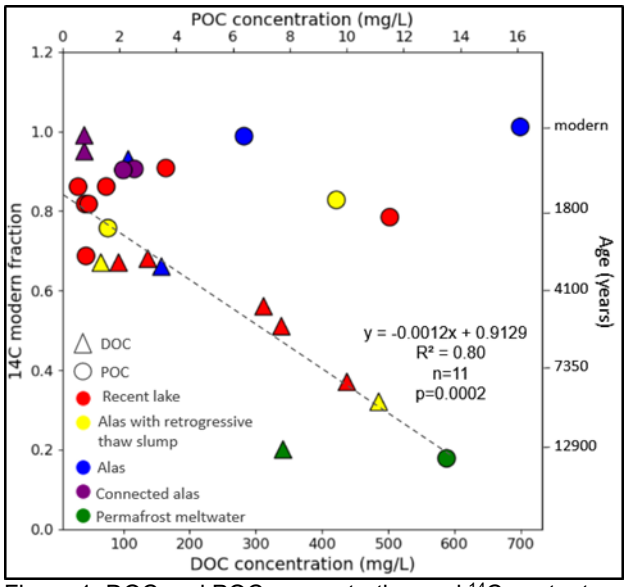

Figure 1. DOC and POC concentration and ^{14}C content.

Moreover, a positive correlation (R^2=0.80, n=11, p<0.005) between DOC concentration and ^{14}C content of DOC can be identified, but not for POC (Figure 1). ^{14}C-DOC values are also related to SUVA values: as the ^{14}C-DOC values decreases, suggesting a higher contribution of permafrost derived carbon, SUVA, and therefore DOM aromaticity decreases (R^2=0.59, n=11, p=0,005).

Connected alases and alases show lower DOC concentrations and ^{14}C content of DOC corresponding to recent atmospheric carbon fixation. This indicates minimal permafrost-derived OM inputs in theses lakes (less than 8% for DOC and from 1 to 11% for POC).

Low ^{14}C-DOC associated with high DOC concentrations and low SUVA values in recent lakes and alases with retrogressive thaw slump indicates that these lake types receive inputs of old and less aromatic DOM previously sequestrated in permafrost. Based on the ^{14}C content, we can state that in recent lakes and alases with retrogressive thaw slumps, most of the DOC (respectively 54% and 61%), but a smaller fraction of POC (20% and 25%) originates from Yedoma.

Conclusion

In Central Yakutia lakes, organic matter composition and origin are related to permafrost degradation history and hydrological connectivity. Recent permafrost thaw led to an important transfer of old organic carbon to lakes, mostly in the dissolved form with a specific composition. Even alases, supposedly inactive, can be considered active when retrogressive thaw slumps are active along their banks.

References

Hughes-Allen, L., Bouchard, F., Laurion, I., Séjourné, A., Marlin, C., Hatté, C., Costard, F., Fedorov, A., and Desyatkin, A. 2021. Seasonal patterns in greenhouse gas emissions from thermokarst lakes. Limnology and Oceanography 66, 98–116. https://doi.org/10.1002/lno.11665

Schuur, E., McGuire, A., Schädel, C., Grosse, G., Harden, J.W., Hayes, D.J., Hugelius, G., Koven C.D., Kuhry, P., Lawrence, D.M., Natali, S.M., Olefeldt, D., Romanovsky, V.E., Shaefer, K., Turetsky, M.R., Treat, C.C., and Vonk, J.E. 2015. Climate change and the permafrost carbon feedback. Nature 520, 171–179. https://doi.org/10.1038/nature14338

Séjourné, A., Costard, F., Fedorov, A., Gargani, J., Skorve, J., Massé, M., and Mège, D. 2015. Evolution of the banks of thermokarst lakes in Central Yakutia (Central Siberia) due to retrogressive thaw slump activity controlled by insolation. Geomorphology 241, 31–40. https://doi.org/10.1016/j.geomorph.2015.03.033

Skachkov, Y.B. 2010. A review of recent climatic and environmental changes in the Republic of Sakha (Yakutia), Climatic parameters: 1-3 (Yakutsk) (In Russian).

Soloviev, P.A. 1973. Thermokarst phenomena and landforms due to frost heaving in Central Yakutia. Biuletyn Peryglacjalny 23: 135–155.

Strauss, J., Laboor, S., Schirrmeister, L., Fedorov, A.N., Fortier, D., Froese, D., Fuchs, M., Günther, F., Grigoriev, M., Harden, J., Hugelius, G., Jongejans, L.L., Kanevskiy, M., Kholodov, A., Kunitsky, V., Kraev, G., Lozhkin, A., Rivkina, E., Shur, Y., Siegert, C., Spektor, V., Streletskaya, I., Ulrich, M., Vartanyan, S., Veremeeva, A., Anthony, K.W., Wetterich, S., Zimov, N., and Grosse, G. 2021. Circum-Arctic Map of the Yedoma Permafrost Domain. Front. Earth Sci. 9, 758360. https://doi.org/10.3389/feart.2021.758360

Vonk, J.E., Tank, S.E., Bowden, W.B., Laurion, I., Vincent, W.F., Alekseychik, P., Amyot, M., Billet, M.F., Canário, J., Cory, R.M., Deshpande, B.N., Helbig, M., Jammet, M., Karlsson, J., Larouche, J., MacMillan, G., Rautio, M., Walter Anthony, K.M., and Wickland, K.P. 2015. Reviews and syntheses: Effects of permafrost thaw on Arctic aquatic ecosystems. Biogeosciences 12, 7129–7167. https://doi.org/10.5194/bg-12-7129-2015

Modeling the fate of carbon and mercury in warming permafrost soils

Christine Olson[1], Kevin Schaefer[1], Benjamin Geyman[2], Elsie Sunderland[2], Colin Thackray[2], Connor Olson[2], Scott Zolkos[3] & David Streets[4]

[1]*University of Colorado Boulder, Boulder, Colorado, United States*

[2]*Harvard University, Cambridge, Massachusetts, United States*

[3]*Woodwell Climate Research Center, Falmouth, Massachusetts, United States*

[4]*Retired, Argonne National Laboratory, Chicago, Illinois, United States*

The Arctic is undergoing dramatic changes in climate driven by human activities and natural processes. In recent decades, average annual surface temperatures in the Arctic have increased at almost twice the global rate and may increase by an additional 3-7°C over the next century. Environmental changes associated with warming in these regions includes increases in soil weathering, soil productivity, carbon mineralization, and subsequent carbon loss (Schuur et al. 2011). Permafrost soils are subject to seasonal thaw and freeze dynamics, thereby providing large inputs to rivers, lakes, and the Arctic Ocean. Over the next century, exports of organic matter are anticipated to increase with major implications for carbon cycling in the Arctic.

Northern permafrost soils contain one of the largest reservoirs of anthropogenic mercury in the world. Increased industrial emissions of mercury during the past 200 years have led to atmospheric deposition of mercury to tundra systems. Soils act as buffers for mercury transfer between atmospheric deposition and runoff to streams and lakes (Lorey 1999). Soils also serve as the main source of mercury to many lakes (Lindqvist et al. 1991). The tundra biome accounts for roughly 6% of the Earth's surface (Bailey 2014), and tundra soils are considered the dominant source of mercury to Arctic rivers and lakes (Fitzgerald et al. 2005). Mercury can be deposited to the tundra through wet and dry deposition and taken up by plants by during photosynthesis. Divalent mercury can bind to thiosulfate within organic matter, which becomes incorporated into the soil pool during plant senescence and litterfall decay. As a result of this process, mercury tends to positively correlate with carbon, which is a useful parameterization for modeling the biogeochemical cycling of mercury and storage within soils.

We will use a process-based, biogeochemical model to quantify how rapid warming of permafrost may alter the behavior and fate of mercury in permafrost soils. Specifically, mercury will be added to the Simple Biosphere Carnegie Ames Stanford Approach (SiBCASA) model, which is a full-physical land surface parameterization model that couples carbon, water, and energy cycles. The model will account for all mercury uptake pathways including wet and dry deposition, plant photosynthesis and through roots. Mercury loss pathways will include microbial decay of soil organic matter, evasion from plants and soils, and export through seasonal permafrost soil thaw. Warming scenarios as defined by the Paris Agreement will be used to simulate mercury biogeochemical cycling into the future through 2300. Improved estimates of mercury storage, cycling, and release from permafrost soils will be critical to understanding the fate of this global pollutant in the future.

References

Bailey, R.G. 2014. Ecoregions: The ecosystem geography of the oceans and continents. New York: Springer. https://doi.org/10.1007/978-1-4939-0524-9.

Fitzgerald, W.F., Engstrom, D.R., Lamborg, C.H., Tseng, C.M., Balcom, P.H., and Hammerschmidt, C.R. 2005. Modern and historic atmospheric mercury fluxes in northern Alaska: Global sources and Arctic depletion. Environmental Science & Technology, 39(2), 557–568. https://doi.org/10.1021/es049128x

Lindqvist, O., Johansson, K., Bringmark, L., Timm, B., Aastrup, M., Andersson, A., et al. 1991. Mercury in the Swedish environment—Recent research on causes, consequences and corrective methods. Water, Air, and Soil Pollution, 55(1–2), xi–261.

Lorey, P.D.C.T. 1999. Historical trends of mercury deposition in Adirondack lakes. Environmental Science & Technology, 33(5), 718–722. https://doi.org/10.1021/es9800277

Schuur, E.A.G., Abbott, B., and Permafrost Carbon, N. 2011. High risk of permafrost thaw. Nature, 480(7375),32–33. https://doi.org/10.1038/48003

Towards landscape-scale carbon isotope-enabled modeling of methane emissions from permafrost

Kevin Rozmiarek[1,2], Youmi Oh[3,4], Irina Overeem[1,2], Bruce Vaughn[1], Valerie Morris[1], Merritt Turetsky[5,6], Nick Hasson[7], Tristian Caro[2], Sebastian Kopf[2], Chuck Smallwood[8] & Tyler Jones[1]

[1]*Institute of Arctic and Alpine Research, University of Colorado Boulder, Boulder, Colorado, United States*

[2]*Department of Geological Sciences, University of Colorado Boulder, Boulder, Colorado, United States*

[3]*NOAA Global Monitoring Laboratory, Boulder, Colorado, United States*

[4]*Cooperative Institute for Research in Environmental Sciences, University of Colorado Boulder, Boulder, Colorado, United States*

[5]*Renewable and Sustainable Energy Institute, University of Colorado Boulder, Boulder, Colorado, United States*

[6]*Department of Ecology and Evolutionary Biology, University of Colorado Boulder, Boulder, Colorado, United States*

[7]*Water and Environmental Research Center, University of Alaska Fairbanks, Fairbanks, Alaska, United States*

[8]*Bioscience Division, Department of Molecular and Microbiology, Sandia National Laboratories, Albuquerque, New Mexico, United States*

Methane flux from biogenic sources in boreal wetlands is largely unconstrained, in part due to the complicating presence of carbon-rich permafrost, which increases the amount of carbon substrate for metabolic activity. Bottom-up inventories of boreal wetland flux observations do not match inversions from atmospheric observation networks (Bruhwiler et al 2021). What is the cause of this mismatch? To understand where this difference occurs, methane inventories must take into account the geochemical and geomorphological variables that change at scales larger than microcosm experiments but smaller than sparse (100s - 1000s of km) atmospheric observations. At present, scientific literature does not adequately describe inventories at intermediate scales due to the heterogeneity of sources, and scientists have been ill-equipped to estimate methane flux from high emitting features. For example, high-latitude climate warming may produce abrupt thaw features such as thermokarst lakes that are high methane-emitting and missed in coarse resolution models (Schneider von Deimling et al. 2015). Understanding the emissions from rapidly changing landforms such as these will help constrain methane flux estimates in boreal wetlands, reconciling mismatches between site-specific ensembles and global methane inversions.

Methane-isotopes (here we consider carbon, denoted $\delta^{13}C{-}CH_4$) record a "fingerprint" of the emission sources and sinks of the measured pool of methane due to mass-based sorting of carbon reservoirs called fractionation. Methane-isotopes from boreal wetlands are often crudely treated in inventory models due to a lack of both observations and modeling of $\delta^{13}C{-}CH_4$ fluxes (Lan et al. 2021). The source side of boreal wetland emissions depends on several factors which all covary strongly with the thermal dynamics of the system: (1) the isotopic composition of precursory organic matter, which is dependent on species, (2) the methane production chemical pathway which depends on microbial dynamics and substrate availability, (3) the transport pathway of produced gases to the surface, and (4) the amount of microbial methane oxidation which depends strongly on the transport pathway. Together, these components must be understood to correctly assign a $\delta^{13}C{-}CH_4$ flux in an isotope enabled geochemical model (Conrad 2005) .

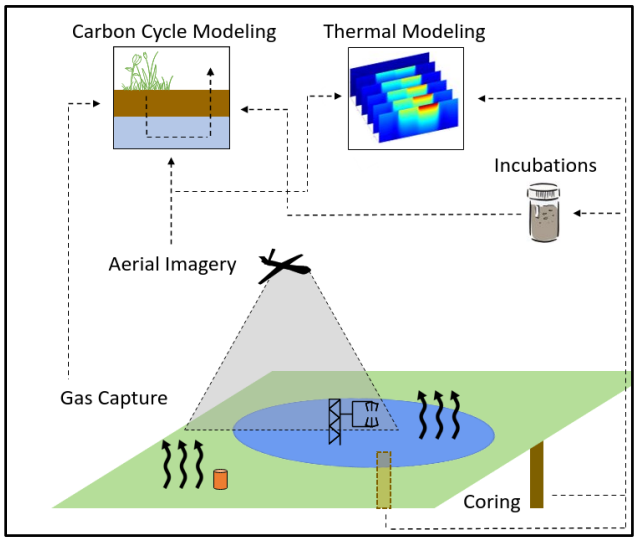

Figure 1. Systematic diagram of interplay between observations for isoTEM parameterization.

Currently, isotope-enabled models are limited to coarse resolution due to the lack of fine scale inputs (Oh et al. 2022). In this work, we seek to establish landscape scale observations and methane-isotope flux modeling for an abrupt thaw lake in Alaska, Big Trail Lake (BTL). To model the methane-isotope emissions

from the BTL system, we use the isotope-enabled version of the Terrestrial Ecosystem Model (isoTEM, (Oh et al. 2022)). The isoTEM model is a processed-based carbon isotope biogeochemistry model for wetlands, including permafrost. Model runs to date have been low resolution, about 0.5° latitude x 0.5° longitude. We increase the resolution of the model to 15 m for the BTL area. Representing ~2 sq. km. A recreation of the 0.5° x 0.5° result from Oh et al. (2022) for the pixel corresponding to the location of Big Trail Lake (Goldstream Valley) can be found below in Figure 2. It is notable that, despite high expected emssions from thermokarst lake, previous results for the area average over it and surrounding features, showing a net sink for the pixel. Higher resolution model runs are needed to capture the dynamics of these high emitting heterogenious sources.

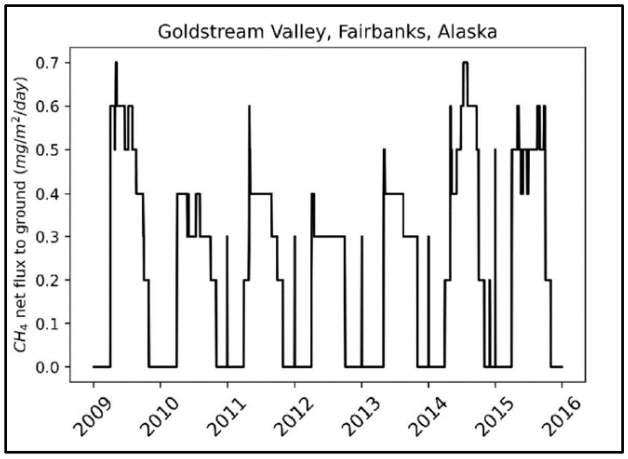

Figure 2. Recreated results from Oh et al. (2022) showing methane flux for the ~1300 sq. km pixel GSV occupies.

To achieve higher resolution parameterization, we use fixed-wing uncrewed aerial system multispectral sensing, soil incubations, and whole-air gas capture compared to equivalent surface measurements (Figure 1). Multispectral data at 5 cm resolution informs vegetation characteristics and water inundation fraction. Incubation of peat cores provides site-specific isotope fractionation parameterization, known to be highly variable in wetlands worldwide (Nisbet et al. 2019). CRU climate reanalysis then drives process-based methane dynamics, producing isotope-flux characteristics at the resolution of interest.

Higher resolution model results are a first step towards appropriately scaled measurements that intergrate accurately over point-source to lake to region footprints. Understanding where and how model scale mismatch exists will, in turn, inform where inventory-inversion scale decoupling exists and provides a deeper understanding of methane-isotope emissions in boreal wetlands. In addition, recommendations for observation networks can be constructed such that we can further further constrain the methane budget at all spatial scales.

REFERENCES

Bruhwiler, L., Parmentier, F.J.W., Crill, P., Leonard, M., and Palmer, P.I. 2021. The Arctic carbon cycle and its response to changing climate. Current Climate Change Reports, 7, pp.14–34.

Conrad, R. 2005. Quantification of methanogenic pathways using stable carbon isotopic signatures: a review and a proposal. Organic geochemistry, 36(5), pp. 739–752.

Lan, X., Basu, S., Schwietzke, S., Bruhwiler, L.M., Dlugokencky, E.J., Michel, S.E., Sherwood, O.A., Tans, P.P., Thoning, K., Etiope, G., and Zhuang, Q. 2021. Improved constraints on global methane emissions and sinks using $\delta^{13}C\text{-}CH_4$. Global Biogeochemical Cycles, 35(6), p.e2021GB007000.

Nisbet, E.G., Manning, M.R., Dlugokencky, E.J., Fisher, R.E., Lowry, D., Michel, S.E., Myhre, C.L., Platt, S.M., Allen, G., Bousquet, P., and Brownlow, R. 2019. Very strong atmospheric methane growth in the 4 years 2014–2017: Implications for the Paris Agreement. Global Biogeochemical Cycles, 33(3), pp.318–342.

Oh, Y., Zhuang, Q., Welp, L.R., Liu, L., Lan, X., Basu, S., Dlugokencky, E.J., Bruhwiler, L., Miller, J.B., Michel, S.E., and Schwietzke, S. 2022. Improved global wetland carbon isotopic signatures support post-2006 microbial methane emission increase. Communications Earth & Environment, 3(1), p.159.

Schneider von Deimling, T., Grosse, G., Strauss, J., Schirrmeister, L., Morgenstern, A., Schaphoff, S., Meinshausen, M., and Boike, J. 2015. Observation-based modelling of permafrost carbon fluxes with accounting for deep carbon deposits and thermokarst activity. Biogeosciences, 12(11), pp.3469–3488.

Tundra ecosystem carbon dynamics and permafrost degradation: Using a novel field experiment to simulate a future warmer world

Edward (Ted) Schuur[1] & Schuur Lab Team

[1]*Center for Ecosystem Science & Society, Northern Arizona University, Flagstaff, Arizona, United States*

Permafrost carbon (C) remains one of the most important C cycle feedbacks to climate, with implications for global society (Schuur et al. 2022, Schuur et al. 2015). Permafrost region soils contain at least 1440-1600 billion tons of C; release of just a fraction of this pool as carbon dioxide and methane can accelerate climate change. Permafrost degradation can change ecosystem C storage by enhancing microbial activity and ecosystem respiration, which depletes the permafrost C pool. At the same time, warming and permafrost degradation can also stimulate plant growth and increase C stored in vegetation and surface soil. The timing and magnitude of these two opposing C fluxes help to determine the ultimate strength of the permafrost C feedback to climate.

The Arctic Carbon and Climate Observatory

We used a novel experiment to warm a tundra ecosystem for fourteen years (2008-2022). This experiment was conducted at a one-of-a-kind permafrost C experimental supersite in Alaska (The Arctic Carbon and Climate (ACCLIMATE) Observatory) that includes observational and experimental studies and high precision methane, carbon dioxide and radiocarbon measurements for detecting greenhouse gas emissions to the atmosphere as a consequence of thawing permafrost (Schuur et al. 2021). This site is located near Healy, Alaska just outside Denali National Park.

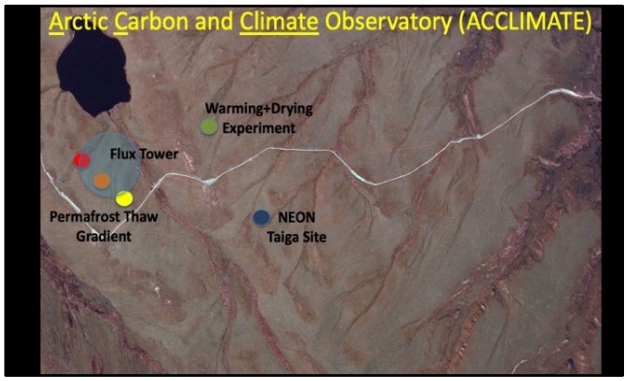

Figure 1. The Arctic Carbon and Climate (ACCLIMATE) Observatory.

Beyond the experimental manipulation, this location is the site of a permafrost thaw gradient that has tracked C exchange where regional permafrost thaw is underway. It is also the location of a National Ecological Observation Network relocatable installation (D19 HEAL). Together this supersite is a central observation location for the Arctic Carbon Warning Network (AWARE), which aims to provide real-time (annual) Arctic carbon emissions updates.

Site Description

The study site is characterized by moist acidic tundra within and around the Eight Mile Lake watershed (63°52'42.1"N, 149°15'12"W; 670 m above sea level). Vascular plant cover is dominated by the tussock-forming sedge Eriophorum vaginatum with deciduous and evergreen shrubs. Non-vascular biomass is dominated by mosses and lichens. Soils are classified as Gelisols, with a thick organic horizon on top of cryoturbated mineral soil. The long-term permafrost temperature record on site indicates warming of the permafrost, which led to ground subsidence and hydrologic redistribution, creating a landscape with different levels of disturbance.

Experimental Warming and Drying Manipulation

The warming manipulation, established in 2008 and called Carbon in Permafrost Experimental Heating Research (CiPEHR, rhymes with viper), uses open-top chambers (OTCs) to increase summer air temperatures by ~0.5°C (treatment called air warming). This established method has been combined with a novel approach to warm the deep soil and degrade permafrost: the installation of snow fences to trap snow as it is redistributed around the landscape by winter wind. Increased snow depth maintains elevated soil and permafrost temperatures because the snow acts as an insulating layer between the soil and the extremely cold air. The accumulated snow is shoveled from the snow fences in early spring, so that the water input and the timing of snowmelt of this treatment (called soil warming) are similar to the control plots. These air and soil warming treatments were applied alone and in combination.

Permafrost degradation is intimately related to changes in surface hydrology because the loss of

ground ice causes ground surface subsidence. Interactions between soil moisture and thaw were examined with a water table manipulation (DryPEHR) established in 2011 within the footprint of the soil warming treatment of CiPEHR. This manipulation altered surface moisture by actively pumping perched water out of plots where barriers were installed down to the permafrost surface. CiPEHR warming alone resulted in wetter soils as a result of ground subsidence, and the drying treatment counteracted that effect by significantly reducing the soil water table. Ground subsidence as a result of soil warming overwhelmed the water table manipulation by 2017; DryPEHR plots were monitored after that point but active water pumping stopped.

RESULTS

The warming treatment had a significant effect of warming surface and deep soils and degrading surface permafrost (Figure 2). End of season soil thaw depth increased from 50 cm at the outset of the experiment in 2009 (after one winter of warming) to over 100 cm by 2017. This doubling of the thaw depth was observed for the soil warming treatment, whereas thaw depth in the air warming treatment with OTCs did not differ from control plots. This matches previous observations that small OTCs can warm air and surface soil, but do not typically affect deeper soil temperatures and permafrost due to the small size of the manipulation plots.

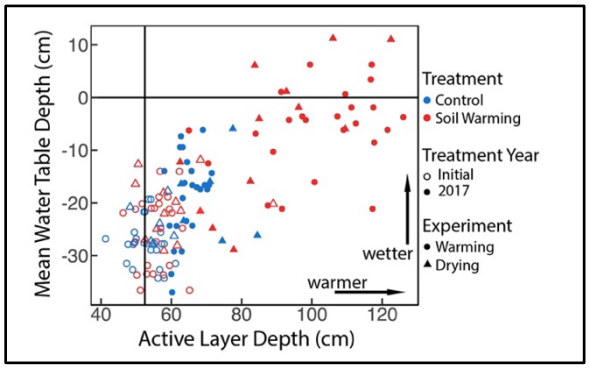

Figure 2. End-of-season soil thaw depth (active layer) and average distance from the moss/soil surface to the surface of the perched water table for individual plots within the warming and drying experiments. Initial values measured in 2009 are represented by the open symbols; closed symbols were measured in 2017 after 9 years of warming.

The distance from the moss/soil surface to the surface of the perched water table decreased over the experiment. Soil water levels were at, or exceeded, the soil surface (depth=0cm). This was primarily due to ground subsidence that occurred as a result of soil warming. Ground ice melted and the soil surface collapsed into the volume previously occupied by ice, lowering the soil into the perched water table. This effect of wetter surface soils was largely achieved by 2017 (Figure 2), whereas soils remained wet but did not get wetter with continued manipulation. In 2022, depth to water table was similar (Figure 3), while thaw depth continued to increase with additional soil warming. Thaw depths >200 cm represented a 400% increase over the intial conditions in 2009.

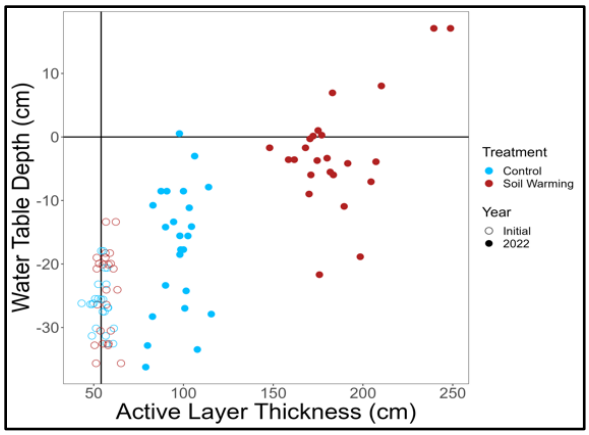

Figure 3. End-of-season soil thaw depth (active layer) and average distance from the moss/soil surface to the water table for the warming experiment only. Initial values in 2009 are represented by the open symbols; closed symbols were measured in 2022 after 14 years.

The physical effects of the warming treatments shown here are synthesized with C pools and fluxes that have been measured over the time course of the experiment. Data show that significant soil C losses have occurred. These losses contain a high proportion of old C stored for hundreds to thousands of years, and the losses were not compensated for by increases in plant growth. This caused experimental plots to be net C sources to the atmosphere of both carbon dioxide and methane.

REFERENCES

Rodenhizer, H., et al. 2023. Abrupt permafrost thaw drives spatially heterogeneous soil moisture and carbon dioxide fluxes in upland tundra. Global Change Biology, 00, 1–17. doi.org/10.1111/gcb.16936

Schuur, E.A.G., et al. 2015. Climate change and the permafrost carbon feedback. Nature 520, 171–179. doi.org/10.1038/nature14338

Schuur, E.A.G., et al. 2021. Tundra underlain by thawing permafrost persistently emits carbon to the atmosphere over 15 years of measurements. Journal of Geophysical Research: Biogeosciences, 126, e2020JG006044. doi.org/10.1029/2020JG006044

Schuur, E.A.G., et al. 2022. Permafrost and climate change: carbon cycle feedbacks from the warming Arctic. Annual Review of Environment and Resources. 47 (1), 343-371. doi.org/10.1146/annurev-environ-012220-011847

Organic carbon characteristics and dynamics in thermokarst terrain on the Alaskan north slope

Fabian Seemann[1,2], Maren Jenrich[1,2], Guido Grosse[1,2], Claire Treat[1], Susanne Liebner[3], Benjamin Jones[4] & Jens Strauss[1]

[1]*Alfred Wegener Institute Helmholtz Centre for Polar and Marine Research, Permafrost Research Section, Potsdam, Germany*

[2]*Institute of Geosciences, University of Potsdam, Potsdam, Germany*

[3]*GFZ German Research Centre for Geosciences, Section Geomicrobiology, Potsdam, Germany*

[4]*Institute of Northern Engineering, University of Alaska Fairbanks, Alaska, United States*

Thermokarst processes have been accelerating since the 1950s in the Alaskan tundra (Chen et al. 2021; Jorgenson et al. 2006) which corresponds to warming permafrost temperatures (Biskaborn et al. 2019) and a disproportional warming climate of the Arctic region (Rantanen et al. 2022). On the Alaskan North Slope, thermokarst is steering the dynamics of thermokarst lakes and drained lake basins (DLBs; Jones et al. 2022), thereby thawing, mobilizing, and sequestering organic carbon. The consequences for the biogeochemical system, which holds significant amounts of organic carbon (Palmtag et al. 2022), remain understudied. In particular, the quality of organic carbon is an important factor for the mobilization potential and rates of release as greenhouse gases (Jongejans et al. 2021). In our study, we aim to investigate the soil organic carbon pool characteristics in a thermokarst terrain close to Utqiaġvik, Alaska.

Study area

The Alaskan North Slope lies within the continuous permafrost zone with a mean annual ground temperature of about -6 °C at the permafrost surface (Obu et al. 2019). Lakes and DLBs cover about 72 % of the landscape (Hinkel et al. 2003). Undisturbed uplands consist of Holocene deposits, which are underlain by Quaternary marine sediments (Eisner et al. 2005).

Methods

Sediment coring took place in 2022 and include permafrost cores from an upland and a DLB. Additionally, unfrozen sediments (i.e., taliks) of two thermokarst lakes (West Twin Lake and East Twin Lake) were cored. The up to 2 m long sediment cores were subsampled in approximately 5 cm steps. The multidisciplinary laboratory approach include bio-, hydrochemical and sedimentological investigations. n-Alkane biomarker analyses are conducted before and after a 12-month-long incubation experiment. Both the anaerob and aerob incubations are kept at 10 °C in dark conditions.

Results

Total organic carbon (TOC) contents are highly variable within the landscape. The upland core is organic-rich with maximum 35 wt% TOC in the upper meter. Below 100 cm depth TOC values are <10 wt%. The DLB has the highest variability of TOC values, ranging from 42 wt% at 8 cm depth to 2 wt% at 129 cm depth. TOC contents in the sediments from both West and East Twin Lake remain <17 wt%. The sediments are generally silty-sandy.

The permafrost is ice-rich in the upland and in the DLB, with minium ice contents of 43 wt% and 21 wt%, respectively. The sediments of West Twin Lake have a water content of >60 wt%. The water contents of the sediments of East Twin Lake range between and 64 (177 cm depth) and 16 wt% (290 cm depth).

All sediment cores reveal an increasing electrical conductivity (EC) with depth. In the upland this increase is observed below 140 cm depth and in the DLB below 98 cm depth. The porewater samples from the sediments of West Twin Lake all had <2 mS/cm, while the porewater from talik sediments of East Twin Lake has EC values of up to 43 mS/cm.

After two months of incubation, the anaerobic experiment indicated distinct developments. Microbial communities in the organic-rich sediments were predominantly producing methane while organic-poor sediments were characterized by primarily carbon dioxide production.

Outlook

The high heterogeneity of the parameters between and within the cores yield an intriguing baseline for further investigations and interpretations of the sediment characteristics. Particularly of interest is the talik of East Twin Lake, as it likely consists of thawed marine deposits that have a high salinity (Jones et al. 2023). The n-alkane patterns from our biomarker analysis will provide key variables for the understanding of organic carbon quality (changes) and mobilization in frozen and thawed sediments.

REFERENCES

Biskaborn, B.K., Smith, S.L., Noetzli, J., Matthes, H., Vieira, G., Streletskiy, D.A., Schoeneich, P., Romanovsky, V.E., Lewkowicz, A.G., Abramov, A., Allard, M., Boike, J., Cable, W.L., Christiansen, H.H., Delaloye, R., Diekmann, B., Drozdov, D., Etzelmüller, B., Grosse, G., Guglielmin, M., Ingeman-Nielsen, T., Isaksen, K., Ishikawa, M., Johansson, M., Johannsson, H., Joo, A., Kaverin, D., Kholodov, A., Konstantinov, P., Kröger, T., Lambiel, C., Lanckman, J.-P., Luo, D., Malkova, G., Meiklejohn, I., Moskalenko, N., Oliva, M., Phillips, M., Ramos, M., Sannel, A.B.K., Sergeev, D., Seybold, C., Skryabin, P., Vasiliev, A., Wu, Q., Yoshikawa, K., Zheleznyak, M., and Lantuit, H. 2019. Permafrost is warming at a global scale. Nat Commun 10, 264. https://doi.org/10.1038/s41467-018-08240-4

Chen, Y., Lara, M.J., Jones, B.M., Frost, G.V., and Hu, F.S. 2021. Thermokarst acceleration in Arctic tundra driven by climate change and fire disturbance. One Earth 4, 1718–1729. https://doi.org/10.1016/j.oneear.2021.11.011

Eisner, W.R., Bockheim, J.G., Hinkel, K.M., Brown, T.A., Nelson, F.E., Peterson, K.M., and Jones, B.M. 2005. Paleoenvironmental analyses of an organic deposit from an erosional landscape remnant, Arctic Coastal Plain of Alaska. Palaeogeography, Palaeoclimatology, Palaeoecology 217, 187–204. https://doi.org/10.1016/j.palaeo.2004.11.025

Hinkel, K.M., Eisner, W.R., Bockheim, J.G., Nelson, F.E., Peterson, K.M., and Dai, X. 2003. Spatial Extent, Age, and Carbon Stocks in Drained Thaw Lake Basins on the Barrow Peninsula, Alaska. Arctic, Antarctic, and Alpine Research 35, 291–300. https://doi.org/10.1657/1523-0430(2003)035[0291:SEAACS]2.0.CO;2

Jones, B.M., Grosse, G., Farquharson, L.M., Roy-Léveillée, P., Veremeeva, A., Kanevskiy, M.Z., Gaglioti, B.V., Breen, A.L., Parsekian, A.D., Ulrich, M., and Hinkel, K.M. 2022. Lake and drained lake basin systems in lowland permafrost regions. Nat Rev Earth Environ 3, 85–98. https://doi.org/10.1038/s43017-021-00238-9

Jones, B.M., Kanevskiy, M.Z., Parsekian, A.D., Bergstedt, H., Ward Jones, M.K., Rangel, R.C., Hinkel, K.M., and Shur, Y. 2023. Rapid Saline Permafrost Thaw Below a Shallow Thermokarst Lake in Arctic Alaska. Geophysical Research Letters 50, e2023GL105552. https://doi.org/10.1029/2023GL105552

Jongejans, L.L., Liebner, S., Knoblauch, C., Mangelsdorf, K., Ulrich, M., Grosse, G., Tanski, G., Fedorov, A.N., Konstantinov, P.Ya., Windirsch, T., Wiedmann, J., and Strauss, J. 2021. Greenhouse gas production and lipid biomarker distribution in Yedoma and Alas thermokarst lake sediments in Eastern Siberia. Glob Change Biol 27, 2822–2839. https://doi.org/10.1111/gcb.15566

Jorgenson, M.T., Shur, Y.L., and Pullman, E.R. 2006. Abrupt increase in permafrost degradation in Arctic Alaska. Geophysical Research Letters 33. https://doi.org/10.1029/2005GL024960

Obu, J., Westermann, S., Bartsch, A., Berdnikov, N., Christiansen, H.H., Dashtseren, A., Delaloye, R., Elberling, B., Etzelmüller, B., Kholodov, A., Khomutov, A., Kääb, A., Leibman, M.O., Lewkowicz, A.G., Panda, S.K., Romanovsky, V., Way, R.G., Westergaard-Nielsen, A., Wu, T., Yamkhin, J., and Zou, D. 2019. Northern Hemisphere permafrost map based on TTOP modelling for 2000–2016 at 1 km2 scale. Earth-Science Reviews 193, 299–316. https://doi.org/10.1016/j.earscirev.2019.04.023

Palmtag, J., Obu, J., Kuhry, P., Richter, A., Siewert, M.B., Weiss, N., Westermann, S., and Hugelius, G. 2022. A high spatial resolution soil carbon and nitrogen dataset for the northern permafrost region based on circumpolar land cover upscaling. Earth Syst. Sci. Data 14, 4095–4110. https://doi.org/10.5194/essd-14-4095-2022

Rantanen, M., Karpechko, A.Y., Lipponen, A., Nordling, K., Hyvärinen, O., Ruosteenoja, K., Vihma, T., and Laaksonen, A. 2022. The Arctic has warmed nearly four times faster than the globe since 1979. Commun Earth Environ 3, 1–10. https://doi.org/10.1038/s43247-022-00498-3

Two decades of permafrost thaw and carbon flux measurements in Alaskan peatlands

Merritt Turetsky

Department of Ecology and Evolutionary Biology, University of Colorado, Boulder, Colorado, United States

Northern peatlands are experiencing some of the most rapid warming on the planet, which is compounded by increases in the extent and severity of climate-related disturbances such as drought, wildfire, and permafrost thaw. Cumulatively these changes lead to both peatland wetting and drying at various scales, making it difficult to predict the fate of northern peatlands and their large carbon stocks.

The current view of northern peatland carbon cycling is that the majority of soil carbon cycling occurs in the acrotelm, the thin, mostly aerated peat layer above the water table. Once carbon is transferred to the deeper, permanently saturated catotelm, carbon mineralization is thought to be negligible due to cold temperatures and anaerobic conditions that inhibit decomposition. Peat carbon below the catotelm can be mineralized anaerobically using a variety of alternative electron acceptors that are energetically less efficient than oxygen and can result in the production of methane. Thus, the position of the water table (and the associated thickness of the acrotelm) is used as a predictor of overall decomposition rates and methane production in peatlands. If climate change leads to a lower or more variable water table in peatlands, either through increased evapotranspiration with warming or changes in precipitation, increased soil carbon turnover in the acrotelm could stimulate soil carbon losses to the atmosphere, change the magnitude of methane flux, and alter the current role of northern peatlands in the Earth's climate system.

The Alaska Peatland Experiment (APEX)

Established in 2004, the Alaska Peatland Experiment (APEX) has been quantifying CO_2 and CH_4 fluxes using eddy covariance measurements and chamber networks in a rich fen, permafrost peat plateau, and several thermokarst bogs in the Tanana River floodplain in interior Alaska. Within the rich fen site, we initiated a factorial design of water table treatments (control, lowered water table position to simulate drying, raised water table position to simulate flooding) and vegetation treatments (plant functional type removal experiments). This has allowed us to compare the effects of experimental drying and wetting with natural changes in hydrology occurring with permafrost thaw.

We initially hypothesized that drying would lead to short-term losses in soil carbon while flooding would inhibit decomposition and stimulate peat accumulation. However, our time series of carbon fluxes at the rich fen suggest that we highly underestimated the role of anaerobic microbial metabolism in the saturated zone (catotelm). Ecosystem respiration of carbon dioxide is not sensitive to our water table manipulations, with the dominant contributions to ecosystem respiration switching from autotrophic respiration in wet years to heterotrophic respiration in dry years. Plant productivity and respiration in wet years is not driven by vascular plants or mosses, as expected, but instead is dominated by an algae-based food web.

Additional evidence for our underestimation of anaerobic soil carbon transformation is that modeled carbon dioxide fluxes based on fixed decomposition constants were less than observed fluxes during wet periods with high water tables. Finally, incubation of fen peat showed that soil carbon dioxide production was comparable under anaerobic and aerobic conditions. This suggests that unknown alternative electron acceptors (possibly humic substances and/or iron) contributed to anaerobic microbial metabolism and suppressed methane production.

Another key APEX finding is that early onset of permafrost thaw, driven by active layer thickening with no evidence of thermokarst, was predicted by changes in the moss community and stimulated methane fluxes 5-fold, accounting for 30% of the total annual thaw-driven increase in methane. Methane emissions were sensitive to rainfall and surface moisture conditions, with spring rain events stimulating soil warming and methane fluxes. Ecosystem respiration exceeded gross primary production at all sites, and winter respiration accounted for up to 25% of carbon dioxide fluxes. Measurements in the rich fen, which experiences extreme flooding and lacks surface permafrost showed the largest atmospheric carbon emissions among all of the APEX sites. In concert with changing permafrost and soil hydrology conditions, changes in plant species composition in response to wetting or drying, such as increases in sedge abundance affects soil redox pool recharge and ultimately controls the ratio of carbon dioxide to methane production.

Given that expansion of thaw will increase hydrologic connectivity and fen expansion, we believe these results provide insights into the future trajectory of carbon fluxes in the floodplain.

New MURI-funded Permafrost Project

A new project was recently funded by the Department of Defense's Multidisciplinary University Research Initiative (MURI) program, sponsored by the Army Research Office. This project seeks to understand the landscape, microbial, and biogeochemical indicators of various thaw processes. We compiled a geodatabase of ground-truthed thaw locations, using all published locations of thaw measurements in Alaska, which will be used to conduct large-scale sampling campaigns to understand the strongest indicators of thaw types. We are particularly interested in understanding the spatial propagation of thaw indicators in streams and the vertical propagation of methane and other types of volatile organic carbon (VOC) from thaw feature surfaces into the boundary layer. At the end of the growing season in 2023, we conducted campaigns at several sites around Fairbanks varying in permafrost ice content. We quantified concentrations of carbon dioxide, methane, and VOCs in vertical increments extending upwards from the ground surface. This information will be used to understand how much VOC emission is driven by methane, how permafrost properties drive variation in VOC profiles, and how methane and other VOCs dissipate in air.

Results from these two studies will be used to frame several forward-looking research questions and approaches urgently needed to better understand the fate of permafrost peatlands and their carbon stocks.

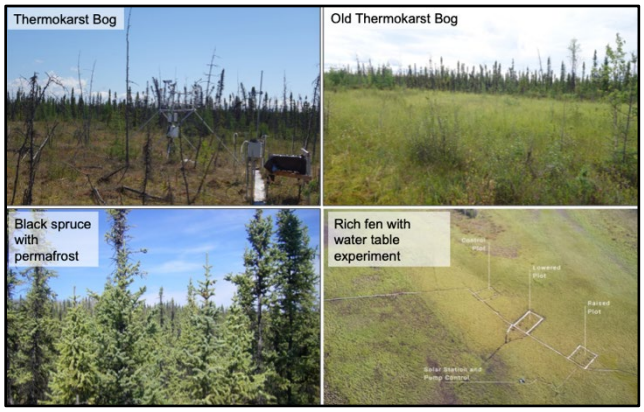

Figure 1. Photographs of four APEX sites that have been monitored for vegetation and carbon fluxes since 2024.

Variations in methane fluxes across a natural permafrost thaw gradient at an upland tundra site

Julia A. Warren[1], Gerardo Celis[2], Justin Ledman[1] & Edward A.G. Schuur[1]

[1]*Center for Ecosystem Science and Society, Northern Arizona University, Flagstaff, Arizona, United States*

[2]*University of Arkansas, Fayetteville, Arizona, United States*

Globally, permafrost soils store 1400 to 1600 Pg of carbon, about three times as much carbon as is in the atmosphere (Schuur et al. 2023). Due to increased global carbon emissions, high northern latitudes are warming twice as fast as the rest of the Earth. Increased warming has contributed to permafrost thaw, exposing a portion of the carbon stored in permafrost to microbial decomposition (Schuur et al. 2023). Aerobic and anaerobic decomposition can emit soil organic carbon as greenhouse gases (i.e., carbon dioxide and methane). In permafrost soils, methane is produced in highly reduced anaerobic zones by methanogens, oxidized to carbon dioxide in aerobic zones by methanotrophs (Abdalla et al. 2016), and emitted to the atmosphere when the balance between the production and consumption is positive. Sustained methane emissions have 45 times the radiative forcing of carbon dioxide over a 100-year time scale (Myhre et al. 2013) and could further lead to a significant positive feedback loop contributing to climate change. In this study, we aim for an improved understanding of the long-term, yearly, and seasonal variations of permafrost methane fluxes.

Site Description

The Arctic Carbon and Climate (ACCLIMATE) observatory is within the Eight Mile Lake watershed located in the interior of Alaska, USA. ACCLIMATE is underlain by discontinuous permafrost and has well drained surface soils consisting of 0.5 m of organic soils overlying mineral soil. This upland tundra site is dominated by low, dwarf shrubs, tussock forming sedges, mosses, and lichen (Schuur et al. 2007). A natural thaw gradient (termed Gradient), housed at ACCLIMATE, has three sites representing different stages of the permafrost thaw (Minimal, Moderate, and Extensive) (Schuur et al. 2007).

Methods

Methane fluxes from 2015 to 2023 were measured at Gradient using an eddy covariance (EC) system. The tower footprint encompasses the Minimal, Moderate, and Extensive sites at Gradient. Methane, carbon dioxide, water vapor, orthogonal wind components, and air temperature were recorded at 10Hz using LI-7500 Analyzer Interface Unit (LI-COR, Biosciences). The calibrations were performed using standard methodology (Taylor et al. 2018). This study focuses on methane flux data collected from the EC system.

Flux data collected from 2015-05-01 to 2023-11-09 was aggregated in half-hourly fluxes and a ± 0.5 µmol s^{-1} m^{-2} filter was applied. Fluxes were dived into years (01 May through 30 April the following year), summer (01 May through 30 September) and nonsummer (01 October through 30 April the following year) (Celis et al. 2017).

Results

Long-term methane flux data collected at Gradient shows a dynamic fluctuation within the permafrost landscape, demonstrating periods of both net methane emission and net methane uptake (Figure 1).

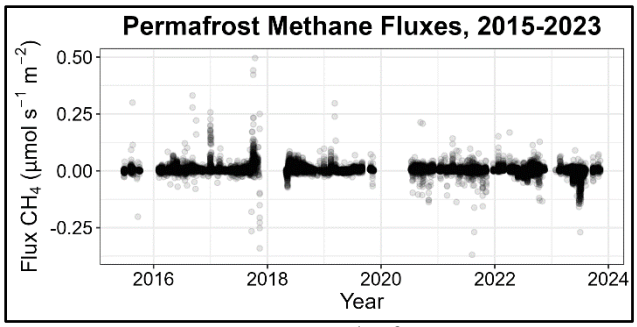

Figure 1. Methane fluxes (µmol s^{-1} m^{-2}) from the EC system collected from 2015-05-01 to 2023-11-09 aggregated in 30-minute fluxes. A positive flux represents a net source, and a negative flux represents a net sink.

Average yearly methane fluxes ranged from 0.002 to 0.006 µmol s^{-1} m^{-2} from 2015 to 2022, with the upper limit of the range being 3 times greater than the lower limit. Average summer methane fluxes ranged from 0.002 to 0.009 µmol s^{-1} m^{-2} from 2015 to 2022. In 2023, the average summer methane flux was -0.008 µmol s^{-1} m^{-2}. Average nonsummer methane fluxes ranged from 0.0007 to 0.006 µmol s^{-1} m^{-2} from 2015 to 2022, with the upper limit being 8.5 times greater than the lower limit.

Discussion

Yearly average methane fluxes have considerable variation. When broken down seasonally, Gradient was a net source of methane in the summer from 2015 to 2022. However, 2023 average summer methane fluxes marked the first time the seasonal average methane flux was a net sink. Average nonsummer methane fluxes exhibited greater variability compared to average summer methane fluxes.

In half of the years from 2015 to 2022, summers were a greater net source of methane than nonsummer, while the other half showed the opposite trend. The frequency and strength of source and sink periods varied considerably throughout the year, highlighting the dynamic nature of methane fluxes on the permafrost landscape.

There was strong interannual seasonal variability indicating that there were other variables that were impacting methane fluxes. Previous studies have shown that there are significant relationships between growing season methane fluxes and different environmental variables (i.e., thaw depth) (Taylor et al. 2018). Future work will include looking at the relationships between methane fluxes and environmental variables over long-term, yearly, and seasonal periods of time.

References

Abdalla, M., Hastings, A., Truu, J., Espenberg, M., Mander, U., and Smith, P. 2016. Emissions of methane from northern peatlands: a review of management impacts and implications for future management options, Ecology and Evolution, 6(19): 7080–7102. doi:10.1002/ece3.2469

Celis, G., Mauritz, M., Bracho, R., Salmon, V.G., Webb, E.E., Hutchings, J., Natali, S.M., Schadel, C., Crummer, K.G., and Schuur, E.A.G. 2017. Tundra is a consistent source of CO_2 at a site with progressive permafrost thaw during 6 years of chamber and eddy covariance measurements, Journal of Geophysical Research: Biogeosciences, 122(6): 1471–185. doi:10.1002/2016JG003671

Myhre, G., Samset, B.H., Schulz, M., Balkanski, Y., Bauer, S., Bernsten, T.K., Bian, H., Bellouin, N., Chin, M., et al. 2013. Radiative forcing of the direct aerosol effect from AeroCom Phase II simulations, Atmospheric Chemistry and Physics, 13(4): 1853–1877. doi:10.5194/acp-13-1853-2013

Schuur, E.A.G, Crummer, K.G., Vogel, J.G., and Mack, M.C. 2007. Plant Species Composition and Productivity following Permafrost Thaw and Thermokarst in Alaskan Tundra, Ecosystems, 10(2): 280–292. doi:10.1007/s10021-007-9024-0

Schuur, E.A.G., Hicks Pries, C., Mauritz, M., Pegorano, E., Rodenhizer, H., See, C., and Ebert, C. 2023. Ecosystem and soil respiration radiocarbon detects old carbon release as a fingerprint of warming and permafrost destabilization with climate change, Philosophical Transactions of the Royal Society A, 381(2261): 20220201. doi:10.1098/rsta.2022.0201

Taylor, M.A., Celis, G., Ledman, J.D., Bracho, R., and Schuur, E.A.G. 2018. Methane Efflux Measured by Eddy Covariance in Alaskan Upland Tundra Undergoing Permafrost Degradation, Journal of Geophysical Research: Biogeosciences, 123(9): 2965–2710. doi: 10.1029/2018JG004444

5C — Reducing Uncertainties for Permafrost Carbon Feedbacks

Session Chairs: Peter Morse[1] & Lexi Mollica[2]

[1]*Geological Survey of Canada, Natural Resources Canada, Ottawa, Ontario, Canada*
[2]*University of Guelph, Guelph, Ontario, Canada*

Surface warming, amplified in the Arctic, is expected to accelerate over time due in part due to greenhouse gas (GHG) emissions from thawing carbon-rich permafrost (primarily CO_2 and CH_4), resulting in permafrost carbon feedbacks that affect the entire Earth system. Permafrost carbon feedbacks involve biogeochemical carbon cycles in three primary environmental settings: near-shore, terrestrial, and aquatic. In addition, there is geologically sourced CH_4 from sedimentary basins that reaches the atmosphere through taliks, which may enlarge as permafrost degrades. A general lack of data and great uncertainty in estimates of Arctic GHG emissions reflect our poor understanding of natural processes in the Arctic.

Though CH_4 is 25 times more powerful a GHG than CO_2 over 100 years and responsible for 30% of global warming since pre-industrial times, there is high uncertainty about Arctic CH_4 emissions because CH_4 quantification to date has focused primarily on anthropogenic sources. Key elements to determining the impact of CH_4 emissions from permafrost on global climate are understanding (1) the amount of carbon stored in permafrost dictated by geological history; (2) the biogeochemical processes in the primary environmental settings that regulate how much CH_4 will be released and over what time frame; (3) the relative emissions of CH_4 versus CO_2; and (4) the relative contributions of CH_4 from biological (biogenic) versus geological (thermogenic) sources.

In this session, we seek presentations about multidisciplinary research to examine CH_4 sources, biogeochemical processes, and fluxes from thawing permafrost across varied spatial and temporal scales.

Determining the influence of eroding thermokarst lake edges on tundra and lake greenhouse gas dynamics

Kathryn A. Bennett[1,2], Carolina Voigt[3], Léa Cornette[1], Roxane Maranger[1], Benjamin Schmidt[1], Christian von Sperber[4], Suzanne Tank[5], Andy Vicente-Luis[1] & Oliver Sonnentag[1,2]

1Université de Montréal, Montréal, Québec, Canada

2Centre d'Études Nordiques, Université Laval, Québec City, Québec, Canada

3Universität Hamburg, Hamburg, Germany

4McGill University, Montréal, Québec, Canada

5University of Alberta, Edmonton, Alberta, Canada

Permafrost-affected soils in the Arctic-boreal region store non-negligible amounts of carbon (C) and nitrogen (N) that can become mobilized with thaw in response to warming air and soil temperatures. This release of organic matter can fuel increased net fluxes of the greenhouse gasses carbon dioxide (CO_2), methane (CH_4), and nitrous oxide (N_2O) to the atmosphere (Miner et al. 2022; Voigt et al. 2020). The patchwork of permafrost characteristics, soil nutrients, vegetation cover, soil moisture conditions, and aquatic features across the heterogeneous Arctic-boreal region make fluxes difficult to estimate at large spatial scales.

Within the Arctic-boreal region, tundra ecosystems specifically are experiencing an increase in shrub biomass and spatial cover, which can increase CO_2 uptake via photosynthesis (Myers-Smith et al. 2011). Simultaneously, warming soil temperature increases microbial CO_2 production (Schädel et al. 2016). Low soil moisture in tundra ecosystems supports minimal emissions of CH_4 while promoting CH_4 uptake that could increase with warming air temperature (Euskirchen et al. 2017; Voigt et al. 2023). Tundra soils are nitrogen limited (Haag 1974), thus plant-microbe competition, in combination with soil moisture, are important controls on tundra N_2O flux (Voigt et al. 2020). Thermokarst processes, thaw of ice-rich permafrost in physically dramatic pulse disturbances (e.g., thaw slumps), release nutrients, alter soil moisture, and can remove vegetation cover influencing tundra CO_2, CH_4, and N_2O flux. Additionally, thermokarst processes can transport sediment and organic matter downstream into tundra lakes, altering lake chemistry (Vonk et al. 2015). Given the increasing prevalence of thermokarst features on the tundra landscape (Farquharson et al. 2019) and the non-negligible contribution of tundra lakes to regional carbon budgets (Wik et al. 2016) and potentially nitrogen budgets (Soued et al. 2016) it is important to determine the underlying mechanisms driving lake and tundra net surface fluxes.

In this study we conducted plot-scale CO_2, CH_4, and N_2O flux measurements from tundra uplands and lakes near Trail Valley Creek, located in the Inuvialuit Settlement Region (ISR), Northwest Territories, Canada, to determine the biogeochemical response of tundra and lake greenhouse gas fluxes to thermokarst processes, and identify underlying mechanisms controlling fluxes across the broader landscape (1 km^2 – 100 km^2). Plot-scale tundra and lake CO_2, CH_4, and N_2O fluxes were measured using manual chamber techniques ~weekly during June – August 2022 and 2023 from four transects (32 plots). The transects span from intact mineral upland tundra, across eroding thermokarst lake edges, and into neighboring lakes. Soil temperature, soil profile CO_2, CH_4, and N_2O gas concentrations, soil moisture, and soil cation and anion concentrations were measured in tandem with plot-scale fluxes.

In July 2023 soil samples were collected to assess soil pH, soil carbon stocks, extractable nitrate (NO_3^-) and ammonium (NH_4^+), and extractable organic and inorganic phosphorus. Lake chemistry was assessed by measuring ~bi-weekly water temperature and dissolved oxygen profiles, surface water dissolved CO_2, CH_4, and N_2O concentrations, and collecting surface water samples to quantify total nitrogen, total dissolved nitrogen, total phosphorus, total dissolved phosphorus, NO_3^-, NH_4^+, dissolved organic carbon, absorbance, and fluorescence. In July 2023 ten additional lakes in the ISR with varying degrees of thermokarst disturbance were sampled at a single moment in time for plot-scale CO_2, CH_4, N_2O diffusive flux and dissolved gas concentrations, and water chemistry. Also in July 2023, two thermokarst eroding lake edges immediately adjacent to two of the ten additional lakes were sampled for CO_2, CH_4, N_2O tundra plot-scale gas flux and soil gas concentrations.

Preliminary results of tundra plot-scale net ecosystem exchange (NEE) ranged from -209.9 to 127.0 mg CO_2 m^{-2} h^{-1} (mean = -3.6 ± 83.4 mg CO_2 m^{-2} h^{-1}, n = 64) at intact mineral upland tundra plots and -1100.6 to 206.4 mg CO_2 m^{-2} h^{-1} (mean = -176.7 ± 345.3 mg CO_2 m^{-2} h^{-1}, n = 64) at disturbed eroding thermokarst lake edge plots. Negative values

indicate net CO_2 uptake and positive values indicate net CO_2 emission. Preliminary results indicate that plots disturbed by thermokarst processes have higher CO_2 flux variability compared to undisturbed mineral upland tundra. Unexpectedly, mean NEE values indicate that thermokarst processes may stimulate CO_2 uptake in the ISR via nutrient release, as long as vegetation cover is intact. Given the sensitivity of tundra CO_2 fluxes to soil temperature, moisture, and organic matter input it is critical to understand the mechanisms driving this potential increase in net CO_2 uptake after disturbance and determine its prevalence in the broader landscape.

Our final results will present CH_4 and N_2O plot-scale fluxes and below-ground concentrations in addition to CO_2. By combining plot-scale CO_2, CH_4, N_2O flux measurements from tundra and lake plots with below-ground environmental variables, soil chemistry, and lake chemistry data we will identify the underlying biogeochemical mechanisms associated with plot-scale flux in the ISR. Our results will contribute to reducing the uncertainty of tundra CO_2, CH_4, and N_2O flux during the snow-free season. These data are important to understand the response of mineral tundra landscapes to rising air temperature, changing precipitation patterns, and increased rates of permafrost thaw.

REFERENCES

Euskirchen, E.S., Bret-Harte, M.S., Shaver, G.R., Edgar, C.W., and Romanovsky, V.E. 2017. Long-Term Release of Carbon Dioxide from Arctic Tundra Ecosystems in Alaska. Ecosystems, 20(5): 960–974. doi:10.1007/s10021-016-0085-9

Farquharson, L.M., Romanovsky, V.E., Cable, W.L., Walker, D.A., Kokelj, S.V., and Nicolsky, D. 2019. Climate Change Drives Widespread and Rapid Thermokarst Development in Very Cold Permafrost in the Canadian High Arctic. Geophys. Res. Lett. 46(12): 6681–6689. doi:10.1029/2019GL082187

Haag, R.W. 1974. Nutrient limitations to plant production in two tundra communities. Can. J. Bot. 52(1): 103–116. doi:10.1139/b74-014

Miner, K.R., Turetsky, M.R., Malina, E., Bartsch, A., Tamminen, J., McGuire, A.D., Fix, A., Sweeney, C., Elder, C.D., and Miller, C.E. 2022. Permafrost carbon emissions in a changing Arctic. Nat. Rev. Earth Environ. 3(1): 55–67. doi:10.1038/s43017-021-00230-3

Myers-Smith, I.H., Forbes, B.C., Wilmking, M., Hallinger, M., Lantz, T., Blok, D., Tape, K.D., Macias-Fauria, M., Sass-Klaassen, U., Lévesque, E., Boudreau, S., Ropars, P., Hermanutz, L., Trant, A., Collier, L.S., Weijers, S., Rozema, J., Rayback, S.A., Schmidt, N.M., Schaepman-Strub, G., Wipf, S., Rixen, C., Ménard, C., Venn, S., Goetz, S., Andreu-Hayles, L., Elmendorf, S., Ravolainen, V., Welker, J., Grogan, P., Epstein, H.E., and Hik, D.S. 2011. Shrub expansion in tundra ecosystems: dynamics, impacts and research priorities. Environ. Res. Lett. 6(4): 045509. doi:10.1088/1748-9326/6/4/045509

Schädel, C., Bader, M.K.-F., Schuur, E.A.G., Biasi, C., Bracho, R., Čapek, P., De Baets, S., Diáková, K., Ernakovich, J., Estop-Aragones, C., Graham, D.E., Hartley, I. P., Iversen, C. M., Kane, E., Knoblauch, C., Lupascu, M., Martikainen, P.J., Natali, S.M., Norby, R.J., O'Donnell, J.A., Chowdhury, T.R., Šantrůčková, H., Shaver, G., Sloan, V.L., Treat, C.C., Turestsky, M.R., Waldrop, M.P., and Wickland, K.P. 2016. Potential carbon emissions dominated by carbon dioxide from thawed permafrost soils. Nat. Clim. Change 6(10): 950–953. doi:10.1038/nclimate3054

Schuur, E.A.G., Abbott, B.W., Commane, R., Ernakovich, J., Euskirchen, E., Hugelius, G., Grosse, G., Jones, M., Koven, C., Leshyk, V., Lawrence, D., Loranty, M.M., Mauritz, M., Olefeldt, D., Natali, S., Rodenhizer, H., Salmon, V., Schädel, C., Strauss, J., Treat, C.C., and Turestsky, M.R. 2022. Permafrost and Climate Change: Carbon Cycle Feedbacks from the Warming Arctic. Annu. Rev. Environ. Resour. 47(1): 343–371. doi:10.1146/annurev-environ-012220-011847

Soued, C., del Giorgio, P.A., and Maranger, R. 2016. Nitrous oxide sinks and emissions in boreal aquatic networks in Québec. Nat. Geosci. 9(2): 116–120. doi:10.1038/ngeo2611

Voigt, C., Marushchak, M.E., Abbott, B.W., Biasi, C., Elberling, B., Siciliano, S.D., Sonnentag, O., Stewart, K.J., Yang, Y., and Martikainen, P.J. 2020. Nitrous oxide emissions from permafrost-affected soils. Nat. Rev. Earth Environ. 1(8): 420–434. doi:10.1038/s43017-020-0063-9

Voigt, C., Virkkala, A.-M., Hould Gosselin, G., Bennett, K.A., Black, T.A., Detto, M., Chevrier-Dion, C., Guggenberger, G., Hashmi, W., Kohl, L., Kou, D., Marquis, C., Marsh, P., Marushchak, M.E., Nesic, Z., Nykänen, H., Saarela, T., Sauheitl, L., Walker, B., Weiss, N., Wilcox, E.J., and Sonnentag, O. 2023. Arctic soil methane sink increases with drier conditions and higher ecosystem respiration. Nat. Clim. Change 13(10): 1095–1104. doi:10.1038/s41558-023-01785-3

Vonk, J.E., Tank, S.E., Bowden, W.B., Laurion, I., Vincent, W.F., Alekseychik, P., Amyot, M., Billet, M.F., Canário, J., Cory, R.M., Deshpande, B.N., Helbig, M., Jammet, M., Karlsson, J., Larouche, J., MacMillan, G., Rautio, M., Walter Anthony, K.M., and Wickland, K.P. 2015. Reviews and syntheses: Effects of permafrost thaw on Arctic aquatic ecosystems. Biogeosciences 12(23): 7129–7167. doi:10.5194/bg-12-7129-2015

Wik, M., Varner, R.K., Anthony, K.W., MacIntyre, S., and Bastviken, D. 2016. Climate-sensitive northern lakes and ponds are critical components of methane release. Nat. Geosci. 9(2): 99–105. doi:10.1038/ngeo2578

Investigating plant-induced priming effects in permafrost soils using a novel plant-soil experimental facility

Nina L. Friggens[1], Gustaf Hugelius[2], Julian B. Murton[3], Gareth K. Phoenix[4] & Iain P. Hartley[1]

[1]*Department of Geography, Faculty of Environment, Science and Economy, University of Exeter, Exeter, United Kingdom*

[2]*Department of Physical Geography, Stockholm University, Stockholm, Sweden*

[3]*Department of Geography, University of Sussex, Brighton, United Kingdom*

[4]*Department of Animal and Plant Sciences, University of Sheffield, Sheffield, United Kingdom*

Thawing permafrost soils are predicted to release 10s of billions of tonnes of carbon (C) by 2100 (Koven et al. 2015), making efforts to limit warming to 2°C all the more challenging. There is little potential for plant biomass gains to offset these losses, with plant biomass changes likely to be small. However, greater plant productivity and increased rooting depths may increase rates of C input into previously frozen soils and thus increase the formation of new soil organic matter (SOM). Alternatively, new inputs may stimulate, or 'prime', the decomposition of previously-frozen organic matter.

Incubation studies have suggested that previously-frozen C may be more vulnerable to priming than near-surface SOM (Wild et al. 2016) and recent modelling work indicates that rhizosphere priming could significantly increase soil C loss from northern permafrost areas by 2100 (Keuper et al. 2020).

Whilst these studies show clear evidence of priming induced by labile C additions to soils, there have, to our knowledge, been no long-term priming study in permafrost soils in which live plants have been used to supply the substrates.

By growing plants in contrasting permafrost soils under a ^{13}C-labelled atmosphere, we directly measure plant-induced priming for the first time.

METHODS

Active layer, mineral and organic permafrost soils where collected from the North West Territories and Yukon, Canada in 2019. A range of gelisols where sampled, including drained thermokarst lake basins, yedomas, turbels and non-lake orthels. These soil types where selected to capture a variety of C contents, soil textures, deposition patterns and cryoturbation.

In order to investigate plant-induced priming in these permafrost soil a bespoke, climate controlled growth and ^{13}C-labelling chamber was designed and built.

This experimental facility includes independent control of both soil and air temperature, programmable grow lights with a wide range of light intensities, and tightly controlled delivery of $^{13}CO_2$ to ensure a consistent atmospheric enrichment across day-night cycles and throughout long-term experiments.

Within the 13C-labelling growth chamber, permafrost soil experiments were set up in mesocosms (Figure 1). The mesocosms were designed to grow Agrostis capillaris in an inert ceramic medium in a central compartment, connected via meshes to four side compartments containing permafrost soil into which the grasses could root. One of the four side compartments was kept as a root free control using a 1 µm mesh to allow water and gas diffusion but prevent root growth into the soil.

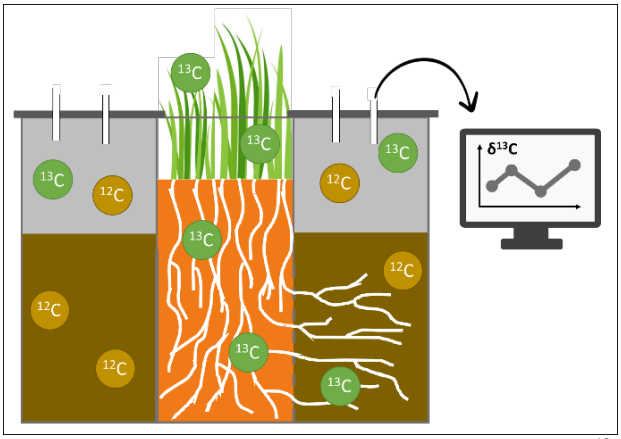

Figure 1. Mesocosm design enabling plant growth in ^{13}C enriched atmosphere whilst rooting into permafrost soils with pull through sampling of soil headspace to measure CO_2 fluxes.

The head space of each soil filled side compartment was sealed and connected to a pull-through respiration system allowing the routine measurement of $^{12\ \&\ 13}CO_2$ fluxes externally to the growth chamber.

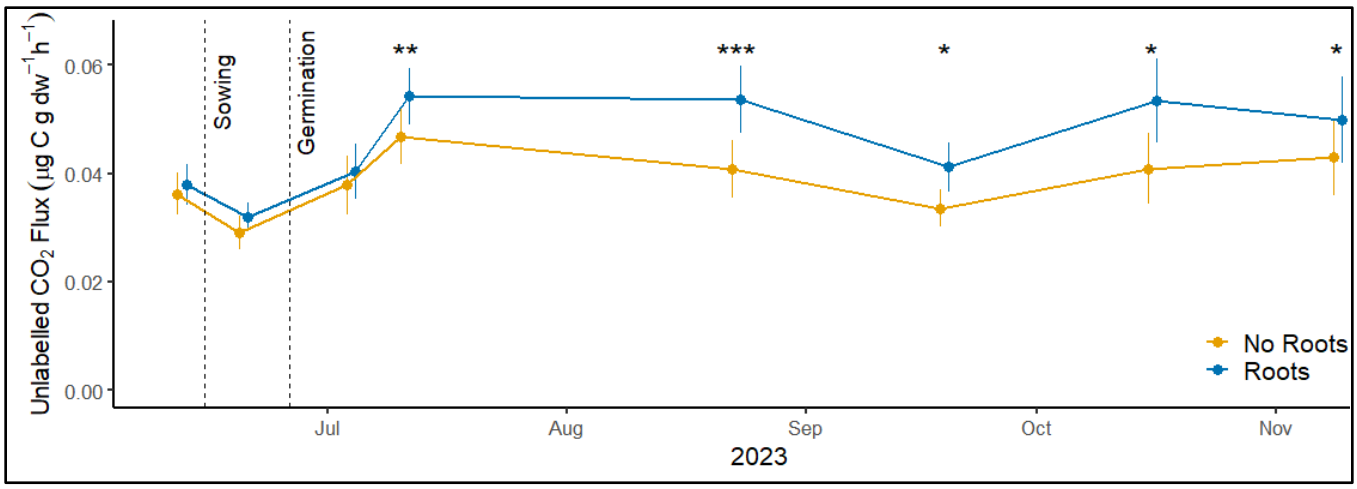

Figure 2. Unlabelled CO_2 flux over time from permafrost soil filled side compartments with and without root access.

Soil priming was derived by the unlabelled CO_2 flux (UCO_2) calculated by the following equation:

$$UCO_2 = \left(\left(\frac{d13C_c - d13C_{sc}}{d13C_c - d13C_{air}}\right) * CO_{2\,sc}\right) * Flow_{air} \qquad [1]$$

Where *c* is the chamber environment, *sc* is the side compartment headspace and *air* is the incoming air flowing into the side compartment.

Results

Prior to the sowing and germination of *A. capilaris* into the mesocosms central compartment there was no significant difference in flux between side compartments. Eight days after germination there remained no difference in the unlabelled CO_2 flux between side compartments with and without root access (Figure 2). By 15 days post germination (mid-July) the unlabelled CO_2 flux in side compartments with roots is significantly higher than in paired side compartments without roots. This difference between roots and no roots remains significant until mid-November (Figure 2).

Discussion

The development, over time since germination, of a significantly higher unlabelled CO_2 flux in soil filled side compartments with roots compared to root-free control side compartments is the first direct evidence of live plant-induced positive priming in thawed permafrost soils.

More analysis is needed to determine how this effect parses within the context of the C content, texture, horizon and cryoturbation of these soils.

Plant-induced priming may result in large scale soil C loss across thawing northern permafrost regions, however, this loss should be placed in the context of potential new SOM formation driven by plant C inputs and soil C stabilisation mechanisms.

Understanding these mechanisms and rates of SOM formation is key, as the balance between new SOM formation and decomposition of previously-frozen SOM will determine how much C is released from these soils and the extent of their contribution to the permafrost carbon feedback.

References

Keuper, F., Wild, B., Kummu, M., Beer, C., Blume-Werry, G., Fontaine, S., Gavazov, K., Gentsch, N., Guggenberger, G., Hugelius, G., Jalava, M., Koven, C., Krab, E.J., Kuhry, P., Monteux, S., Richter, A., Shahzad, T., Weedon, J.T., and Dorrepaal, E. 2020. Carbon loss from northern circumpolar permafrost soils amplified by rhizosphere priming. Nat. Geosci. 13, 560–565. doi:10.1038/s41561-020-0607-0

Koven, C.D., Schuur, E.A.G., Schädel, C., Bohn, T.J., Burke, E.J., Chen, G., Chen, X., Ciais, P., Grosse, G., Harden, J.W., Hayes, D.J., Hugelius, G., Jafarov, E.E., Krinner, G., Kuhry, P., Lawrence, D.M., MacDougall, A.H., Marchenko, S.S., McGuire, A.D., Natali, S.M., Nicolsky, D.J., Olefeldt, D., Peng, S., Romanovsky, V.E., Schaefer, K.M., Strauss, J., Treat, C.C., and Turetsky, M. 2015. A simplified, data-constrained approach to estimate the permafrost carbon-climate feedback. Philosophical Transactions of the Royal Society A: Mathematical, Physical and Engineering Sciences 373. (2054), 20140423 doi:10.1098/rsta.2014.0423

Wild, B., Gentsch, N., Čapek, P., Diáková, K., Alves, R.J.E., Bárta, J., Gittel, A., Hugelius, G., Knoltsch, A., Kuhry, P., Lashchinskiy, N., Mikutta, R., Palmtag, J., Schleper, C., Schnecker, J., Shibistova, O., Takriti, M., Torsvik, V.L., Urich, T., Watzka, M., Šantrůčková, H., Guggenberger, G., and Richter, A. 2016. Plant-derived compounds stimulate the decomposition of organic matter in arctic permafrost soils. Scientific Reports 6 (1), 1–11. doi:10.1038/srep25607

How organo-mineral interactions affect the priming of permafrost soil

Caitlin Hicks Pries[1,2], Fernando Montaño Lopéz[2], Sean Schaeffer[3,4], Sarah Goldsmith[1], Skylar Wilkins[1], Pax Bakke[3,5], Nathan Alexander[3,5], Else Schlerman[3,4], A. Stuart Grandy[3,4,5] & Jessica Ernakovich[3,4,5]

[1]*Department of Biological Sciences, Dartmouth College, Hanover, New Hampshire, United States*

[2]*Ecology, Evolution, Environment, and Society Program, Dartmouth College, Hanover, New Hampshire, United States*

[3]*Center for Soil Biogeochemistry and Microbial Ecology (Soil BioME), University of New Hampshire, Durham, New Hampshire, United States*

[4]*Natural Resources and Earth System Science Program, University of New Hampshire, Durham, New Hampshire, United States*

[5]*Department of Natural Resources and the Environment, University of New Hampshire, Durham, New Hampshire, United States*

The extent to which priming accelerates permafrost organic matter (OM) decomposition upon thaw will depend on interactions between microbes, roots, and minerals. Over 40% of the global stock of permafrost soil OM is found in mineral permafrost (Hugelius et al. 2014). Soil minerals can shield organic matter from microbial enzymatic attack via chemical sorption and complexation processes and via physical protection in microaggregates. While organic matter associated with minerals is not inert (Jilling et al. 2021), on the whole it tends to be older and have longer transit times than unprotected particulate organic matter.

The capacity of a soil to form organo-mineral associations and the strength of those associations are dependent on the minerals' charge and surface area, which are a function of its weathering status (Slessarev et al. 2022). Mineral reactivity peaks at intermediate stages of soil weathering where high surface area and charged secondary 2:1 and poorly crystalline minerals predominate before they further weather into less reactive 1:1 minerals (Torn et al. 1997). Non-crystalline and poorly crystalline minerals have the highest capacity for sorbing to organic matter (Torn et al. 1997). The bioclimatic potential for chemical weathering is lower in the Arctic than in warmer regions. However, the geologic potential varies greatly. There are many recently deglaciated landforms with a high abundance of primary minerals ready to be weathered. Within Alaska's north slope, landforms range in age from 10,000 years old (foothills of Brooks Range) to over 4.5 million years old (Sagwon hills).

The ability of mineral associations to protect soil OM from priming varies. Mineral protection decreases the priming effect induced by new litter and glucose additions (Rasmussen et al. 2007), but can increase the priming effect induced by organic acids, which can mobilize metals and displace native OM bound to minerals (Jilling et al. 2021). Upon its thaw, the magnitude of permafrost OM losses will in part depend on soil mineralogy and the extent to which minerals protect soil OM from warming and priming and in part on the quantity and composition of new organic matter inputs. To quantify the importance of mineral associations in controlling the susceptibility of newly-thawed soil OM to priming, we used the natural variation in mineral types and weathering products (e.g., Fe and Al mineral phases) created by the spatio-temporal heterogeneity of glacial retreat on AK's North Slope.

We had two objectives: 1) We characterized organo-mineral interactions, pH, and soil organic carbon (OC) abundance in active layer and permafrost soil along a glacial chronosequence; 2) We determined how differences in organo-mineral interactions affect the fate of simulated root exudates and the vulnerability of native soil OC to priming in active layer and thawed permafrost soils. We hypothesized that associations between organic matter and poorly crystalline Fe and Al oxides will increase from the youngest to oldest landscape ages and be greater in the active layer than in the permafrost. Thus, soil OC in the active layer of the oldest site would be less susceptible to priming and more likely to retain new exudate-C.

Methods

We sampled permafrost soil across different glacial drifts, where we hypothesized the degree of soil weathering and pedogenesis, and therefore capacity to protect soil OM, would differ by time since deglaciation. We sampled mineral soil from below the O horizon to 20 cm below the permafrost-active layer interface across four sites of different ages— ~11,500 years; ~66,000 years; ~125,000 years; and 4.5 million years—using a Snow, Ice, and Permafrost Research Establishment (SIPRE) corer in August 2021 and '22. These sites were located on the North Slope, AK in the foothills of the Brooks Range south of Toolik Lake (youngest) to the Sagwon Hills 100 km to the north (oldest). We performed selective dissolution to characterize Al and Fe mineral phases and to provide

insights into mineral phases stabilizing OC. Extractions with sodium pyrophosphate release the forms of Al and Fe complexed with OM; acid ammonium oxalate dissolves Al and Fe organic complexes and non-crystalline Al and Fe minerals; and citrate dithionite method solubilizes Al and Fe oxides and hydroxides (more crystalline phases).

We are currently incubating the mineral and active layer soils from the sites described above at 5°C under oxic conditions for 10 weeks, simulating an arctic growing season. We are subjecting the soils to continuous additions of synthetic root exudates or to continuous sterilized water additions as a control (n=4 per soil type and treatment). The exudates are ^{13}C-labeled (x(^{13}C) = 50%) and consist of glucose, oxalic acid, and alanine. Additions of exudates or water are delivered via a microporous artificial root (Rhizon sampler, Rhizosphere Research Product, Germany) at a rate of 5.25µL·h^{-1} to ~40 g of soil through syringe pumps (New Era Pump Systems Inc, USA) in accordance with rates observed under natural conditions. We measure the amount and isotopic enrichment (^{13}C/^{12}C) of respired CO_2 weekly using a Picarro G2201i.

Preliminary results

The youngest site had the highest soil C concentrations. As landscape age increased from 11,500 to 125,000 years, we observed decreasing pH and iron activity ratios which is indicative of increased weathering. The oldest site, Sagwon Hills, was an exception to this trend, likely due to its different parent material (Wang et al. 2019). While we expected active layers would have more poorly crystalline Fe and Al minerals than permafrost soil because they have been subject to more weathering, we found that the opposite. It seems that existing Fe mineral phases undergo state changes due to varying redox conditions in the active layer-permafrost transition zone caused by hydromorphic processes (Barker et al. 2023). Thus, preliminary evidence suggests permafrost-affected soils may be less able to protect OM upon thaw. Our hypothesis on the landscape age gradient was also shown to be incorrect. While there are well documented differences in the pH and cation availability of organic soil along age gradients of Alaska's North Slope (Whittinghill and Hobbie 2011), these patterns do not extend clearly to mineral active layer and permafrost soils.

Three weeks of our incubation has shown that respiration rates in permafrost are higher than in active layers, especially in the exudate treatments. Across ages, the oldest site has the highest respiration rates despite not having intermediate soil C. At the end of the incubation, soil subsamples will be frozen at -80°C for microbial analyses or fractionated into particulate and mineral associated pools by density. A two-pool isotope mixing model of atom fraction values will be applied to separate exudate-derived and native soil C within the respired CO_2, bulk soil, and density fractions. Priming will be calculated as the difference in native C respired from the soils with simulated exudates minus C respired from control soils. We will test how the fate of exudate C—such as the percentage that became mineral associated—and the fate of native soil OC—such as the percentage primed—varies among different extractable Fe and Al concentrations and between active layer and permafrost soil.

References

Barker, A.J., et al. 2023. Iron Oxidation–Reduction Processes in Warming Permafrost Soils and Surface Waters Expose a Seasonally Rusting Arctic Watershed, ACS Earth and Space Chemistry, 7(8), 1479–1495. https://doi.org/10.1021/acsearthspacechem.2c00367

Gentsch, N., et al. 2015. Properties and bioavailability of particulate and mineral-associated organic matter in Arctic permafrost soils, Lower Kolyma Region, Russia, European Journal of Soil Science, 66(4), 722–734. Available at: https://doi.org/10.1111/ejss.12269

Hugelius, G., et al. 2014. Estimated stocks of circumpolar permafrost carbon with quantified uncertainty ranges and identified data gaps, Biogeosciences, 11(23), 6573–6593. https://doi.org/10.5194/bg-11-6573-2014

Jilling, A., et al. 2021. Priming mechanisms providing plants and microbes access to mineral-associated organic matter', Soil Biology and Biochemistry, 158, 108265.https://doi.org/10.1016/j.soilbio.2021.108265

Rasmussen, C., Southard, R.J., and Horwath, W.R. 2007. Soil Mineralogy Affects Conifer Forest Soil Carbon Source Utilization and Microbial Priming, Soil Science Society of America Journal, 71(4), 1141–1150. https://doi.org/10.2136/sssaj2006.0375

Slessarev, E.W., et al. 2022. Rock weathering controls the potential for soil carbon storage at a continental scale', Biogeochemistry, 157(1), 1–13. https://doi.org/10.1007/s10533-021-00859-8

Torn, M.S., et al. 1997. Mineral control of soil organic carbon storage and turnover, Nature, 389(6647), 170–173.

Whittinghill, K.A., and Hobbie, S.E. 2011. Effects of Landscape Age on Soil Organic Matter Processing in Northern Alaska, Soil Science Society of America Journal, 75(3), 907–917. https://doi.org/10.2136/sssaj2010.0318

Methane concentrations and stable carbon isotopes in permafrost cores from western Canadian Arctic

Laura L. Lapham[1], Scott R. Dallimore[2], Peter Morse[3], Jackie Goordial[4] & Lexi Mollica[4]

[1]*Chesapeake Biological Laboratory, University of Maryland Center for Environmental Science, Solomons, Maryland, United States*

[2]*Geological Survey of Canada, Natural Resources Canada, Sydney, British Columbia, Canada*

[3]*Geological Survey of Canada, Natural Resources Canada, Ottawa, Ontario, Canada*

[4]*School of Environmental Sciences, University of Guelph, Guelph, Ontario, Canada*

The Arctic is warming at a pace that is three to four times faster than the rest of the planet (Rantanen et al. 2022). Permafrost responses to climate change include warming and thawing of permafrost, increasing active- layer thickness, and accelerating thermokarst processes such as retrogressive thaw slumping (Kokelj et al. 2017). One consequence of a changing thermal regime of permafrost is the release of dissolved organic carbon which can then be metabolised by soil microbial communities over time to form potent greenhouse gases, carbon dioxide and methane (Schuur et al. 2015).

Whereas many laboratory experiments have focused on understanding what controls these gas production rates (Treat et al. 2015), only a handful have also measured methane residing in the shallow permafrost (e.g., Michaelson et al. 2011). Consequently, there is an inadequate understanding of the methane stored in frozen soils and the fate of this methane when permafrost warms or thaws.

Understanding of the processes, sources, and sinks that govern methane cycling, including the scale of stored methane in the shallow permafrost subsurface, is critical to adequately model atmospheric methane dynamics. Here we report on our investigation of shallow stores of organic matter and methane trapped in various permafrost settings in the Mackenzie Delta region, Northwest Territories, Canada. This project is part of a larger program between Geological Survey of Canada, University of Guelph and University of Maryland Center for Environmental Science focused on understanding the geological, chemical, and biological controls of methane flux in the Mackenzie River Delta region.

METHODS

In August 2021 and 2022, we collected permafrost cores at four sites with different Quaternary histories and surficial geologies (Figure 1). We sampled Holocene-aged deltaic alluvial sediments adjacent to "Lake 520" in the Mackenzie Delta ("Alluvium site"), terrestrial peats overlying Holocene lacustrine deposits at the Permafrost Sentinel Program's Inuvik Peatland ("Terrestrial Peat site") (Ensom et al. 2020), late Wisconsin-aged glacial till deposited at Niglintgak Island ("Glacial Till site"), and Late Wisconsinan glacial outwash sediments at Tuktoyaktuk Island ("Glacial Outwash site"). These sites are in the Inuvialuit Settlement Region, Northwest Territories.

We maintained the permafrost samples in their frozen state from the time of extraction through to delivery at Chesapeake Biological Laboratory, Maryland, United States. Here, frozen cores were sub-sampled every ~10 cm and analyzed to determine methane concentrations, methane stable carbon isotope ratios, gravimetric water contents, bulk densities, and total organic carbon (TOC) concentrations.

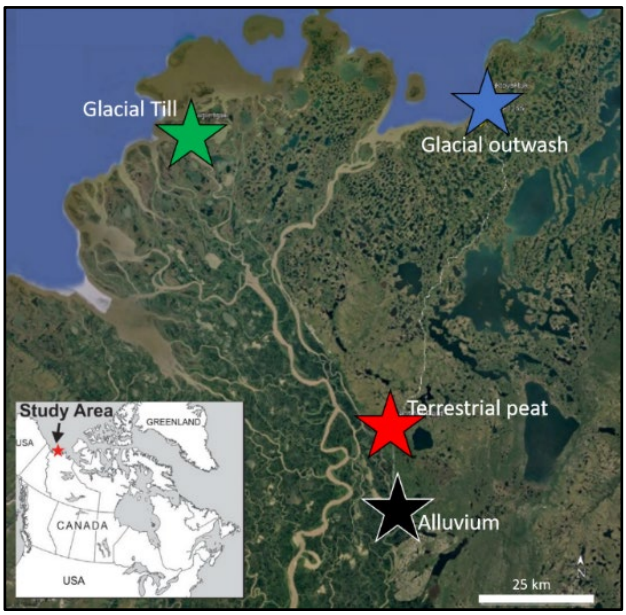

Figure 1. Location of permafrost cores in the Mackenzie River Delta.

Results/Discussion

Despite the varied geological histories, methane concentrations were remarkably high near the top of the permafrost with all sites showing peaks at depths between 50-75 cm below the base of the active layer. Methane concentrations in these frozen soil intervals were consistently above 3 mg kg^{-1} with values reaching 6 mg kg^{-1}. The downcore isotopic composition of this methane ($\delta^{13}C$) averaged -60 ± 7‰ at the Alluvium site, and -68±5‰ in the Terrestrial Peat site. These values suggest a microbial source, being formed through the methanogenic pathway using carbon dioxide (hydrogenotropic) or acetate (acetoclastic) as precursor carbon compounds (data not shown). At the Alluvium site, TOC concentrations are highest at the surface, ~20%, and decrease down core to ~3%. This likely reflects the gradual "stabilization" of the alluvial surface over the Holocene with decreasing frequency of overland sedimentation, vegetative succession, and permafrost aggradation (Gill 1972). In contrast, TOC concentrations were much lower at the Glacial Outwash site, ~5% at the surface and decreased down to 1% at the bottom of the core (Lapham et al. 2021), where initial accumulation of outwash and surface aggradation was likely not accompanied by substantive vegetation succession, but near-surface permafrost likely thawed and re-aggraded in relation to the the Holocene warm interval (Burn 1997). We did not see a strong correlation between TOC and trapped methane, a result which will be further discussed in the presentation.

Conclusions

Whereas the Quaternary histories and surficial geologies of each of our study sites are varied, they share the common trait that methane concentrations are elevated in near-surface permafrost. We suggest that the methane we measured is trapped in permafrost as observed by others (e.g., Michaelson et al. 2011), and that it is likely widespread in other geological settings. We hypothesise that in situ methane is biogenic. It may be sequestered as a result of permafrost aggradation following either surface aggradtion at the Alluvium site or active-layer thinning since the Holocene warm interval at our other sites. Alternatively, the source may be in situ production of methane within ice bonded permafrost at negative temperatures by cold adapted microorganisms. Trapped methane could be released to the atmosphere as the active layer deepens or as permafrost is directly exposed by retrogressive thaw slumping or coastal erosion that are ongoing in the Mackenzie Delta area.

**This is NRCan contribution number 20230399.

References

Burn, C.R. 1997. Cryostratigraphy, paleogeography, and climate change during the early Holocene warm interval, western Arctic coast, canada. Can. J. Earth Sci. 34, 912–925. https://doi.org/10.1139/e17-076

Ensom, T., Morse, P.D., Kokelj, S.V., MacDonald, E., Young, J., Tank, S., Subedi, R., Grozic, E., and Castagner, A. 2020. Permafrost geotechnical borehole data synthesis: 2013–2017.

Inuvik-Tuktoyaktuk region, Northwest Territories. Geological Survey of Canada Open file report 8652.

Gill, D. 1972 The Point Bar Environment in the Mackenzie River Delta. Can. J. Earth Sci. 9, 1382–1393.

Kokelj, S.V., Lantz, T.C., Tunnicliffe, J., Segal, R., and Lacelle, D. 2017. Climate-driven thaw of permafrost preserved glacial landscapes, northwestern Canada. Geology 45, 371–374. https://doi.org/10.1130/G38626.1.

Lapham, L.L., Dallimore, S., Magen, C., Henderson, L.C., Powers, L., Gonsior, M., Clark, B., Cote, M., Fraser, P., and Orcutt, B.N. 2021. Microbial greenhouse gas dynamics associated with warming coastal permafrost, western Canadian Arctic. Frontiers in Earth Sciences. https://doi.org/10.3389/feart.2020.582103.

Michaelson, G.J., Ping, C.L., and Jorgenson, M.T. 2011. Methane and carbon dioxide content in eroding permafrost soils along the Beaufort Sea coast, Alaska. J. Geophys. Res. 116. DOI:10.1029/2010JG001387

Rantanen, M., Karpechko, A.Y., Lipponen, A., Nordling, K., Hyvärinen, O., Ruosteenoja, K., Vihma, T., and Laaksonen, A. 2022. The Arctic has warmed nearly four times faster than the globe since 1979. Communications Earth and Environment 3, 1–10. https://doi.org/10.1038/s43247-022-00498-3

Schuur, E.A.G., McGuire, A.D., Schadel, C., Grosse, G., Harden, J.W., Hayes, D.J., Hugelius, G., Koven, C.D., Kuhry, P., Lawrence, D.M., Natali, S.M., Olfefeldt, D., Romanovsky, V.E., Schaefer, K., Turetsky, M.R., Treat, C.C., and Vonk, J.E. 2015. Climate change and the permafrost carbon feedback. Nature 520, 171–179. DOI:10.1038/nature14338

Treat, C.C., Natali, S.M., Ernakovich, J., Iversen, C.M., Lubascu, M., McGuire, A.D., Norby, R.J., Chowdhury, T.R., Richter, A., Šantrůčková, H., Schädel, C., Schuur, E.A.G., Sloan, V.L., Turetsky, M.R., and Waldrop, M.P. 2015. A pan-arctic synthesis of CH_4 and CO_2 production from anoxic soil incubations. Global Change Biology 21, 2787–2803. https://doi.org/10.1111/gcb.12875

More enhanced non-growing season methane exchanges under warming on the Qinghai-Tibetan Plateau

Zhenhai Liu[1,2], Bin Chen[1], Shaoqiang Wang[1,2,3] & Xiyan Xu[4]

[1]*Key Laboratory of Ecosystem Network Observation and Modeling, Institute of Geographic Sciences and Natural Resources Research, Chinese Academy of Sciences, Beijing, Beijing, China*

[2]*College of Resources and Environment, University of Chinese Academy of Sciences, Beijing, Beijing, China*

[3]*Hubei Key Laboratory of Regional Ecology and Environmental Change, School of Geography and Information Engineering, China University of Geosciences, Wuhan 430078, China*

[4]*Key Laboratory of Regional Climate-Environment for Temperate East Asia, Institute of Atmospheric Physics, Chinese Academy of Sciences, Beijing 100029, China*

Methane (CH_4) has 28 times greater global warming potential than CO_2 over a century and it is the second most impactful greenhouse gas (Shindell et al. 2009). Numerous studies have indicated that climate warming can markedly affect terrestrial ecosystem CH_4 exchanges, producing positive or negative feedbacks on the rate of climate warming (Wang et al. 2022; Yvon-Durocher et al. 2014; Zona et al. 2016). Understanding the response of ecosystem CH_4 exchanges is therefore crucial for assessing and predicting biosphere-atmosphere feedback in a warming world. Qinghai-Tibetan Plateau (QTP) soils have large carbon stocks, with >48 Pg carbon estimated in the top 1 m of soil (Chen et al. 2022). Nevertheless, whether the QTP operates as a CH_4 sink or source and its magnitude still have no consistent conclusion (Wang et al. 2014; Wei and Wang 2017). The uncertainties of CH_4 exchange across the wetlands and grasslands, crucial sources and sinks of CH_4 on the QTP, has increased due to the continuous degradation of permafrost and the asymmetrical seasonal warming (Bibi et al. 2018). Temperature plays a vital role in regulating CH_4 exchange, yet the seasonal patterns of temperature dependencies for CH_4 fluxes over the wetlands and grasslands on the QTP remain poorly understood (Li et al. 2023; Wang et al. 2014; Zhang et al. 2019).

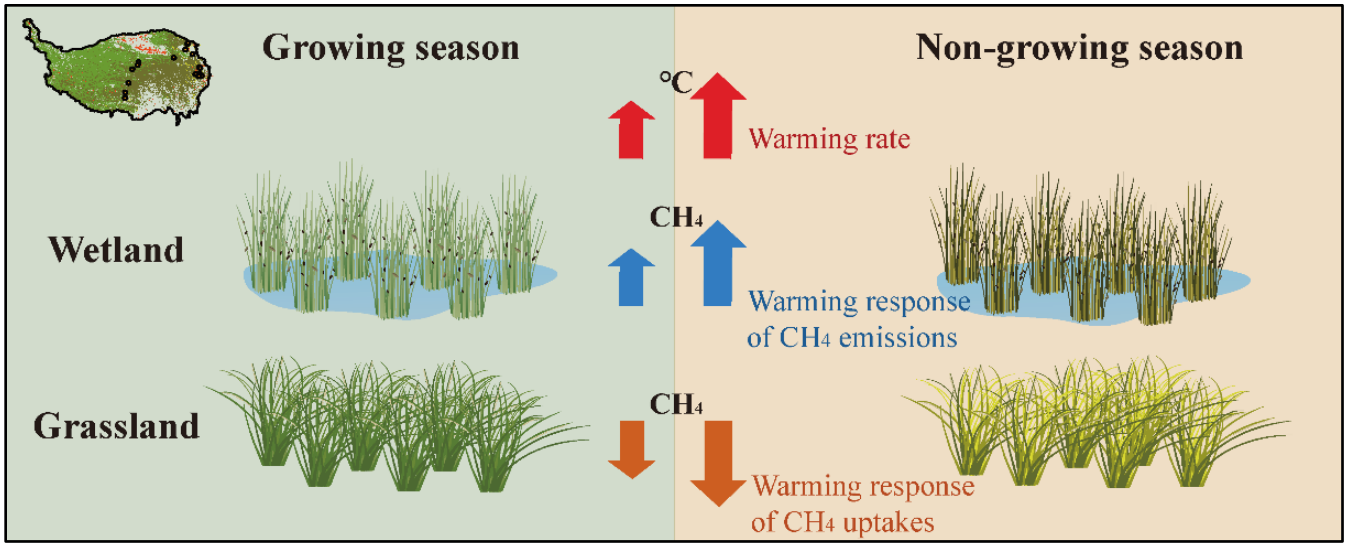

Figure 1. Asymmetric warming and responses of CH_4 exchange jointly regulate QTP being an ecosystem CH_4 source or sink.

Here, we demonstrated a stronger warming response of CH_4 exchanges during the non-growing season compared to the growing season on the QTP (Figure 1). We obtained 9,745 daily observations of CH_4 fluxes from 27 sites across the QTP, encompassing both wetlands and grasslands. The seasonality of CH_4 exchange warming responses in QTP wetlands and grasslands was analyzed based on four methods: regression fitting of temperature-CH_4 flux, temperature dependence calculations based on Boltzmann–Arrhenius functions (Yvon-Durocher et al. 2014), field-based and model-based control experiments. We found that warming intensified CH_4 emissions in wetlands and uptakes in

grasslands. Specifically, the average reaction intensity in the non-growing season surpasses that in the growing season by 1.89 and 4.80 times, respectively. The temperature-driven CH_4 exchange on the QTP displayed different seasonal patterns than global wetlands (Figure 2), which exhibiting stronger dependencies during the warmer growing season (Li et al. 2023). This stronger warming response of CH_4 exchanges during the non-growing season significantly increases the regional CH_4 exchange on the QTP.

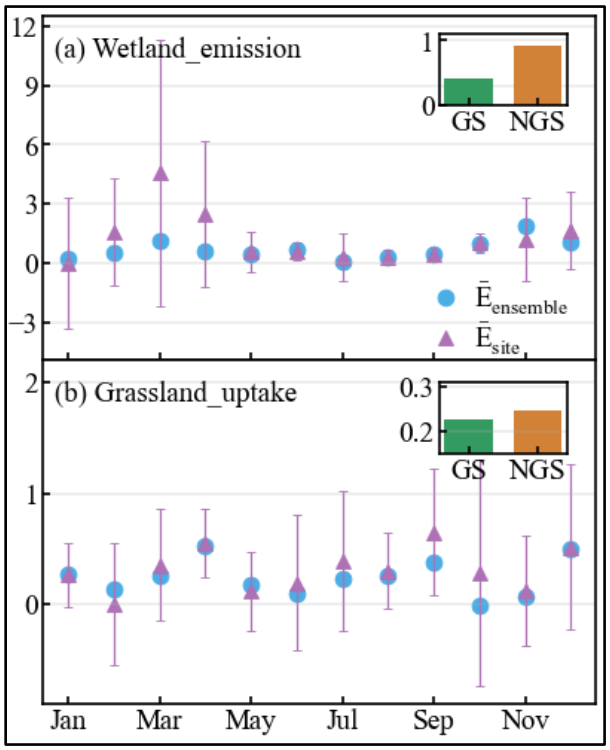

Figure 2. Monthly patterns of the temperature dependence of CH_4 exchanges for ensemble and site level. The bar plot represents the mean activation energy across all sites during growing (GS) and non-growing (NGS) seasons, respectively.

The QTP experiences rapid and asymmetric warming, escalating at 0.4°C per decade over 50 years, with winter warming doubling the annual average (Chen et al., 2022). Our research highlights that non-growing season in the QTP have a stronger warming sensitivity of CH_4 exchanges and a higher warming rate than the annual average. The combined effects of these two factors will significantly alter the CH_4 source/sink on the QTP. Neglecting these impacts would lead to inaccurate estimations of CH_4 source/sink over the QTP under climate warming.

Acknowledgements

We thank the researchers at all stations across the Qinghai-Tibetan Plateau for their work under the harsh climate and efforts to make their datasets publicly accessible. Their contributions regarding the establishment and maintenance of the eddy covariance and manipulative experiments made this study possible.

References

Bibi, S., Wang, L., Li, X., et al. 2018. Climatic and Associated Cryospheric, Biospheric, and Hydrological Changes on the Tibetan Plateau: a Review, International Journal of Climatology, 38(S1): e1–e17. doi:10.1002/joc.5411

Chen, H., Ju, P., Zhu, Q., et al. 2022. Carbon and Nitrogen Cycling on the Qinghai–Tibetan Plateau, Nature Reviews Earth & Environment, 3(10): 701–716. doi:10.1038/s43017-022-00344-2

Li, J., Pei, J., Fang, C., et al. 2023. Opposing Seasonal Temperature Dependencies of CO2 and CH4 Emissions from Wetlands, Global Change Biology, 29(4): 1133–1143. doi:10.1111/gcb.16528

Shindell, D.T., Faluvegi, G., Koch, D.M., et al. 2009. Improved Attribution of Climate Forcing to Emissions, Science, 326(5953): 716–718. doi:10.1126/science.1174760

Wang, P., Wang, J., Elberling, B., et al. 2022. Increased Annual Methane Uptake Driven by Warmer Winters in an Alpine Meadow, Global Change Biology, 28(10): 3246–3259. doi:10.1111/gcb.16120

Wang, Y., Chen, H., Zhu, Q., et al. 2014. Soil Methane Uptake by Grasslands and Forests in China, Soil Biology and Biochemistry, 74: 70–81. doi:10.1016/j.soilbio.2014.02.023

Wei, D., and Wang, X. 2017. Recent Climatic Changes and Wetland Expansion Turned Tibet into a Net CH4 Source, Climatic Change, 144(4): 657–670. doi:10.1007/s10584-017-2069-y.

Yvon-Durocher, G., Allen, A.P., Bastviken, D., et al. 2014. Methane Fluxes Show Consistent Temperature Dependence across Microbial to Ecosystem Scales, Nature, 507(7493): 488–491. doi:10.1038/nature13164

Zhang, H., Yao, Z., Ma, L., et al. 2019. Annual Methane Emissions from Degraded Alpine Wetlands in the Eastern Tibetan Plateau, Science of The Total Environment, 657: 1323–1333. doi:10.1016/j.scitotenv.2018.11.443

Zona, D., Gioli, B., Commane, R., et al. 2016. Cold Season Emissions Dominate the Arctic Tundra Methane Budget, Proceedings of the National Academy of Sciences of the United States of America, 113(1): 40–45. doi:10.1073/pnas.1516017113

Greenhouse gas emissions detected from degrading Arctic permafrost

Lexi Mollica[1], Laura Lapham[2], Claudia Wood[1], Peter Morse[3], Scott Dallimore[4] & Jackie Goordial[1]

[1]*School of Environmental Sciences, University of Guelph, Guelph, Ontario, Canada*

[2]*Chesapeake Biological Laboratory, University of Maryland Center for Environmental Science, Solomons, Maryland, United States*

[3]*Geological Survey of Canada, Natural Resources Canada, Ottawa, Ontario, Canada*

[4]*Geological Survey of Canada, Natural Resources Canada, Sydney, British Columbia, Canada*

Permafrost stores approximately ~50% of soil organic carbon on Earth, and is rapidly degrading in the Arctic (IPCC 2013). Permafrost thaw is a source of greenhouse gases (GHGs) such as carbon dioxide (CO_2) and methane (CH_4), as permafrost microbiota metabolize newly available organic carbon and produce GHGs. This may create a positive feedback cycle that could accelerate climate warming (Schuur et al. 2015). Whereas CO_2 is the most abundant atmospheric GHG, CH_4 has 28 times higher warming potential on a 100-year timescale (IPCC 2013) and is a GHG of concern in permafrost settings.

Incubation experiments on carbon-cycling with permafrost degradation are typically carried out at temperatures >0°C (Schädel et al. 2016; Knoblauch et al. 2018). However, cold-adapted microbiota can actively grow at temperatures as low as -15°C and respire in even colder conditions (Mykytczuk et al. 2013). Additionally, permafrost can release GHGs at sub-zero temperatures (Rivkina et al. 2007; Lapham et al. 2020). Here, we test the hypothesis that ground warming alone may initiate or increase cycling and emission of GHGs from permafrost.

Methodology

Alluvial permafrost cores (3" diameter) were collected in August 2021 near the boundary of the Inuvialuit and Gwitch'in Settlement Regions of the Northwest Territories, Canada (68°18'51.2"N, 133°42'50.9"W). Sediments consisted of organic-rich silts with a 40-cm thick active layer. To determine microbial-mediated flux changes, long-term (>1 year) incubations were carried out on the upper 27 cm of the core at temperatures relevant to permafrost warming and thaw: -8°C, -5°C, and 0°C. Frozen plugs were used to preserve in-situ permafrost structure. Incubations, including autoclaved killed controls, were regularly sampled and CH_4 was measured via gas chromatography. Trapped (in situ) soil CH_4 was also measured.

We additionally carried out highly sensitive radiorespiration assays using 14C labelled acetate (Wood et al. 2023). We incubated samples from the top 5 cm of a replicate permafrost core at -5°C to measure CO_2 production by heterotrophic microbes.

Results and Discussion

We measured trapped CH_4 in all permafrost samples, congruent with the findings of others that permafrost can act as a methane reservoir (Rivkina et al. 2007; Lapham et al. 2020; Michaelson et al. 2011). During anaerobic incubation at 0°C, CH_4 production continuously increased over time and exceeded trapped concentrations after 147 days, suggesting active cryophilic microbial methanogenesis (Figure 1).

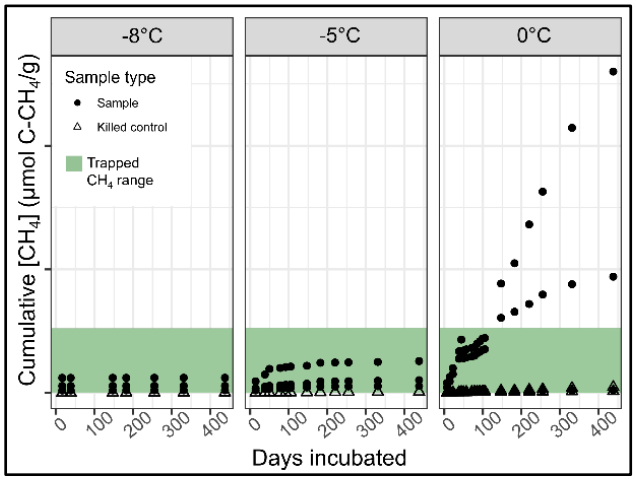

Figure 1. Cumulative sub-zero CH_4 flux from permafrost microcosms. Shaded green area represents range of trapped CH_4 concentrations from all replicate samples.

Incubations at -5°C and -8°C produced low but measurable CH_4 concentrations, plateauing below trapped CH_4 values. This may indicate that CH_4 released at -5°C and -8°C is dominated by gradual off-gassing of trapped CH_4 rather than by new microbial production, as previous studies have reported release of trapped CH_4 during incubation (Rivkina et al. 2007; Mackelprang et al. 2011). It may be that methanogenic microbiota in permafrost are not actively producing CH_4 at these lower temperatures, or that rates of methanogenesis are too low to be detected using these methods.

Aerobic radiorespiration assays by Wood et al. (2023) confirm microbial respiration at -5°C, though the rates were low (10% mineralization after 300 days) and followed a lag phase of ~150 days. In contrast, respiration at 0°C was immediate, and ~50% of the carbon had been mineralised within a year (Figure 2). These data show that permafrost microbiota are active and produce CO_2 at sub-zero temperatures. Thus, labelled substrate addition experiments may facilitate quantification of microbial GHG production in permafrost when rates are low.

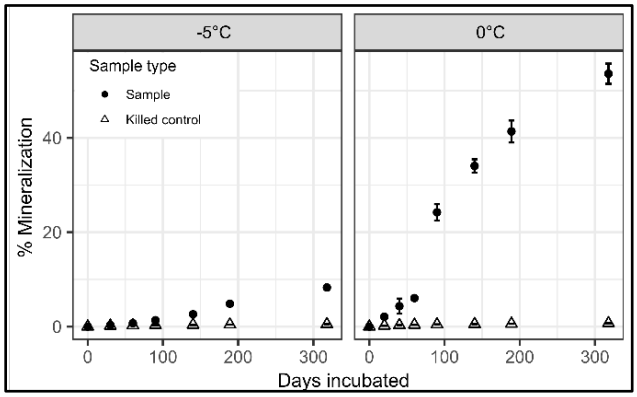

Figure 2. Sub-zero mineralization of radiolabelled acetate to CO_2.

Conclusions

We show that degrading permafrost can emit CH_4 (trapped or newly produced) before complete thaw. We also show that microbiota resident in this alluvial permafrost are active at cryotic temperatures: CO_2 was produced at 0°C and -5°C and CH_4 production was detected at 0°C. Methane emissions were detectable by gas chromatography at -5°C and -8°C, but we attribute this to release of trapped CH_4 overriding signal from new, microbial production. Microbial CO_2 production detected using radiorespiration assays suggests that this approach could be adapted to improve detection of CH_4 from permafrost with previously trapped gas.

Cold-adapted microbiota may be slowly cycling carbon within cryotic ground and potentially accumulating GHGs in permafrost over millennia. Therefore the total influence of permafrost warming and thaw on global carbon cycles is likely underestimated. Elucidating the fate of carbon in warming but still cryotic permafrost is essential to accurately model the permafrost-carbon feedback.

References

IPCC. 2013. Climate Change 2013: The Physical Science Basis, Contribution of Working Group I to the Fifth Assessment Report of the Intergovernmental Panel on Climate Change, Stocker, T.F., Qin, D., Plattner, G.K., Tignor, M., Allen, S.K., Boschung, J., Nauels, A., Xia, Y., Bex, V. and Midgley, P.M. (eds.), Cambridge University Press, Cambridge, United Kingdom and New York, NY, USA.

Knoblauch, C., Beer, C., Liebner, S., Grigoriev, M.N., and Pfeiffer, E.M. 2018. Methane Production as Key to the Greenhouse Gas Budget Of Thawing Permafrost, Nature Climate Change, 8, 309–312. doi:10.1038/s41558-018-0095-z

Lapham, L.L., Dallimore, S.R., Magen, C., Henderson, L.C., Powers, L.C., Gonsior, M., Clark, B., Côté, M., Fraser, P., and Orcutt, B.N. 2020. Microbial Greenhouse Gas Dynamics Associated with Warming Coastal Permafrost, Western Canadian Arctic, Frontiers in Earth Science, 8, 582103. doi:10.3389/FEART.2020.582103

Mackelprang, R., Waldrop, M., DeAngelis, K., David, M.M., Chavarria, K.L., Blazewicz, S.J., Rubin, E.M., and Jansson, J.K. 2011. Metagenomic Analysis of a Permafrost Microbial Community Reveals a Rapid Response to Thaw. Nature 480, 368–371. doi:10.1038/nature10576

Michaelson, G.J., Ping, C.L., and Jorgenson, M.T. 2011. Methane and Carbon Dioxide Content in Eroding Permafrost Soils Along the Beaufort Sea Coast, Alaska, Journal of Geophysical Research,116, G01022. doi:10.1029/2010JG001387

Mykytczuk, N.C., Foote, S.J., Omelon, C.R., Southam, G., Greer, C.W., and Whyte, L.G. 2013. Bacterial Growth at -15°C; Molecular Insights from the Permafrost Bacterium Planococcus halocryophilus Or1, The ISME Journal, 7, 1211–1226. doi:10.1038/ismej.2013.8

Rivkina, E., Shcherbakova, V., Laurinavichius, K., Petrovskaya, L., Krivushin, K., Kraev, G., Pecheritsina, S., and Gilichinsky, D. 2007. Biogeochemistry of Methane and Methanogenic Archaea in Permafrost, FEMS Microbiology Ecology, 61(1), 1–15. doi:10.1111/J.1574-6941.2007.00315.X

Schuur, E.A.G., McGuire, A.D., Schädel, C., Grosse, G., Harden, J.W., Hayes, D.J., Hugelius, G., Koven, C. D., Kuhry, P., Lawrence, D.M., Natali, S.M., Olefeldt, D., Romanovsky, V.E., Schaefer, K., Turetsky, M.R., Treat, C.C., and Vonk, J.E. 2015. Climate Change and the Permafrost Carbon Feedback, Nature, 520, 171–179. doi:10.1038/nature14338

Schädel, C., Bader, M.F., Schuur, E., et al. 2016. Potential Carbon Emissions Dominated by Carbon Dioxide from Thawed Permafrost Soils, Nature Climate Change 6, 950–953. doi:10.1038/nclimate3054

Wood, C., Bruinink, A., Trembath-Reichert, E., Wilhelm, M.B., Vidal, C., Balaban, E., McKay, C.P., Swan, R., Swan, B., and Goordial, J. In press. Active Microbiota Persist in Dry Permafrost and Active Layer from Elephant Head, Antarctica, ISME Communications.

Near-ground aerial surveys and ground-level stationary measurements of methane in a variety of geological settings in the Mackenzie Delta, NT

Jalal Norooz Oliaee[1], Roger MacLeod[2], Chase Sun[1], Laura Lapham[3], Scott Dallimore[2] & Peter Morse[4]

[1]*Metrology Research Centre, National Research Council Canada, Ottawa, Ontario, Canada*

[2]*Geological Survey of Canada, Natural Resources Canada, Sydney, British Columbia, Canada*

[3]*Chesapeake Biological Laboratory, University of Maryland Center for Environmental Science, Solomons, Maryland, United States*

[4]*Geological Survey of Canada, Natural Resources Canada, Sydney, British Columbia, Canada*

Methane (CH_4) has more than 28 times the global warming potential as a greenhouse gas (GHG) than carbon dioxide (CO_2). Consequently, a global effort has recently gained momentum to reduce anthropogenic CH_4 emissions, yet the role of natural sources and sinks of CH_4 is also of great importance. Most notably, Arctic wetlands and permafrost are thought to store enormous amounts of carbon (ECCC 2022), some of which may release CO_2 and CH_4 as climate warms to create positive climate feedback (Schuur et al. 2015). The western Canadian Arctic is experiencing warming that is about three times the global average (Rantanen et al. 2022), but major knowledge gaps exist about the response of thawing permafrost. One of these is an understanding of natural processes releasing CH_4 and challenges related to the quantification of atmospheric flux given the vast and diverse geologic and permafrost settings.

The research discussed in this presentation has been advanced through a collaboration between the Geological Survey of Canada, the universities of Guelph and Maryland and the National Research Council Canada. Our goals are to assess natural sources of CH_4 emissions and appraise their magnitudes in the western Canadian Arctic over different spatial and temporal scales.

This presentation reviews near-ground aerial helicopter surveys using commercial and newly-developed CH_4 sensors, field trials of a newly developed sensor that was mounted on an uncrewed aerial vehicle (UAV), and observations from multi-day stationary monitoring of atmospheric CH_4 concentrations in an area with known hot spots of permafrost CH_4 emissions.

Study Area

Our research was conducted in the Inuvialuit Settlement Region over different geological and permafrost settings to identify regional trends in atmospheric CH_4 concentrations and assess CH_4 hotspots related to active permafrost processes. We are also striving to improve near-surface survey techniques to provide ground-truthing capabilities for airborne surveying (Kohnert et al. 2017; Miller et al. 2019; Barton-Grimley et al. 2022). Our research was conducted in three varied settings in the Mackenzie Delta region: (i) the thin permafrost (<80 m) of the modern Mackenzie Delta, (ii) thicker permafrost (~250-600 m) associated with the Caribou Hills where exposed Tertiary sediments outcrop at the surface, and (iii) across Richards Island comprised of Quaternary and Holocene sediments. Continuous station measurements were conducted in an area of the outer delta where both thermogenic and biogenic CH_4 hot spots had been previously observed (Wesley et al. 2022).

Near-Ground Helicopter-Based Surveys

Near-ground helicopter-based surveys were performed at altitudes between 40 and 250 m above ground level using a Bell 206 LongRanger II (Figure 1). A sampling line (¼" O.D.) was attached to the bottom of the aircraft's nose to sample undisturbed air using a commercially available integrated cavity output spectroscopy-based $CH_4/CO_2/H_2O$ gas analyzer (LGR/ABB, USA), as well as a developmental mid-infrared tunable diode laser absorption spectroscopy-based CH_4/H_2O sensor (Norooz Oliaee et al. 2022), but with an enclosed sample cell. Both instruments feature single-digit parts-per-billion (ppb) resolution.

Helicopter surveys transiting deltaic terrain from Inuvik to the outer delta confirmed a consistent increase of about 100 ppb in low-elevation CH_4 concentrations. A regional increase in concentration was also observed across the outer delta from east to west. At a more detailed scale, we also documented small-scale variability in CH_4 concentrations that were related to geomorphic, geologic, and permafrost features and boundaries including a CH_4 seep, thaw slides, and transitions from the modern delta to the Caribou Hills and Richards Island. Additionally, anthropogenic hotspots of CH_4 were identified including a decommissioned gas facility, a landfill, and a sewage lagoon.

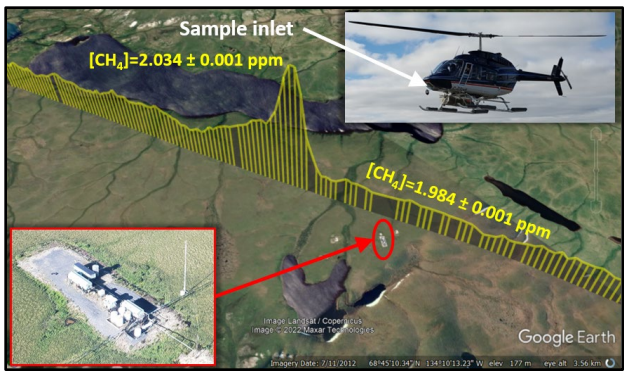

Figure 1. Elevated CH_4 concentration at the Ikhil gas field (68.7431° N, 134.1496° W), as detected by helicopter-based in-situ instruments on 31 July 2022.

Multi-day ground-based stationary monitoring

To study the temporal variability of background CH_4 concentration in the outer Mackenzie Delta away from possible urban emissions, an open-path mid-infrared laser spectroscopy-based CH_4 sensor was stationed for more than five days at a previously identified hot spot of CH_4 emissions (see Figure 2, left). The acquired time series data revealed a considerable increase in local CH_4 concentrations from background levels to values exceeding 5 ppm. The high values were observed during episodes of calm atmospheric conditions, suggesting a significant nearby CH_4 source likely associated with aquatic gas seeps.

Near-surface UAV-based surveys

An ultra-lightweight (<1 kg) laser spectroscopy-based CH_4 sensor with a fast response time of 10 ms in an open-path configuration was developed for UAV deployment. The sensor was deployed atop a DJI Matrice 300 RTK platform. UAV survey missions were carried out downwind of a known natural CH_4 point source and at the edge of a retrogressive thaw slump both to the west of Richards Island. Flight transects across the CH_4 plume allowed its boundaries to be mapped and enabled the estimation of the emission rate. Flights near the headwall of a retrogressive thaw slump identified slightly elevated (≈ 100 ppb) CH_4 concentrations which may be attributed to the release of biogenic CH_4 from the exposed permafrost.

Conclusions and outlook

This work presents the identification of regional spatial and local temporal trends in background CH_4 concentrations in the western Canadian Arctic, and technology development for estimating magnitudes of CH_4 flux. However, it is acknowledged that the subject of CH_4 emissions from thawing permafrost remains poorly understood, stressing the importance of developing and carrying out further measurements to better attribute sources of emissions in complex aquatic-terrestrial permafrost environments.

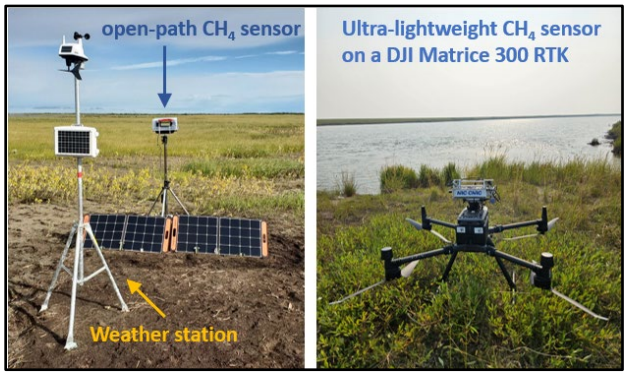

Figure 2. Open-path CH_4 instrument and weather station for multi-day monitoring of concentrations (left). Ultra-lightweight CH4 sensor on DJI Matrice 300 RTK platform beside a gas seepage (right).

References

Barton-Grimley, R.A., et al. 2022. Evaluation of the High Altitude Lidar Observatory (HALO) methane retrievals during the summer 2019 ACT-America campaign, Atmospheric Measurement Techniques, 15(15): 4623–4650. doi:10.5194/amt-15-4623-2022

Environment and Climate Change Canada. 2022. Faster and Further: Canada's Methane Strategy. Accessed December 8, 2023 at https://publications.gc.ca/site/eng/9.915545/publication.html

Kohnert, K., et al. 2017. Strong geologic methane emissions from discontinuous terrestrial permafrost in the Mackenzie Delta, Canada, Scientific Reports, 7(1): 3–8. doi:10.1038/s41598-017-05783-2

Miller, C.E., et al. 2019. An overview of above airborne campaign data acquisitions and science opportunities, Environmental Research Letters, 14(8): 080201. doi:10.1088/1748-9326/ab0d44

Norooz Oliaee, J., et al. 2022. Development of a Sub-ppb Resolution Methane Sensor Using a GaSb-Based DFB Diode Laser near 3270 nm for Fugitive Emission Measurement, ACS Sensors, 7(2): 564–572. doi:10.1021/acssensors.1c02444

Rantanen, M., et al. 2022. The Arctic has warmed nearly four times faster than the globe since 1979, Communications Earth and Environment, 3(1): 1–10. doi:10.1038/s43247-022-00498-3

Schuur, E.A.G., et al. 2015. Climate change and the permafrost carbon feedback, Nature, 520(7546): 171–179. doi:10.1038/nature14338

Wesley, D., et al. 2022. Characterization of atmospheric methane release in the outer Mackenzie River Delta from biogenic and thermogenic sources, EGUsphere [preprint]. https://doi.org/10.5194/egusphere-2022-549

Assessing carbon decomposition dynamics in permafrost peatlands along a 60-year thaw gradient in Northern Norway

Anfisa Pismeniuk[1,2], Peter Dörsch[2,3], Sigrid Trier Kjær[2,3], Mats Ippach[1,2], Norbert Pirk[1,2] & Sebastian Westermann[1,2]

[1]*Department of Geosciences, University of Oslo, Oslo, Norway*

[2]*Centre for Biogeochemistry in the Anthropocene, University of Oslo, Norway*

[3]*Faculty of Environmental Sciences and Natural Resource Management, Norwegian University of Life Sciences, Ås, Norway*

A significant portion of today's permafrost carbon is stored within peat deposits (Hugelius et al. 2020), primarily located along the southern permafrost boundary. In these regions, ground temperatures are already at or near the thawing point, but the insulating effect of a thick organic cover slows the degradation, so that permafrost peat is often referred to as "ecosystem-protected". However, thermokarst processes driven by melting ground ice serve as a major thaw pathway, transforming dry permafrost peat plateaus into permafrost-free mires and bogs. In Scandinavia, permafrost peatlands are expected to largely disappear within the next two to three decades, given current degradation dynamics (Borge et al. 2017). Given the large carbon pool, decomposing peat may trigger significant additional greenhouse gas (GHG) emissions that could further amplify warming. The true decomposition processes occurring after thawing remain unclear, particularly over the decadal to centennial timescales relevant for climate feedbacks. Although the decomposability of permafrost has been investigated in laboratory incubation studies (Elberling et al. 2015; Knoblauch et al. 2018), it is uncertain to what extent these findings are applicable to natural conditions, especially considering their limited time frame of only a few months to a few years. This research addresses this uncertainty through a space-for-time substitution, employing a chronosequence approach along an in-situ thawing gradient of peat plateaus in Northern Norway.

This study focuses on two peat plateaus, Iškoras and Áidejávri, situated in the sporadic permafrost zone in Finnmark, Northern Norway. These peatlands, originally formed as wet fens, have remained permafrost-free for most of the Holocene, with permafrost aggradation occurring during the last millennium (ca. 950–100 cal. yr BP) possibly related to the cooler climatic conditions of the Little Ice Age (Kjellman et al. 2018).

During fieldwork in September 2023, we collected 20 peat cores along four thaw transects. Each core has experienced thawing throughout the past 60 years, either decades ago and more recently. Thermokarst cores were categorized as fresh peat, former active layer, or former permafrost, providing a basis for comparison with permafrost peat in intact peat plateaus. The location of sampling points and the borders of the former peat plateaus in 1955 and 2017 for the Iškoras transect are illustrated in Figure 1.

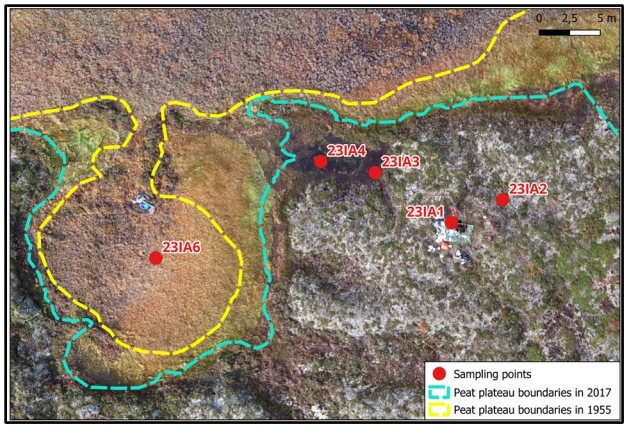

Figure 1. Sampling points location of the one thaw transect in Iškoras, Northern Norway.

To evaluate the dynamics of carbon decomposition in permafrost peatlands, we are conducting incubation experiments with subsamples from all sampled layers (active layer, permafrost peat, thermokarst deposits, mire) in 120 ml serum bottles under oxic and anoxic conditions at 10 °C, using an incubator with automated gas analysis (Molstad et al. 2016). Chemical analyses performed before and after ~1 year incubation include pH, dissolved organic carbon (DOC), elemental composition, and stable isotope ratios of carbon (C) and nitrogen (N).

We hypothesize that i) permafrost peat decomposability and methanogenetic potential increase along the thaw gradient and ii) that mixing of organic material during peat plateau collapse promotes permafrost peat decomposition through carbon priming. Results from the first few weeks of incubation indicate that carbon degradation is markedly inhibited in the absence of oxygen, while there are significant variations in initial respiration rates under aerobic conditions across different peat layers and transects. The highest CO_2 production is observed

in surface samples, including active layer and thermokarst cores, generally decreasing with depth. The exception is deep former permafrost samples in thermokarst cores, showing larger production than former active layer samples, thus supporting the hypothesis that permafrost carbon degradation depends on priming. Intact permafrost samples display the smallest CO_2 production so far. CH_4 production is small and limited to some permafrost samples and deep thermokarst layers.

The collected field and laboratory data on carbon mobilization rates from peat plateaus in Scandinavia can improve our understanding of the carbon cycle in this important permafrost system which can finally contribute to testing and improving the representation of carbon cycling in Earth System Models (ESMs).

REFERENCES

Borge, A.F., Westermann, S., Solheim, I., and Etzelmüller, B. 2017. Strong degradation of palsas and peat plateaus in northern Norway during the last 60 years, The Cryosphere, 11, 1–16. doi:10.5194/tc-11-1-2017

Elberling, B., Michelsen, A., Schädel, C., Schuur, E.A., Christiansen, H.H., Berg, L., Tamstorf, M.P., and Sigsgaard, C. 2013. Long-term CO_2 production following permafrost thaw, Nature Climate Change, 3, 890–894. doi:10.1038/nclimate1955

Kjellman, S.E., Axelsson, P.E., Etzelmüller, B., Westermann, S., and Sannel, A.B.K. 2018. Holocene development of subarctic permafrost peatlands in Finnmark, northern Norway, The Holocene, 28 (12), 1855–1869. doi:10.1177/0959683618798126

Knoblauch, C., Beer, C., Liebner, S., Grigoriev, M.N., and Pfeiffer, E.M. 2018. Methane production as key to the greenhouse gas budget of thawing permafrost, Nature Climate Change, 8, 309–312. doi:10.1038/s41558-018-0095-z

Molstad, L., Dörsch, P., and Bakken, L.R. 2007. Robotized incubation system for monitoring gases (O_2, NO, N_2O N_2) in denitrifying cultures, Journal of Microbiological Methods, 71 (3): 202–211. doi:10.1016/j.mimet.2007.08.011

Methane production in a coastal permafrost region of the Canadian Arctic (Tuktoyaktuk, NWT)

Alexie Roy-Lafontaine[1], Rebecca Lee[2], Dustin Whalen[2], Peter Douglas[3] & André Pellerin[1]

[1]*Institut des sciences de la mer, Université du Québec à Rimouski, Rimouski, Québec, Canada*

[2]*Geological Survey of Canada, Natural Resources Canada, Dartmouth, Nova Scotia, Canada*

[3]*Department of Earth and Planetary Sciences, McGill University, Montréal, Québec, Canada*

Arctic coastal ecosystems are affected by sea level rise, erosion and land submersion, which alters sediment dynamics and organic matter (OM) fluxes along the land-ocean continuum (Tanski et al. 2021). In the Tuktoyaktuk coastlands of the North-West Territories (Canada), retreat rates exceed -4 m/yr due to ground subsidence and submersion, resulting in waterlogged environments (Costa 2022). In waterlogged conditions, the progressive thawing of permafrost exposes long-frozen OM to microbial decomposition, releasing methane (CH_4) (Lapham et al. 2020). The drivers of biogenic greenhouse gas production in sediments are relatively well understood in terrestrial environments but their controls in actively changing landscapes, remain uncertain. This is particularly true in coastal environments with continuous permafrost, where high erosion rates and interaction with seawater strongly influence biogeochemistry and organic matter degradation.

In the Tuktoyaktuk coastlands, inundated tundra flats and polygons dominate the 831 km of coastline (Costa 2022). Ice-wedge polygons are interspersed with lower-lying, wet channels (throughs), underlained by peat deposits and ground ice structures (Martin 2018). Polygons can be categorized as low-centered or as high-centered. These microtopographic formations exhibit significant thermal, hydrological and geochemical gradients (Vaughn et al. 2016). Land submersion by seawater can influence geochemistry, which in turn modifies the microbial communities and organic matter degradation rates. In particular, sulfate anions that are present in seawater cause sulfate reduction to competitively inhibit methanogenesis. This research investigated the impact of seawater on organic matter degradation in this terrain and explores the feasibility of quantifying CH_4 production. The aim was to apply these findings at the landscape level to bridge the knowledge gap in coastal CH_4 biogeochemistry.

Methods

The study was carried out on cores collected from the active layer of an intertidal zone (Toker Point (TP), n=3) and an inland area (Reindeer Point (RP), n=4, about 750 m from coast). Basic environmental parameters such as vegetation type, active layer depth, and waterlogged conditions were assessed in the field. The type of vegetation present can provide insights on the type of organic carbon inputs to soil microbial communities. Both TP and RP featured polygonal terrain, with one low-centered polygon and through sampled at each site. One high-centered polygon was sampled at TP, two were sampled at RP.

Cores were subsampled at intervals of 5 to 10 cm depth, according to shifts in sedimentary units. In the field, samples from each depth were distributed to four 20 mL glass vials with blue butyl rubber stoppers and flushed with N_2 gas to remove oxygen. Anoxic brackish water (collected from the coast) was added to each vial to simulate saltwater input in the coastal sediments. Three vials per depth were used to account for natural variability within each sample. Vials were kept at 4 °C. To understand the variability in CH_4 production within each depth of each site, CH_4 production rates were derived from the accumulation of CH_4 in the headspace over time (Pellerin et al. 2022). These were then integrated over the depth of the active layer. $\delta^{13}C$-CH_4 was measured in the incubation to identify the methanogenesis pathways used by the microbial communities.Geochemical analyses of organic carbon and anions in sediments supported the incubations.

Results and discussion

Sediments from the active layer at the coastal site (TP), produced more CH_4 than the inland site (RP), despite this inland site having a higher concentration in organic carbon (Table 1). It may be due to more recalcitrant organic matter at RP. This is indicated by more negative isotopic signature of ^{13}C-CH_4 (Figure 1), which signals a preferentially hydrogenotrophic pathway for methanogenesis, characteristic of sites with recalcitrant organic carbon (Heffernan et al. 2014). Contrarily, at TP, the coastal site, lower amounts but more labile organic matter in the sediments enhanced CH_4 production. More labile organic matter is indicated by less negative ^{13}C-CH_4 which signals a preferentially acetoclastic pathway for methanogensis, characteristic of sites with labile organic carbon (Heffernan et al. 2014).

Table 1. Intervals of organic carbon, sulfate concentrations and CH_4 production rates for the active layer of the sampled landforms.

Geomorphological forms	C_{org} (% wt.)	SO_4^{2-} (mmol L^{-1})	CH_4 (mmol m^{-2} yr^{-1})
Toker Point (coastal)			
Low-centered polygon (n=3)	2.9 – 4.7	0.3 - 12	17 ± 3.0
Through (n=3)	2.5 – 32	0.07 – 0.8	28 ± 7.4
High-centered polygon (n=3)	30 - 37	0.09 – 3.2	41.5 ± 6.9
Reindeer Point (inland)			
Low-centered polygon (n=3)	37 - 46	0 – 0.1	2.4 ± 1.0
Through (n=3)	39 - 42	0.07 – 0.3	5.0 ± 2.0
High-centered polygon (n=3)	10 - 47	0.07 – 0.2	0.2 ± 0.1

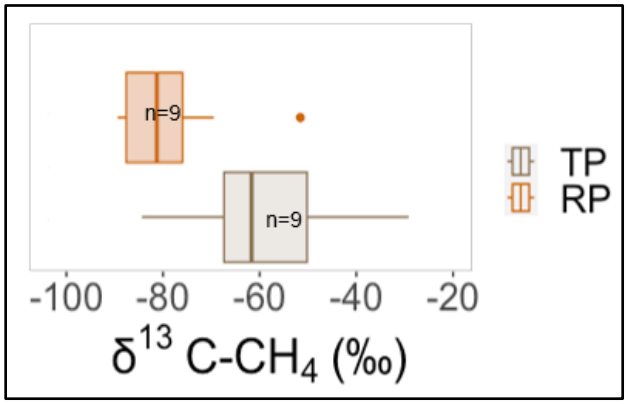

Figure 1. Active layer signature of ^{13}C-CH_4 produced in incubation at Toker Point (coastal) and Reindeer Point (RP).

Sites with a coastal influence thus may produce more CH_4 than inland sites because of more labile organic substrates. This could be due to the presence of a different flora of carex and sedges at TP, which degrade rapidly (Hobbie 1996). Alternatively, a marine input of organic matter from intermittent seawater immersion at the coastal site may also provide an unaccounted source of labile organic matter which could account for higher production rates at TP. However, stable carbon isotopic measurements of organic carbon at TP did not indicate a marine signature for bulk organic matter (data not shown).

Interestingly, CH_4 production did not seem inhibited by the presence of SO_4^{2-} in the incubations. Samples contained a large range of SO_4^{2-} concentrations (Table 1). However, brackish water with a SO_4^{2-} concentration of 5.7 mmol/L was added to all incubations. High CH_4 production rates still occurred (Table 1). CH_4 production under sulfate-rich conditions may result from an imbalance in the microbial community (Adler et al. 2017) and may persist or even be enhanced in surface sediments of coastal systems despite significant interaction with seawater resulting from coastal ground subsidence and submersion.

References

Costa, B. 2022. Remote Sensing Analysis of Recent Coastal Change and Controlling Factors in Tuktoyaktuk Peninsula (Beaufort Sea Coast, Canada). MSc thesis. University of Lisboa.

Heffernan, L., Cavaco, M.A., Bhatia, M., Estop-Aragonés, C., Knorr, K-H., and Olefeldt, D. 2022. High peatland methane emissions following permafrost thaw: enhanced acetoclastic methanogenesis during early successional stages. Biogeosciences. 19, 3051–3071.

Hobbie, S.E. 1996. Temperature and plant species control over litter decomposition in Alaskan tundra. Ecological Monographs, 66, 503–522.

Lapham, L., Dallimore, S., Magen, C., Henderson, L., Powers, L., Gonsior, M., Clark, B., Côté, M., Fraser, P., and Orcutt, B. 2020. Microbial Greenhouse Gas Dynamics Associated With Warming Coastal Permafrost, Western Canadian Arctic. Frontiers in Earth Science. 8:582103.

Pellerin, A., Lotem, N., Anthony, K., Russak, E., Hasson, N., Chanton, J., and Sivan, O. 2022. Methane production controls in a young thermokarst lake formed by abrupt permafrost thaw. Global Change Biology. 28(10), 3206–3221.

Martin, A.F., Lantz, T.C., and Humphreys, E.R. 2018. Ice wedge degradation and CO_2 and CH_4 emissions in the Tuktoyaktuk Coastlands, Northwest Territories. Arctic Science, 4(1).

Tanksi, G., Bröder, L., Wagner, D., Knoblauch, C., Lantult, H., Beer, C., Sachs, T., Fritz, M., Tesl, T., Koch, B., Haghlpour N., Eglinton, T., Strauss, J., and Vonk, J. 2021. Permafrost Carbon and CO_2 Pathways Differ at Constrasting Coastal Erosion Sites in the Canadian Arctic. Frontiers in Earth Science. 9:630493.

Vaughn, L.J.S., Conrad, M.E., Bill, M., and Torn, M.S. 2016. Isotopic insights into methane production, oxidation, and emissions in Arctic polygon tundra. Global Change Biology, 22, 3487–3502.

Environmental drivers of methane oxidation in permafrost peatland and upland soils in the Finnish and Western Greenlandic Arctic

Carolina Voigt[1,2], Wasi Hashmi[2], Christian Knoblauch[1], Jukka Pumpanen[2], Mia M. Teichert[1], Quentin Uttke[1] & Evan J. Wilcox[1]

[1]*Institute of Soil Science, Universität Hamburg, Hamburg, Germany*

[2]*Department of Environmental and Biological Sciences, University of Eastern Finland, Kuopio, Finland*

Arctic wetlands are large sources of methane (CH_4), a strong greenhouse gas. However, the majority of the Arctic land area (over 80 %) is covered by well-drained upland soils, which often are relatively small sources of CH_4, at least during the growing season. Commonly, these drier northern soils are CH_4-neutral, or may act as CH_4 sinks in arctic and boreal regions (Kuhn et al. 2021) where consumption of atmospheric CH_4 causes net CH_4 uptake. A change in moisture conditions, increasing temperatures, and altered nutrient regimes may alter the functioning of such typical CH_4 sinks, and shift landcover types from a net sink to a source of CH_4. For example, the transition from comparably dry landcover types to wetlands due to thawing of ice-rich permafrost is a wide-spread occurrence in the palsa mire region in Northern Fennoscandia (Borge et al. 2017).

Due to the large areal coverage of uplands in the Arctic, soil CH_4 uptake, even if occurring at small rates compared to wetland CH_4 emissions, could be relevant at the pan-Arctic scale and the spatially integrated CH_4 sink could partially compensate for carbon (C) losses to the atmosphere. It is therefore important to understand the abiotic (e.g., temperature, soil moisture, pH, soil structure) and biotic drivers (e.g., vegetation, nutrient availability and microbial functioning) regulating the magnitude of CH_4 uptake rates in arctic soils, in order to improve our understanding of arctic C budgets. While wetland CH_4 production and oxidation processes are known to be sensitive to temperature (Rößger et al. 2022; Knoblauch et al. 2008), the temperature response of high-affinity CH_4-oxidation in drier soils which display CH_4 uptake is poorly known. While the known abiotic drivers, soil temperature and moisture, are established controls on high-affinity CH_4 oxidation, we have recently shown that CH_4-oxidation in upland soils may further be linked to C-substrate supply to methanotrophs: in situ CH_4-uptake correlated with ecosystem CO_2 respiration, and addition of labile C-compounds in laboratory incubations increased CH_4 oxidation (Voigt et al. 2023). Other environmental variables such as N-supply, e.g., ammonium (NH_4^+), as well as soil pH influence the activity of CH_4-oxidizers (Bodelier and Laanbroek 2004; Knief 2015), but responses of CH_4 oxidation to these variables are variable and differ between soils and ecosystems.

Methods

Here, we measured in situ CH_4 fluxes from upland soils and a palsa mire (permafrost peatland) near Kilpisjärvi in Finnish Lapland (68°51′ N, 21°06′ E). Fluxes were measured from different vegetation (shrub-dominated, lichen-dominated) and landcover types (palsa, upland forest, upland tundra) during late summer 2022 using manual chambers combined with a portable gas analyzer (LI-7810). Measurements were repeated within the same week with comparable soil moisture conditions but a 10°C difference in air temperature (at ca. 10°C and 20°C) to roughly assess the in situ temperature sensitivity of CH_4 fluxes. Surface soil samples (0–10 cm) were collected from all flux measurement locations, homogenized, and incubated in the laboratory under two temperatures (4°C, 20°C) and three moisture treatments (20% water-holding capacity [WHC], field moisture, 60% WHC). Additional nutrient addition experiments were performed under the same temperature and moisture conditions (glucose [$C_6H_{12}O_6$] addition, ammonium chloride [NH_4Cl] addition).

Results and discussion

All sites displayed net CH_4 uptake in situ, and CH_4 oxidation rates under field-moist conditions were largest in upland forest (-7.47 ng CH_4–C $(gDW)^{-1}$ h^{-1}, followed by palsa (-3.05 ng CH_4–C $(gDW)^{-1}$ h^{-1}) and upland tundra soils (-1.25 ng CH_4–C $(gDW)^{-1}$ h^{-1}). CH_4 oxidation was slightly larger when shrubs were absent (-4.43 ng CH_4–C $(gDW)^{-1}$ h^{-1}) than under dwarf shrub cover (-3.42 ng CH_4–C $(gDW)^{-1}$ h^{-1}). Oxidation rates did not significantly differ between temperature treatments, but the effect of soil moisture was pronounced, with higher CH_4 oxidation under the 20% WHC than the 60% WHC treatment. Interestingly, elevated soil moisture in the permafrost peatland turned the palsa site from a net sink to a source of CH_4 (Figure 1), pointing towards the

presence of methanogens in the surface layer of these permafrost peatlands. Glucose addition promoted CH_4 oxidation at most sites, but notably only under the 20°C temperature treatment (Figure 1), indicating that the temperature sensitivity of high-affinity CH_4 oxidation can be more pronounced if substrate conditions are favourable. CH_4 oxidation rates further correlated with CO_2 production in most treatments and soils. Our findings additionally point towards a decrease in CH_4-oxidation rates after NH_4^+-addition, but these results are inconclusive as the simultaneous addition of salts may have altered the soil pH with potential inhibitory effects on CH_4-oxidation.

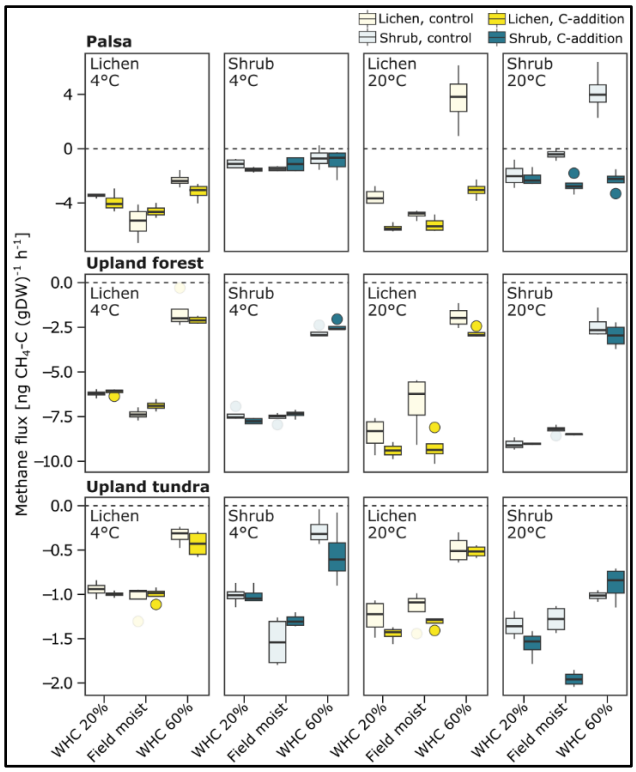

Figure 1. Methane oxidation rates under different soil moisture, temperature, and C-addition treatments in lichen and dwarf-shrub dominated land cover types in Finnish Lapland. C was added as glucose. DW = soil dry weight.

Our study shows that the response of high-affinity CH_4 oxidation to environmental manipulations is complex, and that besides soil temperature and moisture, nutrient regimes and biotic controls may be important drivers behind CH_4 uptake by arctic soils.

Future plans and outlook

To test whether our findings are applicable to a wider range of arctic ecosystems we conducted comparable in situ CH_4 flux measurements at an upland tundra site on Disko Island, Greenland (69°16′ N, 53°27′ W) in late summer 2023. Soil samples have been collected under various vegetation covers at the site, and soil incubations under a wider range of temperature scenarios and more refined nutrient-addition experiments are planned for spring 2024. Results will shed light upon the response of Arctic soils to changing climate, observed in the Arctic with an up to four times faster warming compared to the rest of the globe (Rantanen et al. 2022), leading to widespread permafrost thaw and changes in surface soil moisture and nutrient regimes.

Acknowledgements

This work is funded by the Academy of Finland project MUFFIN (no. 332196) and the BMBF project MOMENT (no. 03F0931A).

References

Bodelier, P.L.E., and Laanbroek, H.J. 2004. Nitrogen as a regulatory factor of methane oxidation in soils and sediments. FEMS Microbiology Ecology 47(3): 265–277. doi:10.1016/S0168-6496(03)00304-0

Borge, A.F., Westermann, S., Solheim, I., and Etzelmüller, B. 2017. Strong degradation of palsas and peat plateaus in northern Norway during the last 60 years. The Cryosphere, 11(1): 1–16. doi:10.5194/tc-11-1-2017

Knief, C., Lipski, A., and Dunfield, P.F. 2003. Diversity and activity of methanotrophic bacteria in different upland soils. Applied and Environmental Microbiology 69(11): 6703–6714. doi:0.1128/AEM.69.11.6703–6714.2003

Knoblauch, C., Zimmermann, U., Blumenberg, M., et al., 2008. Methane turnover and temperature response of methane-oxidizing bacteria in permafrost-affected soils of northeast Siberia. Soil Biology and Biochemistry, 40(12): 3004–3013. doi:10.1016/j.soilbio.2008.08.020

Kuhn, M.A., Varner, R.K., Bastviken, D., et al., 2021. BAWLD-CH4: a comprehensive dataset of methane fluxes from boreal and arctic ecosystems. Earth System Science Data, 13(11): 5151–5189. doi:10.5194/essd-13-5127-2021

Rantanen, M., Karpechko, A.Y., Lipponen, A., et al., 2022. The Arctic has warmed nearly four times faster than the globe since 1979. Communications Earth & Environment, 3(1): 168. doi:10.1038/s43247-022-00498-3

Rößger, N., Sachs, T., Wille, C., Boike, J., and Kutzbach, L. 2022. Seasonal increase of methane emissions linked to warming in Siberian tundra. Nature Climate Change, 12(11): 1031–1036. doi:10.1038/s41558-022-01512

Voigt, C., Virkkala, A.M., Hould Gosselin, G., et al., 2023. Arctic soil methane sink increases with drier conditions and higher ecosystem respiration. Nature Climate Change, 13(10): 1095–1104. doi:10.1038/s41558-023-01785-3

6 Permafrost Hydrology & Wetland Dynamics

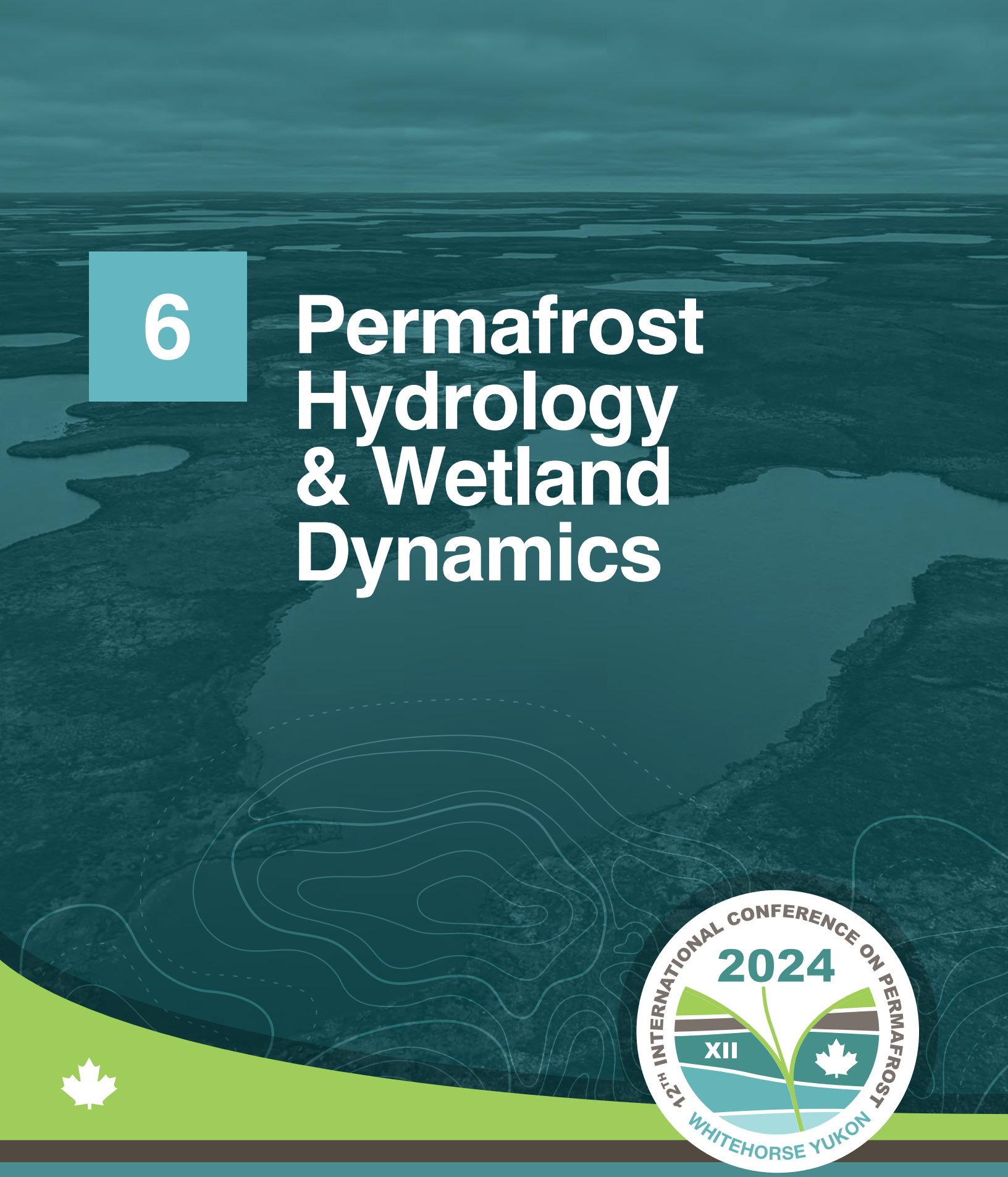

12TH INTERNATIONAL CONFERENCE ON PERMAFROST
2024
XII
WHITEHORSE YUKON

INTEGRATING PERSPECTIVES OF PERMAFROST THAW, CHANGE, AND ADAPTATION

Permafrost Hydrology & Wetland Dynamics

6A — Implications of Thawing Permafrost on Water Resources in Cold Regions

Session Chairs: Stephanie Wright[1], Elliott Skierszkan[2] & Jeffrey McKenzie[3]

[1]*Queen's University, Kingston, Ontario, Canada*
[2]*Carleton University, Ottawa, Ontario, Canada*
[3]*McGill University, Montréal, Québec, Canada*

Permafrost drives surface and subsurface hydrological regimes in northern and mountainous regions. Its thaw is opening new hydrological pathways and activating biogeochemical processes that have substantial ramifications for water availability and water quality. This session aims to unravel the implications of permafrost thaw on water resources, with a special focus on permafrost hydrogeology and the transport of geogenic and anthropogenic contaminants.

We welcome contributions from various themes that centre around water resources in permafrost regions, including physical hydrogeology and hydrology, water quality and water chemistry, management of mining and industrial wastewater, geotechnical considerations of thawing permafrost, and local and indigenous perspectives on water in a changing climate. The anticipated outcome of this session is to provide an overview of the challenges, opportunities, and required adaptations that will accompany the transition from perennially frozen to thawed conditions in the subsurface.

Icings as sentinels and biogeochemical modifiers of wintertime flow in the southern discontinuous permafrost Taiga Shield

Nora E. Alsafi[1], Steven V. Kokelj[2], Mike J. Palmer[3], Maya P. Bhatia[4], Timothy P. Ensom[2], Christopher Spence[5], Maria A. Cavaco[4], Martin R. Kurek[6], Robert G.M. Spencer[6] & Suzanne E. Tank[1]

[1]*Department of Biological Sciences, University of Alberta, Edmonton, Alberta, Canada*

[2]*Northwest Territories Geological Survey, Government of Northwest Territories, Yellowknife, Northwest Territories, Canada*

[3]*North Slave Research Centre, Aurora Research Institute, Yellowknife, Northwest Territories, Canada*

[4]*Department of Earth and Atmospheric Sciences, University of Alberta, Edmonton, Alberta, Canada*

[5]*Environment and Climate Change Canada, Saskatoon, Saskatchewan, Canada*

[6]*Department of Earth, Ocean, and Atmospheric Science, Florida State University, Tallahassee, Florida, United States*

Warming air temperatures and shifting precipitation regimes are changing the dynamics of freshwater systems throughout the Canadian subarctic. Regional air temperatures are increasing at three to four times the global average (Jansen et al. 2020; Rantanen et al. 2022), and this warming has been associated with a shift towards more pluvial runoff regimes and widespread permafrost degradation, including in regions of discontinuous permafrost (Morse et al. 2016; Smith et al. 2022). These changes are altering the seasonality of streamflow and hydrologic flowpaths, as thicker active layers, talik development and expansion, and a longer period of active layer freeze-back allow for expanded surface-groundwater interactions during the frozen season (Walvoord and Kurylyk 2016). Similar to other subarctic regions, increases in late-season flow have been documented within the Taiga Shield (Spence et al. 2015), which typifies “fill-and-spill” hydrology, whereby runoff is only generated when lake basin storage thresholds are exceeded (Woo and Mielko 2007). However, although the Taiga Shield comprises approximately 20% of North America’s permafrost-covered area (Alsafi 2023), we know little about how alterations in winter hydrology might affect the biogeochemistry of this landscape.

In this study, we explore the wintertime biogeochemistry of lake-rich aquatic networks in the southern discontinuous Taiga Shield. We do this using icings, which are sheet-like masses of layered ice that form when winter subsurface flow is forced to the ground surface (Ballantyne 2018). These features can archive water and modify its geochemical composition, and can store a substantial proportion of baseflow within permafrost-affected regions (Crites et al. 2020). To undertake this work, we collected cores from seven icing features in the River Lake and Baker Creek watersheds, both near Yellowknife, NT, Canada. Sampled icing features were variably sourced by large upstream lakes, small upstream lakes, and groundwater. Icing cores were collected during late winter 2021, and were paired with under-ice (i.e., winter-time) and open water measurements of icing source waters. Icing meltwater and source water samples were analyzed for their biogeochemical properties (including general geochemistry, ultra-high resolution dissolved organic matter (DOM) composition, and microbial community composition via 16S rRNA gene sequencing). These biogeochemical analyses were coupled with the analysis of water level time series from two lakes immediately upstream of icing features, and associated game camera images of one developing icing. Instrumented sites had relatively large (Baker Creek) and small (River Lake subwatershed) upstream contributing areas, and analyzed winter seasons were preceded by above- (2020-21) and below-average (2021-22) antecedent (May-October) precipitation.

Across contrasting hydrologic years and catchments, icing formation was limited to years with above average antecedent precipitation (i.e., 2020-21), and – in dry years – sites with larger contributing areas and water storage available in upstream lakes. During the freezing season, persistent water flow and thus icing development showed clear control by air temperature, with sustained, cold conditions causing ice dam formation and elevated hydrostatic pressure in source water lakes (Figure 1a), and warmer temperatures enabling ice dam degradation and rapid rejuvenation of flow, even during periods when surface temperatures remained well below 0 ºC (Figure 1b).

The concentration of geochemical constituents contained within icings was overall dilute compared to source waters, with solute exclusion appearing to preferentially exclude dissolved organic carbon (DOC), total dissolved nitrogen, and trace metals. However, icing geochemistry varied considerably by source water type, with icings sourced by groundwater showing little internal variation, while those sourced by shallow lakes were characterized by pockets of elevated DOC, ammonia, dissolved aluminum, and dissolved iron.

Analysis of water from upstream lakes suggests that this within-icing variability was driven by remobilization of these constituents from lake sediments during low oxygen conditions. Icings were also selectively enriched in aliphatic (i.e., without aromatic structures) DOM relative to source waters, and this aliphatic DOM was preferentially decomposed to CO_2 during a bioincubation. Microbial communities were distinct across seasons and were strongly influenced by measured differences in DOM composition.

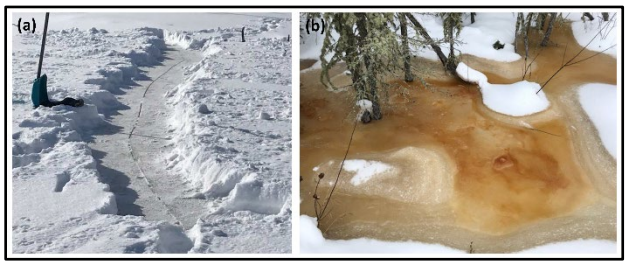

Figure 1. (a) A dilation crack in a lake sourcing an icing in the River Lake watershed, Yellowknife region, NT. (b) Active wintertime overflow immediately downstream of the site of photo (a). Photo credit: Steven V. Kokelj. Photo date: 20 March, 2021.

Our findings illustrate the dynamic nature of winter flow on the Taiga Shield, documenting pulses of water movement with varying geochemical characteristics, well before the traditional spring freshet. They also show that icings can substantially modify the composition of water flowing through connected aquatic networks in the winter, with implications for carbon fate and the composition of microbial communities that form the base of aquatic food webs. Specific consideration of icings and their effect on water movement appears to be critical for understanding the growing hydrological and biogeochemical importance of the winter season in the changing North.

REFERENCES

Alsafi, N.E. 2023. The impact of permafrost thaw on carbon dynamics and microbial communities in the Great Slave Region, Northwest Territories. MSc thesis, University of Alberta, Edmonton.

Ballantyne, C.K. 2018. Periglacial Geomorphology. Wiley-Blackwell, Chichester, United Kingdom.

Crites, H., Kokelj, S.V., and Lacelle, D. 2020. Icings and groundwater conditions in permafrost catchments of northwestern Canada. Scientific Reports, 10(1): 3283. doi:10.1038/s41598-020-60322-w

Jansen, E., Christensen, J.H., Dokken, T., Nisancioglu, K. H., Vinther, B.M., Capron, E., Guo, C., Jensen, M.F., Langen, P.L., Pedersen, R.A., Yang, S., Bentsen, M., Kjaer, H. A., Sadatzki, H., Sessford, E., and Stendel, M. 2020. Past perspectives on the present era of abrupt Arctic climate change. Nature Climate Change, 10(8): 714–721. doi:10.1038/s41558-020-0860-7

Morse, P.D., Wolfe, S.A., Kokelj, S.V., and Gaanderse, A.J.R. 2016. The occurrence and thermal disequilibrium state of permafrost in forest ecotopes of the Great Slave Region, Northwest Territories, Canada. Permafrost and Periglacial Processes, 27(2): 145–162. doi:10.1002/ppp.1858

Rantanen, M., Karpechko, A.Y., Lipponen, A., Nordling, K., Hyvärinen, O., Ruosteenoja, K., Vihma, T., and Laaksonen, A. 2022. The Arctic has warmed nearly four times faster than the globe since 1979. Communications Earth & Environment, 3(1): 168. doi:10.1038/s43247-022-00498-3

Smith, S.L., O'Neill, H.B., Isaksen, K., Noetzli, J., and Romanovsky, V.E. 2022. The changing thermal state of permafrost. Nature Reviews Earth & Environment, 3(1): 10–23. doi:10.1038/s43017-021-00240-1

Spence, C., Kokelj, S.V., Kokelj, S.A., McCluskie, M., and Hedstrom, N. 2015. Evidence of a change in water chemistry in Canada's subarctic associated with enhanced winter streamflow. Journal of Geophysical Research: Biogeosciences, 120(1): 113–127. doi:10.1002/2014JG002809

Walvoord, M.A., and Kurylyk, B.L. 2016. Hydrologic impacts of thawing permafrost—A review. Vadose Zone Journal, 15(6): vzj2016.01.0010. doi:10.2136/vzj2016.01.0010

Woo, M.-K., and Mielko, C. 2007. An integrated framework of lake-stream connectivity for a semi-arid, subarctic environment. Hydrological Processes, 21(19): 2668–2674. doi:10.1002/hyp.6789

Impact of wildfire on above-ground and below-ground processes in discontinuous permafrost peatlands

Maude Auclair[1], William Quinton[1], Oliver Sonnentag[2] & David Olefeldt[3]

[1]*Department of Geography and Environmental Studies, Wilfrid Laurier University, Waterloo, Ontario, Canada*

[2]*Département de géographie & Centre d'études Nordiques, Université de Montréal, Montréal, Québec, Canada*

[3]*Department of Renewable Resouces, University of Alberta, Edmonton, Alberta, Canada*

As climate warms and wildfire activity increases, permafrost in the southern Northwest Territories becomes increasingly vulnerable to thaw (Gibson et al. 2018). In this peatland dominated landscape, permafrost thaw arising from wildfires that occurred in the 1970s and 1980s was found to persist for several decades before pre-fire conditions were restored. Under the current climate, permafrost that is lost due to a wildfire is unlikely to regenerate.

Study Objective

This study examines the impact of a wildfire surface and subsurface energy regimes over the first 8 years post-fire. This is accomplished by assessing changes to a) sub-canopy radiation regimes, and b) the spatial and temporal variability of seasonal ground thaw and permafrost degradation.

Study Site

This study was undertaken near the headwaters of the Scotty Creek Basin (61.3˚N 121.3˚W), Northwest Territories, Canada (Figure 1).

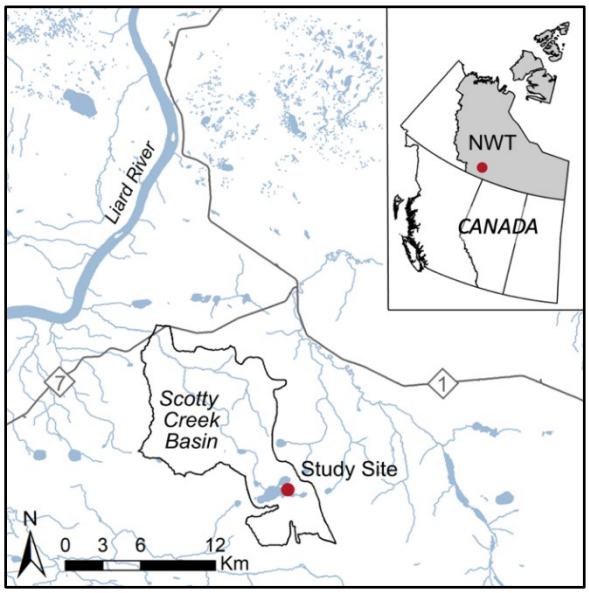

Figure 1. Location of study site within the Dehcho region of the southern Northwest Territories.

Above Ground Processes

Data from meteorological stations located in the burned and unburned (Control) portions of a peat plateau were used to examine changes to four component sub-canopy radiation between 2015-2022. On average shortwave loading over the snow-free season was 12% greater at the Burn station on average over the study period. Net shortwave radiation was consistently higher at the Burn station than the Control. Net longwave radiation was significantly lower at the Burn station than Control, a function of higher outgoing longwave flux due to the higher insolation at the Burn ground surface and the lack of canopy resulting in lower longwave downwelling. The net result of these findings indicate the Burn station maintained a higher net radiation (Q*) on average than the Control over the study period with the most pronounced differences between sites being during the snow-free periods, suggesting that more energy was available to drive the ground heat flux at the Burn. The differences in radiation regimes between sites can largely be attributed to the presence and absence of canopy. Canopy shading reduces the direct incoming solar radiation reaching the ground surface, limiting the available energy for ground thaw (Chasmer et al. 2011; Wright et al. 2009). Conversely, removal of the tree canopy by wildfire may increase ground thaw rates.

Below Ground Processes

Weekly frost probe measurements at the Burn and Control 1 site between 9 June – 25 August, 2021 demonstrated a faster rate of active layer thaw at the Burn compared to the Control. Observations reveal the active layer at the Burn was thinner than the Control, and therefore it required less energy to thaw.

Given this, and the greater Q* at the Burn, a surplus of energy was available to drive other subsurface processes. Specifically, this additional energy may have contributed to the warmer ground temperatures observed beneath the Burn during the snow-free months over the study period. Furthermore, the most notable finding was a near-continuous talik layer beneath Burn where majority of the points surveyed between June-August 2021 overlie a talik, whereas

only about half of the points surveyed at the Control overlie a talik (Figure 2). The presence of a talik (i.e., perennially thawed soil layer between the active layer and permafrost) accelerates permafrost thaw and can even contribute to thaw over the winter months (Connon et al. 2018). This was reflected by annual permafrost table measurements taken near the end of summer each year between 2015-2022, where the burn site demonstrated a significant trend of increasing permafrost table depths, whereas the control site did not show any significant trend. Furthermore, observations demonstrate the permafrost table is more uniform beneath the Burn, whereas the permafrost table beneath the Control is less uniform. Using the absolute elevations of the permafrost table, and assuming a constant rate of thaw between years, we found the annual rate of permafrost thaw to be 9.6 cm/yr beneath the Burn and 5.6 cm/yr beneath the Control.

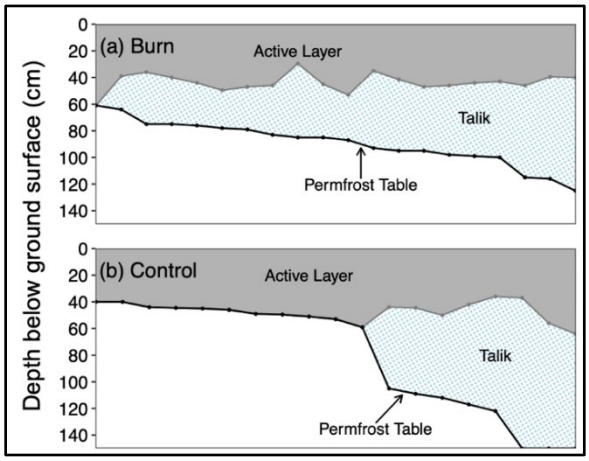

Figure 2. Active layer thickness, talik thickness, and depth to permafrost table measured at the Burn (a) and Control 1 (b) sites in 2021. Values are ranked from shallowest (left) to deepest (right) permafrost table depth relative to the ground surface.

SUMMARY AND CONCLUSION

The wildfire's removal of the tree canopy eradicated the shading effect on the ground surface, facilitating greater and more uniform inputs of energy and moisture to reach the ground at the Burn site. This led to greater and more uniform rates of seasonal active layer thaw and annual permafrost thaw depths that surpass the depth of annual refreeze, resulting in a near-continuous talik layer and more rapid permafrost degradation. By contrast, permafrost beneath the Control maintained relatively effective insulation from the overlying active layer except for limited areas where taliks had formed due to localized inputs of energy and moisture. This assessment provides insight to the impacts of wildfire on permafrost in a peatland dominated landscape in the sporadic-discontinuous permafrost zone. Increasing our understanding on the ways in which permafrost responds to wildfire in different landscapes is an important step in minimizing uncertainties to the trajectory of permafrost thaw.

REFERENCES

Chasmer, L., Quinton, W.L., Hopkinson, C., Petrone, R., and Whittington, P. 2011. Vegetation canopy and radiation controls on permafrost peat plateau evolution within the discontinuous permafrost zone, Northwest Territories, Canada, Permafrost and Periglacial Processes, 22: 199–213 doi:10.1002/ppp.724

Connon, R., Devoie, E., Hayashi, M., Veness, T., and Quinton, W. 2018. The influence of shallow taliks on permafrost thaw and active layer dynamics in subarctic Canada, Journal of Geophysical Research: Earth Surface, 123. doi:10.1002/2017JF004469

Gibson, C., Chasmer, L.E., Thompson, D.K., Quinton, W.L., Flannigan, M.D., and Olefeldt, D. 2018. Wildfire as a major driver of recent permafrost thaw in boreal peatlands, Nature Communications, 9: 3041(2018). doi:10.1038/s41467-018-0547-1

Wright, N., Hayashi, M., and Quinton, W.L. 2009. Spatial and temporal variations in active layer thawing and their implication onrunoff generation in peat-covered permafrost terrain, Water Resources Research, 45: W05414. doi:10.1029/2008WR006880

Increasing discharge trends in a discontinuous permafrost, fractured bedrock watershed

Abigail R. Baran[1], Élise Devoie[1], Ryan F. Connon[2] & Stephanie N. Wright[1]

[1]*Department of Civil Engineering, Queen's University, Kingston, Ontario, Canada*

[2]*Department of Environment and Climate Change, Government of Northwest Territories, Yellowknife, Northwest Territories, Canada*

Across subarctic and Arctic drainage basins, river discharge has increased in recent years, however the rate and pattern of these changes are not consistent. Winter discharge in large, continental-scale basins (e.g., Mackenzie, Yukon, Lena and Kolyma), has increased 0.4-1.8% per year since 1980, while annual mean discharge shows only weakly increasing trends (Liu et al. 2022). St. Jacques and Sauchyn (2009) evaluated 23 rivers in the Northwest Territories (NWT) and found statistically significant increases in winter baseflow in 20 rivers and increasing annual discharge in only 9 rivers. Arctic river peak flows have decreased in magnitude and occur earlier (Bennet et al. 2023). Increased discharge and winter baseflow demonstrate changes to the hydrological regime within a watershed that can lead to altered stream chemistry and temperature and enhanced contaminant pathways (Walvoord et al. 2012).

Study Site

The La Martre River in the central Northwest Territories, flows from Lac La Martre to the Marian River, and ultimately to Great Slave Lake. The gauging station, located below the outlet of Lac La Martre, has a continuous discharge record from 1977 to the present and captures runoff from an area of approximately 14,000 km^2. Unlike other Arctic and subarctic rivers, the La Martre river has seen profound streamflow increases throughout the year. The watershed is underlain by discontinuous permafrost and fractured dolomite bedrock and the landscape is dominated by wetlands, mixed and coniferous forest, and peatlands. The community of Whatì is located at the outlet of Lac La Martre and is one of three NWT communities using groundwater as their primary source of drinking water. The objective of this study is to understand the nature and timing of changes in streamflow, temperature, and precipitation within the La Martre watershed.

Methods

Daily discharge records (1977-2023) for the La Martre river (07TA001) are available from the Water Survey of Canada. The ECCC weather station located at the Whatì airport provides daily temperature records since 1995, and daily precipitation since September 2018. The nearest long-term weather station is in Yellowknife, more than 150 km away. Monthly temperature and precipitation data from four reanalysis products, ERA5-Land (Muñoz Sabater 2019), CMAP, UDEL, and CRU, were compared with the Whatì weather station record and nearby weather stations: Yellowknife, Gameti, and Snare Rapids. ERA5-Land was selected for further analysis as it is available at hourly timescales and compared as well as the other models to the observed data. ERA5-Land is generated from monthly observations at meteorological stations where available, interpolated using a general circulation model, and downscaled to 0.1° by 0.1°.

The reanalysis temperature, precipitation, and observed discharge trends were analyzed using the non-parametric Mann-Kendall trend test and Sen slope indicator at annual, seasonal, and monthly timescales. The seasons were divided as follows: Winter (Nov-Apr), Spring (May-Jun), Summer (Jul-Aug), Autumn (Sep-Oct). The annual period was taken as the hydrological year from Nov-Oct, labeled as the year of the final month. The trend in the ratio of winter baseflow (Jan. 1 to Mar. 31 discharge) to total annual discharge was also calculated.

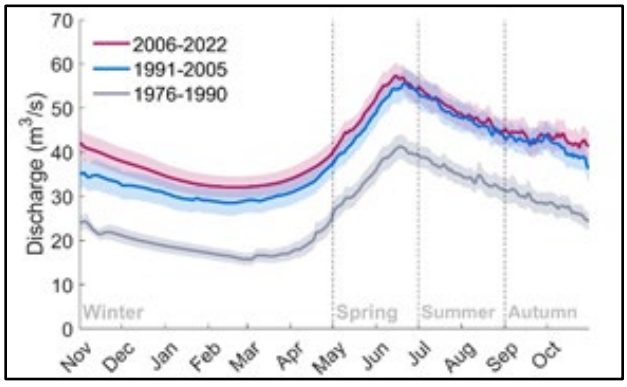

Figure 1. Hydrograph of mean daily discharge in La Martre River for three periods: 1976-1990, 1991-2005, 2006-2022. Shaded area represents the standard error.

RESULTS

From 1950 to 2022, the average annual temperature in Whatì has increased by 2.04°C. Discharge in the La Martre river showed statistically significant increases annually and in every season and month from 1977 to 2022 (see Table 1). The greatest increasing trend was in winter discharge. The percent of discharge as winter baseflow increased significantly from 15% to 21% during the same period. Peak discharge usually occurs in May or June. There was no statistically significant trend in the timing of peak discharge, however in several years since 2010, peak discharge occurred in late summer or autumn. The peak discharge volume also showed a statistically significantly increasing trend.

Increases in precipitation from ERA5-Land match or exceed the increase in specific discharge in the La Martre River. Although the reanalysis precipitation does not compare perfectly to the limited observed precipitation data in Whatì, the ERA5-Land annual precipitation trend is similar to the observed trend in Yellowknife. At the 90% confidence level, only summer, July, and August precipitation show statistically significant increases, and October shows a statistically decreasing trend at the 95% confidence level. The reanalysis precipitation magnitudes are much greater than the limited observed precipitation data available in Whatì. This may suggest that recent years have been drier than average, supported by field conditions and discussions with community members. Throughout the recent dry period, discharge has continued to follow the long-term increasing trend.

Table 1. Trends in precipitation and discharge from 1977–2022. Statistical significance at 95% confidence marked as *, 99% confidence as **.

Parameter	Period	Mean	Slope (mm yr^{-1})
Total Precipitation	Annual	344 mm	1.27 mm/year *
	Winter	102 mm	0.08 mm/year
	Spring	63 mm	0.09 mm/year
	Summer	104 mm	0.88 mm/year *
	Autumn	75 mm	-0.03 mm/year
Specific Discharge	Annual	79 mm	1.15 mm/year **
	Winter	32 mm	0.59 mm/year **
	Spring	17 mm	0.17 mm/year **
	Summer	17 mm	0.16 mm/year *
	Autumn	14 mm	0.17 mm/year **

DISCUSSION AND CONCLUSION

The ERA5-Land data suggest that a primary driver of the increasing annual discharge in the La Martre River is the rising trend in precipitation. However, more substantial increases in winter discharge and the discrepancy between the season with the greatest upward trend in precipitation (summer) and the season with the highest upward trend in discharge (winter) suggest alterations in the routing mechanisms within the watershed. The substantial discharge observed throughout the recent dry period, also implies changes to the landscape storage capacity in the watershed. Permafrost thaw may be responsible for increases in winter baseflow through enhanced summer groundwater recharge accompanying a deeper active layer, expanded groundwater flow paths through vertical and lateral taliks, and altered surface water-groundwater connectivity, especially in wetland dominated landscapes (Wright et al. 2022). Further research is needed to determine which processes are responsible for the hydrological regime shift in the La Martre watershed. The next steps in this study include development of a physically based model of the watershed to better understand the changes resulting in increased winter discharge. This will inform our understanding of current and future landscape changes in the watershed and allow for predictions of the quantity and quality of water accessible to the community of Whatì.

REFERENCES

Bennett, K.E., Schwenk, J., Bachand, C., Gasarch, E., Stachelek, J., Bolton, W.R., and Rowland, J.C. 2023. Recent streamflow trends across permafrost basins of North America. Frontiers in Water 5.

Liu, S., Wang, P., Yu, J., Wang, T., Cai, H., Huang, Q., Pozdniakov, S.P., Zhang, Y., and Kazak, E.S. 2022. Mechanisms behind the uneven increases in early, mid- and late winter streamflow across four Arctic river basins. Journal of Hydrology 606, 127425. https://doi.org/10.1016/j.jhydrol.2021.127425

Muñoz Sabater, J. 2019. ERA5-Land hourly data from 1950 to present. Copernicus Climate Change Service (C3S) Climate Data Store (CDS). doi:10.24381/cds.e2161bac

St. Jacques, J.-M., and Sauchyn, D.J. 2009. Increasing winter baseflow and mean annual streamflow from possible permafrost thawing in the Northwest Territories, Canada. Geophysical Research Letters 36. https://doi.org/10.1029/2008GL035822

Walvoord, M.A., Voss, C.I., and Wellman, T.P. 2012. Influence of permafrost distribution on groundwater flow in the context of climate-driven permafrost thaw: Example from Yukon Flats Basin, Alaska, United States. Water Resources Research 48. https://doi.org/10.1029/2011WR011595

Wright, S.N., Thompson, L.M., Olefeldt, D., Connon, R.F., Carpino, O.A., Beel, C.R., and Quinton, W.L. 2022. Thaw-induced impacts on land and water in discontinuous permafrost: A review of the Taiga Plains and Taiga Shield, northwestern Canada. Earth-Science Reviews 232, 104104. https://doi.org/10.1016/j.earscirev.2022.104104

Water cycle simulations and the effect of permafrost and active layer representations for the Carcajou Watershed, NWT

Melissa Bunn[1], Omar Khader[2], Eric Kessel[2], Andre Erler[2], Hazen Russell[1] & Steven Frey[2]

[1]*Geological Survey of Canada, Natural Resources Canada, Ottawa, Ontario, Canada*

[2]*Aquanty, Waterloo, Ontario, Canada*

In permafrost dominated regions, a gap persists in our understanding of water resources, the influence of groundwater, and the impact of climate change at the regional scale. Regional scale modelling can help to advance the understanding of these impacts by integrating with regional climate models. For regional modelling to be tenable, ongoing development of modelling methods and conceptualizations is required.

By developing a fully integrated numerical groundwater-surface water climate model using HydroGeoSphere (HGS) (Aquanty 2021) for a gauged basin within the discontinuous permafrost zone, this project verifies existing numerical methods and tests conceptualizations of integrated groundwater-surface water flow at the regional scale. This work informs future modelling and forecasting of regional water resources in permafrost regimes.

STUDY AREA

The study area for this modelling exercise is located in the central Mackenzie Valley, southwest of Norman Wells, NWT. The footprint of the model represents the Carcajou River Watershed (CRW) (Figure 1), covering an area of 7800 km^2. The CRW covers varied physiographic regions ranging from the eastern flank of the Mackenzie range (maximum elevation: 2312 m.a.s.l) to the Mackenzie River Floodplain (minimum elevation: 25 m.a.s.l). The watershed is underlain by extensive discontinuous to continuous permafrost with low to moderate ground ice content (Heginbottom et al. 1995).

The CRW was selected for this study as there is a gauging station on the Carcajou River with continuous observations from 1980 to present, the size of the watershed is well suited to regional climate simulations and integration with satellite observations (i.e., GRACE), and there is a transition within the CRW between intermediate and extensive discontinuous permafrost. Additionally, there has been characterization of permafrost hydrogeology and groundwater discharge within a smaller adjacent watershed (Glass 2019).

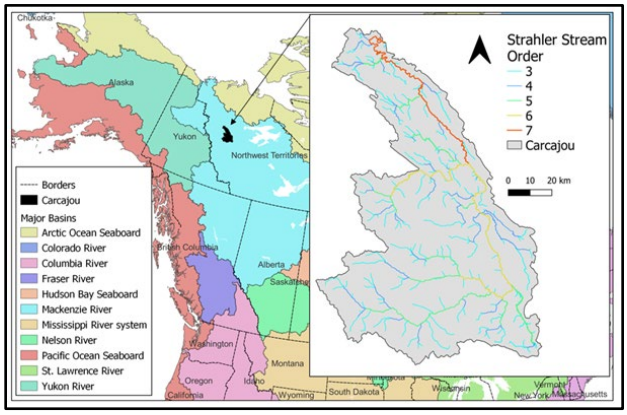

Figure 1. Location of the Carcajou River Watershed (NWT) and surface water classification.

MODEL CONSTRUCTION

Data layers for the model were supported by the data generation for the Canada1Water Project (Publicly available beginning in 2024, https://www.canada1water.ca). This dataset includes nationally harmonized landcover mapping, mineral and peatland soil mapping (including bedrock outcrops), leaf area index, and surface water mapping.

The distribution of Quaternary sediments is mapped according to Fulton (1995), while bedrock is mapped according to Garrity and Soller (2009). The depth to bedrock and subsequent top-of-bedrock geometric surface was generated specifically for this study based on outcrop mapping, and depth to bedrock information within the seismic shothole database (Smith 2011).

An unstructured 3-dimensional finite element mesh (FEM) was constructed to complete the numerical simulations. The mesh included all streams Strahler Order 3 and greater. Along surface water features there is a 250 m resolution in the model. The Maximum distance between finite element nodes is 1000 m.

The subsurface of the CRW model consists of six vertical layers, with two soil layers, two Quaternary layers and two bedrock layers. The model base elevation is fixed at 50 m below sea level.

The historical climatology and weather boundary conditions for the simulation were derived from the

national scale precipitation, temperature, snow water equivalent, and PET data from Canada1Water.

Monthly average soil temperatures were derived from land surface reanalysis datasets averaged over the 1979 to 2020 period to determine seasonal freeze and thaw. Permafrost, when considered, is represented in the CRW model as an impermeable material, with spatial coverage extending across the entire domain, with the exception of the area beneath the Carcajou River.

SCENARIOS

Three initial scenarios have been simulated to evaluate model sensitivity to different conceptual representations of subsurface freezing. These scenarios were selected to illustrate the influence of regional groundwater flow and permafrost representation when simulating hydrologic behavior within permafrost regions. Scenario 1 reflects the simplist approach, with no seasonal or perpetually frozen subsurface materials. Scenario 2 includes seasonal freeze and thaw of the upper two meters of the subsurface, such that active layer dynamics are represented. Scenario 3 advances Scenario 2 by including the representation of uniform permafrost conditions as described above.

RESULTS AND DISCUSSION

The simulations cover the period from 1980 to 2017, representing the times for which climate forcing data was available. Model performance was assessed by comparing simulated versus measured daily and monthly river flow at the Water Survey of Canada Hydrometric Station 10KB001. The Nash-Sutcliffe Efficiency and Percent Bias (Pbias) performance metrics were also used to quantitatively evaluate the model.

All scenarios generally show good agreement with the observed flows given the data support and assumptions needed to generate the model. Where discrepancies between simulated and observed flows occur it is generally following freshet, and during winter baseflow months.

The inclusion of seasonal freeze and thaw in Scenario 2 shows improvement over the simplified Scenario 1, most significantly during fall peak flows, and winter recession to baseflow. When fully impermeable permafrost is added to the simulation (Scenario 3), surface water flows in the months following freshet more closely replicate the observed flows (simulated flow during this period are higher in Scenario 3). However, during winter months, simulated flows in this scenario are higher than observed, and Scenario 2 results are improved relative to Scenario 3. These results suggest that it is not suitable to characterize permafrost as fully impermeable at a regional watershed scale, and that groundwater flow plays a meaningful role in regional water balances in discontinuous permafrost zones throughout the seasonal cycle with the exception of during freshet.

CONCLUSIONS

A well-performing fully integrated groundwater-surface water model was constructed to evaluate model sensitivity to three different conceptualizations of permafrost and active layer dynamics, and to determine the associated impacts on simulated regional scale hydrologic behavior. The model is supporting ongoing research on the regional representation of permafrost within water resources simulation models, and continues to be used to test strategies for enhancing the numerical representation of cold region hydrologic processes.

ACKNOWLEDGEMENTS

This work was funded by the Geological Survey of Canada's GEM-Geonorth program, with in-kind support from the Canada1Water Project.

REFERENCES

Frey, S.K., Miller, K., Khader, O., Taylor, A., Norrison, D., Xu, X., Berg, S.J., Hwang, H.T., Sudicky, E.A., and Lapen, D.R. 2021. Evaluating Landscape Influences on Hydrologic Behavior with a Fully-Integrated Groundwater-Surface Water Model, Journal of Hydrology, 602. https://doi.org/10.1016/j.jhydrol.2021.126758

Fulton, R.J. 1995. Surficial Materials of Canada, Geological Survey of Canada.

Garrity, C.P., and Soller, D.R. 2009. Database of the Geological map of North America – Adapted from the map by C.J. Reef, Jr. and others (2005), Reston, VA.

Glass, B. 2019. Examining Hydrogeological Processes in Freezing Soils using Remote Geophysical and Numerical Techniques. MSc Thesis, University of Waterloo. http://hdl.handle.net/10012/14466

Heginbottom, J.A., Dubreuil, M.A., and Harker, P.T. 1995. Canada, Permafrost in, The National Atlas of Canada, Natural Resources Canada, Geomatic Canada, MCR Series no. 4177 (5th edition). https://doi.org/10.4095/294672

Smith, I.R. 2011. The seismic shothole drillers' log database and GIS for Northwest Territories and northern Yukon, Geological Survey of Canada, Open File 6833. doi:10.4095/288754

Quantifying the impact of cryogenic landslides on lakes in the eastern Mackenzie Delta NT, Canada

Victoria Carroll, Joshua Thienpont & Jennifer Korosi
Faculty of Environmental and Urban Change, York University, Toronto, Ontario, Canada

MACKENZIE DELTA

The Mackenzie River and Delta hydrologically connect vast expanses of Canada's western boreal and subarctic with the Arctic Ocean. Permafrost thaw events, occurring in this region in tandem with rising temperatures and precipitation, can dramatically alter the physical environment (Segal et al. 2016). These landscape changes further impact people and wildlife that rely on the delta and its resources. This research examines how permafrost thaw events in the form of cryogenic landslides have the potential to translocate considerable amounts of terrestrial material, potentially triggering biological and chemical shifts in low-lying receiving waterbodies (Leibman et al. 2014).

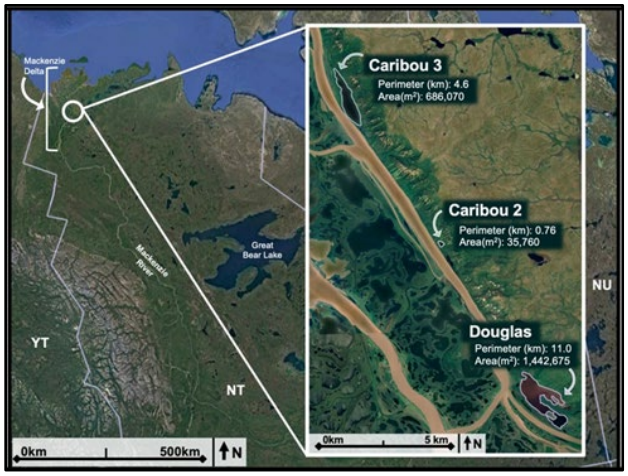

Figure 1. Geographic Context of the Study Lakes.

CARIBOU HILLS LAKES

Our study site is located at the eastern edge of the Mackenzie Delta, ~25 km NNW of Inuvik, NT. To the east, the Caribou Hills are characterized by continuous permafrost and high elevation, and to the west is the low-lying Mackenzie Delta underlain by discontinuous permafrost. Permafrost thaw in the Caribou Hills has resulted in cryogenic landslides depositing terrestrial material into many downslope lakes. During field sampling, these features were pronounced tree-less tracts extending downslope to the edge of the low-lying lakes (Figure 2).


Figure 2. Evidence of cryogenic landslides that occurred during the warm and wet summer of 2017 at Caribou 2. Image taken facing west toward the Mackenzie Delta.

PALEOLIMNOLOGICAL APPROACH

Lake sediments archive a record of changes in a lake and its catchment (the discipline of paleolimnology) that can be used to infer ecosystem changes, particularly where no monitoring data are available (Smol 1992). Using a paleolimnological framework we can identify changes over time by analyzing selected proxy variables preserved in the lake sediments. This research focused on inorganic indicators, measuring total mercury, total organic carbon, inorganic carbon, and nitrogen content, and calculating elemental C/N ratios. Our aim was to understand changes across impacted lake basins and attempt to understand patterns of accumulation of translocated material from upslope landslides. To do this we collected a series of sediment cores across four lakes in the region impacted by landslides in the fall of 2017.

FIELD AND LAB METHODS

Sediment cores were collected in July 2023 at four lakes (all names unofficial) 20-30 km NNW of Inuvik. Three lakes (Douglas, Caribou 2, and Caribou 3) were impacted by cryogenic landslides, and one lake (Caribou Control) located across the East Channel served as a control location. In a boat we collected multiple sediment cores across each basin using a Uwitec gravity corer. Water quality data was collected using a multimeter probe, while lake depths were taken along a transect using an echosounder to provide a rough bathymetry. In addition to core sampling, grab

samples of shoreline sediment were collected from presumed terrestrial landslide material.

Sediment cores, sectioned into 0.5 cm intervals, were kept cool and dark until they were freeze dried. A Milestone DMA-80 direct mercury analyzer was used for total mercury analysis and an Elementar UniCube CN elemental analyzer was used for organic carbon, total carbon, and nitrogen measurements. Samples analyzed for organic carbon content were first acid fumigated with hydrochloric acid for 72 hours, rinsed until neutral, and re-dried. This process removes the inorganic carbon from the sediment. Soil grab samples were processed in an identical manner. Concentrations of total mercury will be expressed both per unit dry weight, and per unit organic carbon. Decreases in organic matter, as might be predicted with an influx of terrestrial material from erosion, can be important for concentrating mercury onto a smaller organic pool of available organic carbon.

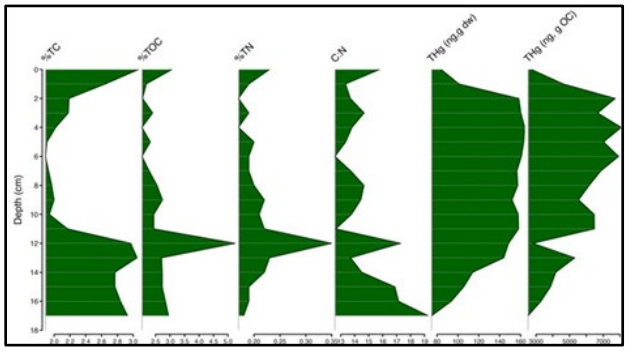

Figure 3. Stratigraphy Caribou 2 – Core 2 (C2-2) - %TC, %TOC, %TN, C:N, THg (ng, g dw), THg (ng, g OC).

PRELIMINARY RESULTS AND NEXT STEPS

Total mercury concentrations are elevated in all three landslide-impacted lakes compared to the control location (Figure 3). The highest concentration recorded was 0.165 mg/kg dw, close to the Interim Sediment Quality Guidelines of 0.17 mg/kg established by the Canadian Council for Minsters of the Environment (CCME, 1999). In both sediment cores from Caribou 2 we record a large pulse in total mercury, the thickness of which varies from ~5 to 20 cm. We infer this pulse to be because of the recent landslide events, translocating material to the lake from the nearby hills. Caribou 2 is the smallest lake and therefore would be expected to record the most significant impacts from the landslide events. Similar increases in total mercury were recorded in Caribou 3 and Douglas, and while the magnitude of increase was smaller, the depth of sediment accumulation also ranged from ~5 to 20 cm, indicating significant deposition to these lakes over the recent past. While the sediment cores collected in 2023 were not dated, 210Pb dating on preliminary cores from the 3 lakes collected in February 2021 showed that the top 20 cm of each core had consistent and low isotopic activity, indicating the material was likely deposited quite rapidly. This supports that these changes are from recent impacts to these lake ecosystems.

Elemental analysis of carbon and nitrogen in the cores provides information to the organic makeup of the sediment and highlights the availability of C, N and Hg in-lake. For example C2-2 shows an increase in THg post landslide followed by a return to background levels in the surface sediment (Figure 3). We additionally will use the C/N ratio to infer production source in lakes (Meyers and Teranes 2001).

IMPLICATIONS

At a local scale, significant landslides in the Caribou Hills were recorded in 2009 and 2017, and thus understanding historic impacts to lakes is essential for characterizing the risk from future thaw-induced landslide events in the western Arctic region. More broadly, this research provides insights regarding the role of rapid mass movement due to permafrost thaw for downstream lake ecosystems. Permafrost degradation, under projected warming, and altered weather patterns is expected to continue, and thus research on this topic is imperative, with implications for aquatic ecosystem health in water-rich northern locations.

REFERENCES

Canadian Council of Ministers of the Environment, 1999. Canadian Sediment Quality Guidelines for the Protection of Aquatic Life Mercury, Canadian Council of Ministers of the Environment. CCME, Hull, QC.

Leibman, M., Khomutov, A., and Kizyakov, A. 2014. Cryogenic Landslides in the Arctic Plains of Russia: Classification, machanisms, and Landforms In World Landslide Forum, Beijing, China, 493–497.

Meyers, P.A., and Teranes, J.L. 2001. Sediment Organic Matter, In Last, W.M. and Smol, J.P. (eds.) Tracking Environmental Change Using Lake Sediments. Dordrecht, The Netherlands: Kluwer Academic Publishers, 239–269.

Smol, J.P. 1992. Paleolimnology: an important tool for effective ecosystem management, Journal of Aquatic Ecosystem Health, 1(1): 49–58. doi:10.1007/bf00044408

Segal, R.A., Lantz, T.C., and Kokelj, S.V. 2016. Acceleration of thaw slump activity in glaciated lands capes of the Western Canadian Arctic, Environmental Reasearch Letters, 11(3): 1–12. doi:10.1088/1748-9326/11/3/034025

Ecosystem effects of recent lake desiccation in permafrost landscapes

Lucile Cosyn Wexsteen[1,3,4], Dermot Antoniades[2,3,4] & Frédéric Bouchard[1,3,4]

[1]*Departement of Applied Geomatics, Université de Sherbrooke, Sherbrooke, Québec, Canada*

[2]*Department of Geography, Université Laval, Québec City, Québec, Canada*

[3]*Centre d'études nordiques (CEN), Université de Laval, Québec City, Québec, Canada*

[4]*Groupe de recherche interuniversitaire en limnologie (GRIL), Université de Montréal, Montréal, Québec, Canada*

Recent climate warming has been up to four times greater in the circumpolar North than the global mean. The Hudson Bay Lowlands (HBL), in the subarctic zone of Canada, represent the second-largest permafrost peatland area in the world and contain thousands of shallow lakes, mostly formed by the thawing of ice-rich permafrost (thermokarst). Three major ecozones are identified in the region: the taiga (boreal spruce forest), an interior peat plateau (palsa bog) and the coastal tundra/fen. The HBL provide vital wildlife habitat for more than 500 different species, including polar bears and migratory birds (Macrae et al. 2014). However, studies and observations highlighted a warming climate in the HBL, leading to a decrease per decade in snow cover between May and June of around 17.8% (Derksen and Brown 2012; Kiest 2016). Furthermore, sea ice surface area and thickness, which are responsible for a negative feedback in winter climate, have also been decreasing (Brand et al. 2014; Hochheim et al. 2011; Rühland et al. 2013). In addition, since the early 21st Century, lake-level drawdown or complete desiccation of many lakes has been observed. This kind of hydrological disturbance could, in the long-term, dramatically impact HBL biodiversity (Bouchard et al. 2013; Rühland et al. 2013).

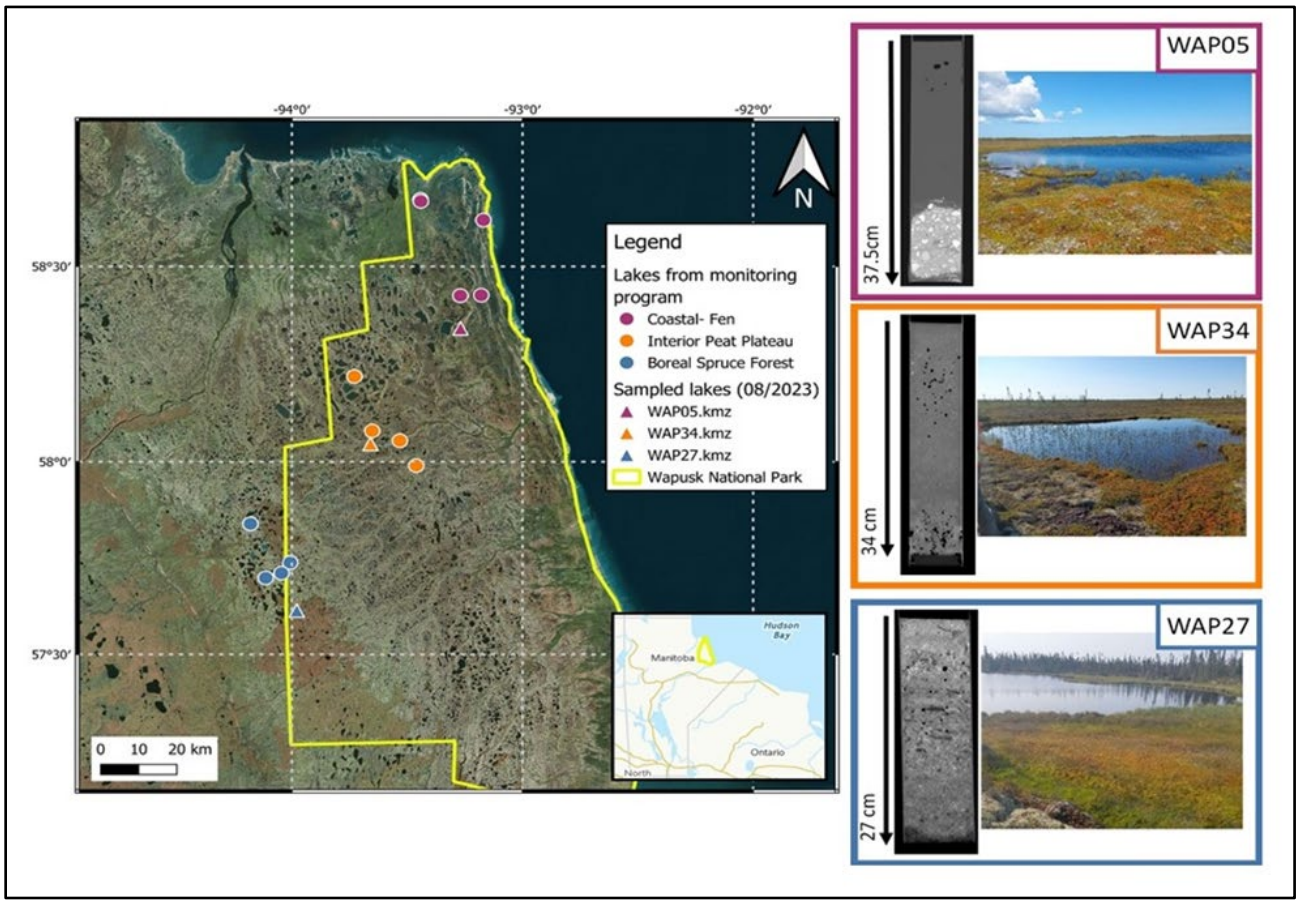

Figure 1. Study area showing the locations of the monitored lakes by Parks Canada. Three of them (WAP05, WAP34 and WAP27), illustrated on the right with accompanying CT-scan images, were sampled in summer 2023.

The main goal of this project is to determine how widespread warming-induced permafrost thawing since the late 20th Century has impacted the regional hydrological balance, including lake connectivity. Interactions between peatlands (which represent more than 35% of the area) and thermokarst lakes, including organic matter accumulation and transfer over time, are also being investigated.

For the study area, data extracted from WorldClim indicate that mean annual air temperature of the region increased by around 1.9°C between 1948 and 2016 (Fick and Hijmans 2017). Preliminary results, based on satellite imagery (Landsat, Sentinel and their products such as Global Surface Water and ESA World Cover 2021), show significant changes in surface water dynamics over the last 30 years in response to this warming, such as the appearance of new seasonal lakes and the loss of many coastal lakes (Pekel et al. 2016). Changes were also detected in land cover, with an important loss of forest in the southern HBL between 2010 and today (Hansen et al. 2013; Zanaga et al. 2022). However, smaller lakes (<1 km^2) are not detected by satellites, but can be assessed using aerial photography. These photographs, with a better spatial resolution, provide an opportunity to reconstruct lake surface change since 1930, 30 years before the first Landsat missions (1960).

The first paleolimnological analysis of cores from the three different ecozones showed differing profiles in terms of composition (sediment, concentration of organic matter). For instance, loss-on-ignition results showed organic matter contents ranging from 10 to 96%. Subfossil diatoms, grain-size and stable isotope analyses will be conducted to reconstruct lake dynamics for the last two centuries.

REFERENCES

Bouchard, F., Turner, K.W., MacDonald, L.A., Deakin, C., White, H., Farquharson, N., Medeiros, A.S., Wolfe, B.B., Hall, R.I., Pienitz, R., and Edwards, T.W.D. 2013. Vulnerability of shallow subarctic lakes to evaporate and desiccate when snowmelt runoff is low. Geophys. Res. Lett. 40, 6112–6117. https://doi.org/10.1002/2013GL058635

Brand, U., Came, R.E., Affek, H., Azmy, K., Mooi, R., and Layton, K. 2014. Climate-forced change in Hudson Bay seawater composition and temperature, Arctic Canada. Chem. Geol. 388, 78–86. https://doi.org/10.1016/j.chemgeo.2014.08.028

Derksen, C., and Brown, R. 2012. Spring snow cover extent reductions in the 2008–2012 period exceeding climate model projections. Geophys. Res. Lett. 39. https://doi.org/10.1029/2012GL053387

Fick, S.E., and Hijmans, R.J. 2017. WorldClim 2: new 1-km spatial resolution climate surfaces for global land areas. Int. J. Climatol. 37, 4302–4315. https://doi.org/10.1002/joc.5086

Hansen, M.C., Potapov, P.V., Moore, R., Hancher, M., Turubanova, S.A., Tyukavina, A., Thau, D., Stehman, S.V., Goetz, S.J., Loveland, T.R., Kommareddy, A., Egorov, A., Chini, L., Justice, C.O., and Townshend, J.R.G. 2013. High-Resolution Global Maps of 21st-Century Forest Cover Change. Science 342, 850–853. https://doi.org/10.1126/science.1244693

Hochheim, K.P., Lukovich, J.V., and Barber, D.G. 2011. Atmospheric forcing of sea ice in Hudson Bay during the spring period, 1980–2005. J. Mar. Syst. 88, 476–487. https://doi.org/10.1016/j.jmarsys.2011.05.003

Kiest, K. 2016. Terrestrial Snow Cover. NOAA Arct. URL https://arctic.noaa.gov/report-card/report-card-2016/terrestrial-snow-cover-7/ (accessed 12.5.23).

Macrae, M.L., Brown, L.C., Duguay, C.R., Parrott, J.A., and Petrone, R.M. 2014. Observed and Projected Climate Change in the Churchill Region of the Hudson Bay Lowlands and Implications for Pond Sustainability. Arct. Antarct. Alp. Res. 46, 272–285. https://doi.org/10.1657/1938-4246-46.1.272

Pekel, J.-F., Cottam, A., Gorelick, N., and Belward, A.S. 2016. High-resolution mapping of global surface water and its long-term changes. Nature 540, 418–422. https://doi.org/10.1038/nature20584

Rühland, K.M., Paterson, A.M., Keller, W., Michelutti, N., and Smol, J.P. 2013. Global warming triggers the loss of a key Arctic refugium. Proc. R. Soc. B Biol. Sci. 280, 20131887. https://doi.org/10.1098/rspb.2013.1887

Zanaga, D., Van De Kerchove, R., Daems, D., De Keersmaecker, W., Brockmann, C., Kirches, G., Wevers, J., Cartus, O., Santoro, M., Fritz, S., Lesiv, M., Herold, M., Tsendbazar, N.-E., Xu, P., Ramoino, F., and Arino, O. 2022. ESA WorldCover 10 m 2021 v200. https://doi.org/10.5281/zenodo.7254221

Mapping change: Regional dynamics of aufeis in northern Alaska

Julian Dann[1], W. Robert Bolton[2], Paul Leonard[3], Kristin Timm[1] & Simon Zwieback[4]

[1]*International Arctic Research Center, University of Alaska Fairbanks, Fairbanks, Alaska, United States*

[2]*Oak Ridge National Laboratory, Oak Ridge, Tennessee, United States*

[3]*U.S. Fish and Wildlife Service, Fairbanks, Alaska, United States*

[4]*Geophysical Institute, University of Alaska Fairbanks, Alaska, United States*

In permafrost regions, the freezing of the seasonal thaw layer, including the downward direction from the surface and upward direction from the permafrost table, can result in increased hydraulic pressure on the unfrozen water between two freezing fronts. This water may be expelled onto frozen ground, river, stream or lake ice or on man-made structures, where it freezes in thin, sheet-like layers (Ensom et al. 2020; Kane 1981). Over the course of a single winter, these individual ice-forming events combine to create a mass of layered ice known as “aufeis”. In German, aufeis translates as “on ice” and is commonly used to refer to all forms of frozen overflow. Other related terms include the English term “icing” and the Russian term “naled”.

Formation processes of aufeis

The formation of aufeis is a function of water availability and freezing conditions, which can be influenced by permafrost, geology, climate, topography, meteorology, and hydrology (Carey 1973; Kane 1981). Climate change processes including rising air temperatures, changes to precipitation, and the associated thaw of permafrost have the potential to change the area, volume, thickness, and timing of aufeis. Interannual variations of aufeis development has been associated with seasonal snow cover thickness (Carey 1973; Yoshikawa et al. 1999), water availability (Carey 1973; Morse and Wolfe 2017, 2015), and winter air temperature fluctuation (Kane 1981; Morse and Wolfe 2015; Sladen 2017; Yoshikawa et al. 2007). Due to the thawing of permafrost and shifts in temperature and precipitation patterns, the distribution and timing of aufeis are expected to change.

Importance of aufeis

An improved understanding and detection of aufeis formation processes and extent is critical to assessing potential socio-economic and environmental risks. Aufeis can be a costly geohazard to infrastructure, including bridges, roads, and culverts. In 2015, large aufeis formations along the Sagavanirktok River on the North Slope of Alaska damaged and closed the Dalton Highway, the only road connecting the Prudhoe Bay oilfield to the Alaskan highway system, for multiple weeks. Transportation and mining activities in the Arctic are commonly required to mitigate the formation of aufeis at drilling pads, bridges, and other stream crossing locations. Conversely, aufeis can play a beneficial role in natural environments by providing a liquid water refuge in winter and maintaining river baseflow throughout summer (Kane and Slaughter 1972; Wanty et al. 2007).

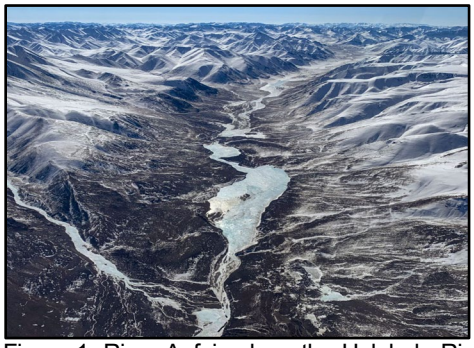

Figure 1. River Aufeis along the Hulahula River of the Arctic Refuge. (Image courtesy of Matt Nolan/Fairbanks Fodar).

Observing aufeis

Mapping of aufeis in North America has focused primarily on the North Slope of Alaska and the Northwest Territory of Canada. Optical satellites (e.g., Dean 1984; Hall and Roswell 1981; Harden et al. 1977; Pavelsky and Zarnetske 2017; Yoshikawa et al. 2007) and synthetic aperture radar (SAR) instruments (e.g., Ajadi et al. 2017; Li Carl Benson et al. 1997; McClernan 2020; Yoshikawa et al. 2007) have been used to study the spatial distribution of aufeis at regional scales. This study uses optical imagery to detect aufeis because it has more established detection algorithms, has a longer timeseries, better resolution, and is more easily interpretable. In the summer, following snowmelt, aufeis is easily discernable in optical satellite imagery due to substantial electromagnetic reflectance contrasts between the land surface, water, and ice. Snow, however, poses a challenge to current detection methods and thus to determining the maximum extent of aufeis.

Current optical detection methods fall into two categories: empirical thresholding of spectral indices

(Morse and Wolfe 2015) or supervised machine learning (Brombierstäudl et al. 2023). We tested both methods on a training dataset containing manually identified land classes (aufeis, ground, snow, etc.). A Bayesian search with K-fold cross validation is used to determine thresholds and fitting hyperparameters. Models are scored using the F1 statistics. Preliminary results show that a random forest approach with 200 trees and a maximum depth of 40 had an F1 score of 0.97 while the empirical approach had an F1 score of 0.84.

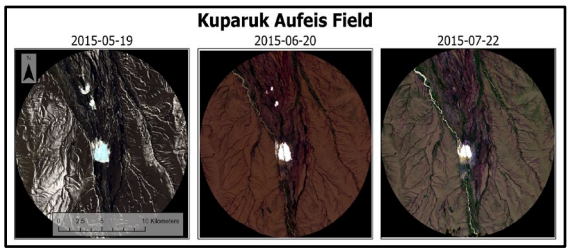

Figure 2. Landsat imagery of the Kuparuk aufeis field during 2015. Images show the melting of aufeis and snow during a two month period between May 19th and July 22nd.

Outcomes of the Project

The purpose of this study is to map the changes in the location, extent, and timing (onset and duration) of aufeis in northern regions of Alaska. It showcases the multispectral capabilities of optical satellite imagery from the Landsat and Sentinel-2 programs in detecting aufeis, even in the presence of snow. This assessment focuses on the visible, near-infrared, and short-wave infrared portions of the electromagnetic spectrum. The goal is to evaluate seasonal and interannual variations in aufeis extent across the North Slope, contributing to a more thorough understanding of ongoing hydrologic changes attributed to a warmer and wetter climate. Additionally, the study anticipates potential impacts on water interconnectivity and habitat dynamics crucial to overwintering and anadromous fish populations.

References

Ajadi, O.A., Meyer, F.J., and Liljedahl, A. 2017. Detection of aufeis-related flood areas in a time series of high resolution SAR images using curvelet transform and unsupervised classification. Presented at the 2017 IEEE International Geoscience and Remote Sensing Symposium (IGARSS), pp. 177–180. https://doi.org/10.1109/IGARSS.2017.8126923

Brombierstäudl, D., Schmidt, S., and Nüsser, M. 2023. Spatial and temporal dynamics of aufeis in the Tso Moriri basin, eastern Ladakh, India. Permafr. Periglac. Process. 34, 81–93.

Carey, K.L. 1973. Icings developed from surface water and ground water.

Dean, K.G. 1984. Stream-icing zones in Alaska. Department of Natural Resources, Division of Geological & Geophysical Surveys.

Ensom, T., Makarieva, O., Morse, P., Kane, D., Alekseev, V., and Marsh, P. 2020. The distribution and dynamics of aufeis in permafrost regions. Permafr. Periglac. Process. 31, 383–395. https://doi.org/10.1002/ppp.2051

Hall, D.K., and Roswell, C. 1981. The origin of water feeding icings on the eastern North Slope of Alaska. Polar Rec. 20, 433–438.

Harden, D., Barnes, P., and Reimnitz, E. 1977. Distribution and Character of Naleds in Northeastern Alaska. ARCTIC 30, 28–40. https://doi.org/10.14430/arctic2681

Kane, D., and Slaughter, C. 1972. Seasonal regime and hydrological significance of stream icings in central Alaska. IAHS Publ 107.

Kane, D.L. 1981. Physical mechanics of aufeis growth. Can. J. Civ. Eng. 8, 186–195. https://doi.org/10.1139/l81-026

Li Carl Benson, S., Shapiro, L., and Dean, K. 1997. Aufeis in the Ivishak River, Alaska, mapped from satellite radar interferometry. Remote Sens. Environ. 60, 131–139. https://doi.org/10.1016/S0034-4257(96)00167-8

McClernan, M.T. 2020. Analysis of the 2015 Sagavanirktok River Flood: Associated Permafrost Degradation Using InSAR and Change Detection Techniques (M.S.). ProQuest Diss. Theses. University of Alaska Fairbanks, United States -- Alaska.

Morse, P.D., and Wolfe, S.A. 2017. Long-Term River Icing Dynamics in Discontinuous Permafrost, Subarctic Canadian Shield. Permafr. Periglac. Process. 28, 580–586. https://doi.org/10.1002/ppp.1907

Morse, P.D., and Wolfe, S.A. 2015. Geological and meteorological controls on icing (aufeis) dynamics (1985 to 2014) in subarctic Canada. J. Geophys. Res. Earth Surf. 120, 1670–1686. https://doi.org/10.1002/2015JF003534

Pavelsky, T.M., and Zarnetske, J.P. 2017. Rapid decline in river icings detected in Arctic Alaska: Implications for a changing hydrologic cycle and river ecosystems. Geophys. Res. Lett. 44, 3228–3235. https://doi.org/10.1002/2016GL072397

Sladen, W. 2017. Icings near the Tibbitt to Contwoyto Winter Road, Great Slave Uplands, Northwest Territories. Carleton University.

Wanty, R.B., Wang, B., Vohden, J., Day, W.C., and Gough, L.P., 2007. Aufeis accumulations in stream bottoms in arctic and subarctic environments as a possible indicator of geologic structure: Chapter F in Recent US Geological Survey studies in the Tintina Gold Province, Alaska, United States, and Yukon, Canada--results of a 5-year project. US Geological Survey.

Yoshikawa, K., Hinzman, L.D., and Kane, D.L. 2007. Spring and aufeis (icing) hydrology in Brooks Range, Alaska. J. Geophys. Res. Biogeosciences 112. https://doi.org/10.1029/2006JG000294

Yoshikawa, K., Petrone, K., Hinzman, L.D., and Bolton, W.R. 1999. Aufeis development and stream baseflow hydrology in the discontinuous permafrost region, Caribou Poker Creek Research Watershed, Interior Alaska, 50th Arctic Science Conference, American Association for the Advancement of Science, 19–22 September 1999, Denali National Park and Preserve, Alaska. Am. Assoc. for the Adv. of Sci. Arctic Div. Fairbanks, pp. 202–203.

The impact of climate and land cover change on permafrost and hydrology in the Mackenzie River Basin

Mohamed Elshamy[1,2], John W. Pomeroy[2,1], Alain Pietroniro[3,2], Howard Wheater[4,1] & Mohamed Abdelhamed[1]

[1]*Global Institute for Water Security, University of Saskatchewan, Saskatoon, Saskatchewan, Canada*

[2]*Centre for Hydrology, University of Saskatchewan, Saskatoon, Saskatchewan, Canada*

[3]*Schulich School of Engineering, University of Calgary, Calgary, Alberta, Canada*

[4]*Department of Civil and Environmental Engineering, Imperial College London, London, United Kingdom*

Continental high latitudes have been warming at higher rates than the global average (DeBeer et al. 2016; Zhang et al. 2019), resulting in extensive permafrost thaw with wide-ranging impacts on soil moisture, hydraulic connectivity, streamflow seasonality, land subsidence, vegetation growth and succession, and wildfire occurrence (DeBeer et al. 2021; Woo et al. 2007; Walvoord and Kurylyk 2016). Earth system models predict that current global warming trends will continue, and some permafrost thaw is projected under all future emission scenarios (Derksen et al. 2019), enhancing global warming through the release of greenhouse gases, mainly methane, stored underground in frozen form (Smith et al. 2022). Accurate simulation of both streamflow and permafrost dynamics is essential for water resources management and climate change impact studies for cold regions. Besides, predicting the state of permafrost and the depth of the active layer is vital for hydrological cycle and river discharge simulations in high latitudes. The permafrost state is intimately linked to hydrological processes, and soil temperature and moisture content (whether frozen or liquid) are directly influenced by the surface water and energy balances. Feedbacks between the surface and the subsurface are complex (Maxwell et al. 2014) and depend on a multitude of factors including changes to precipitation intensity, timing, and phase, as well as soil composition and hydraulic and thermal properties (Walvoord and Kurylyk 2016).

The Mackenzie River Basin (MRB) is the largest river basin in Canada (1.8 M km^2) and is underlain by permafrost of various classes (continuous, discontinuous, and sporadic) for 70-80% of its area. It discharges over 300 km^3 of freshwater annually into the Arctic Ocean's Beaufort Sea, influencing regional and global ocean circulations. The impacts of climate change on this discharge may have implications for ocean ecosystems, salinity, energy budgets, sea ice and global circulation (Yang et al. 2015). Given the large size and hydrological diversity of the basin, ensuring proper simulation of streamflow, seasonal snowpacks, glaciers, evapotranspiration, and permafrost is extremely challenging. As an example of the basin's diversity, the western tributaries of the basin are relatively steep and well-drained, originating from the partially glaciated headwaters in the Canadian Rockies and Mackenzie Mountains, whilst the eastern tributaries drain the level to rolling and poorly drained Canadian Shield of exposed bedrock, lakes, and wetlands. Simulating the permafrost regime requires representation of a deep sub-surface profile (Lawrence et al. 2012; Sapriza-Azuri et al. 2018; Elshamy et al. 2020) with consequently long spin-up periods to properly initialize the energy state at depth.

Here, the MESH distributed hydrological-cryospheric land surface model was set up over the basin to solve for coupled water and energy budgets, forced with bias-corrected, downscaled RCM forcings, and parameterized with snow redistribution by wind and vegetation. It also included a 50 m-deep soil thermophysical profile, organic terrain and glaciers, to couple simulations of hydrological and cryospheric dynamics. The model was partially calibrated against selected river discharge observations and permafrost coverage and validated against discharge and snowpack regimes, permafrost active layer depth and soil temperature observations. The deep profile was initialized by repeating the first 10 years of available forcing data (1951-1960) for 40 cycles to ensure quasi-equilibrium was reached for temperatures in the deepest layers. The resulting high-fidelity model was used to simulate the hydrology, glacier melt and permafrost dynamics over the 21st century under the RCP8.5 climate change scenario using a 15-member GCM-RCM ensemble to assess the uncertainty range.

The results show rapidly increasing rates of permafrost thaw, resulting in an 80% loss by the 2080s, leaving most of the basin permafrost-free (Figure 1). By late century (2071-2100), river discharges are expected to shift to earlier (by 2-6 weeks) and higher peaks (30-50% more) in response to projected increases in precipitation, temperature, snowpack and snowmelt rates, despite increases in evapotranspiration from longer snow-free seasons. Baseflow discharges are expected to increase considerably (doubling or more), due to both enhanced basin connectivity from permafrost thaw and increased precipitation. Soil

moisture storage is expected to rise slightly with a dramatic rise of the liquid moisture fraction and a similar reduction in the frozen one, increasing sub-surface runoff and river discharge. Canadian Rockies deglaciation is projected to reduce summer and annual discharge in the Athabasca and Peace Rivers' headwaters. For example, August discharge for the Athabasca near Jasper is expected at only 30% of its baseline value by late century leading to a reduction of annual flow by 6-16%. Anticipated forest clearing for agricultural land in the south, browning of the boreal forest due to wildfire and disease and shrubification of tundra in the north are expected to amplify climate-induced increases in peak discharge. Downstream and northward of the mountain headwaters, results show that the impacts of climate change on river discharge dominate over those of changing land cover.

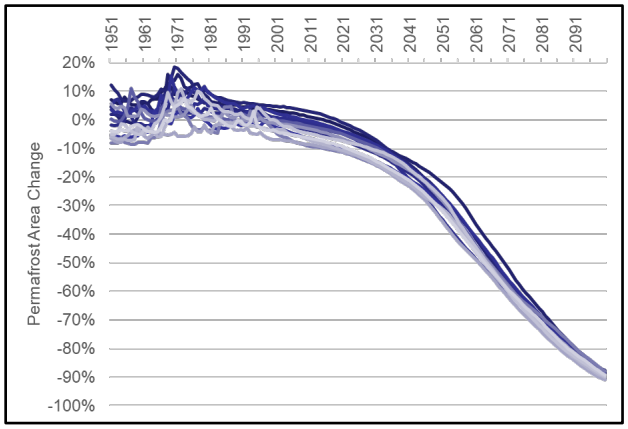

Figure 1. Percentage change in permafrost area within the Mackenzie River Basin compared to 1960-1990 ensemble mean. Different shades are given to different ensemble members.

REFERENCES

DeBeer, C.M., Wheater, H.S., Carey, S.K., and Chun, K.P. 2016. Recent climatic, cryospheric, and hydrological changes over the interior of western Canada: a review and synthesis, Hydrol Earth Syst Sci, 20, 1573–1598. https://doi.org/10.5194/hess-20-1573-2016

Debeer, C.M., Wheater, H.S., Pomeroy, J.W., Barr, A.G., Baltzer, J.L., Johnstone, J.F., Turetsky, M.R., Stewart, R.E., Hayashi, M., Van Der Kamp, G., Marshall, S., Campbell, E., Marsh, P., Carey, S.K., Quinton, W.L., Li, Y., Razavi, S., Berg, A., McDonnell, J.J., Spence, C., Helgason, W.D., Ireson, A.M., Andrew Black, T., Elshamy, M., Yassin, F., Davison, B., Howard, A., Thériault, J.M., Shook, K., Demuth, M.N., and Pietroniro, A. 2021. Summary and synthesis of Changing Cold Regions Network (CCRN) research in the interior of western Canada - Part 2: Future change in cryosphere, vegetation, and hydrology, Hydrol Earth Syst Sci, 25, 1849–1882. https://doi.org/10.5194/hess-25-1849-2021

Derksen, C., Burgess, D., Duguay, C., Howell, S., Mudryk, L., Smith, S., Thackeray, C., and Kirchmeier-Young, M. 2019. Changes in Snow, Ice, and Permafrost Across Canada, in: Canada's Changing Climate Report, 194–260.

Elshamy, M.E., Princz, D., Sapriza-Azuri, G., Abdelhamed, M.S., Pietroniro, A., Wheater, H.S., and Razavi, S. 2020. On the configuration and initialization of a large-scale hydrological land surface model to represent permafrost, Hydrol Earth Syst Sci, 24, 349–379. https://doi.org/10.5194/hess-24-349-2020

Lawrence, D.M., Slater, A.G., and Swenson, S.C. 2012. Simulation of present-day and future permafrost and seasonally frozen ground conditions in CCSM4, J Clim, 25, 2207–2225. https://doi.org/10.1175/JCLI-D-11-00334.1

Maxwell, R.M., Putti, M., Meyerhoff, S., Delfs, J.-O., Ferguson, I.M., Ivanov, V., Kim, J., Kolditz, O., Kollet, S.J., Kumar, M., Lopez, S., Niu, J., Paniconi, C., Park, Y.-J., Phanikumar, M.S., Shen, C., Sudicky, E., and Sulis, M. 2014. Surface-subsurface model intercomparison: A first set of benchmark results to diagnose integrated hydrology and feedbacks, Water Resour Res, 50, 1531–1549. https://doi.org/10.1002/2013WR013725

Sapriza-Azuri, G., Gamazo, P., Razavi, S., and Wheater, H.S. 2018. On the appropriate definition of soil profile configuration and initial conditions for land surface–hydrology models in cold regions, Hydrol Earth Syst Sci, 22, 3295–3309. https://doi.org/10.5194/hess-22-3295-2018

Smith, S.L., O'Neill, H.B., Isaksen, K., Noetzli, J., and Romanovsky, V.E. 2022. The changing thermal state of permafrost. https://doi.org/10.1038/s43017-021-00240-1

Walvoord, M.A., and Kurylyk, B.L. 2016. Hydrologic Impacts of Thawing Permafrost—A Review, Vadose Zone Journal, 15, 0. https://doi.org/10.2136/vzj2016.01.0010

Woo, M.K., Mollinga, M., and Smith, S.L. 2007. Climate warming and active layer thaw in the boreal and tundra environments of the Mackenzie Valley, Can J Earth Sci, 44, 733–743. https://doi.org/10.1139/E06-121

Yang, D., Shi, X., and Marsh, P. 2015. Variability and extreme of Mackenzie River daily discharge during 1973-2011, Quaternary International, 380–381, 159–168. https://doi.org/10.1016/j.quaint.2014.09.023

Zhang, X., Flato, G., Kirchmeier-Young, M., Vincent, L., Wan, H., Wang, X., Rong, R., Fyfe, J., Li, G., and Kharin, V.V. 2019. Changes in Temperature and Precipitation Across Canada; Chapter 4 in Bush, E. and Lemmen, D.S. (Eds.) Canada's Changing Climate Report. Government of Canada, Ottawa, Ontario, pp 112–193.

Thermo-hydrologic processes governing supra-permafrost talik dynamics in discontinuous permafrost near Umiujaq (Québec, Canada)

Philippe Fortier[1,2,3], Nathan L. Young[4], Michelle A. Walvoord[5], Jean-Michel Lemieux[1,2,3] & Aaron A. Mohammed[6]

[1]*Department of Geology and Geological Engineering, Laval University, Québec City, Québec, Canada*

[2]*Centre for Northern Studies, Laval University, Québec City, Québec, Canada*

[3]*Quebec Water Research Centre, Laval University, Québec City, Québec, Canada*

[4]*Department of Sustainable Resource Management, State University of New York, School of Environmental Science and Forestry, Syracuse, New York, United States*

[5]*United States Geological Survey, Earth System Processes Division, Lakewood, Colorado, United States*

[6]*Department of Earth and Environmental Sciences and Department of Civil and Environmental Engineering, Syracuse University, Syracuse, New York, United States*

Widespread supra-permafrost talik formation is currently recognized as a critical mechanism that could accelerate permafrost thaw in the Arctic (e.g., Connon et al. 2018; Farquharson et al. 2022). However, the trajectory of permafrost dynamics following talik formation may prove difficult to predict. Physically-based cryohydrogeologic models provide a powerful tool for understanding processes and factors controlling talik dynamics and, ultimately, how permafrost will respond to climate change. Such models are typically used to represent multiple non-linear processes relevant for groundwater systems in cold regions, such as coupled heat and groundwater movement, including freeze-thaw dynamics and the effects on the surface energy balance and the subsurface thermal and hydraulic properties (Lamontagne-Hallé et al. 2020). Though cryohydrogeologic modeling advances have been made in simulating talik dynamics, few applications have been tested against robust long-term hydrometeorological and subsurface observations.

This study draws on long-term (2000-2022) observations obtained from an extensive instrument network installed at a degrading permafrost mound near Umiujaq (Nunavik, Québec, Canada) (Fortier et al. 2023). Subsurface temperature observations over the last 20 years indicate the permafrost is within the zero curtain (undergoing phase change), while also suggesting possible supra-permafrost talik formation at the site. Observations also indicate a cooler period from 2013 to 2018 (Figure 1) impacted shallow subsurface thermal and hydrologic conditions, although the permafrost temperature observations indicate continued degradation during that period. While Fortier et al. (2023) presented hypotheses for the processes responsible for the observed surface and subsurface dynamics, they were unable to reconcile warming permafrost conditions with the absence of punctuated disturbances or consistent hydroclimatic warming. To further investigate the conditions and physical processes responsible for the degrading permafrost conditions, as well as to better represent infiltration and freeze-thaw dynamics, a 1-D numerical model was constructed using the coupled heat and water transport model SHAW (Flerchinger 2017). Model parameter values reflected the site stratigraphy, namely sand in the 0- to 5-m depth interval and silt in the 5- to 9.25-m interval. Model simulations were run on a daily timestep for the period of October 2000 to October 2020.

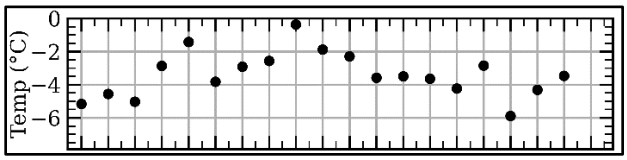

Figure 1. Annual mean air temperature at the study site (after Fortier et al. 2023).

Results

Simulation results (Figure 2) show the formation of a cryotic supra-permafrost talik (< 0°C) which intersected both the initially frozen sand and silt layers and varied in temperature between -0.06 and 0°C. Here, a cryotic talik is defined as a zone where liquid water persists in the pore space above residual saturation levels at temperatures below 0°C, i.e., when temperatures are at a critical transition zone of water-ice phase change, indicating the initial stages of thaw. Valuable insight on the system dynamics can therefore be gained from the model since it captures key processes at the definition threshold between cryotic and non-cryotic (> 0°C) taliks.

As the thaw front penetrates deeper, a seasonal-to-perennial shift in liquid water presence occurs below the active layer due to infiltrated water percolating within the partially frozen pore space,

which impedes frost penetration. The simulated increase in liquid water saturation following ice melt increases the hydraulic and thermal conductivities, allows deeper water movement, and spurs continued thaw and warming. The results of the data-guided simulation also indicate that following a period of colder years, infiltrating water freezes within the talik—as opposed to flowing out of the system when the talik was open—which promotes deeper frost and results in talik closure. The closure of the feature is therefore controlled by thermal conduction, whereas talik formation is driven by thermal advection. While the hydraulic conductivity decreases as pore ice forms, it remains one order of magnitude greater than prior to the talik forming, indicating that the system is more vulnerable to thaw from future warming.

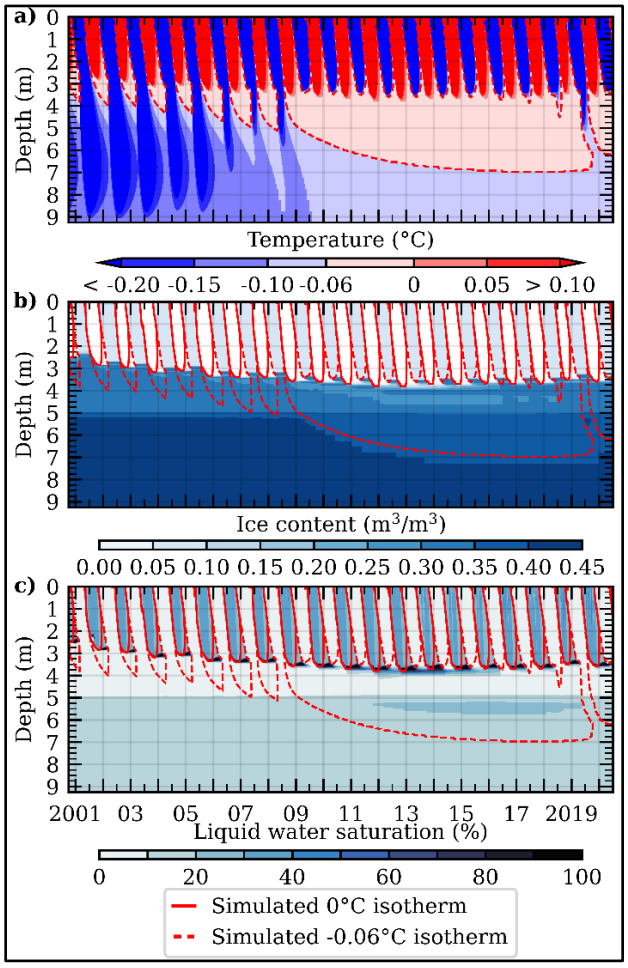

Figure 2. Simulated (a) subsurface temperature, (b) ice content and (c) liquid water saturation between 2000 and 2020. The diverging point of the temperature color scale is centered at -0.06 °C, and not at 0 °C.

IMPLICATIONS

The simulation results suggest that the dynamics of supra-permafrost taliks can reflect the localized effects of high climate variability, particularly in discontinuous permafrost environments characterized by high interannual variability in air temperature. The highly dynamic changes in the hydrogeological structure dictate subsurface water and energy flow in the system in response to multiple feedback loops. Ultimately, this work demonstrates that the trajectories of thermo-hydrologic changes in discontinuous permafrost environments could be less unidirectional and more nuanced than previously thought.

REFERENCES

Connon, R., Devoie, É., Hayashi, M., Veness, T., and Quinton, W. 2018. The Influence of Shallow Taliks on Permafrost Thaw and Active Layer Dynamics in Subarctic Canada. J. Geophys. Res. Earth Surf. 123, 281–297. https://doi.org/10.1002/2017JF004469

Farquharson, L.M., Romanovsky, V.E., Kholodov, A., and Nicolsky, D. 2022. Sub-aerial talik formation observed across the discontinuous permafrost zone of Alaska. Nat. Geosci. 15, 475–481. https://doi.org/10.1038/s41561-022-00952-z

Flerchinger, G.N. 2017. The Simultaneous Heat and Water (SHAW) Model: Technical Documentation (Technical Report NWRC 2017-02). Boise, Idaho, United States Department of Agriculture.

Fortier, P., Young, N.L., Lemieux, J., Walvoord, M.A., and Fortier, R. 2023. Long-Term, High-Resolution Permafrost Monitoring Reveals Coupled Energy Balance and Hydrogeologic Controls on Talik Dynamics Near Umiujaq (Nunavik, Québec, Canada). Water Resour. Res. 59, e2022WR032456. https://doi.org/10.1029/2022WR032456

Lamontagne-Hallé, P., McKenzie, J.M., Kurylyk, B.L., Molson, J., and Lyon, L.N. 2020. Guidelines for cold-regions groundwater numerical modeling. WIREs Water 7, e1467. https://doi.org/10.1002/wat2.1467

Inorganic chemistry of surface waters in palsa mires region of Northern Finland

Joanna Jóźwik[1], Krystyna Kozioł[2], Marcin Frankowski[3], Kamil Nowiński[4], Filip Pawlak[1,5], Żaneta Polkowska[1] & Danuta Szumińska[2]

[1]*Department of Analytical Chemistry, Gdańsk University of Technology, Gdańsk, Poland*

[2]*Department of Geochemistry and Environmental Change, Kazimierz Wielki University, Bydgoszcz, Poland*

[3]*Analytical and Environmental Chemistry Department, Adam Mickiewicz University, Poznań, Poland*

[4]*Department of Hydrology, University of Gdańsk, Gdańsk, Poland*

[5]*Department of Technology in Environmental Engineering, Gdańsk University of Technology, Gdańsk, Poland*

Climate warming in the Northern Hemisphere accelerated permafrost degradation (Streletskiy 2021) and induced the widespread environmental changes in watersheds (Tananayev and Lotsari 2022; Verdonen et al. 2023). In this study, the inorganic chemistry of freshwater (rivers and lakes) in the summer of 2022 in Northern Finland was analysed. The studied water bodies are located at the southern border of permafrost occurrence (sporadic permafrost and isolated patches), in the palsa mires region.

MATERIALS AND METHODS

54 water samples of 10 mL volume were collected between Aug 17th and 25th in the Karasjohka river, their tributary – Viercajohka, seven smaller streams and ten lakes (Figure 1). At selected sites, samples were collected daily or every two days. In lake K5, we also collected water samples from a vertical profile and bottom sediment samples. Each of the collected water samples was filtered using RC syringe filters 0,45 µm.

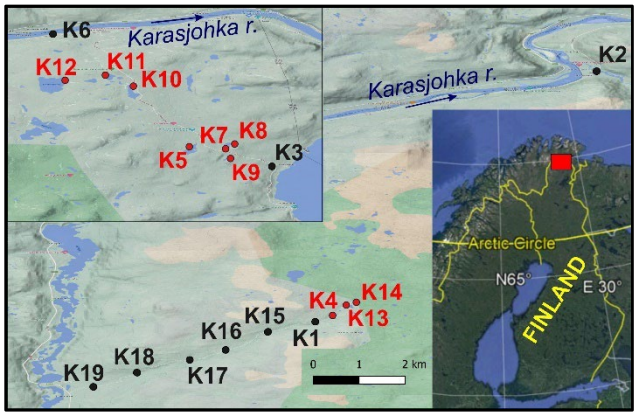

Figure 1. Location of the collected samples. Lake and river sampling points are shown in red and black, respectively. Background: Google Maps.

Bottom sediment samples were mineralised in HNO_3, 65% and HCl, 30% mixture (8:2, v:v, 10 mL per 0.5 g sample), in a microwave pressure digestion device. In case of water samples, we analysed acidified (high-purity HNO_3, Suprapur, Merck Life Science) filtrate. All samples were analysed for elemental concentrations with inductively coupled plasma optical emission spectrometry (ICP-OES 9820, Shimadzu, Japan; for P, S and Ti) and with inductively coupled plasma mass spectrometry (ICP-MS 2030, Shimadzu, Japan; for Ag, Al, As, Ba, Be, Cd, Co, Cr, Cu, Fe, Li, Mn, Mo, Ni, Pb, Sb, Se, Si, Sr, V and Zn). The ICP-MS was calibrated using the ICP IV multielement standard (Merck Life Sciences) and single-element standards of As, Be, Sb, Se, Mo, and V (Sigma-Aldrich), while the ICP-OES was calibrated with single-element 1000 mg/L standards (Sigma-Aldrich). Internal standards controlling for the MS signal were solutions of Sc, Rh, Tb, and Ge in suprapure 1% HNO_3 (Merck). Analytical accuracy was tested against certified reference materials (Sigma-Aldrich) Trace Metals ICP-Sample 1 and Trace Metals ICP-Sample 2, yielding 98-104% recoveries. High-concentration samples were diluted with Milli-Q water (Merck Life Sciences). All measured metal, non-metal and metalloid concentrations have been corrected for a procedural blank value if it exceeded the method limit of quantification (LOQ); otherwise, blank correction was not required.

Total organic carbon (TOC) was determined with a Shimadzu TOC-VCSH/CSN analyser (with catalytic oxidation with oxygen at 720°C, nondispersive infrared spectroscopy detection) and calibrated with a potassium phthalate standard. Coefficient of variation (CV) was below 2% (measured in five replicates). Samples with TOC concentrations exceeding the analytical range were diluted with MilliQ water (18.2 MΩ).

RESULTS AND DISCUSSION

TOC in the collected samples ranged 4.37-25.1 mg/L (mean 12.3 mg/L) in river samples, and 4.76 - 25.7 mg/L (mean 18.1 mg/L) in lake samples. Among the studied elements, iron and aluminium show high concentrations (Fe: 23.4-462 µg/L in rivers,

96-597 µg/L in lakes; Al: 25.8-217 µg/L in rivers, 32.7-155 µg/L in lakes), which is typical for young postglacial areas. For heavy metals, we found low concentrations of As, Cd, Co, Cu, Pb, not exceeding 0.5 µg/L in rivers and lakes, except Cu which were higher in lake K5 (max 2.2 µg/L) and river sample K1 collected in Aug 24th (1.04 µg/L). Hovewer, the higher values were conducted for Ni (0.157-1.59 µg/L in rivers, 0.378-2.76 µg/L in lakes), and Zn (0.259-3.01 µg/L in rivers, 0.611-24.6 µg/L in lakes). The highest concentration of nickel, similarly to copper, were found in water column of lake K5 (at 2- and 3-meters depth). Furthermore, in the bottom sediments of that lake the concentration of Ni, Zn, Cu, Pb and As, amounted to 51, 66.2, 18.9, 5.7, and 3.96 mg/kg, respectively. Such elevated concentrations of elements, including heavy metals, were also indicated in the lakes in Siberia (Szumińska et al. 2023).

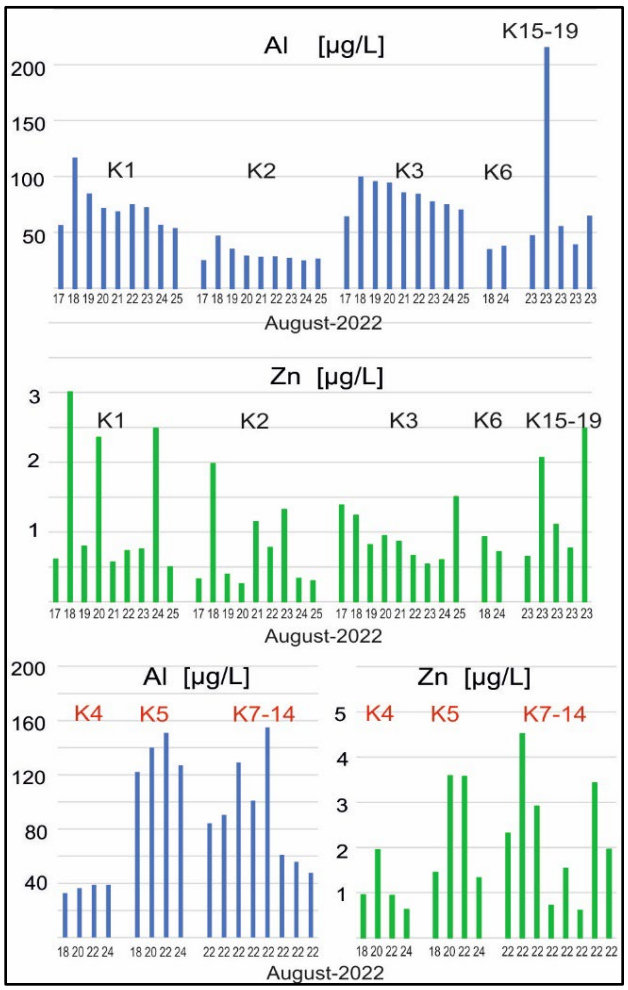

Figure 2. Al and Zn concentration in the collected samples, grouped by sample location (except lakes K7-14 and K15-19, grouped together). All samples were collected between Aug 17th and 25th, 2022.

Al and Zn concentrations showed only occasional variability in time in the sampled rivers within the 9-day sampling window, at a level matched or exceeded by the spatial variability between lakes sampled on the same date (Figure 2). Aluminium concentration increased following an intense rainfall and decreased in the following days. However, zinc concentration noted several peaks. Such different patterns of temporal changes may reflect the varied sources of water feeding the studied rivers and lakes. All sampling sites except K2 (Viercajohka river) and K6 (Karasjohka river) represent small rivers, creeks, and lakes, characterized by the occurrence of palsa mires in their basins.

Conclusions

We found spatial and temporal differences in TOC and elemental concentrations among studied fresh waters, which may reflect connection with the different water sources. An increased concentration of selected elements in vertical profiles and bottom sediments of lake K5 indicate that the lake accumulated metallic pollutants. Further data including organic compounds, cations and anions needs to be analysed to determine the sources of elements, including pollutants, in the studied waters.

Acknowledgements

This research was funded by the National Science Centre of Poland (NCN) grant to project PER2Water, NCN 2021/41/B/ST10/02947, and by the Research Potential Maintenance funds at Gdansk University of Technology.

References

Streletskiy, D. 2021. Permafrost degradation. In: Snow and Ice-Related Hazards, Risks, and Disasters. Elsevier, 297–322. doi:10.1016/B978-0-12-817129-5.00021-4

Szumińska, D., Kozioł, K., Chalov, S.R., Efimov, V.A., Frankowski, M., Lehmann-Konera, S., and Polkowska, Ż. 2023. Reemission of inorganic pollution from permafrost? A freshwater hydrochemistry study in the lower Kolyma basin (North-East Siberia). L. Degrad. Dev., 34; 5591–5605. doi:10.1002/ldr.4866

Tananaev, N., and Lotsari, E. 2022. Defrosting northern catchments: Fluvial effects of permafrost degradation. Earth-Science Reviews, 228, 103996. doi:10.1016/j.earscirev.2022.103996

Verdonen, M., Störmer, A., Lotsari, E., Korpelainen, P., Burkhard, B., Colpaert, A., and Kumpula, T. 2023. Permafrost degradation at two monitored palsa mires in north-west Finland. The Cryosphere, 17, 1803–1819. doi:10.5194/tc-17-1803-2023

Lake-bottom temperature on shallow and deep terraces for sublacustrine open talik assessment near Rankin Inlet, Nunavut, Canada

Anne-Marie LeBlanc, Wendy E. Sladen & Benoit Faucher
Geological Survey of Canada, Natural Resources Canada, Ottawa, Ontario, Canada

Lakes cover about 30% of the region near Rankin Inlet (Nunavut, Canada; Figure 1), and sublacustrine open taliks are expected below several of them (LeBlanc et al. 2022). These may offer pathways for surface and subsurface hydrological interactions and have implications for underground mining operations. Lake-bottom temperature is an important parameter for assessing the potential for open taliks (e.g., Burn 2002). The timing and duration of lake ice contact with sediment beds (bottom-fast ice; BFI), in addition to on-ice snow cover, affect lake-bottom temperature in shallow waters and dictate permafrost presence or absence (Stevens et al. 2010). Most studies on lake-bottom temperatures are mainly on thermokarst lakes in the western Arctic (e.g., Andersen et al. 2021; Roy-Léveillée and Burn 2017). The objective of this study is to characterize lake-bottom temperature on shallow and deep terraces near Rankin Inlet where water depth is less than the maximum ice thickness. This information will improve our efforts to map sublacustrine open taliks in the area.

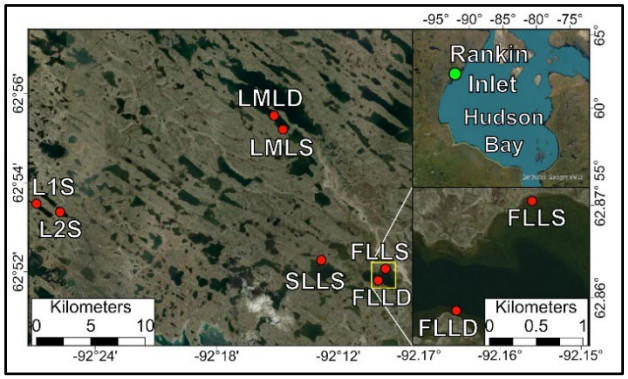

Figure 1. Study sites near Rankin Inlet (Nunavut, Canada). Lakes' name followed by S (shallow) or D (deep terraces).

Study sites and methods

Rankin Inlet is situated within the continuous permafrost zone. Kettle lakes and lakes shaped by glaciofluvial or glacial processes are common in the area, in contrast to thermokarst lakes. The mean annual air temperature (1991–2020) is -9.9°C, and the average annual total precipitation is 314 mm, of which about 40% falls as snow (ECCC 2023). Five lakes were selected to represent a variety of lake sizes, depths, and terrace widths (Figure 1). Maximum lake-ice thickness measured at twelve locations in April 2023 (including three of the study sites) averaged 1.7 m (range of 1.52 to 1.84 m), while the snow cover on lake ice varied from 5 to 40 cm.

Lake-bottom temperature and water level were measured using water level data loggers (Hobo U20L, Onset, accuracy of ±0.44°C and 0.4 cm) at a four-hour interval from mid-June 2019 to early September 2023. Loggers were attached to an anchor and the cable connected to the shoreline and dropped directly on lake terraces about 7-15 m from shoreline. Water depths varied from 0.4 to 0.6 m on shallow terraces and 0.9 to 1.6 m on the deeper terrace areas. Daily mean air temperatures for Rankin Inlet (ECCC 2023) were used to compare climate and lake-bottom freezing and thawing degree days (FDD and TDD).

Results and discussion

Annual mean lake-bottom temperature (T_{lb}) at shallow terraces was below 0°C at all sites except LMLS (Figure 2A). At the two deep terrace sites, T_{lb} was 0°C or higher. There is no apparent relation between water depth and T_{lb}. Positive T_{lb} (or at 0°C) at deep terrace sites is inversely related (R^2 =~0.8) to freezing season length (< 160 days), an association that is likely related to the timing and duration of BFI (Figure 2B). LMLS, with T_{lb} of 0 and 0.8°C at 0.5 m water depth, is the exception with more than 200 days of temperatures below 0°C. At all sites, daily lake-bottom temperatures during the summer are similar between shallow and deep terraces due to water column mixing (Figure 3). Across all sites and years, there is an apparent relation between air and lake-bottom TDD (R^2 =~0.9), while there is none for FDD (Figure 4). At LMLS, lake-bottom TDD is not higher than at other sites (Figure 4) and could not explain high T_{lb}. Over the freezing season, temperatures at FLLD remain slightly above 0°C until late January when BFI forms, while temperatures at FLLS drop rapidly after the onset of the freezing season in early November, reaching a minimum of -10°C (Figure 3). In contrast, at LML, temperatures in shallow waters were higher than in deeper waters. The zero-curtain length was ~20 days higher at LMLS compared to the median length at other sites preventing the sediment bed from freezing rapidly. A thicker snow cover than

the range observed in April 2023 could also explain the positive T_{lb} observed at this site (Roy-Léveillée and Burn 2017) but need to be validated in the field.

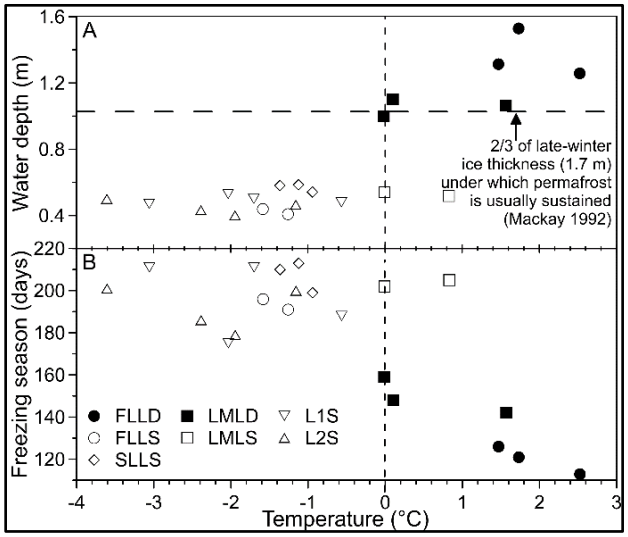

Figure 2. Relations between annual mean lake-bottom temperatures (T_{lb}) for shallow (S) and deep (D) terrace sites and A) water depth, and B) freezing season (temperature below 0°C) at lake-bottom.

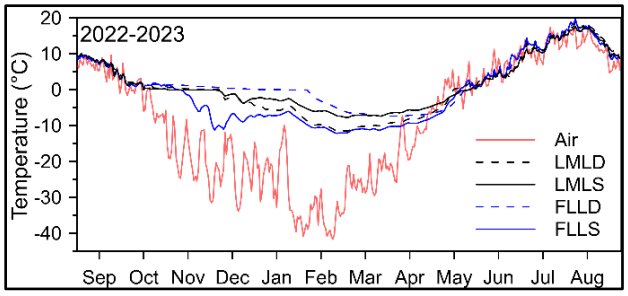

Figure 3. Examples of mean daily temperature at FLL and LML for shallow (S) and deep (D) terraces for 2022-2023. Similar thermal regimes were observed in previous years.

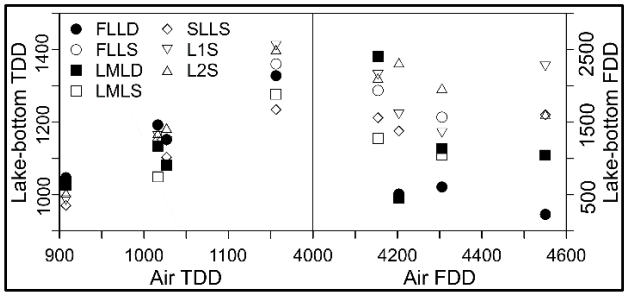

Figure 4. Relation between air and lake-bottom thawing (TDD) and freezing degree-days (FDD) for shallow (S) and deep (D) terrace sites.

The results indicate T_{lb} on terraces deeper than 1 m (~2/3 of maximum ice thickness, Mackay 1992) is insufficient to maintain permafrost. For select terraces <1 m deep, the freezing season length alone may not be indicative of T_{lb} <0°C and that other factors must be considered such as snow. Comparison of these results to our BFI classification (Sladen et al. this volume) will be used to refine SAR imagery dates and the BFI period required to sustain sublacustrine permafrost in this region.

Acknowledgements

This research is supported by Natural Resources Canada, Climate Change Geoscience and GEM-GeoNorth Programs, contribution number 20230343.

References

Andersen, T.S., Jardine, P.A., and Burn, C.R. 2021. Long-term (200-2017) response of lake-bottom temperature to climate variation in two adjacent tundra lakes, western Arctic coast, Canada. In Proceedings of the 19th International Conference on Cold Regions Engineering and the Regional Conference on Permafrost Cold Regions Engineering, Boulder, CO, United States, 1-9.

Burn, C.R. 2002. Tundra lakes and permafrost, Richards Island, western Arctic coast, Canada, Canadian Journal of Earth Science, 39(8): 1281–1298. doi:10.1139/e02-035

ECCC. 2023. Environment and Climate Change Canada. https://climate.weather.gc.ca/, accessed Oct. 15, 2023.

LeBlanc, A.-M., Chartrand, J., and Smith, S.L. 2022. Regional assessment of the presence of taliks below Arctic lakes, Nunavut; Geological Survey of Canada, Scientific Presentation 138, 1 poster. doi:10.4095/330205

Mackay, J.R. 1992. Lake stability in an ice-rich permafrost environment: Examples from the western Arctic coast, in Aquatic Ecosystems in Semi-arid Regions: Implications for Resource Management. In Symposium Series, National Hydrol. Res. Inst., Environ, Saskatoon, Canada: 1–25.

Roy-Léveillée, P., and C.R. Burn. 2017. Near-shore talik development beneath shallow water in expanding thermokarst lakes, Old Crow Flats, Yukon, Journal of Geophysical Research Earth Surface, 122: 1070–1089. doi:10.1002/2016JF004022

Sladen, W.E., LeBlanc, A-M., van der Sanden, J., and Chartrand, J. Using RADARSAT Constellation Mission Imagery to Support Talik Mapping, Rankin Inlet, Nunavut, Canada. In the International Conference on Permafrost 2024, This volume.

Stevens, C.W., Moorman, B.J., and Solomon, S.M. 2010. Modeling ground thermal conditions and the limit of permafrost within the nearshore zone of the Mackenzie Delta, Canada. Journal of geophysical research, 115. doi:10.1029/2010JF001786

Impacts of permafrost thaw below rivers on cryohydrological processes and man-made infrastructure in permafrost regions

Weibo Liu[1], Mingyi Zhang[1], Richard Fortier[2], John Molson[2], Jean-Michel Lemieux[2] & Yan Lu[1]

[1]*State Key Laboratory of Frozen Soil Engineering, Northwest Institute of Eco-Environment and Resources, Chinese Academy of Sciences, Lanzhou, Gansu, China*

[2]*Centre d'études nordiques (CEN), Université Laval, Québec City, Québec, Canada*

Continuous permafrost environments are found at high altitudes such as on the Qinghai-Tibet Plateau, China, and at high latitudes such as in Nunavik (Québec), Canada, which also contain a large number of rivers and lakes. Permanently unfrozen zones within permafrost, called taliks, can form beneath these water bodies which can enhance the flow and exchange between groundwater and river runoff water. The dynamics of these river-talik systems in continuous permafrost environments is complex and not well understood. In summer, when a talik is hydraulically connected to the riverbed, groundwater flow in the river talik can contribute to river baseflow (Liu et al. 2021 and 2022). However, when the riverbed freezes back in winter and the talik is hydraulically disconnected from the riverbed, groundwater pressure can build up in the aquifer at talik constrictions which can crack the frozen riverbed, produce an overflow of suprapermafrost groundwater in the river floodplain, and contribute to icing formation (Liu et al. 2021, 2022). Permafrost degradation beneath a riverbed can also potentially cause riverbed settlement which can subsequently damage bridge foundations.

Objectives

To address the lack of knowledge on the dynamics of river-talik systems in continuous permafrost environments, the following objectives were established : 1) to monitor the thermal regime of a talik beneath a small stream in the Beiluhe River Basin, Qinghai-Tibet Plateau, China, 2) to perform 2D numerical modelling of fully coupled groundwater flow and heat transfer in this river-talik system, and 3) to assess the dynamics of the river-talik system.

Study site

The study site is a small stream at an elevation of about 4628 m in the continuous permafrost zone in the Beiluhe River Basin (34° 49' N, 92° 56' E), Qinghai-Tibet Plateau, China. The mean annual air temperature from 1980 to 2020 was -4.13 °C, with temperature increasing at a rate of about 0.7 °C/10a.

Methods

In late October 2021, a 16 m deep borehole was drilled in the stream bed and a thermistor cable and a water pressure transducer was then installed in the borehole to monitor ground temperature and hydraulic head in the talik (Figure 1).

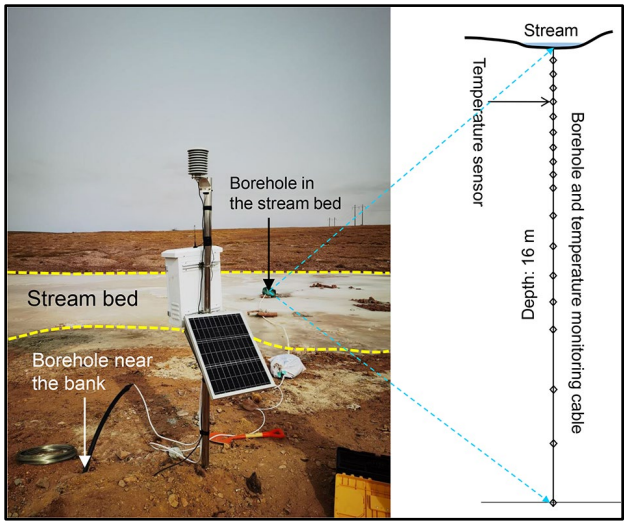

Figure 1. Thermistor cable installed in a borehole drilled in the stream bed in the Beiluhe River Basin, Qinghai-Tibet Plateau, China, along with a meteorological station.

2D numerical modelling of fully coupled groundwater flow and advective-conductive heat transfer using the numerical code Heatflow-Smoker (Molson and Frind 2022) was also undertaken to simulate the cryohydrological processes taking place in the complex river-talik system. Different widths of the riverbed along with future climate warming scenarios at the study site were also considered in the numerical modelling.

Results

Observed air temperature and ground temperature from 2022/01 to 2023/04 is provided in Figure 2. The mean annual air temperature of the study site is -2.01 °C while the permafrost temperature at a depth of 10 m beneath the stream bed is -0.22 °C over that period. There is indeed a 2 m thick talik beneath the

stream bed. The talik base is at a depth of about 4 m with a slight annual change of few decimeters due to the annual cycle of air temperature. The annual variations in the talik base depth are asynchronous with annual air temperature variations due to the phase shift of heat transfer with depth. The freezing front in the stream bed reached a depth of 2.2 m in July 2022. During the field investigations, a significant amount of groundwater was also found in the talik which can be exploited by pumping as a potential source of drinking water for the nearby inhabitants.

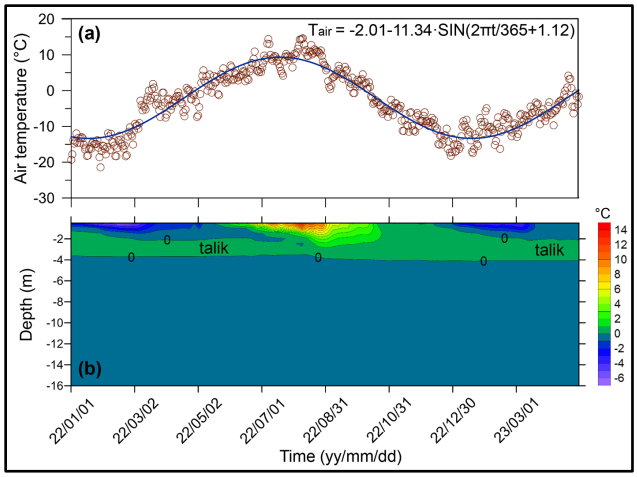

Figure 2. (a) Time series of mean daily air temperature from 2022/01 to 2023/04 and (b) variations in ground temperature beneath the stream bed as a function of depth and time for the same period at the study site in the Beiluhe River Basin, Qinghai-Tibet Plateau, China.

In addition, taking into account anticipated future climate warming scenarios at the study site, the talik and permafrost dynamics were simulated to assess the impacts of climate warming on the cryohydrological processes taking place in the stream-talik system. The simulation results show that, by the middle to late 21st century, permafrost beneath the vast majority of the rivers on the Qinghai-Tibet Plateau will be completely thawed which will form large-scale through-taliks beneath the riverbeds. The specific degree of permafrost thaw and disapperance is related to the river width and local permafrost conditions. Such through-taliks will severely impact the existing water cycle on the Qinghai-Tibet Plateau. Permafrost degradation beneath the riverbeds can also lead to riverbed settlement which will induce thaw subsidence and possible collapse of bridge foundations, resulting in disruption of road traffic and severe economic losses. Most of these bridges were built before the 21st century without considering the possible impacts of climate warming on permafrost dynamics. For instance, thaw induced settlement of about 38 cm of a railway bridge foundation pier of the Qinghai-Tibet Railway occurred over a 4-year period from 2009/02 to 2013/11 (Quan 2017) which seriously affected its performance and safety. Moreover, thawing permafrost near river banks can lead to bank collapse, and river diversion, and can pose threats to near-bank roadways or other infrastructure.

Outcomes

In order to better understand these systems and improve the performance of numerical models, more observations are needed. However, field monitoring work at rivers in permafrost areas is extremly difficult to perform. For instance, drilling boreholes and installing monitoring cables in a river are challenging tasks and pose environmental risk. In addition, numerical modelling of river-talik systems generally needs to consider 3D multi-process coupling which is also very challenging. Research related to rivers in permafrost areas is relatively limited which should receive more attention in future research activities.

References

Liu, W., Fortier, R., Molson, J., and Lemieux, J.-M. 2021. A conceptual model for talik dynamics and icing formation in a river floodplain in the continuous permafrost zone at Salluit, Nunavik (Quebec), Canada, Permafrost and Periglacial Processes, 32(3): 468–483. doi:10.1002/ppp.211

Liu, W., Fortier, R., Molson, J., and Lemieux, J.-M. 2022. Three-dimensional numerical modeling of cryo-hydrogeological processes in a river-talik system in a continuous permafrost environment, Water Resources Research, 58(3), e2021WR031630. doi:10.1029/2021WR031630.

Molson, J.W., and Frind, E.O. 2022. HEATFLOW-SMOKER: Density-dependent flow and advective-dispersive transport of thermal energy, mass or residence time, User Guide. Université Laval, Québec (QC), Canada, and University of Waterloo.

Quan, D. 2017. Cause Analysis of Bridge Pile Foundation Subsidence of the Qinghai-Tibet Railway in Permafrost Region, Railway Engineering, 1: 76–79. doi:10.3969/j.issn.1003-1995.2017.01.17 (In Chinese)

The role of soil moisture on active layer thaw near Yellowknife, NWT

Alana Muenchrath[1], Christopher Spence[2] & Andrew Ireson[1]
[1]*University of Saskatchewan, Saskatoon, Saskatchewan, Canada*
[2]*Environment and Climate Change Canada, Calgary, Alberta, Canada*

Increasing active layer thickness (ALT) is a widespread indication of permafrost degradation due to climate warming. Understanding environmental factors which influence ALT is important for predicting changes in hydrogeological pathways and biogeochemical fluxes. Soil moisture is an important factor influencing active layer thaw because it modifies soil thermal properties and heat transfer into the ground. Soil moisture influences ground thaw in two important ways: i) thermal conductivity: water has a high thermal conductivity which increases four-fold upon freezing, effectively allowing heat to transfer into the ground which can enhance thaw. Conversely, dry soils provide insulation between the surface and subsurface, delaying thaw and decreasing ALT; ii) latent heat: wet soils, with a high ice content, require large amounts of energy to thaw which can decrease ALT, while drier soils may develop thicker active layers. Due to these counteracting effects, and the compounding influence of biophysical factors, empiricial and numerical investigations have produced a divergence of findings on whether high soil moisture has a preserving or degradational effect on near-surface permafrost (Loranty et al. 2018; Smith et al. 2022). In this study we provide empricial evidence to elucidate the role soil moisture has on active layer thaw within a forested valley in the discontinous permafrost region.

METHODS

The study site is located ~7 km north of Yellowknife, NWT (62°35'43'' N, 114°26'28'' W), experiencing a mean annual air temperature of -4°C and annual precipititation ranging between 280–340 mm (Spence and Hedstrom 2018). Observations of soil moisture and temperature were taken at seven vertical profiles (instruments at 0, 15, 30 and 45 cm depth), located 2–10 m from one another and denoted A–G. This was done to minimize the influence of variable biophysical factors (i.e., soil type, vegetation, groundcover) and meteorological conditions. The site is comprised of a ~25 cm upper organic layer overlying silty clay mineral soil. Between the seven instrumented nests, mean organic soil layer thickness was 23 cm (SD = 7.2). Dominant vegetation of the landcover includes black spruce (Picea mariana) and tamarack (Larix laricina), with an understory of Labrador tea (Ledum groenlandicum), green alder (Alnus crispa), willow (Salix spp), moss (Sphagnum spp) and lichen (Cladonia spp).

RESULTS AND DISCUSSION

Despite the proximity of profiles, there was substantial variability in soil water storage (Figure 1A). Pre-freezing storage in the autumn of 2015 ranged from 13 cm (D) to 30 cm (G) (markers, Figure 1A). In the following spring, soil temperatures at 45 cm depth revealed the wettest profile (G) thawed nearly three weeks earlier than the driest profile (D) (markers, Figure 1B). Note that profiles which thaw earlier were found to correlate with greater ALT, as was observed from 2023 measurements (Figure 2).

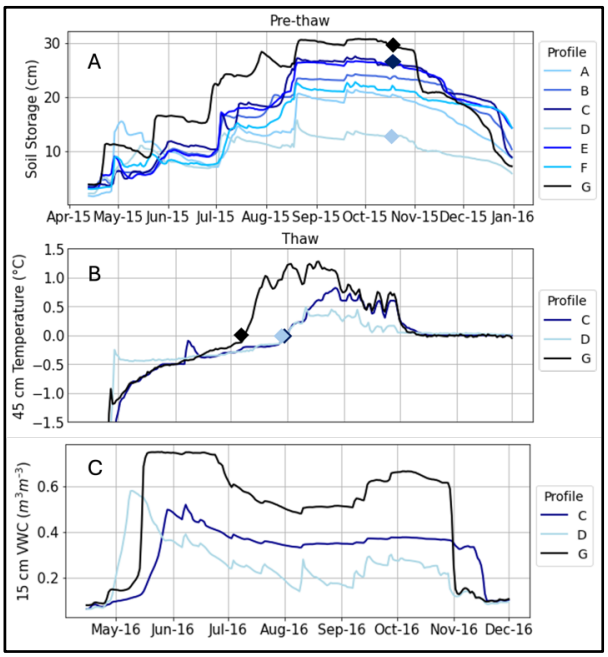

Figure 1. A) 2015 pre-freezing soil storage, B) 2016 soil temperatures at 45 cm, and C) 2016 soil moisture at 15 cm. Markers denote antecedent storage and corresponding thaw of profiles G, C and D.

These findings suggest that wet soils exhibit deeper thaw in response to high thermal conductivity, while low heat transfer in dry soils limits the progression of thaw and thickness of the active layer, dominating over the influence of latent heat.

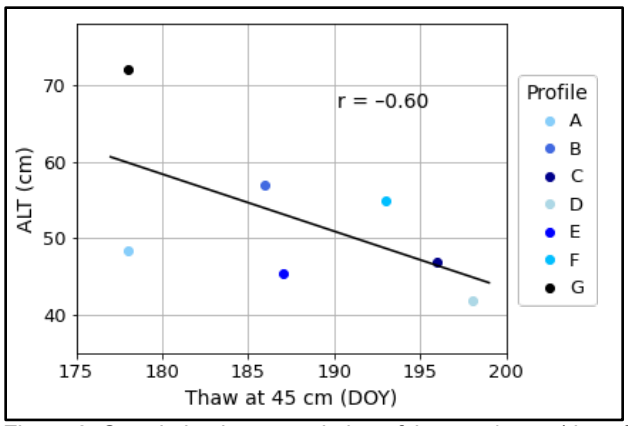

Figure 2. Correlation between timing of thaw at 45 cm (day of year, DOY) and ALT (cm) from 2023 data.

This pattern was exemplified in the wettest and driest profiles, but no consistent relationship between pre-freezing soil storage and progression of thaw was found. For instance, Profile C, with the second highest storage, thawed at a similar time to Profile D (Figure 1 A, B), demonstrating that depth integrated soil storage can not explain thaw dynamics alone.

It is hypothesized that near-surface conditions play an important role in determining thaw progression, and can assist in explaining variability in moisture–ALT dynamics. Profile D and G exhibit very dry and very wet near-surface conditions, with thaw-season water content averages of 0.27, and 0.61, respectively (Figure 1C). The corresponding low and high near-surface thermal conductivities inhibit (and enhance) heat transfer which ultimately dictates ALT, dominating over the effects of latent heat. Whereas in Profile C, with an average near-surface soil moisture of 0.37, had an intermediate thermal conductivity which was insufficient to dominate thaw progression over the large latent heat requirements associated with a high ice content. These findings suggest there may be soil moisture thresholds which determine when one thermal process influences ALT more strongly than the other.

This complex dynamic demonstrates that a straightforward relationship between depth integrated soil moisture and ALT is difficult to resolve, even within one region. This aligns with the findings of Clayton et al. (2021) who reported a negative correlation between ALT and bulk water content, yet positive correlations when assessing water content at 6 and 12 cm depth, indicating both latent heat and thermal conductivity play a role in governing thaw. Similarly, Guan et al. (2010) found near surface moisture to have a postitive yet complex relationship with ground thaw, positing that relationship strength was a function of degree of saturation.

Conclusions

Observations of soil moisture and active layer thaw demonstrate a complex relationship between soil water content and ALT. Findings suggest near-surface soil moisture and corresponding thermal conductivity may dictate ground thaw by limiting or enhancing heat transfer, which may dominate ALT trends over the effects of latent heat. This dynamic was apparent when comparing very wet and dry soils, however no consistent relationship was found between intermediate water contents, suggesting there may be thresholds or constraints for when one thermal processes dominates over the other. These findings emphasize the importance of considering the vertical distribution of soil moisture in the active layer in permafrost models and when assessing the implications of changing landscape wetness.

References

Clayton, L, Schaefer, K., Battaglia, M., Bourgeau-Chavez, L., Chen, J., Chen, R., Chen, A., et al. 2021. Active layer thickness as a function of soil water content, Environmental Research Letters, 16 (5), 055028. doi:10.1088/1748-9326/abfa4c

Guan, X., Westbrook, C., and Spence, C. 2010. Shallow soil moisture – ground thaw interactions and controls – Part 1: Spatiotemporal patterns and correlations over a subarctic landscape. Hydrology and Earth System Sciences, 14(7), 1387–1400. doi:10.5194/hess-14-1375-2010

Loranty, M.M., Abbott, B.W., Blok, D., Douglas, T.A., Epstein, H.E., Forbes, B.C., Jones, B.M., et al. 2018. Reviews and syntheses: Changing ecosystem influences on soil thermal regimes in northern high-latitude permafrost regions. Biogeosciences 15, 5287–5313. doi:10.5194/bg-15-5287-2018

Smith, S.L., O'Neill, H.B., Isaksen, K., Noetzli, J., and Romanovsky, V.E. 2022. The changing thermal state of permafrost. Nat Rev Earth Environ 3, 10–23. doi:10.1038/s43017-021-00240-1

Spence, C., and Hedstrom, N. 2018. Hydrometeorological data from Baker Creek Research Watershed, Northwest Territories, Canada. Eart. Syst. Sci. Data, 10, 1753–1767. doi:10.5194/essd-10-1753-2018

Assessing the fate of toxic metals from permafrost thaw in aquatic ecosystems

Jonathan A. O'Donnell[1], Michael P. Carey[2], Joshua C. Koch[2], Carson Baughman[2], Kenneth Hill[1], Taylor Evinger[3], Benjamin Peterson[3], Sarah E. Janssen[4], Elchin Jafarov[5] & Brett A. Poulin[3]

[1]*National Park Service, Arctic Network, Anchorage, Alaska, United States*

[2]*United States Geological Survey, Alaska Science Center, Anchorage, Alaska, United States*

[3]*University of California Davis, Department of Environmental Toxicology, Davis, California, United States*

[4]*United States Geological Survey, Mercury Research Lab, Madison, Wisconsin, United States*

[5]*Woodwell Climate Research Center, Woods Hole, Massachusetts, United States*

Climate change in the Arctic is altering watershed hydrologic processes and biogeochemistry. Permafrost is thawing in response to rapid warming, shifting surface and subsurface hydrology across Arctic landscapes. Further, permafrost stores large amounts of carbon, nutrients, and metals, many of which are hundreds to thousands of years old. Following thaw, these elements and compounds can be released into terrestrial and aquatic ecosystems. While considerable advances have been made with respect to the permafrost carbon feedback and cycling of permafrost nutrients (Schuur et al. 2015), large uncertainties exist regarding the fate of toxic metals in Arctic ecosystems. Of particular concern is the increased flux of metals to aquatic ecosystems, where metals can degrade water quality and fish habitat, and bioaccumulate across trophic levels in food webs. Here, we discuss two complimentary studies that aim to track the fate of toxic metals released from thawing permafrost to aquatic ecosystems: (1) Rusting Rivers and (2) Permafrost Mercury.

Rusting rivers

Recent evidence indicates that permafrost thaw may impact mobilization of iron from soils to streams (Barker et al. 2023). Here, we have compiled observations of more than 70 streams and rivers that have turned from pristine clear water to orange over the past 10-15 years across Alaska's Brooks Range (O'Donnell et al. In Revision). The "rusting" of Arctic rivers is primarily due to the presence of oxidized iron (Fe(III)) particulates that are transported via stream flow and deposited on stream sediments. In addition to the elevated concentrations of iron, we observed higher acidity, turbidity, sulfate and trace metal concentrations in orange streams compared to clear water reference streams. We also documented impacts to stream biota following an abrupt shift from clear to orange conditions, with a dramatic decrease in benthic macroinvertebrate biodiversity and complete loss of fish species Dolly Varden (Salvelinus malma) and Slimy Sculpin (Cottus cognatus).

Given the recent onset of rusting rivers across the Brooks Range, we contend that climate and permafrost thaw are likely drivers of iron and trace metal mobilization to aquatic ecosystems. Recent climate change in northern Alaska has contributed to widespread warming and thawing of permafrost. We collected surface water samples from orange stream reaches and nearby clearwater reference streams to to assess chemical shifts associated with stream discoloration. Samples were analyzed for metals, anions (e.g., sulfate), and carbon species (dissolved organic carbon (DOC), dissolved inorganic carbon (DIC)). We also collected in situ measurements of water quality, including specific conductivity and pH. Geochemical evidence from these measurements indicates that permafrost thaw is likely exposing sulfide minerals to chemical weathering, a phenomenon that is common in upland mountainous terrain in the region. In lowland terrain, permafrost thaw can affect soil drainage and redox, and the subsequent microbially facilitated mobilization of iron. The consequences of acid and trace metal inputs to streams depends in part on the presence of dissolved organic carbon (DOC) and dissolved inorganic carbon (DIC). DOC can bind with trace metals (e.g., copper, zinc) controlling their bioavailability, and ultimately their toxicity to stream biota. DIC functions to control buffering capacity, or alkalinity, mitigating the magnitude of acid release on stream pH. More work is ongoing to discern how rusting rivers are impacting food web dynamics and habitat quality for resident and anadromous fish.

Permafrost mercury

Permafrost soils of the Arctic contain vast reservoirs of ancient mercury (Schuster et al. 2018), which is being released to freshwater environments following thaw. Inundation of permafrost soils accelerates thaw and creates conditions favorable for anaerobic microbial processes, such as the formation of toxic

methylmercury and methanogenesis. For this study, we are evaluating the relative importance of mercury from ancient permafrost soils versus contemporary mercury from the atmosphere, and how rapidly changing conditions in Arctic landscapes will affect the transformations and food web uptake of these different sources of mercury. To address these questions, we are using a multi-disciplinary approach to track the releases, transformations, and uptake of both carbon and mercury from permafrost soils to fish.

We sampled surface waters, sediment porewaters, and resident fish from beaver ponds and thermokarst lakes in Arctic national parks. Initial findings indicate that inundation from beaver impoundments create methylmercury hotspots, with the highest concentrations observed in sediment porewaters (1-8 ng L^{-1}). Further, we document how redox status decreases with time since beaver pond formation, and older ponds have higher mercury content in fish than younger ponds. Finally, we observed a positive correlation between methylmercury and dissolved methane concentrations, highlighting the potential to model mercury transformations in lakes and ponds. Ongoing work is aimed at (1) using molecular techniques to explore the role of ancient DOC in fueling microbial formation of methymercury, and (2) using radiocarbon and mercury stable isotopes to constrain the contribution of ancient carbon and mercury to aquatic food webs.

IMPLICATIONS FOR WATER QUALITY AND SUBSISTENCE RESOURCES

Together, these findings indicate that the release of mercury and other trace metals from thawing permafrost may represent a novel threat to water quality and subsistence fisheries in Arctic Alaska. For instance, trace metals transported from rusting headwater streams to higher-order rivers may impact drinking water supplies in rural communities. While our initial measurements indicate that metalloids such as arsenic and trace metals of concern did not exceed U.S. EPA drinking water criteria in the impaired reaches tested, this needs to be verified across the Brooks Range. Our preliminary data also suggest that metal mobilization may increase the vulnerability of important subsistence fish species—such as Dolly Varden, chum salmon (Oncorhynchus keta), and whitefish (Coregonus sp.)—to population decline due to both toxic effects and habitat degradation. Further, the potential for mercury to biomagnify through the food web may affect food quality as permafrost thaw increases the pool of actively cycling mercury in Arctic ecosystems. Future work will aim better understanding the causes and consequences of metal mobilization in Arctic watersheds.

REFERENCES

Barker, A.J., et al. 2023. Iron oxidation-reduction processes in warming permafrost soils and surface waters expose a seasonally rustic arctic watershed. ACS Earth Space Chem. 7, 1479–1495.

O'Donnell, J.A., et al. (In Press). Rusting of the Arctic: Metal mobilization from thawing permafrost to aquatic ecosystems. Submitted to Communications Earth & Environment.

Schuster, P.F., et al. 2018. Permafrost stores a globally significant amount of mercury. Geophysical Research Letters 45: 1463–1471.

Schuur, E.A.G., et al. 2015. Climate change and the permafrost carbon feedback. Nature 520: 171–179.

Late-summer sulfate and metal(loid)s mobilization in a continuous permafrost catchment

Elliott K. Skierszkan[1,2], Arsh Grewal[3], Andras J. Szeitz[3], Matthew B.J. Lindsay[2] & Sean K. Carey[3]

[1]*Department of Earth Sciences, Carleton University, Ottawa, Ontario, Canada*

[2]*Department of Geological Sciences, University of Saskatchewan, Saskatoon, Saskatchewan, Canada*

[3]*School of Earth, Environment and Society, McMaster University, Hamilton, Ontario, Canada*

This study evaluates seasonal sulfate and metal(loid) (e.g., Al, Cd, Cu, Ni, Se, Zn) loading in a headwater catchment draining metalliferous shale and overlying continuous permafrost (Slavin Creek, Yukon, Canada). Stream hydrological and chemical monitoring reveals that sulfate and metal concentrations increase from spring through summer, routinely exceeding water-quality guidelines for the protection of aquatic life. The largest seasonal flux of these solutes occurs in spring, yet a second rise in fluxes is observed in late summer under relatively lower stream flows. This late-season mobilization of metal(loid)s and sulfate is consistent with seasonal changes in subsurface flowpaths and their associated chemistry as the active layer expands.

Study area and methodology

The stream studied is Slavin Creek, a ~10 km^2 catchment overlying continuous permafrost along the Dempster Highway, Yukon, Canada (64.706°N, 138.406°W). The catchment drains Palaeozoic marine siliciclastic (shale, siltstone, sandstone, chert, and slate) and carbonate rocks of the Selwyn basin. Slavin Creek has been monitored since 2019 as part of the Tombstone Waters Observatory led by the McMaster University Watershed Hydrology Group. Zero-discharge conditions occur during the coldest months of year (e.g., December to March) but over-winter buildup of channel ice suggests some discharging groundwater.

Thirty-five synchronous stream concentration-discharge (C-Q) samples were collected over the months of May to September, between 2021 and 2023. Discharges were measured using a flow-meter, salt-dilution gauging, and/or inferred from pressure transducers co-located with a stream gauging station. Chemical analyses included: pH, specific conductivity, temperature, alkalinity (by titration with H_2SO_4), major anions (e.g., sulfate, chloride) by ion chromatography, dissolved organic carbon (DOC) by wet oxidation coupled with a carbon analyzer, and metal(loid)s by inductively coupled plasma mass spectrometry (ICP-MS). Samples collected for laboratory analyses were filtered in the field at <0.45 µm using syringes and polyethersulfone syringe-filters. A subset of ICP-MS and DOC samples were also filtered at <0.1 µm and <0.02 µm to assess colloidal metal(loid) transport. All samples were refrigerated prior to analysis, and ICP-MS samples were acidified to pH < 2 using trace-metal grade HNO_3. Statistical significance of C-Q correlations were calculated for each parameter using the power law[1]:

$$\log(C) = \log(a) + b \times \log(Q) \quad [1]$$

"b" is the power law slope, and "log(a)" is the y-axis intercept. Metal(loid) concentrations were compared against Canadian federal guidelines for the protection of freshwater aquatic life (long-term exposure; CCME 2023).

Results

Chemodynamic C-Q behavior describes major solutes (Table 1). C-Q relationships for major solutes are positive, except for DOC and K, which exhibit peak concentrations during spring floods. Stream pH is circumneutral, albeit with significantly lower values in May and June (median pH 7.1, range 5.3–7.6) than July to September (median pH 7.6, range 7.1–7.8; $p < 0.05$, Mann-Wilcox test).

Sulfate and the metal(loid)s Co, Cd, Ni, Se, and Zn have significant negative C-Q slopes reflecting peak concentrations at low discharges in mid- to late summer (Table 1). Concentrations of several metal(loid)s exceed Canadian guidelines for the protection of aquatic life, especially as summer progresses (Table 1).

Sulfate and metal fluxes are seasonally variable, with maxima associated with spring floods in May or June and minima occurring in during periods of low stream flow in July (Figure 1). With the exception of high-flow events driven by summer precipitation, fluxes of sulfate and metal(loid)s increase from July through September.

Colloidal contributions for sulfate and metal(loid)s of environmental concern (e.g., Al, Cd, Co, Cu, Ni, Se, Zn) in the 0.02–0.45 µm size fraction are negligible, although the opposite is observed for DOC and Fe (Table 2).

Table 1. Major constituent and metal(loid) concentrations and C-Q slopes in Slavin Creek, 2021-2023.

Parameter	Concentration Range	C-Q slope† (b)	Water-quality guideline‡ exceedances (%)
Major Constituent (mg/L)			
Ca	2–74	–0.5	–*
Mg	0.1–14	–0.5	–*
Na	0.1–1.3	–0.3	–*
K	0.03–2.0	+0.1	–*
DOC	2.5–25	+0.3	–*
Sulfate	1.5–167	–0.6	–*
Minor and Trace Metal(loid)s (µg/L)			
Al	4.4–647	+0.2	77
Co	<0.1–18	–0.3	–*
Cd	0.23–23	–0.4	100
Ni	6.2–379	–0.4	91
Se	<0.3–2.1	–0.5	20
Zn	38–1,890	–0.4	100

*No guideline value

†All slopes are significant ($p < 0.05$) except those indicated with grey shading.

‡Canadian Environmental Quality Guidelines: Freshwater (long-term exposure; CCME 2023).

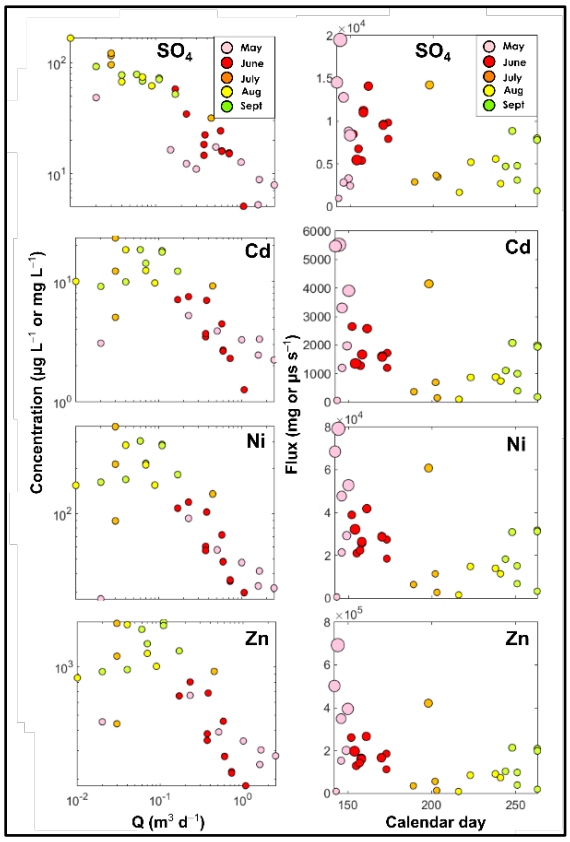

Figure 1. Seasonality of sulfate and metal C-Q patterns (left) and fluxes (right). Symbol color indicates month. Symbol sizes in flux plots are log10-scaled relative to Q. Sulfate mass units are mg, metal mass units are µg.

Table 2. Contribution of major, minor, and trace constituents in the 0.1 to 0.45 µm, 0.02 to 0.1 µm, and <0.02 µm size fractions relative to the concentration obtained at <0.45 µm from staged filtrations completed in July 2023.

Constituent	0.1–0.45 µm (%)	0.02–0.1 µm (%)	<0.02 µm (%)
Major Constituents			
DOC	22	9.8	68
Ca	-1.3	0.7	100
Mg	6.3	1.8	92
Na	0.6	1.0	98
K	4.0	-0.2	96
Si	1.2	-0.2	99
Sulfate†	-1.4	-0.9	102
Minor and Trace Metal(loid)s			
Al	1.0	-21	120*
Cd	-3.1	4.5	99
Co	0.2	0.1	100
Fe	57	21	22
Mn	4.8	0.6	95
Ni	-1.5	1.3	100
Se	-0.9	1.2	100
Zn	-0.1	6.2	94

*Values in excess of 100 % are attributed to contamination in the <0.02 µm filtration step.

†Sulfate inferred from ICP-MS sulfur analysis, assuming negligible contributions from other S species in streams.

Implications for Water Quality in Thawing Permafrost Catchments

Seasonal warming and increased geochemical interaction between infiltration and metalliferous and sulfidic rock can negatively impact streamwater chemistry by contributing sulfate, acidity, and metal(loid)s. Sulfide-mineral oxidation rates are kinetically limited, and may be further increased as thawing permafrost exposes previously frozen rock to rising temperatures and increased infiltration by oxygenated meteoric water. These results suggest that longer-term thaw of permafrost can deteriorate stream-water quality in catchments hosting metal- and sulfide-bearing rock.

References

Canadian Council of Ministers (CCME). 2023. Water Quality Guidelines for the Protection of Aquatic Life, Freshwater.

Quantifying groundwater fluxes in the carbon and water balance of thermokarst ponds

Reginald Somera[1,2] & Jean-Michel Lemieux[1,2]

[1]*Centre d'études nordiques, Université Laval, Québec City, Québec, Canada,*

[2]*Département de géologie et de génie géologique, Université Laval, Québec City, Québec, Canada*

Permafrost mounds develop in discontinuous and sporadic permafrost regions. Ice segregation processes result in these landforms made up of ice lenses, mineral soils, and sometimes, peat. In response to climate warming, permafrost mounds thaw, leaving surficial depressions enclosed by ramparts that accumulate water from precipitation and thawed permafrost. Resulting thermokarst ponds have garnered attention for their biogeochemical cycling of metals and nutrients, and their emissions of greenhouse gasses (GHGs).

Yet, thermokarst ponds have generally been treated as hydrogeologically isolated systems. This assumption may have been previously acceptable since these ponds commonly form in sediments of low hydraulic conductivity, where the presence of permafrost may further reduce groundwater connections. However, sustained permafrost thaw suggests increased surface and subsurface hydrological connectivity (Walvoord and Kurylyk 2016). Under current climate warming conditions, permafrost hydrological systems are anticipated to evolve both on and below the surface, thereby altering groundwater and surface water resources, hydrologic connectivity, and their fluxes.

In Arctic lakes, groundwater discharge is a key mechanism for controlling methane emissions (Olid et al. 2022), underscoring the need to address the implications of groundwater fluxes for pond and lake carbon cycling. As discontinuous permafrost regions are of the most susceptible areas to thaw, this characterization is especially pertinent. In this context, this study will quantify fluxes to thermokarst pond carbon and water balances, with an emphasis on groundwater flow.

METHODS

Hydrological and carbon fluxes between thermokarst ponds and groundwater reservoirs were investigated in the Tasiapik Valley, a 2-km^2 watershed near the Inuit village of Umiujaq (Québec, Canada), located in the discontinuous permafrost zone. Here, lithalsa permafrost mounds at different stages of degradation are abundant, and hydrogeological conditions vary between the resultant ponds of degradation.

At a pond-scale, a water balance equation (Eq. 1) was applied to four thermokarst ponds over the course of one week and is given by:

$$\Delta V / \Delta t = P + G_i - ET - G_o \quad [1]$$

where ΔV is the change in pond volume over change in time Δt, P is precipitation, ET is evapotranspiration, and G_i and G_o are groundwater inflow and outflow, respectively. Eq. 2, a chemical mass balance equation, was equally applied to the four ponds using conservative tracer Cl^- and is given by:

$$\Delta(C_w V) / \Delta t = C_p P + C_{Gi} G_i - C_w G_o \quad [2]$$

where C_w is the concentration of the pond surface water, C_p is the concentration of precipitation, and C_{GI} is the concentration of groundwater inflow. Every parameter was measured, except ET, which was calculated using the Penman-Monteith equation. Certain parameters, like surface inputs and outputs, were negligible for these surficially isolated ponds. Groundwater fluxes were monitored using instrumentation including seepage meters, mini-piezometers, and wells. Hydraulic conductivity (K) values of soils were measured both in-situ and through core laboratory analyses. The four thermokarst ponds were also analyzed for their stable isotopes of water, $\delta^{18}O$ and δ^2H (VSMOW), several times over July and August 2023 to further understand their summer evolution.

At a watershed-scale, samples were taken from groundwater and thermokarst ponds between 2013 and 2016, 2022, and 2023. They were analyzed for major ion chemistry, $\delta^{18}O$ and δ^2H, dissolved inorganic carbon (DIC), dissolved organic carbon (DOC), and their stable isotope ratios ($\delta^{13}C_{DIC}$ and $\delta^{13}C_{DOC}$ (VPDB)). Using $\delta^{18}O$ and δ^2H of pond waters for each year of sampling, an isotopic mass balance approach was applied to trace hydrological inputs and outputs. Through $\delta^{13}C_{DIC}$ of pond waters, permafrost, and sediments, a conceptual model for carbon fractionation between reservoirs is currently being explored, to further inform their carbon cycling.

RESULTS AND DISCUSSION

Hydrogeological, geochemical and geomorphological evidence in the Tasiapik Valley indicate the presence of at least two thermokarst pond types, with contrasting hydrological connectivities to the subsurface. Figure 1 demonstrates a thermokarst pond forming in the permafrost-containing silt substrate; ponds forming in lower permeability substrate, such as this one, are commonly reported elsewhere.

Figure 2 shows a thermokarst pond forming in a sand substrate, underlain by the silt unit.

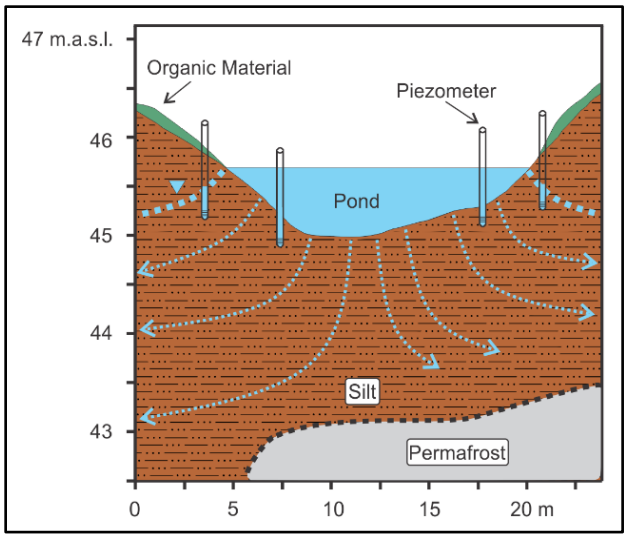

Figure 1. A conceptual model for a thermokarst pond in the Tasiapik Valley, forming from permafrost degradation, in a low permeability silt substrate.

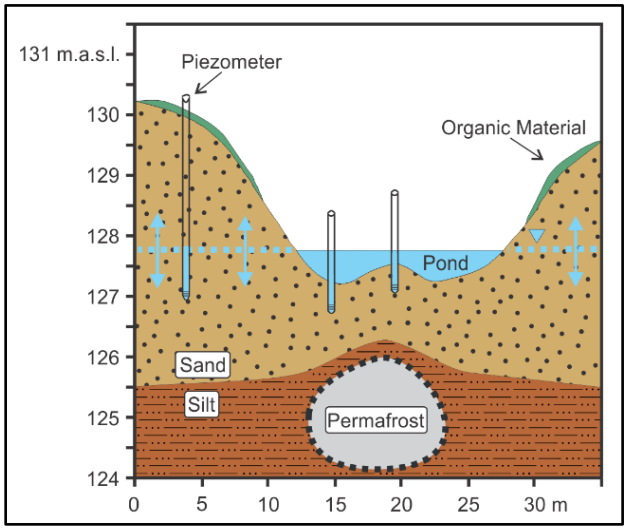

Figure 2. A conceptual model for a thermokarst pond in the Tasiapik Valley, forming from permafrost degradation, in a high permeability sand substrate.

The pond-scale water balance results revealed ponds formed in silt had a net groundwater loss over the experiment period. Mass balance results supported these findings, where Cl^- concentrations of pond waters increased during the experiment. Water levels and geochemistries at the ponds formed in sand, and their associated wells, suggest their water levels respond readily to groundwater fluctuations. Figure 3, which shows $\delta^{18}O$ and $\delta^{2}H$ evolution of the four pond sites across July and August 2023, also indicates different pond inputs and outputs.

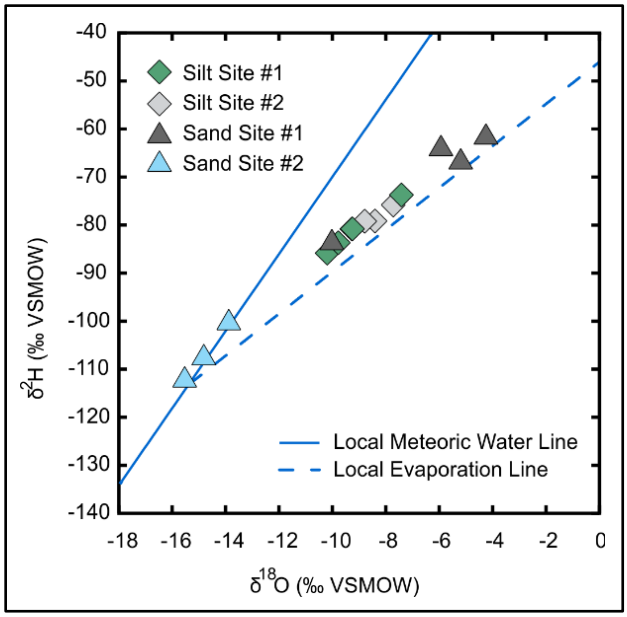

Figure 3. Stable water isotopes of four pond sites across July and August 2023 (n=15). Two ponds occurred in a sand substrate, while the other two occurred in a silt substrate. Values tend to fall near the Local Meteoric Water Line or the 2023 Local Evaporation Line.

Years of stable water isotope data support that most ponds here have evaporative fluxes that are exceeded by hydrological inputs. Positive relationships between historic $\delta^{13}C_{DIC}$ and DOC results suggest the respiration of DOC is a primary source of CO_2 from pond surfaces, however, dissolved carbon dynamics in these groundwater-surface systems and their implications for GHG emissions are still being explored.

REFERENCES

Olid, C., Rodellas, V., Rocher-Ros, G., et al. 2022. Groundwater discharge as a driver of methane emissions from Arctic lakes. Nature Communications. 2022;13(1): 3667. doi:10.1038/s41467-022-31219-1

Walvoord, M.A., and Kurylyk, B.L. 2016. Hydrologic Impacts of Thawing Permafrost—a Review, Vadose Zone Journal, 15(6): 1-20. doi:10.2136/vzj2016.01.0010

Polycyclic aromatic hydrocarbons (PAHs) in surface waters from the lower Kolyma catchment resemble those from permafrost sources

Danuta Szumińska[1], Krystyna Kozioł[1], Małgorzata Szopińska[2], Filip Pawlak[2,3], Joanna Jóźwik[3] & Żaneta Polkowska[3]

[1]*Department of Geochemistry and Environmental Change, Kazimierz Wielki University, Bydgoszcz, Poland*

[2]*Department of Technology in Environmental Engineering, Gdańsk University of Technology, Gdańsk, Poland*

[3]*Department of Analytical Chemistry, Gdańsk University of Technology, Gdańsk, Poland*

Climate change drives rapid thaw of permafrost, thus changing hydrological and hydrochemical regimes of Arctic rivers (Cochand et al. 2019; Suzuki et al. 2021; Koch et al. 2022). We have investigated the PAHs concentrations of potential sources and recipients in the lower Kolyma watershed to test whether thawing permafrost may be a secondary source of PAHs for surface waters in North-Eastern Siberia.

MATERIALS AND METHODS

In July 2021, we collected 28 water samples of 1 L volume in the lower Kolyma watershed (from 4 cross sections of the Kolyma river - sample numbers beginning with K1-4, from its tributaries Omolon and Annuy, and two thermokarst lakes, as well as from permafrost ice and creeks) (Figure 1). Permafrost creeks were rivulets of sediment-laden water discharged from a thawing permafrost cliff, sampled directly below the cliff face.

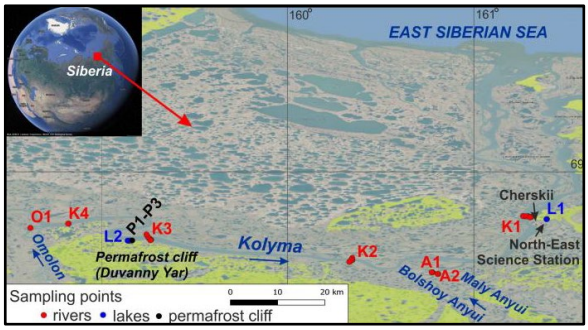

Figure 1. Location of the collected samples. (Yedoma extent in green – after Strauss et al. 2022). Background: Google Maps.

The collected water samples have been filtered in the laboratory of the North-Eastern Research Station, using a pre-cleaned glass filtering unit and pre-combusted (at 400°C) glass fiber filters (pore φ = 0.7 µm). The divided sample was then extracted: the liquid phase with liquid-liquid extraction (from 800 mL aliquot), while the suspended sediment collected on the filterpaper was dried and extracted with solid-liquid extraction, with a clean-up step of solid phase extraction (with SiO_2 and activated copper cartridges). Both liquid extractions were carried out with dichloromethane. Isotope-labelled naphthalene-d8 and benzo(a)anthracene-d12 acted as surrogate standards, while acenaphthene-d10 was an internal standard. Extracts were evaporated to 0.3 and 0.1 mL, for the dissolved and solid fractions, respectively.

Polycyclic aromatic hydrocarbons (PAHs) were determined in extracts from both fractions, using a gas chromatograph (Nexis GC-2030, Shimadzu) coupled with a mass spectrometer (GCMS-QP2020 NX, Shimadzu). The MS operated in selected ion monitoring (SIM) mode. The determined PAHs were (the abbreviations in brackets are used throughout the abstract): naphtalene (NAP), acenaphylene (ACY), acenaphtene (ACE), fluorene (FL), phenanthrene (PHE), anthracene (ANT), fluoranthene (FLA), pyrene (PYR), benz[a]antracene (BaA), chrysene (ChRY), benzo[b]fluoranthene (BbF), benzo[k]fluoranthene (BkF), benzo[a]pyrene (BaP), indeno[1,2,3-c,d]pyrene (IcdP), dibenz[a,h]anthracene (DbA), benzo[g,h,i]perylene (BghiP). Limits of detection (LODs) ranged 2.15 - 3.80 ng/L for the dissolved fraction analysis and 0.84 - 35 ng/L of original sample in the suspended sediment analysis. Limits of quantification (LOQs) were 2.80 - 8.31 and 1.3 - 90 ng/L, respectively.

RESULTS AND DISCUSSION

PAHs concentrations in the collected samples ranged 1.12 - $30.2 \cdot 10^3$ ng/L, of which <LOD-148 ng/L was dissolved fraction and <LOD-$30.2 \cdot 10^3$ ng/L was suspended sediment fraction. The samples with the top concentration levels were two permafrost creeks and the main current of the Kolyma River in a cross-section below a permafrost cliff. Further Kolyma river samples and one thermokarst lake sample also showed high suspended sediment ΣPAHs concentrations.

Since suspended sediment fraction dominated in most collected samples, we focus on its content of particular PAH compounds. The predominant compounds from PAH group in the samples with high concentrations were BaA and PHE, followed by NAP, ChRY, ACY and BbF in single samples (Figure 2).

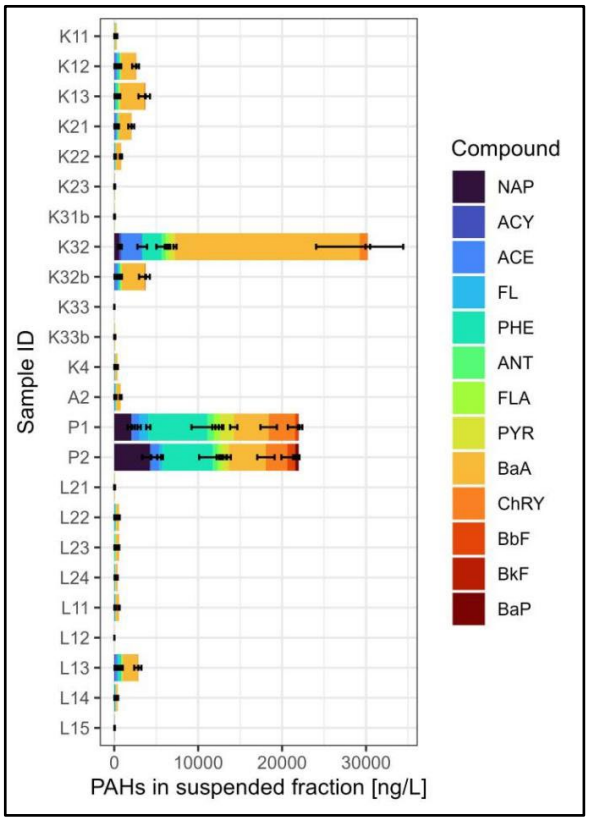

Figure 2. PAH compound concentrations in the collected samples (suspended sediment fraction only). Error bars show analytical procedure uncertainty. Omitted samples showed PAHs concentrations <LOD.

The Kolyma river samples collected, especially those from the main river current below a permafrost cliff (K32, K32b), have shown a similar composition of PAHs compounds as the permafrost creeks (P1 and P2), while the other potential sources of PAHs in the area, such as the tributaries of Kolyma: Omolon, Maly and Bolshoy Annuy, have shown at least two orders of magnitude lower concentrations of PAHs (in Omolon, also of a very different composition, only in the dissolved phase - data not shown). The creeks P1 and P2 have been interpreted as permafrost waters due to both their location and high total dissolved solute, including sodium, chloride and dissolved organic carbon concentrations (Szumińska et al. 2023); however, they most likely contain also chemical components originating from the active layer. The role of hydrological transport in changing PAH composition needs to be fully considered yet.

Conclusions

The PAH suspended sediment loading of permafrost creeks, the Kolyma river, and permafrost lakes as well as their main components in the analysis of particular PAH compounds, show that the main source of PAHs in the Kolyma river is most likely from permafrost thaw, including leaching of the modern active layer. The contributed quantities are closely tied to suspended sediment production at thawing and eroding cliffs, as among the sampled sources this was a strongly dominating one. Further data is urgently needed to estimate the quantitative impact on PAHs fate downstream.

Acknowledgements

This research was funded by INTERACT, H2020-EU.1.4.1.2. (PollAct, grant no. 730938) and the National Science Centre of Poland (NCN) grant no. NCN 2021/41/B/ST10/02947, and supported by the Research Potential Maintenance funds at Kazimierz Wielki Univ. and Gdansk Univ. of Technology.

References

Cochand, M., Molson, J., and Lemieux, J. 2019. Groundwater hydrogeochemistry in permafrost regions. Permafr. Periglac. Process. 30, 90–103. doi:10.1002/ppp.1998

Koch, J.C., Bogard, M.J., Butman, D.E., Finlay, K., Ebel, B., James, J., et al. 2022. Heterogeneous patterns of aged organic carbon export driven by hydrologic flow paths, soil texture, fire, and thaw in discontinuous permafrost headwaters. Global Biogeochemical Cycles, 36, e2021GB007242. doi:10.1029/2021GB007242

Strauss, J., Laboor, S., Schirrmeister, L., Fedorov, A.N., Fortier, D., Froese, D.G., Fuchs, M., Günther, F., Grigoriev, M.N., Harden, J.W., Hugelius, G., Jongejans, L.L., Kanevskiy, M.Z., Kholodov, A.L., Kunitsky, V., Kraev, G., Lozhkin, A.V., Rivkina, E., Shur, Y., Siegert, C., Spektor, V., Streletskaya, I., Ulrich, M., Vartanyan, S.L., Veremeeva, A., Walter A., Katey M., Wetterich, S., Zimov, N.S., and Grosse, G. 2022: Database of Ice-Rich Yedoma Permafrost Version 2 (IRYP v2). PANGAEA. doi:10.1594/PANGAEA.940078

Suzuki, K., Park, H.; Makarieva, O., Kanamori, H., Hori, M., Matsuo, K., Matsumura, S., Nesterova, N., and Hiyama, T. 2021. Effect of Permafrost Thawing on Discharge of the Kolyma River, Northeastern Siberia. Remote Sensing, 2021, 13, 4389. doi:10.3390/rs13214389

Szumińska, D., Kozioł, K., Chalov, S.R., Efimov, V.A., Frankowski, M., Lehmann-Konera, S., and Polkowska, Ż. 2023. Reemission of inorganic pollution from permafrost? A freshwater hydrochemistry study in the lower Kolyma basin (North-East Siberia). L. Degrad. Dev. doi:10.1002/ldr.4866

Water balance of a thermokarst wetland surrounded by thawing discontinuous permafrost; Scotty Creek, NWT

Iain Thomson[1], Ryan F. Connon[2], Oliver Sonnentag[3], Stephanie N. Wright[4] & William L. Quinton[1]

[1]*Cold Regions Research Center, Wilfrid Laurier University, Waterloo, Ontario, Canada*

[2]*Environment and Climate Change, Government of Northwest Territories, Yellowknife, Northwest Territories, Canada*

[3]*Département de Géographie & Centre D'études Nordiques, Université de Montréal, Montréal, Québec, Canada*

[4]*Department of Civil Engineering, Queen's University, Kingston, Ontario, Canada*

Mean annual air temperatures are increasing rapidly in northwestern Canada, which is among the most rapidly warming regions on Earth. Consequently, permafrost thaw within northwestern Canada is proceeding at a rate not found in the historical record (Pelletier et al. 2017), with areal thaw rates especially high in the peatland-dominated southern margin of discontinuous permafrost (Quinton et al. 2019). In this region, forested peat plateaus are underlain by ice-rich permafrost, while wetlands such as collapse-scar bogs and channel fens are permafrost-free. When permafrost thaws, ground surface of peat plateaus subsides, which has caused vast land cover changes and transformed forest to wetland over much of this region (Carpino et al. 2018). This land cover change has altered how water is stored and cycled on the landscape (St. Jacques and Sauchyn 2009). These changes were shown to be driven by the expansion of runoff contributing areas, as permafrost "barriers" are removed with thaw (Connon et al. 2014). The development of ephemeral channels cut through intervening peat plateaus and enables water to cascade from one wetland to the next when storage thresholds are exceeded (Connon et al. 2015). This wetland capture process effectively taps water stored in the interior of plateau-wetland complexes, thereby increasing the contributing area in the basin drainage network.

Study Objectives

This study aims to better understand the implications of permafrost thaw on flow and storage processes of peat plateau-wetland complexes. A detailed water balance was established for wetland complex in the headwaters of the Scotty Creek drainage basin. The specific objectives of this study are to: 1) Measure each water balance component. 2) Compare the observations for the growing season of 2022 with the flux and storage measurements made at the same wetland in 2013 and 2014. 3) Describe how the hydrological functioning of the wetland has changed and can be expected to change with climate warming induced permafrost thaw.

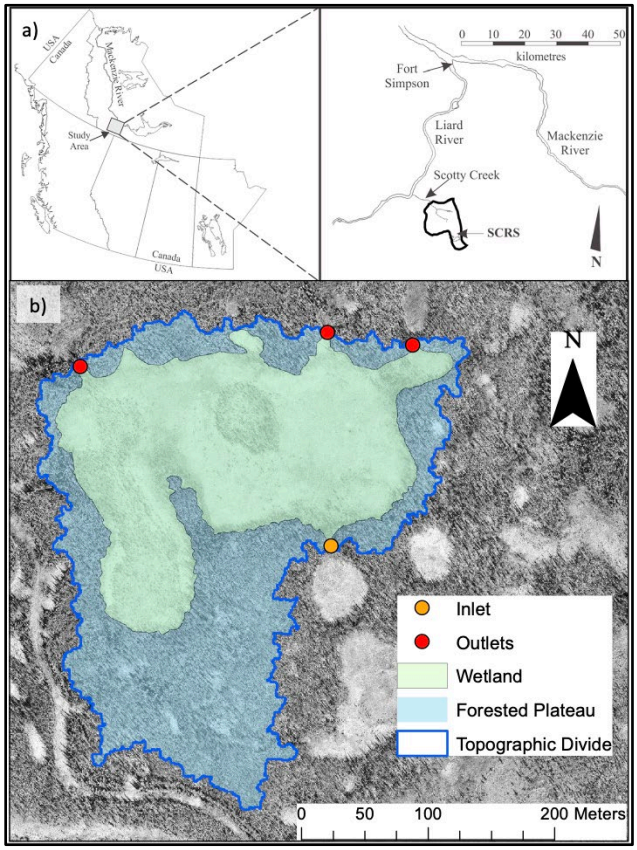

Figure 1. a. Location of the Scotty Creek drainage basin within Canada. Modified from Connon et al. 2018. b. The Wetland within the Scotty Creek Drainage Basin and its forested contributing area, permafrost degradation channels in which allow for overland flow to occur.

Water Balance

During the growing season (April – August) of 2022, measurements of snow water equivalent (SWE) of the snowpack was taken though snow surveys, rainfall was measured by nearby precipitation gauges, evapotranspiration was obtained from eddy covariance measurements, overland flow was measured though a set of weirs and flumes at each of the permafrost degradation channels, vertical groundwater flux was

measured though sets of nested piezometers, subsurface plateau runoff was with monitoring wells along the plateau edge and storage change was measured though an array of water level recorders within the wetland. Discharge from overland flow was greatest during the spring freshet. Water input from the melting snowpack, runoff from adjacent peat plateaus and upstream wetlands contributed to a large increase in water storage within the wetland in the early season. Overland Flow was the greatest source of water loss within the wetland and was greatest during the freshet (419 mm). Discharge was greatly reduced after the spring freshet (44 mm), and by June evapotranspiration was the predominant source of water loss. Evapotranspiration (262 mm) was much greater than precipitation (137 mm) during the growing season. Total precipitation was much lower than the climate normals for 1990-2020 (218 mm). The wetland recorded a water deficit of 103 mm by the end of August.

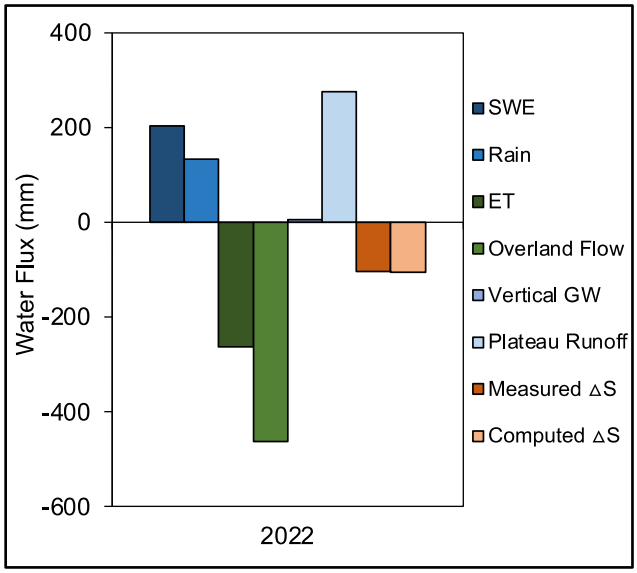

Figure 2. Net water fluxes in sessional (April 1 – August 31) wetland water balance for 2022: snow water equivalent (SWE) of the snowpack on the wetland, direct rainfall (Rain) on the wetland, evapotranspiration (ET) of the wetland, the net overland flow of the wetland, vertical groundwater (GW) flux within the wetland, the subsurface plateau water runoff into the wetland, measured water storage change in the wetland, and computed water storage change from the sum of the measured water fluxes.

Future directions

Comparisons will be made between the 2022 water balance and measurements taken within the same wetland in the 2013 and 2014 seasons. Wetland growth and in turn permafrost loss will be measured using remotely sensed imagery captured in 2013 and 2014 to compare with imagery from 2022. Most notably during this time period was the development of new channels created by permafrost degradation. These channels were developed within the wetland, and in the wetlands upstream. Due to this, the wetland has a greater ability to shed water and the upstream contributing area has become larger. Water balances for the 2013 and 2014 will be conducted utilizing the same methods, taking into account for the changes that occurred within the wetland itself and its contributing area. To further our understanding how water movement and storage within wetlands will change with continued permafrost loss.

References

Carpino, O.A., Berg, A.A., Quinton, W.L., and Adams, J.R. 2018. Climate change and permafrost thaw-induced boreal forest loss in northwestern Canada, Environmental Research Letters, 13: 084018. https://doi.org/10.1088/1748-9326/aad74e

Connon, R.F., Quinton, W.L., Craig, J.R., and Hayashi, M. 2014. Changing hydrologic connectivity due to permafrost thaw in the lower Liard River valley, NWT, Canada, Hydrological Processes, 28: 4163–4178. https://doi.org/10.1002/hyp.10206

Connon, R.F., Quinton, W.L., Craig, J.R., Hanisch, J., and Sonnentag, O. 2015. The hydrology of interconnected bog complexes in discontinuous permafrost terrains, Hydrological Processes, 29: 3831–3847. https://doi.org/10.1002/hyp.10604

Connon, R., Devoie, É., Hayashi, M., Veness, T., and Quinton, W.L. 2018. The influence of shallow taliks on permafrost thaw and active layer dynamics in subarctic Canada, Journal of Geophysical Research: Earth Surface, 123: 281–297. https://doi.org/ 10.1002/2017JF004469

Pelletier, N., Talbot, J., Olefeldt, D., Turetsky, M., Blodau, C., Sonnentag, O., and Quinton, W.L. 2017. Influence of Holocene permafrost aggradation and thaw on the paleoecology and carbon storage of a peatland complex in northwestern Canada, The Holocene, 27(9): 1391–1405. doi:10.1177/0959683617693899

St. Jacques, J.M.S., and Sauchyn, D.J. 2009. Increasing winter baseflow and mean annual streamflow from possible permafrost thawing in the Northwest Territories, Canada, Geophysical Research Letters, 36(1): 1–6. https://doi.org/10.1029/2008GL035822

Quinton, W., Berg, A., Braverman, M., Carpino, O., Chasmer, L., Connon, R., Craig, J., Devoie, E., Hayashi, M., Haynes, K., Olefeldt, D., Pietroniro, A., Rezanezhad, F., Schincariol, R., and Sonnentag, O. 2019. A synthesis of three decades of hydrological research at Scotty Creek, NWT, Canada, Hydrology Earth System Sciences, 23: 2015–2039. https://doi.org/10.5194/hess-23-2015-201

Permafrost groundwater springs

Mikkel Toft Hornum[1,2], Victor Bense[2], Søren Jessen[1], Andy Hodson[2,3] & Ylva Sjöberg[1,4]

[1]*Department of Geosciences and Natural Resource Management, University of Copenhagen, Denmark*

[2]*Arctic Geology Department, The University Centre in Svalbard, Longyearbyen, Svalbard, Norway*

[3]*Department of Environmental Sciences, Western Norway University of Applied Sciences, Sogndal, Norway*

[4]*Department of Ecology and Environmental Science, Umeå University, Umeå, Sweden*

[5]*Hydrology and Environmental Hydraulics, Department of Environmental Sciences, Wageningen University and Research, Wageningen, Netherlands*

A continuous cover of permafrost characterizes the non-glaciated parts of the landscape in Earth's coldest regions. The impervious frozen ground effectively separates hydrological processes into near-surface and deep, sub-permafrost systems. The permafrost seals sub-permafrost groundwater and solutes such as contaminants and greenhouse gases. Groundwater springs located above through-taliks provide exceptional circumstances that allow sub-permafrost groundwater and solutes to reach the ground surface. However, fundamental questions as to the location, persistence and driving mechanisms behind these so-called talik springs remain unanswered. We aim to resolve some of these fundamental questions.

Distribution

Across the continuous permafrost zone talik springs are rare, but they may be regionally common. They are most often located in low-lying parts of high relief landscape and typically in valleys (Crites et al. 2020; Yoshikawa 2013; Yoshikawa et al. 2007) where the current permafrost cover formed during the Holocene because of marine regression, glacial retreat, or climate cooling since the Holocene climate optimum. This relationship points to the transient aspect of the formation of talik springs. Some talik springs are located in close vicinity of glaciers or ice sheets (Grasby et al. 2012), while others in areas where these or other obvious recharge sources are lacking.

Current understanding

Contemplating on the lack of obvious recharge sources for talik springs located in glacier-free areas, we recently proposed a new mechanism for driving talik springs in which groundwater flow and spring discharge are driven by hydraulic pressure generation associated with the formation and downwards aggradation of permafrost (Figure 1; Hornum et al. 2020, Hornum et al. 2023). Using cryohydrological modelling tools, we show that the proposed mechanism related to water's expansion during downwards movement of the freezing front can explain spring outflow with up to a couple of liters per second, and over millennial timescales after surface cooling has ceased.

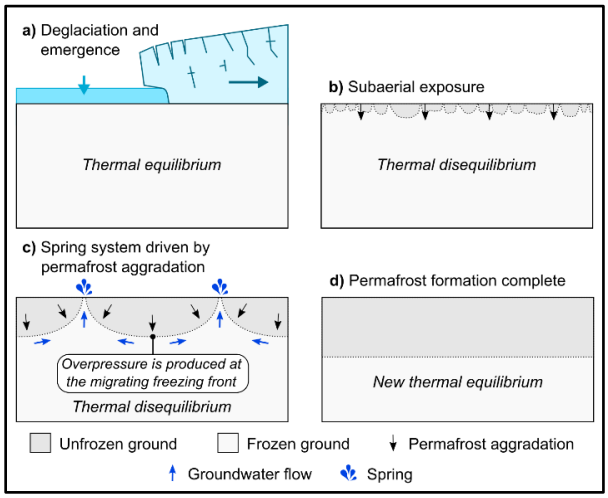

Figure 1. Conceptual model for permafrost-aggradation-driven spring formation. Following permafrost-free conditions during glaciation, sea inundation (a), or temperate climate (not shown), surface temperature drops below 0°C and permafrost starts to form (b). (c) Freezing pressure at the freezing front drives groundwater to the surface through taliks kept open by advective heat transport. (d) If surface temperatures remain constant, the ground eventually reaches a thermal equilibrium and no-flow conditions prevail in lack of other drivers. Modified from Hornum et al. (2023).

Ongoing research

Our ongoing research considers groundwater springs associated with glaciers and ice sheets:

1) In Isortoq Valley, West Greenland, we discovered up to 40 groundwater springs on satellite imagery from 2000-2023 (Figure 2). The groundwater springs are distributed along the margins of ~100-km-long valley from the sea and with a semi-exponential frequency towards Isunnguata Sermia, a major outlet of the Greenland ice sheet (GIS). We visited three of the groundwater springs located ~5 km from GIS. The springs are oxygen depleted, calcium-bicarbonate dominated and with low chloride concentration.

Together, the distribution of groundwater springs and their geochemistry suggest that glacial meltwater produced at the base of the GIS recharges an aquifer system within the valley sediments and below the permafrost. The groundwater springs in Isortoq Valley represent a previously unknown mechanism of meltwater routing from the GIS, whose importance for GIS mass loss and transport of solutes and dissolved gases to the oceans and atmosphere needs to be resolved.

2) In Svalbard, perennial proglacial groundwater springs emerge in the forefields of retreating and often cold-based glaciers (Figure 3). The springs are supersaturated with methane and contribute significantly to the total landscape emissions across Svalbard (Kleber et al. 2023). The cold-based setting at many of the glaciers seems to preclude glacial meltwater as the origin of the spring water. We combine inverse hydrogeochemical modelling and cryohydrological modelling tools to investigate our two prevailing hypotheses as to what drives these peculiar spring systems: I) Hydraulic head generation associated with permafrost beneath the exposed forefield and the thinned glacier (depicted by Figure 1), and II) warm-season sub-permafrost groundwater replenishment from precipitation recharging through glacial and subglacial fracture systems.

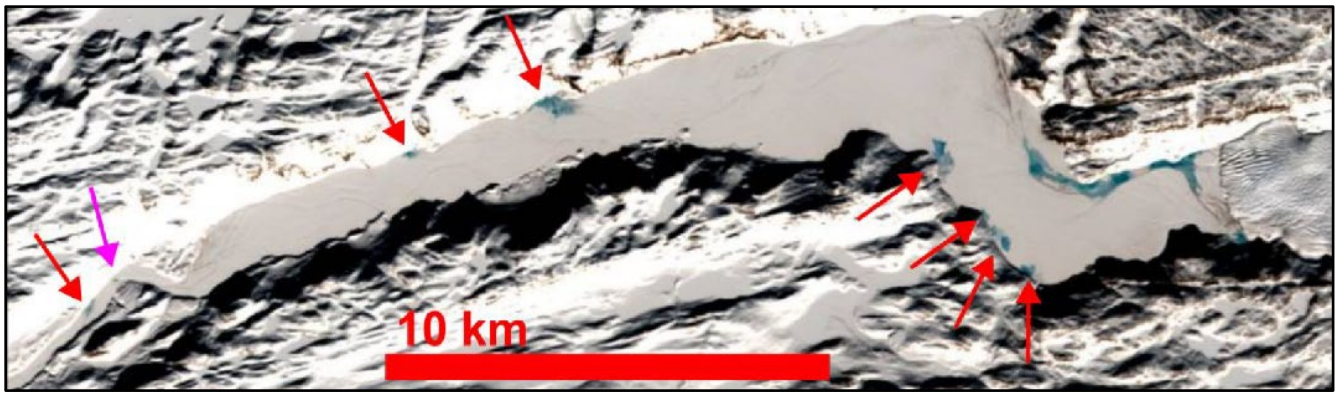

Figure 2. Landsat-7 image of Isortoq Valley (4 April 2001) showing icings that result from groundwater discharge (red arrows). Colors are a false color composite created with bands 3 (green), 4 (red), and 5 (near-infrared). Landsat-7 image courtesy of U.S. Geological Survey (2023).

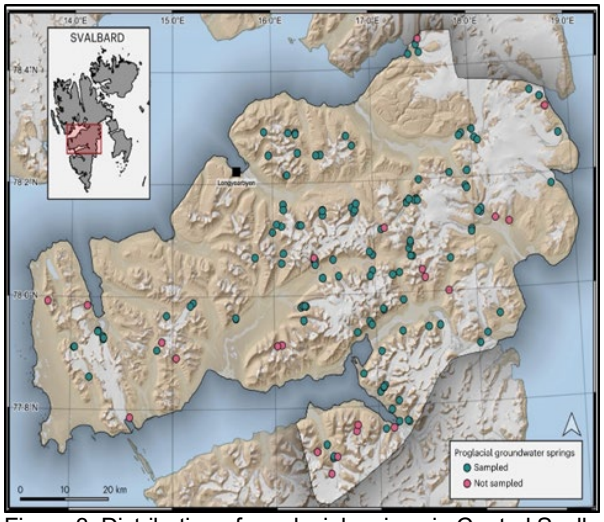

Figure 3. Distribution of proglacial springs in Central Svalbard (modified from Kleber et al. 2023).

REFERENCES

Crites, H., Kokelj, S.V., and Lacelle, D. 2020. Icings and groundwater conditions in permafrost catchments of northwestern Canada, Nature Scientific Reports, 10(3283): 1–11. doi:10.1038/s41598-020-60322-w

Grasby, S.E., Beauchamp, B., and Bense, V. 2012. Sulfuric acid speleogenesis associated with a glacially driven groundwater system-paleo-spring “pipes” at Borup Fiord Pass, Nunavut, Astrobiology, 12(1): 19–28. doi:10.1089/ast.2011.0700

Hornum, M.T., Hodson, A., Jessen, S., Bense, V., and Senger, K. 2020. Numerical modelling of permafrost spring discharge and open-system pingo formation induced by basal permafrost aggradation, The Cryosphere, 14: 4627–4651. doi:10.5194tc-7-2020

Hornum, M.T., Bense, V., van der Ploeg, M., Kroon, A., and Sjöberg, Y. 2023. Arctic Spring Systems Driven by Permafrost Aggradation, Geophysical Research Letters, 50(17): e2023GL104719. doi:10.1029/2023GL104719

Kleber, G.E., Hodson, A.J., Magerl, L., Mannerfelt, E.S., Bradbury, H.J., Zhu, Y., et al. 2023. Groundwater springs formed during glacial retreat are a large source of methane in the high Arctic, Nature Geoscience, 16: 597–604. doi:10.1038/s41561-023-01210-6

Yoshikawa, K. 2013. Pingos, In Treatise on Geomorphology, Academic Press, San Diego, California, USA, 8: 274–297. doi:10.1016/B978-0-12-374739-6.00212-8

Yoshikawa, K., Hinzman, L.D., and Kane, D.L. 2007. Spring and aufeis (icing) hydrology in Brooks Range, Alaska, Journal of Geophysical Research, 112: G04S43. doi:10.1029/2006JG000294

Heterogeneity in aquatic biogeochemical flux and active layer dynamics within a changing Yukon River Basin

Ryan C. Toohey[1], Edda A. Mutter[2] & Nicole Herman-Mercer[3]

[1]*USGS Alaska Climate Adaptation Science Center, Anchorage, Alaska, United States*

[2]*Yukon River Inter-Tribal Watershed Council, Anchorage, Alaska, United States*

[3]*USGS Southwest Climate Adaptation Science Center, Tucson, Arizona, United States*

The Yukon River Basin is at the forefront of climate change in Alaska (Ballinger et al. 2023). Increasing temperatures, permafrost degradation, wildland fire, changing vegetation (Mizukami et al. 2022; Johnstone et al. 2011) and other climate related effects will likely continue to impact the watershed by altering hydrological pathways and subsistence resources within the watershed. Biogeochemical fluxes in the Yukon River, as in many of the other Arctic rivers, have markedly changed over the past several decades (Tank et al. 2023; Drake et al. 2018; Toohey et al 2017; Tank et al. 2016). One of the prevailing hypotheses is that these changes are due to altered hydrological flowpaths as the result of permafrost degradation (Shrogren et al. 2019). In this study, the Indigenous Observation Network has leveraged USGS resources and data to combine, collect and analyze a novel data set of over 3500 samples in its spatial and temporal representation of the Yukon River that span from 1982 to 2019, its tributaries and active layer dynamics (~2009-2019) (Figure 1). This study primarily investigates biogeochemical changes from approximately 2001 to 2019. The ION data collection efforts were of high quality when compared to USGS and Arctic Great River Observatory data (Herman-Mercer et al. 2018).

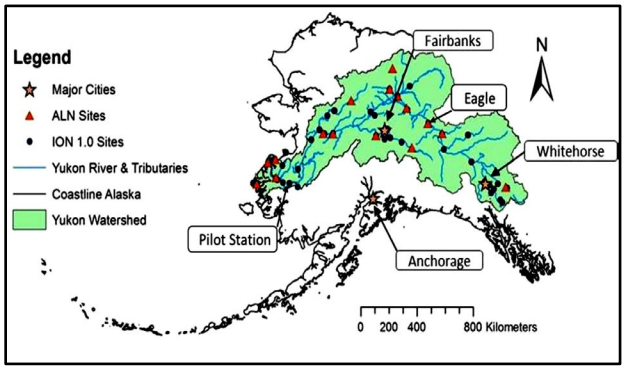

Figure 1. Biogeochemical water quality sites and Active Layer Network sites throughout the Yukon River Basin.

In terms of biogeochemical concentrations, the Yukon River varies both spatially within the river and temporally both seasonally and from year to year. One of the major differences in biogeochemical characteristics along the main stem of the Yukon River occurs between Dawson, YT and Eagle Village, AK. This biogeochemical step change is largest for parameters such as electrical conductivity (EC), alkalinity(ALK), SO_4^- and Mg^+ with concentrations at least doubling between Dawson and Eagle Village. Isotopically, samples east of Eagle Village (i.e., into Canada) are much lighter than the rest of the mainstem Yukon River. Parameters such as dissolved organic carbon (DOC) and NO_3^- increase in concentration more gradually between these two locations. Several Yukon River tributaries (i.e., Stewart and White Rivers) appear to play a significant role in contributing to these within river increase of most constituents. As the river flows downstream of Eagle, parameters such as EC, ALK, DOC, NO_3^-, SO_4^-, and Mg^+ gradually increase in concentration towards the mouth of the river. The isotopic signature of the Yukon River actually decreases from Eagle to Stevens Village revealing similar measurements to the Tanana River(which is overall a slightly heavier signature than the main stem Yukon). Several parameters ($\delta^{18}O$, δD, SO_4^-, NO_3^-) suggest a dilution at Pilot Station with concentrations lower than nearby areas. Mainstem Yukon River pH gradually decreases from Whitehorse to the mouth, with a slightly greater decrease during the winter months. Alkalinity, NO_3^-, SO_4^-, and EC concentrations all increase during the winter months when compared to summer concentrations that suggest a more mineral, groundwater influenced reduced flow. During the months between May and August, SO_4^-, EC, Mg^+, and ALK concentrations increase on a month-by-month basis. While fluxes of these parameters increase during the summer months, fluxes decrease during the winter months.

With good discharge data being limited throughout the watershed, we could not calculate fluxes for each community site. However, we did calculate biogeochemical fluxes where the discharge record matched our biogeochemical data collected by ION and the USGS (approximately 2001-2019). In terms of DOC flux, the Yukon River at Whitehorse and Eagle did not show any particular trend. While Toohey et al. 2017 showed similar findings for over three decades at Pilot

Station and Tanana River, within this shorter time frame, these sites showed an increasing trend for the Tanana and a decreasing trend for the Yukon River. Opposite trends (i.e., decreasing and increasing) for SO_4^- flux within the Tanana and Yukon River were modeled for this time period. Slightly increasing trends of Mg^+ flux were modeled at Eagle Village, Pilot Station and the Tanana River.

ION (combined with USGS efforts) also collects data from several major and culturally important tributaries in the Yukon River Basin such as the Stewart, Tanana, Porcupine, Koyukuk, Anvik and Andreafski Rivers each have unique characteristics (e.g., geological characteristics, permafrost conditions, wildfire history, vegetation characteristics, etc.) within the Yukon River Basin. These tributaries are often significantly different in their biogeochemical concentrations when compared to the main stem of the Yukon River. Within the Porcupine, Chena and Tanana, pH is significantly lower when compared to the mainstem of the Yukon River. EC is relatively higher in the Stewart, Chandalar, Tanana, Koyukuk, and Hess Creek. The Chandalar, Porcupine and Koyukuk rivers all have higher Alkalinity readings. The highest DOC concentrations in the YRB were found in the Porcupine, Chena, Hess Creek, Koyukuk and Anvik rivers. The lowest DOC concentrations were found in the Tanana River. Increased SO_4^- concentrations were found in the Stewart, Chandalar, Porcupine and Koyukuk rivers, with Mg concentrations being relatively high in the Stewart, Chandalar and Koyukuk rivers. The Andreafski and Anvik rivers had the lightest isotopic signatures with the Chandalar and Tanana having some of the heaviest isotopic signatures. Each of these watersheds has climatic or other environmental factors that likely contribute to these differences.

In 2009, ION initiated the Active Layer Network that installed twenty different Active Layer Sites that were located throughout the Yukon River Basin and generally by a local Alaska Native community (Figure 1). Active layer sites upstream of Eagle largely increased active layer depths (Teslin, Dawson and Eagle). However, several of these sites had to be discontinued for various reasons. Interior Alaskan sites such as Nenana, Hess Creek and Nome Creek did not exhibit any trends with mean depths being between 35-65 cm. Many of the sites with the Yukon Delta (Kotlik, Chevak, Emmonak and St. Mary's had some of the deepest mean active layer depths ranging from 45-85 cm. Each of these sites, upstream of Eagle and within the Yukon Delta, exhibited increasing active layer depths over the period of record.

The combination of these data sets allows for novel exploration of biogeochemical and active layer dynamics within large Arctic rivers at multiple scales and with multiple methods.

References

Ballinger, T.J., et al. 2023. Alaska Terrestrial and Marine Climate Trends, 1957–2021. J. Climate, 36, 4375–4391. https://doi.org/10.1175/JCLI-D-22-0434.1.

Drake, T.W., Tank, S.E., Zhulidov, A.V., Holmes, R.M., Gurtovaya, T., Spencer, R.G.M. 2018. Increasing Alkalinity Export from Large Russian Arctic Rivers. Environ. Sci. Technol. 52 (15), 8302– 8308. doi:10.1021/acs.est.8b01051

Herman-Mercer, N., Antweiler, R., Wilson, N., Mutter, E., Toohey, R., and Schuster, P. 2018. Data Quality from a Community-Based, Water-Quality Monitoring Project in the Yukon River Basin. Citizen Science: Theory and Practice, 3(2), p.1. https://doi.org/10.5334/cstp.123

Johnstone, J.F., Rupp, T.S., Olson, M., et al. 2011. Modeling impacts of fire severity on successional trajectories and future fire behavior in Alaskan boreal forests. Landscape Ecol 26, 487–500. https://doi.org/10.1007/s10980-011-9574-6

Mizukami, N., et al. 2022. New projections of 21st century climate and hydrology for Alaska and Hawai'i. Climate Serv., 27, 100312. https://doi.org/10.1016/j.cliser.2022.100312

Shogren, A.J., Zarnetske, J.P., Abbott, B.W., et al. 2019. Revealing biogeochemical signatures of Arctic landscapes with river chemistry. Sci Rep 9, 12894. https://doi.org/10.1038/s41598-019-49296-6

Tank, S.E., McClelland, J.W., Spencer, R.G.M., et al. 2023. Recent trends in the chemistry of major northern rivers signal widespread Arctic change. Nat. Geosci. 16, 789–796. https://doi.org/10.1038/s41561-023-01247-7

Tank, S.E., Striegl, R.G., Mcclelland, J.W., and Kokelj, S.V. 2016. Multi-decadal increases in dissolved organic carbon and alkalinity flux from the Mackenzie drainage basin to the Arctic Ocean, Environ. Res. Lett., 11(5), 1–10. doi:10.1088/1748-9326/11/5/054015.

Toohey, R.C., Herman-Mercer, N.M., Schuster, P.F., Mutter, E.A., and Koch, J.C. 2016. Multidecadal increases in the Yukon River Basin of chemical fluxes as indicators of changing flowpaths, groundwater, and permafrost, Geophys. Res. Lett., 43, 12,120–12,130. doi:10.1002/2016GL070817

A three-decade hydro-meteorological-permafrost dataset from the taiga-tundra ecotone in the western Canadian Arctic

Rosy Tutton[1], Brampton Dakin[1], Branden Walker[1], Gabriel Hould Gosselin[1,2], Jory Griffith[3], Oliver Sonnetang[2], Phillip Marsh[1], Richard Essery[4], Robin Thorne[1] & Vincent Graveline[2]

[1]*Wilfrid Laurier University, Waterloo, Ontario, Canada*

[2]*Université de Montréal, Montréal, Québec, Canada*

[3]*McGill University, Montréal, Québec, Canada*

[4]*University of Edinburgh, Edinburgh, United Kingdom*

Across the Arctic, we are observing complex feedbacks between changing climate, vegetation, snow, permafrost, and hydrology. To better understand these changes there is a need for prolonged and well maintained permafrost observations coupled with hydrological and meteorological monitoring. Trail Valley Creek (TVC) is a long-term research watershed in the Western Canadian Arctic that was established in 1991. Observations and research at TVC integrate meteorological observations, snow studies, eddy covariance measurements of energy and water, permafrost monitoring, streamflow observations, remote sensing and high-resolution spatially distributed modelling. The evolution of research funding, projects and methods since early establishment result in challenges for data management, but form a unique dataset that improves the capacity for permafrost and hydrologic modelling. We summarize TVC monitoring and the steps involved in maintaining and publishing a long-term interdisciplinary data record. This review will outline the recently published open-access datasets and methods used for compilation.

STUDY AREA

The TVC research watershed (68°45'N, 133°30' W) is situated in the southern Tuktoyaktuk Coastal Plains region in the Inuvialuit Settlement Region of the Northwest Territories, Canada (Figure 1). The watershed is underlain with ice-rich continuous permafrost approximately 150 to 350 m in depth with sediments containing ice-wedges, tabular ice, segregated ice, and buried glacier ice (Burn and Kokelj 2009). The surficial geology of the watershed features hummock and rolling moraine consisting of fine-grained lacustrine and coarse-grained glaciofluvial sediments (Rampton 1988). Maximum active layer thickness ranges between 20 to 120 cm and varies by vegetation type, snow and soil conditions (Wilcox et al. 2019; Grünberg et al. 2020).

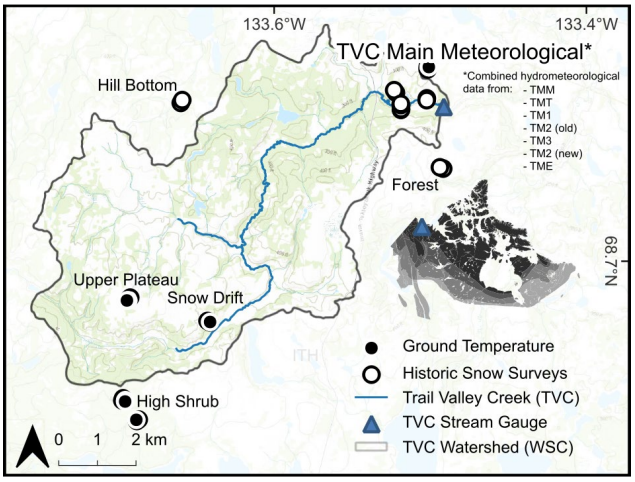

Figure 1. Map of Trail Valley Creek watershed located in the western Canadian Arctic, 50 km north of Inuvik, Northwest Territories. A subset of the many observation stations and repeat survey locations are shown here.

DATA FLOW

We prioritized reproducibility in data flow to ensure data transparency through the three decadal period and to allow future updates to the data sets. Data was processed as follows:

0) Archive: Store all data and metadata available.
1) Format: Convert useable data to standard.
2) Filter: Remove erroneous data.
3) Adjust: Correct data when necessary in order to calculate basic climate variables.
4) Infill: Use gap-filling techniques to create a complete modelling dataset.

All data will be publicly available through Borealis, the Laurier Dataverse data repository.

INTEGRATED DATA COLLECTION

The Water Survey of Canada began collecting streamflow data at TVC in 1985, while the National Hydrology Research Institute, Environment Canada began hydrologic research in 1991. This continued until 2013 when research data collection was taken over by Wilfrid Laurier University (WLU). Environment and

Climate Change Canda (ECCC) continues to collect streamflow data and maintains a weather station in TVC with real time data availability. WLU has expanded and maintained TVC since 2013.

Meteorological data has been collected from multiple weather stations at one central location and combined into a cohesive dataset (Table 1). Details of the data collection varies from 1991 to present, but in general the following data (Table 1) is available over the full record period. This paper presents data from the Trail Valley Creek Main Meteorological station (TMM) that has operated continuously over the full period of record. All original data is available, as well as a complete gap-filled data set typically needed to drive hydrologic, permafrost, and land surface models. The hierarchy of gap-filling sources include linear interpolation (gaps of 3 hours or shorter), adjacent ECCC weather station data, Inuvik airport station data and bias corrected ERA5 reanalysis data (Hersbach et al. 2020).

Table 1. Hydrometeorological measurements from TVC (TMM) (1991-2023), data available from direct measurements before gap filling and their mean annual values. Rainfall and precipitation are based on annual totals.

Variable	Unit	Mean	Data available (%)
Air Temperature	°C	-8.0	94.0
Relative Humidity	%	89	95.8
Wind Speed	m/s	2.6	86.0
Wind Direction	°	190	90.7
Total Rainfall	mm/year	140	92.2
Total Precipitation	mm/year	247	46.3
Snow Depth	m	0.2	84.7
Radiation (SW In)	W/m^2	146.2	65.7
Radiation (LW In)	W/m^2	259.3	49.6

Ground temperature monitoring also began at TMM in 1991 with soil heat flux and volumetric water content added in 1995 and 1997 respectively. Data is quality controlled prior to the assessment of ground thermal conditions, but available as both formatted and filtered data. The top of the permafrost at TMM has decreased from 75 to 114 cm below ground surface from 1991 to 2022. In addition, ground temperature monitoring has been carried out at numerous sites across TVC (Figure 1). These sites have shorter record periods but are extremely useful in considering the influence of variable snow depth and snow water equilvalent (SWE) on ground temperatures. End of winter snow on the ground (depth, density and SWE) is available every year from 1991. This is based on snow surveys across the main vegetation and terrain types, including shrub, forest, tundra, lake, and steep slopes with drifts (Figure 1). Daily TVC streamflow data is available from ECCC for the full period of record. Streamflow typically begins in early May and peaks in late May to early June at, on average, 0.218 m^3/s. Tower based eddy covariance measurements of sensible and latent heat flux are available from a 10 m tower since 2013. Early data sets face challenges such as frost heave, sensor drift and missing legacy metadata.

Conclusion

This long term hydro-meteorological-permafrost data set is unique in the western Canadian Arctic and will be extremely valuable for documenting past changes to climate, permafrost, hydrology, and meteorology in this region. This paper highlights the challenges and benefits of managing a multivariate and interdisciplinary dataset and making these data readily available. This openly-accessible historical TVC data improves our understanding of integrated controlling processes in the Arctic and serves to drive permafrost and hydrological models under future climate scenarios.

References

Burn, C.R., and Kokelj, S.V. 2009. The environment and permafrost of the Mackenzie Delta area, Permafrost and Periglacial Processes, 20(2): 83–105. https://doi.org/10.1002/ppp.655

Grünberg, I., Wilcox, E.J., Zwieback, S., Marsh, P., and Boike, J. 2020. Linking tundra vegetation, snow, soil temperature, and permafrost, Biogeosciences, 17: 4261–4279. https://doi.org/10.5194/bg-17-4261-2020

Hersbach, H., Bell, B., et al. 2020. The ERA5 global reanalysis, Quarterly Journal of the Royal Meteorological Society, 146: 1999–2049. https://doi.org/10.1002/qj.3803

Rampton, V.N. 1988. Quaternary Geology of the Tuktoyaktuk Coastlands, Northwest Territories, Geological Survey of Canada: Ottawa.

Wilcox, E.J., Keim, D., De Jong, T., Walker, B., Sonnentag, O., Sniderhan, A., Mann, P., and Marsh, P. 2019. Tundra shrub expansion may amplify permafrost thaw by advancing snowmelt timing. Arctic Science 5(4): 202–217. https://doi.org/10.1139/as-2018-0028

Permafrost Hydrology & Wetland Dynamics

6B — Drained Lake Basins in Lowland Permafrost Regions

Session Chairs: Helena Bergstedt[1], Juliane Wolter[2,3] & Benjamin M. Jones[4]

[1]*b.geos, Vienna, Austria*
[2]*University of Potsdam, Institute for Biochemistry and Biology, Potsdam, Germany*
[3]*Alfred Wegener Institute Helmholtz Centre for Polar and Marine Research, Potsdam, Germany*
[4]*Institute of Northern Engineering, University of Alaska, Fairbanks, Alaska, United States*

Drained lake basins (DLBs) are some of the most common landforms in lowland permafrost regions. DLB formation and drainage can form complex landscape mosaics that reflect asynchronous periods of permafrost aggradation and degradation. The presence of DLBs and their relative distribution on the landscape influence permafrost-region topography, hydrology, carbon cycling, GHG and nutrient fluxes, habitat availability, geomorphology, and human land use practices including subsistence practices and agriculture.

This session is intended as a forum for current research on DLBs in permafrost-affected landscapes. We seek contributions that reflect diverse scientific fields, approaches, geographic locations and a range of temporal (e.g. decadal to millennial) and spatial scales (e.g., local observation to large-scale studies). We particularly encourage contributions that (1) provide data on DLB geology, cryostratigraphy, geomorphology, and ecology; (2) outline new strategies to improve process understanding; (3) interface with neighbouring fields of science or apply innovative technologies and methods; (4) investigate model validation, model uncertainty, and scaling issues; (5) couple models of diverse processes or scales, and (6) foster our understanding of the geologic history, current state, and future fate of DLBs and associated permafrost conditions and surrounding terrain.

The importance of spatial heterogeneity in landscape characterisation – a case study for drained lake basin mapping

Helena Bergstedt[1,2], Annett Bartsch[1,2], Clemens von Baeckmann[1], Benjamin M. Jones[3], Amy Breen[4], Juliane Wolter[5,6], Louise Farquharson[7], Guido Grosse[8,6] & Mikhail Kanevskiy[3]

[1]*b.geos, Korneuburg, Austria*

[2]*Austrian Polar Research Institute, Vienna, Austria*

[3]*Institute of Northern Engineering, University of Alaska Fairbanks, Fairbanks, Alaska, United States*

[4]*International Arctic Research Centre, University of Alaska Fairbanks, Fairbanks, Alaska, United States*

[5]*University of Potsdam, Institute of Biochemistry and Biology, Potsdam, Germany*

[6]*Alfred Wegener Institute Helmholtz Centre for Polar and Marine Research, Section Permafrost Research, Potsdam, Germany*

[7]*Geophysical Institute, University of Alaska Fairbanks, Fairbanks, Alaska, United States*

[8]*Institute of Geosciences, University of Potsdam, Potsdam, Germany*

Lakes and drained lake basins are common landforms in lowland permafrost regions across the Arctic (Grosse et al. 2013). In permafrost regions, lakes may form as thermokarst lakes as a result of permafrost degradation, ground ice melt, and terrain subsidence in areas with moderate to high ground ice content (Jones et al. 2022). In regions with low ground ice content, lakes can develop in already existing depressions (Jones et al. 2022).

Together lakes and drained lake basins create a heterogeneous and dynamic mosaic of terrain units affected by permafrost aggradation and degradation, providing unique habitats to flora and fauna. Lakes and drained lake basins in permafrost regions play a crucial role in the regions landscape and ecosystem processes, influencing permafrost dynamics, biogeochemical processes, the hydrologic regime, as well as carbon cycling and greenhouse gas emissions (Jones et al. 2022). The formation of drained lake basins leads to permafrost aggradation, increases carbon sequestration and creates a diverse habitat mosaic in Arctic permafrost regions. A better understanding of lake – drained lake basin systems is needed to understand future dynamics, permafrost hydrology linkages, and improve the representation of Arctic permafrost landscapes in climate and Earth system models.

To achieve a better understanding of these complex processes a comprehensive mapping effort is needed to have reliable spatial information on the location of existing drained lake basin systems. In addition to information on spatial extent and location of these landforms, information on their properties is essential to correctly represent them in model setups and to foster our understanding of these landforms on a panarctic scale.

Previously, remote sensing has been used to map existing drained lake basins, monitor changes in surface water area and ongoing lake drainage events. Characterizing drained lake basins with the help of remote sensing has in past studies heavily relied on parameters from multispectral sensors such as the Normalized Difference Vegetation Index (NDVI) (Frohn et al. 2005; Jones et al. 2012), but few studies have also integrated data from radar-based systems (e.g., Regmi et al. 2012). Studies focussing on local scale analysis have shown success in utilizing pattern recognition of basin features to distinguish between basins of different age categories (Hinkel et al. 2003).

Drained lake basin evolution

After lake drainage the newly formed drained basin undergoes changes in surface cover, including vegetation succession, change in surface water presence as well as permafrost aggradation and ground ice formation. The cumulative changes are visible at the surface as a mosaic of terrestrial and aquatic habitats.

Jorgenson and Shur (2007) describe evolution of lakes and drained lake basins, including formation of remnant lakes, infilling ponds, ice wedge polygon development and secondary lake development at later stages after lake drainage. This suggests that drainage basins become more fragmented overtime, exhibiting a more heterogeneous surface cover. It can be assumed that this also translates into an increased spatial heterogeneity of wetness characteristics and vegetation patterns.

Methods and results

Here we investigate the benefit of a remote sensing-based classification and characterization approach considering spatial heterogeneity of drained lake basin complexes instead of a purely pixel-based approach. Our analysis is based on drained lake basin area

derived from Landsat-8 imagery following a method published by Bergstedt et al. (2019) and landcover information based on a data set published by Bartsch et al. (2023). To characterize the basins, we differentiate the complex drained lake basin area into sub-basins using the Copernicus 30 m DEM. To characterize the separate sub-basins, we rely on existing research describing age classification schemes (e.g., Hinkel et al. 2003) for drained lake basins characterization (young, medium, old, and ancient basins). Preliminary results show k-means derived clusters of drained sub-basins differ in vegetation communities present within the basins, allowing for assumptions about the relative time passed since a drainage event occurred. To compliment and verify our remote sensing-based approach, a wide array of field data was collected at multiple sites across the Arctic, including on the Alaska North Slope (e.g., Farquharson et al. 2021). First results show distinct differences between DLBs within the study area, based on the landcover occurring within basins and other surface properties. Characterizing DLBs on a large scale will allow for improved parametrization of regional to pan-Arctic modeling efforts and improve our understanding of DLBs as a crucial landform in Arctic permafrost landscapes.

REFERENCES

Bartsch, A., Efimova, A., Widhalm, B., Muri, X., von Baeckmann, C., Bergstedt, H., Ermokhina, K., Hugelius, G., Heim, B., and Leibmann, M. 2023. Circumarctic landcover diversity considering wetness gradients, EGUsphere [preprint]. https://doi.org/10.5194/egusphere-2023-2295

Bartsch, A., Efimova, A., Widhalm, B., Muri, X., von Baeckmann, C., Bergstedt, H., Ermokhina, K., Hugelius, G., Heim, B., and Leibmann, M. 2023. Circumpolar Landcover Units (1.0) [Data set]. Zenodo. https://doi.org/10.5281/zenodo.8399018

Bergstedt, H., Jones, B.M., Hinkel, K., Farquharson, L., Gaglioti, B.V., Parsekian, A.D., Kanevskiy, M., Ohara, N.; Breen, A.L.; Rangel, R.C., et al. 2021. Remote Sensing-Based Statistical Approach for Defining Drained Lake Basins in a Continuous Permafrost Region, North Slope of Alaska. Remote Sens. 13, 2539. https://doi.org/10.3390/rs13132539

Farquharson, F., Jones, B., Kanevskiy, M., Gaglioti, B., Bergstedt, H., and Hinkel, K. 2021. 14C (Carbon-14) ages of Holocene lake drainage events on the North Slope of Alaska, 2019-2020. Arctic Data Center. doi:10.18739/A29W0913J

Frohn, R.C., Hinkel, K.M., and Eisner, W.R. 2005: Satellite remote sensing classification of thaw lakes and drained thaw lake basins on the North Slope of Alaska. Remote Sens. Environ., 97, 116–126.Grosse, G., Jones, B., and Arp, C. 2013. Thermokarst Lakes, Drainage, and Drained Basins. In: Shroder, J.F. (ed.): Treatise on Geomorphology, 8: 325–353. San Diego: Academic Press. doi:10.1016/B978-0-12-374739-6.00216-5.

Hinkel, K.M., Eisner, W.R., Bockheim, J.G., Nelson, F.E., Peterson, K.M., and Dai, X. 2003. Spatial extent, age, and carbon stocks in drained thaw lake basins on the Barrow Peninsula, Alaska. Arctic, Antarctic, and Alpine Research, 35(3), 291–300. https://doi.org/10.1657/1523-0430(2003)035[0291:SEAACS]2.0.CO;2

Jones, M.C., Grosse, G., Jones, B.M., and Walter Anthony, K.M. 2012. Peat accumulation in a thermokarst-affected landscape in continuous ice-rich permafrost, Seward Peninsula, Alaska. JGR – Biogeosciences, 117: G00M07. doi:10.1029/2011JG001766

Jones, B.M., Grosse, G., Farquharson, L.M., Roy-Léveillée, P., Veremeeva, A., Kanevskiy, M.Z., Gaglioti, B.V., Breen, A.L., Parsekian, A.D., Ulrich, M., and Hinkel, K.M. 2022. Lake and drained lake basin systems in lowland permafrost regions. Nature Reviews Earth & Environment,3(1),85–98. https://doi.org/10.1038/s43017-021-00238-9

Jorgenson, M.T., and Shur, Y. 2007. Evolution of lakes and basins in northern Alaska and discussion of the thaw lake cycle, Journal of Geophysical Research: Earth Surface, 112 (F2). doi:10.1029/2006JF000531

Regmi, P., Grosse, G., Jones, M.C., Jones, B.M., and Walter Anthony, K.M. 2012. Characterizing Post-Drainage Succession in Thermokarst Lake Basins on the Seward Peninsula, Alaska with TerraSAR-X Backscatter and Landsat-based NDVI Data. Remote Sensing, 4(12): 3741–3765. doi:10.3390/rs4123741

Greenhouse gas production potential of drained lake basin sediments from the Yukon coastal plain

Verena Bischoff[1,2,3], Jan Schwarzbauer[1], Jens Strauss[3], Hugues Lantuit[3,4] & Juliane Wolter[2,3]

[1]*Faculty of Georesources and Materials Engineering, RWTH Aachen University, Aachen, North Rhine-Westphalia, Germany*

[2]*Institute of Biochemistry and Biology, University of Potsdam, Potsdam, Brandenburg, Germany*

[3]*Alfred Wegener Institute Helmholtz Centre for Polar and Marine Research, Section Permafrost Research, Potsdam, Brandenburg, Germany*

[4]*Institute of Earth and Environmental Sciences, University of Potsdam, Potsdam, Brandenburg, Germany*

Permafrost carbon pools are vulnerable to climate warming and have the potential to alter both terrestrial and global carbon cycles. Upon permafrost thaw, increased decomposition of organic-rich deposits in the extensive Arctic wetlands could lead to high greenhouse gas production and emission to the atmosphere. This study investigates processes and intensity of organic matter decomposition and associated potential greenhouse gas production in thawed sediments from drained lake basins on the Yukon Coastal Plain in the western Canadian Arctic.

Methods

We conducted one-year low-temperature (4 °C) incubation experiments, assessing the greenhouse gas production potential upon thaw under aerobic and anaerobic conditions in the active layer, transition layer, and permafrost layer of sediment cores from adjacent drained lake basins (Figure 1). The study was supplemented by comprehensive geochemical and biomarker analyses of *n*-alkanes and *n*-alkanols on day 0, 90 and 365 of the incubation experiments.

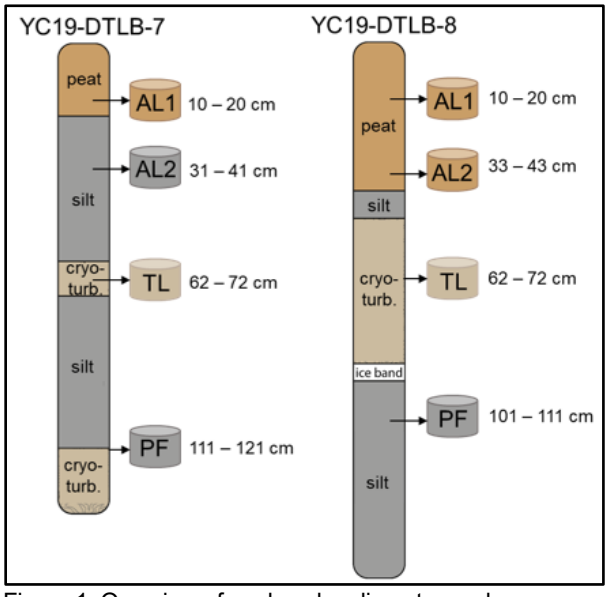

Figure 1: Overview of analyzed sediment samples.

We used one-way ANOVAs to identify differences in greenhouse gas production potential among mineral, organic and cryoturbated samples as well as among active layer, transition layer, and permafrost samples. To test significance of changes in geochemical and biomarker parameters we further performed paired t-tests on before- and after-incubation datasets.

Results

Preliminary results after the first 90 days of incubation revealed the distinct short-term GHG production potential of heterogenous samples under aerobic and anaerobic conditions (Figure 2 and 3).

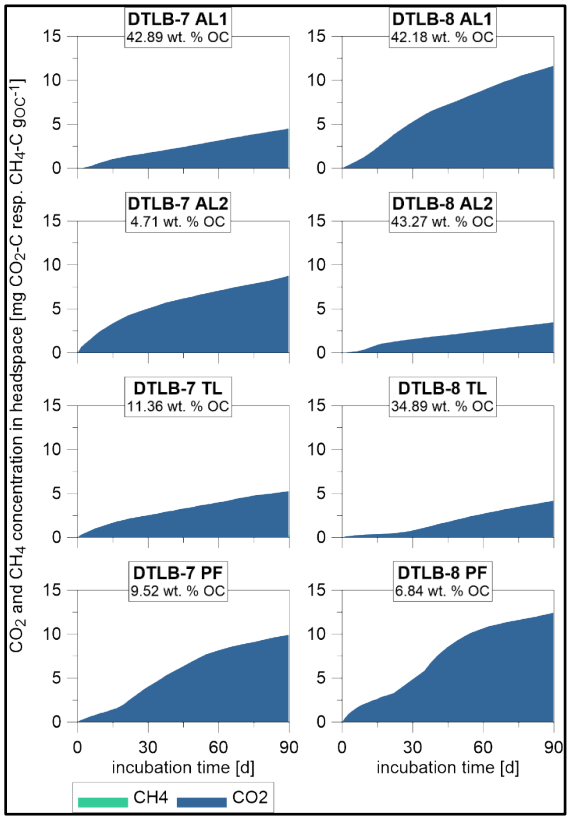

Figure 2. Composition of greenhouse gas production under aerobic conditions.

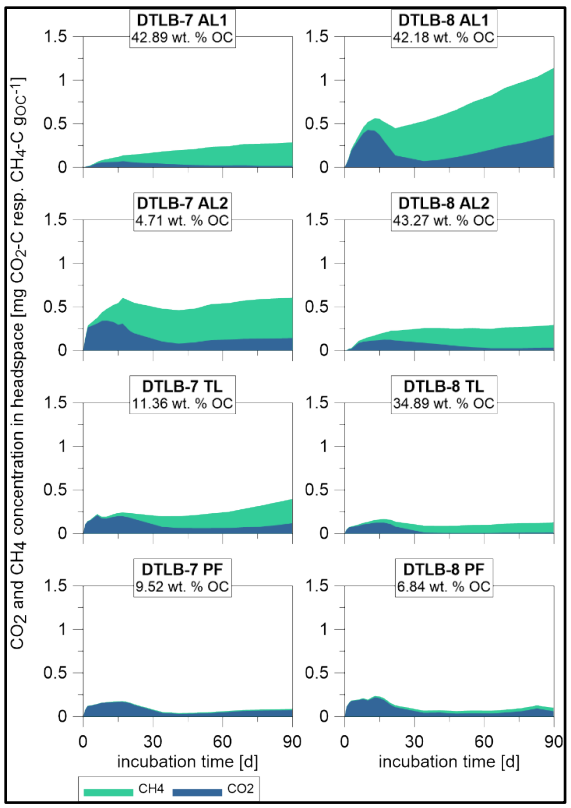

Figure 3. Composition of greenhouse gas production under anaerobic conditions.

The analyzed sediment samples exhibited high C:N ratios, low $\delta^{13}C$ values and distinctive n-alkane and n-alkanol distribution patterns, comprising long-chain lengths and pronounced odd-over-even resp. even-over-odd predominances. After the first 90 days of 4 °C aerobic and anaerobic incubation, changes in geochemical parameters TOC, TN, and C:N ratio were insignificant. n-Alkane and n-alkanol concentrations increased, with higher accumulation of n-alkanols than n-alkanes, reflected in increasing higher plant alkanol indices (HPA) in all samples.

Discussion

Geochemical parameters and biomarker indices pointed to a high input of terrestrial vascular plant waxes to the organic matter of the drained lake basin sediment cores and low degrees of degradation of the material.

Incubation experiments revealed a higher carbon turnover of up to 2.7 % of the available organic carbon to GHG under aerobic conditions within the first three months of incubation. Decompostion of labile carbon pools from mineral permafrost layers matched that of surface peat samples, whereas presumable nitrogen limitation retarded short-term carbon mineralization in pioneer peat layers that accumulated shortly after lake drainage.

On the short term, the GHG production under anaerobic conditions exhibited a high depth-dependency, with permafrost layer samples deviating from the otherwise observed high methanogenesis in active and transition layer samples. The combination of high CH_4 production and short lag times of maximum production rates suggests that the sediments readily provided ideal conditions for methanogenic microbial species or microbial communities were already well established in the sediment. High contributions of the potent greenhouse gas methane of up to 94 % enhanced the climate forcing effect of anaerobic GHG production. Consequently, the determined relative climate forcing is higher under anaerobic compared to aerobic conditions in active and transition layers, suggesting that waterlogged conditions within drained lake basins are more unfavorable in the short term.

While established degradation proxies C:N ratio, $\delta^{13}C$ and CPI did not trace significant degradation of terrestrial organic matter during the first three months of the incubation period, we observed major shifts in the lipid composition.

Conclusion

Carbon pools in drained lake basins on the Yukon coastal plain are highly sensitive to thaw. Trajectories of hydrologic conditions in drained lake basins determine the pace and form of decomposition of the organic carbon pool and hence, potential greenhouse gas emissions. Thaw depth progression under aerobic conditions in drained soils could cause immediate and high peaks in greenhouse gas production, though initially high production rates are expected to decline over time. Further we conclude that drained lake basins could provide perfect conditions for methanogenesis under anaerobic conditions and hence produce a highly unfavourable mix of greenhouse gases.

Post-drainage evolution of an old drained lake basin in Old Crow Flats, Yukon, Canada

Danielle Chiasson, Pascale Roy-Léveillée & Najat Bhiry
Centre d'études nordiques, Université Laval, Québec City, Québec, Canada

Old Crow Flats (OCF) is an ice-rich thermokarst landscape spanning 5,600 km^2 within the continuous permafrost zone of northern Yukon, Canada. It is within the Traditional Territory of the Vuntut Gwitch'in First Nation (VGFN). In 2019, the VGFN declared a climate change state of emergency related to rapid landscape change in their traditional territory. These changes include a reported increase in catastrophic lake drainage events (Lantz and Turner 2015) as well as rapid and persistent willow growth following these drainage events, contributing to landscape-scale shrubification (Lantz 2017). Although contemporary conditions in drained lake basins have been well documented (Lantz 2017; Mackay and Burn 2002), it is difficult to assess the impacts of warming on contemporary post-drainage basin conditions because there are very few paleo-environmental reconstructions of post-drainage basin evolution prior to anthropogenic climate warming.

Methods

This study aims to provide a better understanding of drained lake basin evolution by reconstructing vegetation succession within a large lake basin (5.9 km^2) that drained catastrophically prior to anthropogenic climate warming (Figure 1). Peat samples from the margin and the centre of the basin have been collected to reconstruct local vegetation histories through radiocarbon-dated macrofossil records. Loss on ignition and macrofossil analyses were conducted at 1 cm intervals from the peat surface to the organic/mineral interface. Zones of distinct vegetation change have been identified within the peat profiles and plant macrofossil samples from each zone were submitted for AMS radiocarbon dating. The reconstruction of vegetation histories allows comparison to documented contemporary post-drainage vegetation succession patterns in the region. Key aspects of the evolution of drained basins are examined, such as the local importance and persistence of remnant ponds and different plant assemblages (e.g., sedge fens, large stands of willows, sphagnum bogs), and the relative timing of surface heaving via permafrost aggradation.

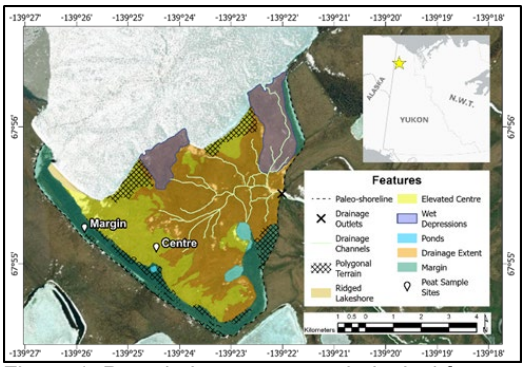

Figure 1. Post-drainage geomorphological features and peat sample sites from a drained lake basin in Old Crow Flats, Yukon.

Results and Discussion

Preliminary results from calibrated radiocarbon dates of basal peat suggest that, following the catastrophic drainage of the lake near 2817 years BP, the margin was exposed while a remnant pond persisted at the centre, which is similar to conditions observed in contemporary basins (Labrecque et al. 2009).

Preliminary results from macrofossil analyses suggest that a hydrosere of wetland communities occurred at the margin (Figure 2), beginning with a wet sedge-shrub marsh, followed by a minerotrophic wet sedge fen, and finally an ombrotrophic string bog. Macrofossil analyses from the centre of the basin suggest a variation in hydroseral succession, beginning with a minerotrophic wet sedge fen, followed by an ombrotrophic bog, and finally a terrestrial tussock tundra community.

The timing of permafrost aggradation at both sites is likely associated with the transition of minerotrophic fen vegetation to ombrotrophic bog vegetation (Ovenden 1982). The relatively rapid succession from fen to bog and tundra vegetation at the centre (compared to the margin) suggests that the establishment and aggradation of permafrost contributed to uplift and drying of the ground surface. Even though the centre of the basin was exposed to subaerial conditions for a shorter period of time than the margin, its wetness decreased over time while it increased in the margin. These conditions are consistent with the landform development model presented by Roy-Léveillée and Burn (2016).

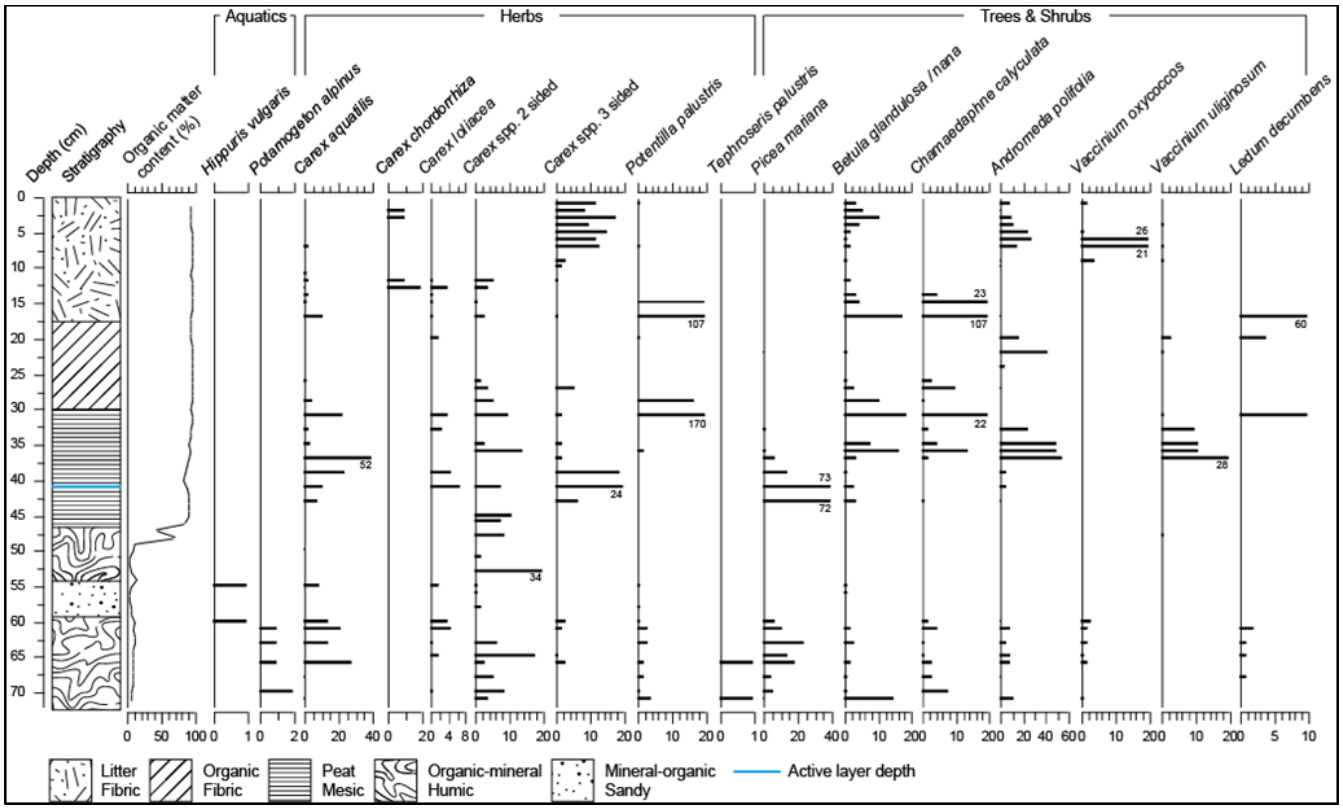

Figure 2. Macrofossil diagram, stratigraphy, and organic matter content of a peat core collected from the margin of a drained lake basin in Old Crow Flats, Yukon. Plant species are presented in number of macrofossils per 1 cm depth.

Further identification of woody material present at the base of the margin sample will help elucidate whether dense thickets of willows have previously represented a seral stage of vegetation succession, as observed in modern basins (Lantz 2017).

CONCLUSIONS

This study provides paleoecological data for a drained lake basin following a catastrophic drainage event prior to anthropogenic climate warming. By reconstructing the history of vegetation succession and its associated permafrost conditions at the margin and centre of the basin, better comparisons of past and present basin evolution can be made. Furthermore, by deepening our understanding of millennial-scale development of basin conditions, better predictions of future basin development can be made and shared with the Vuntut Gwitchin First Nation.

REFERENCES

Labrecque, S., Lacelle, D., Duguay, C.R., Lauriol, B., and Hawkings, J. 2009. Contemporary (1951–2001) Evolution of Lakes in the Old Crow Basin, Northern Yukon, Canada: Remote Sensing, Numerical Modeling, and Stable Isotope Analysis. ARCTIC 62, 225–238. https://doi.org/10.14430/arctic134

Lantz, T.C. 2017. Vegetation Succession and Environmental Conditions following Catastrophic Lake Drainage in Old Crow Flats, Yukon. ARCTIC 70, 177. https://doi.org/10.14430/arctic4646

Lantz, T.C., and Turner, K.W. 2015. Changes in lake area in response to thermokarst processes and climate in Old Crow Flats, Yukon. J. Geophys. Res. Biogeosci. 120, 513–524. https://doi.org/10.1002/2014JG002744

Mackay, J.R., and Burn, C.R. 2002. The first 20 years (1978-1979 to 1998-1999) of active-layer development, Illisarvik experimental drained lake site, western Arctic coast, Canada. Canadian Journal of Earth Sciences 39, 1657–1674. https://doi.org/10.1139/E02-068

Ovenden, L. 1982. Vegetation history of a polygonal peatland, northern, Yukon. Boreas 11, 209–224. https://doi.org/10.1111/j.1502-3885.1982.tb00715.x

Roy-Léveillée, P., and Burn, C.R. 2016. A modified landform development model for the topography of drained thermokarst lake basins in fine-grained sediments. Earth Surf. Process. Landforms 41, 1504–1520. https://doi.org/10.1002/esp.3918

Mercury and methylmercuy concentrations in drained lake basin, Old Crow Flats, Yukon, Canada

Nicole Corbiere[1], Pascale Roy-Léveillée[2], Brian Branfireun[3], Danielle Chiasson[2] & Nathan Basiliko[4]

[1]*Vale Living with Lakes Research Centre, University of Laurentian, Sudbury, Ontario, Canada*

[2]*CRYO-UL: Permafrost Research Laboratory, Université Laval, Québec City, Québec, Canada*

[3]*Department of Biology, University of Western, London, Ontario, Canada*

[4]*Department of Natural Resource Management, University of Lakehead, Thunder Bay, Ontario, Canada*

Lakes and drained basin complexes (LDBC) cover nearly one-fifth of the circumpolar North. In these complexes, drained basins accumulate organic carbon over decades to millennia (Hugelius et al. 2014; Schuur et al. 2008; Schuster et al. 2018). This stored carbon may be associated with atmospherically deposited mercury (Hg) (Lim et al. 2020; Giesler et al. 2017; Schuster et al. 2018). Accelerated landscape changes in permafrost environments may lead to terrain conditions that favour or inhibit Hg methylation - the transformation of inorganic Hg to methylmercury (MeHg), which bioaccumulates and is a neurotoxin (Gordon et al. 2016; Burke et al. 2018). In LDBCs, lake drainages create mosaics of wet and dry environments that evolve as progressive permafrost aggradation heaves the lake bottom. These environments host different microbial communities and are likely to have different Hg methylation potentials. This study examined the net MeHg production potential in drained lake basins of Old Crow Flats (OCF), Yukon (Figure 1). OCF is a vast thermokarst lowland underlain by continuous permafrost that is a crucial part of Vuntut Gwitchin First Nation's traditional territory. Specifically, this study 1) characterized Hg storage in peat and reworked glaciolacustrine deposits in drained lake basins of various ages in OCF of northern Yukon; and 2) analyzed whether delays in permafrost aggregation in drained lake basin could support increased Hg methylation in post drained lake basin evolution environment.

Methods

In June and August 2021 and June 2022, peat and mineral soil samples from the active layer were collected within contemporary and old drained basins in OCF. Samples were frozen, and sent to the Biotron Centre for Experimental Climate Change Research. Soil sample analysis to quantify total Hg content (THg) with a DMA-80 mercury analyzer and MeHg concentration via cold vapour atomic flurescence spectopscopy on a Tekran2700 to identify the methyl-total mercury ratio in drained basin complexes.

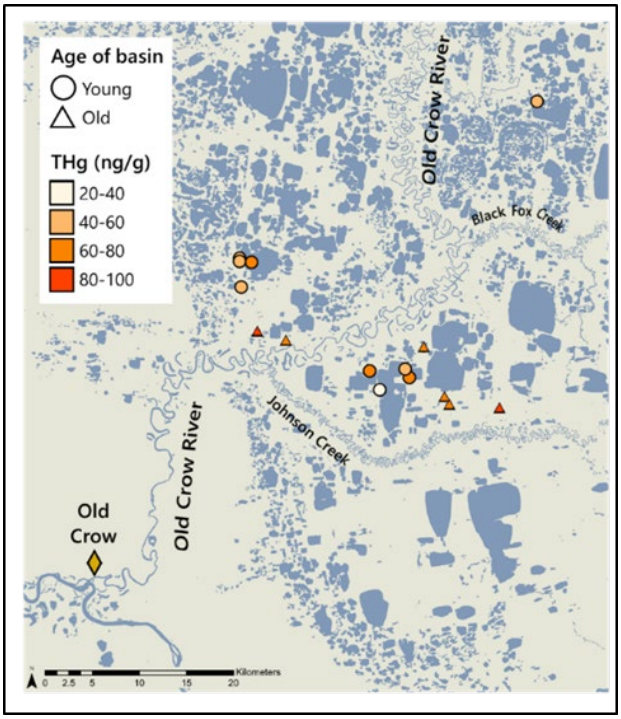

Figure 1. Sampling sites, including contemporary and old drained basins, and total Hg content in the upper 10 cm of the ground.

Preliminary results

Total Hg concentrations were low and comparable to other permafrost peatlands of the Western Arctic. Old drained basins had a slightly higher THg concentration (66 ng/g) than young drained basins (59 ng/g).

Old drained basins had a lower ratio of Hg to soil organic carbon (0.17 µg/g) than young drained basins (0.80 µg/g), where the organic layer had not yet developped or was very thin. The ratio of Hg to soil organic carbon in Old drained basins was relatively low and consistent with observations from other permafrost peat complexes in Siberia (0.15 µg/g, Lim et al. 2020) and in the Hudson Bay Lowlands (0.21 µg/g, Kirkwood et al. 2021). The ratio of Hg to soil organic carbon in young basins was comparable to concentrations reported for mineral soils in Siberia (0.64 µg/g, Lim et al. 2020), but still much lower than the global median

Hg to soil organic carbon of 1.6 µg/g reported by Schuster et al. (2018).

The younger drained basins had a higher MeHg/THg ratio than old basins (2.6 vs 0.8%), associated with wetter conditions and abundant *Carex* sp. These results suggest that, where permafrost fails to aggrade in young drained basins and wet conditions (remnant ponds) persist, extensive marshy vegetations can lead to higher net Hg methylation potential.

COMMUNICATING RESULTS TO COMMUNITY

OCF is a crucial part of Vuntut Gwitchin First Nation's traditional territory, and the communication of results about the presence and cycling of Hg is a sensitive matter. The lead author, Nicole Corbiere, is Anishinaabe from Wiikwemikoong First Nation and produced a series of illustrations incorporating traditional woodland art style to facilitate the presentation of research results in a clear and relatable way to members of the Old Crow community.

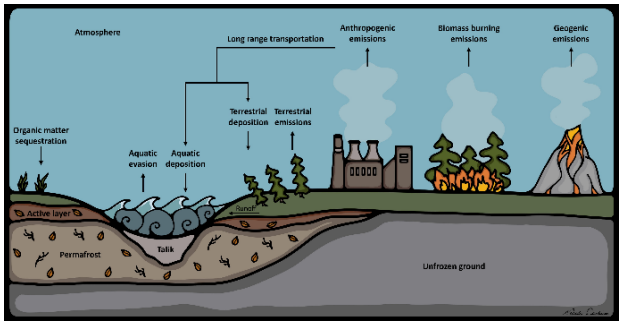

Figure 2. Example of an illustration produced by the lead author to facilitate discussions about the Hg cycle with local community members.

ACKNOWLEDGEMENTS

Mahsi cho Caleb Charlie, Dougie Charlie, Jeneen Njoutli, Nico Njoutli, Robert Linklater, Crystal Linklater, Harlow Linklater, and Mary Jane Moses from Vuntut Gwithcin First Nation. Thank you to Louis-Philippe Roy and Fanny Amyot from Yukon University and Kevin Turner from Brock University. This work was supported by the Natural Science and Engineering Research Council of Canada (NSERC), NSERC PermafrostNet, ArcticNet, Polar Knowledge Canada, Western Canadian Society, Weston Family Foundation and Royal Canadian Geological Society.

REFERENCES

Burke, S.M., Zimmerman, C.E., Branfireun, B.A., Koch, J.C., and Swanson, H.K. 2018. Correction to: Patterns and controls of mercury accumulation in sediments from three thermokarst lakes on the Arctic Coastal Plain of Alaska. Aquatic Sciences, 81(1): 1–15. doi:10.1007/s00027-017-0553-0

Giesler, R., Clemmensen, K.E., Wardle, D.A., Klaminder, J., and Bindler, R. 2017. Boreal Forests Sequester Large Amounts of Mercury over Millennial Time Scales in the Absence of Wildfire. Environmental Science & Technology, 51(5): 2621–2627. doi10.1021/acs.est.6b06369

Gordon, J., Quinton, W., Branfireun, B.A., and Olefeldt, D. 2016. Mercury and methylmercury biogeochemistry in a thawing permafrost wetland complex, Northwest Territories, Canada. Hydrological Processes, 30(20): 3627–3638. doi:10.1002/hyp.10911

Hugelius, G., Strauss, J., Zubrzycki, S., Harden, J.W., Schuur, E.A.G., Ping, C.-L. ., Schirrmeister, L., Grosse, G., Michaelson, G.J., Koven, C.D., O'Donnell, J.A., Elberling, B., Mishra, U., Camill, P., Yu, Z., Palmtag, J., and Kuhry, P. 2014. Estimated stocks of circumpolar permafrost carbon with quantified uncertainty ranges and identified data gaps. Biogeosciences, 11(23): 6573–6593. doi:10.5194/bg-11-6573-2014

Kirkwood, A.H., Pascale Roy-Léveillée, Branfireun, B.A., and Basiliko, N. 2021. Mercury, Methylmercury, and Microbial Communities in a Degrading Palsa of the Hudson Bay Lowlands, Far North Ontario. doi:10.1061/9780784483589.005

Lim, A.G., Jiskra, M., Sonke, J.E., Loiko, S.V., Kosykh, N., and Pokrovsky, O.S. 2020. A revised pan-Arctic permafrost soil Hg pool based on Western Siberian peat Hg and carbon observations. Biogeosciences, 17(12): 3083–3097. doi:10.5194/bg-17-3083-2020

Schuster, P.F., Schaefer, K.M., Aiken, G.R., Antweiler, R.C., Dewild, J.F., Gryziec, J.D., Gusmeroli, A., Hugelius, G., Jafarov, E., Krabbenhoft, D.P., Liu, L., Herman-Mercer, N., Mu, C., Roth, D.A., Schaefer, T., Striegl, R.G., Wickland, K.P., and Zhang, T. 2018. Permafrost Stores a Globally Significant Amount of Mercury. Geophysical Research Letters, 45(3): 1463–1471. doi:10.1002/2017gl07557

Schuur, E.A.G., Bockheim, J., Canadell, J.G., Euskirchen, E., Field, C.B., Goryachkin, S.V., Hagemann, S., Kuhry, P., Lafleur, P.M., Lee, H., Mazhitova, G., Nelson, F.E., Rinke, A., Romanovsky, V.E., Shiklomanov, N., Tarnocai, C., Venevsky, S., Vogel, J.G., and Zimov, S.A. 2008. Vulnerability of Permafrost Carbon to Climate Change: Implications for the Global Carbon Cycle. BioScience, 58(8): 701–714. doi:10.1641/b580807

Recent advances in research investigating permafrost conditions, geomorphology, vegetation, and lake hydrology in Old Crow Flats (YT, Canada)

Samuel Gagnon[1,2], Pascale Roy-Léveillée[1,2] & Kevin Turner[3]

[1]*CRYO-UL: Permafrost Research Laboratory, Université Laval, Québec City, Québec, Canada*

[2]*Centre d'études nordiques, Université Laval, Québec City, Québec, Canada*

[3]*Department of Geography and Tourism Studies, Brock University, St. Catharines, Ontario, Canada*

Old Crow Flats (OCF) is a 5600 km^2 wetland in the traditional territory of the Vuntut Gwitchin First Nation (VGFN), northern Yukon, Canada. Located in the continuous permafrost zone, it contains thousands of thermokarst lakes and drained lake basins (TL-DLB) that have formed in ice-rich glaciolacustrine deposits left after the drainage of glacial lake Old Crow about 15 ka ago. OCF holds immense cultural value for the VGFN and is internationally recognized for its ecological and cultural integrity (Vuntut Gwitchin First Nation and Smith 2009). Like other high-latitude lowland regions, OCF has been changing rapidly due to climate warming, inducing landscape changes largely driven by TL-DLB dynamics. Since TL-DLB provide important habitat for migratory birds, fishes, moose, muskrats, and numerous other species, the VGFN is concerned that the recent environmental changes observed by local residents in OCF will affect the traditional activities and food security of their citizens (Douglas et al. 2014; Wolfe et al. 2011). Research in OCF has intensified over the last two decades, following concerns expressed by the community, and the rapidity and severity of the environmental changes pushed the VGFN to declare the climate change state of emergency in 2019 (Avery 2019). Ice-rich permafrost is sensitive to climate change and surface disturbance, which can interact in synergy to promote thermokarst development. However, changes in environmental conditions can lead to both positive and negative feedbacks involving interactions between permafrost conditions, geomorphology, vegetation, and lake hydrology. As a result, it is necessary to use an interdisciplinary approach to study environmental changes in OCF to better understand current and future changes in the region.

Objectives

This project aims to synthesize previously published and on-going environmental research in OCF to advance knowledge of relations between climate-driven changes in vegetation structure, permafrost sustainability and ground conditions, and hydrological connectivity. In addition to discussing recent observations and examine trends in landscape changes based on existing literature, this project will present updated and new results addressing gaps in the data available in OCF.

Prelimininary results

Preliminary results focussing on thermokarst lake dynamics show that the expansion of shrubs (i.e., shrubification) in OCF can affect the hydrological regime of lakes, shore erosion, lake geometry, the permafrost thermal regime, and the release of carbon, mercury and nutrients through interactions and feedbacks (Figure 1). In areas with sparse vegetation (i.e., low-shrub tundra), permafrost temperatures are lower because of snow redistribution by the wind that reduce snow cover and increases snow density (Roy-Léveillée et al. 2014). While permafrost in such conditions is colder, the lack of vegetation can increase shore bank vulnerability to thermomechanical erosion, resulting in large oriented lakes (Roy-Léveillée and Burn 2015) and enhanced mobilization of permafrost carbon into expanding lakes. Furthermore, lakes in tundra areas tend to be more sensitive to variations in precipitations and to catastrophic drainage (Lantz and Turner 2015; Turner et al. 2014). Conversely, in areas with tall shrubs, the taller and denser vegetation cause permafrost temperatures to increase due to the thicker and less dense snow cover. It can also reduce the hydrological sensitivity of the lakes by dampening the seasonal variations in precipitations (Turner et al. 2014) and increase nutrient input from catchment due to greater snowmelt (Balasubramaniam et al. 2015). The vegetation can also protects shorelines against ice push in spring and wave action during the open summer season (Roy-Léveillée and Burn 2010), which results reduced erosion rates, irregular shorelines, and thaw subsidence as the dominant process affecting lake expansion (Roy-Léveillée and Burn 2017). Therefore, while the shrubification of OCF could lead to permafrost warming and surface disturbances (i.e., thermokarst), it could also increase lake resilience to geomorphological (reduced shore erosion) and hydrological (variations in precipitations) changes.

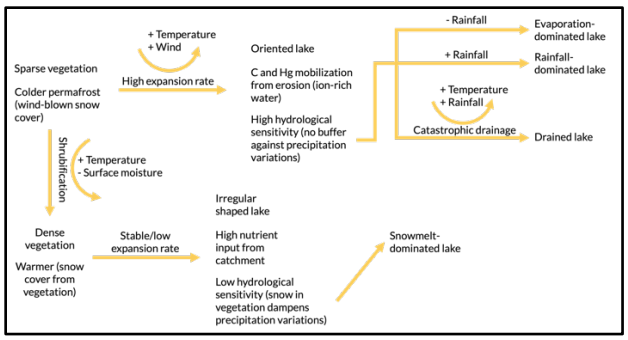

Figure 1. Conceptual model describing the effects of the shrubification on thermokarst lake dynamics.

REFERENCES

Avery, H. 2019. Old Crow declares climate change state of emergency | CBC News. CBC.

Balasubramaniam, A.M., Hall, R.I., Wolfe, B.B., Sweetman, J.N., and Wang, X. 2015. Source water inputs and catchment characteristics regulate limnological conditions of shallow subarctic lakes (Old Crow Flats, Yukon, Canada). Can. J. Fish. Aquat. Sci. 72, 1058–1072. https://doi.org/10.1139/cjfas-2014-0340

Douglas, V., Chan, L., Wesche, S., Dickson, C., Kassi, N., Netro, L., and Williams, M. 2014. Reconciling Traditional Knowledge, Food Security, and Climate Change: Experience From Old Crow, YT, Canada. Progress in community health partnerships : research, education, and action 8, 3. https://doi.org/10.1353/cpr.2014.0010

Lantz, T.C., and Turner, K.W. 2015. Changes in lake area in response to thermokarst processes and climate in Old Crow Flats, Yukon. J. Geophys. Res. Biogeosci. 120, 513–524. https://doi.org/10.1002/2014JG002744

Roy-Léveillée, P., and Burn, C.R. 2017. Old Crow Flats: Thermokarst Lakes in the Forest–Tundra Transition, in: Slaymaker, O. (Ed.), Landscapes and Landforms of Western Canada, World Geomorphological Landscapes. Springer International Publishing, Cham, pp. 267–276. https://doi.org/10.1007/978-3-319-44595-3_19

Roy-Léveillée, P., and Burn, C.R. 2015. Geometry of oriented lakes in Old Crow Flats, northern Yukon. Presented at the GEOQuebec2015: 68th Canadian Geotechnical Conference and the 7th Canadian Permafrost Conference, Québec, QC, Canada, p. 8.

Roy-Léveillée, P., and Burn, C.R. 2010. Permafrost conditions near shorelines of oriented lakes in Old Crow Flats, Yukon Territory. Presented at the GEO2010: 63rd Annual Canadian Geotechnical Conference and the 6th Canadian Permafrost Conference, Calgary, AB, Canada, pp. 1509–1516.

Roy-Léveillée, P., Burn, C.R., and McDonald, I.D. 2014. Vegetation-Permafrost Relations within the Forest-Tundra Ecotone near Old Crow, Northern Yukon, Canada: Permafrost Temperatures within the Forest-Tundra near Old Crow, YT. Permafrost and Periglac. Process. 25, 127–135. https://doi.org/10.1002/ppp.1805

Turner, K.W., Wolfe, B.B., Edwards, T.W.D., Lantz, T.C., Hall, R.I., and Larocque, G. 2014. Controls on water balance of shallow thermokarst lakes and their relations with catchment characteristics: a multi-year, landscape-scale assessment based on water isotope tracers and remote sensing in Old Crow Flats, Yukon (Canada). Global Change Biology 20, 1585–1603. https://doi.org/10.1111/gcb.12465

Vuntut Gwitchin First Nation, Smith, S. 2009. People of the Lakes: Stories of Our Van Tat Gwich'in Elders/Googwandak Nakhwach'ànjòo Van Tat Gwich'in. The University of Alberta Press.

Wolfe, B.B., Humphries, M.M., Pisaric, M.F.J., Balasubramaniam, A.M., Burn, C.R., Chan, L., Cooley, D., Froese, D.G., Graupe, S., Hall, R.I., Lantz, T., Porter, T.J., Roy-Leveillee, P., Turner, K.W., Wesche, S.D., and Williams, M. 2011. Environmental Change and Traditional Use of the Old Crow Flats in Northern Canada: An IPY Opportunity to Meet the Challenges of the New Northern Research Paradigm. ARCTIC 64, 127–135. https://doi.org/10.14430/arctic4092

Assessing sudden drainage in a small lake from the Mackenzie Delta uplands using remotely sensed imagery and lake sediments

Claire O'Hagan, Rachel Pellegrino, Joshua Thienpont & Jennifer Korosi
Faculty of Environmental and Urban Change, York University, Toronto, Ontario, Canada

Climate change is greatly affecting landscapes across the circumpolar north. Near-surface permafrost thaw is a significant consequence of increased temperatures, with enhanced thermokarst activity, including retrogressive thaw slumps, observed due to ongoing permafrost thaw. Retrogressive thaw slumps are mass wasting features that develop along the shorelines of lakes (Burn 1990), affecting the water quality of the impacted lakes (e.g., Kokelj et al. 2009). Thaw slumps are prevalent throghout the Mackenzie Delta, and the slumps can remain active for years before stabilizing.

Permafrost thaw plays a role in lake area change and drainage dynamics. Some areas studied have experienced marked lake expansion, while others experienced drainage, leaving the direction of change largely ambiguous (Hinkel et al. 2007). Given the vast area covered by thermokarst lakes in Arctic regions, the expected increased frequency of drainage events associated with warming air and ground temperatures may play an important role in future potential widespread limnological changes for Arctic surface waters.

METHODS

The aim of this project is to assess the drainage of a small retrogressive thaw slump-impacted lake, Lake 2B (unofficial name), located north of Inuvik, in the continuous permafrost zone of the uplands east of the Mackenzie Delta (Figure 1). The lake comes from the well-studied series of paired lakes established by Kokelj (2005), with 'B' lakes representing slump-impacted lakes, and 'A' lakes representing reference lakes. Based on field observations, it was known that the lake drained sometime between 2008 and 2017, though the timing and drivers of the drainage were unknown. Using remotely sensed imagery, the lake was assessed to determine 1) when drainage occurred, and 2) whether drainage occurred catastrophically. As it was expected that the lake drained during the summer snowmelt season, the approach was taken to examine images from the beginning of the snowmelt season (early June), and visually compare to images from the end of the summer (late August). This was carried out for every year starting with 2017, and working backwards towards 2008. Climate data was also assessed around the inferred timing of drainage, in order to gain climatic context for the time that the drainage event occurred. To assess the impact of the limnology of the lake, diatom-based paleolimnological techniques were employed on a sediment core collected in April 2021. A sediment core from the lake was previously analyzed to assess slump impacts (Thienpont et al. 2013), and could therefore be used to compare to post-drainage limnological inferences from diatom algae using identical methods.

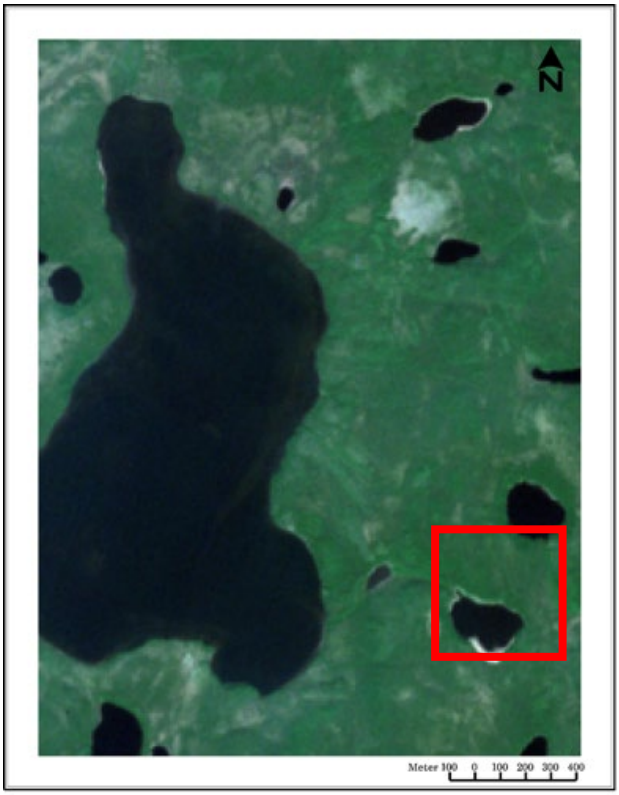

Figure 1. Sentinel 2 Image of Lake 2B (red box), July 2021.

REMOTE SENSING ANALYSIS

Using Landsat 7 and 8 imagery, it was determined that the lake drained between 2012 and 2013. Further imagery analysis, including GVI (Greeness Vegetation Index) analysis, was conducted to analyze the change. GVI was chosen to highlight changes to vegetation and lake surface area, as green vegetation, water, and exposed sediment have notably different GVI values.

The results of the GVI demonstrate Lake 2B likely drained between June 13, 2012 and August 9, 2012.

Climatic context of drainage

Based on analysis of climate data it is clear that July 2012 was a particulary warm, wet month, which we believe led to sudden drainage of the lake. On July 9th 2012, there was a major rainfall event that resulted in 26.7mm of precipitation in a 24 hour period, greater than the combined precipitation in June and August of that year (Figure 2). Similar weather conditions led to a catastrophic lake drainage event in August 1989 in the region, observed by Marsh (2008). They documented a summer that was warmer and wetter than normal, with several extreme precipitation events before drainage of a small, thaw slump-impacted lake. These climate data provide a mechanism for a drainage event occurred between June and July of 2012, supporting our hypothesis that the drainage event on Lake 2B occurred on or around July 9th due to warm temperatures, and extreme precipitation.

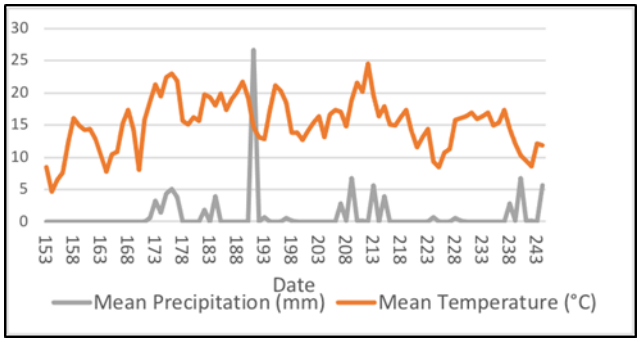

Figure 2. Daily mean precipitation (grey) and daily mean temperature (orange) from the Inuvik weather station, throughout summer 2012.

Lake sediment core analysis

Sedimentary diatoms in sediment intervals dated by 210Pb techniques as post-2012 show a decrease in planktonic taxa, primarily *Cyclostephanos* spp., at the time of inferred lake drainage, as would be expected with rapid water level lowering. These taxa were replaced by species occupying benthic and periphytic habitats, including *Acnanthidium minutissimum* and *Diatoma tenue*. The lowest relative abundance of plankters occurred immediately post drainage, but was observed to rise towards the surface of the sediment core, taken in 2021. This suggests the lake has experienced some re-filling following the initial water level drawdown, which was confirmed during field sampling in the summer of 2023. The most significant change in the diatom assemblage still remained the impacts of thaw slumping from the early 1970s, influenced by the 1968 Inuvik wildfire (Landhausser and Wein 1993), though the 2012 drainage was of a similar scale.

Conclusions and impacts

Our results indicate Lake 2B drained around July 9, 2012, in the context of warm summer temperatures, and a significant precipitation event. Sediment core inferences and field observations indicate the lake has refilled somewhat from the lowest level, immediately post drainage.

Understanding effects of warming temperatures in the Arctic is essential as the area continues to be affected by global change. This includes cases such as Lake 2B with cumulative impacts from multiple and potentially related stressors including shoreline subsidence from permafrost thaw and rapid drainage.

References

Burn, C., and Lewkowicz, A.G. 1990. Canadian Landform Examples- 17 Retrogressive Thaw Slumps. The Canadian Geographer, 34(3), 273–276. https://doi.org/10.1111/j.1541-0064.1990.tb01092.x

Hinkel, K.M., Jones, B.M., Eisner, W.R., Cuomo, C.J., Beck, R.A., and Frohn, R. 2007. Methods to assess natural and anthropogenic thaw lake drainage on the western Arctic Coastal Plain of Northern Alaska. Journal of Geophysical Research, 112(F2), F02S16–n/a. https://doi.org/10.1029/2006JF000584

Kokelj, S.V., Jenkins, R.E., Milburn, D., Burn, C.R., and Snow, N. 2005. The influence of thermokarst disturbance on the water quality of small upland lakes, Mackenzie Delta region, Northwest Territories, Canada. Permafrost and Periglacial Processes, 16(4), 343–353. https://doi.org/10.1002/ppp.536

Kokelj, S.V., Lantz, T.C., Kanigan, J., Smith, S.L., and Coutts, R. 2009. Origin and polycyclic behaviour of tundra thaw slumps, Mackenzie Delta region, Northwest Territories, Canada. Permafrost and Periglacial Processes, 20(2), 173–184. https://doi.org/10.1002/ppp.642

Landhausser, S.M., and Wein, R.W. 1993. Postfire vegetation recovery and tree establishment at the Arctic treeline: climate-change-vegetation-response hypotheses. Journal of Ecology, 665–672.

Marsh, P., Russell, M., Pohl, S., Haywood, H., and Onclin, C. 2009. Changes in thaw lake drainage in the western Canadian Arctic from 1950 to 2000. Hydrological Processes, 23(1), 145–158. https://doi.org/10.1002/hyp.7179

Thienpont, J.R., Ruehland, K.M., Pisaric, M.F., Kokelj, S.V., Kimpe, L.E., Blais, J.M., and Smol, J.P. 2013. Biological responses to permafrost thaw slumping in Canadian Arctic lakes. Freshwater Biology, 58(2), 337–353.

Lake drainage increases snowdrift in Arctic tundra

Rodrigo C. Rangel[1], Noriaki Ohara[2], Andrew D. Parsekian[2,3] & Benjamin M. Jones[4]

[1]*Department of Earth Sciences, University of Toronto, Toronto, Ontario, Canada*

[2]*Department of Civil & Architectural Engineering & Construction Management, University of Wyoming, Laramie, Wyoming, United States*

[3]*Department of Geology and Geophysics, University of Wyoming, Laramie, Wyoming, United States*

[4]*Institute of Northern Engineering, University of Alaska Fairbanks, Fairbanks, Alaska, United States*

Snow storage in drifts is a significant component of the hydrological cycle in the Arctic tundra. Due to prevailing wind direction, snowdrifts tend to form on steep slopes, including the margins of lakes and drained lake basins (DLBs), which comprise vital water storage for the ecosystem when the snow melts during the spring and summer. Here, we combine field measurements, remote sensing observations, lake drainage simulation, and snow modeling to investigate how lake drainage impacts snow redistribution in Inigok on the Arctic Coastal Plain (ACP) of Alaska. Our results show a significant increase in snow storage in drifts after lake drainage.

The Arctic tundra is covered by seasonal snow for more than half of the year and the snow redistribution is mainly controlled by wind. The amount of snow accumulation is a critical component of the hydrological cycle, however, it is still poorly quantified on regional scales (Brown et al. 2021). Due to lake formation, expansion, and drainage, the surface morphology is in constant change, which partially controls the snow accumulation during the cold seasons. Lakes and DLBs combined are estimated to cover >20% of the Northern Hemisphere permafrost region and ~50% of the region <300 m elevation (Jones et al. 2022). Previous work showed that 1 to 2 lakes (>10 ha) have drained per year between 1955 and 2017 and ~1,900 lakes are susceptible to drainage on the western ACP of Alaska (Jones et al. 2020). Under future climate warming, if the lake drainage rate accelerates, it can have a significant impact on the water cycle. In this study, we present an investigation of how lake drainage increases snow/water storage in Arctic tundra.

We studied an area of ~140 km^2 in Inigok on the ACP of Alaska (Figure 1), where the topography is characterized by rolling hills on paleo sand dunes (Carter 1981). In this area, lakes cover ~22% and DLBs ~4% of the land surface. The wind records show a prevailing easterly direction between October 2018 and April 2019.

Methods

We conducted field measurements on April 27 and 28, 2019, near maximum snowpack conditions. We measured snow depth using ground penetrating radar (GPR, 800 MHz) and probe. Probe measurements were used to calibrate the snow radar velocity (0.189 ± 0.023 m ns^{-1}) to perform a time-depth conversion for all GPR traces.

To simulate lake drainage, we followed the work done by Simpson et al. (2021) to estimate bathymetry for 33 lakes in our study area using Landsat images and field-measured bathymetric data from four lakes. We used the SMOOTH (Ohara et al. 2022) to model the snow redistribution before and after lake drainage simulation. Field measurements of snow depth and (nearly) snow-free IfSAR (5 m resolution) digital terrain model were used to calibrate the snow model.

The ACP of Alaska is characterized by an average snow depth <0.5 m (e.g., Ohara et al. 2022), and we assumed snowdrift as any snowpack >1 m depth.

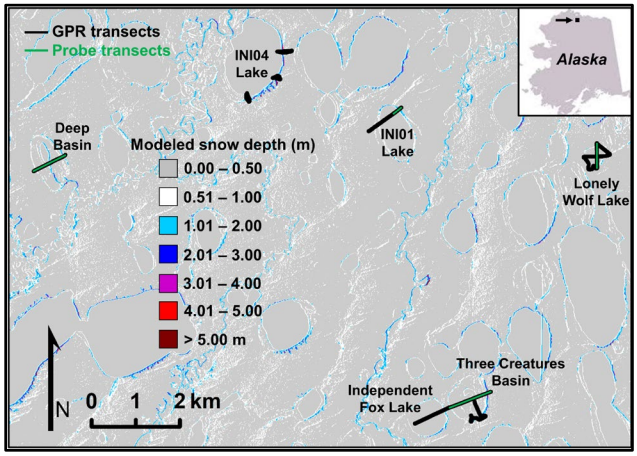

Figure 1. Snow model for the study area in Inigok at the Arctic Coastal Plain of Alaska (adapted from Rangel et al. 2023).

Results and Discussion

Figure 1 shows the snow model results for the whole area and the location of the snow depth measurements using GPR and probe, and Figure 2 shows an example of processed GPR radargram on snowdrift. Based on the lake bathymetry estimation (Figure 3), we modeled the snow redistribution before and after lake drainage simulation (Figure 4).

Our results show an increase in snow storage of up to ~24% at DLBs compared to lakes and ~35% considering only snowdrifts in whole study area. The larger the lake, the higher the amount of snow stored in the basin after drainage. This increase in snow storage could substantially impact the tundra landscape when it melts, including wildlife, vegetation, biogeochemical processes, and cause natural hazards like snow-dam outburst floods.

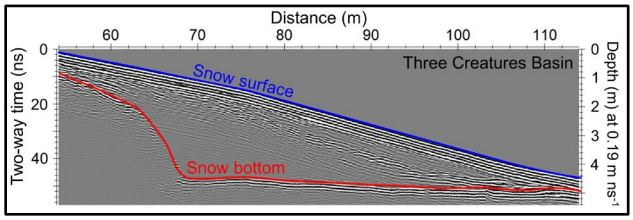

Figure 2. GPR radargram on a snowdrift at Three Creatures Basin (adapted from Rangel et al. 2023).

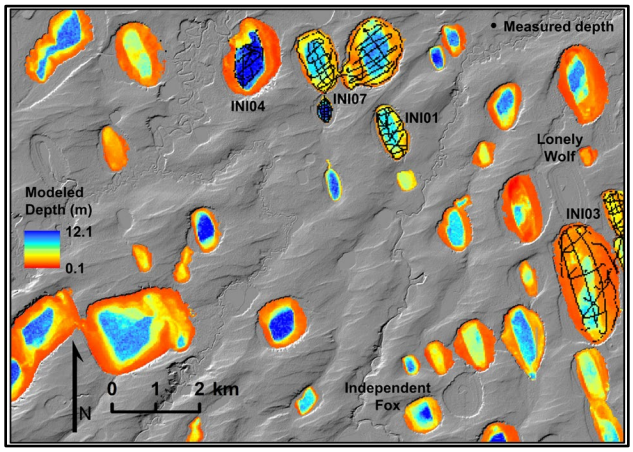

Figure 3. Bathymetry estimation for 33 lakes (adapted from Rangel et al. 2023).

CONCLUSIONS

Our results show a significant increase in snow storage in drifts after lake drainage in the ACP of Alaska, highlighting the impact of lake drainage on snow storage and, consequently, the hydrologic system. This study shows that a combination of field measurements, remote sensing, and modeling of snow properties is effective in understanding and predicting how lake drainage affects snow redistribution on the Arctic tundra, which can be useful for other regions in the world.

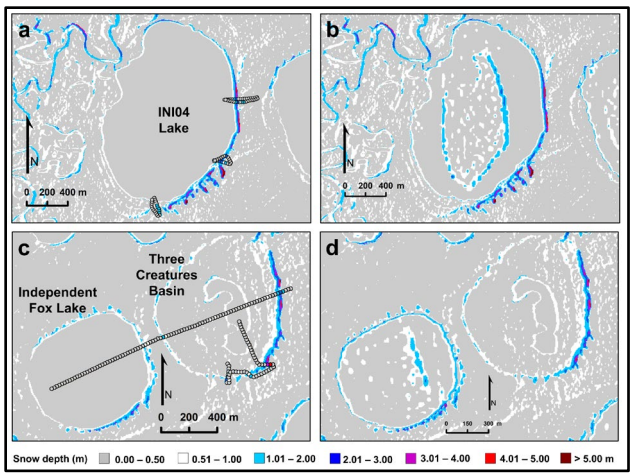

Figure 4. Examples of snow model results before (left) and after (right) complete lake drainage simulation (adapted from Rangel et al. 2023).

ACKNOWLEDGEMENTS

This work was supported by the NSF Office of Polar Programs award numbers 1806202, 1806213, and 1823717.

REFERENCES

Brown, R., Marsh, P., Dery, S., and Yang, D. 2021. Snow cover - Observations, processes, changes, and impacts on northern hydrology. In: Arctic hydrology, permafrost and ecosystems (Yang D., and Kane, D.L., Eds., pp. 61–99). Springer. doi:10.1007/978-3-030-50930-9

Carter, L.D. 1981. A Pleistocene sand sea on the Alaskan Arctic Coastal Plain. Science, 211(4480), 381–383. doi:10.1126/science.211.4480.381.

Jones, B.M., Arp, C.D., Grosse, et al. 2020. Identifying historical and future potential lake drainage events on the western Arctic coastal plain of Alaska. Perm. and Perig. Proc., 31(1), 110–127. doi:10.1002/ppp.2038

Jones, B.M., Grosse, G., Roy-Léveillée, P., et al. 2022. Lake and drained lake basin systems in lowland permafrost regions. Nature Reviews Earth & Env., 3(1), 85–98. doi:10.1038/s43017-021-00238-9

Ohara, N., He, S., Parsekian, A.D., et al. (2022). Spatial snowdrift modeling for an open natural terrain using a physically-based linear particle distribution equation. Hyd. Proc., 36(1), e14468. doi:10.1002/hyp.14468

Rangel, R.C., Ohara, N., Parsekian, A.D., and Jones, B.M. 2023. Arctic tundra lake drainage increases snow storage in drifts. Journal of Geophysical Research: Earth Surface, 128. doi:10.1029/2023JF007294

Simpson, C.E., Arp, C.D., Sheng, et al. 2021. Landsat-derived bathymetry of lakes on the Arctic Coastal Plain of northern Alaska. Earth System Science Data, 13(3), 1135–1150. doi:10.5194/essd-13-1135-2021

Catastrophic lake drainages and landscape evolution in Old Crow Flats, YT

Pascale Roy-Léveillée[1], Fabrice Calmels[2], Kevin Turner[3] & Arianne B. St-Amour[1]

[1]*CRYO-UL: Permafrost Research Laboratory, Université Laval, Québec City, Québec, Canada*

[2]*Yukon University Research Centre, Yukon University, Whitehorse, Yukon, Canada*

[3]*Department of Geography and Tourism Studies, Brock University, Ontario, Canada*

The rates of catastrophic lake drainages are increasing in many thermokarst lowlands. While the impacts of lake expansion and drainage on the development of new thermokarst lakes has been examined (Morgenstern et al. 2011), the effects of catastrophic drainages on the geomorphic evolution of permafrost lowlands remains understudied. This research investigates the impacts of catastrophic lake drainages on the development of channel networks, treeline dynamics, and permafrost sustainability in a warming climate in the Old Crow Flats (OCF) of Northern Yukon.

Old Crow Flats

Located at the eastern edge of Beringia, OCF is an interior basin separated from the Arctic coast by the British and Barn mountains. During the last glacial maximum, it was covered by Glacial Lake Old Crow, which formed in the Bell, Old Crow, and Bluefish basins while drainage was blocked at the McDougall Pass by the Laurentide ice sheet (Figure 1). The glacial lake deposited up to 9 m of glaciolacustrine silts and clays over the thick Pleistocene and Tertiary alluvial sands and silts. It drained catastrophically westward approximately 14.8 ka BP, incising the Porcupine River channel up to 40 m below the plain surface. In the following 1000 years, the Old Crow River and its main tributaries incised the exposed basin sediment, while permafrost aggraded and a peat cover progressively developed (Lauriol et al. 2002). Today, the Old Crow River and five key tributaries meander 20 to 50 m below the flat plain surface where thermokarst lakes cover approximately a third of the land surface.

The first thermokarst lakes of OCF were likely large remnant ponds that began to erode their shores via thermokarst processes (Ovenden 1982). Several generations of thaw ponds and lakes have since developed, expanded, and drained catastrophically leaving drained lake basins and drainage outlets across the landscape. Recently, catastrophic drainages are increasing in frequency in OCF, similar to trends reported from other thermokarst lowlands (Lantz and Turner 2015). However, the role of these catastrophic lake drainages in the geomorphic evolution of this glaciolacustrine plain is poorly understood.

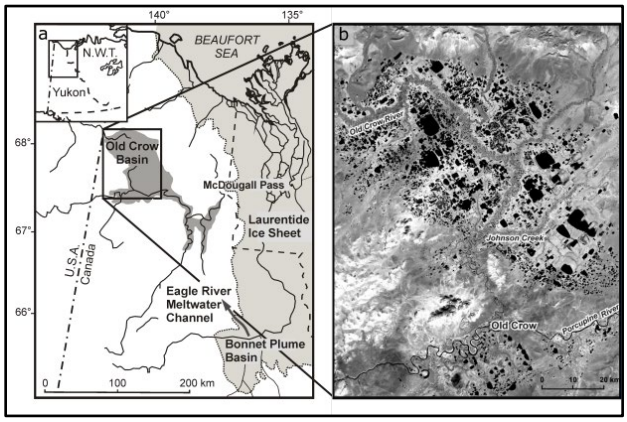

Figure 1. a) Extent of Glacial Lake Old Crow in N Yukon shown in dark grey and max. extent of the Laurentide Ice Sheet shown in light-grey (modified from Roy-Leveillee and Burn 2016). b) Landsat 7 ETM orthoimage of Old Crow Flats acquired on 30 August 2001.

Data and Methods

Old drained lake basins were outlined using the ArcGISPro online Basemap and contemporary basin outlines were added based on Lantz and Turner (2015). All OCF creeks were digitized using 5-m resolution SPOT imagery (acquired in July 2007). The distribution of evergreen, deciduous, and mixed forests as well as woodlands in relation to basin outlines and drainage outlets was assessed using Landsat-derived land cover data from the ABoVE program (Wang et al. 2019). Ground temperatures were monitored near the ground surface (5 cm) and in the top of permafrost (1.25 m) using Onset Hobo U23 proV2 loggers with Onset TMC6-HA sensors in basins drained in the 2010s, 2000s, 1970s and in basins that drained hundreds and thousands of years ago. The distribution of permanently frozen ground in these basins was assessed using electrical resistivity tomography (Wenner and dipole-dipole arrays) with electrodes every 2 m along transects that extended over 100 to 200 m on the basin floor perpendicular to the basin paleoshoreline. Earth augering was used to confirm the presence or absence of frost in the basin floor sediment.

PRELIMINARY RESULTS AND DISCUSSION

Despite a lake coverage of over 30% in Old Crow Flats, total digitized creek length (channelized water only) was 2459 km and drainage density was 0.83. This drainage density is high compared to other thermokarst landscapes with similar or greater slopes and similar or greater age (Arp et al. 2012). Contrary to other areas with similar drainage density, the channels of OCF did not include beaded streams and no signs of headward thermo-erosional gullying where observed in the ice wedge networks. In a 1300 km^2 tundra area of OCF, 87% of the drainage channels either originated from or intersected the boundary of drained lake basins, suggesting that catastrophic lake drainages may have driven drainage channel development in OCF following aggradation of permafrost and peat cover development. The high drainage density resulting from catastrophic drainages in OCF may contribute to permafrost stabilization in the landscape by facilitating lake drainage, limiting the potential for future thermokarst growth, and increasing the extent of bottom-fast ice (Morgenstern et al. 2011; Shaposhnikova et al. 2023).

In the tundra of OCF, the distribution of trees often coincides with paleoshorelines and drainage channels (Figure 2). The latter unique topography in the low grade terrain of Old Crow Flats creates environments favorable for tree growth that may facilitate treeline advance under warming climatic conditions.

Figure 2. Examples of preferential tree growth along paleoshorelines (black arrows) and basin outlets (blue arrows) visible on a) the ABoVE Landsat-derived Land Cover (Wang et al. 2019) with deciduous, coniferous, and mixed forest shown in dark green; and b) on oblique photographs showing tree growth along a drainage outlet (above) and the paleoshoreline of a lake after partial drainage.

Permafrost recovery was progressing well in tundra basins drained in 1980s and 2018. In taiga basins drained in 2007, however, permafrost recovery was partial and delayed with some persistent frozen ground developing only after a recent winter with very low snow precipitation. Catastrophic drainages may thus facilitate the transition from continuous to discontinuous permafrost, as was shown by predictive modelling in other thermokarst lowlands, particularly in parts of OCF with taiga vegetation where snow-vegetation interactions result in higher permafrost temperatures.

REFERENCES

Arp, C.D., Whitman, M.S., Jones, B.M., Kemnitz, R., Grosse, G., and Urban, F.E. 2012. Drainage Network Structure and Hydrologic Behavior of Three Lake-Rich Watersheds on the Arctic Coastal Plain, Alaska. Arctic, Antarctic, and Alpine Research 44: 385–398.

Lantz, T.C., and Turner, K.W. 2015. Changes in lake area in response to thermokarst processes and climate in Old Crow Flats, Yukon. Journal of Geophysical Research: Biogeosciences 120: 2014JG002744.

Lauriol, B., Duguay, C.R., and Riel, A. 2002. Response of the Porcupine and Old Crow rivers in northern Yukon, Canada, to Holocene climatic change. The Holocene 12: 27–34.

Morgenstern, A., Grosse, G., Günther, F., Fedorova, I. and Schirrmeister, L. 2011. Spatial analyses of thermokarst lakes and basins in Yedoma landscapes of the Lena Delta. The Cryosphere 5: 849–867.

Ovenden, L. 1982. Vegetation history of a polygonal peatland, northern Yukon. Boreas 11: 209–224.

Roy-Leveillee, P., and Burn, C.R. 2016. A modified landform development model for the topography of drained thermokarst lake basins in fine-grained sediments. Earth Surface Processes and Landforms 41: 1504–1520.

Shaposhnikova, M., Duguay, C., and Roy-Léveillée, P. 2023. Bedfast and floating-ice dynamics of thermokarst lakes using a temporal deep-learning mapping approach: case study of the Old Crow Flats, Yukon, Canada. The Cryosphere 17: 1697–1721.

Wang, J.A., Sulla-Menashe, D., Woodcock, C.E., Sonnentag, O., Keeling, R.F., and Friedl, M.A. 2019. ABoVE: Landsat-derived Annual Dominant Land Cover Across ABoVE Core Domain, 1984-2014. ORNL DAAC, Oak Ridge, Tennessee, USA.

Wetland characteristics and organic matter in Arctic drained lake basins

Juliane Wolter[1,2], Benjamin M. Jones[3], Matthias Fuchs[4], Amy Breen[5], Ingeborg K. Bussmann[6,7], Boris Koch[8], Josefine Lenz[2], Isla H. Myers-Smith[9], Torsten Sachs[10], Jens Strauss[2], Ingmar Nitze[2] & Guido Grosse[2,11]

[1]*University of Potsdam, Institute of Biochemistry and Biology, Potsdam, Germany*

[2]*Alfred Wegener Institute Helmholtz Centre for Polar and Marine Research, Section Permafrost Research, Potsdam, Germany*

[3]*University of Alaska Fairbanks, Institute of Northern Engineering, Fairbanks, Alaska, United States*

[4]*University of Colorado Boulder, Renewable and Sustainable Energy Institute, Boulder, Colorado, United States*

[5]*University of Alaska Fairbanks, International Arctic Research Center, Fairbanks, Alaska, United States*

[6]*Alfred Wegener Institute Helmholtz Centre for Polar and Marine Research, Section Shelf Sea System Ecology, Helgoland, Germany*

[7]*Alfred Wegener Institute Helmholtz Centre for Polar and Marine Research, Section Marine Geochemistry, Bremerhaven, Germany*

[8]*Alfred Wegener Institute Helmholtz Centre for Polar and Marine Research, Section Ecological Chemistry, Bremerhaven, Germany*

[9]*University of Edinburgh, School of GeoSciences, Edinburgh, United Kingdom*

[10]*GFZ German Research Centre for Geosciences, Section Remote Sensing and Geoinformatics, Potsdam, Germany*

[11]*University of Potsdam, Institute of Geosciences, Potsdam, Germany*

Wetlands in Arctic drained lake basins (DLB) have a high potential for carbon storage as well as for elevated greenhouse gas emissions, making these abundant wetlands especially uncertain elements of the Arctic permafrost carbon budget. After lake drainage both talik and exposed lake sediments refreeze and the former lake bottom is colonized by pioneer graminoids, succeeded by moss-sedge-dwarf shrub vegetation, producing a typical peat sequence. Vegetation composition and organic matter dynamics in DLBs have been studied at few sites around the Arctic and are far from comprehensive.

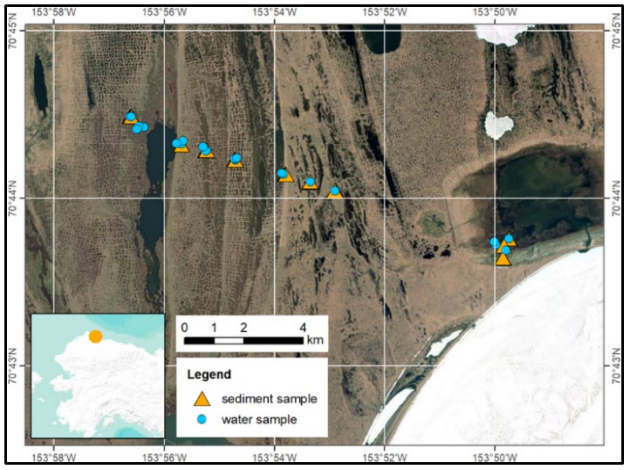

Figure 1. Study area map indicating all sampling sites.

METHODS

We surveyed vegetation, surface sediment, and pond waters from a DLB system with multiple basin generations in northern Alaska (Figure 1). We associated remote sensing-derived eco-hydrological classes with soil organic matter composition and methane concentrations along a post-drainage succession gradient to assess spatial characteristics of soil organic matter and methane. We specifically investigated (i) plots along a transect across a temporal drainage gradient and surveyed vegetation, soil surface sediment, and pond water. We then used (ii) a landcover classification of the main eco-hydrological classes to (iii) upscale from plot to basin scale.

RESULTS AND DISCUSSION

Statistical clustering of vegetation data revealed a strong change in vegetation and organic matter between basins drained within the last decades and all older age classes spanning several thousands of years. We identified five eco-hydrological classes, which corresponded to our remote sensing-based land cover classes. Surface wetness was the main predictor of vegetation composition, and time since drainage was the second most important predictor. Overall, vegetation composition differed more between eco-hydrological classes than between drainage age classes. Surface sediments had very high water contents (>80%), suggesting largely anaerobic conditions, which favour methane production. Our findings suggest moderate to high methane concentrations independent of drainage age, with particularly high concentrations in wet patches beneath shallow water (up to 200 µmol/L, Figure 2) and in pond water (up to 22 µmol/L). In addition, pond water samples had very high concentrations of dissolved organic carbon and total dissolved nitrogen, indicating high biological activity and organic matter decomposition.

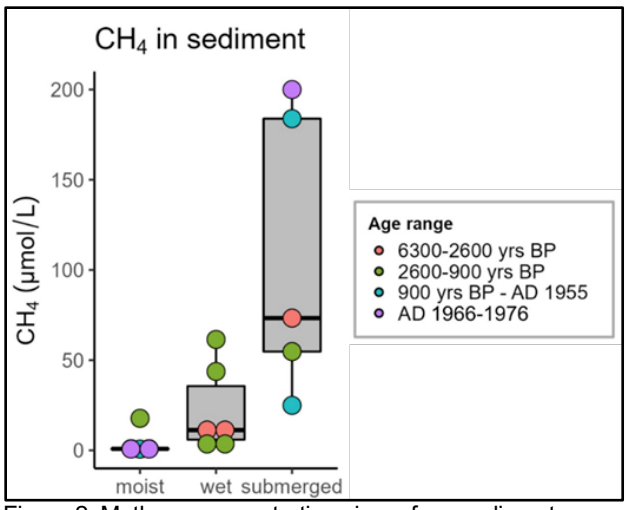

Figure 2. Methane concentrations in surface sediment.

Land cover classification (Figures 3 and 4) yielded seven classes: five vegetation classes, a water class and a bare ground class, which we identified from a machine learning algorithm using object-based image analysis. We found that 42 % of the basin area was occupied by wet patches and water patches with very high methane production.

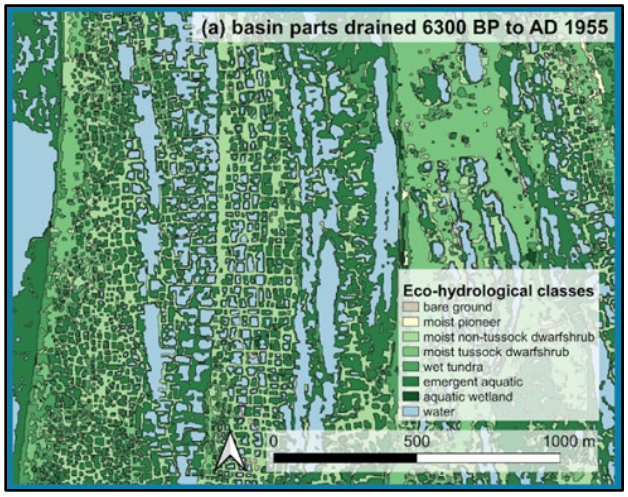

Figure 3. Results of eco-hydrological land cover classification in mature basin parts.

Small-scale heterogeneity in mature basin parts that drained several hundred to thousands of years ago (Fig. 3) replaced the initial pioneer classes, which occupied larger patches with simpler shapes (Fig. 4).

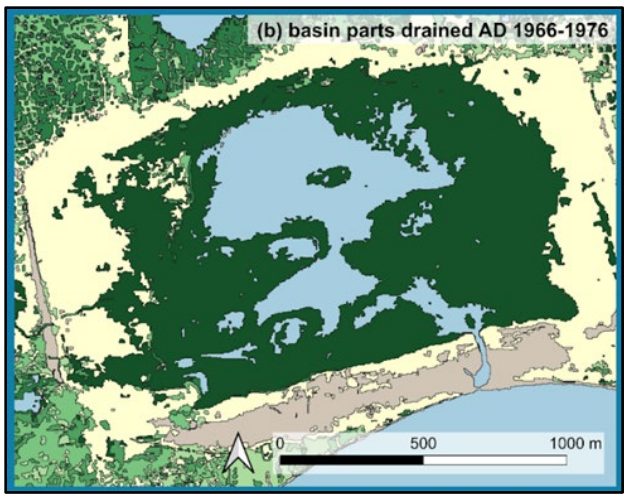

Figure 4. Results of eco-hydrological land cover classification in a recently drained basin part.

CONCLUSIONS

In conclusion, we demonstrate that DLB wetlands have high methane concentrations in ponds and sediments, which may indicate higher production and emissions compared to surrounding upland tundra. Our study shows that remote sensing-based land cover classifications are useful for quantifying wet-vs-moist patches and high-vs-moderate methane production in Arctic drained lake basins. We also confirmed that wetness is a good predictor of both vegetation composition and sediment methane concentrations. Our results indicate that the evolution of vegetation and ground ice formation-driven microtopography such as from ice-wedge polygons alters organic matter composition and local surface wetness on small spatial scales (Figures 3 and 4) We therefore suggest that investigations of vegetation, carbon and nitrogen dynamics in DLBs need to consider this small-scale variability in regional-scale assessments of permafrost region contributions to global budgets. We conclude that the abundant wetlands that form in Arctic DLBs might add substantial natural greenhouse gases to the global carbon cycle. As these basins are abundant in permafrost lowlands, the study highlights the potential for future upscaling methane emissions from such wetland environments.

6C — Arctic Wetlands in a Changing Climate

Session Chairs: Juliane Wolter[1], Claire Treat[2] & Liam Heffernan[3]

[1]*University of Potsdam, Institute of Biochemistry and Biology, Potsdam, Germany*
[2]*Alfred Wegener Institute Helmholtz Centre for Polar and Marine Research, Potsdam, Germany*
[3]*Evolutionary Biology Centre, Department of Ecology and Genetics/Limnology, Uppsala University, Uppsala, Sweden*

Half of the world's wetlands are located in Arctic regions including peatlands, wet tundra, shallow water areas, and coastal marshes. Arctic wetlands are key components of global biogeochemical cycles, especially for carbon and nitrogen, but also for various contaminants. They are biodiversity hotspots and key breeding and moulting habitat for birds. Intact wetlands also have a hydrological storage function. Climate change threatens to alter some of the main functions of these sensitive wetland systems. For example, the hydrological balance of wetlands in permafrost regions is sensitive to changes in thaw depth, precipitation and evapotranspiration, as well as to changes in geomorphology and local topography caused by permafrost thaw. Such changes have effects on all wetland functions. In addition to uncertainties about wetland resilience and adaptability to climatic warming, the current properties of Arctic wetlands are still not comprehensively understood and quantified.

In this session, we invite contributions related to Arctic region and permafrost wetlands from various scientific fields using a wide range of methods, such as field observations, laboratory analyses and experiments, modelling and simulations, and remote sensing. We particularly encourage studies on (1) carbon and nitrogen cycling, including stocks and fluxes; (2) vegetation change and its effects on wetland ecosystems; (3) ecology of wetland organisms; (4) major contaminants such as mercury and their mobility or stability; and (5) wetland ecosystem response to disturbance events such as wildfire, permafrost thaw, and changes in hydrology.

Vegetation succession and its impact on carbon accumulation in a thermokarst landscape in Nunavik (Northern Québec, Canada)

Édith Auclair-Fournier[1,2,3,4], Pascale Roy-Léveillée[1,3] & Michelle Garneau[2,3,4]

[1]*CRYO-UL: Permafrost Research Laboratory, Department of Geography, Université Laval, Québec City, Québec, Canada*

[2]*Department of Geography, Université du Québec à Montréal, Montréal, Québec, Canada*

[3]*Centre for Northern Studies, Québec City, Québec, Canada*

[4]*Geotop Research Centre in Earth System Dynamics, Montréal, Québec, Canada*

Omission of plant physiological adaptation to climate warming in terrestrial systems models has caused an underestimation of primary productivity (Knauer et al. 2023). Permafrost peatlands are vulnerable to warming, yet the net effect of thaw-induced carbon (C) release vs accumulation due to increased primary productivity is still unclear. Despite an abundance of climate and greenhouse gas emissions projections, the permafrost C feedback remains largely uncertain (Miner et al. 2022; Schuur et al. 2022). The scarcity of data on recent vegetation succession and plant productivity in thaw features of permafrost peatlands is one crucial restriction contributing to this uncertainty.

Using a palaeoecological approach, this project aims to document the timing and trajectory of vegetation succession following permafrost thaw in a degrading lithalsa field near Kangiqsualujjuaq, Nunavik, Canada (Figure 1). The main objectives are to i) reconstruct vegetation succession following permafrost thaw, ii) quantify peat and C accumulation since thaw using ^{14}C and ^{210}Pb chronologies, and iii) assess small scale variability.

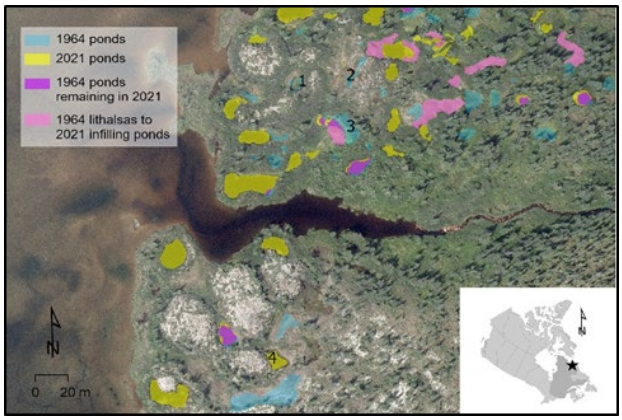

Figure 1. Lithalsas, thermokarst and pond evolution between 1964 and 2021 at the site (Kangiqsualujjuaq, Nunavik, Canada). Scale 1:1800. Projection: NAD1983 CSRS MTM6. Sources: NRCAN (1964), MERN (2021).

METHODS

In the field, short peat cores (n= 23) have been collected from the edges of four thermokarst ponds along outward transects perpendicular to each side of the infilling pond (Figure 2). Metal boxes of 30 to 50-cm length were used to collect subsurface samples, as the focus of the study was recent vegetation succession. In each site, surface vegetation surveys were also conducted.

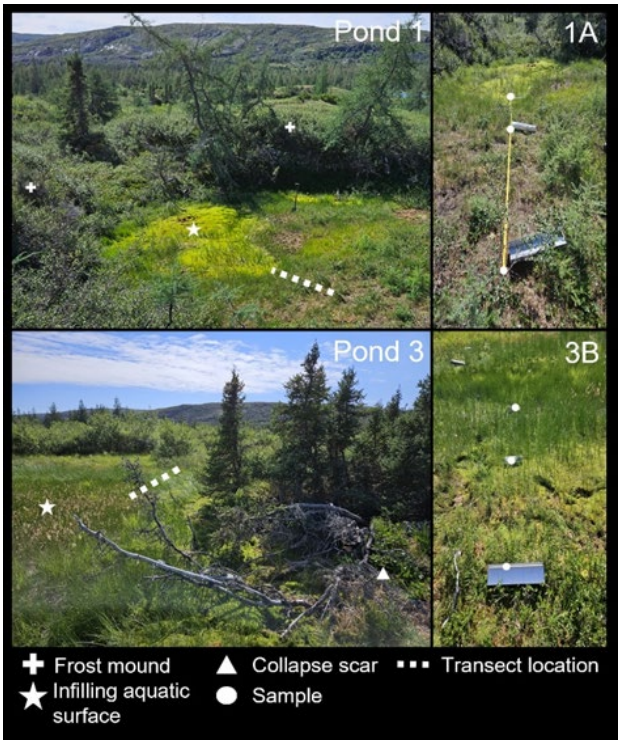

Figure 2. Sample ponds and transects at the permafrost peatland site (Kangiqsualujjuaq, Nunavik, Canada).

On each core, loss on ignition (LOI) at 1-cm interval was performed to quantify organic matter and estimate organic C content (50% of organic matter mass) (Chambers et al. 2011). A Carlo Erba NC 2500 elemental analyzer was used for analysis for total C and nitrogen (N) analysis at 2-cm intervals allowing

information on peat decay (Kuhry and Vitt 1996). Plant macrofossils analyses at a minimum of 4-cm interval was realized to reconstruct historical plant succession and hydrological variations in the peat (Mauquoy et al. 2010). High resolution chronologies using ^{14}C and ^{210}Pb dating supported estimations of the successional changes in relation with climate warming and permafrost thaw. The chronologies were used to compute age-depth models, as well as peat and apparent C accumulation rates.

Preliminary results and discussion

Diachronic analysis of aerial photographs highlighted changes in thermokarst features in the lithalsas site, where numerous ponds have been infilled with vegetation between 1964 and 2021, while new ones have formed (Figure 1). Preliminary results show that recent accumulation and related C content is variable between the vegetated pool edges, as shown in Figure 3. Vertical C content follows similar but offset paths according to sampling position within transects. Peat layers with higher C content were associated with qualitatively greater decomposition and found deeper in cores closest to the pond along a depth gradient.

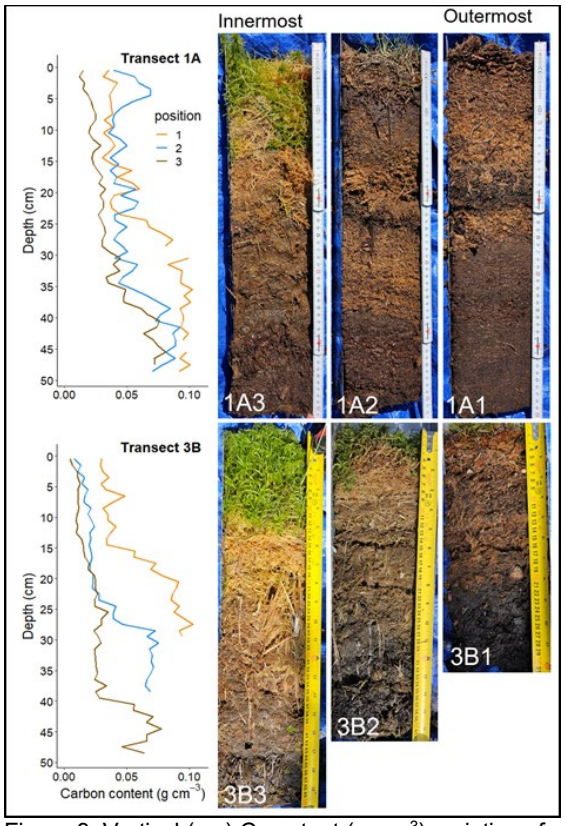

Figure 3. Vertical (cm) C content (g cm^{-3}) variations from LOI of peat cores for one transect along respectively two thermokarst pool banks.

The results suggest an influence of local microtopography and hydrology on the recent post thaw dynamics of the studied sites. The reconstruction of peat and C accumulation rates using ^{14}C and ^{210}Pb chronologies (pending), will support an improved understanding of the vegetation successions and related C dynamics.

Incorporation of spatiotemporal heterogeneity in C accumulation might present challenges in C budget modeling. This study emphasizes the significance of empirical fieldwork in documenting small scale ecological processes under the scope of remote sensing and modeling. Results will be compared with other studies realized across circum-arctic locations and will contribute to the evaluation of the responses of high-latitude peatland ecosystems to climate warming. Additionally, documentation of recent changes in peat accumulation environments in northern latitudes can support conservation decision making, as protection of C stocks and sinks is increasingly recognized as a natured-based solution in global warming mitigation.

References

Chambers, F.M., Beilman, D.W., and Yu, Z. 2011. Methods for determining peat humification and for quantifying peat bulk density, organic matter and carbon content for palaeostudies of climate and peatland carbon dynamics, Mires and Peat, 7(7).

Knauer, J., Cuntz, M., Smith, B., Canadell, J.G., Medlyn, B.E., Bennett, A.C., Caldararu, S., and Haverd, V. 2023. Higher global gross primary productivity under future climate with more advanced representations of photosynthesis. Science Advances, 9(46). https://doi-org.acces.bibl.ulaval.ca/10.1126/sciadv.adh9444

Kuhry, P., and Vitt, D.H. 1996. Fossil carbon/nitrogen ratios as a measure of peat decomposition. Ecology, 77(1), 271-275. doi: https://doi.org/10.2307/2265676.

Mauquoy, D., Hughes, P.D.M., and van Geel, B. 2010. A protocol for plant macrofossil analysis of peat deposits. Mires and Peat, 7(6).

Miner, K.R., Turetsky, M.R., Malina, E., Bartsch, A., Tamminen, J., McGuire, A.D., Fix, A., Sweeney, C., et al. 2022. Permafrost carbon emissions in a changing Arctic. Nature Reviews Earth & Environment, 3(1), 55–67. https://doi.org/10.1038/s43017-021-00230-3

Schuur, E.A.G., Abbott, B.W., Commane, R., Ernakovich, J., Euskirchen, E., Hugelius, G., Grosse, G., Jones, M., et al. 2022. Permafrost and climate change: carbon cycle feedbacks from the warming Arctic. Annual Review of Environment and Resources, 47(1), 343–371. https://doi.org/10.1146/annurev-environ-012220-011847

Methylmercury concentrations in a degrading lithalsa field near Kangiqsualujjuaq, Nunavik (Québec), Canada

Rose-Marie Cardinal[1,2], Pascale Roy-Léveillée[1,2], Sarah Gauthier[1,2], Michael Kwan[3] & Brian Branfireun[4]

[1]*CRYO-UL: Permafrost Research Laboratory, Department of Geography, Université Laval, Québec City, Québec, Canada*

[2]*Centre for Northern Studies, Université Laval, Québec City, Québec, Canada*

[3]*Nunavik Research Centre, Nunavik (Québec) Canada*

[4]*Department of Biology, Western University, Ontario, Canada*

The accelerated degradation of permafrost has sparked widespread interest in its potential impact on biogeochemical cycles. For instance, important stores of atmospherically deposited mercury (Hg) are associated with organic matter in permafrost environments. Concerns have been raised about the potential activation of a previously dormant Hg store with permafrost thaw (Schaefer et al. 2020; Schuster et al. 2018). This thawing could potentially expose stored Hg to microbial activity that can convert inorganic mercury (IHg) to its organic, bioavailable, and neurotoxic methylated form, methylmercury (MeHg). Degradation of ice-rich permafrost alters topography, hydrology, and ecology at the local scales and may create favorable conditions for anaerobic microbial activity such as methylation processes (Gordon et al. 2016; Yang et al. 2016). Yet, the impacts of permafrost thaw on landscape evolution vary drastically depending on terrain characteristics and climatic settings. While field data on total mercury (THg) and MeHg in permafrost terrain are generally scarce, the evolution of net IHg methylation potential through the progressive thaw and stabilization of permafrost features is understudied.

Frost mounds, such as palsas and lithalsas, are formed in peatlands by the aggradation of segregated ice in peat and underlying fine-grained sediment and are widespread in the discontinuous permafrost zone (Allard et al. 1986; Calmels et al. 2008). Near Kangiqsualujjuaq, Nunavik (Canada), the evolution and degradation of frost mound fields create evolving mosaics of hydrological and ecological conditions, where organic matter is redistributed from well-drained elevated surfaces to rim ridges and thaw ponds where the accumulation of organic matter can lead to terrestrialization. This research examines whether the geomorphic and ecological evolution of such a degrading lithalsa field creates environmental conditions conducive to IHg methylation.

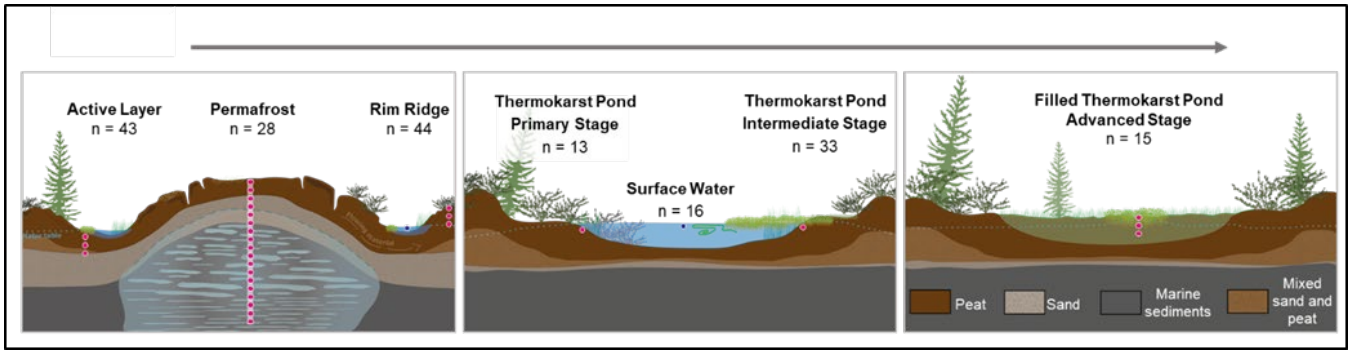

Figure 1. Sampling plan in the expected geomorphic components and environmental conditions associated with frost mound degradation over time. Red dots represent surface soil sampling and a 4 m core from the active layer to the permafrost. Blue dots represent surface water sampling.

METHODS

Remotely sensed imagery from 1964 to 2021 was used to examine geomorphic change and informed the selection of 90 sampling sites, including frost mounds (n = 13), rim ridges (n = 12), and thermokarst depressions at different stages of pond formation and revegetation (n = 65) (Figure 1). Key vegetation components at different successional stages, i.e., dead Betula glandulosa at the primary stage, Cyperaceae and brown mosses for the intermediate stage, and Sphagnum spp. for the advanced stage (Arlen-Pouliot and Bhiry 2005), were used as a proxy to identify stages in the evolution of the thermokarst ponds. Hydrological and ecological conditions including water depth, vegetation cover, and organic layer thickness were assessed in the field. Over 150 soil samples and

16 surface thermokarst pond water samples were collected along the degradation and revegetation toposequence to characterize THg and MeHg concentrations, as well as related soil geochemical parameters (C, N, S).

Table 1. Median concentration of Total mercury (THg), methylmercury (MeHg), and percentage of THg that is MeHg (% MeHg) for all terrain units.

Terrain unit		THg (ng/g)	MeHg (ng/g)	% MeHg
Frost mound		68	0.47	0.57
Rim ridge		95	0.5	0.5
Thermokarst pond		88	3.3	4.8
Evolution stages of the thermokarst ponds	Primary	81	6.0	6.7
	Intermediate	79	3.3	4.8
	Advanced	108	2.6	2.6
Water	Thermokarst ponds	THg (ng/L)	MeHg (ng/L)	% MeHg
Unfiltered Water	Younger	18	4	30
	Intermediate	4.2	0.9	21
	Older	5.2	0.9	17
Filtered Water	Younger	2.8	1.0	37
	Intermediate	2.2	0.7	28
	Older	1.2	0.5	22

RESULTS AND DISCUSSION

The mineral permafrost in the frost mound core had very low median THg concentrations (6.7 ± 0.4 ng/g) (Table 1). MeHg concentrations were below the detection limit of 0.0103 ng/g, indicating no net methylation within the permafrost. While THg was similar (p-value > 0.05) in the top 10 cm of all geomorphic terrain units (median of 68 ± 17 ng/g for lithalsa, 95 ± 12 ng/g for rim ridge, and 88 ± 8 ng/g for thermokarst pond), they showed significantly different net MeHg concentrations ($p < 0.05$). The methylated fraction of THg (%MeHg) was lowest in frost mounds (0,57 ± 0.06 %) and rim ridges (0.5 ± 0.4 %), and highest in thermokarst ponds (4.8 ± 0.7 %), where it was also most variable ($\sigma = 5.3$). Net methylation concentration varied between pond successional stages (p-value > 0.05). It was highest in primary successional stages with submerged dead Betula glandulosa (6.7 ± 1.4 %), when the system was characterized by the highest input of fresh organic matter, nutrients, sediments, and stagnant open water. It then showed a slight decrease with successional stages, where intermediate stage ponds dominated by Cyperaceae and brown mosses (4.8 ± 1.1 %), and ponds at advanced stages of terrestrialization with Sphagnum spp., settling in more nutrient-poor conditions (2.6 ± 1.1 %), had lower MeHg production. THg (p-value > 0.05) and MeHg (p-value < 0.05) in both filtered and unfiltered water followed the signal of the thermokarst pond evolution, with higher % MeHg in younger thermokarst ponds than in older ones. Therefore, as these frost mounds degrade, the highest net MeHg production potential is associated with a temporary phase, which is the earliest stage of thermokarst pond evolution. Net MeHg production potential decreases as pond terrestrialization progresses. This study exemplifies how the combination of permafrost geomorphology, ecology, and Hg biogeochemistry helps to better link permafrost landscape evolution to the effects of warming on Hg cycling.

REFERENCES

Arlen-Pouliot, Y., and Bhiry, N. 2005. Palaeoecology of a Palsa and a Filled Thermokarst Pond in a Permafrost Peatland, Subarctic Québec, Canada, The Holocene, 15(3): 408–419. doi:10.1191/0959683605hl818rp.

Allard, M., Seguin, M.K., and Lévesque, R. 1986. Palsas and mineral permafrost mounds in northern Québec. In V. Gardiner, ed., International Geomorphology, Part II-285-309.

Calmels, F., Allard, M., and Delisle, G. 2008. Development and decay of a lithalsa in Northern Quebec: a geomorphological history, Geomorphology, 97(3-4): 287–299. doi:10.1016/j.geomorph.2007.08.013

Gordon, J., Quinton, W., Branfireun, B.A., and Olefeldt, D. 2016. Mercury and methylmercury biogeochemistry in a thawing permafrost wetland complex, Northwest Territories, Canada, Hydrological Processes, 30(20): 3627–3638. doi:10.1002/hyp.10911

Schaefer, K., et al. 2020. Potential Impacts of Mercury Released from Thawing Permafrost, Nature Communications, 11(1). doi:10.1038/s41467-020-18398-5.

Schuster, P.F., Schaefer, K.M., Aiken, G.R., Antweiler, R.C., Dewild, J.F., Gryziec, J.D., Gusmeroli, A., Hugelius, G., Jafarov, E., Krabbenhoft, D.P., and Liu, L. 2018. Permafrost stores a globally significant amount of mercury, Geophysical Research Letters, 45(3): 1463–1471. doi:10.1002/2017GL075571

Yang, Z., Fang, W., Lu, X., Sheng, G.P., Graham, D.E., Liang, L., Wullschleger, S.D., and Gu, B. 2016. Warming increases methylmercury production in an Arctic soil, Environmental Pollution, 214: 504–509. doi:10.1016/j.envpol.2016.04.069

Coupled experimental and numerical assessment of low arctic vegetation thermal properties: impact of fibrous and porous structure

Simon Cazaurang[1,2], Manuel Marcoux[1], Michel Quintard[1], Sergey V. Loiko[3], Artem G. Lim[3], Oleg S. Pokrovsky[2,3] & Laurent Orgogozo[2]

[1]*Biological porous media research group, Toulouse Fluid Mechanics Institute, Toulouse, France*

[2]*Geosciences & Environmental Laboratory, University of Toulouse (Toulouse III – Paul Sabatier), Toulouse, France*

[3]*BIO-GEO-CLIM Laboratory, Tomsk State University, Tomsk, Russian Federation*

Arctic environments are covered by millions of km² of permafrost-affected wetlands. The lowlands of Western Siberia are one of the largest of such areas. The low vegetation cover of these wetlands consists of *Sphagnum* moss, lichen, and peat. The spatial distribution of this vegetation layer is mainly driven by microtopography (Loiko et al. 2019). This complex patchwork of low vegetation cover has been identified to be the main interface between the atmosphere and the geosphere (Park et al. 2018). Previous general circulation models have shown the importance to study the transfer properties of the low vegetation strata to assess the influence of this fibrous and porous media in the climate change impacts on arctic environments (Porada et al. 2016).

In this work, the vegetation cover is considered and studied as a porous media. Standard techniques of porous media properties assessment are used for the study of transfer properties of 12 samples collected in 2018 at Khanymey Research Station (Western Siberian Lowlands) and dried after their extraction from the research station. The sample lot consists of eight samples of *Sphagnum* (four from permafrost mounds -*Mound* samples- and four other samples from thermokarstic depressions -*Hollow* samples-) with two additional samples of lichen and two samples of peat. Morphological and hydraulic properties of such samples have previously been studied in Cazaurang et al. (2023). The present study focuses on the assessment of effective and intrinsic thermal properties of these samples using an experimental approach coupled with inverse numerical modelling.

Experimental assessment of effective thermal conductivity of the vegetation layer

Thermal properties of the arctic low vegetation are first studied using experimental methods for characterizing the effective properties of the porous media. By effective properties we mean the properties of the global porous medium including every phase present, for instance air phase and vegetation matter phase for a dried sample. For this purpose, an adaptation of the ISO 8301 standard for experimental measurement of thermal conductivity is done. A schematic of the experimental bench is available in Figure 1.

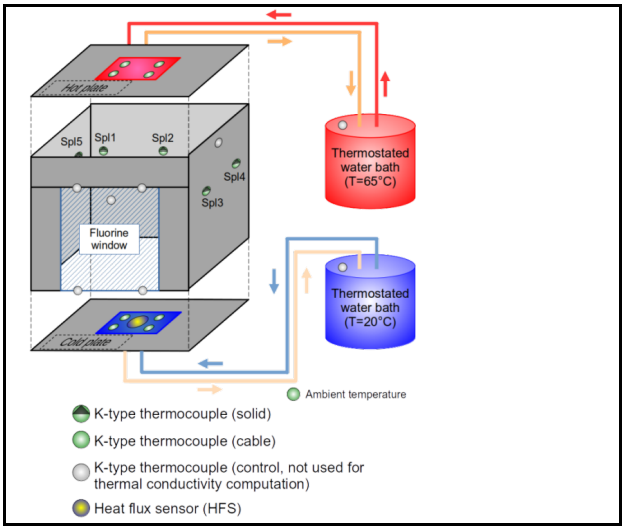

Figure 1. Experimental setup for effective thermal conductivity assessment.

The samples are placed in a confined chamber made of polystyrene. An infrared camera is set up in front of the confinement chamber and a fluorine window allowing monitoring heat front propagation. Samples are heated from the top at 65 °C and let heat up for at least one hour. Effective heat flux is measured on the bottom face, maintained at room temperature (20 °C). When steady-state heat transfer is set, effective thermal conductivity λ_{eff} can be derived from bottom heat flux measurement using Equation 1:

$$\lambda_{eff} = \frac{f e_h d}{T_{hot} - T_{cold}} \quad [1]$$

With f being the conversion factor between voltage and effective heat flux, eh the electric voltage measured with a thermal fluxmeter and d the diameter of the fluxmeter's surface. The computed

effective thermal conductivity λ_{eff} for each sample type is shown in Table 1.

Table 1. Average effective thermal conductivity (λ_{eff}) for each sample type.

Sample	λ_{eff} ($W \cdot m^{-1} \cdot K^{-1}$)
Hollow *Sphagnum*	$6.8 \cdot 10^{-2} \pm 8.8 \cdot 10^{-3}$
Lichen	$5.0 \cdot 10^{-2} \pm 5.4 \cdot 10^{-3}$
Mound *Sphagnum*	$3.7 \cdot 10^{-2} \pm 2.2 \cdot 10^{-3}$
Peat	$4.1 \cdot 10^{-2} \pm 2.2 \cdot 10^{-3}$

From Table 1, one can see that the effective thermal conductivity is of the same order of magnitude for each sample type. The mean effective thermal conductivity for all sample sets at $4.9 \cdot 10^{-2}$ $W \cdot m^{-1} \cdot K^{-1}$. Standard deviation is about 10% of the assessed value, which is within the tolerance margin of the ISO 8301 standard. The obtained values therefore tend to show that this vegetation cover can be considered as a thermally insulative porous medium in spite of its high permeability and porosity.

Numerical inverse modeling of vegetation matter intrinsic thermal conductivity

A numerical twin of the previous experiment is conducted from X-ray tomographic reconstructions of the 3D structure of the previously studied samples. For this purpose, a corresponding numerical case is created on the open-source CFD toolbox *OpenFOAM.* A modified heat diffusion solver is created to account for the multiphase nature of the porous media, allowing describing thermal properties for both air and vegetation matter. A similar heating scenario from the experiment is chosen. Then, the effective heat flux computed at the bottom face of the sample is fitted to the effective experimental heat flux measured for each sample by tuning the intrinsic thermal conductivity of the vegetation matter (λ_{veg}). By intrinsic thermal conductivity we mean the thermal conductivity of the vegetation matter phase only. The results of such intrinsic thermal conductivity fitting are available in Table 2.

Table 2. Intrinsic thermal conductivity of vegetation matter (λ_{veg}) fitted according to the theoretical heat flux (Φ_{exp}) derived from effective thermal conductivities of Table 1.

Sample	Φ_{exp} ($W \cdot m^{-2}$)	Φ_{simu} ($W \cdot m^{-2}$)	λ_{veg} ($W \cdot m^{-1} \cdot K^{-1}$)
Hollow *Sph.*	56.06	54.99	2.2
Lichen	43.05	42.39	$5.0 \cdot 10^{-2}$
Mound *Sph.*	25.60	27.44	$7.1 \cdot 10^{-2}$
Peat	43.03	41.54	$3.3 \cdot 10^{-2}$

The results depicted in Table 2 show that the intrinsic thermal conductivity of the vegetation matter is slightly higher than the thermal conductivity of air (λ_{air} = $2.62 \cdot 10^{-2}$ $W \cdot m^{-1} \cdot K^{-1}$), although the intrinsic thermal conductivity of Hollow *Sphagnum* is a hundred times higher than for the others. This discrepancy can be partly explained by the high porosity and the vertically oriented fibrous structure of the Hollow samples, although further investigation is needed on this point.

Conclusions & perspectives

These results show that the studied samples can be considered as thermally insulative, which is in line with in-field and other laboratory experiments. The inverse modelling gives some clues about the possibility of enclosed air pores to generate most of the insulating effects, which is typically the behaviour found for highly fibrous material (i.e., glass wool). Yet, some further studies are compulsory to evaluate the effects of solar radiative influx, evapotranspiration and water saturation effects in the energy balance of the low vegetation cover, leading to the generation of a computationally-efficient thermal boundary condition that could be used for catchment-scale mechanistic permafrost simulations: *permaFoam* (Orgogozo et al. 2023).

References

Cazaurang, S., et al. 2023. Numerical assessment of morphological and hydraulic properties of moss, lichen and peat from a permafrost peatland. Hydrology and Earth System Sciences, 27(2), 431–451. https://doi.org/10.5194/hess-27-431-2023

Loiko, S.V., et al. 2019. Microtopography Controls of Carbon and Related Elements Distribution in the West Siberian Frozen Bogs.Geosciences, 9(7), 291. https://doi.org/10.3390/geosciences9070291

Orgogozo, L., et al. 2023. Permafrost modelling with OpenFOAM®: New advancements of the permaFoam solver. Computer Physics Communications, 282, 108541. https://doi.org/10.1016/j.cpc.2022.108541

Park, H., et al. 2018. Modeling the Effect of Moss Cover on Soil Temperature and Carbon Fluxes at a Tundra Site in Northeastern Siberia. Journal of Geophysical Research: Biogeosciences, 123(9), 3028–3044. https://doi.org/10.1029/2018JG004491

Porada, P., et al. 2016. Effects of bryophyte and lichen cover on permafrost soil temperature at large scale. The Cryosphere, 10(5), 2291–2315. https://doi.org/10.5194/tc-10-2291-2016

Predicting the hydrology of permafrost catchments: A case study from the western Canadian Arctic

Brampton Dakin[1], Philip Marsh[1], David Rudolph[2], Robin Thorne[1] & Branden Walker[1]

[1]*Cold Regions Research Centre, Wilfrid Laurier University, Waterloo, Ontario*

[2]*Cold Regions Research Centre, University of Waterloo, Waterloo, Ontario*

Earth's dramatically warming climate is impacting many aspects of the Arctic environment at unprecedented rates. We have started to see changes impacting active layer depths and permafrost thaw, shrubs expanding further north, snow free and lake ice durations, lake evaporation and evapotranspiration, and precipitation. These are interacting to produce complex changes to all aspects of Arctic hydrology. Unfortunately, the small number of monitoring stations across the Arctic makes it difficult to understand the overall impacts of these changes on lake levels or streamflow for example. Previous studies have even suggested that it is unknown whether the integrated impacts of these changes will result in the wetting or drying of the Arctic. This study will use a combination of detailed monitoring and hydrologic modelling to study ongoing changes to the hydrology of a site in the western Canadian Arctic with the goal of investigating these complex hydrologic changes.

Field observations were conducted in the Trail Valley Creek research watershed in the western Canadian Arctic. This site is located 50 km north-east of Inuvik, NWT, and has over three decades of research observations. For this study, detailed observations focused on Siksik Creek, a 1 km^2 sub-catchment of Trail Valley Creek. Field observations included measurements of end of winter snow cover, precipitation, evapotranspiration, active layer depths, water table depths, and stream discharge. Data was available for two contrasting summers: 2021, and 2016. The summer of 2021 was likely the 7th warmest summer on record and possibly the driest summer on record with only 3 mm of precipitation recorded for July. The summer of 2016 was considerably wetter than 2021 but had similar air temperatures making it a good comparison to test the influence that changing moisture conditions might have on hydrology and active layer thicknesses.

We applied the GEOtop model to investigate the hydrologic conditions of these two contrasting summers. GEOtop was applied using a high resolution elevation model, vegetation map, end of winter snow distribution map, and discretization of soil properties. GEOtop outputs for soil moisture, active layer depths, evapotranspiration and streamflow were compared to observations.

Results showed that active layer depths, discharge, and soil moisture contents significantly changed across years. These simulations did an excellent job of predicting these changes, and demonstrated that 2021, the drier year, had significantly shallower thaw, while the wetter year, 2016, had deeper thaw and nearly 3x the amount of discharge. When we consider that the drying of Arctic peatlands might lead to shallower thaw throughout the summer, whereas the wetter years lead to deeper thaw depths, these results have direct implications for carbon sequestration or release as well as impacts on tundra fires. Understanding which areas might become wetter or drier will help policy makers make better informed decisions for different parts of the Arctic.

We are currently building upon this work and applying GEOtop to the entire Trail Valley Creek watershed. In doing so we will build a more comprehensive model domain, which tests more landscape types, including forested areas found in the catchment, bare ground, and taller shrub types. This will then be back casted to cover a longer time period, where we have meteorological data that has been gap filled over the last 30 years. This will let us analyze Trail Valley Creek over a 30-year period and to evaluate if the catchment as a whole is becoming more wet or dry, and if different landcover types in the catchment are changing with this.

Ground temperature regime of isolated permafrost in northeastern Mongolia

Yadamsuren Gansukh[1], Yamkhin Jambaljav[2], Masayuki Kawahigashi[1] & Batbayar Nyambayar[3]

[1]*Department of Geography, Tokyo Metropolitan University, Tokyo, Japan*

[2]*Geocryo LLC, Ulaanbaatar, Mongolia*

[3]*Wildlife Science and Conservation Center of Mongolia, Ulaanbaatar, Mongolia*

Permafrost occurs in polar regions and at high elevations (Brown et al. 1997), and globally, the dominant factors for its presence are high latitude, and high elevation, which overlap in certain locations (French 2007). The permafrost in Mongolia fringes the southern edge of Siberia, the world's largest permafrost region; however, it is distinctive from the latitudinal permafrost in Siberia and North America and the mountain permafrost in other regions. In Mongolia, the permafrost is distributed along mountain topography and mosaic-landscape, geology, hydrogeology, and geotectonic patterns. Both continuous and discontinuous permafrost distributions can be confirmed in northern and high-elevation locations within Mongolia. Sporadic and isolated permafrost are present at lower elevations in intermountain valleys.

Yamkhin et al. (2022) have concluded that the lower limits of permafrost in northeastern Mongolia (Hentii Mountain range) are 800 m in the northwest, 1,270 m in the south, and 1,000 m in the east. Below these elevations, permafrost patches exist in peatland areas along vast valleys and depressions, and they exist due to the accumulation of cold air masses in winter. The combination of cold air masses and ground surface covered by peat provides favourable conditions for permafrost development (Shur 2007).

This study aims to determine the thermal state and degradation of permafrost in wetland environments along the permafrost fringe in Mongolia.

Study site

The study area is the Khurkh River valley, located in the isolated permafrost region (Yamkhin et al. 2022) of northeastern Mongolia at the southern boundary of Siberian permafrost (Figure 1). The valley (approximately 1000 m a.s.l) includes a wetland in the centre and is surrounded by pasture and agricultural lands (steppe and forest-steppe landscapes). The mean annual air temperature (MAAT) is about 0.12 ℃ and the mean annual precipitation is about 260 mm during 2018/19 according to the climatic station located at the centre of the valley.

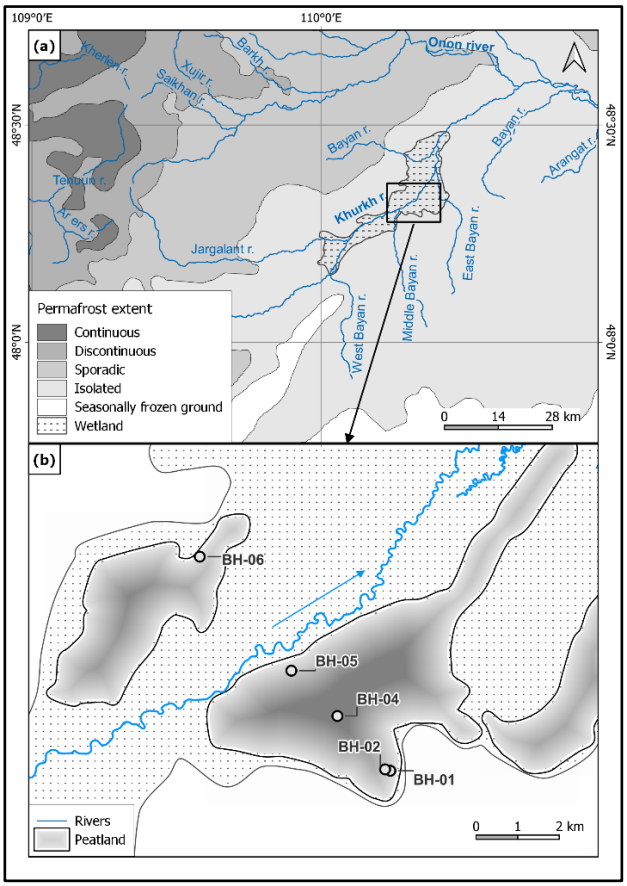

Figure 1. (a) Permafrost extent in north-eastern Mongolia and (b) borehole (BH) locations at Khurkh River valley.

Vertical ground temperature profiles for boreholes have been obtained through continuous temperature recordings at the surface and 1–10 m by 1-m intervals. These profiles represent an envelope of maximum and minimum temperature and are used to calculate permafrost characteristics. The most valuable parameters, indicated by the mean annual ground surface temperature (MAGST), the mean annual ground temperature (MAGT) at a depth of zero annual amplitude (DZAA), thickness of the active layer (ALT), and the seasonally frozen ground (TSF) are useful for determining the thermal state and degradation of permafrost in different environments.

$$DZAA_z = 2(\pi kP)^{1/2}$$

where, k is thermal diffusivity ($m^2 s^{-1}$), P is the period of the wave (one year) in seconds.

$$k = \frac{\pi}{P}\left(\frac{z_2 - z_1}{Ln\, A_1/A_2}\right)^2$$

where A_1 and A_2 are amplitude of different Z_1 and Z_2 depths (Williams and Smith 1989). The gradient of permafrost temperature (GPT) is used to assess the state of permafrost degradation (Ishikawa et al. 2018).

$$GPT = \frac{MAGT - TTOP}{DZAA - ALT}$$

We have analyzed the parameters and classified the permafrost formation process as climate-driven and ecosystem-driven based on the approach of Shur (2007).

Results and Discussions

In boreholes BH-01 and BH-06, located in the transition zone between grassland and wetland, no permafrost was detected. At BH-02, a shallow permafrost horizon of 2 m thickness was found at the wetland edge. The temperature at 10 m depth at BH-04 and BH-05 are -1.1 and -0.4 ℃.

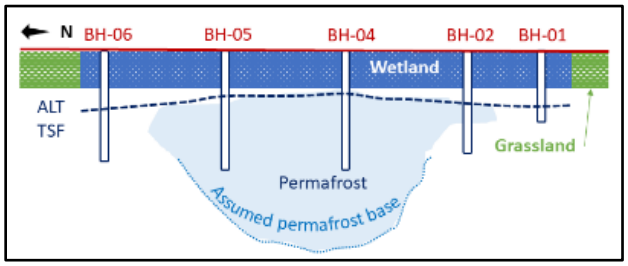

Figure 2. Graphical illustration of a cross-section of the study area and boreholes.

Table 1. Observed and estimated parameters in 2018/2019.

Parameters	BH-01	BH-02	BH-04	BH-05	BH-06
MAGST, ℃	2.1	1.7	0.9	1.9	2.5
MAGT, ℃ (1m)	1.1	-0.5	-1.3	0.9	2.1
TTOP, ℃	-	-0.40	-1.13	-0.12	-
ALT, m	-	3.0	1.6	3.0	-
TSF, m	2.5	-	-	-	3.0
DZAA, m	11.3	7.6	13.3	12.3	12.0
GPT, ℃	-	0.196	0.004	-0.03	-

MAGST at all boreholes range from 0.9 to 2.5 ℃, however, temperatures at 1 m depth have significantly decreased, ranging from -1.3 to 2.1 ℃ (Table 1). In the BH-02 and BH-04, the temperature difference between MAGST and MAGT at 1 m is 2.2 ℃ (thermal offset between surface and 1 m depth), indicating a high thermal offset of the soil horizons. During the drilling of boreholes, no peat layer was observed at BH-06 and BH-01. At the centre of the wetland (BH-04), the peat layer thickness reached 45 cm.

Ishikawa et al. (2018) concluded a notable decrease in mean annual ground temperatures (MAGTs) and a significant increase in the depth of zero annual amplitude. Permafrost characterized by warm and thermally unresponsive conditions, primarily influenced by latent heat, is present in sporadic and isolated zones.

The existence of permafrost depends on many factors, which can be divided into climatic and ecosystem factors. In the high Arctic or high mountain regions, climatic factors are more favourable. In contrast, ecosystem factors are more favourable in the southern edge of the Arctic or the surrounding high mountain regions (Shur 2007). Permafrost with a TTOP equal to or greater than MAGT is warming and in a state of degradation.

For our study area, the ecosystem is a more favourable factor for the existence of permafrost.

References

Brown, J., Ferrians, O.J., Heginbottom. J.A., and Melnikov, E.S. 1997. International Permafrost Association Circum-Arctic Map of Permafrost and Ground Ice Conditions, Map CP-45. US Geological Survey, USA. https://doi.org/10.3133/cp45

French, H.M. 2007. The periglacial environment. John Wiley and Sons, Toronto, Canada.

Yamkhin, J., Yadamsuren, G., Khurelbaatar, T., Gansukh, T.–E., Tsogtbaatar, U., Adiya, S., Yondon, A., Avirmed, D., and Natsagdorj, S. 2022. Spatial distribution mapping of permafrost in Mongolia using TTOP. Permafrost and Periglacial Process.; 33(4): 386–405. https://doi.org/10.1002/ppp.2165

Shur, Y.L., and Jorgenson, M.T. 2007. Patterns of permafrost formation and degradation in relation to climate and ecosystems. Permafrost Periglacial Process., 18: 7–19. https://doi.org/10.1002/ppp.582

Williams, P.J., and Smith, M.W. 1989. The Frozen Earth: Fundamentals of geocryology. Cambridge University Press, Ottawa, Canada.

Ishikawa, M., Jamvaljav, Y., Dashtseren, A., Sharkhuu, N., Davaa, G., Iijima, Y., Baatarbileg, N., and Yoshikawa, K. 2018. Thermal states, responsiveness and degradation of marginal permafrost in Mongolia. Permafrost and Periglacial Process. 29: 271–282. https://doi.org/10.1002/ppp.1990

Exploring MeHg responses to winter warming: A snow fence field experiment in a Swedish sub-arctic peatland

Charlotte Haugk[1], Alyssa Azaroff[1], Margareta Johansson[2], Mingyue Li[3], Lauren Thompson[4,5] & Sofi Jonsson[1]

[1]*Department of Environmental Science, Stockholm University, Stockholm, Sweden*

[2]*Department of Physical Geography and Ecosystem Science, Lund University, Sweden*

[3]*Institute of Tibetan Plateau Research, University of Chinese Academy of Sciences, Beijing, China*

[4]*Department of Renewable Resources, University of Alberta, Edmonton, Alberta, Canada*

[5]*Hatfield Consultants, Calgary, Alberta, Canada*

Permafrost experiences rapid transformations through ongoing thaw, thereby releasing mercury (Hg) and potentially forming hotspots for Hg methylation as organic matter is degrading. Monomethylmercury (MeHg) is a known neurotoxin and of health concern to northern communities if it bioaccumulates in the food chain. Studies have found that with climate warming, winter precipitation is about to increase the northern Scandinavia (Saelthun and Barkved 2003). An increase in snow cover has an insulating effect from cold air temperatures and is leading to active layer deepening and biogeochemical changes in permafrost peatlands. If Hg is remobilized and bioaccumulated as neurotoxic MeHg in the food web and it can pose serious risk to wildlife and human health.

A snow fence long-term field experiment was originally set up on a peatland plateau in 2005 in Abisko, northern Sweden to study the effect of snow cover increase on permafrost and vegetation. The snow fences simulate ongoing permafrost thaw due to increased snow thickness and insulation of the ground. After seven years of treatment, higher ground subsidence and increased active layer thickening were recorded in manipulated plots compared with control plots (Johansson et al. 2013).

While previous studies have explored Hg responses and dynamics in permafrost peatlands (Lehnherr et al. 2012; Fahnestock et al. 2019; Tarbier et al. 2021), our research focus on the effects of winter warming on Hg mobilization as well as seasonal variations in a thawing permafrost mire.

Here, we will present data from two sampling campaigns: 12 soil cores representing “spring” conditions (early June 2022) and 12 cores representing “fall” conditions (September 2022). We concentrated our efforts on determining total mercury (THg, as to sum up the organic and inorganic forms of Hg) and MeHg in soil cores and further conducted incubation experiments to track potential Hg^{II} methylation (k_m) and MeHg demethylation (k_d) at selected soil depths with the use of enriched Hg stable-isotope tracers. Additionally, we sampled pondwater accumulated at some of the plots for analysis of THg and MeHg.

Using this dataset, we will test if increased winter snow cover in permafrost peatlands leads to higher Hg methylation and increased loss of Hg from the soil matrix. Considering the potential ecological and health implications, these findings can hold significant implications for understanding the complex dynamics of Hg in thawing permafrost ecosystems.

References

Fahnestock, M.F., Bryce, J.G., McCalley, C.K., Montesdeoca, M., Bai, S., Li, Y., Driscoll, C.T., Crill, P.M., Rich, V.I., and Varner, R.K. 2019. Mercury reallocation in thawing subarctic peatlands. Geochem. Persp. Let. 11, 33–38. doi:10.7185/geochemlet.1922

Johansson, M., Callaghan, T.V., Bosiö, J., Åkerman, H.J., Jackowicz-Korczynski, M., and Christensen, T.R. 2013. Rapid responses of permafrost and vegetation to experimentally increased snow cover in sub-arctic Sweden, Environmental Research Letters, 8(3), 035025. doi:10.1088/ 1748-9326/8/3/035025

Lehnherr, I., St. Louis, V.L., Emmerton, C.A., Barker, J.D., and Kirk, J.L. 2012. Methylmercury cycling in High Arctic wetland ponds: Sources and sinks, Environmental Science & Technology, 46(19), 10514–10522. doi:10.1021/es300576p

Sælthun, N.R, and Barkved, L. 2003. Climate change scenarios for the SCANNET region NIVA Report SNO: 4663–2003 (Oslo: Norwegian Institute for Water Research).

Tarbier, B., Hugelius, G., Sannel, A.B., Baptista-Salazar, C., and Jonsson, S. 2021. Permafrost thaw increases methylmercury formation in Sub-Arctic Fennoscandia, Environmental Science & 81 Technology, 55(10), 6710–6717. doi:10.1021/acs.est.0c04108

Mercury storage and cycling in thawing permafrost peatlands of the Hudson Bay Lowlands

Adam Kirkwood[1,2], Pascale Roy-Léveillée[2], Nathan Basiliko[3] & Murray Richardson[1]

[1]*Department of Geography and Environmental Studies, Carleton University, Ottawa, Ontario, Canada*

[2]*CRYO-UL: Permafrost Research Laboratory, Université Laval, Québec City, Québec, Canada*

[3]*Department of Natural Resources Management, Lakehead University, Thunder Bay, Ontario, Canada*

Mercury (Hg) is a heavy metal identified as a contaminant of concern by the World Health Organization, and is widespread in soils of the Circumpolar North (Schuster et al. 2018). Circumpolar scale estimates of Hg stored in permafrost-affected soils vary greatly and range from 1,656 ± 962 Gg (Schuster et al. 2018) to 597 Gg (IQR 384-750 Gg) (Lim et al. 2020). The above estimates were made by applying a single ratio of Hg to carbon (C) to previously estimated maps of C storage. These large-scale estimates draw attention to the importance of northern Hg stores, but their resolution and precision at regional and local scales is insufficient to support Indigenous communities and their partners as they strive to make environmental management decisions that are informed by the potential impacts of changes in Hg cycling on their traditional territories and practices.

The Hudson Bay Lowlands (HBL) is the largest wetland in North America (372,000 km^2), hosts the continent's lowest latitude continuous permafrost, and is home to the traditional territory of 11 Indigenous communities (Figure 1). Previous Circumpolar estimates do not account for any field data from the region, yet suggest that it stores a large amount of Hg with >150 mg Hg m^{-2} in the top 300 cm of the ground (Schuster et al. 2018). As permafrost thaws in the HBL, it may release Hg stored in frozen soils to environments such as thermokarst fens, ponds, and lakes where it is more likely to be converted to its organic, bioaccumulative, and neurotoxic form of methylmercury (MeHg). Empirically driven estimates of Hg storage in the HBL at a resolution that can account for variability between landforms and an improved understanding of the impacts of thaw on methylation potential would help inform and support the Indigenous communities who steward this pristine wilderness area. The purpose of this study is to improve estimates of Hg storage and examine the impact of permafrost thaw on Hg storage and methylation across the HBL. Specifically, the objectives were to: 1) estimate Hg storage in soils of the HBL; and 2) assess how warming and associated thaw processes may affect production of MeHg in the HBL.

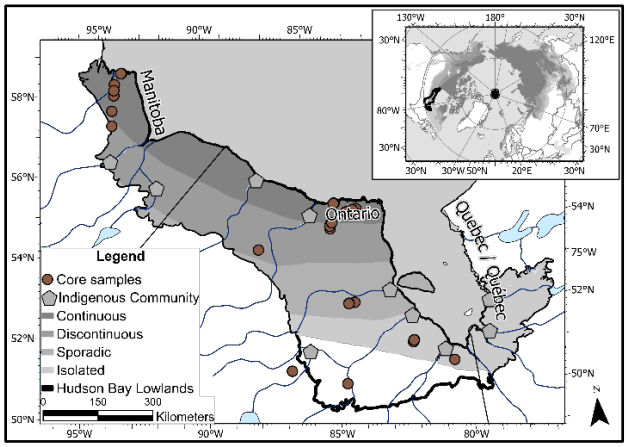

Figure 1. Extent of the Hudson Bay Lowlands with location of core samples and Indigenous Communities.

METHODS

50 peat cores were collected from a total of 39 sites across the HBL from either unfrozen bogs or fens in the southern HBL (<53°N latitude) or from unfrozen bogs, fens, or thermokarst fens adjacent to permafrost features in the northern HBL (>53°N; Figure 1) using a Jeglum-type box corer and Russian pattern side-cutting peat corer (Packalen et al. 2014). In the northern HBL, samples of active layer and permafrost were collected from palsas and peat plateaus, two common permafrost features in the region by cutting the active layer into 10 x 10 cm rectangles to the depth of frost, and collected permafrost cores with a portable permafrost coring system in either end of August 2017–2022 or mid-October 2018–2019 (Calmels et al. 2005). Cores were subsampled in 5 or 10 cm increments along the depth profile, with a total of 980 subsamples. Subsamples were analyzed for total Hg concentration (THg) using a Milestone DMA-80, and elemental composition of carbon (C), nitrogen (N) and sulfur (S) was measured using an Elementar Vario ISOTOPE cube. Estimates of Hg storage in the HBL were made by calculating a region-specific Hg/C ratio from the analysed samples and applying it to a C storage estimate specific to the HBL (Packalen et al. 2014).

A subset of subsamples (n = 280) were analyzed for MeHg concentration, dissolved organic matter (DOM) composition, and microbial community structure to evaluate the impact of permafrost thaw on MeHg production. MeHg was measured following USEPA method 1630 and subsequent analysis on a Tekran 2700. DOM composition was evaluated by extracting pore-water from peat samples, and using an Agilent Cary Eclipse Fluorescence Spectrophotometer to calculate DOM composition indices that indicate humification and the biological contribution to DOM production. DNA was extracted from subsamples and sequenced using the 16s rRNA marker gene to evaluate microbial community composition.

RESULTS AND DISCUSSION

In the HBL, the median Hg/C ratio (±S.E) was 0.08 ± 0.003 µg THg g C^{-1}, which is considerably lower than the Hg/C ratio applied to the region by previous circumpolar estimates (Table 1). Applying this Hg/C value to the estimated 30 Pg of C in the HBL (Packalen et al. 2014) yields a regional store of 2.4 ± 0.12 Gg of THg, compared to an estimated 48 Gg of THg if using the Hg/C ratio applied by Schuster et al. (2018). While the Hg/C ratio used by Lim et al. (2020) yields an estimated THg storage more similar to our region-specific value, a difference of 3.3 Gg (or 3,300,000 kg) is considerable, especially given that Indigenous communities have expressed concerns around Hg in their country foods (Houde et al. 2022).

Table 1. Hg/C ratios specific to this study, Hg/C ratios used in previous models of Hg stored in the Circumpolar North, and associated size of estimated Hg store in HBL.

Study	Hg/C value (µg THg g C^{-1})	Estimated THg storage in the HBL (Gg)
Schuster et al. 2018	1.6	48
Lim et al. 2020	0.19	5.7
This study	0.08	2.4

Concentrations of MeHg (median ± IQR) were higher in thermokarst fens (0.92 ± 0.80 ng/g) than the intact palsas and peat plateaus (0.51 ± 0.77 ng/g). Net MeHg (%MeHg; proportion of THg occurring as MeHg) weakly increases with depth in the palsa profile (R^2 = 0.07, p <0.001), where more THg occurs as MeHg near the bottom of the thawed active layer and top of frozen ground. This suggests that thaw via active layer deepening promotes MeHg production as conditions were anaerobic and the C:N ratio was lower (indicating more labile substrates) in the transient layer.

The composition of microbial communities in thawed portions of palsas correlated to MeHg concentrations (ρ = 0.55, p < 0.001), while there was no correlation in frozen subsamples of palsa cores, or thermokarst subsamples. Random forest models indicate microbial community composition to be an important predictor of MeHg and %MeHg in thawed subsamples of palsas in addition to lower C:N ratios. In thermokarst subsamples, microbial community composition contributed little to explaining MeHg concentrations, while total organic carbon content and DOM composition explain the most. This indicates varying importance of microbial community in relation to MeHg production between active layer deepening and thermokarst encroachment.

IMPLICATIONS AND CONCLUSIONS

This work highlights the importance of regional field data on Hg storage and advances understanding of the impacts of permafrost thaw on Hg cycling. Using regional field data to calibrate the Hg storage model decreased the estimate of Hg storage for the HBL by a factor of 20. As permafrost thaws, active layer deepening and thermokarst encroachment will create environments that are more favorable to methylation than the intact forms. The results from this study can contribute to the decision-making processes of regional authorities or local community in regards to concerns around contaminants and food security and overall health of the local environment.

REFERENCES

Calmels, F., Gagnon, O., and Allard, M. 2005. A portable earth-drill system for permafrost studies. Permafrost and Periglacial processes, 16(3), pp.311–315.

Houde, M., Krümmel, E.M., Mustonen, T., Brammer, J., Brown, T.M., Chételat, J., Dahl, P.E., Dietz, R., Evans, M., Gamberg, M., and Gauthier, M.J. 2022. Contributions and perspectives of Indigenous Peoples to the study of mercury in the Arctic. Science of the Total Environment, 841, p.156566.

Lim, A.G., Jiskra, M., Sonke, J.E., Loiko, S.V., Kosykh, N., and Pokrovsky, O.S. 2020. A revised pan-Arctic permafrost soil Hg pool based on Western Siberian peat Hg and carbon observations. Biogeosciences, 17(12), pp.3083–3097.

Packalen, M.S., Finkelstein, S.A, and McLaughlin, J.W. 2014, Carbon storage and potential methane production in the Hudson Bay Lowlands since mid-Holocene peat initiation. Nature communications 5, no. 1: 4078.

Schuster, P.F., Schaefer, K.M., Aiken, G.R., Antweiler, R.C., Dewild, J.F., Gryziec, J.D., Gusmeroli, A., Hugelius, G., Jafarov, E., Krabbenhoft, D.P., and Liu, L. 2018. Permafrost stores a globally significant amount of mercury. Geophysical Research Letters, 45(3), pp.1463–1471.

Increasing vulnerability of peatlands to wildfire: Insights from a new high-resolution peatland map of Alaska

Mark J. Lara[1,2], Roger Michaelides[3], Duncan Anderson[2], Wenqu Chen[2], Emma C. Hall[2], Caroline Ludden[1], Aiden I.G. Schore[1], Umakant Mishra[4] & Sarah N. Scott[5]

[1]*Department of Plant Biology, University of Illinois, Urbana, Illinois, United States*

[2]*Department of Geography, University of Illinois, Urbana, Illinois, United States*

[3]*Department of Geography, Washington University at Saint Louis, Saint Louis, Missouri, United States*

[4]*Computational Bio & Biophysics, Sandia National Laboratories, Livermore, California, United States*

[5]*Thermal/Fluids Science and Engineering, Sandia National Laboratories, Livermore, California, United States*

Peatlands cover 3% of the global land surface, yet store 25% of the world's soil organic carbon. These organic-rich soils are widespread across permafrost regions, representing nearly 18% of land surface and storing between 500 and 600 PgC (Yu 2012). Peat (i.e., partially decomposed thick organic layers) accumulates due to the imbalance between plant production and decomposition often within saturated, nutrient deficient, and acidic soils, which limit decomposition. As warmer and drier conditions become more prevalent across northern ecosystems, the vulnerability of peatland soils may increase with not only the rate of aerobic respiration, but with the susceptibility of peat-fire ignitions (Turetsky et al. 2015).

During recent summers, anomalously warm and dry climatic conditions increased wildfires across Alaska, elevating the prevalence of peatland fires. Although the combustion of peat has direct impacts on carbon-climate feedbacks, the distribution of peatlands across Alaska remains uncertain. We developed the first wall-to-wall fine-scale (20 m spatial resolution) peatland map of Alaska (~1.5 million km^2), using a (1) peatland suitability model to identify the lowland environments suitable for peat formation and (2) fusion of Sentinel-1, Sentinel-2 and ArcDEM derivatives for machine learning classification of peatland soils. This novel product was used to evaluate the sensitivity of peatlands to ignition by categorizing peatland soils into wet and moist classes and determining the potential spatial patterns and trends of peat-fires on the total area burned between 1985 and 2022 across Alaska.

METHODS

We used a combination of 16 different space-borne remotely sensed fused datasets to derive a statewide 20 m spatial resolution peatland map of Alaska. To determine the terrain suitable for peat accumulation, we generated a peatland suitability model with 30 m elevation data from NASA's Shuttle Radar Topography Mission (SRTM) using a topographic cost function. Within the bounds of suitable peatland terrain, we fused a seamless composite of optical (Sentinel-2), radar (Sentinel-1), and ArcDEM derivatives for peatland mapping, shown to be successful in regional applications (e.g., Karlson and Bastviken 2023).

We trained support vector machine classifiers in Google Earth Engine using hundreds of multispectral and SAR observations. Training samples were selected using ground or aerial reference locations to represent homogeneous spectrally pure pixels for peatlands. The statewide peatland map was validated using both ground-based observations and high-resolution image interpretation. Due to the difficulty in identifying tundra peatlands from aerial or spaceborne observations, only ground-based data were used to evaluate the accuracy of tundra peatlands across the Seward Peninsula, Noatak National Preserve, Brooks Foothills, and the Arctic Coastal Plains. In contrast, both ground-based observations and high-resolution image interpretation was used to evaluate map accuracy across boreal and maritime ecoregions as fens, bogs, marshes, and other predominant wet-moist peatland environments are readily identifiable from imagery. Thus, we included validation data from the Yukon Kuskokwim Delta, Minto Flats, Tanana Flats, Yukon Flats, Cook Inlet basin, Copper River Delta, Noatak National Preserve, and the Tongass National Forest. Within these subregions, we placed between 75 to 1500 points inside and outside of our peatland map extent using a stratified random sampling design, assigned as either peatland or non-peatland categories using traditional image interpretation techniques (e.g., Karlson and Bastviken 2023). Data were used to evaluate map accuracies using contingency tables and kappa coefficients. We used the Alaska statewide fire history data to estimate the spatial patterns and temporal trends in peatland area burned across level 1 and level 2 ecoregions of Alaska. Level 1 ecoregions include the polar, boreal, and maritime ecoregions, comprising 25, 57, and 18% of the total land area, respectively, and level 2 ecoregions include Arctic tundra, Bering tundra, Bering taiga, Intermontane boreal, Alaska range transition, Coast mountains transition, Pacific mountains

transition, Coastal rainforests, and Aleutian meadows (Nowacki et al. 2002). Using our peatland map, we determined the area of peatlands impacted by wildfire over time by calculating the peatland area within AICC historical fire scars.

Results and Discussion

Statewide (overall accuracy and kappa coefficient was 85% and 0.62, respectively, where the user and producer accuracies for peat were 74% and 70% and user and producer accuracies for no peat were 91% and 91%, respectively, suggesting we were able to reliably detect peatlands across Alaska. We used this peatland map to evaluate the potential peatland area impacted by wildfire between 1985 and 2022 within nine polar (i.e., Bering tundra, Bering taiga, and Arctic tundra), boreal (i.e., Coastal mountains transition, Pacific mountains transition, Alaska range transition, and Intermontane boreal), and maritime (i.e., Aleutian meadows and Coastal rainforests) ecoregions. Results identify peatlands in polar, boreal, and maritime ecoregions in Alaska to cover 26,842 (4.6%), 69,783 (10.4%), and 13,506 (5.3%) km^2, respectively.

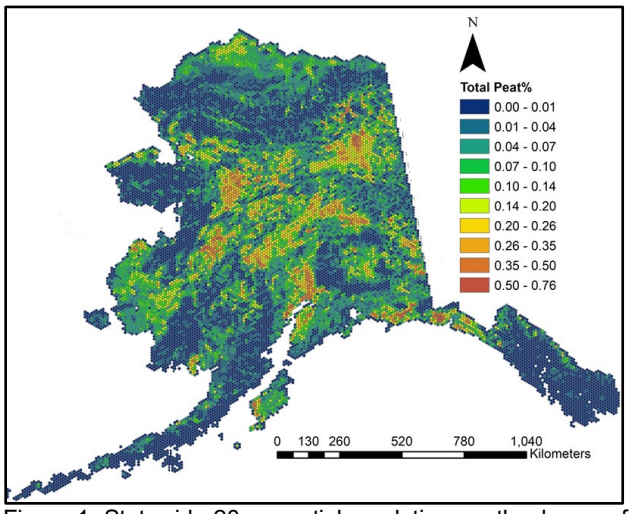

Figure 1. Statewide 20 m spatial resolution peatland map of Alaska (Lara et al. 2023). Tesselated map is displayed at 1 km for visulaization.

Peat-fires increased across polar and boreal ecoregions as temperatures warmed over the last ~40 years. Both the total peatland area burned and the proportion of peatland area burned increased 189 km^2 and 2.2% per degree of warming, respectively (R^2 = 0.24, p <0.05 and R^2 = 0.24, p <0.05). Wildfires occurring in regions with annual temperatures of less than -6°C typically had no peatland areas burned, but regions with annual temperatures of 0°C, the proportion of peatland areas to burn within wildfires increased to 20%; of which nearly 65% occurred in moist peatlands. We posit that decadal warming trends in both polar and boreal ecoregions increased peatland desiccation (greatest in the Intermontane boreal; Bieniek et al. 2014), increasing peat flammability (McCarty et al. 2020) and the prevalence of peat-fires in response to drier summer seasons (Kuklina et al. 2022; McCarty et al. 2020).

New high-resolution peatland products improve our ability to determine the regionally-specific sensitivity, vulnerability, and/or resilience of peatlands (i.e., wet and moist) to drying and ignition. Our first-order analysis of the impact of peat-fire dynamics indicate, indeed, peat-fires in both polar and boreal ecoregions across Alaska will continue to increase with projected warming. These new geospatial datasets (Lara et al. 2023) may not only be important for quantifying historical losses of peatland carbon pools, but also for improving projections of carbon emissions and smoke forecasting of particulate matter, carbon monoxide, and other volatile organic compounds emitted under flaming and smouldering scenarios across Alaska.

References

Bieniek, P.A., Walsh, J.E., Thoman, R.L., and Bhatt, U.S. 2014: Using Climate Divisions to Analyze Variations and Trends in Alaska Temperature and Precipitation. J. Climate, 27, 2800–2818. https://doi.org/10.1175/JCLI-D-13-00342.1

Karlson, M., and Bastviken, D. 2023. Multi-Source Mapping of Peatland Types Using Sentinel-1, Sentinel-2, and Terrain Derivatives—A Comparison Between Five High-Latitude Landscapes. J Geophys Res Biogeosci, 128.

Kuklina, V., Sizov, O., Rasputina, E., Bilichenko, I., Krasnoshtanova, N., Bogdanov, V., and Petrov, A.N. 2022. Fires on Ice: Emerging Permafrost Peatlands Fire Regimes in Russia's Subarctic Taiga. Land, 11, 322. https://doi.org/10.3390/land11030322

Lara, M.J, Michaelides, R., Anderson, D., Chen, W., Hall, E.C., Ludden, C., Schore, A.I.G., Mishra, U., and Scott, S.N. 2023. Alaska Peatland Map (2019-2021). Arctic Data Center. https://doi.org/10.18739/A2NK3667M

McCarty, J.L., Smith, T.E.L., and Turetsky, M.R. 2020. Arctic fires re-emerging. Nat. Geosci. 13, 658–660. https://doi.org/10.1038/s41561-020-00645-5

Nowacki, G.J., Spencer, P., Fleming, M., Brock, T., and Jorgenson, T. 2002. Unified Ecoregions of Alaska: 2001. U.S. Geological Survey, Open-File Report 2002-297. https://doi.org/10.3133/ofr2002297

Turetsky, M.R., Benscoter, B., Page, S., Rein, G., Van Der Werf, G.R., and Watts, A. 2015. Global vulnerability of peatlands to fire and carbon loss. Nat Geosci 8, 11–14. https://doi.org/10.1038/ngeo2325

Yu, Z.C. 2012. Northern peatland carbon stocks and dynamics: a review, Biogeosciences, 9, 4071–4085. https://doi.org/10.5194/bg-9-4071-2012

Plant-derived carbon accelerates methane production in permafrost-affected wetlands

Maija E. Marushchak[1,2], Christina Biasi[2], Suzanna Brauer[3], Wasi K. Hashmi[2], Hannu Nykänen[2], Carlos Palacin-Lizarbe[2], Dhiraj Paul[2], Minna Pääkkönen[2], A. Britta K. Sannel[4], Henri Siljanen[2], Suvi Suurnäkki[1], Lena Ström[5], Carolina Voigt[6], Joel White[5] & Marja Tiirola[1]

[1]*Department of Biological and Environmental Science, University of Jyväskylä, Jyväskylä, Finland*

[2]*Department of Environmental and Biological and Sciences, University of Eastern Finland, Kuopio, Finland*

[3]*Department of Biology, Appalachian State University, Boone, North Carolina, United States*

[4]*Department of Physical Geography, Stockholm University, Stockholm, Sweden*

[5]*Department of Physical Geography and Ecosystem Science, Lund University, Lund, Sweden*

[6]*Institute of Soil Science, Universität Hamburg, Hamburg, Germany*

Although the importance of permafrost carbon (C) for the global climate system has been acknowledged, there are still major uncertainties that hinder accurate quantification of permafrost C feedback. One of the open questions is related to the composition of the gaseous C release: Which proportion of the total C release will occur as CH_4, a GHG ~30 times stronger at a 100-year time horizon than CO_2. Anoxic incubation studies with permafrost-affected soils often report complete absence of CH_4 production or, if the incubation is long enough, substantial lag-times from weeks to years (Treat et al. 2015; Knoblauch et al. 2018). However, this does not accurately represent the insitu conditions, where, following thaw, permafrost-derived organic matter is exposed to a complex environmental setting including plant communities. Plants may enhance mineralization of soil organic matter by fuelling the microbial community with labile C compounds, a phenomenon known as the rhizospheric priming effect. The effect of rhizospheric priming on C gas release under oxic conditions has been shown for permafrost affected soils (Keuper et al. 2020), but the importance of this phenomenon in anoxic soil is not known.

Material and methods

Here, we investigated the effect of plant-derived C on anaerobic decomposition processes in permafrost-affected wetlands in a 1+-year long incubation study. We collected soils from two permafrost-affected wetland sites: mineral subsoils underlying fen and grassland in Zackenberg, Eastern Greenland, and active layer and permafrost from Tavvavuoma palsa mire in Northern Sweden.

We determined the CO_2 and CH_4 production rates and CH_4/CO_2 ratios with and without additions of ^{13}C-enriched glucose and cellulose (n = 5). Based on the ^{13}C-enrichment measured by a cavity ring-down spectroscope analyzer (Picarro G2201-i), we were able to partition the C gas release between the SOM and the added substrate, and thus estimate the priming effect for both CO_2 and CH_4.

Additionally, we conducted molecular analyses to understand whether changes in the microbial community as a result of the anaerobic incubation and C additions might be driving the observed patterns in C gas production. We used 16S rRNA amplicon sequencing to look at overall changes in the microbial community structure. Further, we took a closer look at the microbes participating in CH_4 cycling by targeted sequencing of key functional genes of both CH_4-producing methanogens (mcrA) and methanotrophs (pmoA, mmoX).

Preliminary results

The temporal pattern, magnitude and composition of the C gas release varied greatly between the studied soils. While the fen subsoils showed high rates of CH_4 production and 1:1 CH_4/CO_2 ratios from the beginning of the incubation, in permafrost peat samples the CH_4 production was initiated only after ~1 year of incubation under anoxic conditions. Interestingly, CH_4 production was observed only in the C-amended permafrost samples, while no CH_4 production was observed without C addition. The differences in the CH_4 production and overall decomposition rate between the soils and treatments were partly explained by differences in the microbial community composition and the functional gene abundance.

Taken together, our data suggests that plant-derived C may influence anoxic decomposition processes and the related microbial community composition in Arctic wetlands. This suggests that the interactions between plants and microbes should be considered when estimating future C release from anoxic soils of the permafrost region.

ACKNOWLEDGEMENTS

This research was funded by the Academy of Finland in the frame of projects PANDA (no. 317054) and Thaw-N (no. 349503).

REFERENCES

Keuper, F., Wild, B., Kummu, M., Beer, C., Blume-Werry, G., Fontaine, S., Gavazov, K., Gentsch, N., Guggenberger, G., Hugelius, G., Jalava, M., Koven, C., Krab, E.J., Kuhry, P., Monteux, S., Richter, A., Shahzad, T., Weedon, J.T., and Dorrepaal, E. 2020. Carbon loss from northern circumpolar permafrost soils amplified by rhizosphere priming. Nature Geoscience, 13: 560–565. doi:10.1038/s41561-020-0607-0

Knoblauch, C., Beer, C., Liebner, S., Grigoriev, M.N., and Pfeiffer, E. 2018. Methane production as key to the greenhouse gas budget of thawing permafrost. Nature Climate Change, 8: 309–312. doi:10.1038/s41558-018-0095-z

Treat, C.C., Natali, S.M., Ernakovich, J., et al. 2015. A pan-Arctic synthesis of CH_4 and CO_2 production from anoxic soil incubations. Global Change Biology, 21, 2787–2803. doi:10.1111/gcb.12875.

Potential impact of degrading polygons to thermokarst lake water and carbon cycles in the context of Yedoma, Yukon, Canada

Sarah Ollivier[1], Antoine Séjourné[1], Aurélie Noret[1], Frédéric Bouchard[2] & Laure Gandois[3]

[1]*GEOPS, Université Paris-Saclay, Orsay, France*

[2]*CARTEL, Université de Sherbrooke, Sherbrooke, Québec, Canada*

[3]*Laboratoire Ecologie Fonctionnelle et Environnement, CNRS, Université de Toulouse, Toulouse, France*

Ice-rich Yedoma permafrost is widespread in the Arctic (Strauss et al. 2021). The Arctic has experienced a +0.6°C/decade air temperature increase over the past 30 years (IPCC 2013), causing lake formation by ground subsidence, called thermokarst lakes (Soloviev 1973). Hydrology and geochemistry of hydrosystems are also impacted with drainage modification and inputs of organic and inorganic elements previously stored in permafrost (Vonk et al. 2015). Ancient organic matter (OM) could be released, converted into greenhouse gases, and enhance the positive feedback on climate (Schuur et al. 2015). In this context, the PRISMARCTYC project aims to better understand permafrost thaw impacts, surface/groundwater fluxes and carbon cycle, as well as their controlling factors. It focuses on small inland Arctic watersheds where localized and rapid thermokarst occurrences remain understudied. Here, this work aims at understanding the impact of ice-rich permafrost degradation on water and carbon cycles in thermokarst lakes in Yukon.

Study site

Our study site is located in Western Yukon, Canada, near the Beaver Creek village (Figure 1). Permafrost is discontinuous extensive in southern Yukon and cryostratigraphic investigations revealed the presence of Yedoma deposits (Fortier et al. 2018). We will focus on one large lake (20,000 m^2) possibly formed by thermokarst during the early Holocene. Permafrost degradation around the lake is evidenced by degraded ice-wedge polygonal landscape (Figure 1).

Methods

We sampled the lake, permafrost porewater and ice wedges from the polygon area during two field campaigns, in August 2022 and August 2023. Physico-chemical in situ parameters, water stable isotopes ($\delta^{18}O$, $\delta^{2}H$), major element concentrations, concentrations and ^{14}C isotope of dissolved organic carbon (DOC), specific ultraviolet absorbance of OM (SUVA) have been analyzed. In 2022, water has been sampled following a depth profile in the center of the lake, where the maximal depth has been encountered (11 m). In 2023, we sampled 3 depth profiles following a proximity gradient to the permafrost degradation area: the west bank, center, and east bank (Figure 1).

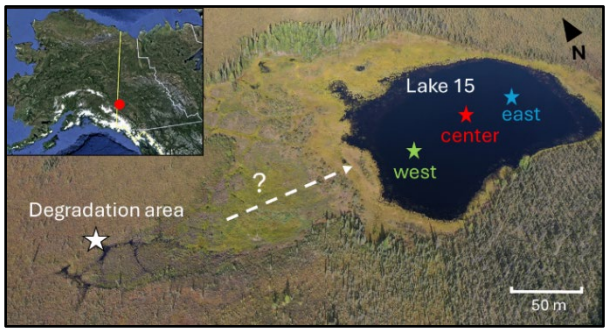

Figure 1. Study region and sampled lake with degradation area along its banks.

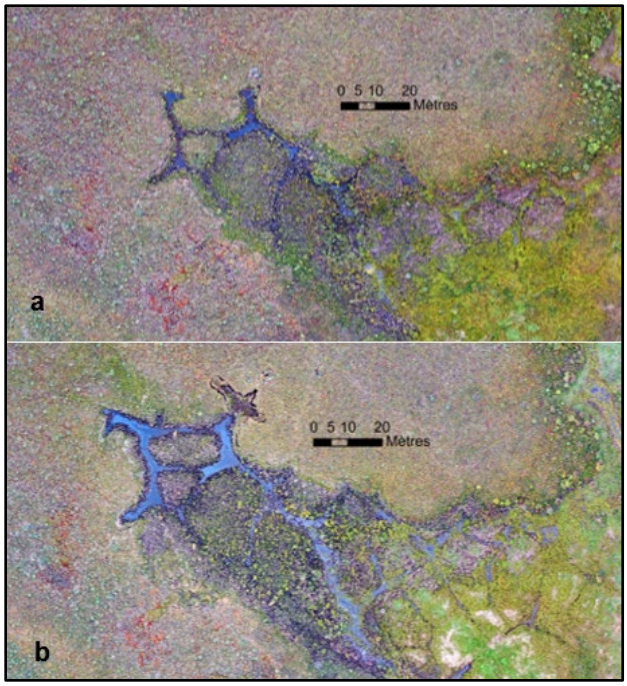

Figure 2. Development of degradation of ice-wedge polygons from a) August 2022 to b) August 2023.

Results and Discussion

Active thermokarst degradation of ice-wedge polygons occurred from 2022 to 2023 (5–10 m growth to the north; Figure 2).

$\delta^{18}O$ values along vertical profiles in the lake for both years range from -17.7 to -20.7‰ and show a noticeable decrease of 1.5–2‰ between 2 and 4 m deep (Figure 3). The same pattern can be identified with $\delta^{2}H$. In contrast, values for the ice wedges and porewater extracted from permafrost core are more depleted (respectively between -23 and -24 ‰ and around -20 ‰). We hypothesize that this is indicative of inputs of more depleted permafrost meltwater to the lake via the active layer (Figure 1). To test this interpretation, we sampled 3 profiles in 2023 close or distant from the degradation area. All profiles show similar decrease indicating either a mixing of the lake or that the input of meltwater propagates to the entire lake. The values show that enrichment by evaporation is not important.

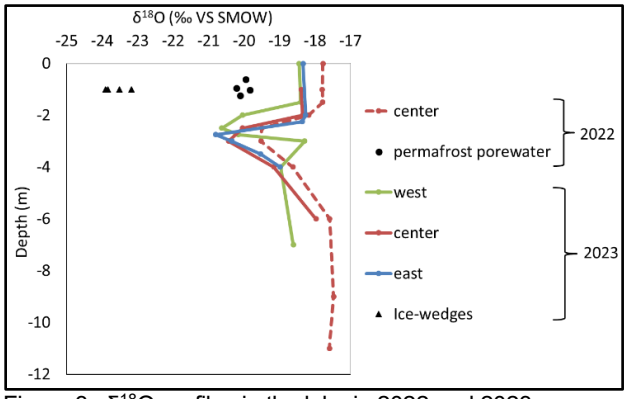

Figure 3. $\delta^{18}O$ profiles in the lake in 2022 and 2023.

DOC values increase slowly with depth from 19.6 to 23.5 $mg \cdot L^{-1}$ in 2022 with a slight decrease at 3 m depth, while in 2023 in the 3 profiles, they range from 22 to 24 $mg \cdot L^{-1}$, with no strong trend with depth. DOC content of ice wedges are lower, between 5 and 15 $mg \cdot L^{-1}$. SUVA values range between 3.2 at the surface and 4.2 at the bottom of the lake both in 2022 and 2023 for all profiles. No strong trend in DOC profiles or differences in parameters related to OM composition (SUVA) have been identified in the lake. This indicates no strong inputs of permafrost OM with meltwater, or permafrost OM signature cannot be detected. The latter can be due to rapid mineralization and production processes by microorganisms in the lake. Only ^{14}C signature of organic carbon could indicate if OM is ancient, i.e., coming from permafrost, or recent, i.e., from the current lake carbon cycle.

Conclusion

Active thermokarst of Yedoma deposits is occurring in Southwestern Yukon. Degradation of ice wedges leads to inputs of depleted meltwater into the studied thermokarst lake. No changes have been detected on dissolved organic carbon cycle in terms of concentration or OM composition. Further analysis of ^{14}C will complete the study and will be presented at the conference. Major element concentrations and other carbon cycle related parameters such as $\delta^{13}C$ isotopes of DOC will be analyzed and soon exploitable to identify potential impacts of permafrost thaw on soil alteration, mixing and biological processes.

References

Fortier, D., Strauss, J., Sliger, M., Calmels, F., Froese, D., and Shur, Y. 2018. Late Pleistocene Yedoma in south-western Yukon (Canada): a remnant of Eastern Beringia. 5th European Conference on Permafrost, Chamonix Mont-Blanc, France, 23rd June-1st July, Book of abstract, pp 637–638.

IPCC in Climate Change. 2013. The Physical Science Basis. Contribution of Working Group I to the Fifth Assessment Report of the Intergovernmental Panel on Climate Change (Eds Stocker, T. F. et al.) 1535 (Cambridge Univ. Press, 2013).

Schuur, E., McGuire, A., Schädel, C., Grosse, G., Harden, J.W., Hayes, D.J., Hugelius, G., Koven C.D., Kuhry, P., Lawrence, D.M., Natali, S.M., Olefeldt, D., Romanovsky, V.E., Shaefer, K., Turetsky, M.R., Treat, C.C., and Vonk, J.E. 2015. Climate change and the permafrost carbon feedback. Nature 520, 171–179. https://doi.org/10.1038/nature14338

Soloviev, P.A. 1973. Thermokarst phenomena and landforms due to frost heaving in Central Yakutia. Biuletyn Peryglacjalny 23: 135–155.

Strauss, J., Laboor, S., Schirrmeister, L., Fedorov, A.N., Fortier, D., Froese, D., Fuchs, M., Günther, F., Grigoriev, M., Harden, J., Hugelius, G., Jongejans, L.L., Kanevskiy, M., Kholodov, A., Kunitsky, V., Kraev, G., Lozhkin, A., Rivkina, E., Shur, Y., Siegert, C., Spektor, V., Streletskaya, I., Ulrich, M., Vartanyan, S., Veremeeva, A., Anthony, K.W., Wetterich, S., Zimov, N., and Grosse, G. 2021. Circum-Arctic Map of the Yedoma Permafrost Domain. Front. Earth Sci. 9, 758360. https://doi.org/10.3389/feart.2021.758360

Vonk, J.E., Tank, S.E., Bowden, W.B., Laurion, I., Vincent, W.F., Alekseychik, P., Amyot, M., Billet, M.F., Canário, J., Cory, R.M., Deshpande, B.N., Helbig, M., Jammet, M., Karlsson, J., Larouche, J., MacMillan, G., Rautio, M., Walter Anthony, K.M., and Wickland, K.P. 2015. Reviews and syntheses: Effects of permafrost thaw on Arctic aquatic ecosystems. Biogeosciences 12, 7129–7167. https://doi.org/10.5194/bg-12-7129-2015

Shift in growing season timing and impact on carbon sequestration on Samoylov Island in the Siberian Arctic between 2002 and 2017

Selina Undeutsch[1], David Holl[1], Lars Kutzbach[1], Christian Wille[2], Torsten Sachs[2] & Julia Boike[3]

[1]*Institute of Soil Science, University of Hamburg, Hamburg, Germany*

[2]*GFZ German Research Centre for Geosciences, Potsdam, Brandenburg, Germany*

[3]*Alfred Wegener Institut Potsdam, Potsdam, Brandenburg, Germany*

Permafrost ecosystems in the Arctic tundra have slowly built up a large stock of organic carbon over millennia. Projected climate warming, which is particularly pronounced in the Arctic, may shift these ecosystems to a net carbon source via permafrost thaw and the subsequent release of previously sequestered carbon. In this study, we investigated the influence of environmental controls on the carbon dioxide exchange for a polygonal tundra ecosystem on Samoylov Island in the Lena River Delta in Northern Siberia, Russia (72°22' N, 126°30' E). Environmental controls, including in situ measurements of soil and air temperature, a vegetation index derived of remote sensing data and snowmelt timing, were compared to the growing season net carbon dioxide exchange and its components gross primary productivity and total ecosystem respiration. Initial results show that Samoylov Island acted as a net carbon dioxide sink during each growing season from 2003 to 2017. However, a significant decrease in net carbon dioxide uptake was observed during the growing season, particularly in the late growing season. This decrease can be attributed to the late snowmelt and the strong warming of the air temperature in autumn.

METHODS

We leveraged the integration of remote sensing, in situ measurements and comprehensive eddy covariance data to investigate environmental factors influencing vegetation development and thereby carbon dioxide exchange on Samoylov Island. To estimate the total net carbon dioxide exchange between soil and atmosphere during growing season, we used half-hourly eddy covariance (EC) carbon dioxide net ecosystem exchange (NEE) fluxes from 2002 to 2017 from Holl et al. (2019). Using combined light and temperature response models at comparably fine temporal resolution (days to weeks), we extended the NEE dataset with modeled values of half-hourly gross primary production (GPP) and total ecosystem respiration (TER) for May to September. The in situ air and soil temperature data we used (Boike et al. 2019) span the entire EC dataset timeframe. A time series of normalized difference vegetation indices (NDVI) from remote sensing with the Moderate Resolution Imaging Spectroradiometer (MODIS) was derived for Samoylov Island. A particular advantage of NDVI is the possible determination of the seasonal vegetation maximum. All days before the maximum annual NDVI was reached were defined as “early growing season”; all days afterwards were defined as “late growing season”. The onset of the growing season was defined as the first day of year (DOY) when mean daily soil temperature rose above 0 °C, and the end was determined when the same temperature fell below 0.1 °C. The measure of growing degree days (GDD5) was used to represent heat accumulation during the unfrozen period, which represent the sum of the positive differences between daily average temperatures and a base temperature of 5 °C. Snow melt timing was visually evaluated using automated time-lapse photographs from Boike et al. (2018), with data available from 2006 onwards. The onset of snowmelt was defined when clear snow-free areas were visible.

RESULTS

Preliminary results indicate a shift in the growing season carbon exchange dynamics between 2002 and 2017. While the onset of the growing season as estimated by the unfrozen soil period shows a trend towards a later start (0.71 ± 9 days/year), the end of the growing season has not changed over time, indicating a trend to an overall shorter growing season. The reason for this appears to be a later timing in snowmelt. The timing (DOY) of snowmelt and the timing of the start of the unfrozen soil period were highly correlated. When studying vegetation dynamics, we observed a clear increase in the NDVI maximum, indicating a clear trend towards greening of the tundra of Samoylov Island, whereas the timing of maximum NDVI did not change. In general, the average daily air temperatures and GDD5 in the late growing season have risen over the 16-year period. In addition, increasing GDD5 in May were observed, thus in the very early growing season and even before the snowmelt. However, these warmer phases in spring do not directly lead to earlier snowmelt, suggesting a possible role of snow thickness

or other energy balance components, which will be further investigated in a later analysis.

Our results indicate that the change in growing season dynamics could strongly influence net carbon dioxide uptake during the growing season, as shown in Figure 1. Net carbon dioxide uptake during the growing season is significantly reduced between 2002 and 2017.

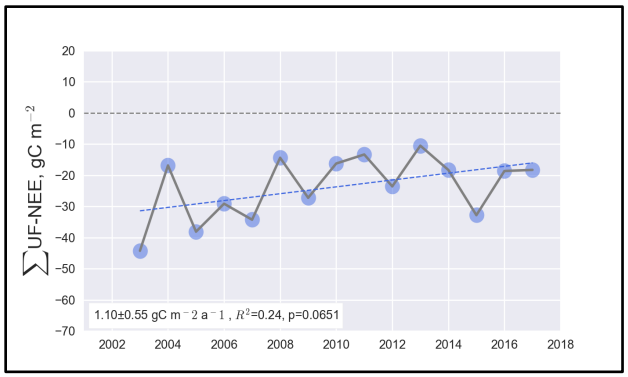

Figure 1. Cumulative sum of net ecosystem exchange of carbon dioxide (CO_2) (NEE; g·C·m^{-2}) during growing season (UF) on Samoylov Island between 2007 and 2017.

Ultimately, although later snowmelt does not hinder greening on Samoylov, it does not necessarily lead to greater carbon sequestration. One possible explanation could be radiation limitation. Although autumn warming is more intense than spring warming, plants lack the ability to sequester increasing amounts of carbon later in the season because they have already exceeded their maximum photosynthetic potential, which follows the seasonal decline of radiation input. Ultimately, ecosystem respiration (TER) reacts more strongly to warming in the fall than gross primary productivity (GPP) (Figure 2).

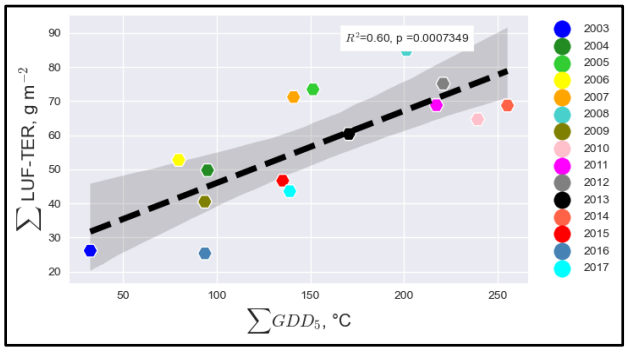

Figure 2. Growing degree days (GDD5, °C) and cumulative sum of total ecosystem respiration (TER, g·C·m^{-2}) between 2003 and 2017 on Samoylov Island in the late growing season (LUF).

In summary, net carbon dioxide uptake during the growing season on Samoylov Island in the North-Siberian Lena River Delta decreased between 2002 and 2017, possibly due to a delay in snowmelt and shortening of the growing season as well as warmer temperatures late in the growing season.

References

Boike, Julia; Nitzbon, Jan; Anders, Katharina; Grigoriev, Mikhail N; Bolshiyanov, Dimitry Yu; Langer, Moritz; Lange, Stephan; Bornemann, Niko; Morgenstern, Anne; Schreiber, Peter; Wille, Christian; Chadburn, Sarah; Gouttevin, Isabelle; Kutzbach, Lars (2019): Measurements in soil and air at Samoylov Station (2002-2018), version 201908. Alfred Wegener Institute - Research Unit Potsdam, PANGAEA. https://doi.org/10.1594/PANGAEA.905236

Boike, Julia; Nitzbon, Jan; Anders, Katharina; Grigoriev, Mikhail N; Bolshiyanov, Dimitry Yu; Langer, Moritz; Lange, Stephan; Bornemann, Niko; Morgenstern, Anne; Schreiber, Peter; Wille, Christian; Chadburn, Sarah; Gouttevin, Isabelle; Kutzbach, Lars (2018): Time lapse camera pictures at Samoylov, LTO, 2002-2017. Alfred Wegener Institute - Research Unit Potsdam, PANGAEA. https://doi.org/10.1594/PANGAEA.891129

Supplement to: Boike, Julia; Nitzbon, Jan; Anders, Katharina; Grigoriev, Mikhail N; Bolshiyanov, Dimitry Yu; Langer, Moritz; Lange, Stephan; Bornemann, Niko; Morgenstern, Anne; Schreiber, Peter; Wille, Christian; Chadburn, Sarah; Gouttevin, Isabelle; Burke, Eleanor J; Kutzbach, Lars (2019): A 16-year record (2002–2017) of permafrost, active-layer, and meteorological conditions at the Samoylov Island Arctic permafrost research site, Lena River delta, northern Siberia: an opportunity to validate remote-sensing data and land surface, snow, and permafrost models. Earth System Science Data, 11(1), 261-299. https://doi.org/10.5194/essd-11-261-2019

Holl, David; Wille, Christian; Sachs, Torsten; Schreiber, Peter; Runkle, Benjamin R K; Beckebanze, Lutz; Langer, Moritz; Boike, Julia; Pfeiffer, Eva-Maria; Fedorova, Irina V; Bolshiyanov, Dimitry Yu; Grigoriev, Mikhail N; Kutzbach, Lars (2018): A long-term (2002 to 2017) record of closed path and open path eddy covariance CO_2 net ecosystem exchange fluxes from the Siberian Arctic. PANGAEA. https://doi.org/10.1594/PANGAEA.892751

Supplement to: Holl, D et al. (2019): A long-term (2002 to 2017) record of closed-path and open-path eddy covariance CO2 net ecosystem exchange fluxes from the Siberian Arctic. Earth System Science Data, 11(1), 221-240. https://doi.org/10.5194/essd-11-221-2

Drained lake basin ages in northern permafrost regions

Juliane Wolter[1,2], Helena Bergstedt[3], Louise Farquharson[4], Benjamin M. Jones[5], Mikhail Kanevskiy[5], Pascale Roy-Léveillée[6], Alexandra Veremeeva[2] & Guido Grosse[2,7]

[1]*University of Potsdam, Institute of Biochemistry and Biology, Potsdam, Germany*

[2]*Alfred Wegener Institute Helmholtz Centre for Polar and Marine Research, Section Permafrost Research, Potsdam, Germany*

[3]*bgeos, Korneuburg, Austria*

[4]*University of Alaska Fairbanks, Geophysical Institute, Permafrost Laboratory, Fairbanks, Alaska, United States*

[5]*University of Alaska Fairbanks, Institute of Northern Engineering, Fairbanks, Alaska, United States*

[6]*Université Laval, Department of Geography, Centre d'études Nordiques, Québec City, Québec, Canada*

[7]*University of Potsdam, Institute of Geosciences, Potsdam, Germany*

Lakes and drained lake basins are abundant landforms in Arctic lowlands with ice-rich permafrost. Many of these lakes formed by thermokarst (thaw of ice-rich permafrost and subsequent subsidence) or when formed by other processes were reshaped by thermokarst dynamics. Growth and gradual expansion of lakes frequently leads to partial of full drainage of the mostly shallow lakes, resulting in complex landscape-scale mosaics of lakes and multiple generations of drained basins across Arctic lowlands (Figure 1).

Figure 1. Lakes and drained lake basins on the Alaskan North Slope.

The age of wetlands in drained lake basins directly affects hydrology, ecology, and biogeochemical cycling (Jones et al. 2022). While lakes variably act as carbon source or sink depending on their age and specific environmental setting, drained lake basins mostly contain wetlands that act as carbon sinks, especially when wetlands have been developing for longer time periods (Jones et al. 2022). Estimations of how thawing and mobilized permafrost carbon contribute to the atmospheric carbon greenhouse gas content should therefore include information on the spatio-temporal distribution of drained lake basins and their age. In this study, we are compiling the first database of lake drainage ages covering lowland regions from northern Siberia, across Alaska to the Canadian Arctic.

METHODS

We cored drained lake basins and used radiocarbon dating of terrestrial peat that formed directly above lacustrine sediments. Specifically, we collected permafrost cores in 123 drained lake basins from Arctic Siberia, Alaska and Canada. After careful stratigraphic assessment, we subsampled the base of the uppermost peat (Figure 2) as the onset of terrestrial conditions after lake drainage.

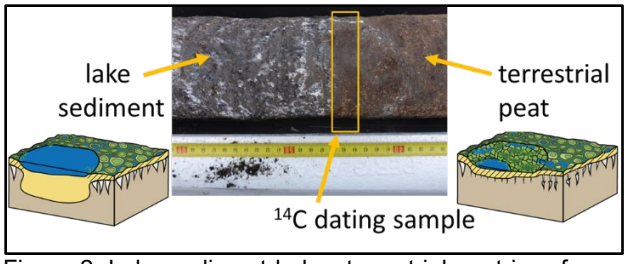

Figure 2. Lake sediment below terrestrial peat in a frozen sediment core retrieved from a drained lake basin.

We assessed the quality of the dates and the stratigraphic, sedimentologic or biogeochemical identification of drainage events for each basin, including published drainage ages. In this way we will provide a region-wide quantification of drained lake.

RESULTS AND DISCUSSION

We sampled and dated 123 dated basins (Figures 3 and 4), of which 89 are from North and West Alaska, 21 are from NW Canada and 13 are from the Lena Delta Region in NE Siberia. Additional dates from the literature are continuously being added.

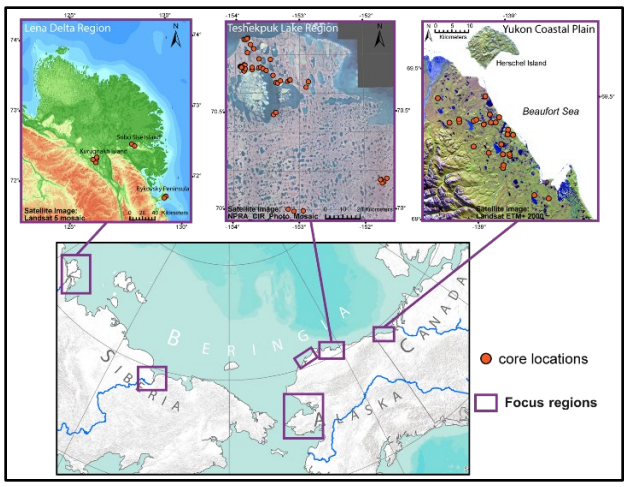

Figure 3: Study region and examples of core locations.

We found that nearly all basins drained during the Holocene, and >90 percent of our studied basins drained after 3000 BP (Figure 4). Remote sensing imagery showed recent increases in lake drainage (e.g., Nitze et al. 2018), which are not detectable using radiocarbon dating, and will complement our data.

Brosius et al. (2021) provided an extensive overview of age distributions for the formation of Arctic lakes. We are developing a database focused on lake drainage ages. This database can then be used to quantify carbon dynamics of drained lake basins in Arctic lowlands. For the first time, the regional spatial scale and the Holocene time scale will ensure representative information for this highly relevant and abundant permafrost landform.

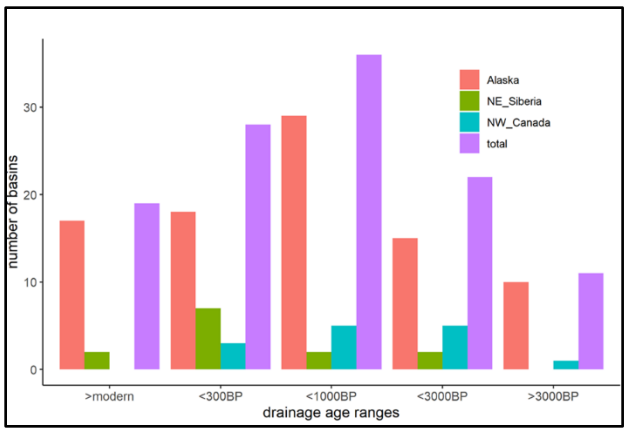

Figure 4. Drainage age distribution among the first 123 cores we verified for our database.

REFERENCES

Brosius, L.S., Walter Anthony, K.M., Treat, C.C., Lenz, J., Jones, M.C., Bret-Harte, M.S., and Grosse, G. 2021. Spatiotemporal patterns of northern lake formation since the Last Glacial Maximum, Quaternary Science Reviews, 253: 106773. doi:10.1016/j.quascirev.2020.106773

Jones, B.M., Grosse, G., Farquharson, L.M., Roy-Léveillée, P., Veremeeva, A., Kanevskiy, M.Z., Gaglioti, B.V., Breen, A.L., Parsekian, A.D., Ulrich, M., and Hinkel, K.M. 2022. Lake and drained lake basin systems in lowland permafrost regions, Nature Reviews Earth and Environment, 3: 85–98. doi:10.1038/s43017-021-00238-9

Nitze, I., Grosse, G., Jones, B.M., Romanovsky, V.E., and Boike, J. 2018. Remote sensing quantifies widespread abundance of permafrost region disturbances across the Arctic and Subarctic, Nature Communications 9: 5423. doi:10.1038/s41467-018-07663-3

Permafrost Hydrology & Wetland Dynamics

6D — The Hydrology of Mountain Permafrost

Session Chairs: Bastien Charonnat[1], Eole Valence[2] & Michel Baraer[1]

[1]Hydrology, Climate and Climate Change, École de technologie supérieure, Montréal, Québec, Canada
[2]Department of Earth and Planetary Science, McGill University, Montréal, Québec, Canada

Permafrost is a critical component of the cryosphere, affecting mountain hydrology and alpine ecosystems. The accelerating permafrost degradation observed in alpine regions raises concerns about potential consequences for downstream water resources. This session aims to bring together researchers and practitioners from diverse fields to discuss the implications of mountain permafrost thaw for mountain water budgets, hydrological processes, and downstream water resources.

The session will cover a range of topics related to the hydrological behaviour and significance of alpine permafrost, the connections of mountain permafrost to surface waters and groundwater, and potential risks associated with mountain permafrost degradation on water resources and downstream communities. The session will cover the different mountain permafrost features such as rock glaciers, periglacial talus, ice-cored moraines, thermokarst, and frozen rock walls.

We invite presentations focusing on field-based studies, modelling and practical applications at both local and global scales. The session will provide an opportunity for participants to exchange ideas, share knowledge and expertise, and discuss challenges and opportunities related to permafrost research. We particularly encourage submissions from early-career researchers and practitioners, and those working in interdisciplinary fields that intersect with permafrost research. The session will foster collaborations and partnerships among participants from diverse backgrounds and identify research priorities and opportunities for future research in the alpine environment.

Rock glaciers are shaping the subsurface drainage of proglacial areas

Bastien Charonnat[1,2,3], Michel Baraer[1,2,3], Janie Masse-Dufresne[1,2,3], Eole Valence[2,4], Jeffrey McKenzie[2,4], Chloé Monty[5], Kaiyuan Wang[6] & Elise Devoie[7]

[1]*Hydrology, Climate and Climate Change laboratory, École de technologie supérieure (ÉTS), Montréal, Québec, Canada*

[2]*GEOTOP (Research Centre on the Dynamics of the Earth System), Montréal, Québec, Canada*

[3]*CentrEau (Quebec Research Water Centre), Québec City, Québec, Canada*

[4]*Department of Earth and Planetary Science, McGill University, Montréal, Québec, Canada*

[5]*Department of Earth Sciences, University College London, London, United Kingdom*

[6]*Department of Earth, Environmental & Planetary Sciences, Brown University, Providence, Rhode Island, United States*

[7]*Civil Engineering Department, Queen's University, Kingston, Ontario, Canada*

The deglaciation of high mountain ranges is leading to the expansion of proglacial areas. Proglacial margins encompass diverse permafrost and ground ice landforms, as glaciers transition to ice-debris complexes and rock glaciers (Harrison et al. 2021). Although they have been traditionally overlooked in mountain hydrology studies, permafrost and ground ice features, including rock glaciers, exert an increased influence on the hydrology and hydrogeology of mountain ranges (Arenson et al. 2022; Harrison et al. 2021), especially in dry climates (Buckel et al. 2022) and in the post-peak water phase of deglaciation (Brighenti et al. 2019).

Rock glaciers are likely to be interconnected with other debris features in a valley system, due to high flow transmissivity in their unfrozen superficial, intra- or sub-permafrost debris layer (Navarro et al. 2023). Therefore, they play a short-term storage and release function in the drainage of alpine valley systems, either towards downstream surface waters, or towards the groundwater system (Bearzot et al. 2023; Reato et al. 2022; Jones et al. 2021; Harrison et al. 2021; Wagner et al. 2020; Falatkova et al. 2020). They can also act as a dam to surface waters, forming ponds (Colombo et al. 2020). However, their role in a proglacial valley system remains poorly documented, especially their control and redistribution of groundwater recharge from glacial meltwater. This study addresses this knowledge gap by investigating how rock glaciers redistribute glacial meltwater in a study catchment.

Shar Shäw Tágà (Grizzly Creek) is a subarctic glacial catchment located in the Kluane National Park and Reserve, St. Elias Mountains (Yukon, Canada), that is experiencing significant glacial retreat. The Shar Shäw Tágà creek is edged by non-relict rock glaciers (Evin et al. 1997). One of them is located at the outlet of a glacial sub-catchment but its front only displays a few springs with minimal discharge. These minor springs contrast notably with the substantial discharge observed at higher elevations above the rock glacier.

The use of dye being proscribed within the national park limits, we based our approach on the analysis of natural tracers and flow monitoring. Water level, water temperature and electrical conductivity variables were monitored in identified springs throughout the summer of 2022. Compared with meteorological data through wavelet coherence analysis, they enable the determination of the springs' origins and drivers of flow variability. Additionally, multiple sampling campaigns were conducted in the summers of 2022 and 2023 to analyze major ions concentrations (Na^+, Ca^{2+}, Mg^{2+} and SO_4^{2-}) and water stable isotopes ($\delta^{18}O$ and δ^2H) signatures in the catchment's streams (Figure 1). These sampling campaigns have been conducted during various hydrological periods in the catchment: 1) in June 2022 at the snowmelt onset; 2) in August 2022 at the end of the summer season, at the peak of glacial ablation; 3) in June 2023 after the snowmelt peak but before the start of glacial ablation as the glaciers were still covered with snow.

The results indicate that the rock glacier serves as a critical obstacle and deflector to subsurface glacial meltwater. Indeed, glacial meltwater originating from the sub-catchment is forced to infiltrate deeper into the subsurface above the rock glacier or flow around it but cannot be found flowing out at the front of the rock glacier. Inversely, lateral subsurface flow coming from Shar Shäw Tágà creek is redirected to resurge at the front of the rock glacier, forcing part of the alluvial floodplain shallow aquifer to reach the surface. This deflector function is likely to be related to the ice-rich basal layer of the rock glacier, as suggested by the cold temperatures of the resurgences at its front. This deflector function might therefore not be permanent in a permafrost degradation context. Other studies would be of interest to determine if a proglacial hydrogeological system will inherit the alternative flow pathways formed by its rock glaciers before they entered their relict phase.

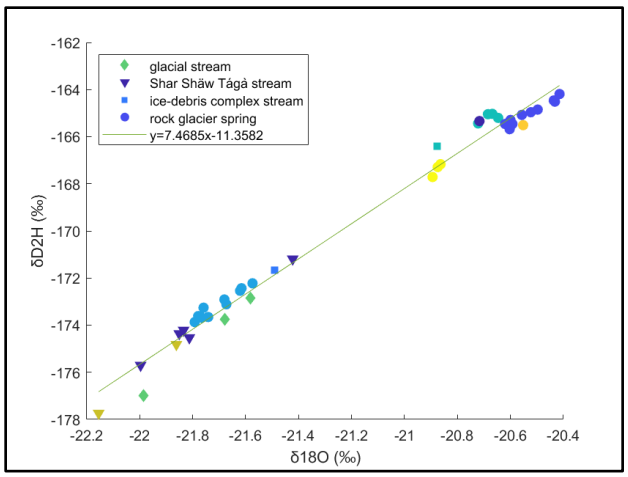

Figure 1. Isotopic ratios for August 2022 samples.

This study highlights the role of rock glaciers as critical deflectors for shallow subsurface flow in proglacial valley systems. By impeding subsurface flow, they can strengthen alternative pathways for glacial meltwater flow toward deep aquifers or lowlands' surface waters. While rock glaciers are often considered as potential water reservoirs, such findings nuance the ability of rock glaciers to store and release glacial meltwater, as they can deflect shallow subsurface flow. The study shows that rock glaciers can force infiltration and resurgence of water at specific locations, affecting the broader mountain hydrogeological system. Furthermore, it highlights their complex and critical role in the future of water resources supplied by high mountain ranges while glaciers are retreating.

REFERENCES

Arenson, L.U., Harrington, J.S., Koenig, C.E.M., and Wainstein, P.A. 2022. Mountain Permafrost Hydrology—A Practical Review Following Studies from the Andes. Geosciences 12, 48. https://doi.org/10.3390/geosciences12020048

Bearzot, F., Colombo, N., Cremonese, E., di Cella, U.M., Drigo, E., Caschetto, M., Basiricò, S., Crosta, G.B., Frattini, P., Freppaz, M., Pogliotti, P., Salerno, F., Brunier, A., and Rossini, M. 2023. Hydrological, thermal and chemical influence of an intact rock glacier discharge on mountain stream water. Science of The Total Environment 876, 162777. https://doi.org/10.1016/j.scitotenv.2023.162777

Brighenti, S., Tolotti, M., Bruno, M.C., Engel, M., Wharton, G., Cerasino, L., Mair, V., and Bertoldi, W. 2019. After the peak water: the increasing influence of rock glaciers on alpine river systems. Hydrological Processes 33, 2804–2823. https://doi.org/10.1002/hyp.13533

Buckel, J., Reinosch, E., Voigtländer, A., Dietze, M., Bücker, M., Krebs, N., Schroeckh, R., Mäusbacher, R., and Hördt, A. 2022. Rock Glacier Characteristics Under Semiarid Climate Conditions in the Western Nyainqêntanglha Range, Tibetan Plateau. Journal of Geophysical Research: Earth Surface 127, e2021JF006256. https://doi.org/10.1029/2021JF006256

Colombo, N., Ferronato, C., Vittori Antisari, L., Marziali, L., Salerno, F., Fratianni, S., D'Amico, M.E., Ribolini, A., Godone, D., Sartini, S., Paro, L., Morra di Cella, U., Freppaz, M., 2020. A rock-glacier – pond system (NW Italian Alps): Soil and sediment properties, geochemistry, and trace-metal bioavailability. CATENA 194, 104700. https://doi.org/10.1016/j.catena.2020.104700

Evin, M., Fabre, D., and Johnson, P.G. 1997. Electrical Resistivity Measurements on the Rock Glaciers of Grizzly Creek, St Elias Mountains, Yukon. Permafrost and Periglacial Processes 8, 11.

Falatkova, K., Šobr, M., Slavík, M., Bruthans, J., and Janský, B. 2020. Hydrological characterization and connectivity of proglacial lakes to a stream, Adygine ice-debris complex, northern Tien Shan. Hydrological Sciences Journal 65, 610–623. https://doi.org/10.1080/02626667.2020.1711913

Harrison, S., Jones, D., Anderson, K., Shannon, S., and Betts, R.A. 2021. Is ice in the Himalayas more resilient to climate change than we thought? Geografiska Annaler, Series A: Physical Geography 103, 1–7. https://doi.org/10.1080/04353676.2021.1888202

Jones, D.B., Harrison, S., and Anderson, K. 2019. Mountain glacier-to-rock glacier transition. Global and Planetary Change 181. https://doi.org/10.1016/j.gloplacha.2019.102999

Navarro, G., Valois, R., MacDonell, S., de Pasquale, G., and Díaz, J.P. 2023. Internal structure and water routing of an ice-debris landform assemblage using multiple geophysical methods in the semiarid Andes. Frontiers in Earth Science 11. https://doi.org/10.3389/feart.2023.1102620

Reato, A., Borzi, G., Martínez, O.A., and Carol, E. 2022. Role of rock glaciers and other high-altitude depositional units in the hydrology of the mountain watersheds of the Northern Patagonian Andes. Science of The Total Environment 824, 153968. https://doi.org/10.1016/j.scitotenv.2022.153968

Wagner, T., Brodacz, A., Krainer, K., and Winkler, G. 2020. Active rock glaciers as shallow groundwater reservoirs, Austrian Alps. Grundwasser - Zeitschrift der Fachsektion Hydrogeologie 25, 215–230. https://doi.org/10.1007/s00767-020-00455-x

Spatial distribution of supra-permafrost groundwater in the Qinghai–Tibet Engineering Corridor using inversion models

Yu Gao[1,2], Mingtang Chai[3], Wei Ma[1,2] & Yutao Gao[3]

[1]*State Key Laboratory of Frozen Soils Engineering, Northwest Institute of Eco-Environment and Resources, Chinese Academy of Sciences, Lanzhou, China*

[2]*School of Engineering Science, University of Chinese Academy of Sciences, Beijing, China*

[3]*School of Civil and Hydraulic Engineering, Ningxia University, Yinchuan, China*

The construction of five major linear projects within the Qinghai-Tibet Engineering Corridor (QTEC) has been carried out in permafrost regions for many years. The operational performance and safety of these important infrastructures are directly related to the stability of the underlying frozen soil foundation. Supra-permafrost groundwater (SPG) is an important hydrogeological element in the permafrost area, and its seepage will significantly affect the thermal stability of permafrost. Therefore, the distribution of SPG in the QTEC is one of the key bases for the analysis of the hydrothermal mechanism, operational risk assessment and road structure design of related projects. However, due to the harsh natural conditions, complex formation mechanisms, and transport characteristics, on-site monitoring is extremely difficult. Currently, on-site monitoring studies mainly focus on single-point monitoring, which greatly limits the spatiotemporal scale and resolution accuracy of research on water on the frozen layer, making it difficult to obtain the distribution characteristics of SPG along the entire QTEC. At the same time, due to the uniqueness of the SPG, the changes in the permafrost environment caused by climate and environmental changes will impact on its migration and distribution. Therefore, there is an urgent need to explore new methods for analyzing the dynamic distribution of SPG at a large scale.

DATA AND METHODS

The QTEC is selected as 10 km wide on each side of the Qinghai-Tibet Highway, with a total width of 20 km. The remote sensing data from the July to September, 2019 Landsat8 OLI images with strip numbers 136/035, 137/035, 137/036, 137/038, 138/037, 138/038, and 138/039. Soil moisture content (SMC) and SPG depth data were collected or read from 12 sampling plots.

The temperature vegetation dryness index (TVDI) inversion method is a soil moisture inversion model based on normalized difference vegetation index and land surface temperature. The remote sensing model for groundwater table distribution (RSMGTD) combines remote sensing techniques and hydrogeologic principles, can used to invert the spatial distribution of groundwater level (Figure 1).

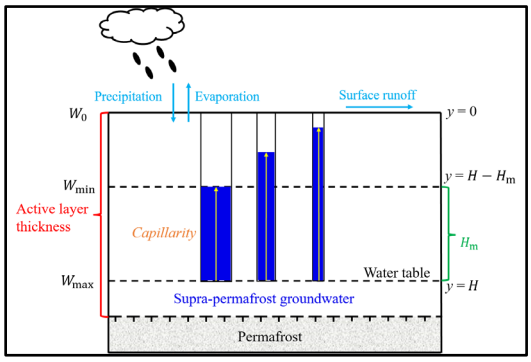

Figure 1. Diagram summarizing the remote sensing model of groundwater table distribution.

SPATIAL DISTRIBUTION OF SMC AND SPG

The simulated SMC based on image-derived TVDI values was classified into five categories: 0–10%, 10%–20%, 20%–30%, 30%–40%, and 40%–50%, accounted for 0.13%, 9.06%, 60.27%, 30.10%, and 0.44% of the entire corridor, respectively (Figure 2). The QTEC areas where SPG was detected at depths <0.5, 0.5–0.8, 0.8–1.0, and 1–1.2 m accounted for 22.48%, 53.73%, 18.25%, and 5.53%, respectively (Figure 3). The average accuracies of the SMC and SPG inversion were 84.77% and 81.42%, respectively.

UNCERTAINTY

The uncertainty of the results mainly comes from two aspects. Firstly, the measured SPG depth fluctuated within a range, whereas the simulated SPG depth was a specific value; hence, there was a certain deviation between the simulated and measured values. Secondly, this study assumes that continuous permafrost exists along the QTEC. However, due to permafrost degradation over multiple years, talik may occur in certain sections of the QTEC. In the talik zone, the SPG flows downward, and the SMC in the active layer is lower than that in the continuous permafrost zone.

Since this study is an exploratory attempt to use a new method to explore the distribution of SPG, some factors that may affect the development of SPG have been simplified, which makes the results have a certain degree of error.

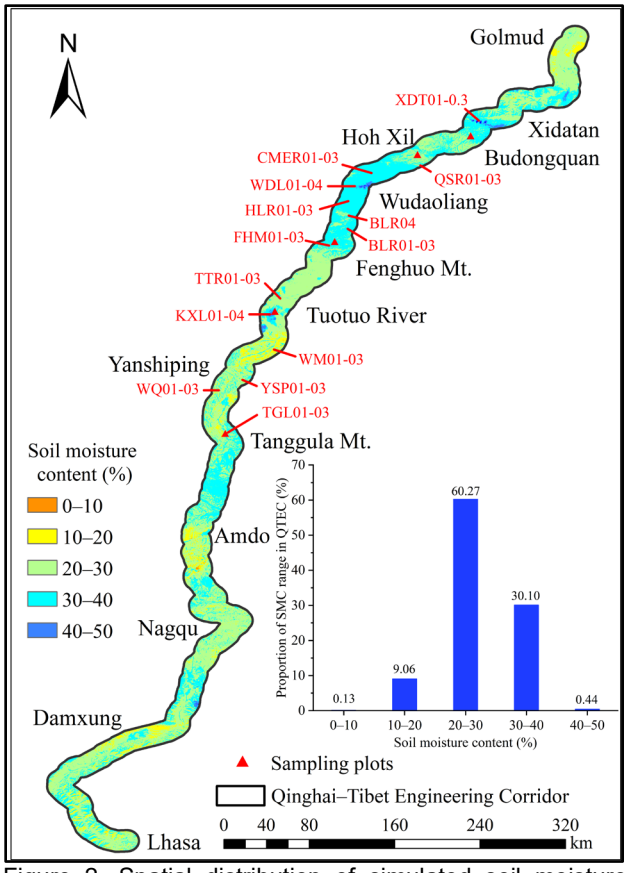

Figure 2. Spatial distribution of simulated soil moisture content in the Qinghai–Tibet Engineering Corridor from Golmud to Lhasa.

CONCLUSIONS

The results of this study are a preliminary exploration of the spatial distribution of SPG at large scales with 30 m resolution, which is a guide on further targeted verification of whether a certain area is endowed with SPG. The results showed an improved spatial resolution of SPG distribution, however, since this study is an exploratory attempt to the distribution of SPG using a new method, some simplification has been done in the assumptions of the model. With the support of more on-site monitoring data in the future, and the continuous correction and improvement of the model, its accuracy and reliability will be greatly improved, which will provide support for the dynamic analysis of the distribution of SPG on a large scale in the permafrost area.

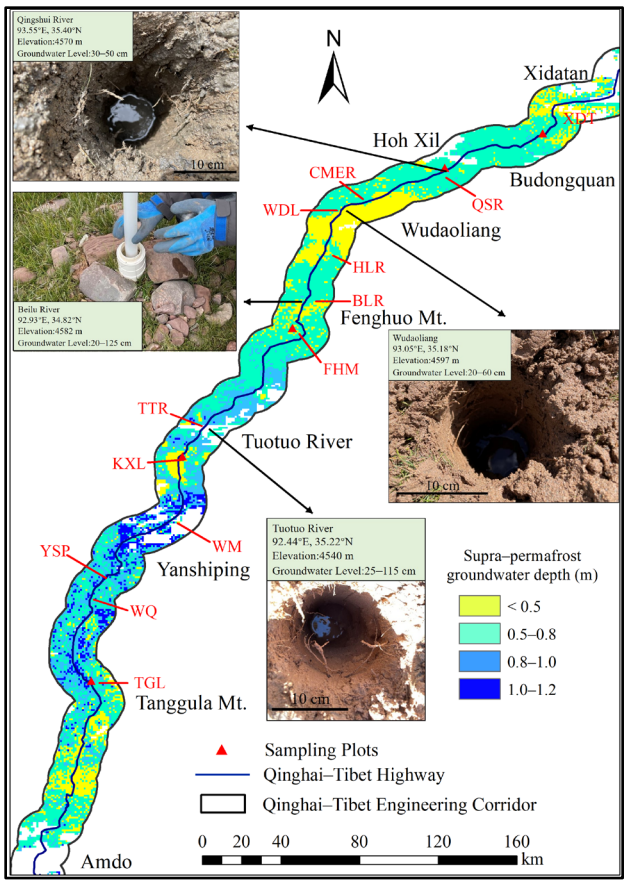

Figure 3. Spatial distribution of supra–permafrost groundwater (SPG) of the Qinghai–Tibet Engineering Corridor from Golmud to Lhasa in the season of thawing active layers.

COPYRIGHTED STATEMENT

These findings were previously published in Advances in Climate Change Research. Further details are provided below: Gao Y., Chai M.T., Ma W., Gao Y.T. 2023. Spatial distribution of supra-permafrost groundwater in the Qinghai-Tibet Engineering Corridor using inversion models. Advances in Climate Change Research.

Disentangling the influence of seasonality and discharge on solute export in permafrost underlain streams

Arsh Grewal & Sean K. Carey
School of Earth, Environment, and Society, McMaster University, Hamilton, Ontario, Canada

Seasonality is an important driver of runoff and solute export processes in cold mountain catchment regions. Seasonal freeze-thaw of the active layer can greatly alter runoff processes in cold regions. During spring, infiltration of relatively large volumes of snow melt water is restricted to the organic rich layer, leading to greater export of DOM and discharge. As the thaw front moves down into the deeper mineral layers and the amount of water in the catchment (and by extension discharge) decreases, the stream concentration of weathering derived solutes increases and the stream concentration of DOM decreases (Carey 2003). Additionally, discharge can also drive solute concentrations, as high flows can reflect soil chemistry of the shallow soil layers and low flows can reflect chemistry of deeper soil layers (Stewart et al. 2022). The influence of seasonal freeze-thaw and discharge on stream chemistry has not been disentangled in permafrost underlain catchments.

Research Questions

Do frost table dynamics drive stream concentrations in permafrost underlain catchments at seasonal scales and can this be quantified via CQ relationships?

How do catchment characteristics influence CQ relationships in permafrost underlain systems?

Study Area and Data Collection

We collected chemistry and discharge data at ten catchments with distinct land covers and areas ranging from 169 km^2 to 5 km^2. We collected specific conductance (SpC), Ca, Mg, Sulphate, and dissolved organic carbon (DOC) at all catchments over a range of seasons and flow conditions. Due to the vast distances between the catchments, sampling frequency and period varied significantly. Four of the catchments are located in Wolf Creek Research Basin (WCRB), just outside of Whitehorse, YT in Kwanlin Dün Territory. WCRB has a large elevational gradient with coniferous forest cover in the lowlands and tundra vegetation in the uplands. The WCRB outlet (WCO) and Coal Lake (CL) subcatchment are relatively large catchments underlain with sporadic permafrost. Buckbrush Ck (BB) and Granger Ck (GC) are smaller alpine subcatchments of WCRB and are underlain with discontinuous permafrost. Six of our study catchments are part of the Tombstone Waters Observatory (TWO) located within Tr'ondëk Hwëch'in territory. These headwater catchments are underlain with continuous and discontinuous permafrost and the outlet of these catchments can be found along the Dempster Highway in Yukon Territory. The catchments are named after the kilometer marker where the stream intersects with the highway. Km 44 (Yin-Yang) and Km 71 (Blackshale Ck) are the most mountainous catchments, Km 99 (Slavin Ck) and Km 104 are relatively flat and overlain with primarily shrubs and tundra vegetation, Km 175 and Km 185 have moderate slopes and are primarily composed of landcover consisting of forests and shrubs.

Methods

The relationship between stream concentrations and discharge is often defined by a power-law relationship (Equation 1; Godsey et al. 2009). Where C is solute concentration, Q is discharge, and a and b are constant parameters. Taking the log of all terms in the relationship allows for the fitting of a linear model (Equation 2). Where the log-log slope (b) can describe the relationship of a particular solute with flow. A positive slope indicates that a solute is transport-limited (flushing), where rising water tables during high flows lead to increased connection between the solute and the stream facilitating lateral transport. A negative slope indicates that a solute is source-limited (dilution), where a particular solute is diluted during high flows. The direction of the slope has shown to be associated with soil profile chemistry, where high flows reflect soil chemistry of the upper soil layers, and low flows reflect the chemistry of the deeper mineral layers (Stewart et al. 2022).

To disentangle the role of discharge and seasonality on stream concentrations we utilize generalized additive models (GAMs). GAMs allow you to add additional terms which can be linear or fit via a spline. The influence of a term on a model can be assessed through partial effect plots and significance values. We add a spline term to the traditional CQ model to assess the effect of DOY on CQ relationships (Equation 3). We also utilize the ratio of coefficient of variation of solute concentrations and discharge (CV_C/CV_Q), which can indicate whether or not a solute

is chemostatic or chemodynamic even when the log-log slopes are close to 0 (Thompson et al. 2011).

$$C = aQ^b \quad [1]$$

$$\log(C) = b\log(Q) + \log(a) \quad [2]$$

$$\log(C) = b\log(Q) + \log(a) + s(\log(DOY)) \quad [3]$$

Results and Discussion

Log-log slopes from the GAM models were generally negative for weathering derived ions and positive for DOC (Figure 1). CV ratios were the highest for DOC, particularly for Km 44 and Km 71, the two most mountainous catchments. The relatively low log-log slopes for DOC at some sites and high CV ratios indicate chemodynamic behaviour via processes other than discharge for DOC.

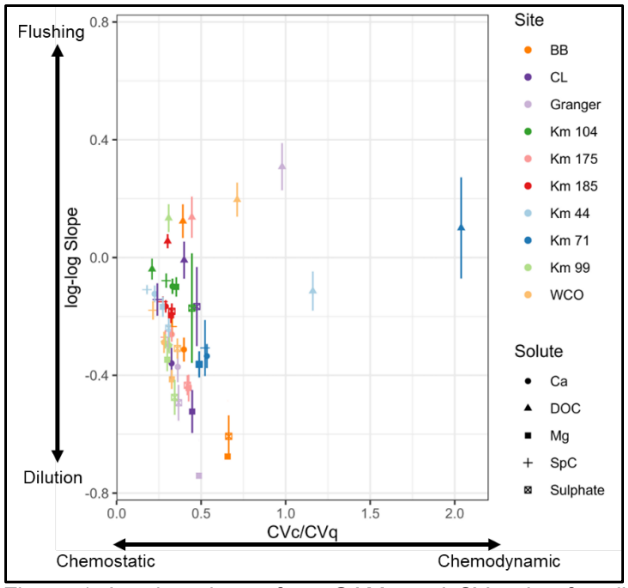

Figure 1. Log-log slopes from GAMs and CV ratios for all solutes and study sites. Vertical line represents the standard error of the slope.

All solutes showed significant seasonality for CQ relationships for most sites (Figure 2). Weathering ions generally increased from Spring to Fall irrespective of flow. DOC generally decreased from Spring to Fall. This seasonal effect can be explained by the thickening of the active layer, where water flows through deeper mineral soils as the thaw front descends. Seasonality was the highest for DOC, particularly for the two mountainous catchments (Km 44 and Km 71). However, log-log slopes which were close to zero for these catchments indicate a homogenous soil profile in terms of organic matter, thus seasonality in DOC is likely driven by processes other than changing flow pathways. The two mountainous catchments had the highest median specific discharge, which may have lead to increased flushing of organic matter from soils leading to decreases in mobile organic carbon pools in the soil profile. This process may be less important in low flow catchments. For example Km 104 has a very low median specific discharge, a log-log slope close to zero but no seasonality in DOC concentrations. This suggests that DOC pools remain equally transport limited throughout the Spring-Fall transition in Km 104.

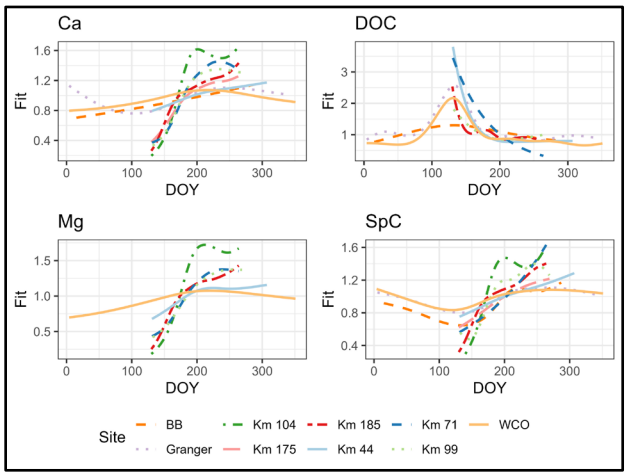

Figure 2. Partial effect plots for DOY term. The y-axis represents the s(DOY) term in $C = s(DOY)aQ^b$ for a particular DOY. Only sites that showed significant seasonality were included (p-value <= 0.05).

References

Carey, S.K. 2003. Dissolved organic carbon fluxes in a discontinuous permafrost subarctic alpine catchment, Permafrost and Periglacial Processes, 14(2); 161–171. doi:10.1002/ppp.444

Godsey, S.E., Kirchner, J.W., and Clow, D.W. 2009. Concentration-discharge relationships reflect chemostatic characteristics of US catchments, Hydrological Processes, 23(13); 1844–1864. doi:10.1002/hyp.7315

Stewart, B., et al. 2022. Streams as Mirrors: Reading Subsurface Water Chemistry From Stream Chemistry, Water Resources Research, 58(1); 1–20. doi:10.1029/2021WR029931

Thompson, S.E., et al. 2011. Relative dominance of hydrologic versus biogeochemical factors on solute export across impact gradients, Water Resources Research, 47(7); 1–20. doi:10.1029/2010WR009605

A high-resolution distributed hydro-thermal coupled hydrological model for cold regions: development and evaluation

Linmao Guo, Genxun Wang, Chunlin Song & Shouqin Sun

State Key Laboratory of Hydraulic and Mountain River Engineering, College of Water Resource and Hydropower, Sichuan University, Chengdu 610065, China

Cold regions, where snow, ice, and frozen soils exert disproportionate significant controls on the hydrological cycle, are primarily distributed in high-altitude, high-latitude, and alpine areas, which provide critical water resources to billions of populations in Europe, Asia, and the Americas. The presence of frozen ground alters the regional thermal-moisture regimes and the movement, storage, and exchange of surface and subsurface water through the freezing-thawing cycles, posing challenges to the quantification and modeling of hydrological processes in cold regions. Researchers have endeavored to integrate empirical hydro-thermal functions into hydrological models to depict the influence of frozen soil on the hydrological processes. These improvements have to some extent enhanced the accuracy of streamflow simulation but cannot represent the mutual feedback of soil water and heat transport processes, resulting in certain limitations in investigating the interactions between permafrost degradation and hydrological processes under climate change.

Here, we have developed a distributed hydro-thermal coupled hydrological model for cold regions (DHTC, Figure 1), the DHTC model fully coupled the moisture-heat transport processes by employing the conduction-advection heat transport equation and Richard equation with the consideration of ice-water phase change. The impact of soil freezing-thawing cycles is considered throughout the infiltration, evapotranspiration, and soil water and heat transport processes. In addition, the DHTC model considers the effect of organic matter on the soil thermal and hydraulic parameters including soil porosity, hydraulic conductivity, thermal conductivity, and heat capacity. Furthermore, a subpermafrost groundwater module is introduced to estimate cold season discharge sustained by subpermafrost groundwater. In addition, the incorporation of cluster and fuzzy membership algorithms has enabled the DHTC model to accurately simulate high-resolution permafrost thermal regimes while conserving computational resources (Figure 2).

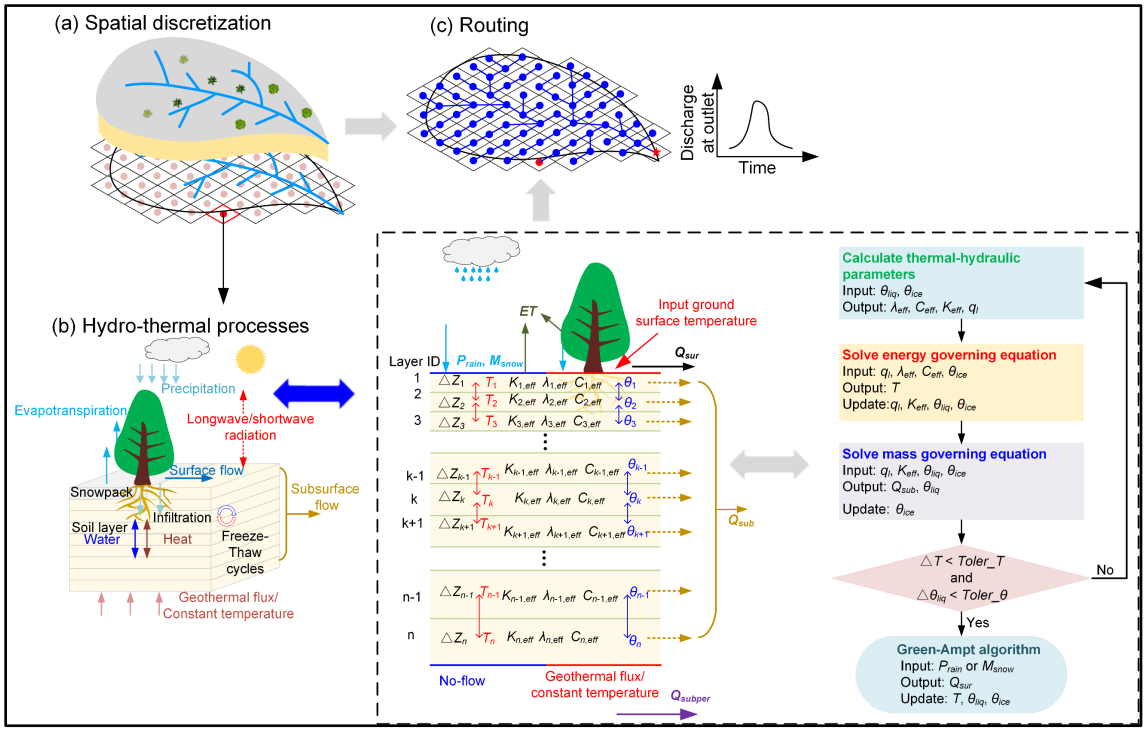

Figure 1. The Overall structure of the DHTC model.

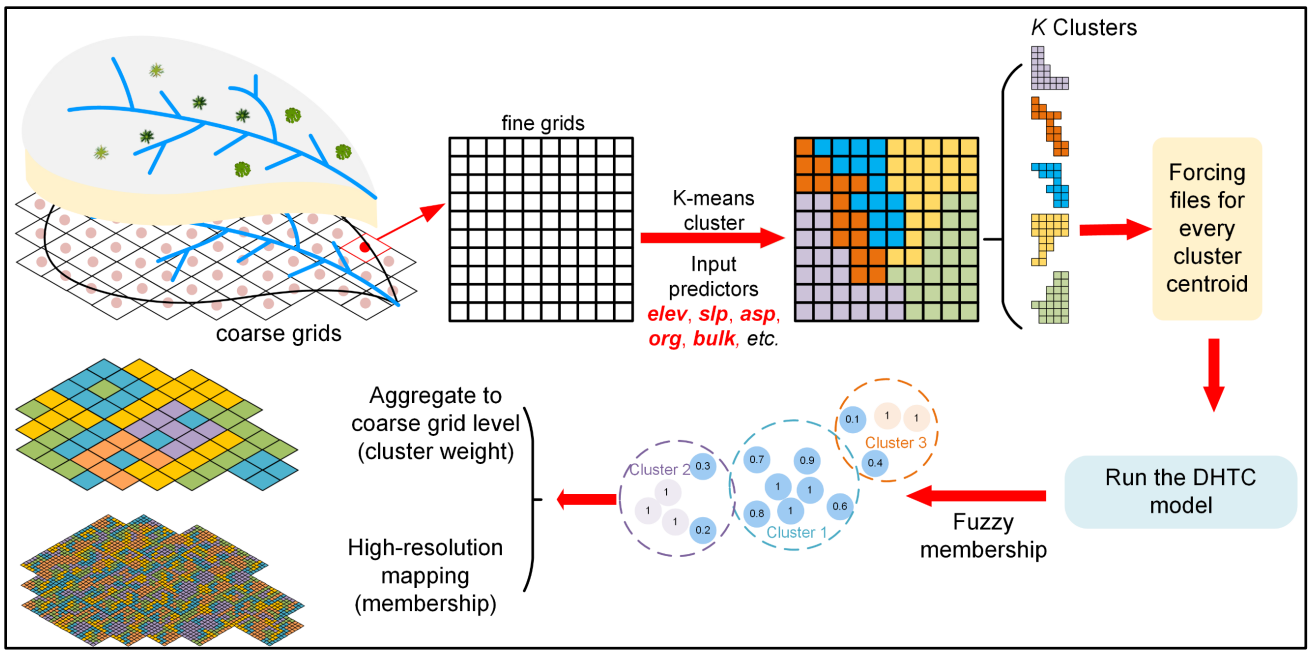

Figure 2. Flowchart of the high-resolution mapping of hydro-thermal regimes of the DHTC model.

A comprehensive evaluation of the hydrothermal process simulation performance of the DHTC model is conducted. At the point scale, the DHTC model accurately reproduces daily soil temperature (R^2=0.98, RMSE = 0.61 ℃) and moisture (R^2=0.87, RMSE = 0.03 $m^3 \cdot m^{-3}$) dynamics. At the basin scale, for the monthly evapotranspiration simulation, the DHTC model (R^2=0.90, RMSE = 15.7 mm) outperformed the GLDAS/Noah, GLDAS/VIC, and PML-V2 models in the Source Regions of Yangtze River (SRYR). The DHTC model reasonably simulated streamflow on the daily, monthly, and multi-year monthly scale in the SRYR with the NSE of 0.67, 0.85, and 0.97 and the KGE of 0.83, 0.90, and 0.93, respectively. The model also successfully reproduced the snow depth in basin-averaged time series and spatial distributions (RMSE =0.86 cm). The DHTC model is a robust tool to investigate the responses of frozen ground thermal-moisture regimes and hydrological processes under climate change.

Modelling permafrost thaw in the central Andes (27°S-34°S)

Cassandra E.M. Koenig[1,2], Christin Hilbich[1], Christian Hauck[1], Lukas U. Arenson[3] & Pablo Wainstein[4]

[1]*Department of Geosciences, University of Fribourg, Fribourg, Switzerland*

[2]*BGC Engineering Inc., Toronto, Ontario, Canada*

[3]*BGC Engineering Inc., Vancouver, British Columbia, Canada*

[4]*BGC Engineering Inc., Calgary, Alberta, Canada*

Hydrological dynamics of the mountain cryosphere are shifting from being controlled by glacial to periglacial processes due to climate change (e.g., Arenson et al. 2022). Altered flow contributions from glacial melt and changes in atmospheric processes collectively influence subsurface thermal and hydrologic regimes via non-linear heat and water transfer feedbacks. Impacts may manifest as altered water flow paths with the degradation of a permafrost aquiclude, or as shifts in runoff and infiltration dynamics with a thickening active layer or supra-permafrost talik formation. Water stored in permafrost may also be affected by changes to recharge and discharge patterns and quantities, or through the release of water from melting ground-ice. In the arid Andes, ongoing degradation of permafrost under climate warming has raised much interest among industry professionals, permafrost researchers and regulators alike. Hydrological implications are of particular interest given rising concerns about water security in the region. Towards understanding the processes controlling permafrost degradation and the associated release of water from ground-ice, the authors previously developed a numerical cryo-hydrogeological model of an ice-rich rock glacier located in the Argentinian Andes (Koenig et. al 2023). Preliminary simulations of the ground thermal and flow regimes illustrated permafrost degradation with melting and draining of ground-ice under existing climatic conditions. In the current submission, the dynamics of simulated supra- and sub-permafrost flow are presented in greater detail.

Conceptual and Numerical Models

The conceptual site model forming the basis of numerical simulations is shown in Figure 1. This includes an ice-rich rock glacier situated on a bedrock slope at a high-altitude site in Argentina. The site is within an extremely arid region, with monthly air temperatures ranging from approximately -10 °C to 15 °C, depending on the season. Permafrost is in a natural state of degradation (i.e., MAAT >0 °C across the site) and progressive melting of ground-ice may contribute to supra- and sub-permafrost flow. This may discharge to the ground surface, depending on local conditions. The base of the rock glacier is subject to regional geothermal heat fluxes and the groundwater table is >200 m deep.

The 2D numerical model, constructed in TEMP/W-SEEP/W (GEOSLOPE 2022), is a 1,600 m-long cross-section through the rock glacier. The model was developed using site-specific topo-climatic and geologic data, and was calibrated to site ground temperatures and borehole temperature gradients. A 25-year simulation was run assuming 100% initial ice-saturation within the rock glacier (conservative assumption) and a temperature-depth profile consistent with borehole temperature data. Surface boundary conditions were derived from local monitoring data and represent current conditions (i.e., without warming). Constitutive relationships that consider conductive and advective heat transport, latent heat, unsaturated water flow, and restricted water flow for ground temperatures ≤0 °C were employed in the simulation.

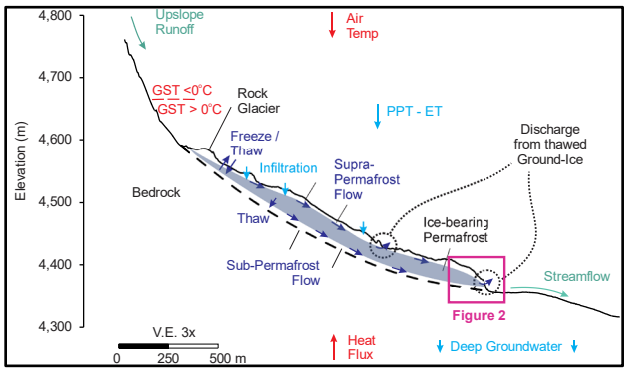

Figure 1. Conceptual Site Model.

Results

Figure 2 depicts simulated groundwater flow and temperature for a 250 m sub-section of the model. Results are shown for 23.5 and 24 years of simulation, illustrating the austral summer (January) and winter (July), respectively. Arrowheads depict flow direction, while the black-white colour legend indicates flow magnitude. Figure 3 illustrates simulated supra- and sub-permafrost flow for modelling years 20 to 25 alongside surface boundary conditions (ground surface temperature, (GST) and potential recharge, (Pot. Rch.)).

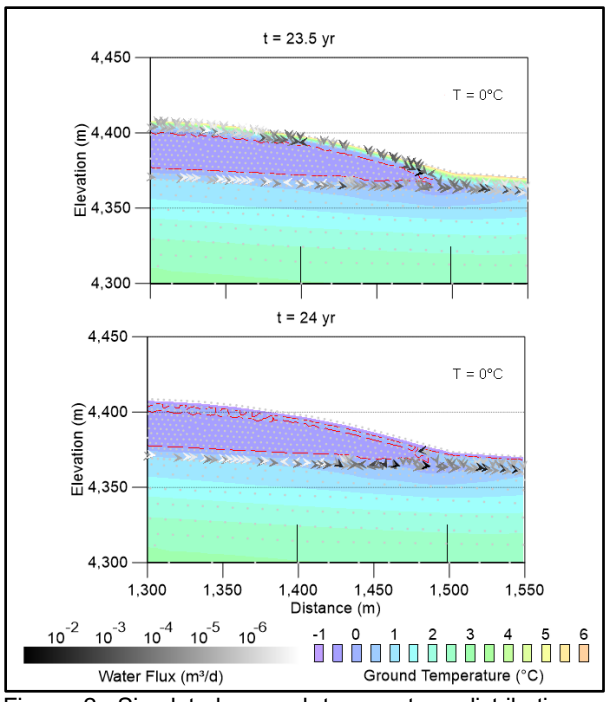

Figure 2. Simulated ground temperature distribution and groundwater flux vectors.

The figures clearly illustrate the model's projection of seasonal flow and temperature patterns. Supra-permafrost flow occurs during the summer (when shallow ground temperatures are >0 °C), whereas sub-permafrost flow occurs year-round. Modelled supra-permafrost water fluxes range from zero flow (<1x10^{-9} m^3/day) to 5 m^3/day with the freezing and thawing of the active layer, while sub-permafrost water flux remains constant at around 0.2 m^3/day. Although neither are significant contributors to the overall water balance, (i.e., neighboring streamflows reach up to 1.3x10^4 m^3/day or 155 L/s), notably higher water fluxes are projected in the supra-permafrost zone than in the sub-permafrost zone. This is partially attributed to greater contributions from melting ground-ice in the supra-permafrost zone, triggered by heat fluxes induced by surface temperatures that reach up to 15 °C each year. Surface infiltration (indicated by the downward arrowheads in Figure 2) also adds water to the supra-permafrost zone. Conversely, water flowing through the sub-permafrost zone originates mostly from melting ground-ice at the base of the rock glacier, where seasonal temperature influences are minimal. This flow is governed mainly by conductive heat fluxes induced by the simulated temperature gradient between the rock glacier and underlying bedrock and is limited by the ice-content assigned within the model domain. However, this is an assumption specific to the 2D model transect; in reality, sub-permafrost flow might also result from 3D surficial and lateral infiltration from adjacent slopes.

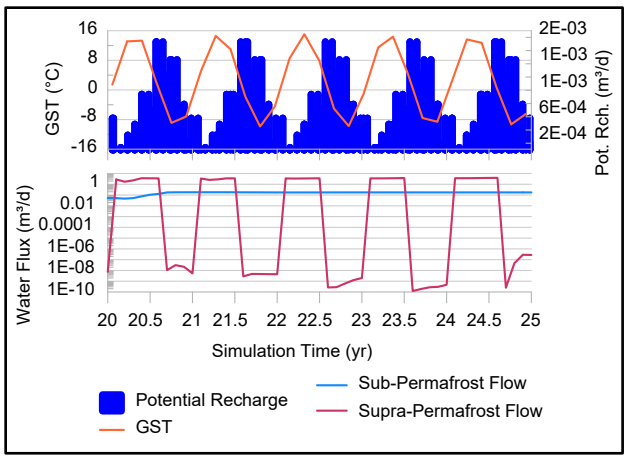

Figure 3. (Top) Surface boundary conditions and (Bottom) simulated supra- and sub-permafrost flow for years 20-25 at 1,400 m along section.

SUMMARY

A numerical cryo-hydrogeological model was used to depict seasonal temperature and flow variations within an ice-rich rock glacier. Supra-permafrost flow was shown to be controlled by seasonal climate variability and sourced from melting of ground-ice and potential recharge. In contrast, modelled sub-permafrost flow was derived from melting ground-ice governed by temperature gradients between the rock glacier and underlying bedrock, and occurs mostly independent from seasonal climate variations that affect supra-permafrost flow.

REFERENCES

Arenson, L.U., Harrington, J.S., Koenig, C.E.M., and Wainstein, P.A. 2022. Mountain Permafrost Hydrology-A Practical Review Following Studies from the Andes. Geosciences, 12(2): 48 pp.

GEOSLOPE International Ltd. 2022. Heat and mass transfer modeling with GeoStudio 2021 (Second Edition). Calgary, Alberta, Canada.

Koenig, C.E.M., Hilbich, C., Hauck, C., Wainstein, P., Pastore, S., and Arenson, L.U. 2023. Modelling Ground-Ice Degradation within a Rock Glacier in Central Argentina. 6th European Conference on Permafrost, Puigcerdà, Catalonia, Spain, 18-22 June 2023.

Permafrost investigations and hydrochemical characteristics of permafrost-influenced surface waters in the Western Pamir

Jan Lentschke[1], Martin Fleischner[1], Sergey Marchenko[2] & Djamshed Abdudhukurov[3]

[1]*Department of Geography, Humboldt-Universität zu Berlin, Berlin, Germany*

[2]*Geophysical Institute, University of Alaska Fairbanks, Fairbanks, Alaska, United States*

[3]*Djamshed Abdudhukurov, Institute of Water Problem, Hydropower and Ecology, Academy of Sciences of Republic of Tajikistan, Dushanbe, Republic of Tajikistan*

The mountainous region of the Western Pamirs reaches up to more than 7,000 m asl, and glaciation partly reaches down to 2,600 m asl. Many large rock glaciers also indicate the existence of permafrost. Some of the valleys draining to the Panj are relatively populated despite harsh climatic conditions in winter.

Only a few permafrost studies are available for the Pamirs. The first permafrost campaigns in the Pamirs were carried out in the 1970s by the Kazakh Permafrost Laboratory in the basins of Lake Karakul, Lake Rangkul and Lake Shorkul. Since 2022, permafrost studies have been taken place in the Eastern Pamir as part of the PAMIR research project of the Swiss Polar Institute Flagship Initiative.

This paper presents the first results of the electrical resistivity tomography measurements for permafrost detection and modelling approaches of permafrost occurrence in the Vanj valley and the hydrochemical characteristics of the river Vanj and its tributaries. The Vanj valley is one of three example valleys for the Western Pamir.

The Vanj river is located in the Western Pamir and drains over a length of approx. 100 km in a south-westerly direction into the Panj. The catchment area is delimitated by the Darvaz range to the north, the Vanj range to the south and the Academy of Sciences range to the east and encompasses surfaces between 1 600 m asl and a maximum of 5 992 m asl. In the Vanj valley live more than 26 000 people. Summers are dry and warm and allow intensive land use based on efficient irrigation systems up to 2 300 m asl: potatoes, fruit, vegetables, cereals, walnuts and much more are grown beyond subsistence level and are sold to lowland markets and consumers outside Gorno-Badakhshan as well. Settlements and cultivated areas are concentrated on alluvial fans that protrude into the valley from north and south. A close relationship between people and the environment is evident in the smallest of spaces. Changes caused by climate change, in particular the melting of the cryosphere, may have a negative impact on water quality. In order to assess these potential effects, an initial investigatory field campaign regarding the hydrochemistry of the Vanj Valley was launched in the summer of 2023.

Methods and results

At five locations in the Langar valley – a southern tributary of the Vanj – with varying altitudes, surface orientation and slope degree (inclination) ERT measurements were carried out. They provide an initial orientation for parameterising the modelling of potential permafrost deposits. With altitude and surface orientation being essential factors for the existence of permafrost, the data analysis showed that slope inclination also has a significant influence on permafrost localization. Despite the higher altitude at equalling surface cover and orientation no indicators of permafrost could be detected. Here, however, the inclination was significantly lower than at a comparison site 200 m asl lower with obvious permafrost influence. These findings were taken into account for modelling the spatial distribution of potential permafrost occurrence. Unfortunately, inclination figures calculated from the available terrain model with a resolution of 30x30m (SRTM 1 Arc) using standard GIS tools do not match the actual field situation. Thus, a special tool was programmed to extrapolate relevant inclination areas and improve the modelling results.

In addition, two ERT measurements were carried out on an active rock glacier. The movement dynamics of the rock glacier can be quantified as 90 m over the past 50 years. The results in the front part with very dynamically active areas characterised by movement bulges on the surface of the rock glacier show a thickness of the block mantle of around 3-4 m. About 100 m asl uphill, at the edge of a dynamically inactive area, no block mantle could be delineated and, above all, no ice content could be verified. These results allow an initial differentiation of the rock glacier in terms of ice content.

For a general hydrochemical characterisation of the Vanj, tributary rivers and sources potentially influenced by permafrost, 21 water samples were analysed regarding content of main ions and heavy

metals. A portable multiparameter meter was used to measure the physico-chemical quality at the time of sampling. For heavy metal analysis, two different samples or sample preparations were taken, one unfiltered and one filtered with 0.45 µm. Both samples were acidified with 1 % 2 mol nitric acid. The comparison of both measurement results confirms that at higher pH values the dissolved heavy metals adhere to the suspension load or combine with each other and are removed from the sample by filtering. The results of the unfiltered and acidified samples showed a higher concentration of almost all elements. The compounds were dissolved by acidification and only filtered under laboratory conditions before the elements were determined.

The sampling sites can be divided into five groups:

a) Vanj River (one sample each of upper, middle and lower section),
b) Langar River (southern tributary to the Vanj with one sample each of upper, middle and lower section),
c) Tributary rivers with glaciers and rock glaciers in the catchment area (7 samples),
d) Tributary rivers without glaciers and rock glaciers in the catchment areas (3 samples) and
e) Springs (5 samples: slope springs, debris springs and rock glacier springs).

Maximum concentration tolerance according to German Drinking Water Ordinance 2023 (GDWO) was used to assess harmful contamination. Nine of the 21 samples showed very high levels of aluminium (concentration 40 times above GDWO limit) and iron (concentration 70 times above GDWO limit). Of these nine samples, eight showed high concentrations of manganese, one of magnesium, one of nickel and one of sulphates. The contaminated samples come from all five groups and no dominant influence of permafrost, rock glaciers or glaciers is evidential. One of the contaminated water samples, even if the concentrations are only slightly above limit, is used directly for irrigating agricultural land. The middle and lower reaches of the Vanj are heavily polluted. Here, too, the water in the lower reaches of the Vanj is used directly to irrigate agricultural land. The extent of contamination of soil or agricultural products will be investigated during the next field campaign. In general, it can be stated for the Vanj that the concentration of all elements increases from the upper to the middle reaches, in some cases significantly.

Conclusions

The results of the first field campaign allow a rough assessment of the permafrost occurrence and the hydrochemical characteristics of the Vanj valley. From a methodological perspective, the results provide a valuable orientation for designing further campaigns in the Vanj and the two other Western Pamir sample valleys.

The focus of the project is not only on physical-geographical and hydrochemical characterisation of the Western Pamirs and the general effects of climate change in this region. Rather, the project focusses on the human-environment relationship and how climate change directly affects the ecology of rural communities in high alpine regions. Living conditions and resource utilisation of local communities will also be empirically investigated in future field campaigns.

Thermal and hydrologic regimes of blocky materials in Tianshan Mountains, Central Asia

Sergey Marchenko[1,3], Huijun Jin[2,3], Martin Hoelzle[4], Jan Lentschke[5], Nikolay Kasatkin[6] & Tomas Saks[4]

[1]*Geophysical Institute, University of Alaska Fairbanks, Fairbanks, Alaska, United States*

[2]*School of Civil Engineering and Transportation and Permafrost Institute, Northeast Forestry University, Harbin, China*

[3]*National Key Laboratory of Cryosphere and Frozen Soil Engineering, Northwest Institute of Eco-Environment and Resources, Chinese Academy of Sciences, Lanzhou, China*

[4]*University of Fribourg, Fribourg, Switzerland*

[5]*Department of Geography, Humboldt-Universität zu Berlin, Berlin, Germany*

[6]*Institute of Geography of the Republic of Kazakhstan, Almaty, Kazakhstan*

Central Asia is a water-stressed area where projected climate change could further reduce stream flow and groundwater recharge (IPCC 2007). General circulation models suggest that the increase in summer diurnal temperatures over Central Asia is likely to be higher relative to that in other regions. Therefore, we expect a further and more intensive retreating of mountain glaciers and more extensive degradation of alpine permafrost and decrease in snow cover. Under continued atmospheric warming, the decrease in snowfall will lead to a decline in snowmelt contribution to river runoff. Increased glacier melting will compensate for this process for some period of time. However, eventually, a further decrease in glacial area and volume would lead to a decline in the contribution of glacier melt to the river discharge. Under persistent climate warming and permafrost degradation in Central Asia, the accelerated melting of ground ice could boost future water supply, and the melt waters from the thawing permafrost could become an increasingly important source of freshwater in this region in the near future.

Mountain permafrost and associated periglacial landforms contain large quantities of stored fresh water in the form of ice. The moraines, rock glaciers and other coarse blocky materials (Figure 1) have especially high ice content (30-70% by volume). The best-studied rock glaciers are situated in the north-central part of the Zailiysky Alatau Range in the Bolshaya and Malaya Almatinka watersheds. The investigations of rock glaciers in northern Tien Shan started in 1923 with the geodetic observations of Russian glaciologist N. Palgov near the front of the Gorodetsky rock glacier. Based on his geodetic net, the observations were repeated ten more times, most recently in 2012. Additional data on the temporal variations of movement have been obtained recently by the use of aerial photographs taken in different years. Recent observations indicate a warming of permafrost in many mountain regions with the resulting degradation of ice-rich permafrost. Permafrost temperature has increased by 0.5 to 3.0°C in Tianshan Mountains, Central Asia during the last 50 years. At the same time, the average active-layer thickness (ALT) increased by 23-30% in comparison to the early 1970s (Marchenko et al. 2007). Runoff from the active layer contributes a significant amount of water during the summertime, when snowmelt has finished and the ground ice melt starts and intensifies. The ALT is one of the dominant factors controlling the subsurface flow conditions. Air temperature, precipitation and ground structure are other components influencing water flow. Blocky materials and other coarse debris, such as protaluses and block fields (kurums), accumulate a significant volume of water in the form of perennial and seasonal ice.

Result and Discussion

We conducted observations on seasonal ground ice accumulation and ablation inside of coarse debris, runoff, precipitation, evaporation, and temperature dynamics in blocky materials of various genesis at elevations of 2500 and 3300 m ASL. The mean annual temperatures inside coarse debris in the Northern Tien Shan Mountains are typically 3-4°C below the regional mean annual air temperatures (MAAT) (Harris and Pedersen 1998; Gorbunov et al. 2004; Marchenko et al. 2007). In such conditions, ice-rich permafrost may develop within coarse debris even in areas with MAATs of above 0°C (in the case of 2500 m ASL site, MAAT is 1.55°C).

Two sites at elevations of 2500 and 3300 m ASL were examined during the last seven years. Sensors for temperature measurements were installed at the depths of 3.0 and 5.5 m inside of blocky material and at 0.3 m in depth in silt beneath blocky debris. One sensor was installed at 2.0 m above blocks for air temperature measurements. The perforated aluminum tube was positioned inside of blocks up to bottom of blocky material at 5.5 m depth for dynamics of ice accumulation measurements. Every five days, the ice accumulation and snow depth measurements were performed. Additionally, during the melting period, the

melted water discharge from blocky materials also was measured.

Because the coarse debris has a high surface roughness, the snow cover appears as discontinuous or temporary snow cover in comparison with surrounding areas of fine-grained soils. In this situation, snow cover exists immediately after snowfall, but then it could quickly disappear during the following 2–3 solar days.

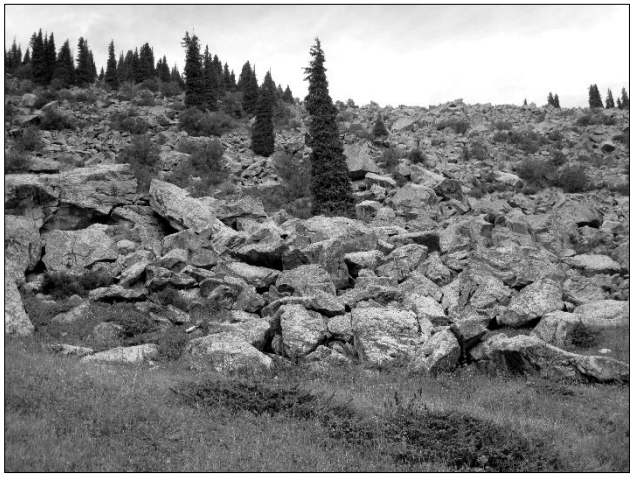

Figure 1. Blocky materials at an elevation of 2500 m ASL in the Northern Tien Shan Mountains, Kazakhstan.

During 2004-2005 and 2009-2010, preliminary investigations of water flow from permafrost were carried out. The discontinuous permafrost site located within the area without glacier runoff near the Kazakhstani permafrost research station in the northern Tien Shan was selected for measurements. Thickness of permafrost in this area varies from 10 to 90 m and the maximum ALT reaches 4.5-5.2 m. There are eight thermometric boreholes varying from 4 to 300 m in depth at this location equipped with data-loggers. The site represents a closed depression confined by mountain ridges. Each set of measurements included recording water discharge and temperature, ground temperature and soil moisture content, ALT, solid/liquid precipitation, evaporation, air temperature and relative humidity. Every ten days, samples of water were collected for further hydrochemical analysis. Preliminary analysis showed an increase of total mineralization and especially ionic concentration of SO_4^{2-}, Ca^{2+}, Mg^{2+}, Na^{+} and K^{+} during the period of intensive ground thawing, with a maximum when the ALT was almost reached, generally in September-October. We hypothesized that the increase in the total mineralization during the intensive period of ground thaw could be related to increased water flow from thawing permafrost. Runoff from the active layer contributes a significant amount of water during the summer time, when snowmelt has finished and the ground ice melt starts and intensifies. The ALT is one of the dominant factors for controlling the subsurface flow conditions.

Conclusion

We have found that the highest rate of ice accumulation inside of coarse debris occurrs during the spring time when air temperature during the day crosses 0°C threshold and has melted and the condensed water penetrates into coarse debris, then freezes and cements the debris. The result is an ice-block mass with ice content as high as 30-50% by volume and sometimes ice may have survived over the summer season. Over the summer season, the water discharge from melting seasonal ice in the upper portion of coarse debris is a very important factor in seasonal redistribution of the total river runoff. The rough estimation of the ice volume in such deposits show that up to 30% of melted snow could be accumulated in the form of ice inside of blocky materials and feed the river runoff during the summer time. This circumstance should be taken into account for hydrologic modeling of individual watersheds.

References

Gorbunov, A.P., Marchenko, S.S., and Seversky, E. 2004. The thermal environment of blocky materials in the mountains of Central Asia. Permafrost and Periglacial Processes 15: 95–98.

Harris, S.A., and Pedersen, D.E. 1998. Thermal regimes beneath coarse blocky materials. Permafrost and Periglacial Processes 9: 107–120.

IPCC 2007. Climate Change 2007: Synthesis Report. Contribution of Working Groups I, II and III to the Fourth Assessment Report of the Intergovernmental Panel on Climate Change [Core Writing Team, Pachauri, R.K and Reisinger, A. (eds.)]. IPCC, Geneva, Switzerland, 104 pp.

Marchenko, S.S., Gorbunov, A.P., and Romanovsky, V.E. 2007. Permafrost warming in the Tien Shan Mountains, Central Asia. Global and Planetary Change, 56: 311–327.

The N-factor at different land cover in discontinuous permafrost zone of Northeastern Mongolia

Nandintsetseg Nyam-Osor[1], Jambaljav Yankhim[2], Ochirkhuyag Jargalsaikhan[1] & Nyambayar Batbayar[1]

[1]*Wildlife Science and Conservation Center of Mongolia, Ulaanbaatar, Mongolia*

[2]*Geocryo LLC, Ulaanbaatar, Mongolia*

Mongolia is one of the fastest-warming regions in the world, with annual average air temperature has rapidly increased by 2.46°C over the last 83 years (BUR2 2023). This change in air temperature has significant effect on the permafrost and active layers (Sharkhuu et al. 2007). The ratio of ground temperature to air temperature is determined, as n-factor, for the thawing (warm) and freezing (cold) seasons (Klene et al. 2001). This study explores the response of different vegetation cover and temporal variations in the n-factors during freeze-thaw periods in peatlands of the Khurkh Valley in northeastern Mongolia.

Study site

The Khurkh Valley is located in the Khurkh-Khuiten Nature Reserve, Khentii province, Mongolia. The permafrost in the area belongs to the Eurasian discontinuous permafrost zone (Yamkhin et al. 2022; Obu et al. 2019). The Nature Reserve is rich in biodiversity and supports a variety of ecosystems including grassland, forest, farmland, peatland and wetland.

As part of the Khurkh Long Term Ecological Research Station's activities, a permafrost monitoring program was created by researchers in 2017. The program was established to study the climate change impact on wetland ecosystems and to monitor the response of permafrost and soil properties in discontinuous permafrost zones in northeastern Mongolia. The site has a network of five boreholes to monitor ground temperatures, and an automatic weather station (AWS) to record meteorological parameters at wetland and unfragmented peatland locations.

In this report, we excluded BH2, since the data is incomplete. Borehole BH1 is located on the southern edge of the wetland. BH4 is located inside the AWS's fence which was in the center of the peatland, where the peat is 40-50 cm thick. BH5 is located on the northern edge of the peatland, where the peat is less than 20 cm thick. BH6 is located inside vegetation monitoring enclosure, which is located on the northern edge of the wetland.

Result and disscusion

The components of the surface energy balance function produce a ground temperature that may differ by several degrees from the air temperature. Predominantly, the freezing n-factor depends mainly on terrain conditions and snow accumulation, while the thawing n-factor depends on land cover and vegetation. Freeze-thaw n-factors are used to separate the effects of snow cover and vegetation on surface temperature into freeze-thaw seasons (Sharkhuu et al. 2007).

In 2018-2019, at the beginning of cold season, the n-factor, which was the same for wetland-BH1, peatland BH5 and wetland BH6, increased until the beginning of February and was stable at the end of the freezing season. In contrast, at BH4 site the n-factor increased sharply in early November and gradually increased in the following months until April. In general, the change pattern of freezing n-factor in 2022–2023 was similar to that in 2018–2019, but all n-factor values were lower compared to 2018–2019. It was noticeably lower for BH4 and BH6 (Figure 1).

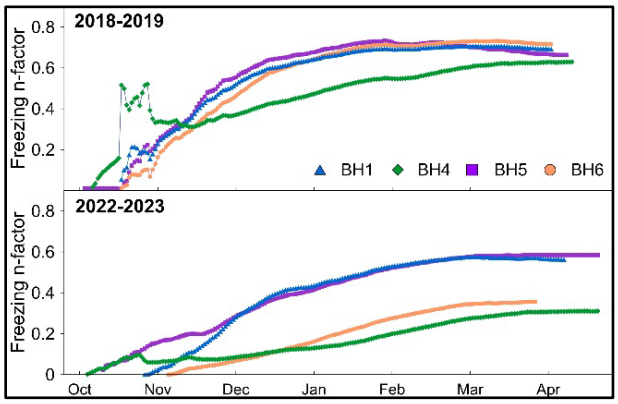

Figure 1. Daily cumulative freezing n-factors at the study sites for winter 2018-2019 and 2022-2023.

Differences in the thawing n-factor increased rapidly at the beginning of the warm season and stabilized towards the end. In 2019, BH1 and BH6 sites had a thaw n-factor of 1.17 and 1.12, respectively. These sites have higher grazing intensity compared to other sites. Whereas, the thaw n-factors at peat rich BH4 and BH5 sites were 0.78 and 0.98, respectively. The peat has much lower thermal conductivity than mineral soils,

under both frozen and unfrozen conditions (Klene et al. 2001). The n-factor thawing pattern was similar at all boreholes between 2019 and 2023, with the exception of BH5 (Figure 2).

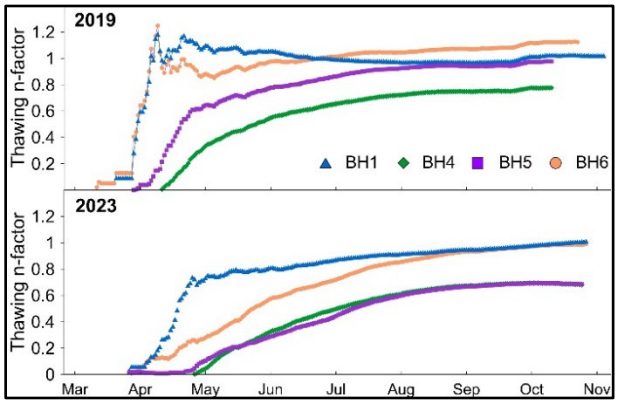

Figure 2. Daily cumulative thawing n-factors at the study sites for summer of 2019 and 2023.

The mean of seasonal snow-induced freezing n-factor was relatively consistent, ranging between 0.46 and 0.64 at all sites, and mean thawing n-factor ranged from 0.74 to 1.09 (Table 1). In addition, the changes in freezing n-factors between 2018 and 2023 was between 0.13 to 0.37.

Table 1. Freeze-thaw n-factors computed using air and ground temperature at the study sites, 2018-2023.

	Year	BH 1	BH 4	BH 5	BH 6
Freezing n-factors	2018-2019	0.71	0.63	0.73	0.73
	2019-2020	0.65	0.49	0.74	0.43
	2020-2021	0.61	0.42	0.57	0.66
	2021-2022	0.50	0.45	0.55	0.61
	2022-2023	0.58	0.31	0.59	0.36
	Mean	0.61	0.46	0.64	0.56
Thawing n-factors	2019	1.17	0.78	0.98	1.12
	2020	1.00	0.82	0.88	1.15
	2021	1.09	0.70	0.86	1.16
	2022	0.92	0.72	0.51	1.01
	2023	1.01	0.69	0.69	0.99
	Mean	1.04	0.74	0.78	1.09

Differences in freezing n-factor between years and between sites were also likely due to the differences in snow depth, and the changes in thawing n-factor were depended on land cover type as well as vegetation patterns.

In our study area, the number of livestock has quadrupled over the past 30 years (Sumiya et al. 2023). Therefore, the n-factors may have been influenced by either on the vegetation cover (snow and vegetation) or on the use of pastures. Because some parts of our study area are used as pasture only during the winter, while others are used for all year round.

Furthermore, some of borehole sites were excluded from the livestock grazing for the entire season by fencing, and this might have been reflected in the n-factor patterns. For example, BH4 site is not often used for grazing during warm season as long as it is located in the middle of the swampy area. Because of it animals do not easily reach the center of the peatland. In the first year, the pattern of daily cumulative freezing n-factor on BH5 was similar to BH1. After 5 years of fencing, the freezing n-factor decreases sharply from 0.63 to 0.31 and the thawing n-factor of thawing changed slightly from 0.78 to 0.69 at BH4. Also, the freezing n-factor dropped sharply from 0.73 to 0.36 on BH6 site, that was located next to a vegetation monitoring fence. Here, snow and vegetation accumulations may have affected the freezing n-factor, because there is a fence on the windward side.

During the thawing season, the n-factor does not change significantly, except for at the BH5 site where it decreases from 0.98 to 0.69. One possible reason for this is that grazing in the area may have decreased due to heavy rainfall in recent years, which has made the area swampy and difficult for animals to enter. In general, the n-factor values for 2022-2023 were similar to those of 2018-2019, but all values were lower. The values for BH4 and BH6 were even lower. It's important to note that n-factors depend not only on land covers like snow and vegetation but also on overgrazing. Additionally, the thawing n-factor is influenced by rain patterns and swampiness.

REFERENCES

BUR2. 2023. Mongolia's Second Biennial Update Report. Under United Nations Framework Convention on Climate Change, Ulaanbaatar, Mongolia.

Klene, A.E., Nelson, F.E., Shiklomanov, N.I., and Hinkel, K.M. 2001. The N-factor in Natural Landscapes: Variability of Air and Soil-Surface Temperatures, Kuparuk River Basin, Alaska, U.S.A. Arct Antarct Alp Res 33, 140–148. doi:10.1080/15230430.2001.12003416

Obu, J., Westermann, S., Bartsch, A., et al. 2019. Northern hemisphere permafrost map based on TTOP modelling for 2000–2016 at 1-km^2 scale. Earth Sci Rev. 193: 299–316. doi:10.1016/j.earscirev.2019.04.023

Sharkhuu, A., Sharkhuu, N., Etzelmüller, et al. 2007. Permafrost monitoring in the Hovsgol mountain region, Mongolia. J Geophys Res Earth Surf 112. doi:10.1029/2006JF000543

Sumiya, V., Yamkhin, J., Tsogt-Erdene, G., et al. 2023. The effects of livestock grazing on soil water content in a wetland of Mongolia. Mongolian Journal of Biological Sciences. 21: 15–21. dio:10.22353/mjbs.2023.21.02

Yamkhin, J., Yadamsuren, G., Khurelbaatar, T., et al. 2022. Spatial distribution mapping of permafrost in Mongolia using TTOP. Permafrost and Periglac Process. 33(4): 386–405. doi:10.1002/ppp.2165

Towards quantifying ice contents in mountain permafrost environments

Julie Røste[1], Andreas Kääb[1] & Sebastian Westermann[1,2]

[1]*Department of Geosciences, University of Oslo, Norway*

[2]*Center for Biogeochemistry in the Anthropocene, University of Oslo, Norway*

In its special report on Ocean and Cryosphere in a Changing Climate (SROCC) the Intergovernmental Panel on Climate Change (IPCC) highlights clear knowledge gaps concerning the extent and ice content of permafrost in mountain regions (Hock et al. 2019). Quantifying sub-surface ice reserves and assessing their changes under a changing climate is crucial, particularly at regional and local scales, due to their implications for, among other factors, mountain biodiversity, geohazards, and water resources.

Understanding the distribution and evolution of sub-surface ice reserves is expected to be especially critical for water resources in dry areas where rock glaciers (tongue-like features of frozen debris that deform under gravity) and sub-surface ice often serve as the sole freshwater reserves in high altitude and continental regions, together with ground water. It is, however, little known where and how large these water resources are, how they could evolve in the future, and what the potential implications could be for the surrounding ecosystems and communities.

Methods and datasets

We aim to investigate a global estimate of the sub-surface ice reserves in mountainous regions and their climatic setting. The first part of this work is to investigate the feature space of mountain permafrost and potentially ice-rich landforms using an empirical (statistical/machine learning) approach. For this purpose, we use climatic and topographic features in combination with existing inventories of rock glaciers, as these are the best visible indicators of mountain permafrost. Rock glaciers contain typically several tens of percent in ice content, which makes them also a good indicator of the presence of sub-surface ice.

Based on such data we create a data-driven model to, among others, predict the probability of where to find potential rock glaciers, similar to the approach of Deluigi et al. (2017) and Karjalainen et al. (2020). We can then investigate the vulnerability of these potentially ice-rich areas under climate change.

In the next step, we move to a smaller geographic scale and model the mountain sub-surface ice of idealised catchments, and investigate the potential climate-change impacts on them. Mountain permafrost, and in particular its ice contents, are data-poor science fields (in opposite to data-rich fields), thus we are interested in obtaining more validation data for our data-driven models. By using physically-based models to produce “synthetic observations" in low-confidence areas, and by re-running the numerical model where the information gain is the highest, we aim to obtain improved results for our data-driven models. This is done using an active learning scheme, where a statistically-based model is informed by a numerical permafrost model. In this work, we use the CryoGrid community model of Westermann et al. (2023).

Finally, we extend the analysis by looking at the potential run-off contribution from mountain sub-surface ice, using the frameworks developed earlier in the project, in order to identify in which areas and feature settings it will be relevant to better consider sub-surface ice within assessments of mountain hydrology regimes. In addition, we analyse the hydrological impact of sub-surface ice in a more global context under different climate scenarios and expand the analyses to relevant mountain ranges.

Outlook

The goal of this research is to advance our knowledge about the distribution of mountain permafrost, including an improved understanding of its characteristics, estimation of ice content, and its hydrological significance. In a methodological context, this project involves the development of new applications of statistical methods and the improvement of existing model frameworks.

References

Deluigi, N., Lambiel, C., and Kanevski, M. 2017. Data-driven mapping of the potential mountain permafrost distribution. Science of The Total Environment 590–591, 370–380. doi:10.1016/j.scitotenv.2017.02.041

Hock, R., Rasul, G., Adler, C., Cáceres, B., Gruber, S., Hirabayashi, Y., Jackson, M., Kääb, A., Kang, S., Kutuzov, S., Milner, A.I., Molau, U., Morin, S., Orlove, B., and Steltzer, H. 2019. High Mountain Areas. In: IPCC Special Report on the Ocean and Cryosphere in a Changing Climate [H.-O. Pörtner, D.C. Roberts, V. Masson-Delmotte, P. Zhai, M. Tignor, E. Poloczanska, K. Mintenbeck, A. Alegría, M. Nicolai, A. Okem, J. Petzold, B. Rama, N.M. Weyer (eds.)]. Cambridge University Press, Cambridge, UK and New York, NY, USA, pp. 131–202. doi:10.1017/9781009157964.004

Karjalainen, O., Luoto, M., Aalto, J., Etzelmüller, B., Grosse, G., Jones, B.M., Lilleøren, K.S., Hjort, J., 2020. High potential for loss of permafrost landforms in a changing climate. Environ. Res. Lett. 15 (10), 104065. doi:10.1088/1748-9326/abafd5

Westermann, S., Ingeman-Nielsen, T., Scheer, J., Aalstad, K., Aga, J., Chaudhary, N., Etzelmüller, B., Filhol, S., Kääb, A., Renette, C., Schmidt, L.S., Schuler, T.V., Zweigel, R.B., Martin, L., Morard, S., Ben-Asher, M., Angelopoulos, M., Boike, J., Groenke, B., Miesner, F., Nitzbon, J., Overduin, P., Stuenzi, S.M., and Langer, M. 2023. The CryoGrid community model (version 1.0) – a multi-physics toolbox for climate-driven simulations in the terrestrial cryosphere. Geoscientific Model Development 16 (9), 2607–2647. doi:10.5194/gmd-16-2607-2023

Increasing sediment supply and massive sediment deposition in Tibetan Plateau rivers

Genxu Wang, Jinlong Li, Chunlin Song, Jiapei Ma & Shouqin Sun

State Key Laboratory of Hydraulic and Mountain River Engineering, College of Water Resource and Hydropower, Sichuan University, Chengdu 610065, China

The high-altitude Tibetan Plateau (TP) boasts the planet's third-largest cryosphere reservoir, encompassing glacier-snow-permafrost, and exhibits heightened sensitivity to global climate change. Not only serving as vital water resources, the rivers originating from the TP play indispensable ecological roles. They convey essential terrigenous materials—ranging from freshwater and sediment to carbon and nutrients—nurturing the vitality of local ecosystems and sustaining the livelihoods of nearly two billion people in downstream regions. Nevertheless, these river systems, uniquely situated in the world's largest area of alpine permafrost (~1.3 × 106 km^2 or 42% of the TP), are currently confronted with escalated threats stemming from the rapid degradation of the cryosphere. While existing research underscores the substantial increase in water and sediment fluxes in Tibetan Plateau rivers, with potential implications for regional ecosystems and biogeochemical cycles, a comprehensive spatiotemporal understanding of changes in sediment yield pattern and transport processes on the TP remains elusive.

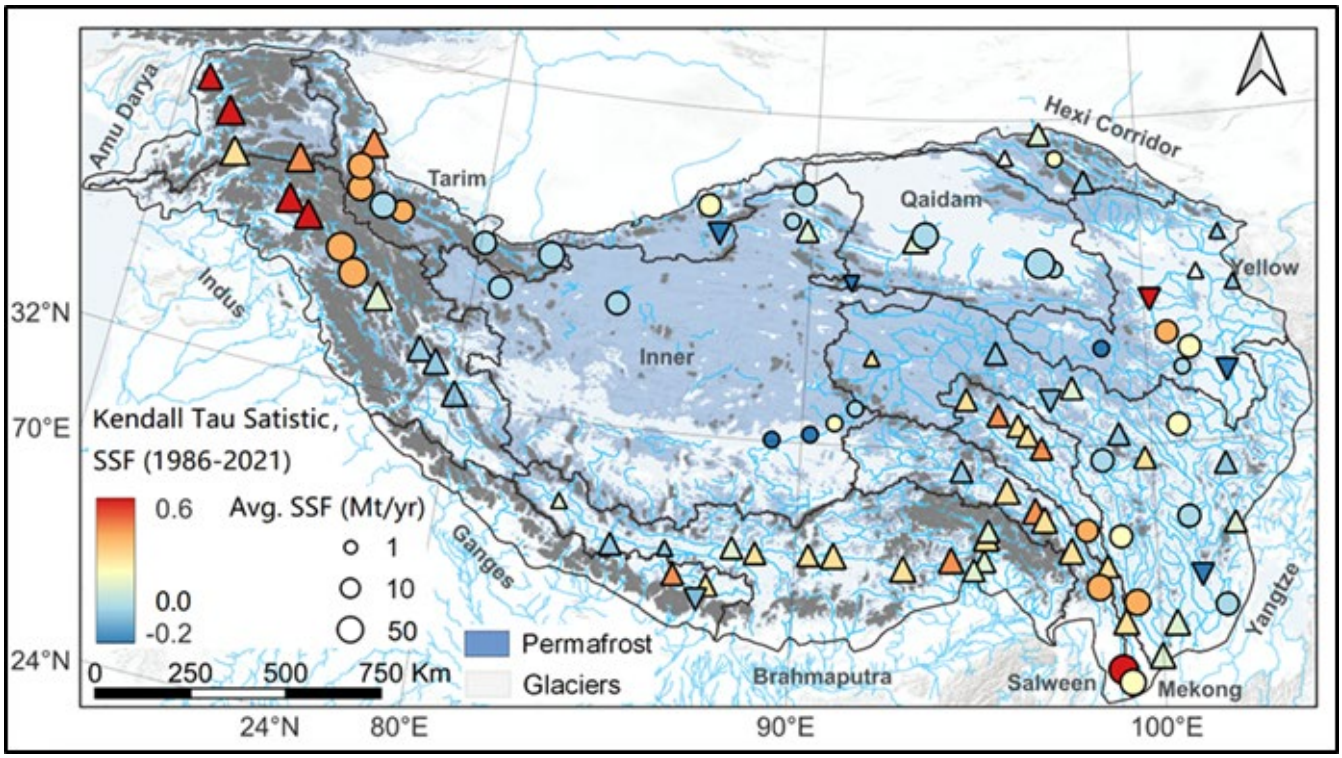

Figure 1. Changes in the annual average suspended sediment flux in 1986-2021 across the Tibetan Plateau.

In this study, we integrated advanced remote sensing techniques with in situ river monitoring to intricately reconstruct the quantitative history of suspended sediment dynamics in the major headwater regions of the TP. Our investigation spanned both the mainstreams and major tributaries of prominent Asian rivers (e.g., the Yangtze, Yellow, Ganges, Indus, Salween, and Mekong Rivers) and inland rivers (e.g., Amu Darya and Tarim Rivers). The outcomes of our research revealed a robust west-east spatiotemporal heterogeneity in basin-scale sediment yield and transport patterns. This heterogeneity is primarily driven by the convergence of climate change and specific hydrogeomorphic processes, such as glacial erosion or collapses, permafrost thaw, associated landslides, and rock-ice avalanches.

In contrast to existing reports based on sediment monitoring stations at basin outlets, our findings indicate a substantial underestimation of the overall sediment flux of each major river. Specifically, the underestimation of suspended sediment concentration ranged from 7.81% to 43.52%, while the underestimated suspended sediment flux fell between 9.01% and 46.85%. This underestimation can predominantly be ascribed to the dynamic redistribution of sediment within each headwater basin, stemming from occurrences of sediment deposition or a lack of transport capability at specific locations—elements not adequately captured by the available station data. All our discoveries are grounded in state-of-the-art advancements in techniques and satellite remote sensing approaches, providing invaluable insights into sediment mobilization, transport dynamics, and delivery mechanisms in cold regions.

7 Permafrost Infrastructure

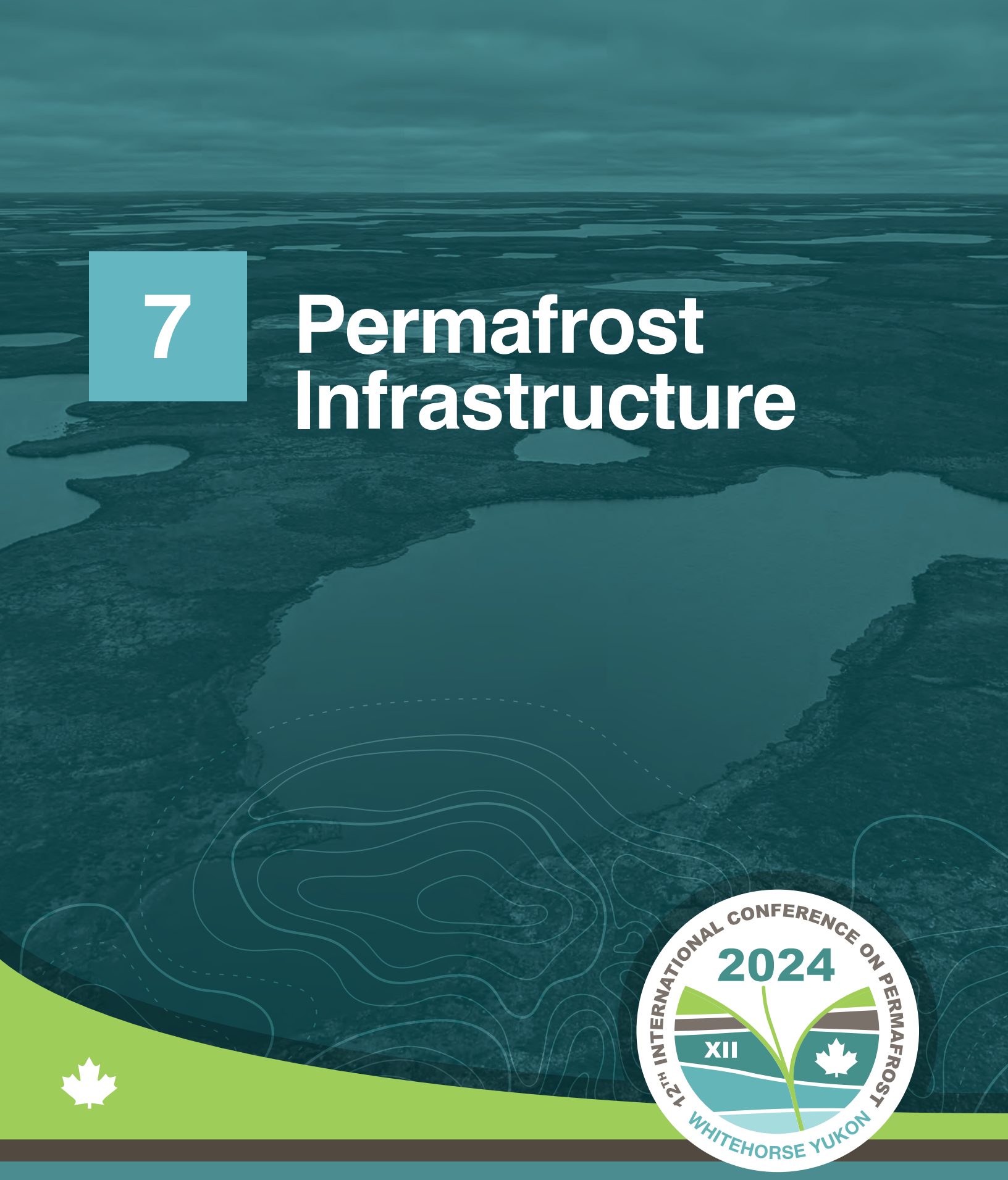

12TH INTERNATIONAL CONFERENCE ON PERMAFROST
2024
XII
WHITEHORSE YUKON

INTEGRATING PERSPECTIVES OF PERMAFROST THAW, CHANGE, AND ADAPTATION

7A — Permafrost Railways

Session Chairs: Brett Young[1,2], Zhanju Lin[3], Pascale Roy-Léveillée[4] & Andy Take[5]

[1]*Hudson Bay Railway, The Pas, Manitoba, Canada*
[2]*Royal Military College of Canada, Kingston, Ontario, Canada*
[3]*Cold and Arid Regions Environmental and Engineering Research Institute, Chinese Academy of Science, Lanzhou, China*
[4]*Centre D'Études Nordiques, Université Laval, Québec City, Québec, Canada*
[5]*Queen's University, Kingston, Ontario, Canada*

Railways built over permafrost terrain are vulnerable to damage arising from ground warming and thaw. They are particularly sensitive to ground subsidence, frost-jacking of piles, and other permafrost processes causing rail bed deformation and negatively impacting rail geometry. Differential settlement and heaving at transition sections (e.g. between road and bridge, excavation and filling, or tunnel and subgrade) are an important cause of railway damage. Additionally, the management of water and prevention of washouts near permafrost railways is complicated by the nature of permafrost hydrology and by warming effects of water accumulation near the embankment foot.

Several mitigation methods can be used to alleviate the impacts of permafrost on railways, including adapted railbed design and improved monitoring and detection of incipient rail deformation. To be effective, these methods should be paired with effective characterization of permafrost distribution and ground-ice content, study of temperature-dependent geotechnical properties, and modelling of expected permafrost and ground surface response to climatic change.

This interdisciplinary session is focused on the characterization, prediction, management, and mitigation of permafrost-related hazards affecting railways in permafrost regions and welcomes research, data, and perspectives from all fields and sectors that aim to increase the resilience of permafrost railways to climatic warming.

Preliminary results of permafrost vulnerability mapping of the Hudson Bay Railway

Nana K. Frimpong Agyei & Jocelyn L. Hayley
Department of Civil Engineering, University of Calgary, Calgary, Alberta, Canada

Temperature increases in the Arctic in the last three decades have led to increased permafrost thaw across the North (Bush et al. 2022). Close to half of Canada's land mass is underlain by permafrost; thus, understanding the response of the permafrost as the climate changes is critical. For example, up to 50% of global infrastructure is expected to be at risk of damage due to permafrost thaw by 2050, translating to billions of dollars in repairs and maintenance costs (Hjort et al. 2022). In Canada, the north is sparsely populated; hence, linear infrastructure, such as the Hudson Bay Railway, is the most at risk of damage due to changing permafrost conditions. The Hudson Bay Railway is a 1009-kilometre-long (627 miles) railway in northern Manitoba that runs from The Pas to Churchill, with a branch line to Flin Flon. The rail line runs on continuous, extensive discontinuous and sporadic discontinuous permafrost zones and has undergone thaw-induced damage in the last three decades. Mitigation measures required to alleviate the effects of permafrost thaw on infrastructures can be expensive to implement and maintain. This paper will focus on identifying critical zones to prioritize resource allocation as permafrost conditions underneath the rail line change.

BACKGROUND

The Hudson Bay Railway (HBR) was completed in 1929, and the line has served as a means to transport hazardous materials, concentrates, fertilizer, automobiles, construction materials, heavy equipment, wheat, and other grain products. Since its construction and operation, the HBR has been affected by permafrost thaw, which results in differential track settlement. Thaw settlement, a function of anthropogenic activities and climate change, can cause train derailment if left unchecked. In 1977, Canadian National Railway (the line operators at that time) contracted EBA Engineering Consultants Limited to help them understand the processes influencing the thaw and implement measures to mitigate this hazard. However, Addison et al. (2015) showed that some previously stable locations have now become susceptible to settlement due to changes in the thermal regime. This has necessitated revisiting the site and developing a hazard map along the HBR to help guide the mitigation measures needed along the track in the coming years.

Hazard mapping helps forecast the impacts of permafrost thaw, with some hazard predictions going as far as 50 years. Most hazard maps are built with geo-hazard indices that assume a fixed relationship between thaw settlement and the factors that affect permafrost thaw. This assumption can be erroneous when dealing with different permafrost zones, as the ecological and climatic factors influencing permafrost degradation are not uniform everywhere. Furthermore, these geo-hazard indices only consider a few factors that impact permafrost thaw at a time. Ground ice, change in active layer thickness and the mean annual ground temperature are commonly considered. At the same time, other variables such as surficial geology, elevation and the snow depth are not accounted for.

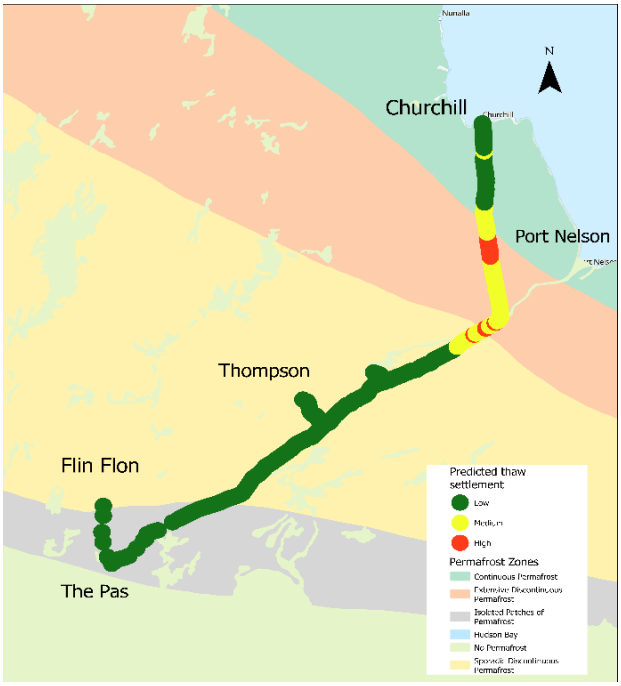

Figure 1. Map showing permafrost zones and the predicted thaw susceptibility along the Hudson Bay Railway as determined by the initial run of the MGWR model using climatic inputs and a dependent variable of observed sinkholes.

METHODS AND DATASETS

To eliminate discrepancies in maps produced by geo-hazard indices, Ni et al. (2021) created a combined

index based on the geo-indices proposed by Daanen et al. (2011) and Xu and Wu (2019). This combined index enhanced the accuracy of hazard maps in the Qinghai-Tibet Plateau. Still, this index is computationally onerous and requires the creation of three initial indices, gridded analysis and a combination of the indices.

In this work, we used Multiscale Geographically Weighted Regression (MGWR). This spatial modelling tool can consider a broader range of climactic and ecological factors impacting permafrost degradation and tie these factors to the currently observed settlement. This allows more influential factors to be considered while determining their statistical significance.

MGWR is a spatially-varying coefficient model developed by Fotheringham et al. (2017) as an extension of the traditional GWR. Being a "local" regression model, the MGWR model accounts for the heterogeneity of a process such as thaw settlement. The benefit of this extension over the traditional GWR is that it eliminates the restriction that relationships between the independent and the dependent variables must vary at the same scale, enhancing our hazard map's accuracy and resolution.

In our model, the dependent variable was sinkholes, i.e., the count of the measured surface depressions on the track's surface. Our initial model only used climactic factors closely associated with permafrost degradation: snow water equivalent, air temperatures, snow depth, and snow cover temperatures. These variables showed statistical significance regarding the count of sinkholes in our model. Other climatic variables that did not have a statistically significant correlation to thaw settlement were discarded. As we advance, we will include other factors such as ground ice abundance (%), bedrock geology, surficial geology units, vegetation cover, elevation, and surface albedo.

Conclusions

Using MGWR allowed us to create a hazard map that implicitly expresses the spatially varying behaviour of permafrost thaw across different permafrost zones, thereby eliminating the assumption of fixed relationships usually in some geo-hazard indices. The resulting hazard map (Figure 1) shows the upward movement of thaw-susceptible areas from extensive discontinuous to continuous permafrost zones. Confirming the changing permafrost boundaries detected by Addison et al. (2015). Hence, this hazard map can help identify areas along the HBR susceptible to thaw settlement and prioritize mitigation measures in these areas.

Acknowledgements

Funding for this project is provided by Transport Canada's National Trade Corridors Fund. We thank Arctic Gateway Group for their ongoing partnership and support of the project.

References

Addison, P., Oommen T., and Lautala P. 2015a. A Review of Past Geotechnical Performance of the Hudson Bay Rail Embankment and Its Comparison to the Current Condition. Proceedings of the 2015 ASME Joint Rail Conference. March 23-26, 2015. San Jose, California.

Bush, E., Bonsal, B., Derksen, C., Flato, G., Fyfe, J., Gillett, N., Greenan, B.J.W., James, T.S., Kirchmeier-Young, M., Mudryk, L., and Zhang, X. 2022. Canada's changing climate report, in light of the latest global science assessment. https://doi.org/10.4095/329703

Daanen, R.P., Ingeman-Nielsen, T., Marchenko, S.S., Romanovsky, V. E., Foged, N., Stendel, M., Christensen, J.H., and Hornbech Svendsen, K. 2011. Permafrost degradation risk zone assessment using simulation models, The Cryosphere, 5, 1043–1056. https://doi.org/10.5194/tc-5-1043-2011

Fotheringham, A.S., Yang, W., and Kang, W. 2017. Multiscale Geographically Weighted Regression (MGWR), Annals of the American Association of Geographers, 107:6, 1247–1265. doi:10.1080/24694452.2017.1352480

Government of Canada, Natural Resources Canada, Canada Centre for Remote Sensing, The Atlas of Canada. Atlas of Canada 1,000,000 National Frameworks Data, Rail Network Geospatial Data Presentation Form: Vector digital data, 2008. http://www.geogratis.gc.ca/download/frameworkdata/rail/

Hjort, J., Streletskiy, D., Doré, G., Wu, Q., Bjella, K., and Luoto, M. 2022. Impacts of permafrost degradation on infrastructure. In Nature Reviews Earth and Environment (Vol. 3, Issue 1, pp. 24–38). Springer Nature. https://doi.org/10.1038/s43017-021-00247-8

Ni, J., Wu, T., Zhu, X., Wu, X., Pang, Q., Zou, D., Chen, J., Li, R., Hu, G., Du, Y., Hao, J., Li, X., and Qiao, Y. 2021. Risk assessment of potential thaw settlement hazard in the permafrost regions of Qinghai-Tibet Plateau. Science of the Total Environment, p. 776. https://doi.org/10.1016/j.scitotenv.2021.145855

Permafrost Atlas of Canada, 5th Edition. Natural Resources Canada.

Xu, X.M., and Wu, Q.B. 2019. Impact of climate change on allowable bearing capacity on the Qinghai-Tibetan Plateau. Advances in Climate Change Research,10(2),99–108. https://doi.org/10.1016/J.ACCRE.2019.06.003

Monitoring frost jacking impacts on infrastructure: A case study of a bridge on the Hudson Bay railway

Natalie Arpin[1], Ryley Beddoe[2] & W. Andy Take[1]

[1]*Department of Civil Engineering, Queen's University, Kingston, Ontario, Canada*

[2]*Department of Civil Engineering, Royal Military College of Canada, Kingston, Ontario, Canada*

When designing pile foundations in cold regions and areas underlain by permafrost, engineers must consider the possibility of frost jacking. The term "frost jacking" is used to describe the upward displacement of a pile when the upward forces exerted by frozen ground surrounding the pile, overcoming the forces which are holding the pile into the ground (Wang et al. 2022).

The forces that uplift the pile are a result of the tangential stresses caused by the freezing of the ground and subsequent heaving around the pile. In areas where the ground is not frozen or in taliks, the friction between the soil pile and the ground interface generates the restraining force. In permafrost regions, the resistance is provided by the adfreeze bond between the pile and the frozen ground (Penner 1974; Wang et al. 2022). Previous controlled studies have examined frost jacking mechanics and impacts under both laboratory and field conditions (Penner 1970; Wang et al. 2017). However, there is a lack of research examining frost jacking impacts on operational infrastructure.

CASE STUDY

The Hudson Bay Railway is a critical piece of linear infrastructure in Canada which runs 1000 kilometres from The Pas to Churchill, Manitoba. Numerous communities in northern Canada depend on the railway as their only form of land-based transportation. Since its construction, the operation of the railway remains challenging because of the extensive presence of muskeg, peat, and various permafrost conditions which underlie it, as depicted in Figure 1.

One of the operational challenges facing the railway because of its location is frost jacking. In the Herchmer division, the Horn Creek Crossing has undergone almost 0.5 metres of frost jacking over a 10-year period. Figure 1 indicates the location of the bridge. The bridge is composed of a 4-span steel ballast deck supported by steel H-piles (Figure 2). In July 2022, the bridge underwent repairs to level the structure, however, these repairs do not prevent future uplift from occurring.

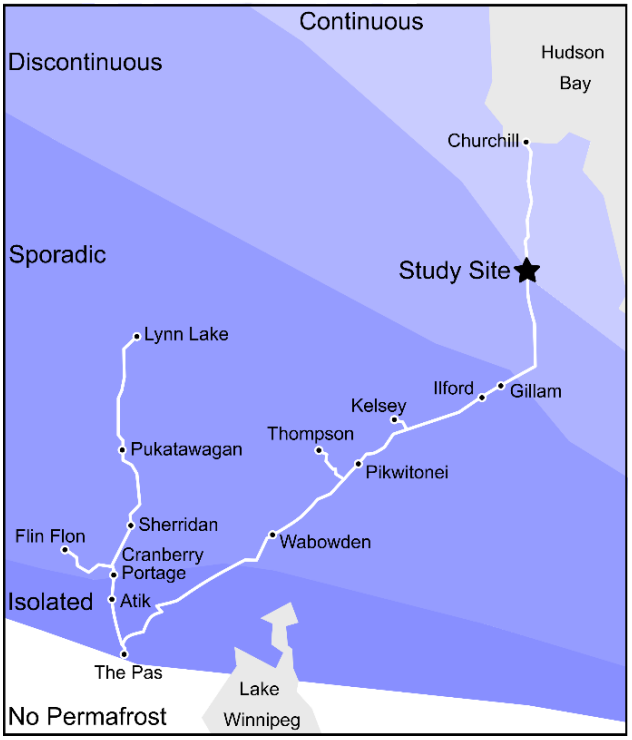

Figure 1. Map of the Hudson Bay Railway indicating the study site and distribution of permafrost (Adapted from O'Neil et al. 2020).

Figure 2. Horn Creek Crossing on the Hudson Bay Railway with 0.5 metres of frost jacking present on the northern pier of the bridge with Span 1 in the foreground pre-repairs made in July 2022.

Limited information is available as to the rate of and seasonality of this movement because of its remote location. A monitoring program has been devised and put into operation at the bridge to determine the consequences of frost jacking on this bridge and the wider implications for the Hudson Bay Railway.

Site Instrumentation

Installation of instruments on the bridge allowed for monitoring of frost jacking. RST Biaxial tiltmeters were attached to each span on both sides of the bridge for hourly monitoring of span movement. A HOBO weather station was placed at the site to monitor daily air temperatures. Trail cameras were installed to monitor water levels and snow cover.

Preliminary Results and Discussion

Monitoring the bridge started in October 2022, post the repair, and is ongoing. Preliminary results from the monitoring are presented in Figure 3. Over the winter, span 1 (Figure 1b) of the bridge underwent 31 mm of upward movement on the east side of the bridge and 38 mm on the west side of the bridge. Span 2 moved up 29 mm on the eastern side, while on the western side, it moved upwards by 32 mm (Figure 1c). An upward trend of movement of the spans is visible throughout the winter and continues until daily mean air temperatures rise above 0 °C (Figure 3d).

A small amount of recovery is present in the spring as daily mean air temperatures increase above 0 °C, allowing the ground around the pile to thaw and for the bridge to settle downwards from its self-weight. This recovery is measured to be an average of 11 mm, which is less than the upwards movement in the winter due to frost jacking. This results in an overall upward seasonal trend in the piers and span's location.

Conclusions and Ongoing Work

Frost jacking is an ongoing process which is impacting the infrastructure of the Hudson Bay Railway. There is recovery of the movement in the spring, however, the movement is less than what is experienced over winter. Monitoring will continue to help develop an understanding of the seasonality and the expected rates of movement.

Acknowledgements

The authors thank Arctic Gateway Group, and especially Brett Young and Nathan Gullacher, for their support and acknowledge the support of Transport Canada (NTCF).

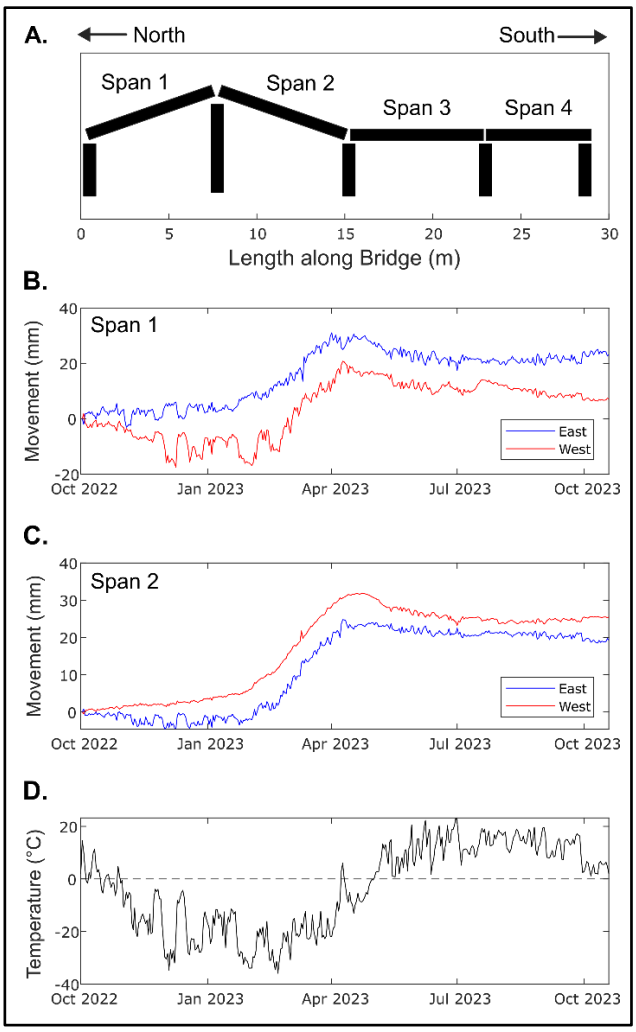

Figure 3. Movement from October 2022 to 2023 with (a) span naming convention, (b) Span 1 movement, (c) Span 2 movement, and (d) daily mean air temperatures.

References

O'Neil, H.B., Wolfe, S.A., and Duchesne, C. 2020. Ground ice map of Canada. Geological Survey of Canada, Open File 8713, 2020, 7 pages (1 sheet). doi:10.4095/326885

Penner, E. 1970. Frost heaving forces in Leda clay. Canadian Geotechnical Journal 7(1): 8–16. doi:10.1139/t70-002

Penner, E. 1974. Uplift Forces on Foundations in Frost Heaving Soils. Canadian Geotechnical Journal, 11(3): 323–338. doi:10.1139/t74-034

Wang, T., Liu, J., Tian, T., and Lv, P. 2017. Frost jacking characteristics of screw piles by model testing. Cold Regions Science and Technology, 138: 98–107. doi:10.1016/j.coldregions.2017.03.008

Wang, T., Qu, S., Liu, J., Luo, Q. and Hu, T. 2022. Frost jacking of piles in seasonally and perennially frozen ground. Cold Regions Science and Technology, 203. doi:10.1016/j.coldregions.2022.103662

The Qinghai-Tibet Railway in China

Zhanju Lin, Fujun Niu, Xingwen Fan & Jing Luo

State Key Laboratory of Frozen Soil Engineering, Northwest Institute of Eco-Environment and Resources, Chinese Academy of Sciences, Lanzhou, Gansu, China

THE HISTORY ON THE QTR

The thought of building a railway to Tibet was first proposed by British explorers in the late 19th century, and China started carefully considering this project until the mid-20th century. The construction of section from Xining city (the capital of Qinghai province) to Golmud city (one of the cities of Qinghai province) was started in 1958, and it was completed to operate in 1984. Because this section has no permafrost, it is not difficult to build. However, due to the existence of high temperature and high ice content permafrost at section from Golmud city to Lhasa city (capital of the Tibet Autonomous Region), it is extremely difficult to build. So, for trying to solve the permafrost problem, the Chinese scientists and engineers have experienced a technological exploration nearly half a century. Finally, this section of railway started to construct in 2001 and finished completely in 2006.

The QTR is the highest railway in the world, reaching an altitude of over 4500 m in permafrost region. The design speed is 100 km/h. The railway spans a total length 1956 km and includes ~550 km continuous permafrost section and 82 km discontinuous permafrost section. There are 58 stations, over 400 bridges, and two tunnels (Kunlun and Fenghuo mountain) within 1142 km from Golmud to Lhasa section. The total length of bridge is 126 km, including a longest bridge of 11.7 km.

THE METHODS ON ACTIVE COOLING ROADBED

Most lines of the QTR are located in high-altitude areas. In 550 km length permafrost zone, the high-temperature permafrost (annual mean ground temperature is higher than -1.0 °C) is about 275 km, the high-ice content permafrost (volumetric ice content exceeds 20%) is ~221 km, and the overlapping section both high-temperature and high-ice content is about 134 km. So, the permafrost along the QTR is very sensitive to the thermal disturbances and easily thawing to cause the surface settlement. In order to protect permafrost and keep a long-term stability, the method of Active Cooling Roadbed was used in construction of QTR. The main embankment includes five type structures as follows.

Crushed-rock roadbeds

Crushed-rock roadbeds include several different forms and configurations, such as the rock-based roadbeds, U-shaped rock roadbeds, embankments with rock revelments, and embankments with the slopes partly covered by crushed-rock. Among them, rock-based embankments (Figure 1a) and embankments with rock revetments (Figure 1b) were mainly adopted in the primary designing. The structure is laid with a rock layer with ~1.5 m thick at the bottom of the roadbed, and the cold wind from the rocks in winter to take away heat.

Duct ventilated roadbeds

Ventilation techniques have been widely used in permafrost regions in the construction of garages, warehouses and storage tanks. The fundamental mechanism is to force air flows in ducts installed in foundations, in order to intensify heat exchange between foundations and underlying permafrost. Key of the method is to ensure that cold air can pass though the buried ducts fluently, taking away the beat of the adjacent earth. Strong wind on the QTP in winter makes it possible for air to effectively move in the ducts. And this has been tested in the railway roadbed construction (Figure 1c).

Thermosyphon installed roadbeds

Along the QTR, there are two rows of iron rods with ~2 m high on both sides of the roadbed. The whole rod body is central controlled and filled with liquid ammonia (named thermosyphon). Thermosyphon can effectively lower the ground temperature using phase changing and circling of media inside it in winter time. Normally thermosyphons are installed in the regions where warm and ice-rich permafrost spreads along the railway, and also in some cut sections (Figure 1d).

Sunshine-shielding roadbeds

The main factor causing rise of air temperature and ground temperature is solar radiation. To shield the ground surface from solar radiation can effectively lower the ground temperature. According to the results of indoor experiments and field monitoring studies, the sunshine-shielding can lower air temperature by a value of 8 °C to 20 °C, and even up to 24 °C

(Figure 1e). As sunshine-shielding can effectively lower the ground surface temperature, it can be adopted to protect the underlying permafrost even in climate warming background.

Land bridges

In some warm and ice-rich permafrost regions, land bridges are suggested to be the necessary method to pass the region, as any of the embankment configurations were hardly to prevent influences of the permafrost. The longest land bridge of 11.7 km shows in Figure 1f. In spite of high cost of land bridges, this method has three advantages to the railway and local environment First of all, land bridges possess good mechanical stability and can support heavy loads. Secondly, bridges can shade the ground from solar radiation, and also air can fluently flow under them. In addition, they can provide migration routes for wild animals on the plateau. This is also very important in the plan, design, construction and services of the railway.

Figure 1. The cooling embankment structures used in Qinghai-Tibet Railway.

THE OPERATION SITUATION AT PRESENT AND POSSIBLE CHANGES IN FUTURE

Since the QTR was put into operation in 2006, the trains in permafrost areas have been running smoothly as the designed speed of 100 km/h, and the permafrost roadbed is generally stable. There has never been a railway shutdown or a traffic accident owing to the permafrost problem. By the end 2022, the railway had transported 260 million passengers, increasing from 6.48 million in 2006 to 18.71 million in 2021.

At present the railway can guarantee regular operation. However, under the impact of global climate warming and warm-wetting tendency of QTP, the railway has also produced some secondary diseases problems. According to the data of monitored ground temperature along the QTR, the annual mean ground temperatures at 1 m depth has been warming as a rate of 0.5 °C/10a over 2002-2020. The active layer thickness has been increasing steadily by 2-9 cm/a, and with an average value of 4.6 cm/a. The temperature near the permafrost table (~2.0 m depth) has been increasing at a rate of 0.1 and 0.6 °C/10a, with an average of 0.3 °C/10a. Permafrost temperatures at 15 m depth has been warming by about 0.1-0.2 °C/10a. The GIPL2.0 model simulation results indicate that the annual mean permafrost temperature at 1 m depth will increase by 0.6-1.8 °C in next 100 year (to 2100) and increase ~40-100 cm in active layer thickness.

According to this tendency of permafrost change, the disease rate of railway subgrade will gradually increase in the future. At present, it is mainly reflected in the uneven subsidence of the high embankment section and the local longitudinal cracks. In particular, the differential subsidence of road and bridge transition section is the main problem affecting the safe operation of railway. Therefore, the safe operation of the QTR in the future will also encounter some serious problems, which will bring severe challenges to the maintenance of the railway. Nowadays, it is more necessary to develop new reinforcement measures to deal with the crisis brought by climate change to the permafrost roadbed.

REFERENCES

Cheng, G. 2005. A roadbed cooling approach for the construction of Qinghai-Tibet railway. Cold Regions Science and Technology. 42: 169–176.

Niu, F., Xu, J., Lin, Z., Wu, Q., and Cheng, G. 2008. Permafrost characteristics of the Qinghai-Tibet Plateau and methods of roadbed construction of Railway. Acta Geological Sinica. 82(5):949–958.

Niu, F., Lin, Z., Lu, J., Liu, H., and Xu, Z. 2011. Characteristics of roadbed settlement in embankment-bridge transition section along the Qinghai-Tibet Railway in permafrost regions Cold Regions Science and Technology. 65: 437–445.

Zhou, F., Yao, M., Fan, X., Yin, G., Meng, X., and Lin, Z. 2022. Evidence of warming from long-term records of climate and permafrost in the hinterland of the Qinghai–Tibet Plateau. Front. Environ. Sci. 10:836085.

The diseases characteristics of the Qaidam-Muli Railway on south slope of the Qilian Mountains

Niu Fujunn,Yin Guoan & Luo Jing

State, Country State Key Laboratory of Frozen Soil Engineering, Northwest Institute of Eco-Environment and Resources, Chinese Academy of Sciences, Lanzhou 730000, China

The Qaidam-Muli Railway is the first local railway built with self-financing funds by the Qinghai provinc. The line runs 140 km from Gangca County and Tianjun County in the north-east of the province, from the Gangca County in the east to Muli district in the west. This section is 140 km from Chaidar station to Muli station, and about 70km of the section is in permafrost region. Now the railway is abandoned and no maintenance works were continued. Therefor serious settlement and collapse happened along the line. Based on SBAS-InSAR technology and field investigation, the disease status of the railway abandoned 4 years ago was analyzed, and the reuse scheme was suggested.

Geotechnical investigations for a proposed new railway – Baffin Island, Nunavut, Canada

Adam Plazek, Kiran Chandra Prakash & Warren Hoyle
Hatch Ltd., Niagara Falls, Ontario, Canada

This abstract presents the changes proposed and successfully executed relative to previous drilling approaches at the site for drilling in permafrost to collect undisturbed frozen geotechnical samples.

PERMAFROST CONDITIONS

Mary River site is in continuous permafrost. The results of previous investigation programs on Baffin Island have indicated that the depth of continuous permafrost extends to over 500 m. The active layer, ranges from 0.5 m in poorly drained low-lying areas to between 2 m and 3 m in well-drained sand and gravel materials.

The permafrost temperature measured along the proposed railway alignment is between -8°C and - 10°C at depths below 8 m. Deep thaw bulbs are present under lakes and rivers with water depths greater than 3 m to 4 m.

PREVIOUS INVESTIGATIONS AND METHODS

Between 2006 and 2012 there were:

- Approximately 758 boreholes completed along the rail alignment; diamond drilling with double tube conventional core barrel was used as the drilling technique with water used as drilling fluid.
- Air photo interpretation
- Geophysical surveys
- A preliminary gravimeter surveys
- Over 450 test pits

Although a significant amount of investigation had been conducted, gaps in the data were still evident. The primary reason for data gaps was that the boreholes were drilled using water as a drilling fluid, which thawed ice-rich soils and washed away sands and fines within the core. There were also changes to the alignment since the previous investigations that required investigation, and structures such as bridges that required further investigation to advance from a conceptual design to a full detailed design.

GEOPHYSICS APPROACH

Geophysical surveys were used to assist in the planning and execution of the drilling program. Ground Penetrating Radar (GPR) scans were conducted along a 40 km segment of the alignment that is exceptionally ice rich. This allowed for planning and execution of boreholes that targeted large subsurface ice bodies, which are a primary geotechnical risk factor for the railway construction as they are particularly vulnerable to thaw and creep settlement (Canadian Standards Association 2019).

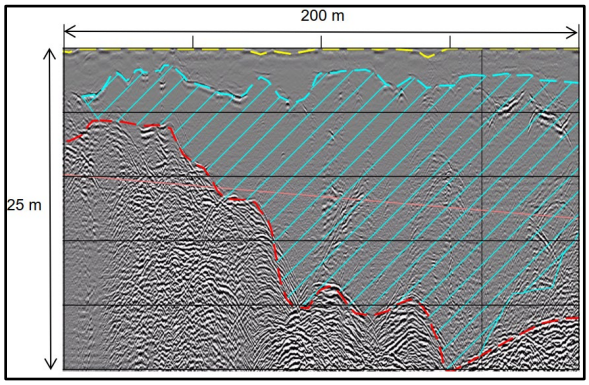

Figure 1. GPR image sample indicated interpreted ice lens (blue), bedrock (red).

2023 DRILLING INVESTIGATION

The planning of the investigation program began with the preliminary selection of locations for geophysical and drilling investigations. The GPR portion of the geophysical work preceded the drilling investigation to facilitate the refinement of borehole locations as previously mentioned. Boreholes were prioritized in locations that were at higher risk such as significant cuts and high embankment fills on suspected ice-rich soils that might need specialized design considerations (Roujanski et al. 2010), or at structures needing further investigation such as bridges and tunnels. The depth of each borehole was carefully selected based upon the requirements for design. For high embankment fills and cuts, this was the extent of the expected zone of influence. For bridges, depth to competent bedrock was confirmed for the design of the deep foundation.

Some borehole locations were also chosen for the installation of thermistor casings to facilitate the future installation of new thermistors to collect ground temperature measurements. These casings were 2-inch PVC casing which were filled with a high salinity brine to prevent freezing.

The drilling investigation utilized two heli portable ZINEX A5 drill rigs on-site, running on both day and night shifts continuously. Continuous operation allowed for a reduced schedule and mitigated the risk of freezing the rods in the borehole if they were not removed at the end of a shift. The drilling was conducted using a 5 ft (1.5 m) triple tube core barrel and a diamond drill bit to core both permafrost soils and bedrock.

Where the permafrost soils were the target of the investigation, chilled brine at a temperature below - 4°C was used as the drilling fluid to allow the soils to stay frozen and prevent washout of fine material. This approach was accomplished by mixing a solution of calcium chloride of high concentration (95% or 98%) and water, with the temperature then being reduced by adding snow or ice until the brine reached the desired temperature.

DRILLING AND COLLECTING SAMPLES

The use of chilled brine proved to be an increasing challenge as the investigation program extended into the mid summer. As air temperatures rose and the snowpack melted, it become difficult to cool the brine on site. The mixing of calcium chloride with water is an exothermic reaction, with temperatures as high as 40°C noted after the mixing of a 1 m^3 water tote. With above freezing air temperatures and a lack of snowpack available on site, cooling the brine to the target temperature was challenging. The brine temperature had to be very closely monitored, as core recovery would reduce significantly when the brine temperature increased above the target temperature.

Grab samples of permafrost cores were collected and placed in sealed plastic jars; plastic wrap and tape used to increase the quality of the jar seal. It was decided that all grab samples would be transported at room temperature and allowed to thaw, and therefore no advanced testing could be undertaken. This decision was based on the logistics of keeping the samples below freezing and the cost and duration of testing was seen as unrealistic for this project.

Field salinity tests and bulk density calculations were conducted during the drilling program. One negative aspect of drilling with brine is that it reduces the reliability of the salinity measurements due to the salts in the brine. Field bulk density measurements were conducted to better quantify the ice content within some core samples. While the accuracy of these tests in the field was limited by the quality of the field instruments and drilling conditions, the data that resulted could be used to relatively measure the volumetric ice content of the permafrost soil, which is critical for design.

Figure 2. Undisturbed ice body recovered from location identified in Figure 1.

DIGITAL DELIVERY

The Hatch team implemented a full digital delivery of the recording, storage, and presentation of the collected geotechnical data using Bentleys OpenGround Cloud data management system and the associated tablet-based collector app. Geospatial data such as borehole locations, water sources, and field observations were recorded using the ERSI Field Maps app which utilized Hatch's ArcGIS Online GIS space. The digital delivery allowed all data to be collected via tablets, integrating the collection of field descriptions, core photos, sample information, and drilling notes into one platform that could then be instantly uploaded to the cloud upon return from the site. This allowed for data to be viewed by any team member with a data connection in near real time, without the need for paper logs into a digital database.

GEOTECHNICAL DESIGN AND ANALYSIS

While Hatch had previous experience Arctic geotechnical investigation and design experience for linear infrastructure (Roghani 2021), the 2023 investigation program closed several data gaps, with improved planning and execution methods that resulted in successful program. The method of using chilled brine as the drilling fluid greatly increased the recovery and the quality of samples, which will be an important input into design calculations such as settlement analysis and bearing capacity.

REFERENCES

Canadian Standards Association. 2019. Technical Guide: Design and construction considerations for foundations in permafrost regions, CSA Group, Toronto, Ontario, Canada.

Roghani, A. 2021. Review of the current state of knowledge regarding the design, construction and maintenance of railway lines over permafrost, National Research Council of Canada, Ottawa, Ontario, Canada.

Roujanski, V.E., Jones, K.W., Haley, J., Hawton, K., and Fitzpatrick, C. 2010. Some Permafrost Related Terrain Features and Associated Design Considerations along the Proposed Southern Rail Alignment, Mary River Project, Baffin Island, Nunavut, In GEO2010, Calgary, Alberta, Canada.

Geocell-supported railway embankment subjected to permafrost degradation

Payam Sharifi[1], Ji Woo Kim[2], Geoff N. Eichhorn[3] & Ryley Beddoe[2]

[1]*GeoTerre Ltd, Brampton, Ontario, Canada*

[2]*Department of Civil Engineering, Queen's University, Kingston, Ontario, Canada*

[3]*Department of Civil Engineering, Royal Military College of Canada, Kingston, Ontario, Canada*

Infrastructure built on permafrost in northern Canada is increasingly threatened by permafrost degradation driven by climate change. The Hudson Bay Railway (HBR) located in northern Manitoba is the only rail built on permafrost in Canada. One mitigation strategy that has been proposed for thaw settlement of rail overlying peat includes the use of geocells for subgrade soil shear strength reinforcement. There is limited design guidelines on the use of geocells as a reinforcement technique in cold regions. For the HBR railway for which the native near surface soil is composed of peat, two construction designs exist. The use of geocell reinforcement directly on top of in situ peat is evaluated under varying permafrost degradation conditions. Alternatively, peat material is sometimes replaced with an engineered fill requiring excavation of in situ ground (that method not discussed here).

Geocells, also called cellular confinement are three-dimensional geosynthetic soil reinforcement systems with honeycomb shaped networks. The space within each honeycomb creates pockets that are typically infilled with cohesionless soil. An example of a geocell is shown in Figure 1.

Figure 1. Set up of geocell layer over the HBR railway embankment foundation (Paradox 2021)

NUMERICAL MODELLING

The use of numerical modelling techniques in permafrost regions for railway embankments is well established. Although plenty of investigations have documented shown the influence of using geocells in a variety of civil projects, there is limited information on the performance of geocell reinforcement in railway engineering (Leshchinsky and Ling 2013). Miao et al. (1995) and Lai et al. (2009) reported that the Mohr-Coulomb failure criterion is appropriate for modelling frozen soils at confining pressures less than 4 MPa. This upper bound value is sufficient to cover the majority of railway embankments founded on permafrost.

A series of numerical models were conducted to simulate and quantify the performance of a typical geocell reinforced embankment founded on peat with underlying permafrost. The finite element software package used in this study was GeoStudio 2021, including TEMP/W, SEEP/W, and SIGMA/W. Only half of the 2D embankment was modelled due to the symmetric geometry. The boundary conditions and mesh grid are shown in Figure 2.

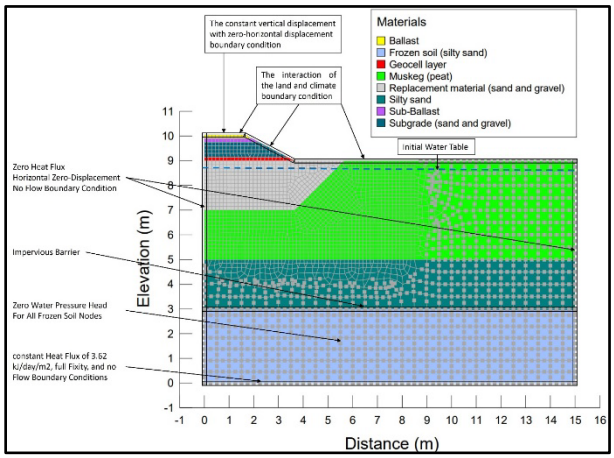

Figure 2. Geometry, boundary conditions and mesh size of a typical numerical model, shown for permafrost condition in year 2070 with active layer depth at 7 mbgs.

RESULTS AND CONCLUSIONS

The permafrost degradation driven by climate change was simulated for 50 years. An example of the thermal analysis in 2020 and 2070 is shown for the rail embankment founded directly on peat in Figure 3. It is evident from the thermal regimes plotted that there is a clear degradation of permafrost over the study period.

These simulations show that the active layer depth slowly increases over the first 20 years, from 0.54 m to 0.73 m below original ground surface. This small change emphasizes the role latent heat is playing in the top few metres in the first 20 years. However, after two decades there is a significant increase in the active layer depth from 0.73 m in 2040 to 8.72 m by 2070.

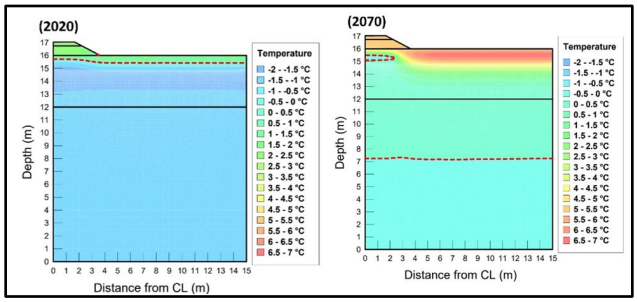

Figure 3. 2D contour plots of ground temperature for the embankment over the peat for 2020 condition and 2070 prediction

From the thermal analysis over the 50 year period, five thaw depths were taken at 1 meter intervals (referred to here as A = 1, corresponding to 1 meter thaw beyond base 2020 model). The thaw depths defined the zone of frozen and unfrozen soil for the bearing capacity analysis. The load-deformation results of peat bed scenarios are shown in Figure 4, which shows the crest settlement of the unreinforced and reinforced railway embankment founded directly on peat for increasing active layer thicknesses. The results show that a uniformly distributed pressure on the embankment founded directly on peat will experience a bearing capacity failure at around 30 kPa. Using a geocell reinforcement increases the bearing capacity to approximately 70 kPa, for a no thaw condition. There is a clear benefit of using the geocell, as it was seen that crest settlement was reduced from 2 meters to 1 meter by using geocell. This method should be compared against other more intensive material removal methods such as the engineered replacement (fill) method (ERM). These results are not presented here but are documented in Sharifi (2022) and Sharifi et al. (2024).

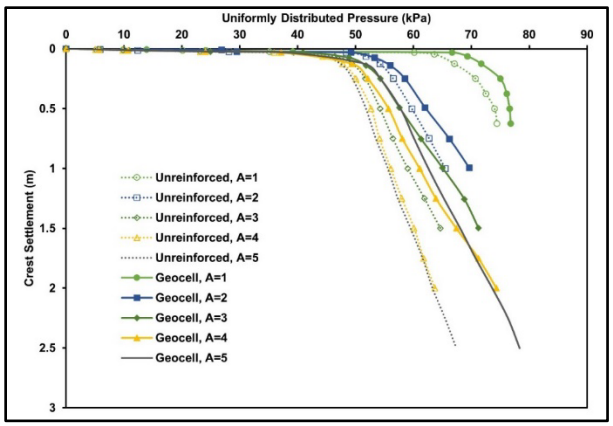

Figure 4. Embankment crest settlement under uniformly distributed pressure for different active layer depths (A=1 to 5 m).

REFERENCES

Lai, Y., Jin, L., and Chang, X. 2009. Yield criterion and elasto-plastic damage constitutive model for frozen sandy soil. International Journal of Plasticity, 25(6), pp.1177-1205.

Leshchinsky, B., and Ling, H.I. 2013. Numerical modeling of behaviour of railway ballasted structure with geocell confinement. Geotextiles and Geomembranes, 36, pp.33–43.

Miao, T., Wei, X., and Zhang, C. 1995. Creep of frozen soil by damage mechanics. Science in China (Scienctia Sinica) Series B, 8(38), pp.996–1002.

Sharifi, P. 2022. Assessing a geocell-supported railway embankment subjected to permafrost degradation and ponding water conditions using numerical modelling techniques. MSc Thesis. Royal Military College of Canada.

Sharifi, P., Eichhorn, G.N., Beddoe, R. 2024. Geocell-supported railway embankment subjected to permafrost degradation. Journal of Cold Regions Engineering. Submitted January 2024).

Yang, Y., Lai, Y., and Chang, X. 2010. Laboratory and theoretical investigations on the deformation and strength behaviours of artificial frozen soil. Cold Regions Science and Technology, 64(1), pp.39–45.

7B — Foundations and Infrastructure on Permafrost: Case Studies and Innovations

Session Chairs: Ming Xiao[1], John Thornley[2] & Ziyi Wang[1]

[1]*Pennsylvania State University, Pennsylvania, United States*
[2]*Williams Sale Partnership Limited, Anchorage, Alaska, United States*

42% of Arctic communities and 70% of Arctic infrastructure lie in permafrost, whose temperature has consistently increased in the past four decades. Infrastructure can itself accelerate the thawing of permafrost. Innovative infrastructure and foundation design are needed to meet the challenges of thawing permafrost.

This session welcomes researchers, practitioners, and government officials to share case studies, innovative technologies, and learned lessons and experiences in designing and constructing foundations of civil infrastructures on permafrost.

Permafrost and geothermal modelling in support of geotechnical foundation design and hazard mitigation: Pretty Rocks Landslide, Denali National Park, Alaska

Heather M. Brooks, Ph.D., P.E.[1], Lukas Arenson, Dr.Sc.Techn.ETH, P.Eng.[2], Earl De Guzeman, Ph.D., P.Eng.[3], Evan Garich, P.E.[4] & Denny Capps, Ph.D.[5]

[1]*BGC Engineering, Inc., Calgary, Alberta, Canada*

[2]*BGC Engineering, Inc., Vancouver, British Columbia, Canada*

[3]*Tetra Tech, Vancouver, British Columbia, Canada*

[4]*Western Federal Lands Highway Division, Vancouver, Washington, United States*

[5]*National Parks Service, Denver, Colorado, United States*

The Denali Park Road is a 92-mile scenic roadway that connects the Denali National Park entrance, near Healy, AK, to Kantishna, AK and is the only access road into the park. In September 2021, the roadway was closed at approximately Mile 45 due to the accelerated movement of Pretty Rocks Landslide in a section of the roadway known as Polychrome Pass. Pretty Rocks Landslide effects approximately 90 m (300 ft) of the Denali Park Road. Since 2021, the National Park Service, Western Federal Lands Highway Division, Jacobs Engineering and BGC Engineering USA Inc. (BGC) were collaborating on the design of a bridge that will provide access to Kantishna by avoiding the landslide hazard. The bridge consists of a 145-m (475-ft), single-span steel truss bridge that will be founded in rock. This extended abstract and work focuses on the East Abutment of the bridge.

SUBSURFACE CONDITIONS AND DESIGN MODEL PURPOSE

In support of this project, BGC completed two site investigations with boreholes, geophysical surveys, instrumentation, and geologic field mapping. The subsurface conditions at the east abutment consist of an approximately 60-degree east-dipping rhyolite, approximately 27 m (90 ft) in thickness, overlying a clay-like, ash tuff material to the extents of the investigations. Permafrost is present throughout with ice observed in joints in the rhyolite and a 0.3 m (1 ft) ice layer (East Abutment ice) present at the basal contact of the rhyolite and the ash tuff. Ground temperatures in this area are approximately -0.5°C (31°F) (BGC, 2022 November 21).

We recognized the importance of the East Abutment ice as a critical feature to be considered in the design of the foundation of the bridge. Given the site was unglaciated from 50,000 to 80,000 years ago (Healy glaciation) and the topography was generally set prior to Riley Creek glaciation (9,500 to 26,000 years ago), permafrost aggraded into the subsurface within this timeframe (Wahrhaftig 1958). Additionally, the hydration of the ash tuff through time and potential heat flow pathways, given the topography, the East Abutment ice is assumed to be present in a continuous layer of varying thickness due to the preferential heat flow pathway through the higher thermal conductivity rock.

This realization required the design team to use geothermal modelling to address three major questions:

- Will changing climate conditions at the site degrade the permafrost at this depth during the service life of the structure? If so, what are the implications of this degradation on the structure?
- Will passive cooling techniques (thermosiphons) function to cool the subsurface to a temperature that will maintain a significant portion of the porewater in a frozen state?
- If both answers are yes, what is the layout of a thermosiphon system around the other foundation elements that will provide this cooling capacity?

Due to the complex topography, a three dimensional (3D) geothermal model was developed to answer these questions.

GEOTHERMAL MODELLING

The model consisted of the development of a 3D geological model in Seequent's Leapfrog Geo software for this section of the site, using borehole, geophysics and lidar data, and structural geological mapping results. This geometry was imported into GeoStudio's Build3D software for the development of the model meshing, application of boundary conditions and material properties. Air temperature boundary conditions were determined from CMIP5 climate data for the site to the year 2100. N-factors were used to modify these air temperatures to ground temperatures based on the aspect, local topography and site photos in summer and winter to characterize the general albedo and snow drifting. A geothermal heat flux of

80 mW/m^2 (0.0253 BTU/hr/ft^2) was used to select the basal boundary condition.

GeoStudio's Temp3D was used for the geothermal modelling. The model was calibrated to match measured ground temperatures throughout the year and active layer extents in the fall. In January 2022, BGC received photos from site showing a significant scarp was present adjacent to the East abutment. These photos were used to alter the topography of the model such that an approximate 15 m (50 ft) scarp was present within the model following the calibration step. Once calibrated and the scarp material removed, projected air temperatures were cycled for 5 years of model time for each climatic timestep (2020-2040, 2040-2060, 2060-2080, 2080-2100). Permafrost conditions at the East Abutment ice will degrade based on the model results with ground temperatures at the depth of the East Abutment ice above 0°C in 2099.

Additional modelling was completed to determine the effectiveness of thermosiphons at the site, and the quantity and location of those thermosiphons to prevent the permafrost degradation of the East Abutment ice. Air temperature projections were updated to CMIP6 data. A thermosyphon boundary condition (encoded in TempW3D) with a 15.8 m^2 (170 sqft) condenser area and extending 33.4 m (110 ft) depth was applied at 22 locations within the model. The geometry of the thermosiphons focused cooling on a trapezoidal prism at the East Abutment. Wind speeds were determined from CMIP6 projections and compared to a limited (2-year duration) on-site dataset and resulted in approximately 1.6 m/s (3.6 mph) constant speeds were applied to the thermosiphon boundary condition. The design ground temperature for the thermosiphons is -2°C as at this ground temperature the majority of the pore water within the ash tuff will be present in solid form. The thermosiphon boundary conditions were active for each of the 5-year duration climatic timesteps.

RESULTS

The thermosiphons cooled the ground temperatures at the base of the thermosiphons from -0.5°C to between -12°C and -5°C (10°F and 22°F) depending on the projected climatic timestep. The thermosiphons meet the design intent and have been included within the bridge foundation design. The location of the thermosiphons was optimized based on discussions with design team members and the contractor, to limit restrictions on temporary construction works. For this reason, approximately 5 of the thermosiphons will be installed at a batter.

CONCLUSION

Three-dimensional geothermal modelling was completed to determine whether degradation of the East Abutment ice will occur during the expected service life of the structure. Modelling proved that degradation is likely at the depth of the East Abutment ice. Thermosiphons were added to the model via thermosiphon boundary conditions at 22 locations to a depth of 33.5 m (110 ft) in a trapezoidal prism around the east bridge abutment. The thermosiphon modelling will reduce the ground temperatures to the extent needed in the design.

REFERENCES

BGC Engineering USA Inc. (2023, June 21). Geotechnical Report 02-23, Polychrome Area Improvements – Geotechnical Report. Prepared for Western Federal Lands Highway Division, Federal Highway Administration, FHWA.

BGC Engineering USA Inc. (2022, November 21). Geotechnical Memorandum 42-22, AK NPS DENA10(49), Polychrome Area Improvements – Instrumentation Data and Geothermal Modeling Update. Prepared for Western Federal Lands Highway Division, Federal Highway Administration, FHWA.

BGC Engineering USA Inc. (2022, March 29). Geotechnical Report 06-22, Polychrome Area Improvements – Geotechnical Modeling Report. Prepared for Western Federal Lands Highway Division, Federal Highway Administration, FHWA.

Wahrhaftig, C.L. 1958. Quaternary Geology of the Nenana River valley and adjacent parts of the Alaska Range (Part A). In Quaternary and Engineering Geology in the Central Part of the Alaska Range. Geological Survey Professional Paper 293.

Building stabilization on warm permafrost in Mongolia

Namdag Choibalsan[1], Yamkhin Jambaljav[2], Byambajav Bayarbat[3] & Avirmed Mukhtsolmon[2]

[1]*NewCon LLC, Ulaanbaatar, Mongolia*

[2]*Geocryo LLC, Ulaanbaatar, Mongolia*

[3]*Golden Progress LLC, Ulaanbaatar, Mongolia*

Mongolia is located on the southern edge of the East Siberian permafrost region, which is the world's largest permafrost area. Almost 29.3% of the country's territory is covered with permafrost from isolated to continuous distribution (Yamkhin et al. 2022). Climate projection models suggest that with future climate change, the most negative impacts for Mongolia could arise from the intensification of drought and aridity, thawing of permafrost, etc (MARCC-2014).

Mongolia is divided into 21 provinces, each province has several administrative units called soums. About 105 soums are located on permafrost, and about 1,400 km of roads pass through the permafrost areas of Mongolia. However, in recent years, buildings on permafrost have been damaged due to permafrost thawing within 1-5 years after construction, both in the north of the country and in the south of the permafrost distribution.

Mongolia has the same rules for construction on permafrost as Russian construction rules (Namdag 1996).

There are several methods to mitigate the effects of thawing permafrost beneath infrastructure, such as convection embankments, thermosyphons, pile foundations and etc.

We used pile foundations, which remove heat from the infrastructure, but recently most buildings with pile foundations in Mongolia are being damaged due to the thawing of permafrost underneath, and buildings with pile foundations are accelerating the rate of permafrost degradation. Most often, permafrost thaws in front of the facades of buildings with pile foundations, after which thawing bowls form underneath it.

Therefore, in recent years, we have combined pile foundations with thermosyphons, and here we present the initial result of the cooling effect of a thermosyphon under a hospital building in Arbulag soum, Hovsgol province, northern Mongolia.

Thermosyphon is a sealed tube containing a two-phase low-temperature liquid under pressure, it is a renewable energy (winter-cold) device that does not require additional energy for operation (Edward et al. 2002). There are several types of thermosyphons developed since the 1960s. In our case, we use inclined thermosyphons.

Site settings

Site is located in soum center of Arbulag, Hovsgol province, Northern Mongolia, where permafrost has a discontinuous distribution. At the local level, the center of the soum is located in valleys with small lakes, springs and small rivers. Therefore, the subsurface materials are dominated by lacustrine sediments with gravel, loam and silt. Permafrost has uneven ice content.

In the center of Arbulag soum there are several buildings, some of which are damaged due to permafrost thawing (Figure 1).

Figure 1. Wooden building in Arbulag soum. The holes in the foundation are for ventilation. Cracks appeared on both the internal and external side walls.

Construction structure

Many of these buildings, built between 1950 and 1990, are predicted to fail due to the weakening load-bearing capacity of the frozen soil in which the concrete piles are installed. Statistics show several large buildings are predicted to fail by 2030 (French 2007). In Mongolia, we used pile foundations on permafrost, and recently these buildings were damaged due to the thawing of the permafrost underneath. Additional cooling of permafrost beneath the infrastructure is currently required.

The new hospital building, 27 meters wide and 33 meters long, stands on 40 concrete pile foundations. On the side of the pile foundation, we placed 50 inclined thermosyphons with a slope of 73 degrees. According to previous practice, permafrost thawing begins from the facade of the building, so we installed additional

inclined thermosyphons between the pile foundations on the front and left sides of the building (Figure 2).

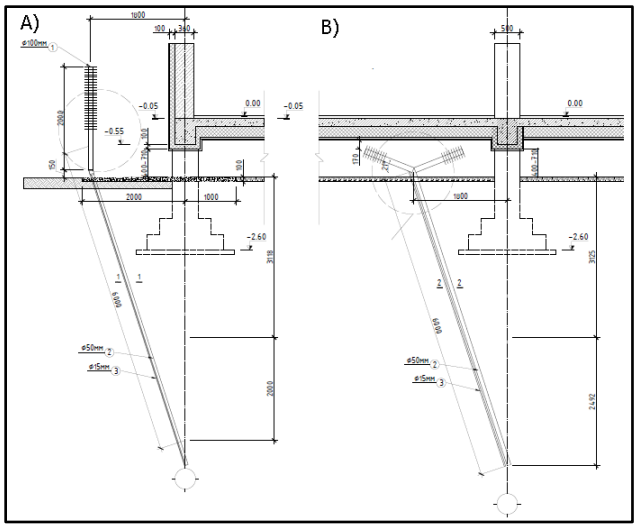

Figure 2. Thermosyphon under the building. A) Thermosiphon outside the building and with the evaporators tilted at 73 degrees. B) Thermosyphon in the crawl of a building with an inclined evaporator and with 2 condensers.

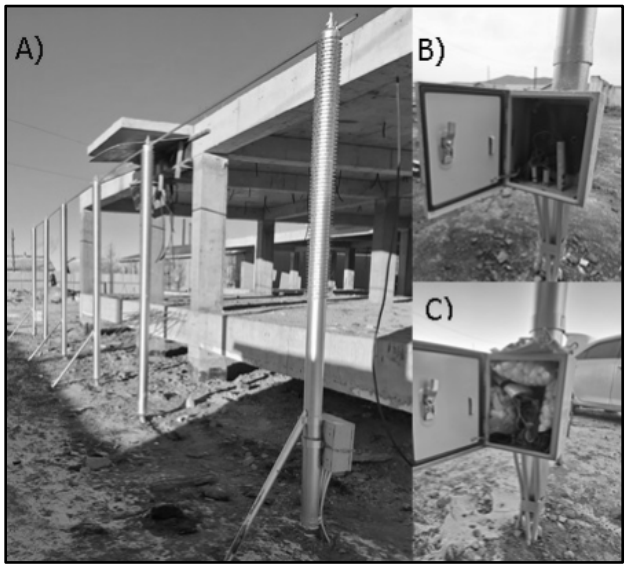

Figure 3. A) Thermosyphons on the facade of the building, B) Control box with tubes with a diameter of 15 mm to control the temperature along the evaporator piles. C) A UX120-006M 4-channel analog recorder from Onset was placed in the control box and recorded data at 1-hour intervals.

RESULTS AND DISCUSSION

The most effective method for stabilizing warm permafrost is thermosyphon cooling beneath the infrastructure (Wagner 2014).

Construction of the hospital building in Arbulag soum began in May 2023. After the construction of the building frame, thermosyphon condensers were installed in Ausgust 2023 (the above-ground part of the thermosyphons). After drilling the holes, a 15 mm diameter pipe was installed along with evaporator piles to control the temperature along the evaporator. Also, 7 control boxes were installed for monitoring of 23 thermosyphons and holes were drilled at 7 points to control the ground temperature at some points on the thermosyphon side under the building (Figure 3). The ground temperatures were measured once along the evaporator tubes before charging, and these temperatures ranged from -1°C to -2°C below 3.5m from ground surface. Mainly in Mongolia, the thermosyphon began to cool the ground from the end of September. In other words, from the end of September the air temperature at night becomes sub-zero.

As of November 30, 2023, the ground temperature along the evaporator pipes ranged from -5.1°C to -11.5°C, while the air temperature was -21°C, the ground temperature on the thermosyphon side was from +0.05°C to -1.5°C.

REFERENCES

Edward, Y., and Erwin L.L. 2002. Recent Developments in Thermosyphon Technology, In 11th International Conference on Cold Regions Engineering, Anchorage, Alaska, USA, 1: 656–662.

French, H.M. 2007. The periglacial environment. 3rd ed., Chichester, UK: John Wiley & Sons Ltd.

Mongolian Second Assessment Report on Climate Change 2014. Ulaanbaatar, MN

Namdag, Ch, 1996. Rules and Norms for Basis of Buildings and Facilities. Ulaanbaatar, MN:

Wagner, A.M. 2014. Review of Thermosypon Applications, Technical Report, ERDC/CRREL TR-14-1

Yamkhin, J, Yadamsuren, G, Khurelbaatar, T, et al. 2022. Spatial distribution mapping of permafrost in Mongolia using TTOP. Permafrost and Periglac Process, 33(4): 386–405. doi:10.1002/ppp.2165

Random finite element model for the freezing effects on soils and underground pipes

A. Shaoyang Dong, Yusheng Jiang & Xiong (Bill) Yu
Department of Civil Engineering, Case Western Reserve University, Cleveland, Ohio, United States

This paper describes the development of a random finite element model (RFEM) to holistically simulate the temperature, stress, and deformation responses of frozen soils. The RFEM model is firstly validated with experimental data and is then implemented to simulate the induced stress in pipes due to ground freezing.

Frost heave in cold regions may cause pavement upheaving and cracking, retaining wall and pipeline failures and other serious damages to civil infrastructure. It is a coupled multi-physical process involving the coupling of the thermal-hydro-mechanical (THM) process. In the microstructural view, frozen soil is a four-phase material that includes soil particles, ice, water, and air, arranged randomly. This paper describes the development and implementation of random finite element model, which can simulate the phase composition of frozen soil and the thermo-hydro-mechanical processes in frozen soils.

METHODS

The theoretical basis, the governing equations of the model, for the thermo-hydro-mechanical processes has been established in previous works by Dong et al. (2021) and were utilized in this work.

The single column freezing experiments were conducted using two identical cylindrical silt specimens. The vertical strain and temperature variation at different depths are measured during both freezing and thawing process.

Based on the physical properties of the silt specimens, the corresponding soil image samples are generated by grey scale pixcels in Matlab. The phase of the image sample is color coded with black, dark grey, light grey, and white to represent soil particles, ice, water and air, respectively. The sample image is then imported to the finite element software COMSOL to assign the material properties (including thermal, mechanical, hydraulic properties) based on the color scale of the image and perform coupling analysis. The Zoomed-in example of specimen images is shown in Figure 1.

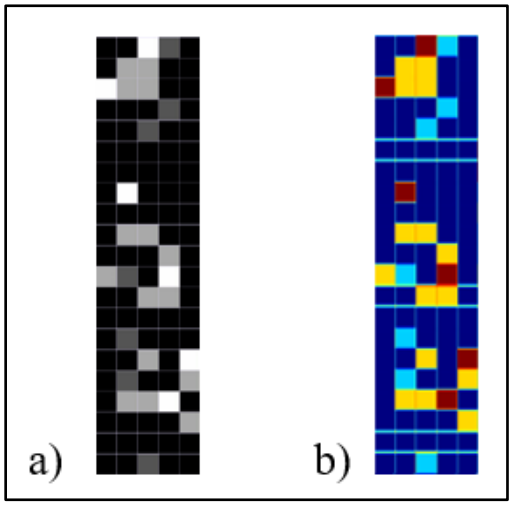

Figure 1. Zoomed-in example of specimen image: a) grey scale phase coded image by MATLAB and b) converted phase coded image by COMSOL.

RESULTS AND ANALYSIS

The comparison between the image-based RFEM modeling and lab experiments validates the performance of the model. Both the vertical strain and temperature distribution show well-matched results as presented in Figure 2 and 3.

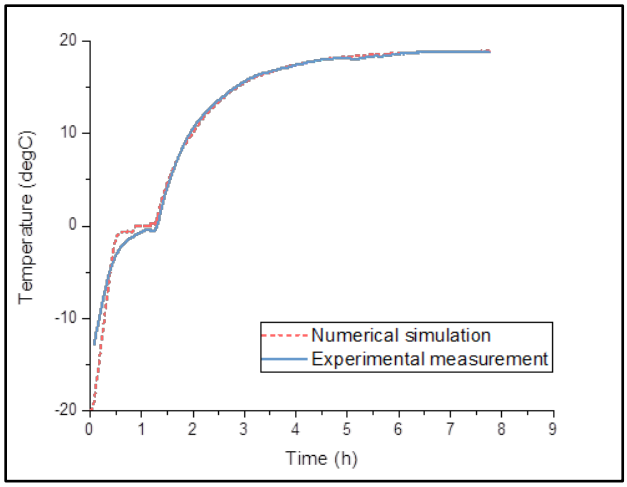

Figure 2. Comparison of the numerical simulation and the experimental measured average sample temperature.

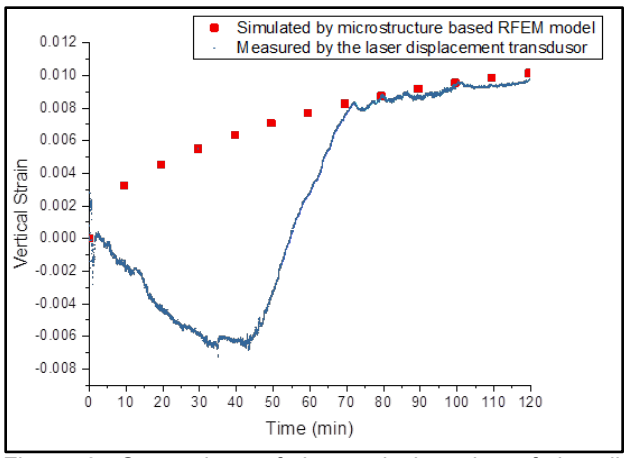

Figure 3. Comparison of the vertical strains of the silt specimen between experimental measurement and numerical simulation during the freezing process.

CASE STUDY OF SOIIL-PIPE INTERACTIONS

To demonstrate the engineering applications of the new model, it is utilized to analyze the interactions between ground and pipeline subjected to freezing conditions. Four different scenarios are considered in the model: intact pipe, pipe with crack, cracked pipe with a 15 kN point load on the ground surface, cracked pipe with 480 kN point load on the ground surface. The results of contact pressure around the pipe before freezing and after freezing are simulated. Examples of the results are shown in Figure 4 and 5.

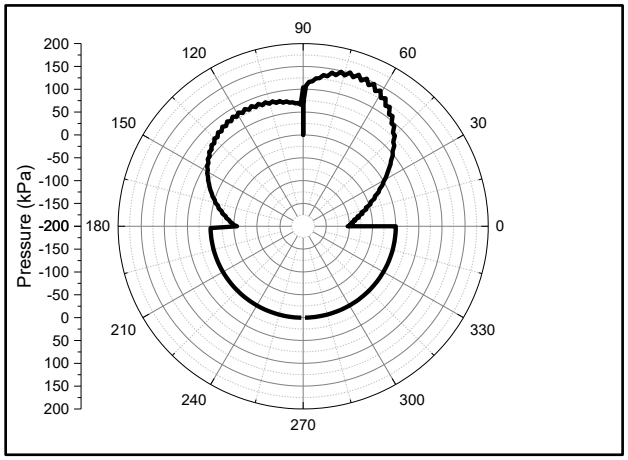

Figure 4. Pressure distribution around the water pipeline buried under ground before freeze.

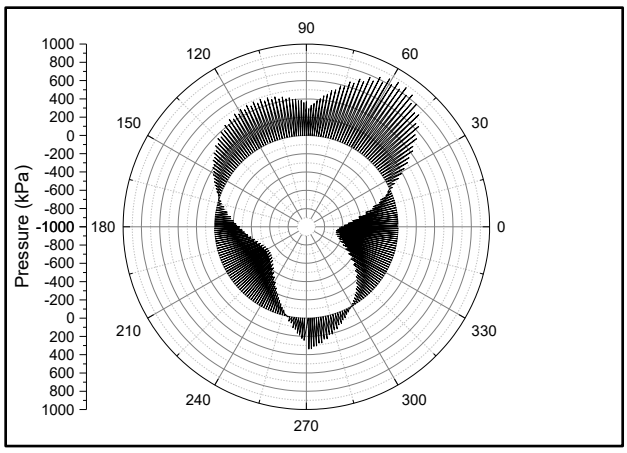

Figure 5. Pressure distribution around the water pipeline buried under ground after freeze.

DISCUSSION

The case results show there are unique characteristics of contact stress variations around the pipe due to soil microstructure. The sensitivity study shows that frost load increases the stress in the underground pipes, which is also affected by the pipeline burial depth, the integrity of the pipe (i.e., cracks), surface load (i.e., by traffic). Ground freezing tends to increase the stress in underground pipes, and therefore accelerate its fatigue damages.

The RFEM model combines the advantages of discrete element model, in describing the microstructure effects, and finite element model, in its high computational efficiency.

REFERENCE

Dong, S., Jiang, Y., and Yu, X. 2021. Analyses of the Impacts of Climate Change and Forest Fire on Cold Region Slopes Stability by Random Finite.

Versatile cooling strategies for mitigating permafrost thaw in varied infrastructure environments

Igor Egorov
National Research Council of Canada, Ottawa, Ontario, Canada

The degradation of permafrost beneath Northern Canada's infrastructure poses significant challenges, leading to an escalation of permafrost-related issues that strain budgets and resources (Chasmer et al. 2017, Smith et al. 2010, Write et at. 2022). Traditional reactive methods for road and building rehabilitation in permafrost-affected areas have proven to be both costly and environmentally detrimental. In response to these pressing challenges, NRC Construction has introduced and tested innovative cooling techniques designed to effectively manage permafrost thaw.

These cooling techniques offer versatile applications in different scenarios, ranging from linear structures like roads (Doré et al. 2016) to specific areas of interest and various foundation types, including pile foundations and shallow foundations. The initial trial in Tuktoyaktuk yielded promising results, showcasing the potential of these techniques to mitigate permafrost thaw.

The objective of this study project is to assess the efficiency of these cooling techniques and evaluate their potential application for Northern infrastructure. By doing so, the project aims to lay a solid foundation for future phases, contributing to the sustainable management of permafrost-related challenges in the region.

Evolving permafrost environments and risks to communities

The ongoing degradation of permafrost is exacting a substantial financial toll, with the associated processes necessitating costly retroactive maintenance measures. These processes include the expansion of thermo erosion, retrogressive thaw slumps, icing, an increase in active layer thickness, talik formation, thermokarst, differential settlements, active layer changes, increased groundwater flow, leaching of chemicals buried in permafrost, frost jacking, frost heave, and heaving, increasing freezing/thawing cycles (Figure 1). The cumulative impact of these permafrost-related challenges underscores the urgent need for effective mitigation strategies to alleviate the economic burden on the affected regions.

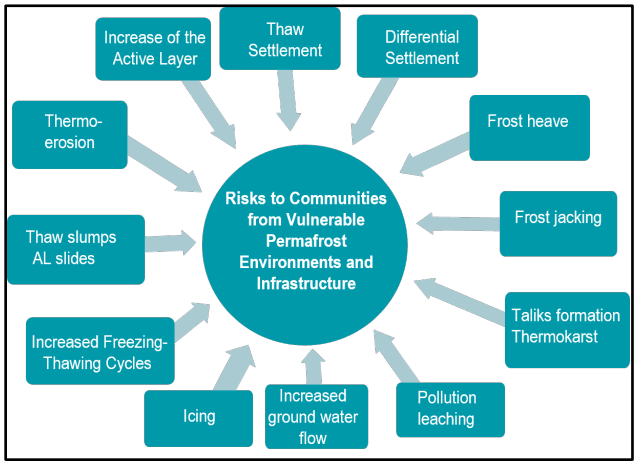

Figure 1. Permafrost thaw-related processes endangering landscapes and infrastructure in permafrost regions.

Study site

The study site for the research on remediating permafrost with active and passive freezing systems is situated in Tuktoyaktuk. This location is characterized by continuous permafrost, with a 2-meter talik in fill material. The freezing index (FDD) are recorded at -4051 degree days, and the thawing index (TDD) stand at 1349 degree days. The mean annual air temperature for the current year (2023) is documented as -7.30°C. The site provides an ideal environment for investigating the effectiveness of various remediation techniques, including liquid-filled thermosyphons (Kazemi et al. 2022) natural and artificial insulation, and phase change material, in addressing permafrost-related challenges (Figure 2)

Preliminary results

This pilot test focuses on assessing the effectiveness of active and passive methods designed to restore permafrost in both existing and future infrastructure projects. The methods under investigation include liquid-filled thermosyphons (LFT), organic solutions (peat moss), and insulation paired with phase change material (PCM). Initiated in the summer of 2022, the pilot field tests aim to refine the performance of each ground cooling technology by monitoring variations in minimum ground temperatures, freezing and thawing indices, winter and summer ground conditions, and adjusted mean

annual ground temperatures. The project assesses the effectiveness of various mitigation methods, such as Active LFT, Active LFT+INS+PCM, Passive LFT+INS+PCM, Peat+PCM, and INS+PCM, as engineered cooling ground solutions. It compares the cooling effects across different stations.

Figure 2. Evaluating freezing techniques - active liquid-filled thermosiphon in action.

Preliminary findings from a 12-month monitoring period (August 2022 to December 2023) reveal that Active LFT exhibited the most substantial reduction in minimum negative ground temperatures at a 1-meter depth, registering at -4.1°C compared to the control station (see Figure 3).

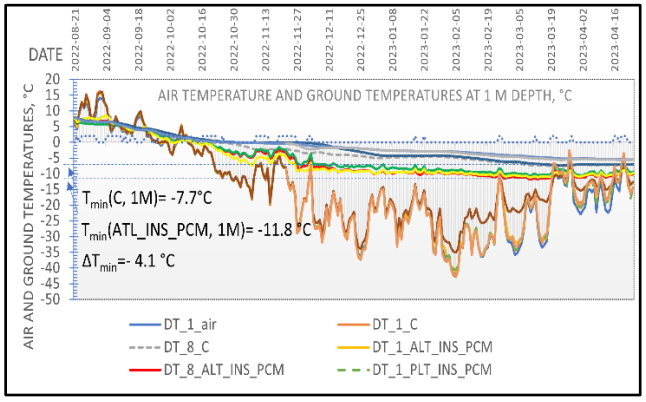

Figure 3. Air and ground temperature data, illustrating the distinct freezing effects achieved by different techniques throughout the winter of 2022/2023.

Engineering Insights

Controlling permafrost thaw involves modifying the properties and heat balance of the Active Layer. Test results indicate that liquid-filled thermosyphons, in conjunction with a "cold battery," insulation, and phase-change materials, exhibit optimal efficiency in permafrost restoration.

These freezing systems have versatile applications, including point freezing (thermopiles), linear freezing ("frozen wall"), and area freezing/thawing ("frozen pad"). They can effectively counteract thermal erosion, slumps, and the differential settlements of roads and shallow foundations.

Liquid-filled thermosyphons, combined with insulation and phase-change materials, can also be utilized in thawing.

Acknowledgement

The author thanks CRBE NRC for financial support and technicians Dennis Crys and Antal Prigli for field assistance and device development

References

Chasmer, L., and Hopkinson, C. 2017. Threshold loss of discontinuous permafrost and landscape evolution. Global Change Biology 23, 2672–2686. https://doi.org/10.1111/gcb.13537

Doré, G., Niu, F., and Brooks, H. 2016. Adaptation Methods for Transportation Infrastructure Built on Degrading Permafrost. Permafrost and Periglacial Processes, 27(4), 352–364. https://doi.org/10.1002/ppp.1919

Kazemi, A., Roostaie, M., Egorov, I., and Leonenko, Y. 2022. An Analytical Solution For Heat Extraction From Shallow Ground Using A Single Phase Closed Thermosyphon: A Model For Artificial Ground Freezing. Journal of Energy Storage, 55(B), 105599. doi:10.1016/j.est.2022.105599. Available at SSRN: https://ssrn.com/abstract=4033757 or http://dx.doi.org/10.2139/ssrn.4033757

Smith, S.L., Romanovsky, V.E., Lewkowicz, A.G., Burn, C.R., Allard, M., Clow, G.D.,Yoshikawa, K., and Throop, J. 2010. Thermal state of permafrost in North America: a contribution to the international polar year. Permafrost and Periglacial Processes 21, 117–135. https://doi.org/10.1002/ppp.690

Wright, S.N., Thompson, L.M., Olefeldt, D., Connon, R.F., Carpino, O.A., Beel, C.R., and Quinton, W.L. 2022. Thaw-induced impacts on land and water in discontinuous permafrost: A review of the Taiga Plains and Taiga Shield, northwestern Canada. Earth-Science Reviews 232,v 104104. https://doi.org/10.1016/j.earscirev.2022.104104

The prospects of using heat pumps in the construction of buildings in the areas with buried table of ice-rich permafrost

Alina Gorbunova[1], Alexey Gunar[1] & Konstantin Ozeritskiy[2]
[1]*Department of Geocryology, Lomonosov Moscow State University, Moscow, Russia*
[2]*Department of Civil Engineering, University of Calgary, Calgary, Alberta, Canada*

Climate warming has a significant impact on built infrastructure in the permafrost region. The increased settlement of buildings, caused by the thawing of permafrost (Khrustalev et al. 2011), necessitates the development and implementation of a monitoring system for the foundation conditions almost at all infrastructure in permafrost areas. However, monitoring and timely resolution of emerging issues are not optimal for the operation of structures. Our task is to develop and implement solutions ensuring the stable operation of structures in permafrost regions.

CLIMATE-INDEPENDENT CONSTRUCTION

The most common method of building infrastructure on perennially frozen soils, developed and implemented in construction practices in the USSR, involves the use of ventilated crawl spaces beneath the structures. In this approach, the ventilated crawl space can be employed both in areas with continuous permafrost and in locations with a buried permafrost table (Khrustalev 2005). In the former case, the crawl space cools the soils, enhancing their load-bearing capacity, while in the latter, it regulates the amount of heat entering the mass, preventing freezing and thawing of the soils beneath the building.

Currently, methods of permafrost stabilization using thermosyphons are widely used—they can be positioned both beneath buildings and along the perimeter of the structure. Technologies managing geocryological parameters, such as snow clearance around the building or the use of insulation to reduce seasonal thawing around structures, are employed to a lesser extent.

However, all the construction methods mentioned above share a common drawback—they are all climate-dependent. With the rise in average annual air temperatures, each of these methods loses its efficiency. If the warming trend persists in the coming years, within 2-3 decades, in regions where perennially frozen soils are prevalent, these methods will become ineffective and require additional financial investments.

ACTIVE FREEZING OF SOILS

It seems that using refrigeration units to maintain the frozen state of the soil mass over the 50-80 years of a structure's operation is initially too expensive. However, the combination of a heat pump and modern insulation materials allows to minimize costs. Insulation materials reduce the heat flow from the structure into the soils, and the use of a heat pump allows the extracted thermal energy to be converted into an additional heat source for heating systems or water supply systems. In Russia, a patent (Khrustalev et al. 2016) has been obtained, and a low-depth slab foundation for light buildings is being developed, incorporating both the cold and warm circuits of a heat pump. The cold circuit of the slab cools the foundation soils, while the heat extracted from the foundation is directed to heating the building's floor (Gorbunova 2023). Heat transfer from the warm circuit to the cold one is minimized by using a layer of thermal insulation (Figure 1).

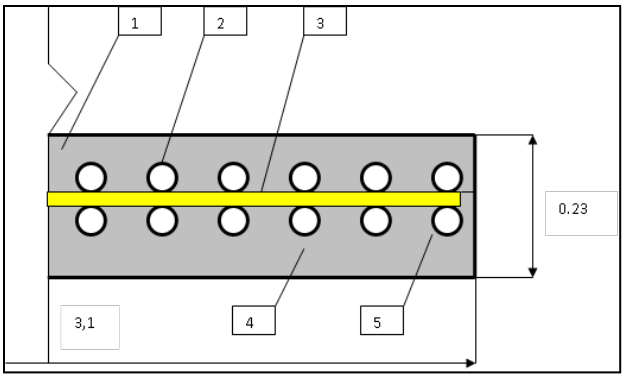

Figure 1. Fragment of a surface foundation. 1 - Upper part of the reinforced concrete slab; 2 - coil of the heating circuit of the heat pump; 3 - thermal insulator; 4 - lower part of the reinforced concrete slab; 5 - coil of the cooling circuit of the heat pump.

However, for the construction of heavy buildings, the proposed technology will not allow for sufficient load-bearing capacity of the soils. The solution to this problem is scaling — it is necessary to place the cooling circuit deep enough into the soil mass. Our calculations show that having the cooling circuit at a depth of 4 meters from the heat-emitting boundary

allows maintaining the soils in a frozen state with 10-15 heat pump activations per year, even in the presence of perennial thawing beyond the structure's perimeter (Figure 2).

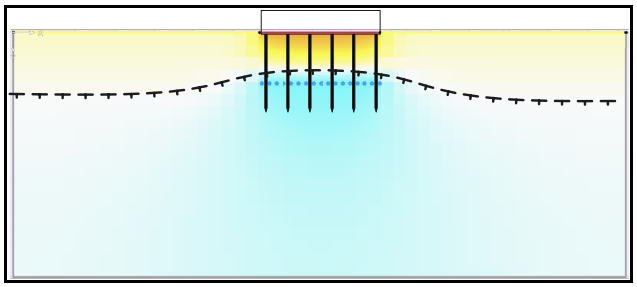

Figure 2. Stabilization of the upper boundary of permafrost soils using a heat pump, simulated by QFrost (Pesotskiy 2016).

CONCLUSION

The choice of one technical solution over another at the project development stage should be based on a technical and economic comparison of options. However, the climate dependence of standard design solutions creates some uncertainty in assessing the reliability of structures throughout their entire service life. The solution to this problem is to incorporate methods of active thermal stabilization of soils into the project. For areas with high embankments, the cooling circuit allows the creation of a buffer zone of cyclically freezing and thawing soils, completely eliminating the heat flow from the building to the buried permafrost table. In areas with confluent permafrost, heat pumps can serve as a backup device. If the climatic parameters specified in the project exceed acceptable limits, turning on the cooling unit installed at the project stage will prevent thawing of the base. The economic feasibility of the proposed solution is determined by the reduction of operating costs and the almost complete elimination of problems associated with the thawing of the frozen base.

REFERENCES

Gorbunova, A.A. 2023. A new way of using high-temperature permafrost soils as the foundations of single-storey buildings in the conditions of global climate warming. Scientific Bulletin of the Yamal-Nenets Autonomous District. № 1. (118). P. 38–54.

Khrustalev, L.N. 2005. Geotechniqal fundamentals for permafrost regions. Moscow MSU, 2005

Khrustalev, L.N., Parmuzin, S.Yu., and Emelianova, L.V. 2011. Reliability of northern infrastructure in a changing climate. Moscow, Universitetskaya kniga, 260 p.

Khrustalev, L.N., Khilimonyuk, V.Z., Perlstein, G.Z., and Kamanin, D.V. 2016. Surface foundation of a structure ensuring the preservation of foundation soils in a frozen state with simultaneous heating of the structure. Patent No. 2583025, Bulletin No. 12

Pesotsky, D.G. 2016. QFrost software for calculating the thermal interaction of structures with permafrost soils. Certificate No. 2016614404. State register of computer programs, 04/22/16.

Longyearbyen ski lift – Geotechnical design

Arne Instanes
Instanes AS Consulting engineers, Bergen, Norway

The world's most northenly ski lift was constructed in Longyearbyen in 2023. The ski lift is located on the eastern sloping hills of the Longyear valley, Svalbard, at 78° north, see Figure 1.

Figure 1. Location of ski lift in Longyearbyen.

The lower station will be approximately 38 metres above sea level (m.a.s.l) with the 460 metres long lift transporting skiers up to approximately 153 m.a.s.l. The lift consists of a lower loading station, an upper unloading station, and seven masts supporting the tow cable. The design and construction of the ski lift is carried out by Doppelmayr Seilbahnen GmbH, Austia. In the Doppelmayr foundation system, each station and mast must have a foundation consisting of a concrete slab buried at a minimum 1.6 m below the terrain surface. Given the presence of permafrost, the standard foundation system could not be used due to the risk of thaw settlement and possible lateral loads acting on the shallow foundations from slope processes.

Instanes AS Consulting Engineers (IAS) investigated a revised foundation design taking into consideration the permafrost conditions at site. A piled foundation system has been designed where the piles are to be drilled to bedrock.

CLIMATE AND CLIMATE CHANGE

The normal air temperature in Longyearbyen increased from -6.7 °C (based on the 30-year period 1961-1990) to -3.8 °C (based on the 30-year period 1991-2020). Figure 2 presents observed annual air temperaures (circles) 2000-2022, observed increase in 30-year mean (bold red line), and RCP8.5 models for Longyearbyen based on Hanssen-Bauer et al. (2019). The RCP8.5-lines presented in the figure represent a modelled linear increase in 30-year mean annual air temperatures from 2071-2000 to 2071-2100.

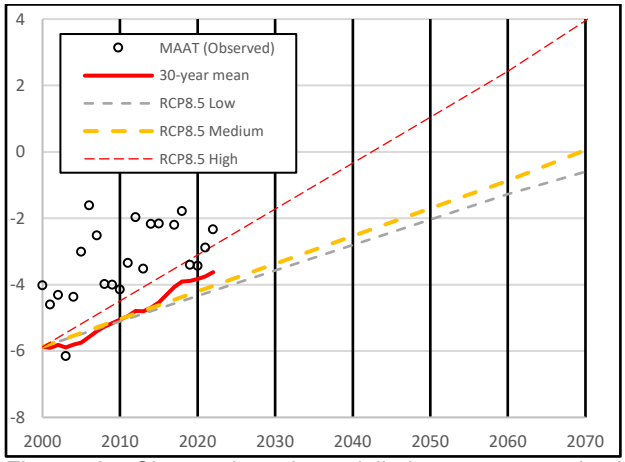

Figure 2. Observed and modelled mean annual air temperature Longyearbyen.

Hanssen-Bauer et al. (2019) have recommended using a medium based RCP8,5 climate scenario as a design basis for engineering projects. This entails the engineering design taking into account that the "normal" annual air temperature in Longyearbyen will be approximately 0 °C in 2070 (30-year mean 2041-2070) compared to the current normal of -3.8 °C.

SOIL INVESTIGATIONS AT THE SITE

In January 2022, the soil investigations were carried out by a subcontractor to IAS, Geofield Svalbard AS. The drilling was carried out with a geotechnical drill rigg Geotech 605. The main purpose of the soil investigations was to determine soil layering and depth to bedrock. Given the presence of permafrost, the transition from soil to weak rock is difficult to access based on drilling data only. Disturbed samples of drill cuttings were collected and were, thus, categorised and analysed for water content in the lab.

The soil investigations indicate that the soils on the slope consist of relatively coarse frictional materials and moraine. The water content (by mass) was found to decrease from approximately 30 % in the surface layers, to less than 10 % at 4 metres depth. Water

contents < 10 % are, based on experience from Longyearbyen, considered to be an indication of weathered sedimentary rock. Figure 3 presents the water contents from the samples that were analysed in the laboratory.

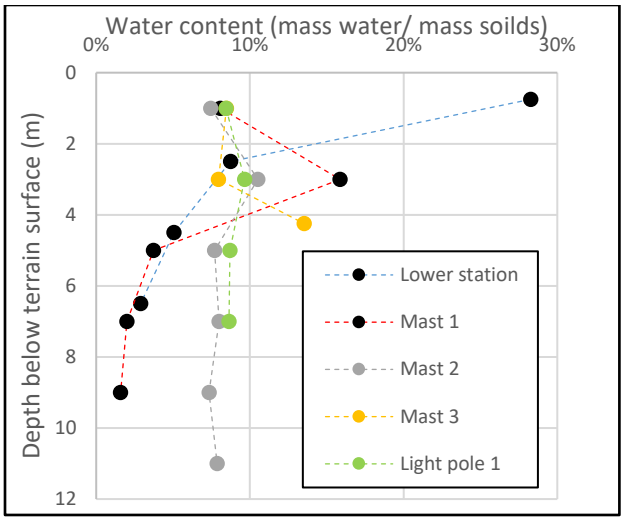

Figure 3. Water content versus depth.

GEOTECHICAL DESIGN

Geotechnical design in Norway must be in accordance with regulations and recommendations in the Norwegian Building Code and Eurocode 0, 7 and 8 (for details, see Norwegian Building Authority, 2017 and Norwegian Standard Series, 2016 a,b,c). This entails that the following items must be included in the geotechnical design:

i) An analysis of the risk and consequences of "acts of nature". Acts of nature includes flooding, snow avalanche, land slide and rock fall.

ii) Safety principle for the geotechnical design including safety class for "acts of nature" and material coefficients to be applied to the characteristic soil parameters in the geotechnical bearing capacity and settlement analyses.

iii) Permafrost response to RCP8.5 medium climate scenario.30-year mean annual temperature of 0 °C in 2070.

The analysis of risk of natural disasters indicated that the annual probability of slides were in general less than 1 ‰. This fulfills the requirements for safety class 2 according to the Nowegian Building Authority (2017). However, the upper part of the slope has an annual probability of snow avalanche greater than 1 %. It is therefore recommended to close the ski slope during avalanche risk in the area. There were also some concerns from the local authorities that snow production in the winter would increase risk of land slides in the area during the thaw season. This study showed that melting of the artificially produced snow would require several weeks and the impact on slope stability would be small. The probability of a sudden melt-off of the whole snowpack in a few days was considered to have an annual probability of occurrence of less than 0.1 ‰.

The standard Doppelmayr foundation system requires that the 7 masts and upper and lower station must be mounted directly on a concrete slab. The slab is designed as gravity foundation with sufficient mass to balance uplift forces from the tow rope. The design vertical stress transferred to the foundation soils is 250 kPa. As part of the geotechnical design, the concrete foundations were checked for bearing capacity and settlements during the design service life time of 50 years.The bearing capacity of the foundation was found to be satisfactory. However, the calculated settlements of the mast and station foundations, exceeded the design values in the lower part of the slope. In the lower part of the ski lift, below approximately 100 m.a.s.l., the depth of bedrock was up to approximately 10 metres, It was recommended that the concrete slabs should be placed on piles to bedrock in this area. In the upper part of the slope, above approximately 100 m.a.s.l., the depth to bedrock was in general approximately 2-4 metres. The soil was then excavated and the concrete foundation was placed directly on bedrock.

REFERENCES

Hanssen-Bauer, I., Førland, E.J., Hisdal, H., Mayer, S. Sandø, A.B., and Sorteberg, A. (editors). 2019. Climate in Svalbard 2100, The Norwegian Centre for Climate Services (NCCS), Oslo, Norway.

Norwegian Building Authority. 2017. Regulations and technical requirements for construction work. www.dibk.no

Norwegian Standard Series. 2016a. Eurocode 0: Basis of structural design. NS– EN 1990 : 2002 + A1 : 2005 + NA : 2016.

Norwegian Standard Series. 2016b. Eurocode 7: Geotechical design. NS- EN 1997 -1 : 2004 + A1 : 2013 + NA :2016.

Norwegian Standard Series. 2016c. Eurocode 8: Design of structures for earthquake resistance. NS-EN 1998-1:2004+A1:2013+NA:2014.

Permafrost degradation along China-Russia crude oil pipeline and mitigative measures

Guoyu Li[1,2], Wei Ma[1], Dun Chen[1,2], Yapeng Cao[1,2], Kai Gao[1,2] & Gang Wu[1,2]

[1]*State Key Laboratory of Frozen Soil Engineering, Northwest Institute of Eco-Environment and Resources, Chinese Academy of Sciences, Lanzhou, Gansu, China*

[2]*Da Xing'anling Observation and Research Station of Frozen-Ground Engineering and Environment, Northwest Institute of Eco-Environment and Resources, Chinese Academy of Sciences, Jagdaqi, Heilongjiang, China*

The 1030-km-long China-Russia Crude Oil Pipeline (CRCOP) starts from the Skovorodino oil station of the Russian East Siberia-Pacific Oil Pipeline, enters China from the Xing'an Town of Mo'he, and ends at Linyuan pump station of Daqing in Northeast China. Its part in Chinese territory has been constructed in two stages. Its first line (CRCOP Ⅰ) and second line (CRCOP Ⅱ) were officially operated in January 2011 and January 2018, respectively, which imported 30 million tons of Russian crude oil each year at ambient temperature. The traditional burial method with the depth of 1.6–2.0 m is employed in the permafrost areas. The pipeline in China has a length of 953 km, including 441 km of discontinuous permafrost from Mo'he-Jagdaqi and 512 km of the deep seasonally frozen ground region (frost depth >1.5 m) from Jagdaqi-Daqing. The permafrost section includes 119 km of warm and ice-rich permafrost and 50 km of permafrost marshland.

The construction of CRCOP faces three challenges: permafrost degradation, severely cold environment and fragile ecology. This paper proposes innovative techniques and systematic solutions aiming at permafrost problems based on years of study experiences and lessons, which ensures the safe operation of CRCOP and provides reference for construction, operation and maintenance of similar projects.

PERMAFROST PROBLEMS ALONG CRCOP

The permafrost problems in the construction and operation of CRCOP are complex and challenging, mainly manifested in the following four aspects.

Permafrost degradation. Permafrost along the CRCOP belongs to the high temperature (−1.8 °C to −0.7 °C from south to north) and high ice content (80%–90%) permafrost. Its continuity varies from 0–20% to 60%–70% from south to north, with poor thermal stability and high sensitivity to disturbances (such as engineering construction, farming and fire). It has degraded due to climate warming and human activities. Its degradation can cause a series of problems, such as pipeline instability, ecosystem degradation and soil erosion.

Open excavation. The CRCOP passes through a large area of forest (coverage of 70%), wetlands and many villages, and the open excavation with depth of 2.5–6 m and width of 2–3 m exposed permafrost and the pipeline ditch accumulated water, which caused melting of under-ground ice and quick permafrost degradation.

High oil temperature. The CRCOP operated at high oil temperature (20.69-30.65 °C in 2021), directly heating the underlying permafrost. Therefore, there was a greater thaw depth (nearly 10 m in 2018) under the pipeline, which increases the risk of pipeline instability and environmental degradation.

Hydrogeological and engineering geological problems. The areas along the pipeline have large snowfall (350 mm in Mo'he) in winter and large rainfall (500 mm in Mo'he) in summer. The high underground water level, abundant surface water and underground water, widespread swamps, dense forests, frequent transitions between permafrost and taliks, and wide distribution of frost- or thaw-sensitive soils posed high risks of frost heaving and thaw settlement on pipeline.

MITIGATIVE TECHNIQUES FOR PIPELINE STABILITY

Thickening pipeline wall. Increasing pipeline wall thickness can directly improve the strength, flexibility, and resistance of pipeline to deformation and damage induced by permafrost thawing. In non-permafrost regions, the wall thickness of CRCOP is designed as 11.9 mm. However, in permafrost regions, it is increased to 12.5–17.5 mm depending on different ice content and sensitivity to thaw settlement.

Replacing foundation soil of pipeline. Frost susceptible soil and thawing unstable permafrost are widely distributed in the subsurface layers along the CRCOP, such as clayey silt and peaty soil. These foundation soils have been widely replaced by non-frost susceptible soils to improve the bearing capacity and reduce thaw settlement.

Restoring surface vegetation. After burying the pipeline, the restoration of surface vegetation on the

right-of-way (ROW) has changed the water and heat transfer conditions on the ground surface, lowered the surface temperature, finally mitigated permafrost from thawing. Meanwhile, it has improved eco-environment affected by pipeline construction.

Thermosyphons have been widely used in pipeline construction and maintenance phases. The monitoring data at a field site showed that the ground temperature at the depth of 4 m and 3 m of the thermosyphon installed segment was 1 °C and 2.5 °C lower than that of the uninstalled section, respectively in 2019. At present, more than 12 000 thermosyphons have been employed in warm and ice-rich permafrost regions along CRCOP.

Longitudinal air-ventilated pipe (LAVP) was an air-ventilated-duct coolig system buried in parallel on both sides of the pipeline like those applied in cold road engineering. In cold season, natural convection heat transfer occurs in the air-ventilated pipe, which releases heat from warm pipeline into atmosphere, lowering the ground temperature of underlying permafrost. In warm season, the LAVP stops working. The numerical simulation tests showed that the thawing depth of permafrost could be reduced by about 4 m after 20-year operation.

U-shaped air-ventilated pipe (UAVP), with the similar cooling principle as that of LAVP, is suitable for cooling the permafrost at a point or a short pipeline sections. A field application of the LAVP w at a permafrost site under the CRCOP demonstrated a good cooling effect in the cold season. The ground temperature 4 m deep below the surface near the LAVP in the cold season was about 0.5 °C lower than that in the area without the LAVP.

W-shaped air-ventilated pipe (WAVP), a similar cooling device as the UAVP adding a air-ventilated pipe in the middle of it with an unpowered ventilator on its top to enhance heat transfer. In non-wind and cold season, the natural convection heat transfer happened in the air-ventilated pipes due to the temperatural gradient between the upper part and lower part of the middle air pipe, where warm pipeline heated the air in the pipe. In the windy and cold season, the natural wind drives the ventilator to suck the air in the middle pipe, which accelerates air flow to quickly release the heat from the pipeline to the atmosphere, slowing down thawing of permafrost. The results of an indoor model test showed that after 6 freeze-thaw cycles, ground temperature at depth of 25 cm below the oil pipeline without and with the WAVP is about 2.4 °C and 0.4 °C, respectively, which proved that the WAVP has a certain cooling effect.

Thermal insulation for pipeline. 8-cm-thick thermal insulation material (hard polyurethane foam) has been coated around pipeline to reduce heat emission from warm oil pipeline to surrounding permafrost. This measure significantly reduces the thawed bulb and thawing rate of permafrost at some field sites.

Air-ventilated pipe and “cold energy” storage system (AVP-CESS), a device combining air-ventilated pipe heat dissipation with cold energy storage utilizing released latent heat of phase change of cooling media, can both control thaw settlement and avoid frost heave. Numerical simulation tests have found that the AVP-CESS had a good controlling effect on permafrost thawing. The actual engineering effect is currently being verified at a field site of the CRCOP.

Air convective (crushed rock-sandwiched) pipline embankment (SCPE), an above ground pipeline laying structure, can avoid trench excavation, permafrost disturbance and thermal impact of wildfire on permafrost thawing. The pipeline is laid in the coarse grain soil embankment. In its lower part, a crushed rock layer is placed to cool the underlying permafrost, and to mitigate its thawing. An indoor model test showed that after 6 freeze-thaw cycles, the maximum thawing depth of permafrost under the SCPE is only 17% of that of the non-crushed-rock soil embankment, indicating that the SCPE has a good control effect on permafrost thawing.

Combinations of various techniques. In the ice-saturated and ice-sandwiched permafrost regions, the combinations of thermal insulation with other measures, such as thermal insulation and soil replacement, thermal insulation and increasing wall thickness, thermal insulation and thermosyphon, thermal insulation and UAVP, and thermal insulation and soil replacement and increasing wall thickness, have better control effect on permafrost thawing. Some of them have also been applied in the field along the CRCOP.

REFERENCES

Jin, H. 2010. Design and construction of a large-diameter crude oil pipeline in Northeastern China: A special issue on permafrost pipeline, Cold Regions Science and Technology, 6(3): 209–212.

Li, G.Y., Ma, W., Wang, X.L., et al. 2015. Frost hazards and mitigative measures following operation of Mohe-Daqing line of China-Russia crude oil pipe-line. Rock and soil mechanics, 36(10): 2963–2973 (in Chinese).

Wang, F., Li, G., Ma, W., et al. 2019 Pipeline-permafrost interaction monitoring system along the China-Russia crude oil pipeline, Engineering Geology, 254: 113–125.

Li, G., Cao, Y., Ma, W., et al. 2021. Permafrost Engineering Problem Along China-Crude Oil Pipeline and Mitigative Measure, Bulletin of Chinese Academy of Sciences (Chinese Version), 36(2): 150–159.

Lateral deformation of expressway embankment on the Qinghai–Tibet Plateau: Field observation and mechanisms discussion

Wei Ma[1,2], Mingde Shen[1,2], Zhiwei Zhou[1] & Yuezhen Xu[1]

[1]*State Key Laboratory of Frozen Soil Engineering, Northwest Institute of Eco-Environment and Resources, Chinese Academy of Sciences, Lanzhou, Gansu, China*

[2]*University of Chinese Academy of Sciences, Beijing, China*

The permafrost accounts for about 23% of the world's land area which is widely distributed in, Canada, China, Greenland, Russia, Antarctica and North America. Many important road engineering were constructed in these permafrost regions, such as the Qinghai-Tibet railway, Alaska highway, Thompson drive, etc. The service performance (such as pavement roughness and pavement cracks) of these roads was directly influenced by the embankment deformation. It is generally accepted that the embankment deformation should be considered as a 2-dimensional problem in most conditions but almost all previous investigations regarding the deformation of road in cold regions only analyzed the vertical settlement. These deformation mechanisms are unable to explain the serious road longitudinal cracks in permafrost regions. The field investigations and previous studies have shown that the lateral deformation of embankment was observed in roads with serious longitudinal cracks. The developed understanding of lateral deformation is crucial for 2-dimensional deformation analysis and road damage formation mechanisms of embankment in permafrost. Therefore, in this study, an observation profile has been constructed in an experimental embankment section of expressway in the Beiluhe region of the Qinghai-Tibet Plateau to explore the potential lateral deformation mechanisms of embankment in permafrost regions. The features and formation mechanisms of lateral deformation of embankment were discussed and a new lateral deformation mechanism was proposed.

SITE DESCRIPTION AND MONITORING SYSTEM

An observation profile including ground temperature and lateral deformation monitoring was established in an experimental road embankment section (34°49′N, 92°54′E) which is built according to the Qinghai-Tibet expressway standards, located in the South Beiluhe Basin and in the Qinghai-Tibet engineering corridor. This site is considered as a typical warm and ice-rich permafrost area. The experimental embankment section had been completed in 2009. To simultaneously monitor the thermal condition and lateral deformation of the road embankment, the flexible inclinometer with high precision (Shape Accel Array, SAA) was installed in the sunny shoulder, as shown in Figure 1.

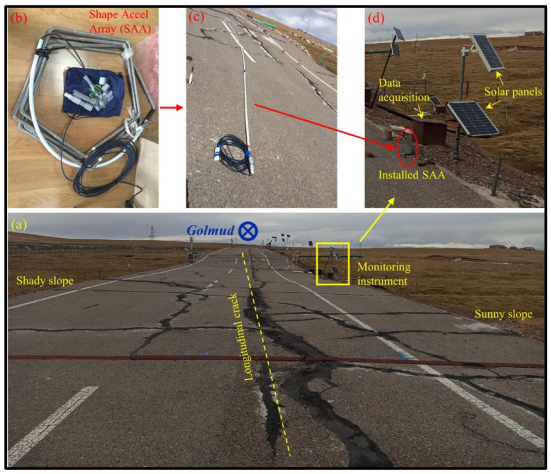

Figure 1. Schematic diagram of the experimental embankment section of the expressway and installed monitoring system.

FEATURES OF GROUND TEMPERATURE

The geothermal contours exhibits the geothermal process of the monitoring profile from December 2018 to April 2021. As shown in Figure 2, the permafrost table is declining: the maximum thawing depth in 2020 is 7.39 m which is deeper than 7.28 m in 2019. Natural ground began to thaw in early July, and reached the maximum thawing depth in mid-November.

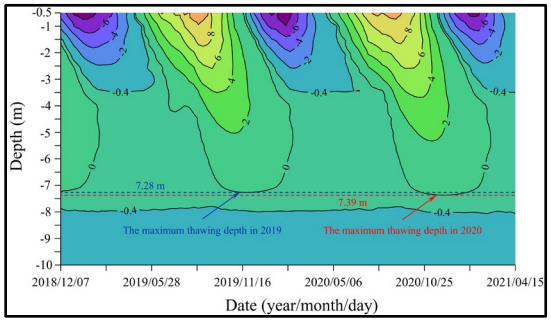

Figure 2. Variations of the ground temperature from December 2018 to April 2021.

FEATURES OF LATERAL DEFORMATION

As shown in Figure 3, the large lateral deformation can be observed in two layers: 0~0.5 m and 3.5~4.5 m. Firstly at the depth of 0.5 m, the cumulative lateral deformation periodically grows in November, 2019 to September, 2020 and decreases in early September to November, 2020. At depths of 3.5~4.5 m, the cumulative lateral deformation decreases in two periods (from mid-February to late-October) and increases in other period. In these two layers, the deformation laws are summarized as follows:

- The lateral deformation is growing continuously and slowly when the ground temperature rising (above 0 ℃, deformation growth lags behind temperature change), decreasing continuously and slowly in freezing period.
- The reduction of lateral deformation in each deformation period is constant.

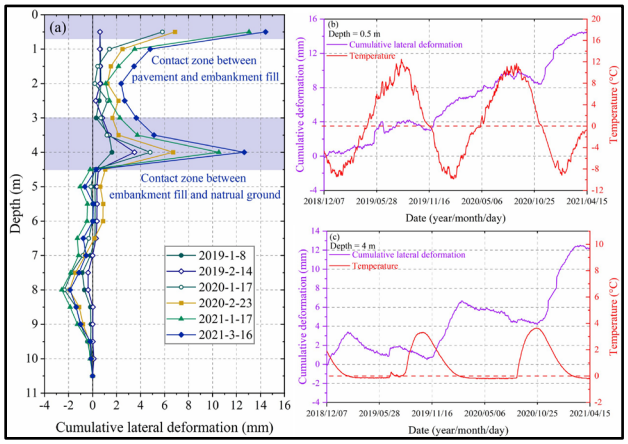

Figure 3. Features of lateral deformation and its relationship with ground temperature.

LATERAL DEFORMATION MECHANISMS DISCUSSION

According to the evolution laws and vertical distribution characteristics of cumulative lateral deformation, the lateral deformation may could be recognized as creep-springback deformation under variable thermal stress conditions. The irrecoverable lateral deformation which is cumulated year by year could be defined as visco-plastic deformation.

MODEL VERIFICATION OF NEW LATERAL DEFORMATION MECHANISM

The elastic visco-plastic model is employed to preliminarily verify whether the key features of accumulative lateral deformation could be described by the presented mechanism. Based on the monitored results in Figure 3 and the corresponding analysis of lateral deformation features, an elastic visco-plastic model has been established, as shown in Figure 4.

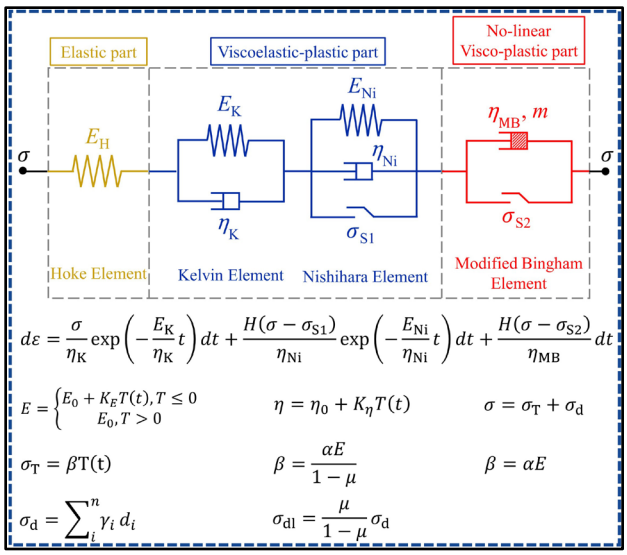

Figure 4. Theoretical mode of lateral deformation.

The theoretical calculation and monitoring results of cumulative lateral deformation at the depth of 4 m is shown synthetically in Figure 5. The calculations indicate that the crucial features of lateral deformation could be explained well by the presented mechanism, such as the maximum, springback and cumulative lateral deformation. Furthermore, the evolution law of lateral deformation with the time is represented well, which is thermally related, periodically deformed and cumulated year by year.

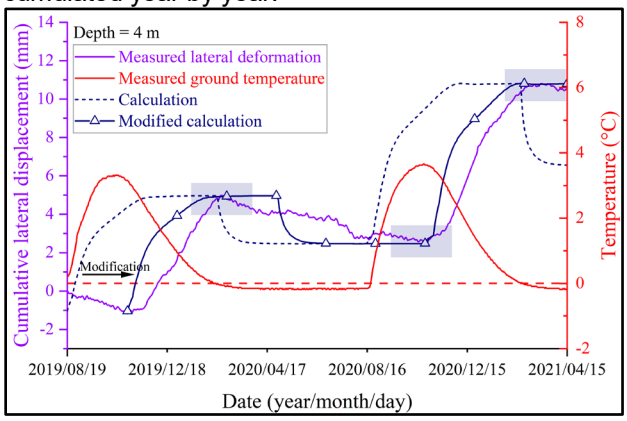

Figure 5. Comparison between the monitored and calculated lateral deformation.

COPYRIGHTED STATEMENT

These findings were previously published in International Journal of Pavement Engineering. Further details are provided below: Shen M.D., Zhou Z.W., Ma, W. and Xu Y.Z. 2023. Lateral deformation of expressway embankment on the Qinghai-Tibet Plateau: field observation and theoretical model, International Journal of Pavement Engineering, 24(1), 2171036. doi:10.1080/10298436.2023.2171036

Heat pipes monitor permafrost temperatures — Trans Alaska Pipeline

Larry Mosley[1], John Zarling, Ph.D., PE[2] & Frank Wuttig, PE[3]
[1]*Alyeska Pipeline Service Company, Fairbanks, Alaska, United States*
[2]*Zarling Aero and Engineering, Fairbanks, Alaska, United States*
[3]*Alyeska Pipeline Service Company, Fairbanks, Alaska, United States*

Two heat pipes (thermosyphons) were installed in each supporting pile, referred to as vertical support member (VSM), on the elevated portion of the Trans Alaska Pipeline System (TAPS) where it crosses warm non-thaw-stable permafrost. Following construction, non-condensable gas (NCG) began to occur in some of the heat pipes, affecting their performance. Alyeska has repaired 55,000 underperforming heat pipes of the 124,000 installed due to NCG issues by recharging heat pipes mainly with carbon dioxide, (CO_2). This paper describes how Alyeska has used repaired heat pipes as thermometers to monitor end-of-thaw-season ground temperatures at the base of thermal VSMs.

TAPS HEAT PIPES

TAPS heat pipes, manufactured by the McDonnell Douglas Corporation, were charged with anhydrous ammonia, (NH_3) and then sealed. They were made of mild steel with an inside diameter of 38 mm and lengths varying from 8.5 m to 22.9 m in 0.91 m increments. Shorter heat pipes have 1.2 m aluminum fin sections and longer units have 1.8 m finned sections which are pressed onto their condensers. VSMs with heat pipes installed on TAPS are called thermal VSMs, (Heuer 1979). Greater details on the TAPS heat pipes and thermal VSMs are provided in (Heuer 1979; Mosley et al. 2022; Heat Pipe Data Sheet C-2).

NH_3 AND CO_2 REPAIRS

Heat pipe repairs to date total 55,000 with 20 out of 255 still recharged with NH_3 and the balance repaired by charging with CO_2. Main steps in the process are welding on a thread-o-let above the finned section, hot tapping into the heat pipe, bleeding-off contaminated ammonia, purging with nitrogen, evacuating, and then charging with a known mass of CO_2 through a CGA 320 manifold valve.

HEAT PIPES AS THERMOMETERS

Because the working fluid, a mixture of liquid and vapor, is in the two-phase zone, temperature and pressure are not independent properties. Measuring absolute pressure at the CO_2 valve and correcting this pressure for hydrostatic head of the CO_2 vapor above the liquid pool yields pressure near the base of the heat pipe. The temperature is easily determined based on this pressure from a saturated pressure-temperature table/chart for CO_2 as shown in Figure 1 [(see Refrigerant 744-saturated liquid and vapor, (ASHRAE 2017)]. In 2003 a program was initiated to measure pressure on several hundred heat pipes along the pipeline corridor during early fall before freezing temperatures occur. These data have been tracked for the last 20 years in order to monitor the impact of climate dynamics on permafrost temperatures at the base of thermal VSMs.

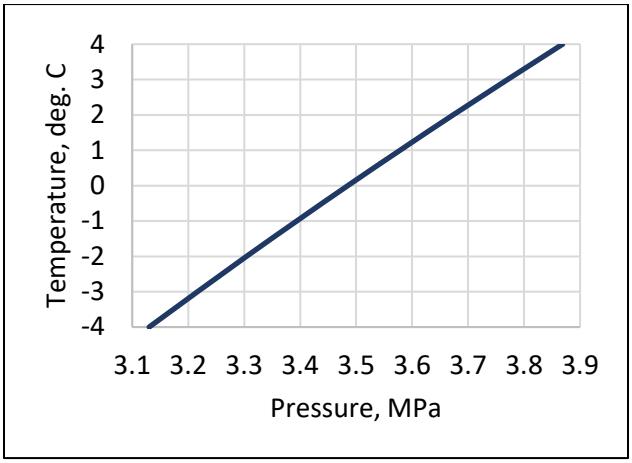

Figure 1. Saturation temperature as a function of saturation pressure for CO_2.

Pressure transducers have been installed above the finned sections on heat pipes on several thermal VSMs along the above ground pipeline. Additionally, a beehive radiation shielded thermistor for measuring air temperature, a near surface ground thermistor, and a vertical thermistor string located within 18-inches of the thermal VSM were also installed at these thermal VSM sites.

Data from a site south of Fairbanks is shown in Figures 2 and 3. The temperatures plotted in Figures 2 and 3 are daily averages and show the processed data for Julian days 60 through 360. The vertical thermistor string is 18 m long at this site.

Figure 2 shows the air, base of heat pipe, and thermistor node at a depth of 10.6 m. It is noted that

base of heat pipe temperatures follows the air temperatures until air temperatures continually exceed base of heat pipe temperatures starting on about day 90. It is also noted that the base of heat pipe temperature continues to warm as the surrounding ground seeks an equilibrium temperature through the summer months. The thermistor node at a depth of 10.6 m which is within few feet of the bottom of the thermal VSM follows a similar trend as the heat pipe. Around day 290 the thermistor starts showing the opposite as temperatures start to decrease from the heat pipe being active.

Figure 3 shows the near ground surface temperatures for this particular site follows air temperature once the ground surface is no longer snow covered.

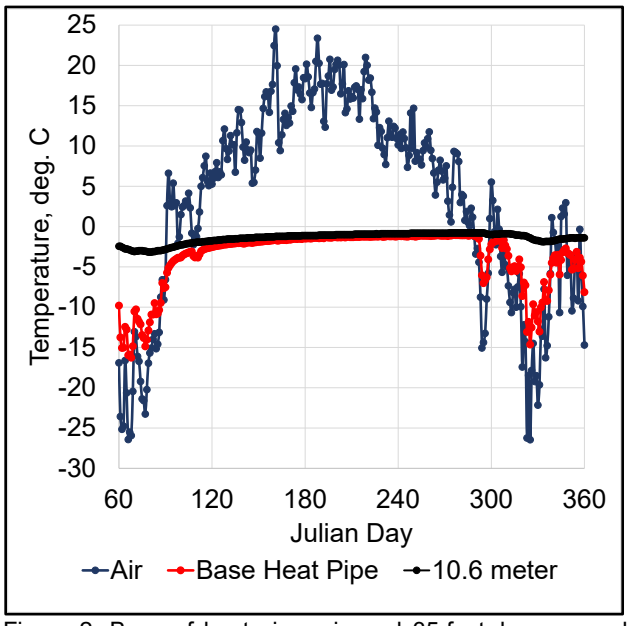

Figure 2. Base of heat pipe, air, and 35-foot-deep ground temperatures.

SUMMARY AND CONCLUSIONS

Alyeska has more than 40 years of heat pipe experience operating an aboveground pipeline system in thaw unstable warm permafrost. Integrity management experience has shown the innovative use of heat pipes as thermometers to monitor end of thaw season ground temperatures at the base of thermal VSMs.

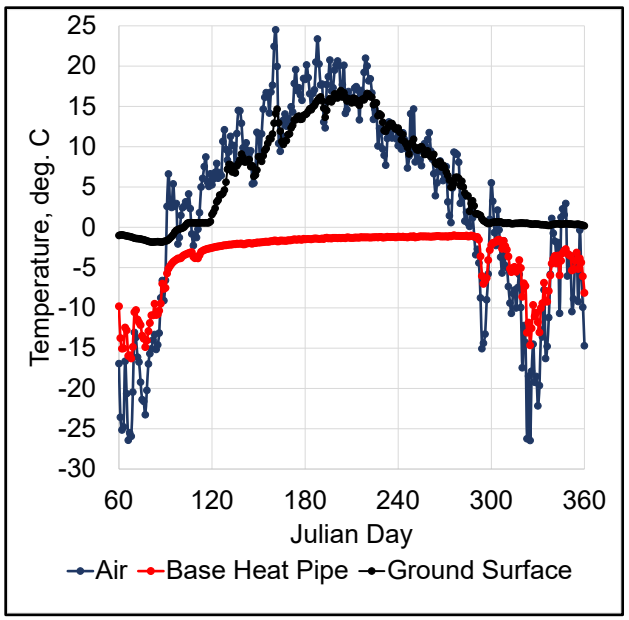

Figure 3. Base of heat pipe, air, and near ground surface temperatures.

REFERENCES

ASHRAE 2017. ASHRAE Handbook Fundamentals, American Society Heating, Refrigerating, Air-Conditioning Engineers, Atlanta, GA.

Heat Pipes, Data Sheet C-2, Alyeska Pipeline Service Company, Anchorage, Alaska.

Heuer, C.E. 1979. The application of heat pipes on the Trans-Alaska pipeline, Cold Regions Research and Engineering Laboratory, Special Report 79–26, Hanover, N.H.

Mosley, L., Zarling, J., Wuttig, F., and Schultz, C. 2021. Alyeska's 40-plus Years of Experience with Heat Pipes on Trans Alaska Pipeline System, Proc. Regional Conf. on Permafrost 2021 – 19th International Conf. on Cold Regions Engineering, ASCE, Reston VA: 327–338.

Temperature and relative humidity of the active layer and permafrost in natural and construction-influenced environments: Case of the Machu Picchu Antarctic research station, King George Island, Antarctic Peninsula

Evelyng Peña-Chávez[1,2], Baclimer Quispe[3] & Wai L. Ng-Cutipa[1]

[1]*Geological Survey of Spain, Madrid, Madrid, Spain*

[2]*Escuela Profesional de Ingeniería Geológica, Universidad Nacional de San Antonio Abad del Cusco, Cusco, Cusco, Perú*

[3]*Instituto Geológico, Minero y Metalúrgico, INGEMMET, Lima, Lima, Perú*

The Antarctic Scientific Station Machu Picchu (ECAMP) in Mackellar Inlet, Admiralty Bay, King George Island (Antarctic Peninsula); conducts data collection during the summer, including soil temperature measurements taken every 30 minutes since 2014 at various depths. Preliminary results from two new boreholes, one exposed to the environment (PERM03) and the other under station infrastructure in the permafrost zone (PERM04), show differing temperature and humidity patterns. The data were analysed using statistical methods and suggest the relevance of understanding permafrost evolution and potential infrastructure risks, especially for structures built in 1989.

Study area and local conditions

Study area has a cold climate that is around 0 °C, minimums of -30 °C and maximums of +16 °C on the surface, and the wind exceeded a speed of 78 km/h; the data recorded in the southern summer of 2020.

The geology of the study area is comprised of marine terraces differentiated into 6 levels of marine terraces, composed of regularly classified, polymictic, subrounded to rounded clast gravels, interspersed with medium to coarse sand levels.

Methodology

This work shows the preliminary results of 2 new boreholes both at 1,75 m depth, one of them directly exposed to the environment (PERM03), and the other one under the station infrastructure, in the permafrost zone (PERM04).

For the recording of temperature and relative humidity, HOBO® U23 Pro v2 Temp/RH sensors were used, installed inside tubes in 0,15; 0,50; 0,7; 1,0; 1,25; 1,50 and 1,75 m depth, during 1 year (February, 2019 to January, 2020). The original recording is every 30 min but for this analysis, we are considered every 1 hour. These data were used to calculate the mean temperatures at different depths.

Likewise, temperature (T°) and relative humidity (HR) data have been analysed using statistical analysis, employing bar charts and box plots in Excel and the R Studio program for each depth.

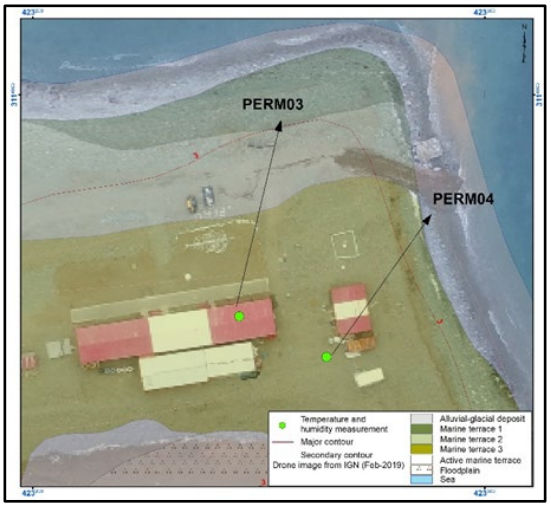

Figure 1. Location of sensors at the Antarctic Scientific Station Machu Picchu (ECAMP) in Admiralty Bay, King George Island, Antarctica.

Results

Mean temperatures. Minimum, media and maximum temperatures are presented for PERM03 and PERM04 (Fig. 2). Mean temperatures of soil in both boreholes are different.

Data in PERM03 shows 2 layers with different range of temperature. Shallow layer is from the surface to 0,98 m deep approximately which it is characterized by minimum temperature below 0 °C. At 0,15 m deep, has 8,06 °C as higher temperature and -2,68 °C as lower temperature. To the 0,98 m, data at 0,50 and 0,70 m deep, show an approach to 1 °C. This shallow layer is an active layer. Under the active layer, there is a layer with all mean temperature greater than 0 °C but near to 1 °C. Temperature tree is closes at 1,75 m deep, and this corresponds to unfrozen soil.

PERM04 show 3 layers. The shallow layer also is an active layer, but from the surface to 0,52 m deep. The base of this layer has minimum and mean temperature below 0 °C, and maximum temperature close to 0 °C.

We considered 0,52 m as the base of active layer and in the same way, the top of permafrost. Second layer, below active layer, has all temperatures below 0 °C until 1,12 m deep. Under permafrost is a layer which is characterized for a temperature increase which, the deeper it is, the more positive it is. This last layer, at 1,25 m deep, has lower temperatures than PERM03 in the same deep.

Permafrost layer is shallow from 0,52 to 1,12 m deep approximately and from -1,46 to -0,33 °C in PERM04 (below the infrastructure). No permafrost is possible to uncover ground because soil temperature is greater than 0 °C.

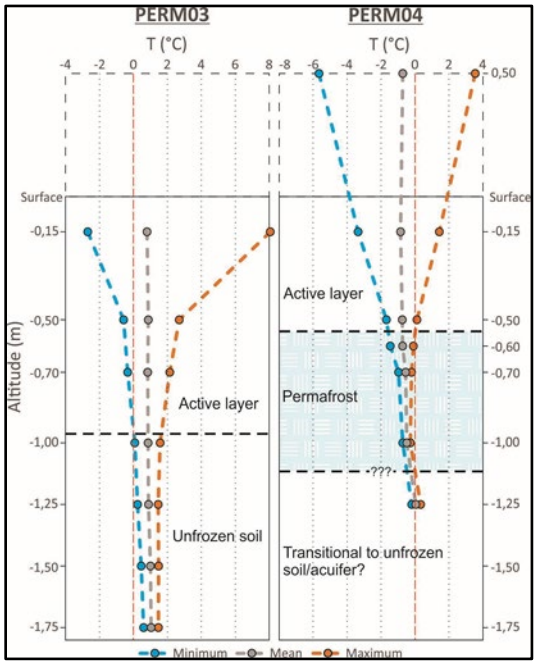

Figure 2. Mean temperature variation in shallow boreholes (PERM03 and PERM04) from February 2019 to January 2020, around ECAMP.

Statistical analyses of temperatures and relative humidity. In the case of temperature in PERM04, values below the median are observed, which is reflected in elongated boxes towards the minimum value, indicating lower temperatures. In contrast, PERM03 displays elongated boxes towards the maximum value, indicating higher temperatures. Furthermore, the box plots show that relative humidity increases with depth in PERM04, while the opposite occurs in PERM03.

In Fig. 3, comparative statistical data between PERM03 and PERM04 is presented. In the case of PERM03, as the depth of sensor location increases, there is a slight decrease in the interquartile range. However, this decrease becomes more noticeable at locations 1,50 and 1,75 m deep. Regarding the median (q2), there is an upward trend as the sensor location deepens, surpassing 0°C. The arithmetic mean, on the other hand, tends to skew lower at greater depths. In contrast, for PERM04, the interquartile range noticeably decreases in size. The median (q2) rises with depth until reaching 0 °C, and the arithmetic median, at greater depths, decreases, behaving very similarly to PERM03 data.

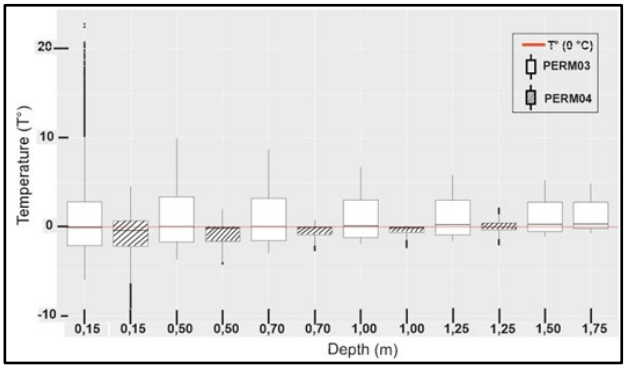

Figure 3. Statistical comparison of soil temperature between PERM03 and PERM04 around ECAMP.

In the case of Figure 4, comparative statistical data for relative humidity is shown. In the case of PERM03, the median (q2) experiences a decline as the sensor location deepens, dropping from 100 to values below 80. Conversely, in the data for PERM04, an inverted representation is observed compared to PERM03, where the median (q2) shows an increase as the sensor location deepens.

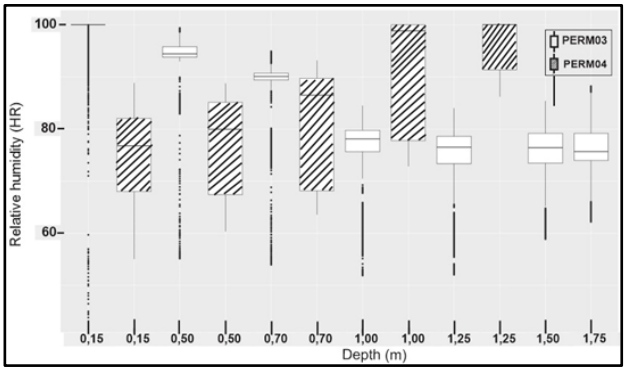

Figure 4. Statistical comparison of soil relative humidity between PERM03 and PERM04 around ECAMP.

CONCLUSIONS

The temperature analysis of boreholes PERM03 and PERM04 reveals distinct thermal profiles. PERM03 has two layers, and PERM04, three layers (one of them, permafrost layer). The statistical analysis of temperature and relative humidity data highlights the significance of variations with depth in wells PERM03 and PERM04. This information is crucial for understanding the evolution of permafrost and anticipating potential risks to ECAMP infrastructure.

Ground temperatures and chemical conditions in an Arctic landfill

Mari Vestland[1], Regula Frauenfelder[1], Gudny Okkenhaug[1] & Gijsbert Breedveld[2]
[1]*Norwegian Geotechnical Institute (NGI), Oslo, Norway*
[2]*The University Center in Svalbard, Longyearbyen, Norway*

Waste disposal in the Arctic presents a variety of challenges connected to the harsh and remote environment, the permafrost conditions, climate change and the vulnerability of the Arctic ecosystem. In 2017, 66.1% of Arctic settlements were located on permafrost (Nordregio 2019). Waste from these settlements is still predominately disposed off in landfills. To guarantee environmentally friendly and safe waste deposition, and ultimately, long-lasting termination of Arctic landfills, factors such as ground thermal state, waste composition, ground stability, hydro(geo)logical conditions and climate change impacts need to be carefully assessed. This to minimize the risk of pollutants from such landfills entering the vulnerable Arctic ecosystem.

Study site

We studied a solid waste landfill located at 78°10.490' N 15°56.303' E in the Advent valley on Svalbard, ca. nine kilometers southeast of the town of Longyearbyen (Figure 1). The landfill rests directly on the ground, without any constructed sealing layer between the original soil and the waste. The landfill covers an area of ca. 30,000 m^2 and is entirely located below the marine limit.

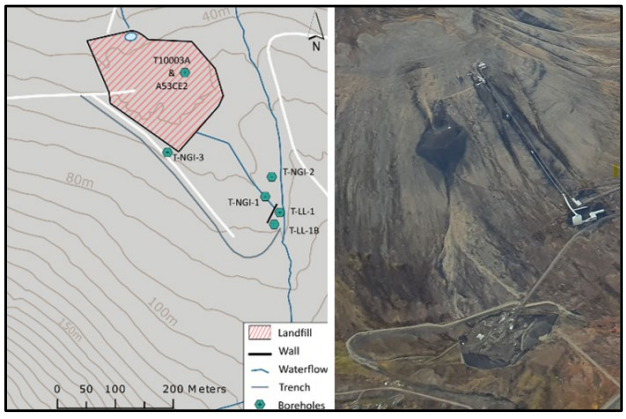

Figure 1. Left: Map of Advent valley landfill (in red) with location of temperature boreholes (in green). Map: Castilla et al. (2022); Right: Aerial photograph of the landfill in 2020, below spoil tip of abandoned coal mine. Photo: Kjersti Olsen Ingerø, Longyearbyen Lokalstyre.

The Governor of Svalbard gave permission the landfill in 1991, and waste disposal started in 1992.

Orders to terminate the landfill by 2023 were given in 2018. The total amount of waste disposed at the landfill today is estimated at 72 tons (NGI 2021). Initially, household waste, waste from building- and construction and electronic waste dominated. Disposal of wet organic waste ended in 1997. From 2008, ash and waste from the energy facility and waste from building- and construction was predominant. Occasionally, mining waste was deposited, and probably also hazardous waste. The latter at unknown amounts. The depth of the landfill at its centre varies between 8 to 11 metres. Waste disposal partly happened in a creek bed. Mitigation attempts to gain control of the associated water ways has only shown limited effect and the site suffers from runoff water, flowing through and below the landfill, especially during the melting season (NGI 2018).

Measurements

Ground temperatures around and inside the landfill are measured within six thermistor-equipped boreholes. Ground temperatures are registered at 0.5–1 m interval, down to 11–12 m. The borehole inside the landfill is ca. 20 m deep (Figure 2). In addition, water temperature, pH and electrical conductivity were measured along several transects outside and crossing the landfill on June 28, 2022 (Figure 3), each transect comprises various measurement locations.

Results

Borehole temperature measurements at the Advent valley landfill reveal that there are no permafrost conditions inside the landfill today (Figure 2, plot T10003A). Comparison with results by Løtveit (2012) imply that the permafrost table within the landfill has been lowered by more than 1 m per year in the past 10 years. Such a dramatic decrease can only be explained by the existence of a significant internal heat source, which suggests the presence of decaying waste, emitting heat. Our results also point to permafrost degradation due to water accumulation at a concrete wall intended to mitigate effects of water-flow (Figure 2, plots T-NGI-1 and T-LL-1).

The water measurements upstream and downstream show that water passing the landfill has a 10x increase in electrical conductivity, which is attributed to the dissolution of solids (Castilla et al.

2022), confirming that there is contaminant transport from the landfill.

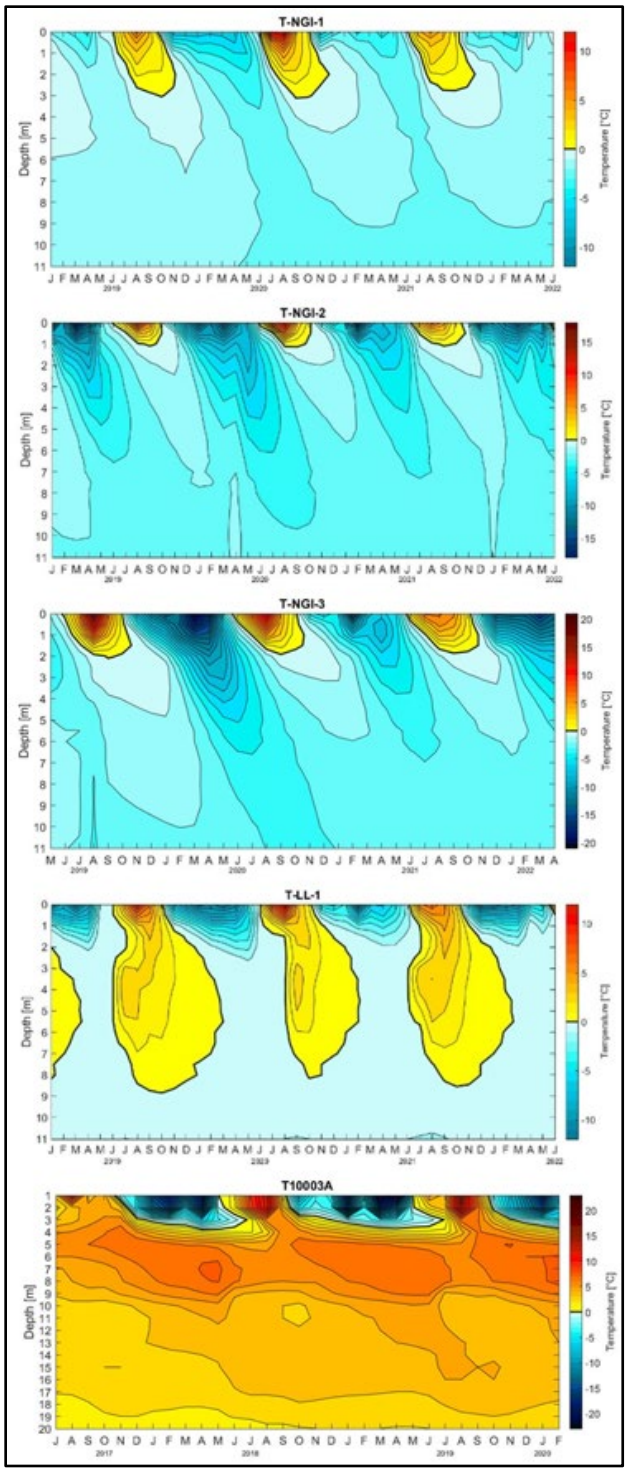

Figure 2. Temperature conditions in five (of six) boreholes (for location see Figure 1 left). T-NGI-2 and T-NGI-3 show the natural conditions outside the creek bed, while T-NGI-1 and T-LL-1 are located within the creek bed. T10003A is located at the centre of the landfill.

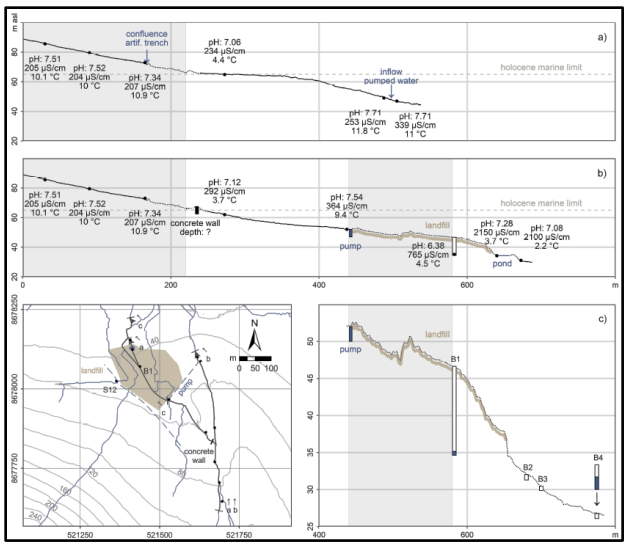

Figure 3. Measurements of field parameters (pH, electrical conductivity, temperature) and water table depths. Grey areas in a), b) and c): overlapping profile sections. Source: Castilla et al. (2022).

CONCLUSIONS

The permafrost does not any longer meet the requirements of a geological barrier at this site. Its degradation in combination with malfunctioning water mitigation structures might open more pathways for pollutants to enter the vulnerable Arctic ecosystem downstream of the landfill.

ACKNOWLEDGEMENTS

We are grateful for financial support from the Research Council of Norway (NGI base funding) and for the very good collaboration with the landfill owner Longyearbyen Lokalstyre, UNIS and the students of course AG-352 2022. Elisabeth Hoffstad Reutz is thanked for help with the temperature plots.

REFERENCES

Castilla, C., Schetselaar, A., Vacek, F., and Wiegand, T. 2022. Permafrost Conditions at the Adventdalen Landfill, Svalbard. Student project report in AG-352 Geohazards and Geotechnics in Permafrost Regions, UNIS, July 2022. Supervision by Mari Vestland, NGI.

Løtveit, S. 2012. Deponiet i Adventdalen. En vurdering av spredning av forurensning og permafrostens egnethet som bunntetting. (Master thesis, 2012).

NGI. 2018. Vurdering av permafrost som geologisk barriere_Delrapport 1. 20180397-01-R.

NGI. 2021. Adventdalen deponi. Plan for avslutning og etterdrift. Rapport 20180689-02-R.

Nordregio, 2017. https://nordregio.org/maps/settlements-on-permafrost-in-the-arctic/

Retrofitting a passively cooled at-grade foundation at Quinhagak, AK, USA

Austen Whitney, EIT & Edward Yarmak, P.E.
Arctic Foundations, Inc., Anchorage, Alaska, United States

Two-phase thermosyphons are the most widely used passive refrigeration devices for cooling and maintaining permafrost soils supporting infrastructure in cold regions. Since 1978, the foundation design for many at-grade structures founded on permafrost have utilized thermosyphons for passive subgrade cooling. A typical design for an at-grade structure utilizing thermosyphons includes a layer of rigid insulation beneath the slab with thermosyphon evaporators installed beneath the base of the subgrade insulation in a layer of Non-Frost-Susceptible material. Passively cooled at-grade foundations rely on cold winter air to remove heat to maintain permafrost and structural stability. As the climate warms in northern latitudes, this natural heat sink is reduced, thus reducing the heat removal capacity of passive systems, and jeopardizing the stability of the structures being protected.

In the Kuskokwim Delta area of western Alaska, the at-grade water treatment plant in Quinhagak was built in 1995 using thermosyphons for passive subgrade cooling. The thermosyphons have always been fully operational. However, the foundation system for this facility was not designed for the warmer climate the region is experiencing today. The structure has experienced differential movement due to warming from areas beyond the perimeter of the foundation. The water treatment plant is a critical piece of infrastructure that cannot be readily replaced. The facility is in an area not connected to the road system where the construction costs are high, and the construction season is shorter due to the climate. This scenario presented a unique opportunity to investigate the feasibility of extending the life of the structure by retrofitting the existing foundation system before the foundation failed to the extent where the structure would become unserviceable and require replacement. To maintain structural stability and usability into the future, Arctic Foundations, Inc. worked with the Alaska Native Tribal Health Consortium (ANTHC) and the Quinhagak community to upgrade the foundation system.

The geotechnical report from 1995 classified the permafrost beneath the site as thaw-unstable and prone to large settlement. The original foundation design used 11 thermosyphons with nominal 80 mm sloping evaporators fitted with 6.5 m^2 condensers (Figure 1). Beneath the structure, the original construction drawings specified 200 mm of rigid insulation to extend 1.2 m outboard of the edge of the structure, with thinner layers of rigid insulation to extend an additional 1.2 m. The design used 2166.67 °C·days for the freezing index and 1777.78 °C·days for the thawing index.

Figure 1. The original thermosyphon system installed at the water treatment plant in Quinhagak, AK, as seen in 2022.

The foundation retrofit work was accomplished over four months during the summer of 2022 (Figure 2 and 3). The passive heat removal capacity of the existing thermosyphon system was increased by retrofitting all existing thermosyphons with larger 15.8 m^2 condensers. Hybrid heat exchangers were added below the condensers, allowing the use of mechanical refrigeration to mitigate future thaw beneath the structure should the need arise. In addition to retrofitting the existing thermosyphon system, a new hybrid flat-loop evaporator thermosyphon (FLET) was installed on the north, east, and south perimeter of the structure. Where the gravel pad was excavated for the FLET, new subgrade insulation and fill material were added, and the subgrade insulation skirt was extended 3.7 m outboard from the edge of the structure (Figure 4).

Figure 2. Upgraded thermosyphon system at the water treatment plant in Quinhagak, AK.

Figure 3. Quinhagak community members and ANTHC installing the flat-loop evaporator thermosyphon system.

Figure 4. Quinhagak community members and ANTHC extending the rigid subgrade insulation around the perimeter of the structure.

After the retrofit work was complete, the mechanical refrigeration capability of the hybrid FLET was initiated in August 2022 to refreeze and stabilize the soils around the perimeter of the structure. Twelve temperature sensors were attached to the more than 128 m of FLET to monitor ground temperatures and refrigeration performance around the perimeter of the structure. The average ground temperatures of the FLET sensors were -9.0 °C after 12 days of operation. Near the end of the thaw season in October 2023, the average ground temperatures of the FLET sensors were -13.5 °C, and there have been no reports of significant differential movement at the site.

The short-term results show that retrofitting at-grade foundations utilizing passive subgrade cooling can be accomplished in a short time frame and successfully reduce the ground temperatures around the perimeter of the structure where heat is coming in from a warming climate. The wider implications of this work provides a potential solution for similar at-grade structures utilizing thermosyphons for passive cooling that have or will have similar issues due to climate warming.

Design, construction and thermal monitoring of a landfill (Tier II Disposal Facility) at FOX-3 DEW Line Site in Canadian Arctic

Guangwen (Gordon) Zhang
WSP Canada Inc., Edmonton, Alberta, Canada

This extended abstract summarizes the design, construction, and long-term thermal monitoring of a landfill (Tier II disposal Facility) at the FOX-3 (Dewar Lakes) DEW (Distant Early Warning) Line Clean-Up (DLCU) site on Baffin Island in Nunavut, Canada.

During the DLCU, existing landfills associated with historic operations at the sites were remediated and new landfills were constructed. Tier II Disposal Facilities were new landfills designed and constructed during the DLCU to contain contaminated soil that exceeded the Tier II DEW Line Clean-Up Criteria.

Design concept of DLCU Tier II Disposal Facility

At each site, the design of these facilities was guided by the characteristics of the contaminants in the soils, the geothermal properties of the area and the local permafrost regime. The design objective was full encapsulation of the Tier II contaminated soil, using permafrost as the primary containment barrier; both the Tier II contaminated soil and the nearly saturated, silty sand/gravel perimeter berms used to contain it were designed to be continuously frozen after initial freeze-back following construction. The perimeter berms were keyed into the permafrost.

Site-specific numerical geothermal analysis was conducted to determine the short-term and long-term geothermal regime of the facilities and the thickness of the cover material required to prevent thawing of the Tier II contaminated soil under projected climate change conditions. A geomembrane (HDPE) liner, protected on each side by a non-woven geotextile, was placed at the base and side slopes of the facilities to provide secondary containment. The liners were selected to be chemically compatible with the contaminated soil and were designed to prevent movement of contaminants during the period required for permafrost aggradation. The designs included specific thicknesses of particular types of granular fill placed on top of the Tier II contaminated soil. A second HDPE liner was placed over the Tier II contaminated soil, and was seamed to the base liner to prevent precipitation from percolating down through the cover fill and into the Tier II contaminated soil.

To monitor permafrost freeze-back following construction, and to assess whether or not the Tier II contaminated soil and perimeter berms remain frozen over time, all Tier II Disposal Facilities were instrumented with ground temperature cables. These instruments consist of individual sensors (thermistor beads) installed at specific depths below the ground surface.

Design of FOX-3 Tier II Disposal Facility

The geotechnical design (by the author) of the FOX-3 Tier II Disposal Facility (FOX-3 DF) was completed in 2007. The FOX-3 DF was designed to encapsulate contaminated soil using perimeter containment berms, top and bottom geomembrane liners, and a granular fill cover. Numerical geothermal analyses were carried out to predict the short-term and long-term ground thermal conditions and the maximum thaw penetration into the granular fill cover under various climatic conditions including mean, 1 in 100 warm year, and projected long-term global warming (climate change) conditions. The recommended minimum fill cover thickness on top of the Tier II soil was 3.1 m (EBA 2007).

Construction of FOX-3 Tier II Disposal Facility

Construction of the FOX-3 DF commenced in the 2009 construction season. Most of the key trench was completed in 2009 and the remainder, including construction of the perimeter berms, was completed in the 2010 construction season. The placement of Tier II contaminated soil was completed by July 2011. The top geomembrane liner system was installed in August 2011. The granular fill was then placed over the liner system. Four vertical thermistor cables (VT-1 to VT-4) with data loggers were installed in this facility on September 7, 2011.

The facility has a rectangular shape and is approximately 5.3 m high and has an approximate top surface area (without landfill slopes) of 6,622 m^2 (77 m in a west-east direction by 86 m in a south-north direction). Figure 1 shows the as-built details and sequence of soil layers for the facility (AECOM and HATCH 2013). Note that the as-built minimum cover thickness over the Tier II soil was 3.15 m. The thickness of the contained contaminated soil is estimated to be in the order of 1.3 to 1.4 m.

THERMAL MONITORING OF FOX-3 DF

Measured ground temperature data from VT-1 to VT-4 during the period of September 2011 to August 2018 was provided by Defence Construction Canada. The data was evaluated to assess the thermal performance of the FOX-3 DF (WSP 2024). Figure 2 presents the measured mid-September temperature profiles at VT-3 in the FOX-3 DF. The key findings from the assessment include the following:

- Freeze-back was achieved by June 2012, less than one year after the final completion of the facility in September 2011.
- The thermal performance of the FOX-3 DF during the period of June 2012 to August 2018 met the design criteria and was satisfactory.
- A satisfactory level of thermal stability was established for the FOX-3 DF during the period of June 2012 to August 2018 under the long-term warming trend of measured air temperatures at the site.

REFERENCES

AECOM and HATCH 2013. FOX-3 Dewar Lakes as-built drawings. Submitted to National Defence by AECOM and HATCH, November 10, 2013.

EBA 2007. Geotechnical design of landfills, FOX-3 (Dewar Lakes) DEW Line site, DEW Line Cleanup Project. Draft report submitted to UMA Engineering Ltd. by EBA Engineering Consultants Ltd., May 2007.

WSP 2024. Assessment of thermal data for landfills at DEW Line sites. Technical report submitted to Defence Construction Canada by WSP E&I Canada Limited, February 2024.

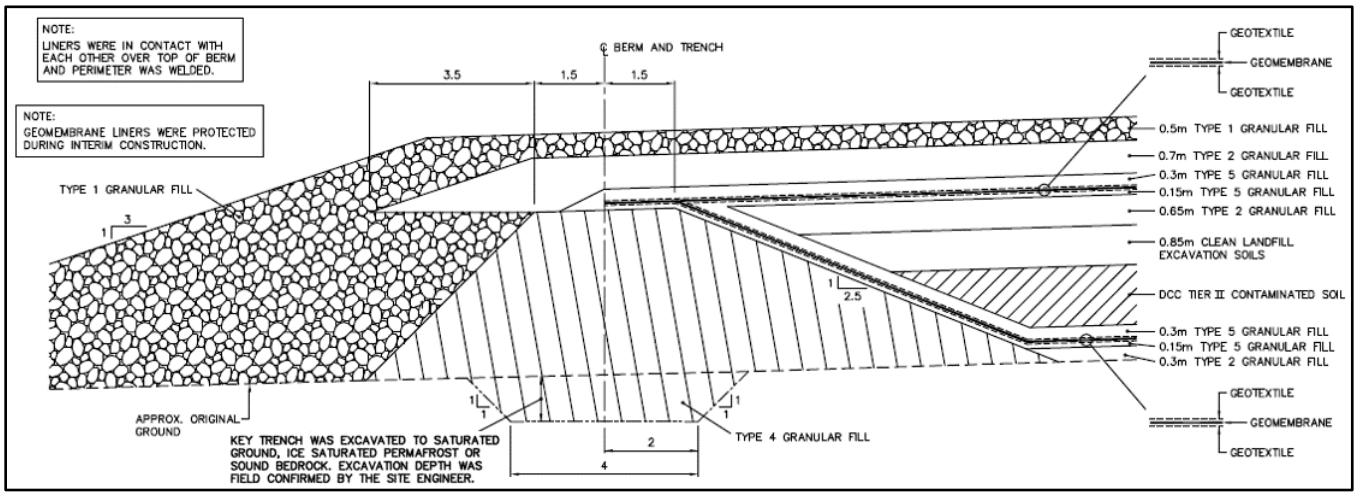

Figure 1. As-built details of FOX-3 Tier II Disposal Facility (AECOM and HATCH 2013).

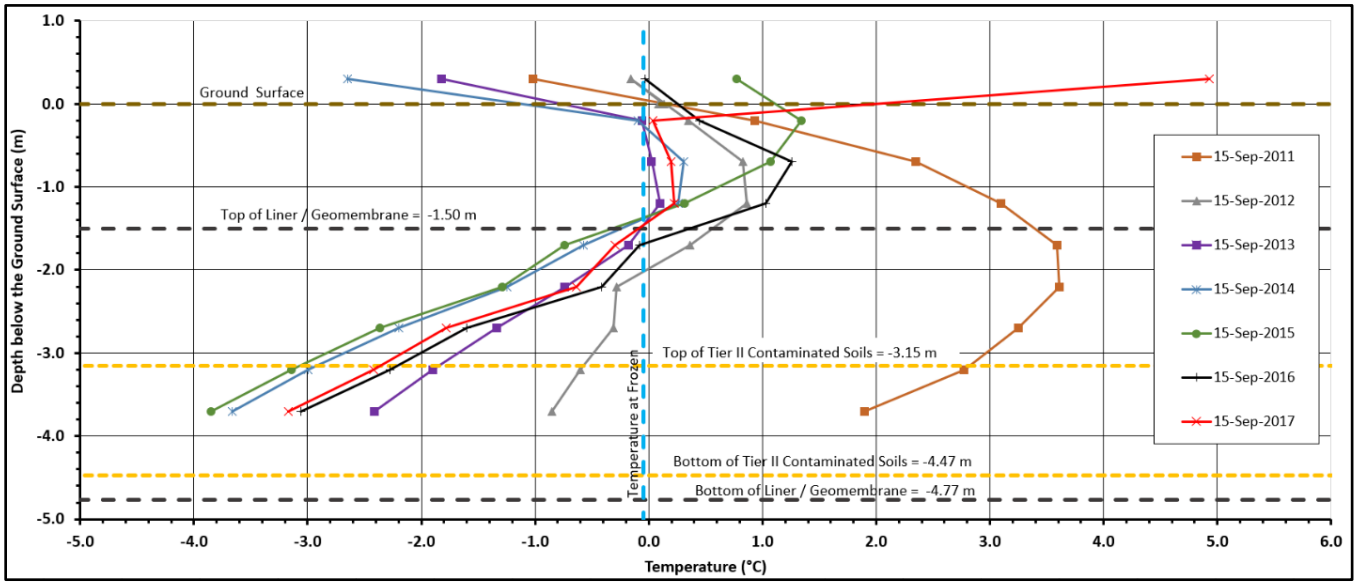

Figure 2. Measured mid-September temperature profiles at VT-3 in FOX-3 Tier II Disposal Facility (WSP 2024).

Field thawing study of high ice content permafrost based on high-power heating tube

Xuwei Zhu, Bo Tian, Lei Quan, Panpan Zhang, Lihui Li, Sili Li & Kaimin Niu
Research Institute of Highway, Ministry of Transport, Beijing, China

The Qinghai-Tibet Plateau (QTP) is densely covered with a globally unique 1.5 million km^2 of mid to low latitudes and high altitudes permafrost. An increasing numbers of engineering structures, such as roads and railways, have been constructed in this region. To ensure the thermal stability of the permafrost foundation, a series of measures have been taken to protect it, including thermosyphon embankment, insulated board embankment, ventilated duct embankment, and block stone embankment (Sha et al. 2022). However, decades of deformation observations on the Qinghai-Tibet Highway and Qinghai-Tibet Railway have revealed that engineering measures designed to protect permafrost face challenges in effectively managing permafrost thaw settlement (Hjort et al. 2022). Furthermore, with global climate warming, the shallow, high ice-content permafrost foundation will inevitably warm or even thaw, posing significant challenges to the long-term operation of infrastructure built on the permafrost layer. Therefore, early thawing of high ice-content permafrost layers is an effective method to reduce later settlement of upper infrastructure.

METHODOLOGY

Figure 1 illustrates a high-power heating tube designed for the thawing permafrost in the field. It was welded from a heater with a power of 10 kW and a steel pipe with a diameter of 10 cm and a height of 100 cm. The upper part of the heating tube had a 2 cm diameter air outlet, which can be connected to the galvanised tube by means of a nut to extend it into the ground. Depending on the thawing depth, the number of galvanised pipes can be increased or decreased by 1 m per section. The QB320 heat transfer oil was added to the cavity of the heating tube, and the temperature of the heating tube was controlled by a thermostat during the test. Heat transfer oil can be rapidly heated to a set temperature in less than 5 minutes using a home-made high power heating tube. In this study, the heating tube was placed 5.5 m underground, and the temperature was set at 260 °C.

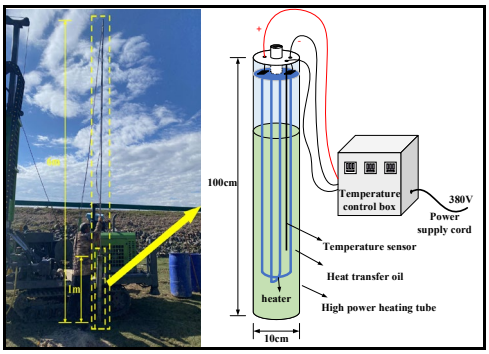

Figure 1. High-power heating tube device for thawing permafrost on site.

The on-site thawing permafrost test was conducted at the Qinghai Province Permafrost Research and Observation Base, located in Maduo County, China. The average elevation of the area is 4260 m, and the annual average temperature is -3 °C, with an average warming rate of 0.46 °C / decade. Table 1 shows the geological distribution of the test site. The Groundwater table and permafrost table were -1.6 and -2.8 m, respectively.

Table 1. Geological conditions of the test site.

Depth (m)	Soil Type	Mass water content (%)
0 - 0.3	silty clay	19.1
0.3 – 2.4*	gravelly sand	14.6
2.4 – 3.1	coarse sand	9.4
3.1 – 4.0	fine sand	13.4
4.0 – 6.5	sandy clay	25.6

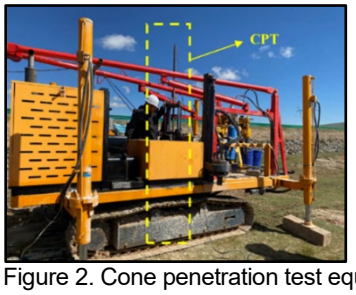

Figure 2. Cone penetration test equipment.

To quickly evaluate whether the permafrost is thawed or not, double bridge cone penetration testing was used to test the cone tip resistance q_c and cone side resistance f_s of soil at different positions from the

heating tube during the thawing process of permafrost in this study. The thawing effect was evaluated by comparing the changes of q_c and f_s before and after heating.

RESULTS AND DISCUSSION

Figure 3 shows the cone tip resistance along the depth of the soil at different distances from the heating tube for different heating times. Since the permafrost table is below 2.8m below ground level, we will only analyse the test results below permafrost table. The cone tip resistance of the soil changes significantly before and after heating. After heating for 2 hours, the average cone tip resistances of the undisturbed soil, the soil at a radial distance of 20 cm and 30cm within the depth range of 4.5 m to 5.5 m were 13.18 MPa, 5.71 MPa and 12.08 MPa, respectively. Therefore, it can be considered that the permafrost at 20 cm has completely melted, and the permafrost at 30 cm has not yet begun to melt. With the increase of heating time, the thawing range was further expanded. When heated for 4.5 hours, the cone tip resistance of the soil in radial direction 35 cm and 60cm at the depth of 4.5~5.5 m were 7.46 MPa and 12.3 MPa, respectively, which indicated that heating for 4.5 hours could thaw the permafrost in the range of 35 cm.

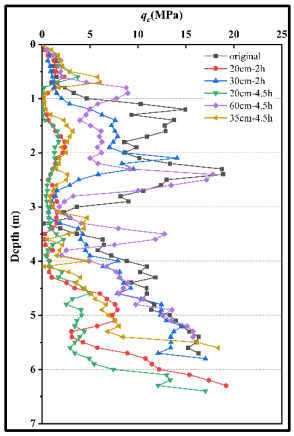

Figure 3. Cone tip resistance of soil at different distances from the heating tube for different heating times.

Figure 4 shows the cone side resistance along the depth of the soil at different distances from the heating tube for different heating times. Cone side resistance and cone tip resistance have similar patterns of change. The maximum cone side resistance of original permafrost at depths of 4.5~5.5 m ranged from 177.6~372.9 kPa, and the cone side resistance of thawed soil at radial 20cm in the same depth range after 2 hours of heating ranged from 7~150.9 kPa. when heated for 4.5 hours, the average cone side resistance values along the radial direction of 35 cm and 60 cm at depths of 4.5~5.5 m were about 38% and 81% of the original permafrost at the same depth, respectively, indicating that the permafrost at the radial direction of 35 cm had also melted. This is consistent with the conclusions drawn from cone tip resistance. Meanwhile, when heated for 4.5 hours, the depth of cone penetration at 20 cm in the radial direction increased by approximately 10 cm compared to heat for 2 hours. This compares with the range of melting in the radial direction, suggesting that the rate of melting along the depth direction is less than in the radial direction.

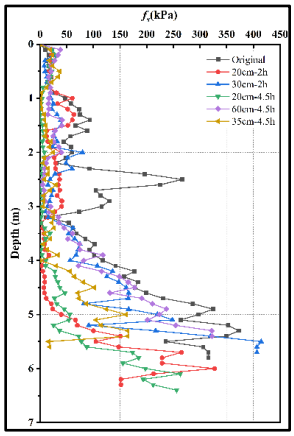

Figure 4. Cone side resistance of soil at different distances from the heating tube for different heating times.

CONCLUSIONS

The cone tip resistance and cone side resistance of the original permafrost changed significantly compared to the melted soil, and the CPT test can be used to rapidly evaluate the extent of permafrost melting in the field. Using the heating tube designed in this study, permafrost with a radius of 35 cm can be melted in 4.5 hours, but the thawing rate along the depth direction is smaller than that in the radial direction. To evaluate the melting range of permafrost more accurately, a quantitative relationship between the heating test parameters and the CPT results needs to be established subsequently.

REFERENCES

Hjort, J., Streletskiy, D., Doré, G., Wu, Q., Bjella, K., and Luoto, M. 2022. Impacts of permafrost degradation on infrastructure. Nature Reviews Earth & Environment, 3 (1): 24–38. https://doi.org/10.1038/s43017-021-00247-8

Qin, S., and Gao, Z. 2017. Developments and Prospects of Long-Span High-Speed Railway Bridge Technologies in China. Engineering, 3 (6): 787–794. https://doi.org/10.1016/j.eng.2017.11.001

7C — Permafrost and Infrastructure Dynamics Along the Inuvik–Tuktoyaktuk Highway, NT

Session Chairs: Jennifer Humphries[1], Charles Klengenberg[2] & Ed Grozic[3]

[1]*Aurora Research Institute, Inuvik, Northwest Territories, Canada*
[2]*Inuvialuit Land Administration, Northwest Territories, Canada*
[3]*Tetra Tech Canada Inc., Calgary, Alberta, Canada*

The Inuvik-Tuktoyaktuk Highway (ITH) is a 140 km-long corridor connecting the Beaufort Delta region to the national highway system. It serves as the only all-weather road to the Canadian Arctic Coast. The highway was built over diverse terrain with varying ice contents and intersects a number of geologic and ecological environments. Across the corridor, permafrost temperatures range from cold (<-4 °C) to warm and near 0 °C. The construction of the ITH provided a unique opportunity to develop a societally-relevant, northern-driven permafrost research agenda. One that supports the planning and maintenance of infrastructure, regulation, and monitoring of climate change impacts and informed adaptation.

This session will showcase the diversity of monitoring and research conducted along the ITH and contributions toward understanding permafrost-infrastructure interactions and developing applied solutions to challenges unique to permafrost terrain. The session has a multidisciplinary focus and welcomes talks highlighting different methods and knowledge sources in monitoring and researching permafrost and infrastructure interactions. This includes the importance of baseline information, its management, analysis, and communication to support decision-making, and the necessity for collaborative or interdisciplinary approaches to address infrastructure management challenges in an ice-rich permafrost environment.

Tracking observed temperatures and projected climate scenarios for an embankment along the Inuvik-Tuktoyaktuk Highway, Canada

Earl de Guzman[1], Marolo Alfaro[2], Lukas U. Arenson[2,3] & Guy Doré[4]

[1]*Tetra Tech Canada Inc., Burnaby, British Columbia, Canada*

[2]*Department of Civil Engineering, University of Manitoba, Winnipeg, Manitoba, Canada*

[3]*BGC Engineering Inc., Vancouver, British Columbia, Canada*

[4]*Département de génie civil et de génie des eaux, Université Laval, Québec City, Québec, Canada*

Thermal performance modelling and climate change assessment of infrastructure in permafrost regions require adequate information on current ground thermal regime prior to embankment design and construction and selection of an appropriate climate scenario. Although climate data is available for different climate scenarios, its selection is based on either an assumed likelihood of occurrence or assuming the worst-case scenario. The worst-case scenario is commonly misinterpreted as the conservative case, but it does not account for any current and future governmental or societal policies aimed to keep the threshold temperature at the end of the century. For infrastructure in the Arctic corridor, limited data is available that monitors the direct impact of embankment construction on the underlying permafrost and how climate change is influencing its performance.

A 5.3 m thick embankment section along the Inuvik-Tuktoyaktuk Highway (ITH) in the Northwest Territories, Canada was instrumented with temperature sensors during its construction in April 2015 and has been continuously monitored to date. The embankment is on continuous permafrost and was built using compacted frozen fill. A numerical model was developed earlier by De Guzman et al. (2021) to simulate the thermal behaviour of this embankment. In their paper, the numerical model was calibrated using temperatures available in the embankment fill and underlying foundation between April 2015 and August 2018, followed by thermal performance forecasting for near-term (i.e., less than 30 years) and long-term (i.e., until 2100) climate scenarios using the second-generation Canadian Earth System Model (CanESM2) under the Coupled Model Intercomparison Project Phase 5 (CMIP5). The CMIP5 scenarios are commonly denoted as the Representative Concentration Pathways (i.e., RCP scenarios).

Since the original thermal assessment for this research site, five years of additional data have been recorded from the temperature sensors. In addition, a newer generation of climate scenarios have been developed under Phase 6 of CMIP, which are represented as Shared Socioeconomic Pathways (i.e., SSP scenarios) that consider different narrative of climate policies and radiative forcings. The model scenarios investigated in this study is summarized in Table 1. GCM in Table 1 indicates a Global Climate Model, while CanDCS means statistically downscaled scenarios. Not all scenarios in CMIP5 and CMIP6 have been downscaled. Additionally, the column 'Ensemble' considers multiple climate models to account for uncertainty and variation between the climate modelling experiments. Only the 50th percentile and multi-model mean for the Ensemble models are presented in this study. The data used in the model is publicly available in https://climate-scenarios.canada.ca/.

Table 1. Model scenarios.

Model Scenario	Canadian Experiment	Ensemble
CMIP5 CanDCS-U5	CanESM2 RCP8.5	RCP8.5
CMIP5 GCM	CanESM2 RCP8.5	RCP8.5
CMIP6 CanDCS-U6	CanESM5 SSP5-8.5	---
CMIP6 GCM	CanESM5 SSP3-7.0, SSP4-6.0, and SSP5-8.5	SSP3-7.0, SSP4-6.0, and SSP5-8.5

The temperature and wind speed projected for each scenario in Table 1 were used in a thermal numerical model using a Surface Energy Balance (SEB) approach. The SEB approach also uses solar radiation, relative humidity, albedo, and snow depth. The solar radiation, albedo, and snow depth were taken to vary each month of the year but were assumed to be cycled for each year until 2100.

Results of the thermal modelling using the climate scenarios in Table 1 are shown in Figures 1 and 2 for CMIP5 and CMIP6, respectively, at the centreline of the embankment and 0.6 m above the natural terrain. The monitored data between 2015 and 2023 is overlain in both figures. For clarity, the time scale presented in these figures is only until 2040. Mean ground temperature to 2100 at the same observation location is shown in Figure 3 for the CMIP6 models.

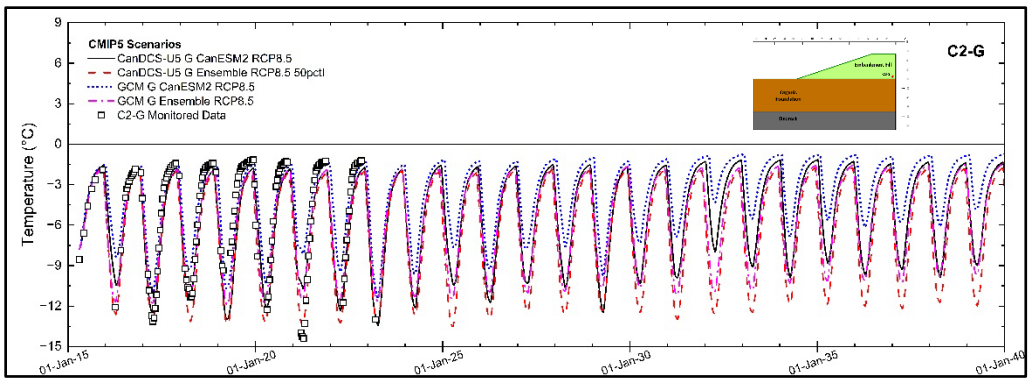

Figure 1. Model results at embankment centreline above natural terrain using CMIP5 scenarios.

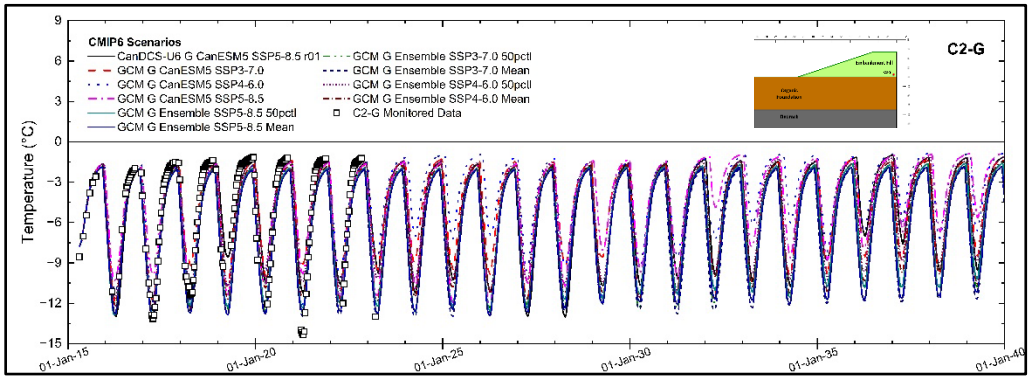

Figure 2. Model results at embankment centreline above natural terrain using CMIP6 scenarios.

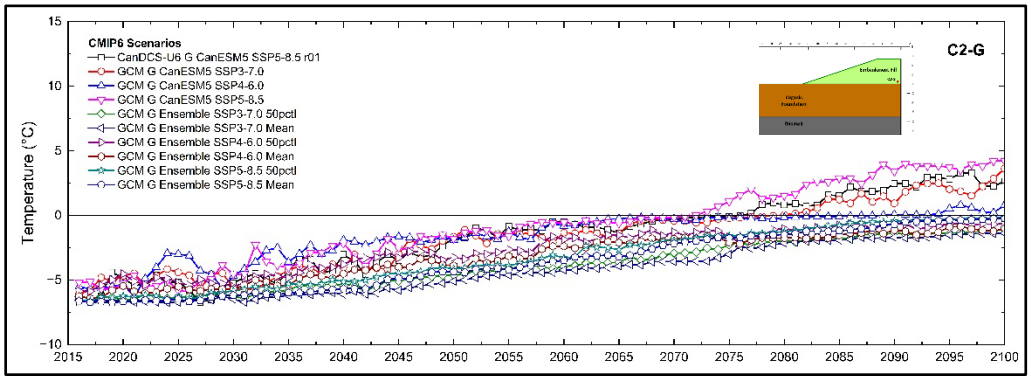

Figure 3. Mean annual ground temperatures at embankment centreline using CMIP6 scenarios.

This study is the first attempt to revisit the original models developed in 2020 and incorporating additional data and improvements in the climate scenarios. Based on the model results, the following observations are made:

- Both CMIP5 and CMIP6 model scenarios reasonably capture the temperatures that have been recorded in the embankment since end-of-construction. This provides confidence in the numerical model developed for this study.
- Although climate models are evolving as climate policies take effect and the science of understanding the climate evolves, the recorded and modelled temperatures demonstrate that the climate is warming and will contribute to the long-term performance of embankments in the Arctic corridor.

REFERENCES

De Guzman, E.M.B., Alfaro, M.C., Arenson, L.U., and Doré, G. 2021. Thermal Regime of Highway Embankments in the Arctic: Field Observations and Numerical Simulations, ASCE Journal of Geotechnical and Geoenvironmental Engineering, 147(6). https://doi.org/ 10.1061/(ASCE)GT.1943-5606.00025

Hydrothermal and terrain effects of a highway on streams in permafrost

Timothy Ensom[1,2], Steven V. Kokelj[3], Philip Marsh[1], Ryan Connon[2], Kelly Kamo McHugh[4] & Jurjen van der Sluijs[5]

[1]*Cold Regions Research Centre, Wilfrid Laurier University, Waterloo, Ontario, Canada*

[2]*Department of Environment and Climate Change, Government of Northwest Territories, Yellowknife, Northwest Territories, Canada*

[3]*Northwest Territories Geological Survey, Government of Northwest Territories, Yellowknife, Northwest Territories, Canada*

[4]*Aurora Research Institute, Aurora College, Inuvik, Northwest Territories, Canada*

[5]*NWT Centre for Geomatics, Government of Northwest Territories, Yellowknife, Northwest Territories, Canada*

Highways in cold regions are often designed to develop and maintain frozen-core embankments to preserve underlying permafrost. Pronounced cooling of terrain can occur beneath highways in winter due to embankment material thermal properties and snow removal (Humphries et al. 2024). During construction and operation of the Inuvik-Tuktoyaktuk Highway (ITH), aufeis growth, winter terrain heave and cracking, spring ponding, subsidence and erosion, and vegetation mortality have been observed at stream crossings. In this work we investigate hydrothermal interactions between highway crossings and streams to better understand these processes. To demonstrate the thermal, hydrological, and terrain effects of bridge structures we present field observations of temperature, water pressure, and terrain dynamics from several stream crossings. On the basis of these data and analyses we develop a conceptual model that shows how bridge structures can accelerate channel freezeback in small streams and initiate a sequence of freeze dam formation, pressure buildup, aufeis development, and terrain instability. While aufeis and injection ice elsewhere have been described (Carey 1973; Kane 1981), we focus on small streams and place this in the context of climate-related increases in winter baseflow that can amplify these processes and effects.

Study region

The ITH was completed in 2017 and traverses 138 km of continuous permafrost on uplands composed primarily of fine-grained, ice-rich till east of the Mackenzie Delta. The region is lake-rich, and there is a northward transition from spruce forest near Inuvik to dwarf-shrub tundra in the Tuktoyaktuk Coastlands (Burn and Kokelj 2009). Small streams are pervasive and catchment areas of investigated highway crossing sites range from 8 to 28 km^2.

Methods

To link continuous in-stream temperature and pressure conditions with observable aufeis and terrain dynamics, we instrumented streambeds with temperature and pressure data loggers at specific ITH crossings and acquired concurrent stream images from bridge-mounted cameras. Thermal data from streams at highway crossings were compared with riparian control sites to assess the thermal influence of bridge structures. Additional data collection at crossings included late-winter snow surveys, drilling in streams to determine aufeis thickness and frozen or thawed substrate extent, slug tests to determine streambed hydraulic conductivity, and stream surveys with remotely piloted aircraft systems (RPAS) to map channel topography.

Results and discussion

Late-winter snow surveys since 2017 have shown that snow accumulation beneath the three southern ITH bridges (mean = 5 cm, StDev = 13 cm) is significantly less than in undisturbed regional riparian terrain (mean = 97 cm, StDev = 50 cm). Near-surface temperature in terrain adjacent to streams under bridges was as low as -40 °C, approximately 20 °C lower than the minimum near-surface temperature for undisturbed riparian terrain. Streambeds beneath bridges with shallow in-stream snow cover were colder than the snow-filled streambed under a bridge that did not block snow. Streams with shallow snow beneath bridges typically froze to their beds.

The freezing of streams beneath bridges caused the hydrostatic water surface elevation (HWSE) upstream of bridges to increase relative to HWSE downstream. The low hydraulic conductivity of the fine-grained substrate beneath streambeds (<2.5 x 10^{-3} m s^{-1}) did not allow the equalization of hydrostatic pressure between the upstream and downstream sides of bridges, so the hydraulic gradient in streams at highway crossings during early winter was higher than summer. Recurrent overflow events in early and mid-winter on the upstream sides of bridges were observed in the field and identified in records from onsite cameras. These overflow events were induced by the high upstream water pressure,

and at one bridge they produced aufeis that grew to within 1.5 m of the span in four of eight monitored years (Figure 1).

Photo sequences have also documented vertical heave of streambanks and riparian vegetation upstream of ITH crossings during winter (Figure 2), sometimes by over 1.5 m, and subsidence the following spring. Terrain heave and subsidence have been observed up to 150 m upstream of the km 8 bridge. In some years injection ice up to 55 cm thick was observed between upper peat and deeper mineral layers in streambanks. Drilling and coring in spring at sites that heaved in winter has revealed a top-down sequence of (i) frozen peat, (ii) a layer of injection ice, (iii) a layer of water or a cavity recently filled with water, and (iv) unfrozen fine-grained mineral soil, similar to frost blisters. Broken roots of riparian shrubs have been observed in the cavity.

Figure 1. ITH km 8 bridge (a) with aufeis on 25 Feb 2017, and (b) without aufeis on 26 Mar 2022.

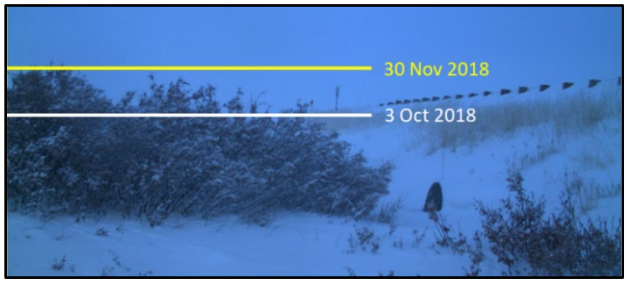

Figure 2. Riparian terrain upstream of a culvert near Tuktoyaktuk, 30 Nov 2018. The lines indicate the tops of the willows on 3 Oct and 30 Nov. Total heave over this period was approximately 1 metre.

The hydrothermal dynamics described here rely on a supply of water from the catchment that persists into the freezing season, and on a freeze dam created by altered stream boundary conditions at a highway crossing. Increases in autumn rainfall associated with climate change appear to increase early winter baseflow in streams and may amplify these processes. The development of injection ice and aufeis has management and safety consequences for transportation infrastructure. Freshet flow over aufeis can scour the highway embankment above elevations armoured to withstand erosion. Freshet streamflow occurred while the aufeis surface remained above the 1:100 year design peak water level in seven of eight years beneath the km 8 bridge and in three of six monitored years beneath the km 26 bridge. Riparian terrain heave has the potential to expose mineral soils and initiate thaw, or damage highway crossing structures. Water that is impounded or diverted by aufeis or ice-filled culverts can lead to thermal erosion of embankments or permafrost terrain adjacent to highways. The preservation of unfrozen conduits for flow in small streams beneath highway crossings in permafrost environments, and active winter monitoring, are key to the reduction and avoidance of such problems.

Conclusion

Highway crossing structures can cause pronounced early-winter stream and streambed cooling. This can lead to freeze damming and, with sufficient winter baseflow, cause elevated water pressure, aufeis, riparian terrain heave, rapid and erosive freshet flow over aufeis, and spring terrain subsidence, posing maintenance and safety challenges at highway crossings. This raises the importance of monitoring to (1) better understand the site and antecedent climate conditions that promote aufies development, and (2) inform maintenance and engineering solutions. This study highlights the need to foster collaboration between scientists, engineers, and practitioners to identify and solve emerging infrastructure challenges in a changing Arctic.

References

Burn, C.R., and Kokelj, S.V. 2009. The environment and permafrost of the Mackenzie Delta area, Permafrost and Periglacial Processes, 20(2): 83–105.

Carey, K.L. 1973. Icings developed from surface water and ground water, Cold Regions Science and Engineering Monograph III-D3. U.S. Army CRREL.

Humphries, J.K., van der Sluijs, J., and Kokelj, S.V. 2024. Embankment evolution of a frozen core road five years after construction: the Inuvik-Tuktoyaktuk Highway, In 12th International Conference on Permafrost, Yukon, Canada.

Kane, D.L. 1981. Physical mechanics of aufeis growth, Can J Civ Eng, 8: 186-195.

N-factor variability across the Inuvik-Tuktoyaktuk Highway treeline: Investigating the influence of snow

M. Alice Wilson[1], Steve V. Kokelj[2] & Emma J. Stockton[3]

[1]*Northwest Territories Geological Survey, Government of Northwest Territories, Inuvik, Northwest Territories, Canada*

[2]*Northwest Territories Geological Survey, Government of Northwest Territories, Yellowknife, Northwest Territories, Canada*

[3]*Department of Geography, Carleton University, Ottawa, Ontario, Canada*

Permafrost temperatures in the western Arctic are increasing and variations in vegetation and snow conditions influence the thermal responses to this warming. To better understand these responses and provide data to calibrate models we require robust datasets to explore the linkages between the climate and ground temperatures.

The transition from forest to tundra is characterised by variations in vegetation and snow cover which influence the ground thermal regime. In the Mackenzie Delta region, snow depth decreases northward due to lower precipitation near the coast and reduced retention capacity in shorter vegetation (Palmer et al. 2012). In winter, snow insulates the ground from air temperatures inhibiting ground heat loss. As a result, ground temperatures are typically higher beneath a deep snowpack (Smith 1975). In this study, our aim was to investigate air-ground temperature relations across treeline and to explore inter-site, and inter-annual differences. We established robust networks of surface thermistors at two mineral soil hilltops with earth hummocks and at two polygonal peatlands within the treeline transition. In 2019-2023, data was collected at hillltop and peatland environments at sites north (Trail Valley) and south (Inuvik) of the treeline (Figure 1). The paired hilltop and peatland sites located north and south of treeline are referred hereafter as the Inuvik and Trail Valley sites.

Ground surface thermistors were installed to 5 cm depth on three hummocks and interhummock depressions at each hilltop site (N=6), and on three polygon centres, edges, and ice-wedge troughs at each polygonal peatland site (N=9).

To explore linkages between air and ground temperatures, n-factors were used. n-factors are a summation of the relation between air and ground temperature for the freezing (n_f) and thawing season (n_t), and have been used to estimate the ground surface temperature from air temperatures (Lunardini 1978). The n-factor is dimensionless and ranges from 0 to ∞ while values near one indicate a close relation between air and ground temperatures. The n-factors were calculated using the methodology in Stockton et al. (2024). Here we present the preliminary results of the n-factors calculated across four years for the hilltop and peatland sites at Inuvik and Trail Valley.

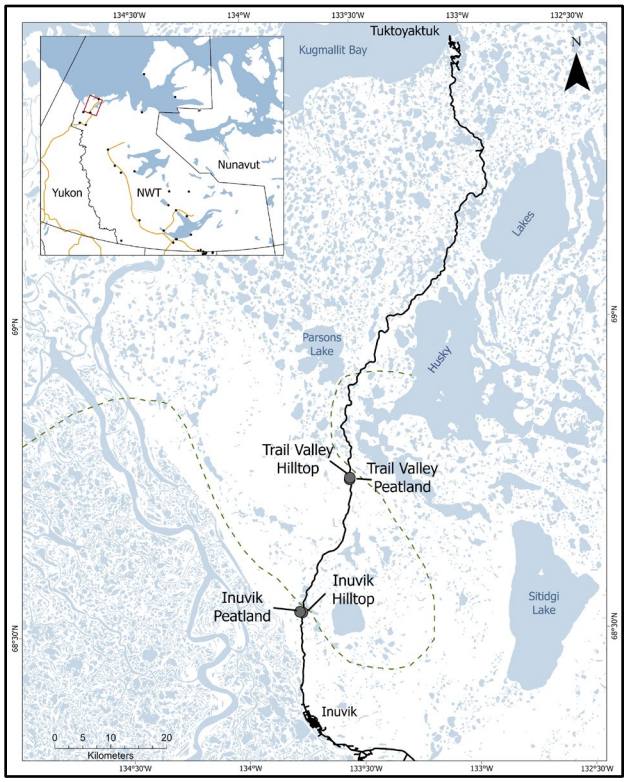

Figure 1. Map of near-surface ground temperature monitoring sites across treeline along the Inuvik-Tuktoyaktuk Highway.

During the study, n_f ranged from 0.05 to 0.67 and n_t from 0.13 to 3.18. The largest within season variation in both n_f and n_t were seen at the polygonal peatland sites (Figure 2), while the hilltop sites were characterised by lower intra-site variation. The large range in n_f in peatlands can be attributed to the ice-wedge troughs, which consistently had lower values than polygon centres. Polygon centres and ice wedge troughs had a median n_f of 0.28 and 0.37, respectively. The troughs can be wet with deeper snow than the other thermistor locations. The Trail Valley sites have higher n_f than the Inuvik sites likely in association with a thinner and denser snow pack north of treeline. For example, snow depth and density was 31 cm and 0.31 g/cm^3 at Trail

Valley Hilltop and 64 cm and 0.24 g/cm^3 at Inuvik Hilltop in March 2020, respectively. The nf values between the two Trail Valley sites were never significantly different over the four winters, and only significantly different between the two Inuvik sites in winter of 2020/2021. For each site, the inter-annual variation in nf was statistically significant between the highest and lowest snow winters except at Inuvik Hilltop. Factors related to timing and amounts of snow in those years will be explored to better understand controls on interannual differences in nf.

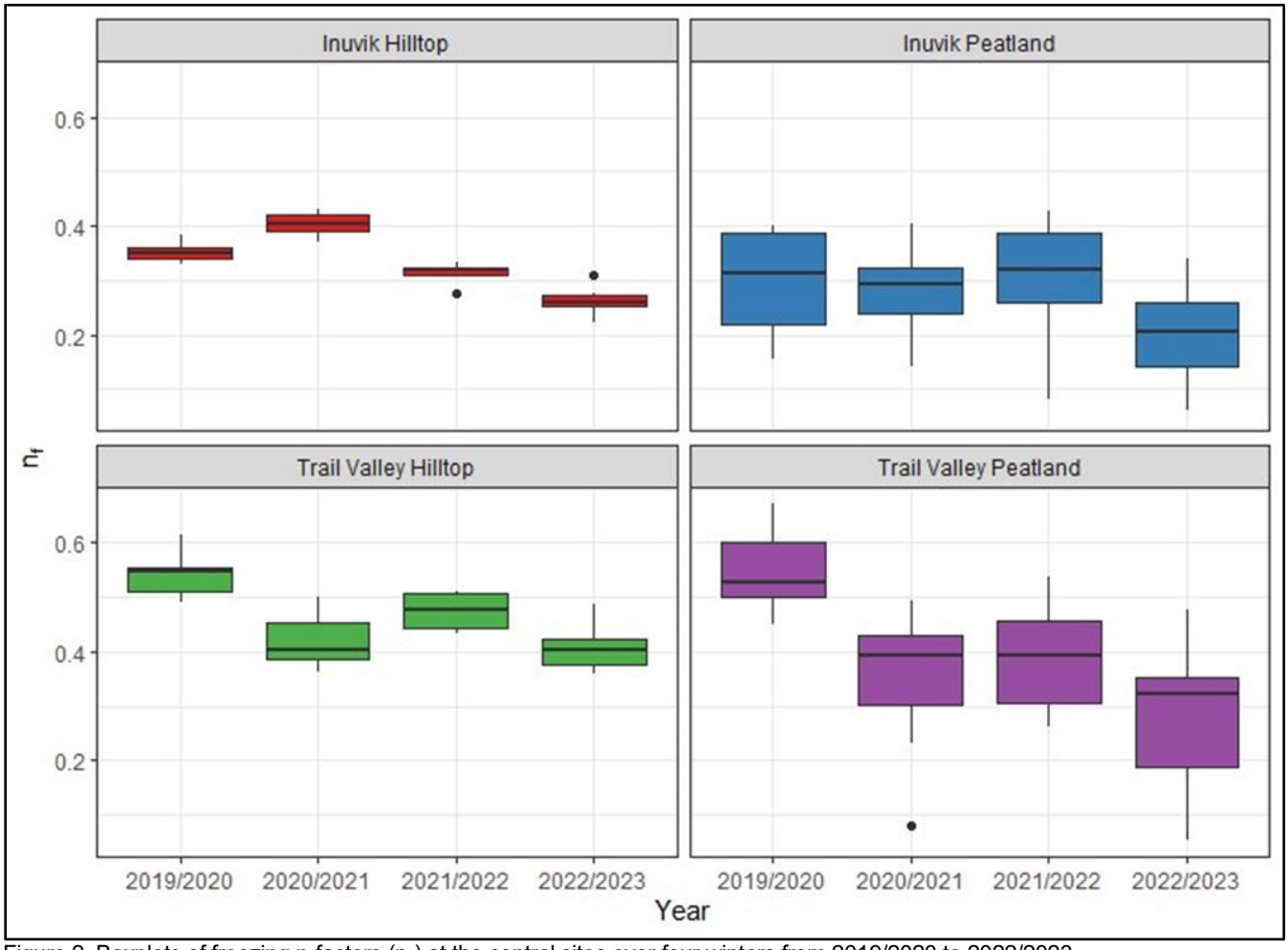

Figure 2. Boxplots of freezing n-factors (n_f) at the control sites over four winters from 2019/2020 to 2022/2023.

REFERENCES

Lunardini, V.J. 1978. Theory of n-factors and correlation of data, In 3rd International Conference on Permafrost, Edmonton, AB, Canada, National Research Council of Canada, 1: 40–46.

Palmer, M.J., Burn, C.R., and Kokelj, S.V. 2012. Factors influencing permafrost temperatures across tree line in the uplands east of the Mackenzie Delta, 2004-2010. Canadian Journal of Earth Sciences, 49:877–894. doi:10.1139/e2012-002

Smith, M.V. 1975. Microclimatic influences on ground temperatures and permafrost distribution, Mackenzie Delta, Northwest Territories. Canadian Journal of Earth Sciences, 12(18): 1421–1438. doi:10.1139/e75-129

Stockton, E.J., Burn, C.R., Wilson, M.A., and Kokelj, S.V. 2024. Road surface n-factors across elevational and latitudinal treelines, Dempster-ITH corridor, western Arctic Canada, In 12th International Conference on Permafrost, Whitehorse, YT

7D — Permafrost Engineering, Geomorphology, Hydrology for Northern Linear Infrastructure Resilience and Safety

Session Chairs: Fabrice Calmels[1], Emmanuel L'Hérault[2] & Thomas Ingeman-Nielsen[3]

[1]*Yukon University, Whitehorse, Yukon, Canada*
[2]*Université Laval, Québec City, Québec, Canada*
[3]*Technical University of Denmark, Kgs. Lyngby, Denmark*

Northern linear infrastructure such as roads and airstrips are vulnerable to natural processes and geohazards. Climate change is contributing to more frequent and intense geohazards which translate to increased maintenance and repair costs, as well as potentially dangerous travelling conditions.

In northern environments, geohazards result from permafrost thaw and permafrost hydrology and commonly cause damage to, or lead to failure of, transportation infrastructures. Some of these geohazards initiate due to thermal disturbances induced by construction of the infrastructures themselves. Other processes that eventually reach and impact infrastructures occur naturally or as a function of climate change, sometimes hundreds of meters away.

In this context, engineering, permafrost geomorphology, permafrost hydrology, and related disciplines are non-exclusively well suited to efficiently assess permafrost thaw-related geohazard risks. By assessing the above- and below-ground preconditions, the processes responsible for the geohazards can be identified. This knowledge supports decision-making about how best to invest in transportation networks in a time when climate change will continue to generate unprecedented extreme conditions associated with permafrost processes.

This session is dedicated to studies using those disciplines to generate new knowledge applicable to improving the resilience and safety of existing northern transportation infrastructure. Transportation infrastructure managers can use this information to augment remediation strategies, develop risk-management procedures and policies to enhance disaster preparedness, and mitigate disaster by implementing appropriate rehabilitation and reconstruction.

Deep foundation replacement and settlement monitoring of airport runway in high-latitude permafrost region

Dun Chen[1,2,3], Guoyu Li[1,2,3], Wei Ma[1,2,3], Chunqing Li[1,2,3], Yapeng Wang[1,2,3], Kai Gao[1,2,3] & Qingsong Du[1,2,3]

[1]*State Key Laboratory of Frozen Soil Engineering Northwest Institute of Eco-Environment and Resources, Chinese Academy of Sciences, Lanzhou, China*

[2]*Da Xing'anling Observation and Research Station of Frozen-Ground Engineering and Environment, Northwest Institute of Eco-Environment and Resources, Chinese Academy of Sciences, Jagdaqi, China*

[3]*International Research Center for China-Mongolia-Russia Cold and Arid Regions Environment and Engineering, Chinese Academy of Sciences, Lanzhou, China*

This study investigates settlement evolution characteristics in high-latitude permafrost regions by analyzing cumulative deformation around the airport's deep foundation pit during construction. It discusses the accuracy and applicability of various settlement prediction methods for runway settlement in permafrost regions. Results indicate that permafrost excavation and filling methods meet construction and deformation requirements, reducing post-construction settlement risk. Curve fitting predicts post-construction runway settlement in permafrost regions, offering insights for airport construction and operation in such environments.

Permafrost airports, due to unique environmental conditions, require special considerations for foundation construction (Liu et al. 2015; Liu et al. 2019). Managing runway settlement is crucial in permafrost regions. Currently, permafrost replacement is widely adopted due to its simplicity and effectiveness. However, deep foundation pit work, inevitable due to varying frozen soil layer thicknesses, disturbs soil layers, leading to frost heave and adjacent surface settlement (Yu and Gong 2002; Shang et al. 2023). Hence, deep foundation pit design and construction must ensure stability and surrounding environment safety. Thorough monitoring and prompt action are essential to address issues and ensure environmental safety.

This paper, based on field monitoring data from Mo'he Airport expansion, elucidates cumulative deformation around the deep foundation pit during construction. It analyzes settlement prediction methods for runway settlement in permafrost regions, offering insights for similar projects in high-latitude permafrost regions.

ENGINEERING BACKGROUND

Mo'he Airport, situated as the northernmost and highest latitude civil airport in China, lies nine kilometers southwest of Mo'he City, Heilongjiang Province, atop low hills. In 2015, an airport expansion project primarily extended the runway by 700 m southeastward and leveled the northwest end by 100 m to the southeast, yielding an effective length of 2,800 m. The standard seasonal freezing depth at this location is 3.0 m, while the frozen soil depth under the extended runway section varies from 8.5 to 15.5 m. Consequently, different reclamation depths are employed based on the stratum and permafrost distribution across the runway area. Thawed permafrost replaces excavated foundation soil to a specified depth, subsequently filled with well-mixed gravel material. Eight monitoring points surround the deep foundation pit to continually track deformation, as depicted in Figure 1.

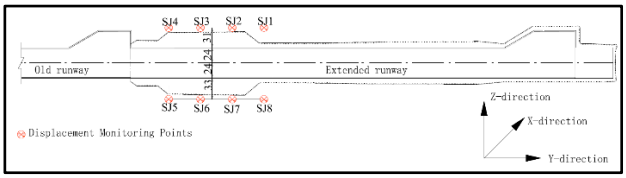

Figure 1. Monitoring points in deep foundation pit (unit: m).

DEFORMATION LAW OF RUNWAY DEEP FOUNDATION PIT

Figure 2 illustrates cumulative deformation curves in X, Y, and Z directions of monitoring points around the deep foundation pit. Over time, cumulative deformation in each direction exhibits a transition from rapid initial increase to gradual convergence, with decreasing curve slopes. Initially, settlement gaps among cumulative deformation monitoring points in all directions are minimal. However, as monitoring progresses, disparities in cumulative settlement among points of the same direction gradually widen. In the X-direction, SJ3 and SJ5 experience more significant deformation, with a maximum of 71 mm. Notably, substantial cumulative deformation occurs at SJ2 and SJ3 in the Y-direction. Throughout the deep foundation pit replacement construction, slope deformation and settlement are controlled within allowable specifications.

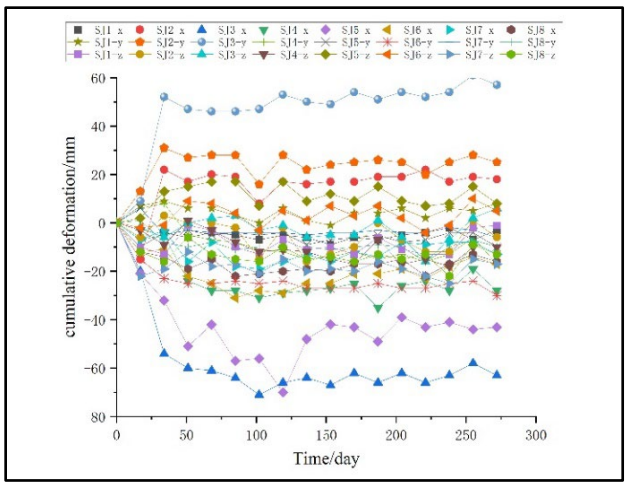

Figure 2. Curves of cumulative deformation of deep foundation pits in different directions with time.

PREDICTION OF DEEP FOUNDATION PIT SETTLEMENT FOR RUNWAY

Utilizing curve fitting, settlement prediction was performed for monitoring point S7 in Mo'he Airport's deep foundation pit, as depicted in Figure 3. Notably, power and logarithmic functions exhibit a high degree of fitting with actual settlement monitoring data. A post-construction (30-year) settlement prediction was conducted for the deep foundation pit monitoring point at Mo'he Airport, revealing a maximum settlement of approximately 26 mm, well within allowable specifications.

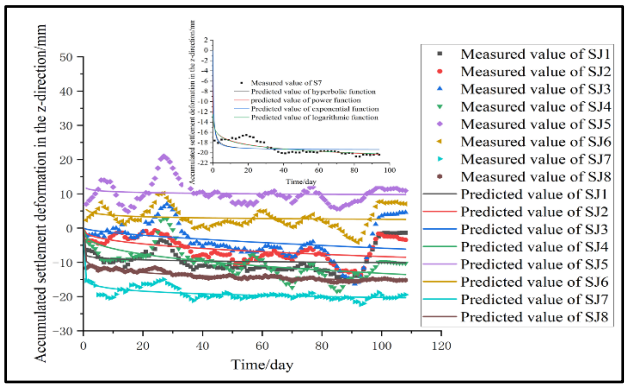

Figure 3. Comparison between the measured points and predicted curves of monitoring site.

CONCLUSION

1. Excavation and replacement measures have effectively addressed runway deformation issues in permafrost regions.
2. Over time, deep foundation pit deformation gradually stabilizes, as indicated by discrete data, meeting specification requirements.
3. Utilizing curve fitting, accurate and applicable predictions for post-settlement of airport deep foundation pits in permafrost regions are achieved with minimal deviation. These results are highly reliable for predicting the settlement of reclaimed runways in permafrost regions.

ACKNOWLEDGEMENTS

Thank you to the Science & Technology Fundamental Resources Investigation Program (Grant No. 2022FY100703), the National Natural Science Foundation of China (Grant No. 42272339), the Foundation of the State Key Laboratory of Frozen Soil Engineering (Grant No. SKLFSE-ZT-202203, SKLFSE-ZQ-202303, Grant No. SKLFSE202010, and Grant No. SKLFSE202010), the program of Gansu Province Science and Technology Foundation for Youths (Grant No. JR5RA089) for funding this work.

REFERENCES

Liu, W.B., Yu, W.B., Chen, L., et al. 2015, Techniques of Airport Runway Construction in Permafrost Regions: A review. Journal of Glaciology and Geocryology, 37(6): 1599–1610.

Liu, G.G., Yang, Y.M., and Niu, F.J., et al. 2019, Influences of Spring Thaw on Working Performance of Airport Soil Field Surface in Cold Region. Journal of Shenzhen University Science and Engineering, 36(6): 621–627.

Yu, J.L., Gong, X,N,. 2002, Research on Deformation of Foundation-pit Engineering. China Civil Engineering Journal, (04): 86–90.

Shang, Y.H., Niu, F.J., Yuan, K., et al. 2023, Freezeback Behavior of a Cast-in-place Pile Foundation Surrounded by Two-phase Closed Thermosyphons in Permafrost Regions. Applied Thermal Engineering, 225: 120151.

Geotechnical field investigations in sporadic, discontinuous permafrost at the Donlin Gold Project in southwestern Alaska

Madeleine Everton[1] & Aaron Weber[2]
[1]BGC Engineering Inc., Calgary, Alberta, Canada
[2]BGC Engineering Inc., Toronto, Ontario, Canada

The Donlin Gold Project (the "site") is a proposed open-pit gold mining project located in the Kuskokwim Mountains of southwestern Alaska, approximately 15 km north of the village of Crooked Creek. Various site investigation methods have been used over a 17-year period to characterize soil, bedrock, and permafrost for the design of project infrastructure. The information is used for the geotechnical design of foundations for infrastructure and facilities, the impacts of frozen ground on seepage potential, and the delineation of thaw-sensitive materials requiring removal. This extended abstract discusses the advantages of each site investigation method and their use cases for permafrost investigations.

Geology, climate, and permafrost

The site remained unglaciated during the most recent glacial maxima. In the valley bottoms, peat overlies alluvium. Thinner organics coat loess and colluvium on the valley walls. Soils are typically clayey silt to silty gravel ranging from 0.3 m to over 15 m thick. Bedrock comprises greywacke, siltstone, and shale deposits, and is highly weathered near surface.

The climate at the site is cold and dry with daily air temperatures ranging on average from -29°C to 22°C, and a mean annual air temperature is -1.9°C. Daily air temperatures are below freezing between October and March. Average annual precipitation is 500 mm, with two-thirds as rain between June and September.

The site is located within a region of sporadic, discontinuous permafrost. Where present, permafrost is warm, typically between -0.5°C and 0°C and varies from less than 2 m to 30 m in thickness. In soil, the permafrost ranges from ice-poor friable soil to ice-rich fine-grained soil, with isolated ice lenses and massive ice up to 1.0 m thick. In bedrock, the permafrost is present as discontinuities filled with ice or frozen infill.

Site access considerations

The site is accessible year-round via a gravel airstrip built to accommodate C-130 Hercules aircraft. Equipment can be transported via barge to Crooked Creek during summer months and by seasonal winter trail using heavy equipment, however this access method is infrequently used. The site has few all-season trails, with temporary winter trails providing the primary land access to the wet valley bottoms and across creeks and streams. As such, summer work is typically restricted to helicopter-portable equipment. Access requirements constrain the equipment types available, and in which seasons they can operate.

Thermal disturbance considerations

Conventional drilling methods introduce thermal disturbance to the samples primarily through the friction from advancing the drill bit or drilling tools, and from fluids used to flush drill cuttings and cool the drill bit. The thermal disturbance affects the ability to recover permafrost, especially when thin or marginally frozen, as it can thaw and melt the permafrost. Drilling fluids can also wash away thawed or ice-poor friable soil.

Auger drilling

Auger drilling at the site has been used to characterize the soils, permafrost, and shallow bedrock. Drilling was conducted in summer and winter seasons, completing over 200 drill holes using a conventional tracked hollow-stem auger drill rig. Holes were drilled to refusal, typically in weathered bedrock. Drilling was completed without the use of fluids, and core was provided continuously when frozen. Where collecting permafrost samples for laboratory testing, a Cold Regions Research and Engineering Laboratory (CRREL) or standard penetration testing barrel was used (Brockett and Lawson 1985). Core samples were 83 mm to 165 mm in diameter. Auger drilling has generally resulted in excellent core recovery, particularly in frozen soils with low gravel content.

Direct push drilling

Direct push drilling at the site has been used to characterize the soils, permafrost, and shallow bedrock, totalling over 130 drill holes during summer and winter campaigns. Direct push drilling involves the use of hydraulics and percussion to advance a sampler, recovering continuous core without the use of fluids. Holes were advanced until refusal, typically in highly weathered bedrock.

The tracked direct push drill rig used at the site was light (under 3000 kg) and relatively compact. It required minimal trail clearing and could be moved in one to three picks with a helicopter, allowing access to wet areas in the late summer or early fall when the active layer (seasonal thaw depth) is greatest. Direct push drilling has provided good sample recovery in both frozen and unfrozen soil, especially when drilling in soils with low gravel content. This method is beneficial for recovering permafrost due to the absence of thermal disturbance from drilling fluids.

DIAMOND DRILLING WITH CHILLED BRINE

Diamond drilling has been completed at the site through most major geotechnical drilling campaigns to characterize the bedrock, using conventional tracked or helicopter-portable equipment configured for mineral exploration. Where characterization of the permafrost within bedrock was desired, a chilled calcium chloride solution (brine) was used as the drilling fluid to reduce the thermal disturbance. Eighty-nine drill holes were selected for brine drilling based on permafrost data from prior site investigations.

The brine was prepared by dissolving calcium chloride pearls in freshwater derived from the creek to depress its freezing point. Refrigeration units were then used to cool the brine to a maximum fluid temperature of -2°C. Thermometers were submerged in the brine tanks and regularly monitored.

This method has proven successful in recovering bedrock discontinuities which were infilled with ice or frozen material. While the intent of the brine drilling campaigns at the site were to characterize frozen conditions within the bedrock, it was occasionally successful in recovering permafrost in soil, where permafrost was thicker and colder, but unsuccessful in thin, warm, or completely unfrozen zones. As such, drill holes were typically paired with other investigation methods to assess surficial soil and ground ice conditions.

This method was useful for the collection of permafrost information within the bedrock. It is more costly than soil drilling methods and requires extensive planning and support infrastructure. It requires close observation to ensure that the brine stays below the maximum allowable temperature. The brine refrigeration system is not widely available and requires drill crews that are familiar with it.

TEST PITTING

Test pits have been used at the site to characterize the soil, permafrost, and shallow bedrock. Test pits were excavated until refusal in bedrock or frozen ground, maximum excavator reach (typically 5 m), or test pit wall instability, using 20-ton to 30-ton excavators equipped with a frost bucket. Material was logged from test pit walls or in the bucket as retrieved by the excavator. To date, more than 350 test pits have been completed at the site.

Test pits are especially useful in characterizing shallow permafrost as they achieve full recovery. Test pitting is relatively quick compared to drilling methods and has a low cost as only an excavator and one operator are required. Because of this, it is possible to cover a large area quickly, complete a large quantity of test pits, and investigate locations that may be difficult for drill rigs to access. It is possible to recover large samples of permafrost and have a broader picture of the subsurface conditions compared to discrete boreholes, such as the pervasiveness, size, and characteristics of ice lenses or massive ice.

Test pitting in the late fall allows for logging the maximum thaw depth, however access may not be possible in wet areas. If test pitting must be completed in the winter for site access, seasonal frost depth must be accounted for when assessing the frozen material recovered. Due to equipment constraints, test pit depths are much shallower than are achievable with drilling. Depth control is not as accurate as with drilling methods, and it is not possible to retrieve undisturbed samples in test pits. Additionally, test pits are generally not conducive to the installation of instrumentation, such as thermistor strings to measure ground temperatures.

CONCLUSIONS

Each investigation method presented herein has its strengths and limitations, and methods are complimentary when combined. Together, they have been successful in determining the extents of permafrost at the site, both laterally and with depth. It is important to recognize when multiple methods, including geophysical methods, may be necessary to assess the complete picture, while also considering the access constraints of the site.

ACKNOWLEDGEMENTS

The authors would like to thank Donlin Gold LLC for their support in sharing these valuable learnings.

REFERENCES

Brockett, B.E., and Lawson, D.E. 1985. Prototype drill for core sampling, fine-grained perennially frozen ground, CRREL Report 85-1. U.S. Army Cold Regions Research and Engineering Laboratory, Hanover, New Hampshire.

Characterizing permafrost conditions in the central Mackenzie Valley corridor using airborne electromagnetic methods (AEM) and ground-based investigations

Duane G. Froese[1], Keytash Moshtaghian[2], Alexandre Chiasson[1], Alejandro Alvarez[1], Lindsey Heagy[3], Joel Pumple[1], Martyn Unsworth[1,2], Steven V. Kokelj[4], Ashley C.A. Rudy[4], Sharon Smith[5] & Joseph M. Young[1]

[1]*Department of Earth and Atmospheric Sciences, University of Alberta, Edmonton, Canada*

[2]*Department of Physics, University of Alberta, Edmonton, Canada*

[3]*Department of Earth, Ocean and Atmospheric Sciences, University of British Columbia, Vancouver, Canada*

[4]*Northwest Territories Geological Survey, Government of Northwest Territories, Yellowknife, Canada*

[5]*Geological Survey of Canada, Ottawa, Ontario, Canada*

The distribution of permafrost and ground ice is typically inferred from relatively sparse borehole measurements, surficial geology or vegetation relationships. However, these approaches are limited in spatial coverage, costly to implement, and can miss significant ground hazards. Ground-based geophysical techniques such as electrical resistivity tomography (ERT) offer advantages in mapping ground ice and permafrost distribution but are only useful for the study of small areas, typically with horizontal extents of hundreds of metres. In contrast to ground-based geophysical methods, airborne electromagnetic (AEM) methods have the capacity to efficiently map permafrost thicknesses to more than 100 m with spatial distributions covering hundreds of kilometres where ground access is difficult. This makes AEM suitable for studies of large, linear infrastructure corridors with complex permafrost–landscape relations. For example, AEM surveys have been used effectively for mapping discontinuous permafrost in Alaska, where the main focus was to understand the influence of surface water and groundwater on permafrost distribution (Minsley et al. 2012). Here, we present the initial results of the AEM survey in the central Mackenzie Valley to infer regional-scale permafrost distribution and to determine drivers of permafrost thaw. We integrate these data with ground-based geophysical and geological investigations of permafrost characteristics from the last several years, in addition to longer-term ground temperature data (Duchesne et al. 2020).

AEM data were acquired over a week in August 2023 using the XCalibur Multiphysics RESOLVE system. The frequency-domain system operates at 6 frequencies in the range 135000 to 400 Hz, flying at an elevation of ~40 m above the surface with an average speed of 120 km/hr. The survey flew between 4 and 6 flight-lines with a spacing of 100 m on the east side of the Mackenzie River, focused along the existing linear infrastructure and winter road corridor between the communities of Wrigley and Norman Wells (Figure 1). In total, ~1340 km of AEM data were flown, covering the 330 km corridor with 3 additional cross-valley surveys. AEM data were processed at a sampling rate of 10 Hz. Therefore, having a nominal aircraft speed of ~30 m/s (~100 km/h), the sampling rate would be 3 meters/sample. The frequency domain AEM data were inverted using SimPEG, an open-source Python package. The 1D models were stitched to create a set of 2D resistivity cross-sections.

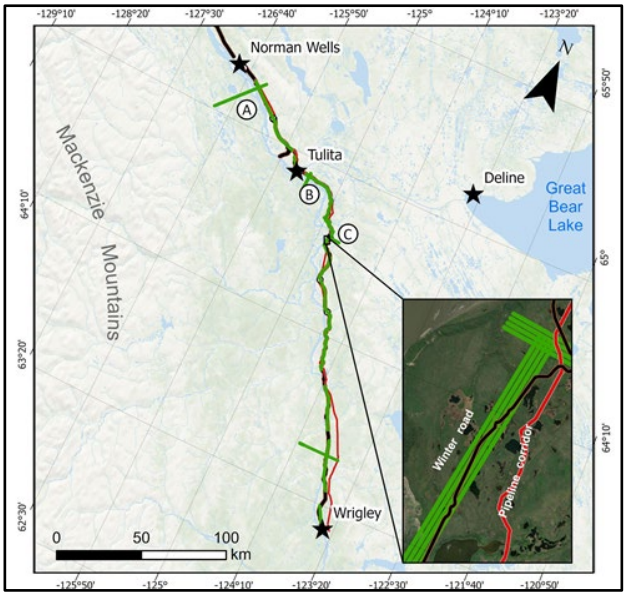

Figure 1. Map of the central Mackenzie Valley corridor. Green lines represent closely spaced (~100 m) AEM survey flight lines. Figure 2 is located southeast of Tulita shown as symbol B. ERT profiles from Figure 3 are shown as symbol A (SL-1) and C (OFP-1).

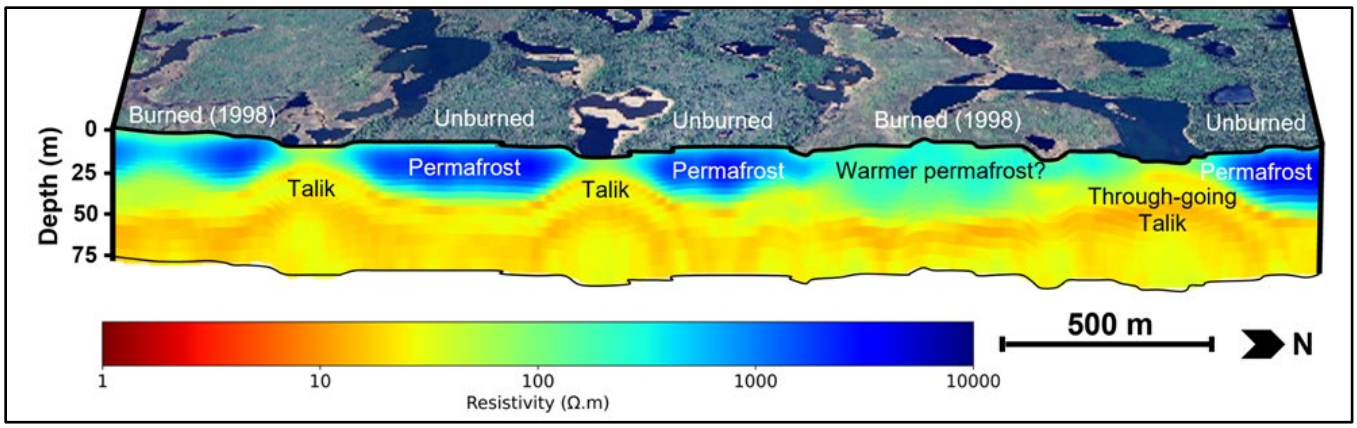

Figure 2. AEM profile of an upland area southeast of Tulita that crosses ice-rich glaciolacustrine sediments of glacial Lake Mackenzie. Permafrost is present along most of the profile to an estimated depth of ~ 25 m with prominent through-going taliks associated with surface water bodies. Less-resistive sediments are associated with an area that burned in 1998.

The AEM data indicate significant permafrost heterogeneity in the central Mackenzie Valley. An inversion model obtained from the AEM data is shown in Figure 2 for part of the cross-valley line immediately southeast of Tulita. The profile traverses sediments from glacial Lake Mackenzie and is marked by irregular lakes that have developed in this ice-rich terrain. The data shows high resistivity in areas that have not been affected by recent forest fires, with permafrost extending to a depth of ~25 m. The permafrost boundary is irregular and marked by the presence of taliks underlying waterbodies and extending through the permafrost. A slightly lower resistivity area, but still on the order of several hundred Ωm, occurs in an area that burned in 1998. This likely reflects the presence of greater unfrozen water content associated with warmer ground temperatures and, thus, lower resistivity.

The model derived from the AEM data is consistent with ground-based observations. At a field site immediately south of the profile (Site B, Figure 1), the subsurface consisted of ice-rich lacustrine sediments in a former drained-lake basin, now occupied by more than one metre of peat (Figure 3A). The model derived from the ERT data indicates permafrost thickness of 8-10 m with a through-going talik associated with a seismic line disturbance that has accumulated surface water (Site A, Figure 1). This contrasts with much deeper permafrost along the winter road near Old Fort Point (Site B, Figure 1), where permafrost is ~30 m thick based on ERT surveys (Figure 3B). These observations are consistent with ground temperatures at the site (Duchesne et al. 2020).

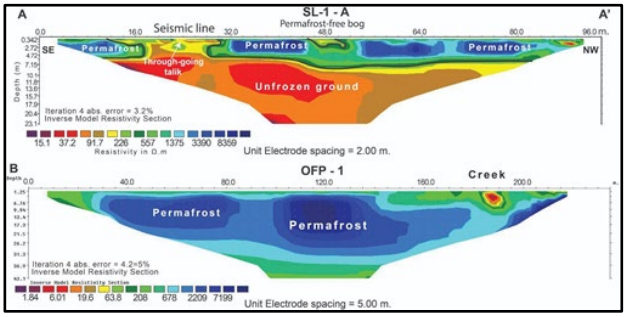

Figure 3. (A) ERT profile from a peat plateau (Figure 1) with ~8-10 m of permafrost and a through-going talik. (B) ERT profile at a site along the winter road near Old Fort Point (Figure 1) indicates permafrost ~35 m thick.

This initial analysis of the 2023 AEM data provides a regional-scale glimpse into the potential for mapping permafrost characteristics through the central Mackenzie Valley. The models derived from the AEM data are consistent with ground-based investigations and regional ground temperature data.

References

Duchesne, C., Chartrand, J., and Smith, S.L. 2020. Report on 2018 field activities and collection of ground-thermal and active-layer data in the Mackenzie corridor, Northwest Territories; Geological Survey of Canada, Open File 8707.

Minsley, B.J., Abraham, J.D., Smith, B.D., Cannia, J.C., Voss, C.I., Jorgenson, M.T., ... and Ager, T.A. 2012. Airborne electromagnetic imaging of discontinuous permafrost. Geophysical Research Letters, 39(2).

UAV-based damage characteristics of the Jagdaqi-Mohe Highway in permafrost regions of Northeast China

Kai Gao[1,2,3], Guoyu Li[1,2,3], Dun Chen[1,2] & Juncen Lin[1,2,3]

[1]*State Key Laboratory of Frozen Soil Engineering, Northwest Institute of Eco-Environment and Resources, Chinese Academy of Sciences, Lanzhou, Gansu, China*

[2]*Da Xing'anling Observation and Research Station of Frozen-Ground Engineering and Environment, Northwest Institute of Eco-Environment and Resources, Chinese Academy of Sciences, Jiagedaqi, Heilongjiang, China*

[3]*University of Chinese Academy of Sciences, Beijing, China*

Under the influence of climate warming and human activities, the high-latitude permafrost in Northeast China is degrading and the road damage is getting worse gradually. However, there are few related road research. Based on field and Unmanned Aerial Vehicle (UAV) surveys, the pavement distresses on the Jagdaqi-Xintian section (JXS) of Jagdaqi-Mohe Highway (JMH) were investigated, and the distribution of pavement distresses, pavement cracks extraction, and pavement smoothness were analyzed. This paper provides an efficient and accurate method for the investigation of road damage in permafrost regions, and explores an evaluation approach for road driving quality in order to design, manage, and maintain road projects in cold regions more scientifically.

Permafrost covers 20% of the exposed land surface in the Northern Hemisphere and has a strong response and feedback to climate change (Hjort et al. 2022). Its gradual warming and degradation under the background of climate warming has increased the risk of thermal hazards (Wu et al. 2021), destabilizing engineering structures in cold regions and causing significant economic losses. Permafrost in Northeast China is a type of latitudinal permafrost in China, termed "Xing'an (Hinggan)-Baikal permafrost" (Jin et al. 2010). This kind of permafrost exhibits poor thermal stability and has degraded quickly in recent years (He et al. 2022; Li et al. 2022). Research on the impact of permafrost degradation on road engineering in Northeast China is less mentioned, especially in terms of road damage characterization. The Jagdaqi-Mohe Highway (JMH) passes through permafrost regions for about 460 km. Under the influence of permafrost degradation and vehicle loads, its serviceability and service life are gradually decreasing. Therefore, for sustainable development, it is of great significance to obtain the damage characteristics of highway and its damage extent.

STUDY AREA AND METHODOLOGY

The investigation road is the Jagdaqi-Xintian section (JXS) of the JMH (Figure 1), which crosses the discontinuous and sporadic permafrost region (Jin et al. 2010). A DJI Matrice M300RTK quadcopter drone equipped with a GNSS RTK receiver and a Zenmuse L1 Lidar lens is used for Lidar and visible light data collection. The distribution of four types of pavement distresses was obtained based on the field and Unmanned Aerial Vehicle (UAV) surveys in 2022 (Figure 2). The Support Vector Machine (SVM) classification algorithm is used to identify and extract the pavement cracks. The standard deviation (Chai et al. 2022) and longitudinal elevation difference are calculated to analyze the pavement smoothness and driving quality. Sampling units and intervals for the data are 10 m and 0.1 m, respectively.

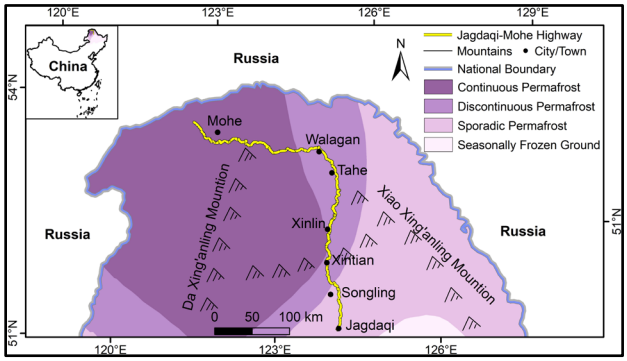

Figure 1. Geographic location of JMH and permafrost distribution along the route.

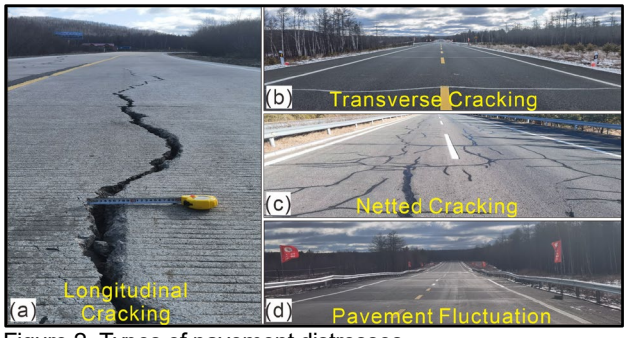

Figure 2. Types of pavement distresses.

The transverse cracking, longitudinal cracking, netted cracking, and pavement fluctuation along the JXS account for 87%, 78%, 32%, and 42%, respectively, and the four types of distress that exceed 200 m length per kilometer account for 66%, 57%, 31%, and 14%, respectively (Figure 3).

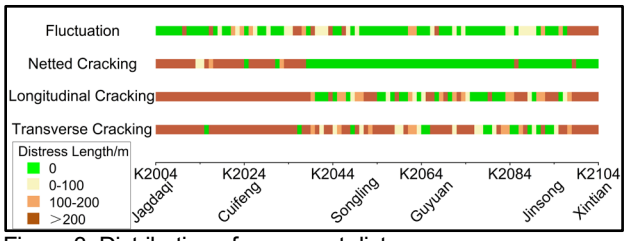

Figure 3. Distribution of pavement distresses.

The overall accuracy of SVM algorithm is 99.78% with a Kappa coefficient of 0.9918 (Figure 4). The area of pavement cracks in the 100 m section is about 64.36 m^2, of which about 86.67% is in the roadway area (Figure 4c). The density of cracks in the roadway is also greater than that in the sidewalk.

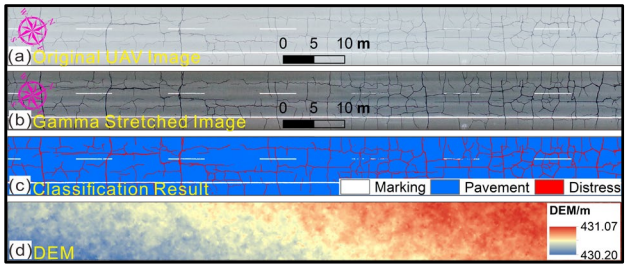

Figure 4. Classification results of pavement cracks in the typical section of 2011 km-300 m~400 m.

By extracting the central elevation of the road surface (Figure 4d), the smoothness and longitudinal height difference of the road surface are calculated (Figure 5). The standard deviation of the pavement elevation of typical section is between 0.018 to 0.041 m, which indicates that the pavement smoothness is good. However, there are still nine pavement bumps in this section, including four light bumps, four medium bumps, and one heavy bump.

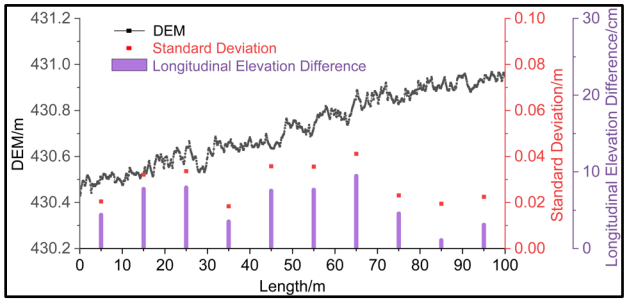

Figure 5. Pavement smoothness of typical section.

CONCLUSION

Based on field and UAV investigation, the pavement damage characteristics on the JXS of the JMH in the permafrost region of Northeast China are conducted. The distribution of pavement distresses, the quantization of cracks areas, and the assessment of pavement smoothness are analyzed. The results show that transverse cracking, longitudinal cracking, netted cracking, and pavement fluctuation account for 87%, 78%, 32%, and 42%, respectively. The pavement crack area of the typical road section is about 64.36 m^2, of which 86.67% is located within the roadway. The pavement of this section is smooth, but there are still 9 pavement bumps.

REFERENCES

Hjort, J., Streletskiy, D., Doré, G., Wu, Q., Bjella, K., and Luoto, M. 2022. Impacts of permafrost degradation on infrastructure, Nature Reviews Earth & Environment, 3(1): 24–38. doi:10.1038/s43017-021-00247-8

Wu, Q., Zhang, Z., and Liu, G. 2021. Relationships between climate warming and engineering stability of permafrost on Qinghai-Tibet plateau, Journal of Engineering Geology, 29(2): 342–352. doi:10.13544/j.cnki.jeg.2020-084

Jin, H., Hao, J., Chang, X., Zhang, J., Yu, Q., Qi, J., Lu, L., and Wang, S. 2010. Zonation and assessment of frozen-ground conditions for engineering geology along the China–Russia crude oil pipeline route from Mo'he to Daqing, Northeastern China, Cold Regions Science and Technology, 64(3): 213–225. doi:10.1016/j.coldregions.2009.12.003

He, R., Jin, H., Luo, D., Huang, Y., Ma, F., Li, X., Wang, H., Li, Y., Jia, N., Li, X., Jin, X., Serban, R., Serban, M., Zhou., C., Liang, Z., and Sun, Y. 2022. Changes in the permafrost environment under dual impacts of climate change and human activities in the Hola Basin, northern Da Xing'anling Mountains, Northeast China, Land Degradation & Development, 33 (8): 1219–1234. doi:10.1002/ldr.4212

Li, G., Ma, W., Wang, F., Jin, H., Fedorov, A., Chen, D., Wu, G., Cao, Y., Zhou, Y., Mu, Y., Mao, Y., Zhang, J., Gao, K., Jin, X., He, R., Li, X., and Li, Y. 2022. A newly integrated ground temperature dataset of permafrost along the China–Russia crude oil pipeline route in Northeast China, Earth System Science Data, 14(11): 5093–5110. doi:10.5194/essd-14-5093-2022

Chai, M., Li, G., Ma, W., Chen, D., Du, Q., Zhou, Y., Qi, S., Tang, L., and Jia, H. 2022. Damage characteristics of the Qinghai-Tibet Highway in permafrost regions based on UAV imagery, International Journal of Pavement Engineering, 1–12. doi:10.1080/10298436.2022.2038381

Woodchip insulation for a buried oil pipeline in permafrost – 40 years experience

Karen Hincks[1], Blake Brodland[2], Ed McRoberts[1] & John Richmond[3]
[1]*WSP E&I Canada, Vancouver, British Columbia, Canada*
[2]*WSP E&I Canada, Calgary, Alberta, Canada*
[3]*Enbridge Pipelines, Edmonton, Alberta, Canada*

A 12-inch (305 mm) diameter oil pipeline, operated by Enbridge Pipelines, was constructed in the early 1980s which runs approximately 869 km from Norman Wells, Northwest Territories to Zama, Alberta. The pipeline, known as Line 21, is buried approximately 1.2 m below ground surface through areas of discontinuous, and sporadic permafrost, with deeper burial at road and water crossings. The geotechnical design of the pipeline was completed by Hardy Associates (1978) Ltd, a predecessor company of WSP, in the late 1970s to early 1980s. WSP and its predecessor companies have provided geotechnical engineering and permafrost monitoring services for Line 21 since construction.

WOODCHIP COVER

To reduce the rate of post-construction permafrost thaw within the pipeline ROW, as a design measure, a layer of woodchips was placed on the ground surface at some of the slopes along the Right-of-Way (RoW) . Woodchips were chosen as they were found to be a good insulator, considered environmentally neutral, relatively cost effective and amenable to deformation, when compared to rigid insulation. The as-built woodchip thickness ranged from 0.5 to 2.2 m.

In the original design for the woodchips, warming within the woodchips due to fungal decay was expected to occur over the first seven years following construction. There was also an assumed decrease in the insulating value of the woodchips over this seven-year period, as the woodchips were expected to decay into a material like peat. Post-construction monitoring data showed that on the majority of the insulated slopes, heating was only significant in the first year or two and on most slopes the woodchips were cooler than expected thereafter. However, the monitoring data did show that significant heating caused by fungal decay of the woodchips occurred on about 10% of the insulated slopes during the second season after completion of construction. All the affected slopes were constructed during the second winter construction season. The heating was attributed to: unapproved inclusion of woodchips from aspen trees which were predicted to have a higher heat generation potential than coniferous trees; rot affected woodchips; and thicker than specified placement of woodchips.

Aside from specific sites where significant fungal decay occurred, the woodchips do not appear to have decayed appreciably since placement in the mid-1980s. This can be attributed to woodchips maintaining an unsaturated condition. In most cases the woodchips physically appear similar to when they were placed in the mid-1980s. Where forest fires have occurred across the RoW, the woodchip surface has been blackened but the fire damage did not penetrate very deep into the woodchip layer. In most cases, Enbridge crews visited the slopes where forest fires occurred and raked over the woodchip surface to disrupt the exposed blackened surface that would warm in the sun more than unburned woodchips. Some areas of woodchip cover are promoting the growth of mushrooms and fungi. In recent years the woodchip surface at some sites has a dimpled or pebbly appearance; this may be attributed to rot and settlement or, at some locations, forest fire impacts.

GROUND TEMPERATURES BELOW THE WOODCHIPS

One important indicator of the effectiveness of the woodchip insulation is the maximum temperature at the ground surface immediately below the woodchip layer. At selected locations along the pipeline, the annual maximum ground surface temperature was determined for each year since construction (except for 1991, 1992 and 1993 for which no data is available), based on the readings collected throughout the year. The maximum, minimum and average temperatures from these thermistors, up to December 2023, are plotted in Figure 1. It should be noted that instrument readings in recent years including 2023 were not as regular as in previous years and, as a result, the data for 2023 may be skewed toward the months where there was data, impacting the overall assessment for the year. The data indicates:

- A slight decrease in the average annual maximum ground surface temperature from approximately +0.6°C to -0.1°C during the first seven years after construction (1984 to 1990, Years 1 to 7; Figure 1).

- No data was available between 1991 and 1993 (Years 8 to 10).
- An increasing trend of average annual maximum temperature from approximately +1°C to +3.7°C from 1994 to 1999 (Years 11 to 17).
- Between 2000 and 2015 (Years 18 through 32) the average annual maximum temperatures have varied in a range between +2.1°C to +4.4°C with no significant trend over time. There does appear to be a cyclical trend with a period of approximately 8 years and a minor increasing trend.
- From the end of 2016 to late 2018 (Years 33 to 35) the pipeline was shutdown. Data during this window may be skewed to temperatures during the operating time of the year.
- From 2019 to present (Year 36 to 39), the average annual maximum surface temperatures ranged from +1.5°C to +5.2°C, which within historical ranges, but with average temperatures slightly higher than historical averages. Of note is that the frequency of instrument readings in recent years has been changing due to manual readings being replaced with daily monitored automated instruments.

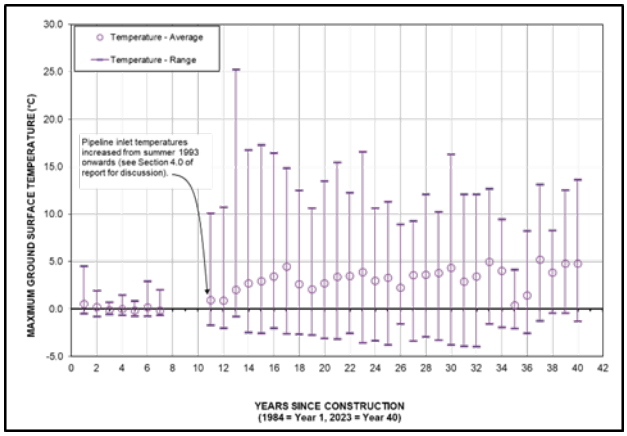

Figure 1. Range and average of maximum ground surface temperature beneath woodchip insulation.

In recent years, many of the thermistors along Line 21 have become automated with satellite linked data loggers. In addition, “thermal fences” equipped with data loggers have been installed at select sites to monitor the 2-D seasonal shape of thaw below the RoW. These new instruments are allowing for insight into in-situ seasonal measurement of the effectiveness of the woodchip cover. An example of the data from a thermal fence is presented in Figure 2.

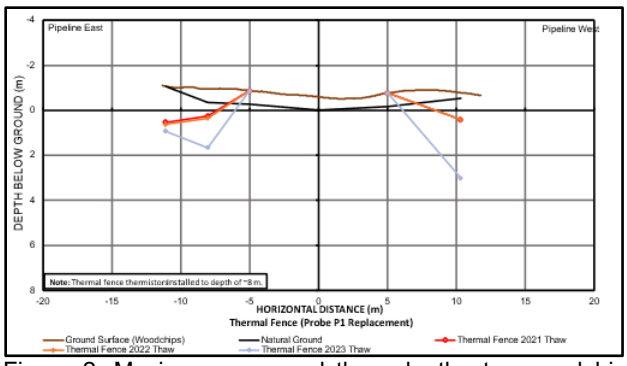

Figure 2. Maximum seasonal thaw depth at a woodchip covered slope.

In the specific example presented in Figure 2, the woodchip cover has delayed the maximum seasonal thaw depth from entering the native soils in the middle of the RoW below the woodchip cover. Conversely, at the edges of the RoW where the woodchip thickness is tapered to zero, maximum seasonal thaw penetration into the native soil is observed.

CONCLUSIONS

The woodchip cover, intended to reduce the impacts from clearing and disturbance in the years immediately following construction, has been effective past the initial post-construction design at some locations. The continued presence of woodchips continues to keep the slopes cooler than if there were no woodchips. Additional benefits of the woodchip cover include a higher albedo surface when compared to vegetation/scrub and insulating the RoW from natural forest fires.

REFERENCES

Monograph on Norman Wells Pipeline Geotechnical Design and Performance. Geological Survey of Canada Open File 3773. 1999

Monograph on the Norman Wells Pipeline Geotechnical Design and Performance – 2006 Update. Geological Survey of Canada Open File 5702. 2007

Freeze-thaw damage investigation of transmission lines in permafrost regions of northeastern China

Juncen Iin[1,2,3], Kai Gao[1,2,3], Guoyu Li[1,2,3] & Yapeng Cao[1,2,3]

[1]*State Key Laboratory of Frozen Soil Engineering, Northwest Institute of Eco-Environment and Resources, Chinese Academy of Sciences, Lanzhou, Gansu, China*

[2]*Da Xing'anling Observation and Research Station of Frozen-Ground Engineering and Environment, Northwest Institute of Eco-Environment and Resources, Chinese Academy of Sciences, Jiagedaqi, Heilongjiang, China*

[3]*University of Chinese Academy of Sciences, Beijing, China*

The freezing and thawing have triggered and accelerated damage to transmission lines in permafrost regions of northeastern China. The freeze-thaw disease characteristics were investigated and summarized as follows: (1) The tilt by upfreezing and water erosion were major threats to tower foundations. They also suffered from crack (4.3%), spalling (2.7%), fissure (2.7%), and fracture (0.5%). (2) The damage to protective caps was much more severe, and 78.2% were affected. (3) The substantial fissures and collapse of utility poles were primarily attributed to frost heaving. Following the results, some reference is provided for the future design and construction of infrastructures in permafrost.

Permafrost degradation is being exacerbated predictably by climate warming and human activity interference. The frost heaving and thaw settlement promoted by degrading permafrost have caused tremendous damage to infrastructures and financial losses (Hjort et al. 2022) and posed a serious and potential threat to the safety of lifeline engineering in service. Typical cases include crude oil pipelines (Wu et al. 2008) and transmission line projects (Wang et al. 2014), progressively arousing people's attention. Further, line facilities are susceptible to frost damage, which considerably impacts on transportation, communication, and energy security. Field investigation can provide positive reference and guidance for subsequent proposed countermeasures, e.g., the detailed distress characteristics of embankment-bridge transition sections in the Qinghai-Tibetan Plateau (He et al. 2023).

Therefore, it is of great significance to recognize the on-site characteristics of freeze-thaw hazards in permafrost, aiming to guarantee the long-term stability of transmission lines.

INVESTIGATION AREA

The permafrost in the northeast of China is discontinuous and sporadic (Jin et al. 2010), covering an area of roughly 400,000 km^2, see Figure 1. The investigations were conducted on the surrounding roads for the sake of safety and convenience. Utility poles and 188 transmission towers along the National Highway (G111) from Jiagedaqi to Mo'he were examined.

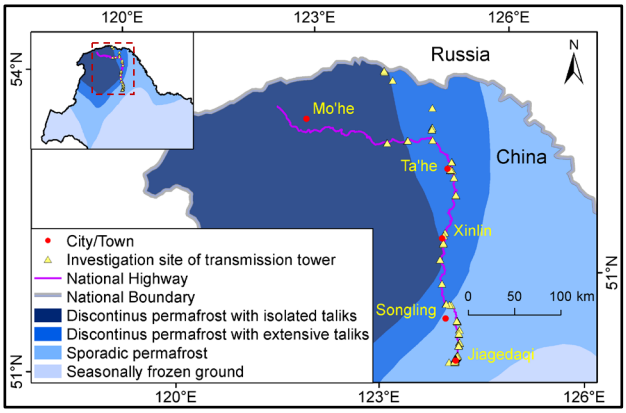

Figure 1. Distribution of permafrost and investigations.

OVERVIEW OF INVESTIGATION RESULTS

The mean annual air temperature gradually rose at a rate of 0.21 °C – 0.40 °C/10a during the past five decades, definitely causing the increase of ground temperature and the thickening of the active layer that subsequently affects the thermal stability of the foundations, as shown in Figure 2. Refreezing produced enormous upward tangential frost-heave force and upfreezed the foundations. There were 34 towers with uniform and non-uniform upfreezing accounting for 8.5% and 9.6%, respectively, approximately five times those with thaw settlement. Additionally, water ponds were obvious for the surrounding soil was over-excavated to backfill foundation pits and improve the stability of towers.

Frost heaving brought much failure to the poles, demonstrated by the substantial fissures and collapse. The inflow of water and air aggravated the erosion of the concrete and internal steel bars. Also, the overturn of a pole drove the adjacent poles to fall as well owing to line connections.

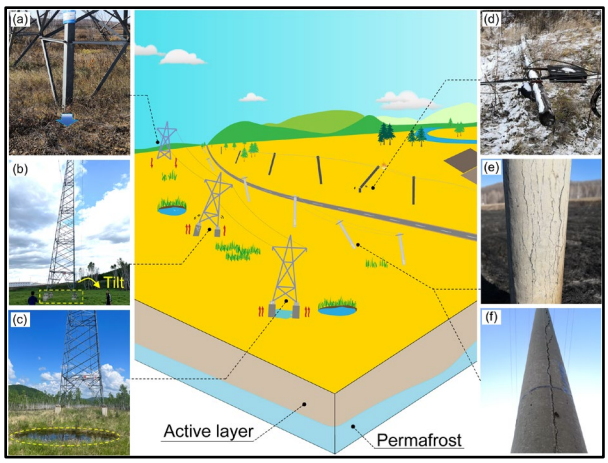

Figure 2. Overview of observed hazards in permafrost.

Additionally, the increased volume by expansion and ice segregation damaged concrete, leading to strength reduction and a series of diseases, as indicated in Figures 3 and 4. It was found that surface damage was more severe and that the most adverse factors affecting towers' safety involved the erosion of ponding water due to soil subsidence and the tilt of a single foundation. Similarly, spalling, cracks, erosion, and fissures also appeared in the protective caps.

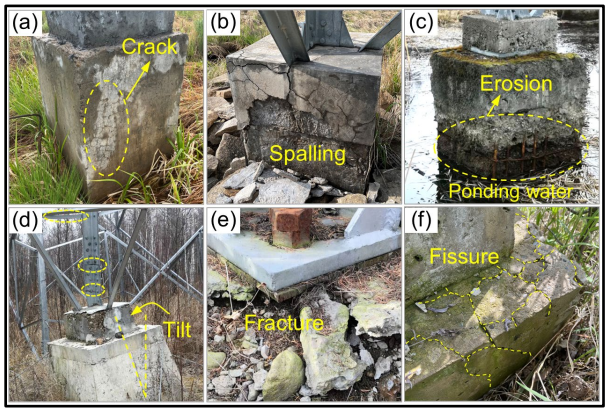

Figure 3. Frost damage to tower foundations.

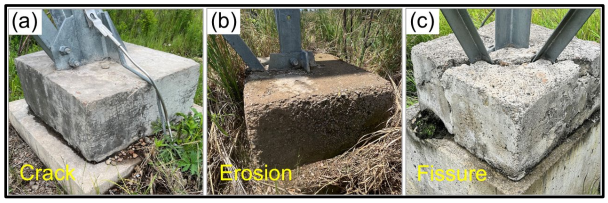

Figure 4. Frost damage to protective caps.

According to the statistics in Table 1, the tower foundations were seriously eroded, with the highest percentage of 5.9%. Defects of protective caps were much more severe than those of the foundations, and 78.2% were affected in total.

Table 1. Number and proportion of towers.

Characteristics	Tower foundations	Protective caps
Fissure	5 (2.7%)	29 (15.4%)
Spalling	5 (2.7%)	16 (8.5%)
Crack	8 (4.3%)	29 (15.4%)
Erosion	11 (5.9%)	109 (58%)
Fracture	1 (0.5%)	-
Tilt	7 (3.7%)	-

CONCLUSION

The investigations exhibited various damage characteristics. The tilt by upfreezing and water erosion were primary threats to tower foundations. They also suffered from crack (4.3%), spalling (2.7%), fissure (2.7%), and fracture (0.5%). The damage to protective caps was much more severe, and 78.2% were affected. Utility poles appeared fissures and collapsed. Implementing countermeasures and carrying out long-term monitoring and maintenance to mitigate disease are highly recommended.

REFERENCES

Hjort, J., Streletskiy, D., Doré, G., Wu, Q., Bjella, K., and Luoto, M. 2022. Impacts of Permafrost Degradation on Infrastructure, Nature Reviews Earth & Environment, 3(1): 24–38. doi:10.1038/s43017-021-00247-8

Wu, Z., Barosh, P.J., Wang, L., Hu, D., and Wang, W. 2008. Numerical Modeling of Stress and Strain Associated with the Bending of an Oil Pipeline by a Migrating Pingo in the Permafrost Region of the Northern Tibetan Plateau, Engineering Geology, 96(1–2): 62–77. doi:10.1016/j.enggeo.2007.10.001

Wang, G., Yu, Q., You, Y., Zhang, Z., Guo, L., Wang, S., and Yu, Y. 2014. Problems and Countermeasures in Construction of Transmission Line Projects in Permafrost Regions, Sciences in Cold and Arid Regions, 6(5): 432–439. doi:10.3724/SP.J.1226.2014.00432

He, P., Niu, F., Huang, Y., Zhang, S., and Jiao, C. 2023. Distress Characteristics in Embankment-Bridge Transition Section of the Qinghai-Tibet Railway in Permafrost Regions, International Journal of Disaster Risk Science, 14: 680–696. doi:10.1007/s13753-023-00506-w

Jin, H., Hao, J., Chang, X., Zhang, J., Hao, Q., Qi, J., Lü, L., and Wang, S. 2010. Zonation and Assessment of Frozen-Ground Conditions for Engineering Geology Along the China–Russia Crude Oil Pipeline Route from Mo'he to Daqing, Northeastern China, Cold Regions Science and Technology, 64(3): 213–225. doi:10.1016/j.coldregions.2009.12.003

Tundra rehabilitation in Alaska's Arctic: An ongoing challenge requiring creative solutions

Lorene Lynn
Red Mountain Consulting LLC., Palmer, Alaska, United States

Oilfield development in Alaska's Arctic vast coastal plain has been underway for nearly 50 years and includes construction of industrial roads, airstrips, pads, and pipelines. Supporting infrastructure such as fiber optic communications were more recently installed. The wetlands of Arctic Alaska are underlain by permafrost, perching water at the surface in a polar desert. The high soil ice content presents challenging conditions for infrastructure development, especially while facing dramatic and sudden effects of climate change.

OILFIELD REHABILITAITON

Oilfield gravel installations require placement of three to five feet of gravel upon the tundra to prevent thawing of the underlying permafrost. When a site is no longer being used, it enters the tundra rehabilitation program at which time contaminants are removed and the gravel is excavated to the level of the surrounding tundra grade, often leaving six inches or more of gravel and low-nutrient silt remaining on the site. While undisturbed tundra typically retains carbon (averaging 20% OC), the disturbed sites have very little to no stored carbon remaining (0-2% OC). Tundra rehabilitation efforts by the author include fertilizing, seeding with locally-collected indigenous seed, and tundra sod transplanting. Factors such as hydrologic conditions, depth of remaining gravel, presence of salts, and proximity to the coastline largely influence the rate of recolonization by indigenous plants. Moss development is common, and while it can prevent colonization of vascular plants, it is likely contributing to improvements in soil quality. With over 10,000 acres now under development, and more construction proposed, rehabilitation techniques are continually being developed to improve soil quality and plant establishment outcomes. This examination of the work completed by the author gives insight into the ongoing development of rehabilitation techniques in this unique setting.

FIBER OPTIC INSTALLATIONS

Fiber optic cables were installed in 2016 and 2017 in trenches along a 240-mile-long stretch of the Dalton Highway to serve the needs of the oil fields and communities near the Arctic coast. The cables were installed mostly in winter with some installation having been completed in summer using various trenching techniques. The region is characterized by continuous permafrost and ecosystems with widely varying ground ice volume from boreal forest to the coastal plain. Shortly after installation, mechanical and thermal erosion was observed to have caused ground subsidence within and adjacent to the trenches.

Trenches dug in permafrost disturb the thermal regime, often causing loss of massive ground ice and surface subsidence. This case study describes the rehabilitation work directed and implemented by the author. A team of science and engineering expertise that includes geocryology, permafrost hydrology, tundra revegetation, restoration ecology, water resources engineering, and remote sensing was assembled in 2020 to address the permafrost degradation using multiple rehabilitation techniques of the tundra surface. Individual rehabilitation plans for each problem location were informed by thermal balance equations, evaluations of watershed hydrology, experience in rehabilitating and revegetating tundra, and repeat photogrammetry by unmanned aerial vehicle (UAV). The sites were evaluated using historic and current aerial photography and visiting sites during high-water spring freshet and during mid-summer.

The subsided trenches commonly capture surface water, creating a heat sink and exacerbating the disturbance of the thermal regime. The lost massive ice, which formed over hundreds or thousands of years, cannot be recreated. Instead, the goals of rehabilitation focus on stabilizing the thermal regime, managing water flow, and creating conditions to promote natural colonization by indigenous plant species. Rehabilitation techniques include backfilling subsided areas with gravel and soil, placing transplanted tundra sod over the backfill, placing water bars in strategic locations, live-staking willows, and placing transplanted tundra sod by hand in highly sensitive areas.

TUNDRA SOD TRANSPLANTING

Taking advantage of an area that was going to be mined for gravel, 1.1 acres of tundra sod was harvested in 2020 and stored for placement at rehabilitation sites. The sod was cut in blocks using a specialized excavator bucket and are approximately 30 cm deep, 1.2 m wide

and long, and weigh approximately 725 kg each. The tundra sod was transported to an established gravel pad for storage. Approximately half of the stored sod has been transplanted to rehabilitation locations.

Where the ground surface can support the use of heavy equipment, the sod is moved onto rehabilitation locations mechanically. In many locations, the ground will not support heavy machinery without causing additional disturbance. Instead, the sod is delivered to the highway embankment, cut into smaller blocks with hand tools, and carried across the tundra to the rehabilitation location. This process is labor-intensive, but often yields excellent results, such that it can be difficult to locate the rehabilitation locations without use of GPS.

Tundra sod provides immediate thermal insulation and revegetation. It can also be used to manage waterflows, returning hydrology to a state similar to pre-disturbance conditions. The harvested tundra sod has been stored for three years and the vegetation present continues to grow, extending roots into the gravel pad below.

Conclusion

There are few or no published scientific studies that address rehabilitating trenches in permafrost and few projects to look to for guidance on successful rehabilitation. Work has been conducted from 2020 through 2023, and will continue forward.

The challenges presented in rehabilitating arctic tundra create a unique opportunity to develop new rehabilitation techniques and to guide future work.

Use of the Peclet number in design of road drainage systems in permafrost

Julie Malenfant-Lepage[1,3,4], Guy Doré[1,4] & Daniel Fortier[2,4]

[1]*Department of Civil and Water Engineering, Université Laval, Québec City, Québec, Canada*

[2]*Department of Geography, Université de Montréal, Montréal, Québec, Canada*

[3]*Department of Civil and Environmental Engineering, Norwegian University of Science and Technology, Trondheim, Norway*

[4]*Centre for Northern Studies, Université Laval, Québec City, Québec, Canada*

Road embankments act as a dam spanning over long distances where the natural flow of water must be redirected to ditches and culverts along the way. However, this commonly used practice can lead to important soil instabilities in the Arctic and subarctic environments (Figure 1). Permafrost degradation can occur due to heat conduction when water is standing at the embankment toe and heat advection when water is flowing into the drainage systems or seeping underneath transportation infrastructure. Advection refers specifically to the process by which heat is transported horizontally by a fluid from one location to another; while convection is the combination of heat transfer by advection, conduction, and vertical motion within a fluid.

Figure 1. Unstable embankment slope due to water ponding at the embankment toe following the blockage of the culvert by ice at km 1462 of the Alaska Highway, Yukon, Canada (Photo: Benoit Loranger, 05-05-2011).

Various engineering methods are currently used to improve drainage conditions in the north (Figure 2). However, the short and long-term impacts on permafrost of water flowing in those drainage systems is poorly documented and no design criteria have been clearly defined to date. Transport infrastructure damages related to water are frequently observed and therefore there is a great need to improve knowledge on the key role of water flow in heat transfer to frozen soils, on thermal erosion in drainage ditches and on the performance of road drainage systems in permafrost regions.

Figure 2. Interceptor ditch located few meters upstream of the Alaska Highway south of Dry Creek, Yukon, Canada. This is one of the drainage methods currently used to keep permafrost degradation that could occur following a ditch construction away from the embankment (Photo: Loriane Périer, 22-05-2013).

The heat flux induced by convection q_c is obtained via the Newton's law of cooling:

$$q_c = h(T_S - T_F) \quad [1]$$

Where h is the coefficient of heat exchange by convection (W/m²°C), T_S is the temperature at the soil surface (°C) and T_F is the temperature (°C) of the fluid (water). Since the convection coefficient for water exhibits a large variability (i.e., between 100 and 900 W/m²°C (Giovannini and Bédat 2012)) and the available data on water temperatures and soil surface temperatures below water bodies is limited, Equation 1 is difficult to apply. Alternatively, dimensionless numbers are useful design parameters for solving heat transfer issues associated with drainage in permafrost areas.

Only a few studies have investigated the application of dimensionless numbers in hydrology of cold regions (e.g., Lunardini et al. 1986; Kane et al. 2001; Costard

et al. 2003), but all have made great leaps in advancing knowledge on convective heat transfer associated with frozen ground. The Peclet number developed for Arctic soils proposed by Kane et al. (2001) is a dimensionless number with great potential for application in permafrost engineering due to the parameters of the equation that can be measured and used for drainage systems around transportation infrastructure. Equation 2 and Figure 3 show the Peclet number for groundwater flow $P_{e(g)}$ adapted from Kane et al. (2001) and used in this study.

$$P_{e(g)} = \frac{\rho c k_h S D \left(\frac{A_L}{L}\right)}{k_t} \quad [2]$$

Where ρ is the water density (kg/m^3), c is the specific heat of water (J/kg·K), k_h is the hydraulic conductivity (m/s), S is the slope of the top of permafrost (m/m), D is the thaw depth in an homogeneous soil layer (m), A_L is the active layer thickness (m), L is the distance travelled by water over which heat transfer occurs (m) and k_t is the soil thermal conductivity (W/m·K).

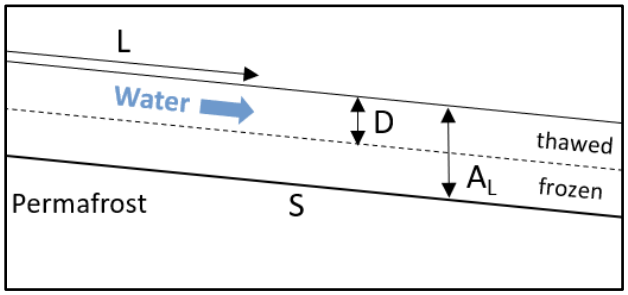

Figure 3. Shema illustrating the parameters used in the Peclet number equation for groundwater flow occurring in a homogenous thawed soil layer in permafrost areas.

A Peclet number value above 1 means that convection is the dominant heat transfer mechanism while a value smaller than 1 indicates that conduction is the dominant mechanism that governs heat transfer. Since convection is a much more effective heat transfer mechanism than conduction, it is important to minimized convection during the design stage of drainage systems by ensuring that the Peclet number remains below 1.

This research project developed drainage design tools based on the Peclet number to mitigate permafrost degradation issues resulting from water flow along and underneath transportation infrastructure. The drainage design tools were validated using observations and data from previous studies (de Grandpré et al. 2012; Chen et al. 2019) conducted at the Beaver Creek road test site in the Yukon (Figure 4) and were applied to the conditions of an additional test site located at km 1895 of the Alaska Highway near the Alaska-Yukon Border.

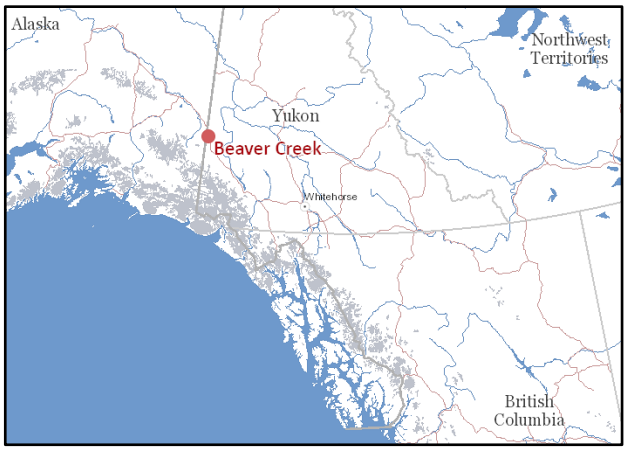

Figure 4. Localisation of the Beaver Creek road test site along the Alaska Highway, Yukon, Canada (GeoYukon).

In this research, the Peclet number has proved to be a solid basis for determining advection hazards. The tools developed allow to calculate the minimum distance required between an embankment and the interception ditch and the allowable change in drainage slope to limit excessive permafrost degradation.

References

Chen, L., Fortier, D., McKenzie, J.M., and Sliger, M. 2019. Impacts on heat advection on the thermal regime of roads built on permafrost. Journal of Hydrology, 34: 1647–1664. doi:10.1016/j.jhydrol.2022.128539

Costard, F., Dupeyrat, L., Gautier, E., and Carey-Gailhardis, E. 2003. Fluvial thermal erosion investigation along a rapid eroding river bank: application to the Lena river (central Siberia). Earth Surface Processes and Landforms, 29: 1349–1359. doi:10.1002/esp.592

De Grandpré, I., Fortier, D., and Stephani, E. 2012. Degradation of permafrost beneath a road embankment enhanced by heat advected in groundwater, Canadian Journal of Earth Sciences, 49: 953–962. doi:10.1139/e2012-018

Giovannini, A., and Bédat, B. 2012. Transfert de chaleur, Éditions Cépaduès, France.

Kane, D.L., Kenneth, M.H., Goering, D.J., Hinzman, L.D., and Outcalt, S.I. 2001. Nonconductive heat transfer associated with frozen soils, Global and Planetary Change Journal, 29(3-4): 275–292. doi:10.1016/S0921-8181(01)00095-9

Lunardini, V.J., Zisson, J.R, and Yen, Y.C. 1986. Experimental determination of heat transfer coefficients in water flowing over a horizontal ice sheet, CRREL Report 86-3, US Army Corps of Engineers, Cold Regions Research and Engineering Laboratory.

Statistical approach for developing a probabilistic estimate of ice wedge occurrence along horizontal alignments

Alyson Mathers[1], Jeremiah Drage[1] & Adam Gabrielson[2]
[1]*WSP USA, Inc., Anchorage, Alaska, United States*
[2]*ConocoPhillips Alaska, Inc., Anchorage, Alaska, United States*

Accurate material estimates for a cross country pipeline project, particularly in remote areas that may be impacted by seasonal access challenges, are essential to meeting project timelines and developing adequate material estimates.

Typical cross-country pipeline construction on the North Slope of Alaska includes installing vertical support members (VSM), steel piles, to design embedment depths in accordance with the project plans and specifications for permafrost soil. The pile lengths are field adjusted based on the cumulative length of massive ice, identified while advancing the VSM (drill) holes, that exceeds the design allowance.

To better accommodate the potential need for these field-identified pile extensions during the construction procurement phase we developed probabilistic equations to estimate necessary pile lengths and quantities to accommodate forecasted occurrences of massive ice that would be statistically expected to be encountered during construction. The objective of the probabilistic approach is to meet the project need and accommodate an estimated contingency while also mitigating the risk of material shortfall or significant material overrun.

The probabilistic estimates were developed based on statistical parameters for massive ice occurrence and thickness (depth) as derived from historical drill hole logs and correlated with terrain type. We conducted terrain unit analyses and used those results to further evaluate the relationship between massive ice occurrence and terrain type.

BACKGROUND

When the cumulative ice thickness identified while advancing VSM holes exceeds the amount of allowable ice, per design, additional VSM embedment is added based on the project specification parameters (referred to as a 'pup' or pile extension). The additional VSM embedment accommodates the reduction in pile capacity through the massive ice zone. Historically, each pile extension would require field-welding, which was time and resource intensive.

To better meet project timelines and ensure sufficient material quantities, we developed a strategy for estimating and procuring pile lengths to accommodate a quantity of forecasted pile extensions. In the event where VSM holes were drilled and no extension was required at that specific hole due to lack of cumulative ice, the drill holes were extended deeper than the design depth to accommodate the extra pile length (excess steel) as opposed to field cutting the steel. Initial efforts to pre-plan pile extensions, and prior to applying this statistical approach, resulted in significant amounts of excess steel.

VSMs for the pipeline alignments can generally range from 12 to 40 inches in diameter and 21 to 38 feet in embedment depth. VSM quantities very from hundreds to thousands depending on the length of the pipeline alignment and VSM spacing.

TERRAIN UNIT ANALYSES

To perform the terrain unit analyses, we analyzed the terrain and developed terrain unit maps that encompassed the drill hole locations. The following geologic terrain units were identified and mapped using available LiDAR, IfSAR, aerial imagery, existing geologic mapping, and geotechnical boreholes where available:

- Alluvium (Qa) ranges in composition from silt and silty sand in sluggish streams, in-filled channels, floodplains, and deltaic areas to gravelly sand and sandy gravel in the larger rivers such as the Colville.
- Alluvial terrace deposits (Qat) are variable in composition from silt to sand and gravel and are typically underlain by marine deposits. Alluvial terrace deposits generally have a surficial cover of thaw lake, eolian sand, or undifferentiated silt and sand deposits.
- Delta deposits (Qu) generally consist of a mix of material resulting from the interaction of coastal processes and the continuing transport of alluvial material near the mouth of the larger rivers on the North Slope. Material ranges from alluvial gravelly sand to fine marine and estuarine silt and clay. Eolian sand and silt deposits commonly form a surface cover together with interbedded organic deposits and peat.
- Thaw Lake deposits (Qt) are present throughout the coastal plain and generally contain a mixture of peat, organic silt, silt, and sand. Successive layers of organic-rich deposits are formed by a combination of lacustrine and eolian processes.

- Undifferentiated silt and sand deposits (Qu) generally contain a mix of marine sediments that have been reworked and inter-layered with alluvial and eolian material. This material generally ranges from ice-rich silt to relatively clean sand and gravelly sand. This unit underlies much of the western portion of the Arctic Coastal Plain and is also present in several locations near the Colville delta.
- Qt/Qu: Thaw Lake deposits overlying undifferentiated silt and sand deposits.

We then analyzed the distributions of the cumulative ice thicknesses using data from 3,123 drill holes distributed across the terrain units. Cumulative ice thickness ranged from zero to 22 feet. Overall, the greatest percentage of drill holes advanced in a terrain unit with greater than three feet of cumulative massive ice (84 percent) were encountered in Qat while lowest percentage (14 percent) were encountered in Qt. The median massive ice thickness for Qat was six feet while that for the other analyzed terrain units was less than three feet.

We fitted probability distributions to the cumulative ice thickness data using the R package "fitditrplus" (Delignette-Muller and Dutang 2020). Exponential distributions were fitted to the data using maximum goodness of fit estimation and Anderson-Darling distances of first and second order to give more weight to the data at the right tail of the distribution (the higher cumulative ice thicknesses). Normal distributions were fitted by maximum likelihood estimation. The uncertainty of the parameter estimates for each of the fitted distributions was estimated using bootstrapped values (2,001 iterations) of the parameters to determine the 95 percent confidence intervals for each of the estimated parameters. Probability distributions were then fitted to each of the individual terrain units and the combined data.

Based on the results of our analyses, it was determined that the distribution of cumulative ice thickness is dependent on terrain type. Exponential probability distributions were then fitted to the following terrain units: Qt, Qu, Qt/Qu, and Qd. While the cumulative ice thickness distribution for Qa appears to fit an exponential distribution, insufficient data was available to adequately fit the distribution for Qa. Normal probability distributions were fitted to the terrain unit, Qat.

DISCUSSION

Based on available drill hole data and terrain unit analyses, the cumulative ice thickness probability distribution is dependent on terrain unit type. The normal cumulative ice distribution of the terrain unit, Qat, indicates that this terrain unit is ice-rich, including a greater presence of ice wedges.

The least amount of ice occurrence was observed in the terrain unit, Qt, when compared to the other terrain units. Relatively less massive ice is likely present overall in Qt because the ground surface exposure to surface air temperature is shorter in duration as compared with ground surfaces that were not previously covered with a shallow lake. Kanevskiy et al. noted that the lower wedge ice-content in young-drained lake basins as compared to mature lake basins and other older terrain units associated with the coastal plain is likely due to modification of permafrost with time related to changes in soil and vegetation (2012). The lower amount of massive ice within Qt is reflected in the fitted exponential distribution and observed distribution of cumulative ice thicknesses. The exponential distribution indicates that there is a higher probability of encountering thinner cumulative ice thicknesses than encountering greater cumulative ice thicknesses.

For future pipeline construction projects, the terrain unit type should be identified along the alignment; then the quantity of vertical support members that will be advanced per terrain unit should be determined. The probabilistic equations should then be applied to estimate the quantities and lengths of vertical support members that may need to accommodate specific ranges of cumulative ice thicknesses. As additional alignments are advanced and new terrain units are encountered, the probabilistic equations should be reevaluated and updated.

CONCLUSION

The presented probabilistic approach can be applied to successfully mitigate schedule and budget risk during the procurement phases of linear pipeline alignment projects in permafrost soils of the North Slope of Alaska. Future applications may include their use in initial infrastructure design by defining an acceptable risk or probability of encountering a thickness of ice and then developing initial designs based on the corresponding ice thickness.

REFERENCES

Delignette-Muller, M.L., and Dutang, C. 2014. fitdistrplus: An R Package for Fitting Distributions. Journal of Statistical Software, Revised May 2020.

Kanevskiy, M., Shur, Y., Jorgenson, M.T., Ping, C.-L., Michaelson, G.J., Fortier, D., Stephani, E., Dillon, M., and Tumskoy, V. 2012. Ground ice in the upper permafrost of the Beaufort Sea coast of Alaska, Cold Regions Science and Technology, 85(2013): 56–70. doi:10.1016/j.coldregions.2012.08.002

Permafrost assessment for the Northern Road Link Project, Ontario

Lynden Penner & Jason Cosford

J.D. Mollard and Associates (2010) Limited, Regina, Saskatchewan, Canada

The Indigenous-led Northern Road Link (NRL) Project will provide access to communities and support economic development in Ontario's Ring of Fire Region by linking the Marten Falls Community Access Road (MFCAR) to the south and the Webequie Supply Road (WSR) to the north. Located on the western margin of the Hudson Bay Lowlands approximately 350 km west of James Bay, the roughly north-south orientation of the project spans several permafrost zones. The NRL route alternatives extend from approximately 20 km north of the sporadic - isolated permafrost zone boundary to about 35 km south of the isolated - non-permafrost zone boundary. Although the southern half of the project is within the non-permafrost zone, palsas and permafrost observed by others indicate the localized presence of permafrost, even toward the southern extent of the study area. Accordingly, assessing the distribution of permafrost is important as the potential degradation of ice-rich permafrost has implications for construction and operation of this transportation infrastructure, which would provide the sole ground transportation link in this region. Moreover, the location of the study area in non- to sporadic-permafrost zones presents a challenge for site-specific permafrost assessment because localized areas of permafrost must first be identified before they can be assessed.

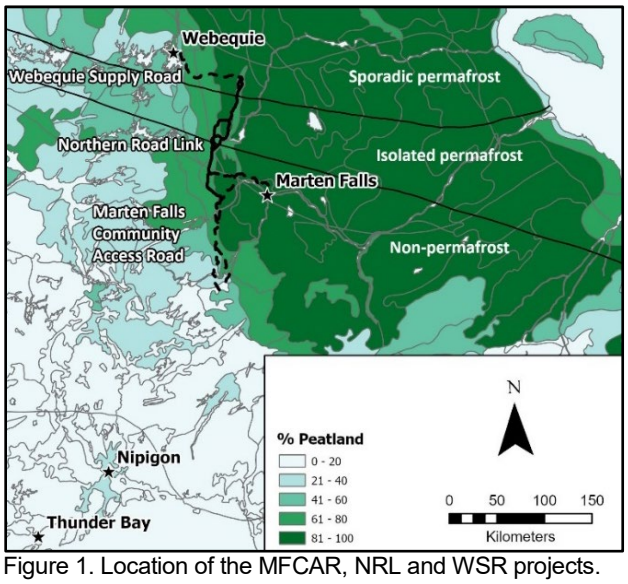

Figure 1. Location of the MFCAR, NRL and WSR projects.

Surficial geology in the study area is characterized by prominent glaciofluvial landforms that extend discontinuously in a roughly north-south direction across almost the entire study area. Glaciofluvial terrain is preferred for road routing from engineering, borrow, construction and maintenance perspectives. Away from these glaciofluvial landforms, peatlands overlying till, glaciolacustrine and glaciomarine deposits extend across nearly 100% of the landscape to the east and west. Route alternatives crossing dominantly peatland terrain are less desirable from an engineering perspective but have been identified to address environmental and community concerns.

Detailed terrain mapping within 2-km-wide alternative road routing corridors delineates a variety of peatland types including multiple types of bogs and fens. Fens are characterized by water tables at or very near the peat surface. Local groundwater gradients are evident in fens from ribbed or string patterns in string and ladder fens, and from water tracks in water track fens. Groundwater flow directions are consistently toward lower lying streams and waterbodies.

Bog types include treed, basin, plateau and net bogs with average peat thicknesses of about 1.5 m in treed bogs, 2 m in basin bogs, 2.7 m in plateau bogs and 3 m in net bogs. Peat thicknesses in fens average about 2 m in horizontal fens, 2.4 m in water track fens and nearly 4 m in string fens. Groundwater levels in bogs tend to be deeper and more variable than in fens, typically ranging from 0-2 m depth based on limited field observations and available borehole data. Water table depth in fens is generally 0-0.5 m.

Given groundwater gradients in fens, the presence of permafrost is expected to be restricted to bogs. Areas where ice-rich permafrost is more likely to occur have been delineated based on thermokarst collapse scars interpreted from satellite imagery and air photos. Thermokarst collapse scars form due to ground subsidence caused by the melting of permafrost ice. In some locations, thermokarst features have little relief compared to the surrounding peat surface. At these locations, permafrost degradation may have been active over a long time and extend well beyond the collapse scars. Elsewhere, sharply defined collapse scars suggest that permafrost thaw is more localized and more recent. At one location, a collapse scar observed in the field in 2022 was not visible in a 1967 air photo, indicating that the collapse scar formed after 1967.

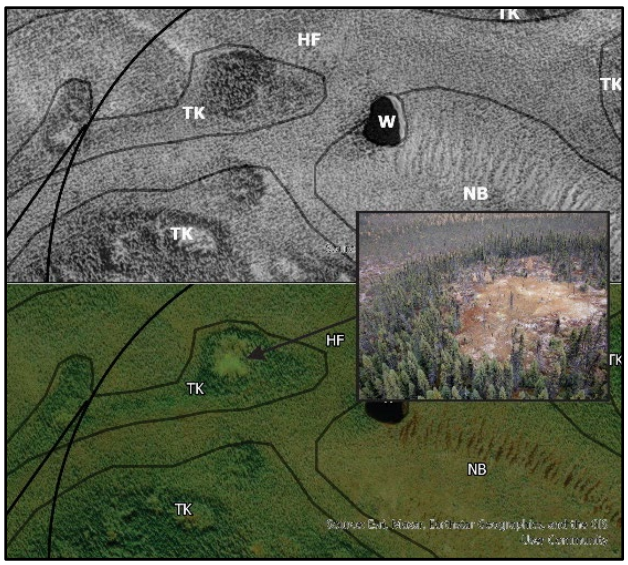

Figure 2. Collapse scar formed after 1967. Upper image: 1967 air photo. Lower image: recent satellite image. Inset: 2022 photograph.

Interpreted thermokarst-affected terrain (TK) was delineated by detailed terrain mapping of 2-km-wide road route corridors using high resolution imagery and LiDAR hillshade and slope maps. TK areas are considered more prone to thawing of permafrost ice during road construction and operation. In some cases, TK terrain mapped within the road corridors matches locations where palsas have been mapped by the Ontario Geological Survey. Palsas are ice cored mounds, while collapse scars form due to thawing of permafrost ice. Therefore, these features are closely related.

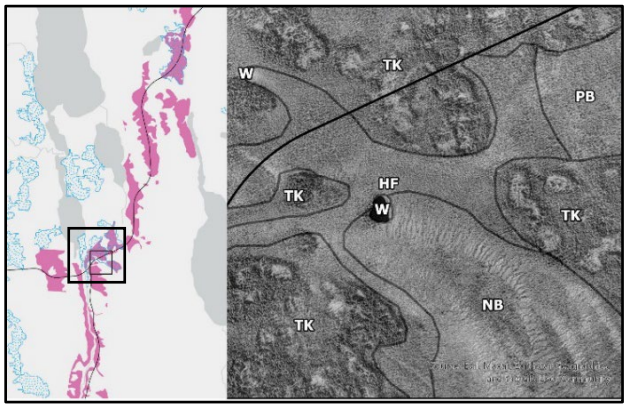

Figure 3. Left: Distribution of thermokarst terrain (pink) and palsas (OGS, blue) along a portion of a corridor alternative. Right: Air photo showing thermokarst areas (TK).

Multiphase desktop and field studies are ongoing to further assess the presence, distribution, and characteristics of ice-rich permafrost within the NRL study area. These studies include change detection using historical air photos and recent satellite imagery, multispectral satellite image analysis and InSAR technology. Targeted field investigations will include borehole drilling to confirm the presence of ice-rich permafrost, peat thickness, peat and mineral soil sampling for geotechnical characterization, and installation of piezometers and thermal sensors for monitoring. Based on peat thicknesses measured to date, boreholes may range up to about 5 m in depth. Geophysical techniques will also be investigated.

Project results will be used to avoid ice-rich permafrost to the greatest degree possible during road route selection, to understand the location and characteristics of ice-rich permafrost where it cannot be avoided, and to take appropriate design measures to mitigate potential impacts and monitor the performance of the road at susceptible locations.

REFERENCES

Barnett, P.J., et al. 2013. Surficial Geology of the Lansdowne House Area Northeast, Northern Ontario; Ontario Geological Survey, 1:100,000. P3697.

Barnett, P.J., Yeung, K.H., and McCallum, J.D. 2013. Surficial geology of the Fort Hope area northeast, northern Ontario; Ontario Geological Survey, P3724, scale 1:100 000.

Barnett, P.J., Yeung, K.H., and McCallum, J.D. 2013. Surficial geology of the Lansdowne House area southeast, northern Ontario; Ontario Geological Survey, P3710, scale 1:100 000.

Permafrost Map of Canada. 1995. The National Atlas of Canada 5th Edition. National Atlas Service, Canada Centre for Mapping, Geomatics Canada, Terrain Sciences Division, Geological Survey of Canada, Natural Resources Canada, Ottawa. Map MCR 4177.

Tarnocai, C., Kettles, I.M., and Lacelle, B. 2011. Peatlands of Canada; Geological Survey of Canada, Open File 6561; CD-ROM. doi:10.495/288786

Vulnerability and resilience of ice-rich permafrost to thermal erosion gullying in the Arctic Foothills infrastructure corridor, Alaska

Eva Stephani[1], Margaret M. Darrow[2] & Mikhail Kanevskiy[2]

[1]*U.S. Geological Survey Alaska Science Center, Anchorage, Alaska, United States*

[2]*Institute of Northern Engineering, University of Alaska Fairbanks, Fairbanks, Alaska, United States*

The Arctic and its permafrost terrains are inherently dynamic, complex, and sensitive environments. Understanding the past and current changes occurring in these systems is key in predicting future variations, including the response of permafrost to climate change and to surface disturbances resulting from natural processes or anthropogenic activities. Here, we focus on advancing our understanding of the drivers controlling terrain vulnerability and resilience to thermal erosion gullying proximal to linear infrastructure in the lowlands of the Arctic Foothills (Alaska). This builds upon our previous work (Stephani et al. 2023) in the infrastructure corridor that includes the Dalton Highway and Trans Alaska Pipeline System (TAPS).

To identify locations affected by thermal erosion gullying and recognize changes in the ~80-km long corridor section that travels through the Arctic Foothills, we compared time series of high-resolution satellite imagery from 2001 to 2023. When we captured the timing of gullying onset and/or growth, we examined prevailing climatic conditions (Sagwon Station) prior to these terrain changes. We integrated our findings with our field-based data (e.g., drilling) described in Stephani et al. (2023).

Results and Discussion

We identified two main settings that increase the terrain vulnerability to thermal erosion gullying in the study area. The first one, advanced in our previous work (Stephani et al. 2023), is related to a widespread formation of thermokarst ditches adjacent to infrastructure in the Arctic Foothills. The Arctic Foothills are characterized by a wide occurrence of an ice-rich layer of the upper permafrost (intermediate layer) that includes the top part of a polygonal ice-wedge network (massive ice). When infrastructure is built over permafrost, it modifies the climate-terrain-permafrost interactions that occur in the natural system, requiring adjustments to conditions changing in the new infrastructure-permafrost system. Typical changes (e.g., surface albedo decrease, increase in snow accumulation, dust) often cause thawing of ice-rich permafrost. As a result, the ground surface subsides and forms a thermokarst ditch at the embankment toe (Figure 1). This ditch is typically affected by shrubification, deeper snow accumulation, and water impoundment, all of which have positive feedback effects. Terrain vulnerability to thermal erosion increases in the thermokarst ditch as it captures and channelizes cross-drainage water, whereas cracks developed in the weakened vegetation mat as the ground surface subsides facilitate water access to ground ice. In summer 2018, we observed the development of a small gully in the thermokarst ditch (Figure 1) following heavy rain events.

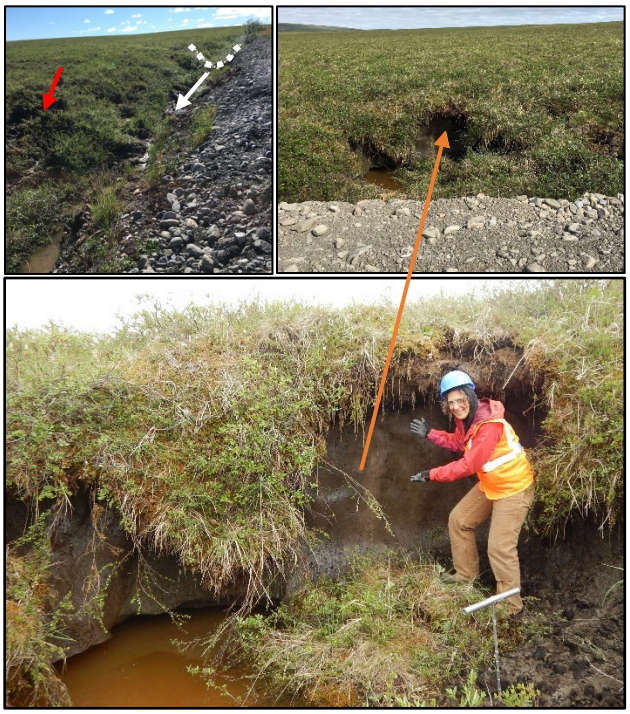

Figure 1. Small gully developed in the thermokarst ditch. The white dashed line highlights the thermokarst ditch with the white and red arrows indicating water flow direction and cracks developed in the vegetation mat, respectively (modified from Stephani et al. 2023).

Although massive ice (wedge ice) became exposed to thermal denudation and thermal erosion in this thermokarst ditch wall, the feature did not expand the following year. We explain this terrain resilience to the lateral discontinuity in massive ice that prompted thaw rates to decrease when reaching the ice-wedge polygon center, and to the low gradient topography and embankment (obstacle) that helped debris to

accumulate, thus allowing the hanging vegetation mat to cover and protect the wall of decreasing slope gradient. This feature left a typical pattern that we observed at a myriad of locations throughout the study area. This suggests that thermal erosion is a dominant permafrost degradation process in the study area, but also that this terrain is resilient as most features stabilized at a relatively small size (typically < 10-m long). A recent larger feature (Figure 2) developed after heavy rains and affected by thaw slumping (Stephani et al. 2023) suggests, however, that there is a risk for gullies to grow to a greater extent than they have in the past.

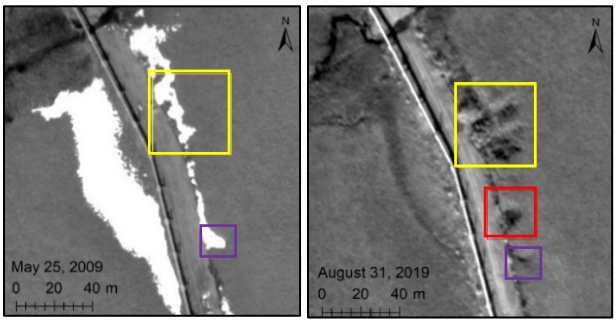

Figure 2. Thermal erosion gullying and slumping developed along the TAPS following heavy rain events in 2014 (yellow box) and 2018 (red box). The purple box indicates a gully that has been stable for at least 17 years. (Modified from Stephani et al. 2023)

Another scenario of thermal erosion gullying in the Arctic Foothills occurs along water tracks. In this case, thermal erosion gullying begins at distance and independently from the permafrost infrastructure interactions, but can progress towards the infrastructure (Figure 3). We have observed a myriad of locations where the linear infrastructure intercepts water tracks along its alignment, but to our knowledge there is only one location where this process is actively affecting the infrastructure (Figure 3). Between 2014 and 2023, starting at a distance of about 200 m upslope from the highway, a section of the gully progressed towards it at an approximate rate of 10 m y^{-1}, except early on when it grew by ~47 m (2014–2015) and again recently by ~25 m (2017–2018). These greater erosion rates occurred at the same time as when we observed an increase in thermal erosion gullying and thaw slumping along the thermokarst ditch (Figures 1 and 2), and more specifically following heavy rainfall events. As of May 2023, the gully reached a total length of ~490 m and width up to ~30 m, with walls now protected by vegetation in the older sections.

Thermokarst ditches and water tracks are both vulnerable to thermal erosion, as water is channelized into zones sensitive to permafrost thaw. Ice-rich permafrost soils in the Arctic Foothills have been, however, relatively resilient to the widespread gullying occurring in thermokarst ditches. This study only identified one location where thermal erosion gullying along water tracks is actively affecting infrastructure, but the myriad of water tracks crossing the alignment suggests that this quiescent status could shift. These gullies also tend to grow at greater extent than those developed in thermokarst ditches, as they are not initially obstructed by the embankment. Gullying exacerbation by heavy rainfall events, both along water tracks and in thermokarst ditches, is concerning in the context of climate change, as precipitation and extreme climatic events are expected to increase. This intensification could be a tipping point in the decline of terrain resilience to thermal erosion gullying in the Arctic Foothills infrastructure corridor.

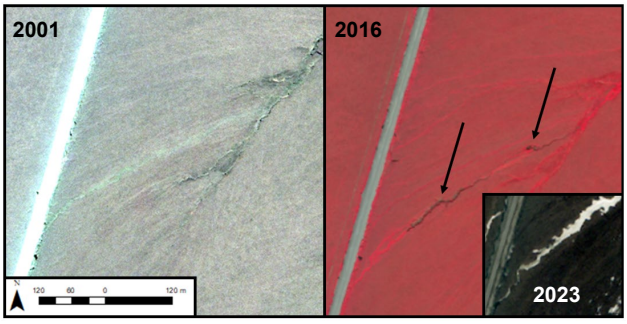

Figure 3. Thermal erosion gullying developed along a water track and progressing towards the Dalton Highway. Black arrows indicate sections of active thermal erosion gullying.

Acknowledgements

The authors wish to thank the co-authors of our previous study (Stephani et al. 2023) upon which this work is built, especially the late Ronnie Daanen.

References

Stephani, E., Darrow, M.M, Kanevskiy, M., Wuttig, F., Daanen, R.P., Scwarber, J.A., Doré, G., Jorgenson, M.T., Croft, P., and Drage, J.S. 2023. Hillslope erosional features and permafrost dynamics along infrastructure in the Arctic Foothills, Alaska. Permafrost and Periglacial Processes, 34(2): 208–228. doi:doi.org/10.1002/ppp.2188

8

Cold Region Engineering Modelling, Characterization, Observations & Testing

INTEGRATING PERSPECTIVES OF PERMAFROST THAW, CHANGE, AND ADAPTATION

Cold Region Engineering Modelling, Characterization, Observations & Testing

8A — Vulnerability of Cold-Region Infrastructure to Permafrost Degradation in a Changing Climate

Session Chairs: Lin Chen[1,2], Yuanming Lai[2], Élise Devoie[3] & Laurent Orgogozo[4]

[1]*Department of Environmental Sciences, University of California, Riverside, California, United States*
[2]*State Key Laboratory of Frozen Soil Engineering, Northwest Institute of Eco-Environment and Resources, CAS, Lanzhou, China*
[3]*Department of Civil Engineering, Queen's University, Kingston, Ontario, Canada*
[4]*Géosciences Environement Toulouse, Observatoire Midi Pyrénées, Université de Toulouse, Toulouse, France*

Globally, permafrost is thawing due to amplified climate warming in cold regions. Permafrost thaw substantially reduces load-bearing capacity of soil and induces differential settlements, leading to potentially catastrophic situations for buildings, pipelines, and roads, as well as increased maintenance costs and reduced lifespans. Nearly 70% of infrastructure built on permafrost is located in areas of high hazard potential. Additionally, construction practices often change or damage vegetation and replace the natural surficial cover with engineered materials such as gravel, sand, and/or asphalt. These surface disturbances result in accelerated permafrost thaw, which is often irreversible. Furthermore, permafrost degradation and talik formation affect the thermal, hydrological, and biogeochemical processes at and below the land surface.

This session is intended as a forum for current research on monitoring and modelling thermal, hydrological, and geotechnical responses of infrastructure built on permafrost to climate change. It addresses (1) investigation of the thermal state of permafrost; (2) recent and upcoming advances in permafrost modelling, including algorithm types, model uncertainties, soil parametrizations, numerical and physical benchmark cases, and land-surface-atmosphere interactions; (3) coupling processes of water, energy, and solute transport through the disturbed ground surface, and their interacting effects on long-term stability of infrastructure, such as permafrost thaw, talik formation, preferential flow; (4) development of mitigation techniques aimed to increase infrastructure resilience against permafrost thawing impacts.

We invite contributions based on laboratory experiments, field observations, or physical and numerical modelling, which advance the characterization, understanding, and models' predictive capacity of cryohydrological processes beneath cold-region infrastructure in a changing climate.

Multi-criteria risk assessment approach for Arctic waste disposal sites

Gijs D. Breedveld[1,2], Regula Frauenfelder[2], Unni Eidsvig[2], Christian Jaedicke[2], Ørjan Nerland[2], Luca Piciullo[2], Kjersti Gisnås[2] & Gudny Okkenhaug[2]

[1]*The University Centre in Svalbard (UNIS), Longyearbyen, Norway*

[2]*Norwegian Geotechnical Institute (NGI), Oslo, Norway*

Management of waste from human settlements as well as from mining activities has been a major challenge in the Arctic. Historic practice has relied on permafrost conditions in the soil to stabilize waste and prevent contaminants from being released into the environment. With increasing climate change, being especially severe in the Arctic, this might result in mobilization of contaminants from historic waste disposal sites. In addition, traditional approaches to handle mine waste may no longer be valid and new solutions need to be developed.

METHOD

We developed a multi-criteria risk assessment approach taking into account various processes that can pose a pressure or act as a driver on a waste disposal system in the future:

- Future climate change can trigger increased erosion
- Permafrost is expected to lose its role as a geological barrier for the containment of contaminants
- Increased landslide and avalanche activity will impact stability and safety at sites
- Geotechnical stability will govern mass movement of the stored waste and release of contaminants
- Hydrological conditions guiding the functioning of barriers between waste and the environment can be corrupted
- Changes in waste properties are the drivers for the release of contaminants and their potential impact on the ecosystem, requiring a clear classification of potential impact

The total risk for a site can be assessed by combining the probability of occurrence of potential adverse events (Table 1) and their consequences in a risk matrix. Adverse events can be evaluated on their potential consequences for Life and health (Lh) and Nature and environment (Nm).

TEST SITES

Our case study sites (Figure 1) are located in the greater Longyearbyen region on Spitsbergen, Svalbard, and comprise a formely active landfill (A) established in 1991, now under closure, and two prospective sites for new landfills (B and C). Site B is intended for masses with low contamination levels and waste primarily from the building and construction industry, while site C is intended for surplus masses (mainly slag and ash) from coal mining. We tested our approach in the context of the planning of sites B and C, while site A was primarily used to help identify potential adverse events.

RESULTS

Figure 2 shows the resulting risk matrix when applying the approach to site C. Our analysis shows that the assessed 18 adverse (Table 1) events and the two consequence categories (Lh and Nm) can be classified as follows (see also Table 2):

1. None of the potential adverse effects are considered to have a high risk.
2. Three potential adverse effects are classified as medium to high risk, where the need for action has to be assessed.
3. Seven incidents are classified as medium risk, where further analyses are required to assess whether action is necessary.
4. Ten incidents are classified as low to medium risk, where the need for further analyses should be considered.
5. Only two incidents are classified as low risk.

Table 1. Compilation of the most important adverse events for a generic future landfill site in the Arctic.

Process		Adverse events	
Climate (K)	K1 Increased precipitation	K2 Increased snow depth	K3 Extreme precipitation
Permafrost (P)	P1 Temperature regime	P2 Deeper active layer	P3 Flow through permafrost
Slides (S)	S1 Slides, Loss of life	S2 Waste transport	S3 Top cover damage
Geotechnical Stability (G)	G1 Shear strength	G2 Fill height	G3 Pore overpressure
Hydrogeology (H)	H1 Material to recipient	H2 Water intrusion	H3 Surface water system
Waste characteristics (A)	A1 Wrong waste classification	A2 Change in waste material	A3 Unknown environmental toxins

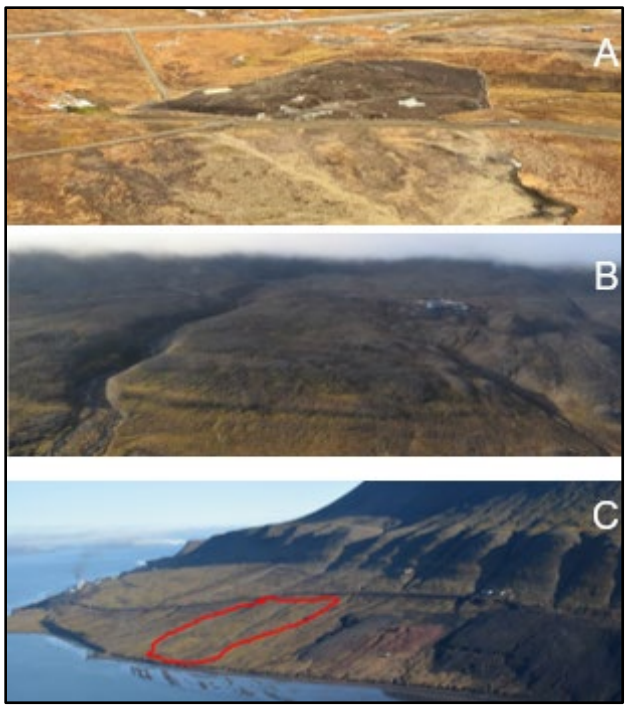

Figure 1. Test sites A, B, C. Further details on these sites are given in the text.

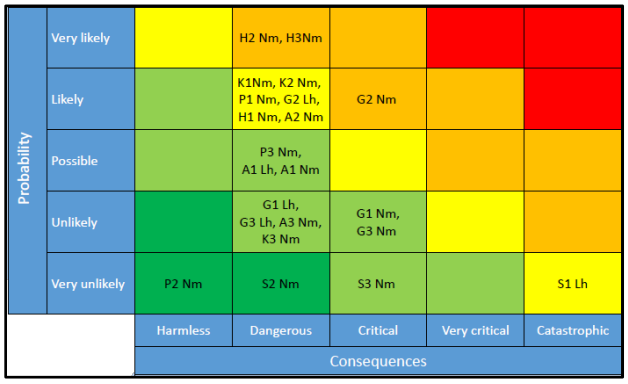

Figure 2. The risk matrix for the establishment of a future landfill at site C.

An aggregated risk can be used to compare different waste sites in relation to each other. Total risk can be assessed based on the number of adverse events that fall into the various categories. By giving high risk e.g., 5 points and low risk 1 point, the total risk can be summed up. In the example here, the total score is 12+21+20+2=55. That sum should be divided by the number of adverse events/consequences that were assessed, in this case 22. This gives a relative score of 55/22=2.5. This relative score can then be compared to scores of other existing landfills or potential new sites.

Pros and cons of the methodology

The presented methodology makes it possible to integrate the risk assessment of six different classes of adverse effects, each of which has its own established methodology for assessing risk. This provides the opportunity to obtain a comprehensive overview in a compact and visual form that makes it easy to identify the need for mitigation measures.

The disadvantage of the method is that, due to differences within the risk classes, it is not possible to make a quantitative assessment without further development into a common risk unit. A monetary parameter is often used to summarise the probability and consequences of various adverse events. In the building and construction industry, the cost of returning to the original state after an adverse event is often used. However, this creates challenges when it comes to valuing nature in terms of biodiversity and environmental quality. This is particularly critical in a vulnerable Arctic environment which is already under significant pressure and strain due to a strong acceleration of climate change.

Conclusions

The proposed integration of criteria allows a qualitative evaluation of the risk from Arctic waste disposal for both human health and the environment. Thereby it is possible to find solutions that are sustainable and take the future climate that is expected in the Arctic in consideration.

Acknowledgements

We are grateful for the financial support from the Svalbard Environmental Protection Fund (grant 18/89).

Table 2. Summary of the most important adverse events associated with the establishment of a future landfill at site C.

Riskcriterion	Description	Adverse events
High risk	Measures must be implemented	None
Medium to high	Need for action has to be assessed	G2Nm, H2Nm, H3Nm
Medium risk	Further analyses required to assess whether action is necessary	K1Nm, K2Nm, P1Nm, S1Lh, G2Lh, H1Nm, A2Nm
Low to medium risk	Further analyses to be considered	K3Nm, P3Nm, S3Nm, G1Lh, G3Lh, G1Nm, G3Nm, A1Lh, A1Nm, A3Nm
Low risk	No action required	P2Nm, S2Nm

Standard on geotechnical site investigations for foundations of building and structures in permafrost zones

Sara Brown

Northwest Territories Association of Communities, Yellowknife, Northwest Territories, Canada

Geotechnical site investigations are essential for the appropriate design, construction and maintenance of buildings. In permafrost zones, these investigations have an added level of complexity due to the potential presence of ice within the soil or bedrock, the influence of climate change, which is modifying the ground thermal regime thereby changing the properties of the permafrost, and the presence of saline soils.

Permafrost zones are subject to specific constraints that geotechnical site investigation should take into account to provide the information that will allow for the design and maintenance of a building within a reasonable timeframe and cost, while ensuring proper risk management.

To that end, a national standard was developed to define a consistent methodology for geotechnical site investigations in a risk management framework, with due consideration of the conditions prevailing at the building site, including the distinctive characteristics of permafrost, the seasonal and interannual climate conditions as well as the projected climate conditions over the service life of the building foundations.

The purpose of this session is to present this tool developed to help Canada's northern regions build a resilient infrastructure despite the uncertainties of a changing climate, and to invite experts to discuss best practices and challenges related to this aspect.

Impact of shading on the structural integrity of cold-region roads and highways

Lin Chen[1,2], Fortier Daniel[3], Jeffrey M. McKenzie[4] & Mingyi Zhang[1]

[1]*State Key Laboratory of Frozen Soil Engineering, Northwest Institute of Eco-Environment and Resources, CAS, Lanzhou, China*
[2]*Department of Environmental Sciences, University of California, Riverside, California, United States*
[3]*Department of Geography, University of Montréal, Montréal, Québec, Canada*
[4]*Department of Earth and Planetary Sciences, McGill University, Montréal, Québec, Canada*

Energy balance is of great importance for evaluating the thermal state of permafrost and the structural integrity of transport infrastructure built on it (Zhang et al. 2019; Chen et al. 2021). For a road embankment, south-facing slopes (*i.e.*, sunny aspect) receive more insolation than north-facing slopes (*i.e.*, shady aspect) (Swift 1976; Revfeim 1978; Tian et al. 2001; Reimchen et al. 2009), shown in Figure 1. Shading effects result in the asymmetric temperature distribution beneath the embankment (Qin et a. 2015; Wang and Yan 2022). This process may lead to the uneven settlement and longitudinal crack (Pei et al. 2016).

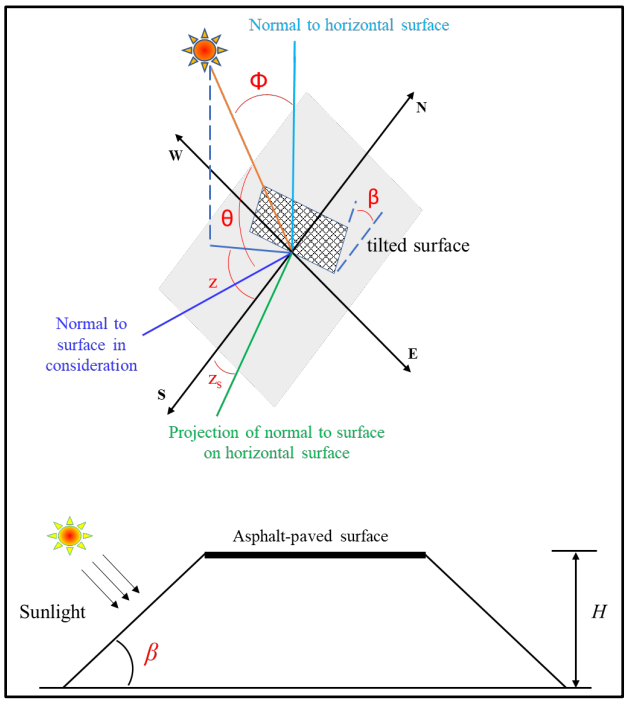

Figure 1. Position of the sun relative to an embankment slope and definition of solar and surface angles.

The role of embankment height (H), slope (β), and orientation on the amount of solar energy absorption on the slope surface has not been quantified methodically. We fully incorporated the surface energy balance model into a coupled groundwater flow and energy transport numerical model (SUTRA-ice) to consider the individual energy processes (e.g., snow insulation, sunny-shady effect, wind convection, etc.) on the land/road surface (Chen et al. 2023). Additionally, we implement an algorithm for the estimation of direct solar radiation on a tilted surface, which enables us to evaluate the thermal response of underlying permafrost to the change of solar radiation caused by the slope aspect and road orientation.

The long-term thermal and meteorological data from Qinghai-Xizang Highway, China are used to validate and calibrate this novel model. Shading effects triggered the asymmetric thermal distributions and promoted the early appearance of a talik on the south-facing side, threatening the structural integrity of roads and highways, particularly, with a north-south orientation.

Our integrated model is applicable to investigate and quantify the shading effect on pan-Arctic infrastructure (e.g., Alaska and Dempster Highways, Canada), or the Qinghai-Xizang Plateau (e.g., Qinghai-Xizang Highway and Railway, China).

KEYWORDS:

Permafrost, Transport infrastructure, Structural integrity, Shading effect, Talik

REFERENCES

Chen, L., Voss, C.I., Fortier, D., and McKenzie, J.M. 2021. Surface energy balance of sub-Arctic roads and highways in permafrost regions. Permafrost and Periglacial Processes 32(4): 681–701. DOI:10.1002/ppp.2129

Chen, L., Fortier, D., McKenzie, J.M., Voss, I.C., and Lamontagne-Hallé, P. 2023. Subsurface porewater flow accelerates talik development under the alaska highway, yukon: a prelude to road collapse and final permafrost thaw? Water Resources Research 59: e2022WR032578. DOI:10.1029/2022WR032578

Pei, W.S., Zhang, M.Y., Li, S.Y., Lai, Y.M., Jin, L., Zhai, W., Wei, Z., Yu, F., and Lu, J.G. 2016. Geotemperature control performance of two-phase closed thermosyphons in the shady and sunny slopes of an embankment in a permafrost region. Applied Thermal Engineering. DOI:10.1016/j.applthermaleng.2016.10.143

Qin, Y.H., Tan, K.H., and Liang, J. 2015. Shading boards with smaller lower-surface thermal emissivity perform better cooling effect. Cold Regions Science and Technology 120: 30–34. DOI:10.1016/j.coldregions.2015.09.005

Reimchen, D., Doré, G., Fortier, D., and Walsh, R. 2009. Cost and constructability of permafrost test sections along the Alaska Highway, Yukon. Presentation Prepared for the annual conference of the Canadian Association of Transportation. Vancouver, Canada: 20.

Revfeim, K. 1978. A simple procedure for estimating global daily radiation on any surface. Journal of applied meteorology 17(8): 1126–1131. DOI:10.1175/1520-0450(1978)017<1126:ASPFEG>2.0.CO;2.

Swift Jr., L.W. 1976. Algorithm for solar radiation on mountain slopes. Water Resources Research 12(1): 108–112. DOI:10.1029/WR012i001p00108

Tian, Y., Davies-Colley, R., Gong, P., and Thorrold, B. 2001. Estimating solar radiation on slopes of arbitrary aspect. Agricultural and Forest Meteorology 109(1): 67–74. DOI:10.1016/S0168-1923(01)00245-3

Wang, T., and Yan, L.E. 2022. A heat-flux upper boundary for modeling temperature of soils under an embankment in permafrost region. Scientific Reports. 12, 13295. DOI:10.1038/s41598-022-17529-w

Zhang, M.Y., Wang, J.W., and Lai, Y.M. 2019. Hydro-thermal boundary conditions at different underlying surfaces in a permafrost region of the Qinghai-Tibet Plateau. Science of The Total Environment 670: 1190–1203. DOI:10.1016/j.scitotenv.2019.03.090

Comprehensive assessment of several data sets related to permafrost occurrence in a fjord system north of Sisimiut, West-Greenland

Tom De Ville[1,2], Anton Berggreen Abrahamsen[1,2], Andrea Securo[3], Marco Marcer[1,2] & Thomas Ingeman-Nielsen[1,2]

[1]*Ilinniarfeqarfik Sisimiut (Arctic DTU), Technical University of Denmark, Sisimiut, Greenland*

[2]*Department of Environmental and Resource Engineering, Technical University of Denmark, Kongens Lyngby, Denmark*

[3]*Department of Environmental Sciences, Informatics and Statistics, Ca' Foscari University of Venice, Venice, Italy*

Permafrost degradation is known to influence landscape alterations, including rock mass and sediment movements (McRoberts and Morgenstern 1974; Mamot et al. 2021). As the Arctic warms at least twice as much compared to the global mean (Smith et al. 2015), it is expected that permafrost will degrade significantly in the near future. This permafrost degradation could potentially lead to soil mass movements posing serious risks on existing infrastructure. Therefore, a good understanding of the evolution of permafrost occurrence and degradation in the Arctic is crucial, which has also been stressed by the latest results from the Nunataryuk project.

Current permafrost models however do not cover the processes influencing permafrost on a sufficiently small scale. This is especially true for complex systems, with large variations in topography and geology in a relatively small region. An excellent example of such systems are fjord systems in Greenland, where permafrost exists in different systems: as lowland sediments, rockwalls and coarse debris. As power lines and hydropower plants in Greenland are typically located in such environments, it is critical to understand the effects of permafrost degradation in these specific areas.

In this context, this study aims to increase our knowledge about the evolution of permafrost occurrence and degradation on a small geographic scale in complex environments in Greenland.

SITE DESCRIPTION

The considered site is the area around the end of the Kangerluarsuq Ungalleq fjord which is located 67°06' N on the west coast, twenty kilometres north from Sisimiut, Greenland's second largest town. This area is characterized by a sedimentary deposit terrace directly next to the fjord with a typical tundra climate. Due to the continuous uplift of Greenland after the last Ice Age, the sedimentary deposits closest to the fjord are melt water deposits, while marine sedimentary deposits are encountered at higher elevations.

The fjord is part of the Aqqutikitsoq mountain area, one of the highest of the whole region between Sisimiut and the ice sheet with elevations reaching 1600 m.a.s.l. Aqqutikitsoq is located in the Nagssugtoqidian fold belt, with the lithological composition mainly existing of a blend of the Sisimiut intrusive suite, gneisses and micashists. These mountains are characterized by steep rockwalls hundreds of meters high, generating

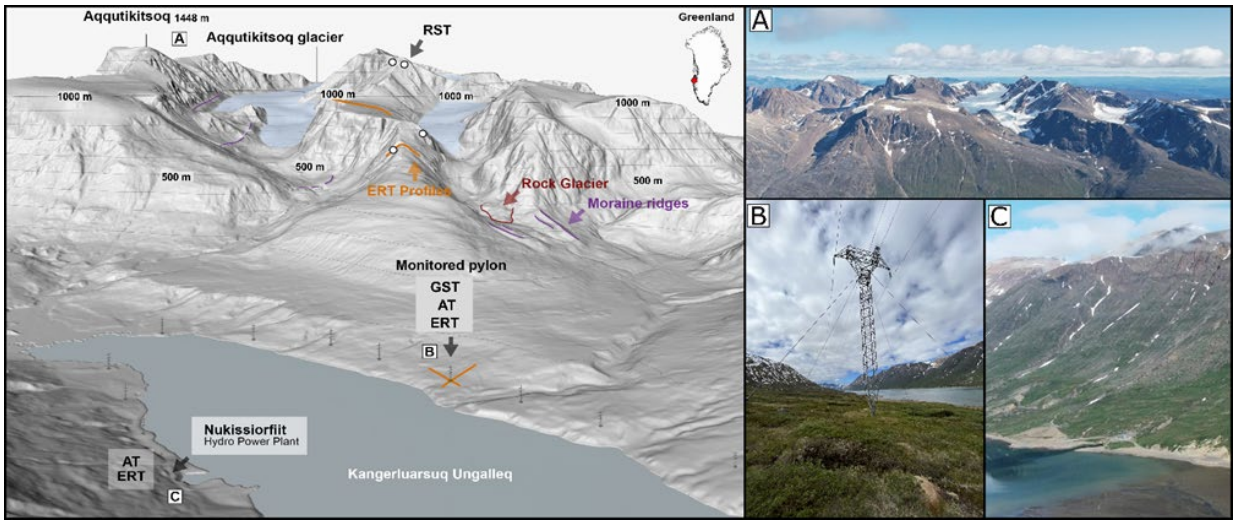

Figure 1. Overview of the Kangerluarsuq Ungalleq – Aqqutikitsoq area. The locations where data is available are indicated on the overview map, illustrated with a picture. Explanation of abbreviations: Electric Resistivity Tomography (ERT); Ground Surface Temperature (GST); Air Temperature (AT); Rock Surface Temperature (RST).

large amounts of debris. Apart from some rock glaciers that mark the landscape, the area also hosts a cluster of approximately 100 valley glaciers. According to Marcer et al (2017), the volume of the glaciers in Aqqutikitsoq decreased approximately 25% in the period 1985–2014, leaving visible frontal and lateral moraines. Overall, this area offers the coexistence of different periglacial systems, with probably a heterogenous occurrence of permafrost.

It is in this complex environment that the powerline and hydropower plant which supply Sisimiut is located. The foundations of the power line masts are both constructed into sedimentary deposits and rocks, while the hydropower plant is constructed deep into a mountain on the northern shore of the fjord. In the recent years, the infrastructure has been enduring damages to the foundations, sparking detailed permafrost research in the area.

DATA

Our dataset explores the three main periglacial systems in the area: sedimentary ice rich permafrost, periglacial landforms in coarse debris and steep bedrock permafrost. The locations where data is available are depicted in Figure 1.

The data set contains time series of Ground Surface Temperatures (GST), Rock Surface Temperatures (RST), Air Temperatures (AT), and Electric Resistivity Tomography (ERT) measurements. Furthermore, the glaciers and rock glaciers in the area have been monitored through a combination of satellite images and drone footage.

RELEVANCE

This data set allows the study of a complex Arctic environment, which leads to a better understanding of the behaviour of permafrost on a small scale, including different landscape and subsurface types, compared to other models such as presented by Obu et al. (2019). A better understanding of the behaviour of permafrost in this type of region will also lead to show the evolution of the landscape in the region, which in turn can be linked to expected risks on infrastructure in the area. For this particular area, this is especially interesting due to the presence of power lines and a hydropower plant. As the geography of Greenland implies that hydropower plants are generally located in regions similar to the studied area, the conclusions from this work can be extrapolated to the whole country as well.

REFERENCES

McRoberts, E.C., and Morgenstern, N.R. 1974. The stability of thawing slopes, Canadian Geotechnical Journal, 11(4): 447-69. doi:10.1139/t74-052

Mamot, P., Weber, S., Eppinger, S., and Krautblatter, M. 2021. A temperature-dependent mechanical model to assess the stability of degrading permafrost rock slopes, Earth Surf. Dynam., 9: 1125–1151. doi:10.5194/esurf-9-1125-2021

Marcer, M., Stentoft, P., Bjerre, E., Cimoli, E., Bjørk, A., Stenseng, L., and Machguth, H. 2017. Three Decades of Volume Change of a Small Greenlandic Glacier Using Ground Penetrating Radar, Structure from Motion, and Aerial Photogrammetry, Journal of Arctic, Antarctic and Alpine Research, 49: 411–425. doi:10.1657/AAAR0016-049

Obu, J., Westermann, S., Bartsch, A., Berdnikov, N., Christiansen, H., Dashtseren, A., Delaloye, R., Elberling, B., Etzelmüller, B., Kholodov, A., Khomutov, A., Kääb, A., Leibman, M., Lewkowicz, A., Panda, S., Romanovsky, V., Way, R., Westergaard-Nielsen, A., Wu, T., Yamkhin, J., and Zou, D. 2019. Northern Hemisphere permafrost map based on TTOP modelling for 2000-2016 at 1km2 scale, Earth-Science Reviews, 193: 299–316. doi:10.1016/j.earscirev.2019.04.023

Smith, S., Edmonds, J., Hartin, C., Mundra, A., and Calvin, K. 2015. Near-term acceleration in the rate of temperature change, Nature and Climate Change, 49: 333–336. doi:10.1038/NCLIMATE2552

Interactions between the built and natural environments in an arctic community: An integrated sensor network in Utqiaġvik, Alaska

Howard Epstein[1], MacKenzie Nelson[1], Mirella Shaban[1], Leena Cho[2], Matthew Jull[2], Hannah Bradley[3], Caitlin Wylie[3], Claire Griffin[4], Luis Felipe Rosado Murillo[5], Lars Nelson[6], Aaron Cooke[7], Chan Charoonsophonsak[7], Georgina Davis[7], Tom Douglas[8], Lauren Bosche[8], Taylor Sullivan[8] & Tobias Gerken[9]

[1]*Department of Environmental Sciences, University of Virginia, Charlottesville, Virginia, United States*

[2]*School of Architecture, University of Virginia, Charlottesville, Virginia, United States*

[3]*School of Engineering and Applied Science, University of Virginia, Charlottesville, Virginia, United States*

[4]*University of Southern Oregon, Ashland, Oregon, United States*

[5]*University of Notre Dame, Notre Dame, Indiana, United States*

[6]*TRIBN Inc., Utqiaġvik, Alaska, United States*

[7]*National Renewable Energy Laboratory, Cold Climate Housing Research Center, Fairbanks, Alaska, United States*

[8]*Cold Regions Research and Engineering Laboratory*

[9]*James Madison University, Harrisonburg, Virginia, United States*

Utqiaġvik, Alaska is home to >4500 residents, with a majority being Indigenous Iñupiat who have occupied the land for >1500 years. Located on the northern coast of Alaska and the Chukchi Sea, and faced with a dynamic natural and anthropogenic environment, the city is managing several issues, such as coastal erosion, water quality changes, and permafrost degradation. Interactions between the infrastructure of the community and the natural environment on which it sits, coupled with the effects of climate change, are driving these system dynamics. A critical question is therefore – how do built (infrastructure) and natural (e.g. ground, water, and atmosphere) system components interact and effect one another within the context of climate change in Arctic communities?

As part of a Navigating the New Arctic grant from the National Science Foundation, academic/agency researchers are collaborating with community participants in Utqiaġvik to answer this critical question, in order to better predict the on-going complexities of these systems and to inform plans for the future of Arctic communities. Project components include complementary terrestrial micro-meteorological and aquatic sensors, along with geophysical surveys at locations throughout and adjacent to the city; design products for future planning; education and outreach; and assessment of our collaborative production of knowledge to inform best practices.

Project objectives and questions

We have three key objectives for this proposed research: 1) The deployment of an array of micro-meteorological and aquatic sensors and geotechnical surveys throughout Utqiaġvik that will measure the interactions among infrastructure, buildings, and nearby landscapes, providing data on how urban system components interact with the surrounding air, ground, and water conditions; 2) The application of sensor data to generate environmental design analysis and design guidelines to address how current and future managements of Utqiaġvik's built environment can be improved; and 3) The study of how our research team and Utqiaġvik residents communicate across disciplines and cultures to co-produce knowledge that is useful for residents and that informs science and social science. Within the framework of these objectives, there are three interrelated research components and associated research questions:

Component #1: Building and infrastructure effects on land-water-atmosphere interactions

To what degree do buildings and infrastructure create micro-meteorological conditions throughout an Arctic city?

Over what spatial and temporal scales are these interactions most prominent?

How do these alterations of micro-meteorological conditions affect the surrounding tundra, and the stability of ground ice and permafrost?

How do buildings and infrastructure (including sewage treatment facilities) influence the hydrology and chemistry of inland surface waters in Utqiaġvik?

How vulnerable are water resources and their associated infrastructure to dynamics in environmental conditions?

Component #2: Design analysis and strategies toward resilient buildings and infrastructure

How can high resolution sensor-based environmental data inform future best practices for design of buildings and infrastructure in an Arctic city?

How can environmental design guidelines be evaluated and enriched by incorporating qualitative data and community input from local and Inupiaq residents?

How can the future design and planning in Utqiaġvik occur in a way to minimize environmental impacts on the landscape and increase the resiliency of the community?

Component #3: Co-production of knowledge through convergent research

How do interdisciplinary researchers and community members align their knowledge, research practices, and values while collaborating?

How do researchers and community members learn from each other about environmental change and sustainability?

How can researchers and community members conduct environmental research that addresses everyone's matters of concern?

Activities and results

The sensor network elements can be divided essentially into four categories (Figure 1): terrestrial micrometeorology at different locations around buildings and a tundra "control;" aquatic conditions in lagoons, lakes, and ponds; geophysical surveying (including ground penetrating radar, electrical resistivity tomography, active layer depth, and LiDAR), and airborne particulate matter. Geophysical surveying have been conducted beginning with the summer of 2021, and the first components of the terrestrial and aquatic sensor arrays were installed in June 2022; we continue to improve upon and expand the measurements. Whereas prior research has shown only a marginally significant urban heat island in Utqiaġvik, our finer scale sensor locations indicate the presence of substantive summer "hot" and "cold" spots, related to aspect and proximity to water. At a residential facility, ground thawed later at a south-facing aspect and ~four days earlier at a north-facing aspect relative to the tundra control. Ground temperatures at 30cm depth were on average 0.99°C (up to ~5.0°C) warmer south-facing and 1.94˚C (up to ~2.5°C) cooler north-facing compared to the tundra. Aquatic sampling indicated generally greater NH_4^+, NO_3^-, and PO_4^- concentrations in urban water bodies compared to the surrounding tundra. Geophysical survey data additionally have mapped the spatial distribution of thaw depth, and the presence of soil water and frozen ground around three major infrastructure facilities (residential housing, hospital, and utilities compound). Very preliminary data on particulate matter identify the dramatic effect of vehicles, as well as the mitigating effect of water deposition (natural and anthropogenic). Our collaborative team includes community members, and our goal is to collectively assess and refine our data collection, in order to ultimately inform future design practices for resilient and sustainable Arctic communities.

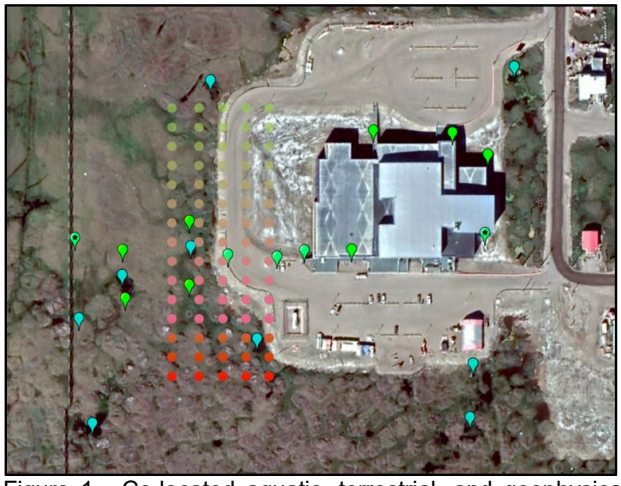

Figure 1. Co-located aquatic, terrestrial, and geophysical sensor arrays at the Samuel Simmonds Memorial Hospital in Utqiagvik, Alaska. Green markers are the terrestrial multiparameter sensors, blue markers are instrumented ponds, and the color-scale grid is the geophysical survey extent (green- low relief terrain to red- thermokarst terrain).

Coastal erosion mapping with a GIS-based indexing tool

Regula Frauenfelder, Elisabeth Hoffstad Reutz, Eivind M. Paulsen, Asgeir O.K. Lysdahl & Ingar Haug Steinholt
Norwegian Geotechnical Institute (NGI), Oslo, Norway

Coastal erosion in the Arctic is a critical problem, leading to damage of infrastructure, threatening coastal communities and releasing organic carbon from permafrost. Arctic coastal erosion is caused by a combination of thermal and mechanical drivers Permafrost thaw and ground-ice melt leads to soil decohesion and degradation, while surface ocean waves mechanically abrade the coast (Nielsen et al. 2022).

Global Arctic-mean erosion rates are projected to increase and very likely exceed their historical range of variability before the end of the century (Nielsen et al. 2022). Yet, Arctic coasts show a large morphological variety and retreat rates vary highly between areas (e.g., Irrgang et al. 2018; Aga et al. 2023). Therefore, being able to model coastal vulnerability depending on local factors would be beneficial to increase the accuracy of local retreat rate estimates.

Here we show the results of a case study where we tested the application of a coastal vulnerability index to a small stretch of Arctic coast in Svalbard.

Study site

Our test study site is located at Isfjord Radio, a radio station, weather station and hotel located at Kapp Linné on the island of Spitsbergen, Svalbard, Norway at 78°03′08″N 13°36′04″E (Figure 1).

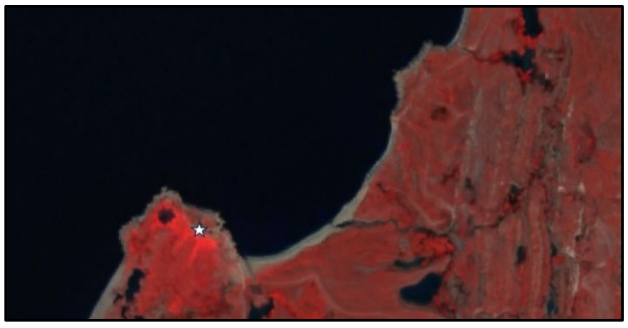

Figure 1. False-colour optical satellite imagery of the case study area. Source: Copernicus Sentinel data [2023]. Isfjord Radio station marked with white asterisk.

On an overarching level, the coast at this site can be characterized as long strand flats east and west of the station, with exposed, finely chiseled bedrock ridges in-between.

Method

We use a Coastal Vulnerability Index (CVI) based on McLaughlin and Cooper (2010) and further developed by SGI/SGU (2020). The CVI is formulated as a function of conditions favourable/non-favourable in the context of erosion, and assets (natural or anthropogenic) that may be vulnerable/ non-vulnerable to erosion. The concept relies on the prerequisite that these conditions and assets are contained within digital maps which serve as input datasets (Figure 2).

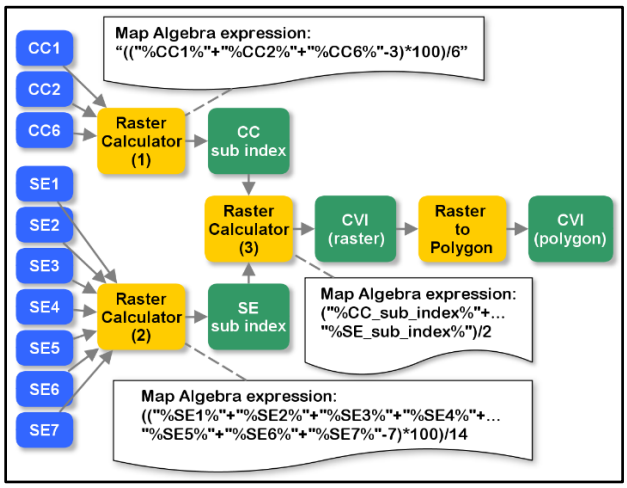

Figure 2. Algorithm developed by SGI/SGU (2020), then modified to identify the vulnerability of coastlines and coastal areas on mainland Norway. The datasets marked in blue are map layers used as input data.

Each input dataset is reclassified to a value between 1 and 3, where 1 is least vulnerable to erosion, and 3 is most vulnerable to erosion. For example, the dataset containing information on sediments is classified so that easily erodible areas are classified as 3, whereas areas with only solid rock are classified as 1.

The coastal vulnerability for every cell is then calculated according to Eq. (1), where the sum of the assumptions used in the final model is normalized.

$$50 * \frac{C_{DTM}+C_{sed}+C_{sho\ \ dist}+C_{wave}+C_{wind}+C_{area}-N_{classes}}{N_{classes}} \quad \text{[Eq1]}$$

The result of the model is written out as a raster dataset, where each cell has a value between 0 and 1, where 0 equals very low vulnerability to coastal erosion and 1 equals very high vulnerability to coastal erosion (example from mainland Norway in Figure 3).

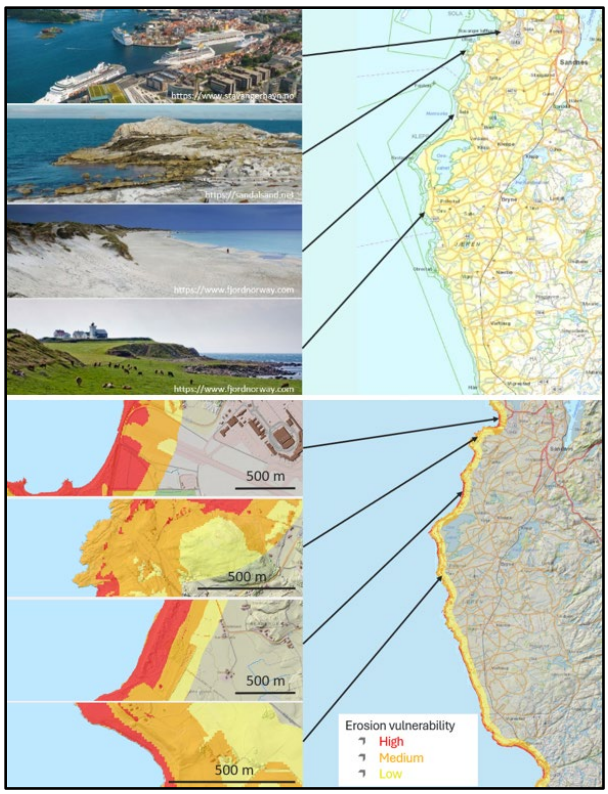

Figure 3. CVI calculation exemplified for the coast of Jæren, Southern Norway. Coast types, from top to bottom: anthropogenic coast (urbanized area), bedrock outcrops, strand flats and sandy beaches, beach terraces and coarse pebble flats. Erosion vulnerability classification: yellow = low, orange = medium, red = high.

Results and Discussion

On Svalbard, several of the map layers available on mainland Norway and originally used in the CVI, are not readily available. Therefore, the CVI had to be adapted and for critical feature layers one had to manually delineate polygons of the different features. In addition, since several differentiating layers are missing, differences in erosion vulnerability become more subtle than on the mainland, and the results had to be visualized in five classes (instead of three) to be able to see significant differences in erosion vulnerability.

Since one of the main points of the CVI modelling is to be able to rely on wide area coverage data layers, the lack of relevant input layers is a clear deficiency when trying to apply the CVI concept to Svalbard. Jaskólski et al. (2018) faced the same problem but circumvented it by applying their CVI model to the town of Longyearbyen, where more map layers are available than for the wilderness areas. However, there exist only two major, permanent settlements on Svalbard today and therefore, areas lacking several of the necessary input layers for the CVI are the norm, rather than the exception.

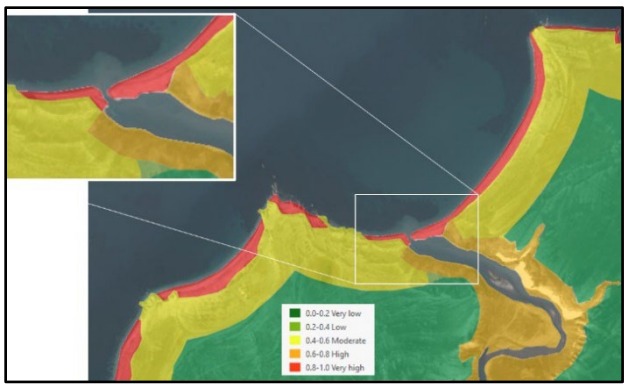

Figure 4. CVI calculation exemplified for a coastal stretch near Isfjord Radio, Spitsbergen, Svalbard.

Conclusions

We tried to transfer and adapt a CVI concept based on McLauglin and Cooper (2010) to map coastal erosion vulnerability on Svalbard. Due to the lack of several relevant input data layers, our attempt was not satisfactory. Computer assisted automatic classification of different land cover types from high-resolution satellite imagery might be a way to mitigate these problems.

Acknowledgements

The CVI implementation for mainland Norway was carried out within the MERRIC strategic project (https://www.ngi.no/en/projects/merric/). We are grateful for the financial support through NGI's base funding from the Research Council of Norway.

References

Irrgang A.M., Lantuit H., Manson G.K., and Günther F. 2018. Variability in rates of coastal change along the Yukon coast, 1951 to 2015. Journal of Geophysical Research: Earth Surface, 2005: 779–800.

Jaskólski, M.W., Pawłowski, L., and Strzelecki, M.C. 2018. High Arctic coasts at risk—the case study of coastal zone development and degradation associated with climate changes and multidirectional human impacts in Longyearbyen. Land Degrad Dev. 2018; 29:2514–2524.

McLauglin, S., and Cooper, J.A.G. 2010. A multi-scale coastal vulnerability index: A tool for coastal managers? Environmental hazards, 9, 233–248.

Nielsen, D.M., Pieper, P., Barkhordarian, A., et al. 2022. Increase in Arctic coastal erosion and its sensitivity to warming in the twenty-first century. Nat. Clim. Chang. 12, 263–270.

SGI/SGU. 2020. Kustens sårbarhet – erosion. Accessible at: https://gis.swedgeo.se/ksi_erosion/

Electrical resistivity tomography (ERT) investigations of drilling-waste sumps within discontinuous permafrost, central Mackenzie Valley, NT

Michelle Landry[1,2], Alexandre Chiasson[1,2], Keytash Moshtaghian[3], Alejandro Alvarez[1,2], Steven V. Kokelj[4] & Duane G. Froese[1,2]

[1]*Department of Earth and Atmospheric Sciences, University of Alberta, Edmonton, Alberta, Canada*

[2]*Permafrost Archives Science Laboratory, Edmonton, Alberta, Canada*

[3]*Department of Physics, University of Alberta, Edmonton, Alberta, Canada*

[4]*Northwest Territories Geological Survey, Government of Northwest Territories, Yellowknife, Northwest Territories, Canada*

Drilling sumps are large pits constructed in permafrost assumed to contain wastes from exploratory oil and gas activities. Widespread throughout the Northwest Territories, nearly 500 drilling sumps and well sites were established between the 1920s to the early 2010s. These sumps were considered an effective in-situ alternative for the indefinite containment of drilling wastes from petroleum operations, such as drill cuttings and saline drilling fluids. Most sumps are located in the Mackenzie Delta and Beaufort region within deep continuous permafrost. However ~190 (~40%) are in the discontinuous permafrost zone of the central Mackenzie Valley. Discontinuous permafrost in this region is particularly vulnerable to future climate change, as the depth of frozen ground is typically thin (10-50 m), and ground temperatures are warm (Smith et al. 2022; Smith et al. 2023). Three sumps in the Sahtu region were examined using Electrical Resistivity Tomography (ERT), testing its application along with Induced Polarization (IP) surveys. Through this, we (1) infer the distribution and extent of permafrost (if present) (2) define the boundaries of solute redistribution and whether these extend within and outside of drilling sump perimeters, and (3) assess whether sumps are performing as intended. ERT can be used as a tool to demonstrate how sumps are performing in warm, discontinuous permafrost in the central Mackenzie Valley, reflecting a tipping point for permafrost thaw over large areas of Northwestern Canada.

Study Area

The central Mackenzie Valley traverses the Taiga Cordillera Low Subarctic Ecoregion (Ecosystem classification group 2010). Common surficial features consist of mega-scale lineations and till plains originating from the Laurentide ice sheet, Holocene post-glacial alluvial and colluvial deposits and late Pleistocene glaciolacustrine deposits (Duk-Rodkin 2002). Permafrost temperatures in the central and southern Mackenzie Valley have experienced warming of ~0.3 °C per decade since the mid-1980s (Smith et al. 2022). Wellsite and sump areas have been cleared of vegetation (~100 m^2) and have not revegetated to their original condition since their construction.

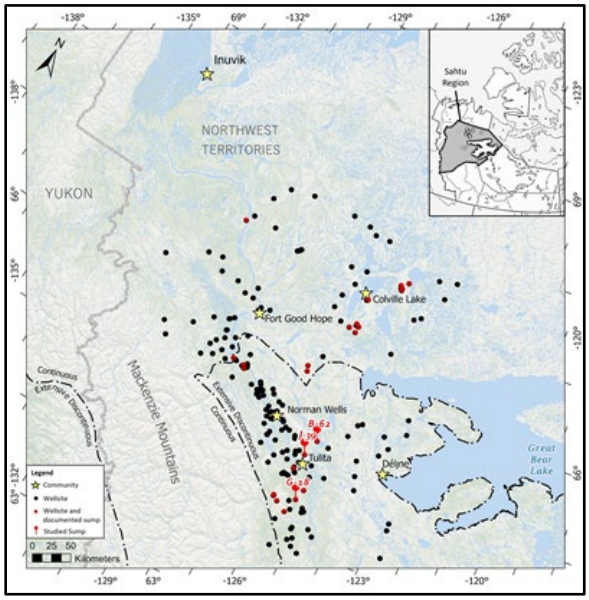

Figure 1. Locations of studied drilling-waste sumps (n=3) among exploratory well/sump sites (n=188) in the central Mackenzie Valley, NT.

Methods

An ABEM Terrameter LS2 multi-electrode ERT system was used to conduct 12 Resistivity (RES) and 10 IP surveys using electrode spacing of 1, 2, or 3 m. We use Wenner arrays to assess the extent of permafrost and saline fluids through RES/IP measurements. These data were processed by extracting resistivity and chargeability values from inverted surveys with the RES2DINV software. Models were run to the 4th iteration or until the root mean squared error was below 5% (Way and Lewkowciz 2015). In addition, soil quality assessments from analytical reports were consulted via the Sahtu Region Public Registry.

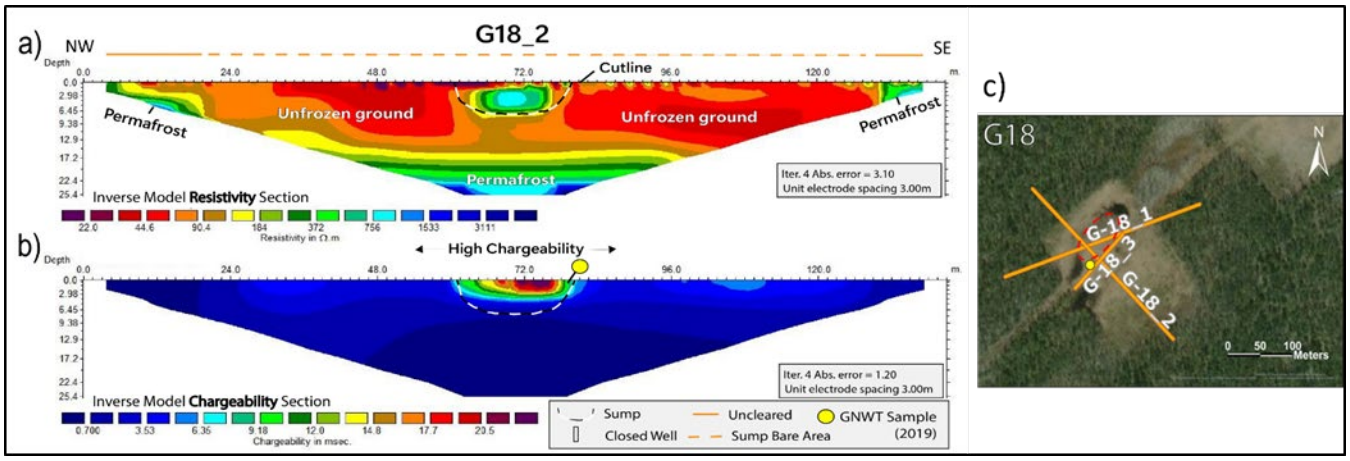

Figure 2. ERT survey of 3.00 m spacing running NW-SE at G18 across the drilling sump. a) Resistivity profile modeling permafrost extent; b) Chargeability profile outlining movement of high chargeability fluids; c) Site map showing resistivity profile lines.

RESULT

ERT surveys were carried out at three sumps across the central Mackenzie Valley. Figure 2 demonstrates the (a) resistivity and (b) chargeability profiles of a 3-m spaced ERT profile of a sump south of Tulita, NT showing evidence of erosion, i.e., cracking and thermokarst ponding. Over this area of fluted glacial till (Tv, Ts) (Duk-Rodkin 2002), resistivities of 20-3500 Ω.m were observed. Directly to the NW and SE of the sump, resistivities are low (20-100 Ω.m) within the first 15 m. In areas of major disturbance around the sump, i.e., areas of ponding and the cutline, the lowest resistivities were observed (20-100 Ω.m). At the sump between 0.5-3 m, high resistivities (100-800 Ω.m) are expressed in a distinctly oval shape. Outside the cleared sump bare area, under tall vegetation, resistivities are moderate (100-800 Ω.m). High chargeabilities of 4-25 msec. are present at the surface directly to the west and east of the sump but were mostly localized to the sump itself (Figure 2b). Values suggest high conductivity fluids are present and concentrated at the sump surface in the active layer and have partially migrated outside the sump and sump bare area. An environmental inspection report conducted in 2019 by the GNWT Department of Lands indicates a soil sample with an salt absorption ratio that exceeds the Canadian Environmental Quality Guidelines (CEQGs) for ecological soil quality and human health (GNWT 2019).

DISCUSSION

Geophysical data shows strong evidence for permafrost absence or degradation at studied sumps, indicating permafrost has likely not recovered following disturbance. IP surveys demonstrate high chargeability materials are present at the surface of sumps and extend into the shallow subsurface, and are likely present outside of sump area perimeters. This project represents the first use of ERT to delineate saline fluid movement and characterise permafrost thaw in drilling-waste sumps in the central Mackenzie Valley. ERT demonstrates its value in understanding the relations between sumps, permafrost, and the mobilization of drilling fluids in a boreal region under a warming climate. Conducting ERT surveys to characterize contaminated sites helps in developing long-term monitoring strategies for sumps in the Sahtu region.

REFERENCES

Duk-Rodkin, A. 2002. Surficial geology, Norman Wells, Northwest Territories. Geological Survey of Canada, A Series Map 1989A. Scale 1:250,000.

Ecosystem Classification Group. 2010. Ecological regions of the Northwest Territories - Cordillera, Department of Environmental and Natural Resources, GNWT, Yellowknife, Canada, p.245.

Government of Northwest Territories. 2019. S99A-015 Oil and Gas Drilling – Wellsite and Sump Environmental Inspection Report.

Smith, S.L. 2022. Terrestrial permafrost cover in State of the Climate in 2019. Bulletin of the American Meteorological Society, 101 (8), S265–S269.

Smith, S.L., O'Neill, H.B., Isaksen, K., et al. 2022. The changing thermal state of permafrost. Nat Rev Earth Environ 3, 10–23.

Way, R.G., and Lewkowicz, A.G. 2015. Investigations of discontinuous permafrost in coastal Labrador with DC electrical resistivity tomography, GéoQuebec: 68th Canadian Geotechnical Conference and 7th Canadian Permafrost Conference. Quebec City, Canada, p.8.

Thaw settlement potential map of Canada

Zakieh Mohammadi, Nana K. Frimpong Agyei & Jocelyn L. Hayley
Department of Civil Engineering, University of Calgary, Calgary, Alberta, Canada

Global warming is causing permafrost degradation, leading to undesirable changes in the mechanical properties of ground material and resulting in instability in natural and built environments. Thaw settlement, caused by permafrost degradation and meltwater expulsion, is a common issue affecting infrastructure in permafrost regions that leads to increased maintenance costs and safety concerns. The objective of the paper is to create a Canada-wide map illustrating the potential for thaw settlement due to the degradation of near-surface permafrost. This map will be a crucial tool for informed decision-making in land use planning, infrastructure design, and resource allocation to mitigate risks and enhance resilience.

Previous studies, including those by Daanen et al. (2011), Hjort et al. (2018), Hong et al. (2014), and Ni et al. (2021), have extensively explored permafrost thaw settlement potential at circumpolar and regional scales, notably in Greenland, Alaska, and the Qinghai-Tibet Plateau. Building on these insights, Mohammadi and Hayley (2023) proposed a method for evaluating thaw settlement potential, introducing the Thaw Settlement Potential Index (TSPI), where ground ice content, surficial deposit unit, and bedrock type were identified as the most important factors. Here, we build on previous work and employ the TSPI approach to develop a thaw-settlement potential map of Canada.

METHODOLOGY

To create a TSPI map for Canada, geospatial data on ground ice, surficial geology, and bedrock were essential, each obtained from different sources.

Acquiring ground ice data involved obtaining a Geotiff file representing volumetric excess ground ice (%) from O'Neill et al. (2021) ground ice map of Canada at a resolution of 1:5000000. Following the approach outlined by Mohammadi and Hayley (2023), the ground ice abundance map underwent reclassification and ascending numerical values from 1 to 9 were assigned, based on the percentage of ground ice present.

Surficial geology map data was obtained from the Geological Survey of Canada at a scale of 1:5000000. The dataset was modified to exclude marine sediments, glacial ice, and snowpacks, considering their irrelevance to permafrost thaw hazards on land. Finally, numerical values ranging from 1 to 9 were assigned to the surficial geology units using the classification proposed by Mohammadi and Hayley (2023).

Bedrock data acquisition involved obtaining shapefiles for the bedrock map of Canada from the Geological Survey of Canada, encompassing variable scales (1:2000000 to 1:5000000) on different sections (Wheeler et al. 1996). These diverse sections were merged to form a unified geological map and underwent modifications, including the removal of all offshore rock units and glaciers or ice packs. The rock units were then categorized into two distinct groups: volcanic, plutonic, and metamorphic rocks were assigned a value of 1, indicating low susceptibility to thaw settlement, while sedimentary rocks received a value of 9, signifying a high susceptibility to thaw settlement.

In the final stage, the modified geospatial files for ground ice, surficial geology units, and bedrock were converted into raster files. These were overlaid in ArcGIS, and TSPI was calculated using Mohammadi and Hayley (2023) weighting scheme: 0.78 for excess ground ice, 0.15 for surficial geology units, and 0.07 for bedrock units.

RESULTS

The TSPI map for Canada is depicted in Figure 1. This map classifies regions into three distinct levels of settlement potential (low, medium, and high) and provides a broad overview of settlement potential across various regions in Canada. In areas characterized as having low settlement potential, there is a minimal likelihood of encountering extensive problematic thaw settlement, often attributed to insignificant ground ice content or the presence of thaw-stable sediments. While widespread thaw settlement is unlikely in these regions, localized occurrences are possible and infrastructure planning may require a more detailed, finer-scale assessment. Regions with medium settlement potential indicate a higher likelihood of problematic settlement, primarily due to moderate ground ice content or the presence of thaw-unstable sediments. To mitigate this risk, an extensive site investigation and cautious engineering design are recommended. Areas with high settlement potential are most susceptible to significant impacts from problematic settlement upon permafrost degradation. These regions, characterized by high ice content and thaw-unstable materials, necessitate

rigorous design measures and a thorough site investigation to minimize the risk of thaw settlement in later project phases. Obtaining high settlement potentials in regions like western Canada and Banks Island aligns with empirical evidence, including widespread subsidence at instrumented sites in northwest Canada and a significant concentration of retrogressive thaw slumps on Bankes Island (O'Neill et al. 2023; Lewkowicz and Way 2019).

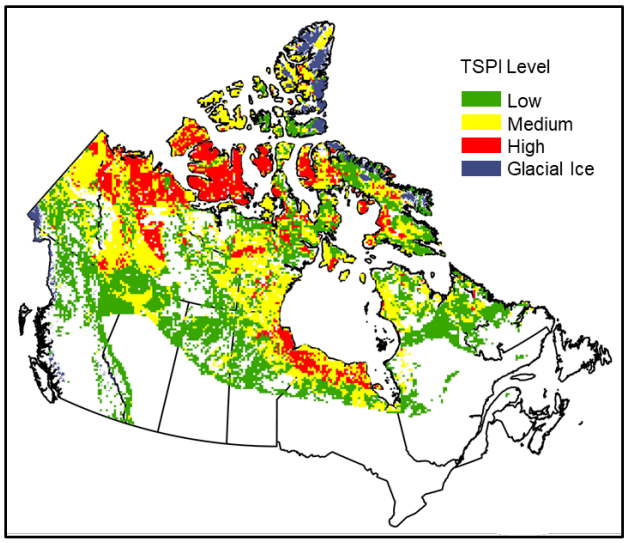

Figure 1. Thaw settlement potential map of Canada.

Due to the high weight assigned to ground ice in TSPI method, the outcomes are predominantly shaped by the ground ice model used for creating the map. Consequently, enhancements in ground ice modelling will directly contribute to an improved evaluation of settlement potential. While the map classifies areas according to their settlement potential, it does not account for the permafrost degradation potential in these regions. To ensure a more comprehensive understanding of potential challenges posed by thaw settlement in different regions of Canada, it is essential to integrate the results with predictions regarding the extent of near-surface permafrost degradation.

Conclusion

The TSPI map for Canada serves as a valuable tool for effective land use planning, site assessment, and the prioritization of route alternatives, particularly for large projects spanning multiple permafrost zones. It enhances our understanding of the potential impact of permafrost degradation on infrastructure across the country. Future studies could explore the integration of this map with climate-related data to develop a comprehensive hazard/vulnerability map for thaw settlement, ultimately overlaying this hazard map with infrastructure maps to create a permafrost degradation risk map for Canada. This integrated approach would provide crucial insights for proactive risk mitigation and resilient infrastructure planning in the face of ongoing climate changes.

Acknowledgements

This research was funded by PermafrostNet, which is supported by the Natural Sciences and Engineering Research Council of Canada (NSERC).

References

Daanen, R.P., Ingeman-Nielsen, T., Marchenko, S.S., Romanovsky, V.E., Foged, N., Stendel, M., et al. 2011. Permafrost degradation risk zone assessment using simulation models. The Cryosphere Discussions, 5(2), 1021–1053.

Geological Survey of Canada. 2014. Surficial Geology of Canada, Canadian Geoscience Map 195, Scale 1:5,000,000. doi:10.4095/295462

Hjort, J., Karjalainen, O., Aalto, J., Westermann, S., Romanovsky, V.E., Nelson, F.E., et al. 2018. Degrading permafrost puts Arctic infrastructure at risk by mid-century. Nature communications, 9(1), 5147.

Hong, E., Perkins, R., and Trainor, S. 2014. Thaw settlement hazard of permafrost related to climate warming in Alaska. Arctic, 93–103.

Lewkowicz, A.G., and Way, R.G. 2019. Extremes of summer climate trigger thousands of thermokarst landslides in a High Arctic environment. Nature communications, 10(1), 1329.

Mohammadi, Z., and Hayley, J.L. 2023. Qualitative evaluation of thaw settlement potential in permafrost regions of Canada. Cold Regions Science and Technology, 216, 104005.

Ni, J., Wu, T., Zhu, X., Wu, X., Pang, Q., Zou, D., et al. 2021. Risk assessment of potential thaw settlement hazard in the permafrost regions of Qinghai-Tibet Plateau. Science of the Total Environment, 776, 145855.

O'Neill, H.B., Wolfe, S.A., and Duchesne, C. 2019. New ground ice maps for Canada using a paleogeographic modelling approach. The cryosphere, 13(3), 753–773.

O'Neill, H.B., Smith, S.L., Burn, C.R., Duchesne, C., and Zhang, Y. 2023. Widespread permafrost degradation and thaw subsidence in northwest Canada. Journal of Geophysical Research: Earth Surface, 128(8), e2023JF007262.

Wheeler, J.O., Hoffman, P.F., Card, K.D., Davidson, A., Sanford, B.V., Okulitch, A.V., and Roest, W.R. 1996. Geological map of Canada. Natural Resources Canada.

Geophysical surveys of ground conditions adjacent to various types of infrastructure in Utqiaġvik, Alaska

MacKenzie Nelson & Howie Epstein

Department of Environmental Science, University of Virginia, Charlottesville, Virginia, United States

Utqiaġvik is the northernmost community in the U.S. Arctic and is a prime example of an Arctic system where the high degree of connectivity between the natural-built environments, projected warming, increasing development and climate uncertainty result in significant challenges for the community. To understand these issues at a finer scale and develop strategies to enhance community resilience, our NSF-NNA project titled *Understanding the Changing Natural-Built Landscape in an Arctic Community: An Integrated Sensor Network in Utqiaġvik, Alaska* uses complementary geophysical surveys to map subsurface characteristics of the permafrost terrain including active layer depth, land surface deformation (subsidence or seasonal fluctuations based on freeze/thaw cycles), as well as structural stability and seasonal variations of underground structures (i.e., foundations and buried utilities) to understand building and infrastructure stabilities in Utqiaġvik. In collaboration with the Cold Regions Research and Engineering Lab (CRREL), electrical resistivity tomography (ERT) and ground penetrating radar (GPR) methods were implemented in the month of August for the last three seasons (2021–2023). Strategic transect locations are informed by previously collected geophysical results and optimized for data quality and proximity to pertinent infrastructure each season. Transect locations focus on the snow accumulation zone from the Taġiuġmiullu Nunamiullu Housing Authority (TNHA) parking lot, the gravel-tundra interfaces surrounding the Samuel Simmonds Memorial Hospital (SSMH), and the Barrow Environmental Observatory (BEO). Coincident seasonal thaw depths were measured using thaw probes along selected transects. The geophysical surveys aim to spatially quantify thaw-vulnerable zones near undisturbed (BEO) and disturbed (TNHA and SSMH) permafrost.

Common offset (CO) 400 MHz GPR configuration with an SIIR 4000 control unit from Geophysical Survey Systems, Inc., produces 2D radar cross sections, i.e., radargrams, that were inspected and the two-way travel time of the radar wave (the round-trip travel time from the transmitter at the surface to the permafrost reflector and back to the receiving antenna at the surface) was selected for optimization. Using thaw depth information from manual probing and corresponding radar travel times we estimated the radar wave velocity within the thawed using thaw depth information from manual probing and corresponding radar travel times. For areas where thaw probing is limited due to gravel, GPR velocities were measured using a common mid-point (CMP) geometry, in which two GPR antennas (pairs of 900 MHz and 400 MHz GSSI antennas) were separated by 0 to 2 m iteratively in 10 cm increments about a center point.

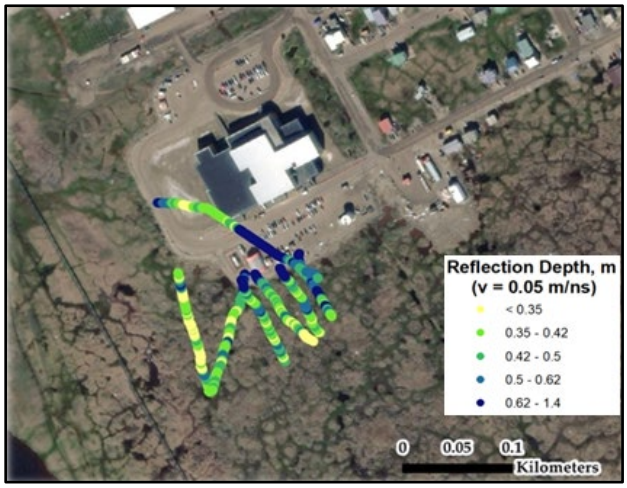

Figure 1. 2022 GPR transects at Samuel Simmonds Memorial Hospital (SSMH).

ERT leverages differences in electromagnetic properties among frozen and thawed soils as ERT is sensitive to changes in electrical resistivity among resistive (frozen) and less resistive (thawed) volumes of the subsurface (Douglas et al., 2008). We used a SuperSting R8 (AGI) ERT meter with 84 electrodes at SSMH, the BEO, and at TNHA. We implemented 2 m electrode spacing across undisturbed tundra at the BEO and SSMH (south transect) in addition to transects with 1 m spacing at TNHA and SSMH (north transect). The ERT cross sections complemented thaw probe and CO- and CMP-GPR /observations with an additional perspective on the distribution of seasonal thaw.

Sensitivity analysis of thawing and freezing n-factors in thermal modeling of permafrost regions under a changing climate: Initial probabilistic results

Khatereh Roghangar & Jocelyn L. Hayley
Department of Civil Engineering, University of Calgary, Calgary, Alberta, Canada

The Arctic landscape is rapidly changing due to climate change which leads to permafrost thaw, the active layer to thicken, and widespread thaw settlement to occur (e.g., De Guzman et al. 2021). In order to maintain the stability of infrastructure on permafrost, frozen ground conditions must be maintained while designing stable infrastructure depends on a thorough understanding and analysis of current and future climate conditions (e.g., Schneider Von Diemling et al. 2021). Climate data can be used as input for thermal models to predict how permafrost may behave under different climatic conditions. However, there is often uncertainty in thermal modelling parameters, and it is important to understand how those uncertainties affect modelled results.

This study presents a sensitivity analysis of how n-factors affect predictions of active layer thickness using a probabilistic thermal model. The goal of this study is to probabilistically assess the critical parameters affecting permafrost degradation in order to optimize data gathered during the investigation.

METHODOLOGY

To investigate the sensitivity of predicted active layer changes to n-factors in soil profiles, a geothermal model was developed. For this purpose, TEMP/W was used for numerical simulations and a Python script was used for probabilistic analysis. The study assumed an active layer thickness of 0.5 m (typical active layer thickness based on literature) and an increase in air temperature an average air temperature ranging from -2 - 6℃ by 2100 (in case of considering the worst-case scenario; SSP-8.5) (IPCC 2021). The thaw settlement was calculated using the following equation:

$$\delta=\varepsilon^{*}\Delta TLD \quad [1]$$

where δ is the thaw settlement (m), ε is the thaw strain and ΔTLD is the change in thawed layer depth (TLD) (m) derived from the thermal modelling results. Thaw strain is calculated based on the dry density of soil in each simulation (Hanna et al. 1978). Thaw settlement is calculated cumulatively from the TLD change between two consecutive years.

We assigned a range of normally and uniform distributed parameter values and performed sensitivity analyses by altering one parameter while holding the rest constant. Tables 1 and 2 provide details of the normal distribution characteristics and uniform distribution characteristics for each parameter derived from literature, respectively (Andersland and Ladanyi 2004; Brooks et al. 2018).

Table 1. Mean and standard deviation of normally distributed parameters used in the sensitivity analysis.

Variable	Mean	Standard Deviation
Water content	0.5	0.1
Dry density	800	10

Table 2. Range of change in uniform distributed parameters used in the sensitivity analysis.

Variable	Range
Particle diameter	0.0000005-0.1
Thawing n-factor	0.73-2
Freezing n-factor	0.25-1

RESULTS AND DISCUSSION

Figure 1 illustrates the changes in TLD associated with changing freezing and thawing n-factors. Increasing thawing and freezing n-factor causes the TLD to increase and decrease, respectively. Based on the definition of n-factor, a higher thawing n-factor means more heat transfer to the ground and a higher freezing n-factor means less heat transfer to the ground which both cause a lower ground temperature and consequently, a lower depth of thaw that can be confirmed using Figure 1. On the other hand, the rate of change of TLD is higher when changing freezing n-factor. There are many reasons for this phenomenon, including the fact that winter cooling tends to be stronger than summer warming. For soil warming to be predicted in ecosystems surrounded by permafrost, ground thermal regimes in the cold season are more critical (Kropp et al. 2021; Frost et al. 2018; Myres-Smith and Hik 2013). In addition, at high latitudes, the winter season is much longer than the summer season. According to Kropp et al. (2021), the resulting year-round cooling will result in less permafrost degradation as temperatures gradually decrease.

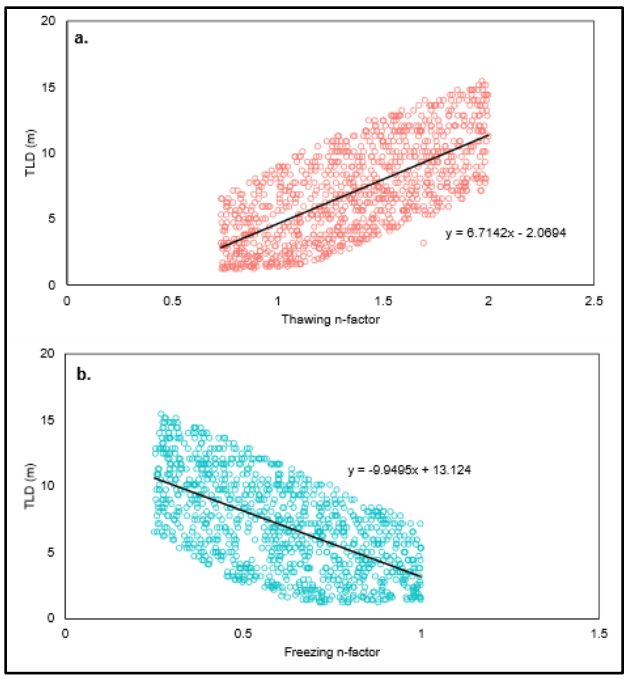

Figure 1. TLD in a. thawing and b. freezing n-factor sensitivity analysis at 2100.

Conclusion

This study investigated the effect of thawing and freezing n-factors parameters on thawed layer depth changes in permafrost regions. Based on the findings of this study, changing freezing n-factor causes bigger changes in the thawed layer depth in comparison to changing thawing n-factor indicating warmer winters are more critical than cooler summers in predicting the thermal regime of permafrost regions.

Acknowledgements

We are grateful to NSERC PermafrostNet for providing funding for this research and appreciate the time and effort Dr. Teddi Herring put into reviewing this manuscript.

References

Andersland, O.B., and Ladanyi, B. 2004. Frozen Ground Engineering Second Edition. The American Society of Civil Engineers & John Wiley & Sons, Inc, 2004.

Brooks, H., Doré, G., and Smith, S.L. 2018. Permafrost geotechnical index property variation and its effect on thermal conductivity calculations. Cold Regions Science and Technology,148, 63–76. https://doi.org/10.1016/j.coldregions.2018.01.004

De Guzman, E.M.B., Alfaro, M.C., Arenson, L.U., and Doré, G. 2021. Thermal Regime of Highway Embankments in the Arctic: Field Observations and Numerical Simulations. Journal of Geotechnical and Geoenvironmental Engineering, 147(6). https://doi.org/10.1061/(asce)gt.1943-5606.0002502

Frost, G.V., Epstein, H.E., Walker, D.A., Matyshak, G., and Ermokhina, K. 2018. Seasonal and Long-Term Changes to Active-Layer Temperatures after Tall Shrubland Expansion and Succession in Arctic Tundra. Ecosystems, 21(3), 507–520. https://doi.org/10.1007/s10021-017-0165-5

IPCC 2021: Summary for Policymakers. In: Climate Change (2021): The Physical Science Basis. Contribution of Working Group I to the Sixth Assessment Report of the Intergovernmental Panel on Climate Change [Masson-Delmotte, V., P. Zhai, A. Pirani, S.L. Connors, C. Péan, S. Berger, N. Caud, Y. Chen, L. Goldfarb, M.I. Gomis, M. Huang, K. Leitzell, E. Lonnoy, J.B.R. Matthews, T.K. Maycock, T. Waterfield, O. Yelekçi, R. Yu, and B. Zhou (eds.)]. Cambridge University Press. In Press.

Kropp, H., Loranty, M.M., Natali, S.M., Kholodov, A.L., Rocha, A.V., Myers-Smith, I., Abbot, B.W., Abermann, J., Blanc-Betes, E., Blok, D., Blume-Werry, G., Boike, J., Breen, A.L., Cahoon, S.M.P., Christiansen, C.T., Douglas, T.A., Epstein, H.E., Frost, G.V., Goeckede, M., and Lund, M. 2021. Shallow soils are warmer under trees and tall shrubs across Arctic and Boreal ecosystems. Environmental Research Letters, 16(1). https://doi.org/10.1088/1748-9326/abc994

Myers-Smith, I.H., and Hik, D.S. 2013. Shrub canopies influence soil temperatures but not nutrient dynamics: An experimental test of tundra snow-shrub interactions. Ecology and Evolution, 3(11), 3683–3700. https://doi.org/10.1002/ece3.710

Schneider Von Deimling, T., Lee, H., Ingeman-Nielsen, T., Westermann, S., Romanovsky, V., Lamoureux, S., and Langer, M. 2021. Consequences of permafrost degradation for Arctic infrastructure - Bridging the model gap between regional and engineering scales. Cryosphere, 15(5), 2451–2471.

Thermal modelling of deep permafrost profiles spanning the Canadian Arctic

Cameron Ross[1,2], Alireza Yaseri[2], Robyn Starycki[2], Greg Siemens[2] & Ryley Beddoe[2]

[1]6 Point Engineering and Avalanche Consulting Ltd., Nelson, British Columbia, Canada

[2]Department of Civil Engineering, Royal Military College, Kingston, Ontario, Canada

There have been numerous studies which have reported on recent warming trends in long-term ground temperature records in the western Arctic; particularly along the Mackenzie River Delta in the Northwest Territories. However, there are fewer studies reporting on ground temperature trends in the central and eastern Arctic where road access is limited and ground temperature data are sparse. In this study, site-specific, long-term ground temperature records were used to first calibrate then simulate the evolution of thermal regimes of three sites spanning the Canadian Arctic.

The three sites are former Distant Early Warning (DEW) Line stations BAR-2 (Shingle Point), Yukon; CAM-M (Cambridge Bay), Nunavut; and FOX-5 (Broughton Island), Nunavut (Figure 1). They represent the western, central and eastern Canadian Arctic respectively, and span a distance of ~3,000 km. All three sites are within the continuous permafrost zone (Heginbottom et al. 1995).

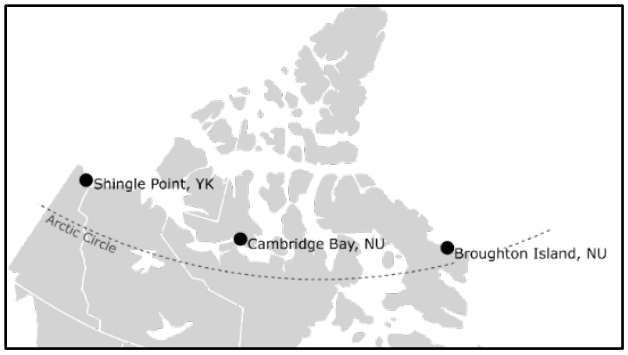

Figure 1. Three thermally monitored former DEW Line station sites spanning the Canadian Arctic at roughly 69° latitude, within the continuous permafrost zone.

GROUND TEMPERATURES AND MODELLING APPROACH

In this study, 50 m-deep, one-dimensional (1D) ground temperature models were developed for each site and calibrated against available thermistor data. The data sets from Shingle Point, Cambridge Bay and Broughton Island were 10, 16 and 5 years respectively. The study's objectives were to reproduce recorded near-surface ground temperature conditions in the top 3-6 metres (m), and to simulate thermal conditions to 50 m depth based on 1970-2000 climate normals. Following calibration and model stabilization methodologies (Ross et al. 2022; McCaw 2019), model domains were extended to 1000 m and future climate change projections were applied in transient analyses to the year 2100. Thermal modelling was conducted using the TEMP/W module of the GeoStudio commercial software suite (versions 2018-R2 and 2021.3) developed by GeoSlope International Ltd.

At the ground surface, a surface energy balance (SEB) was applied using climate projections (CanESM2 for RCP 8.5). Snow-on-ground projection data for each site were reduced by the average snowcover factors developed during calibration (0.4 at Shingle Point and Cambridge Bay; 0.2 at Broughton Island). The bottom boundary condition applied was flux of energy per unit time, Q (e.g., KJ/ day) following the process outlined by Ross et al (2023).

MODEL RESULTS

Full-depth model results are presented in Figure 2 for Shingle Point. The model of the Mean Annual Ground Temperature (MAGT) profile and maximum/minimum temperature envelopes represent the average over the calibration period. The modelled depth of zero-annual amplitude and the projected total depth of permafrost were used to evaluate model performance. The projected total depth of permafrost was calculated based on the thermal gradient at 50 m. At Shingle Point, the modelled depth of zero annual amplitude averaged 23 m below grade over the model calibration period, and the depth of permafrost was calculated to be 334 m at the site based on the gradient of 0.014 °C/m (Figure 2). This is within the range of published values for the Mackenzie Delta near Shingle Point on the Permafrost Map of Canada (Heginbottom et al. 1995), but deeper than those published for the Beaufort Coast northwest of Shingle Point (Smith and Burgess 2002).

The inset in Figure 2 shows a close-up of the phase change boundary over a depth of 20 m, and shows maximum temperature envelopes and active layer thickness (ALT) for the years from 2011 to 2100. The modelled active layer increased from 3.7 m in 2011 to 5.3 m in 2050, and 7.4 m by 2075. By 2075, the ground between 5.5 and 7.4 m did not fully refreeze in winter (not shown, for clarity) indicating the development of a talik.

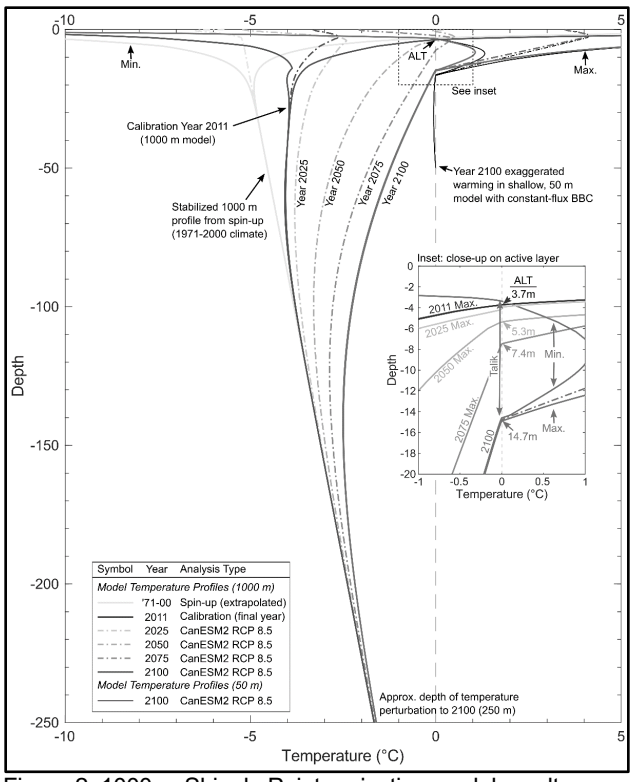

Figure 2. 1000 m Shingle Point projection model results.

Bottom boundary placement at 1000 m in the model reduced simulated warming compared to the same 50 m model due to boundary effects, also shown on Figure 2 and described by Ross et al. (2023). This indicates the importance of available heat storage in deep permafrost models for simulating long-term ground temperature evolution.

Figure 3 displays MAGT versus time for the three sites at depths of 5 m and 12 m (3a and 3b respectively). The initial data points in the Figure are the calibrated model results for 2010. This is then followed by projected temperatures for 2025, 2050, 2075, and 2100. Notably, at the shallower depth of 5 m, closer to the ground surface, all three sites exhibit a consistent and pronounced increase in temperature rates, particularly beyond the year 2075.

CONCLUSION

In this study, 50 m numerical models were developed and calibrated for three distinct Canadian Arctic sites: Shingle Point, Yukon; Cambridge Bay, Nunavut; and Broughton Island, Nunavut. Despite limited subsurface information, the models were effectively calibrated to a depth of 50 m using spin-up techniques. Post-calibration, the now 1000 m models projected climate change effects up to the year 2100 where significant warming was seen over the 90 simulated years.

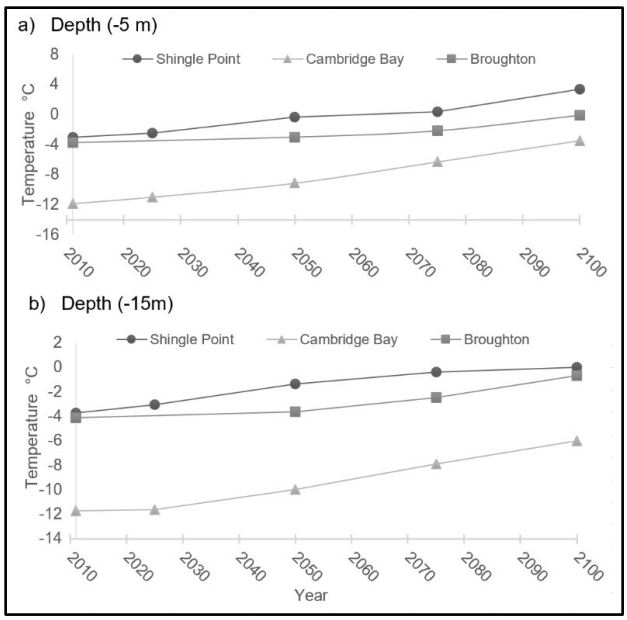

Figure 3. MAGT across three distinct sites.

The resulting models offer a baseline for future sensitivity analyses to consider different projected climate-warming scenarios (e.g., different global climate model outputs and emissions scenarios), collection of additional site-specific data, and extreme weather events.

ACKNOWLEDGEMENTS

This work was supported by numerous consultants, the Canadian Department of National Defence and the Royal Military College of Canada.

REFERENCES

Heginbottom, J.A., Dubreuil, M-A., and Harker, P.A. 1995. Permafrost Map of Canada, National Atlas of Canada 5th Edition (MCR 4177).

McCaw, J. 2019. Development and Calibration of a Permafrost Model Using Finite Element Modelling.

Ross, C., Siemens, G., and Beddoe, R. 2022. Initialization of thermal models in cold and warm permafrost. Arctic Science, 8(2), 362–394.

Ross. C., Beddoe, R., and Siemens, G. 2023. Quantification and practical solution for bottom boundary effects on long-term permafrost models. Cnd Geot. J (Submitted)

Smith, S.L., and Burgess, M.M. 2002. A digital database of permafrost thickness in Canada, Geological Survey of Canada Open File 4173.

Climate warming puts permafrost and infrastructure at risk in the Qinghai-Tibet Plateau

Mingyi Zhang[1,2], Renwei Li[1,2], Weibo Liu[1,2] & Yanqiao Zhou[1,2]

[1]*State Key Laboratory of Frozen Soil Engineering, Northwest Institute of Eco-Environment and Resources, Chinese Academy of Sciences, Lanzhou, Gansu, China*

[2]*University of Chinese Academy of Sciences, Beijing, China*

Meteorological records show that the warming rate of the Qinghai-Tibet Plateau(QTP) over the past five decades is twice the global average (Yao et al. 2019). The climate change has contributed to permafrost degradation and the occurrence of thaw settlement, thereby posing threats to the infrastructure of the QTP permafrost regions (Hjort et al. 2022). We defined the period from the 1900s to 2010s as the historical period, and the period between the 2020s and 2090s was regarded as the future period. Within these defined temporal domains, we thoroughly studied the spatio-temporal change characteristics of climate, permafrost distribution, and thaw settlement hazard risk in the QTP.

In the historical period, the QTP has experienced climate change processes of warming (1900s-1940s), cooling (1950s-1960s), and warming again (1970s-2020s), with the corresponding warming rates of 0.15 °C/10a, -0.30 °C/10a, and 0.22 °C/10a, respectively. For the future period, the average warming trends of the QTP under four shared socio-economic pathway (SSP) scenarios are 0.01 °C/10a (SSP1-2.6), 0.27 °C/10a (SSP2-4.5), 0.45 °C/10a (SSP3-7.0), and 0.52 °C/10a (SSP5-8.5). Overall, permafrost distribution change in the QTP is basically consistent with the climate. For example, climate warming between the 1970s and 2010s has led to a 15% decrease in permafrost area and a 6% increase in the average active layer thickness. Spatially, the Three Rivers Source area and southern Qiangtang Plateau are the regions with significant permafrost changes no matter in the warming or cooling periods.

In the baseline period (2006-2018), areas with high and very high thaw settlement hazard risk levels accounted for 12% and 2% of permafrost regions, respectively. The distribution comparison between subgrade settlement disease along the Qinghai-Tibet Highway (as shown in Wu et al. (2021)) and hazard risk level found that they were highly consistent with each other, which means that the subgrade settlement usually occurred in regions with high and very high hazard risk levels and proves the accuracy of our results. Statistical results indicate that a total of 236,000 individuals resided in regions characterized by high and very high hazard risk levels in the baseline period. Furthermore, these areas also encompassed 1997 km of highway and 494 km of railway. Our study also found that climate warming will aggravate thaw settlement hazard risk, and nearly 15% of permafrost regions are predicted to be at increased hazard risk under the SSP2-4.5 scenario in the 2050s. Spatially, regions with increased hazard risk are mainly located in the Qinghai-Tibet Engineering Corridor, Western Kunlun area, and source region of the Yellow River where permafrost engineerings are widely distributed. For the population, highway, and railway located in high and very high hazard risk regions, they will increase by 22%, 9%, and 2%, respectively, relative to the baseline period.

References

Hjort, J., Streletskiy, D., Dore, G., et al. 2022. Impacts of Permafrost Degradation on Infrastructure, Nature Reviews Earth & Environment, 3: 24–38. doi:10.1038/s43017-021-00247-8

Wu, Q., Zhang, Z., and Liu, G. 2021. Relationships Between Climate Warming and Engineering Stability of Permafrost on Qinghai-Tibet plateau (in Chinese), Journal of Engineering Geology, 29: 342–352. doi:10.13544/j.cnki.jeg.2020-084

Yao, T., Xue, Y., Chen, D., et al. 2019. Recent Third Pole's Rapid Warming Accompanies Cryospheric Melt and Water Cycle Intensification and Interactions between Monsoon and Environment: Multidisciplinary Approach with Observations, Modeling, and Analysis, Bulletin of the American Meteorological Society, 100: 423–444. doi:10.1175/BAMS-D-17-0057.1

Cold Region Engineering Modelling, Characterization, Observations & Testing

8B — Advances in Numerical Modelling of Permafrost

Session Chairs: Anna Pekinasova[1] & Brandon Karchewski[2]

[1]*Department of Civil Engineering, University of Calgary, Calgary, Alberta, Canada*
[2]*Department of Geoscience, University of Calgary, Calgary, Alberta, Canada*

Accurate forecasting of permafrost behaviour under the influence of climate change requires improvements in numerical modelling for simulation and forecasting, including variety of techniques in physics modelling, statistical modelling, and data science.

Permafrost physics modelling may include advances in finite element / difference / volume techniques for simulating the coupled behaviour under changing thermal, hydraulic, and mechanical conditions to predict aspects of ground behaviour such as thaw settlement, talik genesis, and ice lensing. Statistical modelling may include novel techniques for characterizing historical data and/or generating synthetic forecast data under various climate scenarios that may assist in providing realistic boundary conditions to numerical simulations. Data science may include advances in managing remote field data, data pre- and post-processing, and/or machine learning techniques relevant to permafrost monitoring and simulation.

In this session, we invite submissions from a broad range of science and engineering disciplines that use and apply numerical modelling techniques for understanding permafrost behaviour and soil-structure interaction.

Effects of snow and surface material on thermal regime of steep slopes

Pia Blake & Stephan Gruber

Department of Geography, Carleton University, Ottawa, Ontario, Canada

Permafrost occurs in mountains of Western Canada, from southern British Columbia and Alberta to Yukon and the Northwest Territories. Regionally, ground temperature in steep slopes is controlled by elevation, continentality, and latitude, and locally by aspect, slope angle, and ground material. We understand permafrost in near-vertical slopes in Europe and can transfer some of that insight into Canada (Stewart-Jones 2023, Stewart-Jones and Gruber 2023). By contrast, areas where some snow and soil are present have received little research despite their greater relevance in terms of surface area.

Snow warms the ground by insulation during winter, an effect that is reduced with sloughing and avalanching beyond around 40–60° (Wirz et al. 2011; Ishikawa and Sawagaki 2001). Above 60° thin snow cover has been shown to occasionally cool the ground where the effects of increased albedo prevail (Pogliotti 2011). Debris, soil, and organics can accumulate in some slopes up to 50° and above, for example in local concavities. As the water content and latent-heat storage are increase in soil (Morse et al. 2016) compared to rock, this can have additional effects on ground temperature.

On intermediate slopes (30–70°) snow and soil are heterogeneous and systematic observations sparse. This contribution investigates how soil and snow affect mean annual ground surface temperature (MAGST) and surface offset (SO) in slopes and how these effects vary with elevation, aspect, and slope.

Experiments

GEOtop (Endrizzi et al. 2014) is used to simulate ground temperatures for one-dimensional columns, driven with reanalysis data heuristically downscaled using GlobSim (Cao et al. 2019). The example shown here uses ERA5 data for Joffre Peak in British Columbia for the period 1980–2022. The full analysis will include additional locations and re-analyses.

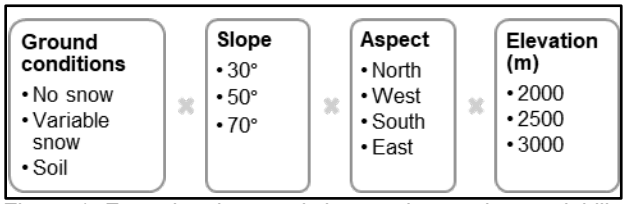

Figure 1. Four site characteristics used to explore variability by simulating the entire set of permutations.

The characteristics explored (Figure 1) were chosen to compare MAGST and SO to existing studies in steeper slopes of Western Canada, while adding lower slope angles and differing ground conditions.

Snow thickness in slopes is driven by precipitation, and overprinted by (1) the cosine of the slope angle, (2) preferential deposition based on wind and local topography, and (3) sluffing and avalanching. GEOtop accounts for (1), and the effects of (2) and (3) can be parameterized using a snow correction factor (SCF) (Pogliotti 2011), used as a multiplier for precipitation, as a first approximation. Here, variable SCF follows Equation 1. Additionally, SCFs of 0.7 for low snow and 1.2 for high snow were used for all slope angles to show cases where snow is removed at low slope angles or increased through deposition at high slope angles dependent on topography.

$$SCF = -0.02 * slope + 1.5 \quad [1]$$

Soil was modelled a 10-cm layer of loam with a volumetric water content of 25%.

Results and Discussion

SO increases with variable snow, and variable snow and soil (Figure 2). MAGST (Figure 3) decreases with increasing slope, increases with increasing snow and soil cover, and the south is warmer than the north. Snow has the largest effect at lower slope angles.

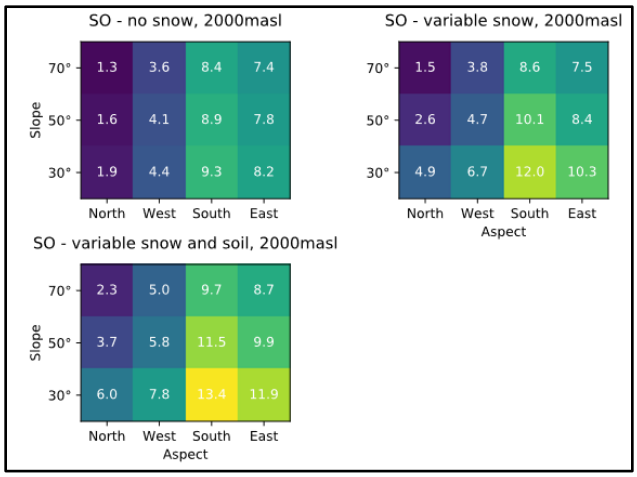

Figure 2. Surface offsets (°C) for simulations at 2000 m with various ground-covers, Joffre Peak, BC.

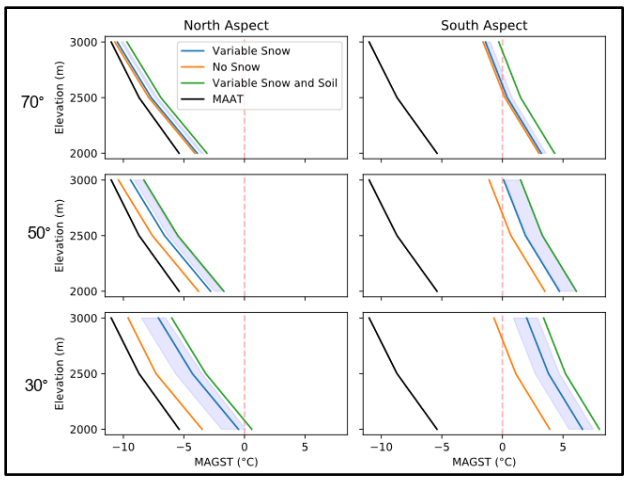

Figure 3. MAGST for different aspects, elevation, slopes, and ground covers, simulated for Joffre Peak BC. Mean Annual Air Temperature (MAAT) is shown for reference. Blue regions represent the region between low and high SCFs.

The 70° 'no snow' SO agrees with values from Stewart-Jones (2023) for steep, snow-free bedrock slopes in the South Interior region, where Joffre Peak is situated. As variable SCFs decrease with increasing slope, SO ranges from near 'snow and soil' conditions to 'no snow' conditions.

SOs are greatest on southern aspects, and smallest on northern aspects, with the largest SOs occurring in variable snow and soil combined. Soil increases the warming effect of snow, even as a thin layer. In the absence of snow and soil, SO only decreases slightly with slope angle. With increasing slope angle and snow present, MAGST approaches MAAT lines in northern aspects.

MAGSTs encompassed by the low and high SCFs center on variable snow MAGSTs at lower slope angles and move towards variable snow and soil cover with increasing slope angles. This shows how snow accumulating in concave sections of topography may impact the ground thermal regime.

REFERENCES

Cao, B., Quan, X., Brown, N., Stewart-Jones, E., and Gruber, S. 2019. GlobSim (v1.0): deriving meteorological time series for point locations from multiple global reanalyses. Geoscientific Model Development, 12(11), 4661–4679.

Endrizzi, S., Gruber, S., Dall'amico, M., and Rigon, R. 2014. GEOtop 2.0: simulating the combined energy and water balance at and below the land surface accounting for soil freezing, snow cover and terrain effects. Geoscientific model development, 7, 2831–2857.

Ishikawa, M., and Sawagki, T. 2001. GIS-simulation of the spatial distribution of snow cover and observed ground temperatures in the Daisetsu Mountains, Japan. Norsk Geografisk Tidsskrift - Norwegian Journal of Geography, 55, 212–218.

Morse, P.D., Wolfe, S.A., Kokelj, S.V., and Gaanderse, A.J.R. 2016. The Occurrence and Thermal Disequilibrium State of Permafrost in Forest Ecotopes of the Great Slave Region, Northwest Territories, Canada: Discontinuous permafrost conditions, Great Slave region, NWT, Canada. Permafrost and periglacial processes, 27, 145–162.

Pogliotti, P. 2011. Influence of snow cover on MAGST over complex morphologies in mountain permafrost regions. PhD, University of Turin.

Stewart-Jones, E. 2023. Modelling surface offsets in rock walls of western Canada. MSc, Carleton University.

Stewart-Jones, E., and Gruber, S. 2023. Transferring Cryosphere Knowledge between Mountains Globally: A Case Study of Western Canadian Mountains, the European Alps and the Scandes. Journal of Alpine Research, 111(2).

Wirz, V., Schirmer, M., Gruber, S., and Lehning, M. 2011. Spatio-temporal measurements and analysis of snow depth in a rock face. The cryosphere, 5, 893–905.

Predicting permafrost presence using an easy to use, adaptable, and scalable machine learning approach

Ghislain de Laplante[1], Elliott Skierszkan[2] & Clément Bataille[1]

[1]*Department of Earth and Environmental Sciences, University of Ottawa, Ottawa, Ontario, Canada*

[2]*Department of Earth Sciences, Carleton University, Ottawa, Ontario, Canada*

Permafrost plays fundamental roles in the Arctic as stable substrate for construction, carbon and pollutant reservoir or hydrological barrier. Permafrost distribution on the landscape varies at high spatial resolution with the influence of local topography, solar exposure, slope, geological substrate, and climate conditions. With the warming of northern latitudes, permafrost is also thawing at an accelerated rate threatening the fragile equilibrium in northern ecosystems. Developing approaches to predict the spatial distribution of permafrost is, therefore, paramount to the sustainability of the north. Currently, only large-scale, low-resolution permafrost distribution maps exist for high latitudes in Canada (Natural Resources Canada 1995; Obu et al. 2019) along with one medium-resolution (30 m^2) model specific to Yukon (Bonnaventure et al. 2012).

While useful for large-scale applications, these low-resolution maps fail to capture the high-resolution patterns of permafrost that are pivotal to understanding local biogeochemical cycles. For example, in west-central Yukon, an area rich in mineral resources, exploration companies and regulators rely on local field surveys to map permafrost distribution at a sufficient resolution for geological, geochemical, and biological research and regulatory oversight. To address the gap between global models and more detailed local surveys, we leverage a novel machine-learning classification approach to map permafrost distribution at high-resolution (~16 m^2) across the west-central portion of Yukon.

We used as training data for the classification a high-resolution, 90 km^2 map produced by extensive field observations and remote-sensing indicators of permafrost distribution and relative ice content produced by Newmont Mining for the Coffee Creek gold mining prospect. This map classifies permafrost into four categories (unfrozen, ice-poor, ice-rich, very ice-rich) and we sampled 10 000 points per category at random to serve as training data. The predictions were then applied over a region that maintains similar topographic and climatic conditions as well as glaciation history as the training area.

We considered a series of geomorphological variables known or suspected of influencing permafrost distribution and ground ice content. Given the small extent of our area of interest we used the ~16 m^2 resolution (at the study site) Canadian Digital Elevation Model (Natural Resources Canada 2013) to calculate these terrain variables. In addition, recognising the key influence of solar radiation, we calculated annual incoming solar radiation across the modelled area using an algorithm that factors in the surrounding land surface and the variable solar elevation and radiative flux throughout the year (Fu and Rich 2002).

To determine which machine learning algorithm and parameterization yielded the most accurate classification, we automated the testing and parameterization of multiple random forest algorithms. In this case study, the *ranger* random forest classification model (Wright and Ziegler 2017) was the most accurate with an overall accuracy of 0.7959 (95% CI: 0.776 – 0.8134).

Table 2. Permafrost model test statistics by class. Training was performed on 70% of data points derived from the mapped polygons with the remaining 30% reserved for testing.

	Ice-poor	Ice-rich	Very ice-rich	Unfrozen
Sensitivity	0.70	0.75	0.62	0.90
Specificity	0.90	0.90	0.999	0.91
Pos pred value	0.76	0.72	0.87	0.87
Neg pred value	0.87	0.91	0.995	0.93
Balanced accuracy	0.80	0.82	0.81	0.90

Our approach was able to predict permafrost presence and relative ice content of frozen ground with high accuracy relative to the training dataset and was highly accurate compared to on the ground observations both within and outside of the training dataset region. Most importantly, we were able to predict exact locations with permafrost and their relative ice-richness, in contrast to previous mapping efforts limited to regional permafrost prevalence.

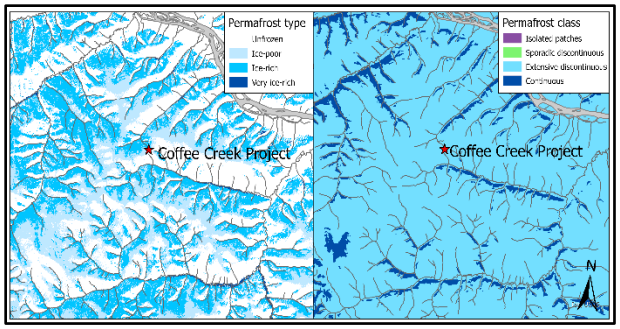

Figure 1. Machine learning output (left) compared to Bonnaventure (2012) modelled permafrost class (right). The machine learning model can predict permafrost occurrence and type with high accuracy at the resolution of the input variables, rather than classifying by general permafrost prevalence.

Based on this successful pilot study and recognizing the potential for our methodology to predict permafrost occurrence at regional scales as well as its applicability to other spatial prediction problems, we have generalized and streamlined our workflow into an R package. This workflow facilitates the integration of new training data from other regions either as points or polygons as well as incorporation of other spatial classifiers (e.g., other geospatial variables or remote sensing products). The refined software can predict categorical or continuous outcomes, accepts point or polygon observations as training data, and can be used to select the best-performing model and model parameterisation from user-specified options.

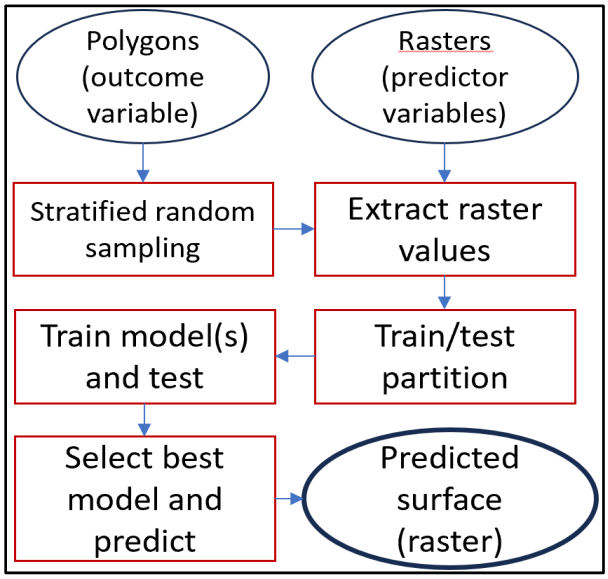

Figure 2. Simplified workflow. Optional steps (not shown) include discarding superfluous variables using random forest selection and running multiple algorithms on down-sampled data; the best model is then run with complete data.

This novel classification tool fills the gap between local data and global permafrost model allowing researchers to leverage existing field surveys into mapping permafrost at ultra high-resolution over regional to continental scales. This framework should considerably enhance the possibility to incorporate permafrost impacts in infrastructure, geological, environmental, and hydrological research in the north increasing the sustainability of northern communities and ecosystems.

REFERENCES

Bonnaventure, P.P., Lewkowicz, A.G., Kremer, M., and Sawada, M.C. 2012. A Permafrost Probability Model for the Southern Yukon and Northern British Columbia, Canada. Permafrost and Periglacial Processes, 23(1), 52–68. https://doi.org/10.1002/ppp.1733

Fu, P., and Rich, P.M. 2002. A geometric solar radiation model with applications in agriculture and forestry. Computers and Electronics in Agriculture, 37(1–3), 25–35. https://doi.org/10.1016/S0168-1699(02)00115-1

Natural Resources Canada. 1995. Canada Permafrost (5th ed.) [Map]. Government of Canada. https://open.canada.ca/data/en/dataset/d1e2048b-ccff-5852-aaa5-b861bd55c367

Natural Resources Canada. 2013. Canadian Digital Elevation Model (1.1) [Map]. Government of Canada. https://open.canada.ca/data/en/dataset/7f245e4d-76c2-4caa-951a-45d1d2051333

Obu, J., Westermann, S., Bartsch, A., Berdnikov, N., Christiansen, H.H., Dashtseren, A., Delaloye, R., Elberling, B., Etzelmüller, B., Kholodov, A., Khomutov, A., Kääb, A., Leibman, M.O., Lewkowicz, A.G., Panda, S.K., Romanovsky, V., Way, R.G., Westergaard-Nielsen, A., Wu, T., et al. 2019. Northern Hemisphere permafrost map based on TTOP modelling for 2000–2016 at 1 km^2 scale. Earth-Science Reviews, 193, 299–316. https://doi.org/10.1016/j.earscirev.2019.04.023

Wright, M.N., and Ziegler, A. 2017. Ranger: A Fast Implementation of Random Forests for High Dimensional Data in C++ and R. Journal of Statistical Software, 77(1). https://doi.org/10.18637/jss.v077.i01

Determining TTOP model parameter importance and TTOP model performance across western Canada

Madeleine Garibaldi[1], Philip Bonnaventure[1], Robert Way[2] & Alexandre Bevington[3]

[1]*Department of Geography and Environment, University of Lethbridge, Lethbridge, Alberta, Canada*

[2]*Department of Geography and Planning, Queen's University, Kingston, Ontario, Canada*

[3]*Ministry of Forests, Lands, and Natural Resource Operations, Government of British Columbia, Prince George, British Columbia, Canada*

The temperature at top of permafrost (TTOP) model is a commonly used equilibrium permafrost model due to its simplicity and transferability across a wide variety of landscapes and permafrost conditions without recalibration. One of the primary challenges of using the TTOP model is determining the values of the scaling factors (N-factors) and soil thermal conductivities which are typically assigned based on field measurements or values presented in the literature. However, few studies have examined the uncertainties, which arise from mischaracterization of TTOP model parameters on the model output. Additionally few studies have looked at the relative importance of each parameter in different permafrost environments using non theoretical data. This study evaluated the sensitivity of TTOP model parameters and permafrost temperature output using a method similar to leave one out cross validation across north-western Canada using in situ data.

Objective

The objective of this study is to determine the performance of the TTOP model across differing environments in western Canada. To accomplish this the sensitivity of each model parameter is examined in each unique environment.

Study area

Sites ranged across western Canada from the High Arctic (Eureka) to Northern British Columbia (Atlin), covering a variety of ecosystems from tundra vegetation to mature mixed spruce forests, and from continuous to sporadic discontinuous permafrost.

Methods

Air, ground surface and ground temperature at depth measurements were recorded hourly or bi-hourly (on even hours) at 193 sites. Record lengths range from 2-16 years. Air temperature was measured about 1.5 meters above the ground surface while ground surface temperature was measured 2-5 cm below the ground surface. Baseline input parameters for the TTOP model and the reference TTOP value were calculated for each site (Equation 1).

$$TTOP = \frac{(rk*nt*TDDa)-(nf*FDDa)}{365} \quad [1]$$

For each year and each site, freezing (FDD) and thawing degree days (TDD) were calculated using daily average air (T_a) and ground surface temperatures (T_s) from September 1st to August 31st of the subsequent year. Following this, freezing (nf) and thawing (nt) N-factors, were calculated for each site. The thermal conductivity (rk) for sites with a depth temperature measurement was calculated using FDD and TDD for both the ground surface (s) and shallow ground depth (g). Once the parameters and reference TTOP value were calculated the sensitivity of the model to changes in each parameter was assessed using a method similar to leave one out cross validation, whereby each parameter was iteratively substituted to assess the changes in the output result. Different methods were used for determining the value to substitute for perturbation. The first method was the direct substitution of selected percentiles (minimum, 5th, 25th, 50th, 75th, 95th and maximum) for each variable determined using he entire dataset. For this method, the tested parameter was assigned the same value at all sites. Additionally, the new value for each parameter was based on the range and values measured in the dataset. For the second method, the new parameter values were determined through a percentage change of the original parameter value. Therefore, for this method the parameter value at each individual site was altered by a magnitude proportional to the initial parameter value for this analysis, each year of data for each site was treated as its own observation and run through the sensitivity analysis resulting in 683 observations. The resulting outputs were then compared to the reference TTOP value to assess the sensitivity of the model to changes in each parameter.

Results

Overall, the TTOP model was most sensitive to changes in freezing parameters nf and FDDa, and least

sensitive to changes in thawing parameters TDDa, nt and rk (Figure 1). However, the importance of specific parameters varied regionally. Regionally the model was most sensitive to changes in the freezing parameters at the more northern regions with an overall increase in sensitivity to the thawing parameters moving south (Figure 2).

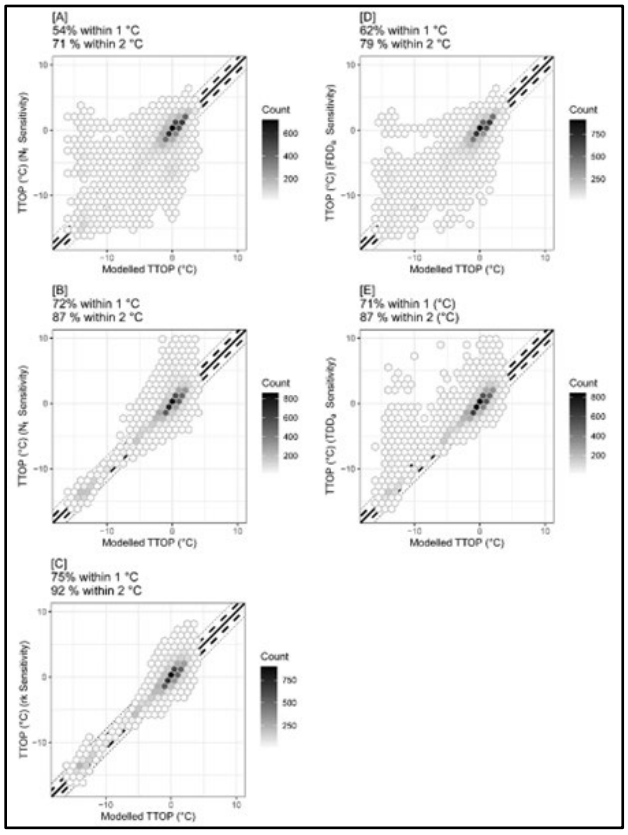

Figure 1. Reference temperature at top of permafrost (TTOP) model values compared to perturbed TTOP model values for all TTOP sensitivity trials for [A] nf, [B] FDDa, [C] nt, [D] TDDa, and [E] rk. Large dashes indicate a ± 1 °C difference while small dashes indicated a ± 2 °C difference.

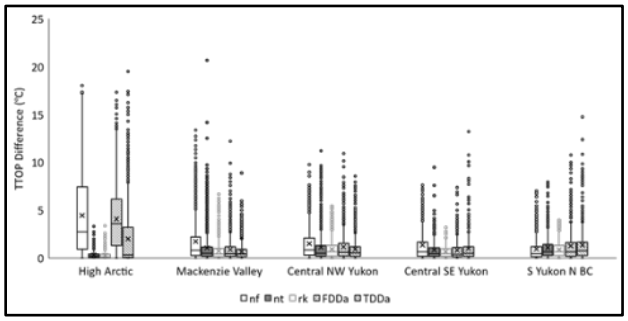

Figure 2. Boxplots for the regional absolute difference between the reference TTOP and the TTOP calculated when parameters were increased or decreased by an assigned amount.

This followed trends in the magnitude difference between FDDa and TDDa. Specifically, where the magnitude of FDDa was much greater than TDDa, the model was most sensitive to changes in freezing parameters and had minimal response to changes in thawing parameters. However, as TDDa became comparable to FDDa the sensitivity to thawing parameters increased. When tested against measured annual mean ground temperature (AMGT), the TTOP model performed well overall likely due to the use of measured in situ data.

The sensitivity and variable importance results using in situ data both supported and refined findings of previous studies, which were based only on theoretical inputs. However, the use of field measured data also provided some additional insight into the relative importance of each parameter. TDDa in the High Arctic region was elevated in importance compared to the other northern regions likely as a result of limited vegetation cover. The findings from this study can aid in parameterization efforts and parameter selection based on modelling location and scale. For example, in locations where FDDa is much greater than TDDa, the impact of incorrect classification of nt, rk, and TDDa was shown to be minimal and therefore, more general assumptions and classifications will not result in a substantial increase in uncertainty or error. As FDDa and TDDa become more similar, generally at locations farther south, the sensitivity of the model to changes in thawing parameters is elevated and accurate classification of nt and rk become more important.

The results of this study highlight the importance of correct parameterization, specifically of the freezing parameters in small-scale national or circumpolar modelling studies, and the increased importance of parameterization of the thawing parameters in locations where the magnitude of FDDa and TDDa are similar. Although these conclusions had been theorized previously the use of a robust network of in situ data to support these assumptions was necessary. Ultimately, the findings of this study help future modelling studies determine parametrization allocation effort based on location and scale and may help explain sources of error and uncertainty in modelled results.

Improving plot-scale prediction of future permafrost change by reducing the bias in climate model-derived driving data

Galina Jonat[1], Alex Cannon[2] & Stephan Gruber[1]

[1]*Department of Geography and Environmental Studies, Carleton University, Ottawa, Ontario, Canada*

[2]*Environment and Climate Change Canada, Victoria, British Columbia, Canada*

Climate-sensitive decisions in the context of permafrost thaw can benefit from seasonal, inter-annual and decadal predictions of relevant permafrost variables at the regional and local scale. Knowledge of the past and projected future states of permafrost enables us to minimize impacts on the natural environment and informs the design of resilient infrastructure (Smith et al. 2022).

Permafrost predictions rely on permafrost models driven by climate model output. However, their coarse grid resolution (tens to hundreds of kilometers), as well as biases and uncertainties arising from internal variability, model inaccuracies, and scenarios (Hawkins and Sutton 2009), can limit their utility for local-scale permafrost studies. This shortcoming can be mitigated by pre-processing climate-model data before using it to drive permafrost models.

The most common pre-processing approach is to bias-correct climate-model data using local observations. As consistent, multi-variable, and long-term observations of climate are sparse in most locations with permafrost, reanalysis data is used instead. Reanalyses are numerical weather prediction models corrected with observations through data assimilation, where available. These reanalyses are themselves subject to uncertainty.

In this study, we present a framework to reduce and quantify the bias from climate model output data and its impact on permafrost simulation results. We compare the quality of de-biased climate model data and investigate whether the best-matched atmospheric time series results in the best-matched permafrost simulations.

Methods and data

The presented approach consists of four steps: (1) downscaling of reanalysis data, (2) de-biasing of daily climate-model output using the reanalysis data, (3) temporal disaggregation of de-biased climate model data, and (4) assessment of processed climate model output and the resulting permafrost simulation results.

As an example, we bias-correct eight climate variables from CanESM2 climate model output for a location near Lac de Gras, Northwest Territories. This area features several water bodies which influence the local climate. We use ERA5 reanalysis data as a reference.

Step 1 uses the software toolkit Globsim, which topographically interpolates and adjusts the reanalysis data to a point scale, addressing the low resolution of reanalysis data and local topography.

Step 2 follows Cannon (2018), performing de-biasing with four algorithms. Univariate quantile delta mapping (QDM) aligns the marginal distributions of each model variable with the reference dataset. The multivariate bias correction (MBC) algorithms MBCp, MBCr and MBCn additionally account for inter-variable dependencies by also correcting Pearson correlation, Spearman rank correlation, and the full multivariate distribution, respectively.

Step 3 makes use of the Teddy-Tool (Zabel and Poschlod 2023) adapted to the needs of this study. For every modelled day, this tool finds the most similar meteorological day at the same time of year in the reference dataset, based on precipitation and a simple rank-sum approach. It then extracts sub-daily patterns from that reference day and applies them to the daily mean of the climate model data. This ensures that seasonal patterns and sub-daily inter-variable dependencies are accounted for. The adaptation includes pre- and post-processing steps for precipitation to remove drizzle bias and to filter days with little or no precipitation. We use the resulting hourly data to drive the permafrost model GEOtop by Endrizzi et al. (2014).

Finally, Step 4 measures the overall model performance. As the climate model is designed to match long-term climatologies and not constrained to be temporally synchronous with observations, we assess the distributions of variable values, rather than using temporally synchronous error statistics. For this, we employ energy distance (D^2) (Rizzo and Székely 2016), a commonly used metric in this context.

Results

Examples of the improved alignment in marginal distributions of climate variables can be seen in the top panels of Figure 1. Looking at air temperature, the warm bias from the climate model is reduced. In precipitation, the extremes are removed and the bias towards more days with no precipitation is reduced.

Turning our attention to Table 1, the cumulative D^2 calculated for 3000 sample days summarizes the alignment of all climate forcing variables' distributions and accounts for the representation of inter-variable dependencies. By only aligning marginal distributions, the cumulative energy distance is improved by 90%. Including inter-variable dependencies further improves energy distance by another ~65%. The same improvement is evident in the mean absolute error (MAE) of the inter-variable correlation matrices (IVC) which is decreased by an order of magnitude.

This improvement does, however, not directly translate to an improvement in modeling ground surface temperature (GST) and thaw depth, summed up in Table 1 and Figure 1. Distributions of GST in MBCn and QDM-driven simulations align worse with GST driven by ERA5 than the original climate model. Considering thaw depth, the distribution alignment looks different as all bias-corrections reduce the energy distance by at least 50%. In both variables, MBCp-corrected climate forcing yield the best-fitting permafrost simulations in the demonstrator case.

Table 1. Performance metrics per debiasing algorithm, for climate forcing, GST, and thaw depth.

	CanESM2	QDM	MBCp	MBCr	MBCn
$D^2\,[10^{-3}]$					
Climate forcing, cumulative	54.202	4.118	1.339	1.416	1.271
MAE(IVC), climate forcing	0.080	0.074	0.006	0.020	0.008
$D^2\,[10^{-3}]$					
GST	1.67	4.02	1.70	0.77	4.47
Thaw Depth	10.88	5.27	2.05	1.27	6.35

Conclusion and Next Steps

The presented approach enables the consistent preparation and quality assessment of climate forcing data for local permafrost models that can be used to predict future change. Given a level of confidence in the reference dataset, this reduces the uncertainty introduced by low model resolution which is important when predicting permafrost change at the local scale. When selecting climate driving data, the impact of bias correction needs to be assessed on the permafrost model level, as an overall better performance in representation of climate forcing does not necessarily yield an overall better performance in permafrost modelling.

Next steps include testing debiasing-data-simulation pairings across a larger number of permafrost variables, across several soil types, and including different permafrost models.

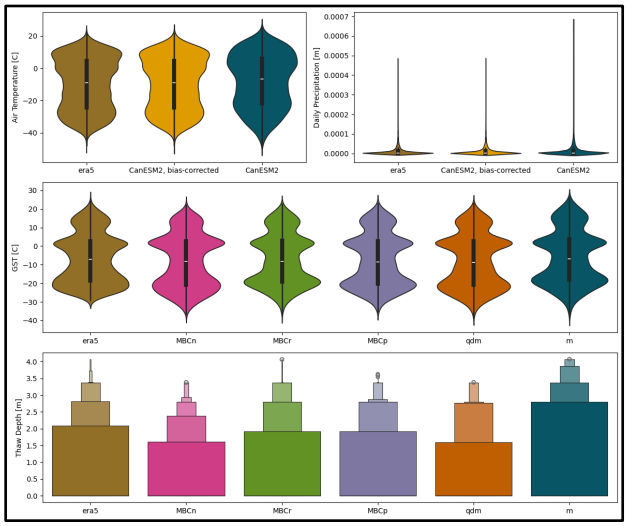

Figure 1. Marginal distributions of daily air temperature and precipitation and modelled daily GST (expressed in violin plots) and thaw depth (expressed in an enhanced box plot). Bias-corrected climate variable distribution is shown for CanESM2 (m), ERA5 as reference data, and the bias-corrected marginal distributions. ERA5 and ERA5-driven data are used as a reference to measure success.

References

Cannon, A.J. 2018. Multivariate quantile mapping bias correction: an N-dimensional probability density function transform for climate model simulations of multiple variables. Climate Dynamics, 50(1–2), 31–49. doi:10.1007/s00382-017-3580-6

Hawkins, E., and Sutton, R. 2009. The potential to narrow uncertainty in regional climate predictions. Bulletin of the American Meteorological Society, 90(8), 1095–1107. doi:10.1175/2009BAMS2607.1

Rizzo, M.L., and Székely, G.J. 2016. Energy distance, WIREs Computational Statistics, 8, 27–38. doi:10.1002/wics.1375

Smith, S.L., O'Neill, H.B., Isaksen, K., Noetzli, J., and Romanovsky, V.E. 2022. The changing thermal state of permafrost. Nature Reviews Earth and Environment, 3(1), 10–23. doi:10.1038/s43017-021-00240-1

Zabel, T., and Poschlod, B. 2023. The Teddy tool v1.1: temporal disaggregation of daily climate model data for climate impact analysis, Geoscientific Model Dev, 16, 5383–5399. doi:10.5194/gmd-16-5383-2023

Modeling the effects of pore-water phase change on ice-wedge cracking

Gabriel Karam[1], Mehdi Pouragha[1] & Stephan Gruber[2]

[1]*Department of Civil and Environmental Engineering, Carleton University, Ottawa, Ontario, Canada*

[2]*Department of Geography, Carleton University, Ottawa, Ontario, Canada*

Ice-wedges are a widespread periglacial feature in the continuous permafrost zones, formed by the repetition of thermal contraction-cracking and infilling of the crack with water. We focus on the thermal contraction-cracking process, which is controlled by the tensile stress generated by the soil. Many environmental factors, such as soil type and air temperature, affect the stress regime, and are well-documented in field research (Mackay 1992; Allard and Kasper 1998; Matsuoka et al. 2018).

Thus far, the effect of the freezing volumetric expansion (FVE) of porewater in soil has not been investigated, as it is difficult to isolate in-situ. For saturated soils of typical porosity, the expansion is around 3% of the total soil volume and can be greater for other soils such as organics.

We present a numerical model to simulate the initial thermal contraction-cracking process in permafrost and identify the effects of the FVE on the ground stress regime.

The model employs the finite element method (FEM), and ground-surface temperatures are imposed on the model surface to drive the thermal contraction-cracking process.

Four soil types with varied particle-size distributions are used in conjunction with four temperature series with different mean annual ground-surface temperatures (MAGST) to perform parametric studies. The selection/calibration of soil material properties was performed using existing laboratory test data.

Apparent coefficient of thermal expansion

Similar to the apparent thermal capacity used to represent latent heat as a component of sensible heat during the freezing and thawing of soils, the apparent coefficient of thermal expansion (CTE) considers the FVE as a component of the CTE already present as a soil property in the numerical model. In the simulation, we use two different CTEs- the first does not account for the FVE and is denoted by α. The second coefficient, α_{FVE}, adds the effect of the FVE to α as shown in Eq. 1.

$$\alpha_{FVE} = \alpha + (-0.09)\,\frac{d\theta_u}{dT} \qquad [1]$$

where θ_u is the proportion of unfrozen water present in the soil and (-0.09) denotes the additional 9% volumetric change upon freezing or melting of water.

Results and discussion

The chosen test metric related to thermal contraction-cracking is tensile stress, expressed as a percentage of the soil fracture strength. This is referred to herein as the “cracking potential”.

The CTE was found to have a pronounced effect on the cracking potential, with an average increase of 41% using α_{FVE} compared to simulations using α.

Despite the non-linearities introduced by the material properties, there is an almost-linear relation between the MAGST at a simulated site and the cracking potential. Relating the above difference in cracking potential to the MAGST of each site shows a difference of roughly 3°C between α and α_{FVE}. This shows that the consideration of the FVE has a significant effect on the model output.

It is hypothesized that the FVE causes increased tensile stress through the sequential expansion with depth and stiffening of the above soil as the freezing front permeates downwards through the active layer.

References

Mackay, J.R. 1992. The frequency of ice-wedge cracking (1967–1987) at Garry Island, western Arctic coast, Canada. Canadian Journal of Earth Sciences, 29(2): 236–248.

Allard, M., and Kasper, J.N. 1998. June. Temperature conditions for ice wedge cracking: field measurements from Salluit, northern Québec. In Permafrost, Proceedings, 7th International Conference, Yellowknife, Canada, Centre d’etudes nordiques, Universite Laval, Collection Nordicana, 57: 5–11.

Matsuoka, N., Christiansen, H.H., and Watanabe, T. 2018. Ice-wedge polygon dynamics in Svalbard: Lessons from a decade of automated multi-sensor monitoring. Permafrost and Periglacial Processes, 29(3): 210–227.

A history of cryohydrogeology modeling and recent advancements through the integration of solute transport

Barret L. Kurylyk[1], Julia A. Guimond[2], Aaron M. Mohammed[3], Victor F. Bense[4], Jeffrey M. McKenzie[5], Michelle A. Walvoord[6], Rob C. Jamieson[1] & Bailey Strong[1]

[1]*Department of Civil and Resource Engineering, Dalhousie University, Halifax, Nova Scotia, Canada*

[2]*Applied Ocean Physics & Engineering, Woods Hole Oceanographic Institution, Woods Hole, Massachusetts, United States*

[3]*Department of Earth and Environmental Sciences and Department of Civil and Environmental Engineering, Syracuse University, Syracuse, New York, United States*

[4]*Hydrology and Environmental Hydraulics, Wageningen University, Wageningen, the Netherlands*

[5]*Department of Earth and Planetary Sciences, McGill University, Montreal, Quebec, Canada*

[6]*U.S. Geological Survey, Water Resources Mission Area, Lakewood, Colorado, United States*

Groundwater flow systems and permafrost are interrelated because permafrost thaw enhances permeability, while groundwater flow can advect heat and accelerate permafrost thaw (McKenzie et al. 2021). Given amplified climate change in cold regions, there is renewed interest in 'cryohydrogeology', the study of groundwater in cold regions. Many data-driven studies have shown that permafrost thaw is leading to activated aquifers and increased baseflow across the Arctic (e.g., Walvoord and Striegl 2007; Evans et al. 2020). Empirical evidence of a subsurface 'replumbing' (Walvoord and Kurylyk 2016) in permafrost regions raises questions about the fate of sequestered contaminants in the North (Langer et al. 2023). We will discuss the history of and emerging opportunities in cryohydrogeological modeling, with a focus on recent contaminant transport modeling.

History and recent developments in cryohydrogeological modeling

1D cold-region groundwater models began emerging in the 1970s to support northern development (e.g., Harlan 1973). Although these research themes combined knowledge from both hydro(geo)logy and geotechnical (permafrost) engineering, many of the early models were developed in distinct disciplines (Kurylyk and Watanabe 2013), leading to redundancy and a failure to integrate knowledge across spheres. With the increase in computational capacity, 2D and 3D cryohydrogeology models began to emerge in the 2000s (e.g., Bense et al. 2009; McKenzie et al. 2007). These models advanced traditional groundwater models by coupling partial differential equations (PDEs) for groundwater flow and heat transfer, with the latter accommodating the latent heat of freeze-thaw. These equations are linked through several processes: (1) the control of temperature on the ground ice distribution and the effective permeability field, (2) the influence of groundwater flow on heat advection and thus permafrost distribution, and (3) the impacts of pore ice on bulk thermal properties. Early multi-dimensional cryohydrogeology models were restricted to saturated medium, but more recent models allow for variably saturated conditions (e.g., Jan et al. 2020). Many cryohydrogeology models were benchmarked through the InterFrost program (Rühaak et al. 2015; Grenier et al. 2018), enabling more collaboration across countries and disciplines (geology, engineering, computer science).

Ongoing challenges

Despite recent advances in cold-regions groundwater modeling, there are challenges that limit the application and utility of these models. First, the non-linear nature of the groundwater flow equation (with permeability dependent on total saturation and ground ice) makes simulation run times prohibitive for most 3D modeling applications. There are efforts to overcome these limitations through massively parallel computing (Orgogozo et al. 2023). Also, several cryohydrogeology model boundary and initial condition concepts are not included in standard groundwater modeling guidelines (Reilly 2001). These include model spin-up time for permafrost generation, the permafrost base depth, geothermal heat fluxes, snow cover dynamics, and temporally focused recharge (snowmelt) in low-permeability frozen soils (Lamontagne-Hallé et al. 2020).

Another ongoing challenge is the lack of solute transport in most cryohydrogeological models and associated knowledge gaps in cold-region contaminant transport. Given the numerical challenges with integrating a reactive transport equation within an existing cryohydrogeological model, Frampton and Destouni (2015) used particle tracking to investigate groundwater travel times under different permafrost degradation scenarios and demonstrated the impact of deepening flow paths due to active layer thaw. More

recently, Mohammed et al. (2021) enhanced a previous cryohydrogeological model within the generic PDE solving framework FlexPDE (Bense et al. 2009) to accommodate reactive solute transport. Their results showed the control of permafrost distributions and transport parameters on plume migration for conservative, degrading, and sorbing solutes. Guimond et al. (2021) included new solute exclusion and solute-dependent freeze-thaw dynamics in FlexPDE, and demonstrated that sea-level rise could lead to saltwater intrusion into Arctic coastal aquifers and trigger the thaw of frozen ground through freezing point depression.

In addition to providing new insight into cold-region contaminant dynamics, these recent modeling studies have highlighted two key challenges associated with contaminant transport modeling in northern groundwater systems. (1) We lack sufficient field or laboratory studies of contaminant transport in cold regions to help parameterise, calibrate, and assess our models. (2) Prohibitive model run times still impede theoretical progress on this topic, but these challenges may be partially overcome through parallel computing.

Acknowledgements

Portions of this research presented was funded by the Government of NWT, the Natural Sciences and Engineering Research Council of Canada (Alliance program), and the National Science Foundation.

References

Bense, V.F., Ferguson, G., and Kooi, H. 2009. Evolution of shallow groundwater flow systems in areas of degrading permafrost, Geophysical Research Letters, 36: L22401. doi:10.1029/2009GL039225

Evans, S.G., Yokeley, B., Stephens, C., and Brewer, B. 2020. Potential mechanistic causes of increased baseflow across northern Eurasia catchments underlain by permafrost, Hydrological Processes. 34: 2676–2690. doi:10.1002/hyp.13759

Frampton, A., and Destouni, G. 2015. Impact of degrading permafrost on subsurface solute transport pathways and travel times, Water Resources Research, 51: 7680–7701. doi:10.1002/2014WR016689

Grenier, C., Anbergen, H., Bense, V.F. et al. 2018. Groundwater flow and heat transport for systems undergoing freeze-thaw: Intercomparison of numerical simulators for 2d test cases, Advances in Water Resources, 114: 196-218. doi:10.1016/j.advwatres.2018.02.001

Guimond, J.A., Mohammed, A.A., Walvoord, M.A., Bense, V.F., and Kurylyk, B.L. 2021. Saltwater intrusion intensifies coastal permafrost thaw. Geophysical Research Letters, 48: e2021GL094776. doi:10.1029/2021GL094776

Harlan, R.L. 1973. Analysis of coupled heat-fluid transport in partially frozen soil, Water Resources Research, 9(5): 1314–1323. doi:10.1029/WR009i005p01314

Jan, A., Coon, E.T., and Painter, S.L. 2020. Evaluating integrated surface/subsurface permafrost thermal hydrology models in ATS (v0.88) against observations from a polygonal tundra site. Geoscience Model Development, 13(5): 2259–2276. doi:10.5194/gmd-13-2259-202

Kurylyk, B.L., and Watnabe, K. 2013. The mathematical representation of freezing and thawing processes in variably-saturated, non-deformable soils, Advances in Water Resources, 60: 160–177. doi:10.1016/j.advwatres.2013.07.016

Lamontagne-Hallé, P., McKenzie, J.M., Kurylyk, B.L., Molson, J., and Lyon, L.N. 2020. Guidelines for cold-regions groundwater numerical modeling. WIREs Water, 7: e1467. doi:10.1002/wat2.1467

Langer, M., von Deimling, T.S., Westermann, S. et al. 2023. Thawing permafrost poses environmental threat to thousands of sites with legacy industrial contamination, Nature Communications, 14: 1721. doi:10.1038/s41467-023-37276-4

McKenzie, J.M., Voss, C.I., and Siegel, D.I. 2007. Groundwater flow with energy transport and water-ice phase change: Numerical simulations, benchmarks, and application to freezing in peat bogs, Advances in Water Resources, 30(40): 966–983. doi:10.1016/j.advwatres.2006.08.008

McKenzie, J.M., Kurylyk, B.L., Walvoord, M.A., Bense, V.F., Fortier, D., Spence, C., and Grenier C. 2021. Invited perspective: What lies beneath a changing Arctic? The Cryosphere, 15(1): 479–484. doi:10.5194/tc-15-479-2021

Mohammed, A.A., Bense, V.F., Kurylyk, B L., Jamieson, R.C., Johnston, L.H., and Jackson, A.J. 2021. Modeling reactive solute transport in permafrost-affected groundwater systems. Water Resources Research, 57: e2020WR028771. doi:10.1029/2020WR028771

Orgogozo, L., Xavier, T., Oulbani, H., and Grenier, C. 2023. Permafrost modeling with OpenFOAM: the permaFoam solver. Computer Physics Communications 282: 108541. doi:10.1016/j.cpc.2022.108541

Reilly, T.E. 2001. System and Boundary Conceptualization, in Ground-Water Flow Simulation, in Techniques of Water-Resources Investigations of the U.S. Geological Survey, Book 3, Applications of Hydraulics, Chapter B8, U.S. Geological Survey, Reston, Virginia.

Rühaak, W, Anbergen, H., Grenier, C. et al. 2015. Benchmarking numerical freeze/thaw models, Energy Procedia, 76: 301–310, doi:10.1016/j.egypro.2015.07.866

Walvoord, M.A., and Striegl, R.G. 2007. Increased groundwater to stream discharge from permafrost thawing in the Yukon River basin: Potential impacts on lateral export of carbon and nitrogen, Geophysical Research Letters, 34. doi:10.1029/2007GL030216

Walvoord, M.A., and Kurylyk, B.L. 2016. Hydrologic impacts of thawing permafrost – A review, Vadose Zone Journal, 15(6). doi:10.2136/vzj2016.01.0010

Development and demonstration of a statistical ranking framework for ground temperature models, tailored towards permafrost environments

Hannah Macdonell & Stephan Gruber
Geography and Environmental Studies, Carleton University, Ottawa, Ontario, Canada

Until recently, the advancement of permafrost modelling has been limited by sparse data for both driving models (surface forcing observations) and evaluating model predictions (observations of the predicted variable). The emergence of reanalysis data products, along with permafrost data sharing and inter-operability, has extended modelling to locations without weather data and led to an increased amount of data in permafrost regions. With this, our capacity to assess modelling applications should also improve, but unfortunately, there exist few systematic approaches for doing so.

Ranking framework

This study proposes a ranking framework to address challenges in evaluating models and serves as an intermediate step towards standardizing the interpretation and comparison of model performance using large observational datasets. There is disagreement in modeling literature regarding which performance metrics to use for ground temperatures and the selection of metrics varies widely. To address this issue, we suggest combining three specific metrics that are suitable for ground temperatures. This framework summarizes model performance using ranks instead of statistical values for clarity. To expose the effects of sparse and short observations and reduce potential bias, a bootstrap method is employed.

The ranking framework is demonstrated using observations and simulations of ground-surface temperature (GST) at three clusters in Figure 1.

Producing simulations for evaluation

GST simulations were produced for plots at three clusters across the Northwest Territories, shown in Figure 1 using GEOtop (Endrizzi et al. 2014). Driving data for simulations include the reanalyses JRA-55, MERRA-2, and ERA-5 (Gelaro et al. 2017; Hersbach et al. 2020; Kobayashi et al. 2015). Plot parameterization combined qualitative field data and geomorphometric indices based on ArcticDEM (Porter et al. 2018). The simulator GEOtop was driven by each reanalysis dataset to produce three different GST simulations and an ensemble mean.

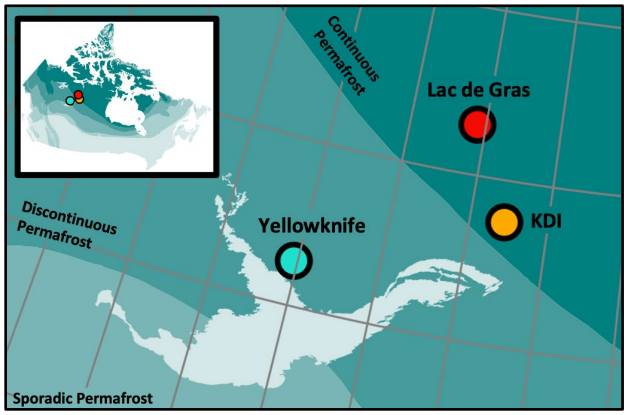

Figure 1. Location of three clusters of ground-surface temperature plots in the Northwest Territories, Canada.

Bootstrapping model performance

Bootstrapping is used to improve the tolerance for incomplete datasets and address bias introduced by unequal spatial or temporal distribution of observations. The bootstrap sample is a set of individual month-long timeseries, comprised of observations and simulation output for a particular plot, that will be referred to as a timeseries. Timeseries data is organized into sets based on terrain and month. Similar surface characteristics such as snow, drainage, vegetation, ground material, and exposure to solar radiation are used to classify plots by terrain type. Each set includes plots from the same terrain type and month, and therefore may contain data from different plots and years.

A bootstrap procedure was performed on each set by randomly selecting a month-long timeseries (comprised of observations and model output) from the set with replacement. The mean value summarizing performance for each model and its relative rank is recorded for each statistical measure (MAE, d_r, and BIAS) through 10,000 repetitions per unique terrain-month set of timeseries.

Statistics

Ground temperatures vary greatly in the uppermost metres. During spring and fall, there can be prolonged intervals near 0˚C. Statistics selected to capture model performance include: a mean absolute error to summarize average magnitude of error,

$$MAE = \sum_{i=1}^{n} |(o_i - p_i)| \quad [1]$$

a mean bias error (*BIAS* in Equation 2) to capture warm or cool bias,

$$BIAS = \sum_{i=1}^{n} (o_i - p_i) \quad [2]$$

and Willmott's index of agreement (d_r in Equation 3) to gauge systematic deviations from observations and variability in predictions, simultaneously.

$$d_r = \begin{cases} 1 - \frac{MAE}{2 \cdot MAD}, & MAE < 2 \cdot MAD \\ \frac{2 \cdot MAD}{MAE}, & MAE \geq 2 \cdot MAD \end{cases} \quad [3]$$

Results

Figure 2 shows the distribution of statistical performance for each model across different sets of terrain-month combinations. After aggregating bootstrap results, a total of 60,000 data points summarize the distribution of model performance.

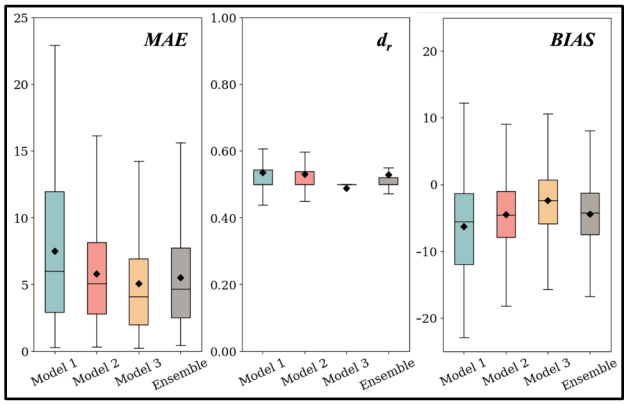

Figure 2. Distribution of performance of three models and their ensemble using (A) MAE, (B) d_r, and (C) BIAS.

Table 1. Ranks with uncertainty for each model and their ensemble across each terrain and season.

Rank:	First	Second	Third	Fourth
Model 1	0.11	0.18	0.21	0.50
Model 2	0.20	0.24	0.33	0.24
Model 3	0.56	0.09	0.08	0.26
Ensemble	0.13	0.49	0.39	0

This translates into a distribution of ranks, which can be analysed by statistic, by terrain, seasonally, or overall, as an aggregated sum of rank distributions (Table 1). Here is an example of how this framework is designed to offer multiple levels of analysis to better understand model performance: Model 3 ranks 1st 56% of the time, but also ranks 4th 26% of the time, indicating that it performs well overall but may not in certain conditions. There may be times of the year or terrain types that are poorly represented by this model. Further analysis reveals that Model 3 ranks 4th 36% of the time in July, August, and September, but excels in winter months. Additionally, Model 3 ranks last 40% of the time for the terrain type with characteristically little to no snow. This may suggest that Model 3 excels in representing snow, which strongly affects ground temperatures in fall, winter, and spring.

Concluding Thoughts

The ranking framework presented is versatile in communicating model performance across different scales. Subsetting by season or terrain type allows for clearer identification of model strengths, weaknesses, and relative performance. Future research can explore tailoring this method to other permafrost variables of interest. An application using multiple permafrost simulators is planned.

Acknowledgements

NSERC PermafrostNet (NETGP 523228-18), Compute Ontario and the Digital Research Alliance of Canada, ArcticDEM from DigitalGlobe (NSF 1043681, 1559691, and 1542736).

References

Endrizzi, S., Gruber, S., Dall'Amico, M., and Rigon, R. 2014. GEOtop 2.0: simulating the combined energy and water balance at and below the land surface accounting for soil freezing, snow cover and terrain effects. Geoscientific Model Development, 7(6), 2831–2857. doi:10.5194/gmd-7-2831-2014

Gelaro, R., McCarty, W., et al. 2017. The modern-era retrospective analysis for research and applications, version 2 (MERRA-2). Journal of Climate, 30(14), 5419–5454. doi:10.1175/JCLI-D-16-0758.1

Hersbach, H., Bell, B., Berrisford, P., Hirahara, S., Horányi, A., Muñoz-Sabater, J., Nicolas, J., Peubey, C., Radu, R., Schepers, D., et al. 2020. The ERA5 global reanalysis. Quarterly Journal of the Royal Meteorological Society, 146(730), 1999–2049. doi:10.1002/qj.3803

Kobayashi, S., Ota, Y., Harada, Y., Ebita, A., Moriya, M., Onoda, H., Onogi, K., Kamahori, H., Kobayashi, C., Endo, H., Miyaoka, K., and Takahashi, K. 2015. The JRA-55 reanalysis: General specifications and basic characteristics. Journal of the Meteorological Society of Japan. Ser. II, 93(1), 5–48. doi:10.1371/journal.pone.0169061

The state and fate of mountain permafrost: Decline of permafrost extent in mountainous regions 1960–2020

Harley R. McCourt[1], William H.G. Roberts[1], Matthew J. Westoby[2], Stuart A. Dunning[3] & Michael Lim[1]

[1]*Department of Geography and Environmental Sciences, Northumbria University, Newcastle upon Tyne, United Kingdom*

[2]*School of Geography, Earth and Environmental Sciences, University of Plymouth, Plymouth, United Kingdom*

[3]*School of Geography, Politics and Sociology, Newcastle University, Newcastle upon Tyne, United Kingdom*

Anthropogenic warming is pronounced in the mountainous regions of the globe (Biskaborn et al. 2019), promoting the initiation and propagation of landslides due to permafrost thaw. Here, a redeveloped high-resolution (30 m^2) global model of permafrost extent and zonation 1960–2020 is presented. Modern reanalysis datasets (JRA-55 and ERA5) are downscaled onto a global digital elevation model (ALOS 3D World) and permafrost extent is calculated as a function of mean annual ground temperature following Gruber (2012). The new high-resolution model can predict future change in permafrost zonation based on the differing scenarios of the IPCC's Shared Socio-economic Pathways.

Permafrost is ground that remains ≤0°C for at least two consecutive years. To monitor the state and fate of permafrost, we require knowledge of its spatial distribution and how it evolves through time. Permafrost is difficult to measure over large areas due to complications in obtaining data through direct observation, particularly in areas of high-altitude (Shi et al. 2018). To address this, permafrost is typically modelled over large areas. The global permafrost zonation model presented by Gruber (2012) is extensively used for model calibration and permafrost extent [PE] estimates due to its high spatial resolution (<1 km) and global coverage despite encompassing a relatively short period 1961–1990. This constraint limits its use for comparison with satellite timeseries data, represented by analysis-ready Landsat data from 1982–onward (Smith et al. 2020).

Here, we extend the temporal coverage and improve the spatial resolution by using modern reanalysis datasets, JRA-55 and ERA5, and a high-resolution (30 m^2) ALOS World 3D digital elevation model [DEM]. This new model provides a global time series of decadal moving-means to highlight regions and catchments where PE has decreased dramatically in recent decades. It has the capability to predict future evolution in permafrost zonation based on the IPCC's differing climate scenarios.

Methodology

Reanalysis datasets comprise atmospheric models based on assimilations of climate observations and provide a source for unique and homogeneous global data including cryospheric regions which are typically inaccessible or sparsely measured (Stewart-Jones and Gruber 2023). Here, two reanalysis datasets are used: JRA-55 and ERA5. Both have a long temporal coverage which can go beyond, the original models time frame 1961–1990 (Gruber 2012). Both datasets comprise of 1.25 resolution which is then downscaled based on the resolution of the 30 m^2 ALOS World 3D DEM, this makes the outputs highly representative of regional mountain geomorphology (Boulton and Stokes 2018).

For both reanalysis datasets, a lapse rate can be calculated based on the difference in height and temperature between the pressure levels for each coordinate grid square. This lapse rate provides a method to downscale the air temperature to the resolution of ALOS World 3D DEM. From this, the MAAT at 0 m can be calculated. Post downscaling, PE is calculated for each pixel as a function of mean annual ground temperature, this is averaged across 30-year windows from 1960–2020 to produce a moving mean to smooth out short-term fluctuations and highlight longer-term trends in change. These newly produced data are compared to a redevelopment of the original PZI model in which lapse rates were derived from the NCEP-NCAR reanalysis data and linear regression of MAAT from CRU TS 2.0 against geopotential heights for the lowermost seven pressure levels (Mokhov and Akperov 2006). These data were then downscaled onto the SRTM30 DEM and the GTOPO30 DEM for areas outside of SRTM30's coverage. Multiple model iterations are used to compare the impact of changing the DEM and temperature source components. These iterations will be compared against point data of GTN-P borehole permafrost presence and accuracies assessed using a receiver operating characteristic curve (Deluigi et al. 2017).

GLOBAL PE CHANGES

Based on the JRA-55-AW3D model, between the contemporary period (1960–1990) and the present (1990–2020), global PE has decreased by 1.4 ± 2% (Figure 1).

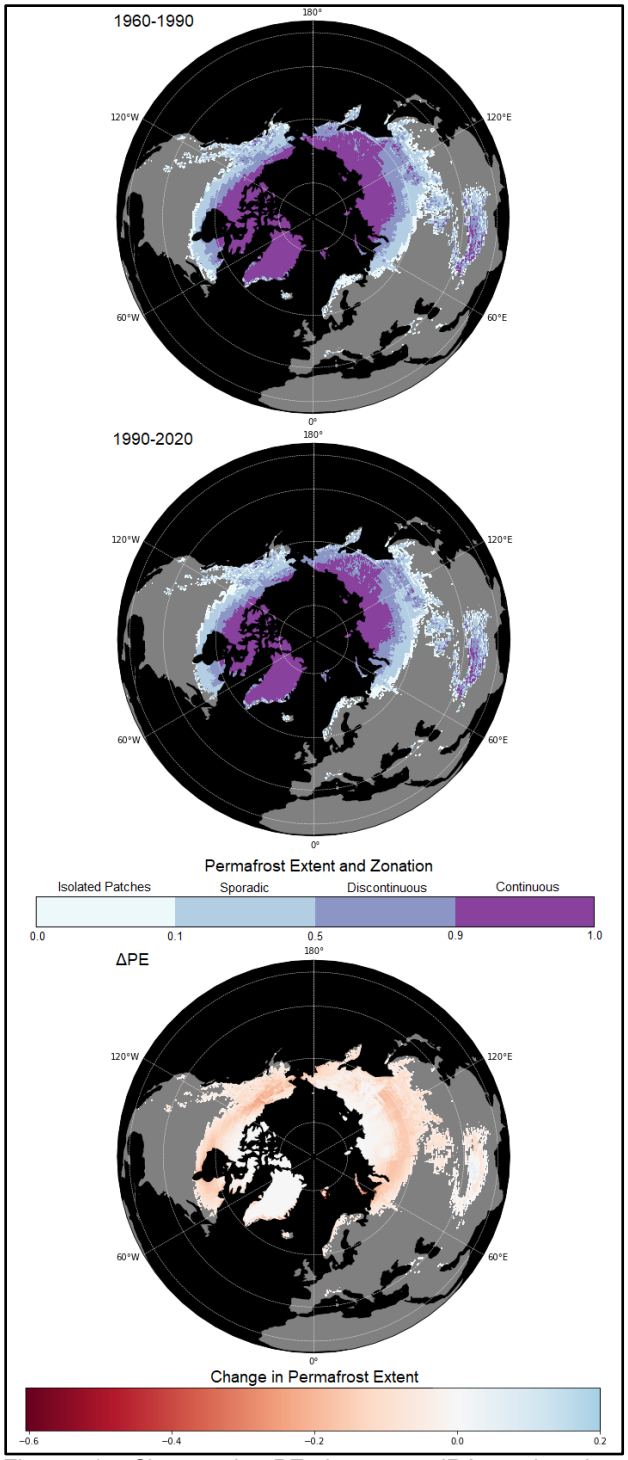

Figure 1. Change in PE between JRA-55 iterations 1960–1990 and 1960–2020 at 0.5° resolution.

This decline in extent is most prevalent within mountainous regions. In the Northern Hemisphere, Alaska and the Himalayas featured an overall average decrease in PE of 9 ± 7% and 3 ± 3.5% respectively. Change in PE is localised within areas where permafrost transitions through characteristic zones, specifically at the sites between continuous and discontinuous permafrost.

REFERENCES

Biskaborn, B.K., Smith, S.L., Noetzli, J., Matthes, H., Vieira, G., Streletskiy, D.A., Schoeneich, P., Romanovsky, V.E., Lewkowicz, A.G., Abramov, A., and Allard, M. 2019. Permafrost is warming at a global scale. Nature communications, 10(1), p.264.

Boulton, S.J., and Stokes, M. 2018. Which DEM is best for analyzing fluvial landscape development in mountainous terrains? Geomorphology, 310, 168–187. doi:10.1016/j.geomorph.2018.03.002

Deluigi, N., Lambiel, C., and Kanevski, M. 2017. Data-driven mapping of the potential mountain permafrost distribution. Science of the total environment, 590, 370–380.

Gruber, S. 2012. Derivation and analysis of a high-resolution estimate of global permafrost zonation. The Cryosphere, 6(1), 221–233. doi:10.5194/tc-6-221-2012

Mokhov, I.I., and Akperov, M.G. 2006. Tropospheric lapse rate and its relation to surface temperature from reanalysis data, Izv. Atmos. Ocean. Phy., 42, 430–438.

Smith, W.D., Dunning, S.A., Brough, S., Ross, N., and Telling, J. 2020. GERALDINE (Google Earth Engine supRaglAciaL Debris INput dEtector): a new tool for identifying and monitoring supraglacial landslide inputs. Earth Surface Dynamics, 8(4), pp.1053–1065.

Stewart-Jones, E., and Gruber, S. 2023. Transferring Cryosphere Knowledge between Mountains Globally: A Case Study of Western Canadian Mountains, the European Alps and the Scandes. Journal of Alpine Research| Revue de géographie alpine, 111–2.

Assessment of permafrost changes in the 21st century in the Alaskan Arctic

Dmitry J. Nicolsky[1], Vladimir E. Romanovsky[1], Louise L. Farquharson[1], Thomas C. Wright[1] & William L. Cable[2]

[1]*University of Alaska Fairbanks, Fairbanks, Alaska, United States*

[2]*Alfred Wegener Institute Helmholtz Centre for Polar and Marine Research, Potsdam, Germany*

The variability in ground temperature across the Arctic landscape is driven by air temperature, snow cover, soil moisture content, vegetation, terrain, soil properties, and related environmental variables. Despite our general sense of currently observed changes in permafrost and their future projections under the future climate scenarios, there is a lack of understanding of how the potential changes in permafrost will affect ecosystems and infrastructure on local and regional scales. A major hurdle in addressing this problem lies in our limited knowledge of local processes due to insufficient spatial and temporal resolution of models, projections of the changing climate, and resulting changes in other environmental characteristics, including permafrost.

In many high-resolution permafrost models, the thermal properties of the mineral and organic soil layers, produce many distinct combinations of the input-data classes, the parameterization of which is a difficult task involving various assumptions and data sets. Here, we consider the ecosystem types, and group existing ground temperature observations into the ecosystem types. This grouping allows estimation of the soil properties using the data assimilation technique for each input-data class (ecotype). Remote sensing and landscape classification is then used to upscale modeling results across the study area.

Justification of this approach is based on the analysis of spatial and temporal variability of near-surface ground temperatures measured in the Selawik region in Alaska (Cable et al. 2016). Later, it was successfully applied to simulate high-resolution permafrost dynamics on the North Slope of Alaska (Nicolsky et al. 2017). Here, we present updated high-resolution mapping of permafrost on the North Slope of Alaska, including southern foothills of the Brooks Range, and the Interior of Alaska.

Using the 1-D transient Geophysical Institute Permafrost Laboratory (GIPL) model (Nicolsky et al. 2007) that accounts for the heat flow and phase change, we simulate the retrospective permafrost evolution and compare it with in-situ observations of the active layer thickness. We employ a monthly averaged CRU TS4.04 data set (Harris et al. 2020) downscaled to a 770-m resolution using the PRISM climatology for 1980-2010 and the delta method (Hijmans et al. 2005). For the future modeling runs with the IPCC RCP 4.5 and 8.5 scenarios, we utilize an average composed of similarly downscaled monthly averaged outputs of five GCMs that perform optimally for Alaska (Walsh et al. 2008).

To parameterize the soil texture, vegetation cover, and their thermal properties, we employ 30-m resolution unified ecological maps by Jorgenson and Heiner (2004) and Jorgenson et al. (2009), supplemented with the soil lithology, surface elevation, wind power datasets.

The considered landscape characteristic maps and related databases include a wide diversity of soil types between foothills of the Brooks Range and the Arctic Ocean. Analyzing the lithology field in the database, we delineate predominant soil texture categories for the top mineral layer in the study area; the elevation dataset allows for characterization of near-surface moisture, while the wind power relates to the snow density.

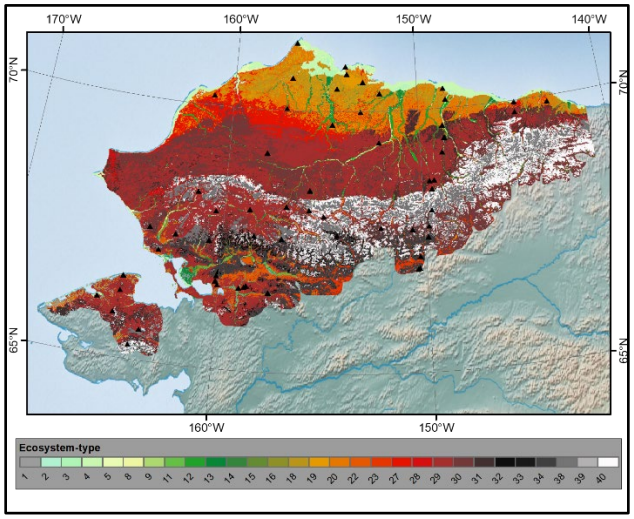

Figure 1. The 30-m unified ecological map by Jorgenson and Heiner (2003) and Jorgenson et al. (2009) delineating local-scale ecosystems (ecotypes). Black triangles indicate locations where ground temperature dynamics was measured and used for parameterization of the ecosystem type properties: thermal properties, soil moisture, snow characteristics.

The methodology developed in this study is believed to be relevant and applicable to many Alaskan and other Circum-Arctic locations to estimate the consequences of permafrost degradation in the 21st century. Modeling results can be found at the project website: http://permamap.gi.alaska.edu.

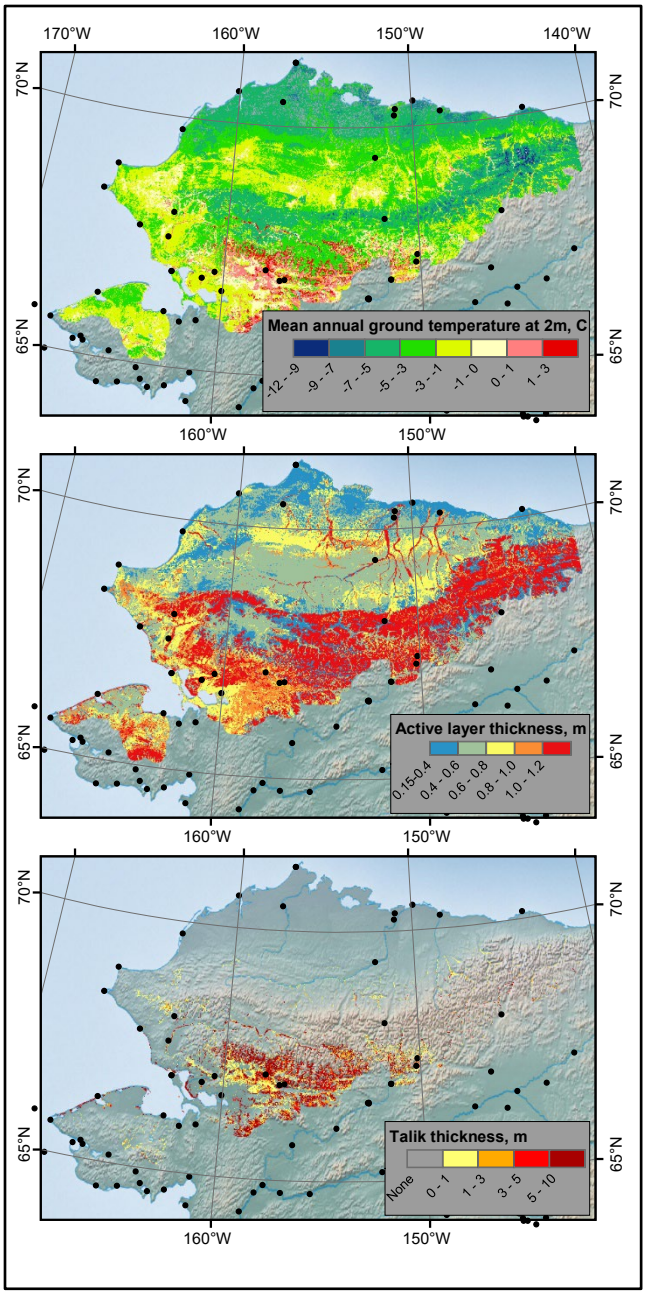

Figure 2. Modeled mean decadal (2010-2019) ground temperature at 2 m (top), thickness of the active layer (middle), and the talik thickness (bottom) for the study area. Black circles indicate locations of communities in Alaska.

References

Cable, W., Romanovsky, V., and Jorgenson, M. 2016. Scaling-up permafrost thermal measurements in Western Alaska using an ecotype approach, The Cryosphere, 10 (5): 2517–2532. doi:10.5194/tc-10-2517-2016

Daly, C., Smith, J., and Halbleib, M. 2018.1981–2010 High-resolution temperature and precipitation maps for Alaska. Final report. Corvallis, OR: PRISM Climate Group, Oregon State University.

Harris, I.C., Jones, P.D., and Osborn, T. 2020. CRU TS4.04: Climatic Research Unit (CRU) Time-Series (TS) version 4.04 of high-resolution gridded data of month-by-month variation in climate (Jan. 1901- Dec. 2019). Centre for Environmental Data Analysis, date of citation. https://catalogue.ceda.ac.uk/uuid/89e1e34ec3554dc98594a5732622bce9

Hijmans, R.J., Cameron, S.E., Parra, J.L., Jones, P.G., and Jarvis, A. 2005. Very high-resolution interpolated climate surfaces for global land areas, International Journal of Climatology, 25(15): 1965–1978.

Jorgenson, T., and Heiner, M. 2004. Ecosystems of Northern Alaska, ABR, Inc., and The Nature Conservancy, Anchorage Alaska, poster.

Jorgenson, M.T., Roth, J.E., Miller, P.F., Macander, M.J., Duffy, M.S., Wells, A.F., Frost, G.V., and Pullman, E.R. 2009. An ecological land survey and landcover map of the Arctic Network. Natural Resource Technical Report NPS/ARCN/NRTR—2009/270. National Park Service, Fort Collins, Colorado.

Nicolsky, D.J., Romanovsky, V.E., and Tipenko, G.S. 2007. Using in-situ temperature measurements to estimate saturated soil thermal properties by solving a sequence of optimization problems, The Cryosphere, 1: 41–58.

Nicolsky, D.J., Romanovsky, V.E., Panda, S.K., et al. 2017. Applicability of the ecosystem type approach to model permafrost dynamics across the Alaska North Slope, Journal of Geophysical Research, 122: 50–75. doi:10.1002/2016JF003852

Walsh, J., Chapman, W., Romanovsky, V., Christensen, J.H., and Stendel M. 2008. Global climate model performance over Alaska and Greenland, Journal of Climate, 21(23): 6156–6174.

Modelling using NEST in valleys prone to intense and frequent surface-based temperature inversions, northcentral Yukon, Canada

Nick Noad[1], Philip Bonnaventure[1] & Yu Zhang[2]

[1]*Department of Geography and Environment, University of Lethbridge, Lethbridge, Alberta, Canada*

[2]*Natural Resources Canada, Ottawa, Ontario, Canada*

Valleys of northcentral Yukon are dominated by a phenomenon known as surface-based temperature inversions (SBIs) (Noad and Bonnaventure 2022; Noad and Bonnaventure 2023). SBIs occur when air temperature (Ta) increases from the surface with increasing elevation (Bradley et al. 1992). SBIs are so frequent and strong that they significantly impact elevational temperature patterns, otherwise known as surface lapse rates (SLRs) (Noad et al. 2023). The resulting patterns of SLRs and mean annual air temperatures (MAAT) impact permafrost distribution in this region where permafrost is more likely to occur in the colder valley bottoms than at higher elevations located near the average top of the SBI (Bonnaventure and Lewkowicz 2013). Permafrost was present at most sites in each valley, except for some slope locations where the SBIs drove SLRs that were 12 °C km^{-1} annually (Noad and Bonnaventure 2022). Permafrost modelling for Yukon began to address the influence of SBIs on SLR patterns and subsequently on permafrost distribution through the development of a new variable called equivalent elevation (Lewkowicz and Bonnaventure 2011). Permafrost probability was then modelled regionally at a resolution of 30 m^2 for northern British Columbia and southern Yukon using an empirical-statistical permafrost model with the influence of SBIs in mind (Bonnaventure et al. 2012).

Since 2016, networks of sensors have been deployed in two dissimilar valleys along the Dempster Highway to allow for elevational transect analysis where characteristics of SBIs and resulting SLRs can be calculated and compared (Noad and Bonnaventure 2022). More recently the deployment of ground temperature nodes (GTNs) (Garibaldi et al. 2021), along with the elevational transects of air, ground surface, and depth temperature sensors have been utilized to model permafrost in these valleys using the TTOP model. With the TTOP model being an equilibrium model, the need exists to apply a one-dimensional numerical process-based permafrost model called the Northern Ecosystem Soil Temperature (NEST) model (Zhang et al. 2003) to predict the transient nature of permafrost over the past century and how it will continue to evolve in the remainder of this century. This will allow for prediction of past, current, and future impact SBIs have on the ground thermal regime.

Objective

To model permafrost and its transient nature in two dissimilar Yukon valleys where SBIs are frequent and strong to predict the impact that SBIs have on permafrost in the past, currently, and in the future.

Study area

The two geomorphically and vegetatively diverse valleys (roughly 65.0° N and 138.3° W) are located roughly 10 km apart along the Dempster Highway at roughly km 150 in a subrange of the Ogilvie Mountains. The study area is 500 km northwest of Whitehorse and 450 km southwest of Inuvik. The closest community is Dawson which is 115 km to the southwest. The sites in the valleys were selected to represent variability of topography and environmental conditions in this mountain region. These valleys are located near the boundary of continuous and extensive discontinuous permafrost zones (Noad and Bonnaventure 2022).

Methods

A network of roughly 27 Ta and 94 GTN sensors have been deployed across the two dissimilar valleys with the objective to collect the data necessary to populate parameters in the NEST model. These sites sample the spatial variation of elevation, topographic index, and landcover type. The in-situ data that is collected, along with field observations and DEM derived variables, will be utilized to populate the NEST parameters for landcover, snow accumulation and redistribution, soil properties, topographic shading, and ground water dynamics. This intensive data collection will allow for the NEST model to be calibrated for the valleys. Once calibrated the influence of SBIs on the ground thermal regime will be tested by adjusting the mean monthly maximum and minimum temperatures to match observations rather than predictions from the MET 1km (Zhang et al. 2020) and ERA5 climate reanalysis data sets. These datasets are used to populate NEST and they largely fail to account for the intensity and frequency of valley SBIs (Noad and Bonnaventure 2022). NEST has been run for each of the 27 Ta sites and the model will be calibrated, and a sensitivity analysis will be run. The ground thermal regime and permafrost characteristics predicted for

each of these sites by the NEST model will then be compared to findings of recent TTOP modelling, and previous statistical-empirical regional permafrost modelling (Bonnaventure et al. 2012). Comparison of future projections of the different models will be made to understand the limits of the equilibrium models when compared with the transient NEST model.

Preliminary Results

Since SBIs are not represented in the coarse resolution climate reanalysis models, there is a cold bias for most high elevation sites. The frequent and intense SBIs drive warmer Ta at higher elevations particularly during the winter season or nighttime when SBIs are most common. This may lead to a warmer ground thermal regime at higher elevations and permafrost that is more susceptible to degradation and loss as the climate continues to warm. Furthermore, permafrost has been measured to be absent at around treeline on the south facing transect of the south valley where intense and frequent inversions drive MAATs that are upwards to 1.2 °C warmer than the valley bottom sites (Noad and Bonnaventure 2022). The NEST model predicts that permafrost was likely present and stable until the active layer began more rapidly thickening in the 1970's and total degradation of the permafrost likely occurred around 1998 (Figure 1). This demonstrates the results the NEST model can produce that can be used to directly measure the impact SBIs are having on the ground thermal regime temporally.

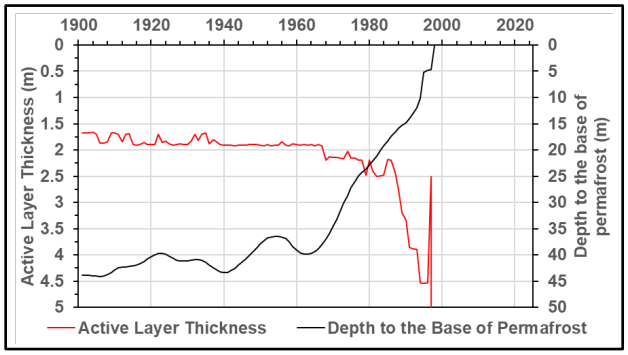

Figure 1. NEST active layer depth and depth of the permafrost base for the site at treeline on the south facing slope of the south valley where permafrost has been measured to likely be absent.

References

Bonnaventure, P.P., and Lewkowicz, A.G. 2013. Impacts of mean annual air temperature change on a regional permafrost probability model for the southern Yukon and northern British Columbia, Canada. CRYOSPHERE, 7(3), 935–946. doi:10.5194/tc-7-935-2013

Bonnaventure, P.P., Lewkowicz, A.G., Kremer, M., and Sawada, M.C. 2012. A Permafrost Probability Model for the Southern Yukon and Northern British Columbia, Canada. Permafrost and Periglacial Processes, 23(1), 52–68. doi:10.1002/ppp.1733

Bradley, R.S., Keimig, F.T., and Diaz, H.F. 1992. Climatology of surface-based inversions in the North American Arctic. Journal of Geophysical Research: Atmospheres, 97(D14), 15699–15712. doi:10.1029/92JD01451

Garibaldi, M.C., Bonnaventure, P.P., and Lamoureux, S.F. 2021. Utilizing the TTOP model to understand spatial permafrost temperature variability in a High Arctic landscape, Cape Bounty, Nunavut, Canada. Permafrost and periglacial processes, 32(1), 19–34. doi:10.1002/ppp.2086

Lewkowicz, A.G., and Bonnaventure, P.P. 2011. Equivalent Elevation: A New Method to Incorporate Variable Surface Lapse Rates into Mountain Permafrost Modelling. Permafrost and Periglacial Processes, 22(2), 153–162. doi:10.1002/ppp.720

Noad, N.C., and Bonnaventure, P.B. 2023. Examining the influence of microclimate conditions on the breakup of surface-based temperature inversions in two proximal but dissimilar Yukon valleys. Canadian Geographies / Géographies canadiennes, N/A, 1–17. doi:10.1111/cag.12886

Noad, N.C., and Bonnaventure, P.P. 2022. Surface temperature inversion characteristics in dissimilar valleys, Yukon Canada. Arctic Science, 8(4), 1320–1339. doi:10.1139/as-2021-0048

Noad, N.C., Bonnaventure, P.P., Gilson, G.F., Jiskoot, H., and Garibaldi, M.C. 2023. Surface-based temperature inversion characteristics and impact on surface air temperatures in northwestern Canada from radiosonde data between 1990 and 2016. Arctic science, 9(3), 545–563. doi:10.1139/AS-2022-0031

Zhang, Y., Chen, W., and Cihlar, J. 2003. A process-based model for quantifying the impact of climate change on permafrost thermal regimes. Journal of Geophysical Research: Atmospheres, 108(D22), 4695–1511. doi:10.1029/2002JD003354

Zhang, Y., Qian, B., and Hong, G. 2020. A long-term, 1-km resolution daily meteorological dataset for modeling and mapping permafrost in Canada. 11(9), 1–27. doi:10.3390/atmos11121363

Developing an open-source modelling tool for predicting large-strain deformation of ground in permafrost regions subject to climate change

Anna Pekinasova[1], Jocelyn L. Hayley[1] & Brandon Karchewski[2]
[1]*Department of Civil Engineering, University of Calgary, Calgary, Alberta, Canada*
[2]*Department of Earth, Energy, and Environment, University of Calgary, Calgary, Alberta, Canada*

Accurate prediction of settlement and heaving of ground subject to freeze-thaw cycling is a vital component of analyzing infrastructure resilience to climate change in permafrost regions. Heaving and settlement are two major causes of infrastructure damage due to water migration from unfrozen to frozen zones, formation of ice-lenses (Yu et al. 2020a), loss of strength due to high pore water pressure, thaw settlement, and formation of thermokarst and talik (cf. Hjort et al. 2018). This leads to an increase in infrastructure maintenance and unreliable operations with negative socioeconomic and environmental impacts on northern regions. There have been significant advances in the modelling of freeze-thaw processes in permafrost terrain and of surface energy boundary (SEB) conditions, but these have not been fully integrated into a practical engineering analysis tool. We are developing an open-source numerical tool that incorporates large-strain thaw consolidation, state-of-the-art physics of ice-rich permafrost terrain, and complex and dynamic heat energy boundary conditions. This modelling tool will assist in the analysis of cold region infrastructure for engineers, geoscientists, climate scientists, owners, policymakers, and other stakeholders.

CLIMATE CHANGE AND SURFACE ENERGY BALANCE

Climate change forcing in permafrost regions (e.g., increases to annual mean temperature, precipitation (rain and snow), relative humidity, surface ponding, runoff, soil moisture, and/or droughts) causes regional and local changes by affecting the ground temperature distribution and the thickness of the active layer (cf. An et al. 2017; Harris et al. 2017). To accurately model the impact of complex climate forcing on long-term ground behaviour, we incorporate surface energy boundary (SEB) conditions including incoming and outgoing short-wave and long-wave radiation, sensible heat flux exchange by convection of air, latent heat flux by evaporation or condensation of water, and ground heat flux by migration of heat into and out of the ground. Each term involves specific formulae and parameters that characterize the SEB (cf. An et al. 2017; Westermann et al. 2023).

THERMO-HYDRO-MECHANICAL MODELLING OF SOIL

The theory of ground freeze-thaw and consolidation involves fully coupled thermo-hydro-mechanical (THM) processes accounting for heat transfer, pore fluid migration, and deformation resulting from a nonlinear void ratio-permeability-effective (total) stress relationship and post-thaw residual stress. In a layer experiencing seasonal variations in the SEB with long-term variations due to climate change, the ground temperature distribution may oscillate with depth, and different parts of the surface layer may experience consolidation or heave processes simultaneously. To model long-term ground behaviour, we cannot assume a single thawing or freezing front at any time. Rather, we track degree of saturation of ice in the pores at integration points throughout the domain, where degree of saturation of ice is related to temperature via an empirical model (e.g., Nishimura et al. 2009). We incorporate the formulations for THM-coupled modelling of soils after Dumais and Konrad (2018) and Yu et al. (2020a; 2020b).

To capture the moving boundary condition due to settlement and heave we use a coordinate transformation described by the change in void ratio between any two reference points which can be mapped onto non-moving Lagrangian coordinates. This transformation also facilitates the calculation of the total settlement of a layer experiencing simultaneous consolidation and heave processes in terms of the void ratio distribution and the initial reference (Lagrangian) coordinates.

We write the heat energy balance in the unfrozen or frozen soil by accounting for conduction, advection, sensible heat storage due to temperature change, and latent heat storage due to phase change (Dumais and Konrad 2018).

The pore fluid flux behaves differently depending on whether the soil is unfrozen or frozen. For unfrozen soil, we assume that fluid flux is governed by the 1D large-strain consolidation process involving the transfer of excess pore pressure to effective stress, since at hydrostatic conditions the flux rate will be zero. We use Darcy's law to relate the pore fluid flux to the gradient of effective stress with a nonlinear void ratio – permeability relationship (Yu et al. 2020b). For frozen soil, we use a water flux function, which has a detailed

history of investigation. The fluid flux in frozen soil depends on several factors including temperature gradient, segregation potential, soil type, void ratio, and stress (cf. Michalowski and Zhu 2006).

For the deformation of the unfrozen soil, we employ a nonlinear void ratio – effective stress relationship that is updated along with the hydromechanical coupled equations following Yu et al. (2020b). For the frozen soil, there is deformation due to fluid migration, phase change, and total stress variation, which introduces some complications owing to the stress-strain relationships (Konrad and Samson 2000; Yu et al. 2020b). We incorporate normal consolidation and unloading-reloading processes together with post-thaw residual stress.

Modelling the full depth of permafrost requires boundary conditions for heat input from geothermal energy. We assume conductive ground heat flux from the geothermal temperature gradient for lower boundary conditions.

Pekinasova et al. (2023) provide a brief overview of the weak form equations for solving the coupled THM system of equations using the finite element method, modified after Yu et al. (2020b).

Results, challenges, and future work

Recent work on fully coupled THM modelling of thaw consolidation (Dumais and Konrad 2018) and freeze-thaw heave and consolidation (Yu et al. 2020a; 2020b) present results and performance of models for relatively thin surface layers <50 cm thick. When scaling simulations to permafrost thickness over multi-annual cycles, selecting a spatial and temporal resolution that suits all aspects of the physics can be a challenge. We ensure acceptable error through adaptive time stepping with iterative correction of model parameters at each time step. We estimate the error using the adaptive half-step method, correct solution variables and modify the time step according to the error estimate at each time step. In this way, we can solve the coupled THM equations at scales of tens to hundreds of metres efficiently. Recent work by Ross et al. (2022) highlights the importance of spin-up stabilization for the ground temperature distribution, which can require simulation of hundreds to thousands of years depending on soil parameters. We will employ our coupled THM model to examine spin-up for both temperature and void ratio in permafrost terrain, which may aid with an estimation of initial void ratio distribution.

This research aims to provide a fully validated THM-coupled code that captures both the thaw consolidation and freeze-thaw processes in soils to predict ground response under complex long-term climate conditions. To invite transdisciplinary collaboration, we implement the numerical code as an open-source Python package frozen-ground-fem available at: https://github.com/annapekinasova/frozen-ground-fem/

In the code repository, we provide examples of usage and encourage those interested in collaboration to reach out for collaborator access.

Acknowledgements

Financial support for this research was provided by the Natural Sciences and Engineering Research Council of Canada (NSERC). We also thank Dr. Teddi Herring for her review and feedback on this manuscript.

References

An, N., et al. 2017. Assessment of the methods for determining net radiation at different time-scales of meteorological variables, Journal of Rock Mechanics and Geotechnical Engineering, 9(2), 239–246.

Dumais, S., and Konrad, J.-M. 2018. One-dimensional large-strain thaw consolidation using nonlinear effective stress – void ratio – hydraulic conductivity relationships, Canadian Geotechnical Journal, 55(3), 414–426.

Harris, S.A., et al. 2017. Geocryology. CRC Press.

Hjort, J. et al. 2018. Degrading permafrost puts Arctic infrastructure at risk by mid-century, Nature Communications, 9(1), 5147.

Konrad, J.-M., and Samson, M. 2000. Hydraulic conductivity of kaolinite-silt mixtures subjected to closed-system freezing and thaw consolidation, Canadian Geotechnical Journal, 37(4), 857–869.

Michalowski, R.L., and Zhu, M. 2006. Frost heave modelling using porosity rate function, Journal for Numerical and Analytical Methods in Geomechanics, 30(8), 703–722.

Nishimura, S., et al. 2009. THM-coupled finite element analysis of frozen soil: formulation and application, Géotechnique, 59(3), 159–171.

Pekinasova, A., et al. 2023. Preliminary results of thermo-hydro-mechanical modelling of large-strain deformation of ground in Canadian cold regions, Proceedings of the 76th Canadian Geotechnical Conference, Saskatoon, SK.

Ross, C. et al. 2022. Initialization of thermal models in cold and warm permafrost, Canadian Geotechnical Journal, 8(2), 362–394.

Westermann, S., et al. 2023. The CryoGrid community model (version 1) - a multi-physics toolbox for climate-driven simulations in the terrestrial cryosphere, Geoscientific Model Development, 16(9), 2607–2647.

Yu, F., et al. 2020a. Frost heave and thaw consolidation modelling. Part 1: A water flux function for frost heaving, Canadian Geotechnical Journal, 57(10), 1581–1594.

Yu, F., et al. 2020b. Frost heave and thaw consolidation modelling. Part 2: One-dimensional thermo-hydromechanical (THM) framework, Canadian Geotechnical Journal, 57(10), 1595–1610.

Mechanistic approach for the spatial ice segregation distribution in non-sorted circles

Xavier Rodriguez-Lloveras, Melanie A. Thurner & Christian Beer

Institute of Soil Science, Department of Earth System Sciences and Centre for Earth System Research and Sustainability, Universität Hamburg, Hamburg, Germany

The current effects of global warming are proven especially critical in arctic regions. Recent studies show that the arctic warms nearly four times faster than the rest of the globe (Rantanen 2022). This rapid warming leads to increased permafrost degradation, enabling a positive permafrost carbon-climate feedback (Koven 2011). The permafrost degradation is uneven across permafrost landscapes, as these are largely governed by the distribution of ground ice and its heterogeneous melting (Lee 2014; Nitzbon 2020). The presence of ice in arctic soils is not restricted to the permafrost, but also present seasonally in the active layer. The seasonality of the active layer dynamically changes the freeze-thaw cycles, which in turn change the soil structure and processes throughout the year and between years at centimetric scale (Rempel 2007). At this scale, the soil particles distribution becomes critical in conditioning the ice segregation and its associated mixing ratios and soil movements, such as organic-rich materials burial to deeper layers or the formation of non-sorted circles (Ping et al. 2015). The final goal of understanding the mechanics of these processes is twofold. Firstly, understanding the current processes shaping the active layer can lead to a better comprehension of the processes leading to the current permafrost landscapes and its carbon storage volume and distribution, which remain largely unknown (Schuur 2015). Secondly, the analysis of the soil-ice relation in time can shed light on the projections of long-term degradation of segregated ice in the permafrost. The long-term soil ice degradation is particularly important in ice dominated landscapes, as the ice melt can lead to thermo-karst or thermo-erosion, shifting arctic ecosystems from neutral or small sink to strong sources of CO_2 (Beer 2023). Focusing on this goal, we developed the Dynamic Soil Model (DynSoM) with two-dimensions simulation capabilities. DynSoM is a new site-level soil model that mechanistically represents the surface energy balance and in particular the soil heat flux and site hydrology processes, adapted to permafrost-affected ecosystems. In addition to soil heat conduction and water flow in the horizontal and vertical dimensions, the model includes the formation of segregated ice, near-ground vegetation processes, and effects of soil texture type in the active layer. DynSoM focuses on the simulation of soil processes at a pedon-scale (cm to m) and sub-hourly to hourly time step. It considers the processes on the full soil column at different levels of detail in the seasonally frozen and thawed active layer, where the formation and growth of segregated ice occur. The input data to obtain the core processes simulated, includes soil properties, meteorological variables, atmospheric conditions, and vegetation properties. To simulate the soil processes, the model considers a set of soil columns on which the soil water and energy balance in the vertical dimension are initially solved, followed by the horizontal dimension in the same time step. On the vertical dimension, the soil water balance is driven by the gravitational potential and the suction on the unsaturated fraction of the soil (matric potential). On the horizontal dimension, the diffusion due to the lateral conductivity and matric potential at the same depth is considered. The energy balance is driven by the net radiation balance at its surface, which is considered as a skin layer. In DynSoM, the skin layer is assumed to be part of the first soil layer. Consequently, the required energy fluxes to balance the net radiation become a boundary condition for the soil heat flux. Through this principle, the model determines the soil temperature through the heat conduction of the columns' layers (vertical dimension) and the layers at the same level in different soil columns (horizontal dimension), during the same timestep. Phase change is included in DynSoM as part of the energy balance, using the concept of excess energy (Ekici et al. 2014). Segregated ice is considered within the model as an integral part of the soil. The model uses a simplified approach based on the capillary theory, combined with the frozen fringe concept and the cryogenic suction principle that under favourable conditions during freezing, water can flow towards the freezing front. Consequently, segregated ice is simulated as frozen water beyond effective saturation of the soil. The model is capable to simulate a wide range of soil compositions and distributions. Nevertheless, to evaluate the model the soil and surface properties of the different layers and columns have been defined following a synthetic typical distribution of the centre and inter-circle of non-sorted circles. The vertical dimension of this synthetic soil is discretized as a 1 m with high

resolution (5 cm layers) followed by layers of lower resolution with a consecutive increase of thickness to a total depth of 50 m. The horizontal dimension is discretized in columns 10 cm wide. The simulation interval has been set for a period of 10 years with an hourly time step. The atmospheric data has been adapted from the CRUNCEP-V7 dataset over Disko Island (Greenland). The ice segregation dynamics results show sensitive differences between the centre and the inter-circle due to its heterogeneity. Seasonally, the larger differences can be seen between Spring and Autumn, when the snow cover is uneven. In this period, the more effective insulation on the inter-circle due the larger accumulation of snow, the plant density and higher porosity of the organic layer, together with the sub-surface eregulate the soil temperature and the thawing depth. Contrastingly the centre's higher exposure to faster temperature changes allow the deeper thaw of the soil and the faster cooling, favouring the conditions for ice segregation. Considering the horizontal dimension, the formation of ice in neighboring columns favour the capillarity towards the lateral freezing front, boosting the water availability towards the centre and depleting the available water in the inter-circle during the freezing period. Contrarily, during the thawing period, the faster thawing of the centre promote the thawing of its immediate neighbouring columns, which combined with the increased porosity created by the thawing of ice excess in the centre, might create an additional water flow from the lateral thawing columns. Due the high organic matter on the inter-circle, the water fluxes towards the centre can be rich in organic matter content, and progressively increase the amount of organic carbon in deeper layers of the centre. If the consecutive winters are warmer, this increased organic carbon in unfrozen soil can boost the carbon emissions due for example, an increased microbial activity. On the contrary, if the consecutive winters are colder, the processes of ice segregation-thawing occur in shallower layers, becoming a carbon sink by burying the carbon-rich layers deeper in the soil. In this last scenario, different generations of ice and carbon rich layers can lead to large emissions of CO_2 in case of a rapid thaw. The results obtained by DynSoM are reasonable and contribute to a deeper understanding of the soil processes that drive the active layer distribution and composition, and ultimately the arctic landscapes. Nevertheless, in its current state the model does not consider important processes such as the ice segregation-induced heave and the heat advection due the warmer water flow towards the freezing front. The inclusion of these processes is in the scope of the future DynSoM development, as they are crucial to correctly assess the soil-ice dynamics, including the soil organic carbon transport within the soil.

Acknowledgements

X.R. acknowledges funding from the German Ministry for Education and Research (project MOMENT, 03F0931A). C.B. and M.T. acknowledge funding by the Deutsche Forschungsgemeinschaft (DFG BE 6485/1-1 and BE 6485/2-1).

References

Beer, C., Runge, A., Grosse, G., Hugelius, G., and Knoblauch, C. 2023. Carbon dioxide release from retrogressive thaw slumps in Siberia, Environmental Research Letters, 18(10): 104053. doi:10.1088/1748-9326/acfdbb

Ekici, A., Beer, C., Hagemann, S., Boike, J., Langer, M., and Hauck, C. 2014. Simulating high-latitude permafrost regions by the JSBACH terrestrial ecosystem model, Geoscientific Model Development, 7(2): 631–647. doi:10.5194/gmd-7-631-2014

Koven, C.D., Ringeval, B., Friedlingstein, P., Ciais, P., Cadule, P., Khvorostyanov, D., et al. 2011. Permafrost carbon-climate feedbacks accelerate global warming, Proceedings of the National Academy of Sciences, 108(36): 14769–14774. doi:10.1073/pnas.1103910108

Lee, H., Swenson, S.C., Slater, A.G., and Lawrence, D.M. 2014. Effects of excess ground ice on projections of permafrost in a warming climate, Environmental Research Letters, 9(12): 124006. doi:10.1088/1748-9326/9/12/124006

Nitzbon, J., Westermann, S., Langer, M., Martin, L.C.P., Strauss, J., Laboor, S., and Boike, J. 2020. Fast response of cold ice-rich permafrost in northeast Siberia to a warming climate, Nature Communications, 11(1): 2201. doi:10.1038/s41467-020-15725-8

Ping, C.L., Jastrow, J.D., Jorgenson, M.T., Michaelson, G. J., and Shur, Y.L. 2015. Permafrost soils and carbon cycling, SOIL, 1(1): 147–171. doi:10.5194/soil-1-147-2015

Rantanen, M., Karpechko, A.Y., Lipponen, A., Nordling, K., Hyvärinen, O., Ruosteenoja, K., et al. 2022. The Arctic has warmed nearly four times faster than the globe since 1979, Communications Earth & Environment, 3(1): 168. doi:10.1038/s43247-022-00498-3

Rempel, A.W. 2007. Formation of ice lenses and frost heave, Journal of Geophysical Research, 112(F2). doi:10.1029/2006jf000525

Schuur, E.A.G., McGuire, A.D., Schädel, C., Grosse, G., Harden, J.W., Hayes, D.J., et al. 2015. Climate change and the permafrost carbon feedback, Nature, 520(7546): 171–179. doi:10.1038/nature14338

A novel analytical-statistical tool for estimating active-layer thickness

Tomáš Uxa[1,2], Filip Hrbáček[2] & Michaela Kňažková[2]

[1]*Institute of Geophysics, Czech Academy of Sciences, Prague, Czech Republic*

[2]*Department of Geography, Faculty of Science, Brno, Czech Republic*

The active layer is the topmost ground layer over permafrost that thaws seasonally from the surface to a depth of up to several meters and then completely refreezes, which is mainly controlled by climate conditions and ground physical properties.

The active-layer thickness has commonly been determined from temperature measurements using data loggers with sensors distributed in vertical arrays across the active layer and near-surface permafrost; geophysical measurements using electric, electromagnetic and/or seismic methods; or thaw-depth measurements using mechanical probing with rigid rods or thaw-tube readings (Burn 1998; Hauck 2002; Bonnaventure and Lamoureurx 2013). Of these methods, temperature measurements using data loggers are the most convenient in terms of accuracy, temporal resolution and/or logistics. At many places, however, temperatures are only measured in the active layer and its thickness must therefore be estimated in these situations. This has been done either through extrapolating the active-layer temperatures using statistical methods or through numerical and analytical models.

Analytical models in particular have become widely popular for estimating the active-layer thickness due to their simplicity, relatively small number of input parameters, computational efficiency and yet sufficient accuracy. However, these tools require several ground physical properties such as thermal conductivity or water content as input parameters in addition to temperature variables, which are seldom available at most sites, thereby limiting their use.

This paper presents and tests a novel simple analytical-statistical tool for estimating the active-layer thickness, which builds on the Stefan (1891) model, but unlike that, it is driven solely by thawing indices at two distinct depths within the active layer.

METHODS

The formula for estimating the active-layer thickness ξ was derived using the Stefan (1891) model and is as follows:

$$\xi = \frac{z_2\sqrt{I_1} - z_1\sqrt{I_2}}{\sqrt{I_1} - \sqrt{I_2}}, \qquad [1]$$

where I_1 and I_2 is the thawing index at the depth z_1 and z_2, respectively ($z_1 < z_2 < \xi$). The validity of Equation 1 was tested using field observations of the active-layer thickness and thawing indices in the active layer from a total of 17 sites situated in contrasting permafrost environments of Antarctica and Alaska. We considered three pairwise combinations of thawing indices from the depth intervals of 0−10 cm, 25−35 cm and 45−55 cm (hereafter referred to as 5 cm, 30 cm and 50 cm, respectively), which provided around two hundred seasons with an active-layer thickness greater than the depth of the temperature sensors (~thawing indices) used.

RESULTS AND DISCUSSION

The active-layer thickness modelled by Equation 1 showed the total mean errors of −2.0 cm (−4.3 %), −1.4 cm (−2.4 %) and −2.6 cm (−4.5 %) using thawing indices at the depth pairs of 5/30 cm, 30/50 cm (Figure 1) and 5/50 cm, respectively.

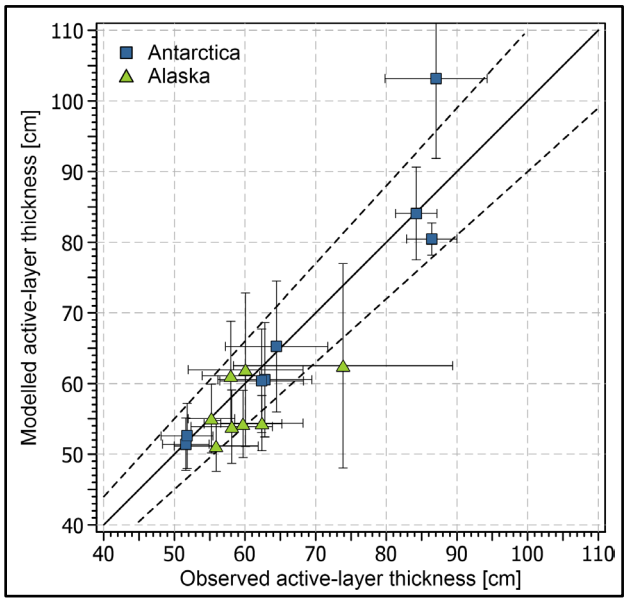

Figure 1. Observed and modelled active-layer thickness using thawing indices at the depth pair of 30/50 cm in Antarctica and Alaska. The black solid and dashed lines represent the line of identity and the error of ±10 %, respectively.

However, the modelled active-layer thickness was more accurate in Antarctica where the mean errors were 5.4 cm (7.1 %), 0.9 cm (0.9 %) and 1.4 cm (1.6 %) for the depth pairs of 5/30 cm, 30/50 cm and

5/50 cm, respectively, while they were −8.6 cm (−14.5 %), −3.6 cm (−5.6 %) and −6.6 cm (−10.5 %) in Alaska. This was largely due to the fact that the active layer tended to be relatively homogeneous at the Antarctic sites, whereas it typically consisted of peat over mineral soil at the Alaskan ones. This is also why the 30/50 cm depth pair showed the lowest errors, as it excluded the surface layer of peat, which is an effective thermal insulator that substantially alters the temperature gradient in the active layer.

Conclusions

The novel analytical-statistical tool for estimating the active-layer thickness worked best when the substrate was homogeneous and the base of the active layer was close below the temperature sensors (~thawing indices) considered. However, its total mean errors were still tested at less than 5 %, which is very promising. The tool can therefore be used wherever at least two temperature measurements are available in the active layer; no ground physical parameters are required. Besides field observations, it can also estimate the active-layer thickness based on various climate reanalyses or climate model products.

Acknowledgement

The research was funded by the Czech Science Foundation (project number GM22-28659M). We acknowledge USDA for access to the soil climate data from Alaska and Antarctica.

References

Burn, C.R. 1998. The Active Layer: Two Contrasting Definitions. Permafrost and Periglacial Processes, 9(4): 411–416. doi:10.1002/(SICI)1099-1530(199810/12)9:4%3C411::AID-PPP292%3E3.0.CO;2-6

Bonnaventure, P.P., and Lamoureux, S.F. 2013. The active layer: A conceptual review of monitoring, modelling techniques and changes in a warming climate. Progress in Physical Geography, 37(3): 352–376. doi:10.1177/0309133313478314

Hauck, C. 2002. Frozen ground monitoring using DC resistivity tomography. Geophysical Research Letters, 29(21): 12-1–12-1. doi:10.1029/2002GL014995

Stefan, J. 1891. Über die Theorie der Eisbildung, insbesondere über die Eisbildung im Polarmeere. Annalen der Physik, 278(2): 269–286. doi:10.1002/andp.18912780206

Mechanistical simulation of permafrost dynamics under climate change at the watershed scale: centennial trends in a catchment of central Siberia

Thibault Xavier[1], Laurent Orgogozo[1], Anatoly S. Prokushkin[2], Esteban Alonso-González[3], Simon Gascoin[4] & Oleg S. Pokrovsky[1,5]

[1]*Géosciences Environnement Toulouse (GET), CNRS, UMR5563, Toulouse, 31400, France*

[2]*V.N. Sukachev Institute of forest SB RAS, Russia*

[3]*Instituto Pirenaico de Ecología, Consejo Superior de Investigaciones Científicas (IPE-CSIC), Jaca, Spain*

[4]*Centre d'Etudes Spatiales de la Biosphère, Université de Toulouse, CNRS/CNES/IRD/INRA/UPS, Toulouse, France*

[5]*BIO-GEO-CLIM Laboratory, Tomsk State University, Tomsk, Russia*

Permafrost dynamic involves non-linear processes and strong coupling between thermal and hydrological transfers (e.g., Hu et al. 2023). A mechanistic approach to solve this stiff problem requires the use of High Performance Computing resources and adapted methodologies. For these reasons, the free, open-source solver permaFoam dedicated to permafrost simulation has been developed within the OpenFOAM framework (Orgogozo et al. 2023).

This paper presents the results obtained with permaFoam on modelling of permafrost dynamics under climate change within a small catchment in Central Siberia. Simulations are carried out until 2100 using CMIP6 scenarios and a quantitative assessment of the thermal equilibrium state of the near-surface permafrost layer (up to 10 m depth) at the end of the century is provided.

The Kulingdakan watershed

The Kulingdakan watershed is located in the East Siberia region (64°31' N, 100°28'E) in the continuous permafrost zone (Figure 1) within a boreal deciduous (larch) forest biome. The watershed, of a total area of 41 km^2, is divided by a East-West river into two slopes, a South Aspected Slope and a North Aspected Slope.

This watershed has been studied and monitored for about two decades (Prokushkin et al. 2007), with in-situ measurements of soil temperature and active layer thickness, and thus is a good candidate for being the subject of a permafrost dynamics study by mechanistical modelling (Orgogozo et al. 2019).

Centennial simulations built on CMIP6 scenarios

Four scenarios are extracted from CMIP6 simulations (SSP1-2.6, SSP2-4.5, SSP3-7.0, SSP5-8.5 from low-forcing sustainable pathway to high-end forcing pathway) and used to provide with the meteorological forcing. Snowpack dynamics under climate change are taken into account by a dedicated degree-day model, calibrated on the observation data translated into snow water equivalent with the use of the MuSA toolbox (Alonso-González et al. 2022). A transfer function model is used to derive empirically the soil surface temperature from the atmospheric conditions by taking into account the insulating effect of both snowpack and moss layers.

The code permaFoam is used on a supercomputing architecture together with a dedicated numerical procedure to efficiently manage and post-process the ensemble of simulations. To obtain the projection of permafrost dynamics through the century for a given climatic scenario on one slope, one month of simulation time is approximately required, using 400k CPU hours and providing 400 GB of data.

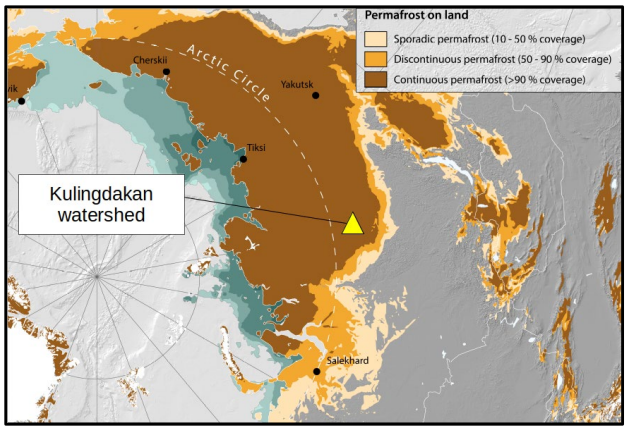

Figure 1. Location of Kulingdakan watershed. Map from GRID-Arendal/Nunataryuk.

Key variables evolution

Several key variables are extracted from the simulations to describe permafrost dynamics, such as active layer thickness, soil temperature or soil water content. The thermohydric dynamics exhibited significantly different responses to the external

forcing depending on both the climate scenario and the slope considered.

Tables 1 and 2 show the change in active layer thickness observed between present climate and 2100 for the four considered climate scenarios. Significant changes are expected at the end of the century with up to +46% in the south-facing slope active layer thickness for SSP5-8.5 scenario. Besides, in this case, the active layer on the north-facing slope could reach a thickness in 2100 comparable to that observed on south-facing slope under present climate (~1 m).

Table 1. Active layer thickness obtained from the simulation for present climate and year 2100.

Active layer thickness (cm)	North-facing slope	South-facing slope
Present climate	64	99
SSP1-2.6 (2100)	72	112
SSP2-3.5 (2100)	76	119
SSP3-7.0 (2100)	88	135
SSP5-8.5 (2100)	92	144

Table 2. Absolute and relative changes in active layer thickness between present climate and year 2100 obtained from the simulations.

Change in active layer thickness (cm / %)	North-facing slope	South-facing slope
SSP1-2.6	+8 / +12	+13 / +13
SSP2-3.5	+12 / +18	+20 / +20
SSP3-7.0	+24 / +37	+36 / +37
SSP5-8.5	+28 / +44	+45 / +46

EQUILIBRIUM STATE AT THE END OF THE CENTURY

To further assess the equilibrium state of the first ten metres of soil at the end of the century, extra 30 years of simulation were run under 2100 conditions and the observed change are discussed.

The simulations demonstrate that under the two scenarios with the highest radiative forcing increase (SSP3-7.0, SSP5-8.5), south-facing slope near-surface permafrost is still far from thermal equilibrium in 2100.

ACKNOWLEDGEMENTS

This work has been funded by the French National Research Agency ANR (grant n° ANR-19 CE46-0003-01), and benefited from access to the supercomputers of CALMIP (project p12166) and GENCI (project A0140410794, TGCC).

REFERENCES

Alonso-González, E., Aalstad, K., Baba, M.W., Revuelto, J., López-Moreno, J.I., Fiddes, J., Essery R., and Gascoin, S. 2022. The Multiple Snow Data Assimilation System (MuSA v1.0), Geosci. Model Dev., 15, 9127–9155. https://doi.org/10.5194/gmd-15-9127-2022

Hu, G., Zhao, L., Li, R., Park, H., Wu, X., Su, Y., Guggenberger, G., Wu, T., Zou, D., Zhu, X., Zhang, W., Wu, Y., and Hao, J. 2023. Water and heat coupling processes and its simulation in frozen soils: Current status and future research directions, CATENA, Volume 222, 106844, ISSN 0341-8162. https://doi.org/10.1016/j.catena.2022.106844

Orgogozo, L., Prokushkin, A.S., Pokrovsky, O.S., Grenier, C., Quintard, M., Viers, J., and Audry, S. 2019. Water and energy transfer modeling in a permafrost-dominated, forested catchment of Central Siberia: The key role of rooting depth, Permafrost and Periglacial Processes, 30: 75–89. https://doi.org/10.1002/ppp.1995

Orgogozo, L., Xavier, T., Oulbani, H., and Grenier, C. 2023. Permafrost modelling with OpenFOAM®: New advancements of the permaFoam solver, Computer Physics Communications, 282. https://doi.org/10.1016/j.cpc.2022.108541

Prokushkin, A.S., Gleixner, G., McDowell, W.H., Ruehlow, S., and Schulze, E.-D. 2007. Source- and substrate-specific export of dissolved organic matter from permafrost-dominated forested watershed in central Siberia, Global Biogeochem. Cycles, 21, GB4003. https://doi.org/10.1029/2007GB002938

Permafrost in basin may face higher degradation risk under warm climates

Xinyao Zhang[1] & Mousong Wu[2]

[1]*Department of Earth System Science, Tsinghua University, Beijing, China*

[2]*International Institute for Earth System Science of Nanjing University, Nanjing, Jiangsu, China*

The Tibetan Plateau (TP), which contains the most extensive permafrost zone at middle and low latitudes, is experiencing a rapid degeneration induced by global warming (Zhao et al. 2020). Permafrost over the TP could be divided into several degradation stages by soil thermal stability (Ran et al. 2021). Complex terrains influence regional hydrological processes by converging the meltwater and precipitation in lowland (Gao et al. 2018), and thus affect permafrost evolution. However, most of the previous studies concentrate on the variations of permafrost thermal states and hydraulic transfer, but neglect the impacts of degradation stage and topography. In this study, CoupModel, a physics-based model coupled soil hydrothermal processes, was calibrated and validated against the borehole data. And three numerical experiments were conducted to simulate the permafrost evolution until 2100 at two sites which are very close to each other but with different degeneration periods and topographies.

Data and method

The Upslope Site (UPS) and the Downslope Site (DWS) are located in Kangqiong small basin (35.26°N, 96.53°E) of the northeastern Tibetan Plateau. The UPS is situated on a gentle slope and represents the final stage of permafrost degradation, while the DWS is nestled in basin and categorized into initial degradation period. Soil temperature and water content were measured at both sites during 2017-2020 at depths of 20, 50, 80, 120, 160, and 200 cm. In order to simulate permafrost evolution, future climate conditions were accessed from the CMIP6 data, which was downscaled and bias-corrected by the CMFD and TPHiPr data. Three scenarios under different Shared Socioeconomic Pathways (SSP): SSP1-2.6, SSP2-4.5 and SSP5-8.5 were considered in this study.

The experiment design could be divided into three steps. Firstly, 8 sensitive parameters were picked out based on previous studies to represent site characteristics. To depict topography induced water inflow, 8.93 times extra precipitation was set at the DWS determined by sensitivity analysis, and just around 0.33 times could be conserved considering the runoff. Secondly, CoupModel was calibrated against the borehole data and showed good performances on both sites. Thirdly, three numerical experiments were conducted to simulate the permafrost evolution until 2100. The first (DWS) and second (UPS) experiments represent the permafrost evolution at the DWS and UPS respectively. And the third experiment (DWS-topo) indicates the permafrost evolution at the DWS without topography impacts.

Preliminary results

Simulation results demonstrate that the permafrost at two sites will suffer distinct degradations under warm climates and the DWS will experience faster degenerations under the same scenario. Figure 1 shows that the mean annual soil temperatures at a depth of 0-20 m (ST20) are projected to increase by 5.4 °C and 2.6 °C during 2040-2100 under SSP5-8.5 at the DWS and UPS respectively. Accompanied by permafrost thawing, soil water storage reduces, evapotranspiration enhances, and runoff increases. According to Figure 3, the soil water storages decrease at a rate of 28 mm/year and 7 mm/year, the mean annual evapotranspirations are 648 mm and 521 mm, and the annual average runoffs are 447 mm and 291 mm during 2050-2090 under SSP5-8.5 at the DWS and UPS individually.

Simulation results also indicate that topography induced water inflow is the predominant factor to accelerate thawing at the DWS under warm climates, and the impacts of other factors such as degradation stages are limited compared to topography. As shown in Figure 2, the ST20 could decrease by 4.2 °C in 2100 at DWS without additional inflow. The possible mechanisms are as follows. The extra inflow consists of precipitation and meltwater, which will bring large amounts of heat into permafrost under warm scenarios. The extra water also makes surface soil moister and enhance evapotranspiration. The ground ice transforms to liquid water and then run off during thawing, causing the reduction of soil water storage. Therefore, more attentions should be paid to the permafrost in basin and lowland over the TP because of the higher degradation risk.

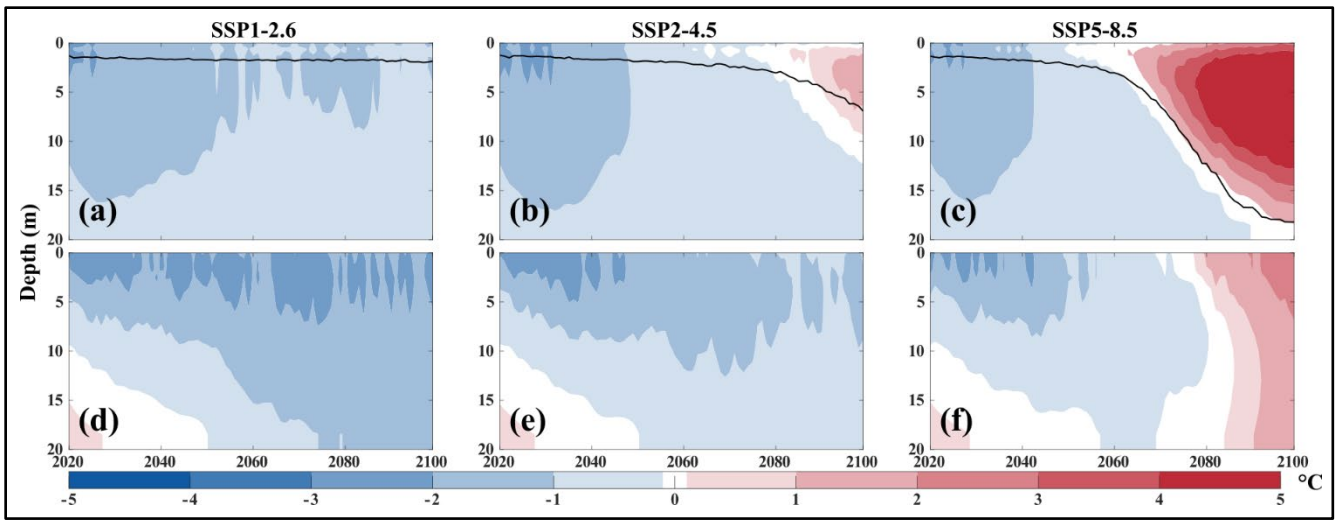

Figure 1. The simulated mean annual soil temperature profiles of the (a)-(c) DWS and (d)-(f) UPS experiments under three scenarios. The black lines represent the Active Layer Thicknesses (ALTs).

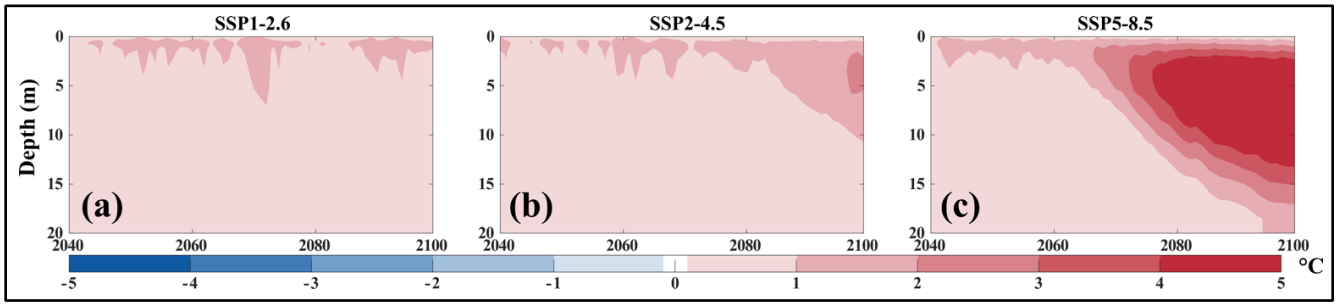

Figure 2. The differences of the simulated mean annual soil temperature profiles between the DWS and DWS-topo experiments (DWS minus DWS-topo) under three scenarios.

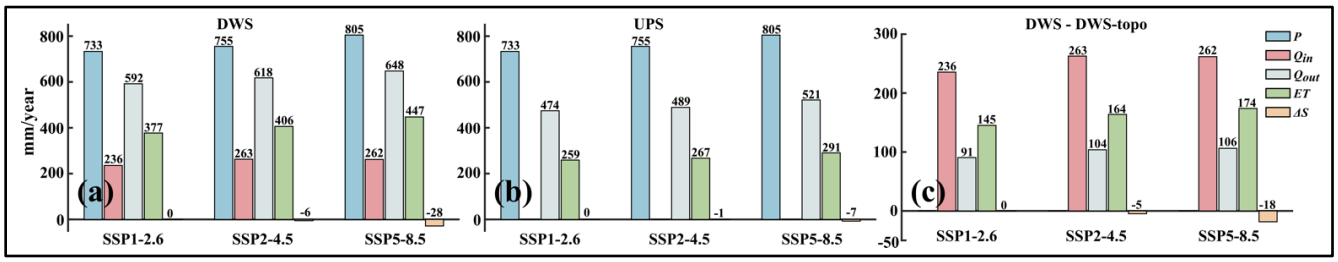

Figure 3. The water budgets of the (a) DWS and (b) UPS experiments, and (c) the water budget differences between the DWS and DWS-topo experiments (DWS minus DWS-topo) during 2050-2090. Where P is precipitation, Qin is water inflow, Qout is water outflow, ET is evapotranspiration and ΔS is change in water storage.

REFERENCES

Zhao, L., et al. 2020. Changing climate and the permafrost environment on the Qinghai–Tibet (Xizang) plateau, Permafrost and Periglacial Processes, 31(3): 396–405. doi:10.1002/ppp.2056

Ran, Y., et al. 2021. Mapping the permafrost stability on the Tibetan Plateau for 2005–2015, Science China Earth Sciences, 64(1): 62–79. doi:10.1007/s11430-020-9685-3

Gao, B., et al. 2018. Change in frozen soils and its effect on regional hydrology, upper Heihe basin, northeastern Qinghai–Tibetan Plateau, The Cryosphere, 12(2): 657–673. doi:10.5194/tc-12-657-2018

Impacts of lateral conductive heat flow on ground temperature and implications for permafrost modelling and mapping

Yu Zhang, Gang Hong & Mitchell T. Bonney

Canada Centre for Remote Sensing, Canada Centre for Mapping and Earth Observation, Natural Resources Canada, Ottawa, Ontario, Canada

Annual mean near-surface ground temperature (Tnsg) in permafrost regions can vary by 5 to 10 °C at a landscape scale due to differences in snow cover, topography, vegetation, water, and soil conditions, particularly due to the effects of water bodies and redistribution of snow by wind (e.g., Zhang et al. 2021). This large spatial variation affects permafrost condition and its response to climate change, which have significant impacts on infrastructure, eco-systems, hydrology, and greenhouse gas emissions. To capture this spatial variation, permafrost distributions have been mapped at increasingly high spatial resolutions. The grid size of the permafrost maps has decreased from tens of kilometers to tens of metres (e.g., Zhang et al. 2012). Most permafrost maps were developed based on one-dimensional (1D) approaches, which explicitly or implicitly assumed that the ground temperature (Tg) is determined by vertical heat flow. The effects of lateral heat flow from surrounding areas were not considered. In this study, we theoretically calculated the impacts of lateral conductive heat flow on Tg under equilibrium and transient conditions and discussed the implications for modelling and mapping permafrost.

Methods and data

We theoretically calculated the impacts of conductive heat flow on Tg based on the method developed by Lachenbruch (1957). This method assumes that the ground is uniform in thermal conductivity and heat capacity, and there is no latent heat involved (i.e., no thawing and freezing). We calculated the Tg below a site O due to the impacts of a) a circular area, b) a square grid, c) a circular annulus (their centres are at point O in all these three cases), and d) a very large area beside the point O. We calculated the Tg profiles under point O for transient and equilibrium conditions. For transient analysis, we assumed that the Tnsg increases at a rate of 0.1 °C/year from an initial equilibrium condition.

To validate the method, we compared calculated Tg profiles with observations in a mining area near Schefferville (54°48'N, 66°49' W) in eastern Canada. Ground temperatures up to 100-m depth were observed at multiple sites in a 20-km by 4-km stripe by the McGill Sub-Arctic Research Laboratory with support from the Iron Ore Company of Canada from 1957 to 1982 (Granberg et al. 1984). The data are from Smith et al. (2003), which include Tg observations at 191 sites measured in various periods from 1957 to 1982.

Results

Under equilibrium condition, the impact of a square on the Tg under its centre point O is directly related to the ratio between the side-length of the square and the depth at which Tg is considered. The impacts of squares with side-lengths of 2z, 4z, 6z, and 10z account for 33%, 59%, 71%, and 82% of the total effects of the entire ground surface on Tg at depth z. A small area affects only the Tg at shallow ground while large areas affect the Tg from near the surface to deep ground.

Similarly, the impact of an annulus on the Tg also depends on the ratios between the size of the annulus and the depth where the Tg is considered. Under equilibrium conditions, there is a depth where the impact has a maximum value, and the maximum impact depth increases with the radii of the annulus, especially the radius of the inner circle. For a unit area of a section of annulus (i.e., the ring width is 1 m and the average arc length of the inner and outer circles of the section of the annulus is 1 m), its maximum impact depth is approximately 0.707 times of the distance from the centre of the unit area to the site.

For transient impacts, increase in Tnsg causes warming of the ground top-down, and the impacts depend on time. The longer the change in Tnsg, the deeper the impacts on Tg. If the increase in Tnsg occurs in the whole area, the impact (using a criterion of 0.1 °C) reaches about 190 and 300 m in 100 and 200 years, respectively. If the increase of Tnsg occurs only in a circular area for certain years, then its impact on the Tg under the centre of the circular area increases with the size of the circular area when it is small. However, the impact gradually becomes independent of the size of the circular area due to the limit of time needed for heat transfer. For timescales of 100 and 200 years, the impacts of the circular areas do not change with the size when the radii of the circular areas are more than about 130 and 200 m, respectively.

Lateral conductive heat flow causes non-linear patterns in the distribution of Tg with depth. Observed Tg profiles near Schefferville show different patterns: Tg increased with depth at most sites where Tnsg was relatively low, but Tg decreased with depth when Tnsg was relatively high. These patterns can generally be explained by the theoretically calculated Tg profiles under circular areas and annulus with different Tnsg.

Implications for permafrost modelling and mapping

One-dimensional permafrost models assume that Tg is determined by conditions in local area. The initial conditions of 1D models are usually determined by running the model iteratively (spinning up) assuming that the Tg is in equilibrium. Our theoretical calculation indicates that the impact of a local grid under equilibrium condition is related to the ratio between the grid size and depth of Tg. To include 59% of the impacts of the entire land surface, the side-length of the grid should be four times of the depth at which the Tg is considered. Permafrost thickness ranges from less than 10 m to nearly a kilometer. The corresponding side-lengths of the grids are 40 m, 400 m, and 2 km for calculating the Tg at 10 m, 100 m and 500 m depths, respectively. These are the grid sizes to include only 59% of the impact of the entire land surface on the Tg at these depths. A larger grid size is needed to include a higher percentage.

The required grid size for 1D modelling can also be estimated based on calculated errors. To keep the errors <1 °C at 10 m, 100 m and 500 m depths, the side-lengths of the grids must be >88 m, >880 m, and >4.4 km, respectively, if the Tnsg of the grids is 5 °C lower than the Tnsg of the surrounding area. Therefore, initializing 1D models needs to use a large grid size.

The required grid size for transient change is smaller than that required at equilibrium conditions. For timescales of 100 and 200 years under an increase rate of Tnsg by 0.1 °C/year, the required radii of the local area are 130 m and 200 m, respectively, to keep the impacts of the surrounding areas less than 0.1 °C. The transient impact areas are small because the impacts of surrounding areas are limited by time (the surrounding areas mainly affect the Tg at deeper depths, which require longer time to transfer the Tnsg disturbance to these depths).

Discussion and conclusions

One-dimensional process-based models are initialized assuming that the Tg is in equilibrium with the Tnsg, and Tg almost linearly increases with depth. Our theoretical calculation and observations near Schefferville show that Tg profiles are non-linear due to lateral heat flow effects. Errors in initial conditions (initial Tg and the corresponding permafrost thickness) directly affect the accuracy of the model results, especially for predicting changes with climate at high spatial resolutions. Such an initialization procedure is valid only when the grid is quite large (i.e., at coarse spatial resolutions). Under transient conditions, lateral conductive heat flows affect relatively small areas and shallow depths for timescales of one or two centuries.

Our calculation shows a large downward heat flux with climate warming and this heat flux increases with time if climate warming continues. This heat flux can be much larger than the upward geothermal heat flux. Therefore, using a constant geothermal heat flux as the lower boundary condition can over-estimate the warming of the ground, especially when the lower boundary of the model is shallow.

Observations show large variations in Tnsg in short distances in permafrost regions; thus, lateral effects on Tg might be quite common. Therefore, it is necessary to consider the effects of lateral heat flows on Tg, especially for modelling and mapping permafrost at high spatial resolutions.

References

Granberg, H.B., Lewis, J.E., Moore, T.R., Steer, P., and Wright, R.K. 1984. Schefferville Permafrost Research. Volume I, Parts 1a and 1b: Summary, Review and Recommendations, and Catalogue of Available Materials. Earth Physics Branch Open File Number 84-7. 92p. doi:10.4095/293687

Lachenbruch, A.H. 1957. Three-Dimensional Heat Conduction in Permafrost Beneath Heated Buildings. U.S. Geological Survey Bulletin, 1052-B, 51–69.

Smith, S., Granberg, H.B., and Burgess, M. 2003. Schefferville Permafrost Temperature Database, Version 1. Geological Survey of Canada, Natural Resources Canada. Data available at https://nsidc.org/data/GGD605/versions/1

Zhang, Y., Touzi, R., Feng, W., Hong, G., Lantz, T.C., and Kokelj, S.V. 2021. Landscape-Scale Variations in Near Surface Soil Temperature and Active-Layer Thickness: Implications for High-Resolution Permafrost Mapping. Permafrost and Periglacial Processes, 32(4), 627–640. doi:10.1002/ppp.2104

Zhang, Y., Li, J., Wang, X., Chen, W., Sladen, W., Dyke, L., Dredge, L., et al. 2012. Modelling and Mapping Permafrost at High Spatial Resolution in Wapusk National Park, Hudson Bay Lowlands. Canadian Journal of Earth Sciences, 49(8): 925–937. doi:10.1139/E2012-031

Cold Region Engineering Modelling, Characterization, Observations & Testing

8C — Geomechanics and Engineering Geophysics for Permafrost Characterization

Session Chairs: Teddi Herring[1], Heather Brooks[2] & Mahya Roustaei[3]

[1]*University of Calgary, Calgary, Alberta, Canada*
[2]*BGC Engineering Inc., Calgary, Alberta, Canada*
[3]*Ghent University, Ghent, Belgium*

Designing and maintaining resilient infrastructure in cold regions is a critical challenge for northern communities and governments. Stakeholders are looking for geotechnical approaches to improve the resilience of existing infrastructure and to enable the design and construction of new, sustainable, climate-resilient infrastructure in changing cold regions. To this end, it is essential to understand the physical and mechanical properties of permafrost, as these properties will determine the future performance of infrastructure in a changing climate.

In this session, we invite contributions in areas of the novel site or material characterization methods, techniques, and tools that further our understanding of the physical and mechanical properties of frozen ground. These include recent advances in geomechanical and geophysical measurement techniques to assess spatial and temporal variation of the ground's physical properties or incorporate these data for next-generation models of frozen ground and its response. These techniques provide new tools to better understand, analyse, and predict the behaviour of frozen ground.

Effects of melting permafrost on earthquake site hazards

Jan Dettmer & Jeremy M. Gosselin

Department of Earth, Energy, and Environment, University of Calgary, Calgary, Alberta, Canada

Permafrost thaw negatively impacts ecosystems and infrastructure throughout northern regions, which are warming more than two times the global average rate. Permafrost thaw increases risk for many natural hazards including landslides and thaw subsidence. Yet, little is known about how melting changes earthquake site hazards; including how ground shaking is affected by temporal changes to subsurface properties. Specifically, ground shaking intensity is affected by the physical phenomena of amplification, resonance, and dynamic liquefaction. These phenomena in turn cause triggering of other geohazards. The effects of climate change on earthquake hazards may be significant long before permafrost layers completely vanish. Seismic site effects generally cause increased hazards since soil rigidity decreases. For example, liquid-state pore fluid at the base of the acive layers may cause significant liquefaction potential. Subsurface shear-wave velocity is an important property in earthquake engineering, and is a proxy for ground rigidity. Low shear-wave velocities result in increased shaking-related hazards.

Permafrost plays a crucial role for soil stiffness and shear strength, and its degradation is a source for increasing risks. During earthquake shaking, the degradation likely causes increased shaking, liquefaction, subsidence, and landslide potential. However, the severities of these impacts remain poorly studied. This work considers seismic site characterization and hazard assessment for discontinuous permafrost environments.

Data and methods

Seismic site classification and ground-motion models typically rely on the travel-time average of seismic shear-wave velocity over the uppermost 30 m of soil (e.g., Boore and Atkinson 2008; Seyhan and Stewart 2014). This common engineering parameter is referred to as VS30, and is implicitly weighted more heavily towards low-rigidity (i.e., low-velocity) soils which increase hazards. The National Building Code of Canada Seismic Hazard Model adopts the site classification scheme of the National Earthquake and Hazards Reduction Program (NEHRP; Table 1). This classification assigns hazard factors which are incorporated in Canada-wide seismic-hazard models (e.g., Adams et al. 2015). Currently, few site-specific measurements from northern Canada are used to inform national hazard models. Furthermore, national seismic hazard models currently do not consider variations in seismic hazard due to climate change (specifically due to permafrost thaw). This work aims to improve seismic hazard assessment for northern Canada, as well as improve understanding of potential site-specific changes in seismic hazards.

Table 1. National Building Code of Canada Seismic Site Classification (Adams et al. 2015).

Site Class	Description	VS30 (m/s)
A	Hard rock	>1500
B	Rock	760-1500
C	Very dense soil and soft rock	360-760
D	Stiff soil	180-360
E	Soil with soft clay	<180
F	Site-specific analysis required	-

Seismic site hazards are analyzed by the common earthquake engineering parameters of linear amplification terms for predicted peak ground velocity (PGV), peak ground acceleration (PGA), and spectral acceleration (SA). These quantities describe the expected amplified response of a particular site to earthquake shaking, with respect to class B (rock) conditions. Furthermore, we employ numerical simulations of seismic waves incident on specific soil profiles (e.g., Boore 2000).

Here, seismic site classification and amplification terms were calculated for a range of hypothetical 1D models representative of discontinuous permafrost environments (Figure 1). Additionally, site-specific seismic hazard assessment is conducted for soil properties inferred from geophysical data (e.g., Molnar et al. 2010; Gosselin et al. 2018) recorded at study sites in western Yukon, in a region of discontinuous permafrost. In collaboration with the Yukon Geological Survey (YGS), passive seismic datasets were recorded at a variety of sites. These include locations with known permafrost, and a variety of types of soil and vegetation cover. Locations with cleared forests (of known clearing date) may provide a proxy for permafrost thaw evolution, as forest removal accelerates permafrost thermal response and degradation. Consequently, we investigate site-specific seismic hazards for varying soil types and permafrost conditions (i.e., thaw state).

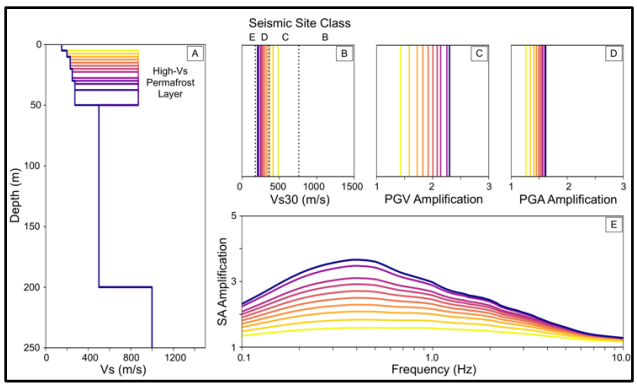

Figure 1. Changes to earthquake site hazards due to varying permafrost degradation. (a) A model with a 5-m thick active layer over 45 m of permafrost is shown in yellow. A model with no permafrost is shown in blue. (b) Sites are classified according to the time-averaged shear-wave velocity of the shallowest 30 m (VS30; Table 1). Linear site terms of earthquake ground-motion prediction equations (Seyhan and Stewart 2014) are shown for (c) expected peak ground velocity (PGV), (d) peak ground acceleration (PGA) and (e) spectral acceleration (SA).

Discussion and Conclusion

Seismic site amplification terms are calculated for hypothetical and inferred 1D models representative of discontinuous permafrost environments. Figure 1 presents expected seismic site amplification (relative to rock conditions) under varying extent of permafrost degradation for a model that is representative of some regions in south-west Yukon. Note that the shear-wave velocity of 850 m/s chosen for the frozen layer is representative of soils with some ice content in pore space. In comparison, ice-rich permnafrosts and permafrosts at lower temperatures can exhibit shear-wave velocities of >1700 m/s (Dou et al. 2014). Consequently, our analysis represents conservative estimates of changes in seismic site hazards due to thaw. This example illustrates that, all else being equal, the removal of high shear-wave velocity permafrost layers can lead to significantly increased amplification of earthquake shaking (up to 4 times). Seismic hazard assessment of inferred soil properties for sites in south-western Yukon provides valuable new constraints for national seismic hazard models. Furthermore, these results illuminate how seismic hazards vary spatially, and potentially through time, in complex (discontinuous) permafrost environments.

Soil seismic properties can be measured or inferred through a variety of methods. The earthquake hazard assessment discussed here is not restricted to passive seismic investigations. However, the methods used to infer 1D models of soil structure for this work are non-invasive and offer a straightforward approach to propagate uncertainty in soil properties into uncertainty in seismic site assessment (e.g., Molnar et al. 2010; Gosselin et al. 2018). Future work may incorporate additional geological constraints and other geophysical data types (e.g., passive electrical resistive measurements).

Our initial results indicate that climate-change likely has, and will, influence earthquake site hazards in northern Canada. Such impacts should be considered in future seismic hazard models.

Acknowledgements

We respectfully acknowledge that data in support of this research are collected in the traditional territory of the Champagne and Aishihik First Nations. We would like to acknowledge financial support from the Yukon Geological Survey and from the Natural Sciences and Engineereing Research Council Discovery Grant to Jan Dettmer, and a postdoctoral fellowship to Jeremy M. Gosselin.

References

Adams, J., Halchuk, S., Allen, T., and Rogers, G. 2015. Canada's 5th generation seismic hazard model, as prepared for the 2015 National Building Code of Canada. In 11th Canadian Conference on Earthquake Engineering, Victoria, BC, Canada, 21–24.

Boore, D.M. 2000. SMSIM--Fortran programs for simulating ground motions from earthquakes: Version 2.0.-- OFR 96-80-A (No. 2000-509). US Geological Survey.

Boore, D.M., and Atkinson, G.M. 2008. Ground-motion prediction equations for the average horizontal component of PGA, PGV, and 5%-damped PSA at spectral periods between 0.01 s and 10.0 s, Earthquake spectra, 24(1): 99–138. doi.org/10.1193/1.2830434

Dou, S., and Ajo-Franklin, J.B. 2014. Full-wavefield inversion of surface waves for mapping embedded low-velocity zones in permafrost, Geophysics, 79(6): EN107–EN124. doi.org/10.1190/geo2013-0427.1

Gosselin, J.M., Cassidy, J.F., Dosso, S.E., and Brillon, C. 2018. Probabilistic seismic-hazard site assessment in Kitimat, British Columbia, from Bayesian inversion of surface-wave dispersion. Canadian Geotechnical Journal, 55(7): 928–940. doi.org/10.1139/cgj-2017-0265@cgj-ec.2018.01.issue-7

Molnar, S., Cassidy, J.F., and Dosso, S.E. 2010. Bayesian inversion of microtremor array dispersion data in southwestern British Columbia, Geophysical Journal International, 183(2): 923–940. doi.org/10.1111/j.1365-246X.2010.04761.x

Seyhan, E., and Stewart, J.P. 2014. Semi-empirical nonlinear site amplification from NGA-West2 data and simulations, Earthquake Spectra, 30(3): 1241–1256. doi.org/10.1193/063013EQS1

A numerical investigation of ice-filled discontinuities relating to rock mass destabilization due to ice-rock detachment

Greg Gambino[1,3], Stephan Gruber[2] & John P. Harrison[3]

[1]*WSP Canada Inc., Mississauga, Ontario, Canada*

[2]*Department of Geography and Environmental Studies, Carleton University, Ottawa, Ontario, Canada*

[3]*Department of Civil and Mineral Engineering, University of Toronto, Toronto, Ontario, Canada*

The detachment of blocks due to the thawing of ice-filled discontinuities (IFDs) in rock is a significant hazard to civil and mining infrastructure, and to other forms of land use. Hazards caused by rockfall events in alpine regions have also been associated with the degradation of ice-filled discontinuities and can have a significant impact high mountain infrastructure stability and landscape evolution (Ravanel et al. 2010). Developing a better understanding of the thermo-mechanical behaviour of IFDs is thus critical to the prediction of rock fall hazards due to the thawing of IFDs.

This paper discusses the discovery of the formation of a detachment crack along an ice-rock interface as an IFD thaws (Gambino, 2023). A novel application of ablation modelling is applied in a numerical simulation to investigate the thermo-mechanical behaviour and associated stress development that is related to the thawing of an IFD.

The numerical modelling applied in this work includes heat transfer along the air-rock, air-ice, and ice-rock boundaries. Importantly, the benefit of the novel application of an ablation modelling technique is that the meltwater can freely drain from the simulated IFD at the free surface. The numerical results show that as the ice and rock warm, a detachment crack forms along the ice-rock interface and can extend along the interface significantly more quickly than the observable exposed ice surface that melts radially inward (Figure 1).

The formation of the detachment crack has significant ramification for the development of stress and mechanical propagation that eventually causes complete separation between ice and rock along the IFD interface. Stresses along the ice-rock interface increase exponentially due to the continued IFD thawing (Figure 2). This significant increase in stress as melting occurs, in addition to the stress concentrations that can occur at a crack tip, are likely to be key contributing factors that destabilize rock masses containing IFDs subjected to melting conditions.

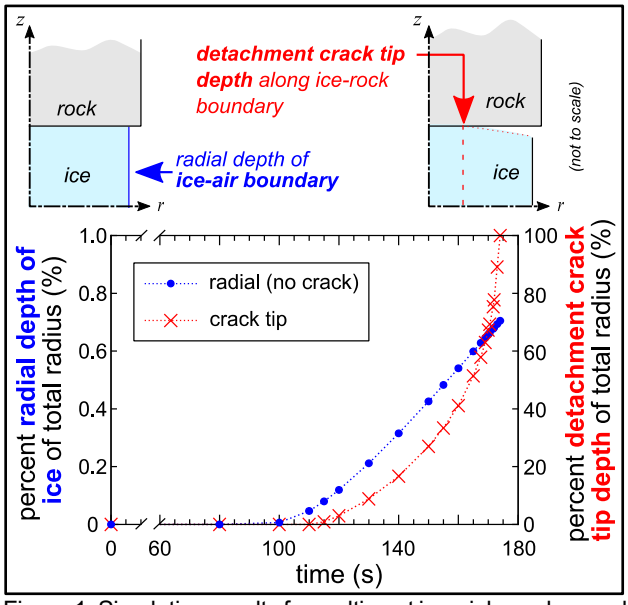

Figure 1. Simulation results for melting at ice-air boundary and the detachment crack depth.

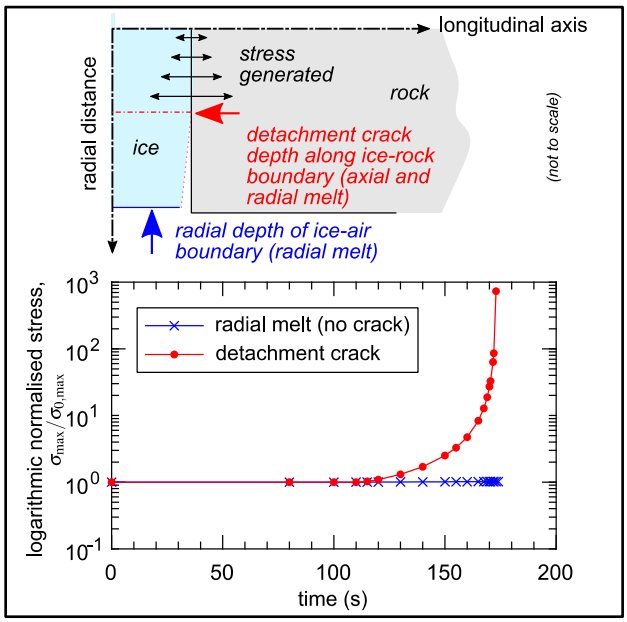

Figure 2. Stress development from detachment crack.

The development and rapid propagation of the crack tip due to ice melting within an IFD and the associated stresses have practical ramifications for assessing and mitigating rock fall hazards in mountainous regions as well as engineering in rock masses containing IFDs. This work demonstrates that the development of a detachment crack is a critical phenomenon to the destabilization of rock masses containing IFDs. Similar to the effect of heat advection by water flow in IFDs (Hasler et al. 2011), the detachment crack is a fracture-scale phenomenon that deviates from the thermal dynamics of the bulk rock mass surrounding it.

REFERENCES

Gambino, G. 2023. Contributions to the thermo-mechanics of ice-filled rock discontinuities for rock engineering design (Doctoral thesis). University of Toronto.

Hasler, A., Gruber, S., Font, M., and Dubois, A. 2011. Advective Heat Transport in Frozen Rock Clefts: Conceptual Model, Laboratory Experiments and Numerical Simulation. Permafr Periglac Process 22, 378–389. https://doi.org/10.1002/ppp.737

Ravanel, L., Allignol, F., Deline, P., Gruber, S., and Ravello, M. 2010. Rock falls in the Mont Blanc Massif in 2007 and 2008. Landslides 7, 493–501. https://doi.org/10.1007/s10346-010-0206-z

A novel inversion of MASW data on saline permafrost soils

Thomas Højland Lorentzen[1], Thomas Mejer Hansen[2] & Thomas Ingeman-Nielsen[1]

[1]*Department of Environmental and Resource Engineering, Technical University of Denmark (DTU), Kgs. Lyngby, Denmark*

[2]*Department of Geoscience, Aarhus University, Aarhus, Denmark*

Permafrost presents unique challenges for near surface geophysical mapping. Multichannel analysis of surface waves (MASW) is a seismic method utilizing the velocity dispersion of surface waves to interpret structure and elastic properties of the subsurface. MASW can be challenged by the multimodal nature of surface waves where higher modes commonly dominate when the subsurface shows large velocity contrast or velocity inversion, i.e. a profile where velocities are not monotonically increasing with depth (Fonti et al. 2018). Such situations can commonly be found in saline permafrost conditions where the porewater salinity may cause layers with high unfrozen water contents beneath fully frozen and ice rich layers. This is the case in Ilulissat, Greenland, where we collected hammer seismic data in April 2021. To gain the best possible dataset, we used both P- and S- wave hammer sources and 3-component geophones to collect a dataset containing both Rayleigh and Love waves. No available MASW inversion scheme was found that could fulfill the requirement of our data from the saline permafrost case, namely: jointly inverting Rayleigh and Love waves, while handling highly multimodal data, to infer a realistic model of the subsurface, and include complex prior information.

The main identified challenge of multimodal MASW lies partly in the high computational demand of evaluating dispersion curves and, more significantly, in our uncertainty about which modes of the synthetic dispersion curves should be compared to the interpreted observed data points. To achieve an inversion scheme that can handle this, we combine the idea of a goodness-of-fit based on the properties of the stiffness matrix (Maraschini and Fonti 2010) with a forward model based on a thin layer approach (Kumar and Naskar 2017), allowing for arbitrarily complex models and thereby similarly complex prior models. We use a rejection sampler (Hansen 2021) to solve the inversion problem. Figure 1 explores the functionality of the inversion process through a synthetic example. The data is a synthetic shot gather that has been transformed to the dispersion spectra shown in Figure 1A and B for Rayleigh and Love waves, respectively. The chosen model is considered realistic for Ilulissat and can be seen in pink in Figure 1C, D and E.

For dispersion data, we propose considering the data as points in the phase-velocity/frequency space rather than the traditional phase-velocity as a function of frequency approach. This implies that we assign an uncertainty to both the frequency and the phase velocity of each point picked in the dispersion spectra. Figure 1A and B also show the picked data points with uncertainties based on the width of the high intensity area in the spectra. By considering the data as two-dimensional, we can capture the information from both flat and steep parts of the dispersion.

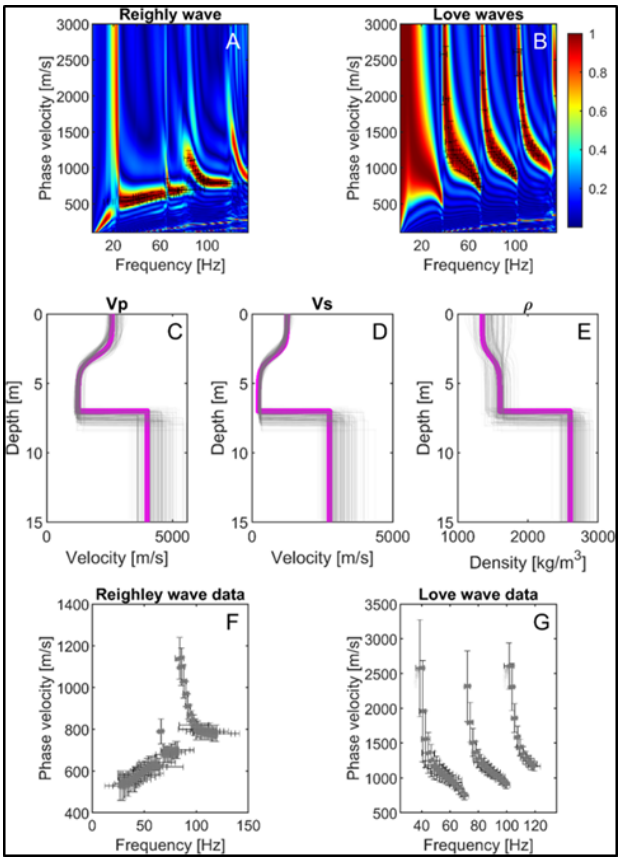

Figure 1. Visualization of a synthetic data set and inversion results. A and B show the dispersion spectra extracted form the synthetic shot gather along with the picked data points and uncertainty estimates. C, D and E show the true model in pink and the accepted inversion models in gray. F and G show the Reighley and Love wave data respectively and the theoretical dispersion curves of the accepted models in gray.

We employ a probabilistic approach to the inverse problem, following Tarantola (2005). This allows for the use of arbitrarily complex 1D models and prior models.

To capture the complexity of Ilulissat case, the prior model describing the subsurface, is made up from discrete thin layers with models parameters of p-wave velocity, s-wave velocity, and density. Specifically, the subsurface was parameterized into a three layer model with a smooth transition from the first to the second layer. The noise model is Gaussian.

Applying a rejection sampling algorithm to solve this problem is not feasible due to the computation time of the dispersion curves. We therefore propose a less computationally heavy approximate likelihood based on the condition number of the stiffness matrix. The approximate likelihood is independent of mode, and allow us to collect a list of models that approximately fit the data.

To evaluate the full likelihood, we assume that the correct mode to associate with a data point is simply the closest mode. Similar to Maraschini and Fonti (2010), we only evaluate the full likelihood for the models collected based on the approximate method, which makes this assumption reasonable. We apply a rejection sampler to the list of models, and thereby find a collection of models fitting the data, representing the posterior distribution, i.e. the solution to the inverse problem. By limiting the number of times the full likelihood has to be evaluated, we end up with a computationally feasible, joint, probabilistic inversion for multimodal surface waves with an informed prior.

The results of the inversion of the synthetic data in Figure 1A and B is shown in Figure 1C, D and E where the accepted models are plotted in transparent gray. The inversion successfully reproduces a good estimate of the Vp and Vs structure of the true model. The density model is poorly resolved, showing a high variability that is mostly constrained by the prior model. Points along the synthetic dispersion curves associated with the data points are shown in Figure 1F and G. A good agreement is demonstrated between the data and the synthetic dispersion curves of the accepted models for both data sets.

The synthetic example demonstrates the effectiveness of the inversion algorithm in handling multimodal data, continuous 1D models, and prior information, while jointly inverting the Rayleigh and Love waves.

REFERENCES

Foti, S., Hollender, F., Garofalo, F. et al. 2018 Guidelines for the good practice of surface wave analysis: a product of the InterPACIFIC project. Bull Earthquake Eng 16, 2367–2420.

Hansen, T.M. 2021. Efficient probabilistic inversion using the rejection sampler—exemplified on airborne EM data, Geophysical Journal International, Volume 224, Issue 1, January 2021, Pages 543–557.

Kumar, J., and Naskar, T. 2017. A fast and accurate method to compute dispersion spectra for layered media using a modified Kausel-Roësset stiffness matrix approach, Soil Dynamics and Earthquake Engineering, Volume 92, Pages 176–182.

Maraschini, M., and Foti, S. 2010. A Monte Carlo multimodal inversion of surface waves, Geophysical Journal International, Volume 182, Issue 3, Pages 1557–1566.

Tarantola, A. 2005. Inverse Problem Theory and methods for model parameter estimation, SIAM.

The need for integrated permafrost science labs and collections, and development of the University of Alberta Permafrost Archives Science Laboratory

Joel Pumple[1,2], Jordan Harvey[1,2], Jeff Kavanaugh[1], Brian Lanoil[1], David Olefeldt[1], Hendrik Poinar[3], Mahya Roustaei[4], Alberto Reyes[1], Suzanne Tank[1] & Duane Froese[1,2]

[1]*Department of Earth and Atmospheric Sciences, University of Alberta, Edmonton, Alberta, Canada*

[2]*Permafrost Archives Science Laboratory, University of Alberta, Edmonton, Alberta, Canada*

[3]*McMaster Ancient DNA Centre, Anthropology and Biochemistry, McMaster University, Hamilton, Ontario, Canada*

[4]*Department of Civil Engineering, Ghent University, Geotechnics Laboratory, Technologiepark, Ghent, Belgium*

The collection of permafrost cores is time-consuming, carbon intensive and often incurs great expense to access remote locations. This work is completed for many reasons, whether engineering, environmental, biological, or palaeobiological, to name a few, but typically cores are collected for a single purpose and commonly discarded following analyses. This is particularly the case for large industrial projects that may spend 100s of thousands of dollars on recovering cores that may be partially or completely consumed during analysis, or discarded for lack of available space to keep samples frozen. However, these cores are potentially of great value with applications in diverse areas of permafrost science and engineering. To meet these needs, we established the Permafrost ArChive Science (PACS) lab funded by the Canadian Foundation for Innovation, Government of Alberta, and hosted at the University of Alberta. PACS Lab is Canada's first integrated permafrost archive and research facility. It provides access to a large collection of permafrost cores from across northern Canada and dedicated research space focused on permafrost science and engineering needs. It supports standardized and comprehensive physical, biogeochemical, and biological characterization and analysis of cores to support new insight into processes and impacts of climate and environmental change in permafrost regions.

At its initial conception there were no labs that addressed the complete use-case that we were proposing but other labs such as the LacCore (lake sediment archive and analytical facility) at the University of Minnesota and National Ice Core Laboratory (NICL) had aspects that were deemed important. These included excellent core archives, trained staff to support users, and analytical facilities to support standardized subsampling and analysis of samples.

In the design of the PACS Lab several capabilities were included:

- Space for archival material available to users across different areas of permafrost science and engineering.
- A cutting room allowing for easy preparation of permafrost samples.
- Imaging facilities to better understand properties of permafrost such as ice content, cryostructures, organic matter distribution and density.
- Analytical facilities for physical properties including grain size, and water isotopes.
- Clean labs specialized for low temperature samples for biogeochemical, microbial or ancient environmental DNA analyses.

Physical and digital permafrost archives

The PACS Laboratory covers about 400 m^2 over the lab areas and archives, with freezers having an estimated capacity for ~2.5 km of 4-inch (~10 cm) diameter core stored in coolers (Figure 1). The physical archive has been used by permafrost and non-permafrost researchers looking to test and develop instrumentation or access material from a particular region present in the archive. At present these requests are made by the staff and evaluated with respect to availability and terms of original collection permits (e.g., Murchie et al. 2021; MacDonald et al. 2021). Access to the archive for these researchers minimizes the cost and carbon footprint of their research. As well, users new to permafrost have access to permafrost-specific expertise and instrumentation and many samples include ancillary data that may reduce costs or increase the context of the new research.

Recently developed non-destructive permafrost specific methods are utilized in the PACS Lab to extend the life and expand the value of the PACS Lab physical archive (Pumple et al. 2023). These non-destructive

methods include the use of Multi-Sensor Core Logging (MSCL) and Computed Tomography (CT) Scanning, which have the ability to rapidly collect bulk density, volumetric ice content and excess ice-content, for example, providing the foundation for a robust digital permafrost archives (Figure 2). In addition to the non-destructive methods, the PACS Lab continues to use traditional analyses to build large permafrost datasets applicable to a range of applications in permafrost science and engineering.

Figure 1. (a) image of PACS Lab archive freezer, (b) image of PACS Lab cutting/core processing room, (c) Nikon XTH 225 ST Industrial CT Scanner (d) Geotek MSCL.

Unlike other areas of geoscience in which communities have come together to build dedicated multi-disciplinary research facilities, no comparable investments have been made for permafrost research. There is need for facilities that can serve the permafrost research communities as attention is increasingly focused on better understanding, predicting and adapting to the ongoing challenges of permafrost change in northern Canada and across the Circumpolar world. The PACS Lab continues to work together with external research groups to develop approaches to integrate instrumentation and methods commonly used in engineering, physics, and chemistry into PACS Lab analyses.

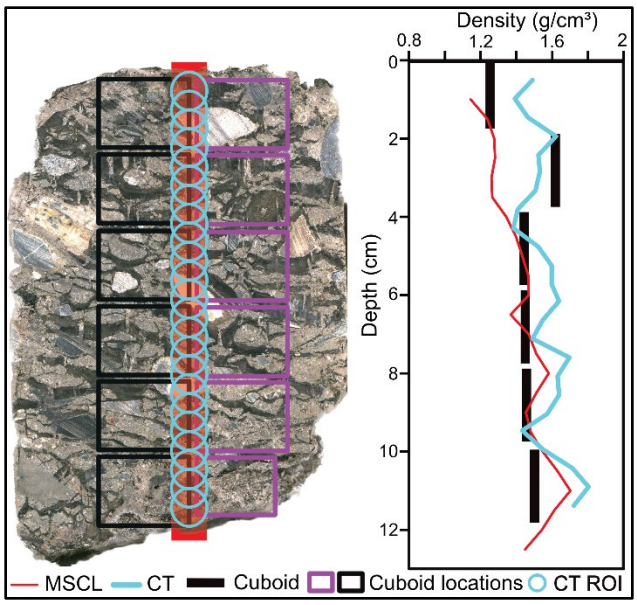

Figure 2. Image of a core highlighting the destructive subsample locations relative to the non-destructive data collection transects.

Conclusions and Future Developments

Permafrost-specific facilities like the PACS Lab foster the development and implementation of destructive and non-destructive methods for collecting physical properties and ultimately result in robust permafrost borehole digital archives. Additionally, these facilities provide increased accessibility to permafrost materials for groups or individuals not working in the north and extend the value of permafrost materials previously collected.

References

MacDonald, E.N., Tank, S.E., Kokelj, S.V., Froese, D.G., and Hutchins, R.H.S. 2021. Permafrost-derived dissolved organic matter composition varies across permafrost end-members in the western Canadian Arctic. Environmental Research Letters, 16(2), 024036.

Murchie, T.J., Monteath, A.J., Mahony, M.E., Long, G.S., Cocker, S., Sadoway, T., Karpinski, E., Zazula, G., MacPhee, R.D.E., Froese, D., and Poinar, H.N. 2021. Collapse of the mammoth-steppe in central Yukon as revealed by ancient environmental DNA. Nature Communications 12, 7120. https://doi.org/10.1038/s41467-021-27439-6

Pumple, J., Monteath, A., Harvey, J., Roustaei, M., Alvarez, A., Buchanan, C., and Froese, D. 2023. Non-destructive multi-sensor core logging allows rapid imaging, measurement of bulk density and estimation of ice content in permafrost cores, The Cryosphere, 2023, 1–27.

Ground ice estimation in permafrost samples using industrial computed tomography

Mahya Roustaei[1], Joel Pumple[2,3], Jordan Harvey[2,3] & Duane Froese[2,3]

[1]*Department of Civil Engineering, Geotechnics Laboratory, Ghent University, Ghent, Belgium*

[2]*Department of Earth & Atmospheric Sciences, University of Alberta, Edmonton, Alberta, Canada*

[3]*Permafrost Archives Science Laboratory, University of Alberta, Edmonton, Alberta, Canada*

The distribution and abundance of ground ice in permafrost is a fundamental property that determines the potential for thaw subsidence and terrain effects of permafrost landscapes. Permafrost is often characterized by the presence of excess ice, or ground ice that exceeds the total pore volume that the ground would have under unfrozen conditions (Van Everdingen 1998). The presence of excess ground ice can affect the permafrost thermal regime, and landscape structure, and is proportional to thaw settlement following disturbance. Widespread thawing of permafrost is expected under a warmer future climate and modeling studies suggest large-scale degradation of near-surface permafrost by the end of this century (Cai et al. 2020). Past studies have illustrated that the presence of excess ice and its distribution in permafrost can significantly affect the rate of permafrost thaw and consequently Arctic ecosystems (Kokelj and Jorgenson 2013). A better estimation of ground ice is important for improving existing methods for mapping the distribution of excess ice at landscape scales, and predicting the impacts of permafrost thaw (Cai et al. 2020). Descriptive systems have been used widely in North America for field and laboratory tests for description of ground ice and excess ice estimation. These approaches are largely visual, accompanied by simple field tests and in some cases more explicit descriptions. Over the last several decades there have been rapid advances in the use of non-destructive methods (e.g., computed tomography) for the investigation of internal textures and physical properties of frozen materials (Calmels and Allard 2004, 2008).

This study uses CT imaging as a non-destructive method to tackle the limitations of traditional ground ice classification methods by measuring frozen bulk density and estimating excess ice and volumetric ice contents quantitatively from five permafrost samples at a high spatial resolution. All the results are compared to a recent study using the same cores but a different non-destructive method, Multi-Sensor Core Logger (MSCL) (Pumple et al. 2023). We show that CT imaging can produce consistent results non-destructively, and provide the added benefit of enhanced digital archives of permafrost physical properties. The development of standardized and interoperable methods for permafrost characterization will build more robust permafrost datasets and strengthen efforts to understand future thaw trajectories of permafrost landscapes.

Methodology

In this study, five cores (one presented here), each representing common materials encountered in permafrost regions, were selected to be scanned by a Nikon XTH 225 ST cabinet-based industrial computed tomography scanner of the Permafrost ArChives Science (PACS) Laboratory (Figure 1A). The 10 cm diameter frozen permafrost half cores were placed in an insulated sample container and were scanned with the reflection target source at 200 Kv and a voxel (3D volume element representing pixel resolution and slice thickness) size of 65 µm (Figure 1B). The subsampled cubes from the cores were scanned with the rotating reflection target source at 225 Kv and a voxel size of 25 µm (Figure 1D). The images were reconstructed into three-dimensional grey-scale volumes using the Nikon CT pro 3D software and analyzed using ORS Dragonfly 2022 image processing software. An internal standard of known density (water) was used in the scans (Figure 1C) to calibrate the resulting linear attenuation coefficients into g/cm^3 using the Nikon CT Pro 3D software. The destructive cuboid method (Kokelj and Burn 2003) was also used to extract the physical properties of samples destructively. The CT extracted results were finally compared to the cuboid methods as well as the recent non-destructive method (Pumple et al. 2023).

Results and discussion

In the image processing step of this study an automatic clustering-based image thresholding, called Otsu method, was used to differentiate materials based on their densities. Image segmentation using the Otsu method resulted in the differentiation of 5 different materials based on their relative densities; air, low ice, high ice, low sediment, and high sediment (shown in Figure 2 for a diamicton core).

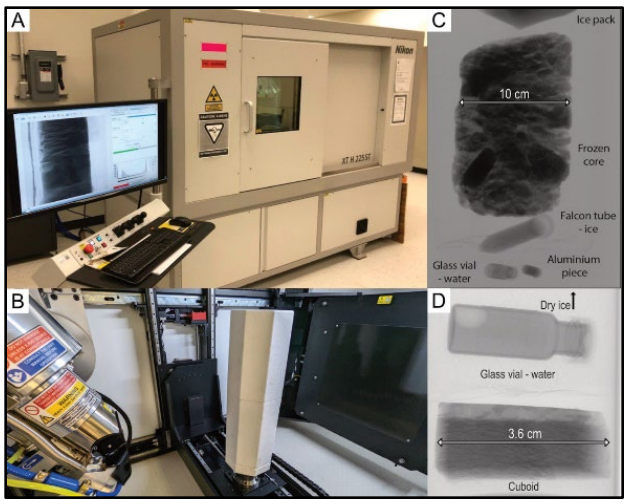

Figure 1. (A) The CT scanner of the PACS Lab.(B) The internal setup for the core scan. (C) X-ray image of the internal setup of the core (D) X-ray image of the internal setup of the cube.

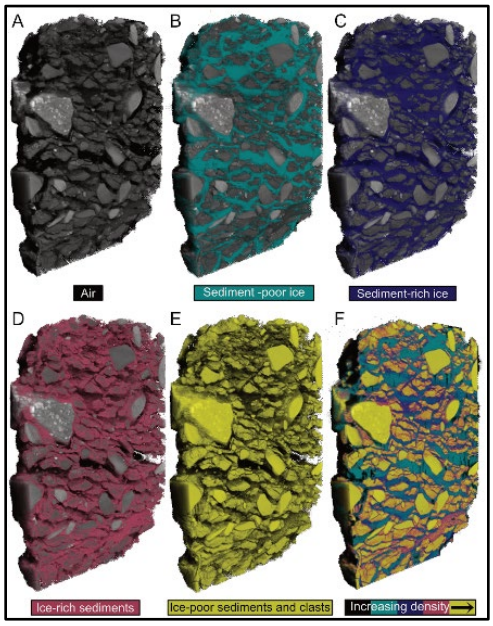

Figure 2. Image segmentation results of the diamicton core.

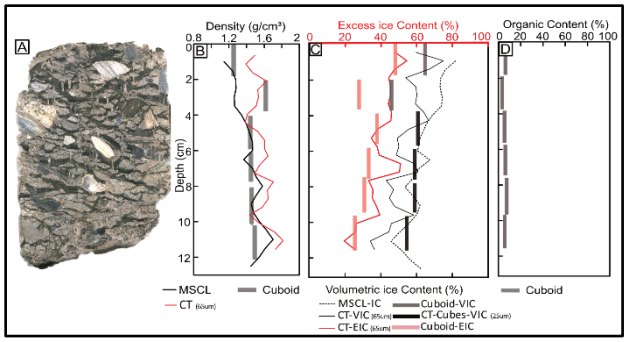

Figure 3. (A) Image of the diamicton core; (B) bulk density; (C) ice contents; (D) organic content distribution in core depth.

Low ice comprises of primary visual or excess ice while high ice mainly results from extraction of pore ice or ice proximal to sediment (sediment-rich ice). Figure 2 illustrates the effectiveness of the Otsu method in generating robust segmentation results while the visual inspection method has its own drawbacks, e.g., inspector's visual acuity and poor reproducibility. The results presented in Figure 3 combine the image processing analysis of CT images of cores and a systematic quantitative comparison between the Cuboid (destructive method) and the recent non-destructive method (Pumple et al. 2023). Physical properties of the permafrost samples, determined from the cuboids, including frozen bulk density, volumetric (VIC) and excess ice contents (EIC), and organic contents are plotted versus the depth of one of the cores (diamicton) and shown as B, C, and D, respectively. The vertical cross-section photo of the core (A) is also presented in this figure. The results showed strong agreement between these methods and demonstrated that these non-destructive techniques can produce consistent and reliable results.

REFERENCES

Cai, L., Lee, H., Schanke Aas, K., and Westermann, S. 2020. Projecting circum-Arctic excess-ground-ice melt with a sub-grid representation in the Community Land Model, Cryosphere, 14, 4611–4626. https://doi.org/10.5194/tc-14-4611-2020

Calmels, F., Clavano, W.R., and Froese, D.G. 2010. Progress on X-ray computed tomography (CT) scanning in permfrost studies, in: GeoCalgary 2010 : the 63. Canadian geotechnical conference and 6. Canadian permafrost conference, Calgary, AB (Canada), 12-15 Sep , 1353–1358.

Van Everdingen, R.O. 1998. Multi-Language Glossary of Permafrost and Related Ground-Ice Terms, Calgary.

Kokelj, S.V., and Burn, C.R. 2003. Ground ice and soluble cations in near-surface permafrost, Inuvik, Northwest Territories, Canada, Permafr. Periglac. Process., 14, 275–289. https://doi.org/10.1002/ppp.458.

Kokelj, S.V., and Jorgenson, M.T. 2013. Advances in Thermokarst Research, Permafr. Periglac. Process., 24, 108–119. https://doi.org/10.1002/ppp.1779

Pumple, J., Monteath, A., Harvey, J., Roustaei, M., Alvarez, A., Buchanan, C., and Froese, D. 2023. Non-destructive multi-sensor core logging allows rapid imaging, measurement of bulk density and estimation of ice content in permafrost cores. EGUsphere, 2023, 1–27.

Cold Region Engineering Modelling, Characterization, Observations & Testing

8D — Investigating Permafrost Using Geophysical Techniques

Session Chairs: Saskia Eppinger[1], Julius Kunz[2] & Burke Minsley[3]

[1]*Technical University of Munich, Munich, Germany*
[2]*University of Wuerzburg, Wuerzburg, Germany*
[3]*US Geological Survey, Denver, Colorado, United States*

Global warming affects Arctic environments and results in changing permafrost characteristics, alteration of permafrost hydrology, release of previously frozen carbon, and amplified morphological changes that can impact both the natural and built environment. Warming or thawing permafrost can multiply potential risks for infrastructure and lead to rapidly changing landscapes. Geophysical techniques are becoming a common field method for detecting internal structures and changes in permafrost and periglacial features or entire landscape units. Ground penetrating radar (GPR), electrical resistivity tomography (ERT), seismic, and electromagnetic (EM) methods have become well-tested and easily applicable to remote Arctic environments.

Due to their robust survey designs, geophysical methods are very useful for detecting and characterizing different permafrost features. Especially multi-dimensional approaches allow the detection of small-scale heterogeneities and can reveal spatial and temporal changes. In recent times, airborne geophysical approaches have been used, which significantly enlarge the spatial extent of measurements. Combined use of geophysics along with other in situ data can contribute to an enhanced understanding of changing permafrost environments and linkages between surface and subsurface changes.

In this session, we welcome contributions focusing on field-based studies on all kinds of Arctic permafrost and periglacial landforms and landscapes, such as thermokarst features (e.g., retrogressive thaw slumps), ice wedges, pingos, or drained lake basins using geophysical techniques. The focus can be on the characterization of internal structure but also on monitoring changes in active layer thickness, coastal erosion, or sub-sea permafrost. Contributions using multidisciplinary approaches of geophysics and other in situ or remote-sensing methods are highly encouraged.

Advantages of different electrical resistivity tomography arrays for mountain permafrost mapping in the Dry Andes of Argentina

Diana Agostina Ortiz[1], Cristian Daniel Villarroel[2] & Lothar Schrott[1]

[1]*Department of Geography, University of Bonn, Bonn, Germany*

[2]*Research Centre of the Geosphere and Biosphere (CIGEOBIO-CONICET). FCEN-UNCUYO, San Juan, Argentina*

In remote regions as the Central Andes, studies on the occurrence and spatial distribution of mountain permafrost are scarce. Since the water contained in periglacial landforms play a significant role in most Andean and sub-Andean ecosystems and human societies, serving as a vital source for irrigation, industrial processes, and domestic use, knowledge about the spatial distribution and its significance holds particular regional importance.

Electrical resistivity tomography (ERT) helps to identify mountain permafrost; however, the most reliable result depends on the type of array applied. The use of different array combinations (Schlumberger, Wenner, Dipole- Dipole) is a very common practice when using ERT as a methodology to investigate the subsurface structures. These arrays have several specific benefits and limitations, and their properties differ in terms of depth of investigation (Barker 1989), lateral and vertical resolution (Barker 1979) and signal-to-noise ratio (Dahlin and Zhou 2004). In this study, we applied three different array configurations (Wenner (W), Dipole-Dipole (DD) and Pole-Pole (PP)) in seven profiles (27 electrodes, 5.4 m spacing), distributed in the upper, middle and lower part of El Colorado rock glacier (Pachon River basin, San Juan, Argentina) (Figure 1). The properties of each array are compared and assessed to determine the potential advantages of using different configurations in order to identify the most suitable and accurate option to map mountain permafrost distribution.

The following characteristics were considered when selecting the arrays: (i) the type of subsurface structures to be mapped (i.e., the sensitivity to vertical and horizontal changes in the subsurface), (ii) the depth of investigation, (iii) the horizontal data coverage, (iv) the sensitivity and potential of the resistivity meter, (v) the background noise level, and (vi) field and time setting. All profiles were iterated 10 times using robust data constrain and robust model constrain. We used the model resolution (Day-Lewis et al. 2005) index section after normalization by the model block area with an index cut-off value of 0.05 (5%) (Loke 2004) to compare the resolution between DD, W and PP arrays.

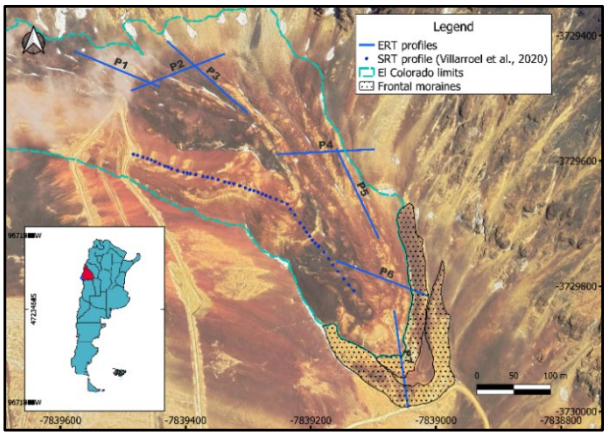

Figure 1. Delimitation and measurements made on El Colorado rock glacier. A modified version of the mapping of possible frontal moraines mapped in Villarroel et al. (2020) was included

Model resolution sections show that the trend of this parameter follows the resistivity distribution in the underground and change abruptly where strong contrasts on the resistivity are present. This parameter also shows a link with the type of array. DD and PP arrays show strong changes in the resolution index, whose pattern is related to resistivities distribution and present index values higher than 5 % for the first 10-15 m decreasing with depth. W array shows a more progressive decrease with depth independently of sharps boundaries. Similar results were found by Martorana et al. (2017).

In terms of internal structure, significant differences were found when comparing the three arrays. An upper layer up to 8 kohm.m for depths < 5.3 m are present in all the profiles (except on profile P7 which is mostly located in the frontal moraines mapped in Figure 1). This near surface layer with relatively low resistivity values and thicknesses lower than 5.3 m can be interpreted as the active layer of the rock glacier. At this depth, a sharp boundary is present showing resistivities reaching ~ 120 kohm.m., being consistent with ice-rich permafrost occurrence. Within this layer two noticeable differences are observed in terms of internal structure and resistivities distribution when comparing the use of different arrays. As can be observed in Figure 2 (P4) a vertical boundary is detected but at very different locations. In DD the gradient becomes sharp around

49 m, while for W the same vertical boundary is present at 81 m and the resistivities within this layer for this array are <24 kohm.m.The first part of 49 m from the beginning of the profile, shows a clear decrease in resistivities for both, the upper and lower layers compared with the rest of the line; this part of the profile is located mostly on the talus slope next to the rock glacier (Figure 1). It corresponds to the transition from the ice-rich permafrost layer present in the ridges of the rock glacier to the less ice-permafrost body represented by a resistivity of 24 kohm.m in the lateral talus slope.

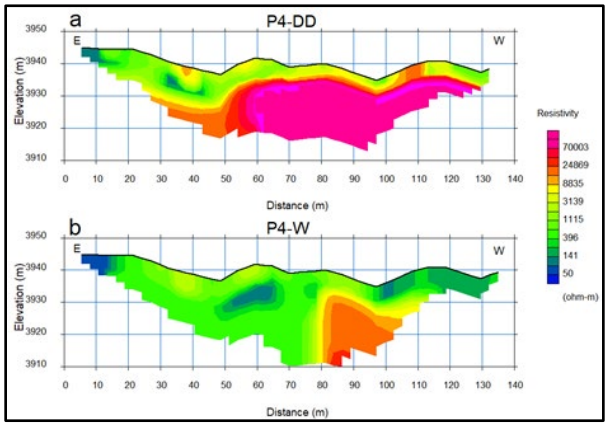

Figure 2. ERT results for a) P4 (DD) and b) P4 (W).

P6 is very different comparing DD and W array in terms of absolute resistivities values, but not in terms of the resistivity pattern (Figure 3). A vertical boundary is observed at around 49 m for both arrays, however for DD this layer starts at ~ 7 m depth and reaches 120 kohm.m, while for W array the same layer has a maximal resistivity of ~ 5 kohm.m. This could indicate completely different lithologies or frozen status of material present in the underground. Resistivities around 5 kohm.m may indicate unfrozen and wet conditions but not presence of permafrost.

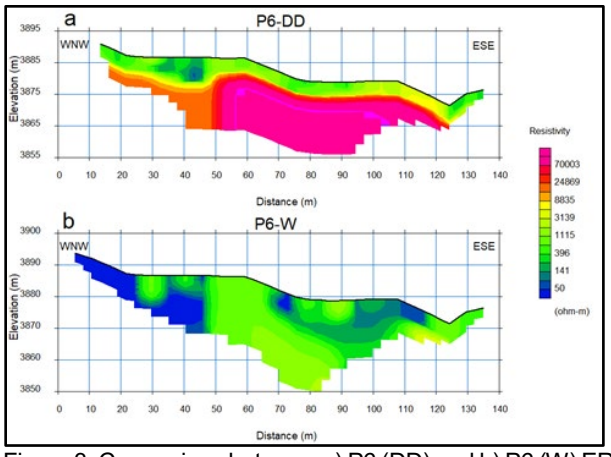

Figure 3. Comparison between a) P6 (DD) and b) P6 (W) ERT results.

Significant differences between the three analyzed arrays were found in terms of absolute resistivities values, distribution of resistivities and resolution indexes. The comparison of resolution per norm unit area between DD, W and PP arrays was, for all profiles in this study, higher for DD array, followed by PP and W. DD arrays showed better resolution index and a more realistic representation of internal structure of the rock glacier. W array reached depths higher than DD arrays, however the resolution index was the poorest. The low resolution may be due to the layout used. PP configurations present the middle index resolution but an important loss of detail within the first meters of depth. The main advantage is the considerable depth it can reach (four times DD).

The internal structure of El Colorado rock glacier has been better represented by DD array. The electrical resistivity values and the distribution of it, locate more realistic structures compatible with active layer thicknesses and rich- ice/ poor-ice permafrost bodies. This study enhances our understanding of the quantitative aspects related to the application of Electrical Resistivity Tomography, thereby enhancing the interpretation of mountain permafrost using different ERT arrays.

REFERENCES

Barker, R.D. 1979. Signal contribution sections and their use in resistivity studies, Geophysical Journal International, 59(1): 123–129. https://doi.org/10.1111/j.1365 246X.1979.tb02555.x

Barker, R.D. 1989. Depth of investigation of collinear symmetrical four-electrode arrays, Geophysics, 54(8):1031–1037. http://dx.doi.org/10.1190/1.1442728

Dahlin, T., and Zhou, B. 2004. A numerical comparison of 2D resistivity imaging with ten electrode arrays, Geophysical Prospecting, 52(5): 379–398. http://dx.doi.org/10.1111/j.1365-2478.2004.00423.x

Day-Lewis, F.D., Singha, K., and Binley, A. 2005. The application of petrophysical models to radar and electrical resistivity tomograms: resolution dependent limitations, Journal of Geophysical Research, 110(B08). https://doi.org/10.1029/2004JB003569

Loke, M.H. 2004. Tutorial: 2-D and 3-D Electrical Imaging Surveys. Geotomo Software, Res2dinv 3.5 Software.

Martorana, R., Capizzi, P., D'Alessandro, A., and Luzio, D. 2017. Comparison of different sets of array configurations for multichannel 2D ERT acquisition, Journal of Applied Geophysics, 137(2017): 34–48. https://doi.org/10.1016/j.jappge

Seismic polarity reversal unveils low-velocity layer above ice-rich permafrost in rock glaciers

Jacopo Boaga[1], Mirko Pavoni[1], Alexander Bast[2,3] & Samuel Weber[2,3]

[1]*Department of Geosciences, University of Padova, Via Gradenigo 6, 35131 Padova, Italy*

[2]*WSL Institute for Snow and Avalanche Research SLF, Flüelastrasse 11, 7260 Davos Dorf, Switzerland*

[3]*Climate Change, Extremes and Natural Hazards in Alpine Regions Research Center CERC, Flüelastrasse 11, 7260 Davos Dorf, Switzerland*

Seismic refraction tomography (SRT) is a common technique to characterize rock glaciers (RG). The boundary between ice-bearing ground and debris represents, in fact, a strong impedance contrast. We observed in several RGs a reversed polarity of the waves refracted by an extended permafrost layer, with respect to the phase of direct wave arrivals. This phase inversion is likely due to interferences in a low velocity layer above the ice-bearing one. Based on SRT, electrical resistivity tomography, and borehole stratigraphy data, we defined a rock glacier model and computed synthetic seismograms to demonstrate that the presence of a low-velocity layer may cause a polarity reversal in the acquisition of a seismic gather.

Rock glaciers are common landforms in permafrost environments. The rising temperatures make them potential mass movement hazards, for both communities and infrastructures in high mountain regions. Various geophysical methods have been used in recent decades to map, characterize, and monitor RGs. Seismic methods are one of the earliest techniques to investigate the near subsurface of these landforms (Barsch 1973). Recently, refraction seismic tomography (SRT; Musil et al 2002) was coupled with ERT in joint-inversion algorithms, to provide more detailed information about ice, water, rock, and air composition in the RGs (Hauck et al. 2011; Pavoni et al. 2023a).

In SRT first arrival times of the direct and refracted waves are studied to infer the velocity structure of the RG (Leopold et al 2011). Low-velocity layer (LVL) in between two faster ones is not visible by the seismic refraction technique as no refraction exists for negative impedance contrast. This is the main drawback of the methodology, but different wave attributes may be analyzed in the raw seismic shot gather. Polarity reversal, or so-called phase change, is a very well-known local attribute anomaly that can indicate the presence of a low-velocity layer in between two faster media (Simm and Bacon 2014) in reflected waves. We observed polarity phase reversal also of the refracted waves with respect to the direct waves collecting SRT datasets in different rock glaciers. Here, we provide experimental evidence in support of our hypothesis and compared our findings in field data with synthetical modelling.

REAL CASE EXAMPLES

For the sake of brevity, we present one real case example from Switzerland (Schafberg RG; Phillips et al. 2023; Boaga et al. 2020). The site was characterized by ERT and SRT data, and a detailed borehole stratigraphy is available. Figure 1 shows the seismic refracted and direct waves, and the reversal polarity in the raw shot gather is indicated by the change from the negative phase (-) to the positive (+) phase. This anomaly is observed only in the zone where the ice-rich permafrost layer is continuous, and not outside the RG.

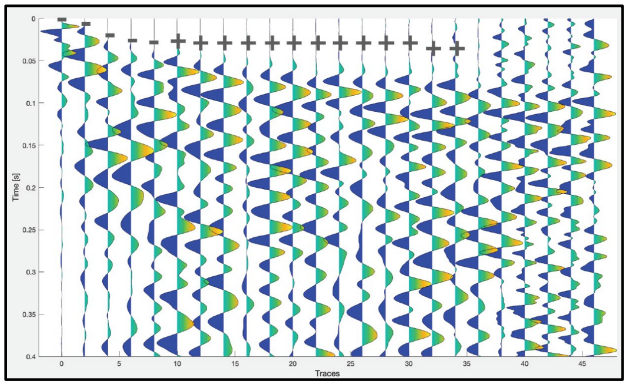

Figure 1. Raw data seismogram highlighting inverse polarity in seismic data collected at Schafberg RG in 2022.

From the borehole stratigraphy, we know that above the permafrost zone, there is a thin fine- to medium-grained sediment layer. This represents the classical low velocity layer (LVL), invisible to seismic refraction technique, and often not visible by ERT due to its limited thickness. We speculate the polarity reversal was induced by interference in this thin finer sediment layer above the ice-bearing permafrost layer. Synthetic examples with different parametrizations were then calculated to simulate the presence or absence of the LVL.

SYNTHETICS EXAMPLES

Considering the existing Schafberg borehole stratigraphy and structure, we computed two seismic synthetic shot gathers adopting the full-waveform spectral element solver Salvus (Mondaic ETH spin off; Afanasiev et al. 2019).

Figure 2 shows the two model outputs, first with the 1 m thick LVL modelled upon the ice-layer (a), then without the LVL (b). It can be seen that the presence of even a thin LVL in the RG stratigraphy strongly affects the seismic shot gather and results in a polarity reversal between direct and refracted waves.

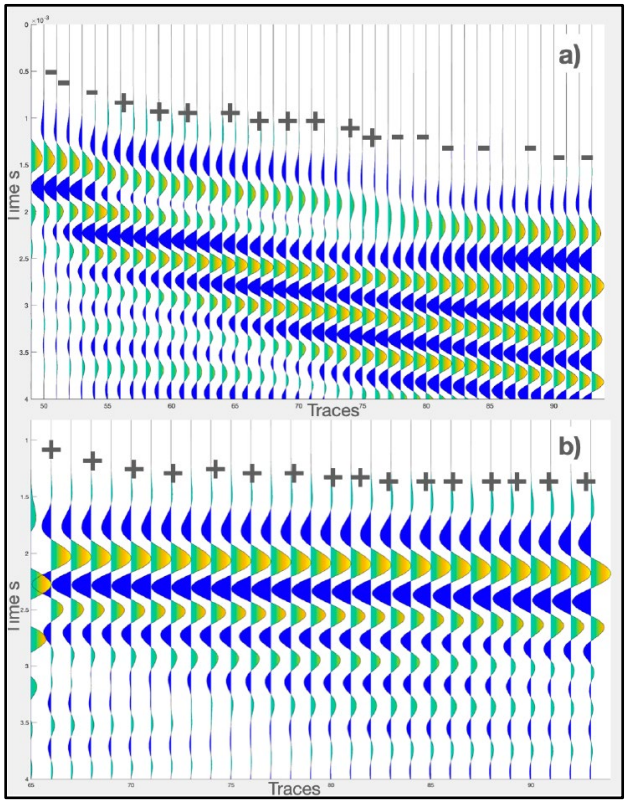

Figure 2. Synthetic shot gathers of the Schafberg site with a LVL thin layer (a) and without the LVL (b).

CONCLUSIONS

It is known that the reversal polarity in reflected seismic waves indicate the presence of a low-velocity layer (LVL) above the reflector. Also refracted waves can present reversal polarity, due to interference with the LVL.

For rock glaciers, this attribute may refer to the presence of a low velocity finer sediment horizon, as demonstrated by our real and synthetic datasets. This LVL might play a relevant role in subsurface hydrology, e.g., acting as an aquiclude (Pavoni et al 2023b) or favoring local water accumulation (Haeberli et al 2001). Phase reversal polarity in shot gather can suggest the presence of fine sediment layers overlying the permafrost ones.

REFERENCES

Afanasiev, M., Boehm, C., van Driel, M., Krischer, L., Rietmann, M., May, D.A., et al. 2019. Modular and flexible spectral-element waveform modelling in two and three dimensions. Geophysical Journal International, 216(3), 1675–1692.

Barsch, D. 1973. Refraktionsseismische Bestimmungen an der Obergrenze des gefrorenen Schuttkörpers in verschiedenen Blockgletschern Graubündens. Zeitschrift für Gletscherkunde und Glaziologie, IX (1-2): 143–167.

Haeberli, W., Kääb, A., Vonder Mühll, D., and Teysseire, P. 2001. Prevention of outburst floods from periglacial lakes at Grubengletscher, Valais, Swiss Alps. Journal of Glaciology, 47(156): 111–122.

Hauck, C., Bottcher M., and Maurer, H. 2011. A new model for estimating subsurface ice content based on combined and seismic data sets. The Cryosphere, 5: 453–468. doi:10.5194/tc-5-543-2011

Leopold, M., Williams, M.W., Caine, N., Völkel, J., and Dethier, D. 2011. Internal structure of the Green lake 5 rock glacier, Colorado Front Range, USA. Permafr. Periglac. Process. 22 (2), 107–119.

Musil, M., Maurer, H., Green, A.G., Horstmeyer, H., Nitsche, F.O., Mühill, D.V., and Springman, S. 2002. Shallow seismic surveying of an Alpine rock glacier. Geophysics 67 (6), 1701–1710.

Pavoni, M., Boaga, J., Wagner, F.M., Bast, A., and Phillips M. 2023a. Characterization of rock glaciers environments combining structurally-coupled and petrophysically-coupled joint inversions of electrical resistivity and seismic refraction datasets, Journal of Applied Geophysics, Vol. 215. doi:105097, ISSN 0926-9851

Pavoni, M., Boaga, J., Carrera, A., et al. 2023b. Mountain permafrost acts as an aquitard during an infiltration experiment monitored with electrical resistivity tomography time-lapse measurements. The Cryosphere 17(4), pp. 1601–1607.

Simm R., and Bacon M. 2014. Seismic Amplitude An Interpreter's Handbook Cambridge University Press, Cambridge, UK.

Permafrost thickness variations on peat plateaus in the central Mackenzie Valley, NWT

Alexandre Chiasson[1], Brielle Andersen[1], Alejandro Alvarez[1], Keytash Moshtaghian[2], Jurjen van der Sluijs[3], Ashley C.A. Rudy[4], Steven V. Kokelj[4] & Duane G. Froese[5]

[1]*Department of Earth and Atmospheric Sciences, University of Alberta, Edmonton, Canada*

[2]*Department of Physics, University of Alberta, Edmonton, Canada*

[3]*NWT Centre for Geomatics, Government of Northwest Territories, Yellowknife, Northwest Territories, Canada*

[4]*Northwest Territories Geological Survey, Government of Northwest Territories, Yellowknife, Northwest Territories, Canada*

[5]*Department of Earth and Atmospheric Sciences, University of Alberta, Edmonton, Alberta, Canada*

Permafrost temperature, thickness and distribution in the central Mackenzie Valley is principally known from the eastern side of the Mackenzie River between Wrigley and Fort Good Hope (Smith et al. 2005; Smith et al. 2010; Smith et al. 2022; Duchesne et al. 2020). These studies reflect the abundance of legacy data and infrastructure from pipeline development and communities over the last ca. 50 years. In contrast, relatively little is known about the lowland permafrost terrain that occupies areas west of the Mackenzie River. Ground temperature data presented from previous studies are more homogeneous, and boreholes tended to be located in areas away from water bodies or peatlands along the pipeline and winter road corridor. This leads bias toward sites appropriate for pipeline or road development away from thaw sensitive terrain. To date, more than 25 ground monitoring stations have been established along the eastern side of the Mackenzie valley, and within deposits that share similarities along the corridor. Smith and Burgess (2002) compiled data on permafrost thicknesses in the Mackenzie Valley, showing that it varied from ~10 and 50 m within 100 kilometers from Norman Wells. The relative lack of permafrost data beyond this corridor limits our regional understanding of permafrost conditions across a diversity of physical environments that characterize the central Mackenzie Valley. This paper investigates the thicknesses of permafrost under peat plateau in the central Mackenzie Valley, through the transition zone from regionally discontinuous to continuous permafrost. Here, we assess the material properties and permafrost thickness across peat plateau sites located at varying elevations, vegetation cover, and geological settings using electrical resistivity tomography.

METHODOLOGY

In this study, our goal is to assess material properties and permafrost thicknesses in peatlands in the central Mackenzie Valley. Electrical Resistivity Tomography (ERT) has been shown to be a useful geophysical tool for investigating subsurface electrical resistivity, especially in discontinuous permafrost (Way and Lewkowicz 2015; Herring and Lewkowicz 2022). Here, we use an ABEM Terrameter L2 using Wenner arrays with an electrode spacing of 1, 2, 4 or 8 meters to achieve a penetration depth of ~10 to 65 m, dependent on electrode spacing. Subsequently, these data were inverted using RES2DINV software, following Loke et al. (2003). The inversion process was iterated until the root mean squared error was below 5% or the fifth iteration (Sjöberg et al. 2015). Frost table depths were determined using a 1.25 m steel probe at each electrode location in the ground. ERT surveys were conducted at three permafrost peat plateaus (MM-1, FGH-1, FGH-2) across the valley to determine the thickness of permafrost.

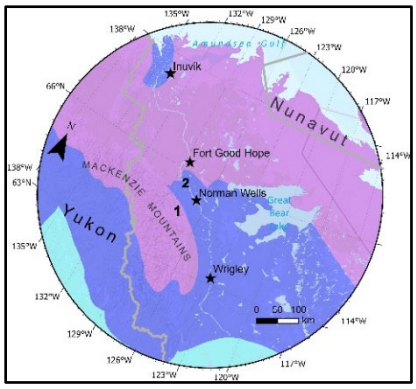

Figure 1. Location of the study area and main communities of interest along the Mackenzie Valley. The permafrost zones are depicted with different colors: continuous permafrost is highlighted in purple, extensive discontinuous permafrost is shown in blue, and sporadic discontinuous permafrost is represented in aqua. Permafrost zones modified from Heginbottom et al. (1995). Number 1 corresponds to site MM-1, 2 corresponds to sites FGH-1 and FGH-2.

RESULTS

At the Mackenzie Mountains site, high resistivity values (>300 Ω.m) characterize the upper 7 m of the profile. Frost probing and ERT values suggest a

permafrost resistivity boundary of >300 Ω.m for frozen peat, similar to values reported in Lewkowicz et al. (2011) and Way and Lewkowicz (2015) for organic soils. The transition from low to high resistivity values observed at depth in MM-1 suggests an estimated permafrost thickness of approximately 5 to 9 meters at this site (Figure 1). The areas with lower resistivity values (<300 Ω.m) correspond to unfrozen ground, aligning with the locations of the channel fens and bog that the survey traverses.

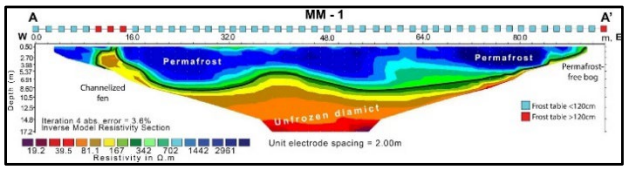

Figure 1. ERT profile (2-m spacing) and frost table probing result across a permafrost peat plateau and a channelized fen.

A 2-m spaced ERT survey was carried out at FGH-1 of the FGH dendritic peat plateau complex, crossing a peat plateau and a channelized fen. The ERT data from FGH-1-A shows high resistivity (>500 - 600 Ω.m) values in the first six meters of the profile. The thickness of the permafrost beneath the peat plateau is estimated to be ~6 m. The boundary contact between unfrozen/frozen ground in this DPP was inferred over 600 Ω.m based on the presence of coarse sands and gravels (high modeled resistivity values). At the upper site (FGH-2), the ERT data showed high-resistivity regions (≥700 Ω.m) under the peat plateau, suggesting that permafrost extends from 12 to 17m depth. The lower ERT values (≥600 Ω.m) agree with frost probe data along the ERT transect, in which the edges and the center of the wetlands yielded the deepest frost probe measurements (Figure 2).

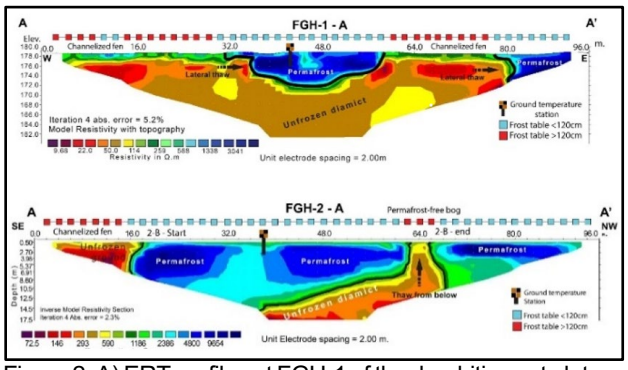

Figure 2. A) ERT profiles at FGH-1 of the dendritic peat plateau near Fort Good Hope. ERT profile (2-m spacing) and frost table probing across permafrost peat plateaus and channelized fens. B) ERT profiles at FGH-2 of the dendritic peat plateau near Fort Good Hope. ERT profile (2-m spacing) across permafrost peat plateaus and a channelized fen, and a bog. Black lines represented the inferred base of permafrost.

Discussion and Conclusion

Permafrost thickness variations of three dendritically-drained peat plateaus and one polygonal peatland in the central Mackenzie Valley indicates thin, patchy permafrost, with estimated thicknesses that are significantly less that those at long-term monitoring sites along the winter road corridor (Smith et al. 2009; Smith et al. 2010; Duchesne et al. 2020). Contrary to our expectations, thicknesses of permafrost under fragmented peat plateaus with collapse scars and fens vary between ~5 and ~15 meters and is less than the permafrost thicknesses reported for well-drained, forested mineral soil sites Our study underscores the sensitivity of saturated organic deposits to thawing, the importance of thaw-driven terrain fragmentation, lateral heat flux, and possibly advection in controlling permafrost thicknesses in dendritically drained peatlands.

References

Duchesne, C., Chartrand, J., and Smith, S.L. 2020. Report on 2018 field activities and collection of ground-thermal and active-layer data in the Mackenzie corridor, Northwest Territories; Geological Survey of Canada, Open File 8707, 84 p.

Lewkowicz, A.G., Etzelmüller, B., and Smith, S.L. 2011. Characteristics of discontinuous permafrost based on ground temperature measurements and electrical resistivity tomography, southern Yukon, Canada. Permafrost and Periglacial Processes, 22(4), 320–342.

Smith, S.L., and Burgess, M.M. 2002. A digital database of permafrost thickness in Canada, Open File 4173. Geological Survey of Canada.

Smith, S.L., Burgess, M.M., Riseborough, D., and Mark Nixon, F. 2005. Recent trends from Canadian permafrost thermal monitoring network sites. Permafrost and periglacial processes, 16(1), 19–30.

Smith, S.L, Chartrand, J., Nguyen, T.N., Riseborough, D.W., Ednie, M., and Ye, S. 2009. Geotechnical database and descriptions of permafrost monitoring sites established 2006–07 in the central and southern Mackenzie Corridor. Geological Survey of Canada Open File6041: (CD-ROM)

Smith, S.L., Romanovsky, V.E., Lewkowicz, A.G., Burn, C.R., et al. 2010. Thermal state of permafrost in North America: a contribution to the international polar year. Permafrost and Periglacial Processes, 21(2), 117–135.

Sjöberg, Y., Marklund, P., Pettersson, R., and Lyon, S.W. 2015. Geophysical mapping of palsa peatland permafrost. The Cryosphere, 9(2), 465–478.

Way, R.G., and Lewkowicz, A.G. 2015. Investigations of discontinuous permafrost in coastal Labrador with DC electrical resistivity tomography. In Proceedings of GéoQuebec: 68th Canadian Geotechnical Conference and 7th Canadian Permafrost Conference. Quebec City, Canada (p. 8).

Way, R.G., Lewkowicz, A.G., and Zhang, Y. 2018. Characteristics and fate of isolated permafrost patches in coastal Labrador, Canada. The Cryosphere, 12(8), 2667–2688.

A geoelectric survey to study the ground state beneath the main facilities of the Peruvian Antarctic Station Machu Picchu

Antonio Correia[1], Wai Hg-Cupita[2] & Pedro Mendes[1]

[1]*Institute of Earth Sciences, University of Evora, Evora, Portugal*

[2]*Geological and Mining Institute of Spain, CSIC, Madrid, Spain*

Under the framework of Project Hydrotomo, funded by the Foundation for Science and Technology of the Ministry of Higher Education of Portugal, the Peruvian Polar Program and the Portuguese Polar Program a geoelectrical survey using electrical resistivity tomographies (ERTs) was carried out in January 2019 under the facilities of the Peruvian Antarctic Station Machu Picchu. The station is located in the Admiralty Bay of King George Island of the South Shetland Islands archipelago. The main objective of the survey was to try to estimate the depth and lateral extent of the permafrost that was found beneath the main buildings of the Machu Picchu station during maintenance works performed in the Antarctic summer of 2018. Two rectangular shaped buildings of the Machu Picchu Antarctic Station were chosen to measure the ground electrical resistivity beneath them. In the biggest building (the main building), the electrical profiles crossed 14 m beneath it along its smallest dimension (Lines 1 and 2 in Figure 1); in the other, (a refuge), the electrical profile crossed 7 m beneath the building also along its smallest dimension (Line 3 in Figure 1).

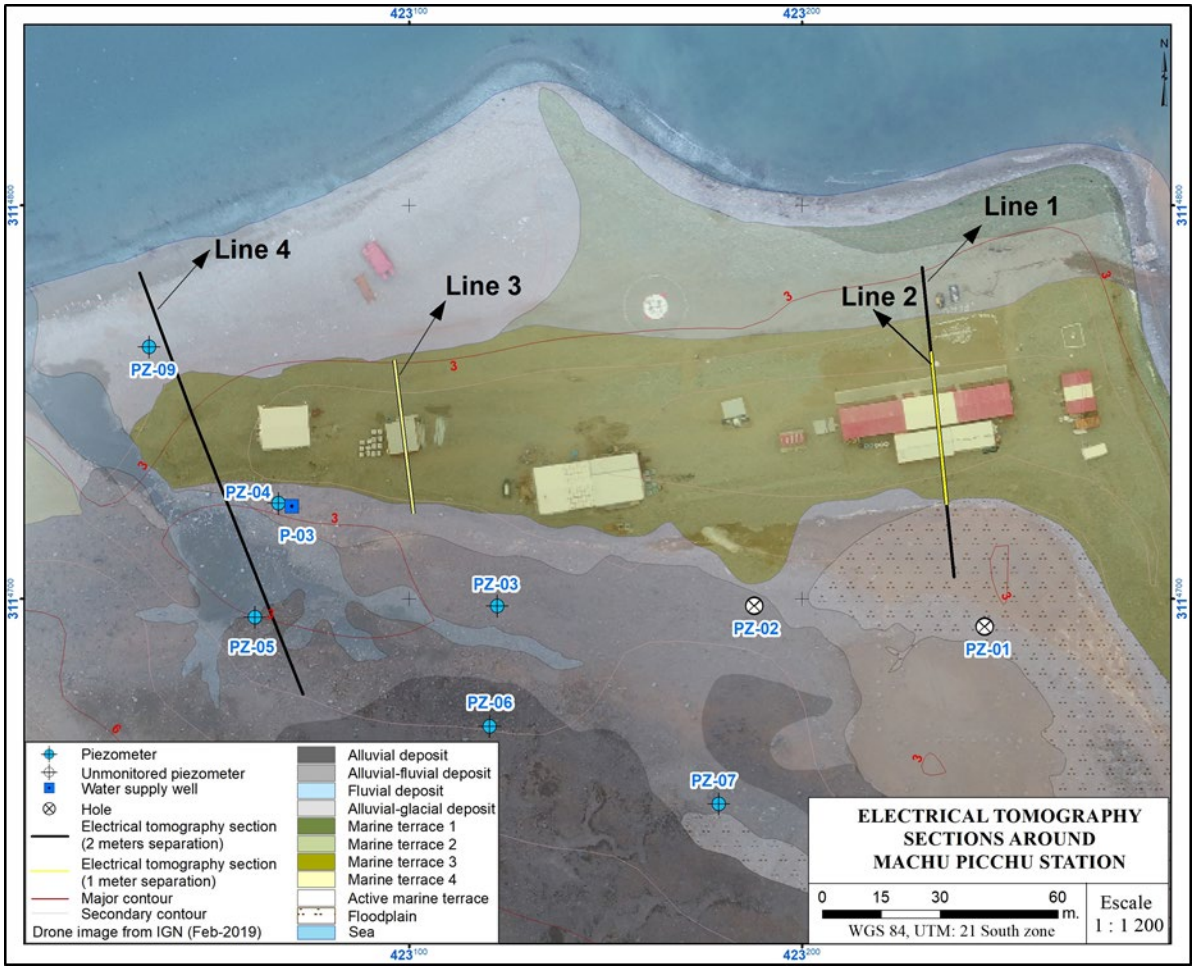

Figure 1. Sketch of the Machu Picchu Antarctic Station with the main facilities in grey. Lines 1 to 4 represent ERT that were carried out to study permafrost in the region. Lines 1 to 3 are the ones discussed here.

GEOLOGY SKETCH OF THE STUDY AREA

The study area is on Barton horst oriented SW-NE with volcanic and volcanogenic rocks which are cut by dykes and intruded by calco-alkaline plutons. Machu Picchu station is built on top of Quaternary deposits. Near Crepin Point, the Cardozo Cove Group consists of volcanic and volcanogenic successions (dacitic-andesitic) differentiated into three sub-units with ages from the Upper Cretaceous to the Paleocene. Cerpa (2015) made a detailed description of Quaternary deposits in Crepin Point, recognizing glacial deposits, fluvial-alluvial system and six marine terraces (Figure 1). Geomorphology wise the zone has marine action geoforms (marine terraces, beach), modeled glaciar geoforms (glacial, morraines, erosioned/ transported glacial-fluvial, gelifraction detritus) and mountain and denudational colin geoforms.

ELECTRICAL RESISTIVITY SURVEY

To carry out the geoelectrical profiles 40 active electrodes were used in a Wenner configuration; 1 m (Lines 2 and 3) and 2 m (Line 1) distances between adjacent electrodes were used for different profiles so that different depths of investigation could be achieved. An LGM Resistivity Meter was used to control the measuring process and record the field data, which were downloaded later for processing. During the acquisition stage, a few problems related to high electrical contact resistances between the ground and the stainless electrodes had to be solved. By eye inspection those problems were the result of frozen ground, pebbles and/ or very dry ground. Those problems were solved by watering with seawater the zone of the electrodes affected by high electrical contact resistance. After processing the raw electrical data, electrical resistivity sections of the ground beneath the building were obtained. The apparent electrical resistivity values were converted into two-dimensional electrical resistivity models (geoelectric sections) of the soil by mathematical inversion, using the EarthImager software. The models obtained by inversion represent geoelectric sections with depths between 6 and 12 m (the latter, Line 1 in Figure 2).

CONCLUSIONS

After processing the raw electrical data, real electrical resistivity sections of the ground beneath the two buildings were obtained. The preliminary interpretation of those electrical resistivity profiles indicate that in both buildings there is a layer of permafrost (high electrical resistivities) almost continuous. However, beneath the permafrost layer, coinciding with the area of both buildings, an isolated low electrical resistivity layer about 1 to 2 m thick, with electrical resistivity values as low as 20 Ω.m was found (see Figure 2); the layer appears to extend sideways perpendicularly to the direction of the ERT profiles. The interpretation of this low electrical resistivity layer is still a challenge. The permafrost layers detected with the ERT profiles show a good correlation with temperature measurements obtained with thermometers installed in 2018, as well as with visual observation after digging a small hole to install new thermometers during the geoelectrical survey.

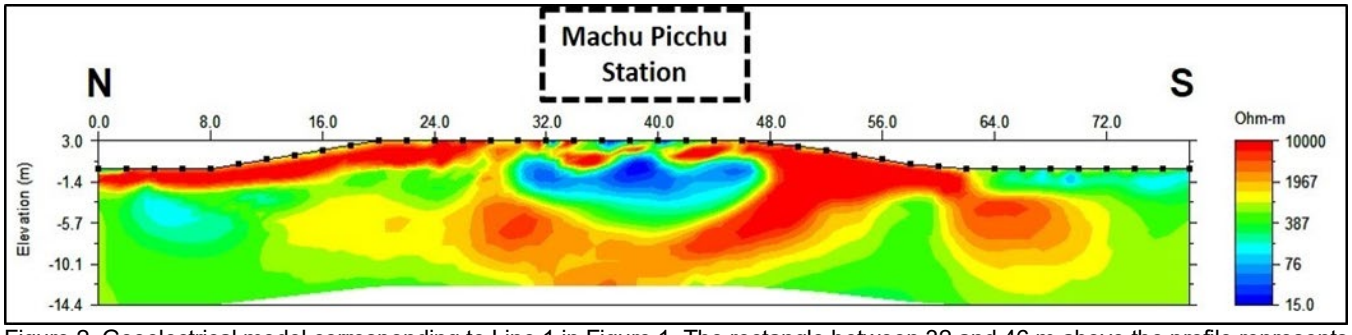

Figure 2. Geoelectrical model corresponding to Line 1 in Figure 1. The rectangle between 32 and 46 m above the profile represents the cross-section of the main facility of Machu Picchu Station. Beneath the facility, there is a low electrical resistivity area above, of which permafrost was found by digging a short borehole.

REFERENCES

Cerpa, L. 2015. Estratigrafía de Punta Crepín, isla Rey Jorge, islas South Shetland, Antártida, Boletín de la Sociedad Geológica del Perú, 110, 59–62.

Probabilistic multiphysics inference for permafrost characterization

Jan Dettmer, Pejman Shahsavari & Jeremy M. Gosselin
Department of Earth, Energy, and Environment, University of Calgary, Calgary, Alberta, Canada

Canada's North concentrates infrastructure along accessible road corridors that harbour permafrost and seismically active regions. Here, climate change occurs at rates over two times greater compared to global averages and is irreversibly degrading permafrost. Permafrost plays a crucial role for soil stiffness and shear strength, and its degradation is a source for increasing risks of natural hazards, including landslides, thaw subsidence, and earthquake-related hazards. The severities of these impacts remain poorly studied, and mitigation efforts require better subsurface characterization and monitoring of temporal permafrost changes, as well as improved constraints on permafrost mechanical (poro-elastic) properties. This work considers the potential of permafrost characterization with probabilistic multiphysics inference (PMPI) of non-invasive geophysical observations. In particular, we study the uppermost shallow Earth using a combination of seismic and magnetotelluric measurements. Our analysis employs a probabilistic (Bayesian) framework for robust characterization of uncertainties in inferred permafrost properties.

DATA AND METHODS

The data considered in this work are observed with passive geophysical methods that do not require a built signal source, but rely on naturally occurring signals. Two types of seismic data are employed. (1) Surface-wave dispersion data (SWD) are obtained by beamforming ambient seismic noise recordings on several instruments arranged in a cross-shaped (surface) array. These measurements are mostly sensitive to Rayleigh waves and constrain shear-wave velocity in the uppermost 10^2 m. (2) Horizontal-to-vertical spectral ratio (HVSR) data are obtained by considering the ratio of seismic-wave spectra on the horizontal and vertical components of a seismograph. These data are predominantly caused by the ellipticity of Rayleigh wave particle motion. Importantly, HVSR data are sensitive to the shallowest (10^0 to 10^1 m) properties compared to SWD data (Hobiger et al. 2013), but suffer a tradeoff between depth of soil layers and shear-wave velocities. Therefore, combining these data types provides excellent resolution for depths relevant to permafrost characterization.

The addition of data sensitive to subsurface electrical resistivity is desirable for improving the resolution of frozen layers. In this work we limit analysis to 1D earth structure and consider magnetotelluric (MT) data at audible frequencies (10^0 to 10^4 Hz).

Significant assumptions are often made for joint analysis of multiple data types that stem from different physical processes (e.g., Moorkamp 2017). For example, since the various data are sensitive to different physical properties, the subsurface discretization should permit decoupling of parameters where required by the data (Piana Agostinetti et al. 2018). Furthermore, data weights are often applied to adjust how much a specific data type contributes to the solution.

We employ a generalized PMPI where Bayesian methods are employed to reduce the assumptions practitioners make during data analysis. The method assumes only depth dependence of geophysical properties (i.e., a 1D approximation), but the parametrization is *trans-dimensional*, treating the number of subsurface layers as unknown (Dettmer et al. 2012). Furthermore, the parametrization permits automated trans-dimensional de-coupling, reducing artefacts due to over-parametrizing the model. The weight of each data type is given by the noise statistics of the data residuals, which are estimated in terms of the data covariance matrices that include the effects of correlated noise due to measurement and modelling errors. The PMPI analysis provides probabilistic resistivity and shear-wave velocity estimates as a function of depth, thereby intrinsically addressing uncertainty quantification. We demonstrate these analyses by considering simulated data that reflect site conditions expected for areas with discontinuous permafrost. Future work will apply the method to existing seismic and magnetotelluric data collected near Haines junction, Yukon.

RESULTS AND CONCLUSION

Data were simulated for a shear-wave velocity profile typical for basin structures with alluvial infill (Figure 1) and permafrost at depths between 5 and 50 m. Analysis is carried out for individual data types which are then compared to PMPI analysis (Figure 1). Inverting only MT data for frequencies between

10 and 8,000 Hz (Figure 1A), shows limited ability to resolve shallow resistivity structure. While the probabilistic results show some evidence of a frozen layer, a high degree of non-uniqueness exists. The active layer is not resolved, but high uncertainty at shallow depths indicate that data have some sensitivity to it. Note that uncertainty estimates appear to be inconsistent with the true model. This is because the inference is largely sensitive to the average of active and frozen layers and represents uncertainties about the ability to estimate that average. This is an undesirable effect.

The analysis of only SWD data between 1 and 10 Hz (Figure 1B) shows sensitivity to the active layer but is not able to resolve the elevated shear-velocity of the frozen layer. Instead, significant non-uniqueness is again observed. Furthermore, uncertainties appear to misrepresent the information content, again being biased toward the average property of multiple layers.

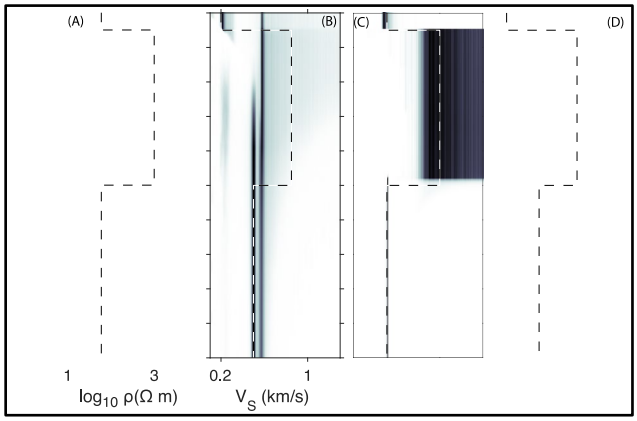

Figure 1. Probabilistic resistivity and shear-wave velocity profiles resolved from simulated data for a 5-m thick active layer and a 45-m layer of permafrost soil. (A) Only MT data, (B) only SWD data, and (C-D) multiphysics inference of MT, SWD, and HVSR data. Dark colors represent high probability.

Finally, Figure 1C-D demonstrates that PMPI of MT, SWD, and HVSR data resolves the active layer, the frozen layer, and the underlying sediments with appropriate uncertainties. Hence, the complementary information contained in the various data types, and the probabilistic estimation of objective data weights, enables higher-resolution inference of shallow subsurface properties than can be achieved by independent inference from individual data types. This may be particularly valuable for permafrost characterization and monitoring, where frozen ground introduces strong elastic (i.e, seismic) and electrical resistive (i.e., MT) signatures. PMPI allows for robust subsurface characterization while avoid subjective inversion practices that preclude meaningful model uncertainty quantification.

Our work represents an initial step towards using PMPI as a reliable tool for probabilistic seismic site hazard assessment in permafrost environments. Future work will consider analysis of existing field data collected at multiple study areas in western Yukon.

ACKNOWLEDGEMENTS

We respectfully acknowledge that data in support of this research are collected in the traditional territory of the Champagne and Aishihik First Nations. We would like to acknowledge financial support from the Yukon Geological Survey and from the Natural Sciences and Engineereing Research Council Discovery Grant to Jan Dettmer, and a postdoctoral fellowship to Jeremy M. Gosselin.

REFERENCES

Dettmer, J., Molnar, S., Steininger, G., Dosso, S.E, and Cassidy, J.F. 2012. Trans-dimensional inversion of microtremor array dispersion data with hierarchical autoregressive error models, Geophysical Journal International, 188(2): 719–734. doi.org/10.1111/j.1365-246X.2011.05302.x

Hobiger, M., Cornou, C., Wathelet, M., Giulio, G.D., Knapmeyer-Endrun, B., Renalier, F., Bard, P.-Y., Savvaidis, A., Hailemikael, S., and Le, B.N. 2013. Ground structure imaging by inversions of Rayleigh wave ellipticity: sensitivity analysis and application to European strong-motion sites, Geophysical Journal International, 192(1): 207–229. doi.org/10.1093/gji/ ggs005

Moorkamp, M. 2017. Integrating electromagnetic data with other geophysical observations for enhanced imaging of the earth: a tutorial and review, Surveys in Geophysics, 38(5): 935–962. doi.org/10.1007/s10712-017-9413-7

Piana Agostinetti, N., and Bodin, T. 2018. Flexible coupling in joint inversions: A Bayesian structure decoupling algorithm, Journal of Geophysical Research: Solid Earth, 123(10): 8798–8826. doi.org/10.1029/2018JB016079

Real-time monitoring of active layer freeze-thaw using automated ERT

Mohammad Farzamian[1], Teddi Herring[2], Antoni G. Lewkowicz[3] & Christian Hauck[4]

[1]*Centre for Geographical Studies, Associate Laboratory TERRA, IGOT, Universidade de Lisboa, Lisbon, Portugal*

[2]*Department of Civil Engineering, University of Calgary, Calgary, Canada*

[3]*Department of Geography, Environment and Geomatics, University of Ottawa, Ottawa, Canada*

[4]*Department of Geosciences, University of Fribourg, Fribourg, Switzerland*

Repeat Electrical Resistivity Tomography (ERT) surveys are increasingly being used to track long-term permafrost change in mountain and polar environments. A single annual survey is generally sufficient for this purpose, providing it is undertaken at the same time each year. However, ERT also has the potential to monitor short-term variations in ground conditions, such as those associated with active layer freezing and thawing, or wetting and drying. While these changes are driven by short-term meteorological events such as snowmelt or rainfall, they can have important cumulative impacts by altering thermal properties such as conductivity and latent heat, by direct transfer of convective heat, and by buffering the ground from air temperature fluctuations in winter. Ground monitoring of this sort requires a much higher survey frequency, one that would be impractical using manual measurements. In this context, we describe a recently-installed robust Automated ERT (A-ERT) system that makes daily measurements at a permafrost site in the southern Yukon, Canada. We also detail the automated workflow developed to process the large amounts of data being received on a real-time basis. The expectation is that this setup will provide deeper insights into active layer and permafrost dynamics.

STUDY SITE AND METHODS

The A-ERT monitoring system was installed in September 2023 at a perennially frozen peat plateau covered by open black spruce forest, near Teslin, Yukon. ERT surveys have been undertaken near-annually at this lowland site (known as MP 788, see Lewkowicz et al. 2011) since 2008. Ancillary information includes ground temperatures in a shallow borehole, air temperature, snow depth, and frost table depths.

The A-ERT system comprises 48 stainless steel plates (each 10 x 30 cm) spaced at 0.5 m, a solar panel, a satellite antenna, and a temperature-rated waterproof box housing the main electronic components (Figure 1). The Wenner electrode configuration was employed for optimized energy consumption and enhanced vertical resolution, aiming to delineate the active layer-permafrost boundary (Farzamian et al. 2020). The array was positioned to include sections of perennially frozen ground and the adjacent seasonally frozen bog. A total of 360 data points are collected during each daily A-ERT survey, providing information on the active layer and the uppermost permafrost to a maximum depth of ~4 m. The data are transmitted via satellite.

Figure 1. A-ERT monitoring system installation at the MP 788 site near Teslin, Yukon. The A-ERT box contains the 4POINTLIGHT_10W resistivity meter connected to a solar-panel-driven battery, multi-electrode connectors, and a satellite datalink. Electrodes (buried in the ground), the solar panel, and the satellite antenna are all connected via buried cables to the A-ERT box using mil-rated connectors. For additional details on the previous version of this setup, refer to Farzamian et al. (2020).

An automated data processing workflow was developed based on Herring et al. (2023) to efficiently identify and filter poor quality and anomalous A-ERT measurements. All data were then inverted using the open-source software pyGIMLi (Rücker et al. 2017), employing a blocky model norm for improved resolution of sharp boundaries and significant resistivity contrasts, as anticipated between the active layer and frozen ground.

Further analyses include time series for a virtual borehole (VB) and a Zone of Interest (ZoI). VB analysis allows real-time visualization of resistivity changes at a specific location, facilitating comparisons with borehole and probed thaw depth data. ZoI analysis assesses the evolution of average resistivity within specific zones of interest, such as the active layer or permafrost (see Herring et al. 2023).

RESULTS

Data collection started on September 21, 2023. Results from the first 75 days of monitoring can be compared to meteorological data recorded at Teslin airport, 25 km to the northwest (Figure 2).

Figure 2a shows the vertical resistivity distribution at the mid-point of the A-ERT profile. Two distinct resistivity zones are observed: the first, extending to approximately 1 m depth with a resistivity below 200 ohm.m, corresponds to the unfrozen active layer. The deeper zone represents warm permafrost (-0.05°C) down to 4 m, with resistivities ranging from 200-400 ohm.m, and increasing with depth. A resistivity increase in the near-surface is evident in late October, coinciding with the air temperature falling below 0°C (Figure 2c) and the onset of seasonal freezing. However, there is no subsequent visible advance of the freezing front.

Average resistivity for the top 50 cm of the ground along the transect varied from 165 to 185 ohm.m over the monitoring period (Figure 2b). Slight reductions in resistivity from the start of the record through to early October are likely linked to rainfall events (not shown) increasing the active layer moisture content. When air temperatures dropped below 0°C in late October (Figure 2c), resistivity increased, indicating the initiation of freezing. However, several factors may have prevented more substantial resistivity changes during the observation period. First, the average daily air temperature from the start of freezing to early December was -6°C, more than 3°C warmer than the 1991-2020 average for this time of year. Additionally, precipitation in November was in the form of snow (Figure 2c), which acts as an insulator, mitigating rapid freezing and promoting an extended zero curtain in the moist active layer. The slight decrease in resistivity in late November is attributed to air temperatures temporarily exceeding 0°C, leading to partial melt of the snowpack. Notably, inversion results are reliable, with a consistently small RMS error range of 5-6% (Figure 2b).

CONCLUSION AND OUTLOOK

The system's performance to date has been excellent, demonstrating its capability to operate in a subarctic environment. The high-resolution ERT data is of good quality, allowing real-time detection of changes in the active layer and upper permafrost horizons. Our results also showcase the processing workflow's efficiency in extracting information from A-ERT data, enabling real-time detection of changes in the active layer.

We plan to continue A-ERT measurements at this warm permafrost site, including calculations of daily, monthly, and annual resistivity changes, enabling the long-term assessment of active layer dynamics and permafrost stability.

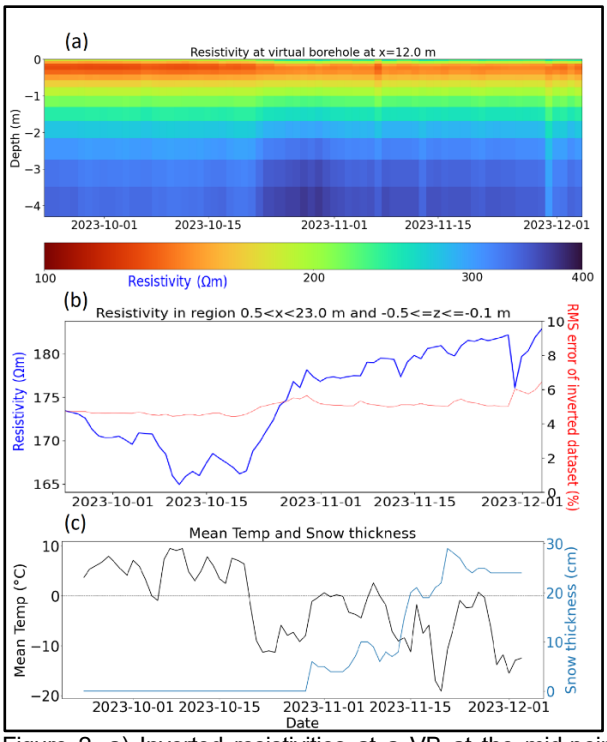

Figure 2. a) Inverted resistivities at a VB at the mid-point of the A-ERT survey, b) Average resistivity within the ZoI, and RMS error of inverted dataset over time c) daily snow thickness and air temperatures at Teslin weather station (https://climate.weather.gc.ca/climate_data/daily_data_e.html?StationID=8985).

REFERENCES

Farzamian, M., Vieira, G., Monteiro Santos, F.A., Yaghoobi Tabar, B., Hauck, C., Catarina Paz, M., Bernardo, I., Ramos, M., and Angel De Pablo, M. 2020. Detailed detection of active layer freeze-thaw dynamics using quasi-continuous electrical resistivity tomography (Deception Island, Antarctica). The Cryosphere, 14(3), 1105–1120. https://doi.org/10.5194/tc-14-1105-2020

Herring, T., Lewkowicz, A.G., Hauck, C., Hilbich, C., Mollaret, C., Oldenborger, G.A., Uhlemann, S., Calmels, F., Farzamian, M., Calmels, F., and Scandroglio, R. 2023. Best practices for using electrical resistivity tomography to investigate permafrost. Permafrost and Periglacial Processes, 34, 4, 494–512, https://doi.org/10.1002/ppp.2207.

Lewkowicz, A., Etzelmüller, B., and Smith, S.L. 2011. Characteristics of discontinuous permafrost based on ground temperature measurements and electrical resistivity tomography, Southern Yukon, Canada. Permafrost and Periglacial Processes, 22(4), 320–342. https://doi.org/10.1002/ppp.703

Rücker, C., Günther, T., and Wagner, F.M. 2017. pyGIMLi: An open-source library for modelling and inversion in geophysics. Computer & Geoscience, 109, 106–123. https://doi.org/10.1016/j.cageo.2017.07.011

Characterization of discontinuous permafrost using ambient vibration techniques in Haines Junction, Yukon

Jeremy M. Gosselin[1], Tess Leishman[2], Jan Dettmer[1], John F. Cassidy[2,3] & Tae-Seob Kang[4]

[1]*Department of Earth, Energy, and Environment, University of Calgary, Calgary, Alberta, Canada*

[2]*School of Earth and Ocean Sciences, University of Victoria, Victoria, British Columbia, Canada*

[3]*Geological Survey of Canada, Pacific, Natural Resources Canada, Sidney, British Columbia, Canada*

[4]*Division of Earth Environmental System Science, Pukyong National University, South Korea*

Haines Junction, Yukon, is situated at the base of the St. Elias mountains. The region is characterized by complex active tectonics, which lead to rapid uplift, erosion, and exhumation (Turner et al. 2016). The region also hosts crustal-scale faults and significant seismicity. Together, these present natural hazards to the region. Evolving, discontinuous permafrost throughout the area causes a complex response to natural hazards that is currently understudied. In collaboration with the Yukon Geological Survey (YGS), we aim to investigate shallow Earth structure in Haines Junction and the surrounding region. This includes the characterization of discontinuous permafrost with the goal of natural hazard mitigation. This work presents preliminary field investigations towards characterizing shallow Earth structure using non-invasive, ambient vibration (AV) methods that are based on recording background seismic noise.

DATA AND METHODS

Background (ambient) seismic signals were recorded at over 20 sites throughout the Haines Junction region. Measurements are between 30 minutes and 3 hours in duration. Site ambient seismic recordings consisted of either a single instrument, or an array of 17 synchronous long-period instruments in a cross orientation with an aperture of approximately 120 m (Figure 1). Instruments recorded ground motion in the vertical, east, and north directions at a sampling frequency of 100 Hz. Sites were selected based on a variety of factors including preliminary community-scale surficial geology mapping and results from recent electrical resistivity surveys provided by the YGS.

Recordings from all instruments are used to compute horizontal-to-vertical spectral ratios (HVSR), which is an established technique for estimating the fundamental resonance frequency of a site and constrain the depth to significant seismic impedance contrasts (i.e., soil layering structure) and (to a lesser extent) soil stiffness properties (Nakamura 1989). The HVSR method has recent applications in permafrost characterization and monitoring (e.g., Lim et al. 2020; Hayes et al. 2022). At most sites considered in this work, we compute reliable HVSR curves over 0.2-50 Hz. HVSR over this wide frequency band is sensitive to both shallow (10^0 m) and deep (10^3 m) soil properties in the subsurface. However, HVSR suffers from trade-offs (non-uniqueness) between soil seismic properties and depth to impedance contrasts (Molnar et al 2018).

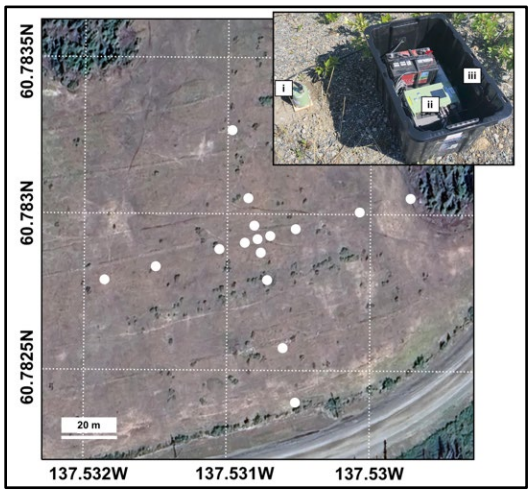

Figure 1. Passive seismic instrument deployment. An example of a multi-instrument deployment is shown for one site. Instrument locations are shown in white. Instruments are positioned along 4 arms/branches and are spaced at approximately 5, 15, 40, and 60 m distances from the centre of the array. Inset showns a single instrument consisting of a 3-component sensor (seismometer) (i) that is mechanically coupled to soil by a ceramic plate. Data are saved on a digital recorder (ii) that uses a GPS antenna (iii) to achieve synchronous timing.

At sites with synchronous multi-instrument (array) recordings, we employ beamforming to measure the propagation velocity of seismic surface waves as a function of frequency (e.g., Wathelet et al. 2004). The velocity-frequency relationship (dispersion curve) can be used to infer subsurface soil properties (e.g., Wathelet et al. 2004). Specifically, dispersion measurements are most sensitive to depth-integrated soil shear-wave velocity. In contrast, HVSR data are sensitive to discontinuous layering at shallow depths.

Complementary information is contained in these data types which are considered jointly here. At most sites considered in this work, dispersion data are reliably measured between 2-12 Hz. This frequency band is a function of the array geometry.

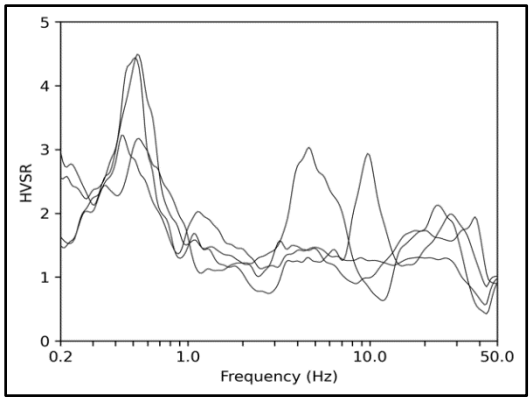

Figure 2. HVSR for sites near Haines Junction, Yukon. Examples of HVSR computed from ambient seismic noise recorded at several different sites are shown. Most sites exhibit a low-frequency (0.2-0.8 Hz) peak due to deep subsurface basin structures. Most sites also exhibit multiple, varying high-frequency (>5 Hz) peaks due to complex soil layering structure, including potential permafrost and seasonally active layers.

Discussion and Conclusion

HVSR curves reveal fundamental resonance frequencies at 0.3-0.8 Hz for most sites throughout the study region (Figure 2), suggesting a thick layer of sediment (of up to several hundred meters) overlies bedrock. The difference in HVSR fundamental peaks suggests subsurface geology varies laterally over larger scales throughout the area, which we attribute to structures associated with the Dezadeash River basin. HVSR curves for most sites exhibit at least one high frequency peak >5 Hz. Additional HVSR peaks indicate additional discrete layering in the overburden between the surface and bedrock layer. High-frequency peaks are indicative of strong impedance contrasts within the uppermost few meters of the subsurface. Permafrost is present but discontinuous throughout the Haines Junction region, and distinct overburden layers observed in HVSR peaks at many sites are likely due to cryospheric processes. This is consistent with recent electrical resistivity surveys conducted in the region by the YGS.

Surface-wave dispersion measurements reveal anomalously high seismic velocities at high frequencies (5-10 Hz). This is indicative of rigid material at shallow depths. Based on surficial mapping and site selection, these measurements may be attributed to frozen material at shallow depths in the subsurface. Future work will estimate robust models of soil seismic structure by jointly analyzing dispersion and HVSR data. Southwestern Yukon hosts complex active geologic processes, which lead to natural hazards. This work presents preliminary analysis of passive seismic data collected in Haines Junction, Yukon, with the aim of characterizing permafrost for improved understanding of natural hazards in the region. Furthermore, this work demonstrates the value of AV measurement techniques for rapid, non-invasive characterization of soil structure. This includes the characterization of permafrost and seasonally active layers.

Acknowledgements

We gratefully acknowledge that we were able to record the data for the research within the Traditional Territory of the Champagne and Aishihik First Nations. This work is supported by the Natural Sciences and by Engineering Research Council. We thank the YGS for providing funding and guidance on local geology. We thank Youngjun Jeon, Min-Hyug Koh, and Minog Kim for their valuable assistance in data collection. We thank Panya Lipovsky and Derek Cronmiller for useful discussions on this work.

References

Hayes, S., Lim, M., Whalen, D., Mann, P.J., Fraser, P., Penlington, R., and Martin, J. 2022. The role of massive ice and exposed headwall properties on retrogressive thaw slump activity, Journal of Geophysical Research: Earth Surface, 127(11): e2022JF006602. doi.org/10.1029/2022JF006602

Lim, M., Whalen, D., Martin, J., Mann, P.J., Hayes, S., Fraser, P., Berry, H.B., and Ouellette, D. 2020. Massive ice control on permafrost coast erosion and sensitivity, Geophysical Research Letters, 47(17): e2020GL087917. doi.org/10.1029/2020GL087917.

Molnar, S., Cassidy, J.F., Castellaro, S., Cornou, C., Crow, H., Hunter, J.A., Matsushima, S., Sánchez-Sesma, F.J., and Yong, A. 2018. Application of microtremor horizontal-to-vertical spectral ratio (MHVSR) analysis for site characterization: State of the art, Surveys in Geophysics, 39(1): 613–631. doi.org/10.1007/s10712-018-9464-4

Nakamura, Y. 1989. A method for dynamic characteristics estimation of subsurface using microtremor on the ground surface, Quarterly Report of Railway Technical Research, 30(1): 25–33.

Turner, D.G., Ward, B.C., Froese, D.G., Lamothe, M., Bond, J.D., and Bigelow, N.H. 2016. Stratigraphy of Pleistocene glaciations in the St Elias Mountains, southwest Yukon, Canada, Boreas, 45(3): 521–536. doi.org/10.1111/bor.12172

Wathelet, M., Jongmans, D., and Ohrnberger, M. 2004. Surface-wave inversion using a direct search algorithm and its application to ambient vibration measurements, Near surface geophysics, 2(4): 211–221. doi.org/10.3997/1873-0604.2004018

Active layer mapping on James Ross Island, Antarctica, using electromagnetic induction system CMD Mini Explorer 6-L

Filip Hrbáček[1], Mohammad Farzamian[2],Karolína Kohoutková[1], Michaela Kňažková[1] & Christian Hauck[3]

[1]*Department of Geography, Faculty of Science, Masaryk University. Kotlářská 2, 611 37 Brno, Czech Republic*

[2]*Instituto Nacional de Investigação Agrária e Veterinária, 2780-157 Oeiras, Portugal*

[3]*Department of Geosciences, University of Fribourg, Switzerland*

Conductivity meters based on electromagnetic induction (EMI) provide solutions for fast geophysical surveying of frozen ground to delineate the active layer-permafrost boundary. An EMI sensor provides measurements of the depth-weighted apparent electrical conductivity (σ_a). Similar to other geophysical techniques, their application is based on the contrast between geological boundaries or material properties, including frozen ground. Yet, the application of EMI in periglacial areas is still sparse (e.g., Kasprzak 2020; Pavoni et al. 2021). This may be due to the limitation of many EMI instruments to 1 to 3 investigation depth levels and the lack of an inversion process, which often prohibits the detection of clear contrast between zones formed by a material with very low electromagnetic conductivities, such as solid rock, dry material and frozen ground. In addition, these low conductivities are often too close to the resolution limit of the instruments to provide unambiguous results concerning the presence and characteristics of frozen ground.

Recently, advancements in multi-coil EM sensors allow the simultaneous collection of σ_a at various coil spacings and orientations in a single reading. Coupled with an inversion process, this technology facilitates the estimation of subsurface conductivity distribution (σ_b), enhancing the delineation of the active layer and permafrost boundary. In this contribution, we present the first results of an EMI survey conducted during the summer season of 2023 with the Multidepth Electromagnetic Conductivity Meter CMD Mini Explorer 6-L (GF Instruments Brno, Czech Republic) on James Ross Island, Antarctica and discuss the pros and cons of the system for the active layer thickness mapping in this area.

Study sites and methods

We did an EMI mapping comprising about 10 km of profiles in February 2023 on James Ross Island. The profiles were located in the northern part of the island. Our objectives encompassed the monitoring of active layer thickness variability across diverse landforms such as pattern ground, solifluction lobes, desert pavements, braidplains, tidal zones and buried ice in the glacier margin. Part of the surveying campaign was conducted on the Circumpolar Active Layer Monitoring sites (CALM-S) located in the vicinity of Johann Gregor Mendel station (CALM-S JGM).

CMD Mini Explorer 6-L has six channels with effective depths down to 2.3 meters allowing precise detection of the surficial layering of the ground. The thaw depth was also measured by manual probing along the EMI surveys in multiple locations. The measured σ_a data was inverted in order to estimate σ_b and was then used to estimate active layer thickness based on conductivity contrast. For validation of the EMI results, we conducted several high-resolution Electrical Resistivity Tomography (ERT) profiles with 0.5 m electrode spacing using a 4-point light 10W instrument (Lipmann GM) using 40 electrodes.

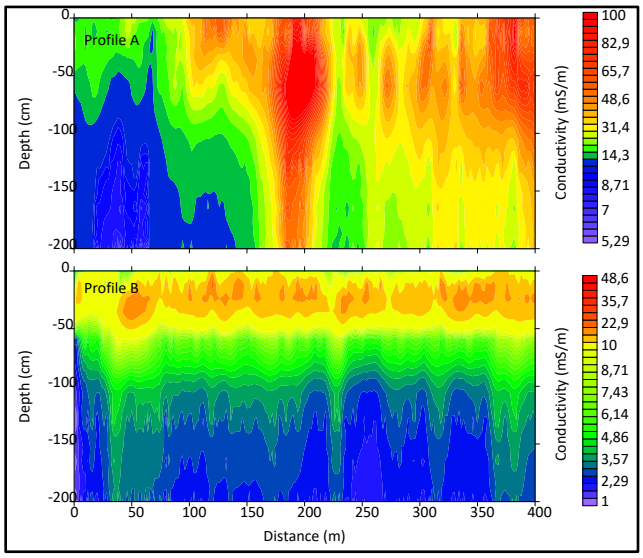

Figure 1. Example of EMI surveying of Berry Hill slopes area on Jams Ross Island in February 2023. To survey was done in two 400 m long profiles in distinctive conditions in terms of topography and lithology. The results are inverted from measured apparent conductivities.

Results and interpretation

Figure 1 shows an example from EMI surveying along two 400 m transects in the Berry Hill slopes area on the northern part of James Ross Island. The distribution of conductivity values highlights a contrast between a more conductive zone (active layer) and

more resistive frozen soil (permafrost) around 80 to 120 cm along profile B. Along profile A, the subsurface conductivities exhibit a rapid increase and a shift in the vertical gradient around 100–150 m. We attribute this change to crossing a braidplain area (150–250 m) where we lost the contrast in vertical gradient. The last section (250–400 m) indicates the effect of a different type of lithological unit having a finer fraction than the first part (0–150 m). Different textures resulted in the conductivities in both unfrozen and frozen ground being about 3 to 4 times higher between both sections.

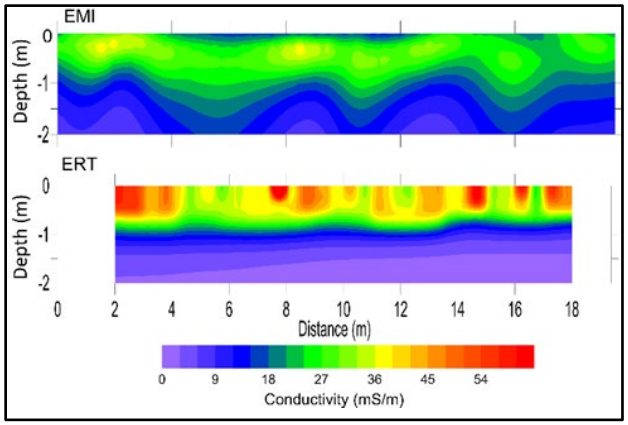

Figure 2. The comparison of the EMI and ERT on the 20 m section on the CALM-S JGM site measured in February 2023. The ERT data are transformed from resitivities to conductivities.

To assess the efficiency of EMI in delineating the active layer/permafrost boundary, Figure 2 presents a comparison between EMI and a very high-resolution ERT model along the same short profile. The EMI modeling results are similar to the one shown in Figure 1b, showing a more conductive zone at the top (active layer) and a more resistive zone at the bottom (permafrost). The pattern of conductivity changes is comparable with the ERT model, indicating that EMI can be used to delineate the active layer relatively well. However, two distinct differences are apparent in this comparison. The ERT model exhibits a larger conductivity contrast, as expected for unfrozen soil versus frozen soil. Additionally, a sharper distinction and smaller lateral change between these zones are detected in the ERT profile, which is also more anticipated along such a small profile. This can be explained by the fewer σ_a depth level measurements and lower sensitivity of EMI compared to the ERT method. In this context, the over-parameterized inverse problem and the smoothing effects from regularization applied in the inversion algorithm make it also more challenging to resolve sharp conductivity contrasts in EMI models. Furthermore, the sensitivity of the EMI signals is limited over the resistive zone, hindering the accurate resolution of the resistive zone (see Farzamian et al. 2021).

Conclusion and Outlook

Preliminary findings from the analysis of the two EMI surveys, shown here, indicate that EMI can yield reliable results, contributing to the detection of active layer thickness over large areas. However, a comparative analysis of EMI modeling with high resolution ERT results suggests that while the EMI method can distinguish these two zones well, it may not precisely identify the boundary between them at a very high resolution. Processing other EMI profiles that were collected across diverse lithologies and conductivity ranges will offer more insights into the circumstances under which EMI performs optimally.

Future works could enhance the inversion process and improve model reliability by incorporating supplementary information such as ground temperature, active layer thaw depth measurements, moisture measurements, ERT, and UAV surveying of detail topography. These data will be also utilized to finetune inversion parameters and potentially establish a conductivity threshold between the active layer and permafrost. This approach will further enable an assessment of the potential of EMI in permafrost studies across different lithologies. Repeating EMI surveys along the same transects and probing in the same locations can provide insights into the potential of using EMI for monitoring thaw depth over large areas.

References

Farzamian, M., Autovino, D., Basile, A., et al. 2021. Assessing the dynamics of soil salinity with time-lapse inversion of electromagnetic data guided by hydrological modelling, Hydrol. Earth Syst. Sci., 25, 1509–1527. https://doi.org/10.5194/hess-25-1509-2021

Kasprzak, M. 2020. Seawater Intrusion on the Arctic Coast (Svalbard): The Concept of Onshore-Permafrost Wedge. Geosciences 2020, 10(9), 349. https://doi.org/10.3390/geosciences10090349

Pavoni, M., Sirch, F., and Boaga., J. 2021. Electrical and Electromagnetic Geophysical Prospecting for the Monitoring of Rock Glaciers in the Dolomites, Northeast Italy. Sensors 2021, 21(4), 1294. https://doi.org/10.3390/s21041294

Monitoring degrading permafrost with single-station passive seismic methods

Stephanie R. James[1], Burke J. Minsley[1], Jack W. McFarland[2] & Mark P. Waldrop[2]

[1]*U.S. Geological Survey, Denver, Colorado, United States*

[2]*U.S. Geological Survey, Menlo Park, California, United States*

As northern latitudes warm, permafrost environments are predicted to undergo widespread degradation. Thawing of permafrost destabilizes the land surface which can have cascading impacts on hydrology, ecosystem functions, human and wildlife communities, and the global carbon budget. Understanding the complex dynamics of when, where, and how permafrost thaws relies on detailed measurements of conditions and changes within the subsurface. Here, we demonstrate the potential value of passive seismic monitoring, using novel single-station methodologies, for tracking changes in water and ice content across multiple timescales.

Methods

In April 2018, we installed nine three-component seismic stations at a thermokarst site near Fairbanks, Alaska. The seismometers continuously recorded the ambient seismic noise wavefield which we used in two ways: 1) coda-wave interferometry (CWI) using cross-component autocorrelations, and 2) horizontal-vertical spectral ratios (HVSR). CWI and HVSR rely on different wave physics, yet both use the three-component seismic records (north-south, east-west, and vertical) from individual stations to sense shear-wave velocity (Vs) changes (James et al. 2021; Köhler and Weidle 2019). Thawed and water-logged soils exhibit significantly slower Vs compared to frozen, permafrost soils; therefore, Vs variations can be a useful proxy for soil moisture and thaw extent. We investigated the relative velocity variations (dv/v) measured by CWI and peak frequency migrations from HVSR, in comparison to soil properties (temperature, water content, thaw depth) to identify spatiotemporal patterns captured by the seismic data.

Results

Both CWI and HVSR results show strong seasonal cycles reflecting active-layer freeze and thaw. Shorter timescale responses to rain events and soil moisture increases in the summer are observed (Figure 1), along with temperature fluctuations in the winter. Spatial patterns were observed across the study site, distinguishing areas with greater thaw and water content at the collapse-scar bog margins compared to more ice-rich stable permafrost locations. CWI proved more advantageous for year-round monitoring, while HVSR displayed a more direct relationship to thaw depth and the presence of talik zones. Lastly, interannual comparisons of seismic results suggest deepening thaw and warming permafrost at select locations, demonstrating the capability for seismic monitoring to capture signs of permafrost degradation.

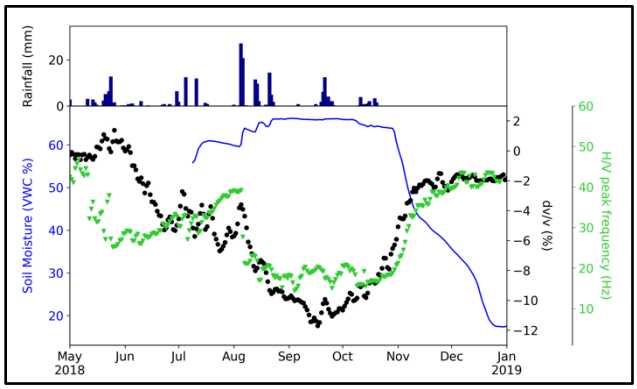

Figure 1. Example seismic results from CWI (dv/v, black dots) and HVSR (peak frequency, green triangles) methods in comparison to soil moisture (blue line) and rainfall (top bar plot).

Conclusions

Both CWI and HVSR methods exhibit sensitivity to soil moisture variations and seasonal active-layer thaw dynamics. These single-station passive seismic methods open new opportunities for scalable and adaptable monitoring of subsurface processes within heterogeneous and dynamically evolving landscapes.

References

James, S.R., Minsley, B.J., McFarland, J.W., Euskirchen, E.S., Edgar, C.W., and Waldrop, M.P. 2021. The Biophysical Role of Water and Ice Within Permafrost Nearing Collapse: Insights from Novel Geophysical Observations. Journal of Geophysical Research: Earth Surface, 126(6). https://doi.org/10.1029/2021jf006104

Köhler, A., and Weidle, C. 2019. Potentials and Pitfalls of Permafrost Active Layer Monitoring Using the HVSR Method: A Case Study In Svalbard. Earth Surface Dynamics, 7(1): 1–16.

A geoelectrical study in the KGL-1 site near the Korean Antarctica Station King Sejong, King George Island, Maritime Antarctica

Kim Kwansoo[1], Joohan Lee[1] & Antonio Correia[2]
[1]*Korean Polar Research Institute, Incheon, South Korea*
[2]*Department of Physics, University of Evora, Evora, Portugal*

In the Antarctic summer of 2017–2018, the KGL-1 site was established to perform several geophysical and biological studies in the Barton Peninsula of King George Island, near the Korean Antarctic Station King Sejong. The geophysical component, in particular the geoelectrical study, was the result of a cooperation between Korean and Portuguese researchers and was intended to be the starting point for a long term monitoring study using electrical resistivity tomography (ERT) methods to evaluate permafrost and active layer spatial and time evolution at the site. Because of the covid pandemic the work came to a halt and, hopefully, will resume in the antarctic summer of 2023-2024.

GEOLOGY SKETCH OF THE STUDY AREA

The Barton Peninsula, where KGL-1 site is located, is composed of volcanic rocks (basalt, basaltic andesite, and lapilli tuff) and plutonic rocks (granodiorite and diorite) as well as sandstones and siltstones. The former result from volcanic activity from Cretaceous to Tertiary times. The KGL-1 site is located on a relatively flat surface at approximately 70 m a.s.l. Geologically, the site is overlaid by the Sejong Formation, which is the lowest stratigraphic unit in Barton Peninsula and can be seen in the southwestern and southern cliffs of the coastline with a thickness of 150-200 m; it mainly consists of congglomerates and sandstones intercalated with basaltic and andesitic lapilli tuff.

THE GEOELECTRICAL SURVEY

In 2017-2018 three tomographic profiles, 3 meters apart, were carried out twice a week for three consecutive weeks to detect possible spatial and time variations in permafrost and active layer thicknesses (Figure 1). Each profile was performed with 40 active electrodes (i.e., computer controlled) separated by 1 meter, using a Wenner configuration; each tomographic profile had a length of 39 m. The equipment used is of the brand Lippmann LG High Power. The electrical resistivity data obtained (pseudosections of apparent electrical resistivity) were processed using an EarthImager™ software to obtain profiles of real electrical resistivity along the larger side of the study area and over time. Small trenches were also dug near the ERT profiles which confirmed the existence of permafrost at depths shallower than 1 meter. All electrical resistivity tomography profiles were oriented along the major side of the rectangle shown in Figure 1.

PRELIMINARY CONCLUSIONS

The models obtained by inversion represent geoelectric sections with 39 m length and about 6 m depth (see example in Figure 2). The results, although preliminary, seem to indicate that there is a correlation between the distribution of zones of high electrical resistivity and the absence of mosses and vice versa. On the other hand, it seems evident that during the period of realization of the repetitions of the several ERTs no significant change was detected in the active layer and in the distribution permafrost. In the future, more data will be collected and will be used to construct two- and three-dimensional models of the electrical resistivity distribution at the study site. Furthermore, interpretation of the ERT profiles indicates that in the KGL-1 site permafrost is discontinuous and its electrical resistivity varies between 8,000 and 10,000 ohm.m; the active layer appears to be partially controlled by a small creek where the water flows from NW towards SE near the middle of the ERT profiles (dark blue zone at the surface of the geoelectrical models of Figure 2). The geoelectric survey allowed the detection of not only permafrost but also groundwater areas.

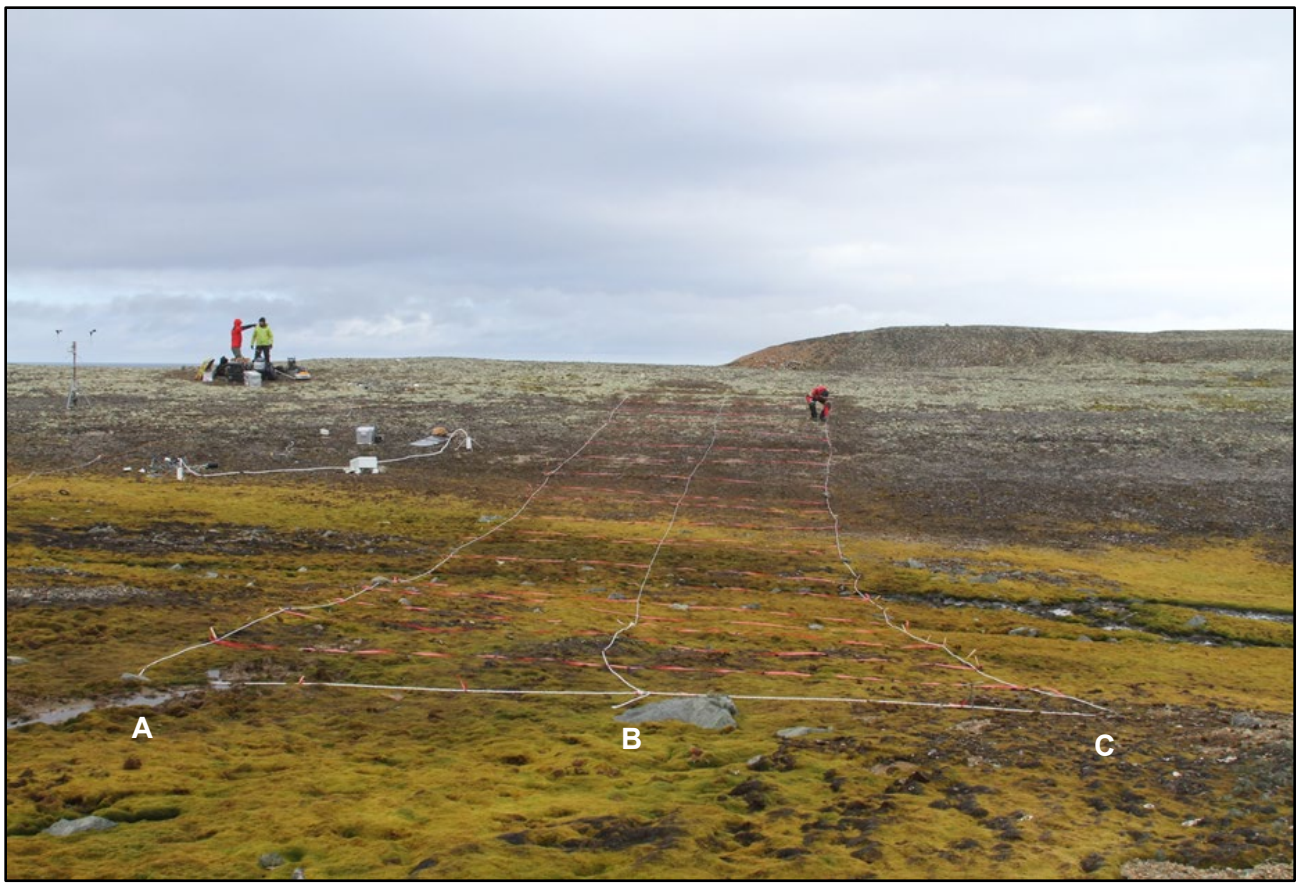

Figure 1. General view of the KGL-1 site in Barton Peninsula near the King Sejong Antarctic Station in King George Island. The white lines indicated by A, B and C represent the three ERT profiles as well as their locations and orientations.

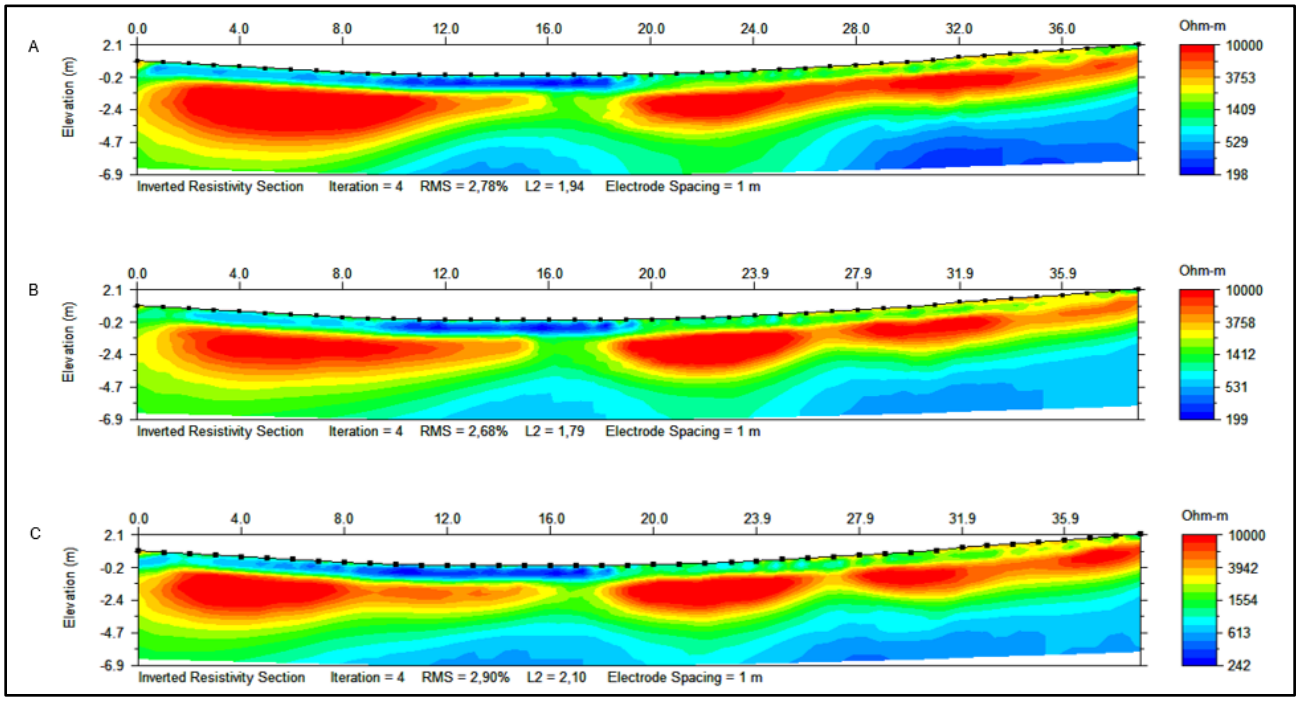

Figure 2. Geoelectric models along lines A, B and C in Figure 1.

Determination of electrical resistivity for frozen soil based on RC circuit

Tianci Liu[1], Feng Zhang[1], Chuang Lin[1], Zhichao Liang[1], Guanfu Wang[1], Decheng Feng[1] & Joey Yang[2]
[1]*School of Transportation Science and Engineering, Harbin Institute of Technology, Harbin, Heilongjiang Province, China*
[2]*Department of Civil Engineering, University of Alaska, Anchorage, Alaska, United States*

To investigate the electrical resistivity characteristics of frozen soils, this paper proposes an indoor frozen soil resistivity testing system based on the RC circuit. The study focused on the silty clay in the permafrost region of the Xiaoxingan Mountain, examining the patterns of unfrozen water content. Subsequently, the proposed resistivity testing system was used to evaluate the soil resistivity under different porosity, temperature, and unfrozen water content.

In Heilongjiang Province, northeast of China, permafrost is concentrated in high-latitude areas such as the Xinganling Mountains, covering nearly half of total area. With the degradation of permafrost. Frozen soil engineering issues pose a global technical challenge (Shan et al. 2015). Soil electrical resistivity is commonly used to anticipate alterations in soil parameters (Sun et al. 2020). The commonly used indoor method for measuring soil electrical resistivity is the volt-ampere method based on Ohm's law (Lyu et al. 2019). The feasible two-electrode method has contact resistance. The four-electrode method in frozen soil is a challenge due to probe insertion. Alternating current can prevent soil melting, but may cause polarization effects. This paper proposes an indoor frozen soil resistivity testing system based on a low-frequency RC circuit. The study investigated the influence of porosity, temperature, and unfrozen water content on frozen soil resistivity. The findings contribute to the understanding electrical properties of frozen soil so that is helpful to employing electrical methods in the geotechnical exploration of frozen soil and analyzing the interface between frozen and unfrozen soil layers.

METHODS AND MATERIALS

This system is based on a series RC circuit, which calculates the resistivity of the tested soil sample. In the interconnected RC circuit, as the alternating voltage fluctuates, the capacitor undergoes a cyclical process of charging, equilibrium, and discharging. The formula for charging and discharging in the series RC circuit can be expressed as in Equation 1.

$$V_C = V_S(1 - e^{\frac{-t}{RC}}) \quad [1]$$

where V_C is the voltage across the capacitor, Vs is the input voltage from the power source, R is the resistance within the circuit, C is the electrical capacity of the capacitor, and t is charging time. when the t=RC, $V_C \approx 0.632V_S$ and the value of can be obtained from the figure in order to calculate the value of resistance R. Testing apparatus setup is shown in Figure 1. The testing system utilizes a signal generator to emit low-frequency alternating current, effectively preserving the structural characteristics of frozen soil samples. Data collection is performed using an oscilloscope, offering better precision compared to existing methods for testing frozen soil resistivity.

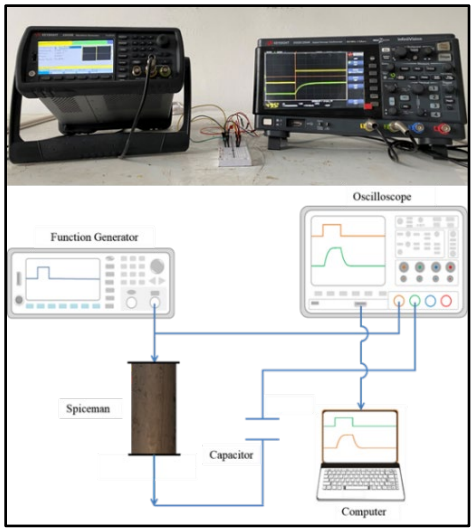

Figure 1. Electrical resistivity testing system based on RC circuit.

The silty clay used in this study was obtained from a discontinuous permafrost region in Xiaoxingan mountain, Heilongjiang province of China. Table 1 shows the basic physical properties of the soil.

Table 1. Characteristics of tested soil.

Properties	Value
Plastic limit (PL)	28.4%
Liquid limit (LL)	39.6%
Plasticity index (IP)	11.2
Specific gravity (Gs)	2.58
Soil classification	Silty clay

The specimens were formed using the slurry consolidation method. The axial pressure and porosity for specimen preparation are listed in Table 2.

Table 2. Consolidation pressure and porosity of specimen.

No.	1	2	3	4	5	6	7	8
Axial pressure(kPa)	20	50	100	150	200	250	300	350
Porosity (%)	75	74.5	73.8	73	72.3	71.5	70.8	70

The specimens were formed using the slurry consolidation method. The axial pressure and porosity for specimen preparation are listed in Table 2. Tested the unfrozen water content of soil specimens at various temperatures during the freezing. Then using proposed system tested the resistivity of frozen soil samples.

RESULTS

Figure 2 shows unfrozen water content variation with temperature in frozen soil samples of different porosities. At the same freezing duration, the unfrozen water content exhibits a gradual increase with rising temperatures.

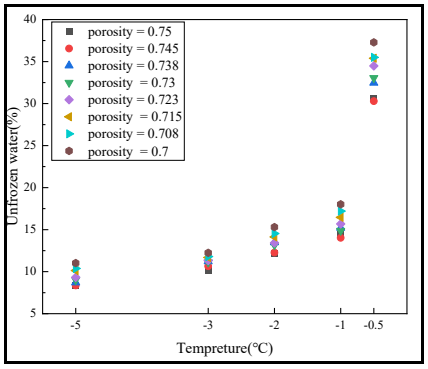

Figure 2. The relationship between unfrozen water and porosity ratio.

Figure 3 shows the relationship between frozen soil resistivity and temperature. As temperature rises, electrical conductivity increases while electrical resistivity decreases.

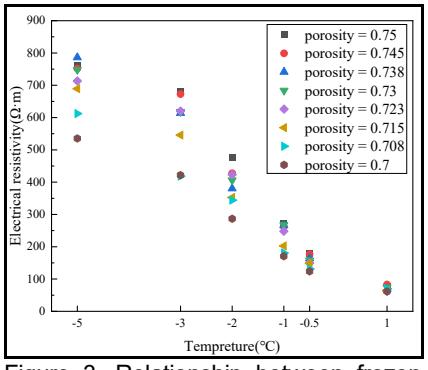

Figure 3. Relationship between frozen soil resistivity and temperature.

Figure 4 shows the typical relationship between electrical resistivity and unfrozen water content. It can be observed that the electrical resistivity of the soil sample changes inversely with the variation in unfrozen water and temperature.

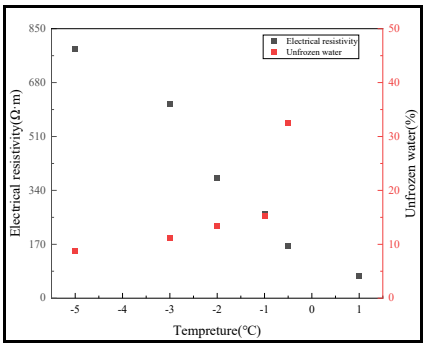

Figure 4. The relationship between electrical resistivity and unfrozen water content, the porosity is 0.738.

CONCLUSION

This study introduces an indoor testing system utilizing an RC circuit for frozen soil resistivity and applies it to experiment, accompanied by unfrozen water content testing. At sub-zero temperatures, soil samples with higher porosity exhibit elevated resistivity. Electrons move through the unfrozen water in pores, with smaller porosity soils relying on soil particle surfaces for cation-assisted electron transfer. For soil samples with same porosity, decreasing temperature correlates with an increase in resistivity. Analyzing electrical resistivity and unfrozen water content changes in soil samples with same porosity as temperature decreases reveals an inverse relationship.

REFERENCES

Lyu, C., Sun, Q., Zhang, W., and Hao, S. 2019. Effects of NaCl concentration on electrical resistivity of clay with cooling. Journal of Applied Geophysics 170, 103843. https://doi.org/10.1016/j.jappgeo.2019.103843

Shan, W., Liu, Y., Hu, Z., and Xiao, J. 2015. A Model for the Electrical Resistivity of Frozen Soils and an Experimental Verification of the Model. Cold Regions Science and Technology 119, 75–83. https://doi.org/10.1016/j.coldregions.2015.07.010

Sun, Q., Lyu, C., and Zhang, W. 2020. The relationship between thermal conductivity and electrical resistivity of silty clay soil in the temperature range -20°C to 10°C. Heat and Mass Transfer 56, 2007–2013. https://doi.org/10.1007/s00231-020-02813-0

On the use of Electrical Resistivity Tomography and Induced Polarization-surveying in arctic landfill assessments

Asgeir Olaf Kydland Lysdahl[1], Regula Frauenfelder[1], Andreas Olaus Harstad[1,2] & Sara Bazin[1,3]

[1]*Norwegian Geotechnical Institute (NGI), Oslo, Norway*

[2]*Now at: Skanska AS, Oslo, Norway*

[3]*Now at: UBO, Institut Universitaire Européen de la Mer, Plouzané, France*

Variations in ground temperature affect the physical properties of permafrost, such as the amount of unfrozen water and ice content. For arctic landfill management, it is important to understand to which extent permafrost can or cannot act as a geological barrier, and how potential barrier characteristics are impacted by climate change. This applies to both existing landfills and future landfills.

Ground-based Electrical Resistivity Tomography (ERT) provides an indirect near-surface indication of permafrost down to a few tens of meters depth. While ERT is very adequate to map the active layer, further interpretation of resistivity profiles is impeded by the lack of resistivity contrast within the permafrost. Indeed, the lithological structures are hidden by the strong resistivity of the frozen layer. We present how combining ERT with Induced Polarization (IP) allows to uncover the interface between the sediments and the bedrock. Although IP is rarely acquired on permafrost, our results show the benefit of measuring it simultaneous to ERT, at no extra costs or time consumption.

We present three examples from the island of Spitsbergen, Svalbard, where combined ERT and IP surveying was used to detect the interface between sediments and bedrock within permafrost, and to investigate potential environmental hazards related to precipitaton and surface water run-off paths from existing and planned landfills.

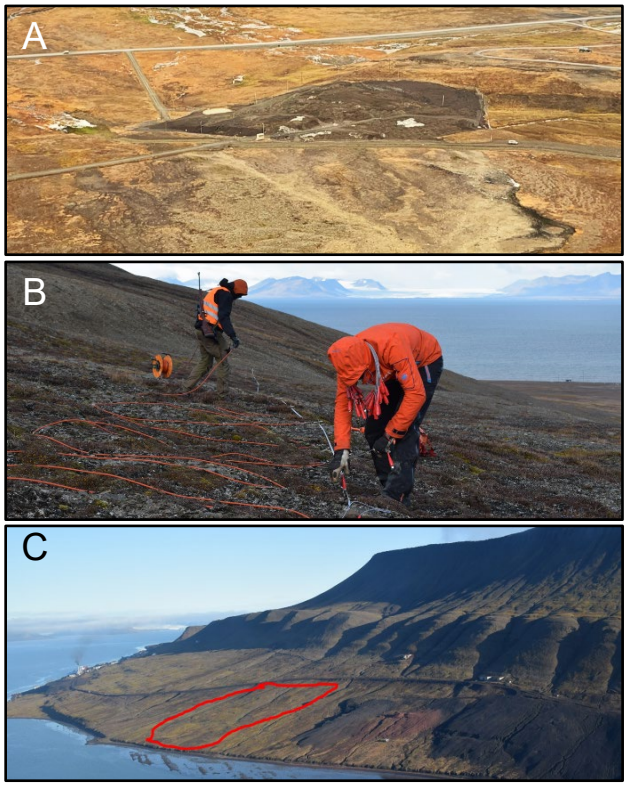

Figure 1. From top to bottom: Oblique image of former active landfill at site A; Outlay of ERT profile at prospective site B; Oblique image of potential site for new landfill (outlined in red) at site C.

Study sites

Our test sites, located in the greater Longyearbyen region on Spitsbergen, Svalbard (Figure 1), are a formely active landfill (site A) established in 1991, now under closure, and two prospective sites for new landfills (sites B and C). Site B is intended for slightly contaminated masses and waste primarily from the building and construction industry, while site C is intended for surplus masses (mainly slag and ash) from coal mining.

Methods and measurements

ERT and IP data were collected at eight profiles in September 2018, when active layer thickness was assumed to be at its maximum. One profile was measured at site A, three at site B, and four at site C. An ABEM Terrameter LS2 with GradientXL acquisition protocol was used for the measurements. For all profiles, 2 m electrode spacing and a layout of four cables, each with 20 connection points, were used. The simultaneous measurement length was thus 160 metres, which gives a penetration depth of around 20–30 metres, depending on ground conditions. For longer profiles, a series of roll-alongs were carried out to cover the entire length of the desired profile. The resolution

is approximately 2 m (equal to the electrode spacing) at surface and deteriorates with depth. Resistivity data was processed with the commercial software RES2DINV, while IP data was processed with Aarhus Work-bench. In the resistivity processing, the measured standard deviation of the voltage data was used to weight the inversion, in order to get a reliable estimate of the survey depth. The 'robust data'- and and 'model-' inversion options were chosen. The raw IP data was of good quality and was inverted directly, without clipping negative attenuation curves.

RESULTS

Investigation depth is 20–30 m for all profiles. The main low-resistivity anomalies come from the unfrozen active layer above the permafrost body, creating a very strong vertical gradient in the upper part of the resistivity models. Due to lack of boreholes for calibration at sites B and C, the transition between unfrozen and frozen ground was defined as the depth where the vertical gradient is highest.

The results show that thickness of the active layer is quite homogenous at site B (Figure 2), but much more variable at sites A and C (Figures 3 and 4).

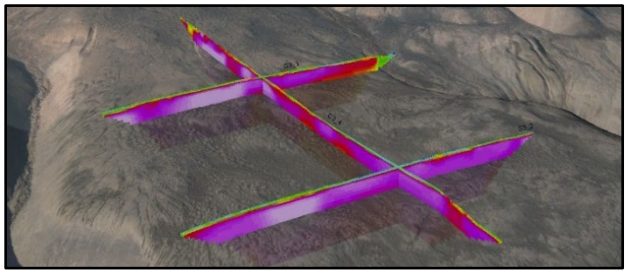

Figure 2. Quasi 3D-composite of resistivity profiles at site B. Colour scale is from 20 to 2000 Ohm-m. The profiles are shown in their correct position, but are raised 15 m above the terrain model.

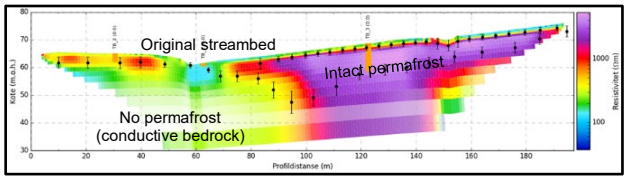

Figure 3. Resistivity profile at site A. Colour scale as in Figure 2. The bottom of the active layer and the top of bedrock are indicated as upper and lower point rows. Orange bars indicate depth to bedrock in drill holes established in November 2018.

We observe a clear influence on the resistivity by creeks draining the hill slopes at sites A (Figure 3) and C (Figure 4). The conductive layer is much thicker where the ERT profiles intersect the creeks, indicating that the ground is unfrozen there.

The IP results show increased chargeability with depth, where bedrock can be expected. Depth to bedrock in boreholes at site A coincides well with the transition from the loose sediment layers to more compact bedrock found in the IP results. At site C, the IP results suggest a terrace-shaped feature, which agrees with the general conception of the bedrock structure at that site. Since the ground is frozen below the active layer, chargeability anomalies at depth are attributed to mineral polarization in the crystalline sediments and capacity effects between large agglomerates of minerals.

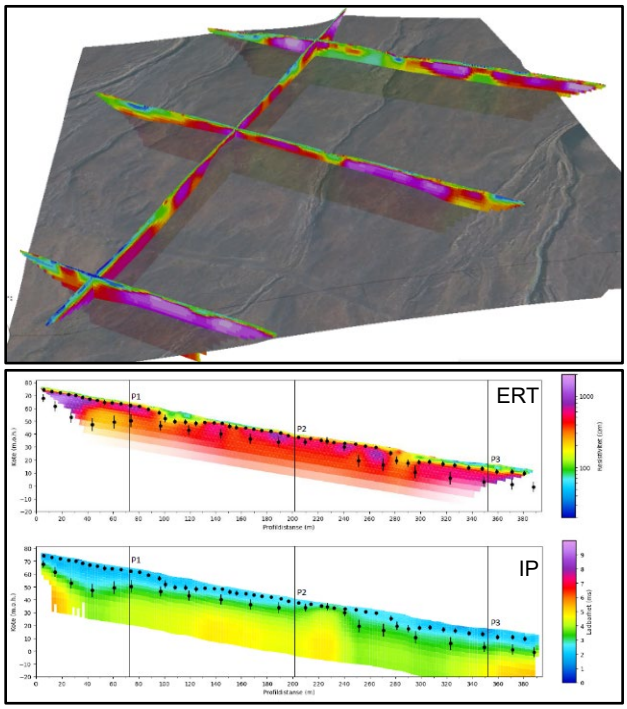

Figure 4. Top: Quasi 3D-ERT composite at site C. Colour scale as in Figure 2; Bottom: Longitudinal resistivity (ERT) and chargeability (IP) profiles, both with interpreted ground conditions. While active layer thickness is interpreted from ERT data, the top of bedrock is based on the IP data.

CONCLUSIONS

Higher temperatures, in combination with more precipitation, will affect both the thickness of the active layer and the properties and extent of permafrost in the ground. Despite the interpreted presence of permafrost in the ground at all investigated sites, ERT/IP data show that there are zones where permafrost is less widespread or absent, particularly in areas with surface drainage in creeks. It seems likely that permafrost as a geological barrier will have a reduced effect in a future warming climate and should not anymore be regarded as a long-term barrier against runoff from man-made landfills in the Arctic.

Combined geophysical and geotechnical investigation to aid in the design of a proposed new railway–Baffin Island, Nunavut, Canada

Ben McClement[1], Adam Plazek[2] & Kiran Chandra Prakash[2]
[1]*Geophysics GPR International Inc., Mississauga, Ontario, Canada*
[2]*Hatch Ltd., Niagara Falls, Ontario, Canada*

As part of a geotechnical investigation program, a geophysical investigation to delineate areas of frozen soils, ice lenses and bedrock was conducted along a proposed new rail alignment in Baffin Island, Nunavut. The geophysical component consisted of ground penetrating radar (GPR) and seismic refraction.

Geophysics GPR International Inc., and Hatch Ltd. assisted in the planning and execution of a geotechnical investigation aimed at addressing gaps in the existing data to advance the design work to the tender stage for a proposed 150 km railway system in Baffin Island, Nunavut.

The results of these geophysical surveys were used to assist in planning and execution of a drilling investigation program.

Ground Penetrating Radar (GPR)

GPR is a non-intrusive geophysical tool that uses electromagnetic pulses to image the subsurface based off the reflections from materials of differing electromagnetic impedances (Daniels 2000).

The GPR data was collected with a GSSI SIR-4000 System and 200HS Digital Antenna with WI-FI connection. This antenna provided a favourable trade off between depth and resolution for ice detection in the upper 15 to 20 m. Positioning was controlled by survey wheel and a GNSS receiver internal to the GPR antenna providing an estimated accuracy on the order of 2 to 5 m (Geophysical Survey Systems, Inc 2022).

The GPR program took place over several weeks in the spring with a two-person survey crew plus support crew between April and May to take advantage of the snow on the ground.

Initial plans were to pull the GPR system by snowmachine; however, the terrain, including snow drifts, steep inclines, and boulders, proved better suited to hand-pulling the antenna.

Additional challenges included site access (helicopter, snow machine) and unpredictable weather conditions. Many other factors influenced the productivity and quality of the data.

The investigation consisted of GPR data collection along approximately 38 km of the proposed rail alignment. Data were collected along profiles parallel with the proposed rail alignment at offsets within the range of 5-8 m on each side. Additional data were collected at proposed bridge and culvert locations and at areas identified to potentially have significant ice lenses.

A total of approximately 120 km of GPR data were collected and interpreted. Results of the survey were presented as interpreted cross-sectional radargrams and georeferenced plan view plots of interpreted ice lens thickness and bedrock elevation.

Overall, the quality of the GPR data was excellent. In some areas signal penetration was greater than 20 m. Interpretation of the GPR data was based primarily on the qualitative analysis of three characteristics of GPR reflections: continuity, amplitude, and shape. The interpreter identifies reflectors and textures within the GPR records that represent subsurface contacts, objects, or zones. The biggest issue relates to the classification of the GPR reflectors. In most areas multiple reflectors were apparent for which the true nature of the material can only be assumed. Borehole data was limited and often offset from the alignment. Figure 1 provides a sample of the interpreted GPR data.

The interpretation of the GPR data identified and delineated potentially significant zones of subsurface ice, providing focus to the subsequent drilling program.

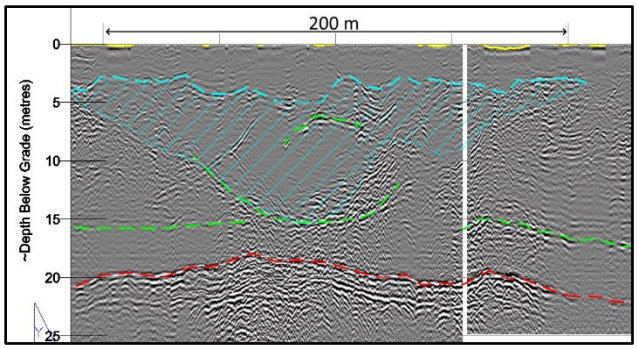

Figure 1. GPR image sample indicated interpreted ice lens (blue), bedrock (red) and unknown/stratigraphic contact (green).

Seismic Refraction

The seismic refraction method relies on measuring the shortest travel time of an induced wave to travel from the source location to a series of receivers, from

which seismic velocities and layer depths can be calculated (Redpath 1973).

The seismic refraction method was employed to map the depth to bedrock and potential permafrost layers at 25 river crossings for proposed bridges or culverts. At each location, one to three seismic spreads were collected along, or perpendicular to, the alignment. The energy source was limited to a sledgehammer.

The seismic program took place over several weeks in the late summer with a three-to-four-person survey crew plus support crew.

Interpretation of the seismic data was completed using both computer aided refraction tomography and with Hawkins' method calculations (Redpath 1973).

The results of the investigation were presented as a compiled interpretation highlighting rock and other refractor profiles with each layer's calculated seismic velocity. Figure 2 provides a sample of the interpreted seismic refraction data with overlain borehole data.

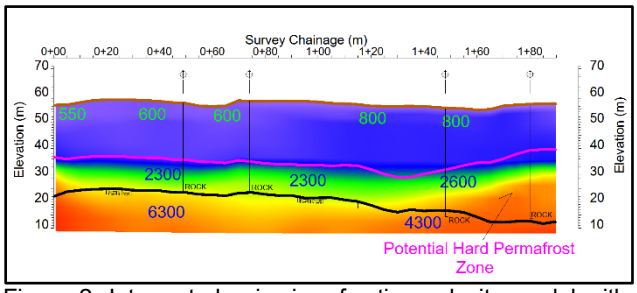

Figure 2. Interpreted seismic refraction velocity model with overlain borehole data.

Overall, the quality of the raw seismic records was exceptionally good, given the energy source limitations and difficult terrain conditions (steep slopes, boulders). The interpretation of the data was complicated by the extremely high velocity of the frozen sand/gravel/boulder material. In some areas, the suspected extremely hard permafrost layer prevented a confident bedrock interpretation.

The seismic refraction results provided interpreted bedrock depths and potential zones of frozen soils or permafrost along with compressional wave velocity information to aid in the design of the bridges and culverts.

DRILLING INVESTIGATION AND DESIGN

The interpreted GPR data was used in the planning process and selection of borehole locations. GPR data has been collected along this rail alignment over the past few years (Roujanski et al. 2010). Based on the previous geophysical data and the 2023 GPR data, Hatch Ltd. was able to identity the minor and massive ice bodies in the subsurface. Hatch Ltd. understands that GPR data is reliable but is influenced by several factors like the experience in interpretation, knowledge of site conditions, etc. (Benedetto 2015).

The 38 km of the alignment scanned with GPR had been identified as a high-risk area with minor to massive ice bodies. Furthermore, the study has proved that GPR can be implemented for the rest of the alignment as drilling boreholes in some areas along the alignment has been challenging.

Most of the massive ice bodies cannot be eliminated completely during the proposed construction, and design considerations would have to be implemented to mitigate the effects of these massive ice bodies (Roujanski et al. 2010). As part of the monitoring program there is a benefit to include the GPR scanning periodically during the life span of the proposed new railway which will help in monitoring the degradation of massive ice bodies, active layer thickness.

The use of seismic refraction allowed for a reduction in number of boreholes required for the design of the deep foundations for bridges by providing a complete bedrock profile, data for the possible thickness of the weathered zone within the bedrock, as well as insight in permafrost conditions. This method was more cost and time effective than the amount of drilling that would have been required to achieve the same result.

REFERENCES

Benedetto, A., and Pajewski, L. (Eds.). (2015). Civil Engineering Applications of Ground Penetrating Radar. Springer.

Daniels, J. 2000. Ground Penetrating Radar Fundamentals. 10.4133/1.2921864

Geophysical Survey Systems Inc. 2022. GSSI GS System Brochure 200HS, Nashua, NH, USA

Redpath, B.B. 1973. Seismic Refraction Exploration for Engineering Site Investigations. Army Engineer Waterways Experiment Station, Livermore, California, USA.10.2172/4409605

Roujanski, V.E., Jones, K.W., Haley, J., Hawton, K., and Fitzpatrick, C. 2010. Some Permafrost Related Terrian Features and Associated Design Considerations along the Proposed Southern Rail Alignment, Mary River Project, Baffin Island, Nunavut, In GEO2010, Calgary, Alberta, Canada.

New approaches to the inversion of frequency domain airborne electromagnetic data to map discontinuous permafrost in the central Mackenzie Valley, NWT, Canada

Keytash Moshtaghian[1], Martyn Unsworth[1,3], Lindsey Heagy[2], Alejandro Alvarez[3], Alexandre Chiasson[3], Joseph M. Young[3], Steven V. Kokelj[4] & Duane G. Froese[3]

[1]*Department of Physics, University of Alberta, Edmonton, Alberta, Canada*

[2]*Department of Earth, Ocean and Atmospheric Sciences, University of British Columbia, Vancouver, British Columbia, Canada*

[3]*Department of Earth and Atmospheric Sciences, University of Alberta, Edmonton, Alberta, Canada*

[4]*Northwest Territories Geological Survey, Government of Northwest Territories, Yellowknife, Northwest Territories, Canada*

More than a third of Canada is underlain by permafrost. In the discontinuous permafrost zone, permafrost distribution and thickness are highly heterogeneous and strongly impacted by local conditions that include vegetation cover and interactions with surface and groundwater (Walvoord and Kurylyk 2016). Conventional geophysical and geological methods are used to locally characterize permafrost thickness and distribution, however, they are not effective at mapping regional-scale variabilities. In this study, we describe the use of airborne electromagnetic (AEM) surveys across a range of landscapes in the central Mackenzie Valley, NWT, Canada. The goal of the project was to map regional permafrost distribution and thickness, and determine the relationship between surface water, groundwater, and permafrost conditions.

AEM surveys are effective in permafrost studies because they can rapidly measure profiles that are hundreds of kilometres long, while also imaging subsurface structures from the surface to depths of hundreds of metres (Figure 1). AEM is suitable for permafrost studies because of the difference in electrical resistivity between permafrost and unfrozen ground. Frequency-domain AEM has been used to map permafrost in Alaska (Minsley et al. 2012). This presentation focuses on the analysis and interpretation of AEM surveys across a key linear infrastructure corridor in the central Mackenzie Valley that identify landscape-scale configurations of permafrost and its relations to surface water and groundwater systems.

METHODOLOGY

The AEM data were collected by XCalibur Multiphysics using a RESOLVE 6 electromagnetic (EM) system, supplemented by a high-sensitivity cesium magnetometer. A GPS electronic navigation system was used to accurately position the AEM measurement points. The RESOLVE system is a symmetrical dipole system that measures data at the 6 frequencies listed in Table 1. The in-phase and quadrature components are recorded for each frequency at 10 samples per second. The depth of investigation varies with frequency, which means that multi-frequency data can determine the variation of resistivity with depth.

The RESOLVE system was flown at an average elevation of 42 m above the surface at a speed of 120 km/h. In total, 47 survey blocks were surveyed between Norman Wells and Wrigley, NWT (Figure 1). Each block included multiple lines with a spacing of 100 m. In total, the AEM survey covered 1340 km of survey lines.

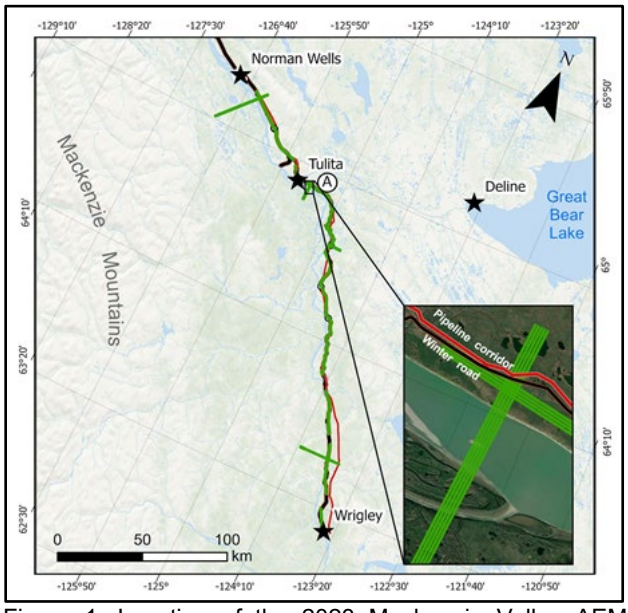

Figure 1. Location of the 2023 Mackenzie Valley AEM surveys (green flight lines) along the winter road (black line) between Wrigley and Norman Wells, NWT, and gas pipeline corridor (red line). The location of the profile in Figure 2 is shown as A.

Data processing by XCalibur involved calibration, background removal for drift, lag correction, spheric and noise rejection, and leveling. Inversion is required to convert the data into a resistivity model of the Earth as a function of depth. This was achieved with a 1-D approach implemented in SimPEG - an open-source Python package (Cockett et al. 2015).

Table 1. The RESOLVE 6 system.

Frequency (Hz)	Coil orientation	Coil separation (m)
135000	Co-planar	7.95
40000	Co-planar	7.93
8200	Co-planar	7.95
3300	Co-axial	9.06
1800	Co-planar	7.94
400	Co-planar	7.93

Each AEM sounding consisted of in-phase and quadrature secondary field measurements at the 6 frequencies listed in Table 1. We used a mesh where the thickness of the first layer was 1 m, and the layer thickness increased with depth by a geometric factor of 1.1. The mesh extended to a total depth of 220 m. The error floor was set to 1%. The inversion began from a model with a uniform resistivity of 1000 Ωm. The average RMS misfit of the 1D models was 2.27, which is a statistically acceptable value. Finally, the 1D models were stitched together to create a 2D resistivity cross-section.

RESULTS

The results are illustrated with an AEM profile across the Mackenzie River near the community of Tulita (Figure 2). High resistivity values (> 500 Ωm) define permafrost extent and are associated with the upland areas of glacial Lake Mackenzie sediments on the south side of the Mackenzie River. Permafrost is also present on islands in the river. The thickness of permafrost in this area is around 30 m, consistent with ground-based electrical resistivity (ERT) and borehole temperature data (Duchesne et al. 2020).

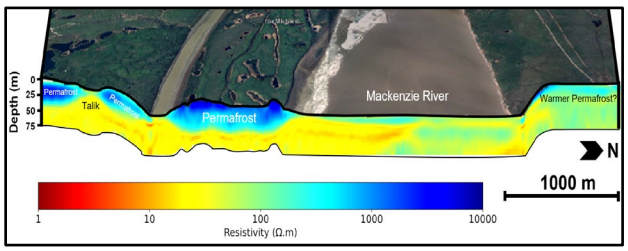

Figure 2. Cross-section of the resistivity model crossing the Mackenzie River near Tulita. Profile shows high resistivity in the upland areas and on an island on the south side of the river, indicating the presence of permafrost.

The AEM model also shows the impact of surface and groundwater on the depth to the top of the permafrost layer. Most notably, permafrost is absent below channels of the Mackenzie River, as indicated by low resistivity. In the upland terraces, areas of low resistivity are associated with water bodies, likely representing talik formation. In addition, the relatively low resistivity values (200-500 Ωm) on the eastern terrace may indicate permafrost at warmer temperatures and increased unfrozen water content.

DISCUSSION AND CONCLUSION

Our initial analysis of 2023 AEM data in the central Mackenzie Valley clearly illustrates the significant potential of airborne geophysical surveys for characterizing the regional distribution of permafrost and improving our understanding of its potential for thaw. Our interpretations of the inversion model are consistent with ongoing ground-based geophysical and geological investigations and borehole temperature profiles in the study area. The relatively low resistivity values on the eastern terrace may correspond to increasing temperature and unfrozen water content of the permafrost table, likely driven by higher regional groundwater gradients than the western terraces of the survey. This model also indicates the presence of frozen sediment under a modern river bar of the Mackenzie River, which suggests this area underwent permafrost aggradation to present thickness during the Holocene.

REFERENCES

Cockett, R., Kang, S., Heagy, L.J., Pidlisecky, A., and Oldenburg, D.W. 2015. SimPEG: An open source framework for simulation and gradient based parameter estimation in geophysical applications. Computers & Geosciences, 85, 142–154.

Duchesne, C., Chartrand, J., and Smith, S.L. 2020. Report on 2018 field activities and collection of ground-thermal and active-layer data in the Mackenzie corridor, Northwest Territories; Geological Survey of Canada, Open File 8707, 84 p.

Minsley, B.J., Abraham, J.D., Smith, B.D., Cannia, J. C., Voss, C.I., Jorgenson, M.T., et al. 2012. Airborne electromagnetic imaging of discontinuous permafrost. Geophysical Research Letters, 39(2).

Walvoord, M.A., and Kurylyk, B.L. 2016. Hydrologic impacts of thawing permafrost—A review. Vadose Zone Journal, 15(6).

Textile instead of steel spike? – A new electrode system for electrical resistivity soundings in harsh and coarse-blocky environments

Mirko Pavoni[1], Jacopo Boaga[1], Matthias Lichtenegger[2,3], Johannes Buckel[4] & Alexander Bast[2,3]

[1]*Department of Geosciences, University of Padova, Via Gradenigo 6, 35131 Padova, Italy*

[2]*WSL Institute for Snow and Avalanche Research SLF, Permafrost Research Group, Flüelastrasse 11, 7260 Davos Dorf, Switzerland*

[3]*Climate Change, Extremes and Natural Hazards in Alpine Regions Research Center CERC, Flüelastrasse 11, 7260 Davos Dorf, Switzerland*

[4]*Institute for Geophysics and Extraterrestrial Physics, Technische Universität Braunschweig, Braunschweig, Germany*

Electrical resistivity tomography (ERT) is frequently used in mountain environments, where debris and coarse-blocky substrates often dominate the surface of rock glaciers, landslide or rockfall deposits. To ensure effective galvanic coupling between the electrodes and the surface substrate, stainless steel spikes are typically employed. However, the installation of these spikes is a difficult and time-consuming task in such harsh environments. To overcome these challenges, we tested conductive textile sachets on a landslide deposit and two rock glaciers in the European Alps. Both, data based on steel and textile electrodes were compared and used to generate inverted resistivity models. These models were found to be nearly identical, suggesting that textile electrodes could serve as a practical substitute to conventional heavy steel electrodes. This would significantly enhance logistics and fieldwork efficiency.

A reliable ERT dataset requires an optimal galvanic contact between the electrodes and the ground surface (Binley 2015). This is particularly challenging in debris and coarse-blocky environments, where high contact resistances between the typically used stainless steel spikes and the surface substrate hinder the electrical current injection. To overcome this challenge, the electrodes are typically coupled with salt water-soaked sponges (Hauck and Kneisel 2008). However, this approach is logistically and temporally demanding since the steel spikes are heavy, have to be precisely hammered in between the boulders, and several liters of salt water are needed per sounding to wet the sponges. Recently, Buckel et al. (2023) used conductive textile sachets as electrodes for ERT measurements on rock glaciers. This approach promises to reduce the logistic and time required to deploy ERT arrays on coarse-blocky surfaces, since the textile electrodes can be easily pushed between the blocks and wetted with a lower amount of salt-water. Here, we tested the textile electrodes by performing three ERT lines on different sites with debris and coarse-blocky surfaces. At each test site, the ERT measurements have been acquired both with steel spikes (coupled with sponges) and conductive textile sachets.

STUDY SITES

The comparative tests were carried out at the Marocche di Drò landslide, the inactive rock glacier of Sadole, and the active rock glacier of Flüelapass. The Marocche di Drò site (Trento, North-East Italy) is a post-glacial landslide deposit, and we focused on the Kas deposit, which ranges from 245 - 265 m a.s.l. The surface consists of calcareous debris, angular blocks and a sparse vegetation cover. The Sadole site (Trento, North-East Italy) is an inactive and partially vegetated rock glacier, consisting of three distinct lobes, ranging from 1820 - 2090 m a.s.l. The comparative test was carried out on the older central lobe. The surrounding rock walls are composed of volcanic ignimbrite, which forms the boulders and debris on the surface of the rock glacier. The Flüelapass rock glacier (Canton of Grisons, Switzerland) is a creeping landform ranging between 2380 to 2800 m a.s.l. It is surrounded by steep walls of metamorphic amphibolite and paragneiss. We focused on the lower part of the rock glacier with a coarse-blocky surface, and a patchy pattern of finer sediments and soil in between.

TEXTILE ELECTRODES

The production of textile sachets is simple and fast, about 10 minutes to make one electrode. We used a conductive polyester fabric metallized with copper (~20%) and nickel (~15%). We cut the textile into 30x30 cm pieces and filled them with ~300 g of fine sand. Finally, the sachets were sealed with cable ties and insulating tape. The cost of producing one electrode is about 15 Euros, which is mainly due to the cost of the conductive textile.

DATA ACQUISITION AND ANALYSIS

At each site, we collected the ERT datasets using steel spike electrodes hammered between the boulders and coupled to sponges soaked in salt water (e.g., Figure 1). Subsequently, we measured the same ERT lines using the conductive textile electrodes, with the sachets pushed between the boulders and moistened with salt water (Figure 1). The datasets were collected with a Syscal Pro resistivity meter (www.iris-instruments.com), 3'542 direct and reciprocal measurements, a dipole-dipole multi-skip acquisition scheme, and stacking range between 3-6 (standard deviation threshold of 5%). All surveys were carried out in the summer of 2023, using different electrode spacings: i) 3 m at Marocche di Drò, ii) 5 m at Sadole, and iii) 2 m at Flüelapass.

Figure 1. Example of a stainless-steel electrode hammered in between the boulders, coupled with salt water-soaked sponges, and a conductive textile sachet electrode placed between the boulders and moistened with salt water (image taken at the Marocche di Drò test site).

To verify the applicability of textile electrodes we compared the contact resistances, the injected electrical current, the measured apparent resistivities, the quality of the ERT datasets (using the reciprocal error check; Binley 2015), and the inverted resistivity models obtained with the measurements collected with the different electrode approaches. Statistical analyses were performed using R (R-core-Team 2022). For data exploration, we used violin plots (Figure 2), which include both the density distribution of the data and notched box plots. The robust Spearman correlation coefficient was calculated for each of the five variables.

To statistically test the accuracy of the textile electrodes we fitted a robust linear regression model with an extended MM estimator within the R package robustbase for all the variables and sites. We performed diagnostic regression plots to analyze the model residuals and ensure that the model assumptions were met. Finally, for each site, the inverted resistivity models are plotted and compared to evaluate the differences.

We present the results obtained and demonstrate that conductive textile sachets electrodes can be successfully used to perform reliable ERT measurements in environments with a coarse-blocky surface substrate, reducing the logistical and time effort of the survey.

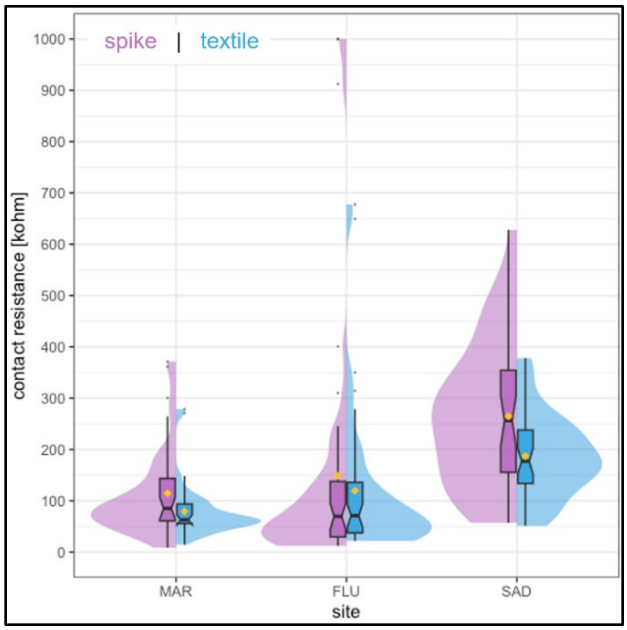

Figure 2. Example of a violin plot for contact resistance values recorded at the three test sites: i) Marocche di Drò (MAR), ii) Flüelapass (FLU), and iii) Sadole (SAD).

REFERENCES

Binley, A. 2015. Tools and Techniques: Electrical Methods, in Treatise on Geophysics, 2nd ed., Schubert, G., Elsevier, Oxford, 233–259. https://doi.org/10.1016/B978-0-444-53802-4.00192-5

Buckel, J., Mudler, J., Gardeweg, R., Hauck, C., Hilbich, C., Frauenfelder, R., Kneisel, C., Buchelt, S., Blöthe, J.H., Hördt, A., and Bücker, M. 2023. Identifying mountain permafrost degradation by repeating historical electrical resistivity tomography (ERT) measurements, The Cryosphere, 17, 2919–2940. https://doi.org/10.5194/tc-17-2919-2023

Hauck, C., and Kneisel, C. 2008. Applied Geophysics in Periglacial Environments. Cambridge: Cambridge University Press.

R-core-Team 2022. A Language and Environment for Statistical Computing, R Foundation for Statistical Computing. https://www.R-project.org (4.2.2) [code].

Geophysical assessment (ERT, SRT) of frozen ground distributions in mountain-road areas of Tierra del Fuego, Chilean Patagonia.

Sebastián Ruiz-Pereira[1,2], Mirko Pavoni[3], Alberto Carrera[3], Jacopo Boaga[3] & Balázs Nagy[4,2]

[1]*DIHA, Pontificia Universidad Católica de Chile, Santiago, Chile*

[2]*PERMACHILE network*

[3]*Università di Padova, Padova, Italy*

[4]Eötvös Loránd University, Budapest, Hungary

Permafrost in southern Patagonia is generally assumed as absent. Nevertheless, Tierra del Fuego (54°S), a shared island between Argentina and Chile named, stands as an extensive area there where dozens of mountains surpass 1,500 m ASL and permafrost probabilistic maps assume it may exist in mountain tops (Figure 1).

In this island, road infrastructure in the Chilean side is being built southwards, trying to reach the southern border and meet the Darwin Range along the Beagle Channel. Thereon, the road is supposed to cross a pass between two peaks, possibly reaching above 900 m ASL. Hence, our prerogative to inspect the warm season regime of subsurface in those critical areas for infrastructure, as recent frozen ground decline may alter compaction and settling of the ground surface, leading to subsidence.

The technical issue here is that even though grounds have consistently different electrical properties when frozen (Hauck and Kneisel 2008), for materials close to zero degrees Celsius, subsurface interpretations may eventually 'mask' the freezing state if materials have 'curtain-effect' type of behaviour due to latent heat constraints. Therefore, geophysical prospection using electrical resistivity tomography (ERT) and seismic refraction tomography (SRT) should stand with enough sensitivity to discretize either partially frozen ground or very shallow lenses pertaining to degrading permafrost profiles. Even shallow lenses could represent risk factors for construction loading inducing vulnerable soil settlement.

The acquisitions will be performed with 24 channel instruments, for the ERT a Syscal Pro (Iris Instrument) while for the seismic method a Geode (Geometrics). In both cases, cables with 5 meters spacing will be used. In this way, the length of the investigation lines can be modified considering the characteristics of the different sites. If higher penetration is required, the full extension of the cables (115 meters) can be used to reach presumably 25-30 meters of investigation depth. On the other hand, if it is necessary to increase the resolution at the near-surface, it is possible to decrease the spacing.

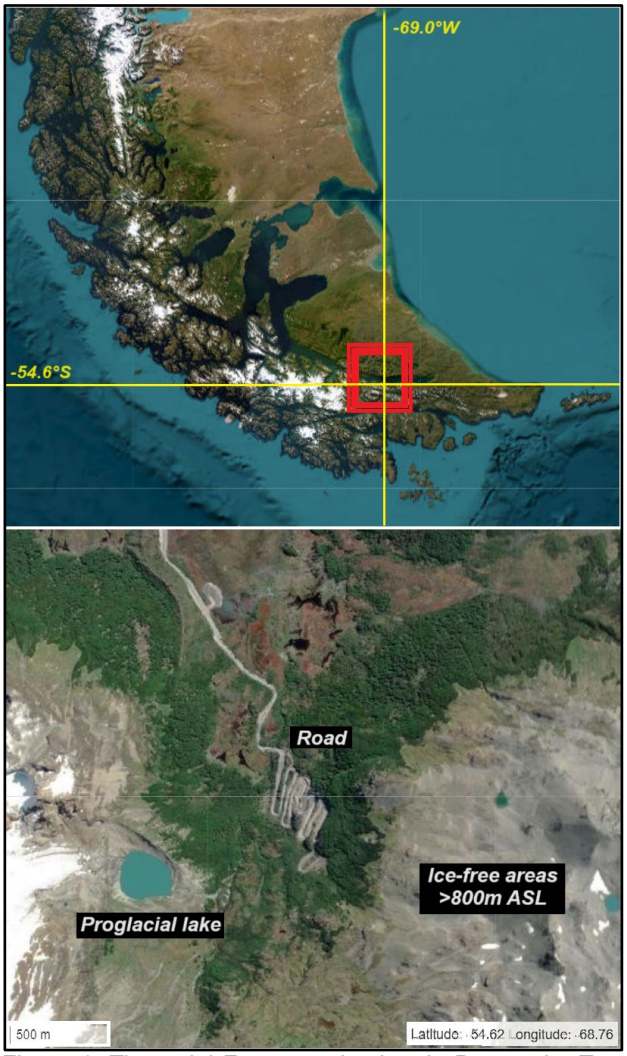

Figure 1. Tierra del Fuego study sites in Patagonia. Top, southern cone context of the island. Bottom, glacial and paraglacial landscapes around road infrastructure. ESRI bedmap 2023.

For the ERT surveys, two different acquisition schemes will be applied, i.e. Dipole-dipole (multi skip) and Wenner-alpha. The datasets will be acquired with stacking and direct-reciprocal measurements. In this way, a reliable evaluation of the data quality will be

possible during the data processing (Binley 2015). To reduce the logistical and time efforts needed to set the ERT arrays, conductive textile sachets (Buckel et al. 2023) will be used as electrodes, wetted with salt water to improve their galvanic contact with the debris surface (Pavoni et al. 2022).

For the seismic acquisition, a 10-kilo hammer will be used as source, and low-frequency vertical geophones (4.5 Hz). In this way, in the data processing phase, it will be possible to perform not only an SRT analysis on the compressive waves (Vp) but also a multichannel analysis of surface waves (MASW – Park et al. 1999) to retrieve a quasi-2D shear wave model. To optimize the lateral resolution, energizations will be performed at each geophone, and to improve the signal-to-noise ratio it is planned to collect several energizations in the same position (stacking).

The ERT and SRT analysis were performed using the open-source Python-based Pygimli library (Rücker et al. 2017), which allows to perform both independent inversions of the datasets and the joint inversion methods, i.e. the datasets acquired with two different techniques on the same investigation line are coupled in a single inversion routine. In particular, we applied the structurally coupled joint inversion (SCCJI – Hellman et al. 2017) and the petrophysically coupled joint inversion (PCJI – Wagner et al. 2019). The SCCJI allows to obtain sharper boundaries in the Vp and resistivity models (e.g., useful to better define the depth of active layer and bedrock), while the PCJI allows to estimate air, water, and ice fractions in the frozen subsurface.

This geophysical evaluation determined subsurface structures as potential permafrost around the permafrost probability limits in Tierra del Fuego around 800 m ASL. In the context of road expansion in the area, more favorable distribution of this feature is examined at lower altitudes nearby the road path.

REFERENCES

Binley, A. 2015. Tools and Techniques: Electrical Methods, in: Treatise on Geophysics, edited by: Schubert, G. (editor in chief), 2nd edn., vol 11, Elsevier, Oxford, 233–259.

Buckel, J., Mudler, J., Gardeweg, R., Hauck, C., Hilbich, C., Frauenfelder, R., ... and Bücker, M. 2023. Identifying mountain permafrost degradation by repeating historical electrical resistivity tomography (ERT) measurements. The Cryosphere, 17(7), 2919–2940.

Hauck, C., and Kneisel, C. 2008. Applied Geophysics in Periglacial Environments. Cambridge University Press.

Hellman, K., Ronczka, M., Günther, T., Wennermark, M., Rücker, C., and Dahlin, T. 2017. Structurally coupled inversion of ERT and refraction seismic data combined with cluster-based model integration. Journal of Applied Geophysics, 143, 169–181.

Park, C.B., Miller, R.D., and Xia, J. 1999. Multichannel analysis of surface waves. Geophysics, 64(3), 800–808.

Pavoni, M., Carrera, A., Boaga, J. 2022. Improving the galvanic contact resistance for geoelectrical measurements in debris areas: a case study. Near Surf. Geophys.

Rücker, C., Günther, T., and Wagner, F.M. 2017. pyGIMLi: An open-source library for modelling and inversion in geophysics. Computers & Geosciences, 109, 106–123.

Wagner, F.M., Mollaret, C., Günther, T., Kemna, A., and Hauck, C. 2019. Quantitative imaging of water, ice and air in permafrost systems through petrophysical joint inversion of seismic refraction and electrical resistivity data. Geophysical Journal International, 219(3), 1866–1875.

Ground penetrating radar survey to study a fragile cultural heritage site at Russekeila, Svalbard

Saman Tavakoli[1], Cristi Nicu Ionut[2], Regula Frauenfelder[1] & Graham Gilbert[1]

[1]*Norwegian Geotechnical Institute, Oslo, Norway*

[2]*High North Department, Norwegian Institute for Cultural Heritage Research (NIKU), Fram Centre, N-9296, Tromsø, Norway*

There are ca. 180.000 cultural heritage sites registered in the Arctic, of which about 4000 are located in Svalbard. Since the discovery of the island of Spitsbergen, Svalbard in 1596, the area has become a hotspot for explorers, hunters and scientists which led to the building of shelters and huts in different parts of Svalbard. The remains of these activities are now protected cultural heritage sites if established prior to 1946. Russian settlements from the Pomor hunters are the most numerous group of cultural heritage sites in Svalbard and spread throughout the archipelago. Pomors lived by the White Sea, and sailed to Norway in the summer season to fish and trade with Norwegians. Previous research has highlighted an archaeological Pomor site at Russekeila, Kapp Linné, Svalbard, as highly vulnerable to cryospheric hazards and coastal erosion. In this study, we investigate this site using a Ground Penetrating Radar (GPR) system, in order to investigate the near-surface stratigraphy of the site, and cultural heritage (CH) remains from 18th century and after.

The study area

The focus of this study is the Russekeila area, an almost 2 km wide bay near the mouth of Isfjorden (Nordenskiöld Land, Svalbard) (Figure 1).

Figure 1. Geographical location of the Russekeila site: Linnéelva river separates the eastern and the western parts of the bay (investigated cultural heritage site in this study in black rectangle).

Russekeila Bay is located approximately halfway between Isfjord Radio and Kapp Starostin. Due to the presence of remarkable geological and quaternary geological features, the area is part of the Fortress Geotop Protection Area. The Linnéelva River divides the bay into a (smaller) western part and a (larger) eastern part. Russekeila hosts the remains of a Pomor wintering station (site 'Russekeila West', RW), which is subject to intense coastal and river erosion. There is also an important Pomor trapper's hut in the centre of Russekeila ('Russekeila East', RE), dating back to the 18th century. In addition, there are two other cabins, a restored grave and a Pomor tree cross from the same period. The main cultural remains are the exposed decaying wooden ruins of a multi-roomed building, the hunting hut and several huts spread around an area of about 200 m^2 (Nicu et al. 2021).

Objectives

The main objectives of the GPR survey in this study were (i) to register the precise surface and subsurface locations of cultural heritage (CH) remains of an 18th century Pomor trapper's hut within the study area, investigate graves and other sub-soil artefacts from the Pomor time, (ii) to determine the impact of coastal erosion on the CH objects, and (iii) to understand the near-surface stratigraphy of the site.

A GPR instrument with two shielded antennas of 500 MHz and 800 MHz, respectively, was used. Initial processing of the GPR data was performed using the Reflex2Dquick-V4.0 (Sandmeier Geophysical Research). In addition, running average and dewow (subtract mean with filter length of 25 ns to eliminate very low frequency components) and Automatic Gain Control (AGC) filters were applied to the data.

Results

Only weak anomalies were observed at the intersections with wooden drifts, which can be explained by the low contrast between the relative dielectric constant values of the driftwood and the background soil. The depth extent of the driftwood within the soil was understood from the processed GPR data to a depth of approximately 25 cm. A near-surface stratigraphy of the site morphology, including thaw depth, saturated and unsaturated sediments and soil cover, was established based on multiple reflectors

observed to 2 m depth. Loose sediments are indicated by reflectors to a depth of approximately 20 cm. Unsaturated fine sediments, which show a stronger signal compared to the underlying saturated sand layers, can be observed from about 1.2 m depth. No reflectors are shown below the thaw depth.

An overview of a representative depth section of one of the profiles (profile 27) which can be considered a high-quality average of all measured profiles in the area after processing, was used to illustrate the dominant near-surface stratigraphy of the site (Figure 2).

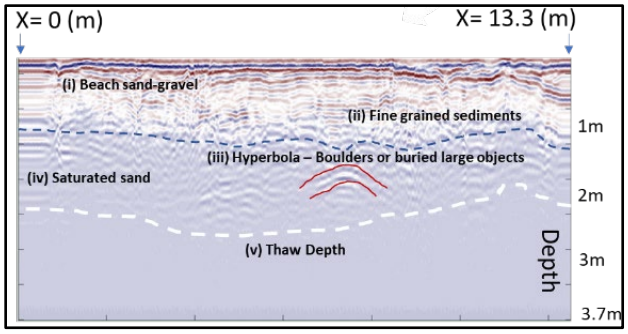

Figure 2. Inferring the dominant near-surface stratigraphy of the study area at the time of measurement (August 2022) based on the GPR measurements. "X" denotes distance along the profile. The presented depth section denotes the processed GPR results from profile 27. Processing is conducted in MATGPR. Conversion to depth was based on V= 0.1 (m/nS). Profile 27 was measured using the 500 MHz antenna.

The following layers were identified after the processing of the GPR data (Tavakoli et al. 2023):

i. Beach sand/gravel: unconsolidated sediments covering the top few centimetres of the subsurface stratigraphy. Stronger reflectors within this part are partly due to the high signal resolution near the surface.

ii. Fine-grained sediments: unsaturated, fine sediments which show a stronger signal compared to their underlying layers. The contrast between the reflectivity of this layer and its overlying parts, which decreases with depth, can be primarily described by variations in grain size.

iii. Large-grained objects: several scattered and weak hyperbolas can be observed across the study area at various depths. These hyperbolas most likely represent larger stones within a fine-grained composition. Alternatively, they may represent unexplored CH objects. Further investigation is required to better understand their origin.

iv. Saturated sand: at approximately 1.2 m depth (Figure 1b), the signal degrades dramatically, most likely due to a shift from the upper, unsaturated layers to the lower, saturated layers.

v. Thaw depth: the weakest reflector in the section is related to the parts of the stratigraphy located below the thaw depth. Frozen ground transmits almost all the energy through itself and therefore no strong reflectors can be observed below the thaw depth.

Conclusion

Based on our GPR measurements and additional visual field observations, the following conclusions can be made: i) strong signals can be observed down to a depth of approximately 0.5 m. After processing, several reflectors can be observed down to a depth of 2 m, but the amplification of the signal is associated with additional noise; ii) the signal deteriorates where the radar pulses hit the wooden drifts of the huts (lower dielectric constant for the wood compared to the sediments). This is the most significant indicative feature of all the cultural heritage features surveyed; iii) understanding the extent of the depth of the graves was challenging due to: the precautions necessary to protect the fragile cultural heritage, signal attenuation due to low S/N ratio over the uneven surfaces of the graves at the site.

Surveying the area with a drone-mounted magnetic sensor, in combination with a ground-magnetic survey could provide significant complementary results to the findings of this study. In light of future work, a combination of additional remote sensing methods, e.g. repeated drone photographs along with detailed geological and geomorphological mapping, and detailed topographical surveys, can be considered. Integrated combination of non-invasive methods would help in managing such fragile Arctic CH sites.

References

Nicu, I.C., Lombardo, L., and Rubensdotter, L. 2018. Preliminary assessment of thaw slump hazard to Arctic cultural heritage in Nordenskiöld Land, Svalbard, Landslides 18 (8) (2021) 2935–2947. doi:10.1007/s10346-021-01684-8

Tavakoli, S., Nicu, I.C., Frauenfelder, R., and Gilbert, G. 2023. First geophysical investigations to study a fragile Pomor cultural heritage site at Russekeila – Kapp Linné), Svalbard, Journal of Cultural Heritage, Volume 63, Pages 187–193.

Detecting massive buried ice using drone-based ground penetrating radar

Adam R. Tjoelker[1,2], Michel Baraër[3,4], Eole Valence[4,5], Bastien Charonnat[3,4], Bryan G. Mark[1,2] & Jeffrey M. McKenzie[4,5]

[1]*Department of Geography, The Ohio State University, Columbus, Ohio, United States*

[2]*Byrd Polar and Climate Research Center, The Ohio State University, Columbus, Ohio, United States*

[3]*Hydrology, Climate and Climate Change (HC3) Laboratory, École de Technologie Supérieure (ÉTS), Montréal, Canada*

[4]*GEOTOP (Research Centre on the Dynamics of the Earth System), Montréal, Canada*

[5]*Department of Earth and Planetary Sciences, McGill University, Montréal, Canada*

Detecting buried ice in deglaciating alpine and high-latitude valleys remains challenging using traditional approaches to manual ground penetrating radar (GPR). The steep and unstable terrain found on debris-covered ice, rock glaciers, talus slopes, moraines and other paraglacial features make terrestrial GPR methods dangerous or cost prohibitive. This study introduces a safe approach for detecting buried ice using a multi-low-frequency drone-based GPR.

Methods

In June 2023, a drone-based monostatic GPR was deployed in Shár Shaw Tagà (Grizzly Creek), a deglaciating valley in Kluane National Park and Reserve in southwest Yukon, Canada (Figure 1).

Figure 1. Location of Shár Shaw Tagà (Grizzly Creek) field site within southwest Yukon, Canada.

Three low frequency antennas of 50, 100, and 200 MHz were flown along a 430 m transect spanning the transition from a debris covered glacier to a steep, talus covered, thermokarst feature (Figure 2). Results from the drone-based survey were compared to manual ground-based GPR measurements using the GPR system configured in a bi-static mode with the same antenna set. The manual surveys were conducted over two sections of the drone transect: one on the debris covered glacier and one above the buried ice at the steep talus slope. Common mid-point (CMP) surveys were also realized at those two locations using the three GPR frequencies.

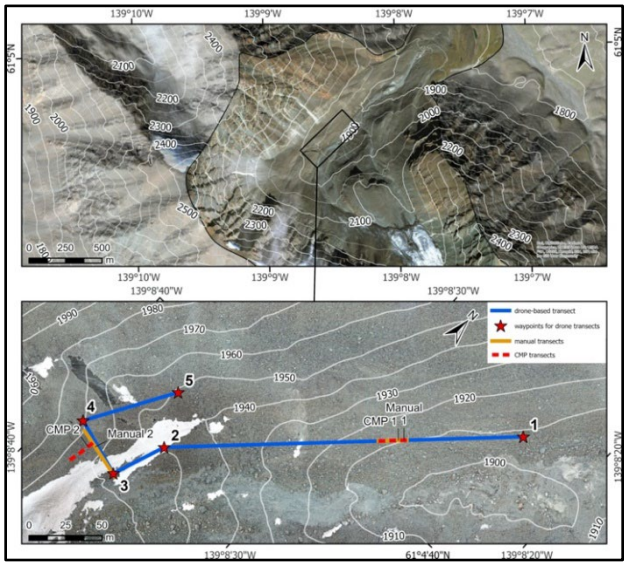

Figure 2. Map showing the location of drone-based and manual GPR transects.

Results

Overall, the drone-based GPR radargrams show good correspondence to the manual GPR comparison surveys, detecting the same layers of buried ice and interface depths (Figure 3 and 4). Buried ice detected at the start of the drone transect near the thermokarst feature (B.I. $_1$) and at the debris covered glacier (B.I. $_2$) are seen in both drone and manual radargrams. CMP results at these two manual GPR transects confirm the characteristics of the detected layers with relative permittivity values of 3.34 to 3.9 for ice and 3.7 to 5.2 for the debris layer. While the drone GPR output generally features greater noise and less detail than that from the manual surveys, the successful detection of the buried ice layers of interest comprises a significant methodological advance.

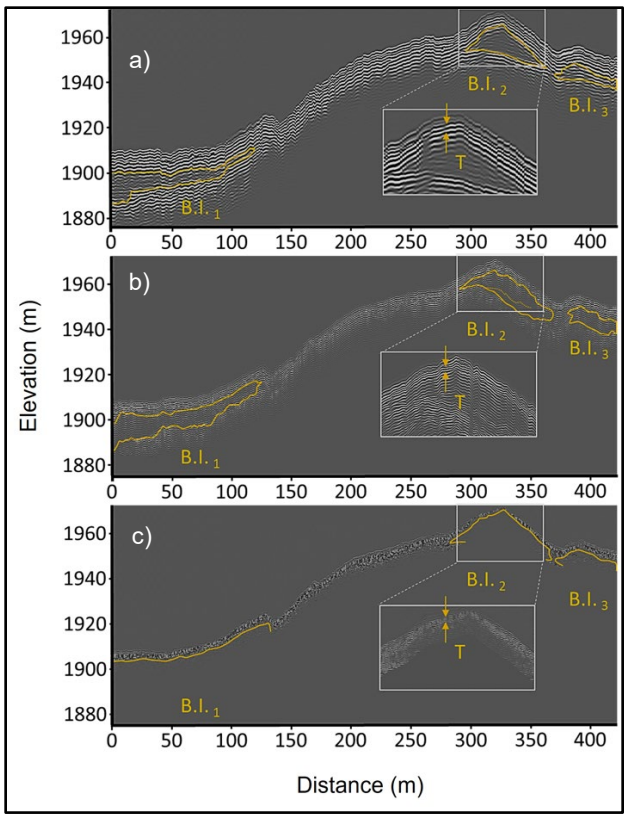

Figure 3. Drone-based GPR radargrams for a) 50 MHz, b) 100 MHz and c) 200 MHz antennas. Orange outlines show areas with buried ice (B.I.) detected with apparent thickness of debris layers indicated by "T" in the boxes.

Conclusion

The multi-low-frequency GPR method applied in this study demonstrates the ability for drone-based surveys to discriminate detail across a range of depths using a multi-antenna approach, where switching frequencies enables characterization of subsurface layers with varying depth and resolution. In deglaciating high mountain regions where traditional ground based GPR methods are not possible, applications of drone-based GPR will unlock new potential for the detection and quantification of buried ice in complex proglacial and periglacial topographies.

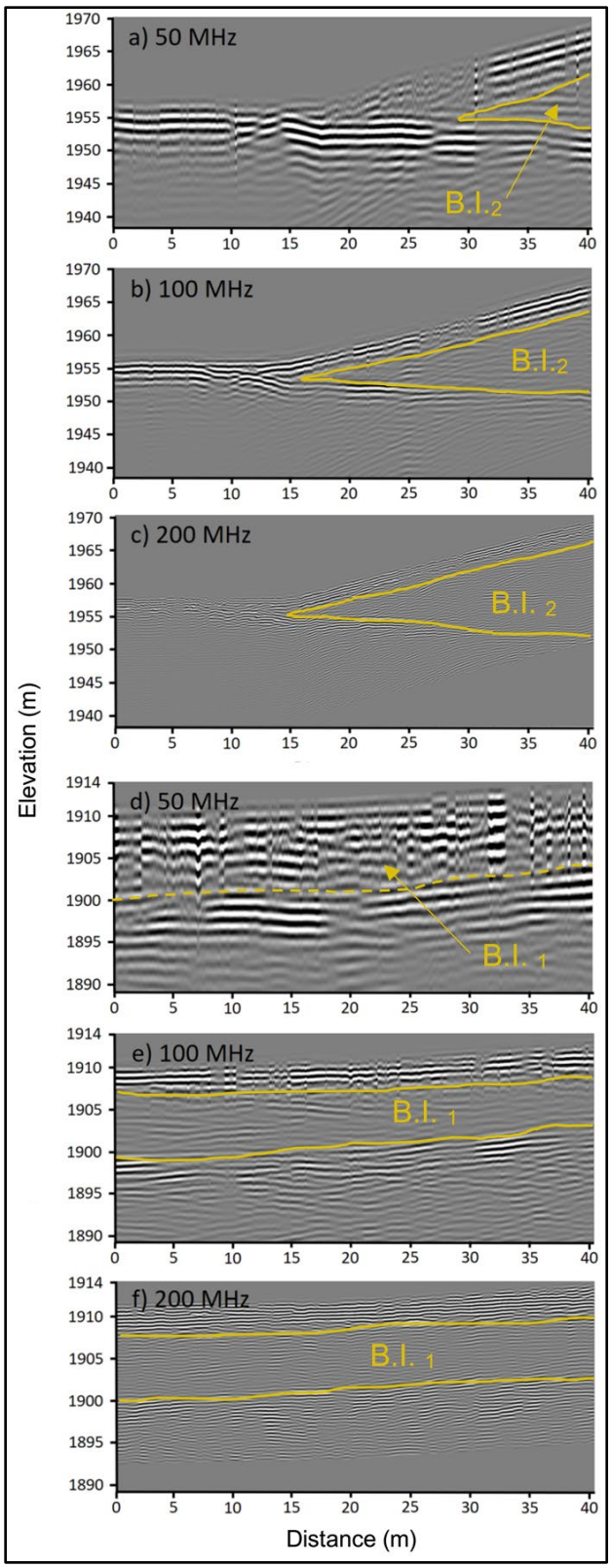

Figure 4. Manual GPR radargrams showing the detection of buried ice at two locations along the drone-based transect at the debris covered glacier ($B.I._2$) in a), b), and c) and the thermokarst slope ($B.I._1$) in d), e) and f).

Cold Region Engineering Modelling, Characterization, Observations & Testing

8F — Laboratory Modelling and Testing of Permafrost Soils

Session Chairs: Geoff Eichhorn[1] & Natalie Arpin[2]

[1]*Royal Military College, Kingston, Ontario, Canada*
[2]*Department of Civil Engineering, Queen's University, Kingston, Ontario, Canada*

This session aims to examine all aspects of the laboratory study of permafrost, at all scales and includes element testing, scaled physical modelling, centrifuge modelling, and full-scale lab testing of permafrost. Maintaining a sample of soil at sub-zero temperatures while also investigating strength, permeability, thermal conductivity, and soil mechanisms presents significant challenges compared to the same testing at temperate, above-freezing states. Both laboratory methods and technological developments to maintain and study cold regions samples are of interest, as well as outcomes of studies if the lab methods used are well examined and discussed. Themes of infrastructure modelling, permafrost soils strength, hydrogeology of cold regions soils, and thermal control and measurement are of interest.

Quantifying frost jacking-induced forces on piled foundations within frozen environments

Natalie Arpin[1], Ryley Beddoe[2], W. Andy Take[1], Sam Stanier[3] & Giulia Viggiani[3]

[1]*Department of Civil Engineering, Queen's University, Kingston, Ontario, Canada*

[2]*Department of Civil Engineering, Royal Military College of Canada, Kingston, Ontario, Canada*

[3]*Department of Civil Engineering, University of Cambridge, Cambridge, England, United Kingdom*

Frost jacking can pose a significant challenge to infrastructure built in any region with a seasonally freezing active layer. The net uplift force resulting from tangential stresses acting on the surface of the pile due to the ground freezing around a structure can overcome the forces holding the pile in the ground. These forces are provided by either the adfreeze bonds in frozen ground or frictional forces in unfrozen ground (Wang et al. 2022). This phenomenon can cause differential movement of structures, which impacts their function and integrity. To design structures able to effectively resist these forces, it is necessary to understand their magnitude and identify the factors that control their formation.

Tsytovich and Sumgin (1937) conducted the first studies on frost jacking to measure adfreeze strength at varying temperatures for concrete and wet wood piles using an anchored reaction frame (Figure 1a). The frame was embedded in bedrock, which limited movement of the pile and generated forces that were measured with a load cell.

In Canada, Penner et al. (1970, 1974) also used a reaction frame to study piles that were embedded in field sites in both Ottawa and Thompson, Canada. The upward force acting on the pile was measured as the ground froze. Johnston and Ladanyi (1972) performed pullout tests on grouted anchors (Figure 1b) in Gillam and Thompson, Manitoba. A hydraulic jack applied a constant load until failure. In each of these studies, the conditions were variable because of the outdoor site locations.

More recent studies have been performed in controlled lab environments. These include studies by Wang et al. (2017) to determine the frost jacking characteristics of screw piles and the impact of a variety of helical pile designs. Jacking forces were measured with load cells and soil heave was measured with a dial gauge. More thoroughly instrumented field experiments using strain gauges and surface monitoring are being conducted by Adajar et al. (2023) on large-scale piles to determine the distribution of stresses impacting the pile (Figure 1c). This test pile can undergo uplift, unlike previous studies.

Controlling factors for frost jacking have so far been determined to include the availability of water, the temperature of the ground and frost-susceptible soils (Wang et al. 2022). Despite previous research, gaps regarding our understanding of the development of and distribution of frost jacking forces still exist and require further study. The study aims to address these gaps at a small-scale in the laboratory.

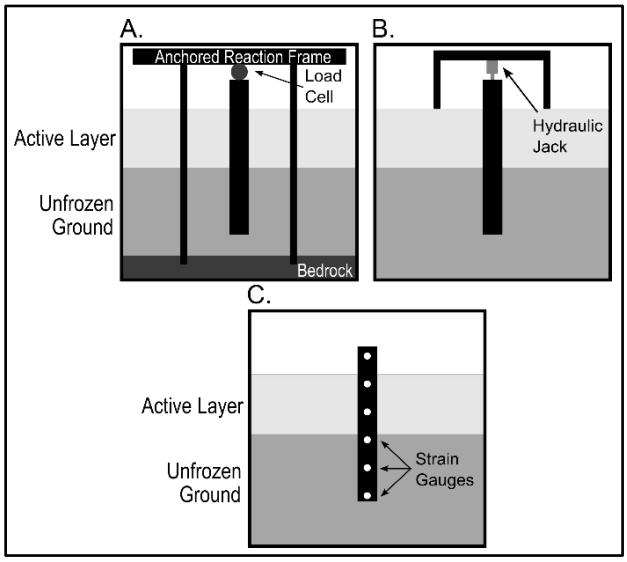

Figure 1. Methods for monitoring frost jacking (a) anchored reaction frame, (b) hydraulic jack for pullout test, and (c) electronic strain gauges.

Experimental methods and preliminary results

The forces associated with frost jacking are being investigated at the University of Cambridge's National Research Facility for Infrastructure Sensing (NRFIS) laboratory. To simulate frost jacking in a pile, a thermally controlled double-walled transparent cell measuring 100 mm in diameter and 100 mm in height, as shown in Figure 2, will be utilized. The cell will be filled with a sand clay mixture, with an 80 mm long, 15 mm diameter miniature pile embedded centrally. Experiments will be conducted at temperatures of -15 °C at the upper boundary and at -2 °C for the lower boundary, creating a top-down propagation of freezing. The confining stress at the top of the cell will also be

varied during testing. Visual monitoring will be conducted using the camera system installed on the cell. Axial strains will be measured within the pile using fiber optics to allow for the determination of the stress and force distribution. Using fiber optics enables the measurement of strains at intervals of 0.26 mm along the pile, with an accuracy of 1 με.

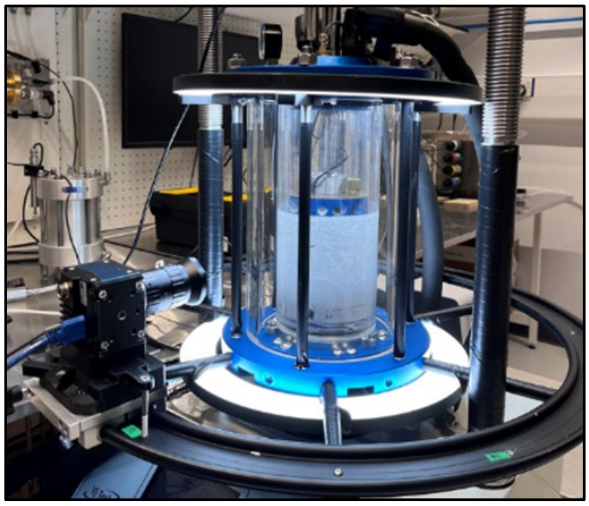

Figure 2. NRFIS lab's thermally controlled triaxial cell.

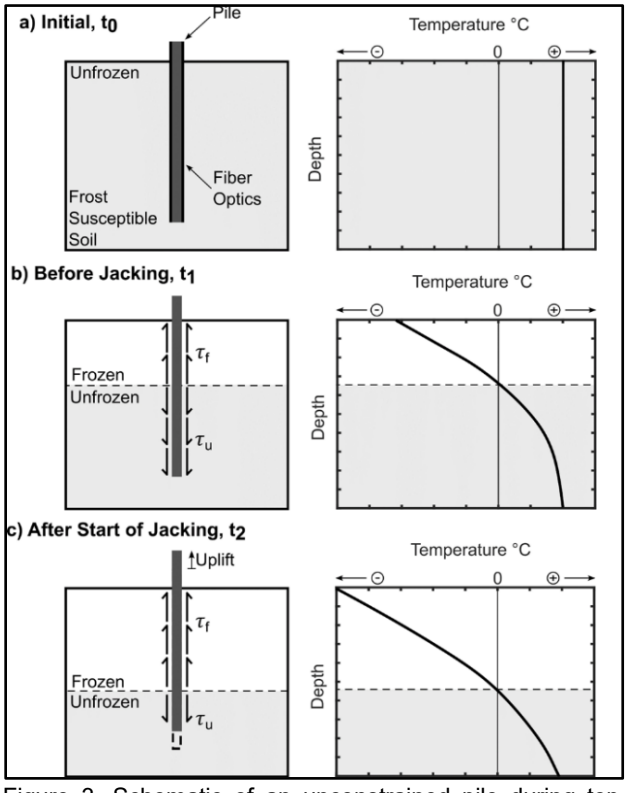

Figure 3. Schematic of an unconstrained pile during top-down freezing, with corresponding temperature profile of the soil (a) the unfrozen system, (b) resisting force from unfrozen soil is greater than the uplift force and (c) uplift force is greater than the unfrozen soils resisting forces.

Preliminary tests have been conducted on a 100 mm long and 6.4 mm diameter pile. The pile was instrumented and placed in water at room temperature before being frozen to a uniform -17 °C. Average maximum induced strains along the length of the pile of 312 με were measured because of both thermal and mechanical strain. Further tests will be conducted on an unconstrained system where the pile can move upward as it freezes (Figure 3).

Tests will also be conducted with the loading to constrain the piles' movement upwards. A load cell will be added to the top of the pile to monitor forces and limit movement. This test will allow for the stresses measured in the unconstrained tests to be validated. Through implementing these tests, a more comprehensive understanding of the extent and distribution of stresses and forces during frost jacking will be attained. This will allow for the better prediction of the rate of and movement of piles from frost jacking.

ACKNOWLEDGEMENTS

The authors acknowledge the support of the University of Cambridge and Queen's Smith School of Engineering.

REFERENCES

Adajar, J.B.Q., Alfaro, M.C., and Arenson, L. U. 2023. Preliminary results from field monitoring of frost heave effects on steel H-piles. In GeoSaskatoon, Canadian Geotechnical Society, Saskatoon, Saskatchewan, Canada: 1-8.

Johnston, G.H., and Ladanyi, B. 1972. Field tests of grouted rod anchors in permafrost. Canadian Geotechnical Journal 9(2): 176–194. doi:10.1139/t72-018

Penner, E. 1970. Frost heaving forces in Leda clay. Canadian Geotechnical Journal 7(1): 8–16. doi:10.1139/t70-002

Penner, E. 1974. Uplift Forces on Foundations in Frost Heaving Soils. Canadian Geotechnical Journal, 11(3): 323–338. doi:10.1139/t74-034

Tsytovich, N., and Sumgin, M. 1937. Principles of mechanics of frozen ground, Izdatel'stvo Akademli Nauk SSSR. Moscow – Leningrad, Russia.

Wang, T., Liu, J., Tian, T., and Lv, P. 2017. Frost jacking characteristics of screw piles by model testing. Cold Regions Science and Technology, 138: 98–107. doi:10.1016/j.coldregions.2017.03.008

Wang, T., Qu, S., Liu, J., Luo, Q., and Hu, T. 2022. Frost jacking of piles in seasonally and perennially frozen ground. Cold Regions Science and Technology, 203. doi:10.1016/j.coldregions.2022.103662

Novel laboratory wave flume experiments on permafrost coastal erosion

Justus Gimsa[1,2], Hugues Lantuit[1,2], Francois Costard[3], David Schürenkamp[4], Nils Michalke[4] & Nils Goseberg[4,5]

[1]*Permafrost Research Section, Alfred-Wegener-Institute Helmholtz-Centre for Polar and Marine Research, Germany*

[2]*Institute of Geosciences, University of Potsdam, Germany*

[3]*Géoscience Paris Sud (GEOPS), CNRS/Université Paris-Saclay, Orsay, France*

[4]*Leichtweiß-Institute for Hydraulic Engineering and Water Resources, Division of Hydromechanics, Coastal and Ocean Engineering, Technische Universität Braunschweig*

[5]*Coastal Research Center, Joint Research Facility of Leibniz Universität Hannover and Technische Universität Braunschweig, Hannover, Germany*

Permafrost coasts are rich in ground ice, that makes them vulnerable to erosion through a combination of thermal (denudation) and mechanical (abrasion) processes. Climate warming leads to rising wave heights, water, and air temperatures. The intensification of these driving processes currently leads to increasing erosion rates, that are expected to further rise in the near future. This threatens Arctic coastal ecosystems, infrastructure, as well as traditional living grounds.

However, the complex interplay between the driving environmental forces and the erosion itself is poorly understood. The main reason for this is the sparse data coverage, caused by the great inaccessibility of Arctic coasts. This prevents a comprehensive process understanding and sound projections for future local and global Arctic coastal erosion rates.

Here, we report on our efforts to establish a novel approach to quantify the effects of environmental drivers on permafrost coastal erosion. This method is based on the framework of physically modelling of coastal processes, a common method to understand low-latitude coastal dynamics. To adapt this onto Arctic coastal conditions, a wave-flume was installed in a climate chamber to reach the first model generation based on a recently published roadmap. The installed air and water cooling allowed us to set distinct constant temperatures, see Figure 1.

The temperature control allowed us to recreate realistic environmental conditions of permafrost coasts. The permafrost specimen for the laboratory simulation was produced by compacting layers of very fine uniform grained sand. The Proctor compaction test was used to define the optimal water content to repeatedly produce identical homogenous frozen samples with fixed densities and without ice segregation.

A piston-type wave maker in the wave flume was used to produce regular waves, which were measured using a set of ultra-sonic wave gauges. Throughout the experiments, a side-view camera observation and a frontal solid-state lidar scanner recorded the niche growth rate above and below the water level elevation. The temperature in the block, as well as air and water temperature were measured by using multiple PT1000 thermocouples.

We tested three different air and water temperature scenarios and observed the subsequent rates of erosion. We triplicated the test experiments to identify error sources.

Thawing and subsequent erosion were mainly observed at the coast-water interface. This contact zone between water and frozen sample was defined by the wave action. The tested permafrost coast specimen are very sensitive towards the water temperature. The findings point towards a great sensivity of the erosional process against the combined action of abrasion and denudation, highlighting the potential for rapidly increasing erosion rates inline with climate warming in the Arctic.

This newly developed method creates an avenue to quantify the main environmental processes and will help to incorporate permafrost coastal erosion in future earth system models. It may also be used in building prognostic capacities to identify local solutions to protect critical infrastructure from coastal erosion.

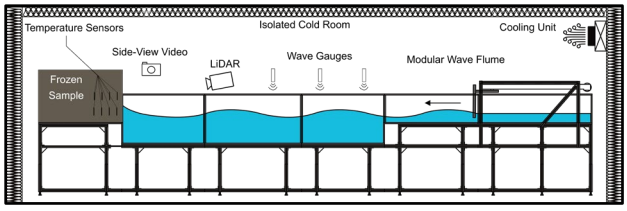

Figure 1. Experimental set-up of the wave flume installed in a climate chamber at the TU Braunschweig to simulate permafrost coastal erosion processes.

Element tests to characterise the behaviour of sandy mixtures under freezing and thawing cycles

Giulia Guida[1], Floriana Anselmucci[2], Francesca Casini[1] & Vanessa Magnanimo[2]

[1]*Department of Civil Engineering, Università degli Studi di Roma Tor Vergata, Rome, Italy*

[2]*Soil Micro Mechanics, Department of Civil Engineering & Management, Faculty of Engineering Technology, University of Twente, Netherlands*

One of the critical issues in permafrost regions is the thawing of subsoil permafrost, exacerbated by climate change. This process occurs as global temperatures rise, causing previously frozen ground to melt. Ice-rich soils may cause instabilities during thawing and other issues related to the trapped biomass release. By 2050, nearly 70% of current structures and infrastructures will be at risk of damages and collapse associated with climate change (Hjort et al. 2022).

EXPERIMENTAL PROGRAMME

This study investigates irreversible phenomena in soil caused by freezing and thawing cycles through laboratory experiments on soil samples. The samples are composed of four sandy mixtures of Fointanbleau sand enriched with Speswhite kaolin at varying weight percentages - specifically 5, 10, 20 and 50% - to explore the impact of fine content. The samples were prepared by dry pluviation of the mixtures into Perspex cylinders (3.6 cm in diameter), and then they were saturated from the bottom by immersion inside a vacuum bell. In the specified preparation procedure, the mixtures with a higher fine content tended to assume more open and loose configurations. The void ratios varied, spanning from 0.6 for the mix with 5% kaolin to 2.0 for the mix with 50% kaolin. After 24 hours of saturation, the samples were sealed at the base with a thermally conductive tape, and a 1 cm film of water was left at the top of the samples as a liquid water reservoir.

The test consisted of placing the sample of sandy mixtures in contact with a cooling plate set at T=-15°C, allowing the frozen front to advance from the bottom to the top of the sample. An insulating coat was installed along the walls of the Perspex cylinder to avoid lateral thermal dispersion and guarantee one-dimensional conditions. The top of the sample was left in contact with the environmental temperature at around 24°C.

Two complete cycles of freezing (for 120 minutes) and thawing (for 60 minutes) were performed for each mixture for an overall 6-hour test. X-ray tomography facilities at TU Delft allowed the scanning of the sample every 40 minutes during freezing and every 30 minutes during thawing. The key states of the sample — namely, the initial, fully frozen, and unfrozen steady state — were imaged using a slower, 10-minute scan at a higher resolution (37.06 µm/px). To minimise image blurring caused by the deformation rate during the freezing-thawing process, the samples were imaged using a faster, 4-minute scan at a lower resolution (74.12 µm/px). The reconstructed three-dimensional images at the different deforming stages offered a powerful tool for a deeper understanding of the complex thermo-hydro-mechanical phenomena involved in the freezing-thawing processes and the microstructure's evolution.

MATERIAL RESPONSE

Figure 1 presents a temporal sequence of images that depict the vertical slice of the three-dimensional computed tomography scan reconstruction of the sample constituted by the sandy mixture with 20% kaolin. The images in the first and second rows show the first and second freezing and thawing cycles, respectively. A lighter greyscale indicates a higher X-ray attenuation corresponding to a denser material state. The brighter dots in the vertical sections of Figure 1 represent two of the five tracers, 1.6 mm diameter glass beads, introduced in the mixtures to track the kinematics along the test. During the freezing process, the soil mixture gradually absorbed the film of liquid water, migrating towards the advancing frozen front. After 120 minutes, with the cooling plate maintained at T=- 15°C, the material was completely frozen, almost doubling its height. The greyscale attenuation reveals that the top part of the sample is denser (appearing lighter in colour) than the lower part. This contrast allows for the detection of the ice front. Once the cooling plate was switched off, thawing began at the sample's top and bottom extremities, in contact with the environmental temperature. Due to gravity, the lower part consolidated, substantially reducing its porosity, while the top part remained suspended, possibly due to friction with the later wall of the Perspex container. Segregation cracks appeared at the beginning of the thawing, when the middle part of the sample remained frozen, and they disappeared with an abrupt collapse when the material was fully thawed. After one freezing-thawing cycle, the

sample showed a residual heave and a thinner water film compared to the initial unfrozen state. In addition, the initial microstructure was significantly modified: the lower part was densified, and the top part remained looser.

In the second freezing cycle, the film of water at the top was absorbed more quickly; it disappeared within 30 minutes, whereas during the first cycle, some water remained even after 80 minutes. In addition, the overall frost heave during the second cycle was less pronounced than the first.

The volumetric response shown in Figure 1 qualitatively represents all the sandy mixtures investigated. As the fine content increases, phenomena such as frost heave, water absorption during freezing, and segregation and collapses during thawing become more pronounced. Furthermore, mixtures with greater fine content are more significantly disturbed due to the extensive deformation experienced during the thermal cycles.

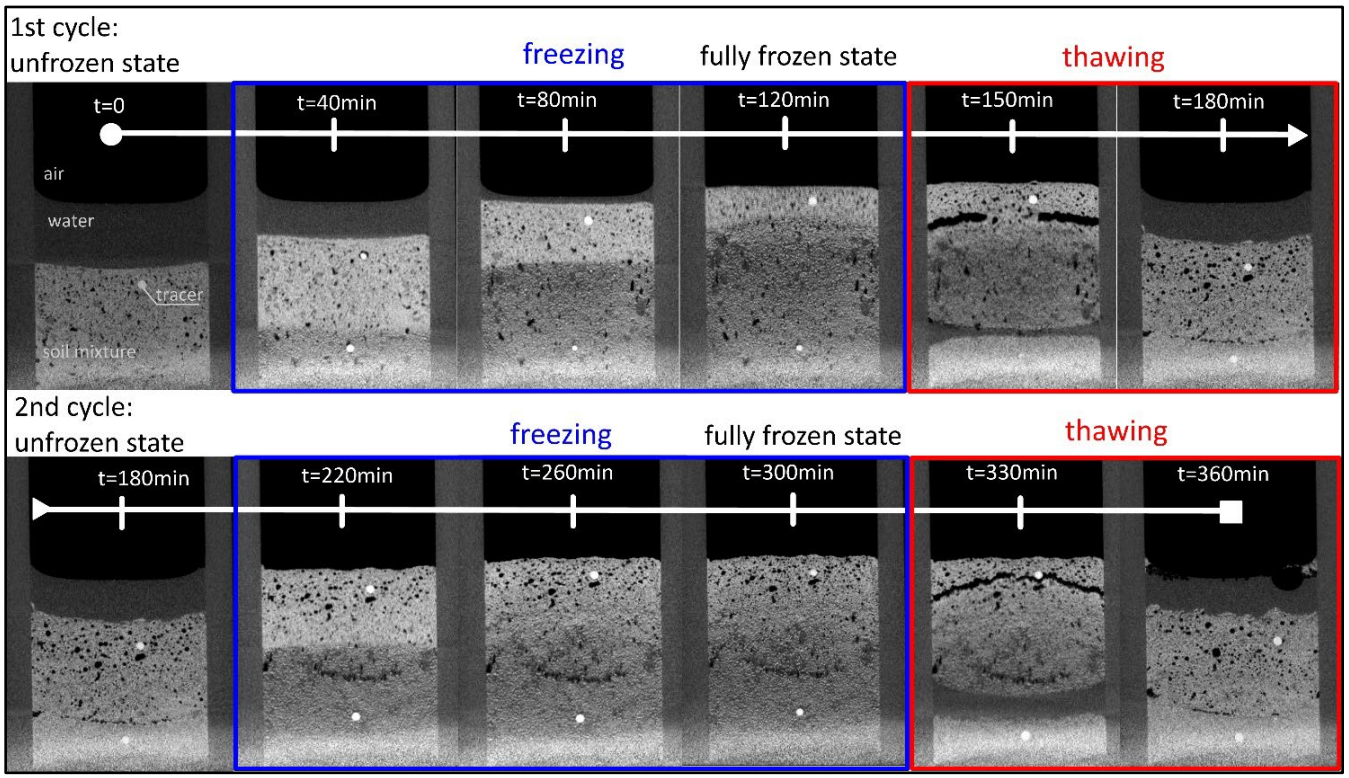

Figure 1. The temporal sequence images represent a vertical slice of the three-dimensional CT-scan reconstruction of a sandy mixture with 20% kaolin during two freezing and thawing cycles.

ACKNOWLEDGEMENT

The authors acknowledge EPOS-NL facilities access (https://epos-nl.nl/), enabling free-of-charge 5-day X-ray tomography scans at TU Delft.

The fixed-term researcher position of Dr Giulia Guida had the financial support of the Regione Lazio (POR-FSE 2014/20 Contributions for the permanence of excellence in the academic world, No. 65629/2020.

REFERENCES

Hjort, J., Streletskiy, D., Doré, G., Wu, Q., Bjella, K., and Luoto, M. 2022. Impacts of permafrost degradation on infrastructure. Nature Reviews Earth & Environment, 3(1), 24–38.

Determination of the critical state line in partially frozen sand

Yawu Liang, Nicholas Beier & David Sego

Geotechnical Centre, Department of Civil & Environmental Engineering, University of Alberta, Edmonton, Alberta, Canada

Recently, the concern with thawing of permafrost associated with climate change in discontinuous permafrost regions was raised by Northern communities (Holubec 2008; Allard et al. 2012; Swanson et al. 2021). The “near surface” soils in those warm regions (ice-rich and/or saline) are in a partially frozen state with unfrozen water and ice coexisting in the internal pore space. To understand the critical state behavior of partially frozen soil, the relationship between critical void ratio and mean effective stress, which is called the critical state line, needs to be established. Here, a newly developed test method is applied to determine CSL in partially frozen sand.

The new triaxial apparatus was originally developed for the measurement of internal PWP within the unfrozen soil by Liang et al. (2022) and was later modified to extend its application into the partially frozen test by Liang et al. (2023a). Temperature control was achieved by circulating a water-glycol mixture (1:1) through two cold baths. PWP was measured by a base pressure transducer and three filter-less rigid piezometers (FRPs) embedded within the specimen.

A series of consolidated undrained (CIU) and drained (CID) triaxial tests, along with internal pore water pressure (PWP) measurements, were conducted on both dense and loose specimens under different strain rates at a temperature of -3 °C. The testing program is summarized in Table 1. The experiments were performed within a controlled cold room environment, following the five-stage procedure meticulously outlined by Liang et al. (2023a). These stages included saturation and consolidation, rapid freezing of the sample, maintaining the sample temperature at approximately -11 °C, subsequent warming of the sample to the testing temperature of -3 °C, confirmation of the continuity in the water phase, and finally, shearing of the sample at a constant strain rate.

RESULTS AND IMPLICATIONS

The results are presented in Figure 1. Similar to unfrozen sand, a unique CSL was established for the partially frozen sand at -3 ˚C, both in stress (q-p') and void ratio (e-p') space. It is recommended to only perform CIU tests to determine CSL in e-p'diagram. This study has contributed to the understanding of and quantification of critical state parameters of partially frozen sand, which can be beneficial for the construction of constitutive models and for engineering design considerations in warm permafrost regions.

Table 1. Summary of the testing program.

Test ID	Initial void ratio	Strain rate (%/min)	Confining pressure (kPa)	Drainage condition
PL-1	0.835	1	100	undrain
PL-2	0.834	1	200	undrain
PL-3	0.835	1	400	undrain
PL-4	0.834	1	400	drain
PL-5	0.834	0.1	100	undrain
PL-6	0.835	0.1	400	undrain
PD-1	0.596	1	100	undrain
PD-2	0.599	1	200	undrain
PD-3	0.594	1	400	undrain

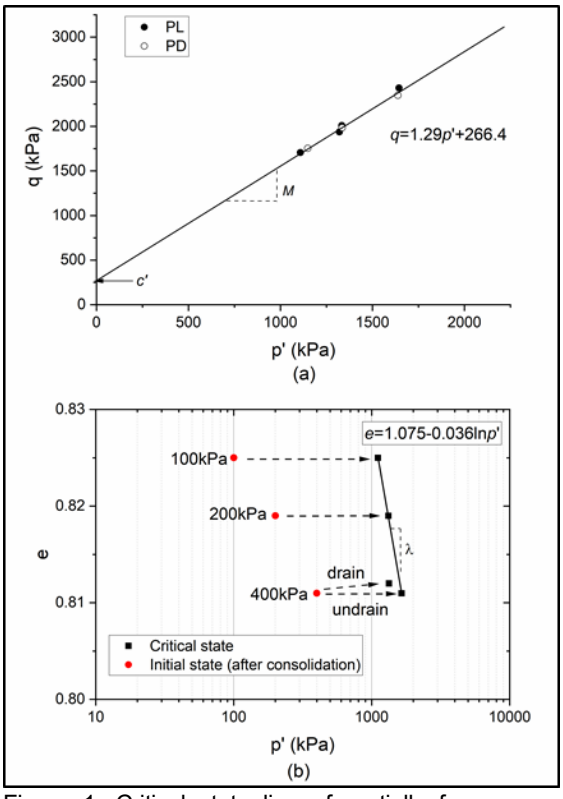

Figure 1. Critical state line of partially frozen specimens (-3ºC). (a) q-p' space and (b) e-p' space (Liang et al. 2023b).

ACKNOWLEDGEMENTS

The financial support of the Natural Sciences and Engineering Research Council of Canada (NSERC) Discovery Grant Program (RGPIN-2019-04573) is gratefully acknowledged.

REFERENCES

Allard, M., Lemay, M., Barrette, C., L'Hérault, E., Sarrazin, D., Bell, T., and Doré, G. 2012. Chapter 6. Permafrost and climate change in Nunavik and Nunatsiavut: Importance for municipal and transportation infrastructures. Nunavik and Nunatsiavut: From science to policy. An Integrated Regional Impact Study (IRIS) of Climate Change and Modernization, ArcticNet Inc. Québec city, Québec, Canada, pp. 171–197.

Holubec, I. 2008. Flat loop thermosyphon foundations in warm permafrost. Government of the Northwest Territories Asset Management Division of Public Works and Services and the Climate Change Vulnerability Assessment of the Canadian Council of Professional Engineers.

Swanson, D., Murphy, D., Temmer, J., and Scaletta, T. 2021. Advancing the Climate Resilience of Canadian Infrastructure: A Review of Literature to Inform the Way Forward. International Institute for Sustainable Development.

Liang, Y., Beier, N., and Sego, D.C. 2022. New Method for Internal Pore-Water Pressure Measurements. Geotechnical Testing Journal, 45(2): 490–502. https://doi.org/10.1520/GTJ20210008

Liang, Y., Beier, N., and Sego, D.C. 2023a. Strength of Partially Frozen Sand Under Triaxial Compression. Canadian Geotechnical Journal, 60 (9): 1277–1288. https: //doi.org/10.1139/cgj-2022-0477

Liang, Y., Beier, N., and Sego, D.C. 2023b. Internal Pore-Water Pressure Measurements and Effective Stress Analysis in Partially Frozen Soil. Ph.D. thesis, Faculty of Graduate Studies and Research, University of Alberta, Edmonton, AB. https://doi.org/10.7939/r3-36s1-jb17

Use of distributed fiber optic sensing for thermal mapping of laboratory permafrost samples

Chelsey Litjens[1], Azin Mardani[2], Geoff N. Eichhorn[2], Ryley Beddoe[1] & Greg Siemens[1]
[1]*Department of Civil Engineering, Royal Military College of Canada, Kingston, Ontario, Canada*
[2]*Department of Civil Engineering, Queen's University, Kingston, Ontario, Canada*

Thermal mapping of laboratory samples pose challenges for capturing the full field state of a cold soil sample. Traditional thermistors which capture discreet temperature points can be physically intrusive to small samples, and full field thermal cameras only allow mapping of soil surface temperature. In contrast, fiber optic strain sensing has been shown as a viable option for high-definition thermal sensing (HD-FOS). The example presented makes use of Rayleigh backscatter strain principles and custom-built sensors, at low cost per sensor, to capture the distributed thermal profile in lab scale and centrifuge scale physical models. The system is deployable at the lab scale, as well as field scale, and has shown to have a strain coefficient of 10 με / °C, and a system accuracy of 1 με, over a range of temperatures from -16°C to +20°C. Considerations of how the sensor can be built and protected from mechanical strain are presented.

BACKGROUND

Historically the measurement of strain within physical models has utilised vibrating wire or foil based strain gauges. These gauges have a substantial size and require data cabling for each individual gauge, so utilising a dense array of instrumentation within a small model, such as those used in geotechnical centrifuge modelling, is problematic. In the last 20 years advances have been made in the use of telecommunication fiber as a strain measurement sensor. Fiber-optic strain measurement techniques allow a dense array of strain measurement points to be located on a single fiber-optic cable leading to simplified installation and wiring. The majority of the experience of utilising this technique to date has involved Fiber-Bragg Grating (FBG) sensors (Correia et al. 2016) which involve measurement of an inscribed grating in the form of a reflected light signal where wavelength of the light is measured. A shift in the wavelength of light from an FBG corresponds to an induced strain in the grating. More advanced distributed fiber optic sensing involves interferometry based on Rayleigh backscatter has the advantage of giving a very dense array of measurement points at modest cost for each model (though the analysers are expensive).

This extended abstract presents the experience of utilising a Rayleigh backscatter based distributed high-definition optical strain sensor, called the Luna Odisi, to measure temperature within a soil sample. Sensor construction, accuracy, and calibration are discussed.

THERMAL MONITORING USING FIBER OPTICS

In contrast to Bragg fiber sensors which are discreet measurements, Rayleigh backscatter is a continuous and distributed measurement, and relies on the inhomogeneity of the silica fiber to act as pseudo-Bragg gratings. The relationship by which strain and spectral shift are related is shown in the fundamental relationship below in Eq.1.

$$\frac{\Delta\lambda}{\lambda} = \frac{\Delta\nu}{\nu} = K_T T + K_\varepsilon \varepsilon \qquad [1]$$

which describes the shift in the optical spectrum (again analogous to a Bragg grating shift), λ (shift in GHz) for the Luna system, or ν (shift in nanometers) for a Bragg grating system (Ferarro & De Natale 2002). These shifts in the optical signal are proportional to the change in temperature T, and mechanical strain ε. K_T and Kε are temperature and strain calibration constants respectively. The environmental parameters which influence the optical signal in the fiber—primarily temperature (which will cause a change in length of the fiber, and to a lesser extent a change in the refractive index of the glass) and mechanical strain.

THERMAL MONITORING OF PERMAFROST

The time and infrastructure required to instrument a large permafrost experiment with traditional resistive based thermocouples or thermistors is significant and scales with the size and complexity of the experiment. In contrast, optical strain sensing for thermal measurement has been used effectively, and is capable of sensor lengths up to 10 meters, with sensing points every 2.6 mm, at measurement rates up to 250 Hz. While this capture frequency is likely unnecessary for permafrost degradation / monitoring activities, the high density measurement makes this method of thermal sensing attractive. A second

benefit is the limited amount of infrastructure required to be installed in a soil model. Only the single fiber optic cable must be installed, and adequately protected from mechanical strain from sources other than temperature change.

A sensor was constructed from scratch using readily available telecommunication single mode (9/125) fiber optic cable. Different fiber cables are available commercially with differing outer plastic coatings (e.g., acyrlate or polyimide). The fiber was then protected within a nylon or polyethelene tube with larger inner diameter than the size of the fiber. The purpose of this 'sheathing' is to isolate the fiber from mechanical strain which may be caused by soil loading, and otherwise cause an interference in the optical signal which is meant to capture the temperature change. The fiber sensor must be terminated with a coreless fiber (for proper signal conditioning), and protected within a larger diameter end structure to adequately allow expansion of the fiber sensor, such that the fiber is not restricted internally in the tubing. This end structure consists of a larger diameter (6 mm OD) nylon tube, which is then capped with epoxy resin to waterproof the sensor.

A temperature calibration of the fiber sensor was performed using a Julabo 900F water bath across a range of temperatures ranging from -20°C to +35°C in steps of 2-5°C. The water bath calibration is shown in Figure 1. Temperature ramps were held constant for at least 5 minutes, and a time averages optical signal taken. The calibration for this type of optical thermal sensor is shown in Figure 2.

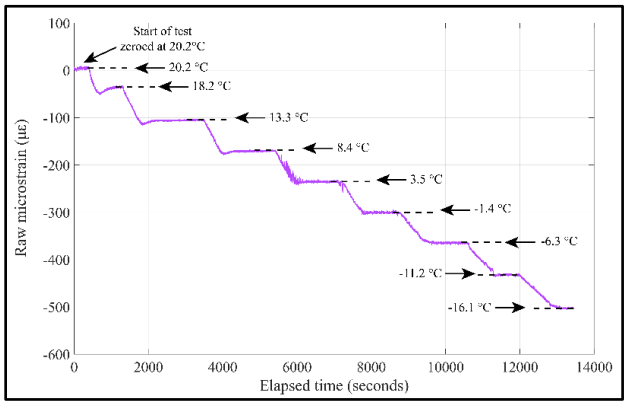

Figure 1. Water bath temperature calibration over time for brass-polyimide, unbonded acrylate and polyimide coated fiber.

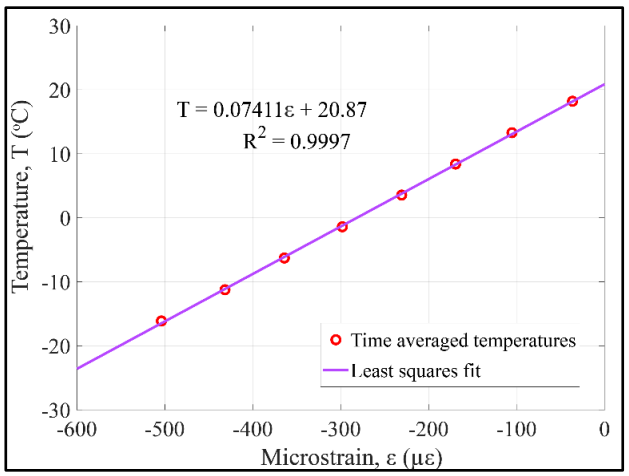

Figure 2. Temperature-spectral shift response for polyimide and acrylate coated fiber optics, and brass bonded polyimide.

System Accuracy and Conclusions

The optical thermal sensing system described here has been utilized at 1g in a cold regions lab, and for accelerated g cold regions experiments in a geotechnical centrifuge. The accuracy of the Luna system and the calibration of the thermal sensor give an optical response of 13.8 [με / °C], giving a sensor resolution of 0.07°C, equivalent or better than resistive based thermocouples. Taken together with the simplicity of installation within a soil sample / model, the use of fiber optical thermal sensing is an attractive alternative to traditional based methods where distributed high resolution sensing is required for cold regions physical modelling. Potential applications of this technology in the field are being explored. Further discussion of this technology is described in Eichhorn (2022).

References

Correia, R., James, S.W., Marshall, A.M., Heron, C.M., and Korposh, S. 2016. Interrogation of fibre Bragg gratings through a fibre optic rotary joint on a geotechnical centrifuge. Sixth European Workshop on Optical Fibre Sensors, 99162B, 1–4. https://doi.org/10.1117/12.2236979

Eichhorn, G. 2022. Landslide-pipeline interaction for onshore slopes in silty sand [Apollo - University of Cambridge Repository]. https://doi.org/10.17863/CAM.99058

Ferarro, P., and De Natale, G. 2002. On the possible use of optical fiber Bragg gratings as strain sensors for geodynamical monitoring. Optics Lasers Engng, 37, 115–1.

Testing the oedometric thaw consolidation core-barrel towards improved practical applicability

Arian Nazeri[1,3], Simon Dumais[1,3] & Jean-Pascal Bilodeau[2,3]

[1]*Département de génie des mines, de la métallurgie et des matériaux, Université Laval, Québec City, Québec, Canada*

[2]*Département de génie civil et de génie des eaux, Université Laval, Québec City, Québec, Canada*

[3]*Centre d'études nordiques (CEN) & Centre de recherche sur la géologie et l'ingénierie des ressources minérales (E4m), Université Laval, Québec City, Québec, Canada*

Characterizing the thaw consolidation properties is essential for the design of infrastructure built on permafrost. The current geotechnical practice for characterizing permafrost involves sampling the frozen ground and conducting thaw consolidation testing in laboratories. Field sampling poses significant challenges, as it requires meticulous preservation of the sample's thermal integrity throughout both the sampling and transportation phases. Additionally, accessing drilling equipment presents limitations in many northern sites, further complicating the process.

In contrast, in-situ testing reduces the need for such measures, simplifying the process and reducing costs. This research aims to contribute engineering knowledge on a testing setup developed by Flécheux et al. (2015) from Guy Doré's research group at Université Laval, Québec, Canada. The apparatus, known as the Oedometric Thaw Consolidation Core-Barrel, is specifically designed for in-situ investigation of the thaw consolidation and thaw settlement properties of permafrost.

PRESENTATION OF THE OEDOMETRIC THAW CONSOLIDATION CORE-BARREL

The study of the thaw consolidation behavior of permafrost has heavily relied on conducting laboratory tests since the 1970s (Morgenstern and Smith 1973; Nixon and Morgenstern 1974). The oedometric thaw consolidation core-barrel presents a practical solution to the existing challenges associated with laboratory testing of permafrost. Its portability and ease of transportation to remote field locations reduce the need for specimen transportation to laboratories for further testing. Moreover, the field deployment of this setup provides flexibility in efficiently investigating different project zones, thus avoiding unnecessary resource expenditure in non-thaw-sensitive areas. The findings derived from this testing approach offer valuable insights for engineers, contributing to informed decision-making throughout the design, construction, and maintenance stages of a project.

The oedometric thaw consolidation core-barrel is engineered for geotechnical investigations within the uppermost layers of permafrost, which are most affected by thaw degradation. Figure 1 represents a schematic illustration of the setup. Each experiment is conducted in two main phases: coring and testing. The initial step involves reaching the permafrost by drilling a hole into the active layer using conventional methods. Subsequently, the coring operation begins using a specialized coring head designed to function in sandy to silty frozen soils. This process is powered by a lightweight 8 hp drill coupled to the driving head of the setup. Once the frozen soil is formed in the core chamber of the setup, the thaw consolidation test begins. The sample first undergoes thawing using an electric heating element that surrounds the core sample. The sample is radially confined and the deformation occurs along the vertical axis. The meltwater generated due to the thawing of ice lenses and pore ice within the frozen soil is drained radially under the consolidation pressure applied by a piston. A pneumatic cylinder allows the operator to adjust the consolidation pressure applied by the piston. In addition to load application, the piston serves another function, which is aiding in the drainage of excess water to the surface once the test is completed. The core sample is surrounded by a porous sintered stainless steel tube filter, which effectively retains the core particles in place during the drainage phase. Throughout the testing process, the axial deformation of the specimen is monitored and recorded. It is to be noted that, based on the design criteria, the load application and thawing process may occur concurrently or in two separate steps during the testing procedure.

The setup allows the estimation of thaw-consolidation and thaw settlement properties of frozen soils. The thaw strain parameter (A_0) and the coefficient of volume compressibility (m_v) could be graphically determined by plotting the curve of relative settlement against the applied pressure (Watson et al. 1973). Using these parameters, the vertical strain of a permafrost layer thawed under stress of σ_0 and loaded to ($\sigma_0 + \Delta\sigma$) is calculated by Equation 1.

$$\Delta H/H_0 = A_0 + m_v \Delta\sigma \quad [1]$$

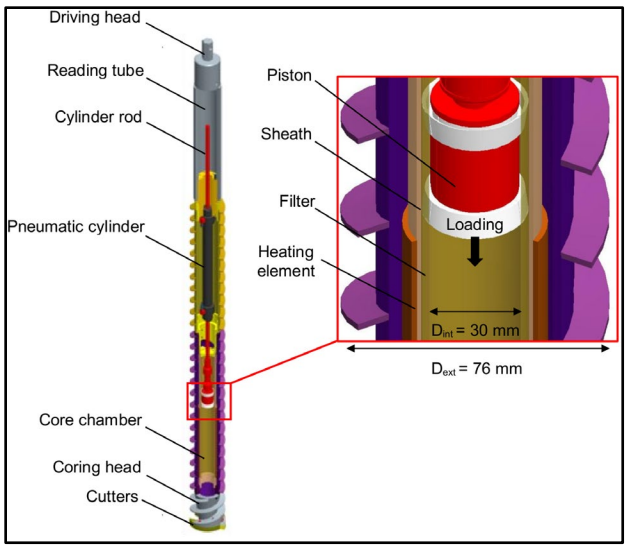

Figure 1. Schematic cross-section view of the setup

Since the initial void ratio e_0 cannot be measured for the soil in the core-barrel chamber, the modified compression index $C_{c\varepsilon}$ is used.

$$C_{c\varepsilon} = \Delta\varepsilon_v / \log(\sigma_2 / \sigma_1) \quad [2]$$

where $\Delta\varepsilon_v$ is the change in vertical strain, and σ_1 and σ_2 are applied stresses on the sample in two different steps.

The coefficient of consolidation for thawing permafrost with radial water outflow (C_{rt}) is another design parameter that could be obtained from the setup using Equation 3.

$$C_{rt} = (T_{90} \cdot R^2) / t_{90} \quad [3]$$

where R denotes the drainage path which equals the core radius, T_{90} and t_{90} denote the dimensionless time factor and time corresponding to 90% average degree of consolidation, respectively.

RESEARCH OBJECTIVES

Although the oedometric thaw consolidation core-barrel is designed to address challenges associated with the standard thaw consolidation testing methodology, a notable knowledge gap still exists concerning the practical implementation of results collected from the setup within geotechnical designs. Permafrost engineering has relied on the methodologies developed in the 1970s for the determination of thaw settlement and thaw consolidation properties using laboratory testing and engineering tools. They have been thoroughly validated and tested in numerous projects. The parameters calculated using the oedometric thaw consolidation core-barrel still need validation. They need to be compared to the parameters obtained from standard methods so they can be used for designs. Additionally, uncertainties persist regarding the formation of samples in the chamber, the thawing process facilitated by the electric heater without the imposition of a temperature gradient, and the overall reliability of the measurements taken during the test. The impact of radial drainage with axial load application needs to be investigated compared to traditional thaw consolidation testing where the load and the drainage are in the axis of the sample. There is a significant anisotropy in permafrost soils due to the orientation of the ice lenses which might impact the time of drainage.

The ongoing study aims to contribute advanced insights into analyzing and properly utilizing data derived from this innovative testing approach while improving the testing procedure. Given the contemporary prominence of the standard thaw consolidation method as the reference for characterizing frozen soil properties in designs, this research concurrently endeavors to establish correlations to create a meaningful link between results obtained from the conventional testing methodology and the oedometric thaw consolidation core-barrel.

REFERENCES

Flécheux, C., Doré, G., Gosselin, L., and Lemieux, C. 2015. Development of a Core Barrel for an In Situ Measurement of the Thaw Consolidation Behavior of Permafrost, In Cold Regions Engineering 2015, ASCE, 68–77.

Morgenstern, N.R., and Smith, L.B. 1973. Thaw–Consolidation Tests on Remoulded Clays, Canadian Geotechnical Journal, 10(1): 25–40. doi:10.1139/t73-003

Nixon, J.F., and Morgenstern, N.R. 1974. Thaw–Consolidation Tests on Undisturbed Fine-grained Permafrost. Canadian Geotechnical Journal, 11(1): 202–214. doi:10.1139/t74-012

Watson, G.H., Slusarchuk, W.A., and Rowley, R.K. 1973. Determination of Some Frozen and Thawed Properties of Permafrost Soils, Canadian Geotechnical Journal, 10(4): 592–606. doi:10.1139/t73-055

Is hysteresis the solution? Bridging the gap between field and laboratory measurements of SFCCs in cryotic soils

Quentin 'Quinn' Sapin & Élise Devoie
Department of Civil Engineering, Queen's University, Kingston, Ontario, Canada

In the face of climate change, permafrost is thawing at an unprecedented rate. This has led to a growing need amongst experts for a better understanding of ice rich soils. The relationship between water content and temperature in soils is hysteretic, but in empirical models of this process, hysteresis is often disregarded for ease of process representation. The goal of this study is to optimize measurement congruency from field to laboratory setting of soil freezing characteristic curves (SFCCs) through the study of the parameters controlling hysteresis in soils. Protocol and sample preparation measurement errors will be quantitatively accessed to reassess the reliability of in lab SFCCs measurements in the current literature.

Anthropogenic climate change is fundamentally jeopardizing the stability of ecosystems on a planetary scale (Fussmann et al. 2014). Amongst the most impacted are polar and subpolar regions which are warming at up to four times the average global rate, leading to permafrost thaw (Rantanen et al. 2022). Though recent studies have improved our understanding of the impact of permafrost degradation on the local hydrology of specific regions (Connon et al. 2014; Jin et al. 2022), questions remain regarding the exact mechanism and parameters that control the observed hydrological changes, especially those relating to the connectivity of landscape (Walvoord et al. 2016). It is well established that the ice content of the soil is the dominant control on the hydrologic connectivity of permafrost landscapes (Connon et al. 2014), and further work is needed to understand the role soil ice content plays on surface water and groundwater movement.

Background

The relationship between unfrozen water content (θ) and temperature (T) in cryotic soils is currently described by a physical relationship called the Soil Freezing Characteristic Curve (SFCC). Water content is measured using nuclear magnetic resonance (NMR), capacitance, calorimetric or other techniques, the availability and feasibility of which depends on whether the data is taken in situ (in the field) versus in a laboratory setting. The presence of hysteresis as soil undergoes freeze-thaw (FT) cycles is ubiquitous and well documented within the scientific literature (Zhou et al. 2019). Hysteresis describes the nonlinear behavior of a system with a 'memory' component whose current state depends on the systems' history. In the case of SFCCs, there is hysteresis in the FT process, where the freezing and thawing limbs are distinct. The four main features that characterize SFCCs are the following: the initial water content θf, residual water content (θ'rwc), the bulk freezing point temperature (Tf) and the freezing/thawing limbs (Figure 1).

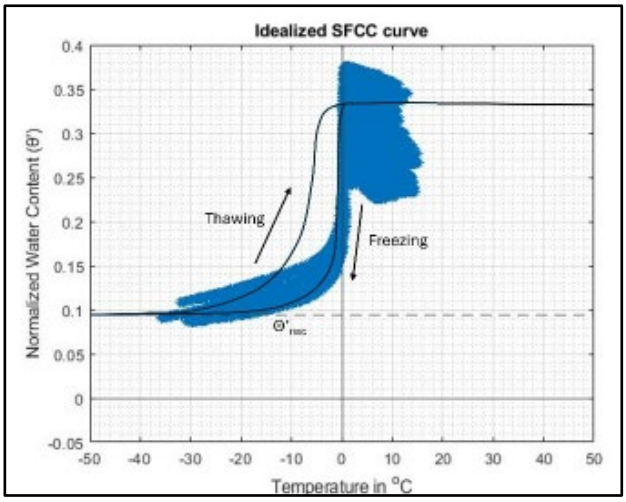

Figure 1. SFCC curve overlaying 20 years of Cape Bounty station field data. A classical hysteric loop can be seen through the freezing and thawing limb of both field and theoretical data.

Methodology

The first part of this project requires in-situ monitoring and field sampling while the second relies on laboratory testing. Data have been gathered from the Cape Bounty Watershed Observatory (74°55′ N, 109°35′ W), and soil samples have been collected at each instrumented site. SFCCs have been extracted from the in-situ temperature and soil moisture monitoring data for each of the 8 Stations assessed. The soil samples collected at these sites will be further characterized in the lab to determine their soil water retention curves and SFCCs under varying sample preparation protocols.

Field sampling and laboratory protocols will be compared based on two main controlling parameters of hysteresis: i) Pore structure and ii) nature of the pore water. Pore structure in both soil particle interaction at

a micro-scale and the arrangement and structural relation of larger particle aggregates at a macro scale plays a large role in water movement and behavior within porous media. (Kolivi et al. 2006) The volume of available pore spaces, their connectivity, shape, nature and distribution is at the core of hysteretic behaviour observed in soils. (Wolfe and et al. 2002) In that regard, pore structure alteration is a core criterion of interest to monitor through soil sampling methods, in-lab sample preparation protocols and the magnitude and cycling of freeze/thaw loops the samples undergo before testing.

The second control on hysteretic FT behaviour is the nature of the pore water. Bulk freezing point depression due to ionic content of water is a well-established and documented phenomenon. Beyond the inherent thermodynamic changes due to ionic content, particle-specific interactions with ions in solution is expected to impact water chemical potential and availability for ice crystal nucleation. (Zhang et al. 2021) Accordingly, the use of native pore water, or properly calibrated water reflecting the original ionic content of the field sample is thought to be critical in laboratory testing.

Parameters of interest will be quantified using available instrumentation at various Queen's University laboratories such as ionic chromatography to characterize ionized content of collected in-situ pore water at variable depths and specific surface area of soil samples. Identically to the field stations, 5TM capacitance-based soil moisture and temperature sensors will be used to monitor water content per temperature during in lab FT cycles. Variability of laboratory results based on soil sampling methods, in-lab sample preparation protocols, magnitude and cycling of freeze/thaw and ionic content of water will be monitored and compared to in-situ measurements.

CONTRIBUTIONS

This work closes the gap between field and laboratory investigations of SFCCs, a critical component in the representation of freezing soils. These enhanced measurement techniques will improve models predicting contaminant transport, streamflow, and other processes caused by the rapid warming of cold regions. The improvements in SFCC data measurement will also be of use in adjacent fields such as mining, civil engineering and water quality control, all of which play a role in ensuring the long-term development and well-being of the population of these regions. Polar and subpolar regions are home to populations that are and will be observing the stability of their environment shift under the rapid changes caused by climate change, and SFCCs are a key piece of this puzzle.

REFERENCES

Connon, R.F., Quinton, W.L., Craig, J.R., and Hayashi, M. 2014. Changing hydrologic connectivity 140 due to permafrost thaw in the lower Liard River valley, NWT, Canada. Hydrol. Process., 28: 4163–4178. https://doi.org/10.1002/hyp.10206

Fussmann, K., Schwarzmüller, F., Brose, U. et al. 2014. Ecological stability in response to warming. Nature Clim Change 4, 206–210. https://doi.org/10.1038/nclimate2134

Jin, H., Huang, Y., Bense, V.F., Ma, Q., Marchenko, S.S., Shepelev, V.V., Hu, Y., Liang, S., Spektor, V.V., Jin, X., et al. 2022 Permafrost Degradation and Its Hydrogeological Impacts. Water. 14(3):372. https://doi.org/10.3390/w14030372

Koliji, A., Laloui, L., Cusinier, O. et al 2006. Suction Induced Effects on the Fabric of a Structured Soil. Transp Porous Med 64, 261–278. https://doi.org/10.1007/s11242-005-3656-3

Rantanen, M., Karpechko, A.Y., Lipponen, A. et al. 2022. The Arctic has warmed nearly four times faster than the globe since 1979. Commun Earth Environ 3, 168. https://doi.org/10.1038/s43247-022-00498-3

Walvoord, M.A., and Kurylyk, B.L. 2016. Hydrologic Impacts of Thawing Permafrost—A Review. Vadose Zone Journal, 15: 1-20. https://doi.org/10.2136/vzj2016.01.0010

Wolfe, J., Bryant, G., and Koster, K.L. 2002. What is 'unfreezable water', how unfreezable is it, and how much is there?. Cryo letters, 23(3), 157–166.

Zhang, Z. et al. 2021. Ion-Specific Effects on the Growth of Single Ice Crystals. The Journal of Physical Chemistry, American Chemical Society. https://doi.org/10.1021/acs.jpclett.1c02601

Zhou, Y. et al. 2019. Practical models describing hysteresis behavior of unfrozen water in frozen soil based on similarity analysis. Cold Regions Science and Technology. 157. 215–223. https://doi.org/10.1016/j.coldregions.2018.11.002

Load dependent thaw strain prediction of fine-grained soils based on index properties

Anthony Valois & Simon Dumais

Département de génie des mines, de la métallurgie et des matériaux, Centre d'études nordiques, et Centre de recherche sur la géologie et l'ingénierie des ressources minérales (E4m), Université Laval, Québec City, Québec, Canada

Thaw consolidation theory has received significant attention in research especially for generalizing the theory to large-strain consolidation (Dumais and Konrad 2018; Yu et al. 2020). A certain consensus has been reached for the formulation and numerical implementation of large-strain thaw consolidation. The formulation has revealed the importance of improving the definition of the volume change characteristics of thawing permafrost for thaw consolidation analysis. The initial thawed state as the soil passes from a frozen to a thawed state is especially hard to define particularly for soils with excess ice content.

Dumais and Konrad (2023a) have proposed a framework to define the relationship between the void ratio and the effective stress for thawing fine-grained soils. The void ratio and the effective stress relationship is defined as a bilinear semi-logarithmic relationship in which a first phase describes the drainage of the excess water and a second phase describes compression of the soil skeleton.

Since discretization of the thawing behaviour at a micro scale is complex and somewhat counterproductive for engineering applications, the model relies on two essential simplifications for ice-rich soils:

- Drainage of the excess water occurs with no compression of the soil skeleton.
- After drainage of excess water, water is drained out of the soil upon compression of the soil skeleton in an ice-poor equivalent manner.

While seemingly trivial, these simplifications are of great importance for the calculation of thaw strain when using the framework because excess ice can be treated separately, and the compression behaviour of ice-rich and ice-poor soils are considered analogous.

Dumais and Konrad (2023b) have also proposed a series of empirical relationships for the thaw consolidation properties of fine-grained soils. They are based on data from the Mackenzie Valley in Canada, but it is believed that they can be used for other locations similarly to the common usage of other spatially specific thaw settlement relationships (Luscher and Afifi 1973; Speer et al. 1973).

The thaw consolidation framework and the empirical relationships can be advantageously combined to predict thaw strain of fine-grained soils. The calculated thaw strain is load-dependent and can be obtained as a function of some index soil properties: the clay content ($\%\mathrm{clay}$), the liquid limit ($\mathrm{w_L}$), or the median grain size of the fine fraction ($\mathrm{d_{50\_FF}}$). This is an improvement over existing thaw settlement relationships which are not load-dependent and only partially account for soil type variation.

Only the empirical relationships from Dumais and Konrad (2023b) as a function of the median grain size of the fine fraction are used herein because it yields the lowest error for the prediction of the volume change characteristics, but the same methodology can be applied with the clay content or the liquid limit.

Calculation of thaw strain

The Dumais and Konrad (2023a) framework consider that thaw strain of permafrost is composed of two stages: strain due to drainage of excess water and load-dependent strain due to compression of the soil skeleton. Strain due to phase change on thawing can be implemented fairly easily but is not considered here for simplicity. The framework considers that ice-poor soils do not contain excess melt water and that all strain other than phase change is load-dependent.

The terminology defined in Dumais and Konrad (2023a) is used hereafter. The strain due to drainage of excess water is:

$$A_i = (e_i^* - e_0^*)/(1 + e_i^*) \quad [1]$$

where e_i^* is the initial thawed void ratio and e_0^* is the thawed void ratio.

The strain due to compression is:

$$A_c = (e_0^* - e(\sigma_v'))/(1 + e_0^*) \quad [2]$$

where $e(\sigma_v')$ is the consolidated void ratio at effective stress σ_v'.

The total thaw strain is the sum of A_i and A_c. The initial thawed void is given by the frozen void ratio divided by 1.09 to account for the volume change due to phase change. The thawed void ratio is the void ratio at the residual stress σ_0' which is the stress that the soil skeleton can sustain on thawing. In ice-poor soils, the thawed void ratio and the initial thawed void ratio are equal. In ice-rich soil, the thawed void ratio indicates how much pore water the soil skeleton can hold on thawing.

CALCULATION OF THAWED VOID RATIO

As explained by Dumais and Konrad (2023b), a thawed ice-rich soil has a compression index for which there is an ice-poor equivalent soil with the same compression index. For a given compression index of a thawed soil, the equations in Table 2 of Dumais and Konrad (2023b) can be used to calculate the thawed void ratio as a function of the initial thawed void ratio.

The thawed void ratio is thus given by:

$$e_0^* \approx 0.39(e_i^*)^{0.11}\left(d_{50\_ff}\right)^{-0.15\log_{10}(e_i^*)-0.13} \quad [3]$$

where d_{50_FF} is expressed in millimetres.

For strain due to compression, the consolidated void ratio is obtained from the void ratio – effective stress relationship defined by:

$$e = -C_c^* \log_{10}(\sigma_v'/\sigma_0') + e_0^* \quad [4]$$

where C_c^* is the compression index of the thawed soil.

The Dumais and Konrad (2023b) empirical relationships used to calculate C_c^* and σ_0' are reproduced here:

$$C_c^* = 0.74\log_{10} e_0^* + 0.22 \quad [5]$$

and

$$\sigma_0' = \exp((e_0^* + 0.25\log_{10} d_{50\_ff} - 0.45)/(0.020\log_{10} d_{50\_ff} - 0.060)) \quad [6]$$

Equations 4 to 6 can be combined to calculate the load-dependent consolidated void ratio from the thawed void ratio. For ice-poor soils, the thawed void ratio is equal to the frozen void ratio divided by 1.09 since there is no excess ice. To obtain the total thaw strain of ice-rich soils, Equations 3 to 6 are used with Equations 1 and 2. For ice-poor soils, only equations 4 to 6 and Equation 2 are used.

Figures 1 and 2 show curves for thaw strain generated using equations 1 to 6 for two arbitrarily chosen types of soil ($d_{50\_ff} = 1e-3$ and $= 4e-3\ mm$). This corresponds to approximately 65% and 30% clay content respectively.

The blue curves are for ice-rich soils with the full line showing thaw strain attributable to excess ice only. The black curves are for ice-poor soils. The dashed lines are for soils subjected to a 20 kPa effective stress. These graphs are expressed as a function of the initial thawed void ratio. For improved practical applicability, they could be expressed in terms of ice content or frozen bulk density. With the methodology described herein, it is possible to generate these types of curves for different types of soils at different loading conditions.

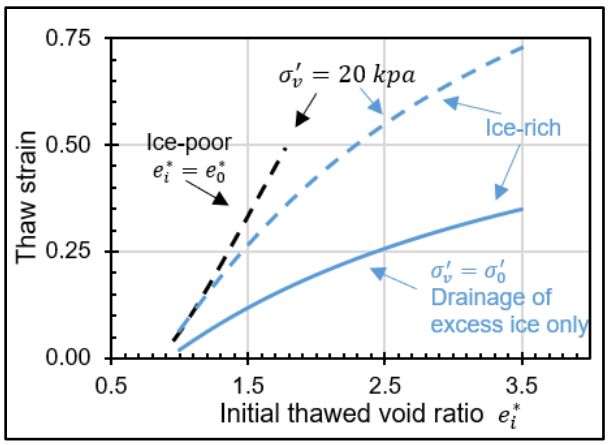

Figure 1. Predicted thaw strain for $d_{50\_ff} = 1e-3\ mm$

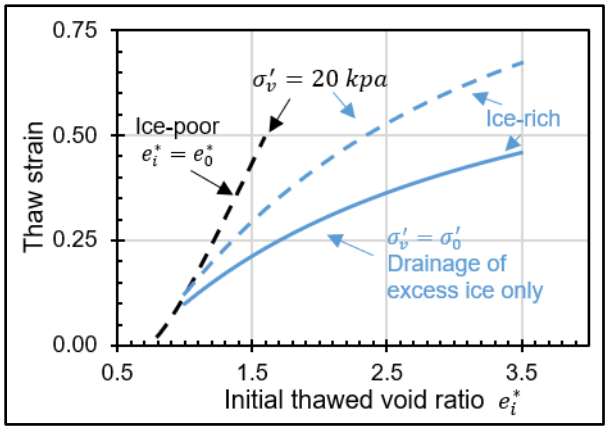

Figure 2. Predicted thaw strain for $d_{50\_ff} = 4e-3\ mm$

REFERENCES

Dumais, S., and Konrad, J.-M. 2023a. Framework for Thaw Consolidation of Fine-Grained Soils. Canadian Geotechnical Journal, Just-IN. doi:10.1139/cgj-2022-0502

Dumais, S., and Konrad, J.-M. 2023b. Thaw Consolidation Properties of Fine-Grained Permafrost Soils of the Mackenzie Valley, Canada. Journal of Cold Regions Engineering. 38(1): 04023020. doi:10.1061/JCRGEI.CRENG-720

Luscher, U., and Afifi, S.S. 1973. Thaw consolidation of Alaskan silts and granular soils. In 2nd Int. Conf. on Permafrost: North American Contribution, 325–334.

Speer, T.L., Watson, G.H., and Rowley, R.K. 1973. Effects of ground-ice variability and resulting thaw settlements on buried warm-oil pipelines. In 2nd Int. Conf. on Permafrost: North American Contribution, 746–752.

Yu, F., Guo, P.,Lai, Y., and Stolle, D. 2020. Frost heave and thaw consolidation modelling. Part 2: One-dimensional thermohydromechanical (THM) framework, Canadian Geotechnical Journal, 57(10): 1595–1610. doi:10.1139/cgj-2019-0306

Thermo-hydro-mechanical behaviour of sand in triaxial test under temperature gradient below zero degrees

Andrea Viglianti[1], Ulrich Schindler[2], Francesca Casini[1] & Roberto Cudmani[2]

[1]*Department of Civil Engineering, Università degli Studi di Roma Tor Vergata, Rome, Italy*

[2]*Technical University of Munich, Chair and Testing Institute of Soil Mechanics and Foundation Engineering, Rock Mechanics and Tunneling, Munich, Germany*

The thawing and freezing of permafrost due to global warming is a persistent challenge and strongly affects these soils' complex thermo-hydro-mechanical (THM) behaviour. The dependence of the mechanical behaviour of frozen soils on the strain rate is generally investigated under a constant, uniform temperature distribution. However, steady-state temperature gradients and transient temperatures also strongly influence the frozen soil behaviour. This work presents the results obtained for Karlsruhe sand tested in frozen conditions obtained with an advanced triaxial apparatus working at temperatures below zero and capable of applying a temperature gradient in the soil specimen.

EXPERIMENTAL SETUP

FROZEN is an advanced triaxial apparatus developed to study the THM behaviour of frozen soils (Bartoli et al. 2019). This apparatus comprises three main components. A mechanical load frame working at controlled displacements, a refrigerating control system, and a triaxial cell (Figure 1).

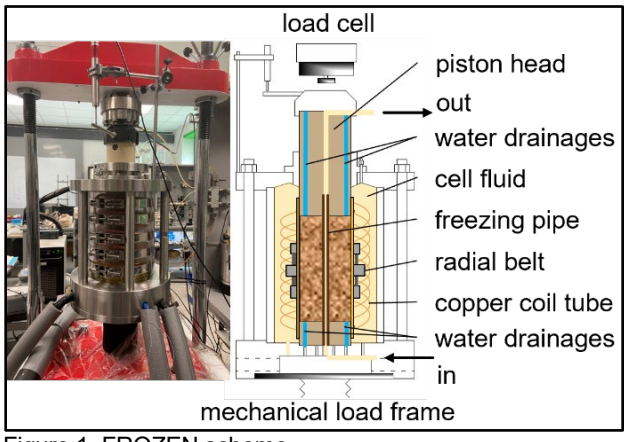

Figure 1. FROZEN scheme.

The triaxial cell is characterised by a piston head and a base in PEEK (PolyEther Ether Ketone) perforated to place thermocouples, water drainages, and the freezing pipe (placed in the middle of the base). A coil copper pipe is placed around the sample. The coolant fluid circulating inside the freezing pipe, the fluid circulating inside the copper pipe, and the cell fluid are a mixture of water (50 %) and glycol (50 %). The temperature of these fluids is controlled by two independent refrigerating systems. The vertical stress is applied by the mechanical load frame. The confining stress and the back pressure are applied through a volume gauge with a pneumatic converter. During the test, the vertical displacement is measured by an LVDT (Linear Variable Displacement Transducer) connected to the piston head in PEEK. The water flow is measured by an LVDT connected to the volume gauge. The local radial strain is measured by a radial belt installed in the middle of the sample. The temperature is monitored with thermocouples located at different points within the specimen. The sample is 100 mm in diameter and 200 mm in height.

MATERIAL AND EXPERIMENTAL CAMPAIGN

The material tested is Karlsruhe sand, characterized by grain size between 0.4 mm and 1.7 mm. The experimental program consisted of 6 tests conducted with 3 different confining effective pressures (50, 200, 800 kPa) and 2 different axial strain rates (0.2 and 0.02 %/min). The specimens were statically compacted at an initial void ratio equal to e_0=0.77 and gravimetric water content of w=0.12. The samples were compacted in four layers of 50 mm each to install the thermocouples. The test phases were the following: saturation, isotropic consolidation, freezing, and axial compression. During the freezing stage, the cooling fluid circulates in the freezing pipe from the bottom up (see Figure 1) with a temperature T= -20 °C, which was maintained constant during the tests. The initial temperature is equal to +5 °C and decreased during the tests until -2 °C. The freezing phase ended when the temperature reached a steady state.

EXPERIMENTAL RESULTS

Figure 2(a) shows the geometry of the sample, of the pipe and the positions of the thermocouples within the specimen. Figure 2(b) shows typical temperature evolutions versus the time during the freezing

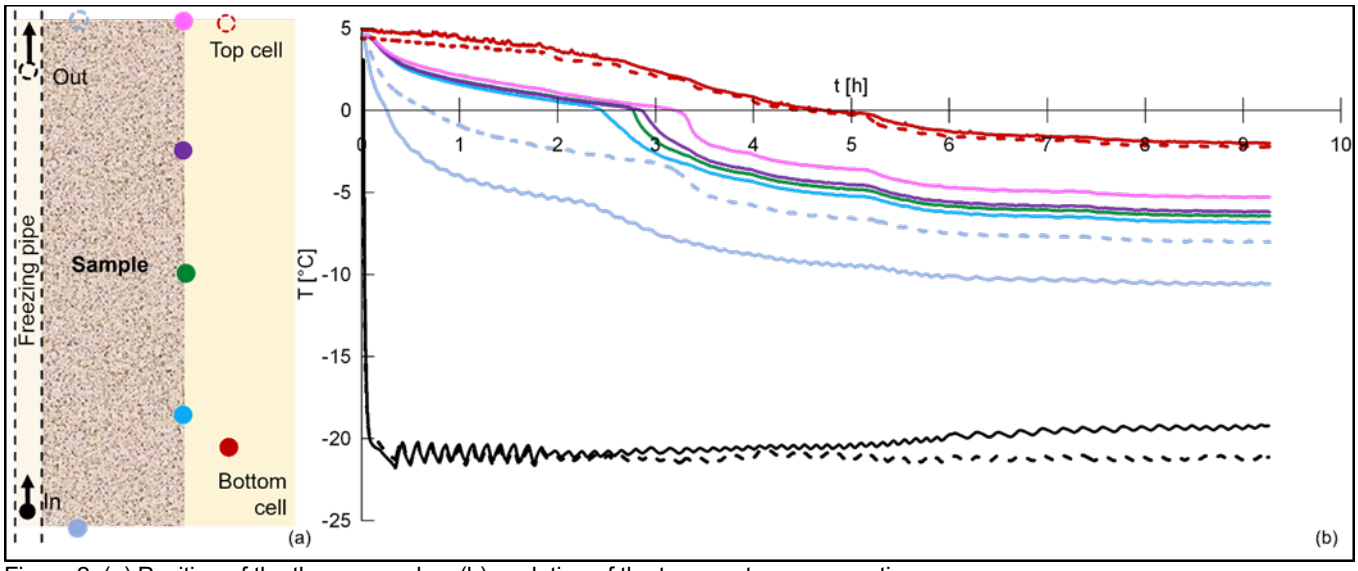

Figure 2. (a) Position of the thermocouples; (b) evolution of the temperatures versus time.

process with a duration of mostly 10 hrs. After the first 15 minutes, the lowest measure point reached 0 °C. After 2 hrs and 25 minutes, the freezing front reached the boundary of the specimen. After 3 hrs and 20 minutes the samples had a T≤0°C. During the freezing phase, water drained out of the sample related to ice formation that pushed out the liquid water.

Figure 3 shows the evolution of the deviatoric stress q versus the axial deformation ε_a during the axial compression phase in the case of σ'_3 = 50 kPa and two strain rates investigated.

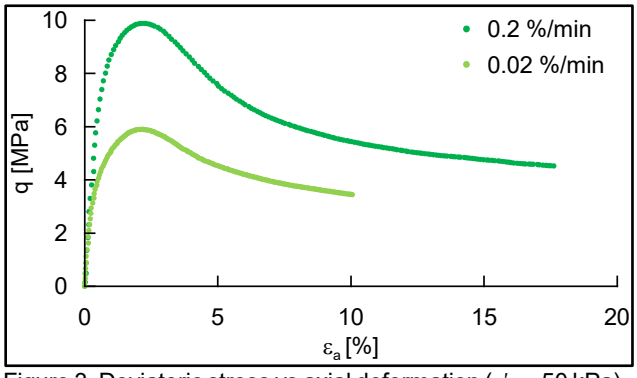

Figure 3. Deviatoric stress vs axial deformation (σ'_3 = 50 kPa).

In both cases, the behaviour is characterised by a peak at $\varepsilon_a \cong 2\%$ of 10 MPa and 6 MPa, respectively, decreasing with the axial strain rate applied. The peak stress increases with the strain rate for each confining pressure applied. The specimen subjected to a higher strain rate exhibits a peak and residual deviatoric stress equal to 10 MPa and to 6 MPa, respectively. Whereas the specimen under a lower strain rate exhibits a peak and residual deviatoric stress equal to 6 MPa and to 3.5 MPa, respectively. The tests at different confining pressures showed a strong effect of the temperature over the deviatoric stress (see Figure 4): the higher σ'_3, the lower q. This behaviour is due to a different temperature distribution within the specimens, with greater σ'_3 corresponding to higher temperatures on average.

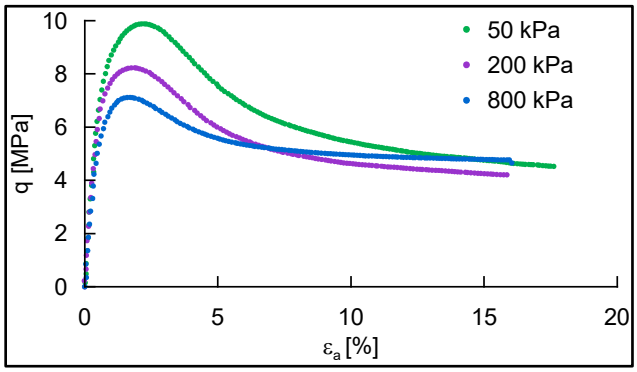

Figure 4. Deviatoric stress vs axial deformation (strain rate = 0.2 %/min).

Furthermore, as the confining pressure increases, it decreases the difference between peak and residual deviatoric stress.

ACKNOWLEDGEMENT

The authors would like to acknowledge DFG Deutch Forschungsgemeinschaft, German Research Foundation for the financial support of the project.

9 Microbial Ecology in Permafrost

INTEGRATING PERSPECTIVES OF PERMAFROST THAW, CHANGE, AND ADAPTATION

Microbial Ecology in Permafrost

9A — Permafrost Microbiology: Combining -omics with Ecological Theory

Session Chairs: Susanne Liebner[1], Rachel Mackelprang[2] & Andrea Soellinger[3]

[1]*GFZ German Research Centre for Geosciences, Potsdam, Germany*
[2]*California State University, Northridge, California, United States*
[3]*Arctic University of Norway, Tromsø, Norway*

Permafrost ecosystem microbiomes are exposed to extreme biotic and abiotic conditions. Unravelling their ecophysiology, genetic potential, community structure, and functional response to environmental change has been at the core of permafrost microbiology research for about a decade. In particular, -omics and trait-based approaches have emerged as promising tools for understanding the functional diversity and ecological processes in permafrost microbiomes. These approaches provide a way to link the characteristics of microorganisms with their roles in ecosystem functioning and to predict how microbial communities respond to environmental change. However, the integration of these approaches with ecological theory and modelling is still in its infancy.

This session provides an opportunity for researchers to bridge this gap by discussing the latest developments in permafrost microbiology covering a range of topics, including: (1) The role of microbial communities in the permafrost carbon cycle and the impact of climate change on these communities; (2) The genetic and physiological adaptations to long-term frozen conditions; (3) Changes in microbial growth, activity, metabolism, and interactions with the environment during thaw; (4) The use of -omics and trait-based approaches to predict the functional diversity and ecological processes in permafrost microbiomes; (5) The integration of -omics and trait-based approaches with ecological theory, such as niche theory and community ecology; and (6) The implementation of genomic, physiological and trait-based data in permafrost carbon feedback models.

This session will provide a valuable platform for researchers to exchange ideas, promote cross-disciplinary collaborations, and advance our understanding of the permafrost microbiomes and their role in the global carbon cycle.

Using multi-omics to link microbial organic matter degradation in active layer soils to fjord sediments in Svalbard, Norway

Fumnanya Abuah[1], Joy Buongiorno[1], Katie Sipes[2], Samantha Peters[3], James Bradley[4], Donato Giovannelli[5], Julia Boike[6], Andrey A. Abramov[7], Tatiana A. Vishnivetskaya[1], Andrew D. Steen[1], Robert Hettich[3] & Karen G. Lloyd[1]

[1]*Department of Microbiology, University of Tennessee, Knoxville, Tennessee, United States*

[2]*Department of Environmental Sciences, Aarhus University, Risø, Denmark*

[3]*Biosciences Division, Oak Ridge National Labs, Oak Ridge, Tennessee, United States*

[4]*School of Geography, Queen Mary University of London, London, United Kingdom*

[5]*Department of Biology, University of Naples "Federico II", Naples, Italy*

[6]*Helmholtz Center for Polar and Marine Research, Alfred Wegener Institute, Postdam, Germany*

[7]*Institute of Physiochemical and Biological Problems in Soil Science, Russian Academy of Sciences, Puschino, Russia*

The degradation of organic matter (OM) within permafrost ecosystems stands as a pivotal aspect of Arctic biogeochemistry, influencing carbon cycling dynamics and climate change feedback mechanisms. This study concurrently examines OM degradation in active layer soils and an adjacent fjord within Ny-Ålesund, Svalbard. By integrating metagenomic assemblies, metagenome-assembled genomes (MAGs), metatranscriptomics, and metaproteomics, our focus was to comprehensively understand microbial communities and their roles in OM degradation across these interconnected ecosystems. Active layer soils were collected using a drill and sub-sectioned at a 2 cm frequency to a depth of 2 meters, preserving the stratigraphy of the active layer, and. Sediment cores from the adjacent fjord were collected and sub-sectioned at a 1 cm resolution. By focusing on MAGs, our approach combines taxonomic descriptions and detailed exploration of the genomic capabilities. Matching predicted functions to metaproteomic data in active layer soils and metatranscriptomic data in fjord sediments allows a direct assessment of functions that were active in situ. Un-binned contigs from the metagenomic assemblies were subjected to the same analysis to provide an in-depth examination of the genetic repertoire present in the under-characterized portion of the metagenomic data. By scrutinizing un-binned contigs, we sought to capture genetic information that might not be incorporated into MAGs, ensuring a more comprehensive understanding of the microbial community's genomic landscape.

We focused on the presence, distribution, and abundance of carbohydrate-active enzymes (CAZymes) and peptidases across all the taxa identified in MAGs, as well as diverse depths and sites across the permafrost active layer soils and fjord sediments. Our results reveal shared microbial taxa and functional pathways participating in OM degradation across permafrost and fjord sediments, suggesting these ecosystems may be better studied as an interconnected system, challenging the conventional compartmentalization of permafrost research. In conclusion, our research contributes to a holistic understanding of OM degradation in Arctic environments, emphasizing the need for integrated, multi-omics approaches to unravel microbial dynamics. As the Arctic undergoes rapid transformations, our findings underscore the interconnected nature of permafrost and marine ecosystems, providing critical insights into the implications for carbon cycling in a changing Arctic landscape.

ACKNOWLEDGEMENTS

This research was funded by the US Department of Energy, Office of Science, Office of Biological and Environmental Research, Genomic Science Program DE-SC0020369

A metagenomic approach on understanding seasonal effects on microbial processes in permafrost-affected soils from West Greenland

Claudia S. Bruhn[1], Parvina Gasimova[1], Carolina Voigt[2], Christian Knoblauch[2,3], Tino Peplau[4], Patrick Liebmann[4], Georg Guggenberger[4], Jan Olaf Melchert[5] & Susanne Liebner[1,6]

[1]*Helmholtz-Centre Potsdam, German Research Centre for Geosciences GFZ, Telegrafenberg, 14473 Potsdam, Germany*

[2]*Institute of Soil Sciences, Universität Hamburg, Allende Platz 2, 20146 Hamburg, Germany*

[3]*Center for Earth System Research and Sustainability, Universität Hamburg, 20146 Hamburg, Germany*

[4]*Institute of Soil Science, Leibniz University Hannover, Herrenhäuser Str. 2., 30419 Hannover, Germany*

[5]*Institute for Geology and Mineralogy, University of Cologne, Zülpicher Str. 49B, 50674 Cologne, Germany*

[6]*Institute of Biochemistry and Biology, University of Potsdam, Karl-Liebknecht-Str. 24-25, 14476 Potsdam, Germany*

The Arctic is warming almost four times as fast as the global average (Rantanen et al. 2022). This is subjecting Arctic permafrost soils, which cover approximately 15 % of the northern land area, to drastically changing conditions. Thawing permafrost enables formerly inactive microbes to produce or oxidize methane. Methane (CH_4) has a 28 times higher global warming potential than carbon dioxide (CO_2), making these processes very relevant for the greenhouse gas (GHG) budget of the Earth's atmosphere. While many studies focus on snapshot studies, we present first data on a season-driven observation of the microbial soil metagenome along tundra soil moisture gradients, including the understudied winter with a final field trip planned for early 2024. This way, we are able to directly compare the winter season to the warmer seasons and the potential influence of this seasonality on community composition and functionality. We further investigate genes involed in methane production and methane oxidation along the moisture gradient.

Methodology

In a first survey in September 2022, soil samples were collected from a total of seven plots (P1 to P7) from two transects (T1 and T2) on Disko Island, West Greenland. Each transect covered relatively dry to relatively wet soils (P1 to P3 on T1, and P4 to P7 on T2). We chose the soil moisture gradients to investigate them as the main drivers of microbial CH_4 oxidation vs. production. Soil samples of all plots were also taken during two field trips in June/July and September 2023. To extend insights into the depth distribution of microbes and to compare microbiomes before and after thawing of the active layer, we additionally drilled soil cores during snow-melt in June/July with a SIPRE corer and used a soil probe ("Pürckhauer") or a spade in the late summer season of maximum active layer depth (September 2023) at two of the plots, P5 and P7. These plots were chosen because they provided a good possibility to compare a relatively dry (P5) to a relatively wet plot (P7). All samples were taken in biological triplicates (three sampling points per plot). Soils at plots P5 and P7 were furthermore sampled from different horizons. All samples were individually extracted for DNA.

The samples from the initial survey in September 2022 were used in an incubation experiment, both under aerobic and anaerobic (i.e., water-saturated) conditions, and subsequently measured for CH_4 and CO_2 production using gas chromatography.

Further, a general overview of the prokaryotic community was gained via 16S rRNA gene metabarcoding (Illumina), while whole-genome metagenomics (i.a. Oxford Nanopore) will reveal information on the entire microbial community composition and will indicate further functional groups and pathways within the next months. Quantitative PCR will be used to employ a targeted approach on functional genes for microbial methane production (mcrA) and methane oxidation (pmoA).

Results and outlook

So far, high-quality DNA was obtained from a total of 172 samples spanning all three sampling times, with further extractions still pending. 16S rRNA gene metabarcoding (Illumina) of samples from the initial field trip in September 2022 revealed the overall composition and transectional differences of the prokaryotic microbiome along the moisture gradients and depths. We show, that the known methane oxidizers and methane-associated genera Beijerinckia, Methylobacter, Methylocapsa, Methylocystis and Methylotenera spp. are ubiquitously occuring at low relative levels throughout the whole soil community in September 2022, generally accounting for <1.5 % of all amplicon sequence variants (ASV, a proxy for different species). However, they notably do increase in relative abundance in the lower depths of

one replicate of P6, which is an intermediately wet site on transect 2. Here, they account for approx. 3.5 % of all ASVs. Within the community of methanogens, we were able to identify the genera Methanobacterium and Methanosaeta spp., which are most present at the wet sites P3 and P7, but also in deeper horizons of P4. In one deeper sample below 51 cm, Methanobacterium spp. accounted for more than 25 % of all ASVs, suggesting high methanogenic potential in deeper horizons, even if the area is relatively dry on the surface. Furthermore, the general distribution of methanogens found in metabarcoding was well in accordance with the observed methane production in the incubation experiments.

In the beginning of the thawing period (June/July 2023), methanogens were also detected in lower horizons and in wetter plots, however they have only been accounting for approx. 2 % of all ASV reads at most. The found genera were Methanobacterium, Methanosaeta, Methanosarcina, and Methanoregula. Methane oxidizers have also been present in lower relative abundances than in September 2022, indicating substantial seasonal changes in community composition.

So far, our survey on the microbial community composition and GHG production along two moisture gradients points towards a widely covered potential for methane oxidation, while the occurrence of methane production is more patchy. Additionally, differences in the community composition between the seasons suggest seasonal changes in the methane oxidation and production potential.

This data set will be complemented by whole-genome metagenomics. Also, the 16S rRNA gene metabarcoding data sets from September 2022 and June/July 2023 are currently complemented with samples taken at the later field trips to compare community changes throughout different seasons. A final qPCR approach will help to quantify the metabarcoding-derived data. One further field trip in April 2024 will complete the seasonal approach and will provide insights into microbial abundances in completely frozen and snow-covered soils utilizing the same methods. This way, we will be able to help to understand the microbial functioning underlying CH_4 oxidation and production in context with seasonal changes, which in turn will be important for constraining the pan-Arctic CH_4 budget.

Acknowledgements and sponsorship

The presented work was supported by the project MOMENT (grant number 03F0931A) funded by the German Federal Ministry of Education and Research and the DFG funded excellence cluster CLICSS (EXC2037).

References

Rantanen, M., Karpechko, A.Y., Lipponen, A., Nordling, K., Hyvärinen, O., Ruosteenoja, K., Vihma, T., and Laaksonen, A. 2022. The Arctic has warmed nearly four times faster than the globe since 1979. Communications Earth & Environment, 3(1): 168. doi:10.1038/s43247-022-00498-3

Microbial limitations lead to underestimated methane production from thawed permafrost

Joanne Heslop[1,2,3], Sizhong Yang[2,4], Matthias Winkel[1,2], Katey Walter Anthony[1], Robert Spencer[5], David Podgorski[6], Phoebe Zito[6] & Susanne Liebner[2,7]

[1]*Water and Environmental Research Center, University of Alaska, Fairbanks, Alaska, United States*

[2]*GFZ German Research Centre for Geosciences, Section Geomicrobiology, Telegrafenberg, 14473 Potsdam, Germany*

[3]*Now at: The Alaska Earthquake Center, University of Alaska, Fairbanks, Alaska, United States*

[4]*Cryosphere Research Station on the Qinghai-Tibet Plateau, State Key Laboratory of Cryospheric Sciences, Northwest Institute of Eco-Environment and Resources, Chinese Academy of Sciences, Lanzhou 730000, China*

[5]*National High Magnetic Field Laboratory Geochemistry Group and Department of Earth, Ocean, and Atmospheric Science, Florida State University, Tallahassee, Florida, United States*

[6]*Pontchartrain Institute for Environmental Sciences, Department of Chemistry, University of New Orleans, New Orleans, Louisiana, United States*

[7]*University of Potsdam, Institute for Biochemistry and Biology, Potsdam, Germany*

Processes that control methane production in thawing permafrost environments are largely unknown. Despite having high-quality organic substrate for potential greenhouse gas (GHG) production, permafrost soils, particularly older yedoma-type permafrost, have low in situ microbial diversity and biomass compared to more modern soils and the overlying seasonally-thawed active laye. The combination of high substrate potential and low microbial biomass and diversity can lead to permafrost soils having unfilled gaps in metabolic pathways, providing niches favorable to the establishment of introduced microbial communities. Laboratory incubations, which are a common method for determining GHG production potentials from thawed permafrost soils, usually maintain in situ soil organic matter (OM) and microbial communities. This is not representative of conditions following permafrost thaw in natural settings, where thawed permafrost can potentially immediately mix with more modern OM and microbial communities. The introduction of microbial communities which fill metabolic pathway gaps has the potential to increase GHG production in thawed permafrost soils. Therefore, shorter term incubations that do not allow mixing of contemporary and old material likely lead to underestimations of GHG production potentials.

We anaerobically incubated samples collected from a 12-m yedoma profile in Interior Alaska (the Vault Creek permafrost tunnel; 65°01’46.3”N, 147°42’22.4”W) at two temperatures (3 °C and 13 °C) to examine: (i) interaction between the molecular composition of thawed OM substrate (Fourier transform ion cyclotron resonance mass spectrometry; FT-ICR MS) and microbial community composition (16S rRNA) and potential function (metagenomics); (ii) how mixing modern CH_4-producing communities with microbial communities present in frozen permafrost affects community composition and function following thaw; and (iii) subsequent effects on anaerobic CO_2 and CH_4 production. We used three treatments: (i) control treatments of unaltered thawed permafrost samples; (ii) inoculated treatments where thawed permafrost samples were inoculated with surface sediment collected from an adjacent thermokarst lake, which contained the methanogens Methanobacteriales, Methanomicrobiales, and Methanosarcinales; and (iii) sterilized inoculated treatments where thawed permafrost samples were inoculated with the same surface lake sediment that had been autoclaved to remove active microbial communities. Additional metagenomic sequencing of ten samples from the 9.0 m and 12.0 m yedoma depths was conducted to further evaluate differing priming effect responses to the same inoculate.

Increased GHG production in both the inoculated (mean 32x more CH_4 and 1.4x more CO_2 compared to the control treatments) and sterilized inoculate (mean 1.3x more CH_4 and 0x more CO_2) treatments indicate traditional laboratory incubations underestimate GHG production potentials. Higher CO_2 and CH_4 production in the inoculated treatments compared to the sterilized inoculate treatments (mean 92x more CH_4 and 1.2x more CO_2 in the inoculated treatment) suggests the increased GHG production was primarily stimulated by the addition of CH_4-producing microbial communities in the inoculate, as opposed to the addition of biolabile substrate. Combined data from our microbial (16S rRNA sequencing and metagenomic functional pathways) and chemical composition of water extractable organic matter (WEOM; FT-ICR MS) analyses show increases in anaerobic GHG production following inoculation are associated with enhanced degradation of more complex OM. However, despite

the inoculated treatment producing more GHG in nearly all samples, differences in how the same inoculate altered WEOM utilization between depths suggest that the metabolic pathway gaps limiting OM processing and GHG production vary with depth.

Our ultra-high resolution OM characterization shows the introduction of contemporary microbial communities in the inoculated treatments enhanced the consumption and degradation of carbohydrates, aliphatic- and peptide-like compounds, and proteins compared to the control treatments. The WEOM utilization trends also show that the sterilized inoculate treatments more closely resemble the control treatments than the inoculated treatments, suggesting microbes in the inoculate drive the changes in OM utilization following inoculation. Our 16S rRNA sequencing data support these observed changes in WEOM utilization following inoculation. Differing microbial communities at the end of the incubation between the three treatments suggest the addition of contemporary microbial communities in the inoculated treatments altered microbial community development following thaw. Several taxa that differed in relative abundance between the control and inoculated treatments are associated with fermentation of sugars to acetate and hydrogen (Ignavibacteriae and Lokiarchaeota) and the consumption and degradation of carbohydrates, peptides, and proteins (Bacteroidetes, Balneolaeota, and Calditrichaeota). The inoculated treatments also had higher relative abundance of methanogens including Methanosarcinales and Methanobacteriales compared to the control and sterilized inoculate treatments.

Metagenomic gene analyses showed differing responses in anaerobic GHG production pathways following inoculation between the two yedoma depths in this study (9.0 m and 12.0 m), despite having similar permafrost history and initial metagenomic profiles. Genes associated with CH_4 production from acetate (1099 ± 145 transcripts per million (TPM); ackA, acs, cdhC/D/E, cooF/S, pta) were initially twice as abundant as genes associated with CH_4 production from CO_2 and H_2 (554 ± 60 TPM; ftr, mch, mer, mrtB, mtrA/C/D/E/G). Following incubation, the inoculated treatments for both yedoma depths showed a similar increase in the relative abundance of genes associated with CH_4 production from CO_2 and H_2 (263 ± 99 TPM increase compared to control treatment). However, at the 9.0 m depth there was a strong decrease in the relative abundance of genes associated with CH_4 production from acetate (1051 ± 250 TPM decrease), while at the 12.0 m depth there was a moderate increase (406 ± 212 TPM increase). Relative abundance of the genes shdA and sdhB, which are associated with degradation of fatty acids (carboxylic acids with an aliphatic chain), were higher in the inoculated treatments compared to control treatments (341 ± 39 TPM increase) at the end of the incubation. Genes associated with mixed acid fermentation (e.g., acnA, fumA, fumC, korA, ppc) also had higher abundance in the inoculated treatments compared to the control treatments (513 ± 39 TPM increase).

While microbial metabolic potentials can yield insights to GHG production and emission potentials, the differing responses in anaerobic GHG production and pathways following inoculation indicates that characterizing microbial communities and metabolic pathways in frozen or freshly-thawed permafrost may not yield accurate estimates of GHG production following thaw. Our results suggest the development of microbial communities following permafrost thaw may serve as a more reliable indicator of GHG production potentials than initial OM or microbial characterizations.

ACKNOWLEDGEMENTS

We thank: P. Anthony, S. Billings, J. Chanton, J. Guerard, N. Haubenstock, F. Horn, T. Howe, A. Kholodov, C. Knoblauch, L. Oliver, A. Saborowski, B. Van Veldhuizen, and M. Zhang for assistance in data collection and/or analysis and S. Skidmore for granting access to the Vault Creek permafrost tunnel. A portion of this work was performed at the National High Magnetic Field Laboratory ICR User Facility, which is supported by the National Science Foundation Division of Chemistry and Division of Materials Research through DMR-1644779 and the State of Florida. Additional funding for J. Heslop has been provided by: a GFZ Discovery Fellowship, a UAF Center for Global Change Student Research Grant with funds from the UAF Center for Global Change, and STAR Fellowship Assistance agreement no. FP-91762901-0 awarded by the US Environmental Protection Agency (EPA). This presentation has not been formally reviewed by EPA. The views expressed in this presentation are solely those of J. Heslop, and the EPA does not endorse any products or commercial services mentioned. K.M. Walter Anthony was supported by NSF NNA-2022561 and NASA ABoVE NNH18ZDA001N-TE. M. Winkel was supported by NSF ARCSS-1300931.

Permafrost microbiology in the past, present, and future

Brian Lanoil[1], Duane Froese[2], Suzanne Tank[1] & Hendrik Poinar[3]

[1]*Department of Biological Sciences, University of Alberta, Edmonton, Alberta, Canada*

[2]*Department of Earth and Atmospheric Sciences, University of Alberta, Edmonton, Alberta, Canada*

[3]*McMaster Ancient DNA Centre, Departments of Anthropology and Biochemistry, McMaster University, Hamilton, Ontario, Canada*

Permafrost, i.e., soils that are frozen for at least two continuous years, is a "repository" for large amounts of organic matter and acts as a dateable "archive" of relict materials from the time of it's formation. It has been used extensively as a source of ancient DNA, allowing the reconstruction of genomes of extinct or extirpated organisms, populations, and even whole ecosystems. It has also been studied extensively to better understand the transformation of organic matter.

Microorganisms such as Bacteria, Archaea, and fungi, are the amongst most important functional biological components of soil. They are involved in nutrient dynamics and transformations, act as plant pathogens and growth promoters, and are responsible for the transformation of organic matter into greenhouse gasses (GHG), producing primarily CO_2 in unsaturated soil conditions and primarily CH_4 in water-saturated soils and sediments.

However, despite their importance in these processes, little is known about how microbial communities change over time, respond to ecosystem changes, or even which microbial communities are responsible for transformation of organic matter into GHG. It is critical that we have a more complete understanding of the role of microbial community structure, function, composition, and interactions if we are to be able to accurately reconstruct past ecosystems, understand the impacts of current climate change and associated permafrost thaw, and predict future interactions between microorganisms, permafrost, and climate.

I will describe past and ongoing research in the Lanoil laboratory focusing on reconstructing microbial communities surrounding the transition between the Pleistocene and Holocene, a time of abrupt climate change and massive ecosystem shifts. I will also describe our research focusing on the impact of permafrost thaw on microbial community structure and function in the field (in contrast to the laboratory). Finally, I will discuss how a better understanding of microbial communities and their processes is critical for better future predictions and modelling of climate change and permafrost thaw interactions.

Reconstructing past soil microbial ecosystems

The Pleistocene-Holocene transition, ca. 11,700 years ago, was a period of abrupt climate change, with massive ecosystem shifts. The Beringia region, and specifically the Yukon Klondike area underwent a shift from cold- and dry-adapted flora and fauna as part of the mammoth steppe biome to woody shrubs and mesic tundra ecosystems. We showed that within permafrost from a particular epoch, microbial communities were quite stable and did not change much over time; however, microbial communities in permafrost from different epochs were distinct in terms of their taxonomy (Figure 1) and in at least one major metabolic pathway, i.e., methanogenesis (Saidi-Mehrabad et al. 2020; Murchie et al. 2023). We interpreted these findings to indicate that soil microbial communities are metabolically flexible and able to adapt to relatively small differences and shifts in their local environment. However, once environmental conditions exceed a threshold, the soil microbial community rapidly shifts to a new steady state condition. These shifts are associated with accompanying shifts in flora and fauna, with an overall change in the ecosystem as a whole. These findings may indicate a similar "tipping point" could occur as a result of modern climate change, with unknown consequences for modern ecosystems. Future work should focus on the pace and timing of such changes, and their implications for ecosystem functioning.

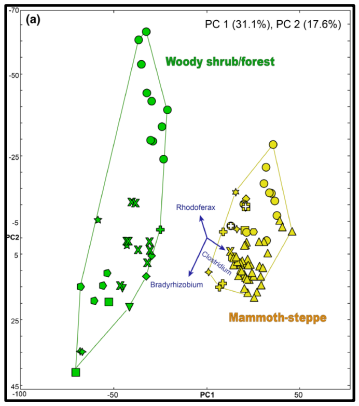

Figure 1. PCoA analysis of metagenomic hits to prokaryotic genus rank hits using a χ^2 ecological index.

IMPACT OF PERMAFROST THAW ON MICROBIAL COMMUNITY STRUCTURE AND FUNCTION IN THE FIELD

Anthropogenic climate warming has a much stronger effect in polar regions—so called "polar amplification". As a result, the Arctic has warmed by ~5°C in the modern period. Permafrost is often at temperatures near thaw; as a result, even relatively small changes in temperature can lead to large regions of thawing permafrost. Permafrost thaw can lead to major landform changes such as land subsidence (thermokarst formation) in regions with ice-rich permafrost. Resulting landscape features such as retrogressive thaw slumps and thermokarst ponds and lakes expose stored organic matter to degradation by microbial communities. Previous work (e.g., Mackelprang et al. 2011) has shown that permafrost microbes are distinct from those in the active layer and that these communities shift in response to thaw; however, many of these studies have been performed in the laboratory without interactions with surrounding ecosystems. We have examined microbial communities in two distinct thawing permafrost ecosystems in the field; a small thermokarst pond that formed ~6 weeks following removal of vegetation for road building in the Klondike region of the Yukon and retrogressive thaw slumps in the Peel River Plateau of the NWT. In the thermokarst pond, we found that while permafrost microbes remained, active layer microbial community members appear to dominate the post-thaw microbial communities (Figure 2; Neuberger et al. 2024). We also found that methanotroph (organisms that consume methane) community membership and activity are more affected by the physical soil disturbance that accompanies permafrost thaw than by shifts in temperature.

Retrogressive thaw slumps (RTS) result from permafrost thaw on a slope. Detachment of these sediments leads to mass wasting of active layer and thawed permafrost into streams and rivers, creating a mixture of microbial communities. We found that microbial activity is correlated with DOM, not POM, in the streams with suspended sediment derived from RTS and that DOM composition is coupled to microbial community structure in these mixed systems. We also found that microbial activity in streamwater increases dramatically in the presence of permafrost thaw sediments, but increases even more dramatically when the indigenous streamwater microbes are removed. Taken together, we interpret these findings to indicate that permafrost associated sediment microorganisms are primarily responsible for degradation of permafrost DOM but do not readily degrade POM in aquatic systems. Furthermore, these sediment associated microorganisms are in competition with aquatic microorganisms in these systems; thus, the amount of sediment input and the composition of organic matter will determine the rate of carbon degradation.

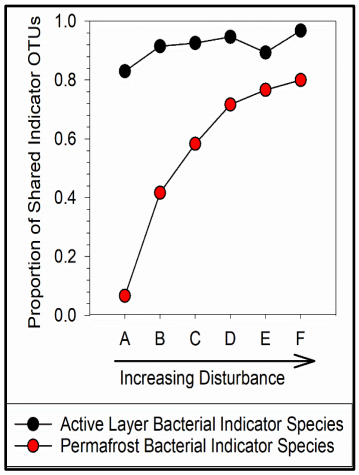

Figure 2. Proportion of active layer indicator species increases with increasing disturbance/thaw.

THE FUTURE OF PERMAFROST MICROBIOLOGY

Altogether, the work in our laboratories (amongst others) indicates that microbial community composition and activity are critical for determining the rate and form of permafrost carbon degradation. Further research into the mechanisms of permafrost microbiome assembly and direct relationships between microbial community composition and permafrost organic matter degradation are critical for modelling of carbon transformation and climate feedbacks in permafrost regions.

REFERENCES

Saidi-Mehrabad, A., et al. 2020. Permafrost Microbial Community Structure Changes Across the Pleistocene-Holocene Boundary. Frontiers Environ. Sci. doi:10.3389/fenvs.2020.00133

Murchie, T., et al. 2023. Permafrost microbial communities follow shifts in vegetation, soils, and megafauna extinctions in Late Pleistocene NW North America. Environ. DNA. 00, 1–21. https://doi.org/10.1002/edn3.493

Mackelprang, R., et al. 2011. Metagenomic analysis of a permafrost microbial community reveals a rapid response to thaw. Nature. 480, 368–371. https://doi.org/10.1038/nature10576

Neuberger, P., et al. 2024. Bacterial community composition changes independently of soil edaphic parameters with permafrost disturbance. Environ. Microbiol. (in press)

What lies beneath: Organic matter decomposition dynamics in thawing subsea permafrost

Constance Lefebvre[1,2], Paul Overduin[1], John Paul Balmonte[3], Susanne Liebner[4,5], Claire Treat[1], Jens Strauss[1], Maria De La Fuente[2] & Sandra Arndt[2]

[1]*Permafrost Research Section, Alfred Wegener Institute Helmholtz Center for Polar and Marine Research, Potsdam, Germany*

[2]*Department of Geosciences, Environment & Society-BGEOSYS, Université libre de Bruxelles, Brussels, Belgium*

[3]*Department of Earth and Environmental Sciences, Lehigh University, Pennsylvania, United States*

[4]*Geomicrobiology, GFZ German Research Centre for Geosciences, Potsdam, Germany*

[5]*Institute of Biochemistry and Biology, University of Potsdam, Potsdam, Germany*

Subsea permafrost (SSPF) on the Arctic shelf is thawing, potentially unlocking up to an estimated 2822 Pg of organic carbon (Miesner et al. 2023). Under continued climate warming, SSPF thaw is expected to accelerate as a consequence of sea ice loss and the warming of ocean bottom waters, intensifying SSPF organic matter decomposition rates and, thus, carbon (as methane CH_4 and carbon dioxide CO_2) and nutrient (nitrite NO_2^-, nitrate NO_3^- and phosphate PO_4^{3-}) production. This may lead to shifts in seafloor carbon and nutrient fluxes, with potentially important, yet unquantified, consequences for the Arctic Ocean primary production and acidification, greenhouse gas emissions and, ultimately, global climate. The magnitude and evolution of these SSPF-derived fluxes are highly dependent (i) on the apparent reactivity of the organic matter and (ii) on the response of the resident, reactivating microbial communities in their changing habitat (frozen to thawed sediment). The assessment of future feedbacks between SSPF thaw, the carbon cycle, and global climate requires the development of numerical reaction-transport models that provide a robust quantification of organic matter decomposition rates in the thawing permafrost, as well as CH_4 consumption and associated biogeochemical dynamics in the overlying unfrozen sediments. However, most existing diagenetic models currently do not explicitly resolve microbial biomass dynamics and bioenergetic limitations, nor are they designed to capture the evolving microbial habitat. Furthermore, direct observational data from SSPF sediment samples are currently lacking. Consequently, critical model parameters such as those that control the response of the microbial community to its changing habitat, as well as the reactivity of the permafrost organic matter, are currently difficult to constrain (Miesner et al. 2023). Here, we adopt an integrated model-data approach to address these knowledge gaps.

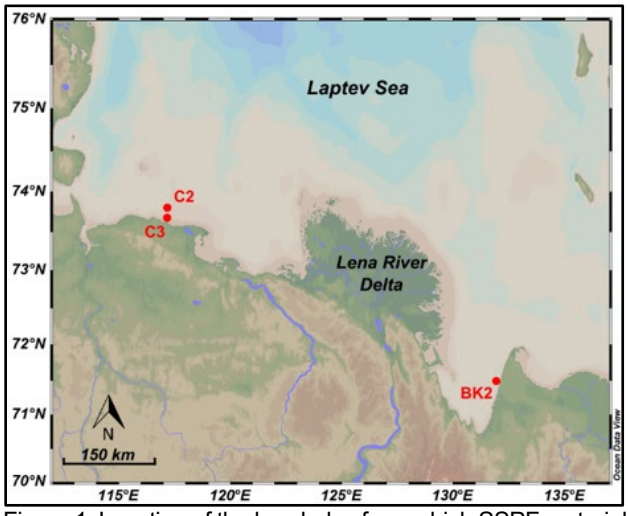

Figure 1. Location of the boreholes from which SSPF material was retrieved in 2005 (C2 and C3) and in 2012 (BK2). Map produced with Ocean Data View.

INCUBATION EXPERIMENTS

We first incubated SSPF material from three different locations in the Laptev Sea (Figure 1). Samples were retrieved in 2005 (cores C2 and C3, Winterfeld et al. 2011) and in 2012 (core BK2, Overduin et al. 2015). Sections representative of different ages and depositional conditions were selected and were incubated under anaerobic conditions at two different temperatures (4°C and 10°C) over a period of one year. Greenhouse gas production (CH_4 and CO_2), extracellular enzyme activity, and biomass evolution were analyzed over time. Methanogenesis rates were determined from CH_4 and CO_2 accumulation in the headspace. Assays for extracellular leucine aminopeptidase, phosphatase, and β-glucosidase offered insight into rates of nitrogen, phosphorus and carbon cycling related to the decomposition of macromolecular organic matter in the thawed permafrost. Cell counts and gene analysis allowed us to determine compositional changes in the microbial community over time.

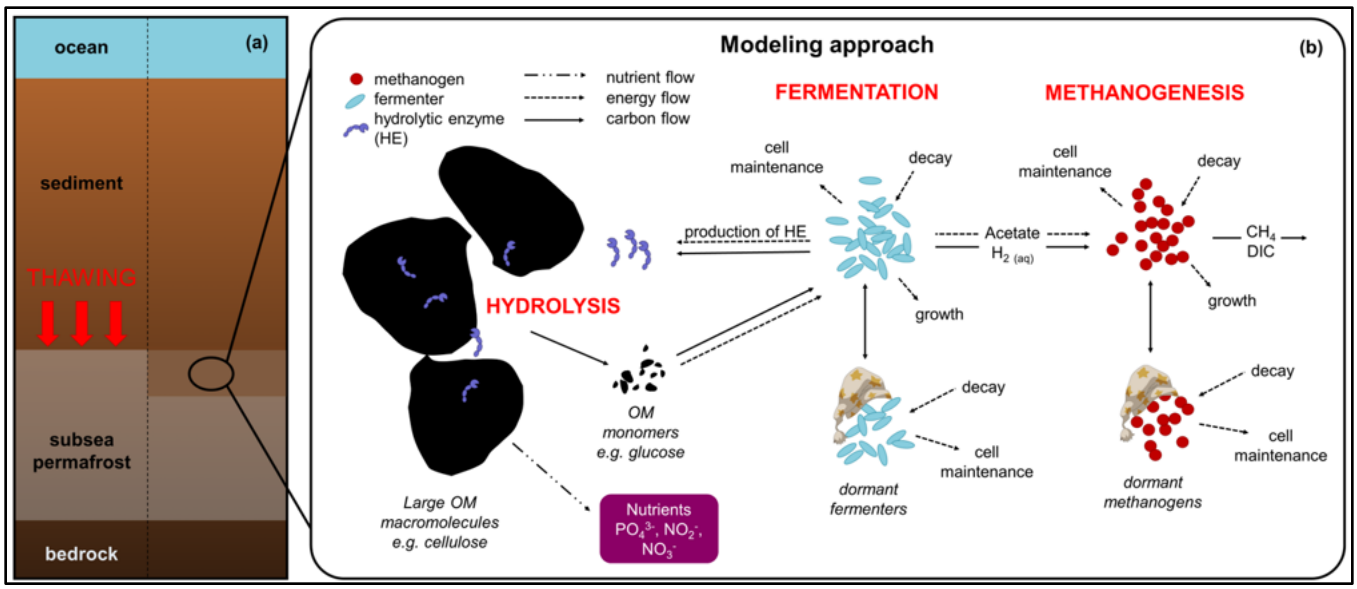

Figure 2. (a) vertical transect of a section of the Arctic shelf containing SSPF and undergoing accelerated thawing under climate change, (b) conceptual 0D model for the decomposition of organic matter in thawed SSPF.

Organic matter decomposition model

An inverse modeling approach was then used to determine the parameters of a reactive continuum model for organic matter decomposition (RCM, Boudreau and Ruddick 1991; Arndt et al. 2013) from measured CH_4 and CO_2 production rates. Inverse model results provide novel insights into the distribution of SSPF organic matter compounds over the entire reactivity spectrum and allow quantifying the evolution of apparent SSPF organic matter reactivity over both incubation (days-months), as well as policy relevant timescales (decades-centuries). This unique experimental and model data will then be used to constrain a bioenergetics-informed kinetic model for organic matter decomposition in thawing SSPF that accounts for extracellular hydrolysis, fermentation, and methanogenesis, following the model concept proposed by Bajracharya et al. (2022) (Figure 2). The model simulates syntrophic relationships between several functional groups of microorganisms in the energy-limited environment of thawing SSPF. The novel model will not only provide more robust predictions of SSPF derived carbon fluxes on a local and regional scale, but will also help explore the response of SSPF microbial communities to changes in substrate availability and their physical environment.

References

Arndt, S., Jørgensen, B.B., LaRowe, D.E., Middelburg, J.J., Pancost, R.D., and Regnier, P. 2013. Quantifying the degradation of organic matter in marine sediments: A review and synthesis. Earth-Science Reviews 123, 53–86. https://doi.org/10.1016/j.earscirev.2013.02.008

Bajracharya, B.M., Smeaton, C.M., Markelov, I., Markelova, E., Lu, C., Cirpka, O.A., and Cappellen, P.V. 2022. Organic Matter Degradation in Energy-Limited Subsurface Environments—A Bioenergetics-Informed Modeling Approach. Geomicrobiology Journal 39, 1–16. https://doi.org/10.1080/01490451.2021.1998256

Boudreau, B.P., and Ruddick, B.R. 1991. On a reactive continuum representation of organic matter diagenesis. American Journal of Science 291, 507–538. https://doi.org/10.2475/ajs.291.5.507

Miesner, F., Overduin, P.P., Grosse, G., Strauss, J., Langer, M., Westermann, S., Schneider von Deimling, T., Brovkin, V., and Arndt, S. 2023. Subsea permafrost organic carbon stocks are large and of dominantly low reactivity. Sci Rep 13, 9425. https://doi.org/10.1038/s41598-023-36471-z

Overduin, P.P., Liebner, S., Knoblauch, C., Günther, F., Wetterich, S., Schirrmeister, L., Hubberten, H.-W., and Grigoriev, M.N. 2015. Methane oxidation following submarine permafrost degradation: Measurements from a central Laptev Sea shelf borehole. Journal of Geophysical Research: Biogeosciences 120, 965–978. https://doi.org/10.1002/2014JG002862

Winterfeld, M., Schirrmeister, L., Grigoriev, M.N., Kunitsky, V.V., Andreev, A., Murray, A., and Overduin, P.P. 2011. Coastal permafrost landscape development since the Late Pleistocene in the western Laptev Sea, Siberia. Boreas 40, 697–713. https://doi.org/10.1111/j.1502-3885.2011.00203

Microbial taxa and functional traits show significant differences in response to permafrost thaw

Rachel Mackelprang[1], Michael W. Snyder[1], Suzi Arzoumanian[1], Serena Hernandez[1], Jonathan Corpeño[1], Sommer Starr[2], John Chodkowski[3], Samuel Barnett[3], Thomas A. Douglas[4], Robert G.M. Spencer[2] & Ashley L. Shade[5]

[1]*Department of Biology, California State University Northridge, Northridge, California, United States*

[2]*Earth, Ocean, and Atmospheric Science Department, Florida State University, Tallahassee, Florida, United States*

[3]*Department of Plant, Soil, and Microbial Sciences, Michigan State University, East Lansing, Michigan, United States*

[4]*Biogeochemical Sciences Branch, Cold Regions Research and Engineering Laboratory, US Army Engineer Research & Development Center, Fairbanks, Alaska, United States*

[5]*Laboratoire Ecologie Microbienne, University of Lyon, Lyon, France*

Permafrost thaw unlocks previously frozen carbon to microbial communities, who decompose the millennia-old organic matter and convert it to CO_2 and CH_4 (Schädel et al. 2016). Crossing the freezing point of water triggers drastic changes in microbial communities (Mackelprang et al. 2011), causing increased growth and metabolism. However, we do not understand the factors controlling community membership, function, and carbon turnover during permafrost thaw. These local-scale interactions between changing microbial communities and a changing environment drive large-scale biogeochemical cycles.

Methods

We disentangled the effects of soil type versus community source during permafrost thaw through a novel in situ thaw experiment. Sterilized active layer soils, Holocene permafrost (~2 kya) or Pleistocene permafrost (~40 kya) were placed into 0.2 micron nylon membrane bags and inoculated with microbial communities from the same soil type (e.g., Holocene communities into Holocene permafrost) or a different soil type (e.g., active layer communities into Pleistocene permafrost). Bags were buried in the active layer to simulate thaw and recovered after two weeks or two months. This allowed samples to experience "real world" conditions, while the filter bags prevented the exchange of microbial communities with the surrounding environment. Microbial community structure was evaluated using 16S rRNA and ITS amplicon sequencing. The functional potential was assessed using metagenome sequencing. Metatranscriptome sequencing and analysis of soil organic matter via FT-ICR MS (Fourier transform ion cyclotron resonance mass spectrometry) are ongoing.

Results

After two weeks of thaw, soil type (active layer, Holocene, or Pleistocene) was more significantly more important than community source in structuring functional genes (KEGG and CAZy, PERMANOVA, $P < 0.05$) (Figure 1). By contrast, both soil type and community source were equally important in 16S rRNA amplicon data ($P < 0.05$). After two months, the effect of community source was no longer significant in functional genes. These "founder effects" were still apparent in 16S rRNA amplicons, though the variance explained decreased (Figure 2).

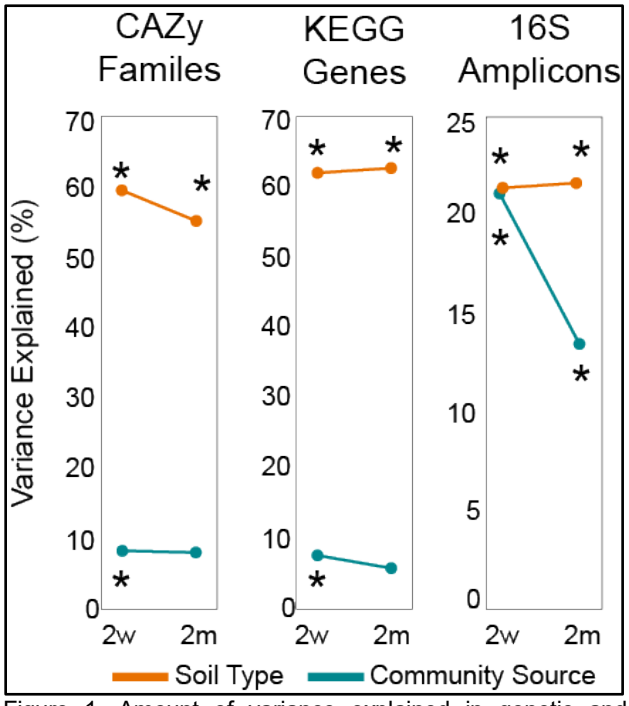

Figure 1. Amount of variance explained in genetic and community structure by soil type and community source after two weeks (2w) and two months (2m) of thaw. *$P < 0.05$.

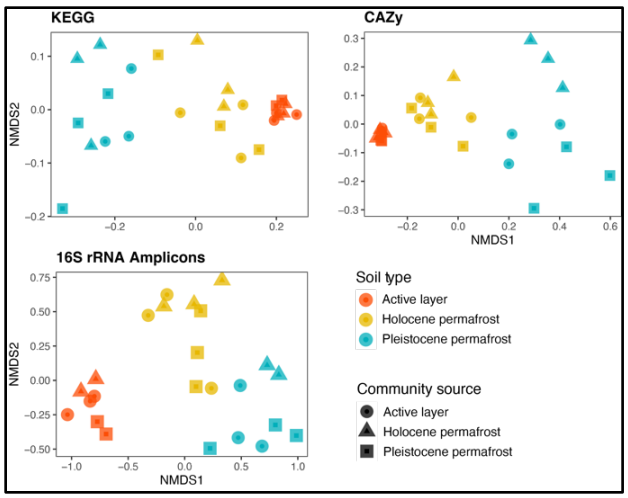

Figure 2. NMDS ordination of 16S rRNA amplicon, KEGG, and CAZy data from samples thawed for two months.

Similar to the 16S rRNA amplicon data, community source and soil type explained the similar amounts of variation in fungal community structure after two weeks of thaw ($P < 0.05$). However, after two months of thaw, opposite trends were observed. Community source was still significant, while the effect of soil type was no longer significant. In particular, soils inoculated with active layer communities clustered separately from samples inoculated with permafrost communities (Figure 3).

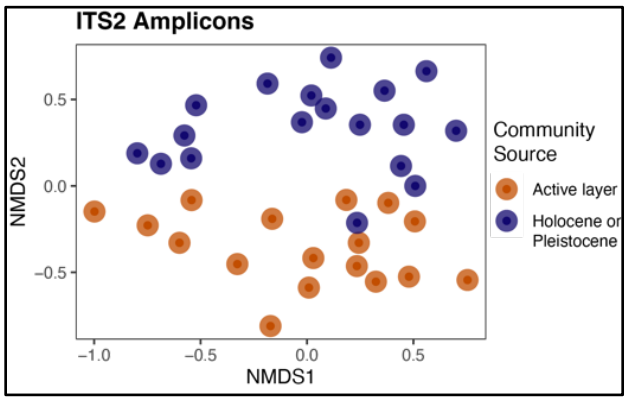

Figure 3. NMDS ordination of ITS2 amplicon data from samples thawed for two months.

Genes significantly more abundant after thaw included those related to metabolism (e.g., TCA cycle, denitrification, carbon substrate use) and "lifestyle" (e.g., motility, biofilm formation, and environment sensing). These data indicate a substantial shift in crucial microbial processes in response to thaw. Ongoing metatranscriptome and FT-ICR MS analyses will reveal the actual function and the corresponding carbon transformations

Conclusions

Response to environmental disturbance is influenced both by both soil characteristics and starting microbial communities. However, the significant differences between genetic and community structure in thaw response suggest decoupling of taxonomy and function. This occurs in communities with high functional redundancy (Martiny et al 2015). These data underscore the importance of investigating microbial function in addition to community structure, and that response to thaw may not be generalizable across permafrost types.

References

Mackelprang, R., et al. 2011. Metagenomic analysis of a permafrost microbial community reveals a rapid response to thaw, Nature 480 (7377). doi:10.1038/nature10576

Martiny, J.B.H., et al. 2015. Microbiomes in the light of traits. A phylogenetic perspective, Science, 350 (6261), aac9323. 10.1126/science.aac9323.

Schadel, C., et al. 2016. Potential carbon emissions dominated by carbon dioxide from thawed permafrost soils, Nature Climate Change, 6 (10): 950–953. 10.1038/nclimate3054.

C-Isotopic analysis of soils and soil emissions on Disko Island

Jan Olaf Melchert[1], André Craveiro Pereira Coelho Faust[1], Tino Peplau[2], Andrea Jaeschke[1], Georg Guggenberger[2], Christian Knoblauch[3,4], Susanne Liebner[5,6] & Janet Rethemeyer[1]

[1]*Institute for Geology and Mineralogy, University of Cologne, Zülpicher Str. 49B, 50674 Cologne, Germany*

[2]*Institute of Soil Science, Leibniz University of Hannover, Herrenhäuser Str. 2, 30419 Hannover, Germany*

[3]*Institute of Soil Science, Universität Hamburg, Allende Platz 2, 20146 Hamburg, Germany*

[4]*Center for Earth System Research and Sustainability, Universität Hamburg, 20146 Hamburg, Germany*

[5]*GFZ German Research Centre for Geosciences, Geomicrobiology, Telegrafenberg, 14473 Potsdam, Germany*

[6]*Institute of Biochemistry and Biology, University of Potsdam, Karl-Liebknecht-Str. 24-25, 14476 Potsdam, Germany*

The northern circumpolar regions are warming faster than the global average and as a result, annual permafrost thaw is prolonging and extending deeper into the ground. This active layer thickening promotes the microbial degradation of previously freeze-locked soil organic matter (SOM) and potentially turns carbon (C) sinks into sources. The release of greenhouse gases (GHG) such as carbon dioxide (CO_2) and methane (CH_4) from previously unavailable C sources may further accelerate the arctic warming and is known as the permafrost carbon feedback. Although arctic permafrost soils were the subject of numerous extensive studies throughout the past, the extent of the potential GHG release upon permafrost thaw is not fully understood. The regulation of GHG production and release through microbial activity and the response to environmental changes through, for example, soil hydrology, freeze-thaw cycles, or the intermixing of substrates through cryoturbation is still incompletely understood. In our study, we approach this knowledge gap by identifying the biological sources of GHG emissions via radiocarbon and stable carbon isotopic analyses. Additionally, the quality of SOM and the diversity of the microbial community along a hydrological gradient are assessed through the analyses of lipid biomarkers.

Methods

This study was conducted in Blæsedalen, on Disko Island, West Greenland and started with sampling campaigns in September of 2022 and 2023, respectively. The study area comprises a transect, with four sampling sites in total, following a slope gradient with changing moisture content. Changes in soil moisture were first assessed by topographical position and validated by the soil water content at each site and the installation of soil moisture sensors. The transect feature Cryosols, consisting of glacial till and basaltic sediments. Soil samples were taken at each of the four sites, from three profiles per site. To assess the carbon isotopic composition of GHGs emitted from the soils in the study area through heterotrophic microbial respiration, vegetation was clipped and carefully removed, and soil collars were installed at each site that allow sampling of total soil CO_2 efflux via respiration chambers. In addition to the active CO_2 sampling, that integrates the carbon isotopy over the whole active layer, passive CO_2 collection probes were installed at each site in the top- and subsoil to target CO_2, emitted through microbial activity from specific soil depths. Dissolved organic C (DOC) was sampled using suction probes that were installed in the uppermost litter layer, top- and subsoil. Pore water was then sampled via syringes, stored in HDPE bottles and shipped back frozen for radiocarbon and lipid analysis. For an initial characterization of soil properties, total organic carbon (TOC), water content and pH values were determined as well as the radiocarbon content of bulk SOM. Lipid biomarkers including n-alkanes and fatty acids and bacterial membrane phospholipid fatty acids (PLFAs) are extracted from bulk SOM and will give evidence on SOM composition and bacterial communities. Radiocarbon analysis of SOM, DOC and CO_2 samples is performed via accelerator mass spectrometry.

Preliminary results and outlook

The results indicate a slight decrease in average active layer pH values from 6.5 at the supposedly driest site to 5.4 at the wettest site along the moisture gradient. The TOC content increased from the drier soils towards the wetter ones. Radiocarbon data of SOM indicate ^{14}C enrichment through bomb-spiked plant litter in the uppermost soil horizons and a decreasing ^{14}C content with increasing soil depth. The averaged and normalized ^{14}C content per soil profile slightly decreases along the moisture gradient from dry to wet. Our data indicate a relationship between ^{14}C and TOC content, which in turn is controlled by water content, i.e., low ^{14}C contents were measured in horizons with low TOC and water content. Furthermore, we found that SOM in cryoturbated soil horizons contains relatively more ^{14}C compared to the SOM from

surrounding horizons. The comparison of ^{14}C content of bulk SOM and pore-space CO_2 emissions from targeted soil depths shows a distinct offset at sites with dryer conditions. Microbes from deeper soil horizons released CO_2 with a relatively higher ^{14}C content compared to the respective bulk SOM, which likely indicates preferential mineralization of fresher substrates such as DOC mobilized in the topsoil, where ^{14}C analysis is in progress. In addition, lipid biomarkers will give further evidence on the state of SOM degradation via ratios of stable and labile lipids. PLFA contents and changes in their distribution will be used as a proxy for the quantity and type of microbial biomass in the soils along the transect, which is work in progress.

FINANCIAL SUPPORT

This study is part of the larger 'MOMENT' research consortium and is financed by the Federal Ministry of Education and Research (BMBF, grants no. 03F0931A, 03F0931C) in Germany.

Determining microbial processes associated with soil organic matter dynamics in rhizosphere and permafrost communities using quantitative stable isotope probing

Sean R. Schaefer[1], Steve Blazewicz[2], Hannah Holland-Moritz[1], Stuart Grandy[1], Caitlin Hicks Pries[3], Fernando Montaño-Lopez[3], Will Wieder[4], Nate Alexander[1], Jennifer Pett-Ridge[2] & Jessica G. Ernakovich[1]

[1]*Department of Natural Resources & Earth Systems Science, University of New Hampshire, Durham, New Hampshire, United States*

[2]*Lawrence Livermore National Laboratory, Livermore, California, United States*

[3]*Department of Biological Sciences, Dartmouth College, Hanover, New Hampshire, United States*

[4]*National Center for Atmospheric Research, Boulder, Colorado, United States*

As tundra vegetation communities change in response to increased temperature and permafrost thaw, so do their root-associated—or rhizosphere—microbial communities. The impact of changing rhizosphere and native permafrost microbial communities on global carbon cycles remains uncertain, despite the potential for significant carbon losses from Arctic soils due to increased microbial decomposition. We aim to enhance mechanistic understanding of how rhizosphere and permafrost microbial community interactions influence belowground carbon dynamics by quantitatively assigning microbial functions to taxa in these communities and assessing their impact on global carbon cycles.

Background

Warming global temperatures are accelerating permafrost thaw and altering landscapes, displacing tussock-forming cotton grass with woody shrubs in a process known as shrubification. Tussocks and shrubs exhibit differences in their life history strategies, which influence belowground carbon dynamics and ecosystem function (Sturm et al. 2001). For example, differences in root phenology, preference of soil horizon, mineralogical interactions, and mycorrhizal associations shape distinct root-associated, or rhizosphere, communities (Lynch et al. 2018) (Figure 1). Divergent rhizosphere communities drive differences in ecosystem functions, such as the storage and decomposition of soil organic matter (SOM). Permafrost-affected regions contain over 33% of global soil carbon stocks (Schuur et al. 2022) and are warming almost four times faster than the global average (Rantanen et al. 2022). There is serious concern that permafrost thaw will continue to result in significant greenhouse gas emissions through increased decomposition of SOM. Permafrost thaw alters the soil environment by introducing nutrients and energy that were previously unavailable to microbes and plants (Ernakovich et al. 2017), increasing microbial metabolism, as well as "awakening" previously dormant microbial communities (Burkert et al. 2019). As plant roots travel deeper in the soil profile following thaw, rhizosphere and permafrost microbial communities collide, forming distinctly new communities. Understanding how these new communities will influence the formation and decomposition of SOM represents a knowledge gap that is critical to better understanding carbon fluxes from thawed permafrost systems.

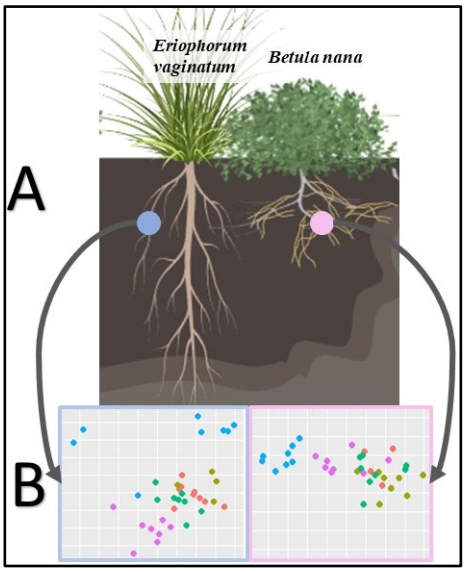

Figure 1. A) Comparison of aboveground and root growth patterns between *E. vaginatum* and *B. nana*. B) Differences in rhizosphere fungal community structures, as shown by non-metric multidimensional scaling 3. Each point is a different rhizosphere community (sample), with colors representing sites on the North Slope of AK.

Methods

To examine how distinct microbial communities from permafrost and rhizosphere coalesce influence

SOM dynamics, we inoculated rhizosphere communities from the shrub *B. nana*, the sedge *E. vaginatum,* as well as a no-plant control, to native permafrost. To select microbes associated with degrading root exudates or SOM, we added either an exudate cocktail (primed) or water (control) to the permafrost or permafrost-rhizosphere samples daily. The samples were incubated at 4°C for 54 days, and CO_2 and CH_4 production were measured throughout the incubation at various time points (Figure 2). To identify specific taxa associated with SOM or exudate degradation from these microbial communities, we performed quantitative stable isotope probing (qSIP). To this end, we added isotopically enriched water (^{18}O-H_2O) or exudates (^{13}C glucose, oxalic acid, alanine) during the final 8 days of the incubation.

The next steps will be to extract and fractionate DNA from our samples at Lawrence Livermore National Laboratory (LLNL). Utilizing their high throughput qSIP pipeline, we will identify taxon-specific microbial traits, such as growth and exudate incorporation rates from different rhizosphere and permafrost microbial communities. From this we will determine how specific taxa influence the formation and decomposition of SOM in rhizosphere and permafrost soils. The findings of this experiment will then be used to help inform the MIcrobial-MIneral Carbon Stabilization model (MIMICS), which will be used to predict SOM dynamics in the tundra.

Results

Initial respiration results suggest differences in microbial community structure and biogeochemical function between the rhizosphere-inoculated permafrost and native permafrost communities, as well as diverging functions for primed versus control groups (Figure 2). Further analysis from qSIP will allow us to identify guilds of microbes associated with degrading root exudates or SOM, as well as their growth rates in different communities and environmental conditions.

Conclusion

Permafrost thaw and rhizosphere intrusion is rapidly altering tundra microbial communities. Understanding how these interactions will influence SOM formation and decomposition rates is critical to predicting the fate of permafrost carbon. This study will advance mechanistic understanding of rhizosphere and permafrost community assembly interactions, and provide insight into areas of microbial ecology by identifying key taxa associated with degrading root exudates and SOM.

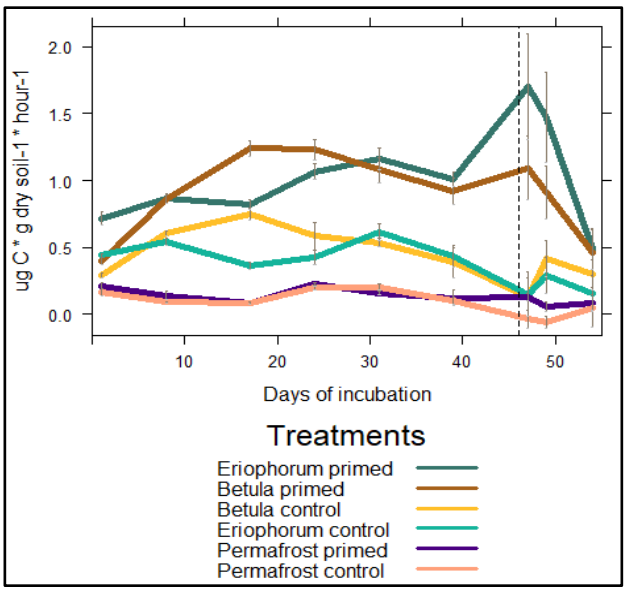

Figure 2. Respiration rates were separated by the inoculant/ priming treatment combination, where primed groups received 5 µL of exudate cocktail (5.7 µg/µL) daily, while control groups received 5 µL of water. The dashed line signifies the point at which isotopes were added, and all treatments received 180 µL amount of exudate cocktail (5.7 µg/µL) or water.

References

Burkert, A., Douglas, T.A., Waldrop, M.P., and Mackelprang, R. 2019. Changes in the Active, Dead, and Dormant Microbial Community Structure across a Pleistocene Permafrost Chronosequence. Applied and Environmental Microbiology 85, e02646-02618. doi:10.1128/AEM.02646-18

Ernakovich, J.G., Lynch, L.M., Brewer, P.E., Calderon, F.J., and Wallenstein, M.D. 2017. Redox and temperature-sensitive changes in microbial communities and soil chemistry dictate greenhouse gas loss from thawed permafrost. Biogeochemistry 134: 183–200. doi:10.1007/s10533-017-0354-5

Lynch, L.M., Machmuller, M.B., Cotrufo, M.F., Paul, E.A. and Wallenstein, M.D. 2018. Tracking the fate of fresh carbon in the Arctic tundra: Will shrub expansion alter responses of soil organic matter to warming? Soil Biology and Biochemistry 120: 134–144. doi:10.1016/j.soilbio.2018.02.002

Rantanen, M. et al. 2022. The Arctic has warmed nearly four times faster than the globe since 1979. Nature Communications Earth & Environment, 3: 168. doi:10.1038/s43247-022-00498-3

Sturm, M., Racine, C., and Tape, K. 2001. Increasing shrub abundance in the Arctic. Nature 411: 546–547. doi:10.1038/35079180

Microbial Ecology in Permafrost

9B — Microbial Pattern and Process in Permafrost Affected Ecosystems

Session Chairs: Mary-Cathrine Leewis[1], Jessica Ernakovich[2] & Sam Bratsman[3]

[1]Agriculture and Agri-Food Canada, Québec City, Québec, Canada
[2]Center of Soil Biogeochemistry and Microbial Ecology, University of New Hampshire, Durham, New Hampshire, United States
[3]Natural Resources and Earth System Science, University of New Hampshire, Durham, New Hampshire, United States

Microbial communities in permafrost-affected ecosystems—from soils to wetlands to rivers and lakes—are a critical component of biogeochemical cycles because they drive the transformation of elements from local to global scales. It is increasingly recognized that studies focused on microorganisms and how they interact with their environment are essential because of the vital role microbes play in driving ecosystem processes. The understanding of the response of microorganisms and their functions to disturbance (such as permafrost thaw, wildfire, shrubification, lake drainage, and glacier retreat to name a few) is limited, however important patterns are beginning to emerge. Major processes which are critical for understanding the effects of disturbance can be categorized as those which explore the interactions of permafrost-affected microorganisms with (1) other microorganisms (e.g., bacteria, archaea, viruses, and fungi) and soil fauna; (2) plant communities; (3) soil minerals; and (4) soil water and ice.This session invites interdisciplinary submissions exploring the complexity of microbial patterns and processes in northern latitude ecosystems. This session invites microbial ecologists and biogeochemists with expertise in laboratory, field, and modelling approaches to explore how interactions between microbial communities and other components of permafrost-affected ecosystems influence cryosphere processes under global change.

Interactions and transformations: Unveiling microbial community responses to permafrost thaw and sediment transport into Arctic streams

Bethlehem Abraham, Brian Lanoil & Suzanne Tank

Department of Biological Sciences, University of Alberta, Edmonton, Alberta, Canada

Permafrost, covering a quarter of the Northern Hemisphere, is undergoing rapid thaw due to climate change, leading to significant consequences for global carbon cycling (Ping et al. 2020). This study investigates the interactions between the terrestrial permafrost-derived microbial community and the aquatic microbial community following permafrost thaw and subsequent transport of sediment into streams. Our project focuses on the Peel Plateau region—an area profoundly impacted by permafrost degradation and among the fastest-warming regions in the Arctic.

Climate change-induced thawing of permafrost liberates previously frozen organic carbon, making it susceptible to microbial degradation (Lee et al. 2012). Microorganisms play a pivotal role in this process, releasing potent greenhouse gases such as carbon dioxide and methane. Retrogressive thaw slumps (thaw slumps) are prominent forms of mass wasting that result from the thaw of ice-rich permafrost (Kokelj and Jorgensen), leading to the mixing of permafrost and active layer soils. This process initiates a cascade of events, including sediment deposition into streams and rivers, with potential ramifications for aquatic ecosystems (Kokelj et al. 2015). Microbial community interactions are important elements for determining greenhouse gas fluxes from the decomposition of permafrost carbon.

This study aimed to investigate the impact of thaw slump sediment deposition on both terrestrial and aquatic microbial community structures and activity. Our approach involved an analysis of the interactions between these two microbial communities, examining the consequences of their mixing, and the influence of the aquatic environment on the slump-derived microbial community. We hypothesized that the interactions between terrestrial and aquatic microbial assemblages would lead to a novel microbial community, with associated increases in secondary production. The predicted microbial community shift would be dependent upon community interactions, and would have direct consequences for the greenhouse gas flux potential from these systems.

Sampling sites

Four retrogressive thaw slump features (CB, FM3, HB and SF) on the Peel Plateau, NT, were sampled over a two-month period in the summer of 2022. These sites were selected to capture the region's geochemical diversity and were all chosen to have debris tongues flowing into intersecting streams resulting from thaw slump outflow. Sediment samples were collected along the debris tongue outflow, complemented by water samples from sites that were upstream (unimpacted) and downstream (impacted) of the slump. Following collection, samples were transported on ice to the laboratory for subsequent analyses.

Sample processing

Water samples from downstream and a subset from upstream were filtered through 0.22 µm sterivex filters and preserved at -80°C for 16S rRNA gene sequencing. Filtrates were aliquoted and stored at -20°C and 4°C for subsequent chemical and nutrient analysis.

Incubation bottles were established with three experimental conditions at 20°C to investigate the microbial response to sediment input: (1) unfiltered upstream water with thaw slump sediment; (2) filtered upstream water (0.22 µm) with thaw slump sediment; (3) whole unfiltered upstream water. Additionally, two controls were included: (4) whole upstream water with thaw slump sediment and 0.1% sodium azide (killed control); and (5) Milli-Q water (blank control). Incubations were initiated immediately following transport to the laboratory. Subsamples for sequencing, chemical, and nutrient analyses were collected at t = 0 days and t = 7 days. Secondary production estimates were determined through a radiolabeled leucine incorporation technique.

The remaining sediment samples were sieved (2 mm) and stored at -80°C for in-depth chemical, nutrient, and 16S rRNA sequencing analyses.

Preliminary results

Initial results revealed a pronounced difference in microbial secondary production post-incubation, which was not associated with the specific slump site but rather correlated with the treatment group (Figure 1).

An anticipated rise in secondary production was observed moving from the whole upstream to the upstream-plus-slump sediment treatment, attributable to the introduction of terrestrial microbes and nutrients that amplify microbial activity. However, the substantial

surge in secondary production in the filtered upstream water and slump sediment treatment was unforeseen. The disparity in microbial activity between filtered and unfiltered treatments suggests that terrestrial and aquatic microbial community interaction modulated community productivity. Absent aquatic microbes, the terrestrial community demonstrated heightened activity, suggesting a competitive dynamic with native aquatic microbes. These findings suggest that the introduction of terrestrial microbes into aquatic systems was significantly influenced by the presence of indigenous aquatic microorganisms. The change in secondary production did not appear to vary much from site-to-site, and were very consistent for each treatment.

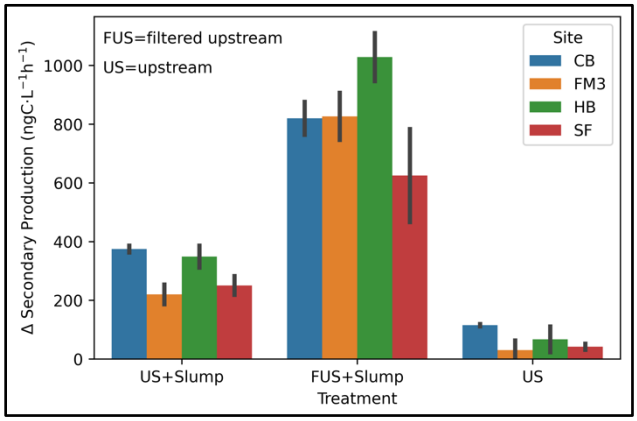

Figure 1. Change in secondary production over 7-day incubation (triplicate) at 20°C. Samples were collected from four thaw slump sites (CB, FM3, HB, and SF). The incubations consisted of the following treatments: 1) upstream water with added thaw slump sediment; 2) filtered upstream water (0.22 µm) with added thaw slump sediment; 3) whole upstream water. Error bars represent standard errors.

Conversely, chemical data presented variation across slump sites that appeared decoupled from treatment effects (Figure 2). Slump sites SF and CB, which are geographically close, exhibited minimal chemical disparities. Together, these data indicate that the secondary production findings may be broadly generalizable, and do not vary between sites and are not strongly influenced by local biogeochemical factors.

While these observations may underscore potential terrestrial-aquatic microbial interactions, ongoing 16S rRNA sequencing aims to characterize the microbial community composition involved and correlate them with the observed production metrics.

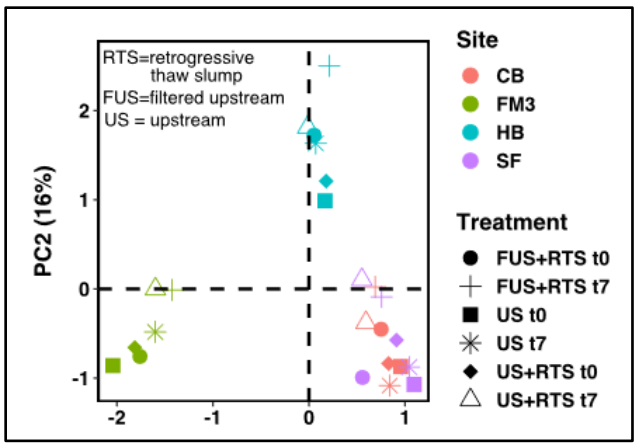

Figure 2. Ordination of incubation water chemistry from four slump sites (CB, FM3, HB, and SF). The incubations were 7-days at 20°C and consisted of the following treatments: 1) upstream water with added thaw slump sediment; 2) filtered upstream water (0.22 µm) with added thaw slump sediment; 3) whole upstream water. Chemistry subsamples were taken at days t = 0 and t = 7.

Conclusion

The incubation experiments shed light on the intricate dynamics between terrestrial permafrost-derived microbial communities and native aquatic microbes. This interplay has substantial implications for carbon degradation in freshwater ecosystems, potentially influencing biodegradation processes and greenhouse gas emissions. These initial findings illustrate the complexity of microbial interactions within the natural environment, underscoring the imperative for further research to fully comprehend permafrost ecosystem dynamics and for projecting the trajectory of permafrost-derived organic carbon in an evolving Arctic.

Reference

Kokelj, S.V., Tunnicliffe, J., Lacelle, D., Lantz, T.C., Chin, K.S., and Fraser, R. 2015. Increased precipitation drives mega slump development and destabilization of ice-rich permafrost terrain, northwestern Canada, Global and Planetary Change, 129: 56–68.

Lee, H., Schuur, E.A., Inglett, K.S., Lavoie, M., and Chanton, J.P. 2012. The rate of permafrost carbon release under aerobic and anaerobic conditions and its potential effects on climate, Global Change Biology, 18: 515–527.

Ping, C.L., Jastrow, J.D., Jorgenson, M.T., Michaelson, G.J., and Shur, Y.L. 2015. Permafrost soils and carbon cycling, SOIL, 1: 147–171.

Bacterial metabolism of nitrogen in Arctic soils (Hornsund Region, Svalbard) as a potential source of high nitrous oxide emissions

Julia Brzykcy[1,2], Jakub Grzesiak[2], Robert Stasiuk[1] & Renata Matlakowska[1]

[1]*Department of Geomicrobiology, Institute of Microbiology, Faculty of Biology, University of Warsaw, Warsaw, Poland*

[2]*Department of Antarctic Biology, Institute of Biochemistry and Biophysics, Polish Academy of Sciences, Warsaw, Poland*

Thawing of permafrost, induced by climate warming, leads to the release of substantial quantities of stored organic matter and mineral compounds. This accelerates the metabolic activity of soil microbiocenoses, particularly microorganisms involved in the decomposition of soil organic matter and the turnover of carbon and nitrogen, leading to the emission of greenhouse gases (GHGs) such as CO_2, CH_4, and N_2O, which create a positive feedback loop on climate (Jansson and Taş 2014). N_2O is a highly potent GHG (300 times more potent than CO_2), that also contributes to the depletion of the ozone layer (Voigt et al. 2020). N_2O emissions from soils affected by permafrost thaw in the Arctic have been recognised as among the highest from natural sources and comparable to rainforests (Altshuler et al. 2019; Repo et al. 2009).

N-cycling includes several microbiological processes, that contribute to N_2O emission (Figure 1). Primary pathways involve direct mechanisms such as denitrification, which accounts for the majority of N_2O production, and nitrifier denitrification. In addition, although to a lesser extent, nitrification, dissimilatory nitrate reduction to ammonium, and anammox may serve as indirect sources of N_2O, releasing it as a by-product. Moreover, N_2-fixation, decomposition of plant matter, and the considerable amounts of nitrogen released from permafrost contribute to the soil active layer N pool. (Butterbach-Bahl et al. 2013; Kuypers et al. 2018; Voigt et al. 2020).

Moreover, N-cycling is regulated by soil and environmental properties. Conditions that promote N_2O production are predominately: low pH, high moisture, anoxic conditions, high C and N content, especially N in mineral form, and low C:N ratio, although these relationships may exhibit variations across different sites (Voigt et al. 2020).

Those complex interactions between groups of microorganisms occurring in the soil microbiocenoses, involved in above-mentioned processes of nitrogen metabolism and environmental factors, indicate that insight into whole N-cycling is crucial to understand further Arctic soils development and implication of N_2O emissions on climate, both at local and global scales. Moreover, it is necessary to further extend the measurements to ecosystems affected by permafrost thaw, that have not been previously studied.

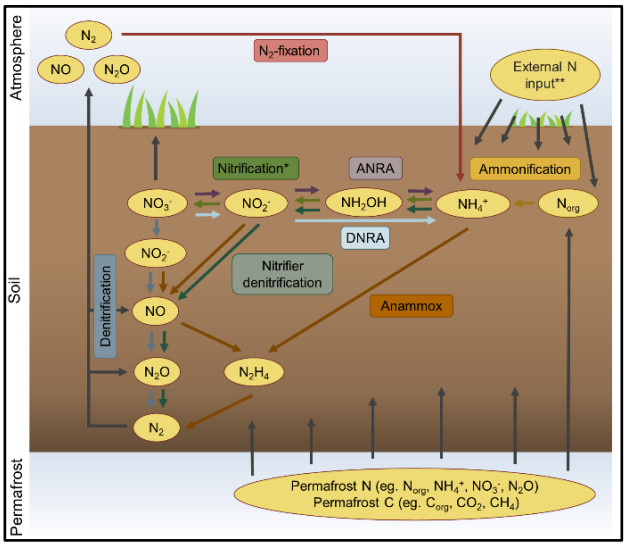

Figure 1. Hypothetical nitrogen cycling in permafrost-affected soils: main biogeochemical processes (does not include by-products). DNRA: dissimilatory nitrate reduction to ammonium, ANRA – assimilatory nitrate reduction to ammonium, *ammonia oxidation by bacteria, ammonia oxidation by archaea, nitrite oxidation by bacteria and comammox., **eg. plant and animal matter, atmospheric deposition.

The objective of this study was to examine Arctic soils, characterise their geochemical properties and microbiological community to identify areas with the highest potential to become hot spots for N_2O emission, and further investigate N-cycling using microcosm approach.

To infer the N_2O-generating potential of permafrost-affected soils, we investigated six soil habitats, reflecting the ecosystem diversity of the Arctic: ornithogenic soil (OS), Hans Glacier lateral moraine (HG), stream area (ST), patterned ground (PG), area with moss vegetation (MC) and soil under anthrophogenic impact (HS). Fieldwork was conducted in the vicinity of the Polish Polar Station Hornsund (Svalbard, High Arctic). Comprehensive interdisciplinary geochemical, microbiological, and molecular study was conducted, including obtaining

taxonomic structure, metabolic versatility, and abundance of the bacterial community. Those factors were combined with geochemical soil background, acquired by colorimetric methods, atomic absorption spectroscopy, gas chromatography (GC/MS) and CHNS elemental analysis.

The results collectively hint at the soil of ornithogenic origin (Little auk *(Alle Alle)* colony) as having the highest potential for N_2O emissions, indicated by the highest concentrations of total N, NH_4^+, NO_3^-, organic N compounds and the lowest C:N ratio of the studied sites (Figure 2). The OS microbial community showed also the highest number of OTUs, and metabolic flexibility.

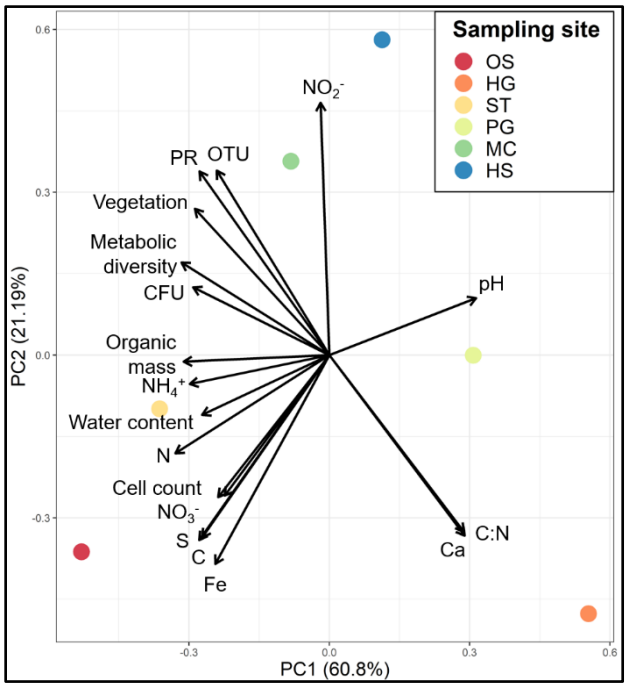

Figure 2. Principal component analysis biplot depicting the physicochemical properties, and microbiological factors. CFU: colony-forming unit on R3A medium, PR: positive responses on Community-Level Physiological Profiling array.

Further analysis included incubation of batch closed microcosms in anoxic conditions, combined with GC/MS measurements of volatile compounds and quantitative determination of concentration of mineral N compounds. Results indicate N_2O emissions from soil along with another GHG – CO_2. In addition, hydrazine – intermediate in anammox pathway was detected, as well as changes in concentration of mineral forms of N. Those results can be linked with identified bacterial taxa potentially involved in N-cycling: N_2-fixation (*Rhizobiales, Frankiales, Oscillatoriales*), nitrification (*Nitrospirae*), denitrification (*Luteitalea pratensis, Bradyrhizobium japonicum, Brachymonas denitrificans, Comamonas denitrifican, Paracoccus denitrificans, Rhodanobacter denitrificans, Pseudomonas frederiksbergensis*) and anammox (*Gemmataceae*).

The data highlight the potential of Arctic ornithogenic soils for extensive microbial N-cycling processes, which also drive increased N_2O emissions, further impacting the climate warming.

References

Altshuler, I., Ronholm, J., Layton, A., Onstott, T.C., Greer, C.W., and Whyte, L.G. 2019. Denitrifiers, nitrogen-fixing bacteria and N_2O soil gas flux in high Arctic ice-wedge polygon cryosols. FEMS Microbiology Ecology, 95(5), 1–12. doi:10.1093/femsec/fiz049

Butterbach-Bahl, K., Baggs, E.M., Dannenmann, M., Kiese, R., and Zechmeister-Boltenstern, S. 2013. Nitrous oxide emissions from soils: How well do we understand the processes and their controls? Philosophical Transactions of the Royal Society B: Biological Sciences, 368(1621). doi:10.1098/rstb.2013.0122

Jansson, J.K., and Taş, N. 2014. The microbial ecology of permafrost. Nature Reviews Microbiology, 12(6), 414–425. doi:10.1038/nrmicro3262

Kuypers, M.M.M., Marchant, H.K., and Kartal, B. 2018. The microbial nitrogen-cycling network. Nature Reviews Microbiology, 16(5), 263–276. doi:10.1038/nrmicro.2018.9

Repo, M.E., Susiluoto, S., Lind, S.E., Jokinen, S., Elsakov, V., Biasi, C., Virtanen, T., and Martikainen, P.J. 2009. Large N_2O emissions from cryoturbated peat soil in tundra. Nature Geoscience, 2(3), 189–192. doi:10.1038/ngeo434

Voigt, C., Marushchak, M.E., Abbott, B.W., Biasi, C., Elberling, B., Siciliano, S.D., Sonnentag, O., Stewart, K.J., Yang, Y., and Martikainen, P.J. 2020. Nitrous oxide emissions from permafrost-affected soils. Nature Reviews Earth & Environment, 1(8), 420–434. doi:10.1038/s43017-020-0063-9

Changes in microbial community composition and physiology in thawing Yedoma induced by rhizodeposits

André Craveiro Pereira Coelho Faust[1], Christoph Rosinger[2,3], Jan Olaf Melchert[1] & Janet Rethemeyer[1]

[1]*Institute for Geology and Mineralogy, University of Cologne, Cologne, Germany*

[2]*Institute of Soil Research, University of Natural Resources and Life Sciences Vienna, Vienna, Austria*

[3]*Institute of Agronomy, University of Natural Resources and Life Sciences Vienna, Tulln an der Donau, Austria*

The ice-rich permafrost sediments that were deposited in the unglaciated areas during the Pleistocene, known as Yedoma, are particularly susceptible to rapid thaw, which can quickly expose large amounts of organic carbon (OC) to microbial decomposition, which in turn leads to the emission of climate-relevant greenhouse gases. It is suspected that the release of this ancient sedimentary OC, particularly by abruptly occurring thaw processes, which are most relevant in the Yedoma area, could be a "tipping element" for the future climate.

The availability of OC in permafrost to microbial degradation is controlled by its molecular composition, the composition of the microbial community and its response to permafrost thaw. Several studies indicate an overall high bioavailability because the material was freeze-locked and, as a result, not subjected to stronger decompositional processes during the Holocene. Previous analyses of microbial communities in deep Yedoma permafrost conducted so far indicate an active but less diverse microbial community. After thawing and exposure of the Yedoma sediments, suitable conditions may activate the dormant microbial communities and change OC decompositions significantly. In addition, Arctic warming will increase the vegetation cover, releasing larger amounts of easily accessible OC and nitrogen through root exudates and plant litter that may accelerate the decomposition of OC in thawed Yedoma. The extent of priming-induced microbial decomposition of ancient OC is however not yet well understood.

In this study, we address this issue by analysing the diversity and activity of the microbial community at different sites on a retrogressive thaw slump comprising freshly thawed Yedoma and mixed Pleistocene and Holocene sediments. We simulate the effect of vegetation growth and related input of rhizodeposits in an aerobic incubation experiment and measure changes in microbial community structure and physiology using different microbial indicators. The data are compared with an existing dataset including bulk sedimentary data, CO_2 fluxes and ^{14}C ages of CO_2.

Methods

The thaw slump is located in the southern part of the Lena River Delta on the Kurungnakh Island Ice Complex in Northeastern Siberia. It comprises Pleistocene-age Yedoma overlain by Holocene polygonal tundra. Study sites on the thaw slump include two thaw mounds of Pleistocene Yedoma and one site on the slump floor containing a mixture of Pleistocene Yedoma and eroded Holocene sediments. Samples were collected during summer in the active thaw layer in 10 cm increments at each site down to the permafrost table. To simulate the effect of rhizodeposition in a warming arctic, samples were amended with a mixture of glucose, cellulose, amino acids and proteins in amounts equivalent to either 1% or 4% OC and incubated at 10°C for 6 weeks.

The microbial community is characterised by bacterial and fungal membrane phospholipid fatty acids. Microbial physiology is assessed by means of CO_2 production during the incubation as well as bacterial and fungal growth rates, determined via the amount of ^{3}H-leucine and ^{14}C-acetate incorporated into bacterial proteins and fungal ergosterol, respectively. Furthermore, enzymatic activities are measured fluorometrically for six specific enzymes targeting carbon, nitrogen and phosphorous containing molecules. Lastly, microbial carbon-use efficiency is evaluated by converting bacterial and fungal growth rates into carbon units and relating it to the amount of carbon respired.

Preliminary results and outlook

The undisturbed Yedoma exposed as thaw mounds and the site where Pleistocene-age Yedoma and Holocene sediments were mixed differ considerably in the elemental composition and CO_2 fluxes measured in the field. The thaw mounds contain less OC (1-2%) compared to the site on the slump floor, where Holocene and Pleistocene sediments were mixed (4-6%). Total N contents were slightly higher in the mixed sediment than in the two thaw mounds corresponding to OC/N ratios of 14-17 and 9-14, respectively indicating a lower stage of organic matter degradation at the slump floor site due to admixtures of

fresh OC from the Holocene terrace. Despite the more advanced state of degradation and lesser OC in the thaw mound, CO_2 fluxes were higher suggesting that decomposer communities may have specifically adapted their composition, size and activity to each site. The ongoing incubation experiment will reveal how the observed differences in organic matter quality influence the microbial community structure and physiology and may explain the differing CO_2 fluxes. In addition, these parameters will change in a warming world where the thawed Yedoma will be vegetated and OC mineralisation will be affected due to carbon and nutrient inputs from roots changing the substrate composition. Fungal and bacterial growth rates will provide insight into the consequences these inputs have on the two decomposer groups, thus revealing potential current carbon or nutrient limitations. Lastly, microbial carbon-use efficiency as well as enzymatic activity will reveal the quality of available OC and nutrients, since recalcitrant compounds require a greater investment in extracellular enzymes before uptake.

FINANCIAL SUPPORT

This study has been financed by the Federal Ministry of Education and Research (BMBF, grant no. 03F0764E and 03F0834D) of Germany.

Nitrogen pools and turnover processes in the land-water transition in two Arctic rivers

Wasi Hashmi[1], Meret Carstensen[2], Marit Ebbinghaus[2], Johanna Kerttula[1], Lukas Kohl[1], Carlos Palacin Lizarbe[1], Jukka Pumpanen[1], Tina Sanders[4], Henri M.P. Siljanen[1], Carolina Voigt[2], Claudia Fiencke[2,3] & Maija E. Marushchak[1]

[1]*Department of Environmental and Biological Sciences, University of Eastern Finland, Kuopio, FI-70210, Finland*

[2]*Institute of Soil Science, Universität Hamburg, Allende-Platz 2 20146 Hamburg, Germany*

[3]*Center for Earth System, Research and Sustainability (CEN) Universität Hamburg, Allende-Platz 2 20146 Hamburg, Germany*

[4]*Institute of Carbon Cycles, Helmholtz-Zentrum Hereon, D-21502 Geesthacht, Germany*

Climate change is altering the biogeochemical cycles in the Arctic, including the terrestrial nitrogen (N) cycle. Nitrogen is of importance, as it is the primary limiting nutrient in Arctic soils. The warming of the Arctic ecosystem has resulted in vast amounts of N being liberated from permafrost and soil organic matter, and part of it may end up in Arctic rivers via leaching and erosion (Sanders et al. 2021). Warmer temperatures may also lead to an increase in N mineralization, catalyzed by microorganisms, which may further result in enhanced nitrification (Ramm et al. 2022). Further impacts are being observed on the liberation of greenhouse gases, such as significant amount of nitrous oxide (N_2O), from these soils (Voigt et al. 2020).

Fluvial soils are important for N cycling, as they represent the land-water transition zone, where terrestrial N leaching from terrestrial ecosystems may be processed before entering into aquatic ecosystems. N losses in form of gaseous emissions may also occur due to higher N availability for mineral N turnover such as nitrification and denitrification as a result of low vegetation (Fiencke et al. 2022). Furthermore soil moisture supports N_2O emissions by forming a gradient between dry to water-logged areas.

In this study we therefore, explored the spatial variability in the N pools and microbial turnover processes in Arctic Fluvisols with the aim to better understand the fate of N in this land-water transition zone.

LOCATION

We collected fluvial soil samples from Teno river Finland (69.6°N, 25.9°W) (Figures 1 and 2) in July 2023 and Disko Island, Western Greenland (69.16°N, 53.28°W) (Figure 3) in September 2023. From Teno riverbank we sampled:

- Unvegetated sandbank between the main river and a river arm.
- A vegetated riverbank in main river shore.

In Greenland we sampled vegetated and bare sites next to a small river. The soil sampling sites represent the same latitude.

Figure 1. Teno River, Northern Finland (Hashmi 2023).

Figure 2. Satelite image (from Google Maps 2023) with highlighed sampling points in Teno river, Northern Finland.

Figure 3. Disko Island, Western Greenland (Fienkcle 2023)

Material and methods

We determined the mineral N, dissolved organic nitrogen (DON) and total soil N pools, as well as the content of dissolved organic carbon (DOC) and total soil carbon (C) in the riverine soil samples. We further determined both net and gross rates of mineralization and nitrification using isotope pools dilution assays. To determine the production of greenhouse gases (carbon dioxide, methane and N_2O), we incubated the soils at field moisture at 5°C for two weeks under both oxic and anoxic conditions.

Moreover, Microbial samples were taken to analyze abundance and expression of ammonia monooxygenase (amoA) gene diversity, associated with the first step of nitrification

Preliminary results

The mineral N turnover rates showed substantial variability between the studied fluvial soils. In oxic conditions, we observed N_2O uptake or small N_2O emissions, while in anoxic conditions N_2O emissions were commonly found from both Finnish and Greenlandic fluvial soils. Methane production was observed only in distinct samples. The results altogether show the role of Arctic fluvial soils as sites of active mineral N turnover.

Funding

This work was funded by DAAD program (German Academic Exchange Service & the Academy of Finland) in the frame of the FinNcycle-project and the Academy of Finland project Thaw-N (No. 349503).

References

Fiencke, C., Marushchak, M.E., Sanders, T., Wegner, R., and Beer, C. 2022. Microbiogeochemical traits to identify nitrogen hotspots in permafros regions, Nitrogen, 3: 458–501. doi:0.3390/nitrogen3030031

Ramm, E., Liu, C., Ambus, P., Butterbach-Bahl, K., Hu, B., Martikainen, P.J., Marushchak, M.E., Mueller, C.W., Rennenberg, H., Schloter, M., Siljanen, H.M.P., Voigt, C., Werner, C., Biasi, C., and Dannenmann, M. 2022. A review of the importance of mineral nitrogen cycling in the plant-soil-microbe system of permafrost-affected soils—changing the paradigm, Environmental Research Letters, 17: 1–35. doi:10.1088/1748-9326/ac417e.

Sanders, T., Fiencke, C., Fuchs, M., Haugk, C., Juhls, B., Mollenhauer, G., Ogneva, O., Overduin, P., Palmtag, J., Povazhniy, V., Strauss, J., Tuerena, R., Zell, N., and Dähnke, K. 2021. Seasonal nitrogen fluxes of the Lena River Delta, Ambio, 51: 423–438. doi:10.1007/s13280-021-01665-0

Voigt, C., Marushchak, M.E., Abbott, B.W., Biasi, C., Elberling, B., Siciliano, S.D., Sonnentag, O., Stewart, K.J., Yang, Y., and Martikainen, P.J. 2020. Nitrous oxide emissions from permafrost-affected soils, Nature Reviews Earth & Environment, 1: 420–434. doi:10.1038/s43017-020-0063-9

Synthesizing thaw microbiomes: Development of a thaw database and initial results

Mark D. McDonald[1], Sarah Bagby[2], Christopher C.M. Baker[3], Robyn Barbato[3], Jiri Barta[4], James Bradley[5], Stacey J. Doherty[3], Liam Heffernan[6], Rebecca Hewitt[7], Hannah Holland-Moritz[1,8], Mincheol Kim[9], Joy O'Brien[10], Ursel Schütte[11], Katherine Shek[1], Tatiana Vishnivetskaya[12], Jana Voříšková[13] & Jessica Ernakovich[1,8]

[1]*Department of Natural Resources and the Environment, University of New Hampshire, Durham, New Hampshire, United States*

[2]*Department of Biology, Case Western Reserve University, Cleveland, Ohio, United States*

[3]*U.S. Army Cold Regions Research and Engineering Laboratory, Hanover, New Hampshire, United States*

[4]*Centre for Polar Ecology, University of South Bohemia, Ceske Budejovice, Czech*

[5]*School of Geography, Queen Mary University of London, London, United Kingdom*

[6]*Department of Ecology and Genetics, Uppsala University, Uppsala, Sweden*

[7]*Department of Environmental Studies, Amherst College, Amherst, Massachusetts, United States*

[8]*Center of Soil Biogeochemistry and Microbial Ecology, University of New Hampshire, Durham, New Hampshire, United States*

[9]*Division of Life Science, Korea Polar Research Institute, Incheon, South Korea*

[10]*Department of Biology, Indiana University Bloomington, Bloomington, Indiana, United States*

[11]*Institute of Arctic Biology, University of Alaska Fairbanks, Fairbanks, Alaska, United States*

[12]*Department of Microbiology, University of Tennessee, Knoxville, Tennessee, United States*

[13]*Department of Microbiology, The Czech Academy of Sciences, Prague, Czech*

Microorganisms play an important role in the biogeochemistry of permafrost such as the degradation of organic matter, nutrient cycling, and their active transformation of substrates within the salty, water-veins of frozen permafrost. However, as permafrost thaws due to global climate change, the microbial communities' structure and function will be altered, potentially resulting in greater production of greenhouse gases and further exacerbation of climate change. Over the last 15 years, a plethora of studies have examined the changes in permafrost microbial community structure and/or function following permafrost warming at single or, at most, a handful of locations. Thus, we can now synthesize these data into a database of relevant studies to seek generalizable trends in microbial responses to thaw across permafrost-affected soils. The initial goal of this database and synthesis study is to develop estimates and predictions of how the structure of the microbiome—as well as its emergent functions—respond under warming permafrost conditions.

We envision that the Permafrost Thaw Microbiome Database will serve as a catalyst and resource for future studies examining thaw dynamics. To accomplish this, we aim to harmonize microbial datasets (amplicon and metagenomic data), bioinformatic pipelines, and metadata across the database, which may then serve as a template for data collection during future explorations into permafrost thaw dynamics.

Methods and current work

Work on this database began prior to 2020 and resumed in early 2023. The work is being conducted under the guidance of the Permafrost Microbiome Network; a working group comprised of several dozen permafrost microbial scientists from around the globe.

Our initial criteria for inclusion in the database included three specific criteria (as discerned from reading the abstract): 1) the data is from permafrost-affected soils; 2) the soils must have undergone thaw (lab thaw, experimental field thaw, or natural thaw); and 3) the study must have analyzed microbial sequencing data (amplicon or metagenomes) collected both pre- and post-thaw. However, as we began to vet research article abstracts, we came to the consensus that a more pluralistic database regarding thaw in the permafrost-affected regions would likely be more beneficial to the public. As such, several studies we plan to include are not necessarily permafrost-affected, or do not have a thaw component.

As of December 2023, more than 450+ studies have been vetted for inclusion in the database. The studies meeting all three criteria as identified by our initial vetting are summarized in Figure 1. At least 55 studies fully met all criteria for inclusion in the database. Of these, the majority of studies (36) included natural thaw (either along a thaw gradient or over time). Another 12 studies contained thaw that was generated in a laboratory setting, mostly during controlled incubations of permafrost soil. Seven studies included thaw

generated as part of in-situ experiments with thaw/warming. Finally, 6 studies fully passing the initial vetting do not contain a thaw component ("NA" category for "Yes"). These 6 studies were identified to contain microbial data that would be highly useful for future database analyses.

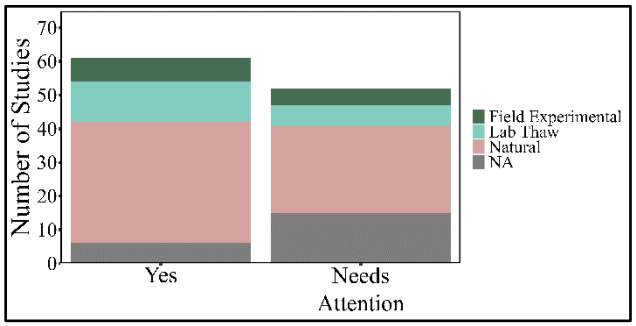

Figure 1. Summary of studies meeting all vetting criteria for inclusion in the thaw database. Studies in the "Yes" column with the category "NA" did not have a thaw component. Studies in the "Needs Attention" column with the category "NA" either did not contain thaw, did not indicate a thaw type in the abstract text, or indicated a thaw type that was not easily categorized into one of the three thaw types.

Fifty-two studies initially appearing to meet the vetting requirements will require further investigation ("Needs attention" column in Figure 1). These studies were denoted as "Needs Attention" if some aspect of the vetting criteria was unclear from the abstract text. These studies, along with all studies passing initial vetting, will be further annotated to harvest the appropriate metadata and confirm their inclusion in the database.

Many of the rejected studies included valuable information regarding soil physicochemical changes associated with thaw but did not meet the criteria for appropriate microbial data—metagenomes or marker genes (16S, ITS/18S). These studies highlight the extensiveness of the work being conducted on permafrost thaw and represent the potential for increasing our engagement of non-microbial permafrost scientists interested in the outcomes of thaw.

Several studies initially excluded from the database were associated with either water columns or sediments from thermokarst lakes. These studies often contained the appropriate microbial data types and were associated with some type of thaw but have been initially excluded because they are not "soils" in the traditional sense. We are still internally discussing whether these types of studies would be useful to include in the database, and plan to further discuss their utility with other permafrost microbial and non-microbial scientists.

PLANS FOR THE DATABASE

The remainder of the database will be vetted and annotated throughout the winter of 2023-2024. The collection and annotation of metadata will be completed in Spring 2024 and will include both study-level metadata (GPS coordinates, thaw type, vegetation, etc.) and sample-specific data where available (soil physicochemistry, depth, length of thaw, primer sets, etc.). The bioinformatic pipelines to be used for the initial synthesis and analysis of the data are being discussed at the time of writing and should be fully developed by the time this conference paper is presented. Finally, we anticipate some initial analyses of community structure pre- and post-thaw by Summer 2024 and aim to include these initial findings in our conference presentation.

The initial manuscript to be developed from this study will comprise a thorough investigation into the complex changes in microbiome composition and function following permafrost thaw, with particular interest in identifying phylogenetic patterns and characteristics that are predictive of the observed changes in post-thaw communities.

We have identified several initial variables of interest that may aid in explaining these patterns including geographically defined ecotypes, vegetation cover type, permafrost type and/or mineral content, depth of permafrost table, moisture availability and redox potential, mean annual temperature, permafrost formation processes, landscape position, and carbon and nitrogen content.

SUMMARY

We have begun the development of a comprehensive database of microbially-focused permafrost thaw studies from high latitude and high-altitude permafrost environments. The work is currently underway, with the majority of initial study vetting completed as of December 2023. Our initial analysis will include a comprehensive reporting of permafrost microbial communities' diverse responses to thaw across the vast regions covered within this database. This synthesis will aid in both our general understanding of how microbial communities will change under climate change scenarios, and potentially help identify areas where this change may cause major shifts in carbon loss.

Finally, we hope to catalyze community engagement with the thaw database and to gather thoughts and suggestions from the permafrost community at-large to help refine and guide the detailed questions we can address with this database.

Is the air in northern Alaska influenced by thawing permafrost? ARCSPIN project overview and possible implications

Marina Nieto-Caballero[1], Kevin R. Barry[1], Thomas C.J. Hill[1], Thomas A. Douglas[2], Christina S. McCluskey[3], Paul J. DeMott[1], Sonia M. Kreidenweis[1] & Jessie M. Creamean[1]

[1]*Department of Atmospheric Science, Colorado State University, Fort Collins, Colorado, United States*

[2]*Cold Regions Research and Engineering Laboratory, U.S. Army ERDC, Fairbanks, Alaska, United States*

[3]*National Center for Atmospheric Research (NCAR), Boulder, Colorado, United States*

Arctic air temperatures are rising up to four times faster than the global rate, rapidly thawing elements of the cryosphere (Rantanen et al. 2022) such as permafrost (i.e., earth materials continuously frozen for at least two years), including melting of ice wedges (i.e., frozen surface water accumulated into ground cracks). Thawed permafrost can be introduced into water systems (Matheus Carnevali et al. 2015) by thermokarst lake (TKL) formation, coastal erosion, and increasingly common permafrost thaw slumps and landslides. Ultimately, these terrestrial elements can be released to the atmosphere through mechanisms such as greenhouse gas bubble-bursting and bubble-bursting from wind-induced wave action on lakes, lagoons, and the open ocean. Once airborne, terrestrial biological particles can be a source of ice nucleating particles (INPs) that can facilitate cloud ice formation at temperatures ≥ -15°C, having the potential to alter cloud properties and dynamics, the radiation budget, and regional climate. Terrestrial particles from permafrost are known to be highly enriched with INPs (Creamean et al. 2020) and persistent in the environment (Barry et al. 2023), highlighting the importance of understanding bioaerosol sources in the region and their implications, particularly for arctic mixed-phase clouds (AMPCs), which are highly sensitive to the quantity and characteristics of INPs, and hence, INP sources.

RESULTS AND DISCUSSION

Here, we present DNA results (16S rRNA gene) and INP spectra from a broad range of samples collected during the ARCtic Study of Permafrost Ice Nucleation (ARCSPIN) field campaign in the Utqiaġvik region (Alaska, U.S.) in September 2021. Samples analyzed include air and multiple potential local bioaerosol sources, such as water bodies (i.e., ocean, lagoon, and thermokarst lake water), terrestrial (i.e., active layer, permafrost, ice wedge, landslide and sediment), and vegetation samples. Microbial taxa show overlap between air samples and the potential local sources (Figure 1), suggesting that part of these bioaerosol populations (i.e., particles of biological origin) have local sources in the region.

Microbial source tracking was performed with SourceTracker2 (Knights et al. 2011). Results show how air collected near different water bodies in Northern Alaska was strongly influenced by seawater and terrestrial elements (Figure 2). In particular, 1) bioaerosols collected near coastal regions were highly influenced by coastal waters and their sediments, 2) air collected near the Elson Lagoon, where terrestrial runoff is visible on satellite, showed terrestrial elements (including permafrost and ice wedges) as predominant sources, and 3) bioaerosols collected near thermokarst lakes were influenced by these water bodies (freshwater), as well as terrestrial elements (soil/frozen soil), and vegetation.

Air				
Water	13.8%			
Foam	7.51%	13.5%		
Terrestrial	20.3%	14.6%	11.9%	
Vegetation	4.11%	1.2%	1.2%	11.8%
	Air	Water	Foam	Terrestrial

Figure 1. Percentage of amplicon sequence variants (ASVs) shared between different sample types, including air, foam, water, vegetation, and terrestrial elements.

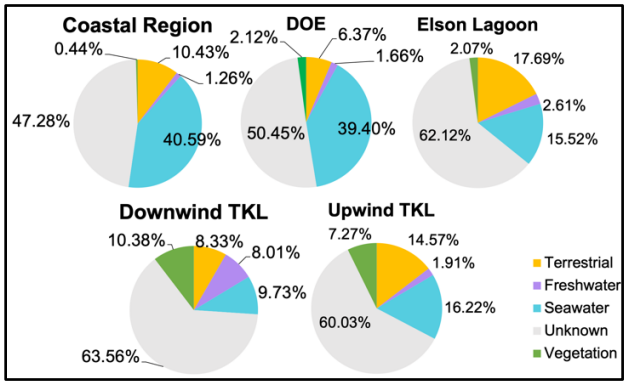

Figure 2. Microbial source tracking of bioaerosol samples with potential local source contribution. Colors correspond to the assessed local sources of bioaerosols in the region.

In addition, the percentage of unknown bioaerosol sources near TKLs shows an inverse linear correlation with wind speed during the time of sampling (multiple correlation coefficient R = 0.830, p-value = 0.021). These lakes were additionally assessed for INP release, by sampling air upwind and downwind of the lakes. INP analysis confirmed that these abundant water bodies in Northern Alaska can enrich the lower atmosphere with INPs (Figure 3). Additionally, total organic carbon (TOC) analysis was performed, showing a positive correlation with INP concentrations. These measures allow for the integration of our results into climate models such as the Community Earth System Model (CESM) to predict climate simulations.

With the ARCSPIN multidisciplinary project we aim to integrate microbiology, atmospheric science, and modeling to gain insight into how the increasing permafrost thawing can be introduced to the lower atmosphere, and how it can affect cloud formation, precipitation, and climate patterns in the region.

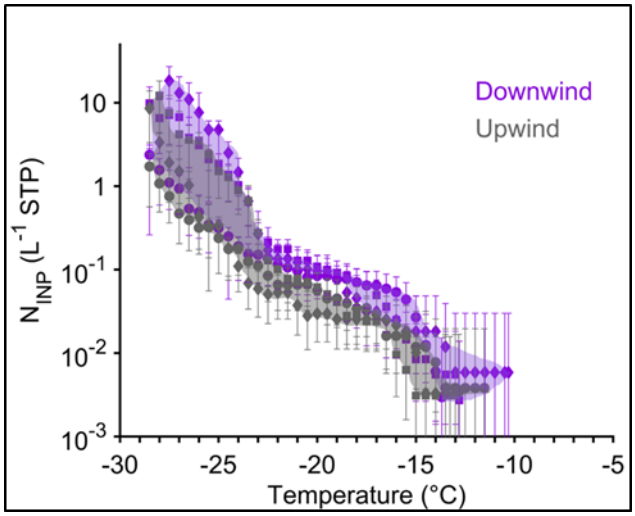

Figure 3. Cumulative INP activation spectra downwind (purple) and upwind (gray) of thermokarst lakes shows an INP enrichment downwind of the lakes.

REFERENCES

Barry, K.R., Hill, T.C.J., Moore, K.A., Douglas, T.A., Kreidenweis, S.M., DeMott, P.J., and Creamean, J.M. 2023. Persistence and Potential Atmospheric Ramifications of Ice-Nucleating Particles Released from Thawing Permafrost. Environmental Science & Technology 57(9): 3505–3515. doi:10.1021/acs.est.2c06530

Creamean, J.M., Hill, T.C.J., DeMott, P.J., Uetake, J., Kreidenweis, S., and Douglas, T.A. 2020. Thawing permafrost: an overlooked source of seeds for Arctic cloud formation. Environmental Research Letters 15(8): 084022. doi:10.1088/1748-9326/ab87d3

Knights, D., et al. 2011. Bayesian community-wide culture-independent microbial source tracking. Nature Methods 8(9): 761–763. doi:10.1038/nmeth.1650

Matheus Carnevali, P.B., et al. 2015. Methane sources in arctic thermokarst lake sediments on the North Slope of Alaska. Geobiology 13(2): 181–197. doi:10.1111/gbi.12124

Rantanen, M., et al. 2022. The Arctic has warmed nearly four times faster than the globe since 1979. Communications Earth & Environment 3(1): 168. doi:10.1038/s43247-022-00498-3

Microbial responses to retrogressive thaw slumping in aquatic systems on the Peel Plateau, NT, Canada

Marina Taskovic[1], Maria A. Cavaco[2], Maya P. Bhatia[2], Brian D. Lanoil[1] & Suzanne E. Tank[1]

[1]*Department of Biological Sciences, University of Alberta, Edmonton, Alberta, Canada*

[2]*Department of Earth and Atmospheric Sciences, University of Alberta, Edmonton, Alberta, Canada*

The metabolism of terrestrial organic carbon is central to biogeochemical cycling and food web dynamics. In streams, heterotrophic microorganisms are drivers of carbon cycling, providing energy (i.e., carbon) to organisms through the decomposition of organic matter. The composition of organic matter and environmental conditions are strong determinants of microbial community composition, which can affect the metabolic pathways of organic carbon that contribute to carbon outgassing through respiration (i.e., CO_2, CH_4) and the microbial biomass available to higher trophic level organisms. As such, assessing the variation in microbial communities and how organic carbon and environmental factors influence community structure and function is central to understanding the effects of global change on food web dynamics and biogeochemical cycling.

Across the circumpolar regions of the world, the impacts of amplified climate warming are exacerbated in northern landscapes underlain by ice-rich permafrost that, upon thaw, results in thermokarst development (i.e., land subsidence) (Kokelj et al. 2021). Thermokarst dramatically alters the terrain, resulting in landforms such as retrogressive thaw slumps that lead to substantial sedimentary fluxes and disruptions to hydrological flow paths. In the ice-rich, glacially conditioned Peel Plateau region of western Canada, retrogressive thaw slumps have rapidly increased in intensity and frequency in conjunction with summer warming and precipitation. The sedimentary and geochemical fluxes from thaw slumps have profound effects on water chemistry and the composition of organic matter in immediate downstream systems, such that the concentration of particulate nutrients and organic carbon (POC) increases relative to dissolved fractions (including dissolved organic carbon; DOC), but with POC that is more degraded and recalcitrant (Shakil et al. 2020). The dominance of particulate organic matter downstream of thaw slumps may influence the structure and function of microbial communities in impacted systems. While there is evidence that POC from thaw slumps is subject to low degradation rates, these findings may be confounded by chemolithotrophy (Shakil et al. 2022), leaving uncertainties concerning the biotic fate of organic carbon in these systems. To better understand the ecological implications of thaw slumping for impacted systems, the structure and function of microbial communities must be assessed.

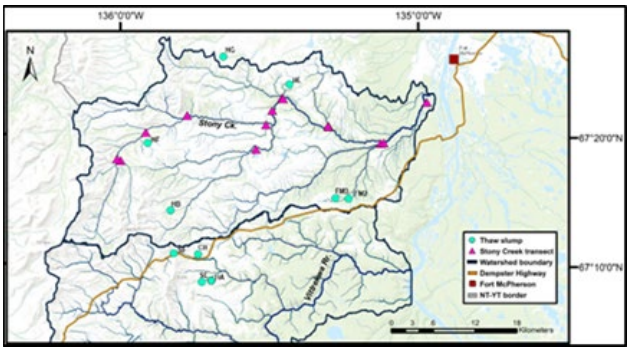

Figure 1. Map of retrogressive thaw slump sites and transect within the Stony Creek and Vittrekwa River watersheds on the Peel Plateau.

This work examines how thaw slumping affects microbial ecology by exploring the relationships between community composition (16S rRNA gene sequencing) and growth (biomass production via tritiated-leucine incorporation) within the stream environment, emphasizing the effects of organic matter composition and water chemistry. Sampling efforts focused on a series of ten thaw slumps in the Stony Creek and Vittrekwa River watersheds (Figure 1), where a rapid increase in the frequency of thaw slumps coupled with a fluvially-incised terrain has intensified downstream connectivity. Between June–August 2022 and 2023, we collected samples from thaw slump runoff and upstream and downstream of the slump debris inflow. In addition, we sampled a transect of Stony Creek from headwaters, inflowing tributaries, and along the main channel. Starting in the Richardson Mountains, the transect extended eastward to the outlet into the Peel River (Figure 1), effectively capturing a gradient of increasing thaw slump activity that reflects the transition from an unglaciated to glacially conditioned terrain across the watershed. While thaw slump activity on the Peel Plateau is most pronounced along headwaters, by expanding our sampling approach to the watershed scale, we recognize the interconnected nature of stream systems and can examine ecological responses as sedimentary materials and geochemical effects propagate through aquatic networks (Kokelj et al. 2021).

FINDINGS

Across thaw slump sites, the influx of sedimentary materials defined a disturbance gradient (Comp. 1, Figure 2) such that thaw slump runoff and downstream systems had greater concentrations of total suspended solids (TSS), total and dissolved nitrogen (TDN, TN), ammonium (NH_4^+), total phosphorus (TP), and major ions (Ca^{2+}, SO_4^{2-}, Mg^{2+}) (Figure 2) that reflect previously reported trends (e.g., Shakil et al. 2020). However, bacterial biomass production did not track with
this disturbance gradient and was found to be significantly correlated with DOC, which does not follow consistent trends in concentration across slump site sampling locations, unlike POC (Shakil et al. 2020). In downstream, receiving waters along Stony Creek, bacterial production responses in 2022 and 2023 continued to track DOC concentrations and consistently increased along the main channel to the Peel River. While DOC is known to be a bioavailable energy source to microorganisms, these observations highlight uncertainties for a region where aquatic systems show orders of magnitude increases in POC at sites impacted by retrogressive thaw slumps.

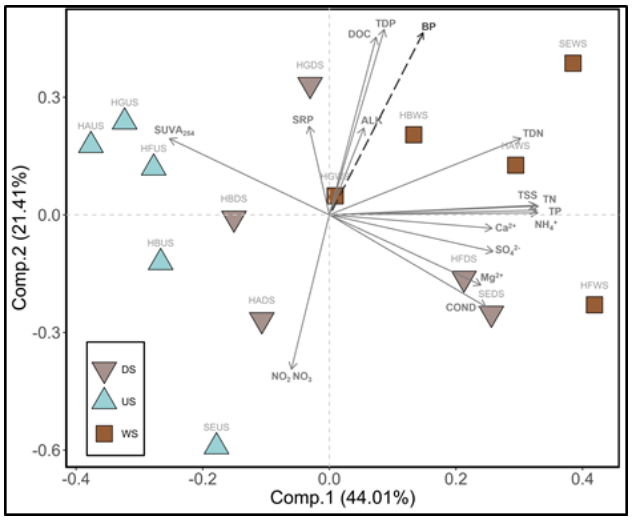

Figure 2. Principal component analysis results for water chemistry and dissolved organic matter (DOC, SUVA254) in thaw slump runoff and stream water (US = upstream, WS = within-slump, DS = downstream). Bacterial biomass production (BP) was correlated to the ordination axes and projected onto the ordination as a vector.

Our interpretation of bacterial biomass production across the study systems will be refined by future incorporation of particulate organic matter concentrations (POC, particulate nitrogen; PN) and molecular characterization of DOM using a parallel factor analysis model (PARAFAC) from absorbance and fluorescence spectra. In addition, ongoing 16S rRNA gene sequencing of stream microbial communities will allow us to assess how organic matter and stream chemistry may control community composition and further enhance our understanding of observed bacterial production in streams.

This work aims to further quantify biotic processes in aquatic systems impacted by thaw-driven mass wasting on the Peel Plateau. This knowledge will be crucial to accurately predict the effects of ongoing permafrost thaw on the carbon cycle and microbially driven freshwater ecosystem services intrinsic to northern communities' culture, sustenance, and economy.

ACKNOWLEDGEMENTS

This research supported by the Northern Scientific Training Program (POLAR Canada), UAlberta North, and Weston Family Award in Northern Research (MT); and NSERC, ArcticNet, and Campus Alberta Innovates Program grants awarded to SET and BDL.

REFERENCES

Kokelj, S.V., Kokoszka, J., van der Sluijs, J., Rudy, A.C.A., Tunnicliffe, J., Shakil, S., Tank, S.E., and Zolkos, S. 2021. Thaw-driven mass wasting couples slopes with downstream systems, and effects propagate through Arctic drainage networks, The Cryosphere, 15: 3059–3081. doi:10.5194/tc-15-3059-2021

Shakil, S., Tank, S.E., Kokelj, S.V., Vonk, J.E., and Zolkos, S. 2020. Particulate dominance of organic carbon mobilization from thaw slumps on the Peel Plateau, NT: Quantification and implications for stream systems and permafrost carbon release, Environmental Research Letters, 15(114019). doi:10.1088/1748-9326/abac36

Shakil, S., Tank, S.E., Vonk, J.E., and Zolkos, S. 2022. Low biodegradability of particulate organic carbon mobilized from thaw slumps on the Peel Plateau, NT, and possible chemosynthesis and sorption effects, Biogeosciences, 19: 1871–1890. doi:10.5194/bg-19-1871-20

Top and subsoil microbial communities along environmental and spatial gradients in high Arctic tundra

Bjorn Tytgat[1], Ruben Van Daele[1], Maaike Dhondt[1], Jill De Visscher[1], Lotte De Maeyer[1], Josef Elster[2,3], Wim Vyverman[1] & Elie Verleyen[1]

[1]*Laboratory of Protistology & Aquatic Ecology, Ghent University, Gent, Belgium*

[2]*Centre for Polar Ecology, University of South Bohemia, Ceske Budejovice, Czech Republic*

[3]*Phycology Centre, Institute of Botany, Czech Academy of Science, Trebon, Czech Republic*

High-Arctic soils are dominated by microorganisms, which are the main primary producers in these (semi-)arid environments. Here, microorganisms are typically assembled into biological soil crusts (BSCs), which form quickly after deglaciation. As early colonizers of barren soil, they therefore initiate succession and ultimately facilitate the establishment of higher plants (Barrera et al. 2022). Indeed, they are considered as ecosystem engineers, since they provide ecosystem services such as water retention, temperature regulation, soil stability and soil erosion resistance (Belnap and Lange 2001). These assemblages also play a key role in nutrient and carbon cycling, and the associated fluxes of greenhouse gases such as carbon dioxide, methane and nitrous oxide.

Despite the importance of microbial communities in these changing environments, the influence of environmental properties such as water content, soil texture, nutrient availability and other edaphic factors related to the underlying bedrock on the diversity and community structure of these microbiomes remains, however, poorly understood. Studies typically focus on small spatial scales and hence environmental gradients, and tend to focus on topsoil bacterial communities, while the eukaryotic and sub-soil components are largely neglected. The relative importance of regional and local factors on the microbial community structure in these soils is therefore largely unknown. This is, however, particularly relevant in this era of climate change, with higher temperatures deepening the active layer and extending the timeframe for heterotrophic activity. In turn, this is predicted to result in higher emissions of greenhouse gases due to the increased microbial breakdown of organic matter stored in permafrost soils. Gathering knowledge on these factors is thus important, since responses to climate change might differ depending on the local community composition, including interactions between prokaryotes and eukaryotes, and environmental conditions.

Here, we studied the top (1 cm) and sub-soil (5-10 cm depth) microbial communities at both large and small spatial scales using a metabarcoding approach (Illumina MiSeq v.3) targeting both bacteria and micro-eukaryotes – including Fungi – using general 16S and 18S rRNA primers. We compared 12 regions in Spitsbergen (western Svalbard), from 78 to 79.5° N (Figure 1), differing in bedrock type.

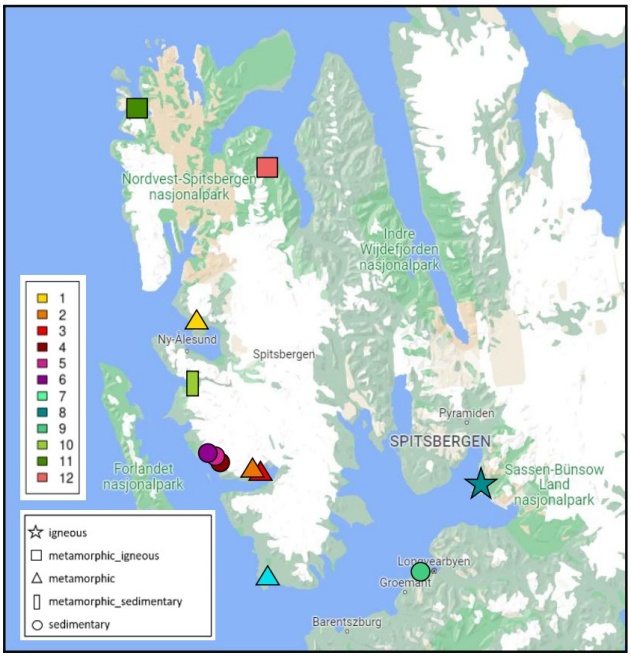

Figure 1. Sampling locations in western Svalbard (colors), with main bedrock type of each location (symbols).

In each site, we compared the microbial community composition along three different stages of soil and vegetation development. Since nitrogen is often a limiting nutrient in these fairly oligotrophic environments, we also investigated the occurrence and diversity of nitrogen fixing (nifH) and nitrite reduction (nirS) genes using dedicated primer sets.

Results

Surface and subsurface layers harbour strikingly different microbial communities for both bacteria and micro-eukaryotes within the sites. At large spatial scales, distance between sites, bedrock type and

related factors, exert, however, a greater impact on the community structure than the different conditions between the surface and subsurface layers. For nifH, however, more overlap between sites was apparent, while differences between top and sub-soil were more pronounced in the sequence diversity of this gene. In general, Chlorophyta and Ciliophora had opposite trends along the vegetation cover gradient. Ciliophora showed the highest average abundance in well-developed vegetation, while Chlorophyta were more abundant in BSCs. Cyanobacteria were also more abundant here, especially in moist conditions.

Given the importance of bedrock type on the microbial community structure, we expect that communities on different bedrock types might respond differently to the predicted changes in temperature and precipitation patterns.

REFERENCES

Barrera, A., Acuña-Rodríguez, I.S., Ballesteros, G.I., Atala, C., and Molina-Montenegro, M.A. 2022. Biological Soil Crusts as Ecosystem Engineers in Antarctic Ecosystem. Front. Microbiol. 13. doi:10.3389/fmicb.2022.755014

Belnap, J., and Lange, O.L. 2001. Structure and Functioning of Biological Soil Crusts: a Synthesis. In: Belnap, J. and Lange, O.L. (eds) Biological Soil Crusts: Structure, Function, and Management. Ecological Studies, vol 150. Springer, Berlin, Heidelberg, Germany. doi:10.1007/978-3-642-56475-8_33

Pushkareva, E., Johansen, J.R., and Elster, J. 2016. A review of the ecology, ecophysiology and biodiversity of microalgae in Arctic soil crusts. Polar Biology 39(12): 2227–2240. doi:10.1007/s00300-016-1902-5

Tytgat, B., Verleyen, E., Sweetlove, M., D'hondt, S., Clercx, P., Van Ranst, E., Peeters, K., Roberts, S., Namsaraev, Z., Wilmotte, A., Vyverman, W., and Willems, A. 2016. Bacterial community composition in relation to bedrock type and macrobiota in soils from the Sør Rondane Mountains, East Antarctica. FEMS Microbiol. Ecol. 92. doi:10.1093/femsec/fiw126

Microbial nitrogen-fixation in active layer and thawing permafrost of high Canadian Arctic

Tatiana A. Vishnivetskaya[1,2], Xiaofen Wu[2], Archana Chauhan[2§], Wyatt A. Cyr[2], Maggie C.Y. Lau Vetter[3†], Brandon T. Stackhouse[3], Lyle Whyte[4] & Karen G. Lloyd[1]

[1]*Department of Microbiology, University of Tennessee, Knoxville, Tennessee, United States*

[2]*Center for Environmental Biotechnology, University of Tennessee, Knoxville, Tennessee, United States*

[3]*Department of Geosciences, Princeton University, Princeton, New Jersey, United States*

[4]*Department of Natural Resource Sciences, McGill University, Montréal, Québec, Canada*

[§]*Present address: Department of Zoology, Panjab University, Chandigarh, India*

[†]*Present address: Laboratory of Extraterrestrial Ocean Systems, Institute of Deep-Sea Science and Engineering, Chinese Academy of Sciences, Sanya, Hainan, China*

Permafrost is warming as a result of climate change, particularly in the Arctic permafrost zone, where the surface temperature is increasing over twice as fast as the global average. Warming lead to permafrost degradation, which occurs through either the increase of active layer thickness or development of thermokarst for ice-rich permafrost. Consequently, permafrost thaw exposes large quantities of preserved soil organic carbon to microbial decomposition, potentially leading to the release of greenhouse gas emissions (e.g., CO_2, CH_4 and N_2O), which again contribute to further global warming.

Nitrogen is an essential element for both plants and soil microbes. However, permafrost is suggested to be an N-limited environment due to the slow N mineralization rates at low temperatures, low rates of atmospheric N deposition and biological N_2 fixation. Microbial populations that can fix N_2 are confined to methanogenic archaea and a diverse group of bacteria, including cyanobacteria and heterotrophs.

This study utilized metagenomic sequencing to examine microbial N_2 fixation across four depths representing active layer (5, 35 and 65 cm) and permafrost (80 cm) soils with low organic carbon, where one-meter intact cores were subjected to 72 weeks of simulated thaw. Permafrost thaw was designed to simulate spring/summer thawing of active layer deepening and waterlogged terrain developing by adding weekly inputs of artificial rainwater (1).

Methods and Current Work

One-meter soil cores were collected while still frozen in May 2011 from the McGill Arctic Research Station (MARS) located on Axel Heiberg Island, Nunavut Canada as described in (1, 2). The cores contained the active layer that experienced seasonal thaw (<70 cm depth) and the permafrost that remained perennially frozen (>70 cm depth). Cores were collected from the polygon interior and polygon edge. The thawing experiment was carried out as previously described (1). Briefly, cores were gradually thawed at 4.5°C for 18 months. The polygon interior core was thawed at conditions of saturation to mimic the waterlogging-affected terrain by adding 40 mL of artificial rainwater weekly from week 2, totaling ~500 mL of water, while the edge core received no water input during thaw (1). Samples from four depths (5, 35, 65, and 80 cm samples) were collected from each of the two cores at 0-time, 1 week and 72 weeks after thaw with the exception of 35 cm, which was only sampled for two time points (0-time and 72 weeks).

Table 1. Pore-water characteristics in saturated core at depths 5, 35, 65 and 80 cm after the layer thawed.

Characteristics	5	35	65	80
Total Carbon, %	1.0	1.4	1.2	1.2
Total Nitrogen, %	0.09	0.1	ND	0.1
pH	6	ND	5.7	5.5
Na, µM	58	498	543	609
Nitrite, µM	0	0	0	0
Nitrate, µM	1.4	1.2	4.6	3.4
Ammonium, µM	8	ND	3.5	27
Acetate, µM	128	74	134	84
Chloride, mM	12.3	0.4	0.3	0.2
CH_4, nM	0	0	182	452

Total community gDNA was extracted using the FastDNA® SPIN Kit for Soil (MP Biomedicals) as previously described (3) and were sequenced on the Illumina HiSeq 2000 platform with paired-end 2 x 100 bp mode. Approximately 30 to 150 million paired reads were generated per sample. Metagenome analyses were done as previously described (2). Metagenome raw reads were trimmed using Trimmomatic v0.36 with default parameters. Trimmed reads were taxonomically classified against GTDB database using kraken2 and bracken. The trimmed reads were also co-assembled

into contigs using Megahit v1.2.9 with a kmer list of 41, 51, 61, 71, 81 and 91 at each depth. The coverage of individual samples in the assembly was defined by mapping the trimmed reads from each sample against co-assembled contigs using bowtie2 v2.2.9 and v2.3.5 and samtools v1.3.1. Metabat v2.12.1 was used to perform binning with a contig length cutoff of 1500 bp. The quality of all the recovered bins was evaluated using CheckM. Recovered bins with a completeness >=70% and contamination <=10% were selected (defined as metagenome assembled genomes (MAGs)). All the selected MAGs were taxonomically annotated using GTDB-Tk v1.0.2 against GTDB database r89. Gene prediction was carried out using Prodigal v2.6.3 in metagenomic mode for each selected MAG. KofamScan v1.2.0 was then used to assign KEGG orthologies (KOs) to predicted genes against HMM profiles from the KEGG database. The percentage of reads mapped to each MAG were obtained by mapping the trimmed reads back to the corresponding MAG. Metabolic pathway reconstruction was performed on nitrogenase positive MAGs. Co-assembled contigs (>= 1000 bp) were annotated against the KEGG database using KofamScan v1.2.0 after genes were predicted with prodigal v2.6.3. Normalized transcripts per million (TPM) values obtained using Salmon v1.0.0 represents reads per million in metagenome study. Heatmaps were generated using ComplexHeatmap. Phylogenetic analyses of nifH gene sequences were carried out on amino acid sequences extracted from the MAGs and co-assembled contigs. The extracted nifH sequences along with sequences from the nifH database were used for constructing a maximum-likelihood phylogenetic tree after alignment with ClustalW using Molecular Evolutionary Genetics Analysis software (MEGA, version 10.2.6).

Summary

The archaeal and bacterial communities from 5 cm active layers remained similar at different time points upon thaw. Lack of observable changes in microbial composition between samples with different thawing times at 5 cm suggests that microbial communities from the 5 cm active layer have already adapted to seasonal thaw and changes in temperature and water regime. In addition, the samples collected after 1-week thaw were similar to the samples obtained at 0-time for 5, 65 and 80 cm. This is likely due to the fact that all the depths remained frozen at week 1, whereas soils thawed by the start of week 3 for 5 cm, the middle of week 4 for 35 cm, and the start of week 10 for 65 cm (1). Samples of the saturated core from 35 and 65 cm were more similar to permafrost at 80 cm after 18-months thaw. Overall, across the thawing period, Proteobacteria was the most abundant taxon for samples at 5 cm (averaging abundance of the two cores 36.65-41.84%), while samples from 35, 65 and 80 cm were dominated by Actinobacteriota (26.99-40.72%) except that Bacteroidota was the dominant taxon for samples collected at 18-months from 65 cm (28.36%). The differences of microbial composition observed between the saturated core and edge core at 35, 65 and 80 cm suggest that the thawing type may be involved in shaping microbial community.

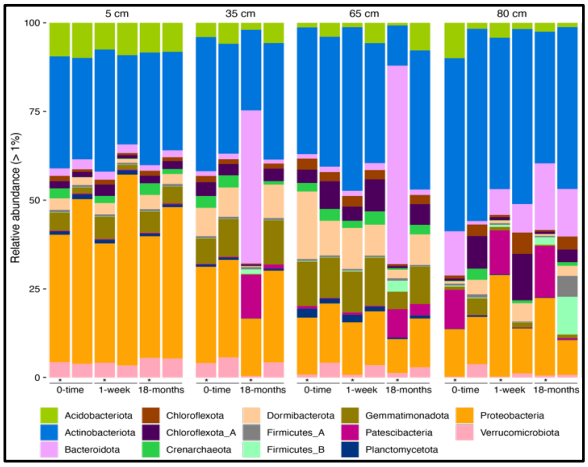

Figure 1. Archaeal and bacterial composition based on metagenomic assemblies. The asterisk symbols indicate samples from the saturated core.

Acknowledgements

The research was funded by the US Department of Energy, Office of Science, Office of Biological and Environmental Research DOE-PS02-09ER09-25 and Office of Biological and Environmental Research, Genomic Science Program DE-SC0020369.

References

(1) Stackhouse, B., Vishnivetskaya, T., Layton, A., Chauhan, A., Pfiffner, S., Mykytczuk, N., Whyte, L., Hedin, L., Saad, N., and Onstott, T.C. 2015. Effects of simulated spring thaw of permafrost from mineral cryosol on CO_2 emissions and atmospheric CH_4 uptake. Biogeosciences 120:1764–1784.

(2) Wu, X., Chauhan, A., Layton, A., Lau Vetter, M.C.Y., Stackhouse, B., Williams, D., Whyte, L., Pfiffner, S., Onstott, T.C., and Vishnivetskaya, T. 2021. Comparative Metagenomics of the Active Layer and Permafrost from Low-Carbon Soil in the Canadian High Arctic. Environmental Science & Technology 55:12683–12693.

(3) Vishnivetskaya, T., Layton, A., Lau, M.C., Chauhan, A., Cheng, K., Meyers, A., Murphy, J., Rogers, A., Saarunya, G., Williams, D., Pfiffner, S., Biggerstaff, J., Stackhouse, B., Phelps, T.J., Whyte, L., Sayler, G., and Onstott, T.C. 2014. Commercial DNA extraction kits impact observed microbial community composition in permafrost samples. FEMS Microbiology Ecology 87:217.

10 Remote Sensing of Permafrost

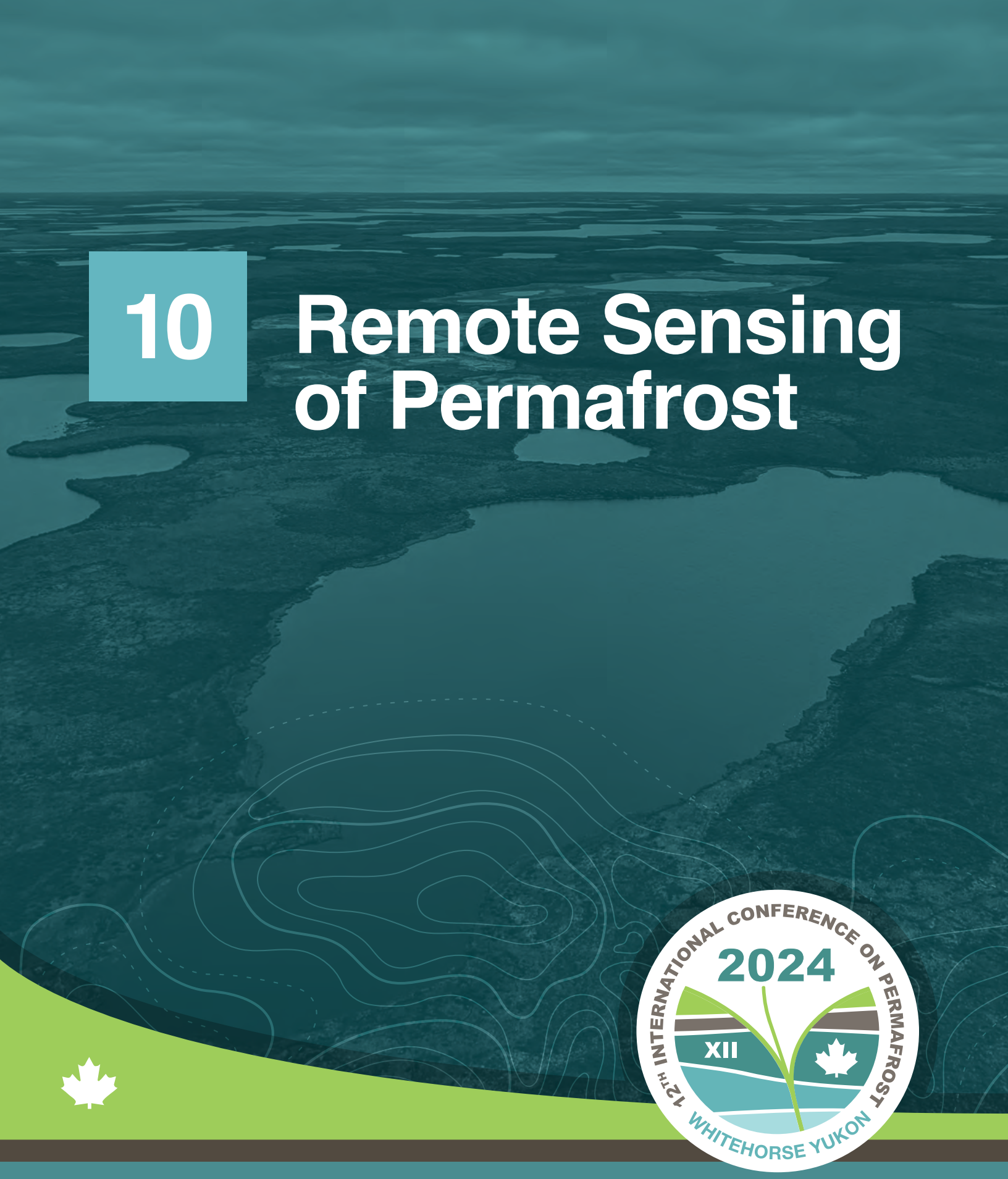

12TH INTERNATIONAL CONFERENCE ON PERMAFROST
2024
XII
WHITEHORSE YUKON

INTEGRATING PERSPECTIVES OF PERMAFROST THAW, CHANGE, AND ADAPTATION

10A — Remote Sensing of Permafrost Processes and Impacts on the Environment

Session Chairs: Tazio Strozzi[1], Santosh Panda[2] & Remya S.N.[3]

[1]GAMMA Remote Sensing, Switzerland
[2]University of Alaska, Fairbanks, Alaska, United States
[3]Divecha Centre for Climate Change, Indian Institute of Science, Bangalore, India

Permafrost is a key component of the northern environment, and it influences major landscape processes including the carbon cycle, geomorphic processes, landscape restructuring, and environmental health. Monitoring surface features of permafrost terrains and typical periglacial landforms are necessary to understand the current and future dynamics of permafrost degradation. Remote sensing techniques are the best to monitor changes across scales, as some of these landforms are typically found in extremely remote and inaccessible locations. Satellite assessments can also bridge the gap between field observations and modelling efforts and support the comprehension of the effects of climate change.

In this session, the entire permafrost community is invited to submit unique advanced remote sensing applications that address evolution and dynamic disturbance processes in permafrost landscapes, both in lowland and mountain regions. We are open to a wide range of remote sensing approaches, including short- and long-term monitoring that makes use of time series analysis, airborne, spaceborne, and machine learning as well as unmanned aerial systems, and is validated from field-based and/or modelling analysis. We also welcome research on landscape disturbances, such as permafrost thaw, active-layer degradation, and talik formation, which affect periglacial landscape processes and the environment.

The Northwest Territories Thermokarst Mapping Collective: Opportunities and challenges of mid-project mapper training

William Bender[1], Steve Kokelj[2], Seamus Daly[3], Alice Wilson[2], Celtie Ferguson[4], Vivianne Pauzé[2] & William Quinton[1]

[1]*Department of Geography and Environmental Studies, Wilfrid Laurier University, Waterloo, Ontario, Canada*

[2]*Northwest Territories Geological Survey, Government of Northwest Territories, Yellowknife, Northwest Territories, Canada*

[3]*North Slave Research Centre, Aurora Research Institute, Yellowknife, Northwest Territories, Canada*

[4]*Western Arctic Research Centre, Aurora Research Institute, Inuvik, Northwest Territories, Canada*

Ice-rich permafrost acts as the frozen foundation for much of the circumpolar North. High rates of warming in the Northwest Territories is accelerating permafrost thaw which is altering the landscape and ecosystems, most notably through land subsidence (Kokelj and Jorgenson 2013). Accelerated thermokarst has become a major stressor on infrastructure, land use and food security for northern communities. The nature of landscape change is dependent on conditions specific to the location and will manifest differently based on those conditions (Jorgenson et al. 2015). Current understanding of thermokarst distribution on a circumpolar-wide scale can be derived from modern modelling products (Olefeldt et al. 2016). However, the model outputs do not describe the distribution of thermokarst features well on a local to regional scale. Decision makers often rely on these products as such levels of confidence in these products at local and regional scales is important. The Thermokarst Mapping Collective (TMC) sets out to create an empirically-based inventory of thermokarst features in the Northwest Territories and adjoining watersheds. Satellite imagery is systematically interpreted by mappers and feature data is stored within GIS software. The project mapping started in 2019 and lessons learned since then continue to shape the study design and mapper training.

STUDY OBJECTIVE

The study objective is to highlight the processes of training for new mappers joining midway through the project. A presentation will comprise of a brief demonstration of mapper training and discussion of opportunities and challenges that still exist to increase future mapper training quality. Preliminary quantitative results of intermapper comparison will be shown to convey interpretation reproducibility.

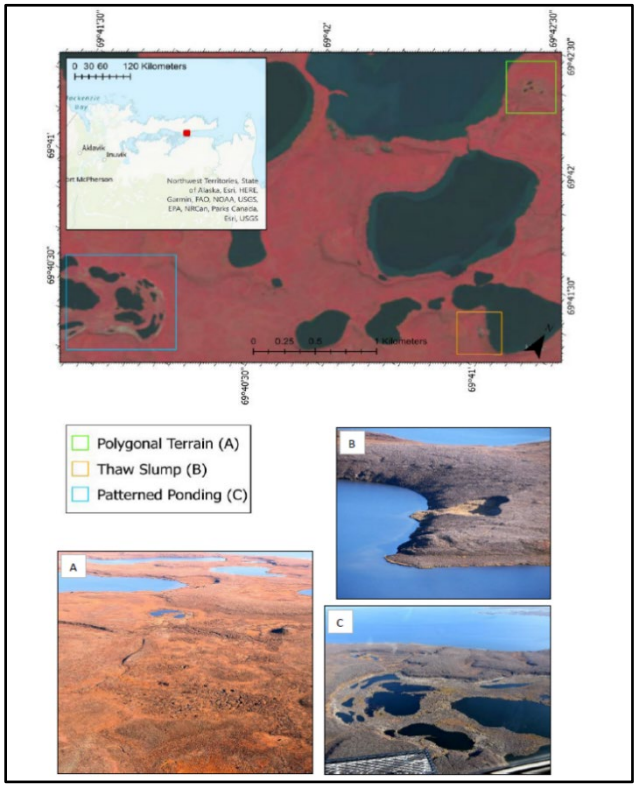

Figure 1. Example of Sentinel 2 satellite false-colour imagery near the Beaufort Delta used to identify thermokarst features at a scale of 1:23,000. (A) Polygonal terrain in the periglacial theme identified by its unique pattern in the imagery. (B) Thaw slump in the mass wasting theme. (C) Patterned ponding in the hydrological theme.

STRENGTHS AND CONTINUED CHALLENGES OF THE CURRENT TRAINING PROCESS

A mapper interpretation rubric is used as the training guideline and was established from consultation with experts and stakeholders. Mapping is subdivided into three themes based on the processes that drive thermokarst: mass wasting, hydrological and periglacial. Initially, mappers were trained on interpreting thermokarst features within a specific spatial range given their research interests or

familiarity with a region. In the summer of 2023, I was trained with the intention of gaining territory-wide experience with the ultimate goal of completing mapping gaps over the territory. As an undergraduate student, I traveled to Yellowknife to receive in-person training to learn the basics of the project and to establish relationships with those involved. Training began with learning and becoming familiar with the various thermokarst features included in the study by reading literature, comparing oblique feature images to mapped features, and gaining knowledge from experienced mappers and experts. The benefit of training mappers with this method is that themes will ideally be consistently mapped regardless of location. A challenge in this process is that a feature, such as polygonal pattern ponding, can appear differently in the satellite imagery in the far north compared with the same feature in a more southern region. This is because the conditions can widely vary over the territory. To reduce individual uncertainty, interpretive skill can be improved through a combination of assistance from the resident experts and gaining a familiarity with the region's landscape through literature, The GNWT ecosystem class framework (GNWT n.d.), available oblique imagery, and on-the-ground observation. Mapped areas provided an opportunity for me to try and map the same cells and compare my interpretation to that of the previous mapper, but also as a moment for a trainer to gauge the quality of the training so far. My training has demonstrated that, although helpful, it is not a requirement for new mappers to have in-depth knowledge of thermokarst processes before onboarding onto the TMC as I had limited previous background knowledge of these processes. Additionally, the experience of traveling to Yellowknife for in-person training allowed me to engage with the experts and learn the landscape in a meaningful way that would have been difficult to recreate remotely.

FUTURE DIRECTIONS

As the mapping is completed through interpretation of satellite imagery, there exists potential for variablility in a mapper's interpretations, even when following the mapping rubric. We are in the early stages of developing an intermapper comparison test with the purpose of comparing new trainee's abilities to those of experienced mappers. Beyond training, the model can be expanded to compare the variability of experienced mappers.

REFERENCES

Jorgenson, M.T., Kanevskiy, M., Shur, Y., Moskalenko, N., Brown, D.R.N., Wickland, K., Striegl, R., and Koch, J. 2015. Role of ground ice dynamics and ecological feedbacks in recent ice wedge degradation and stabilization. Journal of Geophysical Research: Earth Surface 120: 2280–2297. doi:10.1002/2015JF003602

Kokelj, S.V., and Jorgenson, M.T. 2013. Advances in thermokarst research. Permafrost and Periglacial Processes 24: 108–119. doi:10.1002/ppp.1779

GNWT (no date) Ecosystem classification, Ecosystem Classification. Available at: https://www.gov.nt.ca/ecc/en/services/ecosystem-classification#resources (Accessed: 2023)

Olefeldt, D., Goswami, S., Grosse, G., Hayes, D., Hugelius, G., Kuhry, P., Mcguire, A.D., Romanovsky, V.E., Sannel, A.B.K., Schuur, E.A.G., and Turetsky, M.R. 2016. Circumpolar distribution and carbon storage of thermokarst landscapes. Nature Communications 7. doi:10.1038/ncomms13043

Integrating Sentinel-1 and Cosmo-SkyMed InSAR-based information for an improved regional assessment of rock glacier dynamics

Francesco Brardinoni[1], Aldo Bertone[1], Volkmar Mair[2], Nina Jones[3] & Tazio Strozzi[3]

[1]*Department of Biological, Geological and Environmental Sciences, University of Bologna, Bologna, Italy*

[2]*Ufficio Geologia e Prove Materiali, Cardano, Autonomous Province of Bolzano, Italy*

[3]*Gamma Remote Sensing, Gümligen, Switzerland*

In this study, following operational guidelines jointly proposed by ESA Permafrost CCI and IPA Action Group on rock glacier inventories (Bertone et al. 2022), we compare and critically evaluate the InSAR-based kinematic characterization of rock glaciers conducted on Sentinel-1 (S1) and Cosmo-SkyMed (CSK) wrapped interferograms.

The study area is in western South Tyrol (Italy) and includes the so-called (i) Northern Val Venosta, extending over Vallelunga, Val Planol, Val di Mazia and part of Val Senales; and (ii) Southern Val Venosta, extending across Val di Solda, Val di Lasa, Val Martello, and Val d'Ultimo.

Starting from a geomorphologic inventory encompassing 1196 rock glaciers, we consider S1 scenes (2017-2020) and perform relevant InSAR-based kinematic characterization. Subsequently, this activity was replicated using CSK scenes (2016-2020) to obtain an additional kinematic inventory for cross-validation and integration. Temporal baselines in S1 and CSK interferograms range from 6 to 732 days and from 16 to 464 days, respectively. The InSAR processing workflow includes co-registration of SAR images, the computation of interferograms and removal of the topographic-related phase by using a 2005 LiDAR-derived 2.5m gridded-DTM.

Integration of the two inventories, while documenting substantial congruence between S1- and CSK-derived rock glacier dynamic classifications, highlights the complementary nature of the two constellations. On one hand, CSK's high spatial resolution and X-band characteristics made this constellation particularly well suited for investigating slow-moving (e.g., < mm/yr; mm/yr to cm/yr) rock glaciers in greater detail than enabled by S1. For example, 158 slow-moving rock glaciers, not visible on S1 annual interferograms, produced coherent signals on CSK counterparts and consequently, could be classified as permafrost bearing features (see example in Figure 1). On the other hand, S1's C-band characteristics allowed the detection of coherent surface deformation on 16 fast-moving rock glaciers (e.g., dm/yr to m/yr; > m/yr), otherwise not measurable on 16-day CSK interferograms due to decorrelation (Figure 2).

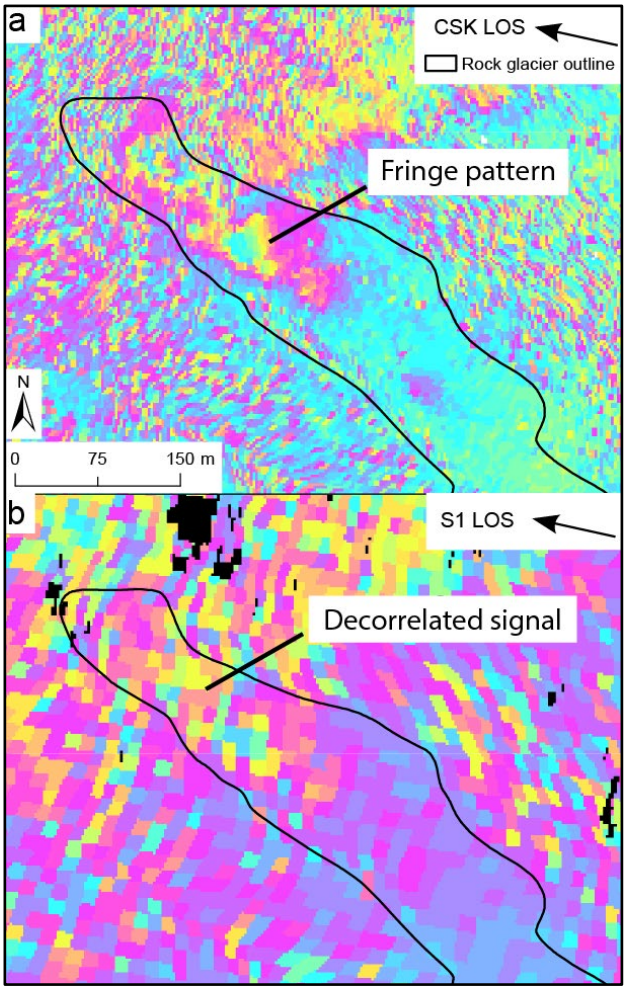

Figure 1. Example showing the geomorphologic outline of a rock glacier (black linework) drawn on: (a) CSK-derived annual interferograms (descending orbit; reference image: 16/08/2017; second image: 03/08/2018; time interval: 352 days; λ: 3.1 cm); and (b) S1-derived annual interferograms (descending orbit; reference image: 26/10/2018; second image: 03/10/2019; time interval: 342 days; λ: 5.55 cm). Note the difference in fringe pattern in panel a, and the decorrelated signal in panel b.

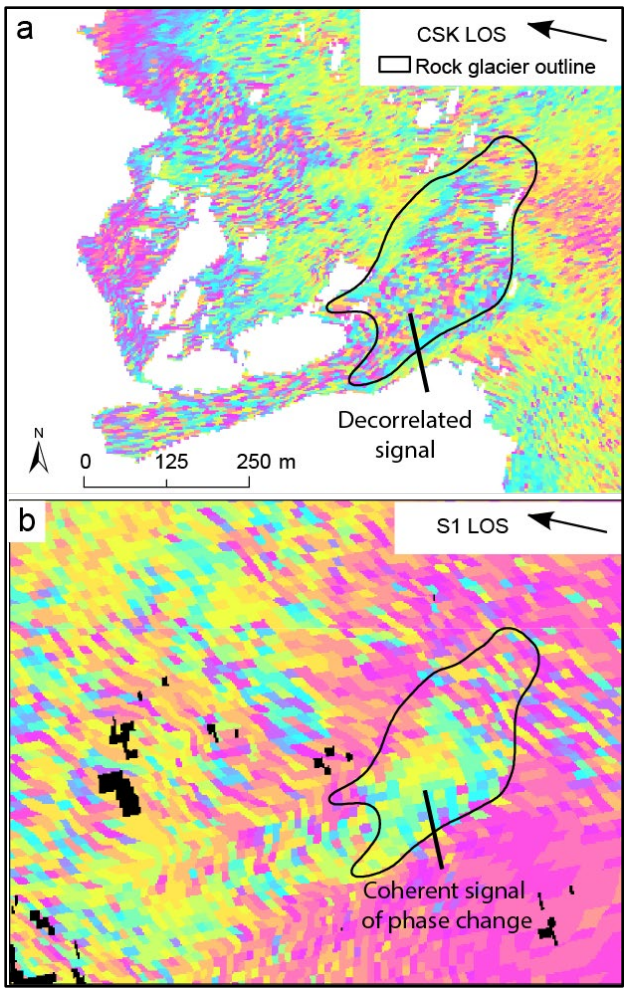

Figure 2. Example showing the geomorphologic outline of a rock glacier (black linework) drawn on: (a) CSK-derived, 16-day interferogram (descending orbit; reference image: 04/08/2018; second image: 20/08/2018; λ: 3.1 cm); and (b) S1-derived, 12-day interferogram (descending orbit; reference image: 28/09/2018; second image: 10/10/2018; time interval: λ: 5.55 cm). Note the difference between the decorrelated signal in panel a, and the coherent pattern of phase change in panel b.

Overall, the combination of kinematic information obtained through CSK and S1 constellations allowed the identification and mapping of rock glacier surface deformation with satisfactory detail. This in turn led to (i) an improvement of our current knowledge of geomorphic process rates, relevant sediment fluxes and geohazard potential; and (ii) the compilation of a more robust and complete rock glacier inventory for an improved appraisal of the spatial distribution of mountain permafrost.

Acknowledgements

CSK scenes were made available to the authors by the Italian Space Agency within the framework of “Cosmo-SkyMed Open Call for Science”, project ID 751. Copernicus freely granted Sentinel-1 scenes.

References

Bertone, A., Barboux, C., Bodin, X., Bolch, T., Brardinoni, F., Caduff, R., Christiansen, H.H., Darrow, M.M., Delaloye, R., Etzelmüller, B., Humlum, O., Lambiel, C., Lilleøren, K.S., Mair, V., Pellegrinon, G., Rouyet, L., Ruiz, L., and Strozzi, T. 2022 Incorporating InSAR kinematics into rock glacier inventories: insights from 11 regions worldwide, The Cryosphere 16: 2769–2792. doi.org/10.5194/tc-16-2769-2022

High spatial heterogeneity in ice-wedge permafrost thaw identified via multi-scale remote sensing

Katherine N. Braun & Christian G. Andresen

Department of Geography, University of Wisconsin-Madison, Madison, Wisconsin, United States

The thawing of permafrost is both spatially and temporally variable. This uneven progression of degradation produces complex spatial patterns of thermokarst and complicates the assessment of permafrost vulnerability and thaw impacts. More accurate remote sensing methods for detecting spatial heterogeneity in permafrost degradation will better allow us to monitor and forecast Arctic landscape evolution and associated land-atmosphere carbon-climate interactions.

Ice-wedge landscapes cover large portions of the Arctic, including over 65% of the Arctic Coastal Plain of Alaska (Lara et al. 2018) and contain multiple scales of thermokarst heterogeneity. While most previous mapping efforts have primarily focused on delineating polygons (e.g., Abolt and Young 2020; Bhuiyan et al. 2020; Zhang et al. 2018), field observations show that an individual polygon can exhibit multiple degradation stages (Jorgenson et al. 2022; Kanevskiy et al. 2017). Ice-wedge degradation stages – ranging from undegraded to degraded to stabilized – provide a means of both classifying the severity of thaw (Jorgenson et al. 2015) and allow examination of spatiotemporal heterogeneity in ice-wedge landscapes. The existing mapping of ice-wedge landscapes, therefore, should be complemented by quantifying both the sub-polygon and kilometer-scale heterogeneity in degradation.

We used a combination of field sampling, drone multispectral surveys, and satellite remote sensing to identify ice-wedge terrain, classify stages of degradation, and examine landscape trends related to permafrost heterogeneity. The mapped study site is located on the Arctic Coastal Plain of Alaska along the Dalton Highway, ~50 km south of Prudhoe Bay, Alaska on the traditional lands of the Inupiat. Both meter-scale and kilometer-scale spatial clustering of ice-wedge degradation stages was delineated in the resulting maps to identify hot spots of permafrost degradation (Figure 1). The spectral and topographic properties of degradation hot spots and cold spots were examined to identify the landscape factors most related to degradation. This spatial analysis revealed that higher elevation portions of the Arctic Coastal Plain contain greater amounts of advanced permafrost degradation, while lower elevation areas have more ice wedges that do not have such intense degradation (Figure 2).

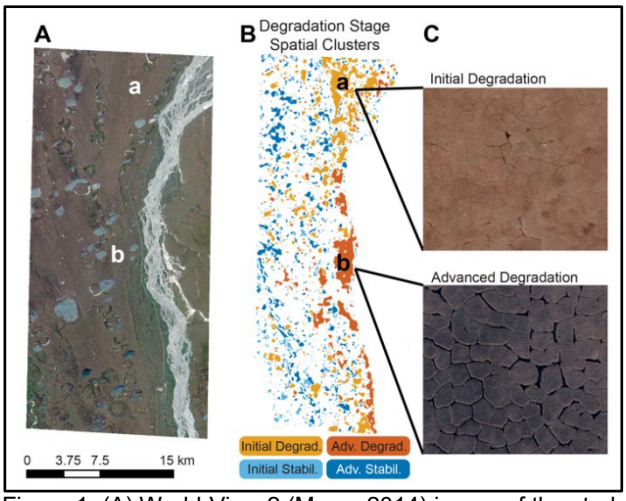

Figure 1. (A) World-View 2 (Maxar 2014) image of the study site, located 50 km south of Prudhoe Bay, Alaska. (B) Ice-wedge degradation stage clusters, identified with Anselin Local Moran's I. Each cluster is defined by statistically significant trends in ice wedge trough width and hydrology, which correspond with degradation stage. (C) World-View 2 from points (a) and (b) demonstrating the different appearance of the initial degradation and advanced degradation stage clusters. Images are at the same scale.

High-resolution maps of ice-wedge degradation are necessary to detangle the interrelated drivers of permafrost thaw and potential impacts. This fine scale understanding of permafrost landscapes is necessary for accurate upscaling of Arctic earth system processes, such as producing better estimates of how permafrost degradation impacts Arctic carbon cycling. These landscapes are highly heterogeneous but are often treated homogenously in earth system models, despite the fact that these landscapes will likely continue evolving in complex ways as the Arctic warms. The high spatial heterogeneity in ice-wedge degradation delineated in this work demonstrates the need to expand beyond single-site and single-scale studies, so that we can improve our understanding of where and why permafrost undergoes thaw and estimate how continued degradation in the Arctic will impact the permafrost-carbon feedback.

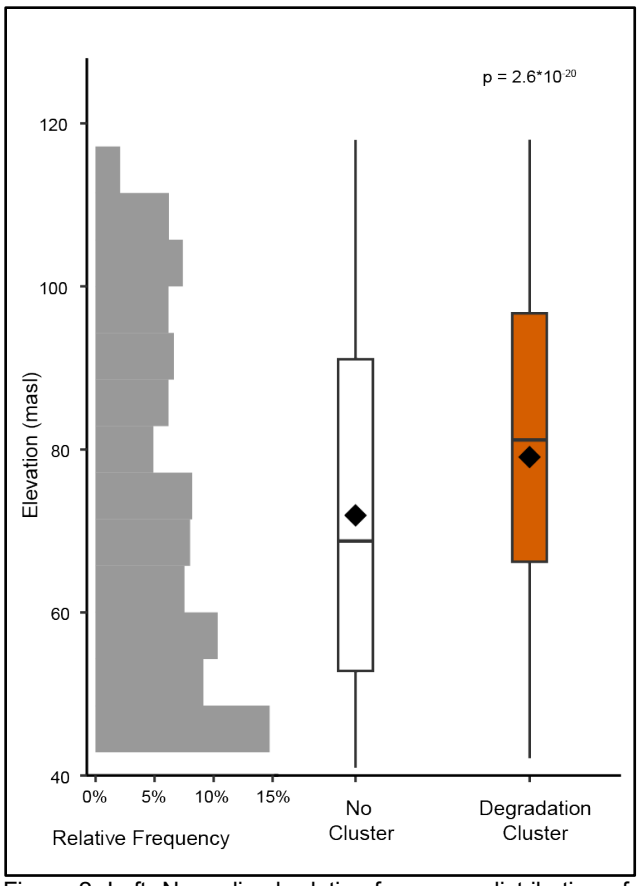

Figure 2. Left: Normalized relative frequency distribution of elevation (in meters over sea level). Right: Box plot of average elevation within the advanced degradation cluster and portion of site without degradation clutering. P-value for the difference in means (diamonds) calculated from Welch's t-test.

ACKNOWLEDGEMENTS

We thank Mark Lara, Caroline Ludden, Jacob May, Shannon Dillard, and Erika Marín-Spiotta for their help in the field and lab. KB was supported by NASA FINESST grant #80NSSC24K0037 and the National Science Foundation Graduate Research Fellowship Program under Grant No. DGE-2137424. Opinions, findings, conclusions, and recommendations expressed in this material are those of the authors and do not necessarily reflect the views of the National Science Foundation. KB was also supported by the University Fellowship, provided by the Graduate School, part of the Office of Vice Chancellor for Research and Graduate Education at the University of Wisconsin-Madison, with funding from the Wisconsin Alumni Research Foundation and UW-Madison. Fieldwork was supported by the UW-Madison Geography Department Trewartha Research Award. Geospatial support for this work was provided by the Polar Geospatial Center under NSF-OPP awards 104681, 1559691, and 2129685. ArcticDEM provided by the Polar Geospatial Center under NSF-OPP awards 1043681, 1559691, 1542736, 1810976, and 2129685.

REFERENCES

Abolt, C.J., Young, M.H., Atchley, A.L., Harp, D.R., and Coon, E.T. 2020. Feedbacks Between Surface Deformation and Permafrost Degradation in Ice Wedge Polygons, Arctic Coastal Plain, Alaska. Journal of Geophysical Research: Earth Surface 125, e2019JF005349. https://doi.org/10.1029/2019JF005349

Bhuiyan, M.A.E., Witharana, C., and Liljedahl, A.K. 2020. Use of Very High Spatial Resolution Commercial Satellite Imagery and Deep Learning to Automatically Map Ice-Wedge Polygons across Tundra Vegetation Types. Journal of Imaging 6, 137. https://doi.org/10.3390/jimaging6120137

Jorgenson, M.T., Kanevskiy, M., Shur, Y., Moskalenko, N., Brown, D.R.N., Wickland, K., Striegl, R., and Koch, J. 2015. Role of ground ice dynamics and ecological feedbacks in recent ice wedge degradation and stabilization. Journal of Geophysical Research: Earth Surface 120, 2280–2297. https://doi.org/10.1002/2015JF003602

Jorgenson, M.T., Kanevskiy, M.Z., Jorgenson, J.C., Liljedahl, A., Shur, Y., Epstein, H., Kent, K., Griffin, C.G., Daanen, R., Boldenow, M., Orndahl, K., Witharana, C., and Jones, B.M. 2022. Rapid transformation of tundra ecosystems from ice-wedge degradation. Global and Planetary Change 216, 103921. https://doi.org/10.1016/j.gloplacha.2022.103921

Kanevskiy, M., Shur, Y., Jorgenson, T., Brown, D.R.N., Moskalenko, N., Brown, J., Walker, D.A., Raynolds, M.K., and Buchhorn, M. 2017. Degradation and stabilization of ice wedges: Implications for assessing risk of thermokarst in northern Alaska. Geomorphology 297, 20–42. https://doi.org/10.1016/j.geomorph.2017.09.001

Lara, M.J., Nitze, I., Grosse, G., and McGuire, A.D. 2018. Tundra landform and vegetation productivity trend maps for the Arctic Coastal Plain of northern Alaska. Sci Data 5, 180058. https://doi.org/10.1038/sdata.2018.58

Zhang, W., Witharana, C., Liljedahl, A.K., and Kanevskiy, M. 2018. Deep Convolutional Neural Networks for Automated Characterization of Arctic Ice-Wedge Polygons in Very High Spatial Resolution Aerial Imagery. Remote Sensing 10, 1487. https://doi.org/10.3390/rs10091487

Post-wildfire surface deformation in Northwest Territories revealed by ALOS-2 and Sentinel-1 InSAR

Zetao Cao[1] & Masato Furuya[2,3]

[1]*Graduate School of Science, Hokkaido University, Sapporo, Hokkaido, Japan*

[2]*Faculty of Science, Hokkaido University, Sapporo, Hokkaido, Japan*

[3]*Arctic Research Center, Hokkaido University, Sapporo, Hokkaido, Japan*

Permafrost thaw has received increasing attention these days due to its high sensitivity to climate change and complex feedback to ecological, hydrological, and biological processes (Schuur et al. 2015). Meanwhile, an increasing number of wildfires has been reported over the Arctic tundra and boreal forests where permafrost usually underlies. Wildfires in these regions could turn boreal forests from carbon sinks into carbon emitters (at least) during the fire (Veraverbeke et al. 2021). In addition, depending on the ice extent, wildfires could initiate an abrupt thaw of permafrost that could last much longer than the period of burning and potentially release the frozen carbon again into the atmosphere (Gibson et al. 2018). However, the details of the post-fire abrupt thaw remain uncertain.

The Northwest Territories, Canada is largely underlain by continuous permafrost. The increasingly prevalent wildfires over the Northwest Territories could greatly alter the underlying permafrost dynamics through dramatic changes in near-surface vegetation and groundwater hydrology and lead to irreversible ground deformation (Travers-Smith et al. 2022). Such deformation would alter the landform and local hydrology, and could be responsible for further carbon emissions to the atmosphere. Therefore, it is worth studying the wildfire-induced deformation in permafrost regions to better understand the intricate interplay between wildfire, permafrost dynamics, and the land surface system. At present, wildfires have increased dramatically in the high-latitude areas in the Northwest Territories, but how they affect permafrost landforms and the extent of deformation there are still unknown. Therefore, the first and foremost work is to investigate the magnitude of these deformations and then look into possible influential factors.

Data, method and study area

In permafrost areas, in-situ deformation measurement data are always hard to acquire due to the harsh environment and poor accessibility, especially in the winter season. The satellite-based interferometric Synthetic Aperture Radar (InSAR) technology, which is widely applied in observing ground deformation all over the world, provides a powerful tool to help us measure post-wildfire deformation in permafrost regions (Liu et al. 2014; Yanagiya et al. 2023; Yanagiya and Furuya 2020).

In this study, by performing differential InSAR (D-InSAR) analysis based on Advanced Land Observing Satellite-2 (ALOS-2) data and time-series analysis based on Sentinal-1 InSAR data, we investigate the post-wildfire deformation responses.

The fire scar is located beside the downstream McKenzie River, Northwest Territories, Canada (Figure 1a). This area is underlain by continuous permafrost with medium to relatively high ground ice content (up to ~20%) (O'Neill et al. 2019). From July 23rd to August 2nd 2019, the wildfire occurred and left a fire scar of about 584 km^2. From InSAR-derived displacement data, we investigate the temporal and spatial patterns of ground deformation, including the span-fire and post-fire signals from June 2019 to October 2020.

Results and discussion

The one-year deformation map generated from ALOS-2 data indicates both uplift and subsidence signals in the burned area from September 2019 to September 2020. Uplift signals were detected in some areas in the middle part of the fire scar, among which most areas experienced an uplift smaller than 5 cm in line of sight (LOS). Such uplift indicates that, after the wildfire, the frost-heave signal in the freezing season may be greater than the subsequent summer subsidence signal in some areas. A possible reason account for such a phenomenon is that the increased soil water after the wildfire is frozen into pore ice or ice lens before drainage, and not fully thawed during the subsequent thawing season, leading to the net uplift one year after the wildfire. Meanwhile, subsidence up to 10 cm along LOS can be found in the northwest and southeast parts of the fire scar. Though soil water content in these areas would also increase after wildfire, the river and pond nearby might provide a favourable condition for water drainage. Therefore, subsidence may happen after the loss of ground ice and thawing water.

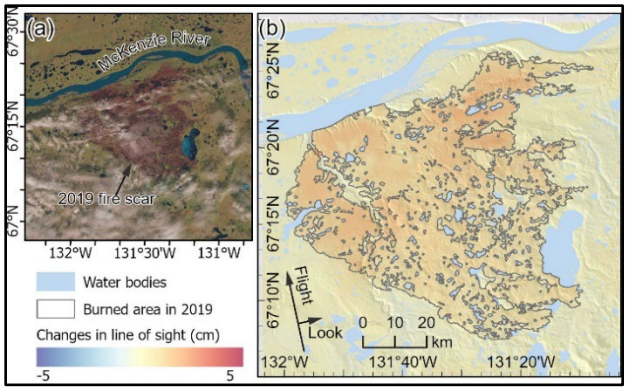

Figure 1. (a) Landsat-8 natural-color image acquired in August 2020 showing the clear wildfire scar one year after the fire. (b) Changes in line of sight (LOS) from August 18 to 30, 2020, that revealed by the Sentinel-1A InSAR image. Positive changes in red indicate subsidence; there is no uplifting area in this InSAR image.

Time-series InSAR based on Sentinel-1 data could provide more temporally detailed deformation signals. In the early freezing season after the fire, the uplift caused by frost heave was enhanced within the burned area, which was possibly due to the loss of the insulation layer and increased soil moisture content from the unburned roots under the ground. The uplift signal was then undetectable in the mid-winter, probably because the freezing front reached the permafrost table. Compared with the unburned areas, some burned areas experienced a larger uplift of up to ~7 cm in LOS. In some parts of the fire scar, uplift in the first frozen season after the wildfire even exceeded the previous summer subsidence, which is consistent with one of the conceptual post-fire transient deformation model proposed by Yanagiya et al. (2023). Then, obvious subsidence signals long LOS were detected in the next summer (Figure 1b), which may caused by the thawing of more ground ice due to the thinner buffer of vegetation and organic layers and a decreasing albedo after the wildfire.

Despite a few unwrapping errors due to low coherence in the fire scar might slightly impact the outcomes, in our preliminary results, the deformation signals in wildfire scars are overall robust and obvious, while negligible in unburned areas. Further studies will focus on dealing with the unwrapping issues and incorporation with models for more insightful investigation.

The study encompasses wildfire-caused ground deformation in permafrost environments, through which, we aim to contribute to a more detailed understanding of the relationships between wildfire impacts and permafrost dynamics.

REFERENCES

Gibson, C.M., Chasmer, L.E., Thompson, D.K., Quinton, W.L., Flannigan, M.D., and Olefeldt, D. 2018. Wildfire as a major driver of recent permafrost thaw in boreal peatlands. Nature Communications, 9(1), 3041. https://doi.org/10.1038/s41467-018-05457-1

Liu, L., Jafarov, E.E., Schaefer, K.M., Jones, B.M., Zebker, H.A., Williams, C.A., et al. 2014. InSAR detects increase in surface subsidence caused by an Arctic tundra fire. Geophysical Research Letters, 41(11), 3906–3913. https://doi.org/10.1002/2014GL060533

O'Neill, H.B., Wolfe, S.A., and Duchesne, C. 2019. New ground ice maps for Canada using a paleogeographic modelling approach. The Cryosphere, 13(3), 753–773. https://doi.org/10.5194/tc-13-753-2019

Schuur, E.a.G., McGuire, A.D., Schädel, C., Grosse, G., Harden, J.W., Hayes, D.J., et al. 2015. Climate change and the permafrost carbon feedback. Nature, 520(7546), 171–179. https://doi.org/10.1038/nature14338

Travers-Smith, H., Lantz, T.C., Fraser, R.H., and Kokelj, S.V. 2022. Changes in surface water dynamics across northwestern Canada are influenced by wildfire and permafrost thaw. Environmental Research Letters, 17(11), 114021. https://doi.org/10.1088/1748-9326/ac97f7

Veraverbeke, S., Delcourt, C.J.F., Kukavskaya, E., Mack, M., Walker, X., Hessilt, T., et al. 2021. Direct and longer-term carbon emissions from arctic-boreal fires: A short review of recent advances. Current Opinion in Environmental Science & Health, 23, 100277. https://doi.org/10.1016/j.coesh.2021.100277

Yanagiya, K., Furuya, M., Danilov, P., and Iwahana, G. 2023. Transient Freeze-Thaw Deformation Responses to the 2018 and 2019 Fires Near Batagaika Megaslump, Northeast Siberia. Journal of Geophysical Research: Earth Surface, 128(2), e2022JF006817. https://doi.org/10.1029/2022JF006817

Yanagiya, K., and Furuya, M. 2020. Post-Wildfire Surface Deformation Near Batagay, Eastern Siberia, Detected by L-Band and C-Band InSAR. Journal of Geophysical Research: Earth Surface, 125(7), e2019JF005473. https://doi.org/10.1029/2019JF00547

Permafrost response to extreme warm summer inferred by InSAR ground deformation

Jie Chen, Simon Zwieback & Franz J. Meyer
Geophysical Institute, University of Alaska Fairbanks, Fairbanks, Alaska, United States

Climate warming and extremes have promoted widespread thawing of ice-rich permafrost, which results in ground subsiding and water cumulative in the surface. These processes alter surface microtopography and moisture conditions, which, in turn, providing feedbacks to permafrost stability in the subsequent years. Yet, the feedbacks of permafrost in response to an extreme warming summer in the following years remains inadequately understood.

We employed Sentinel-1 InSAR-derived ground deformation for evaluating permafrost response to extreme warm summer. Pronounced late-season subsidence has been attributed to the thawing of ice-rich top-of-permafrost due to the extreme warm summer in 2019 in Northwest Alaska (Zwieback and Meyer 2021). Here, intra- and inter-annual ground deformation are quantified during 2017–2023 in Northwest Alaska. The influence of extreme warm summers on the subsequent years is then determined by the joint analysis of spatiotemporal variability of ground deformation and meteorological data.

METHODS

Deformation time series from 2017 to 2023 were estimated from Sentinel-1 IW images using a Small Baseline Subset (SBAS) approach. We constructed intra-annal pairs with a temporal baseline not exceeding 36 days, whereas the inter-annal pairs with thresholds in between 350 to 380 days. A power-spectrum adaptive filter with an exponent value of 0.9 was conducted to mitigate the severe decorrelation. To mitigate the tropospheric artefacts, we manually selected reference points primarily in bedrocks assumed to be stable. We applied Kriging methods to interpolate the tropospheric phase screens based on reference points and subtracted them individually.

To assess temporal variability in ground deformation, we employed three distinct metrics across different stages of thawing: total summer thaw subsidence relative to the thaw onset of each summer, late-season subsidence during late-thaw season, and cumulative interannual deformation relative to the first thaw onset. In our study, based on MERRA2 air temperature data, we determined the dates of thaw onset, late-thaw, and the end of thaw season as June 10, August 5, and September 20, respectively. We identified ice-rich permafrost terrains by applying a late-season subsidence threshold of 2.5 cm/year based on data from 2019 (Figure 1b), which was evaluated against independent ground ice maps (Zwieback and Meyer 2021). Two specific subregions were chosen for evaluating their spatiotemporal variability (the blue polygon in Figure 1a).

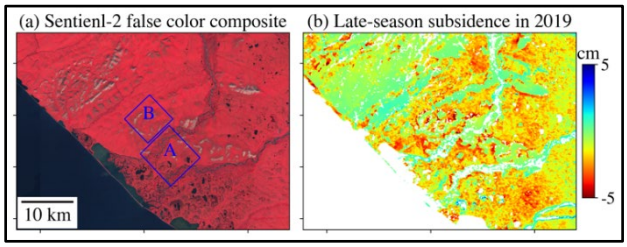

Figure 1. Study area. (a) Sentinel-2 false color composite map. (b) late-season subsidence in 2019.

RESULTS AND DISCUSSIONS

The total summer thaw subsidence in the two subregions for each individual year between 2017 and 2023 is depicted in Figure 2. The degree days of thawing (DDT, ℃·days) were obtained using MERRA2 reanalysis air temperature data (Figure 2a). The largest summer thaw subsidence was observed during the extreme warm summer of 2019 with a DDT value of 1348 ℃·days, followed by the subsequent year of 2020. After 2020, the summer thaw subsidence returned to a level comparable to the pre-extreme years. Although the DDT in 2020 was smaller than 2018 (Figure 2a), the summer thaw subsidence was larger than that in 2018. This suggests a potential legacy of the extreme warm summer in 2019.

The cumulative interannual deformation in the two subregions during 2017-2023 are illustrated in Figure 3. We observed sustained subsidence in geological units with ice-rich permafrost. Furthermore, as illustrated by the pink dashed and green dashed lines in Figure 3, the interannual trajectory of surface position variations showed distinct patterns at the end of thaw season compared to thaw onset. At the end of each thaw season, the most pronounced sustained subsidence was observed in 2019, while subsequent years showed less subsidence. Conversely, at the onset of each thaw period, the surface position consistently decreased and stabilized two years after

the exceptionally warm year of 2019. The InSAR observations point to a significant thaw of ice-rich permafrost during an extreme warm summer, followed by a sustained thaw and then stabilization.

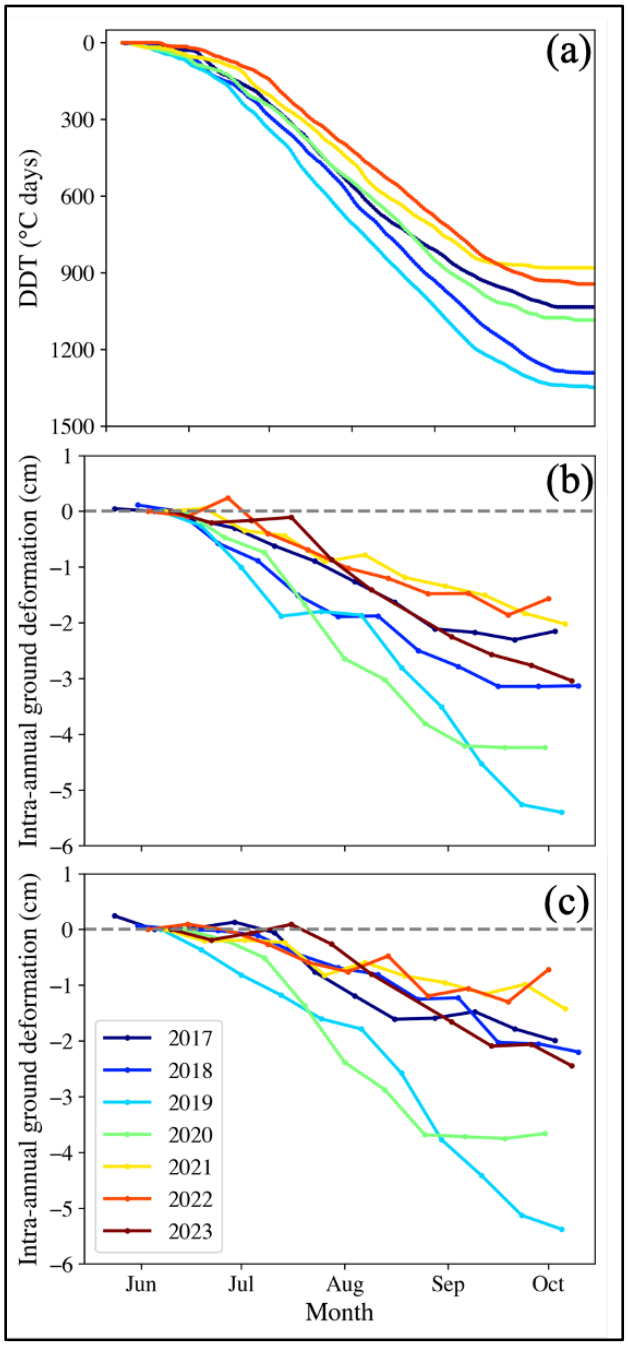

Figure 2. (a) The degree days of thawing (DDT) during 2017–2023 based on MARRA2 reanalysis air temperature data. The time series of mean summer thaw subsidence in the subregions (b) A and (c) B as shown in Figure 1a.

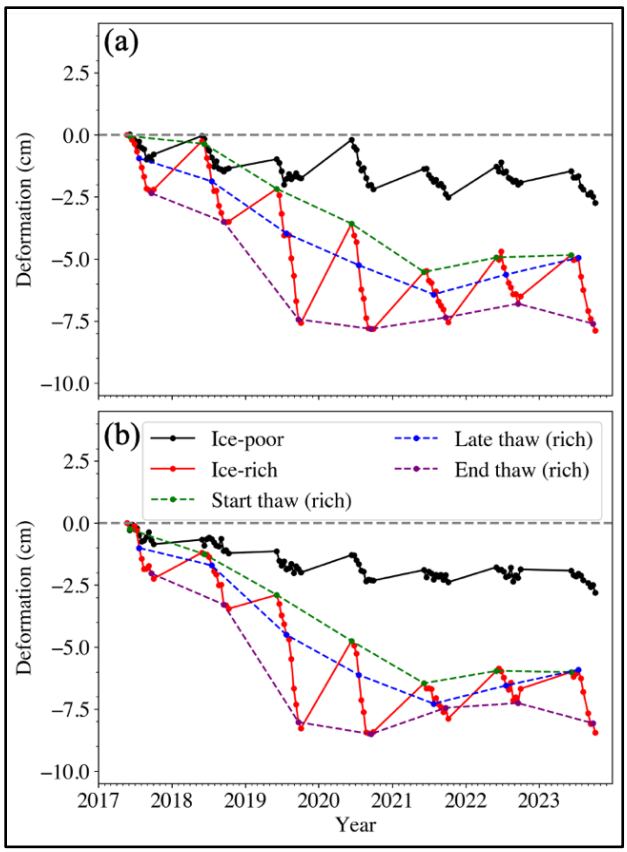

Figure 3. The time series of mean cumulative deformation in the subregions (a) A and (b) B as shown in Figure 1a.

CONCLUSION

We illustrated the deformation trajectory of ice-rich permafrost during and after an extreme warm summer. Our analysis reveals that the cumulative thaw subsidence was elevated in the year following an extreme warm period. Furthermore, we observed that the thawing of ice-rich permafrost may adhere to a pattern involving substantial thaw during extreme warm summers, followed by sustained thaw and, ultimately, stabilization processes. This study contributes novel insights into the understanding of how ice-rich permafrost responds to extreme warm summers in subsequent years.

REFERENCE

Zwieback, S., and Meyer, F.J. 2021. Top-of-permafrost ground ice indicated by remotely sensed late-season subsidence. Cryosphere 15, 2041–2055. https://doi.org/10.5194/tc-15-2041-2021

Intercomparison of land surface temperature time series to support permafrost modelling

Sonia Dupuis[1], Sebastian Westermann[2], Frank-Michael Göttsche[3] & Stefan Wunderle[1]

[1]*Institute of Geography and Oeschger Center for Climate Change Research, University of Bern, Switzerland*

[2]*Department of Geosciences, University of Oslo, Norway*

[3]*Institute of Meteorology and Climatology Research, Karlsruhe Institute of Technology, Karlsruhe, Germany*

Northern high latitudes have experienced pronounced warming throughout the last decades, with particularly high temperatures during winter and spring. This warming, up to four times faster in the Arctic (Rantanen et al. 2022), affects sensitive ecosystems, vegetation dynamics, large-scale circulation patterns and the cryosphere (snow, ice, and permafrost). Permafrost, a crucial component of arctic ecosystems, is particularly sensitive to increasing air temperatures and changes in the snow regime. Land surface temperature (LST) can be used as an indicator of the thermal state of the ground and has, in the last decade, been increasingly used in arctic research and permafrost modelling (Batbaatar et al. 2020; Obu et al. 2019; Westermann et al. 2009). LST observations are available from a few in situ stations or climate models. However, these sources are insufficient to capture small-scale land surface characteristics and their response to climate change on a hemispheric scale (Bartsch et al. 2023).

In contrast, spatially comprehensive LST dynamics can be derived from thermal infrared (TIR) radiation measured by satellites. LST datasets based on MODIS (Moderate Resolution Imaging Spectroradiometer) covering twenty years and having a medium spatial resolution of 1 km are currently the most frequently used for permafrost modelling (Bartsch et al. 2023). To retrieve statistically significant changes in Essential Climate Variables (ECV), time series of at least 30 years are needed. Although a number of satellite LST datasets exist with different temporal and spatial resolutions, only the Advanced Very High Resolution Radiometer (AVHRR) data onboard the NOAA and MetOp satellite series covers more than four decades. In May 2023, EUMETSAT published a new AVHRR global area coverage (GAC) fundamental data record (FDR) (EUMETSAT 2023). Based on this dataset, a new LST product for the northern high latitudes (>50°N) has been produced (Dupuis et al. 2023). This dataset is referred to hereafter as '*Pan-Arctic AVHRR LST*'.

To assess the potential for permafrost modelling of the present Pan-Arctic AVHRR LST product, the AQUA MODIS LST dataset generated within the frame of the ESA LST_CCI project (MYDCCI) (Ghent et al. 2022) is used for comparison. The MYDCCI dataset is stable and suitable for climate analysis (Good et al. 2022).

DATA AND METHODS

The MYDCCI dataset provides LST and associated uncertainties at the satellite pixel level. Observations are provided from 2002 until 2018 at a resolution of 0.01°. The Pan-Arctic AVHRR LST dataset has a spatial resolution of 0.05° and provides LST data from 1981 until 2021. The present study considers the following satellites: NOAA-14, 16, 18, 19, and all MetOp satellites.

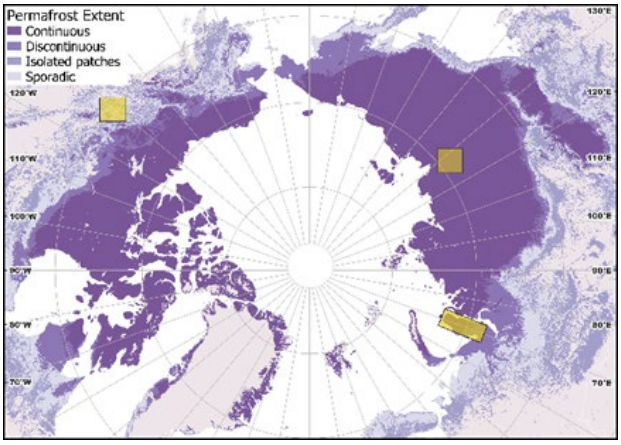

Figure 1. Permafrost extent (adapted from Obu et al. 2019) with AOIs shown in yellow.

The area of interest (AOI) is the whole Northern Hemisphere, but for this study, we selected the following AOI: the Yakutsk region, the Yamal Peninsula, and the Alaska Highway corridor (56° N–61° N) in northwest Canada (see Figure 1). These areas were chosen for their different land covers.

An area corresponding to 3x3 GAC pixels and the corresponding MODIS pixels are extracted. The mean LST value across the AOI is computed. Monthly means are calculated from the daily Pan-Arctic AVHRR LST data. The overlapping period between both datasets (2002-2018) is compared. The Pearson

correlation coefficient (r), the mean difference (MD) and the standard deviation of the MD (SD) are computed to assess the relationship between both datasets.

RESULTS AND DISCUSSION

High correlation coefficients (r >0.9) are found for all three regions (see Table 1). The Yakutsk region has the highest correlation. The predominant land cover for this AOI is dense tree cover. Emissivity retrieval is linked to less uncertainty over dense vegetation, explaining the smaller difference between both LST products.

Table 1. Correlation (r), 95% Confidence Interval (CI), MD and SD for Pan-Arctic AVHRR LST versus MYDCCI.

AOI	Correlation (r) (CI)	MD (SD)
Yakutsk region	0.990 (0.987-0.992)	-1.21 (3.23)
Yamal Peninsula	0.959 (0.947- 0.969)	4.00 (5.11)
Alaska Highway	0.957 (0.941- 0.968)	-6.26 (5.05)

Figure 2 shows the relationship between the two products. Better agreement is found in summer than in winter. This could be due to different thresholds applied to snow cover and different methods for assigning emissivity to snow cover (Ghent et al. 2022).

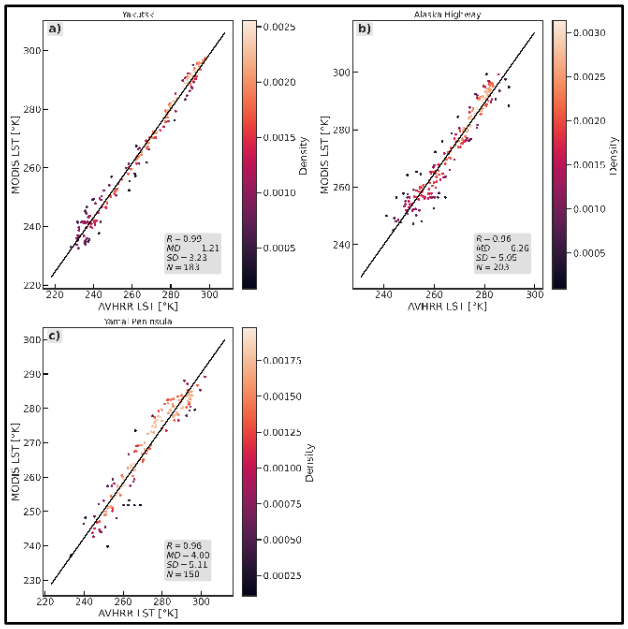

Figure 2. Pan-Arctic AVHRR LST versus MYDCCI relationships.

Overall, the Pan-Arctic AVHRR LST product shows promising performances for the investigated period (2002–2018). This encourages further use AVHRR LST product, starting in 1980, for permafrost modelling. Monthly data are used for the comparisons to have less noisy time series and a more stable density of observations with time, as cloudy pixels in the considered latitudes are frequent. This also motivated Obu et al. (2019) to perform equilibrium permafrost modelling with 8-day temperature averages. In the future, the current 4 km resolution of the AVHRR dataset will be downscaled to 1 km, matching the MYDCCI resolution.

REFERENCES

Bartsch, A., Strozzi, T., and Ingmar, N. 2023. Permafrost Monitoring from Space, Surveys in Geophysics, 44:1579–1613. https://doi.org/10.1007/s10712-023-09770-3

Batbaatar, J., Gillespie, A.R., Sletten, R.S., Mushkin, A., Amit, R., Liaudat, D.T., Liu, L., and Petrie, G. 2020. Toward the detection of permafrost using land-surface temperature mapping, Remote Sensing, 12(4):695. https://doi.org/10.3390/rs12040695

Dupuis, S., Göttsche, F-M., and Wunderle, S. 2023. A Northern hemisphere perspective on Land Surface Temperature variability and trends of the last 40 years, In EMSC, EUMETSAT, Malmö, Sweden.

EUMETSAT. 2023: AVHRR Fundamental Data Record - Release 1 - Multimission, European Organisation for the Exploitation of Meteorological Satellites. http://doi.org/10.15770/EUM_SEC_CLM_0060

Ghent, D., Veal, K., and Perry, M. 2022. ESA Land Surface Temperature Climate Change Initiative (LST_cci): Monthly land surface temperature from MODIS) on Terra, level 3 collated (L3C) global product (2000-2018), version 3.00. NERC EDS Centre for Environmental Data Analysis. 2022. https://dx.doi.org/10.5285/32d7bc64c7b740e9ad7a43589ab91592

Good, E.J., Aldred, F.M., Ghent, D.J., Veal, K.L., and Jimenez, C. 2022. An Analysis of the Stability and Trends in the LST_cci Land Surface Temperature Datasets over Europe, Earth and Space Science, 9(9). https://doi.org/10.1029/2022ea002317

Obu et al., 2019. Northern Hemisphere permafrost map based on TTOP modelling for 2000–2016 at 1 km2 scale. 2019. Earth-Science Reviews, 193: 299–316. https://doi.org/10.1016/j.earscirev.2019.04.023

Rantanen, M., Karpechko, A.Y., Lipponen, A., Nordling, K., Hyvärinen, O., Ruosteenoja, K., Vihma, T., and Laaksonen, A. 2022. The Arctic has warmed nearly four times faster than the globe since 1979, Commun Earth Environ, 3:168. https://doi.org/10.1038/s43247-022-00498-3

Westermann, S., Uers, J.L., Langer, M., Piel, K., and Boike, J. 2009. The annual surface energy budget of a high-arctic permafrost site on Svalbard, Norway, The Cryosphere, 3:245–263. www.the-cryosphere.net/3/245/2009/

Characterization of an "open" ice-wedge polygons network, Rankin Inlet, Nunavut, Canada

Roxanne Frappier & Jorien Vonk
Department of Earth Sciences, Vrije Universiteit Amsterdam, Netherlands

Thawing of permafrost has already caused substantial damages to Arctic ecosystems, some of which are approaching irreversibility (IPCC 2023). It is therefore crucial to better understand permafrost ecosystems, their state and feedback mechanisms. Recently, more attention has been given to the potential role of permafrost thaw in releasing important stocks of soil organic carbon (SOC), further enhancing climatic changes and their impacts (Schuur et al. 2015). The decomposition of SOC after permafrost thaw is influenced by both the SOC composition and the environmental conditions, such as nutrient and moisture availability (Van Huissteden 2020).

Ice-wedge (IW) polygons, which represent one of the most widespread landforms of permafrost environments, have a major influence on permafrost hydrology and carbon cycling (Liljedahl et al. 2016). In polygonal terrain, microtopography, vegetation and soil moisture varies depending on the polygon type (i.e., low- or high-centered) and development stage (i.e., developing, degrading or stabilized) that both influence surface and subsurface conditions (Wainwright et al. 2015; Liljedahl et al. 2016). In order to be able to understand the influence of IW polygons on environmental conditions, the polygons network should be characterized in detail.

In this study, an underexplored coastal permafrost landscape interspersed by IW polygons on the western coast of Hudson Bay (Nunavut, Canada) was investigated. A comprehensive description of the IW polygons network is provided, including 1) a high-resolution mapping of the distribution of the IW network across the study area; 2) a comparison of their distribution with landscape parameters; 3), a characterization of the IWs state; and 4) an estimation of wedge ice volume for the entire IW network.

Study area

The study area is located in Rankin Inlet, a hamlet on the western coast of Hudson Bay in the Kivalliq Region of Nunavut, Canada. After the last deglaciation, the region was submerged by the Tyrell Sea, a post-glacial inland sea that invaded the isostatically depressed Hudson's Bay basin (Randour et al. 2016). Isostatic rebound caused the land to emerge, and cold climatic conditions allowed for permafrost to form. Today, the area still experiences one of the highest rates of isostatic rebound and permafrost is still evolving (Leblanc and Oldenborger 2021).

The area is located within the continuous permafrost zone and is characterized by many periglacial landforms (e.g., IW polygons, mud boils, palsas, solifluction lobes) (GSC 2017). Land cover is dominated by heathlands, graminoids, lichen tundra, and rock complexes (Campbell et al. 2012). Surficial deposits mainly consist of glacial sediments, marine sediments, and bedrock. Topography is low with some undulating bedrock hills, eskers, moraines and drumlins (GSC 2017). The landscape drains towards Hudson Bay via two main fluvial systems (Char and Meliadine rivers). Lakes are widespread and found in relation with bedrock basins and glacial landforms. Mean annual air temperature was -10.3°C for the 1981-2019 period in Rankin Inlet, with an average increase of ca. 0.05°C/year (Leblanc and Oldenborger 2021).

Methods

The IW network was manually mapped in Esri's ArcGIS Pro 3.2.0 from high-resolution satellite imagery (GeoEye-1, Maxar technologies, res.: 0.4 m) by delineating the centerlines of troughs. Then, the distribution of troughs was compared to the distribution of landscape parameters (i.e., elevation, slope, surficial deposits, and landcover) to identify determining factors of IW development in the area and create a map showing frost-susceptible land. Next, the state of IWs was determined based on a characterization of troughs wetness, which was derived from high-resolution near-infrared top-of-atmosphere reflectance. A hot spot analysis was performed and allowed for identification of wetter and drier areas. These hot spots were related to landscape parameters to establish potential relationships and feedbacks between IW troughs hydrological conditions and topography. Finally, the mapped IW troughs network was used to estimate volume of wedge ice in the study area by creating a three-dimensional sub-surface model (3D SSM) representing IWs.

RESULTS AND DISCUSSION

The IW trough network map shows that IWs are unevenly distributed across the study area, and are absent from the islands in the bay. They are particularly concentrated in flat areas, but also along esker ridges and beach crests and spits left behind by the Tyrell Sea as it receded.

Comparison with landscape parameters reveals that IWs develop in diverse elevation ranges and that they preferentially develop on slope ranges of 0-2° and 2-4°. While IWs are typically found in low-gradient terrain, anti-syngenetic IW (i.e., those that develop on denudational slopes) are widespread on hillslopes of the western Canada Arctic coast (Mackay 1995). Here, we find that the steepest IWs developed on the slopes of the main esker ridge, as well as in association with solifluction lobes and paleo-beaches. Two hypotheses can explain the presence of these sloping IWs: 1) They may have formed on the slopes as anti-syngenetic IWs, or 2) they may have formed on beaches when they were flatter and became obscured by slope processes as they became steeper due to preferential post-glacial uplift.

Additionally, we observed that the IWs are associated with all landcover types, but tend to be absent from sand, gravel, and rock deposits. They also preferentially form in organic, glaciofluvial, alluvial and marine deposits, and they are almost absent in glacial deposits reworked by marine waves and current action. This, along with their presence on paleo-beaches, is consistent with IWs developing more easily in finer materials, because these are more susceptible to cracking (French 2018).

We also find a relationship between IW troughs wetness, and the slope on which they develop, with higher slope forming better drained, dryer IWs. We also expect to observe a relationship between polygon sizes, or trough segment lengths, and slope, as better drained terrain has a lower coefficient of thermal contraction, which leads to less cracking, and therefore larger polygons (French 2018).

CONCLUSION

This study characterizes the entire IW network of a coastal permafrost landscape. Not only do the methods provide insight into IW network mapping and characterization, but the results highlight the importance of considering the entire IW network (i.e., including open polygons) to provide a complete portrait of the distribution of IWs. We consider the approach used in this study to be valuable for future investigations of IW terrain to more accurately characterize ground ice content, microtopography, drainage patterns, and the inferred landscape vulnerability to degradation and SOC release.

REFERENCES

Campbell, M.W., Shaw, J.G., and Blyth, C.A. 2012. Kivalliq Ecological Land Classification Map Atlas: A Wildlife Perspective. Government of Nunavut, Department of Environment. Technical Report Series #1-2012.

GSC; Geological Survey of Canada. 2017. Surficial geology, Rankin Inlet, Nunavut, NTS 55-K/16; Canadian Geoscience Map 68, scale 1:50 000.

French, H.M. 2018. The periglacial environment. 4th ed. John Wiley & Sons, Hoboken, NJ, USA.

IPCC; Intergovernmental Panel on Climate Change. 2023. Climate Change 2023: Synthesis Report. Contribution of Working Groups I, II and III to the Sixth Assessment Report of the IPCC [Core Writing Team, H. Lee and J. Romero (eds.)]. IPCC, Geneva, Switzerland.

LeBlanc, A.-M., and Oldenborger, G.A. 2021. Ground temperature, active-layer thickness and ground-ice conditions in the vicinity of Rankin Inlet, Nunavut, In Summary of Activities 2020, Canada-Nunavut Geoscience Office, 63–72.

Liljedahl, A., Boike, J., Daanen, R., et al. 2016. Pan-Arctic ice-wedge degradation in warming permafrost and its influence on tundra hydrology. Nature Geosci., 9, 312–318.

Mackay, J.R. 1995. Ice Wedges on Hillslopes and Landform Evolution in the Late Quaternary, Western Arctic Coast, Canada, Canadian Journal of Earth Sci., 32(8), 1093–1105.

Randour, I., McMartin, I., and Roy, M. 2016. Study of the post-glacial marine limit between Wager Bay and Chesterfield Inlet, western Hudson Bay, Nunavut, In Summary of Activities 2016, Canada-Nunavut Geoscience Office, 51–60.

Schuur, E., McGuire, A.D., Schädel, C., et al. 2015. Climate change and the permafrost carbon feedback. Nature, 520(7546), 171–179.

van Huissteden, J. 2020. Thawing Permafrost, Permafrost Carbon in a Warming Arctic. Springer Nature, Cham, Switzerland.

Wainwright, H., Dafflon, B., Smith, L., et al. (2015). Identifying multiscale zonation and assessing the relative importance of polygon geomorphology on carbon fluxes in an Arctic tundra ecosystem. Journal of Geophys. Res; Biogeosci., 120(4), 788–808.

Lake colour change across northern Canada, 1984–2021

Genevieve George, Anders Knudby & Antoni G. Lewkowicz
Department of Geography, Environment and Geomatics, University of Ottawa, Ottawa, Ontario, Canada

Thawing permafrost in northern Canada can impact the water quality in inland lakes by triggering geomorphic activity that releases sediment and organic matter downstream. This increased input of terrestrial matter can change the physical and chemical properties of lakes, which can affect trophic system dynamics, change carbon fluxes, and affect human activities that depend on clear lake water (Wauthy et al. 2018). Changes to the amount and kinds of particulate matter in lakes also affects their optical properties and can lead to drastic lake colour change (Graneli 2012). Lake colour change has been sporadically identified and studied in northern Canada (Bouchard et al. 2014; Lewkowicz and Way 2019; Watanabe et al. 2011), but its magnitude, as well as any spatial and temporal trends, remains unknown (Wauthy et al. 2018).

Effective monitoring of lakes is useful to understand more far-reaching implications of climate change because lakes can function as sentinels of environmental change (Williamson et al. 2008). The inaccessibility of much of northern Canada is a challenge for Arctic scientists studying the rapidly changing landscape (Canadian Polar Commission 2015), and the geographic distribution and remoteness of northern lakes in Canada makes large scale monitoring of lake water quality change a challenging task. In particular, the spatially and temporally limited coverage of water quality sampling, and the temporal variability of the permafrost environment, make traditional monitoring methods cost-prohibitive if applied across such a large area. However, lake colour change is a phenomenon that can be observed from satellite imagery. Landsat satellite imagery is free to use and available at 30-m resolution since 1982, making it suitable for large-scale and long-term monitoring of lake water. Landsat data can be used to detect differences in water colour and thereby estimate specific water quality parameters such as total suspended solids, Secchi disk depth, dissolved organic carbon, chromophoric dissolved organic matter, and chlorophyll a concentration (Gholizadeh et al. 2016).

Methods

This study used Landsat data from 1984 to 2021 processed in Google Earth Engine to analyze the spatial and temporal pattern of lake colour change in Canada, north of 60°N. We created biennial composite mosaics with the 25th percentile pixel reflectance value from all valid cloud- and ice-free Landsat pixels over each two-year period from 1984 to 2021. Lakes were defined as groups of contiguous water pixels from the Global Surface Water dataset (Pekel et al. 2016) greater than one hectare in size. According to this definition, a total of 1,453,464 lakes were identified and used in this study. We defined five optical change indicators: surface reflectance in the blue, green, red, and near-infrared bands, as well as turbidity calculated from the red band. The pixel values for each lake were first summarized zonally into median values for each lake in each mosaic, and then temporally, into Mann-Kendall statistic and Theil-Sen slope values of each change indicator for each lake across all mosaics. The time series statistics for each lake were then used as inputs to a random forest classifier to assign a value of changed or unchanged to each lake in the study area.

Results

The model classified 22.9% of the lakes as changed, with an overall accuracy of 91.8% and an AUC score of 0.95. Lake size appeared to influence the likelihood of colour change. Almost 23% of smaller lakes (1-500 ha in area) changed colour while only 14% of large lakes (>500 ha) did so. Changing lakes were clustered in coastal areas and several inland regions (Figure 1a). Each changed lake was also assigned a year of change based on the year of greatest absolute interannual change in the time series of green band reflectance. The pattern across the entire study area showed early peaks of change in 1986 and 1994, and more recent smaller peaks of change in 2008, 2012, and 2020. The pattern of temporal change was highly variable by region (Figure 1b).

Areas with many lakes undergoing or having undergone change are geographically diverse, both in terms of their location and their permafrost and substrate conditions. The type of colour change was likewise diverse across these areas, with some lakes undergoing simple and obvious change from one year to the next, and others undergoing gradual or continuous change across an extended time period. These findings indicate that the processes driving lake colour change are likely dependent on local factors, some permafrost-related and some not.

As lake dynamics are important indicators of change in northern landscapes, these findings will help to improve monitoring efforts and increase understanding

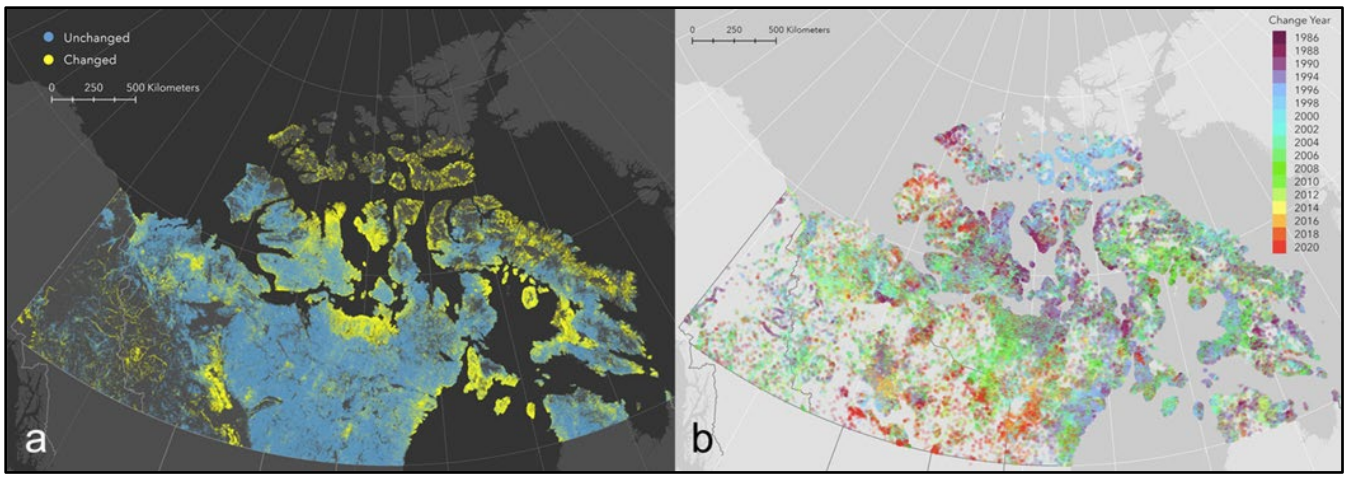

Figure 1. a) Changed and unchanged waterbodies across northern Canada represented by their centroid points. Points are 95% transparent so regions with brighter colours indicate higher waterbody density. Legend symbols enlarged for clarity. b) Maximum year of change in the green band for all changed lakes. The year represents the later of the two years used to calculate the difference, e.g., 2020 indicates that the greatest difference in reflectance values for a particular lake was between 2018 and 2020.

of the spatial and temporal patterns in the landscape's response to a rapidly warming climate. By identifying clusters of significant lake colour change across northern Canada, this study contributes important information for future studies on the local patterns and mechanisms contributing to water colour change and other climate-change driven impacts in the region. The image-processing code for this project will be made publicly available for transparency and to provide a basis for future large-scale water quality monitoring projects.

REFERENCES

Bouchard, F., Francus, P., Pienitz, R., Laurion, I., and Feyte, S. 2014. Subarctic Thermokarst Ponds: Investigating Recent Landscape Evolution and Sediment Dynamics in Thawed Permafrost of Northern Québec (Canada). Arctic, Antarctic, and Alpine Research, 46(1), 251–271. https://doi.org/10.1657/1938-4246-46.1.251

Canadian Polar Commission. 2015. State of Environmental Monitoring in Northern Canada. www.polarcom.gc.ca

Gholizadeh, M.H., Melesse, A.M., and Reddi, L. 2016. A comprehensive review on water quality parameters estimation using remote sensing techniques. In Sensors (Switzerland). https://doi.org/10.3390/s16081298

Graneli, W. 2012. Brownification of lakes. In Bengtsson, L., Herschy R.W. (Ed.), Encyclopedia of Earth Sciences Series (pp. 117–119). Springer Netherlands. https://doi.org/10.1007/978-1-4020-4410-6_256

Lewkowicz, A.G., and Way, R.G. 2019. Extremes of summer climate trigger thousands of thermokarst landslides in a High Arctic environment. Nature Communications, 10(1). https://doi.org/10.1038/s41467-019-09314-7

Pekel, J.-F., Cottam, A., Gorelick, N., and Belward, A.S. 2016. High-resolution mapping of global surface water and its long-term changes. Nature 540 no. 7633: 418–422. https://doi.org/10.1038/nature20584

Watanabe, S., Laurion, I., Chokmani, K., Pienitz, R., and Vincent, W.F. 2011. Optical diversity of thaw ponds in discontinuous permafrost: A model system for water color analysis. J. Geophys. Res, 116, 2003. https://doi.org/10.1029/2010JG001380

Wauthy, M., Rautio, M., Christoffersen, K.S., Forsstr€, L., Laurion, I., Mariash, H.L., Peura, S., Vincent, W.F., Stanley, E., and Del Giorgio, P. 2018. Special Issue-Letter Increasing dominance of terrigenous organic matter in circumpolar freshwaters due to permafrost thaw. Limnology and Oceanography Letters, 3, 186–198. https://doi.org/10.1002/lol2.10063

Williamson, C.E., Dodds, W., Kratz, T.K., and Palmer, M.A. 2008. Lakes and streams as sentinels of environmental change in terrestrial and atmospheric processes. In Frontiers in Ecology and the Environment (Vol. 6, Issue 5, pp. 247–254). John Wiley & Sons, Ltd. https://doi.org/10.1890/070140

Automated mapping of rusting rivers in permafrost landscapes

Emily Graham[1], Julia White[1], Soumitra Sakhalkar[1] & Simon Zwieback[1,2]

[1]*Geophysical Institute, University of Alaska Fairbanks, Fairbanks, Alaska, United States*

[2]*Department of Geosciences, University of Alaska Fairbanks, Fairbanks, Alaska, United States*

In recent decades, there has been a rapid increase in warming within the northern high-latitude regions of the Arctic, leading to increasing permafrost degradation. This response to climate warming could have further implications for the geochemical compositions of rivers and watersheds in the Arctic, via the infiltration and transport of trace elements, increasing carbon mobilization, among other factors (Pokrovsky et al. 2011).

In recent years, orange rivers and creeks have been observed in multiple locations across Alaska. These rusting river reaches are commonly characterized by elevated turbidity, low pH, and red-stained deposits on the floodplains. The rusting disrupts the aquatic ecosystems, alters the water quality, and its ramifications to the local communities who rely on these rivers for sustenance and livelihood, among others.

The causes of the apparent increase in rusting in Arctic Alaska are poorly understood. A potential cause is “acid rock drainage”, a suite of mineral weathering processes resulting in acidic, often orange stained outflow known from many regions across the world (Akcil et al. 2006). Permafrost thaw and attendant increases in subsurface hydrological connectivity could stimulate these weathering processes and microbial activity (Barker et al. 2023; Barker et al. 2014).

Automated remote sensing of river rusting across the Arctic is needed to understand the prevalence, causes and consequences of river rusting across the Arctic.

We mapped rusting river reaches in Northwestern Alaska using machine learning. Toward our goal of obtaining Pan-Arctic maps, we tested the transferability of the Random Forest model in space and time.

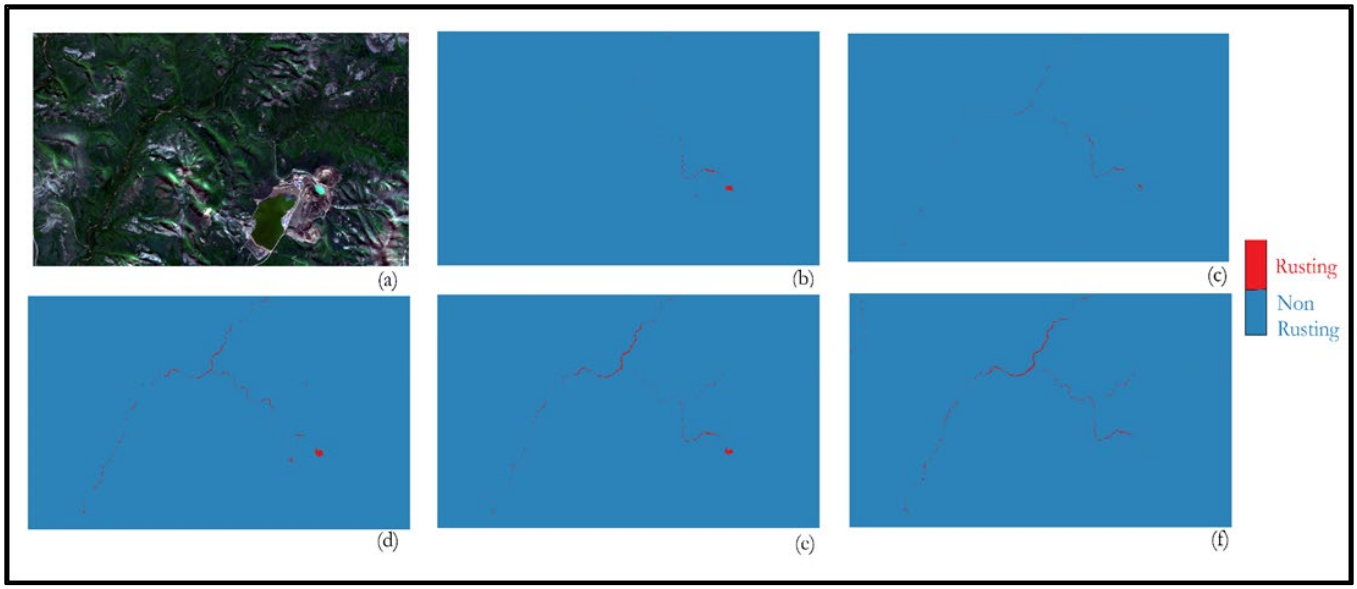

Figure 1. The classification results from one of the sub-regions within the Red Dog mine study site. a) Sentinel-2 composite of year group 1 (2018-2019); b) classified result for year group 1 (2018-19); c) classified result for year group 2 (2019-2020); d) classified result for year group 3 (2020-2021); e) classified result for year group 4 (2021-2022); f) classified result for year group 5 (2022-2023).

METHODS

For the detection and classification of rusting streams, we employed a machine-learning framework. The primary input to the Random Forest are Sentinel-2 imagery (10 and 20 m resolution) and a suite of topographic and hydrographic variables. The output is a binary map of rusting river reaches. To enable upscaling, we used the computational power of Google Earth Engine (GEE).

We trained the Random Forest model on the Red Dog mine area in northwestern Alaska. Training areas were manually delineated along rusting and non-rusting reaches as well as the broader landscape, comprising a total of 4191 training samples. To evaluate the spatial transferability, the model was subsequently tested in basins with contrasting physiographic conditions across the Brooks Range in Alaska. To test the temporal transferability and quantify changes in rusting, we applied the model to imagery from 2018 through 2023, splitting it into five biennial periods (P1: 2018-2019, P2: 2019-2020, P3: 2020-2021, P4: 2021-2022 and P5: 2022-2023).

Results and conclusions

We tested the model's temporal transferability in the Red Dog Mine area (Figure 1) using a total size of 8577 samples, with 1000 to 3000 samples per period. Good transferability is indicated by FScores and Kappa values of up to 0.98 in P5, with lower values in earlier years with less rusting.

The spatial transferability to Anaktuvuk Pass is limited, as the Fscores varied between 0.36 and 0.73. This indicates that the initial training sample is insufficient to transfer the model to the less vegetated, topographically more complex Anaktuvuk Pass region. Preliminary, qualitative results from additional regions in Alaska further indicate adequate spatial transferability across physiographically similar areas.

The preliminary results highlight the potential of machine learning for mapping rusting river reaches from freely available Sentinel-2 imagery. Machine learning enables automated mapping and change detection across the Arctic. Our data products will support process-based studies of the causes and climate drivers and support assessments of the environmental consequences of river rusting in permafrost regions.

References

Akcil, A., and Koldas, S. 2006. Acid Mine Drainage (AMD): causes, treatment and case studies. Journal of cleaner production, 14(12-13), pp.1139–1145. doi:10.1016/j.jclepro.2004.09.006

Barker, A.J., Douglas, T.A., Jacobson, A.D., McClelland, J.W., Ilgen, A.G., Khosh, M.S., Lehn, G.O., and Trainor, T.P. 2014. Late season mobilization of trace metals in two small Alaskan arctic watersheds as a proxy for landscape scale permafrost active layer dynamics. Chemical Geology, 381, pp.180–193. doi:10.1016/j.chemgeo.2014.05.012

Barker, A.J., Sullivan, T.D., Baxter, W.B., Barbato, R.A., Gallaher, S., Patton, G.E., Smith, J.P., and Douglas, T.A. 2023. Iron Oxidation–Reduction Processes in Warming Permafrost Soils and Surface Waters Expose a Seasonally Rusting Arctic Watershed. ACS Earth and Space Chemistry, 7(8), pp.1479–1495. doi:10.1021/acsearthspacechem .2c00367

Duke, C., and Steele, J. 2010. Geology and lithic procurement in Upper Palaeolithic Europe: a weights-of-evidence based GIS model of lithic resource potential. Journal of Archaeological Science, 37(4), pp.813–824. doi:10.1016/j.jas.2009.11.011

Moore, D.W. et al. (1986) 'Geologic setting and genesis of the red dog zinc-lead-silver deposit, Western Brooks Range, Alaska', Economic Geology, 81(7), pp. 1696–1727. doi:10.2113/gsecongeo.81.7.1696

Pokrovsky, O.S., Shirokova, L.S., Kirpotin, S.N., Audry, S., Viers, J., and Dupré, B. 2011. Effect of permafrost thawing on organic carbon and trace element colloidal speciation in the thermokarst lakes of western Siberia. Biogeosciences, 8(3), pp.565-583. doi:10.5194/bg-8-565-2011

The Ka-band interferometric radar mission proposal for cold environments

Irena Hajnsek[1,2], Guðfinna Th Aðalgeirsdóttir[3], Marc Rodriguez Cassola[1], Georg Fischer[1], Guido Grosse[4], Christian Haas[4], Sigurd Huber[1], Katarina Jesswein[5], Andreas Kääb[6], Jung-hyo Kim[7], Gerhard Krieger[1], Benoit Montpetit[8], Alberto Moreira[1], Tobias Otto[5], Kostas Papathanassiou[1], Helmut Rott[9], Tazio Strozzi[10], Volker Tesmer[5], Michelangelo Villano[1], Sebastian Westermann[6], Marwan Younis[1] & Mariantonietta Zonno[1]

[1]*Microwaves and Radar Institute, German Aerospace Center DLR, Germany*

[2]*Institue of Environmental Engineering ETH Zurich, Switzerland*

[3]*University of Iceland, Faculty of Earth Science, Island*

[4]*Alfred-Wegener-Institute, Potsdam, Germany*

[5]*OHB, Germany*

[6]*University of Oslo, Norway*

[7]*Airbus, Germany*

[8]*National Wildlife Research Center, Environment and Climate Change Canada, Canada*

[9]*ENVEO IT, Innsbruck, Austria*

[10]*GAMMA Remote Sensing, Switzerland*

We suggest to present a mission proposal submitted to the Earth Explorer 12 call that aims to address and quantify dynamic processes in cold environments by measuring the static and dynamic topography. This information is essential for understanding, modelling and forecasting the dynamics and interactions within the different elements of the cryosphere and with other Earth system components. The mission proposal will provide very accurate high-resolution, multi-temporal topographic data that will make it possible to derive mass balances and structural changes in the cryosphere, with a focus on permafrost areas as well as glaciers and ice caps, ice sheets and sea ice. At the same time, the mission proposal will enable unprecedented measurements of volume change processes in the geosphere, including volcanic, landslide and seismic activities. In addition, the mission proposal will generate a global digital elevation model (DEM) of about one order of magnitude better, in terms of resolution and height accuracy, then the current reference provided by TanDEM-X.

The instrument consists of a cross-platform Ka-band radar interferometer with two spacecraft that fly in a reconfigurable formation and can dynamically adapt to the needs of scientific observation. Cross-track SAR interferometry is an established remote sensing technique for large-scale measurements of static and dynamic topography and the use of Ka-band minimizes systematic biases and errors that would be caused at lower frequencies due to wave penetration into semi-transparent media.

The mission proposals unique ability to provide time series of highly accurate surface topography measurements allows the mission's primary scientific objectives to be optimally fulfilled, namely:

a) the monitoring of permafrost degradation by means of DEM acquisitions with short repetition intervals and estimates of volume changes in time,

b) the measurement of snow topographic changes to observe different snow regimes to feed hydrological models for a more precise prediction of water availability, and

c) the measurements of glaciers, ice caps, ice-clad volcanoes and their mass balance and modelling of ice dynamics and ice/climate interactions.

At the same time, the SKADI measurements allow to serve a number of secondary science objectives related to floating ice and geosphere applications such as:

a) the measurement of sea ice and fresh water ice topography to define the surface-air-interface,

b) the monitoring of geohazards involving large deformations and volume changes caused by landslides, glacier lake outbursts, rockfalls, mining, landfill, volcanic activities and seismic events,

c) the measurement of a global DEM with unprecedented resolution and accuracy.

The mission proposal will moreover complement and fill critical observation gaps of the current Copernicus and Earth Explorer missions (e.g., Sentinel, Cryosat) by providing frequency diversity and enhanced spatial resolution, while at the same time offering the Earth Observation community and future ESA missions (e.g., Aeolus, EarthCARE) a global topographic reference of superior accuracy and resolution, which enables a major step forward in improving the quality and interpretation of a vast amount of past, present, and future Earth observation

data. A first order performance of the mission products reveal that very accurate DEM change products can be expected, with accuracies in the order of decimetres to centimetres.

In comparison to previous SAR missions, the short wavelength in Ka-band allows a reduction of the size and weight of the antennas and spacecraft and enables the joint launch of two radar satellites with a single medium-sized launch vehicle like Vega C. In this regard, the mission proposal space segment offers also a unique platform to explore and demonstrate new bi- and multistatic SAR techniques, technologies and applications which are expected to shape the future of radar remote sensing.

The mission concept and the associated space segment have been developed in two Pre-Phase 0 studies in close collaboration with Airbus DS and OHB. Both industry partners proposed innovative Ka-band SAR instrument architectures and showed the feasibility of the current mission proposal within the programmatic constraints and the cost cap provided by ESA in its call for Earth Explorer 12 mission ideas. We believe that the versatility and technological innovation of the mission proposal are an important complement to its unique scientific objectives, thereby increasing its impact on societal welfare.

The consolidated mission objectives, the well-defined mission products, the highly accurate performance and the innovative instrument design will be presented. Following the encouraging recommendations provided in the ACEO (Advisory Committee for Earth Observation) report from the EE-11 call, the mission proposal team was submitting a revised version of the mission proposal for the ESA Earth Explorer 12 call in September 2023.

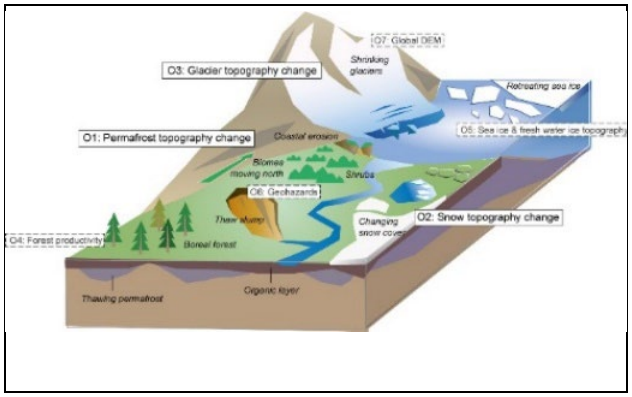

Figure 1. Impact on cold regions due to global warming (modified IPCC scheme) with SKaDI science objectives.

Table 1. Scientific objectives (O1 to O7) of the SKaDI mission.

Objectives Classification	Scientific Objectives
Primary	O1 Permafrost landscape topography
	O2 Snow topographic change
	O3 Topography of glaciers, ice caps, ice-covered volcanos
Secondary	O4 Vegetation structure
	O5 Sea ice & fresh water ice topography
	O6 Geohazards
	O7 Global DEM

The implementation of SKaDI is based on a pair of Ka-band radar satellites that fly in close formation to form a reconfigurable single-pass SAR interferometer with flexible baseline selection. A succinct justification for the selected architecture is given by the two bullets below:

- Why Ka band? The short wavelength of only 0.85 cm ensures a negligible penetration into the media of interest (e.g., snow, ice, soil) and thus prevents systematic errors and biases when measuring the topography and its changes. At the same time, the short wavelength provides sensitivity to small structures together with an excellent geometric and interferometric resolution. Last but not least, the short wavelength allows the size and weight of the antenna and spacecraft to be reduced and enables the joint launch of two satellites with a single medium-sized launch vehicle.
- Why single-pass interferometry with two satellites? SAR interferometry is a cost-effective and well-established remote sensing technique for large-scale measurements of Earth topography and its changes. Moreover single-pass interferometry avoids deteriorations from scene changes, scatterer decorrelation and atmospheric disturbances and is, especially at short wavelengths, a prerequisite for reliable height measurements. Moreover, a twin-platform interferometer, as opposed to a single-platform one, provides a significantly improved height sensitivity and resolution, typically by more than one order of magnitude, while ensuring the flexibility to tune the configuration to the observation needs.

The SKaDI mission proposal builds up on the experience, the know-how and the unique results obtained from the TanDEM-X mission.

REFERENCE

SKaDI proposal submitted to the ESA's EE-12 call, Sep. 2023.

Consequences of wildfires in boreal forests underlain by ice-rich permafrost near Batagay, NE Siberia

Go Iwahana[1,2], Kazuki Yanagiya[3], Masato Furuya[2,4], Petr Danilov[5], Nikolai Fedorov[6], Alexey Desyatkin[7] & Alexander Fedorov[6]

[1]*International Arctic Research Center, University of Alaska Fairbanks, Fairbanks, Alaska, United States*

[2]*Arctic Research Center, Hokkaido University, Sapporo, Hokkaido, Japan*

[3]*Japan Aerospace Exploration Agency, Tsukuba, Ibaraki, Japan*

[4]*Graduate School of Science, Hokkaido University, Sapporo, Hokkaido, Japan*

[5]*Institute of Northern Applied Ecology, North-Eastern Federal University in Yakutsk, Sakha Republic, Russia*

[6]*Yakutsk Permafrost Institute, Yakutsk, Sakha Republic, Russia*

[7]*Institute for Biological Problems of Cryolithozone, Yakutsk, Sakha Republic, Russia*

The increasing frequency of wildfires in the Arctic poses a significant threat to permafrost regions. This study focuses on the irreversible changes wildfires induce in these areas, particularly in regions with ice-rich permafrost. The removal of surface vegetation and organic mat significantly alters the energy and mass balance of these landscapes for decades. Such disturbances can lead to erosion, releasing large amounts of carbon and sediments previously trapped in permafrost for millennia. Global warming has already compromised the stability of Arctic lands, and while numerous studies have reported associated permafrost degradation, our understanding of post-wildfire changes in permafrost landscapes remains limited.

In our research, we examined a series of forest fires that happened up to the year 2019 in the Batagay region of Sakha Republic, Russia. These fires led to increased ground displacement due to thawing permafrost and melting ground ice (thermokarst). Using Interferometric Synthetic Aperture Radar (InSAR) analysis, Yanagiya and Furuya (2020) and Yanagiya et al. (2023) revealed detailed spatio-temporal variations in surface displacement over several years following the wildfires. We extended the analyses of InSAR and also conducted high-resolution optical imagery, coupled with field observations, providing a comprehensive view of the wildfires' overall impact on the landscape and surface soils. The most significant changes observed were gully formations, influenced by natural water cycles and firefighting efforts.

Study areas and methods

Batagay is located in the midstream of the Yana River, NE of Sakha Republic. The area is underlain by at least 50-80 m thick ice-rich permafrost as its interior structure is revealed on the headwalls of a huge thaw slump (Batagaika Megaslump; Murton et al. 2023). Recent wildfires burned an extensive area near Batagay, which triggered prominent thermokarst processes due to the surface disturbance by the fires.

Our study focused on two primary areas of interest for our remote sensing analyses. The first area, referred to as A1, encompasses a 35 km² region impacted by a fire in July 2014, which was partially re-burned in 2019. The second area, A2, includes regions affected by fires in the summers of 2018 and 2019. We established field study sites located at both burned and unburned areas for both areas of interest (Yanagiya et al. 2023).

To analyze ground deformation, we employed InSAR techniques, creating displacement maps of the post-wildfire areas. We used L-band SAR images from ALOS-2/PALSAR-2 (SM3/HH) spanning from 2015 to 2023. To assess long-term ground surface displacement in the burned areas, we utilized a Small Baseline Subset (SBAS)-type time-series analysis with available InSAR data.

In addition to InSAR analysis, we used optical satellite imagery (specifically snow-free and cloud-free) from 2014-2023 to investigate ground surface changes. The 2014 fire perimeter was determined using the difference normalized burn ratio (dNBR; Miller and Thode 2007) from post-fire Landsat 8 images (Collection 2). To identify new gullies and active layer detachment following the 2014 fire, we analyzed changes in the panchromatic band of Landsat 8 images. High-resolution, pan-sharpened optical imagery was also employed to monitor the development of gullies and water drainage patterns in the areas affected by the 2018 and 2019 fires. Furthermore, we conducted fieldwork campaigns over three consecutive thawing seasons from 2019 to 2022. These campaigns involved measuring relative height changes, soil moisture, ground temperature, and thaw depth along established transect lines.

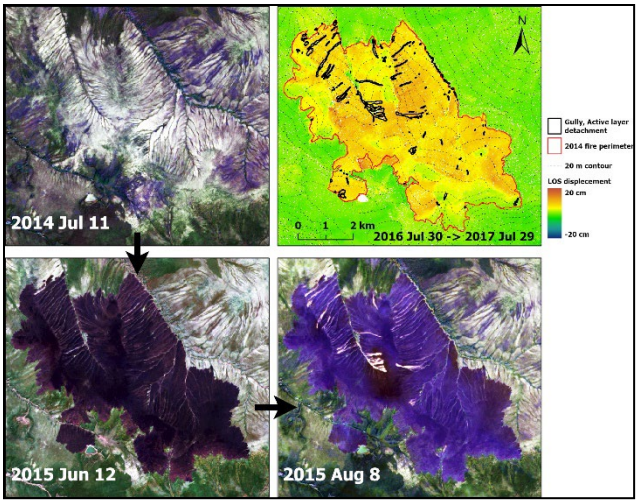

Figure 1. Time series of optical images (Landsat8) over a burn scar by Fire 2014 (A1). InSAR line-of-sight surface deformation map derived from ALOS-2/PALSAR-2 data acquired on 30 Jul 2016 and 29 Jul 2017 (upper right). The positive (reddish colors) and negative (blueish colors) values indicate subsidence and uplift, respectively. The contours are elevated in 20 m intervals. Areas of gully formations and active layer detachment between 12 Jun 2015 and 8 Aug 2015 are also shown as black polygons.

Results and Discussion

InSAR analysis detected long-term trends of ground-surface displacement after the fires. The results indicated that thaw settlement in the first year reached up to 15 cm in the line-of-sight direction, and the interannual trend continued even a few years after the fire with lower magnitudes. The calculated time series indicated that cumulative subsidence has been greater than 30 cm since October 2015 at the area of greatest deformation and the rate of subsidence decreased in the following summers in A1.

In the aftermath of the 2014 and 2019 fires in A1, burned areas experienced a thaw depth about 2.5 times deeper than unburned areas, with shifts in carbon accumulation and higher soil water content. From 2019 to 2021, the thaw depth at burned sites increased significantly more (fourfold) than at unburned sites, along with higher soil moisture levels. The marked differences in physical conditions between burned and unburned sites, including deeper thaw depths and altered soil moisture, are largely attributable to the removal of vegetation and organic matter by wildfires.

In the 2014 burn scar, over 20 gully formations were identified from Landsat 8 images, indicating significant ground surface erosion a year after the fire. These erosions were seen as increased reflectance in satellite imagery and were primarily located along valley lines, especially on northeast-facing slopes. This coincided with areas of greater subsidence post-fire, as observed by InSAR, suggesting that increased soil moisture and thaw depth triggered these erosions.

Soil pit observation and chemical analyses indicated enhanced leaching of ions and micro-elements in the upper active layer at the burned site. In addition, we observed increases in soil moisture and active layer thickness that caused rapid formations of gully and active layer detachment after wildfires in previous sections. This interpretation supports the temporal increase close to a saturated condition in soil moisture in the active layer after wildfires in other permafrost regions.

A2 with the 2018 and 2019 fires, InSAR detected similar enhanced seasonal ground surface displacement and interannual subsidence within the fire scars as observed for A1. In addition to the natural permafrost degradation responding to the fires, fire suppression efforts by local people caused severe gully erosions. Firebreak lines and new roads, stripped of vegetation, acted as drainage channels, leading to rapid erosion, especially during snowmelt.

High-resolution optical images in spring of 2021 revealed overflooding flows and our field observation confirmed new ice-wedge polygon exposures at the gully side walls over 3 meters. These observations suggest that the combination of wildfires and fire suppression activities significantly alters natural runoff and erosion patterns in permafrost ecosystems raising concerns about new large-scale erosions similar to the Batagaika formation.

References

Miller, J.D., and Thode, A.E. 2007. Quantifying burn severity in a heterogeneous landscape with a relative version of the delta Normalized Burn Ratio (dNBR), Remote Sensing of Environment, 109(1), pp. 66–80. https://doi.org/10.1016/j.rse.2006.12.006

Murton, J., et al. 2023. Batagay megaslump: A review of the permafrost deposits, Quaternary environmental history, and recent development, Permafrost and Periglacial Processes, 34(3), pp. 399–416. https://doi.org/10.1002/ppp.2194

Yanagiya, K., and Furuya, M. 2020. Post-Wildfire Surface Deformation Near Batagay, Eastern Siberia, Detected by L-Band and C-Band InSAR, Journal of Geophysical Research: Earth Surface, 125(7), p. e2019JF005473. https://doi.org/10.1029/2019JF005473

Yanagiya, K., et al. 2023. Transient Freeze-Thaw Deformation Responses to the 2018 and 2019 Fires Near Batagaika Megaslump, Northeast Siberia, Journal of Geophysical Research: Earth Surface, 128(2), p. e2022JF006817. https://doi.org/10.1029/2022JF0068

Integration of remote sensing and field observations to map discontinuous permafrost in McGrath, interior Alaska

Alexander Kholodov[1], Pauline Mnev[2], Kelsey Nyland[2], Nikolay Shiklomanov[2], Shauna Burnsilver[3], James Tempte[4], Vera Kuklina[2], Alexander Shiklomanov[5] & Andrey Petrov[6]

[1]*University of Alaska, Fairbanks, Alaska, United States*

[2]*George Washington University, Washington, District Columbia, United States*

[3]*Arizona State University, Phoenix, Arizona, United States*

[4]*Alaska Pacific University, Anchorage, Alaska, United States*

[5]*University of New Hampshire, Durham, New Hampshire, United States*

[6]*Universty of Northern Iowa, Cider Falls, Iowa, United States*

To map detailed permafrost conditions in the vicinity of the city of McGrath in the Alaskan interior on the Kuskokwim River, we employed imagery from the high-resolution SPOT satellite and a ground verification survey. We found permafrost present only within the local black spruce forest with high stand density. The territory surrounding the city of McGrath is transiting from discontinuous to sporadic permafrost zone. While conducting ground verification a ground temperature observation network was established to monitor this transition.

Permafrost extent delineation in the Arctic and Subarctic has significant scientific and applied value. From the perspective of local residents, permafrost is a crucial concern for successful land use planning and maintaining a community's built infrastructure. Within the discontinuous permafrost zone spanning the vast majority of the Interior Alaska, presence or absence of perennially frozen ground is controlled by the ecological conditions, i.e., topography, vegetation and soil (Shur and Jorgenson 2007). Permafrost in this region is usually associated with coniferous forests with a thick organic soil horizon and/or tussocky wetlands. These ecotypes provide significant cooling via shading in summer, snow redistribution in winter (Kropp et al. 2020), and insulation from differences in thermal properties (thermal conductivity and heat capacity) of frozen and unfrozen soils. Any changes of forest coverage or organic layer thickness caused by human's activity or natural processes lead to permafrost degradation. Such strong linkages between land covers and ground thermal regime make remotely sensed products as a good tool for permafrost mapping. But, at the same time, due to high spatial variable and dynamic heat transfer conditions at the ground surface, automation of permafrost mapping cannot be done without ground truth validation.

Research area

The area between the Alaska Range and Kuskokwim Mountains west of Denali is relatively flat with a river terrace 100 m a.s.l. and a sandy aeolian accumulation plain with dunes 145–150 m a.s.l. (Fernald 1960). Recent mean annual air temperatures here are close to 0°C, which means – taking snow cover thermal insulation into account during winter – that mean annual ground surface temperatures are well above freezing (Kholodov et al. 2017). Local vegetation is dominated by coniferous forests of variable stand density, mixed or deciduous forest, shrubs, and grassy wetlands. Part of the mapped area continues to undergo secondary succession following a wildfire in 2000.

Methods

To map land cover in McGrath, Alaska, we modified the algorithm previously used to map permafrost in the village of Telida in 2016–2019 (Panda et al. 2017). A SPOT 4-band pansharpened image at 1.5 m spatial resolution covered the 124 km^2 study area. Running an unsupervised classification, six initial land cover classes were identified: (1) water, (2) built-up areas, (3) shrub/meadow, (4) deciduous forest, (5) coniferous forest, and (6) river banks.

Ground-based validation was performed in October, 2023. The procedure included a geolocated visual survey, vegetation descriptions and thaw depth measurements with a tile probe at 43 points spanning the land classes identified by unsupervised classification. Five out of these 43 points, representing main ecotypes of the area, had been instrumented for long-term measurements of ground temperature using 4-channel HOBO UX120 data loggers with thermistor sensors at 0, 0.5, 1, and 1.5 m depths. We also described and sampled soil profiles at these validation points.

Machine learning pattern recognition was used to analyze contextual features by assessing the

relationship of neighboring pixels at three different extents (4.5, 7.5, and 10.5 m) to discern the optimal resolution for accurately classifying land covers. Subsequently, an additional unsupervised classification was run on the combination of selected contextual features and detailed permafrost observations within specific land covers.

The resulting classified map depicts (1) no permafrost, (2) degrading permafrost/deep seasonal thaw, or (3) stable/intact permafrost conditions within the study area.

Results

We found permafrost at 10 out of 43 validation points, all in undisturbed black spruce forests with high stand density on the river terrace and in depressions between dunes on the aeolian accumulative plain. It this terrain, depth to the permafrost table (active layer) varies from 50 to 100 cm. Sporadic permafrost can potentially be found in spruce forest with medium to low stand density (observed at 6 validation points). Based on other studies conduced in the region (Kholodov et al. 2017) we can assume, that permafrost is also present here, but subject to talik development. Taliks have started to form in Interior Alaska after 2019 (Farquharson et al. 2022). No frozen ground was found within 1.5 m of the surface in grassy wetlands (9 validation points), shrubs (6 points), nor in mixed or deciduous forests (11 points). These last two land covers are typical in areas either disturbed by human activity or wildfires, or in shallow river meander scares on the river terrace.

Based on our studies we conclude, that the city of McGrath and its immediate surroundings is in transition from discontinuous to sporadic permafrost.

Acknowledgements

This research had been done in the frames of the NSF NNA award “Collaborative Research: Frozen Commons: Change, Resilience and Sustainability in the Arctic”. We also appreciate the McGrath Native Village Council and City of McGrath for supporting our studies.

References

Farquharson, L.M., Romanovsky, V.E., Kholodov, A., et al. 2022. Sub-aerial talik formation observed across the discontinuous permafrost zone of Alaska. Nature Geosciences, 15, 475–481.

Fernald, A.T. 1960. Geomorphology of the Upper Kuskokwim region, Alaska. Department of the Interior, Geological Survey Bulletin, 1071-G, 191–279.

Kholodov, A.L., Panda, S.K., and Hanson, T. 2017. December. Permafrost conditions at the Upper Kuskokwim river area and its influence on local communities. In AGU Fall Meeting Abstracts (Vol. 2017, pp. GC34C-04).

Kropp, H., Loranty, M.M., Natali, S.M., Kholodov, A.L., Rocha, A.V., Myers-Smith, I., et al. 2020. Shallow soils are warmer under trees and tall shrubs across Arctic and Boreal ecosystems. Environmental research letters, 16(1), 015001.

Panda, S.K., Kholodov, A.L., Romanovsky, V.E., and Hanson, T. 2017. December. Integrating remote sensing, field observations, and ground temperature modeling to help address permafrost-related societal challenges around native village of Telida, Interior Alaska. In AGU Fall Meeting Abstracts (Vol. 2017, pp. C24A-03).

Shur, Y.L., and Jorgenson, M.T. 2007. Patterns of permafrost formation and degradation in relation to climate and ecosystems. Permafrost and Periglacial Processes, 18(1), 7–19.

Time-series InSAR investigation of surface deformation in urban functional areas in high-latitude permafrost regions

Xianglong Li, Ze Zhang, Yaqian Dong & Qingkai Yan

School of Civil Engineering and Transportation, Institute of Cold Regions Science and Engineering, Permafrost Institute, Northeast Forestry University, Harbin 150040, China

With global climate warming, cities in permafrost regions are facing the risk of surface deformation caused by permafrost degradation. However, due to different human activities, the surface deformation in different functional areas of the city may vary, and research on these aspects is still insufficient. Therefore, this study was designed to investigate the surface deformation in different functional areas of the city. The study area was Yakutsk, and Sentinel-1B data from 2017 to 2021 were used to investigate the surface deformation in different functional areas using PS-InSAR technology. The results showed that although the rate of surface deformation varied, all urban functional areas in Yakutsk were undergoing subsidence. Among several functional areas, roads had the highest surface deformation rate of -7.5 mm/yr, followed by the airport (-5.8 mm/yr), multi-story residential areas (-4.6 mm/yr), individual residential areas (-3.9 mm/yr), and seasonal residential areas (-3.8 mm/yr). Further research results showed that the degradation of ice-containing foundations or permafrost may be the main cause of surface deformation. This study provides a reference for urban planning and construction in permafrost regions and can further enhance our understanding of local and even global climate change.

Due to global climate warming, permafrost degradation has become widespread (Ran et al. 2018; Li et al. 2021). This poses significant surface instability risks for cities located on permafrost. However, the level of human activity varies, leading to inconsistent surface instability risks for different infrastructure areas such as roads, airports, and residential areas in permafrost regions (Azor et al. 2019). Unfortunately, most studies to date have primarily focused on linear engineering in permafrost areas, with limited attention given to urban areas within these regions and the surface deformation of different building facilities. Therefore, it is essential to assess the surface stability of different building facilities, as it plays a crucial role in the development and stable operation of cities (Liu et al. 2010; Li et al. 2023).

In this study, we focused on Yakutsk, the largest city located on permafrost, and investigated the surface deformation of different building facilities using the PS-InSAR technique based on Sentinel-1B data from 2017 to 2021. The findings of this research will guide urban development and planning in permafrost regions and serve as a reference for assessing similar situations in other cities within permafrost areas.

DATA AND METHODS

We obtained 138 scenes of Sentinel-1B C-band VV polarization data between January 2017 and December 2021. The Persistent Scatterer Interferometric Synthetic Aperture Radar (PS-InSAR) method was employed to invert urban surface deformations. Additionally, we acquired the functional zoning data of building facilities in Yakutsk city planning (Figure 1), which was used for deformation comparison among different building facility areas (https://map.yakadm.ru/?ysclid=l7rb46aiql324747660#/app/app/tp/geoportal/task/299dac0cb13c4b4b8892b4ff01542784).

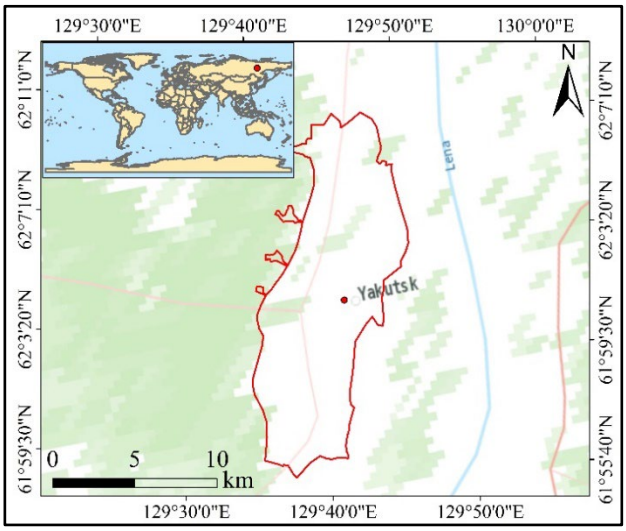

Figure 1. Overview of the study area.

RESULT

Based on the results from PS-InSAR, we compared the surface deformation rates of different building facility areas from January 2017 to December 2021. The deformation analysis revealed that the surface deformations in roads, airports, and residential areas were primarily characterized by subsidence (Figure 2).

Among them, the roads (-7.5 mm/yr) exhibited a higher surface deformation rate compared to the airports (-5.8 mm/yr) and residential areas (-4 mm/yr).

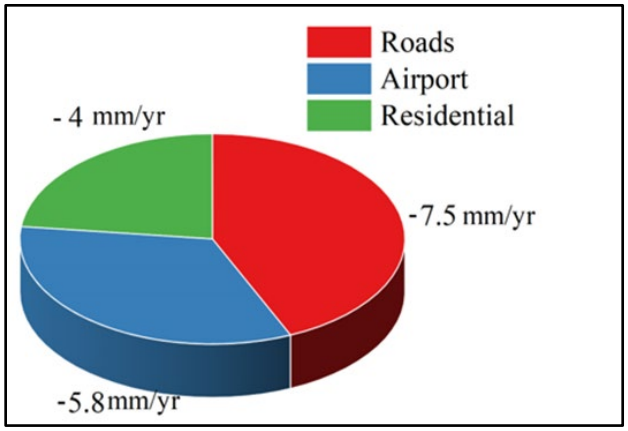

Figure 2. Surface deformation rates in different functional areas of Yakutsk 2017 to 2021.

Further analysis based on the deformation results of residential area types reveals that the surface deformation rate of multi-story residential areas (-4.6 mm/yr) was higher than that of seasonal residential areas (-3.9 mm/yr) and individual residential areas (-3.8 mm/yr) (Figure 3). Overall, regions with frequent human activities exhibited higher degrees of surface deformation.

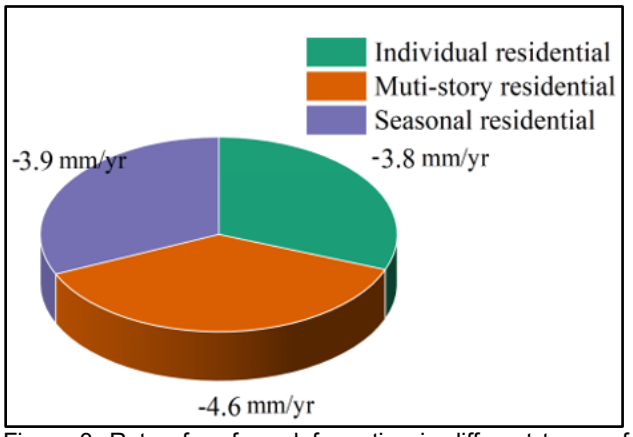

Figure 3. Rate of surface deformation in different types of residential areas of Yakutsk 2017 to 2021.

CONCLUSION

This study was designed to investigate the surface deformation of various building facility areas in Yakutsk, a city located in the permafrost region. The following conclusions can be drawn:

1. From 2017 to 2021, surface deformations were observed in all building facility areas in Yakutsk, primarily characterized by subsidence.
2. When comparing different functional areas, it was found that roads exhibited the highest rate of surface subsidence, while residential areas had relatively slower surface deformation rates.
3. Further differentiation within residential areas revealed that the surface deformation rate in multi-story residential areas is higher than the surface deformation rate in seasonal and individual residential areas.

REFERENCES

Azor, A., Dias da Silva, Í., Gómez Barreiro, J., et al. 2019. Deformation and structure. In The Geology of Iberia: A Geodynamic Approach: Volume 2: The Variscan Cycle (pp. 307–348). Cham: Springer International Publishing. https://doi.org/10.1007/978-3-030-10519-8_10

Ran, Y., Li, X., and Cheng, G. 2018. Climate warming over the past half century has led to thermal degradation of permafrost on the Qinghai–Tibet Plateau. The Cryosphere, 12(2), 595–608. https://doi.org/10.5194/tc-12-595-2018

Li, X., Zhang, Z., Melnikov, A., et al. 2022. Variation of Ground Surface Freezing/Thawing Index in China under the CMIP6 Warming Scenarios. Sustainability, 14(21), 14458. https://doi.org/10.3390/su142114458

Liu, L., Zhang, T., and Wahr, J. 2010. InSAR measurements of surface deformation over permafrost on the North Slope of Alaska. Journal of Geophysical Research: Earth Surface, 115(F3). https://doi.org/10.1029/2009JF001547

Li, X., Zhang, Z., Zheleznyak, M., et al. 2023. Time-series InSAR monitoring of surface deformation in Yakutsk, a city located on continuous permafrost. Earth Surface Processes and Landforms. https://doi.org/10.1002/esp.5736

Automatic segmentation strategies for DEM-based RTS monitoring

Kathrin Maier[1], Philipp Bernhard[1], Ingmar Nitze[2] & Irena Hajnsek[1,3]

[1]*Institute of Environmental Engineering, ETH Zurich, Zurich, Switzerland*

[2]*Alfred-Wegener-Institute, Potsdam, Germany*

[3]*Microwaves and Radar Institute, German Aerospace Center (DLR), Wessling, Germany*

Retrogressive Thaw Slumps (RTSs) are one of the fastest and most drastic changes observed in permafrost regions occurring when permafrost with massive ground ice is exposed and thaws, resulting in the formation of a steep headwall that retreats during the summer season. RTSs have the potential to mobilise large amounts of soil organic carbon and are expected to play a large role in the permafrost-carbon feedback (Turetsky et al. 2020). However, large-scale monitoring of volumetric change rates over the vast Arctic regions is so far limited and their impact on carbon mobilisation and potential release to the atmosphere remains poorly constrained. By differencing Digital Elevation Models (DEM), the direct extraction of volumetric changes of eroded material within the active parts of RTS is possible, and so is the subsequent estimation of mobilized carbon. Single-pass Interferometric SAR (InSAR) techniques applied on observations from the X-Band TanDEM-X mission to generate difference Digital Elevation Models (dDEMs) showed a great potential to enable monitoring of RTS and to track the resulting carbon mobilisation overcoming typical issues of optical imagery-based RTS analysis (Bernhard et al. 2022). In this work, we tested different segmentation methods to enable scalable, automatic detection and delineation of RTS features on dDEMs derived from bistatic InSAR observations based on their performance, efficiency and scalability to be applied on large-scale permafrost areas.

DEM GENERATION AND PROCESSING

We developed an automatic processing pipeline to generate DEMs with InSAR techniques to efficiently process large amounts of TanDEM-X single-pass observations and estimate inherent error magnitudes. Data quality masks are generated for areas experiencing high errors induced by low coherence, layover and shadow, steep incidence angles and water bodies, and a tiling scheme is applied to facilitate data processing with spatial buffering aiming to avoid a potential miss of RTS features at the borders of a tile. Due to an increased error level for observations during the spring and summer months caused by wet vegetation and late laying wet snow, solely winter observations are used (Zwieback et al. 2018). During the winter months in Arctic climate conditions the dry snowpack allows the radar waves to penetrate to the ground. For several winter observations of the same year a weighted average based on the underlying coherences is computed. The averaged DEMs are co-registered and differenced for time steps between 2010 and 2022. The dDEMs are further normalized based on the estimated height error where the impact of erroneous pixels induced during the SAR observation process is reduced, e.g., due to sloped terrain.

TEST SITES AND DATA LABELS

For this investigation we chose nine test sites aiming to represent the heterogeneous landscapes and climate present in the Arctic continuous permafrost region (Figure 1.a).

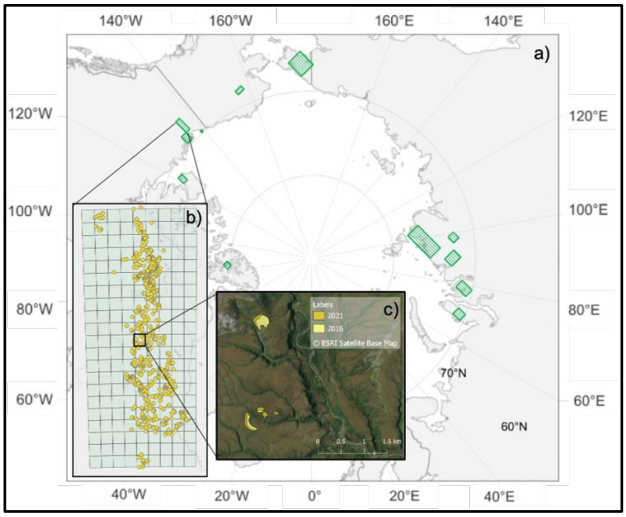

Figure 1. a) Test sites, b) Example of a test site on the Peel Plateau, Canada with c) digitized labels for 2010–2016 and 2010–2021.

Four test sites are located in Canada, namely on Peel Plateau, Tuktoyaktuk, Banks Island and Ellesmere Island, while the remaining sites are located in Russian Siberia, namely on Yamal, Gydan, the Taymyr peninsula and Chukotka. Training data in

the form of labeled RTS features on optical and dDEM data are manually generated (Figure 1.b and c). The labeling accuracy has a strong impact on the segmentation performance; hence, we performed a quantitative evaluation of the label accuracy based on a labelling experiment with three domain experts.

METHOD AND PRELIMINARY RESULTS

Supervised segmentation often outperforms unsupervised methods, yet a lot of training data is needed. Re-using existing labels can be complicated due to different annotation guidelines, and manual labeling is time consuming and error-prone. Furthermore, poor generalisation performance can lead to issues when aiming to apply a trained model across different geographic regions. Hence, we explored both supervised and unsupervised segmentation methods on dDEM images to investigate their potential for large-scale RTS monitoring.

(1) Several automatic 2D image segmentation algorithms including Felzenszwalb's efficient graph-based segmentation, Quickshift, and SLIC, were tested on a small sub dataset to investigate the suitability of the specific task and the optimal parameter settings before applying to all test sites (Figure 2.a).

(2) State-of-the-Art Deep Learning architectures were selected based on their performance for similar segmentation tasks on RTS (Nitze et al. 2018, Huang et al. 2021) with ResNets as encoder with and without pre-trained weights, and UNet and DeepLab3 architectures as decoders (Figure 2.b).

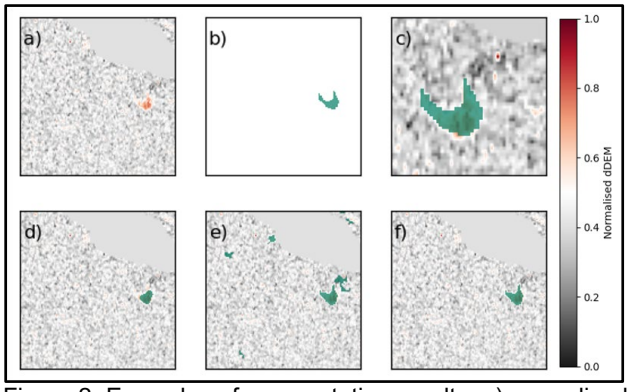

Figure 2. Examples of segmentation results: a) normalised dDEM, b) binary ground truth mask, c) zoom-in to RTS, d) UNet segmentation, Felzenszwalb without e) and with post processing f) segmentation.

Pixel-based accuracy metrics including precision, recall, F1-score, and Intersection over Union (IoU) against the RTS labels were computed for all tested methods to compare their performance. We assessed the accuracy of the Deep Learning segmentation methods within (splitting datasets in train and test sets) and across different test sites (k-fold cross validation), and compared our results to existing Arctic RTS segmentation publications where available (e.g., Nitze et al. 2018).

OUTLOOK

Due to the high-class imbalance of this segmentation task, false positive detections are common. We aim to investigate different post-processing strategies that utilize known RTS properties such as minimum and maximum spatial extents, height change ranges and time-series based logics as they appear as a promising way to improve segmentation accuracies (Huang et al. 2021) as well as if combinations of the best performing model from (2) and algorithm from (1), e.g., through class voting on both individual segmentation results (Zhang et al. 2020), can improve the overall segmentation accuracy. Having a reliable segmentation algorithm to map RTSs on dDEMs would allow us to quantify thaw slumping activity across the Arctic by estimating volumetric change and associated carbon mobilisation rates.

REFERENCES

Bernhard, P., Zwieback, S., Bergner, N., and Hajnsek, I., 2022. Assessing volumetric change distributions and scaling relations of retrogressive thaw slumps across the Arctic. The Cryosphere 16, 1–15. doi:10.5194/tc-16-1-2022

Huang, L., Liu, L., Luo, J., Lin, Z., and Niu, F., 2021. Automatically quantifying evolution of retrogressive thaw slumps in Beiluhe (Tibetan Plateau) from multi-temporal CubeSat images. International Journal of Applied Earth Observation and Geoinformation 102, 102399. doi:10.1016/j.jag.2021.102399

Nitze, I., Heidler, K., Barth, S., and Grosse, G., 2021. Developing and Testing a Deep Learning Approach for Mapping Retrogressive Thaw Slumps. Remote Sensing 13, 4294. doi:10.3390/rs13214294

Turetsky, M.R., Abbott, B.W., Jones, M.C., Anthony, K.W., Olefeldt, D., Schuur, E.A.G., Grosse, G., Kuhry, P., Hugelius, G., Koven, C., Lawrence, D.M., Gibson, C., Sannel, A.B.K., and McGuire, A.D., 2020. Carbon release through abrupt permafrost thaw. Nat. Geosci. 13, 138–143. doi:10.1038/s41561-019-0526-0

Zhang, S., Ma, Z., Zhang, G., Lei, T., Zhang, R., and Cui, Y., 2020. Semantic Image Segmentation with Deep Convolutional Neural Networks and Quickshift. Symmetry 12, 437. doi:10.3390/sym12030427

Zwieback, S., Kokelj, S.V., Günther, F., Boike, J., Grosse, G., and Hajnsek, I., 2018. Sub-seasonal thaw slump mass wasting is not consistently energy limited at the landscape scale. The Cryosphere 12, 549–564. doi:10.5194/tc-12-549-2018

Impact of Arctic sea ice loss on coastal permafrost degradation and its feedback: A remote sensing based case study from the Canadian Arctic Archipelago

Vishnu Nandan[1], Remya Namboodiri[2] & John Yackel[1]

[1]*Department of Geography, University of Calgary, Alberta, Canada*

[2]*School of Sustainable Futures, Amrita University, Kollam, India*

The stability of coastal permafrost when sea ice cover is present, as well as the increased permafrost vulnerability when there is a loss in sea ice, can be explained by changes in both atmospheric heat and moisture transport. Radar remote sensing has demonstrated its capability to characterize coastal permafrost degradation through quantifying changes in active layer thickness and reduction of permafrost extent, in response to rising air temperatures and climate change. In parallel, coastal Arctic sea ice has also declined over the past four decades and radar remote sensing has been instrumental in detecting critical changes in sea ice thermodynamic regimes such as freeze-up, melt-onset etc. across regional- and hemispherical-scales. However, there is a research gap in our understanding of the feedback processes between fluctuating sea ice thermodynamic regimes and the stability of permafrost cover and vice versa. This includes enhanced methane fluxes affecting more sea ice loss. In this study, we show the utility of radar remote sensing to quantify these feedback effects. We use time series of the European Space Agency's C-band Sentinel-1 Synthetic Aperture Radar (SAR) between 2018-23 from selected coastal sea ice and permafrost regions in the Canadian Arctic Archipelago to a) detect sea ice freeze-up, melt- and pond-onset timing and it's differences in the timings during this period, and b) coincidentally use SAR Interferometry tools to detect permafrost thaw subsidence rates and active layer thickness changes in response to sea ice thermodynamic regime changes. We hypothesize that, as the difference in sea ice freeze-up and melt onset timing reduces, the rate of permafrost thaw also increases, suggesting the impact of increased open water season outside the seasonal window affecting the permafrost thaw dynamics. Also, we also investigate the impact of rain-on-snow events on sea ice and its melt effect affecting joint feedback processes on permafrost degradation. This remote sensing-driven study is first of its kind to quantify feedback processes between retreating sea ice and thawing permafrost. Enhanced understanding of key relationships between sea ice and permafrost may give us between information and knowledge about evaluating dynamics of sea ice and permafrost individually and together in vulnerable environments such as the Canadian Arctic Archipelago where communities depend on a stable permafrost cover for infrastructure and stable sea ice cover for hunting, migration etc.

Antarctic Peninsula vegetation monitoring through synergistic remote sensing (1989–2023)

Pedro Pina[1,2], Vasco Miranda[3], Sandra Heleno[3] & Gonçalo Vieira[4]

[1]*DCT, Departamento de Ciências da Terra, Universidade de Coimbra, Portugal*

[2]*IDL, Instituto Dom Luiz, Universidade de Coimbra, Portugal*

[3]*CERENA, Instituto Superior Técnico, Universidade de Lisboa, Portugal*

[4]*CEG, Centro de Estudos Geográficos, Laboratório Associado TERRA, IGOT, Universidade de Lisboa, Lisboa, Portugall*

An approach to classifying vegetation on remotely sensed images in the Antarctic Peninsula is presented. It consists on using recent multiscale imagery (from few centimeters in UAV – Unoccupied Aerial Vehicles to 30 m in Landsat satellites) to build a robust supervised scheme that can used to classify past images when only Landsat datasets were available. The evaluation of how the degradation of the spatial resolution among the different datasets affects the classification performances is also assessed. The classifier is built, calibrated and validated with multiple datasets of the same recent period (2019-2020) and then extrapolated to past and more recent dates. The approach is tested in Barton Peninsula, King George Island (62°S).

Vegetation, in close association with permafrost conditions, is a key element of terrestrial ecosystems in the ice-free areas of the Antarctic (Guglielmin et al. 2014). Its spatial distribution, growth or decline and diversity are closely related to climatic conditions and the topography. Vegetation can be used as a bioindicator as an indirect measure of climate change (Sancho et al. 2019). Mapping it accurately, in space and time, is therefore relevant. The only practical way of achieving this is by using spaceborne remotely sensed images (Fretwell et al. 2011; Miranda et al. 2020), due to the repeatable extended coverage of the surfaces and the availability of multispectral imaging. The occurrence of vegetation in relatively small and sparse patches (metric), makes its identification very challenging at 10-30 m scale (the ones of Sentinel and Landsat, which are the only ones covering large areas and past periods. The details provided by UAV imagery are of great help for overcoming those issues (Pina and Vieira 2022).

METHODOLOGY

The proposed methodology (Figure 1) consists of three processing phases depending on the sizes of the average vegetation patches in relation to pixel image resolutions: 1) Pixel smaller than vegetation patches (UHR images of UAV); 2) Pixel about the same size of vegetation patches (VHR images of WorldView 2) and 3) Pixel larger than the size vegetation patches (HR of Sentinel 2 and Landsat 4 and Landsat 8).

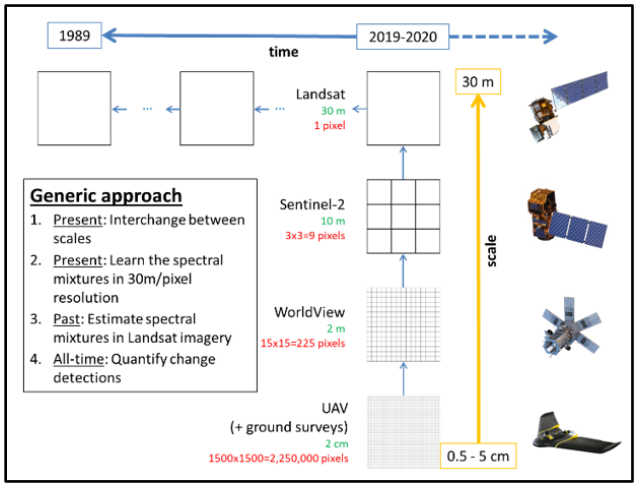

Figure 1. Scheme of classification methodology.

DATA

The datasets used to develop the approach consist of images of 3 different spatial resolutions: ultra-high (UHR, 2 cm, UAV), very-high (VHR, 2 m, WorldView 2) and high-resolution images (HR, 10 m Sentinel 2 and 30 m Landsat 8). The past image is a high-resolution image (HR, 30 m, Landsat 4) and the most recent image is another Landsat 8. The acquisition summer dates can be checked in Table 1.

Table 1. Image datasets.

Platform	Date	Spatial Resolution (m)
UAV	February 2019	0.03
WorldView 2	17 March 2019	2
Sentinel 2	19 January 2020	10
Landsat 8	19 January 2019	30
Landsat 4	28 January 1989	30
Landsat 8	25 February 2023	30

CLASSIFICATION RESULTS

The classes defined in the study area are bare, lichens and mosses (Figure 2).

Figure 2. Classification legend of 3 classes.

The selection of the training and testing samples for the classification of satellite imagery is obtained after the classification of 14 UAV image mosaics located in different sites of Barton Peninsula (Figure 3) with an object-based Support Vector Machine classifier. The average performance on the overall accuracy (*oa*) and kappa coefficient (*k*) is high: *oa*=0.91 and *k*=0.85.

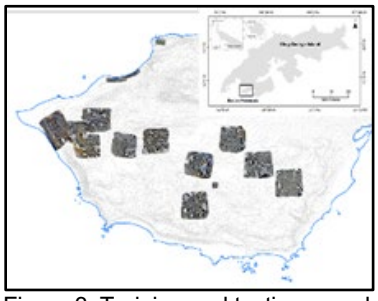
Figure 3. Training and testing samples for the classification of satellite imager, Barton Peninsula.

The samples of bare, lichens and mosses classes are used to train a pixel-based Deep-Learning classifier on the WorldView 2 image, whose thematic map obtained is presented in Figure 4a. The performances are *oa*=0.89 and *k*=0.79.

The creation of end members of the 3 land cover classes were obtained after a processing sequence similar to Shin et al. (2014) where a Linear Spectral Unmixing classifier was applied to Sentinel 2 and Landsat 8 images. Adequate thresholding values allowed selecting the dominating class in each 10m and 30 m pixel. The classified images are presented in Figures 5b and 5c, respectively.

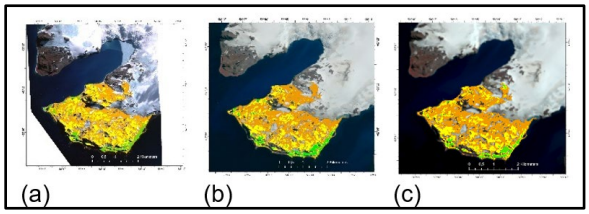

Figure 4. Classified images: (a) WorldView 2, (b) Sentinel 2, (c) Landsat 8.

The lower resolution of Sentinel 2 and Landsat 8, compared to WorldView 2, makes the vegetation to be identified with a deficit of 0.37km^2 and 0.48 km^2, respectively, which is less than 14.6% and 16.2% of the total vegetated area of WorldView 2 reference.

Table 2. Vegetation areas (km^2) in 2019-2020.

Platform	Lichens	Mosses	Total
WordlView 2 (2019)	2.11	0.48	2.59
Sentinel 2 (2020)	1.83	0.39	2.22
Landsat 8 (2019)	1.82	0.36	2.18

Nevertheless, we consider these values to be acceptable, meaning that Landsat images at 30 m of spatial resolution can be used to map vegetation. Therefore, the classification of a Landsat 4 image 1989 and a Landsat 8 image in 2023, gave the results shown in Table 3 (Landsat 8 in 2019 is repeated from Table 2 to make comparisons easier).

Table 3. Vegetation areas (km^2) between 1989 and 2023.

Platform	Lichens	Mosses	Total
Landsat 4 (1989)	1.77	0.27	2.03
Landsat 8 (2019)	1.82	0.36	2.18
Landsat 8 (2023)	1.86	0.38	2.24

CONCLUSIONS

The downscaling of the classification approach is valid and the results at 30m resolution are adequate without major losses in the identified vegetation areas. The approach was generalized to other dates (more ancient and more recent). The approach is also able to discriminate the main types of vegetation (lichens and mosses). The vegetation in Barton Peninsula expanded by 0.2 km^2 (10%) in 34 years (between 1989 and 2023).

REFERENCES

Fretwell, P.T, Convey, P., Fleming, A.H., Hughes, K.A. 2011. Detecting and mapping vegetation distribution on the Antarctic Peninsula from remote sensing data. Polar Biology., 34, 273-281. doi:10.1007/s00300-010-0880-2

Miranda, V., Pina, P., Heleno, S., Vieira, G., Mora, C., and Schaefer, C.E.G.R. 2020. Monitoring recent changes of vegetation in Fildes Peninsula (King George Island, Antarctica) through satellite imagery guided by UAV surveys, Science of the Total Environment. 704, 135295. doi:10.1016/j.scitotenv.2019.135295

Pina, P., and Vieira, G. 2022. UAVs for science in Antarctica, Remote Sensing, 14(7): 1610. doi:10.3390/rs14071610

Sancho, L.G., Pintado, A., and Green, T.G.A. 2019. Antarctic studies show lichens to be excellent biomonitors of climate change. Diversity, 11, 42. doi:10.3390/d11030042

Shin, J-I, Kim, H.C., and Hong, S.G. 2014. Vegetation abundance on the Barton Peninsula, Antarctica: estimation from high-resolution satellite images. Polar Biology, 37, 1579–1588. doi:10.1007/s00300-014-1543-5

UAV LiDAR reveals intra-annual terrain dynamics in Sweden's largest palsa complex

Cas Renette & Heather Reese

Department of Earth Sciences, University of Gothenburg, Gothenburg, Sweden

Palsas, peat mounds with a core of perennially frozen soil, are indicative of permafrost. The degradation of palsas, as a result of climate change, is indicated by both lateral erosion and vertical subsidence. In addition to this, the elevation of permafrost terrain fluctuates cyclically due to annual freeze-thaw cycles within the active layer though this has not been explicitly studied on palsas.

Satelitte remote sensing with InSAR can capture surface deformation trends in palsa mires, but tends to underestimate actual displacement rates due to spatial averaging (de la Barreda-Bautista et al. 2022). The use of UAV (or drone) photogrammetry in permafrost landscapes, including palsa mires, is increasing and has been applied with success. However, regarding small-scale terrain dynamics, this method has limitations. For example, changes due to minor variations in vegetation affect the data. LiDAR (Light Detection and Ranging) sensors for UAVs emerge as a promising tool for obtaining high-resolution (cm-scale) digital terrain models (DTMs). LiDAR can penetrate vegetation and operate effectively in low-light conditions. Another advantage that LiDAR holds over photogrammetry is that ground control points (GCPs) are not required (Harder et al. 2020). This saves both time and costs, especially for repeat flights at high temporal resolution.

Our objective is to quantify the intra-annual vertical heave and subsidence of two palsas in Sweden's largest palsa mire complex, Vissátvuopmi, using repeat measurements of UAV LiDAR data. The two palsas (Dome and Ridge palsa) both rise ca. 4–5 m above the surrounding mire. We conducted five UAV-borne LiDAR scans between September 2022 to September 2023 over these palsas. We scanned on 4 September 2022, 26 April 2023, 18 June 2023, 19 July 2023, and 7 September 2023 with A DJI Matrice 300 RTK UAV, equipped with a YellowScan Mapper+ LiDAR scanner. Our approach allowed us to create digital terrain models (DTMs) from high density point clouds (>1,000 points/m²) and analyze elevation changes over time.

Results and Discussion

We observed seasonal frost heave and thaw subsidence patterns by performing change detection on DTMs from the five campaigns (Figure 1).

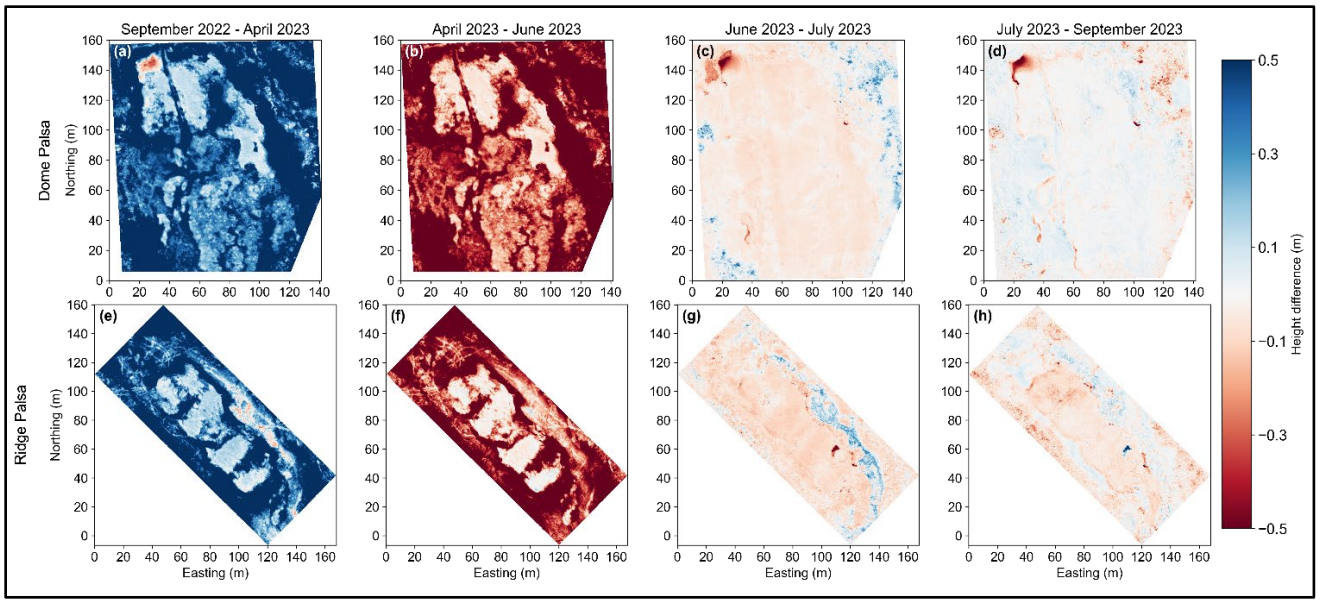

Figure 1. Sequential height difference maps of the palsas between each of the five UAV LiDAR DTMs from September 2022 to September 2023. Each panel showcases the topographical changes over successive intervals. Blue colors indicate elevation gains and red colors indicate elevation losses.

The height of both palsas increased by an average of 0.15 m (and up to 0.30 m) from September 2022 to April 2023, followed by a gradual decrease over the summer (Figure 2). These values are computed at parts of the palsas that were snow-free during the April campaign, so that the effect on the ground surface is isolated.

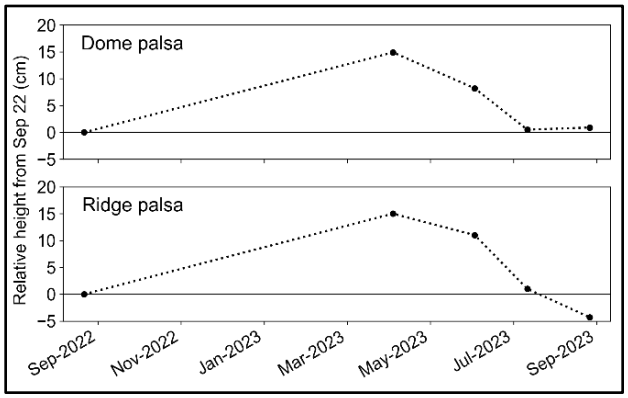

Figure 2. Heave and subsidence on the two studied palsas, relative to September 2022. Values are computed in areas completely snow-free in April 2023.

Additionally, both palsas degraded laterally during the one-year period. In the northwest part of the Dome palsa, we observed a lateral degradation event in a 300 m^2 area, with 0.5–2.0 m height loss (Figure 1a, c and d), likely initiated during the preceding warm and wet summer months. Part of this degradation occurred between September 2022 and April 2023, suggesting that the degradation of these palsas is not limited to the summer months. Figure 3 shows elevation profiles across both palsas for all flights. It shows accurate alignment of the datasets. Figure 3e highlights the rapid subsidence event on the dome palsa. Figure 3f shows frost heave on a snow-free crest on the Ridge palsa, and slight subsidence between September 2022 and September 2023. The ground in Figure 3g was snow covered in April 2023 and subsided after one year than the snow-free ground. The insulating snow pack leads to warmer ground, which is more susceptible to permafrost degradation in the form of inter-annual subsidence.

Freeze-thaw cycles within the active layer cause frost heave and thaw subsidence, partially due to the density difference between water and ice. However, the average observed average heave of 0.15 m cannot be explained alone by this process and requires the formation of seasonal segregation ice (i.e. ice lenses) within the active layer. Alternatively, processes within the core of the palsa, for example, the infiltration and refreezing along meltwater pathways, might result in seasonal heave and subsidence, but required more knowledge of palsas' interior in order to prove.

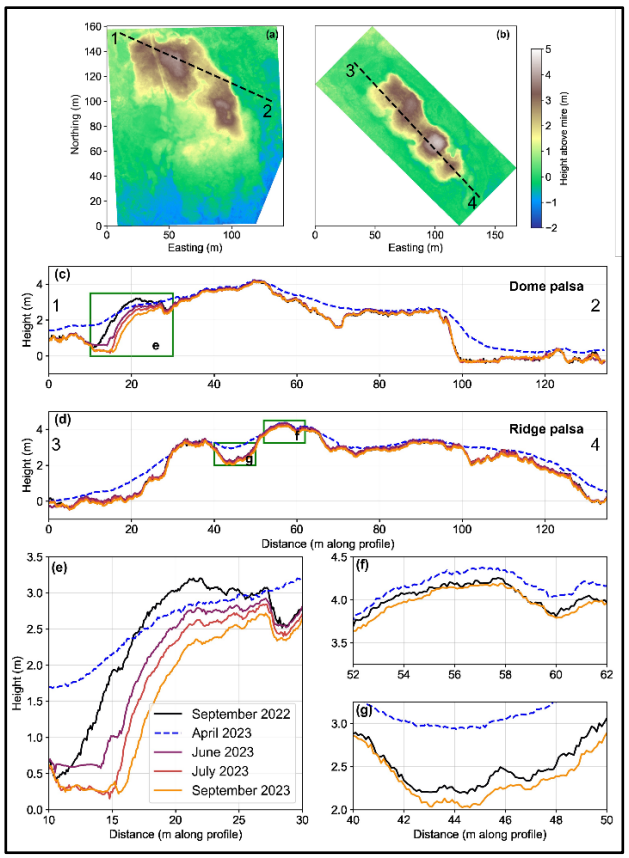

Figure 3. Elevation profiles of the palsas based on UAV LiDAR DTMs from September 2022 to September 2023. (a, b) The dashed lines denote the location of the profiles (c) and (d) provide a general elevation overview of the transect, while (e), (f), and (g) offer zoomed-in views of specific areas of interest, indicated by the green boxes.

This is the first study that covers seasonal terrain dynamics on palsas in such high spatial resolution. The use of repeat UAV LiDAR scanning is a highly effective tool for capturing intra-annual dynamics of palsas, which would not have been observed if only annual measurements had been taken.

References

de la Barreda-Bautista, B., Boyd, D.S., Ledger, M., Siewert, M.B., Chandler, C., Bradley, A.V., Gee, D., Large, D.J., Olofsson, J., Sowter, A., and Sjögersten, S. 2022. Towards a Monitoring Approach for Understanding Permafrost Degradation and Linked Subsidence in Arctic Peatlands. Remote Sensing, 14(3), Article 3. https://doi.org/10.3390/rs14030444

Harder, P., Pomeroy, J.W., and Helgason, W.D. 2020. Improving sub-canopy snow depth mapping with unmanned aerial vehicles: Lidar versus structure-from-motion techniques. The Cryosphere, 14(6), 1919–1935. https://doi.org/10.5194/tc-14-1919-2020

Monitoring the small-scale variability in seasonal deformation on the North slope of Alaska, for InSAR validation

Soumitra Sakhalkar[1], Simon Zwieback[1,2,4], Julia White[1], Jie Chen[1], Andrew Johnson[1,4], Go Iwahana[3] & Franz Meyer[1,2,4]

[1]*Geophysical Institute, University of Alaska Fairbanks, Fairbanks, Alaska, United States*

[2]*Department of Geosciences, University of Alaska Fairbanks, Fairbanks, Alaska, United States*

[3]*International Arctic Research Center, University of Alaska Fairbanks, Fairbanks, Alaska, United States*

[4]*Alaska Satellite Facility, Fairbanks, Alaska, United States*

Northern high-latitude regions like the North Slope of Alaska have been warming rapidly in recent decades. In regions underlain by ice-rich permafrost, long term subsidence can be induced due to permafrost degradation (Nicolsky et al. 2017). In addition, the seasonal freeze induces upward (heave) and seasonal thaw induces downward (subsidence) surface displacement. The seasonal as well as the long-term movement poses a risk to infrastructure and exerts a fundamental influence on the hydrological and ecological functioning of the permafrost landscapes.

Interferometric Synthetic Aperture Radar (InSAR) satellites can measure surface displacements with centimetric accuracy (Liu et al. 2010). However, the accuracy in the Low-Arctic environments is poorly known and draws attention in light of the random and systematic errors associated with dynamic vegetation and soil processes. Accurate in situ measurements are both challenged and necessitated by the sub-resolution variability in surface deformations (Antonova et al. 2018).

We present a ground observation protocol for validating InSAR observations of the upcoming NISAR (NASA-ISRO Synthetic Aperture Radar) and Sentinel-1. The NISAR seasonal permafrost deformation requirement stipulates an accuracy of 4*(1+L^1/2) mm or better, over length scales of 0.1 km < L > 50 km. Our protocol relies primarily on high-precision global navigation satellite system (GNSS) positioning surveys, completed by digital leveling. The elevation changes of ~150 permanently marked points within a 100 m by 100 m NISAR resolution cell are upscaled to obtain the spatially averaged surface deformation.

Methods

To validate the seasonal deformation from satellite InSAR, we conducted kinematic phase-based GNSS surveys at the beginning (late May to early June) and end (mid to late August) of the thaw season of 2022 and 2023. The surface elevations were determined relative to stable benchmarks anchored into the permafrost. Within a resolution cell of 100 m by 100 m, we surveyed 150 permanently marked survey points uniformly distributed along three parallel transects. The elevation differences between the two surveys were determined to estimate the seasonal surface displacement in our field sites on the North Slope of Alaska.

We upscale the point observations to a representative average across the 100 m by 100 m resolution cell. We then form the arithmetic mean and compute its standard error based on the observed variance.

To evaluate the accuracy of the GNSS surveys, we additionally conducted digital levelling surveys in 2023.

The geodetic surveys were complemented by continuous deformation measurements obtained using linear displacement transducers mounted on 2-meter wide metallic frames. The metallic frames were anchored into the permafrost. The continuous observations enable us to temporally match the topographic surveys to the satellite overpasses.

Study sites

The study sites are located on the North Slope of Alaska and underlain by continuous permafrost. The landscape comprises gently rolling hills mantled by ice-rich, fine-grained soils (Iwahana et al. 2020), and elevation ranging between 300 to 600 m. The land cover, located within Arctic bioclimate subzone E , is dominated by vegetation unit 8 (Walker et al. 2005); dwarf shrubs (>0.5 m) and tundra consisting primarily acidic dry tussock-sedges on silt loam to silty clay loam soils, with some occasional gravel (more in one site) or cobbles.

Results and conclusions

The overall seasonal displacements from the geotic surveys and the continuous observations show a general trend of subsidence per year, ranging between 3 to 7 cm.

The initial results presented through this study reveal substantial variability in seasonal groundsurface deformation both in time and space. At our study sites,

where excess ice is abundant in the active layer and upper permafrost, the observed spatial variability necessitates a large number (~150) of observation points for validating the NISAR seasonal permafrost deformation requirement.

Our observations further support enhancing process understanding and the ability to model terrain changes in permafrost regions undergoing increasingly rapid change.

REFERENCES

Antonova, S., Sudhaus, H., Strozzi, T., Zwieback, S., Kääb, A., Heim, B., Langer, M., Bornemann, N., and Boike, J. 2018. Thaw subsidence of a yedoma landscape in northern Siberia, measured in situ and estimated from TerraSAR-X interferometry, Remote Sensing, 10(4): 494. doi:10.3390/rs10040494

Iwahana, G., Busey, R.C., and Saito, K. 2020. Seasonal and Interannual Ground-Surface Displacement in Intact and Disturbed Tundra along the Dalton Highway on the North Slope, Alaska, Land, 10(1): 22. doi:10.3390/land10010022

Liu, L., Zhang, T., and Wahr, J. 2010. InSAR measurements of surface deformation over permafrost on the North Slope of Alaska, Journal of Geophysical Research: Earth Surface, 115(F3). doi:10.1029/2009JF001547

Nicolsky, D.J., Romanovsky, V.E., Panda, S.K., Marchenko, S.S., and Muskett, R.R. 2017. Applicability of the ecosystem type approach to model permafrost dynamics across the Alaska North Slope, Journal of Geophysical Research: Earth Surface, 122(1): 50–75. doi:10.1002/2016JF003852

Walker, D.A., Raynolds, M.K., Daniëls, F.J., Einarsson, E., Elvebakk, A., Gould, W.A., Katenin, A.E., Kholod, S.S., Markon, C.J., Melnikov, E.S., and Moskalenko, N.G. 2005. The circumpolar Arctic vegetation map, Journal of Vegetation Science, 16(3): 267–282. doi:10.1111/j.1654-1103.2005.tb02365.x

Unique contributions of the RADARSAT missions to InSAR monitoring of permafrost terrain

Naomi Short, François Charbonneau & Robert H. Fraser

Canada Centre for Mapping and Earth Observation, Natural Resources Canada, Ottawa, Ontario, Canada

Interferometric Synthetic Aperture Radar (InSAR) uses repeat radar acquisitions to measure displacement of the Earth surface. It is a proven method for mapping displacement of permafrost terrain and gaining insight into periglacial landscape processes. These satellite radar measurements offer wide area mapping and are particularly valuable in remote regions. InSAR measurements of ground displacement can also be incorporated into environmental models and used to estimate geophysical parameters of interest. With falling technology costs the number of spaceborne SAR systems is rapidly expanding and offering users an ever-widening choice of SAR wavelengths, spatial resolutions, product formats and cost models. This paper describes some of the unique capabilities offered by the Canadian RADARSAT missions and their contributions to permafrost terrain monitoring, in particular, high resolution SAR data and compact polarimetric data. We use two sites in the Canadian Arctic to demonstrate RADARSAT's unique capabilities, Banks Island, Northwest Territories and Herschel Island, Yukon.

Spatial resolution

The RADARSAT satellites are C-band SARs (5.6 cm wavelength) and they offer a variety of acquisition beam modes and spatial resolutions. RADARSAT-2 has been operating since 2007 and the RADARSAT Constellation Mission (RCM) since 2019. Collectively, the RADARSAT missions offer Spotlight (1 m), Very High Resolution (3 m), High Resolution (5 m), Fine Resolution (10 m) and Medium Resolution (16 m) modes, as well as many coarser resolutions. The size of the periglacial landforms that can be investigated is limited by the spatial resolution of the data. Figure 1, top panel, shows a WorldView-2 image of low relief, ice-wedge polygons on Banks Island. The lower two panels show the difference in the level of detail between RADARSAT Spotlight mode data (1 m) and moderate resolution Sentinel-1 data processed to 14 m pixel spacing. It can be seen that the higher resolution of RADARSAT has potential to monitor the displacement and geomorphological processes of individual periglacial landforms whereas the moderate resolution data are better suited to the landscape scale.

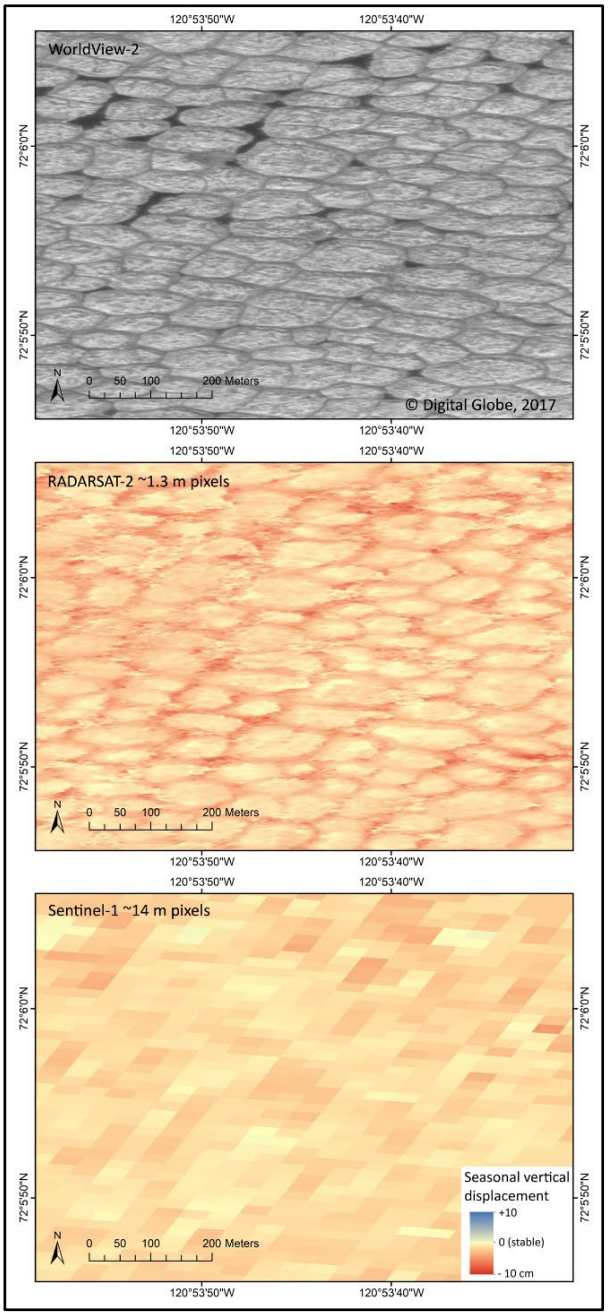

Figure 1. Ice-wedge polygons of Banks Island. Top: WorldView-2 0.5 m resolution panchromatic image; Middle: RADARSAT-2 Spotlight vertical displacement over summer 2019; Bottom: Sentinel-1 vertical displacement over summer 2019.

COMPACT POLARIMETRIC INSAR

The RCM offers a new SAR mode called Compact Polarimetry (CP). In this mode the SAR transmits a right circular wave and receives the horizontal and vertical backscatter returns, while preserving the relative polarimetric phase. Through the creation of the polarimetric and InSAR covariance matrices and the use of a unitary projection vector, it is possible to derive the optimum coherence and the optimum differential phase associated with the optimum polarization for each pixel in an interferogram (Cloude and Papathanassiou 1998). This delivers much higher coherence values for CP-InSAR data sets than for conventional single channel InSAR data sets and hence more complete displacement maps. While the difference may be negligible for short interval and highly coherent InSAR data pairs, it becomes quite noticeable for long interval data pairs. Figure 2 shows the line-of-sight displacement results over a period of 300 days for Herschel Island. The top panel is the result from conventional single channel InSAR (RH) and the lower panel is the result from the CP-InSAR processing using optimum coherence (OC). It can be seen that the optimum coherence terrain displacement map is much more complete, particularly over the unstable slopes of the eroding coastlines and along interior stream channels and gullies. The CP-InSAR method therefore appears to provide new opportunities for detecting long-term terrain displacement without the need for long time series analysis.

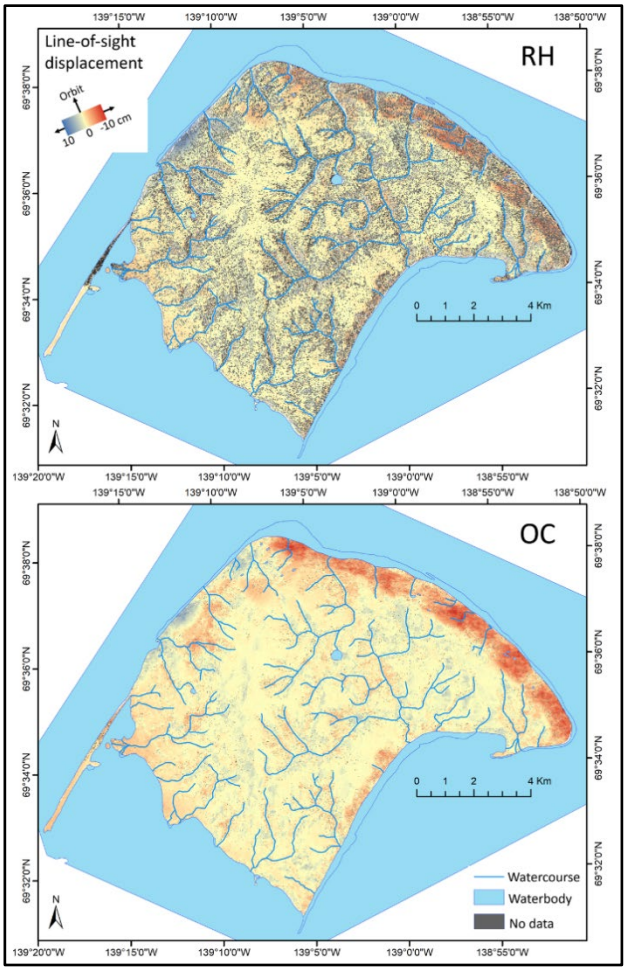

Figure 2. Line-of-sight displacement measured between 20200920 and 20210717 (300 days) over Herschel Island; (RH) using conventional single channel InSAR, and (OC) using CP-InSAR and the optimum coherence method.

ACKNOWLEDGEMENTS

This work was conducted and funded by Natural Resources Canada. RADARSAT-2 data were provided by MacDonald Dettwiler and Associates under the Canadian Government Data Allocation. RCM data were provided by the Canadian Space Agency. Sentinel-1 data were obtained through the Copernicus Data Hub.

REFERENCES

Cloude, S.R., and Papathanassiou, K.P. 1998. Polarimetric SAR Interferometry, IEEE Transactions on Geoscience and Remote Sensing, 36(5): 1551–1565. doi:10.1109/36.718859

Monitoring and numerical modelling of thaw consolidation and subsidence of ice-rich permafrost near Umiujaq, Nunavik (Québec), Canada

Madeleine St-Cyr[1,2], Richard Fortier[1,2] & John Molson[1,2]

[1]*Département de géologie et de génie géologique, Université Laval, Québec City, Québec, Canada*

[2]*Centre d'études nordiques (CEN), Université Laval, Québec City, Québec, Canada*

Permafrost is a major component of northern geosystems and ecosystems, the dynamics of which directly depend on the cold climate at high northern latitudes. Due to climate warming, for example in excess of 3 °C over the last three decades as observed in Nunavik (Québec, Canada), permafrost is currently degrading at a global scale (Fortier et al. 2008). Evidence of this degradation includes thaw subsidence, a natural hazard that affects not only the functioning of northern geosystems and ecosystems, but also the performance of man-made infrastructure built on ice-rich permafrost (Nelson et al. 2001; Fortier et al. 2011; Fortier et al. 2015). Despite its potential impact on the sustainable development of Inuit communities, this natural hazard remains little investigated.

Objectives

To address the knowledge gaps related to thaw subsidence, the following objectives were developed: 1) to monitor the thaw subsidence of ice-rich permafrost near Umiujaq in Nunavik (Québec), Canada, 2) to perform numerical modelling of fully coupled groundwater flow, advective-conductive heat transfer, and thaw consolidation in a discontinuous permafrost environment, and 3) to assess and anticipate permafrost degradation based on past climate variability in Nunavik and different scenarios of climate warming, respectively.

Study site

The Tasiapik Valley, near the Inuit community of Umiujaq (Nunavik, Québec, Canada), is located in a discontinuous permafrost zone. The periglacial valley landscape is characterized by the presence of permafrost mounds called lithalsas. Permafrost degradation takes the form of localized and gradual thaw subsidence on the periphery of the lithalsas. When the subsidence is great enough to produce depressions, they fill with water and form thermokarst ponds which grow over time, extending into the remnant lithalsas (Figure 1, top right). When the permafrost is totally degraded, the lithalsas are completely replaced by thermokarst ponds with peripheral ramparts.

Methods

Surveying and remote sensing methods have been used to monitor permafrost subsidence at Umiujaq. Annual leveling surveys of reference markers on lithalsas in the Tasiapik Valley have been carried out each summer since 2004 using various instruments such as an optical level, a total station, and a Differential Global Positioning System (DGPS). A remote sensing method called LiDAR (Light Detection and Ranging) was also used to scan the study site each summer from 2011 to 2023. In addition, several flights of an Unmanned Aerial Vehicle (UAV) were carried out in summer 2023 to produce a mosaic of high-resolution aerial photographs of the study site and perform digital photogrammetry. Digital Terrain Models (DTMs) and Digital Surface Models (DSMs) were also produced from processing the LiDAR data.

Results

The DTMs and DSMs of 2023 and 2010 were subtracted from each other to assess the spatial distribution of surface elevation variations over this period due to thaw subsidence and shrubification (Lemay et al. 2018), respectively (Figure 1). Thaw subsidence is most pronounced at the periphery of the lithalsas and near the thermokarst ponds. The average thaw subsidence at the study site over this period is 36 cm, but can reach up to 3 m in some places, while the average vegetation growth is 53 cm over the same period. The shrubification is more pronounced at the margins of the thermokarst ponds and in the depressions between lithalsas.

Finally, the numerical code HEAT FLOW/ SMOKER (Molson and Frind 2023) was used to simulate the fully coupled physical processes of groundwater flow, heat transfer, and thaw consolidation taking place in degrading permafrost. Simulated thaw subsidence was compared with observed thaw subsidence to constrain the numerical model. Future thaw subsidence is also predicted according to different scenarios of climate warming.

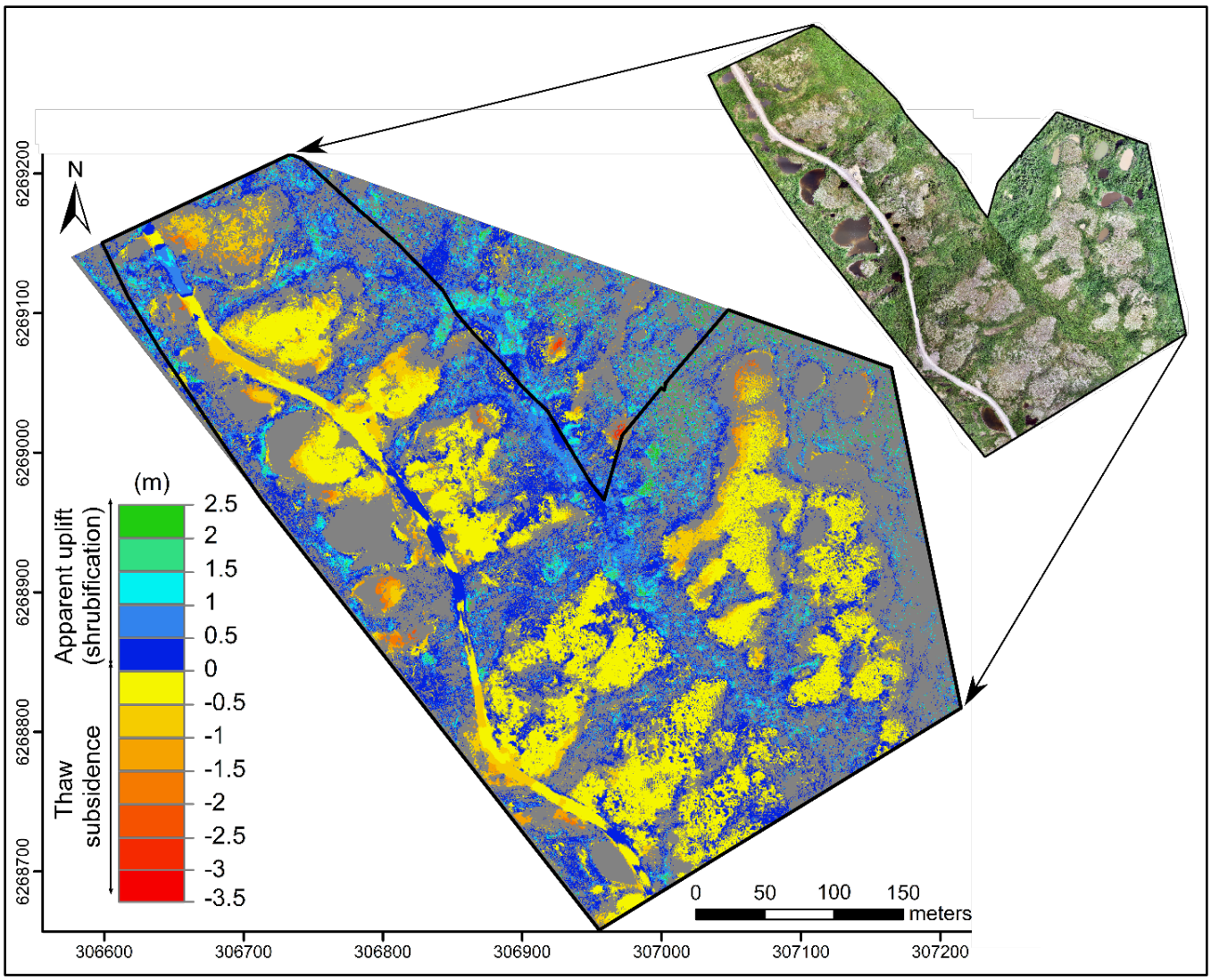

Figure 1. The observed variation in surface elevation from 2010 to 2023. Thaw subsidence was assessed by subtracting the Digital Terrain Model (DTM) of 2023 from that of 2010. Apparent uplift due to shrubification was obtained by subtracting the Digital Surface Model (DSM) of 2023 from that of 2010. The airborne LiDAR survey of 2010 was carried out on behalf of the Ministère des Ressources naturelles et de la Faune (MRNF) of Québec while the terrestrial LiDAR survey of 2023 was performed as part of the present study. The orthomosaic of aerial photographs from a UAV flight carried out in 2023 is provided in the top right corner (note that the orthomosaic is not at the same scale as the map of changes in surface elevation over the 13-year period).

REFERENCES

Fortier, R., and Aubé-Maurice, B. 2008. Fast permafrost degradation near Umiujaq in Nunavik (Canada) since 1957 assessed from time-lapse aerial and satellite photographs, In 9th International Conference on Permafrost, Fairbanks, Alaska, USA, 1: 457–462.

Fortier, R., Guo, S., Lamontagne-Hallé, P., and Yu, W. 2015. High-resolution monitoring of thaw subsidence affecting the access road to Umiujaq Airport in Nunavik (Quebec), In 7th Canadian Permafrost Conference (GeoQuébec 2015), Québec, Québec, Canada: 8 p.

Fortier, R., LeBlanc, A.-M., and Yu, W. 2011. Impacts of permafrost degradation on a road embankment at Umiujaq in Nunavik (Quebec), Canada. Canadian Geotechnical Journal, 48:720–740. doi:10.1139/T10-101

Lemay, M.-A., Provencher-Nolet, L., Bernier, M., Lévesque, E., and Boudreau, S. 2018. Spatially explicit modeling and prediction of shrub cover increase near Umiujaq, Nunavik. Ecological Monographs, 88(3):385-407. doi:10.1002/ecm.1296

Molson, J.W., and Frind, E.O. 2023. HEATFLOW-SMOKER: Density-dependent flow and advective-dispersive transport of thermal energy, mass or residence time, User Guide. Université Laval, Québec (QC), Canada, and University of Waterloo, Waterloo (ON), Canada.

Nelson, F.E., Anisimov, O.A., and Shiklomanov, N.I. 2001. Subsidence risk from thawing permafrost, Nature, 410(6831):889–890. doi:10.1038/35073746

Introducing the CUSP (CommUnity near-Surface Permafrost) dataset

Evan Thaler, Joel Rowland, Jon Schwenk, Lawrence Vulis, Bohan Chen, Charles Abolt, Lauren Thomas & Eve Gasarch

Los Alamos National Laboratory, Los Alamos, New Mexico, United States

Permafrost is a fundamental property of northern high-latitude landscapes. Its presence strongly influences vegetation, hydrology, and the stability of landscapes. Permafrost loss due to warming, land use change, fire, and other disturbances dramatically alters hydrology and ecology and poses a significant risk to critical built infrastructure. Accurate data on where permafrost occurs and how this occurrence may be changing over time is vital to understanding the structure and function of these landscapes and predicting where future loss of permafrost may threaten infrastructure. At present, there are numerous pan-Arctic data products that provide estimates of near-surface permafrost. Unfortunately, over large portions of the Arctic these datasets have poor agreement on the extent and location of permafrost, with disagreement particularly acute in regions of discontinuous permafrost. A major challenge to improving these permafrost datasets and developing new methodologies for permafrost modeling is obtaining enough ground-based observations to train and validate models.

Development of machine learning models to predict the pan-arctic extents of near-surface permafrost and active layer thicknesses (ALT) requires a substantial number of observations across the region. Current statistical models that estimate ALT and permafrost presence at pan-arctic scale are based on a sparse network of borehole data (~1000 observations); however, decades of ALT and permafrost measurements have yielded thousands of observations, which have not currently been used in the development of statistical models. The incorporation of these ground observations in model development has been limited in part by accessibility to the data. Here we present the CommUnity near-surface Permafrost (CUSP) dataset, a community-driven compilation of near-surface permafrost observations. CUSP is an off-the-shelf dataset that provides point-based observations of the presence or absence or permafrost in the near-surface (~130 cm), as well as active layer thicknesses for numerous locations. In addition to information related to the permafrost presence/absence and depth for each observation, CUSP includes a set of environmental features, such as topography, vegetation indices, and climate data, that were extracted from various sources, such as remote sensing and data assimilation models. The features are automatically extracted for each of the observation points using Google Earth Engine. We preserve the temporal component of the observation by extracting multispectral and climate features derived from data representing the date of observation.

We envision CUSP as a resource to help build strong collaborations within the permafrost community, while also providing scientific-quality data for analysis and modeling. For example, one aim of CUSP is to develop the largest training/testing dataset for machine learning approaches to near-surface permafrost modeling. Our current machine learning models built using CUSP have an accuracy of ~90% on the testing dataset.

CUSP is designed to be a living repository, such that new or previously unassimilated data can be uploaded, and the dataset will be updated, including incorporation of the new set of environmental features.

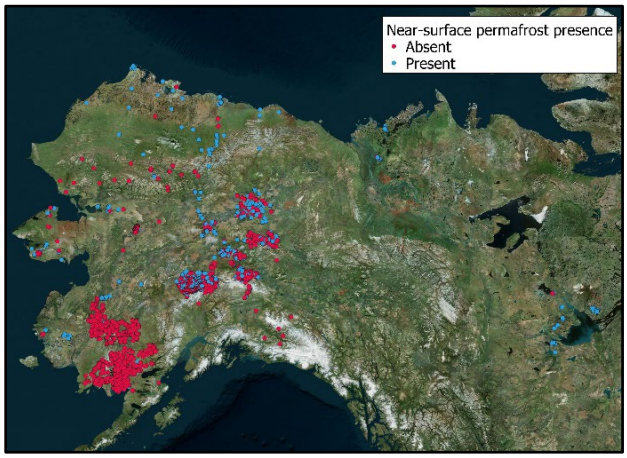

Figure 1. Location of near-surface permafrost observations compiled in the CUSP dataset.

Satellite-based radar interferometry to monitor ground-surface deformation of filtered tailings storage facilities in continuous permafrost

Malte Vöge[1], Regula Frauenfelder[1] & Vincent Boulanger-Martel[2]
[1]*Norwegian Geotechnical Institute, NGI, Ullevål Stadion, Oslo, Norway*
[2]*Université du Québec en Abitibi-Témiscamingue, RIME-UQAT, Rouyn-Noranda, Québec, Canada*

There are an increasing number of mining projects being developed in Canada's Arctic, where continuous permafrost is common. The environmental impacts of mining operations can be significant, especially when large volumes of mine tailings are stored at the surface. The reclamation of tailings storage facilities (TSFs) frequently involves designing engineered covers to control the generation and propagation of contaminants into the environment. These cover systems are designed to remain efficient for an indefinite time and should therefore require minimal long-term monitoring and maintenance. Analysis of the ground conditions and of possible ground deformation is, therefore, necessary to design cover systems accordingly.

The geotechnical behaviour of TSFs and tailings dams is usually monitored using classical geotechnical instrumentation and surveys. However, constraints such as the limited number of measurement points, difficult access to a mine site, or a desire to increase the frequency and resolution of measurements may lead to the use of remote sensing tools to measure ground surface deformation (e.g., Lato 2020).

This study aims to map vertical displacement rates at the surface of the Raglan Mine filtered TSF (located in Nunavik, Québec, Canada, between the Inuit communities of Salluit and Kangiqsujuak) using satellite-based radar interferometry (InSAR). Because snow-free seasons are short in continuous permafrost environments, specifically tailored InSAR processing workflows were necessary to assess potential ground surface deformation at the TSF (Vöge et al. 2022).

Methodology and results

Satellite-based remote sensing technologies such as Synthetic Aperture Radar (SAR) Interferometry (InSAR) have successfully been used to monitor ground-surface deformations of tailings dams and TSFs (e.g., Iannacone et al. 2018). InSAR remote sensing approaches enable monitoring of ground-surface deformations over wide areas, with millimetric precision. In this study, a stack of 44 snow-free images from ESA's Sentinel-1 constellation, covering the period June 2017 to September 2020, has been used to detect potential ground deformations at the Raglan Mine TSF. The data processing has been carried out with the SBAS method (Berardino et al. 2002), which identifies distributed scatterers. The alternative PS approach (Ferretti et al. 2001) focusses on point-like scatterers. SBAS provides better coverage of the TSF and its surrounding area, since both the TSF itself and its neighbourhood feature only few point-like scatterers.

A key aspect of the SBAS technique is the selection of image pairs with small temporal baselines, for which phase differences between the outgoing and incoming radar signals are measured. Images affected by snow cover are usually excluded from the analysis. This to prevent incoherent phase information affecting the analysis. However, because the winter seasons in Artic regions are long, excluding all winter scenes can lead to connection graphs that are not fully connected. Ultimately, this can cause misinterpretation of the seasonal variations as linear subsidence.

Figure 1 shows the connection graph for the dataset used here. Note that only blue connections fulfill the selected requirement of a temporal baseline below 60 days, leading to a not fully connected connection graph.

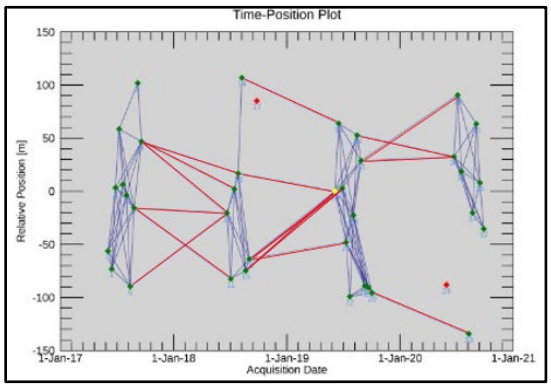

Figure 1. Connection graph for SBAS analysis with manually added winter pairs (red lines).

Subsequently, velocities processed without winter pairs contain considerable artefacts outside of the TSF, in areas which are assumed to be stable (Figure 2, top). The TSF material, however, does not appear to be affected by seasonal variations. In order to improve the interpretation, the temporal baseline was extended to 320 days, thereby allowing connections to span over

the winter period and to allow an average of six connections per acquisition (Figure 1, red lines). This approach clearly yielded more stable velocities outside the TSF (Figure 2, bottom).

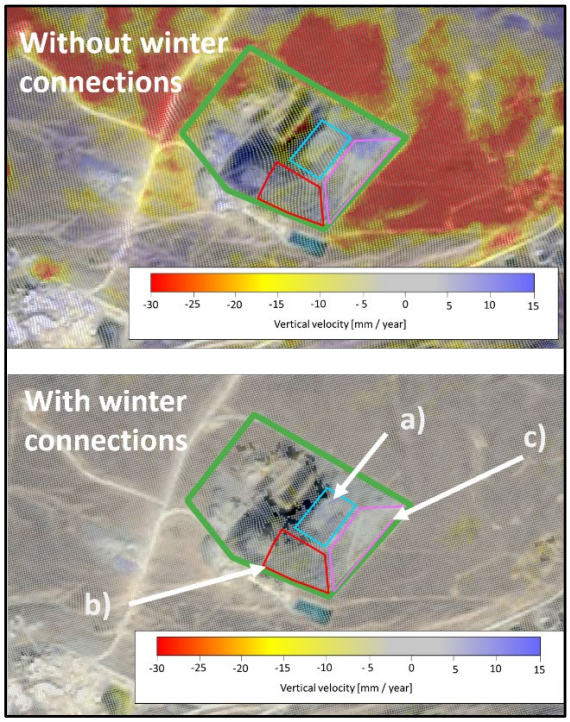

Figure 2. Velocity maps for Raglan Mine TSF from SBAS processing with (bottom) and without (top) winter pairs.

Time series obtained for three sections on the TSF (marked with a), b) and c) in Figure 2, bottom) are shown in Figure 3, together with regression lines showing the fitted linear model.

Conclusion

Mapping of displacements at the Raglan Mine TSF was successfully carried out using InSAR. As expected, the long snow-covered seasons presented the biggest challenge since they result in large data gaps that make consistent measurements across seasons difficult. SBAS processing with a 60-day temporal baseline shows how these data gaps affect the analyses. Increasing the temporal baseline to 320 days, which (among others) allows the analyses to span over the winter period led to clearly improved results.

The TSF surface and the east-facing slope showed slight indications of upward movement during the analyses period, while the south-facing slope showed slight downward movement. However, the measured displacement velocities in the TSF were generally small (<5 mm/year). The presented study is part of a larger study to assess ground deformations at the Raglan Mine TSF. Additional monitoring via field investigations and remote sensing will be conducted to establish the current state of the TSF's deformation, especially with respect to differential settlements.

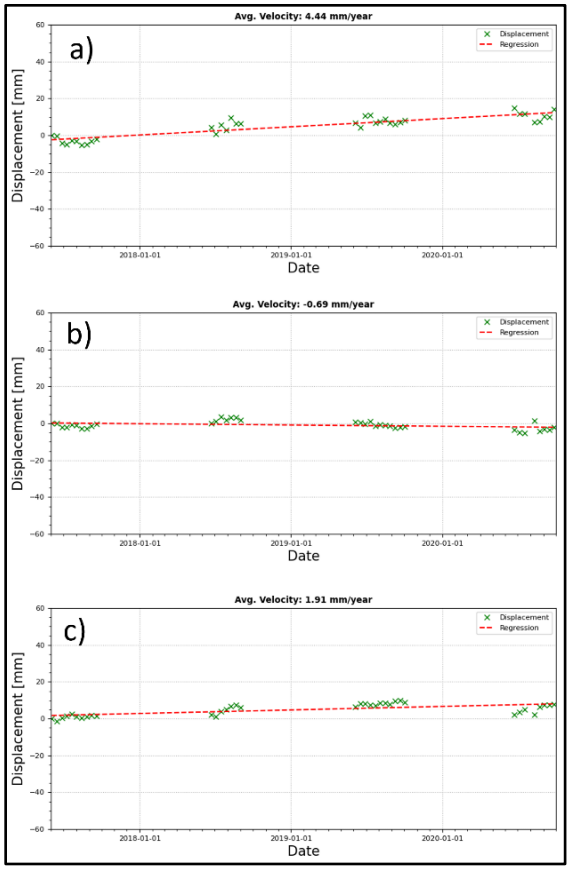

Figure 3. Time series for the areas marked as a) to c) in Figure 2 (bottom) processed with winter pairs.

References

Berardino, P., et al. 2002. A new algorithm for surface deformation monitoring based on small baseline differential SAR interferograms. IEEE Transactions on Geoscience and Remote Sensing, 40(11), 2375–2383.

Ferretti, A., et al. 2001. Permanent Scatterers in SAR Interferometry. IEEE Transactions on Geosciences and Remote Sensing, 39(1), 8–20.

Iannacone, J.P., et al. 2018. InSAR monitoring of active, inactive and abandoned tailings facilities. In Proceedings of the 5th International Seminar on Tailings Management, Santiago, Chile (pp. 11–13).

Lato, M. 2020. Canadian Geotechnical Colloquium: three-dimensional remote sensing, four-dimensional analysis and visualization in geotechnical engineering — state of the art and outlook. Canadian Geotechnical Journal, 58, 1065–1076.

Vöge, M., et al. 2022. Satellite-based radar interferometry for monitoring ground-surface deformation of filtered tailings storage facilities in continuous permafrost regions. 75th Canadian Geotechnical Conference, Calgary, Alberta, Canada.

Global-scale mapping of permafrost in a changing climate

Sebastian Westermann[1,2], Clarissa Willmes[1,2], Lotte Wendt[1,3], Kristoffer Aalstad[1], Juditha Aga[1], Robin Zweigel[1,2], Julie Røste[1], Line Rouyet[3], Frederieke Miesner[4], Birgit Heim[4], Mareike Wieczorek[4], Andreas Kääb[1], Bernd Etzelmüller[1], Tazio Strozzi[5] & Annett Bartsch[6]

[1]*Department of Geosciences, University of Oslo, Norway*

[2]*Center for Biogeochemistry in the Anthropocene, University of Oslo, Norway*

[3]*NORCE Norwegian Research Centre, Tromsø, Norway*

[4]*Alfred Wegener Institute Helmholtz Centre for Polar and Marine Research, Potsdam, Germany*

[5]*GAMMA Remote Sensing, Switzerland*

[6]*BGEOS, Vienna, Austria*

Permafrost is an Essential Climate Variable (ECV) which is defined by the physical variables “permafrost temperature” and “active layer thickness” (as well as “rock glacier velocity” not treated here). In addition, the energetic state of the permafrost is affected by its ground ice content which at present is not part of the permafrost ECV definition, despite its critical importance. In the Permafrost_CCI project funded by the European Space Agency (ESA), we are compiling satellite-based products for the permafrost ECV spanning the last 25 years. To overcome the challenge that ground temperature and thaw depth cannot be directly quantified from space-borne sensors, we have set up a processing chain that can ingest different satellite and reanalysis data sets in a ground thermal model. As a result, we obtain time-resolved 1 km scale maps of ground temperature and thaw depth which can reveal the spatiotemporal patterns of permafrost changes in Arctic and high-mountain environments. In this contribution, we evaluate and discuss the current state of global permafrost mapping efforts and provide perspectives for future improvements.

Algorithms for global permafrost ECV mapping

1. Field observations and statistical methods/ machine learning: The application of machine learning in producing maps of permafrost variables leverages statistical models to analyze spatial datasets from diverse sources (e.g., air temperature, landcover) in order to predict the thermal state of permafrost. These models rely entirely on field observations as training data sets, in particular ground temperature measurements in boreholes (e.g., GTN-P network, Biskaborn et al. 2015) and observations of active layer thickness (CALM network, Brown et al. 2000). In the past decade, several groups have presented global maps of permafrost variables based on this technique (e.g., Karjalainen et al. 2019). The limiting factor is the relative scarcity of permafrost observations and their spatial bias towards few regions - if the observational networks could be extended by one to two orders of magnitude and the spatial coverage improved, this would greatly boost the reliability of perafrost maps derived from machine learning.

2. Field observations and simple heat conduction models: Numerical permafrost models are generally based on the physical laws of heat conduction which makes it possible to derive subsurface temperatures (and thus thaw depth, etc.) from time series of surface variables, e.g., satellite-derived land surface temperatures or snow depths derived from reanalysis data. The key principal problem for spatially distributed application is the large number of model parameters, which vary in space and which again must be constrained using the available spatial data sets, e.g., satellite-derived classifications of the landcover. In practice, numerical permafrost models also rely on training data sets from GTN-P and CALM to constrain unknown model parameters (e.g., Obu et al. 2019). In the ESA Permafrost_CCI project, we use a computationally efficient transient heat conduction scheme in the CryoGrid community model (Westermann et al. 2023) for global permafrost mapping. The scheme is based on remotely sensed data sets of Land Surface Temperature (MODIS LST) and landcover (ESA Landcover_CCI), as well ERA-5 reanalysis. The key practical problem of such approaches in the considerable runtime which not only requires high performance computing clusters, but also limits global application at sufficiently high spatial resolutions (e.g., 1 km) to comparatively simple and process-poor permafrost models. These cannot account for more complex permafrost thaw processes such as excess ice melt or thermokarst.

3. Field observations, permafrost process models and statistical methods/machine learning: In the past decade, sophisticated process models have been developed which can simulate permafrost (thaw) processes even for complex situations. These include the thaw trajectories of ice-rich permafrost landforms (e.g., Nitzbon et al. 2019; Martin et al. 2021), or the

accumulation of segregated ice (Aga et al. 2023). Furthermore, data assimilation makes it possible to ingest satellite data sets into these models to constrain unknown model parameters; as an example snow extent data sets from remote sensors available at 20 m resolution can be used to constrain the height of the insulating winter snow cover which is a key variable in permafrost simulations. As such techniques are computationally expensive, it is not possible to use them for global high-resolution mapping. However, they may be employed to compile spatially distributed, high-quality "synthetic borehole and active layer" to supplement and greatly extend the available field observations, especially in currently data-sparse regions. Such a combined data set could then once again train statistical /machine learning tools, as described in algorithms #1, to achieve upscaling and spatialization of the information content to the global scale.

CONCLUDING REMARKS

In a warming world, permafrost maps must become time-resolved data products to capture the considerable dynamics of permafrost thaw. While numerical modeling, machine learning and satellite-derived data sets play a significant role, systematic field observations, as realized in the GTN-P and CALM networks, will remain of critical importance, underscoring the need for long-term funding to sustain these indispensable data sets. So far, mapping efforts have concentrated on ground temperature and thaw depth, but similar attention needs to be put on ground ice to capture realistic thaw trajectories also in ice-rich permafrost landscapes. Progress may be expected both from InSAR remote sensing which can observe seasonal and multi-annual surface subsidence related to ground ice dynamics, and from improved process models (which could even be combined with remote observations using algorithms #3, see above). Finally, global-scale mapping must develop strategies to account for the considerable small-scale variability of permafrost variables which cannot be captured even by comparatively high-resolution products at 1 km scale. In the Permafrost_CCI algorithm, we therefore simulate not only a single realization for each 1 km pixel, but an ensemble which statistically accounts for subpixel variations in snow depth and ground stratigraphies. To drive such techniques to reality, novel field data sets may be required which not only provide point observations of permafrost parameters, but their distribution over larger areas comparable to the size of a typical model pixel.

REFERENCES

Aga, J., Boike, J., Langer, M., Ingeman-Nielsen, T., and Westermann, S. 2023. Simulating ice segregation and thaw consolidation in permafrost environments with the CryoGrid community model. The Cryosphere, 17, 4179–4206.

Biskaborn, B.K., Lanckman, J.-P., Lantuit, H., Elger, K., Streletskiy, D.A., Cable, W.L., and Romanovsky, V.E. 2015. The new database of the Global Terrestrial Network for Permafrost (GTN-P). Earth Syst. Sci. Data, 7, 245–259.

Brown, J., Ferrians, O.J., Heginbottom, J., and Melnikov, E.S. 1997. Circum-Arctic map of permafrost and ground-ice conditions. U.S. Geological Survey in Cooperation with the Circum-Pacific Council for Energy and Mineral Resources. Circum-Pacific Map Series CP-45, scale 1:10,000,000, 1 sheet.

Brown, J., Hinkel, K.M., and Nelson, F.E. 2000. The circumpolar active layer monitoring (CALM) program: research designs and initial results. Polar geography, 24(3), 166–258.

Karjalainen, O., Aalto, J., Luoto, M., Westermann, S., Romanovsky, V.E., Nelson, F.E., Etzelmüller, B., and Hjort, J. 2019. Circumpolar permafrost maps and geohazard indices for near-future infrastructure risk assessments. Scientific data, 6(1), 1–16.

Martin, L., Nitzbon, J., Aas, K.S., Etzelmüller, B., Kristiansen, H., and Westermann, S. 2019. Stability conditions of peat plateaus and palsas in northern Norway. Journal of Geophysical Research: Earth Surface, 124, 705–719.

Nitzbon, J., Langer, M., Westermann, S., Martin, L., Aas, K., and Boike, J., 2019. Pathways of ice-wedge degradation in polygonal tundra under different hydrological conditions. The Cryosphere, 13, 1089–1123.

Obu, J., Westermann, S., Bartsch, A., Berdnikov, N., Christiansen, H.H., Dashtseren, A., et al. 2019. Northern Hemisphere permafrost map based on TTOP modelling for 2000–2016 at 1 km^2 scale. Earth-Science Reviews, 193, 299–316.

Westermann, S., Ingeman-Nielsen, T., Scheer, J., Aalstad, K., Aga, J., Chaudhary, N., et al. 2023. The CryoGrid community model (version 1.0) - a multi-physics toolbox for climate-driven simulations in the terrestrial cryosphere. Geoscientific Model Development 16 (9), 2607–2647.

HABITAT: High-resolution Arctic Built Infrastructure and Terrain Analysis Tool

Chandi Witharana[1], Elias Manos[1], Amal Perera[1] & Anna K. Liljedahl[2]

[1]*Department of Natural Resources and the Environment, University of Connecticut, Connecticut, United States*

[2]*Woodwell Climate Research Center, Massachusetts, United States*

The Arctic permafrost is experiencing rapid transformations due to warming climate, posing an increasing risk to both natural and human-built environments. Consequently, there is a great need for developing novel monitoring tools to accurately map permafrost landforms and thaw disturbances, track their changes over time, and to assess the economic impact on human-built infrastructure. The entire Arctic has been imaged by very high spatial resolution (VHSR) Maxar satellite sensors at sub-meter resolution multiple times during the last two decades. These images can capture dynamics of individual microtopographic features, thaw disturbances, and human-built infrastructure features without sacrificing the geographical extent and the spatial details. While the data repositories holding millions of VHSR images have reached the petabyte scale, imagery-derived pan-Arctic scale science products are yet rare. Data analysis challenges combined with growing quest for pan-Arctic scale permafrost modelling efforts naturally set the stage for artificial intelligence (AI) algorithms, such as deep learning (DL) convolution neural nets (CNNs). Despite the remarkable performances of DL models in everyday image understanding, bottlenecks still exist when translated to remote sensing image analysis tasks. Image characteristics, landscape variations, and most importantly semantic complexity aggregated into multiple spatial scales pose greater friction on the strengths of DLCNN model inferences. Scalability of automated analysis over millions of square kilometers comprising heterogeneous landscapes reverberates the need for efficient image-to-assessment workflows that center on high performance computing resources. We have developed a novel image analysis tool: High-resolution Arctic Built Infrastructure and Terran Analysis Tool (HABITAT) that enables the integration of operational-scale GeoAI capabilities into Arctic science applications. In this paper, we present four example mapping scenarios of HABITAT: (1) ice-wedge polygons (IWP), (2) Ice-wedge polygon trough network, (3) retrogressive thaw slumps (RTS), and (4) human-built infrastructure features. Our ice-wedge polygon mapping effort stands out as the first-of-its-kind permafrost science use case that capitalizes on thousands of Maxar images to create the first pan-Arctic ice-wedge polygon data set.

ICE-WEDGE POLYGONS

Ice-wedge polygons (IWPs), a common feature in permafrost regions, create a distinctive pattern on the landscape. The exact extent and the prevailing IWP types (i.e., whether the ice wedges experienced melt or not) are largely unknown. Over recent decades, ice-wedge degradation – transformation of low-centered polygons to high-centered polygons due to ice-wedge degradation has been documented at several locations across the Arctic tundra. Understanding of spatiotemporal dynamics behind the evolution of ice-wedge polygonal tundra demands for objective and detailed maps consolidating the ice wedge extent and their prevailing successional stages. The lack of knowledge on the larger geographical extent and successional stage of IWPs introduce uncertainties to regional and pan-Arctic estimates of carbon, water, and energy fluxes. To close this knowledge/data gap, we utilized Maxar satellite images, coupled with AI and HPC resources, to create the first pan-Arctic IWP map. We have detected more than one billion individual ice-wedge polygons across the Arctic tundra. The deep learning model predictions comprise spatial outlining of ice-wedge polygons, coupled with their classification (low-centered vs high-centered IWPs) and geometrical attributes at individual IWP-level.

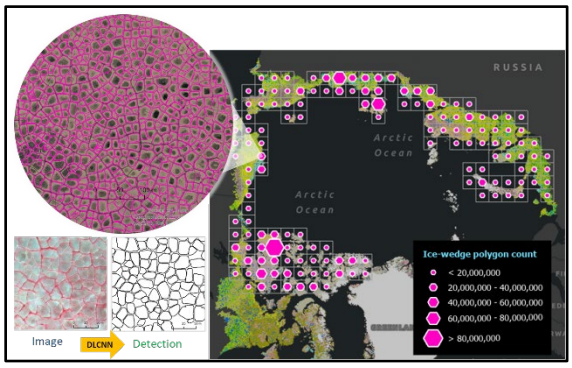

Figure 1. Operational implementation of the deep learning-based IWP mapping algorithm. Large scale map with hexagons summarizes individual IWP detections. Zoomed-in views show outlines of detected individual IWPs.

TROUGH NETWORK

The transition from low-center to high-centered polygons facilitates drainage through new surface runoff pathways provided by development of an integrated drainage network in ice-wedge troughs. Leveraging both contemporary Maxar satellite imagery and historical aerial imagery, we conduct a change detection analysis on ice-wedge polygon terrain with a focus on trough-expansion near Drew Point, Northern Alaska. We trained a U-Net convolutional neural network (CNN) to accurately map troughs from the grayscale average of VHSR multispectral satellite imagery of Point Lonely, Alaska, then applied the model on black-and-white aerial imagery (from 1949 and 2002) and a panchromatic WorldView-2 image (from 2020) of Drew Point, Alaska. Finally, we conducted a graph connectivity analysis that found a 392% and 286% increase in the number of troughs and trough-connections, respectively, from 1949 to 2020. The length of the largest continuously connected trough-network increased by 20-times, suggesting that the landscape has experienced a dramatic increase in lateral drainage.

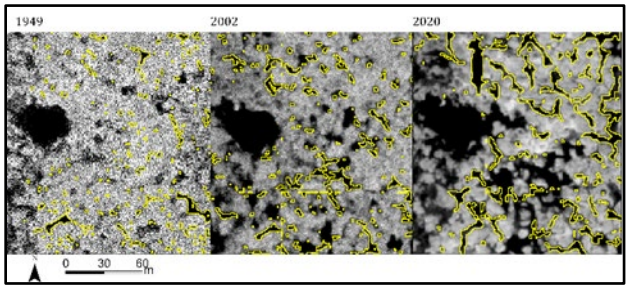

Figure 2. Zoomed-in example of trough detection on imagery of the same location from 1949, 2002, and 2020. Predicted troughs are outlined in yellow. Imagery © Maxar, Inc.

RETROGRESSIVE THAW SLUMPS

Among other permafrost landforms, retrogressive thaw slumps (RTS), also called ground-ice slumps, are recognized as one of the most active, rapid, and dramatic thermokarst landforms in the Arctic. The RTS process creates large open depressions (a horseshoe- or bowl-shaped depression with a steep headwall) on hillslopes due to soil wasting and vegetation displacement. In most cases, the resulting debris flow is terminated by a stream or a lake. The RTS activity poses significant implications on geomorphological, hydrological, biogeochemical, and ecological processes from local to regional scales. Mapping, monitoring, and documentation of abrupt permafrost thaw is crucial to increase our spatio-temporal understanding of permafrost landscape dynamics in the Arctic. We developed a deep learning convolutional neural net model (UNet-based workflow) to automatically detect and characterize RTSs from VHSR imagery.

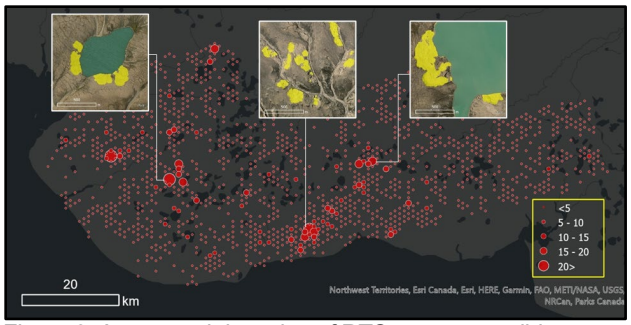

Figure 3. Automated detection of RTSs over a candidate area in Banks Island, CA. The size of the map symbol (red circle) is proportional to the area (in Ha) of the RTS falling inside a hexagonal grid. Each grid cell covers 100 Ha. Yellow shading on zoomed-in views indicate detected RTS. Imagery © Maxar, Inc.

HUMAN-BUILT INFRASTRUCTURE

With approximately 70% of infrastructure across the Arctic located in areas of high potential for near-surface permafrost thaw, there is a pressing need to quantify the economic impacts and occurrence of infrastructure damage caused by permafrost hazards. However, updated, high-resolution geospatial inventories of infrastructure are lacking across the Arctic. We developed an infrastructure detection model, combining the state-of-the-art UNet++ CNN architecture and transfer learning, to map nine types of human-built structures (detached houses, row houses, multi-story blocks, non-residential buildings, roads, runways, gravel pads, pipelines, and storage tanks) in Maxar satellite imagery at a resolution of ≤ 0.5 m.

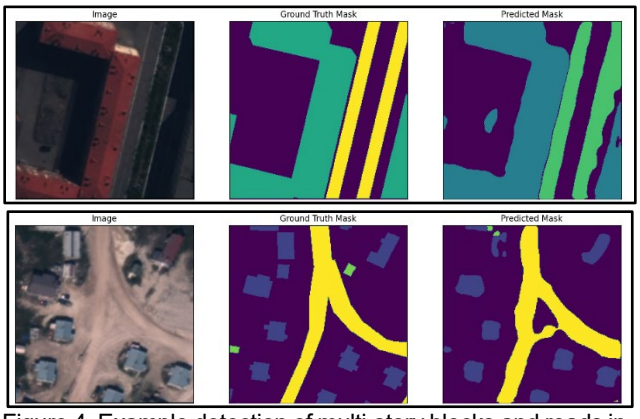

Figure 4. Example detection of multi-story blocks and roads in Norilsk, Russia (top) and detached houses and roads in Coral Harbour, Canada (bottom). The input image is on the left, the ground truth mask is in the center, and the predicted output mask is on the right. Imagery © Maxar, Inc.

Fire-induced spatial heterogeneous thaw subsidence in morainal area of Beaver Creek, Yukon: Detected by ALOS-2 InSAR and field observation

Kazuki Yanagiya[1], Masato Furuya[2,3], Go Iwahana[3,4], Antoine Séjourné[5] & Takeo Tadono[1]

[1]*Japan Aerospace Exploration Agency, Tsukuba, Ibaraki, Japan*

[2]*Faculty of Science, Hokkaido University, Sapporo, Hokkaido, Japan*

[3]*Arctic Research Center, Hokkaido University, Sapporo, Hokkaido, Japan*

[4]*International Arctic Research Center, University of Alaska Fairbanks, Fairbanks, Alaska, United States*

[5]*Geosciences Paris-Saclay, University of Paris-Saclay, Paris, France*

Increasing trends in the frequency and extent of wildfires have been reported in polar regions. These fire regimes may accelerate the positive feedback associated with permafrost soil carbon release (Chen et al. 2021). Consequently, broad monitoring of permafrost thawing is essential for a comprehensive understanding of the carbon cycle in polar terrestrial ecosystems. Interferometric Synthetic Aperture Radar (InSAR) can detect relative ground displacements to the order of centimeters. InSAR enables the observation of spatio-temporal variations in thaw subsidence and frost heave, thus allowing broad monitoring of permafrost freeze-thaw processes (e.g., Yanagiya et al. 2023).

The PRISMARCTYC project aims to better understand the impacts of permafrost thaw on soils, surface/groundwater fluxes and carbon cycle, as well as their controlling factors. Our study focuses on small inland Arctic watersheds where localized and rapid thermokarst occurrences remain under-studied. The study site is Beaver Creek (BC, 62°22'N, 140°52'W), located in the western Canadian discontinuous-extensive permafrost zone. The last glaciation reached the southern area of BC (McConnell Glacier). Cryostratigraphic investigations revealed the presence of a Yedoma deposit (Sliger et al. 2015) between moraine hills at the Beaver Creek Road Experimental Site (BC-RES), located 8 km southeast of BC.

This research focuses on a fire scar that burned in July and September 2019. The scar is located 15 km southeast of BC, and is present in the McConnell moraine deposits. Sentinel-2 optical imagery indicated that the total burned area is approximately 28 km². Additionally, previous core sampling at BC-RES identified the existence of subsurface ice wedges (Stephani et al. 2014). It indicates a potential for rapid, fire-induced permafrost thawing and subsequent ground subsidence around the BC area.

Data and methods

To detect ground deformation around BC, we conducted InSAR image analysis using the data from the Japan Aerospace Exploration Agency's (JAXA) L-band SAR satellite, ALOS-2/PALSAR-2. Annual InSAR images were derived with SM3 data. To further investigate seasonal ground deformation processes with higher spatial resolution, we commenced monthly observations from May to September 2023 with SM1 data, a 5 m spatial resolution in this analysis.

SAR imageries were clipped around the 2019 fire scar, and a quadratic polynomial correction was applied to mitigate the atmospheric and ionospheric phase delay, which can be assumed as the long-wavelength phase trend. The bedrock area outside the 2019 scar was used as the phase reference point.

Additionally, field observations were conducted around BC in August 2022 and 2023. We measured thaw depth, air and surface temperature inside and outside the 2019 scar. A 620 m transect was established on the southern-facing slope of the northern part of the 2019 scar (Site3_P2). Thaw depth was measured at about 30 m intervals with a metal probe. During the 2023 campaign, GNSS measurements were also taken along the transect to verify the InSAR data. Furthermore, orthomosaic images and Digital Surface Models (DSMs) were generated using drone imagery in three areas in the 2019 scars.

Result and discussion

The InSAR imagery, derived from SM3 data, detected annual ground subsidence signals within the 2019 scar. The low interferometric coherence resulted in significant phase noise in the 2019-20 and 2020-21 InSAR pairs. In contrast, 2021-22 and 2022-23 pairs showed ground subsidence signals of up to 6 cm/year (Figure 1a). The spatial pattern of the annual ground deformation is localized to specific areas within the 2019 scar.

In addition, accumulated InSAR images derived from SM1 data detected ground subsidence signals up to 15 cm from June to September 2023 (Figure 1b). The seasonal subsidence signals are also spatially heterogeneous. However, the spatial pattern differs

from the annual deformation, as sporadic subsidence signals are detected even in areas where no annual deformation signal was detected.

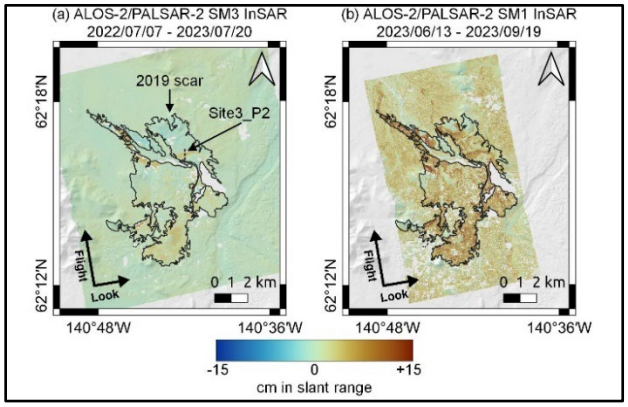

Figure 1. (a) Annual and (b) seasonal displacement map around the 2019 scar. Black line indicates the 2019 scar. Black dashed line indicates the transect established in Site3_P2. Positive value (reddish color) means subsidence signal and negative (bluish color) means uplifting.

In Site3_P2, both seasonal and annual subsidence was detected in the same spatial pattern. Compared with the surficial geology map (provided by Yukon Geological Survey), the spatial extent of both subsidence signals corresponds to the distribution of glaciofluvial sediments covered with poorly decomposed organic layers. In contrast, the surrounding undeformed areas correspond to the morainal till areas. In addition, the annual subsidence signal has been continuously detected from 2019 to 2023 at Site3_P2. It suggests the melting of massive ground ice and the meltwater runoff may have occurred between the moraine hills after the 2019 fire.

Figure 2 indicates the seasonal displacement, elevation, and thaw depth profiles along the transect in Site3_P2. On the mid-slope (white hatch in Figure 2), thaw depth was deepened to 60–111 cm, compared to a depth of 45 cm at the control site, an unburned area adjacent to the 2019 scar. The deepening of thaw depth compared to the control site indicates the progression of permafrost thawing in this area after the 2019 fire. Additionally, the spatial pattern of thaw depth correlates with the pattern of seasonal subsidence, suggesting an increase in the formation and melting of ice lenses within the active layer in areas with deeper thaw depths.

The spatial pattern of seasonal ground subsidence at the central part of the 2019 scar is quite heterogeneous, relating to the distribution of the hummocky moraine. It indicates the seasonal thaw subsidence in the depressed areas in-between moraine mounds/hills. Furthermore, sporadic subsidence signals were also detected outside the fire scar, spatially associated with polygon terrain and small riverbanks. Such sporadic subsidence signals might have been overlooked in the lower-resolution Sentinel-1 and ALOS-2 SM3 InSAR imagery. We will further investigate and verify seasonal and interannual subsidence processes with high-resolution SM1 data, GNSS measurement, and drone imagery.

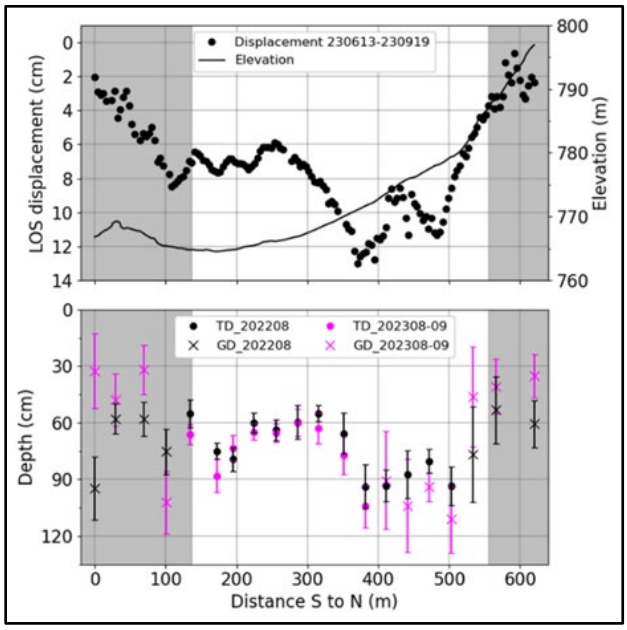

Figure 2. Profiles of seasonal displacement, elevation, and thaw depth change along the transect in Site3_P2.TD and GD mean thaw depth and depth reached on the gravel, respectively. Gray hatch indicates gravel rich moraine till area.

REFERENCES

Chen, Y., Romps, D.M., Seeley, J.T., Veraverbeke, S., Riley, W.J., Mekonnen, Z.A., and Randerson, J.T. 2021. Future increases in Arctic lightning and fire risk for permafrost carbon. Nat. Clim. Chang. 11, 404–410. doi:10.1038/s41558-021-01011-y

Yanagiya, K., Furuya, M., Danilov, P., and Iwahana, G. 2023. Transient Freeze-Thaw Deformation Responses to the 2018 and 2019 Fires Near Batagaika Megaslump, Northeast Siberia. Journal of Geophysical Research: Earth Surface, 128. doi:10.1029/2022JF006817

Sliger, M., Fortier, D., deGrandpré, I., and Lapointe E.L. 2015. Incidence of Late Pleistocene-Holocene Climate on the Concurrent Landscape and Permafrost Development of the Beaver Creek Region, Southwestern Yukon, Canada. GéoQuébec 2015, CGS Québec, QC, Canada, doi:10.13140/RG.2.1.1008.1764

Stephani, E., Fortier, D., Shur, Y., Fortier, R., and Doré, G., 2014. A geosystems approach to permafrost investigations for engineering applications, an example from a road stabilization experiment, Beaver Creek, Yukon, Canada. Cold Reg. Sci. Technol. 100, 20–35. doi:10.1016/j.coldregions.2013.12.006

Enhancing permafrost mapping: The influence of sediment size on permafrost occurrence in the Canadian Rockies

Gerardi Zegers & Masaki Hayashi

Department of Earth, Energy and Environment, University of Calgary, Calgary, Alberta, Canada

Permafrost is a key component of the cryosphere, influencing energy exchanges, hydrological processes, and natural hazards. In mountainous areas, permafrost occurrence is affected by complex topography and surficial geology, resulting in substantial spatial heterogeneity. Mountain permafrost distribution is primarily defined by a combination of climate, topography, and ground conditions: (i) At a regional scale, the climate can generate cold surface conditions governed by latitude and global circulation. (ii) These climate conditions are modified by topography at different scales due to variations in air temperature, solar radiation, and redistribution of snow by wind and avalanches. (iii) Locally, ground properties and their influence on heat and water transfer modify the topographically overprinted climate conditions.

Particularly in discontinuous alpine permafrost zones, the lowest active permafrost is typically found in coarse sediments. These surficial sediments create a unique thermal regime that allows permafrost to persist even under positive mean annual air temperatures. While permafrost mapping methods often incorporate topoclimatic variables, such as altitude, potential incoming solar radiation (PISR), curvature, and normalized difference vegetation index, the influence of sediment size, a recognized critical factor, has been omitted due to the unavailability of datasets or methodologies to estimate this variable.

This study investigated the role of coarse sediments in permafrost occurrence in the Canadian Rockies using field observation and machine learning. The main objectives of this work are: (i) analyze the spatial heterogeneity of permafrost and determine which are the main variables that control permafrost extent at alpine basins, and (ii) find a suitable method to estimate permafrost extent at various alpine basins.

Specifically focusing on alpine landforms such as talus slopes, rock glaciers, and moraines, approximately 380 ground surface temperature sensors were deployed at elevations ranging from 2000 m a.s.l. to 2500 m a.s.l. The permafrost extent was estimated using the basal temperature of snow (BTS) method.

The sensors were deployed across six different sites in the Canadian Rockies—Lake O'Hara, Helen Creek, Lake Louise, Fortress, Ptarmigan Cirque, and Arethusa Valley—and strategically placed to represent different conditions, including altitude, potential incoming solar radiation (PISR), and sediment size.

Conventional manual grain-size sampling methods, such as grid- or line-based pebble counts, are labour-intensive, time-consuming, physically intrusive, and prone to operator sampling bias. These methods are also limited to patch-scale observations, defined as an area of ground measuring approximately 1 m^2.

Since the aim is to generate a distributed permafrost map, an efficient methodology is needed to estimate sediment size at larger scales. Recent methodological advancements aim to enhance the spatial coverage, representativity, and efficiency of surface sedimentological datasets by estimating grain size directly from images. These 'photo-sieving' methods focus on developing non-invasive, semi-automated approaches to obtain grain-size distribution data from ground-based or low-altitude aerial photography.

In this work a new tool was developed to predict the surficial sediment size based on unmanned aerial vehicle (UAV) images, specifically focused on periglacial environments, where angular sediments and broad size ranges are characteristic. At each site, a UAV survey including two types of flights were performed: (i) low-altitude flights (~30 m height) at specific patches to achieve high-resolution ortho mosaics (pixel resolution 5-8 mm) and (ii) high-altitude flights (~100 m height) to cover the whole study area with medium-resolution orthomosaic (pixel resolution 3 cm).

The granulometric distribution curve was first estimated in the high-resolution images using ImageGrain, an image segmentation method. The segmentation is done with the Cellpose algorithm (Stringer and Pachitariu 2021), which is designed for cell and nucleus segmentation in biomedical images. Its segmentation capability is transferred to geoscientific applications through re-training of the model with images of sediment particles. With this methodology, nine characteristic diameters were extracted from each high-resolution image.

Then, a texture-based method, SediNET (Buscombe 2020), was trained to calculate the characteristic diameters using the granulometric distribution curves from 1200 images obtained from the high-resolution images. The final SediNET mode,

specifically trained for alpine landforms, was used to estimate distributed sediment size across each site, obtaining an average error of approximately 15%.

Using this dataset, a machine learning method (random forest) was trained to predict BTS, incorporating sediment diameter and other variables such as PISR, altitude, normalized difference vegetation index, and curvature.

Also, the application of a linear regression model and support vector machine (SVM) were also evaluated obtained greater error than random forest model. Further, feature importance calculated by the random forest model revealed that the sediment size was the second most important variable after altitude to predict the BTS.

Including sediment diameter reduced the permafrost probability prediction errors by 15%, highlighting its significance in predicting permafrost in alpine environments. Further, the obtained permafrost maps show a better correlation with the expected permafrost extent based on geophysics surveys and field interpretation.

This study, employing field measurements and classification methods, demonstrated the important role of sediment size in controlling permafrost occurrence in the Canadian Rockies. Further this newly developed model allow a efficient workflow to estimate permafrost occurrence in new basins. The only requirement is an orthomosaic with resolution of 3 cm that can be generated with flight altitudes of ~100 m depending on the UAV camera. All the other required information is directly extracted from openly available satellite products.

The newly developed mapping tools, which incorporate sediment size as a predicting variable, offer enhanced accuracy and a fast workflow to predict permafrost in alpine landforms. These findings advance the understanding of permafrost dynamics in mountainous regions and provide a valuable tool for estimating permafrost extent at larger scales.

REFERENCES

Buscombe, D. 2020. SediNet: A configurable deep learning model for mixed qualitative and quantitative optical granulometry. Earth Surface Processes and Landforms, 45(3), 638–651.

Stringer, C.A., and Pachitariu, M. 2021. Cellpose: a generalist algorithm for cellular segmentation. Nat Methods 18, 100–106.

10B — High Resolution Remote Sensing Applications in Permafrost Studies

Session Chairs: Stefano Ponti[1], Benjamin Jones[2] & Andreas Kääb[3]

[1]*University of Insubria, Varese, Italy*
[2]*University of Alaska, Fairbanks, Alaska, United States*
[3]*University of Oslo, Oslo, Norway*

Mapping and modelling of permafrost and surface temperatures have become a widespread and shared aim among research groups to project the climate change effects on regional to hemispherical scale. Conversely, the ground validation dataset is still poor and often related to single temperature profiles in boreholes, not well representative of the local scale variability. Even the CALM experiment is restricted to measurements of nodes, knowing that at the inter-node span, the environmental control on permafrost and active layer might change drastically. Therefore, the increase of validated remotely sensed datasets at very high resolution is of scientific interest both for filling the gap between the in-situ measurements and the hemispheric scale (coarser resolution) in modelling and for reaching the closest assessment to the natural variability of permafrost drivers.

This session embraces studies conducted from ground to air-borne and satellite remote sensing of (1) permafrost thermal state; (2) active layer dynamics; (3) surface energy balance; (4) periglacial processes; (5) their interactions and controls. All the contributions aiming to enhance our understanding of the application of multi-spectral cameras, UASs, self-made sensors, space-borne platforms and validation techniques to permafrost science are welcome.

Linear infrastructure and permafrost monitoring with Interferometric Synthetic Aperture Radar (InSAR) and Optical Photogrammetry Data

Usman Iqbal Ahmed[1], Bernhard Rabus[1] & Fabrice Calmels[2]
[1]*SARlab, Simon Fraser University, Burnaby, British Columbia, Canada*
[2]*YukonU Research Centre, Whitehorse, Yukon, Canada*

We aim to exploit synergy in Synthetic Aperture Radar (SAR) and Optical Photogrammetry Structure from Motion (SfM) data for direct and indirect change detection in active permafrost areas. High precision photogrammetric DEMs from airborne optical SfM surveys can be used for direct change analyses. These DEMs also serve as a reference surface for airborne SAR and Interferometric SAR (InSAR) applications. Photogrammetry not only provides high resolution DEMs but the block adjustment parameters can fine-adjust the flight trajectory for enhanced motion compensation for repeat pass Interferometric SAR application, thus producing high precision interferometric change maps for the area of interest. Moreover, spaceborne SAR data based interferometric time series analysis can augment the airborne results at a higher temporal and lower spatial resolution. All these outputs can be combined into highly accurate change maps.

Experimental Setup

We operate a Tri-Band (X, C and L) Band SAR System (called SlimSAR) with a co-incident Optical SfM system (called fodar) mounted on a Helio-courier operated by tourist flight operator in Silver City, Yukon Territory, Canada. The SAR system specifications are shown in Table 1 below:

Table 1. System Specification.

Parameter	X-band	L-band	C-band
Waveform	Pulsed LFM	Pulsed LFM	LFM-CW
Frequency (GHz)	9.35–9.65	1.215–1.4	5.43
Max Bandwidth (MHz)	245	185	160
Transmit Power (W)	25 (+ 50 w/amplifier)	60	1.0
Antennas	1 Tx, 2 Rx	2 Rx/Tx	1 Tx, 2 Rx
Polarizations	VV	HH, HV, VH, VV	VV

The optical system consists of a DSLR (Nikon D850) and an intervalometer which also syncs the camera flash events as IMU events. The experimental setup mounted on the Helio-courier is shown in Figure 1 with the top view of the system installation arrangement on the aircraft.

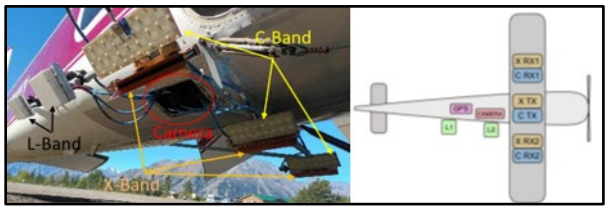

Figure 1. SAR and Optical System mounted on the Helio-courier (Left) Top-view of the system configuration on the aircraft (Right).

Area of Interest

We are interested in Linear Infrastructure change monitoring in active permafrost region. Therefore, we have targeted Alaska Canada Highway near the northern edge of Kluane lake highlighted by a red rectangle in Figure 2.

Figure 2. Area of Interest near Burwash Landing, YT, CA.

Methodology

We are collecting bi-annual SAR and Optical data with our airborne surveys. We will be utilizing DEM derived from the Optical SfM for a direct measure of change occurring in the area coupled with an Interferometric change map based on the SAR data. Bi-annual collection helps in decoupling the seasonal effects/biases in the data.

In addition to the aerial surveys we are also analyzing spaceborne Sentinel-1 (S-1) Interferometric Wide-swath (IW) SAR data over two years for times

series analysis using a Homogenous Distributed Scatterers Interferometry (HDS-InSAR) (Rabus B. et al. 2012).

PRELIMINARY RESULTS

Our airborne interferometric chain is under progress whereas the fodar system output can be used in its present form for precise change detection and monitoring. The DEMs and ortho-mosaics produced by the fodar system are of submeter resolution (~12–24 cm), whereas the slimSAR data is 0.6 m x 1.5 m in resolution (Ahmed et al. 2021). Figure 3 shows different outputs of our system over the Silver City Airstrip.

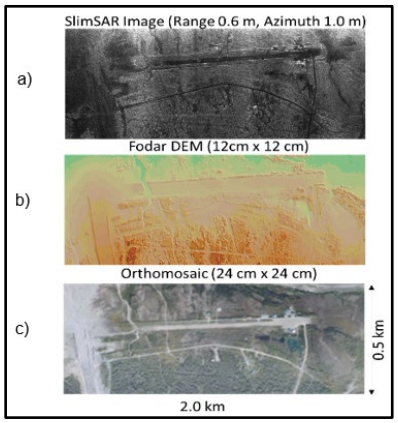

Figure 3. a) Silver City airstrip SAR Image b) corresponding fodar DEM c) Ortho-mosaic.

We collected two datasets over the AOI in quick succession where we parked the car at two different locations during the acquisitions to check the efficacy of the fodar system. Figure 4 below shows that the change of the car location was detected in the difference of the two DEMs. This demonstrates how powerful a tool this can be for change detection.

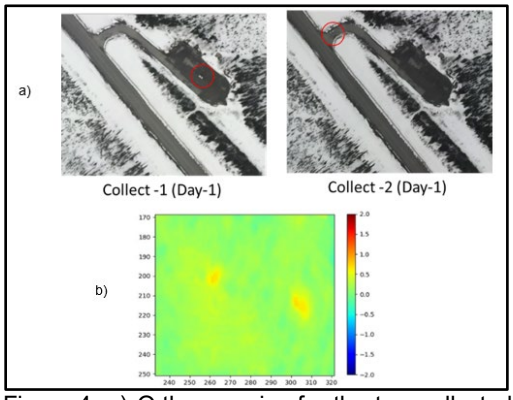

Figure 4. a) Ortho-mosaics for the two collects b) Absolute difference of DEMs for the two acquisitions.

The HDS-InSAR analysis of S-1 IW data presented in Figure 5 shows some interesting trends in the regions where a rock glacier can be seen moving around 5-6 mm over a period of two years in the direction of the SAR acquisition whereas the Highway is deforming about 5 mm away from the look direction of the radar.

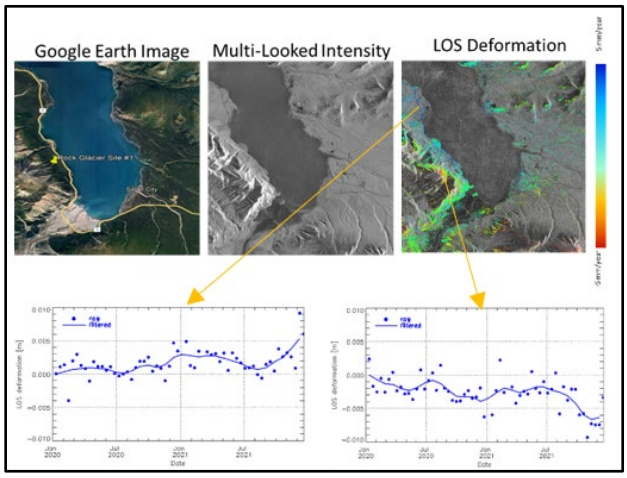

Figure 5. S-1 IW Line of Sight (LOS) Deformation and timeseries trends.

CONCLUSION

Our preliminary results show that our unique methods can be powerful tools to detect and monitor changes due to active permafrost layer. Moreover modelling of the changes based on borehole data, precipitation and temperature data can help in predicting future trends. We will be demonstrating detailed analysis furthering the preliminary finding in during conference.

ACKNOWLEDGEMENT

We acknowledge the support of the Natural Sciences and Engineering Research Council of Canada (NSERC). Additional support for this work comes from NSERC PermafrostNet

REFERENCES

Rabus, B., Eppler, J., Sharma, J., and Busler, J. 2012. Tunnel monitoring with an advanced InSAR technique. In Radar Sensor Technology XVI, 8361: 483–492.

Ahmed, U.I., Rabus, B., and Kubanski, M. 2021. Off-Nadir Photogrammetry for Airborne SAR Motion Compensation: A First Step. In 2021 IEEE International Geoscience and Remote Sensing Symposium IGARSS: 8519–8522.

Large-scale surface deformation dataset derived from InSAR for the permafrost zone of Qinghai-Tibet Engineering Corridor, China

Qingsong Du[1,2,3], Guoyu Li[1,2,3], Fujun Niu[1], Wei Ma[1,2] & Dun Chen[1,2,3]

[1]*State Key Laboratory of Frozen Soil Engineering, Northwest Institute of Eco-Environment and Resources, Chinese Academy of Sciences, Lanzhou, China*

[2]*Da Xing'anling Observation and Research Station of Frozen-Ground Engineering and Environment, Northwest Institute of Eco-Environment and Resources, Chinese Academy of Sciences, Jagdaqi, China*

[3]*College of Resources and Environment, University of Chinese Academy of Sciences, Beijing, China*

Our research focuses on surface deformation in the permafrost region of the Qinghai-Tibet Engineering Corridor (QTEC). Our objective is to gather fully covered and long-term time series data on surface deformation, analyze temporal and spatial variations, investigate influencing factors, and utilize this deformation data for practical engineering applications. Initially, we utilized large-scale InSAR technology to obtain deformation results in the one-dimensional line-of-sight (LOS) direction using ascending and descending SAR satellite data across the study area. Subsequently, we derived two-dimensional deformation information (east-west, EW, and vertical/ up and down, UD) while considering the image acquisition dates as a constraint condition. The accuracy of vertical deformation measurements was validated against in-situ field monitoring results. Our findings indicate that vertical deformation results offer a more precise reflection of real ground surface deformation compared to single LOS deformation results from single ascending or descending orbits. The error in vertical deformation according to UD measurements generally remains within 10 mm, with a maximum deviation of no more than 30 mm, whereas errors in single ascending and descending orbit results frequently exceed 50 mm.

InSAR-based studies have extensively explored surface deformation in the permafrost region of the Tibetan Plateau, providing valuable insights and laying a robust foundation for subsequent research. However, several unresolved issues warrant further investigation as follows (Du 2023):

1. Spatial Scale: Existing studies are predominantly limited to small spatial scales, constrained by SAR image coverage. Only a few studies encompass the entirety of the QTEC, a linear infrastructure project spanning significant east-west and north-south distances, requiring multiple tracks of SAR data. This poses challenges in processing InSAR processing and integrating results, hampering comprehensive monitoring of the entire corridor.
2. Temporal Scale: Despite advancements in MT-InSAR technology and the availability of Sentinel-1 SAR data, most efforts focus on short periods, typically three to four years, with limited monitoring extending beyond five years. This limitation is partly due to constraints such as the launch date of the Sentinel-1a satellite on April 3, 2014, and algorithmic challenges like spatial-temporal incoherence. Additionally, storage and computational constraints hinder the development of long-term InSAR deformation monitoring.
3. Deformation Dimension: Much of the existing research relies on one-dimensional LOS deformation measurements, which may not fully capture actual ground surface deformation. The LOS direction presents challenges in comparing and validating results from different SAR data and orbital configurations. Overcoming these limitations to perform genuine three-dimensional (3D) deformation analysis is particularly challenging. By considering SAR's geometric properties and its limited sensitivity to north-south deformation, we can derive UD and EW surface deformations under the assumption of negligible north-south deformation, utilizing both ascending and descending orbital data.

DATA AND METHODOLOGY

We utilized the LiCSAR product, provided by The Center for Observation and Modelling of Earthquakes (COMET) and accessible at https://comet.nerc.ac.uk/, to process interferometric pair data spanning the entire QTEC (Du et al. 2023a). The LiCSBAS toolkit was employed to derive surface deformation data for the study area from 2015 to 2022. Our analysis included time-series cumulative deformations and deformation rates along the LOS direction for both ascending and descending satellite tracks.

Considering the temporal information extracted from the images as a constraint and assuming minimal or negligible deformation in the north-south direction, we computed the vertical and east-west deformations of the QTEC using Equation 1 in conjunction with the deformation results from both ascending and descending satellite orbits.

$$\begin{bmatrix} d_{insar}^{A} \\ d_{insar}^{D} \end{bmatrix} = \begin{bmatrix} cos_{inc}^{A} & -cos_{azi}^{A} sin_{inc}^{A} \\ cos_{inc}^{D} & -cos_{azi}^{D} sin_{inc}^{D} \end{bmatrix} \begin{bmatrix} d_u \\ d_e \end{bmatrix} \quad [1]$$

Where d_{insar}^{A} and d_{insar}^{D} represent the ascending and descending InSAR monitoring LOS direction results, respectively, θ_{inc}^{A} and θ_{inc}^{D} represent the ascending and descending SAR radar incidence angles, respectively, α_{azi}^{A} and α_{azi}^{D} represent the ascending and descending SAR radar azimuth angles, respectively, d_u represents the vertical direction deformation information, and d_e represents the east-west direction deformation information.

Results

Within the engineering corridor, oriented towards the ascending track data, the rate of LOS deformation ranged from -26.511 mm/yr to 18.367 mm/yr between August 2015 and March 2022. Cumulative deformation over this period varied from -178.08 mm to 147.462 mm, indicating an overall uplift pattern, with more significant settlement occurring in subsidence regions. In contrast, LOS deformation velocity for the descending satellite track displayed a central range from -26.029 mm/yr to 24.251 mm/yr, with cumulative deformation spanning from -187.817 mm to 145.823 mm, indicating a predominant subsidence trend.

From May 25, 2017, to March 31, 2022, the vertical deformation rate of the project corridor's surface primarily ranged between -27.068 mm/yr and 18.586 mm/yr. The mean and median values were -1.06 mm/yr and 0.136 mm/yr, respectively, indicating a slight overall uplift of the corridor over these six years. However, subsidence rates were more pronounced in specific areas, with cumulative deformation mainly ranging from -108.918 mm to 85.867 mm.

In the east-west direction, the deformation rate mainly fell between -21.954 mm/yr and 24.814 mm/yr. The mean and median values were -0.374 mm/yr and 0.323 mm/yr, respectively, indicating a slight eastward tendency for most of the corridor during these six years. However, westward displacement was more significant in intensity, with cumulative deformation concentrated in the range of -21.954 mm to 18.592 mm.

The on-site monitoring dataset revealed that most monitoring points exhibiting significant subsidence aligned well with vertical monitoring results obtained from InSAR. When comparing the one-dimensional LOS deformation results of the ascending and descending satellite orbits with on-site monitoring data, a high degree of consistency was observed in certain areas, where the trends of the ascending and descending orbits matched. However, the error in these areas, compared to the on-site monitoring results, exceeded 30 mm, surpassing that of the vertical results.

In contrast, inconsistencies in the LOS deformation trends between the ascending and descending satellite orbits were observed at some monitoring points. In these areas, relying solely on one-dimensional LOS deformation information may lead to incorrect conclusions. This discrepancy was primarily attributed to variations in the radar beam-ground geometric relationship during satellite imaging, resulting in pronounced geometric attributes within the SAR satellite data (Du et al. 2023b).

Conclusion

By employing the LiCSAR product and the LiCSBAS package, comprehensive and long-term deformation monitoring results for surface changes can be swiftly obtained. This approach presents a novel method and option for conducting wide-ranging surface deformation monitoring. The vertical deformation results consistently align with field-based trends, with errors typically remaining within 10 mm and reaching a maximum of 30 mm in certain cases.

Acknowledgements

Thanks to the Second Tibetan Plateau Scientific Expedition and Research (STEP) program (grant no. 2019QZKK0905) and the Research Project of the State Key Laboratory of Frozen Soils Engineering (grant no. SKLFSE-ZQ-202303) for funding this work.

References

Du, Q.S. 2023. InSAR-based study for surface deformation monitoring and stability evaluation in permafrost areas of Qinghai-Tibet Engineering Corridor in the Qinghai-Tibet Plateau, China. Doctoral Dissertation, University of Chinese Academy of Sciences, Beijing, China.

Du, Q.S., Chen, D., et al., 2023a. Preliminary Study on InSAR-Based Uplift or Subsidence Monitoring and Stability Evaluation of Ground Surface in the Permafrost Zone of the Qinghai–Tibet Engineering Corridor, China. Remote Sensing, 2023, 15, 3728. doi:10.3390/rs15153728

Du, Q.S., Li, G.Y., et al., 2023b. Two-dimensional ground deformation dataset in permafrost zone of the Qinghai-Tibet Engineering Corridor, China (from February 2017 to March 2022). National Tibetan Plateau/Third Pole Environment Data Center. doi: 10.11888/Cryos.tpdc.300400

Thermal photogrammetry on a permafrost rock wall for the active layer monitoring

Stefano Ponti[1,2], Irene Girola[1] & Mauro Guglielmin[1,2]

[1]*Department of Theoretical and Applied Science, University of Insubria, Varese, Italy*

[2]*Climate Change Research Center (CCRC), University of Insubria, Como, Italy*

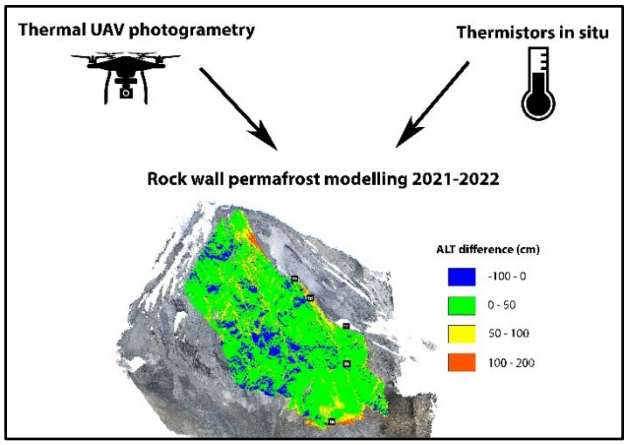

Graphical abstract: use of UAV thermal photogrammetry and installation of thermistors at the rock surface for the ALT modelling.

Permafrost and active layer models often cannot explain the high spatial variability, especially in heterogeneous environments like the mountainous regions due to their scarce resolution, paucity of climatic data and topographic details. This fact, coupled with the consciousness that The European Alps underwent an increase of air temperature of 0.2 – 0.7 °C dec^{-1} during 2000–2019 (Etzelmüller et al. 2020), rises interest in understanding the effect of permafrost degradation at high altitudes. Here, the harshness of the terrain links the permafrost degradation to an increase of the slope instability that lead to high-altitude hazards and risks (Bommer et al. 2010; Duvillard et al. 2019; Duvillard et al. 2020). However, recent unmanned aerial vehicle (UAV) applications and detailed photogrammetry could help solving the modelling issues related to poor topographic details and reaching inaccessible areas.

In this study, we want to introduce a new application of the UAVs in thermal photogrammetry to model the active layer thickness (ALT) of an alpine rock wall through the computation of the thermal inertia that has already been used in permafrost detection but never on Earth (Bandfield and Feldman 2008; Nixon 1990). Subsequently, we want to compare the results with a widespread ALT model (Stefan's solution) and the alpine permafrost index map (APIM) (Boeckli et al. 2012).

On the Gran Zebrù South rock wall (Central Italian Alps, 3851 m a.s.l.), 8 thermal UAV surveys were conducted on 4 different summer days during 2021–2022 to have two 3D thermal models per day at different solar radiation inputs (minimum and maximum). By analyzing topographic data, visible imagery and the thermal models, the apparent thermal inertias (ATIs) (Maltese et al. 2010; Minacapilli et al. 2012) were converted into heat transfer coefficients (HTCs) (Robertson 1988) and then into ALT of 2021 and 2022 through a linear regression obtained with thermistors located in situ and the remotely sensed values. The 3D models of ALT have been validated through the placement of thermistors at different elevations (ranging from 3230 to 3655 m a.s.l.) and with variable depths (2, 15 and 40 cm from the rock surface). These were useful to calculate both the ATI of the rock surface (RS) and the depth of the 0 °C isotherm.

The Stefan's solution model has been developed with the calculated TDDs deriving from the thermistors and the obtained ALT has been compared with the ALT derived from the thermal inertia modelling.

Both the Stefan's solution ALT and the APIM overestimated permafrost occurrence. Mean ALT in 2022 was 228 cm and increased of 29.3 cm from 2021 to 2022 without significant topographic changes (Figure 1). Therefore, we expect sudden rock mass wasting and serious risks for the alpine tourism of this area if this trend is maintained.

Since it is expected that there will be less snowfall on the Alps (Marty et al. 2017; Kotlarski et al. 2023) and permafrost is strictly related to the snow cover distribution/persistence (Magnin et al. 2015), the future trend of permafrost degradation under the climatic change could be extremely variable especially in steep rock walls.

If south-faced rock walls will steepen with the air warming (Zwieback 2021), but less snow will accumulate on steep summits (ALT decrease), what will be the equilibrium in the future? Will the little snow cover cool the RS during winter favoring permafrost formation or anticipate the snowmelt (long-lasting RS warming) favoring permafrost degradation?

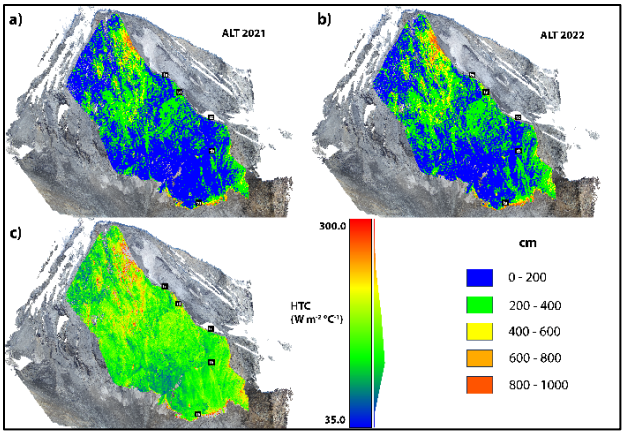

Figure 1. 3D spatial distribution of the modelled ALT in 2021 (a), 2022 (b) and the calculated HTC in 2022 (c). The color classes at the bottom-right of the figure shares the same classes for ALT in 2021 and 2022.

REFERENCES

Bandfield, J.L., and Feldman, W.C. 2008. Martian high latitude permafrost depth and surface cover thermal inertia distributions. J Geophys Res Planets, 113.

Boeckli, L., Brenning, A., Gruber, S., and Noetzli, J. 2012. Permafrost distribution in the European Alps: Calculation and evaluation of an index map and summary statistics. Cryosphere, 6: 807–820. https://doi.org/10.5194/tc-6-807-2012

Bommer, C., Phillips, M., and Arenson, L.U. 2010. Practical recommendations for planning, constructing and maintaining infrastructure in mountain Permafrost. Permafrost and Periglacial Processes, 21: 97–104. https://doi.org/10.1002/ppp.679

Duvillard, P.A., Ravanel, L., Marcer, M., and Schoeneich, P. 2019. Recent evolution of damage to infrastructure on permafrost in the French Alps. Regional Environmental Change, 19: 1281–1293. https://doi.org/10.1007/s10113-019-01465-z

Duvillard, P.A., Ravanel, L., Schoeneich, P., Deline, P., Marcer, M., and Magnin, F. 2021. Qualitative risk assessment and strategies for infrastructure on permafrost in the French Alps. Cold Region Science Technology, 189: 103311. https://doi.org/10.1016/j.coldregions.2021.103311

Etzelmüller, B., Guglielmin, M., Hauck, C., Hilbich, C., Hoelzle, M., Isaksen, K., Noetzli, J., Oliva, M., and Ramos, M. 2020. Twenty years of European mountain permafrost dynamics-the PACE legacy. Environmental Research Letters, 15. https://doi.org/10.1088/1748-9326/abae9d

Kotlarski, S., Gobiet, A., Morin, S., Olefs, M., Rajczak, J., and Samacoïts, R. 2023. 21st Century alpine climate change. Climate Dynamics, 60: 65–86. https://doi.org/10.1007/s00382-022-06303-3

Magnin, F., Deline, P., Ravanel, L., Noetzli, J., and Pogliotti, P. 2015. Thermal characteristics of permafrost in the steep alpine rock walls of the Aiguille du Midi (Mont Blanc Massif, 3842 m a.s.l). Cryosphere, 9: 109–121. https://doi.org/10.5194/tc-9-109-2015

Maltese, A., Minacapilli, M., Cammalleri, C., Ciraolo, G., and D'Asaro, F. 2010. A thermal inertia model for soil water content retrieval using thermal and multispectral images. Remote Sensing for Agriculture, Ecosystems, and Hydrology, 12: 7824, 78241G. https://doi.org/10.1117/12.864672

Marty, C., Tilg, A.-M., and Jonas, T. 2017. Recent evidence of large-scale receding snow water equivalents in the European Alps. Journal of Hydrometeorology, 18: 1021–1031.

Minacapilli, M., Cammalleri, C., Ciraolo, G., D'Asaro, F., Iovino, M., and Maltese, A. 2012. Thermal Inertia Modeling for Soil Surface Water Content Estimation: A Laboratory Experiment. Soil Science Society of America Journal, 76: 92–100. https://doi.org/10.2136/sssaj2011.0122

Nixon, J.F. 1990. Effect of climatic warming on pile creep in permafrost. Journal of Cold Regions Engineering, 4: 67–73.

Robertson, E.C. 1988. Thermal properties of rocks, Open-File Report, U.S. Geological Survey. https://doi.org/10.3133/ofr88441

Zwieback, S. 2021. Topographic Asymmetry Across the Arctic. Geophysical Research Letters, 48: 1–10. https://doi.org/10.1029/2021GL094895

Seasonal comparison of InSAR and PolInSAR observables over a lowland permafrost site

Paloma Saporta[1,2], Alberto Alonso González[3] & Irena Hajnsek[1,2]

[1]*Microwaves and Radar Institute, German Aerospace Center (DLR), Wessling, Germany*

[2]*Institute of Environmental Engineering, ETH Zurich, Zurich, Switzerland*

[3]*Signal Theory and Communications Department, Universitat Politècnica de Catalunya, Barcelona, Spain*

Lowland permafrost studies benefit from the large ground coverage permitted by remote sensing techniques. In particular, Synthetic Aperture Radar (SAR) provides high-resolution imagery of regions of interest at the Earth surface in the radar domain (Moreira et al. 2013). SAR systems consist in an antenna mounted on a moving platform, usually an airplane or a satellite, that transmits and receives an electromagnetic signal. As this system operates in the microwaves domain, the signal is unaffected by the Earth cloud cover. It is an active sensor therefore imagery can also be acquired at night-time, which is a particularly interesting property in the case of Arctic studies.

DLR'S PERMASAR CAMPAIGN

SAR techniques for retrieving bio/geo-physical parameters of the Earth surface can be developed based at first on multi-modal airborne campaigns, covering a small zone of interest with very high spatial resolution. In this context, the German Aerospace Center (DLR) carried out the Permafrost Airborne SAR Experiment (PermASAR) campaign in the Canadian Arctic, as described in Hajnsek et al. (2019). This campaign aimed at investigating the interaction of radar waves with frozen grounds. It was subdivided into two successive missions where SAR datasets were acquired: one in summer 2018 and one in winter 2019, in order to account for both frozen and thawed upper states of the ground. Several antennas onboard allow to image the scene with wavelengths of different bands, namely X (3cm), C (6 cm) and L band (23 cm). The radar signal associated to each wavelength is expected to interact differently with the objects of the scene i.e. the vegetation cover and the ground. In particular, larger wavelengths are expected to penetrate deeper into frozen soils. Additionally, the sensor acquired simultaneously images with four polarization combinations, allowing to separate different types of scattering mechanisms at the Earth surface. Finally, several spatial baselines were flown, which can be combined in an interferometric framework where the resulting phase is sensitive to the structure and dielectric properties of the components of each pixel.

STUDY SITE

The focus of this study is the dataset covering Trail Valley Creek, a well-studied lowland permafrost site located in the North of Inuvik, Northwest Territories, in Canada. The site is characterized by tundra vegetation over continuous permafrost, as described in Grünberg et al. (2020). The imaged area is shown in Figure 1, and one corresponding SAR amplitude image in summer is represented in Figure 2.

Figure 1. Region of interest at the Trail Valley Creek site. The white rectangle delineates the SAR footprint.

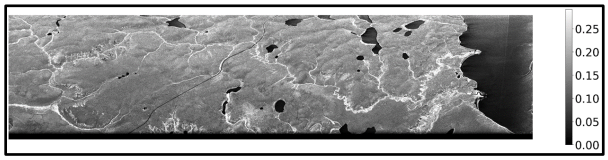

Figure 2. SAR backscatter over the Trail Valley Creek site in summer 2018, L-band, HH polarization.

METHODS

In order to analyze the interaction of the radar waves with the frozen soil, we perform a comparison between radar derived observables during the summer and the winter seasons. For each season, following processing was performed:

- Polarimetric SAR Interferometric coherence region extent. This corresponds to the relative vertical extent spanned by the interferometric phase center heights of all possible polarizations at a given pixel. A scheme is shown in Figure 3.

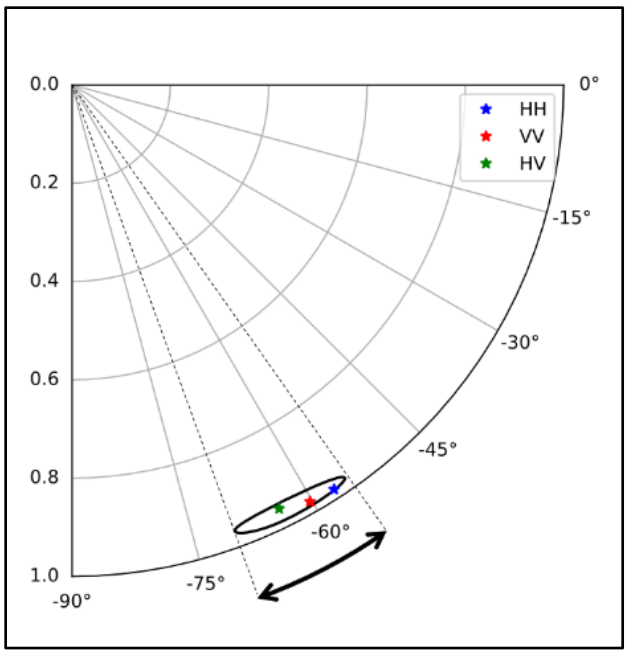

Figure 3. Scheme of the coherence region extent of an example pixel. The coherences associated with a few polarization combinations are plotted as single dots. The boundary of the coherence region is shown in black.

- Absolute phase center height derived from SAR interferometry. The absolute phase center height is the mean scattering height at a given pixel. It is related to the penetration depth of the signal with respect to the ground reference. Phase center heights are taken at VV polarization.

In both cases, the processing was done at L-band. As the absolute phases need to be calibrated with a corner reflector, all plots shown are restricted to the vicinity of the corner reflector. All phase measurements are then converted to height by dividing by the vertical wavenumber. Results are shown in Figure 4.

OBSERVATIONS

The following observations can be made:

- Overall, the coherence region extent increases from summer to winter. This indicates that the phase center heights are more spread in height in winter.
- Positive absolute phases in summer suggest that the calibration is successful as on natural terrain, scattering mainly comes from the vegetation, which is above the ground. In turn, negative phase center heights in winter indicate that the signal penetrates below the corner reflector height.

These observations are indications of penetration into the frozen soil.

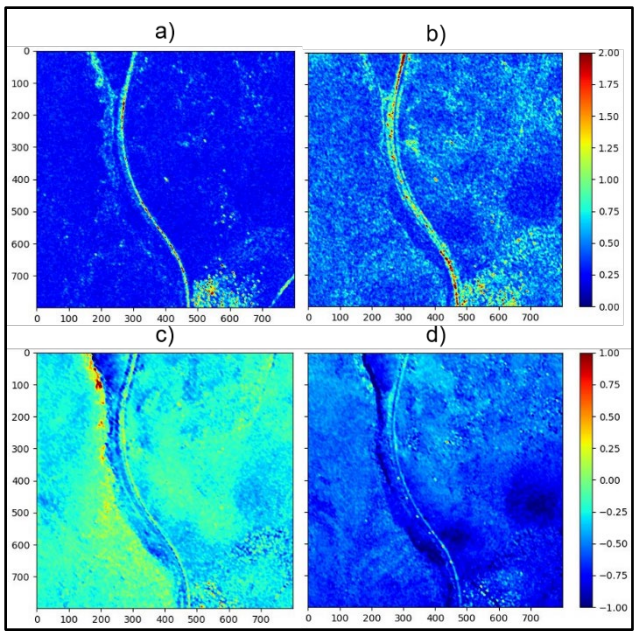

Figure 4. Summary of the results. All scales are in meter. Plots a) and b) represent the vertical extent of the coherence region, in summer and winter respectively. Plots c) and d) represent the absolute phase center heights, with the same season order.

REFERENCES

Grünberg, I., Wilcox, E.J., Zwieback, S., Marsh, P., and Boike, J. 2020. Linking tundra vegetation, snow, soil temperature, and permafrost, Biogeosciences, 17(16), 4261–4279. doi:10.5194/bg-17-4261-2020

Hajnsek, I., Joerg, H., Horn, R., Keller, M., Gesswein, D., Jaeger, M., Scheiber, R., Bernhard, B., and Zwieback, S. 2019. DLR Airborne SAR Campaign on Permafrost Soils and Boreal Forests in the Canadian Northwest Territories, Yukon and Saskatchewan: PermASAR. In POLINSAR 2019; 9th International Workshop on Science and Applications of SAR Polarimetry and Polarimetric Interferometry, Frascati, Italy

Moreira, A., Prats-Iraola, P., Younis, M., Krieger, G., Hajnsek, I., and Papathanassiou, K.P. 2013. A tutorial on synthetic aperture radar. IEEE Geoscience and remote sensing magazine, 1(1), 6–43. doi:10.1109/MGRS.2013.224830

A new ice-rich-permafrost-system observatory on fluvial and lacustrine deposits, Prudhoe Bay Oilfield, Alaska

Donald Walker[1], Amy Breen[2], Billy Connor[3], Ronnie Daanen[4], Olivia Hobgood[1], Torre Jorgenson[5], Anja Kade[6], Benjamin Jones[7], Mikhail Kanevskiy[7], Anna Liljedahl[8], Dmitry Nicolsky[9], Jana Peirce[1], Stuart Rawlinson[10], Martha Raynolds[1], Vladimir Romanovsky[9], Sergei Rybakov[9], Barrett Salisbury[4], Yuri Shur[7], Emily Watson-Cook[1], Julia White[1] & Simon Zwieback[11]

[1]*Institute of Arctic Biology, University of Alaska Fairbanks, Fairbanks, Alaska, United States*

[2]*International Arctic Research Center, University of Alaska Fairbanks, Fairbanks, Alaska, United States*

[3]*Arctic Infrastructure Development Center, University of Alaska Fairbanks, Fairbanks, Alaska, United States*

[4]*Division of Geological and Geophysical Surveys, Fairbanks, Alaska, United States*

[5]*Alaska Ecoscience, Fairbanks, Alaska, Fairbanks, Alaska, United States*

[6]*Department of Biology and Wildlife, University of Alaska Fairbanks, Fairbanks, Alaska, United States*

[7]*Institute of Northern Engineering, University of Alaska Fairbanks, Fairbanks, Alaska, United States*

[8]*Woodwell Climate Research Center, Falmouth, Massachusetts, United States*

[9]*Geophysical Institute, University of Alaska Fairbanks, Fairbanks, Alaska, United States*

[10]*Retired, 7661 Shire Ct, Las Vegas, Nevada, United States*

[11]*Alaska Satellite Facility, University of Alaska Fairbanks, Fairbanks, Alaska, United States*

Long-term permafrost observatories are needed to document and monitor rapid changes to Ice-Rich Permafrost Systems (IRPS) in a variety of geological, climatic, and infrastructure settings. As part of the US National Science Foundation's Navigating the New Arctic (NNA) Program, a new observatory was established near the Deadhorse Airport in the eastern part of the Prudhoe Bay Oilfield (PBO) in 2020–23 (Figure 1).

The NNA-IRPS project has three main research themes: (1) evolution of and degradation of ground ice within the major surficial-geology units; (2) rapid changes in permafrost, landforms, and vegetation due to infrastructure and climate change; and (3) long-term changes in IRPS associated with the calcareous fluvial deposits of the Central Arctic Coastal Plain.

Roadside IRPS studies were previously established at the Colleen and Airport sites in 2014–18 (Walker et al. 2022; Kanevskiy et al. 2022). Natural research sites, relatively unimpacted by oil-development activities, were surveyed at the Jorgenson site in 2011 (Jorgenson et al. 2015; Kanevskiy et al. 2017) and at the Natural Ice-Rich Permafrost Observatory (NIRPO site) in 2020-23 (Walker et al. 2022; 2023). Most of the current NNA-IRPS research is concentrated in the NIRPO-Jorgenson-Colleen (NJC) research area (Figure 1).

The research at the new site builds on a legacy of permafrost, hydrology, vegetation, soil, and remote-sensing research in the PBO and along the Dalton Highway (e.g., Brown 1975; Walker et al. 1980; Walker 1985; Brown and Berg 1980; Osterkamp and Romanovsky 1996; Brown et al. 2000; Jorgenson and Joyce 1994; Bergstedt et al. 2022; Kanevskiy et al. 2022; Walker et al. 2022; Zwieback et al. 2023).

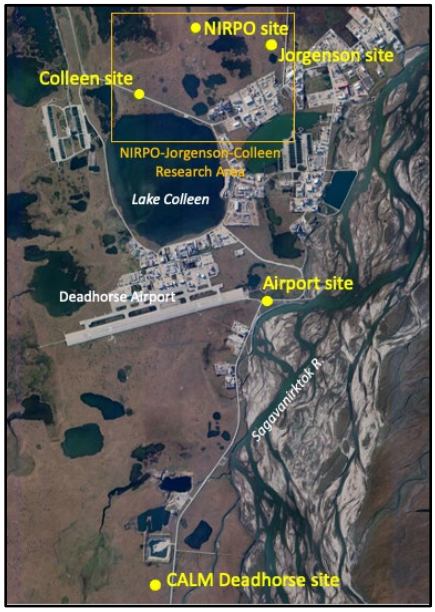

Figure 1. NNA-IRPS research sites near Deadhorse, Alaska. Scale: Deadhorse Airstrip = 2.59 km long. Base map: Google Maxar Technologies image 7/3/2020.

The surficial geology at this site and most of Alaska's Central Arctic Coastal Plain is dominated by thick fluvial gravel deposits from rivers flowing out of the glaciated Brooks Range (Rawlinson 1993). Much of the rest of the northern Alaska's coastal plain is covered by

finer-grained marine and eolian deposits resulting in different ecosystem and permafrost conditions (Jorgenson 2011). Many features related to the gravelly calcareous alluvial deposits are not found at other research sites, including stable gravel-based pingos (M.D. Walker 1990), well-drained nutrient-rich, prairie-like soils (Mollisols), marl-bottomed ponds and lakes, and species-rich calciphilous plant communities (Walker et al. 2001). The new observatory is dedicated to describing, monitoring, and modeling the ongoing changes to permafrost, hydrology, vegetation, and trace-gas fluxes within this geologically diverse and biologically-rich region.

References

Bergstedt, H., Jones, B.M., Walker, D.A., et al. 2022. The spatial and temporal influence of infrastructure and road dust on seasonal snowmelt, vegetation productivity, and early season surface water cover in the Prudhoe Bay Oilfield. Arctic Science, 9: 243–259. https://doi.org/10.1139/as-2022-0013

Brown, J. 1975. Ecological Investigations of the Tundra Biome in the Prudhoe Bay Region, Alaska. Page (J. Brown, Ed.). Biological Papers of the University of Alaska. https://www.arlis.org/docs/vol1/B/3035866.pdf

Brown, J., and Berg, R. 1980. Environmental engineering and ecological baseline investigations along the Yukon River-Prudhoe Bay Haul Road. CRREL Report 80-19. U.S. Army Cold Regions Research and Engineering Laboratory. https://erdc-library.erdc.dren.mil/jspui/handle/11681/9550

Jorgenson, M.T., and Joyce, M.R. 1994. Six strategies for rehabilitating land disturbed by oil development in Arctic Alaska, Arctic 47: 374–390 https://journalhosting.ucalgary.ca/index.php/arctic/article/view/64366/48301

Jorgenson, M.T. 2011, Coastal region of northern Alaska, guidebook to permafrost and related features: Alaska Division of Geological & Geophysical Surveys Guidebook 10, 188 p. https://doi.org/10.14509/22762

Jorgenson, M.T., Kanevskiy, M., Shur, Y., et al. 2015. Role of ground ice dynamics and ecological feedbacks in recent ice wedge degradation and stabilization. Journal of Geophysical Research: Earth Surface 120: 2280–2297.https://doi.org/10.1002/2015JF003602

Kanevskiy, M., Shur, Y., Jorgenson, T., et al. 2017. Degradation and stabilization of ice wedges: Implications for assessing risk of thermokarst in northern Alaska. Geomorphology 297:20–42. https://doi.org/10.1016/j.geomorph.2017.09.001

Kanevskiy, M., Shur, Y., Walker, D.A., et al. 2022. The shifting mosaic of ice-wedge degradation and stabilization in response to infrastructure and climate change, Prudhoe Bay Oilfield, Alaska, USA. Arctic Science. https://doi.org/10.1139/as-2021-0024

Romanovsky, V.E., and Osterkamp, T.E. 1995. Interannual variations of the thermal regime of the active layer and near-surface permafrost in Northern Alaska. Permafrost and Periglacial Processes 6:313–335. https://doi.org/10.1002/ppp.3430060404

Raynolds, M.K., Walker, D.A., Ambrosius, K.J., et al. 2014. Cumulative geoecological effects of 62 years of infrastructure and climate change in ice-rich permafrost landscapes, Prudhoe Bay Oilfield, Alaska. Global Change Biology 20:1211–1224. https://doi.org/10.1111/gcb.12500

Rawlinson, S.E. 1993. Surficial geology and morphology of the Alaskan Central Arctic coastal plain. Alaska Division of Geology and Geophysical Surveys, Report of Investigations 93-1. https://doi.org/10.14509/2484

Shur, Y., Kanevskiy, M., Walker, D.A., et al. 2016. Permafrost-related causes and consequences of Sagavanirktok River flooding in Spring 2015, 11th International Conference on Permafrost, Potsdam, Germany, 10-24 Jun 2016. Book of abstracts, p. 1014–1016. doi:10.2312/GFZ.LIS.2016.001

Walker, M.D. 1990. Vegetation and floristics of pingos, Cantral Arctic Coastal Plain, Alaska. J. Cramer, Berlin. https://www.geobotany.org/library/pubs/WalkerMD1987_thesis.pdf

Walker, D.A., Everett, K.R., Webber, P.J., and Brown, J. 1980. Geobotanical Atlas of the Prudhoe Bay Region, AK, CRREL Report 80-14. Page 69. U.S. Army Cold Regions Research and Engineering Laboratory, Hanover, NH. https://erdc-library.erdc.dren.mil/jspui/handle/11681/9008

Walker, D.A., Raynolds, M.K., Kanevskiy, M.Z., et al. 2022. Cumulative impacts of a gravel road and climate change in an ice-wedge-polygon landscape, Prudhoe Bay, Alaska. Arctic Science 8:1040–1056. https://doi.org/10.1139/as-2021-0014

Walker, D.A. 1985. Vegetation and environmental gradients of the Prudhoe Bay region, Alaska, CRREL Report 85-14. Page 240. CRREL Report 85-14. https://www.geobotany.org/library/reports/WalkerDA1985_crrel_85-14.pdf

Walker, D.A., Bockheim, J.G., Chapin, F.S., et al. 2001. Calcium-rich tundra, wildlife, and the “Mammoth Steppe”. Quaternary Science Reviews 20: 149–163. https://www.sciencedirect.com/science/article/pii/S0277379100001268

Walker, D.A., Epstein, H.E., Romanovsky, V.E., et al. 2008. Arctic patterned-ground ecosystems: A synthesis of field studies and models along a North American Arctic Transect. Journal of Geophysical Research - Biogeosciences, 113:G03S01. https://doi.org/10.1029/2007JG000504

Walker, D.A., and Peirce, J.L. (ed.) 2023. Natural Ice-Rich Permafrost Observatory, Prudhoe Bay, Alaska: 2022 field activities. AGC Data Report 23-02. https://www.geobotany.uaf.edu/library/pubs/AGC23-02_NNA-IRPS_Data%20Report.pdf

Zwieback, S.M., McClernan, M., Kanevskiy, M., et al. 2023. Disparate permafrost terrain changes after a large flood observed from space. Permafrost and Periglacial Processes, 34: 451–466. https://doi.org/10.1002/ppp.2208

Improving simulations of the local ground thermal regime by data assimilation of Sentinel-2-retrieved fractional snow-covered area

Clarissa Willmes[1,2], Sebastian Westermann[1,2] & Kristoffer Aalstad[1]

[1]*Department of Geosciences, University of Oslo, Oslo, Norway*

[2]*Center for Biogeochemistry in the Anthropocene, University of Oslo, Norway*

Increases in permafrost temperatures are observed globally and models predict this increase to continue with climate change, but the timing and magnitude of the projected changes vary considerably between different models and climate scenarios (Smith et al. 2022).

Current regional permafrost models have maximal resolutions of around 1 km, whilst Earth System Models have maximal nominal resolutions of 100 km. At the same time, permafrost landscapes such as thermokarst and high-Arctic permafrost terrain typically show large spatial variability on scales of 1-100 m. Local conditions and processes like snow-redistribution strongly modify the ground thermal state on these scales. For well-informed future projections of permafrost evolution as well as accurate inventories of the present ground thermal state models need to account for these processes.

In-situ observations of the snow cover are sparse in time and space, and satellite remote sensing offers great opportunities to fill these gaps, but can not provide direct information on the subsurface state.

In this study, we combine the CryoGrid community model with satellite retrievals of fractional snow-covered area (FSCA) in a data assimilation framework. Using stand-alone snow models, it has been shown that the timing of snowmelt and the snow depth can be well constrained with the assimilation of fractional snow-covered area (e.g., Aalstad et al. 2018). Assimilating FSCA with a coupled snow-permafrost model such as CryoGrid allows for interaction between the snowpack and the underlying ground.

The validation site

The study site used for validation is a high-Arctic permafrost site close to Ny-Ålesund, Svalbard, Norway. It is characterized by low-relief ridges and trenches at elevations of 10-50 m a.s.l. The area is underlain by continuous permafrost with a permafrost base at about 100 m and active layer thicknesses varying between 1 and 2 m (Humlum 2005).

Due to strong surface winds, snow redistribution plays an important role, leading to large variations in snow depths and snow water equivalent (Zweigel et al. 2021), and consequently in the local thermal regime and hydrology. The snowpack in this area is characterized by wind metamorphism, melt forms and ice layers.

Due to the high spatial variability of the snowpack, mean annual ground surface temperature (MAGST) shows large variability in the study area. An exemplary distribution of MAGST observed by > 100 randomly distributed ground surface temperature (GST) loggers in the area is shown in Figure 1 and highlights the importance of accounting for local processes such as snow redistribution for capturing this variability.

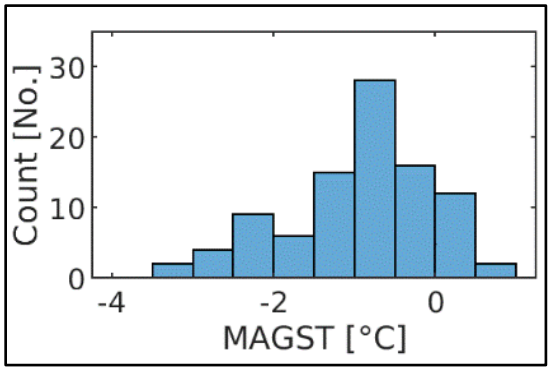

Figure 1. Exemplary distribution of observed MAGST in the study area (2017).

The CryoGrid community model

The CryoGrid community model is a land surface model simulating the ground thermal regime and ice-water balance for permafrost, snow and glaciers (Westermann et al. 2023). It is highly modular and allows for different setups by different process representations and parameterisations (Westermann et al. 2023). In this study, we use a one-dimensional model configuration of the ground and snowpack with lateral interaction according to the chosen processes.

The snowpack is simulated using CryoGrid's implementation of the state-of-the-art snow scheme Crocus (Vionnet et al. 2012). It is a layered snow-scheme, in which snowfall is added with the temperature and wind-speed dependent properties density, grain size, dendricity and sphericity (Westermann et al. 2023). After deposition, snow metamorphism is parameterized in each cell based on time, temperature gradients, water content and overlying snow mass (Westermann et al. 2023).

DATA ASSIMILATION

Data Assimilation (DA) is an uncertainty-aware approach to identify probable system states lying within both the model's and observation's uncertainty based on Bayesian inference. DA is commonly used in operational weather forecasting, but has not yet been widely applied within the framework of permafrost. It is realized by running an ensemble of different model realizations, which are evaluated against the assimilated observations each time for which these are available.

We use an ensemble comprising different atmospheric forcing realizations, leading to different snowpacks. By doing so, we account for snow redistribution by locally producing more/less snow in the model. We apply an adaptive particle batch smoother as the DA-scheme.

ASSIMILATED OBSERVATIONS

We assimilate FSCA retrieved from Sentinel-2 optical imagery. Figure 2 shows a snapshot of the FSCA (between 0 and 1) during a snowmelt season over Brøgger peninsula, Svalbard, including the field validation site. The high spatial variability incl. snow-free ridges and snowdrifts is clearly visible.

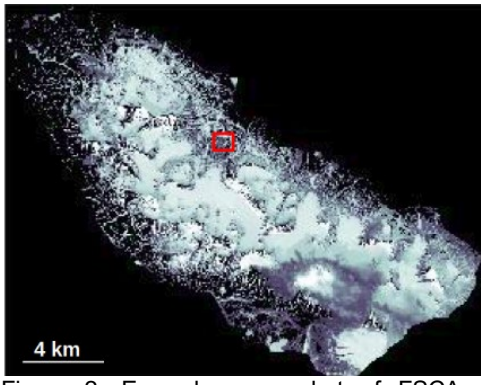

Figure 2. Exemplary snapshot of FSCA over Brøgger peninsula, Svalbard (from Sentinel-2).

RESULTS

The DA improves the representation of the local snow conditions. It picks up on the extremes in snow cover and allows for a better representation of the ground thermal regime of the area. Figure 3 shows the observed GST of an exemplary snowdrift during the melt season 2017 together with the GST without DA (prior, red) and with DA (posterior, blue). The reference run with the snowpack resulting from the original atmospheric forcing clearly underestimates the snow depth, leading to too low temperatures in winter and a too early melt-out of the snowpack. This is improved by the DA scheme.

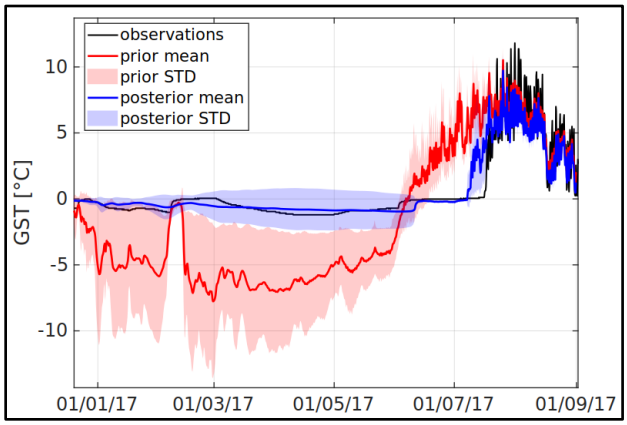

Figure 3. GST during snowmelt season 2017 in a snowdrift.

REFERENCES

Aalstad, K., Westermann, S., Schuler, T.V., Boike, J., and Bertino, L. 2018. Ensemble-based assimilation of fractional snow-covered area satellite retrievals to estimate the snow distribution at Arctic sites, The Cryosphere, 12(1), 247–270. doi:10.5194/tc-12-247-2018

Humlum, O. 2005. Holocene permafrost aggradation in Svalbard, Geological Society, London, Special Publications, 242(1), 119–129. doi:10.1144/GSL.SP.2005.242.01.11

Smith, S.L., O'Neill, H.B., Isaksen, K., Noetzli, J., and Romanovsky, V.E. 2022. The changing thermal state of permafrost, Nature Reviews Earth & Environment, 3(1), 10–23. doi:10.1038/s43017-021-00240-1

Vionnet, V., Brun, E., Morin, S., Boone, A., Faroux, S., Le Moigne, P., Martin, E., and Willemet, J.-M. 2012. The detailed snowpack scheme Crocus and its implementation in SURFEX v7.2, Geoscientific Model Development, 5(3), 773–791. doi:10.5194/gmd-5-773-2012

Westermann, S., Ingeman-Nielsen, T., Scheer, J., Aalstad, K., Aga, J., Chaudhary, N., Etzelmüller, B., Filhol, S., Kääb, A., Renette, C., Schmidt, L.S., Schuler, T.V., Zweige,l R.B., Martin, L., Morard, S., Ben-Asher, M., Angelopoulos, M., Boike, J., Groenke, B., Miesner, F., Nitzbon, J., Overduin, P., Stuenzi, S.M., and Langer, M. 2023. The CryoGrid community model (version 1.0) - a multi-physics toolbox for climate-driven simulations in the terrestrial cryosphere, Geoscientific Model Development, 16 (9), 2607–2647. doi:10.5194/gmd-16-2607-2023

Zweigel, R., Westermann, S., Nitzbon, J., Langer, M., Boike, J., Etzelmüller, B., and Vikhamar Schuler, T. 2021. Simulating snow redistribution and its effect on ground surface temperature at a high-Arctic site on Svalbard, Journal of Geophysical Research: Earth Surface, 126(3), e2020JF005673. doi:10.1029/2020JF005673, 2021

Enhancing ground temperature monitoring network with repeat aerial surveys of ground surface deformation

Thomas C. Wright, Dmitry J. Nicolsky, Vladimir E. Romanovsky & Louise L. Farquharson
University of Alaska Fairbanks, Fairbanks, Alaska, United States

At the present time the Geophysical Institute Permafrost Laboratory (GIPL) has more than 165 Thermal State of Permafrost (TSP) observation sites throughout Alaska (http://permadata.gi.alaska.edu) including 80 sites along the High-Spatial Resolution Alaska Permafrost Transect, 53 sites at the locally distributed permafrost observatories in Selawik area, Imnavait, Fairbanks, Deadhorse, Utqiaġvik, Nome, Kaktovik, Kotzebue and other locations. Some of them are equipped with air and shallow soil temperature and moisture sensors, dataloggers, and automatic climate stations with snow depth sensors. Currently, sites are routinely visited at least once a year to download and service dataloggers.

Despite a general acceptance that ice-rich permafrost degradation leads to thermokarst development, limited work has been done to explore in-situ causality between changes in ground thermodynamics, ground ice melt, and surface subsidence. The ground subsidence is a key element for assessment of damages to infrastructure in the permafrost environment. Many of our monitoring sites have already begun to experience thermokarst development due to a deepening of the active layer, and several others are in regions of warm permafrost that is close to 0°C. As such, our permafrost monitoring network provides an ideal platform upon which to evaluate potential drivers of surface disturbance.

In 2020, we enhanced monitoring capabilities of permafrost observatories in Alaska by conducting repeat geomorphological surveys using unoccupied aerial vehicles (UAVs) at locations where thermokarst is developing already or is expected to develop soon. These ongoing surveys are being conducted using a DJI Phantom 4 RTK equipped with a 20MP CMOS sensor and a DJI Matrice 300 RTK UAV which has dual-payload capability. Typical payloads of the Matrice 300 include a DJI Zenmuse L1 solid-state LiDAR sensor, DJI Zenmuse P1 with a 35 mm lens, and a Micasense RedEdge-P multispectral camera.

The collected temperature and surface subsidence data can constrain hypotheses regarding the thermal mechanisms of thermokarst development and stabilization and help predict thermokarst development in the future. The latter could verify existing models of thermokarst development or demonstrate a need to revise therm.

For each surface observation site, thermokarst landforms are mapped. To characterize changes in surface vegetation and hydrology caused by permafrost degradation we apply several indices, including the Normalized Difference Vegetation Index (NDVI), the Normalized Difference Water Index (NDWI) and the Normalized Difference Moisture Index (NDMI). Data from UAV surveys will be used to create an online, open access, 3-D model library of thermokarst landforms and surface change for a selection of sites. 3-D thermokarst models will be made publicly available through the Geophysical Institute Permafrost Laboratory website (http://permafrost.gi.alaska.edu) or the 3-D content sharing website.

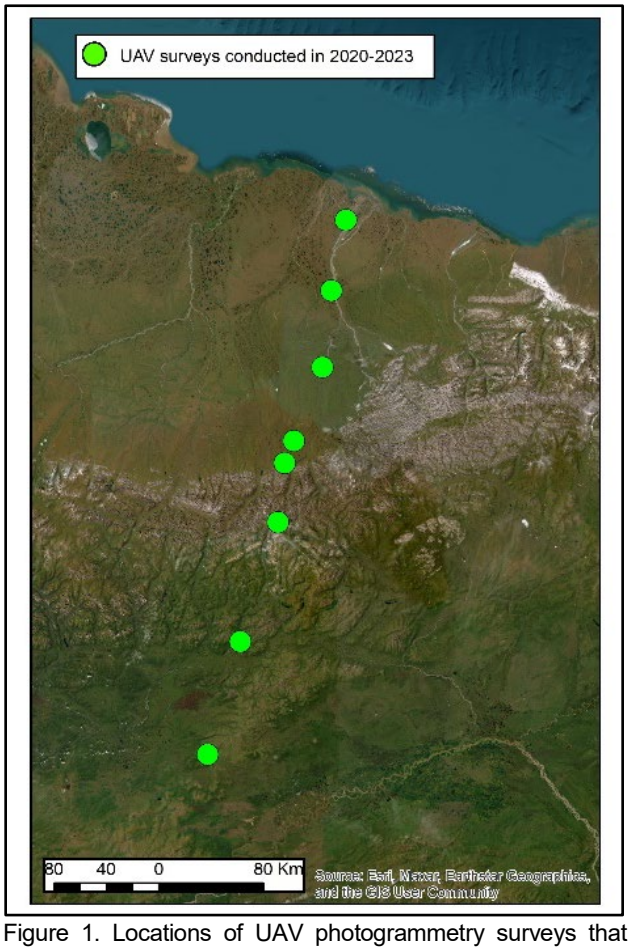

Figure 1. Locations of UAV photogrammetry surveys that have been flown since 2020.

The technology developed in this study is believed to be relevant and applicable to many Alaskan and other Circum-Arctic locations for the estimation of possible consequences of permafrost degradation in the 21st century.

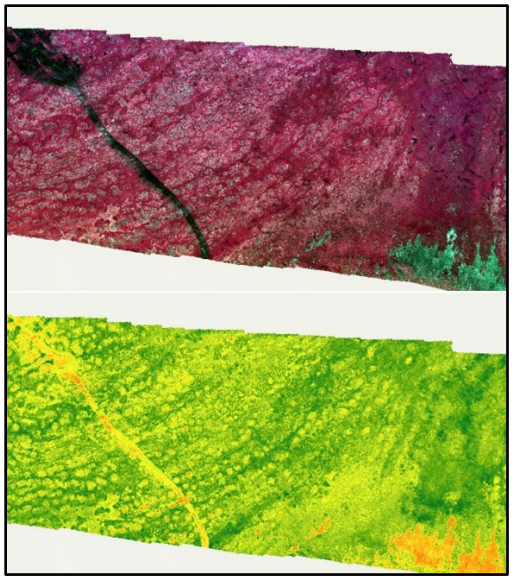

Figure 2. False color infrared (top) and NDVI (bottom) maps from the Pinnell Mountain National Recreation Trail near Fairbanks, Alaska where active tundra restoration is being conducted by the Bureau of Land Management.

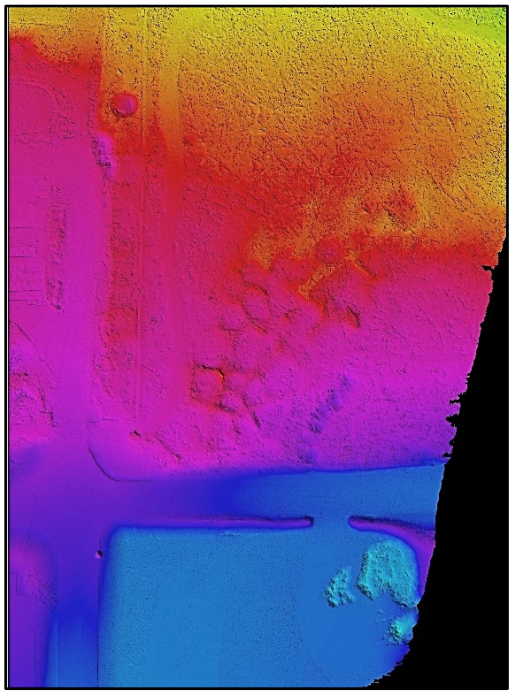

Figure 3. A digital surface model (DSM) produced using UAV LiDAR data shows patterned ground features that are otherwise obscured by dense spruce forest. Data collected at the University of Alaska Fairbanks.

REFERENCES

Cable, W., Romanovsky, V. and Jorgenson, M. 2016. Scaling-up permafrost thermal measurements in Western Alaska using an ecotype approach, The Cryosphere, 10 (5), pp. 2517–2532. doi:10.5194/tc-10-2517-2016

Daly, C., Smith, J., and Halbleib, M. 2018.1981–2010 High-resolution temperature and precipitation maps for Alaska. Final report. Corvallis, OR: PRISM Climate Group, Oregon State University.

Harris, I.C., Jones, P.D., and Osborn. T. 2020. CRU TS4.04: Climatic Research Unit (CRU) Time-Series (TS) version 4.04 of high-resolution gridded data of month-by-month variation in climate (Jan. 1901- Dec. 2019). Centre for Environmental Data Analysis, date of citation. https://catalogue.ceda.ac.uk/uuid/89e1e34ec3554dc98594a5732622bce9

Hijmans, R.J., Cameron, S.E., Parra, J.L., Jones, P.G., and Jarvis, A. 2005. Very high-resolution interpolated climate surfaces for global land areas, International Journal of Climatology, 25(15), 1965–1978.

Jorgenson, T., and Heiner, M. 2004. Ecosystems of Northern Alaska, ABR, Inc., and The Nature Conservancy, Anchorage Alaska, poster.

Jorgenson, M.T., Roth, J.E., Miller, P.F., Macander, M.J., Duffy, M.S., Wells, A.F., Frost, G.V., and Pullman, E.R. 2009. An ecological land survey and landcover map of the Arctic Network. Natural Resource Technical Report NPS/ARCN/NRTR—2009/270. National Park Service, Fort Collins, Colorado.

Nicolsky, D.J., Romanovsky, V.E., and Tipenko, G.S. 2007. Using in-situ temperature measurements to estimate saturated soil thermal properties by solving a sequence of optimization problems, The Cryosphere, 1, 41–58.

Nicolsky, D.J., Romanovsky, V.E., Panda, S.K., et al. 2017. Applicability of the ecosystem type approach to model permafrost dynamics across the Alaska North Slope, Journal of Geophysical Research, 122, 50–75. doi:10.1002/2016JF003852

Walsh, J., Chapman, W., Romanovsky, V., Christensen, J.H., and Stendel, M. 2008. Global climate model performance over Alaska and Greenland, Journal of Climate, 21(23), 6156–6174.

11 Waste Containment in Permafrost

INTEGRATING PERSPECTIVES OF PERMAFROST THAW, CHANGE, AND ADAPTATION

Waste Containment in Permafrost

11A — Mining Geotechnics, Reclamation, Contaminant Behaviour and Nuclear Waste Safety in a Changing Climate

Session Chairs: Vincent Boulanger-Martel[1], Mahsa Malmir[2], Marja Vuorio[3] & Wolfram Rühaak[4,5]

[1]*Université du Québec Abitibi-Témiscamingue, Québec, Canada*
[2]*Université Laval, Québec City, Québec, Canada*
[3]*COVRA N.V., Netherlands*
[4]*Technische Universität Darmstadt, Peine, Germany*
[5]*Bundesgesellschaft für Endlagerung mbH, Peine, Germany*

There are an increasing number of mining projects being developed in regions where continuous permafrost is present. With the development of such mining projects, numerous unique engineering and environmental challenges follow. With respect to geotechnical engineering, mining operations have several critical infrastructures such as tailings dams, tailings, and waste rock storage facilities, which must be designed, operated and reclaimed to ensure optimal mine waste management and minimize environmental risks. The closure of mine waste storage facilities often requires the design and construction of engineered covers which aim to maintain the mine wastes physically and chemically stable.

Such geotechnical infrastructures constructed in continuous permafrost environments require time to freeze-back and reach thermal equilibrium with the natural ground. The aggradation of permafrost conditions within the mine wastes as well as tailings dams and cover systems have the overall beneficial effect of improving their physical stability, reducing water seepage and reducing the potential for the generation and transport of contaminants into the receiving environment. In this context, climate change represents the largest source of uncertainty with respect to the long-term geo-environmental behaviour and performance of mine waste storage facilities and their reclamation strategies.

Cryogenic processes also play a crucial role in the safety assessments of long-term nuclear waste repositories and the transport of other contaminants. Within the timespan for which a safe enclosure of the waste must be ensured, which depending on the regulations, could be more than one million years, numerous climate cooling and warming cycles must be considered. The presence, aggradation, and degradation of permafrost and ice sheets can exert extensive pressure gradients and changes in pathways that impact the transport of radionuclides and other contaminants from the geosphere into the biosphere. Present-day permafrost regions currently serve as analogues for repository sites in a future cold climate, where processes that influence the migration of contaminants can be studied. Numerical modelling approaches of freezing and thawing of soil and rocks are constantly being improved as the interplay between different processes and parameters becomes better understood.

On-going thermal performance of Diavik's A21 Dike

Lukas U. Arenson[1], Alma Ornes[2], Angela G. Küpper[2] & Gord Stephenson[3]

[1]*BGC Engineering Inc., Vancouver, British Columbia, Canada*

[2]*BGC Engineering Inc., Edmonton, Alberta, Canada*

[3]*Diavik Diamond Mines (2012) Inc., Yellowknife, Northwest Territories, Canada*

The Diavik Diamond Mine is located on East Island in Lac de Gras, Northwest Territories (Canada), approximately 300 km northeast of Yellowknife, NT, in a zone of continuous permafrost (Figure 1). The A21 Dike is a water retaining dike constructed within the Lac de Gras to enable dewatering of the area enclosed by the dike and allow open pit mining of the A21 Kimberlite pipe. The A21 Dike is a 2,200 m long zoned rockfill embankment with a seepage cut-off wall. The A21 Dike is founded on permafrost near the lake shore, transitioning to unfrozen foundation in deeper waters, where the presence of the lake created a large talik. In the sections of the dike founded on permafrost, the frozen soil and bedrock are used as hydraulic barrier. Thermosyphons were installed in both the North and South Abutments where the embankment foundation transitions from permafrost to talik. Monitoring of the extent of the permafrost along the foundation of the dike is essential, specially on the South Abutment, where the water is shallow for approximately 400 m along the embankment.

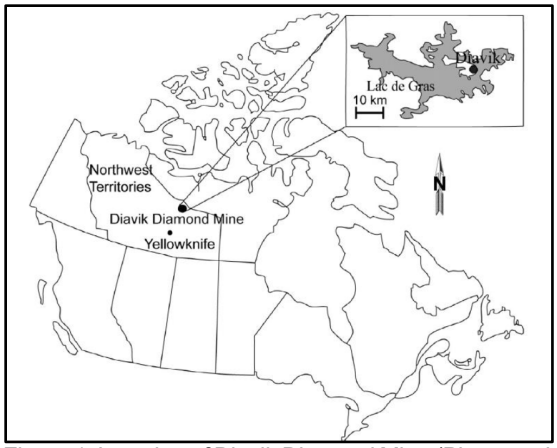

Figure 1. Location of Diavik Diamond Mine (Pham et al. 2013).

Construction of the A21 Dike was completed in 2018, and the open pit was officially opened on August 20, 2018. Extensive ground temperature monitoring has been completed since initiation of construction and during open pit mining. This monitoring has shown the aggradation of permafrost through the initial dewatering phase and the past five years of excavation of the pit walls.

SITE CONDITIONS

The A21 Dike is located about 220 km south of the Artic circle. Based on local weather stations, the mean annual air temperature at the site is about -9 °C (2004 to 2021), the average monthly maximum temperature of 13.5 °C occurs in July, and the average monthly minimum temperature of -28 °C occurs in January/February. The summer of 2022 and 2023 had above average temperature compared to the past 10-year record.

Precipitation at Diavik is typicaly low with an annual average of about 280 mm, 60% of which occurs as snow during the winter (Neuner et al. 2013). The dominant winds are northerly and easterly with an average speed of 17 km/h (Amos et al. 2009). The active layer, i.e. the active freeze-thaw zone, may extend up to approximately 4 m into dry bedrock (Pham et al. 2013).

A21 DIKE AND GROUND MONITORING DESCRIPTION

Description of the individual components of the dike are presented in Küpper et al. (2019). A typical cross-section of the A21 Dike is shown in Figure 2. A plan view of the A21 Dike with the ground temperature monitoring locations is shown in Figure 3. Thermosyphons were constructed on the North Abutment and at the end of the South Arm at Sta. 0+020 m and 1+550 m, respectively. Thermistors were installed along the South Arm from Sta. 1+550 m to 2+000 m to monitor a shallow water area that forms a complex-shaped submerged peninsula with a talik under the permafrost. Additional thermistors were installed near Sta. 0+450 m to monitor a shallow foundation area near Island A.

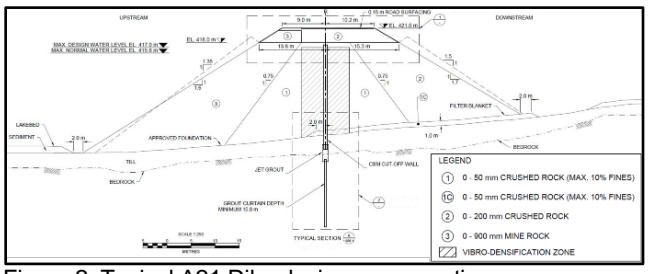

Figure 2. Typical A21 Dike design cross-section.

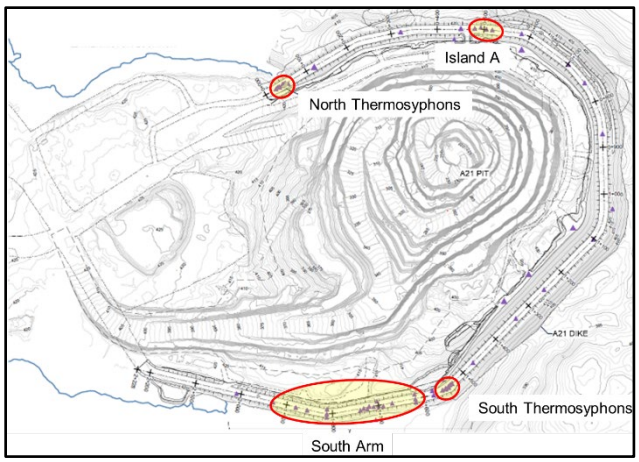

Figure 3. A21 Dike plan view showing location of thermistors for ground temperature monitoring.

TEMPERATURE MONITORING

Ground temperatures for the North Thermosyphons and South Thermosyphons are summarized in Figure 4. The temperatures show substantial cooling of the passive system and seasonal fluctuation with the ground temperature remaining below 0 °C throughout the entire time.

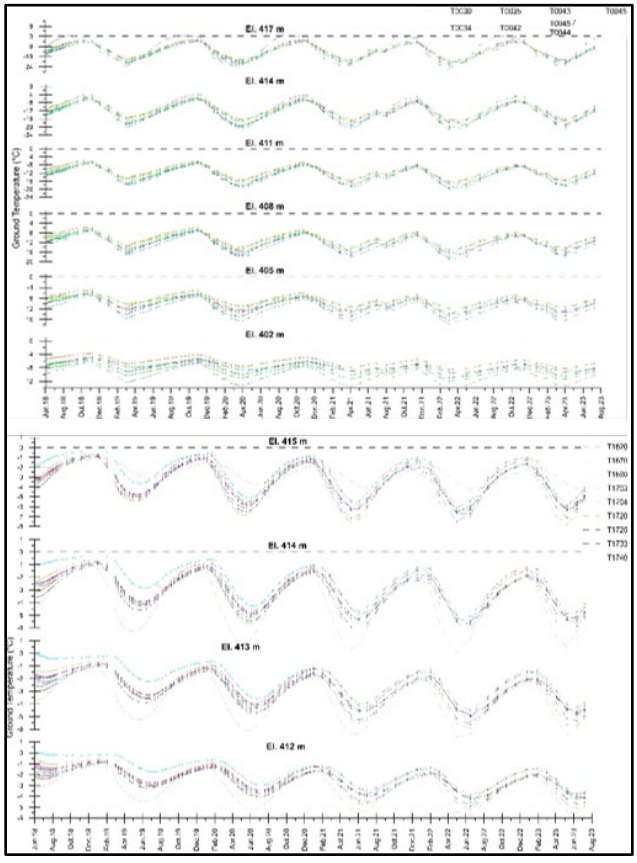

Figure 4. A21 Dike North (top) and South (bottom) Thermosyphons temperature trends.

Some ground temperatures along the shallow foundation areas for Island A and the South Arm are summarized in Figures 5 and 6, respectively. The temperatures show seasonal fluctuations superimposed over a general cooling trend year over year, despite some warm summers recently.

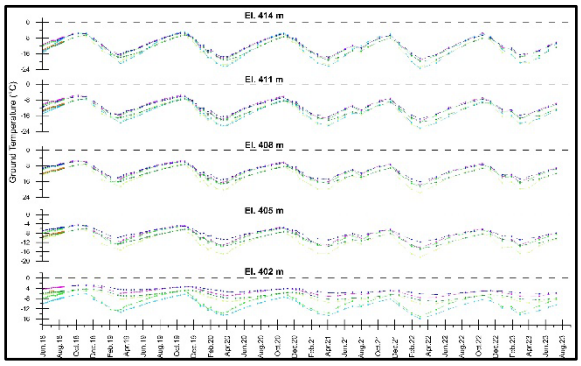

Figure 5. A21 Dike South Arm temperature trends.

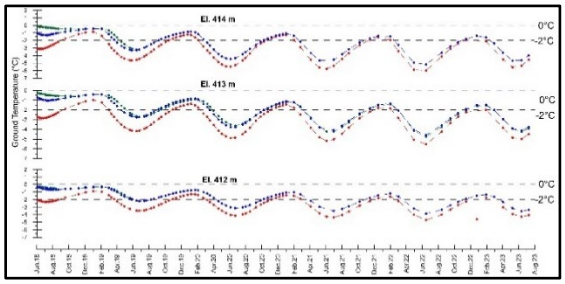

Figure 6. A21 Dike Island A temperature trends.

CONCLUSIONS

Ground temperature monitoring shows on-going cooling of the frozen ground around the A21 Dike and an increase in permafrost depth along the South Arm and Island A area. These data confirm success of the thermal design applied for the A21 Dike.

REFERENCES

Amos, R.T., Blowes, D.W., Smith, L., and Sego, D.C. 2009. Measurement of wind-induced pressure gradients in a waste rock pile. Vadose J., 8: 953–962.

Küpper, A., Roca, J., Wenger, G., and Stephenson, G. 2019. Construction of the A21 Dike at the Diavik Diamond Mine. In Geo St.John's 2019.

Pham, N.H., Sego, D.C., Arenson, L.U., Blowes, D.W., Amos, R.T., and Smith, L. 2013. The Diavik waste rock project: Measurement of the thermal regime of a waste-rock test pile in a permafrost environment. Applied Geochemistry, 36: 234–245.

Neuner, M., Smith, L., Blowes, D.W., Sego, D.C., Smith, L.J., Fretz, N., and Gupton, M. 2013. The Diavik waste rock project: Water flow though mine waste rock in a permafrost terrain. Applied Geochemistry, 36: 222–233.

Design considerations for a non-hazardous-waste facility, Coral Harbour, Nunavut

Aron Piamsalee & Kris Hojka
Stantec Consulting Ltd., Winnipeg, Manitoba, Canada

There are important consideration in the design of waste containment facilities in continuous permafrost environments. A case study is presented, focusing on the aspects of site selection and engineered cover design for a Non-Hazardous Waste (NHW) Facility in Coral Harbour, Nunavut.

BACKGROUND

The Hamlet of Coral Harbour is located on Southampton Island, near the north of Hudson Bay in a region of continuous permafrost. The project site constitutes a former military base decommissioned in the 1970s, situated 10 km northwest of the main townsite. Numerous environmental investigations have been conducted over the past 30 years to assess and characterize contamination at the site. Stantec Consulting Ltd. was retained to prepare the design and specifications for remediation of the project site. Several methods are used for the waste management at the site, one of which includes construction of a NHW Facility to provide long-term containment of non-hazardous waste.

DESIGN FACTORS

Waste materials to be placed within the NHW Facility included stained soil, barrel caches, buried and surface metal and wood debris, scrap metal from vehicles/storage tanks, and asbestos materials (secured within heavy duty bags). The NHW Facility was designed to accommodate a waste volume of approximately 8,000 m^3, however the design capacity was flexible to store additional waste based on actual waste volumes recovered. Infiltration into the waste material was to be controlled by provision of an engineered cover system including a membrane barrier. Design requirements for the engineered cover system included resistance to: surface runoff erosion; action of burrowing animals; damage from occasional vehicular traffic; UV degradation, puncture, and tearing of the membrane barrier. Key design guidelines from The Cold Regions Cover System Technical Guidance Document (AANDC and O'Kane Consultants Inc. 2012) were followed. A major design consideration was site selection for the NHW Facility within the larger project site, weighing factors including: proximity to waste materials (located at distinct Areas of Environmental Concern throughout the project site); availability of borrow materials for construction; NHW Facility location with respect to surface water and flooding risk; and, social acceptance by making the NHW Facility least visible to the public.

SITE PHYSIOGRAPHY

The topography of the site is undulating with numerous shallow lakes filling depressions, and overall surface drainage is southward to Hudson Bay. The surface is generally devoid of vegetation. The active layer thickness ranges from 1.1 to 1.4 m. The surficial geology consists of glaciomarine and marine deposits, including areas of washed till (Geological Survey of Canada 1994). Overburden materials are generally composed of a mixture of sand, gravel, and finer sediment. Gradation results typical of the site, taken from composite samples at potential borrow locations are shown on Figure 1.

NHW FACILITY SITE SELECTION

The selected location for the NHW Facility is near a local topographic high. This provides good drainage away from the NHW Facility. There are no major water bodies upslope of the selected NHW Facility location, and the nearest lake is located 250 m downstream to the southwest, about 10 m lower in elevation. The physiography of the site is not typical of environments prone to evolution of the lake shoreline (Bouchard et al. 2020). Other long-term changes in drainage patterns associated with climate change (e.g., active layer thickening) could however not be ruled out completely. The NHW Facility was therefore sited upslope of any major water bodies to reduce flooding risk. The selected location also scored well considering other factors (i.e., proximity to waste and borrow materials, low public visibility).

NHW FACILITY DESIGN SUMMARY

The NHW Facility has a single containment cell, approximately 80 m by 80 m in area. The cell bottom is approximately 1 m below the existing ground surface to maximize capacity, while protecting permafrost and stopping excavations, whenever permafrost is reached. Materials excavated to achieve the cell bottom can be processed for use as fill materials, thus reducing

the total areas disturbed from borrow material extraction. The waste containment cell is surrounded by berms sloped at 5H:1V. The waste thickness was designed at 1.5 m, which can be increased during construction if required.

ENGINEERED COVER SYSTEM DESIGN

The NHW materials intended for disposal are considered non-reactive, non-hazardous, and leachate generation from the waste is not expected. Nonetheless, an engineered cover system complete with a geomembrane barrier to prevent water infiltration was considered beneficial in reducing seepage and preventing unforeseen geochemical processes from occurring. A Linear Low-Density Polyethylene (LLDPE) geomembrane was selected over other barriers (e.g., compacted clay liner, compacted sand-bentonite, bituminous geomembrane, geosynthetic clay liner, high-density polyethylene). The main factors considered in the selection were local material availability, cost, and durability and ease of installation at low temperatures.

The cover system includes layers of granular fill of specified thicknesses and gradation to protect the LLDPE geomembrane. Three distinct granular fill types (Type 1, 2, and 3) were specified as part of the design, with gradation limits shown on Figure 1.

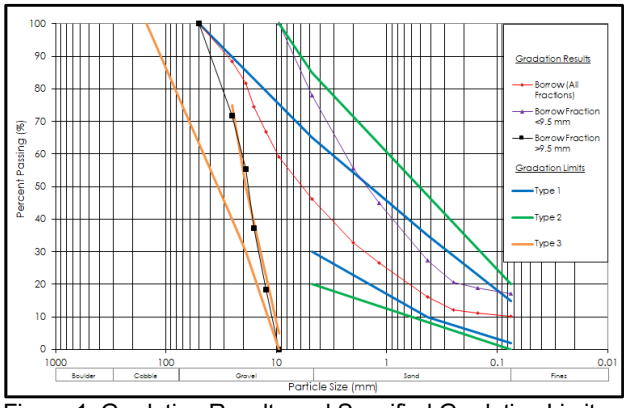

Figure 1. Gradation Results and Specified Gradation Limits.

Development of the gradation limits considered the gradation of available borrow materials to reduce the required effort in processing. Generally, very limited screening of the borrow materials is required to meet the grading limits for Type 1, which is used for bulk buffer protection and construction of the berms. Screening of the borrow material into two separate fractions finer and coarser than the 9.5 mm sieve size yields products approximately meeting the Type 2 and Type 3 granular fill specifications respectively. The finer Type 2 granular fill is used as bedding material to protect the LLDPE geomembrane, while the coarser Type 3 material serves as erosion protection at the surface of the engineered cover system. A non-woven geotextile was recommended above and below the LLDPE geomembrane to cushion against puncture, given the relative coarseness of the Type 2 bedding material. The engineered cover system design from top to bottom, is summarized in Table 1.

Table 1. Engineered Cover System Design.

Layer	Primary Function	Thickness (mm)
Type 3 Granular Fill	Erosion Protection	300
Type 1 Granular Fill	Bulk Buffer Protection	700
Type 2 Granular Fill	Bedding for LLDPE	200
Non-Woven Geotextile	Cushion for LLDPE	-
LLDPE Geomembrane	Infiltration Membrane	1.5
Non-Woven Geotextile	Cushion for LLDPE	-
Type 2 Granular Fill	Bedding for LLDPE	200

Careful selection of gradation limits for the cover system design resulted in 1) minimizing the required processing effort; 2) a straightforward screening procedure to simultaneously produce the Type 2 and Type 3 granular fill products; 3) minimizing the production of castoffs, considering proportions of granular fill types required for the project.

ACKNOWLEDGEMENTS

Project funding was provided by Public Services and Procurement Canada (PSPC) on behalf of Crown-Indigenous Relations and Northern Affairs Canada (CIRNAC).

REFERENCES

Aboriginal Affairs and Northern Development Canada (AANDC) and O'Kane Consultants Inc., 2012, Cold Regions Cover System Design Technical Guidance Document, MEND Report 1.61.5c.

Bouchard, F., Fortier, D., Paquette, M., Boucher, V., Pienitz, R., and Laurion, I. 2020. Thermokarst lake inception and development in syngenetic ice-wedge polygon terrain during a cooling climatic trend, Bylot Island (Nunavut), eastern Canadian Arctic, The Cryosphere, 14, 2607–2627. https://doi.org/10.5194/tc-14-2607-2020, 2020

Geological Survey of Canada, 1994, Canadian Geoscience Map 195 (ed. Prelim., Surficial Data Model V.2.0 Conversion). https://doi.org/10.4095/295462

Water flow in frozen soils with applications to cold region mining dams: Why heterogeneity and coupled analyses matter

Zakary Picard[1,2], Simon Dumais[1,2], Élise Devoie[3] & John Molson[2,4]

[1]*Département du génie des mines, de la métallurgie et des matériaux, Université Laval, Québec City, Québec, Canada*

[2]*Centre d'études Nordiques, Université Laval, Québec City, Québec, Canada*

[3]*Civil Engineering, Queen's University, Kingston, Ontario, Canada*

[4]*Département de géologie et du génie géologique, Université Laval, Québec City, Québec, Canada*

Mining dams are key components of tailings storage facilities and water management plans. In permafrost areas, frozen ground can be used as a cost-effective hydraulic barrier within the dam structure (Andersland and Ladanyi 2004). The thermal stability of frozen hydraulic barriers is crucial to maintain efficiency and to mitigate the risk of failures which can have severe ecological and financial consequences.

Evidence of unexpected seepage across frozen mining dam components has recently been observed at several mining sites in northern Canada. Preliminary work was undertaken to investigate probable causes which include potential preferential water flow which can occur in heterogeneous media (Picard et al. 2023a; b). Soil heterogeneity is an inherent spatial variation in soil properties, resulting in nonuniform soil behaviour (Elkateb et al. 2003; Qin et al. 2013). The objective of this study is to provide preliminary insights into the impact of preferential seepage due to soil heterogeneity on total water flow and heat flow in frozen soil.

A coupled GeoStudio (V2022.1) TEMP/W and SEEP/W numerical model of a simplified soil domain representative of conditions that may be found in frozen dam foundations was developed. The purpose of the model is to simulate water flow from impounded water through a heterogeneous, frozen dam foundation. The domain geometry is 20 m by 10 m, with numerous horizontal soil layers. While the domain is 2D, 1D horizontal water flow is forced by the hydraulic boundary conditions. A hydraulic gradient of 0.5 m/m is applied. This hydraulic gradient was chosen according to the model's size and typical dam geometries. Thermal conditions are defined by the impounded water temperature on the upstream side (Twater) and initial soil temperature (Tsoil). The model was run for three inflow water temperatures (1°C, 5°C and 10°C) and three initial soil temperatures (-0.5°C, -2°C and -5°C) at local equilibrium with pore water and pore ice.

To implement soil heterogeneity, soil type fractions in the horizontal soil layers were varied according to depth. The same methodology was used in Picard et al. (2023b), where a more exhaustive description can be found. This method is thought to be appropriate for preliminary modelling and also replicates the strong vertical anisotropy typical of permafrost foundations of mining dams.

Variations in soil type fractions are associated with changes in soil water characteristic curves (SWCCs). Such methods are common in unsaturated soil predictive modelling (Gitirana 2005). Furthermore, this allowed frozen soil hydraulic and thermal conductivity functions to be defined as a function of sub-zero temperature using the Clapeyron equation. The geometric mean method was used to evaluate the thermal conductivity in marginally frozen, saturated soil. Therefore, this study considered how temperature relates to pore ice and unfrozen pore water content and the impact on the hydraulic and thermal properties.

Figure 1 presents some selected results and illustrates the soil thermohydraulic behaviour. The heterogeneous cases are compared to the equivalent homogeneous cases in the form of ratios. The impact of heterogeneity on preferential water flow is thus illustrated in Figure 1. The red and blue colors are associated with water flow (Q) and heat flow (Φ), respectively. The results indicate that preferential seepage in frozen heterogeneous soil can significantly impact total water flow and heat flow.

The increase in water flow ratios indicates more rapid thaw in heterogeneous soils compared to its equivalent homogeneous case. The results show that water flow in heterogeneous cases can be up to 4 orders of magnitude greater than in equivalent homogeneous cases at certain analysed times. However, at subsequent times, thawing eventually occurs in the homogeneous cases and causes a decrease in ratios as shown in Figure 1.

The water temperature and the initial soil temperature influence the thermohydraulic behaviour. Thawing occurs earlier for warmer inflowing water and higher initial soil temperatures. Furthermore, the strong correlation between water flow and heat flow indicates that heat advection by flowing water strongly impacts heat flow in the model scenarios.

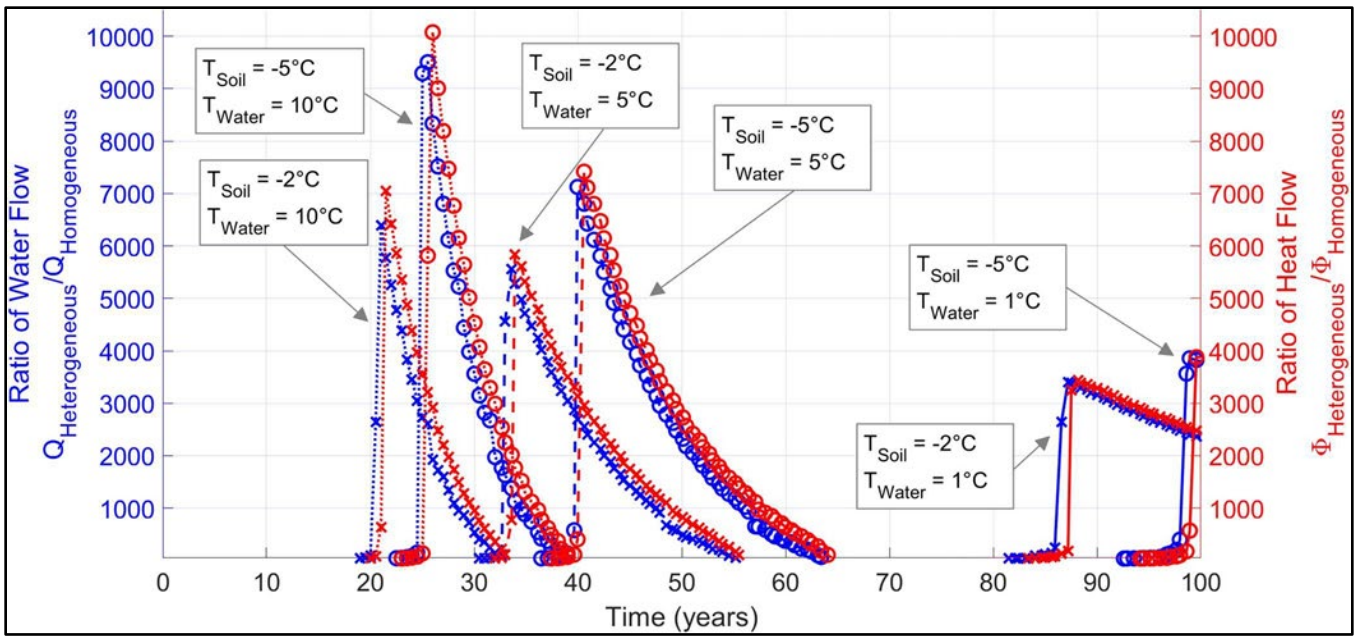

Figure 1. Impact of frozen soil heterogeneity on water flow (in blue) and heat flow (in red).

This highlights the importance of coupled thermohydraulic analyses when assessing long-term thermal and hydraulic fluxes when water flow is involved.

While the authors acknowledge that performing additional analyses with additional soil type variations and different distributions would have been beneficial, the simplified modelling methodology provides valuable insight on the long-term impact of preferential water flow in frozen soil:

- Thermal degradation is initiated faster in heterogeneous cases than in homogeneous cases due to preferential water flow;
- Heat advection by flowing water can be a significant source of heat transfer even at sub-zero temperatures.

Therefore, considering soil heterogeneity and performing coupled analyses are crucial to assess the thermohydraulic behaviour of frozen components of mining dams. Further work should be oriented towards developing and validating a more rigorous heterogeneous thermohydraulic model of a mining dam with frozen components. If a probabilistic approach is adopted, a sensitivity analysis could clarify which variables should be defined in greater detail and which can be treated as deterministic values to simplify the model. These results could also be of interest to engineers when conducting field investigations and lab tests.

REFERENCES

Andersland, O.B., and Ladanyi, B. 2004. Frozen Ground Engineering, 2nd ed. Wiley; ASCE, Hoboken, NJ : [Reston, Va.]

Elkateb, T., Chalaturnyk, R., and Robertson, P.K. 2003. An overview of soil heterogeneity: quantification and implications on geotechnical field problems, Can. Geotech. J., 40 (1): 1–15. https://doi.org/10.1139/t02-090

Gitirana, G. 2005. Weather-related Geo-hazard Assessment Model for Railway Embankment Stability, University of Saskatchewan, Saskatchewan, Canada.

Picard, Z., Dumais, S., and Devoie, É. 2023a. Hydraulic conductivity assessment of mining dams with frozen components, In 76th Annual CGS Conference - GeoSaskatoon 2023, Saskatoon, SK, Canada.

Picard, Z., Dumais, S., Devoie, É., and Molson, J. 2023b. Preliminary Numerical Analysis of the Impact of Heterogeneity on Seepage in Frozen Soils, Submitted to 20th ICCRE, Anchorage, AK, USA.

Qin, T., Lebeau, M., and Konrad J.-M. 2013. Influence of heterogeneity on the hydro-thermal response of an embankment dam, In 66th Annual CGS Conference - GeoMontréal 2023, Montréal, QC, Canada.

Volume change due to thawing/freezing processes in the context of nuclear waste repository safety

Wolfram Rühaak[1,2], Hailong Sheng[1], Markus Schedel[1], Hung Pham[1], Christoph Schüth[1], Ingo Sass[1,3], Eva Schill[1], Marc Wengler[2] & Leonie Peti[2]

[1]*Technische Universität Darmstadt, Germany*

[2]*Bundesgesellschaft für Endlagerung mbH, Germany*

[3]*GFZ German Research Centre for Geosciences, Potsdam, Germany*

In the German safety analysis for a high-level waste repository, the behaviour of the repository system in its entirety is investigated over the assessment period of one million years regarding the safe containment of radioactive waste. In this period, which starts after the planned closure of the repository, ten glacial-interglacial cycles are possible. In particular, the effects associated with this cyclicity, such as glaciations and the formation of permafrost followed by thawing, can have an impact on the geological barrier of the repository, and thus, a possible negative influence on the long-term safety of the repository.

The project presented here, which is embedded in the CatchNet group (see https://skb.de/Catchnet/), aims to address these research questions. The focus lies on the investigation on effects associated with volume changes due to thawing/freezing processes in permafrost regions, which particularly may affect the overburden of the rock containment zone. The project comprises the experimental and numerical analysis of thermo-mechanical coupled processes resulting from the expansion of freezing and thawing, respectively. In a second step, the relevance of this thermos-mechanical process with respect to the regional groundwater flow regime is evaluated by an integrated hydrogeological model.

Introduction

Substantial research has been performed in recent years, both with respect to experiments (Anbergen et al. 2014), as numerical models (Grenier et al. 2018; Rühaak et al. 2015), for a better understanding of the impact of freezing and thawing on rocks. The research has focussed on the effect of latent heat and changes of the relative hydraulic conductivity. However, the resulting stresses and strains due to freezing are not that well studied (Beddrich et al. 2022; Chen et al. 2022).

Surface-subsurface models (Mölders and Rühaak 2002; Beven 2012; Maxwell et al. 2014; Fisher and Koven 2020; Gao and Coon 2022; Torres-Rojas et al. 2022; Hou et al. 2023) are an important tool for studying the relevance of such process.

Today most codes which consider freezing/ thawing are not mechanically coupled. However, freezing (e.g., permafrost) has a mechanical relevance on the subsurface. Other effects like glaciation have also an effect on the subsurface stress-regime, in this case due to the loading of the glacier (Rühaak et al. 2014). All mentioned processes must be considered while assessing the safety of a nuclear waste repository.

Methods and data

In this project both experimental but also numerical studies are planned. An experimental setup has to be developed which is able to measure all relevant properties (e.g., pore-pressure, strain-tensor, relative permeability, saturation) on various samples, like unconsolidated (sand, silt, clay) and consolidated rocks (claystone, crystalline rocks, sandstones). The stresses and strains resulting due to freezing and thawing have to be recorded at various temperature ranges and water saturations (e.g., Mohammed et al. 2021).

Numerical studies are performed aiming to reproduce the experimental behaviour in respective models. Finally, the relevance of the mechanical impact of freezing/thawing will be studied using a catchment scale model.

Conclusions and outlook

For a profound assessment of the safety of a nuclear waste repository numerous effects of future ice ages must be considered.

For a durable analysis natural analogue, experimental studies at various scales and numerical models are important.

This study aims to validate model results by analysing the relevance of volume changes and the respective stresses and strains on rock integrity.

The general study approach together with first results will be presented.

REFERENCES

Anbergen, H., Rühaak, W., Frank, J., and Sass, I., 2014. Numerical simulation of a freeze–thaw testing procedure for borehole heat exchanger grouts. Canadian Geotechnical Journal 14, 1–14. https://doi.org/10.1139/cgj-2014-0177

Beddrich, J., Gupta, S., Wohlmuth, B., and Chiogna, G., 2022. The importance of topographic gradients in alpine permafrost modeling. Advances in Water Resources 170, 104321. https://doi.org/10.1016/j.advwatres.2022.104321

Beven, K., 2012. Rainfall-Runoff Modelling: The Primer. John Wiley & Sons, Ltd. https://doi.org/10.1002/9781119951001

Chen, Y., Lin, H., and Cao, R. 2022. Damage constitutive model considering nonlinear fracture closure of rock under freezing–thawing cycles. Environ Earth Sci 82, 4. https://doi.org/10.1007/s12665-022-10695-0

Fisher, R.A., and Koven, C.D. 2020. Perspectives on the Future of Land Surface Models and the Challenges of Representing Complex Terrestrial Systems. Journal of Advances in Modeling Earth Systems 12, e2018MS001453. https://doi.org/10.1029/2018MS001453

Gao, B., and Coon, E.T. 2022. Evaluating simplifications of subsurface process representations for field-scale permafrost hydrology models. The Cryosphere 16, 4141–4162. https://doi.org/10.5194/tc-16-4141-2022

Grenier, C., Anbergen, H., Bense, V., Chanzy, Q., Coon, E., Collier, N., Costard, F., Ferry, M., Frampton, A., Frederick, J., Gonçalvès, J., Holmén, J., Jost, A., Kokh, S., Kurylyk, B., McKenzie, J., Molson, J., Mouche, E., Orgogozo, L., Pannetier, R., Rivière, A., Roux, N., Rühaak, W., Scheidegger, J., Selroos, J.-O., Therrien, R., Vidstrand, P., and Voss, C. 2018. Groundwater flow and heat transport for systems undergoing freeze-thaw: Intercomparison of numerical simulators for 2D test cases. Advances in Water Resources 114. https://doi.org/10.1016/j.advwatres.2018.02.001

Hou, Y., Guo, H., Yang, Y., and Liu, W. 2023. Global Evaluation of Runoff Simulation from Climate, Hydrological and Land Surface Models. Water Resources Research 59, e2021WR031817. https://doi.org/10.1029/2021WR031817

Maxwell, R.M., Putti, M., Meyerhoff, S., Delfs, J.-O., Ferguson, I.M., Ivanov, V., Kim, J., Kolditz, O., Kollet, S.J., Kumar, M., Lopez, S., Niu, J., Paniconi, C., Park, Y.-J., Phanikumar, M.S., Shen, C., Sudicky, E.A., and Sulis, M. 2014. Surface-subsurface model intercomparison: A first set of benchmark results to diagnose integrated hydrology and feedbacks. Water Resources Research 50, 1531–1549. https://doi.org/10.1002/2013WR013725

Mohammed, A.A., Cey, E.E., Hayashi, M., Callaghan, M.V., Park, Y.-J., Miller, K.L., and Frey, S.K. 2021. Dual-permeability modeling of preferential flow and snowmelt partitioning in frozen soils. Vadose Zone Journal 20, e20101. https://doi.org/10.1002/vzj2.20101

Mölders, N., and Rühaak, W. 2002. On the impact of explicitly predicted runoff on the simulated atmospheric response to small-scale land-use changes-an integrated modeling approach. Atmospheric Research 63. https://doi.org/10.1016/S0169-8095(02)00002-9

Rühaak, W., Anbergen, H., Grenier, C., McKenzie, J., Kurylyk, B.L., Molson, J., Roux, N., and Sass, I. 2015. Benchmarking Numerical Freeze/Thaw Models, in: Energy Procedia. https://doi.org/10.1016/j.egypro.2015.07.866

Rühaak, W., Bense, V.F., and Sass, I. 2014. 3D hydro-mechanically coupled groundwater flow modelling of Pleistocene glaciation effects. Computers and Geosciences 67. https://doi.org/10.1016/j.cageo.2014.03.001

Torres-Rojas, L., Vergopolan, N., Herman, J.D., and Chaney, N.W. 2022. Towards an Optimal Representation of Sub-Grid Heterogeneity in Land Surface Models. Water Resources Research 58, e2022WR032233. https://doi.org/10.1029/2022WR032233

North Country Rock Pile closure cover – Diavik Diamond Mine

Sean Sinclair[1], Gord Stephenson[1], Ben Wickland[2], Hongwei Xia[3] & Chantal Pawlychka[3]

[1]*Rio Tinto, Yellowknife, Northwest Territories, Canada*
[2]*WSP Canada, Vancouver, British Columbia, Canada*
[3]*Tetra Tech, Edmonton, Alberta, Canada*

Rio Tinto's Diavik Diamond Mine is located in the Canadian sub-arctic in an area of continuous permafrost. The mine has been operating since 2003 and is in the final stages of closure planning with the end of Operations in 2026. The mine consists of four diamondiferous kimberlite pipes mined from three open pits, extensive underground workings and with significant surface operations. The mine waste rock is stored in the North Country Rock Pile (NCRP), which covers an area of approximately 1.8 km^2 and contains potentially acid generating (PAG) waste rock. The NCRP will contain an estimated 95 Mm^3 of waste rock after completion. The closure strategy for the NCRP is permafrost aggradation with a thermal cover to promote long term physical and chemical stability in consideration of climate change. The cover construction started in 2017 and had been largely constructed at the end of 2023. The design and construction of the NCRP closure are summarized herein, with early performance monitoring data.

CLOSURE STRATEGY

For the mine site the aspirational strategic objective is relinquishment with no requirement for a permanent site presence and this resulted in the early management decision to operationally segregate all waste rock based on the acid-generating potential of minable units classified based on carbon-sulfur analysis results collected from every blast hole. Segregated PAG waste rock was stored in the NCRP where it would eventually be isolated under a Non-Acid Generating (NAG) rock cover overlying frozen till. Conceptually, the cover is intended to control ARD/ML by sustaining permafrost aggradation in the PAG waste rock, with the additional benefit of reducing infiltration. The till layer has higher volumetric and latent heat and reduced hydraulic conductivity. The NAG waste rock layer provides insulation that limits thaw of the till layer and protects against erosion.

In 2004 Rio Tinto initiated the Diavik Waste Rock Project with the University of Waterloo, University of Alberta, and University of British Columbia which confirmed the operational PAG-NAG segregation program was protective, proved the design concept with thermal modelling, and provided field-scale physiochemical validation of the proposed closure design. Based on this research a strategic decision was made to advance the NCRP closure design to construction-ready engineered detail almost a decade ahead of final closure.

In 2017 Diavik initiated full-scale progressive construction of the final NCRP landform which capitalized on the lower cost of direct haulage and placement of cover materials from the operating open pit rather than an intermediate borrow placement requiring additional drilling, blasting, and loading. The cover construction schedule had to be dynamic but not reactive and was continuously adapted to the outcomes of the operation. Emphasis then shifted from planning, predicting, and executing to monitoring.

THERMAL MODELLING

The initial design was based on temperature measurements collected from the large-scale test pile built at Diavik and numerical simulations conducted by the Diavik Waste Rock Research Project team (Pham 2013). Tetra Tech Canada Inc. (Tetra Tech) was then retained by Rio Tinto to conduct a series of one-dimensional and two-dimensional thermal analyses to inform the closure cover design. Thermal analyses were conducted using Tetra Tech's proprietary two-dimensional finite element software, GEOTHERM. Sensitivity studies of key parameters (i.e., layer thicknesses, climate change, till gravimetric water content (GWC), and heat generation in PAG rock) were also performed to investigate the long-term thermal performance of the cover.

The climate change scenario adopted in the thermal analyses was based on a study conducted by Environmental Modelling and Prediction P/L Australia (EMPA). The climate model used by EMPA predicts an annual mean air temperature warming rate at Diavik of +0.056 °C/year between 1970 and 2060, which was extended out to 100 years in the design basis. The predicted mean annual air temperatures under EMPA's climate model are warmer than those from the Coupled Model Intercomparison Project Phase 5 (CMIP5) for the Representative Concentration Pathway (RCP) 4.5 (e.g., -2.8 °C under EMPA model versus -4.8 °C under CMIP5 RCP 4.5 in 2120).

Thermal results suggest that after wet-up of the till layer (with a minimum 10% GWC maintained) the

seasonal thawing front is expected to remain within the closure cover system, and PAG material is expected to remain in a frozen condition after 100 years under the projected mean climate change scenario.

COVER DESIGN

The NCRP closure cover design and construction package were developed by WSP Canada Inc (WSP). The design includes cover of areas containing PAG rock by re-sloping to a maximum of 3H:1V to allow equipment to work on the slope, then placement of 1.5 m of till and 3 m of NAG waste rock.

CONSTRUCTION

The NCRP was successfully re-sloped and the majority of the cover placed by the end of 2023 (Figure1).

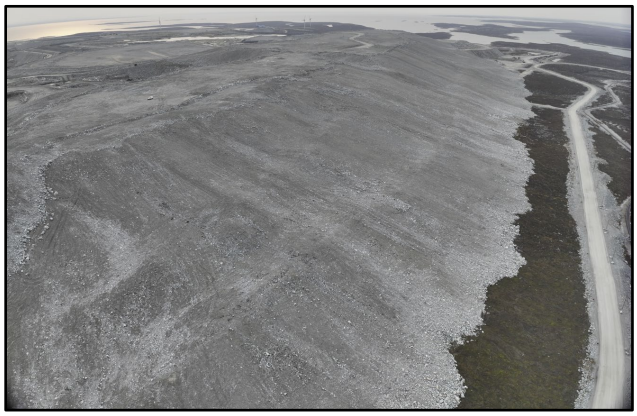

Figure 1. NCRP Closure Cover – North Slope (2023).

Challenges during construction related to the climate included re-sloping the pile and working with till which contained fine grained materials and water. Re-sloping the frozen waste rock pile required blasting and ripping in places. The till borrow sources included an open pit mine, where unfrozen till from the lakebed was hauled run-of-mine, and a till pile that had frozen, and required blasting to excavate. The till cover was required to be overbuilt in areas where frozen till was used due to the frozen condition from the borrow source.

EARLY THERMAL PERFORMANCE AND MONITORING

Time-domain reflectometer (TDR) water content probes (probes) were installed to monitor in-situ GWC throughout the till layer. Data from the TDR probes suggest that areas of fully constructed cover (i.e., till with overlying NAG rock), have started to freeze back, which aligns with thermal modeling predictions. This suggests that the initial stage of thermal cover performance is trending towards meeting the design objectives. Ground temperature cables (GTCs) are to be installed to a minimum 15 m depth below the NCRP surface after full cover construction to monitor the thermal conditions in the closure cover and underlying PAG rock.

LESSONS LEARNED

The progressive closure of the NCRP demonstrates Rio Tinto's commitment, not only to mine closure, but to modern best practices with integrated mine closure. Outcomes of the NCRP project supports the argument that bulk earthworks progressive closure projects can be successfully integrated into operational mine plans if 1) closure concepts are defined early and researched with consideration of evolutionary climate change risks; and 2) closure schedules are aligned with the mine plan allowing for dynamic adjustments which capitalise on evolving opportunities inevitable in an operating mine including direct haulage of materials and optimized continuity of employment and equipment utilization. In order to motivate the integration of closure works into an operation both the cultural and organizational alignments must be supported by appropriate performance metrics and financial mechanisms to ensure united priorities. Climate change creates uncertainty for closure projects: the robust design of the NCRP cover appears to have held up to 15 years of advances in climate change predictions.

This project has resulted in long-term financial savings for the business, a reduced closure schedule, allowed for early delivery of closure objectives and early initiation of closure performance data collection to decrease long-term risk and performance uncertainty. This work has prioritized the establishment of clear expectations of successful closure and external development of predictable regulatory pathways to the complete return of security and relinquishment of the site.

REFERENCES

Pham, H.N. 2013. Heat Transfer in Waste-Rock Piles Constructed in a Continuous Permafrost Region. Ph.D. thesis. University of Alberta.

Numerical modeling framework for contaminant transport from subsurface wastewater treatment systems in cold regions

Ronald Bailey Strong[1], Barret Kurylyk[1], Rob Jamieson[1] & Laurent Orgogozo[2]

[1]*Department of Civil & Resource Engineering, Dalhousie University, Halifax, Nova Scotia, Canada*

[2]*Geosciences Environment Toulouse, Toulouse, France*

Communities within cold regions face ongoing challenges with wastewater treatment (WWT) as conventional mechanical forms of WWT developed for warmer jurisdictions are not appropriate in these environments. There is potential for subsurface wastewater treatment systems, such as rapid infiltration basins, to provide a robust WWT option. While these systems have been widely developed and tested in warmer climates (e.g., Andres and Sims 2013) as a solution for WWT in small remote communities, their effectiveness in colder regions is not well understood due to vast differences in hydrological and hydraulic processes. Such differences can be caused by conditions that are distinct to cold regions, including seasonally and perennially (permafrost) frozen ground that alters the flow of groundwater and contaminants. Additionally, climate change is warming cold regions at an accelerated pace compared to the global average (Rantanen et al. 2022) and is activating dormant groundwater flow systems (Haynes et al. 2019; Lamontagne-Hallé et al. 2020; Lamontagne-Hallé et al. 2018; McKenzie et al. 2021; Walvoord and Kurylyk 2016), accelerating the need for detailed understanding and analysis of these systems. There is currently a lack of tools that can accurately predict the full suite of coupled heat-water-contaminant hydrogeological processes in cold regions, making the design and analysis of these systems difficult and highly uncertain. Available numerical models often fall short in representing all vital cold-region processes, from unsaturated zone dynamics to appropriate freeze-thaw responses and effects on advection, dispersion, sorption and ice ionic exclusion within freezing soils (e.g., Lamontagne-Hallé et al. 2020; Mohammed et al. 2021; Walvoord and Kurylyk 2016). These processes are essential to mathematically represent as they can strongly influence the migration and fate of contaminants. However, coupling the appropriate partial differential equations in a numerical model remains challenging, and model runs are often constrained by simulation time (e.g., Mohammed et al. 2021). Therefore, the purpose of this research is to develop a valid numerical modeling framework for the assessment of contaminant fate and transport in subsurface environments within cold regions under current and future climate conditions.

METHODS

The proposed numerical modelling methodology involves the development and use of a coupled water-heat-contaminant transport numerical model to simulate the mobility and fate of contaminants for different climate and hydrogeologic conditions. The numerical model will consider factors that most available models do not typically include such as unsaturated flow-solute-energy transport, frozen ground, and surface-subsurface interactions. These factors are important coupled mechanisms to consider within cold regions but, to our knowledge, have not been fully considered in previous studies (e.g., Frampton and Destouni 2015; Mohammed et al. 2021). Validated open-source modelling frameworks will be utilized where the theory and framework are well developed such as: the Simultaneous Heat and Water (SHAW) model (Flerchinger et al. 2012) for the appropriate surface-canopy energy balance and shallow moisture fluxes, and the open-access and parallelized code OpenFOAM via the solver permaFoam (Orgogozo et al. 2022; Weller et al. 1998) for the freeze-thaw dynamics in unsaturated soils. New solute transport equations will be tested in OpenFOAM to represent contaminant transport processes based on state-of-the-art understanding of cold region contaminant transport and fate mechanisms that are missing from current numerical models.

STUDY SITE AND DATA COLLECTION

The research will be conducted in Fort Good Hope, Northwest Territories (66° 16' 53", -128° 36' 36", see Figure 1). The site features a monitoring well network near an existing WWT exfiltration trench. These wells have instrumentation (see Figure 2) for measuring hydraulic head, shallow-subsurface temperatures, and can be used for water sample collection.

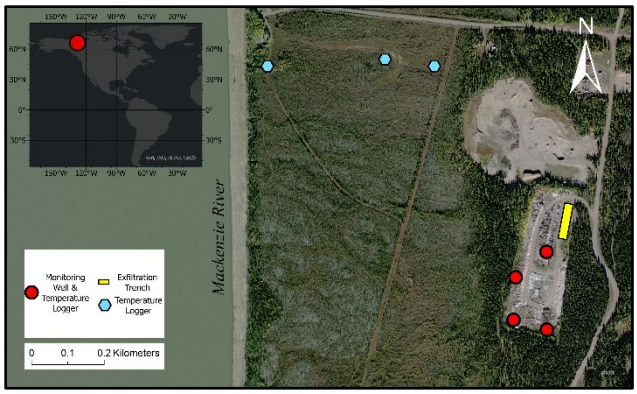

Figure 1. Study site for validating numerical framework.

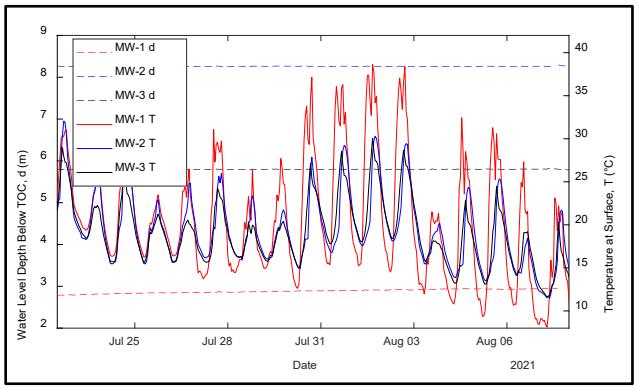

Figure 2. Shallow surface temperature (T) and water level depth (d) below top of casing (TOC) data for several monitoring wells (MW) during a summer period.

Summary and Acknowledgements

The fate of contaminants in northern regions is a growing concern across the Arctic, yet we do not have the modeling capacity to investigate the interactions between groundwater flow, permafrost, and contaminant transport in variably saturated conditions. This study addresses this knowledge and tool gap with the application focused on subsurface wastewater treatment systems. Funding for this research has been provided by the NSERC Alliance Program and the Government of the Northwest Territories. We would like to thank Isabelle de Grandpré and Jeanne Arsenault for their assistance with data collection.

References

Andres, A.S., and Sims, J.T. 2013. Assessing potential impacts of a wastewater rapid infiltration basin system on groundwater quality: a Delaware case study. Journal of Environmental Quality. (42): 391–404. https://doi.org/10.2134/jeq2012.0273

Flerchinger, G.N., Caldwell, T., Cho, J., and Hardegree, S.P. 2012. Simultaneous heat and water (SHAW) model: model use, calibration, and validation. Transactions of the ASABE. (55): 1395–1411.

Frampton, A., and Destouni, G. 2015. Impact of degrading permafrost on subsurface solute transport pathways and travel times. Water Resources Research. (51): 7680–7701. https://doi.org/10.1002/2014WR016689

Haynes, K.M., Connon, R.F., and Quinton, W.L. 2019. Hydrometeorological measurements in peatland-dominated, discontinuous permafrost at Scotty Creek, Northwest Territories, Canada. Geoscience Data Journal. (6): 85–96. https://doi.org/10.1002/gdj3.69

Lamontagne-Hallé, P., McKenzie, J.M., Kurylyk, B.L., Molson, J., and Lyon, L.N. 2020. Guidelines for cold-regions groundwater numerical modeling. WIREs Water. (7): e1467. https://doi.org/10.1002/wat2.1467

Lamontagne-Hallé, P., McKenzie, J.M., Kurylyk, B.L., and Zipper, S.C. 2018. Changing groundwater discharge dynamics in permafrost regions. Environ. Res. Lett. (13): 084017. https://doi.org/10.1088/1748-9326/aad404

McKenzie, J.M., Kurylyk, B.L., Walvoord, M.A., Bense, V.F., Fortier, D., Spence, C., and Grenier, C. 2021. Invited perspective: What lies beneath a changing Arctic? The Cryosphere. (15): 479–484. https://doi.org/10.5194/tc-15-479-2021

Mohammed, A.A., Bense, V.F., Kurylyk, B.L., Jamieson, R.C., Johnston, L.H., and Jackson, A.J. 2021. Modeling reactive solute transport in permafrost-affected groundwater systems. Water Resources Research. (57): e2020WR028771. https://doi.org/10.1029/2020WR028771

Orgogozo, L., Xavier, T., Oulbani, H., and Grenier, C. 2022. Permafrost modelling with OpenFOAM®: New advancements of the permaFoam solver. Computer Physics Communications. (282). https://doi.org/10.1016/j.cpc.2022.108541

Rantanen, M., Karpechko, A.Y., Lipponen, A., Nordling, K., Hyvärinen, O., Ruosteenoja, K., Vihma, T., and Laaksonen, A. 2022. The Arctic has warmed nearly four times faster than the globe since 1979. Commun Earth Environ. (3): 1–10. https://doi.org/10.1038/s43247-022-00498-3

Walvoord, M.A., and Kurylyk, B.L. 2016. Hydrologic impacts of thawing permafrost—a review. Vadose Zone Journal. (15): 1–20. https://doi.org/10.2136/vzj2016.01.0010

Weller, H.G., Tabor, G., Jasak, H., and Fureby, C. 1998. A tensorial approach to computational continuum mechanics using object-oriented techniques. Computer in Physics. (12): 620–631. https://doi.org/10.1063/1.168744

Assessment of frozen foundation conditions of Giant Mine dams

Hung Vu[1], Jason Song[2], Logan Morhart[1] & Greg Misfeldt[1]
[1]*WSP Canada Inc., Saskatoon, Saskatchewan, Canada*
[2]*WSP Canada Inc., Calgary, Alberta, Canada*

Giant Mine (the Site) is an abandoned open pit and underground gold mine located 5 km north of Yellowknife, Northwest Territories. The Northwest Tailings Containment Area (TCA) of Giant Mine was constructed in the 1980s to expand the tailings storage capacity of the Site. Tailings at the Northwest TCA are contained by topographic highs (bedrock outcrops) and tailings dams. Frozen soil condition was encountered in most of boreholes drilled at the dams. At closure, the TCA will be covered and dam slopes will be modified to improve slope stability conditions. An assessment of dam frozen foundation conditions was completed to assess i) the future changes in foundation thermal regime, ii) the potential thaw settlement of the foundation, and iii) the potential effects of thawing process in foundation soils to dam slope stability conditions.

Soil stratigraphy and frozen conditions

The general foundation units encountered at the Site consists of peat/organic soils, silty clay, silt and bedrock. Fill materials used for dam construction includes rockfill of various size, filter material consisting of sand and gravel, and clay fill for the dam core. During the soil investigation, only small amounts of visible ice in some soil samples were observed. The frozen soil samples, where visible ice was observed, contain insignificant ice quantities that were in excess of the volume of water present in the soil in the unfrozen state.

As part of the on-going care and maintenance for the Site, the dams are routinely inspected and monitored. Recent geotechnical inspections indicated no signs of slope movement at the dams, except minor cracking and localized sloughing of downstream slope at some locations.

Thermistor strings were installed in the dams in 2019 to monitor soil temperatures; temperature measurements have been continuous nearly monthly since the thermistor installation. The monitoring results indicate that the frozen zone extends through the dam fill materials, foundation soils and into bedrock.

Thermal analysis

In this thermal study, frozen foundation soils are assumed to be subjected to temperature change at ground surface. It was assumed that the soil stratigraphy and water content in the foundation soils remain unchanged through the modelling periods.

Climate change is considered for thermal analysis of the dam frozen foundations at the Site. The future air temperatures estimates were obtained from a climate change study completed for the Site. A standardized approach was developed for completing climate change assessments which is in line with the best practices being developed by the Mining Association of Canada. The approach provides a description of the current climate baseline and how those values are projected to change under future climate conditions, grounded in the best available climate observations and climate projections. In current sitewide design basis for the Site, the projection at the 50th percentile is used for most design applications and the 95th percentile for critical infrastructure to evaluate climate change impact on the site design applications.

One-dimensional, transient, thermal analyses were conducted to assess soil temperatures under various geometry and boundary conditions. The assessments of thermal regime, in the dam frozen foundation conditions, primarily the depth and rate of change of the active layer due to heat conduction, are divided into three steps, which are described as below:

- Step 1: Calibrate the thermal model based on the measured soil temperatures at thermistor locations. This was achieved by replicating the thermal trends in the subsurface to available site-measured temperatures
- Step 2: Predict the future thermal response at the dam crest using projected air temperatures. This thermal analysis represents future thermal response of dam crest and bench that have rockfill overlying foundation soils.
- Step 3: Predict the future thermal response at the dam toe using projected air temperatures. This thermal analysis represents future thermal response of natural ground soils without overlying rockfill.

All the predictive modelling were run to 2100, in which the projected air temperatures are available.

The results of model calibration indicates that the modelled temperatures agree well with the measured data, indicating the model calibration is satisfactory. The calibration modelling results provide a basis to use the calibrated thermal properties to predict future thermal responses (e.g., thaw depth and thaw rate) of

the frozen dam foundation to the projected air temperatures due to climate change.

The estimated thaw depth by 2100 is between approximately 10 metres below ground surface (mbgs) and 20 mbgs depending on soil stratigraphy of the borehole location. These results indicate that the underlying foundation soils beneath the Northwest TCA dams would thaw to some extent. The foundation soils can be totally thawed by 2100 at the locations where the rockfill layer is thin. When the thickness of the rockfill layer is greater than 20 m, the underlying foundation soils are less likely to thaw. The estimated average thaw rate is between approximately 80 mm/year and 200 mm/year.

THAW SETTLEMENT

The potential thaw settlement of dam foundation (by 2100) in the Northwest TCA is dependent on the thawing depth, underlying stratigraphy, freeze/thaw histories, compressibility of the unfrozen materials (organic content, fine content, and water content) and surcharge load (e.g., thickness of rockfill). From the dam and foundation soil units identified for the thermal analysis, the organic soils/peat layer and silty clay layer would have the greatest potential for settlement as a result of thawing. This is because the organic soils and silty clay have high in situ water contents, which can result in significant settlement if these materials have not been previously exposed to freeze-thaw cycles. Thawing rockfill material would have negligible impact on settlement. Significant settlement can have an impact on the integrity of a dam structure.

The foundation soils at the Northwest TCA contain minor amounts of excess or visible ice (the amount in excess of the volume of water present in the soil in the unfrozen state), the settlement associated with thawing of excess ice is anticipated to be minor. The thaw settlement was estimated based on the thawing depths obtained from the thermal analyses under the projection at the 95th percentile, estimated effective stress of the rockfill layer, and assumed stress-strain modulus for the organic soils and silty clay materials. The stress-strain modulus was assumed to be 500 kPa for the organic soils and 2,000 kPa for the silty clay. The settlement of the silt layer was estimated less than 0.05 m due to large stress-strain modulus. It was assumed that no settlement would occur below the predicted active zone or thawing depth.

SLOPE STABILITY

The thawing of foundation soils (e.g., organic silt, silty clay, and silt) may lead to the build-up of excess pore water pressures in the foundation that may lower the dam slope stability. The development and maintenance of excess pore pressures would depend mainly on the thaw-consolidation ratio, which is a measure of the balance between the rate of generation of excess pore waters, and the ability of the soil to dissipate these waters from the pore space.

The water dissipation rate due to thawing was estimated according to the conventional consolidation theory by considering single drainage, upwards to the rockfill layer. Based on the estimated thaw depth in the foundation soils, the estimated time required to achieve 90% consolidation would be approximately 5 years, at which it was estimated the foundation soils will have the largest thaw thickness (5.5 m). The time required to achieve 90% consolidation at other borehole locations would be less than 5 years due to thinner thaw thickness (i.e., shorter drainage pathway to the rockfill layer) in the foundation soils. The results of thermal analysis indicate that future thawing, due to climate change, would occur at a rate of less than 200 mm/year. It is anticipated that the water generated as a result of thawing will flow from the soil at the same rate as it is produced. No excess pore pressure will be generated, and settlement will occur concurrently with thawing. This suggests that excess pore-water pressures would not develop in the foundation soils when considering thawing will be occurring gradually over 80 years. Thawing of frozen foundation due to climate change would have insignificant effect to the slope stability of the dams.

The process of thawing of frozen soils and compression of thawing soils under loading is complex and difficult to characterize adequately. However, the effect of fast thawing of frozen foundations can be evaluated by considering the potential increase in pore water pressure in the thawing soils. On thawing, the soil is subjected to loading caused by its self-weight and overlying material (e.g., rockfill).

To evaluate the potential impact of fast thawing condition, it was conservatively assumed that excess pore-water pressures exist in all foundation soils. A pore pressure coefficient, B-Bar equaling to 0.5 was used for the slope stability analyses. The analysis results suggest that the factor of safety would meet the minimum slope factor of safety for short term condition of 1.3. The analysis results indicate that the Northwest TCA dams would perform adequately in the event of thawing of foundation soils.

12 Monitoring Permafrost Conditions & Processes

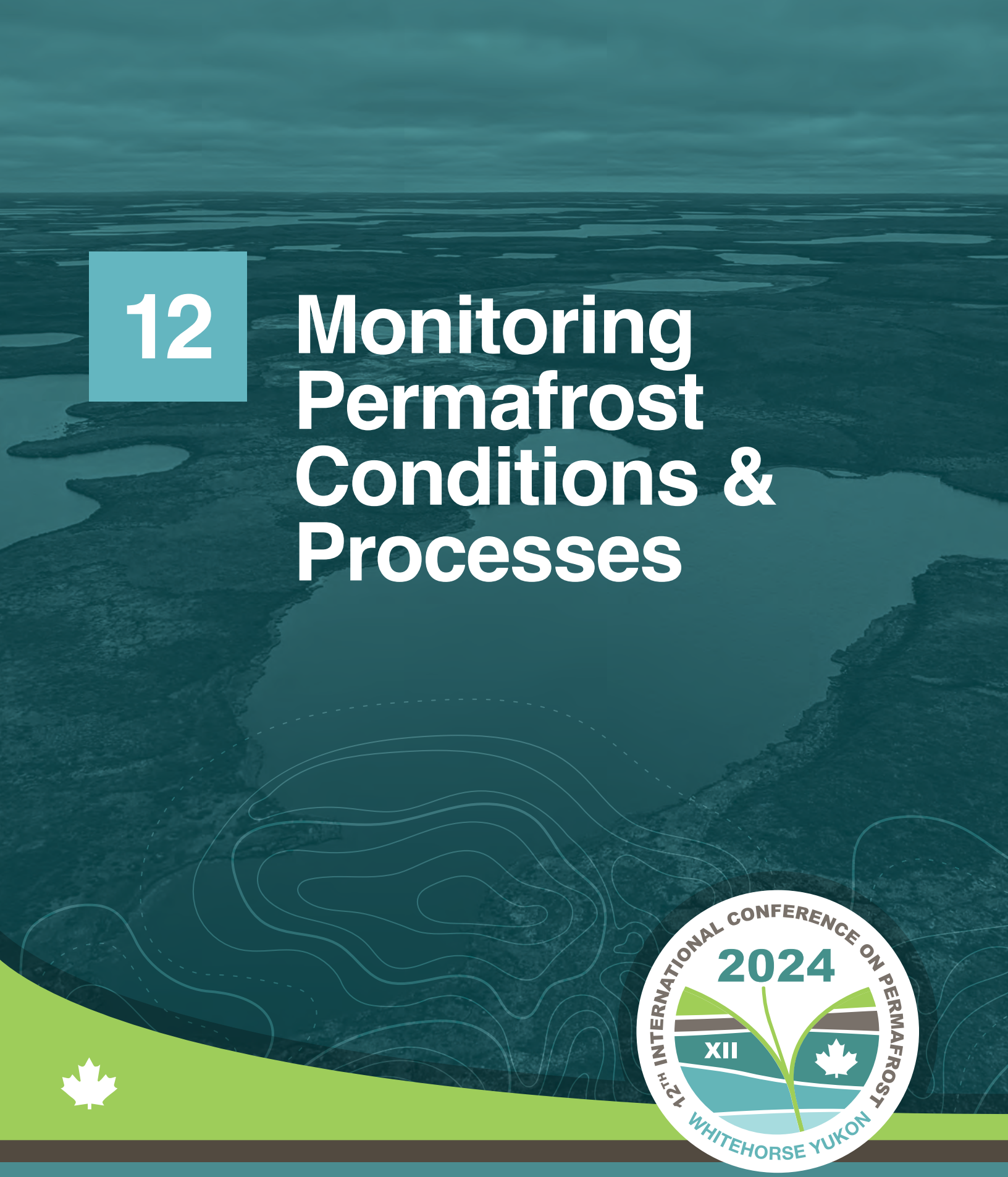

12TH INTERNATIONAL CONFERENCE ON PERMAFROST
2024
XII
WHITEHORSE YUKON

INTEGRATING PERSPECTIVES OF PERMAFROST THAW, CHANGE, AND ADAPTATION

Monitoring Permafrost Conditions & Processes

12A — Monitoring Techniques and Feedback of Snow, Vegetation, and Permafrost

Session Chairs: Anna Wagner[1], Julian Dann[2] & Emma Lathrop[3]

[1]Cold Regions Research and Engineering Laboratory, US Corps of Engineerings, Fairbanks, Alaska, United States
[2]International Arctic Research Center, University of Alaska, Fairbanks, Alaska, United States
[3]Center for Ecosystem Science and Society, Northern Arizona University, Flagstaff, Arizona, United States

Snow, vegetation, and permafrost are intricately linked across the cold regions of the globe. Snow protects the ground during the winter and provides insulation for the permafrost, which guards against cold temperatures from penetrating deep into the soils. Vegetation changes, including shrub expansion, are observed, and linked to increases in snow depth, redistribution of the snowpack, and soil moisture changes. However, the dynamic nature of snow and vegetation mean that these interactions could shift with potential for large climate impacts. While the interactions among snow-dominated landscapes and permafrost are abundant, research efforts linking these disparate fields remain sparse.

Part of the challenge is the paucity of accurate distributed snow measurements and model results. Single-point and remote sensing data collection campaigns are limited in their range and/or resolution in space and time. Meanwhile, recent in situ field- and watershed-scale observations using dense sensor deployments have captured multi-scale transformations of permafrost. Such observations create opportunities to test hypotheses and numerical models.

In this session, we invite papers on snow, vegetation, and permafrost interactions—including advancements in remote sensing and monitoring technologies of such interactions--within cold regions across the globe with particular emphasis on the impacts to the hydrologic cycle and climate change effects. We also encourage contributions on novel advances in the field of in situ sensor technology observing the evolution of permafrost systems.

Spatio-temporally resolved snow distribution estimates using sensor networks and machine learning techniques

Katrina E. Bennett, Claire Bachand, Baptiste Dafflon, Chen Wang Shannon Dillard, Eve I. Gasarch, Ian Shirley, Lauren Thomas, Sarah Maebius & Bob Bolton

In high latitude environments, snow plays a critical role in insulating the ground surface from cold temperatures that impact permafrost (Sturm et al. 1997). As the climate warms, precipitation is anticipated to shift across high latitude ecosystems, leading to changes in snow depth, duration, and extent (Liston and Hiemstra 2011). These changes will strongly influence the permafrost, possibly leading to enhanced thawing and increased carbon release to the atmosphere, intensifying global climate warming (Schuur et al. 2022). An improved understanding of snow distribution patterns and key drivers is essential for accurate representation of the permafrost and the Arctic carbon balance within earth system models. However, observing snow dynamics, especially in remote high-latitude regions, is expensive and challenging (i.e., Bennett et al. 2022).

In this study, we propose a novel method for measuring snow depth using small, cheap, and easy-to-deploy temperature sensors and a machine learning model. Intensive field studies to collect snow, permafrost, and ground surface temperature (GST) data were carried out at sites on the Seward Peninsula of Alaska in 2019, 2022, and 2023. During 2021-2022, snow depth and hourly GST were recorded at ~150 locations using a series of distributed temperature sensors (Dafflon et al. 2022; Léger et al. 2019; Wang et al. 2024). We use these collocated snow depth and GST measurements to train a Machine Learning (ML) random forest (rf) model to predict snow depth from GST features.

Initial results show that the ML-rf can predict snow depth with high accuracy (R = 0.91, Figure 1). We evaluate the transferability of the ML-rf by training at one field site and testing on the other. ML-rf predictions remained robust, but accuracy decreased. We apply this technique to obtain 4-hourly snow depth estimates from 264 iButton and Tiny Tag temperature sensors deployed across a range of topography and vegetation types to capture spatial variations in the snow depths. We additionally have tested our technique across multiple sites in the Arctic, with varying results that will be discussed.

We aim to link this broad set of snow depth time-series estimates to spatially continuous snow depth maps and landscape characteristics to generate spatially and temporally continuous snow depth estimates for our study region. Ultimately, we will use our findings to evaluate earth system model simulations of snow distribution for improved understanding of snow-permafrost interactions, which has implications for increased carbon and ultimately, greater climate impacts for both the Arctic and the globe.

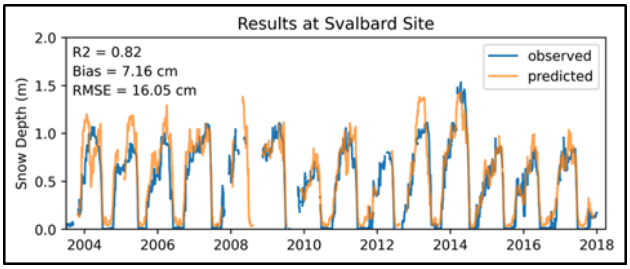

Figure 1. Results of the ML-rf at Svalbard site. Model is trained on Seward Peninsula data and applied to the Svalbard site data set. Data: Boike et al. 2018.

References

Bennett, K.E., Miller, G., Busey, R., Chen, M., Lathrop, E.R., Dann, J.B., Nutt, M., Crumley, R., Dillard, S.L., Dafflon, B., and Kumar, J. 2022. Spatial patterns of snow distribution in the sub-Arctic. The Cryosphere, 17;16(8): 3269–3293. https://doi.org/10.5194/tc-16-3269-2022

Boike, J., Juszak, I., Lange, S., Chadburn, S., Burke, E., Overduin, P.P., Roth, K., Ippisch, O., Bornemann, N., Stern, L., and Gouttevin, I. 2018. A 20-year record (1998–2017) of permafrost, active layer and meteorological conditions at a high Arctic permafrost research site (Bayelva, Spitsbergen), Earth System Science Data, 10(1): 355–390. https://doi.org/10.1594/PANGAEA.880120

Dafflon, B., Wielandt, S., Lamb, J., McClure, P., Shirley, I., Uhlemann, S., Wang, C., Fiolleau, S., Brunetti, C., Akins, F.H., Fitzpatrick, J., Pullman, S., Busey, R., Ulrich, C., Peterson, J., and Hubbard, S.S. 2022. A distributed temperature profiling system for vertically and laterally dense acquisition of soil and snow temperature. The Cryosphere, 16: 719–736. https://doi.org/10.5194/tc-16-719-2022

Léger, E., Dafflon, B., Robert, Y., Ulrich, C., Peterson, J.E., Biraud, S.C., Romanovsky, V.E., and Hubbard, S.S., 2019. A distributed temperature profiling method for assessing spatial variability in ground temperatures in a discontinuous permafrost region of Alaska. The Cryosphere, 13(11): 2853–2867.

Liston, G.E. and Hiemstra, C.A., 2011. The changing cryosphere: Pan-Arctic snow trends (1979–2009), Journal of Climate, 24(21): 5691-5712.

Schuur, E.A., Abbott, B.W., Commane, R., Ernakovich, J., Euskirchen, E., Hugelius, G., Grosse, G., Jones, M., Koven, C., Leshyk, V., and Lawrence, D., 2022. Permafrost and climate change: carbon cycle feedbacks from the warming Arctic, Annual Review of Environment and Resources, 47: 343–371.

Sturm, M., Holmgren, J., König, M., and Morris, K. 1997. The thermal conductivity of seasonal snow, Journal of Glaciology, 43(143): 26–41.

Wang, C., Shirley, I.A., Wielandt, S., Lamb, J., Uhlemann, S., Breen, A.L., Busey, R.C., Bolton, W.R., Hubbard, S., and Dafflon, B. 2024. Local-scale heterogeneity of soil thermal dynamics and controlling factors in a discontinuous permafrost region. Environmental Research Letters, 19(3).

Examining elevational transect analysis sensitivity along the Dempster Highway, Yukon, Canada

Mitch K. Codd, Nick C. Noad & Philip P. Bonnaventure
Department of Geography and Environment, University of Lethbridge, Lethbridge, Alberta, Canada

Understanding the impact of warming climate on permafrost distribution and thermal state in northern and mountainous Canada is critical. Permafrost, a physical state of the lithosphere affected by freezing and thawing processes (French and Williams 2013), is evident in the boreal forest and moss-covered valley along the Dempster Highway in the Yukon's Ogilvie Mountain Range (Noad and Bonnaventure 2022). A thorough examination of the thermal state of permafrost is needed due to the region's shallow underlying permafrost. A complicating factor on thermal conditions in this mountain valley environment is the presence of frequent and intense surface-based temperature inversions (SBIs) which have been observed to impact air and ground temperature patterns (Lewkowicz et al. 2012; Noad and Bonnaventure 2022). SBIs deviate from the typical pattern by exhibiting a temperature increase with increased altitude/elevation, a phenomenon commonly seen in Arctic areas (Ruman et al. 2022). This can drive complex patterns of ground temperatures where the warmest ground temperatures and lowest probability of permafrost occur at middle or high elevations while the coldest ground temperatures and highest probability of permafrost occurs in the valley bottom (Bonnaventure and Lewkowicz 2013). Recent research has been undertaken to test the relationship between SBI characteristics and annual average surface lapse rates (SLR), which describes the rate at which temperature changes with elevation. To achieve this objective, Elevational Transect Analysis (ETA) was utilized, which required the deployment of a large network of sensors that was set up in several valleys along the Dempster Highway (Noad and Bonnaventure 2022, 2023). From this network of sensors, air temperature data and SLR can be compared for the years since deployment. Furthermore, the sensitivity of ETA and resulting SLR to additions and removal of sensors along the transect must be analyzed. This aids in understanding the ideal number of sensors needed to accurately calculate SLR and to better utilize resources in the investigation of future sites.

Objective

This study quantifies SBI in a Yukon valley and examines air temperature variations between sensor locations and interannually. In addition, the number of sensors along the elevational transects will be adjusted and SLR recalculated to determine the optimal number of sensors for maximum accuracy and efficiency.

Study Area

The study site is in a valley (unofficially named WS01) surrounded by a section of the Ogilvie Mountains and is west of the Dempster Highway in northern Yukon, Canada. The valley opens to the east, with slopes to the north, west, and south. Vegetation along the valley floor is comprised mostly of mosses and lichen, stopping primarily at the base of either slope which are covered in weathered block rock. A creak runs down the middle of the valley, before veering off and discharging along the base of the south facing slope. The valley bottom has an elevation of around 990 m asl. with total relief of about 450 m. Permafrost within this area is between continuous and discontinuous (Noad and Bonnaventure 2022).

Methods

In the WS01 valley, an elevational transect analysis is carried out by employing sensors strategically placed on the valley floor and up the surrounding slopes to measure air and ground temperatures. The sensors are placed from the valley bottom and up each surrounding slope at increments of 50 vertical meters from the valley floor, 150 meters from the valley floor, and every 100 vertical meters from that point up to the ridgetops. The WS01 weather station is situated at the valley floor, while the DMP13, DMP05, and DMP11 sensors are positioned at elevations ascending from 997 m, 1059 m, 1147 m, to 1225 m, respectively. Mean annual air temperature (MAAT) is calculated from August 2017 to July 2018 for each sensor location and each subsequent year up to July 2023. Following this, the monthly average SLRs are calculated using linear regression between each monthly average temperature and sensor elevation in Excel. Sensors are then removed from the linear regression analysis to calculate alternative SLRs and compare them to determine the sensitivity of ETA to changing the density of deployed sensors. By observing sensor patterns over multiple elevations and years, the ETA aids in analyzing SBIs in high latitude valleys.

RESULTS

Only results for the north facing transect in the WS01 valley will be presented here. Initial observations between sensors WS01 and DMP05, at elevations 997 m and 1147 m, indicate consistent occurrence of SBIs in fall, winter, and spring, with normal (negative) SLRs in summer months (Figure 1). The WS01 station experienced a malfunction in its air temperature sensor, resulting in missing data for 2023, so the sensitivity analysis for ETA was only done for the year August 2021 to August 2022. On average, we observe a yearly SLR of approximately 10 °C km^{-1} between 2017 and 2023.

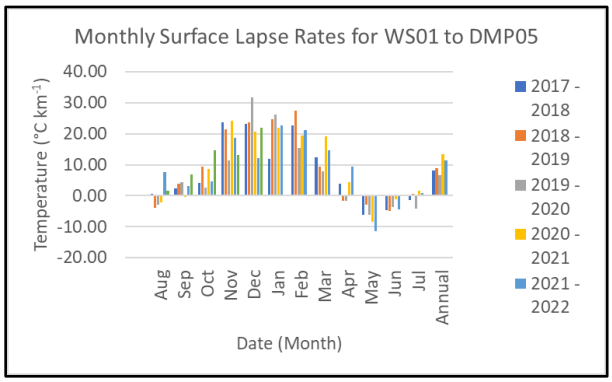

Figure 1. Monthly surface lapse rates, per kilometer, between two sensors, WS01 and DMP05, from 2017 to 2023. WS01 is at the base of the valley, at an elevation of 997 m, and DMP05 is on the north facing slope, at an elevation of 1147 m – a 150 m difference.

When evaluating the northern slope's ETA sensitivity, we consider four sensors: WS01, DMP13, DMP05, and DMP11. This results in six configurations, with WS01 being mandatory in each due to its position at the base of the valley. Upon initial inspection, the DMP13 sensor seems to disrupt SLRs, with unusually high values compared to other setups, particularly in September with the WS01, DMP13, DMP05 configuration, resulting in a positive SLR over 156 °C km^{-1} (Table 1). The configurations yielding average results are between sensors WS01 and DMP05 (configuration 2), WS01, DMP05, and DMP11 (configuration 6), or all 4 stations (configuration 7).

Table 1. Sensor configurations, along the north facing slope, resulting in varying monthly surface lapse rates from 2021 to 2022. WS01 sits at an elevation of 997 m, DMP13 at 1059 m, DMP05 at 1147 m, and DMP11 at 1225 m.

	1	2	3	4	5	6	7
Aug	-2.8	7.6	3.4	8.4	-4.2	-44.1	-42.1
Sep	0.9	3.1	12.1	9.4	156.4	3.3	40.7
Oct	2.2	4.6	14.2	9.1	11.2	3.8	9.8
Nov	13.1	18.6	37.4	22.2	15.8	15.0	16.2
Dec	8.7	12.2	27.5	16.1	11.5	9.9	11.5
Jan	18.0	22.8	39.0	24.7	18.7	19.3	19.2
Feb	16.4	21.1	33.0	22.1	16.7	17.7	17.4
Mar	11.2	14.6	23.9	15.5	11.6	12.2	12.0
Apr	7.6	9.4	10.8	9.4	7.5	8.1	7.9
May	-8.7	-11.4	-17.6	-11.9	-8.9	-9.5	-9.3
Jun	-4.1	-4.5	-4.5	-4.5	-4.1	-4.2	-4.2
Jul	-1.0	0.9	5.9	9.4	-4.2	-3.3	-4.7
Ann	5.4	11.5	15.4	11.6	6.5	9.4	9.4

REFERENCES

Bonnaventure, P.P., and Lewkowicz, A.G. 2013. Impacts of mean annual air temperature change on a regional permafrost probability model for the southern Yukon and northern British Columbia, Canada. Cryosphere, 7, 935–946. doi:10.5194/tc-7-935-2013

French, H.M., and Williams, P. 2013. The Periglacial Environment, Wiley, Somerset, USA.

Lewkowicz, A.G., Bonnaventure, P.P., Smith, S.L., and Kuntz, Z. 2012. Spatial and thermal characteristics of mountain permafrost, northwest canada. Geografiska annaler. Series A, Physical geography, 94, 195–213. doi:10.1111/j.1468-0459.2012.00462.x

Noad, N.C., and Bonnaventure, P.P. 2022. Surface temperature inversion characteristics in dissimilar valleys, Yukon Canada. Arctic Science, 8, 1320–1339. doi:10.1139/as-2021-0048

Noad, N.C., and Bonnaventure, P.B. 2023. Examining the influence of microclimate conditions on the breakup of surface-based temperature inversions in two proximal but dissimilar Yukon valleys. Canadian Geographies / Géographies canadiennes, 1–17. doi:10.1111/cag.12886

Ruman, C.J., Monahan, A.H., and Sushama, L. 2022. Climatology of Arctic temperature inversions in current and future climates. Theoretical and applied climatology, 150, 121–134. doi:10.1007/s00704-022-04147-9

Disentangling the controls on subsurface thermo-hydrological processes across an Arctic watershed with discontinuous permafrost

Baptiste Dafflon[1], Ian Shirley[1], Chen Wang[1], Sebastian Uhlemann[1], Craig Ulrich[1], Stijn Wielandt[1], Sylvain Fiolleau[1], Bob Busey[2], Robert W. Bolton[3], Katrina Bennett[4] & Susan S. Hubbard[3]

[1]*Lawrence Berkeley National Laboratory, Berkeley, California, United States*

[2]*National Oceanic and Atmospheric Administration, Anchorage, Alaska, United States*

[3]*Oak Ridge National Laboratory, Oak Ridge, Tennessee, United States*

[4]*Los Alamos National Laboratory, Los Alamos, New Mexico, United States*

In Arctic regions, understanding the mechanisms controlling soil and groundwater thermo-hydrological behaviors in thawing permafrost is particularly challenging, yet critical for improving the prediction of storage and flux of carbon and water in a changing climate. Here, we analyze the effects of spatial heterogeneity in terrain, soil, permafrost, bedrock and vegetation properties on variability in subsurface heat and water dynamics across a watershed in a discontinuous permafrost environment. In particular, we investigate how snowmelt and rain events are partitioned between surface and subsurface runoff as a function of the thaw layer thickness, talik distribution, and position in the watershed hydrological system. Further, we evaluate the impact of conduction and advection processes associated with changes in water content and flow on the subsurface thermal state. The above analysis relies on a variety of observations, including in-well monitoring data, geophysical imaging, aerial-based mapping of snow depth, a dense monitoring network of soil temperature and snow depth, and stream discharge and weather measurements.

STUDY SITE

The studied watershed located about 40 km northwest of Nome on the Seward Peninsula in Alaska is the subject of extensive investigations by the Next-Generation Ecosystem Experiment (NGEE) Arctic project (Bennett et al. 2022; Léger et al. 2019; Shirley et al. 2022; Uhlemann et al. 2021; Uhlemann et al. 2023). The 2.3 km^2 watershed characterized by a 130 m elevation gradient has three main types of topographic features, including a stream that cuts through the center of the watershed, a midslope region characterized by a series of risers and terraces, and flatter regions at the top and bottom of the watershed characterized by patterned ground (Figure 1). The watershed is covered by low-lying tundra vegetation and patches of deciduous willow shrubs. The mean annual air temperature at Nome Airport (1980–2018; located 35 km from the site) is -2.3°C, and the annual precipitation is 430 mm, with 45% falling as snow (Bennett et al. 2022).

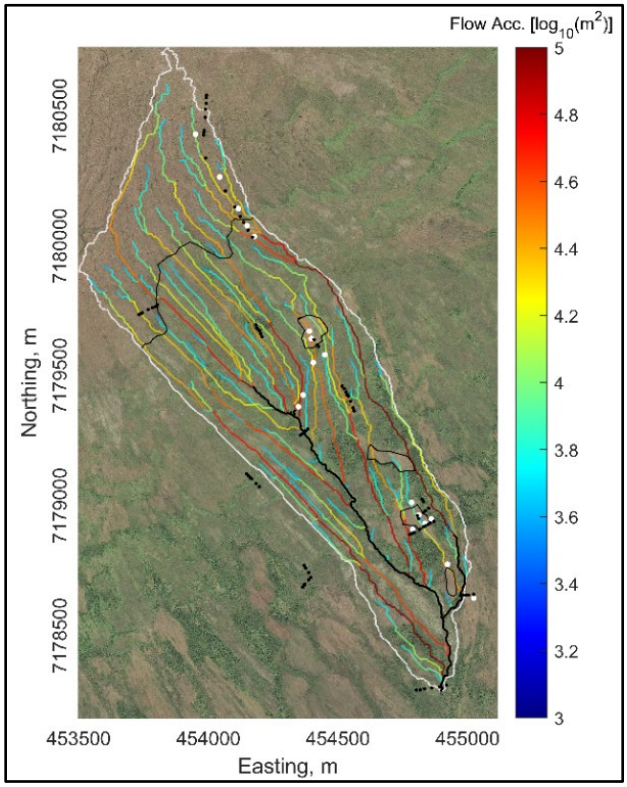

Figure 1. The studied watershed characteristics and monitoring infrastructure. Flow accumulation calculated from a terrain model with streams shown in black. The areas delineated with a black line represent identified permafrost areas. The monitoring infrastructure includes 17 monitoring wells (white dots) and 60 locations with autonomous measurements of snow depth and snow and soil temperature (black dots).

METHOD

We integrate various datasets to investigate the thermo-hydrological dynamics and their controls. Groundwater table and depth-resolved temperature dynamics are monitored at 17 wells (3 to 18 m deep). A network of snow depth and soil temperature measurements (Dafflon et al. 2022) provides soil thaw/freeze depth, snow depth and snowmelt timing at 60 locations. Electrical Resistivity Tomography (ERT)

complements soil temperature data and borehole information to assess bedrock, permafrost and talik distribution across the watershed. Two automated time-lapse ERT transects help capture heat and water dynamics at the interface between permafrost and talik areas. Aerial-based surveys provide snow depth near the peak in Soil Water Equivalent (SWE). Weather stations and discharge data quantify surface hydrological inputs and outputs.

We use the snow depth sensor network, aerial-based maps of snow depth and digital terrain products to estimate the spatio-temporal distribution in SWE and the amount of water released daily during the snowmelt. We compare the estimate with the stream discharge measurements, the soil infiltrability, and the groundwater table fluctuations and gradients to evaluate surface and subsurface runoffs. We similarly assess the partitioning of rain events between surface and subsurface runoffs. Finally, we investigate the mechanisms driving heterogeneity in heat and water dynamics, including topography, snow distribution, subsurface structure and thermal regimes, and groundwater flow across the watershed.

Results and Discussion

Among several results, our observations indicate a strong spatial and temporal heterogeneity in hydro-thermal behaviors driven by soil and permafrost characteristics, position in the hydrological system, and timing and amount of water input. The surface/subsurface water partitioning is strongly impacted by the infiltrability of the soil. While a large fraction of the snowmelt water ends up in surface runoff due to frozen ground limiting infiltration, preferential flow paths in the subsurface enables some surface water to infiltrate into underlying taliks, leading to some cooling effect where a vadose zone is present. As the thawed soil thickness increases during the snow-free season, the amount of water infiltrating into the soil increases, as well as presumably the depth of flowlines. A consistent increase in the difference between the air and stream temperature is observed. During the second part of the thawing season when most taliks are hydrologically connected to the ground surface, water infiltration associated with rain events tends to more strongly impact groundwater dynamics and redistribute heat in the subsurface. Results suggest that this dynamic may accelerate the development of preferential flow paths while reshaping surface and subsurface water distribution that strongly modulates carbon fluxes. Also, the results highlight the critical role of the soil thermal and physical parameters and the topographic position on water and heat transfer.

Furthermore, the results of this study provide insights on the value of surficial indicators for informing on the spatial variability in subsurface thermo-hydrological regimes. Terrain and vegetation structure are revealed as being strong indicators due to their link to subsurface thermal state and soil physical properties, as well as their impact on snow distribution, and surface water flow and accumulation. Overall, our results highlight the heterogeneity and complexity in surface and subsurface hydrology in discontinuous permafrost environments and inform on processes and heterogeneity that need to be represented in ecosystem models to reduce bias in predictions of water and carbon fluxes.

References

Bennett, K.E., Miller, G., Busey, R., Chen, M., Lathrop, E.R., Dann, J.B., Nutt, M., Crumley, R., Dillard, S.L., Dafflon, B., Kumar, J., Bolton, W.R., Wilson, C.J., Iversen, C.M., and Wullschleger, S.D. 2022. Spatial patterns of snow distribution in the sub-Arctic, The Cryosphere, 16: 3269–3293.

Dafflon, B., Wielandt, S., Lamb, J., Mcclure, P., Shirley, I., Uhlemann, S., Wang, C., Fiolleau, S., Brunetti, C., Akins, F.H., Fitzpatrick, J., Pullman, S., Busey, R., Ulrich, C., Peterson, J., and Hubbard, S.S. 2022. A distributed temperature profiling system for vertically and laterally dense acquisition of soil and snow temperature. The Cryosphere, 16: 719–736.

Léger, E., Dafflon, B., Robert, Y., Ulrich, C., Peterson, J.E., Biraud, S.C., Romanovsky, V.E. and Hubbard, S.S. 2019. A distributed temperature profiling method for assessing spatial variability in ground temperatures in a discontinuous permafrost region of Alaska. The Cryosphere, 13: 2853–2867.

Shirley, I.A., Mekonnen, Z.A., Wainwright, H., Romanovsky, V.E., Grant, R.F., Hubbard, S.S., Riley, W.J., and Dafflon, B. 2022. Near-Surface Hydrology and Soil Properties Drive Heterogeneity in Permafrost Distribution, Vegetation Dynamics, and Carbon Cycling in a Sub-Arctic Watershed. Journal of Geophysical Research: Biogeosciences, 127, e2022JG006864.

Uhlemann, S., Dafflon, B., Peterson, J., Ulrich, C., Shirley, I., Michail, S., and Hubbard, S.S. 2021. Geophysical Monitoring Shows that Spatial Heterogeneity in Thermohydrological Dynamics Reshapes a Transitional Permafrost System. Geophysical Research Letters, 48, e2020GL091149.

Uhlemann, S., Shirley, I., Wielandt, S., Ulrich, C., Wang, C., Fiolleau, S., Peterson, J., Lamb, J., Thaler, E., Rowland, J., Hubbard, S.S., and Dafflon, B. 2023. Estimating Permafrost Distribution Using Co-Located Temperature and Electrical Resistivity Measurements. Geophysical Research Letters, 50, e2023GL103987.

High-resolution classified vegetation maps of evolving ice-wedge-polygon terrain, Prudhoe Bay, Alaska

Olivia M. Hobgood[1], Donald A. Walker[1], Martha K. Raynolds[1], Amy L. Breen[2], Julia White[1] & Santosh K. Panda[3]

[1]*Institute of Arctic Biology, University of Alaska Fairbanks, Fairbanks, Alaska, United States*

[2]*International Arctic Research Center, University of Alaska Fairbanks, Fairbanks, Alaska, United States*

[3]*Geophysical Institute, University of Alaska Fairbanks, Fairbanks, Alaska, United States*

Many flat Arctic areas with extensive ice-wedge polygons, such as those of Prudhoe Bay, are undergoing rapid changes due to degradation of top surfaces of ice wedges and formation of a vast number of new ice-wedge thermokarst ponds (Jorgenson et al. 2006; Jorgenson et al. 2015; Raynolds et al. 2014; Liljedahl et al. 2016; Kanevskiy et al. 2022; Walker et al. 2022). A new study in the Prudhoe Bay Oilfield of Alaska is examining landscape evolution in relationship to ice-wedge development and degradation in different surficial-geology units to characterize the evolution of permafrost, ice wedges, landforms, soils, and vegetation and the subsequent degradation of ice wedges and ecosystem changes in this relatively young (ca. 5000 y old) alluvial-plain region of the Central Arctic Coastal Plain (Rawlinson et al. 1993). Vegetation is a key element in the study, and here we present two preliminary classified vegetation maps of: (1) a 5.6-km^2 area at Deadhorse, Alaska, with several different-age surfaces, and (2) a 300-m x 100-m area in one of the oldest portions of the area with abundant thermokarst ponds.

Cover-abundance and environmental data were collected at permanent vegetation plots established in 2021-2022 (Walker et al. 2022). A preliminary vegetation classfication was developed using the vegetation analysis tool JUICE (Tichy 2002). Geospatial analysis was conducted in ArcGIS Pro 3.1 using WorldView-02 pansharpened multispectral imagery with 0.54-m resolution and a LiDAR-derived digital elevation model (DEM) with 0.25-m resolution. Training polygons were drawn on areas of homogenous tundra surrounding the permanent vegetation plots. The WV-02 imagery was normalized for illumination effects (Wu 2004). A coarse resolution DEM was derived from a minimum aggregation of the initial DEM. A “microtopgraphy height” raster file was created by subtracting the aggregation from the initial DEM. A random forest classifier was trained and used to derive the classified output (ESRI 2023).

The classified output is shown at two different scales in Figures 1 and 2. An accuracy assessment is underway and will be included in the poster along with the table analysis, and an area analysis of classified vegetation units by surficial geology units

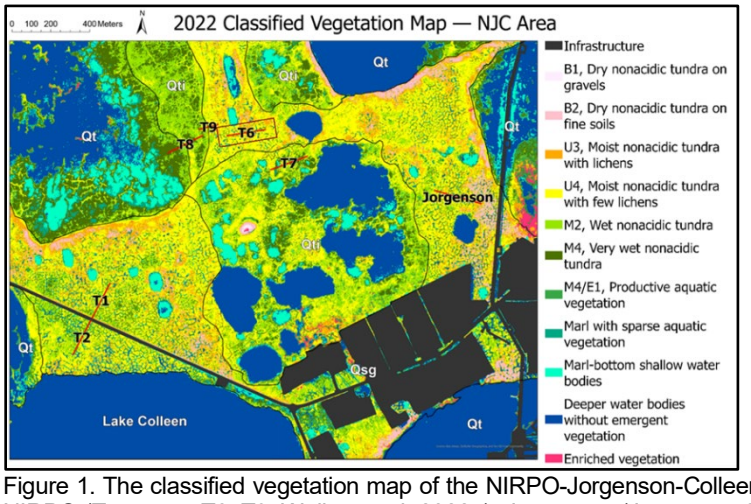

Figure 1. The classified vegetation map of the NIRPO-Jorgenson-Colleen (NJC) Study Area. The area includes the well-described NIRPO (Transects T6–T9, Walker et al. 2022a), Jorgenson (Jorgenson 2015), and Colleen (T1 and T2, Walker et al. 2022b) sites. Study transects T1, T2, T6–T9 and the Jorgenson transect are displayed in red with labels in black. The transects, from which vegetation and training data were collected, are in a variety of different age surficial-geology units mapped by Rawlinson (1993): Qt = lakes and young thaw lake deposits, Qti = ice-rich thaw lake deposits of intermediate age (note that T7 and T8 are present on different age variations of this unit), and Qsg = alluvial plain deposits on older ice-rich surfaces with abundant thermokarst ponds. A detailed vegetation map of T6 is in Figure 2.

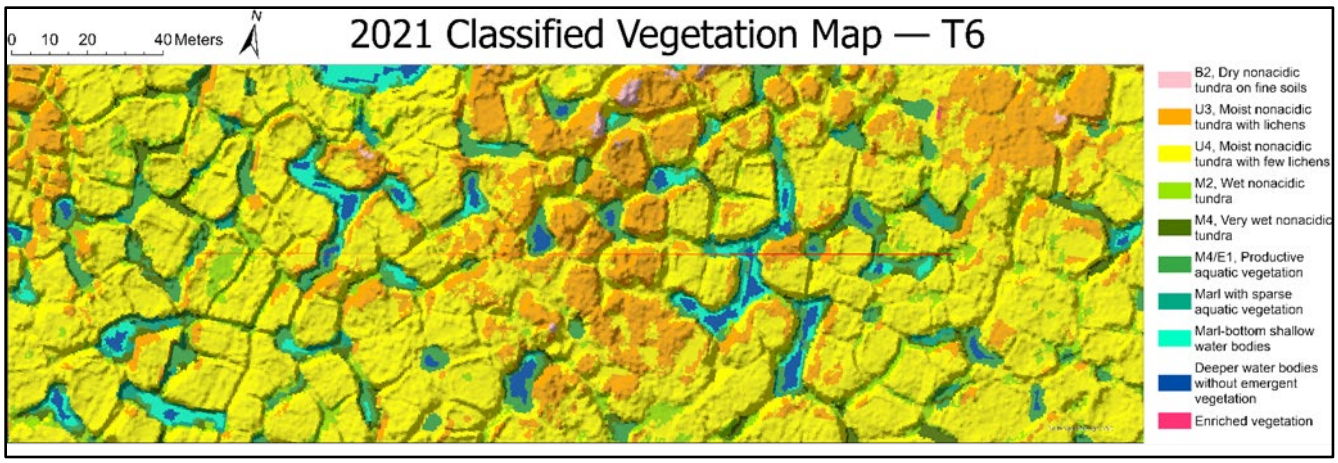

Figure 2. Classified landform and vegetation map shown for the three hectare area surrounding NIRPO Transect 6. The red central transect is 200 m long. 2021 community designations at plot and transect points are overlaid with the same color scheme as the legend to show the overlap between the classification and ground data. A transparent hillshade is overlaid to show topography

This study was funded by the U.S. National Science Foundation Navigating the New Arctic award no. 1928237.

REFERENCES

ESRI. 2023. Forest-based Classification and Regression (Spatial Statistics). URL https://pro.arcgis.com/en/pro-app/3.1/tool-reference/spatial-statistics/forestbasedclassificationregression.htm

Jorgenson, T.M., Shur, Y.L., and Pullman, E.R. 2006. Abrupt increase in permafrost degradation in Arctic Alaska, Geophysical Research Letters, 33: L02503. https://doi.org/10.1029/2005GL024960

Jorgenson, M.T., Kanevskiy, M.Z, Shur, Y.L., et al. 2015. Role of ground ice dynamics and ecological feedbacks in recent ice-wedge degradation and stabilization, Journal of Geophysical Research, 120(11):2280–2297. https://doi.org/10.1002/2015JF003602.

Kanevskiy, M.Z, Shur, Y.L., Walker, D.A., et al. 2022. The shifting mosaic of ice-wedge degradation and stabilization in response to infrastructure and climate change, Prudhoe Bay Oilfield, Alaska, USA, Arctic Science, 8(2):498–530. https://doi.org/10.1139/as-2021-0024.

Liljedahl, A.J., Boike, J., Daanen, R.P., et al. 2016. Pan-Arctic ice-wedge degradation in warming permafrost and its influence on tundra hydrology. Nature Geoscience 9:312–318. https://doi.org/10.1038/ngeo2674

Major, J. 1951. A functional, factorial approach to plant ecology. Ecology 32:392–412. https://doi.org/10.2307/193171

Rawlinson, S.E. 1993. Surficial geology and morphology of the Alaskan Central Arctic coastal plain. Alaska Division of Geology and Geophysical Surveys, Report of Investigations 93-1. https://doi.org/10.14509/2484

Raynolds, M.K, Walker, D.A., et al. 2014. Cumulative geoecological effects of 62 years of infrastructure and climate change in ice-rich permafrost landscapes, Prudhoe Bay Oilfield, Alaska, Global Change Biology, 20(4):1211–1224. https://doi.org/10.1111/gcb.12500.

Tichy, L. 2002. JUICE, software for vegetation classification. Journal of Vegetation Science 13: 451–453. https://doi.org/10.1111/j.1654-1103.2002.tb02069.x

Walker, D.A., Kanevskiy, M., Breen, A.L., et al. 2022a. Observations in ice-rich permafrost systems, Prudhoe Bay Alaska. AGC Data Report AGC22-01. doi:10.18739/A28G8FK0H

Walker, D.A., Raynolds, M.K., Kanevskiy, M.Z., et al. 2022b. Cumulative impacts of a gravel road and climate change in an ice-wedge-polygon landscape, Prudhoe Bay, Alaska. Arctic Science 8:1040–1066. https://doi.org/10.1139/as-2021-0014

Wu, C. 2004. Normalized spectral mixture analysis for monitoring urban composition using ETM+ imagery. Remote Sensing of Environment 93:480–492. https://doi.org/10.1016/j.rse.2004.08.003

Examining permafrost detection and validation techniques in thermally complex, mountainous terrain: a case study in the Ogilvie Mountains north-central Yukon, Canada

Ria Nicholson & Philip P. Bonnaventure

Department of Geography and Environment, University of Lethbridge, Lethbridge, Alberta, Canada

Permafrost thaw-related geohazards are increasing the need for a comprehensive understanding of permafrost distribution. However, precise mapping of permafrost is challenging. Unlike other aspects of the cryosphere, permafrost cannot be directly detected with optical remote sensing (Obu et al. 2019), and the potential for highly variable temperatures over short horizontal distances (Garibaldi et al. 2021) make obtaining sufficient point data difficult. In addition, many logistical constraints are associated with collecting ground temperature data, leading to a reliance on models. However, all models are constrained by the quality of data which inform their parameters, and observations of ground temperature are spatially and temporally fragmented (Anisimov and Zimov 2021). Mountainous permafrost zones are especially challenging to characterize due to extreme thermal heterogeneity. This produces differing land cover types which conduct heat variably over short horizontal distances (Etzelmüller 2013). This issue is especially prevalent in the Ogilvie Mountains, where the continental, high latitude and mountainous terrain has modified the subarctic climate with both topographic shading and intense cold-air drainage (Burn et al. 2015). As a result, the slopes are subject to extremely powerful surface-based temperature inversions (SBIs) which cause temperature to increase with height rather than decreasing (Noad and Bonnaventure 2022). Therefore, the slopes defy expectations of standard elevation-based cooling (-6.5 °C km^{-1}). Instead, the warmest annual temperature averages are seen at mid elevation, while the coldest annual are seen in the valley bottoms (Bonnaventure et al. 2012). This causes them to be at odds with parameter constraints on typical permafrost models.

Objective

The goals of this research are to analyze best practice methodology for ground truthing in thermally complex mountainous terrain. Ground truthing refers to one's ability to validate the presence of permafrost physically or thermally in situ. Additionally, we aim to characterize the permafrost thermal state and distribution within the study area.

Study area

The study area is located in two vegetatively dissimilar valleys approximately 10 km apart along the Dempster Highway (WS01 and WS02) (Noad et al. 2022). These valleys both show extensive presence of wintertime SBI with continuous permafrost. The major difference being that WS01 is treed while WS02 is treeless and dominated by felsenmeer slopes.

Methods

Since 2017, an expanding climatological network of ground temperature nodes (GTNs) and air temperature stations have been installed along elevational transects throughout the valleys with the goal of comparing surface offsets and determining the role of SBIs in permafrost distribution (Noad and Bonnaventure 2022). Although permafrost has been modeled as continuous, substantial thermal heterogeneity exists. The fundamental issue presented in this landscape is validating the presence of permafrost or determining its thermal state due to the nature of the substrate. In 2022, a database of all sites was created to compare offsets between mean annual air and ground temperatures with elevation and land cover type. These land cover types are categorized as: 1) treed organic mat, 2) tundra organic mat, 3) vegetated periglacial facies, 4) periglacial facies, 5) treed clast ground, and 6) ridge top. The thick organic mat at these sites is an extremely significant microclimate variable, as it provides an intense insulating effect which results in ecosystem protected permafrost (Shur and Jorgensen 2007). A preliminary, binary prediction of permafrost was made, with special considerations made towards sites with a mean annual ground surface temperature (MAGST) >0 °C but potential for ecosystem protected permafrost. 50 sites covering different land cover types and elevations throughout the valleys were then selected as cryotic assessment sites (CAS). Several sites were expected to be unviable for ground truthing due to coarse substrates but were chosen for testing for falsification.

The thermal gradients method was chosen as the primary method of investigation. Thermal gradients is

a direct method of permafrost testing which involves placing several sensors in the ground in fixed intervals to extrapolate the probability of permafrost at depth (e.g., Holloway and Lewkowicz 2020). A hollow aluminum avalanche probe was wired to contain three thermistors, placed 25 centimeters apart. Holes were drilled through the aluminum at the depth of each thermistor to reduce insulation. Through ice-point calibration testing, it was determined that the thermistors were accurate to ± 0.3 °C.

At each CAS, a pilot hole was made using a frost probe within 1 meter of the pre-existing temperature sensor on the same land cover type to ensure consistency. The thermistors were connected to an ONSET MX1105 logger and then inserted to the maximum possible depth. A fourth thermistor was placed <1 cm below the ground surface to record surface temperature without influence of solar radiation. The four channels remained in the ground until all four channels reached equilibrium (<0.1 °C/minute) to a maximum of 15 minutes. If the ground temperature reached ≤0.5 °C, permafrost was recorded as present.

Preliminary results

The thickness of the active layer in both valleys hindered field progress throughout the season and resulted in what we believe to be several false negatives. Of the 58 cryotic assessment sites which were tested, 11 were directly confirmed as being positive for permafrost, with temperatures between -0.04 °C and 0.48 °C recorded between 40-184 cm depth below the surface. 2 of these sites had a MAGST greater than 0 °C, at 0.66 °C and 0.98 °C respectively. All these sites were in land cover categories with thick organic mat cover. The reasons for this are twofold. Firstly, CAS with thick organic mat cover were more likely to be penetrable to reasonable depth with ground truthing instruments, without the interference of roots or clasts. Secondly, the insulating nature of the organic mat cover prevented active layer depth from exceeding the length of the probe. Three separate thaw features were discovered in-situ in the field which were not present in 2021, with fissures revealing active layer depths up to 130 cm deep. Permafrost was confirmed 40-50 cm below the base of these fissures at all three sites. Therefore, we believe that a number of the sites which did not produce the ≤0.5 °C isotherm were false negatives, especially those in areas with near-zero MAGST in thick organic mat landcover types. To compensate for this discrepancy, all other CAS will be analysed with simple linear regression, to determine the likelihood of permafrost temperatures at depth based on the gradient derived from field measurements.

References

Anisimov, O., and Zimov, S. 2021. Thawing permafrost and methane emission in Siberia: Synthesis of observations, reanalysis, and predictive modeling. Ambio, 50(11), 2050–2059.

Bonnaventure, P.P., Lewkowicz, A.G., Kremer, M., and Sawada, M.C. 2012. A Permafrost Probability Model for the Southern Yukon and Northern British Columbia, Canada. Permafrost and Periglacial Processes, 2012;23(1); 52–68. doi:10.1002/ppp.1733

Burn, C.R., Moore, J., O'Neill, B., Hayley, D., Trimble, J., Calmels, F., et al. 2015. Permafrost characterization of the Dempster Highway, Yukon and Northwest Territories. In 7th Canadian Permafrost Conference.

Etzelmüller, B. 2013. Recent Advances in Mountain Permafrost Research. Permafrost and Periglacial Processes, 24: 99–107.

Garibaldi, M.C., Bonnaventure, P.P., and Lamoureux, S.F. 2021. Utilizing the TTOP model to understand spatial permafrost temperature variability in a high arctic landscape, cape bounty, Nunavut, Canada. Permafrost and Periglacial Processes, 32(1), 19–34.

Holloway, J.E., and Lewkowicz, A.G. 2020. Half a century of discontinuous permafrost persistence and degradation in western Canada. Permafrost and Periglacial Processes, 31(1), 85–96.

Noad, N.C., and Bonnaventure, P.P. 2022. Surface temperature inversion characteristics in dissimilar valleys, yukon canada. Arctic Science, 8(4), 1320–1339.

Obu, J., Westermann, S., Bartsch, A., Berdnikov, N., Christiansen, H.H., Dashtseren, A., et al. 2019. Northern Hemisphere permafrost map based on TTOP modelling for 2000–2016 at 1 km^2 scale. Earth-Science Reviews, 193, 299–316.

Shur, Y.L., and Jorgenson, M.T. 2007. Patterns of permafrost formation and degradation in relation to climate and ecosystems. Permafrost and Periglacial Processes, 18(1), 7–19.

Preliminary results on the impact of water content on the thermal conductivity of permafrost ground covers

Konstantin Ozeritskiy & Jocelyn L. Hayley
Civil Engineering Department, University of Calgary, Calgary, Alberta, Canada

Permafrost regions, characterized by continuous or discontinuous layers of perennially frozen ground, are crucial components of the Earth's cryosphere. Understanding the thermal behavior of permafrost is essential for environmental studies, infrastructure development, and climate change assessments. A significant factor in the heat exchange within permafrost regions is the role of ground covers, including moss, peat, lichen, and forest litter.

Moreover, ground covers can exist in a range of moisture conditions, which in turn affects their thermal properties. The moisture-dependent thermal conductivity of these ground covers is crucial in determining how heat is exchanged between the Earth's surface and the atmosphere, particularly in permafrost regions. However, these relationships are not well understood. In this study, we addressed these knowledge gaps and focused on developing a relationship between thermal conductivity and water content for different ground covers in permafrost regions. This work is an important step towards quantifying the thermal properties of dynamically changing ground cover in permafrost regions.

Background

The thermal properties of ground covers, such as moss, lichen, and forest litter, have been the subject of several studies. However, most research has focused on their thermal conductivity under unfrozen condition (O'Donnell et al. 2009; Soudzilovskaia et al. 2013), while limited data is available for the cold season. Furthermore, many studies lack comprehensive information on the physical properties (water content and density) at which ground covers were examined (Fukui 2008; Isaev et al. 2022). These gaps in knowledge make it challenging to generalize existing relationships and apply them to real-world situations effectively.

Studies by Chernyadyev et al. (1984) and Gavriliev (2004) have provided insights into the thermal properties of various types of moss (mainly sphagnum) in different arctic regions. Their work has shown variations in thermal conductivity coefficients depending on water content, which emphasizes the importance of considering moisture in understanding the behavior of ground covers.

In the context of understanding the thermal properties of ground covers in permafrost regions, it is essential to highlight the consistent relationship between thermal conductivity and water content, as demonstrated by O'Donnell et al. (2009) and Soudzilovskaya et al. (2013). These findings reveal that this relationship remains stable across various moss types, degrees of organic soil decomposition, and density, indicating a non-species-specific and linear dependency on water content in unfrozen state.

Methodology

Our study employs a comprehensive methodology that includes field sampling, laboratory testing, empirical formula development, model validation, and sensitivity analysis. The primary focus is on developing a relationship between thermal conductivity and water content for different ground covers in permafrost regions.

Moss samples were collected at various sites with thermal boreholes in Northern Manitoba along the Hudson Bay Railway. For laboratory testing, volumetric water content (VWC) was controlled by using soil moisture sensor ECH$_2$O EC-5. Thermal conductivity was measured using a thermal probe KD2PRO. Freezing and subsequent thermal conductivity measurements were also conducted.

Based on laboratory studies, graphs depicting the relationship between thermal conductivity and VWC were built. A comparison was made with previous relationships described in the literature, and data analysis produced an empirical formula for calculating the thermal conductivity of vegetation cover based on VWC. This formula enhances our understanding of how moisture affects thermal conductivity.

Next, this study used a modelling approach using transient analysis in TEMP/W software, employing a Convective Surface boundary condition to simulate soil-climate interactions. The thermal model was validated by comparing simulated temperature fields with field-measured data. Additionally, sensitivity analysis was conducted to assess the impact of thermal conductivity-moisture relationships on frozen soil behavior. This analysis evaluates the effects of water content determination errors on the thermal modelling results, identifying the empirical equation's range of applicability and limitations.

RESULTS AND DISCUSSION

The results of this research provide valuable insights into the thermal conductivity of ground covers in permafrost regions, considering their dependence on volumetric water content. Figure 1 displays the values measured in the laboratory and the trend derived from these data. It also shows the limits of uncertainty resulting from the measurement methods used. When the VWC changes from 7 to 82%, thermal conductivity in the unfrozen state varies from 0.108 to 0.556 W/mK, and in the frozen state with VWC ranging from 12 to 78%, thermal conductivity ranges from 0.125 to 1.883 W/mK.

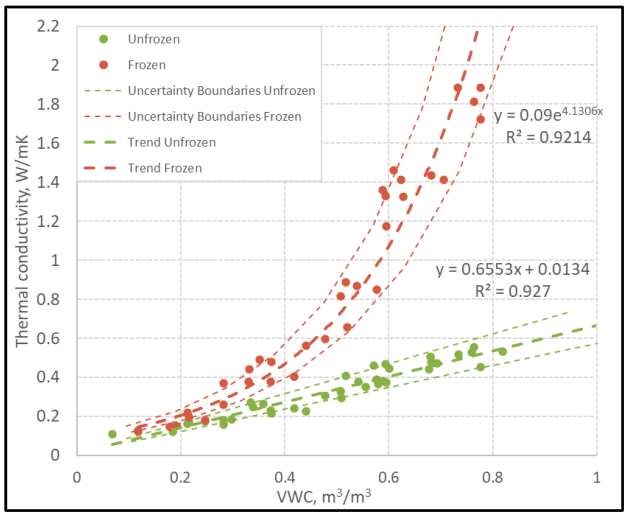

Figure 1. Dependence of thermal conductivity of the ground cover on the volumetric water content.

This dependence can be incorporated into the surface boundary condition of the thermal model by means of the heat transfer coefficient (Eq. 1). Under these circumstances, changes in the water content of ground cover can be determined using satellite data or simulating using Land Surface Models.

$$h_{total} = 1/(1/h+R_{snow}+l_{veg}/\lambda_{veg}) \quad [1]$$

where h is the heat transfer coefficient, W/(m^{2}K), R_{snow} is the thermal insulance of snow cover, (m^{2}K)/W, and l_{veg} is the height of ground cover, m, λ_{veg} is the thermal conductivity of ground cover, W/(mK).

By developing an empirical dependency and validating it through thermal modelling, this study aims to enhance our ability to predict the thermal regime of frozen soils.

CONCLUSION

This research bridges critical knowledge gaps regarding the thermal behavior of ground covers in permafrost regions, particularly during the cold season. By establishing a relationship between thermal conductivity and water content and validating it through thermal modelling, this study contributes to a more accurate understanding of ground cover effects. The practical implication of this work is that it enables more precise modelling of energy balance during design and construction processes, especially when ground covers are removed. This knowledge can inform decisions about thermal regulation in infrastructure projects within permafrost regions, ultimately leading to more sustainable and environmentally conscious construction practices.

ACKNOWLEDGEMENTS

Funding for this project was provided by Transport Canada's National Trade Corridors Fund and the Natural Sciences and Engineering Research Council of Canada (NSERC). We thank Arctic Gateway Group for their ongoing partnership and support of the project.

REFERENCES

Chernyadiev, V.P, Chekhovskiy, A.L., Stremyakov, A.Y., and Pakulin, V.A. 1984. Forecast of the thermal state of soils during the development of northern regions. Nauka, Moscow, Russia.

Fukui, K., Sone, T., Yamagata, K., Otsuki, Y., Sawada, Y., Vetrova, V., and Vyatkina, M. 2008. Relationships between permafrost distribution and surface organic layers near Esso, central Kamchatka, Russian Far East. Permafrost and Periglacial Processes, 19(1): 85–92. doi:10.1002/ppp.606

Gavriliev, R. 2004. Thermophysical properties of natural environment components in permafrost. Russian Academy of Science, Novosibirsk, Russia.

Isaev, V., Kioka, A., Kotov, P., Sergeev, D.O., Uvarova, A., Koshurnikov, A., and Komarov, O. 2022. Multi-Parameter Protocol for Geocryological Test Site: A Case Study Applied for the European North of Russia. Energies (Basel), 15(6): 2076. doi:10.3390/en15062076

O'Donnell, J.A., Romanovsky, V.E., Harden, J.W., and McGuire, A.D. 2009. The Effect of Moisture Content on the Thermal Conductivity of Moss and Organic Soil Horizons from Black Spruce Ecosystems in Interior Alaska. Soil Science, 174(12): 646–651. doi:10.1097/SS.0b013e3181c4a7f8

Soudzilovskaia, N.A., Bodegom, P.M., Cornelissen, J.H., and Schweitzer, J. 2013. Dominant bryophyte control over high-latitude soil temperature fluctuations predicted by heat transfer traits, field moisture regime and laws of thermal insulation. Functional Ecology, 27(6): 1442–1454. doi:10.1111/1365-2435.12127

Unraveling the impacts of snowpack dynamics on soil temperatures and biogeochemical processes in two discontinuous permafrost watersheds

Ian Shirley, Chen Wang, Zelalem Mekonnen, William J. Riley & Baptiste Dafflon
Lawrence Berkeley National Laboratory, Berkeley, California, United States

In high-latitude discontinuous permafrost environments, spatial variation in snow depth plays an important role in shaping landscape heterogeneity. Via its impact on soil thermal regimes, snow depth variation strongly influences hydrological processes, vegetation dynamics, and carbon cycling (Shirley et al. 2022). Better understanding of these links and their landscape variability requires collection of spatially and temporally dense hydro-geochemical data, which is made challenging by remote field locations and harsh environmental conditions. Here, we use a combination of field observations and model experiments to explore the role that snow regime variability plays in shaping variability of other high-latitude ecosystem processes. We analyze spatially and temporally dense measurements of snow and soil temperature collected using novel sensor technology (Dafflon et al. 2022) in two discontinuous permafrost watersheds in Alaska and perform model experiments using ecosys, a state-of-the-art ecosystem model.

Study site

This study focuses on two watersheds underlain by discontinuous permafrost on the Seward Peninsula in Alaska, both of which have been extensively investigated by the Next-Generation Ecosystem Experiment (NGEE) Arctic project (Uhlemann et al. 2021; Shirley et al. 2022; Mekonnen et al. 2021). The first (Teller 27), located about 40 km northwest of Nome, covers an area of approximately 2.3 km^2, exhibits a 130 m elevation gradient, and is covered by low-lying tundra vegetation interspersed with patches of tall willow shrubs. This watershed has a mean annual air temperature of -2.1 °C. The second watershed (Kougarok) is located about 100 km north of Nome, covers an area of approximately 1.4 km^2, exhibits a 40 m elevation gradient, and is covered by low-lying tundra vegetation interspersed with patches of tall alder shrubs. This watershed is colder, with a mean annual air temperature of -3.7 °C.

Methods

We use novel distributed sensor technology to acquire spatially and temporally dense measurements of soil temperature, snow temperature, and snow depth across each watershed (Dafflon et al. 2022). The sensors, which were designed in-house to optimize data accuracy, minimal power consumption, and low total cost, provide collocated temperature measurements from 1.4 m above the ground surface to 1.2 m below the ground surface in 5-10 cm increments every 15 minutes. We deployed these sensors at 98 locations across the Teller 27 watershed, and at 47 locations across the Kougarok watershed. Here we present data collected from each sensor between June 2021 and September 2023.

For the model experiments, we use ecosys, which is a mechanistic, process-rich ecosystem model that has been successfully tested across the high-latitudes (Shirley et al. 2021). North American Regional Reanalysis (NARR) data are bias-corrected using weather station data available at each watershed and used to force the model at an hourly time-step. Observed increases in snow depth throughout the winter were used to generate winter precipitation inputs in order to reproduce spatial variability in snow depths. In addition to varying snow depths, we also perform additional sensitivity analyses, varying soil hydro-thermal properties and vegetation cover to determine how these factors interact with snow depth variation to influence soil temperatures and biogeochemical processes.

Results and discussion

We find that variation in annual maximum snow depth is strongly correlated with mean annual soil temperatures at both the Teller 27 and the Kougarok watersheds. However, this relationship is stronger at the Kougarok watershed, where air temperatures are colder in the winter and snow cover develops later in the fall. We also find that inter-annual variability in snow regimes drives inter-annual variability in near-surface soil temperatures during the growing season. While peak snow depths were similar for the two years of data, later snow melt in 2023 delayed soil thawing and decreased the number of days with warm near-surface soil temperatures.

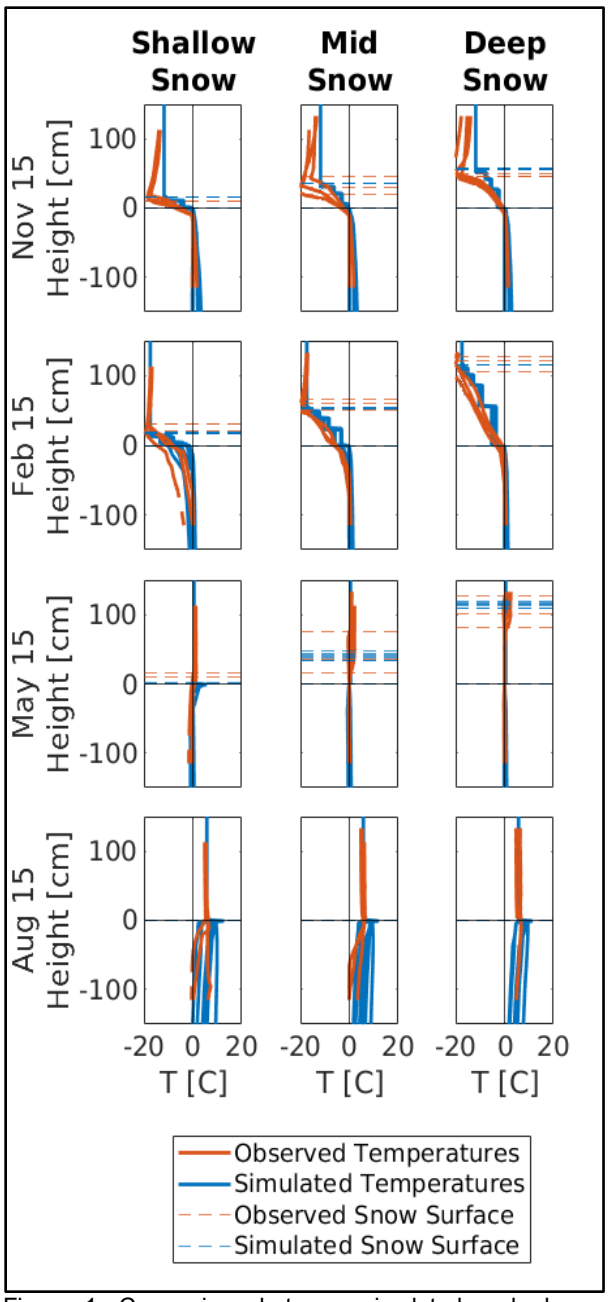

Figure 1. Comparison between simulated and observed snow depth, snowpack temperatures, and soil temperatures. Observed (red) and simulated (blue) snow depths (dashed lines) and snow and soil temperatures (solid lines) are shown for a subset of sensor locations characterized by shallow, mid, and deep snowpacks at the Teller 27 watershed. Daily means of each variable are shown for November 15, 2021, February 15 2022, May 15, 2022, and August 15, 2022.

We find good agreement between modeled and observed snowpack dynamics (snow depths and snow temperature profiles) throughout both years of data. We find that, in addition to snow depth, soil thermal-hydrological characteristics, in particular organic layer thickness and drainage, have a strong impact on simulated soil temperatures. This model result is used to explain why locations with similar snow depths can have different soil thermal regimes. We then use the model to explore the impact of varying snow depths on biogeochemical regimes. We find that spatial variation in snow depths is associated with variation in rates of biogeochemical processes (e.g., more primary productivity in areas of deep snow), and that inter-annual variation in snowmelt timing has a strong impact on growing season dynamics (e.g., leaf out date, growing season length).

The results presented here highlight the strong interaction between snow and soil temperatures in discontinuous permafrost environments, and demonstrate that these interactions vary across watersheds and years. Also emphasized is the important role that subsurface hydrology plays in determining soil thermal and biogeochemical responses to variation in snowpack dynamics. Overall, these results point to the need for more comprehensive environmental monitoring that targets the interaction between snow, water, permafrost, and carbon in high-latitude ecosystems.

References

Dafflon, B., Wielandt, S., Lamb, J., Mcclure, P., Shirley, I., Uhlemann, S., Wang, C., Fiolleau, S., Brunetti, C., Akins, F.H., Fitzpatrick, J., Pullman, S., Busey, R., Ulrich, C., Peterson, J., and Hubbard, S.S. 2022. A distributed temperature profiling system for vertically and laterally dense acquisition of soil and snow temperature. The Cryosphere, 16: 719–736.

Mekonnen, Z.A., Riley, W.J., Grant, R.F., Salmon, V.G., Iversen, C.M., Biraud, S.C., Breen, A.L. and Lara, M.J., 2021. Topographical controls on hillslope-scale hydrology drive shrub distributions on the Seward Peninsula, Alaska. Journal of Geophysical Research: Biogeosciences, 126(2), p.e2020JG005823.

Shirley, I.A., Mekonnen, Z.A., Grant, R.F., Dafflon, B., Hubbard, S.S., and Riley, W.J. 2022. Rapidly changing high-latitude seasonality: implications for the 21st century carbon cycle in Alaska. Environmental Research Letters, 17(1), p.014032.

Shirley, I.A., Mekonnen, Z.A., Wainwright, H., Romanovsky, V.E., Grant, R.F., Hubbard, S.S., Riley, W.J., and Dafflon, B. 2022. Near-Surface Hydrology and Soil Properties Drive Heterogeneity in Permafrost Distribution, Vegetation Dynamics, and Carbon Cycling in a Sub-Arctic Watershed. Journal of Geophysical Research: Biogeosciences, 127, e2022JG006864.

Uhlemann, S., Dafflon, B., Peterson, J., Ulrich, C., Shirley, I., Michail, S., and Hubbard, S.S. 2021. Geophysical Monitoring Shows that Spatial Heterogeneity in Thermohydrological Dynamics Reshapes a Transitional Permafrost System. Geophysical Research Letters, 48, e2020GL091149.

Two decades of subsurface soil moisture and temperature in the active layer above permafrost, north slope of Alaska

Vasily Tolmanov[1] & Frederick Nelson[1,2]

[1]*Department of Geography, Environment and Spatial Sciences, Michigan State University, East Lansing, Michigan, United States*

[2]*Department of Earth, Environmental and Geographical Sciences, Northern Michigan University, Marquette, Michigan, United States*

Active layer thickness (ALT) above permafrost is one of the essential climate monitoring variables (Brown et al. 2000). This highly dynamic layer thaws each summer and re-freezes each winter. Formation of the active layer strongly depends on a variety of environmental factors. The core factors influencing the depth of the summer thaw are the amount of incoming heat penetrating the frozen soil, moisture regime of soils, insulating effect of the snow cover and vegetation, thickness of the transient layer, etc. (Oblogov et al. 2023; Shur 1988; Shur et al. 2005). Soil moisture plays a very important role in active layer formation. The thickness of the active layer can be influenced by soil moisture in two ways: (a) alterations in soil thermal properties and (b) latent heat related to phase transition. Typically, latent heat has a more significant impact, especially when there is increased ground ice content, requiring more heat for phase transitions and resulting in a thinner active layer the subsequent summer.

NRCS-USDA (National Resources Conservation Service, United States Department of Agriculture) soil temperature and moisture records from northern Alaska have been used to assess the impact of both thermal and moisture parameters on the formation of the active layer thickness for almost three decades in different geographic locations. Nine experimental soil stations were implemented on the North Slope of Alaska in 1996. They are located in the Prudhoe Bay area, Sagwon Hills, Barrow, and Atqasuk, and represent typical landscape conditions for two physiographic provinces: the Arctic Coastal Plain and the Arctic Foothills. These stations (Figure 1) measure and record climate parameters that include air temperature, soil temperature at various depths (mostly in the active layer (AL)), as well as soil water content at 10, 25, and 40 cm depths. Vitel sensors were used for measuring the soil moisture in the soil at three depths, Campbell 107b temperature sensors were used at the same depths for the thermal measurements. These sites are located close to the CALM (Circumpolar Active Layer Monitoring) grids or smaller experimental 1 ha plots, so the long-term ALT (Active Layer Thickness) data are available. The CALM Program provides data derived at the end of the thawing season in series of experimental sites representing climatic and landscape conditions for 28 consecutive years using a standardized methodology (Brown et al. 2000). Maintenance of the stations and data collection were performed annually during the CALM field season. Daily averaged data were used.

Data from moisture loggers installed in 2021 and 2022 by CALM personnel are used for verification of the measurements. The data show that most of the summertime uppermost layer of soils stay oversaturated, especially at the sites located on the coastal plain, starting from the rapid snowmelt events. Variation of the temperature and moisture is much stronger in the top 10-15 cm of the soil profile.

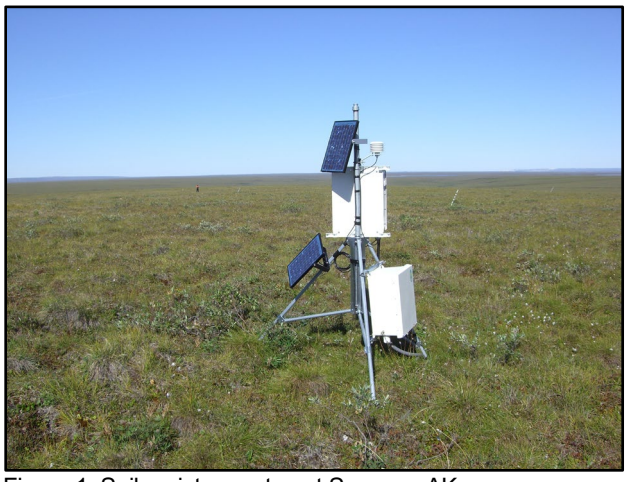

Figure 1. Soil moisture setup at Sagwon, AK.

Data show that in certain years snow cover protects the top of the active layer from winter freezing, promoting a thicker active layer at the Foothills sites. Even with an insufficient amount of heat penetrating the soil during below-average summers, ALT usually is higher than average (above the 20-year mean value). Years with an extremely thin active layer are clearly indicating the lack of the summer heat penetrating the ground and complete refreezing of the active layer during the previous winters. For example, in Sagwon, three absolute active layer minima, 2005; 2014, and

2020, were produced during the three coldest summers (Figure 2). We hypothesize that active layer thickness formation in one record year can impact the system for years afterward. In oversaturated conditions, summers with the extreme amount of heat and extreme active layer thicknesses can lead to extensive ice segregation during the fall freezing, which will not allow formation of a thicker active layer in subsequent summers. This appears to have occurred at the Betty Pingo (U7A) site in 1998 (ALT record for 28 years of observation), which slowed down ALT increase rates for 3 to 5 years afterwards. We observe a drop in soil moisture after the snowmelt and drier conditions of the summer for sites that have more variations in soil moisture during the summer period, which is related to the transpiration effect from the vegetation. The same effect was described at one of the West Siberian and Middle Siberian sites (Oblogov et al. 2023; Grebenets et al. 2021). Generally, this leads to the formation of a thicker ALT. Thus, the record year in Sagwon (2011, 65 cm to 57 cm average at the site for 23 years of observation) shows the cumulative impact of environmental factors: higher soil temperature during the wintertime (including the 40 cm depth, temperature values stayed positive until March), presumably due to thick snow cover, drier and relatively warmer conditions during summer (Figure 2).

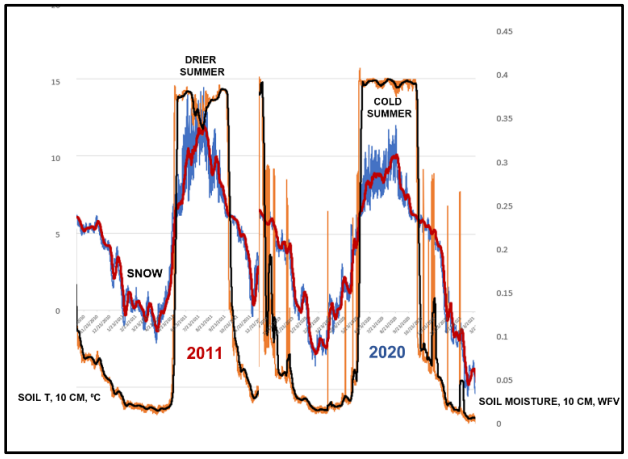

Figure 2. Temperature and moisture records for two extreme years (2011 – red, 2020 - blue) with maximum and minimum ALT at the Sagwon site at 10 cm depth. Blue line and red lines represent temperature and weekly moving average. Orange and black represent soil moisture and weekly moving average.

There is a noticeable lag between thawing at a certain depth and moisture increase at other depths. Moisture variation at 40 cm is less pronounced at all the sites. Soils at this depth remain oversaturated most of the time. Temperature variability is more pronounced and depends on the geographic location of the monitoring site.

Long-term data on the moisture regime and the temperature record of the soils in the active layer at different depths helps to assess thaw progression rates and explain the mechanism of the AL formation every year, which is essential for local and regional permafrost forecasting and modelling.

REFERENCES

Brown, J., Hinkel, K.M., and Nelson, F.E. 2000. The Circumpolar Active Layer Monitoring (CALM) program: research designs and initial results. Polar Geography 24: 165–258.

Grebenets, V.I., Tolmanov, V.A., and Streletskiy, D.A. 2021. Active Layer Dynamics Near Norilsk, Taimyr Peninsula, Russia. GEOGRAPHY, ENVIRONMENT, SUSTAINABILITY.;14(4):55-66. https://doi.org/10.24057/2071-9388-2021-073

Nyland, K.E., Shiklomanov, N.I., Streletskiy, D.A., Nelson, F.E., Klene, A.E., and Kholodov, A.L. 2021. Long-term Circumpolar Active Layer Monitoring (CALM) program observations in Northern Alaskan tundra, Polar Geography, 44, 167–185. https://doi.org/10.1080/1088937X.2021.1988000

Oblogov, G.E., Vasiliev, A.A., Streletskiy, D.A., Shiklomanov, N.I., and Nyland, K.E. 2023. Localized Vegetation, Soil Moisture, and Ice Content Offset Permafrost Degradation under Climate Warming. Geosciences 13, 129. https://doi.org/10.3390/geosciences13050129

Shur, Y.L. 1988. Upper Horizon of Permafrost and Thermokarst. Nauka, Moscow (in Russian).

Shur, Y., Hinkel, K.M., and Nelson, F.E. 2005. The transient layer: Implications for geocryology and climate-change science, Permafrost Periglac, 16, 5–17, https://doi.org/10.1002/ppp.518.

Long-term snow trends in an Alaskan watershed

Anna Wagner[1], Zoe Courville[2], Nawa Raj Pradhan[3] & Ross Alter[2]

[1]*Cold Regions Research and Engineering Laboratory (CRREL), Fort Wainwright, Alaska, United States*

[2]*CRREL, Hanover, New Hampshire, United States*

[3]*Coastal and Hydraulics Laboratory (CHL), Vicksburg, Mississippi, United States*

Precipitation plays a crucial role in shaping ecosystem structures and functions. Snow, specifically, has an outsized influence on the cold region ecosystems' hydrological and thermal energy budgets. When present, snow shields the ground from low winter temperatures. Its arrival and departure influence the surface and subsurface ground energy balance. In Interior Alaska, where permafrost temperatures are at a critical threshold, changes in snow cover can have a negative impact. To assist with predicting the extent of this impact, and how it might influence the ground thermal balance and water runoff, we evaluated 40-year snow trends at an interior Alaska watershed.

Methods

We used SnowModel (Liston and Elder 2006; Liston et al. 2020), a spatially distributed snow model, to simulate daily time series that spanned 40 years from 1 September 1981 to 31 August 2021. Our simulation domain was about 14,700 km^2 and we used 100 m grid cells (n_x = 1490; n_y = 988). The snow model was forced using reanalysis input data sets (air temperature, wind speed and direction, relative humidity, and precipitation) associated with different atmospheric forcing conditions. In our study, we used the European Centre for Medium-Range Weather Forecasts (ECMWF) Reanalysis, 5th Generation (ERA5) forcing dataset. To get an understanding of the difference in applying a variety of forcing datasets, we compared the results with NASA's Modern Era Retrospective analysis for Research and Applications, Version 2 (MERRA-2).

Results

The snow modeling indicates a downward trend in total snow days (Figure 1), mean max snow depths (Figure 2), and snowfall (results not shown). The mean total snow days for the time period averages from about 194 to 258 days over the study area (Figure 1a). The decadal trend of total snow days for the domain is decreasing over the entire domain (Figure 1b). For the MERRA-2 and ERA5 simulations, the domain-average decreases about 7 and 3 days/decade, respectively (Figure 1c). The average difference between the yearly total snow days is about 10 days (-40 to 23 days).

Over the study domain, the mean max snow depth ranged from 23 to 183 cm (Figure 2a). As found with the number of days, the snow depth shows a decadal decrease (Figure 2b). The domain-average max snow depths are decreasing by about 1.5 and 1 cm/decade for the MERRA-2 and ERA5 simulations, respectively (Figure 2c). The yearly average snow depth difference between MERRA-2 and ERA5 is about 22.1 cm (minimum of 7.2 cm and maximum of 47.6 cm).

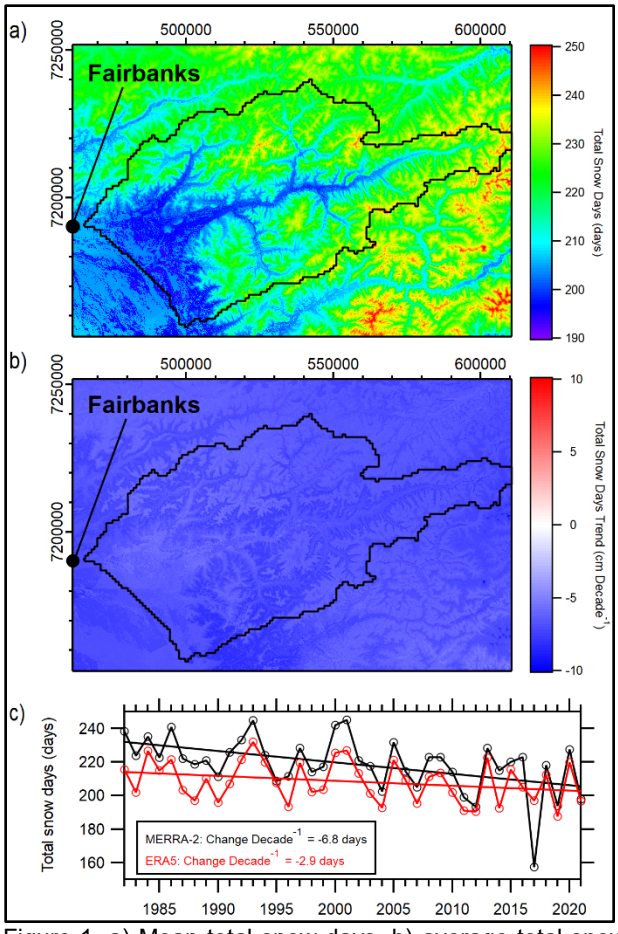

Figure 1. a) Mean total snow days, b) average total snow days trend, and c) yearly domain-averaged number of snow days and trend line for water year (WY) 1982 – 2021. The Chena River watershed is outlined in black.

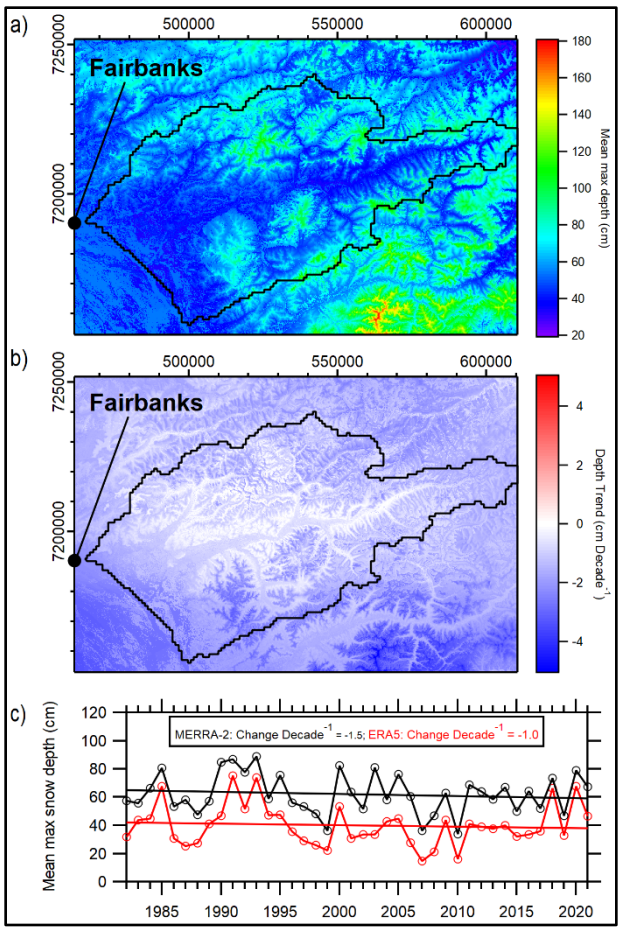

Figure 2. a) Mean max snow depth, b) mean max snow depth trend, and c) yearly domain-averaged max snow depth and trend line for WY 1982 – 2021. The Chena River watershed is outlined in black.

Snowfall also shows a decreasing decadal trend of 0.5 and 0.3 cm for MERRA-2 and ERA5, respectively. We also investigated the trends in rain-on-snow (ROS) events. Up to three ROS events were found in the study domain, with most of these events occurring at lower altitudes (results not shown). We found no apparent trend of the yearly and decadal averages.

Conclusions

Our study has the potential to greatly enhance our understanding of snow distribution in a changing climate. The snowpack dataset presented herein can be used for infrastructure-design purposes. Because the thermal balance of frozen ground is greatly impacted by the snowpack, this dataset is also important when investigating future changes in permafrost degradation. In general, a decreasing trend of both mean max snow depth and total number of snow days is found. There is also a notable difference in trends when forcing the model with the MERRA-2 or the ERA5 atmospheric forcing conditions. Therefore, future studies needs to carefully chose the forcing datasets when simulating snowpacks in cold regions.

Acknowledgements

Funding for this was supported by “Intelligent Environmental Battlespace Awareness” under Project Element Number: 622182 and Project Number 2CX and the US Department of Defense—PE 0602182A and 633463AR4, Applied Research Project ‘Extreme Cold Weather Threats and Dependencies’.

References

Liston, G.E., and Elder, K. 2006. A distributed snow-evolution modeling system (SnowModel). J. Hydrometeorol, 7, 1259–1276.

Liston, G.E., Itkin, P., Stroeve, J., Tschudi, M., Stewart, J.S., Pedersen, S.H., Reinking, A.K., and Elder, K.A. 2020. Lagrangian snow-evolution system for sea-ice applications (SnowModel-LG): Part I—Model description. J. Geophys. Res. Ocean, 125, e2019JC015913.

Monitoring Permafrost Conditions & Processes

12B — Exploring the Roles of Ground Ice on Permafrost Dynamics

Session Chairs: Samuel Gagnon[1], Antoine Séjourné[2] & Daniel Fortier[3]

[1]*Université Laval, Québec City, Québec, Canada*
[2]*Université de Paris Saclay, Orsay, France*
[3]*Université de Montréal, Montréal, Québec, Canada*

Ground ice is one of the main components of permafrost and is often present in excess of the soil's porosity. It is a critical parameter in the permafrost thermal regime due to (1) its high thermal conductivity and latent heat of fusion; (2) dictating thaw settlement potential and therefore thermokarst processes; (3) affecting geotechnical properties to build infrastructure; (4) is an important characteristic to reconstruct climatic conditions and sediment deposition; and (5) plays a central role in periglacial landscape evolution in general. Despite its significance, means of measuring and mapping ground ice accurately remain limited, and its impacts on permafrost landscape dynamics are understudied. With predictions pointing to a warmer, wetter/drier Arctic, it is becoming increasingly important to have a good characterization of ground ice distribution as well as of the processes relating to ground ice formation and melting to better understand the areas that will be most affected.

This session invites speakers to address subjects pertaining (but not limited) to: (1) ground ice characterization (e.g., cryostratigraphic description of the ice, vertical ice distribution, microtomodensitometry (CT-scan)); (2) distribution and detection techniques of ground ice using geophysics (e.g., ERT, GPR, seismic), satellite/airborne remote sensing (e.g., multispectral imagery, LiDAR, UAV), and permafrost drilling and coring; (3) the biogeochemical properties of ground ice (e.g., DOC, major ions, isotopes, etc.) and their impacts on permafrost aggradation/degradation and hydrology; (4) the thermal properties of ground ice and its impact on the permafrost thermal regime; and (5) thermokarst processes (e.g., ground ice related mass movements) and how they affect landscape evolution.

Permafrost Index properties and establishment of a large ground ice potential database for northern Canada

Omid Asghari[1,2], Alexandre Chiasson[1], Mahya Roustaei[3], Joel Pumple[1], Steven V. Kokelj[4] & Duane G. Froese[1]

[1]*PACS Lab, Department of Earth and Atmospheric Sciences, University of Alberta, Edmonton, Alberta, Canada*

[2]*Department of Mining Engineering, University College of Engineering, University of Tehran, Tehran, Iran.*

[3]*Department of Civil Engineering, Ghent University, Geotechnics Laboratory, Technologiepark, Ghent, Belgium*

[4]*Northwest Territories Geological Survey, Government of Northwest Territories, Yellowknife, Northwest Territories, Canada*

Estimation of ground ice is important for improving existing methods of mapping the distribution of excess ice at landscape scales, and predicting the impacts of permafrost thaw (Cai et al. 2020). However, recent permafrost, thermokarst potential and ground ice maps lack field observations leading to incomplete understanding of ground ice distribution and abundance. Here, we present a Permafrost Index Properties database of more than 2500 permafrost cuboid samples from northern Canada. This database includes volumetric and excess-ice content (VIC, EIC), organic content (OC), gravimetric water content (GWC), soil density, and frozen bulk density.

The goal of the research is to establish the relations between GWC and excess-ice in permafrost by building a large dataset to determine index properties of permafrost. We then estimate excess ice using a Beta regression model from extensive geotechnical databases (~100,000 measurements) such as the Permafrost Index Network (PIN) from the Northwest Territories, the Permafrost database of Yukon and permafrost related work in Nunavik (Northern Québec) and Nunavut communities. This aligns with Theme 1 (PermafrostNet) goals to develop a Ground Ice Potential database and contribute to the Ground Ice Map of Canada Network Data Product.

METHODS

EIC is defined as ground ice that exceeds the total pore volume that the ground would have under unfrozen conditions (Brown et al. 1997). Its significance lies in providing insights into potential thaw settlement scenarios. In order to further our understanding of excess ice we have sampled more than 150 permafrost cores from diverse depositional environments, primarily from the western Canadian Arctic. These cores were cut into 3 cm^3 aliquots at two-centimeter intervals as described in Pumple et al. (2023). This method enables the preservation of sample heterogeneity and captures the variability of physical properties.

PACS LAB INDEX PROPERTIES DATABASE

We see a high positive linear correlation (~0.85) between EIC, GWC and VIC (Figure 1), similar to Lin et al. (2020). However, the correlation with soil density and organic content is weak. Database cleaning and variable filters were crucial for evaluating relations between variables. Peat and samples with high organic content (≥17%) pose a challenge due to peat's water absorption properties complicating EIC estimates. As a result, we remove samples classified as peat (≥17% organic content) as defined by the Soil Classification Working Group (1998).

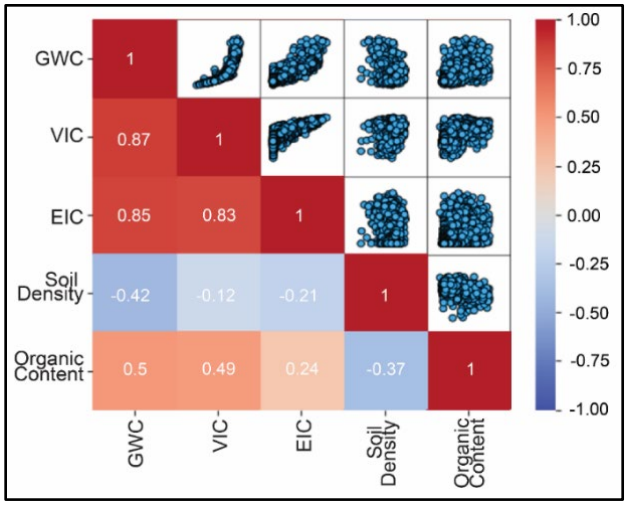

Figure 1. Correlation coefficients of index properties (for ~ 1,600* PACS samples).

STATISTICAL INSIGHTS: EXPLORING PATTERNS THROUGH PCA AND BETA REGRESSION

Given the limited number of consistently sampled variables in the PIN database, our modeling with the PACS database focused on GWC, Depth, Latitude, and Longitude. Principal Component analysis revealed three key findings: 1) GWC as the main predictor of EIC, 2) higher latitudes correlated more positively with EIC than longitude, and 3) EIC decreased with depth.

A statistical regression method for proportions between 0 and 1 known as a Beta regression was

used to estimate EIC in the PIN database based on coefficients derived from the PACS Index Properties data. Residual analysis shows a discernible trend, including instances of overestimation for low EIC values, underestimation for moderate, and overestimation again in high EIC values.

GWC AND EIC RELATION

We define negligible EIC as < 5%, indicating a thaw settlement of less than ~25 cm in 5 m of permafrost. Crucially, the EIC-GWC relation is defined by index properties, leveraging GWC that is present in large geotechnical databases.

Analysis of GWC vs. EIC plots in the PACS database, across various depositional environments, established a threshold value for GWC associated with a 5% EIC threshold. A key takeaway is the adoption of a conservative value of GWC of 30% for most deposits and 20% for till samples (Figure 2). These values are notably conservative when contrasted with the higher ~40% values estimated from the dataset of Kokelj and Burn (2003).

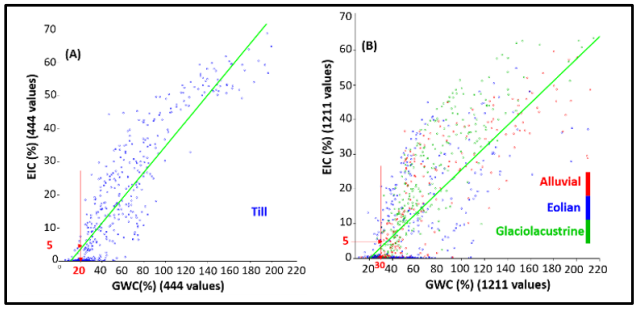

Figure 2. Selecting GWC for Negligible EIC in (A) till sediments (20%) and (B) alluvial, eolian and glaciolacustrine sediments (30%).

EFFECT OF APPLYING <5% EIC TO THE PIN DATABASE

The PIN database (Smith et al. 2005), with ~13,000 boreholes and ~55,000 measurements of GWC, was cleaned based on specific criteria. The data cleaning criteria involved trimming GWC to > 30 % (> 20 % for till) and < 260%, and depth to > 0.5 m and < 10 m, excluding most active layer samples and very deep measurements. Secondly, applying the 5% EIC threshold, defined by PACS Index Properties, excludes around 70% of PIN data. In other words, most of the samples have negligible excess ice.

Biases are apparent across these three separate databases. PIN samples, largely collected to support transportation corridors and infrastructure routing, were likely biased towards ice-poor sites, in contrast to a common focus of permafrost researchers on ice-rich locations.

CONCLUSIONS

Significant strides have been taken in the development of the Ground Ice Potential database, entailing the initial compilation of Permafrost Index Properties and the evaluation of ground ice potential for over 50,000 permafrost measurements. Next steps will require further testing with additional datasets, and constructing typical ground ice profiles for different regions and depositional environments. Moreover, additional work is needed on peat samples that are presently not considered in this study.

REFERENCES

Cai, L., Lee, H., Schanke Aas, K., and Westermann, S. 2020. Projecting circum-Arctic excess-ground-ice melt with a sub-grid representation in the Community Land Model, Cryosphere, 14, 4611–4626. https://doi.org/10.5194/tc-14-4611-2020

Canadian Agricultural Services Coordinating Committee. Soil Classification Working Group, National Research Council Canada, Canada. Agriculture, & Agri-Food Canada. Research Branch. (1998). The Canadian system of soil classification (No. 1646). NRC Research Press.

Brown, J., Ferrians, O., Heginbottom, J., and Melnikov, E.S. 1997. Circum-Arctic map of permafrost and ground-ice conditions. https://doi.org/10.3133/cp45

Kokelj, S.V., & Burn, C.R. 2003. Ground Ice and Soluble Cations in Near-Surface Permafrost, Inuvik, Northwest Territories, Canada, Permafrost and Periglacial. Process. 14: 275–289. doi:10.1002/ppp.458

Lin, Z., et al., 2020. Factors controlling near surface ground-ice characteristics in a region of warm permafrost, Beiluhe Basin, Qinghai-Tibet Plateau, Geoderma,376(1):114540. doi:10.1016/j.geoderma.2020.114540

Pumple, J., Monteath, A., Harvey, J., Roustaei, M., Alvarez, A., Buchanan, C., and Froese, D. 2023. Non-destructive multi-sensor core logging allows rapid imaging, measurement of bulk density and estimation of ice content in permafrost cores, The Cryosphere, 2023, 1–27.

Smith, S.L., Burgess, M.M., and Lawrence, D.E. 2005. Digital Borehole Geotechnical Database for the Mackenzie Valley-Delta Region. Geological Survey of Canada, Open File 4924, 25 p.

Stable isotope development in ground ice along an alpine tundra slope in the Ogilvie Mountains, Yukon Territory

Casey Buchanan[1], Duane G. Froese[2], Trevor Porter[3] & Jeffrey Kavanaugh[2]

[1]*Permafrost and Geosciences Research, Yukon University, Whitehorse, Yukon, Canada*

[2]*Department of Earth and Atmospheric Sciences, University of Alberta, Edmonton, Alberta, Canada*

[3]*Department of Geography, Geomatics and Environment, University of Toronto Mississauga*

Stable isotope ratios of oxygen and hydrogen ($\delta^{18}O$ and δD) from ground ice in permafrost regions have been used to reconstruct paleoclimate spanning the Late Pleistocene and Holocene in subarctic and arctic regions (Porter et al. 2019). This is possible due to the strong relations between the isotopic composition of atmospheric moisture and air temperatures (Dansgaard 1964). However, isotope records from ground ice (specifically, pore and texture ice) are difficult to interpret because their source waters can become isotopically altered by local environmental conditions and processes prior to long-term preservation in aggrading permafrost (Dereviagin et al. 2003; Wetterich et al. 2014). These processes include surface evaporation, soil water mixing, pooling, cryofractionation (Throckmorton et al. 2016), and cryosuction of critically cooled waters. The transition layer might also affect isotopic values due to potential fractionation during partial thaw and refreezing. Currently, the combined effect of these processes on underlying ground ice records, and the role of the transition layer in isotope records, is not well understood.

This study investigates the isotopic relations between source precipitation, active layer waters, transition layer ice, and relict pore and texture ice, to better understand the processes affecting water isotope record formation and preservation in ground ice to improve their effectiveness as a paleoclimate proxy.

Sites and methodologies

The Blackstone uplands 2019 (BS19) study area spans a fen and hillslope peatland located within the Southern Ogilvie Mountains, Yukon Territory, Canada (64.920°N, 138.284°W, 940 m elev. a.s.l.) at kilometer 126 of the Dempster Highway. Regional climate is subarctic continental (Wahl et al. 1987), and permafrost is continuous within the study locale and encompassing valley due to high elevation. Precipitation $\delta^{18}O$ and δD values fall along a Local Meteoric Water Line (LMWL) of $\delta D = 6.8\delta^{18}O - 24.5$ (Baranova 2017).

The study area contains four sites: hilltop (Site 1), hillslope (Site 2), degrading polygons (Site 3), and fen hummock (Site 4). These sites form a catena underlain by pebbly-sandy silt overlain by an organic horizon about 1 m thick. Surface cover is typical shrub-tundra vegetation assemblages of primarily tussock grass, low dwarf birch, and Sphagnum moss.

Permafrost cores and thawed (at time of sampling) active layer soil columns were collected in June, 2019 from each site. The sites were revisited in September, 2019, at which time waters from the base of the thawed active layer were collected in addition to recollecting thawed active layer monoliths. Surface water was also sampled at this time. Precipitation was collected during both visits.

Stable isotope, electrical conductivity, and pH analyses were conducted on the active layer waters, precipitation, surface waters, and thawed ground ice at the University of Alberta PACS laboratory.

Role of slope on isotope formation

Basal active layer water $\delta^{18}O$ and δD increased, while d-excess decreased, with down-slope position, most likely caused by the accumulation of thawed, isotopically enriched basal ice and evaporatively enriched soil moisture flushed downward by rainwater from the acrotelm as active layer water moves down-slope. These changes were reflected in the isotopic composition of the active layer, transition layer, and relict pore and texture ice, that became slightly enriched down-slope.

Active layer isotopic modification

Rayleigh fractionation during bi-directional freezing (Sites 1, 2, and 4) produced 'C'-shaped stable isotope profiles in the active layer. This is supported by δD-$\delta^{18}O$ regressions with slopes around 6.5 to 8. These profiles consist of enriched first ice at the top and base of the active layer with the most depleted values often in the lower-middle of the active layer where the freezing fronts met. In spring and summer, downward melting removes most of this record, such that a thawed, enriched basal first ice remains available for incorporation into the transition layer during subsequent freeze-back.

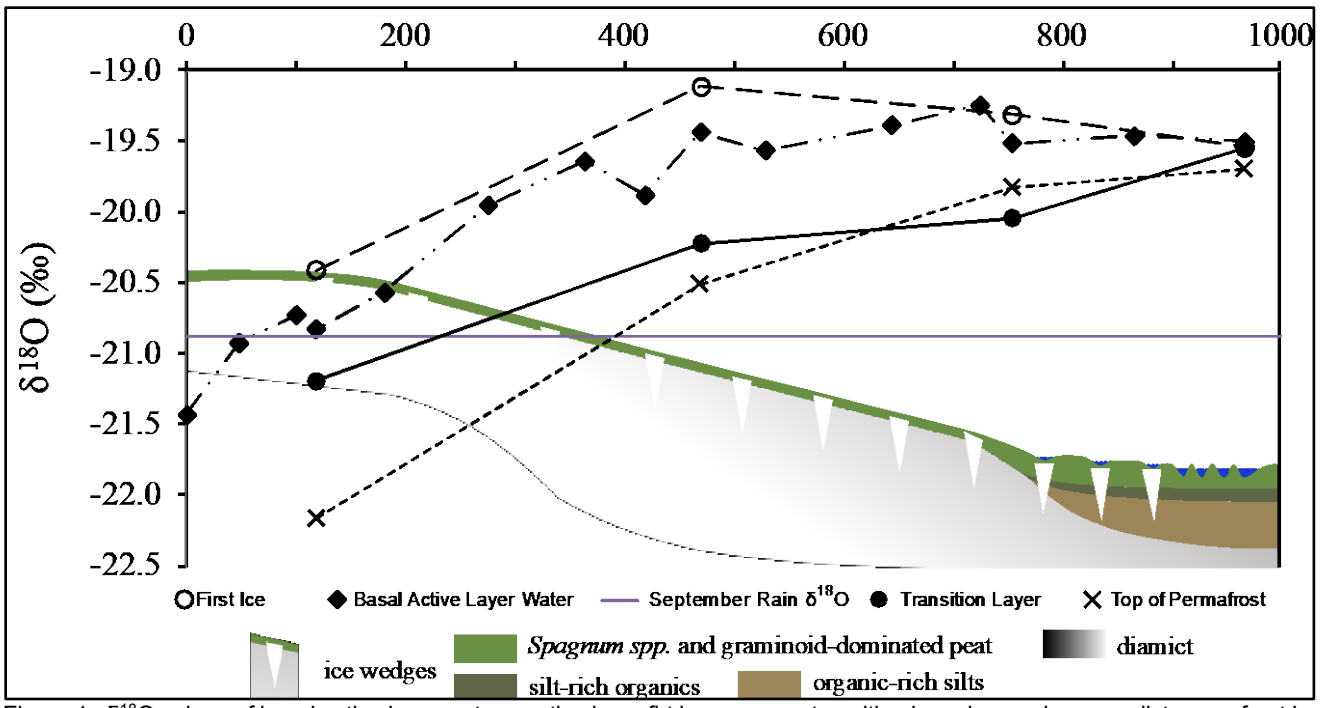

Figure 1. $\delta^{18}O$ values of basal active layer waters, active layer firt ice, average transition layer ice, and upper relict permafrost ice along slope.

TRANSITION LAYER ISOTOPIC MODIFICATION

The transition layer appears to act as an isotopic intermediary between the active layer and relict ice. Sites 1, 3, and 4 represent isotopically 'mature' transition layer values consisting of ice-rich aggradational ice that likely accumulated over many years, but likely most during years that produced deep active layers and thus likely had more enriched waters. Basal active layer ice from deep thaw years have a higher preservation protential due to the lower likelihood of future thawing to the same depth. In contrast, Site 2 represents an isotopically 'immature' transition layer because a C-shaped active layer isotope profile is still visible. This C-shaped profiles will presumably be overprinted by future deep thaw-refreeze events.

Co-isotopic regressions indicate that the style of isotopic fractionation (kinetic vs. equilibrium) exhibited by the uppermost relict pore and texture ice is consistent with the style of isotopic fractionation within the overlying transition layer. Collectively these processes, whereby only the deepest thaw years reach the ice-rich transition layer, provide a compelling mechanism to preferentially preserve more isotopically enriched active layer waters within the aggradational ice at the top of permafrost. These processes lead to the relative homogeneity of the isotopic record of near surface permafrost despite the variability of waters within the active layer at any particular time. This suggests that isotopic values near the top of permafrost are more representative of climatic conditions over decadal to century timescales, as compared to the higher frequency variation within the active layer.

REFERENCES

Baranova, N. 2017. Evaluating Groundwater In a Permafrost Watershed Using Seasonal Geochemical and Isotope Discharge Trends, Ogilvie River, Yukon, doctoral dissertation, University of Ottawa.

Dansgaard, W. 1964. Stable isotopes in precipitation, Tellus, 16(4): 436–468. doi:10.3402/tellusa.v16i4.8993

Dereviagin, A.Y., Chizhov, A.B., Meyer, H., Hubberten, H.-W., and Siegert, C. 2003. Recent ground ice and its formation on evidence of isotopic analysis, In Proceedings of 8th International Conference on Permafrost, Zurich, Switzerland, 8, 21–25.

Porter, T.J., Schoenemann, S.W., Davies, L.J., Steig, E.J., Bandara, S., and Froese, D.G. 2019. Recent summer warming in northwestern Canada exceeds the Holocene thermal maximum, Nature Communications, 10(1), 1631. doi:10.1038/s41467-019-09622-y

Throckmorton, H.M., Newman, B.D., Heikoop, J.M., Perkins, G.B., Feng, X., Graham, D.E., O'Malley, D., Vesselino, V.V., Young, J., Wullschleger, S.D., and Wilson, C.J. 2016. Active layer hydrology in an arctic tundra ecosystem: quantifying water sources and cycling using water stable isotopes, Hydrological Processes, 30(26): 4972–4986. doi:10.1002/hyp.10883

Wetterich, S., Tumskoy, V., Rudaya, N., Andreev, A.A., Opel, T., Meyer, H., Schirrmeister, L., and Hüls, M. 2014. Ice Complex formation in arctic East Siberia during the MIS3 Interstadial, Quaternary Science Reviews, 84: 39–55. doi:10.1016/j.quascirev.2013.11.009

Detecting ground ice content in polycyclic retrogressive thaw slumps

Saskia Eppinger[1], Konrad Heidler[2], Hugues Lantuit[3,4] & Michael Krautblatter[1]

[1]*Chair of Landslide Research, Technical University of Munich, Munich, Germany*

[2]*Chair of Data Science in Earth Observation, Technical University of Munich, Munich, Germany*

[3]*Alfred Wegener Institute Helmholtz Centre for Polar and Marine Research, Potsdam, Germany*

[4]*Institute of Geosciences, University of Potsdam, Potsdam, Germany*

Landforms such as retrogressive thaw slumps (RTS) are vulnerable to a warming climate. Increasing numbers of RTS were observed over the past years in the Canadian Arctic (Lantuit and Pollard 2008; Ward Jones et al. 2019). Massive ice content is an important controlling factor for the occurrence of these landforms (Hayes et al. 2022), yet its distribution underneath the surface is often challenging to determine and map. Since RTS behaviour, including polycyclicity and reactivation, is primarily driven by the presence of ground ice (Hayes et al. 2022; Ramage et al. 2017), it is necessary to find means to better map its occurrence in the subsurface.

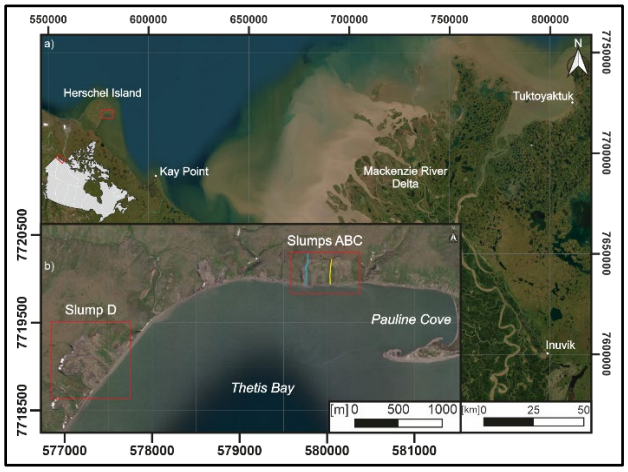

Figure 1. a) location of Herschel Island west of the Mackenzie Delta area; b) investigated retrogressive thaw slumps ABC and D facing Thetis Bay, ERT-profiles in Slump B (yellow) and Slump C (blue) are shown in Figure 2 (Maps were created using Esri Satellite).

Herschel Island (HI) - Qikiqtaruk - was selected for this study because of the occurrence of large bodies of massive ground ice and RTS. HI lies off the Yukon Coast between the Mackenzie Delta region and the Alaskan border (Figure 1) and is part of the Yukon coastal plain. Its stratigraphy is complex and was shaped by ice movement by an advance of the Laurentide Ice Sheet (Rampton 1982). The volumetric ice content on HI exceeds 45% (Couture and Pollard 2017), massive ground ice constitutes up to 70% of the upper permafrost (Pollard 1990) and the active layer depth normally ranges between 40-60 cm (Burn and Zhang 2009). The RTS investigated for this study are among the biggest along the Yukon coast (Ramage et al. 2017) and can be classified as mega slumps according to Kokelj et al. (2013). We focused on three merged RTS, hereby called Slumps ABC — as well as the biggest RTS on HI called Slump D.

METHODOLOGY

Electrical Resistivity Tomography (ERT) is a robust and common method to investigate permafrost. To detect the internal structure of the RTS, we measured longitudinal and shoreline parallel profiles. All profiles were measured using a 5 m spacing. A roll-along setup was used, Wenner- and Schlumberger-array were measured simultaneously, the shown results are a combination of both arrays.

In addition to ERT surveys, UAV-flights were conducted to document the current RTS extent and activity rate during the field campaigns in 2019 (Slump D) and 2022 (Slumps ABC), active layer depth was measured along several ERT profiles and samples were taken from the active headwalls to gain a better understanding of temperature and resistivity relations by laboratory tests. To gain a better understanding of exposure times for different parts of the RTS, we mapped their extent on several Orthophotos and DEMs recorded between 1952 and 2022. All this additional information was then carefully used to interpret the ERT results.

RESULTS

ERT results show a clear structure for all investigated RTS:

1. the area close to the shoreline shows low resistivities, often < 70 Ωm
2. the slump floor, that is already restabilized (in all cases revegetated), shows mediocre resistivities up to approx. 5000 Ωm
3. an area with lower resistivities can be detected in front of the headwall; these areas were unvegetated and wet

4. high resistivities in formerly undisturbed tundra and old slump floor, where massive ground ice is available (see Figure 2a)

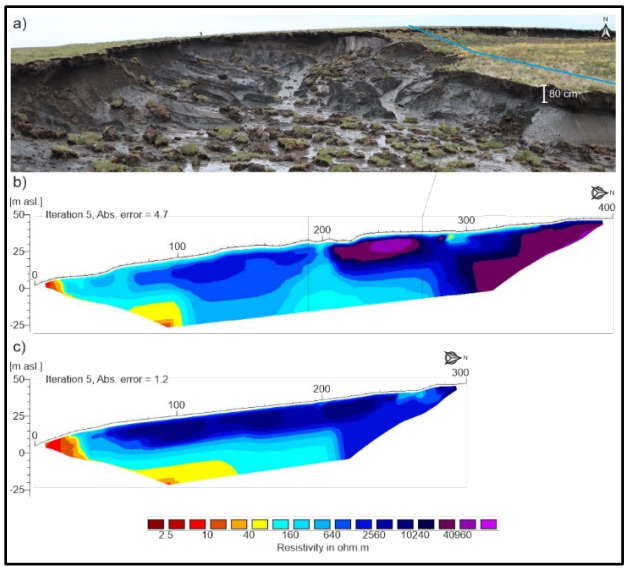

Figure 1. a) View towards active part of Slump C in 2022, active layer depth approx. 80 cm, blue line shows upper part of ERT profile b); b) Slump C (blue in Figure 1), kink in profile (dash lines) due to accessibility during field campaign, headwall at 340 m; c) Slump B (yellow in Figure 1), headwall at 280 m; colour scheme valid for b and c, based on laboratory calibration: blue colours: frozen conditions, red and yellow: likely to be unfrozen or influenced by other factors.

The results clearly show the occurrence of ground ice, also in previously slumped floor, that have restabilized for several decades or were only disturbed by shallow RTS. This has a high impact on the likelihood of polycyclic behaviour.

The interpretation of ERT data should be treated carefully, as the occurrence of liquid water in mud pools and gullies strongly influences the ERT data (e.g., in area (3)). Furthermore, the occurrence of salt and marine layers can lead to masking of underlying structures (area 1), as shown in subsea-permafrost studies (Arboleda-Zapata et al. 2022).

Our results show the capacity of ERT to detect massive ice bodies and estimate the overburden thickness, in contrast to remote techniques such as remote sensing (Hayes et al. 2023). This highlights the need to deploy complementary techniques to correctly depict the characteristics of RTS.

REFERENCES

Arboleda-Zapata, M. Angelopoulos, M., Overduin, P.P., Grosse, G., Jones, B.M., and Tronicke, J. 2022. Exploring the capabilities of electrical resistivity tomography to study subsea permafrost, The Cryosphere, 16: 4423–4445. doi:10.5194/tc-16-4423-2022

Burn, C.R., and Zhang, Y. 2009. Permafrost and climate change at Herschel Island (Qikiqtaruq, Yukon Territory, Canada, Journal of Gephysical Research, 114: F02001. doi:10.1029/2008JF001087

Couture, N.J., and Pollard, W.H. 2017. A Model for Quantifying Ground-Ice Volume, Yukon Coast, Western Arctic Canada, Permafrost and Periglacial Processes, 28: 534–542. doi:10.1002/ppp.1952

Hayes, S., Lim, M., Whalen, D., Mann, P.J., Fraser, P., Penlington, R., and Martin, J. 2022. The Role of Massive Ice and Exposed Headwall Properties on Retrogressive Thaw Slump Activity, Journal of Geophysical Research: Earth Surface, 127(11): e2022JF006602. doi:10.1029/2022JF006602

Kokelj, S.V., Lacelle, D., Lantz, T.C, Tunnicliffe, J., Malone, L., Clark, I.D., and Chin, K.S. 2013. Thawing of massive ground ice in mega slumps drives increases in stream sediment and solute flux across a range of watershed scales, Journal of Geophysical Research: Earth Surface, 118(2): 681–692. doi:10.1002/jgrf.20063

Lantuit, H., and Pollard, W.H. 2008. Fifty years of coastal erosion and retrogressive thaw slump activity on Herschel Island, southern Beaufort Sea, Yukon Territory, Canada, Geomorphology, 95: 84–102. doi:10.1016/j.geomorph.2006.07.040

Pollard, W.H. 1990. The nature and origin of ground ice in the Herschel Island area, Yukon Territory, In Proceedings of the Fifth Canadian Permafrost Conference 1990, Centre d'études Nordiques Université Laval, Québec city, Québec, Canada, 23–30.

Ramage, J.L., Irrgang, A.M., Herzschuh, U., Morgenstern, A., Couture, N., and Lantuit, H. 2017. Terrain controls on the occurrence of coastal retrogressive thaw slumps along the Yukon Coast, Canada, Journal of Geophysical Research: Earth Surface, 122(9): 1619–1634. doi:10.1002/2017JF004231

Rampton, V.N. 1982. Quaternary Geology of the Yukon Coastal Plain, Geological Survey of Canada, Bulletin 317.

Ward Jones, M.K, Pollard, W.H and Jones B.M. 2019. Rapid initialization of retrogressive thaw slumps in the Canadian high Arctic and their response to climate and terrain factors, Environmental Research Letters, 14(5): 055006. doi:10.1088/1748-9326/ab12fd

Thaw settlement and excess ice estimation using computed tomography

Jordan Harvey[1,2], Joel Pumple[1,2], Mahya Roustaei[3], Evan Francis[1,2] & Duane Froese[1,2]

[1]*Department of Earth & Atmospheric Sciences, University of Alberta, Edmonton, Alberta, Canada*

[2]*Permafrost Archives Science Laboratory, University of Alberta, Edmonton, Alberta, Canada*

[3]*Department of Civil Engineering, Geotechnics Laboratory, Ghent University, Ghent, Belgium*

In permafrost research, excess ice, or ground ice that exceeds the pore space of the host sediment, plays a crucial role in the settling processes of permafrost environments during thawing conditions. As northern climates continue to warm, thawing of permafrost will degrade the landscape (e.g., increased slope instability and permeability of soils) and will have negative effects on local infrastructure as excess ice melts out and the remaining material collapses (Mohammadi and Hayley 2023). The accurate estimation of excess ice is important for designing climate-resilient infrastructure and predicting the impacts of permafrost thaw in Arctic Canada (Castagner et al. 2022) and Alaska (Yang et al. 2021).

This study looks to develop and test a method to induce consistent top-down thaw within a custom 3D-printed thaw chamber with synthetic permafrost cores that can be scanned at high resolution via Computed Tomography (CT) to estimate excess ice content when frozen and through the thaw process, and image the resulting thaw settlement (thawed cell scan). We show that (a) we can effectively estimate excess ice non-destructively via 3D CT scanning and (b) these values are consistent with the resulting supernatant water following permafrost thaw. This provides a strong support to move forward with a reliable method to estimate excess ice non-destructively via CT scanning. Future work will involve experiments on natural permafrost samples with greater variance in excess ice abundance from the Permafrost Archives Science (PACS) Lab archive collection.

Methodology

This project utilizes previously developed methods for scanning permafrost cores and introduces the ability to induce unidirectional thaw on cores to investigate the characteristics of the sample both during and following thaw.

Synthetic cores were produced inside the 3D-printed thaw chambers to eliminate any air gaps on the chamber's sides. Six synthetic cores were simultaneously created with interlayered ice lenses and sediment layers of the Devon silt (Azmatch et al. 2011) from the Edmonton area (Figure 1). Sediment layers were created by mixing silt and a known volume of water until the sediment reached its saturation point. Total sediment and water mass were then calculated for each core to be later used to measure volumetric and excess ice contents using the destructive method (Pumple et al. 2023).

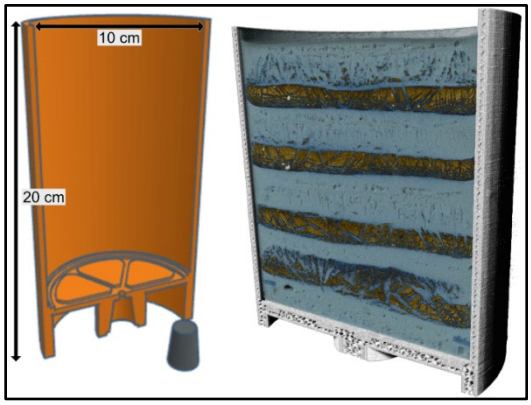

Figure 1. Tinker CAD cross-sectional rendering of 3D-printed cell (left) and a 3D profile of the synthetic core inside the cell (right, via CT). Ice is colourized with light blue and sediment as brown while gas is black.

Two thawing methods were applied to the synthetic cores, one using a uni-directional thawing system and the other thawing in ambient room temperature conditions. Top-down thaw is controlled by housing the sample in a temperature-controlled chest freezer at -2 °C while continuously maintaining a "surface" temperature (top of cell) of 25 °C. Multi-directional thawing involved leaving the core on the lab counter at room temperature (22 °C), with a plastic wrap cover to prevent evaporative loss. Total thawing times ranged from two days at room temperature (multi-directional thaw) and four days for top-down thaw within the -2 °C chest freezer.

Cores were scanned on a Nikon XT H 225ST industrial CT scanner at frozen, partially thawed, fully thawed, drained, and dried states (Figure 2). A voxel resolution of 58 µm was achieved for each of the helical scans, with scan parameters of 200-210 kV. Segmentations and visualizations were created using ORS Dragonfly, where volumes of each segmented material were compared to physical core weights and volumes collected at the frozen, drained, and dry states to produce Excess Ice content (EIC) and Volumetric Ice Content (VIC) measurements.

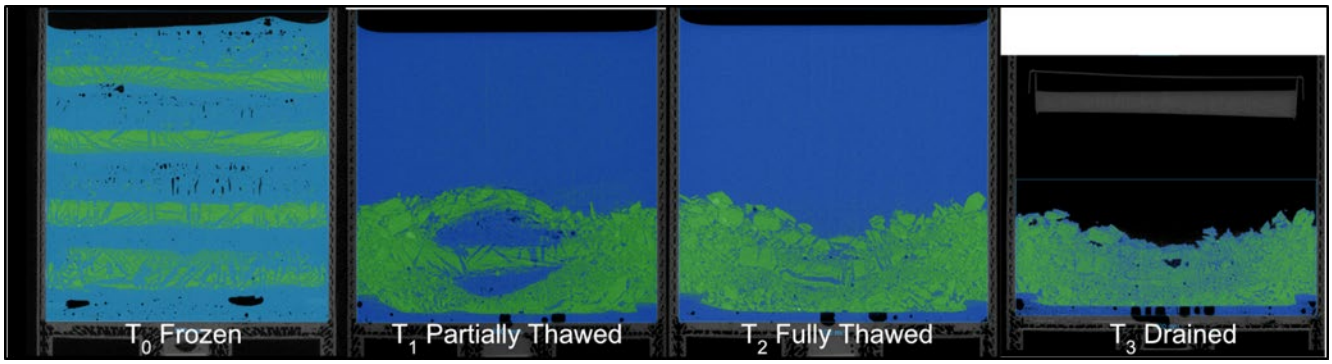

Figure 2. Thaw stages of top-down thaw chamber at frozen (t0), partially thawed (t1), fully thawed (t2), and drained (t3) stages.

Table 1. Measurements of thaw chambers.

Characteristics	Core 1 (Multi-directional)	Core 2 (Top-down)
1. Water added (g)	649	636
2. Water extracted (g)	648	628
3. Supernatant water drained (mL)	519	508
4. CT water volume from fully-thawed scan (mL)	531	530
5. CT Excess Ice Content (%)	74.77	73.52
6 Volumetric Excess Ice Content (%)	70.67	72.61
7. Volumetric Ice Content (%)	89.87	91.52

RESULTS AND DISCUSSION

Table 1 above shows how CT-derived EIC estimates are comparable to conventional destructive methods for estimating volumetric excess ice content. Water volumes estimated from segmented fully-thawed CT data closely match the measured volume of supernatant water from thawed and drained cores.

Vertical settlement of both cores (79.0% and 73.7% loss of height after draining for multi-directional and top-down thaw) corresponds favourably with CT-derived excess ice estimates (Table 1, row 5). The greater difference in the multi-directional thawed core values reflect uneven settlement. Initial observations show that our thaw settlement chamber and CT-derived EIC estimates are consistent with destructive methods, and this approach estimates thaw settlement reliably in high-EIC cores. Moving forward will include thawing natural permafrost cores with and without loads, to better simulate thaw consolidation processes. Alternative thawing conditions (e.g., varying grain size, ice content, organic content, and drainage conditions) will be tested on synthetic cores and natural permafrost cores to determine how other conditions may affect thaw settlement. These experiments will help isolate factors such as organic content, grain size, excess ice content, drainage conditions, rate of loading and rate of thawing that may affect thaw settlement and consolidation.

REFERENCES

Azmatch, T.F., Sego, D.C., Arenson, L.U., and Biggar, K.W. 2011. Tensile strength and stress–strain behaviour of Devon silt under frozen fringe conditions, Cold Regions Science and Technology, 68(1-2), 85–90.

Castagner, A., Brenning, A., Gruber, S., and Kokelj, S.V. 2022. Vertical distribution of excess ice in icy sediments and its statistical estimation from geotechnical data (Tuktoyaktuk Coastlands and Anderson Plain, Northwest Territories), Arctic Science, 9(2), 483–496.

Mohammadi, Z., and Hayley, J.L. 2023. Qualitative evaluation of thaw settlement potential in permafrost regions of Canada, Cold Regions Science and Technology, 216,104005.

Pumple, J., Monteath, A., Harvey, J., Roustaei, M., Alvarez, A., Buchanan, C., and Froese, D. 2023. Non-destructive multi-sensor core logging allows rapid imaging, measurement of bulk density and estimation of ice content in permafrost cores, EGUsphere, 2023, 1–27.

Yang, Z.J., Lee, K.C., and Liu, H. 2021. Permafrost thaw and ground settlement considering long-term climate impact in northern Alaska, Journal of Infrastructure Preservation and Resilience, 2(1), 1–17.

What can we infer about ground ice from induced polarization analysis of mobile electromagnetic observations?

Burke Minsley[1], Stephanie James[1], Neal Pastick[2], Andrea Viezzoli[3], Gianluca Fiandaca[4] & Allesandro Signora[4]

[1]*United States Geological Survey, Geology, Geophysics, and Geochemistry Science Center, Denver, Colorado, United States*

[2]*United States Geological Survey, Earth Resources Observation and Science (EROS) Center, Sioux Falls, South Dakota, United States*

[3]*EMergo, Cascina, Pisa, Italy*

[4]*Department of Earth Sciences, University of Milan, Milan, Italy*

Ground ice is an important parameter in permafrost environments. Ice-rich ground is vulnerable to subsidence and formation of thermokarst, and can also contain large stocks of carbon that may be released to the environment when thawed. Methods for characterization of subsurface ground ice remain limited, however. Remote sensing data are important for identification of ice-rich landscapes over large areas, but do not detect physical properties beneath the land surface. Coring is invaluable for detailed characterization of ground ice, but is limited to point observations and depths that can be reached by drilling. Here, we discuss the role of induced polarization (IP) effects on mobile electromagnetic observations for remote characterization of ground ice at intermediate scales. We consider both airborne and ground-based geophysical instruments that have the potential to contribute to subsurface ground ice characterization at intermediate-to-regional scales.

Geophysical instruments that use electromagnetic induction to map subsurface properties are widely used, including application to permafrost studies. Electromagnetic sensors can be advantageous in remote regions because there is no need for direct contact with the ground, and instruments can be carried or towed rapidly on land, water, or by aircraft. Instruments are often characterized by whether they operate in the time-domain (TDEM) or frequency-domain (FDEM). For either type of instrument configuration, data are typically interpreted to recover estimates of electrical resistivity with depth from a few meters to hundreds of meters below ground. Electrical resistivity can be used to infer permafrost conditions, as resistivity increases significantly as liquid water freezes. However, resistivity alone can be somewhat ambiguous in characterizing ground ice as other factors such as geologic material or unsaturated conditions can also lead to high resistivity.

In some instances, electromagnetic data can be complicated by IP, which causes resistivity to be a complex, frequency-dependent parameter often described by the four-parameter Cole-Cole model (Pelton et al. 1978). IP effects have been previously related to TDEM datasets collected over frozen ground, where the presence of ice is the cause of the IP behavior (Kozhevnikov 2022). Although the presence of IP complicates data interpretation, it provides an opportunity to more directly fingerprint the presence or absence of ground ice compared with resistivity alone. Recent advances in software algorithms incorporate IP parameterizations that estimate the Cole-Cole parameters when data are inverted. Here, we discuss observation and interpretation of IP-impacted TDEM data collected with a backpack-portable instrument at multiple sites in interior Alaska.

Finally, we consider the impact of ground ice and interpretation of IP effects on FDEM data, which has not previously received attention compared with IP in TDEM data. Several large airborne FDEM datasets have already been acquired in permafrost areas (e.g., Minsley et al. 2012), and may benefit from further IP analysis. We will use numerical modeling to understand how IP parameters manifest in FDEM data, and consider the conditions where it could be observable in field data.

REFERENCES

Kozhevnikov, N.O. 2022. On the association between fast induced polarization in frozen rocks and dielectric polarization of ice. Geophysical Prospecting, 70, 1380–1387. https://doi.org/10.1111/1365-2478.13246

Minsley, B.J., Abraham, J.D., Smith, B.D., Cannia, J.C., Voss, C.I., et al. 2012. Airborne electromagnetic imaging of discontinuous permafrost, Geophys. Res. Lett., 39, L02503. doi:10.1029/2011GL050079

Pelton, W.H., Ward, S.H., Hallof, P.G., Sill, W.R., and Nelson, P.H. 1978. Mineral discrimination and removal of inductive coupling with mulifreqnecy IP. Geophysics, 43:3, 588–609.

Ice-wedge development in the barrens of the Hudson Bay lowlands, northern Manitoba

Tabatha Rahman[1,2], Pascale Roy-Léveillée[1,2] & Duane Froese[3]

[1]*CRYO-UL: Permafrost Research Laboratory, Department of Geography, Université Laval, Québec City, Québec, Canada*

[2]*Centre for Northern Studies, Québec City, Québec, Canada*

[3]*PACS Lab: Permafrost ArChives Science Laboratory, Department of Earth and Atmospheric Sciences, University of Alberta, Edmonton, Alberta, Canada*

The Hudson Bay Lowlands (HBL) are a permafrost peatland that hosts 15 communities and crucial linear infrastructure, such as the Hudson Bay Railway. Permafrost in the region aggraded less than 8000 years ago following land emergence from the Tyrrell Sea due to post-glacial isostasy (Dredge 1992). Since land emergence, 25–400 cm of peat has accumulated on underlying glaciomarine sediment, representing an organic carbon reservoir of ~30 Pg (Dredge 1992; Packalen et al. 2014). In northwestern HBL, the Barrens (57.02°N to 58.71°N) form a 50,000 km^2 continuous permafrost region characterized by ice-wedge polygonal tundra, shallow lakes, fens, and bogs (Figure 1). Extensive polygonal terrain is unusual at such low latitudes, particularly in a recently emerged landscape with relatively young permafrost (O'Neill et al. 2019).

Figure 1. a) The Barrens (red) of northern Manitoba in the HBL (white). b) Polygonal terrain in the Barrens. c) Borehole locations (yellow dots) from 57.49–58.33°N.

Ice-wedge volume and the timing and environmental conditions associated with ice-wedge development have not yet been studied in this permafrost lowland. Improving knowledge of ground-ice dynamics is essential for predicting and mitigating risks associated with permafrost thaw around northern communities and infrastructure. This study investigates ice-wedge development in the Barrens, with a focus on 1) ice-wedge volume and distribution within different terrain units; and 2) the timing and environmental conditions associated with ice-wedge development in relation to the evolution of surface conditions.

Methods

In 2022–2023, 63 permafrost cores (4" diameter, 2–5 m length) were extracted from the Barrens along a 100-km latitudinal transect (Figure 1). To determine ice-wedge morphology, depth, and cross-section area, cores were extracted along six short transects perpendicular to ice-wedge troughs. Volume was calculated by multiplying cross-section area by trough length estimated using drone and satellite imagery. To constrain the timing of the marine-terrestrial transition and potential initiation of permafrost aggradation, five basal peat samples from polygon centers were AMS ^{14}C dated. Changes in paleosurface conditions were assessed in cores using visible transitions in vegetation types and charcoal/ash layers. Cryostratigraphic analysis of all cores using CT-scan, and stable water isotope analyses (δ^{18}O and δD) of 100 ice samples, were used to distinguish between different ice types and freezing conditions. Dissolved organic matter from the base of eight distinct ice wedges were AMS ^{14}C dated to determine the timing of ice-wedge aggradation. Morphological evidence of ice-wedge growth (shoulders, ice veins) and degradation (thaw unconformities, tunnels, pool ice) were assessed to reconstruct ice-wedge development in relation to the evolution of surface conditions.

Results and Discussion

The top five meters of cores from ice-wedge polygon centers were characterized by the following bottom-up sequence: fine-grained offshore glacio-marine deposits (>200 cm thick), coarse-grained near-shore marine deposits (40–100 cm thick), and

peat (110–240 cm thick; with a 40–60 cm active layer). Peat thickness decreased in the direction of the Tyrrell Sea retreat (190–240 cm at the three oldest sites, and 110–160 cm at the three youngest sites). Ice wedges were exclusively in mineral soil at younger sites where peat was thin (<1 m), and partially in organic and mineral soil at older sites where peat was thicker (>1 m) (Figure 2). Ice-wedge cross-section area in the top 2.5 m was 1.8 m^2 (σ=1.2 m^2, n=3) for wedges with larger troughs visible on 30 cm/pixel satellite imagery, and 0.64 m^2 (σ=0.26 m^2, n=3) for wedges whose troughs were too small to be visible on 30 cm/pixel imagery. There was evidence of recent ice-wedge cracking at most sites (cracks along troughs at the surface of wedges), including at a site which experienced a wildfire in 2012. In addition, pool and aggradational ice near the permafrost table at all sites were indicative of thaw unconformities and possible ice-wedge truncation. At the southernmost site, a 40-cm tall tunnel under an ice-wedge trough (between thawed peat and underlying pool ice) indicated ice-wedge degradation.

The double-tailed morphology of several ice wedges (Figure 2) suggested that past changes in surface conditions may have led to variations in the freezing-season thermal stress field, thereby altering the location, direction, and angle of cracking (Fortier and Allard 2004).

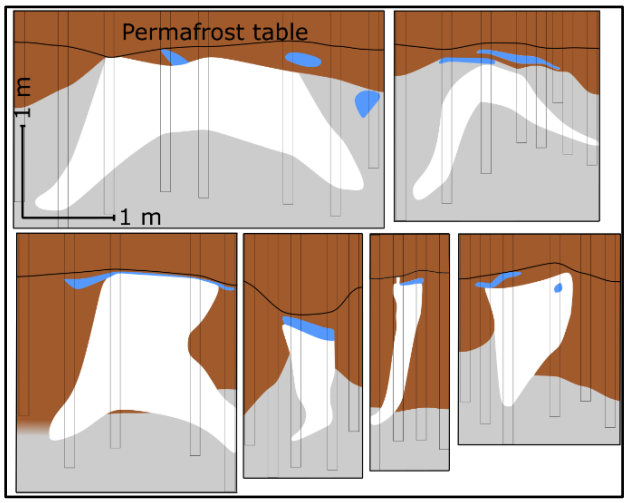

Figure 2. Classic and double-tailed ice wedges based on interpolation of borehole data and $\delta^{18}O$ and δD isotope analysis. Brown is peat, grey is mineral soil, white is wedge ice, and blue is pool or aggradational ice.

Changes in paleoenvironmental surface conditions may be linked to past wildfires. The presence of charcoal deep in the active layer, and large expanses of terrain visibly affected by past fires, indicate a long-term history of wildfires. Further, the abundance of thick woody material (5–15-cm length) in tundra permafrost suggest a transition from taiga to tundra, potentially as a result of increasing continentality, climate changes, paludification, permafrost aggradation, and fires (e.g., Kuhry 2008; Dredge and Mott 2003).

These results on wedge-ice volume, distribution, and development in response to environmental changes will help support predictions of landscape evolution near communities and infrastructure in this recently emerged permafrost lowland.

Acknowledgements

The Barrens are located on the traditional land of the Cree, Dene, Inuit, and Métis Nations (Treaty 5). Thank you to S. Olivier, L. Fishback, and the staff of the Churchill Northern Studies Center (CNSC) for their local insights and guidance; to E.L'Hérault, A. Kirkwood, H. Crisias, T. Herring, K. Ozeritskiy, and F. Brieger for field assistance; and to the CRYO-UL and PACS laboratories for help with sample processing. Financial and logistical support was provided by NTCF (TC), PCSP, NSERC, NSERC PermafrostNet, WCS Canada, Hudson Bay Railway, NSTP, FRQNT, RCGS, and CNSC.

References

Dredge, L.A. 1992. Field guide to the Churchill region, Manitoba: glaciations, sea level changes, permafrost landforms and archaeology of the Churchill and Gillam areas, Miscellaneous report 53, Geological Survey of Canada, Ottawa.

Dredge, L.A., and Mott, R. 2003. Holocene pollen records and peatland development, northeastern Manitoba, Géographie physique et Quaternaire, 57(1), 7–19. doi:org/10.7202/010328ar

Fortier, D., and Allard, M. 2004. Late Holocene syngenetic ice-wedge polygons development, Bylot Island, Canadian Arctic Archipelago, Canadian Journal of Earth Sciences, 41(8), 997-1012. doi:10.1139/e04-031

Kuhry, P. 2008. Palsa and peat plateau development in the Hudson Bay Lowlands, Canada: timing, pathways and causes, Boreas, 37(2) 316–327. doi:10.1111/j.1502-3885.2007.00022.x

O'Neill, H.B., Wolfe, S.A., and Duchesne, C. 2019. New ground ice maps for Canada using a paleogeographic modelling approach, The Cryosphere, 13(3), 753–773. doi:10.5194/tc-13-753-2019

Packalen, M.S., Finkelstein, S.A., and McLaughlin, J.W. 2014. Carbon storage and potential methane production in the Hudson Bay Lowlands since mid-Holocene peat initiation, Nature Communications, 5(1), 1–8. doi:10.1038/ncomms5078

Cryostratigraphy and ground ice distribution in Longyeardalen, Svalbard

Knut I.L. Tveit[1,2] & Hanne H. Christiansen[3]

[1]*Arctic Geology Department, University Centre in Svalbard, Longyearbyen, Svalbard, Norway*

[2]*Arctic Technology Department, University Centre in Svalbard, Longyearbyen, Svalbard, Norway*

[3]*Arctic Geophysics Department, University Centre in Svalbard, Longyearbyen, Svalbard, Norway*

With global warming, the risk of permafrost-related geohazards is expected to increase. The project "Developing a permafrost and meteorological climate change response system to build resilience in Arctic communities" ("PermaMeteoCommunity") at the University Centre in Svalbard (UNIS) is aiming to build a response system to increase resilience towards the increased risk (see also poster by Maaike Weerdesteijn in session 1E). To be able to build such a system, it is important to have a good understanding of the ground ice content and sediment types and distribution in areas exposed to such hazards. In this project we have therefore gathered data on ground ice and sediment distribution in the study area, with an aim to create a map showing the spatial distribution of ground ice.

Study area

This study takes place in the valley Longyeardalen in central Svalbard, which is where the largest settlement in Svalbard, Longyearbyen, is situated. The town is located at 78°N, with about 2500 inhabitants. The valley is in the continuous permafrost zone with a permafrost thickness of 100-200 m (Humlum 2005). The relatively narrow valley is delimited by steep hillsides which are exposed to various permafrost-related geohazards (Figure 1).

Methods

A total of 14 boreholes have been drilled across the study area between October 2021 and May 2023 to obtain core or drill cutting samples for laboratory analyses and to determine sediment thickness above bedrock. The boreholes were placed to have a geographical spread over the study area, and to include the main periglacial landforms as mapped geomorphologically (Rubensdotter 2022). Five of the boreholes were drilled in the valley bottom using the purpose-built UNIS permafrost drill rig (Christiansen et al. 2021) to a maximum depth of 45 m (Figure 1). Samples obtained from these boreholes comprise 20 m of core samples, and 115 m of drill cuttings. Core samples were obtained primarily in the top 10 m below the surface in ice cemented sediments, and drill cuttings were obtained below and in ice-poor sediments to facilitate faster drilling to reach bedrock.

The remaining 9 boreholes were drilled in the hillsides of the valley (Figure 1) with a novel approach using an electric Eibenstock PLD 182.1 NT Powerline drill mounted on a purpose-built platform designed and constructed by Kolibri Geo Services. This drill can deliver rotation speeds up to 4400 rpm, facilitating drilling in coarse sediment which is typically not possible using traditional hand-held drilling techniques. The whole drilling set-up was transported with snowmobiles allowing for access also to the lower slopes. Using this drill set-up, we could core the slopes surrounding Longyearbyen within primarily coarse alluvial and colluvial sediments. The slope boreholes were drilled to a maximum depth of 7.4 m with continuous coring. The core samples were generally of good quality where the ice content was high, and remoulded where the ice content was low. Six of the slope boreholes have been instrumented with thermistor strings, and the active layer thickness has been recorded from the thermistor data.

Laboratory analyses comprising cryostratigraphic logging, gravimetric ice content, excess ice and salt content of meltwater were carried out on selected samples from the boreholes, focusing on the top 5 m below the surface.

In addition to the data gathered from the boreholes, data from publicly available ground investigation reports in Longyeardalen was also included. These reports were accessed through the Norwegian National Database of Ground Investigations (NADAG) and the local municipalities webpage: https://www.lokalstyre.no/fagrapporter.488045.no.html

Results

The core samples collected in the lower slopes in Longyeardalen were drilled in different landforms comprising colluvial deposits and till. The sediment primarily consists of diamict with a mixture of structureless and suspended ground ice. The active layer in these boreholes ranged from 1.6 to 2.2 m, with a sharp increase in ice content typically from (up to 238 %wt) just below the active layer (Figure 1).

Four of the five boreholes drilled on the valley floor were drilled in fluvial deposits, and the last was drilled in a till deposit. The retrieved sediments from the boreholes in the fluvial deposits consisted of gravel with

low ice content from 7 to 13 %wt in the top meter of permafrost (Figure 1). The sediments retrieved from the borehole in the till deposit display suspended ice just below the active layer overlaying diamict with low ice content (typically 10 to 20 %wt).

The active layer thicknesses in the deeper valley bottom boreholes were estimated by the driller during drilling, which took place in October-November 2021. The estimated active layers varied between 1.6 and 1.8 m.

Information on the ground ice, sediment and/or active layer depth were found from 69 external ground investigation points in the studied reports. 42 of these points had active layer depths, ranging from 1 to 3.4 m in natural deposits, and two points in man-made deposits had deeper active layer depths ranging from 3.75 to 5.0 m.

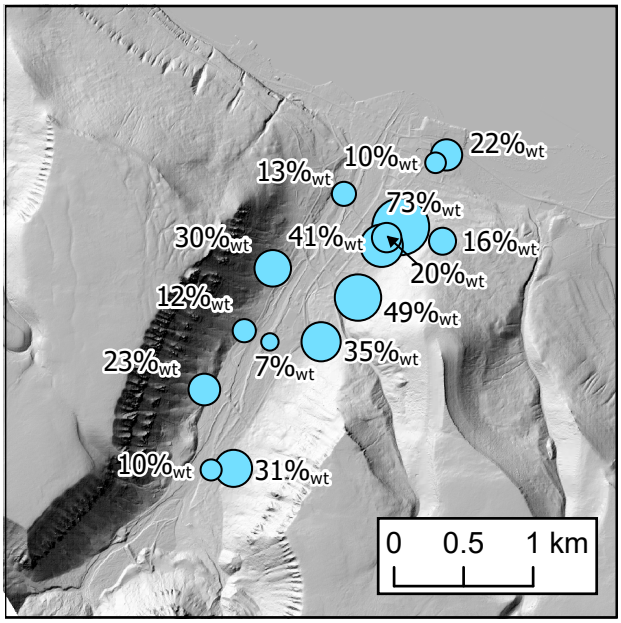

Figure 1. Average ground ice content in the top meter of permafrost at the 14 investigated borehole locations in Longyeardalen. The size of the circles is proportional to the amount of ice.

Discussion

Preliminary data analysis indicates a relation between ground ice content and sediment type in Longyeardalen, with some variation. We have identified four main sediment types from the geomorphological map (Rubensdotter 2022): (1) alluvial, (2) colluvial, (3) marine, and (4) till. The first two types are deposited by modern slope and river processes, while the two last types are deposited during the Quaternary by the sea and by glaciers. The ice content in the top permafrost is highest in the colluvial and marine sediments, and lowest in the alluvial and till sediments, as shown in Figure 2. We have also compared the ground ice content with various topographical factors comprising elevation, aspect, and slope, and have not found a clear relation.

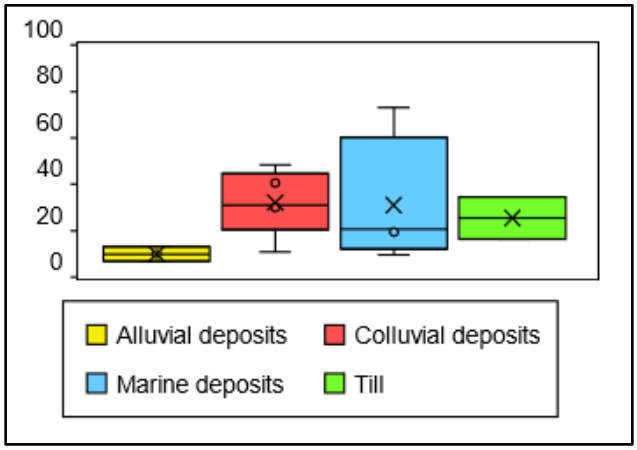

Figure 2. Ground ice content in top 1 m of permafrost from the studied 14 boreholes classified by sediment type in Longyeardalen.

Conclusions and perspectives

Based on the laboratory analyses of the sediment samples from the 14 boreholes and the previously published data, a relation has been found between sediment type and ground ice content, allowing for spatial extrapolation to develop a ground ice map based on the mapped landforms. This conclusion can only be drawn based on the detailed cryostratigraphical studies enabling a characterisation of the sediment thickness related to landform.

References

Christiansen, H.H., Gilbert, G.L., Neumann, U., Demidov, N., Guglielmin, M., Isaksen, K., Osuch, M., and Boike, J. 2021. Ground ice content, drilling methods and equipment and permafrost dynamics in Svalbard 2016-2019 (PermaSval). In: Moreno-Ibáñez et al (eds) SESS report 2020, Svalbard Integrated Arctic Earth Observing System, Longyearbyen, 259–275. https://doi.org/10.5281/zenodo.4294095.

Humlum, O. 2005. Holocene permafrost aggradation in Svalbard, in Harris, C & Murton, J.B (eds.) Cryospheric Systems: Glaciers and Permafrost. London: The Geological Society of London.

Rubensdotter, L. 2022. Preliminary map of Quaternary Geology and Geomorphology in Longyeardalen, Svalbard. Scale 1:10,000. Geological Survey of Norway.

Investigating thermokarst dynamics: A multimethod approach to understand pond formation and ice cliffs degradation in periglacial landscapes

Eole Valence[1,2], Jeffrey M.McKenzie[1,2], Bastien Charonnat[2,3], Michel Baraër[2,3], Timothee Briand[1], Janie Masse-Dufresne[2,3], Adam R. Tjoelker[4,5] & Adrien Dimech[3]

[1]*Department of Earth and Planetary Sciences, McGill University, Montréal, Québec, Canada*

[2]*Geotop, Montréal, Québec, Canada*

[3]*Département du Génie de la Construction, École de Technologie Supérieure, Montréal, Québec, Canada*

[4]*Department of Geography, The Ohio State University, Columbus, Ohio, United States*

[5]*Byrd Polar and Climate Research Center, The Ohio State University, Columbus, Ohio, United States*

Due to climate change, the mountain cryosphere is rapidly evolving. The most perceptible changes outside of the polar regions occur in mountainous areas, which host a significant amount of the cryosphere (Rangwala et al. 2012). In alpine area, the retreat of the cryosphere is even more pronounced as atmospheric warming increases with the altitude. Thus, permafrost and ground ice thawing modify the hydrology of these areas.

Our research focuses on the hydrological behaviour of the Shár Shaw Tagà (Grizzly Creek), a subarctic catchment in the Kluane Range. The catchment is in the south-west of the Yukon at an elevation comprised between 1700 and 2500 m.a.s.l. and is composed by diverse cryospheric elements, including bare glaciers, debris-covered glaciers, ice cored moraine, ground ice, rock glaciers, and permafrost. However, this system shows no significant surface water discharge, indicating potential groundwater flow out of the catchment. Thus, identifying and quantifying the hydrological pathways and fluxes in this type of watershed is crucial to face climate changes in arctic and subarctic mountainous regions.

Thermokarst landforms and ice cliffs are prominent hydrologic and geomorphic features of ice-rich debris complexes. Thermokarst sinks may form after englacial conduits collapse on buried ice (Clayton 1964). Therefore, pond may form at the entrance of the sinkhole when its hydraulic conductivity is not high enough to transmit inflowing precipitation, snow melt, and glacial melt. Ice cliffs are debris-free ice walls highlighting the presence of buried ice.

Sinkholes are hypothesized to promote the formation of ice cliffs, which are generally formed by the sliding of debris from steep slopes or calving at supraglacial pond margins (Miles et al. 2020). Once initialized, ice cliffs expand and grow (back-wasting); as ice is unburied, ice cliffs can locally increase the melting rate of the ice, which may also increase again the ice cliff size.

With climate change, temperatures in mountainous regions are increasing and extreme weather event are occurring more frequently and with greater amplitude. The net result of these changes should increase thermokarst sinkhole depressions and ice cliff formation. However, only a few studies have defined the energy-balance of supraglacial ponds on debris-covered glaciers (Kaab and Haeberli 2001; Miles et al. 2016; Pan et al. 2014), and even fewer studies have clearly defined the impact of precipitations and extreme weather events on these ponds (Figure 1).

Figure 1. Daily image from time lapse camera monitoring pond formation in a thermokarst sinkhole depression.

We present a multi-method approach to quantify the impacts pond formation have on thermokarst sink.

The study utilizes drone-based photogrammetry, with both visible and thermal imagery, to precisely measure surface topographical changes, capturing the evolving nature of thermokarst sinkhole depressions. Autonomous terrestrial Lidar and time-lapse cameras are deployed to monitor pond formation and ice cliffs degradation, providing valuable insights into the temporal dynamics of these critical features. Furthermore, the research integrates advanced geophysical techniques, including drone-based ground-penetrating radar (GPR) and electrical resistivity tomography (ERT). Combining these tools allow for the measurement of changes in buried ice volumes, offering a comprehensive view of subsurface dynamics, such as debris supply and ice degradation.

The results of the research will provide new insights into how rain events affect ground ice melt and ice cliff formation, including implications for understanding glacier retreat and downstream water resource management in glacier-fed regions.

REFERENCES

Clayton, L. 1964. Karst Topography on Stagnant Glaciers. Journal of Glaciology, 5(37), 107–112. https://doi.org/10.3189/S0022143000028628A

Kääb, A., and W. Haeberli (2001) Evolution of a High-Mountain Thermokarst Lake in the Swiss Alps, Arctic, Antarctic, and Alpine Research, 33(4), 385-390. DOI:10.1080/15230430.2001.12003445

Miles, K.E., Hubbard, B., Irvine-Fynn, T.D.L., Miles, E.S., Quincey, D.J., and Rowan, A.V. 2020. Hydrology of debris-covered glaciers in High Mountain Asia. Earth-Science Reviews, 207, 103212. https://doi.org/10.1016/j.earscirev.2020.103212

Miles, E.S., Pellicciotti, F., Willis, I.C., Steiner, J.F., Buri, P., and Arnold, N.S. 2016. Refined energy-balance modelling of a supraglacial pond, Langtang Khola, Nepal. Annals of Glaciology, 57(71), 29–40. https://doi.org/10.3189/2016AoG71A421

Pan, X., Yu, Q., and You, Y. 2014. Role of rainwater induced subsurface flow in water-level dynamics and thermoerosion of shallow thermokarst ponds on the Northeastern Qinghai–Tibet Plateau, The Cryosphere Discuss., 8, 6117–6146. https://doi.org/10.5194/tcd-8-6117-2014

Rangwala, I., and Miller, J.R. 2012. Climate change in mountains: a review of elevation-dependent warming and its possible causes. Climatic Change 114, 527–547. https://doi.org/10.1007/s10584-012-0419-3

Evaluating InSAR sensitivity to in-situ ground ice contents across different landforms

Lotte Wendt[1,2,3], Line Rouyet[2], Hanne H. Christiansen[3] & Sebastian Westermann[1]

[1]*Department of Geosciences, University of Oslo, Oslo, Norway*

[2]*NORCE Norwegian Research Centre AS, Tromsø, Norway*

[3]*Arctic Geophysics Department, The University Centre in Svalbard (UNIS), Longyearbyen, Svalbard*

This field study aimed to assess how well surface movements from Interferometric Synthetic Aperture Radar (InSAR) satellite remote sensing can document variations in active layer ice contents across a range of permafrost lowland landforms. Here we present the results of the comparison between in-situ ground ice contents and InSAR displacements in Adventdalen, Svalbard. The comparison displays an overall good alignment of the InSAR subsidence in the thawing season 2023 to the expected subsidence from ground ice content melt. Late season subsidence from the ice-rich uppermost permafrost is observed, and the diverse active layer stratigraphy leads to a large variability in displacement patterns.

Background

In periglacial landscapes, the thawing and freezing of the active layer induces a seasonal subsidence and heave pattern. These dynamics can be documented with InSAR remote sensing.

Previous studies have investigated large scale InSAR displacement patterns, compared active layer soil water contents to InSAR displacement amplitudes and investigated top-of-permafrost ground ice loss (e.g., Chen et al. 2020; Rouyet et al. 2019; Zwieback and Meyer 2021). However, the sensitivity of InSAR subsidence to in-situ active layer ice content melt has not been studied in any large detail.

Methods

The study area is the lower Adventdalen valley in Nordenskiöld Land, Svalbard (Figure 1A). Its tundra landscape is characterised by continuous permafrost and contains a range of periglacial landforms (Figure 1B).

12 sediment cores from the frozen active layer and uppermost permafrost were retrieved in spring 2023 from different landforms with varying InSAR signals (Figure 1). The cores were analysed for volumetric ice content, excess ice content, porosity, grain size and organic matter content.

The active layer thickness at the end of the thawing season was estimated through manual probing and borehole temperatures.

The InSAR surface displacement timeseries were retrieved through Small Baseline Subset (SBAS) processing of Sentinel-1 imagery. The displacement timeseries start with the thaw onset in May 2023 and are evaluated until the start of the freeze-back period in September 2023.

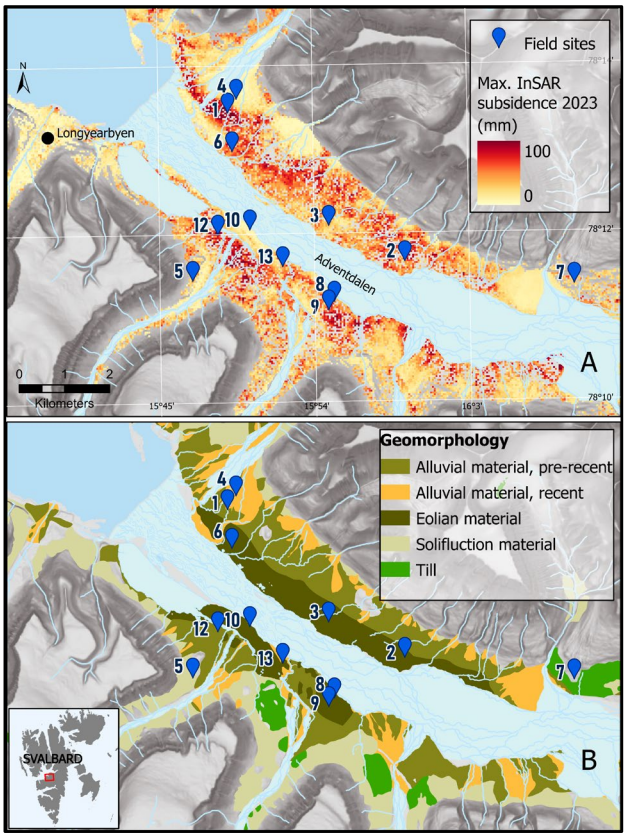

Figure 1. A) Overview map of field sites and maximum InSAR subsidence in the thawing season 2023. B) Geomorphological map of the study area modified from Härtel and Christiansen (2014).

Results

The field measurements reveal a large variability in active layer thickness, ranging from 0.5 – 2 m, reflecting the landform diversity in Adventdalen. The active layer includes sediment layers corresponding to eolian sediment terraces, peatland, solifluction sheets,

active and inactive alluvial fans and till deposits. As a result, the volumetric ice content and especially the occurrence of excess ice is highly heterogeneous, both between sites but also down through the active layer and into the permafrost at the individual sites. Figure 2 shows an example of the diversity of the measured active layer properties.

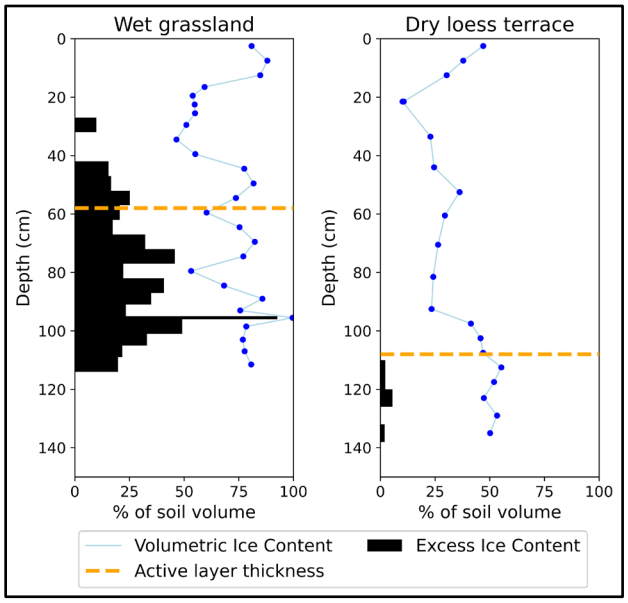

Figure 2. Ground ice contents at site 2 (left) and site 10 (right) through the entire active layer and into the top permafrost.

The InSAR subsidence aligns well with the expected subsidence from the in-situ ice contents. Yet, without considering excess ice layers, the InSAR subsidence cannot be matched. Since 2023 was an exceptionally warm summer, late season subsidence into the ice-rich uppermost permafrost is seen at some sites (Figure 3: wet grassland site).

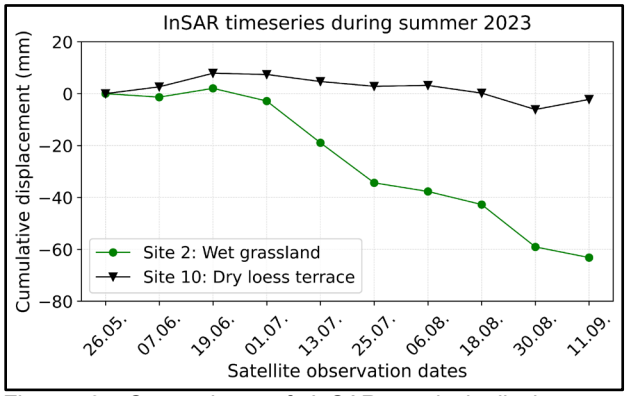

Figure 3. Comparison of InSAR vertical displacement timeseries for the two sites from Figure 2.

Outlook

The evaluation of the field data and comparison to the InSAR timeseries is ongoing.

We will examine the similarities and differences between the InSAR timeseries and point-scale in-situ cryostratigraphies and thereby discuss the ability of InSAR remote sensing to map ground ice.

We plan to test if the InSAR signal can be replicated in the physically-based permafrost model CryoGrid (Westermann et al. 2023). The insights gained from this evaluation will enhance our understanding of the information that can be obtained about ground ice contents from seasonal InSAR timeseries.

Acknowledgements

The fieldwork has been funded through an Arctic Field Grant from the Research Council of Norway (RiS ID 12143). The work is in synergy with the objective of the ESA CCI Permafrost Option 7 IceInSAR (4000123681/18/I-NB).

References

Chen, J., et al. 2020. Active layer freeze-thaw and water storage dynamics in permafrost environments inferred from InSAR. Remote Sensing of Environment 248: 112007. doi:10.1016/j.rse.2020.112007

Härtel, S., and Christiansen, H.H. 2014. Geomorphological and Cryological map of Adventdalen, Svalbard. PANGAEA, doi:10.1594/PANGAEA.833048

Rouyet, L., et al. 2019. Seasonal dynamics of a permafrost landscape, Adventdalen, Svalbard, investigated by InSAR. Remote Sensing of Environment 231: 111236. doi:10.1016/j.rse.2019.111236

Westermann, S., et al. 2023. The CryoGrid community model (version 1.0) – a multi-physics toolbox for climate-driven simulations in the terrestrial cryosphere. Geoscientific Model Development 16: 2607–2647. doi:10.5194/gmd-16-2607-2023

Zwieback, S., and Meyer, F.J. 2021. Top-of-permafrost ground ice indicated by remotely sensed late-season subsidence. The Cryosphere 15: 2041–2055. doi:10.5194/tc-15-2041-2021

Estimating near-surface excess ground ice from InSAR

Simon Zwieback[1,2], Go Iwhana[3], Samantha Taylor[1], Rowan Biessel[4], Soumitra Sakhalkar[1], Qianyu Chang[5] & Franz Meyer[1,2]

[1]*Geophysical Institute, University of Alaska Fairbanks, Fairbanks, Alaska, United States*

[2]*Department of Geosciences, University of Alaska Fairbanks, Fairbanks, Alaska, United States*

[3]*International Arctic Research Center, University of Alaska Fairbanks, Fairbanks, Alaska, United States*

[4]*Department of Earth and Atmospheric Sciences, Cornell University, Ithaca, New York, United States*

[5]*Department of Geography, University of Guelph, Guelph, Ontario, Canada*

The warming and thawing of Arctic permafrost has major impacts on Northern livelihoods, infrastructure, and ecosystems. Where the permafrost is rich in ground ice, thaw can induce terrain instability. We currently lack automated methods to reliably determine near-surface excess ice at fine resolution on regional scales, thus limiting predictions of landscape change and sustainable planning.

We present a satellite-based approach for estimating near-surface excess ground ice profiles. Its primary input are Interferometric Synthetic Aperture Radar (InSAR) observations of thaw-season deformation. It is based on the tenet that subsidence is induced by melting of excess ice at the thaw front; as the thaw front deepens over the summer, we can probe successively deeper strata. We use a fast Bayesian inference method to invert the observed subsidence time series for the unknown excess ice concentrations based on a simple thaw subsidence model.

In years with deep thaw, subsidence at the end of the thaw period provides insight into the (previous years') upper permafrost. We present results from Northwestern Alaska during the exceptionally warm summer of 2019, finding a clear distinction between locations independently determined to be rich or poor in upper-permafrost ground ice.

Methods

The estimation is based on a simple thaw consolidation model according to which surface subsidence is prompted by the melting of subsurface excess ice, with consolidation ensuing from meltwater drainage. The thermal module is based on Stefan-type energy balance considerations and accounts for the coupling between thermal dynamics and subsidence. For a given excess ice profile and ancillary soil stratigraphy, it predicts the position of the thaw front and the surface as a function of time.

The inverse model uses the observed subsidence time series to constrain the volumetric excess ice profile. An ensemble-based Bayesian inversion yields posterior distributions of the excess ground ice profile at each pixel.

Excess ground ice profiles

The accuracy and posterior dispersion of inferred excess ground ice concentrations varied with depth. In simulations, they were best (<0.1) in the central active layer, deteriorating (>0.2) toward the surface and the permafrost table. Validation with in-situ cores at two sites in the Brooks Foothills, Alaska, largely agreed within the observational uncertainty, while the increase in excess ice below the long-term active layer thickness of 40 cm was only reproduced in a warm year.

On regional scales, ice profiles estimated from Sentinel-1 InSAR were spatially associated with the surficial geology in two regions with continuous permafrost. In most geological units, the estimated profiles were ice poor in the central and, to some extent, the upper active layer. In a warm summer, units with ice-rich permafrost had elevated inferred ice contents at depths spanning the base of the active layer and the (previous years') upper permafrost. This suggests that in years with deep penetration of the thaw front, ice-rich materials in the previous years' upper permafrost, including the transient and intermediate layer, can be detected. Conversely, low excess ice was inferred for ice-poor locations such as rubble-covered ridges.

Identifying ice-rich permafrost

Near Kivalina, Northwestern Alaska, we mapped subsidence from Sentinel-1 InSAR during the exceptionally warm summer of 2019 (Figure 1). Elevated late-season subsidence of ~3 cm in ice-rich locations contrasted with ~0 cm in ice-poor locations. A low overlap of 2% between the distributions of late-season subsidence in locations independently determined to be ice-rich and ice-poor, respectively, demonstrates the specificity and sensitivity of the approach for identifying top-of-permafrost excess ground ice.

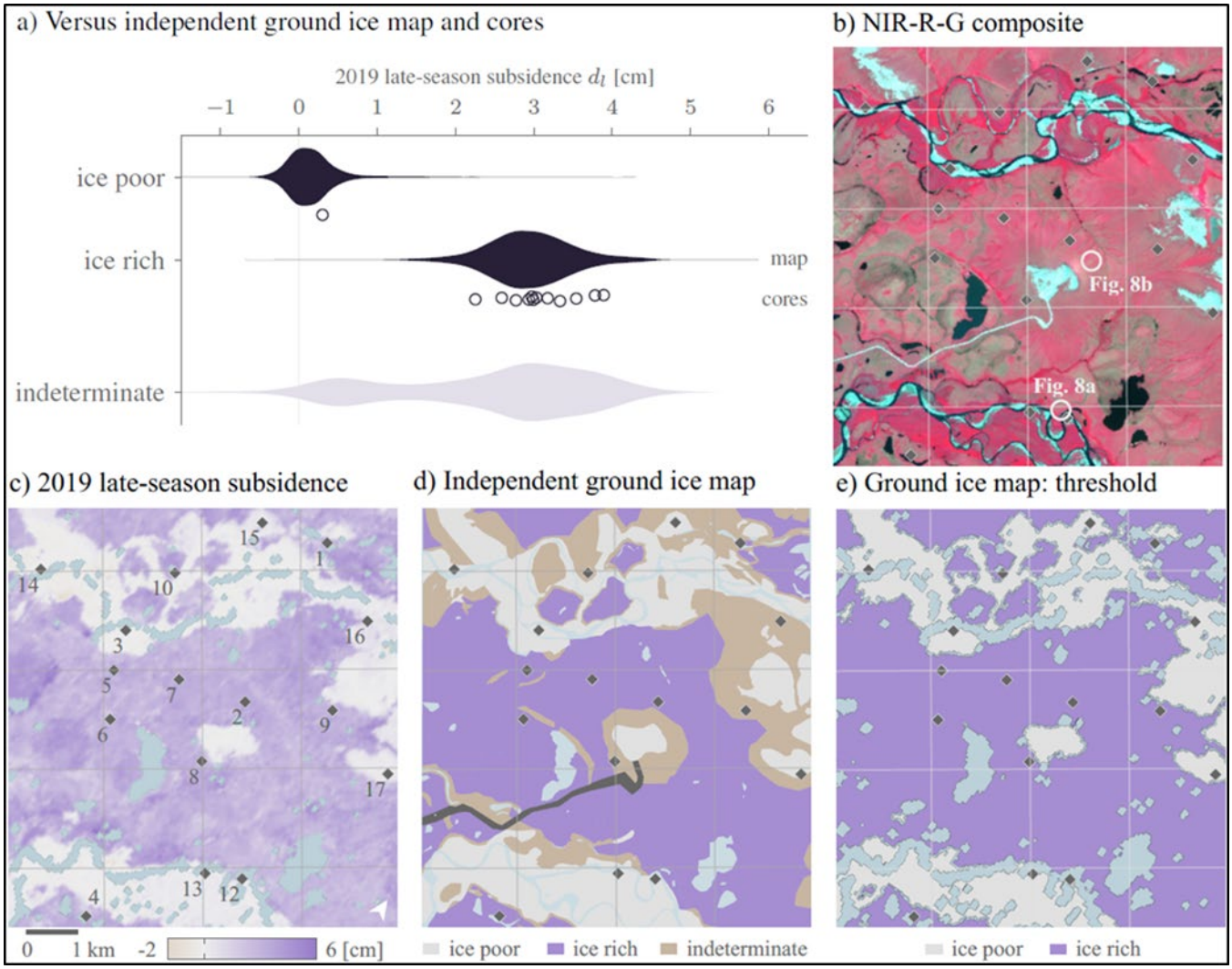

Figure 1. Assessment of late-season subsidence with respect to an independent ground ice map and coring observations. a) Distribution of late-season subsidence; b) Sentinel-2 composite; c) late-season subsidence; d) expert-derived ground ice map based on high-resolution optical imagery, cores, and ancillary information; e) ground ice map obtained by thresholding the InSAR late-season subsidence. From Zwieback and Meyer 2021.

The contrast in late-season subsidence was equally manifest in excess ice contents near the permafrost table inferred by model inversion.

Conclusion

The strengths of this novel method include the ease of automation, the independence of costly ground observations, and its applicability to areas that lack conspicuous manifestations of ground ice. Drawbacks include the insensitivity to excess ice below the thaw front, the dependence on climatic conditions, and observational errors in the InSAR observations. InSAR is thus complementary to ground ice mapping approach based on surficial geology, ground-ice related landforms, and remote sensing of surface proxies such as vegetation.

Pan-Arctic InSAR observations enable novel observational constraints on the controls, drivers and consequences of ground ice formation and loss.

References

Zwieback, S., and Meyer, F.J. 2021. Top-of-permafrost ground ice indicated by remotely sensed late-season subsidence, The Cryosphere, 15, 2041–2055. doi:10.5194/tc-15-2041-2021

Monitoring Permafrost Conditions & Processes

12D — Multiscale Observations of Permafrost Landscape Dynamics

Session Chairs: Simon Zwieback[1], Cornelia Inauen[2] & Mark Lara[3]

[1]*University of Alaska, Fairbanks, Alaska, United States*
[2]*Alfred Wegener Institute, Potsdam, Germany*
[3]*University of Illinois, Champaign, Illinois, United States*

Permafrost landscapes are continually shaped and reshaped by interdependent geomorphic, hydrological, and ecological processes. In light of changing climatic conditions and intensifying disturbance regimes, increased rates of permafrost landscape changes have been reported. However, the spatial distribution, drivers, and controls on these thaw processes remain poorly constrained across spatial and temporal scales. Multiscale observations of dynamic permafrost processes from plot to landscape scales are critical for determining the spatial heterogeneity, scale dependence, and interactions and feedbacks with the water, energy, nutrient, sediment, and carbon cycles.

In this session, we aim to advance permafrost research through novel multiscale observational techniques and analyses. We solicit contributions that (1) quantify geomorphic (e.g., thermokarst, coastal erosion), hydrological (e.g., wetland dynamics) and ecological (e.g., postfire succession, shrub expansion) processes and their interactions; (2) elucidate the drivers, controls and consequences of permafrost landscape change through model-data integration; and/or (3) establish new sensing modalities or analysis techniques that bridge spatiotemporal scales.

Insights into the shallow groundwater system evolution in permafrost-rich alpine environments through aufeis analysis

Michel Baraer[1,2,3], Bastien Charonnat[1,2,3], Eole Valence[2,4], Jeffrey McKenzie[2,4] & Janie Masse-Dufresne[1,2,3]

[1]*Hydrology, Climate and Climate Change laboratory, École de technologie supérieure (ÉTS), Montréal, Québec, Canada*

[2]*GEOTOP (Research Centre on the Dynamics of the Earth System), Montréal, Québec, Canada*

[3]*CentrEau (Quebec Research Water Centre), Québec City, Québec, Canada*

[4]*Department of Earth and Planetary Science, McGill University, Montréal, Québec, Canada*

Alpine environments in cold regions undergo rapid and profound changes due to shifting climates, sparking concerns about the future of ecosystems and downstream water supplies. Traditionally, hydrological studies in these regions have centred on highly visible cryospheric elements like glaciers and snow covers, overlooking buried cryosphere features such as permafrost, ice-cored moraines, and rock glaciers. Similarly, groundwater within cold region alpine valleys has historically been relegated to a minor role in water budget assessments and has consequently received limited attention in research efforts. However, recent investigations reveal that groundwater plays a pivotal role in these environments, exerting significant influence on local watershed dynamics and even broader regional water resources.

Understanding hydrogeology in cold regions' alpine environments presents challenges due to the remote and inaccessible nature of study sites, compounded by harsh winter meteorological conditions. Despite these obstacles, recent studies have highlighted that the winter hydrogeological dynamics of proglacial areas are captured within proglacial aufeis, which are ice formations forming during winter where water sources persist even amidst extended sub-zero air temperatures lasting several months (Terry et al. 2020).

This study aims to investigate aufeis formation within a tributary of the Duke Valley, a glacierized catchment located in the green belt of Mount St-Elias on the Kluane First Nation territory in Yukon. The research employs two distinct methodologies: a field-based approach conducted at the Shar Shäw Tágà (Grizzly Creek) study site and a remote sensing analysis on the same catchment utilizing satellite imagery.

During the field-based phase spanning from 2018 to 2023, our study utilizes time-lapse imagery, hydrochemical tracers, and meteorological records to delineate the key stages of aufeis growth and ascertain the water source contributing to its formation. Our focus area within Shar Shäw Tágà features a segment of the streambed where aufeis forms consistently across most years (Figure 1). When present, the ice spans from the canyon exit at a rock glacier margin to the subsequent meander of the Grizzly Creek River approximately 300 meters downstream. Importantly, the distance between the aufeis formation and the valley's glaciers suggests findings by Chesnokova et al. (2018) regarding the role of groundwater in proglacial riverbed aufeis formation potentially applies to our study area. This supposition gains further support from the recent research of Charonnat et al. (2024), indicating that in the absence of inflow from Grizzly Creek River, the water exiting the canyon originates exclusively from groundwater sources.

Figure 1. Aufeis formation area at the end of the summer (top) and at the 2019 maximum extend.

The field study's results revealed that, over the past three years, aufeis did not form at all. Furthermore, in the years when aufeis did form, there was considerable variability in the dates of formation. Conversely, the ablation consistently occurred within a narrow timeframe, spanning from late May to early June. Interestingly, observations indicated that aufeis growth progressively decelerated or ceased starting around March, despite the sustained subzero air temperatures. During these final months of continuous cold, there were no distinct indications of new ice layer formation, signaling a slowdown or halt in aufeis growth.

The remote sensing part of the study enabled the detection of icing occurrences dating back to 1974. Figure 2 illustrates the relative frequencies of the analyzed aufeis formations spanning the last five decades.

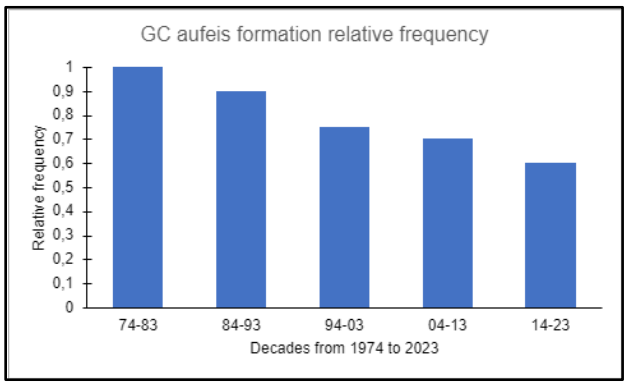

Figure 2. Evolution the Grizzly Creek River aufeis formation occurrence from 1974 to 2023.

The data depicted in Figure 2 reveals a declining trend in aufeis occurrences over time. Recent studies by Pavelsky and Zarnetske (2017) and Zemlianskova et al. (2023) corroborate this negative tendency. However, the literature lacks a consensus regarding the underlying cause of this decline. While some studies, like Zemlianskova et al. (2023), attribute the decrease in aufeis extent or occurrence to fluctuations in fall and winter meteorological conditions, others, such as Dubnick et al. (2023), propose that aufeis occurrence are influenced by water supply and hydraulic conditions beneath the aufeis.

A statistical examination of the relative occurrences of aufeis formation, as obtained from remote sensing data (see Figure 2), suggests a possible connection between the absence of aufeis formation and meteorological conditions from the previous summer. If these results are confirmed, they would provide evidence in favor of the theory that aufeis formation depends on factors affecting groundwater dynamics, such as permafrost degradation or groundwater replenishment. The correlation between aufeis formation and longer-term factors like groundwater dynamics implies that aufeis might serve as a valuable indicator of groundwater evolution in alpine cold regions. Its sensitivity to processes beyond immediate seasonal variations positions aufeis as a crucial source of information regarding the broader changes in groundwater behavior over extended periods in these environments.

REFERENCES

Charonnat, B., Baraer, M., Masse-Dufresne, J., Valence, E., McKenzie, J., Monty, C., Wang, K., and Devoie, E. 2024. Rock glaciers are shaping the subsurface drainage of proglacial areas. 12th International Conference on Permafrost, Yukon, Canada.

Chesnokova, A., Baraer, M., and Bouchard, E. 2020. Proglacial icings as records of winter hydrological processes. The Cryosphere, 14, 4145–4164. https://doi.org/10.5194/tc-14-4145-2020

Dubnick, A., Turcotte, B., Girard, M., and Saal, S., 2023. Control on aufeis formation: lessons from a small Yukon stream. 22nd Workshop on the hydraulics of Ice-Covered Rivers, CGU, Canmore, Alberta Canada.

Pavelsky, T., and Zarnetske, J. 2017. Rapid decline in river icings detected in Arctic Alaska: Implications for a changing hydrologic cycle and river ecosystems. Geophysical Research Letters, 44. https://doi.org/10.1002/2016GL072397

Terry, N., Grunewald, E., Briggs, M., Gooseff, M., Huryn, A., Kass, A., Tape, K., Hendrickson, P., and Lane, J.W. 2020. Seasonal Subsurface Thaw Dynamics of an Aufeis Feature Inferrer From Geophysical Methods. Journal of Geophysical Research: Earth Surface, 125. https://doi.org/10.1029/2019JF005345

Zemlianskova, A., Makarieva, O., Shikhov, A., Alekseev, V., Nesterova, N., and Ostashov, A. 2023. The impact of climate change on seasonal glaciation in the mountainous permafrost of North-Eastern Eurasia by the example of the giant Anmangynda aufeis. Catena, 233, 107530. https://doi.org/10.1016/j.catena.2023.107530

Predicting ice wedge polygons and visible ground ice at regional scales using remote sensing

Qianyu Chang[1], Simon Zwieback[2] & Aaron Berg[1]

[1]*Department of Geography, Environment and Geomatics, University of Guelph, Guelph, Ontario, Canada*

[2]*Geophysical Institute, University of Alaska Fairbanks, Fairbanks, Alaska, United States*

Ice wedge polygon (IWP) networks are a common terrain feature in the western Canadian Arctic (Kokelj et al. 2014), formed by the repetitive thermal cracking of ground and infilling of water that then freezes into wedge ice. IWPs play an important role in the climate and carbon feedback of the Arctic, as their microtopography introduces spatial variations in ground thermal regime, snow cover distribution, hydrological channels, and vegetation composition (Jorgenson et al. 2015; Liljedahl et al. 2016; Wainwright et al. 2015).

Ground ice content, which includes wedge ice, is an important permafrost variable that controls permafrost thaw and is responding rapidly to the changing climate. Thawing of ice-rich permafrost and the consequent landscape change can have pronounced ecological and societal consequences, including changes in drainage pattern, vegetation composition, and greenhouse gas emissions, as well as damages to infrastructure (Becker et al. 2016; Lara et al. 2015; Liljedahl et al. 2016).

However, mapping ground ice over large area is challenging because it is not directly visible on the surface. While some wedge ice can be inferred from active IWPs, some may not have clear surficial expressions. Thus, there is currently almost no regional-scale ground ice or IWP maps, hindering our ability to understand the controls on ground ice content or to effectively map permafrost vulnerability under a changing climate. Mid-resolution remote sensing and topography have the potential to predict IWP and ground ice thanks to the numerous links between surface and subsurface processes. However, such predictability has not been quantified.

We explored the applicability of random forest in predicting IWPs and ground ice occurrence using remote sensing and topographic indices on a regional scale. Out study is focused on the Tuktoyaktuk Coastal Plain in Northwest Territories, Canada, an area underlain by ice-rich continuous permafrost and characterized by numerous IWPs (Kokelj et al. 2014; Lantz et al. 2017). We used IWP inventory data covering the study area (Lantz et al. 2017) and borehole records along the Inuvik-Tuktoyaktuk Highway corridor (Castagner et al. 2022) as reference data for IWP and ground ice occurrence, respectively.

For the IWP prediction model, we generated 60,000 random points across the study area and classified them as either IWP (1) or non-IWP (0) according to the reference data. For the ground ice model, we classified the 564 borehole records as ice-rich (1) or ice-poor (0) based on the presence of visible ground ice in the top 5 m. We used the same set of predictor variables for both the IWP and ground ice models, including a suite of topographic variables derived from the 30 m Copernicus digital elevation model (DEM), Landsat 5 vegetation indices, PALSAR backscatters, distance to the coast, and surficial geologies (Figure 1). To identify the best set of predictors, we tested 5 random forest models, starting with only the most basic DEM variables (Model 1) and then gradually adding more predictors, until all variables were included (Model 5). Each model was optimized with hyperparameter tuning and evaluated by the ROC AUC score, a metric showing how well the model distinguished between positive and negative classes.

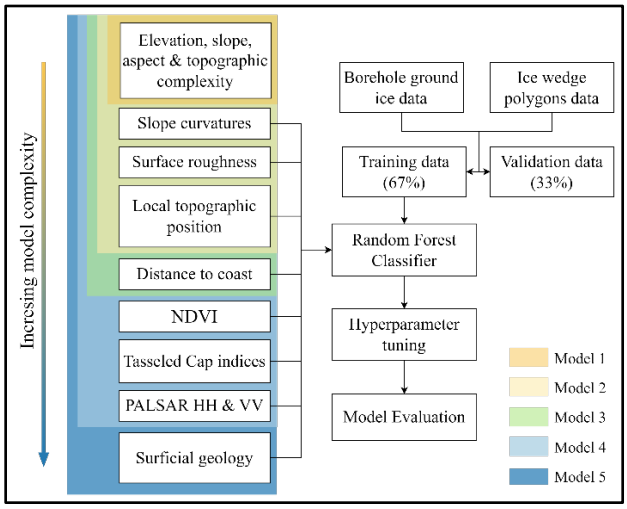

Figure 1. Flowchart of data processing and random forest models.

We found that the model with the best performance for both IWP and ground ice predictions had all predictors but surficial geology. We achieved a ROC AUC score of 0.95 for IWP prediction, with a close alignment of spatial pattern between the model

prediction and the reference data (Figure 2). The topographic variables and distance to the coast were the most important predictors, emphasizing the role of geographic settings in controlling IWP formations. The model also successfully predicted IWP occurrence in elevated areas further away from the coast, which was commonly assumed to have scarce IWPs due to its unfavourable conditions for IWP development.

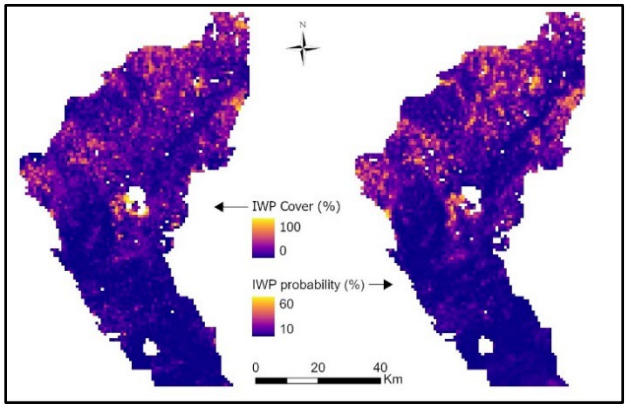

Figure 2. Maps of IWP areal cover based on the reference dataset (left) vs. IWP probability predicted by random forest model (right). Resolution = 900 m for easier visual comparison.

For ground ice prediction, the model achieved a ROC AUC score of 0.70, but with a high false-positive rate (i.e., ice-poor samples were frequently labeled as ice-rich). This skewed result is partially limited by our small number of ice-poor samples (12.3% of all samples), as the study area is dominated by ice-rich permafrost. Our results highlight the potentials of ground ice prediction using surface characteristics, providing abundant and balanced reference data. The results also highlight current challenges in predicting ground ice based on remotely sensible surface characteristics, as they may not accurately reflect the long-term geological and glacial histories that shaped the ground ice conditions in the western Canadian Arctic.

REFERENCE

Becker, M.S., Davies, T.J., and Pollard, W.H. 2016. Ground ice melt in the high Arctic leads to greater ecological heterogeneity. J Ecol 104, 114–124. https://doi.org/10.1111/1365-2745.12491

Castagner, A., Brenning, A., Gruber, S., and Kokelj, S. 2022. Vertical distribution of excess ice in icy sediments and its statistical estimation from geotechnical data (Tuktoyaktuk Coastlands and Anderson Plain, Northwest Territories). Arctic Science 9. https://doi.org/10.1139/AS-2021-0041

Jorgenson, M.T., Kanevskiy, M., Shur, Y., Moskalenko, N., Brown, D.R.N., Wickland, K., Striegl, R., and Koch, J., 2015. Role of ground ice dynamics and ecological feedbacks in recent ice wedge degradation and stabilization. J. Geophys. Res. Earth Surf. 120, 2280–2297. https://doi.org/10.1002/2015JF003602

Kokelj, S.V., Lantz, T.C., Wolfe, S.A., Kanigan, J.C., Morse, P.D., Coutts, R., Molina-Giraldo, N., and Burn, C.R., 2014. Distribution and activity of ice wedges across the forest-tundra transition, western Arctic Canada. Journal of Geophysical Research: Earth Surface 119, 2032–2047. https://doi.org/10.1002/2014JF003085

Lantz, T.C., Steedman, S.V., Kokelj, S.V., and Segal, R.A., 2017. Inventory of polygonal terrain in the Tuktoyaktuk Coastlands, Northwest Territories, Northwest Territories Geological Survey. NWT Open Report 2016-022. https://doi.org/10.46887/2016-022

Lara, M.J., McGuire, A.D., Euskirchen, E.S., Tweedie, C.E., Hinkel, K.M., Skurikhin, A.N., Romanovsky, V.E., Grosse, G., Bolton, W.R., and Genet, H., 2015. Polygonal tundra geomorphological change in response to warming alters future CO2 and CH4 flux on the Barrow Peninsula. Glob Chang Biol 21, 1634–1651. https://doi.org/10.1111/gcb.12757

Liljedahl, A.K., Boike, J., Daanen, R.P., Fedorov, A.N., Frost, G.V., Grosse, G., Hinzman, L.D., Iijma, Y., Jorgenson, J.C., Matveyeva, N., Necsoiu, M., Raynolds, M.K., Romanovsky, V.E., Schulla, J., Tape, K.D., Walker, D.A., Wilson, C.J., Yabuki, H., and Zona, D. 2016. Pan-Arctic ice-wedge degradation in warming permafrost and its influence on tundra hydrology. Nature Geosci 9, 312–318. https://doi.org/10.1038/ngeo2674

Wainwright, H.M., Dafflon, B., Smith, L.J., Hahn, M.S., Curtis, J.B., Wu, Y., Ulrich, C., Peterson, J.E., Torn, M.S., and Hubbard, S.S. 2015. Identifying multiscale zonation and assessing the relative importance of polygon geomorphology on carbon fluxes in an Arctic tundra ecosystem. Journal of Geophysical Research: Biogeosciences 120, 788–808. https://doi.org/10.1002/2014JG002799

Rates and patterns of permafrost thaw induced landcover change in discontinuous permafrost peatlands

Mason Dominico[1], William Quinton[1], Stephanie Wright[2] & Ryan F. Connon[3]

[1]*Department of Geography and Environmental Studies, Wilfrid Laurier University, Waterloo, Ontario, Canada*

[2]*Department of Civil Engineering, Queen's University, Kingston, Ontario, Canada*

[3]*Environment and Climate Change, Government of Northwest Territories, Yellowknife, Northwest Territories, Canada*

The subarctic region of northwestern Canada is undergoing accelerated warming, impacting the stability and presence of permafrost (Smith et al. 2022; Osborne et al. 2018). In peatland-dominated regions of sporadic and discontinuous permafrost, permafrost is often at disequilibrium with the current climate and increasingly susceptible to thaw. In these regions, common permafrost features are peat plateaus, where the permafrost core raises the ground surface 1 to 2 m above surrounding permafrost-free wetlands and creates dry near-surface conditions that support dense stands of black spruce trees. When permafrost thaws, the surrounding wetlands expand at the expense of permafrost supported forests. This landcover change is rapidly transforming the hydrology of these regions, impacting surface-ground water interactions altering the storage, transport and connectivity of water through northern basins (Wright et al. 2022).

Study Objective

To understand the rates and patterns of permafrost thaw at the landscape scale, remote sensing techniques are employed to monitor the shifting areal proportions of permafrost (Philipp et al. 2021). Conversely, intensive in-situ monitoring and data collection provide valuable information to elucidate sub-grid processes influencing thaw rates on a point scale as well as refine numerical modelling efforts (Devoie et al. 2019). This study seeks to integrate landscape and point scale data to improve the understanding of the rates and patterns of permafrost thaw on the landscape.

Plateau Fragmentation– Remote Sensing Analysis

To estimate the reduction in the area of terrain underlain by permafrost, a 4 km^2 area of interest (AOI) was selected in the headwaters of the Scotty Creek basin, located in the southern Dehcho region in the Northwest Territories, Canada. Permafrost was then digitized and inventoried to compare across three reference points (1977, 2010 and 2018) using a combination of air photos, multispectral imagery and LiDAR derived products. The results showed that the proportion of area underlain by permafrost in the 4 km^2 AOI decreased from 51% in 1977 to 43% in 2010, and to 40% in 2018. Results showed that large peat plateau complexes fragmented into a higher number of smaller isolated plateaus, while small permafrost-free wetlands expanded and coalesced into larger wetland networks. Of the 73 plateaus identified in the 1977 baseline image, 29% were no longer detected in 2018 while the total number of plateaus inventoried increased by 60% (121) in 2018 (Figure 1).

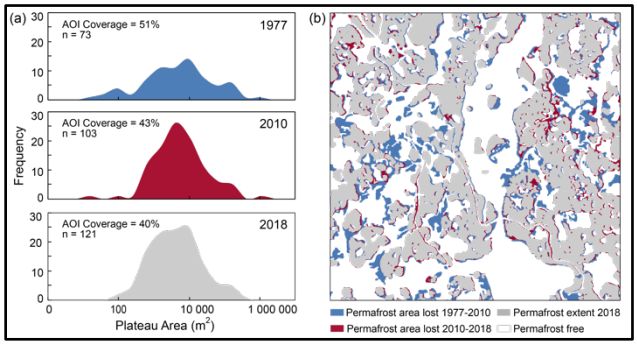

Figure 1. A) Frequency distributions of plateau area as determined by manual delineation. B) Identification of areas within the 2 × 2 km AOI where permafrost was lost during specific time periods.

Integrated Measurements

To integrate the multiple scales of measurement, a stable plateau with baseline data from 2010 to present was selected for intensive study. This baseline data includes geophysical (electrical resistivity tomography) data (2010 to present), ground temperature data (2018 to present), and repeated manual measurements of the depth to permafrost (2011 to present). Geophysical surveys suggest that permafrost beneath the study plateau thawed by 0.5 m at the base of the permafrost between 2010 (McClymont et al. 2013) and 2019 Manual frost probe measurements suggest that depth to permafrost from the ground surface has increased by 0.25 m over the same time period. Combining these in-situ measurements with results from the remote sensing analysis show that the study plateau has lost 13% of permafrost volume over the past decade. Of this loss, basal (5%) and lateral (5%) thaw were the two

most significant factors (Table 1) Should the observed rate of thaw be maintained, linear forecasts predict that this permafrost body will disappear by 2070.

Table 1. Estimated permafrost volume below the Study Plateau in 2010 and 2018.

Parameter	2010	2018	Difference
Surface area (m^2)	16 424	15 581	843 (5%)
Depth to permafrost (m)	0.62	0.88	0.25
Depth to base of permafrost (m)	10	9.5	0.5
Volume of permfrost (m^3)	154 057	134 308	19 749(13%)
Volume lost from above (m^3)	-	-	4051 (3%)
Volume lost from below (m^3)	-	-	7790 (5%)
Volume lost from sides (m^3)	-	-	7266 (5%)

REFERENCES

Devoie, É.G., Craig, J.R., Connon, R.F., and Quinton, W.L. 2019. Taliks: A tipping point in discontinuous permafrost degradation in peatlands. Water Resources Research, 55(11), 9838–9857.

McClymont, A.F., Hayashi, M., Bentley, L.R., and Christensen, B.S. 2013. Geophysical imaging and thermal modeling of subsurface morphology and thaw evolution of discontinuous permafrost. Journal of Geophysical Research: Earth Surface, 118(3), 1826–1837.

Osborne, E., Richter-Menge, J., and Jeffries, M. Eds., 2018. Arctic report Card 2018. https://www.arctic.noaa.gov/Report-Card

Philipp, M., Dietz, A., Buchelt, S., and Kuenzer, C. 2021. Trends in satellite Earth observation for permafrost related analyses—A review. Remote Sensing, 13(6), 1217.

Smith, S.L., O'Neill, H.B., Isaksen, K., Noetzli, J., and Romanovsky, V.E. 2022. The changing thermal state of permafrost. Nature Reviews Earth & Environment, 3(1), 10–23.

Wright, S.N., Thompson, L.M., Olefeldt, D., Connon, R.F., Carpino, O.A., Beel, C.R., and Quinton, W.L. 2022. Thaw-induced impacts on land and water in discontinuous permafrost: A review of the Taiga Plains and Taiga Shield, northwestern Canada. Earth-Science Reviews, 232, 104104.

Remote sensing, geophysics, and ground based surveys quantify top-down and lateral permafrost thaw following fire disturbance

Thomas A. Douglas[1], M. Torre Jorgenson[2], Taylor Sullivan[1] & Caiyun Zhang[3]

[1]*U.S. Army Cold Regions Research and Engineering Laboratory, Fort Wainwright, Alaska, United States*

[2]*Alaska Ecoscience, Fairbanks, Alaska, United States*

[3]*Department of Geosciences, Florida Atlantic University, Boca Raton, Florida, United States*

Climate warming in Interior Alaska has led to the degradation of discontinuous permafrost across the region (Jorgenson et al. 2020; Douglas et al. 2021; Farquharson et al. 2022). Changes in permafrost extent affect hydrology, ecological processes, and the carbon cycle (Douglas et al. 2014) and pose infrastructure challenges. With warming projected to accelerate over coming decades the rates and extent of these changes are expected to increase. However, means of quantifying permafrost thaw across space and time are limited.

Recent research has used repeat imagery and airborne LiDAR to identify hotspots of permafrost thaw and ground surface subsidence (Zhang et al. 2023). These studies leverage differences in surface elevation or vegetation cover as indicators for where permafrost extent has changed in the subsurface. Combining repeat geophysical measurements with surface and subsurface surveys has shown utility in mapping three-dimensional changes in permafrost extent (Minsley et al. 2023).

In this study, we combined perspectives from electrical resistivity tomography, ground validations, and airborne remote sensing measurements to identify rates and morphologies of surface and subsurface permafrost degradation as a function of time since disturbance on the Tanana Flats lowland near Fairbanks, Alaska. The field sites represent three different aged fire scars from wildfires in 1988, 2001, and 2020 and an unburned reference location to identify rates of change attributable to recent climate warming in the area as well as time since wildfire disturbance. Repeat measurements spanning 8 years (2012 and 2020) allowed us to quantify surface subsidence and subsurface thaw of permafrost at the sites and identify how much thaw was likely attributable to recent climate warming (press disturbance) versus thaw associated with wildfires (pulse disturbance).

Study Site

The study focused on four transects located along the northern edge of the Tanana Flats lowland south of Fairbanks, Alaska (Figure 1). Covering 6,000 km^2, Tanana Flats is characterized by a heterogeneous patchwork of forested areas underlain by discontinuous permafrost up to 50 m thick as well as numerous collapse-scar bogs and fens (Douglas et al. 2014). The bogs and fens are not generally underlain by permafrost, but their outside margins are dictated by frozen ground. From the air these wetland features are readily apparent, however, the morphology of their subsurface permafrost boundaries is not well known. Detailed descriptions of the ecology, hydrogeology, and permafrost thermal state are provided elsewhere (Douglas et al. 2016; Jorgenson et al. 2022).

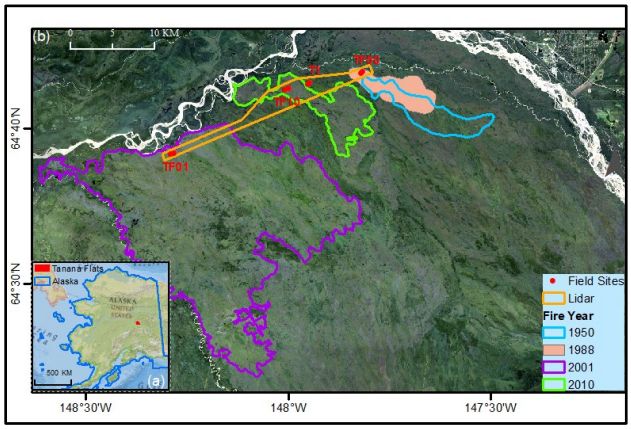

Figure 1. A location map in Interior Alaska with the three fire scars (TF50, TF01, and TF10) and the undisturbed site (T1) identified.

Field Measurements

Electrical resistivity tomography (ERT) measurements were made along ~400 meter-long linear transects at three different aged fire scars “TF50” (1988), “TF01 (2001), “TF10” (2010) and an unburned reference location “TF1.” Measurements were made in 2012 and repeated in 2020. We used an Advanced Geosciences Incorporated (Austin, Texas) SuperSting R8 eight-channel portable induced polarization galvanic earth resistivity meter. More detailed operational information for measurements made in 2012 is provided in Douglas et al. 2016). Resistivity values above 800 Ωm have been shown to represent syngenetic permafrost bodies near Fairbanks (Yoshikawa et al. 2006). Six cables with a total of

84 take-out electrodes were pounded into the ground at 2 m spacings at each site. A dipole-dipole array was used for all measurements due to its lateral sensitivity in permafrost extent (Kneisel 2006). Electrodes were typically 45 cm to 1 m in length.

RESULTS

Cross sections showing changes in ground surface elevation, active layer depth, and resistivity are included in Figure 2.

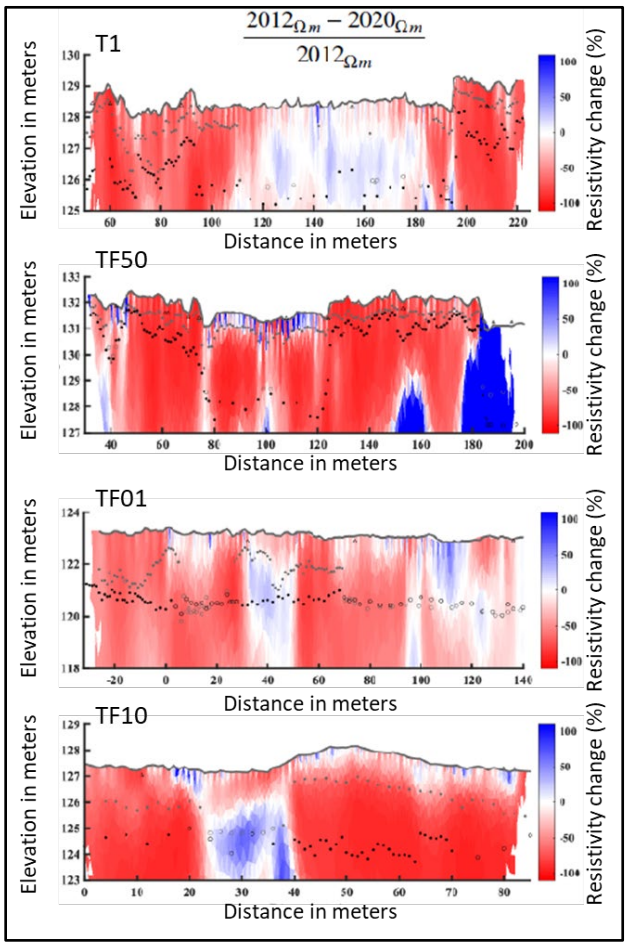

Figure 2. Differences in electrical resistivity inverse solutions from the four Tanana Flats sites. T1 is unburned while TF50, TF01, and TF10, represent fire scars from 1988, 2001, and 2010, Active layer depths (filled circles) and maximum observed unfrozen depths (open circles), are shown with black denoting 2020 and grey denoting 2012.

All four sites exhibited changes in the top of near surface permafrost between 2012 and 2020 as well as lateral thaw expansion of non-permafrost bog features (light colored regions in each transect) into permafrost plateaus. The greatest thaw of top-down permafrost occurred at TF10 (up to 2 meters) followed by TF01 and TF50 with the least top-down thaw (~1 meter) occurring at the unburned site T1. Clearly the wildfire disturbance increased the thaw of near-surface permafrost at greater rates than ongoing climate warming.

REFERENCES

Douglas, T.A., Jorgenson, M.T., Brown, D.R., Campbell, S.W., Hiemstra, C.A., Saari, S.P., Bjella, K., and Liljedahl, A.K. 2016. Degrading permafrost mapped with electrical resistivity tomography, airborne imagery and LiDAR, and seasonal thaw measurements. Geophysics, 81(1), pp.WA71–WA85.

Douglas, T.A., et al. 2021. Recent degradation of interior Alaska permafrost mapped with ground surveys, geophysics, deep drilling, and repeat airborne lidar. The Cryosphere, 15(8), pp.3555–3575.

Farquharson, L.M., Romanovsky, V.E., Kholodov, A., and Nicolsky, D. 2022. Sub-aerial talik formation observed across the discontinuous permafrost zone of Alaska. Nature Geoscience, 15(6), pp.475–481.

Jorgenson, M.T., et al. 2020. The roles of climate extremes, ecological succession, and hydrology in repeated permafrost aggradation and degradation in fens on the Tanana Flats, Alaska. Journal of Geophysical Research:Biogeosciences, 125(12), p.e2020JG005824.

Jorgenson, M.T., Brown, D.R., Hiemstra, C.A., Genet, H., Marcot, B.G., Murphy, R.J., and Douglas, T.A. 2022. Drivers of historical and projected changes in diverse boreal ecosystems: fires, thermokarst, riverine dynamics, and humans. Environmental Research Letters, 17(4), p.045016.

Kneisel, C. 2006. Assessment of subsurface lithology in mountain environments using 2D resistivity imaging. Geomorphology, 80(1-2), 32–44.

Minsley, B.J., Pastick, N.J., James, S.R., Brown, D.R., Wylie, B.K., Kass, M.A., and Romanovsky, V.E. 2022. Rapid and gradual permafrost thaw: A tale of two sites. Geophysical Research Letters, 49(21), p.e2022GL100285.

Yoshikawa, K., Leuschen, C., Ikeda, A., Harada, K., Gogineni, P., Hoekstra, P., Hinzman, L., Sawada, Y., and Matsuoka, N. 2006. Comparison of geophysical investigations for detection of massive ground ice (pingo ice). Journal of Geophysical Research: Planets, 111(E6).

Zhang, C., Douglas, T.A., Brodylo, D., and Jorgenson, M.T. 2023. Linking repeat lidar with Landsat products for large scale quantification of fire-induced permafrost thaw settlement in interior Alaska. Environmental Research Letters. 18(1):015003.

The role of ice-cored landforms in the transformation of proglacial landscapes in periglacial (Svalbard) and non-periglacial (SE Iceland) settings

Marek W. Ewertowski[1], David J.A. Evans[2], David H. Roberts[2], Aleksandra M. Tomczyk[1] & Szymon Śledź[1]

[1]*Faculty of Geographical and Geological Sciences, Adam Mickiewicz University, Poznan, Poland*

[2]*Department of Geography, Durham University, Durham, United Kingdom*

In many polar and mountain environments, proglacial landscapes are especially important as they often contain an abundance of sediments readily available for transport and ice-cored landforms, which may constitute a significant proportion of the ice within the catchments (Schomacker 2008; Evans 2009). As proglacial areas can be highly dynamic, understanding their transformation is crucial for the correct interpretation and reconstruction of past glacial events and prediction of the potential delivery of meltwater and sediments down valleys. In addition, some of the processes observed in proglacial areas might have a character of cryo-conditioned geo-hazards (Kääb et al. 2005). However, our knowledge about the quantitative aspect of landscape changes in front of retreating glaciers remains unsatisfactory (Carrivick and Heckmann 2017).

In this study, we focused on the role of ice-cored landforms (ice-cored moraines, ice-cored eskers, buried ice within outwash plains) in the transformation of proglacial landscapes. The main aim was to quantify the degradation of ice-cored landforms at different temporal (weekly, annual, decadal) and spatial scales (whole glacial foreland, individual landforms) and to evaluate the changing patterns of geomorphological processes responsible for proglacial landscape transformation. In this contribution, we summarise the results of our previous studies conducted in Svalbard and SE Iceland to compare rates and roles of ice-cored landform transformations in periglacial and non-periglacial settings.

Study areas and methods

We quantified the dynamics of ice-cored landforms for glacial forelands in periglacial environments of central Spitsbergen, Svalbard (Ebbabreen, Ragnarbreen, Hørbyebreen) (Ewertowski 2014; Ewertowski and Tomczyk 2015; Ewertowski and Tomczyk 2020; Ewertowski et al. 2019) and non-periglacial settings of SE Iceland (Fjallsjökull, Hrútárjökull, Kvíárjökull, Breiðamerkurjökull) (Evans et al. 2023; Śledź et al. 2023). Volumetric transformation of the landforms was calculated from DEMs of differences (DoDs) constructed based on data collected using topographic surveys and unmanned aerial vehicle (UAV) surveys or generated from stereo pairs of archival aerial photographs. Planimetric transformations were investigated based on all available remote sensing datasets (historical aerial photographs, high-resolution satellite images, UAV-collected data) and field-based data) and therefore covered relatively extended historical timescales.

Results and discussion

Short-term (annual) transformations of ice-cored landforms can be substantial, with elevation lowering ranging from 0.14 m a^{-1} to 1.83 m a^{-1} in the 2012-2024 period in Ragnarbreen and Ebbabreen (Svalbard) (Ewertowski and Tomczyk 2015). Degradation of the ice-cored moraine complex in front of Kvíárjökull (SE Iceland) was at the rate of 0.82 m a^{-1} in 2014-2022 (Śledź et al. 2023). For Ice-cored landforms in the overdeepening of Hrútárjökull and Fjallsjökull (SE Iceland), the average lowering of elevation in the period 2014-2022 was at 0.79 m a^{-1} and 0.63 m a^{-1}, respectively (Evans et al. 2023). Average long-term (decadal) changes of ice-cored moraines were usually lower; for example, in the period 1960-2009, the ice-cored moraine complex at Hørbyebreen degraded at the rate of 0.15 m a^{-1} (Ewertowski et al. 2019) and 0.03 m a^{-1} in case of Ragnarbreen (Svalbard) (Ewertowski 2014).

We also demonstrated that the response of the ice-cored landforms to global and regional climate warming is filtered by local conditions such as topography, thickness of debris cover and abundance of meltwater. Therefore, their role in the transformation of the proglacial landscape is strongly variable in both time and space. Depending on the glacier, some parts of the ice-cored landforms (from ~10% to >50%) were stable in short-term as well as decadal temporal scales, which indicated that they could stay in equilibrium with current climatic and environmental conditions and be a stable landscape component for at least 50-60 years. The remaining parts of ice-cored landforms degraded at different rates, with zones of highest degradation migrating as the ice margins retreated and left unstable, partly ice-cored topography. Such unstable landforms

were first transformed by mass wasting processes and, depending on the degree of coupling between glacifluvial and moraine components, could temporarily store sediments and ice for different time periods (from days to tens of years) until they become fully depleted.

ACKNOWLEDGEMENTS

This research was funded by the National Science Centre, Poland, Grant Number 2019/35/B/ST10/03928.

REFERENCES

Carrivick, J.L., and Heckmann, T. 2017. Short-term geomorphological evolution of proglacial systems, Geomorphology, 287: 3–28. doi:10.1016/j.geomorph.2017.01.037

Evans, D.J.A. 2009. Controlled moraines: origins, characteristics and palaeoglaciological implications, Quaternary Science Reviews, 28: 183–208. doi:10.1016/j.quascirev.2008.10.024

Evans, D.J.A., Ewertowski, M.W., Tomczyk, A., and Chandler, B.M.P. 2023. Active temperate glacial landsystem evolution in association with outwash head/depositional overdeepenings, Earth Surface Processes and Landforms, 48: 1573–1598. doi:10.1002/esp.5569

Ewertowski, M. 2014. Recent transformations in the high-arctic glacier landsystem, Ragnarbreen, svalbard, Geografiska Annaler: Series A, Physical Geography, 96: 265–285. doi:10.1111/geoa.12049

Ewertowski, M.W., Evans, D.J.A., Roberts, D.H., Tomczyk, A.M., Ewertowski, W., and Pleksot, K. 2019. Quantification of historical landscape change on the foreland of a receding polythermal glacier, Hørbyebreen, Svalbard, Geomorphology, 325: 40–54. doi:10.1016/j.geomorph.2018.09.027

Ewertowski, M.W., and Tomczyk, A.M. 2015. Quantification of the ice-cored moraines' short-term dynamics in the high-Arctic glaciers Ebbabreen and Ragnarbreen, Petuniabukta, Svalbard, Geomorphology, 234: 211–227. doi:10.1016/j.geomorph.2015.01.023

Ewertowski, M.W., and Tomczyk, A.M. 2020. Reactivation of temporarily stabilized ice-cored moraines in front of polythermal glaciers: Gravitational mass movements as the most important geomorphological agents for the redistribution of sediments (a case study from Ebbabreen and Ragnarbreen, Svalbard), Geomorphology, 350: 106952. doi:10.1016/j.geomorph.2019.106952

Kääb, A., Huggel, C., Fischer, L., Guex, S., Paul, F., Roer, I., Salzmann, N., Schlaefli, S., Schmutz, K., and Schneider, D. 2005. Remote sensing of glacier-and permafrost-related hazards in high mountains: an overview, Natural Hazards and Earth System Science, 5: 527–554.

Schomacker, A. 2008. What controls dead-ice melting under different climate conditions? A discussion, Earth-Science Reviews, 90: 103–113. doi:10.1016/j.earscirev.2008.08.003

Śledź, S., Ewertowski, M.W., and Evans, D.J.A. 2023. Quantification of short-term transformations of proglacial landforms in a temperate, debris-charged glacial landsystem, Kvíárjökull, Iceland, Land Degradation & Development, 34: 5566–5590. doi:10.1002/ldr.4865

Multi-platform remote sensing for mapping and assessing the optical variability of permafrost thaw ponds in Nunavik, Subarctic Canada

Pedro Freitas[1,2], Gonçalo Vieira[1,2], Diana Martins[1], Teresa Cabrita[1], João Canário[2,3], Diogo Folhas[2,3], Warwick F. Vincent[2,4], Pedro Pina[5,6], Bennet Juhls[7], Birgit Heim[7] & Carla Mora[1]

[1]*Centro de Estudos Geográficos, Laboratório Associado TERRA, IGOT, Universidade de Lisboa, Lisboa, Portugal*

[2]*Centre d'Études Nordiques, Université Laval, Québec City, Québec, Canada*

[3]*Centro de Química Estrutural, Institute of Molecular Sciences and Department of Chemical Engineering, Instituto Superior Técnico, Universidade de Lisboa, Lisboa, Portugal*

[4]*Département de biologie, Université Laval, Québec City, Québec, Canada*

[5]*Departamento de Ciências da Terra, Universidade de Coimbra, Coimbra, Portugal*

[6]*Instituto Dom Luiz, Universidade de Coimbra, Coimbra, Portugal*

[7]*Alfred Wegener Institute, Potsdam, Germany*

Permafrost is warming at the global scale (Biskaborn et al. 2019), and constitutes a significant pool of carbon, nutrients and contaminants (Olefeldt et al. 2016). As permafrost warms and thaws, old carbon is no longer isolated from the climate system, increasing the amount of carbon released as greenhouse gases to the atmosphere. Therefore, permafrost thawing acts as a positive feedback loop that induces yet more climate warming (Schaefer et al. 2014).

Permafrost depletion can occur gradually by active layer deepening, or abruptly with the formation of thermokarst, referring to the subsidence, erosion and collapse of the ground. As opposed to gradual thaw, which is more predictable and easier to model and integrate into Earth System Models, most of the mechanisms related to abrupt permafrost thaw are not yet accurately depicted in such models, because they are diverse and difficult to track and predict in space and time (e.g., thaw slumps, lake/pond formation, ice wedge degradation) (Turetsky et al. 2020). However, abrupt permafrost thaw processes may result in intense soil carbon emissions that are more than twice (≈125 to 190%) those from gradual thaw (Walter Anthony et al. 2018).

The formation of thaw (thermokarst) lakes and ponds results from abrupt permafrost thaw processes. Favoring microbial and photochemical transformations under anoxic conditions, they are known to be dynamic biogeochemical hotspots for the release of carbon dioxide (CO_2), nitrous oxide (N_2O), and especially methane (CH_4) into the atmosphere (Zandt et al. 2020). These active, numerous, diverse and widespread aquatic environments generally exhibit individual sizes below 10,000 m^2 and depths less than 5 m, and they tend to be more active biogeochemically than larger lakes (Abnizova et al. 2012). However, these characteristics impose severe constraints for not only in-situ sampling strategies but also continuous individual monitoring from Earth Observation satellites.

Although successful remote sensing strategies have been developed for global inventorying and tracking large waterbody changes over time (Pekel et al. 2016), efficient strategies are still lacking for ponds, as well as narrow river channels, streams and creeks, due to sensor spatial resolution and data availability limitations (Mullen et al. 2023).

Advances by the Copernicus Program, since 2015, in particular with the launch of two twins Sentinel-2 satellites with worldwide acquisitions at 10/20-m resolution, and more recently, since 2016, Planet Labs launching CubeSat nanosatellites (e.g., PlanetScope Dove, Dove-R and SuperDove) with daily acquisitions at only ≈ 3 m resolution, are improving the global remote sensing detection and monitoring of lakes and ponds, as well as small rivers, streams and creeks. These advances not only allow consistent and detailed water body delineations in space and time (Mullen et al. 2023), but also improve monitoring of their optically active constituents such as algal populations, colored dissolved organic matter and suspended particulate matter (Sagan et al. 2020).

Here, we used native PlanetScope Dove (PS-D) imagery at 3 m pixel size and 4 bands spectral resolution for mapping optically and morphologically diverse small water bodies at the boreal-forest tundra transition zone of Nunavik, Subarctic Canada. In particular, we trained a Mask R-CNN deep learning model using a robust training set of more than 20,000 water bodies located in diverse environmental and limnological contexts of the Arctic and Subarctic Canada (Figure 1).

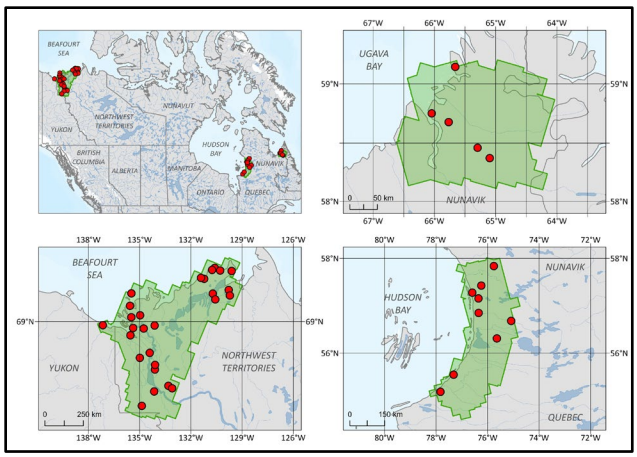

Figure 1. Locations in Canada where the training of the model was performed.

We tested the fully autonomous performance of the model by developing a multi-scale approach using detailed ground truthing from PS-D imagery, and also from ultra high resolution Unoccupied Aerial Systems (UAS) orthomosaics (0.05-0.15 m pixel size) in a variety of landscapes, including peatlands (e.g., fen, bog), wetlands, shrublands and forest sectors in Eastern Hudson Bay, Nunavik, Subarctic Canada. This strategy allowed a full sub-pixel assessment of the performance of the model for automatically mapping small water bodies (< 1 ha).

The results varied according to different landscape units, with mean Intersection over Union (IoU) 0.5 F1 Scores of 0.53-0.71 (results based on the number of classified features) and mean F1 Scores of 0.62-0.95 (results based on the classified area). Considering 166 m^2 as the minimum size detection threshold, the IoU 0.5 F1 Scores were 0.7-0.91 and F1 Scores were 0.76-0.83 when comparing the automated model results with ultra-high resolution manual delineations.

The regional implementation of the algorithm over 400 mosaicked PS-D images in Eastern Hudson Bay, revealed ≈ 300,000 ponds and several very high and optically diverse pond density hotspots, with more than 150 per square kilometer. Besides the deep learning model over PS-D imagery for automatically detecting these hotspots, we feed the model with Sentinel-2 imagery for better evaluating the optical variability, as well as spatial and temporal dynamics of permafrost thaw ponds (Freitas et al. 2019). Finally, we associate the results with in-situ observations on optically active constituents of permafrost thaw ponds (CDOM, Chl-a and SPM) for a better understanding of their biogeochemical significance and regional importance and representativity (Figure 2).

Figure 2. Surface water sample collection of a permafrost thaw pond in a sporadic permafrost degrading shrubland close to Kuujjuarapik, Nunavik.

REFERENCES

Abnizova, A., et al. 2012. Small ponds with major impact: The relevance of ponds and lakes in permafrost landscapes to carbon dioxide emissions, Global Biogeochemical Cycles, 26(2). doi:10.1029/2011GB004237

Biskaborn, B.K., et al. 2019. Permafrost is warming at a global scale, Nature Communications, 10(264). doi:10.1038/s41467-018-08240-4

Freitas, P., et al. 2019. Identification of a Threshold Minimum Area for Reflectance Retrieval from Thermokarst Lakes and Ponds Using Full-Pixel Data from Sentinel-2, Remote Sensing, 11(6). doi:10.3390/rs11060657

Mullen, A.L., et al. 2023. Using High-Resolution Satellite Imagery and Deep Learning to Track Dynamic Seasonality in Small Water Bodies, Geophysical Research Letters, 50(7). doi:10.1029/2022GL102327

Olefeldt, D., et al. 2016. Circumpolar distribution and carbon storage of thermokarst landscapes, Nature Communications. Nature Publishing Group, 7(13043). doi:10.1038/ncomms13043

Pekel, J.F., et al. 2016. High-resolution mapping of global surface water and its long-term changes, Nature. Nature Publishing Group, 540, pp. 418–422. doi:10.1038/nature20584

Sagan, V., et al. 2020. Monitoring inland water quality using remote sensing: potential and limitations of spectral indices, bio-optical simulations, machine learning, and cloud computing, Earth-Science Reviews. Elsevier, 205(103187), pp. 1–31. doi:10.1016/j.earscirev.2020.103187

Schaefer, K., et al. 2014. The impact of the permafrost carbon feedback on global climate, Environmental Research Letters. IOP Publishing, 9(8). doi:10.1088/1748-9326/9/8/085003

Turetsky, M.R., et al. 2020. Carbon release through abrupt permafrost thaw, Nature Geoscience. Springer US, 13, pp. 138–143. doi:10.1038/s41561-019-0526-0

Walter Anthony, K., et al. 2018. 21st-century modeled permafrost carbon emissions accelerated by abrupt thaw beneath lakes, Nature Communications. Springer US, 9(3262). doi:10.1038/s41467-018-05738-9

Zandt, M.H., Liebner, S., and Welte, C.U. 2020. Roles of Thermokarst Lakes in a Warming World, Trends in Microbiology. The Authors, 28(9), pp. 769–779. doi:10.1016/j.tim.2020.04.002

Studying drivers of thermo-erosional gully development based on in-situ measurements, remote sensing data, and modeling

Cornelia Inauen[1], Guido Grosse[1], Moritz Langer[2], Ingmar Nitze[1], Sophia Barth[1], Mackenzie Baysinger[1], William L. Cable[1], Caitlynn Hanna[3], Luis Kremer[4], Tillmann Luebker[1], Anne Morgenstern[1], Tabea Rettelbach[1], Alexandra Runge[5] & Irena Hajnsek[6]

[1]*Alfred Wegener Institute, Helmholtz Centre for Polar and Marine Research, Potsdam, Germany*

[2]*Department of Earth Sciences, Faculty of Sciences, Vrije Universiteit Amsterdam, Amsterdam, The Netherlands*

[3]*International Arctic Research Center, University of Alaska Fairbanks, Fairbanks, Alaska, United States*

[4]*Institute of Geosciences, University of Potsdam, Potsdam, Germany*

[5]*GFZ German Research Centre for Geosciences, Helmholtz Centre, Potsdam, Germany*

[6]*Department of Civil, Environmental and Geomatic Engineering, Institute of Environmental Engineering, ETH Zürich, Zürich, Switzerland*

Thermo-erosional valleys and gullies are widespread and important landscape components in some regions with ice-rich permafrost (Morgenstern et al. 2021). With accelerated arctic warming, channelization and erosion are expected to increase in permafrost regions (e.g., Chartrand et al. 2023). The resulting gully networks not only impact in-situ ground-ice loss through thermo-erosion, but also have far-reaching consequences through changing drainage pathways, modifying the local hydrology as well as sediment, nutrient, carbon, and contaminant fluxes and impacting ecosystems at catchment scale. Only few studies exist that conducted detailed research on thermo-erosional gully development (e.g., Fortier et al. 2007; Godin et al. 2012). However, the underlying process interactions defining incision rates and gully network expansion are complex due to spatially and temporally varying feedback mechanisms and likely are regionally variable. This leads to a lack of predictive tools for future thermo-erosional gully development (Rowland 2023).

In our study, we analyse the thermo-hydrodynamic conditions at two example gullies using in-situ measurements, remote sensing data and modeling at very high spatial resolution. The overall aim is to study driving forces and process interactions impacting further gully deepening or talik formation as well as network expansion in these example settings using permafrost modeling. In particular, we analyse the influence of topography, snow cover, runoff/moisture accumulation, ground ice variation as well as sediment accumulation versus erosion at the gully base. Here we present the analysis of our field data, which will feed into parametrising and validating simulations using the permafrost model CryoGrid.

The two thermo-erosional gully sites are located in West Alaska on the Baldwin Peninsula (BAP) and the Central Seward Peninsula (CSP) in ice-rich permafrost settings, as indicated by ice wedge polygons visible from satellite imagery (Figure 1). BAP is a coastal gully site, where the gully incises more than 10 meters into the surrounding terrain. The gully at CSP was formed following lake drainage and exhibits an incision in the range of one meter (Figure 1a).

At both gully sites, we performed ground temperature, topography (dGPS), active layer thickness (ALT), UAV and LiDAR Backpack surveys. Furthermore, we installed temperature sensors along two transects (T1 and T2), measuring temperature at 15 to 30 min intervals from August 2022 to September 2023. Especially at BAP, the two transects represent different settings where T1 crosses the very upper gully part resembling a shallow water track. Further downstream, the gully gradient makes a step change and levels-out at a deeply incised part with sediment accumulating at the gully center of T2.

Snow cover duration differs significantly across the gullies (Figure 1). During thaw season, snow remains predominantly in snow drifts within the gully and on eastern gully slopes. In contrast, autumn snow layer build-up is delayed in the gully where soil moisture is increased or water is flowing. All this is reflected in the soil surface temperature measurements and is displayed as freezing and thawing degree days (FDD and TDD) in Figure 1b. At all transects, the FDD remain at the highest temperatures at the gully base. In BAP T2, the temperature stays close to the freezing point for the whole winter, whereas in summer the TDD remains comparatively low due to the extended snow cover and snow melt duration. Despite the lower summer temperatures, the ALT exceeds by far the values measured at the other locations. This highlights the complex interactions of snow cover, snowmelt and runoff/moisture accumulation.

In conclusion, the data measured at the two gully sites deliver important insights into the thermo-hydrological processes required to simulate gully deepening driven by the seasonally varying

temperature and moisture regimes at the different gully sections. Furthermore, the BAP site proves to be a good test case for modeling the interaction of water tracks, moisture accumulation and gully network expansion along ice wedge polygons.

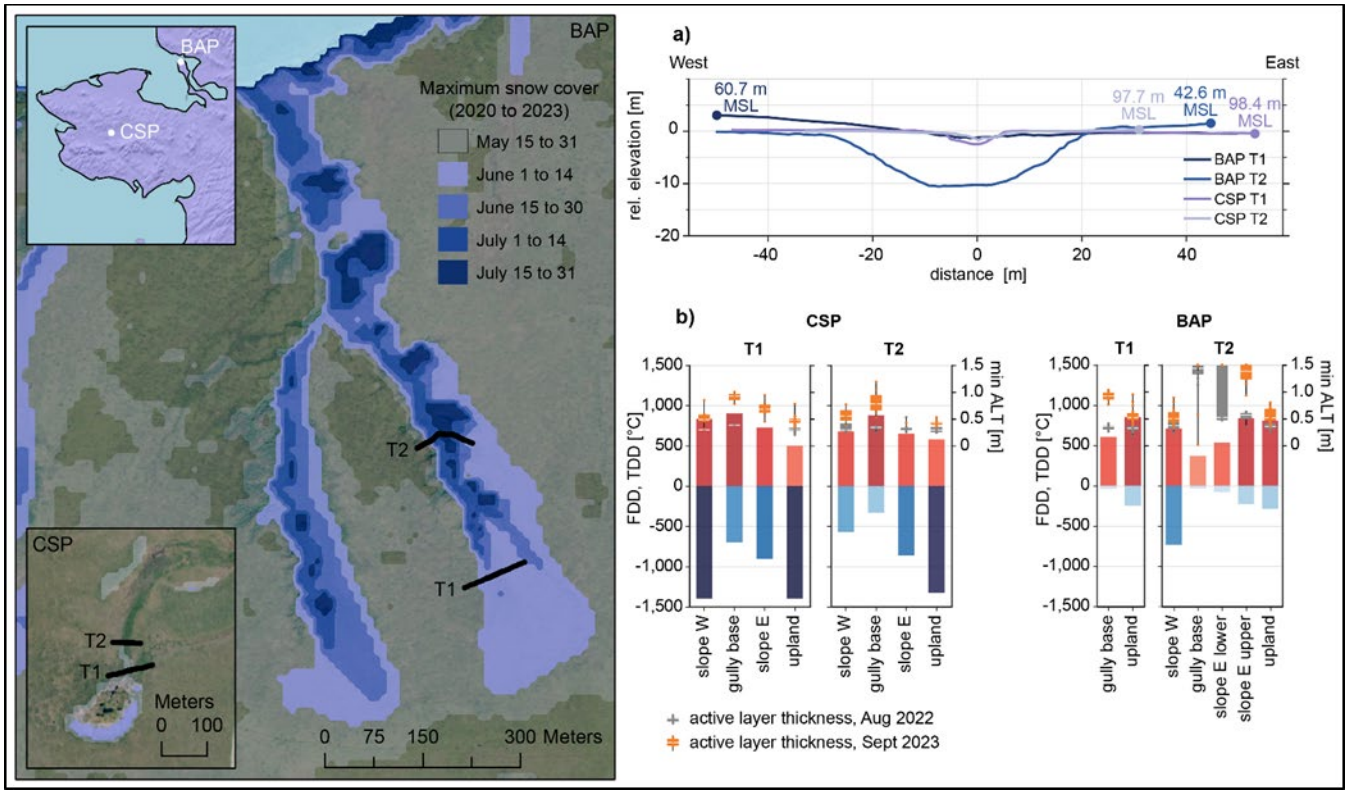

Figure 1. Left: Study site and gully transect locations (T1 and T2) on the Baldwin Peninsula (BAP) and the Central Seward Peninsula (CSP). The blue shading displays the significantly varying snow cover duration along the gully. It was extracted from Sentinel-2 derived NDSI, including imagery from the 2020 to 2023 spring seasons. (Background: Alaska High Resolution Imagery through https://geoportal.alaska.gov/ and Natural Earth hillshade). Right: a) dGPS measurements along the transects, with BAP T2 being significantly deeper incised. b) Annual freezing and thawing degree days (FDD and TDD) derived from soil surface temperature measurements along the four gully transects using 3 to 5 iButton temperature loggers per transect. For all transects the gully base exhibits the highest FDD, with BAP remaining close to the freezing point. In accordance, the active layer thickness (ALT), displayed as boxplots, exceeds the maximum measurable thickness of 1.5 m at BAP T2.

References

Chartrand, S.M., Jellinek, A.M., Kukko, A., Galofre, A.G., Osinski, G.R., and Hibbard, S. 2023. High Arctic channel incision modulated by climate change and the emergence of polygonal ground, Nature Communications, 14(1): 5297. doi:10.1038/s41467-023-40795-9

Fortier, D., Allard, M., and Shur, Y. 2007. Observation of rapid drainage system development by thermal erosion of ice wedges on Bylot island, Canadian Arctic Archipelago, Permafrost and Periglacial Processes, 18(3): 229–243. doi:10.1002/ppp.595

Godin, E., and Fortier, D. 2012. Geomorphology of a thermo-erosion gully, Bylot Island, Nunavut, Canada, Canadian Journal of Earth Sciences, 49(8): 979–986. doi:10.1139/e2012-015

Morgenstern, A., Overduin, P., Gunther, F., Stettner, S., Ramage, J., Schirrmeister, L., Grigoriev, M., and Grosse, G. 2021. Thermo-erosional valleys in Siberian ice-rich permafrost, Permafrost and Periglacial Processes, 32(1): 59–75. doi:10.1002/ppp.2087

Rowland, J.C. 2023. Drainage network response to Arctic warming, Nature Communications, 14(1): 5296. doi:10.1038/s41467-023-40796-8

A thermokarst monitoring network for Alaska

M. Torre Jorgenson[1], Yuri Shur[2], Mikhail Kanevskiy[2], Thomas Douglas[3], Neal Pastick[4] & Benjamin M. Jones[2]

[1]*Alaska Ecoscience, Fairbanks, Alaska, United States*

[2]*Institute of Nothern Engineering, University of Alaska, Fairbanks, Alaska, United States*

[3]*Cold Regions Research and Engineering Laboratory, Fairbanks, Alaska, United States*

[4]*Earth Resources Observation and Science Center, U.S. Geological Survey, Sioux Falls, South Dakota, United States*

Permafrost thawing affects all components of the involved ecosystems, triggering strong positive and negative feedbacks that control further degradation and stabilization pathways. Thermokarst occurs across diverse terrain and ground-ice conditions, develop into a wide range of feature sizes (m^2 to km^2), and have numerous degradation and stabilization stages spanning a wide age range. Grappling with this heterogeneity of terrain, ground ice conditions, transformations, areal extent and ages requires a multi-component and multi-scale approach. Accordingly, we have developed a monitoring network for Alaska that integrates regional, landscape and local scale monitoring strategies (Figure 1). Here we briefly summarize and provide examples of various components of the monitoring strategy.

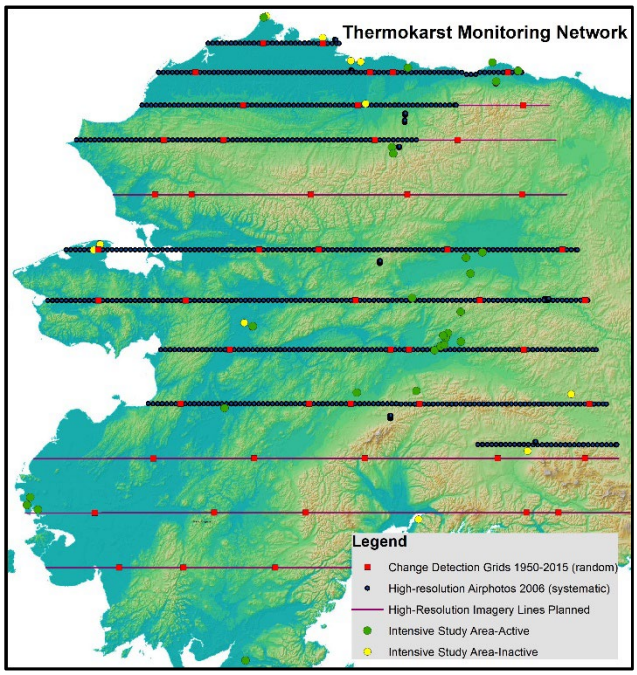

Figure 1. Map of change detection grids and airphoto-interpretation points for remote sensing, and regionally distributed intensive study areas for field monitoring.

Remote sensing

For regional and landscape level assessment of the nature, extent, and trends of thermokarst features, we are using three approaches. First, we acquired high-resolution stereo airphotos at 10-km spacing along longitudinal transects across Alaska in 2006 and determined the absence or presence of thermokarst and its type in the center of each of the 655 airphotos (Jorgenson et al. 2007). Determinations at the systematically distributed points were done through photo-interpretation of vegetation, geomorphology, topography, and pattern recognition based on experience gained from field surveys.

Second, we established 50 random remote sensing monitoring grids (2 x 2 km, with 100 points at 200 m spacing) across northern and central Alaska to quantify historical rates of change back to the 1940s using the same photo-interpretation technique as previously described. These repeat monitoring grids use a time-series of georectified imagery to track changes at 5000 points to provide more robust analyses of thermokarst state transitions.

Third, for landscape-level monitoring of change, we established 33 study areas widely distributed across Alaska with active thermokarst where we have been mapping, or systematically photo-interpreting thermokarst features on systematic grids, within 2–5 km^2 areas at 1:2,000 scale using airphotos and satellite imagery from ~1950, ~1980, ~2010, and ~2020 to document intermediate-term changes.

Field monitoring

For local-scale field monitoring and evaluation of thermokarst processes, a comprehensive set of ecological components have been sampled along 200–300 m transects at the 33 intensive study areas, representing different landscapes. Data collection varies somewhat across study areas, but usually includes information on topography (surveying, ground-based LiDAR, airborne LiDAR, or photogrammetry), thaw depths and permafrost table (probing and geophysical surveys), hydrology and snow (water-table surveys, water-level recorders, and time-lapse photography) (example in Figure 2). Soils and ground

ice data are obtained through coring and sampling (example in Figure 3), following the approach of French and Shur (2010). Paleoecological history is interpreted through peat macrofossils, stratigraphic analysis and radiocarbon dating. Dataloggers are used for quantifying soil and water thermal regimes, and water levels (example in Figure 4). Vegetation cover by species is obtained through ocular estimates or point sampling (example in Figure 5). At most study areas, sampling for the entire suite of components has been stratified into 4–6 degradation/stabilization stages with each stage replicated at three or more plots.

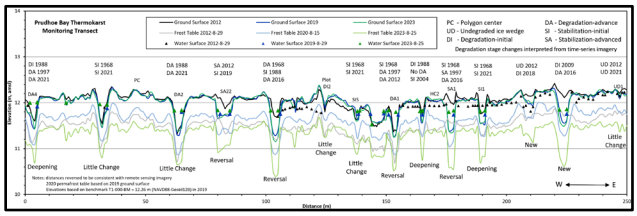

Figure 2. A monitoring transect at Prudhoe Bay showing ground, water, and permafrost surfaces from 2012 to 2023. Also shown are location of plots for sampling permafrost soils, vegetation, gas fluxes, and water chemistry (modified from Jorgenson et al. 2015).

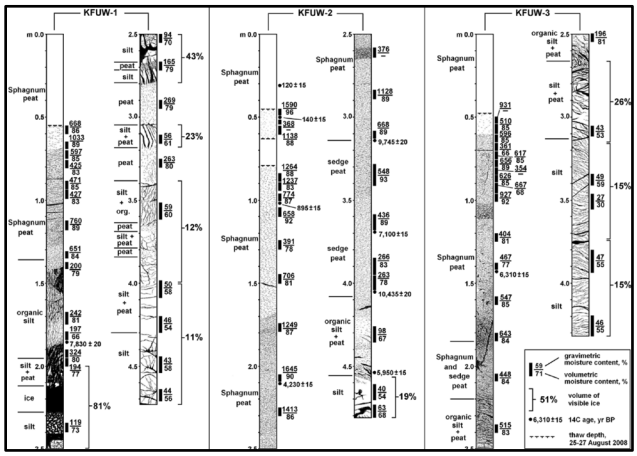

Figure 3. Soil stratigraphy and cryostructures for cores at the Koyukuk Flats study area (Kanevskiy et al. 2014).

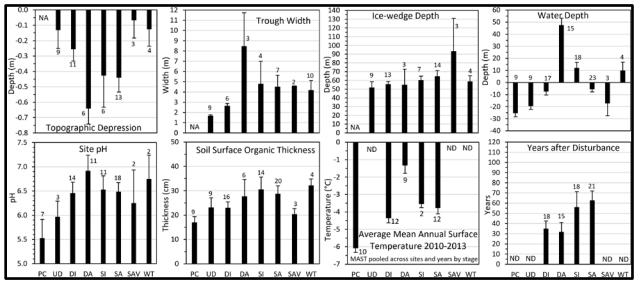

Figure 4. Comparison of environmental factors across a range of ice-wedge degradation and stabilization stages at the Jago monitoring study area (Jorgenson et al. 2022).

These monitoring transects initially were established on state and federal lands as part of NSF-funded studies of permafrost degradation, with the first study areas established in 1994. We have been partnering with agency personnel to continue long-term monitoring at the study areas. The field surveys and remote sensing are designed to be repeated every 5 and 10 years, respectively.

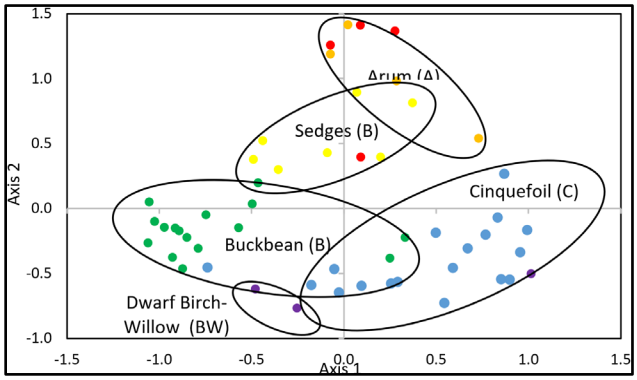

Figure 5. Ordination of vegetation composition showing grouping of plots across five stages of recovery in thermokarst fens on Tanana Flats (Jorgenson et al. 2022).

References

French, H.M., and Shur, Y. 2010. The principles of cryostratigraphy, Earth-Science Reviews 101: 190–206.

Jorgenson, M.T., Shur, Y.L., Osterkamp, T.E., and George, T. 2007. Nature and extent of permafrost degradation in the discontinuous permafrost zone of Alaska. In 7th International Conf. on Global Change: Connection to the Arctic (GCCA-7), International Arctic Research Center, University of Alaska, Fairbanks, AK: 120–125.

Jorgenson, M.T., Kanevskiy, M.Z., Jorgenson, J.C., et al. 2022. Rapid transformation of tundra ecosystems from ice-wedge degradation. Global and Planetary Change 216:103921.

Jorgenson, M.T., Kanevskiy, M.Z., Shur, Y., et al. 2015. Role of ground-ice dynamics and ecological feedbacks in recent ice-wedge degradation and stabilization. JGR-Earth Surface 120: 2280–2297.

Jorgenson, M.T., Kanevskiy, M.Z., Roland, C., et al. 2022. Repeated permafrost formation and degradation in boreal peatland ecosystems in relation to climate extremes, fire, ecological shifts, and a geomorphic legacy. Atmosphere 13(8): 1170.

Kanevskiy, M., Jorgenson, M.T., Shur, Y., et al. 2014. Cryostratigraphy and permafrost evolution in the lacustrine lowlands of West-Central Alaska. Permafrost and Periglacial Processes 25(1): 14–34.

Osterkamp, T.E., and Jorgenson, M.T. 2009. Permafrost conditions and processes. In Geological Monitoring. R. Young and H. Thompson, eds. Geological Society of America, Boulder, CO: 205–227

Rapid rejuvenation of sedimentary and geochemical cascades mark a transition into the Anthropocene in the western Canadian Arctic

Jaedyn L.J. Smith[1], Steven V. Kokelj[2], Duane G. Froese[3], Jon F. Tunnicliffe[4], Jennifer B. Korosi[5], Alexandre Chiasson[3], Alejandro Alvarez[3] & Suzanne E. Tank[1]

[1]*Department of Biological Sciences, University of Alberta, Edmonton, Alberta, Canada*

[2]*Northwest Territories Geological Survey, Government of Northwest Territories, Yellowknife, Northwest Territories, Canada*

[3]*Department of Earth and Atmospheric Sciences, University of Alberta, Edmonton, Alberta, Canada*

[4]*School of Environment, University of Auckland, New Zealand*

[5]*Department of Environmental and Urban Change, York University, Toronto, Ontario, Canada*

Arctic hydroclimactic regimes are in a period of profound change, with warming and wetting causing substantial permafrost thaw throughout the circumpolar North (Mekonnen et al. 2021; Smith et al. 2022). In high relief terrain, degradation of ice-rich permafrost can result in the loss of slope stability, producing a suite of thaw-driven mass-wasting features that can rapidly mobilize sediments and solutes. Retrogressive thaw slumps are a particularly dynamic form of mass wasting that affects ice-rich slopes. These features develop when erosion exposes ground ice, forming a headwall that retreats upslope and a saturated slurry that can flow downslope toward valley-bottom streams (Kokelj and Jorgenson 2013). This dynamic change is particularly pronounced in the Peel Plateau-Richardson Mountains region of the western Canadian Arctic, which is an ice-marginal environment that was briefly covered by the Laurentide Ice Sheet (LIS) during the late Pleistocene (Lacelle et al. 2013). Glaciation has conditioned this landscape by emplacing ground ice, and a cold climate has largely preserved relict ice in permafrost, priming the environment for climate-driven geomorphic change (Ballantyne 2018; Kokelj et al. 2017). Present-day shifts in hydroclimatology coupled with this geologic legacy have led to a reactivation of this formerly dynamic paraglacial environment, making this region among the most geomorphically active in the warming circumpolar world (Kokelj et al. 2021).

This study focuses on the Willow River catchment, which spans from beyond the LIS margin to the western edge of the depositional Mackenzie River Delta, and has an estimated 40% of its present-day stream network affected by thaw-driven mass-wasting features (Kokelj et al. 2021). Resultant downstream sediment transport led to an avulsion of the fan complex at the catchment's valley outlet in 2007, causing the newly-formed outlet channel to flow through a large deltaic lake (Willow Lake). Subsequent deposition of sediment within Willow Lake captures a substantial, but unknown, proportion of sediment load that would otherwise be routed to the Peel River. In the spring of 2021, a team of researchers and Gwich'in land users worked together to collect a series of shallow boreholes across alluvial and floodplain settings, encompassing cores of alluvial and lacustrine sediments within and around Willow Lake (Figure 1). This core collection and analysis was coupled with a Landsat-based assessment of 1986–2021 trends in terrestrial disturbance area and lake turbidity throughout the Willow River catchment. From these data, we use multiple lines of evidence to assess the sedimentary and biogeochemical effects of this recent, "slope-to-sink" threshold change.

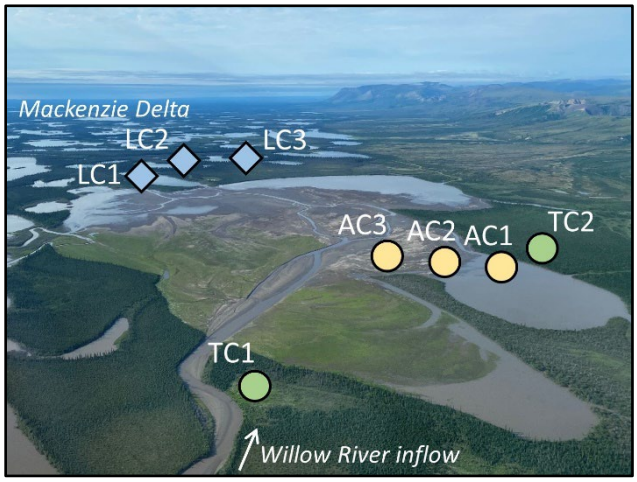

Figure 1. Alluvial surfaces within and around Willow Lake, illustrating the location of cores within the prograding delta (AC1-AC3), in surrounding floodplain environments (TC1 and TC2), and in distal, depositional lakes (LC1-LC3). The Willow River inflow (foreground) and Mackenzie Delta (background) are denoted. Photo location: lat 68.155°, long -135.348°.

Semi-remote sensing analysis reinforce that the Willow River catchment experienced rapid increases in the number (3.8-fold increase), size (9.2-fold), and density (16.3-fold) of thaw-driven mass wasting features between 1986 and 2021, with features developing almost entirely within the margin of LIS glaciation. This rapid intensification caused

pronounced changes in Landsat-inferred turbidity (as Normalized Difference Turbidity Index; NDTI) of catchment lakes. Notably, NDTI increased in delta lakes adjacent to the re-routed inflow to Willow Lake ($p<0.05$), and decreased overall in lakes adjacent to the abandoned channel, but with a break-point between increasing and decreasing trends in 2007 ($p<0.05$).

Cores from alluvial surfaces within the Willow Lake delta (AC1-AC3; Figure 1) and nearby floodplains (TC1 and TC2) indicate coincident shifts in material provenance and character, with a coarsening upward sequence of sediments consistent with the remotely observed delta progradation within Willow Lake. Stratigraphic variation within the cores reveals dynamic post-depositional change in the sediment. Notably, the composition of surficial sediments indicates mineral weathering processes and organic matter accumulation in deposited materials, when compared to parent materials upstream in the catchment. Temperature profiles from thermistor strings installed in 2021 demonstrate the aggradation of permafrost in recently deposited subaerial deltaic sediments, sequestering materials at depth into frozen ground.

This study documents rapid, thaw-driven transformation that has propogated throughout the Willow River catchment. Abrupt and ongoing thaw-driven mobilization of glacial sediments in the central catchment and their subsequent deposition in the Delta represents a prolific redistribution of materials, which is enabling widespread alteration of biogeochemical processes. The Willow River is an exceptional site to document changes across a slope-to-sink continuum; however this pattern of mobilization and changing biogeochemical function is increasingly common throughout the circumpolar north, as thaw-driven mass wasting intensifies throughout regions of ice-rich permafrost.

REFERENCES

Ballantyne, C.K. 2018. Periglacial Geomorphology. Wiley-Blackwell, Chichester, United Kingdom.

Kokelj, S.V., and Jorgenson, M.T. 2013. Advances in thermokarst research. Permafrost and Periglacial Processes, 24(2): 108–119. doi:10.1002/ppp.1779

Kokelj, S.V., Lantz, T.C., Tunnicliffe, J., Segal, R., and Lacelle, D. 2017. Climate-driven thaw of permafrost preserved glacial landscapes, northwestern Canada. Geology, 45(4): 371–374. doi:10.1130/G38626.1

Kokelj, S.V., Kokoszka, J., van der Sluijs, J., Rudy, A.C.A., Tunnicliffe, J., Shakil, S., Tank, S.E., and Zolkos, S. 2021. Thaw-driven mass wasting couples slopes with downstream systems, and effects propagate through Arctic drainage networks. Cryosphere, 15(7): 3059–3081. doi:10.5194/tc-15-3059-2021

Lacelle, D., Lauriol, B., Zazula, G., Ghaleb, B., Utting, N., and Clark, I.D. 2013. Timing of advance and basal condition of the Laurentide Ice Sheet during the last glacial maximum in the Richardson Mountains, NWT. Quaternary Research, 80(2): 274–283. doi:10.1016/j.yqres.2013.06.001

Mekonnen, Z.A., Riley, W.J., Grant, R.F. and Romanovsky, V.E. 2021. Changes in precipitation and air temperature contribute comparably to permafrost degradation in a warmer climate. Environmental Research Letters, 16(2): 024008. doi:10.1088/1748-9326/abc444

Smith, S.L., O'Neill, H.B., Isaksen, K., Noetzli, J., and Romanovsky, V. E. 2022. The changing thermal state of permafrost. Nature Reviews Earth & Environment, 3(1): 10–23. doi:10.1038/s43017-021-00240-1

A framework for classifying permafrost terrain

Niek Speetjens[1], Stephan Gruber[2] & Trevor Lantz[1]

[1]*Department of Environmental Studies, University of Victoria, Victoria, British Columbia, Canada*

[2]*Department of Geography and Environmental Studies, Carleton University, Ottawa, Ontario, Canada*

Permafrost covers roughly 11% of the global land area and significantly influences hydrological processes, soil conditions, vegetation, and the global carbon budget. Rapid climate warming is triggering profound transformations in permafrost environments, impacting water resources, ecosystem services, infrastructure, and carbon and nutrient fluxes. Despite considerable advancements in permafrost science, the lack of a unified interdisciplinary framework hinders collaboration on pressing issues arising from changing permafrost environments.

Groups and individuals with an interest in permafrost have emphasized the importance of synthesizing multidisciplinary observations, creating data products characterizing permafrost change, establishing practices for data sharing, and setting up representative long-term monitoring (Laurie 2017). This is also reflected in elements of a vision forwarded for permafrost knowledge in Canada (Gruber et al. 2023). A foundational element in elevating permafrost science beyond individual sites and disciplines is a shared approach to identifying similar and dissimilar locations.

Permafrost knowledge spans multiple knowledge systems and an ever-increasing number of academic disciplines. This diversity of perspectives is a strength, but their integration is hampered by a range of approaches to classifying and describing permafrost environments. We aim to support incremental progress toward a more unified approach by proposing terminology and a classification framework specifically for permafrost terrain types.

The presence and dynamics of ground ice within permafrost terrain significantly influence its surface expressions and characteristics. Researchers commonly rely on surface features to guide their investigations and categorize, compare, and communicate their results. However, the importance of ground ice necessitates considerations that might not be reflected in terrain classification systems established in different contexts. While some consensus exists regarding pertinent terrain attributes and classes, substantial variations persist across different scales (e.g., The National Wetlands Working Group 1997; Grosse et al. 2006; Olefeldt et al. 2016; Kokelj et al. 2023). The absence of a standardized framework hinders synthesizing information across spatial scales and the comprehensive understanding of permafrost terrain dynamics.

We present a framework for classifying permafrost terrain. It consists of a nested hierarchy of classes for characterizing pattern and process across scales, from continental to local. We review existing classification methods from disciplines such as hydrology, ecology, geomorphology, glaciology, soil science and permafrost science. Based on this, we examine what classes are formed, which variables are used, and what application and purpose this serves. Subsequently we propose a framework that maximizes similarity and usage of existing approaches, employing an 'adopt and adapt' strategy.

The goal of this framework is to facilitate inventorying of permafrost-related stocks (e.g., carbon, nutrients, biodiversity), process domains (e.g., landforms), conditions (e.g., thermal state and ground-ice content), and projected change trajectories (e.g., various modes of permafrost degradation and their impacts). Successful implementation and adoption by permafrost stakeholders across scales will facilitate increased interoperability, enhanced data synthesis, and improved accessibility for modelers. Additionally, it will foster enriched communication with stakeholders outside academia, identifying urgent community, governmental, or industrial concerns and guiding scientific efforts accordingly.

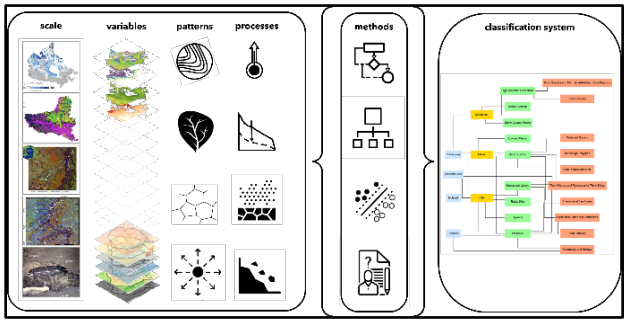

Figure 1. Conceptual figure of the classification framework.

REFERENCES

Grosse, G., Schirrmeister, L., and Malthus, T.J. 2006. Application of Landsat-7 satellite data and a DEM for the quantification of thermokarst-affected terrain types in the periglacial Lena-Anabar coastal lowland. Polar Research, 25 (1). https://doi.org/10.1111/j.1751-8369.2006.tb00150.x

Gruber, S., Hayley, J., Karunaratne, K., King, J., MacLean, T., Marshall, S., and Moore, D. 2023. Considerations toward a vision and strategy for permafrost knowledge in Canada. Arctic Science, 9 (4), 4–8. https://doi.org/10.1139/as-2023-0016

Kokelj, S.V., Gingras-Hill, T., Daly, S.V., Morse, P.D., Wolfe, S.A., Rudy, A.C.A., van der Sluijs, J., Weiss, N., O'Neill, H.B., et al. 2023. The Northwest Territories Thermokarst Mapping Collective: a northern-driven mapping collaborative toward understanding the effects of permafrost thaw. Arctic Science, 9 (4), 886–918. https://doi.org/10.1139/AS-2023-0009

Laurie, M. 2017. Workshop report: toward a Canadian Permafrost Network. Ottawa, Canada. doi:10.22215/pn/10117001

National Wetlands Working Group. 1997. The Canadian Wetland Classification System, 2nd Edition. Warner, B.G. and C.D.A. Rubec (eds.), Wetlands Research Centre, University of Waterloo, Waterloo, ON, Canada. 68 p.

Olefeldt, D., Goswami, S., Grosse, G., Hayes, D., Hugelius, G., Kuhry, P., Mcguire, A.D., Romanovsky, V.E., Sannel, A.B.K., Schuur, E.A.G., and Turetsky, M.R. 2016. Circumpolar distribution and carbon storage of thermokarst landscapes. Nature Communications, 7. https://doi.org/10.1038/ncomms13043

Diverse landscape expressions and patterns of thermokarst observed via systematic aerial inventory and characterization of thaw-sensitive permafrost terrain, Northwest Territories, Canada

Jurjen van der Sluijs[1], Steven V. Kokelj[2], Ashley C.A Rudy[2] & M. Alice Wilson[2]

[1]*Northwest Territories Centre for Geomatics, Government of Northwest Territories, Yellowknife, Northwest Territories, Canada*

[2]*Northwest Territories Geological Survey, Government of Northwest Territories, Yellowknife, Northwest Territories, Canada*

Circumpolar landscapes are among the most climatically sensitive environments in the world due to the effects of permafrost thaw. Thermokarst develops due to the thawing of ice-rich permafrost, and together with periglacial features, comprise a broad suite of landforms that can indicate the thaw-sensitivity of permafrost terrain. There is limited empirical data that describe the patterns in thaw-sensitive terrain for most circumpolar regions, which restricts our understanding and extrapolation of environmental effects of permafrost thaw and limits evaluation of remote sensing and spatial modelling products intended to detect and predict thaw-driven changes. This scarcity of empirical datasets identifies a heightened need to systematically characterize permafrost terrain and efficiently organize collections of permafrost information. For the characterization of permafrost conditions and coupling between remote sensing and field-based observations, it is critical to develop standardized methods for permafrost landform identification and attribution. The Northwest Territories Thermokarst Mapping Collective (TMC) produced a standardized mapping rubric and method to empirically inventory indicators of thaw-sensitive terrain using satellite imagery interpretation of 7.5 × 7.5 km^2 grid cells for a 2 million km^2 region of northern Canada (Kokelj et al. 2023). The TMC approach enabled landscape assessments of 25 thermokarst and periglacial features and attributes, which were validated using Northwest Territories (NWT)-wide aerial inventories of thermokarst and periglacial landforms.

While the aerial inventories were initially conceptualized to directly support TMC validation efforts, it was recognized that the helicopter-based observations enabled a refinement of the TMC mapping rubric. The ability to observe detailed aspects of thermokarst and periglacial features that are difficult to determine with satellite imagery, drove a concurrent effort to document and synthesize the diverse landscape expressions and patterns of thermokarst observed via systematic aerial inventory across NWT.

Integrating the knowledge of several permafrost experts through a data model characterizing terrain features, and supported by web-GIS technologies, this work documents the first systematic aerial inventory of a wide range of thermokarst processes and thaw-sensitive permafrost terrain across a wide range of permafrost environments. Specific goals of the work were: (1) to generate a systematic dataset documenting the thermokarst features and periglacial landforms by means of empirical low-altitude helicopter-based observations, and (2) to develop a standardized permafrost assessment and data recording method.

Methods

Helicopter-based surveys were conducted in the summers of 2020–2022, during the COVID-19 pandemic, supported by the Polar Continental Shelf Project (PCSP). The unique opportunity was capitalized upon as the standardized (satellite-based) TMC mapping rubric was already in place and because northern science and geomatics capacity existed to implement the project at a time when the pandemic restricted other researchers to enter the NWT. The PCSP funding enabled northern TMC project partners to sustain field programs while providing opportunities to work with Indigenous partners for training in permafrost observational methods.

The recording method, implemented using ESRI Survey123, used a custom logic model as a standardized template for identifying a broad suite of thermokarst features and permafrost landforms along with landform attributes organized under mass wasting, hydrological, and periglacial themes. Geotagged photos were acquired to provide a visual record at the time of observation and to act as a mechanism for quality control-assurance and gap-filling of attributes. Several high-quality cameras were used, including a Nikon D5600 24 megapixel digital single-lens reflex (DSLR), a Nikon D750 24 megapixel DSLR, and a Sony RX100 III 20 megapixel 1” sensor compact camera. Observations were typically made using a two- or three-person team, carrying out thermokarst interpretation, photography, data recording, and navigation roles. Observations were not collected opportunistically, rather helicopter transects were planned in such a way as to couple regular travel to field sites with data collection in new regions or corridors. While sampling

was not random, the nature and abundance of features and landform attributes can be summarized on the basis of several environmental stratifications, such as latitude and ecoregion.

RESULTS

Helicopter-based surveys spanned a total of 68 days within the three-year period (37,429 km) across 14 degrees of latitude, enabling collection of 7,597 observations and 41,559 geo-tagged photos. The acquired dataset is novel in the sense of explicitedly linking point coordinates, extensive landform codes and attribute information, as well as a detailed visual reference of thermokarst and periglacial features. The acquired dataset enabled northern organizations to co-lead the production and dissemination of scientific knowledge, leveraging northern-based capacity and research infrastructure along with nation-wide expert knowledge, while providing field-based knowledge sharing opportunities with Indigenous partners.

The dataset consisted of 4,088 periglacial samples (54%), 1,971 hydrological samples (26%), and 1,538 mass wasting samples (20%). Patterns between themes and regions emerged once assessment intensity was taken into account. The proportion of observations per theme differed among ecoregions, with Cordillera ecoregions featuring more mass wasting observations and less periglacial or hydrological observations compared to Taiga Plains and Shield ecoregions. The relative differences between several Cordillera ecoregions did not differ substantially, with approximately 65% of observations belonging to the mass wasting theme and 25% of observations to the periglacial theme. Likewise, Plains and Shield ecoregions as well as the Northern and Southern Arctic landscapes consisted predominantly of periglacial observations (50-75%) with minor mass wasting and hydrological contributions. The observations thus reflect patterns expected from broader Ecoregion-level knowledge and point to the overall quality of the dataset.

Summarized results highlight the nature and diversity of thermokarst and periglacial features in the NWT. For example, diverse morphologies were observed of mass wasting processes, most abundant in western and northern parts of the NWT. The greatest density of thaw slumps occurred in the Tundra Cordillera and southern Arctic, while four other Ecoregions featured relative proportions exceeding 25%. The Boreal and Taiga Cordillera, along with the Northern Arctic, featured greater proportions of shallow slides compared to thaw slumps, while for the Taiga Plains these proportions were similar. Thaw slumps were documented from 62°N northwards, which is further south than other recent works. Within the hydrological theme, results indicated that both lake lowering and expansion were dominant modifiers of lakes in permafrost regions of the NWT, while complete drainage and shoreline collapse were secondary in abundance. Here relative abundance of these four characteristics differed across ecoregions and latitudes, and in some cases all four lake dynamics characteristics were observed (e.g., Mackenzie Delta). Periglacial observations most often included collapse scars and high-centered polygons, along with patterned forest (stringbog) and low-centered polygons. Their dominance, as well as their drainage type and permafrost degradation status, also differed among ecoregions and latitudinally.

SUMMARY

The extensive aerial surveys form one of the first initiatives to document thermokarst and periglacial features across the NWT. Diverse landscape expressions and patterns of thermokarst were observed, including a high degree of diversity in landforms, providing a novel window into the characteristics and dynamics of the warming permafrost environment. This diversity is important to identify and recognize to aid in our understanding of environmental effects, and the evaluation of remote sensing monitoring and predictive spatial modelling outputs. This dataset will provide new insight into the nature and diversity of permafrost landscapes, and a visual, spatially explicit product that can be explored by scientists and the public.

REFERENCES

Kokelj, S.V., Gingras-Hill, T, Daly, S.V., Morse, P.D., Wolfe, S.A., Rudy, A.C.A., van der Sluijs, J., Weiss, N., O'Neill, H.B., Baltzer, J.L., Lantz, T.C., Gibson, C., Cazon, D., Fraser, R.H., Froese, D.G., Giff, G., Klengenberg, C., Lamoureux, S.F., Quinton, W.L., Turetsky, M.R., Chiasson, A., Ferguson, C., Newton, M., Pope, M, Paul, J.A., Wilson, M.A, and Young, J.M. 2023. The Northwest Territories Thermokarst Mapping Collective: a northern-driven mapping collaborative toward understanding the effects of permafrost thaw, Arctic Science. 9(4): 886–918. doi:10.1139/as-2023-0009

Arctic Coastal Hazard Index (ACHI): A framework for assessing vulnerability to permafrost thawing, coastal erosion, and flooding in the Arctic

Ziyi Wang[1], Ming Xiao[1], Dmitry Nicolsky[2], Vladimir Romanovsky[2], Christopher McComb[3] & Louise Farquharson[2]

[1]*Department of Civil and Environmental Engineering, Penn State, Pennsylvania, United States*

[2]*Geophysical Institute Permafrost Laboratory, University of Alaska Fairbanks, Alaska, United States*

[3]*Department of Mechanical Engineering, Carnegie Mellon University, Pittsburgh, Pennsylvania, United States*

In coastal areas, permafrost thaw, talik formation, and thermokarst processes can contribute to coastal erosion, as thawed sediments are more easily eroded than frozen ones. The development of assessment methods for evaluating combined Arctic coastal hazards is relatively rare when compared to their widespread utilization in low-latitude coastal regions. No attempt was made to integrate permafrost thaw, coastal erosion, and coastal flooding into a synthetic hazard assessment of the Arctic coast. To fill this knowledge gap, this study conducted an integrated analysis of the coastal plains of Alaska's northernmost borough, North Slope Borough (Wang et al. 2023).

General methodological framework

We integrate the index-based permafrost thaw potential as an input variable into the Arctic coastal hazard assessment framework. The conceptual framework consists of three steps: 1) assessment of permafrost conditions; 2) assessment of permafrost thaw subsidence; 3) assessment of Arctic coastal hazards. First, in-situ field observations of mean annual ground temperature (MAGT) and active layer thickness (ALT), ground thermal properties, and environmental data serve as inputs for the Geophysical Institute's Permafrost Laboratory (GIPL)-2.0 model. MAGT, ALT and talik thickness projections from the GIPL model for the Representative Concentration Pathway (RCP) 4.5 and 8.4 are visualized in GIS (Geographical Information System)-based maps for the 2020s and the 2060s. Second, using the input from thaw subsidence factors derived from existing ground ice maps (Jorgenson et al. 2014) and the predicted MAGT, ALT, and talik thickness from the GIPL-2.0 model, the ground settlement index is quantified. The hazard indices are then used to delineate areas into five categories of permafrost thaw potential (PTP) caused by the thawing of near-surface permafrost. Third, the erosion and flooding factors combined with the gridded PTP from the second step constitute the input factors of the Arctic Coastal Hazard Index (ACHI). In this study, coastal hazard refers to thaw subsidence, flooding, and erosion caused by storms and permafrost thaw acting upon shorelines. Environmental risk encompasses the product of hazard occurrence and its potential societal consequences. ACHI is determined by incorporating thaw subsidence and erosion-flooding potential.

Assessment of permafrost thaw subsidence

We considered the role of taliks in the potential of permafrost thaw subsidence. In permafrost regions with sub-aerial taliks, talik thickness plays a crucial role in the occurrence of potential thaw settlement. Liquid water resulting from the talik formation drains away from the impacted sites. We propose an improved approach that incorporates changes in talik thickness to accurately estimate ground subsidence. The calculated thaw settlement signifies an upper bound estimate, as the computation assumes a transformation of the thawed permafrost into a non-porous state. Two GIS-based thaw subsidence hazard maps were generated in this study, comparing the 2060s to the 2020s under two climate forcing scenarios, RCP4.5 and RCP8.5 (Figure 1). The two hazard maps exhibit relatively consistent geographic variation. Regions with relatively higher potential for thaw subsidence are primarily concentrated along the west coast of the Beaufort Sea, the middle portion of the North Slope Borough, and low-latitude upland areas. We propose that the spatial patterns for potential thaw subsidence are primarily influenced by the presence and distribution of ground ice, which, in turn, is closely associated with cryolithology and Quaternary depositional environments.

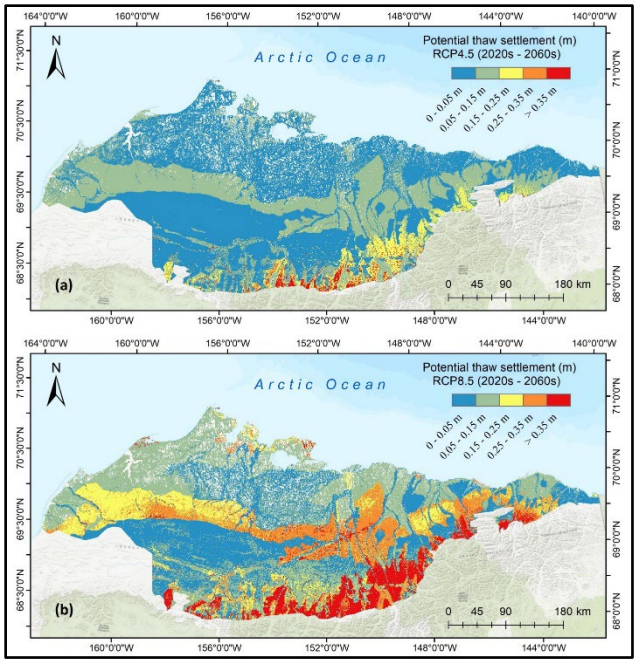

Figure 1. Maximum potential thaw settlement (m) for the 2060s compared against 2020s. (a) predicted results using RCP4.5 climate forcing; (b) predicted results using RCP8.5 climate forcing.

Assessment of Arctic Coastal Hazards

The distributions of the Arctic Coastal Hazard Index (ACHI) are classified into quartiles to represent different levels of coastal hazard scores. The quartiles are defined as follows: high (upper 25%, ranging between 3.5 to 5), moderate (50% to 75%, ranging between 3.2 to 3.5), low (25% to 50%, ranging between 2.8 to 3.2), and stable (lower 25%, ranging from 1 to 2.8); the upper bound of each range is inclusive. Figure 2 shows the predicted ACHI results of coastal hazard potential of North Slope Borough, Alaska by 2060s using RCP4.5 and 8.5 climate forcing. Both hazard maps demonstrate a relatively consistent geographic distribution of ACHI. Regions with relatively higher potential for coastal hazards are primarily concentrated along the west coast of the Beaufort Sea, including the coastline of Point Barrow, Smith Bay, and Pogik Bay. Additionally, the regions between Wainwright and Peard Bay also exhibit elevated levels of potential coastal hazards.

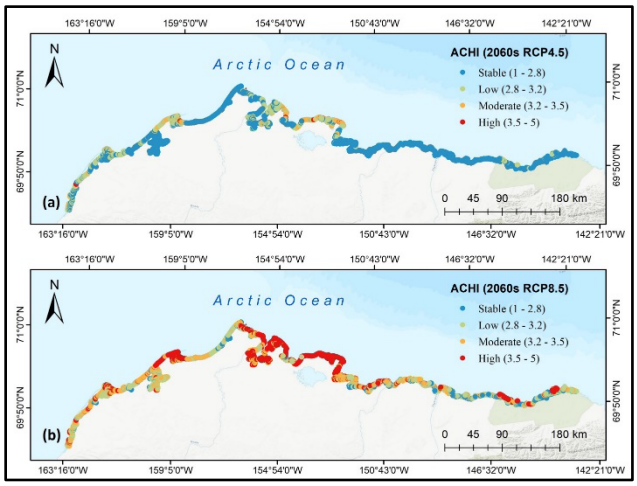

Figure 2. Predicted ACHI results of coastal hazard potential of North Slope Borough, Alaska by 2060s. (a) using RCP4.5 climate forcing; (b) using RCP8.5 climate forcing.

References

Wang, Z., Xiao, M., Nicolsky, D., Romanovsky, V., McComb, C., and Farquharson, L. 2023. Arctic coastal hazard assessment considering permafrost thaw subsidence, coastal erosion, and flooding. Environmental Research Letters, 18(10), p.104003.

Jorgenson, M.T., Kanevskiy, M., Shur, Y., Grunblatt, J., Ping, C.L., and Michaelson, G. 2014. Permafrost database development, characterization, and mapping for northern Alaska.

What is happening to discontinuous permafrost around Yellowknife, NWT?

Niels Weiss[1], Steve Kokelj[1], Steve Wolfe[2], Peter Morse[2], Wendy Sladen[2] & Rosy Tutton[3]

[1]*Northwest Territories Geological Survey, Government of Northwest Territories, Yellowknife, Northwest Territories, Canada*

[2]*Natural Resources Canada, Geological Survey of Canada, Ottawa, Ontario, Canada*

[3]*Wilfrid Laurier University, Yellowknife, Northwest Territories, Canada*

Permafrost is a product of environmental and climatic conditions and inherently sensitive to change. Given the diversity in permafrost types as well as in the manifestations of climate change, the combined effects are highly variable and often uncertain. Although a general warming trend is observed across the Circumpolar North, seasonal temperature extremes and the timing and quantity of precipitation remain uncertain. The North Slave region of the Northwest Territories is characterized by a continental climate and is particularly susceptible to multi-year shifts in precipitation patterns that can yield drought conditions and wildfire. Just like long-term meteorological records are essential to understanding climate change, permafrost characterization and monitoring are crucial to anticipating permafrost change. Robust permafrost monitoring networks that include relevant terrain types, cover important regional gradients, and generate long-term observations are invaluable but require significant resources to establish and maintain. The Northwest Territories Geological Survey (NTGS) and Geological Survey of Canada (GSC) manage a permafrost monitoring network in the North Slave region, consisting of sites and instruments associated with a variety of projects pertaining to permafrost research, environmental monitoring, and infrastructure performance. There are currently 70 sites with a total of 125 boreholes up to 12 m depth. Long-term data records have been disseminated through open data reports (e.g., Duchesne et al. 2016) and will be made available in repositories like the Northwest Territories Permafrost Database in the future.

Permafrost terrain types

The landscape around Yellowknife is a mosaic of lakes, bedrock outcrops, organic terrain, and alluvial and (glacio-)lacustrine deposits. Permafrost is discontinuous and primarily found in peatlands and fine-grained mineral sediments with high ground ice content (Morse et al. 2016; Paul et al. 2021). Lithalsas, which are mineral permafrost mounds raised due to permafrost aggradation and segregated ice, are widespread in the region (Wolfe et al. 2014) and developed following exposure after the retreat of glacial Lake McConnell and current Great Slave Lake (Wolfe and Morse 2017). In the landscape, lithalsas are commonly associated with degradation features called ramparts, occurring as ramparted-lake-lithalsa complexes (Morse et al. 2019). Because of the contrasting surficial materials and site conditions, permafrost characteristics in lithalsas and peatlands differ significantly. Active layers are thick in well-drained mineral lithalsa soils and mean annual ground temperatures are very close to 0°C (Morse et al. 2016). Due to its thermal characteristics, organic peat soils preserve the permafrost table closer to the ground surface through insulation in summer and more effective conductive cooling in winter. Despite the differences in permafrost characteristics between landforms, there are important similarities for permafrost in the North Slave region. Mean annual ground temperatures are warm, on average around -0.5°C, and are increasing (Morse et al. 2016). Furthermore, temperature in many boreholes is approaching 0°C (Duchesne et al. 2016; Morse et al. 2016), which can be indicative of ground ice melt and permafrost loss.

Quantifying the effects of change

To get a more detailed understanding of the processes and effects of climatic variation in contrasting permafrost terrain types, a precipitation manipulation experiment was established in 2022 at two monitoring sites near Yellowknife. At each location, multiple instrument clusters were installed to record soil moisture content in the active layer, and ground temperatures up to 3 m depth. Starting in 2023, an increase in precipitation before freezeback and a decrease in early winter snow accumulation was simulated at each location. However, due to exceptionally dry conditions, the first year of baseline ground temperature and soil moisture observations is informative, but atypical. Therefore, a longer record in conjunction with the field manipulation experiment is needed to better quantify differences in response to precipitation change. In this presentation, we examine decadal scale ground thermal records from lithalsas and peatlands in the Yellowknife region and assess trends and interannual patterns of variation. We also summarize the influence of artificial wetting and drying on freezeback duration in specific terrain types and explore short and long-term implications.

REFERENCES

Duchesne, C., Morse, P.D., Wolfe, S.A., and Kokelj, S.V. 2016. Report on 2010-2015 Permafrost Thermal Investigations in the Yellowknife Area, Northwest Territories; Geological Survey of Canada, Open File 8093; Northwest Territories Geological Survey, NWT Open Report 2016-019, 54 p. doi.org/10.4095/299189 & doi.org/10.46887/2016-019

Morse, P.D., Wolfe, S.A., Kokelj, S.V., and Gaanderse, A.J.R. 2016. The occurrence and thermal disequilibrium state of permafrost in forest ecotopes of the Great Slave Region, Northwest Territories, Canada. Permafrost and Periglacial Processes, 27(2), pp.145–162. doi.org/10.1002/ppp.1858

Morse, P.D., Wolfe, S.A., and Rudy, A.C.A. 2019. Lithalsa degradation and thermokarst distribution, subarctic Canadian Shield, in Proceedings of the 18th International Conference on Cold Regions Engineering and 8th Canadian Permafrost Conference, ASCE Cold Regions Engineering 2019, 308–316.

Paul, J.R., Kokelj, S.V., and Baltzer, J.L. 2021. Spatial and stratigraphic variation of near-surface ground ice in discontinuous permafrost of the taiga shield. Permafrost and Periglacial Processes, 32(1), pp.3–18. doi.org/10.1002/ppp.2085

Wolfe, S.A., Stevens, C.W., Gaanderse, A.J., and Oldenborger, G.A. 2014. Lithalsa distribution, morphology and landscape associations in the Great Slave Lowland, Northwest Territories, Canada. Geomorphology, 204, pp.302–313. doi.org/10.1016/j.geomorph.2013.08.014

Wolfe, S.A., and Morse, P.D. 2017. Lithalsa Formation and Holocene Lake-Level Recession, Great Slave Lowland, Northwest Territories. Permafrost and Periglacial Processes, 28(3), pp.573–579. doi.org/10.1002/ppp.1901

Response of early colonizers in retrogressive thaw slumps on the trajectory of tundra greening

Zhuoxuan XIA[1], Mark J. Lara[2,3] & Lin Liu[1]

[1]*Earth and Environmental Sciences Programme, the Chinese University of Hong Kong, Hong Kong, China*

[2]*Department of Plant Biology, University of Illinois Urbana-Champaign, Urbana, Illinois, United States*

[3]*Department of Geography, University of Illinois Urbana-Champaign, Urbana, Illinois, United States*

Retrogressive thaw slumps (RTSs) are a form of abrupt permafrost thaw, which are widely distributed across the northern hemisphere and have increased in occurrence over recent years. Thaw slumps have a near vertical ice-rich headwall and gentle slump floor often filled with a slurry of mud and water as the headwall retreats over several years to decades following initiation (Ballantyne 2018). During periods of rapid expansion, vegetation is either transported downslope or covered by the RTS debris-tongue. After ice-rich permafrost or ground-ice is either lost or protected, the RTS stabilizes and initiates the process of primary succession, as vegetation gradually recolonizes barren disturbed terrain. However, the rate at which pioneer species may reestablish disturbed RTS terrain and alter local-scale patterns of productivity as inferred by vegetation greenness or the normalized difference vegetation index (NDVI) is poorly understood. We hypothesize that the recovery rate will vary across permafrost zones, limited by climate and nutrient availability. However, the impact of the climate-permafrost zone on the rates of vegetation recolonization in recently initiated RTSs is poorly understood. To fill the gap, we examined sites on the Qinghai Tibetan Plateau (QTP) and Northern America (NA) to compare the patterns and trends in vegetation greenness (i.e., NDVI) within RTSs (Figure 1).

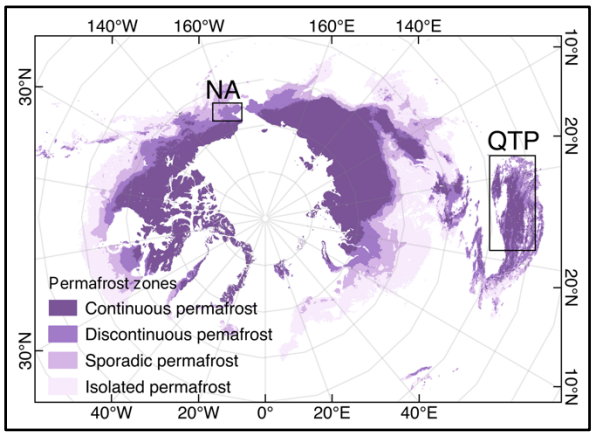

Figure 1. The distributions of the study sites.

Data and methods

We used NDVI computed from PlanetScope (Planet Team 2017)Scenes between 2017 to 2023 to investigate the temporal change in vegetation greenness. We acquired PlanetScope scenes with a resolution of 3–5 m for every year during the peak-growing season. The peak-growing season was estimated for each subregion using long-term (i.e., 2000-2023) local phenological patterns of NDVI from Landsat 7 and 8 (Hall and Lara 2022). Unusable data mask (UDM) layers were applied to the PlanetScope images to remove bad-quality pixels. Like other satellite images, the PlanetScope images are subject to misregistration and the Bidirectional Reflectance Distribution Function (BRDF) effect. To generate consistent time series NDVI values, we first co-registered the scenes based on that in 2023 using AROSICS (Scheffler 2017). Then, we cross-calibrated PlanetScope surface reflectance based on the Harmonized Landsat and Sentinel-2 (HLS) products, which provide the BRDF-adjusted Landsat and Sentinel-2 images. We selected the nearest-day HLS images and checked the QA layer for every band to retain good-quality pixels. Using band-specific histogram matching, we cross-calibrated the PlanetScope scenes based on the nearest-day BRDG-adjusted HLS images. Finally, we calculated the NDVI using red and near-infrared bands. To evaluate the robustness of the calibrated results, we extracted impervious pixels that should have stable surface reflectance yearly.

We computed a metric of relative NDVI, by taking the difference between NDVI for each RTS and year from that of 2017 (i.e., our earliest spectral observation). We selected three RTSs undergoing active headwall expansion or stabilization in both the QTP and NA (Figure 1).

Results

The average standard deviation for the calibrated NDVI on impervious ground was 0.02, which is only 50% of the standard deviation of the NDVI generated based on raw PlanetScope images, indicating our

NDVI time-series stable NDVI values over seven years.

The mean NDVI in stable thaw slumps increased by around 0.08 in Figure 2d and 0.6 in Figure 2e, while only 0.03 in Figure 2f, which has been stable for over 30 years. All of the stable thaw slumps on NA (Figure 2d) and on QTP (Figure 2e, f) had relatively steady NDVI in 2017–2022. However, nearly all stable thaw slumps showed a rapid increase in NDVI in 2023, while the one in NA had a greater increase. In active thaw slumps (Figure 2a, b, c), the NDVI increased following the uniform pattern. Moreover, before the initiation, the NDVI values had already decreased (Figure 2a, b, c).

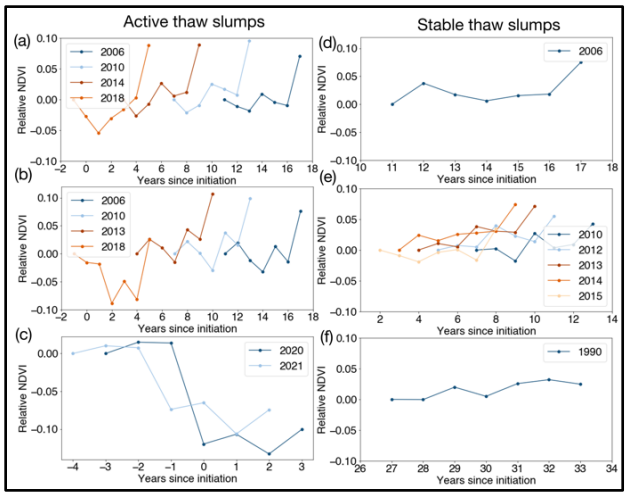

Figure 2. The yearly NDVI time series (from 2017 to 2023) of RTSs in the NA (a,b,d) and the QTP (c,e,f), with locations in Figure 1. Different lines represent the parts in an RTS initiated in different years. (a) Re-activated thaw slump. (b) Re-activated thaw slump. (c) Activated thaw slump. (d) Stable thaw slump. (e) Stable thaw slump. (f) Stable thaw slump with sparse vegetation cover.

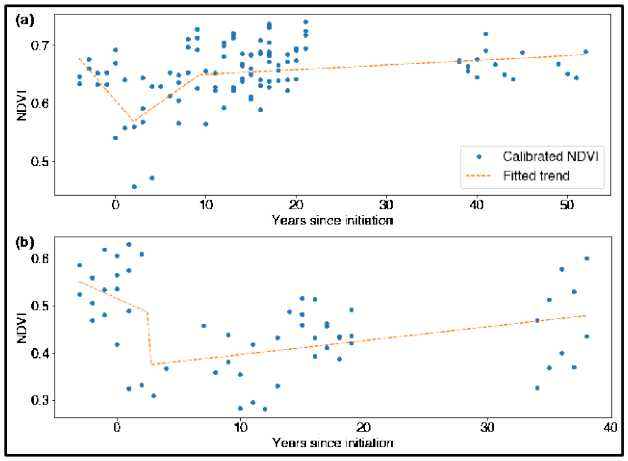

Figure 3. The simulated NDVI trends in Toolik (a) and central QTP (b).

Discussion

Overall, NDVI increased at a faster rate in active RTSs than stabilized RTSs, likely associated with dense vegetation canopy coverage in older thaw slumps. However, NDVI remained lower than that of undisturbed tundra, which suggests RTS disturbance on the QTP is irrecoverable. This is in contrast to RTS in NA as observations suggest NDVI will increase greater than undisturbed tundra as tall-shrubs colonize disturbed terrain.

Summary

We validated the robustness of the NDVI time series generated from the calibrated PlanetScope scenes. Using the time series, we distinctly identify diverse vegetation responses to RTS initiation across permafrost regions in the NA and QTP. In the future, we will conduct a more comprehensive comparison of changes in vegetation greenness by increasing our sample size across spatial domains.

References

Ballantyne, C.K.: Periglacial Geomorphology, 1st edn., Wiley Blackwell, Chichester, 132–134, ISBN 978-1-405-10006-9, 2018.

Hall, E.C., and Lara, M.J. 2022. Multisensor UAS mapping of Plant Species and Plant Functional Types in Midwestern Grasslands. Remote Sens. 14, 3453. https://doi.org/10.3390/rs14143453

Planet Team 2017. Planet Application Program Interface: In Space for Life on Earth.

Scheffler, D. 2017. AROSICS: An Automated and Robust Open-Source Image Co-Registration Software for Multi-Sensor Satellite Data. https://doi.org/10.5281/ZENODO.3743085

13 Thaw, Change & Adaptation

INTEGRATING PERSPECTIVES OF PERMAFROST THAW, CHANGE, AND ADAPTATION

13A — Permafrost Thaw, Change and Adaptation

Session Chairs: Frédéric Bouchard[1], Earl de Guzman[2], Derek Cronmiller[3] & Ylva Sjöberg[4]

[1]*Université de Sherbrook, Sherbrook, Québec, Canada*
[2]*Tetra Tech Canada Inc., Edmonton, Alberta, Canada*
[3]*Yukon Geological Survey, Whitehorse, Yukon, Canada*
[4]*Department of Geosciences and Natural Resource Management, University of Copenhagen, Copenhagen, Denmark*

This session features wide-ranging contributions that delves into the latest findings and on-going global research on permafrost thaw, change, and adaptation. The session spans topics from the geological origins of ice formations to the socio-environmental impacts of permafrost dynamics. The session will also offer valuable insights for scientists, policymakers, and stakeholders interested in the future of cold regions and their role in the global climate system.

Highlights of this broad but comprehensive session include the formation processes of massive ice and ice wedges in Smoking Hills, Northwest Territories, variations in permafrost depth across the Central Andes, and the chronology of cryopeg formation in Adventdalen, Svalbard. The session will also examine landscape characteristics and particulate organic carbon composition in the Peel River watershed, the impact of surface lapse rate changes on mountain permafrost in the Yukon, and the initiation of permafrost research in Bhutan. Addressing the distribution of polycyclic aromatic hydrocarbons in permafrost and thermokarst formation mechanisms and carbon stocks in the Sahtu Region are also presented. Effects of permafrost thawing and climate change on landforms, the active layer, and an existing water supply will be of interest to practicing professionals. Understanding the interplay of science, community, and policy for Arctic justice is also covered in this session.

Exploring the impact of surface lapse rate change scenarios on mountain permafrost distribution in four dissimilar valleys in Yukon, Canada

Philip P. Bonnaventure, Madeleine C. Garibaldi & Nick C. Noad
Department of Geography and Environment, University of Lethbridge, Lethbridge, Alberta, Canada

The distribution of mountain permafrost is complex owing to the extreme spatial variability in surface and near surface characteristics. Distribution of air temperature, however, follows two main patterns of change with elevation. First, in low latitude or maritime mountain ranges, permafrost is generally assumed to be present at high elevations and absent in lowlands, following the spatial topographic distribution of Mean Annual Air Temperature (MAAT) cooling with increased elevation (Bonnaventure et al. 2012). With warming climate, permafrost in these environments is expected to warm and thaw unidirectionally, with the lower elevation limit of permafrost moving upslope (Bonnaventure and Lewkowicz 2013). In these environments, warming is also expected to be amplified at higher elevations due to a variety of mechanisms including changes in albedo, changes in water vapor and latent heat release and aerosols (Pepin et al. 2015). This phenomenon is referred to as elevation-dependent warming (EDW) and has been supported by observations and climate modelling studies in the Andes, Rocky Mountains, and Alps (e.g., Williamson et al. 2020). However, this concept and observations have only been made in regions with normal, linear relations between air temperature and elevation. As a result, the concept of EDW is already thought to be non-inclusive for certain mountain environments.

A second mountain permafrost distribution pattern is more commonly found in high-latitude, continental mountains, where permafrost is present in both valley bottoms and high elevations because of persistent winter temperature inversions (Noad and Bonnaventure 2022). These inversions produce warming air temperatures with increasing elevation up to treeline or higher, resulting in the warmest air temperatures at mid to high elevations. In such locations the surface lapse rate (SLR) or change in temperature with elevation, is said to be inverted. With warming MAAT, this permafrost distribution pattern and the complicated relation between temperature and elevation may not produce the same warming and thawing pattern as in locations with a linear permafrost distribution. As shown for portions of Yukon subject to inverted SLRs below treeline, warming results in a bidirectional loss of permafrost as thaw advances both up and downslope from treeline (Bonnaventure and Lewkowicz 2013). Only uniform changes in MAAT have been applied and potential changes in the strength of the inverted SLR were not considered. With climate change, winter inversions could weaken (become more normal). This complicates the distribution of warming for both the air and the ground. As a result, EDW may not hold true in the high-latitude, continental mountains.

The objectives are to theoretically test using a scenario-based approach potential alternatives to EDW in four dissimilar high-latitude, continental mountain valleys in Yukon through changes in inverted SLR strength.

STUDY AREA

Four valleys with unique temperature inversions strengths, surface characteristics and spatial distributions of air and ground thermal regimes were selected, two along the Dempster Highway (Ogilvie Mountains) and two along the North Canol Road (Selwyn Mountains). Valley WS01 is the southernmost site in the Ogilvie Mountains and has an elevation range of about 700 m with trees on one side. Valley WS02 is the northern most site and, despite being only 10 km away from WS01, is quite different in terms of vegetation being treeless. In the Selwyn Mountains the Mile 222 Valley site is located on the North Canol Highway near the Yukon/ Northwest Territories border in a wide valley. Lastly, Valley MTS is the southernmost site located on the North Canol and amongst the study areas overall. This site has the largest elevation range of the study areas (about 805 m) and is comprised of treed slopes that transition to alpine tundra.

METHODS

Models for current air temperature metrics were created using *in situ* data from air temperature stations in each valley. SLRs were calculated and MAAT was spatially modelled. Ground temperatures were spatially modelled using the temperature at top of permafrost (TTOP) model (Equation 1) (Smith and Riseborough 2002).

$$TTOP = \frac{(rk * n_t * TDD_a) - (n_f * FDD_a)}{P} \quad TTOP \leq 0 \qquad [1]$$

Where: rk is the differential thermal conductivity of the substrate, n_f and n_t are freezing and thawing n-factors, FDD_a and TDD_a are freezing and thawing

degree days in the air and P is the period (365 days). In situ data for this model were sourced from 25 Ground Temperature Nodes (GTN) located in each valley generating TTOP. To assess the potential outcomes of warming and evaluate alternatives to EDW, several potential scenarios were run including both baseline warming coupled with current SLR conditions and weakening of the inverted SLRs in each valley. Using the location of the lowest air station, the baseline magnitude of warming was determined for the shared socioeconomic pathways (SSP) 2-4.5 and 3-7.0 for the 2041-2070 and the 2071-2100 climate normal using ClimateNA. To determine the magnitude of warming, the difference between MAAT for the downscaled current climate (1981-2010) and the predicted MAAT for each climate warming scenario was added to the measured MAAT for the valley. This was done to account for discrepancies between the downscaled climate normal and the measured air temperatures in each valley. For scenarios, annual inverted SLRs were weakened by 1, 2.5, and 5 °C km^{-1} in addition to the baseline warming.

Results

Only results from the SSP2-4.5 scenario are presented. For changes to inversion strength in valleys with highly inverted SLRs at lower elevations, even a 5°C weakening still resulted in annual inverted SLRs in these portions of the valleys (Figure 1). In all four valleys a uniform warming scenario without changes in the SLR, MAAT was predicted to warm evenly maintaining the current spatial distribution pattern of air temperatures. Scenarios involving a uniform warming coupled with a change in SLR strength, altered the spatial distribution of air temperature with elevation, as high elevations became colder relative to temperatures at mid and low elevations. Additionally, due to the reduced warming at high elevations resulting from weaker inverted SLRs or even a transition to normal SLRs, warming over the valleys was less than predicted in the downscaled climate reanalysis data. This reduction in overall warming increased with decreasing inverted SLR strength, becoming most pronounced for the 5 °C weakening scenario. For all scenarios and valleys, the pattern of warming for MAGT was the same as MAGST, with the greatest warming at high elevations in WS01, WS02 and MTS except for the 5 ºC decrease in temperature inversion strength scenario. Under this scenario, MAGT at high elevations warmed relatively little compared to temperatures in the valley bottom (WS01 and WS02) or mid elevations (MTS). In M222, the warming pattern in MAGT was also the same as MAGST. However, there were differences in the spatial distribution of MAGT compared to MAGST and between the warming scenarios in each valley. In Valley WS01, the relatively cold MAGTs were predicted for all scenarios in the valley bottom and at high elevations. This was also true in WS02, where the coldest temperatures were predicted on the west-facing slope and in a small portion of the valley bottom. In M222, the spatial distribution of MAGTs was the most like that of MAGST with the coldest MAGT at high elevations and the warmest in the valley bottom. For these three valleys, the magnitude of warming in MAGST and MAGT were similar, ranging from 1.2-1.9, 1.3-1.8, and 0.9-1.8 ºC for WS01, WS02 and M222, respectively. Lastly, in MTS, MAGT in the valley bottom remained the coldest throughout each warming scenario. This valley also showed the largest difference in the spatial distribution and warming of MAGST and MAGT with a range of average warming of 0.7- 0.8 ºC for MAGT compared to 1.8 to 1.9 ºC for MAGST across all scenarios.

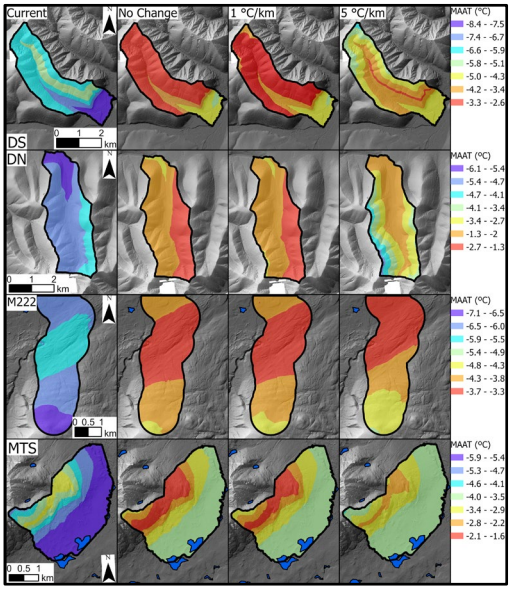

Figure 1. Impact to Mean Annual Air Temperature under investigated scenarios.

References

Bonnaventure, P.P., Lewkowicz, A.G., Kremer, M., and Sawada, M.C. 2012. Permafrost and Periglacial Processes. 23(1); 52–68. doi:10.1002/ppp.1733

Bonnaventure, P.P., and Lewkowicz, A.G. 2013.The Cryosphere. 7(3); 935-946. doi:10.5194/tc-7-935-2013

Noad, N.C., and Bonnaventure, P.P. 2022. Arctic Science. 8(4); 1320–1339. Dx.doi.org/10.1139/AS-2021-0048

Pepin, N., Bradley, R.S., Diaz, H.F., Baraer, M., Caceres, E.B., Forsythe, N. 2015 Nature Climate Change 5(5); 424–430. doi:10.1038/nclimate2563

Smith, M.W., and Riseborough, D.W. 2002. Permafrost and Periglacial Processes. 13(1); 1–15. doi:10.1002/ppp.410

Williamson, S.N., Zdanowicz, C., Anslow, F.S., Clarke, G. K., Copland, L., Danby, R.K., Hik, D.S. 2020.Journal of Climate. 33(8); 3253–3269. Doi:10.1175/JCLI-D-19-040

Origin and age of tabular massive ice and ice wedges in the Smoking Hills, Northwest Territories, Canada

Clody Desjardins[1], Denis Lacelle[1], I. Rod Smith[2], David J.A. Evans[3] & John C. Gosse[4]

[1]*Department of Geography, University of Ottawa, Ottawa, Ontario, Canada*

[2]*Geological Survey of Canada, Calgary, Alberta, Canada*

[3]*Department of Geography, University of Durham, Durham, United Kingdom*

[4]*Department of Earth and Environmental Sciences, Dalhousie University, Halifax, Nova Scotia, Canada*

The origin and age of massive ice within permafrost of the western Canadian Arctic has been the focus of many studies as they can increase our understanding of glacial history and landscape evolution. In other areas of the western Canadian arctic, some studies have identified buried glacial ice from the last (Late Wisconsinan) glaciation (e.g., Lorrain and Demeur 1985; St-Onge and McMartin 1995; Dyke and Savelle 2000), while others attributed the formation of massive ground ice to other processes (e.g., Rampton 1988; Mackay and Dallimore 1992; Lacelle et al. 2004). In the Smoking Hills region, NWT (69°N; 127°W), Evans et al. (2021) suggested that the cryostratigraphy exposed in a thaw slump presented evidence of a complex history of glacial ice burial and epigenetic ice-wedge formation, followed by a deformation of the ice wedges by either a glacial readvance or subsequent glaciation and a thermal unconformity. Our study examined extensive tabular massive ice deposits exposed in the Smoking Hills region, including the Anderson River slump identified by Evans et al. (2021).

Method

Field observations and imagery revealed hundreds of large thaw slumps exposing metres to tens of metres of tabular massive ice and ice wedges. Fieldwork was undertaken in July 2023 to collect samples of ground ice and sediments from the headwalls of four thaw slumps. Samples from ice wedges and massive ice at the Anderson River and Franklin Bay slumps were also collected for $^{14}C_{DOC}$ and ^{10}Be dating. Ice samples were analyzed for major ions and δD-$\delta^{18}O$. Sediment samples collected from debris-rich lenses, and sediments filtered from ice samples were analyzed for major, minor and trace elements, grain size, and carbonate content. The data was used to determine the glaciological and permafrost history of the Smoking Hills region.

Results

During the 2023 field season, the Anderson River slump (68°56'59"N; 128°08'47"W) had changed substantially since first observed by Evans et al (2021). While the headwall was 8-12 m high in 2018, only the upper 3-6 m of it was visible in 2023 due to headwall retreat and infilling of the slump floor by thawed sediments. In 2023, the exposure consisted of a lower unit of tabular, foliated massive ice in which 1.5-2 m wide epigenetic ice wedges had formed. A thermal unconformity defined the top of the ice wedges and massive ice, which could be traced across the 200+ m wide headwall. However, the northwestward deformation of the ice wedges, visible in 2018, was entirely covered in 2023. Overlying this lower unit was icy diamict (up to 3 m thick) and up to 1.5 m of organic-rich colluviated and cryoturbated sediments. The lower unit of massive ice had average $\delta^{18}O$ values of -28.9 ± 0.3‰ and a δD-$\delta^{18}O$ regression slope value near that of the global meteoric water line (GMWL; Figure 1). The ice wedges had $\delta^{18}O$ values that are about 2‰ lower (average of -30.4 ± 1.8‰) than the enclosing glacial ice. A small ice vein and pore ice collected from the icy diamicton had $\delta^{18}O$ values of -23.7 and -23.5‰, respectively. In the near-surface organic-rich sediments, the pore ice had $\delta^{18}O$ values of -20.7 ± 3‰, respectively (Figure 1).

At the Franklin Bay site (69°40'31"N; 126°40'02"W), the thaw slump exposed three units. The lowermost unit consisted of highly foliated and tectonized debris-rich massive ice, the intermediate unit was an icy diamict, and the uppermost unit was colluvial deposits. The massive ice had $\delta^{18}O$ values of -27.4 ± 1.1‰, and the δD-$\delta^{18}O$ regression slope was near that of the GMWL (Figure 1). Ice wedges in the colluvium had $\delta^{18}O$ values of -20.7 to -20.6‰.

The Coal River slump (69°12'43"N; 126°18'52"W) occurs within a belt of glacitectonic thrust moraines and exposed two distinct units: the lower unit was tabular, massive foliated and debris-rich ice and the upper unit consisted of diamict and colluvium. No ice wedges were observed at this site. The $\delta^{18}O$ values in the massive ice were the lowest of all four sites investigated (-31.2 ± 1.4‰), and like the other sites, the δD-$\delta^{18}O$ regression slope value was near the GMWL (Figure 1).

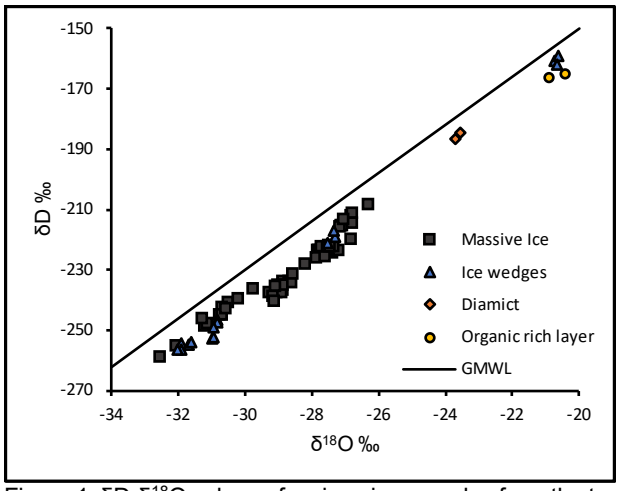

Figure 1. δD-δ^{18}O values of various ice samples from the tree sampled sites in the Smoking Hills, Northwest Territories. GMWL = global meteoric water line.

Discussion

The tabular massive ice at our sampled had low δ^{18}O values (-29.5 ± 3.2‰) and δD-δ^{18}O slopes near the GMWL, suggesting a buried glacial ice origin. The δ^{18}O values were within the range of those measured in other sites with tabular massive ice that developed during the Late Pleistocene in western Canadian Arctic (Mackay and Dallimore 1992; Murton et al. 2004; Lacelle et al. 2018). At the Anderson River slump, epigenetic ice wedges developed in the buried glacial ice. The δ^{18}O values of the ice wedges were 2‰ lower than the enclosing ice, suggesting that they formed in Late Pleistocene during an episode when the glacial ice was further south (MIS3 interstadial?). A glacial re-advance deposited the overlying diamict and likely caused the northwestward deformation of the ice wedges noted previously by Evans et al. (2021). A similar glaciotectonic deformation of warm ice-rich permafrost beneath an advancing Laurentide Ice Sheet was also observed by Murton et al. (2004) in the Tuktoyaktuk Coastland. However, the pore ice in the diamict had δ^{18}O values (-23.6‰) typically associated with Holocene waters. This would suggest a thermal unconformity (likely early Holocene) and that surface waters infiltrated the diamict to form the pore ice. Overlying the buried glacial ice at all sites, and icy diamict in some places, was a colluvium in which ice wedges developed during the Holocene. The 14CDOC and possible 10Be dating of the different types of ice will help to determine with more certainty the timing of their formation. This, combined with ice and sediment chemistry analyses, will help to refine our interpretations of the glacial and permafrost history of the Smoking Hills region.

This abstract is LMS contribution #20230322.

References

Dyke, A.S., and Savelle, J.M. 2000. Major end moraines of Younger Dryas age on Wollaston Peninsula, Victoria Island, Canadian Arctic: implications for paleoclimate and for formation of hummocky moraine, Can J Earth Sci, 37(4), 601–619.

Evans, D.J.A., Smith, I.R., Gosse, J.C., and Galloway, J.M. 2021. Glacial landforms and sediments (landsystem) of the Smoking Hills area, Northwest Territories, Canada: Implications for regional Pliocene – Pleistocene Laurentide ice sheet dynamics, QuatSciRev 262, 1–50.

Lacelle, D., Fisher, D.A., Coulombe, S., Fortier, D., and Frappier, R. 2018. Buried remnants of the Laurentide Ice Sheet and connections to its surface elevation, Scientific Reports, 8(1),1–10.

Lacelle, D., Lauriol, B., and Clark, I.D. 2004. Segregated-intrusive ice of subglacial meltwater origin in retrogressive thaw flow headwalls, Richardson Mountains, NWT, Canada, QuatSciRev, 23(5–6), 681–696.

Lorrain, R.D., and Demeur, P. 1985. Isotopic evidence for relic Pleistocene glacier ice on Victoria Island, Canadian Arctic Archipelago, Arctic and Alpine Research 17(1), 89–98.

Mackay, J.R., and Dallimore, S.R. 1992. Massive ice of the Tuktoyaktuk area, western Arctic coast, Canada, Can J Earth Sci, 29(6), 1235–1249.

Murton, J.B., Waller, R.I., Hart, J.K., Whiteman, C.A., Pollard, W.H., and Clark, I.D. 2004. Stratigraphy and glaciotectonic structures of permafrost deformed beneath the northwest margin of the Laurentide ice sheet, Tuktoyaktuk Coastlands, Canada. J Glaciol, 50(170), 399–412.

Rampton, V.N. 1988. Origin of massive ground ice on Tuktoyaktuk peninsula, Northwest Territories, Canada: a review of stratigraphic and geomorphic evidence. In Proc. of the Fifth Intern. Conf. on Permafrost, Tapir Publishers, Trondheim, Norway, 3: 850–855.

St-Onge, D.A., and McMartin, I. 1995. Quaternary geology of the Inman River area, Northwest Territories, Geological Survey of Canada, Bulletin 446, 1–59.

Permafrost pathways: Connecting science, people, and policy for arctic justice and global climate

John Holdren[1], Sue Natali[2] & Jennifer Spence[1]

[1]*Arctic Initiative – Permafrost Pathways, Harvard Kennedy School, Cambridge, Massachusetts, United States*

[2]*Woodwell Climate Research Center – Permafrost Pathways, Falmouth, Massachusetts, United States*

Permafrost Pathways is in the second year of a 6-year program supported by the TED Audacious Project—a collaborative funding initiative catalyzing solutions to the world's most urgent challenges. Permafrost Pathways brings together leading experts in climate science, policy action, and environmental justice to strengthen the science of permafrost thaw and inform adaptation and mitigation strategies to address the challenges this phenomenon poses for the Arctic and the world.

The project is engaging a diverse and extensive network of scientists, Indigenous knowledge holders, policymakers, and practitioners. Its leaders bring to it an unusual blend of experience and expertise—conducting Arctic research, working with impacted communities, convening stakeholders and policymakers—to guide this endeavor.

This presentation by members of the Arctic Initiative at Harvard Kennedy School and Woodwell Climate Research Center will elaborate on the status of the project two years in and detail efforts to collaborate with Alaska Native communities affected by permafrost thaw to create Indigenous-led climate adaptation plans and ensure permafrost carbon emissions are accounted for in global climate policy. The presentation will also provide insight into one of the project's public-private partnerships with the Alaska Native Tribal Health Consortium (ANTHC) and the importance of working with multidisciplinary experts to amplify Arctic adaptation efforts.

Additional project updates will include:

- Expanded carbon flux monitoring network
- Efforts to enact policy change through community engagement
- Efforts to develop a self-sustaining "community of practice" among Arctic permafrost reseachers and modelers that promotes engagement in national and global climate policy and decision-making processes

It will also provide an opportunity for other experts working on permafrost thaw and its impacts—whether on the science, policy and strategy, or social-justice aspects— to connect with project members and share insights.

Landscape characteristics and particulate organic carbon composition in the Peel River watershed, Canada

Kirsi Keskitalo[1,2], Niek Speetjens[3,2], Pier Paul Overduin[4], Sebastian Westermann[5], Frederieke Miesner[4], Torsten Sachs[6], Ingmar Nitze[4], Lisa Bröder[7], Julie Lattaud[8,7], Negar Haghipour[7,9], Timothy Eglinton[7] & Jorien Vonk[2]

[1]*Department of Geography and Environmental Sciences, Northumbria University, Newcastle upon Tyne, United Kingdom*

[2]*Department of Earth Sciences, Vrije Universiteit Amsterdam, Amsterdam, The Netherlands*

[3]*Department of Environmental Studies, University of Victoria, Victoria, British Columbia, Canada*

[4]*Alfred Wegener Institute Helmholtz Centre for Polar and Marine Research, Potsdam, Germany*

[5]*Department of Geosciences, University of Oslo, Oslo, Norway*

[6]*GFZ German Research Centre for Geosciences, Potsdam, Germany*

[7]*Department of Earth Sciences, Swiss Federal Institute of Technology, Zürich, Switzerland*

[8]*Department of Environmental Sciences, University of Basel, Basel, Switzerland*

[9]*Laboratory of Ion Beam Physics, Swiss Federal Institute of Technology, Zürich, Switzerland*

The Arctic is warming up to four times the rate of the global average (Rantanen et al. 2022). This induces accelerated permafrost thaw, along with intensification of fires, and shifts in hydrology and vegetation (Schuur et al. 2015). The effects of these changes on aquatic networks are diverse and dependent on landscape-specific factors (Tank et al. 2020). The Peel River watershed is underlain largely by continuous permafrost (Figure 1) and covers a diverse set of landscapes from wetlands to barren mountainous areas. The watershed undergoes abrupt permafrost thaw, such as retrogressive thaw slumping, that releases dominantly particulate organic carbon (POC) into fluvial waterways (e.g., Kokelj et al. 2017; Shakil et al. 2020). Thaw slumping increases sediment and POC loads in rivers thus changing their hydrochemical composition. These changes may cascade across entire watersheds (Kokelj et al. 2017). Furthermore, degradation of permafrost-derived organic carbon in the water column may add greenhouse gases to the atmosphere, thus enhancing climate warming (e.g., Schuur et al. 2015).

In this study, we couple landscape characteristics to river POC to better understand its spatial variability and the changes imposed on the watershed by permafrost thaw. We sampled POC in July–August 2019 during a particularly dry summer both in the Peel River mainstem and its tributaries (total n=~100) and used carbon isotopes ($\delta^{13}C$, $\Delta^{14}C$) and lipid biomarkers (n-alkanoic acids and glycerol dialkyl glycerol tetraethers - GDGTs) to characterize its composition, degradation status and sources. Additionally, we used Landsat-based tasseled cap trend indices to illustrate changes in the landscape and to better understand connection between landscape and water column dynamics.

Our preliminary data show an order of magnitude difference in POC concentrations (<0.1 to 800 mg L^{-1}) and large variability in its composition (e.g., $\Delta^{14}C$-POC ranging between -906.4 and -23.4 ‰). There is a stark contrast in POC composition in the Peel River mainstem between the lower part of the watershed, which receives old permafrost carbon from thaw slumping, and the upper watershed, where POC originates mostly from in-river processes and the permafrost active layer (Figure 2). Tributaries, on the other hand, vary in their POC composition, especially in the lower catchment (Figure 2).

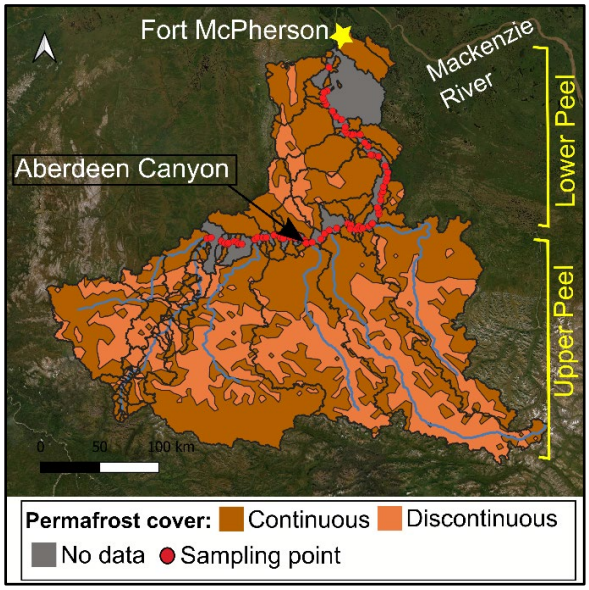

Figure 1. Permafrost cover in the Peel River watershed and sampling points indicated with red circles (following the course of the Peel River mainstem). Permafrost cover is based on Obu et al. (2019). The Peel River catchment is divided by the Aberdeen Canyon (marked with a black arrow) to upper and lower watershed that differ distinctly from each other in their particulate organic carbon composition. Background map source: ESRI.

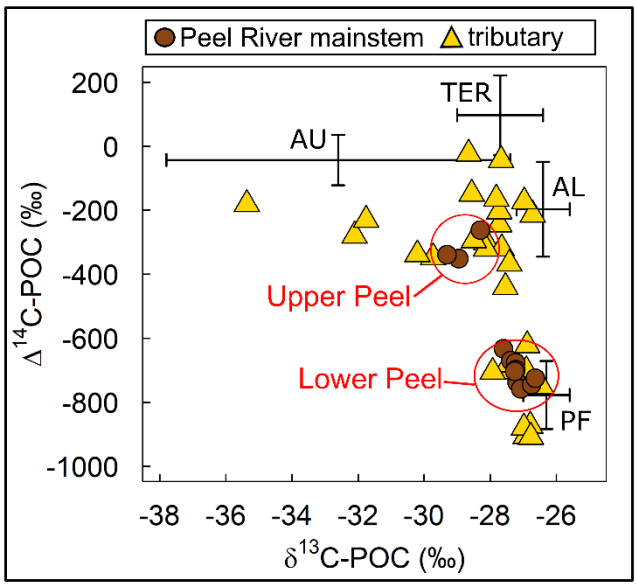

Figure 2. Particulate organic carbon (POC) $\Delta^{14}C$ and $\delta^{13}C$ in the Peel River mainstem (circles) and its tributaries (triangles) across the watershed. Samples from upper and lower Peel River mainstem are highlighted with red circles. Endmembers for different carbon sources are indicated with black lines: AU=autochthonous, TER=terrestrial, AL=active layer, and PF=permafrost. Endmembers are according to Behnke et al. (2023); Vonk et al. (2012); Levin et al. (2013); Wild et al. (2019); and Winterfeld et al. (2015).

The change in the tasseled cap wetness index suggests an increase in soil erosion (between 2001 and 2020) that can be mostly attributed to thaw slumps and landslides as well as other rapid landscape dynamics, such as wildfires and vegetation changes. With these data we aim to better understand ongoing changes in the watershed and reflect how it may change in the future.

References

Behnke, M.I., Tank, S.E., McClelland, J.W., Holmes, R.M., Haghipour, N., Eglinton, T.I., Raymond, P.A., Suslova, A., Zhulidov, A.V., Gurtovaya, T., Zimov, N., Zimov, S., Mutter, E.A., Amos, E., and Spencer, R.G.M. 2023. Aquatic biomass is a major source to particulate organic matter export in large Arctic rivers, Proceedings of the National Academy of Sciences of the United States of America,120(12):1–9. https://doi.org/10.1073/pnas.2209883120

Kokelj, S.V., Lantz, T.C., Tunnicliffe, J., Segal, R., and Lacelle, D. 2017. Climate-driven thaw of permafrost preserved glacial landscapes, northwestern Canada, Geology, 45(4): 371–374. doi:10.1130/G38626.1

Levin, I., Kromer, B., and Hammer, S. 2013. Atmospheric $\delta^{14}CO_2$ trend in Western European background air from 2000 to 2012, Tellus, Series B Chemical and Physical Meteorology,65(1):1–7. doi:10.3402/tellusb.v65i0.20092

Obu, J., Westermann, S., Bartsch, A., et al. 2019. Northern Hemisphere permafrost map based on TTOP modelling for 2000–2016 at 1 km^2 scale, Earth-Science Reviews, 193: 299–316. doi:10.1016/j.earscirev.2019.04.023

Rantanen, M., Karpechko, A.Y., Lipponen, A., Nordling, K., Hyvärinen, O., Ruosteenoja, K., Vihma, T., and Laaksonen, A. 2022. The Arctic has warmed nearly four times faster than the globe since 1979, Communications Earth and Environment, 3(1): 1–10. doi:10.1038/s43247-022-00498-3

Shakil, S., Tank, S.E., Kokelj, S.V., Vonk, J.E., and Zolkos, S. 2020. Particulate dominance of organic carbon mobilization from thaw slumps on the Peel Plateau, NT: Quantification and implications for stream systems and permafrost carbon release, Environmental Research Letters, 15(11): 114019. doi:10.1088/1748-9326/abac36

Schuur, E.A.G., McGuire, A.D., Schädel, C., Grosse, G., Harden, J.W., Hayes, D.J., Hugelius, G., Koven, C.D., Kuhry, P., Lawrence, D.M., Natali, S.M., Olefeldt, D., Romanovsky, V.E., Schaefer, K., Turetsky, M.R., Treat, C.C., and Vonk, J.E. 2015. Climate change and the permafrost carbon feedback, Nature, 520: 171–179. doi:10.1038/nature14338

Tank, S.E., Vonk, J.E., Walvoord, M.A., McClelland, J.W., Laurion, I., and Abbott, B.W. 2020. Landscape matters: Predicting the biogeochemical effects of permafrost thaw on aquatic networks with a state factor approach, Permafrost and Periglacial Processes, 31(3): 358–370. doi:10.1002/ppp.2057

Vonk, J.E., Sánchez-García, L., van Dongen, B.E., Alling, V., Kosmach, D., Charkin, A., Semiletov, I.P., Dudarev, O.V., Shakhova, N., Roos, P., Eglinton, T.I., Andersson, A., and Gustafsson, Ö. 2012. Activation of old carbon by erosion of coastal and subsea permafrost in Arctic Siberia, Nature, 489(7414): 137–140. doi:10.1038/nature11392

Wild, B., Andersson, A., Bröder, L., Vonk, J., Hugelius, G., McClelland, J.W., Song, W., Raymond, P.A., and Gustafsson, Ö. 2019. Rivers across the Siberian Arctic unearth the patterns of carbon release from thawing permafrost, Proceedings of the National Academy of Sciences of the United States of America, 116(21): 10280–10285. doi:10.1073/pnas.1811797116

Winterfeld, M., Goñi, M.A., Just, J., Hefter, J., and Mollenhauer, G. 2015. Characterization of particulate organic matter in the Lena River delta and adjacent nearshore zone, NE Siberia – Part 2: Lignin-derived phenol compositions, Biogeosciences, 12(7): 2261–2283. doi:10.5194/bg-12-2261-2015

Depth to Permafrost in the Central Andes (27°S-34°S)

Cassandra E.M. Koenig[1,2], Christin Hilbich[1], Christian Hauck[1], Lukas U. Arenson[3] & Pablo Wainstein[4]

[1]*Department of Geosciences, University of Fribourg, Fribourg, Switzerland*

[2]*BGC Engineering Inc., Toronto, Ontario, Canada*

[3]*BGC Engineering Inc., Vancouver, British Columbia, Canada*

[4]*BGC Engineering Inc., Calgary, Alberta, Canada*

The global understanding of permafrost's thermal state is based primarily on data from circumpolar regions and mountain environments of the Northern Hemisphere (e.g., Smith et al. 2022). While permafrost has long been known to exist in mountain regions of the Southern Hemisphere (Catalano 1926; Corte 1953), there is a lack of ground temperature data from these regions, particularly from depths greater than a few metres. Historically, this has limited evaluations of the thermal state and the possible degradation of mountain permafrost in the High Andes, excluding them from consideration in global assessments of climate change, or resulting in speculation. This contribution presents preliminary estimates of depth to permafrost from a suite of thermistor strings installed at the Chile-Argentine border, between 27°S and 34°S. Of the 18 boreholes examined, only three locations within rock glaciers showed evidence of permafrost degradation, with a clear deepening of the permafrost table over time and formation of a supra-permafrost talik. These observations are consistent with surface geomorphological evidence of advanced degradation within these particular landforms.

Ground Temperature Data

Ground temperature monitoring data from a series of industrial projects in the Andes were previously compiled, and preliminary attributes of borehole temperatures were presented by Koenig et al. (2023). The full dataset includes 54 boreholes, 31 of which were installed in permafrost or at potential permafrost sites. A subset of the monitoring locations detailing selected characteristics of the boreholes in cryotic ground is included in Table 1.

Monthly variations in ground temperatures and thermal gradients observed within the boreholes are discussed in detail in a companion paper currently in preparation by the authors. The dataset does not clearly indicate secular warming or cooling of the ground, except for three boreholes within rock glaciers. Temporal trends within these landforms are obscured by latent heat effects in the monitoring data. However, there is a clear deepening of the permafrost table over time of monitoring at these locations, implying permafrost degradation.

Table 1. Monitoring Sites and Borehole Characteristics.

Site No.	Lat / Long	No. of Boreholes in Cryotic Ground	Borehole Depth or Depth Range (m)	Depth to Permafrost Range (m)[1]
1	27°44" / 69°14"	2	24 - 25	1.1 - 1.8
2	28°26" / 69°36"	4	38 - 50	0.8 - 1.5
3	29°19" / 70°1"	10	15 - 100	0.6 - 6
4	29°23" / 69°59"	1	25	--
5	30°1" / 69°55"	5	10 - 48	0.9 - 1.8
6	31°43" / 70°30"	5	22 - 35	7.3 - 17.4
7	31°45" / 70°26"	4	27 - 40	~1.6

[1]*Estimated from most recent available data.*

Methods and Results

Depth to permafrost was estimated in boreholes for which the data record encompassed at least one complete freeze-thaw cycle and subsequent seasonal refreezing of the ground. Out of the 31 boreholes in cryotic ground (Table 1), a total of 18 met these criteria. The Active Layer Thickness (ALT) in permafrost boreholes (or maximum thaw depth in boreholes with less than 2 years of data) was estimated by linearly interpolating recorded temperatures between thermistors positioned above and below the zero-degree isotherm at the time of maximum annual thaw. Within two boreholes installed in rock glaciers (Boreholes 6-1 and 6-4), the depth to permafrost exceeded the maximum depth of annual freeze/thaw. Therefore, the measurement of interest at these three locations is more appropriately termed depth to permafrost table as opposed to ALT or thaw depth.

The range in estimated values of depth to permafrost are plotted against time in Figure 1, with results < 4 m deep shown on an expanded vertical scale for increased visibility of variation over time. The figure illustrates that depth to permafrost typically ranges from ~0.5 to less than 4 m for bedrock and colluvium sites, with one location (Borehole 3-5) reaching a depth of 6 m. Notably, the depth to permafrost within rock glaciers is the greatest within the dataset, ranging between 7.3 to 17.4 m below the

ground surface during the 2021 calendar year. This is consistent with surficial evidence of degradation in these landforms.

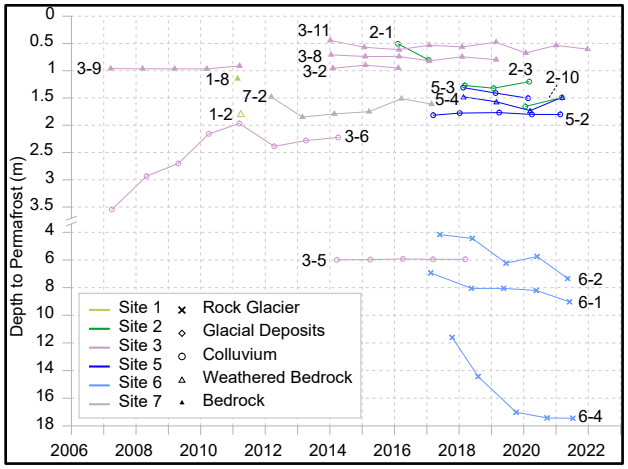

Figure 1. Depth to Permafrost in Cryotic Boreholes.

As with the ground temperature time-series discussed in our companion paper, there is no salient trend in deepening (or shallowing) of the active layer over time across the dataset. Instead, individual locations show signs of shallowing of the active layer (e.g., Boreholes 3-6 and 3-9, and possibly 2-3 and 2-10) whereas others, specifically those installed in rock glaciers (Boreholes 6-1, 6-2, and 6-4), show a deepening of the permafrost table over time.

The evolution of the thermal regime within the three rock glaciers is further illustrated in the diagrams of Figure 2, which show ground temperatures interpolated over the full depth and time span of available measurements within each of the three boreholes. Depth to permafrost is highlighted on these contour plots by black dots, and horizontal lines represent the depth of thermistors used for interpolation. The contour plots show degradation of permafrost through the progressive lowering of the permafrost table in each case, with a clear de-coupling of the top horizon of permafrost from annual freeze/thaw penetration in Borehole 6-1 and 6-4, and formation of a supra-permafrost talik.

SUMMARY

Depth to permafrost was estimated using temperature measurements in 18 boreholes in cryotic ground (between 10 and 100 m deep) in the High Andes of Chile and Argentina. Evidence for permafrost degradation was found only in three rock glaciers, which showed a clear deepening of the permafrost table with time. For the other sites, the depth of permafrost appears to have remained stable in recent years.

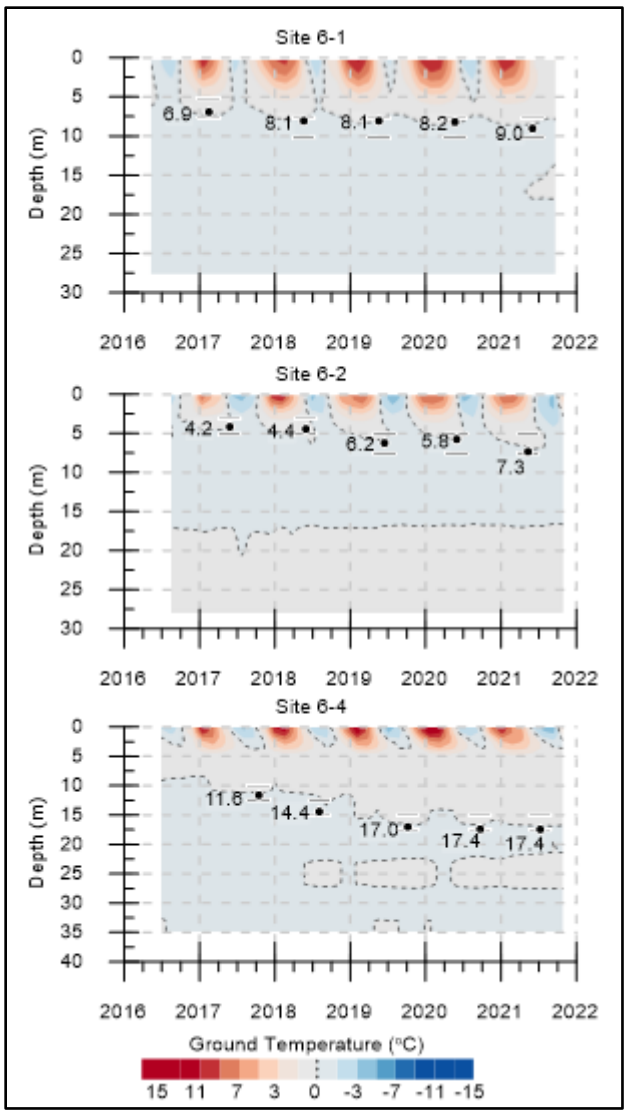

Figure 2. Ground thermal regime within rock glaciers.

REFERENCES

Catalano, L. 1926. Contribución al conocimiento de los fenómenos geofísicos. Dirección General de Minas, Geología e Hidrología, Buenos Aires (Publicación 24), 78 pp.

Corte, A. 1953. Contribución a la Morfología Periglacial de la Alta Cordillera con Especial Mención del Aspecto Criopedológico. Anales del Departamento de Investigaciones Científicas, 1(2): 54 pp.

Koenig, C.E.M., Hilbich, C., Hauck, C., and Arenson, L.U. 2023. Thermal State of Permafrost in the Central Andes. 6th European Conference on Permafrost, Puigcerdà, Catalonia, Spain, 18-22 June 2023.

Smith, S.L., O'Neill, H.B., Isaksen, K., et al. 2022. The changing thermal state of permafrost. Nat Rev Earth Environ 3: 10–23. doi.org/10.1038/s43017-021-00240-1

Landform fingerprints reveal variation in permafrost thaw-sensitivity

Steven V. Kokelj[1], Niels Weiss[1], Anastasia Sniderhan[2], Stephen Wolfe[3], Duane Froese[4], Jurjen van der Sluijs[5], Jennifer Baltzer[2], Trevor Lantz[6], Peter Morse[3], Stephan Gruber[7], H. Brendan O'Neill[3], Alejandro Alvarez[4] & Suzanne Tank[8]

[1]*Northwest Territories Geological Survey, Government of Northwest Territories, Yellowknife, Northwest Territories, Canada*

[2]*Department of Biology, Wilfrid Laurier University, Waterloo, Ontario, Canada*

[3]*Geological Survey of Canada, Ottawa, Ontario, Canada*

[4]*Department of Earth and Atmospheric Sciences, University of Alberta, Edmonton, Alberta, Canada*

[5]*Northwest Territories Centre for Geomatics, Government of Northwest Territories, Yellowknife, Northwest Territories, Canada*

[6]*School of Environmental Studies, University of Victoria, Victoria, British Columbia, Canada*

[7]*Department of Geography and Environmental Studies, Carleton University, Ottawa, Ontario, Canada*

[8]*Department of Biological Sciences, University of Alberta, Edmonton, Alberta, Canada*

Permafrost affects 12–17 million km^2 of the exposed land surface in the Northern Hemisphere (Zhang et al. 2003) and profoundly influences physical and biological processes shaping circumpolar environments. Widespread permafrost thaw is already observed and projected to increase over the coming century (Shukla et al. 2019). This will transform ice-rich landscapes through a broad suite of thaw-driven processes called thermokarst (Kokelj and Jorgenson 2013). However, a conceptual framework for understanding variation in the nature and diversity of thaw-driven landscape change, upscaling field studies, and predicting the consequences for ecosystems, climate, and land use remains a fundamental knowledge gap in permafrost science.

New information on terrestrial Arctic change derived primarily through modeling, remotely sensed, or machine-learned analyses increasingly shapes how the scientific community conceptualizes the nature, distribution, and consequences of permafrost thaw (Hjort et al. 2018; Spence et al. 2021), as well as the perceptions of policymakers and the public. Technological advances to monitor and model terrestrial Arctic change are timely as the effects of permafrost thaw now exceed rates and magnitudes that occurred throughout the late Holocene. However, empirical studies indicate significant heterogeneity in permafrost characteristics and a wide range of spatial and temporal variability in the nature and intensity of thaw-driven landscape change. For example, across ice-rich permafrost regions of North America, an increase in thaw-driven landslides (Lewkowicz and Way 2019), top-down ice-wedge thaw, and pond formation (Fraser et al. 2018), thermokarst lake expansion, rapid lake drainage (Nitze et al. 2020), and peatland degradation (Gibson et al. 2021), are amongst the most recognized processes that shape thawing terrain. These landforms manifest in complex patterns across landscapes reflecting variations in the nature and patterns of thaw-driven change (Figure 1).

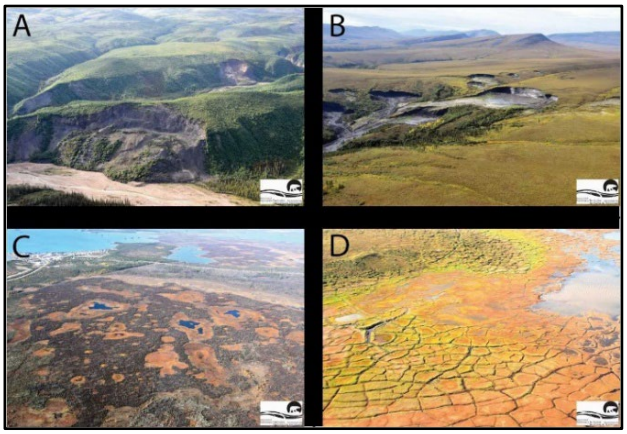

Figure 1. A and B show thaw-driven landslides. A. Deep-seated and bedrock-controlled slides in discontinuous permafrost and B. large thaw slumps and debris tongues in continuous permafrost with melting of relict ice. C and D show lowland thermokarst and periglacial landforms. C. Collapse scars and thermokarst ponds in organic terrain with thin, discontinuous permafrost, and D. high and low-centered polygonal peatlands underlain by ice-wedge networks and a small pingo in cold continuous permafrost.

In Quaternary science, landsystem approaches provide an integrative framework for characterizing landform-sedimentary relationships that manifest as distinct terrain types, and when mapped, contribute significant insight into geological processes, such as the nature of glaciation. As an extension, we propose that geological legacies conditioned by climate and paleoenvironmental history give rise to distinct permafrost landforms that combine as landscape assemblages reflecting stratigraphic, ground ice, and thermal conditions. In this presentation, we explore

the broad-scale (10^6 km^2) patterns of variation in thermokarst and periglacial landforms and determine whether they manifest as distinct, overlapping, or divergent "fingerprints" at finer scales (10^3 km^2). We utilized a subset of data from a systematic grid-based inventory (7.5 x 7.5 km^2, n=1985) of 25 permafrost landforms from across the continental scale eco-climate gradient of northwestern Canada (Kokelj et al. 2023). To assess typical thermokarst and periglacial landform combinations and the influence of climate and terrain predictor variables we employed redundancy analysis (RDA). In brief, RDA axis 1 reflects variation in landform assemblages that characterize organic and lake-rich terrain across the continental climate-permafrost gradient of northwestern Canada. The result demonstrates that major ecoregions can be distinguished based on differences in the permafrost landform indicators of thaw sensitivity. RDA axis 2 reflects differences among sites with lowland thermokarst or periglacial features and those topographically complex landscapes influenced by mass-wasting processes. Stratifying the RDA site scores and examining landform richness indices for higher-level ecoregions that occupy smaller areas indicate that thermokarst fingerprints distinguish observed permafrost terrain sensitivities across a hierarchy of scales. These spatially explicit characterizations of permafrost terrain provide a basis to explore linkages between landforms, ecosystems, underlying permafrost conditions, and their relations with geological and climate legacies. We integrate our landform synthesis with expert knowledge to visualize archetypical permafrost landsystems and highlight the utility of this framework for communicating the holistic nature and variability of permafrost conditions. On this basis, plausible future effects of thaw can be anticipated based on the similarities or differences in terrain fingerprints coupled with process knowledge of mapped locations. Furthermore, the insight gained will help parameterize and calibrate transient simulations of thaw better to quantify its timing, magnitude, and location. We conclude that permafrost landsystem approaches provide an integrative, geologically-based, forward-facing lens for characterizing permafrost terrain towards a deeper understanding of thaw-driven change, and better-informed prediction of the ecological and societal consequences.

REFERENCES

Fraser, R.H., Kokelj, S.V., Lantz, T.C., McFarlane-Winchester, M., Olthof, I., and Lacelle, D. 2018. Climate sensitivity of high arctic permafrost terrain demonstrated by widespread ice-wedge thermokarst on Banks Island, Remote Sensing, 10. doi:10.3390/rs10060954

Gibson, C., Cottenie, K., Gingras-Hill, T., Kokelj, S.V., Baltzer, J.L., Chasmer, L., and Turetsky, M.R. 2021. Mapping and understanding the vulnerability of northern peatlands to permafrost thaw at scales relevant to community adaptation planning, Environmental Research Letters, 16. doi:10.1088/1748-9326/abe74b

Hjort, J., Karjalainen, O., Aalto, J., Westermann, S., Romanovsky, V.E., Nelson, F.E., Etzelmüller, B., and Luoto, M. 2018. Degrading permafrost puts Arctic infrastructure at risk by mid-century, Nature Communications, 9. doi.org/10.1038/s41467-018-07557-4

Kokelj, S.V., and Jorgenson, M.T. 2013. Advances in thermokarst research, Permafrost and Periglacial Processes, 24(2): 108–119. doi.org/10.1002/ppp.1779

Kokelj, S.V., Gingras-Hill, T., Daly, S.V., Morse, P., Wolfe, S., Rudy, A.C., ... and Young, J. 2023. The Northwest Territories Thermokarst Mapping Collective: A northern-driven mapping collaborative toward understanding the effects of permafrost thaw, Arctic Science, 9(4): 886–918. doi.org/10.1139/as-2023-0009

Lewkowicz, A.G., and Way, R.G. 2019. Extremes of summer climate trigger thousands of thermokarst landslides in a High Arctic environment, Nature Communications, 10. doi:10.1038/s41467-019-09314-7

Nitze, I., Cooley, S.W., Duguay, C., Jones, B., Grosse, G., 2020. The catastrophic thermokarst lake drainage events of 2018 in northwestern Alaska: Fast-forward into the future, The Cryosphere, 14(14): 4279–4297. doi:10.5194/tc-14-4279-2020

Spence, C., Norris, M., Bickerton, G., Bonsal, B.R., Brua, R., Culp, J.M., Dibike, Y., Gruber, S., Morse, P.D., Peters, D.L., Shrestha, R., and Wolfe, S.A. 2020. The Canadian water resource vulnerability index to permafrost thaw (Cwrvipt), Arctic Science, 6. doi:10.1139/as-2019-0028

Shukla, P.R., Skea, J., Slade, R. van Diemen, R., Haughey, E., Malley, J., Pathak, M., and Portugal Pereira., J. (eds.) Technical Summary, 2019. In: Climate Change and Land: an IPCC special report on climate change, desertification, land degradation, sustainable land management, food security, and greenhouse gas fluxes in terrestrial ecosystems.

Small, shallow lakes as sentinels of environmental change in discontinuous permafrost peatlands

Jennifer Korosi[1], Kristen Coleman[1], Steven Kokelj[2], Michael Palmer[3], Joshua Thienpont[1] & William Quinton[4]

[1]*Faculty of Environmental and Urban Change, York University, Toronto, Ontario, Canada*

[2]*Northwest Territories Geological Survey, Government of Northwest Territories, Yellowknife, Northwest Territories, Canada*

[3]*Aurora Research Institute, Aurora College, Yellowknife, Northwest Territories, Canada*

[4]*Department of Geography and Environmental Studies, Wilfrid Laurier University, Waterloo, Ontario, Canada*

The Dehcho region of the Northwest Territories straddles the boundary between sporadic and discontinuous permafrost (Figure 1), and is one of the most rapidly warming regions on Earth. The landscape is dominated by permafrost peatlands that have been thawing at unprecedented rates in recent decades, rapidly converting forested permafrost peat plateaus into wetlands, enhancing hydrological connectivity, and reducing wetland water storage (Wright et al. 2022). Small lakes are abundant across boreal permafrost peatlands and offer useful insights into permafrost thaw processes as sentinels of broader landscape change.

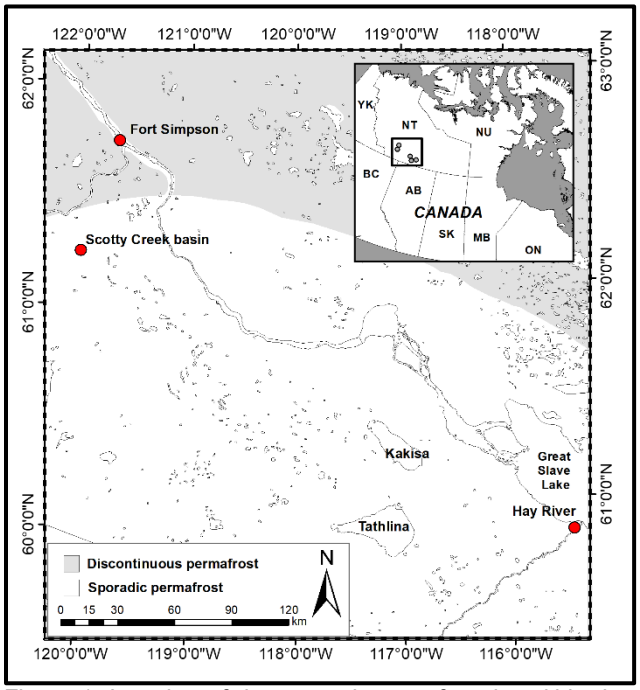

Figure 1. Location of the general area of study, within the Dehcho region of the southern Northwest Territories.

Study objective

The study objective is to understand how loss of permafrost alters limnological conditions in small (0.1-7.0 km^2), shallow (1-2 m) lakes of the Dehcho, so that lake ecosystem changes can be monitored and interpreted as sentinels of permafrost landscape evolution.

Limnology of Dehcho lakes – a preliminary survey

We analyzed surface water chemistry in summer for 60 small, shallow (max. depth 1-2 m) lakes across the Dehcho between 2012 and 2018. The most notable finding was a lack of any correlation, even a weak one, between dissolved organic carbon (DOC) and lake colour, due to the prevalence of lakes with high concentrations (20-50 mg/L) of non-chromophoric DOC. This was reflected in the lake primary producer communities, where two clusters of diatom assemblages (single-celled algae of the class Bacillariophyceae) were evident: one dominated by epiphytic (i.e., attached to plants) diatom taxa characteristic of high water clarity, and a second assemblage dominated by small benthic Fragilariaceae that tolerate low-light conditions in lakes with high chromophoric DOC (Figure 2). The reasons why several lakes exhibit high non-chromophoric DOC are currently being investigated, and preliminary findings could not establish a link with surface water hydrological connectivity (Coleman et al. 2023). Lake "browning", defined as an increase in chromophoric DOC, has been widely projected for northern lakes impacted by permafrost thaw, with implications for global carbon cycling (Vonk et al. 2015). Our findings indicate that DOC in Dehcho lakes is complex, and that predictions of widespread boreal lake browning may not be straightforward for this region. We postulate that the complexity in water chemistry may relate to thin discontinuous permafrost that allows for interaction with subsurface geology.

Paleolimnological reconstruction

Diatoms preserve well in lake sediment cores, providing a paleoenvironmental record of permafrost landscape changes spanning decades to millennia. Diatoms have been analyzed in short gravity cores incorporating the last ~200-500 years in 25 Dehcho lakes. Sediment core findings indicate that diatom assemblage changes mostly remained within the two

identified clusters, except for two lakes that experienced a shift from a high-clarity to a low-clarity diatom assemblage. For one of the lakes, evidence strongly implicated forest fire and subsequent permafrost thaw as the most probable cause (Coleman et al. 2015; Korosi et al. 2015), and preliminary evidence supports a similar cause in the second lake. Overall, this suggests that lake browning may manifest abruptly in response to rapid permafrost thaw, but the underlying mechanisms are not yet understood. First Lake, located at the Scotty Creek Research Station, was unique in exhibiting recent increases in planktonic Cyclotella taxa, which has been widespread elsewhere across the circumpolar North (Rühland et al. 2015).

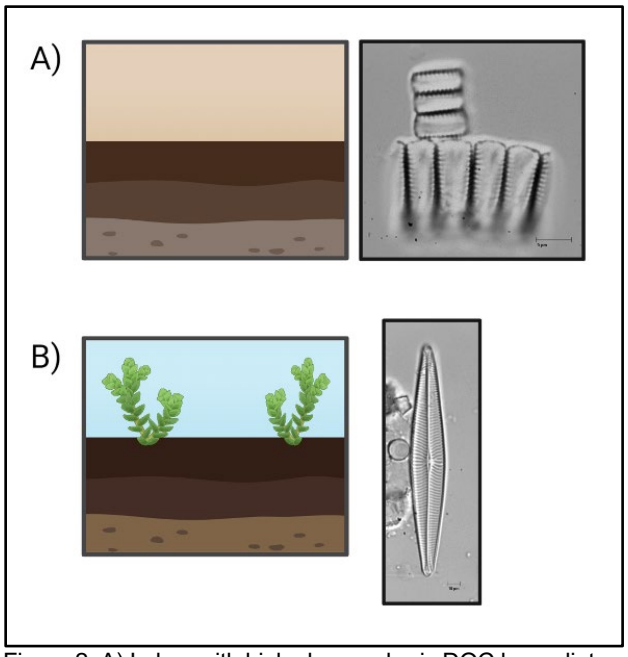

Figure 2. A) Lakes with high chromophoric DOC have diatom assemblages dominated by small benthic Fragilariaceae. B) Clear lakes with high non-chromophoric DOC have diatom assemblages dominated by large benthic Navicula taxa. Created with BioRender.com.

Future directions

We plan to undertake a synoptic water quality survey of small lakes strategically selected to span major gradients in permafrost conditions and surficial geological units in the Dehcho. This will allow us to explore the reasons for unusually high non-chromophoric DOC in Dehcho lakes, and the underlying mechanisms that would explain why permafrost thaw causes lake browning for some lakes but not others. This work will be incorporated into a larger, multi-partner effort to advance a new geologically-based framework for characterizing and classifying permafrost-affected lakes and predicting their sensitivity to climate-related disturbances.

We will pair the lake survey with long-term limnological research on three lakes at the Scotty Creek Research Station, sampling across seasons. The Scotty Creek Research Station was burned in a severe late-season wildfire in October 2022 and is expected to experience rapid permafrost thaw as a result. Scotty Creek has been a site of long-term permafrost and ecohydrological field research going back decades, and the area has been routinely surveyed by the NASA ABoVE Airborne Campaign since 2017. Scotty Creek provides an unprecedented opportunity to enhance process-based understanding of post-fire land and water transformations in discontinuous permafrost peatlands.

References

Coleman, K.A., Palmer, M.J., Korosi, J.B., Kokelj, S.V., Jackson, K., Hargan, K.E., Mustaphi, C.J.C., Thienpont, J.R., Kimpe, L.E., Blais, J.M., Pisaric, M.F., and Smol, J.P. 2015. Tracking the impacts of recent warming and thaw of permafrost peatlands on aquatic ecosystems: a multi-proxy approach using remote sensing and lake sediments, Boreal Environment Research, 20(3): 363–377. http://hdl.handle.net/10138/228213

Coleman, K.A., Hoskin, G.N., Chasmer, L., Thienpont, J.R., Quinton, W.L., and Korosi, J.B. 2023. Limnology and diatom ecology of shallow lakes in a rapidly thawing discontinuous permafrost peatland, Inland Waters, 13(1): 13–29. doi:10.1080/20442041.2022.2144699

Korosi, J.B., McDonald, J., Coleman, K.A., Palmer, M.J., Smol, J.P., Simpson, M.J., and Blais, J.M. 2015. Long-term changes in organic matter and mercury transport to lakes in the sporadic discontinuous permafrost zone related to peat subsidence, Limnology and Oceanography, 60(5): 1550–1561. doi:10.1002/lno.10116

Rühland, K., Paterson, A.M., and Smol, J.P. 2015. Lake diatom responses to warming: reviewing the evidence, Journal of Paleolimnology, 54: 1-35. doi:10.1007/s10933-015-9837-3

Vonk, J.E., Tank, S.E., Bowden, W.B., Laurion, I., Vincent, W.F., Alekseychik, P., Amyot, M., Billet, M.F., Canário, J., Cory, R.M., and Deshpande, B.N. 2015. Reviews and syntheses: Effects of permafrost thaw on Arctic aquatic ecosystems, Biogeosciences, 12(23): 7129–7167. doi:10.5194/bg-12-7129-2015

Wright, S.N., Thompson, L.M., Olefeldt, D., Connon, R.F., Carpino, O.A., Beel, C.R., and Quinton, W.L. 2022. Thaw-induced impacts on land and water in discontinuous permafrost: A review of the Taiga Plains and Taiga Shield, northwestern Canada, Earth-Science Reviews, 232: 104104. doi:10.1016/j.earscirev.2022.104104

Discussing the fate of PAHs distribution in permafrost: combine large scale to local perspective in the warming Arctic

Rachele Lodi[1,2], Gustaf Hugelius[3,4], Elena Argiriadis[2], Jacopo Gabrieli[2] & Carlo Barbante[1,2]

[1]*Department of Environmental Sciences, Informatics and Statistics, Ca' Foscari University, Venice, Italy*

[2]*Institute of Polar Sciences, National Research Council of Italy (CNR), Venice, Italy*

[3]*Department of Physical Geography, Stockholm University, Stockholm, Sweden*

[4]*Bolin Centre for Climate Research, Stockholm University, Stockholm, Sweden*

The study addresses the critical issue of permafrost thawing and its repercussions on the remobilization of organic pollutants, emphasizing the global fractionation process triggered by the cycle of deposition and re-emission. The impacts of these phenomena extend beyond regional boundaries, affecting environmental, economic, political, and societal dynamics on a global scale.

Future permafrost thaw could lead to the release of significant amounts of organic contaminants which may become active in biogeochemical fluxes (Cabrerizo et al. 2018; Chadburn et al. 2017). The extensive research conducted by the Arctic Monitoring and Assessment Program (AMAP) into Arctic organic contaminants serves to demonstrate a comprehensive understanding and wealth of data on contaminants in biota and water (AMAP 2021). However, it also highlights a significant deficiency in data regarding contaminants in Arctic soils, particularly those located below the permafrost table. Improving knowledge gaps and understanding contaminants' fate are recognised as global priorities. Among the priority issues for AMAP, organic compounds stand out. To model the risks associated to permafrost thaw and organic pollutants release, better knowledge of what compounds are stored in permafrost and at which concentrations is needed.

This study aims to identify and discuss potential upscaling factors that are better known and/or easily measured than the presence of organic contaminants in the soil, to create maps of storage and potential release of organic contaminants. Understanding the determinants of changes in contaminants levels observed in the environment is crucial for interpreting trends, drawing valid conclusions regarding policy effectiveness, and ensuring their validity.

Method

To accomplish our objective, we determined that Polyciclic Aromatic Hydrocarbons (PAHs) are an appropriate organic compound class for primary correlation analysis with physicochemical parameters affecting permafrost soil and other indirectly assessed geospatial parameters. To provide geospatial databases, it is crucial to ascertain which landscape features will enable us to accurately measure the levels of contaminants. In particular, the work was characterised by the distinction between Low-Centred Polygons (LCPs) and High-Centred Polygons (HCP) in ice-wedge polygon soils and in peat bogs and rockglaciers. To achieve our research aims, we provide an account of the analyses and scaling of contaminants in a landscape context, with particular attention to the mapping of soil landscape features, organic carbon concentration (%), and depth beneath the surface.

Soil and sediment sampling and analysis were conducted for 22 congeners of PAHs in active layer and permafrost core samples from diverse locations, including Komakuk Beach and Ptarmingan Bay in Yukon, Canada, and Bayelva and Stuphallet in Svalbard, Norway. The concentrations were quantified using Accelerated Solvent Extraction (Thermo Scientific Dionex ASE 350) and Gas Chromatography — Triple Quadrupole Mass Spectrometry (Trace 1310 GC coupled with TSQ9000 TQMS, Thermo Scientific) at CNR-ISP Venice, Italy (Gambaro et al. 2009).

Results

The content of individual PAHs and their total concentration exhibited significant variation between different spatial areas. The contribution of individual PAHs to the overall amount varies. Our findings indicate light 2-4-nuclear and heavy 5-6-nuclear PAHs have distinct vertical distribution patterns, and a significant increase in mass fraction of high molecular weight PAHs down the profile is not observed in any sampled environment.

The different distribution patterns of the PAHs in the permafrost core sections of the different landform classes, emphasizes the influence of hydrology and percolation on contaminant distribution in permafrost soils, which are exacerbated in semi-degraded permafrost landforms. Moreover, it is possible to observe an increase in PAHs concentrations at the permafrost transient layer: it is a dynamic zone that

undergoes a cyclical process of freezing and thawing on decadal timescales; during the freezing phase, the permafrost transient layer solidifies and freezes, trapping organic compounds accumulated from the lower active layer.

Conclusions

The correlation between PAHs and carbon content implies an initial upscaling method for quantifying legacy organic contaminants in permafrost, calibrated on landscape analysis and regional standards. Correlations with physicochemical parameters were assessed also considering relevant literature data, and subsequently employed in regression models applicable to the evolution of landscape analysis maps and Carbon content in permafrost.

The findings contribute to a comprehensive understanding of the complex interactions shaping organic contaminant distribution in Arctic permafrost environments.

References

AMAP. 2021. POPs and Chemicals of Emerging Arctic Concern: Influence of Climate Change. Arctic Monitoring and Assessment Programme (AMAP), Tromsø, Norway. viii+142 pp.

Cabrerizo, A., Muir, D.C.G., De Silva, A.O., Wang, X., Lamoureux, S.F., and Lafrenière, M.J. 2018. Legacy and Emerging Persistent Organic Pollutants (POPs) in Terrestrial Compartments in the High Arctic: Sorption and Secondary Sources. https://doi.org/10.1021/acs.est.8b05011

Chadburn, S.E., Krinner, G., Porada, P., Bartsch, A., Beer, C., Belelli Marchesini, L., Boike, J., Ekici, A., Elberling, B., Friborg, T., Hugelius, G., Johansson, M., Kuhry, P., Kutzbach, L., Langer, M., Lund, M., Parmentier, F.-J.W., Peng, S., Van Huissteden, K., Wang, T., Westermann, S., Zhu, D., and Burke, E.J. 2017. Carbon stocks and fluxes in the high latitudes: using site-level data to evaluate Earth system models. Biogeosciences 14, 5143–5169. https://doi.org/10.5194/bg-14-5143-2017

Gambaro, A., Radaelli, M., Piazza, R., Stortini, A.M., Contini, D., Belosi, F., Zangrando, R., and Cescon, P. 2009. Organic micropollutants in wet and dry depositions in the Venice Lagoon. Chemosphere 76, 1017–1022. https://doi.org/10.1016/j.chemosphere.2009.04.063

Filling the white spots — Initiating permafrost research in Bhutan

Nadine Salzmann[1,2], Cecile Pellet[3], Sonam Lhamo[4], Rebecca Gugerli[5,6], Kathrin Naegeli[7], Karma Karma[4] & DB Gurung[8]

[1]*WSL Institute for Snow and Avalanche Research SLF, Davos, Grison, Switzerland*

[2]*Climate change, Extreme events and natural hazards in mountain regions Research Center CERC, Davos, Grison, Switzerland*

[3]*Department of Geosciences, University of Fribourg, Fribourg, Switzerland*

[4]*National Center for Hydrology and Meteorology, Royal Government of Bhutan, Thimpu, Bhutan*

[5]*Environmental Remote Sensing Laboratory, École Polytechnique Fédérale de Lausanne (EPFL), Lausanne, Switzerland*

[6]*Radar, Satellite and Nowcasting Division, Federal Office of Meteorology and Climatology MeteoSwiss, Locarno-Monti, Switzerland*

[7]*Department of Geography, University of Zurich, Zurich, Switzerland*

[8]*Royal University of Bhutan, College of Natural Resources, Lobesa, Punakha, Bhutan*

In the Himalayas, thawing permafrost is meanwhile widely recognized as a major risk for initiating mass movements, influencing hydrological run off or impacting biodiversity. However, information and knowledge on the occurrence of mountain permafrost in the Himalayas, and even more so its changes are still very scarce or absent in most areas. This is the case for Bhutan. In the recently launched CRYO-SPIRIT project, Bhutan and Switzerland are joining hands to initiate permafrost research in Bhutan and to fill this important white spot. We aim at starting first in-situ measurements and geomorphological mapping, in parallel to initiating related education programs at the university level. Moreover, the awareness of (future) risks related to permafrost thaw, including the development of adaptation strategies, will be a major focus of the project. In this contribution, we present and discuss our approaches.

Available permafrost information in the Himalayas and Bhutan

Except for the Tibetan plateau, where measurements exist along some railway and highway routes (Gao et al. 2021), information on mountain permafrost is mostly lacking for the Himalaya region. For Bhutan, so far only large scale and global assessments provide a rough idea of the occurrence of permafrost (Gruber 2012; Obu et al. 2020; Schmid et al. 2015). In a study across the entire Hindu Kush Himalaya region, Gruber et al. 2017 estimated the land surface covered by permafrost in Bhutan to be about 1.2 (± 0.3–3.5) x 10^3km^2 (compared to glaciers with 1.0 or 1.5 x 10^3km^2, depending on the glacier inventory). This is an important assessment but given the limitations of deriving permafrost indications from climate reanalyses or satellites data, in-situ measurements are importantly required.

CRYO-SPIRIT: A new joint initiative between Bhutan and Switzerland

CRYO-SPIRIT is a recently launched project funded by the Swiss National Science Foundation (https://data.snf.ch/grants/grant/216522). It aims at initiating and establishing new in-situ measurements of the cryosphere in Bhutan using methods that have previously been tested in Switzerland, and with a specific emphasis on permafrost and regarding its related risks and impacts. We focus on compiling the first regional map of potential permafrost occurrence in Bhutan using data from two approaches: (i) measuring in-situ Ground Surface Temperature (GST), and (ii) mapping permafrost characteristic landforms, in particular rock glaciers (cf. Figure 1).

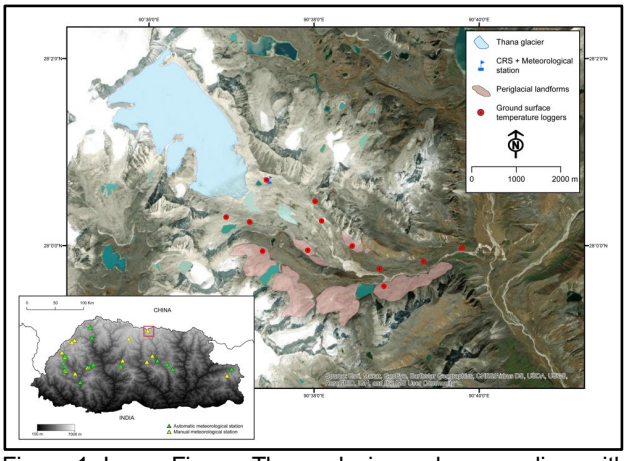

Figure 1. Large Figure: Thana glacier and surrounding, with indicated cryospheric landforms and the approximate locations planed for the installation of the CRS (SWE) and the GST loggers (permafrost). Small Figure lower left: Location of the main study site Thana glacier (red square) and the locations of the NCHM observation sites. Shown elevation is based on the 'High Mountain Asia 8-meter DEM'.

During the first field campaign in autumn 2024, we intend to install UTL-3 loggers, which have been successfully used by the Swiss Permafrost Monitoring Network PERMOS to continuously monitor GST over decades. We will place these loggers along an altitudinal transect from the valley bottom up to Thana glacier, where glacier and climate monitoring is ongoing for several years through the National Center for Hydrology and Meteorology (NCHM) of Bhutan, and additional activities are planned in the frame of CRYO-SPIRIT. Logger installation will start at around 4000 m a.s.l. (i.e., below the expected lower limit of permafrost occurrence in Bhutan) up to around 5200 m a.s.l. with one logger for every 100 m of elevation gained. Additionally, we will place GST loggers at locations which either clearly indicate permafrost occurrence (indicated by landforms) or bear particular risks from thawing permafrost (e.g., moraine-dammed lakes). These locations are identified and selected through our second approach, the landform mapping. The mapping includes the compilation of a Bhutan-wide rock glacier inventory (partly as an update of Schmid et al. 2015) based on DEMs and satellite images.

The inventory will be derived following the recently released guidelines by the International Permafrost Association (RGIK 2022), which were developed and tested using Google Earth images for a worldwide harmonized quality level. In parallel, we also intend to map other landforms and periglacial environments indicating potential permafrost occurrence, such as talus slopes, glacier forefields, (ice-cored) moraines, protalus ramparts, solifluction lobes and patterned grounds using additional satellite imagery. Specially, we focus on spots/locations which indicate potential risks from thawing permafrost, such as ice-cored moraine-dammed lakes associated with risks of GLOFs.

EDUCATION AND OUTREACH

In order to ensure long-term sustainability for our efforts, an important part of CRYO-SPIRIT is dedicated to education and capacity building of young Bhutanese researchers (including two PhD students in Bhutan, jointly supervised by scientists from Bhutan and Switzerland), and thus the next generation of researchers in Bhutan. Currently, the cryosphere and in particular permafrost is not included in any of the available curriculums. We intend to jointly develop and implement teaching modules at the Royal University of Bhutan, provide specific hands-on training session during our field campaigns, and establish research collaborations at an international level.

In our contribution we will present and discuss the concepts of the CRYO-SPIRIT project and intend to foster collaborations with potential other interested actors in the region and internationally.

REFERENCES

Gao, H., Wang, J., Yang, Y., Pan, X., Ding, Y., and Duan, Z. 2021. Permafrost Hydrology of the Qinghai-Tibet Plateau: A Review of Processes and Modeling, Front. Earth Sci. 8. https://doi.org/10.3389/feart.2020.576838

Gruber, S. 2012. Derivation and analysis of a high-resolution estimate of global permafrost zonation, The Cryosphere 6, 221–233. https://doi.org/10.5194/tc-6-221-2012

Gruber, S., Fleiner, R., Guegan, E., Panday, P., Schmid, M.-O., Stumm, D., Wester, P., Zhang, Y., and Zhao, L. 2017. Review article: Inferring permafrost and permafrost thaw in the mountains of the Hindu Kush Himalaya region, The Cryosphere, 11, 81–99. https://doi.org/10.5194/tc-11-81-2017

Obu, J., Westermann, S., Barboux, C., Bartsch, A., Delaloye, R., Grosse, G., Heim, B., Hugelius, G., Irrgang, A., Kääb, A.M., Kroisleitner, C., Matthes, H., Nitze, I., Pellet, C., Seifert, F.M., Strozzi, T., Wegmüller, U., Wieczorek, M., and Wiesmann, A. 2020. ESA Permafrost Climate Change Initiative (Permafrost_cci): Permafrost active layer thickness for the Northern Hemisphere,v2.0. https://doi.org/10.5285/29C4AF5986BA4B9C8A3CFC33CA8D7C85

RGIK 2022. Towards standard guidelines for inventorying rock glaciers: baseline concepts (v. 4.2.2). IPA Action Group rock glacier inventories and kinematics.

Schmid, M.-O., Baral, P., Gruber, S., Shahi, S., Shrestha, T., Stumm, D., and Wester, P. 2015. Assessment of permafrost distribution maps in the Hindu Kush Himalayan region using rock glaciers mapped in Google Earth, The Cryosphere, 9, 2089–2099. https://doi.org/10.5194/tc-9-2089-2015

Practical applications of integrating geohazards in community infrastructure climate change risk assessments

Virginia Sarrazin & Rebekah Richardson-Duffy
WSP Canada Inc, Whitehorse, Yukon, Canada

Across Northern Canada, temperature increases are becoming more pronounced, precipitation patterns are shifting in timing and intensity, and climate-related events are increasingly leading to lasting damages. Average air temperatures in the North are increasing three times faster than the global average and impacts on communities are already being experienced.

In addition to the effects of climate change, remote northern locations are exposed to complex geohazards, such as permafrost thaw, riverine flooding, ice jams, and shifts in groundwater regimes. A comprehensive understanding of the suite of hazards—climatological, environmental, and geological—requires careful consideration of each as independent as well as interdependent actors in a complex and connected system. With climate change, some geohazards may be eliminated, while others may develop.

Limitations for evaluating risk, such as data gaps and limited resources, are also common in northern communities. These unique landscapes and limitations require climate adaptation practitioners to adopt a tailored and contextualized approach for assessing the potential risks posed by climate change and recommending adaptation options for these areas. Probabilistic projections of climate parameters under climate non-stationarity are necessary to inform future design to maintain required levels of service as historical climate records no longer represent future conditions. Historical geohazard assessments may not include considerations of a changing climate.

When making long term community infrastructure decisions, the intersection of these challenges can be explored in a climate risk and resilience assessment (CRRA) as was conducted in this case study for an Indigenous community in central Yukon Territory, Canada. In addition to widespread climate change impacts, the community has been subject to significant shifts in environmental and geological conditions; roads, water distribution infrastructure, sanitary sewers, and homes in the area have already been damaged from warming permafrost and groundwater table increases, and riverine flooding, ice jams, and wildfires continue to threaten the community.

Figure 1 shows the approximate location of the community in reference to the permafrost map completed by NRCAN in 1995. This shows the project area in the extensive discontinuous permafrost zone, where 50-90% of the terrain is underlain by permafrost. Geotechnical investigation reports confirm the presence of permafrost and indications of permafrost emphasize the importance of immediate and continued measure to respond to the hazard.

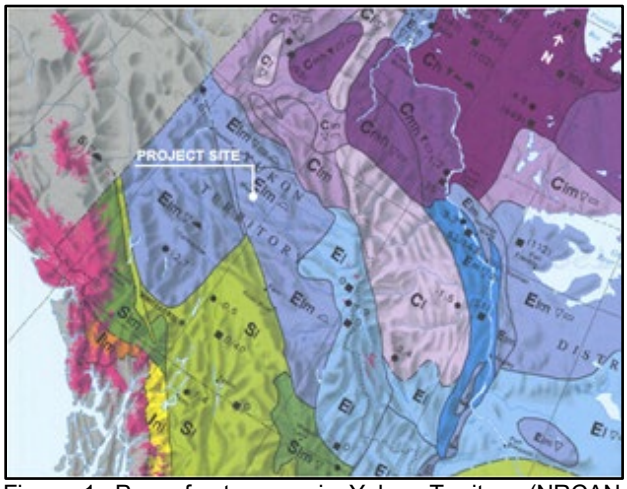

Figure 1. Permafrost zones in Yukon Territory (NRCAN, 1995)

The CRRA evaluates the risk to community infrastructure from projected climate hazards and geohazards. Recommendations are provided to inform community discussions and decisions about future community plans to rebuild aging infrastructure or relocate.

OBJECTIVES

Drawing on the insights from the Yukon CRRA case study, this presentation introduces an approach for integrating geohazards and climate risk for application in community adaptation planning and resilient community infrastructure. We explore the opportunities and drawbacks of using the CRRA approach in this context, highlighting the challenges of evaluating complex systems with limited historical data or broad spatial information to guide the

assessment. We offering lessons learned from the project with the goal of encouraging climate adaptation practitioners to consider how they might navigate similar challenges.

METHODS

The combined geohazard and climate change assessment approach aligns with ISO 31000:2018—a standard framework to assess and manage risk and ISO14091:2021 which forms the basis of many climate change risk assessments. Both approaches consider the components of risk to be exposure, hazard, vulnerability and a product of likelihood of an interaction occurring and the consequence should that event happen. Where risks are deemed too high to accept, recommendations are provided to mitigate unacceptable risk and increase community resilience. Figure 2 shows the methodology used for this assessment.

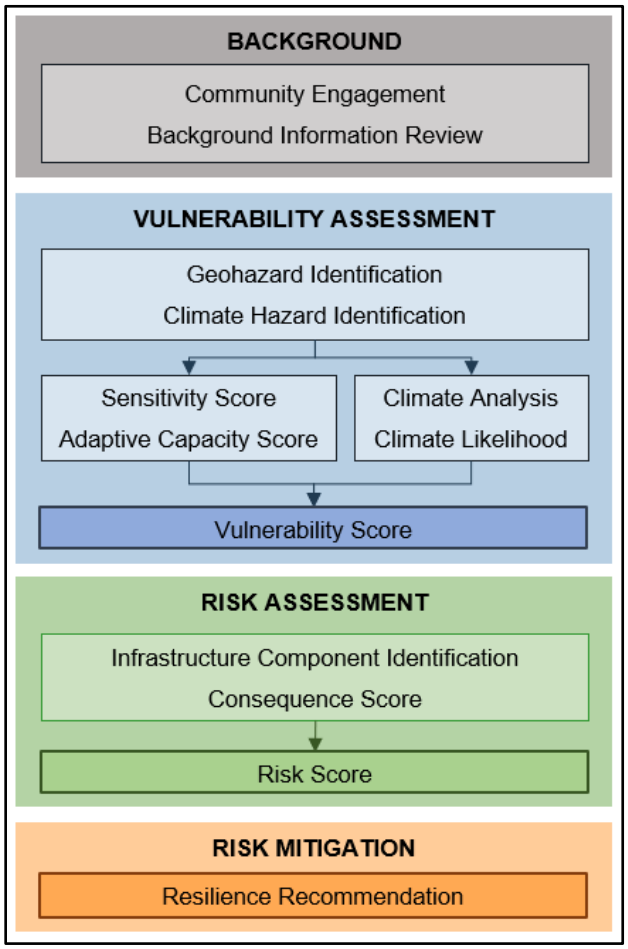

Figure 2. Climate Risk and Vulnerability Assessment Methodology.

The CRRA project incorporates input from community stakeholders to capture Indigenous knowledge and local insights in the initial development of the assessment framework. The assessment is then guided by the input of subject matter experts, including climate scientists, hydrologists, fluvial geomorphologists, permafrost experts, civil and structural engineers to evaluate the combined climate hazards and geohazard interactions that are likely to affect the project site in the present and that are projected to occur in within two future time periods, the 2050s and 2080s.

The difference in this approach is to incorporate geohazard exposure and vulnerability into the early stages of the process to characterize potential risks beyond those driven uniquely by climate change.

FINDINGS

The successful completion of this risk assessment approach relies heavily on a combination of stakeholder engagement, professional judgement, and systematic analysis. Direct communication with community members via a workshop format provides critical information about historical and current conditions in the area, while local knowledge and professional judgement guide the interpretation of future projections and the outcomes of each step in the assessment.

Finally, a structured framework for systematic analysis allows the assessment team to identify information gaps, limitations, and assumptions that ultimately inform the assessment outcomes. The recommendations developed from this approach play a critical role in prioritizing adaptation responses and communicating decision-making processes for a community.

SIGNIFICANCE

The incorporation of geohazards, assessed independently and interdependently, is a novel approach to apply in typical climate change risk assessments for community infrastructure and is an important modification in CRRA methodology as more northern communities face critical decisions in response to substantial environmental change.

REFERENCES

NRCAN. 1995. The National Atlas of Canada 5th edition – Canada Permafrost. National Atlas Information Service, Canada Center for Mapping, Geomatics Canada, Terrain Sciences Division, Geological Survey of Canada. Ottawa, Ontario, Canada.

Mechanisms of thermokarst formation and associated carbon stocks in the Sahtu Region of the Northwest Territories, Canada

Evan Schijns[1], Catherine Dieleman[1], Jennifer Baltzer[2], Adam Gillespie[1] & Merritt Turetsky[3]

[1]*University of Guelph, School of Environmental Sciences, Guelph, Ontario, Canada*

[2]*Wilfrid Laurier University, Department of Biology, Waterloo, Ontario, Canada*

[3]*University of Colorado Boulder, Renewable and Sustainable Energy Institute, Boulder, Colorado, United States*

Northern peatlands are globally significant terrestrial carbon stores that generally absorb more carbon from the atmosphere than they release. These carbon stocks accrue slowly over centuries in part due to chronically cold belowground temperatures that historically have maintained permafrost in ~50% of northern peatlands (Rodenhizer et al. 2020). However, climate change is warming surface temperatures and increasing the frequency and severity of disturbances like wildfire, both of which are causing permafrost thaw events globally (Jungqvist et al. 2014; Turetsky et al. 2011). Following thaw permafrost soils can experience rapid decomposition, releasing their stored carbon back to the atmosphere as carbon dioxide and methane. This relationship between permafrost thaw and the global atmosphere is referred to as the permafrost-carbon feedback and can further the effects of climate change (Schuur et al. 2015). The strength of the permafrost-carbon feedback varies greatly across northern peatlands, most likely reflecting differences in local environmental conditions and thaw formation patterns.

Despite the importance of the permafrost-carbon feedback we have an incomplete understanding of the drivers that govern carbon losses and subsequent recovery following thaw events, particularly in ice-rich permafrost systems that can experience relatively rapid decay (Jones et al. 2017; O'Donnell et al. 2012). Our research addresses this gap by examining 1) time-since-permafrost thaw; where we expect stable bogs to hold greater C stocks than unstable bogs, 2) time-since-peatland establishment; where stable bogs expected to have begun soil C accumulation earlier than unstable bogs, 3) local soil drainage conditions; with different drainage conditions expected to influence C stocks via waterlogging and anoxic soil conditions, and 4) vegetation successional pathways; where differing vegetation regimes over time influencing C losses and recovery. Both stable (BS) and unstable (BU) bog features are compared against intact permafrost regions (PT) within the same site network. We examine these four mechanisms by characterising differences in soil and macrofossil traits in over 150 soil cores collected throughout the Sahtu Region in Northwest Territories, Canada.

Fifteen peatland complexes were selected using aerial imagery across the study region, spanning a gradient of time-since-fire dating back to 1965 that was used to infer a variation of time-since-permafrost-thaw on the landscape. Each peatland complex contained three distinct permafrost features: an intact permafrost plateau; an actively thawing thermokarst bog (i.e., unstable bog) and a stabilized thermokarst bog (i.e., stable bog). Soil cores spanning the entire organic soil horizon to the mineral layer were collected from each feature along a 30 m south to north transect. A total of 45 surface cores were taken from intact permafrost plateaus (15 permafrost plateaus features × 3 replicate soil cores), paired with a total of 15 Snow, Ice, and Permafrost Research Establishment (SIPRE) cores taken at a point representative of mean seasonal thaw depth. From stable and unstable thaw bog features, a composite surface and Russian soil core was collected from the feature's centre and two from its edge (30 thaw bog features × 3 soil cores = 90 cores). In areas too inundated for accurate traditional coring, soil samples were collected using the frozen finger soil collection method (also known as freeze coring) (Wright 1980). These cores were all shipped frozen to maintain moisture content and soil structure.

All cores were divided into 5-10 cm depth increments depending on the soil collection method. Each increment was divided vertically, with one half processed for soil structure and biogeochemistry (i.e. soil horizon type, mineral soil texture, moisture fraction, bulk density, and carbon fraction) to determine C stocks, soil moisture, and surface mineral texture class. The other half of the increment was set aside to quantify shifts in presence of dominant plant growth forms with depth and provide material for radiocarbon dating analysis. Radiocarbon data targeted the transition soil layers between historically frozen silvic peat (pre-thaw generated peat) and modern Sphagnum peat (post-thaw generated peat) to quantify time-since-permafrost-thaw as well as the transition from mineral to organic soils to describe time-since-peatland establishment.

Initial laboratory results indicate local drainage conditions as determined by mineral soil texture likely plays a small role in driving thermokarst C stocks; with

little to no variation in mineral texture class across all sites and features. Preliminary analysis suggests intact permafrost plateaus contain moderately larger C stocks than both stable bogs and unstable bogs, as shown in Figure 1. Remaining data analysis will involve running a series of mixed-effect models testing for differences in time-since-thaw, time-since-initiation, and differing vegetation successional trajectories between the two thermokarst bog types.

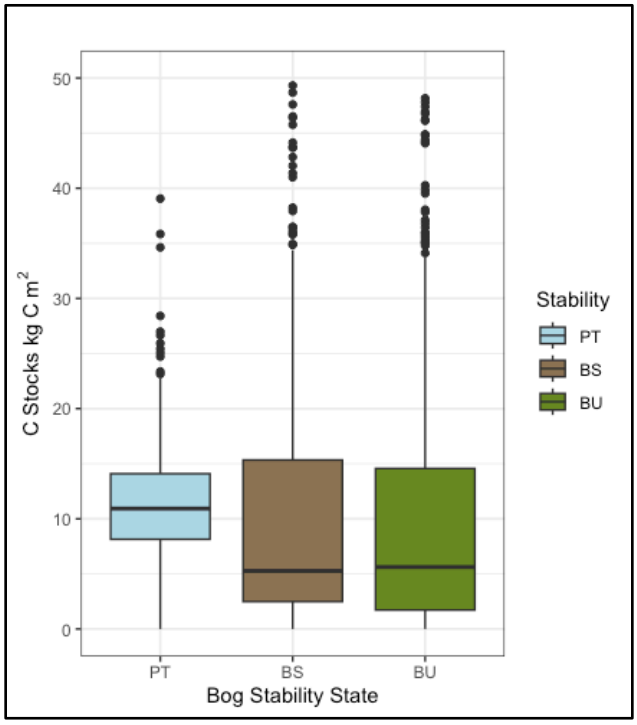

Figure 1. Averaged carbon stocks (kg·C·m^2) across three feature types; intact permafrost plateau (PT), stable bog (BS) and unstable bog (BU).

This research will generate new knowledge on permafrost thaw successional patterns in central NWT, a remote region that is likely to have a unique permafrost history from other more commonly studied regions (Jorgenson et al. 2001). By delineating drivers of post-thaw C cycling, this research can help parameterize both regional and global carbon cycling models used to characterize the impacts of permafrost thaw on the future of Earth's climate.

REFERENCES

Jorgenson, M.T., Racine, C.H., Walters, J.C., and Osterkamp, T.E. 2001 Permafrost degradation and ecological changes associated with a warming climate in central Alaska. Climatic Change, 48, 551–579. https://doi.org/10.1023/A:1005667424292

Jones, M.C., Harden, J., O'Donnell, J., Manies, K., Jorgenson, T., Treat, C., and Ewing, S. 2017. Rapid carbon loss and slow recovery following permafrost thaw in boreal peatlands. Global Change Biology, 23, 1109–1127. https://doi.org/10.1111/gcb.13403

Jungqvist, G., Oni, S.K., Teutschbein, C., and Futter, M.N. 2014. Effect of climate change on soil temperature in Swedish boreal forests. PLoS One, 9(4), e93957. https://doi.org/10.1371/journal.pone.0093957

O'Donnell, J.A., Jorgenson, M.T., Harden, J.W., et al. 2012. The effects of permafrost thaw on soil hydrologic, thermal, and carbon dynamics in an Alaskan peatland. Ecosystems, 15, 213–229. https://doi.org/10.1007/s10021-011-9504-0

Rodenhizer, H., Ledman, J., Mauritz, M., Natali, S.M., Pegoraro, E., Plaza, C., et al. 2020. Carbon thaw rate doubles when accounting for subsidence in a permafrost warming experiment. Journal of Geophysical Research: Biogeosciences, 125(6), e2019JG005528. https://doi.org/10.1029/2019jg005528

Schuur, E.A., McGuire, A.D., Schädel, C., Grosse, G., Harden, J.W., Hayes, D.J., et al. 2015. Climate change and the permafrost carbon feedback. Nature, 520(7546), 171–179. https://doi.org/10.1038/nature14338

Turetsky, M.R., Kane, E.S., Harden, J.W., Ottmar, R.D., Manies, K.L., Hoy, E., and Kasichke, E.S. 2011. Recent acceleration of biomass burning and carbon losses in Alaskan forests and peatlands. Nature Geosciences, 4, 27–31. https://doi.org/10.1038/ngeo1027

Wright, H.E. 1980. Coring of soft lake sediments. Boreas, 9, 107–114. https://doi.org/10.1111/j.1502-3885.1980.tb010

Analyzing factors of micrometeorological variance around infrastructure and aspects in Utqiagvik, Alaska

Mirella Shaban & Howard E. Epstein

Department of Environmental Science, University of Virginia, Charlottesville, Virginia, United States

Warming air and ground temperatures in the Arctic have altered freeze and thaw cycles, deepening the annually thawing ground (active layer). The resulting degradation of the ground and its subsequent subsidence poses major risks for infrastructure and development. Stability of infrastructure in the Arctic is highly dependent on the ground-atmosphere thermal regime (Rowley et al. 2015), which is disturbed by the introduction of materials to the surface and below ground. The disruption of the thermal regulation of the ground-atmosphere interface from infrastructure such as pilings, gravel pads, pipelines, utilidors, snow fences, and roadways in addition to rising air temperatures will severely alter the landscape (Rowley et al. 2015) within the periglacial environment. With a continuing need for new and improved infrastructure to support the ever-growing population and mitigate the increase in thermokarst, there is also a need to intimately understand active layer and permafrost dynamics around infrastructure to ensure the longevity and stability of these buildings and the underlying permafrost.

Infrastructure affects micrometeorological variables by altering the energy budget of the ground surface at fine spatial scales. The absorption of solar radiation by the ground surface is typically dependent on the zenith angle of the sun, the height and distribution of cloud cover, shading by vegetation, and the ground surface properties. Man-made shading from infrastructure can intercept incoming solar radiation depending on the aspect of the building (Klene et al. 2013). Insulating effects, similar to natural insulating properties of snowpack and vegetation, can occur. Air temperatures around buildings have been observed to vary from ambient outdoor air temperatures due to seasonal heating (Nawalany and Sokołowski 2019) and typically create warm zones around infrastructure otherwise absent in adjacent tundra.

Research Focus

Winter heat island effects have been documented in Utqiagvik, AK (Hinkel et al. 2003). Variations in micrometeorology within urban areas may reveal vulnerability of permafrost at certain aspects due to higher ground temperatures. High resolution micrometeorological sensing of ground temperatures and moisture contents from 0 cm – 90 cm, near surface air temperatures, solar radiation, and wind dynamics has been conducted from June 2022 – present. Data gaps due to communication outage during the summer of 2023 limit the data that were collected during July, limiting inter-annual comparisons for summer months. Comparisons between north and south aspects, among urban sites, and urban vs. tundra sites have shown notable differences between north and south facing ground temperatures during summer and fall seasons. There were also notable differences in freezing dates at the urban sites between north and south aspects.

Methods

Time series data from the summer and fall from 2022 and 2023 were analyzed across two urban sites, Tagiuġmiullu Nunamiullu Housing Authority (TNHA) and Samuel Simmonds Memorial Hospital (SSMH), and compared to the Barrow Environmental Observatory (BEO) tundra control site. Daily mean values for ground temperatures at selected depths of 10 cm, 55 cm, and 90 cm were analyzed along with daily averages for ground moisture at depths 0-15 cm, 45-60 cm, and 75-90 cm from Onset® RXW-GP6-900 HOBOnet Multi-Depth Soil Moisture Sensors. Ground temperature data were compared to daily averaged solar radiation and air temperature to assess the meteorological drivers responsible for variability across sites and stations. Diverging trends were noted for north and south facing sensors at the TNHA and SSMH sites.

PCA was conducted to reduce dimensionality and determine the variables of greatest association with differences among sensor locations. Freeze-thaw dates were determined, and relationships between ground and air temperatures were generated. The length of the zero-curtain was compared to Hinkle's' measurements for fall 1995 (Hinkel 2001).

Results

Summer 2022 data showed southern aspects (TNHA-SA) were warmer than northern aspects (TNHA-SC) at the TNHA consistently, while northern aspects at the SSMH (SSMH-SB) were warmer for a short duration of time during the beginning of the season. Data losses for the northern sensor (SSMH-SB) at the SSMH were present between ~ 7/8/2022-

8/15/2022. For Fall 2022, southern aspects at the TNHA were warmer than northern aspects through 65 cm. Urban sites were colder than the tundra control at 90 cm depth for both summer and fall seasons. Heaving of up to 10 cm occurred at the BEO (BEO-B06) ~11/01/2022, reducing the utility of those data after that time. During 2022, the summer season at the SSMH south aspect was on average warmer than the north aspect at 10 cm, 65 cm, and 90 cm. The TNHA south aspect was warmer at all depths for the summer season. Both sites showed warmer southern aspects during the fall at all depths compared to the northern aspect (Figure 1).

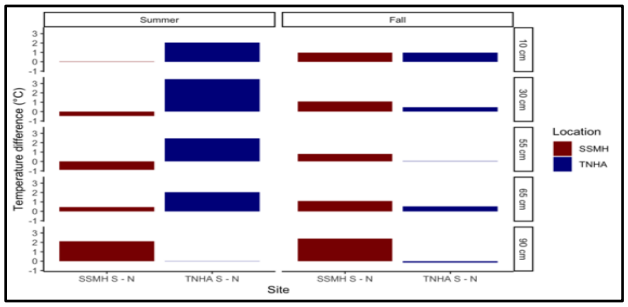

Figure 1. Summer and fall 2022 mean daily averaged ground temperature differences between north and south aspects at two urban sites.

The 2023 summer season showed warmer southern aspects at the SSMH site for all depths compared to summer 2022. The TNHA site showed similar trends at all depths with slightly higher differences between aspects at 10 cm depth. The TNHA during the fall 2023 season had larger temperature differences between these aspects at all depths except 65 cm, compared to the fall 2022 data (Figure 2).

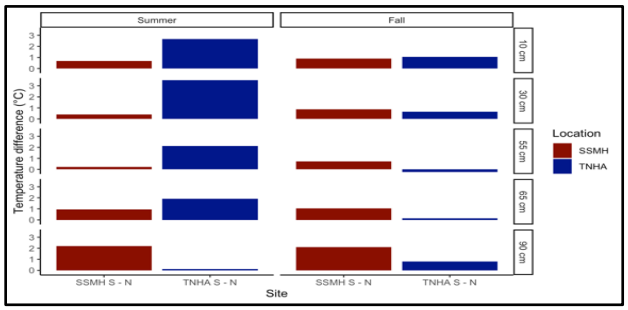

Figure 2: Summer and fall 2023 mean daily averaged ground temperature differences between north and south aspects at two urban sites.

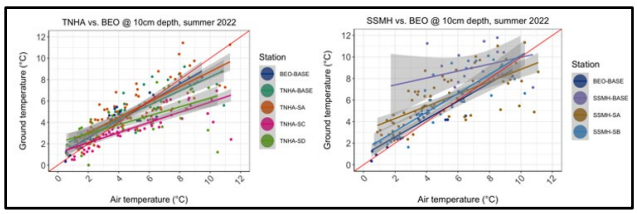

Figure 3: Mean daily average air temperatures and ground temperatures between N and S aspects at urban sites (TNHA, I; SSMH, II) for summer 2022.

Differences in the relationship between air and ground temperatures during summer 2022 were seen when comparing south vs. north aspects at 30 cm depth, particularly at the TNHA site (Figure 3).

Discussion

The changing climate of the Arctic presents unprecedented challenges as well as interactions between humans and the environment. Arctic ecosystems are disproportionately impacted by the effects of warming air and ground temperatures due to their distinctive climatology and pedology. As urbanization expands in Arctic communities, an understanding of how the ground changes due to the influence of infrastructure is imperative. The findings of this research may enhance future studies on micrometeorological scale analysis of infrastructure and anthropogenic inputs on stability of the ground and variability across aspects at high resolution spatial scales.

References:

Hinkel, K.M. 2001. Patterns of soil temperature and moisture in the active layer and upper permafrost at Barrow, Alaska: 1993–1999. Global and Planetary Change, 29(3-4), 293–309. doi.org/10.1016/S0921-8181(01)00096-0

Klene, A.E., Nelson, F.E., and Hinkel, K.M. 2013. Urban–rural contrasts in summer soil-surface temperature and active-layer thickness, Barrow, Alaska, USA. Polar Geography, 36(3), 183–201. doi:10.1080/1088937X.2012.706756

Nawalany, G., and Sokołowski, P. 2019. Building–Soil Thermal Interaction: A Case Study. Energies, 12(15), 2922. doi:10.3390/en12152922

Rowley, T., et al. 2015. Periglacial Processes and Landforms in the Critical Zone | Developments in Earth Surface Processes. 19:397–447. doi:10.1016/B978-0-444-63369-9.00013-6

Active layer deepening predictions in an Arctic landfill due to climate warming

Robyn Starycki[1], Ryley Beddoe[1], Greg Siemens[1], Alison Street[2] & Susan Pfister[2]
[1]*Department of Civil Engineering, Royal Military College of Canada Kingston, Ontario, Canada*
[2]*The Department of National Defence (DND), Ottawa, Ontario, Canada*

The Distant Early Warning (DEW) Line is a series of former radar stations ~80 km apart along the 69th parallel across the Canadian Arctic, Greenland, and Alaska. These sites were built in the 1950s to detect and relay warning of approaching aircraft. The 21 DND DEW Line sites were decommissioned in the 1990s with the subsequent construction of the North Warning System. Environmental and geotechnical investigations were carried out to develop remediation plans resulting in clean-up activities which included remediation of existing landfills, the demolition of infrastructure and excavation of contaminated soil. Large volumes of waste were removed from the sites or stored in a series of engineered landfills constructed during the clean-up. A portion of the engineered landfills were designed to contain contaminated material and waste below the active layer.

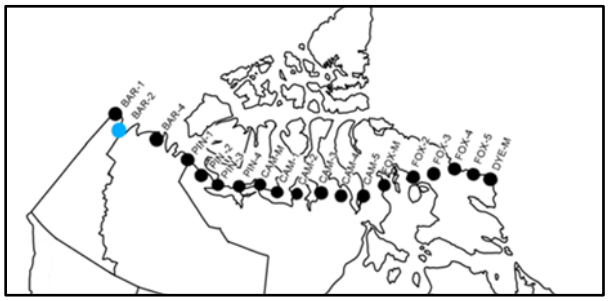

Figure 1. Instrumented Cdn DND Former DEW Line Sites.

Where specified, instrumentation was installed during the site remediation including thermistor strings and monitoring wells. Data loggers connected to the thermistors have been collecting ground temperature data at approximately 12-hour intervals for over two decades at some locations. Figure 1 illustrates the DND site locations spanning across the Canadian Arctic. The significant amount of data being collected to monitor the performance of the landfills provides the opportunity to initialize and validate models of the ground temperature at these various locations.

Given the knowledge of current climate trends and the numerical modeling software available, it is possible to track the progression of the active layer downward as air temperature rise occurs. This is an opportunity to visualize any change in the active layer depth during the one to two decades following landfill construction and predict when the active layer would retread below the cover thickness.

The site chosen for this study (shown in blue in Figure 1) is the former BAR-2 Shingle Point DEW Line station. It is located at the furthest northwest point of the Mackenzie Valley Delta on the coast of the Beaufort Sea in the Yukon, Canada at 68°55'23" N and 137°15'43" W. One engineered landfill instrumented with eight thermistors (USAF Landfill) lies approximately 285 m from the coast. The landfill is an irregular shape approximately 160 m by 136 m and was constructed on a natural east facing slope covered by on site borrow material generally consisting of sand and gravel and silty sand. A geosynthetic liner was tied into the permafrost along the toe of the landfill to prevent contaminant migration. The design included a 3.8 m cover thickness on the landfill slope based on the observed conditions during the pre-construction site visit in 1998 (EBA 1999).

A two-dimensional numerical model was created using GeoStudio 2020 Temp/W representing a 100 m soil column. Soil samples were taken during a 2023 site visit to visual classify the material and estimate thermal properties. The numerical model was initialized using available climate data and estimated soil thermal properties to achieve a model that closely relates to the thermistor data collected. The objectives of the numerical model include 1) creating a calibrated and validated model using 20 years of thermistor data (a validation curve for 2003 and 2014 shown in Figure 2) and 2) understanding the changes in active layer depth at the landfill site using climate predictions.

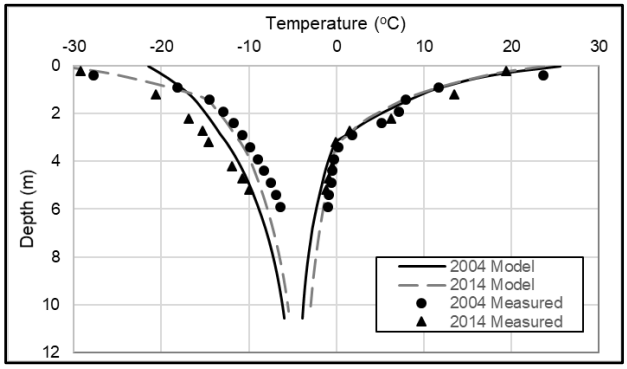

Figure 2. Comparison of measured and model ground temperature for 2003 and 2014.

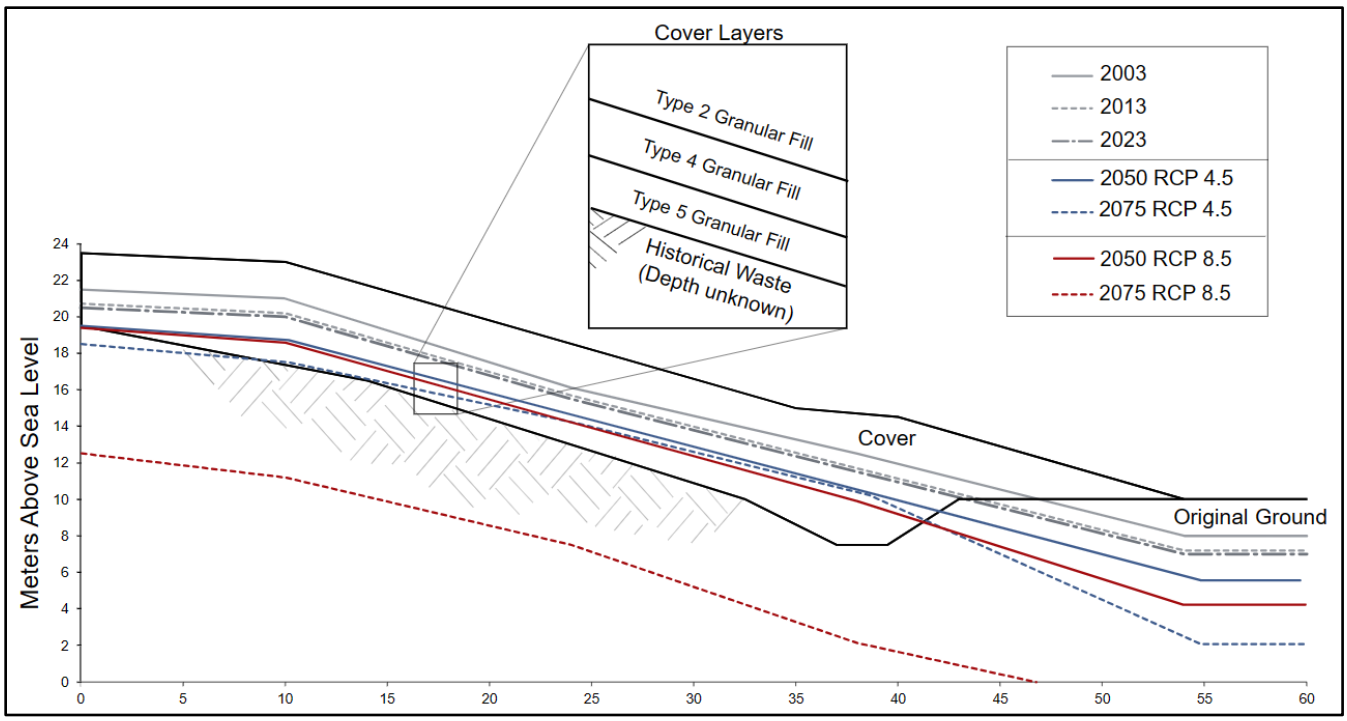

Figure 3. Changes in active layer depth based on RCP 4.5 and 8.5.

The results of the validated model illustrate the change in mean annual ground temperature (MAGT) and minimal active layer depth increasing since the installation of the thermistors during the landfill construction. In the 2D model shown in Figure 3, it is clear that the top of the permafrost is still well within the cover system to date.

Forecasting of ground temperature changes using predicted changes in air temperature and precipitation was completed to understand the changes in the active layer depth over time. In this analysis RCP 2.6, 4.5 and 8.5 were used to determine the effects on the facility. Each of these climate scenarios were modelled resulting in a different increase in active layer depth. Figure 4 illustrates the active layer deepening at the site based on RCP 4.5 and RCP 8.5 climate data. During the RCP 2.6 prediction the active layer remained within the cover system until 2100. Whereas the models using RCP 4.5 and 8.5 show the active layer eventually penetrating below the cover system.

Based on the predicted changes in active layer depth the active layer recedes below the cover in 2075 based on RCP 4.5 and by 2065 based on RCP 8.5 predictions.

This data set has provided an opportunity to look at a ground thermal regime change over the last two decades and make predictions based on a validated model. The numerical modeling completed during this analysis can be used as a prediction tool of the maintenance of infrastructure and to aid in the process of modeling and understanding permafrost degradation as climate change occurs. The potential of calibrating models across a vast climate-driven landscape to an amassed data set is a unique opportunity to understand a changing landscape and its effects on northern infrastructure.

ACKNOWLEDGEMENTS

This work was supported by numerous consultants, the Canadian Department of National Defence and the Royal Military College of Canada.

REFERENCES

EBA Engineering Consultants Ltd. 1999. DEW Line Clean Up Project BAR-2 Shingle Point Pre-Construction Site Visit. Report Submitted to UMA Engineering Consultants Ltd, October 1999.

A framework for understanding the impacts of permafrost thaw-driven disturbance regimes on northern lakes

Joshua Thienpont[1], Claire O'Hagan[1], Grace Hoskin[1], John Smol[2], Steve Kokelj[3] & Jennifer Korosi[1]

[1]*Faculty of Environmental and Urban Change, York University, Toronto, Ontario, Canada*

[2]*Department of Biology, Queen's University, Kingston, Ontario, Canada*

[3]*Northwest Territories Geological Survey, Government of Northwest Territories, Yellowknife, Northwest Territories, Canada*

Permafrost thaw slump disturbances on aquatic ecosystems are intensifying across the Arctic due to anthropogenic climate change. Their location in ice-cored morainal terrain has predisposed many lakes of the western Canadian Arctic (and other similar regions) to thaw slump-driven ecosystem changes. In the Tuktoyaktuk Coastal Plains, most of the recent increase in slump activity has been associated with old slump disturbances, rather than the initiation of new slumps (van der Sluijs et al. 2022). When a new thaw slump forms, it will actively grow and persist for some length of time, typically years to decades, but then stabilizes. After a period of stability, slumps can re-activate and grow further, a repeated process that may occur many times over decades, centuries, and millennia. This process is called slump "polycyclicity." The implications of slump polycyclicity for aquatic ecosystem impacts can only be considered in the context of a disturbance regime, where past exposure to thaw slumping may alter the lake's sensitivity to future slumping. Our aim is to integrate existing knowledge, gain new perspectives, and inform future hypotheses by developing a conceptual model considering the impacts of shoreline thaw slumps on well-studied lakes in the Tuktoyaktuk Coastal Plains region (western Canadian Arctic).

CHANGES IN WELL-STUDIED SLUMPS

Colour aerial photographs (1:30,000) from 2004 were used to classify 66 lakes in the study region according to thaw slump status (active, stable, and ancient), and classifications were verified in the field (Kokelj et al. 2009). Active slumps had thawing headwalls and bare areas, while stable slumps were completely re-vegetated but still had well-defined headwalls. Ancient slumps were re-vegetated and had subdued headwall relief. Thaw slump area and catchment area were estimated by digitization on georeferenced, orthorectified 2004 aerial photos and used to calculate the percentage of the lake catchment disturbed by thaw slumping. 2017 SPOT 1.5 imagery was used to re-classify the 66 lakes by slump status and measure slump enlargement (if any) between 2004 and 2017. In 2005, there were seventeen lakes with stable slumps and thirteen lakes with active slumps (Table 1). By 2017, eighteen lakes had stable slumps and fourteen lakes had active slumps. Two lakes classified as reference lakes in 2005 had new, active slumps by 2017. Of the seventeen lakes with stable slumps in 2005, four lakes experienced slump re-initiation by 2017 (Table 1). Five of the thirteen lakes with active slumps in 2005 had stable slumps by 2017, and a further three lakes showed signs of nearing slump stabilization. Of the eight lakes that had active slumps in both 2005 and 2017, the increase in slump size ranged from 0.41% of the catchment to 11.2% of the catchment.

Table 1. Slump status comparison between 2005 and 2017. Reference lakes are not listed. Naming follows Kokelj et al. (2005).

	Stable - 2017	Active - 2017
Stable – 2005	13 lakes	4 lakes
Active – 2005	5 lakes	8 lakes
No Slump – 2005		2 lakes

LAKEWATER CHEMISTRY CHANGES

We compared regional changes in lake water quality variables known to be impacted by slumping between 2005 and 2017 for 46 of the 66 lakes above. These chemical analyses suggest that timelines to recovery in lake dissolved organic carbon (DOC) following slump stabilization are longer than the time between cycles of slump growth, stabilization, and re-initiation in most lakes. Specific conductivity values in lakes were more variable, with decreases in most of the lakes that were active in 2005 and stabilized by 2017. This suggests conductivity may be more responsive to changing slump activity than DOC.

LAKE SEDIMENT INFERENCES

We analyzed geochemical changes using loss-on-ignition analyses in gravity sediment cores that incorporated the last several hundred years in 18 lakes that span a gradient in thaw slump disturbance, as well as a piston core dating back to ~1365 AD in a lake with an ancient slump. Sediments from lakes with a history of thaw slumping are low in organic matter and

carbonate content, and high in siliciclastic content, compared to reference lakes, which are more variable. Results also suggest that sediment geochemical changes are most pronounced at the initial onset of slumping, with only muted changes in sediment characteristics upon slump growth or re-initiation.

FRAMEWORK FOR SLUMP DISTURBANCE REGIME

The combined sediment core and regional lake survey results were used to guide the development of a new conceptual model on the trajectory of lake change with polycyclic slumping (Figure 1). Under this framework, lakes with no previous history of thaw slump impacts in their catchment (reference lakes in our analyses) exhibit high levels of coloured DOC and low ionic strength (Figure 1, lake type A). The onset of a naïve thaw slump results in an initial, transitional phase (B) characterized by high turbidity from suspended clays and low benthic production. After some duration of time, slump-impacted lakes enter a third phase (C) characterized by clear water, which promotes enhanced macrophyte abundance (Mesquita et al. 2010) and associated periphytic algal growth (Thienpont et al. 2013). Our data suggest lakes have often remained within this state even through cycles of slump stabilization and re-activation, and that previous slumping acts as a form of ecological memory, presenting as a barrier to recovery. Only a few lakes have had slumps stable long enough to "recover" – phase D. As climate warms and slump impacts intensify, several lakes with a history of slumping are exhibiting an enhancement in slump impacts, and a return to conditions like phase B, which is likely to become more prominient in the near future.

This model can be used to guide future investigations into the extent to which lakes with recurring thaw slumps are predisposed to, or buffered against, significant limnological changes under anthropogenic climate warming. In addition, this framework can serve as an important example of how long-term field data collection and studies of a particular permafrost lake type (predisposted to slump disturbance) can inform the nature of disturbance regimes and future trajectories of change. Applying these methods and tools will be important to understand how different permafrost lake types will respond to climate change, and enable us to paint a picture of the mosaic of changing aquatic ecosystems that will characterize a warming circumpolar north.

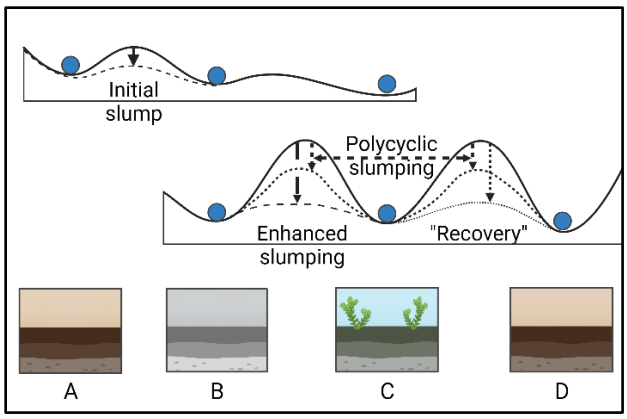

Figure 1. A conceptual diagram of limnological changes associated with retrogressive thaw slump impacts to lakes within a disturbance regime framework that considers polycyclic slump behaviour. Individual lakes will have different predisposition to slumping which can affect the shape of the curves describing behavior in this model. Created with BioRender.com.

REFERENCES

Kokelj, S.V., Jenkins, R.E., Milburn, D., Burn, C.R., and Snow, N. 2005. The influence of thermokarst disturbance on the water quality of small upland lakes, Mackenzie Delta region, Northwest Territories, Canada. Permafrost and Periglacial Processes, 16(4), 343–353. doi:10.1002/ppp.536

Kokelj, S.V., Zajdlik, B., and Thompson, M.S. 2009. The impacts of thawing permafrost on the chemistry of lakes across the subarctic boreal-tundra transition, Mackenzie Delta region, Canada. Permafrost and Periglacial Processes, 20(2), 185–199. doi:10.1002/ppp.641

Mesquita, P.S., Wrona, F.J., and Prowse, T.D., 2010. Effects of retrogressive permafrost thaw slumping on sediment chemistry and submerged macrophytes in Arctic tundra lakes. Freshwater Biology, 55(11). 2347–2358. doi:10.1111/j.1365-2427.2010.02450.x

Thienpont, J.R., Rühland, K.M., Pisaric, M.F., Kokelj, S.V., Kimpe, L.E., Blais, J.M., and Smol, J.P. 2013. Biological responses to permafrost thaw slumping in Canadian Arctic lakes. Freshwater Biology, 58(2), pp.337–353. doi:10.1111/fwb.12061

van der Sluijs, J., Kokelj, S.V., and Tunnicliffe, J.F. 2023. Allometric scaling of retrogressive thaw slumps. Cryosphere, 17, 4511–4533. doi:10.5194/tc-17-4511-2023

Permafrost subsidence around water supply well – Case study

Christopher Valentine[1], Frank Wuttig[2] & Mark Musial[1]
[1]*WSP USA Inc., Anchorage, Alaska, United States*
[2]*Alyeska Pipeline Service Company, Fairbanks, Alaska, United States*

The poster presentation will discuss historical challenges of installing a water well in permafrost under artesian conditions that included loss of well control and abandoning early wells when unexpected warm and artesian conditions were encountered; challenges of maintaining and operating an artesian well in an arctic/permafrost environment, such as maintaining flow reliability and controlling frost heave; and geotechnical and geochemical investigations undertaken to understand the permafrost regime and develop a conceptual site model. The presentation will also summarize remedial measures that were undertaken to stabilize the well and repair the annular void sinkhole. In addition, we will discuss monitoring and performance of the well and repair since installation in 2018.

BACKGROUND

Permafrost soils and ground ice surrounding a drinking water well at a pump station along the Trans Alaska Pipeline System (TAPS), situated in an area of relatively thin permafrost on the northern flanks of the Brooks Range south of Galbraith Lake, have challenged well integrity for a critical water supply for many years. Passive thermosyphons installed at the corners of the wellhouse in 2002 have proven insufficient to stabilize thaw settlement. Warmer winter weather patterns, age, warm aquifer water, and artesian conditions exacerbated permafrost thawing around the well. By 2018, a 17.7-meter-deep annular void sinkhole had formed along well casing that required immediate response and repair.

HISTORY

The water well was originally installed in 1978 after seven attempts to install a water well due to difficult conditions. The water well extends to a depth of 52.1 meters and is completed in limestone bedrock, but the top 30.5 meters consists of ice-rich permafrost. Artesian conditions below the permafrost created difficult drilling and installation, with multiple wells being attempted before completion of the current well.

Water seeping up through the fill around the wellhouse was noted since 1988. An investigation into the source of the water that collected around the wellhouse and the well casing in the winter noted that the soils were thawed around the well casing and confirmed that water at the well head and adjacent spring/pond was from the same sub-permafrost source. It was speculated that the drainage path to adjacent ponds could be restricted in the winter, thereby increasing flow and ponding around the well casing and flow out through thawed soil below the wellhouse to nearby seeps.

Thaw settlement and differential heave of the well house has been a noted problem since 1988; the most visible result being approximately 1.5 meters of increased stickup of the well casing. Past mitigation repair attempts included fill repair completed in 1989 and thermosyphons installed in 2002.

ANNULAR VOID AND REPAIR

A deep water-filled annular void was discovered around the wellhead in December 2018. The void extended to a depth of 17.7 meters below grade and at an estimated lateral extent up to 2 meters from the well casing. The bottom of the concrete seal is only 43.6 meters deep, so a 17.7-meter-deep hole around the well seriously compromised the seal around the well casing. Bubbling water observed in the hole around the existing wellhead indicated communication between the artesian aquifer with a pressure of 30 psi (21.3 meters of head) and the surface.

The cause of the thawing permafrost around the well is likely a result of thermal disturbance cause by the warm artesian water flow (at 7°C) through the 6-inch (170 mm) insulated well casing. Radial thawing of the permafrost layer could extend along the entire length of casing.

Conceptually, as the permafrost around the casing thawed, the solids in the ice rich permafrost settled in the annular space, creating a void near the surface and looser soil at depth, potentially to the base of the permafrost. The bubbling noted around the casing, suggests some flow of sub-permafrost groundwater upward along the well casing that would have further exacerbated thawing due to convective heat transfer. Differences in ice content and soil type around the casing would likely have thawed at different rates, resulting in the variable diameter void that was observed and documented by measurement with a downhole caliper and tracking of fill volume with depth.

Repair work was completed during January 2019. The work included backfilling the annular void with 27 pallets of bentonite chips to provide a flexible seal that will be tolerant of minor movements if the permafrost around the well continues to degrade thermally. Air temperatures were routinely -30°C to -40°C during implementation.

POST REPAIR PERFORMANCE

Annual monitoring has shown the repair to be effective at sealing the well and maintaining integrity of the well following the repairs.

Timing of cryopeg formation in Adventdalen, Svalbard

Yishai Weinstein[1], Dotan Rotem[1,2], Andrew Hodson[2] & Hanne Hvidtfeldt Christiansen[3]

[1]*Department of Environment, Planning and Sustainability, Bar-Ilan University, Ramat-Gan, 529002, Israel*

[2]*Arctic Geology Department, The University Centre in Svalbard, UNIS, N-9171 Longyearbyen, Norway*

[3]*Arctic Geophysics Department, The University Centre in Svalbard, UNIS, N-9171 Longyearbyen, Norway*

Cryopegs are layers of unfrozen ground in the permafrost, which may also include lenses of overcooled brines, where freezing is prohibited due to the brines' high salinity.

In this paper we discuss the chemistry and Ra isotope data of saline pore water and ground ice (hereafter, together: pore water) extracted from a partially frozen 20 m core, drilled into the permmafrost in the Adventdalen valley, 5 km upvalley from the local fjord.

Adventdalen is a fjord valley in central Svalbard (78°N), which is located within the continuous permafrost region. The valley-filling sediments are composed mainly of Early Holocene marine and deltaic sediments, overlain by a thin cover of Late Holocene fluviatile and aeolian deposits. Permafrost thickness in the valley is about 100 m (Humlum et al. 2003), which increases upvalley (Gilbert et al. 2018). Permafrost in the marine part developed epigenetically during the Early to Middle Holocene, following elastic rebound and exposure to the atmosphere (Gilbert et al. 2018; Rotem et al. 2023), while the superficial sediments froze syngenetically.

All pore water samples, but the very shallow ones (2-3 m), show high salinity (e.g., Cl^- concentration between 7,600-27,700 mg l^{-1}, Figure 1a), with composition (i.e. major element ratios) close to that of seawater, e.g., Na/Cl and SO_4/Cl ionic ratios of 0.82-0.94 and 0.046-0.065, respectively (Figures 1a-b).

During drilling, there was a seepage of water into the drillhole at ca. 11m. Cl^- concentration of this water was 50,438 mg l^{-1}, 2.7 that of seawater, and major element ratios were similar to those measured in the pore water (Figures 1a-b). This composition is probably the result of freezing and brine rejection. The similarity in composition between the brine and pore fluid, and the fact that the highest salinity was measured in the infiltrating brine, suggests that it is the brine that intruded through the local permafrost and mixed with the original, freshser pore fluid (or ground ice) to a depth of at least 20m. The mechanism and permafrost conditions that would allow this brine intrusion should be further investigated.

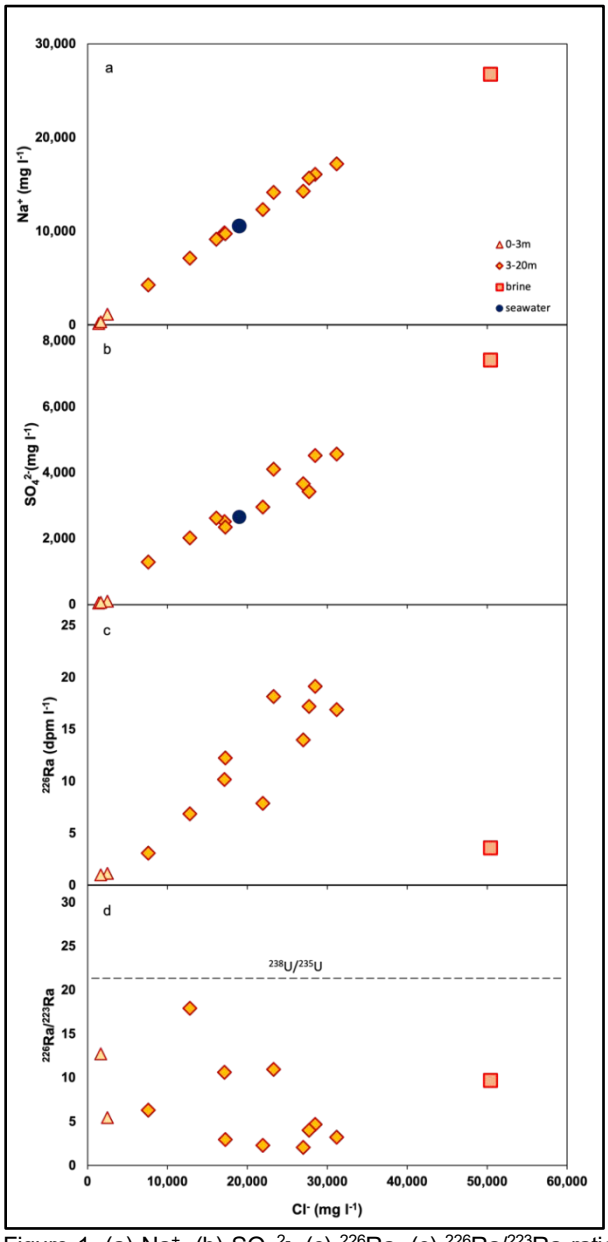

Figure 1. (a) Na^+, (b) SO_4^{2-}, (c) ^{226}Ra, (d) $^{226}Ra/^{223}Ra$ ratios against Cl^- concentrations in ground ice and pore water from the studied Adventdalen site. Also shown are brine composition and seawater composition (in (a) and (b)). In (d), the dashed line is the natural activity ratio of $^{238}U/^{235}U$, which is assumed to be the secular equilibrium ratio of their respective radiogenic daughters $^{226}Ra/^{223}Ra$.

All samples were also measured for their Ra isotope quartet (^{224}Ra, ^{223}Ra, ^{226}Ra and ^{228}Ra) in order to gain insight into the time scales of this intra-permafrost dynamics. All Ra isotope activities (i.e., concentrations, in disintegration per minute per volume) increased with salinity (e.g., Figure 1c), as is commonly observed in groundwater studies (e.g., Gonneea et al. 2008; Kiro et al. 2012). Nevertheless, activities in the seeping brine water were lower than in the high-salainity ground ice/pore water (Figure 1c), which is probably due to the more effetive water-rock interaction (mainly, recoil) in the latter.

The long-lived to short-lived ^{226}Ra/^{223}Ra activity ratios are relatively low (compared with old groundwater, e.g., Weinstein et al. 2021), mostly varying between 2.5-13, and the brine fluid spefically has a ratio of 9.7. While in general, radium activities increase with residence time in the aquifer, this could depend on several water-rock mechanisms, including dissolution, desorption and recoil via the α-decay of the radioactive parent Th isotopes (e.g., ^{230}Th for ^{226}Ra). In the studied samples, in particular the brine fluid, the close to seawater composition precludes major impact of the first two mechanisms (dissolution and desorption), leaving recoil as the main Ra-enriching agent.

Considering the expected secular equilibrium ratios (21.7, which is the natural activity ratio of their radioactive parents ^{238}U/^{235}U, Figure 1d; see Kiro et al. 2015; Weinstein et al. 2021) and the half-life of the long-lived ^{226}Ra of 1600 years, the relatively low ^{226}Ra/^{223}Ra ratio suggests that the residence time of the brine fluid is ≤1500 years, which is much younger than permafrost formation in this area.

This residence time could ultimately mean the time since water introduction (i.e., infiltration) into the subsurface (e.g., Weisntein et al. 2021). Alternatively, an environmental change which will favor a better water-rock interaction or that will allow an interaction with radioactively-enriched sediments could (partly) reset the clock and lower the ^{226}Ra/^{223}Ra ratios in the water. Accordingly, we suggest that the relatively young age of the studied brine is due to its infiltration and interaction with the valley-fill sediments 1000-1500 years ago, post permafrost-formation. The lower ^{226}Ra/^{223}Ra ratios in most of the pore waters, compared with the brine itself, suggest that this was not a unique event, but had been rather a continuous process.

This is supported by the daughter to parent ^{224}Ra/^{228}Ra ratio, which shows steady state values in the brine water (1.65), but is relatively high in sampled pore water (>2), suggesting that pore water reacted with the sediment quite recently (Kiro et al. 2015).

The provenance of this saline water, whether an old deep brine, a relict of the Early Holocene seawater ingression or a Late Holocene seawater intrusion that went through permafrost formation and brine rejection process, should be further studied.

REFERENCES

Gilbert, G.L., O'Neill, H.B., Nemec, W., Thiel, C., Christiansen, H.H., and Buylaert, J.P. 2018. Late Quaternary sedimentation and permafrost development in a Svalbard fjord-valley, Norwegian high Arctic, Sedimentology, 65(7): 2531–2558. https://doi.org/10.1111/sed.12476

Gonneea, M.E., Morris, P.J., Dulaiova, H., and Charette, M.A. 2008. New perspectives on radium behavior within a subterranean estuary, Marine Chemistry, 109(3-4): 250–267. https://doi.org/10.1016/j.marchem.2007.12.002

Humlum, O., Instanes, A., and Sollid, J.L. 2003. Permafrost in Svalbard: A review of research history, climatic background and engineering challenges, Polar Research, 22: 191–215. https://doi.org/10.3402/polar.v22i2.6455, 2003.

Kiro, Y., Yechieli, Y., Voss, C.I., Starinsky, A., and Weinstein, Y. 2012. Modeling radium distribution in coastal aquifers during sea level changes: the Dead Sea case, Geochimica et Cosmochimica Acta, 88: 237–254. https://doi.org/10.1016/j.gca.2012.03.022

Kiro, Y., Weinstein, Y., Starinsky, A., and Yechieli, Y. 2015. Application of radon and radium isotopes to groundwater flow dynamics: an example from the Dead Sea, Chemical Geology, 411: 155–171. https://doi.org/10.1016/j.chemgeo.2015.06.014

Rotem, D., Lyakhovsky, V., Christiansen, H.H., Harlavan, Y., and Weinstein, Y. 2023. Permafrost saline water and Early to Mid-Holocene permafrost aggradation in Svalbard, The Cryosphere, 17(8): 3363-3381. https://doi.org/10.5194/tc-17-3363-2023

Weinstein, Y., Friedheim, O., Odinzov, L., Harlavan, Y., Nuriel, P., Lazar, B., and Burg, A. 2021. Radium isotope dating of saline groundwater and implication to seawater intrusion in shallow and deep aquifers, Journal of Hydrology, 598,126412. https://doi.org/10.1016/j.jhydrol.2021.1264

13B — Observations of Change in the Inuvialuit Settlement Region

Session Chair: Christopher Gruben

Inuvialuit Land Administration, Inuvik, Northwest Territories, Canada

The Inuvialuit Settlement Region (ISR) comprises one of the most climate sensitive permafrost regions in the world, and hosts a high density of road, community and historical oil and gas infrastructure. The region has emerged as a focal area for permafrost and climate change research. The landscape is underlain by ice-rich permafrost and human disturbance or climate-driven thaw that can result in terrain subsidence, slides and slumps. However, shifting permafrost conditions are not happening in isolation from the rest of the environment—they occur alongside changes to ice conditions, fish and wildlife populations, water quality, etc. This session is intended to be an opportunity to learn from two community members, Obie Anikina and Wayne Thrasher, who are experienced land users involved in several monitoring and research programs, about the impacts of climate change on permafrost, the land, infrastructure and communities in the ISR.

13C — Tears of a Rapper: The Science and History Behind the Art of Frozen Debris Lobe Rap Videos

Session Chair: Margaret Darrow

University of Alaska Fairbanks, Fairbanks, Alaska, United States

This special session is in honour of Ronald (Ronnie) Daanen, who died in a helicopter crash on July 20, 2023, on the North Slope of Alaska. Ronnie has been described as a Renaissance Man; he was a husband, father, artist, mechanic, gardener, teacher, scientist...and a rap star. His scientific insights and good-natured humour are embodied in frozen debris lobe (FDL) research and outreach music videos. In this session, his long-time friend and colleague, Margaret Darrow, summarizes over a decade of FDL research including the current collision of FDL-A with the Dalton Highway, all through the lens of five rap/music videos. Please come and celebrate Ronnie's memory by geeking out over these landslides in permafrost.

Cover photo: *Lake in ice-rich terrain in tundra uplands northwest of Inuvik, Northwest Territories. Ice wedge polygons are visible adjacent to the lake (Photo: Rae Landriau).*

12TH INTERNATIONAL CONFERENCE ON PERMAFROST

2024

XII

WHITEHORSE YUKON

INTEGRATING PERSPECTIVES OF PERMAFROST THAW, CHANGE, AND ADAPTATION